ELSEVIER

Talanta 47 (1998) 1

Talanta

Editorial

Aims and scope

The editors are very pleased to announce that Talanta has been experiencing an increase in the number of papers submitted to the journal. This steady increase in submissions will require the journal to become more strict in its editorial policy and to reject papers that do not closely fit the journal's aims and scope. To this effect, authors are encouraged to carefully read the aims and scope of the journal, and to consider the following criteria before submitting a paper to Talanta.

Talanta provides a forum for fundamental studies and original research papers dealing with all branches of pure and applied analytical chemistry.

Classical analytical techniques such as volumetric titrations, UV-visible spectrophotometry (including derivative spectrophotometry), fluorimetry, polarography and related pulsed voltammetric techniques, and so forth, are considered as routine analytical methods, and manuscripts dealing with these methods should be submitted for publication in Talanta only if substantial improvement over existing official or standard procedures is clearly demonstrated. New reagents should demonstrate clear advantages, and their presentation should be comprehensive, rather that generating a series of similar papers.

Solvent extraction methods are well established, and new methods should demonstrate improvements in waste generation, non-hazardous material substitutes, and ease of use (automation).

Application of an original method to real matrices is encouraged, provided that it is properly validated following recommendations of official institutions. The developed method should especially comprise information on selectivity, sensitivity, detection limits, accuracy, reliability and speciation capabilities (e.g. in the case of trace metal analysis). Proper statistical treatment of the data should be provided.

Application of classical analytical approaches such as polarography, voltammetry (pulsed), UV-visible spectrophotometry (and derivative), and fluorimetry to relatively simple matrices having no major interference, such as drug formulations or reconstituted samples, are discouraged unless considerable improvements over other methods in the literature (time saving, accuracy, precision, cleaner chemistry, automation) are highlighted.

Papers dealing with analytical data such as stability constants, pK_a values, etc. should be published in more specific journals, unless novel analytical methodology is demonstrated, or important analytical data are provided which could be useful in the development of analytical procedures.

Gary D. Christian
Jean-Michel Kauffmann
Editors-in-Chief
April, 1998.

0039-9140/98/$19.00 © 1998 Elsevier Science B.V. All rights reserved.
PII S0039-9140(98)00239-2

ELSEVIER

Talanta 47 (1998) 3–10

Talanta

Packed column supercritical fluid chromatographic separation and estimation of acetaminophen, diclofenac sodium and methocarbamol in pharmaceutical dosage forms

Suvarna T. Patil, M. Sundaresan *, Indravadan C. Bhoir, A.M. Bhagwat

Shri. C. B. Patel Research Centre For Chemistry and Biological Sciences, 2nd Floor, Mithibai College Building, Vile Parle (West), Mumbai 400 056, India

Received 25 August 1997; received in revised form 22 December 1997; accepted 2 January 1998

Abstract

A reproducible and fast method has been developed for the assay of acetaminophen, methocarbamol, and diclofenac sodium in bulk and drug forms using packed column supercritical fluid chromatography employing internal standard method. The analytes were resolved by elution with supercritical fluid carbon dioxide doped with 11.1% (v/v) methanol on a Shendon-Phenyl (250 × 4.6 mm) 5 μm column with detection monitored spectrophotometrically at 225 nm. The densities and polarities of the mobile phase were optimised from the effects of pressure, temperature and modifier concentration on chromatograhic figures like retention time (t_R, min), retention factor (k') etc. Modifier concentration proved to be the most effective means for changing both retention and selectivity. Calibration data and recovery of the drug from spiked concentrations were determined to assess the viability of the method. The supercritical fluid chromatography (SFC) method was directly compared to an HPLC assay, developed in the laboratory, of the same analytes. With respect to speed and use of organic solvents SFC was found to be superior, while in all other aspects the results were similar to HPLC. The method has been successfully used for the assay of two formulations containing a combination of (A) acetaminophen and methocarbamol and (B) acetaminophen and diclofenac sodium. There was no interference from excipients. The present work validates the recent proposition that supercritical fluid chromatography using CO_2 and modifiers is a viable, faster alternative to reverse phase HPLC. © 1998 Elsevier Science B.V. All rights reserved.

Keywords: Packed column supercritical fluid chromatography; Acetaminophen; Methocarbamol; Diclofenac sodium; Dosage form; Separation and estimation

1. Introduction

The combination of acetaminophen and methocarbamol is used as an analgesic and muscle relaxant drug and the combination of acetaminophen and diclofenac sodium is used as

* Corresponding author. Tel.: +91 22 6119792; fax: +91 22 6133400.

0039-9140/98/$19.00 © 1998 Elsevier Science B.V. All rights reserved.
PII S0039-9140(98)00045-9

analgesic and anti-inflammatory drug [1]. Various methods [2–7] including HPLC are known for the simultaneous analysis of these drugs in combined dosage forms. Packed column supercritical fluid chromatography (PCSFC) using carbon dioxide with modifiers has recently gained importance in the analysis of drugs and pharmaceuticals. This is evidenced by the large number of papers which have appeared in the last 2 years in which many analyses have been reported not only on bulk drugs but also on pharmaceutical dosage forms [8–12]. Bhoir et al. [13] confirmed the usefulness of packed column SFC for the separation and quantification of metronidazole, tinidazole and diloxanide furoate from dosage form. SFC has the advantage of dramatically changing chromatographic behavior of an analyte by varying temperature, pressure and modifier concentration. The modifier can be a single solvent or binary mixture [14,15]. The present paper attempts at an isocratic separation of acetaminophen, methocarbamol and diclofenac sodium using supercritical fluid carbon dioxide doped with methanol and a simultaneous quantification of the drugs from solid dosage form using internal standard method with exhaustive evaluation of chromatographic figures of merit.

2. Experimental

The apparatus used was a JASCO supercritical fluid chromatograph 900-series configured, for dynamic mixing with a 2-pump system of JASCO-PU 980. The instrument incorporates an on-line organic modifier addition facility to the supercritical fluid mobile phase. The rate of flow of CO_2 and the modifier could be changed from 0.01 to 10.0 ml min^{-1}. The apparatus was capable of giving pressures in the range of 7.2–44.9 MPa and temperatures in the range of 35–80°C. Further the use of a variable restrictor allows for a constant flow rate of the fluid, thus producing stability in system pressure. These system improvements have made SFC more reproducible, accurate and precise. The temperature of the column could be kept at any desired point between 35–80°C using JASCO-CO-965 oven. A Rheodyne injector, model-7125 with a 20 μl external loop was used to introduce the sample into the column. The analytes were separated on a Shendon-Phenyl (250 × 4.6 mm) 5 μm column. The detection was done using UV-Vis detector. Borwin chromatographic software was used for data integration.

2.1. Materials and reagents

Carbon dioxide used was 99.9% pure, obtained from Bombay Carbon Dioxide, Mumbai. Methanol was of E. Merck, HPLC grade. The drug samples of acetaminophen, methocarbamol and diclofenac sodium were received in solid state from reputed UK firms with certified copies of analysis. Separate stock solutions of the individual drugs were prepared by dissolving 100 mg of the analyte in 100 ml of methanol. Mixtures of the drug solutions were prepared by pipetting out appropriate quantities of the individual stock solutions and then mixing them. The final stock solution was containing 10 μg ml^{-1} of acetaminophen, 36 μg ml^{-1} of methocarbamol and 14 μg ml^{-1} of diclofenac sodium.

2.2. Supercritical fluid chromatography of acetaminophen, methocarbamol and diclofenac sodium

Since the elution of acetaminophen, methocarbamol and diclofenac sodium did not occur with neat supercritical fluid CO_2 (7.2–44.9 MPa and 35–80°C) the use of a modifier was warranted for. Methanol was chosen as the modifier as all the three solutes were soluble in this solvent.

In the SFC method development starts with the selection of three parameters, viz., temperature, pressure and modifier concentration. After obtaining an approximate base line resolution and separation of the three compounds, the method development proceeds to optimization. Subcritical parameters like 9.9 MPa and 45°C were utilized for preliminary investigations.

3. Results and discussions

Fig. 1 depicts the effect of wavelength on the peak responses (peak heights) of acetaminophen, methocarbamol, and diclofenac sodium. For this study 20 μl of the individual drug solutions containing 10 μg ml^{-1} of acetaminophen, 36 μg ml^{-1} of methocarbamol, and 14 μg ml^{-1} of diclofenac sodium were injected at an arbitrary pressure of 9.9 MPa, 45°C temperature and with modifier concentration of 13.0% methanol in carbon dioxide at 2.0 ml min^{-1}. The range of wavelength studied was from 210–290 nm. It can be seen from Fig. 1 that an optimised compromise wavelength can be chosen as 225 nm for the simultaneous estimation of all the three drugs.

Chromatographic figures like retention time (t_R, min), resolution (R), retention factor (k'), selectivity (a), asymmetry factor (T) and the number of plates (N) of the three solutes were determined at a minimum of seven points in the range specified of the following parameters: (1) modifier concentration (4.8–16.7%, v/v) (2) temperature (35–70°C) (3) pressure (7.8–24.5 MPa) (4) flow rate of CO_2 (1.00–3.00 ml min^{-1}) with modifier concentration constant at 0.25 ml min^{-1}. Only one parameter was changed while others were kept constant in each of these studies. Modifier concentration causes effective changes in retention and selectivity. Fig. 2 gives the relation between modifier concentration and retention factor at 45°C and 9.9 MPa. As can be seen from Fig. 2, retention factors decrease with the modifier concentrations and nearly merged above 14% concentration. In order to strike a balance between retention time, retention factor and resolution, a modifier concentration of 11.1% was chosen for this study.

A perusal of the collected data showed that retention and retention factor are only modestly affected by temperature. Hence 45°C was chosen for further study. An examination of the results on effect of pressure showed that the retention factor decreases with increase in pressure but there was no effective change in selectivity. Fig. 3 reveals the relation between pressure and retention factor. The best compromise for resolution, selectivity and asymmetry is obtained at 14.7 MPa. The changes in flow rate of CO_2 showed that selectivity and resolution were highest at 3.00 ml min^{-1}. Comparable selectivity and better asymmetry (>1.0) is obtained at a flow rate of 2.0 ml min^{-1} of CO_2.

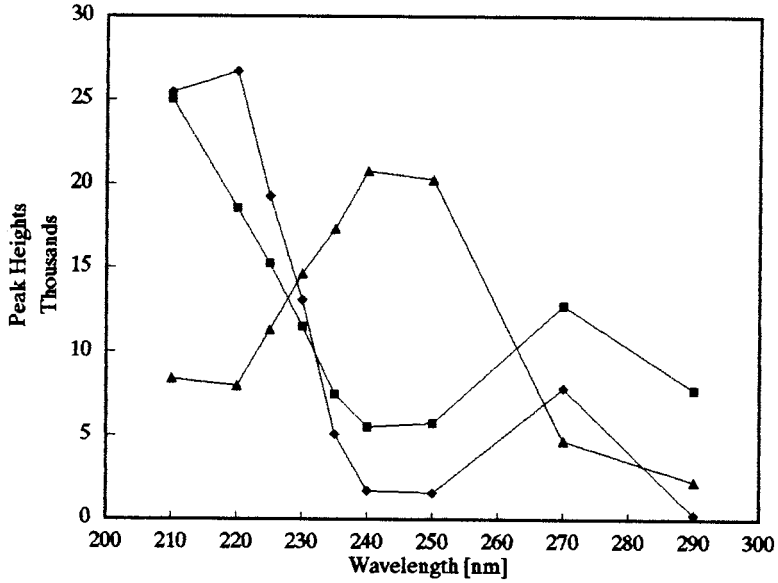

Fig. 1. Wavelength study. 13.0% of methanol in carbon dioxide; 45°C, 9.9 MPa and 20 μl injected. The wavelength range was 210–290 nm. The order was as follows: ▲—acetaminophen, ◆—methocarbamol, ■—diclofenac sodium.

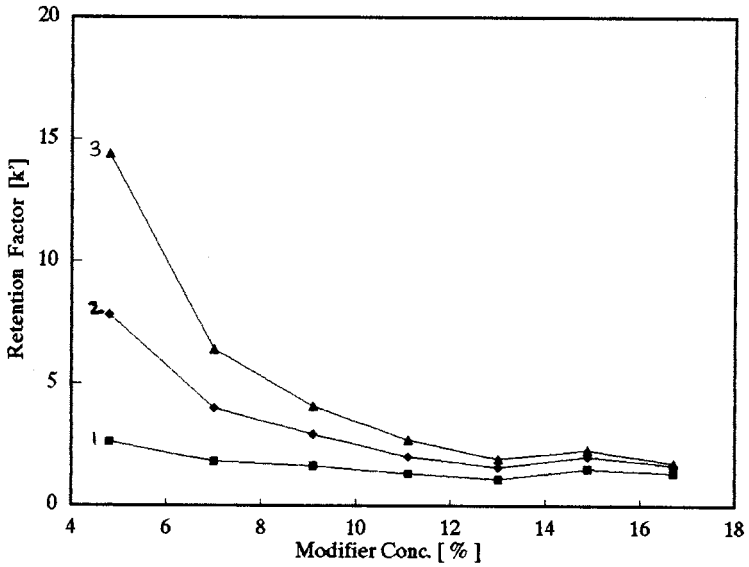

Fig. 2. Effect of modifier concentration on retention factor. 4.8–16.7% of methanol in carbon dioxide (2 ml min^{-1}); 45°C; 9.9 MPa; and 20 μl injected. Detection was by UV analysis at 225 nm. The retention order was as follows: (1) diclofenac sodium (2) methocarbamol (3) acetaminophen.

3.1. Optimisation of parameters

Thus a selection for the best chromatographic conditions among these data leads to a value of 14.7 MPa for pressure, 45°C for temperature, 11.1% (v/v) for modifier concentration and 2.0 ml min^{-1} for flow rate of CO_2. A typical chromatogram containing 10 μg ml^{-1} of acetaminophen, 36 μg ml^{-1} of methocarbamol and 14 μg ml^{-1} of diclofenac sodium, obtained under these conditions is shown in Fig. 4 together with retention times.

3.2. HPLC method for the three drugs

An HPLC method was developed in the laboratory for the separation of acetaminophen, methocarbamol and diclofenac sodium from mixtures. The apparatus used was a JASCO-900 series HPLC chromatograph, with a Shendon-ODS (250 × 4.6 mm) 5 μm column. The mobile phase was methanol: water in the proportion of 80:20 with 0.1% (v/v) of acetic acid in the mixture. The flow rate was 1 ml min^{-1}. The detection was by spectrophotometry at 254 nm. The wavelength of 225 nm used for SFC could not be used here due to spectral interference from acetic acid in the mobile phase.

The comparative chromatographic figures of merit for the chromatograms of the three drugs by SFC and HPLC are listed in Table 1. From this table it is discernible that packed column SFC exhibits, superior or at least good, chromatographic figures of merit as HPLC in the separation and assay of arbitrary group of drugs.

3.3. Linearity study

For linearity studies six different concentrations of acetaminophen(I) and methocarbamol(II) in the range of 0.30–20.00 μg ml^{-1} with diclofenac sodium(III) as the internal standard (5.00 μg ml^{-1}) were assayed ($n = 5$). For linearity of acetaminophen (0.30–20.00 μg ml^{-1}) and diclofenac sodium (0.20–10.00 μg ml^{-1}), methocarbamol (6.00 μg ml^{-1}) was chosen as the internal standard. The detector response (peak height ratios of drug/i.s.) was found to be rectilinear over the concentration ranges studied. The data was analyzed by the linear regression (least

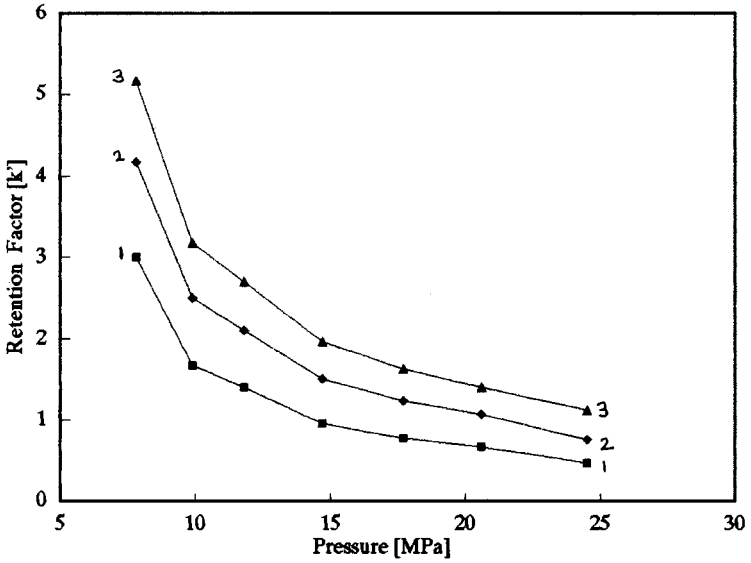

Fig. 3. Effect of pressure on retention factor. 0.25 ml min^{-1} of 11.1% methanol in carbon dioxide; 45°C, 7.9–24.5 MPa pressure and 20 μl injected. Detection was by UV analysis at 225 nm. The retention order was same as in Fig. 2.

squares fit) method and the statistical data are presented in Table 2. The minimum quantifiable concentration listed in Table 2 is a compromise due to selection of one wavelength for all the compounds. It could be improved by a more selective choice of UV-wavelength if only one of the drugs is to be determined Fig. 1.

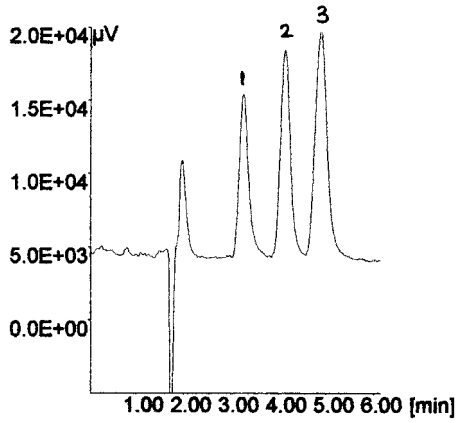

Fig. 4. Typical SFC separation of drugs eluted from a Shendon-Phenyl (250 × 4.6 mm) 5 μm column under steady state conditions. The conditions were as follows: 0.25 ml min^{-1} of 11.1% modifier (methanol) in CO_2, at 45°C and 14.7 MPa outlet pressure. Numbered solutes are indicated in the arbitrary mix and the number indicates retention order. (1) Diclofenac sodium ~ 3.26 min (2) methocarbamol ~ 4.13 min (3) acetaminophen ~ 4.88 min.

3.4. Estimation of the drugs from pharmaceutical dosage forms

Formulation-A: acetaminophen (325 mg) + methocarbamol (400 mg).

Formulation-B: acetaminophen (325 mg) + diclofenac sodium (50 mg).

Twenty tablets of formulation-A were crushed to get fine powdered material [16]. A portion of it which was equivalent to 325 mg of acetaminophen and 400 mg of methocarbamol was weighed accurately and dissolved in 100 ml of methanol. From this solution 0.50 ml of supernatant was mixed with 0.50 mg of the i.s. and was further diluted to get a solution having concentration: 16.25 μg ml^{-1} of acetaminophen, 20.00 μg ml^{-1} of methocarbamol and 5.00 μg ml^{-1} of the i.s. Twenty microliters of this solution was injected in to the chromatograph under the conditions specified. The analyte peaks were identified by comparison with observed retention times with those of respective standards. The peak height ratios (drug/i.s.) obtained were related to slopes

Table 1
Chromatographic figures of merit for the drugs by SFC ($n = 7$) and HPLC ($n = 7$)

Drug	I	RSD (%)		II	RSD (%)		III	RSD (%)
SFC								
Retention time (t_R min)	3.26	0.25		4.13	0.18		4.88	0.39
Resolution (R)	—	—	$R_1 =$	1.67	0.84	$R_2 =$	1.28	1.10
Asymmetry (T)	1.01	0.81		1.00	0.79		1.03	0.82
Retention factor (k')	1.00	0.82		1.50	1.09		1.93	1.11
Selectivity factor (α)	—	—	$\alpha_1 =$	1.50	0.86	$\alpha_2 =$	1.29	1.34
No. of plates (N)	6404	1.31		8432	1.11		8006	1.04
HPLC								
Retention time (t_R min)	2.10	0.29		2.55	0.23		7.25	0.42
Resolution (R)	—	—	$R_1 =$	1.00	0.78	$R_2 =$	10.42	1.08
Asymmetry (T)	1.00	0.64		1.00	0.75		1.02	0.89
Retention factor (k')	1.75	0.91		2.25	1.01		8.50	0.93
Selectivity factor (α)	—	—	$\alpha_1 =$	1.29	0.91	$\alpha_2 =$	3.78	1.41
No. of plates (N)	6628	1.17		8276	1.24		9264	1.32

I, diclofenac sodium; II, methocarbamol; III, acetaminophen.
R_1: resolution between I and II, R_2: resolution between II and III.
α_1: selectivity between I and II, α_2: selectivity between II and III.

and intercepts from calibration data to calculate concentration of both drugs. Formulation-B was treated in a similar way. The final dilution for formulation-B was containing 16.25 μg ml^{-1} of acetaminophen, 2.50 μg ml^{-1} of diclofenac sodium, and 6.00 μg ml^{-1} of the i.s. From a series of eight experiments the mean contents of the tablet were found to be 324.55 ± 0.95 and 399.69 ± 0.93 mg of acetaminophen and methocarbamol, respectively, as against 325 and 400 mg stated for formulation-A. For formulation-B the mean contents of the tablet were found to be 324.60 ± 0.65 and 49.56 ± 0.67 mg of acetaminophen and diclofenac sodium, respectively, as against 325 and 50 mg stated amount. Commonly used excipients like starch, microcrystalline cellulose, talc, lactose, HPMC, etc. do not interfere in the method. Analytical recoveries of the drugs were carried out from a series of spiked concentrations to the pre-analyzed dosage forms.

Table 2
Linear regression (least squares fit) calibration data of acetaminophen (I), methocarbamol (II), and acetaminophen (III), diclofenac sodium (IV) by SFC

	I	II	III	IV
Conc. range (μg ml^{-1})	0.30–20.00	0.30–20.00	0.30–20.00	0.20–10.00
Slope (m)	0.2952	0.0726	0.5339	0.4930
Intercept (b)	0.0150	0.0050	−0.0806	0.0030
SD of slope (S_m)	0.0083	0.0003	0.0068	0.0044
SD of intercept (S_b)	0.0660	0.0024	0.0592	0.0192
Correlation coefficient (r)	0.9999	0.9999	0.9997	0.9998
Standard error (S_{yx})	0.1338	0.0500	0.1191	0.0383
LOD (μg ml^{-1})	0.10	0.20	0.10	0.10

Mean values from $n = 5$.
LOD: limit of detection.
I and II, values of acetaminophen and methocarbamol with diclofenac sodium as the internal standard (5.0 μg ml^{-1}).
III and IV, values of acetaminophen and diclofenac sodium with methocarbamol as the internal standard (6.0 μg ml^{-1}).

Table 3
Analytical recoveries of acetaminophen, methocarbamol, and diclofenac sodium by SFC

Acetaminophen				Methocarbamol				Diclofenac sodium			
Amount added (mg)	Amount found (mg)[a]	Recovery (%)	RSD (%)	Amount added (mg)	Amount found (mg)[a]	Recovery (%)	RSD (%)	Amount added (mg)	Amount found (mg[a])	Recovery (%)	RSD (%)
5.00	4.98	99.67	2.36	5.00	4.97	99.40	2.43	2.00	1.99	99.50	2.69
10.00	10.02	100.16	1.87	10.00	9.89	99.81	1.47	5.00	4.96	99.20	1.87
15.00	15.04	100.25	1.17	15.00	15.03	100.20	0.98	10.00	9.96	99.64	1.23

[a] Each value is mean of five determinations ($n = 5$).

the data listed in Table 3 revealed that the mean recovery was found to be more than 99% for all the three drugs.

4. Conclusions

The HPLC method using 80% methanol has a run time of 8.0 min and generates 8 ml of total effluent (6.4 ml of methanol + 1.6 ml of water) while SFC requires only 6 min and generates 13.5 ml of a mixture of 12.0 ml of CO_2 and 1.5 ml of methanol. Of this 12.0 ml of CO_2 will be spontaneously evaporated to the atmosphere. As CO_2 is eco-friendly SFC will generate only 1.5 ml of effluent. Not only that in the case of HPLC 8 ml of the mixture will have to be freed from moisture before incineration of the organic solvent waste.

The work has shown that packed column supercritical fluid chromatography is ideally suited for the separation and quantitative estimation of the above mentioned drugs in bulk as well as dosage forms. In the present method compromise has been struck between modest speed and modest efficiency for SFC. Apart from merits in separation, this technique offers a viable alternative to HPLC as it is faster and cheaper. In packed column SFC the necessity of preparation of mobile phase is obviated as selectivity can be easily and widely tuned by the proper choice of temperature, pressure and modifier concentration. The technique can be equally useful as HPLC for the analysis of bulk drugs and pharmaceutical dosage forms

Acknowledgements

The authors thank Shri. Kelkar C.P., Director (Admn.), Dr R. Kalyanraman, Professor Emeritus, C. B. Patel Research Centre, Mumbai-56, and co-workers Yagnesh Patel, Viddesh Bari and Mrs Deepali Nadkarni for encouragement in carrying out this work.

References

[1] J.E.F. Reynolds (Ed.), Martindale—The Extra Pharmacopeia, Pharmaceutical Press, London, 1988.
[2] L.A. Carreira, M. Rizk, Y. El. Shabrawy, N.A. Zakhari, S.S. Toubar, J. Pharm. Biomed. Anal. 13 (11) (1995) 1331.
[3] H.L. Rao, A.R. Arora, P.G. Rao, Indian Drugs 28 (6) (1991) 285.
[4] J.L. Chawla, R.A. Sodhi, R.T. Sane, Indian Drugs 33 (4) (1996) 171.
[5] M.S. Bhatia, S.G. Kashedikar, S.C. Chaturvedi, Indian Drugs 33 (5) (1996) 213.
[6] R.T. Sane, R.S. Samant, V.G. Nayak, Indian Drugs 24 (4) (1987) 196.
[7] G. Ramana Rao, A.B. Avadhanulu, D.K. Vatsa, Pontulu, Indian Drugs, 27 (11) (1990) 576.
[8] O. Gyllenhaal, J. Vessman, J. Chromatogr. 628 (1993) 275.
[9] P. Petersson, N. Lundell, K.E. Markides, J. Chromatogr. 623 (1992) 129.
[10] X.J. Lu, M.R. Myers, W.E. Artz, J. Am. Oil Chem. Soc. 70 (1993) 355.
[11] T.J. Jenkins, M. Kaplan, M.R. Simmonds, G. Davidson, M.A. Healy, M. Poliakoff, Analyst 116 (1991) 1305.
[12] Y.P. Patel, M. Sundaresan, U.J. Dhorda, Indian J. Pharm. Sci. 59 (1997) 3.
[13] I.C. Bhoir, M. Sundaresan, A.M. Bhagwat, Bhanu Raman, Anal. Chim. Acta. 354 (1-3) (1997) 123.
[14] T.A. Berger, W.H. Wilson, J. Pharm. Sci. 83 (1994) 281.
[15] C.J. Bailey, R.J. Ruane, I.D. Wilson, J. Chromatogr. 32 (1994) 426.
[16] The United States Pharmacopeia—XXII, Rockville, MD, 2085, 1990.

ELSEVIER

Talanta 47 (1998) 11–18

Talanta

Spectrophotometric flow injection determination of L-ascorbic acid with a packed reactor containing ferric hydroxide

Airton Vicente Pereira, Orlando Fatibello-Filho *

Departamento de Química, Grupo de Química Analítica, Centro de Ciências Exatas e de Tecnologia, Universidade Federal de São Carlos, Caixa Postal 676, CEP 13.560-970, São Carlos, SP, Brazil

Received 6 October 1997; received in revised form 5 January 1998; accepted 6 January 1998

Abstract

A flow injection system with spectrophotometric detection is proposed for determining L-ascorbic acid in pharmaceutical formulations. In this system a column containing $Fe(OH)_3$ immobilized in polyester resin (packed reactor) is inserted before the detector. Fe(III)-1,10-phenanthroline complex is reduced by L–ascorbic acid to produce Fe(II)-1,10-phenanthroline complex which is monitored at 510 nm. Under the optimum analytical conditions, the linearity of the calibration equation for L-ascorbic acid ranged from 5.0×10^{-6} to 6.0×10^{-5} M of added amount. The detection limit was 5.0×10^{-7} M and recoveries between 98.5–102.0% were obtained. No interference was observed from the common excipients of pharmaceutical formulations and other active substances such as acetylsalicylic acid, caffeine and thiamine. © 1998 Elsevier Science B.V. All rights reserved.

Keywords: L-Ascorbic acid; Flow injection spectrophotometry; Pharmaceutical formulations; Ferric hydroxide; Packed reactor

1. Introduction

L-ascorbic acid (one of the most important water-soluble vitamin) is the active agent against scurvy [1] and used for pharmaceutical purposes, as food additives and antioxidants. Numerous analytical methods for the determination of the L-ascorbic acid are based on its redox properties. Most of these methods have been employed 2,6-dichlorophenolindophenol [2,3] or other oxidizing agents such as iodine [3], ceric sulphate [4] and *N*-bromosuccinimide [5]. Titration with 2,6-dichlorophenolindophenol [2] has been found to be the most satisfactory procedure, but this procedure is inaccurate for colored samples due to difficult end-point visualization.

To determine L-ascorbic acid in juices, foods, biological samples and pharmaceutical formulations several flow injection methods have been proposed, most then were based on UV-visible spectrophometry [6–10], amperometry [11–14],

* Corresponding author. Tel.: +55 16 2748208; fax: +55 16 2748530; e-mail: doff@power.ufscar.br

0039-9140/98/$19.00 © 1998 Elsevier Science B.V. All rights reserved.
PII S0039-9140(98)00047-2

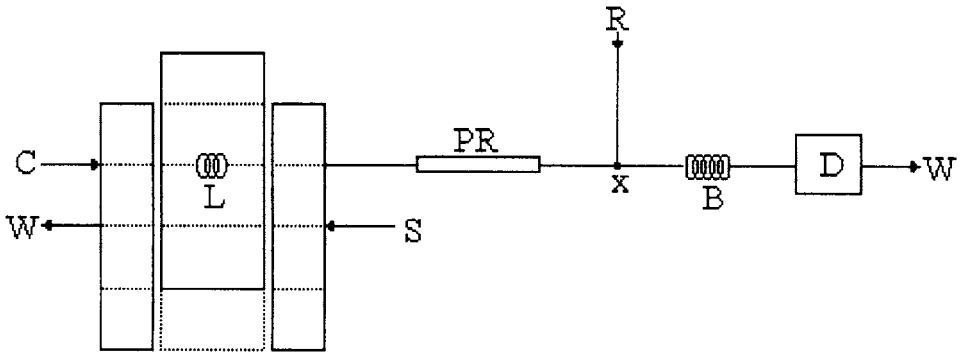

Fig. 1. Flow diagram of the system used for spectrophotometric determination of ascorbic acid. The three rectangular pieces represent a scheme of the sliding bar injector. S, sample or standard solutions; L, sample loop (75 cm long, 0.8 mm i.d.; 375 μl); C, carrier solution, 0.025 M sulfuric acid, flowing at 2.0 ml min^{-1}; R, 0.25% m v^{-1} 1,10-phenanthroline solution, flowing at 0.9 ml min^{-1}; PR, packed reactor containing $Fe(OH)_3$ (20 cm × 1.5 mm i.d.); D, spectrophotometer at 510 nm; B, reaction coil (150 cm long, 0.8 mm × i.d.); x, confluence point; W, waste.

chemiluminescence [15–17], coulometry [18], spectrofluorimetry [19] and voltammetry [20].

The use of reaction catalyzed by Cu(II) or Fe(III) ions for determining L- ascorbic acid have been widely accepted and analytical procedures [21–23] have exploited the fact of L-ascorbic acid to be easily oxidized to dehydroascorbic acid by these ions. An FIA system with spectrophotometric detection was also reported [8] for the determination of L-ascorbic acid. This procedure has been based on the reduction of Fe(III) ion to Fe(II) by L-ascorbic acid. Iron(II) produced in this reaction reacted with 1,10-phenanthroline, forming a colored complex which was detected spectrophotometrically.

The combination of flow injection and packed reactors has proved to be useful in several pharmaceutical analysis [24–26]. In a previous work [26], we have reported a flow injection system with an packed reactor containing copper(II) phosphate, wherein L-ascorbic acid reduced Cu(II) to Cu(I) which has been detected spectrophotometrically using bathocuproine as colorimetric reagent. This paper reports on the application of an FI method for a spectrophotometric determination of L-ascorbic acid in pharmaceutical samples using a packed reactor incorporated in a system containing $Fe(OH)_3$ immobilized in polyester resin. The method is based on the oxidation of L-ascorbic acid with Fe(III) in the presence of 1,10-phenanthroline. The Fe(II) formed was quantitatively and rapidly converted to the stable Fe(II)-phenanthroline complex (ferroin) which was measured spectrophotometrically at 510 nm.

2. Experimental

2.1. Apparatus

A schematic diagram of the flow injection system is shown in Fig. 1. A Femto model 435 spectrophotometer (São Paulo, Brazil) equipped with a glass flow-cell (optical path 1.0 cm) was used to monitor the absorbance of the Fe(II)-phenanthroline complex at 510 nm. Peaks were recorded using a Cole Parmer (Chicago, IL) model 1202-0000 two-channel strip-chart recorder. Solutions were pumped with an twelve-channel Ismatec (Zurich, Switzerland) model 7618-50 peristaltic pump supplied with tygon tubes. A laboratory-constructed three-piece manual injector-commutator made of perspex, with two fixed side bars and a sliding central bar was used to introduce samples into the flowing stream. The manifold and reaction coil tubing was constructed with polyethylene tubes (0.8 mm i.d.).

2.2. Reagents and solutions

All reagents were of analytical grade and all solutions were prepared with water from a Millipore (Bedford, MA) Milli-Q system model UV plus ultra-low organics water.

A 0.025 M sulfuric acid was used as carrier. A 5.0×10^{-3} M L-ascorbic acid stock solution was prepared daily by dissolving L-ascorbic acid (Merck) in 100 ml of 0.01 M sulfuric acid previously de-oxygenated with nitrogen.

Reference solutions containing from 5.0×10^{-6} to 6.0×10^{-5} M of L-ascorbic acid were prepared daily by serial dilutions of appropriate volumes of the standard stock solution with 0.01 M sulfuric acid solution.

A 0.25% m v^{-1} 1,10-phenanthroline solution was prepared by adding 1.250 g of this reagent (Synth) to ~400 ml of deionized water heated to 70°C to aid in dissolving the reagent and after cooling was diluted to 500 ml with water.

A commercial polyester resin solution (Resapol T-208, Resana, SP, Brazil) was used for immobilize the $Fe(OH)_3$ and methyl ethyl ketone (Ibere, Ramires and Cia, Taboão da Serra, SP, Brazil) was used as catalyst.

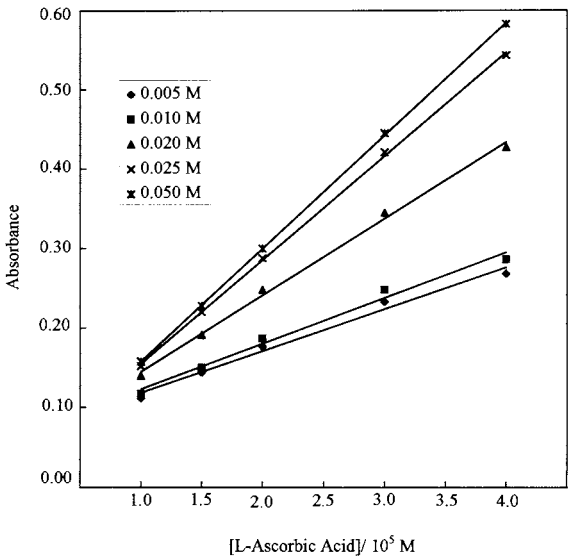

Fig. 2. Effect of the sulfuric acid concentration of carrier (2.0 ml min^{-1}) on absorbance signal. Sample loop 100 cm, 0.25% m v^{-1} 1,10 phenanthroline (1.0 ml min^{-1}, reaction coil of 150 cm and column length of 15 cm × 1.5 mm i.d.

2.3. Methods

2.3.1. Analysis of pharmaceutical samples

The contents of not less than five effervescent tablets were weighed and finely powdered. An accurately weighed portion of powder or accurate volume of oral solutions were transferred into a 100 ml calibrated flask, dissolved and diluted to volume with 0.01 M sulfuric acid. When necessary, these solutions were filtered through a filter paper. Further dilutions were made to obtain an appropriate concentration of L-ascorbic acid that lies in the linear range of the calibration graph. For the flow injection procedure, a 375 μl volume was introduced into the carrier stream via manual injector-commutator. For comparison of results obtained the iodimetric method [3] of the United States Pharmacopoeia was used.

2.3.2. Preparation and immobilization of $Fe(OH)_3$

An amount of 20 g of ferric chloride (Synth) was treated with an excess of ammonium hydroxide (Merck) with continuous manual stirring. The red-brown precipitate of ferric hydroxide formed was filtered and washed several times with distilled water. The resulting material, $Fe(OH)_3$, was dried at 110°C for 4 h, similar to the immobilization procedure used by Rivas and Martínez-Calatayud [27], 10 g of polyester resin solution were transferred to a flask made of silicone rubber and mixed with 10 g of $Fe(OH)_3$. After manual homogenization, 0.5 ml of the catalyst (methyl ethyl ketone) was added and stirred until an increase of viscosity. After 8 h, the resulting rigid solid material was broken with a hammer and a domestic liquefier was used to obtain particles of smaller size. The particle size was selected by passing the particles through known mesh sieves.

About 0.300 g of $Fe(OH)_3$-polyester beads (100–350 μm) were aspired with a help of a syringe into a 20 cm × 1.5 mm i.d. glass tube with one end plugged with glass-wool to prevent the packing material escaping from the column. The column was inserted in the flow manifold between

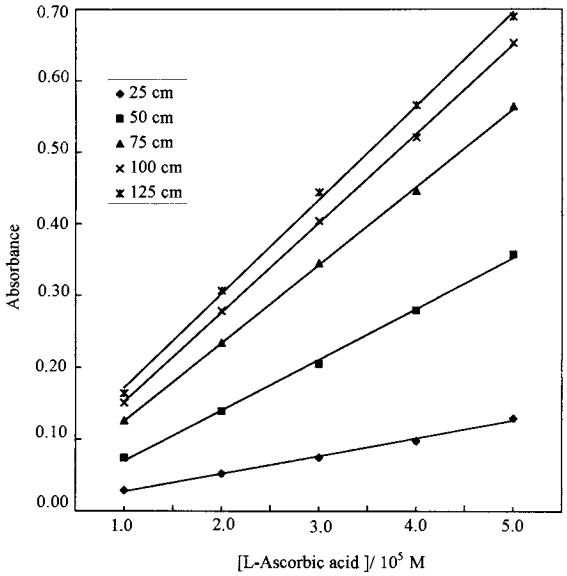

Fig. 3. Effect of the sample volume on the absorbance signal for $1.0–5.0 \times 10^{-5}$ M ascorbic acid with reaction coil of 150 cm and flow rates of carrier and reagent streams of 2.0 and 0.9 ml min^{-1}, respectively.

the injector and the detector. The column was always equilibrated with 0.025 M sulfuric acid before use by pumping this solution through the column for 15 min and was stored in distilled water when not in use.

2.3.3. Flow injection procedure

A flow diagram of the system used for ascorbic acid determination is shown in Fig. 1. The ascorbic acid solution was introduced into the carrier stream with the aid of an injector-commutator. An injection volume of 375 μl was used throughout except in the optimization experiments. The flow rate of the 0.025 M sulfuric acid carrier stream was 2.0 ml min^{-1} and that of the reagent (0.25% m v^{-1} 1,10-phenanthroline solution) stream was 0.9 ml min^{-1} introduced at confluence point x. The sample containing 5.0×10^{-6} to 6.0×10^{-5} M of L-ascorbic acid in 0.01 M sulfuric acid is inserted in the carrier stream and after to pass through the column is mixed at point x with the reagent solution. The Fe(II)-phenanthroline complex formed in the reaction coil B (length 150 cm) is measured spectrophotometrically at 510 nm.

3. Results and discussion

The proposed flow injection system is based on the ability of L-ascorbic acid to reduce Fe(III) to Fe(II), which is rapidly converted to a highly stable and colored Fe(II)-phenanthroline complex.

3.1. Optimization of chemical variables

To optimize the system, various experimental parameters were investigated. The sensitivity of the system depends strongly on the acidity of the carrier stream. In this work, water, 0.01 M hydrochloric acid, 0.01 M sulfuric acid and 0.5 M acetic acid were tested as carrier by injecting 3.0×10^{-5} M L-ascorbic acid solution into the carrier stream. The best results were obtained when 0.01 M sulfuric acid was used as carrier. Thus, 0.01–0.05 M sulfuric acid solutions were successively tested as carrier. The absorbance increased with increasing sulfuric acid concentration as shown in Fig. 2. A sulfuric acid solution of 0.025 M was chosen due its good sensitivity and longer lifetime of the packed reactor containing immobilized $Fe(OH)_3$.

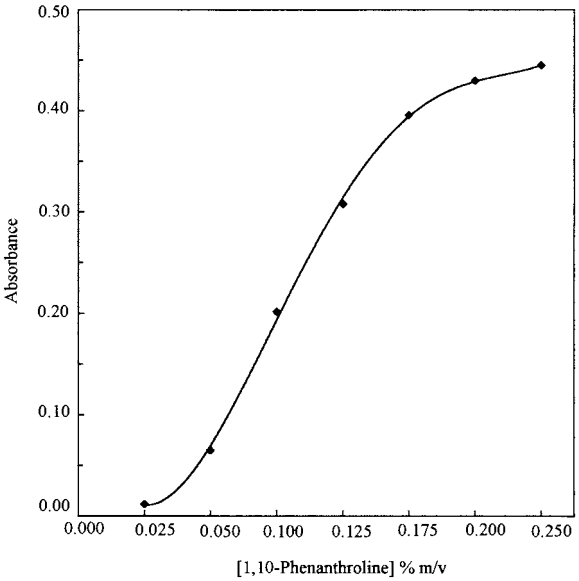

Fig. 4. Effect of the 1,10-phenanthroline concentration on the absorbance signal for 375 μl of 3.0×10^{-5} M L-ascorbic acid, reaction coil of 150 cm and flow rates as indicated in Fig. 3.

Table 1
Results of the recovery tests using pharmaceutical preparations spiked with three different standard concentrations of L-ascorbic acid

Sample	L-Ascorbic acid (μg ml^{-1})[a]		Recovery (%)
	Added	Found	
Redoxon	1.76	1.76	100.0
	3.52	3.57	101.4
	5.28	5.26	99.6
Cebion	1.76	1.74	98.9
	3.52	3.59	102.0
	5.28	5.30	100.4
Cewin	1.76	1.77	100.6
	3.52	3.56	101.1
	5.28	5.20	98.5
Energil C	1.76	1.74	98.8
	3.52	3.50	99.4
	5.28	5.28	100.0

[a] $n = 5$.

The influence of the acidity of the 0.25% m v^{-1} 1,10 phenanthroline solution was also investigated in the sulfuric acid concentration range 0.001–0.01 M. It was observed that with an increase in the sulfuric acid concentration the absorbance decreased. This leads to the conclusion that higher acidity of the carrier stream is important to provide enough solubilization of $Fe(OH)_3$ and the acidity of the final reaction mixture (reaction coil, B) must be sufficiently low to prevent the complete protonation of L-ascorbic acid, since the reducing agent is the ascorbate anion and also to avoid the dissociation of ferroin [28]. Therefore, the reagent 1,10-phenanthroline was prepared in deionized water for all further experiments. The different acidities of the sample, reagent and carrier stream caused no drift in baseline.

3.2. Optimization of the packed reactor

The internal diameters of the glass columns, 1.0, 1.5 and 2.0 mm were tested. Similar to the results obtained in our previous work [26], the 1.5 mm showed the highest analytical signals and was chosen for further experiments. The effect of particle size, < 100 μm, 100–350 μm and 350–500 μm, on the absorbance signal also was studied. Particle size smaller than 100 μm leads to a high hydrodynamic resistance in the system, decreasing the sampling rate. The range chosen was 350–500 μm as a compromise between sensitivity and sample throughput.

The column length was studied in the range of 7–25 cm. Small column length required lower flow rates than large columns to achieve similar results. Consequently, 20 cm was chosen as the optimum length of the column for the reduction of Fe(III) immobilized in the polyester resin. The columns prepared by this procedure gave reproducible results after the injection of at least 600 samples and the reproducibility for four packed reactors shown only a slight variation (3%) of the response slope.

3.3. Optimization of FI variables

The effects of the flow rates of sulfuric acid and reagent streams on the absorbance signal were tested by injecting 500 μl of $1.0–5.0 \times 10^{-5}$ M L-ascorbic acid solutions. In order to establish the optimum flow rates the reagent stream of 1,10-phenanthroline was kept constant at 1.0 ml min^{-1} and the carrier stream (0.025 M sulfuric acid) was varied in the range of 1.3–3.9 ml min^{-1} and optimized with respect to the sensitivity. The lower flow rate implies a longer residence time of the sample within the packed reactor and caused an increase in the sensitivity, but leads to a poor sample frequency. When a higher flow rate of sulfuric acid was employed the absorbance signals decreased and caused an excessive hydrodynamic pressure.

The phenanthroline stream flow rate was studied in the range of 0.9–2.0 ml^{-1} with carrier stream kept constant at 2.0 ml min^{-1}. As a compromise between sensitivity and sample frequency a flow rate of 2.0 ml min^{-1} for the carrier stream and 0.9 ml min^{-1} for the reagent solution were adopted.

The effect of injection volumes from 125 to 625 μl (sample loops of 25–125 cm) on the analytical signals was studied for the L-ascorbic acid concen-

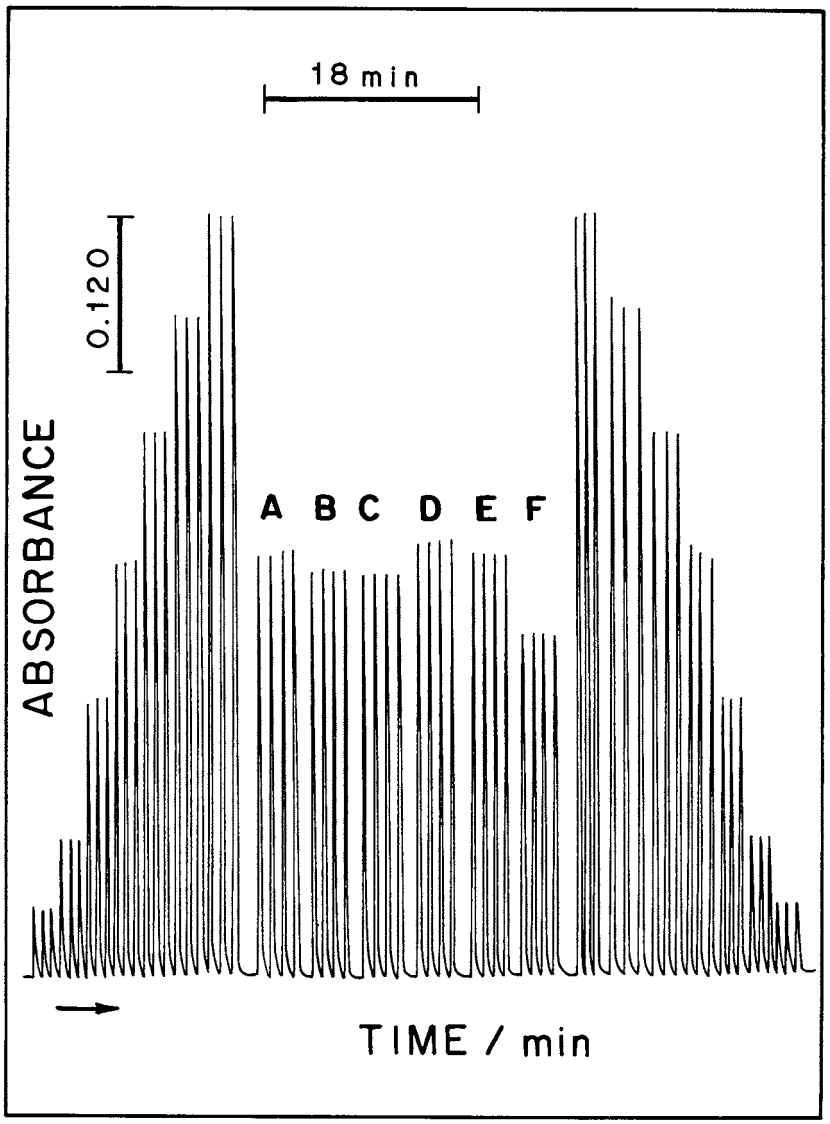

Fig. 5. FIA recording obtained for the injection of L-ascorbic acid reference and pharmaceutical formulations solutions. From left to right triplicate signals for seven reference solutions in the range 5.0×10^{-6}–6.0×10^{-5} M of ascorbic acid followed by four consecutive signals for six pharmaceutical formulations solutions: A, Redoxon; B, Cebion; C, Energil C; D, Cebion Glicose; E, Cewin and F, Aspirina C and reference solutions again.

tration range 1.0–5.0×10^{-5} M. The increase of the sample volume resulted in an increase of absorbance (Fig. 3). A 375 μl injection volume was used since it gives the best linearity and a relatively high frequency sampling.

The effect of reaction coil length was investigated in the range of 50–300 cm. In this reaction coil, Fe(II) is reacting with the phenanthroline to form the Fe(II)-phenanthroline complex ($\lambda_{max} = 510$ nm). The peak heights gradually increased with the increases of the reaction coil up to 300 cm. A 150 cm reaction coil was chosen, taking into account sensitivity and sampling rate.

Table 2
Determination of L-ascorbic acid in pharmaceutical formulations using the iodimetric and flow injection spectrophotometric procedures

Sample	Declared value	Ascorbic acid (mg tablet^{-1})[a]		Relative error (%)	
		Iodimetric method	Flow method	Re_1	Re_2
Redoxon	1000	1025.06 ± 7.72	1001.10 ± 6.5	−2.4	+0.1
Energil C	500	483.71 ± 3.32	493.27 ± 2.2	+2.0	−1.3
Cebion	1000	1011.82 ± 6.85	1007.10 ± 6.10	−0.5	+0.7
Cebion Glicose	1000	1052.30 ± 4.57	1015.5 ± 7.22	−3.5	+1.5
Cewin[b]	200	226.14 ± 2.33	203.29 ± 4.80	−10.1	+1.6
Aspirina C	240	247.62 ± 4.86	236.83 ± 4.96	−4.35	−1.3

[a] $n = 5$, confidence level, 95%.
[b] Value in mg ml^{-1}.
Re_1 FIA-spectrophotometric versus iodimetric value.
Re_2 FIA-spectrophotometric versus declared value.

3.4. Effect of the 1,10-phenanthroline concentration

The effect of the 1,10-phenanthroline concentration in the peak height was examined in the range of 0.05–0.25% m v^{-1} using the system shown in Fig. 4. As can be seen the analytical signal increased continuously with increasing concentration of phenanthroline. The optimum concentration was chosen as 0.25% m v^{-1}. Higher concentrations were not studied due the limited solubility of the reagent in water.

3.5. Interferences and recovery studies

The selectivity of the proposed method was assessed by studing the effect of common excipients used in pharmaceutical preparations and other active substances on the determination of 3.0×10^{-5} M ascorbic acid. No interference in the flow procedure was observed up to a 10–fold excess for lactose, starch, sodium chloride, sucrose, saccharin, glucose, fructose, thiamine hydrochloride, acetylsalicylic acid and caffeine. A slight negative interference for citric acid was obtained when this acid was present at same concentration of ascorbic acid.

Recoveries of 98.5 and 102.0% of L-ascorbic acid from samples of four pharmaceutical formulations ($n = 5$) were obtained using the FI-spectrophotometric procedure. In this study, 1.76, 3.52 and 5.28 μg ml^{-1} of L-ascorbic acid were added to each sample (Table 1). This is good evidence of the accuracy of the proposed procedure.

3.6. Calibration graph and applications

The proposed flow injection system was applied to determining L-ascorbic acid in available pharmaceutical formulations. Fig. 5 shows typical transient signals for L-ascorbic acid determinations using the proposed flow system under the optimum conditions. The results of the analysis of some commercial formulations given in Table 2 compared favorably with those obtained by the standard titration method ($r_1 = 0.9994$) and also agreed with those declared on the labels ($r_2 = 0.9997$) confirming the accuracy of the flow injection spectrophotometric method using an on-line packed reactor containing $Fe(OH)_3$. The calibration graph for ascorbic acid was linear in the concentration range from 5.0×10^{-6} to 6.0×10^{-5} M ($A = 0.01927 + 11.042\ C$; $r = 0.9992$, where A is the absorbance and C the concentration of L-ascorbic acid in M) with a detection limit of 5.0×10^{-7} M. The relative standard deviation for ten successive measurements of 3.0×10^{-5} M ascorbic acid was 0.56%.

4. Conclusion

The FI system with an on-line packed reactor containing $Fe(OH)_3$ immobilized in polyester resin with spectrophotometric detection is precise, accurate and sensitive to permit the determination of ascorbic acid in pharmaceutical formulations. The reactor is stable enough to permit the measurement of more than 600 samples.

Acknowledgements

The financial support granted by FAPESP (Fundação de Amparo à Pesquisa do Estado de São Paulo, Processes 91/2637-5 and 92/2637-5), PADCT/CNPq (Process 62.0060/91-3) and also the scholarship granted by CNPq to A.V.P. are gratefully acknowledged.

References

[1] C.A. Burtis, E.R. Ashwood, Clinical Chemistry, Saunders, Philadelphia, PA, 1994, pp. 1311–1314.
[2] D.E. Hughes, J. Pharm. Sci. 72 (1983) 126.
[3] United States Pharmacopeia XXI, The National Formulary, XXVI, US Pharmacopeial Convention, Rockville, MD, 1985 pp. 75–76.
[4] British Pharmacopeia, 5th edn., HMSO, London, vol. II, 1988, p. 901.
[5] D.F. Evered, Analyst 85 (1960) 515.
[6] F. Lázaro, A. Rios, M.D. Luque de Castro, C. Valcarcel, Analyst 111 (1986) 163–167.
[7] J. Hernández-Méndez, A.A. Mateos, M.J.A. Parra, C. Garcia de María, Anal. Chim. Acta 184 (1986) 243.
[8] S.M. Sultan, A.M. Abdennabi, F.E.O. Suliman, Talanta 41 (1994) 125.
[9] M.I. Albero, M.S. Garcia, C. Sánchez-Pedreño, J. Rodríguez, Analyst 117 (1992) 1635.
[10] J.A. Nóbrega, G.S. Lopes, Talanta 43 (1996) 971.
[11] C.W. Bradberry, R.N. Adams, Anal. Chem. 55 (1983) 2439.
[12] G.M. Greenway, P. Ongomo, Analyst 115 (1990) 1297.
[13] A. Sano, T. Kuwayama, M. Furukawa, S. Takitani, H. Nakamura, Anal. Sci. 11 (1995) 405.
[14] L.E. León, Talanta 43 (1996) 1275.
[15] A.A. Alwarthan, Analyst 118 (1993) 639.
[16] T. Pérez-Ruíz, C. Martínez-Lozano, A. Sanz, Anal. Chim. Acta 308 (1995) 299.
[17] A. Sanz-Martínez, A. Rios, M. Valcárcel, Analyst 117 (1992) 1761.
[18] D.J. Curran, T.P. Tougas, Anal. Chem. 56 (1984) 672.
[19] T. Pérez-Ruiz, C. Martínez-Lozano, V. Tomáz, C. Sidrach, Analyst 122 (1997) 115.
[20] Y. Fung, S. Mo, Anal. Chim. Acta 261 (1992) 375.
[21] W.L. Baker, T. Lowe, Analyst 110 (1985) 1189.
[22] E.S. Contreras-Guzman, F.C. Strong III, O. Guernelli, Quim. Nova 7 (1984) 60.
[23] A. Besada, Talanta 34 (1987) 731.
[24] J. Martínez-Calatayud, J.V.G. Mateo, Trend Anal. Chem. 12 (1993) 428.
[25] S. Emara, S. Razee, A.N. El-Shorbagi, T. Masujima, Analyst 121 (1996) 183.
[26] A.V. Pereira, O. Fatibello-Filho, VII Int. Conf. Flow Analysis, Piracicaba, SP, Brazil, August 1997.
[27] G.A. Rivas, J. Martínez-Calatayud, Talanta 42 (1995) 1285.
[28] T.S. Lee, I.M. Kolthoff, D.L. Leussing, J. Am. Chem. Soc. 70 (1948) 2348.

ELSEVIER

Talanta 47 (1998) 19–24

Talanta

Selective separation of copper with Lix 864 in a hollow fiber module

M.E. Campderrós, A. Acosta, J. Marchese *

Laboratorio de Ciencias de Superficie y Medios Porosos.- Depto de Qca.- Facultad de Química, Bioqca. y Farmacia. Unsl. Conicet, Chacabuco y Pedernera, C.C. 256, 5700-San Luis, Argentina

Received 13 September 1997; received in revised form 5 January 1998; accepted 7 January 1998

Abstract

The transfer and separation of Cu(II), Co(II), Ni(II) and Zn(II) ions across a hollow fiber supported liquid membrane containing LIX 864 as the mobile carrier dissolved in kerosene solvent has been investigated. The flux and selectivity for copper has been studied as a function of the feed flow, the carrier concentration in the liquid membrane and the extraction solution acidity. A maximum copper recovery at 30% of LIX (v/v) in the diluent was obtained. The permeation experiments showed that at pH 2 in the extraction solution a highly selective separation of Cu over the other cations can be achieved. Increasing the acidity of the extraction solution copper selectivity decrease and the grade of recuperation sequence is Cu > Co > Ni > Zn. These results suggest that in selected situations, this membrane system can be competitive with the conventional liquid–liquid extraction process, in particular in leaching solutions with low metal concentration. © 1998 Elsevier Science B.V. All rights reserved.

1. Introduction

The demand for various metals is increasing with the gradual depletion of their proper ores, so it will be necessary to mine and treat even lower grade and/or more complex ores in the near future. Solvent extraction technology is expected to become increasingly important in hydrometallurgy as a desirable process for metal winning from the viewpoints of consumption of natural resources and energy conservation. Recently, membrane separation based on solvent extraction has attracted practical interest due to the simplicity of the operation and its use has been attempted in the recovery of metal, protein and other materials [1–4]. Particularly, the application of a membrane extractor made of hollow fiber has been successfully tested for the recovery of metals from aqueous solutions, becoming competitive with solvent extraction processes [5–7].

The employment of this kind of extractor offers some advantages compared with the current solvent extraction process using mixer-settlers. Among them, shorter time of processing, smaller reactor size, a very large interfacial area per unit extractor volume, no direct mixing of aqueous and organic solutions. Mainly the use of the supported liquid membrane significantly reduces the relative amount of organic phase necessary for

* Corresponding author. Fax: +00 54 652 30224/31217; e-mail: marchese@uns 1.edu.ar

0039-9140/98/$19.00 © 1998 Elsevier Science B.V. All rights reserved.
PII S0039-9140(98)00048-4

the extraction. Hence, highly selective and expensive extractants can also be used, which would not be economical in solvent extraction [8,9]. The kinetics of copper extraction with commercial chelating extractants, especially hydroxyoximes, [10] and back-extraction or stripping of this metal by strongly acidic solutions, [11] has attracted the interest of many investigators due to the practical importance for copper recovery by solvent extraction or by using a liquid membrane which contains a chelating extractant as a carrier.

In this paper the mass transfer of copper(II) is analyzed in a hollow-fiber module (HFM) with reactive supported liquid membrane in which facilitated transport takes place and its selective separation from cobalt(II), nickel(II) and zinc(II). The effects of membrane viscosity and flow rate velocity on copper recovery are investigated.

2. Experimental

2.1. Reagents

The carrier used in these studies was LIX 864 (Chile Harting–Henkel) a strong copper extractant with very good physical performance Fig. 1. This commercial reagent is (1:1) volume blend of LIX 860 (5-dodecylsalicylaldoxime) and HS-LIX 64 (a mixture of 2-hydroxy-5-nonylbenzo phenoneoxime, and 5, 8-diethyl-7-hydroxydodecan-6-oxime), a product of a relative density of 953 kg m^{-3} and a viscosity of 0.608 kg $m^{-1}s^{-1}$ (298 K), used without further purification. Kerosene JP1 grade was used as organic solvent (relative density: 825 kg m^{-3}, viscosity: 0.15 kg m^{-1} s^{-1}, boiling point: 523–573 K)

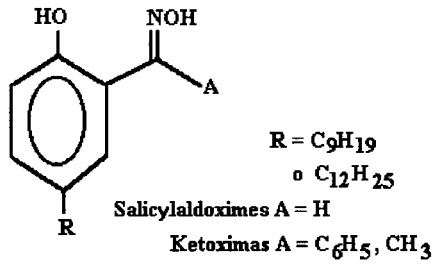

Fig. 1. General chemical structure of the hydroxy oximes used commercially for copper recovery.

Table 1
Characteristics of hollow fiber

Porosity	45–55%
Maximum pore size	1.5–2.0 μm
Inner diameter	0.75–0.85 mm
Outer diameter	1.80 mm
Wall thickness	0.475 mm
Length	15 cm

The feed solution was an aqueous solution of Cu(II) as $CuSO_4.5H_2O$, Ni(II) as $NiSO_4.7H_2O$, Co(II) as $CoSO_4.6H_2O$ and Zn(II) as $ZnSO_4.2H_2O$ (purchased from Merck, Germany), all at an ionic concentration of 0.1 g dm^{-3} in distilled water saturated with kerosene. When buffering was required to maintain a constant pH, acetic-acetate buffer was used. The stripping solution was sulfuric acid 2.7 M. Analytical grade reagents were used throughout.

2.2. Density and viscosity measurements

Densities and viscosities of the LIX-kerosene solutions were measured for comparison of the transport properties of metals with the physical properties of the carrier-diluent organic phase. Viscosities were measured at 298 ± 0.2 K using a Cannon–Feske viscosimeter and densities were determined with a digital densimeter (PAAR DMA 46). The results obtained are showed in Table 2.

2.3. Apparatus for transport measurements

The experimental transport measurements have been carried out with a hollow fiber module (HFM) described in Fig. 2. It has a bundle of five fibers disposed horizontally inside a glass tube. The hollow fiber membrane was a microporous polytetrafluoroethylene fibers (Goretex, Japan). The support has excellent properties such as flexibility and high chemical and mechanical resistance. Some characteristics of the fibers are shown in Table 1. The organic phase was incorporated into the support membrane by capillary action. Donor and stripping solutions are fed in cocurrent by a peristaltic pump, the former through the

inner side of the fiber and the latter by the outer side.

The concentration of the ions in both effluent solutions at steady state were determined by atomic absorption. The tests were carried out over periods of time of 4–5 h. Acidity was measured with a Metrohm–Herisau pH-meter and a combined glass Ag/AgCl electrode.

3. Results and discussion

3.1. Liquid–liquid extraction and stripping measurements

The equilibrium distribution of metal ion between the aqueous and organic phases as a function of pH was determined by contacting equal volumes (10 cm^3) of both phases in a separating funnel for 6 h at 298 ± 0.2 K. The organic phase consisted of 5% solution of LIX in kerosene. After equilibration, a suitable aliquot was withdrawn from the aqueous phase and the metal concentration was determined by atomic absorption.

LIX 864 (denoted as HR) contains in its structure an acid hydrogen ion which is exchanged with the metal ions according to the chemical reaction given in Eq. (1). The experimental results

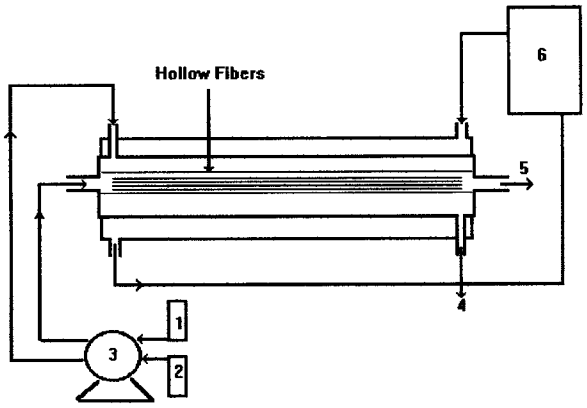

Fig. 2. Schematic representation of the equipment with the hollow fiber module used in permeation experience of metals with LIX 864. (1: donor solution, 2: stripping solution, 3: peristaltic pump, 4: outlet stripping (sample), 5: outlet donor solution (sample), 6: thermostatic bath).

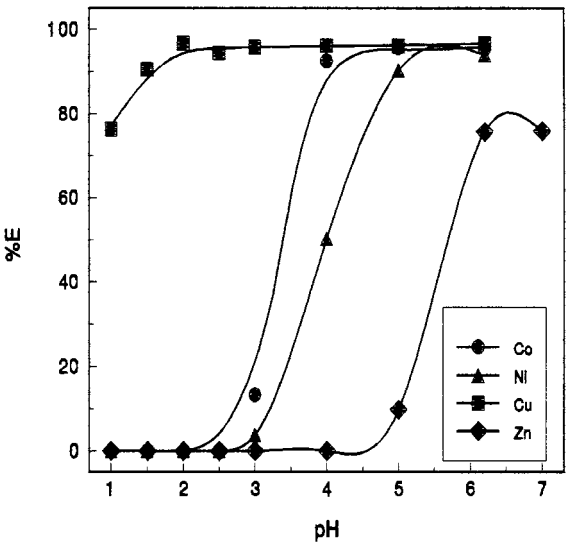

Fig. 3. Extraction of Cu(II), Co(II), Ni(II) and Zn(II) with LIX 864 (5% v/v en kerosene), vs. equilibrium pH ($T = 298 \pm 0.5$ K).

are plotted in Fig. 3 as extraction extent defined in Eq. (2) as a function of equilibrium pH of the aqueous solutions.

$$2HR_{(org)} + Me^{2+}{}_{(aq)} \underset{\text{Stripping}}{\overset{\text{Extraction}}{\leftrightarrows}} MeR_{2\,(org)} + 2H^{+}{}_{(aq)} \quad (1)$$

$$\%E = \frac{[Me]_{org}}{[Me]_{org} + [Me]_{ac}} \times 100 \quad (2)$$

LIX 864 actually is one of the strongest copper extractants capable of complexing Cu(II) even around the pH value of 1 while the Co(II), Ni(II) and Zn(II) extractions increase with increasing pH, reaching a maximum in the pH range of 3.5–6 for Co, 5–6 for Ni and Zn (II) become to be extracted over pH 4.5. It should be noted that a high pH value in the aqueous phase may cause the metal ions to precipitate and these would hinder the extraction. For a selective separation of the metal ion with quite different characteristics as mentioned above, decreasing the pH enhances the selective extraction of copper.

Therefore a qualitative analysis of Fig. 3 allows the selection of the pH operating conditions in each side of the liquid membrane to reach the better selective separation of copper from the other, i.e. for the donor solution (inner side of the

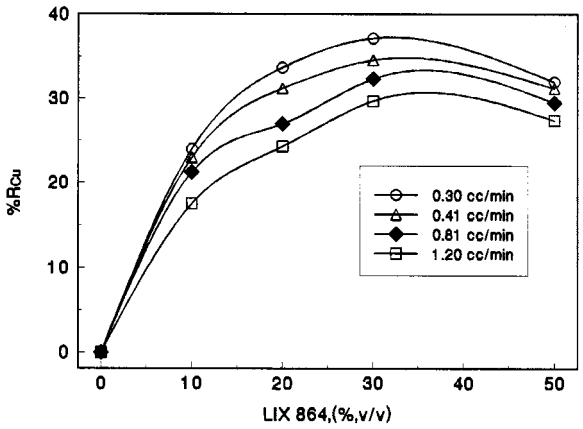

Fig. 4. Effect of LIX 864 concentration in the organic membrane phase and flow rate upon copper recuperation.

fiber) it is convenient to keep the pH around 2. This pH will promote high metal loading in the liquid membrane by means of copper-Lix complex formation. The stripping solution (outer side of the fiber) should be a strong acid solution, which would be conducive to the complex dissociation, stripping in Eq. (1). In these conditions the Zn, Co and Ni transport will be negligible.

3.2. Effect of carrier concentration and flow rate on copper transport in the HFM

Permeation experiments were performed to investigate both the influence of carrier concentration in the HFM and the flow rate of solutions upon copper flux. In all the experiments, the feed solution was an aqueous solution of Cu(II) (0.1 g dm^{-3}) at pH 2. The stripping solution was H_2SO_4 2.7 M and the flow rates of both solutions was varied between 0.3 and 1.2 cc min^{-1}.

The concentration of LIX 864 in the organic solution has a market effect on the cation flux. Fig. 4 shows that, with increasing the carrier concentration, the transport of copper gradually increased, reaching a maximum around 30–35% and then decreased. This effect can be accounted for by analyzing the influence of the viscosity increase of LIX solutions upon the diffusion coefficient of the metal complex in the membrane. Here, both the amount of ion that could be extracted into the membrane and the viscosity of the organic solution increased. An increase in viscosity of the organic phase solution leads to a decrease of the diffusion coefficient and, hence, the permeability of the diffusing species. These opposing effects resulted in maximum transport at an LIX 864 concentration of 30–35% in kerosene.

The viscosity, densities and diffusion coefficients for different carrier concentrations in the hollow fiber are shown in Table 2, where the diffusivity, D_{MeR}, was estimated from Stokes–Einstein equation. In a control experiment without LIX, the same hollow fiber support was used with kerosene alone in the pores. There was no measurable flux of copper.

With increasing feed flow velocity, the amount of transport metal decreases for any analyzed cases. We account for this effect by considering that there is an obvious decrease of contact time between aqueous solution and organic solution in the hollow fiber, i.e. less residence time.

3.3. Selective separation of Cu from Ni, Co and Zn in the HFM

Using the optimized conditions from the obtained results for copper transfer through the

Table 2
Properties of the organic solution, and diffusion coefficients of complex Cu-LIX

[LIX 864] (% v/v)	ρ(298 K) (kg m^{-3})	$^{\mu}$(298 k) (kg m^{-1} s^{-1})	$D_{CuR} \times 10^{11}$ (m^2 s^{-1})
10	807.9	0.178	1.519
20	824.8	0.213	1.269
30	855.5	0.436	0.620
50	903.2	0.589	0.459
100	933.0	0.608	0.444

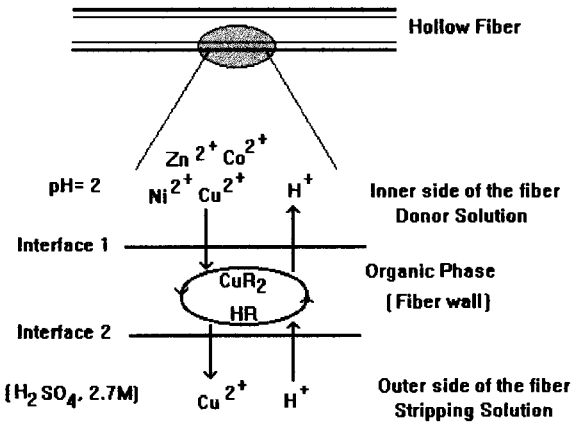

Fig. 5. Schematic representation of the counter coupled transport of ions in the HFM. Selective separation of Cu(II) from Co(II), Ni(II) and Zn(II).

liquid membrane, a series of experiments were carried out to determine the selectivity to separate Cu(II) from solutions containing divalent metals as a function of pH. For this purpose, synthetic solutions containing approximately 0.1 g dm^{-3} of Co(II), Ni(II), Zn(II) and Cu(II) were tested as feed solutions in the range 2–6 pH. The stripping solution, H_2SO_4 2.7 M, was pumped in co-current and LIX 864, 30% (v/v), was incorporated into the hollow fiber.

Fig. 5 shows a schematic representation of the counter coupled transport of the ions in a hollow fiber support. The membrane serves both as a support for the organic phase and as uniform barrier between the two aqueous phases. This results in two aqueous-organic interfaces with well-defined transfer areas.

The experimental results are in accordance with the extraction finding of the above section and are presented in Table 3 as recovery factor (%R) and separation factor $\phi_{A/B}$, as a function of pH, where

$$\%R_A = \left[1 - \left(\frac{[A]_{o1}}{[A]_{i1}}\right)\right] \times 100 \quad (3)$$

and

$$\phi_{A/B} = \left(\frac{[A]_{o2}}{[A]_{o1}}\right) \times \left(\frac{[B]_{o1}}{[B]_{o2}}\right) \quad (4)$$

where [A] and [B] are the metals concentration, the subscripts i and o indicates inlet and outlet at the hollow fiber module, and 1 and 2 are the donor and stripping solution respectively.

Table 3 shows that at pH = 2 in the donor solution maximum Cu/Co, Cu/Ni, Cu/Zn separation occurs. With an increase of pH the metal recovery increases, for all of them, and so the separation decreases. Therefore the proper choice of acidity conditions in the feed solution allows a selective separation of the metals.

4. Conclusions

An experimental study of liquid–liquid extraction and stripping of Cu(II), Co(II), Ni(II) and Zn(II) ions with LIX 864 has been performed. These metal ions were extracted by means of the formation of a complex with the acid hydrogen ion of the reagent which is pH dependent. The stripping was successfully achieved with a solution of sulfuric acid.

With increasing carrier concentration in the organic phase of the membrane, both the amount of metal that can be extracted into the membrane

Table 3
Recovery and separation factors at different extraction solution acidity

pH of donor solution	%R				$\phi_{A/B}$		
	Cu	Co	Ni	Zn	Cu/Co	Cu/Ni	Cu/Zn
2	36.50	—	—	—	total	total	total
4	41.25	36.00	15.00	—	1.25	3.98	total
6	41.15	38.25	27.00	18.50	1.13	2.70	3.08

Stripping solution: H_2SO_4 2.7 M.

and the viscosity of the organic solution increase. These opposing effects result in maximum transport at a LIX concentration of 30% (v/v) in kerosene, for any feed flux analyzed.

Permeation experience with the hollow fiber module showed that keeping up pH 2 in the donor solution, a highly selective separation of Cu over the other cations studied can be achieved. The separation factor with LIX 864 in the hollow fiber decrease with increasing pH, and the grade of recuperation sequence can be written as: $Cu > Co > Ni > Zn$.

With decreasing metal concentration in the leaching (< 1000 mg dm^{-3}), conventional solvent extraction becomes uneconomical. The supported liquid membrane technique offers an alternative and potentially more economical process. In this technique, extraction and re-extraction are carried out in a single step.

References

[1] H. Kishigani, Y. Awakura, H. Majima, Hydrometallurgy 26 (1991) 19.
[2] J. Marchese, M.E. Campderrós, A. Acosta, J. Chem. Biotechnol 64 (1995) 293.
[3] J.T.F. Keurentjes, L.J. Nabuurs, E.A. Vegter, J. Memb. Sci. 113 (1996) 351.
[4] C. Palet, M. Muñoz, S. Daunert, L.G. Bachas, M. Valiente, Anal. Chem. 65 (1993) 1533.
[5] Y. Sato, K. Kondo, F. Nakashio, J. Chem. Eng. Jap. 22 (1989) 200.
[6] J-I Kim, P. Stroeve, J. Memb. Sci. 45 (1989) 99.
[7] J. Havel, C. Moreno, A. Hrdlicka, M. Valiente, Talanta 41 (1994) 1251.
[8] J. Melling, Warren Spring Lab. L.R. (1979) pp. 1–18.
[9] M. Costello, A.G. Fane, P.A. Hogan, R.W. Schofield, J. Memb. Sci. 80 (1993) 1.
[10] I. Komasawa, T. Otake, T. Muraokat, J. Chem. Eng. Jap. 22 (1989) 200.
[11] F. Valenzuela, C. Basualto, Lat. Am. Appl. Res. 24 (1994) 175.

ELSEVIER

Talanta 47 (1998) 25–32

Talanta

Preconcentration with chromatomembrane cell and adsorptive polarographic determination of fluorine in air

Yan-Fei Li, Hong Zhang, Fei Xiao, Zheng-Qi Zhang *

College of Chemistry and Chemical Engineering, Hunan University, Changsha 410082, People's Republic of China

Received 13 September 1997; received in revised form 5 January 1998; accepted 7 January 1998

Abstract

The present paper describes a procedure in which fluorine in the air was preconcentrated in a chromatomembrane cell and its content was determined by adsorptive polarography. In a pH 4.90 buffer solution the fluorine ion can form a ternary complex with La(III) and ALC. The complex can be adsorbed at the mercury electrode and yields a sensitive oscillopolarographic wave at -0.67 V, which can be sensitized by Triton X-100. Over the range 3.0×10^{-8}–1.60×10^{-6} M, the peak currents are linearly proportional to the concentration of the fluoride. The detection limit is 1.0×10^{-8} M. First the fluorine in the air samples was preconcentrated in the chromatomembrane cells using 0.10 M NaOH solution, then its content was determined by complex-adsorptive polarography. © 1998 Elsevier Science B.V. All rights reserved.

1. Introduction

Elemental fluorine is rarely found in industrial waste gases, but fluorine compounds are often, although in low concentration, constituents of industrial emissions. Fluorine occurs mostly as HF and sometimes as SiF_4. Fluorine-containing gaseous pollutants or dust can cause chronic injuries, and cause disturbances in calcium metabolism. Fluorine compounds in the air may lead to appreciable damage to vegetation even when present in very low amounts. Therefore investigation of its quantitative procedure possesses ecological importance.

The earlier procedures are based on the effect of the fluorine ion on color lakes of zirconium with alizarin. The metals are removed from the color lake to form the more stable metal fluoride. The lake is decolorized and the weaker color can be observed on a filter paper or measured with the aid of a spectrophotometer. Kaye [1] described a coulometric procedure for the determination of elementary fluorine. The potentiometry can be used for the determination of fluorides down to 2.0×10^{-6} M [2,3]. Belcher [4–7] recommended a spectrophotometric method for the determination of fluorine with a limit of detection of 5.0×10^{-6} M, which was used to determine the fluoride in air [8]. An impinger containing 70 ml of 0.1 M NaOH solution and 5 ml of 3% H_2O_2 solution was used for the collection of fluoride in an air sample. However, Leithe [9] found that using the impinger for preconcentration of the fluorine in

* Corresponding author.

0039-9140/98/$19.00 © 1998 Elsevier Science B.V. All rights reserved.
PII S0039-9140(98)00050-2

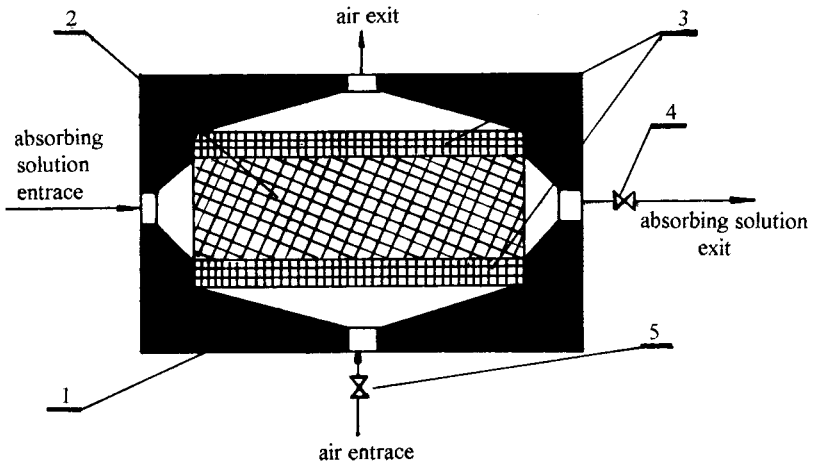

Fig. 1. Chromatomembrane cell: (1) case of the cell; (2) mass-exchange layer; (3) microporous membrane; (4) regulatory valve for absorbing solution; (5) air regulatory valve.

the air at the production sites of superphosphate and aluminum the absorption of fluorine was not complete.

In 1994 Moskvin [11–17], recommended a chromatomembrane method, which is a new technique for separation of a substance. Using the chromatomembrane method the analyte is continuously extracted from a certain phase. The chromatomembrane method combines the main advantages of chromatographic (high efficiency of the mass-exchange process) and membrane (continuous regime) separation method [16]. In this paper, we describe a procedure which illustrates the fact that fluorine in the air is preconcentrated in the chromatomembrane cell and its contents were determined by adsorptive polarography.

2. Principle of chromatomembrane method

The chromatomembrane method is one for mass exchange between a polar liquid phase and a non-polar liquid or gas phase within a chromatomembrane cell [11,12,17]. In a chromatomembrane cell Fig. 1 the mass-exchange process is carried out in the capillary medium of hydrophobic material with two preferential pore types differing in size, which is bounded on two sides by microporous hydrophobic membranes [13]. The mass-exchange layer was made of porous polymer particles such as porous polytetrafluoroethylene(PTFE). The porousity between the particles form macropores with a radius of 0.50–3.0 mm [12]. The polar liquid, which does not wet the surface of the hydrophobic material, fills the macropores of the biporous matrix and moves within them. In the polymer particles there are numerous open micropores with a radius of 0.03–1.0 μm. The non-polar liquid or gas phase moves within the micropores, and contacts with the polar liquid within the macropores, thus the analyte transfer from the original phase into the other.

Throughout the mass-exchange space the gas or non-polar liquid phase does not enter into the macropores because the polar phase pressure is maintained higher than the pressure of the gas phase, and the polar liquid phase also could not penetrate into the micropores because the capillary pressure of micropores can prevent this penetration.

In order to prevent capillary effects, in design of a chromatomembrane cell the capillary pressure should exceed the value calculated from the known expression [13],

$$P_c = (2\sigma \cos \theta)/\Upsilon \quad (1)$$

where P_c is the capillary pressure, σ is the surface tension of the liquid phase, θ is the contact angle between the liquid and the membrane material

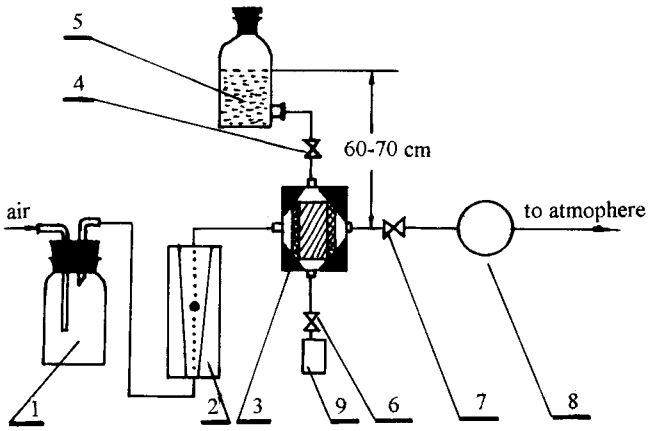

Fig. 2. Scheme of experimental device for absorption of fluorine in air: (1) buffer bottle; (2) rotameter; (3) chromatomembrane cell; (4) and (6) regulating valve for absorbing solution; (5) 0.10 M NaOH; (7) air regulating valve; (8) pump; (9) samples solution collector.

and Υ is the pore radius. In the case of PTFE porous matrix with a contact angle of 108° the capillary effects become negligible within pores of 0.1 mm radius. So it can be guaranteed that the polar liquid phase moves within macropores and the non-polar liquid or gas phase moves within micropores. When we use gas to extract analyte from the polar liquid phase additional conditions have to be guaranteed [13],

$$P_{L1} < P_{G2} + P_c \quad (2)$$

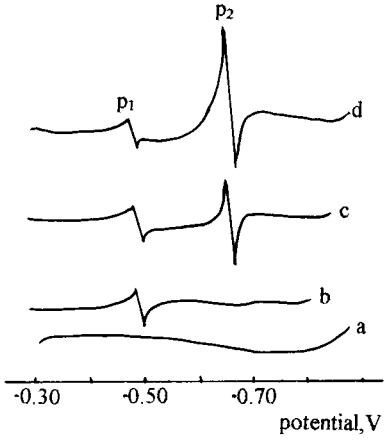

Fig. 3. Polarograms of La(III)–ALC–F^-–Triton X-100 system: (a) pH 4.90, 0.10 M $(CH_2)_6N_4$, 0.10 M KNO_3; (b) a + 1.25 $\times 10^{-5}$ M La^{3+} + 1.0×10^{-5} M ALC; (c) b + 5.0×10^{-7} M F^-; (d) c + 0.0020% Triton X-100.

$$P_{G1} < P_{L2} \quad (3)$$

where P_{L1} and P_{L2} are the liquid-phase pressures at the inlet and outlet of the mass-exchange space of the chromatomembrane cell, respectively, P_{G1} and P_{G2} are the gas-phase pressures at the inlet and the outlet of the mass-exchange space, respectively, and P_c is the capillary pressure in the micropores. Combining Eq. (2) and Eq. (3), and simply transformating, we obtain the following expression,

$$P_{L1} - P_{L2} + P_{G1} - P_{G2} = \Delta P_L + \Delta P_G < P_c \quad (4)$$

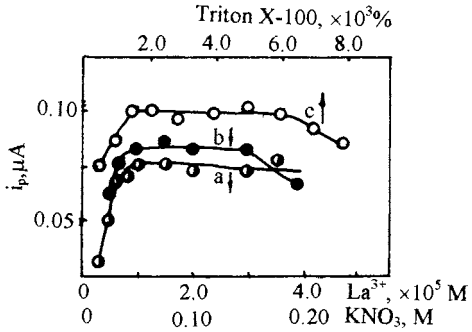

Fig. 4. The composition of the background solution of La(III)–ALC–F^-–Triton X-100 system: pH 4.90, 0.10 M $(CH_2)_6N_4$, 1.0×10^{-5} M ALC, 5.0×10^{-7} M F^- (a) effect of the La(III) concentration: 0.01 M KNO_3, 0.0010% Triton X-100; (b) effect of the KNO_3 concentration: 1.25×10^{-5} M La^{3+}, 0.0010% Triton X-100; (c) effect of Triton X-100: 1.25×10^{-5} M La^{3+}, 0.10 M KNO_3.

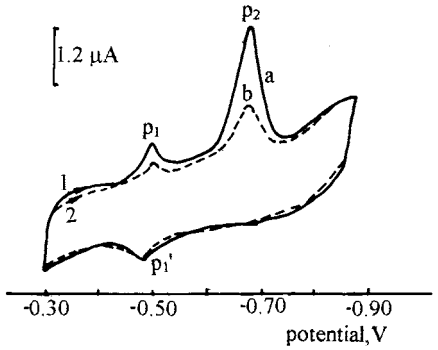

Fig. 5. Cyclic voltammgrams of La(III)–ALC–F^-–Triton X-100 system: pH 4.90, 0.10 M $(CH_2)_6N_4$, 0.10 M KNO_3, 1.25×10^{-5} M La^{3+}, 1.0×10^{-5} M ALC, 1.0×10^{-6} M F^-, 0.0020% Triton X-100, scan rate of 100 mV s^{-1}. (1) first scan; (2) second and repetitive scans.

Obviously, it is neccessary for the chromatomembrane process that the sum of pressure gradients for the liquid and gas phases should be less than the capillary pressure value. Thus the capillary pressure is the main physico-chemical parameter that defines the capabilities of the method [12].

3. Experimental

3.1. Apparatus

3.1.1. Chromatomembrane cell

The experimental chromatomembrane cell Fig. 1 was made of polytetrafluoroethylene. The cell had membranes of 0.8 mm thickness with an average pore size of ~ 0.5 μm. In the mass-exchange units the micropore sizes are as uniform as possible, e.g. 0.5 μm, and the average diameter of macropore size is 0.3 mm. The cells in this study allow variation of the aqueous phase flow within the 0–300 ml min^{-1} range and of the air flow within the 0–1.0 dm^3 min^{-1} range.

3.1.2. Electroanalytical device

The single-sweep polarograms were recorded on a JP-1A oscillopolarograph (Chengdu Instrumental Factory). The polarographic cell has the three electrode system: a dropping mercury electrode(DME) as working electrode, a saturated calomel electrode (SCE) reference electrode and a platitum wire auxiliary electrode. A drop time of 7 s was selected using a knocker, with a rest time of 5 s and a scan time of 2 s, the scan rate being 250 mV s^{-1}. An XJP-821 neopolarograph (Jiangsu Electroanalytical Instrumental Factory) in connection with a LZ3-100 X-Y recorder (Dahua Instrumental Factory) and a JM-01 (manual micro-metric screw delivery) hanging mercury drop electrode (HMDE) were used for cyclic voltammetry measurements. A PAR Model 273 Potentiostat/Galvanostat with a PAR Model 303 static mercury drop electrode, controlled by PAR Model 270 software, was used for normal pulse polarography, linear scan voltammetry and other electrochemical measurements. For pulse polarography the instrumental parameters were as follows: accumulation time, 120 s; accumulation potential, -0.35 V; drop size, medium; pulse amplitude, 50 mV; pulse period, 2 s; equilibrium time, 15 s.

3.2. Reagents

3.2.1. Standard fluoride solution (1.0×10^{-3} M)

A stock solution of sodium fluoride (GR, Changsha Chemicals) was prepared by dissolving 0.0208 g of NaF in 50 ml water, followed by dilution to 500 ml.

3.2.2. Lanthanum(III) solution (1.0×10^{-3} M)

A suitable amount of lanthanum sesquioxide (99.999%, Hunan Institute for Rare Earth Element) was incandesced at 850°C for 2 h, and cooled to room temperature. 0.0408 g of the lanthanum sesquioxide was dissolved in 25 ml of 1.0 M HNO_3 solution, and the solution was made up to 250 ml.

3.2.3. ALC solution (1.0×10^{-3} M)

Alizarin complexone (0.0965 g) (AR, Beijing Chemicals) was dissolved in a suitable volume of 5 M NaOH solution, its pH value was adjusted to 4.90. Then the solution was diluted to 250 ml.

3.2.4. Hexamethylenamine buffer solution (1.0 M)

Hexamethylenamine (70 g) (AR, Changsha Chemicals) and 50 g of KNO_3 were dissolved in 450 ml water. Its pH value was adjusted to 4.90 with 5 M HNO_3 solution, then diluted to 500 ml.

3.2.5. Triton X-100 solution (0.020%)

Triton X-100 (0.10 g) (GR, Beijing Chemicals) was dissolved in 250 ml water, and the solution was diluted to 500 ml.

3.2.6. NaOH solution (0.10 M)

Other reagents were of a suprapure or analytical-reagent grade. Water, redistilled in a fused-silica apparatus, was used throughout.

3.3. Procedures

3.3.1. Preconcentration of the fluoride in air

Fig. 2 presents an experimental device for the preconcentration of the fluoride in air samples. Firstly all valves were closed, and the pump 8 was started. Then the valves 4 and 6 were regulated to control the flow rate of 0.05 ml min^{-1} for absorbing solution (0.10 M NaOH), and then valve 7 was regulated to make the flow rate of air in 0.80 dm^3 min^{-1}. About 3 ml of the solution was collected.

3.3.2. Adsorptive polarographic determination of F^-

3.3.2.1. Polarography of pure sodium fluoride solution. 1.0 ml of the buffer solution, 1.25 ml of 1.0×10^{-4} M La(III) solution, 1.00 ml of 1.0×10^{-4} M ALC solution and 1.00 ml of the Triton X-100 solution were well mixed, and various amounts of standard F^- solution was added. The mixture was diluted to 10 ml with water. After standing for 30 min, the solution was transfered to the polarographic cell, and purged with oxygen-free nitrogen for 10 min. A flow of nitrogen was maintained over the cell throughout the analysis to prevent interference from oxygen. Record the derivative polarograms, starting the potential scan at -0.35 V. The peak potential is -0.67 V.

3.3.2.2. Analysis of air samples. The pH value of the collected solution was adjusted to 5–6 with dilute HNO_3 solution. Analysis was performed as described above for pure sodium fluoride solution.

Table 1
Determination of fluorine in air samples

Samples	F^- found ($\mu g\ m^{-3}$)	Main ($\mu g\ m^{-3}$)	SD (%)
Laboratory 1	0.67, 0.65, 0.68	0.67	2.2
Laboratory 2	0.45, 0.44, 0.47	0.45	3.2
Atmosphere	0.083, 0.089, 0.080	0.084	5.4
Superphosphate plant	2950, 3108, 3032	3030	2.6

4. Results and discussion

4.1. The conditions of preconcentration

4.1.1. Choosing of absorbing solution

The fluorine-containing compounds such as HF in air, are best collected in 0.01–1.0 M sodium hydroxide solution [18]. In this study a 0.10 M NaOH solution was used to absorb fluorine in air samples.

4.1.2. The flow rate of absorbing solution

Using the chromatomembrane cell for the preconcentration of analyte in air samples the flow rate of the absorbing solution depends on the concentration of the analyte in the sample, the sensitivity of the analytical method and the solubility of the analyte.

The hydrogen fluoride in air samples is easy to dissolve in dilute sodium hydroxide solution. If the concentration of fluoride in the sample is higher and the analytical method is more sensitive, the flow rate of the absorbing solution may be larger. In this work, the flow rate of 0.10 M NaOH solution was 0.050 ml min^{-1}.

4.1.3. The flow rate of the air samples

When the analyte is easy to dissolve in an absorbing solution, the larger the flow rate of the sample, the shorter the time of concentration. However, the flow rate of the sample must be less than one which the chromatomembrane cell tolerates. In this study, the flow rate of the air samples was controlled at 0.80 dm^3 min^{-1}.

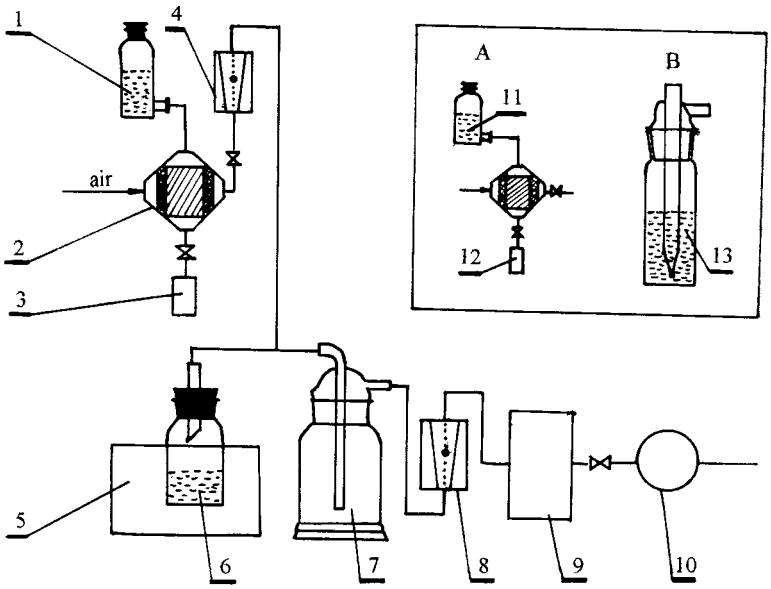

Fig. 6. The device for the comparison between chromatomembrane cell and impinger: (1) 2.0 M NaOH; (2) chromatomembrane cell 1; (3) collector for waste solution; (4) rotameter 1 for free-fluorine air; (5) thermostatical water bath; (6) HF solution (15%) (7) mix chamber; (8) rotameter 2 for sample air; (9) absorbing device (A or B); (10) pump, (11) 0.10 M NaOH, (12) collector for sample solutions, (13) 0.10 M NaOH.

4.2. Adsorptive polarographic determination of F^-

4.2.1. Adsorptive polarography

In a pH 4.3–6.0 buffer solution, the rare earth elements (RE) can form binary complexes with ALC [19,20], which possesses good electroanalytical characteristics and can be used for the determination of RE. Langmyhr [21] investigated in detail the composition of the ternary complex Ce(III)–ALC–F^- with spectrophotometry, and found that the complex is a dipolymer. Li et al. [19,22] investigated the electroanalytical behaviors of the binary complex RE(III)–ALC and the ternary complex RE(III)–ALC–F^-. The results showed that both the binary and the ternary complexes are adsorbed on the mercury electrode. We found that the addition of Triton X-100 into the system of La(III)–ALC–F^- can increase the peak height of the ternary complex. The oscillopolarograms of La(III)–ALC–F^--Triton X-100 system are shown in Fig. 3. In a pH 4.90 buffer solution, La(III)–ALC complex yields a sensitive oscillopolarographic wave p_1 (Fig. 3b). The ternary complex La(III)–ALC–F^- yields a new sensitive polarographic wave p_2 at -0.67 V (Fig. 3c), which can be sensitized by Triton X-100 (Fig. 3d). Its peak potential shifts in the negative direction with increasing pH value of test solution. The p_2 can be used to determine the trace fluoride. Over the range 3.0×10^{-8}–1.60×10^{-6} M, the peak currents are linearly proportional to the concentration of the fluoride. The detection limit is 1.0×10^{-8} M, which was taken as the concentration that gave a signal equal to three times the standard deviation of the blank signal, calculated from the calibration slope. The reproducibility was evaluated by 15 repetitive experiments on a 5.0×10^{-7} M F^- solution. The relative standard deviation was 1.6%.

4.2.2. Effect of pH

The pH value of the test solution affected the peak current and potential of p_2. when the pH value was <4.3 the La(III)–ALC–F^- complex did not yield a polarographic wave, and for pH values >5.5, the p_2 disappeared. In a pH 4.3–5.5 range the peak potential shifts in the negative

Table 2
Comparison between chromatomembrane method and impinger

Mixed gas samples	Temperature of water bath (°C)	Chromatomembrane method		Impinger	
		F^- found (mg m^{-3})	SD (%)	F^- found (mg m^{-3})	SD (%)
1	25	0.41	2.8	0.37	5.1
2	30	0.88	2.2	0.56	4.5
3	40	1.41	2.5	1.24	4.3

direction with increasing pH value of the test solution. In a pH 4.90 solution, the peak potential was -0.67 V. Over the pH range 4.8–5.2 the peak current of the p_2 was the largest and most stable. A pH value of 4.90 was chosen for subsequent studies. The buffers such as HOAc–NaOAc and hexamethylenamine were tested, and the best results were obtained in hexamethylenamine buffer solution, so hexamethylenamine was used as the buffer.

4.2.3. The ratio between ALC and La(III)

In the range of ratio between ALC and La(III) from 0.7 to 1.0 the peak current i_{p2} was the largest and most stable, so the ratio of 0.8 was chosen for subsequent studies.

4.2.4. Effect of La(III) concentration

The La(III) concentration affected the peak current (Fig. 4a). When its concentration is $< 8.0 \times 10^{-6}$ M the i_{p2} increases rapidly with increasing La(III) concentration, and when La(III) concentration is $> 1.0 \times 10^{-5}$ M the i_{p2} remains constant. Accordingly, a concentration of 1.25×10^{-5} M for La(III) was used throughout for maximum sensitivity.

4.2.5. Effect of KNO_3 concentration

Support electrolytes such as KCl, NaCl, KNO_3 and $NaNO_3$ were examined in 5.0×10^{-7} M F^- solution. The best results were obtained with KNO_3 support electrolyte. The effect of its concentration on peak current is shown in Fig. 4b. Over the range 0.050–0.15 M the i_{p2} remains constant. A concentration of 0.10 M for KNO_3 was used throughout.

4.2.6. Effect of Triton X-100 concentration

In order to choose the most suitable surfactant, various surfactants such as cetyl trimethyl ammonium bromide(CTMAB), sidium lauryl sulphate(SLS), *p*-octyl polyethylene glycol phenylether(OP), Tween-80 and Triton X-100 were examined. Triton X-100 showed the best sensitization, so we used it as a sensitizer. The influence of its concentration on the peak current is shown in Fig. 4c. The peak current increases rapidly with increasing Triton X-100 concentration from 0.0005 to 0.0015% and decreases greatly when the concentration of Triton X-100 $>$ 0.006%. A percentage of 0.0020% for the surfactant was chosen for subsequent studies.

4.2.7. Cyclic voltammetry

Fig. 5 shows the cyclic voltammograms for the La(III)–ALC–F^-–Triton X-100 system. The ternary complex La(III)–ALC–F^- gives a cathodic peak at ~ -0.67 V due to its reduction, and no peak was observed on the anodic branch, indicating that the reduction of the ternary complex is irreversible, and the binary complex La(III)–ALC gives both a cathodic peak on the cathodic branch and an anodic peak on the anodic branch, indicating that the reduction of the binary complex is reversible. In Fig. 5 subsequent repetitive scans yielded significantly smaller (but stable) cathodic peaks corresponding to the reduction of dissolved species. This behavior indicates that the adsorption of the binary and ternary complex on the mercury electrode is reactant adsorption [23], which agrees with normal pulse polarographic data.

4.3. Analysis of air samples

The single-sweep polarographic procedure proposed in this paper can be used to determine the fluorine in air samples. According to the procedure described in the section on the preconcentration of the fluoride in air, the fluorine in the samples was collected, and its content was determined by the procedure described in the section on analysis of air samples.

The standard sodium fluoride solutions used for the preparation of calibration line were treated as described in the section on polarography of pure sodium fluoride. The regression equation of the calibration line has the form:

$$Y = 5.50X - 0.094 \quad (5)$$

where Y is the peak currrent in μA and X is the F^- concentration in μg ml^{-1}. The correlation coefficient was 0.999. The results of the determination of the fluorine in the air samples are summarized in Table 1.

4.4. Comparison between chromatomembrane method and impinger

The arrangement shown in Fig. 6 was used for the comparison between the chromatomembrane method and impinger [10]. The chromatomembrane cell 1 was used to prepare a fluorine-free air which is mixed with the gas containing HF (from the HF solution) in the mix chamber. At a certain temperature of water bath the content of HF in the gas may be maintained constant. The flow rate of air in the chromatomembrane cell 1 was constantly maintained at 0.80 dm^3 min^{-1}. The mixed gas sample was absorbed with 0.10 M NaOH solution in the chromatomembrane cell 2 (Fig. 6A) or impinger (Fig. 6B). The results obtained are shown in Table 2. These results show that the chromatomembrane method is more effictive than the impinger for the preconcentration of the fluorine in the air samples.

References

[1] S. Kaye, M. Griggs, Anal. Chem. 40 (1968) 2217.
[2] L.A. Elfers, C.E. Decker, Anal. Chem. 40 (1968) 1658.
[3] P.L. Bailey, Analysis with Ion Selective Electrodes, Heyden, London, 1976, p. 95.
[4] R. Belcher, M.A. Leonard, T.S. West, J. Chem. Soc. (1959) 3577.
[5] M.A. Leonard, T.S. West, J. Chem. Soc. (1960) 4477.
[6] R. Belcher, T.S. West, Talanta 8 (1961) 853.
[7] R. Belcher, T.S. West, Talanta 8 (1961) 861.
[8] W. Leithe, The Analysis of Air Pollutants, Ann Arbor Science, Ann Arbor, MI, 1971, p. 204.
[9] W. Leithe, The Analysis of Air Pollutants, Ann Arbor Science, Ann Arbor, MI, 1971, p. 203.
[10] W. Leithe, The Analysis of Air Pollutants, Ann Arbor Science, Ann Arbor, MI, 1971, pp. 41–43.
[11] L.N. Moskvin, A.N. Katruzov. Russian Patent. 2023488, 1994.
[12] L.N. Moskvin, O.V. Rodinkov, Ecol. Chem. (Russ. Ed.) 4 (2) (1995) 112.
[13] L.N. Moskvin, O.V. Rodinkov, J. Chromatogr. A 725 (1996) 351.
[14] L.N. Moskvin, J. Chromatogr. 669 (1994) 81.
[15] L.N. Moskvin, O.V. Rodinkov, Crit. Rev. Anal. Chem. 24 (1994) 317.
[16] L.N. Moskvin, Talanta 42 (1995) 1707.
[17] L.N. Moskvin, J. Simon, Talanta 41 (1994) 1765.
[18] P.O. Warner, Analysis of Air Pollutants, Wiley, New York, 1976, pp. 218–219.
[19] N.-J. Li, Y.-N. Zhao, X.-X. Gao, Huaxue Xuebao 42 (1984) 1062.
[20] Z.Q. Zhang, Y.C. Zhang, Chin. Chem. Lett. 2 (3) (1991) 237.
[21] F.J. Langmyhr et al., Anal. Chim. Acta, 57: 341.
[22] N.J. Li, X. Shang, Fenxi Shiyanshi 5 (8) (1986) 12.
[23] S. Deng, Fenxi Yiqi 1 (1984) 1.

ELSEVIER

Talanta 47 (1998) 33–42

Talanta

Fluorescence optical fiber sensor for tetracycline

Ying Wang [a,b,*], Wan-Hui Liu [b], Ke-Min Wang [b], Guo-Li Shen [b], Ru-Qin Yu [b]

[a] *College of Chemistry and Chemical Engineering, Southwest China Normal University, Chongqing 400715, People's Republic of China*

[b] *College of Chemistry and Chemical Engineering, Hunan University, Changsha 410082, People's Republic of China*

Received 17 September 1997; received in revised form 5 January 1998; accepted 7 January 1998

Abstract

A new optical fiber sensor for monitoring tetracycline has been described, based on the fluorescence quenching of 1,4-bis(5,5′-dimethylbenzoxazole-1′,3′-yl-2′)benzene incorporated into a thin plasticized polymer film by tetracycline extracted from aqueous phase into film phase. The sensor is fully reversible and highly reproducible. Furthermore, the sensor exhibits a linear response to tetracycline in the range 6.98×10^{-7}–8.73×10^{-5} mol l^{-1} with a detection limit of 1.06×10^{-7} mol l^{-1}, and with the response time < 30 s. The response is also selective to tetracycline, with some common pharmaceutical species, alkali and alkali-earth metal salts being highly discriminated, suggesting that the sensor can be used to monitor tetracycline in three pharmaceutical preparations. The recovery of tetracycline from commercial formulations is 95.3–98.3%. © 1998 Elsevier Science B.V. All rights reserved.

Keywords: 1,4-Bis(5,5′-dimethylbenzoxazole-1′,3′-yl-2′)benzene; Optical fiber sensor; Tetracycline

1. Introduction

Tetracycline (TC), possessing a hydronapthacene skeleton with a variety of functional groups, has been extensively used as a bacteriostatic and antibiotic drug owing to its broad-spectrum antibacterial activity. The human body eliminates 30–60% of the initial administered amount of the unchanged TC through the urine in the first 24 h, and its maximum level in serum is approximately 3–8 μg ml^{-1} [1]. Many reactions and various techniques have been developed for the determination of TC. Spectrophotometry based on the oxidation of TC with ammonium vanadate [2] and sodium cobaltinitrile [3] and the chelation of TC with metal ions and cations [4–11], fluorimetry [12–14] and derivative fluorimetry [15] have been suggested. In general, these methods proposed to determine that TC possesses limited selectivity. Differential-pulse polarography [16,17], absorptive stripping voltammetry [18] and ion-selective electrodes [19] have also been described. Methods based on the use of HPLC [20] as well as diode array [21] and ultraviolet detection [22] after HPLC separation, chemiluminometry [23–25] have been developed for the selective determination of TC. These approaches, however, require special instruments, reagents, precautions and experience.

* Corresponding author.

0039-9140/98/$19.00 © 1998 Elsevier Science B.V. All rights reserved.

PII S0039-9140(98)00049-6

The development and application of optical fiber sensors continue in exciting and expanding areas of analytical research because these sensors offer the advantages of simple design and preparation, reasonable selectivity, fast response, applicability to colored and turbid solutions. Few attempts, however, have been made to develop sensitive optical fiber sensor for TC. The only optosensor based on the TC-europium chelate from temperature phosphorescence energy transfer was published [26].

In this paper, a method for determining TC in commercial pharmaceutical preparations is proposed. The method is based on direct measurement of the sensor film fluorescence quenched by TC. The performance characteristics of the sensor with high sensitivity, good selectivity and fast response for TC were evaluated and used satisfactorily for the direct determination of TC in samples. The results for these samples are in agreement with those obtained by the conventional spectrophotometric method [4].

2. Experimental section

2.1. Apparatus

A Hitachi M-850 spectrofluorimeter was used to acquire fluorescence spectra and perform all fluorescence measurements. Optical fiber sensing experiments were carried out with an in-house-built flow-through cell (Fig. 1) which has been described in detail elsewhere [27]. A randomly distributed bifurcated bundle ($25+25$ quartz glass fibers, 6.0 mm in diameter at the common end) carried the light to and from the flow-through cell. The TC and blank solutions were continuously circulated at a flow rate of 2 ml min^{-1} with a peristaltic pump. The pH of the solution was measured with a commercial pH meter (Model PHS-3C) calibrated with pH standards of 6.86 and 9.18, respectively.

2.2. Materials

Tetrahydrofuran (THF), high-molecular weight poly(vinyl chloride) (PVC) powder, tricresyl phosphate (TCP) (C.P) and bis(2-ethylhexly)sebacate (DOS) were purchased from Shanghai Chemical. The fluorophore 1,4-bis(5,5′-dimethylbenzoxazole-1′,3′-yl-2′)benzene (BMBOB) was synthesized and purified according to the reported method [28] and identified by melting point measurement, infrared spectrum and elemental analysis. Tetracycline hydrochloride was obtained from Changsha Chemical.

Unless specified otherwise, all chemicals used were analytical-reagent grade.

2.3. Preparation of solutions

Stock tetracycline solution (1.46×10^{-3} mol l^{-1}) was prepared from tetracycline hydrochloride by directly dissolving 64.16 mg of the powder in 100 ml of water, and stored and protected from exposure light in a refrigerator, from which other concentrations were freshly obtained by appropri-

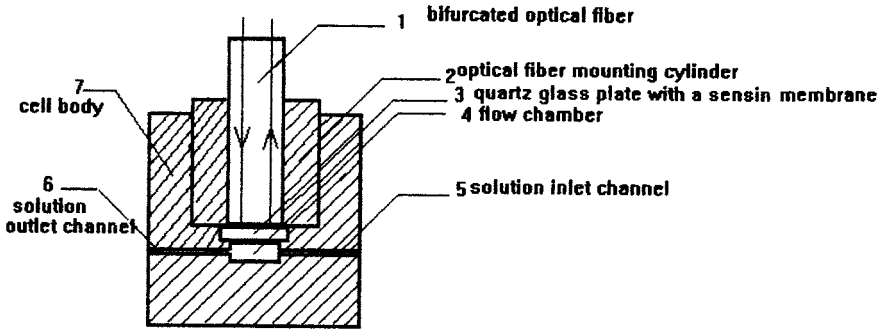

Fig. 1. Schematic diagram of the flow cell arrangement.

ate dilution. Buffer and standard solutions were prepared with deionized water.

2.4. Preparation of the sensor film

A THF film cocktail containing fluorophore was firstly prepared. An aliquot of 0.30 ml of THF solution saturated with BMBOB and additional 0.70 ml of pure THF were used to dissolve 25 mg of PVC and 50 mg of plasticizer (DOS or TCP) to obtain a homogeneous film solution. A film of about 4 μm in thickness was cast from the film solution onto a quartz glass plate of 8 mm in diameter by a spin casting film device [29].

2.5. Basic procedure

The sensor film was positioned on the top of the flow-through chamber. The sensor was conditioned by pumping the blank solution through the chamber for at least 10 min prior to all quantitative measurements, which were made at the maximum excitation and emission wavelengths of BMBOB ($\lambda_{ex} = 345$ nm, $\lambda_{em} = 400$ nm). Samples or standards were pumped through the chamber. Once the fluorescence quenching measurement was taken, blank solution was pumped into the chamber to ensure the sensor film fluorescence recovered before proceeding with the next sample or standard pump.

2.6. Sample preparation

Not less than 20 tablets were weighted and finely powdered. A sample equivalent to ~20 mg of the analyte was weighted accurately and dissolved into 100 ml of water. The powder was sonicated overnight to aid dissolution and then filtered. Working solutions were obtained from this stock solution by appropriate dilution for the final analyte concentration was within the working range.

3. Results and discussion

3.1. Quantitative basis

The extended unsaturated ring system of heterocyclic BMBOB dye produces a strong absorption in the UV region of its electronic spectrum [30], which is the result of $\pi-\pi^*$ transition. Furthermore, the molecule has turned out to be highly luminescent as well. Its emission quantum yield reaches 1.0 in *n*-hexane or 1,4-dioxane solvent [30], making it very attractive for optical fiber sensing and ease of photo detection. The strong fluorescence emission is considered to relate the resonance interaction at different positions of the class of benzoxazole compound [31]. That is, a quinoid structure with separation of positive and negative charges and with a planar configuration in the excited state exists in BMBOB molecule. Thus, the process of the fluorescence emission of BMBOB can be represented as follows:

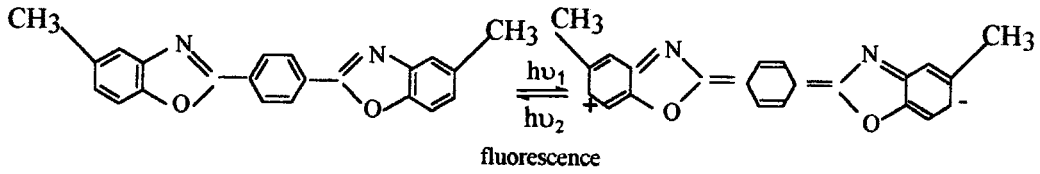

I II

In other words, the $\pi-\pi^*$ excited state reached upon light absorption is much more polar than its ground state, therefore, it may be rationalized by assuming a strong interaction of the polar molecule such as TC with the excited state BMBOB is subject to yield than with the ground state BMBOB. The presence of increasing concentration of TC in water, capable of associating tightly with the BMBOB, will displace the excited state

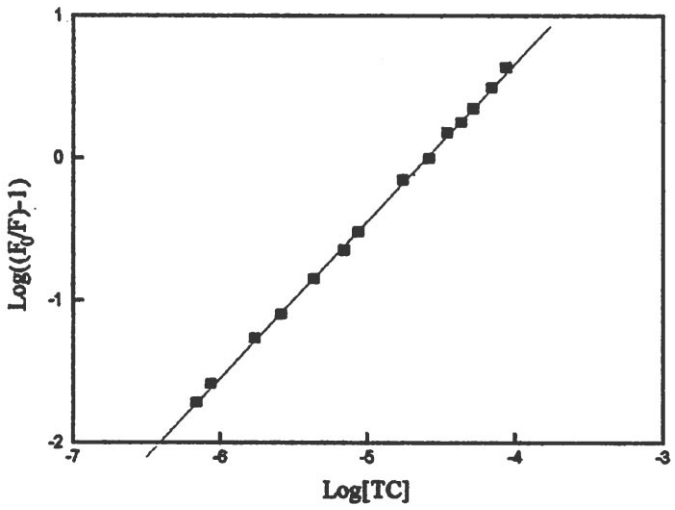

Fig. 2. Calibration curve of logarithm changes in fluorescence intensity measured with the sensor as a function of TC logarithm concentration.

equilibrium toward the formation of nonfluorescent complex. Now, let it be supposed that an extraction equilibrium was established between polymer film and the aqueous phase. For such a system, the overall extraction equilibrium reaction between BMBOB(B) and TC(T) can be written as:

$$mT(\text{aq}) + nB(\text{org}) \overset{K}{\rightleftharpoons} T_mB_n(\text{org}) \quad (1)$$

Where m/n is related to the complex ratio between TC and BMBOB.

In the case of the optical fiber sensor based on fluorescence quenching principle, the quantitative relationship determining the concentration of TC can be described in a modified Stern–Volmer equation and the relative fluorescence value (α) mode [32]:

$$\log\left(\frac{\Delta F}{F}\right) = \log K + (n-1)\log[\text{B}]_{(\text{org})} + m\log[\text{TC}]\Delta F = F_0 - F \quad (2)$$

$$\frac{\alpha^n}{1-\alpha} = \frac{1}{nK[\text{B}]^{n-1}[\text{TC}]^m} \quad (3)$$

Where $[\text{B}]_{(\text{org})}$ and [B] are defined as the equilibrium and total concentrations of BMBOB in the sensor film, respectively. [TC] represents the total concentration of TC in the aqueous sample phase. F_0 and F are the fluorescence intensity of the sensor film contacted with the blank solution and in a given TC concentration, and K is Stern–Volmer quenching constant.

It is obvious from Eq. (2) that a plot of $\log(\Delta F/F)$ versus log[TC] should give a linear relationship in which m is response slope. A log–log linear plot of the signal changes of the sensor film exposed to various concentrations of TC is demonstrated in Fig. 2. As calculated from Fig. 2, a value of $m = 1$ can be obtained. A linear response between TC concentration of 6.98×10^{-7} and 8.73×10^{-5} mol l^{-1} is also achieved by a conversion of logarithm concentration of TC. For n and Stern–Volmer quenching constant K, the different functional relationship between α and the concentration of TC can be governed by giving the different stoichiometric ratios of 1:n and quenching constant K. As shown in Fig. 3, only the curve of theoretical function of 1:1 complex ratio and a reasonable K (equilibrium constant in reaction Eq. (1)) of 4.11×10^4 is the best fit for the experimental data. Namely, the interaction yields a 1:1 complex, which results in the sensor film fluorescence quenching. Obviously, Eq. (2) and Eq. (3) are both chosen as the basis of quantitative determination of TC using the sensor.

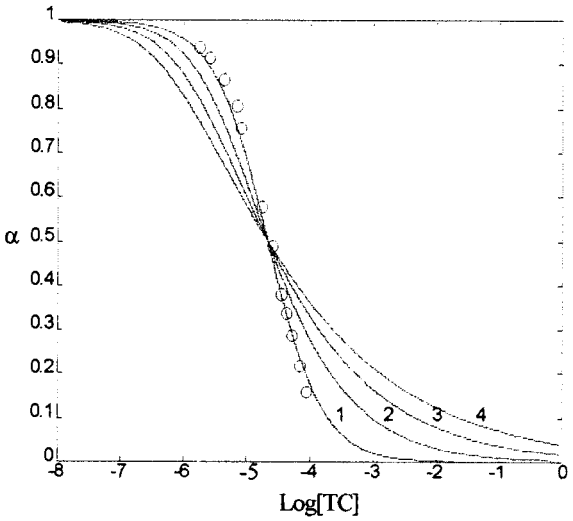

Fig. 3. Relative fluorescence values (α) as a function of log[TC]. The curves fitting the experimental data calculated from Eq. (3). (1) $m{:}n = 1{:}1$, $K = 4.11 \times 10^4$; (2) $m{:}n = 1{:}2$, $K = 1.17 \times 10^8$; (3) $m{:}n = 1{:}3$, $K = 3.09 \times 10^{16}$; (4) $m{:}n = 1{:}4$, $K = 1.97 \times 10^{19}$.

3.2. Spectrum behavior of the sensor film

The fluorescence spectra obtained from the optical fiber TC sensor at different TC concentration are shown in Fig. 4. A slight red shift of fluorescence spectra, two fluorescence maxims with a larger bandwidth, and a dramatic decrease of the fluorescence intensity with the increase of TC concentrations were observed, which is attributed to TC extracted into the sensor film, forming a excited state complex and decreasing the fluorescence emission of BMBOB. Thus, a fluorescence-based sensor for TC could be qualitatively utilized. Monitoring the wavelengths of fluorescence intensity changes centered at 345 nm of excitation and 400 nm of emission were selected for the optical fiber TC sensor described in this paper.

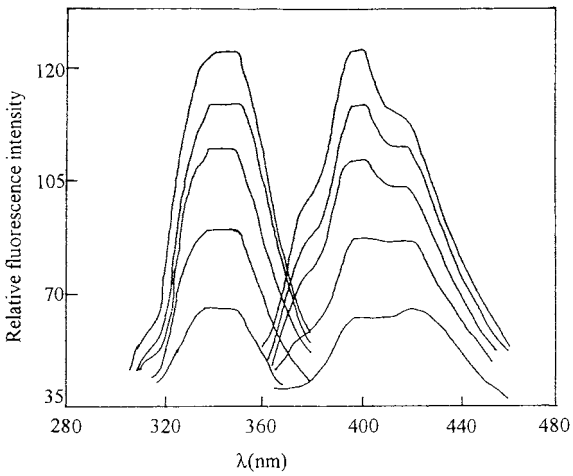

Fig. 4. Fluorescence spectra for an optical fiber TC sensor at different concentrations of TC. From top to bottom: TC concentration ($\times 10^{-6}$ mol l^{-1}): 0, 4.36, 8.73, 17.5, 34.9.

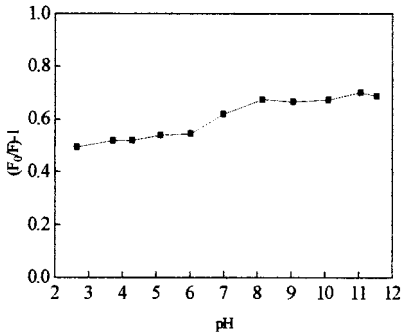

Fig. 5. pH dependence of the response of the sensor exposing to 1.46×10^{-5} mol l^{-1} TC solution.

3.3. Effect of pH

The pH dependence of the fluorescence intensity changes ($(F_0/F) - 1$) of the optical fiber sensing system for 1.46×10^{-5} mol l^{-1} TC solution is shown in Fig. 5. The response of the sensor was strongly influenced by pH. The quenching increased on going from pH 2.65 to 11.06, while decrease of quenching was observed at pH $>$ 11.06. One noted that the quenching reached a maximum value and remained a constant between pH 8.16 and 11.06. With this working pH range, TC exists mainly in molecular form [33], which is subject to being extracted into organic film phase, forming the complex with BMBOB and causing fluorescence quenching of the sensor film. In subsequent experiments, a pH 8.5 NH_3–NH_4Cl buffer solution was used.

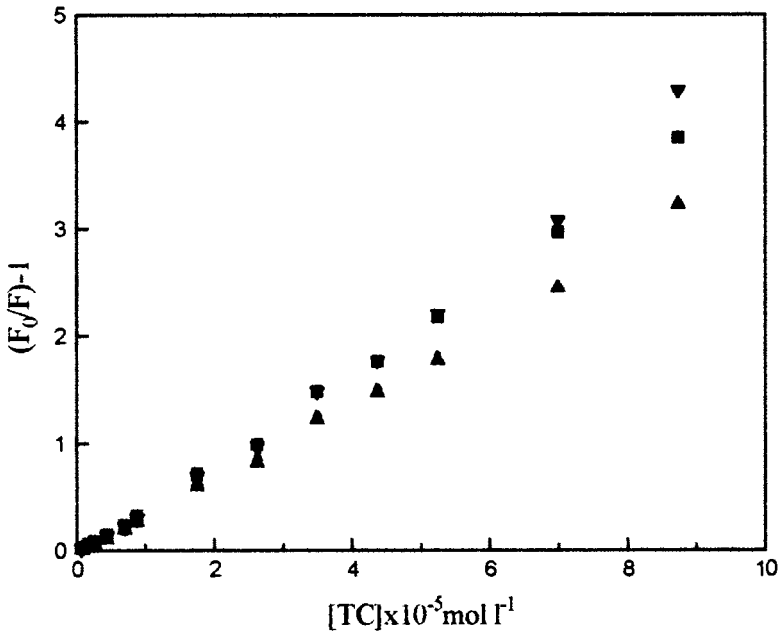

Fig. 6. Effect of plasticizers on the response of the sensor: (▲) dinonyl sebacate; (■) bis(2-ethylhexyl)sebacate; (●) dibutyl phthalate; (▼) tricresyl phosphate.

3.4. Film composition optimum

BMBOB was selected as suitable fluorophore for sensing TC based on the following criteria: high quantum yield [31], strong lipophilicity and good photostability. The BMBOB molecule, processing the planar structure and a strong intermolecular attraction, tends to approach each other and results in fairly low solubility in polar solvent [31], therefore, a volume of THF solution saturated with BMBOB was used instead of the amount optimization of BMBOB.

For film composition optimum, a THF cocktail consisting of fluorophore was firstly prepared as described for optode that contains 25 mg ml^{-1} of PVC and 50 mg ml^{-1} of plasticizer. The different volume of THF solution saturated with BMBOB and additional pure THF were used to dissolve PVC and plasticizer. These sensors made of the aforementioned film cocktails were used to examine the optimum amount of immobilized BMBOB, which was evaluated by optimizing the response of BMBOB under our experimental conditions. The response characteristics include the sensor response sensitivity and reversibility.

BMBOB incorporated in the film influenced the magnitude of the sensor response and its sensitivity. The fluorescence quenching signal of the TC sensor increased with increasing amount of BMBOB doped in the polymer film. However, more BMBOB did not produce better sensitivity. The optimal BMBOB immobilizing for the highest sensitivity was 0.30 ml of THF solution saturated with BMBOB. Further increases in BMBOB concentration resulted in poor reversibility, which was obvious when the sensor was exposed to high concentrations of TC solutions.

The TC sensors consisting of different plasticizers have been prepared. The influences of plasticizers on the sensor responses have also been studied under the present experimental conditions. The best plasticizers of the sensor were found to be DOS and TCP, which exhibited the largest Stern–Volmer quenching constant. Fig. 6 shows the experimental results. The sensitivity observed here is higher than that of the sensor made of dibutyl phthalate and dinonyl phthalate. As a result, DOS or TCP was used exclusively to prepare the sensor described below.

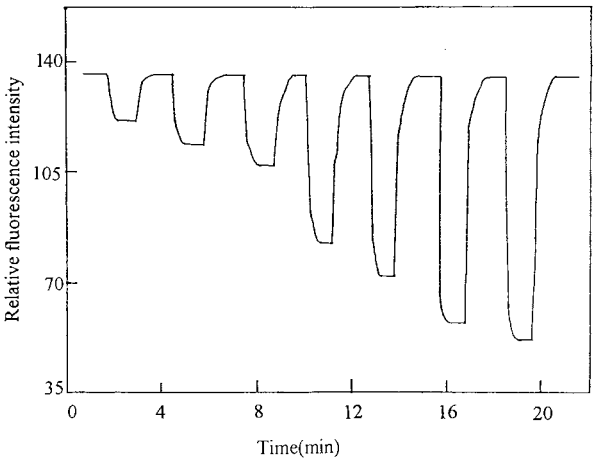

Fig. 7. Response function, response time, and reversibility of the optical fiber sensor, upon step changes of the TC concentration ($\times 10^{-5}$ mol l^{-1}). From left to right: 0.434, 0.698, 0.873, 1.75, 2.62, 3.49, 4.36.

3.5. The response characteristics of the sensor

3.5.1. Response time and reversibility

The response time and reversibility of the sensor were determined by alternating the solution flowing through the cell between any TC concentration and blank solutions. The response time was defined as the period required for the stable fluorescence signal to reach 100% of the total signal change. A response time of less than 30 s and good reversibility of the sensor are shown in Fig. 7. These results indicated that the sensor is able to rapidly and reversibly monitor the TC in sample solutions.

3.5.2. Reproducibility

An estimate of TC sensor response reproducibility was calculated as the relative standard deviations in fluorescence intensities collected from 12 consecutive and alternative measurements of 4.36×10^{-6} and 1.75×10^{-5} mol l^{-1} TC, respectively. The resulting values given in Table 1, suggested that the sensor has a good reproducibility for the determination of TC.

3.5.3. Short-term stability

In defining the short-term stability of the sensor film, blank buffer and 1.75×10^{-5} mol l^{-1} TC solution were continuously pumped through the cell at a flow rate of 1.2 ml min^{-1}. The fluorescence intensities of the sensor film were recorded over a period of 6 h with an interval of 30 min. The relative standard derivations in fluorescence intensity changes were 0.40 and 0.55%, respectively. In addition, no evidence of BMBOB washout was found. To examine this, a sensor film was soaked in a blank solution for 3 h and then removed, and the fluorescence intensity of the remaining solution was measured under the same measurement conditions used for sensing measurements, the measured intensity was only 0.3% of the unquenched intensity from the sensor film in blank solution, which was close to the noise level from the background of the measurement set-up.

3.5.4. Sensitivity

Compared to the other methods such as spectrophotometry [2–4] and chemiluminometry [25], the sensor shows a higher sensitivity (linear range and response slope) to TC. That is, TC sensor based on BMBOB is suitable for measuring a wide range (6.98×10^{-7}–8.73×10^{-5} mol l^{-1}) of TC with a detection limit of 1.06×10^{-7} mol l^{-1}, and with a response slope of 4.11×10^{4} mol $^{-1}$ l.

Table 1
The reproducibility of the sensor for 4.36×10^{-6} and 1.75×10^{-5} mol l^{-1} TC solutions

[TC] (mol l^{-1})	Fluorescence intensity	RSD [a] (%)
4.36×10^{-6}	124.8, 124.5, 124.0, 124.3, 123.5, 123.0, 123.7, 123.8, 123.0, 123.5, 123.4, 123.9	0.45
1.75×10^{-5}	83.7, 83.5, 83.4, 83.0, 82.9, 82.8, 83.0, 82.7, 83.4, 83.7, 83.6, 83.5	0.44

[a] Relative standard deviation.

Table 2
Comparison of sensing performance for tetracyclines

Compound	Linear range (mol l^{-1})	Response slope (l^{-1} mol)
Tetracycline	6.98×10^{-7} – 8.37×10^{-5}	4.11×10^{4}
Oxytetracycline	4.00×10^{-7} – 2.00×10^{-5}	3.31×10^{4}
Chlortetracycline	4.00×10^{-7} – 2.00×10^{-5}	3.53×10^{4}
Doxycycline	4.00×10^{-7} – 8.00×10^{-5}	2.53×10^{4}

3.5.5. Response to other tetracyclines

Under the same experimental conditions, the responses of the sensor to other tetracyclines (TCs) were also compared in terms of linear range and response slope. The data from the calibration graphs of $\log(\Delta F/F)$–log[TCs] are given in Table 2. The difference in response characteristics shows that the film extraction of TC is more favorable than the other TCs, given the maximum response of the sensor to TC.

3.5.6. Selectivity

Based on the possible co-concurrence of TC in the patient body with some common pharmaceutical species, alkali and alkali-earth metals, the response of the sensor to TC in the presence of the interferents was also examined. Selectivity was governed by the relative error of fluorescence intensity changes when the sensor was contacted with 8.74×10^{-6} mol l^{-1} TC as well as standard mixed solution containing 8.74×10^{-6} mol l^{-1} TC and each foreign compound. The data obtained are shown in Table 3. No significant interferences were observed, if a less than $\pm5\%$ relative error was tolerated. The practical application of the sensor for TC seems really feasible.

Table 3
Measured percent change in fluorescence intensity of the sensor for 8.74×10^{-6} mol l^{-1} TC samples varying concentrations of interfering species

Interferent	[TC] = 0.00 mol l^{-1}		[TC] = 8.74×10^{-6} mol l^{-1}	
	Concentration ($\times10^{-3}$ mol l^{-1})	Relative error [a] $(F_0-F/F)\times100$	Concentration ($\times10^{-4}$ mol l^{-1})	Relative error [b] $(F'-F/F)\times100$
KCl	6.00	0.15	530	−2.99
NH_4Cl	6.00	0.10	51.5	−0.27
$MgSO_4$	3.00	0.10	10.5	0.13
$NaNO_3$	3.00	0.00	50.5	0.27
$Ca(Ac)_2.2H_2O$	1.00	−0.30	1.05	−0.66
Ribavirin	1.00	−0.10	4.94	−0.13
Melatonin	5.00	0.10	5.09	−0.27
Theophylline	5.00	0.10	5.00	−1.59
Lidocaine	5.00	0.10	5.00	−4.52
Levamisole	5.00	0.02	6.00	−3.32
Diphenhydramine	10.0	0.03	50.0	−3.72
Amobarbital	10.0	0.00	50.0	−1.86
Ketamini	10.0	0.00	5.00	−2.93
Sulfaguanidine	5.00	0.20	5.00	−2.93
Sulfadiazine	5.00	0.20	5.00	−1.86
Naproxen	0.80	−0.50	1.02	−3.32
Tropicamide	1.00	0.00	5.10	0.13
Clindamycine	50.0	−0.10	5.03	−4.65

[a] F_0 and F are the fluorescence intensities of the sensor film contacted with blank solution and various interferents.
[b] F' and F are the fluorescence intensities of the sensor film when exposed to 8.74×10^{-6} mol l^{-1} TC solutions without and with interferents, respectively.

Table 4
Results for the drugs investigated by the proposed sensor and the spectrophotometry

Generic name and supplier	Nominal composition (mg per tablet)	Mean value ± SD [a] (TC mg per tablet)	
		The proposed sensor	The spectrophotometry
TC tablet Hunan	70 tetracycline. HCl, 80 starch, 50 lactose	70.56 ± 0.249	69.43 ± 0.530
TC tablet Hubei	160 tetracycline. HCl, 50 glucosamine. HCl, 50 starch	161.6 ± 0.533	162.8 ± 0.650
TC tablet Wh	210 tetracycline. HCl, 150 starch, 100 glucosamine. HCl	211.1 ± 0.721	210.7 ± 0.891

[a] Standard deviation of six experiments.

Table 5
Recovery experiments for tetracycline added to sample solutions of commercial pharmaceutical preparations

Generic name and supplier	Amount of tetracycline ($\times 10^{-4}$ mmol)			
	Initially present	Added	Recovered	Recovery [a] (%)
TC tablet Hunan	6.650	4.985	4.900	98.3
TC tablet Hubei	4.212	4.985	4.800	96.3
TC tablet Wh	5.122	4.985	4.750	95.3

[a] Mean value of six measurements.

4. Preliminary application

The main purpose of the investigation was to develop a simple, sensitive, and rapid method having a high degree of specificity for the determination of TC in pharmaceutical preparations. In order to evaluate the proposed sensor for its popular usage in pharmaceutical chemistry, the present sensor was applied to the determination of TC in three commercial pharmaceutical preparations. Tablets were pre-treated as described under sample preparation and analyzed according to the procedure stated under experimental section. The results given in Table 4 are in correspondence with those obtained by the spectrophotometry [4]. In order to determine the efficiency of the proposed method, pure TC was added in known amount samples prior to the assay procedure. The recovery was also satisfactory (Table 5).

Acknowledgements

The authors gratefully thank the Foundation of the Technological Development of Machinery Industry and the National Science Foundation of Hunan Province for their financial supports.

References

[1] D. Damaso, M. Móreno-López, R.M. Daza, Antibiotics Y Quimioteràpicos Antibacterianos Uso Clinico, Grutesa, Madrid, 1984.
[2] M.M. Abdel-Khalek, M.S. Molirons, Talanta 30 (1983) 792.
[3] M.S. Molirons, M.M. Abdel-Khalek, Talanta 31 (1984) 289.
[4] S.M. Saltan, I.Z. Alzamil, N.A. Alarfaj, Talanta 35 (1988) 375.
[5] M. Jelikic-Stankov, D. Veselinovic, Analyst 114 (1989) 719.
[6] M. Jelikic-Stankov, D. Stankov, D. Malesev, Z. Radovic, Microchim. Acta I (1991) 65.

[7] A.A. Alwarthan, S.A. Al-Tamrah, S.M. Sultan, Analyst 116 (1991) 183.
[8] D. Veselinovic, M. Jelikic-Stankov, Pharmazie 42 (1987) 199.
[9] I. Mori, Y. Fujita, H. Kawabe, K. Fujita, T. Tanaka, A. Kishimoto, Analyst 111 (1986) 1409.
[10] M. Jelikic, D. Vaselinovic, Vestn. Slov. Kem. Drus. 33 (1986) 199.
[11] W.B. Chang, Y.B. Zhao, Y.X. Ci, L.Y. Hu, Analyst 117 (1992) 1377.
[12] H. Poiger, Ch. Schlatter, Analyst 101 (1976) 808.
[13] A. Regosz, Pharmazie 32 (1977) 681.
[14] M. Abdel-Hady Elsayad, M.H. Barary, H. Mahgoub, Talanta 32 (1985) 1153.
[15] F. Salinas, A. Muñoz dela Pena, I. Duran Meras, Anal. Lett. 23 (1990) 863.
[16] E.E. Essien, B. Temi-Onadeko, O.F. Olushoga, An. R. Acad. Farm. 51 (1985) 495.
[17] S. Sabharwal, K. Kishore, P.N. Moorthly, J. Pharm. Sci. 77 (1988) 78.
[18] M.A. Ghandour, A.M.M. Ali, Anal. Lett. 24 (1991) 2171.
[19] A.F. Shoukry, S.S. Badawy, Microchem. J. 36 (1987) 107.
[20] N.M. Khan, E. Roets, J. Hoogmarteus, H. Vanderhaeghe, J. Chromatogr. 405 (1987) 229.
[21] T. Galeano Diaz, A. Guiberteau Cabalinas, F. Salinas, Anal. Lett. 23 (1990) 607.
[22] H. Oka, Y. Ikai, N. Kawamura, K. Uno, M. Yamada, J. Chromatogr. 400 (1987) 253.
[23] A.A. Alwarthan, A. Townshend, Anal. Chim. Acta 205 (1988) 261.
[24] T. Owa, T. Masujima, H. Yoshida, H. Imai, Bunseki Kagaku 33 (1984) 568.
[25] S.A. Halvatzis, M.M. Timotheou-Potamia, A.C. Calokerinos, Analyst 118 (1993) 633.
[26] Fausto Alava-Moreno, Marta Elena Díaz-García, Alfredo Sanz-Medel, Anal. Chim. Acta 281 (1993) 637.
[27] Y. Wang, K.M. Wang, W.H. Liu, G.L. Shen, R.Q. Yu, Anal. Sci. 13 (1997) 447.
[28] D.X. Zhang, M.S. thesis, University of Nankai, Tianjin, 1982.
[29] Y. Wang, W.H. Liu, K.M. Wang, G.L. Shen, R.Q. Yu, Analyst 12 (1997) 69.
[30] Y.M. Zhou, D.Y. Zhang, Z.H. Gao, Chem. J. Chin. Univ. 5 (1984) 488.
[31] E. Nyilas, J.L. Pinter, J. Am. Chem. Soc 82 (1960) 609.
[32] Y. Wang, W.H. Liu, K.M. Wang, J.H. Tong, G.F. Li, G.L. Shen, R.Q. Yu, Microchem. J. 58 (1998) 90.
[33] N.E. Piglr, Anal. Chem. 137 (1965) 872.

ELSEVIER

Talanta 47 (1998) 43–52

Talanta

Micellar modified spectrophotometric determination of nitrobenzenes based upon reduction with tin(II), diazotisation and coupling with the Bratton–Marshall reagent

I. Escrig-Tena [a], L. Alvarez Rodríguez [a], J. Esteve-Romero [a,*], M.C. García-Alvarez-Coque [b]

[a] *Area de Química Analítica, E.S.T.C.E., Universitat Jaume 1, 12080 Castelló, Spain*
[b] *Departament de Química Analítica, Facultat de Química, Universitat de València, 46100 Burjassot, Spain*

Received 8 August 1997; received in revised form 5 November 1997; accepted 9 January 1998

Abstract

Nitrobenzenes, such as the antibiotic chloramphenicol, the vasodilator nicardipine, and the herbicides dinitramin, dinobuton, fenitrothion, methylparathion, oxyfluorfen, parathion, pendimethalin, quintozene, and trifluralin, were determined by using a spectrophotometric method in the visible region (540 nm). The method was based on the reduction of the nitrobenzenes to arylamines with tin(II) chloride, diazotisation of the arylamines and coupling of the diazonium ions with the Bratton–Marshall reagent. The two latter reactions were performed in a micellar medium of sodium dodecyl sulphate. The linear calibration range was 2×10^{-6} to 7×10^{-5} M ($r > 0.999$), with limits of detection in the 10^{-7} M level, which is 2–6 fold lower with respect to the corresponding spectrophotometric procedure in non-micellar medium. The procedure was applied to the analysis of the compounds in commercial preparations (pharmaceuticals and herbicide formulations) and in water samples, with good recoveries. © 1998 Elsevier Science B.V. All rights reserved.

Keywords: Nitrobenzenes; Reduction with tin(II) chloride; Azo dye formation; Micellar solution

1. Introduction

The spectrophotometric determination of arylamines, based on diazotisation with nitrite and coupling with the Bratton–Marshall reagent (*N*-(1-naphthyl)-ethylenediamine dihydrochloride, NED), is largely simplified in a micellar medium of sodium dodecyl sulphate (SDS) [1,2]. In this medium, the coupling reactions are accelerated and the protonation constants of the secondary amino group of the azo dyes are shifted to higher pH values. In a non-micellar solution, the diazonium ions are formed at pH < 1, whereas pH > 4 is necessary for coupling, particularly if the diazonium ions lack a strong activating substituent.

* Corresponding author. Tel: + 34 64 345700; fax: + 34 64 345654; e-mail: estevej@nuvol.uji.es

0039-9140/98/$19.00 © 1998 Elsevier Science B.V. All rights reserved.
PII S0039-9140(98)00030-7

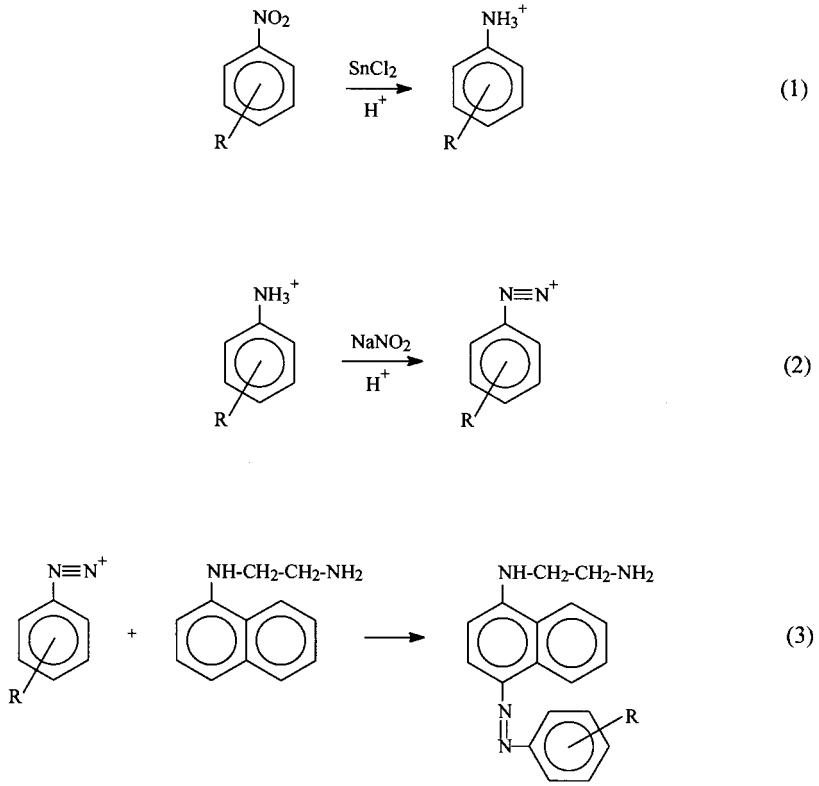

Fig. 1. Derivatisation of nitrobenzenes: (1) reduction, (2) diazotisation of arylamines, and (3) coupling of diazotised arylamines with *N*-(1-naphthyl)ethylenediamine.

Finally, another modification of the pH is usually made in order to measure the absorbance of the azo dyes in their diprotonated form. In the SDS micellar solution, the arylamines can be coupled and measured in a 0.06 M HCl solution, which results from the addition of the reagents to the 0.15 M HCl solution used to diazotise the arylamines.

The Bratton–Marshall procedure in SDS micellar medium was applied to the spectrophotometric determination of sulphonamides in pharmaceuticals [1,2], and aniline in vegetable oils [3]. More recently, a chromatographic procedure was developed for sulphonamides in pharmaceuticals [4] and urine [5]. In this procedure, the azo dyes formed pre-column in an SDS micellar medium were separated with an SDS micellar mobile phase. Another chromatographic procedure was proposed for the determination of diuretics in urine, where these compounds were hydrolysed to the corresponding arylamines in 0.15 M HCl at 100°C, previous to the formation of the azo dyes and separation with an SDS micellar mobile phase [6,7].

Other compounds are also able to produce arylamines after an adequate reaction. For example, nitrobenzenes can be quantitatively reduced to arylamines which can then be determined by the Bratton–Marshall procedure (Fig. 1) [8]. This scheme of analysis, performed in a non-micellar medium, was applied to the determination of chloramphenicol in urine after extraction of the drug in ethyl acetate to increase the selectivity of the spectrophotometric procedure, since degradation products of chloramphenicol still retain the nitro group [9]. Diphenyl ether herbicides were also determined by reduction of the nitrophenyl group to aminophenyl with zinc in ethanol [10].

Other procedures used in these determinations measure the absorbance in the UV region. These procedures are non-selective and subject to matrix interferences, such as humic substances in water samples, making quantitation and identification uncertain [11–13]. High-performance liquid chromatography (HPLC) is commonly used to separate the nitrobenzene compounds from interferences [14–16].

In this work, a colorimetric procedure is reported for the determination in micellar solution of several nitrobenzenes forming azo dyes: the antibiotic chloramphenicol and the vasodilator nicardipine in pharmaceuticals, and the herbicides dinitramin, dinobuton, fenitrothion, methylparathion, oxyfluorfen, parathion, pendimethalin, quintozene, and trifluralin, in several formulations and water samples. The reduction of the compounds to the arylamines was performed with tin(II) chloride, which has the advantage of not requiring filtration or centrifugation to remove the reduction agent, resulting in a considerable decrease in time. The shift to the visible region of the wavelength of maximum absorption (480–560 nm), upon derivatisation, produces an important enhancement in selectivity, which permits adequate analysis of several types of samples. Also, the derivatisation of the nitrobenzenes can be a previous step to be used in a liquid chromatographic separation with micellar mobile phases, for more complex samples.

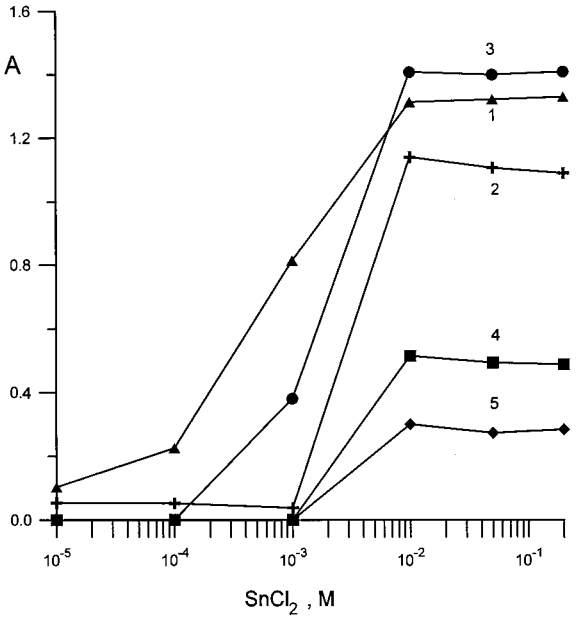

Fig. 2. Influence of the concentration of tin(II) chloride on the absorbance of the azo dyes of several nitrobenzenes: (1) nicardipine (3.5×10^{-5} M), (2) chloramphenicol (2.5×10^{-5} M), (3) nitrobenzene (3×10^{-5} M), (4) dinobuton (4×10^{-5} M), and (5) trifluralin (2×10^{-5} M). Time of reduction was 20 min.

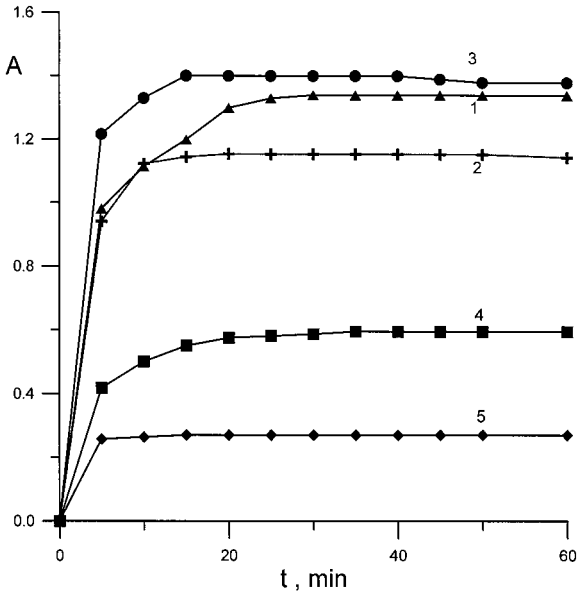

Fig. 3. Dependence of the absorbance for the azo dyes on the time of reduction with 10^{-2} M tin(II) chloride. See Fig. 2 for other details.

2. Experimental

2.1. Apparatus

The absorbance was measured with a UV-visible-near infrared spectrophotometer (Perkin Elmer Model Lambda 19, Norwalk, CT), equipped with 1 cm standard silica cells (Helma, Mülheim-Baden, Germany). The pH measurements were made with a potentiometer provided with a combined Ag–AgCl/glass electrode (Model micropH 2001, Crison, Barcelona). An ultrasonic bath (Selecta, Model 617, Barcelona) was em-

ployed to facilitate the preparation of the solutions.

2.2. Reagents

The following reagents were used: the solvents acetone, ethanol and HCl (Panreac, Barcelona, Spain), the reducing reagents tin(II) chloride (Probus, Badalona, Spain), sodium dithionite (Panreac), sodium sulfide and iron(II) chloride (Merck, Darmstadt, Germany), and the diazotisation and coupling reagents sodium nitrite (Fluka, Buchs, Switzerland), sulphamic acid (Panreac), *N*-(1-naphthyl) ethylenediamine dihydrochloride, and sodium dodecyl sulphate (Merck).

The nitrobenzenes investigated were nitrobenzene (Panreac), chloramphenicol, nicardipine (Sigma, MO), and dinitramin, oxyfluorfen (Rhône-Poulenc Agro, Madrid), dinobuton (Probelte, Barcelona), fenitrothion (Comercial Química Massó, Barcelona), methylparathion, parathion (Bayer Hispania Industrial, Barcelona), pendimethalin (Cynamid Ibérica, Madrid), quintozene (Agrodan, Madrid), and trifluralin (Makhteshim Agan, València). The herbicides were kindly donated by the Spanish laboratories indicated in parenthesis.

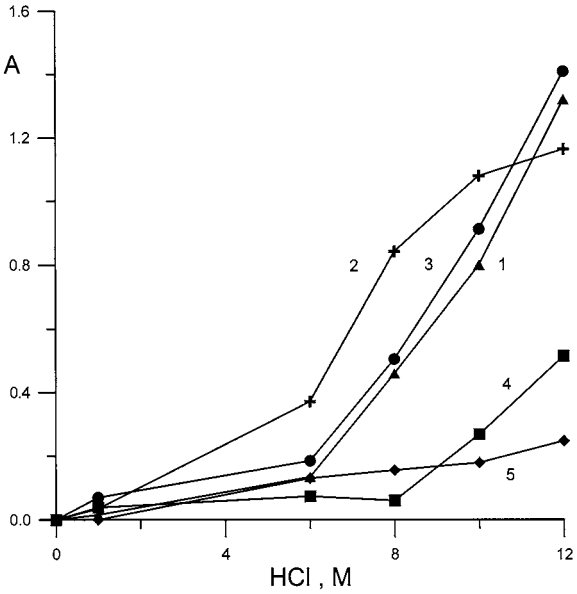

Fig. 4. Influence of HCl concentration on the reduction of the nitrobenzenes with 10^{-2} M tin(II) chloride. See Fig. 2 for other details.

The 10^{-2} M stock solutions of the reducing reagents tin(II) chloride, iron(II) chloride, sodium dithionite and sodium sulfide, were prepared daily. The two former in concentrated HCl. Stock solutions of other reagents were weekly prepared: 0.2 M sodium nitrite, 0.5 M sulphamic acid, 0.07 M SDS and 0.03 M NED. Distilled water was used throughout. The 10^{-2} M stock solutions of chloramphenicol and nicardipine were prepared by adding a small amount of ethanol to dissolve the drugs, and concentrated HCl for dilution. The 10^{-2} M stock solutions of dinitramin, dinobuton, fenitrothion, methylparathion, oxyfluorfen, parathion, pendimethalin, quintozene and trifluralin, were prepared in acetone.

2.3. Procedures

The reduction of nitrobenzenes to arylamines was achieved at room temperature by mixing, in a 25 ml volumetric flask, an aliquot of 1 ml of the compound solutions with 10 ml of 10^{-2} M tin(II) chloride dissolved in concentrated HCl. After 20 min, the volume was completed up to the mark with water. This dilution stopped the reduction process.

For the derivatisation of the arylamines, 2 ml of the reduced nitrobenzenes was introduced into a 25 ml volumetric flask, together with 8 ml of a 0.07 M SDS solution, and 1 ml of 0.2 M sodium nitrite. After 5 min, the excess nitrite was destroyed by reaction with 1 ml of 0.5 M sulphamic acid, and 10 min later, the diazonium ions were coupled with 0.5 ml of 0.03 M NED, to form the azo dye. The volume was made up to the mark with water. Absorbance was measured at 550 nm.

3. Results and discussion

3.1. Optimisation of the experimental conditions

The formation of azo dyes by diazotisation and coupling with the Bratton–Marshall reagent, in an SDS micellar medium, have been extensively described [1,2]. Therefore, the experimental condi-

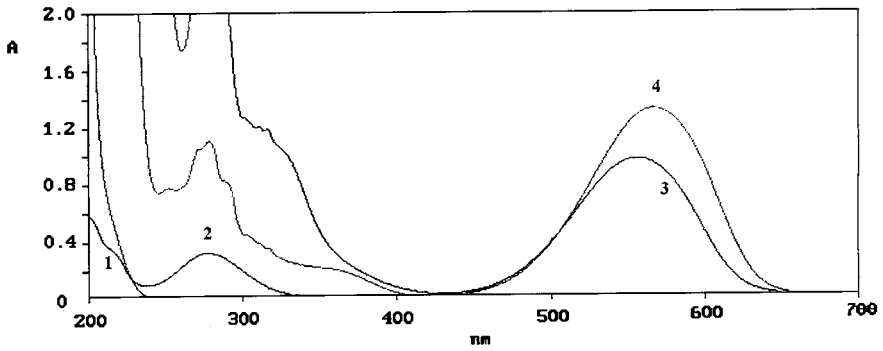

Fig. 5. Absorption spectra of 3×10^{-5} M chloramphenicol: (1) underivatised nitrobenzene, (2) arylamine obtained by reduction, (3) azo dye in non-micellar medium, (4) azo dye in micellar medium.

tions given in these reports were used. However, the previous reduction step required optimisation. This step was carried out in non-micellar solution, since when the surfactant was mixed with concentrated HCl, a turbid solution was obtained. It is well established that SDS is not stable in very acidic media and undergoes hydrolysis to form dodecanol [17].

The optimisation of the reduction step included several parameters: reducing agent concentration, time of reduction and HCl concentration. The reduction procedure consisted in mixing 1 ml of several 10^{-2} M nitrobenzene solutions with 10 ml of the reducing reagent solutions in the 10^{-5} to 0.2 M range, prepared at different HCl concentrations. After a variable time 0–24 h, the volume was made up to 25 ml with water. Four reducing agents: tin(II) chloride, iron(II) chloride, sodium dithionite and sodium sulfide, and five nitrobenzenes: chloramphenicol, dinobuton, nicardipine, nitrobenzene, and trifluralin, were examined.

3.1.1. Selection of the reducing agent

The yellow colour of the iron(III) solution obtained by oxidation of iron(II) chloride interfered with the absorbance measurements of the derivatised arylamines. Thus, this reagent was not further considered. Only tin(II) chloride reduced all nitrobenzenes studied, as shown by the formation of the red azo dyes. However, the dinitrobenzenes dinitramin and pendimethalin, did not give any colour at 550 nm, which is near the wavelength of maximum absorption of the azo dyes in micellar solution. Dinitramin has also an amine substituent, therefore, it is possible that both compounds were reduced but the arylamines produced did not undergo coupling. Dithionite and sulfide only partially reduced nicardipine. The molar absorptivity for this compound was 37000 l^{-1} mol cm^{-1} if reduced with $SnCl_2$, and only 700 l^{-1} mol cm^{-1} if dithionite and sulfide were used.

Fig. 2 shows the absorbance of different azo dyes for varying concentrations of $SnCl_2$. The signal increased up to 10^{-2} M $SnCl_2$ and then remained constant at greater concentrations. $SnCl_2$ is dissolved very slowly in concentrated HCl, especially at concentrations greater than 1×10^{-2} M. Since good reproducibility was achieved for this concentration, it was preferred to greater concentrations of the reagent. A blank prepared in the absence of the nitrobenzenes gave only a negligible absorbance ($A = 0.005 \pm 0.001$, $n = 8$).

3.1.2. Optimisation of the reduction time

The effect of the reduction time was examined. Fig. 3 shows that the absorbance increased for 20 min after the addition of the reducing agent, and then, leveled off. The absorbance was almost the same after 24 h. This indicated that the reduction time was not critical.

3.1.3. Optimisation of the HCl concentration

The concentration of HCl affected the reduction reaction. For this study, $SnCl_2$ was prepared in HCl of varying concentration in the 0–12 M range. Fig. 4 shows that the reduction should be

Table 1
Spectral data and analytical characteristics for the azo dyes obtained after reduction of the nitrobenzenes

Compound	Medium [a]	λ_{max} (nm)	ε (mol^{-1} l cm^{-1})	LOD (M)	C.V. (%), n = 3
Chloramphenicol 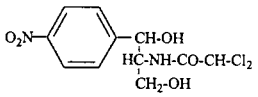	SDS	561	46000	10^{-7}	0.5
	nmm	558	26000	2×10^{-7}	0.8
Nicardipine 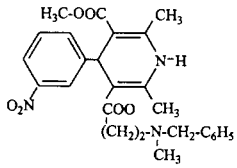	SDS	553	37000	10^{-7}	0.3
	nmm	550	23000	2×10^{-7}	0.8
Dinobuton 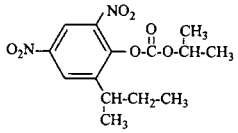	SDS	545	14500	3×10^{-7}	0.2
	nmm	560	4000	10^{-6}	0.3
Fenitrothion 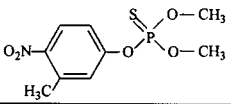	SDS	551	26500	2×10^{-7}	0.3
	nmm	516	4500	10^{-6}	1.7
Methylparathion 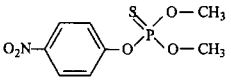	SDS	565	44000	10^{-7}	0.4
	nmm	560	13000	3×10^{-7}	1.3
Nitrobenzene 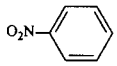	SDS	559	46500	10^{-7}	0.8
	nmm	553	8000	5×10^{-7}	1.2
Oxyfluorfen 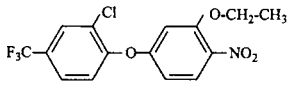	SDS	488	14500	3×10^{-7}	0.5
	nmm	488	9500	5×10^{-7}	1.1
Parathion 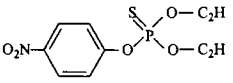	SDS	564	36000	10^{-7}	0.5
	nmm	554	17000	3×10^{-7}	1.7
Quintozene 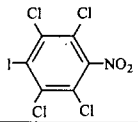	SDS	486	10000	5×10^{-7}	0.6
	nmm	475	9000	6×10^{-7}	0.9
Trifluralin 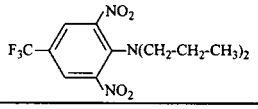	SDS	542	11000	4×10^{-7}	0.1
	nmm	500	7000	7×10^{-7}	0.9

[a] nmm = non micellar medium

Table 2
Determination of nitrobenzenes in pharmaceutical preparations and herbicides

Compound	Preparation (laboratory)	Declared composition	Recovery (%)	C.V. (%) $n = 3$
Chloramphenicol	Colircusi Medrivas Antibiótico (Cusí, Barcelona)	per ml: 20 mg Medroxyprogesterone acetate 0.5 mg tetrizoline Chlorhydrate 7.3 mg Chloramphenicol (sodium succinate)	99.4	0.4
Nicardipine	Lecibral (Nezel, Barcelona)	per pill: 20 mg Nicardipine chlorhydrate excipients	106	0.8
	Dagan (Tedec-Meiji Farma, Madrid)	per pill: 20 mg Nicardipine chlorhydrate excipients	96.8	0.1
	Nicardipino Seid (Seid, Barcelona)	per pill: 20 mg Nicardipine chlorhydrate excipients	99.6	2.8
Fenitrothion	Sumimix (Comercial Química Massó, Barcelona)	per 100 ml: 5 g Fenopatrin 25 g Fenitrothion	81.9	0.2
	Sumicombi 5/25 LE Comercial Química Massó	per 100 ml: 5 g Fenvalerate 25 g Fenitrothion	81.4	0.1
	Sumithion Forte LE (Comercial Química Massó)	per 100 ml: 2 g Fenvalerate 50 g Fenitrothion	81.2	1.8
	Sumithion 50 (Comercial Química Massó)	per 100 ml: 50 g Fenitrothion	94.5	1.0
Parathion	Folidol 20 PM (Bayer Hispania Industrial, Barcelona)	per 100 g: 20 g Parathion	101	1.0
Quintozene	Medeclorex Espolvoreo (Agrodan, Madrid)	per 100 g: 75 g Quintozene	106	1.2
Trifluralin	Agrolan (Agrodan)	per 100 ml: 48 g Trifluralin	91.7	1.7
	Triflurex 48 EC (Makhteshim Agan, Valencia)	per 100 ml: 48 g Trifluralin xylene	104	2.5
	Premerlin 600 EC (Makhteshim Agan)	per 100 ml: 60 g Trifluralin	90.4	0.8

performed in concentrated HCl. After a convenient dilution, this concentration was reduced to 0.3 M, adequate for the diazotisation and coupling reaction of the arylamine products in the SDS micellar medium.

3.1.4. Stability of the azo dyes

The stability of the azo dyes was checked by preparing a stock solution of each, and measuring the absorbance at different times up to a month. The absorbance remained almost constant during this time period, indicating that the azo dyes were highly stable. Therefore, reproducible measurement of the absorbance could be made without a strict control of time. Fig. 5 shows the spectra of the compounds before and after derivatisation in micellar and non-micellar medium.

Table 3
Analysis of water samples

Compound	Water sample	Added (μg ml^{-1})	Found (μg ml^{-1})
Dinobuton	Distilled	1	1.00 ± 0.07
	Cistern		0.90 ± 0.06
	Irrigation ditch		1.00 ± 0.05
	River		0.90 ± 0.05
	Sea		0.98 ± 0.05
	Swimming pool		1.02 ± 0.06
	Tap		1.05 ± 0.06
Fenitrothion	Distilled	0.5	0.43 ± 0.04
	Cistern		0.52 ± 0.04
	Irrigation ditch		0.49 ± 0.03
	River		0.44 ± 0.02
	Sea		0.46 ± 0.02
	Swimming-pool		0.41 ± 0.04
	Tap		0.47 ± 0.05
Methylparathion	Distilled	0.2	0.17 ± 0.01
	Cistern		0.19 ± 0.02
	Irrigation ditch		0.19 ± 0.01
	River		0.18 ± 0.03
	Sea		0.18 ± 0.03
	Swimming-pool		0.17 ± 0.02
	Tap		0.20 ± 0.02
	Distilled	1	0.92 ± 0.09
	Cistern		0.90 ± 0.09
	Irrigation ditch		0.90 ± 0.20
	River		0.75 ± 0.10
	Sea		0.95 ± 0.12
	Swimming-pool		0.95 ± 0.08
	Tap		0.90 ± 0.08
Oxyfluorfen	Distilled	1	0.93 ± 0.04
	Cistern		1.05 ± 0.05
	Irrigation ditch		1.02 ± 0.03
	River		1.10 ± 0.03
	Sea		1.04 ± 0.04
	Swimming-pool		0.98 ± 0.03
	Tap		1.08 ± 0.03
	Distilled	2	2.07 ± 0.05
	Cistern		2.09 ± 0.05
	Irrigation ditch		2.10 ± 0.05
	River		1.95 ± 0.04
	Sea		1.90 ± 0.04
	Swimming-pool		2.01 ± 0.03
	Tap		2.10 ± 0.05
Parathion	Distilled	0.11	0.12 ± 0.01
	Cistern		0.11 ± 0.01
	Irrigation ditch		0.11 ± 0.01
	River		0.10 ± 0.01
	Sea		0.11 ± 0.01
	Swimming-pool		0.11 ± 0.01
	Tap		0.11 ± 0.01

Table 3 (Continued)

Compound	Water sample	Added (μg ml^{-1})	Found (μg ml^{-1})
Quintozene	Distilled	2	2.32 ± 0.03
	Cistern		2.27 ± 0.04
	Irrigation Ditch		2.34 ± 0.02
	River		2.09 ± 0.05
	Sea		2.26 ± 0.04
	Swimming-pool		2.26 ± 0.06
	Tap		2.12 ± 0.03
Trifluralin	Distilled	1	0.94 ± 0.06
	Cistern		1.07 ± 0.05
	Irrigation ditch		1.20 ± 0.10
	River		1.13 ± 0.13
	Sea		0.94 ± 0.15
	Swimming-pool		1.05 ± 0.05
	Tap		1.05 ± 0.05

3.2. Analytical figures

Table 1 shows the wavelength of maximum absorption and molar absorptivities for the azo dyes of several nitrobenzenes. Limits of detection (LODs, 3s criterion) and repeatabilities are also given. The data obtained in SDS micellar and non-micellar media are compared. It may be observed that the sensitivity is enhanced in the presence of micelles, especially for nitrobenzene and fenitrothion with a 6-fold increase in their molar absorptivities.

Trifluralin absorbed at 426 nm without derivatisation, therefore, a more direct spectrophotometric procedure could be used for this compound. However, the molar absorptivity for the underivatised compound was 2400 mol^{-1} l cm^{-1}, lower than the value obtained for the corresponding azo dye. Also, at the shorter wavelength other accompanying compounds in the analysed samples interfered.

3.3. Determination of nitrobenzenes in pharmaceuticals, herbicide formulations and water samples

The optimised procedure was applied to the determination of some nitrobenzenes in commercial pharmaceuticals (pills and drops), herbicide formulations and spiked water samples (Tables 2 and 3). Nicardipine pills were ground in a mortar and dissolved with a mixture of ethanol and HCl (1:9) for analysis. The same solution was used for diluting aliquots of the drops containing chloramphenicol. The solid samples of the herbicide formulations of parathion and quintozene, and the liquid samples of fenitrothion and trifluralin were dissolved with acetone. The analytical procedure was conducted in triplicate for each sample. The data are summarised in Table 2. The recoveries were calculated with respect to the contents declared by the manufacturers.

Finally, some water samples, including distilled, cistern, irrigation ditch, river, sea, swimming-pool and tap water, were collected in the city of Almassora (Castelló, Spain), from which spiked samples were prepared by addition of solutions of several herbicides (dinobuton, fenitrothion, methylparathion, oxyfluorfen, parathion, quintozene, and trifluralin). The results of the analysis are shown in Table 3.

Mutual interference will exist if several different nitrobenzenes are present in the sample solution. Also, interference from arylamines which are diazotised and coupled with the Bratton–Marshall reagent should be expected. Previous work have shown that the azo dyes of sulphonamides [4,5] and some hydrolysed diuretics [6,7] can be ade-

quately separated using micellar mobile phases. Currently, this possibility is being studied in our laboratory for the azo dyes of nitrobenzenes.

Acknowledgements

This work was supported by the DGICYT Project PB94-967 and the BANCAIXA Project P1A97-16 (Spain). I. Escrig-Tena thanks the Universitat Jaume I of Castelló, Spain, for a postdoctoral grant.

References

[1] G. Ramis Ramos, J.S. Esteve Romero, M.C. García Alvarez-Coque, Anal. Chim. Acta 223 (1989) 327.
[2] J.S. Esteve Romero, M.C. García Alvarez-Coque, G. Ramis Ramos, Talanta 38 (1991) 1285.
[3] J.S. Esteve Romero, E.F. Simó Alfonso, M.C. García Alvarez-Coque, G. Ramis Ramos, Anal. Chim. Acta 235 (1990) 317.
[4] M.C. García Alvarez-Coque, E.F. Simó Alfonso, G. Ramis Ramos, J.S. Esteve Romero, J. Pharm. Biomed. Anal. 13 (1995) 237.
[5] E.F. Simó Alfonso, G. Ramis Ramos, M.C. García Alvarez-Coque, J.S. Esteve Romero, J. Chromatogr. Biomed. Appl. 670 (1995) 183.
[6] J.S. Esteve Romero, E.F. Simó Alfonso, M.C. García Alvarez-Coque, G. Ramis Ramos, Talanta 40 (1993) 1711.
[7] S. Carda Broch, M.C. García Alvarez-Coque, E.F. Simó Alfonso, J.S. Esteve Romero, Anal. Chim. Acta 353 (1997) 215.
[8] R.E. Schirmer, Modern Methods of Pharmaceutical Analysis, vol. I, CRC Press, Boca Raton, FL, 1982.
[9] A.J. Glazko, L.M. Wolf, W.A. Dill, Arch. Biochem. 23 (1949) 411.
[10] K. Ishikawa, E. Kamo, A. Sasaki, S. Kuzuoka, Y. Yonekura, K. Suzuki, T. Ito, Eisei-Kagaku 31 (1985) 72.
[11] J.R. Bowser, P.F. Gavin, N.D. Danielson, Microchem. J. 47 (1993) 163.
[12] D.W. Berberich, R.A. Yost, D.D. Fetterolf, J. Forensic Sci. 33 (1988) 946.
[13] H. Huang, H. Li, Yaowu-Fenxi-Zashi 10 (1990) 359.
[14] J.J. Lewis, D.W. Yordy, LC–GC 8 (1990) 54.
[15] P. Cabras, M. Melis, L. Spanedda, C. Tuberoso, J. Chromatogr. 585 (1991) 164.
[16] T.V. Reddy, B.E. Wiechman, E.L. Lin, L.W. Chang, M.K. Smith, F.B. Daniel, G. Reddy, J. Chromatogr. A 655 (1993) 331.
[17] C.J. Garnett, A.J. Lambie, W.H. Beck, M. Liler, J. Chem. Soc. Faraday Trans. 1 79 (1983) 953.

ELSEVIER

Talanta 47 (1998) 53–58

Talanta

pH-Metric determination of acid numbers in petroleum oils without titration

Ya.I. Tur'yan, E. Strochkova, O.Yu. Berezin, I. Kuselman *, A. Shenhar

The National Physical Laboratory of Israel, Danziger A. Building, The Hebrew University, Givat-Ram, Jerusalem 91904, Israel

Received 27 August 1997; received in revised form 21 November 1997; accepted 9 January 1998

Abstract

A new pH-metric method without titration has been developed for determination of acid numbers lower than 0.1 mg (KOH) g^{-1} (oil) in petroleum oils such as White, Transformer and Basic oils. The method is based on rapid and complete extraction of acids from an oil test portion into the novel reagent and measurement of the conditional pH in the 'oil–reagent' mixture by a glass electrode. The method has a quantitation limit equal to 1×10^{-3} mg (KOH) g^{-1} (oil), uses non-toxic reagents, is not time and labor consuming, and is cheap and simple for automation. © 1998 Elsevier Science B.V. All rights reserved.

Keywords: Acid number; Metrological characteristics; Petroleum oils; pH-metry

1. Introduction

The acid number (AN) is an important characteristic of petroleum oil's quality because conductive, corrosive and some other properties of the oils are dependent on AN. The AN is expressed in milligrams KOH necessary for titration of the acids contained in 1 g oil [1–3]. The same characteristic of vegetable oils is named the 'acid value' (AV) [4].

National and international standards for AN determination in petroleum oils [1–3] recommend methods of acid–base titration in nonaqueous systems. These methods are time and labor consuming, and difficult for automation. They use toxic and flammable solvents, for example toluene, as well as nonaqueous alkali titrants which are very sensitive to carbon dioxide contamination from the atmosphere. The difficulties are accentuated for the determination of AN < 0.1 mg (KOH) g^{-1} (oil) (Transformer, White, Basic and other oils). In this case the titration should be carried out in nitrogen atmosphere and, besides the indicator, a color witness is also used for more correct determination of the end point of the titration [1,2].

Alternative methods for AN or AV determination without titration have been considered by us [4]. We believe that pH-metry is the most attractive method for AN determination.

The pH-metric methods are based on the use of a reagent in the form of a weak base in a suitable solvent [5–9]. We consider the solvent to be a

* Corresponding author. Tel.: +972 2 6536534; fax: +972 2 6520797; e-mail: kuselman@netvision.net.il

0039-9140/98/$19.00 © 1998 Elsevier Science B.V. All rights reserved.
PII S0039-9140(98)00031-9

component of the reagent, taking into account the large influence of the solvent on the completeness of the acid–base analytical reaction. Two types of reagents are used. The reagents of the first type dissolve the test portion together with acids [5,6], while the reagents of the second type extract the acids from the test portion [7,8] or from its non-aqueous solution [9]. These last reagents include water in a significant concentration which leads to the following important advantages: (i) reducing the reagent sensitivity to carbon dioxide contamination from the atmosphere (pH drift after sample introduction into the reagent was practically absent); (ii) a rapid response (within 1 min) [10]; and (iii) long (over 1 year) steady work of the pH glass indicator electrode and aqueous reference electrode, which is essential for automatic control on-line. Such a reagent has been developed by us for AV determination in vegetable oils [7,8] and oilseeds [9]. This reagent consists of 0.2 M triethanolamine (TEA), as a weak base, in a mixture of water and isopropanol, 1:1 (vol.%). The reagent forms with the vegetable oil a two-phase system (emulsion) and completely extracts the corresponding acids over 3–4 min. The pH-metric determination of the total concentration of the acids is possible under the following conditions: (i) equilibrium of the reaction between the acids in the oil and the weak base in the reagent should be shifted to the right side; (ii) the weak base (TEA, for example) in the reagent should be greatly in excess in comparison with the total concentration of the acids; and (iii) the ionic strength of the reagent during analysis should be practically constant. To satisfy the last requirement, 0.01 M KNO_3 is used as a component of the reagent.

When all these conditions are fulfilled, the conditional pH value of the 'reagent–oil' mixture, pH′, is dependent linearly on the logarithm of the total acid concentration N_a (eqv l^{-1}) [4]. Such dependence allows AN to be determined by pH′ measurement. The value pH′ is conditional because the measurement of pH is carried out with an aqueous reference electrode and glass indicator electrode calibrated by the usual aqueous buffer solutions.

Several pH-metric techniques for AV determination in vegetable oils have been discussed [7]. The preferable technique consists of AV calculation from results of two pH measurements: the first one is pH'_1 in the 'reagent–oil' system and the second one is pH'_2 after the standard acid (HCl) addition to the system.

The metrological parameters of this technique (repeatability, reproducibility, accuracy and others) are satisfactory [8,11]. It is now transformed into a peer-verified method [12].

Application of the pH-metric approach to petroleum oils met with a number of difficulties. AN values of some petroleum oils, such as White, Transformer or Basic, are 0.002–0.006 mg (KOH) g^{-1} (oil) [1,2], while the limit of quantitation of the method discussed above for vegetable oils is only 0.02 mg (KOH) g^{-1} (oil) [13].

The present paper describes the development of the new reagent for the pH-metric determination of AN in the range 0.001–0.1 mg (KOH) g^{-1} (oil).

2. Experimental

2.1. Apparatus

The pH-meter PHM 95 with a glass electrode G 202 C, Ag/AgCl, KCl 3M electrode REF 251 (Radiometer, Denmark) and a magnetic stirrer for the pH-metric cell 'E. Fried Electric' (Israel) were used for pH measurements. A microburette (2 ml) with 0.01 ml divisions (Bein ZM, Israel) was used for titration with the tip changed by us to decrease the drop size up to 0.008 ml.

2.2. Reagents

Potassium chloride and potassium hydroxide GR were purchased from Merck (Darmstadt, Germany), sodium benzoate (NaBen) GR from Sigma (St. Louis, MO, USA), isopropanol CP and toluene from Frutarom (Haifa, Israel), hydrochloric acid GR and buffers from BDH (Poole, UK), *p*-naphtholbenzein from Aldrich (Milwaukee, WI, USA), naphthenic acid EEC No. 215628 from Fluka (Buchs, Switzerland), light White oil from Sigma (St. Louis, MO, USA), Basic oil from 'Basic Oil' (Haifa, Israel), and Transformer oil from a local supplier.

2.3. Procedures

AN values of purchased commercial White, Transformer and Basic oils were determined by the standard titration method [1]. In accordance with this standard, a weighed oil test portion was added to the solvent consisting of a mixture of toluene, isopropyl alcohol and water. The solution was titrated at a room temperature under nitrogen atmosphere. Titration was performed against standardized 0.01 M potassium hydroxide in isopropyl alcohol using the microburette up to a stable end-point indicated by the *p*-naphtholbenzein indicator.

The naphthenic acid was used for fortification of the oil samples. The acid number of the naphthenic acid $(AN)_{NA}$ was determined by the same titration method. The amount Q (g) of the naphthenic acid which should by added to the amount G (g) of the purchased oil was calculated by the following formula:

$$Q = G[(AN)_p - (AN)_0]/[(AN)_{NA} - (AN)_p] \quad (1)$$

where $(AN)_p$ is the planned AN of the fortified oil; $(AN)_0$ is the AN of the initial (purchased) oil. The AN values of the fortified samples were determined by the standard titration described above.

The same oil samples were analyzed by the proposed pH-metric method. All analyses were performed in five replicates.

3. Results and discussion

3.1. Development of the reagent

The basicity and concentration of the weak base in the reagent have a strong influence on the accuracy of the AN pH-metric determination, especially in the case of low AN (less than 0.1 mg (KOH) g^{-1} (oil)). This fact is explained by the hydrolysis (solvolysis) of the weak base which leads to the same product as the analytical reaction. Therefore, the hydrolysis is a source of positive errors, significant especially for low AN. The decrease of basicity and concentration of the weak base in the reagent allows these errors to be decreased [14] and, hence, to decrease the limit of quantitation of the method.

So, for petroleum oils with low AN, the weak base must have lower basicity and lower concentration than the TEA used in the reagent for vegetable oils [7]. Our choice for the weak base was an anion in the salt of a weak acid and strong base, like benzoate-anion Ben^- in sodium benzoate (NaBen), 0.05 M [15]. In this case the analytical reaction has the following form:

$$\left(\sum_1^m HAn_i\right)_{oil} + m\,Ben^- \rightarrow \sum_1^m An_i^- + m\,HBen \quad (2)$$

where $(\Sigma\, HAn_i)_{oil}$ is the sum of acids in the oil. Corresponding to the above conditions, the dependence of pH′ versus total acid concentration N_a is the following:

$$pH' = A - \log N_a \quad (3)$$

where A is a constant for the given pH-sensor, reagent and temperature:

$$A = A_s^\circ - \log K_S^\circ/(K_B^\circ \cdot C_{NaBen} \cdot f_{Ben^-}) \quad (4)$$

K_S° is the thermodynamic autoprotolysis constant for the given solvent; f_{Ben^-} is the activity coefficient ($f_{HBen} \approx 1$); K_B° is the thermodynamic constant for the basic dissociation of the weak base in the given solvent, and C_{NaBen} is the concentration of the weak base in the reactive mixture. The value A_S° depends on the standard potential of the glass electrode in a given solvent and also on the interfacial potential on the boundary with the aqueous reference electrode.

The influence of the hydrolysis (solvolysis) of the benzoate-anion

$$Ben^- + H_2O \leftrightarrow HBen + OH^- \quad (5)$$

on the results of the analytical reaction is considerably lower in comparison with TEA (for example, in water pK_B° for Ben^- is 9.80 [16], and for TEA is 6.23 [17]), which allows the limit of quantitation to be significantly decreased.

The weak base, i.e., anion of salt NaBen should be greatly in excess of the total concentration N_a of acids in the 'reagent-oil' mixture in order to ensure linearity of the dependence pH versus log N_a (Eqs. (3) and (4)). A considerable excess of the salt also stabilizes the ionic strength of the reagent. Hence, the special addition of an indifferent salt to the reagent for this purpose, as was

done in Ref. [7], was unnecessary in the present case.

The solvent for the reagent was the mixture of isopropanol and water. Its composition is determined by two limiting conditions: (1) the insolubility of oil, but solubility of benzoic acid (formed by the reaction shown in Eq. (2)) in the solvent; and (2) the possibility of using a conventional aqueous pH-metric sensor.

Concentrations of isopropanol below 80% ensure the practical insolubility of petroleum oils in the solvent, and hence the influence of an oil matrix on the solvent properties is absent. An oil sample and the proposed reagent form a two-phase system (emulsion). A decrease of the isopropanol concentration in the solvent below 50% leads to incomplete extraction of the acids. On the other hand, for stable functioning of the pH-metric sensor, the reagent must contain a maximum amount of water in the solvent. Hence, the optimal composition of the reagent is the following: 0.05 M NaBen in the solvent consisting of water and isopropanol, 1:1 (vol.%).

The reagent assures the complete extraction of acids from an oil test portion, when the ratio of the mass (g) of the oil test portion to the volume (ml) of the reagent is equal to or less than 1.1:1.0. The complete extraction of acids into the reagent can be fulfilled during 2–3 min of stirring (dependent on conditions of stirring).

An important characteristic of the reagent is its initial conditional pH (pH'_0). The influence of the pH'_0 value on the result of the analysis is explained by the simultaneous reactions shown in Eqs. (5) and (6):

$$\left(\sum_{1}^{m} HAn_i\right)_{oil} + mOH^- \leftrightarrow \sum_{1}^{m} An_i^- + mH_2O \qquad (6)$$

Because the influence of pH'_0 on equilibrium in Eqs. (5) and (6) is opposite, an optimum pH'_0 value should be found. The latter is reached [5] when the concentrations of [HBen] and [OH^-] in the reagent are equal. In this case the undesirable increase of [HBen] due to Eq. (5) (in addition to the analytical reaction shown in Eq. (2)) is compensated approximately by the decrease of [HBen] concentration in conformity with Eqs. (2) and (6).

The optimum pH'_0 value at the condition [HBen] = [OH^-] has been determined by the potentiometric (pH-sensor) titration of a strong acid (HCl) added to the reagent against KOH solution in the same reagent. The optimum pH'_0 value corresponds to the conditional pH at the equivalence point of the titration (Fig. 1). For the pH-sensor used and ionic strength 0.05, the value of pH'_0 was 9.87 ± 0.02. This value is lower than that for the reagent with TEA. The novel reagent is therefore less sensitive to CO_2 contamination from the atmosphere. For adjustment of the pH of the reagent up to pH'_0 during its preparation, a small volume of aqueous KOH solution is added.

The linear range of the dependence pH′ versus $\log N_a$ with slope 0.999 (square of the correlation coefficient $r^2 = 0.998$) obtained by us was observed for N_a from 2.0×10^{-5} to 3.1×10^{-4} M (Fig. 2). At $N_a < 2.0 \times 10^{-5}$ M, a deviation of the dependence from linearity takes place. It can be explained by the influence of hydrolysis (solvolysis) of the Ben^- anion in Eq. (5). From the low limit of N_a in the linear range of the dependence (2.0×10^{-5} M), it follows that the limit of AN quantitation is $AN_{LOQ} = 1.0 \times 10^{-3}$ mg (KOH) g^{-1} (oil), the maximum mass of an oil sample being 55 g for a reagent volume of 50 ml. This value of the limit of the quantitation is about 20 times smaller than that for the TEA reagent [13] and it is sufficient for the characterization of the petroleum oils with AN $\leqslant$ 0.1 mg (KOH) g^{-1} (oil).

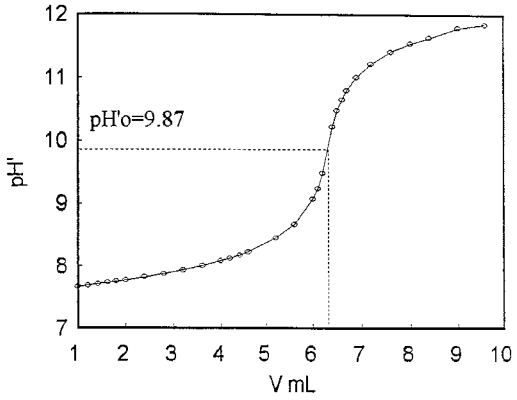

Fig. 1. The curve of titration HCl, 1×10^{-3} M in a mixture of 0.05 M NaBen in a solvent of 50% water + 50% isopropanol (vol.%), against KOH, 1×10^{-2} M.

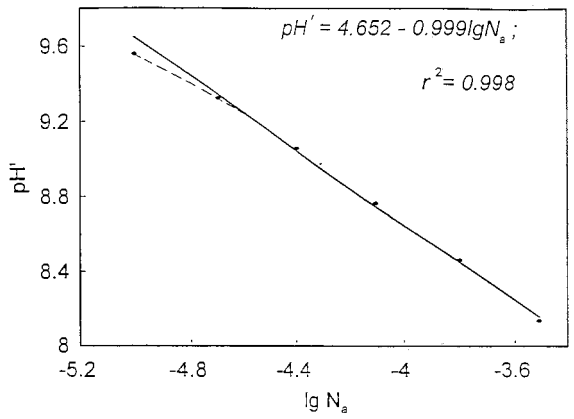

Fig. 2. Dependence of pH′ vs. $\log N_a$ for a reagent consisting of 0.05 M NaBen in a solvent of 50% water + 50% isopropanol (vol.%), $pH'_0 = 9.87$.

As far as the standard addition method is used for AN determination (see below), the maximum N_a under determination should be 2–3 times lower than the upper limit of N_a in the linear range of the dependence pH′ versus $\log N_a$ (3.1×10^{-4} M), i.e., 1.0×10^{-4} to 1.5×10^{-4} M. One can see that the concentration of the salt $C_{NaBen} = 0.05$ M and the same concentration of the weak base (Ben^-) is sufficiently large in relation to these N_a values. Simultaneously, this NaBen concentration ensures the constant ionic strength.

3.2. Test portion preparation

The oil sample should be well mixed and entirely liquid before analysis. The mass of an oil test portion for AN determination should approximately ($\pm$ 10%) correspond to Table 1. According to this mass, the necessary volume of the oil test portion is calculated using the density, which is approximately 0.9 g ml^{-1}. If the expected AN (Table 1) is unknown, the test portion volume can be simply evaluated as an oil volume which should be added to 50 ml of the reagent in order to decrease its pH′ up to 8.7–9.0.

Table 1
Mass of test portion and volume of the standard HCl addition

Expected AN	Mass of test portion for analysis (g)	Addition of 0.05 M HCl (V_{st}) (ml)
0.001–0.005	30–50	0.04–0.1
0.005–0.02	10–25	0.04–0.2
0.02–0.1	1–10	0.05–0.2

The oil test portion, introduced in a beaker, is determined by the difference of the weights of the beaker before and after the oil transfer into the pH-metric cell.

3.3. Measurements

Introduce about 50 ml of the reagent into the pH-metric cell with the oil test portion, and simultaneously turn on the stirrer to provide a good mixing of the components, avoiding pulling air bubbles into the mixture. Introduce the electrodes into the cell and after 3 min read pH'_1. Add a certain volume of the standard 0.05 M HCl aqueous solution (see Table 1), through stirring and again read pH'_2. The optimal $\Delta pH' = pH'_1 - pH'_2 \approx 0.25$–$0.40$.

The calculation of the AN is carried out according to the following formula, obtained from Eq. (3):

$$AN = 56.11 \cdot N_{st} \cdot V_{st} / [m \cdot (10^{\Delta pH'} - 1)] \quad (7)$$

where 56.11 is the molecular weight of KOH; N_{st} is the concentration of the standard HCl solution (M); V_{st} is the volume of the added standard HCl solution (ml); m is the mass of the oil sample (g).

3.4. Precision and accuracy of the results

Table 2 shows: the average results obtained by standard titration and the proposed novel method from $n = 5$ replicates for each sample AN_s and AN_p, respectively; standard deviations for these replicates, S_s and S_p, respectively; $F = S_p^2/S_s^2$; and $t = |AN_s - AN_p|/[(S_s^2 + S_p^2)/5]^{0.5}$.

The critical value for the F-ratio is 6.39 at the 95% level of confidence and the number of degrees of freedom $n - 1 = 4$. For the t-ratio, the critical value is 2.31 at the 95% level of confidence and the number of degrees of freedom $2(n - 1) = 8$. From the comparison of F-data with the critical value, it follows that differences between the precision of results obtained by the standard titration and by the proposed technique are insignifi-

Table 2
Comparison of the results of AN determination by the standard titration method and those obtained by the proposed novel method

No.	Oil	Standard titration		Proposed technique		F	t
		AN_s	S_s	AN_p	S_p		
1	White	0.0028	0.0001	0.0027	0.0001	1.31	2.07
2	White fortified	0.0108	0.0004	0.0105	0.0003	0.47	0.96
3	White fortified	0.1144	0.0011	0.1158	0.0027	5.55	1.07
4	Transformer	0.0020	0.0001	0.0019	0.0001	0.70	1.37
5	Transformer fortified	0.0106	0.0003	0.0105	0.0006	4.48	0.57
6	Transformer fortified	0.1626	0.0039	0.1568	0.0044	1.25	2.21
7	Basic	0.0060	0.0002	0.0061	0.0002	0.82	0.53
8	Basic fortified	0.0153	0.0014	0.0140	0.0006	0.20	1.96
9	Basic fortified	0.1556	0.0069	0.1472	0.0054	0.62	2.13

cant (all F-values are less than 6.39). The accuracy of these techniques is approximately the same, such that the deviations of the average AN results obtained by the proposed method from the average results obtained by the standard technique are insignificant in comparison with the random errors (all t-values are less than 2.31).

Hence, the precision and accuracy obtained by the proposed pH-metric method are sufficient for the quality control of oils.

3.5. Advantages of pH-metric method

The pH-metric method allows AN values to be determined in the range 0.1–0.001 mg (KOH) g^{-1} (oil). The method uses non-toxic reagents, is simple, is not time and labor consuming, has low cost and is facile for automation.

Acknowledgements

The authors would like to express their gratitude to Professor E. Shoenberger for helpful discussions.

References

[1] Standard Test Method for Acid Number of Petroleum Products by Semi-Micro Color Indicator Titration, American National Standard D3339-87, 1987.
[2] Specification for Unused Mineral Insulating Oils for Transformers and Switchgear, IEC Standard 296, International Electrotechnical Commission, Geneva, 1982.
[3] Petroleum Products and Lubricants—Neutralization Number–Color–Indicator Titration Method, ISO-6618-1987 (E), International Organization for Standardization, Switzerland, 1987.
[4] O.Yu. Berezin, Ya.I. Tur'yan, I. Kuselman, A. Shenhar, Talanta 42 (1995) 507.
[5] Ya.I. Tur'yan, O.E. Ruvinskii, S.Ya. Sharudina, J. Anal. Chem. USSR 46 (1991) 661.
[6] T.M. Lapshina, Ya.I. Tur'yan, S.I. Danilchuk, J. Anal. Chem. USSR 46 (1991) 833.
[7] Ya.I. Tur'yan, O.Yu. Berezin, I. Kuselman, A. Shenhar, J. Am. Oil Chem. Soc. 73 (1996) 295.
[8] O.Yu. Berezin, Ya.I. Tur'yan, L. Kogan, I. Kuselman, A. Shenhar, Proc. 11th Int. Conf. Israel Society for Quality, November 19–21, 1996, pp. 536–538.
[9] O.Yu. Berezin, Ya.I. Tur'yan, I. Kuselman, A. Shenhar, J. Am. Oil Chem. Soc. 73 (1996) 1707.
[10] G. Johansson, K. Norberg, J. Electroanal. Chem. 18 (1968) 239.
[11] I. Kuselman, A. Shenhar, Accred. Qual. Assur. 2 (1997) 180.
[12] I. Kuselman, Ya.I. Tur'yan, O.Yu. Berezin, L. Kogan, A. Shenhar, Inside Lab. Management 1 (1997) 36.
[13] O.Yu. Berezin, Ya.I. Tur'yan, L. Kogan, I. Kuselman, A. Shenhar, J. Am. Oil Chem. Soc. 74 (1997) 1339.
[14] Ya.I. Tur'yan, V.F. Pokhodzei, D.A. Krukier, Izv. Vyssh. Uchebn. Zaved., Pisch. Tekhnol., Krasnodar USSR 3 (1989) 39.
[15] E.M. Strochkova, O.Yu. Berezin, Ya.I. Tur'yan, I. Kuselman, A. Shenhar, Israel Patent Applic. No. 120819 (11 May 1997).
[16] Yu.Yu. Lur'e, Reference Book on Analytical Chemistry, Khimiya, Moscow, 1989, p. 299.
[17] R.G. Bates, G. Schwarzenbach, Helv. Chim. Acta 37 (1954) 1437.

ELSEVIER

Talanta 47 (1998) 59–66

Talanta

Titrimetric micro determination of some phenothiazine neuroleptics with potassium hexacyanoferrate(III)

K. Basavaiah [a,*], G. Krishnamurthy [b]

[a] *Department of Studies in Chemistry, University of Mysore, Manasagangotri, Mysore-570006, India*
[b] *Department of Chemistry, PES College of Science, Mandya-571401, India*

Received 18 August 1997; received in revised form 14 January 1998; accepted 15 January 1998

Abstract

Three simple, rapid and accurate titrimetric procedures using potassium hexacyanoferrate(III) have been developed for the micro determination of five phenothiazine drugs in pure form and in dosage forms. The procedures are based on the oxidation of phenothiazines in an acid medium to colourless sulphoxides via orange or purple coloured products. In the first procedure, phenothiazines are titrated directly in H_2SO_4–H_3PO_4 medium to a colourless end point. In the second method, a known excess of the oxidant is added and after a specified time, the residual oxidant is determined iodometrically. The third method employs electrometric end-point detection. The optimum reactions conditions and other analytical parameters are evaluated. The influence of the substrates commonly employed as excipients with phenothiazine drugs has been studied. Statistical comparison of the results with those of an official method shows excellent agreement and indicates no significant difference in precision. © 1998 Elsevier Science B.V. All rights reserved.

Keywords: Phenothiazine drugs; Titrimetry; Potentiometric end-point detection; Potassium hexacyanoferrate(III)

1. Introduction

Phenothiazines represent a major class of drugs used as neuroleptics in the treatment of schizophrenia and other psychotic illnesses [1]. They are also used as antiallergics, antiemetics, analgesics and sedatives. The therapeutic interest in these compounds justifies research to establish analytical methods for the determination of these drugs in pharmaceutical preparations and biological samples. Several methods have been proposed for the determination of phenothiazines and their dosage forms. Titrimetry in non-aqueous media and UV-spectrometry are the recommended procedures for the pure form and formulations, respectively, in the British Pharmacopoeia [2]. Other titrimetric methods include complexometry [3], amperometry [4], thermometry [5], coulometry [6], conductometry [7], potentiometry [8], and bromimetry using a bromate–bromide mixture [9] or *N*,*N*-dibromo dimethyl hyantoin (DBH) [10]. Spectrophotometric methods including differential spectrometry [11], the Fourier function method

* Corresponding author. Tel.: +91 821 515525; fax: +91 821 421263.

0039-9140/98/$19.00 © 1998 Elsevier Science B.V. All rights reserved.
PII S0039-9140(98)00057-5

[12] and derivative spectrophotometry [13] have also been reported. Other methods include fluoroimmunoassay [14], HPLC [15], adsorptive voltammetry [16], spectrofluorimetry [17], GLC [18] and chemiluminescence measurement [19].

Potassium hexacyanoferrate(III) has been used extensively in the determination of a vast number of compounds, particularly, of pharmaceutical interest [20–22]. In this paper we describe three convenient methods for the determination of five phenothiazine-based drugs in the pure form and in pharmaceutical preparations using hexacyanoferrate(III) as an oxidizing agent. The methods are of general applicability and are quick and simple compared with the established procedures [2].

2. Experimental

2.1. Apparatus

Potentiometric titrations were performed using Equiptronics digital potentiometer model EQ-DGM equipped with bright platinum and calomel electrodes.

2.2. Reagents

All chemicals were of analytical reagent grade. A 1×10^{-2} M stock solution of potassium hexacyanoferrate(III) (BDH, Glaxo, India) was prepared by dissolving the required amount of compound in water and standardized iodometrically [23]. A titrant of lower concentration was prepared by dilution and standardized in the same manner.

A 1×10^{-2} M solution of sodium thiosulphate (S.D. Fine Chemicals, India) was prepared by dissolving the requisite amount of the compound in distilled water and standardized iodometrically [24].

Potassium iodide (10%), zinc sulphate (4%), sulphuric acid (10 M), phosphoric acid (10 M) and starch indicator (0.5%) solutions were prepared by using analytical reagent grade chemicals.

2.3. Standard solutions of phenothiazines

Stock standard solutions containing 2000 μg ml^{-1} drug were prepared by dissolving weighed amount of promethazine hydrochloride, PH (Rhone-Poulenc); triflupromazine hydrochloride TPH (Sarabhai); prochlorperazine maleate, PCPM (Rhone-Poulenc); fluphenazine hydrochloride, FPH (Sarabhai) or thioproperazine mesylate, TPPM (Rhone-Poulenc) in distilled water.

For the dissolution of PCPM, a few drops of dilute HCl were used. The solutions were kept in amber coloured bottles and stored in a refrigerator. Working solutions were prepared daily by appropriate dilution of the stock solution in water.

2.4. Analytical procedures

2.4.1. Direct titration (A)

A 5.0 ml aliquot of phenothiazine drug solution containing 1–8 mg PH, 1–7 mg TPH, 1–10 mg PCPM, FPH or TPPM was transferred to a 50 ml titration flask and 10 ml of 10 M sulphuric acid and 2 ml 10 M orthophosphoric acid were added. Potassium hexacyanoferrate(III) (1×10^{-2} M) was added slowly from a 10 ml burette with continuous stirring by magnetic stirrer. At first, a purple or orange colour developed and the titration was continued until the colour discharged completely. From the volume of hexacyanoferrate(III) consumed, the amount of drug was calculated using the following equation:

$$\text{Amount of drug (mg)} = \frac{VMR}{n}$$

where V is millilitres of hexacyanoferrate(III) consumed in the titration, M is the molecular weight of the drug, R is the molarity of hexacyanoferrate(III) solution, and n is the number of moles of hexacyanoferrate(III) reacting with 1 mol of the drug.

2.4.2. Back titration (B)

A known volume (5 ml) of the drug solution containing 1–6 mg PH or TPH, 1–10 mg PCPM, FPH or TPPM was placed in an 100 ml Erlenmeyer flask and 5 ml 10 M sulphuric acid (7 ml in

the case of FPH and TPPM) and 5 ml 1×10^{-2} M hexacyanoferrate(III) (accurately measured) were added. The mixture was shaken occasionally and, after a specific time (Table 1) the mixture was diluted to about 60 ml and 5 ml 4% zinc sulphate and 5 ml 10% potassium iodide solutions were added and the liberated iodine was titrated with 1×10^{-2} M sodium thiosulphate using starch indicator. A blank was run in the same way. The amount of the drug was calculated from the equation:

$$\text{Amount of Drug (mg)} = \frac{(V_1 - V_2)MR}{n}$$

where V_1 is millilitres of thiosulphate solution consumed in the blank titration, V_2 is millilitres of thiosulphate solution consumed in the test sample titration, M is the molecular weight of the drug, R is the molarity of hexacyanoferrate(III) solution, and n is the number of mol of hexacyanoferrate(III) reacting with 1 mol of the drug.

2.4.3. Potentiometric titration (C)

In the potentiometric titration, a 5.0 ml aliquot containing 2–5 mg PH, or TPH 2–10 mg PCPM, FPH or TPPM was transferred to a 100 ml beaker. Sulphuric acid (10 μl 10 M) was added, the mixture was stirred magnetically and the titrant (1×10^{-2} or 1×10^{-3} M) added using a 10 ml burette. From the volume of hexacyanoferrate(III) consumed, the amount of drug was calculated from the same equation given for method A.

2.5. Procedure for pharmaceutical formulations

2.5.1. Tablets

Forty tablets were weighed and pulverised (80 in the case of stemetil, emidoxyn and majeptil). An amount of the powder equivalent to about 200 mg of the pure drug was weighed. The powder was extracted with three 30 ml portions of water (a few drops of dilute HCl were used in the case of PCPM) and filtered into a 100 ml standard flask, the filter was washed and the flask made up to the mark with water. A suitable aliquot of this solution was analysed by either of the above methods.

2.5.2. Ampoules

The contents of 20 ampoules were mixed. An accurately measured volume equivalent to 200 mg of the pure drug was transferred into a 100 ml calibrated flask, made up to the mark with water and an aliquot was analysed as for the tablets. In the case of anatensol and prolinate injections, the contents of the ampoules were treated with a few drops of dilute HCl and warmed before making up to the mark.

3. Results and discussion

Chemical oxidation is a well known reaction that has been extensively exploited for the determination of phenothiazines [25]. The proposed methods are based on the fact that hexacyanoferrate(III) ions in an acidic medium directly oxidise phenothiazine to a purple or orange phenothiazonium radical cation and finally to the colourless sulphoxide. A proposed mechanism is presented in Fig. 1 in conformity with the 1:2 reaction ratio observed. For all the three procedures sulphuric acid was found to be the ideal reaction medium. In direct titration, the presence of phosphoric acid was found to be necessary to sharpen the colour change at the end point. For detection of the end-point in the direct titration as well as the potentiometric titration, the titration should be performed slowly around the end-point. The back titration was attempted to decrease the amount of acid used in the direct titration and the zinc salt was added to ensure quick and irreversible oxidation of iodide by hexacyanoferrate(III) [26] through the removal of ferrocyanide [27]. In all the cases, only 2 mol hexacyanoferrate(III) per mol of the drug were consumed, indicating that the oxidation of phenothiazines stopped at the sulphoxides formation and further oxidation to sulphones did not take place despite a high acid concentration, in contrast to the assumption that sulphones would be formed under high acid conditions [28].

Table 1
Analytical data for the tritration of phenothiazines

Drug	Method A			Method B				Method C					BP method
	Molar ratio	Range (mg)	Recovery (%)	Molar ratio	Reaction time (min)	Range (mg)	Recovery (%)	Molar ratio	Overall potential break (mV)[a]	Steepness near the equivaence point (mV 0.1 ml^{-1})[a]	Range (mg)	Recovery (%)	Recovery (%)
PH	1:2	1–8	98.63	1:2	5	1–6	100.79	1:2	235	225	2–5	100.34	100.34
TPH	1:2	1–7	97.78	1:2	6	1–6	99.84	1:2	255	205	2–5	100.46	99.41
PCPM	1:2	1–10	97.69	1:2	5	1–10	99.52	1:2	215	145	2–10	99.93	100.71
FPH	1:2	1–10	98.26	1:2	10	1–10	99.04	1:2	235	165	2–10	99.63	99.63
TPPM	1:2	1–10	98.84	1:2	15	1–10	98.65	1:2	210	145	2–10	100.66	—

[a] For titrations of 2.5×10^{-3}–3.4×10^{-3} M drug solutions vs. 1×10^{-2} M hexacyanoferrate(III).

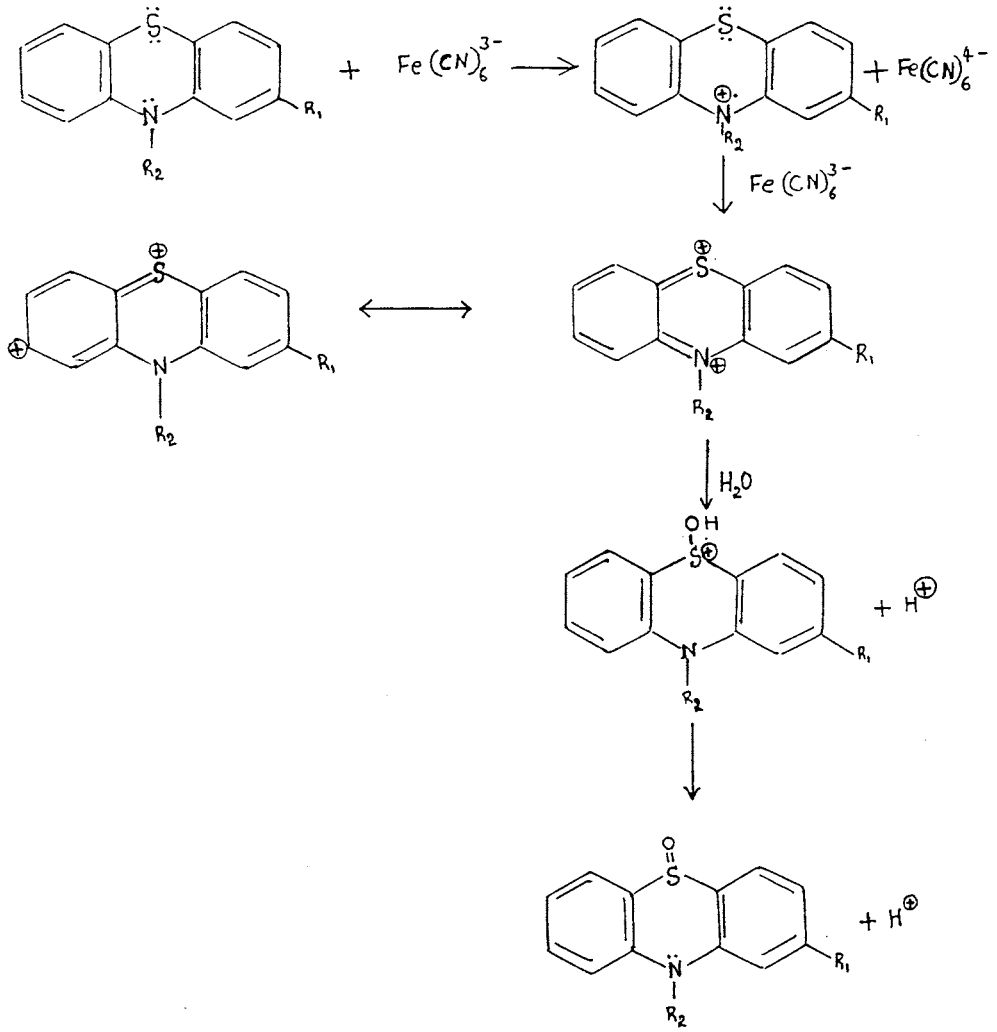

Fig. 1. mechanism of reaction between phenothiazines and hexacyanoferrate(III).

3.1. Interference studies

Interference from the common excipients and additives likely to be present together with the phenothiazines in commercial formulations was studied. Starch, talc, dextrose, magnesium stearate, sodium alginate, gelatin, and sodium sulphite in levels found in formulations did not interfere under experimental conditions.

3.2. Application of the procedures

The proposed methods were applied to the determination of the drugs studied in dosage forms. The results in Table 2 indicate that the methods give good accuracy and precision, with satisfactory agreement with the results obtained by the methods in the British Pharmacopoeia (BP) [2]. The calculated F- and t-values given in Table 3 do not exceed the tabulated values except in

Table 2
Analysis of phenothiazines in various formulations

Formulation	mg/tablet or mg ml^{-1}	Proposed methods									BP method		
		Method A			Method B			Method C			Found (mg)	Recovery[a] (%)	R.S.D. (%)
		Found (mg)	Recovery[a] (%)	R.S.D. (%)	Found (mg)	Recovery[a] (%)	R.S.D. (%)	Found (mg)	Recovery[b] (%)	R.S.D. (%)			
PH													
Phenergan tablets	10	9.86	98.6	0.52	10.09	100.9	1.65	10.15	101.5	0.38	9.98	99.8	0.55
	25	24.60	98.4	0.71	24.78	99.12	1.32	24.90	99.6	0.71	24.90	99.6	0.48
Phena tablets	10	9.70	97.0	1.14	10.14	101.4	0.96	9.87	98.7	0.53	10.01	100.1	0.36
	25	24.80	99.2	0.97	25.01	100.0	0.73	24.78	99.1	0.22	25.20	100.8	0.28
Phenergan injection	25	24.20	96.8	0.62	25.34	101.3	1.14	24.60	98.4	0.84	24.85	99.0	0.71
TPH													
Siquil tablets	10	9.82	98.2	0.39	10.20	102.0	1.04	9.85	98.5	0.72	9.92	99.2	0.35
Siquil injection	10	9.78	97.8	0.60	9.86	98.6	0.85	9.94	99.4	1.14	9.85	98.5	0.52
PCPM													
Stemetil tablets	5	4.92	98.4	0.55	4.96	99.2	0.64	5.02	100.4	0.66	5.02	100.40	0.48
Stemetil injection (as mesylate)	12.5	12.36	98.8	0.49	12.58	100.6	0.85	12.42	99.3	0.48	12.62	100.9	0.49
FPH													
Anatensol injection (as deconate)	25	24.72	98.8	1.56	24.84	99.3	0.84	25.34	101.3	0.22	25.24	101.0	0.53
Prolinate injection (as deconoate)	25	24.66	98.6	1.38	24.62	98.5	0.63	25.12	100.4	0.40	25.13	100.5	0.62
TPPM													
Majeptil tablets	5	4.89	97.8	0.76	4.93	98.6	1.50	4.96	99.2	0.38	—	—	—

[a] Average of five detreminations.
[b] Average of three determinations.

Table 3
Statistical analysis between the proposed and BP methods

Value	PH				TPH				PCPM				FPH				TPPM		
	A	B	C	Official	A	B	C	Official	A	B	C	Official	A	B	C	Official	A	B	C
n	6	6	4	5	6	6	4	5	6	6	4	5	6	6	4	5	6	6	4
Mean	98.63	100.79	100.31	100.34	97.78	99.84	100.46	99.41	97.69	99.52	99.97	100.71	98.26	99.04	99.63	99.26	98.84	98.65	100.66
S.D. (*S*)	0.95	1.21	0.52	0.90	1.07	0.66	0.74	0.46	0.88	1.12	0.82	0.75	0.65	0.76	0.71	0.43	1.05	0.28	0.70
Variance (S^2)	0.90	1.46	0.27	0.81	1.14	0.44	0.55	0.21	0.77	1.25	0.67	0.56	0.42	0.58	0.50	0.18	1.10	0.08	0.49
Student's *t*-test	3.05	0.70	0.06	—	3.63	1.26	2.60	—	4.06	2.09	1.40	—	3.05	0.66	0.97	—			
	(2.26)	(2.26)	(2.36)	—	(2.26)	(2.26)	(2.36)	—	(2.36)	(2.26)	(2.26)	—	(2.26)	(2.26)	(2.36)				
Variance ratio (*F*-test)	1.11	1.80	0.33	—	5.45	2.1	2.62	—	1.38	2.23	1.20	—	2.33	3.22	2.80				
	(6.26)	(6.26)	(9.12)	—	(6.26)	(6.26)	(6.26)	—	(6.26)	(6.26)	(6.59)	—	(6.26)	(6.26)	(6.59)				

Figures in parentheses are the tabulated values at 95% probability level.

respect of the direct titration, hence, there are no significant differences between the proposed and BP methods with respect to accuracy and precision.

4. Conclusion

In conclusion, the results of the titrations indicate that the proposed methods are simpler than and superior to many existing methods and do not require special working conditions. The chloramine-T method [29] is not suitable for micro determination. In the perchloric acid method [30], the medium has to be scrupulously anhydrous. This is inconvenient in practice and even trace amount of water will affect the results. As the reagent is unstable, the *N*-bromosuccinimide method of Pathak et al. [31] is unreliable. The complexometric method [3] involves the filtration of the complex before titrating the unreacted metal. Thermometry [5] requires an expensive experimental set up. Hence, the proposed methods can be recommended for the routine determination of phenothiazines in their pure form and in their preparations. Besides, owing to the stability of the solid reagent and reasonable stability of its solution, hexacyanoferrate(III) can be used for routine analysis.

Acknowledgements

The authors are grateful to the Quality Control Managers of Sarabhai Chemicals, and Rhone-Poulenc, India, for gifts of the pure drug samples.

References

[1] A.S. Horn, Dopamine receptors, in: C. Hansch (Ed.), Comprehensive Medicinal Chemistry, vol. 3, Pergamon Press, Oxford, 1990, pp. 287–288.
[2] The British Pharmacopoeia, HMSO, London, 1993, pp. 552, 1079, 1080, 546, 1074, 1076, 291, 920.
[3] M. Gajewska, Chem. Anal. 18 (1973) 651.
[4] V.I. Tkach and N.G. Timoshenko, Farm. Zh. (Kiev) 2 (1988) 79; Anal. Abstr. 50(10E) (1988) 54.
[5] U.M. Abbasi, M. Siddiqui, M.I. Bhangas, J. Chem. Soc. Pak. 13 (1991) 242.
[6] Z. Feher, I. Kolbe, E. Pungor, Fresenius' Z. Anal. Chem. 332 (1988) 345.
[7] K. Basavaiah, P.G. Ramappa, Indian J. Pharm. Sci. 50 (1989) 231.
[8] S.M. Golabi, M. Showkati-Shishevan, Talanta 38 (1991) 1253.
[9] J. Blazek, Cslka Farm. 15 (1966) 200.
[10] M.I. Walash, M. Rizk, A.-M. Abou-ouf, F. Belal, Analyst 108 (1983) 626.
[11] L. Long, Y. Zhang, Yaowu Fenxi Zarhi, 15 (1995) 45; Anal. Abst. 57(2G) (1995) 175.
[12] H. Mehgrub, M.A. Korany, H. Abdine, E.M. Abdel-Hady, Anal. Lett. 24 (1991) 1797.
[13] P. Ryclovsky, I. Nemcova, Cesk Farm. 38 (1989) 241; Anal. Abstr. 52(6E) (1990) 34.
[14] A. Mounsey, D. Strachan, F.T. Rowell, V. Rowell, J.D. Tyson, Analyst 121 (1996) 955.
[15] D. De Orsi, L. Gagliardi, D. Tonelli, J. Pharm. Biomed. Anal. 14 (1996) 1635.
[16] Z.Q. Zhang, Z.G. Chen, H. Zhang, Microchem. J. 53 (1996) 282.
[17] F.A. Mohamed, Anal. Lett. 28 (1995) 2491.
[18] I.L. Zhuravleva, M.B. Terenina, R.V. Golovnya, M.A. Filiminova, Khim.-Farm. Zh. 5 (1993) 58; Anal Abstr. 56(9G) (1994) 2.
[19] J.L. Lopez Paz, A. Townshend, Anal. Commun. 33 (1996) 31.
[20] M.S. Mehrous, M.M. Abdel-Khalek, M.E. Abdel-Hamid, Talanta 32 (1985) 651.
[21] F.A. Aly, F. Belal, M.I. Walash, J. Pharm Biomed. Anal. 12 (1994) 955.
[22] A. Kojlo, H. Puzanowska-Tarasiewicz, Anal. Lett. 26 (1993) 593.
[23] J. Bessett, R.C. Denny, G.H. Jaffery and J. Mendham, Vogel's Text Book of Quantitative Inorganic Analysis, 4th ed., Longman, Harlow, 1987, p.385.
[24] J. Bessett, R.C. Denny, G.H. Jaffery and J. Mendham, Vogel's Text Book of Quantitative Inorganic Analysis, 4th ed., Longman, Harlow, 1987, p.375.
[25] J. Karpinska, B. Starczewska, H. Puzanowska-Tarasiewicz, Anal. Sci. 12 (1996) 161.
[26] F. Mohr, Annalaus 105 (1958) 60.
[27] F. Feigl, Spot Tests, Elsevier, Amsterdam, 1954, pp. 170, 273.
[28] C. Channegowda, S.M. Mayanna, Indian Drugs 31 (1994) 574.
[29] I.C. Shukla, J. Inst. Chem. (India) 62 (1990) 159.
[30] J. Blazek, M. Pinkasova, Cslka Farm. 23 (1974) 3.
[31] V.N. Pathak, I.C. Shukla, S.R. Shukla, Talanta 29 (1982) 58.

ELSEVIER

Talanta 47 (1998) 67–75

Talanta

Solvent effects on extraction of alkali metal picrates with 15-crown-5 into various organic solvents. Elucidation of fundamental equilibria which govern extraction-efficiency and -selectivity

Yasuyuki Takeda *, Shigeharu Hatai, Hiroshi Hayakawa, Yasumasa Ono, Tsuyoshi Yahata, Kiyokazu Endō, Shoichi Katsuta

Department of Chemistry, Faculty of Science, Chiba University, Yayoi-chō, Inage-ku, Chiba 263-8522, Japan

Received 12 August 1997; accepted 26 January 1998

Abstract

Extractions of alkali metal (Na–Cs) picrates (MA) with 15-crown-5 (15C5) into various diluents of low dielectric constant were conducted at 25°C. Using the extraction data, the ion-pair formation constants (K_{MLA}) in water of 15C5–MA 1:1:1 complexes were determined by an equation derived from the regular solution theory (log K_{MLA} = 4.43 ± 0.27 for Na, 3.27 ± 0.42 for K, 3.58 ± 0.35 for Rb, and 2.78 ± 0.41 for Cs). The actual overall extraction equilibrium constants were obtained by considering the concentrations of the 1:1:1 15C5 complexes and the ion-pair formation between uncomplexed alkali metal and picrate ions in the aqueous phase. The distribution constants of the 15C5 complexes were calculated and their partition behavior is explained by the regular solution theory. Molar volumes and solubility parameters of 15C5 itself and the complexes were determined. Extraction-efficiency and -selectivity of 15C5 for alkali metal picrates were completely elucidated from the standpoint of equilibrium. © 1998 Elsevier Science B.V. All rights reserved.

1. Introduction

It was reported that, for the benzene system, the extraction-selectivity order of 15-crown-5 (15C5) for alkali metal picrates is not determined by the stability order in water, but perfectly by the extractability order of 15C5–alkali metal ion complexes with picrate ions [1]. For further study on molecular grounds of the extraction efficiency and selectivity of 15C5 for alkali metal picrates, thermodynamic parameters for the overall extraction reaction and the distribution of 15C5 were measured for benzene [2] and chloroform [3] systems. The distribution behavior of 15C5, the ion-pair extraction of 15C5–alkali metal picrate complexes, and the overall extraction process were discussed in detail from the thermodynamic point of view [2,3]. The ion-pair extraction consists of the two fundamental chemical processes,

* Corresponding author. E-mail: takeda@scichem.c.chiba-u.ac.jp

0039-9140/98/$19.00 © 1998 Elsevier Science B.V. All rights reserved.
PII S0039-9140(98)00058-7

namely the ion-pair formation in water and the distribution of the 15C5–alkali metal picrate complex. It is next to impossible to determine the two basic equilibrium constants because of the low stability of the 15C5–alkali metal ion complexes in water. The ion-pair formation constants in water give a clue to develop the field of liquid–liquid partition study of electroneutral crown ether–metal salt complexes. In order to determine the ion-pair formation constant of a crown ether–metal salt 1:1:1 complex in water, an equation was derived from the regular solution theory [4] and its predictions were verified experimentally by solvent extraction using benzo-18-crown-6, potassium picrate, and various diluents of low dielectric constant [5]. Then the ion-pair formation constant in water of a 15C5–sodium picrate 1:1:1 complex was determined and the distribution behavior of the 15C5 complex was quantitatively explained by the regular solution theory [6].

In this study, for the final elucidation of fundamental equilibria which govern the highest extraction selectivity of 15C5 for Na^+ among alkali metal ions and of distribution behavior of 15C5–alkali metal picrate 1:1:1 complexes, the partition constants of 15C5, the actual overall extraction equilibrium constants and the ion-pair formation constants in water of the 15C5 complexes were determined at 25°C by a more completed method considering the ion-pair formation between the uncomplexed alkali metal ion and the picrate ion in the aqueous phase.

2. Experimental

2.1. Materials

15-Crown-5 (Nisso) was purified by distillation under vacuum. All the organic solvents were analytical grade. 1,2-Dichloroethane was purified by distillation, but the other solvents were used as received. They were washed three times with deionized water prior to use. Picric acid and alkali metal hydroxides were analytical grade. The abbreviations of the diluents are given in the footnotes of Table 1.

2.2. Extraction of alkali metal (K, Rb, Cs) picrates with 15C5

The experimental procedures were almost the same as those described in the previous paper [6]. Extractions were conducted at 25 ± 0.2°C. Concentrations of 15C5, alkali metal hydroxides, and picric acid were 1.2×10^{-5}–1.9×10^{-1} M, 8.4×10^{-3}–2.0×10^{-2} M and $(1.8–7.2) \times 10^{-3}$ M, respectively. In order to keep the ionic strength in the aqueous phase as constant as possible, the sum of the initial total electrolyte concentrations was held between 1.0×10^{-2} and 2.8×10^{-2} M throughout the extraction experiments. Extractions were carried out at pH 11–12.

3. Theory and results

When an aqueous phase of an alkali metal picrate (MA) and an organic phase of a crown ether (L) attain equilibrium, the equilibrium constants are defined as

$$K_{ex} = [MLA]_o/[M^+][L]_o[A^-], \quad (1)$$

Table 1
Solvent parameters at 25°C

No.	Solvent[a]	δ[b]	V[c]	E_T[d]	ε_r[e]
1	DCM	9.7	63.9	41.1	8.93
2	1,2-DCE	9.8	79.4	41.9	10.36
3	CBu	8.4	104	—	7.39[f]
4	BZ	9.16	89.4	34.5	2.275
5	TE	8.93	106.9	33.9	2.379
6	*m*X	8.80	123.5	—	2.4
7	CB	9.5	102.1	37.5	5.62
8	BB	9.87	105	37.5	5.40
9	*o*-DCB	10.0	112.8	—	9.93
10	CF	9.3	80.7	39.1	4.81[f]
11	Water	17.55[g]	18.1	—	—

[a] DCM, dichloromethane; 1,2-DCE, 1,2-dichloroethane; CBu, chlorobutane; BZ, benzene; TE, toluene; *m*X, *m*-xylene; CB, chlorobenzene; BB, bromobenzene; *o*-DCB, *o*-dichlorobenzene; CF, chloroform.
[b] Solubility parameter ($cal^{1/2}$ $cm^{-3/2}$) Refs. [4,8].
[c] Molar volume (cm^3 mol^{-1}). Ref. [9] (density).
[d] Transition energy (kcal mol^{-1}). Ref. [10].
[e] Ref. [11].
[f] 20°C.
[g] Ref. [12].

Table 2
Extraction equilibrium constants for 1:1:1 15C5–alkali metal picrate complexes at 25°C

No.	Solvent	log K_{ex} [a]				log $K_{ex,ip}$			
		Na[b]	K	Rb	Cs	Na	K	Rb	Cs
1	DCM	4.99 ± 0.02	4.09 ± 0.03	4.22 ± 0.02	3.67 ± 0.01	4.94	3.99	4.24	3.51
2	1,2-DCE	4.82 ± 0.03	4.33 ± 0.01	4.61 ± 0.02	4.05 ± 0.02	4.13	3.60	4.01	3.26
3	CBu	5.09 ± 0.01	3.46 ± 0.03	3.60 ± 0.03	2.66 ± 0.02	3.20	1.52	1.78	0.66
4	BZ[c]	5.05 ± 0.01	2.96 ± 0.03	3.42 ± 0.02	2.43 ± 0.03	3.55	1.41	1.99	0.83
5	TE	5.14 ± 0.01	2.99 ± 0.04	3.38 ± 0.05	2.72 ± 0.03	3.29	1.10	1.61	0.77
6	*m*X	5.18 ± 0.03	2.89 ± 0.02	3.33 ± 0.04	2.29 ± 0.07	3.11	0.78	1.34	0.12
7	CB	5.63 ± 0.01	3.84 ± 0.03	3.89 ± 0.03	3.34 ± 0.01	4.18	2.35	2.52	1.79
8	BB	5.42 ± 0.01	3.49 ± 0.01	3.67 ± 0.02	3.08 ± 0.03	4.27	2.30	2.60	1.83
9	*o*-DCB	5.45 ± 0.01	4.36 ± 0.04	4.48 ± 0.04	3.72 ± 0.03	4.26	3.12	3.37	2.42
10	CF[d]	4.09 ± 0.01	3.69 ± 0.01	3.65 ± 0.01	3.18 ± 0.01	4.31	3.87	3.95	3.30

[a] Each value is the average of 10–30 measurements. The uncertainties are the standard deviations.
[b] Recalculated from the data in Ref. [6].
[c] Recalculated from the data in Ref. [1].
[d] Recalculated from the data in Ref. [3].

$$K_{D,L} = [L]_o/[L] , \quad (2)$$

$$K_{ML} = [ML^+]/[M^+][L] , \quad (3)$$

$$K_{MLA} = [MLA]/[ML^+][A^-] , \quad (4)$$

$$K_{D,MLA} = [MLA]_o/[MLA] , \quad (5)$$

$$K_{MA} = [MA]/[M^+][A^-] , \quad (6)$$

where the subscript 'o' and the lack of a subscript designate the organic and aqueous phase, respectively. The dissociation of MLA into ML^+ and A^- in the organic phases was neglected because of the low dielectric constants (ε_r) of the diluents used in this study. The overall extraction equilibrium constant (K_{ex}) can be written as

$$K_{ex} = K_{D,L}^{-1} K_{ML} K_{MLA} K_{D,MLA} , \quad (7)$$

where $K_{MLA}K_{D,MLA} = [MLA]_o/[ML^+][A^-] = K_{ex,ip}$. The distribution ratio (D) of the metal is expressed by

$$D = [MLA]_o/([M^+] + [MA] + [ML^+] + [MLA]) . \quad (8)$$

In the case that $[M^+] \gg [MA] + [ML^+] + [MLA]$, Eq. (8) is transformed into

$$D = K_{ex}[L]_o[A^-] . \quad (9)$$

From the mass balances, $[M^+]$, $[L]_o$, and $[A^-]$ are given by

$$[M^+] = ([M]_t - [MLA]_o) / \{1 + a[L]_o + (K_{MA} + b[L]_o)[A^-]\} , \quad (10)$$

$$[L]_o = ([L]_t - [MLA]_o) / \{c + (a + b[A^-])[M^+]\} , \quad (11)$$

$$[A^-] = ([HA]_t - [MLA]_o) / \{1 + (K_{MA} + b[L]_o)[M^+]\} , \quad (12)$$

where $a = K_{D,L}^{-1}K_{ML}$, $b = K_{D,L}^{-1}K_{ML}K_{MLA}$, $c = 1 + K_{D,L}^{-1}$, and the subscript 't' represents the total concentration. As a first approximation, it is assumed that $1 \gg a[L]_o + (K_{MA} + b[L]_o)[A^-]$ (Eq. (10)), $c + a[M^+] \gg b[M^+][A^-]$ (Eq. (11)), and $1 + K_{MA}[M^+] \gg b[L]_o[M^+]$ (Eq. (12)). The $[L]_o$ and $[A^-]$ values of Eq. (9) were calculated on this assumption. Plots of $\log(D/[A^-])$ versus $\log[L]_o$ always give a straight line with a slope of 1 in every case. This shows that 15C5 forms a 1:1 complex with the metal ion and the validity of the above assumptions is justified. The first approximate K_{ex} value for each system was determined on these assumptions.

The partition constant ($K_{D,L}$) of the crown ether is estimated by Eq. (13) derived from the regular solution theory [4]:

$$RT \ln K_{D,L}/(\delta_w - \delta_o) = V_L(\delta_w - 2\delta_L) + V_L\delta'_o, \quad (13)$$

where $\delta_o' = \delta_o + RT(1/V_o - 1/V_w)/(\delta_w - \delta_o)$; δ_w, δ_o, and δ_L refer to the solubility parameters of water, the organic solvent, and the crown ether, respectively; V_L, V_o, and V_w are the molar volumes of the crown ether, the organic solvent, and water, respectively. The partition constant ($K_{D,MLA}$) of an MLA ion-pair complex is estimated by

$$RT \ln K_{D,MLA}/(\delta_w - \delta_o) = V_{MLA}(\delta_w - 2\delta_{MLA}) + V_{MLA}\delta_o', \quad (14)$$

where V_{MLA} and δ_{MLA} designate the molar volume and solubility parameter of MLA, respectively. Combination of Eqs. (13) and (14) leads to

$$\log K_{D,MLA} = \{V_{MLA}(\delta_w + \delta_o' - 2\delta_{MLA}) / V_L(\delta_w + \delta_o' - 2\delta_L)\} \log K_{D,L}. \quad (15)$$

Eq. (16) is obtained by adding $\log K_{MLA}$ to both sides of Eq. (15).

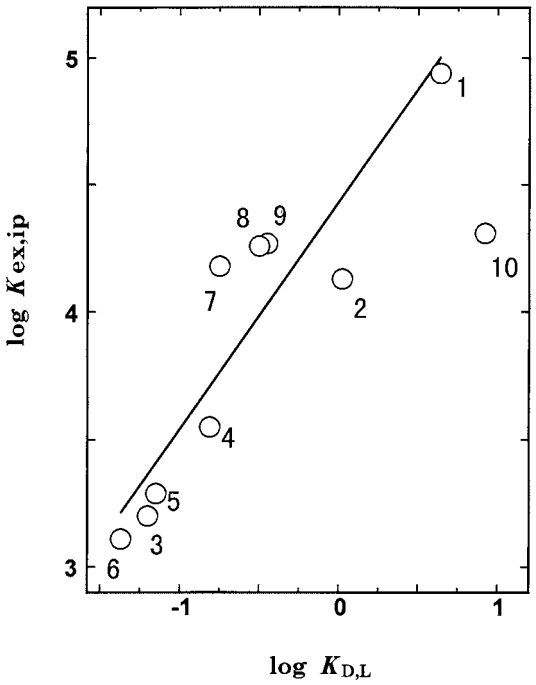

Fig. 1. Plot of actual $\log K_{ex,ip}$ values vs. $\log K_{D,L}$ for the 15C5–sodium picrate system. The solvent numbers correspond to those in Table 1.

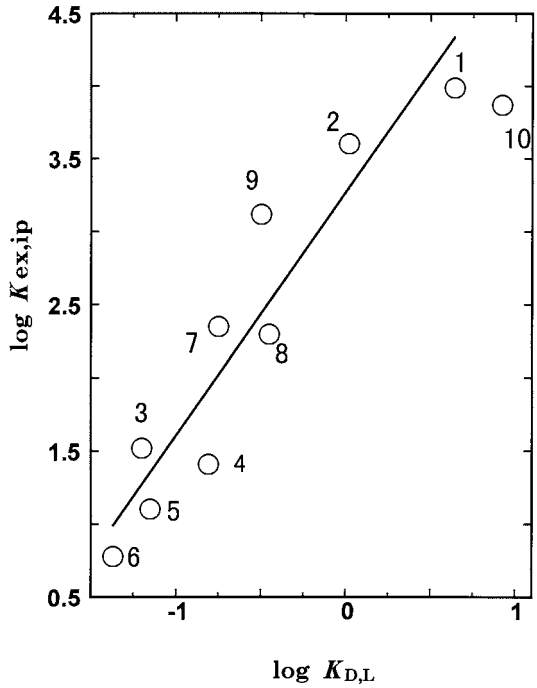

Fig. 2. Plot as in Fig. 1, for the 15C5–potassium picrate system.

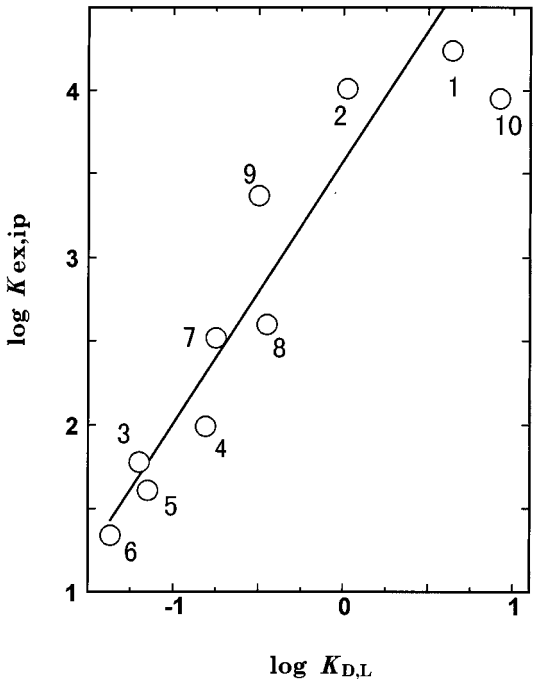

Fig. 3. Plot as in Fig. 1, for the 15C5–rubidium picrate system.

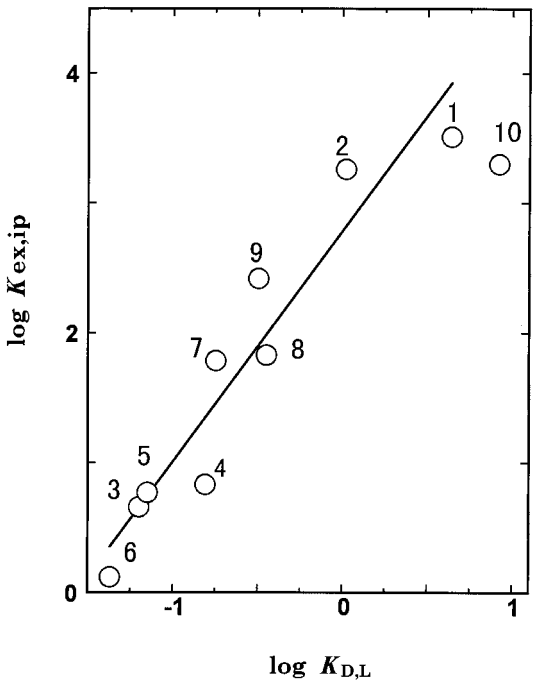

Fig. 4. Plot as in Fig. 1, for the 15C5–caesium picrate system.

$$\log K_{ex,ip} = \{V_{MLA}(\delta_w + \delta_o' - 2\delta_{MLA}) / V_L(\delta_w + \delta_o' - 2\delta_L)\}\log K_{D,L} + \log K_{MLA}. \quad (16)$$

When the δ values of L and MLA are nearly equal, Eq. (16) leads to

$$\log K_{ex,ip} = (V_{MLA}/V_L)\log K_{D,L} + \log K_{MLA}. \quad (17)$$

Plots of the first approximate $\log K_{ex,ip}$ values versus $\log K_{D,L}$ values show a good linear relationship for the respective alkali metals except for CF. The first approximate values of $\log K_{MLA}$ were determined from the intercepts of the $\log K_{ex,ip}$ versus $\log K_{D,L}$ plots. The second approximate $[A^-]$ value was calculated from Eq. (12) by the first approximate values of $[M^+]$, $[L]_o$, and K_{MLA}. The actual $[M^+]$, $[L]_o$, $[A^-]$, K_{MLA}, and K_{ex} values were calculated from Eqs. (1), (7), (10)–(12) and (17) by a successive-approximation method. The $\log K_{ex}$ and $\log K_{MLA}$ values are compiled in Tables 2 and 4, respectively. The plots of the actual $\log K_{ex,ip}$ values versus $\log K_{D,L}$ values also show a good linear relationship for the respective alkali metals except for CF (Figs. 1–4). The correlation coefficients for the Na, K, Rb, and Cs systems are 0.916, 0.937, 0.951 and 0.939, respectively.

4. Discussion

The $\log K_{D,MLA}$ values for 15C5 calculated from the $\log K_{ex,ip}$ and $\log K_{MLA}$ values are summarized in Table 3. The $RT \ln K_{D,MLA}/(\delta_w - \delta_o)$ versus δ_o' plots for the Na(15C5)A complex in Fig. 5 show a linear relationship; those for the potassium, rubidium, and caesium picrate com-

Table 3
Distribution constants for 15C5 and 1:1:1 15C5–alkali metal picrate complexes at 25°C

No.	Solvent	$\log K_{D,L}$ [a]	$\log K_{D,MLA}$			
			Na	K	Rb	Cs
1	DCM	0.64	0.51	0.72	0.66	0.73
2	1,2-DCE	0.02	−0.30	0.33	0.43	0.48
3	CBu	−1.20	−1.23	−1.75	−1.80	−2.12
4	BZ	−0.81	−0.88	−1.86	−1.59	−1.95
5	TE	−1.15	−1.14	−2.17	−1.97	−2.01
6	*m*X	−1.37	−1.32	−2.49	−2.24	−2.66
7	CB	−0.75	−0.25	−0.92	−1.06	−0.99
8	BB	−0.45	−0.16	−0.97	−0.98	−0.95
9	*o*-DCB	−0.50	−0.17	−0.15	−0.21	−0.36
10	CF	0.92	−0.12	0.60	0.37	0.52

[a] Ref. [6].

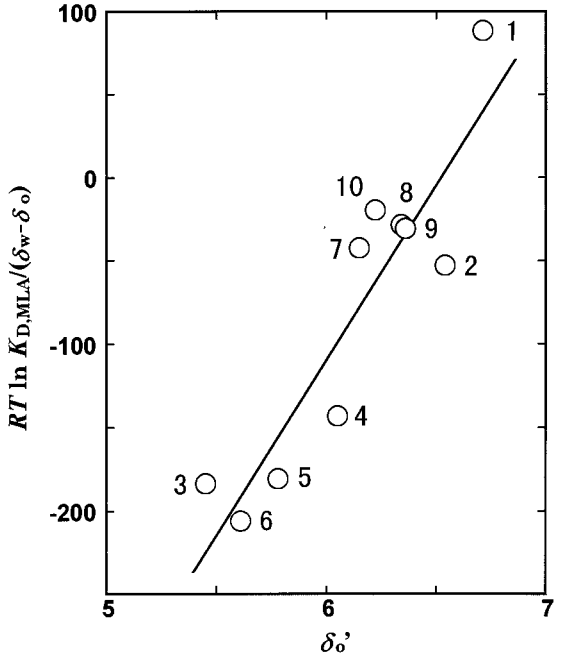

Fig. 5. $RT \ln K_{D,MLA}/(\delta_w - \delta_o)$ vs. δ_o' for 15C5–sodium picrate complex. The solvent numbers correspond to those in Table 1.

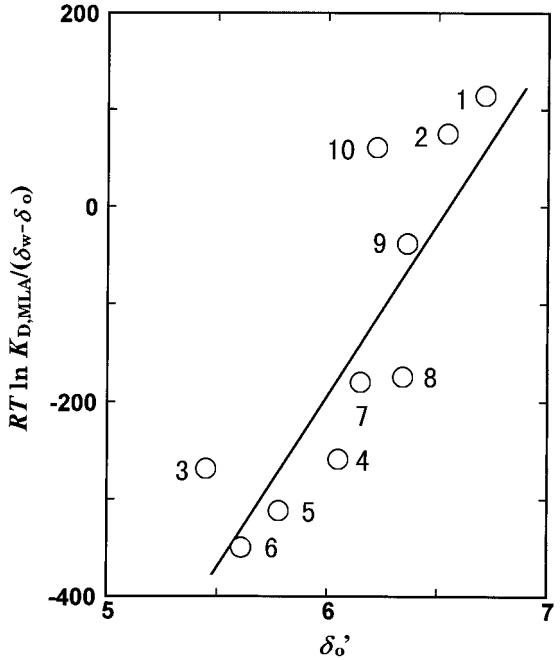

Fig. 7. Plot as in Fig. 5, for 15C5–rubidium picrate complex.

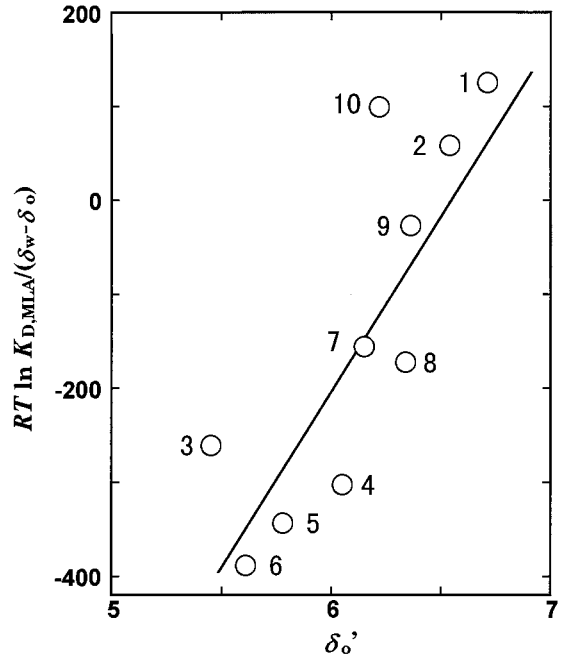

Fig. 6. Plot as in Fig. 5, for 15C5–potassium picrate complex.

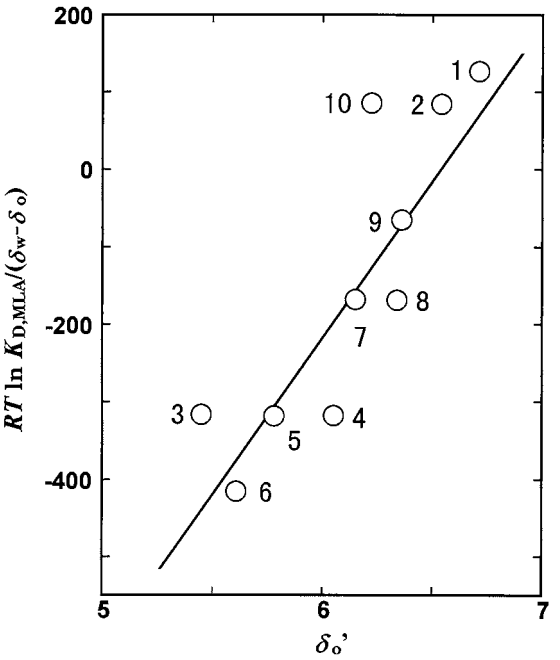

Fig. 8. Plot as in Fig. 5, for 15C5–caesium picrate complex.

Table 4
Fundamental equilibrium constants, molar volumes, and solubility parameters at 25°C

L = 15C5	M				
	Na	K	Rb	Cs	
log K_{MLA}	4.43 ± 0.27	3.27 ± 0.42	3.58 ± 0.35	2.78 ± 0.41	
log K_{MA} [a]	1.38	1.64	1.94	2.07	
log K_{ML} [b]	0.70	0.74	0.62	0.8	
	L	MLA			
V	189 ± 34[c]	210 ± 34	374 ± 76	353 ± 66	386 ± 82
δ	12.0 ± 0.1[c]	12.0 ± 0.1	12.0 ± 0.1	12.0 ± 0.1	12.0 ± 0.1

[a] Ref. [7].
[b] Ref. [13].
[c] Ref. [6].

plexes with 15C5 in Figs. 6–8 also show a linear relationship except for CF. The abnormal behavior of CF is not observed for the Na complex (Fig. 5), but for the K, Rb, and Cs complexes (Figs. 6–8). Except for CF, the correlation coefficients (r) for Na, K, Rb, and Cs complexes are 0.921, 0.880, 0.895, and 0.887, respectively. The Na(15C5)A complex where the Na^+ ion fits most nicely into the 15C5 cavity obeys the regular solution theory best of all the 15C5 complexes.

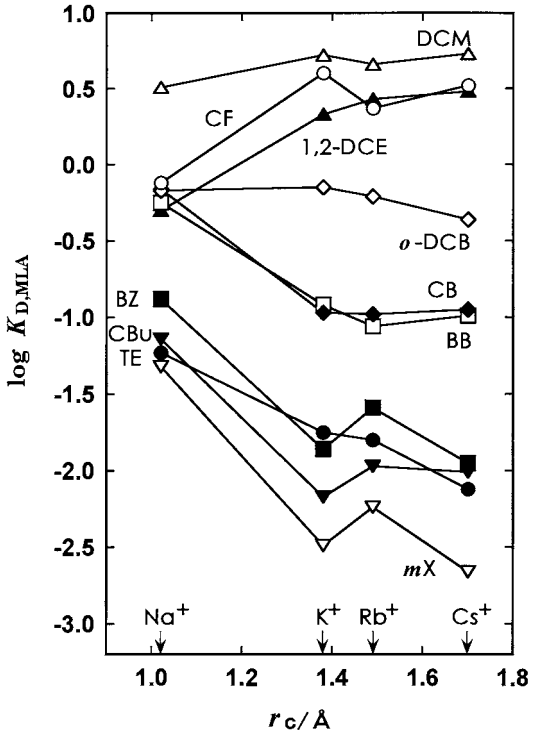

Fig. 9. Plots of log $K_{D,MLA}$ values of 15C5 vs. crystal ionic radii r_c of alkali metals for various diluents.

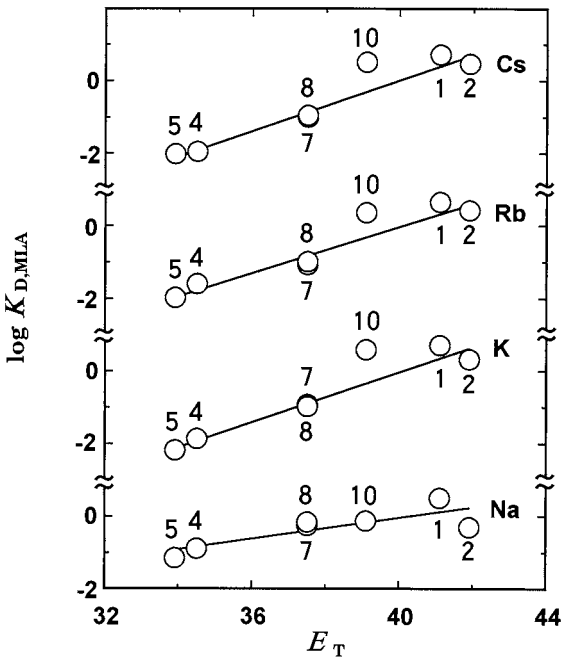

Fig. 10. Log $K_{D,MLA}$ vs. E_T plots for 15C5–alkali metal picrate complexes. The solvent numbers correspond to those in Table 1.

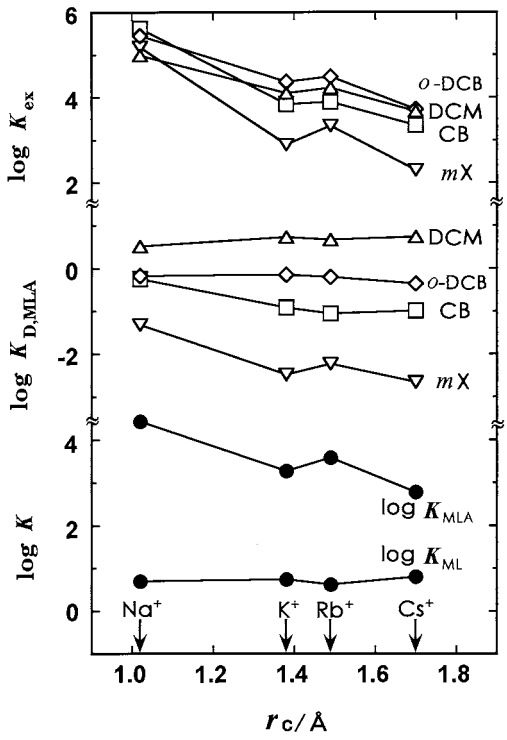

Fig. 11. Plots of $\log K_{ML}$, $\log K_{MLA}$, $\log K_{D,MLA}$, and $\log K_{ex}$ vs. r_c of alkali metals.

The same tendency is found for the 18-crown-6 (18C6) 1:1:1 complex with potassium picrate among the 18C6 complexes with alkali metal (Li–Cs) picrates [1]. This reflects the weaker interaction of the size-fitted MLA complex with some organic solvents (including CF) and/or the smaller variation with the diluent of the number of water molecules attached to the size-fitted MLA complex, compared with the size-misfitted MLA complexes. For K, Rb, and Cs, the M(15C5)A complex does not obey the regular solution theory so closely as the corresponding M(18C6)A complex. This is due to the lower shielding of the central alkali metal ion by 15C5 compared with 18C6. The V and δ values for the M(15C5)A complex were determined from the slope and the intercept, respectively, except for CF. They are listed in Table 4. The δ values of 15C5 and the M(15C5)A complexes are equal. This shows the validity of Eq. (17).

As is to be expected, the V_{15C5} value is smaller than any other $V_{M(15C5)A}$ one. The $V_{M(15C5)A}$ values of K^+, Rb^+, and Cs^+ which are larger in size than the 15C5 cavity are unexpectedly much greater than the $V_{Na(15C5)A}$ value. The magnitude of V_{MLA} value is closely related to that of K_{MLA} value. The greater the K_{MLA} value is, the smaller the V_{MLA} value is. The $\log K_{M(15C5)A}$ value is greater than the corresponding $\log K_{MA}$ value. Stronger hydration of an alkali metal ion causes a smaller $\log K_{MA}$ value [7]. Generally, the order of the $\log K_{M(15C5)A}$ value is the reverse of that of the $\log K_{MA}$ value. This indicates that the more nicely the alkali metal ion fits into the 15C5 cavity, the more water molecules bound to the cation are liberated. For K, Rb, and Cs, the $\log K_{MLA}$ value of 15C5 is lower than that of 18C6, but the reverse is true for Na.[1] The $\log K_{MLA}$ value of 15C5 for Na is nearly equal to that of 18C6 for Cs and smaller than those of 18C6 for K and Rb.[1] It follows from this that in water the picrate ion is not directly in contact with the alkali metal ion in the 15C5 cavity owing to water molecules.

Of all the alkali metals, the $\log K_{D,MLA}$ value of Na is the smallest for DCM, 1,2-DCE, and CF, but the largest for the other diluents (Table 3 and Fig. 9). For alkali metals M_1 and M_2 whose δ_{MLA} values are equal, Eq. (18) is derived from Eq. (14).

$$RT \ln(K_{D,M_1LA}/K_{D,M_2LA}) = (V_{M_1LA} - V_{M_2LA}) \{(\delta_w + \delta_o - 2\delta_{MLA})(\delta_w - \delta_o) + RT(V_o^{-1} - V_w^{-1})\}, \quad (18)$$

where $\delta_{MLA} = \delta_{M_1LA} = \delta_{M_2LA}$. The δ_{MLA} values of Na, K, Rb, and Cs are identical. The V_{MLA} value is smaller for Na than for K, Rb, and Cs. Except for DCM, 1,2-DCE, and CF, the value of $(\delta_w + \delta_o - 2\delta_{MLA})(\delta_w - \delta_o) + RT(V_o^{-1} - V_w^{-1})$ of Eq. (18) is always negative. This is the reason why the $\log K_{D,MLA}$ value of Na is the largest. For DCM and 1,2-DCE, the δ_o values are close to the δ_{MLA}

[1] $r = 0.935$, 0.919, 0.949, 0.920, and 0.943 for Li, Na, K, Rb, and Cs, respectively. Log K_{MLA} values of 18C6 are 3.29 (Na), 4.76 (K), 4.62 (Rb), and 4.49 (Cs). These values are reported in Anal. Sci. 14 (1998) 215.

[2] $RT \ln(K_{D,M_1LA}/K_{D,M_2LA}) = (V_{M_1LA} - V_{M_2LA})\{-(\delta_o - \delta_{MLA})^2 + (\delta_w - \delta_{MLA})^2 + RT(V_o^{-1} - V_w^{-1})\}$.

ones and the V_o values are small, resulting in the positive value of $(\delta_w + \delta_o - 2\delta_{MLA})(\delta_w - \delta_o) + RT(V_o^{-1} - V_w^{-1})$ of Eq. (18).[2] Thus, the $\log K_{D,MLA}$ value of Na is the smallest. Except for DCM and *o*-DCB, the difference in the $\log K_{D,MLA}$ values between Na and the other alkali metal is fairly greater than that between the two alkali metals other than Na. This is attributable to the much smaller V_{MLA} value of Na compared with the other alkali metals, except for CF, because the δ_{MLA} values of Na, K, Rb, and Cs are the same (Eq. (18)). The δ_o value of DCM is close to the δ values of 15C5 and the MLA complexes, whereas that of *m*X is not. The V_o value of DCM is the smallest among all the diluents, whereas that of *m*X is the largest. This is responsible for the fact that the $\log K_D$ values of 15C5 and the MLA complexes are the highest for DCM and the lowest for *m*X, except for CF.

The plots of $\log K_{D,MLA}$ versus E_T for the diluents in Fig. 10 show a linear relationship. Great positive deviations of CF are observed for the size-misfitted K, Rb, and Cs complexes, but not for the size-fitted Na complex.

The magnitude of the K_{ex} value is governed largely by that of the K_{MLA} value. The K_{ex} value varies with the organic solvent. The organic solvent whose δ_o and V_o values are close to the δ values of 15C5 and M(15C5)A and small, respectively, shows a high K_{ex} value (Eq. (7)),[2] because the δ_L and δ_{MLA} values are equal. Fig. 11 shows plots of $\log K_{ex}$ and $\log K_{D,MLA}$ for representative diluents, $\log K_{MLA}$, and $\log K_{ML}$ against crystal ionic radii of alkali metals. The extraction-selectivity order of 15C5 is Na > Rb > K > Cs, except for CF. The same order is observed for the K_{MLA} values and the $K_{D,MLA}$ values for BZ and *m*X. Favorable contributions of the $K_{D,MLA}$ values to the Na extraction selectivity of 15C5 are observed for CBu, BZ, TE, *m*X, CB, and BB, whereas unfavorable contributions and hardly any contribution are found for 1,2-DCE and CF and for DCM and *o*-DCB, respectively (Table 3 and Fig. 9). This is responsible for the fact that the extraction selectivity of 15C5 for Na over for the other alkali metals is fairly higher for CBu, BZ, TE, *m*X, CB, and BB than for DCM, 1,2-DCE, *o*-DCB, and CF (Table 2). Only for BZ and *m*X, the $K_{D,MLA}$ values make contributions to the extraction selectivity of 15C5 for the alkali metals. Scarcely any contribution to the extraction selectivity is found for the K_{ML} values. The extraction selectivity order of 15C5 for the alkali metals is determined completely by the order of ion-pair formation constants of the M(15C5)A complexes in water (Fig. 11).

References

[1] Y. Takeda, H. Goto, Bull. Chem. Soc. Jpn. 52 (1979) 1920.
[2] Y. Takeda, T. Namisaki, S. Fujiwara, Bull. Chem. Soc. Jpn. 57 (1984) 1055.
[3] Y. Takeda, N. Ikeo, N. Sakata, Talanta 38 (1991) 1325.
[4] J. H. Hildebrand, R. T. Scott, The Solubility of Nonelectrolytes, 3rd edn., Dover, New York, 1964.
[5] Y. Takeda, H. Sato, S. Sato, J. Solution Chem. 21 (1992) 1069.
[6] Y. Takeda, C. Takagi, Bull. Chem. Soc. Jpn. 67 (1994) 56.
[7] T. Iwachido, Bull. Chem. Soc. Jpn. 45 (1972) 432.
[8] A.F.M. Barton, Chem. Rev. 75 (1975) 731.
[9] D.R. Lide, Handbook of Chemistry and Physics, 75th edn., CRC Press, Boca Raton, FL, 1994–1995.
[10] C. Reichard, K. Dimroth, Forschr. Chem. Fortsch. 11 (1968) 1.
[11] J.A. Riddick, W.B. Bunger, Organic Solvents, 3rd ed., Wiley, New York, 1970.
[12] T. Wakahayashi, S. Oki, T. Omori, N. Suzuki, J. Inorg. Nucl. Chem. 26 (1964) 2255.
[13] R.M. Izatt, R.E. Terry, B.L. Haymore, L.D. Hansen, N.K. Dalley, A.G. Avondet, J.J. Christensen, J. Am. Chem. Soc. 98 (1976) 7620.

ELSEVIER

Talanta 47 (1998) 77–84

Talanta

Spectrophotometric determination of organic dye mixtures by using multivariate calibration

Patricio Peralta-Zamora [a,*], Airton Kunz [b], Noemi Nagata [b], Ronei J. Poppi [b]

[a] *Departamento de Química, Universidade Federal do Paraná, C.P. 19081, 81531-990 Curitiba-PR, Brazil*
[b] *Instituto de Química, Universidade Estadual de Campinas, C.P. 6154, 13083-970 Campinas-SP, Brazil*

Received 6 October 1997; received in revised form 15 January 1998; accepted 27 January 1998

Abstract

The simultaneous determination of organic dye mixtures by using spectrophotometric methods is a difficult problem in analytical chemistry, due to spectral interferences. By using multivariate calibration methods such as partial least-squares regression (PLSR), it is possible to obtain a model adjusted to the concentration values of the mixtures used in the calibration stage. In this study, the calibration model is based on absorption spectra in the 350–650-nm range for a set of 16 different mixtures of reactive red 195, reactive yellow 145 and reactive orange 122 dyes, and made the determination of the dye concentrations possible in a validation set with significantly greater accuracy than the conventional univariate calibration method. By using the developed model it was possible to monitor the decolorization kinetic of one dye (reactive orange 122), when the mixture of the three dyes was previously submitted to an ozonation process. © 1998 Elsevier Science B.V. All rights reserved.

Keywords: Organic dyes; Spectrophotometric determination; Multivariate calibration

1. Introduction

The spectrophotometric determination of organic dye mixtures is a very complex problem in analytical chemistry due to the spectral interferences, which results in widely overlapped absorption bands. For this determination, the conventional univariate calibration method is impracticable, because of the contribution of one species on the absorption signals of other species, and vice versa.

Several methods have been used for determination of dye mixtures in different matrices. Many procedures are based on electroanalytical [1–4] or electrophoretic [5,6] methods. The resolution of complex mixtures without the use of previous separation of the analytes is a difficult task. For this reason, the application of preliminary separation processes is one of the most recommended alternatives. Over the past years, the method development for resolution of the problems has increased exceptionally, because of the availability of powerful instrumentation and robust numerical methods [1]. For instance, derivative spectropho-

* Corresponding author. E-mail: zamora@quimica.ufpr.br

0039-9140/98/$19.00 © 1998 Elsevier Science B.V. All rights reserved.
PII S0039-9140(98)00073-3

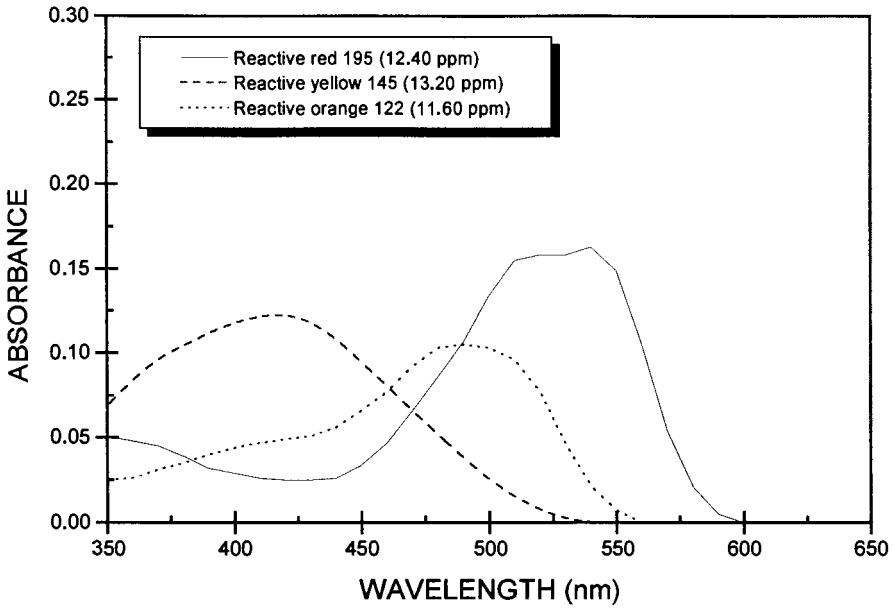

Fig. 1. Typical spectrum of the single dye.

tometry [7–10] and the H-point standard addition method [11,12] have been frequently employed to overcome the problems of interference due to spectral overlapping. However, both procedures are useful for determination of mixtures composed of at most two or three components.

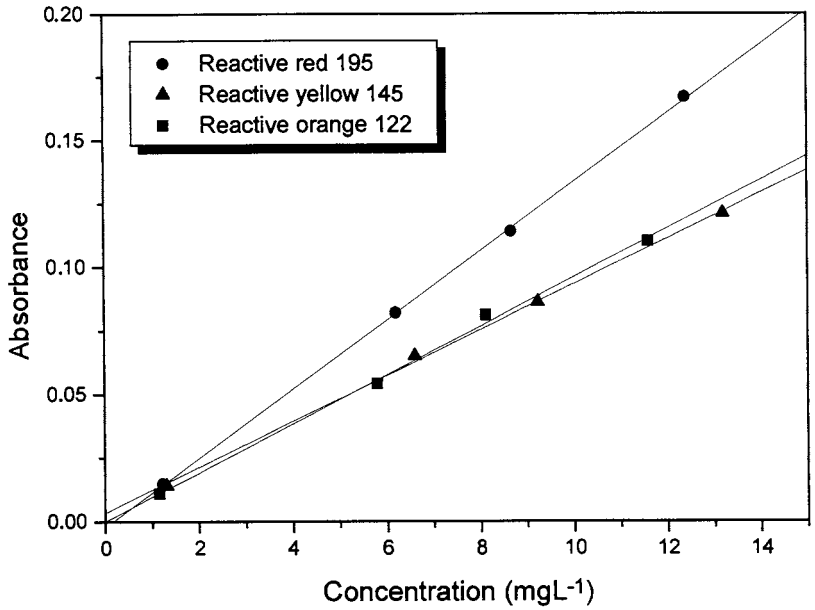

Fig. 2. Analytical curves for univariate determination of synthetic dye mixtures. Reactive red 195: Ab. = 0.0136 × Conc. − 0.0023; $r = 0.99985$; $\lambda = 540$ nm. Reactive yellow 145: Ab. = 0.0089 × Conc. + 0.0034; $r = 0.99933$; $\lambda = 420$ nm. Reactive orange 122: Ab. = 0.0096 × Conc. − 0.000; $r = 0.99868$; $\lambda = 490$ nm.

Table 1
Univariate determination of synthetic dye mixtures

Exp.	Added (mg l^{-1})			Found (mg l^{-1})			Error (%)		
	Red	Yellow	Orange	Red	Yellow	Orange	Red	Yellow	Orange
1	3.72	3.96	3.48	4.81	6.75	8.54	+29	+70	+145
2	2.48	2.64	2.32	3.19	4.30	5.52	+29	+63	+138
3	1.24	1.32	1.16	1.64	2.19	2.71	+32	+66	+134
4	6.20	3.96	2.32	6.87	6.64	9.38	+11	+68	+304
5	7.44	1.32	3.48	8.20	5.08	10.73	+10	+285	+208
6	3.72	6.60	2.32	4.44	8.54	7.92	+19	+29	+241
7	2.48	3.96	5.80	3.70	7.42	9.48	+49	+87	+63
8	2.48	2.64	6.96	4.00	6.64	10.21	+61	+152	+47

The spectrophotometric resolution of mixtures of components with partially overlapped spectra has been the subject of numerous chemometric studies. Several mathematical models can be applied to the analytical data to obtain the model parameters, and then apply this model to estimate the analyte concentration in the samples. Among those, linear regression, partial least-squares regression and principal-components regression, have been used with success in complex determinations such as drugs in pharmaceutical preparations [13,14], lanthanide mixtures [15] and calcium and magnesium in human serum [16].

Table 2
Experimental design for multivariate calibration

Sample	Composition (ml)		
	Red	Orange	Yellow
1	1.0	1.0	8.0
2	1.5	1.5	7.0
3	2.0	2.0	6.0
4	**3.0**	**3.0**	**4.0**
5	4.0	4.0	2.0
6	4.5	4.5	1.0
7	4.0	2.0	4.0
8	2.0	4.0	4.0
9	5.0	2.0	3.0
10	2.0	5.0	3.0
11	7.0	2.0	1.0
12	2.0	7.0	1.0
13	**3.5**	**1.0**	**5.5**
14	1.0	3.5	5.5
15	6.5	1.0	2.5
16	1.0	6.5	2.5
17	**8.0**	**1.0**	**1.0**
18	**1.0**	**8.0**	**1.0**
19	5.5	2.5	2.0
20	**2.5**	**5.5**	**2.0**
21	3.5	3.5	3.0

The entries in bold correspond to samples reserved for validation.
Standard solution concentration (mg l^{-1}): red, 12.4; orange, 11.6; yellow 13.2.

This paper describes an analytical methodology for determination of an organic dye mixture (reactive red 195, reactive yellow 145 and reactive orange 122) using a spectrophotometric method and a multivariate calibration technique (partial least-squares regression, PLSR).

Multivariate calibration methods become very useful in analytical chemistry, principally when it is necessary to determine one species in a complex mixture, and when the analytical information is not selective [17]. Multivariate calibration consists of the establishment of an association between matrices of chemical data. The process is composed of two steps: calibration and prediction. In this case, the calibration step consists of the development of a mathematical model which can reproduce a concentration matrix **Y** (contains 'n' lines which correspond to samples and 'q' columns of different dyes concentrations) from a matrix **X** (with 'n' lines of samples and 'p' columns of selected wavelength values).

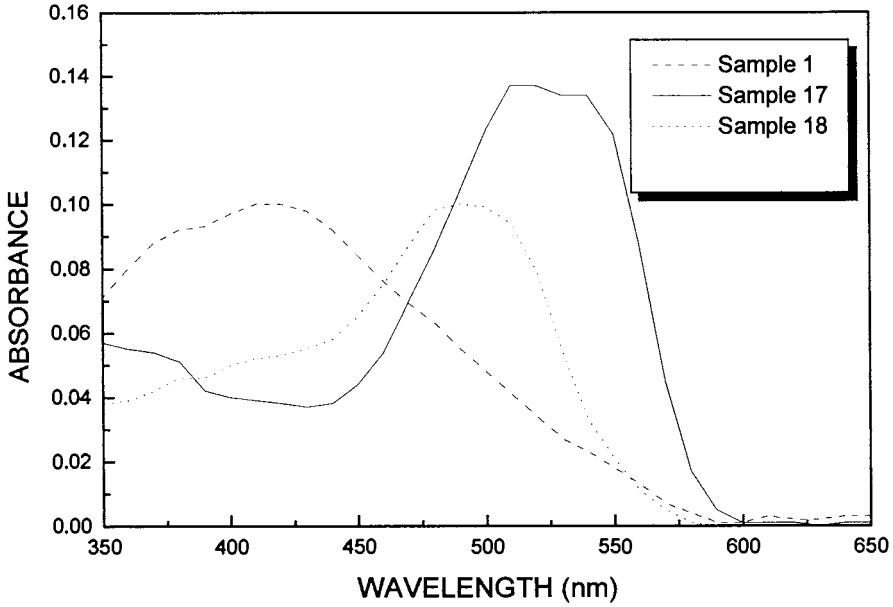

Fig. 3. Spectrum of selected dyes mixtures samples. Sample 1: red (1.24 mg l^{-1}); orange (1.16 mg l^{-1}); yellow (10.56 mg l^{-1}). Sample 17: red (9.92 mg l^{-1}); orange (1.16 mg l^{-1}); yellow (1.32 mg l^{-1}). Sample 18: red (1.24 mg l^{-1}); orange (9.28 mg l^{-1}); yellow (1.32 mg l^{-1}).

2. Experimental

2.1. Reactants and standard solutions

The dyes reactive red 195, reactive yellow 145 and reactive orange 122 were purchased from a textile industry in the Campinas (Brazil) region. Stock solutions of 12.4, 13.2 and 11.6 mg l^{-1}, respectively, were prepared with deionized water (pH 6.5).

2.2. Instrumentation

Spectrophotometric measurements were made with a Hitachi spectrophotometer, model U-2000, using 1 cm quartz cells. Standard solution vol-

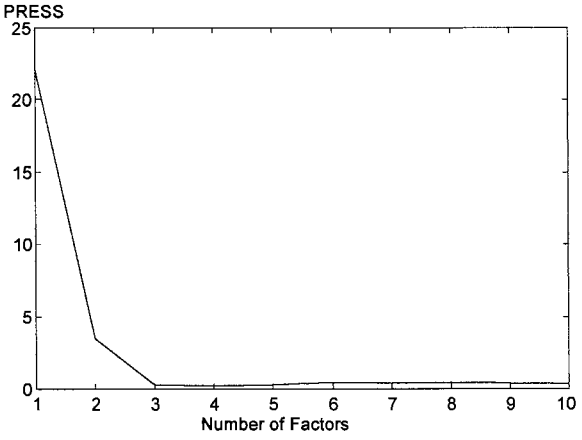

Fig. 4. Cumulative press as a function of number of factors.

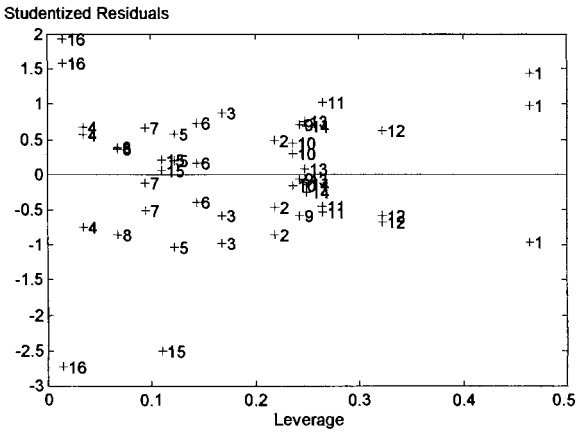

Fig. 5. Studied residuals as a function of leverage.

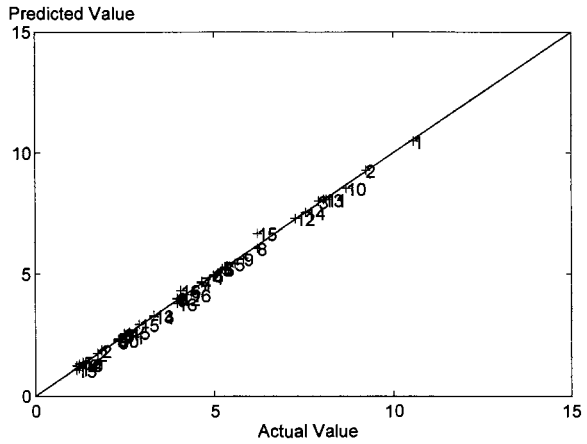

Fig. 6. Real concentration vs. concentration predicted by the PLSR model.

umes were taken in a Metrohm microburette with 0.5000-ml taps. The ozonation process were performed with a OZOCAV ZT-21 Laboratory Ozone Generator.

2.3. Analytical procedure

Known amounts of the standard solutions were placed in a 10 ml volumetric flask and completed to the final volume with deionized water (final pH: 6.5). The final concentration of these solutions varied between 1.0 and 10.6 mg l^{-1} of each dye.

The calibration was made by the conventional univariate method, using the absorbance signals at the maximum absorption wavelength, and by PLSR, using the recorded adsorbance values between 350 and 650 nm as the dependent variables, with intervals of 10 nm.

2.4. Experimental design

The experimental design used for the PLSR is presented in Table 3. The marked lines (samples 4, 13, 17, 18 and 20) correspond to the randomly selected samples reserved for validation of the model.

The preprocessing program was developed in MATLAB 4.0 and the PLSR was performed by using the PLS-toolbox 1.5 [18].

2.5. Ozonation process

Ozonation experiments were carried out at room temperature, in a 500-ml tubular reactor with a sinterized glass dispersor that releases the gas from the bottom to the top of the reactor, using 300 ml of a dye mixture (reactive red 195, 4.1 mgl^{-1}; reactive yellow 145, 4.4 mgl^{-1}; reactive orange 122, 3.87 mgl^{-1}). Ozone was generated by a Laboratory Ozone Generator, using an oxygen flow of 10 l h^{-1}.

3. Results and discussion

3.1. Conventional univariate calibration

The complexity of the spectra given in Fig. 1 shows the problems that can be found in this kind of determination, particularly due to the serious

Table 3
Multivariate determination of the validation samples

Exp.	Added (mg l^{-1})			Found (mg l^{-1})			Error (%)		
	Red	Yellow	Orange	Red	Yellow	Orange	Red	Yellow	Orange
4	3.72	5.28	3.48	3.55	5.29	3.57	−4.6	+0.2	+2.6
4	3.72	5.28	3.48	3.48	5.36	3.48	−6.4	+1.5	0.0
13	4.34	7.26	1.16	4.13	7.60	1.02	−4.8	+4.7	−12.1
17	9.92	1.32	1.16	9.14	1.33	1.74	−7.9	+0.7	+50.0
17	9.92	1.32	1.16	9.27	1.50	1.16	−6.6	+13.6	0.0
18	1.24	1.32	9.28	1.39	1.37	9.08	+12.1	+3.8	−2.2
20	3.10	2.64	6.38	3.07	2.77	6.26	−1.0	+4.9	−1.9

Table 4
Percent errors obtained by the univariate determination of the validation samples

Sample	Error (%)		
	Red	Yellow	Orange
4	+17	+46	+145
13	+7	+23	+538
17	+2	+211	+843
18	+110	+330	+11
20	+31	+137	+53

spectral overlapping. This interference is especially critical for reactive orange 122 dye whose absorption response is influenced by the other two dyes.

For the univariate determination, the following maximum absorption wavelengths were chosen: reactive red 195, 540 nm; reactive yellow 145, 420 nm; reactive orange 122, 490 nm.

By using these wavelengths and pure standard solutions, conventional calibration curves were made, whose equations and correlation coefficients (r) are presented in Fig. 2. By using these calibration curves, determination of eight synthetics mixtures were carried out. The results (Table 1) confirm different degrees of interference and indicate that the univariate process is deficient for this analysis, specially for reactive orange 122 the determination of which leaves errors as high as 300%.

3.2. Multivariate calibration

In the PLSR, a model for calibration was obtained from the experimental design described in Table 2. The spectra of three selected dye mixture samples (Fig. 3) indicate the high degree of the spectral overlapping.

To choose the number of factors to be used in the calibration model a cross-validation procedure was employed. In this procedure, the calibration set is split into 'M' subsets, each time treating one of these subsets as prediction objects. All the calibration objects have been treated as prediction objects and the estimated prediction residual error sum of squares (PRESS) is used to determine the number of factors necessary to establish the more suitable model (Fig. 4). In our case, 10 cross-validation segments were used. Ideally, the predictive capacity of a model can only be assessed by testing on new objects. However, in many cases

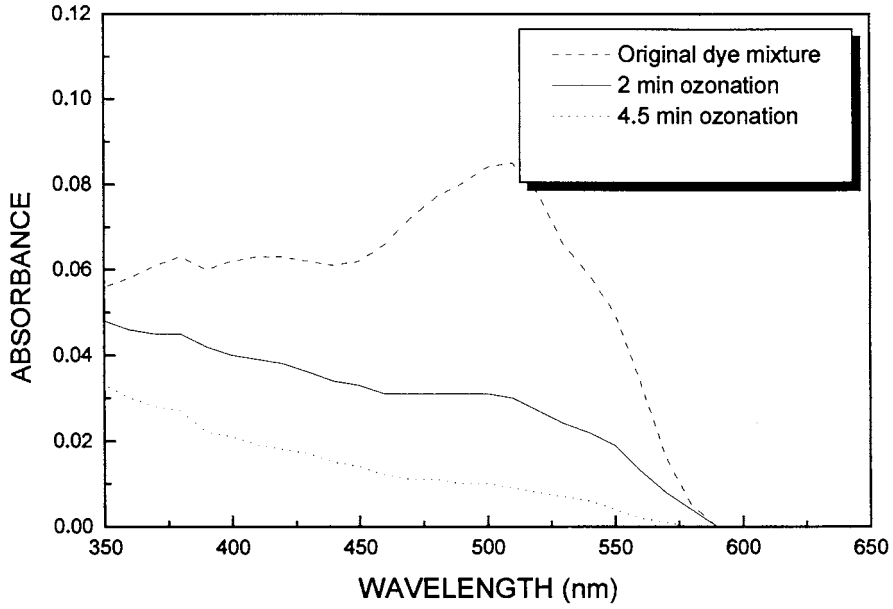

Fig. 7. Spectra of ozonized dye mixture.

cross-validation gives sensible results on the predicting capacity of a model [19].

From Fig. 4 it is possible to verify that the lowest value for the (PRESS) is obtained using three factors. By plotting the residuals as a function of the leverage (relative position of the observations of the independent variables), as shown in Fig. 5, it was possible to verify that there is no existence of anomalous samples (outliers).

The concentrations predicted by the model are very close to the real concentrations, as shown in Fig. 6, which indicates the validity of the calibration model. Using the linear PLSR model developed here, five synthetic mixtures were analysed. The results are presented in Table 3. It can be observed from this set of results that the dye mixture determination is perfectly feasible. The multivariate calibration model allows a significant reduction of the error in relation to the determination by the univariate calibration (Table 4) which demonstrates that the multivariate method is a powerful tool for difficult determinations like this. To check the reproducibility of the proposed method, the determinations of some samples were performed in duplicate. The mean observed relative standard deviation was lower than 2, 5 and 8% for reactive red 195, reactive yellow 145 and reactive orange 122 dyes, respectively.

To investigate the applicability of the multivariate model to more complex samples, a decolorization kinetic study was carried out. For this objective, a sample consisted of a mixture of the three dyes was submitted to ozonation. The evaluation of the efficiency of the remediation process for dye mixtures is a very difficult problem, due to the great difficulty in the determination of one dye in the presence of other dyes or degradation products. Generally, this problem can be overcome only by the use of sophisticated instrumental techniques such as capillary electrophoresis [5,6]. The progressive decolorization of the dye mixture by ozonation can be observed in the spectral sequence presented in Fig. 7.

For reactive red 195 and reactive yellow 145 the decolorization process was very fast. Thus, the concentrations of the dyes in the samples collected at the beginning of the process were lower than the minimal concentration used in the elaboration of the model. Consequently, their evaluation was not possible. On the other hand, the moderate decolorization kinetics of reactive orange 122 dye permitted its complete evaluation. In this particular case, a half-life of about 1.5 min and a complete decolorization of the dye in 3.5 min were observed.

The determination of the dye from a complex mixture that contains, besides the other dyes, unpredictable amounts of several degradation products demonstrates the capability of the multivariate model for such a complex determination.

4. Conclusion

The spectrophotometric determination of three organic dyes can be a difficult problem in view of the complexity of their absorption spectra. The results from the univariate calibration show significant errors, due to the multiple interferences mentioned above. By using a multivariate calibration the accuracy is increased significantly, because by monitoring various wavelengths the contribution of the interference signals is greatly reduced.

References

[1] C. Cruces Blanco, A.M. García Campaña, F. Alés Barrero, Talanta 43 (1996) 1019.
[2] S. Mo, J. Na, H. Mo, X. Qu, Talanta 39 (1992) 1255.
[3] F. Becerro Domingues, F. Gonzales Diego, J. Hernández Mendez, Talanta 37 (1990) 655.
[4] Y. Ni, J. Bai, Talanta 44 (1997) 105.
[5] K.N. Tapley, J. Chromatogr. A 706 (1995) 555.
[6] G.A. Lord, D.B. Gordon, L.W. Tetler, C.M. Carr, J. Chromatogr. A 700 (1995) 27.
[7] N.B. Pappano, Y.C. De Micalizzi, N.B. Debattista, F.H. Ferreti, Talanta 44 (1997) 633.
[8] V.G. Dabbene, M.C. Briñón, M.M. Bertorello, Talanta 44 (1997) 159.
[9] N.X. Wang, Z.K. Si, J.H. Yang, A.Q. Du, Z.D. Li, Talanta 43 (1996) 589.
[10] C.V.N. Prasad, A. Gautman, V. Bharadwaj, P. Parimoo, Talanta 44 (1997) 917.
[11] P. Campíns-Falcó, J. Verdú-Andrés, F. Bosch-Reig, Anal. Chim. Acta 315 (1995) 267.
[12] P. Campíns-Falcó, L. Gallo-Martínez, A. Sevillano-Cabeza, F. Bosch-Reig, Anal. Lett. 29 (1996) 2039.

[13] R.D. Bautista, F.J. Aberásturi, A.I. Jiménez, F. Jiménez, Talanta 43 (1996) 2107.
[14] J.J. Berzas Nevado, J. Rodríguez Flores, G. Castañeda Peñalvo, Anal. Chim. Acta 340 (1997) 257.
[15] R.D. Bautista, A.I. Jiménez, F. Jiménez, J.J. Arias, Talanta 43 (1996) 429.
[16] K. Wróbel, P.L. López-de Alba, L. López-Martínez, Anal. Lett. 30 (1997) 717.
[17] C.E. Miller, Chemometrics Intell. Lab. Syst. 30 (1996) 11.
[18] B.M. Wise, N.B. Gallagher, PLS-Toolbox Version 1.5, Eigenvector Technologies, 1995.
[19] H. Martens, T. Naes, Multivariate Calibration, Wiley, Chichester, 1993.

ELSEVIER

Talanta 47 (1998) 85–93

Talanta

Application of sodium metaperiodate for the determination of ribavirin in pharmaceutical formulations

Chilukuri S.P. Sastry [a,*], Petla Y. Naidu [a], Chilukuri S.R. Lakshmi [b], Manda N. Reddy [b], Ravi Chinthalapati [a]

[a] *Foods and Drugs Laboratories, School of Chemistry, Andhra University, Visakhapatnam 530 003, India*
[b] *Department of Pharmaceutical Sciences, Andhra University, Visakhapatnam 530 003, India*

Received 6 October 1997; received in revised form 15 January 1998; accepted 27 January 1998

Abstract

Three simple and sensitive visible spectrophotometric methods (A–C) have been described for the assay of ribavirin either in pure form or in pharmaceutical formulations. They are based on the oxidation of ribavirin with excess sodium metaperiodate and estimating either the products formed (dialdehyde with MBTH, method A; iodate with metol–sulphanilamide, in the presence of Mo(VI) and iodide, method B) or the amount of periodate consumed (celestine blue in the presence of telurium (IV), method C). All of the variables have been optimized and the reaction mechanisms presented. The concentration measurements are reproducible within a R.S.D. of 1.0%. Recoveries are 99.2–101.2%. © 1998 Elsevier Science B.V. All rights reserved.

Keywords: Sodium metaperiodate; Ribavirin; 3-Methyl-2-benzothia-zolinone hydrazone; Metol; Sulphanilamide; Celestine blue; Visible spectrophotometry

1. Introduction

Ribavirin (RV) is an antiviral agent, widely used in vivo against murine leukemia. It is chemically known as 1-β-D-ribofuranosyl-1H-1,2,4-triazole-3-carboxamide and is officially described in the US pharmacopoeia [1]. A survey of the literature revealed that only a single visible [2] and two ultra violet spectrophotometric methods have been reported [3,4]. Other methods include polarimetry [5], radioimmunoassay [6], GC-MS [7] and high performance liquid chromatography [8–10]. The reported spectrophotometric methods possess deficiencies such as a low λ_{max} value or low sensitivity. It is, therefore, of interest to develop simple and sensitive procedures with higher λ_{max} for the determination of RV in pure and pharmaceutical formulations.

This paper describes three visible spectrophotometric methods for RV determination making use of the vicinol diol presence. Sodium metaperiodate is a selective oxidant for compounds with vicinol diols [11] and, in the case of RV, results in the rupture of carbon–carbon bonds in the ribofuranosyl unit to form a dialdehyde and it's re-

* Corresponding author. Tel.: +91 891 554871; fax: +91 891 555547; e-mail: aulibra@md2.vsnl.net.in

0039-9140/98/$19.00 © 1998 Elsevier Science B.V. All rights reserved.
PII S0039-9140(98)00074-5

duced form, iodate, besides its presence unreacted. Sawicki et al. [12] developed a procedure for determining trace concentration of aldehydes by condensation with 3-methyl-2-benzothiazolinone hydrazone (MBTH) to form an intensely coloured coupling product. Sastry et al. [13] suggested a procedure for determining sulphanilamide by treatment with *p*-methyl aminophenol sulfate (metol) and iodate to form an intensely purple coloured 2:1 charge-transfer complex between *p*-*N*-methyl benzoquinone monoimine (PMBQMI) (formed in situ from metol and iodate) and sulfanilamide. Sastry et al. [14] suggested a procedure for determining several drugs by periodate oxidation, the periodate reacted is determined spectrophotometrically in presence of tellurium (IV) by reaction with coloured oxazine dye, celestine blue (CB) 91-amino carbonyl-7-diethylamino-3,4-dihydroxy-5-phenoxazinium chloride (C.I. No. 51050) through decrease in the intensity of its colour. We have applied the above three reagents ($NaIO_4$–MBTH, $NaIO_4$–M-SA and $NaIO_4$–CB) for the determination of ribavirin in pure and pharmaceutical formulations.

2. Experimental

2.1. Instruments

A Milton Roy spectronic 1201, UV-visible spectrophotometer with matched quartz cells and Elico LI-120 model digital pH meter were used for absorbance and pH measurements respectively.

2.2. Reagents

All the chemicals used were of analytical grade and all of the solutions were prepared with double distilled water. Freshly prepared solutions were always used.

Aqueous solutions of sodium metaperiodate (BDH, 9.35×10^{-3} M), MBTH (Loba, 8.56×10^{-3} M) and acetic acid (BDH, 3.5 M) were prepared for method A. Aqueous solutions of sodium metaperiodate (BDH, 9.35×10^{-3} M), potassium iodide (Merck, 2.40×10^{-1} M), metol (BDH, 8.71×10^{-3} M), sulphanilamide (Wilson Laboratories, 2.32×10^{-2} M), sodium molybdate (Baker, 8.27×10^{-2} M) and potassium acid phthalate buffer (pH 3.0) [15] were prepared for method B. Aqueous solutions of sodium metaperiodate (BDH, 100 μg ml^{-1}), CB (E. Gurr 200 μg ml^{-1}), sodium tellurite (Merck, 1 mg ml^{-1}) and hydrochloric acid (Merck, 5 M) were prepared for method C.

2.3. Preparation of standard drug solution

A 1 mg ml^{-1} solution was prepared by dissolving 100 mg pure RV in 100 ml distilled water and this stock solution was diluted stepwise with distilled water to obtain the working standard solutions of concentrations 100 μg ml^{-1} methods A and B) and 50 μg ml^{-1} (for method C).

3. Analysis of pure samples

3.1. Method A

To a series of 25 ml graduated test tubes containing 1.0–7.0 ml of standard drug solution (100 μg ml^{-1}), 1.0 ml each of $NaIO_4$ (9.35×10^{-3} M) and acetic acid (3.5 M) were added. The total volume in each flask was brought up to 10 ml with distilled water and kept in a boiling water bath for 10 min. After that 1.0 ml MBTH (8.56×10^{-3} M) solution was added and heated further for 2 min. It was later cooled and diluted to 25 ml with distilled water. The absorbance was measured at 660 nm against a reagent blank within the stability period (1–50 min). The amount of RV in a sample was computed from the Beer-Lambert plot.

3.2. Method B

Aliquots of standard drug solution (0.5–3.0 ml, 100 μg ml^{-1}) were put in a series of 25 ml graduated test tubes. Then 1.0 ml sodium metaperiodate (9.35×10^{-3} M) solution was added to each flask. The total volume in each flask was brought up to 6.0 ml with distilled water and kept in a boiling water bath for 10 min. After cooling

to room temperature, 15 ml of buffer solution (pH 3.0) and 1 ml of sodium molybdate (8.27×10^{-2} M) solution were added to each flask. After 10 min, 1 ml potassium iodide (2.40×10^{-1} M) solution was added. After 5 min, 1 ml metol solution (8.71×10^{-3} M) followed by 1 ml sulphanilamide (2.32×10^{-2} M) solution were added. The absorbance was measured at 520 nm against a reagent blank within the stability period (10–50 min). The amount of RV in a sample was computed from the Beer-Lambert plot.

3.3. Method C

Aliquots of standard RV solution (0.5–2.5 ml 50 μg ml^{-1}) were transferred into a series of 25 ml graduated test tubes containing 3.0 ml 5.0 M HCl and 2.0 ml sodium metaperiodate solution (100 μg ml^{-1}). The total volume was brought up to 13 ml with distilled water and kept in a boiling water bath for 10 min. After cooling to room temperature, 2.0 ml Te(IV) (1 mg ml^{-1}) solution and 10.0 ml CB (200 μg ml^{-1}) solution were added successively and the absorbances measured 10 min later at 540 nm against distilled water. In the same way corresponding blank (without the drug) and dye (without the drug and periodate) solutions were prepared and their absorbances measured against distilled water. The decrease in absorbance corresponding to the consumed periodate, and in turn to drug content, was obtained by subtracting the decrease in absorbance of the test solution (dye-test) from that of the blank solution (dye-blank). The amount of RV in a sample was obtained from the Beer-Lambert plot.

3.4. Analysis of pharmaceutical formulations

An accurately weighed or measured amount of sample (capsules or syrup) equivalent to 100 mg of the drug was extracted with isopropyl alcohol (2×15 ml) and filtered. The combined filterate was evaporated to dryness and the residue was dissolved in 100 ml distilled water to achieve a concentration of 1 mg ml^{-1}. This solution was further diluted stepwise with distilled water to working standard solutions (100 μg ml^{-1} for methods A and B and 50 μg ml^{-1} for method C) and analysed under the procedures described for pure samples.

4. Results and discussion

The optimum conditions for the development of the methods (A–C) were established by varying the parameters one at a time [16] and keeping the others fixed, and observing the effect produced on the absorbance of the coloured species.

4.1. Method A

In order to establish the experimental conditions in method A, RV was allowed to react with IO_4^- in the presence of MBTH. The effect of reagent concentrations (IO_4^- and MBTH), volume of acid, temperature, time and the order of the addition of the reagents were studied by means of control experiments. Optimization experiments reveal that 1 ml each of IO_4^-, MBTH and acetic acid solutions were necessary to attain the maximum colour development. A heating time of 10 min initially followed by 2 min after the addition of MBTH in a boiling water bath were necessary to attain the maximum colour development.

4.2. Method B

The most suitable method for determining iodate was considered to be the spectrophotometric determination of iodine produced by the iodate–iodide reaction. It was established [16] that hexamolybdoperiodate and molybdate had no effect on the stoichiometry of this reaction at pH 3.0. The iodine so produced oxidises metol to PMBQMI which in turn forms a coloured charge-transfer complex with SA. The influence of the concentration of $NaIO_4$ and the effect of oxidation time on colour formation in method B have been optimised. The absorbances of the coloured species remain constant within the volume range of 0.9–1.2 ml $NaIO_4$ (9.35×10^{-3} M) and the oxidation time 10–20 min in a boiling water bath. Hence, 1.0 ml of $NaIO_4$ and oxidation time of 10 min were selected for further work. A volume of

15 ml buffer (pH 3.0) and 1.0 ml sodium molybdate (8.27×10^{-2} M) were found to be optimal. A minimum time of 10 min was found to be necessary prior to the addition of 1.0 ml KI (2.40×10^{-1} M). Use 1.0–2.0 ml metol (8.71×10^{-3} M) solution and 0.5–1.5 ml SA (2.32×10^{-2} M) solution afforded the highest absorbance values. A waiting period ranging from 4 to 6 min is necessary between the addition of KI solution for the generation of iodine (by the reaction of iodate and KI) and metol. Maximum colour intensity was attained in 10 min after the addition of SA and remained stable for the next 50 min.

4.3. Method C

This method involves two steps, namely the reaction of the drug with an excess of periodate to give products involving oxidation and the estimation of unreacted periodate using a known excess of CB. The excess dye remaining is then measured with a spectrophotometer at 540 nm. The effect of periodate concentration and acidity at different temperatures for different time intervals in the first step and the effect of sodium tellurite and CB at ambient temperature in the second step, the waiting period in each step with respect to maximum sensitivity, minimum blank, adherence to Beer's law, reproducibility and stability of final colour were studied through control experiments. The studies on the variation of acid concentration indicated that a constant absorbance is obtained in a final acid concentration 0.5–0.7 M HCl at a periodate concentration of 200 μg. In order to ascertain the linear relationship between the concentration of added periodate and the corresponding decrease in the absorbance of CB (2000 μg), experiments were carried out in 0.6 M HCl medium with varying amounts of periodate. As the decreases in absorbance was found to be linear up to 200 μg (2.0 ml of 100 μg ml^{-1}) of periodate, subsequent studies were carried out with 2000 μg (10.0 ml of 200 μg ml^{-1}) of CB and 200 μg of periodate in 0.6 M HCl medium. Different amounts of tellurite were used to minimise the interference of iodate in the periodate determination. The optimum range of sodium tellurite necessary for suppressing the reactivity of iodate in the reaction between CB and periodate was found to be 1.5–3.0 mg. Fixed amounts of periodate (2.0 ml, 100 μg ml^{-1}), CB (10.0 ml, 200 μg ml^{-1}), HCl (3.0 ml, 5.0 M) and sodium tellurite (2.0 ml, 1 mg ml^{-1}) were used in a total volume of 25 ml in further investigations.

Heating on a boiling water bath for 5–15 min in the first step (drug and periodate) and ambient temperature (28 ± 4°C) for 5–20 min in the second step (periodate and CB in the presence of Te(IV)) were found to be necessary. Hence, 10 min heating in a boiling water bath and 10 min at ambient temperature were maintained in further studies of the first and second steps, respectively.

The above optimum experimental conditions were incorporated in the recommended procedures for colour development. Beer's law was found to be valid over the concentration ranges given in Table 1 at appropriate λ_{max} values (Figs. 1–3).

4.4. Analytical data

The Beer's law limits, molar absorptivity, Sandell's sensitivity, detection limits [17], regression equation and correlation coefficients obtained by least squares treatment of these results are given in Table 1. The precision of each method was tested by analysing six replicate samples containing 20, 8 and 4 μg ml^{-1} pure drug for methods A, B and C, respectively. The percent S.D. and the percent range of error at the 95% confidence level of each method are given in Table 1.

4.5. Interference studies

The effect of a wide range of excipients and other additives, usually present in the formulations of RV in the determination (methods A–C), under optimum conditions, were investigated. The commonly used excipients and additives, in the preparation of formulations such as starch, lactose and sugars, are expected to interfere in the determination of RV. Other additives such as talc (up to 250-fold excess (w/w) compared to the drug), boric acid (150-fold), stearic acid (60-fold) and sodium lauryl sulphate (10-fold), do not in-

Table 1
Optical and regression characteristics, precision and accuracy of the proposed methods

Parameters	Methods		
	A	B	C
λ_{max} (nm)	660	520	540
Beer's law limits (mg ml^{-1})	4.0–28.0	2.0–12.0	1.0–5.0
Molar absorptivity (1 mol^{-1} cm^{-1})	0.30×10^{4}	0.70×10^{4}	1.39×10^{4}
Sandell's sensitivity (mg cm^{-2} per 0.001 absorbance unit)	0.074	0.032	0.016
Regression equation (Y)[a]			
Slope (b)	1.35×10^{-2}	3.15×10^{-2}	6.30×10^{-2}
S.D. on slope (S_b)	1.13×10^{-4}	1.82×10^{-4}	5.77×10^{-4}
Intercept (a)	-1.33×10^{-4}	-2.20×10^{-4}	-0.20×10^{-4}
S.D. on intercept (S_a)	1.76×10^{-3}	1.38×10^{-3}	1.91×10^{-3}
S.E. of estimation (S_e)	1.90×10^{-3}	1.40×10^{-3}	1.82×10^{-3}
Correlation coefficient (r)	0.9999	0.999	0.9998
R.S.D. (%)[b]	0.48	0.54	0.62
Percent range of error[b] (95% confidence limit)	0.51	0.57	0.65

[a] $Y = a + bC$ where C is the concentration in mg ml^{-1} and Y is the absorbance unit.
[b] Six replicate samples (concentrations of 20, 8, and 4 mg ml^{-1} of pure drug for methods A, B and C, respectively.

terfere with the determination of RV by the proposed methods (A–C).

Commercial formulations (capsules and syrup) containing RV were successfully analysed by the proposed methods. The interfering excipients (e.g. lactose, starch) should be removed by selectively extracting the RV initially with isopropyl alcohol. The values obtained by the proposed and reference methods [3] for the formulation were compared statistically by the t- and F-tests and found not to differ significantly. As an additional demonstration of accuracy, recovery experiments were performed by adding a fixed amount of the drug to the pre-analysed formulations. These results are summarized in Table 2.

4.6. Chemistry of coloured species

As RV contains a 1,2-diol system, sodium metaperiodate offers a wide scope for analytical determination. The above group is attacked in the manner shown in Scheme 1 giving dialdehyde and iodate besides unreacted periodate. Method A permits the determination of the liberated dialdehyde directly in the reaction medium colorimetrically by an oxidative coupling reaction with MBTH as already illustrated by Sawiki et al. [12].

In method B, RV is determined by a method involving oxidation with sodium metaperiodate, masking the excess periodate with sodium molybdate as hexamolybdoperiodate, and using metol–sulphanilamide at pH 3.0 to determine the iodine released from the iodate formed after the addition of potassium iodide [13,20].

In method C, RV is determined by a method involving oxidation with periodate, masking the iodate formed with tellurium (IV) probably as an ion-pair ($TeCl_3^+$) (IO_3^-) and using CB in 0.6 M HCl to determine the unreacted periodate. From the available information during a literature survey [18,19], it appears that in 0.6 M HCl medium Te(IV) and iodate exist predominantly as oppositely charged ions ($TeCl_3^+$ and IO_3^-), while Te(VI) and periodate exist as neutral species (H_6TeO_6 and H_5IO_6). All these reactions are presented in Scheme 1.

5. Conclusion

Methods A–C are applicable to the intact

Table 2
analysis of pharmaceutical formulations by the proposed and reference methods

Pharmaceutical formulations	Labelled amount (mg)	Amount found by the proposed methods[a] (mg)			Reference method	Recovery by proposed methods[b] (%)		
		A	B	C		A	B	C
Capsules	100	99.6 ± 0.36, $t = 1.21$, $F = 4.93$	99.8 ± 1.25, $t = 0.82$, $F = 2.44$	100.1 ± 0.89, $t = 0.45$, $F = 1.23$	99.7 ± 0.80	99.9 ± 0.44	99.5 ± 0.56	100.24 ± 0.51
Capsules	200	199.6 ± 1.07, $t = 0.70$, $F = 1.58$	200.4 ± 0.86, $t = 1.25$, $F = 1.02$	199.6 ± 0.62, $t = 1.04$, $F = 1.87$	200.4 ± 0.83	99.7 ± 0.41	99.6 ± 0.37	100.21 ± 0.59
Syrup I	50 mg per 5 ml	49.6 ± 1.01, $t = 0.26$, $F = 1.57$	49.7 ± 0.80, $t = 1.08$, $F = 1.0$	50.4 ± 0.70, $t = 0.09$, $F = 1.30$	49.7 ± 0.80	99.0 ± 0.80	99.8 ± 0.95	98.9 ± 0.50
Syrup II	50 mg per 5 ml	50.0 ± 1.80, $t = 0.56$, $F = 4.48$	49.6 ± 0.75, $t = 2.01$, $F = 1.28$	50.8 ± 0.66, $t = 1.07$, $F = 1.28$	50.1 ± 0.85	100.9 ± 0.21	100.2 ± 0.87	99.7 ± 0.14

[a] Average $\pm$ S.D. ($n = 6$). The t- and F-values refer to comparison of the proposed method with the reference method. Theoretical values at the 95% confidence limit, $t = 2.57$, $F = 5.05$.

[b] Recovery of 10 mg added to the pharmaceutical preparation (average of six determinations).

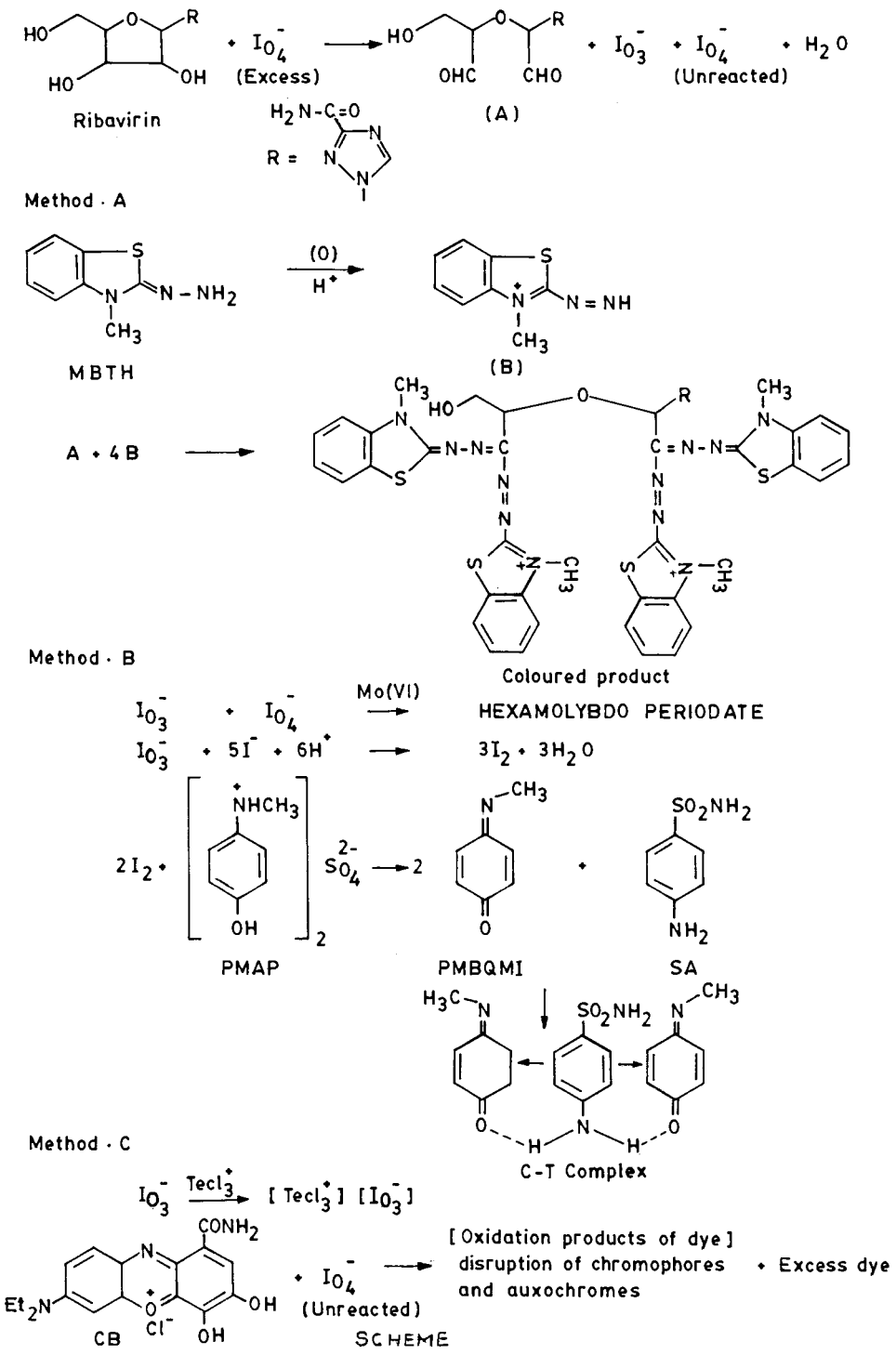
Ribavirin
(Excess)
(A)
(Unreacted)
Method · A
MBTH
(B)
Coloured product
Method · B
HEXAMOLYBDO PERIODATE
PMAP
PMBQMI
SA
C-T Complex
Method · C
[Oxidation products of dye]
disruption of chromophores
and auxochromes
Excess dye
(Unreacted)
CB
SCHEME

Scheme 1.

molecule of RV (obviating the need for any preliminary treatment) and have the advantage of wider range). The sensitivity order of the procedure is C > B > A > reference method and the λ_{max} of the coloured species order is A > C > B > reference method. The proposed methods are advantageous over other reported spectrophotometric methods with respect to higher λ_{max} and sensitivity with reasonable precision and accuracy. The higher λ_{max} values of the proposed methods have a decisive advantage since the interference from the associated ingredients should be generally far less at higher wavelengths than at lower wavelengths. More over only one visible spectrophotometric method has been reported so far. Thus all the proposed methods are simple, sensitive and useful for the determination of RV in pure samples and pharmaceutical formulation. All these methods are selective for compounds containing the 1,2-diol or α-amino-ol portion in their molecules.

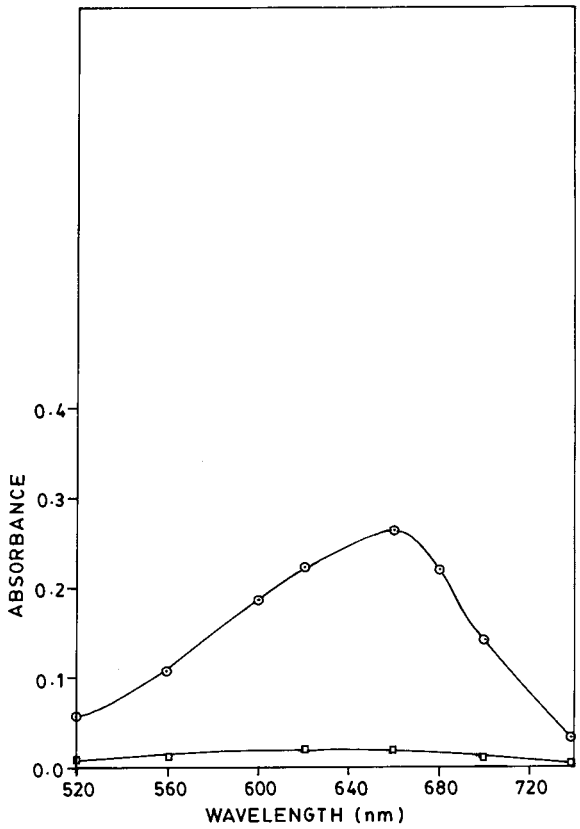

Fig. 1. Absorption spectra of the RV–$NaIO_4$/MBTH system (⊙——⊙) against a reagent blank (□——□) versus distilled water. RV, 9.01×10^{-5} M, $NaIO_4$, 3.74×10^{-4} M; acetic acid, 1.4×10^{-1} M; MBTH, 3.4×10^{-4} M.

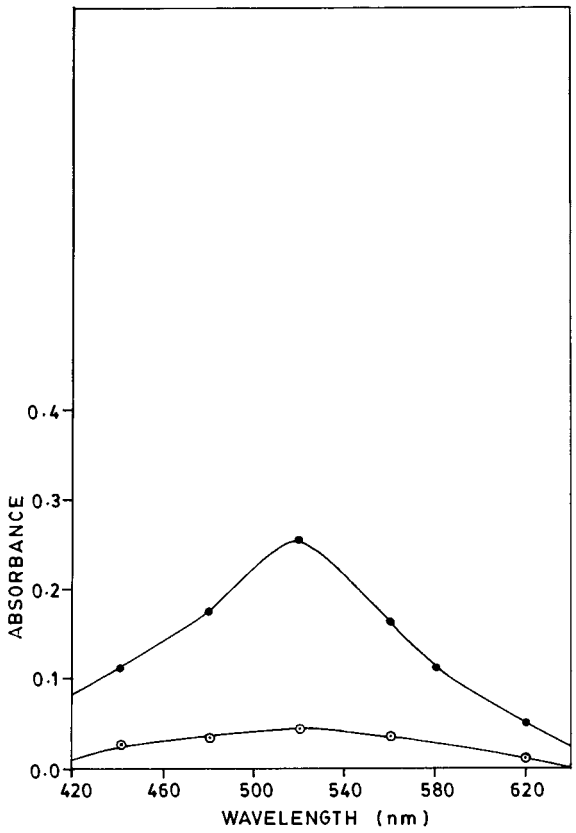

Fig. 2. Absorption spectra of the RV–$NaIO_4$–I^-–PMAP-SA system (●——●) against a reagent blank (⊙——⊙) versus distilled water: RV, 3.60×10^{-5} M, $NaIO_4$: 3.74×10^{-4} M; pH 3.0; Mo(VI), 3.31×10^{-3} M; I^-, 9.63×10^{-3} M; PMAP, 3.48×10^{-4} M; SA, 9.29×10^{-4} M.

Acknowledgements

PYN and CSRL gratefully acknowledge CSIR (New Delhi) and UGC (New Delhi) for providing SRF and JRF, respectively.

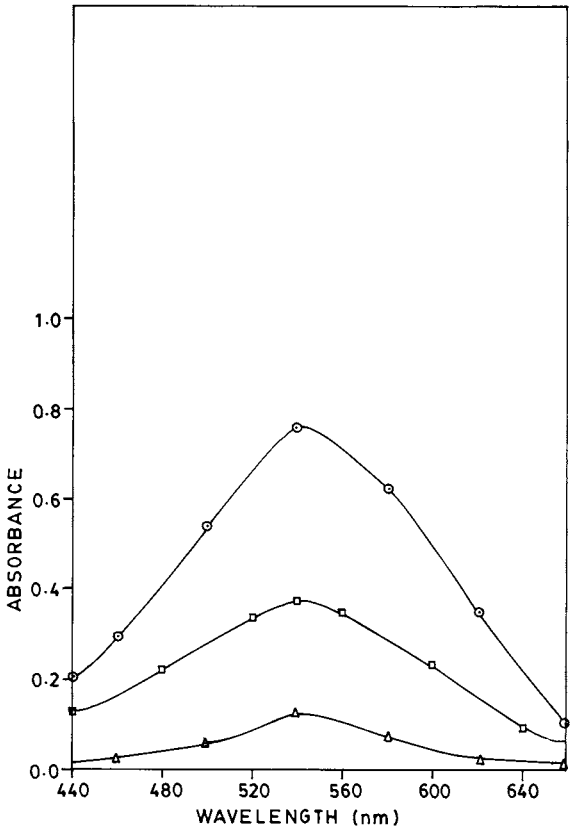

Fig. 3. Absorption spectra of the RV–IO_4^-–CB system (□——□) against a reagent blank (△——△) versus distilled water and dye (CB) (⊙——⊙) versus distilled water: RV, 1.35×10^{-5} M; IO_4^-, 3.74×10^{-5} M; Te(IV), 3.60×10^{-4} M; CB, 2.20×10^{-4} M; HCl, 0.6 M.

References

[1] US Pharmacopoeia, XXIII, Rockville, MD, 1993, p. 1377.
[2] J. Chen, J. Ou, Zhongguo Yiyao Gongye 25 (3) (1994) 124.
[3] Q. Meiling, H. Chumhua, L. Shunrong, Zhongguo Yiyuan Yaoxue Zazhi 24 (7) (1993) 311.
[4] Q. Meiling, H. Chunhua, L. Shunrong, Shenyang Yaoxue Yuanxebao 11 (2) (1994) 133.
[5] W. Wenao, W. Guoxiang, Zhongguo Yiyao Gongye 19 (4) (1988) 178.
[6] K.A. Raleigh, E.T. Park, M. Hintz, D.C. James, F.K. Martin, Antimicrob. Agents Chemother. 24 (5) (1983) 693.
[7] R. John, S. Robert, J. Chromatogr. 160 (1) (1978) 169.
[8] S. Yateen, J. Satish, K.C. Jindal, S. Khanna, Drug Dev. Ind. Pharm. 20 (1) (1994) 85.
[9] W. Gucmin, Z. Jain, Gongye Weishengewu 23 (1) (1993) 36.
[10] R. Paroni, R.C. Sirton, B. Cristina, M.G. Kienle, J. Chromatogr. 420 (1) (1987) 189.
[11] G. Dryhurst, R. Belcher, D.M.W. Anderson (Eds.), Periodate Oxidation of Diol and Other Functional Groups, Pergamon, London, 1970.
[12] E. Sawicki, T.R. Hausen, T.W. Stanley, W. Elbert, Anal. Chem. 33 (1961) 93.
[13] R. Ramakrishna, P. Siraj, C.S.P. Sastry, Acta Cienc. Indic. 6 (1980) 140.
[14] C.S.P. Sastry, S.G. Rao, K.R.S. Rao and P.Y. Naidu, Mikrochimica Acta (in press).
[15] J. Lurie, Handbook of Analytical Chemistry, Mir, Moscow, 1975, pp. 253.
[16] D.L. Massart, B.G.M. Vandegingte, S.N. Deming, Y. Michotte, L. Kaufman, Chemometrics, a Text Book, Elsevier, Amsterdam, 1988, p. 293.
[17] IUPAC, Spectrochim. Acta 33 (1978) 241.
[18] R. Rambabu, P. Vani, N. Sreedevi, L.S.A. Deekshitulu, J. Ind. Chem. Soc. 66 (1989) 906.
[19] R. Ripan, M. Mark, Stud. Cercet. Chem. 14 (1963) 41.
[20] C.S.P. Sastry, N.R.P. Singh, M.N. Reddy, Analusis 14 (1986) 355.

ELSEVIER

Talanta 47 (1998) 95–102

Talanta

Evaluation of the precision and accuracy of an automated sample introduction accessory for the flame atomic absorption spectrometric measurement of calcium in serum

Michael S. Epstein *, Bradley Buehler [1], Margaret F. Bullard [2]

Department of Science, Mount Saint Mary's College, Emmitsburg, MD 21727-7799, USA

Received 29 December 1997; received in revised form 27 January 1998; accepted 27 January 1998

Abstract

The measurement precision and accuracy that results from the use of a sample introduction peristaltic pump system for automated instrument calibration and analysis is compared to manual methods based on traditional gravimetric and volumetric dilution procedures for flame atomic absorption analyses in water and serum matrices. Whilst use of the automated system improves speed of analysis, measurement precision was found to be approximately 2-fold worse than the manual methods based on gravimetric and volumetric dilution procedures. © 1998 Elsevier Science B.V. All rights reserved.

Keywords: Automated sample introduction accessory; Flame atomic absorption spectrometry; Calcium; Serum

1. Introduction

Some 40 years after the first practical demonstration of it's capabilities, flame atomic absorption spectrometry (FAAS) is still unsurpassed as an inexpensive analytical method for the rapid sequential determination of major, minor, and trace metals in solution. Under optimum conditions, relative precision in the range 0.2–0.5% is common, and accuracy better than 1% relative is possible with careful control of the calibration procedures. This is in contrast to the more expensive emission and mass-based spectrometric techniques, which often require internal standardization to compensate for drift and obtain a similar quality of results, particularly in complex matrices. However, the sequential nature of the FAAS method results in a drastic increase in analysis time compared to the simultaneous multi-element emission and mass-based spectrometric techniques.

Automated dilution and calibration devices for atomic spectroscopy can significantly reduce the time and effort required for a FAAS analysis.

* Corresponding author. Present address: Department of Chemistry and Physics, Hood College, Frederick, MD 21701, USA. Tel.: +1 301 6963677; fax: +1 301 6947653; e-mail: epstein@hood.edu

[1] Present address: Department of Forensic Sciences, The George Washington University, Washington, DC20052, USA.

[2] Present address: Department of Chemistry, University of Minnesota, Minneapolis, MN 55455-0431, USA.

0039-9140/98/$19.00 © 1998 Elsevier Science B.V. All rights reserved.
PII S0039-9140(98)00075-7

However, since measurement precision and accuracy are a function of both the reproducibility of the instrument, and the sample and standard preparation and dilution process, the gain in efficiency by automating sample and standard dilution may be at the expense of measurement precision and accuracy. While this was not true for autosamplers used in graphite furnace atomic absorption spectroscopy, where a significant improvement in measurement precision and accuracy was obtained by eliminating manual sample positioning and delivery errors, it is more likely to be true for continuous-flow flame systems. This paper evaluates the effect on measurement precision and accuracy of the use of a two-channel sample introduction pump system (SIPS-20) [1] for automated instrument calibration and analysis using a flame system, compared to manual dilution methods based on traditional gravimetric and volumetric procedures.

2. Experimental

2.1. Instrumentation

For measurements involving copper in dilute acid solutions, manual dilution procedures were used in conjunction with a Perkin-Elmer Model 5000 and a Varian SpectrAA640 atomic absorption spectrometer. Both of these instruments used single-slot burner heads supporting an air–acetylene flame and were carefully optimized for maximum signal-to-noise ratio prior to analysis. Copper hollow cathode lamps from the respective manufacturers were used at the 324.7 nm line for measurements at low concentrations and at 222.6 nm for measurements at high concentrations. Similar analysis conditions were used for automated dilutions with the SIPS-20 and Varian SpectrAA640 atomic absorption spectrometer.

For measurements involving calcium in serum, both manual and automated dilution procedures were used with the Varian SpectrAA640 atomic absorption spectrometer using a single-slot burner head supporting a stoichiometric air–acetylene flame. A Westinghouse calcium hollow cathode lamp was used for all determinations at 422.6 nm.

Table 1
Evaluation of precision: copper in water

Dilution method/instrument	Precision (%R.S.D.) Drift-corrected	Precision (%R.S.D.) Not drift-corrected
Gravimetric (AA640)	0.3	0.5
Gravimetric (PE5000)	0.2	0.5
Volumetric (AA640)	0.6	0.7
Volumetric (PE5000)	0.6	0.6
SIPS (AA640)	—	1.0

2.2. Reagents and materials

High-purity acids obtained by a sub-boiling distillation process and high-purity de-ionized water were used for preparing solutions. Standard solutions of copper and calcium were made from 1000 μg ml^{-1} stock solutions prepared in our laboratory from high-purity copper and calcium carbonate. The superconductor precursor concentrate was obtained from the American Superconductor Corporation. Serum samples were either Standard Reference Materials from the National Institute of Standards and Technology or control samples from the State of New York Department of Health.

2.3. Dilutions

Gravimetric dilutions were made by weighing appropriate amounts of stock solutions into polyethylene bottles on an analytical balance to a precision of at least 1 part per thousand. Unless otherwise noted, solutions were in ~ 0.2 mol l^{-1} HNO_3. Density measurements of these solutions

Table 2
Evaluation of accuracy in a simple matrix: copper in a superconductor precursor concentrate

Dilution method/instrument	Copper (w/w%)[a]
Gravimetric	17.95 ± 0.04
SIPS	17.94 ± 0.09

[a] Uncertainty expressed as 95% confidence limits.

Table 3
Comparison of reference method [2] and modified method for the determination of calcium in serum

Reference method
All solutions are transferred volumetrically using a washout procedure with 10-ml pipets.
500-ml volumetric flasks are used for all dilutions.
Calibration standards are prepared individually from high purity calcium carbonate.
Diluent solution containing La, Na, K, and HCl used as a matrix-match and interference buffer.
Method of bracketing used to determine the Ca concentration in serum samples.
Modified method
Gravimetric transfer of all solutions.
Estimation of unknown density by calibrating micropipet with serum samples of known density.
Calibration standards prepared gravimetrically from laboratory reference stock solution made from high purity calcium carbonate.
Diluent solution containing La, Na, K, and HCl used as a matrix-match and interference buffer.
Calibration curve with drift correction standards (linear fit) used for determination of Ca concentration in serum samples.

were made to a precision of 1 part per thousand using a Paar DMA 35 Density Meter. Volumetric dilutions were made with Class-A pipets into Class-A volumetric flasks. All glassware was individually calibrated for true volume using the weight of de-ionized water contained or delivered.

3. Results and discussion

3.1. Precision evaluation in a simple matrix

Copper was chosen as the test element for precision evaluation. For evaluation of measurement precision in pure water using manual dilution procedures, ten solutions of 5 μg ml^{-1} Cu were prepared by gravimetric dilution and another ten were prepared by volumetric dilution using calibrated Class A 5-ml pipets. Four replicate series of measurements of each of the ten solutions in each set were made on each instrument, for a total of 40 measurements (four per solution) for each set. One of the solutions in each set was designated as a 'drift-correction' standard and was run at the beginning, middle, and end of the data set to correct for signal drift during each measurement set using a linear model. This data provided a baseline precision with which to compare the precision of the SIPS automated dilution system. A similar experimental design was used to evaluate precision using the SIPS. Four sets of 10 sequential dilutions at a concentration of 5 μg ml^{-1} Cu were generated on-line by the SIPS from a 50 μg ml^{-1} Cu stock solution.

The precision obtained for the determination of copper using the different dilution methods is shown in Table 1. Each value is calculated as the mean of the precision of the 4 measurement sets. and is expressed as %R.S.D. in the determined concentrations for each set, with and without drift-correction applied to the manual dilution methods. Statistical significance of results was evaluated at the 95% confidence level using the *t*-test.

There was no significant difference in measurement precision between the two different atomic absorption instruments when the same dilution method was used. However, there was a statistically significant difference between the precision of the gravimetric dilutions and the volumetric dilutions, with the former being more precise. This is expected, since the uncertainty of the gravimetric dilution process is less than 1 part per thousand, which is small compared to the instrument measurement precision. Therefore the measurement precision obtained for the gravimetric dilutions represents the uncertainty introduced by the instrument, due to factors such as lamp or flame instability. The observed precision degrades by approximately a factor of two when volumetric glassware is used, as a result of errors in solution transfer if pipets are not perfectly clean or delivery is inconsistent.

There was also a significant difference in the precision obtained from the SIPS dilutions ($\sim 1\%$ R.S.D.) compared to either the gravimetric or calibrated volumetric dilutions. The measurement precision for the SIPS can be directly compared only to the gravimetric and volumetric data that is not drift corrected. This is because drift correction cannot be applied to the SIPS data, since each SIPS dilution is prepared independently. The

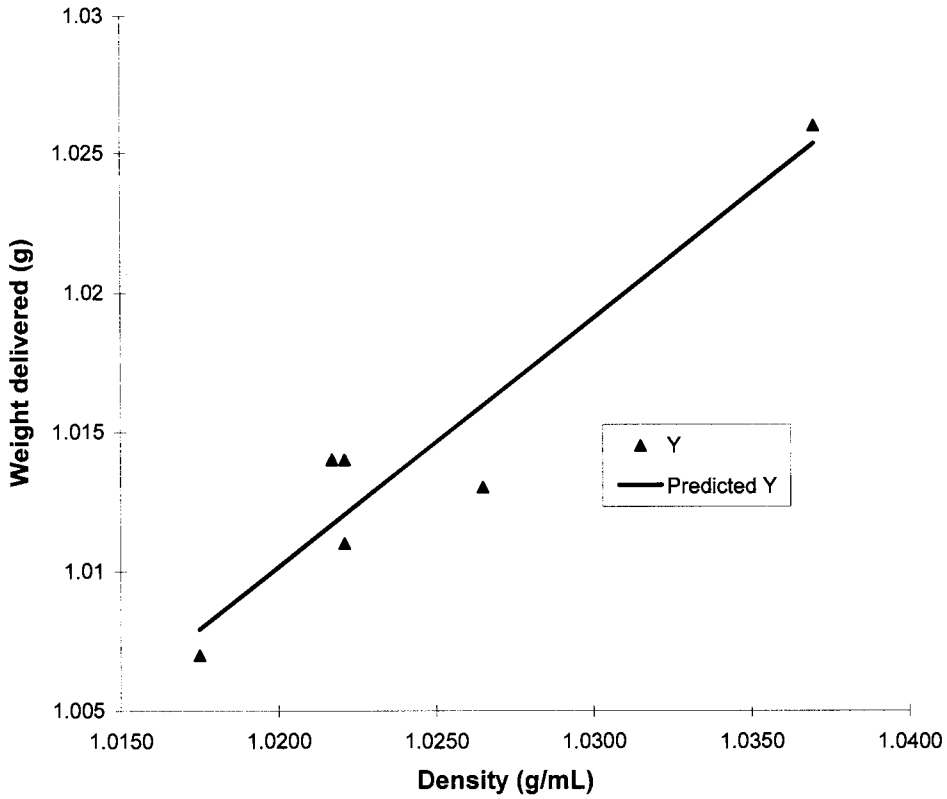

Fig. 1. The determination of density of unknown serum samples based on a linear regression using samples of known density. Unknown serum samples were referenced to the regression line to determine their density.

uncertainty obtained for the SIPS measurements is a function of both the instrument drift and drift in the SIPS dilution process. If there is a significant drift in the SIPS dilution process, such as changes in flexibility of the peristaltic pump tubing that influence flow rate, it will bias any attempt at drift correction.

Another interesting observation is that when drift correction is not used, the precision obtained for the gravimetric dilutions degrades such that it is no longer significantly different from that observed for the volumetric dilutions. This happens as a result of signal drift during the instrumental measurement set, which degrades the gravimetric measurement results. The magnitude of the drift from changes in instrument conditions (i.e. changes in flame stoichiometry, aspiration efficiency, etc.) can be estimated to be approximately 0.4% R.S.D., assuming that the instrument uncertainty and the dilution uncertainty are independent and therefore add quadratically. Elimination of the drift using the linear model reduces the instrument measurement uncertainty to that resulting only from short-term noise sources (flicker and shot components), which then allows us to observe a significant difference in precision between gravimetric and volumetric dilutions.

Under the conditions used in this experiment, where the dilution factor was 10, there is a significant precision difference of about a factor of 2 between careful manual dilution (i.e. gravimetric or volumetric using calibrated glassware) methods and the automated SIPS dilutions. The reproducibility of the SIPS dilution system is approximately 1%, which is somewhat better than the guaranteed precision specification of $< 2.5\%$ when operated with a dilution factor of < 50 [1].

Table 4
Evaluation of accuracy in a complex matrix: calcium in human serum

	Reference value[a] (mg Ca dl^{-1})	Average	%R.S.D.	%Bias
SIPS dilutions				
SRM 909	12.17	12.07	4.1	−0.8
SRM 909a-I	9.31	9.45	1.3	1.5
SRM 909a-II	13.4	13.37	1.1	−0.2
SRM 909b-I	8.89	8.99	2.8	1.1
NY1	8.3	8.15	2.2	−1.8
NY2	14.5	14.85	2.2	2.4
NY3	10.8	10.90	3.6	0.9
NY4	13.1	13.54	0.6	3.4
NY5	6.1	6.24	1.7	2.3
SRM 909b-II NY	14.16	14.26	0.9	0.7
SRM 909b-I NY	8.89	9.11	4.5	2.4
Average			2.3	1.1
Gravimetric dilutions				
SRM 909	12.17	12.03	0.8	−1.2
SRM 909a-I	9.31	9.27	0.8	−0.4
SRM 909a-II	13.4	13.31	0.2	−0.7
SRM 909b-I	8.89	8.97	0.2	0.9
NY1	8.3	8.10	1.6	−2.4
NY2	14.5	14.71	1.0	1.4
NY3	10.8	10.71	1.6	−0.8
NY4	13.1	13.37	1.4	2.1
NY5	6.1	6.28	0.6	2.9
SRM 909b-II NY	14.16	13.99	0.9	−1.2
SRM 909b-I NY	8.89	8.81	3.5	−0.9
Average			1.1	0.0

[a] Reference values for calcium (certified values for SRMs) in the serum samples.

3.2. Accuracy evaluation in a simple matrix

Although the SIPS dilutions were less precise than careful manual dilution procedures, the effect of that imprecision on accuracy can be reduced by increasing the number of measured dilutions if the variation introduced by the SIPS dilutions is random (i.e. there is no unidirectional bias introduced by the SIPS dilution process). This was evaluated by the determination of copper in a superconductor precursor concentrate, a highly concentrated solution of an element that used in the manufacturer of superconducting materials and whose concentration must be known to better than 1% relative. A comparison was made using standard gravimetric dilution procedures that were compared to SIPS-generated dilutions and analysis.

For this study, a 0.823 g aliquot of the Cu concentrate was diluted with 995.1 g of $\sim$0.2 mol l^{-1} HNO_3. A standard of 200.8 μg g^{-1} Cu was prepared by gravimetric dilution of a 993.5 μg g^{-1} Cu stock solution. Cu was measured at 222.6 nm, with 5 standards (prepared online with the SIPS) from 40 to 200 μg g^{-1} Cu. Three analysis sets of 10 replicates each were measured, and the results reported in Table 2 are based on all measurements. The results from manual gravimetric dilutions that were measured using the PE 5000 instrument are also reported in Table 2.

Although the degraded measurement precision of the SIPS-generated dilutions compared to gravimetric dilutions is still apparent, the excellent agreement of average copper content in the concentrate using the different dilution schemes and different instruments indicates that no systematic bias was introduced by the SIPS-generated dilu-

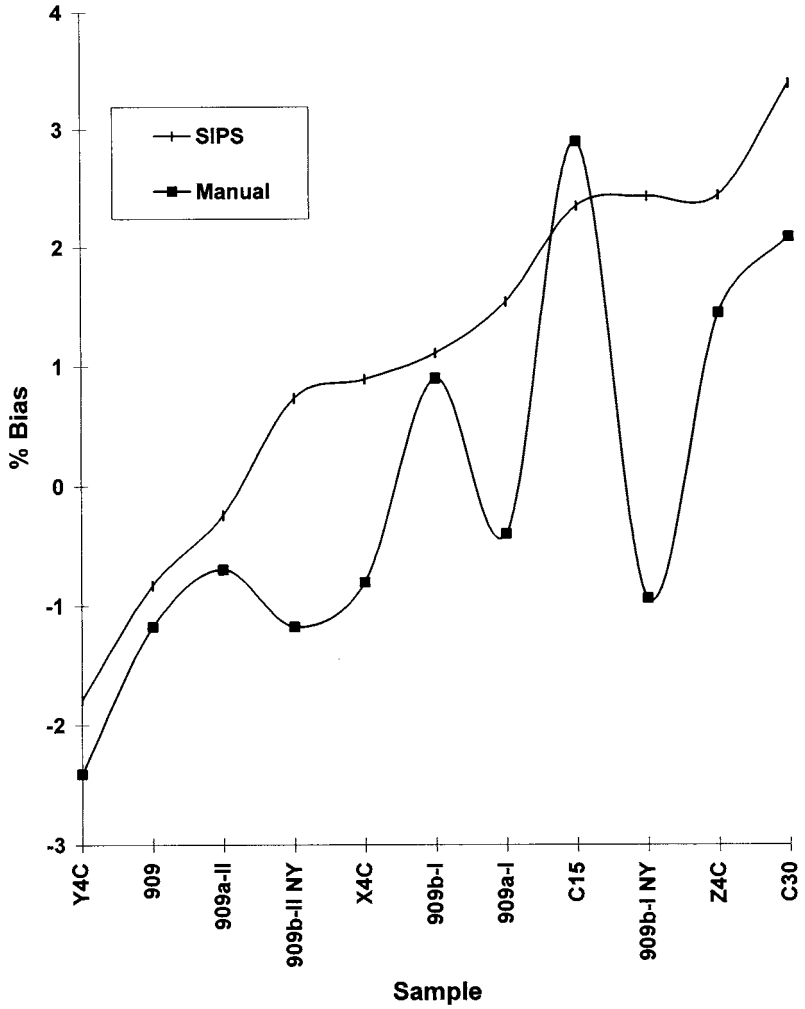

Fig. 2. A plot of sample ID vs. %bias from the reference value for calcium in serum determinations using SIPS and manual gravimetric dilutions. A comparison illustrates a small bias between the two techniques, which is also indicated by a *t*-test using the data pairs.

tions, and that the increased measurement throughput gained by automating dilutions can, if necessary, be used to improve precision by increasing the number of instrumental measurements, thus reducing the relative measurement uncertainty to less than one percent.

3.3. Accuracy and precision evaluation in a complex matrix

The determination of electrolytes in human serum for clinical evaluation requires a measurement process that is both accurate and precise. NIST has published reference methods for the determination of calcium [2], lithium [3], potassium [4], and sodium [5] that are the result of interlaboratory studies [6] using flame atomic absorption and emission spectrometry. These studies are benchmarked to isotope-dilution mass spectrometry [7] or other definitive method [8] determinations to assure accuracy. Depending on the element, the maximum imprecision of the referee methods can be no greater than from 1 to 3% relative with a maximum bias no greater than from 1.5 to 6% relative.

A modified version of the referee method for the determination of calcium in human serum was chosen to evaluate the SIPS performance in a complex matrix. The original reference method [2] was changed to simplify the procedure without any loss in accuracy or precision. Table 3 compares the two methods. The original reference method required large volume pipets and volumetric flasks, as well as solution washout procedures to reduce volumetric transfer errors. These time-consuming procedures were eliminated by careful gravimetric transfer of all solutions. Standards were prepared by gravimetric dilution from a laboratory reference stock solution of calcium prepared from high-purity $CaCO_3$, rather than preparing the standards individually from high-purity $CaCO_3$. A calibration curve with drift correction standards was used rather than the method of bracketing.

Serum samples consisting of reference materials from the National Institute of Standards and Technology and the New York Department of Health were diluted by weighing from 0.5 to 1.0 g of sample into the diluent solution containing La as an interference buffer and HCl. The density of the serum samples was determined by calibrating the delivery of a Rainin EDP2 automated micropipet with serum samples of known density, as shown in Fig. 1. The analysis was corrected for drift using a linear fit to drift-correction standards at the beginning, middle, and end of the analysis run.

The samples were run in three separate analysis sets using a manual introduction procedure, with standards from 1 to 3 μg ml^{-1} Ca prepared gravimetrically. The procedure was then repeated with the SIPS generating the same standards from a stock solution of 10 μg ml^{-1} Ca. The results are shown in Table 4. The precision, expressed as %R.S.D., and the bias, determined from the reference values and expressed as percent bias (%bias), are shown for both methods. The average precision of the SIPS measurements is approximately a factor of 2 worse than the manual gravimetric dilutions, and the difference is statistically significant at the 95% probability level.

A *t*-test (paired two sample for means) indicates a statistically significant difference at the 95% probability level between the %bias of the two methods. A plot of sample ID versus %bias, shown in Fig. 2, also visually indicates this small bias between manual dilutions and the SIPS dilutions. We believe this difference results from the manner in which the SIPS dilutions were performed. For the manual dilutions, each standard contained the same concentration of lanthanum diluent and sodium–potassium matrix-matching elements. For the SIPS dilutions, only the 10 μg ml^{-1} Ca stock solution contained the diluent and matrix matching elements. Since the SIPS diluent solution (the solution used to dilute the higher concentration stock solution to prepare working standards) was water, the standards did not contain exactly the same concentrations of lanthanum, sodium and potassium as the samples, which may have slightly biased the measurements. Unfortunately, it was not possible to use a solution of lanthanum, sodium and potassium as the SIPS diluent solution, so that all standards and samples contained the exact same concentrations. This procedure significantly increased the instrument drift during a measurement set and made it impossible to obtain satisfactory analytical results.

4. Conclusions

In this study, we used the SIPS up to a dilution factor of 10×, and under those conditions, we found its use for automating dilutions for AA analysis degraded precision by approximately a factor of 2 compared to gravimetric or volumetric dilution procedures. Use of the SIPS introduced a uncertainty of approximately 1% into the measurement process, making it satisfactory for all but the most demanding applications.

Acknowledgements

Thanks are due to Doug Shrader of Varian Analytical Instruments for the loan of the SpectrAA 640 and the SIPS system, as well as for many helpful discussions, to Mary Frances Verostek, State of New York Department of

Health, for providing reference serum samples, and to Martin Rupich of the American Superconductor Corporation, for providing the superconductor precursor solutions for evaluation.

References

[1] Sample Introduction Pumping System (SIPS), SpectrAA brochure 85-101340-00, Varian Optical Spectroscopy Instruments, March, 1995.
[2] J.P. Cali, J. Mandel, L. Moore, D.S. Young, A Referee Method for the Determination of Calcium in Serum, NBS Special Publication 260-36, US Department of Commerce, May, 1972.
[3] R.A. Velapoldi, R.C. Paule, R. Schaffer, J. Mandel, L.A. Machlan, E.L. Garner, T.C. Rains, A Reference Method for the Determination of Lithium in Serum, NBS Special Publication 260-69, US Department of Commerce, July, 1980.
[4] R.A. Velapoldi, R.C. Paule, R. Schaffer, J. Mandel, L.A. Machlan, J.W. Gramlich, A Reference Method for the Determination of Potassium in Serum, NBS Special Publication 260-63, US Department of Commerce, May, 1979.
[5] R. A. Velapoldi, R.C. Paule, R. Schaffer, J. Mandel, J.R. Moody, A Reference Method for the Determination of Sodium in Serum, NBS Special Publication 260-60, US Department of Commerce, August, 1978.
[6] J. Mandel, Med. Instrum. 8 (1974) 26.
[7] G.N. Bowers Jr., J.D. Fassett, E. White V, Anal. Chem. 65 (1993) 475R.
[8] J.R. Moody, M.S. Epstein, Spectrochim. Acta B 12 (1991) 1571.

ELSEVIER

Talanta 47 (1998) 103–108

Talanta

Simultaneous determination of phenobarbital and phenytoin in tablet preparations by multivariate spectrophotometric calibration

Héctor C. Goicoechea [a,b], Alejandro C. Olivieri [b,*]

[a] *Departamento de Química, Facultad de Bioquímica y Ciencias Biológicas, Universidad Nacional del Litoral, Paraje El Pozo, Santa Fe, 3000, Argentina*

[b] *Departamento de Química Analítica, Facultad de Ciencias Bioquímicas y Farmacéuticas, Universidad Nacional de Rosario, Suipacha 531, Rosario, 2000, Argentina*

Received 13 October 1997; received in revised form 20 January 1998; accepted 28 January 1998

Abstract

The use of multivariate spectrophotometric calibration for the simultaneous determination of the active components of antiepileptic tablets is presented. The resolution of binary mixtures of phenobarbital and phenytoin has been accomplished by using partial least squares (PLS-1) regression analysis. Although the components show an important degree of spectral overlap, they have been simultaneously determined with high accuracy, with no interference from tablet excipients. A comparison is presented with the related multivariate method of classical least squares (CLS) analysis, which is shown to yield less reliable results due to the severe spectral overlap presented by the studied compounds. A statistical measure for the spectral overlap is proposed. © 1998 Elsevier Science B.V. All rights reserved.

1. Introduction

Phenobarbital is a long-acting barbiturate. It is an effective sedative anticonvulsivant for the treatment of generalized tonic–clonic, simple–partial, and complex–partial seizures. The drug is also effective in *status epilepticus*, alcohol withdrawal syndromes, anxiety, and sleep disorders [1]. On the other hand, phenytoin is an anticonvulsivant structurally related to barbiturates for the treatment of seizures. It was introduced in 1937 as one of the most effective agents in the treatment of resistant epilepsy [2]. It is a useful antiasthmatic agent used either alone or as adjuvant therapy [3], and has been reported to promote wound healing when applied as a topical agent [4]. Its usefulness in the treatment of rheumatoid arthritis has also been reported [5]. The dosage is very important since long-term anticonvulsant treatment produces abnormal bone mineral metabolism [6]. Phenytoin administration can result in insulin insensitivity by inducing a post-binding defect in insulin action [7]. Antiepileptic drugs have been implicated in elevation of serum estradiol and reproductive dysfunction in men with epilepsy [8].

* Corresponding author. Fax: + 54 41 253423; e-mail: aolivier@fbioyf.unr.edu.ar

0039-9140/98/$19.00 © 1998 Elsevier Science B.V. All rights reserved.
PII S0039-9140(98)00070-8

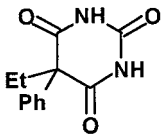

Phenobarbital

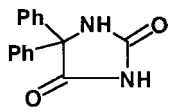

Phenytoin

Multivariate calibration methods [9–11] applied to spectral data (both absorptive and emissive) are being increasingly used for biomedical and pharmaceutical analysis [12–19]. We have recently reported the simultaneous determination of mixtures of urinary metabolites of aspirin [18] and styrene [19] using classical least squares (CLS) analysis. The latter is one of the simplest multivariate methods, and can be performed with easily accessible statistical software. In the present report we discuss the possibility of simultaneously quantitating phenobarbital and phenytoin in antiepileptic tablets, by applying electronic absorption measurements together with multivariate calibration analysis. The results show that partial least squares (PLS) regression using the PLS-1 formalism allows one to accomplish this goal, whereas CLS does not give reliable results. A comparison between both methods is discussed in light of the severe spectral overlap for both studied compounds.

2. Experimental

2.1. Apparatus

Electronic absorption measurements were carried out on a Beckman DU-640 spectrophotometer, using 1.00 cm quartz cells. All spectra were saved in ASCII format, and transferred to a PC 80486 microcomputer for subsequent manipulation by either CLS or PLS programs. CLS analysis was performed by importing the spectra files to Sigmaplot (version 2.0) and processing them with the standard curve fit package. PLS was applied with an in-house program written in Quick Basic according to the algorithm described in ref. [9].

2.2. Reagents

All experiments were performed with analytical-reagent grade chemicals. Doubly distilled water was used. Stock solutions of phenobarbital and phenytoin were prepared by dissolving the compounds in NaOH 0.01 mol l^{-1}. For the analysis of the active components of the antiepileptics Dantoinal and Lactominal, 20 tablets of each pharmaceutical were ground and mixed. The amounts corresponding to the equivalent to half a tablet were dissolved, in each case, in 1000.0 ml of NaOH 0.01 mol l^{-1}. The solutions were then stirred for 15 min and filtered.

2.3. Solutions for multivariate calibration

2.3.1. CLS method

In order to obtain the calibration matrix for applying CLS analysis, five solutions of each of the pure components phenobarbital and phenytoin were prepared, with concentrations in the range $1.9–15.1 \times 10^{-5}$ mol l^{-1}. This range was previously verified to obey Beer's law for each of the studied compounds. The absorbance data (in the range 220–280 nm, digitized every 1.0 nm, 61 points per spectrum) were subjected to least squares analysis in order to obtain the calibration **K** matrix (see below). Unknown mixtures were prepared either from the studied tablet preparations or by mixing known amounts of each stock solution.

2.3.2. PLS method

A training set of ten standard binary mixtures of phenobarbital and phenytoin were prepared for calibration, with the concentrations of both components lying in the known linear absorbance–concentration range. The spectral region, interval and number of points were the same as for the CLS analysis. The data were subjected to PLS-1 analysis.

3. Results and discussion

Fig. 1 shows the electronic absorption spectra of both studied compounds. As can be seen, an

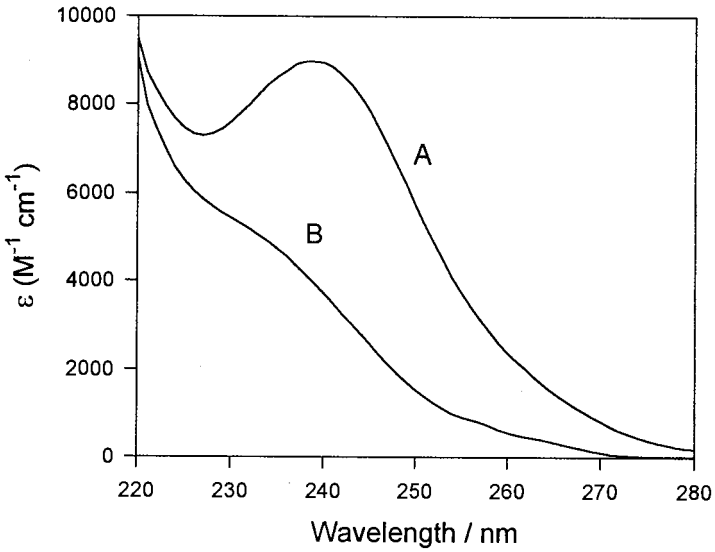

Fig. 1. Electronic absorption spectra of: (A) phenobarbital and (B) phenytoin in NaOH 0.01 mol l^{-1}.

important degree of spectral overlap occurs in the useful region 220–280 nm. A convenient method for resolving mixtures, which can in principle be applied to the present case, is least-squares analysis [9–11]. In the classical (CLS) version, a linear relationship between the absorbance and the component concentrations at each wavelength is assumed. In matrix notation, the model for m calibration standards containing l chemical components with spectra at n digitised wavelengths is given by $\mathbf{A} = \mathbf{CK} + \mathbf{E}$ ($\mathbf{A}$ is the $m \times n$ matrix of calibration spectra, $\mathbf{C}$ is the $m \times l$ matrix of component concentrations, $\mathbf{K}$ is the $l \times n$ matrix of absorbance-concentration proportionality constants, and $\mathbf{E}$ is the $m \times n$ matrix of spectral errors or residuals not fit by the model). During calibration, $\mathbf{K} = (\mathbf{C}^t\mathbf{C})^{-1}\mathbf{C}^t\mathbf{A}$, and during prediction, the vector of unknown component concentrations is $\boldsymbol{c} = (\mathbf{K}\mathbf{K}^t)^{-1}\mathbf{K}\boldsymbol{a}$ ($\boldsymbol{a}$ is the spectrum of the unknown sample) [9–11].

Several mixtures, both synthetic and real, were subjected to the present analysis with the results shown in Table 1. Full-spectrum methods such as CLS usually provide significant improvement in precision over methods restricted to a small number of wavelengths. However, it can be confidently applied provided there is no extensive overlapping between the component spectra. In order to study the effect of spectral overlapping, the following procedure can be adopted. After obtaining the best fit parameters (the unknown component concentrations), CLS programs usually yield the magnitude of the dependency D_i, defined for each of the refined parameters as:

$$D_i = 1 - \frac{\sigma_i^2(\text{marg})}{\sigma_i^2(\text{cond})} = 1 - F_i^{-1} \tag{1}$$

where σ_i^2(marg) and σ_i^2(cond) are the marginal and conditional variances for the parameter c_i respectively. They are obtained through eqs. (2,3):

$$\sigma_i^2(\text{marg}) = \sigma_{\text{fit}}(\mathbf{B}^{-1})_{ii} \tag{2}$$

$$\sigma_i^2(\text{cond}) = \sigma_{\text{fit}}(\mathbf{B}_{ii})^{-1} \tag{3}$$

where $\mathbf{B}$ is a matrix whose elements are defined by $B_{ij} = [(d\boldsymbol{a}_{\text{pred}}/dc_i)(d\boldsymbol{a}_{\text{pred}}/dc_j)^t]$, and $\sigma_{\text{fit}} = \sqrt{\Sigma\,(a_{\text{act}} - a_{\text{pred}})^2/(n-2)}$. For a two component mixture, $\boldsymbol{a} = \boldsymbol{k}_1 c_1 + \boldsymbol{k}_2 c_2$, $\boldsymbol{k}_{1,2}$ being the column vectors of individual component absorptivities. Hence, from eqs. (2,3) it can be shown that:

$$D_i = \frac{\left(\sum \boldsymbol{k}_1 \boldsymbol{k}_2^t\right)}{\sum \boldsymbol{k}_1 \boldsymbol{k}_1^t \sum \boldsymbol{k}_2 \boldsymbol{k}_2^t} \tag{4}$$

Table 1
Results obtained in the determination of binary mixtures by applying the CLS method

Mixture	Component	Actual	Found mol $l^{-1} \times 10^5(\sigma)$[a]	Recovery (%)	σ_{fit} [b]
Synthetic	Phenobarbital	2.50	2.3(1)	92	0.015
	Phenytoin	2.50	2.7(1)	108	
Synthetic	Phenobarbital	1.98	1.7(1)	86	0.012
	Phenytoin	2.94	3.4(1)	116	
Dantoinal[c]	Phenobarbital	2.25	2.3(1)	102	0.012
	Phenytoin	4.00	3.4(1)	85	
Lactominal[c]	Phenobarbital	1.08	1.35(5)	125	0.009
	Phenytoin	3.08	3.4(1)	110	

[a] σ = Marginal standard deviation for the refined parameters.
[b] $\sigma_{fit} = \sqrt{\Sigma(a_{act} - a_{pred})^2/(n-2)}$, n = number of data points.
[c] Actual concentrations calculated from the content of each component in the tablets, as reported by the manufacturing laboratories.

The latter equation shows that $\sqrt{D_i}$ is a convenient measure of the degree of spectral overlap (notice that D_i only depends on the spectral characteristics of each component). In the case of the presently studied compounds, the spectra shown in Fig. 1 lead to $D_i = 0.85$, implying a 92% of spectral overlap. A better statistical approach is to compare the obtained values of F_i from Eq. (1) with the maximum $F(\alpha,v_1,v_2)$ values given in standard statistical tables, where a is the confidence level and v_1 and v_2 are the degrees of freedom for both variances. We may take $v_1 = v_2$ as the number of digitised wavelengths minus one, so that $F(0.01,60,60) = 1.84$. In the present case $F_i = 6.7$, and hence $F_i > F(\alpha,v_1,v_2)$. This means that CLS analysis is to be considered unreliable in order to obtain the component concentrations for the presently studied mixtures. This fact is also reflected in the poor recoveries obtained (Table 1). Nevertheless, the latter study indicated that the tablet excipients did not interfere with the analysis, since spectra for synthetic mixtures closely matched those for comercial tablets with comparable concentrations.

One alternative to analysing mixtures when severe spectral overlapping occurs involves the use of PLS methods. Briefly, the data matrix $\mathbf{A}$ is decomposed into $\mathbf{A} = \mathbf{T}_a\mathbf{B}_a$ ($\mathbf{B}_a$ and $\mathbf{T}_a$ are the $h \times n$ loading and $m \times h$ scores matrix respectively, and h is the number of PLS factors). The calibration mixture matrix $\mathbf{C}$ is similarly decomposed: $\mathbf{C} = \mathbf{T}_c\mathbf{B}_c$. During calibration, the following equations are solved by least-squares: $\mathbf{T}_c = \mathbf{T}_a\mathbf{V}$ ($\mathbf{V}$ is the $h \times h$ calibration matrix). During prediction, the component score is obtained from the unknown spectrum $\boldsymbol{a}$ as $\boldsymbol{t} = \boldsymbol{a}\ (\mathbf{B}_a)^t$, and the unknown concentration from $c = \boldsymbol{t}\mathbf{V}\boldsymbol{b}_c$, where $\boldsymbol{b}_c$ is the appropriate hx1 vector associated with the component of interest. Notice that individual components are independently modelled by PLS-1, using an optimum h value for each of them [9].

For the presently studied mixtures, the calibration matrix was designed with concentration ranges of $0.50–3.20 \times 10^{-5}$ mol l^{-1} for phenobarbital and of $1.00–4.50 \times 10^{-5}$ mol l^{-1} for phenytoin, since the accuracy of the analysis is affected by the appropriate choice of component concentration in the standards. The latter concentrations lie within the linear range, as previously verified for CLS analysis. The calibration design used for the analysis is shown in Table 2. For the selection of the optimum number of factors, the cross validation method proposed by Haaland and Thomas was used. It involves computing the PRESS (Prediction Error Sum of Squares) for each value of h, selecting the one which yields the minimum PRESS (h*), and computing the following F ratio [9]: $F(h) = \text{PRESS}(h)/\text{PRESS}(h*)$, where $h < h$* and $\text{PRESS} = \Sigma_1^m (c_{act} - c_{pred})^2$. The optimum number of factors is suggested to corre-

Table 2
Mixture design for the application of PLS analysis and statistical parameters for the calibration

Mixture	Phenobarbital (mol $l^{-1} \times 10^5$)		Phenytoin (mol $l^{-1} \times 10^5$)	
	Actual	Predicted[a]	Actual	Predicted[b]
M1	1.00	0.96	2.00	1.97
M2	2.10	2.14	2.30	2.31
M3	2.40	2.39	1.00	0.85
M4	0.50	0.50	3.30	3.40
M5	3.20	3.16	2.80	2.90
M6	1.90	1.84	3.70	3.71
M7	1.50	1.50	4.50	4.40
M8	2.80	2.86	4.00	3.94
M9	1.50	1.52	3.00	3.09
M10	1.80	1.87	3.00	2.99
Statistical parameters				
	Phenobarbital[a]	Phenytoin[b]		
PRESS	0.0062	0.0576		
$F(h)$ (Prob.)	1.03 (0.519)	1.00 (0.500)		
RMSD	0.024	0.076		
r^2	0.999	0.994		
REP, %	1.28	2.57		

[a] Computed with four factors (see text).
[b] Computed with three factors (see text).

spond to a probability of less than 75% that $F(h) > F(h^*)$. In the present case, four factors were used in predicting the concentration of phenobarbital, and three for phenytoin (see Table 2). This latter table also gives the values of PRESS, $F(h)$ and probability for the optimum number of factors, and of the root mean square difference ($\mathrm{RMSD} = [1/m\ \Sigma_1^m\ (c_{\mathrm{act}} - c_{\mathrm{pred}})^2]^{1/2}$), square of the correlation coefficient ($r^2 = 1 - \Sigma_1^m(c_{\mathrm{act}} - c_{\mathrm{pred}})^2 / \Sigma_1^m(c_{\mathrm{act}} - \bar{c})^2$, $\bar{c}$ is the average component concentration in the m calibration mixtures) and relative error of prediction ($\mathrm{REP},\% = 100/\bar{c}[1/m\ \Sigma_1^m(c_{\mathrm{act}} - c_{\mathrm{pred}})^2]^{1/2}$), which give an indication of the quality of fit of all the data.

It should be noticed that two other related multivariate factor-based methods, PCR and PLS-2, were also applied to the present samples, with essentially the same results as those reported here.

Table 3 summarises the results after applying the PLS method to both real and synthetic samples. As can be appreciated, the recoveries are more satisfactory than using CLS analysis.

4. Conclusions

The content of phenobarbital and phenytoin, usual components of antiepileptics tablet formulations, were simultaneously determined using electronic absorption measurements, together with PLS-1 multivariate calibration analysis. Synthetic binary mixtures as well as two commercial tablets were studied, with excellent recoveries in all cases. A related multivariate method, CLS, has been shown to be unreliable in quantitating the studied compounds in their mixtures, due to extensive spectral overlapping.

Acknowledgements

Financial support from CONICET (Consejo Nacional de Investigaciones Científicas y Técnicas), the University of Rosario and Fundación Antorchas is gratefully acknowledged. We also thank Elvetium, Dr. Rafael Quesada and Gramon laboratories for supplying Dantoinal, Lactominal and sodic phenytoin respectively. H.C.

Table 3
Results obtained by applying PLS-1 analysis to both synthetic and real binary mixtures of phenobarbital and phenytoin.

Mixture	Component	Actual (mol $l^{-1} \times 10^5$)	Found (mol $l^{-1} \times 10^5$)	Recovery (%)
Synthetic	Phenobarbital	2.00	2.05	103
	Phenytoin	2.80	2.82	101
Synthetic	Phenobarbital	2.50	2.49	100
	Phenytoin	2.50	2.57	103
Synthetic	Phenobarbital	2.50	2.43	97
	Phenytoin	1.50	1.40	93
Dantoinal[a]	Phenobarbital	2.25	2.24	100
	Phenytoin	3.08	3.49	113
Lactominal[a]	Phenobarbital	1.08	1.06	98
	Phenytoin	2.97	3.00	99

[a] Actual concentrations calculated from the content of each component in the tablets, as reported by the manufacturing laboratories.

Goicoechea thanks FOMEC (Programa para el Mejoramiento de la Calidad de la Enseñanza Universitaria) for a fellowship.

References

[1] A. Goodman-Hilman, T. Rall, A. Nier, P. Taylor, The Pharmacologycal Basis of Therapeutics, McGraw-Hill, New York, 1996.
[2] P. Rajma, J. Veres, J. Vitray, Ther. Hung. 39 (1991) 30.
[3] S. Jain, K. Jain, J. Asthma 28 (1991) 201.
[4] A. Pendse, A. Sharma, A. Sodani, S. Hada, Int. J. Dermatol. 32 (1993) 214.
[5] M. Naidu, K. Ramesh, R. Anuradha, U. Rao, Drugs Exp. Clin. Res. 17 (1991) 271.
[6] C. Alderman, C. Hill, Ann. Pharmacother. 28 (1994) 47.
[7] K. al-Rubeaan, E. Ryan, Diabet. Med. 8 (1991) 968.
[8] A. Heroz, L. Levesque, F. Drislane, M. Ronthal, D. Schomer, Epilepsia 32 (1991) 550.
[9] D.M. Haaland, E.V. Thomas, Anal. Chem. 60 (1988) 1193.
[10] H. Martens, T. Naes, Multivariate Calibration, Wiley, Chichester, 1989.
[11] K.R. Beebe, B.R. Kowalski, Anal. Chem. 59 (1989) 1007A.
[12] A. Espinosa-Mansilla, A. Muñoz de la Peña, F. Salinas, M. Martínez Galera, Anal. Chim. Acta 276 (1993) 141.
[13] M. Sánchez Peña, A. Muñoz de la Peña, F. Salinas, M.C. Mahedero, J.J. Aaron, Analyst 119 (1994) 1177.
[14] A. Espinosa-Mansilla, F. Salinas, A. Zamoro, Analyst 119 (1994) 1183.
[15] A. Guiberteau Cabanillas, T. Galeano Díaz, A. Espinosa-Mansilla, P.L. López de Alba, F. Salinas López, Anal. Chim. Acta 302 (1995) 9.
[16] K. Mahalanabis, D. Basu, Analyst 114 (1989) 1311.
[17] A. Bozdogan, A.M. Acar, G.K. Kunt, Talanta 39 (1992) 977.
[18] P. Damiani, G. Ibáñez, M.E. Ribone, A.C. Olivieri, Analyst 120 (1995) 443.
[19] M.E. Ribone, A.P. Pagani, A.C. Olivieri, Anal. Lett., submitted.

ELSEVIER

Talanta 47 (1998) 109–120

Talanta

Data-, knowledge- and method-bases in chemical sciences I. BAQOR—database for equilibrium constants in aquo-organic media

A. Braibanti [a,*], R. Sambasiva Rao [1,a], G. Nageswara Rao [b], N. Satyanarayana [b]

[a] *Physical Chemistry Section, Pharmaceutical Department, University of Parma, I-43100 Parma, Italy*
[b] *School of Chemistry, Andhra University, Visakhapatnam-530003, India*

Received 16 July 1997; received in revised form 23 January 1998; accepted 28 January 1998

Abstract

BAQOR is a computer readable database for equilibrium constants in presence of different percentages of water miscible cosolvents. The present version with user friendly software in dBase III + contains 740 records and runs on any IBM compatible PC. The physico-chemical properties of binary and ternary water-cosolvent mixtures, the equilibrium constants of proton– and metal–ligand complexes are retrievable through pop-up menus. Specific searches by metal-, ligand-, solvent-, and stoichiometry-wise and their combinations is possible. Several display modes—monitor, file and hard copy—are available for the numerical fields as well as for literature citation. © 1998 Elsevier Science B.V. All rights reserved.

Keywords: Database; Equilibrium constant; Aquo-organic mixtures; dBase III +

1. Introduction

Most of the passive databases for equilibrium constants of proton–ligand and metal–ligand complexes available are for systems in aqueous solution. The first series contains all the published data without deleting any systems and leaving the decision to the investigator. The critical stability constants by Martell [1] are based on peer scrutiny, quality of data and ambient conditions. Williams [2–4] prepared a computer readable thermodynamic stability constant database. May et al. [5–7] in their project JESS developed a thermodynamic stability constant database and 50000 lines of Fortran code was developed for the interpretation for variation of stability constant with temperature and ionic strength. Pettit and Pettit [8] also prepared a database for equilibrium constants in non-aqueous and mixed solvents. Izutsu [9] brought out a passive database for stability constants in pure non-aqueous solvents. This contains very few systems at different aquo–organic compositions.

* Corresponding author. Tel.: + 39 521 905024; fax: + 39 521 905006; e-mail: braiban@ipruniv.cce.unipr.it

[1] On leave from the School of Chemistry, Andhra University, Visakhapatam, India.

0039-9140/98/$19.00 © 1998 Elsevier Science B.V. All rights reserved.
PII S0039-9140(98)00059-9

In spite of the progress in understanding the role of water in chemical/biochemical reactions with the aid of the equilibrium, kinetic and spectroscopic parameters at different ionic strengths, temperatures, cosolvent contents, micelles, or cryptands, no unified theory has yet evolved. The chromatographic studies [10] in aquo–organic mixtures to separate the isomers changed the facet of equilibrium chemistry from basic research to that essential in industrial processes. Further Sigel [11] proposed a new application of equilibrium constants in aquo–organic media to determine the effective dielectric constant at the biological cavity for similar reactions. The equilibrium constants in aquo–organic mixtures have been studied since the initial attempts by Calvin [12] in the early 1940's. A perusal of the literature revealed that hitherto there is no printed form of equilibrium constants data in aquo–organic media. An upgradable database and method-base paves the way for progress in this direction. Keeping these aspects in view a database (BAQOR) was developed in dBASE III+.

2. Experimental

The stability constant data incorporated in the present database are from the published original research papers. With today's speed (66/100 MHz), primary memory (4/8/16 MB RAM) and auxiliary storage devices (540 MB hard disk) of a 486 system, the performance to price ratio is very high. This is adequate for many of the chemical tasks. Hence, a microcomputer in a DOS environment was chosen.

In recent times dBASE III+, dBASE IV and FOXBASE have become popular in academic and R&D organizations. However in corporate bodies and international organizations like the International Atomic Energy Agency, fourth generation languages like SYBASE and ORACLE are in use for mega projects [10]. dBASEIII+ requires approximately 200 KB of RAM and occupies around 800 KB of disk space. The maximum number of records handled is more than a million. The other unique features which made it popular are that

- SYBASE can access dBASE III+ files. Hence small databases developed by different groups of chemists can be integrated into a corporate body.
- It can be interfaced with EXSYS [13], an expert system environment where the rules for the data trends can be generated.
- The retrieval and interpretation programs written in dBASE III+ are convertible to executable modules running in DOS (without dBASE III+) through CLIPPER.

2.1. Creation of BAQOR

An ideal database is one which occupies minimum memory and whose retrieval/search time is fast. Each item in the database, called a record, is a complete source of information useful in chemical or biochemical research/teaching. Thus, all the fields pertaining to numerical data, literature cita-

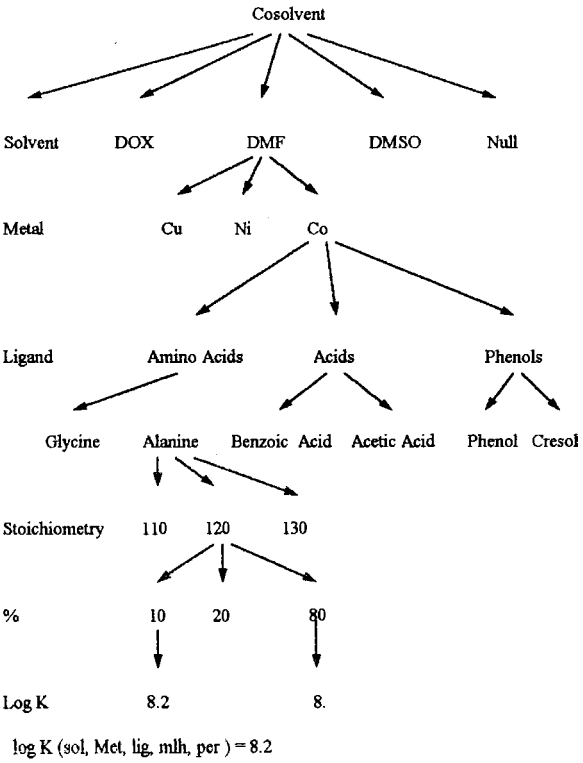

Fig. 1. Hierarchical representation of stability constant database in aquo-organic media.

Table 1
Different categories of literature in the bibliographic citations

Journals	*Regular	Original research papers
	*Irregular	
Books	*Edited	
	*Texts/Advanced	Condensed form of information
	*Monographs	The last few years
	*Bench mark papers	
	*Current opinion	
Dissertation abstracts		Details of research work
Theses		All over the globe
Proceedings	*Full paper	
Current awareness	*Abstracts	
	*Titles	
Private/personal communications		Data/programs
News papers, magazines		Essential in disciplines like AIDS and human genome studies

tion, experimental conditions and statistical analysis in BAQOR (Beta in AQuo–ORganic mixtures) should be in a single record. The stability constant information of a chemical system can be depicted by a hierarchical structure (Fig. 1), an object or even in relational mode. However, the relational database management approach requires large disk space which is disadvantageous. The large disk space is due to the following reasons:

- The same author may perform analysis of more than one system and thereby the literature citation is repeated many times.
- The ambient conditions of the experiment and instrumental characteristics are also the same for many chemical systems.
- Except in a few cases the statistical parameters are not reported which results in gaps in the record.

Keeping these factors in view to optimize the disk space, several structures for the database of equilibrium constants in aqueous, micellar, and aquo–organic media have been developed. Based on the changing scenario of hardware and software, it is thought at the moment that separate structures are the optimum for aquo–organic mixtures, aqueous solution and single/mixed micellar media. Hence, separate databases for the literature (exclusive files for books and references, Table 1), experimental conditions, and statistical parameters, are created. Different database files created

Table 2
Database files in BAQOR

Database	No.of records	Description of the File
BAQOR	740	Stability constants in mixtures of water and one cosolvent
REF-AQOR	300	Bibliographic citations for journals
BAQOR2	100	Stability constants in mixtures of water and two cosolvents
WS1CHAR	25	Macroscopic characteristics of mixtures of water and one cosolvent
WS1S2CHAR	10	Macroscopic properties of mixtures of water and two cosolvents
	Index files	
BAQOR	REF, LIGAND1, METAL1, S1NAME, MLHXYM2M	
REF-AQOR	JOURNAL, A1, A2	
WS1CHAR	S1	
WS1S2CHAR	S12	

Table 3
The condensed structure of the databases

Field name	Field type (length)	Field name	Field type (length)
BAQOR		BAQOR2	
REF	N (4)	REF	N (4)
LIGAND1	C (30)	LIGAND1	C (30)
LIGAND2	C (30)	LIGAND2	C (30)
METAL	C (2)	METAL	C (2)
OXSTATE	N (2)	OXSTATE	N (2)
S1NAME	C (20)	S1NAME	C (20)
VWX	C (1)	S2NAME	C (20)
MLHXYM2M3	C (8)	VWX	C (1)
P1	N (6.2)	MLHXYM2M3	C (8)
LogB1	N (7.3)	P1S1	N (6.2)
SD1	N (5.3)	P1S2	N (6.2)
—		LogB1	N (7.3)
—		SD1	N (5.3)
P10	N (6.2)	—	
LogB10	N (7.3)	—	
SD10	N (5.3)	P10S1	N (6.2)
LINKCOND	N (4)	10S2	N (6.2)
LINKSTAT	N (4)	LogB10	N (7.3)
		SD10	N (5.3)
		LINKCOND	N (4)
		LINKSTAT	N (4)
WS1CHAR		WS1S2CHAR	
S1NAME	C (10)	S1NAME	C (10)
VWX	C (1)	S2NAME	C (10)
P1S1	N (6.2)	VWX	C (1)
D1	N (6.2)	P1S1	N (6.2)
DENSITY1	N (6.4)	P2S2	N (6.2)
NX1	N (6.4)	D1	N (6.2)
CH2O1	N (6.3)	DENSITY1	N (6.4)
—		NXS11	N (6.4)
—		NXS21	N (6.4)
P1S8	N (6.2)	CH2O1	N (6.3)
D8	N (6.2)	—	
DENSITY8	N (6.4)	—	
NX18	N (6.4)	P1S8	N (6.2)
CH2O8	N (6.3)	P2S8	N (6.2)
		D8	N (6.2)
		DENSITY8	N (6.4)
		NXS18	N (6.4)
		NXS28	N (6.4)
		CH2O8	N (6.3)
		F5	C (15)
REF_LIT		A5	C (25)
REF	N (4)	ETC	L (1)
F1	C (15)	JOURNAL	C (30)
A1	C (25)	VOLUME	C (6)
—		YEAR	N (5)
—		PAGES	C (15)

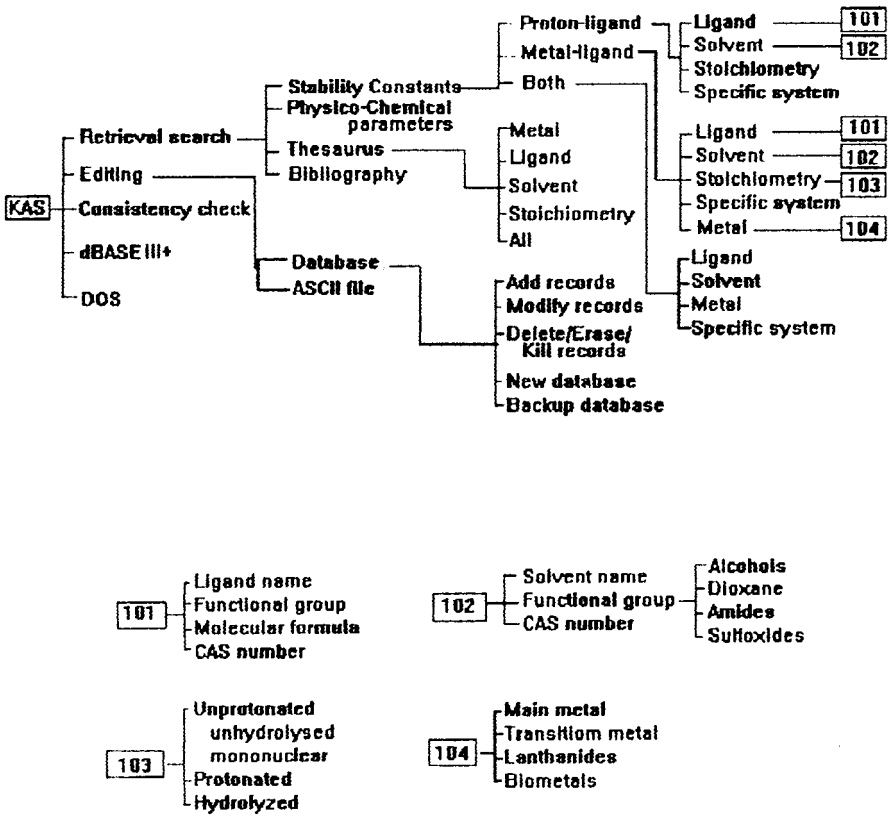

Fig. 2. User choosable options in KAS for the retrieval of the contents of BAQOR.

in this connection are depicted in Table 1. It is useful for modifying the structure, creating similar databases and developing software. Intelligent integrity checks and detection of wild values are also provided in the present software.

The execution of INSTALBAQ in dBASE III + creates a thesaurus and index files for the numerical and the literature databases. The thesaurus contains lists of unique names of metal, ligand, solvent journals, the first and last names of the authors, etc. Index files are used in dBASE III + for quick retrieval without scanning the entire database sequentially.

They contain the information where the record physically exists in the database file. During retrieval, the database and index files together mimic a random access file with low seek time. The relevant index files are shown in Table 2.

2.2. Software for BAQOR

During the preliminary planning of the package KAS (K in Aquo-Solvents) for data retrieval, features like centering the heading with variable window sizes, scrolling the menu option with a light bar, automatic (prefixed/user chosen time delay) or prompt based screen displays, etc. (Menu) have been identified. In order to increase the speed of execution they are joined in a procedure, making use of the dBASE III + intrinsic facility. Task independent modular programs have been written to display screens (Table 1, Short_1, Pauthor), search the data and unique contents in a field (Uniq_), output, check consistency of the database, and edit program/database files.

The databases and retrieval programs are available on a bootable 1.2 MB floppy disk (5.25“) which shall be provided on request. After insert-

Table 4
Physico-chemical parameters of aquo–cosolvent mixtures

(a) Binary solvent systems

Solvent (%)	Dielectric constant	mole_fraction	Density
0.00	78.540	0.0000	0.9971
10.00	77.320	0.0250	0.9965
20.00	74.860	0.0520	0.9961
30.00	72.400	0.0890	0.9959
40.00	69.520	0.1310	0.9956
50.00	65.950	0.1820	0.9950
60.00	61.740	0.2470	0.9928
0.00	56.730	0.3320	0.9878

(b) Ternary solvent systems

S1 (%)	S2 (%)	Dielectric constant	S1 mole_fraction	S2 mole_fraction	Con_of_H20 %	Density
7.00	3.00	71.580	0.0158	0.0142	50.153	0.9990
14.00	6.00	64.560	0.0339	0.0306	44.964	1.0010
21.00	9.00	57.420	0.0551	0.0497	39.752	1.0026
28.00	12.00	50.0 80	0.0802	0.0724	34.446	1.0025
35.00	15.00	42.810	0.1107	0.0999	29.079	1.0013

ing the floppy in drive A the system can be soft booted by pressing Ctrl + Alt + Del simultaneously.

3. Results

3.1. Description of BAQOR

BAQOR contains the magnitudes of equilibrium constants at different cosolvent contents pertaining to 9 metals and 193 ligands with 8 types of species in 28 solvents present in 740 records. WS1CHAR and WS1S2CHAR contain the physico-chemical properties—macroscopic dielectric constants (D1, D2,..., D8), mole fraction (NX1, NX2,..., NX8), concentration of cosolvent (P1S1, P1S2,..., P1S8) and that of water (CH2O1, CHO2,..., CH2O8)—in the presence of one and two cosolvents, respectively. SOLVENT contains the name of the solvent and its physico-chemical characteristics at a single temperature. Each record of the bibliographic database (REFBAQ) contains primary fields for the first (F) and last (A) names up to a maximum of five authors and the source of publication. The fields like LINKLIG, LINKSTAT, etc. are used to connect the data items present in physically separate databases while retrieving the integrated information. The structures of these databases are briefly described in Table 3.

3.2. Retrieval of data from BAQOR

The running of KAS in a dBASE III + environment results in the appearance of the screen containing the main menu. Scrolling freely forward or backward through the cursor keys followed by selection of an option by pressing the ENTER key leads to a submenu. From here onwards retrieval of one of several options is possible. Each menu is displayed through built-in intelligence with an optimum size of the window and highlighted bar menu. Fig. 2 depicts the various options available.

By choosing physico-chemical parameters under the retrieval search option, the user has to give a number of solvents and their names. It

Table 5
Abridged screen dump of proton–ligand stability constants of glycine: Natural Query Language: can I get only proton ligand complexes of glycine in all aquo–organic media? Retrieval keys: Retrieval, stability constants, aquo–cosolvent, proton–ligand, ligand, ligand name: glycine

Met(OX)	Ligand	Solvent	mlh	Ref.	
H(1+)	GLYCINE	DOX	011	1048[a]	
H(1+)	GLYCINE	DOX	012	1048	
H(1+)	GLYCINE	ETOH	011	1080[b]	
H(1+)	GLYCINE	ETOH	012	1080	
H(1+)	GLYCINE	ISOP	011	1080	
H(1+)	GLYCINE	ISOP	012	1080	
H(1+)	GLYCINE	MEOH	011	1048	
H(1+)	GLYCINE	MEOH	012	1048	
Short display of stability constants					
GLYCINE	mlh	011	DOX	Ref: 1048	
(V)	0.00	20.00	40.00	50.00	60.00
Log K011	2.33	2.60	2.94	3.17	3.45
(V)	70.00	75.00	80.00		
Log K011	3.81	4.05	4.33		
GLYCINE	mlh	012	DOX	Ref: 1048	
(V)	0.00	20.00	40.00	50.00	60.00
Log K012	9.60	9.64	9.70	9.76	9.84
(V)	70.00	75.00	80.00		
Log K012	9.98	10.07	10.23		
GLYCINE	mlh	011	ETOH	Ref: 1080	
(W)	0.00	8.00	16.40	25.30	34.40
Log K011	2.33	2.55	2.66	2.70	2.88
(W)	44.00	54.10	64.70	76.00	
Log K011	3.05	3.38	3.53	3.73	

[a] 1048, K. Mui and W.A.E. McBryde, Can. J. Chem. 52 (1974) 1821.
[b] 1080, B.P. Dey and S.C. Lahiri, Ind. J. Chem. 27A (1988) 1979.

results in a table (Table 4a) with dielectric constant, mole fraction, and concentration of water at each composition of DMF. The number of cosolvents and their mole fractions are displayed in addition to other properties (Table 4b).

For retrieval of stability constants in aquo–organic media, three options, viz., proton–ligand, metal–ligand or both are available for a ligand, solvent, stoichiometry, metal, or a combination of them. As an illustration, an abridged form of the screen dump for glycine is shown in Table 5. Here the proton–ligand stability constants of glycine at all stoichiometries in the presence of any cosolvent are displayed. It is followed by the display of the percentage of cosolvent, the corresponding stability constant and S.D. if available. A full literature citation is also displayed.

Similarly the database can be searched for a cosolvent or stoichiometry. A part of the screen dump is shown in Table 6. A search on the combination of ligand, solvent and stoichiometry is useful to find whether a system has been investigated or not. Table 6c describes the user action and systems response for this narrow search. In this case, there are two options namely, the screen-wise display and the tabular summary.

The retrieval procedure for metal–ligand complexes is similar to that of proton–ligand, except that the searches are possible metal-wise also. Table 7a illustrates the retrieval of zinc complexes and Table 7b searches for both proton–ligand and metal–ligand complexes in a specific solvent. The narrow search, say zinc–glycine complexes (ML) in DMSO is described in Table 7c. Here

Table 6
Display of ligand protonation of user's choice

Met(OX)	Ligand	Solvent	mlh	Ref.
(a) Retrieval of proton–ligand complexes in aquo–DMSO				
H(1+)	ALANINE(L−)	DMSO	011	999
H(1+)	ALANINE(L−)	DMSO	012	999
H(1+)	DIT	DMSO	011	1420
H(1+)	DIT	DMSO	012	1420
H(1+)	DIT	DMSO	013	1420
H(1+)	GLYCINE	DMSO	011	1420
H(1+)	GLYCINE	DMSO	012	1420
H(1+)	MIT	DMSO	011	1420
H(1+)	MIT	DMSO	012	1420
H(1+)	MIT	DMSO	013	1420
H(1+)	PYRIDINE	DMSO	011	1420
H(1+)	Phenylalanine,3,4-dihydroxy	DMSO	011	997
H(1+)	Phenylalanine,3,4-dihydroxy	DMSO	012	997
H(1+)	Phenylalanine,3,4-dihydroxy	DMSO	013	997
H(1+)	Proline	DMSO	012	97009
H(1+)	Tryptophan	DMSO	011	97009
H(1+)	Tryptophan	DMSO	012	97009
H(1+)	Histidine	DMSO	012	97009
H(1+)	Histidine	DMSO	013	97009
(b) Retrival of proton–ligand complexes with stoichiometry 012				
H(+)	8-hydroxyquinoline,5-SO_3H	DOX	012	1045
H(+)	8-mercaptoquinoline	DOX	012	1045
H(+)	ACETYLACETONE	DOX	012	999
H(+)	ALANINE	DOX	012	71
H(+)	BUTYRIC ACID	DOX	012	999
H(+)	CITRIC ACID	DOX	012	1074
H(+)	GLYCINE	DOX	012	1048
H(+)	Heptanoic acid	DOX	012	999
H(+)	Hexanoic acid	DOX	012	999
H(+)	Phenyl hydroxylamine, *N*-benzoyl	DOX	012	999
H(+)	ACETYLACETONE	ETOH	012	999
H(+)	Aspartic acid	ETOH	012	3018
H(+)	GLUTAMIC ACID	ETOH	012	3018
H(+)	GLYCINE	ETOH	012	1080
H(+)	L-HISTIDINE	ETOH	012	3018
H(+)	L-SERINE	ETOH	012	3018

Table 6 (continued)

Met(OX)	Ligand	Solvent	mlh	Ref.
H(+)	L-TRYPTOPHAN	ETOH	012	3018
H(+)	LEUCINE	ETOH	012	1080
H(+)	Phenylhydroxylamine,*N*-benzoyl	ETOH	012	999
(c) Retrieval of protonation equilibria of glycine with stioichiomety 011 in aquo–DMF				
011	PL		Glycine	HL
DMF–H2O				
V Solvent	Log Beta	SD		
00.00	2.34			
20.00	2.50			
40.00	2.78			
50.00	2.97	K. Mui and W.A.E. McBryde, Can. J. Chem. 52 (1974) 1821		
60.00	3.26			
70.00	3.65			
75.00	3.96			
80.00	4.28			

also either screen-wise display or tabular mode can be chosen. The option for both corresponding to proton–ligand and metal–ligand complexes is provided, keeping in view of the routine literature search.

In spite of the fact that a list of unique items in a field, (metal ion, journal, etc.) are retrievable, the thesaurus has several advantages apart from their instantaneous display. They are useful for consistency checking and the development of a hierarchical/network/object representation of keywords in intelligent database management systems. Table 8 briefly describes a few contents at the beginning and end of each of the files of the thesaurus.

4. Discussion

BAQOR is the first computer readable database for equilibrium constants in the presence of varying amounts of water miscible cosolvents. The present version is fast enough even on a minimum hardware configuration. It can be exported into EXSYS, B+ trees and as ASCII files. Heuristics and object oriented programs are under development in TURBOPROLOG, PASCAL6 and C++.

Just like any algorithmic procedure, the speed of retrieval of the data/information depends primarily upon the hardware characteristics viz., processor/clock speed, seek time, cooperativity of operating system, detection and implementation of parallel processes on even a sequential machine, built-in constructs with optimum speed, and the efficient application of the programs. The last, but not least, is the size of the database. It has been observed the recovery rate versus specificity to follow a hyperbolic relationship [14] and the shape for a specific system depends upon the preciseness of the keywords, the abstractor's competence and the retrieval strategy.

4.1. Quality index

Collecting data from different laboratories, or through reports in the literature, can lead to associated problems of varying quality and incomplete auxiliary information. The quality index (QI) [15] is an empirical multidigit number useful

Table 7
Partial screen dumps of metal–ligand systems

Met(OX)	Ligand	Solvent	mlh	Ref.
(a) Retrieval of complexes of Zn				
Zn(2+)	Ethylenediamine	CH3CN	110	1048
Zn(2+)	Ethylenediamine	CH3CN	120	1048
Zn(2+)	Ethylenediamine	CH3CN	130	1048
Zn(2+)	Glycine	CH3CN	110	1048
Zn(2+)	Glycine	CH3CN	120	1048
Zn(2+)	Glycine	CH3CN	130	1048
Zn(2+)	Ethylenediamine	DMF	110	1048
Zn(2+)	Ethylenediamine	DMF	120	1048
Zn(2+)	Ethylenediamine	DMF	130	1048
Zn(2+)	Glycine	DMF	110	1048
Zn(2+)	Glycine	DMF	120	1048
Zn(2+)	Glycine	DMF	130	1048
Zn(2+)	8-Hydroxyquinoline	DOX	110	1045
Zn(2+)	8-Hydroxyquinoline	DOX	120	1045
Zn(2+)	8-Hydroxyquinoline,5-SO_3H	DOX	110	1045
Zn(2+)	8-Hydroxyquinoline,5-SO_3H	DOX	120	1045
Zn(2+)	8-Hydroxyquinoline,5-acetyl	DOX	110	1045
Zn(2+)	8-Hydroxyquinoline,5-acetyl	DOX	120	1045
Zn(2+)	8-Hydroxyquinoline.5-chloro	DOX	110	1045
(b) Retrieval of stability constants in aquo–EtOH				
Cu(2+)	ACETIC ACID	ETOH	110	16179
Zn(2+)	ACETIC ACID	ETOH	110	16179
H(1+)	ACETYLACETONE	ETOH	011	2193
H(1+)	ACETYLACETONE	ETOH	011	999
H(1+)	ACETYLACETONE	ETOH	012	999
H(1+)	AMMONIA	ETOH	011	77
H(1+)	AMMONIA	ETOH	011	98
H(1+)	ANILINE	ETOH	011	77
H(1+)	ANILINE	ETOH	011	77
H(1+)	ACETIC ACID	ETOH	011	16179
H(1+)	Ammonia,dimethyl	ETOH	011	77
H(1+)	Ammonia,ethyl	ETOH	011	98
H(1+)	Ammonia,monomethyl	ETOH	011	77
H(1+)	Ammonia,monomethyl $T = 298$	ETOH	011	98
H(1+)	Ammonia,trimethyl	ETOH	011	77
H(1+)	Ammonia,trimethyl $T = 298$	ETOH	011	98
H(1+)	Ammonia,dimethyl	ETOH	011	98
H(1+)	Aniline,*N*,*N*-dimethyl	ETOH	011	77
H(1+)	Aniline,*N*,*N*-dimethyl $T = 298$	ETOH	011	98
(c) Retrieval of data of Zn(II)–glycine system in aquo–DMF				
110	Zn	2	Glycine	HL
DMF–H2O				
V Solvent	Log Beta	SD		
20.00	5.460			
40.00	5.740			
50.00	5.920	K. Mui and W.A.E. McBryde, Can. J. Chem. 52 (1974) 1821		
60.00	6.100			
70.00	6.440			
75.00	6.650			
80.00	6.920			

Table 8
Abridged screen dumps of the thesaurus

Metal
1. Ca
2. Co
3. Cu
4. Fe
5. Mg
6. Mn
7. Ni
8. Pb
9. Zn

Stoichiometry
1. 00-1
2. 011
3. 012
4. 013
5. 110
6. 120
7. 130
8. 131

Journals	
1. Anal.Chem.	10. J .Inorg. Nucl. Chem
2. Anal.Chim.Acta	11. Mikrochim. Acta
3. Chemistry and Industry	12. Polyhedron
4. Chemomet.Intel.Lab.Syst.	
5. Comput.& Chem.	
6. Fresenius Z Anal.Chem	
7. J. Chem. Soc.	
8. J Chem. Educ.	
9. J Chemomet.	

Cosolvent	
1. 1,2-DIETHOXY ETHANE	2. 1,2-DIMETHOXY ETHANE
3. 1-PROPANOL	4. 2-ETHOXY ETHANOL
5. 2-METHOXY ETHANOL	6. ACETAMIDE
7. ACETONE	8. ACETIC ACID
9. ACETONITRILE	10. DIMETHYL ACETAMIDE
11. DME	12. DMF
13. DMSO	14. DOX
15. ETHYLENE GLYCOL	16. ETOH
17. FORMAMIDE	18. HCOOH
19. HYDRAZINE	20. ISOP
21. METHANOL	22. N-BUTYL ACETAMIDE
23. N-METHYL ACETAMIDE	24. N-METHYL FORMAMIDE
25. SULFOLANE	26. SULFONE
27. THF	28. tBuOH

Ligand

1. (+)-PROPRANOLOL	2. 1,2 -Dimethoxyethane
3. 2,2-DI(THIOETHYL)-SULFIDE	4. 2,3-NAPTHALINE
5. 2,3-diCH3, Salicylidineaniline	6. 2,4-diCH3, Salicylidineaniline
7. 2,4-diOCH3, Salicylidineaniline	8. 2,5-diCH3, Salicylidineaniline
9. 2-Amino ethanol	10. 2-Furoic acid hydrazide
11. 2-Methoxy ethanol	12. 3,4-diCH3, Salicylidineaniline
13. 3,5-diOCH3, Salicylidineaniline	
....	....
18. 8-HYDROXYQUINOLINE, 5-acetyl	19. 8-HYDROXYQUINOLINE, 5-SO3H
20. 8-HYDROXYQUINOLINE, 5-chloro	21. 8-HYDROXYQUINOLINE, 5-nitro
22. 8-MERCAPTOQUINOLINE	23. ACETIC ACID
24. ACETYL ACETONE	25. Adipic acid dihydrazide
26. ALANINE	27. ALAINE (beta-)
28. ALANINE, PHENYL(L-)	29. AMMONIA
....	....
181. PYRIDINE, trimethyl	182. Pyridinium, 2-bromo
183. Pyridinium, 3-bromo	184. Pyridinium, 4-bromo
185. SALICYCLIC ACID	186. SALICYCLIC ACID, 3,5-dinitro
187. SALICYCLIC ACID, 5-bromo	188. SALICYCLIC ACID, 5-chloro
189. SALICYCLIC ACID, 5-fluoro	190. SALICYLOYL HYDRAZINE
191. SEBACIC ACID	192. SERINE(L-)
193. SULFOSALICYLIC ACID	

to discriminate different sets of data on the same chemical system. Although QI is a relative measure, it throws light on sophistication of instruments, quality of data and reputation of the investigator/laboratory. The QI develops into a more complicated function and requires expertise when one handles parameters derived from primary data. Although instrument characteristics play a role in primary data, other physico-chemical parameters, model assumptions, noise characteristics, procedures and heuristics contribute in assessing the quality of chemical parameters. A four digit empirical QI is proposed in this laboratory for the equilibrium constants. It takes into account:

- sample characteristics (matrix, concentration, stability and composition)
- instrument (single/multisensor/hyphenated, operating conditions, readability and reproducibility)
- experimental conditions (number of experiments, number of points, metal to ligand ratio and range of metal concentration)
- processing (pre-processing/pruning of primary data, $\log K$ estimation statistical analysis and optimization method)

The magnitude of each digit in turn indicates the details regarding the sub classes. FFFF represents an ideal system while 0000 is at the other extreme. A critical evaluation of the systems reported and modelling of the variation of equilibrium constants of different groups with solvent parameters using least median squares and fuzzy logic is in progress. CHEMNETS [16], a hybrid technology of theoretical and empirical models is utilized.

The limitations of the present version of the database is that it is a relational one. As the keyboard search in this discipline is not yet fool proof, there is a chance that some of the literature citations might have missed our attention. However, we have adopted a cover-to-cover manual search of some of the relevant journals.

Acknowledgements

The authors (AB and RSR) thank the Council of National Research, Italy for partial financial support in the form of a bilateral project.

References

[1] A.E. Martell, R.M. Smith, Critical Stability Constants, vol. 1–4 (1974), Supplement (1982), vol. 5 (1982), vol. 6 (1989), Plenum, New York, NIST Standard Reference Database 46, NIST Critically Selected Stability Constants of Metal Complexes (version 3.0), Gaithersburg, MD 20899.
[2] J.R. Duffield, F. Masicano, D.R. Williams, Polyhedron 10 (1991) 1105–1111.
[3] J.R. Duffield, F. Marsicano, M. Waters, D.R. Williams, Polyhedron 10 (1991) 1113–1120.
[4] J.R. Duffield, J.R. Johns, F. Marsicano, D.R. Williams, Polyhedron 10 (1991) 1121–1129.
[5] P.M. May, K. Murray, Talanta 38 (1991) 1409–1417.
[6] P.M. May, K. Murray, Talanta 38 (1991) 1419–1426.
[7] P.M. May, K. Murray, Talanta 40 (1993) 819–825.
[8] L.D. Pettit and G. Pettit, Stability Constants Database Management System, IUPAC Commission on Equilibrium Data, 1990.
[9] K. Izutsu, Acid-Base Dissociatation Constants in Dipolar Aprotic Solvents, IUPAC Commission on Analytical Chemistry, Blackwell Scientific Publications, Oxford, 1990.
[10] M.C. Garcia Alvarez-Coque, E. Bonet-Domingo, J.R. Torres Lapasio, M.J. Medina Hernandez, Anal. Chim. Acta 287 (1994) 201–210.
[11] H. Sigel, R.B. Martin, R. Tribolet, U.K. Haring, R. Malini Balakrishnan, Eur. J. Biochem. 152 (1985) 187.
[12] M. Calvin, K.W. Wilson, J. Am. Chem. Soc. 70 (1948) 3270.
[13] EXSYS, EXSYS Inc., P.O. Box 11247, Albuquerque, NM 87192.
[14] R.E. Dessy, M.K. Starling, Anal. Chem. 51 (1979) 924A.
[15] S.R. Heller, Anal. Chim. Acta 210 (1988) 81.
[16] Z. Wang, J. Hwang, B.R. Kowalski, Anal. Chem. 67 (1995) 1497.

ELSEVIER

Talanta 47 (1998) 121–126

Talanta

Enzymatic flow-injection determination of L-phenylalanine using the stopped-flow and merging-zones techniques

M.J. Almendral Parra *, A. Alonso Mateos, M. Martín Mata, C. García de María

Department of Analytical Chemistry, Nutrition and Food Sciences, Faculty of Chemistry, University of Salamanca, 37008 Salamanca, Spain

Received 14 October 1997; received in revised form 27 January 1998; accepted 28 January 1998

Abstract

A flow injection enzymatic method for the spectrophotometric determination of L-phenylalanine has been developed. L-phenylalanine is deaminated in the presence of L-amino acid oxidase and the keto acid formed is made to react with borate to give a coloured enol–borate complex that can be detected at 282 nm. Catalase is added to the catalyzed reaction to prevent the keto acid being destroyed by the hydrogen peroxide generated. Kinetic determinations are performed by measuring the change in absorbance between 2 and 4 min. The proposed procedure, involving both merging-zones and stopped-flow techniques, can be applied to the quantitation of L-phenylalanine between 10 and 260 mg l^{-1}. Detection limit and R.S.D. are 1.1 mg l^{-1} and 3.0%, respectively. © 1998 Elsevier Science B.V. All rights reserved.

Keywords: Phenylalanine; Enzymatic analysis; Flow injection; Serum

1. Introduction

Many methods have been described for the quantitative determination of amino acids [1–4]. This is because of the interest in these compounds in the fields of medicine and biochemistry, where the analysis of amino acids has often been used to detect genetic mutations in their metabolism [5]. Such interest has recently been extended to the field of food technology since amino acids are useful for determining the nutritional properties of foods and are also intimately linked to their sensory characteristics [6]. Amino acids may also be used to control the manufacturing [7], the adulteration [8–11] or the geographic origin [12,13] of foods.

Among the methods described for the determination of amino acids, enzymatic methods [14–22] are of special interest because of their high selectivity. Such methods are often based on L-amino acid oxidase-catalyzed reactions where hydrogen peroxide is also produced.

The analysis of L-phenylalanine (Phe) is of interest in the early detection of phenylketonuria in

* Corresponding author. Tel.: + 34 23 294483.

0039-9140/98/$19.00 © 1998 Elsevier Science B.V. All rights reserved.
PII S0039-9140(98)00061-7

neonates [23–25]. Many methods have been reported for the detection of this amino acid. Ion exchange column chromatography [26], gas chromatography [27,28], HPLC [29,30] and fluorimetric methods [31] are outstanding. Enzymatic methods based on the use of the enzyme phenylalanine dehydrogenase have recently been developed [32–34].

This study reports on an enzymatic flow-injection procedure for the determination of Phe. This is first transformed into phenylpyruvic acid. In this reaction, catalyzed by the enzyme L-amino acid oxidase, hydrogen peroxide is also produced. In a later step, the phenylpyruvic acid generated is made to react with borate giving an enol–borate complex that is measured spectrophotometrically at 282 nm [35]. The presence of catalase is required to prevent oxidation of phenylpyruvic acid by hydrogen peroxide.

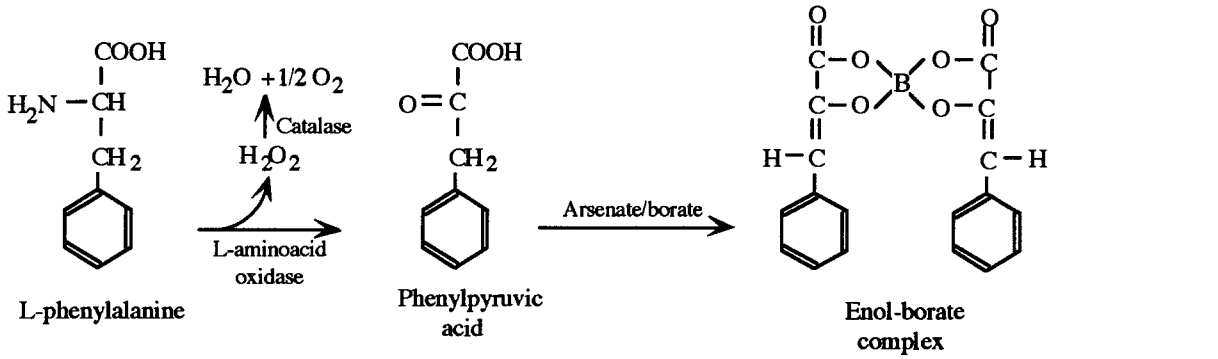

The use of the merging-zones technique permits a drastic reduction in the cost per analysis. Interferences by tyrosine and tryptophan, the main drawback of the enzymatic methods, are prevented by kinetic discrimination using the stopped-flow technique [36,37].

2. Experimental section

2.1. Reagents

Phosphate buffer: 0.2 M disodium phosphate (Probus) at pH 6.5; borate–arsenate–phosphate buffer (BAP buffer): 1.0 M orthoboric acid (Probus) and 2.0 M disodium arsenate (Probus) in 0.2 M phosphate buffer at pH 6.5; standard solutions: Phe (Sigma) in phosphate buffer; reagent solutions: L-amino acid oxidase (E.C. 1.4.3.2, Sigma) and catalase (E.C. 1.11.1.6, Sigma) in BAP buffer.

2.2. Apparatus and materials

A SPD-6AV UV-vis spectrophotometric detector (Shimadzu) with a C-R5A Chromatopac data processor and a 8 μl flow cell of 10 mm optic pathway; a double PTFE rotatory injection valve (Tecator L-100-1) fitted with loops of 115 μl for sample solutions and 198 μl for reagent solutions; an Eyela MP3 and Gilson Minipuls 2HP4 peristaltic pump with silicone or vinyl pump tubes; a microburette and a chronometer for flow-rate measurements; 0.5 mm i.d. PTFE tubing with normalized tube endings (Rheodyne); a water-circulation thermostatic bath.

2.3. Flow system and experimental procedure

Experiments were carried out in the flow system depicted in Fig. 1. Phosphate buffer is pumped through C_1 and C_2 at a flow rate of 0.80 ml min^{-1} for each channel. Standard or sample solutions of Phe are injected (115 μl) into valve V_S. The reagent solution (0.41 U ml^{-1} of L-amino acid oxidase and 2.2×10^3 U ml^{-1} of catalase in BAP buffer at pH 6.5) is injected into valve V_R (198 μl). Both injections are simultaneous so that Phe and reagent solutions mix and begin to react in reactor R (300 cm long, 0.5 mm i.d.). A programmed timer, interconnecting the peristaltic

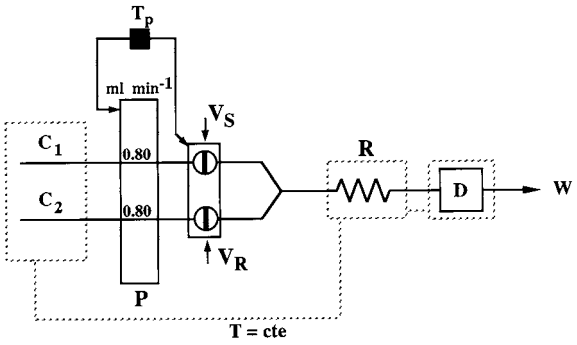

Fig. 1. Flow system. P, peristaltic pump; C_1, C_2: 0.2 M phosphate buffer, pH 6.5, 0.80 ml min^{-1}; V_S: sample injector, 115 μl; V_R: reagent injector, 198 μl; R: coiled PTFE tube, 300 cm long, 0.5 mm i.d.; T_p: timer; D: detector; W: waste; working temperature is kept constant by means of a water-circulation thermostatic bath.

pump and the injection valves, allows the flow to be stopped at 0.68 min after each injection, when the reacting mixture is in the detector flow cell. All the solutions, the reactor R and the flow cell are kept at a fixed working temperature by means of a water-circulation thermostatic bath.

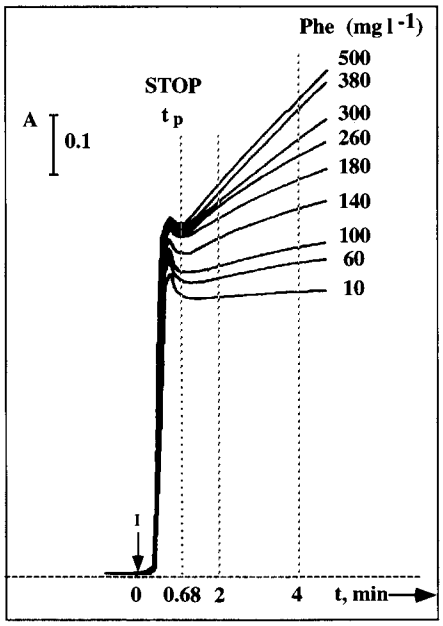

Fig. 2. Analytical signal registered for different concentrations of L-phenylalanine. pH 6.5; L-amino acid oxidase = 0.41 U ml^{-1}; catalase = 2.2×10^3 U ml^{-1}; $T = 45$°C.

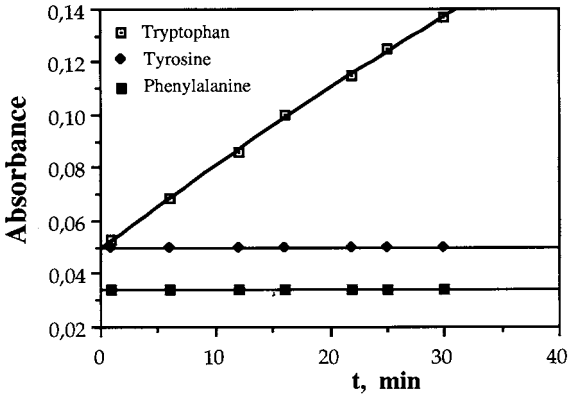

Fig. 3. Kinetic curves of phenylalanine, tyrosine and tryptophan in BAP buffer at pH 6.5 and 350 nm. L-amino acid oxidase = 0.36 U ml^{-1}; catalase = 5.6×10^2 U ml^{-1}. Filled square, Phenylalanine, 20.0 mg l^{-1}; Filled diamond, tyrosine, 20.0 mg l^{-1}; Open square with bullet, tryptophan, 6.0 mg l^{-1}.

The registered signal (Fig. 2) shows an initial peak due to the absorbances of Phe, catalase and the enol–borate complex produced in the reactor R. Once the flow is stopped, the slope represents the reaction rate. Under the proposed experimental conditions, absorbance at 282 nm increases linearly with time, at least between 2 and 4 min after each injection. The increase in absorbance in this interval is measured for samples and standards and the calculated slope is taken as the analytical parameter.

3. Results and discussion

3.1. Spectrophotometric characteristics of the enol–borate complexes of phenylalanine, tyrosine and tryptophan

Tyrosine and tryptophan, as well as phenylalanine, undergo L-amino acid oxidase-catalyzed deamination. This can be followed spectrophotometrically through the coloured compounds formed between the keto acids generated and borate. Within the pH 6.0–7.5 range, the absorption spectra of these compounds depend on pH, and they also change with time. Thus, at pH 6.5 and 350 nm, the absorbance due to the complex of tryptophan differs increasingly with time from

those of the other two complexes (Fig. 3). At pH 6.5 and 282 nm, the absorbance due to the Phe complex increases more rapidly than those of the tyrosine and tryptophan complexes (Fig. 4).

As pH 6.5 and a wavelength of 282 nm seemed to lead to the most favourable kinetic discrimination of Phe, these conditions were chosen for subsequent experiments on the determination of this amino acid.

3.2. Optimization of experimental variables

To optimize the proposed flow system and the working conditions, the effect of some chemical and hydrodynamic variables on the analytical signal were studied. Based on preliminary qualitative experiments, flow rates of channels C_1 and C_2 were fixed in 0.80 ml min^{-1} and a coiled tube of 300 cm in length and 0.5 mm i.d. was chosen as reactor R. These conditions provide enough reaction time for the reaction to be initiated in reactor R and to be significant before reaching the flow cell. The flow is stopped 48 s (0.68 min) after each injection. The volume of standard or sample solutions injected in valve V_M was conventionally fixed at 115 μl.

Temperature was investigated between 20 and 65°C. The carrier, reagent (0.36 U ml^{-1} of L-amino acid oxidase and 1.0×10^3 U ml^{-1} of catalase) and the standard (300 mg l^{-1} Phe) solutions were kept at the working temperature in a thermostatic bath. Reactor R and the flow cell were also kept at the fixed working temperature by means of water-circulation jackets. The volume of reagent solution was 198 μl in all the experiments. Changes in temperature were observed to modify the flow in channels C_1 and C_2. The flow rates were readjusted in each experiment in order to get the same reaction time in all cases, so that the measurements would be comparable. The maximum value of the slopes was obtained at temperatures between 45 and 55°C. A working temperature of 45°C was chosen for all subsequent experiments.

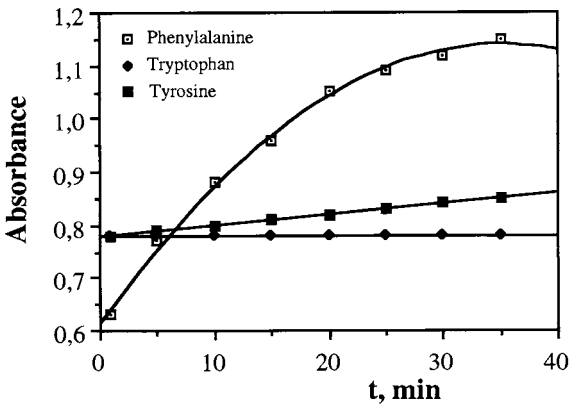

Fig. 4. Kinetic curves of phenylalanine, tyrosine and tryptophan in BAP buffer at pH 6.5 and 282 nm. L-amino acid oxidase = 0.36 U ml^{-1}; catalase = 5.6×10^2 U ml^{-1}. Open square with bullet, phenylalanine, 20.0 mg l^{-1}; filled square, tyrosine, 20.0 mg l^{-1}; filled diamond, tryptophan, 6.0 mg l^{-1}.

The volume of the reagent solution (0.36 U ml^{-1} of L-amino acid oxidase and 2.2×10^3 U ml^{-1} of catalase in BAP buffer) injected into V_R was varied between 115 and 572 μl. A standard solution containing 300 mg l^{-1} Phe was used in all the experiments. The measured slopes were found to increase with the injected volume along the whole experimental range. This effect was very pronounced for volumes below 200 μl, approximately. Above 300 μl, the measured slopes were almost independent of the volume injected. A loop of 198 μl was chosen for the injection of the reagent solution in the later experiments. This volume provides a good compromise between reagent consumption and sensitivity.

The presence of catalase improves the formation of the enol–borate complex and hence the analytical signal. This enzyme catalyzes the decomposition of the hydrogen peroxide generated during deamination of Phe, thus preventing oxidation of phenylpyruvic acid by this peroxide. The effect of the concentration of catalase was investigated between 0.40 and 1.60 mg ml^{-1} (1.1×10^3–4.5×10^3 U ml^{-1}). Three series of experiments, with standards of 100, 300 and 400 mg l^{-1} Phe, were performed. The concentration of L-amino acid oxidase in the reagent solution was 0.36 U ml^{-1} in all cases. The maximum slope in each series was observed for concentrations of catalase between 1.5×10^3 and 2.5×10^3 U ml^{-1}

The fact that the maximum slope values were found at intermediate concentrations of catalase can be explained by taking into account that the

measurements were carried out at a preset time. On increasing the concentration of catalase, the reaction rate first increases but later decreases as a steady state is approached. A concentration of catalase of 2.2×10^3 U ml^{-1} was chosen for the later experiments.

The effect of the concentration of L-amino acid oxidase was studied within the 0.40–1.20 mg ml^{-1} range (0.20–0.61 U ml^{-1}). Three series of experiments, with standards of 100, 300 and 400 mg l^{-1} Phe, were performed. In each series, the slope was found to be a maximum for concentrations of L-amino acid oxidase of 0.4 U ml^{-1} or higher. A concentration of 0.41 U ml^{-1} of L-amino acid oxidase in the reagent solution was chosen for the subsequent experiments.

3.3. Analytical parameters

Under the optimal experimental conditions proposed in the previous section, Phe can be detected at concentrations of higher than 1.1 mg l^{-1} (the detection limit is considered as the minimum concentration of Phe injected that affords an increase in absorbance of twice the noise). The relationship between the concentration of Phe injected and the measured slope is linear in the 10–260 mg l^{-1} range ($S = 1.5 \times 10^{-3} + 3.0 \times 10^{-4}\ C$; $r = 0.996$; S: slope, AU min^{-1}; C: concentration, mg l^{-1}). The R.S.D. ($n = 10$) for 40.0 mg l^{-1} Phe is 3.0%.

3.4. Interference

The interference of tyrosine and tryptophan were investigated under the proposed working conditions. The injection of solutions containing up to 100 mg l^{-1} tryptophan did not give measurable slopes in any case. So, tryptophan causes no interference. The effect of the presence of tyrosine was investigated with standard solutions containing both 40.0 mg l^{-1} Phe and concentrations of tyrosine between 0 and 100 mg l^{-1}. The results (Table 1) indicate that concentrations of tyrosine lower than 20 mg l^{-1} do not interfere. This is an important fact since normal concentrations of this amino acid in clinical samples range between 7 and 12 mg l^{-1}.

Table 1
Interference of tyrosine in the determination of 40.0 mg l^{-1} of L-phenylalanine

Tyrosine added (mg l^{-1})	Slope (AU min^{-1})[a]
—	0.012
10.0	0.013
20.0	0.014
30.0	0.018
50.0	0.023
100.0	0.026

[a] Mean value of three determinations.

4. Analysis of clinical samples

The proposed procedure was applied to the determination of Phe in samples of serum provided by the Department of Pediatrics at the University Teaching Hospital of Salamanca. One of the samples was a mixture of sera from adults and the rest were sera from healthy newborns or from patients with different pathologies (e.g. high bilirubin levels). In the proposed procedure, none of the components of the blood, such as proteins, organic metabolites and inorganic components, which absorb at the working wavelength, caused interference; their presence only modified the height of the peak registered when the flow was on, but not the value of the slope once the flow was stopped.

The method gave satisfactorily precise and reproducible results in all cases, with Phe contents lower than 20 mg l^{-1}. For serum containing 12.0 mg l^{-1} the R.S.D. ($n = 20$) was 2.5%.

Table 2
Recovery of L-phenylalanine in supplemented serum

L-Phenylalanine (mg l^{-1})		Recovery (%)[a]
Added	Found[a]	
—	12.0	—
10.0	21.8	98
20.0	30.8	94
40.0	53.7	104
60.0	76.0	107
120.0	129.0	98

[a] Mean value of three determinations.

Serum containing 12.0 mg l^{-1} Phe was supplemented with this amino acid to give final concentrations of 22.0–192.0 mg l^{-1}. Recoveries were in the 94–107% range, as shown in Table 2.

To compare the results obtained using the proposed method with those afforded by liquid chromatography, 10 samples in the 10–250 mg l^{-1} concentration range were analyzed. The calculated linear regression and correlation coefficient were $y = 1.32 + 0.994x$ and $r = 0.996$, respectively.

References

[1] P.D. Wentzell, S.R. Crouch, Anal. Chim. Acta 224 (1989) 263.
[2] S.A. Corcoran, S.C. Rutan, Anal. Chem. 60 (1988) 1146.
[3] H.V. Malmstadt, T.P. Hadjioannou, Anal. Chem. 35 (1963) 14.
[4] Y.-S. Hsieh, S.R. Crouch, Anal. Chim. Acta 296 (1994) 333.
[5] H.J. Bremmer, M. Duran, J.P. Kamerling, H. Przyrembel, S.K. Wadman, Disturbances of Amino Acid Metabolism: Clinical Chemistry and Diagnosis, Urban and Schwarzenberg, Baltimore, 1981.
[6] D. Blanco Gomis, A.M. Picinelli Lobo, M.D. Gutierrez Alvarez, Quim. Anal. 10 (1991) 321.
[7] A.P. Williams, HPLC in food analysis, in: R. Macrae (Ed.), Food Science and Technology, chap. 12, Academic Press, New York, 1988.
[8] S. Wallrauch, Fluess. Obst. 48 (1981) 197.
[9] J.J. Navarro, L. Izquierdo, M. Aristoy, J.M. Sendra, Int. Fruchtsaft-Union Wiss.-Tech. Komm. (Berl) 19 (1986) 357.
[10] I. Hibbret, R.A. Lawrie, J. Food Technol. 7 (1972) 333.
[11] N.H. Poulter, R.A. Lawrie, Meat Sci. 4 (1980) 21.
[12] W. Ooghe, H. Kastelijn, A. de Waele, Ann. Fals. Exp. Chim. 74 (1981) 381.
[13] W. Ooghe, A. de Waele, M.P. Derde, D.L. Massart, J. Autom. Chem. 5 (1983) 136.
[14] G.G. Guilbault, E. Hrabankova, Anal. Chem. 42 (1970) 1779.
[15] K.V. Dyke, C. Szustkiewicz, Clin. Chem. 15 (1969) 155.
[16] G.G. Guilbault, J.E. Hieserman, Anal. Biochem. 26 (1968) 1.
[17] L.A. Lichtenberg, D. Wellner, Anal. Biochem. 26 (1968) 313.
[18] M. Nanjo, G.G. Guilbault, Anal. Chim. Acta 73 (1974) 367.
[19] S. Igarashi, W.L. Hinze, Anal. Chim. Acta 225 (1989) 147.
[20] G.G. Guilbault, G.J. Lubrano, Anal. Chim. Acta 69 (1974) 183.
[21] G.G. Guilbault, G. Nagy, Anal. Lett. 6 (1973) 301.
[22] M. Mascini, G. Palleschi, Anal. Chim. Acta 100 (1978) 215.
[23] J.R. Henry, D.C. Cannon, J.W. Winkelmann, Clinical Chemistry: Principles and Techniques, 2nd ed., Harper and Row, New York, 1974.
[24] C. R. Scriver, L.E. Rosemberg, Problemas actuales de la pediatría clínica, Tomo IX: Metabolismo de los aminoácidos y sus trastornos, Edit. Científico-médica, Barcelona, 1979.
[25] R. E. Dickerson, I. Gris, The Structure and Actions of Proteins, Harper and Row, New York, 1969.
[26] K.A. Piez, L. Harris, Anal. Biochem. 1 (1960) 187.
[27] C.W. Gehrke, K. Leimer, J. Chromatogr. 58 (1971) 219.
[28] G. Ramis Ramos, A.R. Mauri Aucejo, M.C. García Alvarez-Coque, Microchem. J. 36 (1987) 113.
[29] R.A. Roesel, P. Blankenship, Clin. Chim. Acta 156 (1986) 91.
[30] T. Teerlink, P.A.M. Van Leeuwen, A. Houdijk, Clin. Chem. 40 (1994) 245.
[31] M.W. McCarman, E. Robins, J. Lab. Clin. Med. 59 (1962) 885.
[32] R.S. Campbell, R.D. Hollifield, H. Varsani, T.P. Milligan, Ann. Clin. Biochem. 31 (1994) 140.
[33] S. Keffler, R. Denmeade, A. Green, Ann. Clin. Biochem. 31 (1994) 134.
[34] N. Kiba, A. Itagaki, M. Furusawa, Talanta 44 (1997) 131.
[35] B.N. La Du, J. Michael, J. Lab. Clin. Med. 55 (1960) 491.
[36] M. Valcárcel. M.D. Luque de Castro, Flow Injection Analysis: Principles and Applications, Ellis Horwood, Chichester, 1987.
[37] J. Ruzicka, H. Hansen, Flow Injection Analysis, 2nd ed., Wiley, New York, 1988.

ELSEVIER

Talanta 47 (1998) 127–136

Talanta

Sorption of proton and heavy metal ions on a macroporous chelating resin with an iminodiacetate active group as a function of temperature

Raffaela Biesuz [a], Maria Pesavento [b,*], Anna Gonzalo [c], Manuel Valiente [c]

[a] *Dipartimento di Chimica Generale Università degli Studi di Pavia, Viale Taramelli 12, I-27100 Pavia, Italy*
[b] *Istituto di Scienze Mat., Fis., Chim., Università degli Studi di Milano, via Lucini 3, I-22100 Como, Italy*
[c] *Quimica Analitica, Universitat Autonòma de Barcelona, E-08193 Bellaterra, Barcellona, Spain*

Received 4 November 1997; received in revised form 27 January 1998; accepted 28 January 1998

Abstract

A macroporous resin containing iminodiacetic groups (Lewatit) was investigated for its sorption properties towards proton and nickel(II) and cadmium(II). Different compositions of the aqueous phase, and different temperatures were examined. The stoichiometry, the exchange coefficients and the intrinsic constants of the sorption equilibria were obtained from the experimental data by using the Gibbs–Donnan model for the ion exchange resin. The intrinsic constants were found to be independent of the composition of the solution, so that they were used for characterizing the sorption equilibria. While the first intrinsic protonation constant of the active groups in the resin was found to depend on the temperature, the second one was independent. The sorption equilibrium of nickel in the resin was different from that of cadmium, being ascribable respectively to the formation of the complexes NiL and $Cd(HL)_2$. inside the resin. Their intrinsic complexation constants were found to be $10^{-1.84}$ and $10^{-3.64}$ at 25°C. Compared to those of another resin with the same active groups, but not macroporous, they are higher. The dependence of the intrinsic constant on the temperature was also different for the two metals, allowing to evaluate a $\Delta H°$ of $+30.9$ and of $+13.7$ kJ mol^{-1} respectively. When a comparison is possible, these values are near to those in aqueous solution for the complexation with ligands of similar structure. These results can be used to achieve metal ion separation based on temperature variations. © 1998 Elsevier Science B.V. All rights reserved.

Keywords: Chelating resin; Sorption mechanism; Intrinsic complexation; Protonation constant; Temperature dependence; Selectivity

1. Introduction

The importance of the iminodiacetic resins for preconcentration and speciation of metal ions in natural waters is well known. Many applications have been proposed and some work has also been

* Corresponding author. Tel.: +39 382 507580; fax: +39 382 528544; e-mail pesaven@ivp.36.unipv.it

0039-9140/98/$19.00 © 1998 Elsevier Science B.V. All rights reserved.
PII S0039-9140(98)00060-5

done to elucidate the sorption equilibria. For instance the properties of one of these resins, Chelex 100, towards several metal ions were studied in detail, [1,2] at 25°C, from pH 2 to 10. It was found that the Gibbs–Donnan model, also tested for a completely different chelating resin, [3,4] successfully describes the behaviour of this iminodiacetic resin. The model was applied not only to simple solution but even to a complicated matrix such as artificial seawater [5].

Once the equilibria of the sorption of a metal ion has been elucidated, the model allows us to foresee the sorption behaviours in conditions different from those chosen for the specific experiment, which is very useful for practical applications.

Investigations on the metal sorption properties of iminodiacetic resins at different temperatures are only very recent [6], even though information of this kind is very interesting in order to better elucidate the sorption reactions and with a view to the applications. For instance it has been suggested that sorption and desorption procedures at different temperatures should permit almost reagentless separation. [6–8]

In the present paper an iminodiacetic resin was examined for its sorption properties towards metal ions not only for different conditions, but also for different temperatures. The resin is commercially available from Bayer Hispanica and called Lewatit TP-207. The sorption equilibria of Ni(II) and Cd(II) from 0.1 mol kg^{-1} NaCl solutions up to pH 5 was investigated at 25, 45 and 65°C according to a well established procedure [1–5]. Since the active group is a weak acid the determination of the intrinsic protonation constants preceded the sorption studies.

2. Experimental

2.1. Apparatus and reagents

A PHM 84 research pH meter (Radiometer, Copenhagen) with an ABU 80 autoburet and a combined Radiometer glass electrode (ref. GK2401C) were used for the acid–base titrations. A Perkin-Elmer 1100B flame AAS was used for the metal ions determinations. All chemical were analytical reagent grade.

2.2. Preparation of Lewatit TP-207

The resin obtained in Na^+ form was converted in H^+ form according to a procedure described elsewhere [1,2], left to dry in the open air and stored in sealed bottles. The humidity was around 33% and was checked weekly. The H^+ form is more suitable for acid–base titrations, besides being recognized as giving the lowest blank values in AAS determinations [9].

2.3. Acid–base titrations and determination of capacity

The capacity of an ion exchanger is the number of ion exchange sites per unit of mass or volume. Here the total capacity is defined as the mmol of iminodiacetate groups per g of dry resin obtained from an acid–base titration. It was performed in a conventional way, already described in detail elsewhere [1–5], at constant temperature (T) with a slight N_2 overpressure. The electrode was standardized in H^+ concentration, at the considered T, before starting the resin titration. Standard sodium hydroxide was added to a known volume containing a known excess of acid and a weighted amount of resin. The pH was recorded when the potential was steady (0.1 mV drift in 3 min).

The amount of water sorbed and the amount of counter ion in the resin phase as a function of degree of deprotonation were determined as described previously [1–5].

The acid–base titrations allow the evaluation of the protonation coefficients (K_{aj}) according to a previously described procedure [1–5].

2.4. Sorption curves

The sorption curves were determined by a batch procedure. A known amount of the considered metal ions were left to equilibrate in 0.1 mol kg^{-1} NaCl solution containing a known amount of resin. The concentration of the active group was always in large excess with respect to the total concentration of the metal ions. The pH was

varied with small additions of concentrated HCl or NaOH. After equilibration the pH was measured and recorded. A small amount of solution (usually 100 μl) was diluted to 5–10 ml with 0.1 mol kg^{-1} HNO_3 and analysed by flame AAS. The amount of metal sorbed was calculated by difference from the total.

The sorption curves were obtained by plotting the fraction of sorbed metal ion (f) as function of pH values of the aqueous phase.

2.5. Calculations of the intrinsic constants.

The method is based on the Gibbs–Donnan model of the resin, which allows us to relate the sorption equilibrium coefficient calculated from the sorption curves to the complexation constants of the active group in the resin with the considered metal ion.

Suppose that the sorption reaction is

$$M + nH_rL' \leftrightarrow MH_pL'_n + qH \quad (1)$$

the corresponding exchange coefficient is

$$\beta_{1npex} = \frac{[MH_pL'_n][H]^q}{[H_rL']^n[M]} \quad (2)$$

The concentration of the species is expressed in mol kg^{-1} (molality) both in the solution and in the resin phase and the species with the primes are those in the resin phase.

The fraction of sorbed metal ion f is given by the relation

$$f = \frac{c}{c_{tot}} = \frac{[MH_pL'_n]w}{[MH_pL'_n]w + [M]V\alpha_{M(I)}} \quad (3)$$

which can be transformed in the following form

$$f = \frac{1}{1 + \dfrac{\alpha_{M(I)}}{\dfrac{\beta_{1npex}[H_rL']^n w}{[H]^q V}}} \quad (4)$$

where c is the concentration of metal sorbed on the resin, i.e. the quantity calculated by difference from the total; c_{tot} is the total metal concentration originally present in the sample; w indicates the g of water sorbed per g of dry resin; and V the ml of solution; $\alpha_{M(I)}$ represents the coefficient of the side reactions of M with complexing substances in solution, being the sorption on the resin the main reaction. $\alpha_{M(I)}$ is equal to 1 when the metal is only present as free hydrated ion in the aqueous solution.

The exchange coefficient β_{inpex} and q can be determined from the sorption curves, if $\alpha M(I)$ is known.

The exchange coefficients β_{inpex} can be related to the thermodynamic complexation constants in the resin phase $\beta^*_{T(1np)}$ through the following relationship, obtained from the Gibbs–Donnan equilibria [1–5]

$$\beta_{1npex} = \beta^*_{T(1np)} \frac{\gamma_M \gamma_{H_rL'}}{\gamma_{MH_pL'_n}\gamma_H^q} \frac{\{C'\}^{(m-q)}}{\{C\}^{(m-q)}} \quad (5)$$

where the thermodynamic complexation constant in the resin phase is

$$\beta_{T(1np)} = \frac{\{MH_pL'_n\}\{H'\}^p}{\{M'\}\{H_rL'\}^n} \quad (6)$$

Eq. (5) holds when the counter ion C, is a monovalent cation, and the charge of the sorbed metal is $m.\gamma_Y$ and $\{Y\}$ indicate the activity coefficient and the activity of the specie Y respectively.

According to the Gibbs–Donnan model the thermodynamic complexation constants in the resin are expected to be equal to those in aqueous solution with soluble ligands with a structure similar to that of the active group since the same reference and standard state are assumed in the two phases [5]. For instance in the case of Chelex 100, the methyliminodiacetic acid (MIDA) and the iminodiacetic acid (IDA) were shown to be a good model for describing the complexation property of the resin, at least in the acid region [1,2].

However the activity coefficients are not experimentally obtainable and they depend on the structure of the resin. Nevertheless the quantity

$$\beta^*_{T(1np)} \frac{\gamma_{H_2L'}\gamma'^{(m-q)}_{C'}}{\gamma_{MH_pL'_n}},$$

called the 'intrinsic complexation constant' [5], determined experimentally, can be used to characterize the sorption equilibria of that particular resin since it is independent of the conditions of the external solution. This is important because, if the sorption equilibrium and the corresponding exchange coefficient are known, it is possible to

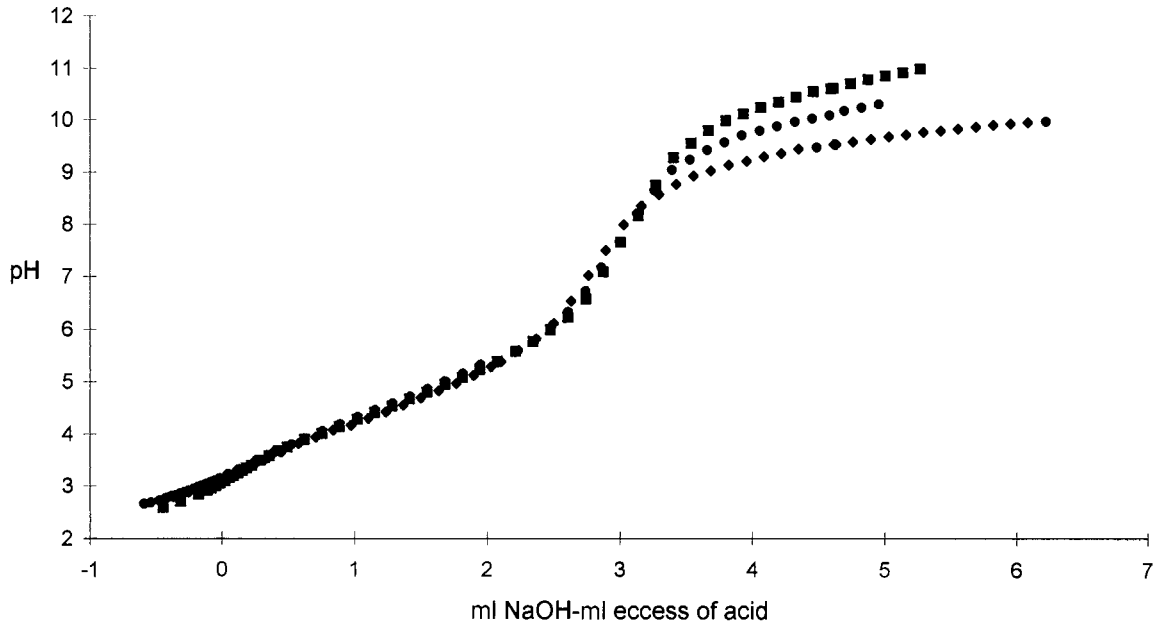

Fig. 1. Titration curves for Lewatit TP-207, 0.15 g as dry resin in H^+ form, 0.1 mol kg^{-1} NaCl. 0.173 mol kg^{-1} sodium hydroxide as the titrant solution. ■, $T = 25$°C and $V(0) = 35.1$ ml; ●, $T = 45$°C and $V(0) = 51.3$ ml; ◆, $T = 65$°C and $V(0) = 52.2$ ml. Abscissa: ml of base to titrate the active group of the resin.

predict the sorption rate for a solution of a given composition.

In the present investigation, the sorption equilibria at different temperatures were investigated according to the Gibbs–Donnan model, in order to determine the stoichiometry of the sorption reactions and their equilibrium coefficients.

According to Eq. (5), the intrinsic complexation constant can be evaluated from the exchange coefficient. The concentration of the r-protonated free ligand (H_2L) is evaluated from the free active groups, when the protonation equilibria are known.

Similar relationship exist also for the protonation coefficients. They are related to the intrinsic protonation constant(K_{Taj}) by an equation similar to Eq. (5) [1–4]

$$K_{aj} = K_{Taj} \frac{\gamma_H \gamma_{H_{x-1}L'}}{\gamma_{H_xL'}} \frac{\{C'\}^{(m-q)}}{\{C\}^{(m-q)}} \quad (7)$$

according to the definitions reported above in the case of complexation. Consequently the intrinsic protonation constant is $K_{Taj}\gamma_{H_{(x-1)}L'}\gamma_{C'}/\gamma_{H_xL'}$, and is independent on the composition of the aqueous phase.

3. Results and discussion

3.1. Protonation equilibria

The iminodiacetic groups in the resin are twice protonated at pH 2 and the protons can be neutralized by addition of a base up to pH 10. Typical titration curves at $T = 25$, 45 and 65°C of Lewatit TP-207 from NaCl 0.1 mol kg^{-1} solutions are shown in Fig. 1.

From Eq. (7) it is possible to estimate the intrinsic protonation constant if the concentration of the counter ion in the resin phase and the water sorbed by the resin are known. The counter ion concentrations was calculated as previously described [2,3]. The quantity of water sorbed per g of dry resin, q, as function of the protonation degree, a, was found to be $q = 0.92\ (0.05) + 0.41\ (0.04)a$ for $a < 1$, while it was constant, $q = 1.4$ for

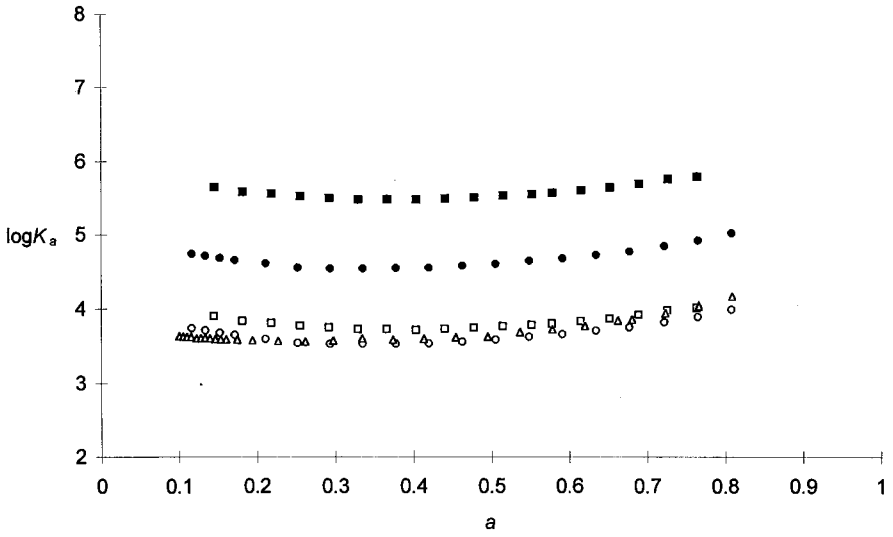

Fig. 2. Protonation coefficients (full symbols) and intrinsic protonation constant (empty symbols) as function of the deprotontion degree. Square, NaCl 0.01 mol kg^{-1} solution; circle, NaCl 0.1 mol kg^{-1} solution; triangle, NaCl 1 mol kg^{-1}.

$a > 1$. Similar results were obtained at all the considered T. It should be notice that this determination of water represents the total amount of water present in the resin. Dealing with a macroporous resin, it is the water in the resin phase, but also the water in the macropores which properly belongs to the solution phase.

The capacity, in terms of mmol of active groups per g of dry resin, was found to be 3.46 ± 0.15 mmol g^{-1} and it was independent of T.

The protonation coefficients obtained experimentally from solutions of NaCl at different concentrations are shown in Fig. 2 as a function of the protonation degree (a). They strongly depend on the concentration of the counter ion in solution, as expected from the Gibbs–Donnan model. This shows that Lewatit TP-207 is a matrix permeable to ions [10] to which the model can be correctly applied. The values of the intrinsic complexation constants $\log K_{\mathrm{Ta}j}\gamma_{\mathrm{H}_{(x-1)}\mathrm{L}'}\gamma_{\mathrm{C}'}/\gamma_{\mathrm{H}_x\mathrm{L}'}$ calculated on the basis of the model are shown in Fig. 2 with open symbols. They are calculated from Eq. (7) and the agreement of values obtained at different concentration of NaCl is very good.

The intrinsic protonation constants found at different temperatures are reported in Table 1 together with the estimated $\Delta H°$(kJ mol^{-1}). This values were obtained from the van't Hoff equation by plotting 2.303 $\log K$ versus $1/T$ (°K) assuming that the temperature interval is sufficiently low that $\Delta H°$ (kJ mol^{-1}) and $\log \gamma_{\mathrm{H}_{(x-1)}\mathrm{L}'}\gamma_{\mathrm{C}'}/\gamma_{\mathrm{H}_x\mathrm{L}'}$ are not dependent on T. Here the intrinsic protonation constant, not the thermodynamic one was used for the evaluation (i.e. $\log K = \log K_{\mathrm{Ta}j}\gamma_{\mathrm{H}_{(x-1)}\mathrm{L}'}\gamma_{\mathrm{C}'}/\gamma_{\mathrm{H}_x\mathrm{L}'}$). The term $\log \gamma_{\mathrm{H}_{(x-1)}\mathrm{L}'}\gamma_{\mathrm{C}'}/\gamma_{\mathrm{H}_x\mathrm{L}'}$ appears in the constant parameters of the straight line.

The values of the protonation enthalpy obtained here are not very different from those found in aqueous solution for IDA, a ligand having the same chelating group as Lewatit TP-

Table 1
Intrinsic protonation constant of Lewatit TP-207 at different temperature and estimated protonation enthalpy values

T (°C)	$\log K_{\mathrm{Ta}1}\gamma_{\mathrm{L}'}\{\mathrm{Na}'\}/\gamma_{\mathrm{HL}'}$	$\log K_{\mathrm{Ta}2}\gamma_{\mathrm{HL}'}\{\mathrm{Na}'\}/\gamma_{\mathrm{H_2L}'}$
25	9.06 (0.15)	3.63 (0.04)
45	8.66 (0.05)	3.61 (0.03)
65	7.97 (0.07)	3.53 (0.05)
$\Delta H°$(kJ mol^{-1})	-54.61 ± 9.21	-4.75 ± 1.84
Intercept $\cdot R$ (kJ mol^{-1})	-7.32 (2.59) 10^{-3}	$+53.93$ (0.52) 10^{-3}

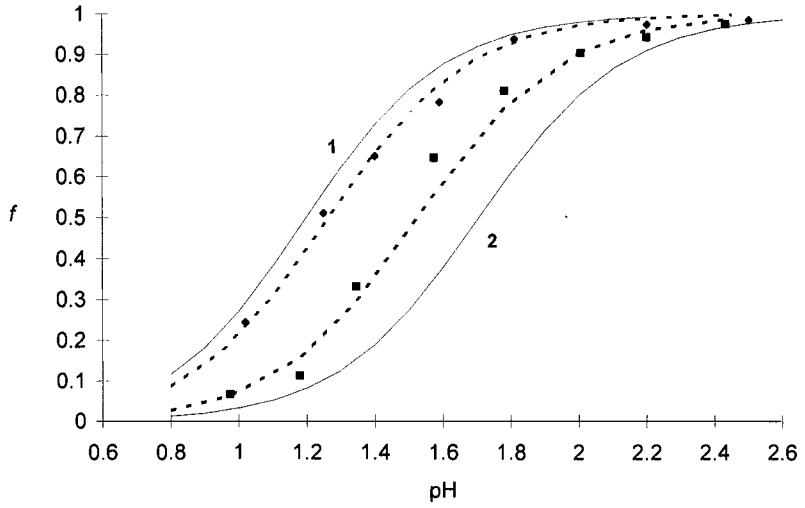

Fig. 3. Experimental sorption curves of Ni on Lewatit TP-207. $V = 35$ ml of 0.1 mol kg^{-1} NaCl, [Ni] = 2.47 10^{-3} mol kg^{-1} and 0.74 g of dry resin at $T = 25°C$ (■) and $V = 35$ ml of 0.1 mol kg^{-1} NaCl, [Ni] = 3.18 10^{-3} mol kg^{-1} and 0.55 g of dry resin at $T = 65°C$ (◆). Dotted curves are calculated on the basis of Eq. (4) with the intrinsic complexation constant reported in Table 2. Curves 1 and 2 are calculated for $T = 80$ and 5°C, respectively.

207. ΔH_1° was estimated to be -34.1 kJ mol^{-1} by Anderegg in 1964 [11] from calorimetric studies, -32.3 and $\Delta H_2^\circ = -3.2$ kJ mol^{-1} by Bonomo et al. in 1979 [12]. From the protonation constants of IDA at different T recently published [13], it was possible to estimate $\Delta H_1^\circ = -41.76$ kJ mol^{-1}.

While $\log K_{Ta1}\gamma_{L'}\gamma_{Na'}/\gamma_{HL'}$ is in good agreement with the protonation constant of IDA [12] or MIDA [14], the value of $\log K_{Ta2}\gamma_{HL'}\gamma_{Na'}/\gamma_{H_2L'}$ is considerably higher than that of the monomeric model in aqueous solution. Other resins containing the same active groups present this difference. The second protonation constant was found to be 3.0 for Chelex 100 from a $NaNO_3$ solution [1], 3.10 for a synthesized resin with an IDA group from 1 M KCl solution [15], ranging from 2.95 to 3.20 for an IDA supported on highly crosslinked agarose (Novarose™) from 0.1 M $NaNO_3$ solution [16], and 3.74 for a Rohm and Haas IRC 718 from KCl solution (R. Biesuz, M. Muhammed, personal communication).

At the moment there is no satisfactory explanation of this effect that seems higher when chloride is the co-ion. It was observed [17] that an uncorrected evaluation of the water in the resin phase can easily occur when a macroporous resin such as Lewatit TP-207 are examined and this can lead to an incorrect evaluation of the concentration of the counter ion in the resin phase (cf. Eq. (7)).

3.2. Complexation equilibria with Ni and Cd

In Figs. 3–5 the sorption curves of Ni and Cd obtained from 0.1 mol kg^{-1} NaCl solution at different T are reported. Since the solution contains a high concentration of chloride, the complexation reactions of chloride should be considered as side reactions. The values of $\alpha_{M(Cl)}$ coefficients for both metals at the considered T were evaluated to be $\alpha^{25°}_{Cd(Cl)} = 5.86$, $\alpha^{45°}_{Cd(Cl)} = 6.24$, $\alpha^{65°}_{Cd(Cl)} = 6.33$ and $\alpha^{25°}_{Ni(Cl)} = 1.11$, $\alpha^{45°}_{Ni(Cl)} = 1.09$, $\alpha^{65°}_{Ni(Cl)} = 1.07$ [18,19].

The stoichiometry and the equilibrium coefficients of the sorption reactions of each of the considered metal ions on the resin are determined from experimental points f versus pH, considering the capacity and the protonation coefficient previously found and the side reaction coefficients.

Typical sorption curves of Ni on Lewatit TP-207 are reported in Fig. 3. The sorption reaction was found to be:

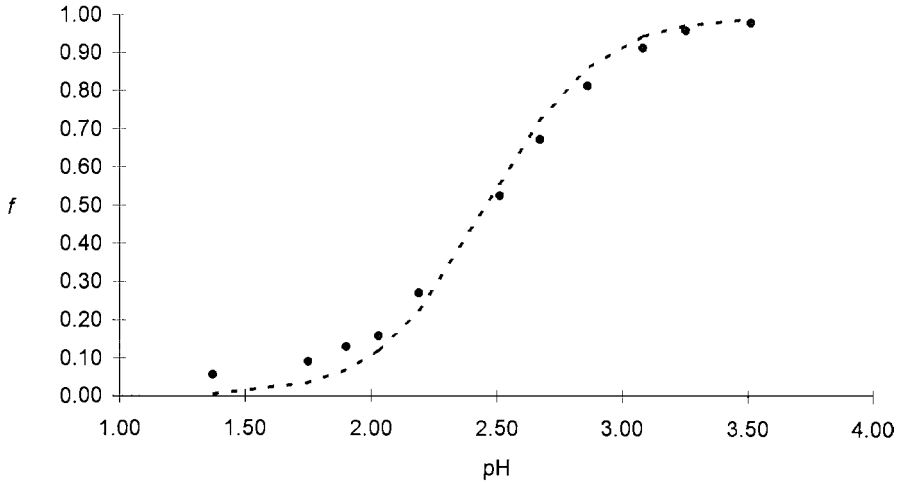

Fig. 4. Sorption curves of Cd on Lewatit TP-207 at $T = 45$°C. $V = 50$ ml of 0.1 mol kg^{-1} NaCl, [Cd] = 3.48 mol kg^{-1} and 0.50 g of dry resin. The dotted curve is calculated on the basis of Eq. (4) with the intrinsic complexation constant reported in Table 2.

$$Ni + H_2L' \leftrightarrow NiL' + 2H \quad (8)$$

The intrinsic complexation constants and the estimated value of ΔH°_{110} (kJ mol^{-1}) are reported in Table 2. The stoichiometry is the same found for the sorption on Chelex 100 [1]. The value of the intrinsic complexation constant $\beta^*_{T(110)}(\gamma_{H_2L'})/(\gamma_{NiL'})$ is higher then that found in the case of Chelex 100. This characteristic of Lewatit TP-207 was also observed in the case of copper(II). The sorption under experimental conditions similar to those used for Ni was higher then 90% at pH 1, while it was expected to be around 50% considering the 1:1:2 complex found with Chelex 100 [1]. This means that the intrinsic complexation constant of copper is higher for Lewatit TP-207 then for Chelex 100, and according to Eq. (5) this can be ascribed to a difference in $\gamma_{H_2L'}/\gamma_{ML'}$. Another reason could be an inaccurate evaluation of water in the resin phase, due to the fact that Lewatit TP-207 is macroporous. This point was discussed above in the case of the protonation, for which a similar effect was observed.

On the other hand the estimated value of ΔH°_1 is in quite good agreement with the values found in literature for IDA: $\Delta H^\circ_1 = -21.13$ kJ mol^{-1} was reported by Anderegg [11] and $\Delta H^\circ_1 = -34.91$ kJ mol^{-1} was calculated from the values reported in [13]. This could show that the same complexation takes place in the two resins and in the soluble monomer.

The sorption of cadmium was found to take place according to

$$Cd + 2H_2L' \leftrightarrow Cd(HL)'_2 + 2H \quad (9)$$

The complex $Cd(HL)_2$ is the same as found in Chelex 100 and the value of the intrinsic complexation constant is in good agreement with that of Chelex 100 and with that in aqueous solution with acetate as already noted [1]. The intrinsic complexation constants obtained at different temperature are reported in Table 2. In Fig. 4 a typical sorption curve for Cd is shown. The dotted line is calculated using the intrinsic complexation constant reported in Table 2.

The formation of complex $Cd(HL)_2$ in the resin phase is slightly dependent on T, i.e. different to Ni. Indeed a different kind of complex is involved in the sorption reaction of the two metal ions. The difference between the complexation of Ni and that of Cd is particularly evident if the comparison is made between ΔH° pertinent to the complex formation which are reported at the end of Table 2. No comparison can be made with the complexation in the aqueous phase since nothing is reported about $Cd(HL)_2$. In water solution only the complex CdL was found to be formed with $\Delta H^\circ_1 = -6.11$ kJ mol^{-1} [19].

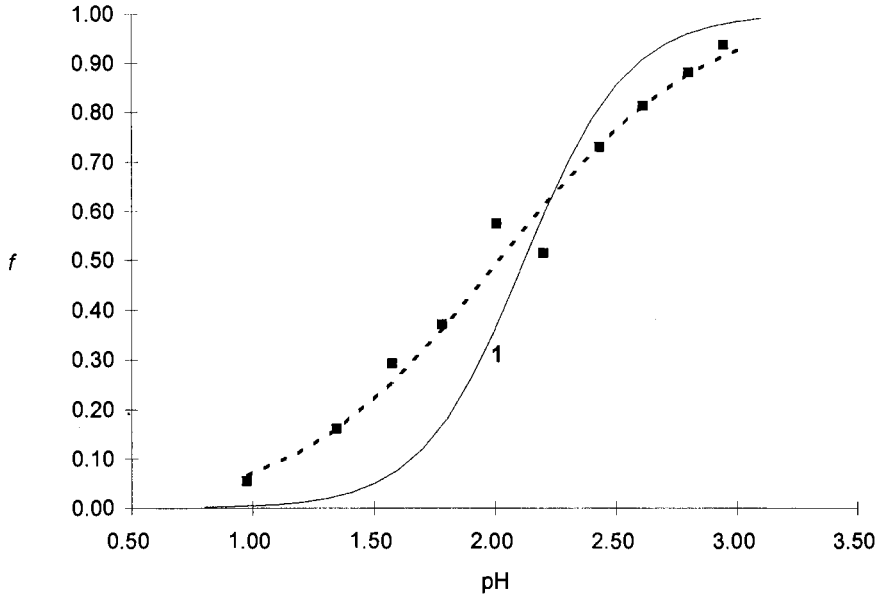

Fig. 5. Sorption curves of Cd on Lewatit TP-207 at $T = 25°C$. $V = 35$ ml of 0.1 mol kg^{-1} NaCl, [Cd] = 2.44 mol kg^{-1} and 0.74 g of dry resin. The dotted curve is calculated on the basis of Eq. (4) considering $\beta^*_{T(111)}\gamma_{H_2L'}/\gamma_{CdHL'}$. Curve 1 is calculated only considering $\beta^*_{T(122)}\gamma^2_{H_2L'}/\gamma_{Cd(HL)_2}$ reported in Table 2.

It is interesting to note that a different sorption equilibrium involving different complexation inside the resin was found in a more acidic solution. In Fig. 5 a sorption curve obtained with a ratio V/w half of that used in the experiment shown in Fig. 4 is reported. The shape of the curve is different from that calculated if only the complex $Cd(HL)_2$ were formed (curve 1). In this condition (cf. Eq. (4)) sorption is shifted to a lower pH and takes place according to the following:

$$Cd + H_2L' \leftrightarrow CdHL' + H \quad (10)$$

The intrinsic complexation constant was found to be $\beta^*_{T(111)}(\gamma_{H_2L'}\gamma_{C'})/(\gamma_{CdHL'}) = -1.16$. The dotted curve is calculated using only the sorption through the reaction in Eq. (10).

4. Conclusion

The Gibbs–Donnan model allows us to describe the sorption of nickel(II) and cadmium(II) on Lewatit TP-207 in a satisfactory way. It was found that the intrinsic complexation and protonation constants do not agree with those of similar soluble ligands as found in the case of a resin containing iminodiacetic groups, Chelex 100. The reason for this could be the macroporous nature of Lewatit TP-207 that causes an incorrect evaluation of the water in the resin phase. Another reason for this difference could be that, compared to Chelex 100, there is a relative high concentration of active sites in Lewatit TP-207. This could have an influence on the ratio of the activity coefficients of the 1:1 complex that could not be evaluated. On the other hand the values of the reaction enthalpy are in satisfactory agreement with those found in solution for IDA, so confirming that there is a similarity between the complexation in the resin and that in the monomeric model.

The formation of 1:2:2 complex with Cd, identified for the first time with Chelex 100, was confirmed from the sorption study on Lewatit TP-207. The possibility of the formation of this complex makes the resin containing the iminodiacetate active group less selective then expected, in particular for preconcentration and speciation from sea water [1,5], since alkaline earth metals are strongly sorbed through the formation of

Table 2
Intrinsic complexation constants of Lewatit TP-207, from 0.1 mol kg^{-1} NaCl solution at different temperature and the estimated complexation enthalpy values

T (°C)	[NaCl] (mol kg^{-1})	Nickel	Cadmium
		$\beta^*_{T(110)}(\gamma_{H_2L'})/(\gamma_{NiL'})$	$\beta^*_{T(122)}(\gamma^2_{H_2L'})/(\gamma_{Cd(HL)_2})$
25	0.1	−1.84 (0.12)	−3.64 (0.09)
	1.0		−3.64 (0.03)
45	0.1	−1.53 (0.09)	−3.38 (0.10)
	0.1		−3.37 (0.14)
65	0.1	−1.25 (0.11)	−3.34 (0.18)
$\Delta H°$(kJ mol^{-1})		+28.43 (0.19)	+13.71 (2.99)
Intercept · R (kJ mol^{-1})		60.11 (0.05) 10^{-3}	−22.84 (1.64) 10^{-3}
$\Delta H°$[a] (kJ mol^{-1})		−30.94 (10.86)	+3.89 (1.69)
Intercept · R (kJ mol^{-1})		106.75 (2.99) 10^{-3}	13.50 (0.66) 10^{-3}

[a] Referred to the complex formation reaction $M + x\overline{H_rL} \leftrightarrow \overline{M(H_rL)x}$.

these complexes. In the present study it is shown that the sorption equilibria are better characterised by the intrinsic constants than by the thermodynamic constants. Moreover, the intrinsic constants can be evaluated experimentally while the thermodynamic ones cannot.

The present study offers the possibility to give a satisfactory explanation of the selectivity based on the temperature response that otherwise in not easily justified [6]. The sorption on Lewatit TP-207 of the two metal ions is through the formation of different complexes.

When the sorption equilibria are known exactly, it is possible to predict the best conditions for a of separation Cd–Ni. As an example, in Fig. 3 the sorption curve, calculated with the exchange coefficients obtained from the van't Hoff equation at 80 and 5°C are reported as solid lines. The conditions considered were as follows: pH 1.3, 50 ml NaCl 0.1 mol kg^{-1} containing $[Ni] = 1 \times 10^{-3}$ mol kg^{-1} and 0.5 g dry resin. It is expected that Ni is selectively sorbed at 80 and desorbed at 5°C. Under the same conditions Cd is not sorbed, either at 80 or at 5°C.

Acknowledgements

This work was partially supported by MURST (Ministero deu' Università e della Ricerca Scientifica e Techologica) of Italy. A.G. is a recipient of a fellowship from CIRIT (Commission for Science and Technology of Catalunya).

References

[1] M. Pesavento, R. Biesuz, M. Gallorini, A. Profumo, Anal. Chem. 65 (1993) 2522–2527.
[2] M. Pesavento, R. Biesuz, Anal. Chem. 67 (1995) 3558–3563.
[3] M. Pesavento, A. Profumo, R. Biesuz, Talanta 35 (1988) 431–437.
[4] M. Pesavento, R. Biesuz, J.L. Cortina, Anal. Chim. Acta 298 (1994) 225–232.
[5] M. Pesavento, R. Biesuz, Anal. Chim. Acta 346 (1997) 381–391.
[6] D. Muraviev, A. Gonzalo, M. Valiente, Anal. Chem. 67 (1995) 3028–3035.
[7] D. Muraviev, A. Gonzalo, M.J. Gonzàlez, M. Valiente, Ion exchange developments and applications, in: J.A. Greig (Ed.), Society of Chemical Industry, Cambrige, 1996, pp. 516–523
[8] , D. Muraviev, A. Gonzalo, N.A. Tikhonov, M. Valiente, J. Chromatogr. 1998 (in press).
[9] F. Baffi, A.M. Cardinale, R. Bruzzone, Anal. Chim. Acta 270 (1992) 79–86.
[10] A. Chatterjee, J.A. Marinsky, J. Phys. Chem. 67 (1963) 41.
[11] G. Anderegg, Helv. Chim. Acta 47 (1964) 1801–1814.
[12] R.P. Bonomo, R. Calì, F. Riggi, E. Rizzarelli, S. Sammartano, G. Siracusa, Am. Chem. Soc. Inorg. Chem. 18 (1979) 3417–3422.
[13] M.J. Gonzales, M. Muhammed, V. Romano, G. Ruggirello, R. Zingales, Abstr. of XIII Congresso Nazionale di Chimica Analitica, Viterbo, Italy, 7–11 September 1997, pp. 82–85.

[14] G. Schwarzenbach, G. Anderegg, W. Schneider, H. Senn, Helv. Chim. Acta 38 (1955) 1147–1151.
[15] Ö. Szabadka, J. Inczédy, J. Chromatogr. 201 (1980) 59–66.
[16] P. Hashemi, Å. Olin, Talanta 44 (1997) 1037–1053.
[17] J.A. Marinsky, T. Miyaajima, E. Högfeldt, M. Muhammed, React. Polym. 11 (1989) 279.
[18] Stability Constants of Metal Ions Complexes, Chem. Soc., Special Pub. No. 17, 1964.
[19] M.H. Hutchinson, W.C.E. Higginson, J. Chem. Soc. Dalton Trans. 1973, 1247–1253

ELSEVIER

Talanta 47 (1998) 137–142

Talanta

Simultaneous determination of copper, cadmium and nickel by ratio derivative polarography

Yongnian Ni *

Department of Chemistry, Nanchang University, Nanchang Jiangxi 330047, People's Republic of China

Received 6 October 1997; received in revised form 4 February 1998; accepted 5 February 1998

Abstract

Ternary mixtures of metals can be resolved by using the ratio derivative polarography without the need for any pre-separation step. The method is based on the simultaneous use of the first derivative of ratios of polarograms and measurements of zero-crossing potentials. The polarogram of the mixture is obtained and the amplitudes of the current at appropriate potentials are divided by the corresponding amplitudes in the polarogram of a standard solution of one of the components, and the subsequent derivation against potential results to the first derivative of the ratio polarogram. The concentrations of the other two components are then determined from their respective calibration graphs established by measuring the ratio derivative analytical signal at the selected zero-crossing points. The method has been successfully applied for resolving ternary mixtures of copper, cadmium and nickel, which have overlapped polarograms in pH 2.87 Britton-Robinson buffer. The concentration ranges to be determined are 0.30–1.40 mg l^{-1} for copper, 0.90–4.50 mg l^{-1} for cadmium and 0.20–1.20 mg l^{-1} for nickel, and the recoveries are 88.3–101.9% for copper, 92.2–105.4% for cadmium and 95.0–107.0% for nickel. © 1998 Elsevier Science B.V. All rights reserved.

Keywords: Ratio derivative polarography; Metals

1. Introduction

Electroanalytical techniques, such as differential pulse polarography, anodic stripping voltammetry and adsorptive voltammetry, generally have high sensitivity, though their applicabilities to the determination of mixtures of several components are rather limited when they display a strongly partially overlapped polarograms or voltammograms. Several methods have been proposed to overcome this limitation and resolve the overlapped polarograms or voltammograms. Turnes et al. [1] have applied multiple linear regression (MLR) to resolve highly overlapped peaks of mixed metal ions produced by differential pulse polarography and anodic stripping voltammetry. Recently, Garcia et al. [2] have also applied MLR to the treatment of high overlapped peaks obtained from the mixture of cadmium, copper and nickel by differential pulse polarography. In that work the baseline should be subtracted and the authors reported that the results could be further

* Corresponding author. E-mail: ynni@ncu.edu.cn

0039-9140/98/$19.00 © 1998 Elsevier Science B.V. All rights reserved.
PII S0039-9140(98)00076-9

improved by employing smoothed polarograms. Brown and Brown [3] demonstrated the application of the Kalman filter to the resolution of an overlapped multicomponent linear sweep voltammograms of cadmium, indium and lead system. Henrion et al. [4] applied partial least squares (PLS) to resolve quantitatively overlapped responses obtained from differential pulse anodic stripping voltammetry. PLS was also used for resolve the overlapping polarograms of organic compounds, pyrazine and its methyl derivatives [5]. Recently, Cabanillas et al. [6,7] have used PLS to resolve the differential pulse polarographic signals of binary and ternary mixtures of nitrofuran derivatives. Ni et al. [8] have applied PLS to resolve the overlapping voltammograms of food colorants.

Salinas et al. [9] developed a new spectrophotometric method, named the 'ratio derivative spectrum' for resolving binary mixtures. This method has then been widely applied to resolve binary and ternary spectropotometric problems [10–16].

We have extended this alternative method to the area of electroanalysis and to resolve the overlapping voltammograms of amaranth and sunset yellow [17]. In this paper a further work for resolution of ternary mixtures of metals has been done, with the aim of demonstrating the ease with which the derivative method circumvents the problem of overlapping polarograms, so allowing the simultaneous determination of mixtures of copper, cadmium and nickel.

2. Principle

For a ternary mixture containing components A, B and C, the polarogram of the mixture can be defined by Eq. (1):

$$I_i = a_{A,i}\ C_A + a_{B,i}\ C_B + a_{C,i}\ C_C + I_{i0} \quad (1)$$

where I_i is the polarographic current of the mixture at potential E_i, C_A, C_B and C_C are the concentrations of A, B and C, $a_{A,i}$, $a_{B,i}$ and $a_{C,i}$ are the proportional coefficients of A, B and C at potential E_i, and I_{i0} is the residual current at E_i, which can be simply denoted as $I_{i0} = k_0 + k_1E_i + k_2E_i^2$ (k_0, k_1 and k_2 are constants here) in a limited potential region.

If Eq. (1) is divided by the proportional coefficient of one of the component (e.g. $a_{A,i}$), the following equation can be obtained (Eq. (2)):

$$I_i/a_{A,i} = C_A + C_B(a_{B,i}/a_{A,i}) + C_C(a_{C,i}/a_{A,i}) + I_{i0}/a_{A,i} \quad (2)$$

By using the first derivative approach, the following equation can be written:

$$\mathrm{d}(I_i/a_{A,i})/\mathrm{d}E = C_B\mathrm{d}(a_{B,i}/a_{A,i})/\mathrm{d}E + C_C\mathrm{d}(a_{C,i}/a_{A,i})/\mathrm{d}E + \mathrm{d}(I_{i0}/a_{A,i})/\mathrm{d}E \quad (3)$$

where $\mathrm{d}(I_{i0}/a_{A,i})/\mathrm{d}E$ is independent on the concentrations of each component and is a constant at any given potential point. Eq. (3) indicates that the amplitude of the 'ratio derivative polarogram' of the mixture is independent on the value of C_A and is dependent on the values of C_B and C_C in the mixture.

In practical work, the polarogram of component A with known concentration, C_A^0, is used to replace the proportional coefficient (i.e. $a_{A,i}$, the polarogram of unit concentration) as divisor, and the polarogram of residual current which is obtained from a real blank solution is used in ratio derivative calculation. Thus Eq. (3) can be written as:

$$(1/C_A^0)\mathrm{d}((I_i - I_{i0})/a_{A,i})/\mathrm{d}E = (C_B/C_A^0)\mathrm{d}(a_{B,i}/a_{A,i})/\mathrm{d}E + (C_C/C_A^0)\mathrm{d}(a_{C,i}/a_{A,i})/\mathrm{d}E \quad (4)$$

Note that the term of 'residual current' is moved to the left side of Eq. (4) in order to omit the intercept. Method of 'zero-crossing point' can be applied to Eq. (4) to obtain the concentrations of B and C. The principle of further treatment procedure was completely explained by Berzas Nevado et al. [11] and will not be described here.

3. Experimental

3.1. Apparatus

The polarograms were obtained with an electroanalyzer (BAS 100A) equipped with a model PARC 303A cell stand (EG and G). A three-electrode cell, containing a mercury drop electrode (function of a static mercury drop electrode, SMDE, was used in this work) as the working electrode, a Ag-AgCl (3 mol l^{-1} KCl) electrode as the reference electrode, and a platinum wire as the counter electrode, was used. The polarographic spectra were plotted by using a plotter (DMP 40, Houston Instrument), and the current data were recorded by a computer connected to BAS 100A. The pH of the solution was measured by the use of a pH meter (Orion SA720). All experiments were performed at 25°C.

3.2. Reagents

All reagents used were of analytical reagent grade. Stock solutions of copper and nickel (10.0 mg l^{-1}) and the solution of cadmium (30.0 mg l^{-1}) were prepared from their nitrate or chloride salts according to the classical method. The solution of potassium thiocyanate (4.0 mol l^{-1}) was prepared by dissolving 388.72 g crystal of this salt in water and diluting to 1 l. Britton-Robinson buffer solution (pH 2.87) was prepared from phosphoric acid, acetic acid, boric acid and sodium hydroxide [18]

3.3. Procedure

Analysis was performed by pipetting a suitable amount of mixture of metals, together with 3.0 ml of the Britton-Robinson buffer solution (pH 2.87) and 1.0 ml of 4.0 mol l^{-1} solution of potassium thiocyanate into a cell and made up with deionized water to 10.0 ml. The solution was purged with purified nitrogen gas for 480 s. After a 10 s quiet time, the potential was scanned from -250 to -850 mV versus Ag-AgCl reference electrode using differential pulse polarography (DPP) at a static mercury drop electrode (SMDE). The pulse amplitude potential was -50 mV, The drop time interval was 2000 ms, and the sweep rate was 2 mV s^{-1}. After sweeping, the instrument plotted the polarograms and printed the response current data automatically. The data were sampled at 225 points by a computer, in the range of -300– -750 mV with 2 mV intervals, and all these data were used in calculations.

The ratio derivative polarograms were calculated according to Savitzky-Golay method through the use of seven experimental points [19–21]. Fig. 1 shows the polarographic waves of copper, cadmium and nickel. It can be seen that the waves are overlapped, especially for cadmium and nickel.

4. Results and discussion

4.1. Selection of measurement potentials

Fig. 2 shows the first derivatives of the ratio polarograms of copper and nickel when cadmium is as a divisor. It can be seen that there is not any polarogram overlap between these two components, so it can easily be found that copper can be determined by measuring at 472 mV (maximum amplitude peak potential for copper) and nickel at 672 mV (minimum amplitude peak potential for nickel). Fig. 3 shows the first derivatives of ratio

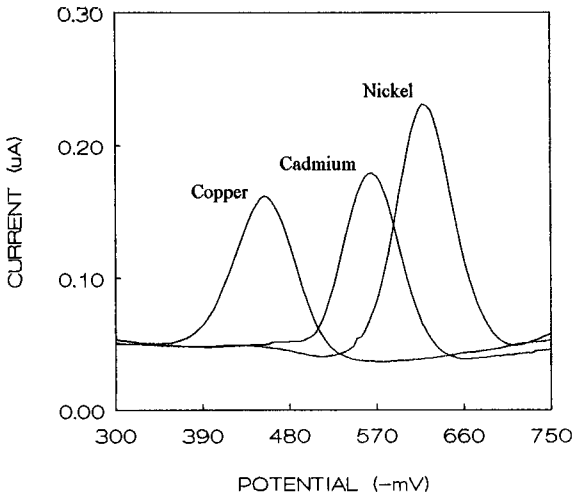

Fig. 1. The polarographic waves of copper (0.8 mg l^{-1}), cadmium (2.0 mg l^{-1}) and nickel (0.8 mg l^{-1}).

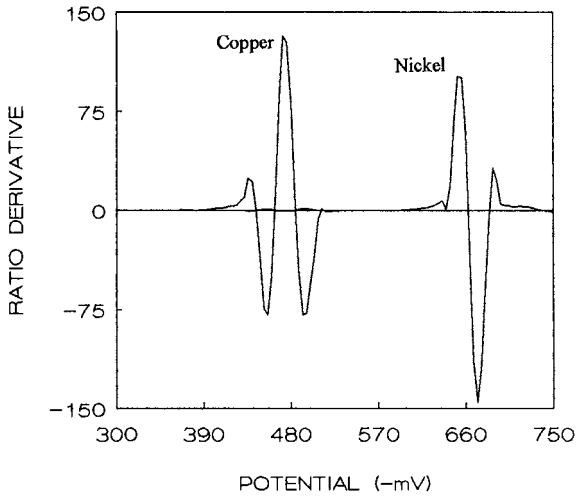

Fig. 2. First derivatives of ratio polarograms of copper (1.8 mg l^{-1}) and nickel (1.8 mg l^{-1}) when cadmium (2.7 mg l^{-1}) is used as a divisor.

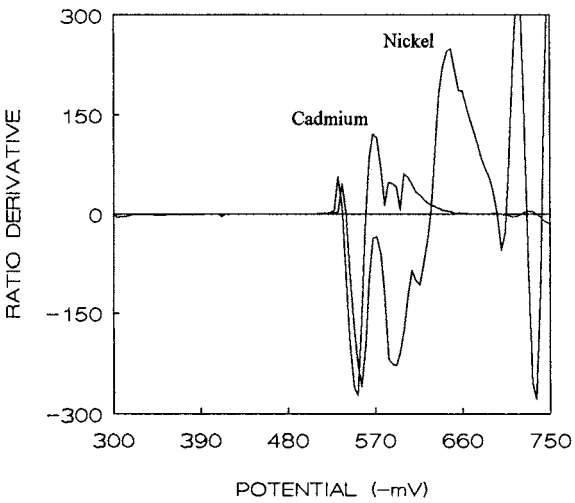

Fig. 4. First derivatives of ratio polarograms of cadmium (1.8 mg l^{-1}) and nickel (1.8 mg l^{-1}) when copper (0.9 mg l^{-1}) is used as a divisor.

polarograms of copper and cadmium when nickel is as a divisor. It can be seen that cadmium can be determined by measuring at 564 mV (minimum amplitude peak potential for cadmium and no overlap from copper at this potential point), and it is difficult to find suitable measuring potential for determination of copper for its polarogram is seriously overlapped by the one of cadmium and no satisfied zero-crossing point can be found. Fig. 4 shows the first derivative of ratio polarograms of cadmium and nickel when copper is as a divisor. It can be seen that 646 mV can be used as measuring potential for determination of nickel, however, no suitable zero-crossing potential point can be used for determination of cadmium. As described above, two potential points can be selected for determination of nickel, however, in this work, 672 mV (cadmium as divisor in Fig. 2) was selected, because this potential point gave better results than the one used in Fig. 4 in practical analysis.

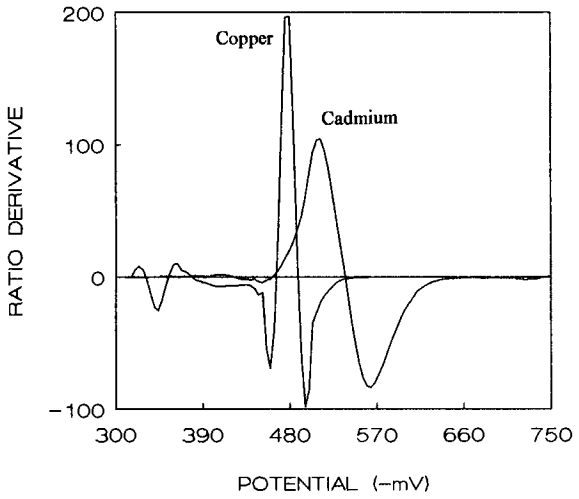

Fig. 3. First derivatives of ratio polarograms of copper (0.9 mg l^{-1}) and cadmium (1.8 mg l^{-1}) when nickel (0.9 mg l^{-1}) is used as a divisor.

4.2. Determination of copper, cadmium and nickel in synthetic mixtures

The calibration graph for each metal was obtained by preparing a set of six standard solutions with different concentrations and then treated as described above. The obtained calibration graphs and some parameters are listed in Table 1. In this work, nine synthetic mixtures of copper, cadmium and nickel with different concentration levels were prepared and resolved by the proposed method. The results are given in Table 2. It can be seen that most of them are satisfactory.

Table 1
Calibration graphs for copper, cadmium and nickel[a]

	Copper	Cadmium	Nickel
Standard solutions (mg l^{-1})	0.3, 0.6, 0.9, 1.2, 1.5, 1.8	0.9, 1.8, 2.7, 3.6, 4.5, 5.4	0.3, 0.6, 0.9, 1.2, 1.5, 1.8
Divisor (mg l^{-1})	2.7 of cadmium	0.9 of nickel	2.7 of cadmium
Measuring potential (mV)	472	564	672
Calibration graphs	$D=2.46+73.64C$	$D=3.02-16.19C$	$D=-3.53-78.21C$
Regression coefficient	0.9995	0.9996	0.9991
S_m	1.53	0.47	2.01
S_b	2.19	2.01	2.87

[a] S_m is the standard deviation of the slope and S_b is the standard deviation of the intercept [22]

Table 2
Results obtained for the determination of synthetic mixtures of copper, cadmium and nickel by the proposed method

Sample	Added (mg l^{-1})			Found (mg l^{-1})			Recovery (%)		
	Copper	Cadmium	Nickel	Copper	Cadmium	Nickel	Copper	Cadmium	Nickel
1	0.300	0.900	1.200	0.285	0.830	1.225	95.0	92.2	102.1
2	0.300	4.500	0.600	0.265	4.650	0.591	88.3	103.3	98.5
3	0.300	2.500	0.200	0.298	2.635	0.214	99.3	105.4	107.0
4	1.400	0.900	0.600	1.426	0.850	0.603	101.9	94.4	100.5
5	1.400	4.500	0.200	1.369	4.525	0.203	97.8	100.6	101.5
6	1.400	2.500	1.200	1.350	2.569	1.186	96.4	102.8	98.8
7	0.900	0.900	0.200	0.915	0.883	0.190	101.7	98.1	95.0
8	0.900	4.500	1.200	0.845	4.486	1.156	93.9	99.7	96.3
9	0.900	2.500	0.600	0.830	2.436	0.630	92.2	97.4	105.0

4.3. Determination of copper, cadmium and nickel in aluminum alloy

A sample (0.1000 g) of aluminum alloy was transferred into a 150-ml flask. A 10-ml volume of 5 mol l^{-1} sodium hydroxide was added to the flask and the sample was dissolved by warming. Several drops of 30% hydrogen peroxide was then added and the solution was kept warming for 2 min. When action had ceased, the sample solution was allowed to cool and 10 ml of concentrated hydrogen nitrate was added and the solution was boiled up to the elimination of nitrogen oxides. After cooling, ca. 20 ml of deionized water was added and the sample was dissolved completely. Ten percent of sodium hydroxide was then carefully added to adjust the pH to 2.8, and the solution was diluted to 50 ml with deionized water. The solution was taken for the determination using the procedure described previously. The results obtained were 0.47% for copper, 0.22% for cadmium and 0.16% for nickel. These results are in agreement with the values obtained by atomic absorption spectrometric method (0.45% for copper, 0.24% for cadmium and 0.17% for nickel), thus confirming the reliability of the proposed method.

5. Conclusions

The results show that the proposed method is effective for resolving ternary mixtures and suitable for the simultaneous polarographic determination of copper, cadmium and nickel in the concentration range of 0.2–4.5 mg l^{-1}. This work indicates that some electroanalytical problems, such as resolution of overlapping polarographic waves, can benefit from the mathematical methods used in spectrophotometry.

Acknowledgements

The author thank the National Natural Science Foundation of China (NSFC) and the Jiangxi Provincial Natural Science Foundation (JXNSFC) for financial support.

References

[1] G. Turnes, A. Cladera, E. Gomez, J.M. Estela, V. Cerda, Electroanal. Chem. 338 (1992) 49.
[2] J.M. Garcia, E. Martin, A.I. Jimenez, F. Jimenez, J.J. Arias, Anal. Lett. 27 (1994) 1763.
[3] T.F. Brown, S.D. Brown, Anal. Chem. 53 (1981) 1410.
[4] A. Henrion, R. Henrion, G. Henrion, F. Scholz, Electroanalysis 2 (1990) 309.
[5] Y. Ni, S. Kokot, M. Selby, M. Hodgkinson, Electroanalysis 4 (1992) 713.
[6] A.G. Cabanillas, T.G. Diaz, A. Espinosa-Mansilla, P.L. Lopez-de-Alba, F.S. Lopoz, Anal. Chim. Acta 302 (1995) 9.
[7] A.G. Cabanillas, T.G. Diaz, A. Espinosa-Mansilla, F.S. Lopez, Talanta 41 (1994) 1821.
[8] Y. Ni, J. Bai, L. Jin, Anal. Chim. Acta 329 (1996) 65.
[9] F. Salinas, J.J. Berzas Nevado, A. Espinosa Mansilla, Talanta 37 (1990) 347.
[10] J.J. Berzas Nevado, C. Guiberteau Cabanillas, F. Salinas, Anal. Lett. 23 (1990) 2077.
[11] J.J. Berzas Nevado, C. Guiberteau Cabanillas, F. Salinas, Talanta 39 (1992) 547.
[12] B. Morelli, Anal. Lett. 27 (1994) 2751.
[13] B. Morelli, Talanta 41 (1994) 673.
[14] J.J. Berzas Nevado, J. Rodriguez Flores, M.J. Villasenor Llerena, Talanta 40 (1993) 1391.
[15] J.J. Berzas Nevado, C. Guiberteau Cabanillas, A.M. Contento Salcedo, Talanta 41 (1994) 789.
[16] J.J. Berzas Nevado, C. Guiberteau Cabanillas, A.M. Contento Salcedo, Talanta 42 (1995) 2043.
[17] Y. Ni, J. Bai, Talanta 44 (1997) 105.
[18] Handbook of Analytical Chemistry, Chinese Chemical Industry Press, Beijing, 1983.
[19] A. Savitzky, M.J.E. Golay, Anal. Chem. 36 (1964) 1627.
[20] J. Steinier, Y. Termonia, J. Deltour, Anal. Chem. 44 (1972) 1906.
[21] P.A. Gorry, Anal. Chem. 62 (1990) 570.
[22] J.N. Miller, Analyst 116 (1991) 3.

ELSEVIER

Talanta 47 (1998) 143–151

Talanta

Laser induced breakdown spectrometry of vanadium in titania supported silica catalysts

P. Lucena [a], L.M. Cabalín [a], E. Pardo [b], F. Martín [b], L.J. Alemany [b], J.J. Laserna [a,*]

[a] *Department of Analytical Chemistry, Faculty of Sciences, University of Málaga, E-29071, Málaga, Spain*
[b] *Department of Chemical Engineering, Faculty of Sciences, University of Málaga, E-29071, Málaga, Spain*

Received 17 September 1997; received in revised form 4 February 1998; accepted 10 February 1998

Abstract

The capability of laser induced breakdown spectrometry (LIBS) for vanadium determination in a xV–2TiO_2–SiO_2 catalyst is presented. The microplasma was generated onto the sample surface using a pulsed Nd:YAG laser operating in the second harmonic (532 nm). Laser produced plasmas were collected and detected using a charge-coupled device (CCD). In order to minimize the complex spectral interferences of emission lines and matrix effects a wide spectral range (210–660 nm) was studied. The focusing of the laser beam on the surface was optimized to improve the signal-to-background ratio, and consequently the limit of detection. The analytical lines selected were used to evaluate the calibration curve. The detection limit for V was estimated to be 38 μg g^{-1} in 2TiO_2–SiO_2. The method precision expressed as relative standard deviation (RSD) was better than 6% in the concentration range 200–1000 μg g^{-1}.
© 1998 Elsevier Science B.V. All rights reserved.

Keywords: LIBS; Vanadium analysis; Catalysts; Quantitative determination

1. Introduction

TiO_2-supported vanadium oxides have been extensively studied and used due to their high catalytic activity and selectivity in many chemical reactions [1–7]. For instance, V/TiO_2 is one of the most effective catalysts in the selective catalytic reduction (SCR) of NO_x by NH_3 [7,8]. Industrially, in these catalysts the anatase, a polymorph form of TiO_2, is used as support for vanadium oxide. Titania is the support more widely used for this purpose, although alumina, and to a lesser extent silica are also used. In spite of its wide use, titania suffers several drawbacks, including limited surface area, poor mechanical strength and a low sintering resistance. On the other hand, the interaction of vanadia with silica is weak and, consequently it results in a higher tendency to thermally induced aggregation with a poor dispersion of the active phase, while alumina-supported vanadia catalysts are susceptible to sulfation. The binary TiO_2–SiO_2 system, in principle, seems an ideal candidate to overcome the above disadvantages [9].

* Corresponding author. Tel.: +34 5 2131881; fax: +34 5 2132000; e-mail: Laserna@uma.es

0039-9140/98/$19.00 © 1998 Elsevier Science B.V. All rights reserved.
PII S0039-9140(98)00063-0

It is envisaged that ternary V–Ti–Si systems display similar characteristics to those of binary V–Ti catalysts. In addition to the economic benefits, the presence of silica grants much better mechanical properties to the system, which may allow its application in fluidized bed reactors or extrusion into monolith reactors. The bulk, the surface physico-chemical properties and the reactivity of V–Ti–Si systems are strongly dependent on the method used for their preparation and the precursors used in the vanadia distribution. Vanadium loading determines the nature and distribution of vanadia species on the titania support. Therefore the structure and morphology of the TiO_2–SiO_2 substrate will determine to a large extent the dispersion of vanadia. In contrast to binary systems, ternary catalysts are still not fully understood.

For V–Ti–Si systems, it is very interesting to evaluate the dispersion and possible diffusion of vanadium into the support. Knowledge of the quantitative microstructure and composition are of great importance in understanding the possible correlations of distribution and composition with catalytic properties. Consequently, the development of analytical methods for these materials is of great practical interest.

The capability of laser induced breakdown spectrometry (LIBS) for materials characterization has been widely demonstrated [10–14]. Recent analytical applications of LIBS include the determination of aluminum in zinc alloy [15], the simultaneous determination of aluminum, copper, iron, nickel, and zinc in alloys [16], the determination of copper in steel [17], and the detection of lead in concrete [18]. Surface analysis of photonic-grade silicon has been demonstrated [19,20]. However, no applications of LIBS for vanadium determination in catalysts have been previously reported. For this purpose, other surface analysis techniques (such as secondary ion mass spectrometry; X-ray photoelectron spectroscopy) can be used [21]. In comparison with those techniques, LIBS presents a number of advantages including the need for little or no sample preparation, the minute sample quantities needed, the possibility of work without controlled atmospheres and the rapid analysis time. In this paper, LIBS has been evaluated for the quantitative determination of vanadium in xV–2TiO_2–SiO_2 catalysts.

2. Experimental section

2.1. Apparatus

The LIBS system has been described in previous works [22,23]. Briefly, it consisted of a pulsed Nd:YAG laser operating in the second harmonic (Continuum, model Surelite SLI-20, $\lambda = 532$ nm, pulse width 5 ns), which was used to generate the microplasma. The laser energy at the sample was 4 mJ pulse^{-1}. The laser beam was focused at normal incidence onto the sample surface using a planoconvex glass lens with a focal length of 100 mm and f-number of 4. The plasma image was collected by a planoconvex quartz lens with focal length of 100 mm and dispersed by an imaging spectrograph (Chromex, model 500 IS, fitted with three indexable gratings of 300, 1200 and 2400 grooves mm^{-1}). Two of the three gratings (300 and 2400 grooves mm^{-1}) were employed in this study. The reciprocal linear dispersion was 20 and 2.5 nm mm^{-1}, respectively. These values gave spectral coverages of 120 nm for the 300 grooves mm^{-1} grating and 15 nm for the 2400 grooves mm^{-1} grating with the detector used. The entrance slit width was 10 μm and the height was 10 mm.

The spectrally resolved light was detected with a solid-state two-dimensional charge-coupled device (CCD) system (Stanford Computer Optics, model 4 Quik 05). The CCD consists of 752(h) × 582(v) elements. The photoactive area is 6×4.5 mm^2. The spectral resolution of the system was 0.16 and 0.02 nm pixel^{-1} using the 300 grooves mm^{-1} and the 2400 grooves mm^{-1} gratings, respectively. The CCD is equipped with an S 20 Q photocatode (spectral response from 180 to 820 nm) and an intensifier system (microchannel plate, MCP). Operation of the detector was controlled by 4 Spec 1.20 software. Shutter and delay times can be selected in 50 ns steps. A fast photodiode was used as external trigger for exact synchronization of the incident laser pulse and opening of the camera shutter. The emission signal was corrected

by subtraction of the dark current of the detector, which was separately measured for the same exposure time. Calibration of the detector system was conducted by using a mercury emission lamp and several lines emitted from a laser induced titanium plasma. Samples were placed on a manual X–Y–Z translation stage to be moved with respect to the laser beam.

2.2. Samples

Catalysts were prepared using $2TiO_2$–SiO_2 as a carrier for the ternary systems xV–$2TiO_2$–SiO_2. Silica microspheres (Aerosil 200 from Degussa) with size ca. 13 nm diameter and surface area of 200 m^2 g^{-1} were used as starting material. The resulting xV–$2TiO_2$–SiO_2 material was obtained by co-deposition of titania and vanadia on the silica surface by incipient wetness impregnation, as described by Geuss et al. [24] and others [25–28]. The impregnation was made by adding a methanolic solution containing variable amounts of titanium tetraisopropoxide and vanadium acetil-acetonate to the support particles. The suspension was ultrasonically dispersed to ensure a good homogeneity. The superficial precipitation on silica occurs in a few minutes at room temperature. Powders were then washed and dried in air at 373 K overnight, and afterwards they were calcined at 773 K in air for 2 h. This procedure allows deposition of oxo-hydrated titanium–vanadium, which yields dispersed TiO_2, with vanadium incorporated into the TiO_2 crystal lattice. Several samples with different vanadium loads were prepared, and they are labelled as xV–$2TiO_2$–SiO_2, where 'x' denotes the theoretical vanadium loading in μg g^{-1} and $2TiO_2$, two theoretical monolayers incorporated onto the silica surface. A monolayer was considered as the loading of titania for completed covering of silica surface by a 0.38 nm thick [26] film of TiO_2, which corresponds to the longest axis of the rutile unit cell. The titanium oxide incorporated on silica remains as small crystals of anatase covering the silica surface, as previously reported by Galán-Fereres et al. [26].

A set of six sample pellets were grounded with a mortar and pelletized at a pressure of 7.5 Ton cm^{-2} for 15 min. Approximately 0.15 g of mixture was pressed leading to samples of 13 mm in diameter and about 0.5 mm thick. Concentration of the calibration standards was in the range 200–10000 μg g^{-1} vanadium in the $2TiO_2$–SiO_2 support. In addition, for qualitative analysis other series of three pellets was prepared: one pellet with a $2TiO_2$–SiO_2 support, the second one with vanadium in form of V_2O_5 and the third one with a 1:1 (w/w) V_2O_5–TiO_2 mixture. As precision and accuracy of LIBS are highly dependent on sample composition, homogeneity, and surface condition, samples were carefully prepared according to the described methodology.

3. Results and discussion

3.1. Spectral analysis

In the analysis of solid samples by LIBS, the resulting plasma includes lines corresponding to the sample elements and matrix constituents. Thus, the goal in the quantitative determination of an element by LIBS is to find a well-resolved line for the element of interest, free of matrix interferences. In the determination of V in xV–$2TiO_2$–SiO_2 samples, silica can be easily identified. A simple study of spectral range permits the choice of the optimal region for observing vanadium without spectral interferences of Si and O emission lines. The main problem in this kind of sample is the presence of TiO_2. The large number of Ti lines along the UV-VIS region and their high intensities can complicate the qualitative and quantitative analysis. Five different spectral regions were studied for the most important emission lines of Ti and V in the range 210–660 nm. The spectral window covering the range 404–418 nm was chosen since it contains the most intense vanadium peak (411.18 nm) free from interference of neighbouring spectral lines. Fig. 1(a–c) shows, respectively, the LIBS spectra corresponding to the $2TiO_2$–SiO_2 matrix, to neat V_2O_5 and to a 1:1 (w/w) V_2O_5–TiO_2 mixture. As shown in Fig. 1(c), the main peaks for Ti and V are clearly distinguished. In these figures, only the most intense emission lines were labelled [29]. Spectra were

obtained using a single laser shot. Integration time and delay time were 1 μs and 300 ns, respectively.

3.2. Effect of laser beam focusing on the signal-to-background ratio

It is well-known that performance of LIBS for quantitative analysis is related among other factors to the signal-to-background ratio (S/B) [30]. Since the background in LIBS depends on the laser fluence used, a study on the effect of laser focusing conditions on the S/B was performed. Fig. 2 shows the variation of the average signal-to-background values and their precision (in terms of relative standard deviation, RSD) as a function of the relative lens-target distance. The values were calculated taking the background as the mean background signal along 30 pixels in an interference free region and close to the peak of interest. In Fig. 2, the distance '0' indicates that the sample was placed at the lens focal length. Positive values of the relative focusing lens-target distance refer to the beam focused at a distance above the sample surface, while negative values refer to the beam focal position placed inside the material.

From this figure, it is interesting to note that the S/B precision appeared approximately constant for relative lens-target distances from -2 to $+4$ mm. However, the S/B reached a maximum when the focal point was placed 1–2 mm above the target surface. This value decreases drastically when the laser beam was defocused a few millimeters onto the sample surface because the laser fluence decreases. Scanning electron micrographs of the craters produced by laser ablation in the 10000V–$2TiO_2$–SiO_2 pellet surface at two differ-

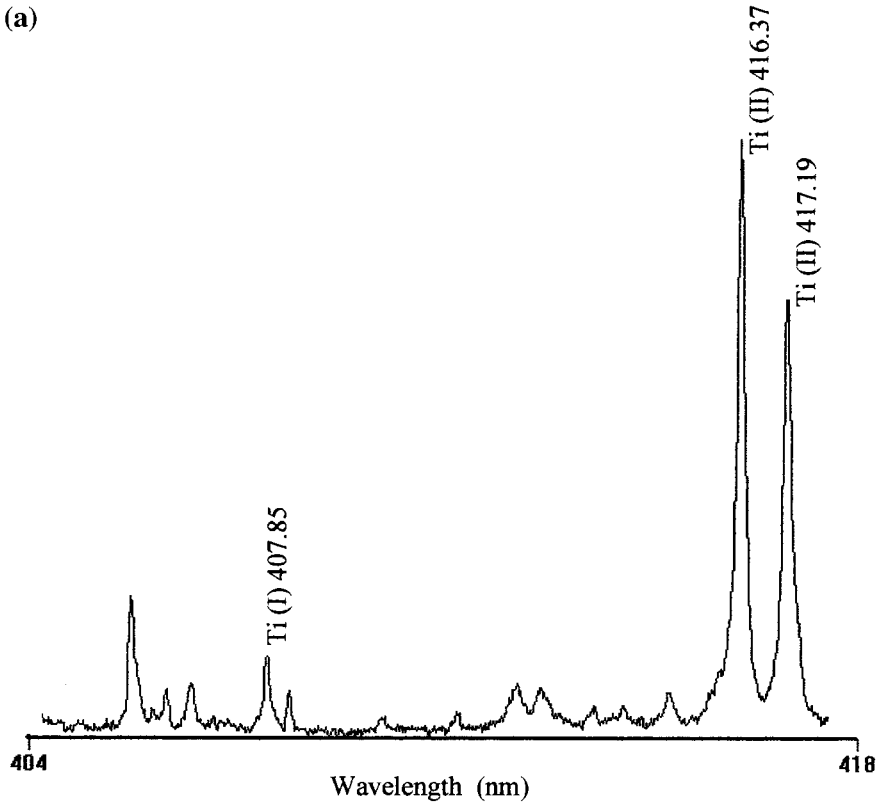

Fig. 1. Single-shot LIB spectra corresponding to (a) $2TiO_2$–SiO_2 support, (b) V_2O_5 and (c) 1:1 (w/w) V_2O_5–TiO_2 mixture. The delay time was 300 ns. Acquisition time was of 1 μs. MCP gain: 700 V.

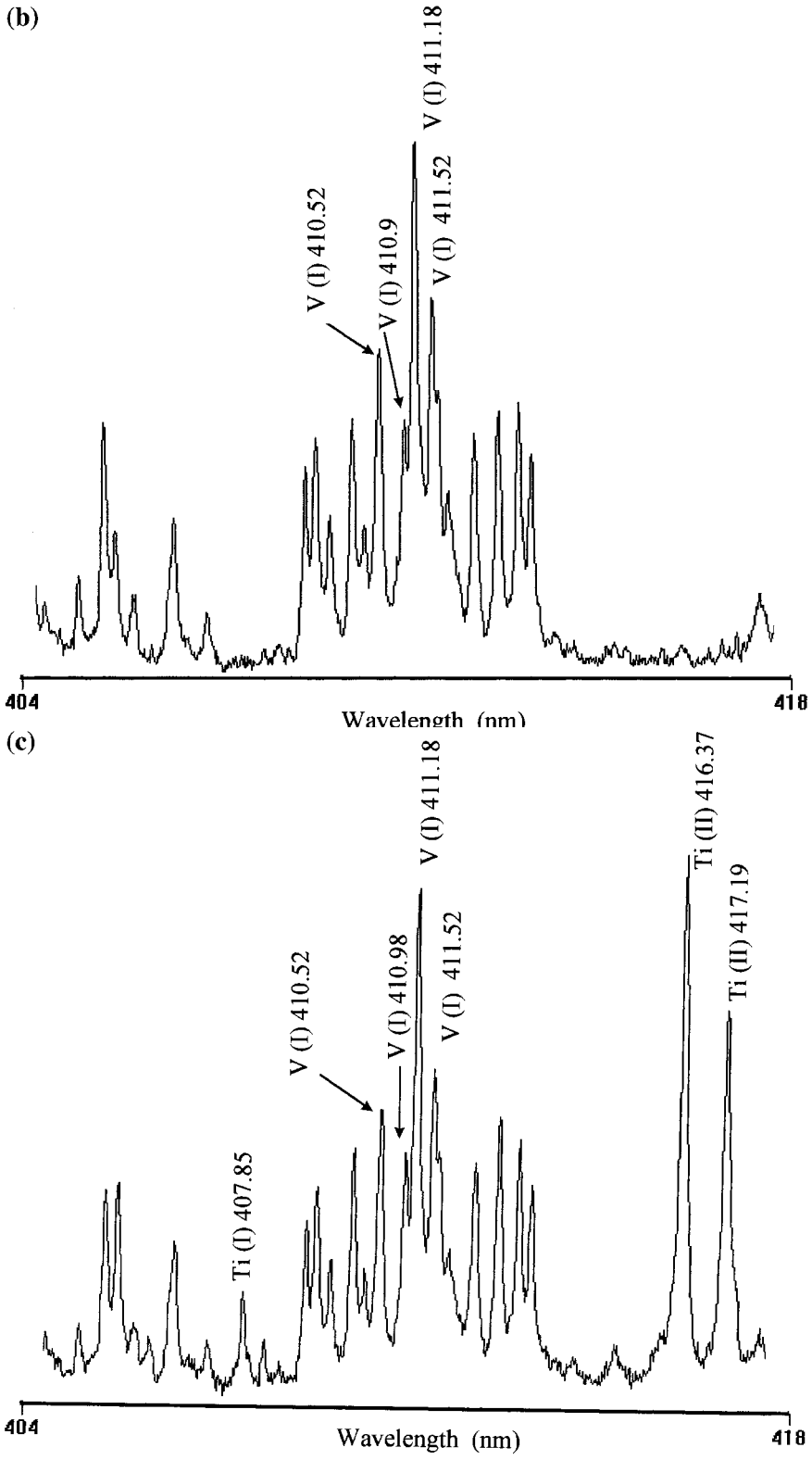

Fig. 1. (*Continued*)

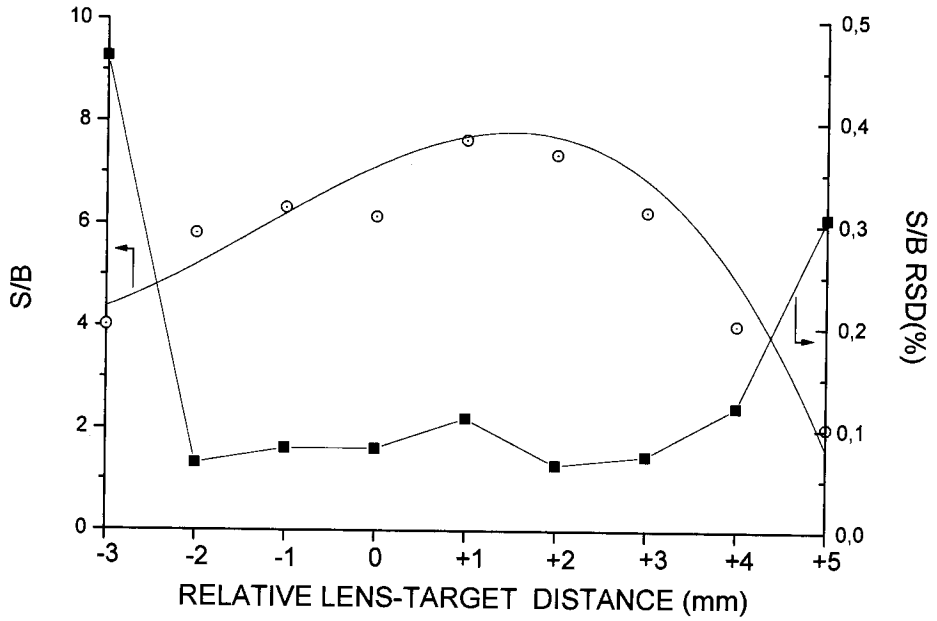

Fig. 2. Signal-to-background ratio and its RSD (%) vs relative focusing lens-target distance. The V(I) line at 411.18 nm was used for the measurements and the results were obtained using the pellet 10000V–$2TiO_2$–SiO_2 support. Other conditions as in Fig. 1.

ent focusing distances are shown in Fig. 3. Micrographs A and B were taken respectively at the focal point and at a relative lens-target distance of + 2 mm, respectively. Two cumulative laser shots were used. Micrographs confirm that the '0' position presents the smallest irradiated surface. However, the efficiency in ablating the sample, and consequently the S/B, can be increased when the laser beam is focused above the focal point (+ 2 mm) because the laser energy is still enough to allow ablation and the beam has a larger area of contact with the target surface. When further defocused, the laser fluence becomes lower and it is less efficient in ablating the sample. Consequently, the optimum focal condition for both maximum ablation and higher signal-to-background ratio is at a focusing lens-target distance of + 2 mm.

The irradiated areas and the laser fluences for each focusing distance are summarized in Table 1. The ablated areas were calculated assuming an elliptical shape of the crater. As shown, a fluence of 2.6 J cm^{-2} with ablated area of 18.6×10^{-2} mm^2 were found for the optimum focusing conditions. It should be to noted that although the plasma is formed at atmospheric pressure and above the focal point, the laser fluence used is below the threshold fluence for breakdown of air, and hence no lines corresponding to its several components are observed.

3.3. Quantitative analysis

It is well known that at early times following plasma formation, the LIBS spectrum is dominated by an intense radiation continuum and ionic emissions. Emission lines are broadened by the Stark effect. Temporal resolution was found to improve both linearity and signal reproducibility of the catalyst analysis. In this case, to compensate for the decreased signal at delayed integration, ten laser shots were accumulated. The optimal delay was estimated to be 1.3 μs after the laser shot. The use of internal standardization was necessary to compensate for the pulse-to-pulse variability and to minimize matrix effects. At delayed integration, continuum emission was reduced, but the intensity of the lines of the internal standard were also affected. For instance, the ionic Ti (II) line intensity at 416.37 nm decreased

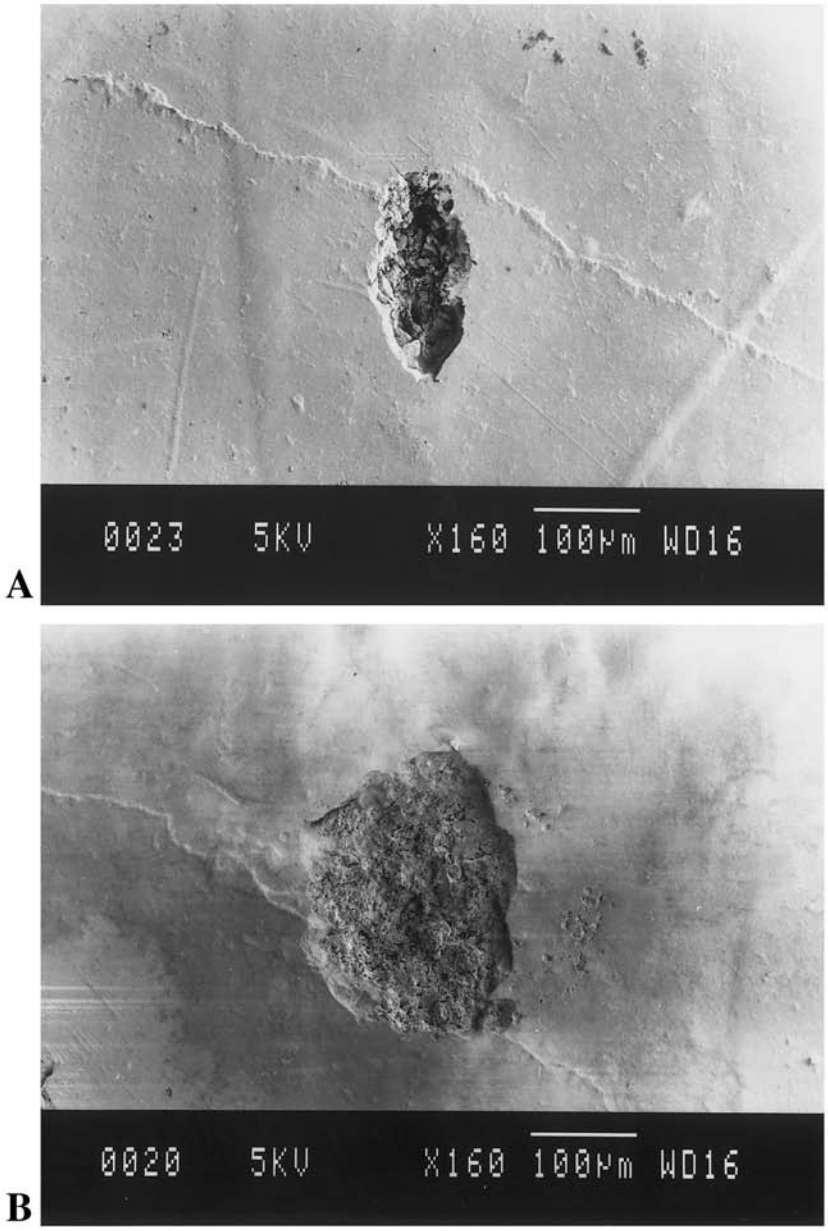

Fig. 3. Scanning electron micrographs of 10000V–$2TiO_2$–SiO_2 sample, showning the craters produced after two cummulative laser shots. (A) Sample placed at the focusing lens focal position. (B) Sample placed 2 mm below the focusing lens focal position.

significantly, while the intensity of the neutral Ti line at 407.85 nm increased. For this reason, the atomic emission line of Ti was then chosen for internal standardization. In addition, this line satisfies the regular requirements of an internal standard, i.e. proximity to the analyte line and freedom from interference with the neighbouring spectral lines.

Several lines of V were evaluated to construct the calibration graph. The V(I) line at 411.18 nm was finally selected as it provides the largest sensitivity with the smallest standard deviation, thus

Table 1
Irradiated areas and laser fluences at different focusing lens-to-sample distances

Focusing lens-target distance (mm)	Crater area (mm^2, $\times 10^{-2}$)	Fluence (J cm^{-2})
−3	42.1	1.0
−2	15.7	2.6
−1	6.5	6.2
0	5.0	8.0
+1	15.6	2.7
+2	18.6	2.6
+3	30.8	1.3

The sample was 10 000 μg g^{-1} V in a TiO_2–SiO_2 support.

leading to the best limit of detection. Fig. 4 shows the calibration graph for V in the $2TiO_2$–SiO_2 support. This figure presents the ratio between the net line intensities of vanadium and internal standard as a function of V concentration. The net peak signal was obtained by subtraction of the background signal. As shown in Fig. 4, the curve presents good linearity, with correlation coefficient $R^2 = 0.9966$. Deviation from linearity was found at concentrations above 1000 μg g^{-1}, probably due to self-absorption [31,32].

The detection limit (CL) was calculated from the formula:

$$C_L = 3s/S$$

where s is the standard deviation of the V to Ti signal ratio at low concentration and S represents the method sensitivity calculated from the slope of the linear section of the calibration curve. The LOD from the time-resolved calibration graph using the s value at 200 μg g^{-1} V was 38 μg g^{-1} V. This value is well below the V level expected in xV–$2TiO_2$–SiO_2 catalysts. The method precision was better than 6% RSD in the concentrate range 200–1000 μg g^{-1}.

To check for the accuracy of the proposed method, a recovery experiment was performed. The results are summarized in Table 2. As shown, recovery values are satisfactory, better than 90%

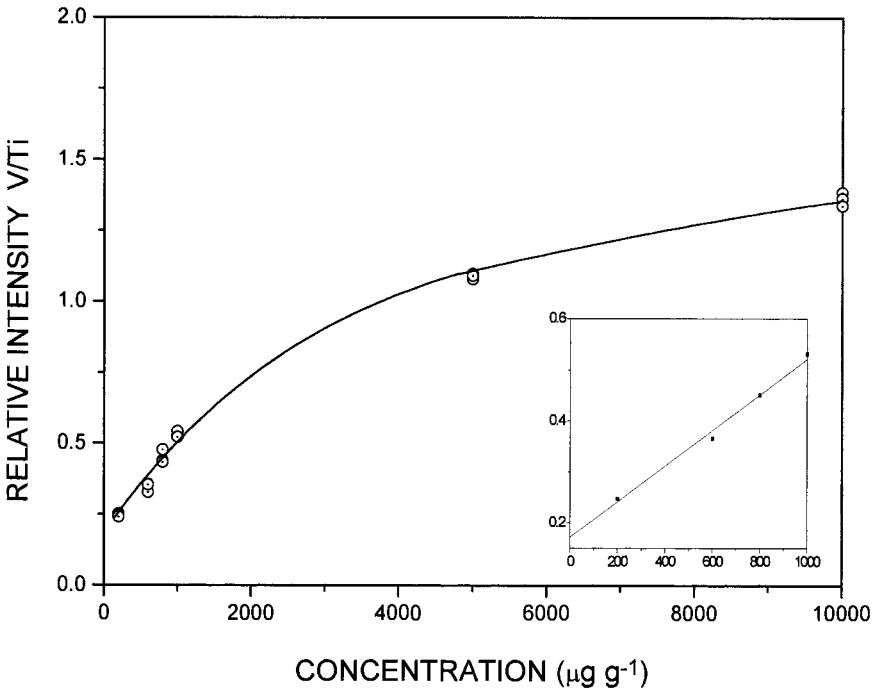

Fig. 4. Time-resolved calibration curve of V in a $2TiO_2$–SiO_2 support. The intensity of the 411.18 nm V(I) line was ratioed to that of the 407.85 nm Ti(I) line. For construction of the calibration curve, mean values were calculated from six repeated measurements, each measurement representing an average of ten shots, from different target locations. The Inset shows the linear portion of calibration curve where each point represents the mean value.

Table 2
Recovery of V in $2TiO_2$–SiO_2 catalysts using laser-induced breakdown spectrometry

Sample	Added V concentration (μg g^{-1})	Found V concentration (μg g^{-1})	Recovery (%)
1	200	215.1	107.5
2	600	554.0	92.3
3	800	798.0	99.75
4	1000	1030.3	103.3

Acknowledgements

Research supported by Projects # PB94-1477 and PB93-1009 of the Dirección General de Investigación Científica y Técnica (Ministry of Education and Science, Madrid).

References

[1] M.A. Bañares, L.J. Alemany, M.C. Jiménez, M.A. Larrubia, F. Delgado, M. López Granados, A. Martínez Arias, J.M. Blasco, J.L.G. Fierro, J. Solid State Chem. 124 (1996) 69.
[2] G.C. Bond, S. Flamerz, Appl. Catal. 71 (1991) 1.
[3] S. Jansen, Y. Tu, M.J. Palmieri, M. Sanati, A. Andersson, J. Catal. 138 (1992) 79.
[4] H. Knözinger, E. Taglauer, Catalysis 10 (1993) 1.
[5] J. Haber, T. Machej, E.M. Serwicka, I. E Wachs, Catal. Lett. 32 (1995) 101.
[6] J.M. Gallardo Amores, V. Sánchez Escribano, G. Busca, V. Lorentzelli, J. Mater. Chem. 4 (1994) 965.
[7] J. M Jehng, I.E. Wachs, Catal. Lett. 13 (1992) 9.
[8] Y. Cai, J. Ozkan, Appl. Catal. 78 (1991) 241.
[9] L.J. Alemany, R. Mariscal, M. Galan-Fereres, M.A. Bañares, J.A. Anderson, J.L.G. Fierro, Chem. Matet. 7 (1995) 1432.
[10] L.J Radziemski, D.A. Cremers, in: L.J. Radziemski, D.A. Cremers (Eds.), Laser-induced Plasmas and Applications, chapter 7, Dekker, New York, 1989.
[11] L. Moenke-Blankenburg, Laser Microanalysis, chapter 5, Wiley, New York, 1989.
[12] L.J. Radziemski, D.A. Cremers, in: L.J. Radziemski, R.W. Solarz, J.A. Paisner (Eds.), Laser Spectroscopy and its Applications, chapter 5, Marcel Dekker, New York, 1987.
[13] E.H. Piepmeier, Analytical Applications of Lasers, chapter 19, Wiley, New York, 1986.
[14] S.A. Darke, J.F. Tyson, J. Anal. At. Spectrom. 8 (1993) 145.
[15] D.E. Kim, K.J. Yoo, H.K. Park, D.W. Kim, Appl. Spectrosc. 51 (1997) 22.
[16] T.L. Thiem, R.H. Salter, J.A. Gardner, Y.I. Lee, J. Sneddon, Appl. Spectrosc. 48 (1994) 58.
[17] W.E. Ernst, D.F. Farson, D.J. Sames, Appl. Spectrosc. 50 (1996) 306.
[18] A.V. Pakhomov, W. Nichols, J. Borysow, Appl. Spectrosc. 50 (1996) 880.
[19] M. Hidalgo, F. Martín, J.J. Laserna, Anal. Chem. 68 (1996) 1095.
[20] J.M. Vadillo, S. Palanco, M.D. Romero, J.J. Laserna, Fresenius J. Anal. Chem. 355 (1996) 909.
[21] G.C. Bond, S.F. Tahir, Appl. Catal. 71 (1991) 1–31.
[22] M. Milán, J.M. Vadillo, J.J. Laserna, J. Anal. At. Spectrom. 12 (1997) 441.
[23] J.M. Vadillo, M. Milán, J.J. Laserna, Fresenius J. Anal. Chem. 355 (1996) 10.
[24] J.W. Geuss, in: G. Poncelet, P. Grange, P.A. Jacobs (Eds.), Preparation of Catalysts III, Elsevier, Amsterdam, 1983, p. 1.
[25] N.E. Quaranta, V. Cortes Corberán, J.L.G. Fierro, Stud. Surface Sci. Catal. 72 (1992) 147.
[26] M. Galán-Fereres, R. Mariscal, J.A. Anderson, L.J. Alemany, J.L.G. Fierro, J. Chem. Soc. Faraday Trans. 90 (1994) 3711.
[27] M. Galan-Fereres, L.J. Alemany, R. Mariscal, M.A. Bañares, J.A. Anderson, J.L.G. Fierro, Chem. Mater. 7 (1995) 1342.
[28] L.J. Alemany, M.A. Bañares, E. Pardo, F. Martín, M. Galán-Fereres, J.M. Blasco, Appl. Catal. 13 (1997) 289.
[29] J. Reader, C.H. Corliss, W.L. Wiese, G.A. Martin, Wavelengths and Transition Probabilities for Atoms and Atomic Ions. NRDS-NBS 68, US Government Printing Office, Washington, DC, 1980.
[30] T.R. Harville, R.K. Marcus, Anal. Chem. 65 (1993) 3636.
[31] F. Leis, W. Sdorra, J.B. Ko, K. Niemax, Mikrochim. Acta 2 (1989) 185.
[32] K.J. Grant, G.L. Paul, J. O'Neill, Appl. Spectrosc. 45 (1991) 701.

ELSEVIER

Talanta 47 (1998) 153–160

Talanta

Kinetic determination of atrazine in foods based on stopped-flow fluorescence polarization immunoassay

B. Sendra [a], S. Panadero [a], S. Eremin [b], A. Gómez-Hens [a,*]

[a] *Department of Analytical Chemistry, Faculty of Sciences, University of Córdoba, Avenida San Alberto Magno s/n, Córdoba, E-14004, Spain*

[b] *Department of Chemistry, Division of Chemical Enzymology, M.V. Lomonosov Moscow State University, Moscow 119899, Russia*

Received 15 October 1997; received in revised form 29 December 1997; accepted 10 February 1998

Abstract

A very simple and fast method for the direct determination of atrazine in food samples based on the use of stopped-flow fluorescence polarization immunoassay is described. Unlike other immunoassay methods where the analytical signal is obtained when the immunochemical reaction has reached or is close to the equilibrium, this method uses the initial rate of this reaction as the analytical parameter, which is measured in only 4–5 s. This approach minimizes the static signal from the sample matrix, allows the direct analysis of the samples and can be easily adapted to the routine automatic determination of atrazine. The dynamic range of the calibration graph was 0.7–100 ng ml^{-1} and the detection limit was 0.2 ng ml^{-1}. The precision and selectivity of the method were also studied. The analytical recoveries obtained by applying the method to white and red wine, orange juice and tea samples ranged from 80 to 104%. © 1998 Elsevier Science B.V. All rights reserved.

Keywords: Fluoroimmunoassay; Kinetic method; Atrazine; Foods; Stopped-flow mixing technique

1. Introduction

Immunoassay techniques continue gaining popularity in environmental and food analysis, as shown by the numerous methods reported in recent years, the determination of pesticides being one of the areas which is receiving a great deal of attention. This is justified by the widespread use of these compounds in agriculture, and the persistence of many of them in the environment, so that they could be easily present in foods, and the fact that the chromatographic methods usually used for this purpose, although well established, are also time-consuming and expensive.

Among pesticides, 1,3,5-triazine compounds are a widely used herbicide group of which atrazine is a representative component. Although the application of this compound has been banned or restricted in some countries [1–3], it is still one of the most extensively used pesticides worldwide. Immunoassay methodology, and particularly heterogeneous enzyme immunoassay, has been specially applied to the determination of atrazine as a

* Corresponding author. Tel.: +34 57 218614; fax: +34 57 218606.

0039-9140/98/$19.00 © 1998 Elsevier Science B.V. All rights reserved.
PII S0039-9140(98)00064-2

response to the growing need to monitor the potential contamination caused by this compound, which can produce adverse effects on the immune system [4]. Numerous methods [5–15], which feature very low detection limits (0.001–0.3 ng ml^{-1}) have been developed for this purpose. However, one of the main limitations of these heterogeneous methods is that they have too many incubation, separation and wash steps, so that automation for continuous determinations is not easily achieved. The use of flow injection immunoassay [14,15] allows the assay time to be reduced, but each measurement requires about 20 min. On the other hand, although a homogeneous immunoassay such as fluorescence polarization immunoassay (FPIA), which has shown its usefulness in clinical analysis [16], can overcome the numerous steps involved in the heterogeneous methods, a disadvantage of this alternative is that the detection limits obtained are relatively high. Thus, the detection limit reported by applying FPIA to the determination of atrazine was 10 ng ml^{-1} [17].

As is known, one of the factors that mainly contributes to the relatively high detection limits obtained in FPIA is the background signal from the sample matrix so that, at low analyte concentrations, its discrimination from the analytical signal obtained when the competitive immunochemical reaction of the analyte and the tracer with the antibody have approached equilibrium is difficult. However, if this background signal does not change with time, its negative effect on the analytical signal can be minimized by measuring the initial rate of the reaction between the tracer and the antibody, instead of the fluorescence polarization signal obtained near equilibrium. Although this initial rate is generally very high, it can be easily measured by using stopped-flow mixing technique (SF), which also allows the automation of the measurement step of the analytical process. The usefulness of kinetic methodology in clinical analysis by using FPIA has been shown for the determination of therapeutic and abuse drugs in serum and urine [18,19], where the detection limits were notably better than those reported by conventional FPIA. SF-fluoroimmunoassay has been recently applied to the determination of the pesticide 2,4-dichlorophenoxyacetic acid (2,4-D) in fruit juice samples [20]. In this instance, the method was based on the measurement of the initial rate of the reaction between the tracer (fluorescein-labelled 2,4-D) and the antibody, which was directly monitored by the fluorescence quenching of the fluorescein.

With the aim of extending the application field of kinetic homogeneous immunoassay in pesticide determination, this paper shows the results obtained by applying SF-FPIA to the direct determination of atrazine in white and red wine, orange juice and tea samples. Although the polyclonal antibodies used here showed a relatively high affinity for other triazine derivatives, the main purpose of this study was to show that the negative effect of the sample matrix can be minimized by measuring the initial rate of the immunochemical reaction, thus allowing the direct analysis of the samples.

2. Experimental

2.1. Instrumentation

An SLM-Aminco (Urbana, IL) Model 8100 photon-counting spectrofluorimeter, equipped with a 450-W xenon arc source, three polarizers (Gran-Thompson calcite prism-type) and two R928 photomultiplier tubes was used. Polarization data were obtained by placing one of the polarizers in the excitation lightpath and the other two in the emission channels of the T-format configuration of the instrument. The excitation wavelength was set at 490 nm by means of the excitation monochromator. The emission wavelength was selected by placing a Schott OG-550 filter on each of the two emission channels. The instrument was fitted with an SLM-Aminco Milliflow stopped-flow reactor which was furnished with an observation cell of 0.2-cm path length. This module was controlled by the associated electronics, the computer and a pneumatic syringe drive system. The solutions in the stopped-flow module were kept at a constant temperature of 25°C by circulating water from a thermostated tank.

2.2. Reagents

A stock solution (100 μg ml^{-1}) of atrazine (Dr Ehrenstorfer, Augsburg, Germany) was prepared in methanol and stored at 4°C. More diluted solutions of this pesticide were prepared daily by dilution with Tris [tris(hydroxymethyl)aminomethane] buffer solution (0.01 M, pH = 8). Polyclonal anti-atrazine antibodies were obtained as described elsewhere [17,21]. The concentration of IgG was calculated by UV measurements based on the absorbence value obtained for 1 mg ml^{-1}, which is 1.3. All other chemicals were of analytical-reagent grade.

2.3. Synthesis of tracers

Five tracers were synthesized (Table 1). Tracers I and II were obtained by reaction of fluoresceinthiocarbamyl ethylenediamine (EDF), which was synthesized as described previously [22], with the corresponding carboxylic acid derivative of the atrazine [17]. Tracers III–V were obtained by dissolving 5 mg of 5-[(4.6-dichlorotriazin-2-yl)-amino]-fluorescein (DTAF) in a mixture of 1 ml of methanol and 50 μl of triethylamine and, then, 10 mg of $RNH_2 \cdot HCl$ (R = methyl, ethyl, i-propyl) was added. After overnight reaction at room temperature, the solvent was evaporated. The product was dissolved in a small volume of methanol and purified by TLC, using $CHCl_3$/methanol (4:1). The concentration of each tracer was determined by using $\varepsilon_{492} = 8.78 \times 10^4$ M^{-1} cm^{-1} for fluorescein. Tracer solutions were prepared in Tris buffer.

2.4. Procedure

Two solutions were prepared to fill the two 2-ml drive syringes of the stopped-flow module. One of them contained the tracer (8×10^{-9} M) and atrazine standard or sample at a final concentration between 0.7 and 100 ng ml^{-1}. The other solution contained the antibody (100 μg ml^{-1}). These solutions were prepared in Tris buffer solution. In each run, 40 μl of each solution was mixed in the mixing chamber at a flow rate of 20 ml s^{-1}. The variation of the fluorescence intensity with time in each emission arm of the T-format configuration of the instrument was monitored by placing the two polarizers perpendicular to each other. The kinetic curves thus obtained were processed by the microcomputer to record the variation of the degree of polarization (P) with time. The initial rate ($V_P = dP/dt$) of the reaction between the tracer and the antibody, which depends on the atrazine concentration, was determined in about 4–5 s by running a program for application of the reaction-rate method. Each sample was assayed in triplicate. All measurements were carried out at 25°C.

Table 1
Chemical structures of the immunogen, atrazine tracers and triazines

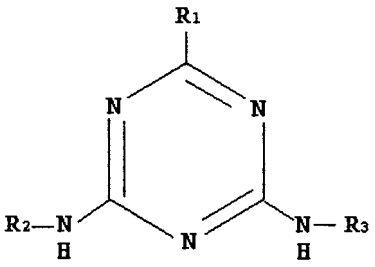

Compounds	Substituents		
	R_1	R_2	R_3
Immunogen	–S–$(CH_2)_2$– –CO–NH–P–	Et	i-Pr
Tracer I	Cl	–$(CH_2)_5$– –CO–EDF	i-Pr
Tracer II	Cl	–$(CH_2)_5$– –CO–EDF	Et
Tracer III	Cl	Fl	Me
Tracer IV	Cl	Fl	Et
Tracer V	Cl	Fl	i-Pr
Atrazine	Cl	Et	i-Pr
Simazine	Cl	Et	Et
Terbutylazine	Cl	Et	t-Bu
Terbutryn	S-Me	Et	t-Bu
Prometryn	S-Me	i-Pr	i-Pr
Atraton	O-Me	Et	i-Pr

EDF, fluoresceinthiocarbamyl ethylenediamide; Et, ethyl; Fl, fluorescein; i-Pr, iso-propyl; Me, methyl; P, carrier protein; t-Bu, tert-butyl.

2.5. Determination of atrazine in food samples

Several samples (white and red wine, orange juice and tea) were spiked with appropriate amounts of atrazine. No sample pretreatment was required for these analyses other than an adequate dilution. All samples were diluted 30 times, except the red wine, which required a 50 times dilution. After dilution, each sample was treated as described above.

3. Results and discussion

3.1. Study of the kinetic behaviour of the atrazine immunochemical reaction

The numerous enzyme immunoassay methods described for atrazine determination above cited are based on the measurement of the analytical signal when the immunochemical reaction has reached or is close to the equilibrium, unlike SF-immunoassay where the analytical signal is obtained at the beginning of the immunochemical reaction. By using a competitive immunoassay, such as FPIA, the initial rate (V_P) of the tracer-antibody reaction, which is obtained by measuring the variation of the degree of polarization $\{P = [(A/B) - 1]/[(A/B) + 1]\}$ with time, decreases when increasing the analyte concentration and is therefore a function of the analyte concentration. As A and B are the fluorescence intensities measured with the emission polarizer parallel and perpendicular, respectively, to the excitation polarizer, the variation of A and B with time is simultaneously measured with a spectrofluorimeter in a T-format configuration with the emission polarizers placed perpendicular to each other and the value of V_P is obtained by processing both kinetic curves by the microcomputer. Although this initial rate is very fast, it is easily measured by using SF, so that the analyte and the tracer are placed in one syringe of the module and the antibody in the other.

In addition to the role played by the immunoassay format used, the features of a competitive immunochemical method for the determination of a hapten such as atrazine depend on the hapten derivatives used as the immunogen and the tracer. The immunogen must imitate as far as possible the analyte in order to obtain the desirable degree of selectivity. The tracer has to be also recognized by the antibody but it may have lower affinity to the antibody than the analyte to tolerate lower analyte concentration and obtain an adequate detection limit. The lack of suitable reaction groups in the atrazine molecule requires its previous modification, which usually involves the introduction of a carboxy-group in the molecule [21]. Thus, the polyclonal antibodies used here were obtained through the immunogen showed in Table 1 where the chlorine atom of atrazine was substituted by thiopropionic acid. The carboxylic acid hapten was treated with *N*-hydroxysuccinimide and dicyclohexylcarbodiimide and, finally, bound to the carrier protein. Five tracers (Table 1) were prepared in order to check their kinetic behaviour with these antibodies. By using SF-FPIA, the measurement of the variation of the degree of fluorescence polarization with time showed that tracer I gave the highest initial rate (100%), followed by tracers V (75%) and IV (30%), while no reaction was observed with tracers II and III. These results show that the isopropyl group in atrazine was preferably recognised by these antibodies, so that tracer I was chosen to develop the kinetic immunoassay method.

Before checking the effect of other variables in the immunochemical system and taking into account that the main purpose of this study was to show the utility of kinetic methodology, in order to obtain fast analytical data avoiding the effect of the sample matrix, the kinetic curves of solutions containing different atrazine concentrations were obtained in the absence or presence of a white wine sample. Fig. 1 shows the results obtained where it can be seen that the initial rate can be measured in only 4–5 s and is not affected by the presence of the sample, while the fluorescence polarization obtained close to the equilibrium decreases by about 10%.

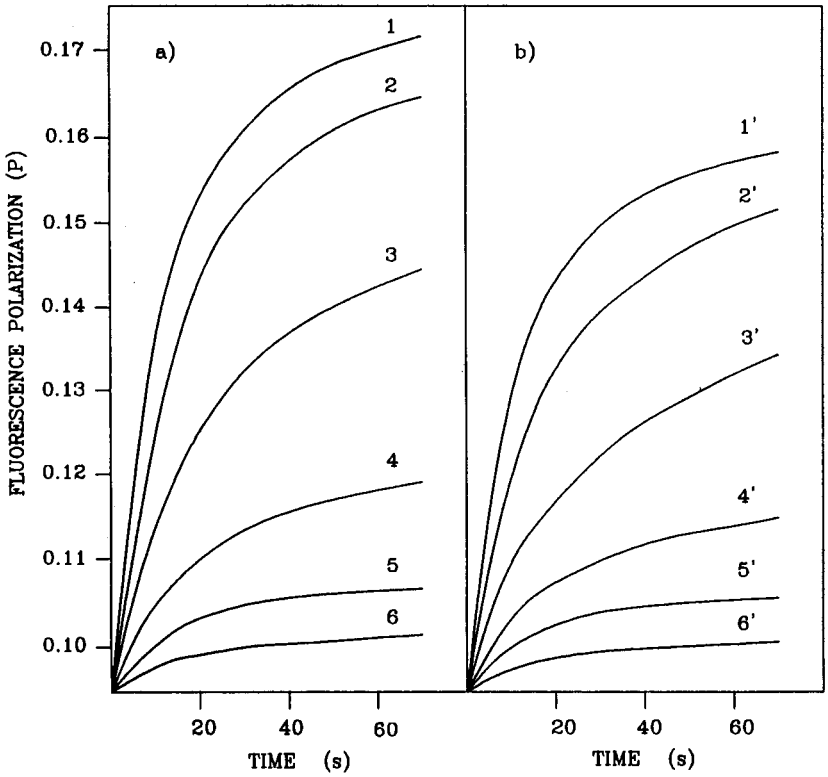

Fig. 1. Kinetic curves obtained for different atrazine concentrations in the absence (a) and presence of white wine (3.3%) (b). [atrazine] (ng ml^{-1}): 0 (1,1′), 1 (2,2′), 3 (3,3′), 10 (4,4′), 100 (5,5′) and 1000 (6,6′). [tracer I] = 8×10^{-9} M, antibody = 100 μg ml^{-1}.

3.2. Optimization of variables

The immunochemical system was optimized by applying the univariate method to initial rate measurements. All concentrations given here are initial concentrations in the syringes (twice the actual concentrations in the reaction mixture at time zero after mixing). Each kinetic result was the average of three measurements.

The appropriate performance of a competitive immunoassay depends on the tracer and antibody concentrations selected. The tracer concentration must be as low as possible, in order to obtain a low detection limit but, also, must give an adequate initial rate with a low noise in the absence of the analyte. A 8×10^{-9} M concentration was chosen, which gave a fluorescence intensity three times higher than the blank in the absence of tracer. By using this tracer concentration, the antibody concentration was selected by measuring the initial rate of solutions containing decreasing amounts of antibody, in order to obtain the dilution curve (Fig. 2). A 20-fold dilution of the antibody, equivalent to 100 μg ml^{-1}, was chosen. Although this concentration is relatively high, only 0.04 ml of the antibody solution is required in each determination. The effect of the temperature in the system was studied in the range 20–40°C. The initial rate was independent of this variable between 20 and 30°C, but decreased by about 20% at 40°C. Thus, a temperature of 25°C was chosen.

3.3. Features of the proposed method

The calibration graph (Fig. 3) was obtained by using the initial rate method. In order to study the effect of the sample matrix, atrazine solutions were prepared in the absence or presence (3.3%) of white wine, obtaining the same initial rate

values in both instances. The dynamic range of the calibration graph was 0.7–100 ng ml^{-1}, equivalent to 0.02–3.0 μg ml^{-1} in the white wine sample. The detection limit was calculated according to IUPAC recommendations [23] and in the presence of the same white wine sample. The value obtained was 0.2 ng ml^{-1}, equivalent to 6 ng ml^{-1} in the sample. The precision of the method was studied by assaying replicates of the white wine sample, which were spiked with two different concentrations of atrazine, namely 30 and 300 ng ml^{-1}. The relative standard deviations obtained ($n = 11$) were 8 and 6%, respectively.

The slight differences between the structure of atrazine and those of other related 1,3,5-triazines, give rise to the fact that the immunoassay methods for atrazine generally show a relatively high cross-reactivity (CR) for other triazines, which also depends on the atrazine derivative used to prepare the immunogen. By using the formula %CR = ([F]/[A]) × 100, where [F] is the apparent atrazine concentration found in the calibration graph from the initial rate of the reaction between the interferent and the antibody and [A] is the interferent concentration added, the effect on the immunochemical system of five triazines containing different substituents (Table 1) was studied at a concentration of 10 ng ml^{-1}. The %CR was relatively low for simazine (30%) and terbutylazine (20%), but very high for terbutryn (100%), prometryn (120%) and atraton (100%). These results are logical taking into account the immunogen used to obtain the antibodies, which contained the isopropyl and thio substituents. Thus, the antibodies do not distinguish between atrazine, terbutryn and atraton, and show a higher response for prometryn, which contains two isopropyl substituents. The selectivity of the method was also studied by assaying other pesti-

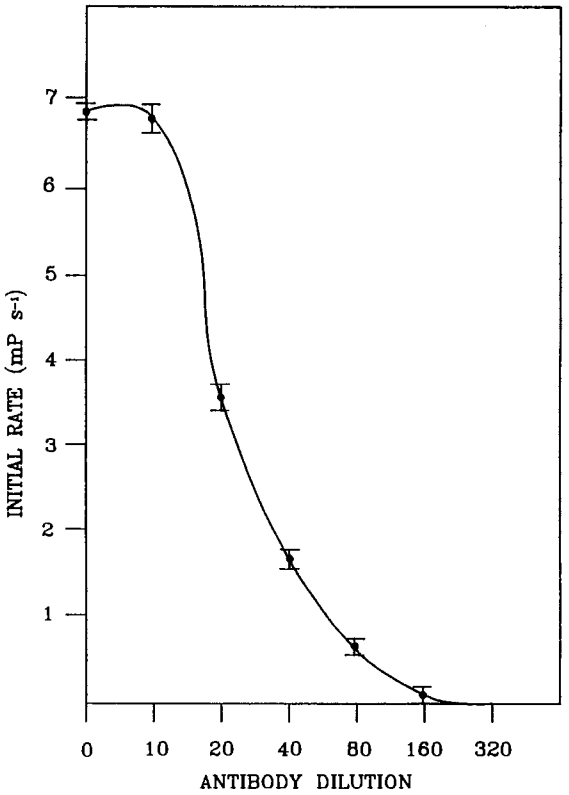

Fig. 2. Antibody dilution curve obtained with 8×10^{-9} M tracer I.

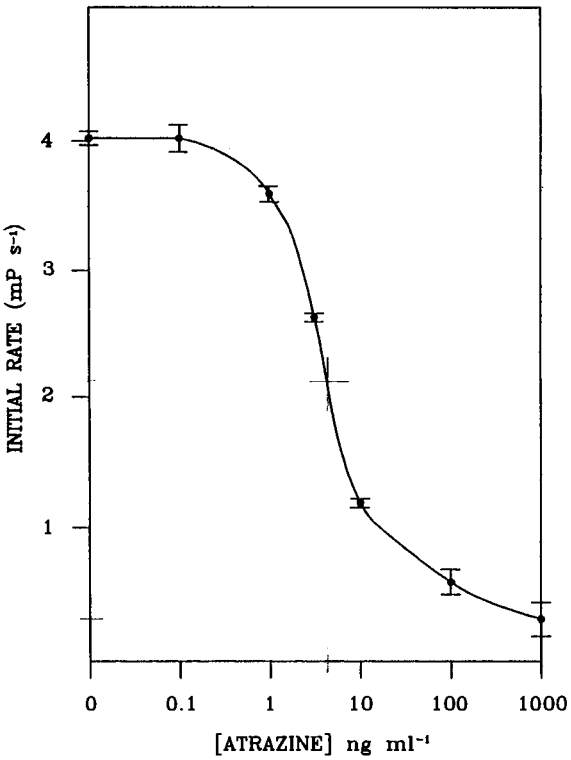

Fig. 3. Calibration graph obtained for atrazine in the absence and presence or white wine (3.3%). [tracer I] = 8×10^{-9} M, [antibody] = 100 μg ml^{-1}.

cides such as carbaryl (1-naphthyl *N*-methylcarbamate), ziram (zinc dimethyldithiocarbamate), bromadiolone {3-[3-(4-bromodiphenyl-4-yl)-3-hydroxy-1-phenylpropyl]-4-hydroxycoumarin} and dimethoate [*o*,*o*-dimethyl-*S*-(*N*-methylcarbamoylmethyl)phosphorodithioate], but none of them interfered with the atrazine system.

The use of the initial rate of the immunochemical reaction as analytical parameter in SF-FPIA allows a high throughput to be obtained. The time required to carry out each measurement is only 4–5 s, so that numerous samples could be analyzed during 1 h. Taking into account the time needed to perform three replicate analyses and changeover on the system, the practical throughput is about 60 samples h^{-1}.

3.4. Analysis of food samples

In order to evaluate the method in relation to the matrix where the atrazine residues should be determined, various amounts of this analyte were added to samples of white and red wine, orange juice and tea. The only treatment required was a 30-times dilution of each sample, except the red wine sample, which required a 50-times dilution. Table 2 lists the analytical recoveries obtained by adding three different amounts of atrazine to each sample. The recoveries ranged from 80 to 104%, with a mean of 91%.

Table 2
Determination of atrazine added to food samples

Sample	Atrazine ($\mu g\ ml^{-1}$)		
	Added	Found[a]	Recovery (%)
White wine	0.2	0.16 ± 0.01	80
	0.5	0.40 ± 0.05	80
	1	1.0 ± 0.2	100
Red wine	0.2	0.17 ± 0.03	85
	0.5	0.40 ± 0.06	80
	1	0.99 ± 0.08	99
Orange juice	0.2	0.16 ± 0.02	80
	0.5	0.49 ± 0.08	98
	1	1.0 ± 0.2	100
Tea	0.2	0.18 ± 0.03	90
	0.5	0.52 ± 0.04	104
	1	1.0 ± 0.2	100

[a] Average of three determinations.

4. Conclusions

The proposed SF-FPIA method shows the utility of kinetic methodology in order to improve some of the features of other immunoassay methods described for atrazine determination. Thus, the dynamic measurements minimize the static signal from the sample matrix, which is one of the main causes of the relatively high detection limit obtained by conventional FPIA. While the detection limit of this method is 10 ng ml^{-1} [17], the value afforded by the kinetic method is 0.2 ng ml^{-1}, which is comparable to those obtained in some of the enzyme immunoassay methods described for atrazine determination. Another outstanding feature of this method is its rapidity: while heterogeneous immunoassays require a delay for the development of the immunochemical reaction, which takes at least 10–30 min [5–15], the measurement step in the kinetic method takes only 4–5 s as it is carried out at the beginning of the reaction. The SF-FPIA reduces reactant manipulations and offers a high sample throughput, so that it is a useful approach to the automatic routine determination of atrazine.

The main aim of this study was to show the advantages of SF-FPIA in comparison with the conventional FPIA and the enzyme immunoassay methods described for atrazine determination. However, in addition to the type of immunoassay chosen, the selectivity afforded in an immunoassay depends on the hapten derivative used to obtain the immunogen, which must imitate the target molecule. A general limitation of the immunoassay methods reported for atrazine is the high CR of other 1,3,5-triazine derivatives [15] and, although monoclonal antibodies allow the selectivity to be improved, attaining specificity is difficult as they also exhibit an appreciable cross-reaction with other triazines [11]. For this reason, a general trend in the determination of triazine residues by immunoassay [24] is to obtain antibodies with high levels of CR so that broad screening can be performed.

Acknowledgements

The authors are grateful to the CICyT (Comision Interministerial de Ciencia y Tecnología) for financing this research in the framework of Project PB96-0984.

References

[1] S.R. Müller, M. Berg, M.M. Ulrich, R.P. Schwarzenbach, Environ. Sci. Technol. 31 (1997) 2104.
[2] M. Wortberg, M.H. Goodrow, S.J. Gee, B.D. Hammock, J. Agric. Food Chem. 44 (1996) 2210.
[3] H. Färber, K. Nick, H.F. Schöler, Fresenius' J. Anal. Chem. 350 (1994) 145.
[4] B. Hileman, Chem. Eng. News 18 (1996) 23.
[5] R.J. Bushway, B. Perkins, S.A. Savage, S.L. Lekousi, B.S. Ferguson, Bull. Environ. Contam. Toxicol. 42 (1989) 899.
[6] B.M. Kaufman, M. Clower Jr., J. Assoc. Off. Anal. Chem. 74 (1991) 239.
[7] R.J. Bushway, L.B. Perkins, H.L. Hurst, B.S. Ferguson, Food Chem. 41 (1992) 283–284.
[8] Y.Y. Wigfield, R. Grant, Bull. Environ. Contam. Toxicol. 51 (1993) 171.
[9] C. Wittmann, B. Hock, J. Agric. Food Chem. 41 (1993) 1421.
[10] K.S. Nam, J.W. King, J. Agric. Food Chem. 42 (1994) 1469.
[11] M. Fránek, V. Kolár, S.A. Eremin, Anal. Chim. Acta 311 (1995) 349.
[12] J. Gascón, E. Martínez, D. Barceló, Anal. Chim. Acta 311 (1995) 357.
[13] C. Wittmann, U. Bilitewski, T. Giersch, U. Kettling, R.D. Schmid, Analyst 121 (1996) 863.
[14] B. Bjarnason, N. Bousios, S. Eremin, G. Johansson, Anal. Chim. Acta 347 (1997) 111.
[15] J. Gascón, A. Oubiña, B. Ballesteros, D. Barceló, F. Camps, M.P. Marco, M.A. González-Martínez, S. Morais, R. Puchades, A. Maquieira, Anal. Chim. Acta 347 (1997) 149.
[16] M.C. Gutiérrez, A. Gómez-Hens, D. Pérez-Bendito, Talanta 36 (1989) 1201.
[17] S.A. Eremin, in: J.O. Nelson, A.E. Karu, R.B Wong (Eds.), Immunoanalysis of Agrochemicals, ACS Symposium Series 586, American Chemical Society, Washington DC, 1995, p. 223.
[18] A. Gaikwad, A. Gómez-Hens, D. Pérez-Bendito, Anal. Chim. Acta 280 (1993) 129.
[19] D. Pérez-Bendito, A. Gómez-Hens, A. Gaikwad, Clin. Chem. 40 (1994) 1489.
[20] E.G. Matveeva, M.P. Aguilar-Caballos, S.A. Eremin, A. Gómez-Hens, D. Pérez-Bendito, Analyst 122 (1997) 863.
[21] M.H. Goodrow, R.O. Harrison, B.D. Hammock, J. Agric. Food Chem. 38 (1990) 990.
[22] M. Pourfarzaneh, G.W. White, J. Landon, D.S. Smith, Clin. Chem. 26 (1980) 730.
[23] G.L. Long, J.D. Winefordner, Anal. Chem. 30 (1984) 751.
[24] M. Winklmair, M.G. Weller, J. Mangler, B. Schlosshauer, R. Niessner, Fresenius' J. Anal. Chem. 358 (1997) 614.

ELSEVIER

Talanta 47 (1998) 161–167

Talanta

Flame AAS and UV-VIS determination of cobalt, nickel and palladium using the synergetic effect of 2-benzoylpyridine-2-pyridylhydrazone and thiocyanate ions

George A. Zachariadis, Demetrius G. Themelis, Despina J. Kosseoglou, John A. Stratis *

Department of Chemistry, Laboratory of Analytical Chemistry, Aristotle University, 54006, Thessaloniki, Greece

Received 21 November 1997; received in revised form 9 February 1998; accepted 10 February 1998

Abstract

A quantitative synergetic extraction procedure for cobalt, nickel and palladium from thiocyanate aqueous solutions into methyl isobutyl ketone (MIBK), containing 2-benzoylpyridine-2-pyridylhydrazone (BPPH), was studied by flame atomic absorption spectrometry (FAAS) and molecular absorption spectrometry (UV-VIS). Using FAAS, linear calibration graphs were obtained from 0.0–0.5 mg l^{-1} Co(II), 0.0–1.5 mg l^{-1} Ni(II) and 0.0–2.0 mg l^{-1} Pd(II). The reproducibilities were $s_{r,\,Co(II)} = 2.0\%$, $s_{r,\,Ni(II)} = 1.0\%$ and $s_{r,\,Pd(II)} = 1.3\%$ and the limits of detection were $c_{L,\,Co(II)} = 0.004$ mg l^{-1}, $c_{L,\,Ni(II)} = 0.009$ mg l^{-1} and $c_{L,\,Pd(II)} = 0.012$ mg l^{-1}. Using UV-VIS method the linear calibration graphs were 0.0–0.5 mg l^{-1} for Co(II), 0.0–1.0 mg l^{-1} for Ni(II) and 0.0–2.0 mg l^{-1} for Pd(II). The reproducibilities were $s_{r,\,Co(II)} = 1.3\%$, $s_{r,\,Ni(II)} = 1.7\%$ and $s_{r,\,Pd(II)} = 1.0\%$ and the limits of detection were $c_{L,\,Co(II)} = 0.001$ mg l^{-1}, $c_{L,\,Ni(II)} = 0.004$ mg l^{-1} and $c_{L,\,Pd(II)} = 0.002$ mg l^{-1}. The extraction method is almost free from interferences and has been successfully applied to the determination of cobalt, nickel and palladium in dental alloys. © 1998 Elsevier Science B.V. All rights reserved.

Keywords: Cobalt; Nickel; Palladium; Spectrometry

1. Introduction

A great number of nitrogen-containing heterocyclic hydrazone compounds have been synthesized and proposed as sensitive and selective analytical reagents for the spectophotometric determination of trace quantities of many transition elements, through their coloured or colourless complexes [1,2]. The complexes are usually stable and they have high molar absortivities. The majority of the chelate ligands used in extraction are weak acids which react in the form of their conjugate bases with metal ions, and give chelates, soluble to water and extractable to organic solvents [3].

2,2′-Dipyridyl-2-pyridylhydrazone (DPPH) was used for the FIA spectrophotometric determina-

* Corresponding author. Tel: + 30 31 997843; fax: + 30 31 997719; e-mail: zacharia@chem.auth.gr

0039-9140/98/$19.00 © 1998 Elsevier Science B.V. All rights reserved.
PII S0039-9140(98)00062-9

tion of Co(II) [4] and the spectrophotometric determination of Pd(II) [5]. Monohalogeno-benzoylhydrazones were also used for the atomic absorption spectrometric determination of Co(II) and Ni(II) [6].

2-Benzoylpyridine-2-pyridylhydrazone (BPPH) was proposed as analytical reagent for the direct spectrophotometric determination of Fe(II), Co(II), Ni(II), Cu(II) and Zn(II) in aqueous solutions [1]. The extraction of Cu(II)-BPPH complex into chloroform [7] and the extraction of the Cd(II)-BPPH complex using methyl isobutyl ketone (MIBK) were reported [8].

The synergetic effect of SCN^- ions on BPPH-Cd(II) for extraction of Cd from stong acidic aqueous solutions into MIBK and its FAAS determination was reported previously [8]. Similar synergetic effect of the same counter ion SCN^- with DPPH for the extraction of Cu(II), Ag(I) and Au(III) complexes of DPPH-M(II)-SCN type, from aqueous solutions into MIBK, and their subsequent FAAS determination, was also reported [9].

The aim of this work was to study the synergetic effect of BPPH and SCN^- ions on the extraction of Co(II), Ni(II) and Pd(II) into MIBK, and to apply this extraction system to the pre-concentration and subsequent determination of the mentioned analytes, using flame atomic absorption (FAAS) and ultaviolet visible spectrometry (UV-VIS). The studied complexes were stable ion-pair complexes of the type LMA [3,6], where L is the ligand (BPPH), M(II) is the metal ion (Co(II), Ni(II) or Pd(II)) and A is the counter ion (SCN^-). The effects of BPPH, SCN^- and H^+ ion concentrations on the percent extraction of the metal complexes were studied and the optimum extraction conditions were investigated.

2. Experimental

2.1. Instrumentation

A Perkin Elmer model 403 Atomic Absorption Spectrometer was used for atomic absorption measurements, equipped with the appropriate hollow cathode lamps. The analytical lines used for atomic absorption measurements were: 240.7 nm for cobalt, 232.0 nm for nickel and 247.6 nm for palladium. An oxidizing air-acetylene flame was used for atomization of the cations and the fuel was properly adjusted to maintain optimum atomization of the injected MIBK extracts. The flow rate of sample consumption was 4 l min^{-1} and a 10-cm slot burner head was used. For the spectrophotometric measurements, a Zeiss Model PMQ 3 spectrophotometer was used.

An Orion 701 A pH-meter was used for the pH measurements with absolute accuracy limits at the pH measurements being defined by NIST buffers.

2.2. Reagents

All reagents and solvents were of analytical reagent-grade and were provided either by Merck (Darmstadt, Germany) or BDH Chemicals (UK). MIBK was also analytical grade reagent and it was used without further purification, after being saturated by double de-ionized water. The double de-ionized water used in the extraction procedure was also saturated by MIBK.

BPPH was synthesized and purified following the procedure previously reported [1]. Stock solution of 0.015 mol l^{-1} BPPH were prepared by dissolving the required amount of BPPH in MIBK. These solutions were stable for several months, if they were stored in amber glass bottles and kept in the dark.

Solutions of HCl (6 mol l^{-1}), NaOH (1 mol l^{-1}) and NaH_2PO_4 (0.1 mol l^{-1}) were used for pH adjustment. The stock 1 mol l^{-1} Na_2SO_4 and NH_4SCN solutions were made up in de-ionized water. Concentrated HCl (12 mol l^{-1}) and HNO_3 (16 mol l^{-1}) solutions were used for dissolution of alloys.

Working solutions of Co(II), Ni(II) and Pd(II) in the range 0–2.0 mg l^{-1}, were prepared by dilution from their stock solutions (1000 mg l^{-1} each, Merck, Titrisol) immediately before use.

2.3. Procedure for extraction from aqueous solutions

Into 50 ml beakers, 10 ml of a solution containing between 0–2 mg l^{-1} Co(II), Ni(II) and Pd(II)

standard solutions were placed. Then, the appropriate amount of the NH_4SCN solution, (final concentration ranging between 0 and 7×10^{-2} mol l^{-1}, according to the experiment) was added and the solution was adjusted to the required pH value using HCl or NaOH together with the phosphate buffer solution. The ionic strength of the solutions was kept constant with the addition of Na_2SO_4 solution (final concentration 0.1 mol l^{-1}). The resulting solutions were transferred into a series of 50 ml calibrated flasks and diluted to the mark with doubly de-ionized water.

The extractions were done in 20-ml extraction funnels. Each aqueous solution ($V_{aq} = 10$ ml) was extracted with MIBK ($V_{org} = 5$ ml) containing the appropriate concentration of BPPH (final concentration ranging between 0 and 3.4×10^{-3} mol l^{-1}, according to the experiment). The two phases were shaken gently for 2 min and were left for 5 min before separation and measurement. All the extracts are stable at least for 72 h, especially if they are not left in contact with the aqueous solution. The development of all colours is almost immediate but in case of Ni(II) extraction some turbidity is expected and the measurements must be taken after complete disappearing of the emulsion.

The distribution ratios between aqueous and organic phases were calculated. The concentration of elements in both phases was measured by FAAS against matrix-matched calibration graphs (i.e. organic extracts were used for calibration when studying the organic phase, whereas aqueous solutions containing buffers and known analyte additions and saturated with the organic solvent were used for calibration when studying the aqueous phase). The calibration curve of each element was calculated both by FAAS and UV-VIS from the same matrix-matched calibration standards. For each method, the blank solutions contained all the appropriate reagents except the determined analyte.

2.4. Procedure for dissolution of dental alloys

An accurately weighed quantity of the alloy (0.1 g) is treated by 25 ml of concentrated HCl (for cobalt-chromium) or 25 ml of aqua regia (for nickel-chromium) or 10 ml concentrated HNO_3 followed by 25 ml concentrated HCl (for palladium-gold), and heated repeatedly until all the sample was completely dissolved. The resulting solution was diluted appropriately with doubly de-ionized water. The pH of the diluted solution was adjusted by the use of 0.1 mol l^{-1} phosphate buffer and 1 mol l^{-1} NaOH, at the optimum pH value for each determination. After that, the procedure was followed as described above under procedure for extraction from aqueous solutions.

3. Results and discussion

3.1. Spectral characteristics of the complexes

Thiocyanate aqueous solutions of Co(II), Ni(II) and Pd(II) ions, react with BPPH into MIBK forming the following coloured complexes: BPPH-Co(II)-SCN (rose-red, $\lambda_{max} = 510$ nm), BPPH-Ni(II)-SCN (orange–red, $\lambda_{max} = 495$ nm) and BPPH-Pd(II)-SCN (violet, $\lambda_{max} = 585$ nm), the maxima of which, in the visible region, are shown in Fig. 1. When the BPPH and SCN^- ions concentrations were fixed at $[BPPH] = 4 \times 10^{-3}$ mol l^{-1} and $[SCN^-] = 2.6 \times 10^{-2}$ mol l^{-1}, the spectra of the complexes were obtained using the following experimental variables: pH = 4.5 and [Co(II)] = 0.8 mg l^{-1} for BPPH-Co(II)-SCN; pH = 8.3 and [Ni(II)] = 2.0 mg l^{-1} for BPPH-Ni(II)-SCN; pH = 5.5 and [Pd(II)] = 5.0 mg l^{-1} for BPPH-Pd(II)-SCN.

The molar absorptivities of the above examined complexes in MIBK are very high ($\epsilon_{\text{BPPH-Co(II)-SCN, } (\lambda max = 510 \text{ nm})} = 14.95 \times 10^4$ l^{-1} mol^{-1} cm^{-1}, $\epsilon_{\text{BPPH-Ni(II)-SCN, } (\lambda max = 495 \text{ nm})} = 5.04 \times 10^4$ and $\epsilon_{\text{BPPH-Pd(II)-SCN, } (\lambda max = 585 \text{ nm})} = 3.50 \times 10^4$ l^{-1} mol^{-1} cm^{-1}) and these absorptivities are considerably higher than others reported for the determination of these elements by similar ligands [3,6].

3.2. Synergetic effect of SCN^- ions and BPPH on the extraction of metal ions

The values of distribution ratios $D_{C(\text{M(II)-BPPH})}$, $D_{C(\text{M(II)-SCN})}$ and $D_{C(\text{BPPH-M(II)-SCN})}$ for Co(II),

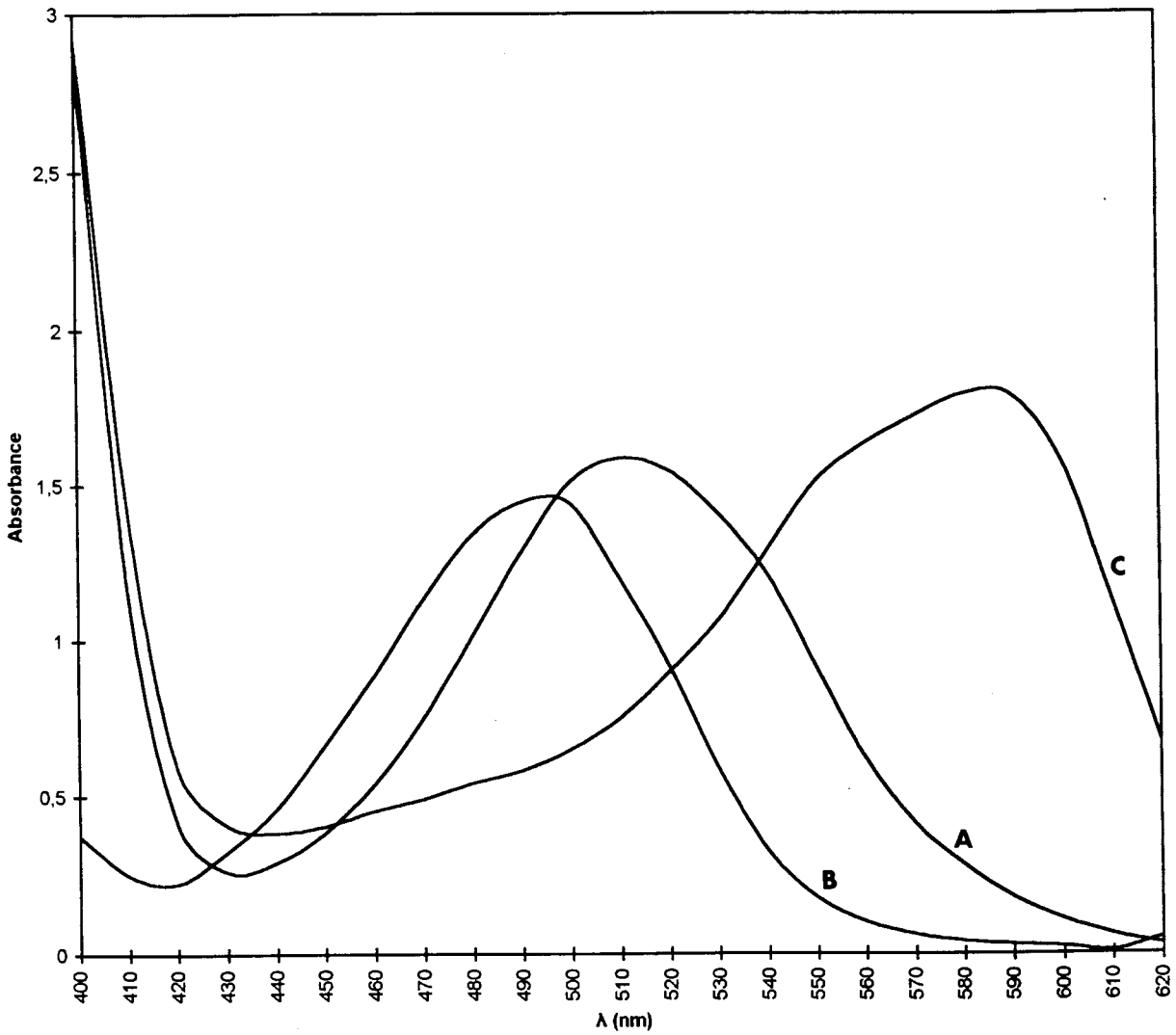

Fig. 1. Molecular spectra of the BPPH-M(II)-SCN complexes for $[BPPH] = 4 \times 10^{-3}$ mol l^{-1}, $[SCN^-] = 2.6 \times 10^{-2}$ mol l^{-1}. BPPH-Co(II)-SCN, $[Co(II)] = 0.8$ mg l^{-1}, pH = 4.5 (A); BPPH-Ni(II)-SCN, $[Ni(II)] = 2.0$ mg l^{-1}, pH = 8.3 (B); BPPH-Pd(II)-SCN, $[Pd(II)] = 5.0$ mg l^{-1}, pH = 5.5 (C).

Ni(II) and Pd(II) are given in Table 1. These values were calculated from separate extractions either in the presence of BPPH only or SCN^- ions only or in the presence of both BPPH and SCN^- ions respectively.

The factors of synergetic effect [10] were calculated according to the ratio:

$$\frac{D_{C(\mathrm{BPPH-M(II)-SCN})}}{D_{C(\mathrm{M(II)-BPPH})} + D_{C(\mathrm{M(II)-SCN})}}$$

where: $D_{C(\mathrm{BPPH\text{-}M(II)\text{-}SCN})}$ is the distribution ratio of the studied cation in the presence of both SCN^- ions and BPPH under the optimum conditions, $D_{C(\mathrm{M(II)\text{-}BPPH})}$ is the distribution ratio in the presence of BPPH only, and $D_{C(\mathrm{M(II)\text{-}SCN})}$ is the distribution ratio in the presence of SCN^- ions only.

The synergetic effect between BPPH and SCN^- for cobalt(II) (factor 158) is greater than for nickel(II) (factor 68) and palladium(II) (factor 58).

Table 1
Distribution ratios of cobalt, nickel and palladium and factors of synergetic effect of BPPH and SCN^- ions on metal extraction in MIBK

Ion	λ_{max} nm	V_{org}/V_{aq}	pH	$D_{C(M(II)\text{-}SCN)}$	$D_{C(M(II)\text{-}BPPH)}$	$D_{C(BPPH\text{-}M(II)\text{-}SCN)}$	$D_{C(BPPH\text{-}M(II)\text{-}SCN)}/D_{C(M(II)\text{-}BPPH)} + D_{C(M(II)\text{-}SCN)}$
Co(II)	510	1:1	4.5	0.60	0.02	98	158
Ni(II)	495	1:1	8.3	0.94	0.50	98	68
Pd(II)	585	1:1	5.5	1.63	0.05	98	58

3.3. Extraction of cobalt, nickel and palladium

In the presence of excess of thiocyanate ions, e.g. $[SCN^-] = 5 \times 10^{-2}$ mol l^{-1} and [BPPH] = 5×10^{-3} mol^{-1}, the influence of the pH on the extraction of the coloured complexes in MIBK from aqueous solutions was studied. The maximum extent of each extraction was observed at pH: 4.5 for cobalt, 8.3 for nickel and 5.5 for palladium (Fig. 1), which were chosen for further work.

In order to optimize the SCN^- ions concentrations on the effectiveness of the extraction, the following experimental variables were used: [Co(II)] = 1.0 mg l^{-1}, [BPPH] = 1×10^{-3} mol l^{-1}, pH = 4.5 for cobalt, [Ni(II)] = 2.0 mg l^{-1}, [BPPH] = 3.4×10^{-3} mol l^{-1}, pH = 8.3 for nickel, and [Pd(II)] = 0.8 mg l^{-1}, [BPPH] = 7.5×10^{-4} mol l^{-1}, pH = 5.5, for palladium. It was found that the minimum concentrations of SCN^- ions were: $[SCN^-] = 1.4 \times 10^{-2}$ mol l^{-1} or $[SCN^-]/[Co(II)] = 800$ for cobalt, $[SCN^-] = 1.8 \times 10^{-2}$ mol l^{-1} or $[SCN^-]/[Ni(II)] = 500$ for nickel, and $[SCN^-] = 1.5 \times 10^{-3}$ mol l^{-1} or $[SCN^-]/[Pd(II)] = 200$ for palladium, which were chosen for further work. In the absence of SCN^- ions, the extraction of Co(II)-BPPH complex was only 25%, while for Ni(II)-BPPH was only 30% and for Pd(II)-BPPH was only 40%.

Using the chosen conditions for pH, SCN^- ions concentrations and the above mentioned analyte concentrations, the minimum BPPH concentrations were: 8.8×10^{-4} mol l^{-1} or $[L]/[Co(II)] > 50$ for cobalt, 3.4×10^{-3} mol l^{-1} or $[L]/[Ni(II)] > 100$ for nickel and 7.5×10^{-4} mol l^{-1} or $[L]/[Pd(II)] > 100$ for palladium. In the absence of ligand, the extraction of all analytes was negligible.

3.4. Calibration curves and precision

Two calibration curves for Co(II), Ni(II) and Pd(II) solutions were recorded under the optimum conditions described above. The calibration graphs were linear and were described by the regression equation $A = i + S_{c_{M(II)}}$, where A is the absorbance as measured by the detector, $c_{M(II)}$ is the concentration of the metal ion in the aqueous solution, i is the intercept and S is the slope of the regression line. The results are summarized in Table 2. The calculated detection limits, $c_{L(k=3)}$, were obtained according to recommendations reported previously [11–13], using the propagation of errors approach [11]. A 1:2 V_{org}/V_{aq} volume ratio was used.

The relative standard deviations of the slopes of the calibration curves s_r for each individual metal, were calculated from the ratio of the standard deviation of each slope to the slope. The s_r is a measure of reproducibility of each method.

3.5. Interference studies

The interference effects of various metallic ions on the UV-VIS and FAAS determination of cobalt, nickel and palladium (1 mg l^{-1} each) were examined following the complexation and extraction procedures described above.

The results are summarized in Table 3. The following metal ions were studied, in addition to those included in Table 3: Cr^{3+}, Mn^{2+}, Pb^{2+}, Sn^{2+}, Zn^{2+}, which do not interfere at an ion/analyte molar ratio of 100:1 and Na^+, K^+, Mg^{2+}, Ca^{2+}, Sr^{2+}, Ba^{2+}, Al^{3+}, which do not interfere at an ion/analyte molar ratio of 500:1. Also, NH_4^+, Cl^-, CO_3^{2-}, NO_3^-, SO_4^{2-}, PO_4^{3-}, and

Table 2
Regression analysis data for cobalt, nickel and palladium determination in MIBK extracts by UV-VIS and AAS

MetalIon	Co(II)	Ni(II)	Pd(II)
AAS			
Linear range, mg l^{-1}	0.0–0.5	0.0–1.5	0.0–2.0
i	0.64×10^{-2}	0.11×10^{-2}	0.28×10^{-2}
S	0.367	0.133	0.071
r	0.99828	0.99977	0.99960
s_r ($n=5$)	2.0%	1.0%	1.3%
c_L ($n=7$), mg l^{-1}	0.004	0.009	0.012
UV-VIS			
Linear range, mg l^{-1}	0.0–0.5	0.0–1.0	0.0–2.0
i	1.88×10^{-2}	0.05×10^{-2}	0.30×10^{-2}
S	2.517	0.858	0.326
r	0.99960	0.99979	0.99980
s_r ($n=5$)	1.3%	1.7%	1.0%
c_L ($n=7$), mg l^{-1}	0.001	0.004	0.002

HPO_4^{2-} do not interfer even at an ion/analyte molar ratio of 1000:1.

The criterion for interference was fixed at a s_r of less than $\pm 2\%$ of the average absorbance signal taken for an analyte concentration corresponding to 1 mg l^{-1}. According to this study, it can be seen that only in case of UV-VIS determinations some significant intereferences are present (Cu^{2+}, Fe^{3+}) while for FAAS determinations no such interferences were found. The explanation for this fact is that some of the interfering ions form similar coloured BPPH complexes extracted in MIBK (Cu^{2+}, Pt^{4+}), while others (Fe^{3+}) form only coloured thiocyanate complexes extracted in MIBK. Finally, some of the ions form colourless complexes either extracted or not in MIBK layer but acting antagonistically to the analytes in ligand complexation, thus eliminating the available concentration of the ligand.

3.6. Applications

The proposed procedures for the determination of cobalt, nickel and palladium were successfully applied to the analysis of commercial dental alloys used in ceramic or acrylic dental works. The samples were dissolved as described above in section 2.4, procedure for dissolution of dental alloys. The available commercial alloys were: V6519, Vitalium Austenal, USA, with 60.6% cobalt; Heranium NA, Heraus, Germany, with 59.3% nickel; and Palgold Keramik SF2 Palkoyannis, Greece, with 78.5% palladium. Using the UV-VIS method, the calculated recoveries ($n=4$) were 95% ($s_r=2.8\%$) for cobalt, 96% ($s_r=3.8\%$)for nickel and 96% ($s_r=2.2\%$) for palladium, while, using the FAAS method, the calculated recoveries were 104 ($s_r=2.1\%$), 105 ($s_r=3.4\%$), and 97% ($s_r=3.0\%$) respectively.

4. Conclusion

The proposed extraction method offers many significant improvements over other direct FAAS

Table 3
Effect of various ions on the determination of cobalt, nickel and palladium (1 mg l^{-1} each) with UV-VIS and AAS, using the optimum conditions given under procedure for extraction from aqueous solutions

Ion added[a]	Molar ratio of ion to Co(II) or Ni(II) or Pd(II)					
	Co(II)		Ni(II)		Pd(II)	
	UV-VIS	AAS	UV-VIS	AAS	UV-VIS	AAS
Au^{3+}	100	100	50	100	100	100
Cd^{2+}	50	50	25	50	100	100
Cu^{2+}	10	10	10	10	50	100
Fe^{3+}	5	10	5	10	25	100
Pt^{4+}	25	100	50	100	50	100

[a] These ions in the stated ratio caused a relative error of less than $\pm 2\%$.

and UV-VIS spectrometric methods e.g. better reproducibilities, lower detection limits, no complicated procedures before the determination of the analyte and few interferences. The presence of SCN^- ions increases the extractability of the studied ions. Cobalt and palladium are quantitatively extracted at pH 4.5 and 5.5 respectively, but the colored complexes have different wavelengths. Nickel is quantitatively extracted at pH 8.3 and not at low pH, while palladium can be extracted from very low pH, thus it can be effectively separated from nickel. Finally, the method is convenient for the determination of micromolar concentrations of the above metals in aqueous solutions as well as in dental alloys.

Acknowledgements

The authors are thankful to Professor P. Garefis for useful discussion and S. Palkoyannis, T. Vougiouklis and C. Poulkas Companies, Thessaloniki, Greece, for supplying the Palgold, Vitallium and Heraus dental alloys used at this work.

References

[1] J.E. Going, R.T. Pflaum, Anal. Chem. 42 (1970) 1098.
[2] H. Alexaki-Tzivanidou, Ph. D.Thesis, University of Thessaloniki, 1972.
[3] A.G. Asuero, M.J. Navas, J.M. Bautista, D. Rosales, Microchem. J. 28 (1983) 183.
[4] D.G. Themelis, G.A. Zachariadis, J.A. Stratis, Analyst 120 (1995) 1593.
[5] J.A. Stratis, A.N. Anthemidis, G.S. Vasilikiotis, Analyst 109 (1984) 373.
[6] S. Arpadjian, I.A. Karadjova, D.L. Tsalev, M.I. Uzunova, J.A. Stratis, I.A. Tossidis, Analyst 113 (1988) 1699.
[7] J.A. Stratis, I.N. Papadoyannis, A.N. Anthemidis, Anal. Lett. 17 (1984) 2359.
[8] I.A. Kafritsas, C.A. Alexiades, J.A. Stratis, Toxicol. Environ. Chem. 20-21 (1989) 169.
[9] J.A. Stratis, D.G. Themelis, D.G. Zatkas, I.A. Kafritsas, Anal. Lett. 22 (1989) 1779.
[10] Z. Aneva, S. Arpadjian, S. Alexandrov, K. Kovatcheva, Mikrochim. Acta 1 (1986) 341.
[11] G.L. Long, J.D. Winefordner, Anal. Chem. 55 (1983) 713A.
[12] ACS Committee on Environmental Improvement, Anal. Chem. 52 (1980) 2242.
[13] Analytical Methods Committee, RSC, Analyst 112 (1987) 199.

ELSEVIER

Talanta 47 (1998) 169–181

Talanta

Luciferin incorporation in the structure of acrylic microspheres with subsequent confinement in a polymeric film: A new method to develop a controlled release-based biosensor for ATP, ADP and AMP

P.E. Michel, S.M. Gautier-Sauvigné, L.J. Blum *

Laboratoire de Génie Enzymatique, UPRESA CNRS 5013-Université Claude Bernard Lyon I, Bât. 308, 43, Bd du 11 Novembre 1918, F-69622 Villeurbanne cedex, France

Received 02 December 1997; received in revised form 02 February 1998; accepted 11 February 1998

Abstract

The controlled release of coreactants at the sensing tip of a biosensor is a possible approach to develop self-contained devices. For luciferin which is a firefly luciferase cosubstrate, a new method of retention is evaluated. The two-step procedure consists of incorporating the substrate in acrylic microspheres during their formation, these last being then confined in a PVA SbQ film. When associated with a compartmentalised trienzymatic sequence (adenylate kinase, creatine kinase and luciferase), such a complex matrix ensures the internal delivery of the cosubstrate in the enzymatic microenvironment at a controlled rate. For the three adenylic nucleotides (ATP, ADP and AMP), the self-containment working time is 3 h of continuous and reproducible assays. The sensitivity of the fibre optic biosensor represents, for ATP, 30% of that obtained when luciferin is supplied in solution whereas for ADP and AMP, the values are about 80% of the reference ones. © 1998 Elsevier Science B.V. All rights reserved.

Keywords: Firefly luciferase; Reagentless fibre-optic biosensor; Compartmentalised sensing layer; Flow injection analysis

1. Introduction

The development of reagentless devices able to sense the target analytes by a simple immersion in the sample is one of the requirements for making true operational enzymatic biosensors.

In the past few years, among the great number of works devoted to enzyme-based biosensors, the integration of the required coreactants (enzymatic cofactors, cosubstrates, mediators, for example) to the sensing layer takes an increasing interest. Two main approaches can be distinguished in the sensing layer design but both involve the retention of the coreactants either with the enzyme molecules or in the vicinity of the immobilised biocatalysts.

* Corresponding author. Tel: + 33 472 431397; fax: + 33 472 442834; e-mail: Loic.Blum@univ-lyonl.fr

0039-9140/98/$19.00 © 1998 Elsevier Science B.V. All rights reserved.
PII S0039-9140(98)00068-X

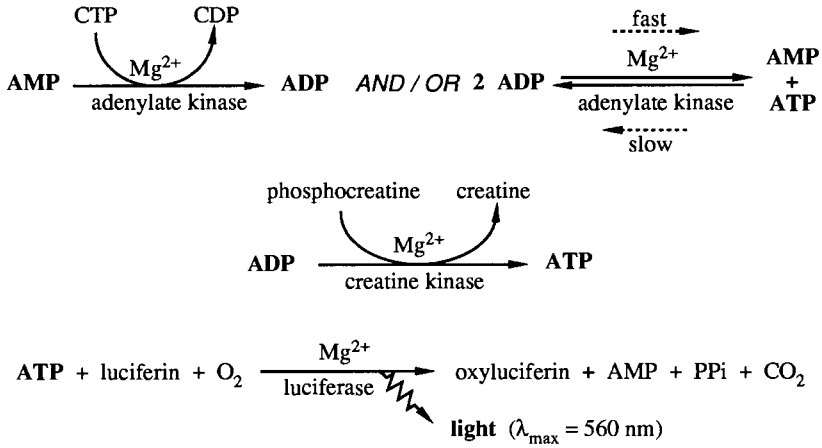

Fig. 1. Scheme of the reactions catalysed by adenylate kinase, creatine kinase and firefly luciferase for the measurement of the three adenylic nucleotides AMP, ADP and ATP. CTP, cytidine 5′-triphosphate, CDP, cytidine 5′-diphosphate. CTP is used to enhance the phosphorylation rate of AMP by adenylate kinase.

The first approach is based on the regeneration of the coreactant which is usually the enzymatic oxidised cofactor, NAD^+. In response to the molecular recognition (mediated by a dehydrogenase), the cofactor is reduced and its regeneration is achieved either by an electrochemical method or by an enzymatic reaction. The coreactant can be included in a polymer [1], immobilised on a membrane-type support [2], confined in solution at the end of the transducer [3,4] or immobilised at the surface of the transducer [5]. The enzymes are either co-immobilised with the reagents or immobilised separately in their vicinity.

In the second approach, the coreactants are confined in a synthetic matrix which is able to release them at a controlled rate, thus playing the role of a microreservoir. When located close to the enzymatic sensing layer, the coreactants are internally delivered in the microenvironment of the immobilised enzymes where they are consumed but not regenerated. This concept has been used in our group for the development of reagentless fibre-optic biosensors for NADH, based on the bacterial bioluminescence reaction [6–8]. The sequential bienzymatic system involved (NAD(P)H: FMN oxidoreductase and bacterial luciferase) requires the simultaneous presence of FMN and an aliphatic aldehyde (decanal). The two coreactants have been co-entrapped in PVA gels either chemically reticulated with glutaraldehyde or polymerised by a cyclic freezing-thawing process. Their use, in association with the immobilised bienzymatic membrane at the sensing tip, allow the sensor to work with reliability during 1–1.5 h.

Recently, a trienzymatic fibre-optic sensor has been developed for the alternate and specific determination of ATP, ADP and AMP [9]. The sensing element consists of a compartmentalised sensing layer involving adenylate kinase (AK), creatine kinase (CK) and firefly luciferase (FL) (Fig. 1). Depending on the target nucleotide, different enzymatic sequences are involved. Indeed for ATP, only the luciferase activity is required to catalyse the bioluminescence indicator reaction whereas for ADP two different bienzymatic sequences may function (AK-FL and/or CK-FL). Finally, for AMP, the assay implies that the three enzymes work sequentially.

When the three adenosine nucleotides are simultaneously present in the same sample, the specificity of the measurements is guaranteed by the modulation of the composition of the reaction medium with regard to (a) the cosubstrates necessary for the expression of the enzyme activities and (b) the presence of adenosine 5′-monosulfate, a competitive inhibitor of AK. Consequently, three different reaction media are used to discriminate between the three nucleotides. However, all of them contain luciferin since FL catalyses the indicator reaction.

For the measurement of ATP, ADP and AMP with the same probe, the design of a reagentless fibre-optic biosensor based on a unique sensing layer which should integrate both the trienzymatic system and all of the required coreactants is incompatible with the criterion of specificity.

The work presented in this paper is focused on the entrapment of luciferin, the common and also the most onerous reactant, in a matrix ensuring its internal and controlled delivery in the sensing tip. Luciferin has been incorporated in acrylic resin microspheres which have been then confined in a photopolymerised PVA film. Different factors affecting the retention and/or the release of luciferin have been identified. The synthetic matrix has then been associated with a membrane bearing FL in order to characterise the release process.

Finally, the performance of the biosensor equipped with the luciferin-containing matrix and the compartmentalised AK-CK-FL system has been studied for the alternate measurements of ATP, ADP and AMP.

2. Material and methods

2.1. Enzymes and reagents

Crystalline recombinant firefly luciferase (FL), (EC 1.13.12.7, 30 units $\times$ mg^{-1} protein) was obtained from Calbiochem. One unit is defined as the amount of enzyme that releases 1 nM pyrophosphate from ATP in the presence of 540 μM ATP and 100 μM D-luciferin per min at 25°C.

Adenylate kinase from chicken muscle (AK), (EC 2.7.4.3, 1500 U $\times$ mg^{-1} lyophilisate, 1500 U $\times$ mg^{-1} protein), creatine phosphokinase from rabbit muscle (CK), (EC 2.7.3.2, 250 U $\times$ mg^{-1} lyophilisate, 250 U $\times$ mg^{-1} protein), dithiothreitol (DTT), adenosine 5′monophosphate (AMP, sodium salt, 99%), adenosine 5′-monosulfate (AMS, sodium salt, 90%), adenosine 5′-triphosphate (ATP, sodium salt, 99%), cytidine 5′-triphosphate (CTP, sodium salt, 98%), phosphocreatine (sodium salt, 98%) and magnesium acetate were supplied by Sigma.

Adenosine 5′-diphosphate (ADP, potassium salt, 84%) and fatty acid-free bovine serum albumin, fraction V (BSA) was obtained from Boehringer Mannheim.

D-luciferin (synthetic, sodium salt) was from Biosynth.

Eudragit® RL 30 D and Eudragit® RS 30 D (aqueous acrylic polymer dispersions, 30% (w/w)) were supplied by Rohm Pharma.

Poly(vinyl)alcohol (PVA) (98–99% hydrolysed, average molecular weight 31000–50000 and 99% hydrolysed, average molecular weight 85000–146000) were from Aldrich.

Photosensitive PVA (PVA SbQ) [stilbazolium (SbQ)-pendant PVA (SPP)] (11 wt % solid content, degree of polymerisation 2300, degree of saponification 88, SbQ content 1.06 mol %, pH 6.2) was obtained from Toyo Gosei Kogyo.

All other reagents were of analytical grade.

2.2. Enzyme immobilisation

The enzymes are covalently immobilised onto bovine type I collagen membranes (Cellagen ™ membranes, ICN). Prior to the enzymatic coupling, disks (11 mm in diameter) are cut out of the membrane and are activated by the acyl-azide mild method described by Coulet et al. [10]. Thereafter, the activated disks are immersed for 3 h at + 4°C into enzymatic coupling solutions composed of 0.5 M glycine-NaOH solution, pH 7.7 plus 4 mM DTT (to prevent enzyme inactivation). To immobilise FL alone, the coupling solution contains the soluble activity of 21 units $\times$ ml^{-1}. For the co-immobilisation of AK and CK on the same membrane, the coupling solution contains 450 U $\times$ ml^{-1} AK and 2500 U $\times$ ml^{-1} CK. The different enzyme activities are chosen with regard to the activities exhibited, after immobilisation, by the bioactive membranes and correspond to the optimal ones recently reported [9].

After coupling, the bioactive membranes are thoroughly washed at room temperature first, for 20 min in a stirred 0.1 M phosphate-NaOH buffer, pH 7.0 containing 4 mM DTT (buffer A) and then, twice in buffer A plus 1 M KCl in order to eliminate the enzymatic molecules only adsorbed. Finally, the disks are washed in buffer A for removing the excess of KCl before storage at + 4°C in 0.1 M phosphate-NaOH buffer, pH

7.0 containing 5 mM DTT, 1% (w/v) BSA and 20% (v/v) glycerol.

2.3. Preparation of the luciferin-containing matrix

The luciferin-containing matrices are prepared according to a two-step procedure which consists in firstly incorporating luciferin into Eudragit® microspheres during their preparation process and secondly confining the luciferin-containing microspheres in a photo-cross-linked PVA film.

2.3.1. Incorporation of luciferin in acrylic micromatrices

Eudragit®RL 30 D and RS 30 D are copolymers of acrylic and methacrylic esters with a low content of quaternary ammonium groups. The mean molecular weight is ~ 150000 (Röhm Pharma, information prospectus). These acrylic resins are widely used as coating agents for pharmaceutical preparations.

The luciferin-containing microspheres have been prepared according to the solvent evaporation technique described by Barkai et al. [11].

A solution of 0.8% (w/v) PVA (average molecular weight of either 31000–50000 or 85000–146000) is extemporaneously prepared in distilled water. A mixture composed of 15% (w/w) Eudragit® in distilled water (156 mg), methylene chloride (625 µ1) and luciferin (1–9.3 mg) is then added to 6.25 ml of the aqueous PVA solution after its complete cooling at room temperature. The resulting emulsion (Eudragit®-methylene chloride-luciferin-PVA) is stirred (500 rev × min^{-} l) at room temperature in darkness for 4 h. During this process, the microspheres form themselves with simultaneously a complete evaporation of the solvent. Eudragit® RL 30 D and RS 30 D have been used either separately or mixed in a 1:1 (w/w) ratio.

The luciferin-containing microspheres are allowed to settle by centrifugation (3 min at 10000 g) and washed five times in distilled water.

2.3.2. Confinement of the luciferin-loaded microspheres in a PVA SbQ film

The microspheres, re-suspended in distilled water (50–150 µl), are mixed with an aqueous solution of PVA SbQ to a final volume of 360 µl and a PVA SbQ content of 1.8% (w/w). The homogeneous mixture is spread onto a cellulosic membrane (1.5 × 1.5 cm) (Spectrapor™, MW cutoff: 6,000–8,000, from Spectrum) and is allowed to dry for 2 h under a tungsten lamp. After an exposure to UV radiation (254 nm) for 45 min, the film is kept overnight at + 4°C in darkness before cutting out disks (11 mm in diameter) for use.

2.4. Apparatus and sensor tip design

The light intensity measurements have been performed with a fibre-optic sensor consisting of a 1 m long glass fibre bundle (8 mm in diameter) [12]. One end (the sensing part) is equipped with the bioactive membrane(s) maintained in close contact with the bundle by a screw cap whereas the other end is directly connected to the photomultiplier tube of the luminometer (Biocounter M 2500, Lumac).

The sensing part is inserted in a specially designed black flow-cell comprising a reaction chamber with a volume of 125 µl. Samples (50 µl) are injected in the flowing stream using an injection valve (Model 5020, Rheodyne). Reliable homogenisation of the sample and of the reagents is obtained by direct magnetic stirring in the flow cell.

The changes in luminescence intensities (expressed in relative light units (RLU)) are recorded on a Servotrace recorder type PE (Sefram).

When ATP measurements are carried out with FL immobilised alone, the co-reactant containing matrix is inserted between the enzymatic membrane and the surface of the fibre bundle (Fig. 2A). When using the compartmentalised AK-CK-FL layer for assaying the three adenylic nucleotides, the additional membrane on which AK and CK are co-immobilised is placed so that it faces the reaction medium (Fig. 2B).

For reference measurements, the sensor is only equipped with the enzymatic membrane(s) and luciferin is continuously supplied by the flowing stream of the reaction medium at the optimal concentration of 0.3 mM.

2.5. Bioluminescent assays of ATP, ADP and AMP

All the measurements are performed in the presence of 50 mM Tris-acetate buffer, pH 7.75 containing 4 mM DTT and 30 mM acetate magnesium at 23°C [9].

Standard solutions of ATP, ADP and AMP are prepared daily in distilled water.

2.5.1. ATP assays performed with only a luciferase membrane

With entrapped luciferin, the carrier is simply composed of the buffered solution.

The flow-rate and the stirring speed are fixed at their optimal values of 0.53 ml $\times$ min^{-1} and 1200 rev $\times$ min^{-1}, respectively [13].

2.5.2. ATP, ADP and AMP measurements with the compartmentalised AK-CK-FL system

As previously stated [9], the specific analysis of each of the three nucleotides involves the use of three different reaction media due to the interference caused by the activity of AK. For the specific determinations of ATP and ADP, adenosine 5′ monosulfate (AMS) is added to the appropriate reaction media in order to inhibit temporarily the activity of AK. Consequently, the required reaction media are composed as follows: for ATP, 5 mM of AMS are present in the buffered solution whereas for ADP, the reaction medium contains 35 mM phosphocreatine in addition to AMS (5 mM). For AMP, the assays require the activity of AK and are performed without AMS using a buffered solution containing in addition 35 mM phosphocreatine and 0.5 mM CTP.

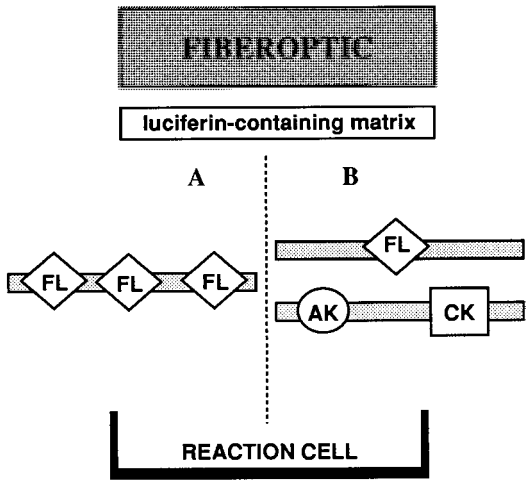

Fig. 2. Location at the sensing tip of the fibre-optic sensor of the luciferin-containing matrix when associated with the firefly luciferase membrane alone (A) and with the compartmentalised adenylate kinase-creatine kinase-firefly luciferase system (B).

The flow-rate and the stirring speed are fixed at 0.2 ml $\times$ min^{-1} and 1200 rev $\times$ min^{-1}, respectively.

Luminescence measurements of the adenylic nucleotides are performed either with standard nucleotide solutions (i.e. containing only one of the three nucleotides) or with 'complex' samples that are containing the three nucleotides simultaneously.

3. Results and discussion

3.1. Principle of luciferin entrapment

Luciferin is incorporated into the Eudragit® microspheres during their preparation according to the solvent evaporation process which has been previously described for drug incorporation [11]. The structure of the microspheres depends on the amount of micromatrices which is prepared. Indeed, when prepared on a large scale, spherical micromatrices comprise an internal void space and a polymeric membrane containing the drug. When prepared on a small scale, the microspheres are dense and homogeneous spherical polymer micromatrices in which the drug is either dispersed or dissolved.

The experimental conditions we have employed for incorporating luciferin (small laboratory scale) should lead to the formation of dense and homogeneous microspheres with a mean size of $\sim$500 μm.

The confinement of the luciferin-containing micromatrices in the polymeric structure of a photo-cross-linked PVA film has been carried out in order to facilitate the handling and to favour the control of the internal delivery rate of luciferin. Indeed, luciferin must diffuse first, out of

the microspheres into the PVA SbQ film and second, out of the PVA film before being released into the enzymatic microenvironment.

3.2. Factors influencing the preparation of the microspheres and their confinement in a PVA Sbq film

Three different factors which may affect the preparation and the confinement of the microspheres are studied. For evaluating their effect on the performance of the biosensor, it is equipped with the luciferin-containing matrix associated with a FL membrane. The responses of the sensor, measured consecutively to the injections of 25 pmol ATP, are compared to the reference ones obtained when luciferin is delivered by the flowing stream of the buffered solution. The self-containment period of the biosensor, defined as the time during which the measurements are reproducible, is determined.

3.2.1. Effect of the molecular weight of the PVA polymer used during the micro-sphere preparation

During the solvent evaporation process, PVA forms a stable emulsion of methylene chloride in water. Indeed, it plays a protective role by acting as a steric barrier at the oil–water interface of the droplets, thus preventing their coalescence [11].

Two PVA polymers differing in their average molecular weight (31000–50000 and 85000–146000) are used to prepare the microspheres.

In both cases, the micromatrices are made using an emulsion containing 6.2 mg luciferin and a mixture of equal parts of Eudragit® RS 30 D and RL 30 D dispersions. Their subsequent confinement in PVA-SbQ films is performed with 100 μl of the microsphere suspensions.

When the microspheres are obtained using the PVA polymer of 31000–50000 molecular weight, the responses of the sensor are 40% of the reference values. However, they decrease slowly to represent finally 50% of the initial value after 30 consecutive assays performed in two h.

When the micromatrices are prepared using the PVA polymer of 85000–146000 molecular weight, the sensor responses represent only 20% of the control ones but they are stable during 2 h before decreasing.

Afterwards, the microspheres will be prepared using a PVA polymer of 85000–146000 molecular weight.

3.2.2. Effect of the type of Eudragit® dispersion.

Two types of Eudragit® dispersions marketed by Röhm Pharma (Eudragit® RL 30 D and RS 30 D) are tested. They differ in their permeability properties (RL: high permeability, RS: low permeability), the molar ratio of the ammonium groups being twice higher in the case of the RS 30 D dispersion than that in the case of Eudragit® RL 30 D.

The release of luciferin from the microspheres being expected to depend on the type of acrylic resin used, three different types of microspheres are made. For the first type, RL30 D dispersion is used alone whereas for the second type the two dispersions are mixed in a 1:1 (w/w) ratio. The third type is made using RS 30 D dispersion alone.

In all cases, the emulsions contain a solution of PVA of 85,000–146,000 molecular weight and 6.2 mg luciferin. The confinement of the microspheres is performed with 100 μl of each suspension.

When the microspheres are prepared with Eudragit® RL 30 D alone, the response of the sensor represents 9% of the reference signal and the assays are reproducible over 1.5 h.

When using the RS and RL dispersions mixed in a 1:1 (w/w) ratio, the relative response of the sensor represents 20% of the control value and remains constant for 2 h.

The best results are obtained when the microspheres are prepared with Eudragit® RS 30 D alone. In this case, the response of the sensor represents 30% of the reference one and the self-containment period was evaluated to be 2 h of reliable measurements.

The microspheres will then be prepared with Eudragit® RS 30 D alone.

3.2.3. Selected volume of micro-sphere suspension to be confined in the PVA SbQ film

Microspheres are made in the conditions determined as optimal i.e. using a solution of PVA of 85,000–146,000 molecular weight and Eudragit® RS 30 D alone. The loading amount of luciferin in the emulsion was 6.2 mg.

The confinement of the luciferin-containing micromatrices in a PVA SbQ film is performed with microsphere suspension volumes ranging from 25 to 150 μl.

The maximum response of the sensor (30% of the control value) is obtained with the films prepared using 100 and 150 μl of the luciferin-containing microspheres. The self containment is evaluated to be 2 and 2.5 h of continuous measurements, respectively.

Consequently, a microsphere volume suspension of 150 μl was selected optimum for the confinement in a film of PVA SbQ.

3.3. Effect of the location of the luciferin-containing matrix on light transmission and on luciferase stability

Due to its location between FL membrane and the fibre bundle surface, it is necessary to check that the matrix in which luciferin is entrapped, does not significantly decrease the transmission of light.

For this purpose, microspheres are made without luciferin and are then confined in a PVA SbQ film. The different steps of the overall preparation process are carried out in the conditions previously determined.

For light intensity measurements, the biosensor is equipped with the 'neutral' matrix stacked on the luciferase membrane and the flowing reaction medium contains 0.3 mM luciferin. The sensor responses to injections of 25 pmol ATP are compared to those obtained when the sensing tip was equipped with an FL membrane alone.

A 20% decrease in light transmission is observed. After a prolonged contact with the 'neutral' matrix the activity exhibited by the bioluminescent membrane is unchanged indicating that FL stability is preserved.

3.4. Selected loading amount of luciferin

Prior to the evaluation of the effect of the loading amount of luciferin on the biosensor response and self-containment, we have checked that the reactivity of luciferin was not affected by the experimental conditions used for the incorporation in the micromatrices and the photopolymerisation of PVA SbQ.

Microspheres are prepared using luciferin amounts ranging from 1 to 9.3 mg. In each case, both the preparation and the confinement of the micromatrices are achieved in the conditions previously determined as optimal. The luciferin-containing matrix is associated with a FL membrane at the end of the sensor and light intensity is measured for injections of 25 pmol ATP.

The biosensor response which increases with the loading amount of luciferin, reaches a maximum value for 3.1 mg luciferin and remains constant up to 9.3 mg. The response of the biosensor represents then 30% of the control value determined when the sensing tip of the sensor is only equipped with a FL membrane, the luciferin being free in solution in the reaction medium.

A slight increase in the self-containment working time of the biosensor (2–2.5 h) occurs when the loading amount of luciferin increases from 1 to 3.1 mg Above 3.1 mg, higher amounts have no effect on the self-containment working time which remains equal to 2.5 h. Therefore, the optimum amount of luciferin selected for loading is 3.1 mg.

3.5. Reproducibility of the preparation of the luciferin containing matrices

For estimating the reproducibility of the preparation of the luciferin-containing matrices with respect to both the microspheres preparation batch process and their confinement in a PVA SbQ film, five different matrices are simultaneously made in the same conditions. Each of them is associated with the same FL membrane at the sensing tip of the sensor and the biosensor responses are monitored for five consecutive ATP injections (50 pmol). For each set of experiments, the mean value of the biosensor responses is calculated and the five mean values thus obtained are taken into account to calculate the RSD value of the overall process of preparation of the luciferin-containing matrices. With a RSD value of 6.3%, the reproducibility of the preparation process is considered as quite satisfactory.

3.6. Characteristics and performance of the reagentless monoenzyme-based sensor for ATP

When the fibre-optic sensor is equipped with a luciferin-containing matrix and a FL membrane, it can be regarded as a reagentless biosensor for ATP.

3.6.1. Calibration for ATP

The reference calibration graph is established using luciferin in solution (0.3 mM) in the flowing stream, the sensor being then equipped with the enzymatic membrane alone.

When luciferin is internally released from the synthetic matrix, the calibration graph is linear from the detection limit (2.5 pmol)–2.5 nmol whereas the linear range of measurements of the reference graph extends from 0.5 pmol (detection limit)–2.5 nmol.

With soluble luciferin, the detection limit is 5-fold better than that obtained with entrapped luciferin. This result is not surprising since with a luciferin-containing matrix the response of the biosensor is about three times lower than that measured when the luciferin is supplied by a buffered solution.

In both configurations, the upper limits of linearity are identical which suggests that the concentration of luciferin is not a limiting factor when the substrate is internally released from the synthetic matrix.

3.6.2. Characteristics of the light signals

Compared with the reference signals, no difference in the shape and in the cycle time (i.e. the time necessary for the light intensity to return to the background level) is observed using a luciferin-containing matrix. For example, the average cycle time was 3–4 min for injections of 25 pmol ATP.

3.6.3. Biosensor self-containment and characteristics of the release process

For estimating the self-containment working time of the biosensor, repetitive injections of 25 pmol ATP are performed at regular intervals until the biosensor responses decrease significantly.

From the first ATP injection, the responses of the biosensor are stable (Fig. 3) suggesting that the release of luciferin in the microenvironment of immobilised FL occurs at a constant rate as soon as the sensing tip of the sensor is immersed in the reaction medium. Consequently, the internal release of luciferin would be characterised by a zero-order kinetic.

During 2.5 h, the measurements are reproducible (zone I) as shown by the homogeneous distribution of the 32 points around the average value (105.0 RLU) and by the RSD value of 5.4%. The magnitude of the biosensor response then represents 30% of the reference one. Thereafter, a constant decrease in the biosensor responses occurs (zone II) indicating a depletion of luciferin in the microenvironment of the bound luciferase.

After its removal from the sensing tip, the substrate matrix exhibits a green colour which demonstrates that it still contains luciferin. Thereby, the decrease in the biosensor responses is postulated to result from the release of only a limited amount of luciferin incorporated in the microspheres rather than from an exhaustion of the matrix. This hypothesis is in agreement with the observations reported by Liebowitz et al. [14] about the inability to obtain a complete release of salicylic acid from various acrylic resin films.

3.7. Compartmentalised trienzymatic sequence-based biosensor for the alternate measurements of ATP, ADP and AMP using a luciferin-containing matrix

A luciferin-containing matrix is associated with the compartmentalised AK-CK-FL system at the sensing tip of the biosensor (Fig. 2B) for the continuous flow measurements of ATP, ADP and AMP. For reference assays, luciferin is supplied by the carrier stream and the sensing tip of the sensor is equipped with the same two enzymatic stacked membranes.

As recently described [9], the discriminating analysis of the three nucleotides requires the use of three reaction media differing from one another in the enzymatic cosubstrates and/or the effector they contain. This use of different reac-

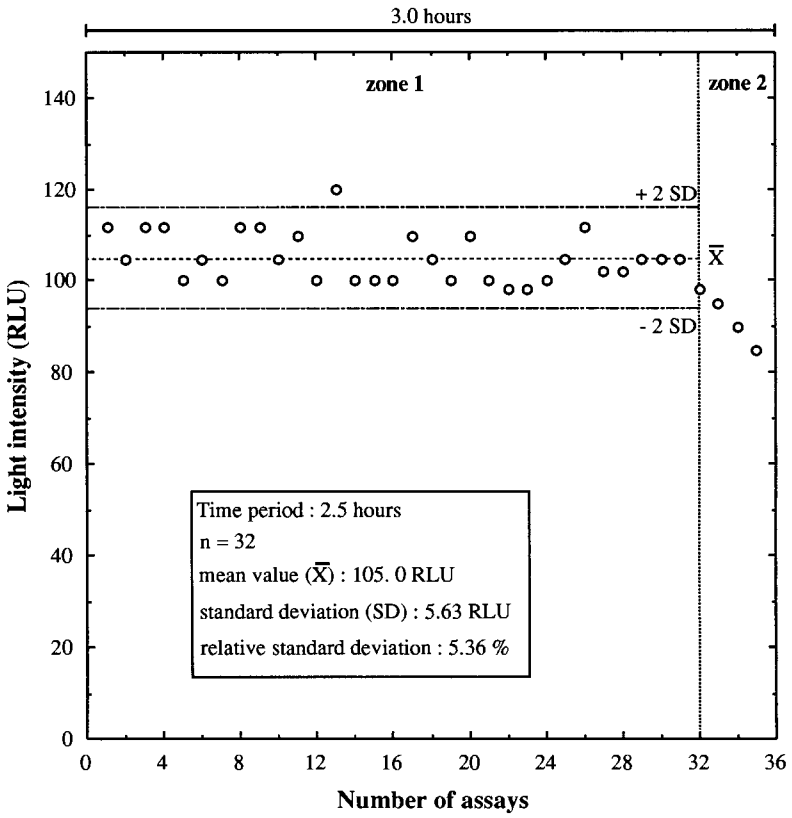

Fig. 3. Repeatability of the assays of ATP performed using the biosensor including the luciferin-containing matrix and the luciferase membrane. Light intensity is measured upon injections of 25 pmol ATP. Zone 1: self-containment working time corresponding to the period during which the assays are reproducible. Zone 2: decrease in biosensor response after the self-containment working time.

tion media is necessary to activate the enzymes or the enzymatic sequences specifically required for the assay of each target nucleotide.

The main results obtained are summarised in Table 1.

3.7.1. Dynamic ranges of measurements for ATP, ADP and AMP

Whatever the adenine nucleotide to be assayed, the detection limit represents the lower limit of linearity. For ATP, the detection limit (10 pmol) is 4-fold higher than the reference value obtained with an external supply of luciferin (2.5 pmol) whereas the upper limit of linearity (2.5 nmol) is not modified by the internal release of the coreactant. The normalised value of the response is 30% of the control one. In the case of ADP, the detection limit (50 pmol) and the dynamic linear range of measurements (up to 2.5 nmol) are identical to those determined when luciferin is free in solution in the reaction medium. Moreover, in the presence of the luciferin-containing matrix, the response of the biosensor represents 80% of the control one. Concerning the assays of AMP, linear measurements range from 25 pmol to 5 nmol as for those performed with an external supply of luciferin. Over the dynamic linear range, the biosensor responses measured with the luciferin containing matrix represent 75% of the control values.

The comparison of the two luciferin supply processes in the vicinity of the bound FL (internal release and external delivery) shows that in both cases the local concentrations of luciferin are very close since neither the upper limit of linearity nor the sensitivities of the biosensor (defined as the

slope value of the linear part of the calibration curve) are modified, irrespective of the adenylic nucleotide to be determined.

Concerning the magnitude of the biosensor responses for each nucleotide (which are normalised with respect to those determined with the conventional supply of luciferin), it appears that the values obtained for ADP (80%) and for AMP (75%) are about 2.5-fold higher than that determined for ATP (30%). A priori, the simplest explanation is that the AK-CK membrane is a diffusional barrier limiting the ATP access to the luciferase membrane. The AK-CK membrane being in direct contact with the reaction medium, the binding of both ADP and AMP on CK and AK will be favoured compared with that of ATP on luciferase. Indeed, ATP must first diffuse through the kinase membrane before reaching its binding site. However, this assumption is inconsistent with the results obtained with the biosensor equipped with only an FL membrane. In that case, the luciferase membrane faces the reaction medium, and the magnitude of the normalised biosensor response is also 30%, that is identical to that obtained with a compartmentalised sensing layer. A plausible interpretation is that the increase of the relative biosensor response results from an activation of CK, involved in both the assays of ADP and AMP, by an unknown compound released from the luciferin matrix.

In an attempt to prove that the enhancement of the magnitude of the biosensor response for both ADP and AMP is due to an activation of the reaction catalysed by the immobilised CK, 'neutral' microspheres (i.e. without luciferin loading) are prepared and are then confined in a PVA SbQ film.

In addition to such a 'neutral' matrix, the sensing tip of the biosensor is equipped with the two enzymatic layers (on the one hand the FL membrane and on the other hand the co-immobilised AK-CK membrane). A calibration curve for ADP is established by immersing the sensing tip into a carrier stream containing 0.3 mM luciferin, 35 mM phosphocreatine (for CK activity) and 5 mM AMS (for AK inhibition).

For comparison, another calibration graph is established using the same reaction medium but with the sensor only equipped with the compartmentalised trienzymatic layer i.e. in the absence of the 'neutral' matrix.

The sensitivity of the biosensor, obtained in the presence of the 'neutral' matrix represents 140% of that measured in its absence (3.3×10^{12} RLU $\times$ mol^{-1} instead of 2.3×10^{12} RLU $\times$ mol^{-1}) instead of 80% as expected if no activation occurred, since as stated above, the presence of a 'neutral' matrix leads to a 20% decrease in light transmission.

Such a result confirms the activation phenomenon of CK.

Table 1
Performance of the partly reagentless biosensor for ATP, ADP and AMP

Parameter	Target analyte		
	ATP	ADP	AMP
Dynamic linear range (pmol)	10–2 500	50–2 500	25–5 000
Sensitivity [a] (RLU $\times$ mol^{-1})	5.5×10^{12}	2.8×10^{12}	2.8×10^{12}
Normalised biosensor response [b] (%)	30	80	75
Self-containment working time (h)	3	3	3
RSD (%)	4	4.3	6.0
for n assays	$n = 16$	$n = 16$	$n = 14$

[a] the sensitivity is defined as the slope value of the linear part of the calibration graph.
[b] percentage of the reference value determined with luciferin free in solution when the sensing tip is equipped with only the compartmentalised AK-CK-FL sequence.

3.7.2. Characteristics of the light signals

As for the ATP biosensor, with the ADP or AMP biosensor, both the shape of the signal and the cycle-times are unchanged compared with those obtained with luciferin free in solution. The maximum peak light emission is obtained about 1 min after sample injection and the base width of peak, i.e. the cycle-time, is about 8–9 min.

3.7.3. Self-containment working times

The self-containment working time of the biosensor is evaluated for each of the three nucleotides by performing repetitive injections of the

Table 2
Determination of ATP, ADP and AMP in complex samples with the partly reagentless biosensor

Sample	Real (I) and experimentally determined (II) concentrations (μM)					
	ATP		ADP		AMP	
	(I)	(II)	(I)	(II)	(I)	(II)
A	2	2.1	2	2.15	5	4.75
B	2	4.3	20	21.8	20	21.6
C	20	21.8	20	18.6	5	3.2
D	20	20.6	2	5.4	20	18.5

adenylic nucleotide (50 pmol ATP, 50 pmol ADP or 100 pmol AMP). For each adenine nucleotide tested, the sensor is equipped with a new luciferin-containing matrix. The results are presented in Table 2.

Whatever the nucleotide, the responses of the sensor are stable from the first injection. The self-containment working time is estimated to be 3 h of reproducible measurements ($4\% < RSD < 6\%$) before observing a decrease of the response. Compared with the self-containment working time of the reagentless sensor for ATP which was only equipped with the FL membrane (2.5 h), a slight improvement is obtained when using a compartmentalised sensing layer. It can be easily explained by the presence of the additional AK-CK membrane which acts as a diffusion barrier and thus slows down the luciferin release-process into the flowing stream of reaction medium.

3.7.4. Determination of ATP, ADP and AMP in complex samples

Four samples containing simultaneously the three nucleotides in different concentration ratios are made using standard solutions with known concentrations. The nucleotides are specifically determined according to the three-step experimental procedure described in the experimental section and their concentrations are then compared with the real ones. The change of reaction medium was associated to a renewal of the luciferin-containing matrix.

As shown by the results presented in Table 2, the experimental and expected results are in good agreement except in the cases where one nucleotide concentration is much lower than the two others. For example, sample B is a mixture of ADP and AMP at the same concentration (20 μM) and ATP at a concentration ten times lower (2 μM). For this sample, the measured ADP and AMP concentrations are consistent with the real values whereas the measured ATP concentration is twice the real value.

4. Conclusion

As an attempt for developing a reagentless enzymatic sensor based on the control delivery of a reactant included at the sensing tip, we have evaluated a new method of preparation of the reagent-containing matrix. It consists of the incorporation of luciferin in the structure of acrylic (Eudragit®) microspheres subsequently confined in a photopolymerised PVA film. The procedure is very simple and quite reproducible provided that the parameters such as, for example, the stirring applied during the solvent evaporation process are strictly controlled.

When integrated at the sensing tip of a mono or tri-enzymatic firefly luciferase-based sensor, such a matrix ensures the internal release of the contained-reactant in the microenvironment of the immobilised enzymes. Due to the method employed for preparing the matrix which involves a double-entrapment of the reagent, first in the acrylic microspheres and then in the meshes of the photopolymerised PVA, the release process is expected to be complex. However it occurs at a zero order rate which allows reliable measurements from the first contact of the sensor with the target analyte. The self-containment working time is es-

timated to be 2.5 h in the case of the monoenzymatic FL based biosensor for ATP and 3 h of continuous assays for ATP, ADP, and AMP when using the biosensor equipped with the compartmentalised trienzymatic sequence. The little improvement of the self-containment working time is attributed to a slower release of luciferin into the carrier stream due to the presence of the bienzymatic AK-CK membrane which plays the role of an additional diffusion barrier.

The short self-containment working time is postulated to result from the release of only a limited amount of luciferin incorporated in the microspheres. Further experiments should be focused on the selection of modifier agents able to markedly enhance the amount of luciferin released while preserving a zero order release kinetics.

Although the self-containment working time is still too short for allowing intensive use of the (partly) reagentless sensor, the possibility of renewing the luciferin-containing matrix without significant variation of the performance of the sensor is an efficient way for circumventing this shortcoming.

The unexpected drawback is the decrease in the magnitude of the biosensor response for ATP compared with the reference value obtained when luciferin is free in solution (30 instead of 100%). Due to the matrix location at the sensing tip, the light transmission is only 80%. Consequently, the maximum value of the biosensor response will never exceed 80% of the reference one. However, this value is about 2.5-fold higher than that determined (30%) when using the luciferin-containing matrix. Such a result could have been explained by the absorption of a part of the emitted light by the luciferin-containing matrix but no incompatibility has been found between the absorption spectral properties of luciferin, Eudragit, PVA SbQ and the spectral properties of the light emission (the respective absorption maxima occur at wavelengths very different from that of the light emission). Another possible explanation lies in changes of pH in the microenvironment of FL caused by the release of luciferin (which is an acidic molecule) from the unbuffered matrix. These small variations might induce either a decrease in the activity of FL and/or a shift in the wavelength of the maximum light emission. However, no experimental result supports such an hypothesis at the present time.

Nevertheless, with regard to the sensitivity, to the extent of the linear range of measurement and to the cycle time, the performance of the reagentless sensor for ATP and especially these of the partly reagentless sensor for the three adenylic nucleotides are quite satisfactory. Indeed, compared with the results obtained with the conventional supply of luciferin, neither the sensitivity of the sensors nor the cycle time are affected. For the dynamic range of assays, a reduction of its extent is observed for ATP due to a higher detection limit value but no modification is observed for ADP and AMP. For these nucleotides, the best results obtained (with respect to the detection limit compared with the case of ATP) proceed from an enhancement of the immobilised creatine kinase activity by a compound which is released from the mixed acrylic resin/PVA SbQ matrix and which is not identified for the present time.

Finally, one can underline that with regard to the cost of an analysis cycle, this approach allows significant savings since the needed amount of luciferin is 2.5-fold lower than that requires for performing the same number of assays when luciferin is freely soluble in the buffered carrier stream.

References

[1] B. Leca, J.L. Marty, Anal. Chim. Acta 340 (1997) 143.
[2] X. Xie, A.A. Suleiman, G.G. Guilbault, Biotechnol. Bioeng. 39 (1992) 1147.
[3] C. Schelp, T. Scheper, F. Buckmann, K.F. Reardon, Anal. Chim. Acta 255 (1991) 223.
[4] T. Scheper, A.F. Buckmann, Biosens. Bioelectr. 5 (1990) 125.
[5] H. Gunasingham, C.H. Tan, J.K.L. Seow, Anal. Chem. 62 (1990) 755.
[6] S.M. Gautier, L.J. Blum, P.R. Coulet, Anal. Chim. Acta 243 (1991) 149.
[7] S.M. Gautier, L.J. Blum, P.R. Coulet, Anal. Chim. Acta 266 (1992) 331.
[8] S.M. Gautier, P.E. Michel, L.J. Blum, Anal. Lett. 27 (11) (1994) 2055.

[9] P.E. Michel, S.M. Gautier-Sauvigne, L.J. Blum, Anal. Chim. Acta 360 (1998) 89.
[10] P.R. Coulet, J.H. Julliard, D.C. Gautheron, Biotechnol. Bioeng. 16 (1974) 1055.
[11] A. Barkai, Y.V. Pathak, S. Benita, Polyacrylate (Eudragit retard) microspheres for oral controlled release of nifedipine: formulation design and process optimization, in: J.I. Wells, M.H. Rubinstein (Eds.), Pharmaceutical Technology-Controlled drug release, 2, Ellis Horwood, UK, 1991, p. 105-117.
[12] L.J. Blum, S.M. Gautier, P.R. Coulet, Anal. Lett. 21 (5) (1988) 717.
[13] S.M. Gautier, L.J. Blum, P.R. Coulet, Anal. Chim. Acta 235 (1990) 243.
[14] S.M. Liebowitz, K. Ichizura, J.W. McGinity, Physicochemical factors influencing drug release from acrylic resin films, in: M.H. Rubinstein (Ed.), Pharmaceutical Technology-Controlled drug release, Ellis Horwood, UK, 1987, p. 9-16.

ELSEVIER

Talanta 47 (1998) 183–191

Talanta

Urea potentiometric biosensor based on urease immobilized on chitosan membranes

Júlia M.C.S. Magalhães, Adélio A.S.C. Machado *

LAQUIPAI, Faculdade de Ciências, R. Campo Alegre 687, Porto P4150, Portugal

Received 12 September 1997; received in revised form 5 February 1998; accepted 11 February 1998

Abstract

Potentiometric biosensors based on urease (E.C. 3.5.1.5.) immobilized on chitosan membranes coupled to all-solid-state nonactin ammonium ion selective electrodes are described. The enzyme was immobilized on the chitosan membranes by four procedures: (A) adsorption; (B) adsorption followed by reticulation with dilute aqueous glutaraldehyde solution; (C) activation with glutaraldehyde followed by contact with the enzyme solution; and (D) activation with glutaraldehyde, contact with the enzyme solution and reduction of the Schiff base with sodium borohydride. The response characteristics of the biosensors obtained with these enzymatic membranes were determined and compared. The biosensor with best response characteristics, obtained by procedure (B), showed the following characteristics of response to urea: (i) linearity in the 10^{-4} to 10^{-2} M range; (ii) slope of up to 56 mV per decade; (iii) response time between 30 s and 2 min; and (iv) lifetime of 2 months. This biosensor was tested in the determination of urea in blood serum samples. © 1998 Elsevier Science B.V. All rights reserved.

Keywords: Urea potentiometric biosensor; Urease; Chitosan membrane; Blood serum

1. Introduction

Urease is an important enzyme in biological systems, where it catalyses the conversion of urea to carbon dioxide and ammonia. The coupling of this catalytic reaction with different tranducers has allowed the development of thermal [1–6], amperometric [7–10], conductimetric [11–14], optical [15–18], piezoelectric [19], potentiometric [20–44], and FET based [45,46] biosensors. Such biosensors have been receiving attention since their introduction in 1969 [20,21], but recently a upsurge of interest can be detected in the literature (almost 25% of the papers listed under References were published in or after 1995).

Potentiometric biosensors, based on the detection of either ammonium ion [20–31], ammonia gas [32–37], carbon dioxide [38] or pH change [39–41] produced by the enzymatic reaction, are among the most attractive biosensors for urea, because of the simplicity of their construction procedure and the general availability of the instrumentation required for their utilization. Commercial self-contained electrode probes based on ammonia gas selective electrodes coupled to im-

* Corresponding author. Tel.: +351 2 6082874; fax: +351 2 6082959; e-mail: amachado@fc.up.pt

0039-9140/98/$19.00 © 1998 Elsevier Science B.V. All rights reserved.
PII S0039-9140(98)00066-6

mobilized urease are available [47]. Previous work [29,30] showed that all-solid-state nonactin based ammonium ion selective electrodes are among the most adequate transducers for the development of potentiometric urea biosensors, due to their fast and reproducible response [26], and their long lifetime, up to 12 months [27]. The development of such potentiometric biosensors for determination of urea in blood serum deserves much interest, since urea is a biological product that is monitored in blood as an indicator of renal function.

Enzyme immobilization plays a fundamental role in the performance characteristics of biosensors based on ion selective electrodes. Ideally, a large amount of the active enzyme should be directly attached to the surface of the electrode membrane in a matrix without a diffusional barrier. However, the development of a biosensor for blood serum analysis not only requires that the sensing membrane polymer has adequate functional moieties for stable enzyme immobilization, but also that this polymeric material shows good compatibility with blood serum. PVC membranes do not fulfil these two conditions but sensing membranes made of polymers with better compatibility with blood proteins, like silicone [48], or with membranes of modified polymers to allow better enzyme immobilization, for instance modified PVC [49], usually show a less selective response than PVC based electrodes. Moreover membranes have been coupled to ion selective electrodes to modify the selectivity of their response, in which the pore size molecular cut-off of dialysis membranes [26] or transient electrostatic effects, for example in anion exchange membranes [28], are explored. The immobilization of urease on a membrane matrix with good blood compatibility and with good permeability to ammonium is desirable for the development of potentiometric enzyme biosensors based on ammonium selective electrodes.

Chitin, a linear polymer composed of near straight chains of β-(1→4)2-acetamido-2-deoxy-D-glucopyranose, kept together by strong interchain hydrogen bonding, is the second most abundant natural polysaccharide after cellulose. Upon deacetylation of chitin a related substance, chitosan, is obtained [50]. Both substances have been used for enzyme immobilization for industrial applications [51] and, as they are non-toxic and biocompatible [52], they are suitable as support materials for the construction of biosensors for measurements in blood serum samples. Very recently, enzymatic sensors with chitin and chitosan supports have been reported for determination of glucose [53], lactate [54], ethanol [55] and urea [56]. The literature on immobilization of urease on chitosan is dominated by the use of beads [57], but Krajewska et al. [58] immobilized urease on membranes of chitosan activated with glutaraldehyde. However, the chemistry of chitosan/glutaraldehyde reactions is complex [59] and the permeability of the membranes to several ions, including ammonium, decreases when the ratio of glutaraldehyde/chitosan used in the preparation is increased [60]. On the other hand, when the immobilization is based on Schiff base formation, leaching of the enzyme from the membrane can occur due to the reversibility of this reaction [61].

The aim of the present work was to develop a potentiometric urea biosensor, based on urease immobilized on a chitosan membrane, applied to an all-solid-state ammonium electrode. To obtain membranes with high enzyme loadings, with adequate permeability towards ammonium ion and without significant enzyme leaching, four different procedures of enzyme immobilization were attempted: (A) adsorption; (B) adsorption followed by reticulation with dilute aqueous glutaraldehyde solutions; (C) activation with glutaraldehyde followed by contact with the enzyme solution; and (D) activation with glutaraldehyde, contact with the enzyme solution and reduction of the Schiff base with sodium borohydride. The characteristics of the biosensors assembled with these membranes were studied and compared. A preliminary report of this work [56] included only results obtained by procedure (A). Biosensors with type B membranes showed the best response characteristics and were tested for the determination of urea in real samples of blood sera.

2. Experimental

2.1. Preparation of chitosan membranes

A solution was prepared by overnight stirring of 1 g of chitosan (Sigma) in 100 ml of 0.8% (w/v) acetic acid. The membranes were cast on polyethylene plates on a nylon mesh from a measured volume per surface area of 0.34 ml/cm^2, and formed upon drying at 60°C overnight. The next day they were neutralized with 1% NaOH solution for 30 min and washed with water. The membranes were kept under water until use for enzyme immobilization.

2.2. Enzyme immobilization

The procedures described below were used.

2.2.1. Adsorption based procedures

2.2.1.1. Procedure A (physical adsorption) [62]. The membranes were dipped in a pH 4 acetic acid solution, washed with water and then left overnight at ca. 5°C, in contact with an urease solution containing 2 mg of the enzyme (urease III, Sigma) per ml of a pH 5.6 phosphate buffer. The next day, the membranes were washed with water and with a pH 7.0 phosphate buffer solution.

2.2.1.2. Procedure B (adsorption followed by reticulation) [63]. Type A membranes were reticulated with a 0.01% glutaraldehyde solution for 60 min and then washed with water.

All the membranes, types A and B, were kept in a pH 7.0 phosphate buffer until use.

2.2.2. Activation based procedures

2.2.2.1. Procedure C (activation with glutaraldehyde) [64]. One of the sides of a membrane (2 cm^2) was activated with 0.02 ml of a 1% glutaraldehyde solution and was allowed to dry. Then, 0.02 ml of an urease solution with 2 mg/ml in a pH 5.6 phosphate buffer was spread on the same surface and left until dry. The membrane was washed with water and kept in a pH 7.0 phosphate buffer until use.

2.2.2.2. Procedure D (activation followed by reduction with sodium borohydride) [65]. Membranes of type C were treated with a sodium borohydride solution (5 mg/ml) dissolved in a pH 9.0 borate buffer. The reduction with this solution was carried out at ca. 5°C for 10 min. The membrane was washed with water and kept in a pH 7.0 phosphate buffer until use.

2.3. Determination of the activity of the immobilized enzyme

Measurements were made with an ammonium selective electrode (see Section 2.4) following a procedure described by Mascini and Palleschi [37]. Fifty milliliters of 0.1 M urea solution in 0.1 M (pH = 7) TRIS buffer were placed in a cell and, after stabilization of the potential difference, a piece of membrane with area previously measured (2–4 cm^2) was introduced into the solution and the variation of potential with time was recorded. The amount of ammonium ion produced along the time was calculated from a previously obtained calibration curve and the specific immobilized activity per unit area was calculated in μmol min^{-1} cm^{-2} (unit cm^{-2})

2.4. Construction of the ammonium electrode

All-solid-state ammonium ion selective electrodes with a nonactin cocktail dispersed in a PVC membrane applied on a conductive epoxy support [66] were used as base electrodes. Graphite powder (< 50 μm, Merck) was used to make the epoxy (Epoxy Technology, H54-UNF) conductive.

The membranes were constituted by evaporation of the solvent from a THF (Merck p.a.) solution of nonactin (Fluka Selectophore, Ionophore I) (2%), bis(2-ethylhexyl)adipate (Fluka, Selectophore) (68%) and PVC (Fluka, selectophore) (30%).

2.5. Assembly of the biosensors

The membranes with immobilized urease were applied to the tip of the ammonium electrodes (Φ = 10 mm) with a silicone ring.

2.6. Evaluation of the biosensors

Calibration curves in the range 0.02–20 mM were obtained by titration of 20 ml of a 0.1 M (pH = 7) TRIS buffer with a 0.1-M urea solution prepared with the same buffer as solvent.

2.7. Other equipment

The electrodes were calibrated at 25 ± 0.2°C and an Orion 90.02 double junction reference electrode (with TRIS buffer in the external compartment) was used.

The calibrations were carried out with an automatic system controlled by a Compaq personal computer, Prolinea 325S. The potential difference values were acquired with the AD converter of a Lab Master DMA (Scientific Solutions) card, through a high impedance circuit. A Crison Microbu2030 microburete, controlled via the RS 232C interface of the computer, was used for the addition of the standard solution.

2.8. Blood serum analysis

For the determinations, a urea biosensor and an ammonium electrode were used simultaneously and a differential measurement was made both in calibration and sample measurement [67]. A solution [26] containing ammonium chloride (0.0003 M), potassium chloride (0.002 M) and sodium chloride (0.140 M) was diluted tenfold with 0.1 M (pH = 7.0) TRIS buffer and used as a matrix for the calibration of the urea biosensor in the range 0.0001–0.02 M. Blood serum samples were also diluted (1:10) with 0.1 M (pH = 7.0) Tris buffer.

The blood serum samples were kindly provided by the Laboratório de Análises Clínicas of the Faculty of Pharmacy of Oporto. The results provided by this laboratory were used for comparison. They were obtained with an automatic analyzer using a two step enzymatic method based on urea to ammonium transformation by urease, followed by reaction of this ion with α-ketoglutarate in the presence L-glutamic dehydrogenase and NAD (nicotinamide adenine dinucleotide).

3. Results and discussion

3.1. Effect of the chitosan membranes on the ammonium electrode response

Similarly to cellulosic membranes, chitosan membranes are water swollen gels that can affect the response characteristics of the enzymatic electrodes. Calibration curves of the ammonium electrode showed that the slope of its response to ammonium was slightly lowered (Table 1) when the electrode was assembled with chitosan membranes without immobilized enzyme and that the lower limit of linear response was shifted from 5×10^{-5} to 1×10^{-4} M. Chitosan membranes with urease immobilized by adsorption (procedure A) showed no influence on the response to ammonium ion, but for electrodes assembled with membranes reticulated with glutaraldehyde (procedure B), the response was affected in about the same way as for the chitosan membrane (Table 1).

Table 1
Effect of the chitosan membranes on the response of the ammonium selective electrode[a]

Membrane	R	s	E^o
Without chitosan membrane	0.99996	57.9 ± 0.4	212.6 ± 0.9
	0.99991	57.4 ± 0.3	208.6 ± 0.8
	0.99997	57.9 ± 0.4	213.6 ± 1.0
Chitosan	0.9998	51.9 ± 0.5	197.8 ± 1.2
	0.9998	52.7 ± 0.4	197.3 ± 1.0
	0.9995	52.3 ± 0.3	196.5 ± 0.8
A	0.9998	58.4 ± 0.5	213.0 ± 1.4
	0.9997	58.3 ± 0.5	212.9 ± 1.4
	0.9996	57.8 ± 0.7	210.4 ± 1.6
B	0.9999	51.2 ± 0.9	192.1 ± 0.9
	0.9999	55.0 ± 0.4	201.2 ± 0.9
	0.9992	56.6 ± 2.0	202.7 ± 5.2

[a] Parameters obtained in the concentration range 5×10^{-4} to 10^{-2} M. R, correlation coefficient ($n = 6$); s, slope in mV/decade; E^o in mV, with reference to an Orion 90-02 reference electrode, both given with standard deviation.

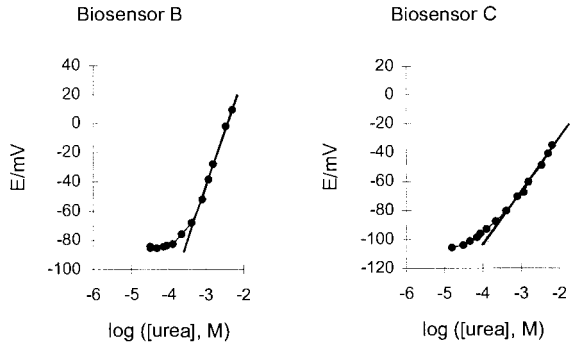

Fig. 1. Calibration curves of (urea) biosensors of types B and C.

3.2. Response characteristics of the urea biosensors

The immobilization of urease on chitosan by physical adsorption (procedure A) produced membranes with high activity of immobilized enzyme (19 units cm^{-2}). Reticulation of these membranes with glutaraldehyde (procedure B) decreased slightly the enzyme activity to 17 units cm^{-2} (with SD = ± 1.5, $n = 3$). Both activation based procedures rendered membranes with much lower activity (1–2 units cm^{-2} with SD = ± 0.3, $n = 3$).

Despite of this large difference in enzymatic activity, all the membranes produced urea biosensors with potentiometric response. Biosensors of types A and B showed linear response (response potential versus logarithm of urea concentration) in the range 1×10^{-4} to 1×10^{-2} M, while biosensors of types C and D showed linear response in the range 5×10^{-4} to 1×10^{-2} M (Fig. 1). This difference in the range of linear response is related to the permeability characteristics of the membranes [68] and the large difference in their enzymatic activity [69]. Besides the different values for the lower limit of linear response, Fig. 1 also shows a marked difference in the shape of the calibration curves obtained for biosensors of types B and C, which is a consequence of the large difference in enzymatic activity of the two types of membranes [69].

Table 2 summarizes the calibration parameters of the urea biosensors obtained along the time, during a couple of months. Biosensors of type B showed lifetimes longer than 2 months, while those of type A showed lifetimes of 1 month. Biosensors of type B showed higher slopes of response to urea than those of type A. The stability along time of the response potential of these biosensors to urea solutions (Table 2 and Fig. 2) showed that the response of biosensors of type B was more stable. The differences observed in the

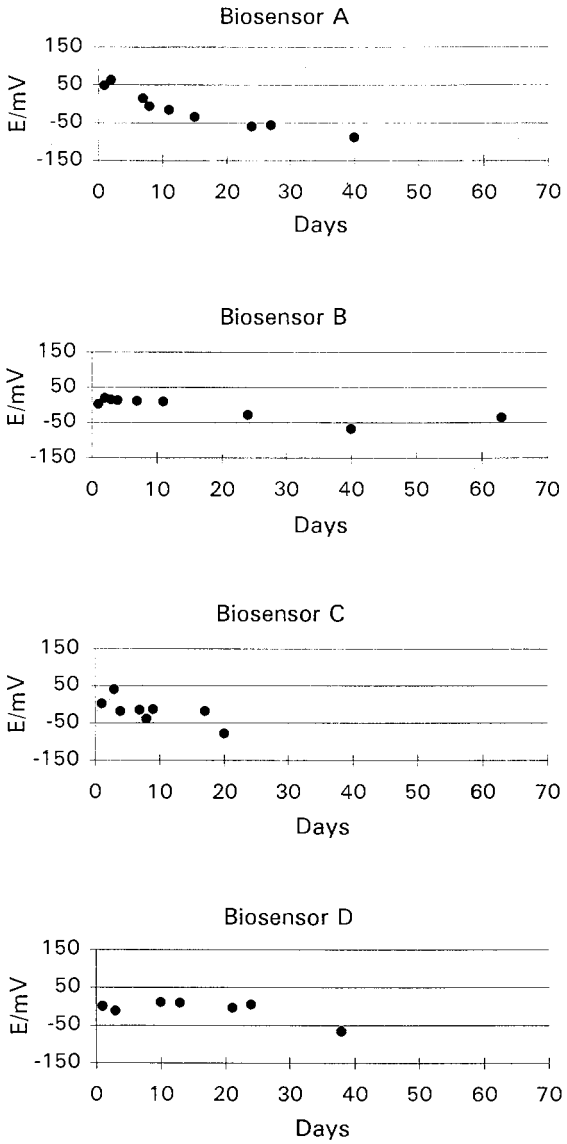

Fig. 2. Variation along the time of the response to a 2×10^{-3} M urea solution of biosensors of the four types.

Table 2
Calibration parameters of the urea biosensors A–D obtained on different days[a]

Biosensor A				Biosensor B				Biosensor C				Biosensor D			
Days	R	s	E°	Days	R	s	E°	Days	R	s	E°	Days	R	s	E°
1	0.9992	43.9 ± 0.9	167.0 ± 2.2	1	0.9997	52.3 ± 0.4	142.8 ± 1.3	1	0.9996	47.4 ± 1.5	71.4 ± 4.0	1	0.9997	52.3 ± 1.4	142.8 ± 3.5
2	0.9991	47.4 ± 1.3	192.1 ± 3.3	2	0.9995	45.8 ± 1.2	145.7 ± 2.7	3	0.9983	31.6 ± 1.2	29.0 ± 3.2	3	0.9997	37.8 ± 1.6	91.14.3 ± 4.1
7	0.9997	36.6 ± 0.9	112.7 ± 2.2	3	0.9997	52.2 ± 1.2	156.4 ± 3.2	4	0.9999	46.9 ± 2.0	60.9 ± 5.0	10	0.9997	37.3 ± 2.3	15.713.0 ± 5.9
8	0.9992	42.4 ± 0.9	107.1 ± 2.4	4	0.9993	56.6 ± 0.7	140.9 ± 1.7	7	0.9999	54.2 ± 1.6	5.9 ± 4.3	13	0.9990	35.8 ± 1.2	106.2 ± 3.0
11	0.9988	39.5 ± 1.3	89.6 ± 3.2	7	0.9997	43.3 ± 0.6	128.5 ± 0.9	8	0.9980	58.3 ± 2.2	81.5 ± 5.8	21	0.9996	38.0 ± 1.4	99.3 ± 3.7
15	0.9998	46.5 ± 0.8	90.2 ± 2.2	11	0.9992	40.8 ± 0.7	101.1 ± 1.6	9	0.9973	31. 8 ± 1.5	34.0 ± 4.0	24	0.9998	39.1 ± 0.9	110.7 ± 2.3
24	0.9996	41.4 ± 1.5	39.1 ± 3.5	24	0.9993	48.1 ± 0.8	101.7 ± 2.6	17	0.9999	36.3 ± 2.2	96.7 ± 5.7	38	0.9997	32.0 ± 2.4	20.7 ± 6.2
27	0.9990	47.6 ± 1.4	71.3 ± 3.5	40	0.9995	43.1 ± 0.7	147.5 ± 1.9	20	0.9900	29.2 ± 1.3	−15.1 ± 3.4				
40	0.9990	34.5 ± 2.0	52.3 ± 5.1	63	0.9999	46.9 ± 0.7	161.8 ± 1.7								

[a] See Table 1 footnote.

patterns of variation in Fig. 2, which shows a more marked decrease for type A than for type B biosensors, are related to the reticulation step in the procedure of enzyme immobilization. Biosensors of types A and B showed good response reproducibility within an working day, with standard deviations of the slope and E^o obtained in three consecutive calibrations lower than 1.5 mV/decade and 4 mV, respectively.

Biosensors of type C had a lifetime of only 2 weeks and showed a noisy response as shown by the values obtained for the parameters of the calibration curves (Table 2) and by the marked oscillations of the potentials in response to a 2×10^{-3} M urea solution obtained on different days (Fig. 2). The results obtained with biosensors of type D showed that reduction of the Schiff base with sodium borohydride produced no improvement of the response characteristics. Indeed biosensors of type D showed much lower slopes than those of type C except on the first day (Table 2).

The response time of the present urea biosensors varied from 30 s to 3 min depending on the urea concentration and on the type of the biosensor. The shortest response times were obtained for biosensors of type A (30 s to 2 min) and the longest for biosensors of type C (2–3 min). The response times for type B biosensors varied between 30 s and 2 min.

These results show that the best procedure for urease immobilization on chitosan membranes for obtaining potentiometric urea biosensors is adsorption of the enzyme followed by reticulation with dilute aqueous glutaraldehyde solutions. The urea biosensors assembled with these membranes (type B), showed characteristics competitive with those of other potentiometric urea biosensors based on coupling immobilized urease to ammonium selective electrodes [20–27]. Type B biosensors show longer lifetimes than biosensors based on urease immobilized in polyacrilamide [23,24]. The results also show that reticulation of the adsorbed enzyme significantly improves its stability as shown by the reproducibility of response and lifetime of type B biosensors. The linear response range and response time of type B biosensors are identical to most potentiometric biosensors based on coupling of urease to ammonium ion selective electrodes based on nonactin [23–27].

Table 3
Results obtained in the determination of urea in samples of blood sera

Sample	Urea (mg/100 ml)	
	Provided[a]	Found[b]
1	39	38.2 ± 0.9
2	62	64.0 ± 2.0
3	46	44.0 ± 1.0
4	19	23.0 ± 0.4
5	23	24.9 ± 0.2
6	38	37.0 ± 1.0
7	28	31.2 ± 0.6
8	32	33.2 ± 0.7
9	63	62.0 ± 2.0
10	27	29.0 ± 0.4
11	62	63.0 ± 1.0
12	45	46.9 ± 0.8

[a] See text.
[b] Average of three determinations with standard deviation.

3.3. Analysis of blood sera

Table 3 summarizes the results obtained in the determination of urea in samples of blood sera using a biosensor of type B. The value of the correlation coefficient (R) for the least squares linear regression of the urea concentration values determined with the potentiometric biosensor versus the values provided by the clinical analysis laboratory was 0.994, showing a good correlation between the results obtained by the two methods. The slope of the regression line is rather low, 0.94, but falls within the confidence limits (95% level) of 0.87 and 1.02. The value of the intercept for the regression line is 3.3 with confidence limits (95% level) of 0.15 and 6.49. This suggests that the method used for matrix correction, based on the results obtained in simultaneous measurements of ammonium with a ion selective electrode and urea with the biosensor of type B, is not fully adequate for the purpose of matrix correction.

4. Conclusions

Chitosan is an adequate material for the preparation of potentiometric urea biosensors based on coupling of enzymatic membranes with all-solid state PVC membrane ammonium electrodes with nonactin as sensor. The characteristics of response of these urea biosensors depend on the procedure used for enzyme immobilization. The biosensors with urease immobilized on chitosan membranes by adsorption followed by crosslinking with dilute aqueous glutaraldehyde solutions, showed the best characteristics of response, including the longest lifetime (more than 2 months).

Acknowledgements

Dra. Laura Pereira of the Laboratório de Análises Clínicas of the Faculty of Pharmacy of Oporto is thanked for providing serum samples and results of spectrophotometric measurements of their urea contents.

References

[1] B. Danielsson, K. Gadd, B. Mattiasson, K. Mosbach, Anal. Lett. 9 (1976) 987.
[2] C. Tran-Minh, D. Vallin, Anal. Chem. 50 (1976) 1874.
[3] S. Rich, R.M. Ianello, N.D. Jespersen, Anal. Chem. 51 (1979) 204.
[4] B. Xie, M. Mecklenburg, B. Danielsson, O. Ohman, P. Nolin, F. Winquist, Analyst 120 (1995) 155.
[5] B. Xie, B. Danielsson, Anal. Lett. 29 (1996) 1921.
[6] S.P. Fulton, C.L. Cooney, J.C. Waever, Anal. Chem. 52 (1980) 505.
[7] D. Kirstein, F. Scheller, Anal. Chim. Acta 171 (1985) 345.
[8] P.C. Pandey, A.P. Mishra, Analyst 113 (1988) 329.
[9] S.B. Adeloju, S.J. Shaw, G.G. Wallace, Anal. Chim. Acta 323 (1996) 107.
[10] P. Bertocchi, D. Compagnone, G. Palleschi, Biosens. Bioelectron. 11 (1996) 1.
[11] S.R. Mikkelsen, G.A. Rechnitz, Anal. Chem. 61 (1989) 1737.
[12] D.C. Cullen, R.S. Sethi, C.R. Lowe, Anal. Chim. Acta 231 (1990) 33.
[13] K. Chen, D. Liu, L. Nie, S. Yao, Talanta 41 (1994) 2195.
[14] N.F. Sheppard Jr., D.J. Mears, A. Guiseppi-Elie, Biosens. Bioelectron. 11 (1996) 967.
[15] T.K. Rhines, M.A. Arnold, Anal. Chim. Acta 227 (1989) 387.
[16] X. Xie, A.A. Suleiman, G. Guilbault, Talanta 38 (1991) 1197.
[17] C. Stamm, K. Seiler, W. Simon, Anal. Chim. Acta 282 (1993) 229.
[18] H. Li, O.S. Wolfbeis, Anal. Chim. Acta 276 (1993) 115.
[19] Y. Xu, C. Lu, Y. Hu, L. Nie, S. Yao, Anal. Lett. 29 (1996) 1069.
[20] G. Guilbault, J. Montalvo, Anal. Chem. 41 (1969) 1897.
[21] G. Guilbault, J. Montalvo, J. Am. Chem. Soc. 91 (1969) 2164.
[22] G. Guilbault, E. Hrabankova, Anal. Chim. Acta 52 (1970) 287.
[23] G. Guilbault, E. Nagy, Anal. Chem. 45 (1973) 417.
[24] G. Guilbault, E. Nagy, S.S. Kuan, Anal. Chim. Acta 67 (1973) 195.
[25] K. Yasuda, H. Miyagi, Y. Tanaka, Analyst 109 (1984) 61.
[26] G. Palleschi, M. Mascini, E. Martinez-Fábregas, S. Alegret, Anal. Lett. 21 (1988) 1115.
[27] S. Alegret, E. Martinez-Fábregas, Biosens. Bioelectron. 4 (1989) 287.
[28] S.A. Rosário, G.S. Cha, M.E. Meyerhoff, Anal. Chem. 62 (1990) 2418.
[29] Z. Zamponi, B. Lo Cicero, M. Mascini, L. Della Ciana, S. Sacco, Talanta 43 (1996) 1373.
[30] J. Grácia, M. Poch, D. Martorell, S. Alegret, Biosens. Bioelectron. 11 (1996) 53.
[31] M.H. Gil, A.P. Piedade, S. Alegret, J. Alonso, E. Martinez-Fábregas, A. Orelana, Biosens. Bioelectron. 7 (1992) 645.
[32] A. Llenardo, G.A. Recknitz, Anal. Chem. 46 (1974) 1109.
[33] M. Mascini, G. Guilbault, Anal. Chem. 49 (1977) 795.
[34] L. Campanella, M. Pia-Sammartino, M. Tomassetti, Analyst 115 (1990) 827.
[35] K. Narinesingh, R. Mungal, T.T. Ngo, Anal. Chim. Acta 249 (1991) 387.
[36] S.B. Butt, K. Camman, Anal. Lett. 25 (1992) 1597.
[37] M. Mascini, G. Palleschi, Anal. Chim. Acta 145 (1983) 213.
[38] G. Guilbault, Anal. Chem. 44 (1972) 2161.
[39] I. Wacerz, R. Konki, E. Leszczynska, S. Glab, Anal. Chim. Acta 315 (1995) 289.
[40] S. Glab, R. Koncki, E. Kopczewska, I. Wacerz, A. Hulaniki, Talanta 41 (1994) 1201.
[41] R. Koncki, E. Kopczewska, S. Glab, Anal. Lett. 27 (1994) 475.
[42] S.B. Adeloju, S.J. Shaw, G.G. Wallace, Anal. Chim. Acta 28 (1993) 1611.
[43] S.B. Adeloju, S.J. Shaw, G.G. Wallace, Anal. Chim. Acta 28 (1993) 621.
[44] E.C. Hernandez, A. Witkowski, S. Daunert, L.G. Bachas, Mikrokim. Acta 121 (1995) 63.
[45] F. Winquist, A. Spetz, I. Lundstrom, Anal. Chim. Acta 163 (1984) 143.
[46] N. Kazanskaya, A. Kukhtin, M. Manenkova, N. Reshetilov, L. Yarysheva, O. Arzhakova, A. Volynskii, N. Bakeyev, Biosens. Bioelectron. 11 (1996) 253.

[47] S.S. Kuan, G.G. Guilbalt, Ion-selective electrodes and biosensors based on ISEs, in: A.P.F. Turner, I. Karube, G.S. Wilson (Eds.), Biosensors, Fundamentals and Applications, Oxford Science, Oxford, 1989, p. 150.
[48] G.S. Cha, D. Liu, M.E. Meyerhoff, H.C. Cantor, A.R. Midgeley, H.K. Goldberg, R.B. Brown, Anal. Chem. 63 (1991) 1666.
[49] V.V. Cosofret, W.W. Olson, S.A.M. Marzouk, M. Erdosy, T.A. Johnson, R.P. Buck, Analyst 119 (1997) 2283.
[50] R.A.A. Muzzarelli, Chitin, Pergamon, London, 1977, p. 62.
[51] S. Hirano, Production and application of chitin and chitosan in Japan, in: G. Skja-Braek, T. Anthonsen, P. Sandford (Eds.), Chitin and Chitosan, Sources, Chemistry, Biochemistry, Physical Properties and Applications, Elsevier, Amsterdam, 1988, p. 37.
[52] M. Nakajima, K. Atsumi, K. Kifune, Development of absorbable sutures from chitin, in: J.P. Zikakis (Ed.), Chitin, Chitosan and Related Enzymes, Academic Press, New York, 1984, pp. 407–410.
[53] E. Ohashi, T. Koriyama, Anal. Chim. Acta 262 (1992) 19.
[54] S. Hikima, T. Kakizaki, M. Taga, K. Hasebe, Fresenius' J. Anal. Chem. 34 (1993) 607.
[55] Y. Kurauchi, T. Yanai, N. Egashira, K. Ohga, Anal. Sci. 10 (1994) 213.
[56] J.M.C.S. Magalhães, A.A.S.C. Machado, Enzyme immobilization on chitin and chitosan for the construction of enzymatic sensors, in: G. Guilbault, M. Mascini (Eds.), Uses of Immobilized Biological Compounds for Detection, Medical, Food and Environmental Analysis, Kluer, Dordrecht, 1993, p. 191.
[57] P.A. Sandford, Chitosan: commercial uses and potential applications, in: G. Skja-Braek, T. Anthonsen, P. Sandford (Eds.), Chitin and Chitosan, Sources, Chemistry, Biochemistry, Physical Properties and Applications, Elsevier, Amsterdam, 1988, p. 51.
[58] B. Krajewska, J. Chem. Technol. Biotechnol. 52 (1991) 157.
[59] R.A.A. Muzzarelli, Analyst 119 (1997) 136.
[60] S. Nakatsuka, A.L. Andry, J. Appl. Polym. Sci. 44 (1992) 17.
[61] K. Peters, F.M. Richards, Ann. Rev. Biochem. 46 (1977) 523.
[62] A. Roosevear, J.F. Kennedy, J.M.S. Cabral, Immobilized Enzymes and Cells, Adam Hilger, Bristol, 1987, p. 89.
[63] A. Roosevear, J.F. Kennedy, J.M.S. Cabral, Immobilized Enzymes and Cells, Adam Hilger, Bristol, 1987, p. 95.
[64] A. Roosevear, J.F. Kennedy, J.M.S. Cabral, Immobilized Enzymes and Cells, Adam Hilger, Bristol, 1987, p. 109.
[65] A. Roosevear, J.F. Kennedy, J.M.S. Cabral, Immobilized Enzymes and Cells, Adam Hilger, Bristol, 1987, p. 110.
[66] A.A.S.C. Machado, Analyst 119 (1994) 2263.
[67] E.A.H. Hall, Biosensors, Open University Press, Buckingham, 1990, p. 276.
[68] M.L. Davies, B.J. Tighe, Selective Electrode Rev. 13 (1991) 159.
[69] E.A.H. Hall, Biosensors, Open University Press, Buckingham, 1990, p. 271.

ELSEVIER

Talanta 47 (1998) 193–202

Talanta

The H-point and generalized H-point standard additions methods for flow injection procedures

P. Campíns-Falcó *, F. Blasco Gómez, F. Bosch-Reig

Departament de Química Analítica, Facultat de Química; Universitat de Valencia, C/ Dr. Moliner 50, E46100, Burjassot, Valencia, Spain

Received 26 November 1997; received in revised form 9 February 1998; accepted 11 February 1998

Abstract

This paper establishes the fundamentals of the H-point standard additions method (HPSAM) and generalized H-point standard additions method (GHPSAM) in the flow injection technique. Two kinds of analytical signals can be employed, FIA peaks and spectra. Different analytical problems have been studied: determinations of one analyte in the presence or absence of matrix effect when different blank features are present, and determination of two analytes in the presence of blank bias error affecting the development of one of them. The determination of chloride with mercury thiocyanate which presents a matrix effect, and the determinations of calcium and/or magnesium with arsenazo III are examined. The methods were compared with conventional data treatment and proved able to isolate the analyte signal from the global one, thus providing accurate and precise results in the determination of the above mentioned species in bottled waters. No additional experimental work is needed to apply the methods. © 1998 Elsevier Science B.V. All rights reserved.

Keywords: Flow injection; Blank bias error; Chloride determination; Calcium and magnesium determination

1. Introduction

The H-point standard additions method (HPSAM) proposed by us [1–3] makes it possible to evaluate and eliminate the systematic error that the excess of reagent introduces in determinations which use absorbent reagents [4–6]. The method can isolate the blank signal from the total analytical signal using absorbance increments that only depend on the analyte concentration.

In this report the basis of the HPSAM method is established when an on-line technique (flow injection) is used. In addition it is demonstrated that the generalized H-point standard additions method (GHPSAM), proposed in ref. [3] for analyte determinations in unknown samples, can be effectively used to solve a specific blank feature in flow injection. In order to avoid the blank signal it is usually subtracted from the total analytical signal [7] or eliminated from a chemical or physical process [8]. This topic has received little attention in the literature.

* Corresponding author. Tel.: +34 6 3983002; fax: 34 6 3864436; e-mail: pilar.campins@uv.es

0039-9140/98/$19.00 © 1998 Elsevier Science B.V. All rights reserved.
PII S0039-9140(98)00067-8

In order to adapt the method to flow injection, a new variable, time, which is not taken into account in the batch method, is introduced. The signals provided by this technique are the variation in the absorbance with time and variation in the absorbance with wavelength. When the first records are used it is necessary to define the equations that will allow the concentration of the analyte to be calculated. On the other hand, if the data used, are spectra, the HPSAM equations defined in previous studies are effective.

The HPSAM and the GHPSAM are used to determinate of chloride with mercury thiocyanate and iron(III), and to simultaneously determine calcium and magnesium with arsenazo III. The determinations were carried out in mineral and synthetic waters.

2. Theoretical background

The two kinds of data to be treated are FIA peaks and the spectra recorded at the time which provides the maximum signal for the formed derivate:

2.1. FIA peaks

X is the analyte to be determined and Y the response of the blank. The FIA peaks are shown in Fig. 1 for a given concentration. There are two possible situations to deal with. The first (case a) is the treatment of data in which the Y signal can be considered constant, and the other one (case b) is the treatment of data in which the Y signal can be considered a line with a slope different from zero at given time range.

In the first case (case a) a straight line with a zero slope will be obtained when the reagent is injected (external blank). This signal should agree with the register obtained by plotting the ordinate of the calibration graphs calculated at each time if no consumption of the blank is produced through the calibration graph.

The concentration of the analyte can be calculated without systematic error by selecting a couple of times (t_1 and t_2) at which the signal of the blank ($A_{Y,t1}$ and $A_{Y,t2}$) presents the same intensity and the analyte absorbance values are different. The HPSAM calibration graph is the increment in the absorbance of standards at t_1 and t_2 as a function of the concentration. This equation is the same even if a different blank consumption is produced in terms of the analyte concentration. The method can be described as multivariate because there are several pairs of times that fulfil that condition.

The analyte concentration (C_x) can be calculated according to the following equation:

$$C_H = \frac{A_{S,t_1} - A_{S,t_2}}{M_{t_1} - M_{t_2}} = \frac{(A^0_{X,t_1} - A^0_{X,t_2}) + (A_{Y,t_1} - A_{Y,t_2})}{M_{t_1} - M_{t_2}} = \frac{A^0_{X,t_1} - A^0_{X,t_2}}{M_{t_1} - M_{t_2}} = -C_X \quad (1)$$

where $A_{S,t1}$ and $A_{S,t2}$ are the measured absorbance of the sample at t_1 and t_2; $A_{X,t10}$ and $A_{X,t20}$ are the absorbances of the analyte in the sample at t_1 and t_2; $A_{Y,t1}$ and $A_{Y,t2}$ are the absorbances of the interferent in the sample at t_1 and t_2, and, M_{t1} and M_{t2} are the slopes obtained

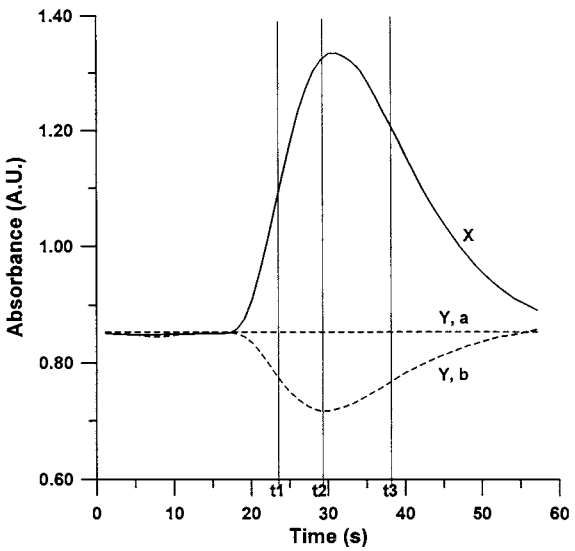

Fig. 1. Theorethical FI peaks, for an injection of a standard (X), and an injection of the reagent (Y). Y, a case: The reagent signal can be considered as linear. Y, b case: Due to the concentration gradient and the consumption of the reagent the signal is not constant.

from the calibration curve at t_1 and t_2. If matrix effect is known not to be present, standard additions are not needed.

$A_{S,t1}$ and $A_{S,t2}$ are equal to:

$$A_{S,t_1} = A^0_{X,t_1} + A_{Y,t_1} \quad (2)$$

$$A_{S,t_2} = A^0_{X,t_2} + A_{Y,t_2} \quad (3)$$

Case b is specific for the flow injection technique because a concentration gradient with time is produced. To resolve case b it is necessary to locate a time range in which that signal could be considered linear. This is easy when derivative spectrophotometry is used, as is demonstrated in ref. [3], where the generalized HPSAM (GHPSAM) was proposed for analyte determinations in unknown samples for the spectrophotometric field. The method locates the linear behaviour for the global interference without any previous data on it.

In order to locate linear profiles for the reagent in the calibration set, it is only necessary to calculate the quotient of the second derivative of the sample ($A''_{S,ti}$) spectra and the second derivative of the analyte molar absorption (ϵ''_{ti}) at each measured time. The time interval in which the quotient can be considered constant is the linear interval for the reagent signal. ϵ''_{ti} is calculated from the slopes of the calibration lines obtained from the second derivative spectra of the different solutions. After this, the method validates the linearity supposition and estimates the analyte concentration free from bias error.

Two different situations can appear, one in which this signal is the same regardless of the analyte concentration, and another in which the signal varies as a function of the amount of analyte. The two options can be solved by the method, as will be demonstrated in the next section.

To resolve the problem in flow injection analysis (FIA), the absorbance must be measured at three times (t_1, t_2 and t_3) instead of three wavelengths. In this way the analytical signals to be processed are absorbance increments ($\Delta A_{S(t3-t2)}$ and $\Delta A_{S(t2-t1)}$), and the calibration graph includes two lines. The crossing of both curves, which is called the H-point, gives the concentration of the sample analyzed.

The only condition needed is that the analyte can not present a linear behaviour at the three times selected. As can be deduced from Fig. 1, it is possible to choose from a large range of times and to select different trios of times. The unknown concentration can be calculated by means of the following equation:

$$C_H = \frac{q\Delta A_{S(t_2,t_1)} - p\Delta A_{S(t_3,t_2)}}{p(M_{t_3} - M_{t_2}) - q(M_{t_2} - M_{t_1})} = \frac{q(A^0_{X,t_2} - A^0_{X,t_1}) - p(A^0_{X,t_3} - A^0_{X,t_2})}{p(M_{t_3} - M_{t_2}) - q(M_{t_2} - M_{t_1})} = \frac{A^0_{X,t_2} - qA^0_{X,t_1} - pA^0_{X,t_3}}{qM_{t_1} + pM_{t_3} - M_{t_2}} = C_X \quad (4)$$

$\Delta A_{S(t3-t2)}$ and $\Delta A_{S(t2-t1)}$ are the absorbance increments of the sample; $A_{X,t3}$ is the absorbance of the analyte in the sample at t_3; $A_{Y,t3}$ is the absorbance of the interferent at t_3 and M_{t3} is the slope of the calibration curve at t_3.

$\Delta A_{S(t3-t2)}$ and $\Delta A_{S(t2-t1)}$ are equal to:

$$\Delta A_{S(t_2-t_1)} = A_{S,t_2} - A_{S,t_1} = (A^0_{X,t_2} + A_{Y,t_2}) - (A^0_{X,t_1} + A_{Y,t_1}) \quad (5)$$

$$\Delta A_{S(t_3-t_2)} = A_{S,t_3} - A_{S,t_2} = (A^0_{X,t_3} + A_{Y,t_3}) - (A^0_{X,t_2} + A_{Y,t_2}) \quad (6)$$

p and q are defined by the expressions:

$$p = \frac{t_2 - t_1}{t_3 - t_1} \qquad q = \frac{t_3 - t_2}{t_3 - t_1} \quad (7)$$

and if t_2 is the central value between t_1 and t_3, then $p = q = 1$. As mentioned above, if there is no matrix effect, M_{t1}, M_{t2} and M_{t3} values correspond to the slopes of the calibration graphs with standards at t_1, t_2 and t_3. Case a shown in Fig. 1 can be also solved following this method.

2.2. Spectra

By selecting a time which provides the maximum signal during the injection, we obtain the spectrum of the derivate at the measured wavelengths. In this case the HPSAM or GHPSAM can be employed in the same way as those pro-

posed for batch procedures. The analytical signals used are different if the goal is to solve a mixture of an analyte with the absorbent reagent [4,5] than if the goal it is to solve the mixture of two analytes with the absorbent reagent [6,9].

2.2.1. Determination of one analyte

The method works with pairs of reagent wavelengths with the same absorbance values. The absorbance increments depend only on the analyte concentration. Hence, plotting $\Delta A_{\lambda 1,\lambda 2}$ vs. C_i leads to a straight line with zero intercept and a slope of $M_{\lambda 1} - M_{\lambda 2}$. This line shows no influence of the free reagent, because at each point its absorbance is cancelled, even when its contribution to the absorbance value differs from one solution to another. The analyte concentration can be calculated according to the following equation:

$$
\begin{aligned}
-C_H &= \frac{A_{S,\lambda_1} - A_{S,\lambda_2}}{M_{\lambda_1} - M_{\lambda_2}} \\
&= \frac{(A^0_{X,\lambda_1} - A^0_{X,\lambda_2}) + (A_{Y,\lambda_1} - A_{Y,\lambda_2})}{M_{\lambda_1} - M_{\lambda_2}} \\
&= \frac{(A_{X,\lambda_1} - A^0_{X,\lambda_2})}{M_{\lambda_1} - M_{\lambda_2}} = -C_X
\end{aligned} \tag{8}
$$

where $A_{S,\lambda 1}$ and $A_{S,\lambda 2}$ are the absorbances of the sample at the two selected wavelengths λ_1 and λ_2; $A^0_{X,\lambda 1}$ and $A^0_{X,\lambda 2}$ are the absorbances of the analyte in the sample, and $A_{Y,\lambda 1}$ and $A_{Y,\lambda 2}$ are the absorbances of the reagent. $M_{\lambda 1}$ and $M_{\lambda 2}$ are the slopes of the calibration graphs with standards or with the standard additions method if a matrix effect is present, at the two selected wavelengths.

2.2.2. Determination of two analytes

When the reagent Z is used to determine two analytes, X and Y, the problem can be solved by the HPSAM as a ternary mixture. For solving the X concentration, pairs of wavelengths where the following equation is satisfied must be selected.

$$
\frac{A_{Y,\lambda_1}}{A_{Y,\lambda_2}} = \frac{A_{Z,\lambda_1}}{A_{Z,\lambda_2}} = r_{Y,Z} \tag{9}
$$

Only one spectrum of species 'Y' and another of species 'Z' are needed. The quotient between the two spectra is then applied and the wavelength pairs that show the same value for this quotient are sought. This relationship is equal at the two selected wavelengths, regardless of the Y and Z concentrations chosen. There are generally several pairs of wavelengths to choose from. The $r_{Y,Z}$ factor transforms situation (a) into (b), as can be seen in Fig. 2.

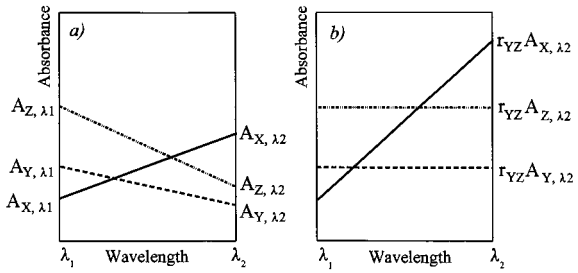

Fig. 2. Signals of the three components of the sample (X, Y and Z) at the wavelengths λ_1 and λ_2 before the employement of the correction r_{YZ} factor (a case) and final signals after using the r_{YZ} factor (b case). Since the r_{YZ} factor operates in λ_2 $A_{X,\lambda 1}$, $A_{Y,\lambda 1}$ and $A_{Z,\lambda 1}$ are the same in a and b cases.

The concentration of X can be calculated from the equation:

$$
-C_H = \frac{A_{S,\lambda_1} - r_{Y,Z}A_{S,\lambda_2}}{r_{Y,Z}M_{X,\lambda_1} - M_{X,\lambda_2}} = \frac{A^0_{X,\lambda_1} - r_{Y,Z}A_{X,\lambda_2}}{r_{Y,Z}M_{X,\lambda_1} - M_{X,\lambda_2}} \tag{10}
$$

where $A_{S,\lambda 1}$ and $A_{S,\lambda 2}$ are the absorbance values presented by the sample at the two chosen wavelengths and $M_{X,\lambda 1}$ and $M_{X,\lambda 2}$ are the slopes of the standard additions method for X or, if the matrix effect is known not to be present, the molar absorption coefficients for species X at the two wavelengths. $A^0_{X,\lambda 1}$ and $A^0_{X,\lambda 2}$ are the absorbance values of species X in the sample. Therefore, the calculated concentration corresponds to compound X.

Similar equations for solving species Y from $r_{X,Z}$ factor can be described.

3. Experimental

3.1. Apparatus

A detection system consisting of a Hewlett-Packard HP8453 UV-Visible spectrophotometer,

equipped with a 10 mm pathlength quartz cell was used. The FIA peaks were recorded every second from 0 to 60 s, and the spectra every nanometer from 200 to 800 nm. The spectrophotometer was interfaced to a Hewlett-Packard Vectra XM 5/90 personal computer, equipped with G1115AA software.

The pH was measured with a Crison micropH 2000 pH-meter.

3.2. Reagents

The following reagents were used: $Hg(SCN)_2$ (Riedel-de Haën AG) 2×10^{-3} M; $Fe(NO)_3 \times 9H_2O$ 0.12 M (Panreac, Montplet and Esteban, Barcelona, Spain); Cl^- stock solution of NaCl (Probus, Badalona (Barcelona), Spain) 0.085 M; Ca (II) stock solution of $CaCl_2$ (Probus) 0.125 M; Mg (II) stock solution from $MgCl_2 \times 6H_2O$ 0.125 M (Probus); Arsenazo III 0.245 g l^{-1}; 0.1M NH_3/NH_4^+ pH = 8.5 buffer and 10 M NH_3/NH_4^+ pH = 10 from NH_3 (Probus) and NH_4Cl (Probus); NaOH (Probus); HNO_3 60% (Panreac); $CaCl_2$ (Probus); $Mg(NO_3)_2$ (Probus); Na HCO_3 (Merck); Methanol (Scharlau, Barcelona, Spain); Ethylendiamintetraacetic acid disodium salt, EDTA (Probus); Eriochrome black T and murexide (Probus, used as solid reagents diluted in NaCl). Water was distilled and then deionized using a Sybron/Barnstead (IZASA, Madrid, Spain) Nanopure II purification system, followed by filtration over a Hollow Fibre Filter 0.2 μm (Barnstead D3750).

Two samples of water were processed for chloride determination, the first one was a commercial water (Cardó®) and the second was a synthetic water prepared in our laboratory.

Their compositions were: 400.2 ppm of HCO_3^-, 85.7 ppm of Ca^{2+}, 33.5 ppm of Mg^{2+}, 16.0 ppm of Cl^-, 20.0 ppm of SO_4^{2-} and 7.2 ppm of Na^+ for Cardó® water and 406.6 ppm of HCO_3^-, 85.6 ppm of Ca^{2+}, 33.4 ppm of Mg^{2+}, 15.2 ppm of Cl^-, 20.7 ppm of SO_4^{2-} and 9.9 ppm of Na^+ for the synthetic water.

The calibration sets for the determination of calcium and magnesium consisted in five standards, their concentrations were; 0, 3.1, 6.2, 9.3 and 12.4 ppm for Calcium and 0, 1.8, 3.7, 5.5 and 7.3 ppm for Magnesium. For the determination of Calcium and Magnesium simultaneously a calibration set of 25 standards was built, the composition of the standards was derived from all the possible combination of the above mentioned concentrations. Five commercial waters and another one synthetic were tested, and the results were compared with those obtained by the complexometric titration with EDTA. The tritations were done three times a day for three consecutive days. The spectrophotometric results correspond to nine replicates done on different days.

3.3. Procedures

The reagent employed for the chloride determination was prepared by mixing the appropriate amount of $Hg(SCN)_2$ dissolved in methanol with the appropriate amount of $Fe(NO)_3 \times 9H_2O$ dissolved in distilled water in an acidic medium (HNO_3). The final concentrations were: $Hg(SCN)_2$ 2×10^{-3} M, $Fe(NO)_3 \times 9H_2O$ 0.12 M, methanol 15% (v/v) and HNO_3 0.4% (v/v).

The chloride determination was carried out following the standard additions method because of the known presence of matrix effect.

The total hardness of the waters by using EDTA titration was measured at pH = 10, buffered with NH_3/NH_4^+ buffer; Eriochrome black T was used as an indicator. Calcium determination by using EDTA titration was performed at pH > 12, and murexide was used as an indicator. The magnesium concentration was then obtained by subtracting.

The commercial waters were diluted with NH_3/NH_4^+ pH = 8.5 buffer, to give concentrations of Ca^{2+} and Mg^{2+} included in the calibration set.

3.4. Fi assembly

The FI assembly is shown in Fig. 3. The same assembly was employed for both determinations (Cl^- and, Ca^{2+} and Mg^{2+}). For the chloride determination the reagent was the mixture previously described and the carrier was distilled water.

For the Ca^{2+} and Mg^{2+} determinations the employed reagent was Arsenazo III and the carrier was NH_3/NH_4^+ 0.1 M pH = 8.5 buffer.

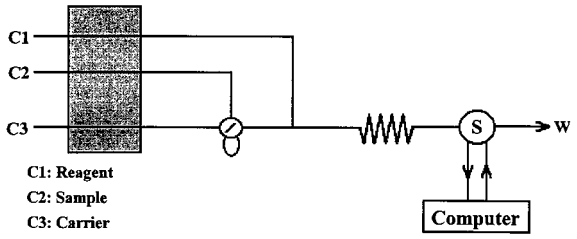

Fig. 3. FI assembly employed for the determination of Cl^-, Ca^{2+}, Mg^{2+} and Ca^{2+} and Mg^{2+}. Loop volume: 50 μl, coil length: 100 cm. Flow rate: 1.75 ml min^{-1}. W: Waste, S: Spectrophotometer.

In both cases the loop was 50 μl and the coil was 100 cm long. The flow rate was 1.75 ml min^{-1}.

4. Results and discussion

4.1. Chloride determination

4.1.1. Study of the blank shape

In Fig. 4 can be seen a FIA peak for a given concentration of chloride of the synthetic sample (see experimental section) and the FIA peak of the internal blank, defined in ref. [5] as the intercept of the analyte calibration lines at the different times in the range of times at which the peak appears. This value represents the behaviour of the blank in the calibration step because it is obtained by extrapolation from the calibration data on the analyte in the presence of the reagent. The synthetic sample is used because the exact chloride concentration is known. As can be seen, it corresponds to case b, postulated in the fundamentals section. The GHPSAM could then be employed to eliminate the blank bias error in the analyte determination.

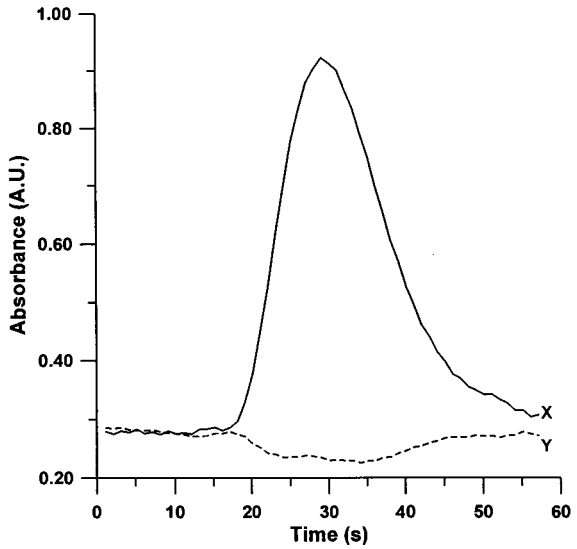

Fig. 4. FI peaks for an injection of the chloride sample (synthetical water) added with 7 ppm of Cl^- from a standard solution (X). Intercept or internal blank, obtained by regression of the calibration set at each time (Y).

4.1.2. Location of the linear interval for the reagent

Fig. 5 shows the plot employed for testing the linear behaviour of the reagent. The possible divisions by zero (inflexion points for the analyte) of the lines must be considered in order to eliminate them because of the abnormally high or low values that can be calculated. It can be seen that the linearity interval is similar for the different concentrations tested. The quotient $A''_{S,ti}/\epsilon''_{ti}$ is equal to C_X (analyte concentration) if the analytical signal of the reagent is linear in a given interval of time, $t_i \in [t_1, t_2]$. The C_X value obtained from the quotient $A''_{S,ti}/\epsilon''_{ti}$ versus t_i should be considered an approximate value, not a definitive one, as was demonstrated in ref. [3].

4.1.3. Determination of chloride in waters

Two waters were analyzed. The first one was a commercial water (Cardó®) and the second was a synthetic water prepared in the laboratory. Their composition are given in the experimental section.

The data was treated following the conventional calibration, GHPSAM and HPSAM (in this case approximating the blank signal to the case a of the Fig. 2). The calibration curve equations were: $y = 0.0151x - 0.0382$, $r^2 = 0.9975$ measuring at $t = 30$ s for the conventional method; $y = 0.0243x - 0.0076$, $r^2 = 0.9975$ for the GHPSAM using 47–34–17 absorbance increment and $y = 0.0131x - 0.0088$, $r^2 = 0.9899$ for the HPSAM using 30–55 absorbance increment. The best value for the ordinate corresponds to that provided by the GHPSAM. Both the GHPSAM

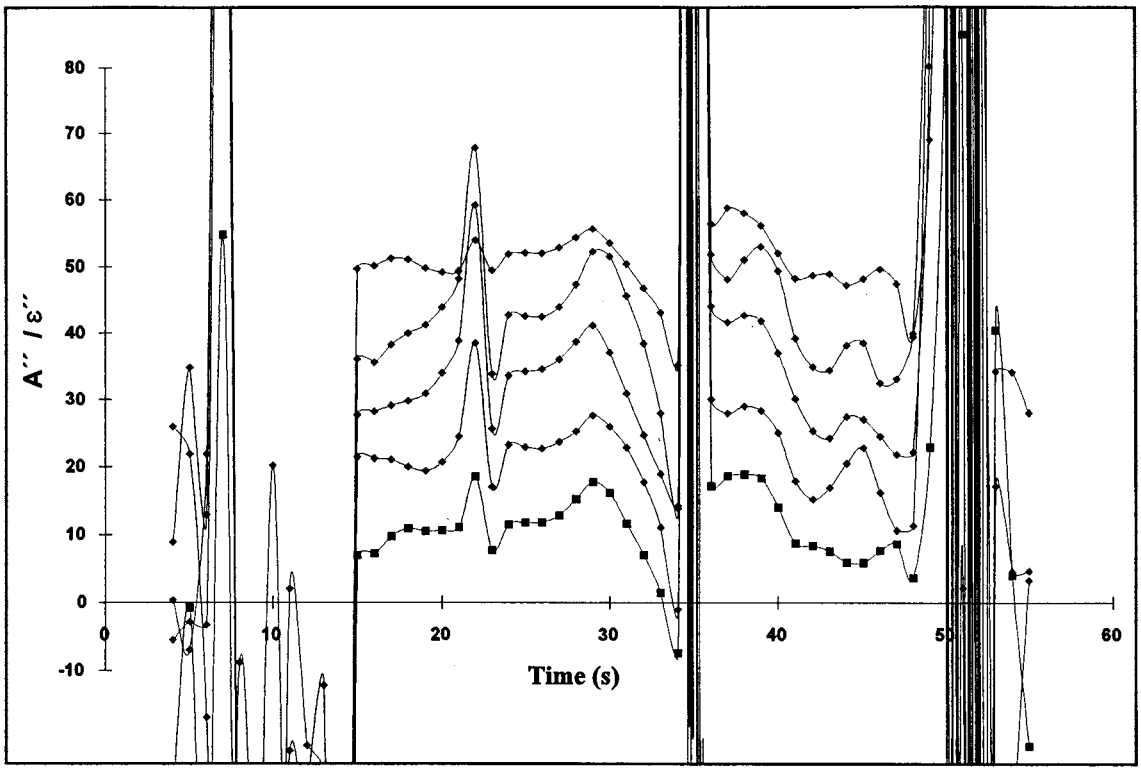

Fig. 5. Quotients between the second derivative spectra of the calibration set solutions and the second derivative molar absorption of the analyte quotient vs time. Sample: (■), additions: (◆). Cl^- in the sample: 15.2 ppm ($C_X = 15.2$). Additions of 0, 6.8, 12.6, 18.7 and 24.9 ppm of Cl^-. $A''_{S,ti}/\epsilon''_{ti}$ is approximately equal to C_X in the time interval in which this quotient value can be considered constant.

and HPSAM methods can eliminate the blank analytical signal from the total analytical signal even if it varies with the analyte concentration. The HPSAM also provides a good calibration graph because the record of the blank does not vary greatly. The worst ordinate value is obtained when the data are treated in the conventional way.

With the GHPSAM it is possible to predict the sample and the additions used to construct the model. The prediction of the concentrations of the different standard additions can serve as a measurement of the quality of the model. The trios of times used were: 41–30–17, 41–32–17, 41–34–17, 47–30–17, 47–32–17, 47–34–17, 47–38–17, 48–30–17, 48–30–17, 48–38–17 and 49–34–17. The estimated concentration is calculated as a mean value. GHPSAM offers advantages over conventional calibration that result in a smaller error in the additions prediction. The decrease in the prediction error is more important the lower the standard concentration assayed (4.6 and 11.1% of relative error, for the GHPSAM and conventional method respectively, for the most diluted standard). The increased accuracy in the standard prediction means a better prediction of the unknown sample.

When the synthetic water (exact concentration known) was analyzed, very good results were obtained. The prediction error was 1.4%, while the results achieved with the conventional method with standard addition were affected by an error of 17.1%. The error in the prediction of Cardó® water was 17.1 and 27.6% for the GHPSAM and conventional method respectively, using the declarated values on the bottle. The standard deviation for both waters and both methods was about 1 mg l^{-1}.

4.2. Calcium and magnesium determination

These determinations were carried out employing as data sources the spectra at the time of maximum signal during the injection. Three kinds of determinations for calcium, magnesium and calcium and magnesium simultaneously were done.

4.2.1. Selection of the analytical signals

When the aim was to determine one of the ions in the presence of the reagent (arsenazo III) the HPSAM for binary mixtures [4,5] was used (Eq. (8)), while if both ions were to be measured simultaneously the HPSAM for ternary mixtures [6,9] was employed (Eq. (10)). For M values we used the slopes of calibration graphs with standards because no matrix effect is present. As in the previous case the classic calibration method and the HPSAM will be compared. In both cases the data were treated to adjust them to a linear curve and a polynomial of two-degree curve. To compare the modelling capacity of the data by each method when only calcium or magnesium were to be measured, the standards were predicted after the fitting of the data, employing their corresponding equations.

The results obtained with the HPSAM (Eq. (8)) are suitable using the linear or polynomial regression. The relative errors using the increments 518–597, 434–649, 523–595, 514–600 and 282–609 for calcium determination were about 2% (value calculated from the mean of the predictions) for all the standards; 291–607, 436–648 and 441–646 were selected for the determination of magnesium, all the relative errors were lower than 10%. The results using the polynomial regression were quite similar to those. In contrast, when the classic calibration method is employed the results are suitable when the polynomial regression is applied (measuring at 649 nm for calcium and 646 nm for magnesium all relative errors were lower than 7%) while the results provided by the linear regression are affected by a large error when the assayed concentrations are low (11.6% for 3.1 ppm of calcium and 39.6% for 1.8 ppm of magnesium measuring at the same wavelengths).

When both analytes were determined together, the HPSAM for ternary mixtures was applied (Eq. (10)). For this purpose it was necessary to find two wavelengths where the two other species considered interferents present the same absorbance relationship. These wavelengths are easy to find if a quotient spectrum of both interferents is plotted, as is discussed in the fundamentals section. There are several pairs of wavelengths that fulfil that condition. For Ca determination the pairs of wavelengths are: 655–681, 655–685, 655–686, 655–687 and 655–688, while for Mg determination they are 597–627, 599–630, 604–631, 609–630 and 611–626.

4.2.2. Determination of calcium and magnesium in water samples

The calibration graph for calcium in presence of different amounts of magnesium best fitted to a second degree polynomial, the equation was $y = -0.0022x^2 + 0.0877x - 0.0053$, $r^2 = 0.9971$ ($n = 25$). As can be observed, the calibration curve does not depend on the magnesium concentration, so any sample can be predicted using its equation. The same occurs when the method is used in the batch mode, but in this case the calibration graph is linear [9].

In Table 1 are given the results of calcium determination in every sample, as can be seen, the HPSAM provides accurate and precise results.

The calibration curve for magnesium depends on the amounts of calcium present in the sample. The same occurs with the batch procedure developed in ref. [9]. Because the absorbance increments are small if the HPSAM for ternary mixtures is applied, the accuracy is not fully satisfactory, and it is therefore better to work in another way.

It is possible to eliminate the Ca analytical signal from the sample analytical signal. Then the problem can be solved by the HPSAM as a binary mixture by choosing two wavelengths at which Arsenazo III absorbs the same value. These wavelengths are 622–478, 621–479, 618–484, 621–478 and 624–475. Fig. 6(a) shows that when Mg is absent, the analytical signal is zero. This indicates that the HPSAM completely eliminates the presence of the reagent and Ca complex. The analyti-

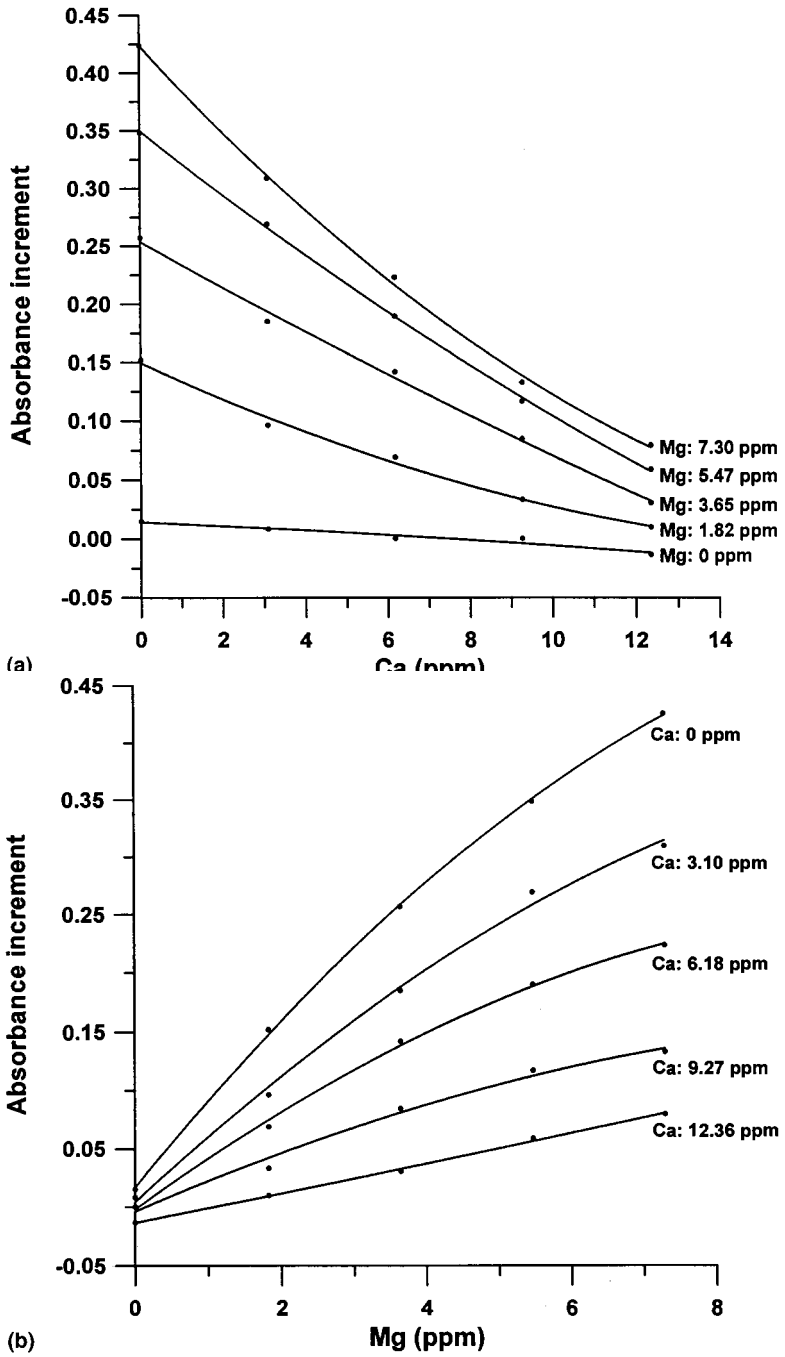

Fig. 6. (a) Absorbance increment ($A_{622}-A_{478}$), after the subtraction of the absorbance of the calcium at those wavelengths, vs Ca concentration for different concentrations of magnesium. Variation on the magnesium response as a function of the calcium present in the sample. (b) Calibration curves for the determination of Mg in the presence of different amounts of calcium. Absorbance increment: $A_{622}-A_{478}$.

Table 1
Results obtained for the prediction of calcium and magnesium with the tritimetric method and the HPSAM

Water/method	EDTA		HPSAM	
	Calcium (ppm)	Magnesium (ppm)	Calcium (ppm)	Magnesium (ppm)
Font vella	37.6 ± 0.9	9.0 ± 0.1	39 ± 1	11 ± 2
Lanjaron	24.8 ± 0.2	8.9 ± 0.7	25.1 ± 0.8	10 ± 1
Synthetic	86 ± 1	33.7 ± 0.7	84 ± 4	33 ± 9
Solàn de Cabras	53 ± 1	26.1 ± 0.9	52 ± 2	26 ± 6
Solares	72.4 ± 0.7	13 ± 2	76 ± 2	20 ± 4
Viladrau	18.6 ± 0.7	3.9 ± 0.2	19.6 ± 0.7	4.5 ± 0.6

cal signal provided by Mg decreases depending on the Ca present. This figure allows the construction of any calibration graph for Mg in presence of a given Ca concentration. Fig. 6(b) shows the calibration graphs for Mg at different Ca concentration present in the sample. The points fitted a two-order polynomic equation. By interpolating the absorbance increment value for the sample in the corresponding polynomic equation, it is possible to obtain the Mg concentration.

To determine Mg it is necessary to make a calibration graph considering the Ca concentration estimated previously or to have of a series of standards that make it possible to obtain the calibration graph as in the example. The results obtained are given in Table 1. As can be seen, they are satisfactory.

5. Conclusions

The basis of the HPSAM and GHPSAM methods when an on-line technique like flow injection is employed has been established.

It has been proven that the GHPSAM can correct the blank signal regardless of its feature, even when a matrix effect is also present in the determination.

It has also been demonstrated that HPSAM is able to isolate the signal of the analyte from the global signal, even if there are two analytes interfering simultaneously. The calibration graphs obtained are only dependent on the analyte concentration, because the other species are cancelled at each point, even when their contribution to the absorbance value differs from one solution to other. The HPSAM and GHPSAM methods can work as multivariate methods because there are generally several pairs or trios of wavelengths/times to choose. The present report also shows the versatility of the method in providing the best solution in each case.

The results obtained demonstrate that the two methods provide better results than the classic calibration method. This improvement is more obvious at lower concentrations.

Acknowledgements

The authors are grateful to the DGICYT (Project No. PB 94-0984) for financial support.

References

[1] F. Bosch Reig, P. Campíns Falcó, Analyst 113 (1988) 1011.
[2] F. Bosch Reig, P. Campíns Falcó, Analyst 115 (1990) 111.
[3] P. Campíns Falcó, J. Verdú Andrés, F. Bosch Reig, C. Molíns Legua, Anal. Chim. Acta 302 (1995) 323.
[4] P. Campíns Falcó, F. Bosch Reig, J. Verdú Andrés, Anal. Chim Acta 270 (1992) 253.
[5] F. Bosch Reig, J. Verdú Andrés, P. Campíns Falcó, C. Molíns Legua, Talanta 41 (1994) 39.
[6] P. Campíns Falcó, J. Verdú Andrés, F. Bosch Reig, Anal. Chim. Acta 348 (1997) 39.
[7] J. Verdú Andrés, F. Bosch Reig, P. Campíns Falcó, Analyst 120 (1995) 299.
[8] S. Igarashi, T. Aihara, T. Yotsuyanagi, Anal. Chim. Acta 323 (1996) 63.
[9] P. Campíns Falcó, J. Verdú Andrés, F. Bosch Reig, Anal. Chim. Acta 348 (1997) 39.

ELSEVIER

Talanta 47 (1998) 203–212

Talanta

LA-ICP-MS, IC and DPASV-DPCSV determination of metallic impurities in solar-grade silicon

Pier Luigi Buldini [a,*], Anna Mevoli [b], Jawahar Lal Sharma [c]

[a] *C.N.R.-Lamel, Via P. Gobetti n. 101, 40129, Bologna, Italy*
[b] *PASTIS SCpA, S.S. 7, km. 7,300, 72100, Brindisi, Italy*
[c] *K.M. College, University of Delhi, Delhi, 110007, India*

Received 2 October 1997; received in revised form 11 February 1998; accepted 11 February 1998

Abstract

Stringent specifications are laid down for the silicon used for solar cells. The present work deals with the application of different techniques to the simultaneous determination of most common metallic impurities like iron, copper, nickel, zinc, lead and cadmium, in industrial process control. Laser ablation inductively coupled plasma mass spectrometry is quite expensive in apparatus, but it directly performs the analysis of solid silicon with very good sensitivity, even if coupled to considerable standard deviation, probably due to the material defects. Both ion chromatography and voltammetry need sample pre-treatment, but they are characterized by cheap and simple apparatus, suitable detection limits, good sensitivity and small standard deviation. © 1998 Elsevier Science B.V. All rights reserved.

Keywords: Solar-grade silicon; Metallic impurities; Laser ablation inductively coupled plasma mass spectrometry; Ion chromatography; Voltammetry

1. Introduction

In the current decade, photovoltaic industry has established its own identity as a result of the increasing relevance of alternative energies. The actual trend is to produce silicon ingots or ribbons suitable for fabricating large area (>100 cm^2) and thin (<150 μm) photovoltaic cells, thereby reducing the cost factor, without affecting their efficiency. Solar-grade silicon is characterized by an intermediate level of quality in respect of semiconductor-grade and most of the metallic impurities that can be present, cause a considerable reduction in minority carrier lifetime if overcoming the low ppm range. The most favourable result is achieved when a tolerable impurity content is counter balanced by the low cost of the starting material coupled with the minimum manipulations resulting from the crystal growth technique and the melt replenishment strategy.

In electronic-grade materials, the content of metallic impurities is generally monitored by spectrography [1], spark source mass spectrometry

* Corresponding author. Tel.: +39 051 6399203; fax: +39 051 6399216, +39 054 720267.

0039-9140/98/$19.00 © 1998 Elsevier Science B.V. All rights reserved.
PII S0039-9140(98)00065-4

(SSMS) [2], secondary ions mass spectrometry (SIMS) [3] or neutron activation analysis (NAA) [4] which, coupled with radiochemical separation and measurements, provide the lowest detection limits. These techniques, however, are very expensive and relatively long time is required for analysis, in addition their use in industrial process is unusual.

The permissible limits of metallic impurities in solar-grade silicon, made it possible the use of techniques much more cheap and easy to manage, for process control, like flameless atomic absorption spectrometry (FAAS) [5], polarography [6], ion chromatography (IC) [7] or inductively coupled plasma mass spectrometry (ICP-MS) [8]. These techniques are very attractive for trace analysis owing to their ease of operation and satisfactory sensitivity in process control coupled with the advantage of simultaneous determinations.

In the present work, laser ablation inductively coupled plasma mass spectrometry (LA-ICP-MS), ion chromatography (IC) and pulsed voltammetries (DPASV-DPCSV) are applied to the simultaneous determination of iron, copper, nickel, zinc, lead, cadmium, and cobalt in solar-grade silicon.

LA-ICP-MS requires only minimal sample preparation: silicon ingots or ribbons must be cut and the wafer is ablated by laser pulses and ions analyzed in inductively coupled plasma.

IC and DPASV-DPCSV require pieces or coarse powder dissolution in a mixture of hydrofluoric and nitric acids, that are successively volatilized at the same time of the silicon matrix (as hexafluorosilicic acid). The residue is then dissolved in water and analyzed.

2. Experimental

2.1. Reagents and standards

Sodium hydrogencarbonate, sodium acetate, oxalic acid, lithium hydroxide, 2-dimethylaminoethanol, 4-(2-pyridylazo)-resorcinol monosodium salt (PAR) and pyridine-2,6-dicarboxylic acid (PDCA) were chromatographic grade (Novachimica, Milan, Italy), ammonium hydroxide (30%), glacial acetic acid, hydrofluoric acid (50%), nitric acid (70%), trichloroethylene, acetone and methanol were Erbatron electronic grade (Carlo Erba Reagenti, Milan, Italy), while ammonium acetate, catechol, dimethylglyoxime and ethyl alcohol (95°) were ACS reagent grade. 2 M ammonium acetate (pH = 5.5) was chelation grade (Dionex, Sunnyvale, CA). Ultrapure water with conductivity < 0.1 μS (DI water) was obtained from a MILLI-Q system (Millipore, Bedford, MA). Working standards for use in analysis by IC and DPASV-DPCSV were prepared daily by diluting Carlo Erba Reagenti Normex atomic absorption standards (1.000 g l^{-1}), while for ICP use, AccuStandard solutions (1.000 g l^{-1}) were used.

Polytetrafluoroethylene (PTFE) labware was cleaned by refluxing in hot and concentrated nitric acid, then carefully washed with DI water and finally dried with filtered air in a clean atmosphere. Details of cleaning procedures and apparatus are reported in the standard texts. Normal precautions for trace analysis were observed throughout. Reagents, standards and sample solutions were prepared and stored in fluorinated ethylene propylene labware. Polypropylene calibrated equipment was used

Table 1
Laser and inductively coupled plasma mass spectrometric conditions

Laser mode	Q switched
Laser power	850 V
Focus	Sample surface
Laser energy (J $shot^{-1}$)	0.2
Repetition rate (Hz)	4
Raster	7×7
Aerosol gas path length (m)	2.5
Aerosol Ar gas flow rate (l min^{-1})	0.98
Auxiliary Ar gas flow rate (l min^{-1})	0.40
Coolant Ar gas flow rate (l min^{-1})	13.0
Inductively coupled plasma power (W)	1200
Multichannel analyzer (channels)	4096
Dwell time (μs)	160
Sweeps per acquisition	100
Pre-ablation time (s)	120
Ablation time (s)	180
Acquisition time (s)	60

Table 2
Ion chromatographic conditions

Column	Dionex IonPac CG5+CS5
Eluent 1 [Fe^{3+}, Cu^{2+}, Ni^{2+}, Zn^{2+}]	6 mM PDCA +50 mM CH_3COOH +50 mM CH_3COONa (pH = 4.6)
Eluent 2 [Pb^{2+}, Cd^{2+}, Co^{2+}]	50 mM $(COOH)_2$ +95 mM LiOH (pH = 4.8)
Eluent flow rate	1.0 ml min^{-1}
Injection volume	150 μl
Detection	Visible absorbance
Post column reagent	0.3 mM PAR in 1 M 2-dimethylaminoethanol +0.5 M NH_4OH +0.5 M $NaHCO_3$
PCR flow rate	0.5 ml min^{-1}
Wavelength	520 nm

throughout in order to prevent leaching and/or adsorption effects. Manipulations were done on a laminar-flow clean bench to avoid fortuitous pollution.

2.2. Voltammetric complexing solutions

For the determination of iron(III), a 0.1 M catechol solution was used as complexant. It was prepared by dissolving 2.750 g of pyrocatechol in ultrapure water under a nitrogen flow in a dark bottle. The solution was stored under nitrogen atmosphere to prevent its oxidation, which otherwise causes the shift and decrease of the iron peak thereby influencing the response linearity.

For the determination of nickel(II) and cobalt(II), a 0.043 M dimethylglyoxime solution was prepared in ethyl alcohol (95°).

2.3. Chromatographic eluent and post-column reagent solutions

A mixture of 6 mM PDCA, 50 mM acetic acid and 50 mM sodium acetate (pH = 4.6) was employed for the determination of iron(III), copper(II), nickel(II), and zinc(II). For the analysis of lead(II), cadmium(II), and cobalt(II) a mixture of 50 mM oxalic acid and 95 mM lithium hydroxide (pH = 4.8) was used as the eluent. The post-column reagent used with both eluents was 0.3 mM PAR dissolved in 1 M 2-dimethylaminoethanol, 0.5 M ammonium hydroxide and 0.5 M sodium hydrogencarbonate.

2.4. Instrumentation

For ion chromatographic and voltammetric analyses, a laboratory mill (Spex, Edison, NJ) fitted with an agate cell, was the standard apparatus used to prepare the samples. Then they were microwaving digested in a MLS 1200 system (Milestone, Sorisole, Italy) equipped with a FAM 40 acid scrubber module. Dissolution was performed using 40% power and programming temperatures as a function of the values dictated by the factorial design.

Mass spectrometric analyses were performed on a VG PlasmaQuadII + (VG Elemental, Thermo Instruments, Winsford, UK) inductively coupled plasma mass spectrometer equipped with a fine focused LaserProbe ablation module. The LaserProbe is based on a 500 mJ pulsed Nd:YAG laser operating at a wavelength of 1064 nm. The fine focus optics facilitate the production of laser craters of about 100 μm in the Q-switched mode for silicon. A full description of the laser and ICP-MS instrumentation and analysis methodology is reported in the standard texts [9]. ^{29}Si is used as the internal standard isotope. Most instrumental functions are controlled by an 80386 based computer (Epson, Sesto S. Giovanni, Italy) with VG PlasmaQuad software.

All the mass spectrometric conditions are listed in Table 1.

Chromatographic analyses were performed on a metal-free Dionex DX-300 ion chromatograph equipped with: an AGP gradient pump, a Post-column Pneumatic Controller for post-column reagent addition and a DSA UV-Vis multiple-wavelength detector.

All the chromatographic conditions are listed in Table 2.

All measurements were made at room temperature and in all cases, injection of the sample was done at least in triplicate. All the samples were filtered through 0.45 μm filter.

Data manipulation and the operation of all components in the system were controlled by AI-450 Dionex chromatographic software interfaced via an ACI-2 Advanced Computer Interface to an 80386 based computer (Epson, Sesto S. Giovanni, Italy).

Table 3
Voltammetric conditions

Electrode type	MME operated as HMDE, Hg drop size 0.60 mm^2.
Electrode stirring speed (during deposition time)	1920 rpm
Zn(II), Cd(II), Pb(II), Cu(II)	Deposition (at −1.450 V) 120 s, quiet time before potential scan 20 s, DPASV from −1.450 to −0.100 V, pulse amplitude 60 mV, potential scan rate 10 mV s^{-1}.
Fe(III)	Deposition (at −0.650 V) 60 s, quiet time before potential scan 20 s, CSV from −0.650 to −1.100 V, potential scan rate 60 mV s^{-1}.
Ni(II), Co(II)	Deposition (at −1.100 V) 35 s, quiet time before potential scan 30 s, DPCSV from −1.100 to −1.450 V, pulse amplitude −40 mV, potential scan rate 10 mV s^{-1}.

Voltammetric measurements were performed on a Metrohm (Herisau, Switzerland) 646 VA processor equipped with a 647 VA stand, a 675 VA sample changer, a 677 drive unit and Dosimat 665 automatic addition burettes. A conventional three-electrode arrangement consisting of a multimode electrode (MME) working electrode, an Ag/AgCl [3 M KNO_3] reference electrode and a 6.5 cm long platinum wire auxiliary electrode was used.

All the voltammetric conditions are listed in Table 3.

2.5. Mass spectrometric working conditions

LA-ICP-MS requires only minimal sample preparation: (a) the slicing of a flat piece off the silicon ingot or the cutting of a ribbon piece that fits inside the laser cell and is no more than 5 mm above the motorized X–Y sample stage, (b) the degreasing of the sample, such as usually performed on semiconductor wafers, in order to remove any residue of the cutting process and (c) the pre-ablation of the sample site for removing any surface contamination caused by the handling of the slice in order to insure that impurities result from the silicon ablation. A pre-ablation step two minutes long proved to be sufficient to remove any surface contaminant. Then ablation is carried out for 3 min, because this time was sufficient to insure the generation of a stable aerosol density prior to acquisition time (last 60 s), long enought to provide an high intense spectrum when scanning in the m/z 20–210 range. Any sample is at least ablated at three different sites in order to reject spurious data and to ensure better precision. Particularly important is to analyze silicon samples without variations in the characteristics of the physical matrix because of variations in volatilized sample mass, so causing apparent variation of the analytes concentration. Due to the absence of silicon wafers standards, LA-ICP-MS operating parameters were optimized by using NIST SRM 610 and 614 glass wafers as the most similar standard matrix possible. Once optimization was achieved, in-house reference silicon samples were used in order to insure data intercomparability on short and long term.

2.6. Ion chromatographic working conditions

Silicon pieces or coarse powder is dissolved with an hydrofluoric–nitric acid mixture before the injection on to the chromatographic column. Effectively, cations can be determined by simply reducing acid concentration in the sample solution, but its plain dilution is not desirable because of the low amount of metallic impurities usually present in solar-grade silicon. It is therefore highly recommended to remove mineral acid excess, that is necessary for the complete dissolution of the sample, through its volatilization.

In addition, the volatilization process is not only quite effective for the removal of the reagent excess, but also for eliminating the matrix without affecting most of the metallic ions. Silicon is removed as hexafluorosilicic acid, which distils as an azeotrope with water and hydrofluoric acid at about 110°C. The residue is then dissolved in the same chromatographic eluent, filtered and injected.

Table 4
Ion chromatographic recovery of metal standards added to semiconductor silicon, dissolution in $HF–HNO_3$ mixture and volatilization to dryness at 130°C

	Fe(III) μg kg^{-1} Si	Cu(II) μg kg^{-1} Si	Ni(II) μg kg^{-1} Si	Zn(II) μg kg^{-1} Si	Pb(II) μg kg^{-1} Si	Cd(II) μg kg^{-1} Si	Co(II) μg kg^{-1} Si
Added[a]	80	80	150	80	80	80	80
Found[a]	82 ± 2	81 ± 2	150 ± 3	80 ± 2	79 ± 2	79 ± 1	80 ± 2
Rec. (%)	102	102	100	100	99	99	100
Added[a]	200	200	500	200	200	200	200
Found[a]	199 ± 3	202 ± 2	495 ± 8	201 ± 4	199 ± 2	200 ± 4	198 ± 3
Rec. (%)	99	101	99	101	99	100	99
L.O.D.[b]	50	50	100	50	50	50	50

[a] Mean value calculated on ten samples $\pm s$-triplicate injection each. Chromatographic conditions as reported in Table 4.
[b] Limit of detection calculated as 3σ+average noise.

Table 5
Voltammetric recovery of metal standards added to semiconductor silicon, dissolution in $HF-HNO_3$ mixture and volatilization to dryness at 130°C

	Cu(II) μg kg^{-1} Si	Pb(II) μg kg^{-1} Si	Cd(II) μg kg^{-1} Si	Zn(II) μg kg^{-1} Si	Fe(III) μg kg^{-1} Si	Ni(II) μg kg^{-1} Si	Co(II) μg kg^{-1} Si
Added[a]	150	80	80	150	150	150	80
Found[a]	152 ± 4	80 ± 1	80 ± 1	148 ± 4	156 ± 7	150 ± 4	79 ± 1
Rec. (%)	102	100	100	99	104	100	99
Added[a]	500	200	200	500	500	200	200
Found[a]	507 ± 10	199 ± 2	199 ± 2	490 ± 10	509 ± 15	200 ± 5	196 ± 3
Rec. (%)	102	100	100	98	102	100	98
L.O.D.[b]	100	50	50	100	100	100	50

[a] Mean value calculated on ten samples $\pm s$. Voltammetric conditions as reported in Table 5.
[b] Limit of detection calculated as 3σ+average noise.

Table 6
Metallic impurities determined in NBS SRM 57a silicon metal and in solar-grade silicon of different origin

Impurity	Analytical Technique	NBS SRM 57a		Samples			
		Certified value[a]	Found[b]	A[b]	B[b]	C[b]	D[b]
Fe	IC	5000 ± 100	4990 ± 57	1100 ± 14	440 ± 6	250 ± 3	170 ± 2
	CSV	5000 ± 100	5020 ± 85	1120 ± 23	448 ± 10	255 ± 7	172 ± 3
	LA-ICP-MS	5000 ± 100	—[c]	1095 ± 100	440 ± 42	247 ± 26	168 ± 17
Cu	IC	40 ± 10	41 ± 1	81 ± 2	53 ± 1	9.0 ± 0.2	<0.05
	DPASV	40 ± 10	40 ± 3	80 ± 3	54 ± 1	9.0 ± 0.2	<0.1
	LA-ICP-MS	40 ± 10	—[c]	79 ± 8	53 ± 4	9.5 ± 1	<0.01
Ni	IC	80 ± 20	79 ± 2	200 ± 3	81 ± 2	<0.1	<0.1
	DPASV	80 ± 20	82 ± 4	200 ± 5	80 ± 3	<0.1	<0.1
	LA-ICP-MS	80 ± 20	—[c]	198 ± 20	79 ± 8	<0.01	<0.01
Zn	IC	(<10)	<0.05	8.2 ± 0.2	<0.05	<0.05	<0.05
	DPASV	(<10)	<0.1	8.3 ± 0.2	<0.1	<0.1	<0.1
	LA-ICP-MS	(<10)	—[c]	8.5 ± 1.0	<0.01	<0.01	<0.01
Pb	IC	<10	<0.05	5.6 ± 0.2	<0.05	<0.05	<0.05
	DPASV	<10	<0.05	5.5 ± 0.2	<0.05	<0.05	<0.05
	LA-ICP-MS	<10	—[c]	5.5 ± 0.5	<0.01	<0.01	<0.01
Cd	IC	—	<0.05	5.2 ± 0.1	<0.05	<0.05	<0.05
	DPASV	—	<0.05	5.1 ± 0.1	<0.05	<0.05	<0.05
	LA-ICP-MS	—	—[c]	5.0 ± 0.6	<0.01	<0.01	<0.01
Co	IC	—	<0.05	3.2 ± 0.1	<0.05	<0.05	<0.05
	DPCSV	—	<0.05	3.1 ± 0.1	<0.05	<0.05	<0.05
	LA-ICP-MS	—	—[c]	3.0 ± 0.3	<0.01	<0.01	<0.01

[a] Values in μg g^{-1} Si.
[b] Values in μg g^{-1} Si. Mean value calculated over ten samples $\pm s$.
[c] NBS SRM 57a is in the form of a fine powder and laser ablation is unreliable.

As shown in Tables 4 and 5, it was found that iron(III), copper(II), nickel(II), zinc(II), lead(II), cadmium(II), and cobalt(II) are not affected by acids and matrix volatilization at 130°C and their recovery results in the 98–102% range.

2.7. Voltammetric working conditions

The same dissolution procedure used for the ion chromatographic analysis proved to be suitable for the voltammetric one, too, because it well succeeds in the complete removal of the reagent excess. Hydrofluoric acid traces are particularly dangerous owing to the use of glass mercury drop electrodes in voltammetry. In this case the residue is dissolved in DI water and the solution is transferred to the electrolytic cell.

The best voltammetric conditions for the simultaneous determination of zinc, cadmium, lead, copper, iron, nickel and cobalt were experimentally established [10]. The procedure consists of three steps at different pH. First of all, the determination of zinc, cadmium, lead and copper by differential pulse anodic stripping voltammetry (DPASV) is performed at pH 5.5 (acetate buffer), then the determination of iron by cathodic stripping voltammetry (CSV) of its catechol complex follows at pH 9.5 (ammonia–ammonium acetate buffer) and at the same pH nickel and cobalt are determined by differential pulse cathodic stripping voltammetry (DPCSV) of their dimethylglyoxime complexes.

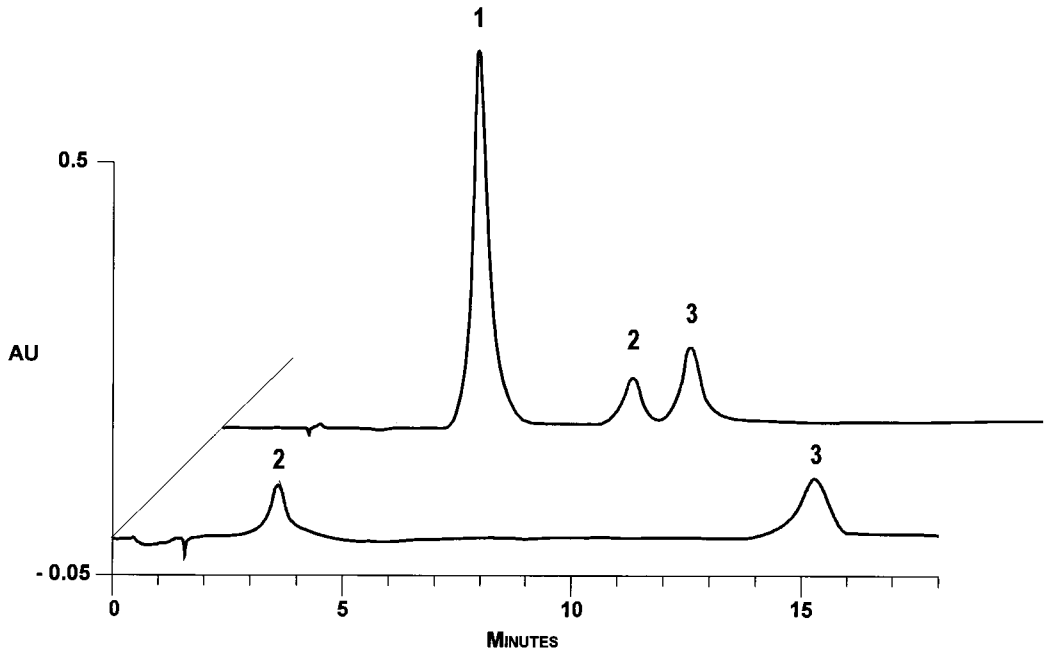

Fig. 1. Chromatogram, using oxalic acid eluent (front) and PDCA eluent (rear), of cations present in a solar-grade silicon sample dissolved as described under Experimental. Chromatographic conditions as in Table 2. Peaks: 1. Fe(III) 438 μg g^{-1}, 2. Cu(II) 54 μg g^{-1} and 3. Ni(II) 80 μg g^{-1}; oxalic acid eluent: Pb(II), retention time 2.7 min, Cd(II), retention time 4.3 min, and Co(II), retention time 8.1 min, not found; PDCA eluent: Zn(II), retention time 11.1 min, not found.

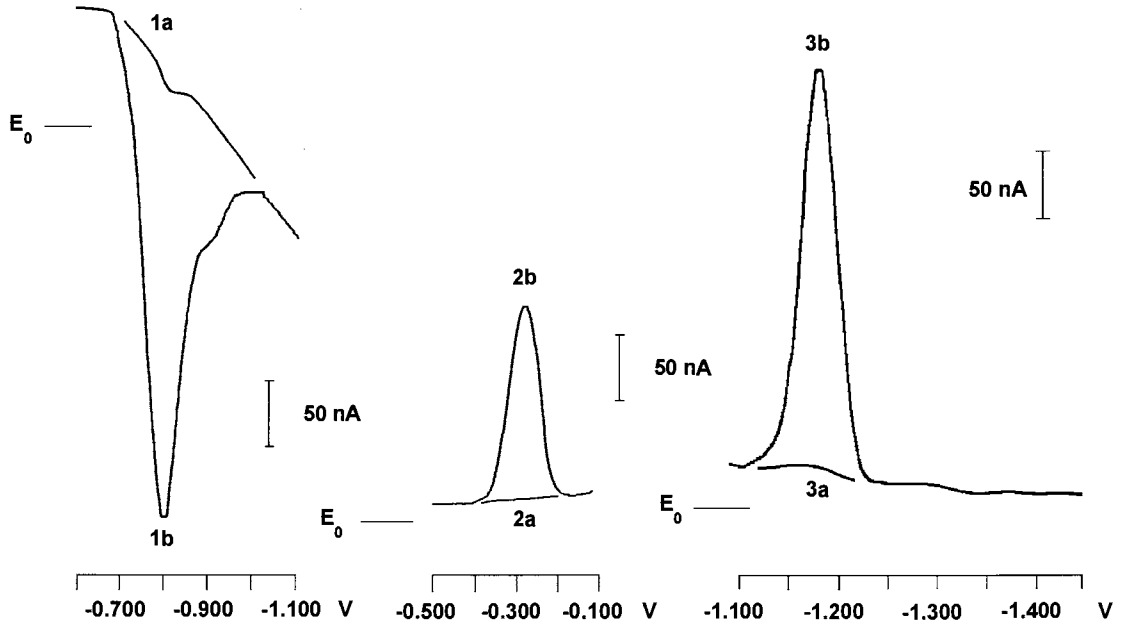

Fig. 2. Voltammogram of cations present in a solar-grade silicon sample dissolved as described under Experimental. Voltammetric conditions as in Table 3. DPASV peaks in ammonium acetate buffer (pH 5.5): 2. Cu(II) Ep −0.270 V 55 μg g^{-1}; Zn(II) Ep −1.230 V, Cd(II) Ep −0.800 V, and Pb(II) Ep −0.650 V, not found. CSV and DPCSV peaks in ammonia–ammonium acetate buffer (pH 9.5) 1. Fe(III) Ep −0.800 V 452 μg g^{-1}, 3. Ni(II) Ep −1.175 V 82 μg g^{-1}, Co(II) Ep −1.290 V, not found. a. reagents blank, b. solar-grade silicon sample.

pH value and ligand concentration were optimized to ensure a complete and fast cation complexation and a reproducible complex deposition onto the hanging mercury drop electrode (HMDE), during the pre-electrolysis step. The blank observed in iron and nickel/cobalt determinations is essentially due to the fact that both catechol and dimethylglyoxime are electroactive in the same potential range in which the respective complexes with iron(III) and nickel(II) are reduced back.

2.8. Procedure

Silicon ingots and ribbons are properly cut and slices are cleaned by ultrasonic washing and degreased with trichloroethylene, acetone and methanol [11]. After rapid etching with 1 + 1 hydrofluoric–nitric acid mixture at room temperature in order to remove the surface layer, the slices are washed in DI running water and dried in pure nitrogen flow.

The sample is directly inserted in the laser chamber, if LA-ICP-MS is used, or it is ground, in a mill fitted with an agate cell, for the successive acid dissolution, when ion chromatography or voltammetry are performed. Then, in a PTFE vessel, 10–100 mg of sample are added with 2 ml of 12 M HNO_3 and 3 ml of 28 M HF and heated to 110°C for 5–10 min, then the temperature is raised to 130°C and acidic fumes are completely scrubbed off (20 min).

The small residue is dissolved in: (a) 5 ml of eluent and directly injected on to the ion chromatograph fitted with on line filter or (b) 10 ml of DI water and transferred to the electrolytic cell.

For voltammetric analysis, the equipment operations consist of a 300 μl addition of 2 M ammonium acetate buffer (pH 5.5) followed by the determination of zinc, lead, cadmium and copper, a further addition of 300 μl of 5 M ammonia–ammonium acetate buffer (pH 9.5) and 50 μl of 0.1 M catechol for iron determination and, at last, 50 μl of 0.043 M dimethylglyoxime for the determination of nickel and cobalt.

3. Results and discussion

Because no solar-grade silicon standards were found, NBS SRM silicon metal was analyzed (see Table 6) and the detection limits and linear ranges were determined by spiking ultrapure semiconductor silicon with various amounts of the determined species, subjecting them to microwave digestion and then analyzing them by means of the proposed procedures. Some data are summarized in Tables 4 and 5, while in Fig. 1 their chromatographic behavior and in Fig. 2 their voltammetric behavior is reported.

Some results obtained on solar-grade silicon ingots fused in a tentative run of refining raw material are summarized in Table 6, too.

In absence of standards, the results obtained by the three considered techniques were compared each other and they were found in good agreement.

No interference of the impurities usually found in silicon was found, the only drawbacks being the heat dissolution treatment over volatile species, like arsenic and antimony [12], thus making impossible their quantitation.

4. Conclusions

All of the selected analytical techniques revealed suitable for the determination of metallic impurities in solar-grade silicon process control.

LA-ICP-MS is quite expensive in apparatus, but it permits the direct analysis of solid silicon coupled with very good sensitivity even if connected to considerable standard deviation, probably due to the polysilicon defects. It requires only minimal sample preparation and the single standard calibration technique used, enables the determination of trace to major element content without reference to matrix matched standards. The principal component of the matrix is used as the internal standard isotope (^{29}Si).

Both IC and DPASV-DPCSV need sample pretreatment, but cheap and simple apparatus, suitable detection limits and small standard deviation characterize them. In both cases run time is about 1/2 h, plus the sample pre-treatment. It is neces-

sary to match sample results with standards. Voltammetry reveals a bit complicated if compared to ion chromatography.

Acknowledgements

One of the authors (J.L.S.) acknowledges financial support from the International Center for Theoretical Physics (Trieste, Italy).

References

[1] V.G. Protasov, Spectrographic analysis of technical and used silicon, Zavod. Lab. 55 (1989) 54–55.
[2] I.U.P.A.C. Analytical Chemistry Division, General aspects of trace analytical methods. VI. Trace analysis of semiconductor materials, A. Bulk analysis, Pure Appl. Chem. 57 (1985) 1133–1152.
[3] A.B. Tolstogouzov, T.I. Kitaeva, S.S. Volkov, SIMS imaging: apparatus and applications, Mikrochim. Acta 114-115 (1994) 505–510.
[4] E.L. Lakomaa, P. Manninen, R.J. Rosenberg, R. Zilliacus, Neutron-activation analysis of semiconductor materials, J. Radioanal. Nucl. Chem. 168 (1993) 357–366.
[5] D.A. Stewart, D.C. Newton, Determination of iron in semiconductor-grade silicon by furnace atomic-absorption spectrometry, Analyst 108 (1983) 1450–1458.
[6] P.L. Buldini, A. Toponi, Q. Zini, Polarographic determination of metallic impurities on lapped silicon wafers, Microchem. J. 38 (1988) 241–245.
[7] P.L. Buldini, S. Cavalli, A. Mevoli, E. Milella, Application of ion chromatography to the analysis of high-purity CdTe, J. Chromatogr. 739 (1996) 131–137.
[8] W. Hub, H. Amphlett, Application of ETC-ICP-MS in semiconductor process control, Fresenius J. Anal. Chem. 350 (1994) 587–592.
[9] W.T. Perkins, N.J.G. Pearce, in: P.J. Potts, J.F.W. Bowles, S.J.B. Reed, M.R. Cave (Eds.), Microanalytical Techniques in the Geosciences, Chapman and Hall, London, 1995, pp. 291–325.
[10] P.L. Buldini, D. Ferri, D. Nobili, Determination of transition metals in natural waters by microprocessor-controlled voltammetry in comparison with graphite furnace atomic absorption spectrometry, Electroanalysis 3 (1991) 559–566.
[11] P.L. Buldini, Q. Zini, D. Ferri, Anodic oxidation of polysilicon, J. Electrochem. Soc. 128 (1981) 1062–1064.
[12] S. Niese, K. Icker, D. Birnstein, J. Dubnack, M.L. Boettger, Semiconductor silicon samples for inter-laboratory comparison, Isotopenpraxis 25 (1989) 237–239.

ELSEVIER

Talanta 47 (1998) 213–221

Talanta

Determination of microquantities of thiosulfate by kinetic method

I.V. Pulyayeva *, N.L. Yegorova, L.P. Experiandova, A.B. Blank

Institute for Single Crystals, National Academy of Sciences of Ukraine, 60 Lenin Ave., 310001 Kharkov, Ukraine

Received 23 June 1997; received in revised form 9 February 1998; accepted 12 February 1998

Abstract

A new redox indicator reaction between Cu^{2+}, Mn^{2+} and $S_2O_3^{2-}$ in the presence of 2,2′-bicinchoninic acid is investigated. Optimum reaction conditions are determined. The influence of nonaqueous solvents on the reaction rate is studied. It is shown that in the presence of acetone the $S_2O_3^{2-}$ determination limit is lowered 0.005 μg ml^{-1}. Random errors lie within the limits allowable at the determination of microconcentrations. To raise the sensitivity of the determination of $S_2O_3^{2-}$ in some inorganic salts (KCl, KNO_3, $CsNO_3$), this impurity was concentrated by low-temperature directed crystallisation. Metrologic characteristics of the developed technique are presented. © 1998 Elsevier Science B.V. All rights reserved.

1. Introduction

At present, the development of sensitive methods to determine cationic and anionic microimpurities in scintillation and optical crystals has turned out to be a topical problem. This is explained by the fact that crystals with pre-specified properties cannot be obtained without knowledge of the presence and distribution of impurities both in crystal samples and in materials used in their growth. High-purity inorganic salts used as initial components in the crystal growth may have oxygen-containing impurities such as carbonates, sulfites, sulfates or thiosulfates. Their presence causes changes in the physical properties of crystals, for instance, to an essential decrease of the optical transparency. In this connection, sensitive methods for their determination should be developed.

There are some literature data on the determination of thiosulfate microamounts by different techniques, in particular, by spectrophotometric methods. However, in most cases thiosulfate is determined in water.

These techniques are based for the most part on thiosulfate oxidation to sulfate or tetrathionate [1–4] or on its reduction to hydrogen sulfide [5]. The spectrophotometric method [1] using a complex of Fe^{3+} with 1,10-phenanthroline allows the determination of thiosulfate in high concentrations (40–650 μg ml^{-1}). The spectrophotometric determination of thiosulfate by its reaction in the presence of formaldehyde with iodine in organic phase and solvent extraction of iodide with methylene blue is reported in [3]; the thiosulfate

* Corresponding author. Tel.: +380 572322331; fax: +380 572320273; e-mail: name@isc.kharkov.ua

0039-9140/98/$19.00 © 1998 Elsevier Science B.V. All rights reserved.
PII S0039-9140(98)00077-0

determination range is $(0.1–6) \times 10^{-6}$ M. However, it should be noted that the use of extraction and re-extraction, as well as other stages of the analysis process increases essentially the duration of the thiosulfate determination procedure. A method for thiosulfate analysis within the concentration range from 0.6 to 42.0 μg ml^{-1} based on the oxidation by permanganate is described in [4].

Kinetic methods are very seldom used to determine inorganic anions as compared to metal ions. Therefore, it is important to widen the range of indicator reactions used for thiosulfate analysis. Moreover, the determination of thiosulfate impurity in inorganic salts is a matter of particular interest. The kinetic method based on the iodine-acid reaction is characterised by a high sensitivity but it is mainly used for analysis of water [6].

Authors [7] describe a method for thiosulfate determination based on its inhibiting effect on the formation of silver ternary complex with 1,10-phenanthroline and brompyrogallol red. In this case, the range of determinable thiosulfate concentrations is 0.3–1.8 μg ml^{-1}.

In the present paper, we describe a kinetic method which allows the analysis of thiosulfate in some inorganic salts (KCl, $CsNO_3$, KNO_3) using the system Cu^{2+}-Mn^{2+}-2,2′-BCA. In this method the sensitivity of analysis is raised by the concentration of thiosulfate impurity by means of low-temperature directed crystallisation [8].

2. Experimental

2.1. Reagents and apparatus

All chemicals used, except for organic solvents, were of analytical grade and were used without further purification. Organic solvents (acetone, isopropanol, propanol, ethanol, dimethylformamide, dimethylsulfoxide) were purified using the procedure described in [9]. The 5×10^{-3} M solution of 2,2′-BCA (4,4′-dicarboxy-2,2′-biquinoline) was obtained by dissolving the weight (0.1722 g) of the substance in water under addition of potassium hydroxide solution (0.5 ml, 6.5 M). The standard solution of thiosulfate containing 1000 μg ml^{-1} of $S_2O_3^{2-}$ was prepared by dissolving sodium thiosulfate in freshly boiled and cooled bidistilled water, and standardised by the iodatometric method [10]. The working solutions containing 100, 10 and 1 μg ml^{-1} of $S_2O_3^{2-}$ were prepared daily by diluting the initial solution.

Buffer solutions as required for adjusting the pH of the reaction solutions to 6.4–8.5, were prepared by mixing the required quantities of acetic acid (1 M) with sodium acetate (1 M). Stock solutions of Mn^{2+} (1.6×10^{-3} M) and Cu^{2+} (1.6×10^{-3} M) were obtained by dissolving accurate weights of $MnSO_4 \cdot 5H_2O$ and $CuSO_4 \cdot 5H_2O$ salts, respectively.

High-purity salts KCl, $CsNO_3$, KNO_3 of MERCK were used.

In this work, a SF-46 spectrophotometer (LOMO, Leningrad) with temperature-controlled cuvette chamber and a NBE thermostat (GDR) with temperature control accurate up to ± 0.1°C were used. pH values were controlled by a pH-meter pH 673 M (ZIP, Homel'). For kinetics studies, the reaction was performed in special mixers. The mixer consists of a glass vessel of 15 volume provided with four test tubes with their neck welded into the vessel bottom.

2.2. Procedure

To investigate the kinetics of the proposed reaction, 1 ml Cu^{2+} stock solution and 1 ml buffer solution were placed into one of the test tubes of the mixer. The second test tube was used to receive 1 ml of manganese stock solution. The solution of 2,2′-BCA and organic solvents (in case when their influence on the reaction rate was to be studied) were placed into third test tube. The fourth test tube was used for necessary amounts of $S_2O_3^{2-}$. The total volume of solutions in the test tubes was brought up to 10 ml by bidistilled water. The mixer was then placed in the thermostat and kept there for 30 min at a preset temperature (25°C). Then it was turned upside down, thermostated solutions were mixed for exactly 15 s and the mixer was transferred into the cuvette of SF-46. The absorbance was measured during 3 min (taking results every 30 s).

The absorbance of the Cu^{+}-2,2′-BCA complex solution was measured against bidistilled water at

557 nm wavelength. The reaction rate was determined by the initial rates method (the method of tangents, a differential variant of kinetic methods) [11]. The said parameter is characterised by the slope of a straight line (tg α) in absorbance (A)–time (t) coordinates. In parallel, the reaction rate for the solution without $S_2O_3^{2-}$ (blank solution) is evaluated. The difference between the reaction rates value in the presence (sample) and absence (blank) of $S_2O_3^{2-}$ (all other conditions being the same) is considered as the kinetic reaction rate.

3. Results and discussion

The system Cu^{2+}-Mn^{2+}-2,2′-BCA is proposed as an indicator reaction for thiosulfate ion determination.

Prior to the analysis, complexes Cu^{+}-2,2′-BCA (curve 1), Mn^{2+}-2,2′-BCA (curve 2), Cu^{2+}-2,2′-BCA (curve 3) and 2,2′-BCA (curve 4) were obtained (Fig. 1). As is seen from this figure, it is practically only the Cu^{+}-2,2′-BCA complex that absorbs in the region of 557 nm. In view of this fact the reaction rate was determined from the formation of a violet complex Cu^{+}-2,2′-BCA.

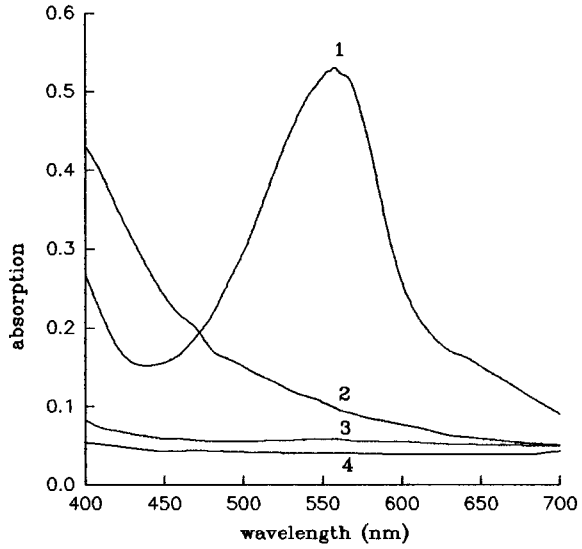

Fig. 1. Absorbance spectra of Cu^{+}-2,2′-BCA (1), Mn^{2+}-2,2′-BCA (2), Cu^{2+}-2,2′-BCA (3) and 2,2′-BCA (4). Conditions: pH 7.0, 3.75×10^{-4} M of 2,2′-BCA and (1) 1.6×10^{-4} M Cu^{+}; (2) 1.6×10^{-4} M Mn^{2+}, (3) 1.6×10^{-4} M Cu^{2+}.

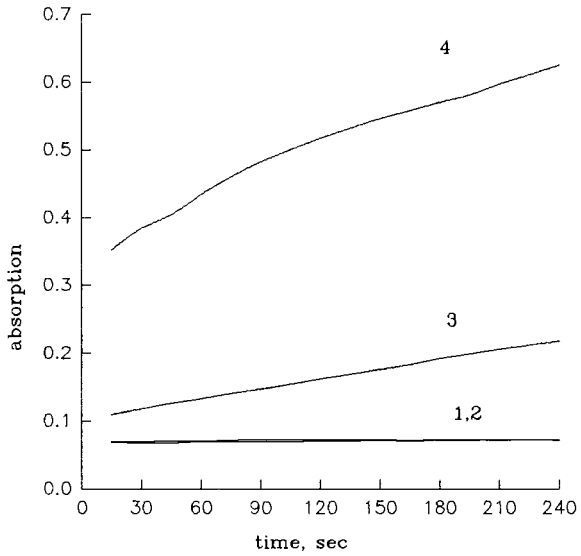

Fig. 2. Time dependence of absorbance. pH 7.0, 1.6×10^{-4} M Cu^{2+}, 1.6×10^{-4} M Mn^{2+}, 3.75×10^{-4}M 2,2′-BCA; 7 μg ml^{-1} $S_2O_3^{2-}$; curve 1: Cu^{2+}-2,2-BCA, curve 2: Cu^{2+}-2,2-BCA-$S_2O_3^{2-}$; curve 3: Cu^{2+}-2,2-BCA-Mn^{2+}; curve 4: Cu^{2+}-2,2-BCA-Mn^{2+}-$S_2O_3^{2-}$.

(2,2′-BCA is a sensitive and selective reagent to determinate Cu^{+} [12]).

The reaction rate is known to be defined by ionic interactions taking place in the solution, concentrations of reacting components and hydrogen ions, as well as by on temperature.

3.1. Time dependence of absorbance

The time dependence of the reaction rate is shown in Fig. 2. It has been found in our experiments, that Cu^{+}-2,2′-BCA complex is not formed in such circumstances (curve 1). Curve 2 shows that thiosulfate does not reduce Cu^{2+} to Cu^{+}, i.e. the violet complex Cu^{+}-2,2′-BCA (curve 1) is not obtained. The reaction rate of copper reduction with manganese in the presence of 2,2′-BCA is low (curve 3). The introduction of thiosulfate raises the reaction rate (curve 4). These data testify that the chosen indicator reaction allows the determination of thiosulfate microimpurity in the system Cu^{2+}-Mn^{2+}-2,2′-BCA. As follows from the data presented in Fig. 2, the investigated reaction rate proceeds varies in time and 'absorbance-time' dependence is linear within the

interval from 0.5 to 4.0 min. The reaction time is chosen to equal 3 min.

3.2. Influence of hydrogen ions

The reaction rate dependence on pH was studied in the interval from 6.4 to 8.5 (Fig. 3). As is seen from the figure, this dependence is described by a curve having a maximum. In the absence of thiosulfate, the reaction rate varies only slightly (curve 1). The introduction of thiosulfate results at first in its increases, and the maximum value is observed at pH 6.9–7.0 (curve 2). Such a behaviour of the dependence is caused by changes in the reacting particles' composition in the solution, in particular, by the state of copper and manganese ions defined by pH. At the further pH increase, the reaction rate becomes lower, and this seems to be connected with the formation of inactive hydrolised particles. The pH value of 6.9 was chosen as the optimum one.

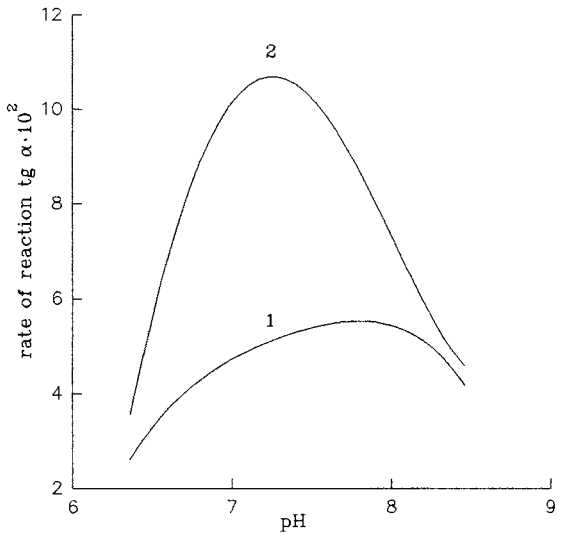

Fig. 3. Effect of pH on the reaction rate. 7 μg ml^{-1} $S_2O_3^{2-}$, 3.75×10^{-4} M of 2,2′-BCA, 1.6×10^{-4} M Cu^{2+}; 1.6×10^{-4} M Mn^{2+}, curve 1 in the absence of $S_2O_3^{2-}$, curve 2 in the presence of 7 μg ml^{-1} $S_2O_3^{2-}$.

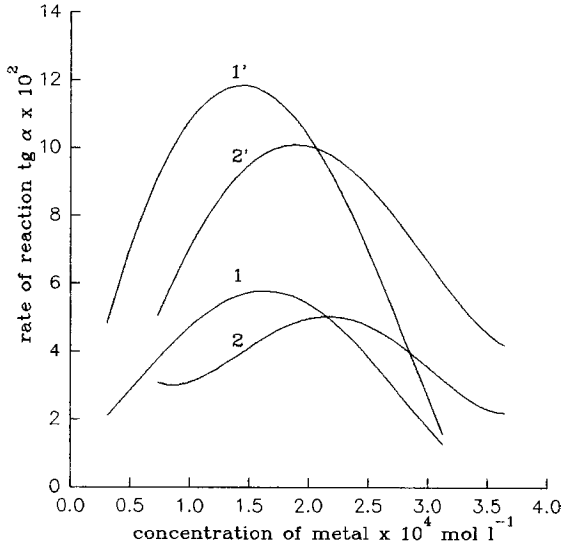

Fig. 4. Effect of Cu^{2+} (curve 1, 1′) and Mn^{2+} (curve 2, 2′) concentrations on the reaction rate. Conditions: 3.75×10^{-4} M 2,2′-BCA, curves 1, 2 in the absence of $S_2O_3^{2-}$, curves 1′, 2′ in the presence of 7 μg ml^{-1} $S_2O_3^{2-}$, pH 7.0.

3.3. Dependence of the reaction rate on copper(II) and manganese(II) concentration

The dependence of the reaction rate on concentrations of Cu^{2+} and Mn^{2+} was studied at the above-stated optimum value of pH (6.9); concentrations were varied from 0.25 to 3.5×10^{-4} M (Fig. 4). As follows from the figure, in the presence of thiosulfate (curves 1′,2′) the reaction rate highest at 1:1 ratio of Cu^{2+} and Mn^{2+} concentrations. In the absence of thiosulfate (curves 1,2), the reaction rate varies insignificantly.

3.4. The reaction rate as a function of 2,2′-BCA concentration

The dependence of the reaction rate on 2,2′-BCA concentration is shown in Fig. 5. The experiments were carried out in a $1–7 \times 10^{-4}$ M range of 2,2′-BCA concentrations, pH, 6.9; the concentration of Cu^{2+} and Mn^{2+} metals in the presence of 7 μg ml^{-1} of thiosulfate was 1.6×10^{-4} M.

It is seen from the figure, that the value of 2,2′-BCA concentration above, which the reaction

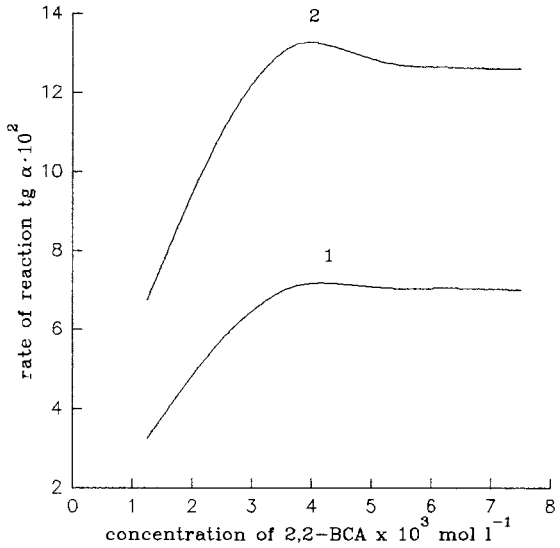

Fig. 5. Effect of the 2,2′-BCA concentration. Conditions: pH 7.0, 1.6×10^{-4} M Cu^{2+}, 1.6×10^{-4} M Mn^{2+}, curve 1 in the absence of $S_2O_3^{2-}$, curve 2 in the presence of 7 μg ml^{-1} $S_2O_3^{2-}$.

rate does not change both in the presence of thiosulfate (curve 2) and in its absence one (curve 1), is 3.75×10^{-4} M. This is obviously associated with the formation of coordinately saturated complexes at an excess of 2,2′-BCA. The working concentration of 2,2′-BCA was chosen to be equal to 3.75×10^{-4}M.

3.5. Influence of temperature

It is not expedient to raise the temperature above 25°C, since under such conditions the rate of the reaction in the absence of thiosulfate, increases substantially.

3.6. Calibration graph in aqueous medium

Under the optimum reaction conditions, the reaction rate dependence on thiosulfate concentration was obtained for 3–10 μg ml^{-1} range. That a dependence is the straight line described by the equation presented in Table 1.

3.7. Influence of organic solvents

To raise the sensitivity of thiosulfate determination, the influence of some organic solvents on the rate of the considered reaction was studied under the optimum conditions.

In the present paper we studied the influence of protic solvents (ethanol, propanol, isopropanol) and aprotic ones (dimethylformamide, dimethylsulfoxide, acetone). Their maximal content did not exceed 30%, since under such conditions the solution pH is defined by the aqueous phase [13]. Dependences of reaction rate on the content of

Table 1
Metrological characteristics of $S_2O_3^{2-}$ determination ($n = 7$, $P = 0.95$)

	Aqueous medium	Aqueous-acetone medium			
			KCl	$CsNO_3$	KNO_3
Linear range, μg ml^{-1}	3–10	0.05–5.0	0.08–3.0	0.05–3.0	0.1–3.5
Calibration graph equations	tg $\alpha = 0.0108^c - 0.0147$	tg $\alpha = 0.0505^c + 0.0042$	tg $\alpha = 0.069^c + 0.0003$	tg $\alpha = 0.0414^c + 0.0022$	tg $\alpha = 0.0663^c + 0.0055$
Detection limit[a], c_L, μg ml^{-1}	1.8	0.002	0.006	0.01	0.08
Regression coefficient	0.9878	0.9979	0.9986	0.9986	0.9971
Relative standard deviation	0.006[b]	0.002[c]	0.010[c]	0.020[c]	0.020[c]

[a] 3σ.
[b] $n = 7$, for 5 μg ml^{-1} $S_2O_3^{2-}$.
[c] $n = 7$, for 1.5 μg ml^{-1} $S_2O_3^{2-}$.

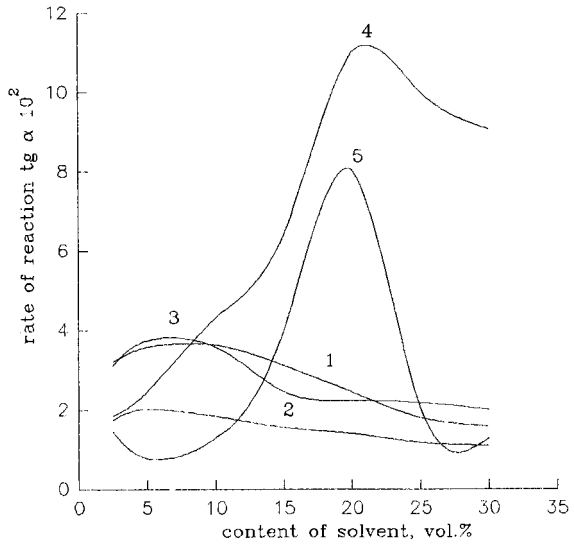

Fig. 6. Effect of alcohol content on the reaction rate; conditions as in Fig. 2, pH 7.0, curve: 1, ethanol; 2, propanol; 3, isopropanol; 4, acetone; 5, DMFA.

solvents have the form of curves with maxim (Fig. 6). The strongest influence on the rate of reaction was observed at 20% content of acetone (curve 4).

Aqueous-acetone medium was used in further investigations for the determination of $S_2O_3^{2-}$.

3.8. Calibration graph in aqueous-acetone medium

The calibration plot is linear within 0.05–3.00 μg ml^{-1} interval of thiosulfate concentration (Table 1). The use of acetone decreases the thiosulfate determination limit down to 0.005 μg ml^{-1}. The metrologic characteristics of the thiosulfate detection in salts are presented in Table 1, also. It follows from this table, that the use of aqueous-acetone medium essentially lowers the detection limit for $S_2O_3^{2-}$.

3.9. Study of interferences

Table 2 contains the data illustrating the hampering influence of foreign ions. Alkali metal ions present in quantities exceeding 500 times the thiosulfate content, are seen to have no hampering effect, Pb^{2+}, Ni^{2+}, Cr^{3+}, Zn^{2+} do not influence the reaction rate, if present in 10–30 μg ml^{-1} concentrations. Zr^{4+} and Cd^{2+} present in amounts twice as high as the thiosulfate content do not hamper either. However, Fe^{3+}, Co^{2+} ions contained in concentration comparable with that of thiosulfate, affect essential by the analysis results. The hampering effect of these metal ions is explained by their redox properties with respect to metals participating in the investigated indicator reaction.

As to anionic impurities, it should be noted that fluoride and phosphate ions affect essentially the reaction rate (apparently due to the formation of stable complexes with Mn^{3+} [14]). I^- can reduce copper(II) to copper(I) CuI formation, thereby decreasing the reaction rate. Sulphur containing anions $S_2O_3^{2-}$ and SCN^- have an effect similar to that of thiosulfate. This fact may be used in the future investigations of simultaneous determination of the said anions.

3.10. Determination of thiosulfate in inorganic salts

The procedure under determination was intended to $S_2O_3^{2-}$ determination in high-purity KCl, $CsNO_3$, KNO_3. Therefore, it was granted that at the study of the hampering influence of anions and cations their 500-fold surplus in the said salts did not take place.

The presented experimental data allowed the development of a technique for the determination of $S_2O_3^{2-}$ in potassium chloride, potassium nitrate and cesium nitrate. To determine $S_2O_3^{2-}$ in salts, an accurate weight of salt (0.50 g KNO_3, KCl or $CsNO_3$) was dissolved in 10 ml of bidistilled water and 1 ml of the obtained solution was introduced into the first test tube of the mixer. Then operations as described above (see procedure) were carried out. The correctness of this technique was controlled by the 'added-found' method [5] (see Table 3). Metrologic characteristics of the determination of $S_2O_3^{2-}$ in some inorganic salts are presented in Table 1.

3.11. Proposed mechanism

On the base of hydrolysis constants [15], states of copper(II), manganese(II), manganese(III) and copper(I) were preliminarily determined at a pH

Table 2
Effect of interfering ions on the $S_2O_3^{2-}$ (2.5 μg ml^{-1}) determination by the recommended procedure

Ion added	μg ml^{-1}	$S_2O_3^{2-}$ found, μg ml^{-1}	Ion added	μg ml^{-1}	$S_2O_3^{2-}$, found μg ml^{-1}
Na^+	500	2.43	Cl^-	500	2.49
K^+	500	2.44	NO_3^-	500	2.52
Cs^+	500	2.43	Ac^-	500	2.50
Mg^{2+}	100	2.45	SO_4^{2-}	50	2.43
Pb^{2+}	30	2.50	CO_3^{2-}	20	2.51
Ni^{2+}	20	2.49	NO_2^-	10	2.43
Cr^{3+}	20	2.47	ClO_4^-	5	2.56
Zn^{2+}	10	2.48	PO_4^{3-}	3	2.43
Cd^{2+}	5	2.43	SO_3^{2-}	2.5	2.56
Fe^{3+}	2.5	2.43	F^-	0.5	2.44
Co^{2+}	2.5	2.43	IO_3^-	0.5	2.45
VO^{2+}	2	2.44	Br^-	0.25	2.57
Sn^{2+}	1	2.47	I^-	0.1	2.50
Hg^{2+}	0.5	2.43	SCN^-	0.1	2.54

equal to 6.5–7.5. For instance, copper(II) was found to exist in the form of Cu^{2+} and in the hydrolysed form $CuOH^+$. Under such conditions, manganese(II) is not hydrolysed, whereas manganese(III) exists in the form of $MnOH^{2+}$.

The proposed mechanism of the studied reaction can be described by the following scheme.

$$Cu^{2+} + 2S_2O_3^{2-} \rightarrow Cu(S_2O_3)_2^{2-}, \quad (1)$$

$$Cu(S_2O_3)_2^{2-} + MnOH^+ \rightarrow Cu(S_2O_3)_2^{3-} + MnOH^{2+}, \quad (2)$$

$$Cu(S_2O_3)_2^{3-} + 2(2,2' - BCA)^{2-} \rightarrow Cu(2,2' - BCA)_2^{3-} + 2S_2O_3^{2-}, \quad (3)$$

$$8MnOH^{2+} + S_2O_3^{2-} \rightarrow 8Mn^{2+} + 2SO_4^{2-} + 2H^+ + 3H_2O. \quad (4)$$

At the first stage Eq. (1) copper(II) forms a stable complex with $S_2O_3^{2-}$ ion ($\lg \beta \approx 12.9$). This complex is further oxidated by Mn^{2+} (reaction 2), and Cu^{2+} is transformed into Cu^+. Such a reaction Eq. (2) can take place due to the fact that the potential of $MnOH^{2+}/Mn^{2+}$ pair at the given pH value is lower ($E = 0.805$) [16] than that of Mn^{3+}/Mn^{2+} one ($E = 1.51$).Further, the complex Cu(2.2′-BCA)$_2^{3-}$ ($\lg \beta \approx 16.20$) is formed Eq. (3).

$MnOH^{2+}$ forms a no complex with 2,2′-BCA (Fig. 1). At the last stage (Eq. (4)), $MnOH^+$ seems to be reduced by $S_2O_3^{2-}$. This assumption is confirmed by the calculation of constants according to recommendations [17].

It is known, that the introduction of organic solvents may change the dielectric permittivity of aqueous medium [18] as well as influence the redox and acid-base properties of the system [18,19].

Papers devoted to the systematic investigation in the influence solvents nature on kinetics and mechanism of complexation are very small in number. Using data given in [20], we suppose the following mechanism of organic aqueous medium influence on the rate of reaction being investigated. The change of reaction kinetics is associated immediately with changing stability of complexes involved in that system (Eqs. (1)–(4)). These changes may be caused by entering organic solvent molecules into the inner solvent shell of central ions [21].

We suppose, that the main effective factor in the system under study is the solvation component of the complexation process, influencing significantly the system activation energy [20]. The organic solvent effect on the rate of reaction is shown in Fig. 6. If the alcohol concentration is less than 50%, alcohol molecules do not enter into solvation shells of metals [21] and their influence on the reaction rate is insignificant. Dependences of the reaction rate on aprotic solvent content are described by curves with maxima. This can be

Table 3
Correctness verification of $S_2O_3^{2-}$ determination in salts

Salt	Added, μg ml^{-1}	Found, μg ml^{-1}		s_r
		Proposed method	Spectrophotometric method [5]	
KCL	0.20	0.19 ± 0.04	—	0.010
	0.5	0.54 ± 0.04	—	0.010
	1.0	1.03 ± 0.06	1.1 ± 0.2	0.008
	1.5	1.49 ± 0.03	1.5 ± 0.1	0.006
KNO_3	0.5	0.53 ± 0.06	—	0.015
	1.0	0.99 ± 0.06	0.9 ± 0.1	0.010
	1.5	1.52 ± 0.05	1.6 ± 0.1	0.008
	2.0	1.96 ± 0.06	2.0 ± 0.2	0.007
$CsNO_3$	0.5	0.53 ± 0.06	—	0.010
	1.0	1.03 ± 0.05	1.1 ± 0.1	0.008
	1.5	1.52 ± 0.03	1.5 ± 0.1	0.007
	2.0	1.97 ± 0.03	1.9 ± 0.1	0.003

explained by the entering of DMFA (or acetone) molecules into the inner solvent shell of Cu(II), resulting in a decreased stability of $Cu(S_2O_3)_2^{2-}$ complex (Eq. (1)); and the rate of process (Eq. (2)) is increased as compared with that in aqueous medium. The maximum reaction rate in the presence of DMFA and acetone is observed 20% content of organic phase. The further raising organic solvent content leads to the reaction rate decrease caused by steric effect.

3.12. Raising the thiosulfate determination sensitivity

To lower the limiting of $S_2O_3^{2-}$ amount determinable in inorganic salts, this impurity was concentrated by the method of low-temperature directed crystallisation of water-salt eutectics (DC WSE) [8]. This method is characterised by numerous merits. First of all, it may be applied to impurities of a different nature, including homologous ones. Moreover, distribution coefficients of different impurities in the same matrix have similar values under similar conditions, and the total background level is low due to the absence of chemical reagents in the preconcentration step. In view of all the mentioned facts, the contribution of the preconcentration procedure to the total analysis error is very small. The process of crystallisation (directed from the bottom upwards) was carried out using the automated apparatus with a compression type refrigerator described in [8]. This allowed to overcool the mixture by 8–10°C with respect to the eutectic melting temperature. The distribution coefficients (K) were estimated from the basic equation of directed crystallisation. The parameters of crystallisation of water–salt eutectic are presented in [8].

Distribution coefficients of arsenazo I in KNO_3, KCl, $CsNO_3$ were determined before using the DC WSE method [8]. Their values were found to be equal to 0.11, 0.32, 0.08, respectively. As is established in our investigations, the segregation of $S_2O_3^{2-}$ impurity in these solutions is characterised by the distribution coefficients 0.12, 0.30, 0.09, respectively. The reduction of c_L due to concentration is estimated from the formula

$$R = q(G/M)$$

where G and M is the mass of the initial salt and the concentrate, respectively, q is the share of the concentrate taken for the analysis. The R values for various salts are presented in Table 4. As is said above, the contribution of the preconcentration error to the total error of the analysis is insignificant. Therefore the technique of $S_2O_3^{2-}$ determination is characterised by an s_r level simi-

Table 4
Increase of $S_2O_3^{2-}$ determination sensitivity by DC WSE method

Salt	G^a (g)	M^b (g)	m^c (g)	q	R	c_L (μg ml^{-1})
KNO_3	11.0	0.11	0.050	0.45	26	0.007
KCl	19.7	0.20	0.025	0.14	3.5	0.04
$CsNO_3$	8.0	0.08	0.025	0.31	20	0.012

$q = m/M$.
$R = q(G/M)$.
[a] Mass of the initial salt in 100 ml of solution taken for concentrating.
[b] Mass of the salt in the concentrate.
[c] Mass of the salt necessary for carrying out the analysis.

lar to that typical for methods where the preconcentration is not used.

Thus, the preconcentration of impurities allows a 3–30 times decrease of the lower determination limit for thiosulfate ions.

References

[1] S. Koch, S. Peisker, Z. Chem. 30 (1990) 261.
[2] T. Koh, H. Wakabayashi, Y. Yonemura, Bull. Chem. Soc. Jpn. 67 (1994) 119.
[3] T. Koh, H. Wakabayashi, Anal. Sci. 10 (1994) 671.
[4] M. Yasuyuki, H. Koumi, T. Koh, J. Chem. Soc. Jap. Chem. Ind. Chem. 2 (1991) 125.
[5] T. Okutani, S. Utsumi, Anal. Abstr. 14 (7) (1967) 24, Ref. 3950.
[6] A. Ensafi, G. Bagherian Dehaghi, Indian J. Chem. A. 34 (1995) 489.
[7] D. Masakadzu, A. Rikiya, Bunsaki Kagaku 18 (1969) 124.
[8] A. Blank, Analysis of Pure Substances using Crystallisation Concentrating, Khimia, Moscow, 1986, p. 194 (in Russian).
[9] A. Weisseberger, E. Proscauer, Organic Solvents. Physical Properties and Methods of Purification, Interscience publishers, New York, 1955.
[10] I. Kolthoff, E. Sandell, Quantitative Chemical Analyses, 4, Macmillan, London, 1969, p. 556.
[11] H. Muller, M. Otto, G. Werner, Katalytische Methoden in der Spurenanalyse, Akademische verlagsgesellschaff Geest und Portig, K.G., Leipzig, 1980, 196.
[12] A. Gershuns, V. Koval, Vestnik Kharkov University, ser. khim. 1 (1970) 64, 69. (Chem. Abstr. 75 (26) (1970) 437 Ref. No 157906w); 69, (ibid 75 (8) 1971 Ref. No 58124h).
[13] V. Alexandrov, Acidity of Non-Aqueous solutions, Kharkov University, Kharkov, 1981, 151p.
[14] J. Barec, A. Berca, Chemicke Listy 10 (1975) 1056–1072.
[15] L.G. Sillen, A.E. Martell, Stability Constants. Special Publication N 17, The Chemical Society, Burbington House, London, W 1, 1964, 734p.
[16] I. M. Issa, M.M. Choneim, Talanta 20 (1973) 517.
[17] M.K. Karapet'yanz, M.L. Karapert'yanz, The Main Thermodynamic Constants of Inorganic and Organic Substances, Khimia, Moscow, 1968, 264p.
[18] V. Gutmann, Coordination Chemistry in Non-Aqueous Solutions, Springer–Verlag, New York, 1968.
[19] Edward. S. Amis, Solvent effects on reaction rates and mechanisms, Academic Press, New York, 1966, 234p.
[20] V. Fedorov, I. Isayev, M. Ackae, Coord. Khim. 15 (1989) 1162–1167.
[21] V. Matveev, Zh. Struct. Khim. 27 (1986) 134.

ELSEVIER

Talanta 47 (1998) 223–228

Talanta

Short Communication

Flow injection-spectrophotometric determination of metoclopramide hydrochloride

M. Royo Herrero, A. Mellado Romero, J. Martínez Calatayud *

Departamento de Química Analítica, Universidad de Valencia, Valencia, Spain

Received 22 September 1997; received in revised form 11 February 1998; accepted 11 February 1998

Abstract

The determination of metoclopramide hydrochloride is spectrophotometrically determined by the Bratton-Marshall method in a flow injection assembly. The required nitrite is prepared on-line in the flow assembly by reducing a nitrate solution with the aid of a copperised cadmium solid-phase reactor. The calibration graph is linear over the range 0.5–85 mg l^{-1}, with a relative standard deviation (RSD) of 0.89%, and sample throughput of 51 samples h^{-1}. The method is easy and simple, and it is applied to determination of metoclopramide in some pharmaceutical formulations. The method eliminates the need for frequent preparation of unstable nitrite solutions. © 1998 Elsevier Science B.V. All rights reserved.

Keywords: Metoclopramide; UV-vis; Pharmaceuticals; Flow injection

1. General introduction

Metoclopramide hydrochloride is a white or almost white crystalline powder, is odourless, and 1 g is soluble at 25°C in 0.7 g of water, 3 g of ethanol (96%) and 55 g of chloroform, though it is practically insoluble in ether. It is soluble in dilute hydrochloric acid. It shows two ionisation constants; $pK_1 = 0.42$ and $pK_2 = 9.71$ [1].

* Corresponding author. Departamento de Química, Colegío Universitario CEU, 46113 Moncada (Valencia), Spain. Tel.: +349 6 3864062; fax: +349 6 3692684; e-mail:jose.martinez@uv.es

1.1. Formulae

Metoclopramide hydrochloride is used as an anti-emetic in the treatment of some forms of nausea and vomiting and to increase gastrointestinal motility. It is of little benefit in the prevention or treatment of motion sickness or in the treatment of nausea and vertigo due to Ménière disease or other labyrinth disturbances [2].

Many analytical methods have been developed for analysis of metoclopramide hydrochloride, most based on spectrophotometric [3–8], fluorimetric [9–11], electrometric [12–14], or chromatographic [15–17] techniques.

0039-9140/98/$19.00 © 1998 Elsevier Science B.V. All rights reserved.
PII S0039-9140(98)00069-1

The colorimetric assays have been the most widely used especially to determine metoclopramide in pharmaceutical preparations. Some of them [3,4] are based on the classical Bratton-Marshall procedure. In this method, the aryl primary amine is determined by diazotisation with $NaNO_2$ in acidic medium and coupling with *N*-(1-naphthyl)ethylendiamine dihydrochloride (NED). The pink coloured complex formed can be monitored spectrophotometrically. The main difficulty is that solutions of nitrite are unstable and have to be stored in the refrigerator and frequently replaced. No flow procedures for metoclopramide determination have been published.

The use of solid-phase reactors in continuous flow assemblies is advantageous for the in situ preparation of an unstable reagent [3]. The proposed manifold uses nitrate solutions for in-line conversion into nitrite thus avoiding problems associated with nitrite oxidation. The nitrite solution generated is used as a spectrophotometric reagent. Our group and others used such a flow injection (FI) assembly to generate unstable oxidants and reductants [18,19].

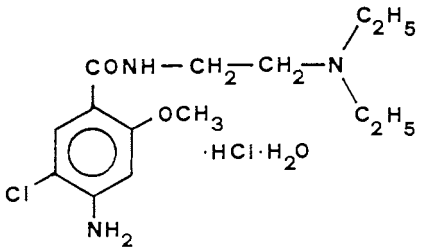

2. Experimental

2.1. Reagents

The reagents used were: metoclopramide hydrochloride (Guinama, pure); *N*-(1-naphtyl)ethylenediamine dihydrochloride (NED) (Sigma, pure); cadmium (Aldrich, pure); sorbitol (Acofarma, pure); lactose (d'Henio, pure); dextrose, fructose (Panreac, a.r.); sodium saccharine, glucose, pyridoxine, sodium bicarbonate, diazepam, pepsin, pancreatine (Guinama, pures); magnesium carbonate, bismuth sub-nitrate, sucrose (Probus, a.r.); oxazepam (Boehringer). Other reagents (acids, salts) were of analytical grade unless stated otherwise.

2.2. Flow-injection assembly

Fig. 1 depicts the manifold used. The sample injector was from Rheodyne, Model 5041, and a Gilson Minipuls 2 peristaltic pump was used. The determination of metoclopramide hydrochloride was carried out by means of a Model Lambda 16 UV-Vis spectrophotometer from Perkin Elmer at 539 nm, using a quartz flow-cell of 18-μl volume and 1-cm path length (Hellma). PTFE tubing was 0.5 mm i.d. and the reducing column was a 15-cm × 6-mm i.d. glass tube.

2.3. Sequential optimisation of experimental parameters

Optimisation of experimental parameters was carried out by a sequential procedure of successive optimisations. After preliminary optimisation of several parameters (media of the sample and the different streams; concentration of HCl and NED) the modified simplex method (MSM) was used for optimisation of the manifold parameters. The modified simplex program was based on the method of Nelder and Mead [20]. After the first set of 21 experiments within the MSM, a new MSM was applied (18 experiments) by adjusting new limits for every tested parameter according to results obtained in the first set. Then and in order to obtain the best compromise of sensitivity (peak

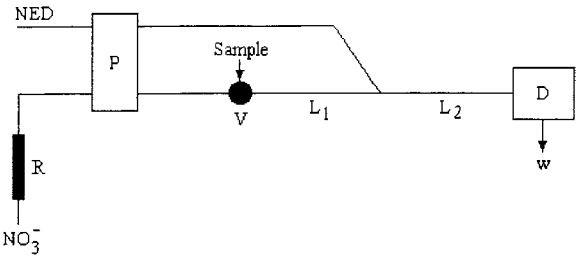

Fig. 1. Flow injection assembly for metoclopramide hydrochloride determination. D, spectrophotometer; L, reactor lengths; P, peristaltic pump; R, solid-phase reactor; V, injection valve.

height), reproducibility (RSD, %) and sample throughput, some points from the simplex producing the best transient signals were selected and compared by recording a series of 20 injections. Final optimisation of chemical parameters was achieved by the univariate method.

2.4. Preparation and study of the solid-phase reactor

The copperised cadmium particles were prepared according to [18] and by adding 2% $CuSO_4$ solution to the cadmium particles, previously washed with 6 M HCl and rinsed with pure distilled water. After 5 min, or when the blue colour faded, the solution was decanted and the procedure repeated with freshly prepared $CuSO_4$ solution until a brown colloidal precipitate developed. Finally the particles were washed copiously with water (at least 10 times) to remove all precipitated Cu.

The column was filled by hand and was placed and used vertically in the flow-manifold to avoid the blocking of the flow by small released Cd or Cu particles. The reduction of nitrate to nitrite was performed in a buffered ammonia-ammonium chloride and sodium EDTA solution according to [21].

The efficiency of the prepared reactor to reduction was tested with the aid of the flow assembly depicted in Fig. 1. FI outputs obtained with KNO_3 10^{-2} M flowing through the reactor were compared with those obtained by passing a freshly prepared solution of KNO_2 10^{-2} M. The calculated efficiency in terms of $R =$ (absorbance by reduction of KNO_3/absorbance by KNO_2) $\times$ 100, gave 99.02%.

2.5. Preparation of real samples

Three different commercially available samples were studied: a syrup, an injection and a tablet.

Ten tablets were taken and powdered in a agate mortar and pestle. Then 3.74 g was exactly weighed and dissolved in HCl 0.05 M and levelled to 250 ml; aliquots of 25 ml were taken and levelled to 100 ml.

Aliquots of syrup and injectable samples (10 and 2 ml, respectively) were taken and diluted to 100 ml with 0.05 mol l^{-1} HCl; aliquots of 25 ml of the resulting solution were then taken and levelled to 100 ml. In all cases the final solution was about 25 mg l^{-1}.

3. Results and discussion

3.1. Preliminary investigations

The stability of the aqueous solution of metoclopramide was previously studied by preparing solutions containing 20 mg l^{-1} of the active principle in 0.05 M HCl and by periodic recordings of its UV-vis absorption spectra for up to 8 days; there were no changes in absorbance up to 25 h; up to 8 days changes were small, less than 20% in absorbance values but without changes in the spectra profile.

Other preliminary experiments were aimed at preparing a suitable manifold; batch tests showed the critical influence of the order of addition of reagents; the addition of NED last resulted in greater absorbances. Different FI assemblies were tested by keeping the order of reagent addition as selected in the preliminary batch experiments. Fig. 1 depicts the selected flow injection analysis (FIA) configuration.

We performed some preliminary tests to select a set of initial conditions that would be subsequently refined. The different acids used as media of metoclopramide hydrochloride solution were: HCl, $HClO_4$, H_3PO_4 and CH_3COOH, all in 0.1 M (metoclopramide solution was 20 mg l^{-1}, KNO_3 10^{-2} M in NH_4^+-NH_3 and Na_2EDTA buffer, NED 500 μg ml^{-1}). Reactor length was 12 cm, flow-rates of KNO_3 and NED streams were 1.9 ml min^{-1}, L_1 and L_2 were 159 cm and 66 cm, respectively, and sample volume was 285 μl. Transient outputs were obtained at 525 nm. Hydrochloric acid was chosen at this stage. The influence of the HCl concentration in metoclopramide solution was tested over the range 0.05–0.2 M (lower limit of HCl concentration was due to metoclopramide solubility); the best results were provided by a 0.05 M concentration of the acid.

Table 1
Studied ranges and obtained results in the multivariate optimisation of FIA parameters

Parameter tested	1st Simplex	2nd Simplex	Selected value
Sample volume (μl)	151.9–544.6	309.0–446.4	388.8
NO_3^- flow-rate (ml/min)	0.6–4.6	1.4–2.1	1.7
NED flow-rate (ml/min)	0.6–4.6	2.0–3.9	2.5
Coil length L_1 (cm)	50.0–200.0	100.0–200.0	129.7
Coil length L_2 (cm)	6.0–150.0	90.0–120.0	103.8

Further experiments were done with different NED concentrations over the range 500–1500 μg ml^{-1}. Absorbance differences (analytical signal minus blank signal) were smaller the greater the reagent concentration; a concentration of 500 μg ml^{-1} proved to be optimal. This NED concentration was selected for further work and tested in water and in 0.05 M HCl; absorbances were greater in pure distilled water, 0.1207 in water and 0.0531 in HCl medium.

3.2. Optimisation

The influence of reduction column length was also tested; outputs were obtained with columns of 5, 10, 12 and 14 cm and different concentrations of the drug (10, 25 and 50 mg l^{-1}) for each tested length (20 replicates). No significant differences were observed on the height of FIA peaks. The shortest column was selected because it provided the best reproducibility (RSD) for the outputs.

The next step involved the optimisation of the experimental variables for the FIA system. Table 1 lists the ranges over which those variables were studied (using the modified simplex method) and the selected values. The procedure was repeated twice as described in Section 2.

At a later stage, chemical variables were re-optimised. Fig. 2 shows the results obtained in the study of the influence of NO_3^-, NED and HCl concentrations; 10^{-2} M NO_3^-, 250 mg l^{-1} NED and 0.05 M HCl were selected for further work.

Finally, a re-optimisation of wavelength was performed; the range studied was from 500 up to 560 nm. The value selected as the best was 539 nm.

4. Analytical applications

The calibration graph was linear over the range 0.5–85 mg l^{-1} of metoclopramide, with the equation: Peak height absorbance $(A) = -0.0176 + 0.0231 \times C$ (C is the metoclopramide concentration in mg l^{-1}) and the detection limit (defined as the average peak height of the blank solution series plus three times its RSD (%)) was 0.5 mg l^{-1}. The correlation coefficient was 0.9997.

The reproducibility of the method, as RSD, was 0.89% for 50 replicates of 25 μg ml^{-1} metoclopramide. The throughput was 51 samples h^{-1} and the residence time, 46 s.

The day-to-day reproducibility was tested by obtaining 12 independent calibration graphs on different days, with independent freshly prepared

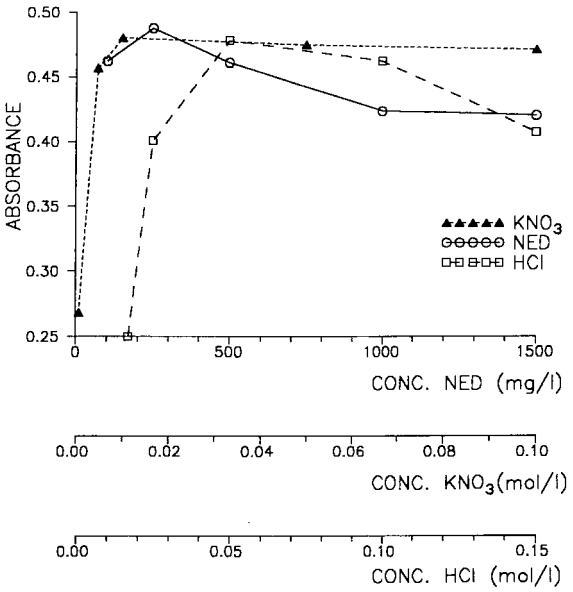

Fig. 2. Influence of different chemical parameters.

Table 2
Influence of foreign compounds

Compound	Concentration (mg l^{-1})	Error (%)
Lactose	1000	2.9
Sorbitol	1000	1.9
Dextrose	1000	0.5
Sodium saccharin	1000	0.2
Sucrose	1000	0.5
Glucose	1000	2.6
Pepsin	1000	2.9
Diazepam	1000	1.7
Fructose	600	0.8
Oxazepam	500	0.1
Pancreatine	200	1.1
Piridoxine	100	2.7
Sodium bicarbonate	100	2.4
Magnesium carbonate	100	2.5
Bismuth sub-nitrate	40	2.9

reagent solutions and two different columns: the average of 12 slopes was 0.02314 with an RSD of 2.0%, and with an average of the correlation coefficient of 0.9996 and RSD 0.04%.

The influence of foreign compounds that are commonly found in pharmaceutical formulations containing metoclopramide was investigated by preparing solutions containing 25 mg l^{-1} of active principle and different concentrations of each potential interferent (not exceeding 1000 mg l^{-1}). The analytical responses provided by these solutions were compared with that obtained from a metoclopramide solution containing 25 mg l^{-1} concentration of the pure drug. The results in terms of concentration and relative error are depicted in Table 2.

Finally, the proposed method was applied to the determination of metoclopramide in three different pharmaceutical formulations: 'Primperan Inyectable' and 'Primperan Oral' (Delagrange, S.A.) and 'Aeroflat' (Biosarto, S.A.). The obtained results were compared with those obtained with the official recommended method [22]. This procedure is based on the extraction of the drug from the alkaline aqueous solution by chloroform; the aliquots from the organic layer were spectrophotometrically tested at 305 nm. The obtained results (average of five replicates) were as follows: (a) 'Primperan Inyectable': label claim, 100 mg per ampoule; FIA, 106.9 mg; and BP, 109.0 mg; (b) 'Primperan Oral': label claim, 100 mg per 100 ml of syrup; FIA, 100.8 mg; and BP, 102.7 mg; and (c) 'Aeroflat': label claim, 5 mg per tablet; and FIA, 5.1 mg.

5. Conclusions

A simple and easy FIA procedure is proposed for the first time for metoclopramide determination.

The method is based on the classical Bratton-Marshall method in which the unstable nitrite solution is prepared on line by means of a copperised cadmium column.

The procedure is applied to metoclopramide determination in three different pharmaceutical formulations with competitive precision and accuracy.

References

[1] D. Pitrè, R. Stradi, in: K. Florey (Ed.), Analytical Profiles of Drug Substances, vol. 16. Academic Press, Orlando, 1982, p. 327.
[2] Martindale, The Extra Pharmacopoeia, 28th edn., The Pharmaceutical Press, London, 1982, p. 964.
[3] A. Mellado Romero, C. Gómez Benito, J. Martínez Calatayud, Anal. Chim. Acta 308 (1995) 451.
[4] D.M. Shingbal, K.V. Sawant, Indian Drugs 19 (1982) 239.
[5] F.M. Abdel Gawad, N.M. El Guindi, Anal. Lett. 28 (1995) 1437.
[6] A.E. El Gendy, Spectrosc. Lett. 25 (1992) 1297.
[7] C.S.P. Sastry, P.L. Kumari, B.G. Rao, Chem. Anal. (Warsaw) 30 (1985) 461.
[8] D.M. Shingbal, S.V. Joshi, Indian Drugs 21 (1984) 517.
[9] M. Buna, J.J. Aaron, P. Prognon, G. Mahuzier, Analyst 121 (1996) 1551.
[10] H.L. Rao, A.R. Aroor, P.G. Rao, Indian Drugs 28 (1991) 195.
[11] V.C. Alka, V. Bozidar, M. Zoran, P. Franjo, Acta Pharm. Jugosl. 38 (1988) 213.
[12] C. Díaz, J.C. Vidal, J. Galban, J. Lanaja, J. Electroanal. Chem. Interfacial Electrochem. 258 (1989) 295.
[13] S.S. Badawy, A.F. Shoukry, Y.M. Issa, Analyst 111 (1986) 1363.

[14] A.A. Badwan, O.A. Jawan, L. Owais, Int. J. Pharm. 28 (1986) 41.
[15] T.G. Venkateshwaran, D.T. King, J.T. Stewart, J. Liq. Chromatogr. 18 (1995) 117.
[16] K.W. Riggs, A. Szeitz, D.W. Rurak, A.E. Mutlib, F.S. Abbott, J.E. Axelson, J. Chromatogr. B. Biomed. Appl. 660 (1994) 315.
[17] N.H. Foda, Anal. Lett. 27 (1994) 549.
[18] J. Martínez Calatayud, Flow Injection Analysis of Pharmaceuticals. Automation in the Laboratory, Taylor and Francis, London, 1996.
[19] J. Martínez Calatayud, J.V. García Mateo, Trends Anal. Chem. 12 (1993) 428.
[20] J.A. Nelder, R. Mead, Comput. J. 7 (1965) 808.
[21] Standard Methods for Water and Wastewater, 15th edn., American Public Health Association, Washington DC, 1981.
[22] British Pharmacopoeia, Her Majesty's Stationary Office, London, 1993, p. 1010.

ELSEVIER

Talanta 47 (1998) 229–236

Talanta

The solvent extraction of alkali metal picrates with 4,13-*N*,*N*′-dibenzyl-4,13-diaza-18-crown-6

Candan Hamamcı [a,*], Halil Hoşgören [b], Sait Erdoğan

[a] *Department of Analytical Chemistry, Faculty of Science, University of Dicle, TR-21280 Diyarbakir, Turkey*
[b] *Department of Organic Chemistry, Faculty of Science, University of Dicle, TR-21280 Diyarbakir, Turkey*

Received 11 December 1997; received in revised form 13 February 1998; accepted 20 February 1998

Abstract

Extraction of alkali metal picrates with *N*,*N*′-dibenzyl-18-crown-6 was carried out, with dichloromethane as water-immiscible solvent, as a function [ligand]/[metal cation]. The extractability of metal picrates (Li^+, Na^+, K^+, Rb^+, Cs^+) was evaluated as a function of [L]/[M^+]. The extractability of complex cation–picrate ion pairs decreases in this sequence: $Li^+ > Rb^+ > Cs^+ > K^+ > Na^+$. The overall extraction equilibrium constants (K_{ex}) for complexes of *N*,*N*′-dibenzyl-18-crown-6 with alkali metal picrates between dichloromethane and water have been determined at 25°C. The values of the extraction constants ($\log K_{ex}$) were determined to be 10.05, 6.83, 7.12, 7.83, 6.73 for Li^+, Na^+, K^+, Rb^+ and Cs^+ compounds, respectively. DB186 shows almost 2-fold extractability against Li^+ compared to the other metal picrates, whereas it shows no obvious extractability difference amongst the other metal cations when [L]/[M^+] is 0.2–1. However, an increasing extractability is observed for Cs^+ when [L]/[M^+] [1]. © 1998 Elsevier Science B.V. All rights reserved.

Keywords: Diaza-crown ether; Solvent extraction; Alkali metal picrate

1. Introduction

Solvent extraction separation methods for alkali metals have been limited. It has been demonstrated that macrocyclic polyethers can behave as highly selective complexing agents for alkali metal cations, and are of potential significance in the separation of ions using solvent extraction procedures. These methods can not only be applied in the separation of ions but can also provide information concerning the nature of the complex formed between the ion and the ligand. Solvent extraction is an available and convenient method for investigating the complexing ability of crown

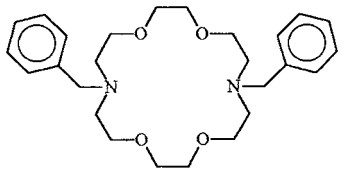

DB18C6

Scheme 1. Schematic representation of 4,13-*N*,*N*′-dibenzyl-4,13-diaza-18-crown-6.

* Corresponding author. Fax: +90 412 2488039.

0039-9140/98/$19.00 © 1998 Elsevier Science B.V. All rights reserved.
PII S0039-9140(98)00082-4

Table 1
Solvent extraction of aqueous metal picrates with 4,13-*N*,*N*′-dibenzyl-4,13-diaza-18-crown-6 as a function of [L][M^+][a]

$[L]_o[M^+]_o$	Extractibility[b] (%)					Selectivity[c]	
	Li^+	Na^+	K^+	Rb^+	Cs^+	M^+	Li^+/M^+[d]
0.2	31.3	15.7	14.5	13.5	14.0	Na^+	70.6
0.4	52.3	29.5	24.0	20.3	27.0	K^+	86.38
0.6	66.6	32.0	33.2	32.3	33.0	Rb^+	57.40
1.0	78.0	39.0	41.4	43.6	38.0	Cs^+	23.89
1.5	84.6	46.9	45.0	48.3	54.0		
2.0	98.9	56.0	51.0	61.3	79.0		

[a] Temperature, 25 ± 0.1°C; aqueous phase (10 ml): [picrates] $= 3 \times 10^{-4}$ M, organic phase (CH_2Cl_2), 10 ml.
[b] Defined as percent picrate extracted into the organic phase.
[c] Relative cation selectivity determined by the distribution ratio of metal ion between the organic and aqueous phases.
[d] Selectivity is calculated when $[L]/[M^+] = 2$.

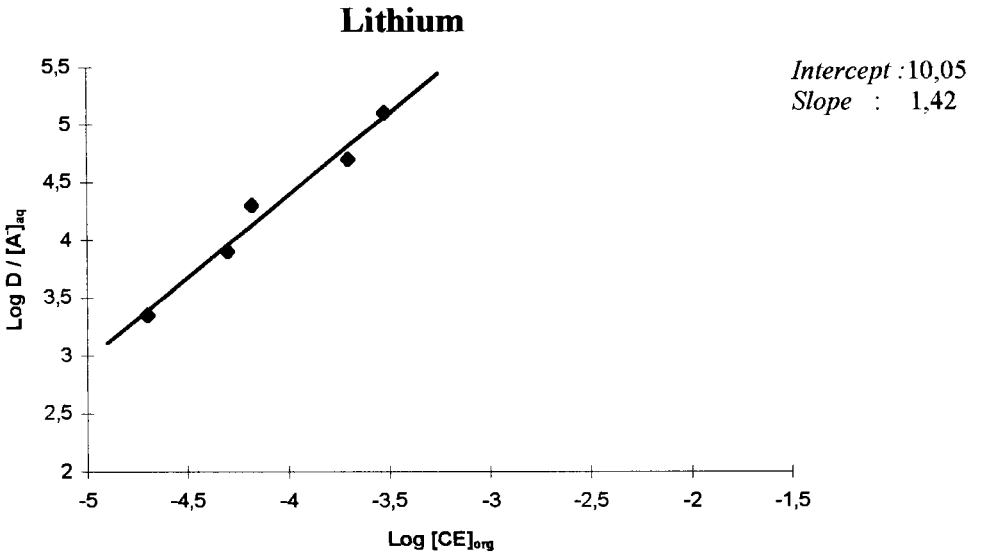

Fig. 1. Plots of $\log(D_M/[A^-])$ vs. $\log[CE]_{org}$ for the univalent metals–*N*,*N*′-dibenzyl-18-crown-6 system at 25°C.

ethers for various cations, and several extraction studies have been reported to date [1].

Macrocyclic polyethers, which are commonly called crown ethers, have recently been utilized as neutral extracting reagent. The complexation of macrocyclic polyethers to alkali metal and other cations has been well documented and several types of ligands have been synthesized to enhance the stability of the cation–ligand complex and to achieve better selectivity [2] (Scheme 1).

Diaza crown ethers are highly potential complexing reagents because of their affinity for cations and hydrophobic properties for solvent extraction and they can be optimised by introducing suitable substituents on the nitrogen atoms. Macrocyclic diaza crown ethers bearing various ligating donor side arms have been employed in solvent extraction of metal perchlorates by using ion-selective electrodes [2,3]. The study is based on modification of parent ligands, and experiments are carried out using equal concentrations of metal/ligand. This gives limited information on cation extraction properties, such as extractability and selectivity, of those armed crown ethers.

Table 2
Complexation ratios and extraction equilibrium constants of alkali metal picrates with *N*,*N*′-dibenzil-18-crown-6 into CH_2Cl_2 phase at 25°C

Cation	Crystal ionic radius (Å)	log K_{ex}	L/M$^+$ complexation ratio
Li^+	0.60	10.05	2:3
Na^+	0.95	6.83	1:1
K^+	1.33	7.12	1:1
Rb^+	1.48	7.83	1:1
Cs^+	1.69	6.73	1:1

Methodology for developing techniques to measure therapeutic lithium levels in the treatment of manic depressive psychosis which must be kept in the range of 0.5–1.5 mM in the blood in the presence of 140 mM sodium, is of great importance. There are several techniques dealing with synthesis of various reagents for achieving high lithium selectivity over sodium, and for blood lithium measurements [3,4]. These include spectrophotometric, polarimetric ion-selective reagents that can be selectively employed for determination of lithium in the presence of sodium. In this work, we used an armed crown ether for the selective extraction of lithium over alkali metals including sodium, a system may be regarded as an indirect method in the quantitative analysis of lithium in serum; that is, lithium can be selectively removed from serum by solvent extraction and then quantitatively analysed by conventional methods. The selectivity extraction of lithium by *N*,*N*′-dibenzyl-18-crown-6 over other alkali metals may be compared with other crown ethers [4].

2. Experimental

N,*N*′-Dibenzyl-18-crown-6 was synthesised in our laboratory according to procedure described previously [5]. The alkali metal picrates were prepared by adding a corresponding carbonate solution to an aqueous solution of picric acid, the resulting precipitates of alkali metal picrates were recrystallized from water as outlined by Coplan and Fuoss [6]. They were dried under vacuum and stored in the dark. Distilled dichloromethane and demineralized water were used. The solvents were saturated with each other before use in order to prevent volume changes of the phases during extraction.

Equal volumes (10 ml) of dichloromethane solution of crown ether and aqueous alkali metal picrate solution were introduced into a stoppered

Table 3
Selectivity of alkali metal picrates with *N*,*N*′-dibenzil-18-crown-6 to [L^0]/[M$^+$]

[L^0]/[M$^+$]	Li^+/Na^+	Li^+/K^+	Li^+/Rb^+	Li^+/Cs^+	Na^+/K^+	Na^+/Rb^+	Na^+/Cs^+	K^+/Rb^+	K^+/Cs^+	Rb^+/Cs^+
0.2	2.44	2.68	6.77	2.89	1.09	2.77	1.18	2.52	1.07	0.42
0.4	2.62	3.47	4.28	2.94	1.32	1.63	1.12	1.23	0.85	0.68
0.6	4.25	4.02	4.19	4.08	0.94	0.98	0.95	1.04	1.01	0.97
1.0	3.11	2.82	2.58	3.29	0.90	0.83	1.05	0.91	1.16	1.27
1.5	6.25	6.74	5.93	4.72	1.08	0.95	0.75	0.88	0.70	0.79
2.0	70.60	86.38	57.40	23.89	1.22	0.81	0.33	0.66	0.27	0.41

Table 4
Extraction of lithium picrate with *N*,*N*′-dibenzil-18-crown-6 into CH_2Cl_2 ([M$^+$] = [Li$^+$] = 3×10^{-4} M)

[L^0]/[M^0]	$[M^+]_{aq}$	$[MLA]_o$	Extraction % (%E = [A]/[M^0]×100)	D	log $D/[A^-]_{aq}$	log$[L]_{org}$
0.2	2.06	0.94	31.3	0.456	3.35	−4.88
0.4	1.43	1.57	52.3	1.098	3.89	−4.38
0.6	1.00	2.00	66.6	2.00	4.30	−4.09
1.0	0.66	2.34	78.0	3.545	4.73	−3.73
1.5	0.46	2.57	84.6	5.521	5.08	−3.49

Table 5
Extraction of sodium picrate with *N,N′*-dibenzil-18-crown-6 into CH_2Cl_2 ($[M^+] = [Na^+] = 3 \times 10^{-4}$ M)

L^0/M^0	$[M^+]_{aq}$	$[MLA]_o$	Extraction % ($\%E = [A]/[M^0] \times 100$)	D	$\log D/[A^-]_{aq}$	$\log[L]_{org}$
0.2	2.530	0.470	15.7	0.186	2.87	−4.89
0.4	2.114	0.885	29.5	0.420	3.29	−4.50
1.0	1.821	1.178	39.0	0.646	3.55	−3.74
1.5	1.591	1.408	46.9	0.884	3.74	−3.51
2.0	1.308	1.692	56.0	1.293	3.99	−3.36

Table 6
Extraction of potassium picrate with *N,N′*-dibenzil-18-crown-6 into CH_2Cl_2 ($[M^+] = [K^+] = 3 \times 10^{-4}$ M)

L^0/M^0	$[M^+]_{aq}$	$[MLA]_o$	Extraction % ($\%E = [A]/[M^0] \times 100$)	D	$\log D/[A^-]_{aq}$	$\log[L]_{org}$
0.2	2.563	0.437	14.5	0.172	2.83	−4.80
0.4	2.269	0.730	24.0	0.322	3.15	−4.33
0.6	2.002	0.998	33.2	0.498	3.39	−4.10
1.0	1.756	1.243	41.4	0.707	3.60	−3.76
1.5	1.647	1.352	45.0	0.821	3.70	−3.50
2.0	1.467	1.532	51.0	1.044	3.85	−3.35
10.0	0.659	2.341	78.0	3.546	4.73	−2.56
17.0	0.398	2.602	86.7	6.537	5.21	−2.32

flask, and shaken for 20 min at 25 ± 0.1°C. This period of shaking was enough to establish equilibrium between the two phases. The phases were than left for 4 h to separate and clarify. The range of the crown ether was from 6.10^{-5} to 6.10^{-4} M. The concentrations of the picrates in the organic and aqueous phases were determined spectrophotometrically at 375 and 356 nm, respectively [1]. The spectrophotometric measurements were made with Shimadzu model 160 UV-visible spectrophotometer. A Heildoeph Type RZR 50 model mechanical stirrer and a Grand Type W14 model water circulator thermostatic bath were used in solvent extraction experiments.

3. Results and discussion

The results of solvent extraction of alkali metal picrates from aqueous phase into dichloromethane phase with DB18C6 are summarized in Table 1. The use of DB18C6 having an 18-membered crown ring system, as an extractant, produces a surprising selectivity in the extraction of Li^+. It is known that 18-membered all-oxygen crown ethers have high selectivity for K^+ ion. DB18C6 shows approximately similar extractability against the other metal cations (Na^+, K^+, Rb^+, Cs^+) and shows no selectivity for these cations when $[L]/[M^+]$ is 0.2–1.0. But when $[L]/[M^+] > 1$, a selectivity becomes apparent as in the order $Li^+ > Cs^+ > Na^+ > Rb^+ > K^+$. The other striking fact observed is the increasing extractability of Cs^+ cation when the ligand concentration is increased beyond $[L]/[M^+] > 1$.

Previous investigations on solvent extraction of alkali metal cations from aqueous phase into organic solvents with all-oxygen crown ethers such as 12-crown-4,15-crown-5 and 18-crown-6 indicate that the following orders are common trends, $Li^+ \geq Na^+ \gg K^+ > Rb^+ > Cs^+$, $Na^+ \gg K^+ > Rb^+ > Cs^+ > Li^+$, $K^+ \gg Rb^+ > Cs^+ > Na^+ > Li^+$, respectively. These orders are explained in terms of the relationship between the crystal radius of metal ions and the size of crown ethers [1,7]. DB18C6 indicates a similar behavior in solvent extraction of alkali metal perchlorates (Li^+, Na^+, K^+, Cs^+) into $CHCl_3$ phase to those of all-oxygen crown, except Cs^+, which was not extracted at all. This observation was associated

Table 7
Extraction of rubidium picrate with *N*,*N*′-dibenzil-18-crown-6 into CH_2Cl_2 ($[M^+] = [Rb^+] = 3 \times 10^{-4}$ M)

L^0/M^0	$[M^+]_{aq}$	$[MLA]_o$	Extraction % (%$E = [A]/[M^0] \times 100$)	D	log $D/[A^-]_{aq}$	$\log[L]_{org}$
0.2	2.81	0.19	6.3	0.067	2.38	−4.38
0.4	2.39	0.61	20.3	0.255	3.03	−4.23
0.6	2.03	0.97	32.3	0.477	3.37	−4.08
1.0	1.69	1.31	43.6	0.775	3.66	−3.77
1.5	1.55	1.45	48.3	0.935	3.78	−3.51
2.0	1.16	1.84	61.3	1.840	4.13	−3.38

Table 8
Extraction of cesium picrate with *N*,*N*′-dibenzil-18-crown-6 into CH_2Cl_2 ($[M^+] = [Cs^+] = 3 \times 10^{-4}$ M)

L^0/M^0	$[M^+]_{aq}$	$[MLA]_o$	Extraction % (%$E = [A]/[M^0] \times 100$)	D	log $D/[A^-]_{aq}$	$\log[L]_{org}$
0.2	2.59	0.41	14.0	0.158	2.79	−4.72
0.4	2.16	0.84	27.0	0.384	3.25	−4.44
0.6	2.01	0.99	33.0	0.492	3.39	−4.09
1.0	1.87	1.13	38.0	0.604	3.51	−3.73
1.5	1.38	1.62	54.0	1.174	3.93	−3.56
2.0	0.63	2.37	79.0	3.770	4.78	−3.44

with a cavity-size relationship. However, we have found higher extractability for all metal picrates and remarkable Li^+ selectivity in all $[L]/[M^+]$ ranges and Cs^+ selectivity after $[L]/[M^+] > 1$. The extractability difference may be attributed to the counter-ion effect but the difference in the selectivity cannot be attributed to this effect [1]. We believe that the cavity-size relationship fails to explain the selective extraction of Li^+ with DB18C6. Some other factors may be accounted for the complex stability of alkali metal cations with BIBLEs (bibracial lariat ethers), such as DB18C6: there are the number of donor atoms [8], effective radii and the molecular topography of complexes [9–14]. Our results are in agreement with the this hypothesis because Li^+, amongst alkali metal cations, is selectively extracted with DB18C6 from aqueous phase into the CH_2Cl_2 phase (see Table 1). This is consistent with the fact that the number of oxygen donor atoms rather than the cavity-size relationship is the key factor for the selective extraction of alkali metal picrates with DB18C6. The steric effect may also be considered as a reason for the selective extraction of Li^+ with DB18C6. The increasing extractability of Cs^+ and the regularity in the selective extraction of the other metal cations when $[L]/[M^+] > 1$ may be ascribed to 1:2 (metal:ligand) stoichiometry that is, metal is 'sandwiched' between two ligand molecules, thus providing sufficient oxygen donor atoms for complexation [9].

In an equilibrium between an aqueous solution of a univalent metal ion, M^+, a picrate anion, A^-, and a dichloromethane solution of a crown ether, CE, the equilibrium constants may be defined by the following equations [10–14].

$$K_{ex} = [M(CE)A]_o[H^+]/[M][CE]_o[HA]_o \quad (1)$$

$$K_{D,CE} = \frac{[CE]_o}{[CE]} \quad (2)$$

$$K_{ex}(HA) = [HA]_o/[H^+][A^-] \quad (3)$$

$$K_{M(CE)} = [M(CE)^+]/[M^+][CE] \quad (4)$$

$$K'_{ex} = [M(CE)A]_o/[M(CE)^+][A^-] \quad (5)$$

Where the subscript 'o' and the lack of subscript designate the organic phase and the aqueous phase, respectively; square brackets indicate the molar concentrations. Thus, K_{ex} can be written as follows:

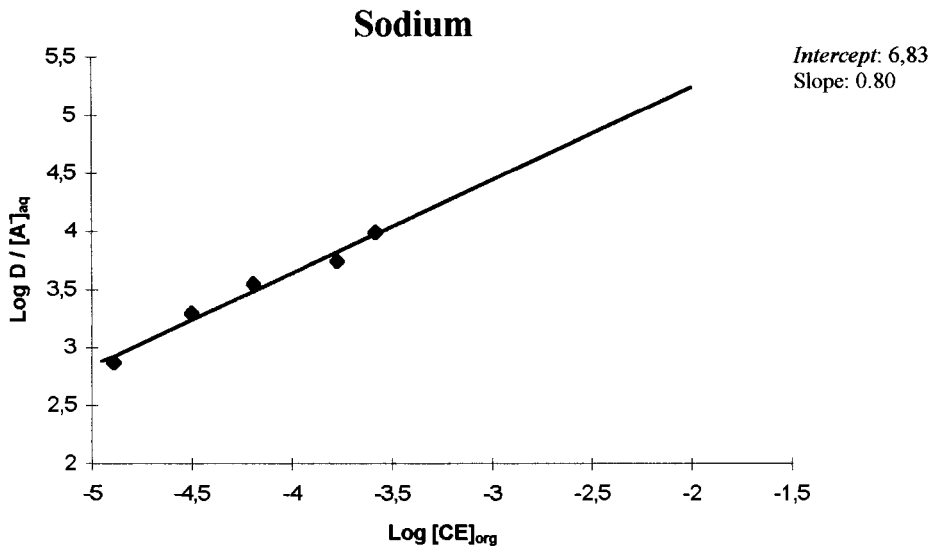

Fig. 2. Plots of $\log(D_M/[A^-])$ vs. $\log[CE]_{org}$ for the univalent metals–*N*,*N*′-dibenzyl-18-crown-6 system at 25°C.

$$K_{ex} = K^{-1}_{D(CE)} K^{-1}_{ex(HA)} K_{M(CE)} K'_{ex} \quad (6)$$

The distribution ratio of the univalent metal may be represented by:

$$D_M = [M(CE)A]_o/([M^+] + [M(CE)^+]) \quad (7)$$

In the case of $[M^+] \gg M(CE)^+]$, Eq. (7) becomes

$$D_M = K_{ex} K_{ex(HA)} [CE]_o [A^-] \quad (8)$$

The $-\log(D_M/[A^-]$ vs. $-\log(CE)_o$ plot in Fig. 1 shows a linear relationship with a slope of 1 in every case, indicating that *N*,*N*′-dibenzyl-18-crown-6 forms a 1:1 complex with the alkali metal ion. The values of $[CE]_o$ and $[A^-]$ in Eq. (8) were

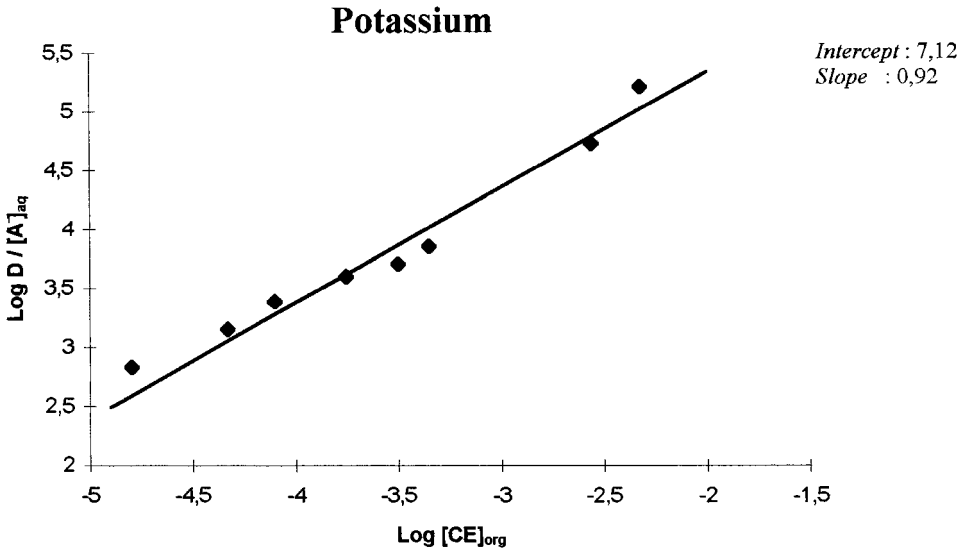

Fig. 3. Polts of $\log(D_M/[A^-])$ vs. $\log[CE]_{org}$ for the univalent metals–*N*,*N*′-dibenzyl-18-crown-6 system at 25°C.

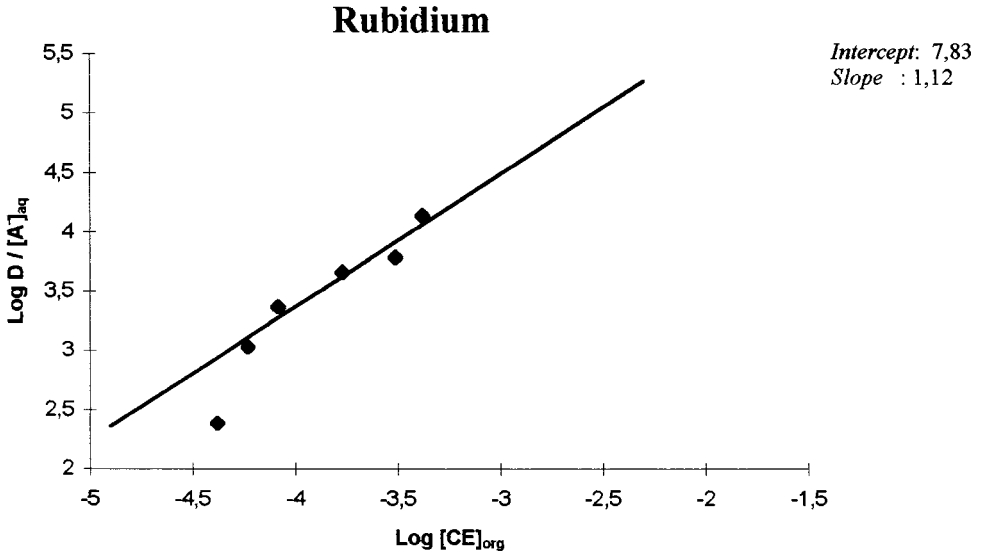

Fig. 4. Plots of $\log(D_M/[A^-])$ vs. $\log[CE]_{org}$ for the univalent metals–*N*,*N*′-dibenzyl-18-crown-6 system at 25°C.

calculated by means of Eq. (9) and Eq. (10), respectively.

$$[CE]_o = ([CE]_t - [M(CE)A]_o/(1 + K_{D,CE}^{-1}) \quad (9)$$

$$[A^-] = \frac{([HA]_t - [M(CE)A]_o)}{[1 + (K_{HA} + K_{ex}(HA)[H^+]]} \quad (10)$$

Where the subscript 't' denotes the total concentration.

Extraction studies were carried out to determine the extraction equilibrium constants (K_{ex}). The extraction equilibrium constant (K_{ex}) between an aqueous solution of alkali metal picrate and a

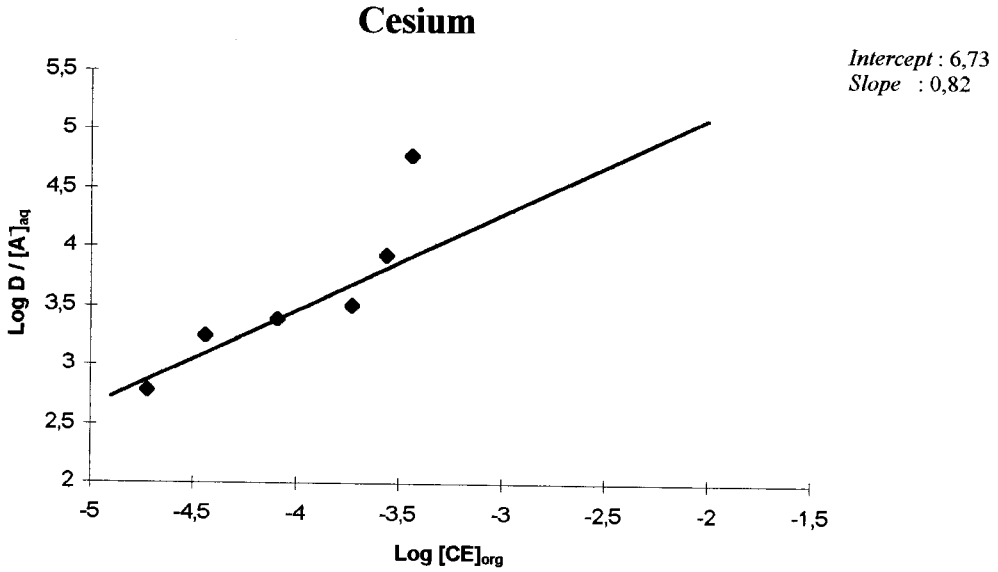

Fig. 5. Plots of $\log(D_M/[A^-])$ vs. $\log[CE]_{org}$ for the univalent metals–*N*,*N*′-dibenzyl-18-crown-6 system at 25°C.

dichloromethane solution of crown ether (CE) for an n:1 crown ether–cation complex can be obtained from Eq. (11). D_M represents the distribution

$$\log(D_M/[A^-]) = n \log[CE]_{org} + \log K_{ex} \quad (11)$$

ratio of a metal cation between the two phases ($D_M = [M(CE)_nA]_{org}/[M^+]_{aq}$The plot of $\log(D_M/[A^-])$ as a function of $\log[CE]_{org}$ should give a straight line with a slope of n ($n = 1$ or 2) and $\log K_{ex}$ as an intercept [15–17]. The plots gave straight lines with a slope of unity for all cations employed over the entire concentration range. Results are shown in Tables 2–8. The K_{ex} values thus obtained are given in Figs. 1–5 along with those for N,N'-dibenzyl-18-crown-6.

In conclusion, it has been shown that the host armed molecule, DB18C6 can be successfully used as a ligand in the selective solvent extraction of Li^+ from other alkali metal ions, which may be considered as an indirect method for determination of lithium levels in serum. The effect of sidearm and the cavity size in the armed crown ethers on the extraction of alkali metal picrates may be an interesting further project to study.

Acknowledgements

This work has been supported in part by a grant (DUAP-96-FF-317) from the Dicle University Research Funds.

References

[1] K. Kimura, T. Maeda, T. Shono, Talanta 26 (1979) 945.
[2] L.-M. Tsay, J.-S. Shih, S.-C. Wu, Analyst 108 (1983) 1108–1113.
[3] I. Cho, S. Chang, Chem. Lett. (4) (1981) 515.
[4] G.D. Christian, J. Pharm. Biomed. Anal. 14 (1996) 899–908.
[5] H. Hoşgören, M. Karakaplan, M. Toğrul, Collect. Czech. Chem. Commun. 61 (1996) 622.
[6] M.A. Coplan, R.M. Fuoss, J. Phys. Chem. 68 (1964) 1177.
[7] S. Kitazawa, K. Kimura, H. Yano, T. Shono, J. Am. Chem. Soc. 23 (1984) 6978.
[8] M. Hiraoka, Crown Compound, Elsevier, Tokyo, 1982.
[9] A. Sadakane, T. Iwachido, K. Toei, Bull. Chem. Soc. Jpn. 48 (1975) 60.
[10] S. Shinkai, T. Nakaji, T. Ogawa, K. Shigematsu, O. Manabe, Chem. Lett. (3) (1980) 283.
[11] S. Shinkai, T. Nakaji, T. Ogawa, K. Shigematsu, O. Manabe, J. Am. Chem. Soc. 103 (1981) 111.
[12] P.D. Beer, E.L. Tite, J. Chem. Soc. Dalton Trans. (9) (1990) 2691–2696.
[13] M. Ouchi, Y. Inoue, T. Kanzaki, T. Hakushi, J. Org. Chem. 49 (1984) 1408–1412.
[14] K.A. Arnold, J.C. Hernandez, C. Li, J.V. Mallen, A. Nakano, O.F. Schall, J.E. Trafton, M.T. Sesarakaja, B.D. White, Supramol. Chem. 5 (1995) 45–60.
[15] M. Ouchi, Y. Inoue, A. Sakamoto, M. Yoshinaga, T. Hakushi, J. Org. Chem. 48 (1983) 3168.
[16] K. Kimura, T. Maeda, T. Shono, Anal. Lett. A11 (10) (1978) 821–827.
[17] B. Vaidy, J. Zak, G.J. Bastiaans, M.D. Porter, Anal. Chem. 67 (1995) 4101–4111.

ELSEVIER

Talanta 47 (1998) 237–238

Talanta

Obituary

The death of David Newton Hume on 2 March 1998 marks the passing of an era in Analytical Chemistry. In their greetings to Professor I.M. Kolthoff on the occasion of his 90th birthday, Laitinen and Meehan [1] stated that 'Through 1982, Kolthoff has produced close to 1100 Ph.D. 'offspring'. They continued by citing three examples of scientific lineage (Professor to Ph.D. student) that spanned four or more generations. These three lines began with J.J. Lingane, H.A. Laitinen, and D.N. Hume, who obtained their Ph.D.'s with Professor Kolthoff in 1938, 1940, and 1943, respectively.

David Hume was born in Vancouver, British Columbia, Canada on 22 December 1917. He moved to the US where he attended Los Angles City College (1935–1937) and UCLA, earning his B.A. in 1939 and his M.A in 1940. It was at a meeting of a poetry-reading club that Dave met Aloyse Bottenwiser, a fellow classmate who was taking a double major in Psychology and English Literature. They were married in Minneapolis in 1941 while Dave was a Ph.D. student and du Pont Fellow at the University of Minnesota. The Humes have two children, Robert and Rebecca. Upon obtaining his degree in 1943 Dave was briefly a Research Associate on the Plutonium Project at the University of Chicago Metallurgical Laboratory, then became a group leader (1943–1944) and section chief (1945–1946) at the Atomic Energy Commission Clinton Laboratories in Oak Ridge, TN.

After WWII, Dave was an assistant professor at the University of Kansas for 1 year and then moved to M.I.T. where he rose from Assistant Professor (1947–1950), to Associate Professor (1950–1959), to Professor (1959–1980). He became an Emeritus Professor of Analytical Chemistry in 1980. His expertise was sought by many groups and Dave served on the Advisory Committee for the Oak Ridge National Laboratory and the Advisory Panel for Chemistry of the National Science Foundation. He was a member of the Committee for Analytical Chemistry of the National Research Council and the Commission on Equilibrium Data of the international Union of Pure and Applied Chemistry, and was a guest investigator at the Woods Hole Oceanographic Institute. He was a Guggenheim Fellow at the Technical University of Denmark (1954–1955) and a Senior NSF Fellow at the Swiss Federal Institute of Technology (1964–1965). His research interest spanned the entire field of analytical chemistry and he made major contributions to the area of radioanalytical and electroanalytical chemistry, complex ions, environmental trace analysis, and chemical oceanography. Following his retirement in 1980 he developed an interest in forensic science.

At the ACS meeting in Los Angeles in 1963, Dave received the Fisher Award in analytical chemistry. Many of his former students took part in the award symposium. The striking thing about that symposium was that none of us reported on research that was remotely related to work that we had done for our Ph.D. theses. In his quiet way Dave imparted a love of analytical chemistry to his students, a love which embraced the entire

0039-9140/98/$19.00 © 1998 Elsevier Science B.V. All rights reserved.
PII S0039-9140(98)00187-8

discipline. He was an excellent teacher who was equally good at teaching introductory and graduate courses. He directed his graduate students with a gentle hand, allowing the student to set his/her own pace. Dave was always available to advise and counsel; he was a good friend. I think that I express the feelings of all his former graduate students when I say that my wife and I looked forward to Thanksgiving Day for it meant that Aloyse and Dave would entertain us all at their home for a traditional holiday feast.

In 1989 Dave was diagnosed with Alzheimer's disease. He continued to live in his home in Wellesley Hills until about a year before his death when he moved to a nursing home. With his passing we mourn the loss of a mentor, a model, and a friend. Our heartfelt condolences and prayers go out to Aloyse, Rob (Katheryn), and Becky (Edward Fitzgerald) at this time.

William C. Purdy
Sir William Macdonald Professor
Dpeartment of Chemistry
McGill University
801 Sherbrooke Street West
Montreal, Que.
Canada H3A 2K6

References

[1] H.A. Laitinen, E.J. Meehan, Anal. Chem. 56 (1984) 248A.

ELSEVIER

Talanta 47 (1998) 239

Talanta

Erratum

Erratum to 'Kinetic determination of organic vapor mixtures with single piezoelectric quartz crystal sensor using artificial neural networks' [Talanta 44 (1997) 959][1]

Xi-Wen He *, Wan-Li Xing

Department of Chemistry, Nankai University, Tianjin 300071, People's Republic of China

The publisher regrets an error in p. 961 of the above article. Some text was missing from the line 13, second column. It should read:

From the initial reaction time, the frequency values ($f(t)$) at every 10 s were recorded. Of particular interest were the 10 min period after injection of the samples and 15 min after purging the detection cell.

* Corresponding author.

[1] [1]PII of original article: S0039-9140(96)02142-X.

0039-9140/98/$19.00 © 1998 Elsevier Science B.V. All rights reserved.

PII S0039-9140(98)00146-5

ELSEVIER

Talanta 47 (1998) 241

Talanta

Corrigendum

Corrigendum to 'Scattering dilution method in Fourier transform infrared spectrometry' Dedicated to: Professor Baiulescu [Talanta 45 (1998) 1049][1]

Mikio Kaihara [a,*], Yohichi Gohshi [b]

[a] *Department of Chemical Engineering, Inchinoski National College of Technology, Aza-Takanashi, Hagisho, Ichinoseki, Iwate 021, Japan*

[b] *Department of Applied Chemistry, School of Engineering, The University of Tokyo, 7–3–1, Hongo, Bunkyo-ku, Tokyo 113, Japan*

The authors would like to apologise for the following mistake in the above paper.

When scattering coefficient S was assumed constant in the infrared region in the paper, the linearity of the obtained calibration curve became excellent. However, S does not necessarily equal 1.0 in the mid infrated region.

* Corresponding author.

[1] [1]PII of original article: S0039-9140(97)00225-7.

0039-9140/98/$19.00 © 1998 Elsevier Science B.V. All rights reserved.

PII S0039-9140(98)00145-3

ELSEVIER

Talanta 47 (1998) 243

Talanta

Corrigendum

Corrigendum to "An optical fiber sensor for berberine based on immobilized 1,4-bis(naphth[2,1-d]oxazole-2-yl) benzene in a new copolymer" [Talanta 46 (1998) 679][1]

Wan-Hui Liu [a,b], Ying Wang [a], Jiang-Hong Tang [a], Guo-Li Shen [a], Ru-Qin Yu [a,*]

[a] *Department of Chemistry and Chemical Engineering, Hunan University, Changsha, 410082, People's Republic of China*
[b] *Analytical Center, Yantai University, Yantai, 254005, People's Republic of China*

The authors would like to apologise for the following error in the above paper.
Reference [13] should be [13] S. Tadao, O. Noriko, Talanta 35 (1986) 415.

* Corresponding author.
[1] PII of original article: S0039-9140(97)00330-5.

0039-9140/98/$19.00 © 1998 Elsevier Science B.V. All rights reserved.
PII S0039-9140(98)00224-0

ELSEVIER

Talanta 47 (1998) 245

Talanta

Book review

Reactions in Solution—An Applied Analytical Approach by B. Trémillon, Wiley, Chichester, 1997. xi + 554 pp. £120.00. ISBN 0-471-95307-5.

The book, a translation of the original French text, is devoted to the understanding and the subsequent controlling, for separative reasons, of the physiochemical processes governing the solubility of solutes in both aqueous and other solvent systems.

In part I the basic principles, theory and factors affecting the aqueous solubility and hence the separation of solutes are covered in considerable depth. Topics covered include complexation, pH effects, partitioning phenomena and the use of ion-exchange resins. Perhaps what separates this from other texts is the excellent coverage of solubility related electrochemical phenomena.

Part II is devoted to the theory, rationale and the use of other solvents to achieve a separation not realisable in aqueous solution. Throughout the text the author emphasises industrial applications and their control and as a consequence the topics covered in part II include a substantial, excellent chapter on reactions in molten salts.

Throughout the book theoretical concepts are clearly and logically presented. Many figures are used (some are difficult to read) to show applications of the theory. As an aid to self-study each chapter has its own bibliography and some also have references. References for many of the names of authors and dates in the text are not given. At the end of the book, linked to each chapter, is a challenging set of theoretical problems for the reader to try. No answers are provided.

Although the English translation is a bit stilted in places the text is relatively mistake free and is a worthy educational learning source on solubility phenomenon for the attention of both under— and post-graduates in chemistry and of practising industrial chemists and engineers.

R.R. Moody

0039-9140/98/$19.00 © 1998 Elsevier Science B.V. All rights reserved.
PII S0039-9140(98)00054-X

ELSEVIER

Talanta 47 (1998) 247

Talanta

Book review

Directory of Capillary Electrophoresis-TrAC Supplement No. 3, Elsevier, Amsterdam, 1996. 190 pp. Softback. US$ 99.50.ISBN 0-44-82600-9.

The new and completely revised Directory of Capillary Electrophoresis (CE) is divided into four sections. The first contains the names and addresses of researchers in the field together with their special interests and one or two key publications. In the second section these names are sorted by country and displayed using a grid showing the main techniques and applications. Section 3 contains details of equipment manufacturers and suppliers of CE accessories and services. In the final section, researchers are listed under their specialisms, e.g. isotachophoresis, drug analysis, instrumentation, etc.

Typical of other successful new analytical techniques, CE has seen an exponential rise in publications. This directory will be particularly useful to new entrants in the CE field who may find an experienced worker in their locality or who may find key authors in their popular field whose work can be searched in the literature.

As with any such directory, it is dependent on researchers replying to requests for information and any publication of this sort is out of data before it is published. Also some notable workers in the UK for examples are missing. Research students are included who by now have completed their thesis and moved on to pastures new.

However this directory mostly achieves what it sets out to do, it is easy to use, and will prove a useful resource to new and existing workers in this exciting and expanding field.

A. Morrisson

0039-9140/98/$19.00 © 1998 Elsevier Science B.V. All rights reserved.
PII S0039-9140(98)00052-6

ELSEVIER

Talanta 47 (1998) 249–250

Talanta

Book review

Sampling and Sample Preparation by M. Stoeppler (editor), Springer–Verlag, Berlin, 1997. xiv + 202 pp. DM 148.00. ISBN 3-540-61975-5

It would seem that here would be a prime case for a multi-author work, where the complexities and intricacies of so many different types of materials and sources have to be dealt with in useful and meaningful detail. So, bearing in mind the possible pitfalls of multi-author works—heterogeneous style, overlap of common ground, repetition of basis principles, I read with curiosity turning to enthusiasm and finally to satisfaction that the final product of this team is indeed a success. The chapters fall into two groups—those dealing with sampling, filing 60% of the book, and those covering sample preparation i.e. in most cases, sample dissolution.

While there is a common theme underlying the sampling essays—how to achieve one's end of representativeness without introduction of contamination—it is interesting to see that in each area, a different special problem has to be dealt with. Thus, with taking of human samples, it is how to handle the samples, which may after all carry pathogens, and how to handle the live subject while sampling. With rain and snow, on the other hand, we have to make the decision as to whether we want the solid, the liquid or the gaseous phase. Handling of freshwater samples revealed that how the sample vessels were cleaned was more important than the choice of container material. The contamination problem—or perhaps our success these days in coming to terms with—is nicely demonstrated by a history of values for 'lead in seawater' showing a very marked decrease over the last forty years, which is, of course, not what one would expect from our general impression of the increasing levels of environmental pollution.

When we come to soils we begin to understand the real difficulties of the soil scientists, for what a gardener understands by 'soil' is but a fraction of the breadth of this class of substances as understood by the environmental scientists. We read here 'in the presence of residual pollution from armaments, the brave sampler should take special care…' Yes indeed. I had begun to wonder if a statistical consideration of sampling would be presented in this book—sample size versus particle size and so on—and in the next chapter, on waste, we find it, though I doubt whether even the most advanced statistics can help us out when we consider the incredible heterogeneity of domestic and industrial waste, with individual particles including complete cars and refrigerators. Still, this work also has to be done by someone. I would like to mention here the fascinating new field of volatile organometallic compound release from sewage and waste tips.

The chapter on Marine samples gives us a good account of the German Environmental Specimen Bank—with a preliminary investigation of methodology dating back to 1976, several years before collection of samples began in 1985. We learn here of the importance of management, training of personnel, financial control, and, most difficult of all, making non-scientists aware of the need for this programme and the huge difficulties in guaranteeing high quality data so that the project will achieve its aim i.e. revealing genuine long-term trends in the state of the environment.

By the time we get to Biological sampling, some repetition is creeping in, but the mention of the

0039-9140/98/$19.00 © 1998 Elsevier Science B.V. All rights reserved.
PII S0039-9140(98)00053-8

importance of selecting the best species as indicators of pollution or of the general state of the environment is an interesting counterbalance to the usual problems of contamination during handling and sample preparation. The first part ends with an account of sampling in industry. We think we know what cement is, so in the cement factory we are more concerned with the accurate balance of inputs and outputs of toxic trace elements—chemical accounting with the accuracy of $\pm 0.2\%$ in order to know what is being emitted from the plant.

The chapter on food analysis leads us to the problems of sample decomposition where the problem lie in the wide rang of procedures, worked out over many years, for dealing satisfactorily with so vast a range of sample types, some of them remarkable resistant to chemical attack. This challenge has been met by the selection of new sample dissolution techniques which have, in the years since the publication of Bock's book in 1972/79, produced workable solutions to many of the old intractables. Pressure digestions and microwave assisted digestions in particular get detailed practical attention here, and when we return to cement, we see that the pioneering work of Tölg stands as respected as ever alongside the results of later investigations.

So back to our opening question: has the book achieved its goals? I think it has. Many very up-to-data literature citations, useful cross-referencing between chapters, little overlap between contributions, and on the whole an admirable standard of English from the German team. Perhaps I may be permitted a small complaint: only a few chapters obliged with references to sources of equipment. When so much of the apparatus for sampling and sample decomposition is obtainable from a few specialised makers, it would be helpful to mention their names and addresses—and they deserve the little publicity for the good work they do. I found only one wrong translation—*Gewinde* (on the neck of a bottle) should be 'thread', not… Well, you should buy the book to find out, because when you do buy it you will find yourself dipping into it very often, and will usually find the answers to your questions on sampling. Strongly recommended.

L. Marr

ELSEVIER

Talanta 47 (1998) 251–252

Talanta

Book review

Lasers in Chemistry, third edition by D.L. Andrews, Springer–Verlag, Berlin, 1997, xiv + 232 pp. Softback. ISBN 3-540-61982-8.

The layout of the third edition of this undergraduate textbook, follows closely to that of its predecessors. An initial chapter on the nature of light, the interaction of light and matter and the principles of laser operation is followed by examples of various practical and commercial lasers in Chapter 2. Chapter 3 is rather a mix of topics, loosely entitled 'Laser Instrumentation in Chemistry.' The chapter combines techniques used to modify laser light, background on associated equipment, and some instruments which utilise lasers mainly via scattering processes. Chapters 4 and 5 provide the main bulk of the applications, with Chapter 4 focusing on spectroscopic processes and the final chapter concentrating on lasers and chemical reactions.

Having used the book myself to help deliver a course on lasers and chemical reactions, I can confirm that the text is well liked by students and offers a relatively clear explanation of the principles of laser operation and descriptions of practical systems. I would, however, question the author's intended audience—second year undergraduate. With the current changes in school and university teaching, courses that would utilise this text are probably more appropriate for levels 3 or 4.

Considering this more mature audience as being more realistic of the readership, I find the referencing somewhat disappointing. The earlier chapters contain very few references either direct, or in the appended bibliography. Whilst Chapters 4 and 5 do contain significantly more references, many of these are old, and the reader is 'thrown in at the deep end', i.e. there are very few references to other more advanced texts or more general articles from *Science*, *Nature*, *New Scientist* etc., which would help to bridge the gap from this text to the, sometimes daunting, primary literature.

Chapters 1 and 2 are the highlight of the book, providing clear explanations of laser operations. The relevant mathematics is not ignored but is treated at a relatively low level making the material approachable to a wide range of students. One or two sections could be improved further and brought up to date, but these chapters provide ideal background material for any course which involves lasers.

Chapter 3 contains a number of very useful sections on modification of laser output pulse shaping, frequently mixing, polarisation) and associated experimental equipment. However, for the sake of clarity and organisation this material might be more appropriate in either Chapter 2 or separate Chapter.

Chapter 4 is a relatively comprehensive review of the applications of lasers within spectroscopy. The sections on Raman and associated techniques are particularly detailed, although the earlier points on referencing should be reiterated. Despite comments on the fly sheet regarding analytical applications, the main focus and thrust of this chapter is on fundamental research.

Chapter 5—Laser Induced Chemistry—is somewhat disappointing. Many of the cited examples on unimolecular and bimolecular reactions has been superseded by more selective experiments which really focus on and illustrate the fundamental processes occurring during reaction.

0039-9140/98/$19.00 © 1998 Elsevier Science B.V. All rights reserved.
PII S0039-9140(98)00051-4

The work of Fleming Crim, Dick Zare, Brad Moore, Ian Smith and Ahmed Zewail (briefly mentioned) would provide more illustrative and modern examples, however, one should also recognise the author's disclaimer in the preface that there is not sufficient room to do justice to all the practitioners in the field.

In summary, Lasers in Chemistry is an ideal text for just that course, a general overview of the use of lasers given at either levels 3 or 4. The generally low level mathematical treatment makes the material approachable, although it does mean that some topics are not treated quite as rigorously as they could be. Major reservations exist about the nature of some of the Chapter 5 and the referencing for all sections of the book.

P.W. Seakins

ELSEVIER

Talanta 47 (1998) 255–260

Talanta

Application of infrared spectroscopy to the assessment of authenticity of tea

G. Budínová, D. Vláčil, O. Mestek, K. Volka *

Department of Analytical Chemistry, Institute of Chemical Technology, CZ-16628 Praha 6, Czech Republic

Received 27 May 1997; received in revised form 16 January 1998; accepted 23 January 1998

Abstract

Diffusion reflectance fourier transform infrared spectroscopy in the mid-IR region was used to assess the authenticity of tea varieties. The differences between the spectra of 12 different tea varieties (seven black, two green, three semifermented grades) were sufficient to allow their discrimination by the soft independent modelling of class analogy classification method or linear discriminant analysis, despite a significant heterogeneity of the samples as revealed by variance analysis. © 1998 Elsevier Science B.V. All rights reserved.

Keywords: Tea; Infrared spectroscopy; Soft independent modelling of class analogy; Linear discriminant analysis

1. Introduction

Tea is among the most popular beverages worldwide. Tea is prepared from leaves of tea plants, grown in the tropical and subtropical zones of various continents. Major producers include India, China, Japan, Sri Lanka, Indonesia, Vietnam, Venezuela, Brazil, Georgia, Azerbaijan and Kenya. Botanical classification is not unique. Two species are usually distinguished, viz. Chinese tea (*Camellia sinensis*) and Assamic tea (*Camellia assamica*). These differ both morphologically and chemically [1].

Tea is usually classified based on sensoric evaluation. Until now, few attempts have been made to apply the chemometric approach to the analysis of tea samples. Palmer [2] used multivariate methods to select flavour terms characterising different tea species, and Liu et al. [3] applied principal component analysis to chemical data of different types of tea in order to differentiate between them. The authors [4] investigated data of the chemical composition of tea leaves to differentiate between two classes of green and black tea. The procedure was based on the following variables: aqueous extract, total polyphenols, total free aminoacids, caffeine, theobromine, and theophylline, which had to be obtained by chemical analysis (gravimetry, spectrophotometry, chromatography).

In this context it is worth mentioning that spectroscopy in the mid-infrared region has been applied recently to qualitative analysis of green coffee [5], and near-infrared spectroscopy, to the authentication of Arabica and Robusta coffee

* Corresponding author. Tel.: +4202 3112828; fax: +4202 3112828; e-mail: Karel.Volka@vscht.cz

0039-9140/98/$ - see front matter © 1998 Elsevier Science B.V. All rights reserved.
PII S0039-9140(98)00055-1

Table 1
Codes, origin and features of tea samples for SIMCA and LDA

Tea (Origin, feature)	Object no.	Tea (Origin, feature)	Object no.
Sri Lanka, green (OP, leaf)	1	Indian, Assam, black (GFOP, leaf)	7
Sri Lanka, black (OP, leaf)	2	India, Darjeeling, black (TGFOP, leaf)	8
China, Keemun, black (congou, leaf)	3	Japan, Sencha, green (leaf)	9
China, Yunnan, black (FOP, leaf)	4	Java, black (leaf)	10
China, Gunpowder, green (leaf)	5	Kenya, Marynin, black (broken)	11
China, Oolong, semiferm. (POGOF, leaf)	6	Taiwan, Oolong, semiferm. (POGOF, leaf)	12

from 27 countries [6]. The present work was aimed at examining the possibility of discriminating between different tea varieties based on their diffusion reflectance fourier transform mid-infrared spectra.

2. Experimental

2.1. Samples

Twelve samples of leaf tea and broken tea as specified in Table 1 were selected for analysis.

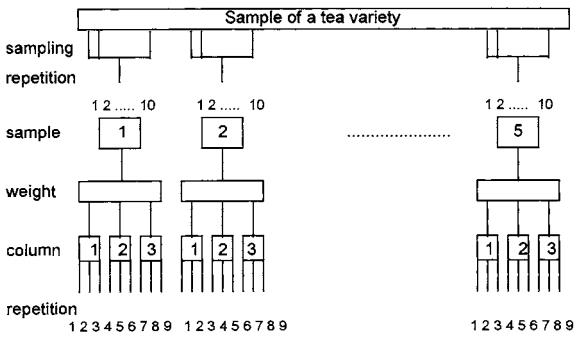

Fig. 1. Experimental design for sampling.

2.2. Chemicals

KBr for infrared spectroscopy (Sigma–Aldrich).

2.3. Apparatus and measuring parameters

Infrared spectra were scanned on a Nicolet 210 FTIR spectrometer, using a Baseline™ Diffuse Reflectance Accessory (Spectra-Tech.) for DR measurements. Samples were weighed on a METTLER AE 240 automatic balance with a precision of 0.1 mg. Tea samples were ground in an ETA 0067 coffee grinder (Elektro–Praga, Hlinsko), finer grinding and homogenization with KBr were achieved by using a 'vibrator' ball mill (Narva, Germany). Sieves 0.071 and 0.500 mm mesh size were used to fractionate the samples and KBr.

The IR measurements were performed within the region 4000–400 cm^{-1}. Gain was selected automatically. Happ–Genzel apodization was applied, mode zero filling was disabled, and the interferometer mirror speed was set at 1.5825 cm s^{-1}. The number of scans was 64, resolution 4 cm^{-1}. The maximum energy at the DTGS detector was adjusted by rotating the DR accessory head, and the beam-splitter position was

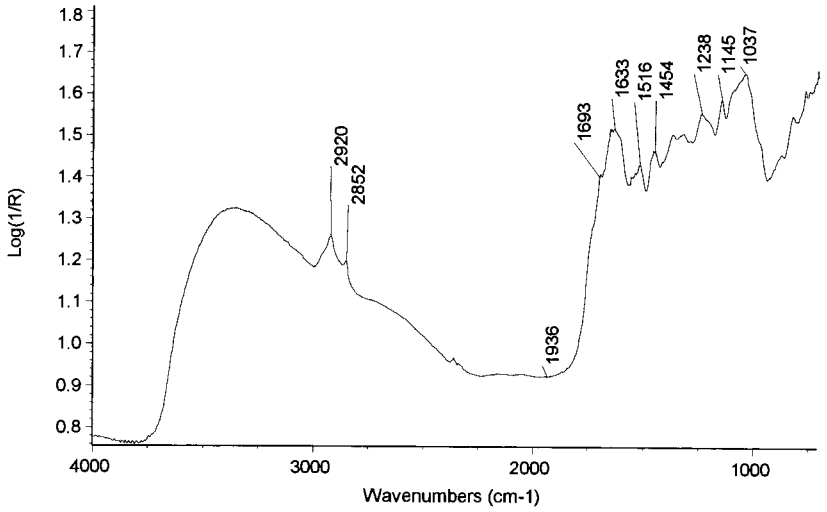

Fig. 2. Absorption maxima and baseline employed for calculation of the basic statistical parameters and variance analysis.

Table 2
SIMCA result: model distances between PCA models for the individual tea varieties

Tea variety	1	2	3	4	5	6	7	8	9	10	11	12
1	1	105	308	119	91	98	108	78	56	60	40	238
2	105	1	76	43	108	44	**13**	40	146	71	12	45
3	308	76	1	16	96	181	80	84	**325**	228	94	197
4	119	43	16	1	77	88	59	53	158	82	66	108
5	91	108	96	77	1	107	101	61	111	84	70	223
6	98	44	181	88	107	1	60	48	88	102	28	59
7	108	**13**	80	59	101	60	1	47	126	67	**8**	70
8	78	40	84	53	61	48	47	1	73	25	34	111
9	56	146	**325**	158	111	88	126	73	1	95	66	152
10	60	71	228	82	84	102	67	25	95	1	26	209
11	40	12	94	66	70	28	**8**	34	66	16	1	64
12	238	45	197	108	223	59	70	111	152	209	64	1

adjusted to the maximum energy at the beginning of each measuring session.

2.4. Software

The instrument was controlled by the OMNIC™ code. This software product of Nicolet company also provided for a complete processing of the spectra measured. The data so obtained were processed by using the tools Excel 5.0a (Microsoft), Unscrambler 6.1 (Camo AS, Trondheim, Norway), and LDA (Institute of Analytical Chemistry, Prague).

2.5. Analytical procedure

Taking into consideration the heterogenity of the tea specimens, major attention was paid to the sampling stage. The specimens were first freed from dust and tiny broken pieces on a 0.500 mm sieve and then poured into a box whose bottom accommodated a paper sheet with a grid of 10×10 squares 2.5 cm edge. Two series of ten random numbers within the interval of [1,10] were obtained by using the random number generator of the Excel 5.0a tool; these determined the vertical and horizontal co-ordinates of 10 sampling

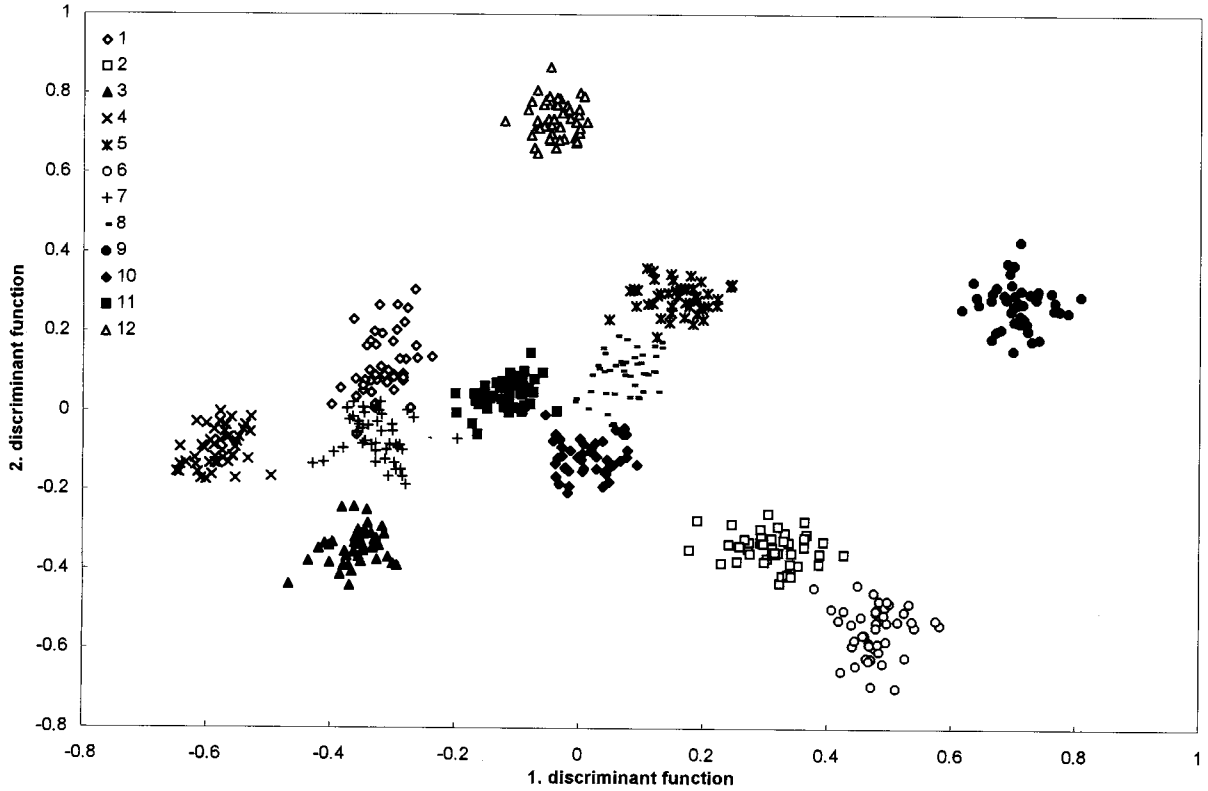

Fig. 3. LDA results for ten parameters: scatter plot in the axis of the first two discriminant functions.

squares. The weight of each sample was from 2.0 to 2.5 g. Subsequently, the remaining tea was again spread homogeneously over the bottom and a next sample was taken. Five samples were prepared in this manner.

Each sample was first ground in the coffee grinder in two steps, coarsely (level 4) and finely (level 1), and subsequently ground in two portions in the ball mill for 3 min. A grain size fraction below 0.071 mm was obtained by sieving and mixed with KBr which had been treated in the same manner. Two portions 1 g each, containing 5% w/w tea, were prepared. Homogenisation was achieved by grinding in the ball mill for 3 min.

Table 3
LDA results: dependence of poorly discriminated samples on the number of discriminant functions *r*

r	Poorly discriminated samples		Variance explained (%)
	%	Number	
1	28.8	155	55.0
2	1.7	9	78.1
3	0.2	1	88.3
4	0	0	93.7

The diffusion reflectance (DR) spectra of the homogenised mixture were obtained by the column method described previously [7]. A column of the tea–KBr mixture approximately 16 mm high, 4 mm in diameter, was compressed by applying a pressure of 5.85 MPa for 1 min. The metallic mirror served as the background. The DR measurement was performed in the column centre and at two spots 2 mm shifted to either side. Three columns were prepared from each homogenized sample mixture, hence, nine spectra were obtained for each sample. A total of 45 DR spectra were thus scanned for each tea variety, following the scheme shown in Fig. 1.

3. Results and discussion

3.1. Variance analysis [8]

To evaluate the statistical significance of the tea sampling factor, ten wave numbers were selected to read the $\log(1/R)$ value. Nine of them, viz. 2920, 2852, 1695, 1633, 1516, 1454, 1238, 1145, and 1038 cm^{-1}, corresponded to the absorption peaks, the tenth, at 1936 cm^{-1}, characterised the baseline. Their positions in the DR spectrum are shown in Fig. 2.

We tested the hypothesis that repeated tea sampling at ten sites gives spectra that are not statistically significantly different. Single-factorial variance analysis was performed at the ten wave numbers for the set of 45 spectra for each tea variety, the F criterion having five levels (five-fold sampling at ten sites) and nine repetitions (three columns, each measured at three spots).

Only in eight cases, i.e. 3.2% of all results, the F criterion was lower than the tabulated value of $F_{1-0.05}(5-1;45-5) = 26060$ for the $\alpha = 5\%$ significance level; mostly, the F_{crit} value was multiply exceeded. The residual variance s_R^2, however, was largely in the order of 10^{-4}–10^{-5}, indicating that the various columns within one sampling were not different. The samplings were statistically significantly different, apparently due to the large heterogeneity of the tea analysed. The use of the $\log[1/R(v)] - \log[1/R(1936\ cm^{-1})]$ difference in place of the $\log[1/R(v)]$ values did not improve the F criterion values appreciably; in fact, 68.5% values were even poorer.

3.2. Soft independent modelling of class analogy (SIMCA)

The soft independent modelling of class analogy (SIMCA) classification approach [9] was employed for qualitative discrimination between the different tea varieties.

Prior to the analysis, the data were reduced by averaging the three spectra measured on each column. In this manner, each of the 12 tea varieties was characterised by 15 average spectra. The objects were labelled by numbers corresponding to Table 1 to facilitate the tea variety identification. Eight spectra chosen at random for each tea variety constituted the training set. The remaining spectra ($7 \times 12 = 84$ spectra) constituted the test set.

The classification proceeds in two steps.

In the first step, a principal component analysis (PCA) model is set up for each class (tea variety) in the training set of samples [10]. Twelve PCA models were set up applying the following conditions: two principal components, full cross validation. The variables (wave numbers in this case) that affect most the variability of the data set were identified from the PCA models based on the loadings plots for the first principal component. The spectral region of 1278–1738 cm^{-1}, exhibiting the largest variability, was chosen to characterise the tea varieties.

The second step of SIMCA classification consists in classifying the test samples, i.e. fitting each sample to each model and deciding whether or not the sample belongs to the corresponding class. As the classification table shows all the test samples were attributed to the appropriate tea varieties at the 5% significance level.

The differences between the individual models of each tea variety are shown as the model distances in Table 2. A model distance > 3 indicates that the two classes concerned are significantly different and can be mutually well distinguished. All of the tea varieties were found to be mutually significantly different. Least different are variety 7 (India, Assam, black, GFOP, leaf), variety 11 (Kenya, Marynin, black, broken), and variety 2 (Sri Lanka, black, OP, leaf), whereas the largest differences were found between variety 3 (China, Keemun, black, congou, leaf) and variety 9 (Japan, Sencha, green, leaf).

SIMCA classification of all samples without averaging (540) failed due to software problems. The results also showed a good discrimination between the tea varieties but due to limitations they could not be compared with the LDA results and are not presented here.

3.3. Linear discriminant analysis (LDA)

Linear discriminant analysis [11] was the second method employed for qualitative discrimination between the different tea varieties. The data matrix, chosen based on the PCA, contained 540 objects (12 tea varieties × 45 spectra) and ten parameters (wave numbers)—1278, 1290, 1338, 1415, 1460, 1519, 1539, 1633, 1693 and 1737 cm^{-1}. The 'leave-one-out' method was applied to the validation of the model.

The LDA result Fig. 3 displays clusters of identical indices, each cluster corresponding to one tea variety. The clusters appear to be sufficiently separated from each other. This fact is confirmed by Table 3, where the numbers of poorly discriminated samples and the values of variance explained are shown.

4. Conclusions

The results give evidence that different tea varieties can be distinguished based on their mid-infrared spectra. In this respect, the spectral method provides a higher information content than chemical analysis, where discrimination between green and black tea is only possible [4]. The differences in the tea characteristics might be made still more pronounced by optimisation of the sampling procedure.

Acknowledgements

The authors wish to thank Mr Jaromír Skdcel (JHP a.s.) and Mr Ivan Šimkovič (CENTROCOM a.s.) for tea specimens and information on tea.

References

[1] P.K. Mahanta, CEMTECH. May (1996) 38.
[2] D. H. Palmer, J. Sci. Food Agric. 25 (1974) 153.
[3] X. Liu, P. Van Espen, F. Adams, S.H. Yan, M. Vanbelle, Anal. Chim. Acta 200 (1987) 421.
[4] P. Valera, F. Pablos, A.G. Gonzáles, Talanta 43 (1996) 415.
[5] M. Suchánek, H. Filipová, K. Volka, I. Delgadillo, A.N. Davies, Fresenius J. Anal. Chem. 354 (1996) 327.
[6] G. Downey, J. Boussion, Proc. Int. Conf. Near Infrared Spectrosc. 7th (1995) 410.
[7] M. Hrebičík, G. Budínová, T. Godarská, D. Vláčil, S.B. Vogensen, K. Volka, J. Mol. Struct. 527 (1997) 410–411.
[8] G. Kateman, F.W. Pijpers, Quality Control in Analytical Chemistry, Wiley, New York, 1981.
[9] S. Wold, Pattern Recognition 8 (1976) 127.
[10] P. Geladi, R. Kowalski, Anal. Chim. Acta 185 (1986) 1.
[11] W.W. Cooley, P.R. Lohnes, Multivariate Data Analysis, Wiley, New York, 1974.

ELSEVIER

Talanta 47 (1998) 261–266

Talanta

Determination of cadmium, lead, and nickel by simultaneous multielement flame atomic absorption spectrometry in burned and unburned Venezuelan crude oil

Jenifer L. Hammond [a], Yong-Ill Lee [a,b], Charles O. Noble [a], James N. Beck [c], C. Edward Proffitt [d], Joseph Sneddon [a,*]

[a] *Department of Chemistry, McNeese State University, PO box 90455, Lake Charles, Louisiana 70609-0455, USA*
[b] *Department of Chemistry, Changwon National University, Changwon 641-773, South Korea*
[c] *Department of Physical Sciences, Nicholls State University, Thibodeaux, Louisiana 70301, USA*
[d] *Environmental Research Centre, McNeese State University, Lake Charles, Louisiana 70609, USA*

Received 24 December 1997; received in revised form 10 February 1998; accepted 10 February 1998

Abstract

This work describes the use of simultaneous multielement flame atomic absorption spectrometry for the determination of cadmium, lead, and nickel in burned and unburned Venezuelan crude oil (5 ml volumes) in controlled laboratory experiments. The simultaneous detection limits were 0.010 μg ml^{-1} (Cd), 0.04 μg ml^{-1} (Pb), and 0.40 μg ml^{-1} (Ni) with precision's of these elements at concentrations of 10 × above these detections limits, and in the crude oil, of 1–2%. Loss of elemental concentrations in the crude oil in a 3–5 ml volume when burned were 4% (Cd), 50% (Pb), and 22% (Ni). These results suggest that the form of the elements and the temperature attained in the burning crude oil effect the removal of the elements. The type of surface affected the volume of oil removed. Soil gave a 15% and a smooth surface almost 50% volume reduction. © 1998 Elsevier Science B.V. All rights reserved.

Keywords: Simultaneous multielement flame atomic absorption spectrometry; Burned and unburned crude oil; Cd; Pb; Ni

1. Introduction

Oils spills (defined as 10000 gallons or more) have caused destruction to vital ecosystems around the world for almost half a century. Most spills come from oil well blowouts or tanker/barge incidents. The Gulf of Mexico is highly susceptible to oil spills because more oil is transported though its ports than through all of the other United States ports combined [1]. More than 80000 tankers/barges enter the Gulf of Mexico annually transporting 272 million ton of crude oil and refined products. Since 1954, approximately

* Corresponding author. Tel.: +318 4755781; fax: +318 4755234; e-mail: jsneddon@acc.mcneese.edu

0039-9140/98/$ - see front matter © 1998 Elsevier Science B.V. All rights reserved.
PII S0039-9140(98)00071-X

25000 off-shore oil wells have been drilled in the Gulf of Mexico. Adjacent to most of these ports are productive marine or estuary areas [1].

The preservation of these areas requires immediate and effective remediation techniques when an oil spill occurs in an estuary or marine area. Traditionally, chemical, mechanical and biological remediation techniques have been used for emergency remediation techniques [2,3]. Burning of oil has been proposed as a form of remediation and removal, with the recent Gulf War in 1991 providing real life information of its effectiveness [4].

To date, most work has been concerned with organics in the burning crude oils with little or no information on the fate of elements during or after the burning process as a form of remediation. The concentration of elements in crude oil can be significant ranging from trace to several hundred parts per million.

This work presents the results of a study involving laboratory experiments of selected metals found in Venezuelan crude oil before and after burning. The determination was performed using simultaneous multielement flame atomic absorption spectrometry [5–7].

2. Experimental

2.1. Instrumentation

A Smith–Hieftje 8000 automatic atomic absorption spectrometer (Thermo Jarrell Ash–Baird, Franklin, Massachusetts) was used with a long path burner and air-acetylene flame. The instrument was operated in the simultaneous mode with a detailed description of the system described elsewhere [6,7]. The samples were introduced via a conventional pneumatic nebulizer, with hindsight suggesting a high solids or Meinhard nebulizer (J.E. Meinhard, Santa Ana, California) may have been more suited to this work. In all three matrices the uptake rate of the solution was similar, to within ± 0.1 ml min^{-1}. The experimental conditions for simultaneous determination were a compromise, as described elsewhere [6], and shown in Table 1.

2.2. Reagents

1000 ± 5 μg g^{-1} metallo organic standards in mineral oil were obtained from High Purity Standards (Charleston, South Carolina) and diluted with methyl isobutyl ketone (MIBK) as required. Venezuelan crude oil was obtained from a local refinery (Citgo Petroleum, Westlake, Louisiana) and stored in a five gallon acid rinsed/deionized water plastic container. The crude oil was a random sample taken directly from a tanker. Venezuelan crude oil contains significant concentrations of vanadium and nickel (>100 ppm), sub-ppm concentrations of many elements including lead, copper, and zinc, as well as trace concentrations of selected elements such as cadmium [8]. It is unclear whether the elements are in a pure state, organometallic or in the form of the stable oxides. The concentrations vary considerable and are dependent on the actual location where the crude oil is originally obtained. Crude oil samples were poured from the original storage container into acid rinsed/deionized water beaker prior to experimentation.

2.3. Procedure

A detailed description of the burning process is described elsewhere [9]. Aluminum foil cups were used for the burning of crude oil. When MIBK was burned in the cup, no levels of cadmium, lead, and nickel were found, at least above the detection limit. The cups were approximately 6 cm in diameter with 12 mm sides. This allowed plenty of air to flow around the flame of the burning oil. A volume of 5 ml of crude oil provided a depth of approximately 2 cm in the cup

Table 1
Experimental conditions for multielement flame atomic absorption determination of cadmium, nickel, and lead in crude oils

Element	Cadmium	Lead	Nickel
Wavelength (nm)	228.8	217.0	232.0
Bandpass (nm)	0.15	0.15	0.15
Lamp current (mA)	2.5	4.0	5.0
Background current (mA)	2.3	3.8	3.0

and required approximately 250 s before the flame became extinguished.

The concentrations of the three elements were determined in the crude oil. A volume of 5.0 ml was added to the cup and burned until the flame extinguished. After cool down, the unburned oil was removed (with the aid of MIBK) and brought to volume with MIBK prior to determining the elements. When standard additions was used, the appropriate organometallic standard was added, and then brought to volume with MIBK before determining the elements.

Several surfaces were investigated including the aluminum foil weighing cups, soil (10 g) from the Lake Charles, Louisiana area (25 mesh and 150 mesh) at a depth of 2 cm, and water at a depth of 2 cm. A 5.0 ml volume of oil was accurately weighed and deposited on the appropriate surface and burned as previously described.

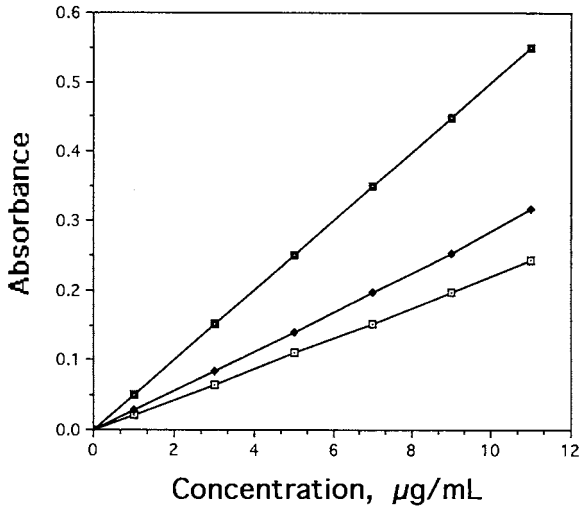

Fig. 1. Calibration curve for simultaneous multielement flame atomic absorption spectrometry of lead (with cadmium and nickel not shown) in three different matrices, ■, aqueous standards; ■, organometallic standards with MIBK as solvent; and ⊡, spiked (with organometallic standards) Venezuelan crude oil.

3. Results and discussion

3.1. Figures of merit of the proposed method

Quantitative elemental determination based on simultaneous flame atomic absorption spectrometry (and other atomic spectroscopic techniques) is obtained by comparison of signals from samples with those of obtained from standards of known composition, typically and most conveniently using aqueous solutions. Various calibration curves of the elements were established using aqueous standards, organometallic standards with methyl isobutyl ketone (MIBK) as the solvent, and Venezuelan crude oil spiked with the elements. The determination of the three elements in the three matrices were performed simultaneously but the results for only one element (lead) in the three different matrices is shown separately for clarification in Fig. 1. Results for cadmium and nickel (not shown) were similar to that of lead. The use of aqueous standards would clearly give inaccurate results. The calibration curves obtained with the use of MIBK as the solvent with organometallic standards is more comparable to crude oil spiked with organometallic standards, than aqueous solutions. However, there was sufficient differences to cause concern over accuracy of using MIBK standards for crude oil determination. For these reasons, standard additions was used throughout the determination of the three elements in unburned crude oil. When the burned oil was removed from the cups with the use of MIBK and made to volume, or the NIST standards were determined, then a calibration using MIBK as the solvent was used for improved accuracy.

The multielement detection limits for the three elements were 0.010 μg ml^{-1} (Cd), 0.04 μg ml^{-1} (Pb) and 0.40 μg ml^{-1} (Ni). This was a reduction in a factor of two to three compared to the optimised single element detection limits but comparable to previous studies [6]. However, the detection limits found were sufficiently low as to determine the elements in the crude oil.

The determinations were performed at least three and as much as ten times. Precision for the determinations in crude oil at 10× above the detection limit and in the concentrations of the three elements in the crude oil were in the 1–2% range. The precision of the results of the volume reduction were in the 3–5% range, except in the

Table 2
Accuracy of simultaneous multielement flame atomic absorption spectrometry for the determination of cadmium, lead, and nickel in crude oils

	Certified values (μg ml^{-1})			Experimental values (μg ml^{-1})		
Standard	Cd	Pb	Ni	Cd	Pb	Ni
NIST 1084a	NC	101.1 ± 1.3	99.7 ± 1.6	32.3 ± 1.6	102.7 ± 2.6	101.0 ± 1.3
NIST 1085a	NC	297.4 ± 9.6	302.9 ± 6.8	83.3 ± 2.2	314.8 ± 8.8	307.1 ± 5.5

NC, Non-certified.

case of the cup containing water. In this case the precision was ~20%. This was attributed to the sputtering and splashing of the burned oil on the water surface with potential for loss and poor precision was to be expected. The precisions are not shown on the calibration curves on Fig. 1 for clarification.

Accuracy was assessed by comparison to National Institutes of Science and Technology (NIST) (Gaithersberg, Maryland)-standard reference material (SRM) 1084a and 1085a crude oil. Dilution with MIBK was used where necessary to be on the linear part of a calibration curve and standard additions used to determine concentrations. The results are shown in Table 2. The cadmium concentration was non certified but a comparison between the lead and nickel concentrations gave good agreement suggesting acceptable accuracy.

3.2. Loss of cadmium, lead, and nickel

The results for the loss of cadmium, lead and nickel in unburned and burned Venezuelan crude oil is shown in Table 3. The concentrations of the three elements remaining in the burned oil were approximately 96% for Cd, to 50% for Ni, and 78% for Pb. Large scale burnings (thousands of gallons) over several to many hours can have much of the mass, in excess of 99% (and presumably organics) removed [10]. There is little or no information on the fate of elements in a large scale burning in the literature. The more volatile Cd (compared to the less volatile Pb and Ni) has the greatest percentage of element in unburned oil. This suggests that the elements are not in a volatile form such as the elemental or organometallic form but most likely in the stable oxide form. Temperatures in a large scale oil burn are estimated to be in excess of 900°C. The temperature will rise from ambient conditions to the maximum over a period of time and this could take several minutes to hours, depending on the volume of oil. In the laboratory experiments, the volume of oil was limited to 3–5 ml and the flame was extinguished in all cases in less than 240 s. It is possible that the temperature of the burning oil did not reach a high enough temperature to volatilise the elements. This suggests that the elements are not in the more volatile organometallic form. The fact that some elements were removed during the burning process (this has been con-

Table 3
Comparison between concentrations of cadmium, lead, and nickel in burned and unburned crude oil.

Element	Concentration in unburned oil (μg ml^{-1})	Concentration in burned oil (μg ml^{-1})	Percentage of element in residue
Cadmium	0.089	0.086	96 ± 0.015
Lead	0.20	0.10	50 ± 0.008
Nickel	1.10	0.86	78 ± 0.012

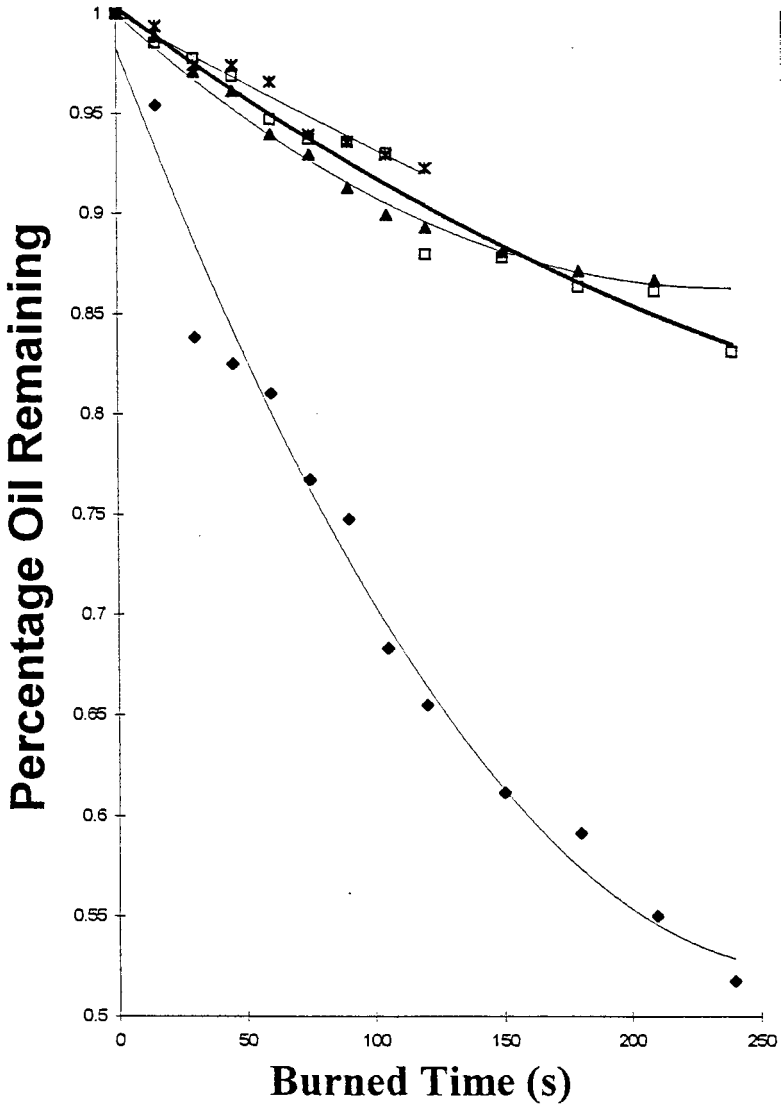

Fig. 2. Volume reduction study for 5 ml of Venezuelan crude oil burned on: ◆, foil cups; □, 25; ▲, 150 mesh soil; and *, water.

firmed by determining lead in burning smoke in the laboratory [9]) suggest that the elements may be present in various forms. The more volatile forms being removed during burning and the less volatile forms remaining. Some preliminary work using gas chromatography-mass spectrometry (GC-MS) suggest this kind of situation but work in this area is very preliminary at this time and will be reported in due course.

3.3. Effect of surface

The results of this study are shown in Fig. 2. When the surface was water, the oil floated and stayed cohesive. Upon ignition, the oil sparked and spattered causing a significant loss. The oil would not stay lit beyond 120 s. When the oil was added to the cup, a volume reduction of approximately 50% occurred over the flame lifetime of

240 s. When burning the oil on the coarse (25 mesh) soil, approximately 85% of the oil remained behind after the flame was extinguished at around 200 s. Initially, the oil seeped into the soil, making it difficult to ignite. Samples with short burn times had a solid cake like crust on top and unburned oil underneath. The samples with longer burn times could be removed from the cup in one piece. The results reported here are when no oil remained in the cup. Similar results were obtained for the fine soil of around 85% remaining after a burn time of around 200 s. However, when the oil was placed on the fine soil (150 mesh) it did not seep into the soil but remained on the surface in a puddle. After burning, all the oil formed a cake-like solid regardless of burn time. The shorter the burn time had some soil underneath that was not affected or come in contact with the oil.

The results from this study are somewhat preliminary but suggest that the volume of oil will be reduced with burning ranging from around 50% from the cup to 85% from the two grades of soil and water. While this is high compared to field studies, it is due to the small volumes of oil burned in the laboratory experiments. A larger volume of oil burns longer and the temperature will increase allowing for more complex and less volatile molecules to be removed. Based on the two sizes of soils used in these experiments, the size of the soils does not affect the final volume reduction. This implies that various sizes (and mixtures) of soil will not effect the final volume reduction. No attempt was made to investigate different types of soil.

4. Conclusion

This work has shown that simultaneous multi-element atomic absorption spectrometry can be used to determine selected elements in burned and unburned crude oil, although standard additions is required for improved accuracy to compensate for various matrices. The results are preliminary and provide some useful insight into the fate of selected elements when burning as a remediation technique is proposed. However, extrapolation to a large scale burning could not be recommended due to the variation in temperature with small volumes compared to large volumes.

Acknowledgements

This work was supported, in part, by United States Environmental Protection Agency (EPA) Grant Number R-824-143-01-00. The authors gratefully acknowledge the support of the Thermo Jarrell Ash–Baird Corporation, in particular Gerald R. Dulude, J. Sotero and Korea Science and Engineering Foundation, Grant Number 971-0304-024-2.

References

[1] P. Ray, Proceedings of Ninth Annual Gulf of Mexico Information Transfer Meeting, Gulf of Mexico production trends and deepwater potential, 1988, p. 6.
[2] W.A. Kucharski, P. Kostecki, Symp. Prococeedings: Gulf of Mexico and Caribbean Oil Spills in Coastal Ecosystems: Assessing effects, natural recovery and progress in remediation research, remediation techniques: an overview, 1994, p. 136.
[3] R.Z. Hoff, Symp. Proceedings: Gulf of Mexico and Caribbean Oil Spills in Coastal Ecosystems: Assessing Effects, natural recovery and progress in remediation research, responding to oil spills in marshes: the fine help between help and hindrance, 1994, p. 146.
[4] B. Hardegree, D.W. Hicks, J.W. Tunnel, Symp. Proceedings: Gulf of Mexico and Caribbean Oil Spills in Coastal Ecosystems: Assessing Effects, natural recovery and progress in remediation research, evaluation of burning as an oil spill clean up technique in high marsh community along the south Texas coast, 1994, p. 195.
[5] K.S. Farah, J. Sneddon, Appl. Spectrosc. Rev. 30 (4) (1995) 351.
[6] K.S. Farah, J. Sneddon, Talanta 40 (6) (1993) 879.
[7] K.S. Farah, J. Sneddon, Anal. Lett. 26 (4) (1993) 709.
[8] L.O. Edwards, Trace Metals and Stationary Conventional Combustion Sources, Volume 1, Technical Report Radian Corporation, Austin, Texas, Contract 68-02-2608, 1980.
[9] C.O. Noble, J.L. Hammond, J.N. Beck, C.E. Proffitt, J. Sneddon, Microchem. J. 57 (3) (1997) 361.
[10] G. Stacey, III, Symp. Proceedings: Gulf of Mexico and Caribbean Oil Spills in Coastal Ecosystems: In-situ burn as an oil response technique, 1994, p. 191.

ELSEVIER

Talanta 47 (1998) 267–273

Talanta

A new piezoelectric response model for population growth of bacteria

Lili Bao, Huwei Tan, Le Deng, Wanzhi Wei *

College of Chemistry and Chemical Engineering, Hunan University, Changsha 410082, People's Republic of China

Received 1 December 1997; received in revised form 11 March 1998; accepted 12 March 1998

Abstract

A piezoelectric response model on the population growth of microorganism is proposed. This model is based on a novel population growth model, which has a more obvious ecological meaning and the fact that the series piezoelectric quartz crystal (SPQC) sensor responses to conductivity changes of the medium during the growth of the microorganism. From the response model four parameters can be obtained including the maximum specific growth rate μ_m, saturated population size N_m, and two constants C and K_1. The influence of the parameters on the response curve is discussed in which the influences of μ_m and N_m are more obvious. With the proposed model the quantitative determination of bacteria may be more accurate than the frequency detection time (FDT) method. Then the growth of *Escherichia coliform* (*E. coli*) monitored with a SPQC sensor is compared with the simulated growth curve obtained by the proposed model and a good agreement is obtained. © 1998 Elsevier Science B.V. All rights reserved.

Keywords: Piezoelectric response model; Population growth; Bacteria; *Escherichia coliform*

1. Introduction

Since the piezoelectric quartz crystal (PQC) sensor oscillates successfully in liquid phase, it has been applied to increasingly wide fields including the life sciences, such as determination of biomacromolecules [1,2], monitor of blood clotting [3] and determination of pharmaceutical compounds [4]. Recently, PQC sensor was utilized to determine microorganism and has attracted the attention of many analysts because it is rapid and the operational process is simple [5–9]. There are mainly two types of PQC methods for microorganism detection: the piezoimmunological method and the methods utilizing the response of the sensor to conductivity including the separate electrode piezoelectric quartz crystal (SEPC) sensor method and the series piezoelectric quartz crystal (SPQC) method. The latter methods rely on the fact that the metabolizing bacteria transform uncharged or weakly charged substrates into highly charged end products. These charged substrates cause an alteration of the conductance of the medium and so the resonant frequency of the PQC sensor changes. The frequency detection time (FDT) is the time required for the initial inoculum to reach the threshold value at which the frequency signal produced can be detected by

* Corresponding author.

0039-9140/98/$ - see front matter © 1998 Elsevier Science B.V. All rights reserved.
PII S0039-9140(98)00134-9

the instrument and acceleration can be observed in the frequency shift value. The FDT is linearly related to the logarithm of the initial concentration of bacteria and so is used to determine the bacteria quantitatively. However, the accurate determination of FDT relies on the experience of the analysts and so is not very easy. Therefore a response model utilizing the whole response curve to present accurate information of the growth are needed.

The relationship between the population growth rate and population density, and the relationship between the growth and nutrient have been an object of discussion for many years. Many models have been proposed to portray these relationships [10–15] in which a Logistics model and a Monod model are typical and have been widely used in both biological theory and practice. In this work, the non-linear limit of food to population growth reflected by the Monod model is combined with the concept of potential for further growth of population presented by Smith to derive a new model of population growth of microorganism [16]. It is more reasonable from the view of ecology. Then the response model of SPQC sensor was derived based on the response of the sensor to conductivity. The response curve can be obtained through the resolve of a differential equation.

The response model has the following advantages: the response model utilizes all the information of the whole response curve to estimate the parameters such as saturated population size N_m, the maximum specific growth rate μ_m, and the constants C and K_1, which are more accurate and so when the model is used to detect bacteria, it will be more accurate than the FDT method. On the other hand the growth model which it is based on has a more obvious ecological meaning and hence is more reasonable ecologically.

2. Theory

2.1. Growth model

Monod model [11] is a classical model for population growth (Eq. (1)):

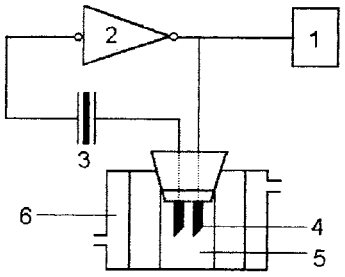

Fig. 1. Schematic diagram of the SPQC system. (1) Frequency counter; (2) IC-TTL oscillator; (3) quartz crystal; (4) conductivity electrodes; (5) detection cell; (6) thermostatic water-jacket.

$$dx/x dt = \mu_m s/(k_m + s) \quad (1)$$

where x is the population density at time t; μ_m is the maximum value of specified growth rate μ ($\mu = dx/x dt$); s is the remained food concentration at t; and k_m is called the Michaelis–Menten constant. If s is considered as the potential for further growth of the population, the Monod equation can be rewritten as (Eq. (2)):

$$dx/x dt = \mu_m P/k_1 + P \quad (2)$$

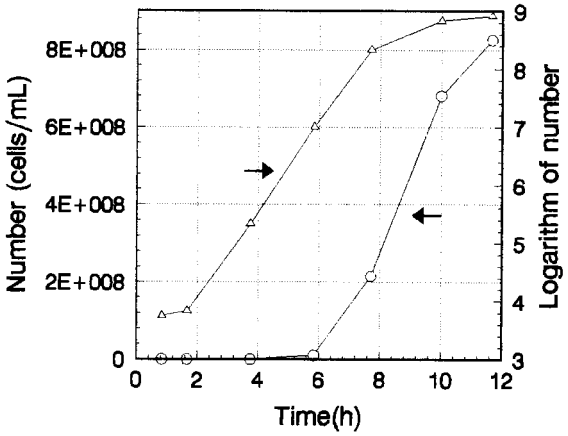

Fig. 2. Growth curve of *E. coli* in the medium. '○' is the number and '△' is the logarithm of number of the bacterium. The initial concentration of *E. coli* is 6.6×10^3 cells ml^{-1}.

Table 1
Calculated μ value by Eq. (9a) and Eq. (9b)

N (cells ml^{-1})	μ (calculated by Eq. (9a))	μ (calculated by Eq. (9b))
34	1.25	0.26
49	0.92	0.22
69	0.72	0.18
109	0.58	0.11
146	0.53	0.06

The parameters used are: $\mu_m = 0.44$, $C = 0.127$, $N_m = 228$, $K_1 = 0.40$.

where k_1 is a constant and P is the potential for further growth of the population. It is obvious that the Monod model reflects a non-linear limit of food to population growth.

However, as pointed out by Smith, on the condition that the growth of the population is limited by food, the potential for further growth of the population should be the portion of the rate of food supply not momentarily being used by the population. It should not be the amount of food (s) [16]. If the rate at which the population utilizes food is represented by F and the total rate of food utilization at saturation is represented by T, then P can be expressed as

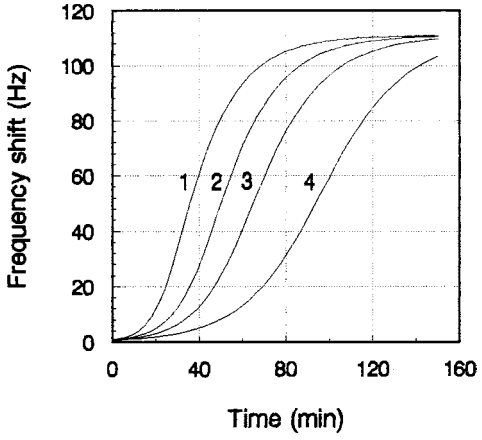

Fig. 3. Simulated response curves with different μ_m. (1) $\mu_m = 0.24$, (2) $\mu_m = 0.16$, (3) $\mu_m = 0.12$, (4) $\mu_m = 0.08$, and other parameters: $C = 0.064$, $K_1 = 0.57$, $N_m = 5.4 \times 10^8$, $N_0 = 3.4 \times 10^6$.

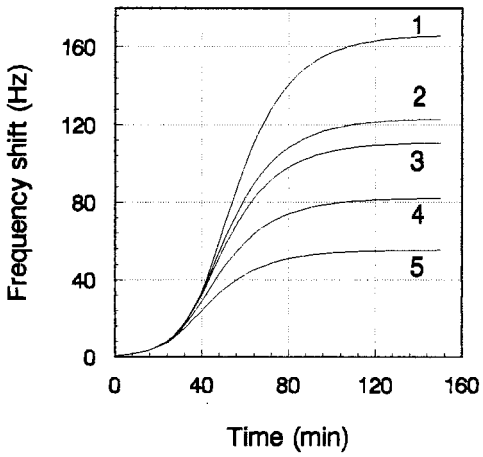

Fig. 4. Simulated response curves with different N_m. (1) $N_m = 8.1 \times 10^8$, (2) $N_m = 6.0 \times 10^8$, (3) $N_m = 5.4 \times 10^8$, (4) $N_m = 4.0 \times 10^8$, (5) $N_m = 2.7 \times 10^8$, and other parameters: $\mu_m = 0.17$, $K_1 = 0.57$, $C = 0.064$, $N_0 = 3.4 \times 10^6$.

follows (Eq. (3)):

$$P = 1 - F/T \quad (3)$$

F is certain to be related to the population size N and the growth rate of population (dN/dt). One simple supposition of F is (Eq. (4)):

$$F = C_1 N + C_2 dN/dt \quad C_1 > 0,\ C_2 > 0 \quad (4)$$

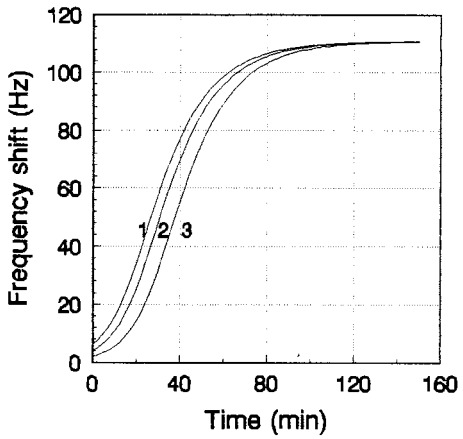

Fig. 5. Simulated response curves with different N_0. (1) $N_0 = 3.0 \times 10^7$, (2) $N_0 = 2.0 \times 10^7$, (3) $N_0 = 1.0 \times 10^7$, and other parameters: $\mu_m = 0.17$, $C = 0.064$, $K_1 = 0.57$, $N_m = 5.4 \times 10^8$.

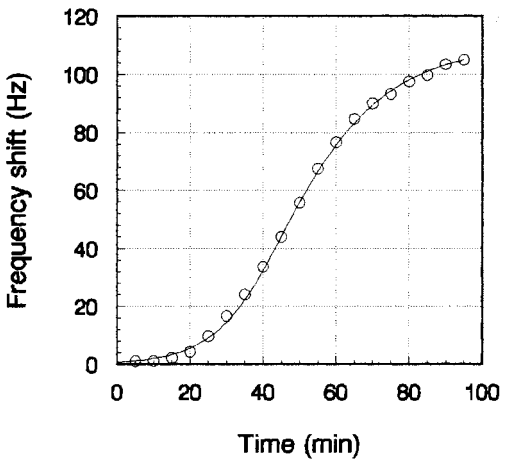

Fig. 6. Simulated response curves and practical response curves of *E. coli*. The lines are simulated curves and the points are experimental data. The initial concentration of *E. coli* is 6.0×10^6 cells ml^{-1} and the process was carried out with a stirring of the suspension.

$$\frac{dN}{N dt} = \mu_m \frac{1 - F/T}{K_1 + (1 - F/T)} = \mu_m \frac{1 - \dfrac{CN + dN/dt}{CN_m}}{K_1 + 1 - \dfrac{CN + dN/dt}{CN_m}} \quad (7)$$

This expression, although derived from the Monod model in terms of the rates of food supply and utilization, is more complicated than the Monod equation. If specified growth rate is expressed as $\mu = dN/N dt$, then Eq. (7) is a quadric order equation of μ.

$$N\mu^2 + (CN - CN_m K_1 - CN_m - N\mu_m)\mu + CN_m\mu_m - CN\mu_m = 0 \quad (8)$$

The two roots are as follows:

$$\mu_1 = \frac{CN_m K_1 + CN_m + (\mu_m - C)N + \sqrt{[CN_m K_1 + CN_m + (\mu_m - C)N]^2 + 4C\mu_m N^2 - 4CN_m\mu_m N}}{2N} \quad (9a)$$

$$\mu_2 = \frac{CN_m K_1 + CN_m + (\mu_m - C)N - \sqrt{[CN_m K_1 + CN_m + (\mu_m - C)N]^2 + 4C\mu_m N^2 - 4CN_m\mu_m N}}{2N} \quad (9b)$$

With such a regression to relate population size and the growth rate of the population food utilization rate, it is evident that, at saturation, since the specific growth rate is zero, $T = C_1 N_m$, where N_m is the saturated population size, and using ratios to express the portion of food supply being utilized, the number of constants needed to express this regression can be reduced from two to one (Eq. (5)):

$$\frac{F}{T} = \frac{C_1 N + C_2 dN/dt}{C_1 N_m} = \frac{CN + dN/dt}{CN_m} \quad (5)$$

and so P can be expressed as [16]:

$$P = 1 - \frac{F}{T} = 1 - \frac{CN + dN/dt}{CN_m} \quad (6)$$

Substituting this expression into the Monod model gives the following expression:

Eq. (9b) is chosen because of the correct relationship between μ and N which will be discussed below. The K_m in the Monod equation is changed to K_1, because the meaning of the two constants are different. In the Monod model, K_m is called the Michaelis–Menten constant and equals to the concentration of the food when the specific growth rate reaches half of the maximum value. It has the dimension of concentration, while in the new model, K_1 represents the portion of the rate of food supply not momentarily being used by the population when the specified growth rate reaches half of the maximum value. K_1 is a constant which is dimension free.

Although this new model has been derived with no attention to the properties or possible biological interpretations of the new constant, C, examination of the model suggests a simple definition.

In Eq. (6), the second item, being a portion, must be dimension free, so CN and CN_m must have the dimension of size/time if they are to be consonant with the population growth rate dN/dt, and thus the new constant C is evidently a rate with the dimension time^{-1}.

As $\mu = dN/Ndt$, (Eq. (9b)) can be written as follows:

$$\frac{dN}{dt} = \frac{CN_mK_1 + CN_m + (\mu_m - C)N - \sqrt{[CN_mK_1 + CN_m + (\mu_m - C)N]^2 + 4C\mu_mN^2 - 4CN_m\mu_mN}}{2} \quad (10)$$

If the items on the right side of the equation is represented by $f(N)$, Eq. (10) can be written as: $(dN)/(dt) = f(N)$, and so

$$N = \int f(N)dt \quad (11)$$

2.2. Response model

As pointed out previously, the metabolizing bacteria transform uncharged or weakly charged substrates into highly charged end products. These charged substrates cause an alteration of the conductance of the medium with a resulting change of the resonant frequency of SPQC sensor. According to Shen et al. [17], when the parameters of the circuit and crystal are fixed and dielectric constant of a solution varies little, the change in conductivity between sample and reference solutions (ΔG) is much less than G_0 and the relationship between frequency shift ΔF and the conductivity change ΔG is linear, $\Delta F = K\Delta G$, where K is a constant. As during the growth of the bacterium, the conductivity change of the medium is proportional to the number of the bacterium, $\Delta G = K'N$, where K' is a constant and N is the number of the bacterium. So $\Delta F = K_{FN}N$, where K_{FN} is a constant. From Eq. (10) and Eq. (11), it can be obtained:

$$\Delta F = K_{FN}\int \frac{CN_mK_1 + CN_m + (\mu_m - C)N - \sqrt{[CN_mK_1 + CN_m + (\mu_m - C)N]^2 + 4C\mu_mN^2 - 4CN_m\mu_mN}}{2} dt \quad (12)$$

A solution of Eq. (12) can give a piezoelectric response curve to bacteria growth and if fitting of the simulated data to the experimental data is made, the parameters of the growth curve can be estimated. As Eq. (12) is very complicated, the functional relation of population size and time is difficult to obtain. So a numerical evaluation of the equation is necessary to get the response curve. After the initial condition (N_0, initial population size) is given, the Euler method is used for the numerical evaluation.

As there is a threshold value of the bacteria at which the frequency signal produces, when the initial concentration is below the threshold value, another parameter λ (lag time) has to be added and t can be corrected by $t' = t - \lambda$, where t' is the corrected time and t is the real time.

3. Experimental

3.1. Apparatus and reagents

The experimental set-up employed is illustrated in Fig. 1. The SPQC sensor was constructed by connecting an AT-cut 9-MHz quartz crystal and a conductivity electrode in series to make up the feedback circuit of the oscillator. One of the crystal lead wires was connected to the input terminal of the oscillator, another crystal lead was connected to one of the lead wires of the conductivity electrode and a third lead wire was connected to the output terminal of the oscillator. A model SC7200 Isutaz universal frequency counter

was employed to monitor the growth of *E. coli*. A thermostat was used to control the growth temperature at 37°C. A PC computer was used to perform the numerical evaluation.

The composition of the culture medium is as follows: proteose peptone, 10.0 g; yeast extract, 6.0 g; lactose, 20.0 g; sodium desoxycholate, 0.1 g; sodium lauryl sulfate, 1.0 g; bile salts, 1.0 g; and distilled water, 1000 ml. The medium was sterilized by autoclaving at 121°C for 15 min.

3.2. Stock culture and detection

Four loops of *E. coli* on agar slant was inoculated into the liquid medium and was incubated at 37°C for 24 h. Then the mixture was preserved in a refrigerator. As the medium used is complicated, a parallel stock culture process was monitored by conventional pour plate count (PPC) method in order to study the growth of *E. coli* in this medium. In detection of growth curve, 0.5 ml stock culture *E. coli* suspension was added to 5 ml medium and a full mixture was made. Then the growth process was monitored by a SPQC sensor with a time interval of 5 min at 37°C. And for a rapid growth, a stirring of the suspension was made during the detecting process.

3.3. Computation and data analysis

After the initial condition (N_0, initial population size) is given and the parameters are chosen, the Euler method is used to obtained the numerical evaluation of Eq. (8) and the programs are written in FORTRAN.

4. Results and discussion

4.1. The growth of E. coli in the medium

The medium used is complicated as there are nitrogen and carbon sources in it. The growth of *E. coli* in this medium is examined by the conventional PPC method. The result is shown in Fig. 2. It can be seen that although the medium is complicated, the growth of *E. coli* in it is simple.

4.2. Selection of right expression of μ

As Eq. (8) is a quadric equation of μ, the resolution of the equation gives two roots (Eq. (9a)) and (Eq. (9b)) and so it is necessary to determine the correct expression of μ. In order to choose the correct expression of μ, the μ values are calculated at given N values according to Eq. (9a) and Eq. (9b). It can be seen from Table 1 that the μ values calculated by Eq. (9a) are larger than μ_m, a result which is not reasonable, while the values calculated by Eq. (9b) are all less than the μ_m value. So Eq. (9b) is chosen as the correct expression of μ.

4.3. Simulated response curve

A numerical evaluation of Eq. (12) gives a response curve. As shown in Fig. 3, the frequency shift increases slowly at first, then accelerates to a maximum slope, then the slope decreases and finally a saturated value is reached and the whole process gives a sigmoidal curve.

4.4. Influence of parameters to response curve

In order to test the influence of the parameters to the growth curve, curves with different parameter values were presented.

Effect of μ_m on the growth curve are shown in Fig. 3. It can be noted that the slope of the curves at initial time points are different. With the increase of μ_m, the initial slope of the curves become more steep and the saturation is more rapid. This is because μ decreases with the increase of N, so μ_m is corresponding to the μ value at initial points. As N_0 values are the same, μ_m is determined by dN_0/dt. With the increase of μ_m the value of dN_0/dt increases and so the initial slope of the curves becomes more steep, and the higher the μ_m, the more rapid the growth of the population and the more quickly the population saturates.

It can be seen from Fig. 4 that N_m obviously influences the curves. The initial part of the curves coincide with each other, then the difference of the curves appear and become obvious gradually. The larger the N_m value, the higher the plateau of

the curve. This is because that N_m is the saturated population size which is permitted by the nutrients in the environment, and the larger saturated value gives a higher plateau of the growth curve.

Influence of N_0 to growth curves are shown in Fig. 5. The initial height of the curves is different. But with the development of time, the curves coincide with each other gradually. The reason is that N_0 is the initial population size and the larger initial size caused higher initial heights of curves. As the saturated values are the same, the curves coincide with each other eventually.

Curves with different C values coincide with each other at the initial part, then the curve with the higher C value increases and saturates more rapidly. For different K_1 values the curves coincide with each other at the initial part, but with the increase in time the curve with the higher K_1 value increases and saturates more slowly. As the biological meanings of C and K_1 are not so obvious, the explanation of the influence will be complicated.

4.5. Verification of the simulation in experiments

The growth of *E. coli* is monitored by SPQC sensor and the results were shown in Fig. 6. It can be seen that the simulated growth curve is in good agreement with the practical growth curve.

5. Conclusions

A piezoelectric response model on the population growth of microorganism is proposed based on a novel population growth model, which has a more obvious ecological meaning. With this response model the quantitative determination of bacteria may be more accurate than the FDT method. It will be very useful for the study of the population growth of microorganism. And if the fitting of the model to the practical growth is made, the various parameters of the microorganism growth can be obtained. The evaluation of the parameters and its application to determine the bacterium will be reported elsewhere.

Acknowledgements

This work is financially supported by the Hunan Natural Science Foundation.

References

[1] H. Muramatsu, E. Tamiya, I. Karube, Anal. Chim. Acta 215 (1988) 741.
[2] L. Deng, L.H. Nie, S.Z. Yao, J. Microb. Methods 23 (1995) 229.
[3] S.H. Si, T.A. Zhou, D.Z. Liu, L.H. Nie, S.Z. Yao, Anal. Lett. 11 (1994) 2027.
[4] L.H. Nie, T.Q. Wang, S.Z. Yao, Talanta 39 (1992) 155.
[5] H. Maramatsu, Y. Wantanabe, M. Hikuma, T. Akata, I. Kubo, E. Tamiya, I. Karube, Anal. Lett. 22 (1989) 2155.
[6] L. Deng, F.J. He, T.J. Jiang, L.H. Nie, S.Z. Yao, J. Microb. Methods 23 (1995) 229.
[7] F.J. He, L. Deng, Q.J. Xie, L.H. Nie, S.Z. Yao, Anal. Lett. 28 (1995) 213.
[8] F.J. He, Q. Geng, W.H. Zhu, L.H. Nie, S.Z. Yao, M.F. Chang, Anal. Chim. Acta 289 (1994) 313.
[9] F.J. He, W.H. Zhu, Q. Geng, L.H. Nie, S.Z. Yao, Anal. Lett. 27 (1994) 655.
[10] R. Pearl, Introduction to Medical Biometry and Statistics, 3rd ed., Saunders, Philadelphia, 1940, 459.
[11] J. Monod, Recherches sur la Croissance des Cultures Bacteriennes, Hermann et Cie, Paris, 1942.
[12] F.J. Richards, J. Exp. Bot. 10 (1959) 290.
[13] W.E. Ricker, Fish Physiol. 8 (1979) 677.
[14] J. Schnute, Can. J. Fish. Aquat. Sci. 38 (1981) 1128.
[15] C.J. Stannard, A.P. Williams, P.A. Gibbs, Food Microbiol. 2 (1985) 115.
[16] F.E. Smith, Ecology 44 (1963) 651.
[17] D.Z. Shen, W.H. Zhu, L.H. Nie, S.Z. Yao, Anal. Chim. Acta 276 (1993) 87.

ELSEVIER

Talanta 47 (1998) 275–283

Talanta

Development of an Hg(II) fibre-optic sensor for aqueous environmental monitoring

Musa Ahmad *, Harun Hamzah, Elya Sufliza Marsom

Chemistry Department, Faculty of Physical and Applied Science, Universiti Kebangsaan Malaysia, 43600 Bangi, Selangor, Malaysia

Received 27 May 1997; received in revised form 9 March 1998; accepted 16 March 1998

Abstract

An optical sensor for Hg(II) monitoring using a complex of zinc dithizonate immobilised on XAD 7 which is based on reflectance spectrophotometry has been developed in this study. Measurements were made using a kinetic approach whereby the reflectance signal is measured at a fixed time of 5 min. The sensor could be regenerated using a saturated solution of KCl in 1 M sulphuric acid. The sensor was found to have an optimum response at pH 3.0 with respective measurement repeatability and probe-to-probe reproducibility of 1.53% and 5.26%. A linear response was observed in the Hg(II) concentration range of 0.0–180.0 ppm with a calculated limit of detection (LOD) of 0.05 ppm. The results obtained for aqueous Hg(II) determination using this probe were found to be comparable with the well-established method of atomic absorption spectrometry. © 1998 Elsevier Science B.V. All rights reserved.

Keywords: Optical sensor; Hg(II); Aqueous environmental monitoring

1. Introduction

Environmental contamination of Hg(II), a widely known toxic heavy metal can result in death or severe damage to the brain. In the past, the tragedy that happened at Minamata and Niigata, Japan, claimed the lives of many victims [1]. For determination of Hg(II), a method based on amalgamation on gold and cold vapour atomic adsorption spectrophotometry (CVAAS) was described in literature [2]. Theoretically, it is sensitive but experimentally it is difficult due to absorption interference by molecular oxygen and background absorption by molecules produced in the atomization process. Another method is interference-free determination of Hg(II) using a gold-plated piezoelectric crystal detector but this method has a detection limit which is a little too high for general applicability [2]. A few spectrophotometric methods were considered unsatisfactory due to the reagents' stability and sensitivity to variations in laboratory conditions and changes in acidity [3]. Conventional methods of determining Hg(II) are found to be tedious and time-consuming using large instruments. The development of a new kind of sensor, namely a fibre optic chemical sensor, brings about an alternative for environmental monitoring especially for hazardous contaminants such as Hg(II). The sensor is

* Corresponding author. Tel: +60 3 8250001; fax: +60 3 8256086.

0039-9140/98/$ - see front matter © 1998 Elsevier Science B.V. All rights reserved.
PII S0039-9140(98)00135-0

small and can be built using a low-budget. Furthermore, it can be made into a portable instrument for in situ measurements.

Dithizone, a sulphophilic reagent, has been known as a selective solvent extraction reagent for heavy metal ions and the complexation reactions can be monitored easily by its sensitive colour change [4]. Nevertheless, the instability of the reagent proved to be a major problem. This problem could be overcome by complexing the reagent with a metal ion such as zinc to form a metal dithizonate complex [4,5]. In this paper, we discuss the possibility of using such a complex as a reagent phase for the development of an optical fibre Hg(II) sensor. The complex of zinc dithizonate was immobilised on XAD 7, a porous polymer of methylmethacrylate.

2. Experimental

2.1. Reagents

Dithizone 0.01% (w/v) was prepared by dissolving 0.0100 g of dithizone in carbon tetrachloride and making up to 100 ml. The complex of zinc dithizonate was prepared by mixing 100 ml of 0.01% (w/v) dithizone with 100 ml 1% zinc sulphate solution. The mixture was stirred using a mechanical stirrer for 30 min.

A stock solution of Hg(II) 1000 μg/ml was prepared by dissolving mercury(II) nitrate, $Hg(NO_3)_2.H_2O$ in 0.2 M nitric acid. Lower concentrations of Hg(II) solutions were obtained by serial dilution of the stock solution.

Regenerating solution was prepared by dissolving an excess amount of potassium chloride in 1.0 M sulphuric acid to form a saturated solution. A buffer solution of pH 3.0 was prepared by mixing 500 ml of 0.1 M potassium hydrogen phthalate and 223 ml of 0.1 M hydrochloric acid. Distilled-deionised water was used throughout the experiment for solution preparation.

2.2. Instrumentation

Optical Spectrum Analyzer (Model ANDO 6310B, Japan) was used to measure the reflectance signal from the probe. Red laser (5 mW, 635 nm; Melles Griot, Electrooptic Div., Boulder, CO) was used as the light source. Fig. 1 shows the schematic diagram of the instrumentation used. The reflectance signal measurement was taken at wavelength of 636.93 nm and a mechanical stirrer was used to stir the analyte solution at a constant rate.

An atomic absorption spectrometer (Perkin-Elmer model 3100) was used for atomic absorption measurement of the aqueous Hg(II) sample.

2.3. Procedure

Amberlite XAD 7 beads (2.0000 g) were soaked in 10.0 ml of zinc dithizonate solution and stirred for 1 h at room temperature. The mixture was left

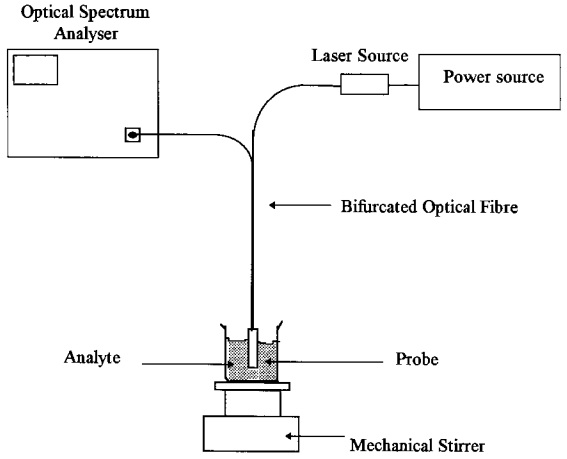

Fig. 1. Schematic diagram of the mercury(II) fibre-optic sensor instrumentation.

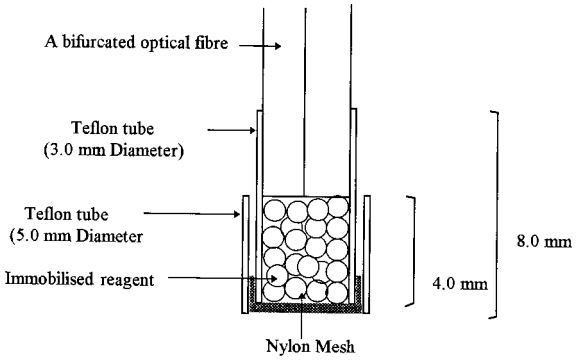

Fig. 2. The design of the mercury(II) probe.

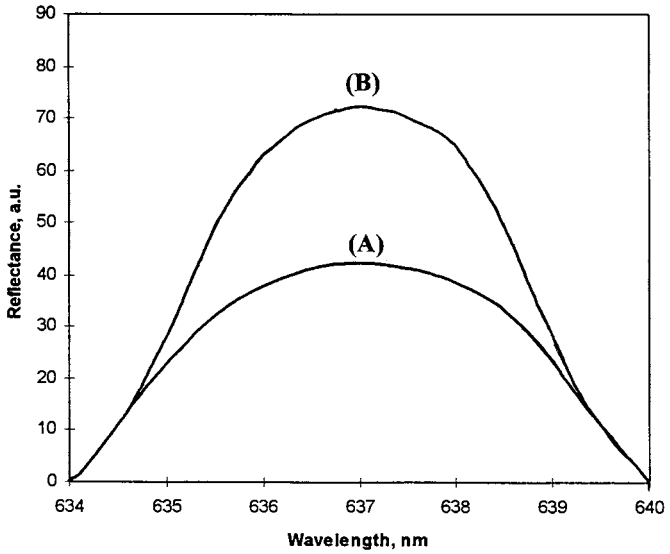

Fig. 3. Reflectance spectra of immobilised Zn(II)-dithizonate complex before (A) and after (B) reaction with Hg(II).

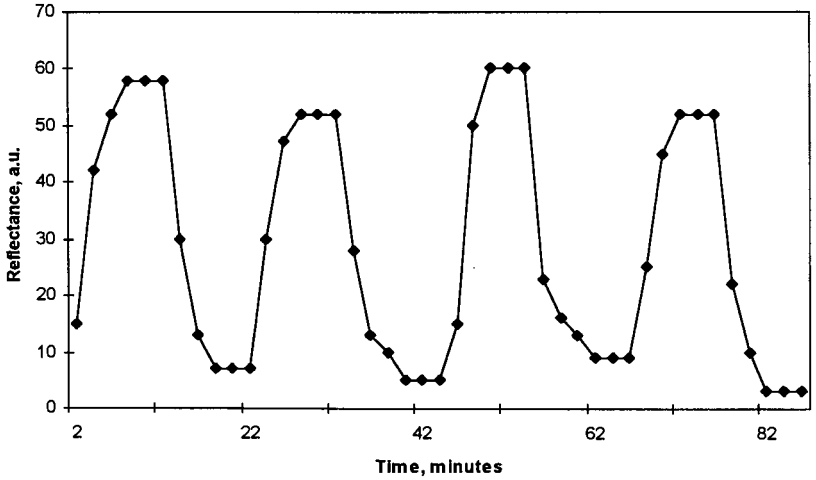

Fig. 4. The response of the sensor to the same concentration (100 ppm) of Hg(II) after regeneration of the probe using saturated KBr solution in H_2SO_4.

standing overnight before the beads were rinsed several times with distilled-deionised water. The beads then were left to dry in a desiccator and kept in a dry container. XAD 7 was used without further grinding. Prior to use, the XAD 7 beads had to be washed thoroughly with distilled-deionised water, soaked in ethanol and washed thoroughly with distilled-deionised water again.

Fig. 2 shows the design for the Hg(II) probe. The probe was built using two Teflon tubes with different diameters. Teflon tube with a diameter of 3.0 mm was cut into 8.0-mm lengths while Teflon tube with a diameter of 5.0 mm was cut 4.0-mm lengths. One end of the 8.0 mm tube was covered with nylon mesh and inserted into the 4.0 mm tube. The shorter but wider tube served the purpose of holding the nylon mesh in place so that the beads with immobilised reagent could be entrapped inside the tube. Nylon mesh was selected with reference to fibre optic aluminium(III)

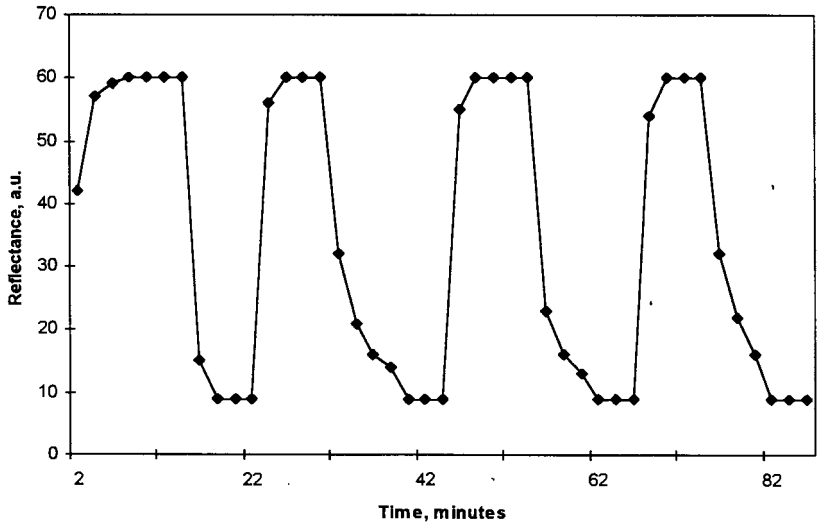

Fig. 5. The response of the sensor to the same concentration (100 ppm) of Hg(II) after regeneration of the probe using saturated KCl solution in H_2SO_4.

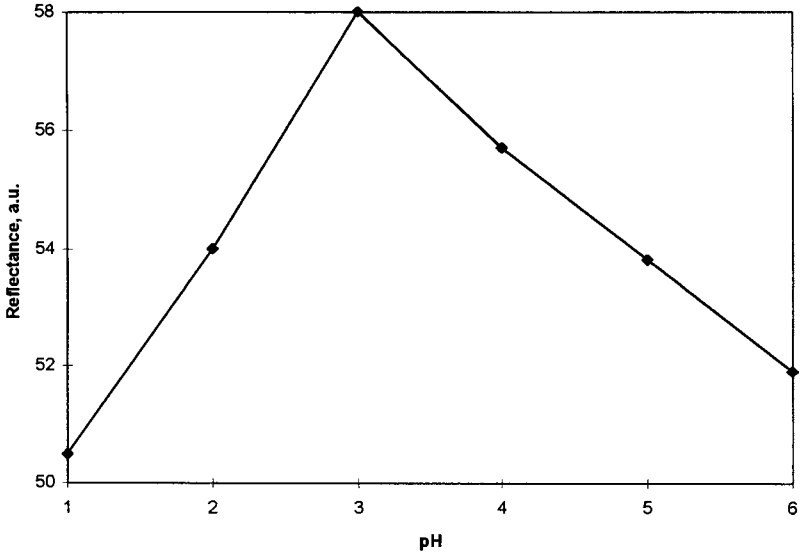

Fig. 6. The effect of pH on the formation of Hg(II) dithizonate complex with immobilised Zn(II) dithizonate complex on XAD 7.

sensor [6]. Ahmad and Narayanaswamy reported that their Al(III) sensing probe using polytetrafluoroethylene (PTFE) membrane, which was based on the conventional design of an optical sensor (e.g. pH sensor) did not give any response. The PTFE membrane was then replaced by nylon mesh and this improved design gave good results. The selection of nylon membrane is also important because it will increase the diffusion rate of the analyte to the reagent phase and hence improve the response time of the probe. The design of the probe used in this study is of a disposable type as the immobilised reagent could easily be replaced. The probe was later attached to the distal end of a bifurcated fibre optic made from plastic (Keyence) before the measurement was made.

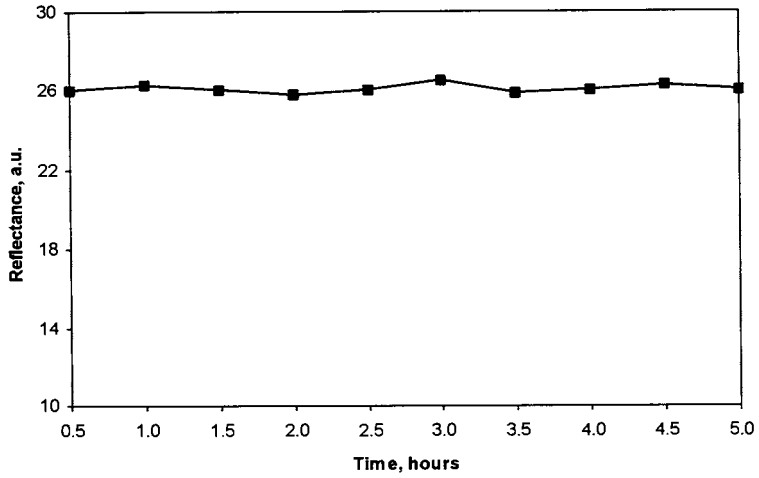

Fig. 7. The photostability of the Hg(II) sensor.

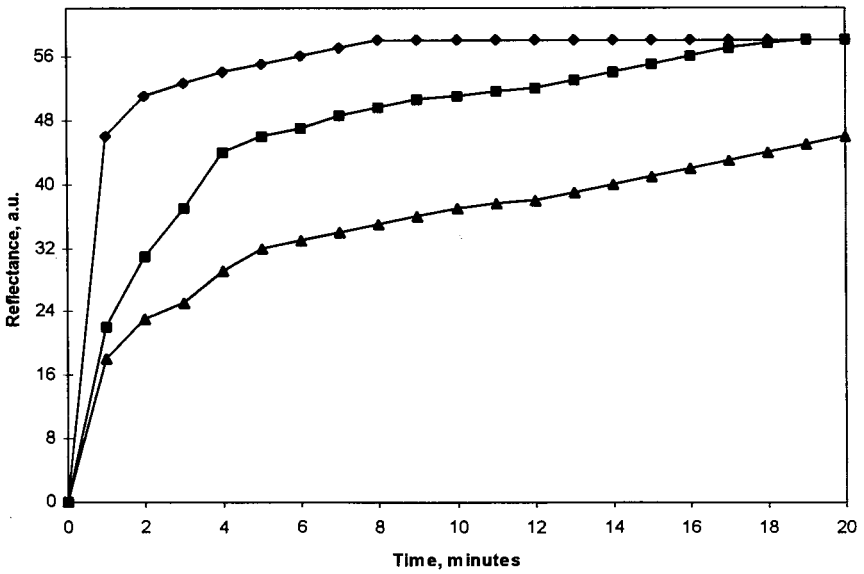

Fig. 8. The steady state response of the sensor for three different concentrations of Hg(II) i.e. 10 ppm (▲), 50 ppm (■) and 100 ppm (●).

A kinetic approach was used for the reflectance measurement where the signal was measured 5 min after insertion of the probe in Hg(II) solution. The measurements were expressed as reflectance difference which is defined as the difference in the reflectance signal of the immobilised Zn(II)–dithizonate complex in the presence and absence of Hg(II).

Interference from foreign ions was studied by introducing a known amount of interfering ions (at 1:1 mole ratio) to the sensing probe during Hg(II) determination. The degree of interference of these ions was evaluated by measuring the reflectance signal of the sensor in the presence and absence of the interfering ions.

For validation of the sensor results, a series of standard Hg(II) solutions with concentrations of 0.0, 30.0, 60.0, 90.0, 120.0, 150.0 and 180.0 ppm

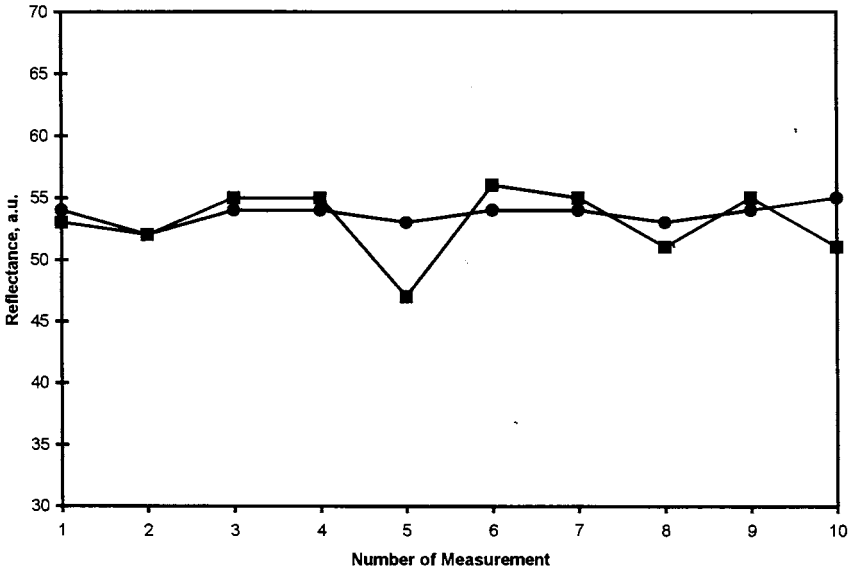

Fig. 9. The measurement repeatability (●) and probe-to-probe reproducibility (■) of the Hg(II) probe.

was prepared by dissolving a definite amount of mercury(II) nitrate in 0.2 M nitric acid solution. These solutions were then analysed using both atomic absorption spectrometer and also the optical fibre Hg(II) sensor which has been developed in this study. Calibration graphs for both methods were plotted. These graphs were later used for determination of known concentrations of Hg(II) samples (70.0 ppm) and the results obtained from both methods were statistically tested for their comparability.

Table 1
Degree of interference by some foreign ions at a 1:1 mole ratio of ion:Hg(II)

Interfering ions	Degree of interference, %
CH_3COO^-	−20.3
I^-	−2.0
Br^-	−3.5
Cl^-	−2.3
EDTA	+4.3
Cu^{2+}	−7.5
Pb^{2+}	−18.8
Ag^+	−12.0
Fe^{2+}	−8.4
Fe^{3+}	0.0

3. Results and discussion

Fig. 3 shows the reflectance spectra of zinc dithizonate before and after reaction with Hg(II). Reaction with Hg(II) caused an increase in the reflectance intensity due to the change in colour of the reagent phase from pink to orange after reaction with Hg(II) ions. The reflectance difference was found peak at 637 nm. All reflectance measurements in this study were therefore carried out at this wavelength.

Regeneration time is defined as the time taken for the probe to reach its base line response soon after it has been dipped in the regenerating solution [6]. Earlier in this study, regenerating solution was chosen based on the eluent used by Sekizuka et al. [7]. In their work, they had used a mixture of sulphuric acid and potassium bromide, KBr solution to elute metal ion from chromatographic column of dithizone immobilised on gel particles. The result (Fig. 4) however shows that although there is a pattern of regeneration, the steady state and the base line response were found to be inconsistent and fluctuated every time regeneration of the probe was carried out. Replacement of KBr with potassium chloride, KCl gives much

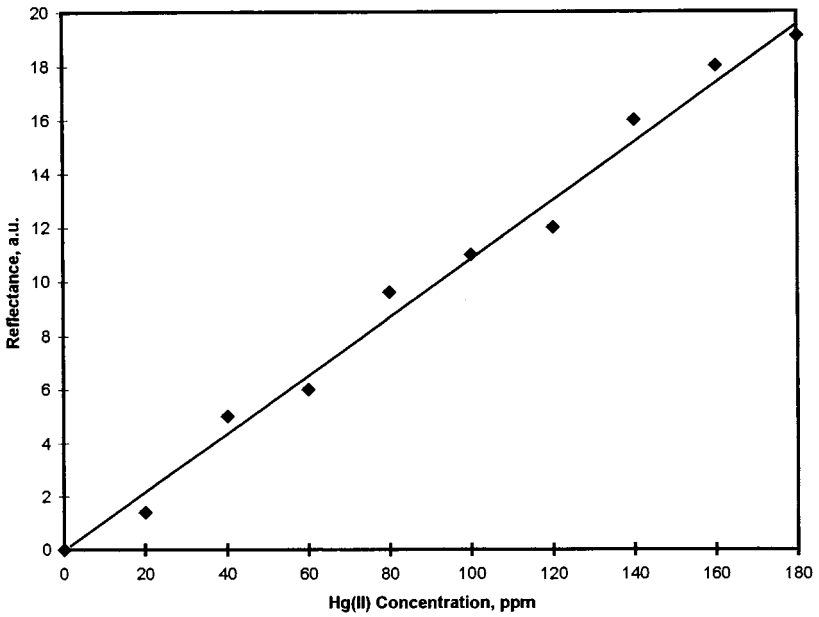

Fig. 10. The dynamic range of Hg(II) concentration which produced a linear sensor response ($r = 0.9901$).

better results (Fig. 5) where the sensor response was found regenerable with good based line and steady state response attainment. There is also a difference in the time taken for probe regeneration. Regeneration time taken when using KBr–H_2SO_4 mixture was between 16–20 min while regeneration using KCl–H_2SO_4 mixture took only 7–9 min. This observation may be explained by the fact that chloride ion is smaller and more reactive than bromide ion. A longer regenerating time of immobilised eriochrome cyanine R after reaction with Al(III) ions using EDTA solution compared to a smaller size ion such as fluoride has been reported in the literature [6].

The reflectance intensity of the Hg(II) sensor was governed by the pH of the analyte (Fig. 6). Basic and neutral media were not investigated in this study because the reaction between Hg(II) ion and dithizone in those media produced a secondary Hg(II)–dithizonate complex [7,8] which could not be differentiated distinctively from the colour of zinc dithizonate immobilised on XAD 7. At lower pH, the probe was found to produce a low reflectance signal because the medium is too acidic and there is a tendency for the reagent to leach from the support. Meanwhile, at higher pH, the reaction of Hg(II) ion and dithizone tends to produce a secondary complex which caused the reflectance signal to decrease. The response of the Hg(II) sensor was found to peak at pH 3.0.

A study on the photostability of the probe was carried out to monitor the possibility of photoleaching or photodecomposition of the reagent phase when it was continuously exposed to the light source for a long period of time. For a continuous monitoring period of 5 h, the result shows that the reagent phase is stable and no leaching had occurred (Fig. 7).

Fig. 8 shows the result of steady state response analysis using three different concentrations of Hg(II). It is shown here that the time taken to achieve the steady state response depends on the concentration of Hg(II). The steady state response was achieved within 5 min for a Hg(II) concentration of 100 ppm, whereas for a Hg(II) concentration of 50 ppm, the time taken was about 20 min. A much longer time was needed for a Hg(II) concentration of 10 ppm to achieve the same steady state response. Therefore, a kinetic approach was used in this study to quantify the Hg(II) concentration where the reflectance signal was measured 5 min after insertion of the probe

into the analyte solution. The same pattern of results was also reported for the Al(III) probe [9].

Measurement repeatability and probe-to-probe reproducibility are two important characteristics for the probe being developed. Alabbas et al. [10] had defined measurement repeatability as the successive runs made using a single sensor to evaluate discrepancies in its response while probe-to-probe reproducibility refers to the discrepancies in response between individual members of a batch of similarly constructed sensors. Fig. 9 shows the result of measurement repeatability and probe-to-probe reproducibility of the probe. It can be seen that the repeatability of the probe is better than its reproducibility. The RSD of the measurement repeatability was found to be 1.53% while for probe-to-probe reproducibility it was 5.26%. The higher RSD value obtained for probe-to-probe reproducibility compared to measurement repeatability is caused by variation in quantity of matrix, particle size and also shape of the probe [10]. The same pattern of results was also reported for the Al(III) probe [11].

The degree of interference measured from some foreign ions at a 1:1 mole ratio of ion:Hg(II) is summarised in Table 1.

Interference from anions such as iodide, bromide and chloride are expected since they are chemically reactive and capable of forming metal halide compounds [12] whereas acetate ion is known as a good electron donor. Table 1 shows that the main anion interference was obtained from CH_3COO^-. Meanwhile EDTA gives positive interference and this could possibly be due to the capability of EDTA to form a mixed ligand complex with unidentate ligands such as chloride which is available in the buffer solution. Formation of such a complex has been reported in the literature [13]. All cations listed in Table 1 except for Fe^{3+}, were reported to be capable of forming coloured metal dithizonate complexes with the immobilised reagent [14]. This explained why Fe^{3+} was found not to interfere in this study.

Fig. 10 shows that the sensor produced a linear response when the Hg(II) concentration determined ranged from 0.0–180.0 ppm with a computed regression coefficient value, r of 0.9968. The use of the Hg(II) sensor and atomic absorption spectrometer for determination of known Hg(II) concentration of 70.0 ppm produced mean values of 71.32 ppm and 69.19 ppm, respectively with corresponding RSD values of 5.25% and 0.49%. Although the latter method was more precise, the result obtained from both methods seems to be comparable. The LOD for this method, defined as the concentration of sample that yields a detector response equal to three times the detector noise was calculated to be 0.05 ppm.

4. Conclusion

An optical fibre Hg(II) sensor has been developed in this study based on immobilised zinc dithizonate on XAD 7. The sensor produced an optimum response at pH 3.0 and could be regenerated using a saturated solution of KCl in 1.0 M H_2SO_4. On reaction with the same concentration of Hg(II), the probe shows good measurement repeatability and probe-to-probe reproducibility with corresponding RSD values of 1.53% and 5.26%, respectively. The probe was found to give a linear response in the Hg(II) concentration range of 0.0–180.0 ppm with a calculated LOD value of 0.05 ppm. The study also indicates that the results obtained for Hg(II) determination using this sensor were comparable to those obtained using the established method of atomic absorption spectrometry. At the 1:1 mole ratio of interfering ion:Hg(II), CH_3COO^- and Pb^{2+} produced the highest interference of 20.30% and 18.8%, respectively.

Acknowledgements

The authors would like to thank Universiti Kebangsaan Malaysia for financial support under UKM research grant S/1/95.

References

[1] J.O. Nriagu (Ed.), The Biogeochemistry of Mercury in the Environment, Elsevier/North Holland Biomedical Press, The Netherlands, 1979.
[2] M. Stoeppler (Ed.), Techniques and Instrumentation in Analytical Chemistry, Vol. 12, Hazardous Metals in the Environment, Elsevier, Amsterdam, 1992.

[3] M. Tsubouichi, Amounts of mercury(II) by extraction with Bindshedler's Green, Anal. Chem. 42(9) (1970).
[4] K. Ueno, T. Yano, T. Kojima, Anal. Lett. 5 (7) (1972) 439.
[5] V. Spevackova, M. Krivanek, Proc. Anal. Chem. Conf., Budapest, Hungary, 1970, p. 121.
[6] M. Ahmad, R. Narayanaswamy, Anal. Chim. Acta 291 (1994) 255.
[7] Y. Sekizuka, T. Kojima, T. Yano, K. Ueno, Talanta 20 (1973) 979.
[8] Y.K. Lee, K.J. Whang, K. Ueno, Talanta 22 (1975) 535.
[9] M. Ahmad, R. Narayanaswamy, Sci. Total Environ. 163 (1995) 221.
[10] S.H. Alabbas, D.C. Ashworth, R. Narayanaswamy, Anal. Proc. 26 (1989) 373.
[11] M. Ahmad, R. Narayanaswamy, Talanta 42 (1995) 1337.
[12] F.A. Cotton, G. Wilkinson, Advanced Inorganic Chemistry: A Comprehensive Text, 3rd ed., Interscience, New York, 1972.
[13] R. Pribil, Analytical Applications of EDTA and Related Compounds. International Series of Monographs in Analytical Chemistry, Vol. 52, Pergamon Press, New York, 1972.
[14] E.B. Sandell, H. Onishi, Photometric Determination of Traces of Metals—Part I. Wiley-Interscience, New York, 1978.

ELSEVIER

Talanta 47 (1998) 285–290

Talanta

Rapid detection of *Escherichia coliform* with a bulk acoustic wave sensor based on the gelation of *Tachypleus* amebocyte lysate

Xiaoge Qu, Lili Bao, Xiaoli Su, Wanzhi Wei *

New Material Research Institute, College of Chemistry and Chemical Engineering, Hunan University, Changsha, 410082, People's Republic of China

Received 6 October 1997; received in revised form 9 March 1998; accepted 16 March 1998

Abstract

A new sensing method (BAW–TAL technique), which combined the bulk acoustic wave (BAW) technique with the gelation reaction of *Tachypleus* amebocyte lysate (TAL), was used for viscosity and density measurement and applied to the detection of *Escherichia coliform* (*E. coli*). This method depended on the fact that the viscosity and density of the mixture increased, and as a result, the resonance frequency decreased correspondingly after TAL was mixed with the heated *E. coli* solution that contained endotoxin. Results showed that the frequency shift was linearly related to the logarithm of *E. coli* concentration in the range of 2.7×10^4–2.7×10^8 cells/ml. The correlation coefficient was 0.996. This BAW–TAL method was compared with the standard pour plate counts (PPC) method. The proposed method was much more rapid and simpler for detection of *E. coli* than the traditional methods. © 1998 Elsevier Science B.V. All rights reserved.

Keywords: *Escherichia coliform*; Biosensors; Bulk acoustic wave sensors; *Tachypleus* amebocyte lysate; Gelation reaction

1. Introduction

E. coli is one of the most important types of normal bacteria in human and animal intestines, and some types of *E. coli* exhibit pathogenicity toward the human body. Therefore, the determination of *E. coli* is very important in food hygiene, clinical medicine and environmental monitoring. Standard methods employed for estimating *E. coli* include the most probable number (MPN) technique and the pour plate counts technique with Violet Red Bile Agar (VRBA) [1]. Both techniques are relatively troublesome and time-consuming. Up to 72 h is required to obtain confirmable results.

The bulk acoustic wave (BAW) sensor has been extensively used as a kind of highly sensitive chemical and biological sensor in various fields, since it oscillated successfully in liquid phase in the 1980s [2–4]. Recently, the use of a BAW sensor as an *E. coli* detector was reported [5]. In

* Corresponding author.

0039-9140/98/$ - see front matter © 1998 Elsevier Science B.V. All rights reserved.
PII S0039-9140(98)00136-2

this sensor, an AT-cut piezoelectric crystal modified with anti-*E. coli* antibody exhibited a shift in oscillation frequency by binding *E. coli*. The sensitivity of the method is relatively low and the concentration range of *E. coli* that can be detected by the method is narrow (10^6–10^8 cells/ml). He and coworkers [6,7] used a separated electrode BAW sensor and a series electrode BAW sensor to determine the number of *E. coli* based on the impedance alteration of the medium in which the inoculated *E. coli* was cultured. Although the concentration range of *E. coli* was augmented, the time required for determination was still relatively long because frequency shifts were detectable only when the concentration of *E. coli* exceeded the threshold values of 1.5×10^6–3.5×10^6 cells/ml and 1×10^6–1.5×10^6 cells/ml, respectively, and both methods were cumbersome.

BAW sensors have also been used as viscosity detectors recently. Muramatsu and coworkers have applied these detectors for the continuous measurement of viscosity changes, thus determining endotoxin using the gelation reaction of *Limulus* amebocyte lysate [8,9], determining the fibrinogen based on its gelation reaction with thrombin [10], and monitoring the process of blood coagulation [11].

E. coli is Gram-negative, and its cell wall is mainly composed of endotoxin (a lipopolysaccharide). The endotoxin is released when *E. coli* has died. Levin and Bang discovered that a horseshoe crab's blood coagulated when the animal was infected [12], and demonstrated that Gram-negative bacterial endotoxins could rapidly induce gelation of *Limulus* amebocyte lysate [13]. Owing to its extreme sensitivity to endotoxins, *Limulus* lysate has been employed to detect and semiquantitate contaminating lipopolysaccharide (LPS) pyrogens in pharmaceuticals and drugs intended for human use [14]. But up to now, there is still no report about its use in detecting the bacteria marked by LPS. In this work, a BAW sensor was used for monitoring viscosity and density changes of the gelation reaction of TAL with endotoxin and applied to detect *E. coli*. This method depended on the fact that after TAL was mixed with the heated *E. coli* solution that contained endotoxin, the viscosity and density of the mixture increased and as a result, the resonance frequency decreased. The proposed method was simple and rapid (the time for detection was less than 90 min); the amount of *E. coli* solution required for detection was very small.

2. Experimental

2.1. Culture medium

The composition of the culture medium for *E. coli* is as follows: Beef extract, 1.0 g; Yeast extract, 2.0 g; Peptone, 5.0 g; NaCl (free of pyrogen), 5.0 g; Pyrogen-free water, 1000 ml. The medium was dispensed into bottles and sterilized by autoclaving at 121°C for 15 min.

2.2. Stock culture

Four loops of *E. coli* in slant agar were inoculated into a 50-ml sterilized conical vial which contained 20 ml of sterilized culture medium. After being incubated for 24 h at 37°C, the conical vial was taken out of the incubator and preserved in a refrigerator. The culture gave an approximate concentration of 2.7×10^8 cells/ml.

2.3. Apparatus

The measuring system was constructed from an Ag-plated (diameter 5.5 mm), AT-cut 9 MHz quartz crystal (diameter 12.5 mm) with a well-type cell to position one side of the crystal at the bottom. A laboratory-made TTL-IC oscillator was designed to drive the crystal at its resonance frequency [15], and the oscillation signal was fed to a universal frequency counter (Iwatsu, Model SC-7201). A thermostat was used to control the reaction temperature at 37°C through a thermostatic water jacket. A schematic diagram of the detection system employed is illustrated in Fig. 1.

2.4. Materials

E. coli strain was provided by Hunan Medical University, Changsha, Hunan. TAL (0.1 ml, 0.25 EU/ml, 970301) was produced by Zhanjiang

Ocean-biological Product Factory in Guang-Dong Province.

The cell was rinsed with endotoxin-free water followed by ethanol. All glassware was heated at 180°C for 3 h before use. After each detection, a thin film on the crystal surface must be removed with 0.1 mol/l hydrochloric acid [4].

2.5. Frequency curve measurement

E. coli sample solutions were prepared by diluting the initial *E. coli* solution. After being heated at 60°C for 30 min, 0.2 ml of the sample solution was incubated at 37°C and added to solute lyophilized TAL. The mixture was injected into the well-type cell, and the resonance frequencies were recorded after incubation at 37°C.

2.6. Estimation of E. coli

The procedure for estimating *E. coli* is as follows: first, obtain frequency curves of various *E. coli* concentrations; second, derive the frequency shifts from the curves; then draw the frequency shift versus the logarithm of the concentration of *E. coli* and get the calibration curve. After this, when the frequency shift of *E. coli* of unknown concentration is determined, the concentration of *E. coli* can be calculated by a regression equation.

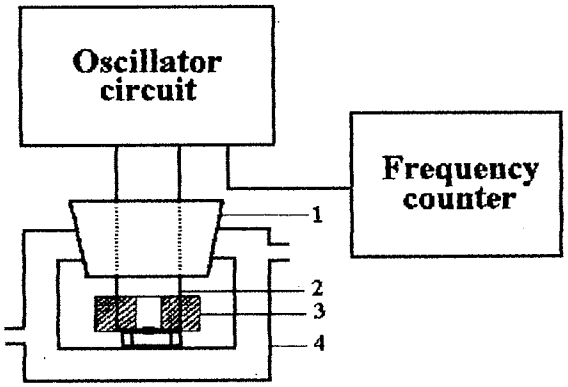

Fig. 1. Schematic depiction of the system for detection of *E. coli*. (1) Rubber plug. (2) Leading wire. (3) Well-type detection cell. (4) Thermostatic jacket.

2.7. Comparison of BAW–TAL method with standard pour plate counts technique

The frequency shifts of *E. coli* solutions of various concentrations were measured by the BAW–TAL technique. From Eq. (2), which is presented below, the cell numbers were obtained. At the same time, the same amount of *E. coli* was also measured by the standard pour plate counts method.

3. Results and discussion

3.1. Principle

BAW sensor as a non-mass one can respond to the viscosity and density of a liquid. According to Kanazawa and Gordon's equation [16]:

$$\Delta F = -F_s^{3/2}(\eta\rho_L/\pi\mu\rho_Q)^{1/2} \quad (1)$$

with ΔF, the resonance frequency shift of the BAW sensor, F_s, the resonance frequency, η, the viscosity of the liquid, ρ_L, the density of the liquid, μ, the shear modulus of quartz, and ρ_Q, the density of quartz. The detection of *E. coli* with the BAW–TAL method proposed in this work is mainly based on the change of viscosity and density. This method depends on the fact that the viscosity and density of the mixture increase after TAL is mixed with the heated *E. coli* solution, as the endotoxin in the cell wall of *E. coli* is released when *E. coli* is dead and the resonance frequency decreases correspondingly. The frequency change is related to the initial number of the bacteria.

3.2. Typical response curve

Fig. 2 shows the responses of the frequency shift to the concentration of *E. coli* samples. The resonance frequency shifts indicate the shift from the resonance frequency measured in the air. At first, the frequency decreases very slowly after an initial lag time according to the progress of gelation of TAL, then drops quickly and a sudden change (its mechanism is still under investiga-

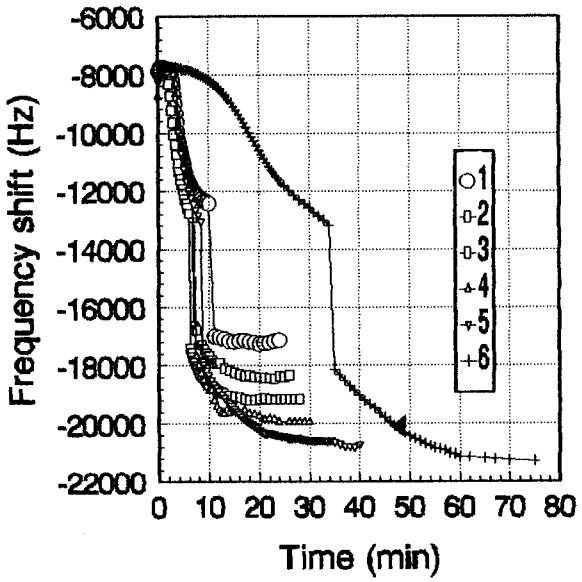

Fig. 2. Frequency curves of different concentrations of *E. coli*. (1) 2.9×10^8, (2) 2.9×10^7, (3) 2.9×10^6, (4) 2.9×10^5, (5) 2.9×10^4, (6) 0 cells/ml.

tion) follows, with finally a constant value after the completion of the gelation.

3.3. Effect of temperature

According to Young et al. [17], the gelation process of TAL with endotoxin involves several enzymatic reactions, which amplify the scale of the reaction at each stage (cascade reaction) and induce rheological change. So 37°C was chosen as the detection temperature.

3.4. Effect of liquid volume on detection

Aliquots of 0.1, 0.15, 0.2 ml of the mixture of TAL and heated *E. coli* solution were injected into the detection cell respectively. Frequency curves were obtained and results are shown in Fig. 3. It can be seen that the mixture volume affects the $\Delta F'$ significantly. The frequency shift is larger while the volume is lower. But when the volume is smaller than 0.1 ml, the surface of the quartz crystal cannot be covered completely. So, 0.1 ml of the mixture was used throughout the whole work.

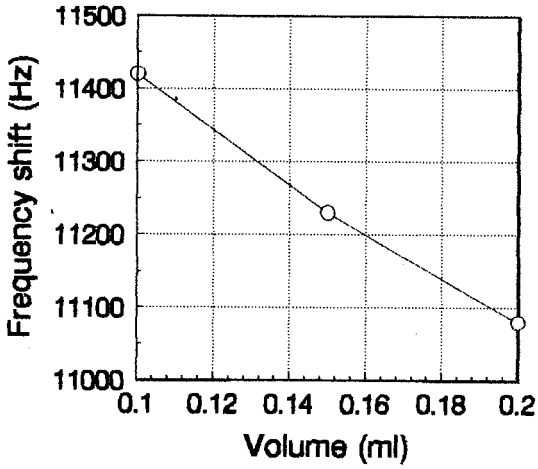

Fig. 3. Effect of liquid volume. (1) 0.1 ml, (2) 0.15 ml, (3) 0.2 ml. Concentration of *E. coli*: 2.7×10^6 cells/ml.

3.5. Detection of E. coli by BAW–TAL technique

In order to estimate the number of *E. coli* by this method, a calibration curve should be established (Fig. 4). The results showed that $\Delta F'$ (which is the difference between the initial frequency shift and the final constant frequency shift) was linearly related to the logarithm of the *E. coli* concentration in the range of 2.7×10^4–2.7×10^8 cells/ml. The regression equation is

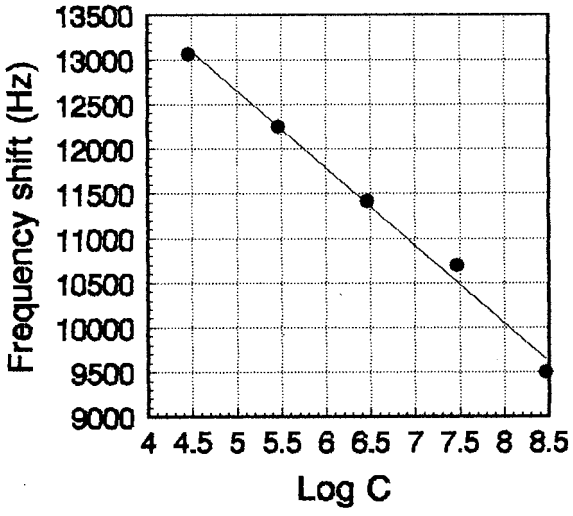

Fig. 4. Calibration curve for $\Delta F'$ and log *C*.

Table 1
Comparison of the *E. coli* concentration predicted by the BAW–TAL technique with that obtained from the PPC method

No.	Concentration predicted by BAW–TAL technique (cells/ml)[a]	Concentration obtained from PPC method (CFU/ml)
1	$(6.4 \pm 1.3) \times 10^4$	6.7×10^4
2	$(3.1 \pm 0.7) \times 10^5$	4.2×10^5
3	$(5.4 \pm 1.0) \times 10^5$	4.9×10^5
4	$(1.3 \pm 0.2) \times 10^6$	1.5×10^6
5	$(5.3 \pm 0.9) \times 10^7$	5.8×10^7
6	$(7.8 \pm 1.5) \times 10^7$	8.1×10^7
7	$(2.0 \pm 0.3) \times 10^8$	2.9×10^8

CFU, colony forming units.
[a] Calculated by Eq. (2).

$$\Delta F' = 16\,997.4 - 868.3 \text{ Log } C \pm 142.4 \quad (2)$$

where C is the concentration of *E. coli* (cells/ml), and $\Delta F'$ is the frequency shift (Hz). The correlation coefficient is 0.996 ($n = 5$). Hence, if the $\Delta F'$ is determined, the number of *E. coli* can be calculated according to Eq. (2). The concentration of the stock culture solution of *E. coli* was obtained by the standard pour plate counts technique. The solutions used in the determination were obtained by a serial dilution of the stock culture solution. Thus, the initial concentrations of the serial bacteria solutions were calculated according to the dilution.

3.6. Limit of detection

Although the linear range of *E. coli* detected is 2.7×10^4–2.7×10^8 cells/ml, the limit of detection can be lowered to 10 cells/ml by culturing the low-concentration *E. coli* solution to 2.7×10^4 cells/ml.

3.7. Comparison of the BAW–TAL technique with the standard pour plate counts method

The proposed method was compared with the conventional pour plate counts method for determining *E. coli*. The results are given in Table 1. It can be seen that all the pour plate counts values fall within the 95% confidence area of the concentration predicted by the BAW–TAL technique. Moreover, *F*-test showed that these two methods were not significantly different ($\alpha = 0.025$). So it can be concluded that the BAW–TAL method is in good agreement with the pour plate counts technique.

4. Conclusions

As described above, the BAW–TAL method proposed offers a new way for efficient estimation of *E. coli*. In comparison with other methods, this method is very simple to perform and good frequency curves are easily obtained. The detection time (< 90 min) is much shorter than that required with the previous methods. Finally, and most importantly, it can be concluded that the methodology in this work is very promising. Its application in other Gram-negative and some Gram-positive microbes is also feasible.

Acknowledgements

This work was supported by the National Natural Science Foundation of China.

References

[1] M.L. Speak, Compendium of Methods for the Microbiological Examination of Foods, American Public Health Association, Washington, DC, 1976.
[2] T. Nomura, M. Maruyama, Anal. Chim. Acta 147 (1983) 365.
[3] K.K. Kanaeawa, J.G. Gordon, Anal. Chim. Acta 175 (1985) 99.
[4] S.Z. Yao, T.A. Zhou, Anal. Chim. Acta 212 (1988) 61.

[5] H. Muramatsu, Y. Watanabe, M. Hikuma, T. Ataka, I. Kubo, E. Tamiya, I. Karube, Anal. Lett. 22 (1989) 2155.
[6] F.J. He, Q. Geng, W.H. Zhu, L.H. Nie, S.Z. Yao, M.F. Chang, Anal. Chim. Acta 289 (1994) 313.
[7] F.J. He, W.H. Zhu, Q. Geng, L.H. Nie, S.Z. Yao, Anal. Lett. 27 (4) (1994) 655.
[8] H. Muramatsu, E. Tamiya, M. Suzuki, I. Karube, Anal. Chim. Acta 215 (1988) 91.
[9] R. Homma, Y. Takada, I. Karube, K. Kimura, H. Muramatsu, Anal. Biochem. 204 (1992) 398.
[10] H. Muramatsu, E. Tamiya, M. Suzuki, I. Karube, Anal. Chim. Acta 217 (1989) 321.
[11] H. Muramatsu, K. Kimura, T. Ataka, R. Homma, Y. Miura, I. Karube, Biosensors & Bioelectronics 6 (1991) 353.
[12] J. Levin, F.B. Bang, Thromb. Diath. Haemorrh. 19 (1968) 186.
[13] J. Levin, F.B. Bang, Bull. Johns Hopkins Hosp. 11 (1964) 337.
[14] J.F. Cooper, H.D. Hochstein, E.B. Seligmann, Bull. Parenter. Drug Assoc. 26 (1972) 153.
[15] S.Z. Yao, Z.H. Mo, Anal. Chim. Acta 193 (1987) 97.
[16] K.K. Kanazawa, J.G. Gordon, Anal. Chim. Acta 175 (1985) 99.
[17] N.S. Young, J. Levin, R.A. Prendergast, J. Clin. Invest. 51 (1972) 1790.

ELSEVIER

Talanta 47 (1998) 291–299

Talanta

Separation and determination of thorium, uranium and mixed rare-earth elements as their UV/Vis absorbing complexes by capillary zone electrophoresis

Bi-feng Liu, Liang-bin Liu, Jie-ke Cheng *

Department of Chemistry, Wuhan University, Wuhan 430072, China

Received 12 November 1997; received in revised form 9 March 1998; accepted 16 March 1998

Abstract

Separation and determination of thorium, uranium and mixed rare-earth elements (RE) as their 2-(2-arsenophenylazo)-1,8-dihydroxyl-7-(4-chloro-2,6-dibromophenylazo)-naphthalene-3,6-disulfonic acid (DBC-As) complexes by capillary electrophoresis is presented in this paper. The pre-column derivitization conditions are discussed. Some separation parameters such as pH value, type of carrier electrolyte, applied voltage, the concentration of ligand in buffer and the sample size are also optimized. Under the selected conditions, the complete separation of thorium and uranium from mixed RE was accomplished in 10 min. Quantitative analyses exhibited an excellent linear dynamic relationship in the range of over two orders of magnitude. Detection limits of 4.81×10^{-8}, 7.23×10^{-8}, and 59.4×10^{-8} mol l^{-1} for RE, Th and U were obtained, respectively. This method was applied to the determination of these metal ions in ore samples. © 1998 Elsevier Science B.V. All rights reserved.

Keywords: Capillary zone electrophoresis; Direct UV/Vis detection; Metal ions

1. Introduction

Over the past decade, capillary electrophoresis (CE) has proved to be a very powerful technique for the separation and simultaneous determination of inorganic cations, due to its ultra-high performance and low reagent consumption. Although the first reported metal ions separation by CE can be dated as early as 1967 [1], two main difficulties were encountered in the initial development: (1) Sensitivity. Most metal ions are transparent in UV/Vis region; (2) Selectivity. It seems to be very difficult to resolve two ions that have similar or identical mobility relying only on the migration behaviour as their free forms. Some other sensitive detection methods have been designed to improve the sensitivity like laser-induced fluorescence (LIF) [2], and chemical luminescence (CL) [3], etc. However, UV/Vis detection is more popular and easy to manipulate. In general, a universal indirect UV detection mode introduced by Foret et al. [4] was employed. The enhancement of selectivity was achieved mainly by on-

* Corresponding author. Tel: + 86 27 7882712; fax: + 86 27 7882661.

0039-9140/98/$ - see front matter © 1998 Elsevier Science B.V. All rights reserved.
PII S0039-9140(98)00137-4

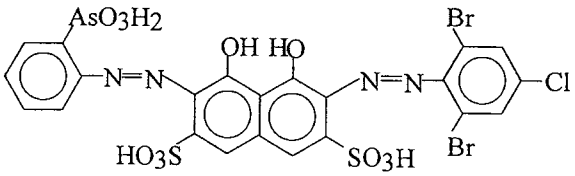

Fig. 1. Molecular structure of DBC-As.

column complex-forming equilibria, ion inclusion and solvent effect, etc. Jandik et al. [5] reported the separation of 24 metal ions using CE in 5 min, including alkali metals, alkali-earth metals, some transitions and lanthanoids. Recently, there has been increasing interest in the application of another approach—direct UV/Vis detection mode of metal ions after complexation with suitable UV/Vis absorbing ligands such as 8-hydroxyquinoline-5-sulphonic acid (HQS) [6], 4-(2-pyridylazo)resorcinolato (PAR) [7], EDTA [8,9], CDTA [10,11], ArsenazoIII [12], 2-(5-bromo-2-pyridyazo) - 5 - (*N* - propyl - *N* - sulfopropylamino)-phenol (5-Br-PAPS) [13], 5-NO_2-PAPS [14], 1,10-phenanthroline [15], as well as some inorganic ligands like cyanide [16,17] and chloride [18]. Micellar interaction, ion association, solvent effect, etc. can be conveniently applied to improving the resolution, as well as differences by the formation of complexes (e.g. differences in the mass, charge and volume of the complex). Compared with the indirect mode, the latter approach seems to be more preferable in view of its greater selectivity, sensitivity and the elimination of interference from complicated sample matrices, and has been applied successfully to some real samples in food [19], industrial [16], geological [17], environmental [10], nuclear technical and biological chemistry applications [8,15].

It is very important to screen a suitable chelating reagent for specific ions in CE with pre-column derivitization. The following three points should be considered carefully: (1) Chelating reagent can only form a single-state complex with an ion under controlled conditions; (2) The complex should remain stable during the electrophoresis in the capillary; (3) The maximum absorptive wavelengths of complexes investigated should be near to each other and be far away from that of the chelating reagent for the demand of the detection.

Although many papers have been published focusing on the separation and determination of

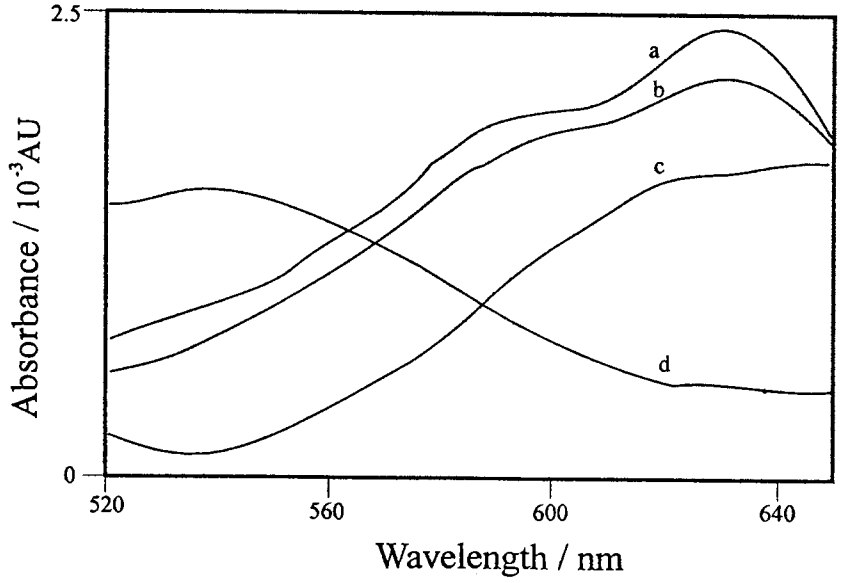

Fig. 2. Absorbance spectra: (a) complex of RE; (b) complex of Th; (c) complex of U; (d) DBC-As, pH 3.0.

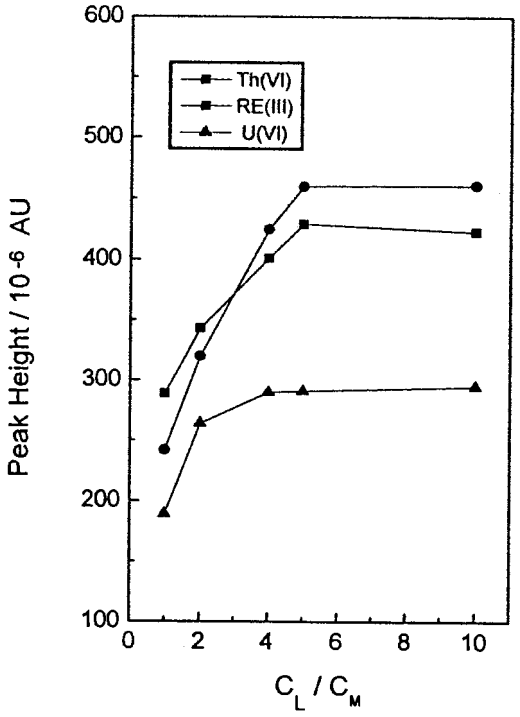

Fig. 3. The influence of concentration ratio of ligand to metal on detection sensitivity.

inorganic cations by CE, no attention has been paid to the simultaneous analysis of thorium, uranium and RE which always interfere with each other in the determination, and often coexist in nature. 2-(2-Arsenophenylazo)-1,8-dihydroxyl-7-(4 - chloro - 2,6 - dibromophenylazo) - naphthalene-3,6-disulfonic acid (DBC-As), synthesized by Yu and co-workers [20], is a very sensitive color reagent for rare-earth elements (RE), thorium and uranium, and relevant spectrophotometric characteristics were reported [21]. However, no reference for the application of this reagent in CE was found.

This paper first presents a novel method for the separation and determination of RE, thorium and uranium as their DBC-As complexes. The pre-column derivitization conditions, optimization of separation parameters and the effect of foreign ions on the quantification were investigated. The application of the method to the analysis of ore samples is also demonstrated.

2. Experimental

2.1. Apparatus and procedure

Analyses were performed on the Spectra-PHORESIS 1000 CE system (Thermal Separation Products, USA) equipped with an untreated fused silica capillary column of 75 μm i.d. (Yongnian Optical Fiber Factory, China). Equipment control and data process were manipulated on an IBM 386 computer using Spectraphoresis software with OS/2 as the operation system. Detection was carried out by on-column spectrophotometric measurement at 630 nm. Samples were introduced at the cathodic side by applying a vacuum for a specified period of time. Prior to use, the capillary was flushed with 1 mol l^{-1} NaOH, H_2O for 15 min at 60°C, respectively, then washed with buffer for 30 min at room temperature. After five injections, the rinse cycle was repeated to ensure reproducibility. Electroosmotic flow (EOF) was determined at 270 nm using acetone as neutral marker.

2.2. Chemicals

The stock solutions of RE and thorium were prepared from their 'Spec Pure' oxides (Matthey Spec Pure, Johnson Matthey, UK), and uranium was prepared from uranylnitrate hexahydrate. The stock solution of mixed RE was prepared by mixing a stock solution of La_2O_3, Ce_2O_3, Pr_2O_3, Nd_2O_3, Sm_2O_3 (20:50:5:20:5, the proportion of RE in a fluocerite ore, China). The chelating reagent DBC-As (as shown in Fig. 1) was synthesized by the Laboratory of Analytical Chemistry (Wuhan University, China). The solution of DBC-As was prepared by dissolving it directly in pure water. All other reagents were of analytical grade with doubly distilled water for preparation of all solutions. Three carrier electrolytes were investigated for optimization, including NaAc–HCl, NaAc–HAc and H_3PO_4–NaH_2PO_4. Carrier electrolyte was prepared daily, and filtered through a 0.45-μm membrane prior to use.

Table 1
The dependencies of the migration time on the pH value

Metal ion	Migration time (min)					
	pH 3.0	pH 3.5	pH 4.0	pH 4.5	pH 5.0	pH 6.0
Th[IV]	4.64	5.09	5.68	7.78	11.45	16.05
RE[III]	5.20	5.65	6.26	8.42	12.14	16.68
U[VI]	8.29	8.86	9.62	11.72	15.52	Not found

2.3. Sample preparation

Standard samples were prepared by mixing appropriate volumes of 1000 μg ml^{-1} RE, thorium and uranium stock solution, 0.1 mol l^{-1} NaAc–HCl electrolyte and 5×10^{-3} mol l^{-1} DBC-As solution at room temperature.

The preparation of ore samples was as follows. An accurately weighed flucite ore sample was immersed with sulfuric acid (1:1) after being torrefied at 850°C for 2 h, and then filtered. The filtrate was treated with 10% H_2O_2 solution. The remaining procedure was the same as the preparation of the standard samples.

3. Result and discussion

3.1. Pre-column derivitization condition

It was reported [21] that RE could chelate with DBC-As in a strongly acidic medium. We found that RE(III), Th(IV), U(VI) could also form sensitive color complexes with DBC-As in a weak acidic environment. The effect of pH on the chelating reaction investigated by the spectrophotometric method showed that the absorbance of complexes changed only slightly from pH 2.0 to pH 6.0. The absorbance spectra of complexes of RE, Th and U with DBC-As are shown in Fig. 2. From these, we could conclude that DBC-As was a suitable chelating reagent for RE, Th and U. There is a large bathochromic shift (about 100 nm) of the maximum absorption wavelength of free ligand owing to the formation of a metal complex. Thus, excessive ligand in buffer is possible and will have a very low background at the wavelength of maximum absorption of the complex, which is added to the buffer to prevent the complexes from dissociating. Furthermore, the maxima of the three complexes are quite close, which leads to the best detection sensitivities for all the three complexes. In this experiment, we chose 630 nm as the detection wavelength for balanced sensitivities.

In our research, the concentration ratio of chelating ligand to metal ion in the sample had a large effect on the formation of complexes, and accordingly on the sensitivities as shown in Fig. 3. With the increase of the ratio value (C_L/C_M), the peak height detected in the detection window of the capillary increased until it reached a constant state. This means that all the metal ions were chelated, and a single-state complex for each cation was formed. The phenomenon as shown in Fig. 3 was very similar to that found in the conventional spectrophotometry measurement, but no free ligand actually occurred in the sample zone at the moment when the complex reached the detection window. It might relate to the existence and concentration of free ligand in the running buffer, which will be discussed in Section 3.2.4. Haumann and Bächmann [22] reported an on-column derivitization method for cations with EDTA. Our further experiment was also performed without ligand in the sample. The cations were directly injected into the capillary, and reacted with the ligand in the buffer when electrophoresing. Although a schematic voltage polarity switch from positive to negative (utilized because the cations migrated in the opposite direction from the formed complexes in the capillary) was employed with varying switch time to accomplishing the on-column derivitization, no

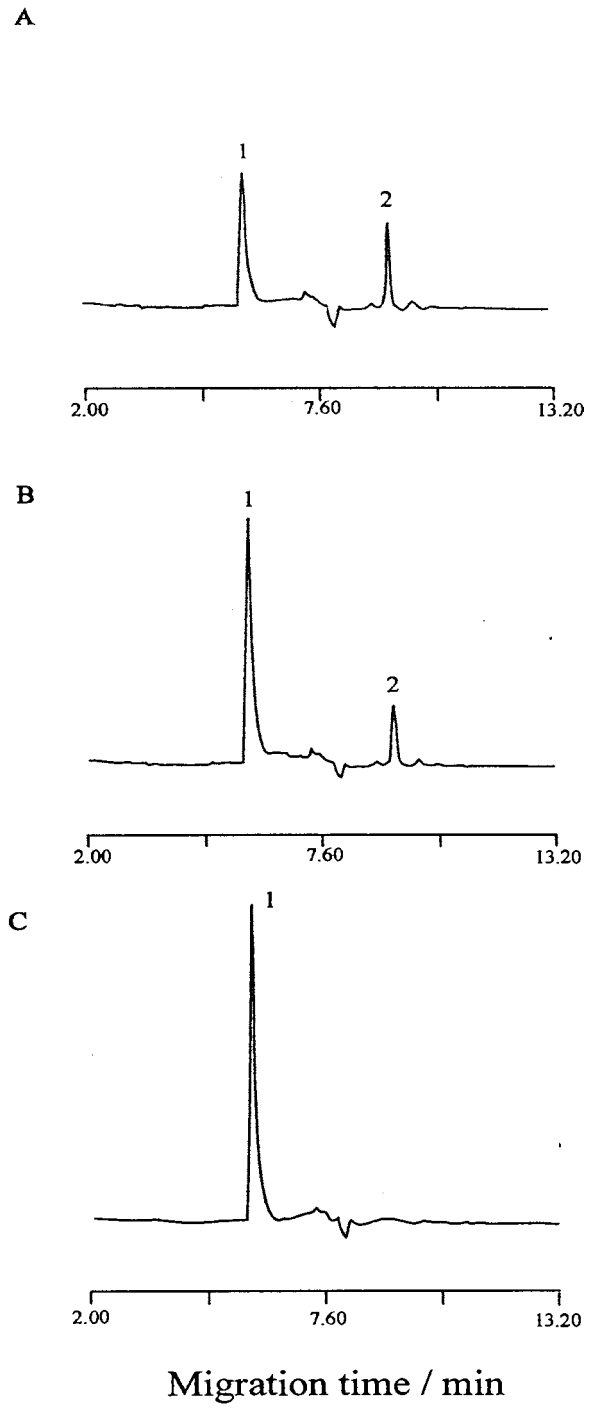

Fig. 4. The effect of concentration of ligand in buffer on separation. Conditions: 20×10^{-3} mol l^{-1} NaAc–HCl buffer, pH 3.0; 30°C; $\lambda = 630$ nm; -30 kV (-29.45 μA); introduction time: 5 s; capillary: 70 cm × 75 μm, effective length: 62.5 cm; the concentration of ligand in buffer: A: 0.05×10^{-3} mol l^{-1}; B: 0.1×10^{-3} mol l^{-1}; C: 0.2×10^{-3} mol l^{-1}; Peak identification: 1: RE(L_2); 2: RE(L).

peak was found. It was believed to be attributable to the reaction kinetics of the formation of the complex. Time was too short to form a complex. It indicated that an excess of DBC-As in sample solution was necessary for the complete chelation and stability of the complexes. A ratio of concentration of 5:1 was selected for further experiments.

3.2. Optimization of separation

3.2.1. pH value

The effect of pH value of the buffer on the migration was investigated. The range of pH was controlled within 3.0–6.0 to guarantee the stability of the complex. Because our work was carried out under the counter-electroosmotic mode [23], the migration time was determined by the following equation:

$$t_{obs} = LL_d/V(U_{ion} - U_{EOF})$$

where t_{obs}, L, L_d, V, U_{ion} and U_{EOF} are the migration time, the total length of the capillary, the effective separation length of the capillary, applied voltage, the migration mobility of complex and EOF, respectively. With increasing pH, the migration time of sample ions increased because of the enhancement of EOF. Table 1 gives the dependencies of the observed migration time on the pH value. When the pH value is over 5, the complex of uranium could not be detected because the mobility of EOF surpassed that of the complex. We chose pH 3.0 to shorten the analysis time.

3.2.2. Type of carried electrolyte

The type of electrolyte played an important role in this experiment. We studied the effects of three electrolytes on the separation, including NaAc–HCl, NaAc–HAc and phosphate. The results showed that NaAc–HCl was more preferable for the separation due to the more complete and more stable complexation, better detectibility, reproducibility and efficiency. It was related to the

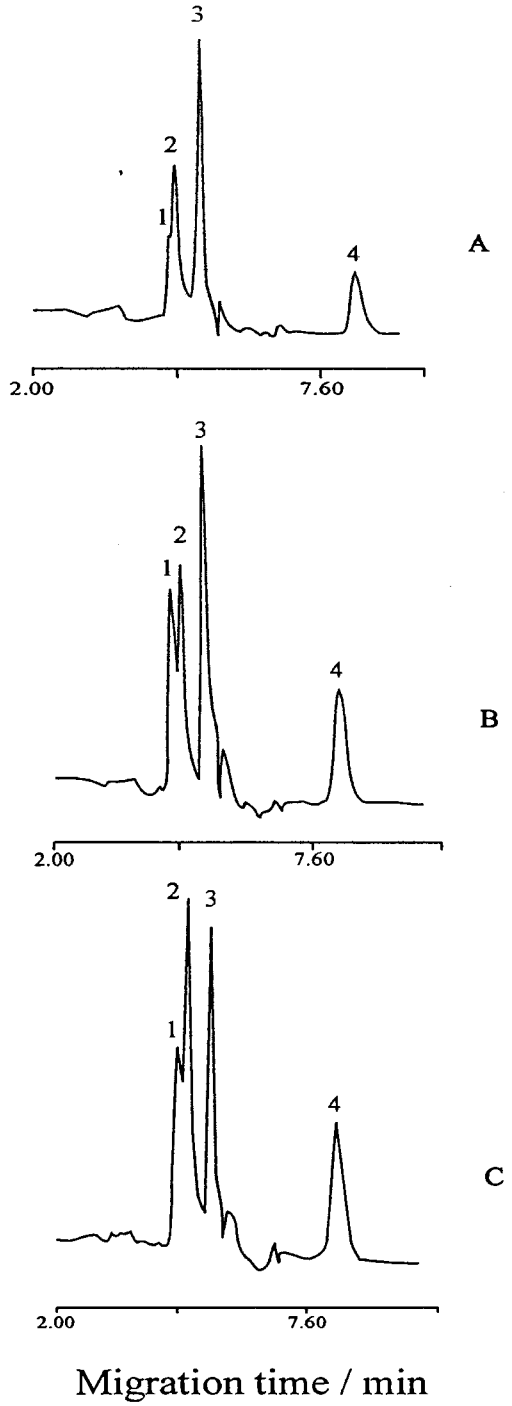

Fig. 5. The effect of sample size on separation. The concentration of ligand in buffer: 0.2×10^{-3} mol l^{-1}; introduction time: A: 10 s; B: 20 s; C: 30 s; other conditions are the same as Fig. 4. Peak identification: 1. DBC-As (system peak); 2. The complex of Th(IV); 3. The complex of RE(III); 4. The complex of U(VI).

formation of a mixed ligand complex. Ac^- acted as a second ligand to form a binary mixed ligand complex, which is more thermodynamically stable. Although the same phenomenon occurred to NaAc–HAc buffer which also contained Ac^-, the buffer caused non-reproducible results. Phosphate buffer led to larger peak broadening. It tended to bring about instability of the complex. We chose 20×10^{-3} mol l^{-1} NaAc–HCl as the running buffer.

3.2.3. Applied voltage

Increasing applied voltage could not improve the efficiency of separation owing to the Joul heating effect as the voltage was over -25 kV. Although a higher voltage could bring about a slight decrease of peak height as a result of peak broadening, we tended to neglect this effect. In this work, -30 kV was chosen mainly for rapid separation.

3.2.4. Ligand in buffer

Because a dynamic equilibrium is established among metal, complex and ligand, a complex can form multiple peaks or no peak during the electrophoresis, due to the dissociation of the complex in the capillary, even though a complete chelation was performed by pre-column derivatization. Therefore, unless single-state complex could be controlled, it would be impossible to carry out the qualitative and quantitative analyses. In general, free ligand was added to the buffer to avoid the dissociation of the complex and the formation of multiple peaks. Fig. 4 shows the tendency of the RE complex and the complex of Th had similar properties. If the concentration of DBC-As was lower than 0.1×10^{-3} mol l^{-1}, the complex of U could not be detected. A concentration of 0.2×10^{-3} mol l^{-1} seemed to be very convenient. Higher concentrations caused more background absorption and a less stable baseline.

3.2.5. Sample size

The sample size investigated in this paper was varied from 0.5 s to 30 s using the hydrostatic injection. Increasing the sample size could increase the sensitivity without the loss of resolution between the complexes. When the injection time

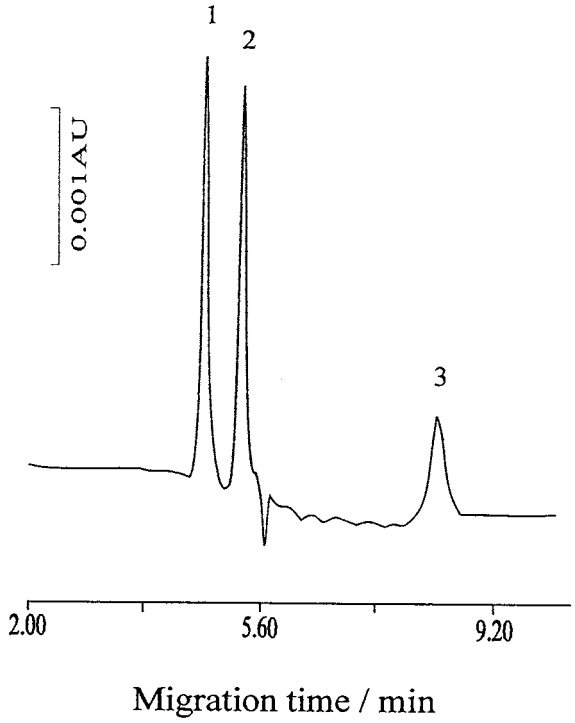

Fig. 6. Electropherogram under the optimized conditions. The concentration of ligand in the buffer: 0.2×10^{-3} mol l^{-1}; other conditions are the same as Fig. 4; Peak identification: 1. The complex of Th(IV): 1 μg ml^{-1}; 2. The complex of RE(III)): 0.4 μg ml^{-1}; 3. The complex of U(VI)): 1.5 μg ml^{-1}.

was lower than 1 s, the reproducibility of the peak height or area was poor. If the injection time was over 5 s, a system peak [12]—the peak of the chelating reagent occurred and gradually overlapped the peak of Th as shown in Fig. 5 because of the so-called electrostacking effect [23], which was popular and useful as a type of on-column pre-concentration method in CE. The complexes and the ligand are negatively charged. Their migration rates are greater and opposite in direction than that of EOF. So, the buffer in the sample plug was backed out into the running buffer container as the analytes stacked at the boundary of the running buffer. Thus, a very long sample plug was concentrated to be a narrow zone. In this experiment a time of 5 s was selected for further quantification.

Table 3
Detection limits

Metal ion	Detection limits (S/N = 2)			
	Concentration		Amount	
	(ng ml^{-1})	(10^{-8} mol l^{-1})	(fmol)	(fg)
Th[IV]	16.8	7.23	1.45	335.4
RE[III]	6.80	4.81	0.96	135.8
U[VI]	142	59.4	11.9	2829

Introduction time: 5 s; introduction volume: 20 nl.

Under the optimum conditions discussed above, Th(IV), U(VI) and RE(III) were completely separated successfully in 10 min (Fig. 6).

3.3. Quantification

Calibration curves were established from six concentration levels of sample that exhibited a linear dynamic range of over two orders of magnitude between the relative peak areas and sample concentrations (see Table 2 for details). The relative peak area was defined as the ratio of area to migration time:

$$S_{rel} = S_{int}/t_{obs}$$

where S_{rel}, S_{int}, and t_{obs} represent relative area, integration area and observed migration time, respectively. It could markedly decrease the influence of diffusion produced by Joul heating on the peak area. Table 3 gives the detection limits deter-

Table 2
Calibration data between the relative peak area and the concentration of the metal ion

Metal ion	Slope	Intercept	γ	Linear range (μg ml^{-1})
Th[IV]	7522	−497.5	0.9993	0.1–50
RE[III]	11 359	266.4	0.9992	0.1–50
U[VI]	800	35.6	0.9989	0.8–100

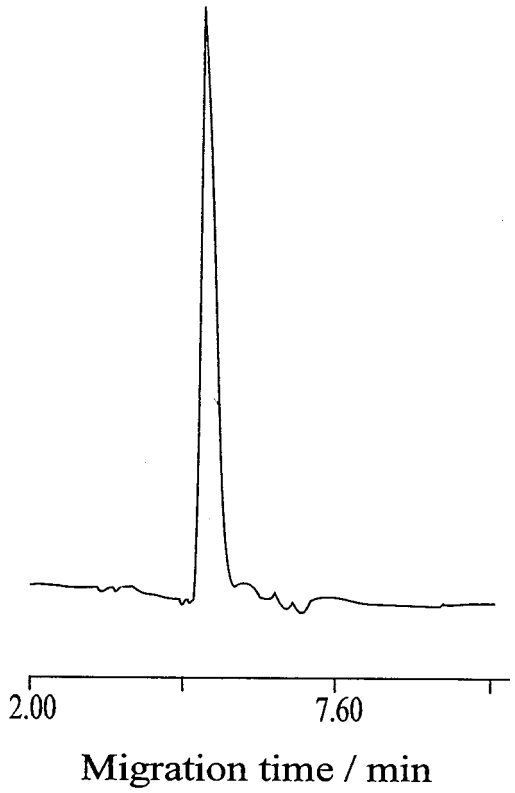

Fig. 7. Electropherogram of the ore sample.

mined under optimum conditions. Detection limits were calculated based on a peak height of twice the baseline noise.

3.4. Effect of foreign ions

DBC-As can chelate with many other ions in weak acidic media such as Be(II), Sr(II), Ba(II), Ti(II), Pd(II), Pb(II), Fe(III), Ga(III), Al(III) (after heating in a boiling water bath) and Zr(IV). They could consume the pre-column reagent, although no peak was found because of the instability of their complexes during electrophoresis except for Zr(IV), which formed a broadening peak, and interferes with the detection of RE and Th; 10 μg ml^{-1} Zr(IV) could affect the peak areas of 0.1 μg ml^{-1} RE and 0.1 μg ml^{-1} Th with errors of 6% and 10%, respectively.

3.5. Application

This method was applied to assaying the ore sample for RE in order to evaluate the quantitative performance. Fig. 7 shows the electropherogram. Although the high ionic strength in the real sample broadened the peak band as a result of electrodispersion effect, it seemed to have minor effect on the peak area according to the quantitative results at the expense of the loss of sensitivity. The assay results are listed in Table 4.

4. Conclusion

This paper demonstrates the separation and determination of RE, Th and U as their DBC-As

Table 4
Assay results for the ore sample

Metal ion	Certified value (μg ml^{-1})	Added (μg ml^{-1})	Found (μg ml^{-1})	Recovery (%)
RE(III)	7.49	0	7.42	99.1
		10.00	17.15	98.1
		20.00	27.56	100.3
		40.00	47.92	100.9
Th(IV)	0.028	0	Not found	
		10.00	10.14	101.1
		20.00	20.61	102.9
		40.00	39.44	98.5
U(VI)	0	0	0	
		10.00	10.43	104.3
		20.00	20.51	102.6
		40.00	39.80	99.5

complex. In this study, DBC-As proved to be a promising chelating reagent for the analysis of metal ions by capillary electrophoresis. It indicates that the combination of a high performance separation method with a highly sensitive color chelating reagent has a bright future for development in the analytical field of rapid, highly selective and highly sensitive separation of inorganic cations.

References

[1] S. Hjerten, Chromatogr. Rev. 9 (1967) 122.
[2] P.F. Swaile, M.J. Sepaniak, Anal. Chem. 63 (1991) 179.
[3] B. Hang, J. Li, L. Zhang, J. Cheng, Anal. Chem. 68 (1996) 2366.
[4] F. Foret, S. Fanali, A. Nardi, W.R. Jones, P. Bocek, Electrophoresis 11 (1990) 780.
[5] P. Jandik, W.R. Jones, A. Weston, P.R. Brown, LCGC 9 (1991) 634.
[6] A.R. Timerbaev, W. Buchberger, O.P. Semenova, G.K. Bonn, J. Chromatogr. A 630 (1993) 379.
[7] T. Saitoh, H. Hoshino, T. Yotsuyanagi, J. Chromatogr. A 469 (1989) 175.
[8] S. Motomizu, M. Oshima, S. Matsuda, Y. Obata, H. Tanaka, Anal. Sci. 8 (1992) 619.
[9] B. Baraj, M. Martinez, A. Sastre, M. Aguilar, J. Chromatogr. A 695 (1995) 103.
[10] A.R. Timerbaev, O.P. Semenova, G.K. Bonn, Analyst 119 (1994) 2797.
[11] A.R. Timerbaev, O.P. Semenova, S. Fritz, J. Chromatogr. A 756 (1996) 300.
[12] B.A. Colburn, M.J. Sepaniak, E.R. Hinten, J. Liq. Chromatogr. 18 (1995) 3699.
[13] S. Motomizu, M. Ohima, M. Kuwabara, Y. Obata, Analyst 119 (1994) 1787.
[14] S. Motomizu, N. Mori, M. Kuwabara, M. Ohima, Anal. Sci. 10 (1994) 101.
[15] J. Xu, P. Che, Y. Ma, J. Chromatogr. A 749 (1996) 237.
[16] W. Buchberger, O.P. Semenova, A.R. Timerbaev, J. High Resol. Chromatogr. 16 (1993) 153.
[17] M. Aguilar, A. Ferran, M. Martinez, J. Chromatogr. 635 (1993) 127.
[18] H.W. Zhang, L. Jia, Z.D. Hu, J. Chromatogr. A 704 (1995) 242.
[19] A. Theobald, L. Dunemann, J. High. Resol. Chromatogr. 19 (1996) 608.
[20] X.M. Yu, R.X. Cai, S.Z. Tian, Y.E. Zeng, Chem. J. Chinese Univ. (Eng. Ed.) 2 (1986) 2.
[21] H. Li, R.X. Cai, X.M. Yu, Y.E. Zeng, Fenxi Huaxue 13 (1985) 651.
[22] J. Haumann, K. Bächmann, J. Chromatogr. A 717 (1995) 385.
[23] P. Jandik, G.K. Bonn, Capillary Electrophoresis of Small Molecules and Ions, VCH, New York, 1993.

ELSEVIER

Talanta 47 (1998) 301–304

Talanta

Pulse injection analysis with chemiluminescence detection: determination of citric acid using tris-(2,2′-bipyridine) ruthenium(II)

He Zhike *, Gao Hua, Yuan Liangjie, Lu Shaofang, Meng Hui, Li Xiaoyan, Zeng Yun'e

Department of Chemistry, Wuhan University, Wuhan 430072, People's Republic of China

Received 1 December 1997; received in revised form 13 March 1998; accepted 16 March 1998

Abstract

A chemiluminescence method for the determination of citric acid was developed. The method is based on the enhancement of citric acid on the chemiluminescence light emission of tris-(2,2′-bipyridine)ruthenium(II). In the presence of tris-(2,2′-bipyridine)ruthenium(II), upon the addition of Ce(IV), resulted in intense light emission. The emission intensity is greatly enhanced by the presence of citric acid. The linear range and detection limit of citric acid are $3.0\times10^{-8}\sim6.0\times10^{-6}$ mol l^{-1} and 3.0×10^{-8} mol l^{-1}, respectively. The precision of the proposed method is determined by analyzing 11 samples containing 1.0×10^{-7} mol l^{-1} citric acid. The relative standard deviation is 3.0%. The enhanced mechanism of citric acid was studied. The method was evaluated by carrying out an interference study with common ions and compounds, by a recovery study and by analysis of human urine and orange juice. A satisfactory result was obtained. © 1998 Elsevier Science B.V. All rights reserved.

Keywords: Chemiluminescence; Citric acid; Tris-(2,2′-bipyridine) ruthenium(II)

1. Introduction

Citric acid is a very important compound in nature. The determination of citric acid has become an important subject in the fields of biochemistry and commercial foods. A large number of methods for the determination of citric acid have been reported [1–5]. Common methods for the determination of citric acid can be classified into three main groups: photospectrometric analysis, electroanalysis and chromatographic determinations, mainly high-performance liquid chromatography (HPLC). The main limitations of these methods have been the relatively low sensitivity.

The chemiluminescence method has been an attractive detection means for trace analysis due to its low detection limits and wide linear working ranges, with relatively simple instrumentation. $Ru(bipy)_3^{2+}$ electrogenerated chemiluminescence has received considerable attention in chemical

* Corresponding author. E-mail: hubwhuphys@hubei.shspt.chinamail.sprint.com

0039-9140/98/$ - see front matter © 1998 Elsevier Science B.V. All rights reserved.
PII S0039-9140(98)00138-6

analysis. In recent years, some analytical applications that use it as chemiluminescence reagent has also been developed. In alkaline medium, it can be applied to determine 6-mercaptopurine [6]. In sulphuric acid medium, chemiluminescence light emission is generated upon continuous oxidation of $Ru(bipy)_3^{2+}$ by Ce(IV). Some hydroxyl/carbonyl carboxylic acids and surfactants can enhance the light emission intensity [7–9].

This paper describes a new analytical method based on a reaction of $Ru(bpy)_3^{2+}$, Ce(IV) and organic acids, proposed and demonstrated by us this year. In the present work, automatic injection CL methodology has been developed and the reaction and experimental conditions optimized to allow the sensitive and selective determination of citric acid to low limits of detection. The linear range and detection limit are $3.0 \times 10^{-8} \sim 6.0 \times 10^{-6}$ and 3.0×10^{-8} mol l^{-1}, respectively. The precision of the proposed method is determined by analyzing 11 samples containing 1.0×10^{-7} mol l^{-1} citric acid. The relative standard deviation is 3.0%. The enhanced mechanism of citric acid was studied. The method was evaluated by carrying out an interference study with common ions and compounds, by a recovery study and by analysis of human urine and orange juice. A satisfactory result was obtained.

2. Experimental

2.1. Apparatus and reagents

LKB-1251 luminometry, dispenser SVD and dispenser controller DC (Pharmacia LKB Biotechnology AB, Sweden), with a Epson LX-800 printer (Seiko Epson, Japan) were used.

A 0.4 mmol l^{-1} stock solution of citric acid were prepared by dissolving 6.3 mg citric acid in 100 ml water. A 1.2 mg ml^{-1} stock solution of $Ru(bipy)_3Br_2$ (prepared in our laboratory [3]) was prepared by dissolving 1.2 g $Ru(bipy)_3Br_2$ in water and diluting with water to 1 l. All other reagents were analytical grade or better and all water used was doubly distilled in fused-silica apparatus.

2.2. Procedures

A 0.4 ml portion of mixed solution of 3.0×10^{-6} mol l^{-1} citric acid and 0.4 ml 7.3×10^{-6} g ml^{-1} $Ru(bipy)_3^{2+}$, were mixed in sample cuvettes, and then moved into the measuring chamber with a constant temperature of 298 K. After the start button pushed, a 0.2 ml of 0.6 mmol l^{-1} Ce(IV) (0.07 mol l^{-1} H_2SO_4) was injected into the reaction cuvettes automatically and the chemiluminescence light emission produced was measured immediately. The calibration graph of emission intensity versus concentration of citric acid was constructed. The peak time of citric acid was at 10 s (Fig. 1).

3. Results and discussion

3.1. Optimization of conditions

3.1.1. Effect of concentration of $Ru(bipy)_3^{2+}$

The study of this is carried out with the solution containing a variable amount of $Ru(bipy)_3^{2+}$, 1.2×10^{-6} mol l^{-1} citric acid, 0.12 mmol l^{-1} Ce(IV) (0.014 mol l^{-1} H_2SO_4) in order to get 9.7×10^{-7} to 2.4×10^{-5} g ml^{-1} concentration. The maximum signal-to-background ratio is obtained at a 2.9×10^{-6} g ml^{-1} concentration (Table

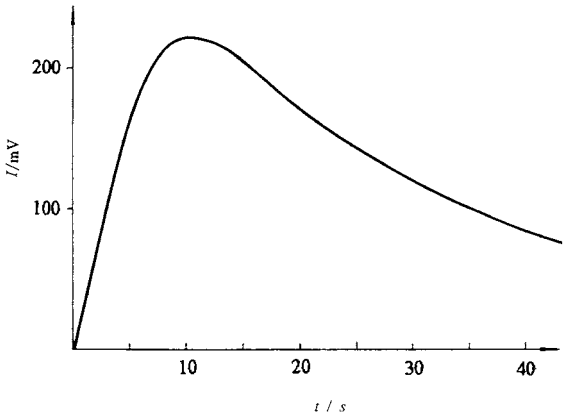

Fig. 1. CL intensity versus time profile obtained in the determination of 1.2×10^{-6} mol l^{-1} citric acid. Conditions: 2.9 μg ml^{-1} $Ru(bipy)_3^{2+}$, 1.2×10^{-4} mol l^{-1} Ce(IV) and 0.014 mol l^{-1} H_2SO_4.

Table 1
Effect of the concentration of $Ru(bipy)_3^{2+}$ on CL intensity

Concentration of $Ru(bipy)_3^{2+}$ (g ml^{-1})	Blank signal (mV)	CL intensity in the presence of citric acid[a] (mV)	Signal-to-background
9.7×10^{-7}	34	79	2.3
1.9×10^{-6}	37	132	3.6
2.9×10^{-6}	41	219	5.3
4.9×10^{-6}	79	313	4.0
1.9×10^{-5}	250	762	3.0
2.4×10^{-5}	352	1004	2.8

[a] 1.2×10^{-6} mol l^{-1} citric acid, 0.12 mmol l^{-1} Ce(IV) in 0.014 mol l^{-1} H_2SO_4.

1). It is shown that the intensity increase with increasing $Ru(bipy)_3^{2+}$ both in the presence of citric acid and in the absence of it. Which implies that the luminophor is $Ru(bipy)_3^{2+}$.

3.1.2. Effect of the concentration of H_2SO_4

The CL emission depends on the concentration of H_2SO_4. The study of this influence is carried out in the range of 0.01–0.018 mol l^{-1} concentration of H_2SO_4 under the standard conditions shown above. The maximum intensity is obtained at a 0.014 mol l^{-1} H_2SO_4 concentration. In the solution of strong acid, the plot of I vs. $1/[H_2SO_4]^2$ is a straight line which indicate that the rate of reaction is inversely proportional to the square of the concentration of sulphuric acid. This is consistent with the conclusion of reference [5].

3.1.3. Effect of the concentration of Ce(IV)

The CL light intensity also depends on the concentration of Ce(IV). The study of this is carried out in the range of 4.0×10^{-5}–3.6×10^{-4} mol l^{-1} concentration of Ce(IV) under the standard conditions shown above. The maximum intensity is obtained at a 1.2×10^{-4} mol l^{-1} Ce(IV) concentration.

3.2. Comparison with other methods

Common methods for the determination of citric acid can be classified into three main groups: gravimetric and volumetric methods, enzymic analyses and chromatographic determinations, mainly high-performance liquid chromatography (HPLC). The main limitations of these methods have been the relatively low sensitivity. Under the optimum conditions, the proposed method allows the determination of citric acid with a $2\sim3$ orders of magnitude higher sensitivity than other reported methods based on various analytical techniques (Table 2).

4. Calibration and detection

Under the optimum conditions, the linear range is $3.0\times10^{-8}\sim6.0\times10^{-6}$ mol l^{-1} for citric acid with a regression equation, $I=13.8+1.37\times10^{8}C$, $r=0.9993$, $n=11$. The detection limit is 3.0×10^{-8} mol l^{-1}, which is calculated as the minimum concentration of citric acid resulting in statistically I value according to (Eq. (1))

Table 2
Comparison of the dynamic linear range for citric acid afforded by the proposed CL method and other reported methods

Methods	Dynamic linear range mol l^{-1}	Reference
Ions chromatography	$8.0\times10^{-6}\sim8.0\times10^{-5}$	[1]
Ions chromatography	$4.7\times10^{-6}\sim4.7\times10^{-5}$	[2]
Kinetic analysis	$2.3\times10^{-6}\sim1.1\times10^{-5}$	[5]
Polarography	6.6×10^{-7} (DL)	[4]
Spectrophotometry	$2.5\times10^{-6}\sim1.25\times10^{-5}$	[3]
Proposed CL method	$3.0\times10^{-8}\sim6.0\times10^{-6}$	

$$C_{DL} = I_{DL}/m \quad (1)$$

where I_{DL} is the minimum value statistically obtained with three times the standard deviation of the measured parameter in the absence of citric acid, and m is the slope of the calibration graph (analytical sensitivity). The precision of the proposed method is determined by analyzing 11 samples containing 1.0×10^{-7} mol l^{-1} citric acid. The relative standard deviation is 3.0%.

5. Effect of other species

The experimental results showed that a 1000-fold K^+, Na^+, Al^{3+}, Zn^{2+}, Cl^-, SO_4^{2-}, NO_3^-, Ni^{2+}, Co^{2+}, Sr^{2+}, Ba^{2+}, Ca^{2+}, F^-, Ac^-, alcohol, 500-fold SiO_3^{2-}, Mg^{2+}, glucose, 100-fold Bi^{3+}, Pb^{2+}, Cu^{2+}, 50-fold Cr^{3+}, 30-fold Mn^{2+}, 10-fold Br^- and one-fold lactic have no effect on the determination of 1.2×10^{-6} mol l^{-1} citric acid.

5.1. Determination of citric acid in human urine and orange juice

The developed methods were applied to the determination of citric acid added to human urine and orange juice. It was found that the blank human urine and orange juice provide a high signal ($\equiv 2.5 \times 10^{-3}$ mol l^{-1} and 15 g l^{-1} citric acid, respectively), so it was necessary to subtract this signal from the total signal. In this way recoveries of 106.7 ($n = 5$) and 93.7% ($n = 5$; Table 3) were obtained for citric acid. It is likely that the effect of interferents present in human urine and orange juice can be circumvented by using liquid chromatography with chemiluminescence detection, as was used for pyruvic acid [10]. The method for the separation and determination of citric acid in human urine and orange juice were investigated by single-column ion exchange chromatography. A 1.0 ml portion of human urine or orange juice was diluted with water to 10 ml. A solution of 0.2 mol l^{-1} Na_2SO_4 was used as the eluant, and the eluate was monitored by chemiluminescence.

Table 3
Recovery of citric acid (CA) in human urine and orange juice

Samples	CA added (μg)	Recovered (μg)	Recovery (%)
Urine A	0.126	0.124	98.4
	0.252	0.250	99.2
Urine B	0.126	0.118	93.7
	0.252	0.269	106.7
Juice A	0.884	0.882	99.8
	1.768	1.66	93.8
Juice B	0.884	0.922	104.3
	1.768	1.71	96.6

Acknowledgements

The authors gratefully acknowledge the support for this research by the Nature Science Foundations from the State and Hubei province of the People's Republic of China.

References

[1] R.P. Singh, S.A. Smesko, G.H. Nancollas, J. Chromatogr. Biomed. Appl. 87 (1989) 239.
[2] Z. Yan, Y. Gengsheng, Huaxue Shijie 31 (4) (1990) 75.
[3] B.D. Lewis, Clin. Chem. 36 (3) (1990) 578.
[4] K. Hasebe, S. Hikama, H. Yoshida, Fresenius J. Anal. Chem. 336 (3) (1990) 232.
[5] F. Grases, A. Costa-Bauza, J.G. March, Analyst 116 (1) (1991) 59.
[6] H. Zhike, L. Xinglian, L. Qingyao, Y. Ximao, Z. Yun'e, Anal. Sci. 11 (3) (1995) 415.
[7] H. Zhike, M. Rongming, L. Qingyao, Y. Ximao, Z. Yun'e, Acta Chimica Sinica 54 (10) (1996) 1003.
[8] G. Hua, H. Zhike, L. Qingyao, Z. Yun'e, Fenxi Huaxue 24 (11) (1996) 1363.
[9] H. Zhike, Y. Liangjie, M. Rongming, L. Qingyao, Y. Ximao, Z. Yun'e, J. Wuhan Univ. (Nat. Sci. Ed.) 43 (2) (1997) 191.
[10] L. Liansheng, H. Zhike, C. Ruxiu, Chem. J. Chin. Univ. 18 (12) (1997) 1963.

ELSEVIER

Talanta 47 (1998) 305–310

Talanta

Anion selective polymeric membrane electrodes based on cyclopalladated amine complexes

Concepción Sánchez-Pedreño *, Joaquín A. Ortuño, Domingo Martínez

Department of Analytical Chemistry, Faculty of Chemistry, University of Murcia, 30071 Murcia, Spain

Received 23 July 1997; received in revised form 3 March 1998; accepted 18 March 1998

Abstract

The potentiometric anion selectivity of two polymer membrane based electrodes (I and II) formulated with two new cyclopalladated amine complexes as the active components are examined. The electrodes exhibit a non-Hofmeister selectivity pattern with a significantly enhanced response towards thiocyanate, iodide and nitrite. The graph potential versus log c is linear over the concentration range 10^{-6}–6×10^{-2} M thiocyanate with electrode I and 10^{-6}–10^{-3} M with electrode II; 10^{-5}–10^{-2} M iodide with electrode I and 10^{-3}–6×10^{-2} M with electrode II; and 10^{-3}–6×10^{-2} M nitrite with both electrodes. The influence of the plasticizer and pH are studied. The potentiometric selectivity coefficients for I, II and blank membrane electrodes are reported. The selective interaction between Pd(II) thiocyanate, iodide and nitrite is postulated to be the reason for its higher response. © 1998 Elsevier Science B.V. All rights reserved.

Keywords: Ion-selective electrodes; Cyclopalladated amine complexes; Non-Hofmeister selectivity

1. Introduction

Anion-selective membrane electrodes using conventional anion exchangers, such as quaternary ammonium salts, respond to anions following the Hofmeister selectivity sequence: decreasing response for decreasing lipophilicity (i.e. $ClO_4^- > SCN^- > I^- > NO_3^- > Br^- > NO_2^- > Cl^-$) [1].

Several ionophores have been found that alter this order: Co(III) cobyrinates [2–5]; Mn(III) [1,6–8], Sn(IV) [9,10], In(III) [11], Ru(II) [5] and Co(III) porphyrins [5,6,12,13]; a hydrophobic vitamin B_{12} derivative [14]; Co(II) electropolymerized porphyrin [15]; Sn(IV) [16–19] Hg(II) [20] and Pd(II) [21] organocompounds and metallocenes [22]. The selectivity of these electrodes is not governed by simple anion lipophilicity but by specific chemical interactions between the organometallic compounds and the anions.

The first optically active cyclopalladated primary amines were easily prepared [23]. In this paper we report the use of two of these cationic cyclopalladated amine complexes of Pd(II), I and II (Fig. 1) to prepare anion selective membrane electrodes. These compounds induce an anti-Hofmeister selectivity pattern with a significantly enhanced response toward iodide, thiocyanate

* Corresponding author. Tel.: +34 68 307100 ext. 2170; fax: +34 68 364148.

0039-9140/98/$ - see front matter © 1998 Elsevier Science B.V. All rights reserved.
PII S0039-9140(98)00132-5

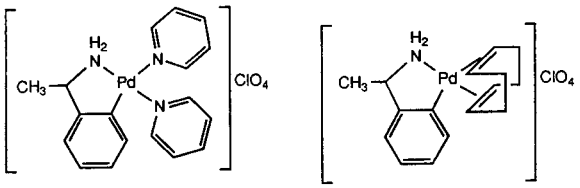

Fig. 1. Structures of cyclopalladated amine complexes, ionophores I and II.

and nitrite. This suggests a selective interaction of the Pd(II) complexes with these anions.

2. Experimental

2.1. Apparatus

Potentials were measured with an Orion (Boston, MA) Expandable Ion Analyzer EA940. The recorder output of the analyzer was connected to a personal computer via a DGH Corporation analogue-to-digital converter (Manchester, UK) 1121 module. An Orion 90-02 double junction silver–silver chloride reference electrode was used.

2.2. Reagents and solutions

The cyclopalladated amine complexes [2-(α-methylbenzylamine) bis(pyridine) palladium(II)] perchlorate and [2-(α-methylbenzylamine) (1,5-cyclooctadiene) palladium(II)] perchlorate, I and II, respectively, were synthesized according to the method of Vicente et al. [23]. Poly(vinyl chloride) (PVC) high molecular mass, 2-nitrophenyl octyl ether (2-NPOE) and tetrahydrofuran (THF) were Selectophore products from Fluka (Buchs., Switzerland). Dibutyl phthalate (DBP) was purchased from Merck. All other reagents used were of analytical reagent grade (Merck) and doubly distilled water was used throughout. Iodide, thiocyanate, nitrite, perchlorate, bromide, chloride, nitrate and sulphate solutions were prepared from sodium or potassium salts.

2.3. Construction and calibrations of the electrodes

Membrane composition was typically 1.3% (w/w) ionophore (as perchlorate salt), 32.9% (w/w) PVC and 65.8% (w/w) plasticizer (NPOE or DBP). The membranes were prepared by dissolving 4 mg ionophore, 100 mg PVC and 200 mg plasticizer in 2 ml of tetrahydrofuran. This solution was poured into a flat bottomed flask (3 cm diameter and 10 cm height) which was covered with filter papers on which a weight was placed for about 48 h to allow the evaporation of the solvent. An 8-mm diameter piece was cut out with

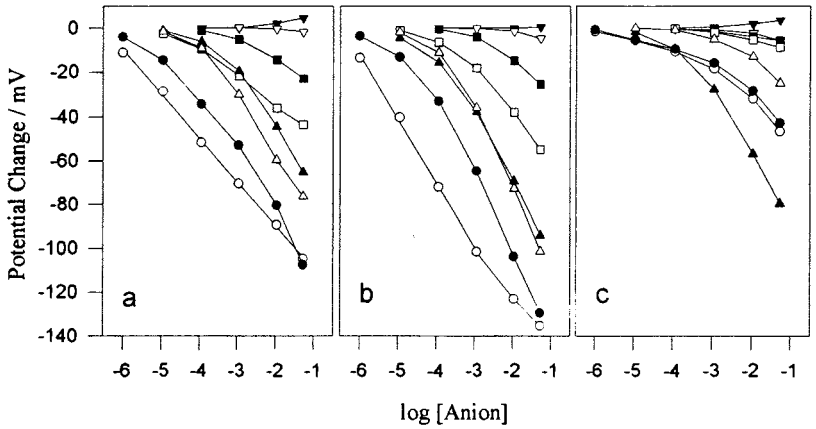

Fig. 2. Calibration graphs for the following anions at pH 4.3: (○) thiocyanate, (●) iodide, (△) nitrite, (▲) perchlorate, (□) bromide, (■) chloride, (▽) nitrate, (▼) sulphate. Membrane prepared with: ionophore I (a); ionophore II (b); and blank membrane (c).

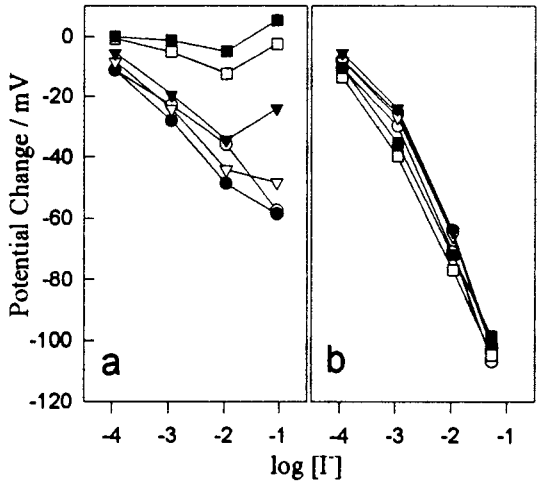

Fig. 3. Calibration graphs for iodide at different values of pH: (○) 1.57, (●) 2.91, (▽) 5.06, (▼) 7.00, (□) 9.21, (■) 11.40. (a) membrane containing ionophore I; and (b) membrane containing ionophore II.

a cork borer and incorporated into a Philips IS-561 electrode body containing 3.8 M KCl saturated with excess AgCl as internal filling solution.

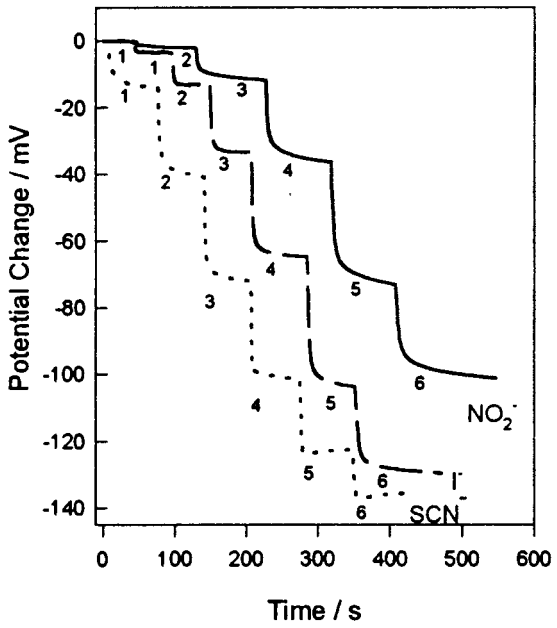

Fig. 4. Dynamic response of electrode prepared with ionophore II towards: (1) 1×10^{-6}; (2) 1×10^{-5}; (3) 1×10^{-4}; (4) 1×10^{-3}; (5) 1×10^{-2}; (6) 6×10^{-2} M.

The electrodes were conditioned by soaking with constant stirring in 50 ml of 0.01 M perchlorate solution with the selected buffer composition until the electrodes gave a constant potential. The calibration of the electrodes was carried out by adding, while stirring, aliquots of known concentrations of the different anion standard solutions to 50 ml of buffer. The buffers used were 0.1 M acetate-acetic acid and 0.1 M Britton-Robinson of various pH. The electrodes were conditioned as described above before calibration with the different anions. The electrodes were stored dry and conditioned before use.

3. Results and discussion

Palladium(II) is commonly thought of as a class-b acceptor or alternatively as a 'soft' acid. This type of acceptor is little electropositive, has relatively full d orbitals, and forms the most stable complexes with ligands which, in addition to possessing lone-pairs of electrons, have empty p orbitals available to accommodate some charge

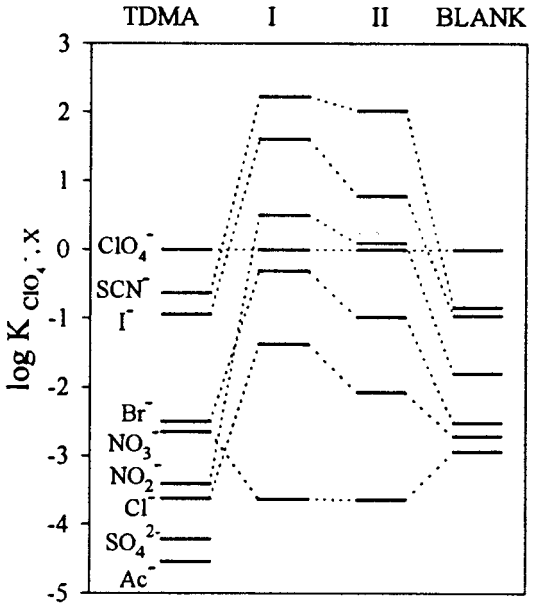

Fig. 5. Potentiometric selectivity coefficients of polymer membrane doped with tridodecylmethylammonium chloride (TDMA), ionophore I (I) and ionophore II (II); and of a blank membrane (BLANK).

from d orbitals of the metal. For instance the stability of the Pd(II) complexes with halide ions increases with the increasing accessibility of empty d orbitals in the heavy halide ions $Cl^- < Br^- < I^-$ [24]. Thiocyanate and nitrite also form stable complexes with Pd(II) in aqueous solution.

The most of Pd(II) complexes are square planar; however, Pd(II) can also exist in the five-coordination. For example, Pd(II) undergoes substitution by an associative path via five-coordinate transition state or intermediate. The tendency for square-planar complexes of Pd(II) to become five-coordinate depends on ligand size, this process being facilitated by smaller ligands and probably also by electronic factors. There is some evidence that softer ligands form five-coordinate complexes more readily than harder ligands [25].

The selective interaction between Pd(II) and some ligands and the tendency of some four-coordinate Pd(II) complexes to become five-coordinate suggest that they can be used as selective carriers for some preferred anions in the development of ion-selective electrodes. Only one paper dealing with the use of Pd(II) complexes as selective carriers in ISEs has been found [21], in which 'neutral' palladium organophosphine complexes are used.

In the present paper 'positively charged' Pd(II) organocomplexes in the form of perchlorate salts are introduced as selective 'charged carriers' in the development of anion selective electrodes.

3.1. Response characteristics of membranes doped with Pd(II) complexes

The theoretical potential response functions of ion-exchange membrane electrodes initially prepared in, or converted to, the form containing an ion '*i*' towards foreign ions '*j*' have been studied by several authors [26–28]. The corresponding models proposed predict a region of enhanced potential response at low concentrations of foreign ions when a discriminated ion is initially present in the membrane ($K_{ij}^{pot} \gg 1$). This is in excellent agreement with experimental findings. The non-equilibrium steady-state potential which is produced has been successfully exploited by Meyerhoff et al. [28] to develop polyion-sensitive membrane electrodes (e.g. an electrode containing chloride as discriminated anion in the membrane for the determination of the polyanionic heparin. In an analogous way a new conditioning procedure for neutral carrier-based cation-selective electrodes, which involves conditioning the electrode membrane in discriminated ion solutions before measurement, has been described [29].

In accordance with all these theoretical and experimental considerations, we have experimentally found that when electrodes containing Pd(II) complexes I and II are conditioned in perchlorate solution (as discriminated ion) the potential response towards thiocyanate, iodide and nitrite is greater than when they are conditioned in the corresponding anions, and permits the determination of lower concentrations of these anions.

The calibration graphs obtained following the procedure described in the Experimental, of two membranes containing the Pd(II) complexes, I or II, in a PVC/NPOE matrix (membranes I and II) for different anions in a 0.1-M acetic-acetate buffer of pH 4.3, are shown in Fig. 2(a and b), respectively. As can be seen the anion-selectivity pattern obtained for both membranes was: $SCN^- > I^- > NO_2^- > ClO_4^- > Br^- > Cl^- > NO_3^- > SO_4^{2-}$ which differs from the Hofmeister series, and represents a significantly enhanced response towards thiocyanate, iodide and nitrite.

Linear response was observed in a wide concentration range for thiocyanate with both membranes, 10^{-6}–6×10^{-2} M (slope -19.9 mV/dec) for membrane I, and 10^{-6}–10^{-3} M (-29.1 mV/dec) for membrane II. The linear range for iodide was 10^{-5}–10^{-2} M (-21.6 mV/dec) with membrane I, and 10^{-4}–6×10^{-2} M (-36.3 mV/dec) with membrane II. The linear range for nitrite was 10^{-3}–6×10^{-2} M with both membranes (-27.6 and -38.9 mV/dec, respectively).

The response obtained was higher for membrane II than I, which emphasizes the role played by the ligands of Pd(II) in controling the behaviour of Pd(II) complexes as anion carriers.

For comparison purposes the calibration graphs of a blank membrane (containing only PVC and NPOE were also studied (Fig. 2(c)). The blank membrane presented a low response and its maximum response was obtained for perchlorate.

The influence of membrane plasticizer of PVC membranes doped with the Pd(II) complexes on the potentiometric response was studied by comparing the above obtained results for NPOE (dielectric constant 23.9) with the potentiometric response of membranes containing dibutyl phthalate, a much less polar plasticizer (dielectric constant 6.44). The anion-selectivity pattern obtained was the same as that obtained for NPOE, but the potentiometric response was much lower. No simple rule can explain the observed influence of the plasticizer on the potentiometric response of membranes containing ionophores that form complexes with the anions. It is likely that changes in both anion partition coefficients and anion-ionophore complexation constants can occur with plasticizer of different dielectric constants, and both effects contribute to the potentiometric response [30]. NPOE was therefore selected as the plasticizer and used in further studies.

3.2. Influence of pH

The influence of pH on the potentiometric response to iodide of membranes I or II was studied using Britton-Robinson buffers of different pH values between 1.57 and 11.40. At each pH, a calibration graph for iodide was obtained. The results are shown in Fig. 3(a and b). As can be seen the response of membrane I was lower than that obtained with the acetic-acetate buffer of similar pH (Fig. 2(a)). At $pH > 9.2$ the response became almost null. The pH had little effect on the response of membrane II over the whole pH range studied. This could be explained by the OH^- entering as a fourth ligand at high pH values to replace the pyridine ligand. This type of reaction is more difficult in Pd(II)-complex II due to the chelate effect of the cyclooctadiene ligand. Taking all this into account, an acetate-acetic medium of pH 4.3 was selected.

3.3. Dynamic response

The typical dynamic response to thiocyanate, iodide and nitrite in acetic-acetate buffer pH 4.3 of an electrode with membrane II is shown in Fig. 4. As can be seen the electrode reaches the equilibrium response in a relatively short time. A similar dynamic response was obtained with the electrode containing membrane I. Potential drifts were obtained from the corresponding derivative dynamic responses, as described in [31]. The drifts obtained varied between 0.1 and 1.5 mV min^{-1}.

3.4. Selectivity

Selectivity coefficients for the different anions with respect to perchlorate were calculated for electrodes containing membranes I, II and blank membrane using the activity ratio method [18], in which the selectivity coefficient is measured as the ratio for ion activities, or concentrations, that generate the same membrane potential when measured in a separate solution type experiment. The calibrations described above (Fig. 1(a–c)) were used to calculate the concentration of perchlorate that corresponds to the potential change observed for a concentration of 10^{-2} M of the interfering ion (10^{-4} M for thiocyanate and iodide in the case of membranes I and II). The selectivity coefficients were then calculated as the ratio of these concentrations, i.e. $K_{ClO_4^-,X^-} = C_{ClO_4^-}/C_{X^-}$.

The resulting selectivity coefficients are shown in Fig. 5. For comparison purposes the selectivity coefficients of a classical anion exchanger-based membrane electrodes are also provided (1.0% (w/w) triclodecylmethylammonium chloride (TDMA)). As can be seen, the anion selectivity with respect to perchlorate of membranes containing the cyclopalladated amine complexes increases for thiocyanate, iodide, nitrite, bromide and chloride with respect to the classical anion exchanger. This deviation suggests that these anions interact preferentially with the Pd(II) complexes within the membrane phase, which is in agreement with the soft type of acceptor and donor described above.

4. Conclusions

The incorporation of cationic cyclopalladated amine complexes of palladium(II) in plasticized PVC membranes shows a marked anti-Hofmeister potentiometric selectivity. Resulting membrane electrodes exhibit an enhanced and potentially

useful analytical response to thiocyanate, iodide and nitrite. The potentiometric response is believed to be due to selective interaction between Pd(II) and these anions.

Acknowledgements

We would like to thank Professor Vicente of the Department of Inorganic Chemistry at the University of Murcia for supplying the cyclopalladated amine complexes. We gratefully acknowledge the Dirección General de Investigación Científica y Técnica, Spain (Project PB93-1139) for supporting this work.

References

[1] D. Ammann, M. Huser, B. Kräutler, B. Rusterholz, P. Schulthess, B. Lindemann, E. Halder, W. Simon, Helv. Chim. Acta 69 (1986) 849.
[2] P. Schulthess, D. Ammann, W. Simon, C. Caderas, R. Stepánek, B. Kräutler, Helv. Chim. Acta 67 (1984) 1026.
[3] P. Schulthess, D. Ammann, B. Kräutler, C. Caderas, R. Stepánek, W. Simon, Anal. Chem. 57 (1985) 1397.
[4] R. Stepánek, B. Kräutler, P. Schulthess, B. Lindemann, D. Amman, W. Simon, Anal. Chim. Acta 182 (1986) 83.
[5] M. Huser, W.E. Morf, K. Fluri, K. Seiler, P. Schulthess, W. Simon, Helv. Chim. Acta 73 (1990) 1481.
[6] N.A. Chaniotakis, A.M. Chasser, M.E. Meyerhoff, J.T. Groves, Anal. Chem. 60 (1988) 185.
[7] A. Jyo, H. Egawa, Anal. Sci. 8 (1992) 823.
[8] D. Gao, J. Gu, R. Yu, G. Zheng, Anal. Chim. Acta 302 (1995) 263.
[9] N.A. Chaniotakis, S.B. Park, M.E. Meyerhoff, Anal. Chem. 61 (1989) 566.
[10] C.E. Kibbey, S.B. Park, G. Deadwyler, M.E. Meyerhoff, J. Electroanal. Chem. 335 (1992) 135.
[11] S.B. Park, W. Matuszewski, M.E. Meyerhoff, Y.H. Liu, K.M. Kadish, Electroanalysis 3 (1991) 909.
[12] A. Hodinár, A. Jyo, Chem. Lett. (1988) 993.
[13] X. Li, D.J. Harrison, Anal. Chem. 63 (1991) 2168.
[14] S. Daunert, L.G. Bachas, Anal. Chem. 61 (1989) 499.
[15] S. Daunert, S. Wallace, A. Florido, L.G. Bachas, Anal. Chem. 63 (1991) 1676.
[16] V.M. Shkinev, B.Y. Spinakov, G.A. Varobeva, Y.A. Zolotov, Anal. Chim. Acta 167 (1985) 145.
[17] S.A. Glazier, M.A. Arnold, Anal. Chem. 60 (1988) 2540.
[18] S.A. Glazier, M.A. Arnold, Anal. Chem. 63 (1991) 754.
[19] N.A. Chaniotakis, K. Jurkschat, A. Rühlemann, Anal. Chim. Acta 282 (1993) 345.
[20] M. Rothmainer, W. Simon, Anal. Chim. Acta 271 (1993) 135.
[21] I.H.A. Badr, M.E. Meyerhoff, S.S.M. Hassan, Anal. Chem. 67 (1995) 2613.
[22] H. Hisamoto, D. Siswanta, H. Nishihara, K. Suzuki, Anal. Chim. Acta 304 (1955) 171.
[23] J. Vicente, I. Saura-Llamas, P.G. Jones, J. Chem. Soc. Dalton Trans. (1993) 3619.
[24] N.N. Greenwood, A. Earnshaw, Chemistry of the Elements, Pergamon, Oxford, 1993, p. 1066.
[25] P.M. Maitlis, P. Espinet, M.J.H. Russell, in: G. Wilkinson, F.G.A. Stone, E.W. Abel, (Eds.), Comprehensive Organometallic Chemistry, vol. 6, Pergamon, Oxford, 1982, p. 235.
[26] A. Jyo, N. Ishibashi, private communication, in: W.E. Morf (Ed.), The Principles of Ion-selective Electrodes and of Membrane Transport, Elsevier, Amsterdam, 1981, pp. 248–252.
[27] M. Maj-Zurawska, T. Sokalski, A. Hulanicki, Talanta 35 (1988) 281.
[28] M.E. Meyerhoff, B. Fu, E. Bakker, J. Yun, V.C. Yang, Anal. Chem. 68 (1996) 168A.
[29] E. Bakker, Anal. Chem. 69 (1997) 1061.
[30] R. Eugster, T. Rosatzin, B. Rusterholz, B. Aebersold, U. Pedraza, D. Ruegg, A. Schmid, U.E. Spichiger, W. Simon, Anal. Chim. Acta 289 (1994) 1.
[31] C. Sánchez-Pedreño, J.A. Ortuño, M.C. López, Anal. Chim. Acta 315 (1995) 63.

ELSEVIER

Talanta 47 (1998) 311–323

Talanta

Experimental design for the study of two derivatization procedures for simultaneous GC analysis of acidic herbicides and water chlorination by-products

Cécile Boucharat [a], Valérie Desauziers [a,*], Pierre Le Cloirec [b]

[a] *Laboratoire Génie de l'Environnement Industriel, Ecole des Mines d'Alès, 6, avenue de Clavières, F-30319 Alès cedex, France*
[b] *Ecole des Mines de Nantes, DSEE, 4, rue Alfred Kastler, B.P. 20722, F-44307 Nantes cedex 03, France*

Received 9 October 1997; received in revised form 6 March 1998; accepted 18 March 1998

Abstract

Two well known derivatization procedures, pentafluorobenzylation and BF_3/methanol esterification, were compared for their applications to GC analysis of acidic water micropollutants (chloroacetic and phenoxyalkanoic acids). A two-level factorial design was used to determine the influence of different parameters and their interactions on each derivatization process. The studied parameters are the reaction time, the amount of reagent (PFBBr) or catalyst (BF_3) and the temperature. Considering pentafluorobenzylation, the most influential factors are the concentration of PFBBr and the interaction 'temperature-time', which improve the derivatization efficiency. However, a PFBBr concentration of 250 mg l^{-1} in the reaction medium cannot be exceeded because of the increase in interfering by-products in GC/ECD. Moreover, chloroacetic acid derivatives are co-eluted with these compounds. This disadvantage was not observed in the operating conditions of GC/MS. The improved pentafluorobenzylation procedure allows the direct determination of the derivatives in GC/ECD without any purification step. The average detection limits are 1.6 and 80 μg l^{-1}, respectively in GC/ECD and in GC/MS. The reproducibility is 13%. For the BF_3/methanol esterification, the interactions 'BF_3 concentration-temperature' and 'BF_3 concentration-reaction time' are significant and have a negative effect on the derivatization yield. A linear model was therefore proposed and validated in the experimental area under study. All the compounds studied were detected in GC/MS, and the average detection limit is 2 μg l^{-1}. The reproducibility is around 7%. Therefore, after optimization, BF_3/methanol esterification followed by GC/MS is as sensitive as pentafluorobenzylation used with GC/ECD, and more reproducible. © 1998 Elsevier Science B.V. All rights reserved.

Keywords: Pentafluorobenzylation; BF_3/methanol esterification; Experimental design; Carboxylic acids

1. Introduction

Carboxylic organic acids represent about 5–8% of the dissolved organic matter identified in natural water [1–3]. These compounds essentially have

* Corresponding author. Tel.: + 33 4 66782766; fax: + 33 4 66782701; e-mail: vdesauzi@ensm-ales.fr

0039-9140/98/$ - see front matter © 1998 Elsevier Science B.V. All rights reserved.
PII S0039-9140(98)00133-7

Table 1
PFBBr derivatization: experimental matrix and response (y)

Exp. no.	PFBBr (mg l^{-1})	Temperature (°C)	Reaction time (h)	y (A.U.)[a]
1	250	70	5	20223
2	250	20	5	39664
3	250	70	0.5	63343
4	250	20	0.5	20358
5	125	70	5	3860
6	125	20	5	12186
7	125	70	0.5	13709
8	125	20	0.5	982

[a] A.U.: Area Unit.

natural origins (fatty acids) [4]. However, a small proportion of them (1%), are anthropogenic and can be toxic at trace level. Examples include phenoxyalkanoic acids, used as herbicides and chloroacetic acids, which are the main by-products of the drinking water chlorination process [2,5,6]. The chemical properties of these compounds are very different and therefore they are generally analyzed separately by using specific methods [7–9]. In this study, a different approach was envisaged. It consisted of a procedure able to simultaneously analyze chloroacetic and phenoxyalkanoic acids.

As these compounds need to be determined at trace level, the first step of the protocol consists of an extraction/concentration procedure (this step will not be studied here). Then, the extract is analyzed by chromatography. GC/MS and GC/ECD were chosen in this study because, respectively, of the possibility of molecular identification of the extracted compounds, and because of the specific and sensitive detection.

GC analysis of organic acids is widely used, but a preliminary derivatization step is needed because of the thermal unstability and the low volatility of these compounds [10,11]. Several derivatization processes are possible and the most representative are esterification, alkylation, acylation or silylation [12]. Esterification involves nucleophilic substitution generally catalyzed by a strong acid (HCl or H_2SO_4) or by a Lewis acid (BF_3) [11]. The other derivatization methods also consist of nucleophilic substitution but a bimolecular mechanism is involved, without formation of a carbocation. This is the case of alkylation by pentafluorobenzyl bromide (PFBBr) or by diazomethane. All these methodologies differ according to the stability of the derivatives formed, the presence of interfering by-products and their rapidity. Thus, diazomethane derivatization is known to be dangerous, and the reagent presents impurities [11,13]. The same disadvantage is observed for pentafluorobenzylation which generally needs a supplementary purification step on a silica cartridge [10,14]. However, the derivatives are stable and can be detected at very low concentrations by electron capture [11,15]. Mass spectrometry of PFBBr derivatives is also interesting, because of the detection of a specific ion m/z 181 [16].

On the other hand, the derivatization methods involving esterification by BF_3/alcool are also widely applied according to their ease of use, and

Table 2
PFBBr derivatization: effect of the factors and interactions on the response (y)

Factor/interaction	Effect	
	Designation	Value
Average	b_0	21790
Temperature (X_1)	b_1	3493
Reaction time (X_2)	b_2	−2807
PFBBr concentration (X_3)	b_3	14106
Temperature/time (X_1X_2)	b_{12}	−10434
Temperature/PFBBr (X_1X_3)	b_{13}	2392
Time/PFBBr (X_2X_3)	b_{23}	−3146
Temperature/time/PFBBr ($X_1X_2X_3$)	b_{123}	−5172

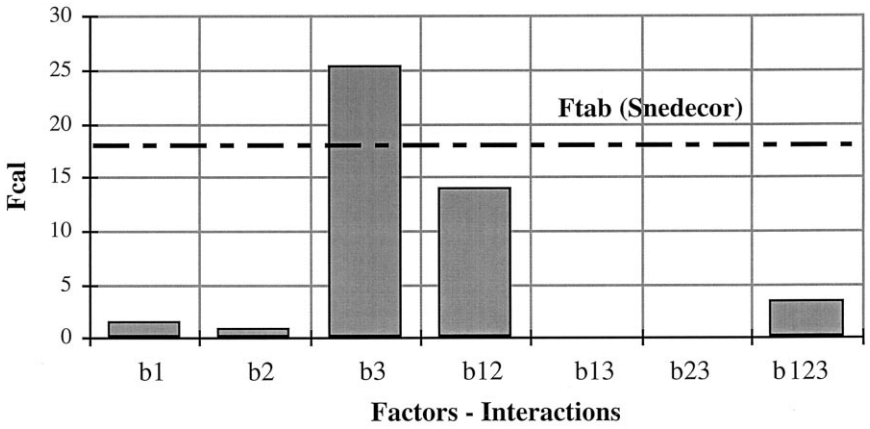

Fig. 1. PFBBr derivatization. Signification of the different factors studied and their interactions.

because no further purification procedure is needed. Moreover, GC/MS identification of a wide range of organic acids is possible. Thus, methyl esters are generally available in mass spectra libraries, unlike PFBBr derivatives. However, no specific ion can be observed and the sensitive GC/ECD is not really suitable except for chlorinated acids.

According to the literature, the detection limits determined for BF_3/methanol derivatization followed by GC/MS analysis range from 5 to 50 μg l^{-1} for acidic herbicides and the average reproducibility is 9% [11]. Considering the PFBBr alkylation, the detection limits in GC/ECD range from 1 to 13 μg l^{-1} for acidic herbicides [11,17], and is close to 10 μg l^{-1} for fatty acids with a reproducibility of 7–11% according to the compounds [16]. These results show that these two methods are suitable for trace GC analysis of organic acids. However, it can be noted that these data concern different families of acids studied separately. Consequently, these procedures (BF_3/methanol esterification and PFBBr alkylation) were tested in this study with a view to their application to organic acids in a wide range of chemical properties. To this aim, a two-level experimental design was applied to each procedure in order to check the most influential factors and interactions, and try to improve the sensitivity of the methods. Detection limits were determined for chloroacetic acids and phenoxyalkanoic herbicides in GC/ECD and GC/MS after PFBBr alkylation, and by GC/MS after BF_3/methanol esterification. Considering pentafluorobenzylation, the elimination of the solid-phase purification step was envisaged by reducing the content of the different reagents.

2. Materials and methods

2.1. Reagents

Solvents were purchased from commercial sources. Methanol, hexane and acetone were RS pesticide grade (Carlo Erba Farmitalia, Milan, Italy), and toluene was 99.5%-grade (Riedel de Haën, Seelze, Germany): potassium carbonate was 99%-grade (UCB): pentafluorobenzyl bromide (PFBBr), 18-crown-6, BF_3/methanol (12/88, m/m) and BF_3/methanol (50/50, m/m) were 99%-grade (excepted BF3/methanol; Aldrich, Milwaukee, WI). Standard of benzoic acid was Pestanal grade (Riedel de Haën, Seelze, Germany), dichloro-, trichloro-acetic acids and d_5-benzoic acid were 99%-grade (Aldrich, Milwaukee, WI), 2-Cl-benzoic acid, 2,4-D, MCPA, 2,4-DP, MCPP, 2,4,5-T and decafluorobiphenyl were 99%-grade (Alltech, Deerfield, USA). Ultrapure water was prepared by purifying demineralized water using a Milli-Q filtration system (Millipore, Bedford, MA).

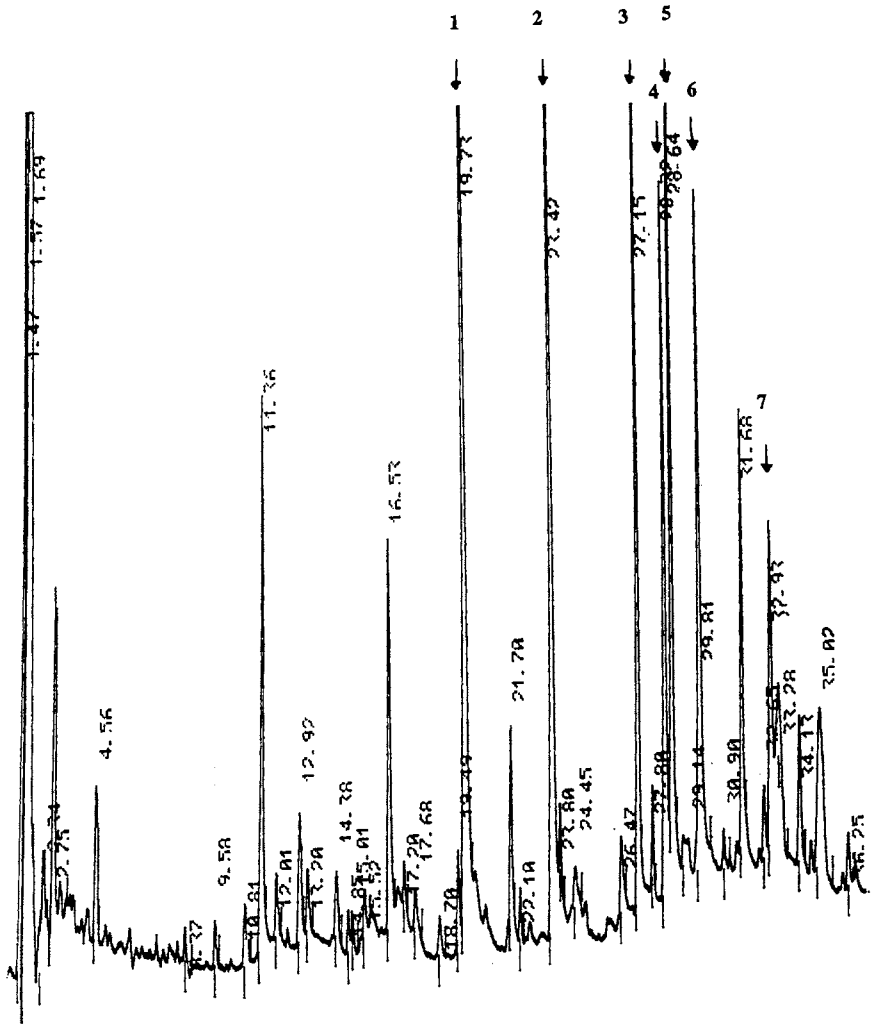

Fig. 2. GC/ECD chromatogram of PFBBr dérivatives (5 h at ambient temperature). 1. benzoic acid; 2. 2-chlorobenzoic acid; 3. MCPP; 4. MCPA; 5. 2,4-DP; 6. 2,4-D; 7. 2,4,5-T. (Detector: attenuation 2; sensitivity 10).

2.2. Standard solutions

The following compounds were used: chloroacetic acids (dichloroacetic and trichloroacetic acids), aromatic acids (benzoic and 2-chlorobenzoic acids), and phenoxyalcanoic acids (2-(4-chloro 2-methylphenoxy) propanoic acid (MCPP), 4-chloro 2-methyl phenoxyacetic acid (MCPA), 2-(2,4-dichlorophenoxy) propanoic acid (2,4-DP), 2,4-dichlorophenoxyacetic acid (2,4-D), 2,4,5-trichlorophenoxyacetic acid (2,4,5-T). These compounds were dissolved in methanol and working solutions were prepared by diluting stock solutions in the derivatization medium. Two internal standards were used. Decafluorobiphenyl was added to the PFBBr reaction medium before GC injection. For BF_3/methanol derivatization, d_5-benzoic acid was used.

2.3. PFBBr derivatization

The PFBBr derivatization was performed in 2 or 4 ml acetone containing the studied acids. The concentrations are 10 μg l^{-1} for phenoxyalcanoic

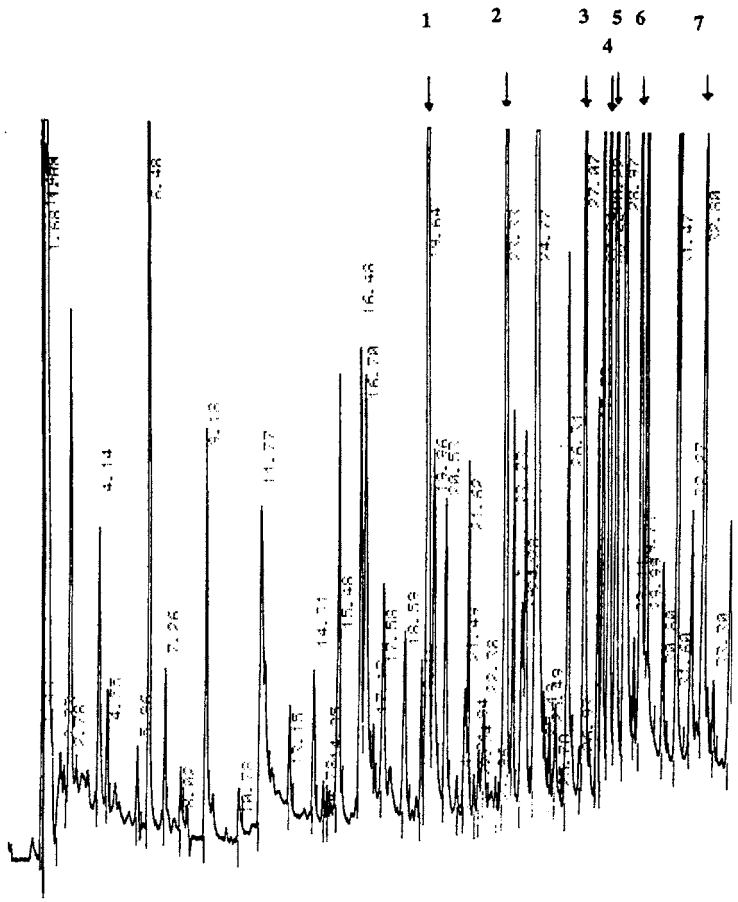

Fig. 3. GC/ECD chromatogram of PFBBr dérivatives (10 min at 70°C). 1. benzoic acid; 2. 2-chlorobenzoic acid; 3. MCPP; 4. MCPA; 5. 2,4-DP; 6. 2,4-D; 7. 2,4,5-T. (Detector: attenuation 2; sensitivity 10).

and aromatic acids and 20 μg l^{-1} for chloroacetic acids. Potassium carbonate was added, together with the catalyst (18-crown-6) and the PFBBr. The concentrations of these different reagents will be studied and discussed in the following paragraphs. Then the glass reaction flask was connected to a micro-refrigerant (Wheaton-33). Several temperatures and reaction times were tested (Section 3.1). The sample was then evaporated in a gentle nitrogen stream and the derivatives were dissolved in 1 ml hexane before GC/ECD or GC/MS injection. The main disadvantage of this protocol is the presence of numerous impurities. Consequently, a purification step should be added to the procedure. It could consist in washing the derivatization medium, by adding 4 ml of ultrapure water with 1 ml of hexane. The mixture was shaken using a Vortex (Heidolf REAX 2000). The hexane extract can be also purified on a solid-phase silica cartridge (Bond Elut 100 mg; Merck, Darmstadt, Germany). The elution of the PFBBr derivatives was carried out by percolating a toluene/hexane solution (30/70, v/v) after rinsing with toluene/hexane (10/90). The elution yield of the derivatives was around 80%. The elimination of these time-consuming steps will be studied further.

2.4. BF_3/methanol derivatization

The reaction was performed in 2 ml of methanol by using different amounts of the BF_3

Table 3
Detection limits of PFBBr derivatives in GC/ECD and GC/MS

Compounds	L.D. GC/ECD (μg l^{-1})	L.D. GC/MS (μg l^{-1})	tr (min) (GC/MS)	m/z ions
Dichloroacetic acid	nd[a]	136	22.0	48-83-181
Trichloroacetic acid	nd[a]	1000	24.8	82-117-181
Benzoic acid	1.6	103	28.8	77-105-181
2-Chlorobenzoic acid	1.5	50	33.6	111-139-181
MCPP	1.6	41	36.5	141-169-181
MCPA	0.9	30	37.9	125-141-181
2,4-DP	1.2	125	38.2	162-181-189
2,4-D	3.6	55	39.8	111-175-181
2,4,5-T	0.8	97	44.0	145-181-209

[a] Not detected.

Table 4
BF_3/methanol derivatization: experimental matrix and response (y)

Exp. no.	BF_3 (%)	Temperature (°C)	Reaction time (h)	y (A.U.)[a]
1	50	70	2	3083
2	50	20	2	1882
3	50	70	0.16	2852
4	50	20	0.16	1641
5	10	70	2	4204
6	10	20	2	2293
7	10	70	0.16	3766
8	10	20	0.16	2508

[a] A.U.: Area Unit.

catalyst (Section 3.2). The concentrations of the studied acids were 800 μg l^{-1} for chloroacetic acids and 400 μg l^{-1} for the other compounds. After derivatization (the temperature and the reaction time will be studied below), 2 ml of ultra-pure water were added and the esters formed were extracted by 1 ml hexane.

Table 5
BF_3/methanol derivatization: effect of factors and interactions on the response (y)

Factor/interaction	Effect	
	Designation	Value
Average	b_0	2704
Temperature (X_1)	b_1	772
Reaction time (X_2)	b_2	161
BF_3 amount (X_3)	b_3	−339
Temperature/time (X_1X_2)	b_{12}	6
Temperature/BF_3 (X_1X_3)	b_{13}	−169
Time/BF_3 (X_2X_3)	b_{23}	−43
Temperature/time/BF_3 ($X_1X_2X_3$)	b_{123}	−9

2.5. Chromatographic instrumentation

PFBBr derivatives were injected both in GC/ECD and GC/MS, whereas methyl esters were only injected in GC/MS.

GC/ECD: a Varian 3400 gas chromatograph was used, equipped with a ^{63}Ni electron-capture detector fixed at 300°C. One microliter of the extract containing the derivatives was injected in a split/splitless injector (splitless mode) fixed at 230°C. The GC column was a PTE-5 (Supelco, Bellefonte, PA), 30 m × 0.32 mm I.D., thickness 0.25 μm. Nitrogen (U) was the carrier gas (flow rate 2.5 ml min^{-1}). The GC oven was programmed from 80 to 220°C at 5°C min^{-1}.

GC/MS: a Varian 3400 chromatograph was used, equipped with a septum programmable in-

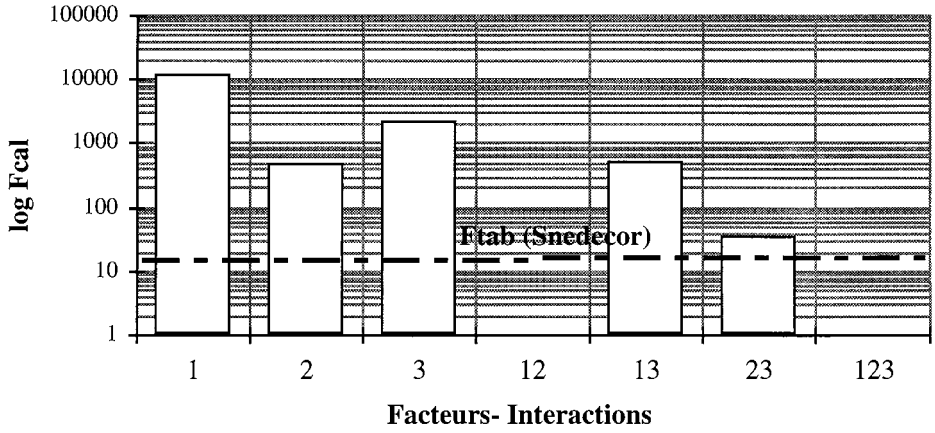

Fig. 4. BF_3/methanol derivatization. Signification of the different factors studied and their interactions.

jector Varian SPI 1093 and coupled with a thermostated transfer line with a mass spectrometric detector Varian saturn II [18]. The GC column was a DB-5 MS (J&W Scientific, Folsom, CA), 60 m $\times$ 0.25 mm I.D., thickness 0.25 μm. Helium (N60) was the carrier gas (flow rate 1.2 ml min^{-1}). For PFBBr derivatives, the GC oven was fixed at 80°C for 2 min, then programmed from 80 to 250°C at 5°C min^{-1}, the final temperature being maintained for 19 min. For methyl ester analysis, the GC oven was fixed at 70°C for 10 min, then programmed from 70 to 250°C at 5°C min^{-1}, the final temperature being maintained for 2 min. The transfer line and ion source were maintained at 220 and 180°C, respectively. For PFBBr derivatives, the injector was programmed from 80 to 220°C at 200°C min^{-1} whereas for methyl esters, it was fixed at 80°C for 1 min and then programmed from 80 to 250°C at 100°C min^{-1}. The mass spectrometer was used in Electron Impact (EI) mode. EI mass spectra were obtained at an ionisation energy of 70 eV. Derivatives were qualified by specific ion mass spectrometry in full scan ionisation mode. The acquisition was performed from 40 to 349 amu at 1 scan per second.

One microliter of extract was injected using a Varian 8200 CX autosampler.

Table 6
Detection limits of methyl ester derivatives in GC/MS

Compounds	L.D. (μg l^{-1})	tr (min)	m/z ions
Dichloroacetic acid	6.8	9.2	59-83-85
Trichloroacetic acid	3.0	12.7	59-82-117
Benzoic acid	0.6	21.7	77-105-136
2-Chlorobenzoic acid	0.8	27.5	111-139-170
MCPP	0.8	36.0	142-169-228
MCPA	1.3	36.4	77-141-214
2,4-DP	1.6	37.7	162-189-248
2,4-D	1.8	38.0	111-199-234
2,4,5-T	2.1	41.8	233-235-268

2.6. Experimental design

The influence of different parameters (or factors) and their interactions on the derivatization procedures were studied by using the experimental design methodology [19,20].

For each derivatization procedure studied, a complete two-level factorial design 2^3 (three parameters) was applied. A complete factorial design consists in testing all the combinations of the levels of the different parameters and their interactions with the minimum of experimentation. Two levels, expressed as coded values ($+1$) and (-1), were defined for each parameter studied [19]. This leads to the determination of an experimental area involving eight (2^3) experimentations, which can be represented by an experimental matrix, where the coded values of the parameters are replaced by their real experimental values (Tables 1 and 4). The parameters and their

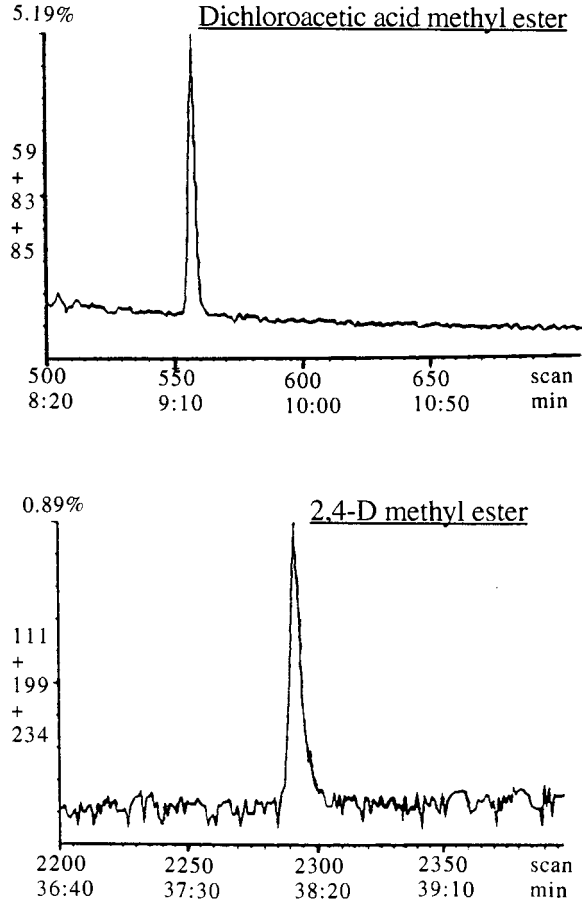

Fig. 5. GC/MS chromatograms of dichloroacetic acid methyl ester (500 μg l^{-1}) and 2,4-D methyl ester (40 μg l^{-1}) (as specific m/z ions).

levels (which delimit the experimental area) were chosen from the literature.

The effects of the parameters and their interactions were evaluated on the average area of the chromatographic peaks (response). The effect of a factor i is represented by the coefficient b_i, obtained by comparing the response values when the factor goes from (-1) to $(+1)$ (Eq. (1)). The interaction between the two factors i and j is expressed as the coefficient $b_{ij,m}$ (m = factor number). It should be considered when the effect of the first factor depends on the level of the second factor.

$$B_{ij} = \frac{1}{n} \sum_k \pm y_k \quad (1)$$

where n is the number of experiments (here, 8), and y_k the response corresponding to the kth experiment.

To represent the response (y), a polynomial equation (Eq. (2)) can be proposed:

$$y = b_0 + \sum_i b_i X_i + \sum_{ij} b_{ij} X_i X_j + \ldots \quad (2)$$

b_0 is the average effect, X_i the coded variable which corresponds to the factor i, and b_i the effect of the factor i on the response y.

Generally, the values of the coefficients b do not allow to directly estimate if the considered factor has a significant effect on the response y. Therefore, a variance analysis was used. The basis hypothesis corresponds to a non-influence of the factor i. In this case, it can be demonstrated that the ratio $F_{cal} = (V_i)/(V_r)$, where V_i is the variance of the factor i and V_r the residual variance follows the Snedecor law [19]. The residual variance V_r represents the variance of a non-controled factor (experimental error), or the variance of a factor which has been not considered in the study (noise factor).

If the influence of the factor is significative (for a given confidence interval), the ratio F_{cal} is higher than the value $F_{tab(\alpha,\beta)}$ given by the Fisher-Snedecor tables. F_{tab} was considered here with a confidence interval of 95%, α and β being the degrees of liberty of the considered factor and of the residue, respectively.

3. Results and discussion

3.1. PFBBr derivatization

3.1.1. Elimination of interferents

The reagents and the reaction medium (organic solvent) were chosen from the literature. Chau and Terry [10] have shown that the amount of esters formed increases with the polarity of the solvent. Therefore, acetone is the most used due to its polarity and volatility which allows an easy evaporation before solvent change and GC injection [10,17,21]. Methanol and other protic solvents are not suitable because they would not

favor bimolecular nucleophilic substitution. Only one reference mentioned the use of ethanol [22]. The solvent where esters are redissolved is less polar than the derivatization solvent: benzene, hexane and isooctane [10,14]. Hexane is the most used and was hence chosen in this study.

A base was added to the derivatization mixture, leading to acid dissociation and reaction on the electrophilic carbon of the pentafluorobenzyl bromide. Several basis were tested [23], and it was shown that potassium carbonate (K_2CO_3) is most suitable because it permits an easier derivatization of carboxylic acids. A catalyst is also involved in the procedure in order to enhance the nucleophilic substitution. The catalyst, generally 18-crown-6 [23,24], would allow the amount of PFBBr to be limited and consequently, the contribution of interfering products.

The protocol defined by Chau and Terry [10] is the basis of numerous studies related to the PFBBr derivatization. The derivatization was performed in 4 ml acetone containing the different model compounds (1 mg l^{-1} each), K_2CO_3 (2 g l^{-1}), 18-crown-6 (0.5 g l^{-1}) and PFBBr (125 mg l^{-1}). The reaction was carried out at the ambient temperature over 5 h. After solvent evaporation and redissolution in hexane, the derivatives were injected in GC/ECD.

However, this procedure induced a lot of interferents. This result is not surprising and confirms the observations previously mentioned in the literature about the problem of impurities. In the case where the responses of the target compounds are higher than those of impurities, a dilution of the extract can simplify the chromatogram. A purification procedure was however envisaged. A water rinse was first performed (Section 2.3). An improvement in the elimination of interferent was observed, but the dilution of the extract (100 times) was still necessary. Moreover, this procedure was not reproducible (RSD = 130% for four experimentations) and the detection limit after dilution was not satisfactory for trace analysis (around 500 μg l^{-1} for 2,4-D). A solid-phase purification was therefore tested (Section 2.3), but the dilution step remains necessary to reduce the contribution of interfering peaks on the chromatogram.

Another possibility consisted in decreasing the amount of reagents. Indeed, Fogelqvist [25] noted an increasing of the baseline noise due to an excessive quantity of 18-crown-6. But the same derivatization yield can be observed by using smaller concentrations of catalyst [23,25]. The quantity of the derivatization reagents was therefore decreased in order to reduce impurities. This procedure was hence carried out until the areas of the target compounds started to diminish so as not to decrease sensitivity. In these conditions, the purity of the extract did not require any further purification or dilution before GC/ECD injection. The composition of the reaction mixture was as follows: 2 ml acetone containing the acidic compounds, K_2CO_3 (50 mg l^{-1}), 18-crown-6 (10 mg l^{-1}) and PFBBr (125 mg l^{-1}).

3.1.2. Experimental design

This study was performed by using the previously described derivatization procedure. The following parameters (factors) were tested: PFBBr concentration, temperature and reaction time. Earlier works mentioned very different experimental conditions: the temperature varies according to a wide scale (ambient or 70°C with controled reflux) and the reaction time ranged from 30 min and 5 h [10,24]. These values were hence retained as the levels (-1) and $(+1)$ for the temperature and time factors. PFBBr was studied in a concentration range where the interferents did not create very much baseline noise. However, the reagent was introduced in excess compared to the total concentration of acids (100 times higher). The response measured is the average area of the chromatographic peaks obtained after injection of the derivatives in GC/ECD. These areas were corrected by using an internal standard (Section 2.2).

The experimental matrix of the complete factorial design studied is described in Table 1.

The response (y) only concerns the aromatic acids and chlorophenoxyalcanoic acids. Chloroacetic acids were not identified according to the experimental conditions applied here.

The values calculated for the effect of the factors and their interactions are described in Table 2.

The following polynomial equation can be therefore proposed (Eq. (3)):

$$y = 21790 + 3493X_1 - 2807X_2 + 14106X_3 - 10434X_1X_2 + 2392X_1X_3 - 3146X_2X_3 - 5172X_1X_2X_3 \quad (3)$$

This model was therefore not acceptable because the predicted values did not match experimental results (difference around 250%).

The significations of the factors and their interactions after comparison of the F_{cal} values with F_{tab} are presented in Fig. 1.

The effects of the interactions X_1X_3 and X_2X_3 are smaller than those of the other interactions. Therefore, they were not considered in the variance calculation [19]. In this case, $F_{tab1,2} = 18.51$ and the residue is 4%. This latter shows that all the factors supposed to have an influence on the derivatization were considered.

The derivatization efficiency increases with the PFBBr concentration which is the most significant factor. However, this concentration could not be further increased because of the possibility of increasing interfering by-products. The 'temperature/time' interaction is quite significant and shows that good results are obtained by applying short reaction time at 70°C, or long reaction time at the ambient temperature. Indeed, it is possible that a long derivatization time at 70°C leads to the degradation of the pentafluorobenzyl esters.

The best result is obtained for a reaction with 250 mg l^{-1} of PFBBr at 70°C over 30 min. A good response is also observed for a derivatization at the ambient temperature during 5 h (Fig. 2). According to the increasing of interfering products when the reaction mixture is heated (Fig. 3), it would be preferable to perform the derivatization at the ambient temperature over 5 h.

Compared to the conditions generally used, which are based on the protocol performed by Agemian and Chau [14], the K_2CO_3 concentration was reduced ten times and the catalyst concentration was diminished from 0.5 g l^{-1} to 10 mg l^{-1}. This allows the derivatives to be analyzed without a further purification step. According to the results of the experimental design, the best conditions were achieved for a PFBBr concentration of 250 mg l^{-1}. This is twice as high than the concentration generally cited in the literature [10,14,17]. However, the temperature and derivatization time (5 h at ambient temperature) were found as previously defined by several authors [10,14,24].

The reproducibility calculated for five experiments corresponding to these conditions is 13%. Good sensitivity and detection limits were obtained in GC/ECD (1–4 μg l^{-1}). These are of the same order as those obtained by Hajslova et al. [11], but in our case, no further purification was used. The detection limits are also considerably lower than those achieved by Gurka et al. (10 μg l^{-1}) [17] and Agemian and Chau (100 μg l^{-1}) [14]. However, chloroacetic acids were not detected. This could be explained by a co-elution of these compounds with the solvent or with interfering by-products because chloroacetic acids were unambiguously identified by GC/MS, using mass spectra available from the literature [10,26,27] (pentafluorobenzyl esters are not listed in mass spectra library). The specific ion m/z 181 also helps to make the identification easier. The sensitivity of GC/MS is not very satisfactory however (40 μg l^{-1} to 1 mg l^{-1}), and is not appropriate for trace analysis in water. Therefore, another derivatization method was studied.

The detection limits in GC/ECD and GC/MS are given in Table 3, together with the characteristic m/z ions used for the ester derivative identification.

It can be noticed that only the average area of all the acids was determined. Thus the chosen conditions are optimized for most acids but not necessarily for some of the individual ones. This could explain the high detection limit for the PFBB derivative of trichloroacetic acid. In this case, the yield for the PFBBr and trichloroacetic acid reaction may be low under the conditions optimized for phenoxyalkanoic acids.

3.2. BF_3/methanol derivatization

The BF_3/methanol derivatization does not need, a priori, any purification step before injection in GC [28–30], but in order to increase the partition coefficient during hexane extraction of the esters, it is necessary to add water to the derivatization mixture [28].

A two-level experimental design similar to that described for PFBBr derivatization was carried out. Three factors likely to have an effect on the derivation efficiency were studied: catalyst amount (BF_3), temperature and reaction time. The response 'y' studied was the average area of the chromatographic peaks obtained by GC/MS (Total Ionic Current). The parameter levels were chosen from the literature [11,13,28,31].

The experimental matrix of the complete factorial design is described in Table 4.

The values calculated for the effect of the factors and their interactions are described in Table 5.

The following polynomial equation can be therefore proposed (Eq. (4)):

$$y = 2704 + 772X_1 + 161X_2 - 339X_3 + 6X_1X_2 - 169X_1X_3 - 43X_2X_3 - 9X_1X_2X_3 \quad (4)$$

This relationship was verified at the center of the experimental area (65 min reaction at 45°C and with 30% BF_3 in methanol). According to these operating conditions, the predicted value matched the experimental response well: the difference is 7.8%. This value is of the same order as the reproducibility (7%) calculated for five experiments carried out at the center of the experimental area. The linearity of the response was also verified with another point (60 min reaction at 40°C with 15% BF_3). The proposed linear model can therefore be validated and the response can be predicted without any further experimentation within the experimental area limits.

The significations of the factors and their interactions after comparison of the F_{cal} values with F_{tab} are presented in Fig. 4.

The interactions X_1X_2 and $X_1X_2X_3$ were not considered in the variance calculation because the corresponding coefficients (b_{12} and b_{123}) were negligible (Table 5). Therefore, according to the PFBBr derivatization, $F_{tab1,2} = 18.51$ [19]. The residue value corresponding to the non-explained variance is 0.01%. This result is satisfactory and shows the correct choice of the influential parameters.

The three considered factors under consideration and two interactions concerning the catalyst content are significant. It appears that the influence of the catalyst content is negative, especially when the temperature and the reaction time are maxima. It can be therefore pointed out that the absence of catalyst leads to a decrease of the peak areas (30%). It is hence necessary to use BF_3, but at low content.

The maximum average of peak areas was obtained for a 2-h derivatization at 70°C with 10% BF_3 in methanol. These conditions correspond to those stated in the literature [11,13], i.e. a small concentration of BF_3 (around 10%) and a derivatization temperature of 70°C. However, the factorial design indicated that better results were achieved with a 2-h reaction, whereas in the literature, shorter times were used (10–20 min) [11,13]. The detection limits obtained after injection in GC/MS are of the order of 1 μg l^{-1}, and vary between 1 and 10 μg l^{-1}, for chlorophenoxyalkanoic and chloroacetic acids, respectively. Considering herbicides, the detection limits are 5–50 times lower than those established by Hajslova et al. [11]. These limits are therefore very low and permit this procedure to be applied to trace analysis in water after a preconcentration step. A procedure has been developed in our laboratory and will be published elsewhere. It consists of a solid-phase preconcentration using a non-specific extraction followed by a specific ion-exchange reconcentration of the acids. After methanolic elution, the compounds are directly methylated by adding BF_3 in the elution solvent. The detection limits thus obtained in GC/MS ranged from 20 ng l^{-1} for phenoxyalkanoic acids and 80 ng l^{-1} for chloroacetic acids. These values are in good agreement with European pesticide regulations for drinking water (100 ng l^{-1}).

The detection limits in GC/MS are given in Table 6, together with the characteristic m/z ions used for the identification of the ester derivatives.

As examples, GC/MS chromatograms of dichloroacetic acid- and 2,4-D-methyl esters are presented in Fig. 5.

4. Conclusion

Two derivatization procedures were compared in order to find the best compromise for trace GC analysis of organic acids. Chloroacetic and phenoxyalcanoic acids were studied simultaneously, ensuring that procedures were applicable to the main acidic micropollutants found in drinking water.

A two-level factorial design enabled us to check the influence of derivatization parameters such as temperature, reaction time and reagent content, and contributed to an improval in reaction efficiency.

This work has shown that GC/ECD analysis of PFBBr derivatives is possible without any purification step. The sensitivity obtained is suitable for trace analysis. However, chloroacetic acids were not analyzed although they were detected in GC/MS. Moreover, the application of this method to natural samples could be limited because of the presence of numerous interfering by-products. Pentafluorobenzyl bromide derivatization is also not really specific to organic acids. Indeed, phenolic compounds may be derivatized by this procedure, and their derivatives could be co-eluted with those of the acidic compounds. GC/MS analysis permits the identification of all the acids studied but it is not sensitive enough for trace analysis.

BF_3/methanol derivatization is easier to perform and does not induce interfering by-products. The derivatives are also easily identified by GC/MS according to their mass spectra which are available in the software library, on the contrary of PFBBr derivatives. Moreover, this methodology does not require any evaporation step and hence, does not induce any compound losses.

In conclusion, BF_3/methanol appears to be a suitable method for GC/MS analysis of carboxylic acids. The low detection limits (1 $\mu g\ l^{-1}$) and the satisfactory reproducibility (7%) make this method suitable trace analysis in water after a preconcentration for step.

References

[1] E.M. Thurman, Organic Geochemistry of Natural Waters, Martinus Nijhoff, Dordrecht, 1985.
[2] M. Doré, Chimie des Oxydants—Traitement des Eaux, Tech. & Doc. Lavoisier, Paris, 1989.
[3] B. Legube, Analusis 19 (1991) i15–i16.
[4] B. Martin, La Matière Organique Naturelle des eaux de Surface: Fractionnement, Caractérisation et Réactivité, Thèse de l'Université de Poitiers, 1995.
[5] H. Ben Amor, J. De Laat, M. Doré, Environ. Technol. Lett. 9 (1988) 1105–1114.
[6] P.C. Singer, J. Environ. Eng. 120 (1994) 727–744.
[7] US Environmental Protection Agency, Test Methods: Methods for Nonconventional Pesticides. Chemical Analysis of Industrial and Municipal Wastewater, EPA440/1-83/079C, No. 615, Washington DC, 1983.
[8] US Environmental Protection Agency, Test Method for Evaluating Solid Waste Physical/Chemical Methods, No. 8150, NTIS, 3rd ed., Washington DC, 1986.
[9] R.C. Barth, P.S. Fair, J. AWWA 84 (1992) 94–98.
[10] A.S.Y. Chau, K. Terry, J. Assoc. Off. Anal. Chem. 59 (1976) 633–636.
[11] J. Hajslova, W.H. Tahtah, Z. Jehlickova, V. Kocourek, P. Curha, Sci. Total Environ. 132 (1993) 259–274.
[12] K. Blau, J.M. Halket, Handbook of Derivatives for Chromatography, Wiley, Chichester, 1993.
[13] J. Horner, S.S. Que Hee, R.G. Sutherland, Anal. Chem. 46 (1974) 110–112.
[14] H. Agemian, A.S.Y. Chau, J. Assoc. Off. Anal. Chem. 60 (1977) 1070–1076.
[15] A.S.Y. Chau, B.K. Afghan, Analysis of Pesticides in Water, vol. II, CRC Press, Boca Raton, FL, 1982.
[16] H.B. Lee, T.E. Peart, J. Chromatogr. 498 (1990) 367–379.
[17] D.F. Gurka, F.L. Shore, S.T. Pan, J. Assoc. Off. Anal. Chem. 69 (1986) 970–975.
[18] J.M. Deroux, C. Gonzalez, P. Le Cloirec, G. Kovacsik, Talanta 43 (1996) 365–380.
[19] G. Sado, M.C. Sado, Les Plans d'Expériences—De l'Expérimentation à l'Assurance Qualité, Afnor Technique, Paris, 1991, p. 266.
[20] M. Pillet, Introduction aux Plans d'Expériences par la Méthode Taguchi, Les Editions d'Organisation, Paris, 1992, p. 224.
[21] L.G. Johnson, J. Assoc. Off. Anal. Chem. 56 (1973) 1503–1505.
[22] F.K. Kawahara, Environ. Sci. Technol. 5 (1971) 235–239.
[23] B. Davis, Anal. Chem. 49 (1977) 832–834.

[24] M. Tanaka, Y. Yasaka, H.L. Wu, T. Shono, Fresenius J. Anal. Chem. 336 (1990) 515–516.
[25] E. Fogelqvist, B. Josefsson, C. Roos, J. HRC & CC 3 (1980) 568–574.
[26] J. De Beer, C. Van Peteghem, A. Heyndrickx, Vet. Hum. Toxicol. 21 (1979) 172–177.
[27] C. Li, R. Magee, B.D. James, Anal. Chim. Acta 255 (1991) 187–196.
[28] A. Zhu, G.Y. Xu, Chromatographia 314 (1984) 421–428.
[29] L.S. Clesceri, A.E. Greenberg, Standard Methods for the Examination of Water and Wastewater, 17th ed., R. Rhodes Trussell, Washington, 1989.
[30] K. Kawamura, Anal. Chem. 65 (1993) 3505–3511.
[31] L. Marinelli, M.F. Feil, A. Schait, A.S.B.C. Proc. (1968) 113–117.

ELSEVIER

Talanta 47 (1998) 325–333

Talanta

Tensammetric determination of non-ionic surfactants combined with the BiAS separation procedure Part 3. Determination in the presence of hydrocarbons[1]

Bogdan Wyrwas, Andrzej Szymanski, Zenon Lukaszewski *

Technical University of Poznan, Institute of Chemistry, PL-60965 Poznan, Poland

Received 18 April 1997; received in revised form 6 March 1998; accepted 19 March 1998

Abstract

A method for the determination of non-ionic surfactants (NS) in the presence of an excess of hydrocarbons is developed. The modified BiAS procedure combined with the indirect tensammetric method (BiAS-ITM) is applied for this purpose. The method consists of extraction of NS into ethyl acetate, precipitation of ethoxylates with modified Dragendorff reagent, removal of adsorbed hydrocarbons by washing with isooctane and the determination of NS in the dissolved precipitate by the ITM. The method is characterised by 96–100% recovery and RSD of 0.02–0.04 at a 1000-fold excess of hydrocarbons. The detection limit of the procedure is 1.5 μg and the linear dynamic range is 2–20 μg in the sample, which facilitates work within the range of 2–1000 μg through the use of aliquots. The non-modified version of the BiAS-ITM exhibits a loss of NS due to their extraction by droplets of residual hydrocarbons trapped in the precipitate. Isooctane as a washing agent is found to be the best among eight tested media: methanol, ethyl acetate, diisopropyl ether, chloroform, water, glacial acetic acid, benzene and isooctane.
© 1998 Elsevier Science B.V. All rights reserved.

Keywords: Non-ionic surfactants; Hydrocarbons; Waters; Tensammetry; Indirect tensammetric method; Bismuth-active substances

1. Introduction

As a result of liquid hydrocarbons covering water surfaces, the oxygen supply to the bulk of the water is cut off causing environmental disasters such as the death of oxygen-dependent organisms. The use of surfactants is among the most effective ways of removing hydrocarbons from the environment. Oil spills can be removed using different mixtures of surfactants [1–4]. Surfactants of adequate chemical structure at sufficient concentration can emulsify liquid hydrocarbons and restore the aerobic conditions of water. Under aerobic conditions, emulsified liquid hydrocarbons are more easily biodegradable. Another possibility is the solubilization of hydrocarbons. In concentrations above a critical micelles concentra-

* Corresponding author. Tel: +48 61 8782786; fax: +48 61 8782571; e-mail: lukasz@et.put.poznan.pl

[1] Dedicated to Professor Zenon Kublik of Warsaw University on the occasion of his 75th birthday.

0039-9140/98/$ - see front matter © 1998 Elsevier Science B.V. All rights reserved.
PII S0039-9140(98)00131-3

tion (cmc), surfactants solubilize different hydrophobic substances, including liquid and solid hydrocarbons. The recent tendency is solubilization of hydrocarbons in contaminated aquifers. Non-ionic and anionic surfactants are used for this purpose [5,6]. Apart from different petroleum products, polycyclic aromatic hydrocarbons (PAH) can also be effectively treated this way [7,8]. A negative side effect of the application of surfactants for the removal of oil spills or remediation of contaminated aquifers may be secondary contamination of the environment by surfactants.

Surfactants have negative influence on aquatic organisms, although their toxic effects are lower compared with those of oil spills or PAH. Lethal concentrations for fish (LC_{50}) of different classes of non-ionic surfactants was determined at 0.25–1.5 mg l^{-1} [9]. The lowest observed effect concentration for non-ionic surfactant $C_{14-15}AE_7$ (oxyethylated alcohol having C_{14-15} hydrophobe and 7 oxyethylene subunits) on some aquatic invertebrates was evaluated at only 160 μg l^{-1} [10]. The maximum tolerable risk level for oxyethylated alcohols was determined by the National Institute of Public Health and Environmental Protection of the Netherlands at 110 μg l^{-1} while the negligible risk level was only 1.1 μg l^{-1} [11].

Two factors should be taken into account concerning the use of surfactants for the emulsifying or the solubilization of hydrocarbons in the environment: (1) surfactants should be used in relatively high concentration; (2) relatively slowly biodegradable surfactants should be applied. The biodegradation rate of surfactants used for emulsifying or solubilization should be at least slightly slower than that of emulsified or solubilized hydrocarbons. If the surfactant was biodegraded quickly, the originally emulsified or solubilized hydrocarbons would rebuild a surface layer after the biodegradation of surfactant. Therefore assurances concerning the high biodegradability of surfactants used to treat hydrocarbons should be considered a little critically. Taking into account these reasons, the behaviour of surfactants used for the removal of oil spills or remediation of hydrocarbons from the aquifer should be carefully controlled.

The determination of surfactants in the presence of hydrocarbons may be more complex than in other water samples due to the heterogeneity of such samples. Even a simple potentiometric titration used for the determination of anionic surfactants required a special approach in the presence of an oily-phase [12]. The separation of NS from hydrocarbons required the use of a sophisticated separation scheme [13]. Recently, a simple solid phase extraction scheme for the separation of low-oxyethylated non-ionic surfactants and the oily-phase was published [14]. However, glycerol fatty acids partial esters remain in the surfactants fraction and cannot be separated.

The Bi(smuth) A(ctive) S(ubstances) procedure is the commonly accepted method used in Western Europe for the determination of NS in surface water, sewage, effluents from sewage treatment plants and biodegradation studies [15–18]. This method is also recommended for the determination of NS in water in Poland [19]. However, no information was found concerning BiAS applicability in the presence of hydrocarbons. Recently a more advanced version of the BiAS procedure was developed. In this modified procedure, NS are determined in the final stage instead of bismuth(III) in the classical version [20,21]. The indirect tensammetric method (ITM) is used for NS quantification. Here, the modified version will be called 'BiAS-ITM'. The analytical signal in the BiAS-ITM is optimal within the range of 2–25 μg of NS in the sample during the final measuring stage. However the method as a whole may be used within the range of 2–1000 μg by processing a larger initial water sample and application of different aliquots [21]. The BiAS-ITM procedure is characterised by a detection limit of 1.5 μg in the sample [21] with in the classical BiAS, approximately 50 μg [22]. The ITM can be used as a sole method [23]. The BiAS-ITM exhibits better specificity than the ITM [21] due to the separation of ethoxylates by specific precipitation with modified Dragendorff reagent [20,21].

According to the data of Novotny and Kalvoda [24], petroleum products should not be adsorbed on the mercury surface for potentials more negative than −1.0 V vs. SCE. Therefore, at the potential of −1.2 V used in the ITM measure-

ments, hydrocarbons should be replaced by water from the mercury surface. Preliminary experiments show that hydrocarbons up to 1 mg in the sample (25 ml) have no influence on the height of the tensammetric peak of ethyl acetate, used as the monitoring substance. Therefore, the first attempt was to ascertain whether this procedure, without any modification, may be applied for the determination of NS in the presence of hydrocarbons. These initial results showed unsatisfactory recovery of the method. This is why the next stages constituted a search for the reason for the loss and the means of its removal. The development of a method for the determination of NS in the presence of excess of hydrocarbons was the main aim of the work.

The ITM as well as adsorptive stripping tensammetry (AdST) were applied for analytical control at every stage of the investigation. The ITM produces one common signal for a mixture of NS (total concentration) [23,25–27] while the AdST produces specific signals of different surfactants [28–32]. However, the AdST is hardly useful for mixtures of non-ionic surfactants [33,34] and therefore it is rather recommended for model investigations, as in part of the present work. On the other hand the AdST signal may be useful in distinguishing the model NS from the other components of the system. Therefore, apart from the BiAS-ITM, the combination of the AdST with the BiAS separation scheme (BiAS-AdST) was also applied.

The 1:1 mixture of C_{12} and C_{16} hydrocarbons was used as a model of a petroleum product. Oxyethylated alkylphenol Triton X-100 was selected as a representative ethoxylate. This surfactant is frequently used as a model. Triton X-100's behaviour has been clearly recognised in both the ITM and the AdST [25,32,33,35,36], as well as in classic tensammetry [37].

2. Experimental

2.1. Apparatus and reagents

A Radelkis OH-105 polarograph and ECO Chemie General Purpose Electroanalytical System μAUTOLAB were alternatively used for tensammetric measurements. A common mode of measurement (without phase sensitivity), a frequency of 60 Hz, a superimposed alternating voltage amplitude of 2 mV and a scan voltage rate of 400 mV min^{-1} were applied. Controlled-temperature HMDE equipment (Radiometer), having an additional platinum wire auxiliary electrode, was used. A quartz beaker was used instead of a glass one with protection of a ceramic frit on the end of a salt bridge to prevent adsorptive loss of surfactant [38]. All potentials cited are against the saturated calomel electrode.

A G5 (Schott-Geräte) glass filter was used. Triton X-100 (Rohm and Haas) was used without additional purification. Methanol, diisopropyl ether, benzene, isooctane (2,2,4-trimethylpentane), glacial acetic acid and sodium hydrogencarbonate all Analar grade were also used. Purified sodium sulphate and sodium chloride were used for preparation of the aqueous base electrolytes. All solutions were prepared in water triply distilled from quartz apparatus. Only freshly distilled water was used. Ethyl acetate and chloroform purified by distillation were used. Only freshly distilled reagents were used.

The modified Dragendorff reagent [39] was prepared by mixing solutions A and B before use. Solution A: 1.7 g of basic bismuth(III) nitrate, 65 g of potassium iodide and 220 ml of glacial acetic acid/1000 ml. Solution B was an aqueous solution containing 290 g of barium chloride dihydrate in 1000 ml.

The solution for dissolving the precipitate (solution C) was prepared from 12.4 g of tartaric acid and 18 ml of ammonia solution (25%) made up with water to 1000 ml. A silica gel cartridge (Bakerbond spe silica gel 7086-03) was used for the purification of this solution.

2.2. Procedures

2.2.1. The ITM measurement: Procedure A

The mixture containing NS, ethyl acetate and hydrocarbons was vigorously shaken and transferred into the voltammetric cell. The mixture was stirred to evaporate excessive ethyl acetate until droplets and turbidity disappeared (approximately

for 10 min in open cell). The saturated solution of ethyl acetate was made in this way. The droplets of excess ethyl acetate can extract surfactants and cause their loss. Therefore this excess must be removed, as evidenced by the disappearance of turbidity or droplets. The amounts of hydrocarbons used in the experiments do not form visible droplets. After a quiescent period (30 s) the tensammetric curve of ethyl acetate was recorded in the cathodic direction using a new mercury drop and starting from −1.20 V (vs. SCE). The difference between the height of the peak of ethyl acetate (recorded in a separate measurement) and the peak height of ethyl acetate in the presence of NS was the analytical signal. The results were quantified using a calibration curve of Triton X-100.

2.2.2. Determination of Triton X-100 by the AdST: Procedure B

The measured solution was transferred into the voltammetric cell. The preconcentration procedure was done with a new mercury drop in a stirred solution at −1.20 V (vs SCE). The preconcentration time (5 min) was measured from the moment of drop formation. No deaeration was used. The tensammetric curve was recorded in the cathodic direction after a 30-s quiescent period. The analytical signal was the height of the 'wide' tensammetric peak of Triton X-100 [32,33]. The results were quantified using a calibration graph of Triton X-100.

2.2.3. Determination of NS in the precipitate by the BiAS-ITM: Procedure C

Spikes of hydrocarbons and Triton X-100 were dissolved in 2 ml of methanol. A volume of 16 ml of water was added causing emulsion formation. Solution A (8 ml) and solution B (4 ml) of modified Dragendorff reagent were mixed and added to the sample. The reacting mixture was stirred for 20 min and left for 10 min. Orange coloured precipitate was filtered through a G5 glass filter. In the initial series of experiments no washing of the precipitate was done, while in the other experiments four 5-ml portions of isooctane were used. In the series of experiments concerning the optimum way of treating the precipitate, the use of nine different media for this purpose was checked.

The precipitate was dissolved in 20 ml hot solution C. Then the filter and the beaker were washed with 3–4 ml of water. This portion of water was added to the solution containing the dissolved precipitate. After cooling the solution, the volume was made up to 25 ml with water.

An aliquot of the solution was transferred to a 25-ml volumetric flask, 2.5 ml of 5 M aqueous sodium chloride and 1.8 ml of ethyl acetate were added and the flask was filled to the mark with water. The further procedure was performed according to procedure A.

2.2.4. Determination of Triton X-100 in the precipitate by the BiAS-AdST: Procedure D

Spikes of hydrocarbons and Triton X-100 were dissolved in 2 ml of methanol. Precipitation, washing and dissolution of the precipitate was performed according to procedure C. An aliquot of the obtained solution was transferred to a 25-ml volumetric flask, 12.5 ml of 1 M aqueous sodium sulphate was added and the flask was filled to the mark with water. The AdST measurement was run. The further procedure was performed according to procedure B.

2.2.5. Determination of NS in the washing media by the ITM

2.2.5.1. Organic solvents: Procedure E. The whole solvent used for washing of the precipitate or its aliquot was evaporated. The residue was dissolved in 1.5 ml of ethyl acetate and transferred to a 25-ml volumetric flask. A volume of 12.5 ml of 1 M aqueous sodium sulphate was added and the flask was filled to the mark with water. The ITM final determination of NS was performed according to procedure A.

2.2.5.2. Precipitating mixture, glacial acetic acid and water: Procedure F. The mixed portions of solution used as a washing agent were collected in a 100-ml volumetric flask and the flask was filled

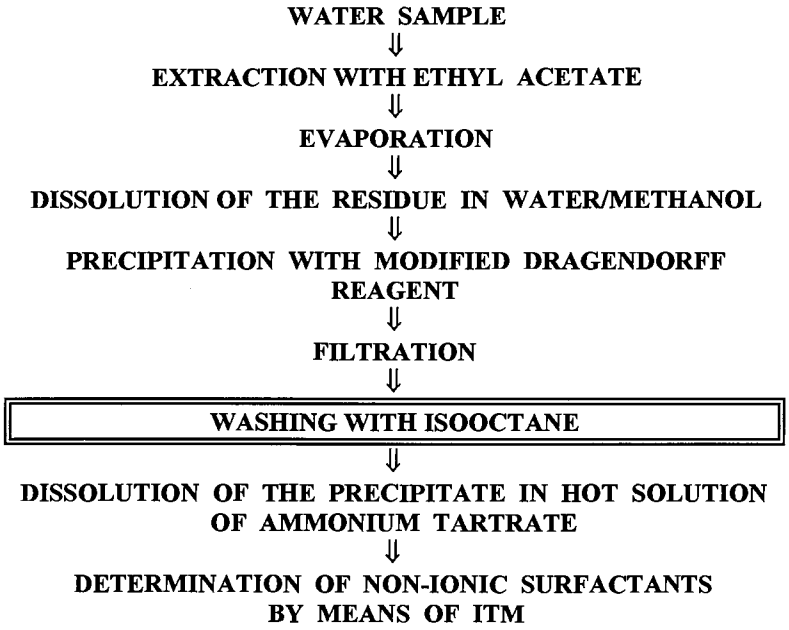

Fig. 1. Scheme of modified BiAS-ITM procedure for the determination of non-ionic surfactants in the presence of hydrocarbons.

to the mark with water. A portion of 20 g of sodium chloride was dissolved in the sample. NS were consecutively extracted from the sample with 15 ml and 10 ml of ethyl acetate. The extracts were mixed in a 25-ml volumetric flask and filled to the mark with ethyl acetate. The whole extract or its aliquot was evaporated. The residue was dissolved in 1.5 ml of ethyl acetate, transferred to a 25-ml volumetric flask, 12.5 ml of 1 M aqueous sodium sulphate was added and the flask was filled to the mark with water. The ITM final determination of NS was performed according to procedure A.

2.2.6. Determination of Triton X-100 in the washing media by the AdST

2.2.6.1. Organic solvents: Procedure G. The whole solvent used for washing the precipitate or its aliquot was evaporated. The residue was dissolved in several portions of 0.5 M aqueous sodium sulphate and transferred to a 25-ml volumetric flask. The flask was filled to the mark with 0.5 M aqueous sodium sulphate. The AdST final determination of Triton X-100 was performed according to procedure B.

2.2.6.2. Precipitating mixture, glacial acetic acid and water: Procedure H. Separation of Triton X-100 from the washing media was performed according to procedure F. The aliquot of ethyl acetate extract was evaporated and further processed according to procedure G with the AdST final determination according to procedure B.

2.2.7. Full cycle procedure (according to Fig. 1): Procedure I

Sodium chloride (60 g) and sodium hydrogencarbonate (0.2 g) were added to 200 ml of water sample and the solution was consecutively extracted with 25 and 20 ml of ethyl acetate. The extracts were mixed in a 50-ml volumetric flask and filled to the mark with ethyl acetate. An aliquot or the whole ethyl acetate solution was evaporated and the residue was dissolved in a mixture of 2 ml methanol and 16 ml water.

The further procedure was performed according to procedure C (Section 2.2.3).

3. Results and discussion

3.1. Model investigations with Triton X-100 and the 1:1 mixture of C_{12} and C_{16} hydrocarbons

The first step was to check whether the BiAS-ITM would be able to determine ethoxylates in the presence of excess of hydrocarbons without any modification. Spikes of 10 and 100 mg of the 1:1 mixture of C_{12} and C_{16} hydrocarbons were added to the solution containing 100 μg of Triton X-100 and processed according to the BiAS procedure (Procedure C, Section 2.2.3). In contrast to the original BiAS procedure recommending the washing of the precipitate with glacial acetic acid [39], the obtained precipitate was not washed. This step was omitted because washing with glacial acetic acid causes a serious loss of the precipitate [40]. The amount of 94.5 μg of Triton X-100 was determined in the presence of 10 mg of hydrocarbons in the sample and only 87 μg in the presence of 100 mg of hydrocarbons, showing the recovery of 94.5% and 87% respectively. To distinguish whether this error appears at the stage of separation or due to the influence of hydrocarbons on the ITM measurement, the experiments were repeated but the AdST was applied for the quantification of Triton X-100 separated according to procedure D (Section 2.2.4). The amounts of 94.5 μg and 88 μg of Triton X-100 were determined for 10 mg and 100 mg of hydrocarbons in the samples, respectively. These almost identical results as in the BiAS-ITM show that the error is not caused by the final measurement. On this basis the hypothesis was formulated that the error is caused by the extraction of NS by droplets of hydrocarbons trapped by the precipitate.

The next series of experiments should show whether a relatively small amount of hydrocarbons really does cause the lowering of concentration of Triton X-100. The spikes of 1, 10 or 100 mg of the 1:1 mixture of C_{12} and C_{16} hydrocarbons and 100 μg spike of Triton X-100 were introduced into the 100-ml volumetric flask. The aliquots of this solution were taken and Triton X-100 was determined both by the AdST and ITM. In the case of the AdST measurement the aliquot was added to the solution of 1 M aqueous sodium sulphate. The mixture was diluted to a concentration of supporting electrolyte equal to 0.5 M. After transferring the solution to the voltammetric cell the AdST measurements were performed according to Procedure B (Section 2.2.2).

In the case of the ITM measurement the aliquot was added to the solution of 1 M aqueous sodium sulphate, 1.5 ml of ethyl acetate was added and the mixture was diluted to a concentration of supporting electrolyte of 0.5 M. After transferring the mixture to the voltammetric cell the ITM measurements were performed according to procedure A (Section 2.2.1).

The recoveries determined by the AdST and ITM were almost identical: 95 and 96 μg of Triton X-100 in the presence of 1 mg of hydrocarbons, 87 and 89 μg of surfactant for 10 mg of hydrocarbons and 75 and 75 μg of Triton X-100 in the presence of 100 mg of hydrocarbons.

The conclusion was obvious: recovery is not complete; the higher the spike of hydrocarbons, the poorer the recovery. These results confirm the hypothesis of the extraction of Triton X-100 by droplets of the emulsion of hydrocarbons.

Another hypothesis for these results might be the influence of hydrocarbons on the analytical signals in the ITM or AdST due to their adsorptive competition with ethyl acetate or Triton X-100 on the mercury surface; however, this is highly improbable. Different effects should be observed in the case of the ITM on the one hand and in the AdST, on the other, if this hypothesis was true. The solubility of hydrocarbons in the base electrolytes used in both methods is different. On the other hand, the behaviour of mixtures of different substances is different in the AdST than in the ITM [27,34]. Therefore, the same degree of lowering of the Triton X-100 peak in the AdST and the ethyl acetate peak in the ITM, caused by the given total concentration of hydrocarbons, might appear only due to the compensation of both effects, which seems to be highly improbable.

An attempt was undertaken to find a washing medium to remove the residue of hydrocarbons from the precipitate based on the presumption

that this residue is responsible for the loss of surfactant-to-be-determined. Taking into account that this stage might be the source of serious loss of precipitated surfactant [40], nine different media for washing the precipitate, including glacial acetic acid and precipitating mixture, were tested. Apart from organic solvents, water and precipitating mixture were tested to obtain wider knowledge concerning the solubility of the precipitate. Concentration of Triton X-100 was measured both in the precipitate (procedures C and D) as well as in the washing medium (procedures E, F, G and H). To make certain, both the ITM and AdST were applied for quantification. The average results with the 95% confidence limits are shown in Table 1. The tested media have been ordered in the sequence of decreasing ability to dissolve the precipitate of Triton X-100 with modified Dragendorff reagent.

Methanol almost totally decomposes the precipitate. Though this solvent is useless as a potential washing medium it can be recommended for dissolution of the precipitate in any further modifications of the BiAS procedure. Ethyl acetate, diisopropyl ether, chloroform and water, used for washing, cause significant losses of the precipitate. The results for glacial acetic acid support the previous conclusion concerning its role as a source of loss and error [40]. The use of benzene and especially isooctane as a washing agent leads to quite acceptable results, although the best washing agent is the precipitating solution.

Table 1
Recovery of spike of 100 μg Triton X-100 precipitated with modified Dragendorff reagent and washed with different solvents or with precipitating mixture

Washing medium	Found (μg) in:	
	Precipitate	Washing medium
Methanol	<d.l.	98.5 ± 0.7
Ethyl acetate	72.8 ± 1.7	28.1 ± 1.4
Diisopropyl ether	76.9 ± 1.9	21.4 ± 1.1
Chloroform	77.6 ± 2.1	20.5 ± 1.0
Water	82.5 ± 1.9	16.0 ± 0.8
Acetic acid (glacial)	92.8 ± 1.9	8.2 ± 0.6
Benzene	96.9 ± 0.9	3.1 ± 0.5
Isooctane	98.1 ± 1.2	<d.l.
Precipitating mixture	98.5 ± 1.3	<d.l.

d.l., detection limit (1.5 μg in the sample).

The further use of isooctane as the washing medium seems to be a good choice taking into account the need to dissolve the residual hydrocarbons adsorbed on the precipitate. It is necessary to stress a good conformity of results concerning Triton X-100 distribution between the precipitate and the corresponding washing solutions. The total average recoveries of the processed 100 μg spike of Triton X-100 were between 98.1 and 101.0 μg.

A series of experiments with the use of isooctane as a washing medium were performed. The precipitation of Triton X-100 with the modified Dragendorff reagent was applied as in the previous case, though in this case the precipitate was washed with isooctane (four times with 5 ml). As in the previous series, the spike of Triton X-100 was 100 μg and the 1:1 mixture of C_{12} and C_{16} hydrocarbons, 1, 10 and 100 mg, respectively. The corresponding excess of hydrocarbons to Triton X-100 was 10, 100 and 1000, respectively. The results, determined both by the ITM and AdST, show the recoveries of Triton X-100 at 95 and 96 μg (the ITM and AdST, respectively) in the presence of 1 mg of hydrocarbons, 97.5 and 97 μg of surfactant for 10 mg of hydrocarbons and 97 and 96 μg for 100 mg of hydrocarbons in the sample. They show that the loss caused by the presence of hydrocarbons or by using glacial acetic acid as a washing medium was eliminated. These experiments show again that hydrocarbons trapped in the precipitate were the cause of the error in the experiments where washing was not performed.

To check the recovery and precision of crucial stages of the investigated procedure, a series of experiments was performed with precipitation of 100 μg spike of Triton X-100 in the presence of a 10 mg spike of the 1:1 mixture of C_{12} and C_{16} hydrocarbons (ratio 1:100) with subsequent washing and dissolution of the precipitate, as well as final determination of Triton X-100. The results of five independent measurements show the recovery of 97.6% of the spike, with a standard deviation of 2.1 μg which corresponds to the relative standard deviation of 2.1%. These results are satisfactory in terms of precision and recovery.

Table 2
Recovery and precision of the determination of Triton X-100 in the presence of C_{12} and C_{16} (1:1) hydrocarbon fraction under river water conditions

No. of measurements	Added		Expected	Found (μg)	Recovery (%)	S (μg)	S_r (%)
	Triton X-100 (μg)	Hydrocarb. (mg)	Triton X-100 (μg)				
2	—	—	—	18	—	—	—
5	100	100	118	118	100	4.5	3.8
5	100	1000	118	102	83	1.9	1.6
5	1000	1000	1018	976	96	1.9	1.9

Therefore the analytical scheme for the determination of non-ionic surfactants in the presence of hydrocarbons shown in Fig. 1 is proposed. The scheme consists of a sequential performance of procedures I, C and A (Sections 2.2.7, 2.2.3 and 2.2.1). The framed stage in the scheme is different from the normal version of the BiAS-ITM procedure as well as the classical BiAS procedure.

3.2. Experiments with real samples

Real samples were the next step after satisfactory results were obtained for model solutions. Recovery and precision in the full cycle measurement (according to Fig. 1) were checked in three series of experiments. Triton X-100 and the 1:1 mixture of C_{12} and C_{16} hydrocarbons were spiked to river water samples and processed in the full cycle measurement. In contrast to the model investigations, river water contained all possible interferents and also native NS (18 μg in a 200-ml sample used for processing). The results are shown in Table 2. Precision of measurements is satisfactory and very similar to those under model conditions. Recovery is satisfactory in the cases when the ratio of NS and hydrocarbons is 1:1000, for both spikes of Triton X-100 used. However, higher excess of hydrocarbons (1:10000) creates a noticeable loss. A decrease of this loss might well be the aim of further improvements in the procedure. On the other hand, traces of NS are not very significant when real samples contain high concentrations of hydrocarbons.

In order to confirm the real applicability of the developed method, 12 real samples containing hydrocarbons emulsified with a commercial mixture of NS and treated with different bacteria species were investigated for the content of NS. Results within the range 48–630 μg in the sample were obtained. Samples contained 48–204 mg hydrocarbons. The ratio of NS to hydrocarbons in the measured samples were within the range of 1:1000 to 1:250. No operational difficulties were observed.

Acknowledgements

This work was supported by the Committee of Scientific Research (institutional grant for the Faculty of Chemical Engineering of the Technical University of Poznan, No DS 31-516/97). Professor A. Olszanowski from the Technical University of Poznan is gratefully acknowledged for providing 12 real samples.

References

[1] M.S. Diallo, L.M. Abriola, W.J. Weber, Environ. Sci. Technol. 28 (1994) 1829.
[2] Y. Ouyang, R.S. Mansell, R.D. Ryue, Crit. Rev. Environ. Sci. Technol. 25 (1995) 269.
[3] R. Martel, P.J. Gelinas, Ground Water 34 (1996) 143.
[4] S.J. Bury, C.A. Miller, Environ. Sci. Technol. 27 (1993) 104.
[5] K. Scheibenbogen, R.G. Zytner, H. Lee, J.T. Trevors, J. Chem. Technol. Biotechnol. 59 (1994) 53.

[6] K.D. Pennell, L.M. Abriola, W.J. Weber, Environ. Sci. Technol. 27 (1993) 2332.
[7] S. Guha, P.R. Jaffe, Environ. Sci. Technol. 30 (1996) 605.
[8] S. Laha, R.G. Luthy, Biotechnol. Bioeng. 40 (1992) 1367.
[9] P. Schöberl, K.J. Bock, L. Huber, Tenside Surf. Det. 25 (1988) 86.
[10] W.B. Gillespie, J.H. Rodgers, N.O. Crossland, Environ. Toxicol. Chem. 15 (1996) 1418.
[11] A.M. Nielsen, INFORM 8 (1997) 28.
[12] J. Gronsveld, M.J. Faber, Tenside Surf. Det. 27 (1990) 231.
[13] J.M. Rosen, Anal. Chem. 35 (1963) 2074.
[14] N. Buschmann, F. Hülskötter, Tenside Surf. Det. 34 (1997) 8.
[15] W.K. Fischer, Tenside Deterg. 17 (1980) 250.
[16] D. Brown, H. De Henau, J.T. Garrigan, P. Gerike, M. Holt, E. Keck, E. Kunkel, E. Matthijs, J. Waters, R.J. Watkinson, Tenside Deterg. 23 (1986) 190.
[17] D. Brown, H. De Henau, J.T. Garrigan, P. Gerike, M. Holt, E. Kunkel, E. Matthijs, J. Waters, R.J. Watkinson, Tenside Deterg. 24 (1987) 14.
[18] E. Matthijs, E.C. Hennes, Tenside Surf. Det. 28 (1991) 22.
[19] Polish Standard PN-88-C04550/11, Determination of non-ionic surfactants in waters by spectrophotometric method using Dragendorff reagent, Polish Committee for Standardization, Measures and Quality Control, 1988.
[20] B. Wyrwas, A. Szymanski, Z. Lukaszewski, Talanta 41 (1994) 1529.
[21] B. Wyrwas, A. Szymanski, Z. Lukaszewski, Talanta 42 (1995) 1251.
[22] E. Matthijs, E.C. Hennes, Tenside Surf. Det. 28 (1991) 22.
[23] A. Szymanski, B. Wyrwas, Z. Lukaszewski, Anal. Chim. Acta 305 (1995) 256.
[24] Novotny, R. Kalvoda, Collection Czechoslovak Chem. Commun. 51 (1986) 1595.
[25] A. Szymanski, Z. Lukaszewski, Anal. Chim. Acta 260 (1992) 25.
[26] A. Szymanski, Z. Lukaszewski, Anal. Chim. Acta 273 (1993) 313.
[27] A. Szymanski, Z. Lukaszewski, Anal. Chim. Acta 293 (1994) 77.
[28] M.K. Pawlak, Z. Lukaszewski, Anal. Chim. Acta 202 (1987) 85.
[29] A. Szymanski, Z. Lukaszewski, Electroanalysis 3 (1991) 17.
[30] A. Szymanski, Z. Lukaszewski, Electroanalysis 3 (1991) 963.
[31] A. Szymanski, Z. Lukaszewski, Electroanalysis 6 (1994) 1094.
[32] A. Szymanski, Z. Lukaszewski, Electroanalysis 7 (1995) 114.
[33] Z. Lukaszewski, H. Batycka, W. Zembrzuski, Anal. Chim. Acta 175 (1985) 55.
[34] M.K. Pawlak, Z. Lukaszewski, Anal. Chim. Acta 202 (1987) 97.
[35] E. Bednarkiewicz, Z. Kublik, Anal. Chim. Acta 176 (1985) 133.
[36] N. Batina, B. Cosovic, D.J. Tezak, Anal. Chim. Acta 199 (1987) 177.
[37] H. Jehring, A. Weiss, Tenside 9 (1969) 251.
[38] A. Szymanski, Z. Lukaszewski, Anal. Chim. Acta 231 (1990) 77.
[39] R. Wickbold, Tenside Deterg. 9 (1972) 173.
[40] B. Wyrwas, A. Szymanski, Z. Lukaszewski, Anal. Chim. Acta 278 (1993) 197.

ELSEVIER

Talanta 47 (1998) 335–342

Talanta

Development of a system with enzyme reactors for the determination of fish freshness

M.-A. Carsol, M. Mascini *

Dipartimento di Sanità Pubblica, Epidemiologia e Chimica Analitica Ambientale, Sezione di Chimica Analitica, Via Gino Capponi 9, 50121, Firenze, Italy

Received 26 November 1997; received in revised form 6 March 1998; accepted 19 March 1998

Abstract

A continuous system for the determination of fish freshness with double enzyme reactors was developed and applied to the determination of the freshness indicator K

$K = 100(\mathrm{HxR} + \mathrm{Hx})/(\mathrm{IMP} + \mathrm{HxR} + \mathrm{Hx})$,

where IMP, HxR and Hx are Inosine monophosphate, Inosine and Hypoxanthine, respectively. The system was assembled with a three electrode screen-printed element (graphite as working electrode, silver as counter and silver, silver chloride as reference electrode) placed in a flow cell, a sample injection valve and two enzyme reactors. The determination of the total amount of HxR and Hx is realized by flowing the sample through two reactors in series: one reactor was packed with nucleoside phosphorylase (Np) and the other with xanthine oxidase (XO) immobilized on aminopropyl glass. Similarly, the other term of the equation was evaluated by flowing through the two reactors the sample treated by Alkaline phosphatase (AlP) for 5–10 min at 45°C. One assay could be completed within 5 min. The system for the determination of fish freshness was reproducible within 2–3% ($n = 4$). The immobilized enzymes were fairly stable for at least 3 months at 4°C. More than 200–300 samples could be analyzed in about one month by using these enzyme reactors provided the disposable screen-printed electrode should be changed every 30–40 real samples. The results obtained suggest that the proposed sensor system provides a simple, rapid and economical method for the determination of fish freshness (K). We applied the present system with two reactors for the determination of K values in fish samples and compared the results with those obtained by the XO-reactor. Correlation factor and regression line between the two methods were 0.992 and $Y = -3.14 + 1.03X$ respectively. We concluded that the present flow injection analysis (FIA) system with XO and Np reactors was suitable as a simple, easy to handle and reliable instrument for quality control in the fish industry. © 1998 Elsevier Science B.V. All rights reserved.

Keywords: Fish freshness; Enzyme reactors; Screen-printed electrodes; Xanthine oxidase; K values; Flow injection analysis; Quality control

* Corresponding author. Tel.: + 39 55 275 7267; fax: + 39 55 2476972; e-mail: mascini@cesit1.unifit.it

0039-9140/98/$ - see front matter © 1998 Elsevier Science B.V. All rights reserved.
PII S0039-9140(98)00129-5

1. Introduction

The establishment of a simple, rapid and accurate method for the determination of fish freshness is required in food industry [1]. After the death of fish, adenosine-5′-triphosphate (ATP) starts to degrade to uric acid (UA) through the following pathway:

$$\mathrm{ATP} \rightarrow \mathrm{ADP} \rightarrow \mathrm{AMP} \rightarrow \mathrm{IMP} \rightarrow \mathrm{HxR} \rightarrow \mathrm{Hx} \rightarrow \mathrm{X} \rightarrow \mathrm{UA}$$

where ADP is adenosine-5′-diphosphate, AMP is adenosine-5′-monophosphate, IMP is Inosine monophosphate, HxR, Inosine, Hx, Hypoxanthine and UA, uric acid.

To indicate fish freshness, the *K* value based on the degradation of these compounds in fish meat is defined as:

$$K = 100(\mathrm{HxR} + \mathrm{Hx})/(\mathrm{IMP} + \mathrm{HxR} + \mathrm{Hx})$$

[2] as ATP, ADP and AMP generally disappear around 24 h after the death.

Enzyme sensor for the determination of Hx, HxR and IMP has been developed for the purpose of *K* determinations [3–6].

In this paper, an attempt to produce a simple and long-lived system based on enzyme reactors and FIA enough stable for a rapid and easy determination of the *K* is described and applied to several kind of fishes.

IMP, HxR and Hx determinations are based on the following enzyme reactions:

$$\mathrm{IMP} \xrightarrow{\mathrm{AlP}} \mathrm{HxR}$$

$$\mathrm{HxR} + \mathrm{P}_i \xrightarrow{\mathrm{Np}} \mathrm{Hx} + \mathrm{Ribose} - 1\mathrm{Phosphate}$$

$$\mathrm{Hx} + 2\mathrm{O}_2 \xrightarrow{\mathrm{XO}} \mathrm{UA} + 2\mathrm{H}_2\mathrm{O}_2$$

where AlP is alkaline phosphatase, Np nucleoside phosphorylase and XO xanthine oxidase.

The final measurement assembly consists of two reactors with a flow cell equipped with a screen-printed graphite electrode and a sampling injection valve.

Graphite electrodes are insensitive to hydrogen peroxide and we showed how this electrode can be useful for the determination of uric acid [7]. Total amounts of IMP, HxR and Hx are determined as the current increase corresponding to uric acid formation in the final step. We tried to realize all enzymatic reactions through reactors with immobilized enzymes, but the best results have been obtained by performing the first reaction with Alkaline phosphatase in batch and then the other two with immobilized enzyme-based reactors.

2. Experimental

2.1. Chemicals

Hypoxanthine, Inosine, Inosine monophosphate, Uric acid, phosphate potassium dihydrogenphosphate, Imidazole and Phosphatase alkaline (EC 3.1.3.1; from Bovine Intestinal Mucosa; 22 U mg^{-1}) were purchased from Sigma, St Louis, MO, Xanthine oxidase (EC 1.1.3.22; from buttermilk; 0.4 U mg^{-1}) and Nucleoside phosphorylase (EC 2.4.2.1; bacterial; 9.7 U mg^{-1}) from Fluka, Glutaraldehyde (25% aqueous solution), $ZnCl_2$ and $MgCl_2$ from Merck.

2.2. Screen-printed electrode

The screen-printed electrodes used in a 3-electrode configuration were realized by several steps corresponding to the deposition of different layers:

1. A first layer of silver ink for the conductive pad (counter electrode).
2. A carbon pad positioned over a part of the silver track (working electrode).
3. A silver/silver chloride over the silver track (reference electrode).
4. And finally an insulating layer with openings to allow electrical contact on a polyester flexible film [8].

2.3. Preparation of enzyme reactors

AlP, Np and XO have been immobilized on controlled pore glass beads (aminopropyl glass, average pore size 700 Å, particle size 80–120 mesh obtained from Sigma) activated by glutaraldehyde. 50 mg of pore glass were gently stirred in a 2.5% glutaraldehyde solution (500 μl

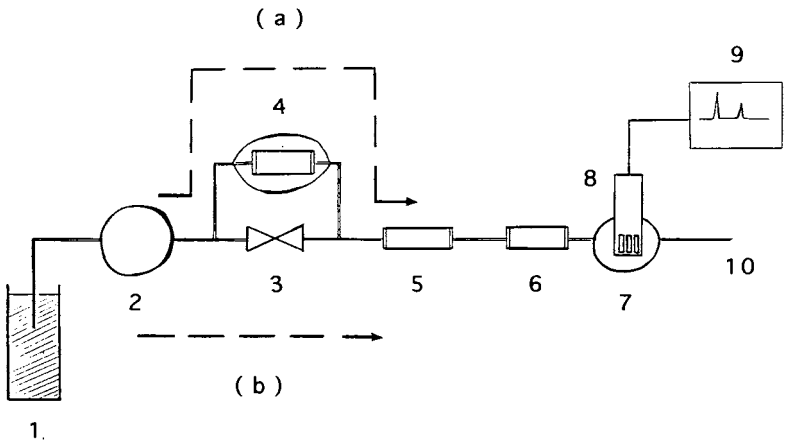

Fig. 1. Schematic diagram of the system. 1, buffer tank; 2, peristaltic pump; 3, injection port; 4, AlP-reactor thermostated; 5, Np-reactor; 6, XO-reactor; 7, flow cell; 8, screen-printed electrode; 9, recorder; 10, waste. (a) the sample flows through the AlP-reactor and the current obtained is proportional to the sum of IMP, HxR, Hx and UA. (b) the sample flows through the valve and the current obtained is proportional to the sum of HxR, Hx and UA.

of buffer pH 7.8) for 1 h at room temperature. After the reaction, this mixture was carefully washed with water. To this, 1.2 mg of XO, 4.0 mg of Np or 4.0, 6.0 and 13.0 mg of AlP is added and stirred at 4°C for 24 h.

The immobilized enzyme glass is packed in Tygon™ tube of 3.50 mm internal diameter and 40 mm long.

The working buffer for the procedure is 0.05 M Imidazole containing 0.1 M KCl and 50 mM KH_2PO_4 at pH 7.8. The reactor is stored at about 4°C in the working buffer when not in use.

2.4. Amperometric determinations

The FIA system included a peristaltic pump (Minipuls 3 Peristaltic Pump Gilson), a sampling device (Rheodyne 5020) and an amperometric biosensor detector (Universal) used as potentiostat and connected with an Amel model 868 recorder.

The screen-printed 3 electrode was placed in a suitable flow cell. The carrier buffer solution is continuously transferred to the flow cell at a constant rate by the peristaltic pump. When the current reaches a stable value (drift less than 1% in 10 min), a known volume of sample solution is injected through the sampling valve. The best flow rate and the sample loop were found 0.5 ml min^{-1} and 100 μl.

IMP, HxR, Hx and UA standard solutions were prepared by dissolving reagent in Imidazole buffer 0.05 M containing 0.1 M KCl–50 mM KH_2PO_4 and were diluted with the buffer solution.

In the first part of the research we tried to realize a measurement of K through only reactors, therefore the measurement system for the total amount of HxR, Hx and UA was prepared by combining Np-reactor and XO-reactor (way b). The system for total amount of IMP, HxR, Hx and UA was prepared by combining AlP-reactor, Np-reactor and XO-reactor (way a). A schematic diagram of the reactors system is shown in Fig. 1.

Hypoxanthine and related compounds determination were based on uric acid detection at a potential of 450 mV vs Ag/AgCl with carbon-based screen-printed electrode [7]. This potential value avoids high background current and several interferences from electroactive compounds. This system is more selective if compared with Platinum electrode for H_2O_2 detection held at 700 mV. This new procedure developed for determination of K values is more suitable for routine analysis than the conventional method (HLPC, Ehira's method) more complicated and time consuming.

2.5. Preparation of samples for fish freshness determination

Several authors proposed a treatment of fish sample according to Ehira's methods [6]. A simpler method has been used. 10 μl of exudate of fish muscle obtained by press treatment were diluted with 5 ml of buffer Imidazole 0.05 M pH 7.8 containing 0.1 M KCl and 50 mM KH_2PO_4. After filtration through 0.45 mm pore filters, exudates from fishes were used immediately as the sample without any pretreatment by injection into the sampling valve.

Samples for the determination of fish freshness were prepared from the specie gilthead bream obtained from Greece and Italy and stored at 4°C with or without ice, 48, 72, 96 or 120 h from death.

3. Results and discussion

3.1. FIA with XO and Np reactors

A first reactor loaded with XO and a second with Np were introduced into the FIA assembly. The current obtained with standard solutions of hypoxanthine (Hx) and inosine (HxR) are linear related with the concentration values and showed high reproducibility and fast recovery. The sampling rate is about 10 samples h^{-1}.

The response curves to HxR, Hx and UA were compared. After the output current reached a steady baseline, an aliquot of each compound was injected through the sampling valve into the reactor and the flowing electrode cell. Any appreciable difference was observed in the output currents and in the response time for HxR, Hx and UA.

In Fig. 2 the calibration curves for HxR, Hx and UA are reported in the range 1–12 μM indicating a total conversion of HxR and Hx to UA. The detection limits was 0.10 μM for all species when a 100 μl was injected. The correlation coefficients for HxR, Hx and UA were 0.998, 0.996 and 0.997, respectively.

The relative standard deviations for four replicate injections were 2–3% for a concentration of 10 μM.

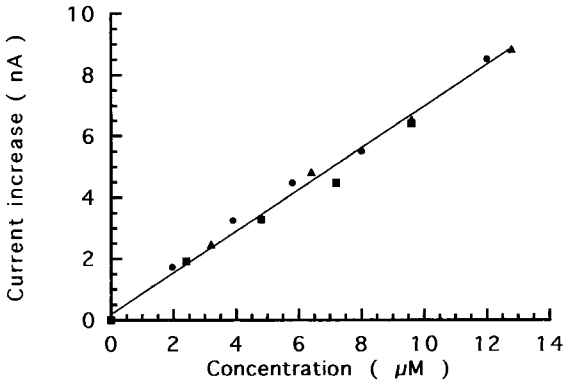

Fig. 2. Amperometric detection with immobilized Xanthine oxidase (XO) and Nucleoside phosphorylase (Np) reactors. Calibration curves for determination of (●) UA, (■) Hx and (▲) HxR. Flow rate, temperature, pH and sample volume were 0.5 ml min^{-1}, 20°C, 7.8 and 100 μl, respectively.

The XO and Np immobilized enzyme reactors were used repeatedly to evaluate the lifetime (Table 1). The system shows linear response after repetitive use even after 2 months with standard solutions. After 3 months, the XO-reactor has always the same behaviour (total transformation of Hx to UA) whereas the Np-reactor lost its performance (about 50%).

3.2. FIA with XO, Np and AlP reactors

We tried to obtain the same results for IMP by adding a reactor with AlP immobilized. The AlP-reactor was placed before the Np-reactor, line (a) of Fig. 1.

Table 1
Effect of the storage time on the output of the HxR and Hx sensors after 2 months

	Concentration of (μM)			
Hx	3.6	7.2	10.8	14.3
0 month (%)	100	100	100	100
2 months (%)	92	82	86	93
HxR	3.3	6.6	9.9	13.1
0 month (%)	100	100	100	100
2 months (%)	75	95	106	99

Sample volume, pH and flow rate were 100 μl, 7.8 and 0.5 ml min^{-1}, respectively.

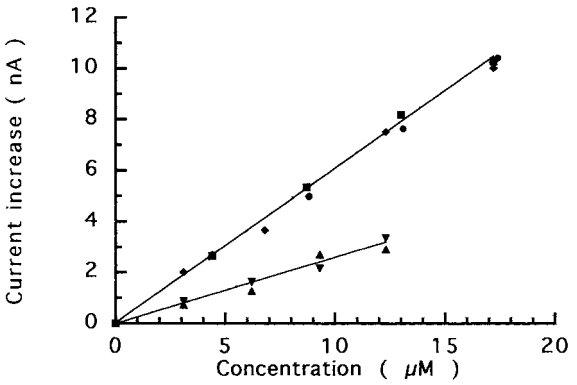

Fig. 3. Calibration curves for determination of (■) Hx, (●) HxR and IMP using (▲) 0.8 mU or (◆) 1.6 mU of AlP added in solution or (▼) AlP-reactor. pH 7.8; T, 20°C; flow rate, 0.5 ml min^{-1}; sample volume, 100 μl.

Standard solutions of IMP, HxR and Hx were injected into the three reactors in series, but the current values obtained from the same concentration were different. HxR and Hx gave the same current valve but IMP gave about the half of the value expected.

We tried to increase the temperature of the AlP reactor using a water thermostat and keeping it at 45°C. But also in this case the current value obtained by IMP was lower than expected.

Then we tried to use AlP in solution, mixing it with the standard solutions of IMP and leaving for 10 min at 45°C in a suitable thermostat.

We add 0.8 or 1.6 mU of AlP in 1 ml of standard solution and only with the higher concentration, total conversion of IMP was reached in the range 1–15 μM.

In Fig. 3 several results have been assembled, with AlP immobilized in reactors or kept in solution at the two concentrations values.

Linear relationships was obtained for IMP below 15 μM with a detection limit of 0.5 μM when a 100 μl was injected. The correlation coefficient and the regression line were 0.999 and $Y = 0.035 + 0.606X$ respectively.

Using the AlP reactor, the enzyme reaction was not complete. No appreciable difference was observed between the response obtained with the AlP immobilized or in solution at 0.8 mU. The calibration graph for IMP was linear below 12 μM using AlP in solution (0.8 mU) or immobilized, with 0.996 and 0.992.

The time for a single measurement was less than 3 min. This rapidity was mainly due to the smaller size of the reactors (70–80 μl).

To increase the extent of the enzymatic reaction, the AlP-reactor has been also placed in the 'loop' arm of the sampling valve in order to vary the contact time with the IMP solution.

In this arrangement the sample containing IMP fill the loop arm with the sampling valve in the position 'load'. After a suitable time (where the sample was in contact with the reactor), the sampling valve was shifted in the position 'inject' and the sample flowed in the other two reactors and then into the electrochemical detector cell.

Four different types of AlP reactor were prepared:

1. Type I, 81 U of AlP was immobilized.
2. Type II, 130 U of AlP.
3. Type III, 277 U of AlP.
4. Type IV, 81 U of AlP activated by $MgCl_2$ and $ZnCl_2$ (100 U ml^{-1} in the presence of 1 mM Mg^{2+} and 0.1 mM Zn^{2+}).

Optimal activity of AlP depends upon the concentration of Mg^{2+} and Zn^{2+} in the reaction mixture. Some Zn^{2+}, bound at a catalytic site, is required for catalytic activity. Mg^{2+} acts as an allosteric activator of AlP, binding to a site on the enzyme distinct from the Zn^{2+} site. However, Zn^{2+}, if present in excess of the amounts necessary for catalysis, will also bind to the Mg^{2+} site (with greater affinity than Mg^{2+}) and thereby reverse the Mg^{2+} activation effect [9].

The efficiencies of the different types of AlP reactor were determined by using a standard IMP solution (3 μM).

The results (Fig. 4) showed that the extent of the enzymatic reaction was not complete although the time was also very long. Any AlP-reactor at 45°C didn't permit to obtain the total enzymatic reaction.

Therefore only the procedure involving the addition of AlP for 10 min at 45°C allows the total enzymatic reaction. We are not convinced that the completeness of the reaction happens in the

preincubation step, but we think that the presence of AlP dissolved in the sample completes the first reaction when the sample passes in the reactor with Np immobilized.

These results showed that a simple, a suitable approach for the K determination can be obtained by using only two reactors with XO and Np immobilized on the aminopropyl glass and by adding a suitable amount of AlP directly to the sample exudate.

3.3. Real samples

The exudates diluted 500 times with the buffer show linear behaviour in the range 0–20 μM with a detection limit of 0.1 μM. Therefore a detection limit of 0.05 mM in the exudate is obtained. After 40 assays with real samples the sensor has to be discarded and substituted with a new one. Therefore a disposable sensor is suitable for such kind of measurement [7].

K value was estimated by analyzing the two response peaks obtained under two different conditions, as shown in Fig. 5. The total amount of HxR, Hx and UA was evaluated by flowing the sample through to the two reactors in series. The amount of IMP, HxR, Hx and UA can be determined by flowing the sample where AlP was added and kept 10 min at 45°C.

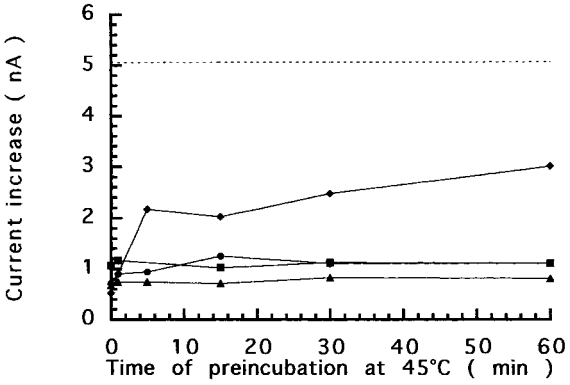

Fig. 4. Effect of the time of preincubation at 45°C on the output of the IMP sensor. (●) 81 U, (■) 130 U, (▲) 277 U and (◆) 81 U with 1 mM Mg^{2+} and 0.1 mM Zn^{2+}. (· · ·) current increase expected with a standard UA solution. pH, flow rate and standard IMP solution were 7.8, 0.5 ml min^{-1} and 3 μM, respectively.

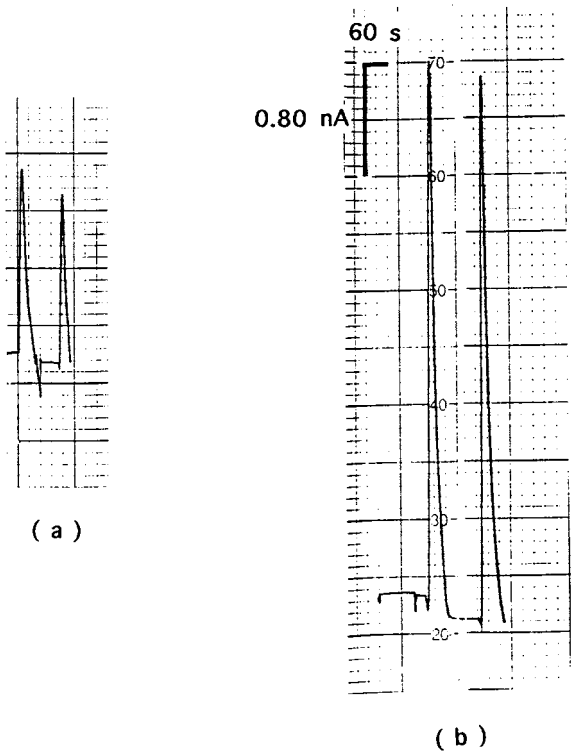

Fig. 5. Response curves of the sensor system using immobilized XO and Np reactors. Typical signals for 100 μl injections of samples solution. (a) The sum of UA, Hx and HxR and (b) the sum of UA, Hx, HxR and IMP. Carrier solution (0.05 M Imidazole buffer at pH 7.8 containing 0.1 M KCl and 0.05 M KH_2PO_4) was pumped at a flow rate of 0.5 ml min^{-1}.

The first and the second peaks of Fig. 5 correspond to the sum of UA, Hx and HxR concentrations (K_1) and UA, Hx, HxR and IMP concentrations (K_2), respectively. The K value was determined by the ratio $(K_1)/(K_2)$.

Three samples of exudates of gilthead bream with different values of K were repeatedly analyzed using a carrier solution (0.05 M Imidazole buffer at pH 7.8 containing 0.1 M KCl and 0.05 M KH_2PO_4) pumped at a flow rate of 0.5 ml min^{-1}. In Table 2 we report a study on the determination of K% of real samples stocked at 4°C with or without ice, 48, 72, 96 or 120 h from death.

The freshness was determined with the proposed reactors system and the results were compared with results obtained by the XO reactor

Table 2
Results obtained with real samples (Gilthead bream from Greece) stored at 4°C

Time from death (h)	K_1	K_2	$K(\%) = K_1/K_2$
48	0.77	4.07	18.9
	0.75	4.06	18.5
72	1.27	3.83	33.2
	1.22	3.83	31.8
96	1.51	3.86	39.1
	1.62	4.15	39.0

system and an uric acid detection [7]. These data were also determined with an amperometric procedure based on platinum electrode and hydrogen peroxide detection [10] in Table 3. Good agreement was observed between K values determined by the three procedures.

The present system based on FIA and two reactors has the advantage of simplicity of manual operation and of a good operational stability during 2 months for at least 700 assays. These conditions are obtained if the reactors are stored at 4°C in the working buffer when not in use and the sensor changed after 40 assays with real samples. The proposed prototype appeared promising for routine determination of fish freshness.

4. Conclusion

An amperometric detection based on FIA procedure using enzymes reactors (Np and XO reactors) and a carbon based screen-printed electrode is proposed for freshness detection. Exudates of fish can be only diluted and injected directly into the FIA system, therefore any preparation step is avoided.

Screen-printed electrode can be used for 30–40 assays without further calibration. The reactors can be exploited for 2 months or at least 700 samples.

Therefore K values can be obtained in 5 min with CV of 3–4% if the concentration is around 2 mM in the original sample; quality studies on fish samples can be easily performed. Good comparative results were observed between the K values determined by the XO reactor [7] and by the new system developed.

Acknowledgements

We acknowledge Prof. B.M. Poli (department of Scienze Zootecniche, University of Florence, Italy) for obtaining the real samples, for the results reported in Table 2 and for the useful discus-

Table 3
Comparison of K values obtained by the screen-printed electrode with one or two reactors and K values obtained by the platinum electrode

Storage method	Time from death (h)	K (%)		
		Pt electrode	SPC/XO reactor	SPC/XO–Np reactors
Gilthead bream from Greece				
4°C	48	21.5	22	19
	72	30	33	32.5
	96	—	41.5	39
4°C with ice	96	30	23	26
	120	24	39	33
Gilthead bream from Italy				
4°C	72	20	22	20
	96	28	24	22
	120	23	26	24
4°C with ice	48	9	11	15
	72	19	18	17
	96	28	21	23

sion. M.-A. Carsol acknowledges ECC Programm (Contract FAIR GT-97-3791).

References

[1] H. Okuma, H. Takahashi, S. Yazawa, S. Sekimukai, Anal. Chim. Acta 260 (1992) 93.
[2] I. Karube, H. Matsuoka, S. Suzuki, E. Watanabe, K. Toyama, J. Agric. Food Chem. 32 (2) (1984) 314.
[3] E. Watanabe, K. Toyama, I. Karube, H. Matsuoka, S. Suzuki, Appl. Microbiol. Biotechnol. 19 (1984) 18.
[4] E. Watanabe, K. Toyama, I. Karube, H. Matsuoka, S. Suzuki, J. Food Sci. 49 (1984) 114.
[5] H. Okuma, H. Takahashi, S. Sekimukai, E. Watanabe, Nippon Shokuhin Kogyo Gakkaishi 38 (1991) 1019.
[6] S. Ehira, H. Uchiyama, Bull. Jpn. Soc. Sci. Fish. 35 (1969) 1080.
[7] M.-A. Carsol, G. Volpe, M. Mascini, Talanta 44 (1997) 2151–2159.
[8] A. Cagnini, I. Palchetti, I. Lionti, M. Mascini, A.P.F. Turner, Sens. Actuators B 24–25 (1995) 85–89.
[9] J. Keesey, Biochemica Information, 1st edn., Boehringer Mannheim, Indianapolis, 1987, pp. 8–9.
[10] G. Volpe, M. Mascini, Talanta 43 (1996) 283–289.

ELSEVIER

Talanta 47 (1998) 343–348

Talanta

Co-ordination ability of Cu^{2+} ion toward the nucleobase-amino acid willardiine

Elzbieta Chruscinska [a], Eugenio Garribba [b], Giovanni Micera [b,*], Angelo Panzanelli [b], Marco Biagioli [b]

[a] *Institute of General Food Chemistry, Technical University of Lodz, Stefanowski Street 4/10, 90-924 Lodz, Poland*
[b] *Department of Chemistry, University of Sassari, Via Vienna 2, 07100 Sassari, Italy*

Received 16 December 1997; received in revised form 18 March 1998; accepted 19 March 1998

Abstract

The complex formation between Cu^{II} and DL-willardiine [1-(2-amino-2-carboxyethyl)uracil], an analog of phenylalanine containing the uracil residue, was investigated by potentiometric and spectral studies. The results indicate that the primary metal binding site of the ligand is the α-amino-carboxylate chelating set. The uracil moiety, however, can coordinate the metal ion in basic solution giving rise to intermolecular bridging. © 1998 Elsevier Science B.V. All rights reserved.

Keywords: Willardiine; [1-(2-Amino-2-carboxyethyl)uracil]; Uracylalanine; Cu(II) complexes

1. Introduction

The interaction of metal ions with amino acids and nucleic bases is of great interest because of their relevance to the essential, medicinal, or toxic bioactivity of metal centres. One of the main concerns in this area is the nature of the complex species that may be formed in solution. Speciation studies are aimed at determining the distribution and the structure of the complexes formed by the interaction of the metal with the ligand. This may be a rather difficult task and often needs the use of a combination of techniques, preferably analytical and spectroscopic methods. A case study is presented here. In the Cu(II)–willardiine system, only the combined use of pH-potentiometry and EPR can address satisfactorily the problem of nature and nuclearity of the complex species.

Willardiine (Wil) [1-(2-amino-2-carboxyethyl)-uracil] or uracylalanine, see Scheme 1, is an analog of phenylalanine that has been isolated from certain plants and is known to be a specific and potent agonist [1–6]. The ligand exhibits quite interesting structural features, including the functional groups distinctive of both an α-amino acid and the nucleobase uracil. Three different coordination sites, the amino nitrogen, the carboxyl oxygen(s), and the negatively charged imide nitrogen are available to metal ions and, presumably, they compete with each other.

* Corresponding author. Tel.: +39 79 229541; fax: +39 79 229559; e-mail: micera@ssmain.uniss.it

0039-9140/98/$ - see front matter © 1998 Elsevier Science B.V. All rights reserved.
PII S0039-9140(98)00130-1

A study on the metal complexes of the Wil ligand offers the opportunity of comparing the binding properties of an α-amino acid and the nucleobase uracil. The only study so far available on the ligand behaviour of willardiine is the report on a 'unique' multinuclear complex, with formula $[Na_2Cu_2Pd(Wil)_4(H_2O)_4]\cdot 9H_2O$, isolated in the solid state [7]. In the complex structure each copper atom is coordinated by two Wil ligands, each of them chelated through the amino carboxylate moiety. The arrangement of the ligands is such that the palladium ion can assume a square planar geometry by coordinating the four imide nitrogens of the uracil moieties. The structure, therefore, substantiates the feasibility of both the donor sites of the ligand as chelating moieties. Namely, it confirms the preference of the copper(II) for the amino carboxylate donor set with respect to the monodentate imide site.

In many cases, solid-state studies on metal complexes are scarcely representative of the ligand behaviour in solution. For instance, this happens if the species isolated in the solid state is only a minor component of the complex system. Therefore, we have examined the solution behaviour of the binary Cu(II)–Wil system in water over a wide pH range. Potentiometric and spectroscopic data for the interaction of Cu^{2+} with the ligand were measured and compared to those of related systems.

2. Experimental

2.1. Chemicals

DL-Willardiine (Wil) was used as obtained from Sigma (St. Louis, MO).

2.2. Potentiometric study

Concentration stability constants $\beta_{pqr} = [M_pA_qH_r]/[M]^p[A]^q[H]^r$ for H^+ and Cu^{2+} complexes were calculated from pH titration curves obtained at 25°C using a total volume of 2.0 cm^3. Alkali was added from a 0.1-cm^3 micrometer syringe that was calibrated by both weight titration and titration of standard materials. Experimental details were: ligand concentration, 2×10^{-3} mol dm^{-3}; metal-to-ligand molar ratios, 1:2 and 1:3; ionic strength, 0.1 mol dm^{-3} KNO_3. The experimental method was as follows: pH-metric titrations on a MOLSPIN pH-meter system using a micro combined glass/calomel electrode (Russell, CMAWL) calibrated in concentration using HNO_3 [8]; number of titrations, 4; method of calculations, SUPERQUAD program [9]. The samples were titrated from pH 2.3 to 11.1.

Standard deviation (σ values) quoted were computed by SUPERQUAD and refer to random errors only. They are, however, a good indication of the importance of the particular species in the equilibrium.

2.3. Spectroscopic measurements

EPR spectra were recorded on a Varian E-9 spectrometer at the X-band frequency (9.15 GHz) at 120 K. Absorption spectra were recorded on a Jasco Uvidec 610 spectrophotometer. The values of ϵ are evaluated for the maximum concentration of the particular species, as obtained from potentiometric data. The metal-to-ligand ratio was 1:2 and the metal concentration was 5×10^{-3} mol dm^{-3}.

3. Results and discussion

Three deprotonation constants (Table 1) were measured for the ligand (H_3A^+). These may be attributed, in order of decreasing acidity, to the carboxylic ($pK_{a1} = 1.465$), the α-ammonium ($pK_{a1} = 7.883$), and the imide ($pK_{a3} = 9.776$) groups. A comparison with literature data indicates that the carboxylic and ammonium groups are distinctly more acidic than in L-alanine [10], as an effect of the substitution by the nucleic base moiety. On the contrary, the imide group of Wil is less acidic than in uracil [11] because of the negative charge of the HA^- form that disfavors the further proton dissociation process.

Calculations based on potentiometric data indicate the formation of six monomeric complexes in the presence of Cu^{II} (Table 1, model I).

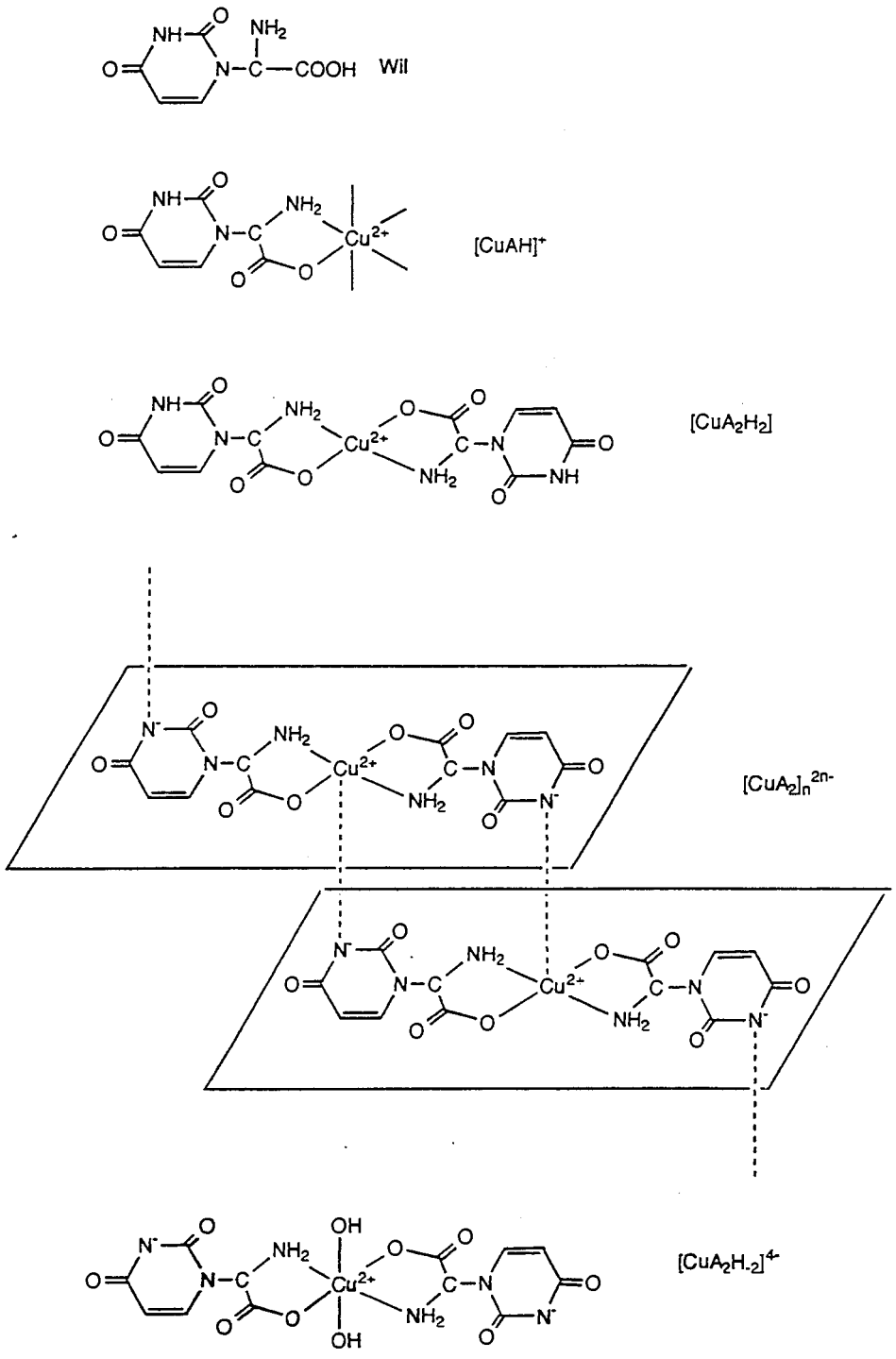

Scheme 1.

Table 1
Stability constants ($\log\beta$) of the proton and Cu^{II} complexes of DL-willardiine at $t = 25°C$ and $I = 0.1$ mol dm^{-3} (KNO_3)

Species	DL-Willardiine		L-Ala[a]	Uracil[b]
	Model I	Model II		
H_3A	19.124(1)			
H_2A	17.659(1)		12.071	
HA	9.776(1)		9.721	
p_a^K (COOH)	1.465		2.350	
pK_a (NH_3^+)	7.883		9.721	
pK_a (imide)	9.776			9.4–9.5
CuAH	16.631(4)	16.663(11)		
CuA			8.087	
CuA_2H_2	31.973(7)	32.066 (13)		
CuA_2H	23.182(9)	23.4 51(18)		
CuA_2	13.68(1)		14.761	
Cu_2A_4		30.969(39)		
CuA_2H_{-1}	2.12(3)	2.60(6)		
CuA_2H_{-2}	−8.37(1)	−8.11(3)		
pH range	2.3–11.1			
DL-Wil (model II)				
$Cu^{2+} + HA^- \rightleftharpoons [CuAH]^+$		$\log K_1 = 6.887$		
$[CuAH]^+ + HA^- \rightleftharpoons [CuA_2H_2]$		$\log K_2 = 5.628$		
$\log K_1/K_2$		1.259		
L-Ala				
$Cu^{2+} + A^- \rightleftharpoons [CuA]^+$		$\log K_1 = 8.087$		
$[CuA]^+ + A^- \rightleftharpoons [CuA_2]$		$\log K_2 = 6.684$		
$\log K_1/K_2$		1.413		

[a] Ref. [10].
[b] Ref. [11].

The complexation process starts with the 1:1 species $[CuAH]^+$ that is the main component at pH ca. 4.5. The bis complex $[CuA_2H_2]$ is the species predominant around pH 7. In both the complexes the Wil molecule is bound to the copper ion through the α-amino acid (COO^-, NH_2) chelating moiety. However, the imide groups remain undissociated in these complexes. Spectral and equilibrium data support this assignment.

The spectral parameters of the species (Table 2) are in very good agreement with those measured on the mono- and bis-chelated species formed by Cu^{II} with alanine in aqueous solution. The stability constants are in the range measured for the copper(II) complexes of α-amino acids [12]. However, a comparison of the equilibrium constants calculated for the complexation reactions (see Table 1) indicates that the mono- and bis-chelated complexes of alanine [10] are significantly more stable than those of willardiine. Most likely, this reflects the less basic strength of the chelating set of willardiine, as measured by the pK_a values of the free ligands.

In basic solution, the deprotonation of the bound ligands occurs to yield $[CuA_2H]^-$ and $[CuA_2]^{2-}$. The calculated pK_a values are 8.791 and 9.502 and they can be attributed to the dissociation of the imide protons. Compared to the free ligand (pK_a value of 9.776), the process is favoured slightly by the presence of the metal. This could be an effect of the electron-withdrawing properties produced by the metal ion bound to the amino carboxylate site or by the direct involvement of the deprotonated imide group in

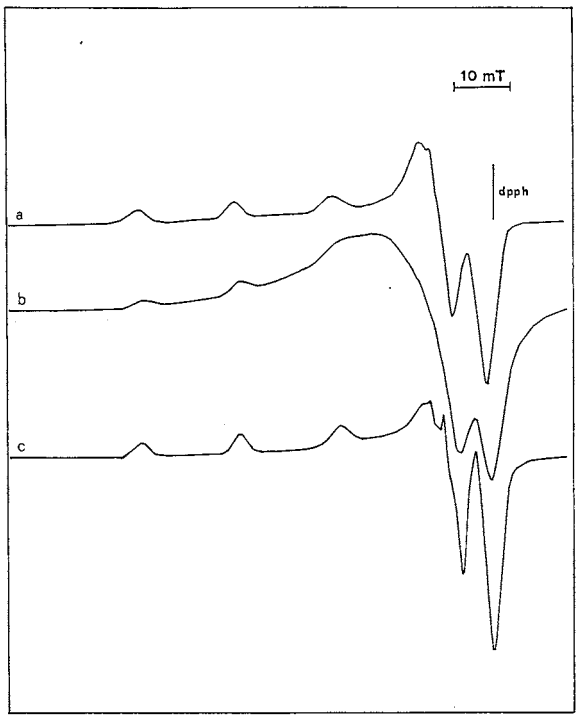

Fig. 1. X-band EPR spectra of the Cu(II)–Wil system, $c_{Cu(II)} = 5 \times 10^{-3}$ mol dm^{-3} and metal-to-ligand molar ratio 1:2, recorded at 140 K and pH 6.70 (a), 10.75 (b) and 11.75 (c).

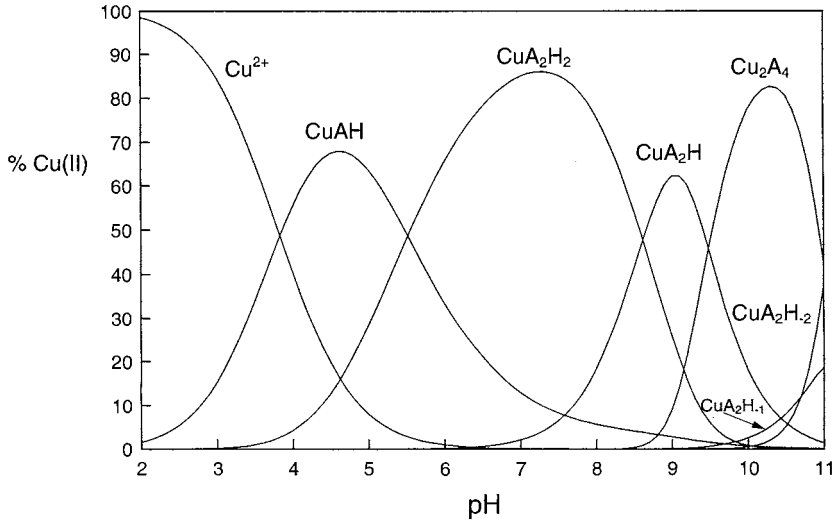

Fig. 2. Distribution curves of the complexes formed in the Cu^{II}–Wil system at the metal ion-to-ligand molar ratio 1:2, $c_{Cu(II)} = 2 \times 10^{-3}$ mol dm^{-3}.

copper(II) binding. A support to the latter hypothesis is given by EPR spectra. In fact, glassy EPR spectra typical of magnetically dilute (e.g. monomeric) species are detected in the presence of $[CuAH]^+$ and $[CuA_2H_2]$. Instead, in the pH range 9–11 an unresolved broad resonance centered at g ca. 2 accompanies the signals of monomeric species (Fig. 1). The finding strongly suggests that, concomitant to the deprotonation of the imide groups, the complex units interact with each other through the uracil nitrogen donor to yield polymetallic species. The pH-metric titration data could be fitted equally well by the formation of a monomeric $[CuA_2]^{2-}$ or a dimeric $[Cu_2A_4]^{4-}$ species, which was chosen to simulate the polymerization process (Table 1, model II, and Fig. 2). However, when both the monomeric and the dimeric species were assumed and refined simultaneously in the pH-metric calculation, the former was always rejected by the computer program.

Noticeably, the EPR features distinctive of purely monomeric species are restored in the high pH range upon formation of $[CuA_2H_{-2}]^{4-}$. Both $[CuA_2H_{-1}]^{3-}$ and $[CuA_2H_{-2}]^{4-}$ can be assumed as species formed by the binding of one or two hydroxo ions, respectively, to the copper(II) center of $[CuA_2]^{2-}$. This additional binding destroys the polymeric arrangement and restores magnetically dilute complexes. The metal environment in $[CuA_2H_{-2}]^{4-}$ is significantly different from that

Table 2
EPR and absorption parameters for the Cu^{II} complexes formed by DL-willardiine

Species	$g_\parallel$	$A_\parallel$ (10^{-4} cm^{-1})	λ_{max} (nm)	ϵ^{a}_{max} (dm^3 mol^{-1} cm^{-1})
$[CuAH]^+$	2.315	168	690	30
$[CuA_2H_2]$	2.260	184	[b]	
$[CuA_2H]^-$				
$[CuA_2]^{2-}$			630	55
$[CuA_2H_{-1}]^{3-}$				
$[CuA_2H_{-2}]^{4-}$	2.253	190	640	40

[a] Measured at the maximum extent of formation.
[b] Not measurable because of the turbidity of the solution.

of $[CuA_2H_2]$ as indicated by the increase of $A_{\parallel}$ and the decrease of $g_{\parallel}$ in the EPR spectra.

It is also worth noting that, in the binary uracil–Cu^{II} system, at the 2:1 ligand-to-metal molar ratio, the EPR resonances attributable to a single complex species ($g_{\parallel} = 2.290$ and $A_{\parallel} = 175 \times 10^{-4}$ cm^{-1}) are detected to a maximum extent at pH ca. 9. The signals, most likely due to a complex with two uracil nitrogens bound to copper, exhibit parameters different from those measured in the system containing Wil. Therefore, the only involvement of the uracil in the metal binding may be excluded in the latter system.

4. Conclusions

From the results of the present study it is worth concluding that, similarly to α-amino acids, Wil can form mononuclear species through the involvement of the amino carboxylate donor set. The imide group can also act as a donor in basic solution. Because of the absence of chelating properties, uracil is not effective in displacing the metal ion from the amino acid site. However, the imide group could be responsible for intermolecular bridging and favour the assembly of monomeric units in polymetallic structures. The polymeric arrangement is clearly shown by EPR spectral measurements.

Acknowledgements

This work was supported by the Polish State Committee for Scientific Research (KBN, 3 T09A 05708) and M.U.R.S.T (Project 40%).

References

[1] A.P. Martinez, W. Lee, J. Org. Chem. 30 (1965) 317.
[2] M.T. Doel, A.S. Jones, R.T. Walker, Tetrahedron 30 (1974) 2755.
[3] J.D. Buttrey, A.S. Jones, R.T. Walker, Tetrahedron 31 (1975) 73.
[4] M.A.S. Ahmmas, C.S. Maskall, E.G. Brown, Phytochemistry 23 (1984) 265.
[5] C.F. Zorumski, L.L. Thio, D.B. Clifford, Mol. Pharmacol. 40 (1991) 45.
[6] F. Ikegami, S. Horiuchi, M. Kobori, I. Morishige, I. Murakoshi, Phytochemistry 31 (1992) 1991.
[7] M. Mizutani, K. Jitsukawa, H. Masuda, H. Einaga, J. Chem. Soc., Chem. Commun. (1996) 1389.
[8] H.M. Irving, M.G. Miles, L.D. Pettit, Anal. Chim. Acta 38 (1967) 475.
[9] P. Gans, A. Vacca, A. Sabatini, J. Chem. Soc. Dalton Trans. (1985) 1195.
[10] M. Branca, G. Micera, T. Kiss, M. Sinibaldi, J. Chem. Res. (1990) 392.
[11] H. Lönnberg, Proton and metal ion interaction with nucleic bases, nucleosides, and nucleoside monophosphates, in: K. Burger (Ed.), Biocoordination Chemistry, ch. 7, Ellis Horwood, London, 1990, p. 294.
[12] T. Kiss, Complexes of amino acids, in: K. Burger (Ed.), Biocoordination Chemistry, ch. 3, Ellis Horwood, London, 1990, p. 56.

ELSEVIER

Talanta 47 (1998) 349–353

Talanta

Kinetic determination of trace cobalt(II) by visual autocatalytic indication

Masatoshi Endo [a,*], Shigeki Abe [a], Yuji Deguchi [b], Takao Yotsuyanagi [b]

[a] *Department of Materials Science and Engineering, Yamagata University, Yonezawa 992, Japan*
[b] *Department of Molecular Chemistry and Engineering, Tohoku University, Sendai 980-77, Japan*

Received 15 September 1997; received in revised form 24 March 1998; accepted 25 March 1998

Abstract

A highly sensitive and simple visual autocatalytic method has been developed for the determination of trace cobalt. The cobalt ion released by the oxidative decomposition of inert bis[2-(5-bromo-2-pyridylazo)-5-(*N*-propyl-*N*-sulfopropyl-amino-phenolato] cobaltate (Co(III)-5-Br-PAPS) with peroxomonosulfate acts as a catalyst for the oxidative degradation of the complex. Thus a definite time lapse of degradation is observed by the sudden disappearance of colored Co(III) complexes. The degradation time varies inversely with the logarithm of the initial concentration of cobalt(II). The determination range of cobalt(II) was from 3×10^{-9} to 2×10^{-7} M in the presence of 5×10^{-6} M of 5-Br-PAPS. The relative standard deviation of the spot size method (10 μl) was 3.5% at 1×10^{-7} M cobalt(II). This autocatalytic indicator reaction system has been successfully applied for the visual determination of urinary cobalt. © 1998 Elsevier Science B.V. All rights reserved.

Keywords: Autocatalytic indication reaction; Autocatalytic oxidation of cobalt(III)–pyridilazo dye complex; Automultiplication of catalyst; Kinetic determination of urinary cobalt; Visual method of analysis

1. Introduction

In rapidly expanding analytical fields such as environmental monitoring of trace metals, there is an increasing need to develop simple and sensitive analytical techniques that do not use expensive and/or complicated test equipment. Thus various simplified reaction-rate methods have been developed; the use of Landolt reaction and metal ion-catalyzed reactions was reported for the determination of V and Mo [1,2]. Catalytic substitution reaction was also applied to the visual determination of total heavy metals in fresh water [3]. These kinetic techniques, however, were devised without resort to their attainable analytical sensitivity.

Recently, a combined approach of chemical amplification and catalytic reaction has been proposed for ultra-trace metal analysis; the concept of the constant sensitivity of determination was introduced and its analytical utility has been demonstrated by theoretical and experimental considerations [4,5]. In the decomposition of the

* Corresponding author. Fax: +81 238 263413; e-mail: te027@dip.yz.yamagata-u.ac.jp

0039-9140/98/$ - see front matter © 1998 Elsevier Science B.V. All rights reserved.
PII S0039-9140(98)00139-8

inert bis[2-(5-bromo-2-pyridylazo)-5-(*N*-propyl-*N*-sulfopropyl-amino-phenolato] cobaltate (Co(III)-5-Br-PAPS) complexes with peroxomonosulfate, the inflection time is indicated spectrophotometrically by the sudden disappearance of colored cobalt(III) complexes. This degradation time can be conveniently determined by substituting a stopwatch for a spectrophotometer. The present investigation extends this novel autocatalytic indication system to the simple chronometric determination of trace cobalt(II). Moreover, the method is adopted to various sample sizes (i.e. macro, micro and spot size scales), which permits cobalt(II) determination down to 10^{-9} M.

2. Experimental

2.1. Apparatus

A Toa Model HM-26s pH meter was used for pH measurements. A Taiyo Model CL-80 thermostat was used to control the temperature. An Hitachi double-beam spectrophotometer, Model U-3000, equipped with a constant-temperature cell holder and magnetic stirrer was used to obtained basic spectrophotometric data. A Carbolite Model ESF3-ELP electric furnace was used to decompose urine samples.

2.2. Reagents

All chemicals used were analytical-reagent grade. Standard cobalt(II) solutions were prepared by dissolving cobalt(II) chloride hexahydrate in water. The solution of Co(III)-5-Br-PAPS was prepared from 2×10^{-3} M 5-Br-PAPS and 1×10^{-3} M cobalt(II) at 70°C. Potassium peroxomonosulfate (Oxone, Sigma) was used as an oxidizing agent. A phosphate buffer (pH 7.0) was prepared from potassium dihydrogenphosphate and disodium hydrogenphosphate.

2.3. Procedures

2.3.1. Macro scale method

Reactants were taken to a 100 ml Erlenmeyer flask in the following order: 10.0 ml of the reagent solution containing 4.0×10^{-5} M Co(III)-5-Br-PAPS, 1.0×10^{-5} M 5-Br-PAPS and 0.2 M phosphate buffer, and 2.0 ml of water. The reaction was started by the simultaneous addition of 5 ml of 2% Oxone and 3 ml of sample solution. The degradation time (t_d) of the violet cobalt(III) complex was followed visually using a stopwatch. The temperature was controlled at 25°C during the measurements.

2.3.2. Micro scale method

Reagent solution (100 μl) and water (20 μl) were placed on an assay plate (350 μl, 96 wells) and stirred. The reaction was started by the simultaneous addition of 50 μl of 2% Oxone and 30 μl of sample solution. The t_d value was measured as described above.

2.3.3. Spot size method

Reagent solution (5.0 μl) and water (1.0 μl) were placed on a Teflon sheet, which was vibrated mechanically. The reaction was started by the simultaneous addition of 2.5 μl of 2% Oxone and 1.5 μl of sample solution. The t_d was measured as above. The reaction temperature was maintained at 25°C by using a thermostat and a heating copper plate. Experiments were done in an air-conditioned room (25°C).

2.3.4. Determination of cobalt in urine

Urine samples were decomposed by the recommended dry method [6]. Briefly, 5 ml of each sample were taken in a porcelain crucible and evaporated to dryness. To remove the coexisting organic compounds, it was heated in a electric furnace at 450°C for 2 h and at 600°C for 6 h. First 1.0 ml of 1 M HCl was added to the mineralized sample for dissolution, then 2.2 ml of 1 M NaOH, 0.05 ml of anhydrous acetic acid and 0.75 ml of deionized water were added to the solution. A calibration curve was made under the same conditions.

3. Results and discussion

3.1. Autocatalytic decomposition of Co(III)-5-Br-PAPS complex

The autocatalytic degradation of the cobalt(III)

complex with peroxomonosulfate was followed spectrophotometrically in phosphate buffer media (Fig. 1). The degradation point for the decomposition of cobalt(III) complexes shifts with an increase in the initial cobalt(II) concentration and a similar sigmoidal reactant concentration–time profile was obtained. As the time required for the completion of degradation is very short and the colored complex suddenly disappears, visual detection of a degradation time is easily done. This time-dependent response resembles that observed in titrimetric analysis.

The inert violet Co(III)-5-Br-PAPS chelate was selected as an autocatalytic indication substrate; it is stable over the wide pH range and its high molar absorptivity (9.8×10^4 l mol^{-1} cm^{-1} at 590 nm) permits the visual observation of reaction processes. Accurate measurements of the degradation time with a stopwatch are done by a color change from violet to colorless.

3.2. Effect of reaction variables

The rate of autocatalytic reactions was found to decrease with an increase of the Co(III)-5-Br-PAPS concentration [5]. As a compromise, 2×10^{-5} M Co(III)-5-Br-PAPS was used for visual indication. Peroxomonosulfate was most suitable as an oxidant for the present purposes. An increase in the Oxone concentration causes a decrease in the inflection time as shown in Fig. 2. The Oxone concentration was selected at 0.5%.

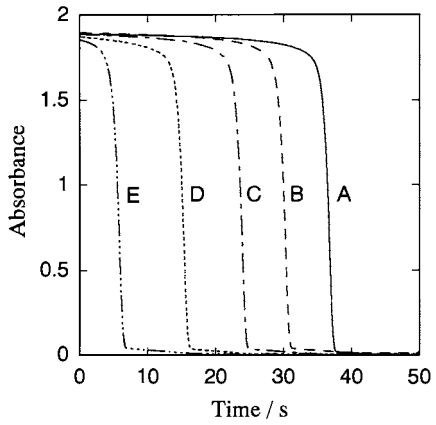

Fig. 1. Autocatalytic reaction curves for decomposition of the Co(III)-5-Br-PAPS complex. [Co(II)]: (A) 0, (B) 1.5×10^{-8}, (C) 3×10^{-8} M, (D) 7.5×10^{-8}, (E) 1.5×10^{-7} M. [Co-5-Br-PAPS]: 2×10^{-5} M. [5-Br-PAPS]: 1.5×10^{-5} M. [Oxone]: 0.5%. Wavelength: 590 nm.

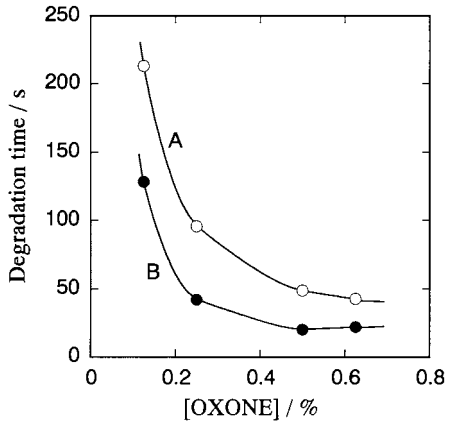

Fig. 2. Effect of Oxone concentration on the degradation time: (A) in the absence of cobalt, (B) in the presence of cobalt. [Co-5-Br-PAPS]: 2.0×10^{-5} M. [5-Br-PAPS]: 1.5×10^{-5} M. [Co]: 7.5×10^{-8} M. [Phosphate buffer]: 0.025 M (pH 7).

When the autocatalytic oxidative decomposition of Co(III) complex with peroxomonosulfate was conducted in phosphate buffer media, a pH change was observed in the course of the reaction. A high buffer concentration (0.025 M) is preferred to analyze the kinetic data at pH 7. Although the limit of cobalt(II) determination is lower at high buffer concentrations, the formation of insoluble blue Co(III)-5-Br-PAPS salt was also proceeded.

The degradation time decreases about 10% by raising the reaction temperature 1°C in the presence of cobalt. The reaction condition was selected at 25°C for further study. When a small quantity of sample solution was measured, the effect of diffusion can not be negligible. The mixing of the reaction solution by a vibration method is preferable when a small reaction volume is used.

The degradation time increased in the presence of free 5-Br-PAPS (Fig. 3). We have ascertained that the coordinating ligands were oxidized competitively, although they contributed to stabilize the cobalt(III) chelates. Thus a high sensitivity

Table 1
Maximum allowable foreign ions for the determination of cobalt

Ion	Maximum mole ratio, [Interferant]/[Co(II)]	Ion	Maximum mole ratio, [Interferant]/[Co(II)]
V(V)	100	Cl^-	10000 [a]
Cr(III)	100	Br^-	100
Cr(VI)	100	NO_3^-	10000 [a]
Mn(II)	100	ClO_4^-	10000 [a]
Fe(II)	100	SO_4^{2-}	10000 [a]
Ni(II)	100	Oxalate	10
Cu(II)	10	Phthalate	100
Zn(II)	100	Citrate	50
		Tartrate	500

[Co(II)]: 1×10^{-7} M. [5-Br-PAPS]: 1×10^{-5} M.
[a] Effects of interferant above this concentration were not investigated.

was obtained when small amounts of 5-Br-PAPS were added. EDTA and trans-1,2-cyclohexanediamine-*N*,*N*,*N*′,*N*′-tetraacetic acid showed similar behavior.

3.3. Comparison of macro and micro methods

It is desirable to choose the reaction volume arbitrarily in routine analysis. Our primary concern is the minimum use of reagent and the reduction of waste. Good analytical results were obtained when an Erlenmeyer flask, an assay plate and a Teflon sheet were used as reaction media. The degradation time was found to be almost equal, regardless of the reaction volume. Thus measurements can be done in various reaction volumes (20 ml to 10 μl). In particular, the assay plate and the Teflon sheet methods afford multiple analysis of samples.

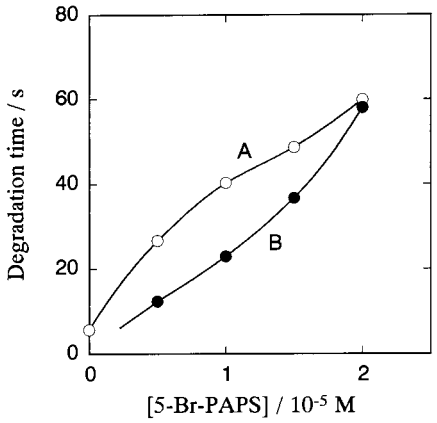

Fig. 3. Effect of free 5-Br-PAPS concentration on the degradation time: (A) in the absence of cobalt, (B) in the presence of cobalt. [Co-5-Br-PAPS]: 2.0×10^{-5} M. [Co]: 7.5×10^{-8} M. [Oxone]: 0.5%. [Phosphate buffer]: 0.025 M (pH 7).

3.4. Calibration and selectivity

The degradation time against the logarithm of analyte concentration gave a linear calibration graph from 3×10^{-9} to 2×10^{-7} M cobalt(II) in the presence of 5×10^{-6} M 5-Br-PAPS. The relative standard deviation was 3.5% ([Co(II)] = 1×10^{-7} M, $n = 5$) including personal error for the spot size method (10 μl).

Metal ions such as V(V), Mn(II), Fe(II), Ni(II) and Zn(II), when present at more than 10^{-5} M, affected the determination of 1×10^{-7} M

Table 2
Determination [a] of cobalt in urine samples

Sample no.	Urine excreted (ml)	Cobalt concentration ($\times 10^{-6}$ M)
1	100	0.10
2	250	0.28
3	70	1.15
4	180	1.17
5	160	0.43
6	270	0.28
7	50	2.02

[a] Analytical data according to the micro method.

cobalt(II) in the presence of 1×10^{-5} M 5-Br-PAPS (Table 1). Relative errors of less than 5% was considered negligible. Chloride, nitrate, sulfate and perchlorate anions did not interfere. Bromide ion accelerated the reaction at concentrations above 1×10^{-5} M. Tartrate, phthalate, citrate and oxalate anions inhibited as reductants. Thus, the autocatalytic indicator reaction showed good selectivity.

3.5. Determination of trace cobalt in urine

The proposed micro scale method was applied to the determination of cobalt in urine samples. The samples were decomposed by the dry method [6] to remove the coexisting organic compounds. The analytical data are shown in Table 2. The samples were collected from a healthy adult male (22 years) successively during 48 h. The concentration range of cobalt in the urine was $0.1–2.0 \times 10^{-6}$ M. Interestingly, the amount of cobalt present in the urine was almost 4–6 μg, although the excreted concentration of cobalt varied considerably. The reliability of the method was confirmed by the standard addition technique. The recovery of 0.81×10^{-6} M cobalt in real urine sample was 105%. The relative standard deviation for urine analysis (1.1×10^{-6} M cobalt) was 7.0% ($n = 3$). The method could be useful for monitoring cobalt in biological processes.

4. Conclusion

In the autocatalytic oxidation of colored substrate containing specified catalyst, the completion of the reaction was precisely estimated by visual observation of the induction period. The determination of trace cobalt(II) was possible through the autocatalytic oxidation of an indication substrate, i.e. Co(III)-5-Br-PAPS complex. This simple method is applicable down to 1.5 μl of a sample drop, cobalt(II) being detectable at 10^{-14} mol levels. The analytical utility of an autocatalytic indication in trace metal analysis will motivate further development of new types of metal complexes participating in the specified catalytic reaction.

References

[1] Cai Qihua, Gu Bo, Zhang Yuyong, Talanta 36 (1989) 665.
[2] S. Kawakubo, K. Ogihara, M. Iwatsuki, Bunseki Kagaku 45 (1996) 965.
[3] S. Abe, A. Kanno, K. Hasegawa, M. Endo, Int. J. Environ. Anal. Chem. 42 (1990) 45.
[4] M. Ishihara, M. Endo, S. Igarashi, T. Yotsuyanagi, Chem. Lett. 1995 (1995) 349.
[5] M. Endo, M. Ishihara, T. Yotsuyanagi, Analyst 121 (1996) 391.
[6] M.G. Angelova, A.A. Alexiev, Anal. Chim. Acta 290 (1994) 363.

ELSEVIER

Talanta 47 (1998) 355–359

Talanta

Synthesis of amido black diazoaminoazobenzene and its application to the spectrophotometric determination of micrograms of cadmium

Peng-Fei Zhang *, Hong-Wen Gao [1], Yong Li

Department of Chemistry, Huaibei Coal Teachers College, Anhui 235000, People's Republic of China

Received 1 December 1997; received in revised form 6 March 1998; accepted 27 March 1998

Abstract

A new azoamino reagent amido black diazoaminoazobenzene (ABDAB) has been synthesized, and found to be a good chromogenic reagent for cadmium. In pH 10.4 $Na_2B_4O_7$NaOH buffer solution cadmium reacts with ABDAB to form an orange-red chelate (1:2), exhibiting an absorption maximum at 520 nm. The apparent molar absorptivity is 1.62×10^5 l mol^{-1} cm^{-1}. Beer's law is obeyed in the range 0–8 μg/25 ml Cd. The method is simple and rapid, with high sensitivity and good selectivity and is applied to the determination of trace amounts of cadmium in waste water and metal materials with satisfactory results. © 1998 Elsevier Science B.V. All rights reserved.

Keywords: Amido black diazoaminoazobenzene; Cadmium; Spectrophotometry

1. Introduction

An azoamino reagent is a good chromogenic reagent for the spectrophotometric determination of cadmium [1–5]. In this paper, the preparation of amido black diazoaminoazobenzene (ABDAB), and the chromogenic reaction of this reagent with cadmium in aqueous solution are reported. Its structure is:

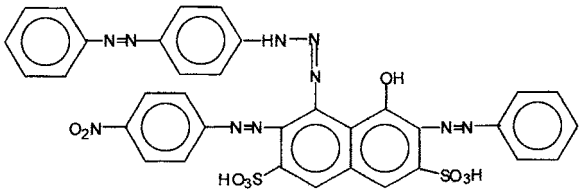

It reacted with cadmium in pH 10.4 $Na_2B_4O_7$–NaOH buffer solution to form an orange-red chelate(1:2).The absorption maximum is at 520 nm and the molar absorptivity is 1.6210^5 l mol^{-1} cm^{-1}. Beer's law is obeyed in the range 0–8 μg/25 ml Cd(II). The method is simple and rapid for the determination of cadmium. In addition, it give a high sensitivity in the presence of both

* Corresponding author.

[1] Huaibei Institute of Environment Science.

0039-9140/98/$ - see front matter © 1998 Elsevier Science B.V. All rights reserved.
PII S0039-9140(98)00150-7

sodium fluoride–sulfocarbamide and sodium citrate. It was used to determine trace amounts of cadmium in waste water and metal samples with the following results: the recovery was between 97–104% and the R.S.D. $< 2.8\%$.

2. Experimental

2.1. Reagents

The following reagents were used: Cd(II) standard solution, 1.0000 g of pure cadmium (99.99%) was dissolved in 30 ml hydrochloric acid. It was transferred to a 1000 ml volumetric flask and diluted to the mark with water. The concentration of this solution was 1.000 mg ml^{-1}, and it was diluted with water to contain 5.0 μg ml^{-1} Cd as required. An ABDAB ethanol solution (0.24‰), a pH 10.4 $Na_2B_4O_7$–NaOH buffer solution, a 1% Triton X-100–SDBS (10:1) solution and a 1% sodium fluoride–sulfocarbamide–sodium citrate reagent.

All the above chemicals were of analytical-reagent grade, and all solutions were prepared with redistilled water.

2.2. Apparatus

Absorbances and absorption spectra were recorded with a model 723G (Shanghai Analytical Instrument) with 1 cm cells, respectively. The pH measurements were made with a model pHS-3D pH meter (Chengdu Electroanalytical Instrument). Elemental analysis were done with a CE model CE-1106 analyzer. A model PE-683 infrared spectrophotometer and a Bruker model AC-80 NMR spectrometer were used for recording IR and NMR spectra.

2.3. Synthesis of ABDAB

Dissolve 1.0 g (1.6 mmol) of amino black 10B in 20 ml hydrochloric acid solution (8%), and cool the solution to 0°C, then add 0.24 g sodium nitrite with vigorous stirring for 20 min and the diazotate is formed. Dissolve 0.32 g (1.6 mmol) aminoazobenzene in 10 ml ethanol solution (95%), and add 5 ml 10% sodium carbonate solution, then add the diazotate solution drop wise to this solution with vigorous stirring, stir for 30 min and adjust the solution pH to 3–5 with 10% sodium carbonate solution. Stir for 1 h at room temperature, adjust the solution to neutral pH with 10% sodium carbonate solution, and then let the mixture stand overnight. Filter off the precipitate. Wash with ethanol and recrystallize from saturated sodium carbonate solution and concentrated hydrochloric acid. Yellowish brown flakes were obtained (m.p. 116°C, decomposition), and the yield was about 65%. The structure has been verified by thin-layer chromatography, elemental analysis, IR and ^1H NMR. TLC (silica gel GF254): a yellow spot is obtained in spreading agent (cyclohexane–ethyl acetate (9:1)), $R_f = 0.45$.

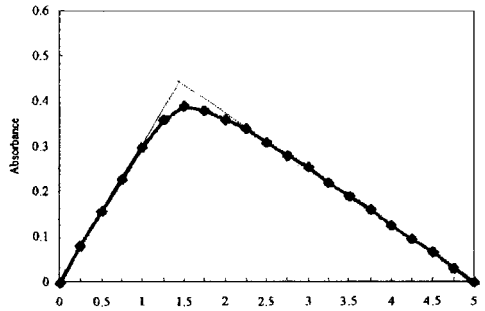

Fig. 1. The molar ratio method, [Cd] = [ABDAB] = 8.2×10^{-5} mol l^{-1}.

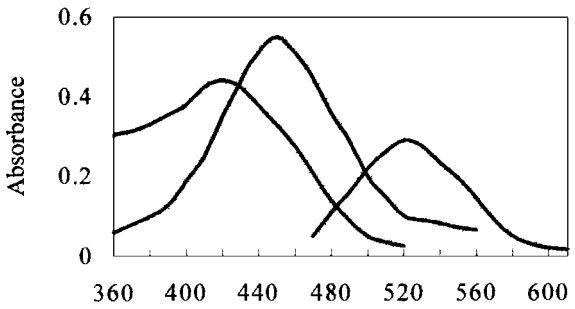

Fig. 2. Absorption spectra of ABDAB and its cadmium chelate, 1 cm cell: (1) ABDAB (2.98×10^{-5} M) vs. H_2O; (2) Cd(II) chelate (1.78×10^{-6} M) vs. reagent blank; (3) Cd(II) chelate (1.78×10^{-6} M) vs. H_2O.

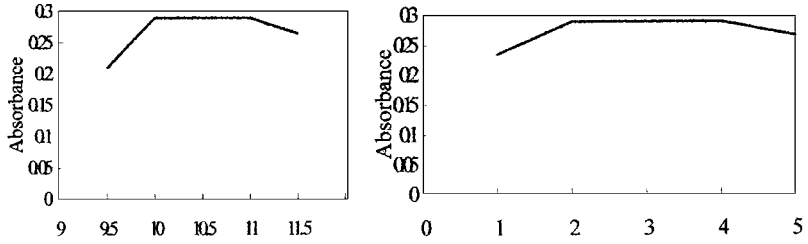

Fig. 3. Effect of pH and surfactant active agent.

Elemental analysis: $C_{34}H_{24}N_{10}O_9S_2$ requires C 52.31; H 3.10; N 17.94%; found C 52.06; H 2.97; N 17.21%. IR ν(KBr): 3456 (OH), 3385 (NH), 3058 (ArH), 1601, 1507, 1467, 1408 (C=C, N=N), 1336 (NO_2), and 1288 (C–N) cm^{-1}. ^1H NMR (solvent: d_6-DMSO, TMS as internal standard) δ 9.19 ppm (2H, s, SO_3H), δ 7.15–7.32 ppm and 7.437.82 ppm (20H, m, ArH), 5.57 ppm (1H, s, OH), δ3.87 ppm (1H, br, NH).

2.4. General procedure

Transfer 5 μg Cd(II) to a 25 ml volumetric flask. Add 5.0 ml of pH 10.4 $Na_2B_4O_7$NaOH buffer solution, 3.0 ml 1% Triton X-100–SDBS solution, 1.0 ml 0.24‰ ABDAB solution and 1.0 ml sodium fluoride–sulfocarbamide–sodium citrate solution. Dilute to volume with water and mix well. After 10 min record the absorbance at 520 nm in a 1 cm cell against a reagent blank.

3. Results and discussion

3.1. Properties of the reagent

The reagent was soluble in DMF (red-brown), acetone (grass green), dioxane (green-yellow), ethyl alcohol (yellow-brown), water (violet-brown), acid solution (pale red) and basic solution (deep green-yellow).

The composition of the chelate and complex constant were determined by the continuous variation method, the molar ratio method (Fig. 1) and the β-correction spectrophotometric method [6]. All the experiments indicated that a 1:2 cadmium chelate was formed, and the complex constant was $K = 5.95 \times 10^5$. For example, in Fig. 1 the chelate (Cd–ABDAB (1:2)), $\alpha = (0.45 - 0.39)/0.45 = 0.133$, $K = (1\text{-}\alpha)/C\alpha^2 = (1 - 0.133)/8.2 \times 10^{-5} \times (0.133)^2 = 5.95 \times 10^5$.

3.2. Absorption spectra

The absorption spectra of ABDAB and its cadmium chelate were recorded as shown in Fig. 2. The absorption maximum of the reagent lies at 420 nm (H_2O) and that of the chelate at 520 nm (reagent blank). 520 nm was chosen for the measurements as its sensitivity is higher, and the absorbance of the reagent itself is very small.

3.3. Effect of the reagent concentration

The absorbances of a series of solutions containing 5.0 μg cadmium and various amounts of 0.24‰ ABDAB solution were measured. It was found that 0.5 ml 0.24‰ ABDAB solution sufficient to complex 5.0 μg Cd; with 2.0 ml reagent

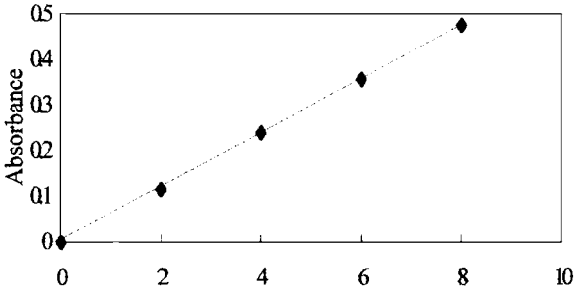

Fig. 4. Calibration graph for the determination of cadmium.

Table 1
Tolerance limits for the determination of cadmium[a]

Ion added	Amount tolerated (μg)	Ion added	Amount tolerated (μg)
Hydroxylamine hydrochloride	2000	Mn(II)	400
Citrate	2000	Mg(II)	400
CNS	2000	Al(III)	150
Tartrate	1000	Ca(II)	150
Salicylic acid	1000	Zn(II)	125
Thiourea	1000	Bi(III)	50
F^-	1000	Tl(III)	50
Cl^-	1000	Hg(II)	50
Br^-	1000	Zr(II)	30
I^-	1000	Ce(IV)	25
K^+	1000	W(VI)	20
Na^+	1000	U(VI)	15
Li^+	1000	Pd(II)	12
NH_4^+	1000	Pb(II)	9 (50[b])
NO_2^-	1000	Ni(II)	7 (35[b])
Cr(III)	800	Fe(III)	5 (25[b])
Ba(II)	1000	Co(II)	5 (20[b])
$C_2O_4^-$	550	Ag(I)	5 (25[b])
SO_4^{2-}	800	Au(III)	4 (15[b])
V(V)	900	Cu(II)	4 (15[b])
Sr(II)	400		

[a] The solution contained 5.0 μg of Cd(II).
[b] Amount tolerated of added marking reagent.

Table 2
Results of cadmium determination in the sample[a]

Sample	ABDAB method[b]		Standard method	R.S.D. (%)	Recovery (%)
	Introduced	Found			
0113Water	0	0.157	0.160	2.4	104
	0.100	0.261			
CW0104	0	0.0118	0.0123	2.8	98
	0.0100	0.0216			
BY02171-1	0	0.148	0.150	2.1	97
Zinc sheet	0.100	0.245			
By0421-2	0	0.112	0.105	2.6	103
Zinc alloy	0.100	0.215			

[a] A measuring unit of standard water and alloy is mg ml^{-1} and percent respectivity.
[b] Average of six determinations.

concentrations the absorbance was essentially constant. Therefore 1.0 ml of the reagent solution was used. The time for the absorbance to reach a stable value was only 5 min at room temperature and the absorbance was stable for at least 24 h.

3.4. Effect of buffer solution and surfactant concentration

The absorbances of a series of solutions containing 5.0 μg cadmium and 1.0 ml 0.24‰ ABDAB were measured adding various buffer

solutions and surfactant concentrations. Fig. 3 shows that the cadmium reacts strongly with ABDAB and their solution reaches maximum sensitivity between pH 10.0–11.0 and 2.0–4.0 ml 1% Triton X-100–SDBS. Hence pH 10.4 $Na_2B_4O_7$–NaOH and 3.0 ml 1% Triton X-100–SDBS were selected in the present study.

3.5. Calibration graph

The calibration graph obtained by the general procedure gives good linearity over the range 0–8 μg/25 ml cadmium as shown in Fig. 4. The linear regression equation was: $A = 0.0597C - 0.0006$ (C = μg/25 ml Cd) and the correlation coefficient was 0.9996. The apparent molar absorptivity was 1.62×10^5 l mol^{-1} cm^{-1}, and the Sandell sensitivity was 6.94×10^{-4} μg cm^{-2}.

3.6. Effect of diverse ions

Numerous cations and anions were examined by applying the method to a fixed amounts of cadmium in the presence of increasing amounts of the ion being studied. The tolerance limit was taken as the amount that caused an error of 5% in the absorbance. For the determination of 5.0 μg cadmium by this method, the foreign ions can be tolerated at the levels given in Table 1. It was shown that cations and anions can be masked in the determination of cadmium by adding 1% sodium fluride–sulfocarbamide–sodium citrite solution.

3.7. Samples analysis

As a test of the method, cadmium was determined in waste water and metal materials. The results were listed in Table 2. The recovery of cadmium was 97–104% and the R.S.D. $< 2.8\%$.

3.8. Structure of chelate

The experiment shows that the absorption spectrum were moved to red wavelength by adding basic solution and the infrared spectrum of ABDAB in 3300 cm^{-1} (ν N–H) were obviously weakened in Cd(II) to form the chelate. It was added at sensitivity by anion surfactant and it move to negative pole. According to Refs. [7,8] the probable structure of chelates is as follows:

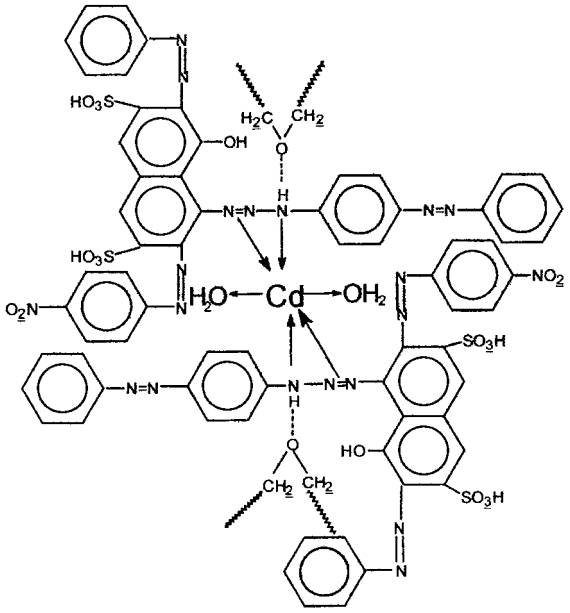

4. Conclusion

Relatively large conjugate systems and polar functional groups are led into the azoamino molecule, the reagent property is improved for solubility in water and in selective sensitivity in the determination of cadmium. The colour reaction of cadmium with ABDAB in the presence of pH 10.4 $Na_2B_4O_7$–NaOH buffer solution provides a simpler, easier and more rapid determination of cadmium than atomic absorption, atomic emission and X-ray fluorescence. The method has good reproducibility and excellent colour stability. It has high sensitivity and good selectivity when applied to the determination of micrograms of cadmium.

References

[1] H. Watanabe, H. Ohmori, Talanta 26 (1979) 959.
[2] G. Papa, A.F. Danet, M. Popescu, Talanta 25 (1978) 546.
[3] P. Ghavanne, C. Geronim, Anal Chim. Acta 19 (1958) 377.
[4] L. Wang, P.P. Sun, N.K. Shen, Fenxi Huaxue 20 (1992) 648.
[5] P.F. Zhang, H.W. Gao, Can. J. Appl. Spectrosc. 41 (1996) 1.
[6] H.W. Gao, P.F. Zhang, Ind. Lab. 62 (1996) 335.
[7] L. Wang, N.K. Shen, Huaxue Xuebao 51 (1993) 1111.
[8] L. Wang, P.P. Sun, Huaxue Xuebao 53 (1995) 923.

ELSEVIER

Talanta 47 (1998) 361–366

Talanta

The study and application of biomimic peroxidase ferric 2-hydroxy-1-naphthaldehyde thiosemicarbazone (Fe^{III}-HNT)

Bo Tang [a,*], Ming Du [b], Ying Sun [b], Hai-ling Xu [a], Han-xi Shen [b]

[a] *Department of Chemistry, Shandong Normal University, Jinan, 250014, China*
[b] *Department of Chemistry, Nankai University, Tianjin, 300071, China*

Received 28 October 1997; received in revised form 18 March 1998; accepted 27 March 1998

Abstract

Ferric 2-hydroxy-1-naphthaldehyde thiosemicarbazone (Fe^{III}-HNT) has been synthesized and used to mimic the active group of horseradish peroxidase (HRP). The catalytic characteristics of this mimic-enzyme catalyst in the oxidation reaction of ascorbic acid with hydrogen peroxide has been studied. The experimental results showed that this peroxidase model compound has similar catalytic activity that of HRP. The catalytic activity of Fe^{III}-HNT has been compared with those of HRP and common mimic-enzymes, metalloporphyrins (e.g. metal tetrakis(sulphophenyl)porphyrin (Me-$TPPS_4$)). Though the catalytic activity of Fe^{III}-HNT is 75% of that of HRP, it can be used as a new kind of mimic-enzyme catalyst in determination of trace H_2O_2. By coupling this mimetic catalytic reaction with the catalytic reaction of glucose oxidase, glucose can be determined indirectly. Under experimental conditions the linear relationship between ΔA_{265} and glucose concentration was in the range of 2.0–40.0 μg ml^{-1}, The correlation coefficient (r) was 0.9996. The R.S.D. ($P = 0.05$, $n = 6$) was 0.24%. The detection limit was determined to be 0.238 μg ml^{-1}. It was applied successfully to the determination of glucose in normal human and diabetic urine. The values of determination by the proposed method were compared with those of a routine method (enzymic glucose determination) applied in an hospital clinical laboratory. The agreement was very good. © 1998 Elsevier Science B.V. All rights reserved.

Keywords: Fe^{III}-HNT; Mimetic enzyme; Catalytic spectrophotometric method; Glucose

1. Introduction

Enzymatic assays have been widely used in analytical biochemistry because of their rapidity and high selectivity [1,2], but many enzymes are expensive and their solutions are not very stable. Hence, researchers hope to substitute common chemicals for bio-enzyme in clinic analysis. They have been more interested in mimetic enzyme [3–6], e.g. the metalloporphyrin system has been widely used as the model to mimic peroxidase [7–11]. As common ligands, Schiff bases are easy to synthesise and the chemicals used are cheap. They dissolve easily and the solutions are stable.

* Corresponding author.

0039-9140/98/$ - see front matter © 1998 Elsevier Science B.V. All rights reserved.
PII S0039-9140(98)00149-0

They easily form metal complexes and are widely used in metal analysis [12,13], but are little used in enzymatic analysis. We have found that the complex of ferric 2-hydroxy-1-naphthaldehyde thiosemicarbazone (Fe^{III}-HNT) has similar catalytic activity as metalloporphyrins or horseradish peroxidase (HRP) have even though they do not have same structure. Fe^{3+} can add extra ligands with HNT to form a square-pyramidal five-coordinate structure and a an octahedral six-coordinate structure [14,15]. The structure of the complex is shown in Scheme 1.

The electronic structure, the oxidation state of the central metal Fe^{3+} and the affinity of the complex for extra ligands are three important factors which determine the catalytic activity [16]. In this catalytic system, the central metal Fe^{3+} is the key factor, which is similar to metalloporphyrins. It functions as a mimic of HRP. In this paper, the catalytic behaviour of Fe^{III}-HNT was studied, and the kinetic characteristics of Fe^{III}-HNT was compared with those of HRP and iron tetrakis(sulphophenyl)-porphyrin (Fe-$TPPS_4$). The oxidation reaction of ascorbic acid with hydrogen peroxide under the catalysis of Fe^{III}-HNT was applied successfully to the determination of glucose in human normal and diabetic urine.

2. Experimental

2.1. Apparatus

All absorbance measurements were carried out on a Shimadzu UV-265 spectrophotometer equipped with 1.0 cm quartz cells. All pH measurements were made with a pHS-3C digital pH-meter (Shanghai Lei Ci Device Works, Shanghai, China) with a combined glass-calomel electrode. The elemental analyses were carried out on a Yanaco (Japan) model MF-3 elemental analyzer.

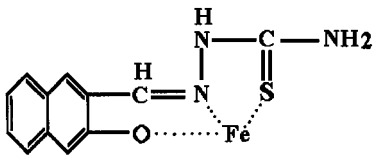

Scheme 1. The structure of the Fe^{III}-HNT complex.

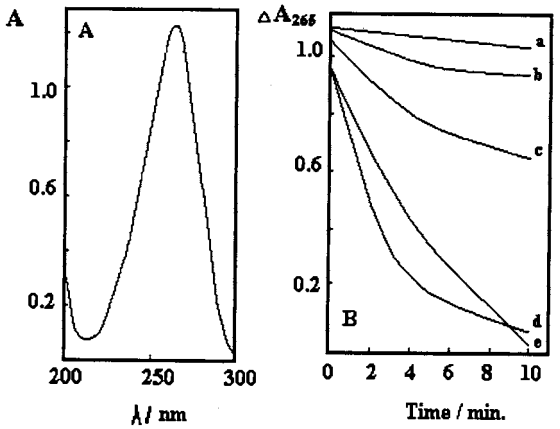

Fig. 1. Absorbance of AsA and absorbance change at 265 nm during AsA oxidation catalyzed by Fe^{III}–HNT (A) and HRP (B). a, AsA + H_2O_2 + Fe^{3+}; b, AsA + H_2O_2 + HNT; c, AsA + H_2O_2; d, AsA + H_2O_2 + HRP; e, AsA + H_2O_2 + Fe^{3+} + HNT. AsA, 4.0×10^{-5} mol l^{-1}; H_2O_2, 5.0×10^{-4}%; Fe^{3+} and HNT, 4.0×10^{-6} mol l^{-1}; HRP, 1.0×10^{-8} mol l^{-1}.

2.2. Reagents

HRP and glucose oxidase (GOD) were purchased from Sino-American Biotechnology, Beijing. Other chemicals used were of analytical reagent grade.

An ascorbic acid (AsA) stock solution (5.0×10^{-2} mol l^{-1}) was prepared every week. The working solution (5.0×10^{-4} mol l^{-1}) was prepared daily by diluting a stock solution kept in a refrigerator. Hydrogen peroxide solution (0.3%) was prepared by dilution of a 30% solution with distilled deionized water (standardized by titration with potassium permanganate). Tris(hydroxymethyl)aminonethane–HCl (Tris–HCl) buffer (0.2 mol l^{-1}, pH 7.0) was used. HRP and GOD were applied at 1.0×10^{-6} mol l^{-1} and 94 U ml^{-1} respectively. HNT was synthesized following the method in the literature [14] (mp 245°C, anal. found (calc.): C, 58.82; (58.75), H, 4.58;(4.52)) and was dissolved in dimethylformamide (DMF), the working solution (4.0×10^{-4} mol l^{-1}) was diluted with distilled deionized water.

Table 1
Comparison of the catalytic characteristics of Fe^{III}-HNT, metalloporphyrins and HRP

Option	Fe-HNT	Mn-TPPS$_4^a$	Fe-TPPS$_4^a$	HRP[a]
C_0 (mol l^{-1})	4.0×10^{-6}	1.0×10^{-5}	1.0×10^{-5}	1.0×10^{-7}
V_{max} (s^{-1})	9.32	8.60	6.00	0.0124
K_{cat} (10^6, l mol^{-1} s^{-1})	1.86	1.72	1.20	2.48
Relative activities (%)[b]	75	69	48	100

Determined at at 265 nm.
[a] [8].
[b] Relative activity is the ratio of K_{cat} metal complexes to that of HRP.

2.3. Procedure

In a 10 ml colorimetric tube, 2.5 ml Tris–HCl buffer, 0.1 ml Fe^{3+}, HNT (4.0×10^{-4} mol l^{-1}) solution and 0.8 ml AsA (5.0×10^{-4} mol l^{-1}) were added. The tube was then diluted to the mark with distilled deionized water. The solution (3 ml) was put in a 1.0 cm quartz cell. The initial absorbance (A_i) at 265 nm was recorded and the reaction was initiated by adding 5.0 μl 0.3% H_2O_2. The absorbance was then recorded at various time intervals for the kinetic calculation. The final absorbance (A_f) was recorded after 10 min. The absorbance difference was defined as $\Delta A_{265} = A_i - A_f$.

2.4. Application to glucose determination

Glucose can react with dissolved oxygen to produce H_2O_2 under the catalysis of GOD. In a 10 ml colorimetric tube, 2.5 ml Tris–HCl buffer (pH 7.0), 0.2 ml 94 U ml^{-1} GOD and appropriate amounts of glucose standard solution were added. After 5 min, the solutions were cooled to 0°C immediately to stop the oxidation reaction. Then 0.1 ml 4.0×10^{-4} mol l^{-1} Fe^{3+}, 0.1 ml 4.0×10^{-4} mol l^{-1} HNT and 0.8 ml 5.0×10^{-4} mol l^{-1} AsA were added and the mixture was diluted with distilled deionized water to the mark. The A_i was recorded immediately. After 10 min, the A_f was recorded and the ΔA_{265} was calculated.

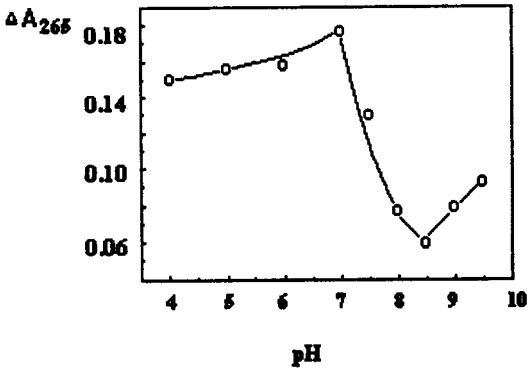

Fig. 2. Effect of pH on ΔA_{265}. AsA, 4.0×10^{-5} mol l^{-1}; Fe^{3+} and HNT, 4.0×10^{-6} mol l^{-1}; H_2O_2, 5.0×10^{-4}%.

3. Results and discussion

3.1. The development of the Fe^{III} catalytic system

AsA has a maximum absorbance at 265 nm in the aqueous phase [8] (Fig. 1A), and its oxidation by H_2O_2 was catalyzed by HRP and Fe^{III}-HNT, but Fe^{3+} and HNT themselves have no catalytic activity (Fig. 1B).

3.2. Stoichiometry of the Fe^{III}-HNT complex

The stoichiometry of the Fe^{III}-HNT complex was studied by molar ratio and continuous variation method. The results obtained by both methods indicated that composition of the complex is 1:1 (Fe^{3+}:HNT).

3.3. Comparison of catalytic activities of Fe^{III}-HNT, metalloporphyrin and HRP

The kinetics enzymatic reaction has been studied by the Michaelis equation [17]. The maximum

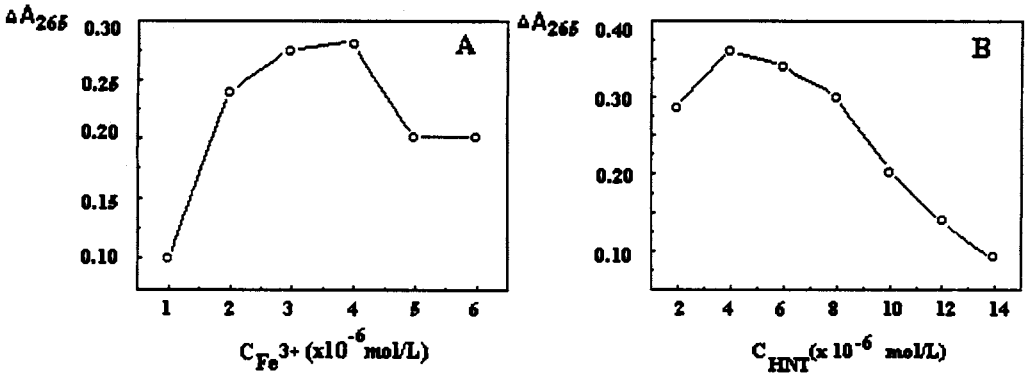

Fig. 3. Effect of Fe^{3+} (A) and HNT (B) concentrations. AsA, 4.0×10^{-5} mol l^{-1}; H_2O_2, 5.0×10^{-4}%; pH 7.0.

rate V_{max} was obtained from Lineweaver–Burk plots [18] ($1/V$ versus substrate, Table 1). The transformation constant K_{cat} was obtained from $V_{max} = K_{cat} \times C_0$. Where C_0 is the initial concentration of the enzyme. The K_{cat} values represent the catalytic activities. Although the catalytic activity of Fe^{III}-HNT is 75% of that of HRP, it can be also used as a substitute for HRP in enzymatic analysis. Their catalytic activities were compared and are shown in Table 1.

To examine the catalytic activity of Fe^{III}-HNT, it was used as a catalyst to determine glucose in human urine.

3.4. Optimization of experimental variables

The experimental variables were optimized by applying the univariate method. The pH dependence of the system was studied over the ranged 4.0–9.50. The optimum pH range for the system was found to be between 6.50 and 7.20, outside of which smaller parameter values were observed, so pH 7.0 was chosen as the experimental pH (Fig. 2).

The effect of the Fe^{3+} and HNT concentrations on the catalytic system are shown in Fig. 3 which demonstrates that the initial ΔA_{265} value (Fig. 3A) increased with increasing Fe^{3+} concentration from 1.0×10^{-6} to 4.0×10^{-6} mol l^{-1}, then decreased. The initial ΔA_{265} value (Fig. 3B) increased with increasing HNT concentration from 2.0×10^{-6} to 4.0×10^{-6} mol l^{-1}, then decreased gradually with increasing HNT concentration from 4.0×10^{-6} to 14.0×10^{-6} mol l^{-1}. In this study, the optimum concentrations of Fe^{3+} and HNT were chosen as 4.0×10^{-6} mol l^{-1}.

The influence of AsA concentrations and reaction time were studied. The results showed that the optimum concentration of AsA was 4.0×10^{-5} mol l^{-1} and the reaction time was chosen as 10 min.

3.5. Analytical characteristics

The calibration graph for the determination of glucose was obtained. The linear relationship between the ΔA_{265} and the concentration of glucose was 2.0–40.0 μg ml^{-1} with a correlation coefficient (r) of 0.9996. The linear regression equation was $\Delta A_{265} = 4.95 \times 10^{-5} C + 1.436$. The R.S.D.($P = 0.05$, $n = 6$) was 0.24% obtained from a series of 10 standards each containing 4.2 μg ml^{-1} glucose. The S.D. was 0.00386 obtained from a series of 10 blank solutions. The detection limit as defined by IUPAC was determined to be 0.238 μg ml^{-1}.

To examine the possible interferences of various constituents of the body fluids and urine, the concentration of H_2O_2 was fixed at 5 μg ml^{-1} and the tolerable error was $< \pm 5\%$, the permitted concentrations of various constituents were 20 times D-fructose, D-galactose, L-phenylalanine, L-isoalanine, sucrose, L-histidine and L-serine; 10 times L-valine, D-glucose, L(+)arabinose and L-aspartate; 6 times L-lysine, L-arginine, L-alanine; 2 times VB_1, VB_2 and VB_6; and 1 times L-cysteine and L-glutamate.

Table 2
Glucose determination in human urine

Sample No.	Glucose added (μg ml^{-1})	Found[a] (μg ml^{-1})		Glucose average content in human urine (mg 100 ml^{-1})
		Proposed method	Refernce method[d]	
I[b]	0	10.00 ± 0.03	10.10 ± 0.01	100.5
	2.0	12.05 ± 0.03	12.18 ± 0.04	
	4.0	13.97 ± 0.01	14.01 ± 0.02	
II[c]	0	28.32 ± 0.04	27.54 ± 0.01	280.7
	2.0	30.11 ± 0.01	30.54 ± 0.04	
	4.0	31.87 ± 0.02	31.01 ± 0.04	
III[c]	0	50.16 ± 0.02	50.32 ± 0.02	503.5
	50	101.6 ± 0.3	100.0 ± 0.1	
	100	145.5 ± 0.5	154.4 ± 0.4	
IV[c]	0	64.25 ± 0.02	65.12 ± 0.02	647.1
	50	114.3 ± 0.1	114.7 ± 0.1	
	100	165.0 ± 0.1	164.8 ± 0.1	

[a] Each sample was diluted 100 times and analyzed six times.
[b] Normal human urine.
[c] Diabetic urine.
[d] [19].

3.6. Sample analysis

The inorganic ions in dilute human urine did not interfere in the determination of glucose, so the glucose amount of human normal and diabetic urine were determined in 0.1 ml samples. The results were compared with those of the official method used in an hospital clinical laboratory and summarized in Table 2.

4. Conclusions

The results obtained in this work verified that the Fe^{III}-HNT complex has similar catalytic activity as that of HRP or metallporphrins, and the proposed method for the determination of glucose indirectly is simple, rapid and inexpensive.

Acknowledgements

This work was supported by the Youth Natural Science Foundation of Shandong Province, China.

References

[1] G.G. Guilbault, Handbook of Enzymatic Methods of Analysis, Marcel Dekker, New York, 1976.
[2] P.W. Washko, R.W. Welch, K.R. Dhariwal, Y. Wang, M. Levine, Anal. Biochem. 204 (1992) 1.
[3] Y.X. Ci, F. Wang, Fresenius' J. Anal. Chem. 339 (1991) 46.
[4] Y. Saito, M. Mifune, J. Odo, Y. Tanaka, M. Chikuma, H. Tanaka, React. Polym. 45 (1986) 243.
[5] B. Chance, Arch. Biochem. 22 (1949) 224.
[6] Y. Saito, M. Mifune, T. Kawaguch, et al., Chem. Pharm. Bull. 34 (1986) 2885.
[7] Y.X. Ci, L. Chen, S. Wei, Fresenius' Anal. Chem. 334 (1989) 36.
[8] X.M. Huang, M. Zhu, L.Y. Mao, H.X. Shen, Anal. Sci. 13 (1997) 145.
[9] F. Wang, Y.X. Ci, Analyst 116 (1991) 297.
[10] S.S. Sun, A.M. Wan, Fen Xi Hua Xue China 18 (1990) 329.
[11] F. Wang, X. Wu, S.S. Shang, Y.X. Ci, Fresenius' J. Anal. Chem. 344 (1992) 556.

[12] D. St. Black, A. Hartshorn, J. Coor, Chem. Rev. 9 (1973) 219.
[13] D. St. Black, N.E. Aust, J. Chem. 36 (1983) 1149.
[14] H. Kato, N. Ban, S. Kawai, Jpn. Anal. 20 (1971) 1315.
[15] M. Degughi, T. Ogi, K. Morisihge, Jpn. Anal. 30 (1981) 104.
[16] Y.X. Ci, F. Wang, Talanta 37 (1990) 1133.
[17] G.E. Brigg, J.B.S. Haldene, Biochem. J. 19 (1925) 338.
[18] Lineweaver, H.D. Burk, J. Am. Chem. Soc. 56 (1934) 658.
[19] Shanghai Medical Inspection Institute, Clinical Biochemical Inspection, Shanghai Science and Technology Press, Shanghai, 1979, p. 61.

ELSEVIER

Talanta 47 (1998) 367–376

Talanta

Amperometric measuring cell for the determination of putrescine oxidase activity

Gèza Nagy [a], Clarke X. Xu [a], Vasile V. Cosofret [a], Richard P. Buck [a,*], Ernö Lindner [b], Michael R. Neuman [c], Robert H. Sprinkle [d]

[a] *Department of Chemistry, University of North Carolina, Chapel Hill NC 27599–3290, USA*
[b] *Department of Biomedical Engineering, Duke University, Durham NC 27708–0295, USA*
[c] *Department of OB/GYN, Metro Health Medical Center, Case Western Reserve University, Cleveland OH 44109–1998, USA*
[d] *School of Public Affairs, University of Maryland, College Park MD 20742, USA*

Received 15 December 1997; received in revised form 19 March 1998; accepted 27 March 1998

Abstract

A microfabricated, flat form, amperometric microcell (microchip) is used in a simple, two-electrode arrangement for putrescine oxidase enzyme activity determinations. The cell contains a platinum microdisk working electrode and an Ag/AgCl reference electrode covered by a porous, hydrophilic membrane. An electrochemically-prepared size-exclusion layer is applied on the working electrode surface, to avoid the effect of electroactive interferences in the sample. The hydrophilic membrane, resting on the bottom of the cell, is soaked with a small volume of buffered substrate solution and a few μl enzyme containing sample solution is dispensed over the electrodes. During the enzyme activity measurement a catalytic reaction takes place in the membrane-supported liquid film over the working electrode surface. The hydrogen peroxide produced in the reaction is detected amperometrically. The amperometric current-time curves are used for evaluation. In our work putrescine was used as a substrate to determine the unknown putrescine oxidase enzyme activity of the sample. Elevated diamine oxidase enzyme activity in the vaginal milieu can indicate premature rupture of the amniotic membrane. Results with membrane discs, containing all the necessary chemicals in solid or lyophilized form, are very encouraging with respect of a single use, 'reagentless' biosensor for home care. © 1998 Elsevier Science B.V. All rights reserved.

Keywords: Amperometric microcell; Platinum microdisc; Putrescine oxidase; Hydrophilic membrane

1. Introduction

Enzyme-based probes are widespread in different areas of quantitative chemical analysis. Most of these probes have been worked out for the selective determination of organic molecules, using enzyme(s) incorporated in the sensing element of the probe. The signal of the enzyme-based sensors normally depends on the rate of substrate transport to the enzyme catalyzed layer when enzyme activities are high. However, at high substrate and low enzyme activities the signal can be dependent on the rate of the enzyme catalyzed

* Corresponding author. Tel.: +1 919 9622304; fax: +1 919 9622388; e-mail: richard_buck@unc.edu

0039-9140/98/$ - see front matter © 1998 Elsevier Science B.V. All rights reserved.
PII S0039-9140(98)00141-6

reaction. Therefore, a probe of similar construction can be made for enzyme activity measurements using a special, enzyme-free reaction layer of high substrate concentration and appropriate reaction conditions (buffer composition, pH, etc.). The biocatalytic reaction is started as the sample of unknown enzyme concentration is introduced.

The development of truly self-contained enzyme sensing 'substrate' probes have proven to be extremely difficult. These 'reversed' enzyme sensors were not sensitive enough to measure the low enzyme activities of practically important samples. Therefore classical substrate-measuring enzyme electrodes are often used indirectly, for enzyme activity measurements. In this kinetic analysis for enzymes, the rates of substrate consumption in the enzyme-catalyzed reaction are followed with the enzyme-containing probe and evaluated in the conventional way [1–4]. Cholinesterase enzyme activity was measured with both potentiometric [5] and amperometric [6,7], choline electrode. The amperometric method was adapted to measure an organophosphorus insecticide (Paraoxon), heavy metals in water samples [8] and acetylcholinesterase and butyrylcholinesterase activities in amniotic fluid [9].

Montalvo [10,11], used a thin layer cell on the surface of an ammonium ion-selective electrode to measure urease activity. Due to the low ammonium ion collection efficiency of his design, it could not be used for measuring low enzyme activities.

1.1. Practical importance

The goal of this work is to show, that the combination of planar microsensor fabrication and simple amperometric detection can dramatically improve the performance of electrochemical enzyme activity measuring biosensors. Such devices will integrate the simplicity and sensitivity of amperometry and the cost effective manufacturing of photolithographic microfabrication [12–15].

Presently enzyme activity determinations are routinely carried out in central clinical laboratories, using high speed, cost efficient, automated analyzers. The simple amperometric enzyme activity sensor described in this paper is not intended to compete with these analyzers. However, there are other areas of health care diagnosis where the need for quick decision making, personal care, self test or the lack of well established, centrally performed methods make a simple, but accurate enzyme activity measuring tool practical. The detection of the premature rupture of the fetal membranes may be one of these applications. If the integrity of the fetal membrane is lost before the onset of labor it is called premature rupture. This happens in 3–14% of all births [16–18]. Premature rupture of the membrane can cause amnionitis, premature labor, and maternal [19–21], fetal and infant [22–25] morbidity and mortality.

Diamine oxidase (E.C.1.4.3.6.) is an enzyme whose activity is normally low in the human plasma. However, it increases considerable in pregnancy [26]. The amniotic fluid also contains diamine oxidase in variable activity [27]. Therefore, the diamine oxidase activity of the vaginal fluid can be used to detect the rupture of fetal membrane in the absence of vaginal bleeding [18]. In designing the amperometric microcell for bedside examination of diamine oxidase activity in cervicovaginal secretions, diagnosis of premature rupture of the fetal membranes was envisioned as a potential field of application. Putrescine oxidase (E.C.1.4.3.10) was used as a model for diamine oxidase (E.C.1.4.3.6).

2. Experimental

2.1. Apparatus

Computer controlled EG&G PAR model 273A electrochemical measuring system was used for most of the studies. However, for electroplating an EG&G PAR model 363 potentiostat/galvanostat was used.

2.2. Preparation of the electrodes

Photolithographically fabricated, individually accessible gold plate twin electrodes with surface areas of 3.0 mm^2 on flexible polyimide film (125 μm thickness, Kapton®, DuPont) were used for

the sensing element of the cell. The description of the fabrication procedure was given earlier [12–14]. To provide good adherence, a chromium layer was sputtered first onto the polyimide surface, and then covered by a sputtered gold layer. Photodefinable polyimide defined the pattern of the electrode surfaces, bonding pads, and insulates connecting leads. Twenty seven (3×9, e.g. rows × columns) microcells equipped with two or three electrodes are manufactured on a 3×3 square inch wafer. Before use, a single cell was cut from the wafer. Next, connecting wires were attached to the bonding pads with silver epoxy (Epoxy Technology). Finally, another epoxy layer was employed over the bonding pads for insulation.

One of the gold plate electrodes was electroplated with a shiny platinum layer [28] while the other was electrochemically converted to an Ag/AgCl reference electrode [29]. A well-known method was followed to prepare the platinization solution [30].

To provide size exclusion-based permselectivity for amperometric hydrogen peroxide detection, an electrochemically-formed, thin poly(*m*-phenylenediamine) film was deposited on the platinum working electrode surface [31,32]. The electrode was placed in 0.01 M phenylenediamine solution in 0.1 M phosphate buffer of pH 7.2. Cyclic voltammetric scans were made in the range of $+0.2$–0.8 V versus Ag/AgCl reference electrode with 2 mV s^{-1} scan rate. The electrodes were individually checked. They were accepted for further use if they detected hydrogen peroxide at 0.6 V, but showed < 5 nA current when challenged with 0.2 mM ascorbic acid [29].

2.3. Fabrication of the cell

The polyimide (Kapton®) film holding the two electrodes was secured on a supporting plate. Microscope slides or special ceramic plates could be used. A thin insulating blacktape cover of ~ 200 μm thickness was stretched and pasted over the plate to hold down the polyimide film. A circular opening (with a diameter of 7 mm) was previously punched out of the blacktape and then it was placed centrally over the electrode area. In this way, the slightly recessed circular region in the center of the cell was increased by the thickness of the blacktape. The small volume space, called 'reaction well' above the electrodes, can hold the reagent-containing porous membrane disc, or liquid reagent film. The cell is supplied with a fitting top 'plate'.

A more advanced version of the cell is shown in Fig. 1. The polyimide film, holding the two electrodes, was embedded in a poly(methyl methacrylate) plastic body. A special mould was made from a flat ground, thick walled glass ring placed on a glass plate. A flat plastic disc (6 mm diameter and 800 μm thickness) was fixed centrally over the electrode area, with water soluble Elmer's glue, to protect the electrode surfaces and shape the well. Next, the Kapton-based cell was pasted inside the ring and the electrode connecting wires were arranged. Finally, the poly(methyl methacrylate) casting slurry was poured inside of the mould. The preparation of the casting mixture is described below. After 24 h the mould was soaked in water and could be taken apart. Following removal of the spacer disk a cylindrical cell body with a shallow, flat bottom reaction well was obtained. The electrochemical deposition of the

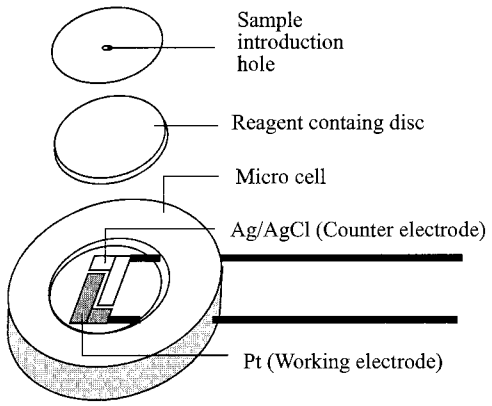

Fig. 1. Amperometric microcell for enzyme activity measurements. The microfabricated electrochemical cell (on flexible polyimide Kapton® with traces, and bonding pads) is embedded in a poly(methyl methacrylate) plastic body. The small volume space, (6 mm diameter and 800 μm thickness) holds the reagent-containing porous membrane disc and/or liquid reagent film. To avoid solvent evaporation a plastic cover slide was used during measurements.

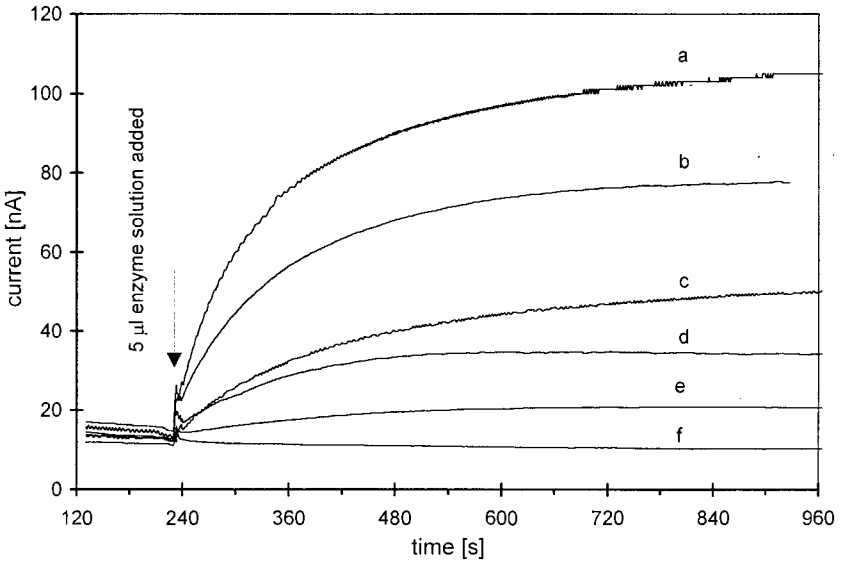

Fig. 2. Putrescine oxidase response: current-time curves recorded after 5 µl aliquot of a putrescine oxidase solution was added to 10 µl 100 mM putrescine solution on the disk. Each curve was recorded with a new reagent disk. Sample activities: (a) 220 mU ml^{-1}; (b) 116 mU ml^{-1}; (c) 57 mU ml^{-1}; (d) 28 mU ml^{-1}; (e) 14.2 mU ml^{-1}; (f) sample blank.

size exclusion membrane on the working electrode was made after the planar cell was embedded into the poly(methyl methacrylate) cell body. To avoid solvent evaporation, the reaction well was covered with a screw cap of a small vial or a plastic cover slide (Fig. 1) during measurements.

2.4. Preparation of the casting slurry

Methyl methacrylate monomer (13 g), 9 g of poly(methyl methacrylate) polymer (both Polysciences) and a few drops of commercial nail polish were mixed together to prepare the casting slurry. The role of the nail polish was to give an attractive color. Benzoyl peroxide (0.05 g) and 3 drops of *N*, *N* dimethyl-*p*-toluidine (both Aldrich) were added to the mixture using continuous agitation. When the mixture achieved a honey like viscosity, it was poured into the mould. A curing time of 10–12 h was usually long enough to obtain a shiny solid body.

2.5. Preparation of the reagent disks

The formation of a well defined layer of reagent on the bottom of the reaction well is one of the key issues of this application. A hydrophilic thin porous matrix, employed at the electrode surfaces, simplifies the film formation and improves its stability. Surface tension decreasing additives, like 1% hydroxypropyl cellulose, carboxymethyl cellulose, Triton or Tween 20, and a film holding window, placed in front of the sensing surface, helped the formation of a homogeneous film. Well functioning 'disposable' cells were prepared by coating the reaction well bottom with layers made of Kiselgel, cellulose acetate and alumina powder using carboxymethyl cellulose as binding material. However, to make multiple measurements with the same cell, a replaceable matrix layer in the form of thin paper tissue disk were used in our experiments. The filter paper disks were punched out from different brands of paper tissue membranes (Whatman P81 filter paper, Kimwipes EX-L delicate task wipers or Olympus lens cleaning tissue) and they were used as the porous matrix. All three filter papers tested in this work were appropriate in facilitating homogeneous spreading of the reagent in the reaction well. Only small differences in the rate of solution uptake (the Whatman paper was considerably slower compared to the other two) and the mechanical stabil-

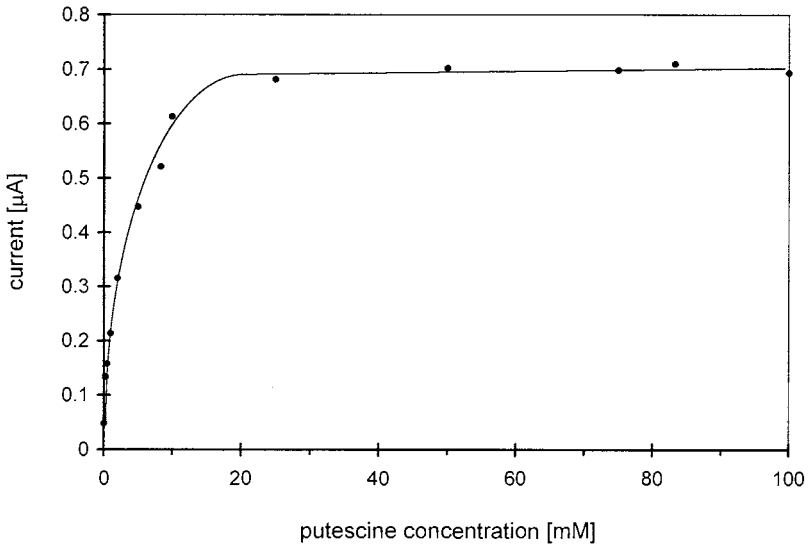

Fig. 3. Effect of the substrate (putrescine) concentration on the current, measured with a sample of 6 mU putrescine oxidase enzyme activity (5 μl enzyme solution of 1.2 U ml^{-1} activity). The current values were measured on the plateau of the response curves.

ity (the Kimwipes paper rolls up easily) were experienced.

2.6. Procedure

A small volume, typically 5–10 μl of buffered putrescine reagent solution was added into the amperometric sensor well. The current-time curves were recorded at a potential of 0.6 V versus Ag/AgCl reference electrode. After obtaining a steady background current, 3–5 μl, of putrescine oxidase standard solution of known enzyme activity was added to the reagent. The reaction chamber was covered after each addition to avoid evaporation related changes in the solution volume. The procedure was repeated with each standard solution and with each the sample. The cell shown in Fig. 1 is 'user friendly'. The fill-up with reagent, the introduction of the standard or sample and later cleaning needs only ordinary care or skill.

The simple two electrode configuration was selected to avoid frequent problems with the three electrode amperometric mode, due to lost contact to the reference electrode. An open circuit can happen easily in a cell holding no more than a few microliters of electrolyte, and can damage the photolithographically prepared thin layer working electrode, unless a special potentiostat or guarding circuit is used.

2.7. Chemicals

The putrescine oxidase [E.C.1.4.3.10] enzyme prepared from *Micrococcus roseus* was a generous gift of Amano Pharmaceutical (Nagoya, Japan). To determine the activity of the enzyme solutions used in our experiments, the procedure described in Toyobo enzymes product catalog (Toyobo, Osaka Japan 1994) was used. In the procedure, the rate of hydrogen peroxide formation is measured through Eq. (1). by detecting the quinoneimine spectrophotometrically at 510 nm :

$$\text{Putrescine} + O_2 + H_2O \xrightarrow{\text{putrescine oxidase}} \text{4-aminobutyraldehyde} + NH_3 + H_2O_2 \quad (1)$$

$$2H_2O_2 + \text{4-Aminoantipyrine} + \text{2,4-Dichlorophenol} \xrightarrow{\text{peroxidase}} \text{Quinoneimine dye} + 4H_2O \quad (2)$$

For the enzyme activity measurements 20.0 ml, 10 mM aqueous putrescine solution, 97.0 ml 0.1

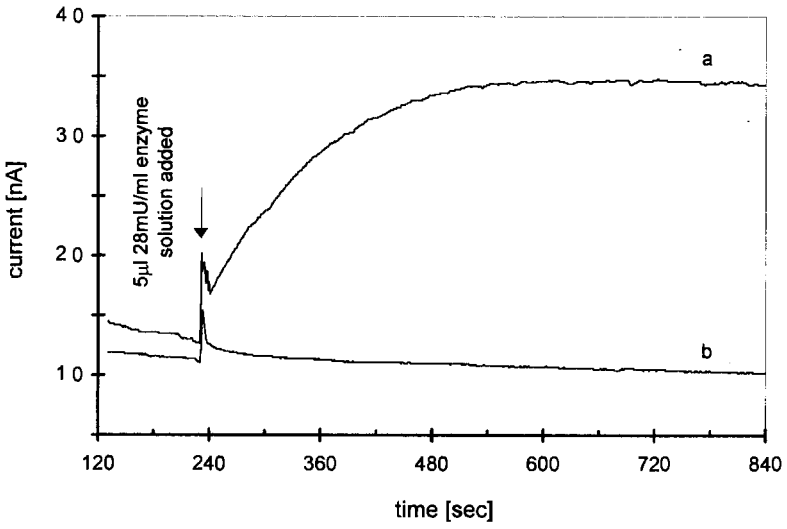

Fig. 4. Putrescine oxidase response curves recorded with and without enzyme substrate (putrescine) on the reagent disk. A 5 µl (28 mU ml^{-1}) aliquot of putrescine oxidase solution was added to 10 µl 100 mM putrescine solution (a) or 10 µl buffer solution (b) on the disk.

M Tris–HCl buffer (pH = 8.0), 1.0 ml 1.2% 4-aminoantipyrine solution, 1.0 ml 0.48% 2,4-dichlorophenol solution prepared with 40% V/V ethanol water solvent and 1.0 ml horseradish peroxidase (E.C.1.11.1.7) solution (400 U ml^{-1}) were mixed together. A 2.85 ml portion of this solution was pipetted into a cuvette ($d = 1.0$ cm) and mixed with 0.15 ml of the enzyme or blank solution after thermal equilibration. The absorbance-time curve was recorded at 510 nm and 30°C. To calculate the enzyme activity of the solution, the change in the initial slope (compared to the blank), the stochiometric and dilution factors and the extinction coefficient (29 cm^2 µmole^{-1}) were used. A 20 mM Tris–HCl buffer (pH = 8.0) was used as solvent for the preparation and dilution of the enzyme solutions.

3. Results and discussion

Putrescine oxidase (PO) catalyzes the following reaction:

$$H_2N\text{-}(CH_2)_4\text{-}NH_2 + O_2 + H_2O \xrightarrow{\text{putrescine oxidase}} H_2N\text{-}(CH_2)_3CHO + NH_3 + H_2O_2 \quad (3)$$

A well functioning amperometric enzyme electrode has been worked out recently for putrescine determinations by detecting the hydrogen peroxide formed in this reaction [33]. Measuring the decrease of putrescine concentration in time by the putrescine sensor, enzyme activity determinations can be made. However, much higher sensitivity, or a much lower detection limit can be achieved if the formation rate of hydrogen peroxide is measured directly in a microcell. It is obvious, that the smaller the dilution of the sample, the more sensitive the determination can be. To meet the sensitivity requirements of clinical samples, the volume of the reaction chamber was minimized. The photolithographically made planar electrode allowed making amperometric determinations in a thin solution film of a few microliters (15–25 µl).

3.1. Measurements with preprepared reagent film

To perform one measurement, the cell was opened and the reaction film supporting disc was placed on the sensing surface. A small volume (5–15 µl) of buffered putrescine solution (pH = 8.0) of known concentration was added onto the disc. The putrescine solution was prepared with

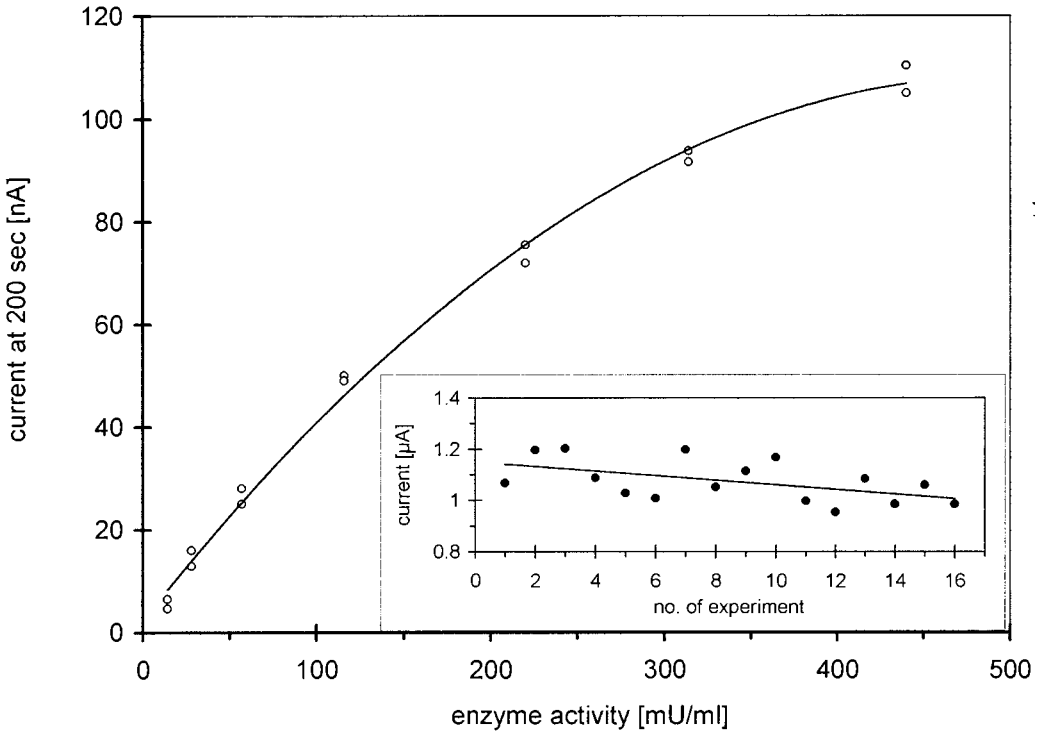

Fig. 5. Putrescine oxidase calibration curve. The current intensities were measured 200 s after the introduction of the enzyme solution. The plotted values are corrected with the background current value. Insert: Reproducibility of the enzyme activity measurements: 5 μl enzyme solution of 6 mU total activity was dispensed on a freshly prepared reagent disk, soaked with 10 μl of 100 mM putrescine solution. The procedure was repeated 16 times.

1% carboxymethyl cellulose, surface tension decreasing additive. The cell was closed and connected to the measuring apparatus. The amperometric current was followed at 0.6 V applied potential. After the current dropped to its steady value, a small aliquot of the enzyme-containing solution was dispensed into the reaction film, through the hole in the plastic cover. Typical current-time response curves are shown in Fig. 2. In these experiments 10 μl of 100 mM putrescine solution and 5 μl of sample, of different enzyme activities, were dispensed onto the Olympus lens cleaning tissue resting on the cell bottom. Due to the experimental arrangement and the small volumes, the sample becomes mixed with the reagent only through diffusion. There is no external agitation after the sample is injected onto the reagent soaked filter paper. Each curve in Fig. 2 was determined with a new filter paper and a new aliquot of substrate and sample solution. The cell was disassembled, washed and reassembled between each measurement.

The shape of the current-time transients depends on the enzyme activity/substrate concentration ratio. At very high enzyme activities or low putrescine concentration (not shown in the figure) the curve achieves an early maximum and then the current sharply falls back [28,34]. However, in the range of diagnostically important low enzyme activities, the current-time curves often show a linear characteristic with enzyme activity dependent slopes. In Fig. 3, the current intensities at the plateau of the response curves are plotted as the function of the putrescine (substrate) concentration when 5 μl of enzyme solution of 1.2 U ml^{-1} (6 mU) activity was added to 10 μl of putrescine solution of a different concentration. At this enzyme activity range, the maximum values of the

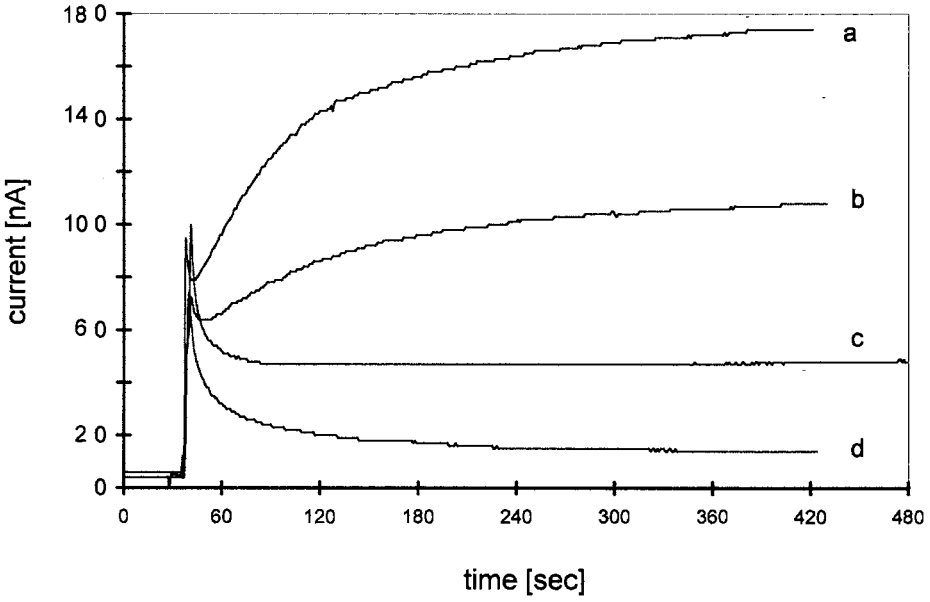

Fig. 6. Putrescine oxidase current-time response curves recorded with dry chemistry reagent kits. Enzyme solution (6 μl) added on a dry filter paper disk (previously pretreated with 5 μl of 100 mM putrescine solution in pH 8 TRIS HCI buffer and dried under infrared lamp). Enzyme activities in 6 μl sample: (a) 1.64 mU; (b) 1.09 mU; (c) 0.54 mU; (d) sample blank.

response curves, do not show putrescine concentration dependencies above 20 mM. However, if samples of higher enzyme activity were added to the same putrescine solution (volume and concentration) the response became smaller and the peak shape of the curve indicated the depletion of putrescine. If the putrescine solution was replaced with buffer solution (i.e. blank run without the enzyme substrate), no enzyme response could be detected, as shown in Fig. 4.

An enzyme activity calibration curve (current response versus enzyme activity) is shown in Fig. 5. The current intensity values plotted in the figure, were measured 200 s after the introduction of the enzyme solution. The amperometric signal shows a well defined dependence on the putrescine oxidase enzyme activity in the range of 6–450 mU ml^{-1}. In kinetic enzyme activity measurements most often the initial slopes are plotted as a function of the enzyme activities. In this special case, the lack of intensive mixing makes the slope method at the very early section of the transient curves uncertain. The larger the portion of the curve that is used for the slope evaluation the less effect the initial uncertainties have. For simplicity, the slopes were determined from only two points (current measured at the start and after a pre-selected 'set-time' period; e.g. after 200 s). Further extension of the 'set time' or using a section of each curve with maximum linearity for the slope determination did not improve the quality of data (calibration curve and reproducibilities).

To determine the reproducibility of the method, enzyme activity measurements were repeated 16 times. Each time, a 5 μl enzyme solution of 6 mU activity (a 5 μl enzyme solution of 1.2 U ml^{-1}) was added to the freshly prepared reagent film (Kimwipes Ex-L tissue paper soaked with 10 ml of 100 mM putrescine reagent solution). The current intensity values measured 200 s after the introductions of the enzyme solution are shown in the insert of Fig. 5. A relative standard deviation of 7.6% was achieved. The drift in the current values correlates with the gradual loss of enzyme activity during the measurements. The latter, unfavorable affects the standard deviation. By correcting the data for drift, the relative standard deviation decreases to 6.1%.

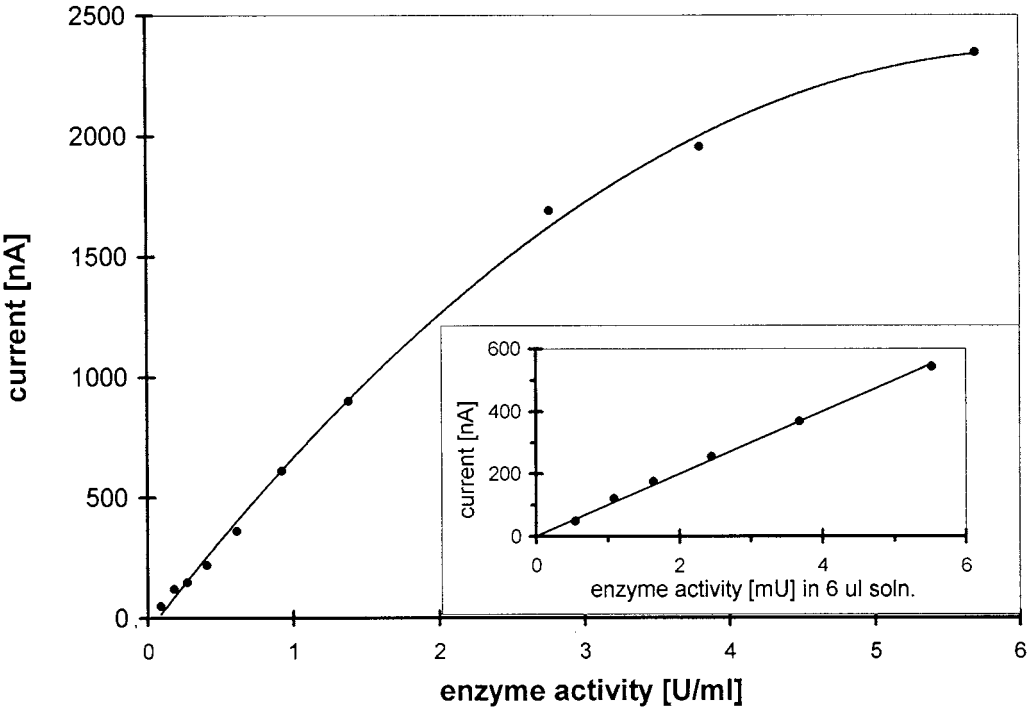

Fig. 7. Putrescine oxidase calibration curve recorded with dry chemistry kit. Enzyme solution (6 μl) added on a dry filter paper disk. The filter paper was previously pretreated with 5 μl of 100 mM putrescine solution in pH 8 Tris–HCl buffer and dried under infrared lamp. Insert: Calibration curve in the low enzyme activity ranges (6 mU in 6 μl corresponds to 1 U ml^{-1}).

3.2. Measurements with dry reagent discs

Considering prospective applications, it is important to make the procedure as simple as possible. If all the reagents are incorporated in advance as solids into the reaction film supporting disk, (i) the reagent handling is simplified, (ii) the extended reagent storage becomes less critical and (iii) the sample dilution is minimized. To prepare dry chemistry kits, Whatman filter paper discs were cut out and soaked with 5 μl 100 mM putrescine solution prepared with pH 8 Tris–HCl buffer. The disks were dried under an infra red lamp. One of these dry reagent discs was introduced into the thin layer enzyme activity measuring cell and 0.6 V voltage was applied. As long as no electrolyte film was on the electrodes there was no current. However, upon wetting the porous matrix with the sample solution (3–20 μl), a sharp current spike could be observed. After this, the response curves were very similar to the wet reagent film membrane response curves.

Fig. 6 shows response curves recorded with dry reagent discs. It was shown that without putrescine on the disc, no enzyme response could be detected. The dependence of the amperometric signal on the putrescine amount employed on the disc was tested by doing measurements with 6 μl putrescine oxidase solution samples of 2.54 U ml^{-1} activity. No influence of the putrescine amount was found in the range 50–1000 nmole. However, below 50 nmole/disc the response dramatically decreased.

Repeating the experiment 21 consecutive times with 6 μl putrescine oxidase solution samples of 2.54 U ml^{-1} activity, the relative standard deviation of the current peak values was 6.6%. Fig. 7 shows a putrescine oxidase enzyme activity calibration curve measured with the dry reagent discs using 6 μl enzyme sample solutions. The lower limit of detection is below 0.01 U ml^{-1}.

4. Conclusions

A new, microfabricated, two-electrode amperometric cell, equipped with a porous reagent disk, has been made and characterized for 'kinetic' enzyme activity measurements. The example system is putrescine oxidase that can be determined in typically 3–6 μl samples for activities down to 0.01 U ml^{-1}. For the bedside diagnosis of premature rupture of the fetal membrane, dry chemistry kits were also tested. These use impregnated reagent disks containing all the necessary reagents in solid form. Using 6 μl samples a relative standard deviation of 6.6% ($n = 21$) was achieved.

Acknowledgements

This work was supported by NSF/Whitaker Foundation Grant BES-9520526. The authors thank to Mr Stefan Ufer of the Biomedical Microsensors Laboratory, North Carolina State University, for the microfabrication of the base electrodes, as well as the partial support by the NSF Engineering Research Center Grant CDR-8622201.

References

[1] G.G. Guilbault, Analytical uses of Immobilized Enzymes, Marcel Dekker, New York, 1984, p. 208.
[2] P.W. Carr, L.D. Bowers, Immobilized enzymes in analytical and clinical chemistry, in: P.J. Wiving, J.D. Winefordner (Eds.), Chemical Analysis, a Series Monographs on Analytical Chemistry and its Applications, vol. 56, Wiley–Interscience, New York, 1980.
[3] D.G. Buerk, Biosensors, Theory and Applications, Technomic Publishing Company, Lancaster, Basel, 1993.
[4] E.A.H. Hall, Biosensors, Prentice–Hall, Englewood cliffs, NJ, 1991.
[5] G.G. Guilbault, A. Iwase, Anal. Chim. Acta 85 (1976) 295.
[6] G. Palleschi, M.G. Lavagnini, D. Moscone, R. Pilloton, D. D'Ottavio, M.E. Evangelisti, Biosens. Bioelectron. 5 (1) (1990) 27–35.
[7] P. Skladal, Anal. Chim Acta 269 (1992) 281–287.
[8] M. Bernabei, S. Chiavarini, C. Cremsini, G. Palleschi, Biosens. Bioelectron. 8 (5) (1993) 265–271.
[9] R.M. Morelis, P.R. Coulet, A. Simplot, C. Boisson, G. Guilbaud, Clin. Chim. Acta 203 (2–3) (1991) 295–305.
[10] J.G. Montalvo, J. Anal. Chem. 41 (1969) 2093.
[11] J.G. Montalvo, J. Anal. Biochem. 38 (1970) 357.
[12] E. Lindner, V.V. Cosofret, S. Ufer, R.P. Buck, R.P. Kusy, R.B. Ash, H.T. Nagle, J. Chem. Soc. Faraday Trans. 89 (1993) 361–367.
[13] M.B. Madaras, I.C. Popescu, S. Ufer, R.P. Buck, Anal. Chim. Acta 319 (1996) 335–345.
[14] V.V. Cosofret, M. Erdosy, T.A. Johnson, R.P. Buck, R.B. Ash, M.R. Neuman, Anal. Chem. 67 (1995) 1647–1653.
[15] R.P. Buck, V.V. Cosofret, E. Lindner, S. Ufer, M.B Madaras, T.A. Johnson, R.B. Ash, M.R. Neuman, Electroanalysis 9 (1995) 846–851.
[16] J.W. Larsen, Obstet. Gynecol. Annu. 8 (1979) 203–221.
[17] Anonymous, Br. Med. J. 1 (1979) 1165–1166.
[18] W.A. Gahl, T.J. Kozina, D.D. Fuhrmann, A.M. Vale, Obset. Gynecol. 60 (1982) 297–304.
[19] R.C. Burchell, Am. J. Obstet. Gynecol. 88 (1964) 251–255.
[20] R.L. Naeye, J. Am. Med. Assoc. 238 (1977) 228–229.
[21] J.A. Fayez, A.A. Hasan, H.S. Jonas, G.L. Miller, Obstet. Gynecol. 52 (1978) 17–21.
[22] G.A. Webb, Am. J. Obstet. Gynecol. 98 (1967) 594–601.
[23] G.C. Gunn, D.R. Mishell Jr., D.G. Morton, Am. J. Obstet. Gynecol. 103 (1970) 469–483.
[24] L.R. Lanier Jr., R.W. Scarbrough, D.W. Fillingim, R.E. Baker Jr., Am. J. Obset. Gynecol. 93 (1965) 398–404.
[25] G.S. Merki-Feld, D. Passweg, et al., Geburtshilfe Frauenheilkd. 52 (12) (1992) 778–779.
[26] N. Tryding, B. Willert, Scand. J. Clin. Lab. Invest. 22 (1968) 29–32.
[27] A. Tornquist, F. Jonassen, P. Johnson, A.M. Fredholm, Acta Obstet. Gynecol. Scand. 50 (1971) 79–82.
[28] G. Nagy, C.X. Xu, R.P. Buck, E. Lindner, M.R. Neuman, R.H. Sprinkle, Anal. Chim. Acta, submitted April, 1998.
[29] D.J.G. Ives, G.J. Janz, Reference Electrodes, Academic Press, New York, 1961.
[30] W. Blum, G.B. Hogaboom, Principles of Electroplating and Electroforming, 3, McGraw-Hill, New York, 1949, p. 382.
[31] S.A. Emr, A.M. Yacynich, Electroanalysis 7 (1995) 913.
[32] S.A.M. Marzouk, V.V. Cosofret, R.P. Buck, H. Yang, W.E. Cascio, S.S.M. Hassan, Talanta 44 (1997) 1527.
[33] C.X. Xu, S.A. Marzouk, V.V. Cosofret, R.P. Buck, M.R. Neuman, R.H. Sprinkle, Talanta 44 (1997) 1625.
[34] G. Nagy, C.X. Xu, R.P. Buck, E. Lindner, M.R. Neuman, Anal. Chem., 70 (1998) 2156.

ELSEVIER

Talanta 47 (1998) 377–385

Talanta

Ribonucleic acid as a novel ionophore for potentiometric membrane sensors of some transition metal ions

Saad S.M. Hassan *, Wagiha H. Mahmoud, Abdel Hammeed M. Othman

Department of Chemistry, Faculty of Science, Ain Shams University, Cairo, Egypt

Received 21 November 1997; received in revised form 20 March 1998; accepted 29 March 1998

Abstract

Ribonucleic acid (RNA) is used as a novel ionophore in plasticized poly(vinyl chloride) matrix membrane sensors for some transition metal ions. Membranes incorporating RNA and doped in Cu^{2+}, Cd^{2+} and Fe^{2+} display fast near-Nernstian and stable responses for these ions with cationic slopes of 31.1, 31.3 and 35.5 mV per decade, respectively, over the concentration range 10^{-6}–10^{-2} M and pH range 4–6.5. The cadmium RNA-based sensor shows no interference by Cu^{2+}, Fe^{2+} Hg^{2+} and Ag^{+}, which are known to interfere significantly with the solid-state CdS/Ag_2S membrane electrode. The copper RNA-based sensor displays general potentiometric characteristics similar to those based on macrocyclic ionophores and organic ion exchangers and has the advantage of a better selectivity for Cu^{2+} over some alkaline earth, divalent and transition metal ions. The iron RNA-based membrane sensor exhibits no interference by Hg^{2+} and Zn^{2+}, which are known to interfere with other previously suggested sensors. The nature and composition of the RNA ionophore and its cadmium complex are examined using electrophoresis, Fourier-transform infrared analysis, elemental analysis and X-ray fluorescence techniques. © 1998 Elsevier Science B.V. All rights reserved.

Keywords: Copper, cadmium and iron potentiometric sensors; Poly(vinyl chloride) matrix; Ribonucleic acid ionophore

1. Introduction

Since the introduction of liquid/polymer membrane-type ion-selective electrodes in the 1970s, many cyclic and acyclic macromolecules have been suggested as electroactive ionophores. Of these, crown ethers [1,2], aza [3] and thia compounds [4], polyamines [5,6], calixarenes [7,8], antibiotics [9,10], mycobactins [11], metalloporphyrins [12,13], metallophthalocyanines [14,15] and metallocenes [16] have been shown to bind some organic and inorganic cations and anions reversibly and to transport them across organic membranes by carrier translocation. Polymeric membrane potentiometric sensors based on these ionophores are found to show excellent electroactive properties, a near-Nernstian response over a wide range of concentrations and pH, and to display good selectivity. The recognition of specific ions by these receptors is determined by the cavity size, type of functional group and geometry of the molecules. However, little is known about

* Corresponding author. Fax: +20 2 831836.

0039-9140/98/$ - see front matter © 1998 Elsevier Science B.V. All rights reserved.
PII S0039-9140(98)00142-8

the use of such compounds for transition metal ions.

Nucleic acids are condensation linear natural multisite polymeric ligands of ribose phosphates that carry four purine and pyrimidine bases arranged mainly in double-helical strands (DNA) or single strands (RNA). The organized centres of charges, N-donor bases, grooves, cavities, loops and geometry of these molecules can selectively bind or preferentially encapsulate some organic and inorganic ionic species [17,18]. These characteristics make RNA and DNA unique ligands, with a combination of stereoselectivity and chemical recognition, which offer a novel entry into the field of selective binding [19]. The application of nucleic acids in chemical analysis is a new area of investigation with only a few specific clinical diagnostic examples. Separation based on binding to target molecules such as organic dyes, amino acids, theophylline, vitamin B_{12}, biological cofactors, thrombin, antibodies and drugs has been reported [19]. Since chemical sensors often use selective binders that are immobilized at the sensor surface to generate an analyte-dependent signal [20], this suggests that nucleic acid is a suitable candidate for the selective sensing of some ionic species.

The present study provides a novel approach to the use of RNA as a natural ionophore in potentiometric polymer membrane sensors responsive to some transition metal ions. It is evident from the present work that RNA, a commercially available natural product, has the ability to effect ion-selective extraction from an aqueous solution to a hydrophobic membrane phase and to transport these ions by ionophore translocation. Plasticized poly(vinyl chloride) (PVC) membranes incorporating RNA and doped in Cd^{2+}, Cu^{2+} and Fe^{2+} solutions displayed a stable near-Nernstian response over a wide range of concentrations and pH for these ions.

2. Experimental

2.1. Apparatus

All potentiometric measurements were made at 25 ± 1°C with an Orion Model SA 720 digital pH/millivoltmeter. A PVC membrane electrode was based on RNA in conjunction with a double junction Ag/AgCl reference electrode (Orion 90-20) containing 10% (w/v) potassium nitrate in the outer compartment. A Ross glass pH electrode (Orion 81-02) was used for all pH measurements. Electrophoresis was carried out using a Minnine Gel Cicle, Submarine Agarose GE unit HE 33 instrument (Hoefer). X-Ray fluorescence measurements were made using a Philips PW1480 X, UNIQ II X-ray spectrophotometer with a PW1530 sample changer. A Unicam Fourier-transform infrared (FTIR) spectrometer (Model Mattson 1000), using the KBr technique, was used for infrared measurements.

2.2. Reagents and materials

Analytical reagent grade chemicals and doubly distilled deionized water were used for preparing all aqueous solutions. High molecular weight poly(vinyl chloride) powder (PVC) and spectrally pure KBr were obtained from Aldrich. Dioctylphthalate (DOP), *o*-nitrophenyloctyl ether (*o*-NPOE), dibutylsebacate (DBS) and tetrahydrofuran (THF) were obtained from Fluka. Ribonucleic acid (rRNA) sodium salt, DNA disodium salt, 5′-adenosine monophosphate (5′-AMP) sodium salt and 5′-nucleoside monophosphate (5′-NMP) sodium salt were obtained from BDH. Salts (mainly chloride or nitrate) of metals such as Ag^{+}, K^{+}, NH_4^{+}, Rb^{+}, Cs^{+}, Hg^{2+}, Cu^{2+}, Cd^{2+}, Zn^{2+}, Co^{2+}, Ni^{2+}, Fe^{2+}, Mg^{2+}, Pb^{2+}, Ba^{2+}, Sr^{2+} and Al^{3+} were obtained from BDH. Stock solutions (10^{-1} M) of these metal ions were prepared and standardized by complexometric titrations. Agarose, molecular biology grade, was obtained from Sigma.

RNA in free acid form was prepared by dissolving 0.5 g of its sodium salt in 20 ml of distilled water acidified with a few drops of 10% HCl; the solution was stirred for about 15 min to precipitate the acid form, and the product obtained was filtered, washed with cold water and dried at room temperature.

2.3. RNA membrane sensors

Unless otherwise specified, the PVC membranes were prepared in the following way: 2 wt.% RNA, 67 wt.% plasticizer (DOP, DBS or *o*-NPOE) and 31 wt.% PVC were transferred to a glass petri dish (5 cm diameter) and dissolved in 5 ml of THF. The solution was allowed to evaporate overnight at room temperature to give a transparent flexible membrane (≈ 0.1 mm thick). A disc of 6-mm diameter was cut out from the PVC membrane and glued to a polyethylene tube (3 cm × 8 mm. i.d.) as previously described [20,21]. Internal reference solutions containing equal volumes of 10^{-2} M NaCl and 10^{-2} M of the metal ion solution were used. An Ag/AgCl internal reference wire electrode (1.0 mm diameter) was immersed in the internal solution. The sensors were conditioned by soaking in 10^{-3} M metal chloride solution overnight. The external reference electrode was Ag/AgCl. The composition of the electrochemical cell was: Ag/AgCl | 10^{-2} M sodium chloride + 10^{-2} M metal ion ‖ PVC membrane ‖ sample solution | Ag/AgCl reference electrode. The sensors were stored in 10^{-3} M metal solution when not in use, and protected from light to avoid any possible photodegradation of the ionophore. The sensors were washed with doubly-distilled deionized water and blotted with tissue paper between measurements.

2.4. Potentiometric measurements

The functions of the membrane sensors were investigated at 25°C. Thirteen different metal ion (Mg^{2+}, Ba^{2+}, Pb^{2+}, Cu^{2+}, Co^{2+}, Zn^{2+}, Cd^{2+}, Mn^{2+}, Ni^{2+}, Hg^{2+}, Fe^{2+}, Cr^{3+} and Al^{3+}) PVC membrane sensors were prepared. Each sensor in conjunction with a double-junction Ag/AgCl reference electrode was immersed in a 50-ml beaker containing 9.0 ml of doubly-distilled deionized water followed by the addition of 1.0-ml aliquots of 10^{-6}–10^{-1} M standared metal ion solutions. The potential readings after each addition were recorded and the e.m.f. was plotted as a function of the logarithm of the metal ion concentration. The lower detection limit was taken at the point of intersection of the extrapolated linear segments of the calibration curve. Potential repeatability was measured by immersing the sensor alternately into 10^{-2} and 10^{-3} M metal ion solutions.

The pH–e.m.f profiles of 10^{-3} and 10^{-2} M test solutions (i.e. containing Cu^{2+}, Cd^{2+} or Fe^{2+}) were obtained by immersing a combined glass electrode and the respective metal sensor in conjunction with a double-junction Ag/AgCl reference electrode into the metal ion solutions. The potential change due to variation of pH over the range 2–8 by the addition of drops of dilute NaOH and/or HCl was recorded.

The values of the selectivity coefficients $K^{pot}_{Cd^{2+},B}$, $K^{pot}_{Cu^{2+},B}$ and $K^{pot}_{Fe^{2+},B}$ were determined by the separate solution method [20,22] and calculated from the rearranged Nicolsky equation:

$$\log K^{pot}_{M,B} = \frac{E_M - E_B}{S} + \left(1 + \frac{Z_M}{Z_B}\right) \log M^+$$

where E_M is the potential measured in 10^{-2} M Cd^{2+}, Cu^{2+} or Fe^{2+} metal ion solution, E_B is the potential measured in 10^{-2} M solution of the interfering cation, Z_M and Z_B are the charges of Cd^{2+}, Cu^{2+} or Fe^{2+} and the interfering ions, respectively, and S is the slope of the electrode calibration plot.

2.5. Cadmium–RNA complex

The complex was prepared by mixing an aliquot (20 ml) of 1% RNA disodium salt with 10 ml of 10^{-2} M cadmium nitrate solution. The mixture was thoroughly stirred for 10 min and filtered through Whatman filter paper no. 42, washed with deionized doubly-distilled water, dried at room temperature for 24 h and powdered. The complex was examined by Fourier-transform infrared analysis, elemental analysis and electrophoresis.

3. Results and discussion

3.1. Potentiometric response

RNA is a natural multisite ligand with a three-dimensional geometry containing pseudoknot, hair pine and stem-loop/bulge [19,23–25] struc-

tures. Cavity widths, lining atoms of the cavities (which act as donors) and the support structure behind the cavities offer a unique structure either as a host to accommodate guest ions or as a chelating agent to bind these ions. Different types of sites particularly suited for binding transition metal ions are expected to be present or generated by folding of the RNA molecule. Sensors based on RNA–PVC plasticized membranes doped with transition metal ions were prepared and their potentiometric response characteristics were investigated. The composition of the membranes was 31 wt.% PVC, 2 wt.% ribonucleic acid and 67 wt.% solvent mediator. The potentiometric response of sensors based on RNA ionophore is greatly influenced by the polarity of the membrane medium, which is in turn defined by the dielectric constant of the solvent mediator. Three different plasticizers having dielectric constants ranging from 4 to 24 (i.e. DBS, DOP and *o*-NPOE) have been used. Since RNA ionophore is partially soluble in these plasticizers, it was incorported by dispersion in the PVC membrane. Dispersion of metal–RNA complexes in the PVC membrane gives a weak response, probably due to their poor solubility in the lipophilic plasticizers.

RNA dispersed in PVC membranes plasticized with DOP and doped with Cd^{2+} and Cu^{2+} exhibited linear stable responses for Cd^{2+} and Cu^{2+} with calibration slopes of 29.5 and 20.3 mV per decade, respectively, over the concentration range 1×10^{-2}–1×10^{-5} M (Fig. 1 and Table 1). The response times ranged from 20 to 50 s for

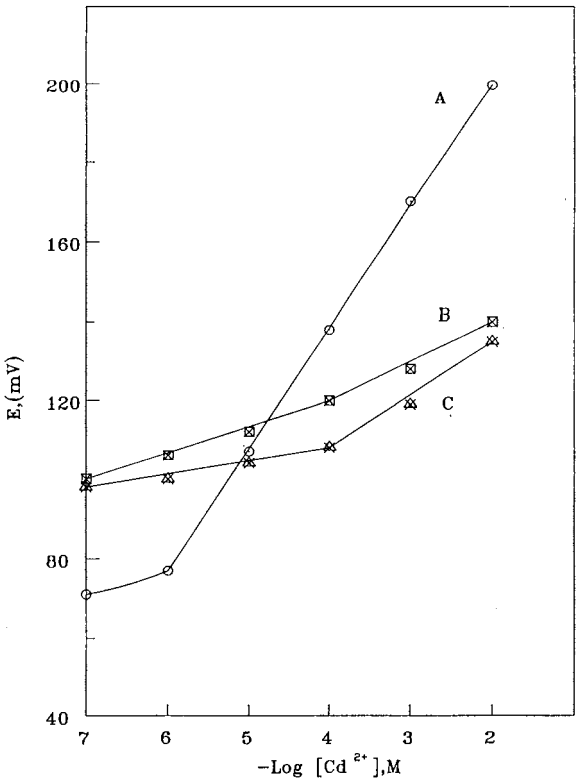

Fig. 1. Potentiometric response of cadmium PVC membrane sensors based on (A) RNA, (B) 5′-AMP and (C) DNA ionophores using *o*-NPOE plasticizer.

10^{-3}–10^{-5} M metal ion solution concentrations. A significantly weak response with limited range of linearity was obtained with many other transition metal ions. Over the concentration range of 10^{-2}–10^{-4} M, RNA membranes doped with Co^{2+} and Ni^{2+} displayed calibration slopes of

Table 1
The potentiometric response characteristics of Cd^{2+}, Cu^{2+} and Fe^{2+} PVC membrane sensors based on RNA ionophore[a]

Parameter	Cd^{2+} membrane (NPOE)	Cu^{2+} membrane (DBS)	Fe^{2+} membrane (NPOE)
Slope (mV per decade)[b]	31.1 ± 0.5	31.3 ± 0.6	35.5 ± 0.1
Intercept (mV)[b]	233 ± 0.3	252 ± 0.2	251 ± 0.4
Correlation coefficient (r)	0.996	0.997	0.996
Working pH range	4–6.5	4–6.5	4–6.5
Lower limit of detection (M)	1×10^{-6}	2×10^{-6}	9×10^{-6}
Response time for 1×10^{-3} M (s)	30	40	40
Lower limit of linear range (M)	1 ± 10^{-5}	1×10^{-5}	1×10^{-5}

[a] Results represent the average of five measurements.
[b] $\pm$ S.D.

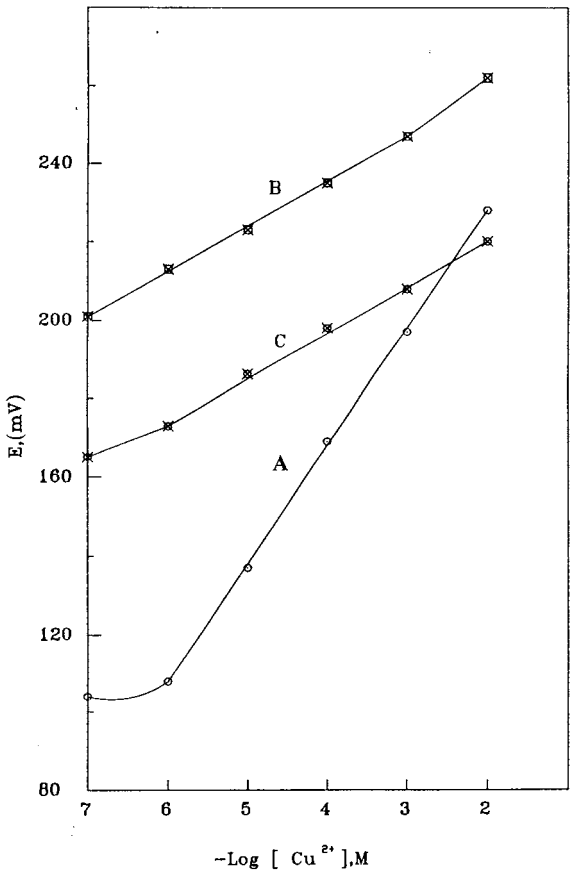

Fig. 2. Potentiometric response of copper PVC membrane sensors based on (A) RNA, (B) 5′-AMP and (C) DNA ionophores using DBS plasticizer.

only 9.2 and 8.5 mV per decade, respectively. No response was detected by membranes doped with Ba^{2+}, Mn^{2+}, Pb^{2+} and Zn^{2+} at concentrations as high as 10^{-2} M of these metal ions.

PVC membranes containing RNA, plasticized with DBS and doped with Cd^{2+} and Cu^{2+} responded to Cd^{2+} and Cu^{2+} within the working concentration range of 10^{-2}–10^{-5} M, with cation slopes of 37.0 and 30.3 mV per decade, respectively (Table 1 and Fig. 2). Responses to Cr^{3+} and Fe^{2+} at concentrations of 10^{-2}–10^{-5} M by RNA–PVC membranes doped with these ions were linear, with slopes of 28.2 and 37.1 mV per decade, respectively. These slopes are higher than those expected for the trivalent Cr^{3+} and divalent Fe^{2+}. The super-Nernstian slopes can probably be attributed to the presence of some metal oxonium hydroxo species such as $[Cr(OH)_2(H_2O)_4]^+$ and $[Fe(OH)(H_2O)_3]^+$ [26]. There was no appreciable response to Co^{2+}, Zn^{2+} and Ni^{2+} by membranes doped with these ions; they displayed calibration slopes of 5.0–19.1 mV per decade for 10^{-2}–10^{-5} M metal ion solutions. No response was displayed by Pb^{2+}, Ba^{2+} and Mn^{2+}.

Membranes incorporating RNA, plasticized with *o*-NPOE and doped with Co^{2+}, Cu^{2+}, Fe^{2+} and Cr^{3+} responded to these ions over the concentration range 10^{-2}–10^{-4} M for Co^{2+} and Cu^{2+} (slopes of 20.3 and 24.1 mV per decade, respectively) and over the concentration range 10^{-3}–10^{-6} M (slopes of 35.5 and 23.5 mV per decade, respectively) for Fe^{2+} and Cr^{3+} (Table 1 and Fig. 3). Cd^{2+} displayed a favourable response of 31.1 mV per decade over the concentration range 10^{-2}–10^{-6} M (Table 1 and Fig. 1). Membranes doped with Mg^{2+}, Ba^{2+}, Pb^{2+}, Zn^{2+}, Mn^{2+} and Ni^{2+} gave either a poor response (not more than 10 mV per decade over the range 10^{-2}–10^{-4} M of metal ions) or no significant response.

It has been reported that individual nucleic acid components, such as 5′-AMP and 5′-NMP, interact with divalent 3d transition metal ions to form macro-chelates with highest stability for Cd^{2+} and Cu^{2+} [27]. PVC matrix membranes plasticized with DBS and *o*-NPOE, doped with Cd^{2+}, Cu^{2+} and Fe^{2+} derivatives of 5′-AMP, respectively, were prepared and examined as sensors for these metal ions. The results obtained (Figs. 1–3) show a weak response over the concentration range 10^{-2}–10^{-7} M metal ions, the calibration slopes being 9, 14 and 15 mV per concentration decade for Cd^{2+}, Cu^{2+} and Fe^{2+}, respectively. PVC membranes containing DNA and doped with Cd^{2+}, Cu^{2+} and Fe^{2+} were also examined. A weak response was noticed for Cd^{2+} and Cu^{2+}, with a slope of ≈ 11 mV per decade of concentration (Figs. 1–3). A linear response (slope of 35 mV per decade) was observed for Fe^{2+} in the range 10^{-3}–10^{-5} M (Fig. 2). Membranes without RNA, DNA and 5′-AMP showed no e.m.f. response for various transition metal cations at different concentration levels.

No trials were made to incorporate ion-exchangers in the sensor membrane. On one hand, ion-exchangers for copper, cadmium and iron ions are very limited and are difficult to prepare. On the other hand, the developed sensors are sensitive enough to measure metal concentrations down to 10^{-6} M.

3.2. Membrane selectivity

It can be seen from this study that RNA–PVC membranes, plasticized with *o*-NPOE, DBS and *o*-NPOE and doped with Cd^{2+}, Cu^{2+} and Fe^{2+}, respectively, are sufficiently selective for these metal ions with excellent potentiometric performance characteristics. Potentiometric selectivity coefficients of Fe^{2+}, Cu^{2+} and Cd^{2+} RNA–PVC membranes were determined by the separate solution method using 10^{-3} M of the primary metal ion and the interferents. Selectivity patterns of these membranes are shown in Fig. 4. Selectivity sequences of the membrane systems were dependent on the plasticizer used and the structural flexibility of the RNA ionophore.

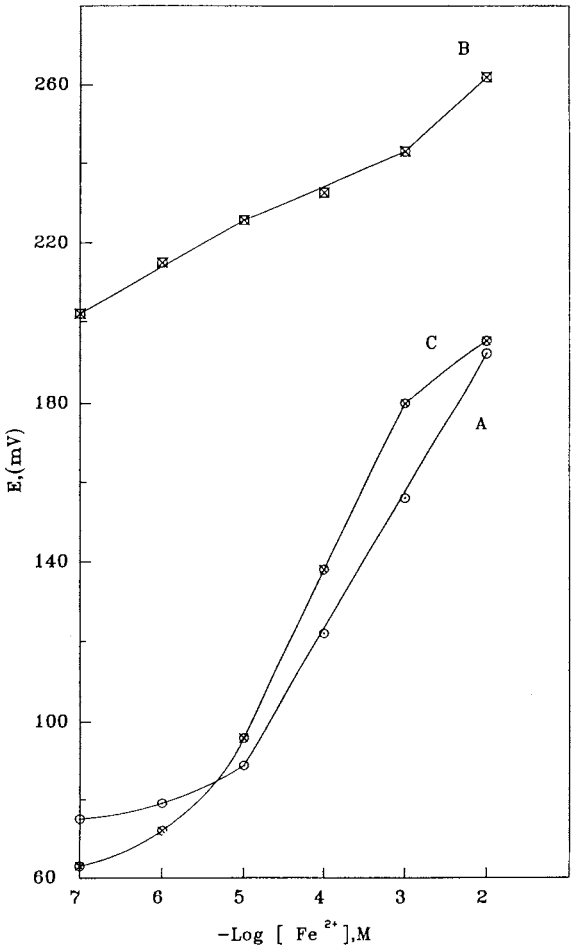

Fig. 3. Potentiometric response of iron PVC membrane sensors based on (A) RNA, (B) 5′-AMP and (C) DNA ionophores using *o*-NPOE plasticizer.

The selectivities of the sensors which depend on the ion-exchange process at the membrane interface and the stability of the metal–ionophore complexes are highly influenced by the composition of the membrane and the inner sensor solution. It may be noticed that the selectivity sequence between Cd^{2+} and Fe^{2+} sensors is quite different in spite of the use of the same ionophore and plasticizer. This is mainly due to the different nature of the membrane composition after soaking in its primary metal ion and the composition of the inner reference solutions of the sensors.

These results revealed that metal ions with ionic radii of less than 0.75 Å (e.g. Zn^{2+}, Co^{2+}, Cr^{3+}, Ni^{2+}, Mg^{2+}) and those of ionic radii greater than 1.0 Å (e.g. Ba^{2+}, Pb^{2+}, Ca^{2+}) display either a weak response over a narrow concentration range or no response. RNA doped membranes based on these systems are of little value. However, good extended Nernstian responses over the concentration range of at least 10^{-2}–10^{-5} M were obtained for metal ions with ionic radii in the range 0.82–0.92 Å (e.g. Cd^{2+}, Cu^{2+}, Fe^{2+}). This can be explained in the light of the conventional idea of the cation cavity size relationship, assuming that RNA at the time of complexation with these metal ions can adopt cavity-like structures to accommodate or encapsulate guest ions of ionic radii in the range of 0.82–0.92 Å. Other factors, including solubility equilibria, ion-exchange at the membrane interface, stability of the cation–RNA complexes and the presence of ionic clusters connected by small channels suitable for ion diffusion, play definite roles in imposing the observed cation selectivity.

The effect of some anions on the response of a cadmium sensor based on a RNA–PVC membrane plasticized with *o*-NPOE was also exam-

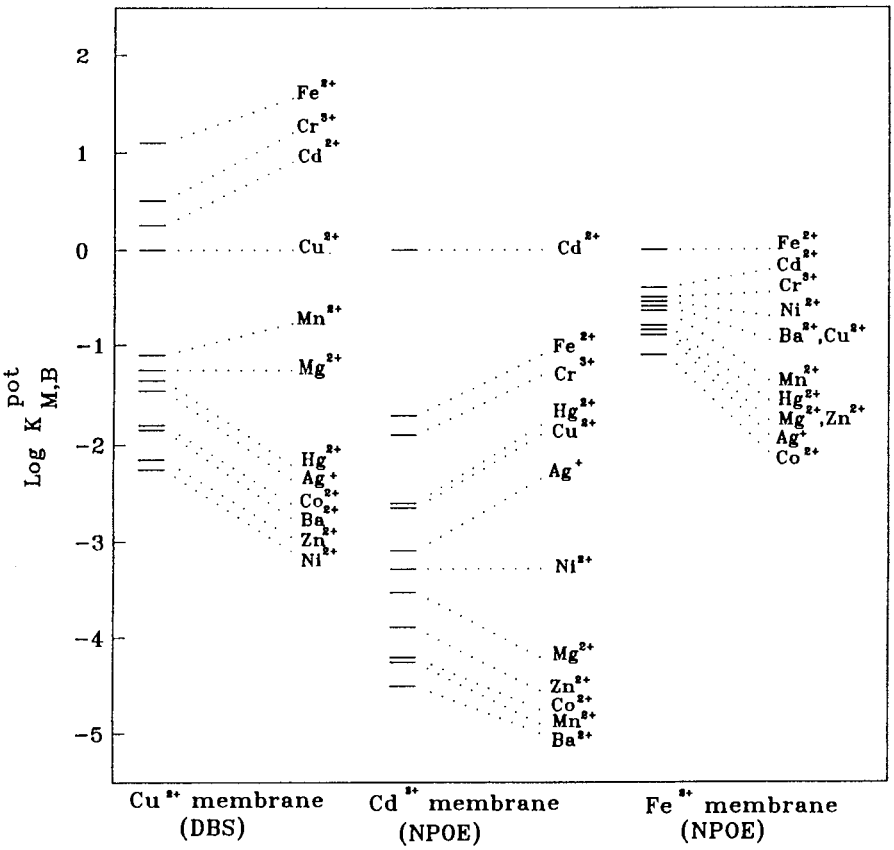

Fig. 4. Selectivity coefficient log $K^{pot}_{M,B}$ patterns for Cu^{2+}, Cd^{2+} and Fe^{2+} PVC membrane sensors based on RNA ionophore.

ined. The anionic response was weak and in the order $S^{2-} > Br^- > I^- > Cl^-$.

3.3. Effects of pH and response time

The effect of H^+ concentration on the responses of RNA–PVC membranes doped with Fe^{2+}, Cu^{2+} and Cd^{2+} was studied in 10^{-2} and 10^{-3} M metal solutions. The pH was adjusted with HCl and NaOH. As seen in Fig. 5, Fe^{2+}, Cu^{2+} and Cd^{2+} sensors responded only to metal solutions in the pH range 4–6.5. Above pH 6.5, the metal signal significantly diminished, probably due to precipitation of metal hydroxides. At higher acidity ($pH < 5$) the membranes extract H^+ in addition to M^{2+} ions and the sensor response increases sharply. Thus, the optimum pH range for determination of these metal ions is 4–6.5. The response times of Cd^{2+}, Cu^{2+}, and Fe^{2+} sensors were tested by measuring the time required to achieve a steady potential (within 1-mV fluctuation) in 10^{-2} and 10^{-3} M Cu^{2+}, Cd^{2+} and Fe^{2+} solutions by a rapid ten-fold increase in metal concentration (dynamic response). Steady potentials were achieved within 30–40 s. The sensors were found to respond effectively for at least 6 weeks after preparation. During this period the calibration slope declined ≈ 2 mV per decade and the potential reading decreased by 2–3 mV.

3.4. Nature and composition of the ionophore

RNA was allowed to react with cadmium(II) and the reaction product was isolated, examined by elemental analysis, X-ray fluorescence, elec-

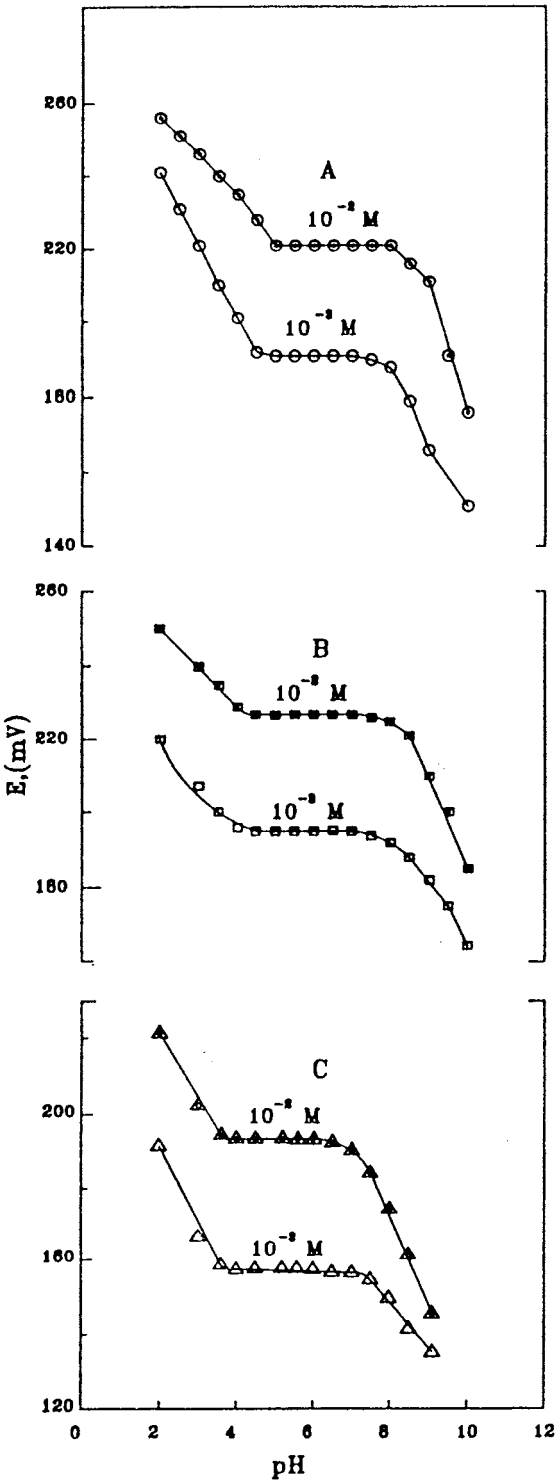

Fig. 5. Effect of pH on the potentiometric responses of RNA PVC membrane sensors for (A) Cd^{2+}, (B) Cu^{2+} and (C) Fe^{2+}.

trophoresis and FTIR. Elemental analysis of RNA (free acid) and its cadmium derivative shows, respectively: C 30.6%, H 5.1%, N 13.8%; and C 24.7%, H 5.1%, N 10.8%. The cadmium content of the RNA–cadmium complex as measured by X-ray fluorescence was 7%. Electrophoresis of RNA free acid and its cadmium derivative was carried out on 5% formamide agarose gel stained with ethidium bromide and scanned at a constant voltage of 50 V for 1–5 h. Electrophoresis of a standard RNA molecular weight marker consisting of 9.5, 4.4, 3.4, 1.4, and 0.24 kilobase (kb) was carried out in a parallel experiment.

The results revealed that the molecular weight of RNA used in the present study is ≈ 2.4 kb and the mobility of the free acid on the gel is 5–10% greater than that of the cadmium-containing acid, which is in good agreement with the X-ray fluorescence measurement (7% cadmium content). FTIR spectrum of RNA (sodium salt) displayed strong signals at 3385, 3206 and 1642 cm^{-1} due to –OH, –NH and –C=N stretching vibrations, respectively. These bands appeared at 3408, 3229 and 1657 cm^{-1}, respectively, in the FTIR spectrum of the RNA–cadmium complex. This indicates participation of these functional groups in the binding with transition metal ions. Since guanine, cytosine and adenine constituents of RNA contain –NH, C–OH and C=N groups, it is more likely that these compounds contribute in the complex formation. It has been reported that cytosine and guanine are regarded as the main binding sites of some nucleic acids [28].

4. Conclusions

Potentiometic PVC membrane sensors based on RNA ionophore are sensitive for the detection of Cd^{2+}, Cu^{2+} and Fe^{2+} over a wide range of concentrations (10^{-6}–10^{-2} M) and pH values (4.6–7). These sensors exhibit enhanced analytical responses for these ions over many transition metal ions. With the cadmium–RNA sensor, no interferences are caused by divalent metal ions such as Pb^{2+}, Cu^{2+}, Fe^{2+}, Hg^{2+} and Ag^{+}, which are known to interfere significantly with

solid state CdS/Ag_2S membrane sensors [29,30]. A wider concentration range (four decades) is also offered by the proposed sensors compared with two concentration decades obtained with other PVC membrane sensors [31,32]. The copper–RNA sensor displays similar characteristics to sensors based on macrocylic ionophores and organic exchangers [33–36]. The proposed copper sensor has the advantage of better selectivity for copper over some alkaline earth, divalent and transition metal ions. However, interferences are caused by Pb^{2+}, Cd^{2+}, Cr^{3+} and Fe^{2+}. These ions are also known to cause serious interference with many other copper membrane sensors, [33–36]. The iron(II)–RNA sensor has a slope of 35.5 mV per decade over a wide concentration range (10^{-6}–10^{-2} M). The lower limit of detection is 9×10^{-6} M and no interferences are caused by many cations (e.g. Hg^{2+}, Zn^{2+} and Sn^{2+}) that are known to interfere with the previously suggested sensors based on tetrachloroferrate(III) aliquate and stannic arsenate [37,38]. In addition, these sensors have the disadvantages of low sensitivity (limit of detection $> 10^{-4}$ M) and sub-Nernstian response.

References

[1] H. Tamura, K. Kimura, T. Shono, Anal. Chem. 54 (1982) 1224.
[2] S.S.M. Hassan, E.M. Elnemma, Anal. Chem. 61 (1989) 2189.
[3] A. Jyo, R. Weber, H. Egawa, Anal. Sci. 9 (1993) 599.
[4] S. Kamata, K. Yamasaki, M. Higo, A. Bhale, Y. Fukuaga, Analyst 113 (1988) 45.
[5] U. Oesch, Z. Brzozka, A. Xu, B. Rusterholz, G. Suter, H.V. Pham, D. Amman, E. Pretsch, W. Simon, Anal. Chem. 58 (1986) 2285.
[6] L. Cazaux, P. Tisnes, C. Picard, C. D'Silva, G. Williams, Analyst 119 (1994) 2315.
[7] K. Odashima, K. Yagi, K. Tohda, Y. Umezawa, Anal. Chem. 65 (1993) 1074.
[8] E. Malinowska, Z. Brzozka, K. Kasiura, R.J.M. Egberink, D.N. Reinhoudt, Anal. Chim. Acta 298 (1994) 245.
[9] K. Suzuki, K. Tohda, H. Aruga, M. Matsuzoe, H. Inoue, T. Shirai, Anal. Chem. 60 (1988) 1714.
[10] S.S.M. Hassan, W.H. Mahmoud, A.H. Othman, Talanta 44 (1997) 1087.
[11] D. Midgley, J. Chem. Soc. Faraday Trans. I 82 (1986) 1187.
[12] N.A. Chaniotakis, A.M. Chasser, M.E. Meyerhoff, J.T. Groves, Anal. Chem. 60 (1988) 188.
[13] I.H.A. Badr, M.E. Meyerhoff, S.S.M. Hassan, Anal. Chim. Acta 321 (1996) 11.
[14] C. Sun, Y. Sun, X. Zhang, H. Xu, J. Shem, Anal. Chim. Acta 312 (1995) 207.
[15] J. Li, X. Dang, D. Gao, R. Yu, Talanta 42 (1995) 1775.
[16] H. Hisamoto, D. Siswanta, H. Nishihara, K. Suzuki, Anal. Chim. Acta 304 (1995) 171.
[17] C. Tuerk, L. Gold, Science 249 (1990) 505.
[18] A.D. Ellington, J.W. Szostak, Nature 346 (1990) 818.
[19] L.B. McGown, M.J. Joseph, J.B. Pitner, G.P. Vonk, C.P. Linn, Anal. Chem. 663A (1995) 1.
[20] T.S. Ma, S.S.M. Hassan, Organic Analysis Using Ion Selective Electrodes, vols. 1 and 2, Academic Press, London, 1982.
[21] S.S.M. Hassan, S.A. Marzouk, Talanta 41 (1994) 891.
[22] IUPAC Analytical Chemistry Division, Commission on Analytical Nomenclature, Pure Appl. Chem. 67 (1995) 507.
[23] M. Sassanfar, J.W. Szostak, Science 364 (1993) 550.
[24] C. Tuerk, S. Mac Dougal, I. Gold, Proc. Natl. Acad. Sci. USA 89 (1992) 6988.
[25] I.C. Bock, L.C. Griffin, J.A. Latham, E.H. Vermass, J. Toole, Nature 355 (1992) 564.
[26] F.A. Cotton, G. Wilkinson, Advanced Inorganic Chemistry, 3rd ed., Interscience, New York, 1972, D. 863.
[27] H. Sigel, S.S. Massoud, R. Tribolet, J. Am. Chem. Soc. 110 (1988) 6857.
[28] H. Richard, J.P. Schreiber, M. Daune, Biopolymers 12 (1973) 1.
[29] G.Yu. Valsov, E.Yu. Ermolenko, V.V. Kolendikov, Zh. Anal. Khim. 36 (1981) 880.
[30] M. Athara, S. Kanetake, Y. Fukuda, Bull. Chem. Soc. Jpn. 58 (1985) 1617.
[31] K.Q. Emmanuel, V.P.Y. Gadzekpo, Analyst 117 (1992) 1899.
[32] M.P. Isabel, L.V.O. Ferrieza, L.F.C. Jose, Analyst 119 (1994) 209.
[33] Z. Brzozka, Analyst 113 (1988) 1803.
[34] K. Ren, Talanta 36 (1989) 767.
[35] S.X. Xia, D. Xiao, R.Q. Yu, Fenxi Huaxue 22 (1994) 892.
[36] A.K. Jain, V.K. Gupta, B.B. Sahoo, L.P. Singh, Anal. Proc. 32 (1995) 99.
[37] R.W. Cattarall, P. Chin-Poh, Anal. Chem. 47 (1975) 93.
[38] P.S. Thind, S.K. Mittal, Bull. Electrochem. 4 (1988) 431.

ELSEVIER

Talanta 47 (1998) 387–399

Talanta

Effect of cationic micelles on the formation of the complex oxalate–Alizarin Red S–Zr(IV) Application to the sensitive fluorescence determination of oxalate ion

Juan Aybar Muñoz, Ana M. García Campaña *, Fermín Alés Barrero

Department of Analytical Chemistry, Faculty of Sciences, Avd. Fuentenueva s/n., University of Granada, E-18071 Granada, Spain

Received 16 September 1997; received in revised form 24 March 1998; accepted 29 March 1998

Abstract

The effect of several surfactants on the formation of the fluorescent ternary complex oxalate–Alizarin Red S–zirconium(IV) has been studied. In weakly acidic medium and in the presence of cationic surfactants, such as cetylpyridinium chloride, total complex formation is achieved, whereas in aqueous medium or in the presence of non-cationic micelles no significant changes are obtained in comparison with the formation of the non-fluorescent binary complex Alizarin Red S–zirconium(IV). The fluorescence characteristics of this system allowed the establishment of a simple and very sensitive method for the spectrofluorimetric determination of oxalate. The ternary complex formed exhibits its highest fluorescence signal at 605 nm with excitation at 490 nm. In these conditions, the method presents a IUPAC detection limit of 4.4 ng ml^{-1}. The procedure has been satisfactorily applied to a biological fluid and a vegetal tissue. © 1998 Elsevier Science B.V. All rights reserved.

Keywords: Biological samples; Fluorescence; Micellar medium; Oxalate

1. Introduction

The addition of certain surfactants has been regularly used in luminescence analysis in order to improve or modify the properties of the analytical methods [1]. Although there is no general theory to explain the effects of the micelles on fluorescence, Sanz Medel et al. have studied the mechanism of cationic surfactant-modified fluorescence of metallic complexes with flavone derivatives and other reagents in an attempt to clarify the effect by which this enhancement takes place [2].

The large amount of literature on ternary complexes showing fluorescence characteristics applied to the determination of different species has been meticulously summarized by Haddad [3]. The improvements in selectivity and sensitivity that often accompany this complex formation in spectrofluorimetric analysis have been improved in recent years by the use of surfactants. This has lead to the greater development of methods using

* Corresponding author. Tel.: +34 958 248594; e-mail: amgarcia@goliat.ugr.es

0039-9140/98/$ - see front matter © 1998 Elsevier Science B.V. All rights reserved.
PII S0039-9140(98)00144-1

micellar media and to better elucidation of the interactions between tensioactives and complexes.

Alizarin Red S (ARS) is a reagent that has recently been used for the spectrofluorimetric determination of metals in the presence of cationic surfactants [4–6]. It has been also found that the fluorescence intensity of the EDTA–ARS–Zr(IV) complex can be strongly enhanced by cetyltrimethylammonium bromide, providing a method for the determination of EDTA with high sensitivity and excellent selectivity [7]. In this sense, a similar study has been carried out on the effect of surfactants on the absorption and fluorescence phenomena of the oxalate–ARS–Zr(IV) complex due to the increasing interest in the determination of oxalate in biological materials. It is directly involved in some methabolic pathways and several diseases since it is one of the principal chelates in the human diet [8]. Oxalate ion forms sodium, potassium, ammonium and lithium chelates that inhibit blood coagulation. It is also closely associated with hyperoxaluria, a genetic disorder that results in excessive generation of urinary oxalate and frequently leads to death, and with urolithiasis, because of its strong capacity to form chelates with calcium which lead to calcium oxalate stone formation. The determination of oxalate in body fluids, particularly blood serum and urine, is therefore of clinical interest for the diagnosis of genetic disorders of oxalate metabolism.

Although a wide variety of methods for the determination of oxalate have been developed, there is a demand for an inexpensive, sensitive and simple procedure in order to obtain more accurate information about oxalate levels not only in biological fluids but also in other matrixes such as vegetables.

The methods applied to urine are usually based on direct precipitation, solvent liquid–liquid extraction, isotope dilution, chromatography, enzymatic reactions and flow injection [9–11]. Although oxalate and its complexes are colourless, variations in absorbance can be produced when oxalate reacts with a metal ion, dissociating the coloured complex initially present. Such a method has been developed, for example, using the uranium–4-(2-pyridylazo)resorcinol complex [12]. In order to increase the selectivity, Salinas et al. [13] used a method to determine oxalate in blood serum and urine, combining separation and spectrometry, by extracting a vanadate–mandelohydroxamate–oxalate complex into toluene. More specificity is achieved by determining oxalic acid by dissociation of the Zr(IV)–chloranilate complex [14].

However, there is still a need for more sensitive, inexpensive and simpler methods for the analysis of oxalate at trace levels. Although spectrofluorimetry has the basic advantage of greater sensitivity, few methods has been proposed using this technique and are mainly based on the quenching by oxalate of the fluorescence of different systems or on its enhancing effect on the oxidation reactions, implicating the formation of a fluorescent specie or the decrease of the fluorescence of the oxidized specie [11,15,16]. The most sensitive method involves the quenching of Zr–flavonol chelate by oxalate, giving a detection limit of 5 ng ml^{-1} [15]. Recently, a flow-injection

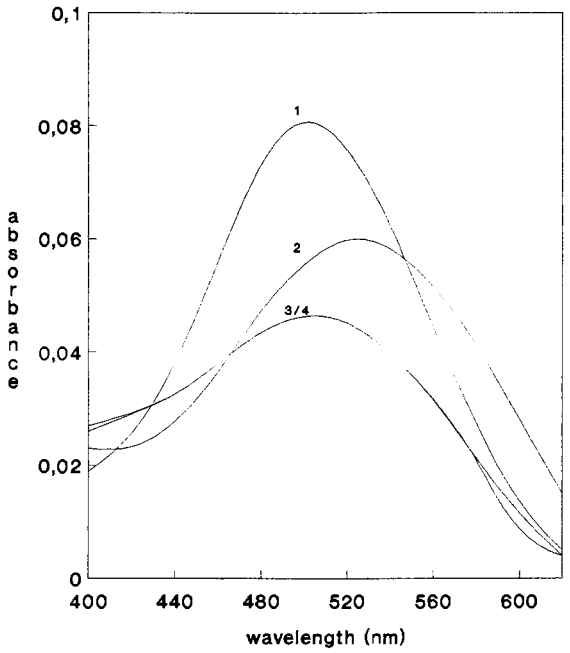

Fig. 1. Absorbance spectra of (1) oxalate–ARS–Zr(IV) in CPC medium; (2) ARS–Zr(IV) in CPC medium; (3) oxalate–ARS–Zr(IV) in aqueous medium; (4) ARS–Zr(IV) in aqueous medium.

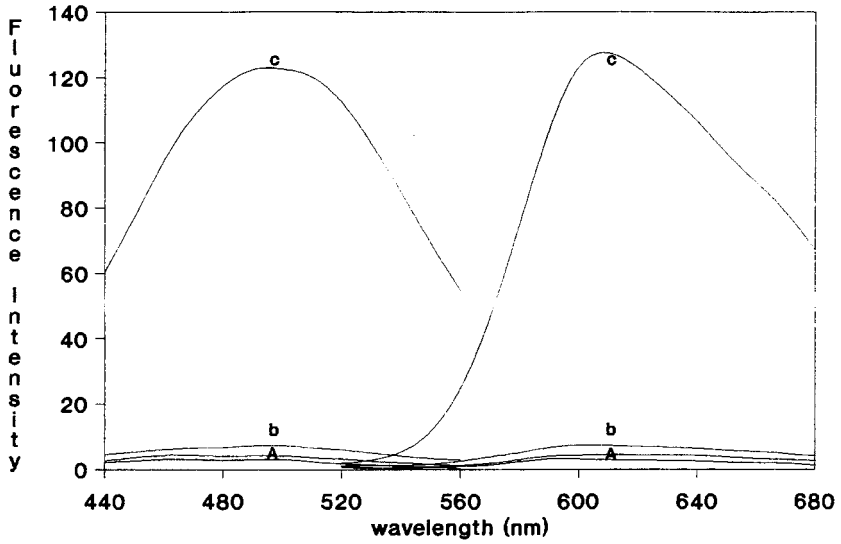

Fig. 2. Fluorescence spectra of (c) oxalate–ARS–Zr(IV) in CPC medium; (b) ARS–Zr(IV) in CPC medium; (a) oxalate–ARS–Zr(IV) and ARS–Zr(IV) in aqueous medium.

configuration has been proposed for a spectrofluorimetric determination in which oxalate is determined indirectly by its effect on the oxidation of Rhodamine B, and is suitable for concentrations between 1.76 and 88 mg ml^{-1} [11]. In all the above determinations, oxalates are separated by precipitation or using an extraction process. In this paper we present a more sensitive and direct spectrofluorimetric determination of oxalate ion in a cationic micellar medium based on the formation of a ternary complex with Zr(IV) and ARS, and the method has been satisfactorily applied to urine and spinach leaves.

2. Experimental

2.1. Apparatus

Fluorescence was monitored with a Perkin-Elmer (Norwalk, CT) Model MPF-66 spectrofluorimeter, equipped with a 150-W Xenon arc lamp and a R-928 photomultiplier. All measurements were performed in standard 10-mm pathlength quartz cells, thermostatically controlled at 25 ± 0.5°C with a water bath circulator (Frigiterm S-382; J.P. Selecta, Spain).

Spectrophotometric measurements were performed on a Perkin-Elmer Lambda 5 ultraviolet/visible spectrophotometer with 1.0×1.0 cm quartz cells.

The pH values were measured with a Crison Digit-501 pH meter.

The spectrofluorimeter was connected to a Perkin-Elmer Model 7300 professional computer provided with PETLS application software (C 646-0280). A 101 Rhodamine quantum counter sample (Perkin-Elmer) was used for source intensity adjustment. Fluorescence data are given without spectral correction.

2.2. Reagents

All experiments were carried out with analytical reagent grade chemicals using doubly distilled and demineralized water.

Alizarin Red S (sodium 1,2-dihydroxyanthraquinone 3-sodium sulphonate) was obtained from Carlo Erba, and a 1.0×10^{-3} M solution was prepared by weighing exactly 0.171 g of the reagent and diluting to 500 cm^3 with doubly distilled water. Other solutions were prepared by dilution.

Oxalate ammonium salt was obtained from Merck. The oxalate stock solution was prepared by dissolving 0.1615 g of analytical grade $(NH_4)_2C_2O_4$ in 100 ml of doubly distilled water. All standard solutions were then prepared by dilution using doubly distilled water.

The zirconium(IV) solution was purchased as $ZrOCl_2 \cdot H_2O$ (Merck) and prepared by weighing exactly 0.3226 g and diluting to 1 l with 1 M HCl (final concentration 10^{-3} M).

Buffer solution (pH 5) was prepared from 1 mol l^{-1} acetic–sodium acetate.

The surfactant solutions were all obtained from Merck. Stock solutions of the following reagents were prepared in water: sodium dodecylsulphate (SDS) 5% (w/v), polyoxyethylene-(9,5)-*p*-tert-octylphenol (Triton X-100, TX-100) 10% (w/v), hexadecyltrimethylammonium bromide (HTAB, 5% w/v), cetylpyridinium chloride (CPC) 5% w/V.

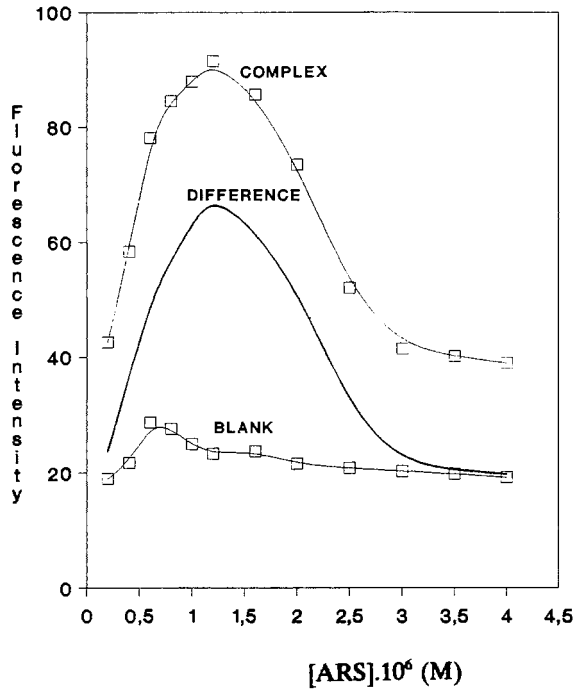

Fig. 3. Influence of the ARS concentration on the fluorescence intensity of the oxalate–ARS–Zr(IV) complex at pH 5. [oxalate] = [Zr(IV)] = 10^{-6} M, [CPC] = 0.3%.

Table 1
Performance characteristics calculated from the calibration data set (three replicates for each standard)

Feature	Value
Linearity (1−RSD(*b*) %) [a]	97.31
Analytical sensitivity (ng ml^{-1}) [b]	3.90
Detection limit (ng ml^{-1}) [c]	8.43
Quantitation limit (ng ml^{-1})	28.11
Precision (%) [d]	
60 ng ml^{-1}	4.0
300 ng ml^{-1}	3.7
Detection limit (IUPAC) (ng ml^{-1})	4.4
Quantitation limit (IUPAC) (ng ml^{-1})	14.8

[a] RSD(*b*), relative standard deviation of the slope.
[b] Quotient between standard deviation of the residuals and slope.
[c] Standard deviation of the blank from regression analysis equations.
[d] Relative standard deviation of the concentration.

2.3. General procedure

Into a 10 ml calibrated flask, transfer a suitable aliquot containing 0.08–1.0 mg of oxalate. Add 0.1 ml of 1.0×10^{-4} M Zr(IV) solution, 1 ml of buffer solution pH 5.0, 0.6 ml of 5% CPC and 0.1 ml of 1.0×10^{-4} M ARS solution and dilute to the mark with doubly distilled water. Allow the mixture to stand at 25°C to achieve total complexation and measure the fluorescence intensity after 15 min at 605 nm with excitation at 490 nm.

2.4. Determination of oxalate in spinach leaves

A spinach sample of 2 g was perfectly cleaned with distilled water, carefully shredded and dried at 80°C for 4 h. Total recovery of free oxalate is achieved following the procedure recommended by Ishii [17] by which all free oxalic acid is extracted by immersion of the vegetal tissue for 20 min in boiling water. To avoid the main interfering substances existing in the spinach sample as some transition metal ions, the oxalate has been isolated by precipitation as calcium oxalate at pH 5 [18].

After the supernatant liquid has been discarded, the precipitate is washed with ammonia solution and dissolved with 4 ml of 0.5 N H_2SO_4 and taken

Table 2
Summary of fluorimetric methods for oxalate

Reagent used	Monitored species	Conc. range or detection limit (mg ml^{-1})	Ref.
$Cr_2O_7^{2-}$, Rodamine	Rodamine (quenching, using flow injection system)	1.8-88	[11]
Zn, resorcinol	Acid glyoxylic–resorcinol complex (indirect detection)	0.08	[24]
$ZrOCl_2$, flavonol	Zr(IV)–flavonol complex (quenching)	0.0055	[15]
$ZrOCl_2$, flavonol	Zr(IV)–flavonol complex (using flow injection system)	0.9–31	[16]
Ce(IV), OsO_4	Fluorescence of Ce(III) (indirect detection)	0.088–0.44	[25]
Zr, Alizarin Red S	Zr(IV)–oxalate–ARS complex	0.004	This work

to 250 ml with doubly distilled water. The proposed procedure is then applied to this sample solution.

2.5. Determination of oxalate in urine

A 5 ml sample of urine at a pH adjusted to 5.0 was precipitated following the above procedure [18]. The $Ca(C_2O_4)_2$ precipitate was separated by centrifugation. The supernatant fluid was decanted and the precipitate was washed with a diluted ammonia solution and then dissolved with 0.5 ml of 0.5 N H_2SO_4 and water diluting the solution to 25 ml with doubly distilled water. Aliquots of this solution were used to determine oxalate content.

Table 3
Tolerance concentration for the determination of 60 ng ml^{-1} oxalate

Foreign specie	Maximum tolerated ratio (w/w)
Li^+, Na^+, K^+, Rb^+, Cs^+, Cd^{2+}, NH_4^+, NO_3^-, alanine	>1000
Sr^{2+}, Pb^{2+}, Cl^-, I^-, SCN^-, glutamic acid, cysteine, histidine	500
Mg^{2+}, Ca^{2+}, Mn^{2+}, Br^-, SO_4^{2-}, Sb^{5+}	100
Co^{2+}, ascorbate	50
La^{3+}, Ni^{2+}, Bi^{3+}	10
Y^{3+}, Hf^{4+}, Mo^{6+}, W^{6+}, Cu^{2+}, Zn^{2+}, B^{3+}, Sn^{2+}, Se^{4+}, citrate, EDTA, PO_4^{3-}	1
As^{5+}, F^-, H_2O_2, tartrate	0.5
V^{5+}, Fe^{3+}, Ti^{4+}, Al^{3+}	≤0.1

3. Results and discussion

The proposed method is based on the complexation of Zr(IV) by ARS and oxalate. It is well known that oxalic acid forms stable complexes with zirconium in acidic media, with the formula $Zr(Ox)_n^{(2n-n)-}$ $(n=1–4)$ [12]. We have observed that, in the presence of surfactant agents and using ARS as reagent, a fluorescent ternary complex is formed in weakly acidic medium.

3.1. Effect of micellar media

This study was carried out by addition of different micellar solutions of anionic (SDS), cationic (HTAB and CPC) and non-ionic (TX-100) surfactants to the oxalate–ARS–Zr(IV) complex, with fixed concentrations of Zr(IV) and ARS (10^{-5} M) and oxalate ion (5×10^{-5} M) using both absorbance and fluorescence measurements. It was observed that the formation of the complex does not take place either in the aqueous medium or in those solution treated with SDS and TX-100, where very slight changes in the measurement signal of the complex and the reagent blank were observed in both absorbance and fluorescence.

When a cationic surfactant is used, the absorbance and the fluorescence intensity of the

Table 4
Determination of oxalate in spinach leaves

Parameters for AC1, AC2, SC and YC Parameter	AC1	AC2	SC	YC
n	8	8	18	5
a	37.31	46.45	22.81	29.90
b	0.3237	0.2997	0.4604	10.60
s	0.9793	0.9164	1.7972	
F-test for slope similarity comparison (ANCOVA)				
s_N^2	40.40			
s_D^2	2.231			
F_{cal}	18.11 [a]	$P = 0.002\%$		
Bonferroni t-test for slope comparison				
b(SC) vs b(AC1)	$t_{cal} = 4.017$ [b]	$P = 0.04\%$		
b(SC) vs b(AC2)	$t_{cal} = 4.849$ [b]	$P = 0.004\%$		
b(AC1) vs b(AC2)	$t_{cal} = 0.620$ [b]	$P = 54.04\%$		
Pooled slope, corrected ordinates and Youden blank				
Corrected ordinates	$a'_{A1} = 37.62$			
	$a'_{A2} = 45.73$			
Pooled slope (AC1, AC2)	$b_p = 0.3135$			
Youden blank	YB = 7.09			
Analyte content calculation, t-test for trueness				
Parameter	AC1	AC2		
c_x (ng ml^{-1})	24.63	50.51		
f	1.250	0.625		
C (mg g^{-1})	30.79	31.57		
s_p	0.9956			
$t(c)$ [c]	0.512		$P = 61.7\%$	

[a] Critical value $F_{tab} = 3.34$ (5%; 2,28 DF).
[b] Critical value $t_{tab} = 2.763$ (1%; 28 DF).
[c] Critical value $t_{tab} = 2.160$ (5%; 13 DF).

complex are strongly enhanced. The corresponding reagent blanks are small and unaffected by the addition of surfactants. Fig. 1 shows the absorption spectra of the binary complex ARS–Zr(IV) and the ternary complex oxalate–ARS–Zr(IV) under different conditions. No changes were observed in the absence of the cationic surfactant in relation to the binary complex ARS–Zr(IV) in aqueous medium. However, in the presence of CPC the formation of ternary complex is achieved, as well as a significant increase in the absorbance of the binary system.

The influence of cationic surfactant on the fluorescence intensity of both binary and ternary complexes is shown in Fig. 2. The formation of the highly fluorescent ternary complex oxalate–ARS–Zr(IV) requires the presence of cationic micelles and no modification is produced to the binary non-fluorescent ARS–Zr(IV) system. This property can be satisfactorily used to establish a sensitive fluorimetric determination of oxalate ions. Comparing the two cationic micellar solutions checked, CPC produces the most important increase in the fluorescence intensity with no changes in excitation and emission maxima. This ternary complex has its excitation maximum at 490 nm while the emission spectrum shows its maximum at 605 nm.

Table 5
Determination of oxalate in urine

Parameters for AC1, AC2, SC and YC Parameter	AC1	AC2	SC	YC
n	8	8	18	4
a	42.34	45.55	22.81	35.90
b	0.1808	0.2138	0.4604	9.923
s	1.4105	0.9002	1.7972	
F-test for slope similarity comparison (ANCOVA)				
s^2_N	201.64			
s^2_D	2.446			
F_{cal}	82.4 [a]	$P = 0.00\%$		
Bonferroni t-test for slope comparison				
b(SC) vs b(AC1)	$t_{cal} = 10.33$ [b]	$P = 0.00\%$		
b(SC) vs b(AC2)	$t_{cal} = 9.11$ [b]	$P = 0.00\%$		
b(AC1) vs b(AC2)	$t_{cal} = 0.942$ [b]	$P = 35.40\%$		
Pooled slope, corrected ordinates and Youden blank				
Corrected ordinates	$a'_{A1} = 41.84$			
	$a'_{A2} = 46.04$			
Pooled slope (AC1, AC2)	$b_p = 0.1973$			
Youden blank	YB = 13.09			
Analyte content calculation, t-test for trueness Parameter	AC1		AC2	
c_x (ng ml^{-1})	30.11		51.41	
f	1.250		0.833	
C (mg l^{-1})	37.64		42.84	
s_p		1.3543		
$t(c)$ [c]		1.514		$P = 15.2\%$

[a] Critical value $F_{tab} = 3.34$ (5%; 2,28 DF).
[b] Critical value $t_{tab} = 2.763$ (1%; 28 DF).
[c] Critical value $t_{tab} = 2.160$ (5%; 13 DF).

From this study, it is possible to conclude that the interaction that can take place between the polar group of the surfactant, above its critical micellar concentration (c.m.c.), and the sulphonic group of the reagent, together with other hydrophobic interactions between the long hydrophobic alkyl chain in the CPC and the hydrophobic part of the complex, will probably bring about a more rigid environment that will produce an enhanced fluorescence signal because of the hindrance to non-radiative processes [2]. These favourable ionic interactions will not occur when a different kind of surfactant is used. Moreover, these hydrophobic interactions between the solubilized complex and the micelle would be operative in the interface and, as a consequence, water and/or hydroxide ligands will be eliminated from the chelate [19]. Thus, oxalate or other ligands could coordinate zirconium more easily.

Enhancement of the fluorecence starts only when the c.m.c. has been overcome, a plateau appearing well above this concentration. Above the c.m.c., the surfactant concentration has no influence on the fluorescence signal of the complex. For this reason a concentration of 0.3% is recommended.

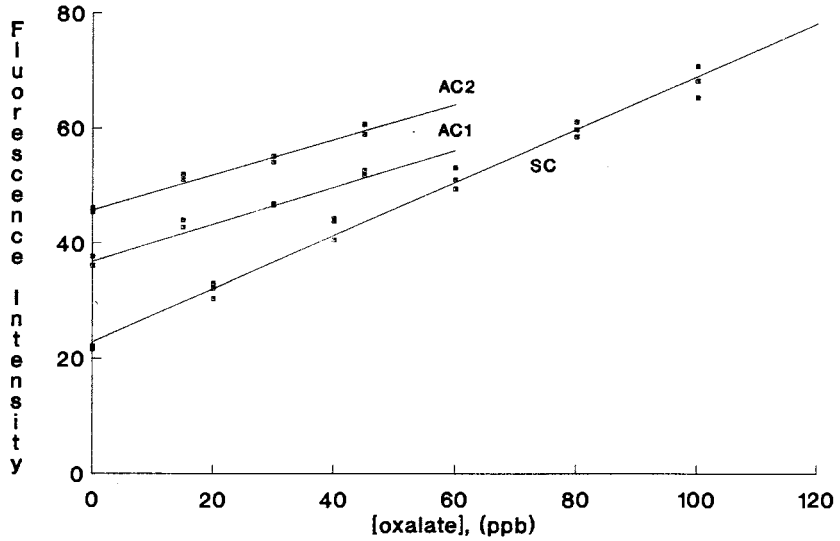

Fig. 4. Calibration curve plots for spinach sample. SC, standard calibration; AC1, AC2, standard addition calibrations with sample portions of 0.8 and 1.6 mg ml^{-1}, respectively.

3.2. Optimum experimental conditions

Once the surfactant medium was selected, a study to select the best pH value for the formation of the complex was carried out. The working pH range is 4.5–5.5; the control of this variable is very important because the fluorescence signals drop dramatically when the pH value is outside the plateau. For all measurements a pH of 5.0 has been selected; this is achieved with an acetic acid–acetate buffer solution of this pH. The buffer concentration has a very slight influence on the signal; 0.1 M was chosen as the most suitable.

The order of addition of the reagents is a critical feature in the optimization procedure. In order to assure a complete and fast development of the fluorescence of the ternary complex, we have found that the prior formation of the non-fluorescent binary complex oxalate–Zr(IV) must be carried out avoiding the consecutive addition of ARS and Zr(IV) solutions. The previous formation of the non-fluorescencent binary complex ARS–Zr(IV) impedes the efficient incorporation of oxalate ions to form the ternary complex, and a longer time is therefore necessary to achieve full fluorescence development. Once the binary oxalate–Zr(IV) complex has been formed, the order of addition of reagent, buffer solution and surfactant has no influence. For the rest to the experimental work we have used the following order: oxalate + Zr(IV) + buffer + surfactant + reagent.

Maximum fluorescence intensity is achieved in 15 min after sample preparation, remaining almost constant for 4 h. A few minutes are allowed to permit the total formation of the complex.

The effect of temperature on the fluorescence measurements was studied by heating the cell thermostatically between 15 and 50°C. The fluorescence intensity decreases gradually as the temperature rises. A temperature of 25°C was chosen for further experimental work.

The effect of the concentration of zirconium ions and ARS on the fluorescence of the complex was also studied using a constant oxalate concentration of 10^{-6} M. The intensity of the fluorescence signal is enhanced with the gradual increment of the Zr(IV) concentration until 10^{-6} M, after which a gradual decrease begins. A zirconium concentration of 10^{-6} M was selected. The effect of ARS concentration was studied in the same way using oxalate and zirconium concentrations of 10^{-6} M. The results observed in Fig. 3 were very similar to those obtained with Zr(IV); thus a 10^{-6} M concentration of ARS was chosen

for the rest of the experiments. From both experiments it is possible to conclude that when the ARS and/or Zr(IV) concentrations are higher than the oxalate concentration, the ternary complex is partially destroyed as the concentrations of these reagents increase, favouring the formation of binary non-fluorescent species. Thus a 1:1 ratio of ARS–Zr(IV) seems the most adequate for complete development of the fluorescence of the ternary system.

The stoichiometry of the ternary complex was studied spectrofluorimetrically and spectrophotometrically under established conditions using the Yoe and Jones method [20]. Continuous variations of oxalate ion were performed in the presence of a constant concentration of the non-fluorescent binary complex Zr(IV)–ARS at 1:1 ratio, as previously found in the literature [21]. Evidence of complexes with stoichiometries of 3:1:1, 2:1:1 and 1:1:1 (oxalate–Zr(IV)–ARS) was found. This is in complete agreement with the coordination characteristics of the bidentate complexant ARS, the analyte and the metal. Nevertheless, the best definition was found for the 3:1:1 complex.

3.3. Analytical parameters

For the calibration graphs we established two ranges with different instrumental sensitivity conditions. Three replicates for each concentration, including the blank as an additional point, are used to calculate the regression line equation. The performance characteristics were obtained from the calibration data set [22].

The established ranges were 8.4–100 ng ml^{-1} (excitation and emission slits set at 15 nm, lack-of-fit P-value = 37.0%) and 35–500 ng ml^{-1} (excitation and emission slits set at 12 nm, lack-of-fit P-value = 17.5%). All the performance characteristics are summarized in Table 1, including the IUPAC detection and quantitation limits [23].

The detection limit achieved in this work is lower than that observed in other relevant papers based on fluorescence methods [11,15,16,24,25] (Table 2), as well as in other simple and inexpensive methods [12–14].

For the subsequent application of the method to the determination of oxalate in some biological matrixes, the effect of several possible interfering ions on the fluorescence of the complex was studied. These possible interfering substances were selected to evaluate the applicability of the method in matrixes likely to hold different amounts of them. In the determination of 60 ng ml^{-1} of oxalate, foreign ions can be tolerated at the levels reported in Table 3. The tolerance criterion used was a value of $\pm t_{\alpha} s_R$ (s_R is regression standard deviation of the mean value of three measurements of the analytical signal, and t_{α} is Student's t one-tail for an $\alpha = 0.05$ significance level) [26]. The first level of interference proved to be a ratio of 1000 (w/w) with respect to the oxalate concentration. If there was interference, the ratio was progressively reduced until the interference disappeared.

Exhaustive study of the literature available on spectrofluorimetric and spectrophotometric determination of oxalate demonstrates that nearly all metal cations seriously interfere [11–14]. Only alkali metal ions and alkaline earth metal ions can be readily tolerated in large amounts. For this reason, the employment of different techniques for separation, such as extraction [13] or precipitation [11], are quite extensive. Here we use an inexpensive and easy to perform technique for separation of the oxalate ion, which makes the work presented comparable in terms of selectivity to most of the above mentioned papers [18].

4. Applications

The applicability of the proposed method has been checked in two biological samples in which it is of interest to control the oxalate content: spinach leaves and urine.

The validation and analysis of samples has been carried out using the statistical protocol proposed by García-Campaña et al. [27], based on the application of the standard addition methodology in the presence of corregible constant and proportional systematic errors. Constant errors are due to response variations that are not attributable to the analyte and are independent of sample size,

while proportional errors are produced by response variations that depend on the matrix–analyte interaction, which is proportional to the matrix–analyte ratio present. The presence of these kinds of errors can be detected by diagnostic statistical techniques and the value used to correct the analytical results.

This simple and rigorous methodology is able to detect both types of error and, where proportional errors exist, seeks a complete interval of sample portions for which saturation of the matrix–analyte interactive effect is obtained. It thus avoids the effects of this interference and arrives at a correct analytical result for the selected experimental region. The method, once validated, can be used in routine analysis with the standard solution addition method, provided that the sample concentration introduced into the calibration curve lies within the saturation interval of the matrix–analyte interactive effect.

The applied protocol implies the use of the data set of three experiments: standard calibration (SC), standard addition calibration to two different constant portions of sample (AC1 and AC2), and Youden calibration (YC), obtained from continuous sample variations and not including the value corresponding to sample portion 'zero'. The statistical parameters for these calibration are shown in Tables 4 and 5 for spinach and urine, respectively. As can be seen in these tables, there is a difference between the intercepts of the curves SC and YC, a_S and a_Y, which indicates the existence of a bias component due to the sample matrix effect. As a_Y is not included in the confidence interval value of a_S, the constant bias component (total Youden blank) has been subtracted from the whole analytical signal to estimate the analyte content of the solution in both analysed samples. The presence of proportional errors due to any matrix–analyte interaction was detected by applying an analysis of covariance (ANCOVA) to compare simultaneously the slopes of the three calibration curves established with standard solution (SC) and with standard additions (AC1 and AC2). To do this, an F-test comparing two means of squares is performed ($F_{cal} = s_N^2/s_D^2$, where the numerator measures the contribution of the differences observed between the three slopes to the sum of squares of the deviations of all the data, considered as one unique data set, from the linear model, and the denominator measures these same deviations but considering each calibration to be independent). The conclusions obtained from this statistical test in both samples are indicated in Tables 4 and 5, from which it is possible to observe a significant difference between the three compared slopes (P-value $< 5\%$), which implies a proportional error to the matrix–analyte relation. This kind of error can be corrected if the slopes of AC1 and AC2 are similar, which is checked using the Bonferroni t-test (see Tables 4 and 5). This has been the conclusion obtained for both analysed samples, being possible to establish a zone of sample portions delimited by those used in these two standard addition calibrations in which this error can be considered constant and so the protocol can be applied. In this case, a pooled slope, b_p, can be estimated as representative for both AC1 and AC2, being estimated the new intercepts of these curves (a'_{A1} and a'_{A2}, respectively). As can be seen in Fig. 4, this is the situation in the application of the proposed procedure for the analysis of oxalate in spinach leaves, in which the content of oxalate is calculated from AC1 and AC2, showing non-significant differences between both calculated values. Similar results were obtained for urine samples.

The trueness of the analytical result was checked by statistical comparison on the analyte contents calculated from AC1 and AC2. No significant difference between these contents was obtained applying the Student's t-test ($P \geq 5\%$). Tables 4 and 5 show the results obtained in the determination of oxalate for spinach and urine samples, respectively. All expressions in Tables 4 and 5 are included in the Glossary (Section 5) and the mathematical equations for the statistical protocol are summarized in Appendix A.

Once the method was validated, three replicates for each selected sample were analysed using sample portions included in the above mentioned intervals. The results obtained as the mean of three determinations were 43.7 ± 6.7 mg g^{-1} for spinach and 29.0 ± 2.6 mg l^{-1} for the urine sample. The standard method [28] to determine oxalates based on the precipitation of the analyte

with $CaCl_2$, dissolution and titration with $KMnO_4$ was used on the spinach samples in order to check the proposed methodology, obtaining a result of 30.4 ± 4.5 mg g^{-1}. No significant difference was observed when the results were compared using Student's t-test ($P \geq 5\%$).

5. Glossary

a	Intercept of each calibration
a'_{A1}	Corrected intercept of AC1
a'_{A2}	Corrected intercept of AC2
AC1	Standard addition calibration to test portion 1
AC2	Standard addition calibration to test portion 2
b	Slope of each calibration
b_p	Pooled slope between AC1 and AC2
(cc)	Corrected sum of squares of concentrations
(cR)	Corrected crossed product of sum of squares of concentrations and analytical signals
$c_{i,A1}$	Concentration of added-standard set used in AC1
$c_{i,A2}$	Concentration of added-standard set used in AC2
$\bar{c}_A$	Average concentration of added standard set used in each AC
C	Sample analyte concentration
DF	Degrees of freedom
f	Multiplicative factor to obtain C from c_x
n	Number of measurements in the calibration
R	Measured analytical signal
(RR)	Corrected sum of squares of analytical signals
$_{A1}$	Average analytical signal for AC1 measurement set
$_{A2}$	Average analytical signal for AC2 measurement set
R_i	Each analytical signal value of calibration measurement set
P	Percentage of the Student's t or F distributions (P-value)
s	Regression standard deviation
SC	Standard calibration
SS	Sum of squares
MS	Mean of squares
s_p	Pooled standard deviation
$t(c)$	Statistic for concentration
YB	Youden blank
YC	Youden calibration

Appendix A

A.1. Checking the kind of error using ANCOVA

A.1.1. General mathematical model

$$R_{ij} = \alpha_i + \beta_i c_{ij} + \epsilon_{ij}$$

where $i = 1,2,\ldots,r$ is each one of the calibration curves, $j = 1,2,\ldots n_i$ is the total number of pairs of data for each calibration, α is the intercept, β is the slope and ϵ is the normally distributed error of model.

A.1.2. Null hypothesis for the statistic test

$$H_0 \cong \beta_1 = \beta_2 = \ldots = \beta_r$$

A.1.3. Steps in the realization of the test

(a) Initial calculations: corrected sums of squares and products for each individual regression(cc) $= \Sigma(c_i - \bar{c})^2 = \Sigma c_i^2 - (\Sigma c_i)^2/n$

$$(\mathrm{RR}) = \sum(R_i - \bar{R})^2 = \sum R_i^2 - (\sum R_i)^2/n$$

$$(\mathrm{cR}) = \sum(c_i - \bar{c})(R_i - \bar{R}) = \sum c_i R_i - (\sum c_i)(\sum R_i)/n$$

(b) Regression deviations: sums of squares (SS) and means of squares (MS) of the residuals

$$\mathrm{SS} = (\mathrm{RR}) - (\mathrm{cR})^2/(\mathrm{cc})$$

$$\mathrm{MS} = \mathrm{SS}/(n-2)$$

(c) Full regression deviations: full degrees of freedom (DF), full sum of squares (SS) and full mean of squares (MS) of the residuals

$$\text{Full DF} = (n_\mathrm{S} - 2) + (n_{\mathrm{A}1} - 2) + (n_{\mathrm{A}2} - 2) = (n_\mathrm{S} + n_{\mathrm{A}1} + n_{\mathrm{A}2} - 6)$$

$$\text{Full SS} = (\mathrm{SS})_\mathrm{S} + (\mathrm{SS})_{\mathrm{A}1} + (\mathrm{SS})_{\mathrm{A}2}$$

$$\text{Full MS} = (\text{Full SS})/(\text{Full DF})$$

where n_S, $n_{\mathrm{A}1}$ and $n_{\mathrm{A}2}$ are the number of pairs of values for each calibration curve, respectively.

(d) Reduced regression: pooled slope (b_p), reduced degrees of freedom (DF), sum of squares (SS) and residual mean of squares (MS)

$$b_\mathrm{p} = \frac{(\mathrm{cR})_\mathrm{S} + (\mathrm{cR})_{\mathrm{A}1} + (\mathrm{cR})_{\mathrm{A}2}}{(\mathrm{cc})_\mathrm{S} + (\mathrm{cc})_{\mathrm{A}1} + (\mathrm{cc})_{\mathrm{A}2}}$$

$$\text{Reduced DF} = [(n_\mathrm{S} - 1) + (n_{\mathrm{A}1} - 1) + (n_{\mathrm{A}2} - 1) - 1] = (n_\mathrm{S} + n_{\mathrm{A}1} + n_{\mathrm{A}2} - 4)$$

$$\text{Reduced SS} = [(\mathrm{RR})_\mathrm{S} + (\mathrm{RR})_{\mathrm{A}1} + (\mathrm{RR})_{\mathrm{A}2}] - \frac{[(\mathrm{cR})_\mathrm{S} + (\mathrm{cR})_{\mathrm{A}1} + (\mathrm{cR})_{\mathrm{A}2}]^2}{(\mathrm{cc})_\mathrm{S} + (\mathrm{cc})_{\mathrm{A}1} + (\mathrm{cc})_{\mathrm{A}2}}$$

$$\text{Reduced MS} = (\text{Reduced SS})/(\text{Reduced DF})$$

(e) Comparison of K slopes: F-test

$$F_\mathrm{cal} = s_\mathrm{N}^2/s_\mathrm{D}^2$$

($\alpha = 0.05$, $\upsilon_1 = k - 1$, $\upsilon_2 =$ full DF, degrees of freedom)

$$s_\mathrm{N}^2 = [(\text{Reduced SS}) - (\text{Full SS})]/(k-1)$$

$$s_\mathrm{D}^2 = (\text{Full MS})$$

A.2. Situations

(e.1) Existence of a constant systematic error: equal slopes. If the null hypothesis is not rejected, there is no proportional systematic error component, at least if the method is applied within the interval of the sample portion under study.

(e.2) Existence of a proportional systematic error: different slopes. Comparisons by pairs. Test of comparisons by pairs using the Bonferroni method:

$$t(b) = \frac{|b_\mathrm{S} - b_{\mathrm{A}1}|}{s_\mathrm{D}\sqrt{\dfrac{1}{(\mathrm{cc})_\mathrm{S}} + \dfrac{1}{(\mathrm{cc})_{\mathrm{A}1}}}}$$

using a 'penalized' Student t-test considering an error α divided among the q possible comparisons performed (error α/q). The null hypothesis (that the two slopes compared do not differ significantly) is not rejected for a level of significance greater than 1%.

(e.2.1) b_s is different from $b_{\mathrm{A}1}$ and $b_{\mathrm{A}2}$, but $b_{\mathrm{A}1}$ and $b_{\mathrm{A}2}$ are similar: component of proportional error becomes constant using the interval of sample portions between these used in AC1 and AC2. The determination of the analyte content as determined by:

$$c_{x,\mathrm{A}1} = \frac{a'_{\mathrm{A}1} - a_\mathrm{Y}}{b_\mathrm{p}}$$

$$c_{x,\mathrm{A}2} = \frac{a'_{\mathrm{A}2} - a_\mathrm{Y}}{b_\mathrm{p}}$$

where $a'_{\mathrm{A}1}$ and $a'_{\mathrm{A}2}$ are estimated by:

$$a'_\mathrm{A} = \overline{R_\mathrm{A}} - b_\mathrm{p}\overline{c_\mathrm{A}}$$

A.2.1. Check of the trueness

The analyte content of each sample portion used, $c_{x,\mathrm{A}1}$ and $c_{x,\mathrm{A}2}$, is then related with the final analyte concentration in the original sample, $C_{\mathrm{A}1}$ and $C_{\mathrm{A}2}$. The intention is to test the trueness of the results, comparing the two values using a

t-test with $(n_{A1}+n_{A2}-3)$ degrees of freedom, calculated according to the following equation:

$$t(c)=\frac{|C_{A1}-C_{A2}|}{\frac{s_p}{b_p}\sqrt{\frac{1}{n_{A1}}+\frac{1}{n_{A2}}+\frac{(\overline{R_{A1}}-\overline{R_{A2}})^2}{b_p^2[(cc)_{A1}+(cc)_{A2}]}}}$$

where s_p is the pooled standard deviation of regression of calibrations AC1 and AC2, obtained by:

$$s_p=\sqrt{\frac{(n_{A1}-2)s_{A1}^2f_1^2+(n_{A2}-2)s_{A2}^2f_2^2}{n_{A1}+n_{A2}-4}}$$

where f_1 and f_2 represent the respective dilution factors (numbers that multiply $c_{x,A1}$ and $c_{x,A2}$ to obtain C_{A1} and C_{A2}, the final sample content). The null hypothesis (the two results do not significantly differ) is not rejected with a level of significance that is greater than 5%.

(e.2.2) b_S is similar to b_{A1} and not to b_{A2}. The component of proportional error can be avoided using a sample portion in the analysis equal to that used to establish the first calibration curve with standard addition to the lesser sample portion (AC1).

(e.2.3) No pair of slopes compared presents similarity. This case may arise when there is a non-constant proportional systematic error and the experimental region in which this effect is saturated has not been localized. To find this saturation zone becoming constant this proportional systematic error, new calibrations must be performed with standard addition using sample portions that are intermediate to those previously considered for the AC1 and AC2 calibrations. The object of this is to test whether, on varying the matrix–analyte relation, the saturation zone is bounded.

References

[1] L.J. Cline Love, J.G. Habarta, J.G. Dorsey, Anal. Chem. 56 (1984) 1133A.
[2] A. Sanz-Medel, R. Fernández de la Campa, J.J. García Alonso, Analyst 112 (1987) 493.
[3] P.R. Haddad, Talanta 24 (1977) 1.
[4] A.M. García Campaña, F. Alés Barrero, M. Román Ceba, A. Fernández Gutiérrez, Analyst 119 (1994) 1903.
[5] A.M. García Campaña, F. Alés Barrero, M. Román Ceba, Anal. Sci. 12 (1996) 647.
[6] C. Cruces Blanco, A.M. García Campaña, F. Alés Barrero, M. Román Ceba, Talanta 42 (1995) 1037.
[7] A.M. García Campaña, F. Alés Barrero, M. Román Ceba, Anal. Chim. Acta 329 (1996) 319.
[8] A. Hodgkinson, Oxalic Acid in Biology and Medicine, Academic Press, New York, 1977, p. 230.
[9] M.D. Luque de Castro, J. Pharm. Biomed. Anal. 6 (1988) 1.
[10] J.A. Infantes, M.D. Luque de Castro, M. Válcarcel, J. Pharm. Biomed. Anal. 10 (1992) 95.
[11] T. Pérez-Ruiz, C. Martínez Lozano, V. Tomás, R. Casajú, Analyst 120 (1995) 2111.
[12] R.E. Neas, J.C. Guyon, Anal. Chem. 44 (1972) 799.
[13] F. Salinas, J. Martínez Vidal, V. González Murcia, Analyst 114 (1989) 1685.
[14] A.M. Dona, J.F. Verchère, Analyst 116 (1991) 533.
[15] D.A. Britton, J.C. Guyon, Anal. Chim. Acta 44 (1969) 397.
[16] E. Gaetani, C.F. Laureri, M. Vitto, L. Borghi, G.F. Elia, A. Novarini, Clin. Chim. Acta 15 (1986) 71.
[17] Y. Ishii, Anal. Sci. 7 (1991) 263.
[18] J.M. Meola, Methodol. Anal. Toxicol. 3 (1985) 147.
[19] A. Sanz-Medel, M.M. Fernández Pérez, Anal. Chem. 58 (1986) 2161.
[20] J.H. Yoe, A.L. Jones, Ind. Eng., Chem. Anal. Ed. 16 (1944) 111.
[21] B.I. Intorre, A.E. Martell, J. Am. Chem. Soc. 82 (1960) 358.
[22] L. Cuadros Rodríguez, A.M. García Campaña, C. Jiménez Linares, M. Román Ceba, Anal. Lett. 26 (1993) 1243.
[23] IUPAC, Analytical Chemistry Division, Nomenclature, symbols, units and their usage in spectrochemical analysis II, Spectrochim. Acta B 33 (1978) 242.
[24] P.M. Zaremski, A. Hodgkinson, Biochem. J. 96 (1965) 717.
[25] G.F. Kirkbright, T.S. West, C. Woodward, Anal. Chim. Acta 36 (1966) 298.
[26] A.M. García Campaña, L. Cuadros Rodríguez, C. Jiménez Linares, F. Alés Barrero, M. Román Ceba, Anal. Lett. 28 (1995) 369.
[27] A.M. García Campaña, L. Cuadros Rodríguez, J. Aybar Muñoz, F. Alés Barrero, J. Assoc. Off. Anal. Chem. 80 (1997) 657.
[28] Royal Society of Chemistry, Official and Standardized Methods of Analysis, 3rd ed., The Royal Society of Chemistry, Cambridge, 1994.

ELSEVIER

Talanta 47 (1998) 401–412

Talanta

The acidobasic and complexation properties of humic acids Study of complexation of Czech humic acids with metal ions

P. Lubal, D. Široký, D. Fetsch [1], J. Havel *

Department of Analytical Chemistry, Faculty of Science, Masaryk University, Kotlářská 2, 61137 Brno, Czech Republic

Received 24 November 1997; received in revised form 24 March 1998; accepted 29 March 1998

Abstract

The acid–base and complexation properties of humic acids (HAs) extracted from bohemian brown coals were studied. The acid–base behavior corresponds with the model of HA as a mixture of mono- and diprotic acids. This model was also verified on commercial HA substances (Aldrich and Fluka). HA binds strongly with heavy metal ions and the highest stability constant of HA–metal ion complexes was observed for copper(II). Stability constant values were found to decrease in the order: $Cu^{2+} > Ba^{2+} > Pb^{2+} > Cd^{2+} > Ca^{2+}$. Both acidobasic models for HA alone and those for HA–metal ion interactions were proposed and the computational methodology for polyelectrolyte equilibria studies demonstrated. © 1998 Elsevier Science B.V. All rights reserved.

Keywords: Complexation; Humic acids; Metal ions; Modeling

1. Introduction

Humic acids (HAs) and related fulvic acids (FAs) occur in soils, natural waters, marine and lake sediments, peats, lignins, brown coals and other natural deposits ([1] and references therein). These substances form a group of polyfunctional acids, which have a yellow to brown color and a molecular size ranging from hundreds to hundreds of thousands of daltons. They represent a heterogeneous mixture of compounds, which do not have a uniform structural formula, but can be divided into three groups [1,2]: (1) humic acids, which are soluble in alkaline solution, but precipitate in acid solution; (2) fulvic acid, which is soluble in both alkaline and acid solution; (3) humin, which is insoluble in both solutions. The characteristic properties are shown in Fig. 1, modified and adapted according to the literature [1,2].

The basic structural units of HAs are aromatic rings of two- or three-phenol type, which are connected by such groups as –COOH, –O–, $-CH_2-$, –NH–, =N–, –S–, and usually contain two free hydroxyl groups [1].

* Corresponding author. Tel.: +42 5 41129568; fax: +42 5 41211214; e-mail:havel@chemi.muni.cz

[1] On leave from ULP-CNRS UMR 7512, LPCB, Strasbourg, France.

0039-9140/98/$ - see front matter © 1998 Elsevier Science B.V. All rights reserved.
PII S0039-9140(98)00143-X

The HAs containing functional groups (–COOH, –OH, $-NH_2$, etc.) can influence the bonding distribution of cations in trace metals in the environment. Complexation of trace metals with HAs can cause a decrease in the metal's toxicity (e.g. copper) or an increase in its solubility (e.g. iron), making the metal ion more available for plants. Humic substances can decompose some soil minerals (mica, illite, kaolinite) [3]. In natural waters, humic substances bind cations. The knowledge of stability constants is very important for the prediction of the complexation properties of soils and to explain the transport of metal ions in the environment.

Several different models in the literature describe the nature of HAs. The so-called 'discrete' model (assuming single binding sites) in which HAs are treated using three basic approaches: multisite, multidentate and electrostatic. The evaluation of titration curves is currently by the Gran linearization procedure [4,5]. In this model, HA is considered as a mixture of some monoprotic acids [4,5]. The second is the 'continuous' model (assuming overlapping of binding sites) in which HAs are considered according to the normal distribution model and the affinity spectrum approach.

In order to describe the acidobasic and complexation properties of HAs, we have tried to evaluate the validity of a 'discrete' model referring to a Czech HA extracted from bohemian brown coal and commercial HAs. Certain parts of this work were briefly and preliminarily reported elsewhere [6,7].

2. Experimental

2.1. Apparatus and reagents

2.1.1. Characterization of HAs

The sample of HA '193 MAR' used in this work was supplied by the Research Institute of Inorganic Chemistry (VÚANCH, Ústí nad Labem, Czech Republic). The HAs were extracted from high-quality oxihumolite which originated from the Northern Bohemia coal mine near Bílina; the HAs were precipitated several times. The sample has a molecular weight distribution known from gel-permeation chromatography results ($M_n = 10189$ g mol^{-1}, $M_w = 19301$ g mol^{-1}). The content of water was 5.99% (relative) and the ash content in dried material 4.13%. The content of HA in the sample, which was determined gravimetrically, represents 89.88%, with total acidity 8.44 mmol g^{-1} and carboxyl content 3.65 mmol g^{-1} determined using the described methods [1]. The presence of inorganic traces (Al_2O_3, SiO_2, Fe_2O_3, etc.) was checked by X-ray fluorescence. A relatively high free radical concentration (3.2×10^{16} spins g^{-1}) was shown by electron paramagnetic resonance. Characteristic peaks in the infrared (IR) spectrum of HA correspond to following wavenumbers (vs, very strong; w, weak; m, medium; sh, shoulder): 2925 cm^{-1} vs, sh; 2851 cm^{-1} vs; 1957 cm^{-1} w; 1706 cm^{-1} m; 1615 cm^{-1} m; 1463 cm^{-1} s; 1377 cm^{-1} s; 1254 cm^{-1} m; 722 cm^{-1} m [1].

The commercial samples of HA were Fluka no. 53680 (Analysis 38537/1293; Buchs, Switzerland) and Aldrich no. 1,675-2 (Analysis 61700-096; Steinheim, Germany).

2.1.2. Preparation of solutions and chemicals

HA '193 MAR' was exposed to ammonia vapors in a desiccator for 24 h and the ammonium salt formed was dissolved in CO_2-free double-distilled water. The stock solution contained 2.0 g l^{-1}. The sodium salt stock solution was prepared by dissolving Czech HA with 0.1 mol l^{-1} NaOH. The other samples of HA in the form of sodium salts (Aldrich and Fluka) were also dissolved (but without ammonia exposure) in CO_2-free double-distilled water.

FULVIC ACID		HUMIC ACID
	-- increasing in degree of polymerization ->	
2000	-------- increasing in molecular weight ----->	300000
45 %	----------increasing in carbon content ------>	62 %
48 %	--------- decreasing in oxygen content ------>	30 %
14 mmol g^{-1}	-------- decreasing in exchange acidity ----->	5 mmol g^{-1}

Fig. 1. Characteristic properties of humic substances.

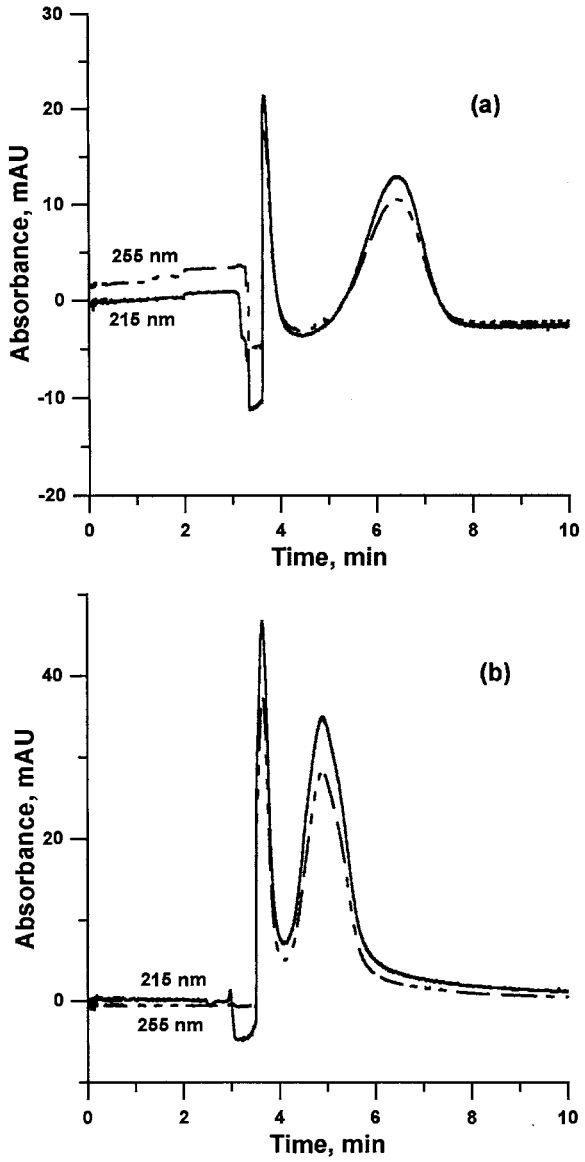

Fig. 2. Capillary zone electrophoresis: electropherogram of HA '193 MAR' (a) and HA Fluka (b) in 60 mM D,L-alanine with 8 mM HCl background electrolyte at pH 3.20, 15 kV, 40°C and 20 s hydrodynamic injection. c('193 MAR') = 101 mg l^{-1}; c(Fluka HA) = 250 mg l^{-1}.

Diluted HA solutions (0.1–0.2 g l^{-1}) and the mixture of metal ions ($\approx 4 \times 10^{-4}$ mol dm^{-3}) and HA (0–1.0 g l^{-1}) were titrated acidimetrically in the pH range 3.5–9 to ensure that no precipitation occurred. Small additions of hydrochloric acid were made and a long cycle time was allowed to ensure that equilibrium had been reached.

All the chemicals used were of analytical grade purity.

2.1.3. Equipment

The potentiometric titrations were carried out on Radiometer titration equipment (Copenhagen, Denmark), which contained pH-meter PHM 84, automatic burette ABU 80 and a digital titrator TTT 81 with a microprocessor unit. The electrometric cell consisted of a reference electrode Radiometer K 401 and indicator electrode which was either glass Radiometer G 202 C or copper(II) or barium(II) ion-selective electrodes (ISE; both from Monokrystaly, Turnov, Czech Republic). The calibration of the cell was done by standard buffer solutions or diluted standard solutions of corresponding metal salts (for the ISE). The accuracy of the measurements was ± 0.02 pH unit. The ionic strength was adjusted to 0.1 mol l^{-1} by adding NaCl solution (except for Ba^{2+}-ISE, where Na^{+} interfere). All experiments were carried out at 25°C.

Capillary zone electrophoresis (CZE) was carried out using SpectraPHORESIS 2000 (Thermo Bioanalysis, CA) with an untreated fused-silica capillary, 75 mm ID (Avery Dennison, MA). The total capillary length was 43.5 cm and the length up to the detector window was 35.5 cm. The applied voltage was 15 kV and the temperature was maintained at 40°C. Prior to use, the capillary was washed for 1 min with HCl 0.1 mol l^{-1}, 1 min with bidistilled water, 1 min with 0.1 mol l^{-1} NaOH and 1 min with bidistilled water. Before each measurement, the capillary was washed with the working electrolyte (D,L-alanine 60 mM and HCl 8 mM, pH 3.20 ± 0.05) for 2–4 min. The samples were injected hydrodynamicaly for 20 s, using a vacuum (10.342 kPa relative to the ambient pressure).

The IR spectra were recorded within the range 400–4000 cm^{-1} on Perkin-Elmer 783 equipment. All samples were carefully dried in a vacuum at elevated temperature to remove water traces. Then samples were dissolved in nujol oil and the solution was measured in a KBr cuvette.

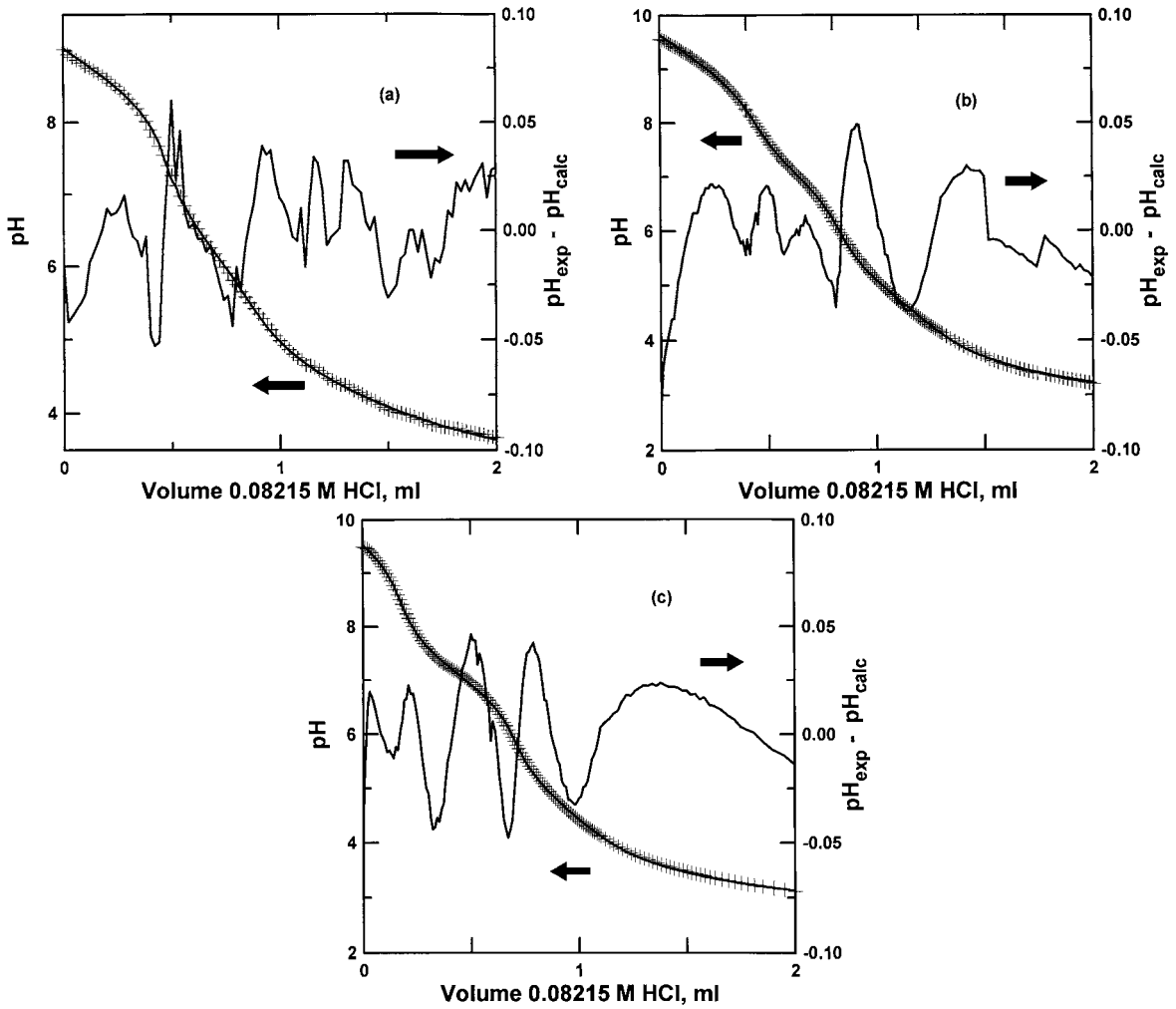

Fig. 3. Titration and residual model curve of humic substances. (a) HA '193 MAR' ($c = 0.1$ g l^{-1}, $V_0 = 200$ ml). (b) HA Fluka ($c = 0.2$ g l^{-1}, $V_0 = 100$ ml). (c) HA Aldrich (0.2 g l^{-1}, $V_0 = 100$ ml). Crosses: experimental points; curve: simulated function for the given model.

2.2. Calculation

For the 'discrete' model, in which the HA is considered as a mixture of different polyprotic acids (e.g. HX, HY and HZ) being studied, calculations were done by means of the programs SUPERQUAD [8,9], HYPERQUAD [8,9] and STATGRAPHICS Version 2.1 [10].

Assuming the equilibria:

$$n\mathrm{H}^+ + \mathrm{X}^{n-} \overset{\beta_{\mathrm{p1},n}}{\rightleftarrows} \mathrm{H}_n\mathrm{X} \qquad \text{(A)}$$

total and stepwise acidity constants can be formulated as:

$$\beta_{\mathrm{p1},n} = \frac{[\mathrm{H}_n\mathrm{X}]}{[\mathrm{H}^+]^n[\mathrm{X}^{n-}]} \qquad (1)$$

$$K_{\mathrm{p1},n} = \frac{[\mathrm{H}_n\mathrm{X}]}{[\mathrm{H}^+][\mathrm{H}_{n-1}\mathrm{X}^{n-1}]} \qquad (2)$$

where n represents the number of bound protons for a given fragment, $n[\mathrm{H}^+]$ is the total amount of extra protons in solutions, β is the

Table 1
Protonation constants of HA '193 MAR' obtained by means of SUPERQUAD and HYPERQUAD programs [8,9]

Model [a]	log $K_{i,j}$	$n(\mathrm{ACID}_i)$ (mmol)	$n(\mathrm{H}^+)$ (mmol)	$s(E)$ [b] (mV)
Mixture of three acids				
HW	$\log \beta_{p1,1} = 8.78 \pm 0.03$	0.058 ± 0.002		
HX	$\log \beta_{p2,1} = 4.33 \pm 0.02$	0.0560 ± 0.0008		
HZ	$\log \beta_{p3,1} = 6.25 \pm 0.02$	0.03151 ± 0.0004	0.018 ± 0.001	1.22
Mixture of one monoprotic and one diprotic acid				
H_2X	$\log \beta_{p1,1} = 8.78 \pm 0.01$			
	$\log \beta_{p1,2} = 13.08 \pm 0.02$	0.0564 ± 0.0008	0.0166 ± 0.0008	1.21
	$\log K_{p1,2} = 4.30 \pm 0.02$			
HZ	$\log \beta_{p2,1} = 6.25 \pm 0.02$	0.0316 ± 0.0004		
Single diprotic acid				
H_2X	$\log \beta_{p1,1} = 8.49 \pm 0.05$			
	$\log \beta_{p1,2} = 13.81 \pm 0.08$			
	$\log K_{p1,2} = 5.32 \pm 0.09$	0.058 ± 0.001	0.011 ± 0.001	7.92
Single triprotic acid				
H_3X	$\log \beta_{p1,1} = 8.43 \pm 0.05$			
	$\log \beta_{p1,2} = 14.20 \pm 0.07$			
	$\log \beta_{p1,3} = 18.1 \pm 0.1$			
	$\log K_{p1,2} = 5.77 \pm 0.09$	0.043 ± 0.001	0.0009 ± 0.001	4.58
	$\log K_{p1,3} = 3.94 \pm 0.16$			
Single tetraprotic acid				
H_4X	$\log \beta_{p1,1} = 8.44 \pm 0.04$			
	$\log \beta_{p1,2} = 14.28 \pm 0.07$			
	$\log \beta_{p1,3} = 18.1 \pm 0.1$			
	$\log \beta_{p1,4} = 21.5 \pm 0.2$			
	$\log K_{p1,2} = 5.84 \pm 0.08$	0.043 ± 0.001	0.0008 ± 0.001	4.17
	$\log K_{p1,3} = 3.8 \pm 0.1$			
	$\log K_{p1,4} = 3.4 \pm 0.2$			

[a] W, X and Z are reaction sites of HA defined in the text.
[b] *Gs(E)* is the standard deviation of weighted fit for the model in mV, defined in [8,9].

total protonation constant, K is the stepwise protonation constant, and X is the anion of the humic acid for the given acid HX.

3. Results and discussion

3.1. Capillary zone electrophoresis (CZE)

The CZE separation of the HA samples ('193 MAR' and Fluka) shows two fractions (Fig. 2). These results are in agreement with those in the literature [11]. The separation of HA into two or three fractions was used for the CZE determination of HA at pH 3.20 ± 0.05 [12] and for a CZE 'fingerprint' characterization of FA and HA (pH 8.9). The number of peaks is dependent on pH but no difference is observed between HA in the form of ammonium or sodium salts.

3.2. Spectroscopic methods

The IR spectrum of the '193 MAR' sample was measured in an attempt to identify the structural fragments of HA. The following bands were assigned [1]: 2900 cm^{-1} (aliphatic C–H stretching, H-bonded OH or NH groups, position of peak is shifted according to bonding force), 1706 cm^{-1}

Table 2
Protonation constants of HA Fluka and HA Aldrich obtained by means of SUPERQUAD and HYPERQUAD programs [8,9]

Model [a]	$\log K_{i,j}$	$n(\mathrm{ACID}_i)$ (mmol)	$n(\mathrm{H}^+)$ (mmol)	$s(E)$ [b] (mV)
(A) Fluka HA				
Mixture of three acids				
HW	$\log \beta_{p1,1} = 9.16 \pm 0.05$	0.040 ± 0.001		
HX	$\log \beta_{p2,1} = 4.86 \pm 0.02$	0.0356 ± 0.0004		
HZ	$\log \beta_{3,1} = 7.03 \pm 0.02$	0.0327 ± 0.0004	0.004 ± 0.002	2.53
Mixture of one monoprotic and one diprotic acid				
H_2X	$\log \beta_{p1,1} = 9.07 \pm 0.04$			
	$\log \beta_{p1,2} = 13.93 \pm 0.05$	0.0363 ± 0.0004	0.0005 ± 0.0007	2.63
	$\log K_{p1,2} = 4.86 \pm 0.03$			
HZ	$\log \beta_{p2,1} = 7.04 \pm 0.03$	0.0324 ± 0.0004		
Single diprotic acid				
H_2X	$\log \beta_{p1,1} = 8.19 \pm 0.05$			
	$\log \beta_{p1,2} = 13.69 \pm 0.08$			
	$\log K_{p1,2} = 5.50 \pm 0.07$	0.0433 ± 0.0006	-0.0112 ± 0.0008	9.69
Single triprotic acid				
H_3X	$\log \beta_{p1,1} = 9.09 \pm 0.04$			
	$\log \beta_{p1,2} = 16.12 \pm 0.07$			
	$\log \beta_{p1,3} = 20.95 \pm 0.08$			
	$\log K_{p1,2} = 7.03 \pm 0.06$	0.0344 ± 0.0004	-0.0004 ± 0.0009	2.97
	$\log K_{p1,3} = 4.83 \pm 0.04$			
(B) Aldrich HA				
Mixture of three acids				
HW	$\log \beta_{p1,1} = 9.5 \pm 0.1$	0.017 ± 0.002		
HX	$\log \beta_{p2,1} = 7.106 \pm 0.009$	0.04334 ± 0.0002		
HZ	$\log \beta_{3,1} = 4.73 \pm 0.02$	0.0309 ± 0.0003	0.003 ± 0.002	1.43
Mixture of one monoprotic and one diprotic acid				
H_2X	$\log \beta_{p1,1} = 7.68 \pm 0.04$			
	$\log \beta_{p1,2} = 12.34 \pm 0.07$	0.0288 ± 0.0008	-0.0088 ± 0.0002	4.16
	$\log K_{p1,2} = 4.66 \pm 0.06$			
HZ	$\log \beta_{p2,1} = 6.62 \pm 0.05$	0.023 ± 0.001		
Single triprotic acid				
H_3X	$\log \beta_{p1,1} = 9.95 \pm 0.06$			
	$\log \beta_{p1,2} = 17.04 \pm 0.07$			
	$\log \beta_{p1,3} = 21.46 \pm 0.08$			
	$\log K_{p1,2} = 7.09 \pm 0.04$	0.0431 ± 0.0004	0.0282 ± 0.0008	4.48
	$\log K_{p1,3} = 4.42 \pm 0.04$			

[a] W, X and Z are reaction sites of HA defined in the text.
[b] Defined in [8,9].

(C=O stretching of COOH and/or ketonic groups), 1615 cm^{-1} (stretching of aromatic C=C bonds, H-bonded C=O groups), 1463 cm^{-1} (C–H deformations of methylene or methyl groups), 1377 cm^{-1} (OH deformation, methyl bonding, C–O stretching), 1250 cm^{-1} (C–O stretching,

OH deformation of COOH groups). Thus, the analyzed HA sample can be included in class A according to the common classification, because there are bands at the positions described above and the band intensities at 1615 and 1706 cm^{-1} are equal [1].

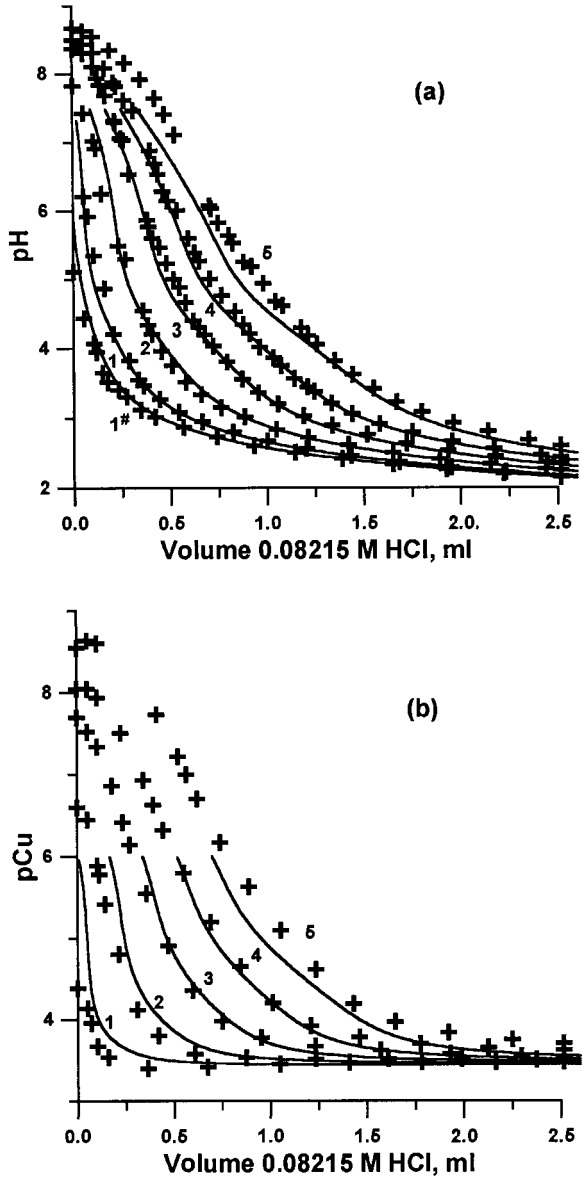

Fig. 4. Experimental values (crosses) fitted by curves of final model (model 7 in Table 3) of the copper(II)–HA ('193 MAR') system using: (a) glass electrode, (b) copper ion-selective electrode; $c_M = 4.02 \times 10^{-4}$ M; c_L (in g l^{-1}): **1** #, 0.1; **1**, 0.2; **2**, 0.4; **3**, 0.6; **4**, 0.8; **5**, 1.0.

3.3. Potentiometry

3.3.1. The acidobasic property of HA

Examples of the titration curves are given in Fig. 3. In the first model (Table 1), HA '193 MAR' was considered as a mixture of three acids (HW, HX and HZ) in accordance with discrete modeling [4,5]; the acidity constants and the concentrations of the acids were determined by means of a computer program. This model was quite successful with a very good fit. The concentrations of HW and HX acids (W, X and Z are reaction sites of HA behaving as isolated bases) in this model are almost the same. In the second model (Table 1), the fit is a little better than the first one and 'unexplained' acidity (proton concentration—due to the presence of acids with $pK < 3$ as was shown [13,14]) accounts for about 10% of the total acidity. The SUPERQUAD program is limited to a number of species because more than three acids cannot be simultaneously present in the model. If this is the case, they must be tested by means of a non-linear regression module in STATGRAPHICS package [10]. In order to check the results obtained by both of the programs, the model with three acids (HW, HX and HZ) was tested. The protonation constants 4.21, 8.84 and 6.16, respectively, were calculated. These were similar to acid concentrations in the first model (Table 1). In the model with four acids (HX, HY, HW and HZ) the calculated protonation constants are 3.31, 4.70, 6.35 and 8.93, respectively. The fit for this model is much worse (the standard deviation values are higher than for the previous model).

The parameters of the third, fourth and fifth models (Table 1) were determined using the SUPERQUAD program and it became clear after comparison of all fit values that the second model was the 'best' of all models as the standard deviation value was minimalized. The diagram of the residuals for this model is shown in Fig. 3. The residuals are randomly distributed and all of them lie within three times standard deviation of pH

Table 3
Survey of testing of different models for the equilibria in the system H^+–copper(II)–HA '193 MAR'

			$s(E)$ (mV)
Indicator electrode: monocrystal Cu^{2+} ISE			
Model 1	CuX	$\log \beta_{1,1} = 7.7 \pm 0.1$	8.21
Model 2	CuX	$\log \beta_{1,1} = 7.75 \pm 0.07$	4.90
	CuX_2	$\log \beta_{1,2} = 12.8 \pm 0.1$ ($\log K_2 = 5.0$)	
Model 3	CuX	$\log \beta_{1,1} = 7.96 \pm 0.05$	2.96
	CuZ	$\log \beta_{2,1} = 6.39 \pm 0.06$	
Model 4	CuX, CuX_2, CuZ	No convergation	
Indicator electrode: glass electrode			
Model 5	CuX	$\log \beta_{1,1} = 7.77 \pm 0.09$	26.78
	CuX_2	$\log \beta_{1,2} = 11.7 \pm 0.2$ ($\log K_2 = 3.94$)	
	CuZ	$\log \beta_{2,1} = 5.7 \pm 0.1$	
Both kinds of titration data: Cu^{2+}–ISE and glass electrode treated simultaneously			
Model 6	CuX	$\log \beta_{1,1} = 7.7 \pm 0.1$	13.94
	CuX_2	$\log \beta_{2,1} = 5.8 \pm 0.1$	
Model 7	CuX	$\log \beta_{1,1} = 7.3 \pm 0.1$	12.87
	CuX_2	$\log \beta_{1,2} = 11.6 \pm 0.2$ ($\log K_2 = 4.32$)	
	CuZ	$\log \beta_{2,1} = 6.2 \pm 0.1$	

$s(E)$, standard deviation of weighted fit for the model in mV defined in [8,9]. $\log \beta$, stability constant for HA–copper(II) complex. Model 2 was considered as the acidobasic model representing HA (Table 1); this means that the acidobasic behavior of HA by this model was approximated as a mixture of one diprotic acid (H_2X) and a second but different monoprotic acid (HZ). The acidobasic protonation constants used for the calculations are given in Table 1.

measurements (0.06 pH unit) which was never exceeded. The total acidity of 8.1 mmol g^{-1} (0.1610 mmol in 200 ml of solution) is almost equal to the 8.44 mmol g^{-1} determined by the analytical procedure described elsewhere ([1] and references therein). Also the carboxylic content declared (45.3%) is almost equal to the acid content ($pK \approx 4.3$ and $pK < 3.0$) calculated as 43.3%. The acid for which $pK \approx 8.8$ is probably a phenolic group and the acid for which $pK \approx 6.25$ could be another less strong carboxylic group of a dicarboxylic fragment (such as citrate, malonate, etc.) [15,16].

The model containing a mixture of acids was tested on the commercial HA samples from Fluka and Aldrich. The models were tested in the same way as '193 MAR'. The survey of these models is shown in Table 2. The best models represent the fitted curves through the experimental points in Fig. 3a and c. The residuals are not in any case higher than 0.06, which shows good fitting through experimental data. HA Fluka and '193 MAR' can be approximated as mixtures of monoprotic and diprotic acids, as was shown in the paragraph about electrophoretic behavior of HA. The components with titratable groups could represent the two fragments observed in CZE and discussed above. In the case of the Fluka sample, the content of phenolic and carboxylic groups is almost equal and the content ratio of carboxylic and ester groups is similar. The Aldrich HA behaves as a mixture of three monoprotic acids and this was also shown by capillary zone electrophoresis [11,12]. The calculated content of titratable groups has been published for the similar region of HA concentrations [4,5] and these are also in agreement with the published data.

A similar approach of non-linear regression fitting to experimental data by the computer program BSTAC was applied [17]. The authors have also fitted the acidobasic titration curve of a river sediment. The best model for this was considered to be mixture of one monoprotic (acidic) and one diprotic (basic) components, but they have not considered this model for the prediction of complexing properties of HA.

3.3.2. Interaction of metal ions with HA

The complexation properties of '193 MAR' were studied by titrations with solutions of different metal ions. From the primary data (Fig. 4) complexation curves of copper for different amounts of HA can be calculated (Fig. 5). The release of copper begins at pH values lower than 5. For higher pH values than 5, the complexation dependence curve tends to become a saturation curve for all HA concentrations. This means that all possible sites in reaction centers are occupied at the given copper concentration 4×10^{-4} mol l^{-1}. Considering this copper(II) concentration as being limiting for HA and assuming it occupies all sites for 0.5 g l^{-1}, the number of active sites of approximately $2 \times 4 \times 10^{-4}/0.5 \approx 1.6 \times 10^{-3}$ mol g^{-1} (in pH region higher than 5) can be found. The value found is in agreement with the results ($1–2 \times 10^{-3}$ mol g^{-1}) [18] obtained from dialysis measurements. Permeable Nafion and Cuprophane membranes were used for the separation, and free metal ion concentration was detected by means of atomic absorption spectrometry. It was found that 50% of free copper was still bound at very low pH values and we can estimate that '193 MAR' is a strong chelating agent with a lower occurrence of protonated metal–humate species.

Furthermore, different models were tested for the proton–copper(II)–HA system (Table 3). The most suitable one is the last model, which assumes species CuX and CuX_2 for one reaction center and species CuZ for the second reaction center (the model was tested in pH region lower than 7.5 where the formation of copper–ammine complexes is negligible):

Table 4
Survey of the best models for the copper(II)–HA (Fluka, Aldrich) systems using glass electrode.

(A) Fluka HA		
Acidobasic parameters		
H_2X	$\log \beta_{p1,1} = 9.07$	Exchange capacity 3.3 mmol g^{-1}
	$\log \beta_{p1,2} = 13.93$	
HZ	$\log \beta_{p2,1} = 7.04$	Exchange capacity 1.5 mmol g^{-1}
Model		
CuX	$\log \beta_{1,1} = 4.8 \pm 0.3$	$s(E)$ 50.03 mV
CuZ	$\log \beta_{2,1} = 8.9 \pm 0.4$	
(B) Aldrich HA		
Acidobasic parameters		
HX	$\log \beta_{p1,1} = 9.5$	Exchange capacity 0.8 mmol g^{-1}
HW	$\log \beta_{p2,1} = 7.106$	Exchange capacity 2.0 mmol g^{-1}
HZ	$\log \beta_{3,1} = 4.73$	Exchange capacity 1.4 mmol g^{-1}
Model		
CuX	$\log \beta_{1,1} = 6.5 \pm 0.1$	$s(E)$ 25.87 mV
CuW	$\log \beta_{2,1} = 6.05 \pm 0.07$	
CuZ	$\log \beta 3,1 = 4.89 \pm 0.06$	

$s(E)$, standard deviation of weighted fit for the model in mV defined in [8,9]. $\log \beta$, stability constant for HA–copper(II) complex.

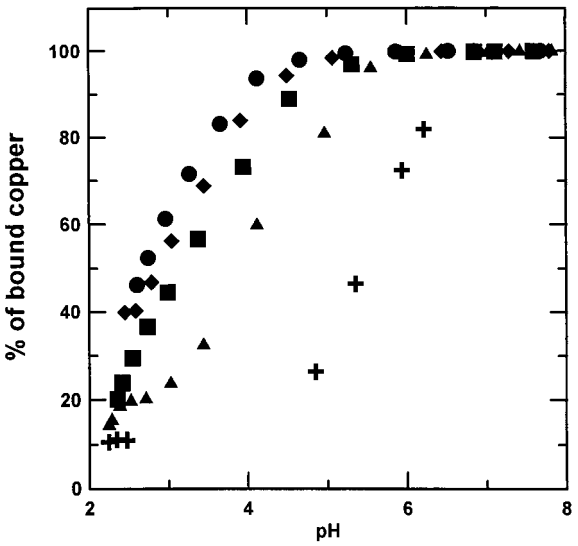

Fig. 5. Formation curves for copper(II) (4.02×10^{-4} M)–HA ('193 MAR') system. HA concentration (in g l^{-1}): +, 0.2; ▲, 0.4; ■, 0.6; ◆, 0.8; ●, 1.0.

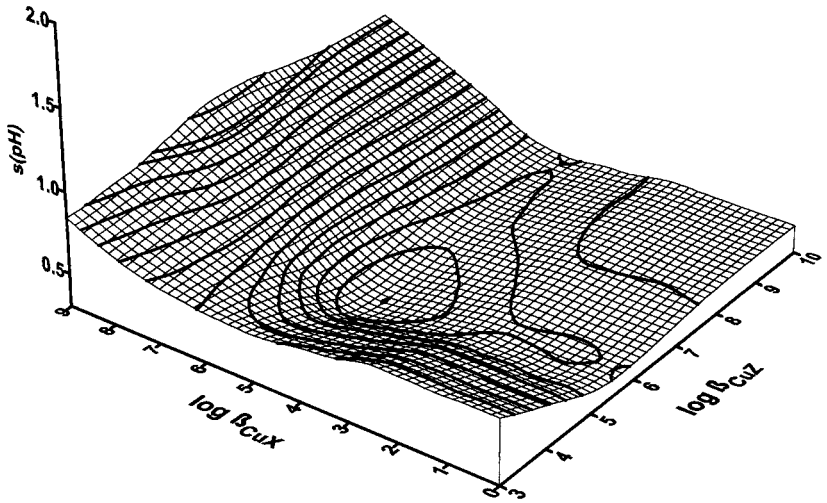

Fig. 6. The residual square function three-dimensional plot for model with CuX and CuZ species for the copper(II)–HA (Fluka) system.

$$Cu^{2+} + X \overset{\beta_{1,1}}{\rightleftarrows} CuX \quad (B)$$

$$Cu^{2+} + 2X \overset{\beta_{1,2}}{\rightleftarrows} CuX_2 \quad (C)$$

CuX, CuX_2: complex formed from a diprotic acid (H_2X) bound Cu(II) in ratio 1:1 and 1:2, respectively.

$$Cu^{2+} + Z \overset{\beta_{2,1}}{\rightleftarrows} CuZ \quad (D)$$

CuZ: complex formed from a monoprotic acid (HZ) bound Cu(II) in the ratio 1:1.

From our model it can be proposed that HAs have two different reaction centers according to the stability constants. They depend on the molecule skeleton, on the molecule bulk and the statistical distribution of each fraction in solution of HA. Stability constant values were compared with the literature data [19] and obtained values were found to be in the range of published results.

Table 5
Survey of the calculated stability constants of HA '193 MAR' with various metal ions ($\log \beta$ are loaded by given standard deviation 0.30)

Metal ion	Indicator electrode	$\log \frac{[MACID_i]}{[M][ACID_i]}$
Ba^{2+}	Ba^{2+}–ISE	BaX: 5.4
		BaZ: 5.3
Pb^{2+}	Glass electrode	PbX: 4.4
		PbZ: 3.4
Cd^{2+}	Glass electrode	CdZ: 3.2
Ca^{2+}	Glass electrode	CaX: 3.1

Similar models were tested for the copper–HA system (Fluka, Aldrich) (Table 4). In the case of the Aldrich sample, only CuX, CuW and CuZ species have been found and this model is considered as the best one. In the case of the Fluka sample, the search for the correct solution was very difficult. The first reason was that the residual square sum function valley was not clearly defined (Fig. 6) and the computer program had difficulty in finding the correct stability constants, as can be seen from the high values of standard deviations for the calculated parameters. Secondly, the low and uncertain proton concentration as one of the fixed parameters (others are protonation constants and concentrations of fragments) causes divergence of minimization. Considering the protonation and stability constants found for the copper–HA system, we can suppose that all three samples of HA can probably have different structural fragments and we are able to describe acidobasic and complexation behavior by the unified model.

Copper(II) was used as the model cation for the study of metal ion interactions with HA, but, generally, each cation is bound in a different way [3,19,20]. A survey of stability constants of HA for various metal ions is given in Table 5. HAs play the role of a multiligand substance with polyreaction centers as it is possible to see in the case of different metal ions (Table 5). For instance, calcium(II) or barium(II) react most probably with one or two carboxylic groups close to each other in one reaction center (as in the case of aliphatic carboxylic acids, oxalic, malonic and/or succinic acid) or with neighboring hydroxyl or carboxylic groups in two strands. Cadmium(II) and lead(II) seem to form the same species as copper, but a less stable one. The statistical probability of metal bonding by HA must be considered and is proportional to the degree of polydispersion.

Our approach is similar to the attempt to describe copper complexation by FA and HA using the 'cascade binding' model [16] where model of FA and/or HA is considered to be a mixture of ligands (acetylacetone, 3-methoxy-*N*-2-(hydroxybenzylsarcosine) or glycylaspartate, and organic acids such as citric, tricarballylic, malic and salicylic).

Also, if logarithms of stability constants values for different metal ions are arranged in the range 3–8, an order similar to the Tipping–Hurley order [18] can be seen: $Cu^{2+} > Ba^{2+} > Pb^{2+} > Cd^{2+} > Ca^{2+}$. The highest stability of HA complexes is observed for copper(II).

Knowledge of stability constants for metal–humate interactions is very important for modeling natural processes [21]. Furthermore, these results can be used for the industrial utilization of humic substances in the future [22]. The methodology given here can be useful for study of the other complexing substances (ligands) whose structures are still not known precisely.

Acknowledgements

We wish to thank Laurence Benjamin, for help with language correction of the manuscript and Profesor L. Sommer for his very interesting comments and discussions about this work. We wish thank Dr M. Ćerník and Professor J. Toužín from the Department of Inorganic Chemistry, Faculty of Science, Masaryk University, for recording the IR spectrum, and Prof. P. Kubáček, of the Department of Theoretical and Physical Chemistry, for recording the EPR spectrum. VÚANCH (Ústi nad Labem, Czech Republic) is thanked for the supplying humic acid samples. This work was supported by the bilateral scientific Czech–French project BARRANDE. The Czech Ministry of Education, the French Ministry of Foreign Affairs and Haut-Rhin General Counsil (Colmar, France) are thanked for their support to David Fetsch.

References

[1] F.J. Stevenson, Humus Chemistry, Wiley, New York, 1982.
[2] S.M. Shevchenko, G.W. Bailey, Crit. Rev. Environ. Sci. Technol. 26 (2) (1996) 95.
[3] J. Buffle (Ed.), Anal. Chim. Acta 232 (Special Issue Humic and Fulvic Compounds) (1990).
[4] L.M. Aleixo, O.E.S. Godinho, W.F. Da Costa, Anal. Chim. Acta 257 (1992) 35.
[5] J.C. Masini, Talanta 41 (1994) 1383.
[6] D. Široký, D. Fetsch, P. Lubal, J. Havel, Chemometrics '95, 3–7 July 1995, Pardubice, Czech Republic.
[7] D. Fetsch, P. Lubal, D. Široký, A.M. Albrecht-Gary, J. Havel, Inorganic Reaction Mechanisms Meeting 95, 4–6 January 1996, Le Bischenberg, France.
[8] P. Gans, A. Sabatini, A. Vacca, J. Chem. Soc. D 1195 (1985).
[9] P. Gans, A. Sabatini, A. Vacca, Talanta 43 (1996) 1739.
[10] STATGRAPHICS, Version 2.1, Statistical Graphics Corporation, 1985–1986.
[11] S. Pompe, K.H. Heise, H. Nitsche, J. Chromatogr. A 723 (1996) 215.
[12] A. Rigol, J.F. López-Sánchez, G. Rauret, J. Chromatogr. A664 (1994) 301.
[13] J.A. Leenheer, R.L. Wershaw, M.M. Reddy, Environ. Sci. Technol. 29 (1995) 393.
[14] J.A. Leenheer, R.L. Wershaw, M.M. Reddy, Environ. Sci. Technol. 29 (1995) 399.
[15] L. Šůcha and S. Kotrlý, Chemical Equilibria in Analytical Chemistry, SNTL Prague, 1988.
[16] R.M. Town, H.K.J. Powell, Anal. Chim. Acta 279 (1993) 221.

[17] M. Gulmini, V. Zelano, P.G. Daniele, E. Prenesti, G. Ostacoli, Anal. Chim. Acta 329 (1996) 33.
[18] J. Komárek, K. Novotný, V. Kubáň, Proceedings Colloqium Analytische Atomspektroskopie CANAS '95, 2–7 April 1996, pp. 435–440.
[19] F.J. Stevenson, A. Fitch, Soil Sci. Soc. Am. (Special Publication) 17 (1986) 29.
[20] E. Tipping, M.A. Hurley, Geochim. Cosmochim. Acta 56 (1992) 3627.
[21] J. Havel, Research Report of Grant GA 1487/93, The Czech Ministry of Environmental Protection, Brno, 1994.
[22] D. Fetsch, J. Havel, XXXIInd International Conference on Coordination Chemistry, 24–29 August 1997, Santiago, Chile.

ELSEVIER

Talanta 47 (1998) 413–419

Talanta

Separation of scandium(III) and yttrium(III) by tris(2-ethylhexyl)phosphate (TEHP)

Mangesh H. Chhatre, Vijay M. Shinde *

Analytical laboratory, Department of Chemistry, The Institute of Science, 15, Madam Cama Road, Mumbai-400 032, India

Received 6 November 1997; received in revised form 30 March 1998; accepted 30 March 1998

Abstract

Tris(2-ethylhexyl)phosphate is proposed as an extractant for scandium(III) and yttrium(III) from salicylate media. The optimum extraction conditions are evaluated and described. The method permits mutual separation of scandium(III) and yttrium(III) and can be used for the separation and determination of scandium(III) and yttrium(III) from binary and multicomponent mixtures. © 1998 Elsevier Science B.V. All rights reserved.

Keywords: Scandium(III); Yttrium(III); Extraction; Separation; TEHP

1. Introduction

Scandium and yttrium are important elements from an industrial point of view. They are extensively used in astronavigation, electronic and metallurgical industries. Both elements are also important in nuclear energy programmes, hence the separation and purification of scandium(III) and yttrium(III) is desired. The preconcentration and purification of scandium(III) and yttrium(III) can be achieved by solvent extraction.

A critical survey of literature reveals that various oxygen containing compounds such as dibutyl phosphate [1], dibutyl hydrogen phosphate [2,3], tri-*n*-butyl phosphate [4–9], tri-*n*-butyl phosphine oxide [10], tri-*n*-octylphosphine oxide [11–14], tri-*n*-phenyl phosphine oxide [15–17], bis(2-ethylhexyl) phosphate [18–20], bis(2-ethylhexyl) hydrogen phosphate [21–24], tetraphenyl imido phosphate [25,26] and mesityl oxide [27,28] have been used for liquid–liquid extraction studies of both scandium(III) and yttrium(III). However, existing methods have limitations such as longer extraction periods [19,26], critical temperature control [8,18–20,26], incomplete extraction [23], the use of salting out agents [7] and synergistic extraction [11,12]. Also, most of these methods work in mineral acid media. In this article a method is proposed for solvent extraction of scandium(III) and yttrium(III) from salicylate media using TEHP as an extractant. The aromatic group in salicylate and its ability to form salt as well neutral ion pair complexes causes extraction. The highlights of the proposed method are:

1. The method is simple, precise and rapid.
2. The method facilitates mutual separation of scandium(III) and yttrium(III).

* Corresponding author.

0039-9140/98/$ - see front matter © 1998 Elsevier Science B.V. All rights reserved.
PII S0039-9140(98)00151-9

3. The method has been successfully applied to the separation of scandium(III) and yttrium(III) from associated elements and recoveries of the elements are $>99.0\%$.
4. The analysis involving the extraction and spectrophotometric determination of scandium(III) and yttrium(III) requires 20 min.

2. Experimental

2.1. Apparatus

Absorbance and pH measurements were carried out on a Shimadzu UV-VIS 160 A spectrophotometer and Control Dynamics digital pH meter with combined glass electrode, respectively.

2.2. Reagents and chemicals

The stock solutions of scandium(III) and yttrium(III) are prepared by dissolving 0.15 g of scandium oxide (BDH) and 0.19 g of yttrium oxide (BDH) in 5 ml of concentrated hydrochloric acid. After evaporation the residue is taken up in 100 ml of 0.1 M hydrochloric acid. The solutions are standardised by known methods [29] and finally diluted as required for the working solutions.

A 0.05% aqueous solution of 4-(2-pyridylazo)resorcinol (PAR) [30] and 20% ammonium acetate buffer are used for the spectrophotometric determination of scandium(III).

A 0.1% aqueous solution of thoron-1 [31] is used for the spectrophotometric determination of yttrium(III).

Tris(2-ethylhexyl)phosphate (TEHP) (Fluka) dissolved in toluene is used for extraction without further purification.

All other chemicals used are of analytical reagent grade.

2.3. General extraction procedure

An aliquot of solution containing microgram amounts of scandium(III) and yttrium(III) is taken and sodium salicylate is added to obtain the desired molarity in a total volume of 25 ml. The pH of the solution is suitably adjusted with 0.1 N hydrochloric acid and 0.1 N sodium hydroxide solutions. The solution is transferred to a separatory funnel and extracted for a required period with TEHP dissolved in toluene. The optimum extraction conditions are reported in Table 1. After phase separation, scandium(III) is re-extracted from the organic phase with 2×5 ml of 2.5×10^{-2} M hydrochloric acid and estimated spectrophotometrically with 4-(2-pyridylazo)resorcinol [30] as follows: adjust the pH 6.0–7.0 with 2.5 ml of 20% ammonium acetate buffer, add 2 ml of 0.05% PAR and dilute to 25 ml with distilled water. Measure the absorbance of the orange red complex after 5 min at 515 nm against the reagent blank prepared analogously.

Yttrium(III) from the TEHP phase is re-extracted with 2×5 ml of distilled water and determined spectrophotometrically with thoron-1 [31] as follows: add 2 ml of 0.1% thoron-1, adjust pH to 4.0 with 0.1 N hydrochloric acid and 0.1 N sodium hydroxide solutions, dilute to 25 ml with distilled water and measure the absorbance at 530 nm against the reagent blank prepared analogously.

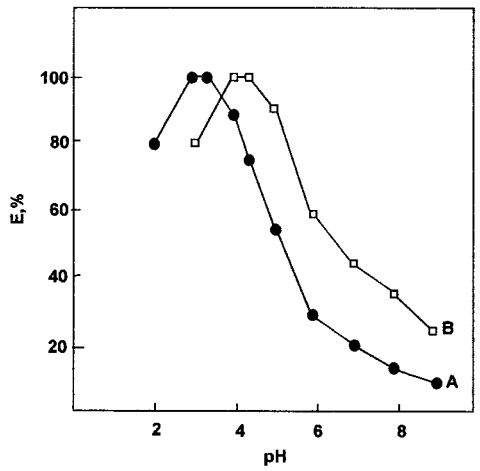

Fig. 1. (A) Extraction behaviour of scandium(III) as a function of pH from 5×10^{-2} M sodium salicylate with 1.7×10^{-1} M TEHP. (B) Extraction behaviour of yttrium(III) as a function of pH from 2.5×10^{-2} M sodium salicylate with 2.1×10^{-1} M TEHP.

Table 1
Optimum extraction conditions for scandium(III) and yttrium(III)

Metal ion	Aqueous phase		Organic phase	Extraction period (s)	Stripping solution	Estimation procedure
	[Sal] (M)	pH				
Sc(III), 10–50 μg	3.5×10^{-2}–5.62×10^{-2}	2.9–3.2	5 ml of 1.7×10^{-1} M TEHP in toluene	30	2×5 ml 0.025 M HCl	PAR [30]
Y(III), 25–100 μg	2.5×10^{-2}–3.75×10^{-2}	4.1–4.4	5 ml of 2.1×10^{-1} M TEHP in toluene	50	2×5 ml distilled water	Thoron-1 [31]

The recoveries of scandium(III) and yttrium-(III) are computed from the previously drawn calibration plots. The distribution ratios are calculated using following relationship:

$$D=\frac{V_a/V_o\cdot E}{100-E}$$

Where V_a and V_o are the volumes of the aqueous and organic phase, respectively, and E is % extraction.

3. Results and discussion

In order to establish the optimum conditions for the quantitative extraction of scandium(III) and yttrium(III) the extraction of scandium(III) and yttrium(III) are performed at various pH (2.0–9.0) shown in Fig. 1, sodium salicylate concentrations (1.25×10^{-4}–5.75×10^{-2} M) shown in Fig. 2 and TEHP concentrations (5×10^{-3}–2.55×10^{-1} M) using toluene as the diluent. The optimum extraction conditions are reported in Table 1. Variation in equilibration time showed that shaking periods of 30 and 50 s are adequate for quantitative extraction of scandium(III) and yttrium(III). However, prolonged shaking had no adverse effect on extraction. The suitability of various diluents such as toluene, xylene, benzene, chloroform and carbon tetrachloride are studied. It was observed that TEHP dissolved in toluene or xylene gives quantitative extraction for both scandium(III) and yttrium(III). With other diluents extraction is incomplete. Toluene was used for further extraction studies as it gave better and quick phase separation.

Various stripping agents are tried in order to re-extract scandium(III) from the organic phase. It was found that 2×5 ml of 2.5×10^{-2}–2.0 M of sulphuric acid, nitric acid, hydrochloric acid and perchloric acid strip scandium(III) completely from the TEHP phase. Distilled water does not strip scandium(III) from the TEHP phase at all. Yttrium(III), however, re-extracts with 2×5 ml of water.

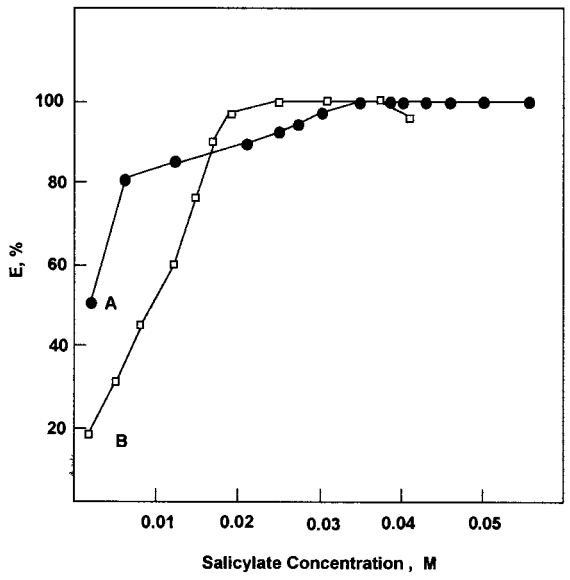

Fig. 2. (A) Extraction behaviour of scandium(III) as a function of sodium salicylate concentration at pH 3.0 with 1.7×10^{-1} M TEHP. (B) Extraction behaviour of yttrium(III) as a function of sodium salicylate concentration at pH 4.1 with 2.1×10^{-1} M TEHP.

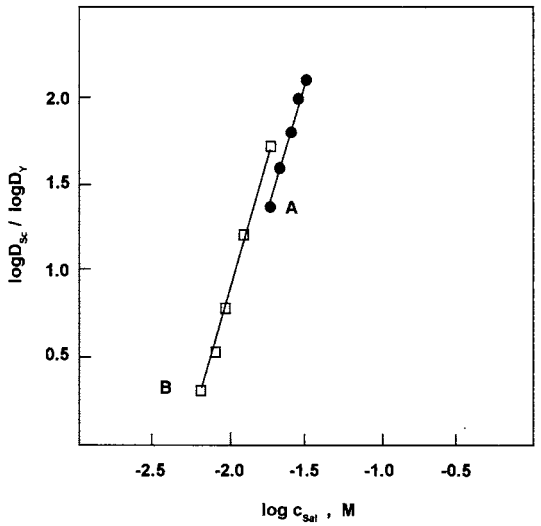

Fig. 3. Plot of log of distribution ratio (D_{Sc}) versus log of salicylate concentration for (A) scandium(III) at pH 3.0 and 1.7×10^{-1} M TEHP and (B) yttrium(III) (D_Y) at pH 4.1 and 2.1×10^{-1} M TEHP.

3.1. Nature of extracted species

An attempt is made to ascertain the nature of the extracted species using log–log plots. A plot of the log of the distribution ratio versus the log of salicylate concentration (at fixed pH and fixed TEHP concentration) gives a slope of 3.0 for both scandium(III) and yttrium(III) (Fig. 3), thus indicating a molar ratio of 1:3 with respect to salicylate.

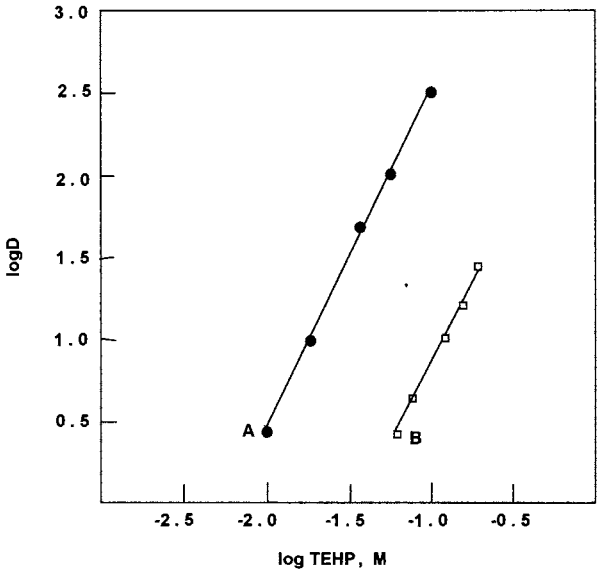

Fig. 4. Plot of log of distribution ratio versus log of TEHP concentration for (A) scandium(III) at pH 3.0 and 5×10^{-2} M sodium salicylate concentration and (B) yttrium(III) at pH 4.1 and 2.5×10^{-2} M sodium salicylate concentration.

Similarly a plot of the log of the distribution ratio versus the log of TEHP concentration (at a fixed pH and a fixed sodium salicylate concentra-

Table 2
Effect of foreign ions

Metal ion	Tolerance limit (μg)	
	Scandium(III)	Yttrium(III)
Mg(II)	5000	4000
Ba(II)	5000	4000
Mn(II)	5000	100
Cd(II)	3000	200
Zn(II)	2000	1000
Ni(II)	250	100
Co(II)	500	500
Hg(II)	100	100
Pb(II)	100	5000
Cu(II)	100	None
Sn(II)	250	250
Fe(III)	200	200
Al(III)	2000	1500
Sb(III)	4000	250
Bi(III)	None	None
Au(III)	1000	1000
V(V)	500	500
Zr(IV)	500	200
Hf(IV)	250	250
Th(IV)	100	250
Mo(VI)	100	250
Cr(VI)	500	1500
U(VI)	1500	1000
Os(VIII)	250	500
Sulphate	4000	2500
Nitrate	4000	2500
Thiocynate	4000	2000
Thiourea	3000	2500
Thiosulphate	2000	2000
Chloride	3000	4000
Nitrite	2500	4000
EDTA	None	None
Oxalate	None	None

Sc(III): 20 μg; salicylate: 5×10^{-2} M; pH: 2.9–3.2; TEHP: 1.7×10^{-1} M.
Y(III): 50 μg; salicylate: 2.5×10^{-2} M; pH: 4.1–4.4; TEHP: 2.1×10^{-1} M.

Table 3
Separation of scandium(III) from binary and multicomponent mixtures

Composition of mixture (μg)	Recovery[a] of scandium(III) (%)	RSD (%)	Recovery[a] of added ion (%)	RSD (%)	Estimation procedure for added ion
Sc (20), Fe (50)	99.8	0.19	99.3	0.14	Thiocyanate [32]
Sc (20), V (50)	99.4	0.22	99.4	0.19	PAR [33]
Sc (20), Cr (50)	99.8	0.12	99.8	0.24	DPC [34]
Sc (20), Nd (50)	99.6	0.10	99.8	0.14	Xylenol orange [35]
Sc (20), Y (50)	99.6	0.21	99.6	0.14	Thoron-1 [31]
Sc (20), La (50)	99.2	0.14	99.6	0.10	Thoron-1 [36]
Sc (20), Sm (50)	99.9	0.095	99.8	0.14	Xylenol orange [35]
Sc (20), Ce (50)	99.3	0.18	99.4	0.14	Arsenazo(III) [37]
Sc (20), Fe (50); Cr (50), Zr (50); Hf (50), Mo (50)	99.5	0.11	—	—	—
Sc (20),V (50); Ti (50), Fe (50); Th (50), Re (50)	99.4	0.23	—	—	—

[a] Average of triplicate analysis.

Table 4
Separation of yttrium(III) from binary and multicomponent mixtures

Composition of mixture (μg)	Recovery[a] of yttrium(III) (%)	RSD (%)	Recovery[a] of added ion (%)	RSD (%)	Estimation procedure for added ion
Y (50), Fe (100)	99.3	0.14	99.1	0.21	Thiocyanate [32]
Y (50), V (100)	99.3	0.21	99.8	0.09	PAR [33]
Y (50), Cr (100)	99.3	0.24	99.3	0.24	DPC [34]
Y (50), Sc (100)	99.8	0.14	99.3	0.24	PAR [30]
Y (50), U (100)	99.6	0.14	99.2	0.28	PAR [38]
Y (50), Th (100)	99.4	0.23	99.4	0.28	Thoron-1 [37]
Y (50), Zr (100)	99.3	0.42	99.3	0.37	Arsenazo(III) [37]
Y (50), Fe (100), U (100), Th (100), Sc (100)	99.4	0.28	—	—	—
Y (50), Cr (100), V (100), Fe (100), Zr (100)	99.4	0.23	—	—	—

[a] Average of triplicate analysis.

tion) give a slope of 2.0 for scandium(III) and 2.1 for yttrium(III), indicating a molar ratio of 1:2 with respect to TEHP (Fig. 4). The extraction involves the following mechanism.

$$M_{aq}^{+3} + 3\ HSal_{aq}^{-} \rightleftharpoons M\ (HSal)_{3\ aq}$$

$$M(HSal)_{3aq} + 2TEHP_{org} \rightleftharpoons M(HSal)_3 \cdot 2TEHP_{org}$$

(solvated metal salicylate salt)

Where M is scandium(III) or yttrium(III), $HSal^-$ is salicylate ion and TEHP is tris(2-ethylhexyl)phosphate. Hence, the probable extracted species is $M(HSal)_3 \cdot 2TEHP$. The salicylate salts are solvated which favours mass transfer of the solute in TEHP.

3.2. Effect of foreign ions

Varying amounts of foreign ions are added to a fixed amount of scandium(III) (20 μg) and yttrium(III) (50 μg) to study their interference in the extraction and spectrophotometric determination of scandium(III) and yttrium(III) by the proposed method. The tolerance limit is set at the amount

required to cause a $\pm 2\%$ error in the metal recoveries. The results are reported in Table 2.

3.3. Binary separation of scandium(III) from yttrium(III), iron(III), vanadium(V), chromium(VI), neodymium(III), lanthanum(III), samarium(III) and cerium(III)

Yttrium(III) (80%) co-extracts with scandium(III) which is selectively re-extracted with 2×5 ml of water. This facilitates the separation of yttrium(III) and scandium(III). Yttrium(III) is determined with thoron-1 [31] and scandium(III) from TEHP is stripped with 2×5 ml of 2.5×10^{-2} M hydrochloric acid and then determined spectrophotometrically with PAR [30].The separation of scandium(III) from lanthanum(III), samarium(III) and cerium(III) is also based on selective stripping. Lanthanum(III), samarium(III) and cerium(III) co-extract with scandium(III) but they are re-extracted with water and determined by known methods [35–37]. Scandium(III) is finally re-extracted with 2.5×10^{-2} M hydrochloric acid and determined as described in the general extraction procedure.

Ions such as iron(III), vanadium(V), chromium(VI), and neodymium(III) do not show any extraction in TEHP and are determined in the aqueous phase by known methods [32–35]. The recoveries of scandium(III) and that of added ions are $> 99.0\%$. The results are reported in Table 3.

3.4. Binary separation of yttrium(III) from scandium(III), iron(III), vanadium(V), chromium(VI), thorium(IV), uranium(VI) and zirconium(IV).

Metal ions such as iron(III), vanadium(V) and chromium(VI) do not extract into TEHP They are determined in the aqueous phase [32–34]. But metal ions such as thorium(IV), uranium(VI) and zirconium(IV) show co-extraction with yttrium(III). Yttrium(III) is selectively stripped with water and determined as described in the general extraction procedure. Co-extracted thorium(IV), uranium(VI) and zirconium(IV) are removed from TEHP by selective stripping with 2.0, 0.8 and 0.5 M hydrochloric acid, respectively [37,38]. The recoveries of yttrium(III) and that of added ions were $> 99.0\%$.The results are reported in Table 4.

Acknowledgement

The authors thank the Department of Science and Technology (DST), New Delhi, India for financing the project.

References

[1] O. Navratil, P. Linhart, Collect. Czech. Chem. Commun. 40 (1975) 3436.
[2] E. Upor, L. Gorbicz, G. Nagy, Magy. Kem. Foly. 75 (1969) 166.
[3] E. Upor, Magy. Kem. Foly. 75 (1969) 205.
[4] C. Rozycki, S. Waldemar, Chem. Anal.(Warsaw) 17 (1972) 1209.
[5] S.S. Corovin, P.G. Berezhko, A.M. Reznik, Zh. Vses. Khim. Ova. 15 (1970) 464.
[6] C. Rozycki, L. Elwira, Chem. Anal. (Warsaw) 15 (1970) 255.
[7] L. Rosicky, J. Hala, J. Radioanal. Chem. 80 (1983) 43.
[8] I.S.EI. Yamini, E.I. Shabana, J. Radioanal. Nucl. Chem. 84 (1984) 307.
[9] R. Kopunec, T.N. Manh, J. Radioanal. Nucl. Chem. 163 (1992) 131.
[10] J. Goffort, Duyckaerts, Anal. Chim. Acta. 46 (1969) 91.
[11] K. Sasayama, M. Mastui, Anal. Chim. Acta. 149 (1983) 253.
[12] T. Shigematsu, M. Mastui, Bull. Inst. Chem. Res. Kyoto Univ. 46 (1968) 269.
[13] C. Krueger, B. Gorski, A.F. Novgorodov, Zfl-Milt 165 (1991) 10.
[14] T.N. Manh, R. Kopunec, J. Radioanal. Nucl. Chem. 159 (1992) 219.
[15] N.G. Bhilare, V.M. Shinde, Fresenius J. Anal. Chem. 354 (1996) 122.
[16] M.A. Qureshi, M. Ejaz, Arabian J. Sci. Eng. 8 (1983) 9.
[17] N.G. Bhilare, V.M. Shinde, Fresenius J. Anal. Chem. 357 (1997) 462.
[18] M. Erdei, B.V. Gromov, Trudy Mosk. Khim. Tekhnol. Inst. 58 (1968) 71.
[19] G.W. Mason, D.N. Metta, J. Inorg. Nucl. Chem. 38 (1976) 2077.
[20] L.N. Moskvin, V.I. Portnyagin, Atomn. Energ. 24 (1968) 568.
[21] M. Csovary, B. Czegledi, I.A. Kuzin, Magy. Kem. Lap 24 (1969) 596.
[22] P. Sladek, O. Navratil, P. Linhart, Collect. Czech. Chem. Commun. 57 (1992) 165.

[23] K. Rengan, H.C. Griffin, Radiochem. Radioanal. Lett. 24 (1976) 1.
[24] R. Kopunec, T.N. Manh, J. Radioanal. Nucl. Chem. 117 (1993) 51.
[25] O. Navratil, E. Herrmann, G. Grossmann, J. Teply, Collect. Czech. Chem. Commun. 55 (1990) 364.
[26] O. Navratil, E. Herrmann, Collect. Czech. Chem. Commun. 57 (1992) 1655.
[27] S. Kalyanaraman, S.M. Khopkar, Anal. Chem. 49 (1977) 1194.
[28] A.D. Langade, V.M. Shinde, Anal. Chem. 52 (1980) 2031.
[29] F.J. Welcher, The Analytical uses of EDTA, Van Nostrand, New York, 1958, pp. 175, 185.
[30] A.I. Busev, F. Chang, Vestn. Mosk. Univ. Ser. Khim. 6 (1960) 46.
[31] S.P. Sangal, Microchem. J. 8 (1964) 304.
[32] A.I. Vogel, A Textbook of Quantitative Inorganic Chemistry, 3rd edn, Longman, London, 785.
[33] S.D. Shete, V.M. Shinde, Anal. Chim. Acta 125 (1981) 165.
[34] C.K. Mann, J.C. White, Anal. Chem. 30 (1958) 989.
[35] D. Prajshar, Chem. Anal. (Warsaw) 8 (1963) 71.
[36] S.P. Sangal, A.K. Dey, Chim. Anal. 46 (1964) 223.
[37] Z. Marczenko, Spectrophotometric Determination of Elements, Ellis Horwood, Chichester, 1976, p. 441, 611, 539.
[38] M.B. Dalvi, S.M. Khopkar, Talanta 25 (1978) 599.

ELSEVIER

Talanta 47 (1998) 421–437

Talanta

Spectrophotometric method for determination parts per million levels of cyclohexylamine in water

A.G. Kumbhar, S.V. Narasimhan *, P.K. Mathur

Water and Steam Chemistry Laboratory (WSCL), Chemistry Group, BARC, Indira Gandhi Centre for Atomic Research Campus, Kalpakkam, Tamil Nadu, 603 102, India

Received 6 January 1998; received in revised form 31 March 1998; accepted 31 March 1998

Abstract

UV–vis spectrophotometric method for the analysis of cyclohexylamine (CHA) in aqueous medium in the range of 0.3–20 ppm was developed by coupling CHA with sodium 1,2-naphthaquinone-4-sulphonate (NQS). At 470 nm a calibration slope of 0.028 OD ppm^{-1} was observed. Minimum detection limit was 0.3 ppm with standard deviation of 0.1 ppm. Reagent concentration and solution pH for the analysis are optimised by studying its effect on absorbance at 470 nm. The method was applied to analyse CHA for evaluating the performance of ion exchange resin used in condensate purification plant (CPP) of power station where, CHA is used as all volatile treatment (AVT) reagent to inhibit steam generator (SG) corrosion. Structure of the adduct formed by coupling CHA with NQS is elucidated using NMR (^{1}H and ^{13}C) and IR spectra, CHN analysis and mole ratio variation method. © 1998 Elsevier Science B.V. All rights reserved.

Keywords: Cyclohexylamine; Sodium 1,2-naphthaquinone-4-sulphonate; Condensate purification plant; Steam generator

1. Introduction

Volatile amines are added in the feed water of steam generators (SG) of power industry to raise the pH of the water and to provide protection against the corrosion. These amines volatilise along with the steam and are partly carried away to the turbine and condenser part, there by, providing protection against corrosion to the entire steam–water circuit. The treatment is called as an all volatile treatment (AVT) and the amines used as AVT reagents. CHA is presently used as one of the AVT reagent [1,2].

In aqueous medium amine hydrolyses as follows:

$$\underset{\text{Amine}}{RNH_2} + H_2O \rightarrow \underset{\text{Amminium ion}}{RNH_3^+} + OH^-$$

The steam condensate containing CHA and other impurities is purified by condensate purification plant (CPP), using mixed bed ion exchange resins (cation and anion). Amminium (RNH_3^+) ions from condensate act as cation impurities and convert the hydrogen form of cation resin (RH^+)

* Corresponding author. Tel.: +91 4114 40397; fax: +91 4114 40360.

0039-9140/98/$ - see front matter © 1998 Elsevier Science B.V. All rights reserved.
PII S0039-9140(98)00152-0

to Amminium form (RNH_3^+). Although, on conversion to amminium form, the impurity (e.g. sodium) removal performance of the CPP resin bed gets deteriorated, the CPP can be still further operated beneficial with amminium form of cation resin. This requires monitoring and controlling precisely the influent CHA concentration and keeping the track of influent impurity (Na) concentrations and percentage bed loading. Thus, time taken to convert the hydrogen form (H/OH) of CPP resin in the cyclohexylaminium (CHA/OH) form and impurity leakage behavior when CPP operates in CHA/OH form is critically dependent on the influent CHA concentration. CHA concentration used for SG water treatment are in the range of 0–10 ppm. In this paper a simple spectrophotometric method for routine lab analysis of CHA using sodium 1,2-naphthaquinone-4-sulphonate (NQS) is described.

2. Experimental

2.1. Apparatus

Spectrophotometric measurements were made on 'Chemito 2500' UV–vis recording spectrophotometer using 1 cm quartz cells. An ION-85 ion analyser with a Seibold combination glass electrode was used to measure pH.

Condensation product of Sodium 1,2-naphaquoinone-4-sulphonate (NQS) and CHA (adduct) was extracted in chloroform and evaporated to dryness at room temperature. The dried product was further purified by recrystalising from mixture of chloroform and methanol This product was again dissolved in chloroform and loaded on silica gel column. The column was then eluted with a mixture of 10% methanol and 90% $CHCl_3$ to get pure adduct with orange colour. The purity of the adduct was further tested on TLC as single compound. This elute was initially dried at 50–60°C for several hours and then dried in vacuum oven at 60°C overnight. The infrared (IR) spectra of the adduct and NQS recorded by pellatizing with KBr and using Bomem Michelson Series FTIR spectrometer. IR spectra of CHA was recorded by using zinc selenoid cells. The nuclear magnetic resonance (NMR) spectrum of CHA and adduct was recorded in $CDCl_3$ medium and NQS was recorded in D_2O medium using Avance Spectrospin Bruker 300 MHz/52 MM NMR spectrometer. The CHN analysis was carried out by using Perkin Elmer (PE 2400) analyser.

2.2. Reagents

All chemicals used in reagent preparation were GR grade. For all preparations deionised (DM) water (triple distilled in quartz) with specific conductivity less than 0.1 μS cm^{-1} was used. 1000 ppm (ppm = mg l^{-1} solution) stock solution of CHA was prepared by dissolving 1000 mg of CHA in freshly prepared DM water and making it up to 1 l. From this stock solution the 100 ppm CHA solution was prepared as working solution for every set of analyses. Reagent solution (0.6% by wt.) was freshly prepared by dissolving 0.15 g of Sodium 1,2-naphthaquinone-4-sulphonate (NQS) in DM water and making it up to 25 ml as and when required. 1 M NaOH solution was prepared as stock solution and 0.5 M NaOH was used as working solution.

2.3. Procedure

75 μl of NaOH (0.5 M) was added to the sample containing CHA in a 25 ml standard volumetric flask and well stirred, then 0.5 ml of reagent (NQS) solution was added to the flask and was well stirred and made up to 25 ml with DM water. Calibration standards of 1–10 ppm were also prepared in the same manner by taking suitable aliquots (0.25–2.5 ml of 100 ppm solution). After a waiting period of 1 h, absorbance values of sample and standards were measured at 470 nm and from the calibration curve, the CHA concentration of the sample was determined. The calibration and sample measurements were carried out at 25°C.

3. Results and discussions

3.1. Analytical method for CHA estimation

Cyclohexylamine (CHA) was found to react with sodium 1,2-naphthaquinone-4-sulphonate (NQS) to form a reddish orange coloured adduct with maximum absorbance at 470 nm (λ_{max}). Fig. 1(a) shows UV–vis spectra of the adduct formed with a 5 ppm CHA solution recorded against reagent blank. Fig. 1(b) shows the variation of absorbance of the adduct at 470 nm as a function of time. After a waiting period of 40–60 min the absorbance was found to be constant. The molar

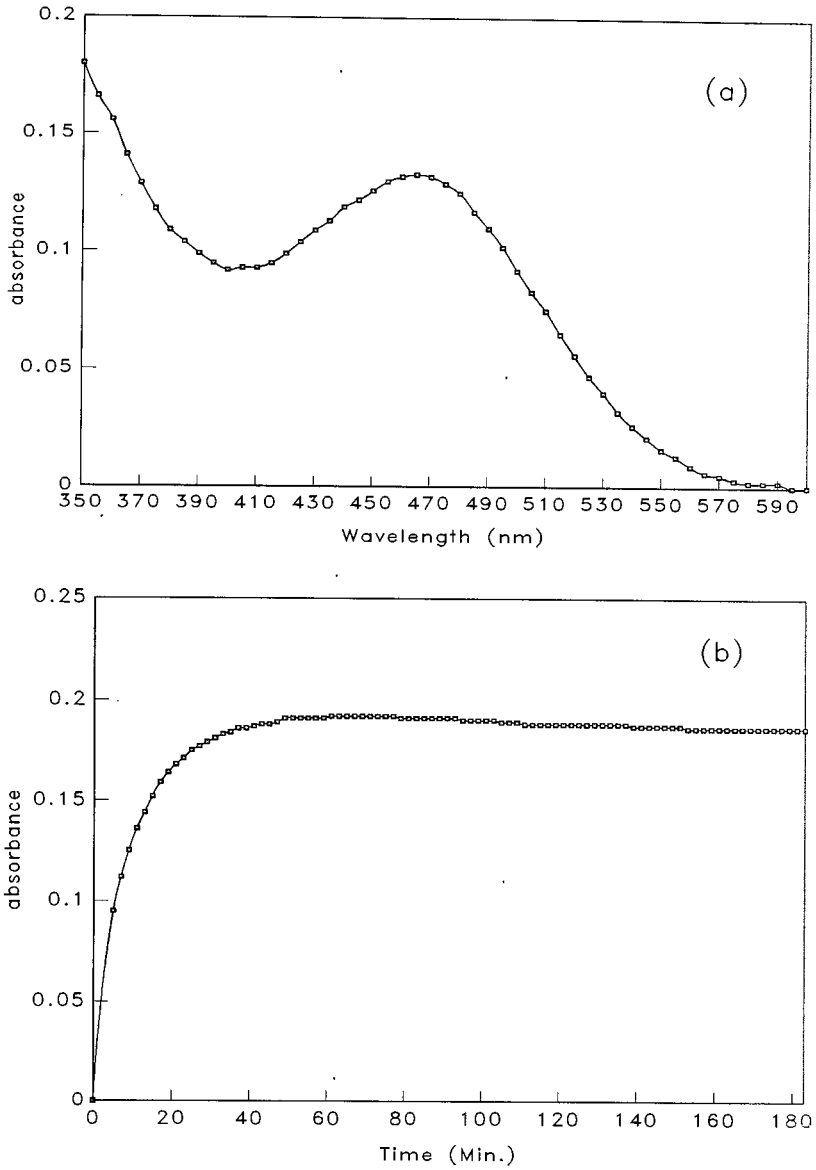

Fig. 1. (a) UV–vis spectrum of CHA-NQS adduct in solution. Path length: 1 cm, NQS (0.6%): 0.5 ml and NaOH (0.5 M): 75 μl, in 25 ml. Final CHA concentration: 5 ppm. (b) Variation of absorbance of CHA-NQS adduct as a function of time after its formation. Path length: 1 cm, NQS (0.6%): 0.5 ml and NaOH (0.5 M): 75 μl, in 25 ml. Final CHA concentration: 5 ppm.

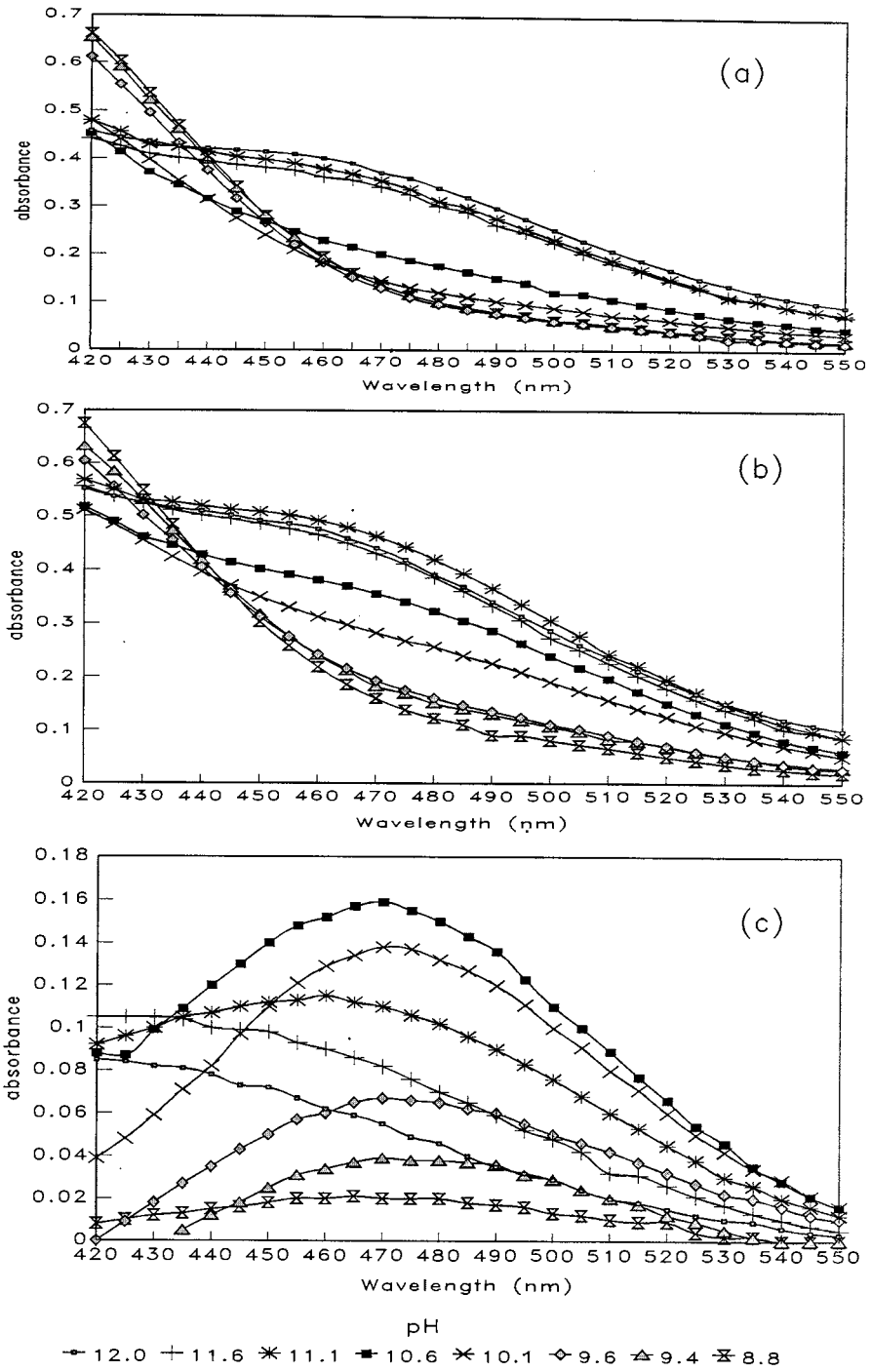

Fig. 2. (a) UV–vis spectra of reagent blank solution vs. DM water at various pH values, Path length: 1 cm, NQS (0.6%): 0.5 ml. (b) UV–vis spectra of 5 ppm CHA-NQS adduct vs. DM water at various pH values. Path length: 1 cm, NQS (0.6%): 0.5 ml. Final CHA concentration: 5 ppm. (c) UV–vis spectra of CHA-NQS adduct vs. reagent blank at various pH values. Path length: 1 cm, NQS (0.6%): 0.5 ml. Final CHA concentration: 5 ppm.

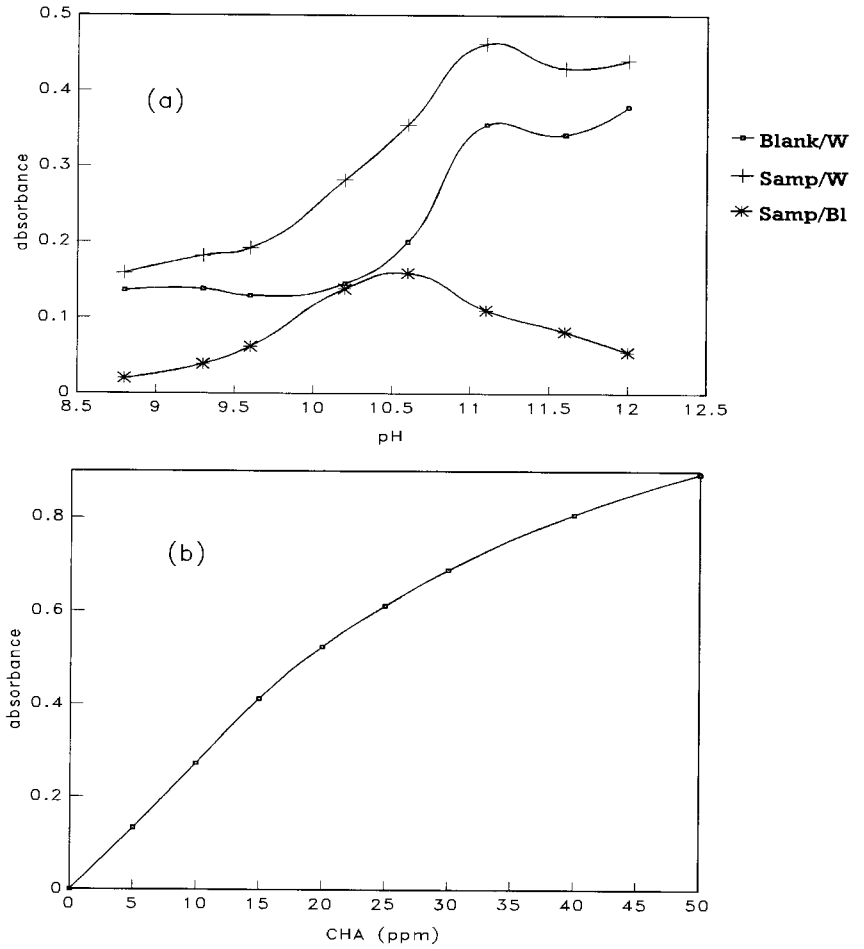

Fig. 3. (a) Variation of absorbance at 470 nm of CHA-NQS adduct solution as a function of pH. Path length: 1 cm, NQS (0.6%): 0.5 ml in 25 ml. Final CHA concentration: 5 ppm. (b) Plot of CHA concentration (0–50 ppm) vs. absorbance. Path length: 1 cm, NQS (0.6%): 0.5 ml and NaOH (0.5 M): 75 μl, in 25 ml.

Table 1
Absorbance values at 470 nm of 0–10 ppm standard of CHA for ten different measurements

No. of measurements	CHA Concentration (ppm)										
	Blank	1	2	3	4	5	6	7	8	9	10
1	−0.004	0.016	0.042	0.071	0.089	0.132	0.148	0.174	0.200	0.237	0.259
2	−0.001	0.022	0.047	0.063	0.087	0.127	0.149	0.18	0.204	0.239	0.263
3	0.001	0.022	0.044	0.074	0.086	0.127	0.162	0.182	0.200	0.244	0.267
4	−0.003	0.019	0.047	0.064	0.092	0.132	0.152	0.179	0.202	0.240	0.272
5	−0.004	0.015	0.049	0.072	0.088	0.127	0.155	0.184	0.209	0.242	0.264
6	0.005	0.015	0.048	0.066	0.092	0.137	0.157	0.188	0.207	0.246	0.266
7	0.000	0.020	0.042	0.069	0.094	0.127	0.161	0.184	0.208	0.247	0.265
8	0.003	0.026	0.042	0.067	0.081	0.123	0.149	0.184	0.201	0.244	0.261
9	0.004	0.022	0.042	0.061	0.088	0.129	0.148	0.184	0.207	0.250	0.273
10	0.002	0.022	0.046	0.072	0.088	0.133	0.156	0.185	0.211	0.249	0.266
Avg.	0.000	0.020	0.045	0.068	0.089	0.129	0.154	0.182	0.205	0.244	0.266
Std.	0.003	0.003	0.003	0.004	0.003	0.004	0.005	0.004	0.004	0.004	0.004

absorptivity at 470 nm was found to be 2600 ($\pm$30) l mol^{-1} cm^{-1}. The molar absorptivity of morpholine-NQS adduct was reported to be 4880 l mol^{-1} cm^{-1} [4]. There was a decrease by a factor of two for CHA-NQS adduct indicating probably the slight difference in adduct structure between morpholine and cyclohexylamine cases. The molar absorptivity value of CHA-NQS adduct, 2600 ($\pm$30) l mol^{-1} cm^{-1}, indicates that it could be due to the transition of nonbonding electrons. Nevertheless, it is sufficient enough to be applied for quantitative analysis.

No appreciable change in OD at 470 nm was observed by varying the excess reagent (NQS) in

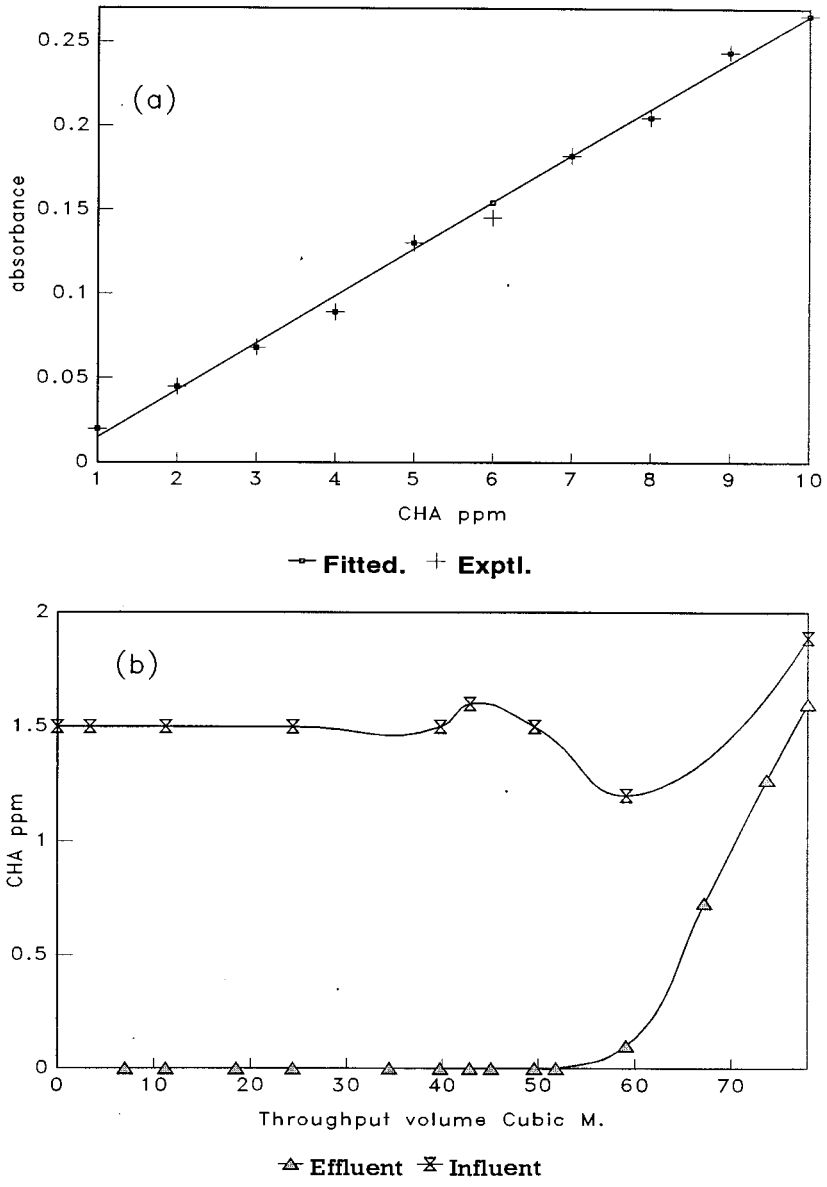

Fig. 4. (a) Calibration plot for 0–10 ppm CHA. Path length: 1 cm, NQS (0.6%): 0.5 ml and NaOH (0.5 M): 75 μl, in 25 ml. (b) CHA break through curve of a ion exchange resin bed used in a simulate CPP system.

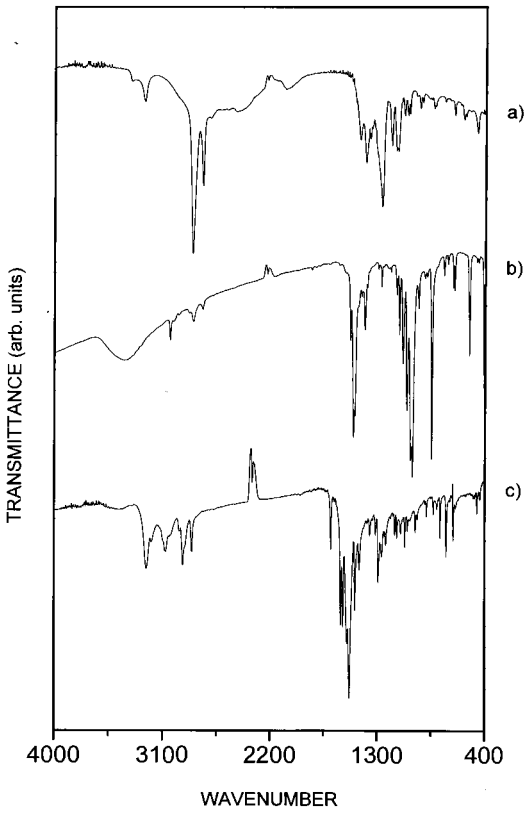

Fig. 5. IR spectra of (a) CHA, (b) NQS and (c) adduct.

range of 0.5–1.0 ml (of 0.6% solution) per 25 ml of sample solution. However, due to high background absorption of the reagent itself, it was necessary to keep the reagent concentration constant for a set of samples and standards to get results within the experimental error.

Absorbance at 470 nm was found to be varying as a function of sample pH which was essentially due to the transformation to the quinonoid structure. In Fig. 2(a) UV–vis spectra of reagent blank with various pH values against DM water are shown. The significant increase in absorbance for blank at 470 nm is observed as sample pH increases above 10.6. In Fig. 2(b) UV–vis spectra of solution containing 5 ppm CHA and reagent against DM water at various pH values are shown. Above pH 9.6 the absorbance at 470 nm was found to be increasing significantly. Below the sample pH 9.6 conversion of the reagent to quinonoid form and further the formation of condensation product with CHA might not be favored. Above pH 11.6 the absorbance at 470 nm did not increase significantly with increase in pH. Fig. 2(c) shows UV–vis spectra of 5 ppm CHA against reagent blank at various pH values. For pH 10.6 the absorbance at 470 nm was found to be maximum. This overall effect of pH on absorption is summarised in Fig. 3(a), here at pH 10.5 the absorbance was found to be the highest. Hence, for all analytical purposes, 0.5 ml of reagent for 25 ml sample was used and pH of the sample was adjusted to 10.5 ± 0.2 by adding 75–100 μl of 0.5 M NaOH to the sample. The selected quantity of the reagents was suitable for a maximum final concentration of CHA of 0–50 ppm.

A plot of absorbance vs. CHA concentration (0–50 ppm) is shown in Fig. 3(b). It can be seen from the figure that the method can be applied for CHA analysis in the range of 0–20 ppm, due to

Table 2
Prominent IR absorption frequencies of CHA, NQS and adduct

S. No.	CHA		Condensation product (adduct)		NQS	
1	3405	$-NH_2$ Str.	—	—	—	
2	3308	$-NH_2$ Str.	—	—	—	
3	2930	$-CH_2$ Str.	2929	$-CH_2$ Str.	—	
4	2855	$-CH_2$ Str.	2854	$-CH_2$ Str.	—	
5	—	—	1604	>C=N Str.	1674	Orthoquinone Str.
6	1631	—	1450	—	1319	Sulphonate band
7	1581	—	1342	—	1289	Sulphonate band
8	1387	—	1047	—	1258	Sulphonate band
9	1341	—	770	—	1218	Sulphonate band
10	—	—	—	—	1069	Sulphonate band

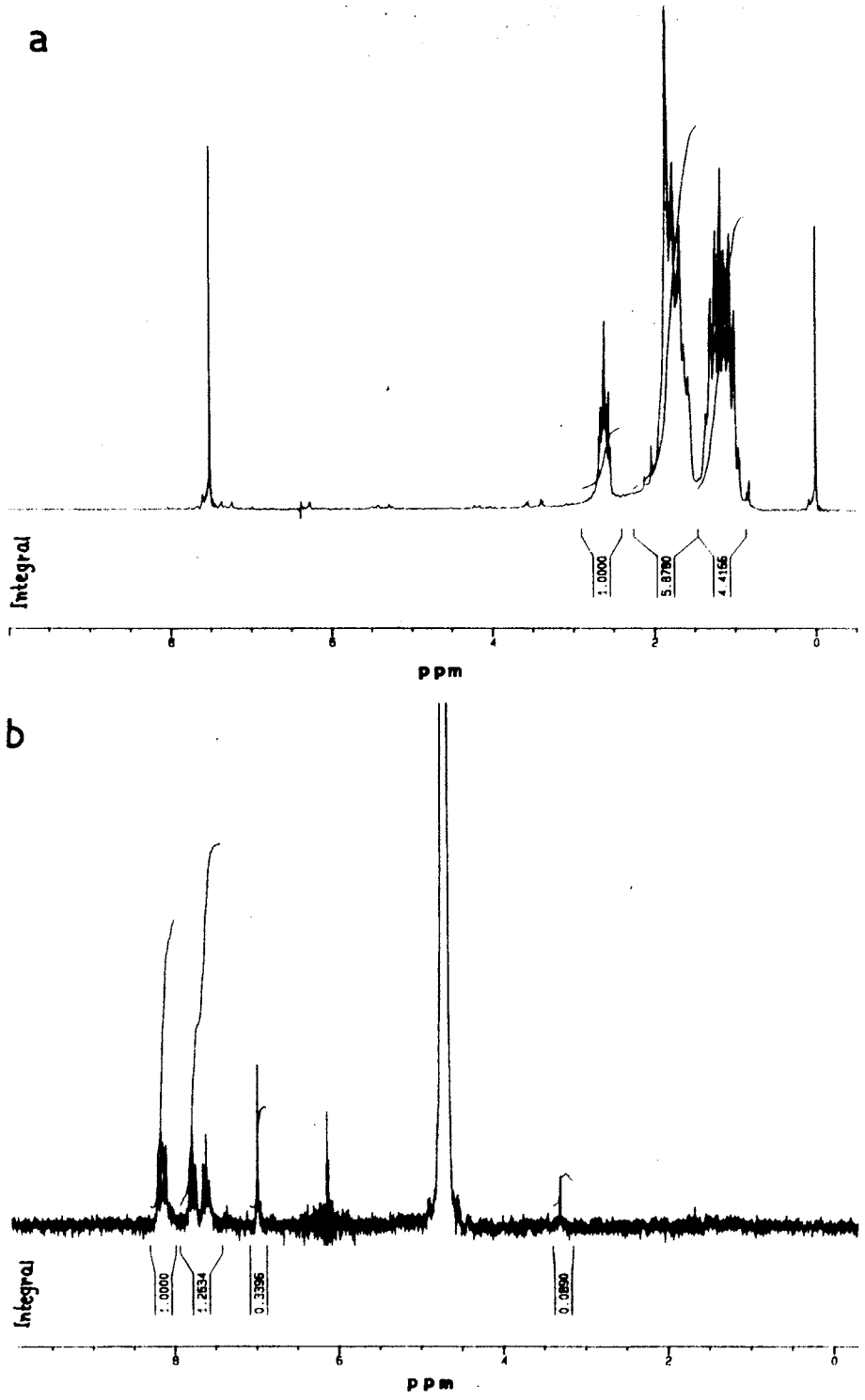

Fig. 6. ^{1}H-NMR spectra of (a) CHA, (b) NQS.

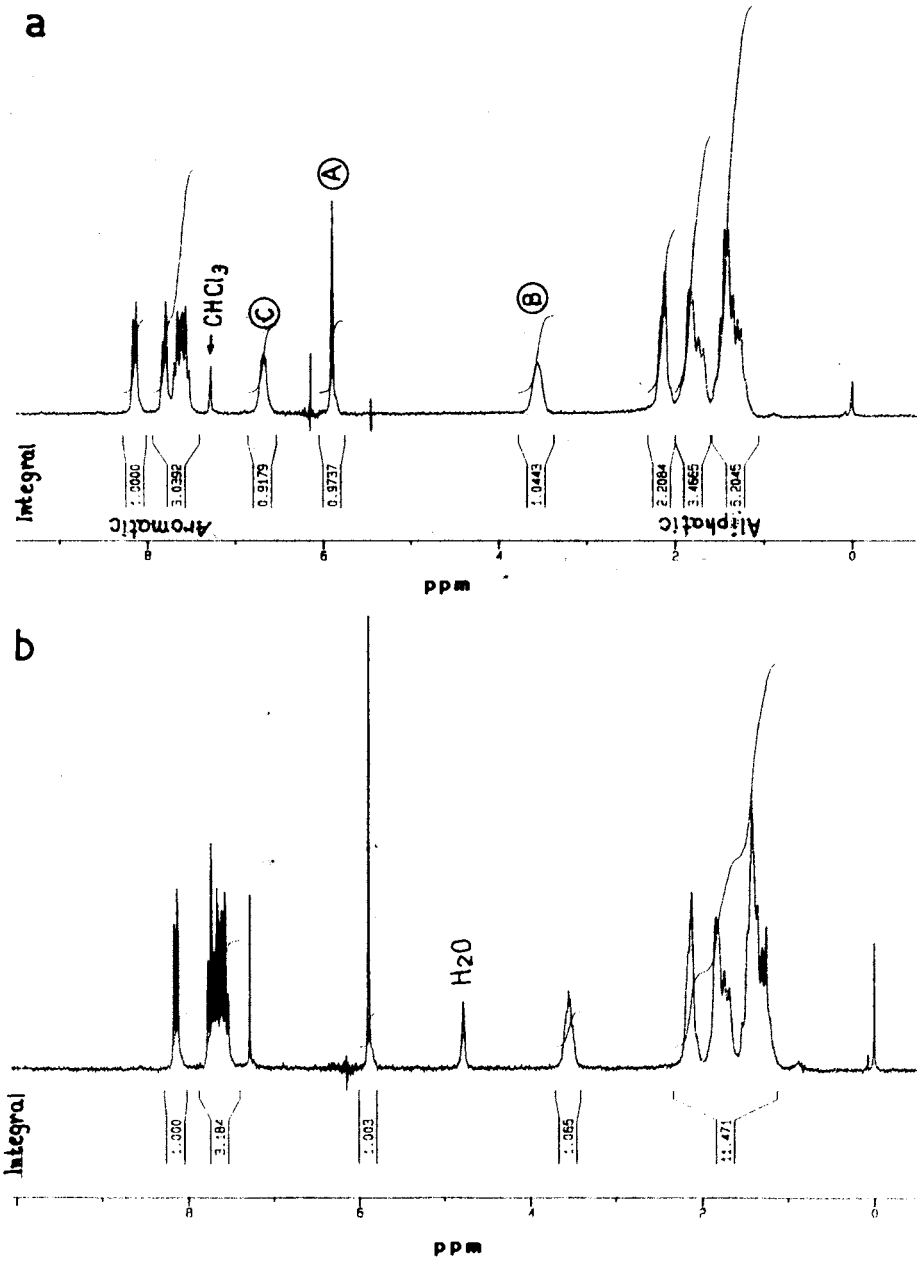

Fig. 7. Proton NMR spectra of (a) adduct in $CDCl_3$ and (b) adduct b in $CDCl_3 + 2–3$ drops of D_2O.

the linear nature of the plot in this range. Concentration range of interest to power plant CPP lies in the range 0–10 ppm CHA. The method was further standardised by taking ten measurements of absorbance for blank and for every ppm of CHA and finding out the standard deviation (σ). The data is given in Table 1. Fig. 4(a) shows the calibration plot of the data. The detection limit ($3 \times \sigma_{blank}$) was found to be 0.3 ppm for a $\sigma_{bank} =$ 0.003 OD units. The slope of the calibration curve is 0.027 absorbance units per ppm. Thus, with this calibration CHA concentration in the range of

1–10 (± 0.1) ppm can be measured. Since, the CHA is added to the DM water and CHA eluting out of mixed ion exchange bed is measured, the possibility of any other interference does not exists here. Hence in the domain of the specific applications the analytical procedure complies adequately.

3.2. Structure elucidation of the adduct

In addition to the analytical calibration, structural investigation of the reaction product of CHA and NQS was also carried out using the IR and NMR spectra, in order to understand the nature of the adduct in comparison to that observed earlier for the morpholine–NQS case [4].

Table 3
Proton peak positions of adduct ^{1}H-NMR spectrum and their attributes to respective carbon atoms

Peak position (ppm)	No. of proton integral	Proton attributed to carbon
1.26	5.2	C3 and C5 CHA proton (four Nos)
1.30	5.2	C3 and C5 CHA proton (four Nos)
1.35	5.2	C3 and C5 CHA proton (four Nos)
1.40	5.2	C3 and C5 CHA proton (four Nos)
1.44	5.2	C3 and C5 CHA proton (four Nos)
1.49	5.2	C3 and C5 CHA proton (four Nos)
1.69	3.5	C2 and C6 CHA protons (four Nos)
1.74	3.5	C2 and C6 CHA protons (four Nos)
1.82	3.5	C2 and C6 CHA protons (four Nos)
1.85	2.2	C4 CHA protons (two No.s)
2.13	2.2	C4 CHA protons (two No.s)
3.57	1.0	C1 CHA proton (one No.)
5.90	0.97	C3 NQS OH proton (one No.)
6.69	0.92	C2 NQS OH proton (one No.)
7.5–8.2	4.04	C5, C6, C7, C8 NQS proton (four No.s)

Subsequent to the coupling reaction, the product solution tested positive for sulphate indicating that the SO_3Na group of naphthaquinone reagent has been released as a sulphite which got oxidised to sulphate. This was further confirmed from the following features observed from IR spectra of CHA, NQS and the adduct given in Fig. 5.

1. The absorption frequencies observed in IR spectrum of CHA corresponding $-CH_2$ asymmetric stretching (2940–2915 cm^{-1}) and symmetric stretching (2860–2840 cm^{-1}) (Fig. 5(a)) are retained in IR spectrum of adduct (Fig. 5(c)).
2. The absorption frequencies corresponding sulphonate (1300–1030 cm^{-1}) observed in IR spectrum of NQS (Fig. 5(b)) are absent in the IR spectrum of the adduct.
3. The strong absorption due to N–H stretching (3350–3300 cm^{-1}) and N–H deformation (1600 cm^{-1}) observed in CHA IR spectrum (Fig. 5(a)) was not found in the adduct. The absorption frequency corresponding to C=N stretch (1610–1550 cm^{-1}) of C=N is observed in adduct indicating the CHA might have been coupled to NQS through >C=N bonding.
4. The absorption frequency at 1674 cm^{-1} corresponding to >C=O in ortho quinone observed in NQS was absent in the adduct. Instead a peak at 1604 cm^{-1} was observed which might be due to >C=N. The prominent absorption frequencies (expressed as wavenumbers, cm^{-1}) are given in Table 2.

The negative absorbance peaks observed in all spectra in the range of 2200–2500 cm^{-1} are due atmospheric CO_2

IR spectral data does not categorically prove the structures, because certain frequencies can be interpreted as belonging to more than one group. e.g. >C=C and >C=N, etc. In view of this it became difficult to contradict a structure similar to that proposed for morpholine–NQS adduct [4], namely

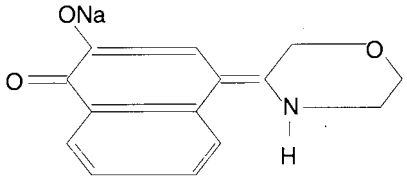

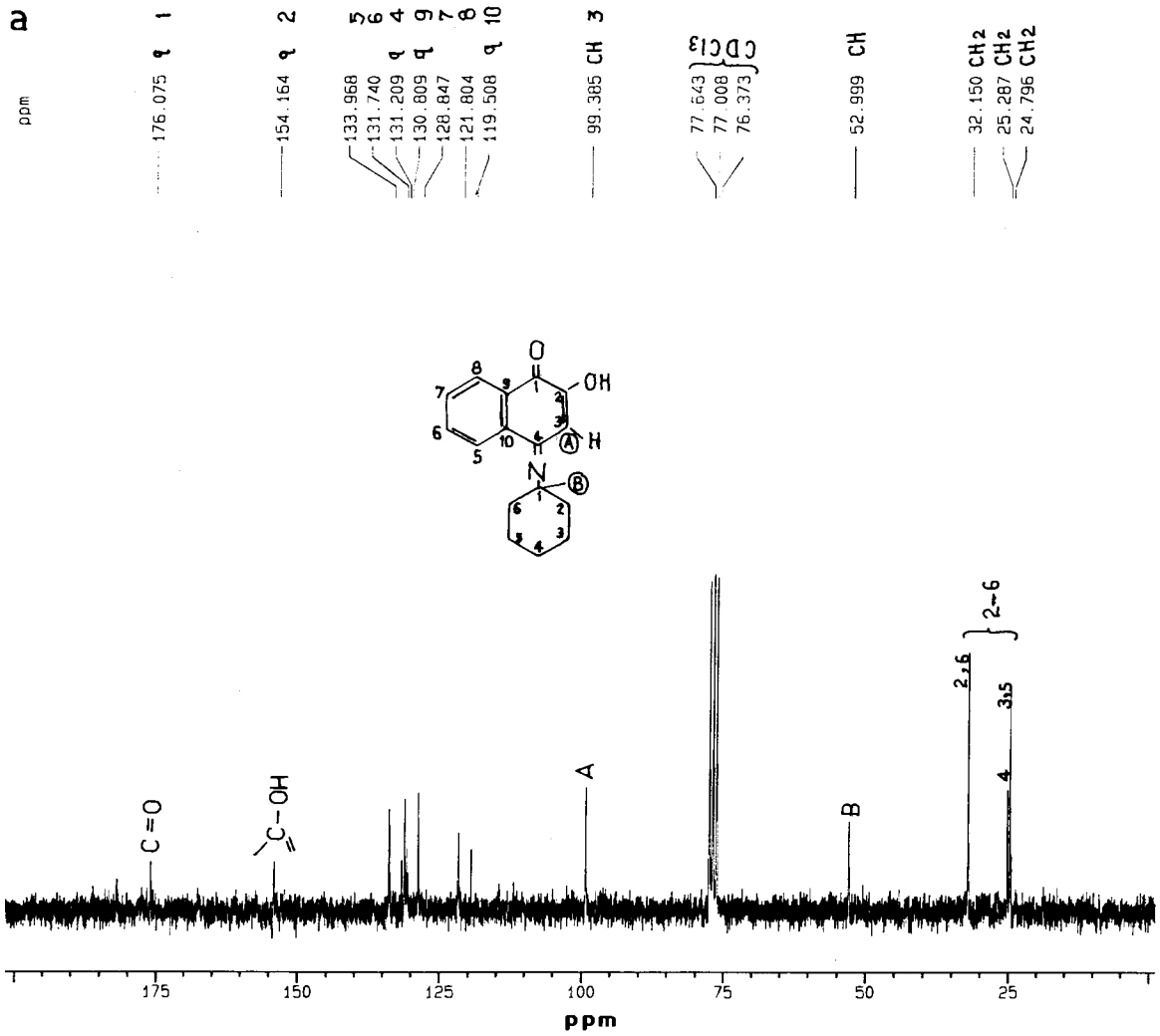

Fig. 8. (a) ^{13}C-NMR spectrum of adduct and (b) DEPT-135 ^{13}C-NMR spectrum of adduct.

It should also be noted that the absence of $-NH_2$ group and N forming a part of a ring in morpholine might have made the orthro $-CH_2$ group to couple NQS. Nevertheless detailed structural investigation for structural ellucidation was lacking in the reference [4]. Earlier piperidine coupling with NQS to give a scarlet p-quinonoid condensation product with limit of detection of 0.6 ppm was also reported [3], where structure elucidation was again not available.

To further investigate the structure of the adduct, NMR spectra of the CHA, NQS and adduct were recorded. Three peaks in the NMR spectrum of CHA (Fig. 6(a)) can be attributed to the following groups of CHA protons. The peak in the range of 2.40–2.89 ppm amount to one proton area and is due to the single hydrogen atom attached to the carbon atom at position 1 to which $-NH_2$ group is attached. The peaks in the range of 1.46–2.26 ppm amount to 5.878 proton area and is due to the six hydrogen atoms attached to the carbon atoms at positions 3, 4 and 5. The peaks in the range 0.864–1.46 ppm amount to 4.48 proton area and is due to the four hydrogen atoms attached to the carbon atoms at positions 2 and 6. The peak due to the two

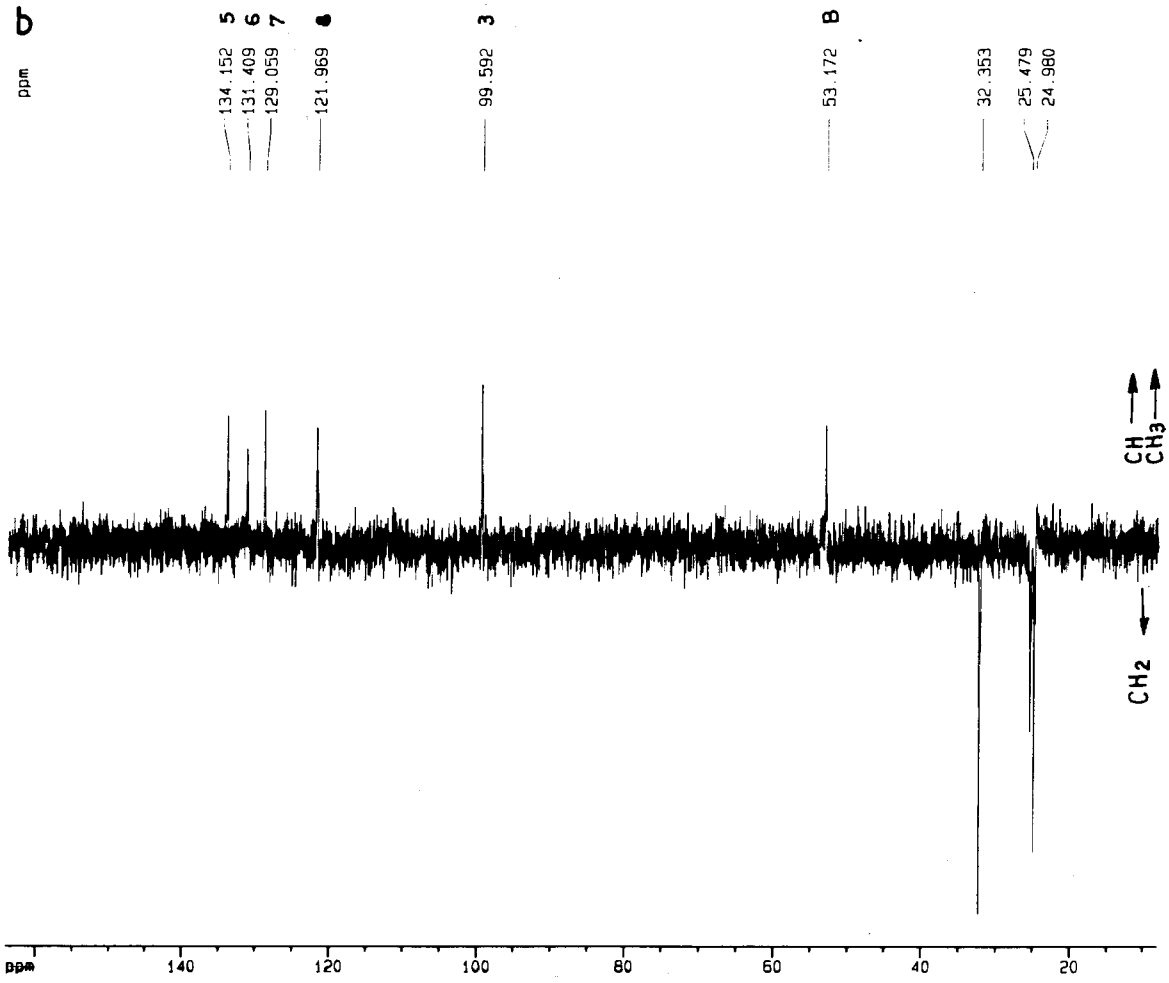

Fig. 8. (*Continued*)

hydrogen atoms of NH_2 groups may be far down field has not been recorded in the spectrum range (0–10 ppm). All these hydrogens attached to alkyl –C appear between 0 and 4 ppm.

Fig. 6(b) shows the NMR spectra of NQS. The peaks observed in the spectrum are above 6 ppm, and can are attributed to the hydrogens attached to aromatic carbons of NQS. The peaks in the integral region 7.981–8.297 ppm and that in 7.414–7.932 ppm range are due to hydrogens in C5 and C8 and C6 and C7 positions. The peak at 6.980 ppm is due to hydrogen in C3 position. The area integration is not however very ideal. However, the splitting pattern confirms above.

Fig. 7(a) shows the NMR spectra of purified adduct. Peaks due to the both CHA (alkyl) and NQS (aryl) protons can be seen in the spectrum. The proton peak attribution for proposed adduct structure given in Table 3. Proposed structure of the adduct is as given below.

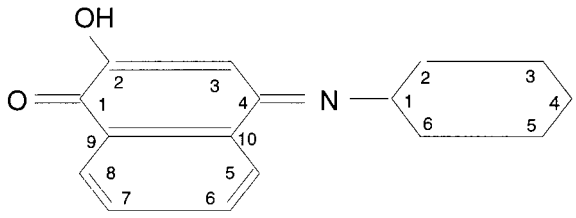

Table 4
Carbon peak positions of adduct ^{13}C-NMR spectrum and their attributes to respective groups

Peak position (ppm)	Attribute	C– bonding
176.07	Quaternary C1 of NQS	>C=O
154.16	Quaternary C2 of NQS	>C–OH
133.97	C5 of NQS	CH
131.74	C6 of NQS	CH
131.21	Quaternary C9 of NQS	>C<
130.81	Quaternary C10 of NQS	>C=
128.85	C7 of NQS	–CH
121.80	C8 of NQS	–CH
119.51	Quaternary C4 of NQS	>C=N
99.38 (A)	C3 of NQS	–CH
52.99 (B)	C1 of CHA	–CH
32.15	C2 and C6 of CHA	$-CH_2$
25.29	C3 and C5 of CHA	$-CH_2$
24.79	C4 of CHA	$-CH_2$

The presence and position (C-2 of NQS) of OH proton at 6.69 ppm was confirmed by taking NMR spectrum of above sample after addition of 2–3 drops of D_2O (Fig. 7(b)). It is seen from the spectrum that due the exchange of OH hydrogen the peak at 6.69 ppm (Fig. 7(a)) has disappeared and a new peak at 6.00 ppm due to H_2O is generated (Fig. 7(b)). Flame photometric test of adduct solution in methanol water mixture for sodium also did not show presence of sodium indicating OH attachment to C-2 of NQS and not ONa as shown earlier in morpholine–NQS adduct case [4].

An integral proton area ratio of 2.37 was observed for peak areas of alkyl (11.90) to aryl (5.01) protons from the adduct NMR spectrum. The good agreement with ratio of alkyl to aryl protons (2.2) for the suggested structure of the adduct indicate that one CHA molecule is attached to one NQS molecule in the adduct.

Fig. 8(a) is the ^{13}C-NMR spectrum of adduct and the peak positions identified in the spectrum are given in Table 4.

Fig. 8(b) is the DEPT-135 (distortionless enhancement by polarisation transfer-flip angle 135°) ^{13}C-NMR spectra. Lines corresponding to =CH– and CH_3 are in the positive *Y* axis while that belonging to $-CH_2-$ appear on negative *Y* axis. Quaternary carbons do not appear in this spectrum.

Further co-relation of the proton NMR and ^{13}C-NMR was done by the taking heteronuclear correlation (HETCOR) NMR spectra (Fig. 9) The peak positions of the ^{13}C and ^{1}H signals are listed in Table 5.

Scan clearly shows six alkyl carbon atoms of CHA in the range of 0–60 ppm (^{13}C-NMR) with their associated protons in the range of 0–4 (^{1}H-NMR) ppm and five aryl carbon atoms of NQS in the range of 80–140 (^{13}C-NMR) ppm with their associated protons in the range of 5–10 (^{1}H-NMR) ppm.

Fig. 10(a) shows the mole ratio variation (Job's method) analysis, in which the concentrations CHA and NQS are varied from 0 to 1 mM in the steps of 0.1 mM in opposite direction to each other and the absorbance at 490 nm is measured against the reagent blank. The observed intercept of the tangents from both sides of bell shaped curve at mole ratio of 1 also, indicates the formation of adduct with 1:1 ratio of NQS and CHA

Results of carbon, hydrogen and nitrogen (CHN) analysis (average of three values) of the adduct is given as below:

Formula of suggested adduct: $C_6H_{17}NO_2$ (mol.wt. = 255.3158 g)

Element	Formula wt. (g)	Formula (%)	Observed (%) (by analysis)
Carbon	192.1760	75.23	76.2 $\pm$ 0.1633
Hydrogen	17.1343	06.71	06.8 $\pm$ 0.2546
Nitrogen	14.0067	05.75	05.5 $\pm$ 0.1074

The above data shows a good agreement between the percentage composition of CHN values obtained from proposed molecular formula of adduct and that of obtained by analysis. This also

confirms the 1:1 presence of CHA and NQS in the adduct.

Fig. 10(b) is UV–vis spectrum of solution of the isolated pure adduct in water methanol mixture. Thus, adduct formation reaction of CHA with NQS in alkaline medium to give reddish orange solution with absorption maxima at 470 nm and the structure of the adduct are established as follows:

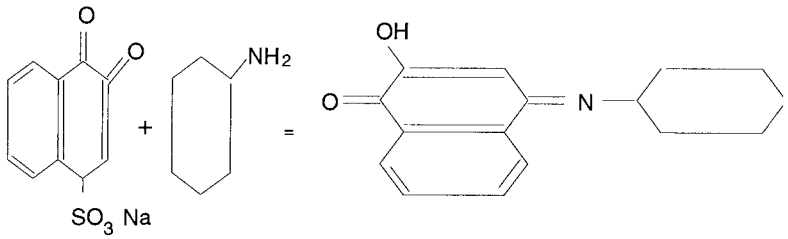

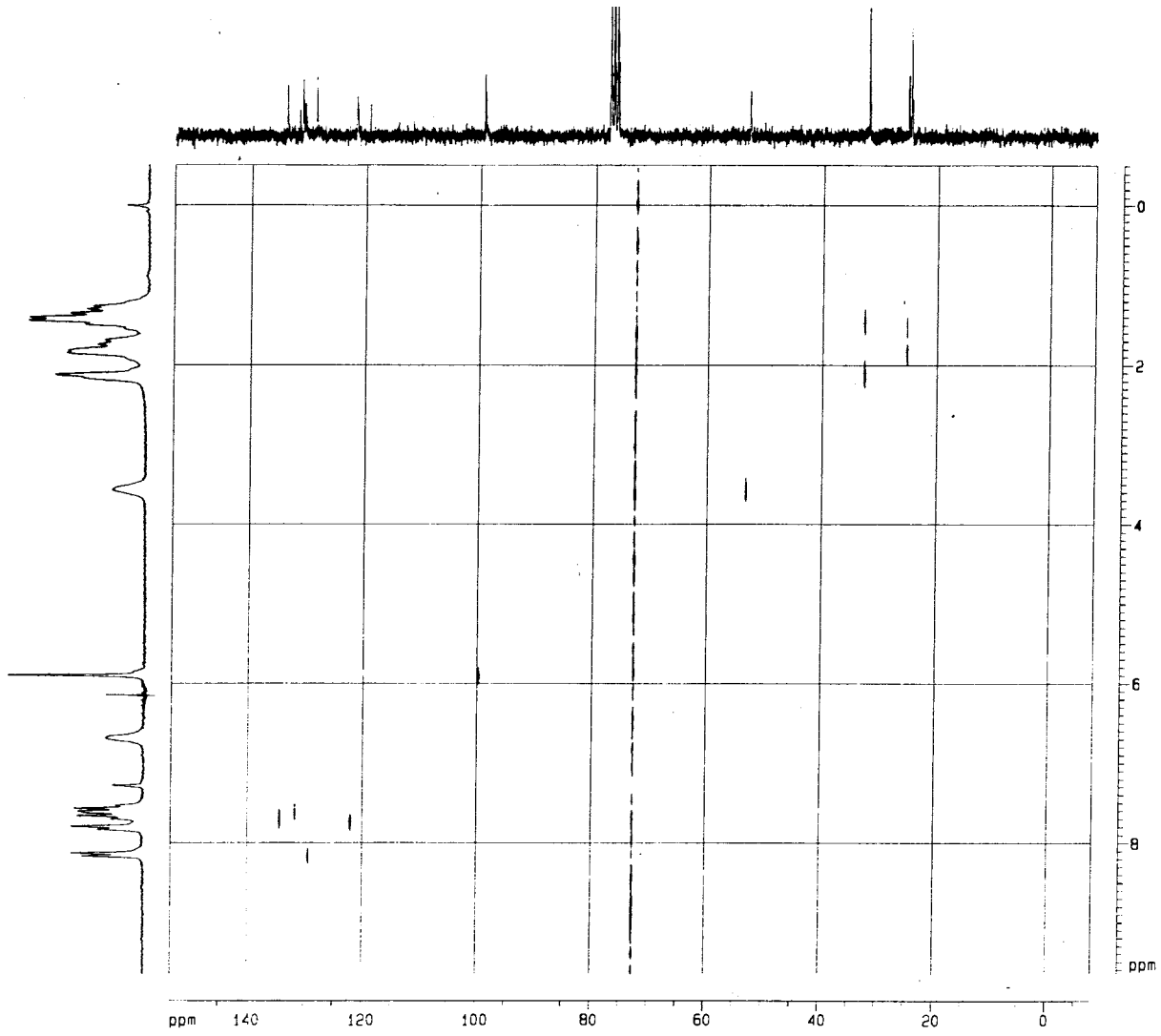

Fig. 9. Heteronuclear (^{1}H and ^{13}C) NMR scan of adduct.

Table 5
Heteronuclear (HETCOR) NMR spectrum (^1H and ^{13}C) of adduct

^1H peaks				^{13}C Peaks	
ppm	Integral area	Expected No. of H	Group	ppm	No. of carbons
Alkyl part of the adduct					
1.49		8	C2, C3, C4, C5 and C6		
1.44		8	C2, C3, C4, C5 and C6		
1.40		8	C2, C3, C4, C5 and C6		
1.35	5.2	8	C2, C3, C4, C5 and C6		
1.30		8	C2, C3, C4, C5 and C6		
1.26		8	C2, C3, C4, C5 and C6	32.15	2C
			C2, C3, C4, C5 and C6	25.29	1C
1.85			C2, C3, C4, C5 and C6	24.79	2C
1.82	3.47	8	C2, C3, C4, C5 and C6		
1.74		8	C2, C3, C4, C5 and C6		
1.69		8	C2, C3, C4, C5 and C6		
2.13	2.2	2	C2, C3, C4, C5 and C6		
3.57	1.01	1	C1	52.99	1C
Aryl part of the adduct					
5.90	0.97		C3	99.39	1C
7.83	3.04	4	C5, C6, C7, C8		
7.79	3.04	4	C5, C6, C7, C8		
7.69	3.04	4	C5, C6, C7, C8	133.97	
7.66	3.04	4	C5, C6, C7, C8	131.74	4C
7.62	3.04	4	C5, C6, C7, C8	128.85	
7.61	3.04	4	C5, C6, C7, C8	121.80	
7.57	3.04	4	C5, C6, C7, C8		
7.53	3.04	4	C5, C6, C7, C8		
8.12	1.0	4	C5, C6, C7, C8		
8.13		4	C5, C6, C7, C8		
6.69	0.92	1	C2	99.39	1C
			C1	176.05	1C
			C9	131.21	1C
			C10	130.81	1C
			C4	119.51	1C

4. Application of the analytical procedure

In power industry CHA is added to the steam generator (SG) water for corrosion prevention. CHA gets volatilised and is carried to the turbine and condenser portion of steam–water circuit. The steam condensation is done by using either river or sea water as a coolant. Generally it is very difficult to have leak tight condensers. There will be always some minor leakage of this cooling water in steam condensate. Moreover, the condensate also contains the corrosion products and other impurities imparted by steam–water circuit surface during its passage. All theses impurities (soluble and insoluble) can get accumulated in SG unless otherwise they are removed before this condensate is fed to SG. This impurity removal is done in a plant using mixed bed ion exchange columns known as condensate polishing plant (CPP). The CHA in condensate gets hydrolysed to CHA^+ and hydroxide ions. When condensate passes through the mixed bed the CHA^+ ion displaces hydrogen of cation resin ion by converting the bed into CHA^+ form ($RH^+ + CHA^+ = RCHA^+ + H^+$). This conversion results in the poor performance of the bed for Na^+ pick up and under certain conditions instead of removing Na^+ ions, the CPP, releases Na^+ ions to the

condensate. The economic criteria demands the operation of CPP even in amminium (CHA/OH) cycle for its optimum use. This can be achieved to by monitoring and controlling the effluent CHA concentrations along with other impurities. In our laboratory a test loop was made operational [5] in which the linear flow rates and impurity ingress conditions similar to the CPP of power plant were simulated. The results of the experimental runs from this loop were used to predict the performance of actual plant CPP.

The method of CHA analysis described in this paper was applied for monitoring the influent and effluent CHA concentrations of the test bed in the above loop. The CHA break through capacity of a cation ion-exchange resin was determined. The effluent impurity variations as a function of influent CHA concentrations were studied and the

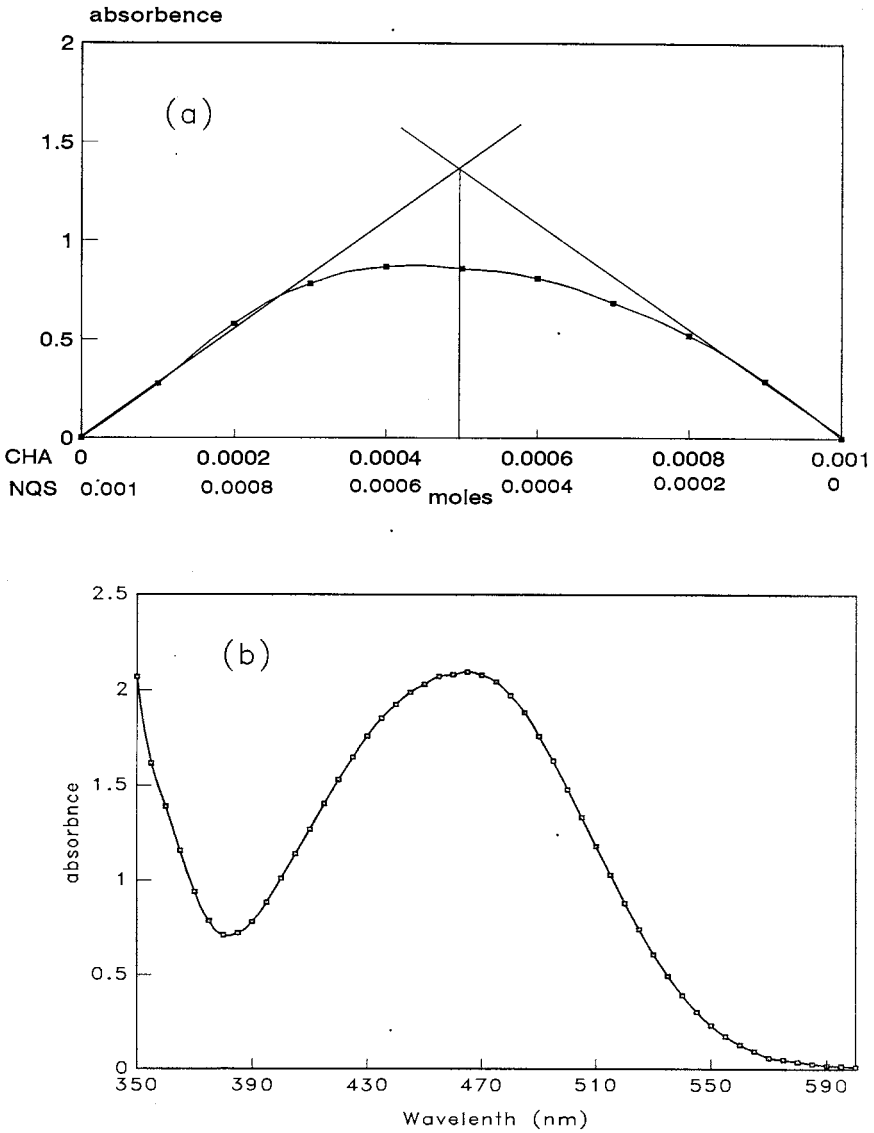

Fig. 10. (a) Mole ratio variation method for determination of CHA:NQS ration in the adduct. (b) UV–vis spectrum of a very dilute solution of isolated and purified adduct in methanol water mixture.

results were used in achieving the optimum performance of a CPP of a nuclear power station. The details regarding the performance of the bed under CHA-OH cycle is outside the scope of the present paper and are under preparation for publication [6]. A typical CHA break through curve is shown in Fig. 4(b). This demonstrates the wide applicability of this easy method to the power industry for analytical estimation of CHA.

5. Conclusions

An easy Spectrophotometric method for estimation of Cyclohexylamine concentration in aqueous medium in the range of 0.3–20 ppm was developed. By analysing IR and NMR spectra, mole ratio variation analysis method and CHN analysis, the structure of adduct formed between CHA and NQS is established. The method was applied to study behavior of ion exchange resin system of CPP in presence of CHA.

Acknowledgements

Authors are thankful to Dr P.N. Moorthy Associate Director, Chemistry Group, BARC for his support and encouragement for this work. Authors are thankful to Dr K.S. Viswanathan, Shri K. Sankaran and Shri K. Sundarajan, IGCAR and Shri. SVS Rao, CWMF for their help in obtaining and interpretation of IR spectra and to Dr V.K. Jain and Dr A.K. Tyagi Chem. Div., BARC and Dr S. Narasimhan and Dr G.N. Krishnakumari, SPIC for their help in the interpretation of NMR spectra and to Dr. V.P. Venugopalan (WSCL) for his help in CHN analysis.

References

[1] K.B. Sung, C.W. Jeong, K.J. Lee, in: Proceedings of JAIF International Conference in Water Chemistry in Nuclear Power Plants, JAIF, 1991, p. 642.
[2] E.T. Swindell, in: Proceedings of JAIF International Conference on Water Chemistry in Nuclear Power Plants, JAIF, 1988, p. 55.
[3] F. Feigl, Spot Tests in Organic Analysis, 6th ed., Elsevier, Amsterdam, 1960, p. 314.
[4] W.H. Stevens, K. Skov, Analyst 90 (1965) 182.
[5] S.V. Narasimhan, K.S. Venkateswralu, K.S.K. Rao, in: Proceedings of JAIF International Conference on Water Chemistry in Nuclear Power Plants, JAIF, 1988, p. 105.
[6] A.G. Kumbhar, S.V. Narasimhan, P.K. Mathur, Chemistry of condensate polishing in combination with AVT, in press.

ELSEVIER

Talanta 47 (1998) 439–445

Talanta

Immobilization of 8-hydroxyquinoline onto silicone tubing for the determination of trace elements in seawater using flow injection ICP-MS

S.N. Willie [a,*], H. Tekgul [b], R.E. Sturgeon [a]

[a] *Insititute for National Measurement Standards, National Research Council of Canada, Ottawa, Ont. K1A OR9, Canada*
[b] *Chemistry Department, Istanbul Technical University, 80626, Maslak, Istanbul, Turkey*

Received 27 January 1998; received in revised form 31 March 1998; accepted 31 March 1998

Abstract

A rapid and simple on-line method is described for the preconcentration of Mn, Co, Ni, Cu, Zn, Cd and Pb from sea water using 8-hydroxyquinoline immobilized onto silicone tubing (Sil-8-HQ) via the Mannich reaction. Recoveries between 35 and 95% and limits of detection in the ppt range were obtained using a 2 m long Sil-8-HQ tube with a sample flow rate of 1.0 ml min^{-1}. A tube could be subjected to sample loading and elution cycles over 200 times. The capacity was 1.5 and 1.3 μg cm^{-2} for Cu and Mn, respectively. Cu, Cd, Co, Pb, Mn, Zn and Ni were determined in coastal and open ocean seawater using flow injection inductively coupled plasma mass spectrometry (FI-ICP-MS). Good agreement with certified values for the certified reference materials NASS-4 and CASS-3 was demonstrated when quantitation was undertaken by the method of additions. © 1998 Elsevier Science B.V. All rights reserved.

Keywords: Flow injection; Preconcentration; ICP-MS; Trace analysis; Immobilized 8-hydroxyquinoline

1. Introduction

The affinity of 8-hydroxyquinoline (oxine) for transition metals while rejecting the alkaline earths has made this chelating agent a popular choice for the preconcentration of trace elements from sea water. As a result, it has been successfully immobilized onto various polymeric and inorganic supports for use in ion-exchange or chromotographic applications [1–9].

The most common supports for immobilization are silica and contolled pore glass. Various immobilization methods have been developed and the properties of the products investigated [1–9]. Silica based supports have been used in many applications [10–16] and possess the advantage of good mechanical strength and resistance to swelling. They are, however, unstable at high pH as hydrolysis of the surface can lead to contamination and loss of capacity due to cleavage of the chelate from the surface [10].

The immobilization of oxine onto polymeric substrates has also been investigated [17–21].

* Corresponding author. Tel.: +1 613 9932359; fax: +1 613 9932451; e-mail: scott.willie@nrc.ca

0039-9140/98/$ - see front matter © 1998 Elsevier Science B.V. All rights reserved.
PII S0039-9140(98)00153-2

These substrates are quite stable over a wide pH range and can be produced with high exchange capacity. Although, it has been reported that overall exchange rates are slow for some materials [20], they have been used successfully in column applications [21,22]. Alternative supports for oxine include cellulose [23] and a polysulfone membrane [24].

The objective of this study was to immobilize oxine onto the inner wall of silicone tubing and evaluate its use as a support for the concentration of trace metals from seawater. This system offers an alternative to packed columns as it is well-suited to low pressure flow injection procedures since back pressure problems can be avoided.

2. Experimental

2.1. Instrumentation

The flow injection inductively coupled plasma mass spectrometry (FI-ICP-MS) system consisted of a Perkin-Elmer Sciex ICP-MS, Model ELAN 6000 (Thornhill, Ont.) and a Perkin-Elmer FIAS 400 FI accessory (Norwalk, CT). The instrument was optimized daily and operated under typical conditions as recommended by the manufacturer. Data acquisition was accomplished using peak hopping with a dwell time of 50 ms and peak height measurement. A Perkin-Elmer 4100ZL atomic absorption spectrometer (Norwalk, CT) equipped with an AS-70 autosampler was used for the analysis of solutions for selected recovery and capacity measurements. The isotopes chosen for monitoring were ^{55}Mn, ^{59}Co, ^{60}Ni, ^{63}Cu, ^{66}Zn, ^{114}Cd and ^{208}Pb.

The immobilization procedures and off-line experiments were carried out using a single four-channel Gilson Minipuls 3 (model M-312, Gilson, Middleton, USA) peristaltic pump.

2.2. Reagents and samples

Deionized, distilled water (DDW) was produced by a commercial mixed-bed ion-exchange system (Barnsted Nanopure, Boston, MA) fed with distilled water. Concentrated HNO_3 and HCl were prepared by sub-boiling distillation in a quartz still using reagent grade feedstocks. An acid mixture of HCl–HNO_3, 10:1% (v/v), was used for the elution of the trace metals. 1 l Of a 1.5 M NH_4Cl buffer solution was prepared by slowly adding 150 ml of NH_4OH (environmental grade, Anachemia, Montreal, Quebec) to 120 ml HCl, both solutions were diluted with DDW prior to mixing. The pH was adjusted to 9 with excess NH_4OH.

Stock solutions (1000 μg ml^{-1}) of Cu, Cd, Co, Pb, Mn, Zn and Ni were prepared by dissolution of the high-purity metals or their salts. Sample preparation was conducted in a Class 100 clean room, although the analysis was performed in a regular laboratory environment. The National Research Council of Canada (NRCC, Ottawa, Ontario) certified reference materials for open ocean and coastal seawater, NASS-4 and CASS-3, respectively, were used to validate the accuracy of the procedure.

Pt or peroxide cured silicone tubing (Cole Parmer, Vernon Hills, IL) having a 0.05 cm i.d. was used as the substrate.

2.3. Immobilization procedure

Oxine immobilized silicone tubing (Si-8-HQ) was synthesized using the Mannich reaction [14,15]. A 10% solution of (3-aminopropyl) triethoxysilane in 50 ml dry toluene was pumped (1 ml min^{-1}) through the silicone tubing for 4 h at 40°C. Following silanization, the tube was washed with dry toluene and dried overnight at 50°C in a vacuum oven. A solution of 50 ml aqueous formaldehyde (40%) containing 1 ml glacial acetic acid was then pumped through the tube for 3 h at room temperature and subsequently rinsed with ethanol. A 2.5% solution of 8-hydroxyquinoline in dry ethanol was adjusted to pH 9 by adding a few drops of tetramethylammonium hydroxide. The functionalization was completed by pumping the oxine solution through the tube for 4 h at 40°C followed by rinsing with ethanol and 1 M HCl.

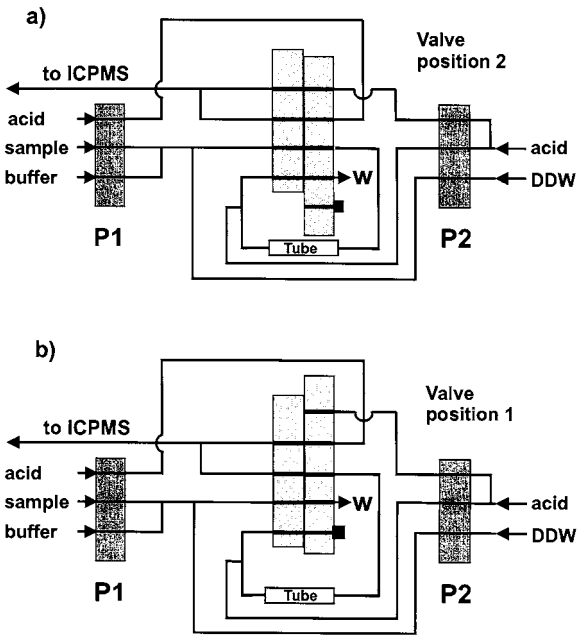

Fig. 1. FI manifold for on-line trace metal separation and preconcentration. P1, pump 1; P2, pump 2; W, waste. (a) Sample loading and wash; (b) elution.

2.4. FI manifold

The FI manifold was constructed from 1/8 in. and 1/16 in. Teflon FEP tubing using low pressure Tefzel flangeless fittings (Upchurch Scientific). Tygon pump tubing was used for all solutions: red-red (1.14 mm i.d.) for the sample and acid lines, blue-yellow (1.52 mm i.d.) for the DDW wash line and orange-green tubing (0.38 mm i.d.) for the buffer.

A schematic diagram of the FI manifold and the sequence of its operation are presented in Fig. 1 and Table 1, respectively. A prefill or priming step flushes the tubing leading from the sample vial with the new sample solution. In step 1, the sample is buffered on-line to pH 8.5 and passed through the Sil-8-HQ tube (3.2 ml min^{-1}). The time selected for this step controls the volume of sample passed through the column. Following sample loading the tube is washed with DDW to remove any salt residue and the sample is eluted into the plasma in step 3. In step 4 the valve is returned to the wash position to return the tube to a neutral pH in preparation for loading the next sample.

The FI manifold was configured such that the acid solution was pumped to the plasma during all steps.

2.5. Recovery and lifetime experiments

Recovery and capacity experiments were performed off-line. Aliquots of sea water were adjusted to pH 8.5 and a 1 ml sample spiked with 0.5 ppb of all analytes of interest was passed through the Si-8-HQ tubing at a nominal flow rate of 0.5 ml min^{-1}. After washing the tubing with DDW the trace metals were eluted with 1 ml 10% HCl (v/w) and 1% HNO_3 (v/w).

Capacity measurements were performed after saturating the surface sites by passing a 10 ppm solution of Cu and Mn (separately) through the tubing, washing with DDW, eluting the sequestered analyte and measuring the total absolute amount recovered per unit surface area (cm^2).

The lifetime of a 2 m tube was established by monitoring analyte recovery during repetitive cycles through the FI program using a solution of seawater spiked with 0.5 ppb of the trace elements. Eluted samples were analysed at 20 run intervals.

Table 1
Flow injection program

Step	Time (s)	Pump 1 (rpm)	Pump 2 (rpm)	Valve position	Description
P	30	50	0	1	Prefill
1	60	50	0	2	Load
2	90	0	50	2	Wash
3	90	0	50	1	Elute
4	40	0	50	2	Wash

Table 2
Recovery, limits of detection and blanks

Element	Recovery* (%)	Limit of detection** (ng ml^{-1})	Blank (ng ml^{-1})
Mn	73 ± 4	0.028	0.035
Co	35 ± 4	0.003	0.009
Ni	95 ± 6	0.054	0.162
Cu	98 ± 5	0.010	0.034
Zn	77 ± 4	0.022	0.165
Cd	90 ± 6	0.004	0.006
Pb	82 ± 2	0.003	0.011

* Mean $\pm$ S.D. ($n = 4$).
** For processing a 3.2 ml sample, defined $3\sigma_{\text{blank}}$.

3. Results and discussion

Common methods used to immobilize oxine are variations of the Hill procedure [1] where the first step in the synthesis involves the immobilization of an aliphatic aminosilane onto the surface of a silica gel substrate. Subsequent reactions of the aminopropyl silica gel are benzoylation, reduction and final coupling of the oxine by diazotisation. Silicone tubing would, however, be destroyed using this method as the benzoylation step consists of prolonged heating of the substrate in chloroform. By comparison, the Mannich reaction involves very gentle heating using an IR heat lamp and the use of organic solvents is limited to toluene in the silanization step. Although toluene causes some swelling of the silicone tubing this was not found to be detrimental to the final product. The Si-8-HQ is yellow in appearance and less elastic than unreacted silicone but sufficiently flexible to be wound in tight spirals. Silicone tubing of 0.05 cm i.d. was used as it provided large surface-to-volume ratio and minimal back pressure. The calculated total exchange capacity of the oxine immobilized silicone tubing was 1.5 and 1.3 μg cm^{-2} of Cu and Mn, respectively. No difference in performance or analytical characteristics were obtained between Pt and peroxide cured formulations of silicone tubes.

3.1. Recovery efficiency

The recovery of analyte spikes added to sea water samples at pH 8.2 is shown in Table 2 using a 2 m length of tube at a flow rate of 1.0 ml min^{-1}. Recovery experiments performed at pH 5.3 using an ammonia–ammonium acetate buffer produced poor results with no recovery for Mn and Pb and less than 10% recovery for Cd and Ni. At pH 1.6, the pH used to stabilize the trace metals in the seawater samples, there was $< 1\%$ recovery for all elements studied except Cu where a $47 \pm 6\%$ recovery was obtained. The limited availability of metal free buffers prevents a more comprehensive pH evaluation between pH 1.6 and 9. Metal uptake and release on unreacted silicone tubing was $< 1\%$ for all elements studied at pH 8.3. Due to incomplete recovery for all metals of interest, the method of standard additions was required for calibration.

The effect of 8-Si-HQ tube length on the uptake and release of trace metals from sea water was studied. Two elements are selected for discussion purposes as they were found to be representative of the two extremes in performance, i.e. Pb is relatively easily collected whereas Mn is most weakly bound to oxine. At a sample flow rate of 3 ml min^{-1} no difference in Pb recovery was observed for tube lengths between 0.5 and 2.0 m. For Mn, the recovery obtained using a 0.5 m tube was increased by 30% with a 2 m long tube. A tube 2 m in length was used for all subsequent work, longer tubes were not examined.

The sample flow rate was varied between 0.5 and 5 ml min^{-1} to determine the effect on recovery. Between 1 and 4 ml min^{-1} there was no effect on Ni, Cu, Co, Pb and Zn results. Cd and Mn showed a decrease between 1 and 2 ml min^{-1}

Table 3
Analytical Results for NASS-4 and CASS-3

Element	NASS-4 (μg l^{-1})		CASS-3 (μg l^{-1})	
	Determined*	Certified**	Determined*	Certified**
^{55}Mn	0.436 ± 0.037	0.380 ± 0.023	2.70 ± 0.06	2.51 ± 0.36
^{59}Co	0.019 ± 0.005	0.009 ± 0.001	0.069 ± 0.011	0.041 ± 0.009
	0.011 ± 0.004***		0.050 ± 0.006***	
^{60}Ni	0.256 ± 0.054	0.228 ± 0.009	0.430 ± 0.060	0.386 ± 0.062
^{63}Cu	0.270 ± 0.029	0.228 ± 0.011	0.582 ± 0.061	0.517 ± 0.062
^{66}Zn	0.134 ± 0.034	0.115 ± 0.018	1.43 ± 0.09	1.24 ± 0.25
^{114}Cd	0.017 ± 0.006	0.016 ± 0.003	0.032 ± 0.007	0.030 ± 0.005
^{208}Pb	0.019 ± 0.002	0.013 ± 0.005	0.012 ± 0.007	0.012 ± 0.004

* Mean $\pm$ S.D. ($n = 4$).
** Mean and 95% confidence limits.
*** Acetic acid wash.

but constant recovery between 2 and 4 ml min^{-1}. At flow rates less than 1 ml min^{-1} recoveries were slightly improved but 3 ml min^{-1} was chosen as a compromise between adequate recovery and rapid sample throughput. A study of the lifetime of the Sil-8-HQ tube was accomplished by repeated loading, washing and elution of the Sil-8-HQ tube. After 200 cycles the signal for Mn Cu, Cd and Pb had decreased by 15%. The signals for Co, Ni and Zn decreased slowly to 50% of the original signal. The overall results indicate the tube continues to be useful beyond 200 cycles.

Lower flow rates and a longer Sil-8-HQ tube result in increased recovery; however, this was not required as a sufficient signal could be obtained using a 60 s load step. A 90 s wash time was necessary to remove residual matrix components of the sample and to obtain similar $^{64/66}Zn$ and $^{63/65}Cu$ ratios for seawater and aqueous standards. The high matrix retention is likely to occur as a result of unreacted amino groups binding the Na, Mg and Ca. Although a 90 s DDW wash was sufficient for the analysis of most trace metals, determination of Co at the low concentrations present in these seawater samples was hampered by an isobaric interference arising from $^{24}Mg^{35}Cl^{+}$, due to the retention of Mg which overlaps with ^{59}Co. Replacing the DDW wash in Step 2 (Table 1) with 1% acetic acid (approximately pH 2.8) decreased the amount of Mg in the acid eluate and permitted the accurate determination of Co.

The precision using peak height measurement was found to be between 3 and 5% R.S.D. for the elements of interest: this was superior to peak area measurement where precision $> 5\%$ was generally obtained. This arose as a result of the nature of the baseline correction method utilized with the commercial software program. Since baseline correction is performed using the first ten points, small deviations over the 60 s elution period resulted in larger errors using peak area than peak height.

3.2. Analytical blanks and detection limits

Analytical blanks and detection limits (3σ of the blank) are presented in Table 2. The blank values (primarily for Ni and Zn) could be lowered by purifying the buffer solution; however, this was neither attempted nor required for these studies. The good precision attainable with FI permits the analysis of seawater at concentration levels only an order of magnitude above the detection limits.

3.3. Analysis of sea water

The accuracy of this procedure was evaluated by the analysis of two seawater reference materials. Analytical results are given in Table 3 for NASS-4 and CASS-3. For most elements, the

results are in good agreement with the certified values. Two results for Co, using either a DDW or acetic acid wash, are reported. Those using an acetic acid wash for elements other than Co (not shown) were with the exception of Zn (high blank) and Mn (no recovery), also acceptable. The results are reported with a combined Type A uncertainty from the sample, blank and calibration [25].

Fig. 2 shows a multielement scan obtained for CASS-3. The Mn signal is attenuated by a factor of 10 and the scans are separated into two figures for clarity. Tailing of the Cu peak requires an elution time of 90 s to return the signal to the original baseline.

Attempts to differentiate between the surface of a treated and untreated (8-Si-HQ) tube using either microscopy-Fourier transform infrared spectroscopy (FTIR), photoacoustic-FTIR or X-ray photoelectron spectroscopy (XPS) were unsuccessful. Although, a visual difference in the surfaces can be observed, the concentration of the microlayer of hydroxyquinoline on the surface is below the limit of detection of these surface techniques.

The methodology and results presented here demonstrate the potential of using a chelating tube for the sequestration of trace elements. This approach provides for the processing of 10 samples h^{-1} with multielement detection. Future developments in low pressure FI analysis using this novel approach may occur through use of alternative chelating agents and improvements in coupling techniques.

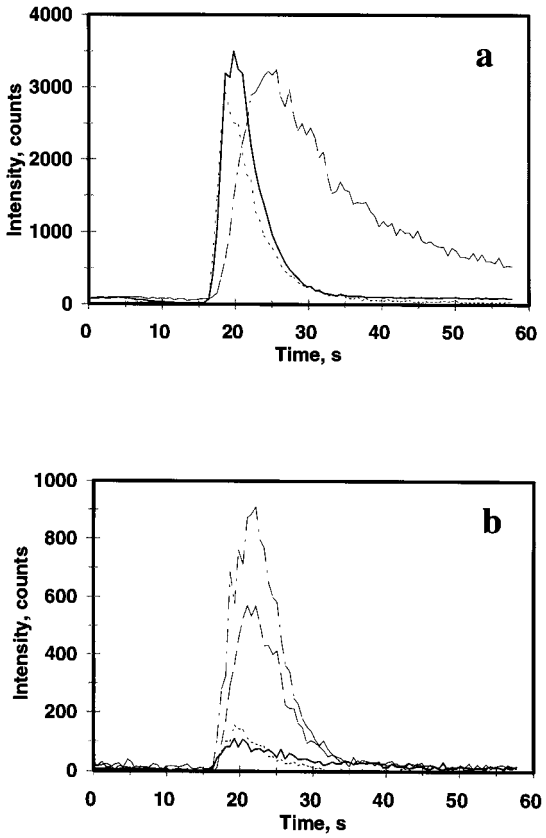

Fig. 2. Multielement scans for the elution of CASS-3. (a): (——) Mn (10 × attenuation); (···) Zn; (– • –) Cu; (b): (– • -) Co; (- - -) Ni; (···) Pb; (– • –) Cd.

Acknowledgements

The authors would like to thank Gerald Pleizier and Anna Delgado for surface analysis of the Sil-8-HQ tube and financial support for HT from The Scientific and Technical Research Council of Turkey.

References

[1] J.M. Hill, J. Chromotogr. 76 (1973) 455–458.
[2] M.A. Marshall, H.A. Mottola, Anal. Chem. 55 (1983) 2089–2093.
[3] C. Fulcher, M.A. Crowell, R. Boyliss, K.B. Holland, J.R. Jezorek, Anal. Chim. Acta 129 (1981) 29–47.
[4] M.A. Marshall, H.A. Mottola, Anal. Chim. Acta 129 (1984) 369–373.
[5] M.A. Marshall, H.A. Mottola, Anal. Chem. 57 (1985) 729–733.
[6] K.F. Sugawara, H.H. Weetall, G.D. Schucker, Anal. Chem. 46 (1974) 489–492.
[7] J.R. Jezorek, H. Freiser, Anal. Chem. 51 (1979) 366–373.
[8] C.R. Lan, M.H. Yang, Anal. Chim. Acta 287 (1994) 101–109.
[9] U. Pyell, G. Stork, Fresenius' J. Anal. Chem. 324 (1992) 281–286.
[10] R.E. Sturgeon, S.S. Berman, S.N. Willie, J.A.H. Desaulniers, Anal. Chem. 53 (1981) 2337–2340.
[11] C.R. Lan, M.H. Yang, Anal. Chim. Acta 287 (1994) 111–117.
[12] J.W. McLaren, J.W.H. Lam, S.S. Berman, K. Akatsuka, M.A. Azeredo, J. Anal. At. Spectrom. 8 (1993) 279–286.

[13] G.M. Greenway, S.M. Nelms, I. Skhosana, S.J.L. Dolman, Spectrochim Acta B 51 (1996) 1909–1915.
[14] S.M. Nelms, G.M. Greenway, R.C. Hutton, J. Anal. At. Spectrom. 10 (1995) 929–933.
[15] D. Yuan, I.L. Shuttler, Anal. Chim. Acta 316 (1995) 313–322.
[16] L.C. Azeredo, R.E. Sturgeon, A.J. Curtius, Spectrochim. Acta B 45 (1993) 91–98.
[17] W.M. Landing, C. Haroldson, N. Paxéus, Anal. Chem. 58 (1986) 3031–3035.
[18] S.N. Willie, R.E. Sturgeon, S.S. Berman, Anal. Chim. Acta 149 (1983) 66–69.
[19] F. Vernon, H. Eccles, Anal. Chim. Acta 63 (1973) 403–414.
[20] J.R. Parrish, Anal.Chem. 54 (1982) 1890–1892.
[21] A. Seubert, G. Petzold, J.W. McLaren, J. Anal. At. Spectrom. 10 (1995) 371–379.
[22] E. Beinrohr, M. Cakrt, M. Rapta, P. Tarapci, Fresenius' J. Anal. Chem. 335 (1989) 1005–1007.
[23] K.-L. Yang, S.-J. Jiang, T.-J. Hwang, J. Anal. At. Spectrom. 111 (1996) 139–143.
[24] M. Kan, M.D. Guiver, G.P. Robertson, S.N. Willie, R.E. Sturgeon, React. Func. Polym. 31 (1996) 207–218.
[25] Guide to the Expression of Uncertainty in Measurement, International Organization for Standardization, Geneva, Switzerland, 1993.

ELSEVIER

Talanta 47 (1998) 447–454

Talanta

Determination of total polar parts with new methods for the quality survey of frying fats and oils

Martina Hein, Hariette Henning, Heinz-Dieter Isengard *

Institute of Food Technology, University of Hohenheim, Garbenstrasse 25, 70593 Stuttgart, Germany

Received 11 August 1997; received in revised form 30 March 1998; accepted 2 April 1998

Abstract

During the frying process the fat undergoes several chemical and physical changes caused by heat, water and atmospheric oxygen. With prolonged heating time the accumulation of deterioration products leads to organoleptic failures and a decrease of the nutritive value. For the quality control of frying fats or oils the determination of total polar parts by preparative column chromatography is an approved standard method. Many attempts were undertaken to replace this time and chemical consuming method. To substitute for the determination of polar components by column chromatography the measurement of dielectric properties with a food oil sensor, nuclear magnetic resonance spectroscopy (NMR) and near infrared spectroscopy (NIR) proved to be suitable. © 1998 Elsevier Science B.V. All rights reserved.

Keywords: Deep fat frying; Heat abuse; Polar parts; Analytical techniques

1. Introduction

Within the past thirty years our habit of food consumption changed significantly. The steadily growing consciousness of scientifically balanced nourishment and the need for a faster way of food preparation led to a change in food processing techniques in almost all areas of food production. Owing to this development the production of fried foodstuffs has steadily increased. Today deep fat frying is a very important method of cooking in the food service industry. It is estimated, that nearly one-half of all lunch and dinner food orders in commercial restaurants and canteens include one or more deep fried items [1]. During the frying process the fat or oil undergoes several chemical and physical changes. As a result of oxidation, polymerisation, hydrolysis, pyrolysis, isomerisation and cyclisation a great number of reaction products are formed. They accumulate with prolonged heating time and lead to organoleptic failures and a decrease of the nutritive value, caused by the decomposition of essential fatty acids. Nutritional and physiological effects were investigated and reported in several publications [2–5]. Most of them indicated that

* Corresponding author. Tel.: +49 711 3974670; fax: +49 711 3974674; e-mail: isengard@uni-hohenheim.de

0039-9140/98/$ - see front matter © 1998 Elsevier Science B.V. All rights reserved.
PII S0039-9140(98)00148-9

only strongly overheated frying fats or oils may cause harmful effects. Those used in normal frying operations do not produce significant changes in animal consumption or animal health.

For the survey of frying fat or oil quality the determination of total polar components by preparative column chromatography, developed by Guhr and Waibel [6], is an approved standard method of IUPAC and AOAC. With prolonged heating time the amount of polar substances rises steadily. It has been suggested that the determination of total polar parts is the most reliable method for the measurement of fat deterioration during frying [7]. The limit of the beginning heat abuse is about 24%, whereas the absolute limit is 27% polar parts. As the preparative column chromatography method is very time and chemical consuming, a lot of attempts have been undertaken to find simple and rapid analyses for the determination of polar parts. The survey of several frying processes under different conditions proved, that a determination of polar components by near infrared (NIR) spectroscopy is possible. There also exists a good correlation between the results obtained by the determination of dielectric properties with a food oil sensor and, respectively, the determination of the relaxation time by nuclear magnetic resonance (NMR) spectroscopy and the results obtained by preparative column chromatography. In comparison to the customary preparative column chromatography technique these three methods are faster, easier to carry out and need no chemicals. Therefore NIR spectroscopy, food oil sensor measurement and NMR spectroscopy can be useful tools to substitute preparative column chromatography and to investigate heat abuse of frying fats and oils in routine analysis in fat industry.

2. Experimental data

2.1. Material

For the following analyses soya bean oil, peanut oil and palm oil were obtained from the manufacturer. As foods peanuts, snack products, cuttlefish and French fries were used for deep fat frying.

2.2. Heating experiments

The frying oils were heated at 190°C for 60 h (21 h with foodstuff) without interruption in a commercial deep fat fryer without any foodstuff. Every 5 h (every 1.5 h if food was fried) a 50 g sample was taken and stored at a temperature of -12°C to avoid further chemical changes.

2.3. Methods

2.3.1. Total polar parts by column chromatography

The determination of total polar parts by column chromatography was carried out according to the 'DGF-Einheitsmethoden' [8]. Analyses were performed in a glass column packed with silica gel. Using a mixture of light petroleum ether and diethyl ether (87:13) the polar and the nonpolar parts of the frying fats and oils can be separated. Unchanged nonpolar triglycerides are eluted by this mobile phase, while polar substances are adsorbed on the silica gel. For the elution of the polar compounds pure diethyl ether has to be used. The amount of each fraction has to be determined by weight after evaporating the solvent.

2.3.2. Food oil sensor measurement

Dielectric measurements were undertaken with a food oil sensor from Northern Instruments (NI-21 A, $3\times$ sensitivity) at a temperature of 63°C with a frequency of 5 MHz. Calibration was carried out either with fresh corresponding oil or with a calibration oil obtained from the manufacturer.

2.3.3. NIR spectroscopy

The instrument used for this analysis was an FT-NIR universal spectrometer (NIRVIS) from Bühler. Spectra of the frying oils were taken from 4000 to 10000 cm^{-1} using a cuvette of optical glass (5 mm).

All samples were preheated at a temperature of 40°C. For the calibration about 50 samples from each frying oil—palm, peanut and soya bean oil—were used. These calibration samples were previously analysed using preparative column

chromatography for the determination of total polar parts.

2.3.4. NMR spectroscopy

Measurements were conducted with an instrument from Bruker (Minispec 120, Table 1) The analysis were performed with 18 mm sample tubes. The samples were filled in these tubes to a height of 1.5 cm. All tubes were tempered at a temperature of exactly 40°C to avoid the influence of temperature on the relaxation time of the samples.

3. Results

Sensory evaluation is still the most reliable method for the quality survey of used frying fats and oils. If chemical analysis can be carried out, judgement is commonly made on the basis of acid number, viscosity, content of carbonyls or conjugated double bounds. None of these methods proved to be completely satisfying—especially if different foods are prepared in the same frying operation—but some can be used to characterize the quality of frying fats or oils roughly. Observing the regulations used for frying fats and oils in different countries [9] it is obvious that in almost all countries the determination of polar parts by preparative column chromatography is used for the quality control of fats and oils. It has been suggested, that the determination of total polar components is the most reliable method for the measurement of fat deterioration during frying [10]. In practise this method proved to be very suitable, although it does not correlate exactly with sensory judgement [11]. The amount of the polar fraction in percent of mass is a criterion for the quality of used frying fats and oils. The limit of acceptance differs slightly from country to country. In most of the countries the limit of heat abuse is 25% polar parts.

As the preparative column chromatography method is very time and chemical consuming, a number of attempts has been undertaken to find simpler and more rapid techniques for the determination of polar parts. The survey of several frying processes under different conditions—different frying oils, different character and amount of foodstuffs—proved that a determination of the polar components by the use of a food oil sensor and by near infrared spectroscopy and by nuclear magnetic resonance is possible. In comparison to the customary preparative column chromatography all the methods presented are easier to carry out, more reproducible, need less time and avoid the use and the disposal of chemicals.

3.1. Food oil sensor

A suitable method to substitute for the customary preparative column chromatography is the determination of the polar parts with a so called food oil sensor [12,13]. When frying fats or oils decompose thermally and by oxidation processes, their dielectric constant increases. The dielectric constant of a substance is its ability to transfer electrical energy as compared with a vacuum. As the number of polar molecules increases, the dielectric constant of the oil or fat increases. At the same time the frying quality of the oil or fat decreases proportionally. In a food oil sensor the frying fat or oil is used as dielectric substance in a patented capacitor sensor. The patented sensor

Table 1
Parameters of the Minispec measurement

Parameter	Value	Parameter	Value
Instrument	Minispec 120	Gain (dB)	89
Recycle delay (s)	2	Scans	15
Analogue bandwidth	Narrow	Digital bandwidth (kHz)	100
Offset compensation	Off	Detection mode	Real
Digital resolution	High	Pulse sequence	CPMG
Temperature (°C)	40		

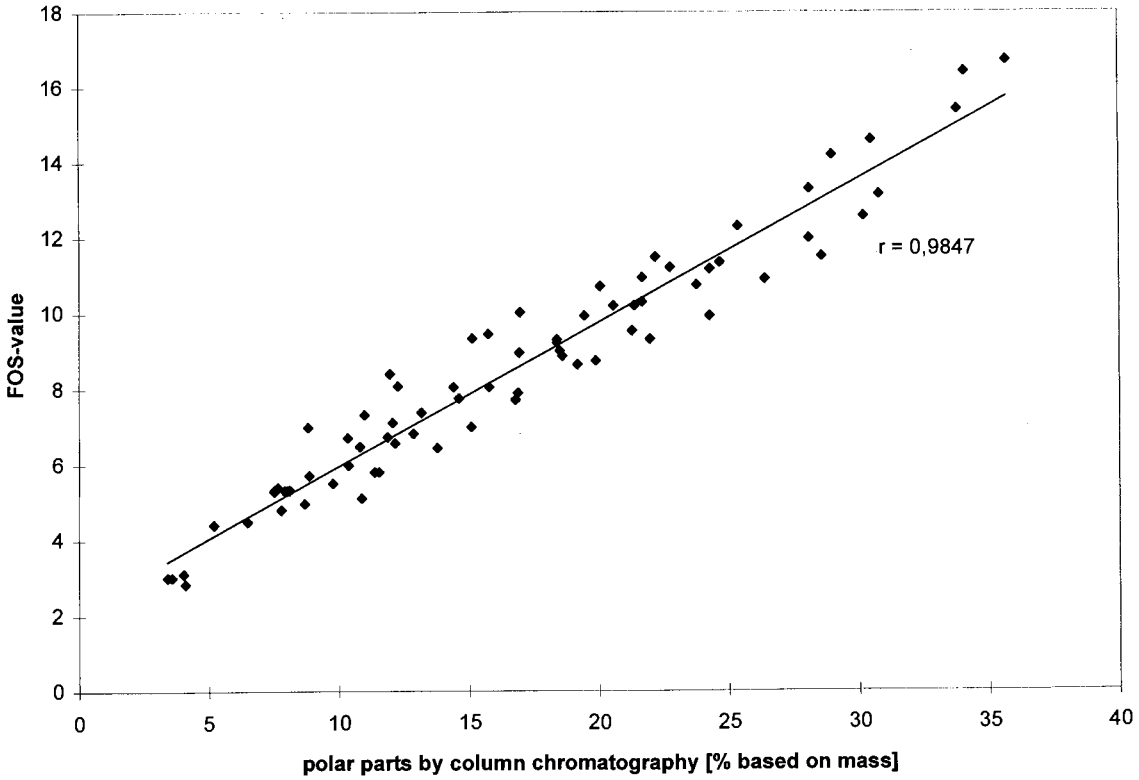

Fig. 1. Correlation between the polar parts determined by preparative column chromatography and food oil sensor values for different oils which were heated with different foodstuffs (all results are average values of triple analyses).

pattern is designed to be extremely sensitive to changes in the permittivity of the capacitor dielectric caused by the degradation of the frying oil or fat. As the changes of dielectric properties of fats and oils are due to the increasing amount of polar molecules it is possible to make a correlation between the amount of polar parts determined by preparative column chromatography and the food oil sensor value.

There are two ways to calibrate the food oil sensor. If only one single sort of frying fat or oil has to be analysed calibration is carried out with the corresponding fresh fat or oil. For palm oil, peanut oil and soya bean oil correlation coefficients for the calibration between food oil sensor value and polar parts determined by preparative column chromatography differ from 0.992 to 0.994 if the calibration is carried out for every single type of oil. If unknown frying fats or oils have to be analysed or if different fats and oils must be analysed together the food oil sensor has to be calibrated with a so-called zero-oil. In this case the correlation is not as good as if the calibration is carried out with fresh oil but still is sufficient (Fig. 1). With the regression line obtained it is possible to screen the amount of polar parts in percent of mass by measuring the food oil sensor value.

In a study with three different laboratories, each consisting of four laboratory assistants, the repeatability r of the food oil sensor measurement was 0.80 and the reproducibility R was 2.21. In comparison, the repeatability of the preparative column chromatography was 2.33 and the reproducibility was 3.79.

3.2. NIR spectroscopy

Another easy and fast way to judge frying fat or oil quality is the use of near infrared spec-

troscopy. In 1996 a quantitative Fourier transformed infrared-analysis (FTIR) was published for the determination of anisidine values and aldehydes in thermally stressed oils [14]. In this study a Fourier transformed near-infrared (FTNIR) transmission-based spectroscopic method for the measurement of polar parts in stressed frying fats and oils was investigated. This method eliminates the use and disposal of solvents and reduces the analysis time. The spectra of several palm oil samples which were heated for different times at 190°C and therefore contain different amounts of polar parts were registered. The spectra (average spectra of 10 measurements) vary noticeably (Fig. 2), especially at the wavenumber range specific for hydroxyl or aldehyde groups (Fig. 3). These changes in the spectra are due to the formation of aldehydes, ketones and hydroxy peroxides during the process of deep fat frying. The spectra were normalised and then the first derivative was formed. The calibration between spectral information and amount of polar parts based on mass determined by preparative column chromatography was developed using the bcap 6.0-software from Bühler. With partial least squares calibration (PLS) [15] as the chemometric method it was possible to obtain a very good correlation for each oil with correlation coefficients from 0.990 to 0.998. To verify the calibration, frying oils heated with different foodstuffs were analysed by preparative column chromatography and by NIR spectroscopy. The results obtained with both methods do not differ significantly (Fig. 4). The correlation between the amount of polar parts determined by column chromatography and NIR spectroscopy was close to 1. It could, thus, be shown that it is possible to determine the amount of polar compounds by NIR spectroscopy instead of preparative column chromatography, even independently of the foodstuff fried in it, if a good calibration

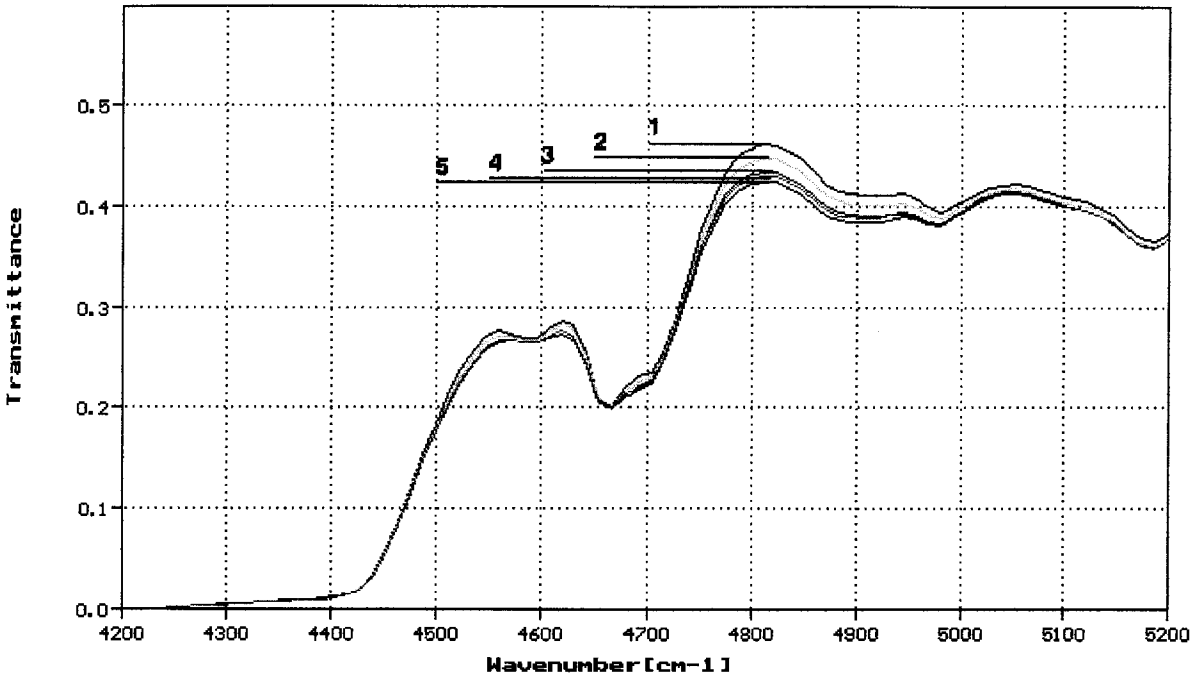

Fig. 2. NIR spectra (wavenumber 4200–5200 cm^{-1}) of heated palm oils: (1) palm oil containing 9% polar parts; (2) palm oil containing 20% polar parts; (3) palm oil containing 29% polar parts; (4) palm oil containing 35% polar parts; (5) palm oil containing 42% polar parts.

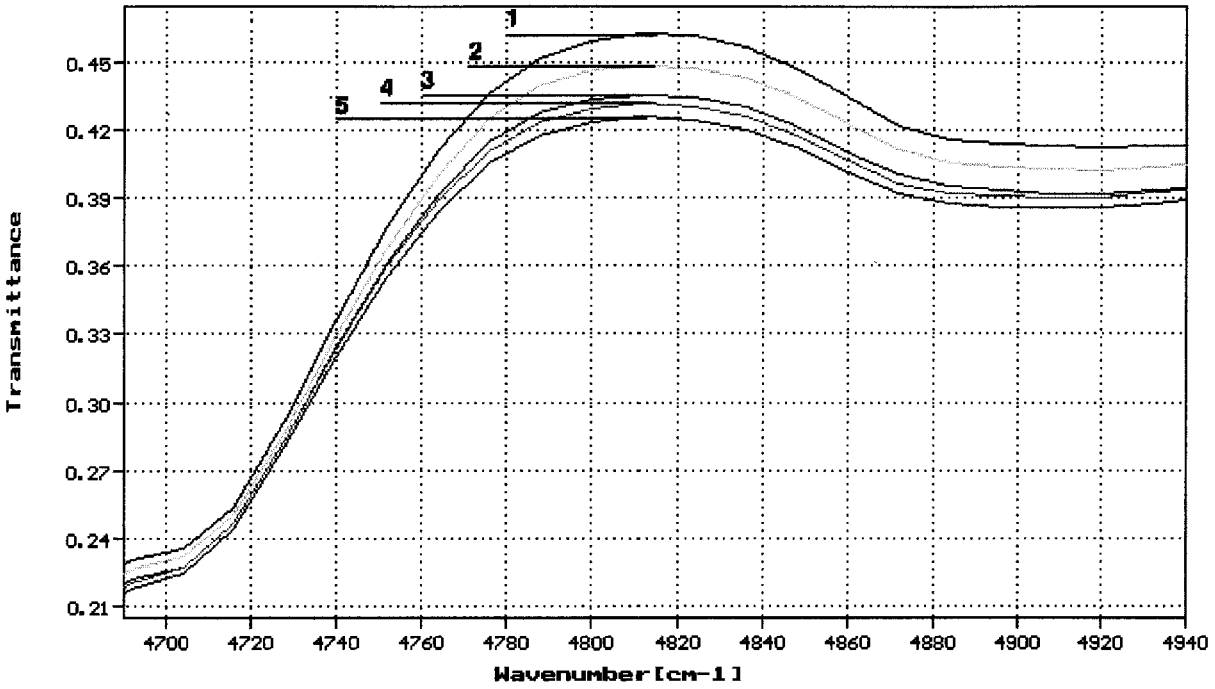

Fig. 3. NIR spectra (wavenumber 4700–4940 cm^{-1}) of heated palm oils: (1) palm oil containing 9% polar parts; (2) palm oil containing 20% polar parts; (3) palm oil containing 29% polar parts; (4) palm oil containing 35% polar parts; (5) palm oil containing 42% polar parts.

has been established. Repeatability of the NIR spectroscopy measurement was 1.01.

3.3. NMR spectroscopy

NMR spectroscopy is a fast, nondestructive way to screen fat and oil quality without using chemicals. The amount of polar parts can be measured because the relaxation time of an oil or fat in NMR spectroscopy will be influenced by the content of the polar parts. The higher the amount of polar parts, the shorter is the relaxation time. Therefore a correlation can be found between the relaxation time and the amount of polar parts determined by preparative column chromatography. For the analysis the frying fat or oil is simply filled into a sample tube. After a constant temperature of 40°C is reached the relaxation time of the sample can be measured in 1 min. Different frying oils were heated with different foodstuffs and analysed by both methods. The correlation between the amount of polar parts determined by preparative column chromatography and the relaxation time for palm oils which were heated with different foods is shown in Fig. 5. The correlation coefficient obtained for one single oil is good, it differs from 0.931 to 0.944. In case where the analysis is carried out with several different frying fats or oils the correlation coefficient is only moderate (correlation coefficient = 0.885, repeatability = 1.36). NMR spectroscopy can nevertheless be used as a fast screening method for the quality control of used frying fats and oils.

4. Discussion

In comparison to the customary preparative column chromatography the three methods pro-

posed need less analysis time and eliminate the use and the disposal of chemicals. The most economic method proposed for the determination of polar compounds is the application of a food oil sensor because the instrument is quite cheap. It can be used in smaller laboratories or even in canteens or restaurants. The equipment for NIR and NMR spectroscopy is more expensive.

The determination of polar parts by food oil sensor, NIR or NMR spectroscopy takes only about 2 min, whereas preparative column chromatography takes 7–8 h.

Sometimes the origin of a frying fat or oil is unknown. Therefore the possibility of using one single calibration for different frying fats and oils is an important criterion for the determination of the polar parts. By using a food oil sensor it is possible to determine the amount of polar components with one correlation line regardless of the sort of frying oil or fat. When applying NIR spectroscopy, it is necessary to create separate calibrations for every frying fat or oil. When using NMR spectroscopy it is possible to use the same calibration line for different oils and fats but in this case the correlation coefficient is not as good. Therefore it is advisable to use different calibration lines for different frying fats and oils.

For the substitution of preparative column chromatography the most important criterion, of course, is the correlation between the analytic results and the amount of the polar parts determined by preparative column chromatography. The correlation between the amount of polar parts determined by column chromatography and by NIR was nearly 1. NIR is therefore a good alternative to preparative column chromatography. Using a food oil sensor and NMR a rough determination of the polar parts is possible. Both methods can be used as screening methods for the polar parts.

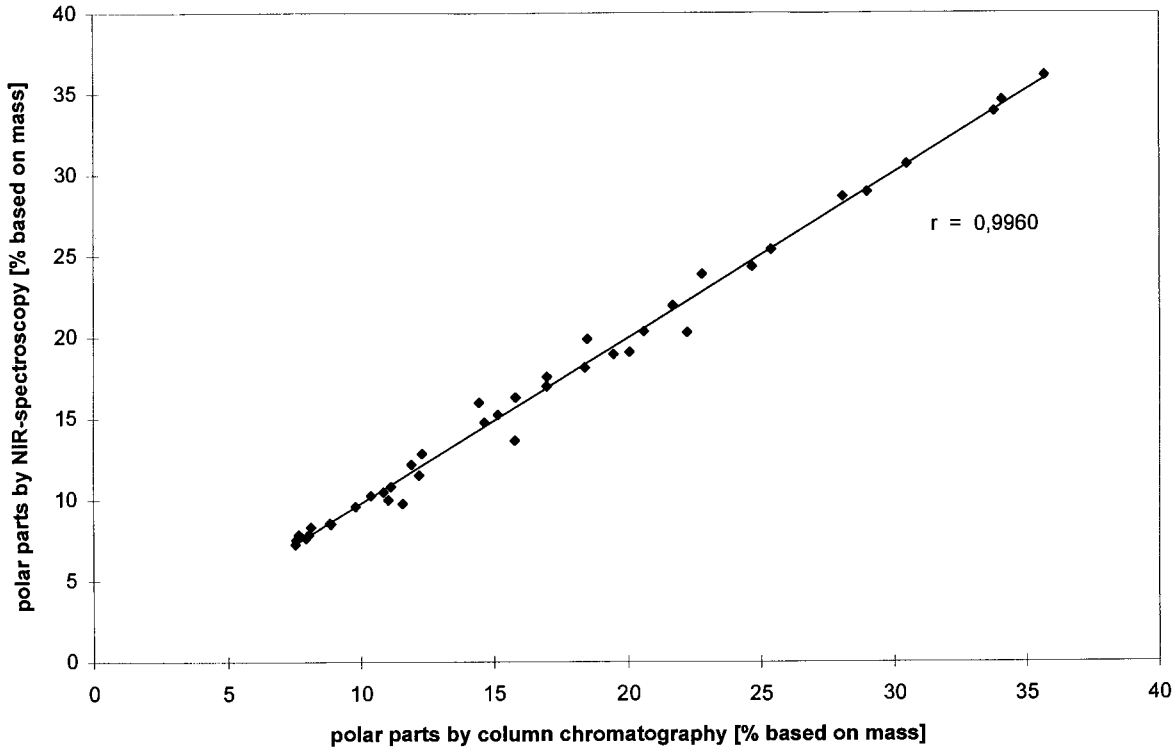

Fig. 4. Correlation between the polar parts determined by preparative column chromatography and by NIR spectroscopy for different palm oils which were heated with different foodstuffs (all results are average values of triple analyses).

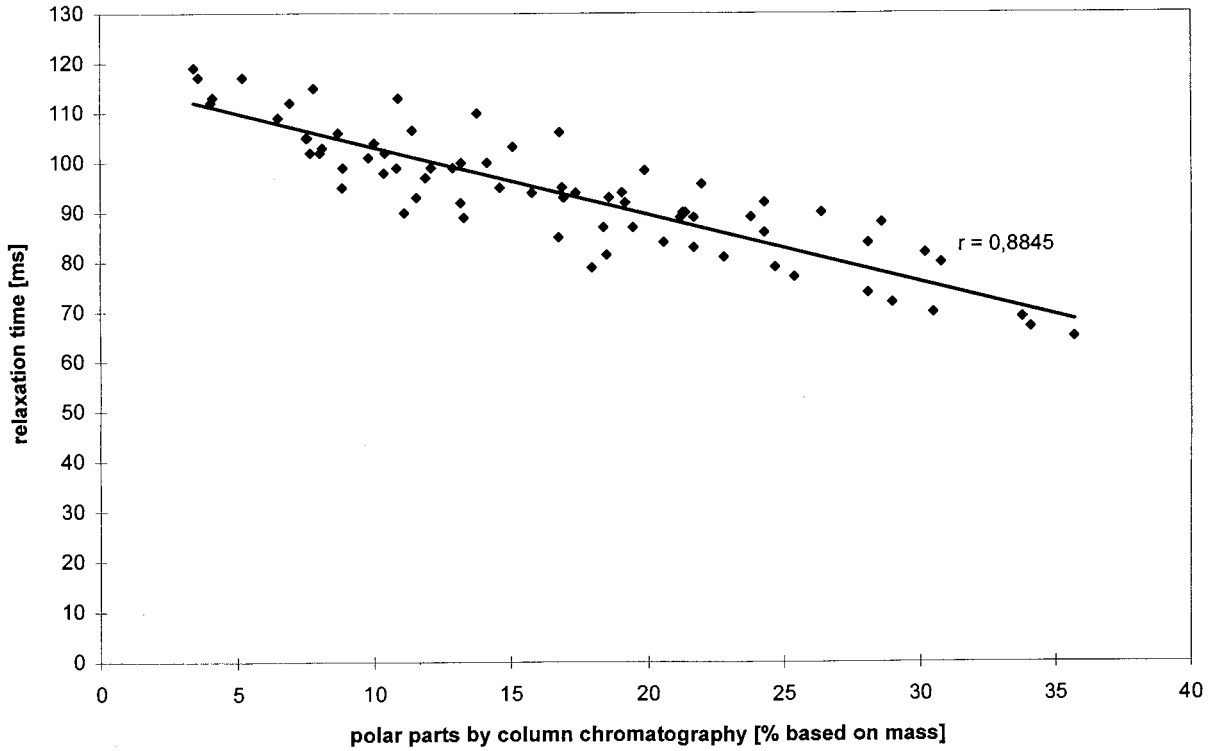

Fig. 5. Correlation between the polar parts determined by preparative column chromatography and relaxation time determined by NMR spectroscopy for palm oils which were heated with different foodstuffs (all results are average values of triple analyses).

References

[1] H.W. Lawson, Standards for Fats and Oils, III. Series, The AVI Publishing Company, Westport, Connecticut, 1985, p 51.
[2] N. Matuso, Biochemistry 41 (1954) 647.
[3] F.W. Quackenbusch, Oil Soap 22 (1945) 336.
[4] P.B. Addis, Food Chem. Toxicol. 24 (1986) 1021.
[5] M.K. Logani, R.E. Davies, Lipids 15 (1980) 485.
[6] G. Guhr, J. Waibel, Fette Seifen Anstrichm. 80 (1978) 106.
[7] C.W. Fritsch, J. Am. Oil Chem. Soc. 58 (1981) 272.
[8] Bestimmung der polaren Anteile in Fritierfetten, DGF-Einheitsmethode C-III 3b (81), Wissenschaftliche Verlagsgesellschaft, Stuttgart.
[9] D. Firestone, R.F. Stier, M.M. Blumenthal, Food Technol. 45 (1991) 90.
[10] G. Billek, Nutr. Metab. 24 (1979) 200.
[11] C. Gertz, Fette Seifen Anstrichm. 81 (1979) (Sonderheft).
[12] S.M. El-Shami, I.Z. Selim, I.M. El-Anwar, M.H. El-Mallah, J. Am. Oil Chem. Soc. 69 (1992) 873.
[13] H.A. Al-Kahtani, J. Am. Oil Chem. Soc. 68 (1991) 859.
[14] J. Dubois, F.R. van Voort, J. Sedman, A.A. Ismail, H.R. Ramaswamy, J. Am. Oil Chem. Soc. 73 (1996) 787.
[15] M.P. Fuller, G.L. Ritter, C.S. Draper, Appl. Spectrosc. 42 (1988) 217.

ELSEVIER

Talanta 47 (1998) 455–462

Talanta

Determination of phenylpropanolamine and methoxamine using flow-injection with fluorimetric detection

P. Viñas, C. López-Erroz, F.J. Cerdán, M. Hernández-Córdoba *

Department of Analytical Chemistry, Faculty of Chemistry, University of Murcia, E-30071 Murcia, Spain

Received 18 November 1997; received in revised form 31 March 1998; accepted 14 April 1998

Abstract

A new flow-injection procedure for the determination of phenylpropanolamine and methoxamine is proposed. The method is based on the derivatization reaction of the primary amine group with *o*-phthalaldehyde in the presence of 2-mercaptoethanol using fluorimetric detection. The calibration graphs based on peak areas were linear in the ranges 5–200 ng ml^{-1} for phenylpropanolamine and 0.2–6 ng ml^{-1} for methoxamine. The detection limits were 3.8 and 0.13 ng ml^{-1}, respectively. The methods were applied to the determination of the drugs in commercial pharmaceutical preparations. © 1998 Elsevier Science B.V. All rights reserved.

Keywords: Phenylpropanolamine; Methoxamine; Flow-injection; Fluorimetry

1. Introduction

Pharmaceutical analysis involves the determination of bulk pure drugs as well as the quality control of the final pharmaceutical formulations. It is therefore necessary to carry out a substantial number of routine analyses of samples of similar composition. Automation obviously plays an important role in this, as it does in other industries, where the quality control laboratory is regarded as an essential part of its operation. Fluorimetry is particularly useful in drug analysis, and the non-fluorescence of many compounds has stimulated the development of reagents which aid the formation of fluorescent derivatives. Fluorescent methods are advantageous due to their excellent detection limits, their selectivity and the possibility of combining them with flow-injection (FI) techniques in automatic or semiautomatic methods using inexpensive instrumentation. For the fluorescent detection of amines, the reagent *o*-phthalaldehyde (OPA) is generally used in combination with a thiol compound, usually 2-mercaptoethanol (ME) [1–4].

The sympathomimetic amines as well as the antagonist of the adrenergic receptors, constitute two of the most extensively studied groups of pharmacological agents, whose determination has been of most interest in the field of clinical chemistry. Methoxamine (MA) is used in the treatment of hypotensive states [5] and phenylpropanolamine (PPA) is used for the relief of nasal congestion. The analytical methods which

* Corresponding author. Tel.: +34 68 307100, ext. 2177; fax: +34 68 364148; e-mail: hcordoba@fcu.um.es

0039-9140/98/$ - see front matter © 1998 Elsevier Science B.V. All rights reserved.
PII S0039-9140(98)00154-4

have been proposed for the determination of PPA are spectrophotometry [6–10], liquid chromatography [11–19] and mass spectrometry [20], while only two methods have been proposed for the determination of methoxamine using nuclear magnetic resonance [21] and capillary electrophoresis [22]. No reference could be found concerning the determination of these drugs using FI or fluorimetric techniques.

The aim of the study described in this paper was the determination of phenylpropanolamine and methoxamine, both substances of interest to the pharmaceutical industry, by the FI technique. Because these substances have no natural fluorescence, fluorescent derivatives were developed using the reagents OPA and ME. The proposed procedures were applied with excellent results to the determination of the drugs in commercial pharmaceutical preparations.

2. Experimental

2.1. Instrumentation

A Kontron (Zurich, Switzerland) SFM 25 fluorescence detector set at wavelengths of 336/455 nm (excitation/emission) was used to measure the fluorescence of the derivatized products. The peaks were recorded and integrated using a PC integration pack (Kontron). For comparison purposes, a Perkin-Elmer 550-SE spectrophotometer set at 340 nm was also used. The flow injection system consisted of a Gilson (Worthington, OH) Minipuls HP4 peristaltic pump; an Omnifit (Cambridge, UK) injection valve; a Hellma (Jamaica, NY) 176.052-QS fluorimetric flow cell, 0.8 mm i.d.; and PTFE tubing and various end fittings and connectors (Omnifit). The temperature of the reactor coil was controlled by a laboratory-made electronic thermostat.

2.2. Reagents

All solutions were prepared using distilled water. A fluorogenic reagent containing 2 mM OPA (Fluka, Buchs, Switzerland) and 0.5 mM ME (Sigma, St. Louis, MO) was prepared in 4% methanol and 0.05 M phosphate–borate buffer (pH 9.2). This solution was kept in a dark bottle at 4°C. Stock solutions of 200 μg ml^{-1} PPA and MA were prepared in water and kept at 4°C. More diluted solutions were prepared by dilution with the 0.05 M phosphate–borate buffer just before use.

2.3. Procedure

A schematic diagram of the two channel flow manifold selected is shown in Fig. 1A. The sample containing the drug (360 μl) was injected into a channel through which flowed 0.05 M phosphate–borate buffer (pH 9.2), and mixed with the fluorogenic reagent (containing 2×10^{-3} M OPA and 5×10^{-4} M ME) by means of a T-piece. The resulting solution flowed through a reactor coil (1.5 m × 0.8 mm i.d.) thermostated at 25 ± 0.1°C and then passed into the flow cell for its fluorescence (336/455 nm) to be recorded. Both streams were pumped at the same flow rate by a peristaltic pump with a total flow rate of 0.9 ml min^{-1}. Calibration graphs were obtained by plotting the peak area against the drug concentration.

For the determination of the drugs in pharmaceutical products, a tablet/capsule or an appropriate aliquot of syrup was treated with water followed by mixing for 10 min, then filtered using a chromatographic filter (Millipore, 0.4 μm) to remove solvent non-soluble adjuvants, and diluted with water in a volumetric flask of the required volume depending on the sample. For ampoules, the whole amount was dissolved with water; an aliquot was subsequently diluted, if necessary, and injected into the FI system. The concentration of the drug in the pharmaceutical was calculated by referencing to a preestablished calibration curve.

3. Results and discussion

PPA and MA are sympathomimetic amines with the following structures:

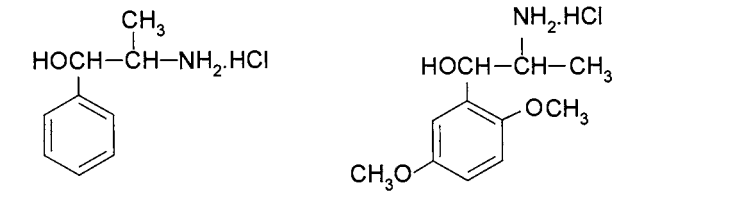

α-[Aminoethyl]benzenemethanol (PPA)

α-[1-Aminoethyl]-2,5-dimethoxybenzyl alcohol (MA)

The mechanism proposed to explain the reaction of OPA and ME with amino acids involves the formation of 1-alkylthio-2-alkylisoindoles as products [23]. The sequence of the reaction is important; the best analytical results were obtained by mixing OPA and ME before addition of

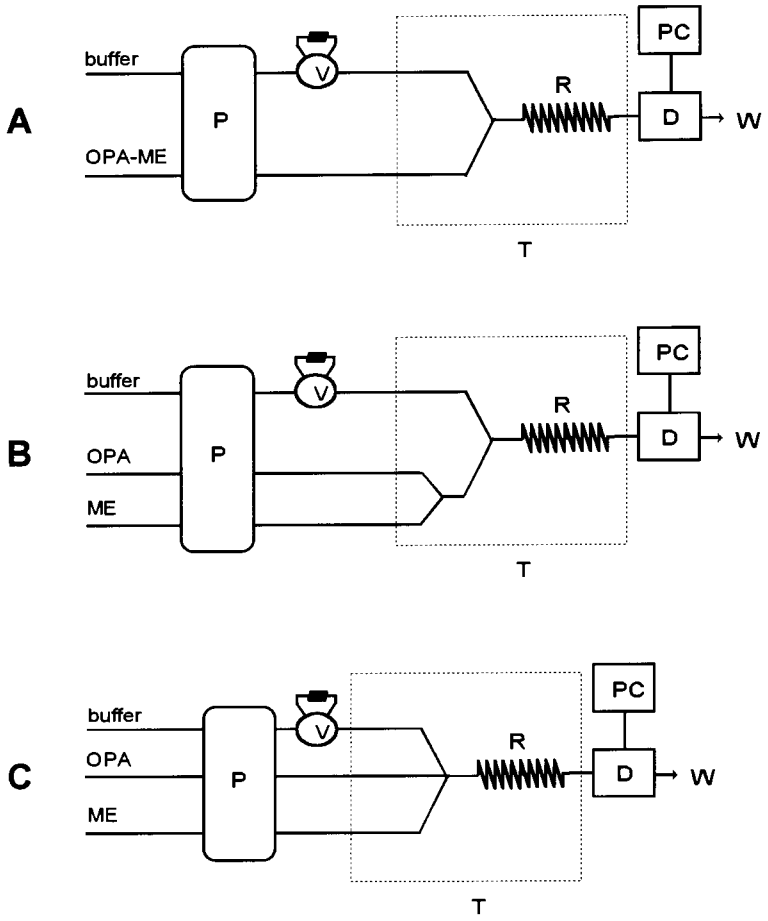

Fig. 1. FI systems used for the determination of amines using the OPA–ME reaction. A, manifold selected; P, peristaltic pump (total flow-rate 0.9 ml min^{-1}); V, injection valve (sample-loop 360 μl); R, reactor coil (1.5 m long and 0.8 mm i.d.); T, thermostat at 25°C; D, fluorimeter (336/455 nm (excitation/emission)); PC, personal computer; W, waste.

the amine. Consequently, several FI systems were tried in an attempt to obtain the optimal configuration. The first (A) was a two-channel system while the other two assays (B and C), both had three channels (Fig. 1). In manifold A, the injection valve was located in a flowing buffer solution which merged with another channel containing the fluorogenic reagent (OPA–ME) by means of a T-piece. The resulting solution flowed through a thermostated reactor coil and then passed to the flow cell. Manifold B was a three channels system, in which the drug was again injected into a buffer which merged at a T-piece with the fluorogenic reagent. This manifold differed from manifold A in that this reagent was obtained by merging, at a second T-piece, the OPA solution with a stream of ME dissolved in the buffer. The rest of the system was similar to the one described above. Manifold C also consisted of three channels. These contained the buffer solution (in which the drug was injected), OPA and ME, respectively. This differed from system B in that the two successive T-pieces were replaced by a 4-way connector which permitted the simultaneous mixture of the buffer, OPA and ME solutions.

Manifold C was less sensitive than the others because the drug solution was diluted more in the 4-way connector. Manifolds A and B were of similar sensitivity and so manifold A was chosen for the experiments because of its greater simplicity.

3.1. Optimization of the chemical variables

The experimental parameters were optimized to obtain maximum fluorescence, i.e. maximum sensitivity in the chemical analytical procedure. The fluorescence intensity was monitored as a function of pH by using different phosphate–borate buffer solutions of between pH 6 and 11. The OPA–ME solution was prepared using the same buffer solutions. Fig. 2 shows that no fluorescence appeared below pH 6, while it increased with increasing pH up to about 9.2, when it levelled off. Consequently, this value was selected as optimal. The effect of the buffer solution concentration was

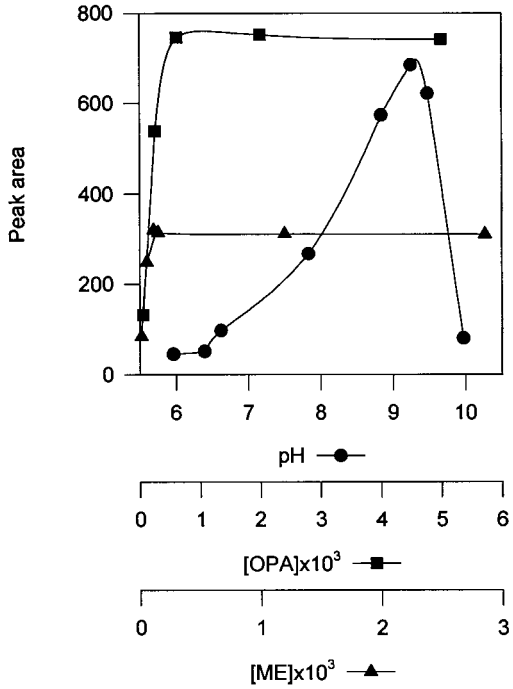

Fig. 2. Influence of pH and OPA and ME concentrations on the fluorescence intensity. Sample loop size 160 μl, reactor length 1.5 m, flow-rate 0.3 ml min^{-1}, PPA injected 10 ng ml^{-1}.

studied in the range 0.02–0.20 M. Fluorescence decreased with increasing buffer concentrations and 0.05 M was selected since this value made it possible to control the pH with no loss of sensitivity. The influence of the OPA concentration was studied between 5×10^{-5}–5×10^{-3} M, while the concentration of ME was maintained at 1.4×10^{-3} M in phosphate–borate buffer (pH 9.2). The fluorescence intensity rapidly increased up to about 6×10^{-4} M (Fig. 2) and then remained constant; an OPA concentration slightly over (2×10^{-3} M) was therefore used in all subsequent investigations. It was observed that when ME solutions of varying concentrations (1.1×10^{-5}–2.9×10^{-3} M) were passed through the FI manifold (Fig. 2), the highest fluorescence intensity was obtained at concentrations of 5×10^{-4} M. Above this concentration there was a very slight drop in fluorescence. Room temperature was selected in order to simplify the experimental work and all

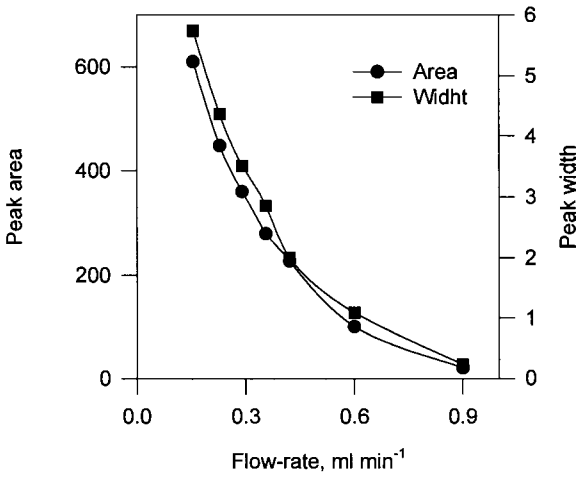

Fig. 3. Effect of the flow-rate on both the area and the width of the FI peaks. 2×10^{-3} M OPA, 5×10^{-4} M ME, pH 9.2, PPA 10 ng ml^{-1}, loop size 360 μl, reactor length 1.5 m.

the experiments were carried out whilst thermostating the reactor at 25 ± 0.1°C.

3.2. Optimization of the FI variables

Utilizing the optimized conditions, the influence of the FI variables was studied. The total flow rate was varied from 0.1 to 0.9 ml min^{-1} to obtain a compromise value leading to maximum fluorescence intensity and sensitivity as well as giving a reasonable throughput rate. An increase in fluorescence was observed when the flow-rate decreased (Fig. 3) since the reaction between the amine and the fluorogenic reagent occurred to a greater extent. However, under these conditions, the peaks were considerably broader and the sample throughput decreased. Fig. 3, plotting the peak width against flow-rate, also shows this effect. A flow-rate value of 0.9 ml min^{-1} was chosen since this resulted in sharp FI peaks, low detection limits and reasonable sampling frequency.

The length of the reactor is an important physical variable. A certain length is required for the reaction to happen, but if this distance is too long, the sample will inevitably be dispersed. The influence of this variable was studied using tubing of 0.8 mm i.d. and by varying the length from 0.3 m (the minimal distance between the mixing point and the flow cell) to 5.8 m. Fig. 4A shows that fluorescence increased up to 1 m and remained constant up to 4 m; greater lengths produced a decrease probably due to sample dispersion. An optimal value of 1.5 m was selected. Fig. 4B shows the effect of varying the sample loop size between 35 and 490 μl. Fluorescence increased over the whole range studied. A volume of 360 μl was selected to avoid broadening of the peaks when higher volumes were injected.

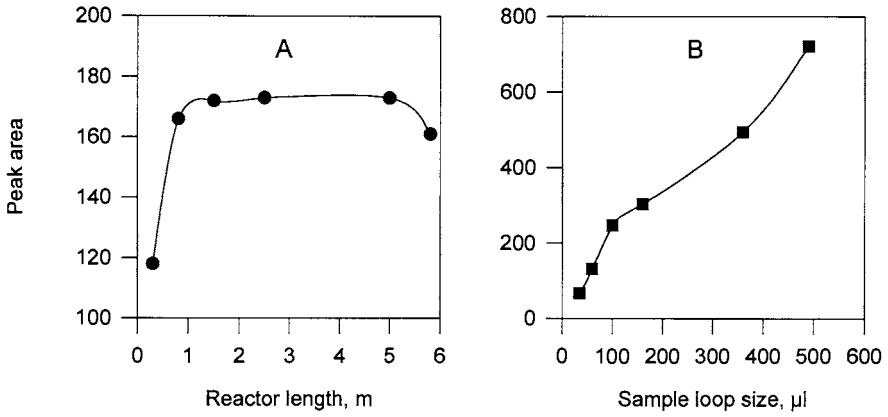

Fig. 4. Influence of the reactor length (A) and the sample loop size (B). 2×10^{-3} M OPA, 5×10^{-4} M ME, pH 9.2, PPA 10 ng ml^{-1}, flow-rate 0.3 ml min^{-1}.

Table 1
Calibration parameters for PPA and MA

Parameter[a]	Drug	
	PPA	MA
Slope (ml ng^{-1})[b]	1.3034 ± 0.0195	36.955 ± 0.296
Intercept[b]	1.8591 ± 0.0241	−1.7868 ± 0.021
Regression coefficient	0.9998	0.9997
Detection limit (ng ml^{-1})	3.8	0.13

[a] Parameters calculated using the peak area.
[b] Mean ± S.D. ($n = 5$).

3.3. Calibration, interferences and applications

Calibration was carried out by plotting concentration against the area or height of the peaks. Linearity between 5 and 200 ng ml^{-1} PPA was obtained for both analytical signals; calibration graphs for MA gave linearity between 0.2 and 6.0 ng ml^{-1}. Table 1 shows the data obtained for the calibration graphs and the regression coefficients. The detection limits were calculated on the basis of 3σ using the regression lines obtained for aqueous standards [24]. These values are also given in Table 1. The precision and accuracy of the methods were demonstrated by repetitive analyses and by calculating the S.D. and average R.S.D. for 10 replicate determinations at different concentration levels. Table 2 shows the statistical parameters obtained for both analytes. As can be seen, repeatability was very similar when either area or height were taken as the analytical signal.

Table 2
Statistical parameters for comparing either area or height as signals

Drug (ng ml^{-1})	Analytical signal	S.D. (ng ml^{-1})	R.S.D. (%)
PPA (7.2)	Area	0.190	2.64
	Height	0.199	2.76
PPA (55.2)	Area	0.861	1.56
	Height	0.922	1.67
MA (0.67)	Area	0.019	2.88
	Height	0.026	3.90
MA (3.37)	Area	0.074	2.20
	Height	0.051	1.51

A comparison of the proposed fluorimetric-FI method with UV-FI analysis based on the same derivatization reaction was carried out. The concentrations of OPA and ME necessary to obtain suitable absorbance signals at a wavelength of 340 nm were higher than those needed for the fluorimetric procedure. Values selected were 0.07 and 0.005 M, respectively. Linearity was obtained between 5 and 50 μg ml^{-1} for both drugs. As can be seen, the sensitivity using the fluorimetric-FI procedure was much more higher than that for the UV-FI method.

Interferences caused by some common adjuvants used in the pharmaceutical industry were studied by injecting solutions containing a fixed amount of PPA (10 ng ml^{-1}) or MA (1 ng ml^{-1}) and different amounts of these compounds. The tolerance limit was taken as the concentration causing an error of no more than ± 3% in analyte recovery. No interference was induced by glucose, saccharose, galactose, citrate, *p*-hydroxybenzoic acid ethyl ester (ethyl paraben) or *n*-propyl *p*-hydroxybenzoate (propyl paraben) at interferent/drug ratios up to 100/1. Higher concentrations were not assayed. Tolerance limits were 100/1 for ascorbic acid, caffeine, lactose and salicylic acid, 50/1 for paracetamol and 10/1 for sorbitol. Other drugs with amine functionality which are present in any of the formulations have also been tested. No interference was found for both carbinoxamine and chlorpheniramine at ratios of 100/1 because these drugs have secondary or tertiary amine groups which did not react with OPA–ME. As can be seen, the proposed procedures are quite selective.

To assess the reliability of the methods, several commercial pharmaceutical preparations were analysed. Table 3 shows the results obtained as well as the composition of the drug formulations. The validation of the method has been carried out by comparing the results obtained using both fluorimetric-FI and UV-FI methods and by means of a recovery study which was carried out by the standard addition method. As can be seen, the

Table 3
Determination of PPA and MA in pharmaceutical formulations

Sample (Laboratory)[a]	Labeled	Found*		
		Fluorimetry-FIA	Standard additions	UV-FIA
PPA				
Senioral (Semar)	30 mg/Tablet	29.8 ± 0.8	30.9 ± 1.0	30.8 ± 1.1
Coricidin Fuerte (Schering-Plough)	25 mg/Capsule	25.3 ± 0.5	24.2 ± 0.6	24.6 ± 0.8
Rinoretard Suspensión (Pfizer)	3.333 mg/ml Suspension	3.36 ± 0.03	3.40 ± 0.04	3.28 ± 0.03
Baby Rinol (Marion Merrell Dow)	2 mg/ml Suspension	1.90 ± 0.02	1.86 ± 0.03	1.84 ± 0.02
Ornade (Syntex Latino)	50 mg/Tablet	49.5 ± 0.7	50.5 ± 0.9	49. 9 ± 1.0
MA				
Metoxamina Gotas (Gayoso Wellcome)	2.5 mg/ml Suspension	2.53 ± 0.01	2.50 ± 0.01	2.60 ± 0.02

[a] Composition: Senioral (PPA 30 mg, clocinizine 5 mg, excipient); Coricidin-F (PPA 25 mg, chlorpheniramine 4 mg, paracetamol 500 mg, excipients); Rinoretard (PPA 3.333 mg, carbinoxamine 0.266 mg, excipients: citrate, ethyl paraben, propyl paraben, sorbitol); Baby Rinol (PPA 0.2 g, chlorphenamine 0.015 g, paracetamol 2.4 g, saccharine 0.125 g, saccharose 40 g, ethanol 7 g, excipients); Ornade (PPA 50 mg, isopropamide 2.5 mg, cinarizine 10 mg, saccharose 200 mg, lactose, excipients); Metoxamina (MA 2.5 mg, excipient).
* Mean ± S.D. ($n = 6$).

recovery was quantitative and there were no significant differences between the results obtained using different methods.

4. Conclusion

Fluorescent derivatization of the drugs PPA and MA using the OPA–ME method proved to be a simple procedure with excellent sensitivity. The use of flow injection methodology to automate the reaction led to considerable savings in analysis times. The procedure might be of use in the pharmaceutical industry for the routine quantitative analysis of drugs.

Acknowledgements

The authors are grateful to the Spanish DGICYT (Project PB96-1100) and Comunidad Autónoma de la Región de Murcia (Project PB/7/FS/97) for financial support.

References

[1] M. Roth, Anal. Chem. 43 (1971) 880.
[2] N. Ichinose, G. Schwedt, F.M. Schnepel, K. Adachi, Fluorometric Analysis in Biomedical Chemistry, Wiley, New York, 1991.
[3] C. López-Erroz, P. Viñas, M. Hernández-Córdoba, Talanta 41 (1994) 2159.
[4] P. Viñas, N. Campillo, C. López-Erroz, M. Hernández-Córdoba, J. Pharm. Biomed. Anal. 16 (1997) 453.
[5] G.A. Goodman, L.S. Goodman, T.W. Rall, F. Murad, The Pharmacological Basis of Therapeutics, 7th ed., Macmillan, New York, 1985.
[6] K.W. Street, M.B. Abrenica, Anal. Lett. 19 (1986) 597.
[7] J. Zhang, Z. Deng, H. Zeng, Yaown Fenxi Zazhi 4 (1984) 157.
[8] H.S.I. Tan, G.C. Salvador, Anal. Chim. Acta 176 (1985) 71.
[9] H.S.I. Tan, G.C. Salvador, Anal. Chim. Acta 188 (1986) 295.
[10] H.S.I. Tan, M. Kolmonpunporn, Anal. Chim. Acta 226 (1989) 159.
[11] V. Das Gupta, A.R. Heble, J. Pharm. Sci. 73 (1984) 1553.
[12] S.I. Sa'sa, K.A. Momani, I.M. Jalal, Microchem. J. 36 (1987) 391.
[13] D.R. Heidemann, K.S. Groon, J.M. Smith, LC-GC 5 (1987) 422.
[14] J. Aranjo, J.F. Boyer, M.L. Probecker, S.T.P. Pharma 4 (1988) 598.
[15] S.S. Yang, R.K. Gilpin, J. Chromatogr. Sci. 26 (1988) 416.
[16] S.K. Pant, B.K. Maitin, C.L. Jain, Indian Drugs 28 (1990) 105.
[17] A.E.H.N. Ahmed, Anal. Lett. 26 (1993) 1153.
[18] K.P. Shah, M. Chang, C.M. Riley, J. Pharm. Biomed. Anal. 13 (1995) 1235.

[19] G. Indrayanto, A. Sunarto, Y. Adriani, J. Pharm. Biomed. Anal. 13 (1995) 1555.
[20] A.P. Snyder, C.W. Cross, S.A. Liebman, G.A. Eiceman, R.A. Yost, J. Anal. Appl. Chim. Acta 226 (1989) 159.
[21] M. de Arment, M. Eastabrooks, K.S. Venkatasubban, R. Benshafrut, R. Rothchild, H. Wyss, Spectrosc. Lett. 27 (1994) 533.
[22] Z. Wang, A.J. Huang, Y.L. Sun, Z.P. Sun, J. High Resolut. Chromatogr. 19 (1996) 478.
[23] S.S. Simons, D.F. Johnson, J. Org.Chem. 43 (1978) 2286.
[24] J.C. Miller, J.N. Miller, Statistics for Analytical Chemistry, 2nd ed., Ellis Horwood, Chichester, 1988.

ELSEVIER

Talanta 47 (1998) 463–470

Talanta

Simultaneous determination of iron, cobalt, nickel and copper by UV-visible spectrophotometry with multivariate calibration

A.M. Garcia Rodriguez, A. Garcia de Torres, J.M. Cano Pavon *, C. Bosch Ojeda

Department of Analytical Chemistry, Faculty of Sciences, University of Malaga, E-29071, Malaga, Spain

Received 19 December 1997; received in revised form 2 April 1998; accepted 14 April 1998

Abstract

A method for the simultaneous spectrophotometric determination of the divalent ions of iron, cobalt, nickel and copper based on the formation of their complexes with 1,5-bis(di-2-pyridylmethylene) thiocarbonohydrazide (DPTH) is proposed. The resolution of quaternary mixtures of these metallic ions was accomplished by several chemometric approaches. A comparative study of the results obtained for simultaneous determinations in mixture by using principal component regression (PCR) and partial least-squares regression (PLS-1 and PLS-2) for absorbance, first-derivative and second-derivative data is presented. In general, the best recovery values are obtained by the PLS-2 method for absorbance data. This procedure allows the simultaneous determination of the cited ions in alloys and biological materials Good reliability of the determination was proved. © 1998 Elsevier Science B.V. All rights reserved.

Keywords: Spectrophotometry; Multivariate analysis; Iron; Cobalt; Nickel; Copper; Determination

1. Introduction

Iron, cobalt, nickel and copper are metals which appear together in many real samples. Several techniques such as X-ray fluorescence [1], atomic fluorescence spectrometry [2], polarography [3], chromatography [4], atomic absorption spectrometry [5], etc., have been used for the simultaneous determination of these ions in different samples. Among the most widely used analytical methods are those based on the UV–visible spectrophotometry techniques, due to both the resulting experimental rapidity and simplicity and the wide application. However, the simultaneous determination of these ions by the use of the traditional spectrophotometry techniques is difficult because, generally, the absorption spectra overlap in a bright region and the superimposed curves are not suitable for quantitative evaluation.

Quantitative spectrophotometry has been greatly improved by the use of a variety of multivariate statistical method, particularly principal component regression (PCR) and partial least

* Corresponding author. Tel.: +34 5 2131887; fax: +34 5 2132000; e-mail: JM_CANO@UMA.ES

0039-9140/98/$ - see front matter © 1998 Elsevier Science B.V. All rights reserved.
PII S0039-9140(98)00157-X

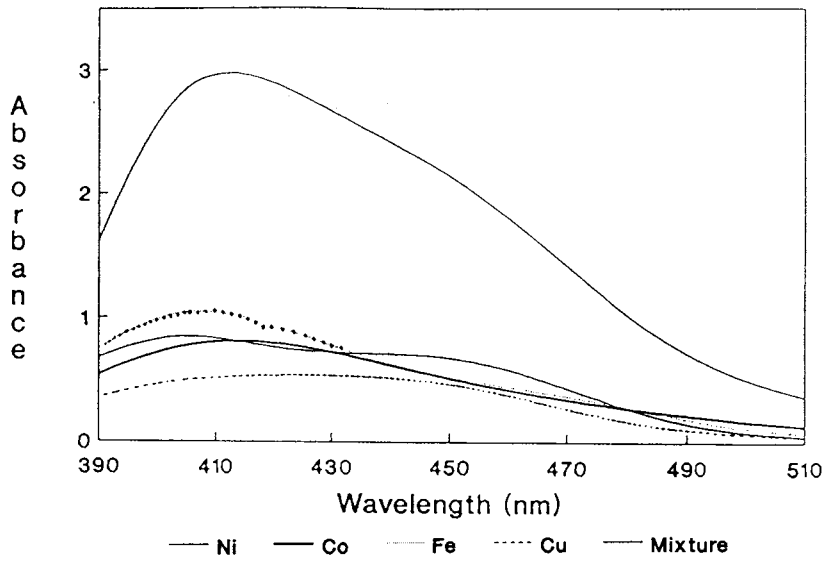

Fig. 1. Absorbance spectra of the cobalt, nickel, iron and copper complexes and their mixture. Concentration of each ion is 1 μg ml^{-1} and the pH is 6.0.

squares regression (PLS). The widespread use of these methods is due to the proliferation of commercial software for laboratory computers and to the development of photodiode array detectors capable of recording full spectra very rapidly.

The theory and application of PCR and PLS in spectrometry have been discussed by several workers [6–9]. Also several multicomponent determinations of inorganic substances based on the application of these methods to spectrophotometric data have been reported [10,11]. A particularly detailed study of multivariate calibration by PLS was carried out for the spectrophotometric determination of metals [12]. The simultaneous determination of iron, cobalt, nickel and copper, among other metals, in aqueous solutions was carried out by Vitouchova et al. [13], who developed a method based on the spectrophotometric response of the metallic complexes formed with 2-(5-bromo-2-pyridylazo)-5-diethylaminophenol (Br-PADAP) and using multivariate calibration with PLS evaluation of absorbance data. Ni [14] later reported a method for the simultaneous determination of these metals in aqueous solutions using a two-component mixture of chromogenic reagents, Br-PADAP and 4-(2-pyridylazo)-resorcinol (PAR), and analysis of spectral data by conventional least squares, PCR and PLS regression methods. The best results were obtained by use of either the PCR and PLS approach. Also, Mac Laurin et al. [15] investigated the practical application of some multivariate calibration routines to visible spectra for the simultaneous multicomponent determinations of the cited ions.

This paper reports the simultaneous spectrophotometric determination of iron, cobalt, nickel and copper with 1,5-bis(di-2-pyridylmethylene) thiocarbonohydrazide (DPTH). This ligand is a good chromogenic reagent [16]. It can react with various metallic ions to form stable complexes with high sensitivity, but unfortunately these reactions are usually not selective. Co(II), Ni(II), Fe(II) and Cu(II) react with DPTH to form different complexes but the absorption curves overlap severely. For overcoming the drawback of spectral interferences, calculation of the metal concentrations is performed using multivariate calibration approaches. With this aim, PCR, PLS-1 and PLS-2 algorithms are applied to the simultaneous determination of the cited ions. The results obtained by the three methods are compared and discussed.

Table 1
Concentration data of the training set and test set for the four-component system (μg ml^{-1})

Sample No.	Nickel	Cobalt	Iron	Copper
1	0.2	0.4	0.6	0.8
2	0.2	1.0	0.4	1.2
3	0.2	0.6	0.8	0.4
4	0.2	0.8	0.4	0.6
5	0.2	1.0	1.2	0.4
6	0.4	0.2	1.2	1.0
7	0.4	0.8	0.2	0.6
8	0.4	1.2	1.0	0.6
9	0.4	0.6	1.0	0.8
10	0.4	1.0	0.2	1.2
11	0.4	0.3	0.7	0.9
12	0.4	0.4	0.4	0.4
13	0.4	0.6	1.0	0.2
14	0.4	0.8	0.8	1.2
15	0.4	0.6	0.8	—
16	0.6	0.8	1.0	1.2
17	0.6	0.2	0.8	0.4
18	0.6	1.0	0.8	1.2
19	0.6	0.4	0.8	1.0
20	0.6	1.2	0.8	0.2
21	0.6	0.6	0.6	0.6
22	0.6	0.5	0.3	1.0
23	0.6	0.8	—	—
24	0.6	0.9	0.3	0.5
25	0.8	0.6	0.4	0.2
26	0.8	0.4	1.2	0.2
27	0.8	0.2	0.6	0.4
28	0.8	1.2	0.2	0.4
29	0.8	0.3	0.5	0.7
30	0.8	—	1.0	0.4
31	0.8	0.7	0.9	0.8
32	1.0	1.2	0.2	0.4
33	1.0	0.6	1.2	0.8
34	1.0	0.2	0.6	0.8
35	1.0	0.4	0.2	1.2
36	1.0	0.8	0.6	0.2
37	1.0	0.4	0.4	1.0
38	1.0	0.5	0.3	0.7
39	1.0	0.4	—	0.8
40	1.2	0.4	1.0	0.2
41	1.2	0.8	0.2	1.0
42	1.2	0.6	0.4	0.8
43	1.2	0.2	1.0	0.6
44	—	0.8	0.2	0.6
Test set				
A	0.5	a0.5	0.5	0.5
B	0.4	0.7	0.3	0.5
C	0.8	0.4	0.6	0.6
D	0.3	0.8	0.8	0.4
E	0.7	0.3	0.9	0.3
F	0.8	0.6	0.3	0.5
G	—	0.8	0.5	0.7
H	0.6	—	0.7	0.4
I	0.5	0.4	—	0.9
J	0.4	0.7	0.8	—
K	0.9	0.5	0.6	0.8
M	0.6	0.9	0.4	0.7

2. Experimental

2.1. Reagents

All chemicals were of analytical-reagent grade and deionized water was used throughout.

Stock solutions of cobalt(II), nickel(II), copper(II) and iron(II) were prepared from their commercial salts (nitrate or sulphate) and standardized titrimetrically or gravimetrically. Standards of working strength were made by appropriate dilution daily as required.

A stock DPTH solution (2.3×10^{-3} M) in DMF was prepared by dissolving solid reagent samples prepared and purified by the authors [16]. This solution was spectrophotometrically stable for at least a week.

Buffer solutions (pH 4.0) was prepared by mixing 9 ml of 0.2 M sodium acetate with 41 ml of 0.2 M acetic acid and diluting to 100 ml with deionized water.

Ascorbic acid solution, 0.1% m/v. This solution was prepared fresh daily.

2.2. Apparatus and software

A Hewlett Packard Model 8452 A diode-array spectrophotometer equipped with glass or quartz cells of 1-cm path length was used for recording absorbance spectra. An HP Vectra QS/165 personal computer was used to control the spectrophotometer and collect data from it via an HP-IB interface.

The programs used to obtain and process the spectra were supplied by the spectrophotometer manufacturer as bundled software. PCR and PLS were carried out using the Lab Calc software package v. A 1.01 and the PLS plus v. 2.0 (Galactic Industries, Salem, NH).

2.3. Procedures

2.3.1. Sample preparation

The certified materials (CRM_s) analyzed to determine the accuracy of the proposed procedure were: National Institute of Standards and Technology (NIST) Standard Reference Materials (SRM_s) 1577a Bovine Liver; Community Bureau

Table 2
Statistical PRESS and F parameters for the PLS-2 and PCR models

Method	Factor	PRESS	Probability ($F \leq F_{cal}$)	Spectrum[a]
PLS-2	12	1.2564	0.73	A
	10	1.1650	0.73	D1
	9	1.2548	0.61	D2
PCR	19	1.1852	0.55	A
	17	3.9361	0.63	D1
	13	1.2057	0.61	D2

[a] A, D1 and D2 represent absorbance, first-derivative and second derivative data, respectively.

of Reference (BCR), CRM_s 186 Pig Kidney; National Research Council Canada (NRCC) CRM_s DOLT-1 Dogfish Liver; Bureau of Analysed Samples LTD 44q Iron Pyrites. These samples were prepared according to the following procedure:

2.3.1.1. Alloy. Dissolve a known amount of accurately weighed sample (0.1 g) in about 30 ml of aqua regia; evaporate the resulting solution to dryness and add 1 ml of hydrochloric acid (1 + 1); then dilute with distilled water to 250 ml.

2.3.1.2. Biological materials. The samples were first dried in accordance with the norms of the respective analysis certificates and mineralized as follow: in a reaction flask were placed 0.2–0.6 g of weighed sample and 10 ml of concentrated nitric acid, and the mixture was heated under reflux up to the disappearance of nitrous fumes. Then, 3 ml of hydrogen peroxide was added and the mixture was concentrated (this step was repeated until the solution was completely colourless). After digestion, the pH of the solutions were adjusted to 4.0 with concentrated NaOH and buffer solutions and finally, the samples were diluted to 25 ml with deionized water in a calibrated flask. Analysis of each sample, in triplicate, was carried out as described in Section 2.3.2.

2.3.2. Recommended procedure for the simultaneous determination of Fe(II), Co(II), Ni(II) and Cu(II)

Standards or samples were prepared in 25 ml standard flasks by taking the required volume of the solution to be analyzed to obtain Co, Ni, Fe and Cu concentrations over their respective linear determination ranges (0.2–1.3 μg ml^{-1} for Co, 0.1–1.2 μg ml^{-1} for Ni, 0.1–1.1 μg ml^{-1} for Fe and 0.2–1.2 μg ml^{-1} for Cu) and so that the final solution contained a total metal concentration lower than 3 μg ml^{-1}. Then, 0.4 ml of 0.1% m/v ascorbic acid, 3 ml of 0.1% m/v DPTH solution in DMF, 12 ml of DMF (to prevent precipitation of the reagent) and 5 ml of buffer solution (pH 4.0) were added. The volume was made up to the mark with deionized water, after a thorough mixing, the solutions were allowed to stand for 30 min and their absorbance, first-derivative and second-derivative spectra, in triplicate, were recorded against a blank reagent, with an integration time of 1 s, a slit-width of 2 nm and a scan range from 390 to 510 nm. The spectra were averaged and their means were stored for use in calibration/prediction.

The optimized calibration matrices, calculated by application of the PCR, PLS-1 and PLS-2 methods, were used to analyze the spectra of the samples under study and to calculate the concentrations of Co(II), Ni(II), Fe(II) and Cu(II) in the mixture.

3. Results and discussion

3.1. Selection of the optimum chemical conditions

Iron(II), cobalt(II), nickel(II) and copper(II) react with DPTH to form intensely coloured complexes. In a previous study [16], the characteristics of these chelates were described and a method was proposed for the simultaneous determination of Co(II) and Ni(II) in binary mixtures [17], this method was successfully applied to the determination of both metal ions in alloys.

With the aim of investigating the possibility of determining Co(II), Ni(II), Fe(II) and Cu(II) in mixtures, the optimum working conditions were studied under the conditions previously established for each metal ion. A sodium acetate buffer solution of pH 4.0 was selected because in this

Table 3
Statistical PRESS and F parameters for PLS-1

Element	Factor	PRESS	Probability ($F \leq F_{cal}$)	Spectrum[a]
Ni	18	0.1160	0.55	A
Co	13	0.2225	0.50	
Fe	12	0.1097	0.69	
Cu	8	0.7339	0.69	
Ni	2	2.8667	0.74	D1
Co	10	0.3782	0.68	
Fe	18	0.6048	0.64	
Cu	11	3.7991	0.63	
Ni	7	0.1457	0.72	D2
Co	9	0.3774	0.60	
Fe	8	0.1611	0.70	
Cu	8	0.6090	0.72	

[a] A, D1 and D2 in Table 2.

medium the absorbance of a Co–Ni–Fe–Cu mixture was maximum (the volume of DMF added in the preparation of the solutions increased the pH over 2.0 unit). The effect of DPTH concentration was also investigated, a reagent concentration of 2.8×10^{-4} M was chosen because its ensures a sufficient reagent excess. The absorbance depends critically on the order of addition of reactants, the most suitable order of addition was: metal ions solutions, ascorbic acid solution, DPTH, DMF and buffer. Under these optimum working conditions the absorbance spectrum of a Co–Ni–Fe–Cu mixture remains constant, after 30 min, for at least 12 h and the Lambert–Beer law is obeyed in the concentration range 0.2–1.3 μg ml^{-1} for Co, 0.1–1.2 μg ml^{-1} for Ni, 0.1–1.1 μg ml^{-1} for Fe and 0.2–1.2 μg ml^{-1} for Cu. The absorption curves are shown in Fig. 1, from this figure it can be seen that the absorption curves are very similar in shape and overlap very severely through the scanning range. It is impossible to determine them simultaneously or selectively by traditional spectrophotometric methods.

3.2. Calibration

The calibration matrix was statistically designed over the concentrations ranges of 0.2–1.2 μg ml^{-1} of metal ions, according to the following basic rules. First, the calibration standards should be mixtures of the components in order to compensate for effects on absorbance from interaction between the components. Second, the peak absorbance of each standard should be less than 2.5 in the analytical wavelength range. Finally, the concentration of all of the components must be independently varied within the set of standards. The calibration matrix used for the analysis is shown in Table 1.

It is also well known [18,19] that the quality of the results obtained in multicomponent analysis from extensively overlapping spectra depends on the wavelength range used. There are mathematical methods that can aid the experimenter in selecting the best spectral region for calibration. One of there is to compute the correlation of the absorbance at every wavelength in the training spectra to the concentrations of every component. Regions that show high correlation are the regions that should be selected. Regions that show low or no correlation should be ignored. Thus, the spectral region between 404 and 510 nm, which implies working with 54 experimental points per spectrum, was selected for analysis. This range include the significant absorbance peaks of the four complexes.

3.3. Selection of the optimum number of factors

The optimum number of factors (latent variables) to be included in the calibration model was determined by computing the prediction error

Table 4
Root-mean squared error of prediction (RMSEP) values for the four-component system

	PCR			PLS-1			PLS-2		
	A[a]	D1[a]	D2[a]	A	D1	D2	A	D1	D2
Ni	0.064	0.047	0.040	0.111	0.048	0.037	0.068	0.031	0.036
Co	0.103	0.088	0.094	0.123	0.069	0.076	0.113	0.076	0.049
Fe	0.025	0.060	0.081	0.026	0.090	0.068	0.031	0.030	0.069
Cu	0.106	0.083	0.075	0.123	0.076	0.078	0.107	0.073	0.073

[a] A, D1 and D2 in Table 2.

sum of squares (PRESS) for cross-validated models using a high number of factors (half the number of total standards + 1). The cross-validation method employed was to eliminate only one sample at a time [20] and then PCR and PLS-calibrate the remaining standard spectra. By using this calibration the concentration of the sample left out was predicted. This process was repeated until each standard had been left out once. One reasonable choice for the optimum number of factors would be that number which yielded the minimum PRESS. Since there are a finite number of samples in the training set, in many cases the minimum PRESS value causes overfitting for unknown samples that were not included in the model. A solution to this problem has been suggested by Haaland et al. [7] in which the PRESS values for all previous factors are compared to the PRESS value at the minimum. The ratio between these values can be calculated and assigned a statistical significance based on the number of samples used in the calibration set. The *F*-statistical test can be used to determine the significance of PRESS values greater than the minimum.

The maximum number of factors used to calculate the optimum PRESS was selected as 23 and the optimum number of factors obtained by the application of PCR and PLS models are summarized in Tables 2 and 3. In these tables, the PRESS and the *F* values obtained by use of the optimum number of factors, are also included. In all instances, the number of factors for the first PRESS value whose *F*-ratio probability drops below 0.75 was selected as the optimum.

3.4. Determination of Fe, Co, Ni and Cu in synthetic mixtures

The predictive ability of each method was determined using twelve four-component metallic ion mixtures (their compositions are given in Table 1). The trace concentrations of each component in these mixtures were in the range 0.3–0.8 μg ml^{-1}. The root-mean-squared prediction errors (RMSEP) for the three calibration methods used for the four-component system using absorbance, first-derivative and second-derivative data are given in Table 4. The use of first derivative data with PLS-2 leads to significantly more precise predictions than absorbance data and the PCR and PLS-1 methods for absorbance and first and second derivative data. There was no significant difference in the precision of the predictions from the absorbance and first or second-derivative data with PCR. With PLS-1 the absorbance data yielded significantly less precise results.

3.5. Effect of foreign ions

The interference due to several cations and anions was studied in detail. For these studies different amounts of the ionic species were added to a mixture of Co, Ni, Fe and Cu containing 0.4 μg ml^{-1} of each. The starting point was a 2500 fold m/m ratio of interference to metal ions, and if the interference occurred the ratio was progressively reduced until interference ceased. The tolerated limits were taken as those concentrations causing changes no greater than ± 5% in the concentration of analytes.

Table 5
Tolerance ratio for foreign ions in the determination of 0.4 μg ml^{-1} of Ni(II), Co(II), Fe(II) and Cu(II)

Tolerated ratio	Foreign ion without masking agent	Foreign ion with masking agent	Masking agent (ppm)
>2500	$S_2O_3^{2-}$, SO_4^{2-}, tartrate, citrate, Cl^-		
1250	Br^-		
500	SCN^-, I^-		
250	$C_2O_4^{2-}$		
100	S_2^-, PO_4^{3-}, F^-		
50	Mo(VI), Sr(II), Ba(II), Zr(IV), Mg(II), Li(I), Ca(II), Y(III), Sb(III)		
40	Cr(III)	Mn(II), Hg(I), Ag(I), Hg(II)	Citrate (800), $S_2O_3^{2-}$ (800), $S_2O_3^{2-}$ (800)
25	UO_2(II), SeO_3^{2-}, WO_4^{2-}, Ce(III)		
20		Pb(II)	Citrate (800)
10	NO_2^-, AsO_4^{3-}		
5	Pb(II), AsO_2^-, Ag(I)		
2		Cd(II)	$S_2O_3^{2-}$ (800)
1	EDTA, Al(III), Bi(III)		
<1	Zn(II)		

The ions which interferes most strongly were Zn and Cd because they form coloured complex with DPTH.

The tolerance limits are depicted in Table 5. The tolerance level for some metal ions can be increased by addition of thiosulphate or citrate. Thus, 800 ppm of thiosulphate will mask 16 ppm of Hg(I), 16 ppm of Ag(I), 16 ppm of Hg(II) and 0.8 ppm Cd(II); 800 ppm of citrate will mask 16 ppm Mn(II) and 8 ppm Pb(II).

3.6. Determination of Fe, Co, Ni and Cu in real samples

In order to test the applicability and matrix interferences of the proposed method to the analysis of real samples, the method was applied in a variety of situations. For this purpose, diverse spiked samples and reference materials were analyzed. Thus, standard solutions containing Co, Cu and Ni were added to 0.1 g of pyrite or to 0.2–0.6 g of DOLT-1, Pig Kidney and Bovine Liver so that the final solution contained between 0.1 and 0.3 ppm of these ions. These samples were prepared and analyzed as described under Experimental. The results of the prediction are summarized in Table 6. It can be seen that the best recovery values are obtained by the PLS-2 method for absorbance data. These satisfactory results indicate that the method would be effective for the analysis of samples of similar complexity. On the other hand, with all three calibration methods the second derivative data yielded significantly poor results, specially for copper and cobalt.

4. Conclusions

The iron–cobalt–nickel–copper mixture is an extremely difficult complex system due to the high spectral overlapping observed between the absorption spectra for these components. For overcoming the drawback of spectral interferences PCR, PLS-1 and PLS-2 multivariate calibration approaches are applied and compared. Analysis of the results for the four-component system revealed no significant difference in the accuracy of prediction between the three procedures for first-derivative data. The use of second derivative data consistently leads to significantly less accurate predictions owing to the much poorer signal-to-noise ratio. The best recovery values are obtained by the application of PLS-2 model for absorbance

Table 6
Recoveries of Fe, Ni, Co, and Cu by the calibration methods

		PLS-2			PCR			PLS-1		
		A	D1	D2	A	D1	D2	A	D1	D2
M1[a]	Fe	91	93	102	91	104	100	87	96	102
	Ni	98	98	98	77	98	98	63	138	77
	Co	100	100	45	100	55	50	120	70	60
	Cu	101	138	130	119	104	123	100	111	138
M2[a]	Fe	101	101	90	101	88	85	103	97	90
	Ni	95	92	95	100	92	100	95	100	100
	Co	100	100	132	95	107	135	93	105	120
	Cu	107	117	123	103	143	115	112	135	120
M3[a]	Fe	109	138	128	130	109	135	123	97	130
	Ni	102	90	76	100	86	68	100	100	76
	Co	107	97	100	100	100	95	100	107	100
	Cu	102	150	167	123	137	180	112	162	170
M4[a]	Fe	90	112	92	97	110	56	99	51	51
	Ni	115	100	90	123	71	84	136	79	100
	Co	102	83	145	100	145	145	75	157	145
	Cu	99	102	145	86	118	150	85	136	154

[a] M1, M2, M3 and M4 are pyrite, DOLT-1, pig kidney and bovine liver, respectively.

data. The good agreement clearly demonstrates the utility of this procedure for the simultaneous determination of iron, cobalt, nickel and copper without tedious pretreatment in complex samples such as biological materials.

Acknowledgements

The authors are grateful to Junta de Andalucia for financial support.

References

[1] O.W. Lau, S.Y. Ho, Anal. Chim. Acta 280 (2) (1993) 269.
[2] V. Rigin, Anal. Chim. Acta 283 (2) (1993) 895.
[3] Z. Shen, Z. Wang, Fensi Huaxue 21 (11) (1993) 1313.
[4] N. Xie, C. Huang, H.D. Fu, Sepu 8 (2) (1990) 114, Chem Abstr. 113 (1990) 094170.
[5] Z. Shen, F. Nie, Y. Chen, Fensi Huaxane 19 (11) (1991) 1272.
[6] H. Martens, T. Naes, Multivariate Calibration, Wiley, Chichester, 1989.
[7] D.M. Haaland, E.V. Thomas, Anal. Chem. 60 (1988) 1193.
[8] K.R. Beebe, B.R. Kowalski, Anal. Chem. 59 (1987) 1007A.
[9] S. Wold, P. Geladi, K. Esbensen, J. Ochman, J. Chemom. 1 (1987) 41.
[10] L.G. Hargis, J.A. Howell, Anal. Chem. 64 (1992) 66R.
[11] J.A. Howell, L.G. Hargis, Anal. Chem. 66 (1994) 445R.
[12] M. Otto, W. Wegscheider, Anal. Chem. 61 (1989) 1847.
[13] M. Vitouchová, L. Jancar, L. Sommer, Fresenius J. Anal. Chem. 343 (1992) 274.
[14] Y.N. Ni, Anal. Chim. Acta 284 (1) (1993) 199.
[15] P. MacLaurin, P.J. Worsfold, M. Crane, F. Norman, Anal. Proc. 29 (1992) 65.
[16] J. Bonilla Abascal, A. Garcia de Torres, J.M. Cano Pavon, Microchem J. 28 (1983) 132.
[17] C. Bosch Ojeda, A. Garcia de Torres, J.M. Cano Pavon, Analyst 110 (1985) 1137.
[18] D.T. Rossi, H.L. Pardue, Anal. Chim. Acta 175 (1995) 153.
[19] L.L. Juhl, J.H. Kalivas, Anal. Chim. Acta 207 (1988) 125.
[20] M. Stone, J. Roy Statis. Soc. B (1974) 111.

ELSEVIER

Talanta 47 (1998) 471–478

Talanta

Permanganate-based chemiluminescence analysis of cefadroxil monohydrate in pharmaceutical samples and biological fluids using flow injection

Fatma A. Aly [a], Nawal A. Alarfaffj [a], Abdulrahman A. Alwarthan [b,*]

[a] *Department of Chemistry, College of Science, Women Student-Medical Studies, Sciences Section, King Saud University, PO Box 22452, Riyadh 11495, Saudi Arabia*

[b] *Department of Chemistry, College of Science, King Saud University, PO Box 2455, Riyadh 11451, Saudi Arabia*

Received 1 December 1997; received in revised form 8 April 1998; accepted 14 April 1998

Abstract

A chemiluminescent method using flow injection is described for the determination of cefadroxil monohydrate. The method is based on the chemiluminescence reaction of cefadroxil with potassium permanganate in sulphuric acid, sensitized by quinine. The proposed procedure allows the determination of cefadroxil over the concentration range 0.1–30 μg ml^{-1} with a detection limit of 0.05 μg ml^{-1} and a sample measurement frequency of 150 samples h^{-1}. The method was successfully applied to the determination of cefadroxil in pharmaceutical preparations and biological fluids. © 1998 Elsevier Science B.V. All rights reserved.

Keywords: Chemiluminescence; Cefadroxil; Potassium permanganate; Pharmaceutical analysis; Biological fluids

1. Introduction

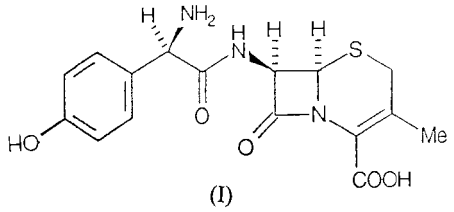

(I)

Cefadroxil monohydrate (I) is a semi-synthetic cephalosporin recently introduced into clinical practice. It is active by oral route on the sensitive gram-positive and gram-negative organisms [1]. Numerous analytical procedures have been reported for its determination either in pure form, in pharmaceutical preparations or in biological fluids. The US P XXIII [2] recommends an HPLC assay, for the evaluation of the raw material and its dosage forms. Other reported methods include: spectrophotometric [3–11], fluorimetric [12–14], polarographic [15], TLC [16] and HPLC [17–20]. Reviewing the literature revealed that, up to the

* Corresponding author. Tel.: +996 1 4676005; fax: +966 1 4679089.

0039-9140/98/$ - see front matter © 1998 Elsevier Science B.V. All rights reserved.
PII S0039-9140(98)00155-6

present time nothing has been published concerning the chemiluminescence (CL) determination of cefadroxil.

Analytical procedures applying (CL) measurements in flow-injection (FI) setups combine the advantages of instrument simplicity (no monochromator required), rapidity in signal detection (normally 0.1–10 s), sensitivity and ease of use. Since many CL reactions are very fast, they give rise to imprecise measurements as a result of irreproducible mixing of sample and reagents, but the reproducibility and selectivity of the CL analysis can be improved by combination with an FI method.

FI chemiluminometric methods based on potassium permanganate oxidation have been reported for the determination of many drugs e.g. morphine [21], loprasolam [22], isoprenaline [23], catecholamines [24] and anaesthetics[25].

Chemiluminescent methods have been used for the determination of some antibiotics e.g. tetracyclines [26–28], cephalothin [29] and penicillins [30].

The present paper describes the development of an FI method based on the CL reaction of potassium permanganate sensitized by quinine for the routine determination of cefadroxil in bulk, in dosage forms and biological fluids.

2. Experimental

2.1. Instruments and flow system

The flow system used for determination and CL detection of cefadroxil, shown schematically in Fig. 1. A Gilson Minipuls 3MP4 peristaltic pump (two channels, variable speed) was used to drive the carrier and the reagent streams through the flow system. Each stream was pumped at a constant flow rate of 3.7 ml min^{-1} using PTFE tubing (0.8 mm i.d.). Cefadroxil solution was injected through the sample injection valve which allows mixing of the sample with the acid and then combination with the $KMnO_4$ solution just before the detector. The emitted light was measured by a photomultiplier tube (Thorn EMI, 9789QB). The signal was recorded by a Yokogawa model 3021 recorder (Yokogawa, Japan). Peak heights were measured.

2.2. Reagents and materials

Analytical reagent grade chemicals and double distilled water were used throughout. Cefadroxil was kindly provided by Bristol-Myers, Squibb, Egypt and used as received. Dosage forms containing cefadroxil being purchased from commercial sources. Cefadroxil standard solution, 1 mg ml^{-1} was prepared in distilled water. Working standard solutions of cefadroxil were prepared by appropriate dilution immediately before use.

Aqueous potassium permanganate (Fluka, UK), 5×10^{-4} M solution.

Sulphuric acid (BDH, Poole, UK), 0.5 M solution.

Aqueous quinine sulphate solution (BDH, Poole, UK) 50 μg ml^{-1} was prepared from 1 mg ml^{-1} stock solution.

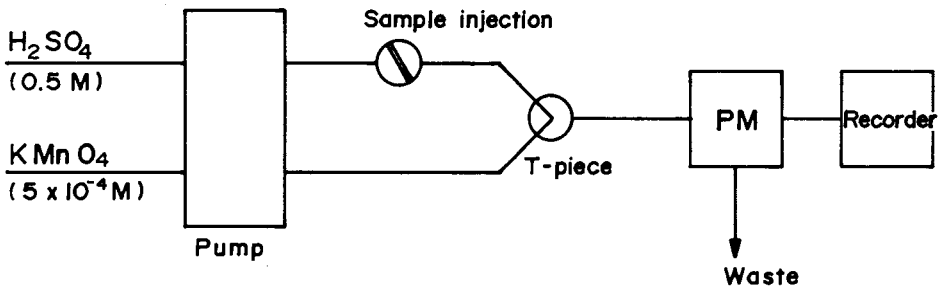

Fig. 1. FI manifold for the chemiluminescent determination of cefadroxil monohydrate: P, peristaltic pump; S, sample port; T, perspex T-piece; L, luminometer; W, waste.

2.3. Procedure

2.3.1. Procedure for calibration

Working cefadroxil-quinine-solution containing cefadroxil in the range of 0.1–30 μg ml^{-1} and quinine sulphate, 50 μg ml^{-1} were prepared from the stock solutions. A 200 μl portion of the above solution was injected into a stream of 0.5 M H_2SO_4 solution which then combined with a stream of 5×10^{-4} M $KMnO_4$ and the resulting peak height was measured. A calibration graph was prepared by plotting the peak height against the concentration of cefadroxil.

2.3.2. Procedure for dosage forms (capsules and suspensions)

Weigh accurately a quantity of the mixed contents of 10 capsules (Ultracef 500 mg per capsule: Bristol-Myers, Squibb, USA) or measure accurately a suitable volume of oral suspension (Ultracef 125 mg per 5 ml: Bristol, Myers, Squibb, USA) equivalent to 10 mg of the drug. Transfer into a 100 ml volumetric flask and dilute to the mark with distilled water. Sonicate for 5 min. Proceed as described above under procedure for calibration. Calculate the nominal content from the corresponding calibration graph or regression equation.

2.3.3. Procedure for biological fluids

2.3.3.1. Procedure for spiked plasma. Add an aliquot of standard aqueous solution of cefadroxil (1 mg ml^{-1}) to 5.0 ml of plasma sample. Add 1.0 ml of 10% (w/v) trichloroacetic acid for each ml of the plasma for deproteination. Blend on a vortex mixer and centrifuge at 3000 rpm for 10 min. Transfer 5.0 ml of the protein-free supernatant into a 25 ml volumetric flask and dilute to volume with distilled water. Proceed as described above. A blank value was determined by treating antibiotic-free plasma in the same way.

2.3.3.2. Procedure for spiked urine. Add a quantity of cefadroxil to the urine to obtain a concentration of 10.0 mg ml^{-1}. Transfer 1.0 ml of this solution into a 100 ml volumetric flask and dilute to volume with distilled water. Proceed as described above. A blank value was determined by treating the antibiotic-free urine in the same way.

3. Results and discussion

The flow-injection chemiluminometric determination of cefadroxil was studied using different oxidants such as potassium dichromate, sodium persulphate, potassium iodate, cerium(IV) sulphate, potassium permanganate and *N*-bromosuccinimide in acidic or basic media. The CL of cefadroxil was obtained only when potassium permanganate was used as an oxidant in an acidic medium.

3.1. Configuration designs

The FI configuration used for the determination of cefadroxil was so designed to provide different reaction conditions for magnifying the CL signal generated by the reaction of cefadroxil with $KMnO_4$. Maximum CL intensity was obtained when the sample was injected into a stream of 0.5 M H_2SO_4 and then mixed with $KMnO_4$ just before the detector.

3.2. Optimization of experimental variables

A series of experiments were conducted to establish the optimum analytical variables. The parameters optimized included reagent concentrations and some physical variables including the total flow rate and the sample injection volume.

3.2.1. Effect of different acid concentrations

Four different acids (i.e. H_3PO_4, CH_3COOH, HCOOH and H_2SO_4) of different concentrations in the range 1×10^{-3}–5.0 M were tested in order to ascertain which was the most suitable. Maximum CL intensity was obtained with 0.5 M H_2SO_4 (Table 1). This was further established using different concentrations of H_2SO_4 with different concentrations of the drug (10–80 μg ml^{-1}).

Table 1
Effect of different acid concentrations on the CL intensity of cefadroxil monohydrate (20 μg ml^{-1})

Concentration of acid (M)	CL intensity[a] (mV)			
	H_2SO_4	H_3PO_4	CH_3COOH	HCOOH
1×10^{-3}	0.3	0.1	0.0	0.0
1×10^{-2}	2.9	0.9	0.0	0.2
0.1	9.0	2.4	0.3	0.8
0.5	12.8	3.2	1.0	3.2
2.0	12.0	3.2	1.8	4.5
5.0	12.0	3.2	2.7	6.6

[a] Each result is the average of three separate determinations.

3.2.2. Effect of potassium permanganate concentration

Fig. 2 shows the effect of $KMnO_4$ concentration on the CL intensity. The greatest CL response was obtained with 5×10^{-4} M. Larger concentrations of $KMnO_4$ lowered the CL intensity. Therefore, 5×10^{-4} M $KMnO_4$ was used.

3.2.3. Effect of sensitizers

Based on the observation that some of the fluorescing compounds can be used for energy-transfer in the CL reactions with an enhancement of the intensity [31,32], various fluorophores were investigated for obtaining maximum yields in CL intensity. Different concentrations (0.5–100 μg ml^{-1}) of rhodamine-B, fluorescein and quinine sulphate dissolved in the drug solution or in the carrier or in the $KMnO_4$ solution were investigated. It was found that only quinine enhanced the CL signal when dissolved in the drug solution. About 50 μg ml^{-1} of quinine gave rise to the most intense signal, so this concentration of quinine was used in all subsequent studies.

Quinine sulphate was previously tested as an energy transfer-reagent in the CL reaction of Ce(IV) with thiol-containing drugs [33,34].

3.2.4. Effect of reagents flow-rate

The flow rate of the reagent solutions was optimized in order to obtain satisfactory CL emission. The flow-rate is conveniently controlled by the peristaltic pump. The effect of total flow-rate was studied, keeping all other conditions constant, over the range 3.6–10.5 ml min^{-1}, with equal flows in each channel. The results obtained show that the CL intensity continues to increase with increasing the total flow-rate up to 7.4 ml min^{-1} (3.7 ml min^{-1} for each channel). Above this flow-rate, the emission intensity started to be constant as shown in Fig. 3.

3.2.5. Effect of sample injected volume

An increase in sample volume normally leads to an increase of emitted CL signal. Fig. 4 shows that a change in loop size from 10–200 μl can improve the CL intensity by a factor of 3, further increase in sample volume from 200–800 μl in-

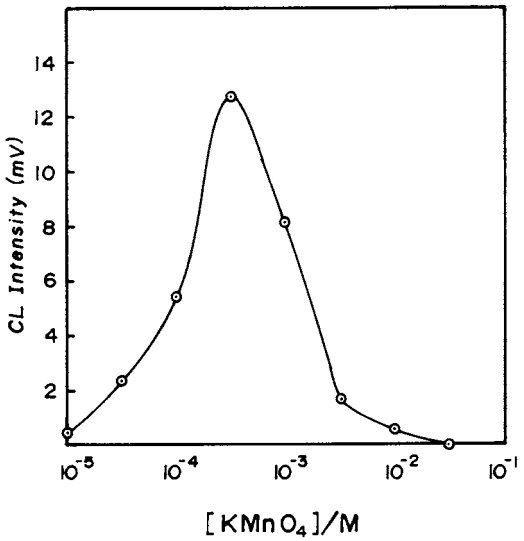

Fig. 2. Effect of potassium permanganate concentration on the cefadroxil CL emission. Injected drug solution (200 μl), 20 μg ml^{-1}, flow-rate 3.7 ml min^{-1}.

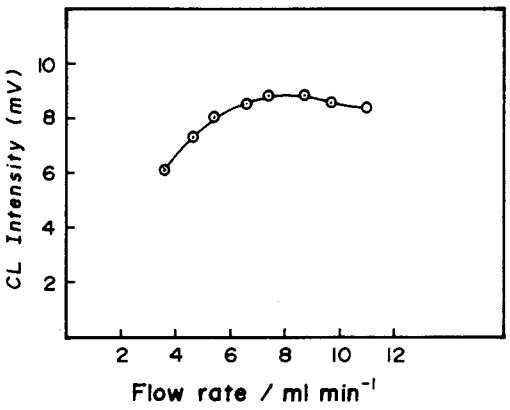

Fig. 3. Effect of total flow-rate on CL intensity of cefadroxil. Injected drug solution (200 μl), 20 μg ml^{-1}.

creases the CL intensity much slower. Therefore, 200 μl was considered the optimum sample injected volume in the FI system.

3.2.6. Effect of some micellar solutions

The effect of some organized systems, including neutral surfactants (Triton X-100), cationic surfactants (cetyltrimethylammonium bromide, cetylpyridinium bromide and cetylpyridinium chloride), and anionic surfactants (sodium dodecyl sulphate) on the CL reaction was investigated.

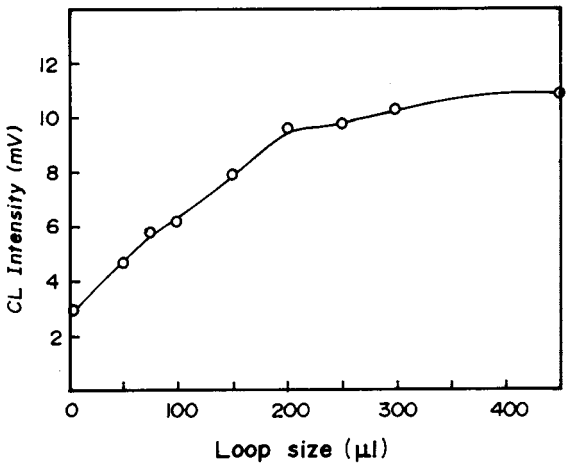

Fig. 4. Effect of sample volume of cefadroxil on CL emission. Injected drug solution 20 μg ml^{-1}.

All these surfactants had no effect on the CL intensity.

4. Determination of cefadroxil monohydrate

Under the described experimental conditions, a standard calibration curve for cefadroxil was constructed. The CL intensity (I, mV) was linearly related to cefadroxil concentration over the range of 0.1–30 μg ml^{-1} with a minimum detectability ($S/N = 2$), of 0.05 μg ml^{-1}. Linear regression analysis of the results gave the following equation.

$$C = -0.494 + 1.988I \quad (r = 0.9999, n = 8)$$

The precision of the method was evaluated by analyzing pure samples of cefadroxil. The results in Table 2 were in accord with those obtained by the USP XXII [35].

5. Possible CL mechanism

The CL mechanism may be attributed to the following reactions:

$$\text{Cefadroxil} + MnO_4^- + 8H^+$$

$$\rightarrow \text{Oxidized cefadroxil}^* + Mn^{+2} + 4\ H_2O$$

In the presence of quinine, the energy resulting from the redox reaction can be effectively transferred to quinine which in turn generates CL emission.

$$\text{Oxidized cefadroxil}^* + \text{Quinine}$$

$$\rightarrow \text{Oxidized cefadroxil} + \text{Quinine}^*$$

$$\text{Quinine}^* \rightarrow \text{Quinine} + \text{light}$$

The CL emission of oxidized cefadroxil(II) may be ascribed to the oxidation of the phenolic group in the para position of the benzene ring to form a cyclohexadienone structure (II). This was further confirmed by unsuccessful trials for the determination of cephalexin, which has a similar structure to cefadroxil but without the phenolic group, by the proposed method. This indicates that the presence of a phenolic group is essential for the CL signal of cefadroxil.

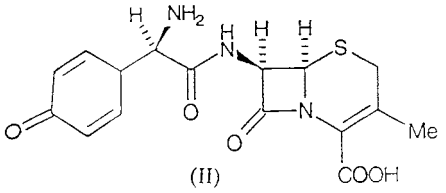

(II)

6. Application of the method

6.1. Analysis of pharmaceutical preparation

The proposed method was successfully applied to the analysis of some dosage forms containing cefadroxil. The results in Table 2 are in accordance with those obtained by the official method [35].

Statistical analysis [36] of the results reveals that there is no significant difference between the two methods as regards to accuracy and precision.

6.2. Analysis of spiked urine and plasma samples

The high sensitivity attained by the proposed method allows the determination of cefadroxil in biological fluids. About 88% of a dose of cefadroxil is excreted in the urine unchanged [37]. Mean peak serum concentrations of cefadroxil in healthy subjects after 0.5 and 1.0 g doses were 15 and 26 μg ml^{-1}, respectively, 2 h after administration [37]. Thus the proposed method proved to be satisfactory for the kinetic studies and routine estimation of cefadroxil in human urine and plasma. For plasma only a deproteination process was carried out using trichloroacetic acid as a sample pre-treatment, an extraction procedure was not necessary [38].

Antibiotic-free urine samples gave a relatively high CL intensity, so a dilution of 1:100 (v/v) was required to minimize this interference. The diluted urine gave a very low CL intensity. Table 3 shows the results of the recovery studies of cefadroxil from spiked plasma and urine.

Table 2
Application of the proposed and official methods to the determination of cefadroxil monohydrate and its dosage forms

Drug form	Taken (μg ml^{-1})	Found (μg ml^{-1})	Recovery (%)	Official method [35] recovery (%)
Cefadroxil (pure sample)	0.5	0.500	100.0	
	1.0	0.997	99.7	
	2.5	2.488	99.5	
	10.0	9.843	98.4	
	20.0	20.179	100.9	
Mean ± SD			99.7 ± 0.9	100.5 ± 1.4
Ultracef capsules[a] (500 mg cefadroxil capsule)	1.0	1.000	100.0	
	2.5	2.500	100.0	
	5 0	5.000	100.0	
	10.0	10.130	101.3	
	20.0	20.240	101.2	
Mean ± SD			100.5 ± 0.7	100.2 ± 0.8
Ultracef suspension[a] (125 mg cefadroxil/5 ml)	1.0	1.000	100.0	
	2.5	2.500	100.0	
	5.0	5.055	101.1	
	10.0	10.230	102.3	
Mean ± SD			100.9 ± 1.1	100.5 ± 0.9

[a] Bristol-Myers, Squibb, USA.

Table 3
Determination of cefadroxil in spiked urine and plasma

Concentration taken (μg ml^{-1})	Found (%)	
	Urine	Plasma
5.0	100.0	96.7
10.0	100.0	96.3
15.0	100.0	95.1
20.0	100.0	95.4
25.0	99.3	94.7
Mean ± SD	99.9 ± 0.3	95.7 ± 0.8

7. Conclusion

A simple, rapid and highly sensitive chemiluminometric method is described for the determination of cefadroxil in dosage forms and in biological fluids. The method described requires only a deproteination of plasma samples and dilution of urine samples to avoid the liable interference. The method can be used for HPLC detection. Trials were made for the determination of other cephalosporins (e.g. cephalexin, cephradine and cefotaxime) and other antibiotics (e.g. kanamycin and neomycin) by the proposed method but no CL signals were obtained.

Acknowledgements

The authors are very grateful to King Abdul Aziz City for Science and Technology (KACST) for the grant supporting this project (AT-17-T16).

References

[1] R. Reiner, Antibiotics, Roche Scientific Service, George Thieme Verlag, Stuttgart, 1982, p. 114.
[2] The United States Pharmacopoeia XXIII, National Formulary XVIII. Rockville, MD, USP Convention, 1995.
[3] P.B. Issopoulos, Acta Pharm. Hung. 61 (1991) 205.
[4] S.S. Badawy, F.M. Abdel-Gawad, M.M. Ibrahim, Anal. Lett. 26 (1993) 478.
[5] M.M. Abdel-Khalek, M.S. Mahrous, H.G. Daabess, J. Pharm. Sci. 7 (1993) 211.
[6] A.A. Al warthan, F.H. Metwally, S.A. Al tamimi, Anal. Lett. 26 (1993) 2619.
[7] F.A. Aly, M.I. Walash, F. Belal, Anal. Lett. 27 (1994) 2677.
[8] M.I. Walash, S. Toubar, S.M. Ahmed, N.A. Zakhari, Anal. Lett. 27 (1994) 2499.
[9] G.A. Saleh, Analyst 121 (1996) 641.
[10] Y.M. Issa, A.S. Amin, Mikrochim. Acta 124 (1996) 203.
[11] C.S.P. Sastry, K.R. Rao, D.S. Prasad, Mikrochim. Acta 126 (1997) 167.
[12] M.A. Korany, M.A.H. El-sayed, S.M. Galal, Spectrosc. Lett. 22 (1989) 619.
[13] J.H. Yang, G.J. Zhou, N.Q. Tie, R.J. Han, C.G. Lin, J.T. Hu, Anal. Chim. Acta 325 (1996) 195.
[14] J.H. Yang, G.J. Zhou, G.L. Zhang, Z.K. Si, J.T. Hu, Anal. Commun. 33 (1996) 167.
[15] A. Ivaska, F. Nordstrom, Anal. Chim. Acta 146 (1983) 87.
[16] H. Fabre, M.D. Blanchin, D. Lerner, B. Mandrou, Analyst 110 (1985) 775.
[17] M.C. Hsu, Y.W. Chang, Y.T. Lee, J. Chromatogr. 609 (1992) 181.
[18] C. Hendrix, Y.X. Zhu, C. Wijsen, E. Roets, J. Hoogmartens, J. Chromatogr. 634 (1993) 257.
[19] C. Hendrix, C. Wijsen, L.M. Yunn, E. Roets, J. Hoogmartens, J. Chromatogr. 628 (1993) 49.
[20] Y.P. Patel, U.J. Dhorda, M. Sundaresan, A.M. Bhagwat, Indian Drugs 34 (1997) 43.
[21] R.W. Abbott, A. Townshend, R. Gill, Analyst 111 (1986) 635.
[22] A.R.J. Andrews, A. Townshend, Anal. Chim. Acta 227 (1989) 65.
[23] A.A. Al-tamrah, A.A. Al-warthan, A.S. Al-amri, J. Saudi Chem. Soc. 1 (1997) 1.
[24] N.T. Deftereos, A.C. Calokerinos, C.E. Efstathiou, Analyst 118 (1993) 627.
[25] X.R. Zhang, W.R.G. Baeyens, G. Van Der Weken, A.C. Calokerinos, K. Imai, Anal. Chim. Acta 303 (1995) 137.
[26] A.A. Al-Warthan, A. Townshend, Anal. Chim. Acta 205 (1988) 261.
[27] C.A. Halvatzis, M.M. Timotheou-Potamia, A.C. Calokerinos, Analyst 118 (1993) 633.
[28] X.R. Zhang, W.R.G. Baeyens, A. Van Den Borre, G. Van Der Weken, A.C. Calokerinos, S.G. Schulman, Analyst 120 (1995) 463.
[29] S.G. Schulman, J.H. Perrin, Guo FanYan, Shagsian Chen, Anal. Chim. Acta 255 (1991) 383.
[30] S. Ventura, M. Silva, D. Perez-Bendito, Anal. Chim. Acta 266 (1992) 301.
[31] K.W. Sigvardson, J.M. Kennish, J.W. Birks, Anal. Chem. 56 (1984) 1096.
[32] K. Honda, K. Miyaguchi, K. Imai, Anal. Chim. Acta 177 (1985) 111.

[33] Z.D. Zhang, W.R.G. Baeyens, X.R. Zhang, G. Van Der Waken, Analyst 121 (1996) 1569.
[34] Y. Zhao, W.R.G. Baeyens, X. Zhang, A.C. Calokerinos, K. Nakashima, G. Van Der Waken, Analyst 122 (1997) 103.
[35] The United States Pharmacopoeia XXII, National Formulary XVII, Rockville MD, USP Convention, (1990).
[36] D.H. Sanders, A.F. Murph, R.J. Eng, Statistics, McGraw-Hill, New York, 1976.
[37] Martindale, The Extra Pharmacopoeia, J.E.F. Reynold (Ed.), 30th Edn., The Pharmaceutical Press, London, 1993.
[38] F.A. Aly, M.M. Hefnawy, F. Belal, Anal. Lett. 29 (1996) 117.

ELSEVIER

Talanta 47 (1998) 479–485

Talanta

Simultaneous kinetic spectrophotometric determination of vanadium(V) and iron(III)

Hossein Tavallali, Ali Massoumi *

Department of Chemistry, Faculty of Sciences, Shahid Beheshti University, Tehran, 19839, Iran

Received 1 December 1997; received in revised form 8 April 1998; accepted 14 April 1998

Abstract

Vanadium(V) and iron(III) can be determined simultaneously at pH 2 and 25°C by a single experiment using their kinetic effect on the oxidation of indigo carmine by bromate which goes through an induction period and then decreases in absorbance, at λ_{max}, 612 nm. The rate of the color-fading of indigo carmine is proportional to the concentration of vanadium and is independent of the concentration of iron. The length of the induction period of the reaction is related to the concentration of iron and is independent of the concentration of vanadium. Concentrations of 0.3–2 (μg ml^{-1}) vanadium(V) and 6–12 (μg ml^{-1}) iron(III) were determined with mean relative errors of 2.7 and 1.6%, respectively. The interference effects of various cations and anions on determination of mixtures of vanadium and iron is reported. Application of the method to real samples and several mixtures of standard solutions are performed which gave acceptable results. © 1998 Elsevier Science B.V. All rights reserved.

Keywords: Kinetic method; Simultaneous determination; Vanadium(V); Iron(III); Determination

1. Introduction

Differences in kinetic behavior have been used extensively for the simultaneous determination of two or more components in mixtures. Many differential kinetic methods have been proposed for the analysis of mixtures of closely related species without prior separation [1], however, most of them have relied on two or more kinetic runs under optimum reaction conditions [2–5]. Simultaneous determination of components by common indicator reaction through a single kinetic run is generally difficult.

We recently determined vanadium(V) based on kinetic effect on the reaction of oxidation of indigo carmine (IC) by bromate [6]. This oxidation reaction was characterized by an induction period. In a certain range, the length of the induction period only depends on the concentration of iron(III). Changes in the iron(III) concentration has no influence on the rate of color-fading of IC. Only changes in the vanadium(V) concentration influences the rate of the color-fading although, it dose not cause changes in the induction period.

This work presents a method which concentrates on the simultaneous determination of mix-

* Corresponding author. Tel.: +98 21 2401765, +98 21 2043041; fax: +98 21 2403041; e-mail: Massoumi@Beheshti.sbu.ac.ir

0039-9140/98/$ - see front matter © 1998 Elsevier Science B.V. All rights reserved.
PII S0039-9140(98)00156-8

tures of vanadium(V) and iron(III) using only one kinetic run, without prior separation or any restriction during the reaction. Although it is less sensitive in comparison to some of the kinetic-catalytic methods reported previously, but, it offers a simple and selective determination of vanadium(V) and iron(III) in mixtures of standard solutions and real samples.

2. Experimental

2.1. Apparatus

A UV–visible spectrophotometer (Shimadzu UV-2100) was used. The change in absorbance by time was displayed on the screen. A mechanical stirrer (Janke and Kunkel, IKA-Werk) was used for mixing when using the procedure of data collection by spectrophotometer. pH was adjusted by a 691 Metrohm pH meter. The temperature was kept constant at 25 ± 0.1°C by a thermostat (Shimadzu TB-85). All the solutions were previously brought to this temperature. The temperature was maintained constant in the reaction cell by circulating water at appropriate temperature around the cell compartment of the spectrophotometer during the experiment.

2.2. Reagents

All reagents were of analytical-reagent grade and triply distilled water was used throughout.

A 1000 μg ml^{-1} stock solution of vanadium(V) was prepared by dissolving 0.2393 g of sodium monovanadate ($NaVO_3$, Merck) in 100 ml of distilled water and standardized it [7]. Working standard solutions were prepared by diluting aliquots of stock solution.

A 1000 μg ml^{-1} stock solution of iron(III) was prepared by dissolving 0.7234 g of ($Fe(NO_3)_3.9H_2O$, Merck) in 100 ml of distilled water and standardized by potassium dichromate [8]. Working standard solutions were prepared by diluting aliquots of stock solution.

Stock solution of IC (1.0×10^{-3} M) was prepared by dissolving 0.0233 g of recrystalized IC (Merck) in distilled water and diluting to 50 ml. Solution of pH 1–3 were prepared by adding appropriate amounts of 0.1 M nitric acid (Merck) and 0.1 M acetic acid (pH 4) to sodium acetate (Merck), respectively and pH was adjusted with pH meter.

Potassium bromate solution (0.03 M) was prepared by dissolving 0.5010 g of $KBrO_3$ (Merck) in distilled water, and diluting to 100 ml.

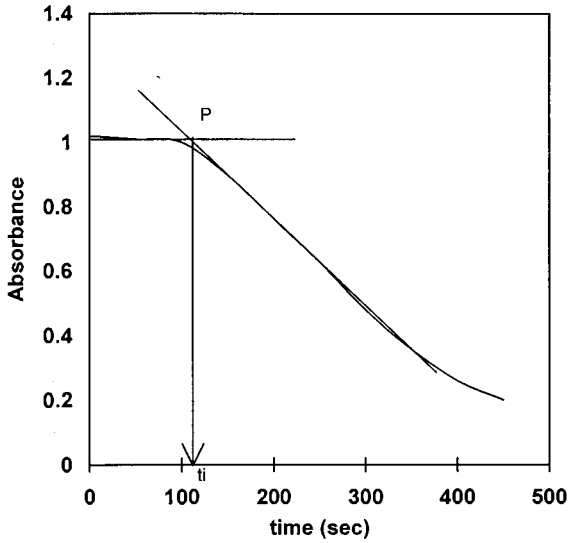

Fig. 1. Change in absorbance during the oxidation of indigo carmine by bromate in the presence of 1.7 μg ml^{-1} vanadium(V) and 8 μg ml^{-1} of iron(III), see text.

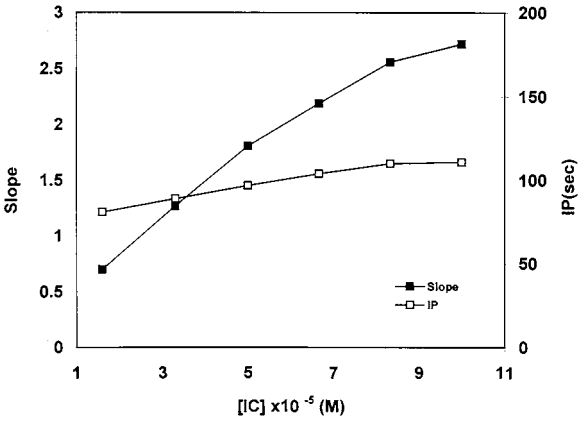

Fig. 2. Effect of indigo carmine concentration on the reaction rate and induction period (IP) in the presence of 1.5 μg ml^{-1} vanadium(V) and 8 μg ml^{-1} of iron(III).

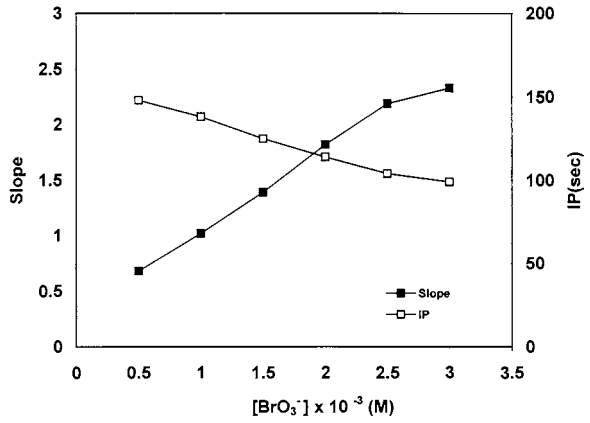

Fig. 3. Effect of bromate concentration on the reaction rate and induction period (IP) in the presence of 1.5 μg ml^{-1} vanadium(V) and 8 μg ml^{-1} of iron(III).

A 3 M stock solution of ionic buffer was prepared by dissolving an appropriate amount of sodium nitrate (Merck) in distilled water and stock solution (5000 μg ml^{-1}) of each interfering ion was prepared by dissolving appropriate amounts of suitable salt in distilled water.

2.3. Recommended procedure

The catalytic reaction was monitored spectrophotometrically by measuring the change in absorbance of the reaction mixture at 612 nm. The solutions were prepared in 1 cm, 4 ml glass cell.

A 1.5 ml of buffer solution (pH = 2) was added to a sample solution containing 200 ml of IC (1.0×10^{-3} M), 250 μl of bromate (0.03 M) and 650 μl of distilled water. The cell was inserted in the cell compartment of the spectrophotometer,

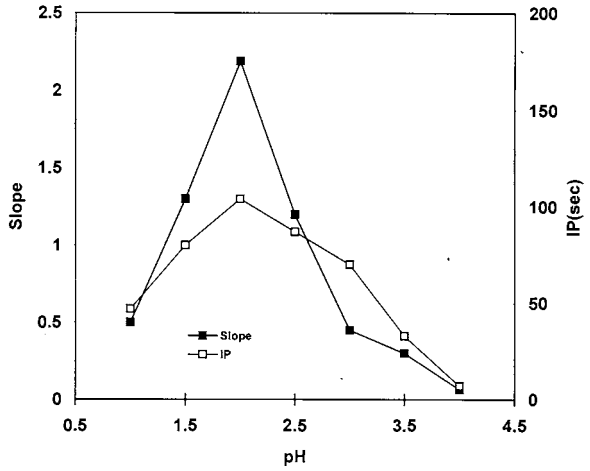

Fig. 4. Effect of pH on the reaction rate and induction period (IP) in the presence of 1.5 μg ml^{-1} vanadium(V) and 8 μg ml^{-1} of iron(III).

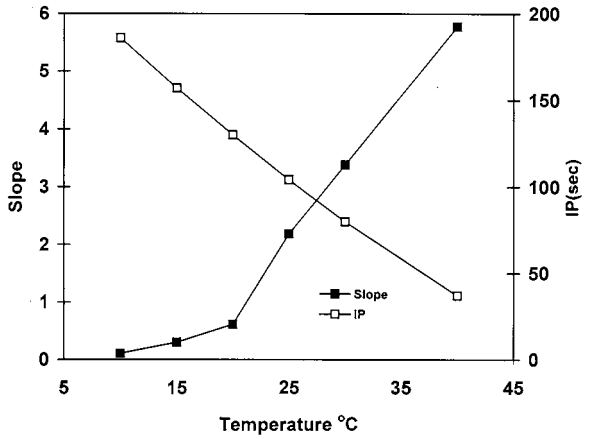

Fig. 5. Effect of temperature on the reaction rate and induction period (IP) in the presence of 1.5 μg ml^{-1} vanadium(V) and 8 μg ml^{-1} of iron(III).

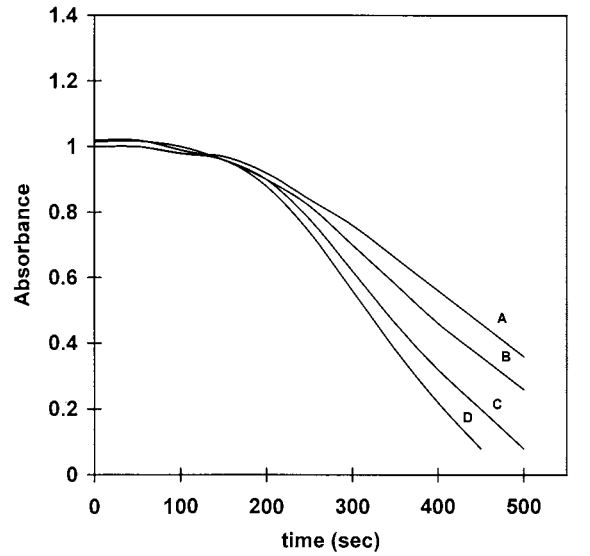

Fig. 6. Effect of changing vanadium concentration, A: 0.9, B: 1.3, C: 1.7, D: 2 μg ml^{-1} , when the iron(III) concentration was kept constant 8 μg ml^{-1}, at optimum conditions.

where its temperature was kept constant at 25°C for 15 min. A mechanical stirrer was used to mix the solution in the cell. After 10 s 200 μl of vanadium and 200 μl of iron (which taken from appropriate concentration) was added simultaneously to the cell by a variable 1000 μl samplers, and the variation of absorbance versus time was measured during a 10 min interval. The cell was cleaned and dried after each use by distilled water and acetone, respectively.

2.4. Results and discussion

Two separate measurements were made. The first was based on the graphical measurement of induction period and the other on the slope method. The linear part of the color-fading, shown in Fig. 1, was prolonged and intersected the extrapolation of the line at the initiation of the curve, shown as point *P*. The time corresponding to point *P* was defined as the induction period t_i , which depends on iron(III) concentration. The rate of the color-fading reaction v was characterized by the slope of the linear part of the curve that depends on vanadium(V) concentration.

Indigo carmine is a dye (C.I.NO. 73015) and is used as a redox indicator [9]. Its oxidized form is produced by oxidants such as bromate [10], forming a colorless product.

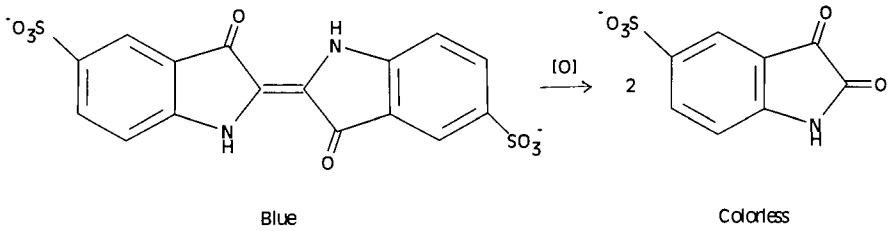

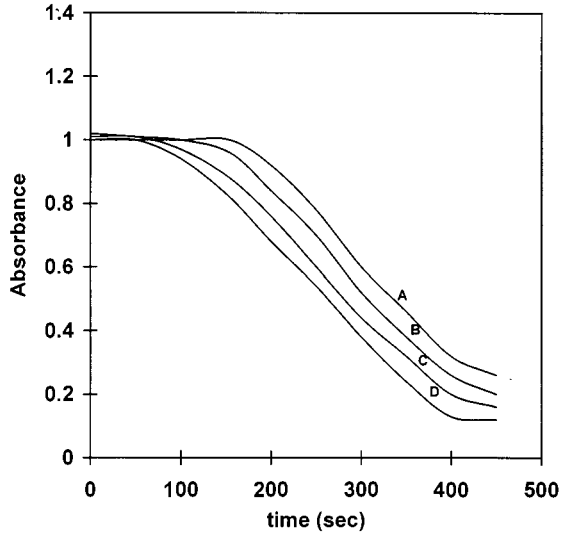

Fig. 7. Effect of changing iron concentration, A: 6, B: 8, C: 10, D: 12, μg ml^{-1}, when the vanadium(V) concentration was kept constant, 1.7 μg ml^{-1}, at optimum conditions.

Table 1
Effect of foreign ions on simultaneous determination of 1 μg ml^{-1} vanadium(V) and 6 μg ml^{-1} iron(III) under optimum conditions

Species	Tolerance limit of ion to
	V(V) ($W_{ion}/W_{V(V)}$)
Co^{2+}, Mg^{2+}, Ag^{+}, W^{6+}, CH_1C^{-}, $H_2PO_4^{-}$, SO_4^{2-}, HPO_4^{2-}, ClO_4^{-}, HCO_3^{-}, Cl^{-}, NO_3^{-}, PO_4^{3-}	500[a]
Al^{3+}, SCN^{-}, IO_3^{-}	250
Cu^{2+}, Fe^{2+}, Hg_2^{2+}, Cr^{3+}, SO_3^{2-}	100
F^{-}, As^{3+}, V^{4+}, $S_2O_7^{2-}$, Ce^{4+}, Mo^{6+}, I^{-}	35
Cr^{6+}, $S_2O_8^{2-}$	1
	Fe (III) ($W_{ion}/W_{Fe(III)}$)
Co^{2+}, Mg^{2+}, Ag^{+}, W^{6+}, Fe^{2+}, CH_3COO^{-}, SO_4^{2-}, Cl^{-}, NO_3^{-}, HPO_4^{2-}, $H_2PO_4^{-}$, PO_4^{3-}, HCO_3^{-}, CLO_4^{-}	100
Al^{3+}, SCN^{-}, IO_3^{-}, SO_3^{2-}	45
Cu^{2+}, Hg_2^{2+}, Cr^{3+}	20
Ce^{4+}, Mo^{6+}, As^{3+}, V^{4+}, F^{-}, I^{-}, $S_2O_7^{2-}$, $S_2O_8^{2-}$	13
Cr^{6+}	0.5

[a] Largest amount tested.

Table 2
Analysis of mixtures of vanadium(V) and iron(III)

Vanadium(V) (μg ml^{-1})			Iron(III) (μg ml^{-1})		
Added	Found	Relative error (%)	Added	Found	Relative error (%)
2.00	2.01	−0.5	7.5	7.4	1.3
1.80	1.85	−2.8	9	8.9	1.1
1.60	1.56	2.5	6.0	5.8	3.3
1.50	1.48	1.3	6.5	6.4	1.6
1.30	1.25	3.8	6.9	7.0	1.4
1.00	1.03	−3.0	7.0	7.1	1.4
0.90	0.93	−3.3	8.3	8.4	1.2
0.80	0.81	−1.3	9.7	9.9	−2.0
0.70	0.67	4.3	10.8	11.0	−1.9
0.50	0.48	4.0	11.5	11.6	−0.9
0.40	0.39	2.5	12.0	11.8	1.7

This reaction proceeds very slowly, but in the presence of traces (μg ml^{-1}) of vanadium and iron, after an induction period, it becomes colorless quickly, as shown in Fig. 1.

The following optimization were undertaken to achieve maximum sensitivity and large linear dynamic ranges.

2.5. Effect of variables

The effect of indigo carmine concentration on the reaction rate and induction period is shown in Fig. 2. The initial absorbance increased with increasing IC concentration. Over the range of 1.6×10^{-5}–1.0×10^{-4} M of IC, the reaction rate increased, but induction period was almost unchanged. Both slope and induction period were maximum when the concentration of IC was selected higher than 6.66×10^{-5} M, but the optimum concentration of IC was chosen as 6.66×10^{-5} M in order to avoid absorbance error due to high molar absorbtivity of IC.

The effect of bromate concentration on the reaction rate and induction period was investigated in the range of 5.0×10^{-4}–3.0×10^{-3} M of bromate shown in Fig. 3.

The reaction rate increased and the induction period shortened with an increase in bromate concentration. Therefore the sensitivity for the determination of vanadium(V) increased and the sensitivity for the determination of iron(III) reduced. A concentration of 2.5×10^{-3} M bromate was therefore adopted for this work.

The effect of ionic strength on the reaction rate was investigated. The ionic strength was varied from 0.01 to 0.1 M, using $NaNO_3$ solution. The results showed that this parameter had no effect on the reaction rate up to 3.3×10^{-2} M.

The effect of pH on the rate of the reaction and induction period were studied in the pH range 1–4 that is shown in Fig. 4. As it is seen from the figure the reaction rate and induction period were maximum at pH 2. So pH 2 was used as optimum pH because higher sensitivity was achieved for the determination of vanadium(V) and iron(III).

The effect of temperature was studied in the temperature range 10–40°C. Fig. 5 shows that the reaction rate increased and induction period decreased with increasing temperature. Also the sensitivity for the determination of vanadium(V) increased and the sensitivity for the determination of iron(III) reduced. The 25°C temperature was selected as optimum conditions of the experiment.

The effect of vanadium(V) and iron(III) on each other was studied. When the iron(III) concentration was kept constant, changing the vanadium(V) concentration only caused a change in the slope of the curve (Fig. 6). On the other hand, changing the iron(III) concentration while the concentration of vanadium(V) was kept constant, gave rise to induction period (Fig. 7). So it was possible to determine these two ions simultaneously.

Table 3
Determination of vanadium(V) and iron(III) in vicalloy and petroleum crude

Method	Sample	Vanadium(V) μg ml^{-1}		Iron(III) μg ml^{-1}	
		Content	RSD (%)	Content	RSD (%)
Proposed method	Vicalloy	1.730	1.20	6.800	1.10
Atomic absorption spectrometry	Vicalloy	1.700	1.00	6.830	1.10
Proposed method	Petroleum crude	1.300	1.30	10.540[a]	1.12
Atomic absorption spectrometry	Petroleum crude	1.310	0.80	10.510[a]	1.10

RSD = relative standard deviation for $n = 6$.
[a] After addition of 10.500 μg ml^{-1} of iron(III) to samples.

2.6. Calibration graphs and precision

Calibration graphs were obtained by slope and induction period for vanadium(V) and iron(III), respectively. For determination of vanadium the calibration curve was linear in the range 0.3–2 μg ml^{-1} with regression equation of $v = 1.064C + 0.597$ and correlation coefficient, r, of 0.9985, where C is the concentration of vanadium in μg ml^{-1} and v is the change in mAbs s^{-1}. The length of the induction period was proportional to the iron(III) concentration, and the calibration curve was linear in the range 6–12 μg ml^{-1} with regression equation of $t_i = -12.463C_i + 203.32$ and correlation coefficient, r, of 0.9978, where C_i is concentration of iron in μg ml^{-1} and t_i is the induction period (s).

To evaluate the precision, and the detection limit, a series of independent standard samples with fixed IC concentration, was used. In the determination of vanadium, six replicate measurements using 0.4 and 1.5 μg ml^{-1} of vanadium with a constant concentration of iron equal to 8 μg ml^{-1}, were made. RSD and recovery for 0.4 μg ml^{-1} of vanadium were 2.1 and 100.1%, respectively, while those for 1.5 μg ml^{-1} of vanadium concentration gave values of 1.3 and 98.0%, respectively. RSD and recovery for four times determinations of 0.4 μg ml^{-1} of vanadium, while the concentration of iron solutions were (6, 8, 10, 12, μg ml^{-1}) were 3.2, 102.3% respectively.

In the determination of iron, the relative standard deviation, RSD, and recovery for six replicate determinations of 8 μg ml^{-1} of iron while the concentration of vanadium kept constant 1.7 μg ml^{-1} were 1.12 and 97.0% respectively. RSD and recovery for four times determinations of 8 μg ml^{-1} of iron, while the concentration of vanadium solutions were (0.4, 0.8, 1.3, 1.7, μg ml^{-1}) were 4.2, 101.7%, respectively.

The limit of detections, which can be calculated on the basis of $Y_{DL} = Y_B + 3S_B$ [11], in which Y_{DL}, Y_B, and S_B are signal of detection limit, blank signal, and standard deviation of the blank, respectively, was 0.27 μg ml^{-1} for vanadium and 4.2 μg ml^{-1} for iron.

2.7. Interference study

To study the selectivity of the proposed method the effect of various cations and anions on the reaction rate and induction period of mixtures, 1 μg ml^{-1} of vanadium and 6 mg ml^{-1} of iron was tested under the optimum conditions. The results are summarized in Table 1 with maximum tolerance limit for each ion.

2.8. Determination of vanadium(V) and iron(III) in mixtures

Various mixtures of standards of iron(III) and vanadium(V) solutions, were prepared and tested according to the recommended procedure. The test was carried out covering concentrations within the dynamic ranges of the species, using different concentration ratio of these elements. These concentrations covered maximum concentration of vanadium(V) with minimum concentration of iron(III) and vice versa with other proportions indicated in Table 2. The relative

error of measurements were less than 5%. The maximum relative errors for vanadium(V) and iron(III) were 4.3 and 3.3%, respectively. The values for the mean relative error were 2.7 and 1.6% for vanadium(V) and iron(III), respectively.

As it is observed, the method is applicable for the determination of iron(III) and vanadium(V) in the mixtures contain each proportions of these two metal ions. Based on the results of previous study [6] it seems that IC is oxidized by bromate with vanadium(V) acting as catalyst. The species formed between IC and vanadium(V) requires an induction period for its formation prior to the oxidation process by bromate. It could be highly probable that formation reaction is promoted by the presence of iron(III) in the system. This is also further indicated by the reduction of induction period prior to oxidation when iron(III) is present. Owing to the complexity of the mechanism, some steps of the reaction are still unclear.

3. Application

The proposed method was applied for the determination of vanadium(V) and iron(III) in vicalloy and petroleum crude, which gave satisfactory results in comparison to atomic absorption spectrometry data (Table 3).

3.1. Vicalloy

An accurate weighed quantity of vicalloy is dissolved in 1:4 H_2SO_4 by heating followed by 10 ml concentrated HNO_3 according to an established procedure [12], after dissolution the solution was diluted and its iron(III) and vanadium(V) contents were determined according to the proposed procedure.

3.2. Petroleum crude

The petroleum crude samples (Named Furouzan) were treated with concentrated sulfuric acid followed by combustion of carbonaceous ash at 526 ± 30°C. The inorganic residues were digested with HCl (1:1) for 15 min. After concentration, a few drops of concentrated HNO_3 and H_2SO_4 were added and the solutions were gently heated until white fumes were formed. The small carbonaceous residues that had not been ignited were destroyed. The solution was finally diluted to 50 ml in a 50-ml volumetric flask and the vanadium(V) and iron(III) contents were measured via the recommended procedure.

Acknowledgements

The authors wish to express their gratitude to Shahid Beheshti University Research council for the support of this work.

References

[1] D. Perez-Bendito, M. Silva, Kinetic Methods in Analytical Chemistry, Ellis Horwood, Chichester, 1988.
[2] K.B. Yatsimirskii, L.P. Raizman, Zh. Anal. Khim. 18 (1963) 829.
[3] J.B. Worthington, H.L. Pardue, Anal. Chem. 42 (1970) 1157.
[4] A. Moreno, K.M. silva, D. Perez-Bendito, Anal. Chem. Acta 159 (1984) 319.
[5] P.A. Rodringun, H.L. Pardue, Anal. Chem. 41 (1969) 1376.
[6] A. Massoumi, H. Tavallali, Anal. Lett. 31 (1) (1998) 193–206.
[7] A.I. Vogel, A Text Book of Quantitative Inorganic Analysis, Longman, 5th edn., pp. 698–699.
[8] A.I. Vogel, A Text Book of Quantitative Inorganic Analysis, Longman, 5th edn., pp. 376–377.
[9] A. Safavi, B. Haghighi, Fresenius J. Anal. Chem. 357 (1997) 870–873.
[10] B.F. Shraydeh, M.A. Abueid, N.A. Zatar, A. Abuobeid, M. Khamis, K. Kanan, Instrum. Sci. Technol. 22 (4) (1994) 355–363.
[11] J. C. Miller, J. N. Miller, Statistical for Analytical Chemistry, Ellis Horwood, New York, 1984.
[12] A.I. Vogel, A Text Book of Quantitative Inorganic Analysis, Longman, 5th edn., p. 699.

ELSEVIER

Talanta 47 (1998) 487–495

Talanta

Immobilization of single-stranded deoxyribonucleic acid on gold electrode with self-assembled aminoethanethiol monolayer for DNA electrochemical sensor applications

Xingyan Sun, Pingang He, Shenghui Liu, Jiannong Ye, Yuzhi Fang *

Department of Chemistry, East China Normal University, Shanghai 200062, People's Republic of China

Received 9 October 1997; received in revised form 17 February 1998; accepted 25 February 1998

Abstract

A synthesized 24-mer single-stranded deoxyribonucleic acid (ssDNA) was covalently immobilized onto a self-assembled aminoethanethiol monolayer modified gold electrode, using water-soluble 1-ethyl-3(3-dimethylaminopropyl)-carbodiimide (EDC). The covalently immobilized ssDNAs were hybridized with complementary ssDNA (cDNA) or yAL_3 gene in solution, forming double-stranded DNAs (dsDNA). Meanwhile, daunomycin as an electrochemical active intercalator in the hybridization buffer solution was intercalated into the dsDNA to form a dsDNA/daunomycin system on the gold electrode surface, which was used for DNA electrochemical sensor. The cathodic waves of daunomycin bound to the double-stranded DNA (dsDNA) by linear sweep voltammetry were utilized to detect the cDNA. The cathodic peak current (i_{pc}) of duanomycin was linearly related to the concentrations of cDNA between 0.1 μg ml^{-1} and 0.1 ng ml^{-1}. The detection limit was about 30 pg ml^{-1}. © 1998 Elsevier Science B.V. All rights reserved.

Keywords: Electrochemical sensor for DNA; Immobilization of DNA; Self-assembled monolayer; Hybridization; Intercalation

1. Introduction

The detection of specific DNA sequence is of significance in many areas including clinical, veterinary, medico-legal, environmental, and food industry. A growing interest has arisen in the simple, cheap, rapid, and quantitative detection of specific DNA sequence. Various novel nonradio isotopic labels including avidin/biotin [1], digoxigenin [2], fluorescent dye [3], and chemiluminescent agent [4] have been developed to replace the traditional method using radioactive labels [5]. However, these techniques have usually been applied to the traditional southern transfer and dot blot experiments. Recently, much attention has been devoted to the development of DNA biosensors capable of selectively detecting DNA [6]. For example, piezoelectric biosensors [7,8], optical

* Corresponding author. Fax: +86 212576217.

0039-9140/98/$ - see front matter © 1998 Elsevier Science B.V. All rights reserved.
PII S0039-9140(98)00108-8

biosensors [9,10], fiber optical biosensors [11,12] and electrochemical biosensors [13–18] have been used for the detection of specific DNA sequence.

Electrochemical detection is a highly sensitive and rapid method. Hashimoto et al. [13,14] reported a DNA electrochemical sensor based on an intercalator as a hybridization indicator. Millan and Mikkelsen [16,17] described a sequence-selective biosensor using a DNA-modified glassy carbon electrode and $Co(bpy)_3^{3+}$ as an electroactive hydridization indicator. The authors also reported the voltammetric detection of sequence- specific DNA using covalently immobilized DNA probes on graphite electrode and using ethidium bromide as a hydridization indicator [18]. In order to prepare a DNA electrochemical sensors, the immobilization of DNA probes should first be considered. The traditional immobilization of DNA onto the electrode surface has a disadvantage. The DNA molecules are immobilized onto the electrode surface at multiple sites resulting in poor hybridization efficiency. The ideal immobilization of ssDNA onto the surface is one point attachment of the ssDNA molecule by 5′ or 3′ end, as a result, higher efficiency of the hybridization reaction will be obtained compare with multiple-site attachment. Recently, molecular self-assembly has become a popular surface derivatization procedure, mostly due to its simplicity, versatility, and establishment of a high level of order on a molecular scale [19–22]. Hashimoto et al. reported that the ssDNA was immobilized on the gold electrode at a site of the 5′ end through a mercaptohexyl group and got a higher sensitive sequence-specific DNA electrochemical sensor [23].

In this work, we report the immobilization of ssDNA monolayer on the gold electrode surface with self-assembled aminoethanethiol monolayer for the applications of voltammetric detection of sequence-specific DNA. In the presence of water-soluble carbodiimide reagent, the 5′-terminal phosphate end of ssDNA formed a phosphoramidate bond with the primary amino group of aminoethanethiol monolayer on the gold electrode surface. The immobilized ssDNAs were hybridized with complementary ssDNAs (cDNA) in solution, forming double-stranded DNAs (dsDNA). Meanwhile, in the hybridization buffer solution daunomycin as an electrochemical active intercalator was intercalated into the dsDNA monolayer to obtain the dsDNA/daunomycin system on the gold electrode surface, which was then used as a DNA electrochemical sensor. Detection of cDNA was thus achieved by measuring the cathodic peak current of daunomycin on the DNA sensor with linear sweep voltammetry.

2. Experimental

2.1. Apparatus

IR spectra were recorded on a FT-IR 5DX spectrometer (Nicolet analytical instruments) at room temperature. The spectra of the membranes in dry state were gained by the reflection method. Linear sweep voltammetry (LSV) and cyclic voltammetry (CV) were performed on Princeton applied research model 173 potentiostat/galvanostat and Model 175 Universal Programmer (EG&G, Princeton, USA) in conjunction with a model LZ 3-204 X-Y recorder (Shanghai Dahua Instrument Factory). The working electrode was a gold electrode with diameter of 2 mm; the reference electrode was a Ag/AgCl electrode, and the auxiliary electrode was a platinum electrode. All the experiments were carried out in a 30 ml electrochemical cell.

2.2. Materials

Both deoxyoligonucleotide (5′-dGCCCCTTCCCTATGAGAATTCGGG-3′) and its complementary target DNA (5′-dCCCGAATTCTCATAGGGAAGGGGC-3′) with a length of 24 nucleotides were synthesized with an applied biosystems model 391 Automatic DNA synthesizer using the solid phase (β-cyanoethyl phosphoramidite chemistry method [24]. The purification of deoxyoligonucleotides was carried out with NAP columns (Pharmacia Sephadex G-25). A model target gene, 400 bp yAL_3 gene containing a sequence complementary to the deoxyoligonucleotide, was provided by Shanghai Institute of cell biology [25]. Denatured and fragmented PNC_3 DNA were prepared by Department of Biology,

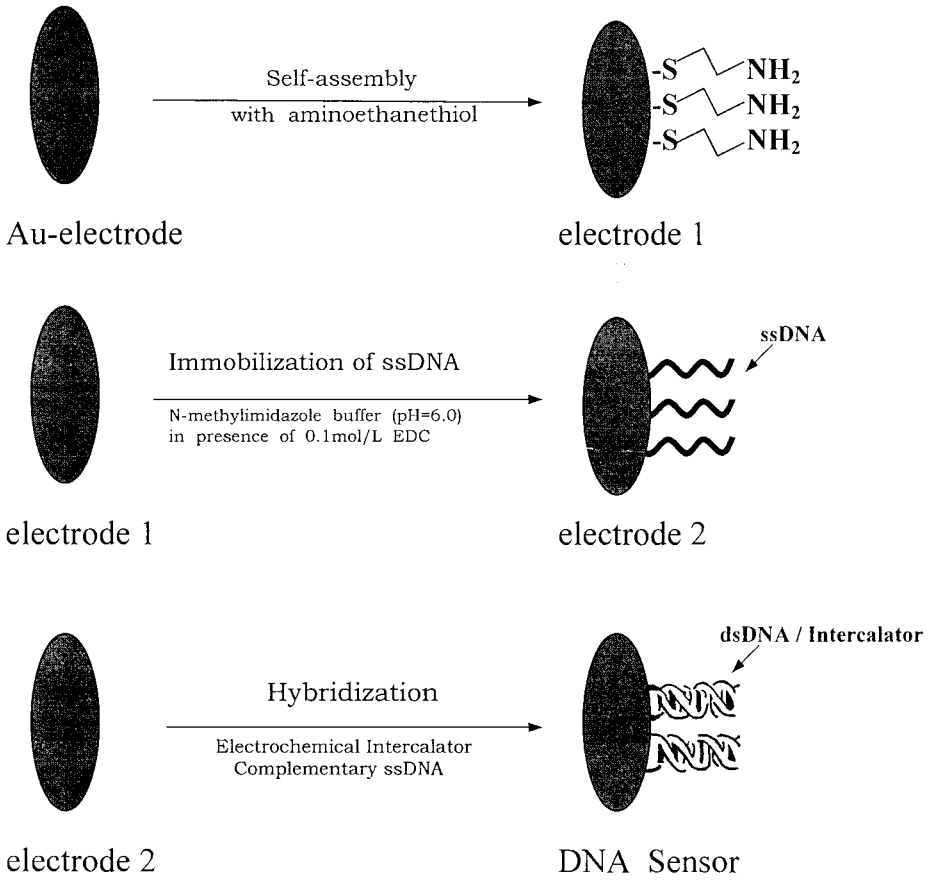

Fig. 1. The procedure of preparation of DNA sensor.

East China Normal University [26]. Daunomycin was obtained from Shanghai Medicine Examination Institute. Aminoethanethiol and hexylmercaptan were purchased from Tokyo Chemical. 1-ethyl-3-(3-dimethylaminopropyl) carbodiimide hydrochloride (EDC) was obtained from Sigma. *N*-methylimidazole and sodium dodecylsulfate (SDS) were provided by Jiangshu Guangyao Chemicals. Other reagents were commercially available and were all of analytical grade.

2.3. Preparation of the DNA sensor

The procedure for the preparation of DNA sensor is schematically illustrated in Fig. 1.

2.3.1. Preparation of a self-assembled monolayer of aminoethanethiol on gold electrode

The surface of the gold electrode was polished by 0.05 μm alumina suspension to mirror finish. The electrode was then washed with 1:1 HNO_3, acetone, and distilled water, respectively, with the aid of ultrasonics for 2 min. The gold electrode was soaked in a 5 mmol l^{-1} aminoethanethiol hydrochloride/ethanol solution for 10 h at room temperature. The surface of the electrode was washed with distilled water and ethanol, and was air dried. After these treatments, self-assembled monolayer with primary amino group was formed on the gold electrode surface as electrode 1.

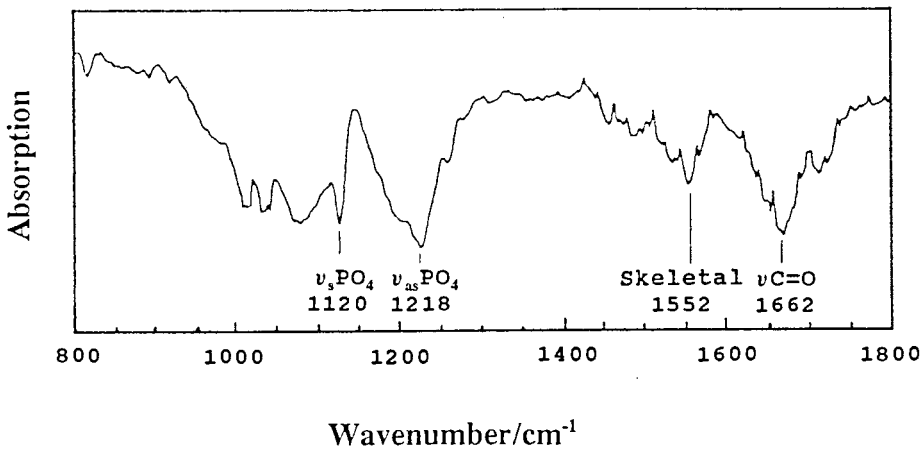

Fig. 2. IR spectra for ssDNA monolayer on gold electrode surface.

2.3.2. Immobilization of ssDNA monolayer

The electrode 1 was immersed in pH = 6.0, 0.1 mol l^{-1} *N*-methylimidazole buffer containing 0.1 mol l^{-1} EDC and 0.1 mg ml^{-1} ssDNA. The electrode was incubated for 3 h at 25°C. These conditions allow immobilization through the 5′-phosphate groups of ssDNA by the formation of a phosphoramidate bond with the amine groups of the electrode 1 surface. The modified electrode was soaked with washing solution (**I**) (0.4 mol l^{-1} NaOH + 0.25% SDS heated 40°C) for 5 min, and then was washed three times to remove free ssDNA which was not immobilized. The electrode immobilized ssDNA monolayer is denominated as electrode 2.

2.3.3. Hybridization and intercalation

Different concentrations of cDNA, which was complementary to the immobilized ssDNA, were added to 30 ml hybridization buffer (300 mmol l^{-1} NaCl + 30 mmol l^{-1} sodium citrate) containing 3×10^{-5} mol l^{-1} daunomycin. The electrode 2 was immersed into the hybridization buffer and incubated in a water bath at 42°C for 1 h with shaking. In the period of hybridization, the specific dsDNAs were formed, and daunomycins were intercalated into the dsDNAs to form dsDNA/daunomycin system on the gold electrode surface. The daunomycins, which were non-selectively adsorbed or blockaged on the surface, were removed by washing three times in 20 ml washing solution (**II**) (750 mmol l^{-1} NaCl + 75 mmol l^{-1} sodium citrate) for 30 min (10 min each time) at 25°C. The electrode is used as DNA sensor.

2.4. Electrochemical measurements

LSV and CV were carried out in a 30 ml electrochemical cell with the above pretreated gold electrode as working electrode, a Ag/AgCl as the reference electrode, and a platinum wire as the counter electrode. Unless otherwise stated, voltammetry was performed at 100 mV s^{-1} in the blank PBS solution (8 g l^{-1} NaCl + 0.2 g l^{-1} KCl + 1.44 g l^{-1} Na_2HPO_4 + 0.2 g l^{-1} KH_2PO_4, pH 7.0) at 25.0 ± 0.2°C. Each measurement was performed using a fresh solution and properly cleaned cells.

3. Results and discussion

3.1. Immobilization of ssDNA on gold electrode

The molecular of aminoethanethiol can be strongly adsorbed on gold surface through their thiol group, forming a very stable self-assembled monolayer [20]. In the presence of 0.1 mol l^{-1} water-soluble carbodiimide (EDC), ssDNA was covalently immobilized onto the aminoethylthiol-coated gold electrode by a phosphoramidate bond between the 5′-end of the ssDNA and primary

amino group on the electrode surface in 0.1 mol l^{-1} *N*-methylimidazole buffer (pH 6.0).Fig. 2 shows the IR spectra of the surface of the electrode 2 in the range of 1800–800 cm^{-1}. The absorption peaks at 1120 and 1218 cm^{-1} might be caused by the symmetry stretching and asymmetry stretching modes of the phosphate of the DNA fragments, and the absorption peaks at 1552 and 1662 cm^{-1} correspond to the C–O stretching vibration of the skeletal and base, respectively. Meanwhile, Maeda et al. suggested that the DNA on the electrode blocked the electrochemical reaction by an electrostatic repulsion between the polyanionic ssDNA and anionic redox couple ions [27]. Therefore, we employed a 1.0×10^{-2} mol l^{-1} $K_3[Fe(CN)_6]$ 0.01 mol l^{-1} KCl solution to investigated the immobilized ssDNA on the gold electrode. The peak current of redox couple of $[Fe(CN)_6]^{3-}/[Fe(CN)_6]^{4-}$ obviously decreased and the peak–peak separation (ΔE_p) increased when the electrode 2 was used compared with that of the electrode 1. On the other hand, the electrode 1 treated with the ssDNA in the absence of EDC gives no significant changes in both current and ΔE_p. These results showed that the DNA fragments could be immobilized on the electrode 1 through a phosphoramidate bond between the 5′-terminal phosphate groups of ssDNA and the amine groups on the aminoethanethiol monolayer on the gold electrode in the presence of EDC.

3.2. Electrochemical response of the DNA sensor

Fig. 3 shows the cyclic voltammograms of the 3×10^{-6} mol l^{-1} daunomycin solution in PBS (pH 7.0). The nearly reversible redox waves were obtained on both the bare gold electrode and the electrode 1. For the DNA sensor, the electrode 2 was hybridized in the hybridization buffer solution containing 3.0×10^{-2} μg ml^{-1} complementary DNA and 3.0×10^{-5} mol l^{-1} daunomycin at 42°C for 1 h. After the electrode was washed three times with 20 ml washing solution (**II**), the linear sweep voltammetry was performed with the DNA sensor as working electrode in the blank PBS solution. As shown in Fig. 4 curve B, apparent cathodic peak current was observed on the

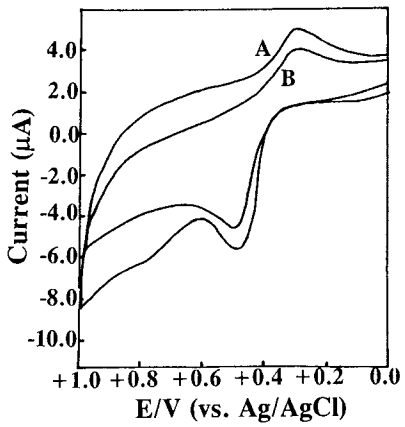

Fig. 3. Cyclic voltammograms of daunomycin on bare gold electrode (A) and the elctrode 1 (B). The concentration of daunomycin: 3×10^{-6} mol l^{-1} in PBS (PH 7.0) solution. Scanning speed: 100 mV s^{-1}.

DNA sensor. It is considered that the i_{pc} value was derived from daunomycin bound to the dsDNA on the DNA sensor through intercalation between base pairs. On the other hand, in the

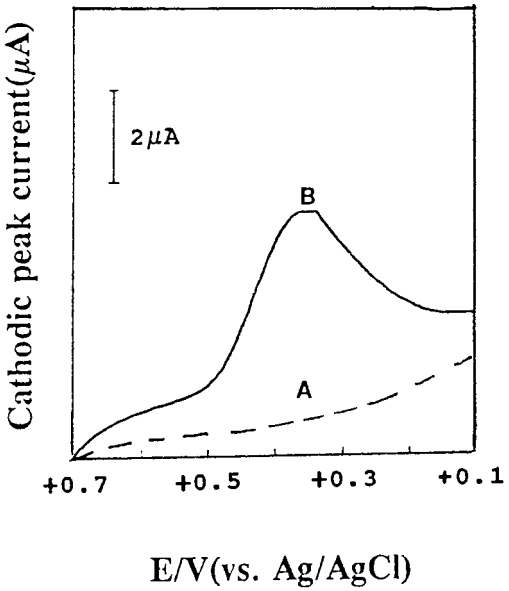

Fig. 4. Linear sweep voltammograms of daunomycin intercalated between base pairs of dsDNA on electrode 2 after hybridization under the following conditions (A) containing no DNA in hybridization buffer solution. (B) containing 3.0×10^{-2} μg ml^{-1} complementary DNA in hybridization buffer solution.

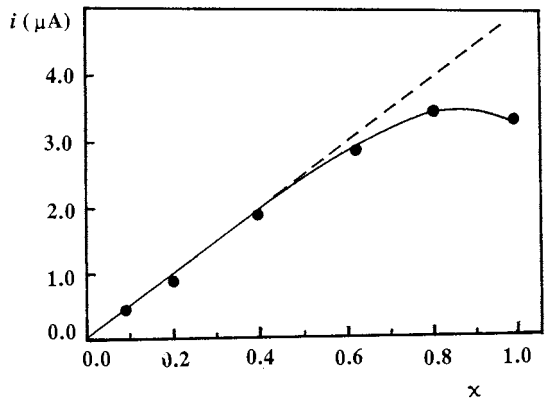

Fig. 5. Electrochemical responses of the DNA sensors which were prepared with different molefraction of aminoethanethiol in each electrode 1. The values of x is the mole fraction of aminoethanethiol on the mixed self-assembled monolayer containing aminoethanethiol and hexylmercuptan, normalized to $x=1$ for the monolayer containing only aminoethanethiol. The concentration of aminoethanethiol plus hexylmercuptan is 1.0×10^{-4} mol l^{-1}. The concentration of cDNA is 3.0×10^{-2} μg ml^{-1} in hybridization buffer solution.

same experimental conditions, the electrode 2 was immersed into the hybridization buffer solution containing only 3×10^{-5} mol l^{-1} daunomycin at 42°C for 1 h, then was washed three times with the washing solution (**II**). The linear sweep voltammogram shows that the i_{pc} of daunomycin was not observed on the electrode (Fig. 4 curve A). This is because daunomycins absorbed or blockaged on the surface of electrode 2 could be washed away by the washing solution (II). The results suggest that the sensor can selectively respond to DNA fragments.

3.3. The efficiency of the hybridization of cDNA

The efficiency of the hybridization of cDNA is one of important factors of affecting the sensitivity of the DNA sensor. It is obvious that the quantity and form of the ssDNA immobilized onto the electrode surface affect the hybridization efficiency [23]. In practice, in order to control the immobilization of the ssDNA, we can regulate the fraction of aminoethanethiol of the self-assembled monolayer on the electrode 1 by using aminoethanethiol and hexylmercaptan to form a mixed self-assembled monolayer on the gold electrode [28,29]. Fig. 5 shows the relation between the electrochemical responses (the cathodic peak current i_{pc} of the intercalator) of the DNA sensors and the fraction of aminoethanethiol on the electrodes 1. It is known that the electrochemical response is directly proportional to the hybridization efficiency of cDNA. Therefore, the results indicate that when the fraction of aminoethanethiol (χ) is lower than 0.5, the hybridization efficiency is lineally increased with the quantity of the immobilized ssDNAs, which are increased with the increase of the fraction of aminoethanethiol of the mixed self-assembled monolayer on the electrode 1. However, in higher fraction of aminoethanethiol (when $\chi>0.5$), the efficiency of the hybridization of cDNA with the ssDNA is increased slowly, and even decreases when $\chi=1.0$. So we can speculate upon that in higher fraction of aminoethanethiol, a lot of ssDNAs have been immobilized on the electrode surface by the aminoethanethiol, some of which are partially folded on the electrode 1 surface, resulting in decrease of the relevant bases freely available for the reaction with cDNA.

3.4. Effect of hybridization time and daunomycin concentration

The efficiency of hybridization is also dependent on the ionic strength, temperature, the concentration of hybridization indicator, as well as the hybridization time. We have discussed the effects of ionic strength and temperature previously [18,25]. Fig. 6 gives the cathodic peak current of daunomycin at various durations for hybridization time when daunomycin concentration is fixed as 3×10^{-5} mol l^{-1}. As hybridization proceeded, the cathodic peak current increases due to the increase of the local concentration of double-stranded DNA on the gold electrode surface, allowing more daunomycin to be intercalated into dsDNA. However, the hybridization reaction completed after a hybridization time of 60 min. Fig. 7 shows the effect of daunomycin concentration to the response of the DNA sensor. As can be seen, when the concentration is high enough, a plateau or maximum value of the peak current is obtained. Therefore 3×10^{-5} mol l^{-1} daunomycin was chosen as the optimum concentration of the hybridization indicator.

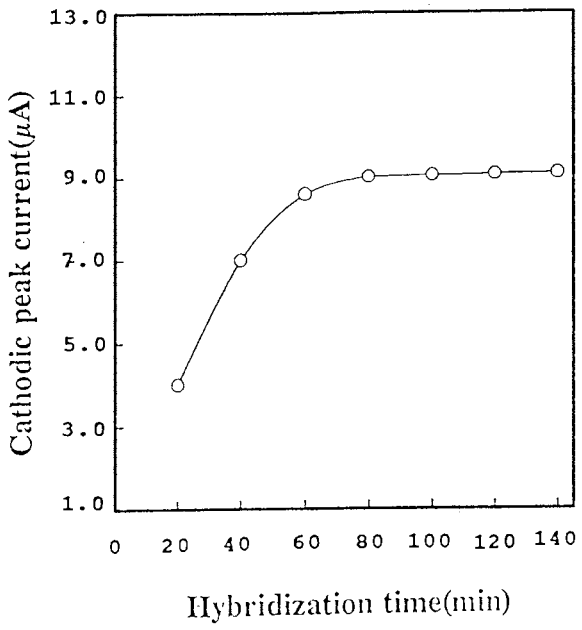

Fig. 6. Electrochemical responses of the DNA sensor as a function of hybridization time. The concentration of cDNA is 7.0×10^{-2} μg ml^{-1} in hybridization buffer solution.

3.5. Response to sequence-specific DNA and stability

The response to 24-mer complementary DNA(cDNA) was investigated in a series of experiment in which a constant amount of immobilized ssDNA on the electrode 2 was hybridized

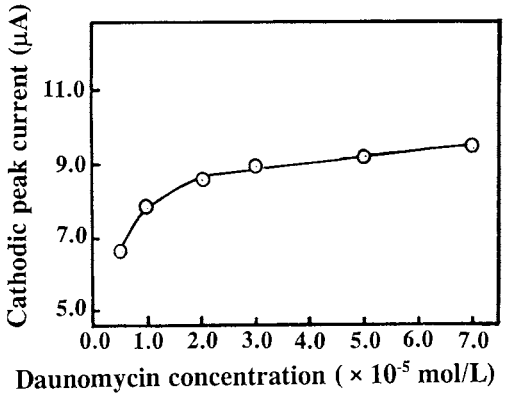

Fig. 7. Electrochemical responses of the DNA sensor as a function of the concentration of intercatator. The concentration of cDNA is 7.0×10^{-2} μg ml^{-1} in hybridization buffer solution.

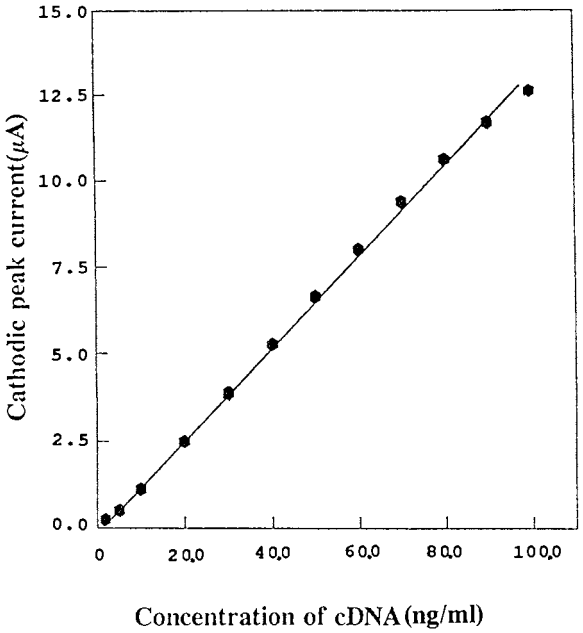

Fig. 8. The calibration curve of the DNA sensor for concentration of cDNA.

with different quantity of the 24-mer cDNA. After intercalation of daunomycin, the corresponding cathodic peak current of daunomycin was found. The calibration curve (Fig. 8) indicates that the peak current is linear to the amount of cDNA ranging from 0.1 μg ml^{-1} to 0.1 ng ml^{-1} with correlation coefficient of 0.9927. The detection limit is about 30 pg ml^{-1} ($S/N = 3$). When the electrode 2 was stored in the TE buffer solution for 1 month and then was hybridized with cDNA and intercalated with daunomycin, the response of the resultant sensor was decreased by about 15%. The DNA sensor was also used for specific gene detection. 400 bp yAL_3 gene which contains a sequence complementary to the immobilized ssDNA on the electrode 2 and PNC_3 DNA which is non-complementary to the immobilized ssDNA on the electrode 2 were first denatured as follows: the solution was heated for 5 min in a boiling-water bath and then rapidly cooled in an ice bath for 5 min. The hybridization and intercalation procedures are identical to those used for the investigation of ssDNA–cDNA hybridization on the surface of the electrode. The results of the

Table 1
Response of the ssDNA-electrode to sequence-specific DNA

Sample	Concentration (mg ml^{-1})	i_{pc} of Daunomycin (μA)
24 base cDNA	6.5×10^{-5}	9.0 ± 0.2
400 bp yAL_3 gene[a]	6.5×10^{-5}	8.6 ± 0.4
PNC_3 DNA[b]	6.5×10^{-5}	—

[a] 400 bp yAL_3 gene contains a sequence complementary to the immobilization ssDNA on the electrode.
[b] PNC_3 DNA is non-complementary to the immobilization ssDNA.

investigation are summarized in Table 1. As shown in Table 1, the response to 400 bp yAL_3 gene was slightly decreased comparing cDNA, while the sensor treated with a similar concentration of non-complementary PNC_3 DNA essentially provided no response.

4. Conclusion

The self-assembly monolayer technique can be conveniently used for the molecular design of electrode with specific functions. In this work, aminoethanethiol was strongly adsorbed on a gold electrode surface, forming an stable, active monolayer, on which DNA fragments could be immobilized by a phosphoramidate bond between the 5′-terminal phosphate groups of ssDNA molecular and amino groups of aminoethanethiol. The method has been demonstrated to be useful for controlling the immobilization of DNA on the electrode surface in the molecular-level. The immobilized DNA on the gold electrode can be applied to prepare a DNA electrochemical sensor by using the hybridization with a complementary DNA and the intercalation of daunomycin as a hybridization indicator to form a dsDNA/daunomycin system on the gold electrode surface. The DNA sensor was shown to be stable and sensitive.

Acknowledgements

We would like to thank the National Natural Science Foundation of China (NSFC) which financially supported this work.

References

[1] K. Jacobs, S.F. Woif, L. Haines, J. Fisch, J.N. Kremsky, J.P. Daugherty, Nucleic Acids Res. 15 (1987) 2911.
[2] A. Reisfeld, J.M. Rothenberg, E.A. Bayer, M. Wilchek, Biochem. Biophys. Res. Commun. 142 (1987) 519.
[3] S. Girotti, E. Ferri, S. Ghini, M. Musiani, M.L. Zerbini, D. Gibellini, G. Gentilomi, Anal. Chim. Acta 255 (1991) 387.
[4] P.O. Part, E. Lopez, G. Mathis, Anal. Biochem. 195 (1991) 283.
[5] J.L.J. Arnod, P.W. Hanonond, N.C. Neison, Clin. Chem. 35 (1989) 1558.
[6] M.E.A. Downs, S. Kobayashi, I. Karube, Anal. Lett. 20 (1987) 1897.
[7] N.C. Fawcett, J.A. Evans, L.C. Chien, N. Flowers, Anal. Lett. 21 (1988) 1099.
[8] Y. Okahata, Y. Matsunobu, K. ijiro, M. Mukae, A. Murakami, K. Makino, J. Am. Chem. Soc. 114 (1992) 8299.
[9] C.F. Mandenius, A. Chollet, M. Mecklenburg, I. Ludstrom, K. Mosbach, Anal. Lett. 22 (1989) 2961.
[10] T. Vo-Dinh, K. Houck, D.L. Stokes, Anal. Chem. 66 (1994) 3379.
[11] P.A.E. Piunno, U.J. Krull, R.H.E. Hudson, M.J. Damha, H. Cohen., Anal. Chim. Acta 288 (1994) 205.
[12] P.A.E. Piunno, U.J. Krull, R.H.E. Hudson, M.J. Damha, H. Cohen, Anal. Chem. 67 (1995) 2635.
[13] K. Hashimoto, K. Miwa, Y. Ishimori, Supramol. Chem. 2 (1993) 265.
[14] K. Hashimoto, K. Ito, Y. Ishimori, Anal. Chim. Acta 286 (1994) 219.
[15] K.M. Millan, A.J. Spurmanis, S.R. Mikkelsen, Electroanalysis 4 (1992) 929.
[16] K.M. Millan, S.R. Mikkelsen, Anal. Chem. 65 (1993) 2317.
[17] K.M. Millan, A. Saraullo, S.R. Mikkelsen, Anal. Chem. 66 (1994) 2943.
[18] S.H. Liu, J.N. Ye, P.G. He, Y.Z. Fang, Anal. Chim. Acta. 335 (1996) 239.
[19] T.T. Li, M.J. Weaver, J. Am. Chem. Soc. 106 (1984) 6107.
[20] C.E.D. Chidsey, C.R. Bertozzi, T.M. Putvinski, A.M. Mujsee, J. Am. Chem. Soc. 112 (1990) 4301.
[21] P.G. He, J.N. Ye, Y.Z. Fang, I. Suzuki, T. Osa, Electroanalysis 91 (1997) 68.
[22] P.G. He, Y.N. Ye, Y.Z. Fang, J. Anzai, T. Osa, Talanta 44 (1997) 885.
[23] K. Hashimoto, K. Ito, Y. Ishimori, Anal. Chem. 66 (1994) 3830.

[24] M.D. Matteucci, M.H. Caruthers, J. Am. Chem. Soc. 103 (1981) 3185.
[25] Y.Z. Fang, S.H. Liu, P.G. He, Chem. J. Chinese Univ. 17 (1996) 1222.
[26] Z. Wu, B.J. Qi, R.Q. Jiao, F.L. Chen, L.F. Wang, Gene 106 (1991) 103.
[27] M. Maeda, Y. Mitsuhashi, K. Nakano, M. Takagi, Anal. Sci. 8 (1992) 83.
[28] K.L. Prime, G.M. Whitesides, Science 252 (1991) 1164.
[29] G.K. Rowe, S.E. Greager, Langmuir 7 (1991) 2307.

ELSEVIER

Talanta 47 (1998) 497–501

Talanta

Flow-injection catalytic spectrophotometric determination of nitrite using the redox reaction between naphthol green B and potassium bromate

Zhang Zhi-Qi *, Gao Lou-Jun, Zhan Han-Ying

Central Laboratory, Shaanxi Normal University, Xi'an 710062, People's Republic of China

Received 24 October 1997; received in revised form 17 February 1998; accepted 25 February 1998

Abstract

A flow injection catalytic spectrophotometric method is proposed for the determination of nitrite based on its catalytic effect on the redox reaction between naphthol green B and potassium bromate in phosphoric acid medium. The reaction is monitored spectrophotometrically by measuring the decrease in absorbance of naphthol green B at the maximum absorption wavelength of 722 nm. The detection limit is 0.5 ng cm^{-3} in a sample volume of 90 mm^3. Up to 50 samples can be analyzed per hour with a relative precision of ca. 2%. The method is free from most interferences, especially from large amounts of nitrate. The procedure was successfully applied to the determination of trace nitrite in natural waters. © 1998 Elsevier Science B.V. All rights reserved.

Keywords: Catalytic method; Spectrophotometry; Flow injection; Nitrite; Water

1. Introduction

There has been an increasing need for a highly sensitive and rapid method for the determination of trace nitrite in natural water because of its environmental, agricultural, geochemical and ecological importance. The most widely used methods for determination of nitrite are spectrophotometry based on the diazotization of an aromatic amine and subsequent coupling to form an azo dye [1–4]. These methods are generally highly sensitive but often have drawbacks of serious interferences, toxicity of the reagent used and a relatively long coupling time. Other methods such as electrometry [5,6], liquid chromatography [7], fluorimetry [8] are also used but suffer from more or less time-consuming procedures and complicated instrumentation. In view of sensitivity, the catalytic kinetic method is one of the most attractive approaches for the ultratrace determination of nitrite [9–13], but manual operation, which requires close control of conditions, is unsuitable for routine application in terms of rate of analysis and precision. The flow injection technique, which is rapid, reproducible and suitable for on-line analysis, has been employed for the determination of nitrite spectrophoto-metrically. However, few methods of the flow injection have

* Corresponding author.

0039-9140/98/$ - see front matter © 1998 Elsevier Science B.V. All rights reserved.
PII S0039-9140(98)00109-X

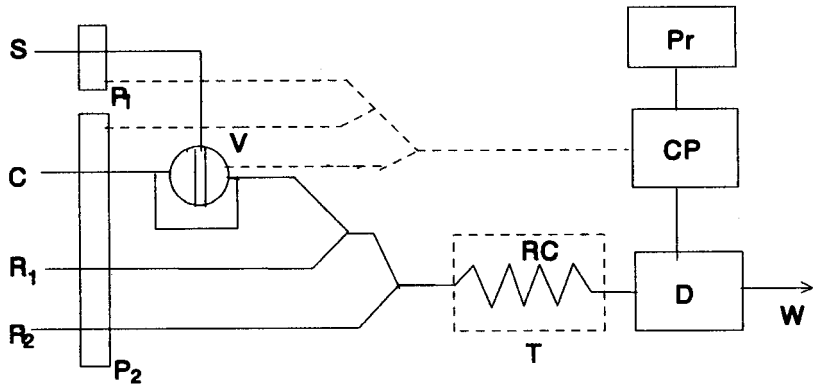

Fig. 1. Schematic diagram of the flow-injection system used for the determination of nitrite. S, sample; C, carrier; R_1, potassium bromate in phosphoric acid solution; R_2 , naphthol green B; P_1, P_2, peristaltic pumps; V, injection rotary valve; RC, reaction coil; T, thermostatic water bath; D, detector; CP, computer controlling and data processing system; Pr, printer.

been described for the determination of nitrite by a catalytic method [14,15].

In the work reported here, a sensitive catalytic method based on the catalytic oxidation of naphthol green B by potassium bromate has been established with a flow injection system. So far there has been no report on the naphthol green B as an indicator for catalytic determination. The proposed procedure is very simple, rapid and suitable for the determination of nitrite in natural waters.

2. Experimental

2.1. Apparatus

A 600 MC flow-injection analyser (Shanghai) with an 18 mm^3 flow cell (light paths, 10 mm) was used to measure the decrease in absorbance (ΔA) at 722 nm, which is equipped with two peristaltic pumps and one rotary valve and controlled by a computer. A schematic diagram of the flow injection system is shown in Fig. 1. The sample solutions were injected into the carrier C stream with the aid of a rotary valve V having a 90 mm^3 loop. This stream was merged 20 cm downstream with a stream of R_1 at a PTFE Y-piece and merged again 5 cm downstream with a stream of R_2 at second PTFE Y-piece. The three merged zones travelled 450 cm (reaction coil 400 cm) at the total flow-rate of 5.4 cm^3 min^{-1} for each channel 1.8 cm^3 min^{-1}. The measurement results were recorded by means of a PP40 printer. A model 501 thermostat was employed to keep the reaction temperature at 50 ± 0.1°C.

2.2. Reagents

All chemicals were of analytical reagent grade. Solutions were made up in deionized water.

A stock standard solution of nitrite (1.0 mg cm^{-3}) was prepared by dissolving the required amount of sodium nitrite in water. Working solutions were freshly prepared by diluting the stock solution.

Naphthol green B (NGB) solution (0.020 mol dm^{-3}) and potassium bromate solution (0.40 mol dm^{-3}) were prepared by dissolving the required amounts in water, respectively. Phosphoric acid solution (5.0 mol dm^{-3}) was prepared from the 85% reagent.

Reagent R_1 was obtained by mixing 25 cm^3 potassium bromate solution with 20 cm^3 phosphoric acid solution and diluting to 100 cm^3.Reagent R_2 was obtained by diluting 2.00 cm^3 NGB solution to 100 cm^3. Carrier C contained 3% (w/v) of ammonium sulfate.

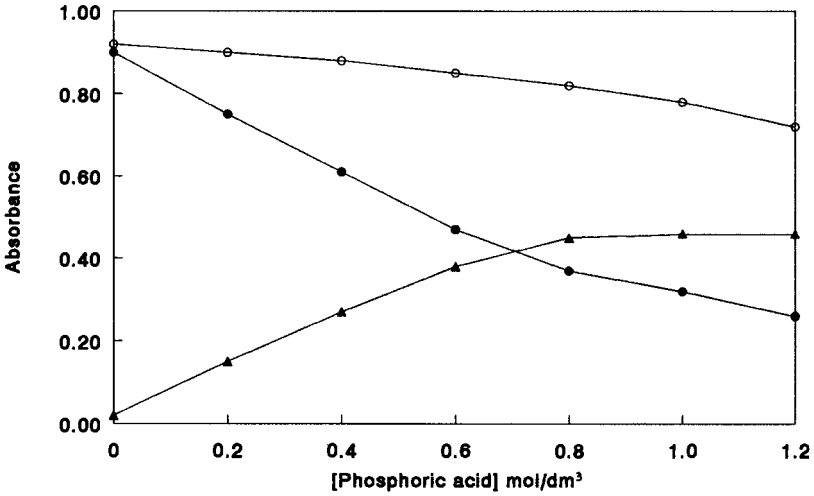

Fig. 2. Effect of phosphoric acid concentration. The absorbances were measured against an R_2 stream of deionised water. potassium bromate, 0.10 mol dm^{-3}; naphthol green B, 4.0×10^{-4} mol dm^{-3}. ○, blank; ●, 200 ng cm^{-3} nitrite; ▲, analytical signal (ΔA).

3. Results and discussion

3.1. Optimization of manifold parameters

The variables studied were volume of sample solution injected, flow rate, length and controlled temperature of the reaction coil. The conditions used in these experiments were as follows: R_1, 0.10 mol dm^{-3} potassium bromate in 0.8 mol dm^{-3} phosphoric acid solution; R_2, 3.0×10^{-4} mol dm^{-3} NGB solution; C, 3% of ammonium sulfate; S, 200 ng cm^{-3} nitrite solution.

The injected sample volume of a 100 ng cm^{-3} nitrite standard was varied between 30 and 150 mm^3. The analytical signal ΔA increased with increasing sample volume up to 85 mm^3,above which no significant increase was observed. The sample volume to be injected was selected as 90 mm^3.

Different flow rates were obtained by changing the pump tube diameters. Experiments indicated that the decrease in absorbance obviously depended on the residence time of the sample zone in the flow system, i.e. on the total flow rate and the coil length. The lower flow rates and longer coil gave higher ΔA but the reproducibility was poor and the peaks were so broad that the sample throughput was very slow. A reaction coil of 400 cm, a total flow-rate of 5.4 cm^3 min^{-1} (1.8 cm^3 min^{-1} for each channel) were chosen as a compromise between sensitivity and sampling rate.

The effect of reaction temperature was studied in the range 20–70°C. The results showed that ΔA increased with temperature but at higher temperature (>50°C) the uncatalysed reaction between NGB and $KBrO_3$ would accelerate and nitrite catalyst was not necessary for the reaction. The later would result in a decrease in the sensitivity for nitrite. The optimum reaction coil temperature was controlled by a thermostatic water bath at 50°C.

3.2. Optimization of reagent concentrations

The effects of reagent concentrations were tested in the optimized flow system.

Experimental results showed that the catalytic reaction could proceed only in strongly acidic media. Among sulfuric, hydrochloric and phosphoric acids, the highest sensitivity could be obtained in a phosphoric acid medium.

ΔA increased with increasing concentration of H_3PO_4 in R_1 up to 0.8 mol dm^{-3} (Fig. 2), above which it remained virtually constant. 1.0 mol dm^{-3} phosphoric acid in R_1 was chosen.

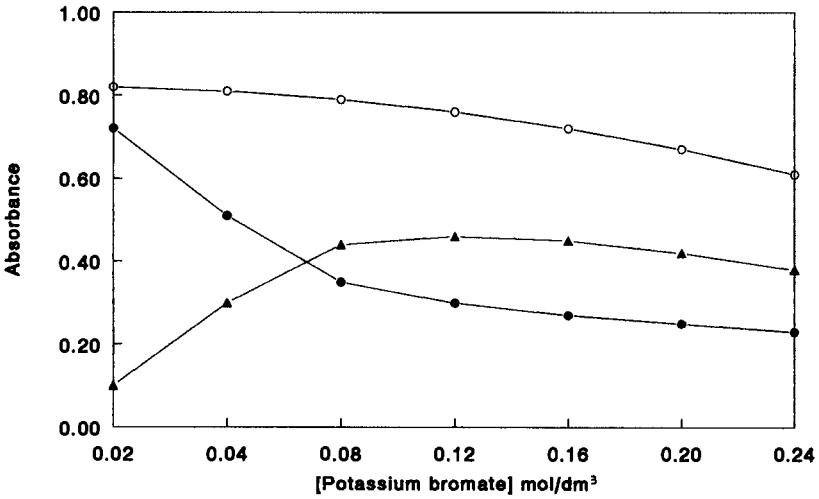

Fig. 3. Effect of potassium bromate concentration. The absorbances were measured against an R_2 stream of deionised water. phosphoric acid, 1.0 mol dm^{-3}; naphthol green B, 4.0×10^{-4} mol dm^{-3}. ○, blank; ●, 200 ng cm^{-3} nitrite; ▲, analytical signal (ΔA).

The effect of $KBrO_3$ concentration in R_1 on obtaining a constant and maximum sensitivity was investigated. The optimum concentration of $KBrO_3$ was in the range 0.08–0.16 mol dm^{-3} (Fig. 3) and above that the sensitivity for nitrite decreased slightly. As such 0.10 mol dm^{-3} $KBrO_3$ in R_1 was adopted in subsequent work.

NGB is the indicator for monitoring the catalytic decolorization reaction. Lower concentration can obtain higher sensitivity but narrower linear range for determination of nitrite. The working solution (R_2) chosen was 4.0×10^{-4} mol dm^{-3} as a compromise between sensitivity and linear range.

The catalytic reaction would be accelerated and the sensitivity for nitrite could be enhanced by the present of ammonium. The optimum condition chosen was 3% (w/v) of ammonium sulfate in carrier stream which could enhance the sensitivity to about 50%.

3.3. Analytical parameters

Under the chosen experimental conditions, the decrease in absorbance of NGB varied linearly with the concentration of nitrite between 2.0 and 200 ng cm^{-3}, and fitted the equation

$$\Delta A = 3.27 \times 10^{-3} c + 0.0014 \quad r = 0.9992$$

The detection limit was 0.5 ng cm^{-3} with the signal to noise ratio value of 3. Relative standard deviation of six replicate determinations is 1.8% for 80 ng cm^{-3} nitrite.

The sampling rate is about 50 samples per hour.

3.4. Interference of foreign species

The interference of several foreign species normally found in association with nitrite was studied

Table 1
Tolerance limit of diverse species in the determination of 80 ng cm^{-3} nitrite

Tolerance ratio $C_{ion}/C_{nitrite}$	Species
1000[a]	Na^+, K^+, NH_4^+, Ca_2^+, Mg^{2+}, Ba^{2+}, Sr^{2+}, Pb^{2+}, SO_4^{2-}, NO_3^-, $C_2O_4^{2-}$, CO_3^{2-}, PO_4^{3-}, Cl^-, F^-
500	Mn^{2+}, Co^{2+}, Cu^{2+}, Ag^+, Al^{3+}, Zn^{2+}, Cd^{2+}
100	Ni^{2+}, Cr^{3+}, Fe^{3+}, Fe^{2+}
50	SO_3^{2-}, Br^-, Hg^{2+}
1	I^-, S^{2-}, V(V)

[a] Maximum concentration tested.

Table 2
Results for the determination of nitrite in some natural waters

Sample	Nitrite added (μg cm^{-3})	Nitrite found (μg cm^{-3})		Recovery[c] (%)
		This method[a]	Reference[b]	
Well water	—	—	—	
	0.050	0.051		102
River water 1	—	0.041 ± 0.001	0.042	
	0.050	0.090		98
River water 2	—	0.096 ± 0.002	0.102	
	0.050	0.144		96
Lake water	—	0.158 ± 0.002	0.162	
	0.020	0.177		95

[a] Average of six determinations ± S.D.
[b] Obtained by standard method in [16].
[c] Average of six determinations.

by using a solution containing 80 ng cm^{-3} nitrite and adding various concentration of the foreign species. The maximum concentration at which the species caused an error of $\leq 5\%$ was taken as its tolerance limit. The results are summarized in Table 1.

3.5. Applications

The proposed method was applied to the determination of nitrite in some natural waters. The samples were collected from Xi'an and its environs. Prior filtration of the sample is necessary due to the interference of turbidity. The results which were compared with those obtained by spectrophotometry [16] are given in Table 2.

4. Conclusion

A sensitive catalytic spectrophotometric method for the determination of nitrite was developed with a indicator reaction of the oxidation of naphthol green B by potassium bromate in a flow injection system. The results demonstrated that this method is very simple and rapid and is useful for the practical analysis of natural waters.

References

[1] S. Flamerz, W.A. Bashir, Analyst 110 (1985) 1513.
[2] M. Nakamura, T. Mazuka, M. Yamashita, Anal. Chem. 56 (1984) 2242.
[3] P.K. Tarafder, D.P.S. Rathore, Analyst 113 (1988) 1073.
[4] A. Kojlo, E. Gorodkiewicz, Anal. Chim. Acta 302 (1995) 283.
[5] L. Ganghan, Y. Shenglai, Anal. Lett. 22 (1989) 1743.
[6] Z. Gao, Z. Zhao, Anal. Chim. Acta 241 (1990) 161.
[7] W. Zhai, N. Cao, Fenxi Huaxue 13 (1985) 708.
[8] N. Jie, J. Yang, F. Meng, Talanta 40 (1993) 1009.
[9] R. Montes, J.J. Laserna, Talanta 34 (1987) 1021.
[10] M. Jing, F. Jiang, X. Tang, Z. Zhao, Anal. Chim. Acta 234 (1990) 403.
[11] A.A. Ensafi, M. Saminifar, Talanta 40 (1993) 1375.
[12] B. Liang, M. Iwatsuki, T. Fukasawa, Analyst 119 (1994) 2113.
[13] A. Zhang, H. Wang, S. Wang, Fenxi Huaxue 24 (1996) 292.
[14] G. Zhang, S. Liu, X. He, H. Shi, Goadeng Xuexiao Huaxue Xuebao 14 (1993) 492.
[15] J. Wang, R. He, Huajing Kexue 16 (1995) 71.
[16] Standard method of analysis for hygiene chemists, Pharmaceutical Society of Japan, Kanehara, Tokyo, 1980, p. 69.

ELSEVIER

Talanta 47 (1998) 503–507

Talanta

Short communication

Sensitivities of selenite, selenate, selenomethionine and trimethylselenonium ion in aqueous solution and in blood plasma—ETAAS compared with ICP-MS.

Bente Gammelgaard [a,*], Erik H. Larsen [b]

[a] *Department of Analytical and Pharmaceutical Chemistry, The Royal Danish School of Pharmacy, Universitetsparken 2, DK-2100 Copenhagen, Denmark*

[b] *Danish Veterinary and Food Administration, Institute for Food Research and Nutrition, Mørkhøj Bygade 19, DK-2860 Søborg, Denmark*

Received 11 December 1997; received in revised form 26 January 1998; accepted 27 January 1998

Abstract

Aqueous solutions and blood plasma spiked with selenite (Se(IV)), selenate (Se(VI)), selenomethionine (SeMet) or trimethylselenonium (TMSe) iodide were analyzed by Zeeman-corrected electrothermal atomic absorption spectrometry (ETAAS) using palladium as a chemical modifier, and by inductively coupled plasma mass spectrometry (ICP-MS). Using ETAAS, the sensitivities for Se(IV), SeMet and TMSe in aqueous solution were similar, whereas the sensitivity of Se(VI) was 63% of that value. In blood plasma, the ETAAS sensitivities of Se(IV) and Se(VI) were equal, whereas the sensitivities of SeMet and TMSe were 87 and 56%, respectively, of that value. In contrast, the ICP-MS sensitivities obtained for Se(VI), TMSe and SeMet were between 96 and 98% of that obtained for Se(IV) in aqueous solution and in blood plasma. It is concluded, that ICP-MS is superior to ETAAS as the problem of differences in sensitivity of the selenium species when using ETAAS are not prevalent when using the ICP-MS technique. © 1998 Elsevier Science B.V. All rights reserved.

Keywords: Selenium; ICP-MS; Atomic absorption

1. Introduction

In biological samples, selenium occurs as a variety of species. In human plasma proteins, selenium is present as selenocysteine (SeCys) in selenoprotein P and glutathione peroxidase, while selenium in albumin is present as selenomethionine (SeMet). The distribution of selenium in various body pools is dependent on the level of selenium intake and on the species of selenium consumed [1]. In human urine, selenium has been identified as selenite (Se(IV)) and trimethylselenonium (TMSe) [2]. However, it has been questioned

* Corresponding author. Tel.: +45 35 370850; fax: +45 35 375376; e-mail: bg@mail.dfh.dk

0039-9140/98/$ - see front matter © 1998 Elsevier Science B.V. All rights reserved.
PII S0039-9140(98)00056-3

Table 1
Graphite furnace programme and instrumental conditions for the determination of selenium

	Step					
	1	2	3	4	5	6
Temperature (°C)	80	130	1100	2200	2600	20
Ramp time (s^{-1})	1	20	10	0	1	1
Hold time (s^{-1})	15	15	20	5	5	10
Internal gas flow (ml min^{-1})	300	300	300	0	300	300
Recorder				−5		
Read				−1		

Instrumental conditions: light source, EDL; lamp current, 10 mA; power supply, 5 W; wavelength, 196.0 nm; slit-width, 0.7 nm; sample volume, 10 μl; chemical modifier volume, 5 μl.

if TMSe constitutes a quantitatively significant urinary excretory product under low dosing conditions [3].

A commonly used analytical method for the determination of selenium at trace levels is electrothermal atomic absorption spectrometry (ETAAS). As selenium volatilizes in the electrothermal atomizer at temperatures below 700°C, a chemical modifier which thermally stabilizes the element is therefore mandatory. Several chemical modifiers have been proposed, including nickel, copper and palladium, often in combination with magnesium nitrate. Palladium in combination with magnesium nitrate has even been proposed as a universal modifier for a large number of elements in different matrices [4].

The selenium analytes are stabilized differently in the graphite furnace of the ETAAS instrument even though the temperature programme and use of modifier have been optimized carefully. This may lead to erroneous results if the selenium species present in the sample are different from that of the calibration standard. Several investigations have dealt with this problem [5–9], but a modifier which equally stabilizes all selenium species in different matrices has never been proposed.

The purpose of this study was to compare ETAAS and inductively coupled plasma mass spectrometry (ICP-MS) with respect to the sensitivities obtained for a variety of biologically important selenium species. The inorganic selenium species Se(IV) and selenate (Se(VI)) as well as organically bound selenium (oxidation state −2) as SeMet and the TMSe ion were chosen as the test substances.

2. Experimental

2.1. Apparatus and operating conditions

A Perkin-Elmer Zeeman 5000 atomic absorption spectrometer (Perkin-Elmer, Norwalk, CT) equipped with an HGA-500 electrothermal atomizer and an AS-40 autosampler was used for the ETAAS measurements. Pyrolytic graphite coated tubes with inserted platforms were used throughout. Argon was used as the purge gas. The instrumental conditions and temperature programme are shown in Table 1.

The ICP-MS system used was a Perkin-Elmer SCIEX ELAN 5000 (Perkin-Elmer SCIEX, Concord, Ont.). The operating parameters used are given in Table 2. In addition to measuring the selenium signal intensity the ICP-MS was set to sample the ion intensity for yttrium (Y) which was added to all samples as an internal standard.

2.2. Reagents

All reagents were of analytical reagent grade or higher. Milli-Q water from a Milli-Q deionization unit (Millipore, Bedford, MA) was used throughout. The palladium modifier was prepared by

dilution of a commercial solution at 10 ± 0.2 g l^{-1} Pd in 15% nitric acid (Merck) with nitric acid and water to a final concentration of 4 g l^{-1} Pd in 7.5% nitric acid.

2.3. Standards

Aqueous standard solutions were prepared as follows. A Se(IV) solution was diluted from a 1.000 g l^{-1} Se Titrisol selenium dioxide solution (Merck, Darmstadt, Germany). A solution of Se(VI) was prepared from sodium selenate (Fluka, Buchs, Switzerland) and a solution of SeMet was prepared from (D, L) selenomethionine (Sigma, MO). The solution of TMSe was prepared from trimethylselenonium iodide, which was synthesized and characterized in-house [9].

2.4. Samples

For the ETAAS measurements working solutions at 100 μg l^{-1} Se were prepared from each of the aqueous standard solutions by dilution with a mixture of 0.1% Triton X-100 (Merck, Darmstadt, Germany) in 10^{-3} mol l^{-1} nitric acid. An in-house pool of human blood plasma was diluted 1:3 with the same mixture, and was spiked with each selenium standard at 100 μg l^{-1} Se in the final solutions. Prior to the ICP-MS measurements all samples were further diluted 1:10 with acetic acid and water to a final concentration of 5% acetic acid, and yttrium (Teknolab, Drøbak, Norway) was added to a final concentration of 10 μg l^{-1} Y. All solutions were analysed by each analytical technique in triplicate.

Table 2
Operating parameters of the ICP-MS

ICP-MS instrument	
R.f. power (W)	1300 W
Sampler and skimmer cones	Platinum
Argon flow rates	
Outer (l min^{-1})	15
Intermediate	0.8
Nebulizer (l min^{-1})	1 (variable)
Mass-to-charge ratios detected (m/z)	82 (^{82}Se) and 89 (^{89}Y)
Data acquisition	
Graphics mode (signal intensity versus time)	
Dwell time per mass (ms)	1000
Sweeps per reading	1
Readings per replicate	1
Number of replicates	10
Estimated time (s)	21
Scanning mode	Peak hop
Sampling system	
Peristaltic pump speed (ml min^{-1})	1.3
Sample introduction	Glass cyclonic spray chamber with a Meinhard (type TR-30-K3) concentric nebulizer

3. Results and discussion

The result of the sensitivity measurements by ETAAS and ICP-MS are shown in Table 3. In aqueous solution, the ETAAS sensitivity of Se(VI) is 63% of that obtained for the three other species. In the blood plasma samples, the sensitivities of SeMet and TMSe are 87 and 56%, respectively, of the equal sensitivities obtained for Se(IV) and Se(VI). The results show that when using the ETAAS technique the selenium species are not stabilized to the same extent and that the sensitivity is sample dependent. The selection of the amount of the palladium chemical modifier for the ETAAS measurements was based on the results obtained in a previous study in which the influence of palladium and magnesium concentrations on the stabilization of Se(IV), Se(VI), SeMet and TMSe in aqueous solution and in blood plasma was studied [10]. Even after careful optimization of the temperature programme and amounts of modifier it was not possible to find a modifier which was able to stabilize all species equally. The results showed that the addition of 20 μg palladium gave the best result in terms of equal stabilization, while the additional use of magnesium was not useful as this substance only increased the background absorbance. The degree of stabilization of the four selenium species was

Table 3
Sensitivities for four selenium species using ICP-MS and ETAAS given as mean values ± S.D. of 3 replicates

Species	ICP-MS			ETAAS	
	Counts (s^{-1})	Se/Y ratio (10^2)	Selenite (%)	Abs*s	Selenite (%)
Aqueous solution					
Se(IV)	9023 ± 33	2.81 ± 0.01	100	0.219 ± 0.002	100
Se(VI)	8762 ± 59	2.72 ± 0.02	97	0.137 ± 0.003	63
SeMet	8705 ± 23	2.74 ± 0.01	97	0.222 ± 0.001	101
TMSe	8713 ± 17	2.70 ± 0.01	96	0.219 ± 0.003	100
Blood plasma					
Se(IV)	9839 ± 68	3.42 ± 0.02	100	0.244 ± 0.004	100
Se(VI)	9628 ± 64	3.29 ± 0.01	96	0.244 ± 0.001	100
SeMet	9564 ± 3	3.32 ± 0.01	97	0.213 ± 0.005	87
TMSe	9777 ± 29	3.23 ± 0.01	95	0.136 ± 0.002	56

ETAAS measurements were performed using 100 μg l^{-1} Se, whereas the ICP-MS measurements were performed using the same solutions diluted 1:10 in 5% acetic acid.
Abs*s: integrated absorbances.

different in the two matrices studied. This palladium modifier was, however, used as the best, although not satisfactory, modifier in the present experiments. In contrast, the recorded ICP-MS sensitivities of the selenium species are almost equal in the aqueous solutions as well as in the plasma samples. However, small differences in sensitivities do occur for Se(VI), SeMet and TMSe which are 95–97% of the sensitivity obtained for Se(IV). By normalizing the ICP-MS signal responses for selenium against the yttrium internal standard, errors due to drift in sensitivity were alleviated. The same result, however, was obtained without normalization to the internal standard.

A marked positive matrix effect is caused by carbon from the 5% acetic acid which was added to all samples (A. Stroh, personal communication (1997), unpublished results). The selenium (^{82}Se) sensitivity in this matrix would be equivalent to 99250 counts s^{-1} for a 100 μg l^{-1} Se(IV) solution, whereas in aqueous solution the sensitivity for Se(IV) at the same concentration was 12100 counts s^{-1}. This corresponds to a sensitivity enhancement of 8.2-fold which is useful for ultra-trace-level determinations of selenium by ICP-MS [11].

Several papers have stressed the importance of careful optimization of the amount of chemical modifiers in order to achieve equal stabilization of selenium species in ETAAS work [5–8]. In digests of biological reference materials, it was shown that the amount of modifier needed was highly dependent on the type of matrix analysed [8]. Similar results have been reported for the direct determination of Se(IV) in urine, where the amount of chemical modifier needed for the stabilization of selenium in a urine matrix was 5-fold higher than that needed for water. Furthermore, the sensitivities obtained for SeMet and TMSe in urine were dramatically different from that of Se(VI) [12]. The amount of chemical modifier should therefore be optimized for each selenium species and sample type. This is however, highly time consuming and may not be possible if the selenium species present in the sample are unknown. To circumvent this problem, the matrix of the samples should be digested [12], and the selenium species present should be converted into the same chemical form as used for the calibration standard. However, the direct determination of selenium in blood plasma is still possible because lower limits of detection may be obtained in this way.

4. Conclusion

The results of the present study show that the problem of differences in sensitivity of selenium

species using ETAAS, are not prevalent when using the ICP-MS technique. All selenium species tested in this study may be analysed using direct injection into the ICP-MS of aqueous solutions or diluted blood plasma. The sensitivity difference of selenium in the aqueous and in the blood plasma matrices observed for both analytical techniques is due to the intrinsic selenium content of blood plasma. In conclusion, ICP-MS is superior to ETAAS with regard to equal sensitivities of the different selenium species in the two matrices tested.

References

[1] J.T. Deagan, M.A. Beilstein, P.D. Whanger, J. Inorg. Biochem. 41 (1991) 261.
[2] R. Hasunuma, T. Ogawa, Y. Kawanishi, Bull. Environ. Contam. Toxicol. 50 (1993) 19.
[3] X. Dauchy, M. Potin-Gautier, A. Astruc, M. Astruc, Fresenius J. Anal. Chem. 348 (1994) 792.
[4] G. Schlemmer, B. Welz, Spectrochim. Acta 41B (1986) 1157.
[5] H. Docekalova, B. Docekal, J. Komarek, I. Novotny, J. Anal. At. Spectrom. 6 (1991) 661.
[6] B. Welz, G. Schlemmer, U. Voellkopf, Spectrochim. Acta 39B (1984) 501.
[7] J. Neve, S. Chamart, L. Molle, Trace Elem. Anal. Chem. Med. Biol. 4 (1987) 349.
[8] M. Deaker, W. Maher, J. Anal. At. Spectrom. 10 (1995) 423.
[9] J.K. Johannessen, B. Gammelgaard, O. Jǿns, S.H. Hansen, J. Anal. At. Spectrom. 8 (1993) 999.
[10] B. Gammelgaard, O. Jǿns, J. Anal. At. Spectrom. 12 (1997) 465.
[11] E.H. Larsen, S. Stürup, J. Anal. At. Spectrom. 9 (1994) 1099.
[12] A. Leblanc, J. Anal. At. Spectrom. 11 (1996) 1093.

ELSEVIER

Talanta 47 (1998) 509–524

Talanta

Review

Inorganic and methylmercury speciation in environmental samples

J.E. Sánchez Uría *, A. Sanz-Medel

Department of Physical and Analytical Chemistry, University of Oviedo, c/Julián Clavería 8, 33006 Oviedo, Spain

Received 3 November 1997; received in revised form 25 February 1998; accepted 16 March 1998

Abstract

The different strategies for mercury species analysis in environmentally-related samples are reviewed. After consideration of the main different steps involved in the speciation of mercury, such steps are discussed with more extension for mercuric ion and methylmercury. The different approaches for preservation of these mercury species during the storage of samples are considered. Different ways for the extraction of mercury species from the several possible environmental compartments and the possibilities for preconcentration of such species after previous derivatization reactions are discussed. Mercuric ions and methylmercury chromatographic and non-chromatographic separations along with different techniques used for sensitive and selective detection of mercury are also critically reviewed. Ranges of published detection limits achievable for such species determination, by using hyphenated techniques between a chromatographic separation and a specific atomic detector are also given. © 1998 Elsevier Science B.V. All rights reserved.

Keywords: Mercuric ion; Methylmercury; Speciation; Environmental samples

1. Introduction

Mercury is considered by the Environmental Protection Agency (EPA) as a highly dangerous element because its accumulative and persistent character in the environment and biota. Calculations of 1973 assessing the antropogenic atmospheric contamination by mercury estimated a total mercury emissions to the atmosphere of around 10000 tones. These emissions came from the calcination of sulphide ores, fossil fuels combustions and heating of other mercury-containing materials [1]. Similar data were published by Nriagu [2] 10 years later. Today, both inorganic and organic mercury compounds are produced in industrial processes for agriculture, paper industry, pharmaceutical uses, etc. and they are responsible for the vast majority of present antropogenic contamination of our environment with this toxic metal.

* Corresponding author. Tel.: +34 8 5103480; fax: +34 8 5103125.

0039-9140/98/$ - see front matter © 1998 Elsevier Science B.V. All rights reserved.
PII S0039-9140(98)00116-7

Moreover, mercuric ion can be converted into methylmercury. It should be stressed that the most numerous cases of human poisoning by an organometal have involved the ingestion of methylmercury compounds. This organometallic species is neurotoxic, causes blockage of binding sites of enzymes, interferes proteine synthesis, impides thymidine incorporation into DNA, etc. [3]. Reports of such cases have come from many areas of the world, but those from Asia have been the most numerous. Particularly disastrous were the widespread methylmercuric compound poisoning cases of Minamata Bay, Japan, from which the name 'Minamata disease' derived to describe methylmercury poisoning [4]. These organomercurials can be consumed in two classes of foods: fish and shellfish accumulating the poison from waters or sediments; and grain seeds coated with antifungal methylmercuric preparations. These dangerous methylmercury species can be antropogenic, but also inorganic mercury can be biologically converted into methylmercury in algae [5], humic substances [6], etc. via methylation of mercuric derivatives by bacteria [7–10]. Both inorganic and organic mercury tend to be accumulated in sediments and biota [11,12], particularly fish and molluscs [13–15]. In this way, neurotoxic methylmercury would eventually reach our food chain specially from sea food [16]. The high affinity of methylmercury to sulphydril groups and lipids of animals would explain its accumulation in living organisms, particularly in lipidic tissue of mammals. Conversely, it appears that sulphide groups in the sediment would be responsible for the binding and final preconcentration of mercury species [17] in sediments.

Nowadays it seems accepted that the rate and extent of methylation of Hg(II) in the waters and sediments depends upon factors such as: the compound of Hg(II) (acetate is easier to methylate than mercuric chloride), the methylation agent [18], the chemical composition of the sediment, its oxygen concentration and the pH [19].

In the waters it is interesting to note that levels of methylmercury are usually much lower than those of inorganic mercury. This is due to the difficulty of methylation reactions in aqueous phases, from one side, and to the easy decomposition by solar UV light [20,21] of organomercury compounds from the other. Recent reports [22] estimate a total mercury concentration in natural waters, ranging from 0.2 to 100 ng l^{-1}, while methylmercury levels are much lower, around 0.05 ng l^{-1} [23]. Of course, higher values can be found in waters from heavily industrialized areas [22]. The upperlimit for total mercury concentration in drinking water recommended by the EC is 1 μg l^{-1}.

In sediments and biota the levels of methylmercury are higher than in waters because of accumulative phenomena [24]; while methylmercury in sea water is only found in highly contaminated areas and amounting only to around 1% of total element present [25], inorganic mercury and methylmercury seem to be preconcentrated in sediments and are found at relatively high levels in fish [14,15,26,27].

Several authors have found the presence of dimethylmercury in fish [24,28–31]. However, Puk and Weber have pointed out that most analytical methods published would not provide reliable results, or even detect dimethylmercury species, if present [27]. Studies on the occurrence of other organic mercury compounds in the environment are comparatively scarce, even if some recent references have been published on the presence of ethylmercury in water samples [32], soils and sediments [29,33,34]. Cai et al. attribute this lack of observations of these species to present analytical methodologies mainly focused to develop methods just for methylmercury [34].

Nowadays it is worldwide recognized that the toxicity of an element (e.g. Hg) is determined by its particular species occurring in the sample. In general terms the organic forms of metals (more hydrophobic) go through biological membranes quite easily as compared to inorganic forms. Thus, organomercuric compounds are much more toxic than inorganic mercury. Therefore, today we are witnessing a growing interest in analytical speciation of trace elements [35–37] and of mercury in particular in samples of environmental origin.

Considering the present knowledge, the main species or forms of mercury to be identified and determined in the environment are mercuric ion

(inorganic mercury), methylmercury and, only occasionally, dimethylmercury. The various reviews appeared in the last few years about this topic [27,38–41] give evidence of the great scientific interest arisen by mercury speciation.

A possible revival of older disastrous episodes of 1953 in Minamata [4], and other parts of the world in the 1960s, could happen now in the Amazonia as a result of the new 'gold rush' of the so-called 'garimpeiros' or gold-diggers. Their techniques of amalgamation on gold-ore and further open 'burning' of the possibly formed gold amalgam is responsible for 80% of the total mercury emission into atmosphere in Brazil (168 tonnes of the metal according to estimations of 1989). Investigations to evaluate total mercury contamination in waters, sediments and biota in Amazonia rivers are already in progress [26,42,43] and a cooperative project to assess the extent of methylation of such mercury (volatilized into atmosphere and then deposited in soils, flora and rivers) is due to start this year [44].

In this paper a revision of the different steps to speciate mercury, particularly inorganic and methylmercury, in environmental samples is carried out. Precautions to be taken at each step (extraction, preconcentration, separation and specific detection), analytical strategies and particular techniques proposed to tackle this modern problem of mercury speciation are thoroughly discussed.

2. The main steps to consider for mercury speciation in environmental samples

It is quite obvious that the ideal analytical strategy for speciation of mercury and other toxic elements would be direct 'in-situ' analysis of the sought species in the desired sample. In this way the most stringent challenge of speciation, namely preservation of the original nature of the sought species, would be nearly secured by avoiding sample manipulations of any type. Electrochemical and optical (bio)-sensors could be in the future viable approaches for metal speciation [45,46]. At present, however, 'in-situ' direct species-specific techniques are seldom useful to solve speciation problems in real-life situations because of lack of the sensitivity. In such situations previous sample treatments, preconcentrations, separations, etc., before final detection are usually needed.

In order to achieve a reliable determination of the two main environmentally relevant species of mercury, Hg(II) and CH_3Hg^+, there are four different steps to be considered individually:

1. Mercury species 'extraction' from the environmental sample (e.g. from soil, sediment or biota) securing the integrity of the sought species as they are in the sample;
2. Mercury species 'preconcentration' from the obtained extract (again, preserving the identity of those components) to achieve a final concentration level matching the detection limits accessible with the detection technique selected;
3. Inorganic mercury and methylmercury 'separation' without disturbing their relative original concentration levels;
4. Individual 'detection' (determination) of each of the previously separated species.

Of course, in filtered aqueous samples only the last three steps should be considered. However, to speciate a given toxic metal in an aquatic environment non-dissolved materials (solids in suspension, sediments and soil) and biota (plants, fish, shellfish and plankton) should be dealt with as well.

As a result of the extremely low levels of mercury compounds in such real samples the coupling of the four different steps to develop an integrated mercury speciation strategy in those particular samples is almost mandatory. All the four steps should be 'tamed' to such a degree that risks of contamination, losses, degradations or changes in the mercury species nature and their relative concentrations are avoided (or at least, well assessed to allow for eventual corrections).

Table 1 summarizes the 'more common techniques' used to assemble an integrated strategy made of 'the four mentioned steps required for speciation in environmental samples'.

Table 1

Pretreatment	Preconcentration	Separation	Detection
Homogenization	Criogenic trapping	G.C.	CV-AAS
Acidic preservation	Column chromatography	HPLC	ETAAS
Extraction of species	Non-chromatographic columns	Non-chromatographic	MIP-AES
	—Alumina		ICP-AES
	—Cotton sulphydril		ICP-MS
	—Dithiocarbamate		ECD
	—Ditizone		Electrochemical
	Set-pack cartridges		AFS
	Electrochemical methods		

3. Inorganic and methylmercury extractions

To start with, the environmental sample (water, sediment or biota) should be made homogeneous and perhaps preservative agents could be needed in order to prevent species degradation before final analysis. It is well known that organometallics (e.g. methylmercury, methylarsenic compounds, tributhyltin) can be degraded in many ways including microorganisms action, oxidation, or even UV irradiation. This is why preservation of CH_3Hg^+ in its original form and relative concentration can represent a difficult task, particularly when its extraction from a solid is required; the matrix of the sample can play an important role in the stability of the sought compound. For instance, it has been shown that CH_3Hg^+ in fish (dry or wet) exhibits a remarkable stability with time at room temperature, while in shellfish samples a prolonged storing in the refrigerator, or several freezing and de-freezing of such samples, may bring about significant CH_3Hg^+ losses [47].

The stability of mercury species in waters is rather controversial. There is, however, a sort of consensus on the positive effects of low pH and high ionic strength to stabilize mercury species in solution, particularly when in the solution exists an oxidizing and complexing environment [48]. Oxidants and complex forming agents appear to contribute to stabilize Hg(II), while low pH and high ionic strength prevent cation deposition on the containers wall. Thus, it is advisable to add such preservative agents [49] if the analysis is going to be performed with a delay after sampling. Interestingly, the efficiency of such reagents to stabilize mercury species seems to be related with the water matrix (distilled, fresh water or sea water). Losses of methylmercury in sea water at the ng l^{-1} level have been reported to be caused by adsorption onto the container walls and conversion into the inorganic form [50].

Mineral acids are probably the most common reagents added to water in order to maintain unaltered mercury species in solution, e.g. solutions with 1–2% of HCl or HNO_3 [50,51], or 1% HNO_3 containing 0.05% (m/v) of $K_2Cr_2O_7$ [52]; other preservative reagents proposed include humic acids [53], freezing in liquid nitrogen and further storage at -80°C [28], Au(III) in diluted HNO_3 acid [54], etc. It has been shown [48] that the stability of CH_3Hg^+ in waters depends critically on its concentration level, matrix of the water, containers material and its pretreatment for cleaning, temperature, etc. For instance, it appears that low concentration of CH_3Hg^+ (lower than 10 ng ml^{-1}) are very unstable, while its stability at around 100 ng ml^{-1} levels improves substantially [48]. Likewise, the effect of container material is also stressed in the literature; PTFE containers are preferred to PVC or glass made flasks, provided their previous cleaning with nitric acid [55]. The paper by Leermarkers et al. [48] is recommended in this respect as it is the paper by Lepine and Chamberland [56] about the filtering of water samples immediately after sampling. If a filtration of sample is required, it is necessary to do it at the very moment of sampling, because freezing and filtration after de-

freezing originates a lost of both, inorganic mercury and methylmercury.

In biota and sediments, immediate freezing of samples after collection is recommended as a rule in order to retard microbiol activities [57]; doubts arise sometimes, though, about the possibility of species changes if samples are then de-freezed or dried in the air before speciation measurements (e.g. in the case of deep sediments originally surrounded by a reducing environment). Liofilization processes appear to be risky for biota speciation because some volatile species can be lost and some metal-bound proteins can degrade [58].

Extracting the sought species of methylmercury from the solid environmental sample is a delicate process depending on both, the nature of the species and of sample matrix. While in water samples this process is not so troublesome [28,59–63], in biota or sediments the extraction is probably the most crucial step of the whole speciation strategy designed: a complete extraction of Hg(II) and CH_3Hg^+ should be aimed at without changing the nature of those species. Of course this is very difficult and demands a great deal of care in order to preserve the original speciation. Moreover, the dissolved extracts can be unstable, e.g. they should be kept out of UV light which could cleave the bond Hg–C [20,64,65]. As a general rule, this bond Hg–C should be safe during pretreatment or extraction with added reagents. For example, reagents used for extractions from biota and sediments should be able to break bonds of the mercury species with clay materials, humic substances, sulphides, etc., but the Hg–C bonds should be left unaltered.

The techniques published for pretreatment extraction of mercury species in environmental samples can be grouped into three categories.

1. Acid digestion with solvent extraction: this digestion type was proposed long ago for Westöö as a means for the extraction of methylmercury in foodstuffs with HCl as acidic medium and benzene as the solvent; the extraction needs several steps in order to get a 'clean' solution of CH_3Hg^+ in benzene [66,67]. Later on many modifications of Westöö's methods were proposed for selective extraction of methylmercury from a mineral acidic medium containing NaCl [68,69], KBr [62,70,71] and iodoacetic acid [72], generally using successive extractions with organic solvents such as benzene [73,74], toluene [75,76], chloroform [62,77] or dichloromethane [28,78]. It seems that benzene is not well suited for CH_3Hg^+ extractions at low concentrations down to 0.5 ng l^{-1} [63]. Several authors recommend a back-extraction of the mercury species from the benzene or toluene phase to the aqueous phase, in order to clean or preconcentrate the extracted species, using cysteine or sodium thisulphate [66,67,76]. Problems derived from solvent background may arise when toulene is used and the detection is carried out by microwave-induced plasma-atomic emission spectrometry (MIP-AES) [79]. In the case of CH_3Hg^+ speciation using chloroform, addition of complexing agents to facilitate the extraction of methylmercury to the chloroformic phase has been proposed [62,77], while addition of $HgCl_2$ [25,80] or $CuCl_2$ [81] solutions has been recommended to release the CH_3Hg^+ from the –SH groups complexing the mercury species in the solid.
2. Alkaline digestion and extraction: both KOH-methanol [28,54–56,59,60] and NaOH-Cysteine [59] treatments have been proposed to release methylmercury from sediments while maintaining original Hg–C bonds. In many cases, this alkaline extraction appears troublesome as compared to acidic ones, because alkaline solutions are much more difficult to get in pure form as compared to acidic solutions. Moreover, serious problems encountered in subsequent steps (preconcentration, separation or detection) are derived from the high levels of organic matter, sulphides or ferric ions co-extracted with the sought methylmercury species using this sample treatment [81].
3. Acidic volatilization and preconcentration: an alternative approach is to avoid organic solvent extraction by producing a volatile derivative of the sought species [72,81]. Vapor distillation, in a stream of air or nitrogen at 150°C, of a homogeneate of the solid sample in diluted H_2SO_4 with excess of NaCl is

strongly recommended to allow a non-chromatographic separation of Hg(II) and CH_3Hg^+. The more volatile $CH_3Hg^+Cl^-$ compound formed is so distilled and is collected in a closed tube. This tube is water-cooled and stored in the dark in order to keep extracted methylmercury degradation at a minimum before its final determination with the various atomic detectors [53,82,83].

Comparative studies of the performance of the three extraction approaches cited, from 1 to 3, to extract methylmercury in the same samples are scarce. Horvat et al. [81] carried out such type of studies by applying the three extraction approaches to two certified sediments. They concluded that distillation of methylmercury from a 8-M H_2SO_4 solution containing KI, at 145°C in a nitrogen stream of 60 ml min^{-1} was a most convenient system to isolate and preconcentrate this mercury species from sediments. In a later paper [84] the same authors compared both, solvent extraction and distillation, methods for methylmercury extraction from water samples concluding that distillation method gives consistent and high recoveries of MeHg in various samples. However, recent investigations showed that the distillation procedure used to separate methylmercury from both water and sediment samples generates artificially MeHg aided by the presence of natural organic substances. The magnitude of this artifact appears to be related to the amount and the type of organic mater present in the samples [85]. Horvat et al. [81] propose also the ethylation of the methylmercury before the final detection of mercury by atomic fluorescence spectrometry (AFS). It should be noted, however, that sulphide is the most serious interference for the ethylation reaction [28]. Moreover artifact formation of CH_3Hg^+ may occur because the ethylation reagent might induce methylmercury formation from inorganic mercury if it is present at much higher concentrations [81]. In any case, the use of HCl alone for this distillation is not advisable because it may not be able to release completely the CH_3Hg^+ contained in the sediment, the amount of final mercury recovered depends on total organic carbon [48] and also on sulphide content [86,87] of the analyzed sediment.

4. Preconcentration/derivatization

As said before, the low analytical concentrations of organic or methylmercury expected (typically in the range of pg l^{-1}) determine very often the need to carry out preconcentration of such species in order to allow for concentration levels measurable by the atomic detector used.

Sometimes liquid–liquid extraction have been proposed after acid treatments of sediment, biota or water samples [62,67,70,73,74,80,88,89]. When the final detection is carried out by gas chromatography (GC) with an electron capture detector (ECD), back-extraction to an aqueous phase and further re-extraction to the organic solvent is recommended to clean up the extracts (atomic detection is less critical and so some of the cleaning steps can be disregarded).

Of course, the above mentioned gas–liquid procedures of volatile mercury species formation and distillation from environmental samples [28,82,83] are most appropriate for methylmercury preconcentration and derivatization by ethylation as a mean to enhance the separation/sensitivity attainable before final specific detection. This concept has been well developed in papers by Bloom [28], Rapsomanikis et al. [90,91], Craig et al. [92], etc. during this decade.

Solid-phase extraction can also be employed for preconcentration of extracted mercury species. Lee and Mowrer [63] proposed the use of sulphydryl cotton fiber (SCF) packings as sorbents of methylmercury from an aqueous solution; after trapping/preconcentration in the minicolumn the methylmercury is released of the column with 2 M HCl solution to be then extracted into benzene for final GC-ECD determination. This system was later extended to a flow injection analysis configuration with final detection by CV-AFS [93] or MIP-AES [94]. The group of Jiang [95] applied these cotton sulphydryl minicolumns to the 'field sampling' of inorganic mercury and methylmercury in waters with interesting results, using a field sampling kit consisting of an on-line filter (0.45 μm), a SCF column and a syringe.

Similarly, other groups have investigated the use of immobilized dithiocarbamates, packed in minicolumns, for methylmercury preconcentration

[86,96–98]; then, this species is eluted of the column with an acidic solution of thiourea followed by its extraction into toluene. There, the organomercurial is derivatized using the Grignard reagent before its final separation/determination by several possible techniques, particularly gas chromatography with microwave-induced plasma-atomic emission spectrometry (GC-MIP-AES) [59,69,86,98].

Non-chromatographic separations can be also successful as proposed some time ago by Minegawa et al. [97]: using cold vapor generation these authors described the separation of Hg(II) (with $SnCl_2$ in KOH solution) from CH_3Hg^+ (with a mixture of $SnCl_2 + CdCl_2$ in KOH solution) and final determination by CV-AAS.

Cryogenic trapping of both hydride and ethylide derivatives of mercury species constitute one of the more successful approaches to mercury compounds preconcentration [24,28,29]. While the use of $NaBH_4$ is more common for cold vapor and hydride generation, the ethylide generation reaction is usually achieved by derivatization 'in-situ' (in the solution or acting on a slurry of the sample) of the Hg(II) and CH_3Hg^+ at pH = 4.9 with $NaB(C_2H_5)_4$ to form volatile diethylmercury and methylethylmercury, respectively [24,90,91]. It is worth noting that ethylation reactions of mercury are considerably slower than the corresponding hydride generation reactions with $NaBH_4$. However, $NaB(C_2H_5)_4$ does not generate the great excess of hydrogen characterizing $NaBH_4$ decomposition in acidic solutions. Once the ethylation step has concluded, the species of derivatized mercury are preconcentrated by cryogenic trapping with liquid nitrogen using a coiled borosilicate glass column, previously cleaned and silanized with a solution of 5% dichlorodimethylsilane in toluene, then the column is packed with 10% OV-101 on Chromosorb W AW-DMCS 40–60 mesh. A Nichrom resistance wire surrounding the column, connected to a variable transformer coupled to a temperature controller, raised the temperature of the column (once this is void of liquid nitrogen) and the ethylated mercury species leave the column according to their boiling points. The sequential detection of mercury species was carried out by AAS using a quartz tube as atomization cell.

Modifications proposed by Liang et al. [99] allow to dispense with the use of cryogenic temperatures for trapping. They proposed to trap the ethylated derivatives formed in chromatographic columns at room temperature and then the different ethylated species are separated there, on heating the column, to be eventually detected by AFS.

Of course, other less popular approaches have been published for methylmercury preconcentration including temperature-controled evaporation in a vacuum [80], electrochemical preconcentration [100] or the 'tandem on-line continuous separation' technique [101]. In this last approach the preconcentration is achieved by continuously extracting the CH_3Hg^+ of the samples with iodide into xylene; the organic extract is continuously merged with a solution of $NaBH_4$ in dimethylformamide, to form the volatile mercury species, which are continuously drawn into an ICP-AES by a stream of argon [101]. In this way the first liquid–liquid separation operates the selective extraction of $CH_3Hg^+ \cdot I^-$ (while inorganic mercury remains in the aqueous phase) and its preconcentration, while the second liquid–gas separation step allows for an important increase in the sensitivity of the specific mercury detection in the ICP-AES via cold vapor generation. Once the methylmercury has been separated, inorganic mercury of the aqueous phase can be analyzed afterwards by cold vapor formation from this phase in a flow system [101].

5. Mercury species separation techniques

As a rule, chromatography is a more powerful separation technique than non-chromatographic approaches [102]. Therefore chromatographic separations are more popular for speciation purposes than non-chromatographic ones. However, simple non-chromatographic approaches can be successful to separate adequately one or two species in a given sample [45]. This is the case for Hg(II) and CH_3Hg^+ speciation and we will refer briefly to this particular speciation.

5.1. Non-chromatographics separations

The described method of 'tandem on-line continuous separations' for methylmercury speciation [101] constitutes a good example of the possibility of solving simple speciation problems by resorting to non-chromatographic separations. The principle of using selective liquid–liquid extractions to separate methylmercury from inorganic mercury by using halogenated acids and organic solvents is quite common and has been carried out usually in an 'off-line' mode for the final detection of mercury, usually with CV-AAS technology [62].

Flow injection analysis (FIA) systems are the most adequate for this type of simple separations. Thus the differential behavior of Hg(II) and CH_3Hg^+ versus reducing agents (i.e. while Hg(II) is reduced to Hg^0 by $SnCl_2$, the methylmercury species is not [21,22,103]) can be used to achieve a simple speciation scheme using CV-AAS detection. Similarly the minicolumns previously described [63,93–95] of sulphydril cotton fibers are also good examples of non-chromatographic approaches to separate inorganic and methylated mercury; in this latter FIA system [93], CH_3Hg^+ seems to be retained in the column while Hg(II) goes through it. The retained organic mercury is then released of the column, oxidized to inorganic mercury (in a flow with acidic $KBr/KBrO_3$), reduced to 'cold vapor' and detected by AFS [93]. This sulphydryl cotton fibers are not commercially available and reported extraction efficiency for CH_3Hg^+ in benzene from these columns is close to 65% [63].

Other non-chromatographic schemes proposed include the use of photo-oxidation [103,104]: firstly only inorganic mercury is detected by conventional CV-AAS; secondly, the organic mercury present is photo-oxidized to inorganic mercury and the total content of mercury is evaluated; in this way methylmercury is calculated by substraction. Recently, Madrid et al. [105] have proposed the use of microorganisms to achieve this separation of inorganic and organic monomethylmercury. Using *Saccharomices cerevisiae* in a suspension, they showed that CH_3Hg^+ seems to bind quite selectively to these cells, after incubation at 37°C during 30 min, while Hg(II) showed no affinity to *S. cerevisiae* yeast.

5.2. Chromatographics separations

Admittedly that non-chromatographic simple technologies of separation may solve particular problems of speciation [45] it is undebatable that the most powerful approach to real-life speciation consists of coupling a chromatographic separation with a sensitive atomic detection. In fact, the speciation of mercury in environmental samples is mainly carried out by the vast majority of workers by resorting to chromatographic separation techniques, particularly employing GC for this purpose [25,55,63,66,72,73,90,98,106]. Table 2 shows a schematic of the chromatographic separation type to be selected depending upon the nature of the species to be separated and quantified by hybrid speciation techniques [45].

As can be seen, GC is to be preferred for species being volatile or able to form easily volatile derivatives without uncontroled changes of the compound in the derivatization/separation processes involved. Thus GC is the more popular separation technique for mercury and organomercury compounds speciation using stationary phases consisting of columns of variable length (15–30 m and 0.3–0.75 cm i.d.) packed with OV

Table 2
Chromatographic-specific (atomic) detection for speciation analysis

Problem:	Volatile, thermostable, neutral species (or able to produce them by derivatization) GC → Interface → Atomic detector
Problem:	Non-volatile/Thermally unstable/charged compounds HPLC → Interface → Atomic detector
HPLC Characteristics	
	Direct separation (no derivatization possible)
	Integrity of species can be more easily preserved
	Liquid chromatography is more versatile than GC
HPLC drawbacks	
	HPLC provides liquid samples
	Atomic detector prefer gaseous samples (less sensitivity)
	HPLC-Atomic detector interfaces with increased sensitivity needed

101, in variable concentration adsorbed on a solid support of Chromosorb W-HP (80–100 mesh) [107] or silanized glass columns packed with 5% DEGS-PS on 100–120 mesh Supelcoprt (Supelco Inc.) [108]. GC techniques have been already used for the speciation of mercury in natural gases and gas condensates [109].

There is, however, a clear trend today to the use of open capillary columns, of the non-polar type, coated with a thin film of phenyl or methyl silicone [110,116]. It appears that this type of columns provide more efficient separations and better resolution, as compared with the above mentioned Chromosorb-type GC columns. Of course, the disadvantage of capillary columns is the general restriction of the small sample volume accepted (usually around 1 μl of sample). Moreover the more common GC detectors might be lacking the required selectivity to be used in speciation of mercury in environmental samples. For instance, the well-known ECD have been proposed for methylmercury speciation. However, the ECD unselective response determined the need to resort to laborious cleaning-up processes of the extract in the organic phase used for the mercury compounds extraction from the sediments. Preliminary work, using GC-ECD for mercury speciation [70], used packed columns to separate the methyl and ethyl mercury halides in toxicological samples and ill-defined and non-reproducible chromatographic peaks were reported. This behavior was ascribed to the polar character of these mercury halides which would therefore interact too strongly with the packing material of the column. A possible way-out to this unfavorable situation is the previous column 'pasivation' by its pretreatment with a solution of $HgCl_2$ in benzene or toluene [70,106]. Apart from the risk of using high concentrations of Hg(II) for this pasivation (before final analysis of low levels of mercury compound in the sample) this pretreatment is not durable and must be repeated rather frequently. Therefore, alternatives to this classical mercury speciation strategy have been investigated in recent years particularly capillary columns.

Other alternative approaches involve the use of pre-column derivatization of mercury species in order to transform them into non-polar dialkylderivatives. These latter compounds exhibit much better chromatographic properties than the original mercury species to be separated with capillary columns [69,71,111,112]. Capillary columns were also used for organomercury separation after the ethylated analyses were preconcentrated on a wide-bore fused-silica column and then desorbed by heating of the trap [113]. It should be stressed, however, that this derivatization approach demands the use of an atomic detector (specific detector for mercury) instead of the conventional ECD. Of course, now the halide, which brings about the measured ECD responses, is no longer there with the mercury sought compound after derivatization. Perhaps the most popular specific detector in this connection has been the Microwave Induced Plasma in the hybrid technique GC-MIP-AES [69,72,77,70,86,93,96,98,114]. Multicapillary columns for GC-MIP-AES, recently proposed for speciation analysis of butyltin compounds [115] allowing for ultra-rapid (30 s instead of about 10 min) and more sensitive analysis, perhaps may offer a good alternative for future mercury speciation.

In an attempt to overcome the numerous drawbacks associated with the gas chromatographic determination of organomercury compounds [110,111,117] many authors have resorted to alternative separation procedures. Particularly HPLC techniques [75,88,118–126] have been tried with the final aim of establishing a reliable procedure for the speciation of such compounds in environmental samples. Of course, HPLC techniques, usually being less sensitive for detection, are more suited for polar species and therefore could be advantageous for organomercury and inorganic mercury speciation. Moreover, the flexibility of liquid chromatography, with more separation mechanisms available, is considerably higher than that of GC in order to achieve satisfactory separations of inorganic and organic mercury compounds in complex environmental samples. Although detection at the exit of the liquid chromatographic column has been proposed with different common HPLC detectors including UV-Vis absorptiometry [75], fluorimetry, electrochemistry, etc., the most effective detection incorporates an

atomic/mercury specific detector in the so-called hybrid approaches which couple the HPLC with atomic spectrometry. AAS [120,123,124], plasma detection using photons measurements as in ICP-AES [101] or MIP-AES [127,128] and mass spectrometry with on-line ICP-MS measurements [121,129,130] have been proposed. The lack of sensitivity is usually a main limitation [45]. Using CV-AFS detection better detection limits for mercury speciation can be obtained [28,71,81,84,93,99,112,131].

There is not doubt that hybrid techniques, using an atomic detector on-line with the column, are becoming the most popular approaches to tackle the modern problem of trace element speciation and this trend is now being noticed in the case of mercury speciation. The main analytical task is to couple the separative column (GC or HPLC) with the atomizer and this operation is achieved via an adequate 'interface'. Of course gas chromatographic columns are compatible with any on-line atomizer (where atomic vapors are produced) in a straightforward manner. Thus the gaseous effluent from the column is directly introduced into the atomizer. The only problem encountered can be the possible condensation of vapors in the interface due to the difference in temperatures between the column in the chromatograph oven, the interface itself and the atomizer. Therefore, a heating and thermostating device to maintain the interface at a temperature slightly higher than that of condensation of expected vapors is usually mandatory for GC-Atomic Detection hybrid approaches [29,40,132].

The interface to couple HPLC columns with the atomiser can be very simple, via the direct connection with a teflon tubing, of the exit of the column with the nebuliser of the AAS [133,134] or plasma detector [135,136]. Care should be exercised just to make compatible the flow rate from the HPLC column with the normal flow rates of the nebuliser used [137,138]. Unfortunately, the efficiency of liquid samples transport attainable using nebulisers is very low (1–3% for plasma nebulisers and 5–10% at most for AAS common nebulisers). As a consequence, the sensitivity observed is limited particularly using flame-AAS detection where attainable detection limits are too high to approach real-life speciation problems (demanding detection limits below 1 $\mu g\ l^{-1}$). The use of on-line conventional nebuliser AFS or ICP-AES detection would find similar limitations of the required sensitivity.

A general way-out to this lack of sensitivity of HPLC separation coupled to atomic detectors is to resort to on-line derivatization at the exit of the column to form 'cold vapor of mercury' to enhance the transport of the metal to the atomic detector. So, HPLC has been used in connection with AFS detection for organomercury species analysis. After the distillation and preconcetration of the mercury species they were separated onto the HPLC column, derivatized to mercury cold vapor and finally detected by AFS [139,140]. The use of 'organized media' in the mobile phase may help cold vapor formation and so enhance the sensitivity of the determination [125]. In fact, the use of vesicles exerts a synergic effect for the speciation of mercury using AAS or ICP-AES [141], particularly for MIP-AES detection [128]. Vesicle-mediated HPLC can be coupled on-line with flame-AAS and particularly with plasma detectors offering both, more flexibility in the mechanism of HPLC separation [142] and increased detectability (because of the beneficial properties of surfactants to on-line formation of hydrides and cold vapor of mercury before their introduction into a plasma). The usefulness of this approach has been demonstrated for the speciation of inorganic and methylmercury in sea water [128,142,143].

Continuous oxidation of mercury in the eluent and on-line further reduction to cold vapor of mercury, which is then introduced into the atomic spectrometric detector, has also been reported recently [144].

Of course, other derivatization procedures such as ethylation in aqueous phases [90,91] can be employed as well.

6. Other separation approaches

There are other separation approaches possible for mercury speciation. For instance, capillary electrophoresis (CE), is rapidly becoming popular for speciation of ionic species and biomolecules,

although its use for chemical speciation and environmental analysis is comparatively scarce [145]. Recently, Medina et al. [146] developed a rapid CE method for speciation of organo-mercury compounds in biological samples of marine origin. This technique allows a very convenient method for mercury speciation in a routine basis and has been validated for methylmercury determinations in tuna freeze-dried materials [147].

Finally, the possibility of resorting to off-line couplings of separation techniques and atomic detection should also be cited here, particularly in connection with the use of the high sensitive technique ETAAS to which we will refer later on.

7. Detectors for mercury speciation

As pointed out before, the analytical selectivity and sensitivity requirements for reliable speciation of trace and ultratrace amounts of toxic metals in environmental compartments (atmosphere, water, soil, sediments and also biota) are extremely high. Therefore, it appears obvious that detectors used should exhibit exceptional selectivity and sensitivity to the element to be speciated. Moreover, 'hybrid' techniques are preferred for speciation and, thus, such detectors should operate ideally 'on-line' with the chromatographic column, providing continuous, real-time information on the trace element sought for speciation. Most chromatographic detectors incorporated in commercial instruments are universal or selective but lacking the required specificity to mercury in environmental samples. In many instances those common chromatographic detectors do not provide the required sensitivity either. To make matters worse, typical electrochemical or molecular spectroscopic detectors are lacking the necessary ability to detect organometallics in general or methyl mercury in particular [137,138].

It is worldwide recognized that in most cases of real-life analytical speciation we have to resort to combine a chromatographic separation technique with an atomic (element-specific) detector. The case of methylmercury is illustrative in this respect: probably the most common technique formerly used for separation and determination of this compound has been GC with ECD. Problems encountered using this mercury unselective detector have been addressed previously. Such problems favored GC-MIP-AES because of its high element-specificity towards mercury [69,146,148]. There is no question that the availability of a commercial instrument for GC-MIP-AES measurements [149] has been decisive to explain the general acceptance of this 'hybrid' technique using plasma detection for speciation purposes.

Table 3
Desirable features for an 'ideal' detector to be used in a hybrid technique for trace element speciation

High sensitivity
High specificity
Ability to handle gases (in GC)
Ability to handle liquids (in HPLC and FIA systems)
On-line continuous operation with the separation column
Real-time information on the sought element
Broad linear dynamic range
Multi-element capacity
Multi-isotopic capacity

Analytical plasmas, both at atmospheric and reduced pressure [150], offer great analytical potential as 'element-specific' detectors. Some of them, particularly the ICP-MS, are now approaching many of the main desirable features for a detector in hybrid chromatographic techniques (Table 3).

Probably the MIP-AES is the plasma detector more frequently used for mercury speciation [69,72,77,86,96,98,114,119,127,128,148,158] as the direct nebulisation of liquid samples into the ICP-AES [101,141,151] lacks the required sensitivity for real-life mercury speciation. However, perhaps the atomic detector closest to the 'ideal' features for speciation (Table 3) is the ICP-MS whose importance in environmental analysis has been rocketing during the last few years [152–155]. Thus, the increasing number of papers devoted to the use of ICP-MS detection for mercury speciation is not surprising [121,130,156–158]. Table 4 resumes the different atomic (specific) detectors used for mercury speciation so far. It is apparent that the detector type more common is still AAS in its different forms of 'high sensitivity' measurements (cold vapor generation in flame quartz

Table 4
Hyphenated techniques with element 'specific' detection for mercury speciation

Separation	Atomic spectrometric detector	References	Detection limits (range)
GC	(CV)-AAS	[47,83,90–92,118]	5–167 pg
HPLC	(CV)-AAS	[120,142,143]	4–16 μg l^{-1}
GC	ETAAS	[73]	0.04 ng
GC	(CV)-AFS	[71,81,84,85,93,99,158]	0.01–6 ng l^{-1}; 0.6–1.3 pg
HPLC	(CV)-AFS	[33,34,139,140]	0.015–0.1 μg
GC	MIP-AES	[69,72,77,86,93,96,98,114,127]	0.04–10 ng l^{-1}
HPLC	(CV)-MIP-AES	[128]	0.35 ng ml^{-1}
GC	ICP-AES	[113,151]	3 pg, 0.6 ng l^{-1}
HPLC	ICP-AES	[142]	0.1 ng ml^{-1}
GC	ICP-MS	[19,129]	0.12–1 pg
HPLC	ICP-MS	[121,126,130,156]	16–400 ng l^{-1}

GC, Gas Chromatography;
HPLC, High Performance Liquid Chromatography;
CV, Cold Vapor;
AAS, Atomic Absorption Spectrometry;
ETAAS, Electrothermal Absorption Atomic Spectrometry;
AFS, Atomic Fluorescence Spectrometry;
MIP-AES, Microwave Induced Plasma Atomic Emission Spectrometry;
ICP-AES, Inductively Coupled Plasma Atomic Emission Spectrometry;
ICP-MS, Inductively Coupled Plasma Mass Spectrometry.

tubes (CVAAS) and electrothermal vaporization in a graphite furnace (ETAAS)) while AFS detection of mercury is also rather popular.

As said previously, any of these atomic detectors will need an appropriate interface to connect the exit of the column with the atomization cell. When using HPLC as a separation technique, the low efficiency of nebulisers demands usually a derivatization technique, on-line with the flow of the mobile phase, to enhance the efficiency of the transport of mercury species to the atomiser. For this purpose the use of $SnCl_2$ and $NaBH_4$ to generate hydrides and the cold vapor of mercury are the most popular derivatization reactions to form volatile species. Recently, the use of $NaB(C_2H_5)_4$ for metal ethylation from an aqueous phase has also been proposed [90,91] and can also be most useful to increase the sensitivity by forming a volatile compound.

Of course, this volatile species formation, particularly of Hg^0, has proved most useful for the preconcentration step of mercury and methylmercury by amalgamation [109] or in adequate traps [29,120]. As Fig. 1 represents schematically, the final detection to provide the 'speciation result' is only a final step in mercury speciation in environmental materials, where the extremely low levels of the element and the complexity of the matrix of the sample render previous preconcentration and separation stages virtually mandatory.

Sensitivity enhancements of atomic detection by resorting to volatile species generation is not restricted to AAS measurements. The extremely high sensitivity of AFS coupled to 'cold vapor' generation provides one of the more sensitive and selective atomic detectors for mercury [159], with instruments providing excellent features [160,161] available today in the market.

ETAAS detection constitutes a different picture. The very low limits of detection affordable by ETAAS for mercury (in the low μg l^{-1} level) and the high selectivity of today's ETAAS technology favor the use of this AAS methodology for mercury speciation [73]. However, the discontinuous character of ETAAS determinations (drying, ashing, atomization and cleaning-up) should be stressed in this respect. In other words, the use of this particular detector is limited because of its 'off-line' obliged operation. Notwithstanding that drawback, there are good examples of speciation

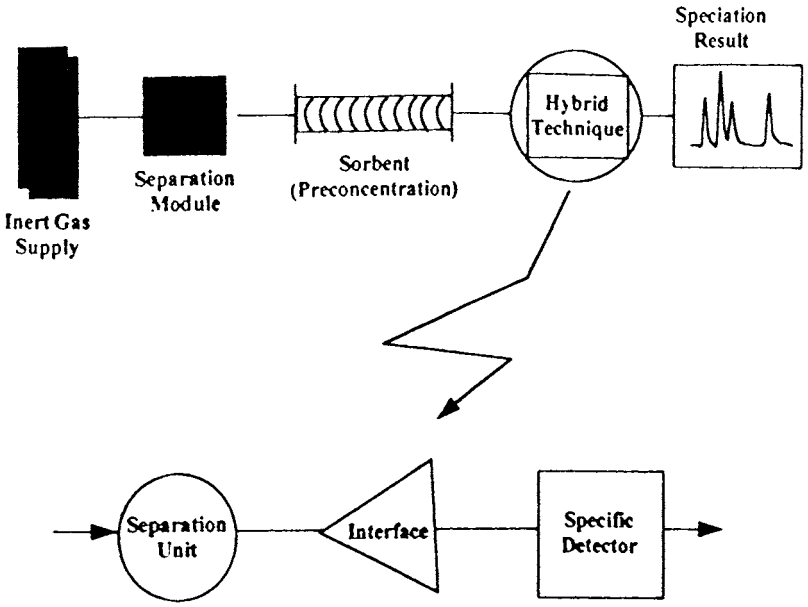

Fig. 1. Schematically representation of several steps involved in mercury speciation in environmental samples.

by collecting one or various (species) coming out of the column and then carrying those separated sample fractions to the corresponding ETAAS 'off-line' analysis for mercury [73]. In any case, the discontinuous nature of ETAAS operations make this detector more appropriate for the analysis 'off-line' of fractions separated by discontinuous (non-chromatographic) techniques particularly with the help of FIA strategies [162].

8. Conclusion

To conclude, the need of several analytical important steps (Table 1) for reliable mercury speciation should be stressed. Errors can occur in any of those basic steps. Therefore, each step (extraction, pretreatments, preconcentration, separation and detection) should be validated adequately, whichever the final strategy selected for mercury speciation in environmental samples. The present need for quality assurance and quality control of all speciation results in general [45] and of mercury speciation data in environmental matrices in particular [147] cannot be overemphasized and should be extensively addressed in the near future by analytical scientists developing in the field of chemical speciation of trace elements in environmental materials.

References

[1] E.L. Kothny, in: E.L. Kothny (Ed.), Trace Elements in the Environment, American Chemical Society, Washington DC, 1973, p 48.
[2] L. Nriagu, Nature 338 (1989) 47.
[3] J.S. Thayer, Organometallic Compounds and Living Organisms, Academic Press, Orlando, FL, 1984.
[4] T. Tsubaki, K. Irukayama (Eds.), Minamata Disease: Methylmercury Poisoning, Kodensha, Tokyo, 1977.
[5] J. Stary, H. Hanusova, B. Havlik, K. Kratzer, J. Prasilova, Acta Hydrodinamica Microbiol. 8 (1980) 29.
[6] H. Nagase, T. Ishikawa, Y. Ose, T. Sato, Sci. Total Environ. 25 (1982) 133.
[7] C.C. Gilmour, E.A. Henry, R. Mitchell, Environ. Sci. Technol. 26 (1992) 2281.
[8] J.M. Wood, F.S. Kennedy, C.G. Rosen, Nature 220 (1968) 173.
[9] R.G. Fischer, S. Rapsomanikis, M.O. Andreae, Environ. Sci. Technol. 29 (1995) 993.
[10] T. Matilainen, Water Air Soil Pollut. 80 (1995) 757.
[11] P. Chapman, G. Romberg, G. Vigers, J. Water Pollut. Control Fed. 54 (1982) 292.
[12] A. Jernelov, in: R. Hartung, B. Dinnan (Eds.), Mercury Chain in Environment Mercury Contamination, Ann Arbor Science Publishers, Ann Arbor, MI, 1972, p. 174.

[13] J.W. Huckabae, J.W. Elwood, S.G. Hildebran, in: J.O. Nriagu (Ed.), Accumulation of Mercury in Freshwater Biota. In the Biogeochemistry of Mercury in the Environment, Elsevier Holland Biomedical Press, New York, 1979, p. 227.
[14] M. Aceto, A.M. Flogizzo, E. Mentasti, G. Sacchero, C. Sarzanini, Int. J. Environ. Anal. Chem. 60 (1995) 1.
[15] R.P. Mason, J.R. Reinfelder, F.M.M. Morel, Water Air Soil Pullut. 80 (1995) 915.
[16] G. Topping, I.M. Davies, Nature 290 (1981) 243.
[17] P.G. Craig, P.A. Moreton, Water Res. 20 (1986) 1111.
[18] P.G. Craig, P.A. Moreton, Environ. Pollut. Series B Chem. Phys. 109 (1985) 141.
[19] H. Hintelmann, R.D. Evans, J.Y. Villeneuve, J. Anal. Atom. Spectrom. 10 (1995) 619.
[20] P.G. Goulden, B.K. Afghan. An Automated Method for Deterring Mercury in Water. Technical Bulletin No. 27, in Land Waters Branch Dept. of Energy, Mines and Resources, Otawa, Canada 1970.
[21] I. Suda, M. Suda, K. Hirayama, Arch. Toxicol. 67 (1993) 365.
[22] D. Cossa, J. Sanjuan, J. Cloud, P.B. Stockwell, W.T. Toms, J. Anal. Atom. Spectrom. 10 (1995) 287.
[23] M. Horvat, L. Liang, N.S. Bloom, Anal. Chim. Acta 282 (1993) 153.
[24] N.S. Bloom, Can. J. Fish Aquat. Sci. 49 (1992) 1010.
[25] R. Cela, R.A. Lorenzo, E. Rudi, A. Botana, M. Valino, C. Casals, M.S. Garcia, M.C. Mejuto, M.H. Bollain, Environ. Technol. 13 (1992) 11.
[26] O. Malm, F.J.P. Branches, H. Akagi, M.B. Castro, W. Pfeiffer, M. Harada, W.R. Bastos, H. Kato, Sci. Total Environ. 175 (1995) 141.
[27] R. Puk, J.H. Weber, Appl. Organom. Chem. 8 (1994) 293.
[28] N.S. Bloom, Can. J. Aquat. Sci. 46 (1989) 1131.
[29] R. Puk, J.W. Webber, Anal. Chim. Acta 292 (1994) 175.
[30] R.P. Mason, W.F. Fitzgerald, Water Air Soil Pollut. 56 (1991) 779.
[31] P. Quevauviller, O.F.X. Donard, J.C. Wasserman, F.M. Martin, J. Schneider, Appl. Organomet. Chem. 6 (1992) 221.
[32] Y. Cai, R. Jaffe, A. Alli, R.D. Jones, Anal. Chim. Acta 334 (1996) 251.
[33] H. Hintelman, M. Hempel, R.D. Wilken, Environ. Sci. Technol. 29 (1995) 1845.
[34] Y. Cai, R. Jaffe, R. Jones, Environ. Sci. Technol. 31 (1997) 302.
[35] First Symposium of Speciation of Elements in Environmental and Biological Sciences, Loen, Norway, June 1991.
[36] The Second International Symposium on Speciation of Elements in Toxicology and in Environmental and Biological Sciences, Loen 1994, Analyst 120 (1995) 30N.
[37] 3th International Symposium on Speciation of Elements in Biological, Environmental and Toxicological Sciences, Port Douglas, Australia, September 1997.
[38] P. Quevauviller, I. Draback, H. Muntau, B. Griepink, Appl. Organom. Chem. 7 (1993) 413.
[39] K. Matsumoto, ACS Symposium Series 445 (1991) 279.
[40] R.-D. Wilken, Fresenius J. Anal. Chem. 342 (1992) 795.
[41] R. Lobinski, Appl. Spectrosc. 51 (1997) 260A.
[42] H. Akagi, O. Malm, F.J.P. Branches, Y. Klnjo, Y. Kashima, J.R.D. Kato, Water Air Soil Pollut. 80 (1995) 85.
[43] L.D. Lacerda, E.D. Bidone, A.F. Guimaraes, W.C. Pfeiffer, Ann. Acad. Bras. Sci. 66 (1994) 373.
[44] R. Sarkis Müller, J.E. de Souza Sarkis, J.I. Garcia Alonso, J.E. Sánchez Uría, A. Sanz-Medel, Distribuçao e Comportamento do Mercurio no Ambiente Amazonico, University of Para, Brasil, 1997.
[45] A. Sanz-Medel, Spectrochim, Acta Part B (in press).
[46] C. Camara, C. Perez-Conde, M.C. Moreno-Bondi, C. Rivas, Fiber optical sensors applied to field measurements, Chapter 7, in: P. Quevauviller (Ed.), Quality Assurance for Environmental Analysis, Elsevier, Amsterdam, 1995.
[47] M. Horvat, A.R. Byrne, Analyst 117 (1992) 665.
[48] M. Leermakers, P. Lansens, W. Baeyens, Fresenius J. Anal. Chem. 336 (1990) 655.
[49] W. Baeyens, Trends Anal. Chem. 11 (1992) 245.
[50] R. Ahmed, M. Stoeppler, Anal. Chim. Acta 192 (1987) 109.
[51] R. Ahmed, K. Hay, M. Stoepler, Fresenius J. Anal. Chem. 326 (1987) 510.
[52] Analytical Quality Control Committe, Analyst 110 (1985) 103.
[53] R.W. Heiden, D.A. Aikens, Anal. Chem. 55 (1983) 2327.
[54] Certificate ORMS-1 National Research Council of Canada, Otawa, Ontario 1982.
[55] P. Lansens, C. Meuleman, W. Baeyens, Anal. Chim. Acta 229 (1990) 281.
[56] L. Lepine, A. Chamberland, Water Air Soil Pollut. 80 (1995) 1247.
[57] D.E. Wells, Mikrochim. Acta 109 (1992) 13.
[58] J.M. Bayona, I Simposium Sobre Técnicas de Especiación en Análisis Medioambiental, University of Huelva, Spain, October 1994.
[59] C.E. Oda, J.D. Ingle Jr., Anal. Chem. 53 (1981) 2305.
[60] L. Magos, Analyst 86 (1971) 847.
[61] L. Magos, T.W. Clarkson, J. Assoc. Off. Anal. Chem. 55 (1972) 966.
[62] M.C.R. Rezende, R.C. Campos, A.J. Curtius, J. Anal. Atom. Spectrom. 8 (1993) 247.
[63] Y.H. Lee, J. Mowrer, Anal. Chim. Acta 221 (1989) 259.
[64] R. Ahmed, M. Stoeppler, Analyst 111 (1986) 1371.
[65] Y.K. Chau, P.T.S. Wong, Fresenius J. Anal. Chem. 339 (1991) 640.
[66] G. Westöö, Anal. Scand. 20 (1966) 2131.
[67] G. Westöö, Anal. Scand. 21 (1967) 1790.
[68] S. Padberg, M. Burow, M. Stoepler, Fresenius J. Anal. Chem. 346 (1993) 686.
[69] E. Bulska, D.C. Baxter, W. Frech, Anal. Chim. Acta 249 (1991) 545.

[70] M. Horvat, A.R. Byrne, K. May, Talanta 37 (1990) 207.
[71] A. Alli, R. Jaffe, R. Jones, J. High Resolut. Chromatogr. 17 (1994) 745.
[72] P. Lansens, W. Baeyens, Anal. Chim. Acta 228 (1990) 93.
[73] M. Filipelli, Anal. Chem. 59 (1987) 116.
[74] G.B. Jiang, H.B. Hau, Z.M. Ni, S.R. Wang, Fresenius J. Anal. Chem. 334 (1989) 27.
[75] M. Hempel, H. Hintelman, R.-D. Wilken, Analyst 117 (1992) 669.
[76] P. Beauchemin, K.W.M. Siu, S.S. Berman, Anal. Chem. 60 (1988) 2587.
[77] Y. Telmi, V.E. Norwell, Anal. Chim. Acta 85 (1976) 203.
[78] Y. Thibaud, D. Cossa, Appl. Organomet. Chem. 3 (1989) 257.
[79] H. Emteborg, H.-W. Sinemus, B. Radziuk, D.C. Baxter, W. Frech, Spectrochim. Acta 51B (1996) 829.
[80] G. Westöö, Acta Chem. Scand. 22 (1968) 2277.
[81] M. Horvat, N.S. Bloom, L. Liang, Anal. Chim. Acta 281 (1993) 135.
[82] M. Floyd, L.E. Sommers, Anal. Lett. 8 (1975) 523.
[83] M. Horvat, K. May, M. Stoepler, A.R. Byrne, Appl. Organom. Chem. 2 (1988) 515.
[84] M. Horvat, L. Liang, N.S. Bloom, Anal. Chim. Acta 282 (1993) 153.
[85] Y. Cai, R. Jaffe, A. Alli, R. Jones, Anal. Chim. Acta 334 (1996) 251.
[86] H. Emteborg, D.C. Baxter, M. Sharp, W. Frech, Analyst 120 (1995) 69.
[87] P.G. Craig, P.A. Moreton, Water Res. 20 (1986) 1111.
[88] W. Holak, Analyst 107 (1982) 1457.
[89] M. Schintu, F. Jeancaurant, J.C. Amiard, Ecotoxicol. Environ. Saf. 24 (1992) 95.
[90] S. Rapsomanikis, P. Craig, Anal. Chim. Acta 248 (1991) 563.
[91] R. Fischer, S. Rapsomanikis, M.O. Andreae, Anal. Chem. 65 (1993) 763.
[92] P.T. Craig, D. Mennnie, N. Otash, O.F.X. Donard, F. Martin, Analyst 117 (1992) 823.
[93] W. Jian, C.W. McLeod, Talanta 39 (1992) 1537.
[94] M.L. Mena, C.W. McLeod, P. Jones, A. Withers, V. Mingauti, R. Capelli, P. Quevauviller, Fresenius J. Anal. Chem. 351 (1995) 456.
[95] W. Jiang, M.L. Mena, R.W. McLeod, J. Rollins, J. Environ. Anal. Chem. 57 (1994) 99.
[96] P. Lansens, C. Meuleman, M. Leermakers, W. Baeyens, Anal. Chim. Acta 234 (1990) 417.
[97] K. Minegawa, Y. Tokizawa, I. Kifuce, Anal. Chim. Acta 115 (1980) 103.
[98] H. Emteborg, D.C. Baxter, W. Frech, Analyst 118 (1993) 1007.
[99] L. Liang, M. Horvat, N.S. Bloom, Talanta 41 (1994) 371.
[100] C. Ergucyener, O.Y. Ataman, S. Aygun, A. Temizer, J. Anal. At. Spectrom. 3 (1988) 177.
[101] A. Menéndez García, M.L. Fernández Sánchez, J.E. Sánchez Uría, A. Sanz Medel, Mikrochim. Acta 122 (1996) 157.
[102] M. Valcárcel, M.D. Luque de Castro, Non-Chromatographic Continuous Separation Techniques, The Royal Society of Chemistry, Cambridge 1991.
[103] R.H. Atallah, D. Kalman, J. Anal. Toxicol. 17 (1993) 87.
[104] H. Morita, M. Sugimoto, S. Shimomura, Anal. Sci. 6 (1990) 91.
[105] Y. Madrid, C. Cabrero, T. Pérez-Corona, C. Cámara, Anal. Chem. 67 (1995) 345.
[106] S.C. High, J. Assoc. Off. Anal. Chem. 70 (1987) 667.
[107] S. Williams (Ed.), Official Methods of Analysis of the Association of Analytical Chemists, Arlington VA, 1984, p. 472.
[108] R. Pinel, Analusis 19 (1991) T19.
[109] W. Frech, D.C. Baxter, B. Bakke, J. Snell, Y. Thomassen, Anal. Comm. 33 (1996) 74.
[110] R. Cela, R.A. Lorenzo, M.C. Mejuto, M.H. Bollain, M.C. Casais, A. Botana, E. Rubi, I. Medina, Mikrochim. Acta 109 (1996) 111.
[111] E. Bulska, H. Emteborg, D.C. Baxter, W. Frech, D. Ellingsen, Y. Thomassen, Analyst 117 (1992) 657.
[112] R.D. Jones, M.E. Jacobson, R. Jaffe, J. West-Thomas, C. Arfstrom, A. Alli, Water Air Soil Pollut. 80 (1995) 1285.
[113] M. Ceulemans, F. Adams, J. Anal. At. Spectrom. 11 (1996) 201.
[114] M. Johansson, M. Emteborg, H. Glad, F. Reinholdsson, D.C. Baxter, Fresenius J. Anal. Chem. 351 (1995) 461.
[115] V.O. Schmitt, I.R. Pereiro, R. Lobinski, Anal. Comm. 34 (1997) 141.
[116] E. Rubi, R.A. Lorenzo, C. Casais, A.M. Carro, R. Cela, J. Chromatogr. A 605 (1992) 69.
[117] R.A. Lorenzo, A.M. Carro, E. Rubí, C. Casais, R. Cela, J. AOAC Int. 76 (1993) 608.
[118] R. Falter, H.F. Scholer, Fresenius J. Anal. Chem. 353 (1995) 34.
[119] M. Fernández García, R. Pereiro Garcia, N. Bordel García, A. Sanz Medel, Talanta 41 (1994) 1833.
[120] R. Falter, H.F. Scholer, Fresenius J. Anal. Chem. 354 (1996) 492.
[121] B.S. Bushee, Analyst 113 (1988) 1167.
[122] E. Munaf, H. Haraguchi, D. Ishii, T. Takouchi, M. Goto, Anal. Chim. Acta 235 (1990) 399.
[123] J.C.G. Wu, Spectroscopy Lett. 24 (1991) 681.
[124] X.D. Yao, J.C. Llu, J.K. Cheng, Y. Zeng, Anal. Sci. 8 (1982) 255.
[125] B. Aizpun Fernández, M.R. Fernández de la Campa, A. Sanz-Medel, J. Anal. At. Spectrom. 8 (1993) 1097.
[126] S.C.K. Sum, H. Pangand, R.S. Houk, Anal. Chem. 64 (1992) 2444.
[127] A.M. Carro Díaz, R.A. Lorenzo Ferreira, R. Cela Torrijos, J. Chromatogr. A 683 (1994) 245.
[128] J.M. Costa, F. Lunzer, R. Pereiro, A. Sanz-Medel, N. Bordel, J. Anal. At. Spectrom 10 (1995) 1019.
[129] A. Prange, E. Jantzen, J. Anal. At. Spectrom. 10 (1995) 105.

[130] M.J. Bloxham, D. Gachenja, S.J. Hill, P.J. Worsfold, J. Anal. At. Spectrom. 11 (1996) 145.
[131] C.C.Y. Chan, R.S. Sadana, Anal. Chim. Acta 282 (1993) 109.
[132] L. Ebdon, R.W. Ward, D.A. Leathard, Analyst 107 (1982) 129.
[133] N. Yoza, S. Ohaski, Anal. Lett. 6 (1973) 595.
[134] J.R. Van Loon, B. Radzink, N. Kahn, J. Lichwa, F.J. Fernández, J.D. Keber, At. Absorpt. Newsl. 16 (1977) 79.
[135] D.M. Fraley, D. Yates, S.E. Manahan, Anal. Chem. 51 (1979) 2225.
[136] K. Yoshida, T. Hasenagua, H. Hgaruchi, Anal. Chem. 55 (1983) 2106.
[137] L. Ebdon, S. Hill, R.W. Ward, Analyst 112 (1978) 1.
[138] L. Ebdon, S. Hill, P. Jones, Analyst 112 (1987) 437.
[139] M. Yoshino, H. Tanaka, K. Okamoto, Bunseki Kagaku 44 (1995) 691.
[140] R. Falter, G. Ilgen, Fresenius J. Anal. Chem. 358 (1997) 407.
[141] B. Aizpun, M.R. Fernández de la Campa, A. Sanz Medel, J. Anal. At. Spectrom. 8 (1993) 1097.
[142] A. Sanz-Medel, B. Aizpun, J.M. Marchante, E. Segovia, M.L. Fernández, E. Blanco, J. Chromatogr. A 683 (1994) 233.
[143] B. Aizpun, M.L. Fernández, E. Blanco, A. Sanz-Medel, J. Anal. At. Spectrom 9 (1994) 1279.
[144] C. Schickling, J.A.C. Broekaert, Appl. Organomet. Chem. 9 (1996) 29.
[145] C.L. Ng, H.K. Lee, S.F.Y. Li, J. Chromatogr. A 652 (1993) 547.
[146] I. Medina, E. Rubí, M.C. Mejuto, R. Cela, Talanta 40 (1993) 1631.
[147] A.M. Carro, R.A. Lorenzo, R. Cela, Mikrochim. Acta 123 (1996) 73.
[148] H. Emteborg, E. Bjorklund, F. Odman, L. Karlson, L. Mathison, W. Frech, D.C. Baxter, Analyst 121 (1996) 19.
[149] B.D. Quimby, J.J. O'Sullivan, Anal. Chem. 62 (1990) 1027.
[150] J.M. Costa, R. Pereiro, A. Sanz-Medel, N. Bordel, J. Anal. At. Spectrom. 10 (1994) 649.
[151] T. Kato, T. Uehiro, A. Yasuhara, M. Morita, J. Anal. At. Spectrom. 7 (1992) 15.
[152] S.J. Hill, Anal. Proc. 29 (1992) 399.
[153] M.S. Cresser, J. Armstrong, J. Cook, J.R. Dean, P. Watkins, M. Cave, J. Anal. At. Spectrom. 9 (2) (1994) 25R.
[154] M.S. Cresser, J. Armstrong, J.M. Cook, J.R. Dean, P. Watkins, M. Cave, J. Anal. At. Spectrom. 10 (2) (1995) 9R.
[155] M.S. Cresser, L.M. Garden, J. Armstrong, J.R. Dean, P. Watkins, M. Cave, J. Anal. At. Spectrom. 11 (2) (1996) 19R.
[156] C.-W. Huang, S.-J. Jian, J. Anal. At. Spectrom. 8 (1993) 681.
[157] R. Lobinsky, F.C. Adams, Spectrochim Acta 52B (1997) 1865.
[158] G.K. Zoorob, J.W. McKiernan, J.A. Caruso, Mikrochim. Acta 128 (1998) 145.
[159] L. Liang, M. Horvat, E. Cernichiari, B. Gelein, S. Balogh, Talanta 43 (1996) 1883.
[160] P.B. Stockwell, K.C. Thompson, A. Henson, E. Temermman, C. Vandecasteele, Int. Lab. 14 (1989) 45.
[161] C.C.Y. Chan, R.S. Sadana, Anal. Chim. Acta 282 (1993) 109.
[162] Z. Fang, Flow Injection Atomic Absorption Spectrometry, Chapter 9, Willey, Chichester, 1995.

ELSEVIER

Talanta 47 (1998) 525–530

Talanta

First and second order derivative spectrophotometric determination of benzyl alcohol and diclofenac in pharmaceutical forms

Y.C. de Micalizzi, N.B. Pappano, N.B. Debattista *

Department of Pharmacy and Department of Chemistry, San Luis National University, Chacabuco 917, 5.700 San Luis, Argentina

Received 22 October 1997; accepted 29 December 1997

Abstract

Diclofenac sodium is a drug with analgesic, antipyretic and anti-inflammatory properties. It is present in numerous pharmaceutical preparations. In injectable forms, it is usually accompanied by benzyl alcohol as an excipient, which is used as a blocking anesthetic (4%) and an antiseptic (4–10%). In this work spectrophotometric methodology was used in order to determine diclofenac and benzyl alcohol in injectable formulations by applying, on the one hand, the first-derivative method of crossing zero for diclofenac sodium and on the other, second derivative for benzyl alcohol. The results obtained show that this method has a significant advantage over other techniques and it is appropriate for routine pharmaceutical analysis. © 1998 Elsevier Science B.V. All rights reserved.

1. Introduction

UV-vis spectrophotometry is frequently used for drug and excipient quality controls before and after formulation as well as for quantitative analysis [1].

Spectral overlap and non-specific irrelevant absorption affect the interpretation of data for even the simplest single-component drug systems, leading to variable intercepts on the absorbance axis and systematic errors in the graphs of absorbance versus concentration.

Particularly, diclofenac sodium, a non-steroid drug with analgesic, antipyretic and anti-inflammatory properties [2], is usually accompanied by benzyl alcohol as an excipient when used in injectable form [3]. Even though benzyl alcohol is present as an excipient, it is important that its concentration does not exceed limit values for each formulation type, since it can produce fatal toxic syndromes, allergies and undesirable effects over the nervous system.

Generally, benzyl alcohol is quantitatively determined by gaseous chromathography and diclofenac sodium by gaseous chromathography and high performance liquid chromathography (HPLC) [4]. These drugs present partially overlapping spectra. One elegant approach to the problem of solving spectral overlap that has received attention in pharmaceutical analysis is derivative spectroscopy [5], whereby the first, second or

* Corresponding author. Tel.: +54 65224689; fax: +54 65230224.

0039-9140/98/$ - see front matter © 1998 Elsevier Science B.V. All rights reserved.
PII S0039-9140(98)00080-0

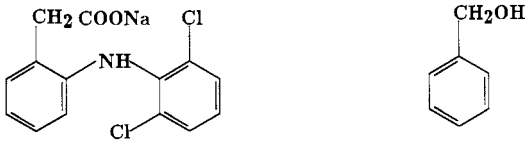

DICLOFENAC SODIUM BENZYL ALCOHOL

Fig. 1. Structural formulae of diclofenac sodium and benzyl alcohol.

higher derivative of spectral band absorbance or intensity is generated with respect to wavelength at all points in the spectrum.

Derivative methods have been seriously applied to the quantitative assay of drugs [5] and metals [6] in mixtures.

This paper describes the application of first and second derivative ultraviolet-visible spectrophotometry for the quantitative assay of benzyl alcohol and diclofenac in their dosage forms.

2. Experimental

2.1. Apparatus

Ordinary and derivative spectrophotometric analyses were performed on a Shimadzu UV-vis spectrophotometer UV 160A with standard 1.0 cm quartz cuvettes.

Absorption spectra of samples were recorded at a scan speed of ~ 480 nm min $^{-1}$ between 230–300 nm.

The first and the second derivative spectra were recorded with a $\Delta\lambda = 7.2$ and $\Delta\lambda = 0.7$ nm, respectively.

2.2. Reagents

Stock benzyl alcohol solution, prepared by dissolving benzyl alcohol (Sigma) in distilled water Fig. 1.

Stock diclofenac sodium solution, prepared by dissolving diclofenac sodium (Sigma) in distilled water Fig. 1.

Commercial injectable form: diclofenac sodium (75 mg) and excipients (mannitol, sodium metabisulfite, benzyl alcohol, propylene glycol, sodium hydroxide sufficient amount for pH 8.4, and distilled water apyrogene), sufficient amount for 3 ml.

2.3. Sample preparation and procedures

Samples (5 ml) were prepared in 8-ml test tubes

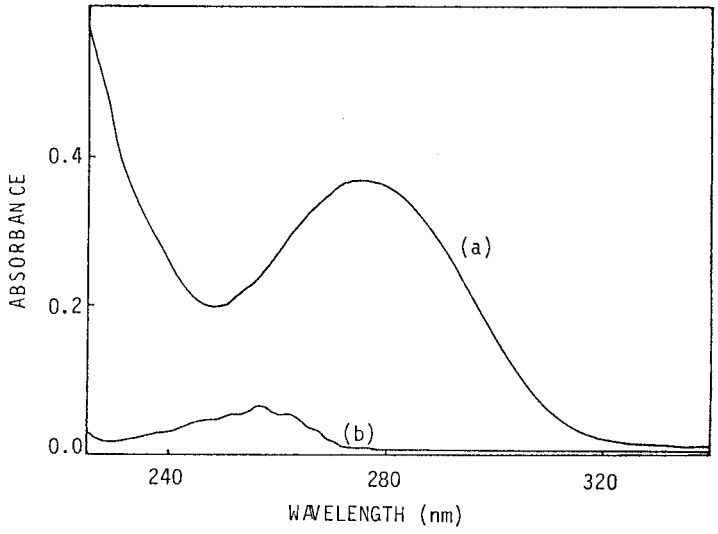

Fig. 2. Absorption spectra of (a) diclofenac sodium and (b) benzyl alcohol.

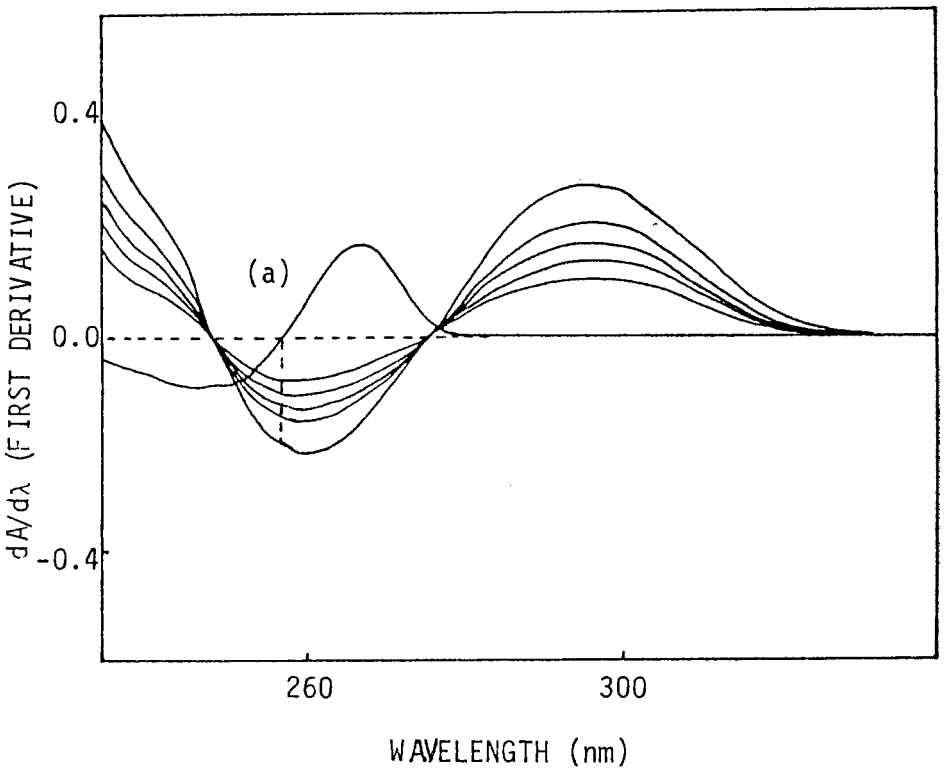

Fig. 3. A series of first derivative spectra with varying concentrations of diclofenac sodium (15.1–40.2 μg ml^{-1}) and constant benzyl alcohol concentration (16.0 μg ml^{-1}). (a) First derivative spectrum of benzyl alcohol.

Table 1
Calibration graph data of diclofenac sodium

[D] (μg ml^{-1})	15.1	20.1	25.1	30.2	40.2
A (h_{257})	0.078	0.100	0.122	0.146	0.200

Slope = 4.907×10^{-3}.
Intercept = 8.138×10^{-4}.
Correlation coefficient = 0.999.

containing 15.0–50.0 μg ml^{-1} of diclofenac sodium in the presence of benzyl alcohol at a constant concentration (16.0 μg ml^{-1}) and all the other excipients present in the injectable preparation.

On the other hand, samples containing 40.0–130.0 μg ml^{-1} of benzyl alcohol in the presence of diclofenac sodium at a constant concentration (52.0 μg ml^{-1}) and all other excipients were prepared in our laboratory.

The absorption spectra were recorded against a reagent-blank (excipients in water).

The absorbance calibration graphs were constructed on chart paper against the corresponding concentrations

The absolute values of the derivatives were obtained by a zero-crossing technique with measurements at 257.0 nm for diclofenac (first derivative) and ΔA (h_{277}–h_{271}) for benzyl alcohol (second derivative), respectively.

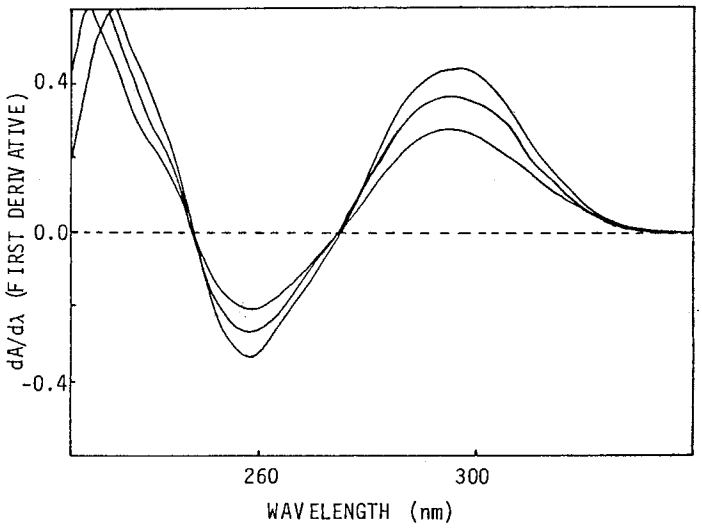

Fig. 4. First derivative spectra of injectable dilutions.

3. Results and discussion

Fig. 2 shows the closely overlapping absorption spectra of diclofenac and benzyl alcohol in the region of 225.0–340.0 nm.

This fact makes it extremely difficult to determine diclofenac in the presence of benzyl alcohol by conventional spectrophotometry. When derivative UV spectra were recorded, sharp bands of large amplitudes of diclofenac sodium were produced which may offer more selective identification and specific determination of this drug.

Fig. 3 shows the first derivative spectra of diclofenac sodium (15.1–40.2 μg ml^{-1}) with constant benzyl alcohol concentration (16.0 μg ml^{-1}).

The zero-crossing for benzyl alcohol appears at 257.0 nm. This value was selected as optimum to determine diclofenac in the presence of the benzyl alcohol.

Table 2
Determination of diclofenac sodium in an injectable solution

A (h_{257})	[D] known (μg ml^{-1})	[D] found (μg ml^{-1})	Recovery (%)
0.202	39.2	40.0	102.0
0.258	51.8	52.4	101.2
0.318	63.9	64.6	101.1

In the determination of diclofenac sodium a calibration graph (Table 1) was constructed from the first derivative signals by measuring at 257.0 nm for standard samples containing between 15.1 and 40.2 μg ml^{-1}, in the presence of 16.0 μg ml^{-1} of benzyl alcohol.

It can be verified (Fig. 3) that all curves which contain the same concentration of benzyl alcohol converge twice to an abscissa value corresponding to the zero crossing wavelength of the diclofenac sodium (248.0 and 276.0 nm).

Once the calibration curve was obtained, injectable solutions were prepared and diclofenac sodium concentration were determined from the first derivatives (h_{257}) (Fig. 4,Table 2).

Due to total spectra overlapping, the second derivative spectrophotometry was applied for the determination of benzyl alcohol. In contrast, the second derivative spectrum $d^2A/d\lambda^2$ is inverted with respect to the zero order spectrum and features two satellite maxima S and L and one minimum coinciding with the λ_{max} for the normal absorption band [7]. In principle both peak height and amplitude (ΔA) measurements [(h_{277})–(h_{271})] are proportional to benzyl alcohol concentration [8].

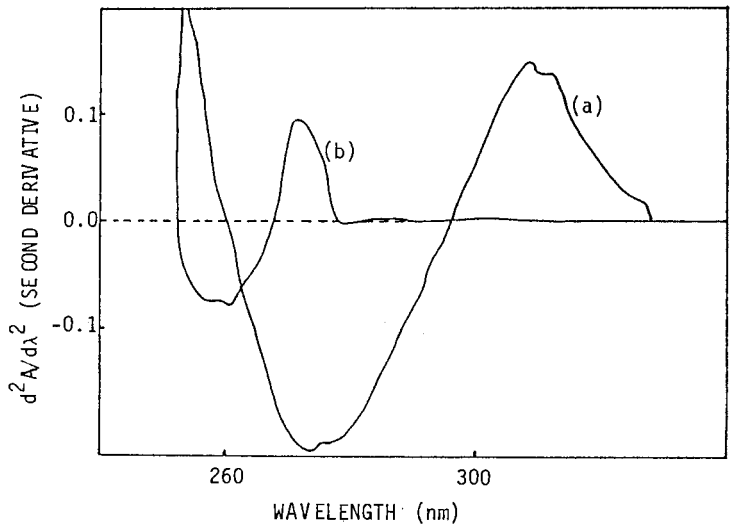

Fig. 5. Second derivative spectra of (a) diclofenac sodium and (b) benzyl alcohol.

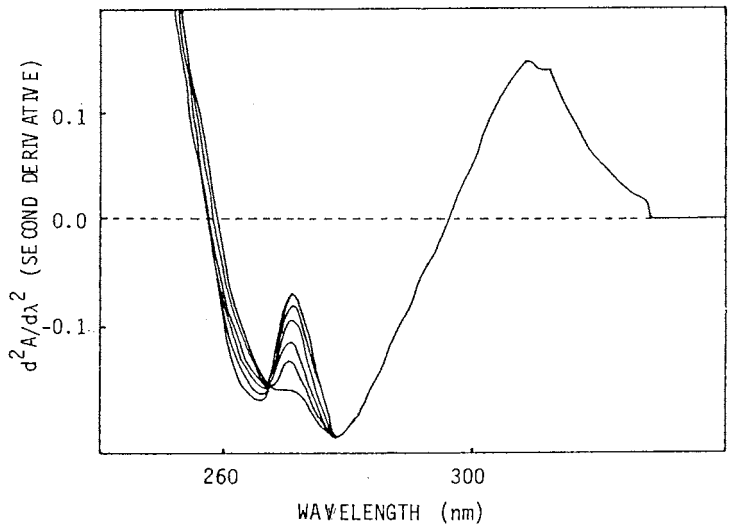

Fig. 6. A series of second derivative spectra of binary mixtures with varying concentrations of benzyl alcohol (40.8–126.3 μg ml^{-1}) and constant diclofenac sodium concentration (52.0 μg ml^{-1}).

Fig. 5 shows the second derivative spectra for diclofenac sodium and benzyl alcohol. Fig. 6 shows a series of second derivative spectra of binary mixtures with varying concentrations of benzyl alcohol (40.8–126.3 μg ml^{-1}) and constant concentration of diclofenac sodium (52.0 μg ml^{-1}) (scan speed: medium, $\Delta\lambda = 0.7$ nm). In this case a ΔA ($h_{277}-h_{271}$) is measured which is proportional to the concentration of benzyl alcohol present in the mixtures.

The ΔA and concentration values are seen in Table 3. The calibration graph was obtained and it was used to evaluate the benzyl alcohol concentration in the injectable solution (Table 4).

These applications illustrate the relative ease and simplicity offered by first and second deriva-

Table 3
Calibration graph data of benzyl alcohol

[B] (μg ml^{-1})	40.8	65.7	81.3	97.3	113.0	126.3
$\Delta A(h_{277}–h_{271})$	0.049	0.075	0.091	0.109	0.127	0.138

Slope = 1.112×10^{-3}.
Intercept = 1.358×10^{-3}.
Correlation coefficient = 0.999.

Table 4
Determination of benzyl alcohol in standard mixtures and in an injectable solution

ΔA ($h_{277}–h_{271}$)	[B] known (μg ml^{-1})	[B] found (μg ml^{-1})	Recovery (%)
0.064	57.1	56.3	98.6
0.081	71.5	71.6	100.1
0.097	89.4	87.1	97.4
0.119	105.6[a]	105.8[a]	100.2

[a] Injectable dilution.

tive spectrophotometry for the assay of spectrally interfering components.

Second derivative spectrophotometry generates inverted, sharpened spectra with improved resolution of overlapping peaks. The amplitude of carefully selected peaks may be quantitatively related to the studied compound concentrations in mixtures [9,10].

From the results obtained it can be stated that first and second derivative spectrometry offers a relatively simple, sensitive and inexpensive method for analysis of pharmaceutical products.

Acknowledgements

This work was supported by the funds of San Luis National University, San Luis, Argentina.

References

[1] A.F. Fell, Anal. Proc. (1978) 260.
[2] R.N. Brogden, R.C. Heel, G.E. Pakes, T.M. Speight, G.S. Avery, Drugs 20 (1980) 24.
[3] J.C. Boylan, J. Cooper, Z.T. Chowhan (eds.), Handbook of Pharmaceutical Excipients, p. 17. American Pharmaceutical Association, Washington, USA, 1986.
[4] Clarke's, Isolation and identification of Drugs. 2nd ed. p. 533, The Pharmaceutical Press, London, 1986.
[5] F. García Montelongo, M J. Sánchez, J.C. García Castro, A. Hardisson, Anal. Lett. 24 (1991) 1875.
[6] C.M. García, M.A. Lage-Yusty, J. Simal Lozano, Fresenius J. Anal. Chem. 338 (1990) 703.
[7] T.C. O'Haver, Anal. Chem. 51 (1979) 91A.
[8] F. Sánchez Rojas, C. Bosch Ojeda, J.M. Cano Pavon, Talanta 35 (1988) 753.
[9] S.M. Hassan, A.G. Davidson, J. Pharm. Pharmacol. 36 (1984) 7.
[10] M.E. Abdel-Hamid, M.M. Abdel-Khalek, M.S. Marhous, Anal. Lett. 17 (1984) 135.

ELSEVIER

Talanta 47 (1998) 531–536

Talanta

Indirect spectrophotometric determination of ascorbic acid with ferrozine by flow-injection analysis

A. Molina-Díaz *, I. Ortega-Carmona, M.I. Pascual-Reguera

Department of Physical and Analytical Chemistry, Faculty of Experimental Sciences. University of Jaén, E-23071 Jaén, Spain

Received 27 May 1997; received in revised form 9 February 1998; accepted 12 February 1998

Abstract

A FIA indirect spectrophotometric determination of ascorbic acid was developed using its reducing action on Fe(III) in acidic medium and following the spectrophotometric determination of the reduced iron by using sodium 3-(2-pyridyl)-5,6-diphenyl-1,2,4-triazine-4′,4″-disulphonate (ferrozine) as chromogenic reagent in buffered medium (pH 5.5) and monitoring the absorbance signal at 562 nm. A three-line manifold with two reaction coils was used: in the first reaction coil, ascorbic acid reduces Fe(III) to Fe(II); and in the second one, the complexation reaction is developed. The linear range of the method was 0.5–10 μg ml^{-1} of ascorbic acid, the detection limit being 0.028 μg ml^{-1}. The proposed method was sensitive, rapid (sampling rate of 90 samples h^{-1}) and reproducible (RSD 0.19%, $n = 10$). Satisfactory results were obtained in the determination of ascorbic acid in pharmaceutical preparations, fruit juices and urine testifying the applicability of the method to real samples. © 1998 Elsevier Science B.V. All rights reserved.

Keywords: Ascorbic acid; Ferrozine; Pharmaceutical preparations; Fruit juices

1. Introduction

Ascorbic acid participates in many different biological processes and is an essential compound in the human diet. There is a need for fast, selective and automated method for its determination, particularly in routine analyses. Several analytical techniques have been proposed, e.g. electroanalytical [1], chemiluminescence [2], spectrofluorimetric [3] and spectrophotometric [4–7] techniques, the latter being the most used.

Flow injection analysis (FIA) has been applied to determine ascorbic acid in a large number of samples, including foods, pharmaceuticals and biological samples, by using potentiometric [8], coulometric [9], amperometric [10], spectrofluorimetric [11], kinetic [12] and spectrophotometric [13–15] detection systems.

By spectrophotometry, in order to overcome the problem of interferences in the UV region, indirect determination of ascorbic acid by reagents which produce specific colour reactions is used.

One of the most sensitive approaches to the determination of ascorbic acid is based on the

* Corresponding author. Tel.: + 34 53 212147; fax: + 34 53 212526; e-mail: amolina@ujaen.es

0039-9140/98/$ - see front matter © 1998 Elsevier Science B.V. All rights reserved.
PII S0039-9140(98)00085-X

reduction of Fe(III) to Fe(II) by ascorbic acid, followed by the determination of Fe(II). Fe(II) can be conveniently measured after its complexation with the chromogenic specific reagent 3-(2-pyridyl-5,6-bis(phenylsulfonic acid)-1,2,4 triazine (ferrozine). The advantages of ferrozine over other Fe(II) selective reagents are higher molar absorption coefficient, water solubility, stability and low viscosity. It also reacts readily with iron (II) in a wide pH range [16]. On the other hand, with the reduction of Fe(III) to Fe(II), there is an amplification factor of two, leading to an increase in the sensitivity of this indirect determination. Ferrozine has been used for ascorbic acid analysis in citrus fruits [16], urine [17] and tissue extracts [18].

The present paper reports a simple, fast and selective indirect spectrophotometric method of the determination of ascorbic acid at 562 nm, via reduction of Fe(III) to Fe(II), followed by the determination of Fe(II) with ferrozine using flow injection techniques. This method was applied, with good results, to the routine determination of ascorbic acid in pharmaceutical preparations, fruit juices and urine.

2. Experimental

2.1. Reagents and chemicals

All reagents were of analytical-reagent grade and bidistilled water was used throughout.

L(+)-ascorbic acid solutions (Merck). Only aqueous fresh solutions, prepared from a 4.8×10^{-5}-M solution, were used for the spectrophotometric measurements.

Ferrozine, (sodium 3-(2-pyridyl)-5,6-diphenyl-1,2,4-triazine-4′,4″-disulphonate; Fz; Fluka). Solutions of various concentrations of Fz were prepared by dissolving Fz in water. These solutions were stored under refrigeration at 5°C. Under these conditions the solutions are stable for at least 30 days.

Buffer solutions (pH 5.50) were prepared by dissolving 4 g of hexamethylentetramine (HMTA) in 200 ml of water containing 2 ml of 1 M hydrochloric acid.

Iron (III) (1.79×10^{-4} M) solution was prepared by dissolving ammonium sulphate (Panreac R.A.) in 0.01 M of sulphuric acid.

2.2. Instrumentation and apparatus

All spectral measurements and real-time data acquisition of flow injection peaks were obtained using a double beam microprocessor controlled Lambda 2 UV-VIS Spectrophotometer (Perkin Elmer). The instrument was interfaced to an IBM PS/2 mod. 30-286 running Perkin-Elmer computerised spectroscopy software (PECSS V 4.1).The FI system consisted of a GILSON MINIPULLS-3 peristaltic pump, a Reodhyne type 50 four-way injection valve, a Hellma 178.011-OS flow cell with a 80-μl internal volume and a 10-mm light pathlength and the above spectrophotometer as detector. The pH measurements were made with a Crison Model 2002 pH-meter fitted with a glass-saturated calomel electrode assembly and a temperature probe

2.3. Flow injection procedure

A three-line system (Fig. 1) was used for the determination of ascorbic acid constructed with PTFE tubes of 0.8 mm i.d. The sample (300 μl) containing 0.5–10 μg ascorbic acid ml^{-1} at pH 2 was injected into the carrier (bidistilled water) stream by a four-way injection valve Reodhyne to which a volume control loop was attached. In the first merging point, the stream was mixed with the acidic Fe(III) solution 1.79×10^{-4} M in the 100-cm reaction coil (RC_1). At this point the reduction of Fe(III) to Fe(II) was achieved. The 1×10^{-2} M ferrozine solution buffered at pH 5.5 with HMTA/HCl was pumped at a flow rate of 4.3 ml min^{-1} and mixed in the 150-cm reaction coil (RC_2) where the formation of coloured complex between Fz and Fe(II) took place. The absorbance of the complex in the flow cell at 562 nm was monitored and a calibration graph was obtained by plotting the peak-absorbance versus the concentration of ascorbic acid in the range from 0.5 to 10 μg ml^{-1}.

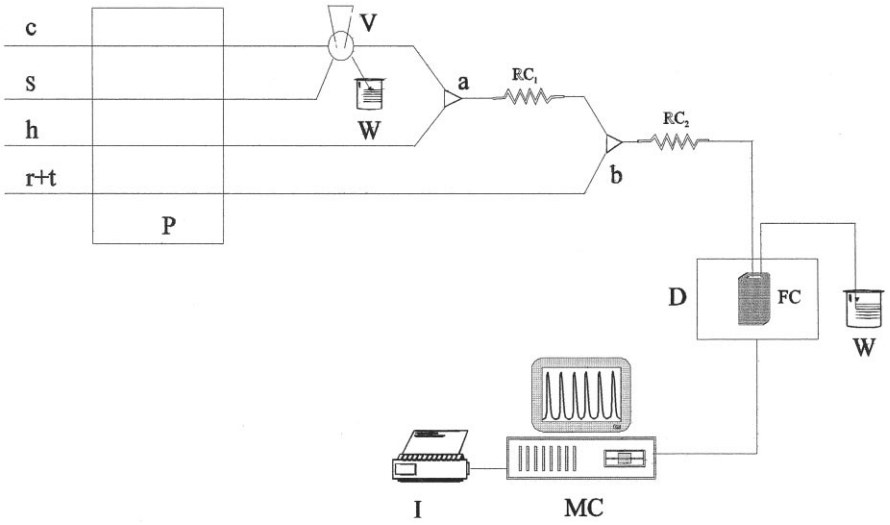

Fig. 1. Manifold configuration. S, sample (ascorbic acid); c, carrier solution (water), flow rate 4.6 ml min^{-1}; h, Fe(III) solution, flow rate 4.6 ml min^{-1}; r + t, buffered solution (pH = 5.5) of Fz (10^{-2} M), flow rate 4.3 ml min^{-1}; P, pump; V, four-way rotary injection valve equipped with teflon tube loop of 300 μl; a and b, confluence points; RC_1, reaction coil (0.8 mm i.d; 100 cm long); RC_2, reaction coil (0.8 mm i.d; 150 cm long); W, waste; D, photometric detector equipped with flow cell (FC); MC, microcomputer; I, impresor.

2.4. Pretreatment of the samples

2.4.1. Pharmaceutical samples

No sample pre-treatment was needed. An accurately weighed powder obtained from the tablets or the granular packets was transferred into a 1000-ml calibrated flask and the volume was made up to the mark with distilled water. After adequate dilution the sample was injected in the FIA system.

2.4.2. Urine samples

Urine sample was obtained from an individual 2 h after having a pharmaceutical compound (Citrovit) containing 1000 mg of ascorbic acid dissolved in 50 ml of water. An equivalent volume of 0.6 M trichloroacetic acid solution was added in order to deproteinise the urine [19] and the sample was filtered through a 0.45-μm membrane filter (Millipore). The analysis was performed immediately after diluting to an appropriate volume.

2.4.3. Fruit juices

Fresh fruits were purchased from the local market squeezed mechanically and the juices centrifuged at 3500 rpm for 4 min at 4°C. Finally, the obtained solutions were filtered through Whatman no. 42 filter and diluted to the appropriate volume.

3. Results and discussion

The indirect proposed procedure of determination of ascorbic acid was based in its reducing reaction on Fe(III) in acidic medium and following the spectrophotometric determination of the reduced iron by using Fz as chromogenic reagent. Fe(II) forms only one coloured (magenta) chelate at pH 5.5 whose absorption spectra measured against a reagent blank shows its maximum absorption at 562 nm [21].

3.1. Optimisation of the FIA system

Flow injection and chemical variables were optimised for the proposed FI method. This study was carried out by altering each variable in turn while keeping the others constant.

The effect of pH, buffer system and its concentration on the formation of the iron complex had been studied in a previous paper [20], the optima being 5.5 and 0.14 M HMTA.

3.1.1. Reagent concentration

The influence of Fz concentration was studied in the range 1.0×10^{-4} to 1.0×10^{-2} M, the optimum value being 1.0×10^{-2} M.

3.1.2. Influence of iron concentration

The influence of Fe(III) concentration was studied in the range 1.02×10^{-4} to 9.0×10^{-3} M the optimum value being 1.79×10^{-4} M. This represents a molar ratio Fe(III)/ascorbic acid of 3.

3.1.3. Influence of sample pH

The influence of sample pH was studied in a range of 1.0–9.5 (Fig. 2). Absorbance values were constant in the range 1.5–8.5, not being necessary to adjust the pH of the sample.

3.1.4. Influence of acidity of iron solution

For the completion of the reaction, the pH of iron solution must be below 2.5 (Fig. 3). The absorbance decreases drastically for pH values higher than 2.5 probably due to the hydrolysis of Fe(III). On the other hand the reduction of Fe(III) by ascorbic acid requires high acidity (this result agrees with that described by other authors [22]).

3.1.5. Sample volume

The influence of the sample volume was investigated by injecting volumes in the range of 50–500 μl. A 300-μl volume was selected as optimum because the signal of absorbance reaches its maximum value and remains constant from 200 μl.

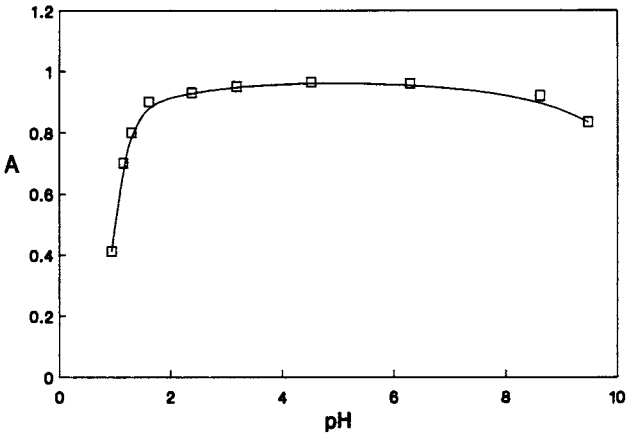

Fig. 2. Effect of sample acidity. (Ascorbic acid) = 5.65×10^{-5} M; (Fe(III)) = 1.79×10^{-4} M; (Fz) = 1.0×10^{-2} M.

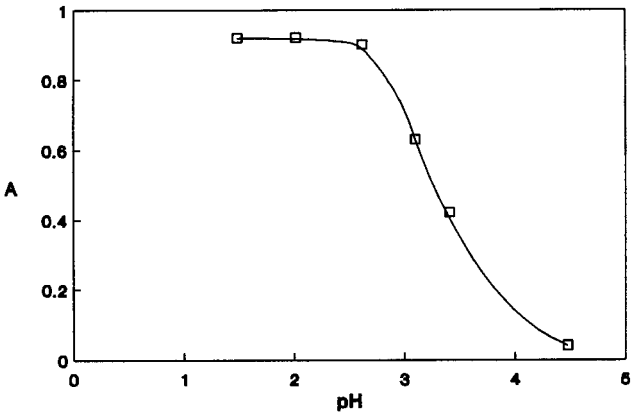

Fig. 3. Effect of iron solution acidity. (Ascorbic acid) = 5.67×10^{-5} M; (Fe(III)) = 1.79×10^{-4} M; (Fz) = 10^{-2} M.

3.1.6. Effect of the reaction coil lengths

The effect of the length of the reaction coils (RC_1 and RC_2 in Fig. 1) was also examined. The results indicated that reduction (RC_1) and formation of coloured chelate compound (RC_2) reactions were fast because the influence of reaction coil lengths was not very significant. If the lengths of both coils were shortened by 50%, the signal decreases only by 10%. The chosen length were 100 and 150 cm, respectively.

3.1.7. Effect of flow-rate

The effect of the flow-rate was examined by changing in the range from 2.6 to 5.3 ml min^{-1}. Since the absorbance value reaches its maximum and remains constant for rates higher than 4.0 ml min^{-1}, the optimum value chosen was 4.6 ml min^{-1}.

3.2. Calibration graph

With the manifold described above and under the selected experimental conditions, viz., 1.0×10^{-2} M Fz and 1.79×10^{-4} M Fe(III), a linear calibration graph 0.5–10 μg ml^{-1} ascorbic acid was obtained. The analytical parameters are summarised in Table 1. The regression equation found was $A = 0.095$(ascorbic acid) + 0.017, where A is

Table 1
Analytical parameters for the determination of ascorbic acid

Linear dynamic range (μg ml^{-1})	0.5–10
Intercept	0.017
Slope (ml μg^{-1})	0.095
Detection limit ($K=3$; μg ml^{-1})	0.028
Determination limit ($K=10$; μg ml^{-1})	0.095
RSD[a] (%; $n=10$)	0.19

[a] Value for a concentration of ascorbic acid of 4.54×10^{-5} μg l^{-1}.

the absorbance and (ascorbic acid) is expressed in μg ml^{-1}, with a correlation coefficient (r) of 0.9994. Sampling rate was 90 samples h^{-1}.

3.3. Interferences

In order to asses the possible analytical applications of the spectrophotometric method described above, the influence of concomitant species on the determination of ascorbic acid in real samples was studied by analysing synthetic sample solutions containing 8 μg ml^{-1} of ascorbic acid and various excess amounts of the common excipients used in pharmaceutical preparations and other species commonly found in fruit juices and organic acids. The tolerance limit was taken as the amount which caused an error of $\pm5\%$ in each peak height. The tolerance limits for the ions studied are shown in Table 2. Interferences from saccharose, glucose, starch, caffeine, thiamine, fructose, sulphate and chloride were not found. Of the species tested, the only major interferences were PO_4^{3-}, SO_3^{2-} and S^{2-}, probably due to their reactions of complexation (PO_4^{3-}) and reduction (SO_3^{2-} and S^{2-}) with Fe(III).

Table 2
Effect of foreign species on the determination of 8 μg ml^{-1} ascorbic acid

Foreign species	Tolerance level (μg ml^{-1})
SO_4^{2-}, Cl^-, saccharose, glucose, starch, thiamine, caffeine, fructose	>1000
NO_3^-	500
$C_2O_4^{2-}$	25
NO_2^-	20
Tartrate	10
Uric acid	8
PO_4^{3-}	2
SO_3^{2-}	1
S^{2-}	0.1

Table 3
Determination of ascorbic acid in pharmaceuticals

Ascorbic acid content[a]			
Sample	Stated	Proposed method[b]	Reference method[b]
Redoxon[c]	1000	1018 (0.1)	993 (0.4)
Efferalgan[d]	200	197 (0.5)	195 (0.3)
Cebion 500[e]	500	493 (0.1)	495 (0.4)
Frenadol[f]	250	245 (0.6)	253 (0.8)
Algidol[g]	500	504 (0.1)	498 (0.4)
Citrovit[h]	1000	990 (0.1)	1009 (0.3)

[a] Values for samples in mg/tablet or sachet.
[b] Values in parentheses are relative standard deviations in % ($n=3$).
[c] Redoxon tablets (Roche Nicholas, Barcelona, Spain): vitamin C, 1 g; sodium saccharin, 20 mg; saccharose, 1305 mg; plus excipient up to 4.4 g.
[d] Efferalgan tablets (Upsa Médica): ascorbic acid, 200 mg; paracetamol, 330 mg; plus excipient up to 3 g.
[e] Cebion 500 granular sachets (E. Merck-Darmstadt IGODA, Barcelona, Spain): vitamin C, 500 mg; sodium saccharin, 4.2 mg; plus excipient up to 6 g.
[f] Frenadol sachets (Abello Laboratories, Madrid, Spain): ascorbic acid, 250 mg; paracetamol, 650 mg; dextrometorfane, $HBr\cdot H_2O$, 20 mg; caffeine citrate, 30 mg; chlorpheniramine maleate, 4 mg; saccharose, 8.2 mg; plus excipient up to 10 g.
[g] Algidol granular sachets (Berenguer-Infale, Prodesfarma Group Laboratories, Barcelona, Spain): vitamin C, 500 mg; paracetamol, 650 mg; codeine phosphate, 10 mg; plus excipient up to 5.5 g.
[h] Citrovit granular sachets (Abello Laboratories, Madrid, Spain): vitamin C, 1 g; saccharose, 7.09 g; glucose, 0.599 g; invert sugar, 0.178 g; plus excipient up to 10 g.

3.4. Applications

The method was applied successfully to the determination of ascorbic acid in pharmaceutical preparations, juices fruits and urine.

In every case the sample was analysed by both the proposed method and the official AOAC [23] method, the latter used as a reference method.

3.4.1. Pharmaceuticals

In Table 3 the composition for each compound analysed is shown. Since no matrix effect was

Table 4
Determination of ascorbic acid in fruit juices and urine

Sample	Added μg ml^{-1}	Found[c] μg ml^{-1}	Recovery (%)	Found by the reference method[d] μg ml^{-1}
Urine[a]	—	4.3 ± 0.2	—	4.3 ± 0.3
	2	6.3 ± 0.3	98.6	
	4	8.5 ± 0.3	100.6	
Lemon juice[b]	—	78 ± 2	—	75 ± 1
	40	120 ± 3	106.5	
	100	175 ± 5	97.4	
Orange juice[b]	—	147 ± 4	—	145 ± 5
	40	187 ± 6	102	
	80	229 ± 7	105	

[a] Values referred to a dilution of the sample 3/500.
[b] Values referred to a dilution of the sample 4/25.
[c] Average of three determinations.
[d] 2,6-Dichloroindophenol method.

found, the determination of ascorbic acid in pharmaceutical samples was performed by applying the standard calibration graph method. The results obtained were compared with those found by the reference method (based in the titrimetric determination with 2,6-dichloroindophenol) and the concordance was excellent.

3.4.2. Urine

The standard addition calibration graph method was applied owing to the matrix effect observed. This effect could be evaluated from the ratio of the slopes of the standard addition calibration graph to that of the standard calibration graph. The ratio was 0.71. To check the accuracy, a recovery study was made (Table 4).

3.4.3. Fruit juices

Orange and lemon juice were analysed. Here, also a matrix effect was observed and the standard addition calibration graph method was applied. The ratios were 0.021 and 0.016 for orange and lemon juice, respectively. To check the accuracy, a recovery study was also made (Table 4).

References

[1] M.J. Esteve, R. Farre, A. Frigola, Fresenius J. Anal. Chem. 351 (1995) 4.
[2] A.A. Alwarthan, Analyst 118 (1993) 639.
[3] J. Peinado, F. Toribio, D. Pérez-Bendito, Analyst 122 (1987) 775.
[4] M. Sakar, A.R. Sakar, Analusis 22 (1994) 155.
[5] E. Tutem, B. Ulkeseven, R. Apak, Anal. Lett. 25 (1992) 471.
[6] S.Z. Qureshi, A. Saeed, S. Haque, M.A. Khan, Talanta 38 (1991) 637.
[7] E.Y. Backheet, K.M. Emara, H.F. Askal, G.A. Saleh, Analyst 116 (1991) 861.
[8] B. Karlberg, S. Thelander, Analyst 103 (1978) 1154.
[9] D.J. Curran, T. Tougas, Anal. Chem. 56 (1984) 672.
[10] W. Matuszewski, M. Trojanowicz, L. Ilcheva, Electroanalysis 2 (1990) 147.
[11] J. Vardersclice, D. Higss, Micronutr. Anal. 6 (1989) 109.
[12] M.I. Karayannis, D.I. Farasoglou, Analyst 112 (1987) 767.
[13] J. Hernández-Mendez, A. Alonso, M.J. Almendral, C. García de María, Anal. Chim. Acta. 184 (1986) 243.
[14] F. Lázaro, M.D. Luque de Castro, M. Valcárcel, Analusis 15 (1987) 183.
[15] I. Albero, M.S. García, C. Sánchez-Pedreño, J. Rodríguez, Analyst 117 (1992) 1635.
[16] B. Jaselkis, S.J.J. Nelapaty, J. Anal. Chem. 44 (1972) 379.
[17] W.C. Butts, H.J. Mulvihill, Clin. Chem. 21 (1975) 1493.
[18] E.L. McGrown, M.G. Rusnak, C.M. Lewis, J.A. Tillotson, Anal. Biochem. 119 (1982) 55.
[19] S. Amlathe, V.K. Gupta, Analyst 113 (1988) 1481.
[20] M.I. Pascual-Reguera, I. Ortega-Carmona, A. Molina-Díaz, Talanta 44 (1977) 1793–1801.
[21] L.L. Stookey, Anal. Chem. 42 (1970) 779.
[22] Z. Marczenko, H. Kalowska, Anal. Chim. Acta 123 (1981) 279.
[23] Official Methods of Analysis, AOAC, vol. II, 15th ed., 1990, p. 1058.

ELSEVIER

Talanta 47 (1998) 537–545

Talanta

Analysis of binary mixtures of flufenamic, meclofenamic and mefenamic acids by derivative synchronous fluorescence spectrometry

Tomás Pérez Ruiz *, Carmen Martínez Lozano, Virginia Tomás, José Carpena

Department of Analytical Chemistry, University of Murcia, 30071 Murcia, Spain

Received 9 September 1997; received in revised form 9 February 1998; accepted 12 February 1998

Abstract

Second-derivative synchronous fluorescence spectrometry was used to develop a simple, rapid and sensitive spectrofluorimetric method for the determination of binary mixtures of the nonsteroidal antiinflammatory drugs flufenamic (FFA), meclofenamic (MCFA) and mefenamic (MFA) acids in serum and pharmaceutical formulations. The method is based on the intrinsic fluorescence of these compounds in chloroform. A $\Delta\lambda = 105$ nm was used for the resolution of FFA–MFA and MFA–MCFA mixtures, whereas the FFA–MCFA mixture was determined at $\Delta\lambda = 40$ nm. Serum samples are treated with trichloroacetic acid to remove the proteins, and the analytes are extracted in chloroform prior to determination. Pharmaceutical preparations were analysed without prior separation steps. © 1998 Elsevier Science B.V. All rights reserved.

Keywords: Second-derivative synchronous fluorescence spectrometry; Flufenamic acid; Mefenamic acid; Meclofenamic acid; Binary mixtures; Serum; Pharmaceutical preparations

1. Introduction

Flufenamic acid (FFA, *N*-(α,α,α-trifluoro-*m*-tolyl) anthranilic acid), meclofenamic acid (MCFA, *N*-(2,6-dicloro-*m*-tolyl) anthranilic acid) and mefenamic acid (MFA, *N*-(2,3-xylyl) anthranilic acid) belong to a family of nonsteroidal antiinflammatory drugs (NSAIDs) that are derivatives of *N*-phenylanthranilic acid. They are used as potent analgesic and anti-inflammatory agents in the treatment of osteoarthritis, rheumatoid arthritis and other painful musculosketal illnesses. The fenamates appear to owe their properties primarily to their capacity to inhibit cyclooxygenase. Unlike other NSAIDs, they may also antagonize certain effects of prostaglandins [1].

Fenamic acids are readily absorbed after oral administration and metabolized to twp major and at least six minor metabolites. The drugs are metabolized by oxidation of the 3′-methyl group to a pharmacologically active 3′-hydroxymethyl metabolite, which may be further oxidized to an

* Corresponding author. Tel.: + 34 68 307100; fax + 34 68 364148.

0039-9140/98/$ - see front matter © 1998 Elsevier Science B.V. All rights reserved.
PII S0039-9140(98)00086-1

inactive 3′-carboxy metabolite. To a lesser extent, ring hydroxylation and monodehalogenation also occur. Several methods have been recommended for the determination of these fenamic acids, which depend on titrimetric [2,3], polarographic [4], spectrophotometric [5–10], chromatographic [11–13] and flow injection [14] techniques.

The native fluorescence shown by these *N*-phenylanthranilic acid derivatives in organic solvents has also been used for their detection and determination [15]. The formation of complexes with aluminium [14,16], and the cyclisation reactions using formaldehyde or sulfuric acid to give benzoxazines or a mixture of acridones, respectively, have also been found to be useful for the fluorimetric determination of fenamic acids [17,18]

Binary drugs mixtures are increasingly used in therapy for a variety of diseases [19]. The simultaneous control of NSAIDs in serum is of great importance, however, no reports were found concerning the simultaneous determinations of the fenamic acids. The application of luminescent techniques to the analysis of complex mixtures is particularly attractive due to the high sensitivity that can be achieved. However, conventional spectrofluorimetry has an extremely restricted scope of application in the analysis of complex mixtures because it's selectivity is reduced by extensive spectral overlap, although it can be substantially improved by using synchronous [20,21] and derivative [22] luminescence spectrometric techniques.

The combination of synchronous scanning fluorimetry and derivatives is more advantageous than differentiation of the conventional emission spectrum in terms of sensitivity, because the amplitude of the derivative signal is inversely proportional to the band width of the original spectrum. In addition, the selectivity is greatly increased by the joint use of both techniques, as has been demonstrated in the analysis of mixtures of polycyclic aromatic hydrocarbons [23], vitamins [24], drugs [25–27], pesticides [28], rodenticides [29] and inorganic ions [30,31]

In the method described here, the binary mixtures of FFA, MCFA and MFA are determined directly and simultaneously by their natural fluorescence in chloroform solution. However, as the conventional and synchronous fluorescence spectra of the three fenamic acids completely overlap, the determination is carried out using second-derivative synchronous fluorescence spectrometry.

2. Experimental

2.1. Reagents

All chemicals were of analytical-reagent grade.

2.1.1. Standard drug solutions

Stock solution containing 250 mg ml^{-1} of the fenamic acids were prepared in a 100 ml calibrated flask by dissolving 25 mg of each acid obtained from Sigma (St. Louis, MO) in chloroform. Working standard solutions were prepared by suitable dilution of the stock solutions with chloroform.

Table 1
Fluorescence data for FFA, MFA and MCFA

Drug	Solvent	λ_{ex} nm	λ_{em} nm	I_F^a
FFA	Chloroform	286; 348	423	100
	1,2-Dichloroethane	260; 323	425	50
	Ethanol	310; 373	421	5
	Butanol	309; 373	434	8
	1% (w/v) Triton X-100	286; 347	426	20
MFA	Chloroform	290; 355	460	25
	1,2-Dichloroethane	266; 327	460	12
	Ethanol	322; 383	463	6
	Butanol	320; 385	460	9
	1% (w/v) Triton X-100	286; 353	439	8
MCF	Chloroform	286; 340	403	60
	1,2-Dichloroethane	279; 332	403	24
	Ethanol	324; 370	403	9
	Butanol	325; 370	403	8
	1% (w/v) Triton X-100	322; 337	403	12

[a] Relative fluorescence intensity. The response of FFA in chloroform was normalized to 100.

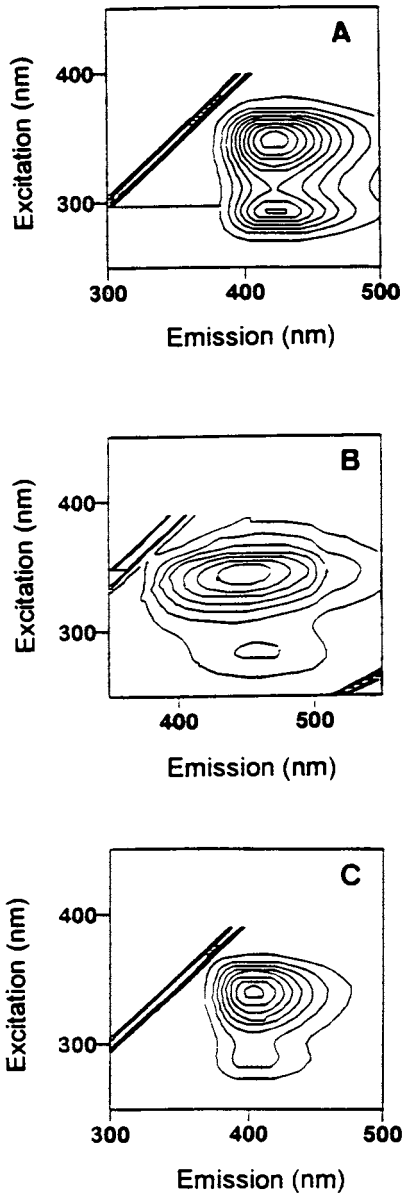

Fig. 1. Contour plot of the excitation-emission matrix of (A) flufenamic acid, (B) mefenamic acid, (C) meclofenamic acid in chloroform. The contours join points showing the same fluorescence intensity.

2.2. Apparatus

An Aminco Bowman (Urbana, IL) series 2 spectrofluorimeter fitted with a 150 W xenon lamp and interfaced to a DTK computer was used for the collection of all fluorescence spectra and intensity measurements. The software provides mathematical manipulation of the spectra and calculates first and second derivatives by the simplified least-squares procedure of Savitzky and Golay [32]. A spectral band-pass of 4 nm was set for the excitation and emission monochromators. For synchronous fluorescence measurements, both excitation and emission monochromators were locked together and scanned simultaneously at a rate of 2 nm s^{-1}. A Colora thermostatic water-bath circulator was used to control the cell compartment temperature at 25°C.

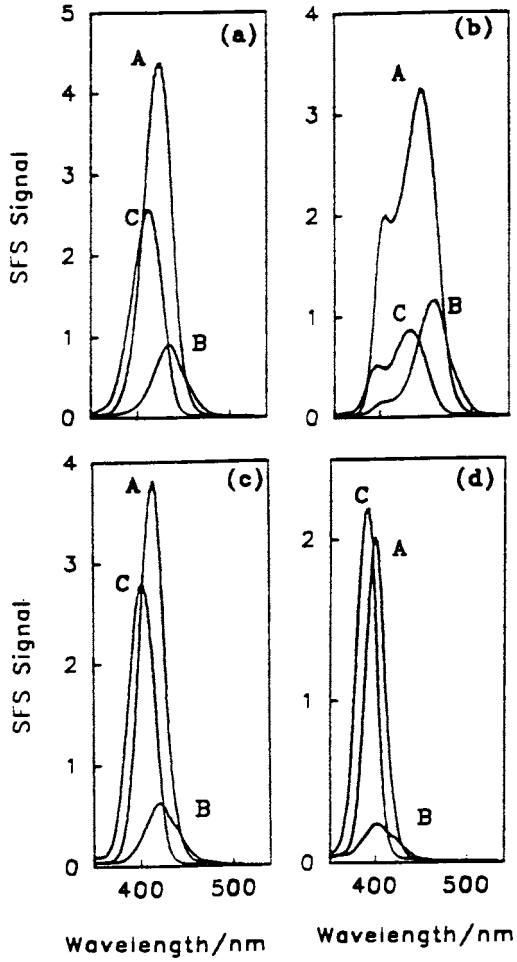

Fig. 2. Synchronous fluorescence spectra of FFA (A), MFA (B) and MCFA (C). (a) $\Delta\lambda = 75$ nm; (b) $\Delta\lambda = 105$ nm; (c) $\Delta\lambda = 63$ nm; (d) $\Delta\lambda = 40$ nm.

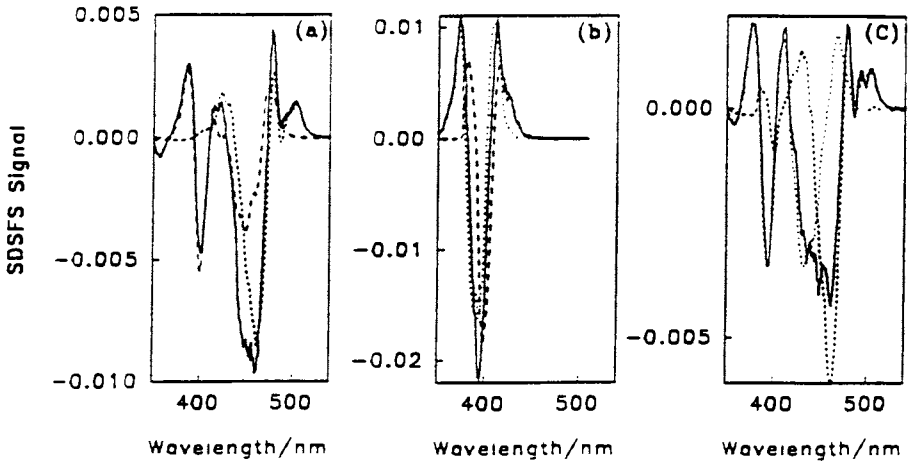

Fig. 3. Second derivative synchronous fluorescence spectra of FFA (—— ——), MFA (- - -) MCFA (···) and binary mixtures (solid lines). (a) FFA–MFA mixture, $\Delta\lambda = 105$ nm; (b) FFA–MCFA, $\Delta\lambda = 40$ nm; (c) MFA–MCFA, $\Delta\lambda = 105$ nm.

2.3. Procedures for the determination of binary mixtures

2.3.1. FFA–MFA mixtures

A sample containing 1.12–11.2 μg FFA and 1.93–9.65 μg MFA was placed in a 10 ml standard flask and the volume was made up to the mark with chloroform. The synchronous fluorescence spectrum, was recorded by scanning both monochromators together with a 105 nm constant difference between them and a scan speed of 2 nm s^{-1}. The excitation monochromator was scanned from 225 to 415 nm and the emission monochromator from 330 to 520 nm. Hereafter all wavelengths referring to synchronous spectra are taken as equal to those of the corresponding emission wavelength. The second-derivative time was smoothed and calculated by Savitzky and Golay method [32] The second-derivative analytical signal was taken as the vertical distance from the second-derivative synchronous spectrum to the base line at 386 nm for FFA and 504 nm for MFA. These signals are directly related to the concentration of each compound from the calibration lines previously obtained using standard solutions.

2.3.2. FFA–MCFA mixtures

A sample volume containing FFA (2.25–9.00 μg) and MCFA (2.36–9.47 μg) was diluted in a 10 ml standard flask with chloroform. The synchronous fluorescence spectra were recorded by scanning both monochromators simultaneously with a constant 40 nm difference between them. The excitation monochromator was scanned from 300 to 410 nm and the emission monochromator from 340 to 450 nm. The vertical distance from the second-derivative synchronous spectrum to zero line were measured at 426 nm for FFA and at 366 nm for MCFA.

2.3.3. MFA–MCFA mixtures

Samples containing MFA (1.93–9.65 μg) and MCFA (1.18–11.8 μg) were diluted to 10 ml with chloroform as described for the other mixtures. The synchronous spectrum was recorded by scanning simultaneously the excitation monochromator from 215 to 425 nm and the emission monochromator from 320 to 530 nm. The derivative signal is obtained by measuring the vertical distance from second-derivative synchronous spectrum to the zeroline at 377 nm for MCFA and at 504 nm for MFA.

2.4. Determination of the binary mixtures of fenamic acids in serum

100 μl Serum was placed in a 10 ml glass-stopped centrifuge tube and 1 ml 0.05 M trichloroacetic acid and 1 ml chloroform were

Table 2
Simultaneous analysis of synthetic binary mixtures of flufenamic, mefenamic and meclofenamic acids

Mixture	Ratio	Amount of FFA (ng ml^{-1})		Amount of MFA (ng ml^{-1})		Amount of MCFA (ng ml^{-1})	
		Taken	Found[a]	Taken	Found[a]	Taken	Found[a]
FFA–MFA	1:1	112	109 ± 1	112	110 ± 1		
		560	551 ± 1.5	560	550 ± 2		
	1:4	224	213 ± 1	896	920 ± 2		
	1:9	112	104 ± 1	1008	1012 ± 3		
	3:2	336	320 ± 1.5	224	226 ± 1		
	4:1	896	878 ± 2	224	220 ± 1.5		
	9:1	1008	1002 ± 2	112	101 ± 1		
FFA–MCFA	1:1	224	220 ± 1			224	218 ± 1
		560	549 ± 2			560	546 ± 2
	1:4	224	209 ± 1			896	902 ± 2
	3:2	336	322 ± 1			224	216 ± 1.5
	4:1	896	872 ± 2			224	232 ± 1
MFA–MCFA	1:1			224	220 ± 1	224	212 ± 1.5
				560	550 ± 2	560	534 ± 2
	1:4			224	216 ± 1	896	874 ± 2
	3:2			336	328 ± 2	224	210 ± 1
	4:1			896	912 ± 2	224	214 ± 1
	9:1			1008	1030 ± 2	112	108 ± 1

[a] Average of three separate determinations $\pm$ S.D.

added successively. The mixture was mechanically vortexed for 3 min and the phases were separated by centrifugation (3 min at $1000 \times g$). After removing the organic phase, chloroform (1 ml) was added and the above treatment was repeated. The two chloroform layers were combined and diluted with chloroform to an appropriate volume in a calibrated flask. The binary mixtures were determined following the above procedures.

2.5. Determination of fenamic acids in pharmaceutical preparations

Representative samples of finely ground tablets or opened capsules were stirred with 20–30 ml distilled water and 2 ml 2 M hydrochloric acid. The mixture was equilibrated twice with 5 ml chloroform and the combined organic extracts were made up to a known volume with chloroform. Appropriate dilutions were made before analysis, so that the concentration of the fenamic acids in the sample solution remained within the range recommended for standard solutions.

3. Results and discussion

The influence of the different media on the spectrofluorimetric characteristics of FFA, MFA and MCFA are summarized in Table 1. The three fenamic acids show two excitation maxima and an emission maximum. None of the solvents is suitable for the resolution of the binary mixtures of these compounds by conventional fluorimetry because of the broadly overlapping spectra.

A different approach, synchronous spectrofluorimetry, was used for the resolution of these binary mixtures. Chloroform was selected because in this solvent the three compounds yielded the highest fluorescence intensity with the lowest blank signal.

In order to determine the optimum $\Delta\lambda$ value for the resolution of the binary mixtures of the fenamic acids, the total fluorescence spectra of FFA, MFA and MCFA were obtained. The two-dimensional (contour plots) representation of these spectra (Fig. 1) show a strong overlapping, which means that the resolution of the binary

Table 3
Determination of binary mixtures of FFA, MFA and MCFA in synthetic serum samples

	Serum concentration (μg ml^{-1})			Concentration found[a] (μg ml^{-1})			Recovery ± S.D.(%)		
	FFA	MFA	MCFA	FFA	MFA	MCFA	FFA	MFA	MCFA
FFA–MFA	5.6	20.0		5.4	19.8		96 ± 2	99 ± 2	
	14.0	12.5		13.5	12.3		96 ± 3	98 ± 1	
	22.4	5.0		21.9	4.9		99 ± 1	98 ± 3	
FFA–MCFA	5.6		24.0	5.3		24.1	95 ± 1		100 ± 2
	14.0		15.0	13.6		14.6	97 ± 2	97 ± 3	
	22.4		6.0	21.8		5.8		97 ± 2	97 ± 1
MFA–MCFA		5.0	24.0		4.8	23.6		96 ± 2	98 ± 2
		12.5	15.0		12.4	14.5		99 ± 2	97 ± 1
		20.0	6.0		20.2	5.8		101 ± 3	97 ± 3

[a] Average of three determinations.

mixtures of fenamic acids using synchronous spectrofluorimetry was not feasible. Fig. 2 shows the synchronous fluorescence spectra at different $\Delta\lambda$ values corresponding to the difference between the emission and excitation maxima for FFA ($\Delta\lambda = 75$ nm), MFA ($\Delta\lambda = 105$ nm) and MCFA ($\Delta\lambda = 63$ nm) and at a lesser $\Delta\lambda$ value of 40 nm.

The spectral overlap can be resolved, however, by applying derivatives techniques to the synchronous spectra.

3.1. FFA–MFA mixture

In order to achieve the simultaneous analysis of the mixture, the system was optimized by changing one variable at a time whilst keeping the others constant. The optimum value taken for each variable was such that the following requirements were met: (i) The fluorescent signal for each compound should not depend on the signal for the other compound. (ii) The signal for each peak (ΔI_{FFA} and ΔI_{MFA}) should be as high as possible.

The most important parameter in the simultaneous analysis of the mixtures is the selection of the optimum wavelength difference between both monochromators. Second-derivative synchronous fluorescence spectra were obtained over a range of $\Delta\lambda$ from 30 to 140 nm. The spectral distribution is a function of $\Delta\lambda$. Spectra were compressed or expanded by decreasing or increasing, respectively, this experimental parameter to which the number of peaks is also related. In addition, $\Delta\lambda$ has a strong influence on the fluorescence intensity. There is an appreciable extent of spectral overlap for $\Delta\lambda < 90$ nm which increases with decreasing $\Delta\lambda$. Above this $\Delta\lambda$ value the fluorescence intensity for each compound, obtained at its corresponding wavelength, was independent of the fluorescence intensity of the other compound. A $\Delta\lambda = 105$ nm was chosen for the simultaneous analysis of the FFA–MFA mixture. The scan speed selected was 2 nm s^{-1}, after verifying that this parameter hardly affected the derivative signal obtained.

Fig. 3a shows the second-derivative synchronous fluorescence spectra of FFA and MFA and a mixture of both drugs. The analytes can be determined by measuring the value of the peak of the second-derivative at 386 and 504 nm, which are proportional to FFA and MFA concentrations, respectively.

3.2. FFA–MCFA mixture

The optimization of each variable was carried out according to the considerations made for the FFA–MFA mixture.

The effect of $\Delta\lambda$ on the second-derivative synchronous fluorescence spectra of both FFA and

Table 4
Determination of fenamics acids in pharmaceutical preparations

Product (laboratory)[a]	Labelled			Proposed method[b]			Reference method[c]		
	FFA	MFA	MCFA	FFA	MFA	MCFA	FFA	MCFA	MCFA
Tablet I (home made)	50	50	48 ± 1	48 ± 1		49 ± 1[d]	51 ± 1[d]		
Tablet II (home made)	75		75	76 ± 1.5		74 ± 1	75 ± 1[d]		76 ± 1.5[d]
Tablet III (home made)		100	100		99 ± 1.5	98 ± 1.5		101 ± 1[d]	99 ± 1[d]
Coslan (capsules) (Park-Davis)		250		251 ± 1.5			251 ± 1[d]		
Movilisin (solution) (Alfarma)	30				30 ± 1		29 ± 1[e]		
Meclomen (capsules) (Parke-Daves)			100			98 ± 1			98 ± 1.5[d]

[a] Composition of samples: Tablet I: flufenamic acid, 50 mg; lactose (excipient), 350 mg. Tablet II: mefenamic acid, 75 mg; lactose, 150 mg and methyl celulose, 200 mg. Tablet III: meclofenamic acid, 100mg; methyl celulose, 350 mg. Coslan (capsules): mefenamic acid, 250 mg; lactose (excipient), 100mg. Movilisin (solution): 1 ml, contain flufenamic acid, 30 mg; glucosaminegluconate polisulphate, 2 mg; salicylic acid, 20 mg. Meclomen (capsules): meclofenamic acid, 100 mg; lactose and other excipient c.s.
[b] Average of four determinations ± S.D.
[c] Average of three deterninations ± S.D.
[d] Non-aqueous alkalimetry [35].
[e] Ion-pair partition chromatography [13].

MCFA shows that the resolution of this mixture is feasible for $\Delta\lambda$ values between 55 and 30 nm, although the greatest sensitivity was at $\Delta\lambda = 40$ nm and this value was selected. Variations in the scanning speed of both monochromators had a similar effect to that described for the preceding mixture.

Fig. 3b shows the second-derivative synchronous fluorescence spectra of FFA and MCFA and a mixture of the two compounds using $\Delta\lambda =$ 40 nm. The distances to the zero line at 366 and 426 nm are proportional to the FFA and MCFA concentrations, respectively.

3.3. MFA–MCFA mixture

Resolution spectral and fluorescence intensity on the scan derivative synchronous fluorescence spectra of MFA and MCFA were also affected by the wavelength difference between the excitation and emission monochromators. A $\Delta\lambda$ value of 105 nm was chosen as ideal in order to establish a rapid and simple analytical method. This $\Delta\lambda$ value made it possible to determine simultaneously both compounds with the greatest sensitivity, using the signal that appears at 377 nm for MFA and at 504 nm for MCFA. Fig. 2c shows the second derivative synchronous fluorescence spectra of MFA, MCFA and a mixture of both.

3.4. Features of the proposed methods

The determination of FFA, MFA and MCFA in their binary mixtures is carried out in only one scan. The method involves the construction of independent calibration graphs for each compound in the mixture. The analysis of samples containing various concentrations of two of these compounds shows that the determination of their mixtures is feasible over the following concentration ranges: FFA–MFA mixture, FFA (0.11–1.12 μg ml^{-1}, % R.S.D. = 0.62), MFA (0.19–0.96 μg ml^{-1}, %R.S.D. = 0.82); FFA–MCFA mixture, FFA (0.22–0.90 μg ml^{-1}, %R.S.D. = 0.96), MCFA (0.23–0.95 μg ml^{-1}, %R.S.D. = 0.73); MFA–MCFA mixture, MFA (0.19–0.96 μg ml^{-1}, %R.S.D. = 0.74), MCFA (0.11–1.18 μg ml^{-1}, %R.S.D. = 1.5). The values of R.S.D. was established at the same concentration levels (0.5 μg ml^{-1}) for all drugs. The limit of detection (LOD) was estimated from the equation $C_L = kS_B/m$, where the S.D. (S_B) from 16 blank determinations, the slope of the calibration curve (m) for each fenamic acid and $k = 3$ were employed [33]. The LOD calculated were 0.006, 0.009 and 0.012 μg ml^{-1} for FFA, MFA and MCFA, respectively. Table 2 summarizes the results obtained in the resolution of several synthetic binary

mixtures containing two of these drugs in different ratios.

3.5. Serum samples

The second-derivative synchronous fluorescence spectra obtained from the serum samples were similar to those corresponding to pure standard samples in the region of interest. The amounts of each drug present in the binary mixtures were calculated either by interpolation on the working lines or by the standard addition method.

Serum samples were spiked with different quantities of two of the three fenamic acids, so that their concentrations were in the range 5–25 μg ml^{-1}. The concentrations for FFA, MFA and MCFA were selected from pharmacokinetic data of these compounds from healthy adults following oral administration of a single 1 g dose of the drugs [34]. The recovery percentages found by application of the proposed method are shown in Table 3. Three spectra of the three different samples at the same concentration were used for each concentration level included in the Table. Analytical recoveries ranged from 95 to 99% for FFA, from 96 to 101% for MFA and from 97 to 100% for MCFA. The absence of detectable blanks in drugs-free serum indicates that the constituents of normal serum extracted in chloroform do not interfere with fluorescence measurements. The two major metabolites (3'-hydroxymethyl and 3'-carboxy) of each fenamic acid should likely interfere in the determination of the binary mixtures of these drugs.

3.6. Pharmaceutical preparations

The results obtained by applying the recommended procedures to pharmaceutical preparations are given in Table 4. The contents of FFA, MFA and MCFA measured by this method are in good statistical agreement with those obtained by the reference method. Routine analyses of the drugs in their commercial dosage forms were also performed in order to demonstrate the applicability of this method for the quality control of the formulations. It is worth noting that the presence of salicylic acid is tolerated. The commercial formulation Movilisin, which contained FFA and salicylic acid was analysed with good results. The high sensitivity and selectivity of the method permit it to be used without prior separation steps. Excipients and preservatives do not interfere.

4. Conclusions

The results obtained in determining the binary mixtures of the fenamic acids show that derivative synchronous fluorescence spectrometry can be useful when analysing binary mixtures of drugs of very similar analytical properties. The proposed method, for example, permits us to determine FFA, MFA and MCFA and their binary mixtures in serum and in pharmaceutical dosage forms. It is worth emphasizing that salicylic acid is not an interferent in the determination of the fenamic acids. The proposed method is applicable to the analysis of these drugs wherever simplicity, rapidity and cost-effectiveness are sought as alternatives to chromatography.

Acknowledgements

The authors are grateful to the Dirección General de Investigación Científica y Técnica for financial support (grant no. PB96-1101).

References

[1] P.A. Insel, in: Goodman, Gilman, A. (Eds.), The Pharmacological Basis of Therapeutics, chap. 27, McGraw-Hill, New York, 1996.
[2] Y.K. Agrawal, Sci. Cult. 46 (1980) 309; Anal. Abstr. 41 (1981) 4E9.
[3] S.T. Hassib, H.M. Safwat, R.I. El-Bagry, Analyst 111 (1986) 45.
[4] O.R. Pryakhin, V.A. Vdoviko, S.A. Pokhmelkina, V.V. Petrenko, V.A. Golovkin, Khim. Farm. Zh. 15 (1981) 93; Anal. Abstr. 43 (1982) 6E46
[5] M. El-Sadek, M. Baraka, A. Aboul Khier, Indian J. Pharm. Sci. 49 (1987) 97.
[6] M.S. Mahrous, M.M. Abdel-Khalek, M.E. Abdel-Hamid, Talanta 32 (1985) 651.
[7] A.S. Issa, Y.A. Beltagy, M. Gabr Kassem, H.G. Daabees, Talanta 32 (1985) 209.

[8] C.S.P. Sastry, A.S.R. Prasad Tipirneni, M.V. Suryanarayana, Analyst 114 (1989) 513.
[9] S. Das, S.C. Sharna, S.K. Talwar, P.D. Sethi, Analyst 114 (1989) 101.
[10] A. Aboul Kier, M. El-Sadek, M. Barak, M. Barak, Analyst 112 (1987) 1399.
[11] L.J. Dusci, L.P. Hackett, J. Chromatogr. 161 (1978) 340.
[12] L. Cotellessa, R. Riva, P. Salva, F. Marcucci, F. Mussini, E. Mussini, J. Chromatogr. 192 (1980) 441.
[13] W.M. Adams, J. Assoc. Off. Anal. Chem. 66 (1983) 1178.
[14] M.I. Albero, C. Sánchez-Pedreño, M.S. García, J. Pharm. Biomed. Anal. 13 (1995) 1113.
[15] A.C. Mehta, S.G. Schulman, Talanta 20 (1973) 702.
[16] Y. Hattori, T. Arai, T. Mori, E. Fujihira, Chem. Pharm. Bull. 18 (1970) 1063.
[17] H.D. Dell, R. Kamp, Arch. Pharm. 303 (1970) 785.
[18] W. Schmollack, U. Wenzel, Pharmazie 29 (1974) 583.
[19] Goodman, Gilman, A., The Pharmacological Basis of Therapeutical, 9th ed., McGraw-Hill, New York, 1996.
[20] J.B.E. Lloyd, Nature 231 (1971) 64.
[21] T. Vo-Dinh, Anal. Chem. 50 (1978) 396.
[22] G.L. Green, T.C. O'Haver, Anal. Chem. 46 (1974) 2191.
[23] T. Vo-Dinh, Appl. Spectrosc. 36 (1982) 576.
[24] A. Petidier, S. Rubio, A. Gomez-Hens, M. Valcarcel, Anal. Biochem. 157 (1986) 212.
[25] F. García Sánchez, C. Cruces Blanco, A.L. Ramos Rubio, M. Hernández López, J.C. Marques Gómez, C. Carnero, Anal. Chim. Acta 205 (1988) 149.
[26] A. Muñoz de la Peña, F. Salinas, M.S. Durán, Anal. Chim. Acta 255 (1991) 317.
[27] E.S. Lianidou, P.C. Ioannou, C.K. Polydorou, C.E. Efstathiou, Anal. Chim. Acta 320 (1996) 107.
[28] F. García Sánchez, C. Cruces Blanco, Anal. Chem. 60 (1988) 323.
[29] S. Panadero, A. Gómez-Hens, D. Pérez Bendito, Talanta 40 (1993) 225.
[30] S. Rubio, A. Gómez-Hens, M. Valcarcel, Anal. Chem. 57 (1985) 1101.
[31] E. Ureña Pozo, A. García de Torres, J.M. Cano Pavón, Anal. Chem. 59 (1987) 1129.
[32] A. Savitzky, M.J.E. Golay, Anal. Chem. 36 (1964) 1627.
[33] G.L. Long, J.D. Winefordner, Anal. Chem. 55 (1983) 713A.
[34] A.C. Moffat, Clarke's Isolation and Identification of Drugs in Pharmaceuticals, Body fluids, and Post-Mortem Material, 2nd ed., The Pharmaceutical Press, London, 1986.
[35] British Pharmacopoeia, HMSO, 1988 pp 354 and 641.

ELSEVIER

Talanta 47 (1998) 547–559

Talanta

Spectrophotometric and complexometric methods for the determination of thorium and fluoride using bromocresol orange reagent

Magdi E. Khalifa *, Medhat A.H. Hafez

Department of Chemistry, Faculty of Science, University of Mansoura, Mansoura, A.R., Egypt

Received 30 September 1997; received in revised form 10 February 1998; accepted 12 February 1998

Abstract

The ternary purple coloured complex formed between Th^{4+}, bromocresol orange (BCO) and cetylpyridinium bromide (CPB) in acidic medium was investigated spectrophotometrically. Results obtained revealed the formation of 1:1:1, Th:BCO:CPB complex in aqueous solution at pH $\approx$ 0.5 with a logarithmic conditional stability constant of 12.04 ± 0.1, $I = 0.1$ at 25°C. The colour of the ternary complex was used for the determination of thorium(IV) in the range of 0.02–2.6 μg ml^{-1} Th^{4+}, $\epsilon = 9.2 \times 10^4$ l mol^{-1} cm^{-1} at 560 nm. Beside its high sensitivity, the reaction was also proved to be highly selective for Th^{4+}. Thorium(IV) was determined in presence of great number of transition metal ions, rare earths and different anions. Th^{4+} was also determined with high accuracy and precision by its titration with disodium ethylenediaminetetraacetate (Na_2EDTA) using BCO as an indicator at pH $\approx$ 0.5. The endpoint was detected either visually or spectrophotometrically ($\lambda = 550$ nm). The proposed procedures were successfully applied for the determination of Th^{4+} in standard Th-U ores and in a series of naturally occurring ores or minerals containing thorium. A spectrophotometric method was also described for the determination of fluoride ion, which was based upon the decrease in colour intensity of the Th-BCO complex on mixing it with F^- ion. The proposed method was convenient, rapid and sensitive for fluoride. It could be used for the determination of fluoride ion in the 0.02–3.00 μg ml^{-1} range (S.D. $\pm$ 0.9%). The proposed method was successfully applied for direct determination of F^- ion in water obtained from different origins and the results were satisfactory. © 1998 Elsevier Science B.V. All rights reserved.

Keywords: Thorium and fluoride determination; Bromocresol orange; Cetylpyridinium bromide

1. Introduction

Thorium is an important element. It is often used as a fuel for nuclear reactors besides its industrial applications. Thorium(IV) occurs in nature in the Earth's crust in the form of the mineral monazite with different proportions of most of the rare earth minerals. The determination of Th^{4+} in presence of these ions is of special interest. Many direct and indirect complexometric methods have been used for its determination

* Corresponding author. Fax: + 20 50 346781; e-mail: sinfac@mum.mans.eun.eg

0039-9140/98/$ - see front matter © 1998 Elsevier Science B.V. All rights reserved.
PII S0039-9140(98)00078-2

[1–5]. Also, the application of various organic reagents for the spectrophotometric determination of Th^{4+} is well known. Among the reagents employed for this purpose are thoron and arsenazo(III) [6,7]. The complex formation of thorium with methylthymol blue [8], 8-hydroxyquinoline [9], chrome azurol S [10], xylenol orange [11], xanthene dyes and bromopyrogallol red [12] has been investigated. The analytical application of mixed ligand complexes for the determination of Th^{4+} has also been reported [13]. Such mixed systems often provides special sensitivity and selectivity of analytical importance. Recently we have prepared the bromocresol orange (BCO) dye and used it successfully for the determination of some toxic mixtures of ions [14].

In this paper, a spectrophotometric study on the interaction of Th^{4+} with bromocresol orange, BCO, (**I**) is conducted. Moreover the influence of the cationic surfactant cetylpyridinium bromide (CPB) on the absorbance of the Th-BCO complex has been investigated and a very sensitive spectrophotometric method for the determination of Th^{4+} is proposed. The use of the dye BCO as an indicator for the complexometric titration of Th^{4+} with ethylenediaminetetracetic acid disodium salt, Na_2EDTA, is also studied. Furthermore, the application of Th-BCO complex for the determination of fluoride has been tested. The proposed procedures are highly selective and have been satisfactorily applied for the determination of thorium in some standard U-Th certified ores and in a series of naturally occurring minerals. Also the thorium complex is applied for the determination of fluoride in water samples supplied from variable sources.

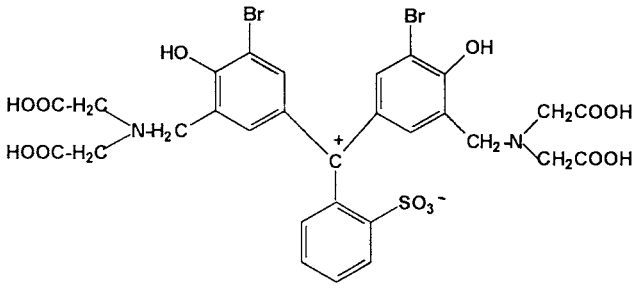

(I)

2. Experimental

2.1. Apparatus

A unicam UV2-100 UV-Visible spectrometer (V 3.32), UK, was used for recording the absorption spectra in the range 340–700 nm with matched 1.0 cm quartz cells.

Spectrophotometric micro-titrations were performed on an Extech digital spectrophotometer (Boston, MA). A removable plastic cap with small holes for a stirring rod was provided. The stirring rod has a PTFE propeller, which was driven by a small electric motor powered by a 1.5-V battery. The capillary tip of a micro-burette was also inserted into a hole in the cap. A 5-ml glass micro-burette was also used, adapted to give a volume of 5–10 μl for each increment.

A Hanna digital pH meter (Italy) with glass and saturated calomel electrodes calibrated on the operational pH scale with standard buffer solutions, was used.

2.2. Reagents and solutions

All reagents used were of analytical reagent grade. Doubly distilled water were used throughout. Purified sample of the free acid form of BCO dye obtained by liquid–liquid extraction procedures [15] was used. The product formed by Mannich condensation at 55°C (10 h) of bromophenol red, iminodiacetic acid and para-formaldehyde was extracted several times with pure n-butanol (organic phase) and 0.1 mol l^{-1} $NaHCO_3$ (aqueous phase). The components in the aqueous phase (semibromocresol orange, SBCO and bro-

mocresol orange, BCO) were extracted several times using n-butanol and 0.1 mol l^{-1} hydrochloric acid as described previously for other similar dyes [15]. SBCO was isolated in the organic phase (raffinate) and BCO was extracted into the aqueous one. The purity of the obtained BCO dye was ascertained with HPLC (LKB, Bromma, Switzerland) instrument using n-butanol–acetic acid–water (4:1:2 by volume) as a mobile phase. For freshly preparing 0.01 mol l^{-1} solution of BCO dye, the corresponding mass of the free acid form of the dye was dissolved in doubly distilled water. This solution was stable for at least 7 days after which its orange colour was slightly changed to red indicating the start of decomposition of the BCO dye. A 5×10^{-3} mol l^{-1} stock solution of Th^{4+} was prepared using Analar thorium nitrate (Prolabo-France) and was standardised as recommended [16]. Sodium fluoride, dried at 140°C for 48 h was used to prepare 100 mg l^{-1} fluoride stock solutions. A 0.02-mol l^{-1} CPB solution was prepared by dissolving the required mass of reagent in pure methanol. All fluoride solutions were stored in polyethylene containers. Working solutions of the above reagents were obtained as required by accurate dilution. Nitric acid (2.0 mol l^{-1}) and hexamine solution (1.0 mol l^{-1}) were used to adjust the pH of the medium. Solutions of diverse ions used for interference studies were prepared from nitrate or sulphate salts of cations and the sodium salts of anions. L-ascorbic acid solution, 10%, (A.R. Cambrian Chemicals) is used for controlling the interference of Fe(III) and Tl(III).

2.3. Procedures

2.3.1. Spectrophotometric determination of Th^{4+}

Into a 10-ml calibrated flask, transfer a suitable aliquot containing between 0.05 and 5 μg of Th^{4+}, dilute to ≈5 ml with 2 ml of 2 mol l^{-1} HNO_3 acid solution adjusting the pH of the solution to be ≈0.5. Add 1 ml of L-ascorbic acid solution, 2 ml of 0.001 mol l^{-1} BCO solution and 0.4 ml of 0.005 mol l^{-1} CPB. Dilute to the mark with doubly distilled water. Mix well and measure the absorbance at 560 nm against a reagent blank reference.

2.3.2. Titration of Th^{4+} with Na_2EDTA using BCO by visual and/or spectrophotometric indication

Into a 15-ml titration cell transfer an aliquot containing not less than 10 μg of Th^{4+}, dilute with a little amount of doubly distilled water, adjust the pH to be ≈0.5, add 1 ml of 0.001 mol l^{-1} of the BCO dye followed by 0.4 ml of 0.005 mol l^{-1} CPB solution. The absorbance of this solution is measured at 560 nm, on adding different precisely measured increments of 0.001 mol l^{-1} Na_2EDTA solution. The endpoint was located graphically from multipoint titration curves (Fig. 1), by plotting the absorbance versus the added titrant volume, microliters. The experiment was repeated several times ($n = 6$) to evaluate the precision of the end point. Alternatively a visual titration was carried out for samples containing greater than 2.5 μg ml^{-1} Th^{4+}.

2.3.3. Determination of fluoride

The thorium reagent used in these tests was prepared by mixing 1.0 ml of 2.2×10^{-4} mol l^{-1} thorium solution with 0.5 ml of 0.001 mol l^{-1} BCO solution adjusting the pH of solution to be ≈0.5 using 2 mol l^{-1} HNO_3 solution, the volume was made up to 10 ml in a calibrated flask. The absorbance of this solution was measured at 530 nm against reagent blank (A_o). Samples containing between 0.5 and 8×10^{-5} mol l^{-1} F^- were prepared in the same manner. The absorbance of these sample solutions (A_i) were also measured at 530 nm. The lowering in the absorbance of these sample solutions compared to the thorium reagent ($A_o - A_i$) was correlated to the concentration of fluoride in samples. Alternatively the fluoride samples could be titrated with standard thorium solution at pH ≈0.5 using BCO as indicator. The endpoint was detected either spectrophotometrically or visually by observing, the change of colour from yellow to bright red. A blank determination was required to avoid errors.

2.3.4. Decomposition of samples

The process of crushing, grinding (150 mesh), weighing (80–150 mg), decomposition by different fusion mixtures of various naturally occurring and certified thorium ores were carried out as

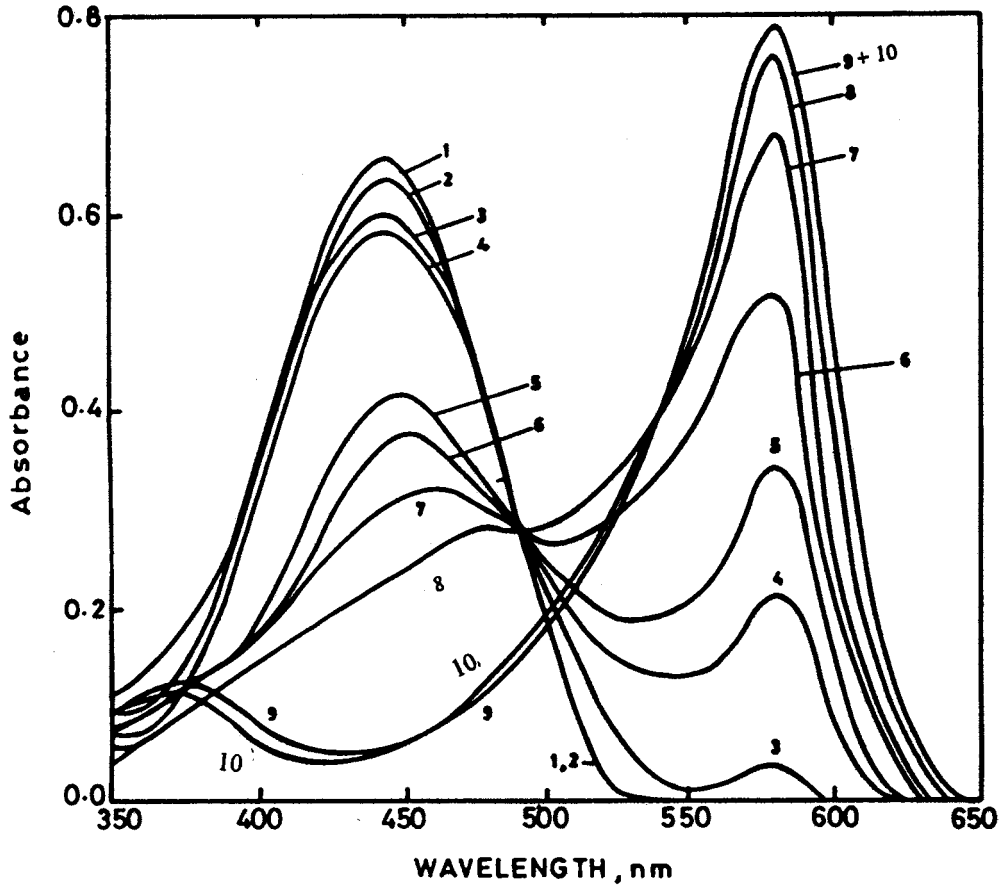

Fig. 1. Effect of pH change on the absorption spectra of BCO indicator. Conditions: (1) pH 0.5; (2) pH 1.0; (3) pH 2; (4) pH 2.5; (5) pH 3.0; (6) pH 4; (7) pH 5; (8) pH 6; (9) pH 8 and (10) pH 10; $C_{BCO} = 1.8 \times 10^{-5}$ mol l^{-1}, $b = 10$ mm.

described previously [1,2,14,16]. Silica was completely removed by treating the fused ore in a platinum crucible with an excess hydrofluoric acid and little sulphuric acid. The cations present first converted to fluoride and next into sulphate salts. The residue was retreated with slight excess sulphuric acid to insure the complete conversion of fluoride to sulphate salts. Short (5–10 min), ignition at 800–850°C converts the sulphate to corresponding oxide. The formed oxides were boiled with nitric acid till nearly dryness, cooled and diluted up with doubly distilled water in 100 ml calibrated flask.

2.3.5. Computation and statistical evaluation of experimental data

The number of determinations (n) for Th^{4+} or F^- ions either by spectrophotometric measurements or by complexometric titrations was eight. The standard deviation and the mean values were calculated and the values which show significant deviations were eliminated using Q-test.

3. Results and discussion

3.1. Effect of pH change on the absorbance of BCO dye in aqueous medium

The pH dependence of the absorbance of BCO aqueous solution has been qualitatively investigated. The absorption spectra of each species caused by the acid dissociation of the BCO dye are shown in Fig. 1. The spectral features of this

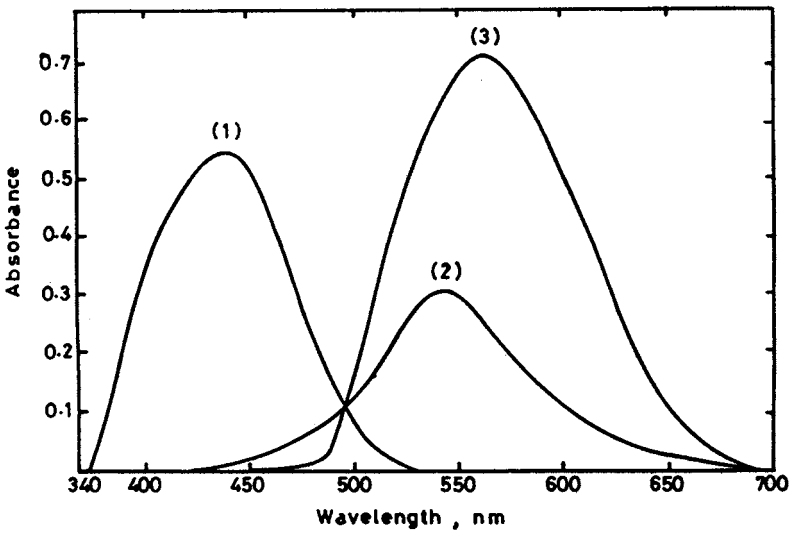

Fig. 2. Absorbance—wavelength curves of BCO indicator, binary Th-BCO and ternary BCO-Th-CPB complexes. Conditions: (1), $C_{BCO} = 1.5 \times 10^{-5}$ mol l^{-1}, pH = 0.5; (2) $C_{Th4+} = 8 \times 10^{-6}$ mol l^{-1} + $C_{BCO} = 1.5 \times 10^{-5}$ mol l^{-1}, pH = 0.5; (3); (2) + $C_{CPB} = 1.5 \times 10^{-5}$ mol l^{-1}, $I = 0.1$, $b = 10$ mm. The absorbances of mixtures (2) and (3) are measured against reagent blank.

figure are similar to that reported for xylenol orange (XO), [17] with the exception that the equilibria between different ionic species take place at lower pHs in the case of BCO dye. Inspection of these data indicates that the dye BCO exists in different ionic forms depending on the pH of the medium. The yellow-orange cationic species of the dye protonated imino-nitrogen (LH^+, λ_{max} 444 nm) predominates in strongly acidic media (pH < 2). The red form of BCO exists as a mixture of the pink and the yellow species in the pH range of 2.5–6 (λ_{max} 444 and 578 nm). The pink anionic form of the dye predominates at pH ≥ 7. These species are characterised by the disappearance of the band present at 444 nm and the sharpness of the 578 nm band. The lower pH part of the graphs indicates the prevalence of the protonated form of BCO, LH^+ species. The predominance of the red form begins to be effective at pH ≥ 2.5. Under these conditions the red colour of the dye interferes with the determination.

It was aimed therefore to establish the optimum conditions favourable for the spectrophotometric determination of Th^{4+} using the proposed ternary system at pH < 2. Preliminary investigation indicated that on mixing Th^{4+} solution with BCO in acidic medium (pH 0.4 ± 0.2) a bright red colour was spontaneously developed, the intensity of which was increased with the increase of Th^{4+} concentration. Further, additional drops of 0.005 mol l^{-1} solution of the cationic surfactant CPB caused an extra intensification of the colour followed by an obvious shift to longer wavelength, however, the use of higher concentrations of CPB ($> 2 \times 10^{-2}$ mol l^{-1}) made the solution slightly turbid. The produced colour was stable for at least 2 weeks.

3.2. Absorption spectra

The visible absorption spectra of BCO solution exhibited an absorption band at 444 ± 2 nm in the pH range of 0.2–2 (Fig. 2). The absorption spectrum of the reagent blank (BCO-CPB mixture) coincided with that of BCO itself; thus it seemed that there was no interaction between BCO and CPB under the proposed working conditions. The maximum absorption wavelengths of both the binary Th-BCO and the ternary Th-BCO-CPB complexes were found to be at 530 and 560 nm, respectively. It was also noticed that the addition of CPB to the Th-BCO complex gave rise to a bathochromic and large hyperchromic effects. It followed that the sensitivity of the procedure

increased remarkably. The absorption spectra of BCO, Th-BCO and Th-BCO-CPB were measured against reagent blanks (Fig. 2).

3.3. Stoichiometry of the ternary complex

Job's method of continuous variations was applied to establish the components ratio of the ternary complex. The mole fractions of two of the components were varied continuously, keeping their final combined concentration constant at 2×10^{-4} mol l^{-1} and keeping the third component in a large constant excess (2×10^{-3} mol l^{-1}) for all solutions in the series. Under these conditions the ternary system was modified to a quasi binary system [18]. The obtained results indicated that the overall ratio for Th^{4+} :BCO:CPB was 1:1:1 at pH $\approx$ 0.5. Further confirmation of this ratio was ascertained by applying the molar ratio method using equimolar mixture of BCO and Th^{4+} (1×10^{-3} mol l^{-1} for each) as the first partner [19]. The experiment was elaborated by keeping the concentration of this mixture constant while changing that of CPB (from 0.1 to 3×10^{-3} mol l^{-1}) as the second partner, and measuring the absorbance of samples at 560 nm against the Th^{4+}-BCO mixture as a reference blank. The absorbance increased steadily until it reaches to the molar ratio 1:1:1 (Th:BCO:CPB) and then attains a more or less constant value. The conditional stability constant of this complex was calculated using the Harvey and Manning method [20] and was found to be $1.1 \times 10^{12} \pm 1.26$ ($\log K' = 12.04 \pm 0.1$, $I = 0.1$) at 25°C.

3.4. Validity of Beer's law and reproducibility

Under the optimum conditions, a linear calibration graph was obtained for 0.02–2.6 μg ml^{-1} Th^{4+} at 560 nm ($r = 0.995$, $n = 8$). The regression equation of the calibration graph obtained by the least square method is (Eq. (1)):

$$A = \log P_o/P_t = 92186.9\,[Th^{4+}] + 0.006 \quad (1)$$

The molar absorptivity of the ternary Th-BCO-CPB complex is 9.2×10^4 l mol^{-1} cm^{-1}, which corresponds to Sandell sensitivity index [21] of 2.5 ng cm^{-2} of Th^{4+}. The detection limit calculated from (2 s + blank) value is found to be 0.03 μg ml^{-1} Th^{4+}. The reproducibility of the procedure was checked by analysing two series of solutions (eight identical samples for each series) having final Th^{4+} concentration of 4×10^{-6}, 7×10^{-6} mol l^{-1}. The mean absorbance values were 0.365 and 0.642 with a standard deviation of 0.006 and 0.005 absorbance units, respectively. Worth mentioning, that higher concentrations of Th^{4+} could be determined using the binary Th-BCO system at pH $\approx$ 0.5. Beer's law is obeyed also for this binary system in the range of 0.05–6.0 μg ml^{-1} Th^{4+}, $\epsilon = 4.2 \times 10^4$ l mol^{-1} cm^{-1} at 530 nm with a detection limit of 0.08 μg ml^{-1} Th^{4+}.

3.5. Effect of diverse interfering ions on the spectrophotometric determination of Th^{4+}

The influence of several ions which might introduce a large error in the determination of Th^{4+} was examined. An aliquot containing 1.5 μg ml^{-1} Th^{4+} and excess amounts of diverse interfering ions was treated as in the procedure. The tolerance levels are shown in Table 1.

Table 1
Maximum tolerance ratio for foreign ions in the spectrophotometric determination of 1.5 mg μl^{-1} Th^{4+}

Tolerance ratio	Interferent
1000	Br^-, NO_3^-, IO_3^-, Cl^-, acetate, tartrate, ascorbic acid, phthalate, borate, thiourea, alkali and alkaline earth metal ions
500	I^-, SO_3^{2-}, SO_4^{2-}, IO_4^-, lanthanides, Al^{3+}, Cd^{2+}, Co^{2+}, Cr^{3+}, Cu^{2+}, Fe^{2+}, Ga^{3+}, Hg^{2+}, Mn^{2+}, Ni^{2+}, Pd^{2+}, Ru^{3+}, UO_2^{2+}
100	CN^-, $(Fe^{3+})^a$, $(Tl^{3+})^a$, $(Bi^{3+})^b$, $(In^{3+})^c$.
5	$(PO_4^{3-})^c$, $(Zr^{4+})^c$, $(Ti^{4+})^c$
<1	EDTA, $C_2O_4^{2-}$, F^-

Ratio (w/w) of diverse ions to Th^{4+}: [a] In presence of L-ascorbic acid; [b] in the presence of iodide; and [c] the pH of the final solution must not exceed 0.4.

Table 2
Comparison of some spectrophotometric methods for Th^{4+}

Reagent	Condition or pH	Wavelength λ_{max} (nm)	Molar absorptivity, $\epsilon \times 10^{-4}$ l mol^{-1} cm^{-1}	Remarks	Reference
Eriochrome cyanine R (ECR)+CPB	4.3	590	6.6	Numerous metal ions interfere e.g.	[22][a]
Pyrocatecol violet (PV)+CPB	7.5	660	6.2	Al^{3+}, Ga^{3+}, In^{3+}, Fe^{3+}, Sc^{3+}, UO_2^{2+}, Rare earths. Hence	[22][a]
Chrome Azurol S (CAS)+CPB	5.2	630	14.0	Th^{4+}, should be separated prior to the determination	[22][a]
Xylenol orange (XO)+CTAB	2.5–4	560–570	5.6	Al^{3+}, Bi^{3+}, Ce^{4+}, Cr^{3+}, Cu^{2+}, Fe^{3+}, Ti^{4+}, Tl^{3+}, UO_2^{2+}, V^{5+} interfere.	[23]
Arsenazo III	8N $HClO_4$	660	8.6	SO_4^{2-}, PO_4^{3-}, F^-, Ti^{4+}, Zr^{4+} interfere.	[24]
Chlorophosphonazo III	1–2	690	4.31	Ti^{4+}, UO_2^{2+}, Bi^{3+}, rare earths interfere.	[25]
BCO+CPB	0.5–1	560	9.2	F^-, oxalate, Zr^{4+} interfere	Present method

[a] Measurement is carried out after 30 min, i.e. the method is time dependent.

3.6. Evaluation of the proposed procedure compared to other sensitive methods for Th^{4+}

Ternary thorium complexes with some triphenylmethane reagents and cationic surfactants had been studied by Jarosz [22]. The present method is compared with these systems and with other sensitive methods for Th^{4+}, Table 2.

Inspection of the data of Table 2 indicates that, the proposed procedure is one of the most sensitive for determining thorium. It has also the advantage of higher selectivity compared to other triphenylmethane reagents. Fortunately, the possibility of elaborating the experiments at lower pHs, enhanced such selectivity. The procedure may be considered specific in the presence of U(VI), rare earth elements and great number of transition metal ions. Beside the good reproducibility and the stability of the produced colours, these reactions are proved to be spontaneous. Moreover, the presence of the electron withdrawing Br-atoms in the *m*-position to the iminodiacetic groups in the BCO reagent, makes the easier ionization of the carboxylic acid protons, it follows that the BCO reagent is easily soluble in water even in highly acidic solutions, $pH < 1$. Other triphenylmethane reagents, e.g. xylenol orange (XO), methylthymol blue (MTB), etc. precipitate completely in acid solution ($pH \leq 1$) and so do their thorium complexes.

3.7. Complexometric titration of Th^{4+} with Na_2EDTA using BCO as indicator

Results obtained from the study of interference indicated that the presence of Na_2EDTA in equimolar amount to Th^{4+} causes a complete change of the colour of the Th^{4+} complex from bright red to lemon yellow. So, a trial for the determination of Th^{4+} with higher precision and accuracy by titration with Na_2EDTA, BCO and with visual and/or spectrophotometric indication of endpoint was carried out. It was concluded the Th^{4+} could be determined by titration with Na_2EDTA in a HNO_3-KNO_3 medium of pH 0.4 ± 0.2 in the presence of a great number of rare earth metals or transition metal ions without any interference. Such acidic solutions caused a considerable control on the behaviour of EDTA, making it possible to titrate quantitatively the

Table 3
Statistical evaluation of a series of spectrophotometric microtitrations of Th^{4+} in the presence of different interfering ions with 0.001 mol l^{-1} Na_2EDTA using BCO as an indicator, $n = 6$

Series no.	Metal ion M^{n+}	(M^{n+}) μmol 15 ml^{-1}	Taken (Th^{4+}), μg 15 ml^{-1}	Mean (Th^{4+}), μg 15 ml^{-1}	s μg^{-1}	s_r (%)	Recovery (%)
1	Th^{4+}	0.15	34.8	34.9	0.2	0.6	100
	Gd^{3+}	0.50					
	Cu^{2+}	2.50					
2	Th^{4+}	0.10	23.2	23.2	0.3	1.3	100
	Fe^{3+}	1.00					
	Zn^{2+}	4.00					
3	Th^{4+}	0.05	11.6	11.5	0.5	4.3	99.1
	UO_2^{2+}	0.80					
	Pb^{2+}	1.50					
4	Th^{4+}	0.20	46.4	46.1	0.1	0.2	99.4
	Zr^{4+}	0.50					
	In^{3+}	1.00					
5	Th^{4+}	0.25	58.0	58.1	0.2	0.3	100
	Tl^{3+}	0.80					
	Bi^{3+}	2.00					

metal ions which form highly stable M^{n+}-EDTA complexes ($n = 3$ or 4, log $K_{MY^{n-4}} > 22$), without interference from other ions [14,26]. The interference caused by Fe^{3+} or Tl^{3+} was cancelled by the reduction of Fe^{3+} to Fe^{2+} and Tl^{3+} to Tl^{+} using L-ascorbic acid solution, which must be added before the addition of the dye BCO. In^{3+} was reduced to the metallic state using magnesium powdered and boiling hydrochloric acid (1:1). The interference of Bi^{3+} was eliminated in the presence of excess KI. The presence of Zr^{4+} at threefold excess compared to Th(IV) caused positive interference. F^- must be absent. Oxalate ion was decomposed by boiling the sample with 5 ml concentrated nitric acid. Five series of microtitration of Th^{4+} in presence of different ions are shown in Table 3. Typical spectrophotometric titration curves for Th^{4+} determination by either direct titration or back titration are shown in Fig. 3(a and b), respectively. From this figure it is clear that there is no difficulties in the determination of the endpoint for the two types of titrations (a and b). The reliability of the linear extrapolation of the endpoint in the spectrophotometric titrations with 0.001 mol l^{-1} Na_2EDTA is significantly affected by the choice of wavelength only if various complexes of the indicator (BCO) with the titrated thorium exist in equilibrium during the course of the indicator change (metal-indicator species in solution). A wavelength of 550 nm was found to be suitable for the micro-titration of Th^{4+}. The results of the statistical evaluation of the data (Table 3) show that the determination of Th^{4+} is highly precise and accurate. The detection limit, i.e. (2 s + blank) is 8 μg of Th^{4+} per 15 ml, i.e. 0.53 μg ml^{-1}. The detection limit of the visual titration is $\sim$2.5 μg ml^{-1} Th^{4+}. A 0.5% precision was attained under these conditions.

The proposed procedures were satisfactorily applied for the determination of thorium in three standard Th-U certified ore samples and in a series of naturally occurring ores or minerals of thorium. Results of analysis are given in Table 4. These results (average of eight determinations) are in good agreement with the values obtained by standard classical methods.

4. Application of Th-BCO complex for the determination of fluoride

The procedure of determining trace amounts of fluoride is based on the bleaching of the red

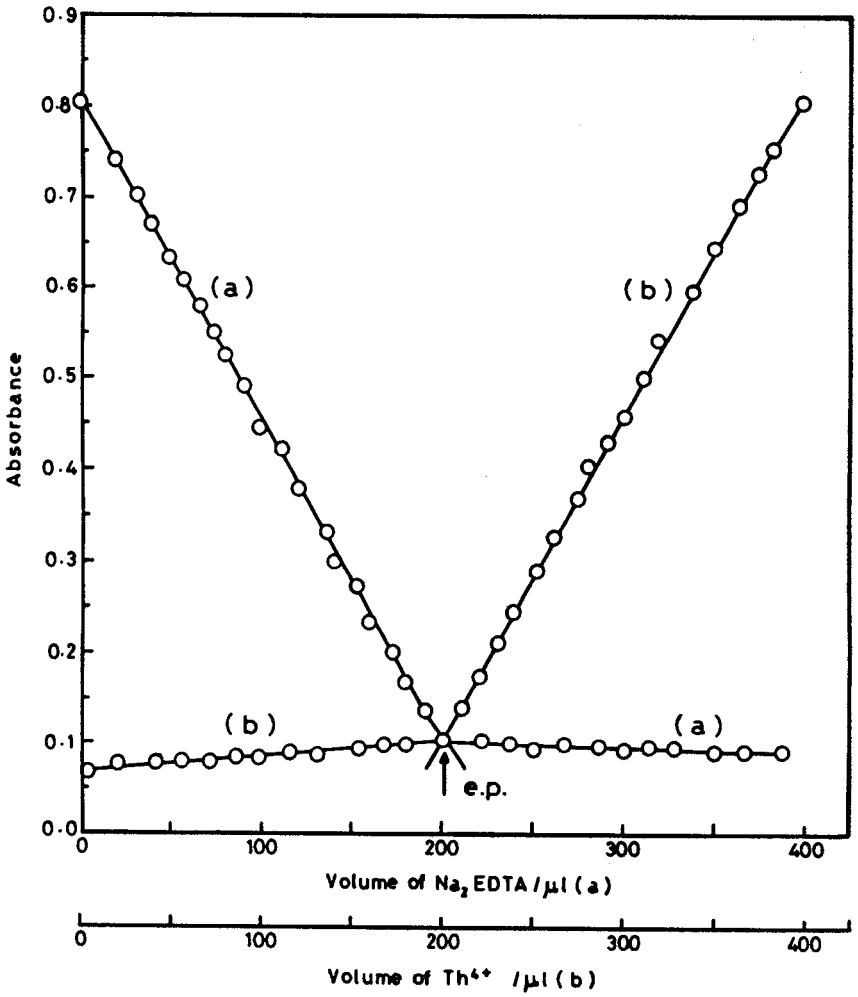

Fig. 3. Spectrophotometric microtitrations of Th^{4+} with 1×10^{-3} mol l^{-1} Na_2EDTA (a) and/or 1×10^{-3} mol l^{-1} Th^{4+} solution (b) using BCO and CPB reagents. Conditions $C_{Th^{4+}} = 1.33 \times 10^{-5}$ mol l^{-1}; $C_{BCO} = 4 \times 10^{-5}$ mol l^{-1}; pH = 0.5; $\lambda = 550$ nm, $b = 18$ mm (curve a). For back titration (curve b), Th^{4+} was determined by adding 0.4 ml of 1×10^{-3} mol l^{-1} Na_2EDTA to the titrated Th^{4+} solution. $C_{CPB} = 2 \times 10^{-5}$ mol l^{-1} in both cases.

Th-BCO complex by fluoride ions, which are strongly coordinated to the thorium ion in the complex [27] and thus liberate the free yellow BCO indicator. It was established that the stoichiometry of the reaction between Th^{4+} and F^- ions is 1:4 under the proposed working conditions (Fig. 4). The initial operation conditions were chosen arbitrarily and it was found that, the reaction was greatly affected by the acidity of the solution. In very acidic solutions (pH $\approx$ 0.5); the reaction took place spontaneously, while it was relatively slow in solutions having pH > 1.0.

4.1. Calibration graph and sensitivity

A linear calibration graph was obtained in the range of 0.02–3.0 μg ml^{-1} F^- ($r = 0.997$, $n = 10$). The relative standard deviation for the determination of 1.8 μg ml^{-1} F^- was 0.85% (eight replicates). The limit of detection was 0.02 μg ml^{-1}.

4.2. Spectrophotometric and visual titrations of fluoride with standard thorium solution using BCO as indicator

The feasibility of these titrations was studied

Table 4
Results of determination of thorium in monazite ores, minerals and in some certified samples by the proposed spectrophotometric and/or complexometric methods

Sample	The mean ThO_2 (%), $\bar{X}_1$ spectrophotometric method	s_1, % ($n=5$)	The mean ThO_2 (%), $\bar{X}_2$, titration method	s_2, % ($n=5$)	ThO_2 (%) classical method[a]
1. Asian monazite	6.12	0.15	6.13	0.18	6.10
2. South African monazite	5.61	0.15	5.62	0.20	5.58
3. Indian monazite	8.77	0.10	8.8	0.15	8.75
4. Esgynite	15.0	0.20	15.1	0.25	14.9
5. Monazite concentrate black sand (Rosetta, Egypt)	5.87	0.18	5.91	0.20	5.86
6. Brazilian monazite	6.67	0.11	6.71	0.15	6.70
7. U-Th certified ore DH-1a[b]	0.92	0.15	—	—	0.91
8. U-Th certified ore DL-1a[b]	0.007	—	—	—	0.007
9. Rare earth—Th ore OKA-2[b]	2.86	0.18	2.79	0.22	2.88

[a] Th(IV) is determined using arsenazo III method [7].
[b] Radioactive materials, from Canadian Certified Reference Materials Project (CCRMP).

under the conditions applied for the usual spectrophotometric measurements. It was found that working at higher acidities (pH ≈ 0.5) was preferable. Such prevalence was due to the sharpness of the colour change between red and yellow. The detection limit in the spectrophotometric titration was 0.15 μg ml^{-1} of F^-, while for the visual titration it was raised to ~2.5 μg ml^{-1} of F^-. Results of a series of five determinations are shown in Table 5. During calculations the volume of Th^{4+} equivalent to F^- ion at endpoint should be multiplied by a factor of 4. In parallel with each test series, a series of standard fluoride solutions should be titrated under the same condition of the sample to avoid the effects due to the fluctuations of the acidity of the medium, instability of the reagents and also to serve as a blank for visual endpoint detection.

4.3. Study of interference

The effect of diverse cationic and anionic species which commonly interfere with fluoride was investigated. Results of measurements indicated that increasing the acidity (pH ≤ 0.4) canceled the interference caused by Al^{3+} and Be^{2+}. The interference of iron(III) on the determination of F^- was removed by the addition of L-ascorbic acid. Large amounts of phosphate interfered because of its reaction with thorium in a way similar to fluoride. This effect was minimised at higher acidity. At pH ≈ 0.4, 1.5 μg ml^{-1} fluoride was determined in presence of 15 μg ml^{-1} phosphate with a reasonably small analytical error (about 5%). For samples containing phosphate in excess to the ratio mentioned above, i.e. (10:1, PO_4^{3-}:F^-), it could be simply separated as silver phosphate by addition of silver nitrate solution. The usual components of water do not interfere with the determination. No interference was observed with 200 μg ml^{-1} Ca^{2+} or Mg^{2+}. The presence of very large concentrations of bicarbonate or hydroxide ions (alkalinity) caused a reduction of the acidity of the medium, thereby increasing the colour of Th-BCO complex and also the colour of the BCO alone. Such effect was cancelled by careful adjustment of pH of sample solution. Large concentrations of chloride or sulphate did not interfere.

In order to test the applicability of the proposed procedures to water, six samples of water

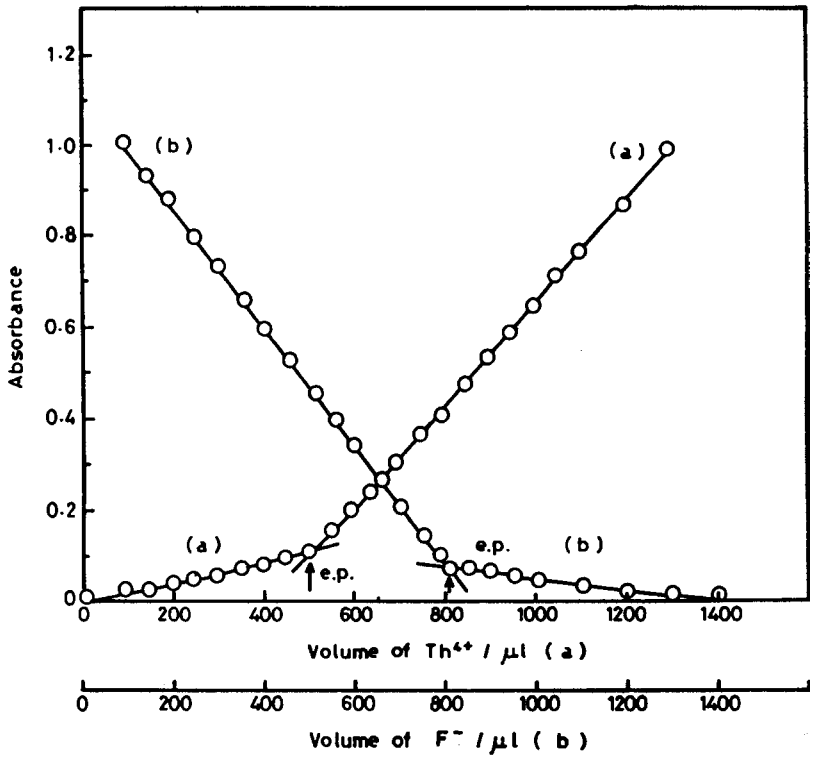

Fig. 4. Spectrophotometric microtitrations of F^- with 1×10^{-3} mol l^{-1} Th^{4+} (a) and/or Th^{4+} with 5×10^{-3} mol l^{-1} F^- (b) using BCO as indicator. Conditions: $C_{F^-} = 1.33 \times 10^{-4}$ mol l^{-1}, pH $\approx$ 0.3, $\lambda = 530$ nm, $b = 18$ mm (a) $C_{Th^{4+}} = 6.67 \times 10^{-5}$ mol l^{-1}, $C_{F^-} = 5 \times 10^{-3}$ mol l^{-1}, $C_{BCO} = 6 \times 10^{-4}$ mol l^{-1} (a and b).

(Table 6) were analysed in duplicate using both the calibration graph method or the direct titration method. For the spectrophotometric method; 1 ml of water sample was mixed with the thorium reagent at the optimum conditions and the lowering in the absorbance of the reagent at 530 nm was observed. On the other hand, fluoride could be determined by the spectrophotometric titration

Table 5
Statistical evaluation of five series of determinations of fluoride by spectrophotometric titration (SP) or by calibration graph (CG) methods

Series no.	Sample, μg ml^{-1}	F^- taken (μg 10 ml^{-1})	Mean found, $\bar{X}$, F^- (μg 10 ml^{-1})		Average recovery (%)
			SP method	CG method	
I	1.5 F^- +15 Al^{3+} +75 Cu^{2+}	15.0	15.6	15.1	102
II	1 F^- +20 Be^{2+} +50 Gd^{3+}	10.0	10.4	9.9	102
III[a]	0.5 F^- +15 Fe^{3+} +15 Tl^{3+}	5.00	5.1	5.0	101
IV	0.2 F^- +20 SO_4^{2-} +0.6 PO_4^{3-}	2.00	—	1.9	95.0
V	0.15 F^- +20 Ca^{2+} +10 Mg^{2+} +10 Mn^{2+}	1.50	—	1.5	100

Conditions as described in Section 2.
[a] In presence of excess L-ascorbic acid.

Table 6
Determination of fluoride in different water samples using the proposed procedures

Source	F^- added, μg ml^{-1}	F^- found by titration with Th^{4+} μg ml^{-1}, I	F^- found from calibration graph μg ml^{-1}, II	Recovery of the standard F^- added			
				μg ml^{-1}		(%)	
				I	II	I	II
Tap water	0	0.78	0.82	—	—	—	—
	0.3	1.09	1.12	0.31	0.3	103	100
Nile water	0	0.93	0.95	—	—	—	—
	0.3	1.22	1.24	0.29	0.29	96.7	96.7
Bottled water	0	0.71	0.70	—	—	—	—
(I) Siwa (mineral water, Egypt)	0.5	1.20	1.19	0.49	0.49	98.0	98.0
Bottled water	0	0.65	0.67	—	—	—	—
(II) Baraka (mineral water, Egypt)	0.4	1.06	1.06	0.41	0.39	103	98.0
Synthetic water	0	0.5	0.51	—	—	—	—
(0.5 ppm F^- added) A*	0.5	1.01	1.02	0.51	0.51	102	102
Synthetic water	0	0.21	0.19	—	—	—	—
(0.8 ppm F^- added) B*	0.8	1.02	0.99	0.81	0.80	101	100

Conditions pH ~ 0.4, $\lambda = 530$ nm.
*Analysis of synthetic water, mg ml^{-1}: Total alkalinity 32, total hardness $SO_4^{2-} = 60$, $Cl^- = 56$, $Fe^{3+} = 1.0$, $Al^{3+} = 0.2$, $SiO_3^{2-} = 10$, $PO_4^{3-} = 3.0$, $Na^+ = 80$, F^- [0.5(A), 0.2(B)].

of 5 ml of water sample with 2.2×10^{-4} mol l^{-1} $Th(NO_3)_4$ solution using BCO as an indicator. Results of analysis are shown in Table 6. The recovery of the standard fluoride added to the water samples confirmed the high accuracy, precision and applicability of the proposed method.

5. Conclusion

The reaction of Th^{4+} with BCO dye in the presence of the cationic surfactant CPB is highly selective and sensitive. It could be used, as a non-nuclear method, for the determination of traces of thorium in uranium ores containing radioactive species. A versatile applications of the reaction using both spectrophotometric measurements and complexometric titration technique is of great importance since it permits a feasible determination of Th^{4+} in variable concentration ranges.

Beside its stability and solubility in aqueous medium, the Th-BCO complex has been successfully applied for the determination of fluoride in water obtained from different origins. The advantages gained with this application are connected with the rapid equilibrium between the Th-BCO reagent and fluoride ions at room temperature. Also, the proposed procedure is markedly more sensitive and less subject to interference compared to the well known thorium and zirconium reagents [28–30], used for the same purpose.

Acknowledgements

We express our sincere gratitude to Dr H. Mohamed Sirag, Lecturer, Nuclear Materials Authority, a branch of the Egyptian Atomic Energy Organisation for providing us with the certified ores and minerals of thorium.

References

[1] M.A.H. Hafez, I.M.M. Kenawy, M.A.M. Ramadan, Analyst 119 (1994) 1103.
[2] M.A.H. Hafez, A.M.A. Abdallah, N.E.S. Abd El Gany, Analyst 115 (1990) 221.
[3] M.A.H. Hafez, Anal. Lett. 25 (9) (1992) 1779.
[4] H.E.L. Palmieri, Spectrophotometric analysis of Th^{4+} with high precision, M.Sc. Thesis, Minas Gerias Univ., Belo Horizonte, M.G. (Brazil), INIS-BR-2668, 1983.
[5] T.S. West, Complexometry with EDTA and Related Reagents, 3rd ed., Broglia Press, Bournemouth, 1966, pp. 208,
[6] A.I. Busev, V.G. Tiptsova, V.M. Ivanov, Analytical Chemistry of Rare Elements, Mir, Moscow 1981, pp. 112.
[7] Z. Marczenko, Separation and Spectrophotometric Determination of Elements, 2nd ed. Ellis Horwood, Chichester, UK, 1986, pp. 574–577.
[8] M. Otmo, Bunseki Kagaku 14 (1965) 229.
[9] K. Goto, D.S. Russell, S.S. Berman, Anal. Chem. 38 (1966) 493.
[10] H. Shi, J. Li, Z. Zhang, Fenxi Houxi 11 (1983) 826.
[11] A.K. Mukhergi, Mikrochem. J. 11 (1966) 243.
[12] V.D. Vasilenko, M.V. Shanyo, V.I. Bolbas, Zh. Anal. Khim. 22 (1967) 1818.
[13] K.A. Idriss, M.M. Seleim, M.K. Hassan, M.S. Abu Bakr, H. Sedaiva, Analyst 110 (1985) 705.
[14] M.A.H. Hafez, M.E. Khalifa, Talanta 44 (1997) 787.
[15] M.A.H. Hafez, I.M.M. Kenawy, M.A.M. Ramadan, Egypt. J. Anal. Chem. 4 (1994) 55.
[16] A.I. Vogel, Text Book of Quantiative Inorganic Analysis, 3rd ed., Longman, London, 1972, pp. 277, 483, 610, 502.
[17] M. Murakami, T. Yoshino, S. Harasawa, Talanta 14 (1967) 1293.
[18] M.M. Seleim, K.A. Idriss, M.S. Saleh, E.Y. Hashem, Polyhedron 10 (1986) 1525.
[19] M.E. Khalifa, Chem. Anal. (Warsaw) 40 (1995) 797.
[20] A.E. Harvey, D.L. Manning, J. Am. Chem. Soc. 72 (1950) 4488.
[21] E.B. Sandell, Colorimetric Determination of Traces of Metals, 3rd ed., Interscience, New York, 1959.
[22] M. Jarosz, Analyst 111 (1986) 681.
[23] T.V. Ramakrishna, R.S.S. Murthy, Talanta 26 (1979) 499.
[24] B. Budensinsky, K. Haas, D. Vrzalova, Collect. Czech. Chem. Commun. 30 (1965) 2372.
[25] V.I. Fadeeva, I.P. Alimarin, Zh. Anal. Khim. 17 (1962) 1020.
[26] D.A. Skoog, D.M. West, Analytical Chemistry, 3rd ed., Saunders Golden Sunburst Series, Philadelphia, PA, 1980, pp. 262.
[27] Ju, Lurie, Handbook of Analytical Chemistry, Mir, Moscow, 1975, 292 pp.
[28] T.J. Cardwell, R.W. Cattrall, M. Mitri, I.C. Hamilton, Anal. Chim. Acta 214 (1–2) (1988) 433.
[29] J.A. Ruzicka, H. Jakshova, L. Mrklas, Talanta 13 (1966) 1341.
[30] Y. Shimoishi, T. Hayami, Bull. Chem. Soc. Jpn. 40 (1967) 1139.

ELSEVIER

Talanta 47 (1998) 561–567

Talanta

Amperometric glucose enzyme electrode by immobilizing glucose oxidase in multilayers on self-assembled monolayers surface

Shi-Feng Hou, Ke-Sheng Yang, Hui-Qun Fang, Hong-Yuan Chen *

Department of Chemistry, the State Key Laboratory of Coordination Chemistry, Nanjing University, Nanjing 210093, PR China

Received 21 October 1997; received in revised form 11 February 1998; accepted 13 February 1998

Abstract

A novel and robust amperometric enzyme electrode for the determination of glucose was constructed by immobilizing glucose oxidase (GOD) and $Os(bpy)_2Cl$–poly(4-vinyl)pyridine (Os–PVP) complex multilayers on thiol self-assembled monolayers surface. The apparent Michaelis-Menton constant K'_m increased with increasing the number of Os–PVP/GOD multilayers. The concentration range of linear response and detection limit were 0.1–10 and 0.05 mM, the interference of ascorbic acid and uric acid were eliminated by the presence of SAMs and the enzyme electrodes were stable over 3 weeks. The preparation technique may be useful for controlling the performance of multilayer enzyme electrodes by changing the enzyme content. © 1998 Elsevier Science B.V. All rights reserved.

Keywords: Multilayer film; Glucose oxidase; Self-assembled monolayers; $Os(bpy)_2Cl$–PVP complex

1. Introduction

Enzyme-based amperometric biosensors have attracted increasing interest in the last two decades. In order to fabricate the enzyme layer, considerable efforts have been devoted to the development of various techniques for immobilizing enzyme [1–4]. The most common includes adsorption, covalent attachment, gel|polymer entrapment, etc. However, each of these methods has its own advantages and disadvantages. For example, physical adsorption of the enzyme on the electrode surface requires no reagents and has a fast response, but it is susceptible to a change of environment [5]. Gel|polymer entrapment uses mild conditions and a wild variety of gel|polymers are available; most enzymes can be easily incorporated into a polymer. But it suffers from disadvantages: many experimental factors must be controlled, possible deactivation of enzyme occurs during polymer formation, and it is limited by the size and structure of the polymer; there is an increase in response time due to a large diffusional barrier [6]. This is because the thickness of polymer is usually thicker. To obtain a fast response, one method is to form an ultrathin polymer film at the electrode surface, the other is to use a mediator. Recently, a redox polymer for

* Corresponding author. E-mail: HYChen@.nju.edu.cn

0039-9140/98/$ - see front matter © 1998 Elsevier Science B.V. All rights reserved.
PII S0039-9140(98)00081-2

immobilizing enzymes has been studied [7–9]; the enzymes are immobilized in a redox polymer film to provide the sample and sensitive amperometric biosensors. The redox polymer usually has two functions, one is as matrix to immobilize the enzyme, and the other is to enhance the electron transfer rate between the enzyme and electrode surface. However, the preparation procedure was complicated, and an ultrathin film could not be obtained by using this method. Recently, a protein–polyelectrolyte complex multilayer assembly by alternative electrostatic adsorption was reported [10–13]; a thin multilayer film could be obtained using this method, because the thickness of one pair of protein–polyelectrolyte multilayers is only about several nm. The multilayer film formed by the protein and polyelectrolyte could be used as a novel biological active material.

The present paper describes the preparation and application of $Os(bpy)_2Cl$–poly(4-vinyl)pyridine/glucose oxidase complex multilayer (Os–PVP|GOD) at self-assembled monolayers (SAMs). The multilayer of Os–PVP|GOD was successively placed on the SAMs gold electrode surface. This enzyme electrode basically does not suffer from the interference of ascorbic acid and exhibits high performance, such as rapid response and high stability.

2. Experimental section

2.1. Materials

$OsCl_3 \cdot xH_2O$(Aldrich), poly(4-vinyl)pyridine (PVP, Aldrich), 3-mercapto-1-propan-sulfonic acid sodium salt (MPS, Aldrich), and glucose oxidase (EC 1.1.3.4) from *Aspergillus niger* (GOD, Sigma) were used as received without further purification. All other chemical reagents were analytical grade. All solutions were prepared with double-distilled water. The solution was deaerated by pure nitrogen before tests. Unless otherwise noted, all experiments were performed in phosphate buffer, pH 6.88.

Cis-bis(2,2-bipyridine-*N*,*N*)dichloride osmium was synthesized from the literature [7,8]. Cis-bis(2,2-bipyridine-*N*,*N*)dichloride osmium and PVP were heated under nitrogen at reflux in an ethylene glycol for 8 h, after the solution was cooled to room temperature the DMF and *N*-(2-bromo ethyl)pyridine were added under stirring, and the stirring was kept at 50°C for 12 h. The polymer was obtained by pouring the above solution into rapidly stirred acetone and then purified. The $Os(bpy)_2Cl$–poly(4-vinyl)pyridine structure is shown in Scheme 1.

2.2. Apparatus and procedures

All electrochemical measurements were performed on model 270 Electrochemistry System (EG&G) using a three-electrode system at 25 ± 1°C: saturated calomel electrode (SCE) as reference electrode, platinum plate as counter electrode and gold disk electrode ($r = 0.5$ mm) as working electrode.

A SAMs of MPS at the gold electrode surface was formed by immersing the gold electrode into ethyl alcohol solution containing 1.0 mM MPS for 48 h. The formation procedure of Os–PVP|GOD multilayers at SAMs surface was as follows: firstly, one Os–PVP layer was adsorbed on the SAMs surface by immersing the SAMs electrode in 1 mg ml^{-1} Os–PVP solution for 30 min, drying at vacuum, then immersing in 10 mg ml^{-1} GOD solution for 1 h; thus, a GOD layer could adsorb on to the Os–PVP layer's surface. The multilayer of Os–PVP and GOD (Os–PVP|GOD) could be formed by alternately immersing the electrode into Os–PVP and GOD solutions, respectively. The resulting electrode (SAMs|Os–PVP|GOD) is denoted here as the enzyme electrode. In this paper, both there are five Os–PVP and GOD layers in the multilayers, if without special note. The structure of the resulting electrode is illustrated in Scheme 1.

3. Results and discussion

3.1. The electrochemical characteristics of enzyme electrode.

Fig. 1a shows the cyclic voltammograms of enzyme electrode in phosphate buffer, the anodic

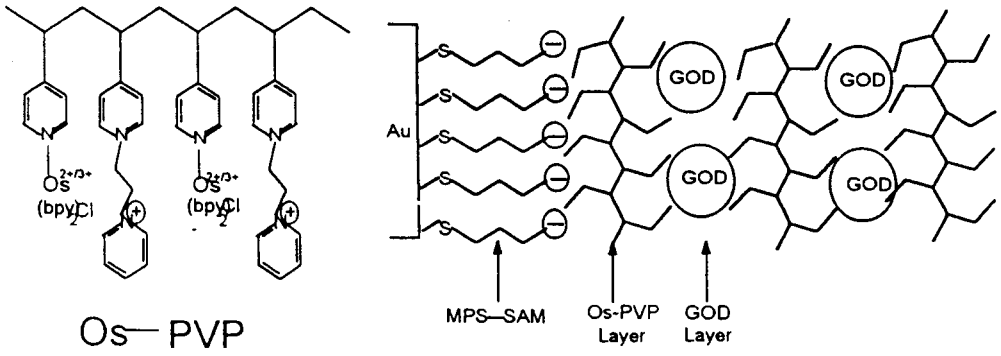

Scheme 1. The structure of the enzyme electrode.

peak and the cathodic peak potentials were 0.28 and 0.24 V (at scan rates of 20 mV s^{-1}), respectively, the difference between the anodic and cathodic peak potential (ΔE_p) was 40 mV. Both the peak currents (i_p) were proportional to the scan rates in the range of 10–60 mV s^{-1}, which indicated the process possesses a surface adsorption property [14]. The surface coverage of redox active center ($Os^{3+/2+}$ complex) (Γ) at the electrode surface was calculated by integrating the charges passing through the anodic or cathodic peak [13].

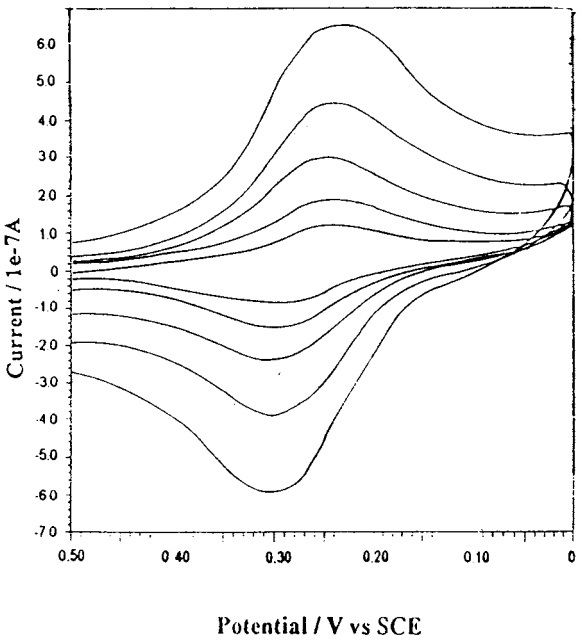

Fig. 1. The cyclic voltammograms of enzyme electrode. Scan rates from inner to outer: 10, 20, 40, 60, 100 mV s^{-1}.

Fig. 2 shows the relation between the Γ and the number of Os–PVP layers. It was clearly that Γ was proportional to the number of Os–PVP layers. This result implies the formation of the multilayers on the SAMs, and the amounts of each Os–PVP layer were roughly the same. Moreover, the experiments showed that the presence of the enzyme does not appreciably affect the electrochemical properties of the Os–PVP.

3.2. The response of enzyme electrode to the glucose

Fig. 3 shows the cyclic voltammograms of the enzyme electrode in the presence of glucose, a typical catalytic oxidation wave was observed, and it appeared that the Os–PVP could act as an efficient electron transfer relay system between the $FAD|FADH_2$ centers of GOD and the SAMs electrode surface. The Os complex can expedite electron transfer between the GOD and the elec-

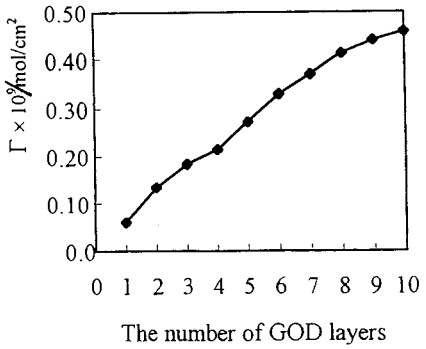

Fig. 2. relation between Γ and the number of Os–PVP layers.

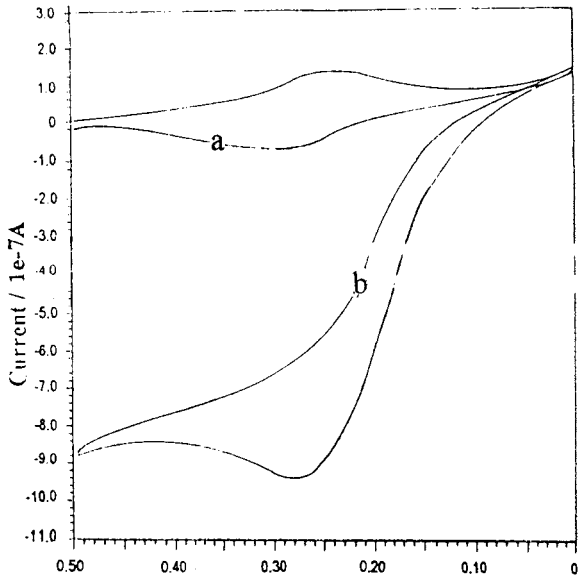

Fig. 3. The cyclic voltammograms of enzyme electrode both in the presence and in the absence of glucose (50.0 mM); scan rate, 20 mV s^{-1}: (a) in the absence of glucose, (b) in the presence of glucose.

trode surface [7,8]. The mechanism can be expressed as follows:

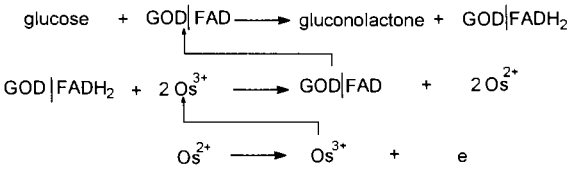

Where GOD|FAD and GOD|$FADH_2$ represent the oxidized and reduced form of flavin adenine dinucleotide within GOD, and Os^{3+} and Os^{2+} are the different redox forms of the Os complex in the Os–PVP layer.

3.3. Constant potential response to glucose

The stable currents of the enzyme electrode to glucose are shown in Fig. 4. The currents increased immediately after injecting glucose into the sample solution. As can be seen, the enzyme electrode showed a rapid response time reaching 95% of the steady-state currents in 10 s. The response times were shorter than those of most

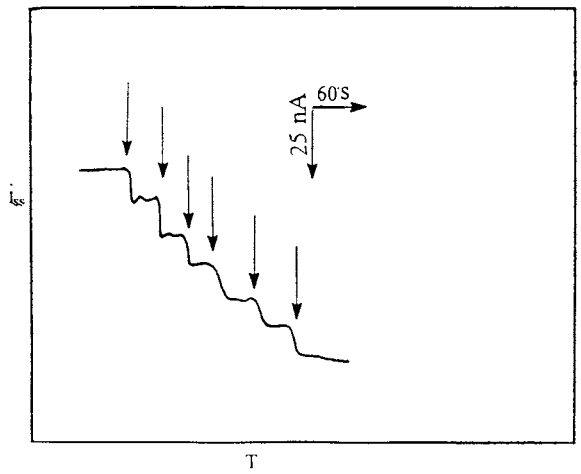

Fig. 4. The amperometric response of enzyme electrode for successive addition of glucose (1.0 mM each time); working potential, 0.24 V.

polymer-immobilized GOD electrodes [15,16], and the fast response should be attributed to the Os-complex because of electron transfer relay, with thin active film and short penetration depth. It was found that the response times were prolonged with increasing Os–PVP and GOD layers, indicating that the time dependence of response may be determined by the thickness or the number of multilayers.

Fig. 5 shows the dependence of the stable response currents on glucose concentration at various numbers of Os–PVP|GOD multilayers. The

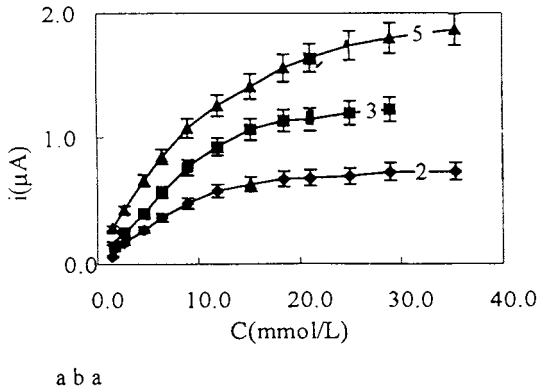

Fig. 5. The dependence of stable response currents of the enzyme electrodes on the number of Os–PVP|GOD multilayers. The number of multilayers are indicated.

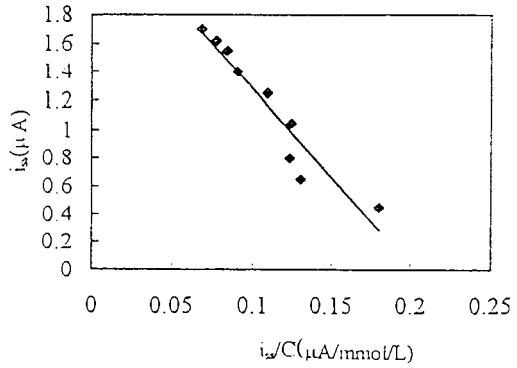

Fig. 6. The plot of i_{ss} vs. i_{ss}/C for various GOD layers.

increased number of the multilayers resulted in an increase in the response currents. Obviously, this is due to the increase of the amounts both GOD and Os–PVP. However, experimental results showed that, when there were five Os–PVP|GOD multilayers, the curve of response currents vs. glucose concentration was found to be a linear one in the range of 0.1–10 mM, and the curve starts to decline when the concentration of glucose is higher than 10 mM. When the enzyme electrode had two or three Os–PVP|GOD multilayers, its sensitivity was less than that with five Os–PVP|GOD multilayers, and the linear ranges were reduced. Thus, the increase of the number of multilayers may improve the sensitivity and response range of the enzyme electrode but prolong the response time.

3.4. The apparent Michaelis-Menten constant K'_m at various numbers of GOD layers

The linear response range of the enzyme electrode can be estimated from a Michaelis-Menten analysis of the glucose calibration curves. The apparent Michaelis-Menten constant K'_m can be determined from the electrochemical Eadie-Hofstee form of the Michaelis-Menten equation [17,18]

$$i_{ss} = i_{max} - K'_m(i_{ss}/C)$$

where i_{ss} is the steady-state currents, i_{max} is the maximum current measured in the case of enzyme saturation and C is the glucose concentration. Fig. 6 shows a plot of i_{ss} vs. i_{ss}/C. The slope of the line gives the value of K'_m. K'_m is 8.5 mM for two GOD layers and is 13.5 mM for five GOD layers. These values are in agreement with that obtained at the enzyme electrode by immobilizing GOD directly on the electrode surface [19], and the results indicate that K'_m increases with increasing of the number of multilayers.

K'_m increases with the number of GOD layers, indicating that the linear range of glucose concentration at the enzyme electrode was extended with GOD layers, these results were in agreement with other authors' results who found that K'_m increases when the enzyme layers were covered by polymer or K'_m is inversely proportional to the enzyme concentration in polymer films [3,7,8]. The real reason is not clear, one reason may be that the addition of the multilayer provides an additional resistance for diffusion of glucose to the inner enzyme layer, and the overall kinetics is controlled by this diffusion process. The linear ranges of these electrodes could be increased substantially by increasing the number of multilayers, these results mean that this technique may be used for controlling the performance characteristics of enzyme electrodes, such as the detection limit and magnitude of the output currents.

3.5. Interference studies

When the concentrations of glucose were in the range of 1–10 mM, the interference effects were investigated by testing the response of the enzyme electrode to fructose, galactose, ethylene glycol, ascorbic acid and uric acid at a concentration of 1.0 mM; it was found that these substances did not cause any observable interference in the determination of glucose.

Ascorbic acid usually interferes with the determination of glucose, because ascorbic acid could be oxidized at the applied potential. However, the MPS SAMs had a negatively charged surface; ascorbic acid was repelled from the SAMs because of the electrostatic repulse force [20]. It was found that the oxidation current of ascorbic acid at SAMs electrodes was only 5% of that at a bare electrode when its concentration was 1.0 mM, and was 12% when its concentration was 10.0 mM. Moreover, the current of ascorbic acid was apparently inversely proportional to the number of

Table 1
Results of the determination of glucose in diabetic urine

Glucose in urine (mg ml^{-1})	Glucose added (mg ml^{-1})	Amounts determinated (mg ml^{-1})	Recovery (%)
0.87[a]	0.50	1.33	92
	1.00	1.90	103
	1.50	2.32	96.7
1.40[b]	1.0	2.34	98
	1.50	2.96	104
	2.00	3.30	96

[a] The result was determined by a spectrophotometric method in diabetic urine (from a subject with an empty stomach).
[b] The result was determined by a spectrophotometric method in diabetic urine (from a subject after dinner).

multilayers. If there were five Os–PVP|GOD multilayers, 1.0 mM ascorbic acid had no oxidation currents at this enzyme electrode, and 10 mM ascorbic acid only caused an increase in current for 7%. So, interference of the ascorbic acid could be eliminated at the enzyme electrode with five layers of Os–PVP|GOD.

3.6. Stability studies

In order to evaluate the long-term stability of the enzyme electrode, the storage stability of the enzyme electrode was examined by determining 2.0 mM glucose five times every 3 days while stored dry at 4°C; the response currents were 90% of the original value after 3 weeks, and 84% after 5 weeks. The operational stability of this enzyme electrode was performed by determining 2.0 mM glucose continuously; the response currents had no obvious change after continuous testing (100 times).

3.7. Determination of glucose in urine of diabetics

It is well known that the amounts of glucose in diabetic urine change greatly in a diabetic with an empty stomach and after dinner. Experiments were carried out in order to test the performance of the enzyme electrode against a standard clinical method of glucose analysis. Ten ml urine from a diabetic were mixed with 10 ml phosphate buffer, then response currents of glucose were determined (the results are shown in Table 1). It is obvious that the results obtained at this enzyme electrode were in good agreement with those obtained by spectrophotometric methods, and the results reflected the changing glucose concentration in diabetic urine.

4. Conclusion

In conclusion, we have demonstrated the feasibility of a novel robust amperometric glucose biosensor by constructing multilayer enzyme membranes, using an osmium redox polymer as mediator. The polymer relay system described in this work effectively mediated the electron transfer from reduced GOD to the thiol SAMs gold electrode surface. The amounts of enzyme immobilized on the electrode surface could be adjusted by controlling the number of multilayers. The alternate and repeated deposition of Os–PVP and GOD layers provides a useful method for regulating the performance of enzyme electrodes, such as response sensitivity and time. Especially, there is little interference from ascorbic acid because of the ionic selectivity of SAMs. The enzyme electrode is more rapid in comparison with polymer-immobilizing GOD enzyme electrodes, and it can be applied to the determination of glucose in biosamples.

Acknowledgements

This project was supported by the Natural Science Foundation of China, Laboratory of Electroanalytical Chemistry, Changchun Institute of Applied Chemistry, Chinese Academy of Science

and the Natural Science Fund of Jiangsu province.

References

[1] A.E.G. Gass, G. Davis, G.D. Francis, H.A.O. Hill, W.J. Aston, I.J. Higgins, E.V. Plotkim, Anal. Chem. 56 (1984) 667.
[2] P.D. Hale, L.I. Boguslavsky, T. Inagaki, H.K. Karan, H.S. Lee, T.A. Skotheim, Anal. Chem. 63 (1991) 677.
[3] T. Hoshi, J. Anzai, T. Osa, Anal. Chim. Acta 289 (1994) 321.
[4] D.M. Zhou, H.Y. Chen, Sensors Actuators 40 (1997) 89.
[5] J.M. Dicks, W.J. Aston, G. Davis, A.P.F. Turner, Anal. Chim. Acta 182 (1986) 103.
[6] S. Iijima, F. Mizutami, S. Yahuki, Y. Tanaka, M. Asai, T. Katsura, Anal. Chim. Acta 281 (1993) 483.
[7] B.A. Gregg, A. Heller, Anal. Chem. 62 (1990) 258.
[8] M.R. Pishko, A.C. Michael, A. Heller, Anal. Chem. 63 (1991) 2268.
[9] C. Bourdillon, C. Demaille, J. Moiroux, J-M Savéant, J. Am. Chem. Soc. 116 (1994) 10328.
[10] Y. Lvov, K. Ariga, T. Kunitake, Chem. Lett. (1994) 2323.
[11] E. Keleinfeld, G. Fergusion, Science 265 (1994) 370.
[12] Y. Lvov, G. Decher, H. Möhwald, Langmuir 9 (1993) 481.
[13] Y. Lvov, K. Ariga, I. Ichinose, T. Kunitake, J. Am. Chem. Soc. 117 (1995) 6117.
[14] W. Kong, L. Wang, M. Gao, H. Zhou, H. Zhang, W. Li, J. Shen, J. Chem. Soc. Chem. Commun. (1994) 1297.
[15] F. Mizutani, S. Yabuki, Y. Hirata, Anal. Chim. Acta 314 (1993) 233.
[16] K. Yokoyama, E. Tamiya, I. Karube, Anal. Lett. 22 (1989) 2949.
[17] G.L. Gorton, H.I. Karan, P.D. Hale, T. Inagaki, Y. Okamoto, T.A. Skotheim, Anal. Chim. Acta 228 (1990) 23.
[18] R.M. Ianniello, A.M. Yacynych, Anal. Chem. 55 (1981) 2090.
[19] G. Jönsson, L. Gotrton, L. Petterson, Anal. Lett. 20 (1987) 839.
[20] F. Malem, D. Mandler, Anal. Chem. 65 (1993) 37.

ELSEVIER

Talanta 47 (1998) 569–583

Talanta

Determination of arsenic in ambient water at sub-part-per-trillion levels by hydride generation Pd coated platform collection and GFAAS detection

Lian Liang [a,*], Steven Lazoff [a], Cornelius Chan [a], Molena Horvat [b], James S. Woods [c]

[a] *Cebam Analytical, Incorporated, 3927 Aurora N., Seattle, WA 98103, USA*
[b] *Department of Environmental Sciences, J. Stafan Institute, Jamova 39, 1000 Ljubljana, Slovenia*
[c] *Department of Environmental Health, University of Washington, Seattle, WA 98105, USA*

Received 20 November 1997; received in revised form 12 February 1998; accepted 13 February 1998

Abstract

A method for trace determination of total arsenic in ambient waters is described. Arsenic is separated on-line from a large volume water sample by hydride generation and purging, pre-collected on a Pd coated pyrolytic platform cuvette using a simple and inexpensive system, and finally detected by GFAAS. Instrument parameters, hydride generation, transportation, and collection were optimized. The analytical behavior for major species including As^{3+}, As^{5+}, monomethyl As (MMA), and dimethyl As (DMA) were investigated individually. Problems arising from use of the system were discussed and eliminated. The necessity of sample digestion and an efficient digestion method were studied. Sample digestion for water with low organic content such as tap water and clean ground water and some clean surface water can be omitted. The method detection limit (MDL) is 0.3 ng l^{-1} for a 25 ml water sample. Recoveries close to 100% with R.S.D. $< 5\%$ can be easily achieved. Typical aqueous samples including tap, ground, lake, river, rain, sewage effluent, and saline water from different origins in the US, China, and Canada were collected and analyzed using ultra clean sampling and analysis techniques. The background levels of As in most water analyzed were established for the first time, and found to be far above the EPA's health effect criteria, 18 ng l^{-1}. © 1998 Elsevier Science B.V. All rights reserved.

Keywords: Hydride generation; Pd coated platform; GFAAS; Arsenic species; Sample digestion; Typical levels

1. Introduction

Arsenic is a teratogen and carcinogen that can traverse placental barriers and produce fetal death and malformations in many species of mammals including human beings [1–3]. Arsenic occurs in air, water, soil, plants and all living tissues. Human exposure to arsenic is by several pathways. Among them, drinking water is one of the major sources. In order to protect human health and assess the chronic effects of arsenic, it is necessary to quantify concentrations of the element in drinking water and other ambient water. This will

* Corresponding author. Tel.: +1 206 6329097; fax: +1 206 6322417; e-mail: Cebam@hotmail.com

0039-9140/98/$ - see front matter © 1998 Elsevier Science B.V. All rights reserved.
PII S0039-9140(98)00079-4

Table 1
Furnace program for Pd deposition, hydride collection, and As detection

Step and performance	Temperature (°C)	Ramp (s)	Hold (s)	Argon (ml min^{-1})	
				P-E 5000	Hitachi 9000
1. Inject and dry Pd solution, insert introduction tubing at end of step	160	5	50	300	200
2. Collect hydrides	160	1	180	300	200
3. Remove introduction tubing	30	1	20	300	200
4. Atomize hydrides	2500	1	6	0	30[a]
5. Clean furnace	3000	1	3	300	200

Lamp current 8 W; wavelength 193.7, 197.3 nm; slit 0.7 nm; signal mode: area; background correction P-E:deuterium Hitachi:Zeeman.
[a] The Hitachi recommended conditions for general metal analysis, and it is not necessary to make a change for higher sensitivity for this work.

Table 2
Conventional graphite furnace program[a]

Step	Temperature (°C)	Ramp (s)	Hold (s)	Argon (ml min^{-1})
1	160	10	40	200
2	50	1	10	200
3	2500	0	6	30
4	3000	1	3	200

[a] A fast furnace program [26].

provide necessary data for calculations of human ingestion of and other exposure to arsenic.

However, because existing methods for the analysis of As are not capable of yielding detection and quantification at ambient water levels, most results are reported as undetectable. Standard reporting limits are less than 1–3 μg l^{-1} (the limit of detection using the EPA GFAA method), or lower than 50 μg l^{-1} (the EPA regulatory criteria for drinking water). Also, without the use of ultra clean sampling and analysis techniques [4,5], some of the results reported in the past were most likely higher than the actual sample concentrations [6,7]. This existing data is not suitable for the correct assessment of the human health effects of the element, suggesting the necessity to develop a sensitive and reliable method that will provide data at or preferably below the EPA health effect criteria of 18 ng l^{-1}.

What is the target detection limit for methods to be developed? The EPA's lowest water quality criteria for As is 18 ng l^{-1}, and because As is a carcinogen, the limit should be combined with at least $\times 10$ safety factor, resulting in a MDL of 1.8 ng l^{-1}. Thus, methods with MDLs at or lower than 1.8 ng l^{-1} are needed.

The most sensitive existing EPA method is Method 1632 [8] for determination of inorganic arsenic in water, which is based on hydride generation/quartz furnace atomic absorption [9]. The MDL of the method is 3 ng l^{-1} being slightly higher than the target MDL. Also this is a speciation method requiring liquid nitrogen and a GC column for the collection and separation of the species, and a quartz furnace in which an air H_2 flame burns for hydride decomposition. For the speciation of As, it is adequate to use this technique. However, when analyzing total As, a simple and sensitive method for total determination should be used. A recent published method for determination of As in fresh and saline water by electrothermal vaporization inductively coupled plasma mass spectrometry [10] provides a DL of 6.9 ng l^{-1}. This is higher than the target MDL

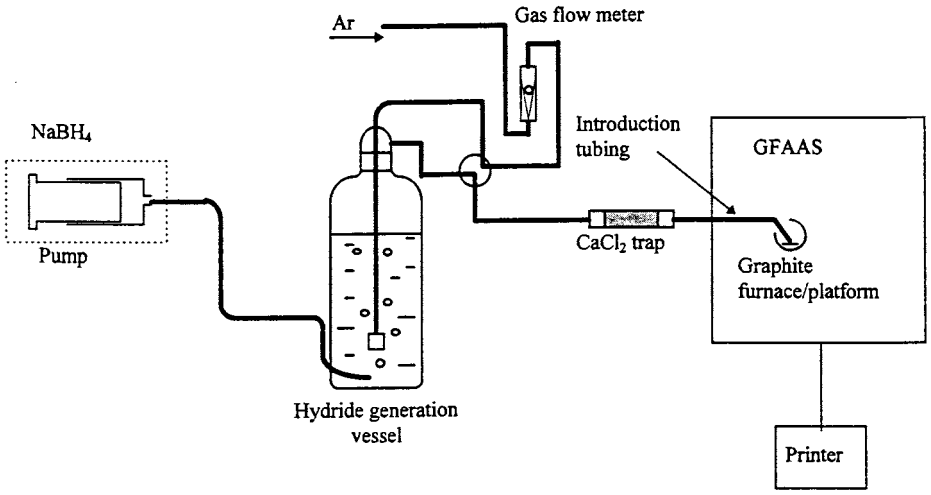

Fig. 1. Schematic of the hydride generation, introduction, deposition and atomization.

Table 3
Stock standard solutions preparation

Standard	Concentration (mg ml^{-1})	Volume (ml)	From	Weight (g)
As^{3+}	1.00	100	As_2O_3	0.1320[a]
As^{5+}	1.00	100	As_2O_5	0.1534[a]
MMA	1.00	100	$CH_3AsO(ONa)_2 \cdot 6H_2O$	0.3924
DMA	1.00	100	$(CH_3)_2AsO_2Na \cdot 3H_2O$	0.2910

[a] First dissolve in 20 ml DDW containing 0.4 g NaOH, then acidify to containing 10% HCl.

and the requirement for sophisticated instruments makes the method difficult to use for most commercial laboratories.

To fill the gap between existing EPA methods and the target MDL of 1.8 ng l^{-1}, we developed this method based on the technique of hydride generation and GFAAS detection [11–13] using a simple and inexpensive system for hydride generation, and transport. Hydride generation is a classic technique for isolation and pre-concentration of hydride forming elements [14]. To increase the sensitivity further several different techniques including liquid nitrogen trapping/quartz furnace atomization [9,15,16] and platform in situ trapping/GFAAS atomization [11–13] have been used. Among them, the platform in situ trapping/GFAAS atomization is much less complex and labor intensive because using this method the hydride is collected on the platform of the furnace which is a part of GFAAS instrument, making the use of liquid nitrogen, three additional gases, and a quartz furnace unnecessary. Moreover, using this method, the hydride is atomized by fast electrothermal heating at stabilized temperatures up to 3000°C resulting in atomization efficiencies above 95% [17]. However, if the hydride is atomized by an air H_2 flame heating at 300–500°C in a quartz furnace, this results in only 10% atomization efficiency and matrix interference [18,19]. Thus, the hydride generation-GFAAS method takes advantage of modern GFAAS instruments, high sensitivity, precision, and convenience [20].

The technique has been applied to determination of As and other hydride forming elements in a variety of environmental samples [21–25], and shown excellent sensitivity and reliability. However, except for Willie [25], few papers paid attention to organo-arsenic compounds. Some of the species such as MMA, DMA were known to be hydride forming species [9,25], but some like ar-

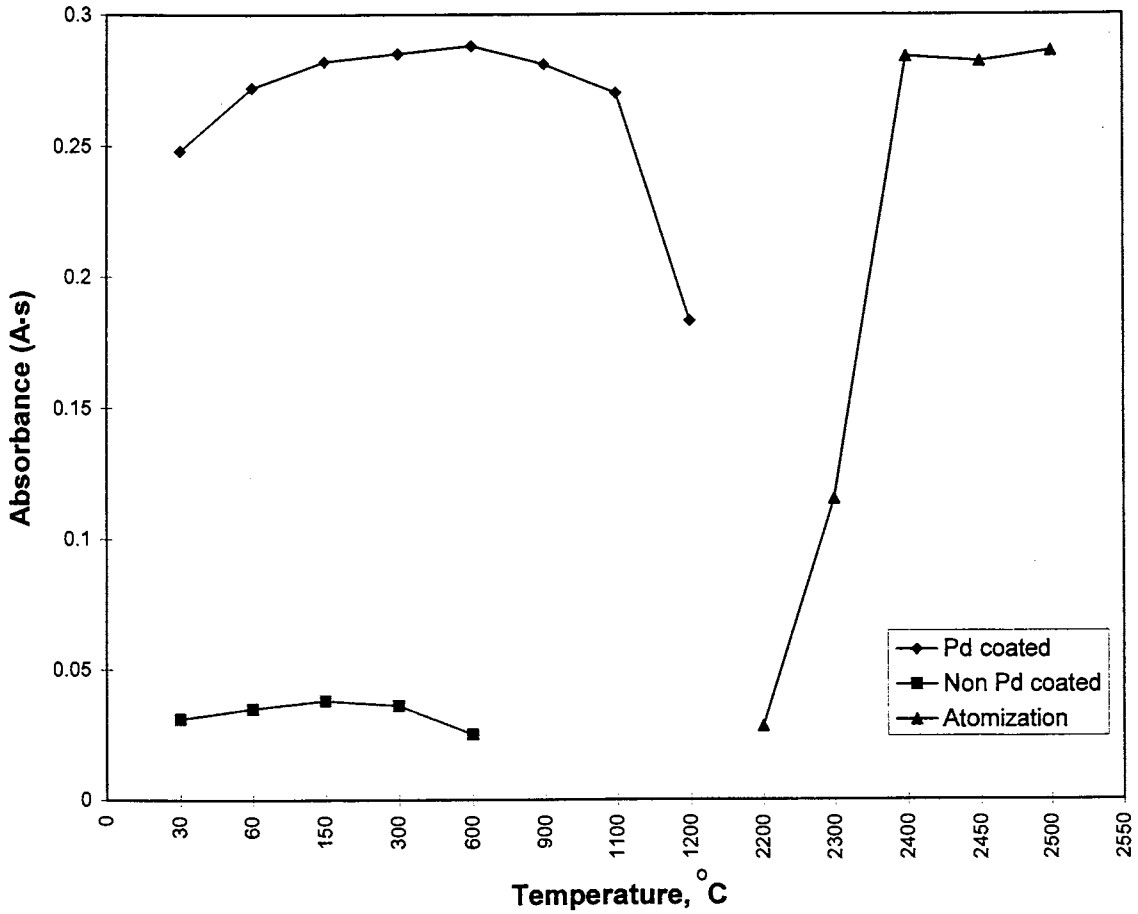

Fig. 2. Collection and atomization temperature curves for 1 ng of As^{3+} by hydride generation, Pd coated and non-coated platform collection GFAAS (using PE 5000).

senobetaine (AsB), arsenocholine (AsC), and tetramethylarsenic (TmA) were not [25]. In order to obtain recoveries close to 100%, organic species need to be investigated individually. Moreover, in a few papers seawater [21,22] and natural water [25] were involved, but not specifically focused upon, and the samples analyzed were limited to CRMs only. In the field of ambient water the technique seems to be the best choice for analysis of some elements due to its low MDL, therefore it warrants further investigation.

Willie [25] used a flow injection system, hydride forming species, As^{3+}, As^{5+}, MMA, and DMA were recovered completely with no hydride transport problems. However the transport of DMA hydride was a problem when our system was used. Willie used UV irradiation or micro wave digestion to decompose non-hydride forming species, AsB, AsC, and TmA to obtain good recoveries. In our work, since a different system was used, the analytical behaviors of some species such as DMA exhibited different patterns. In order to obtain accurate results, the analytical behaviors of individual species were investigated and hydride transport problems were eliminated. Good recovery of DMA and non-hydride forming species was obtained using a simplified and efficient acid digestion method.

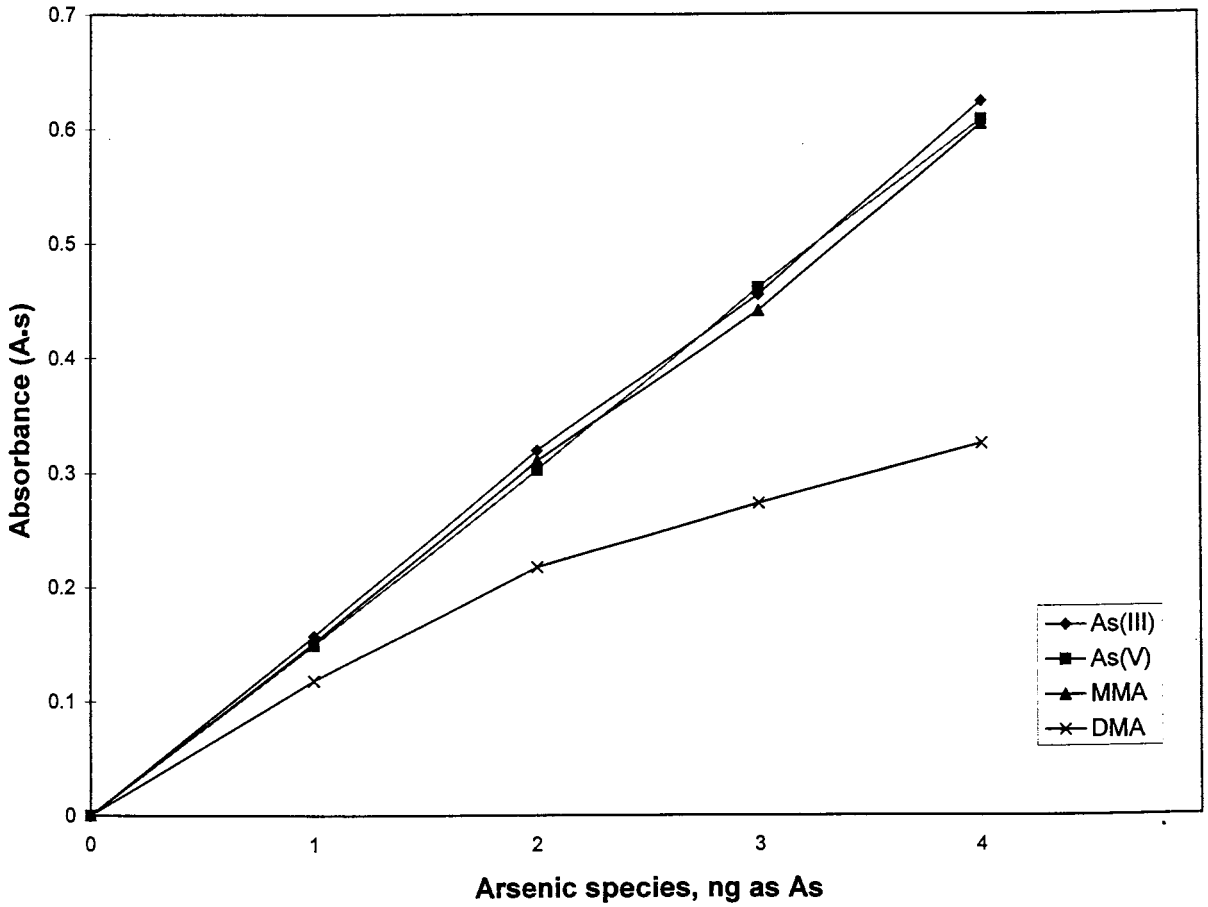

Fig. 3. Calibration curves of different species, As^{3+}, As^{5+}, MMA, DMA.

Compared to the previous work based on this technique, our work makes a useful contribution to the determination of As focused on ambient water at ultra low levels which meets the requirement of the EPA's Health Effect Criteria. The lowest MDL and recoveries close to 100% were obtained using a simple and inexpensive system, and optimized conditions of both instrument and hydride generation/transport/collection. All general laboratories with GFAAS can set up the system at any time without the need to purchase additional equipment such as flow injection, UV irradiation or microwave digestion systems. The necessity of water sample digestion was investigated. The adequacy of the method has been evaluated by analyzing a variety of ambient waters collected using ultra-clean sampling methods [4] from different origins of three countries including the USA, China and Canada. The background levels for most waters were established for the first time and found to be far above the EPA's Health Effect Criteria, indicating the associated populations may be exposed to a risk of As from drinking waters.

High quality data are particularly important for health risk assessment. This method will provide data for health risk assessment from the lowest effect levels to no-effect levels.

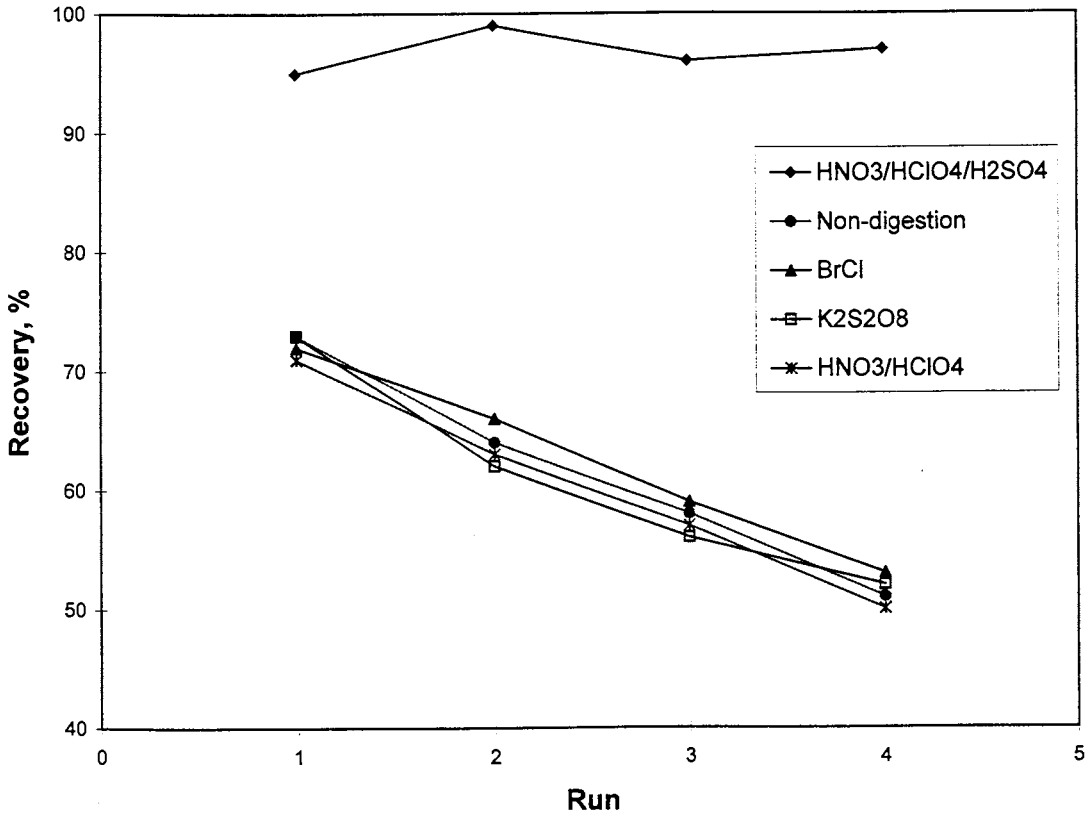

Fig. 4. Recoveries of 50 ng of DMA, as As, digested with different methods.

2. Experimental

2.1. Apparatus

The method was developed previously using a Perkin-Elmer 5000 AAS with HGA-600 graphite furnace for optimization of instrument conditions. A Hitachi 9000 Zeeman GFAAS was used for other investigations. Both instruments worked well and were used based on availability. A pyrolytic graphite platform furnace cuvette and conventional hollow cathode lamps were used. The hydride generation GFAAS program and instrument parameters are listed in Table 1.

In order to evaluate the efficiency of hydride generation and Pd platform collection, a conventional GFAAS and a fast program [26] on the Hitachi 9000 were used (Table 2).

Before each run, 30 μl of the Pd solution is deposited on the platform, the instrument is started, at the end of step 1, the instrument is stopped, a standard or a sample is injected, and then the instrument is started again for the analysis.

2.2. Hydride generation, collection, transportation, and decomposition system

The system in Fig. 1 was constructed for on line hydride generation, purging, transportation, collection, decomposition and GFAAS detection.

A Harvard Syringe Infusion Pump is used for pumping the $NaBH_4$ solution. A 60 ml standard taper 24/40 glass bottle with a four-way valve sparging-tube cap-assembly and an injection port with a silicone rubber septum was used as the hydride generation vessel. The i.d. of the vessel is 28 mm. A trap made of Teflon tubing, 10 cm long and 0.9 cm i.d. containing $CaCl_2$,

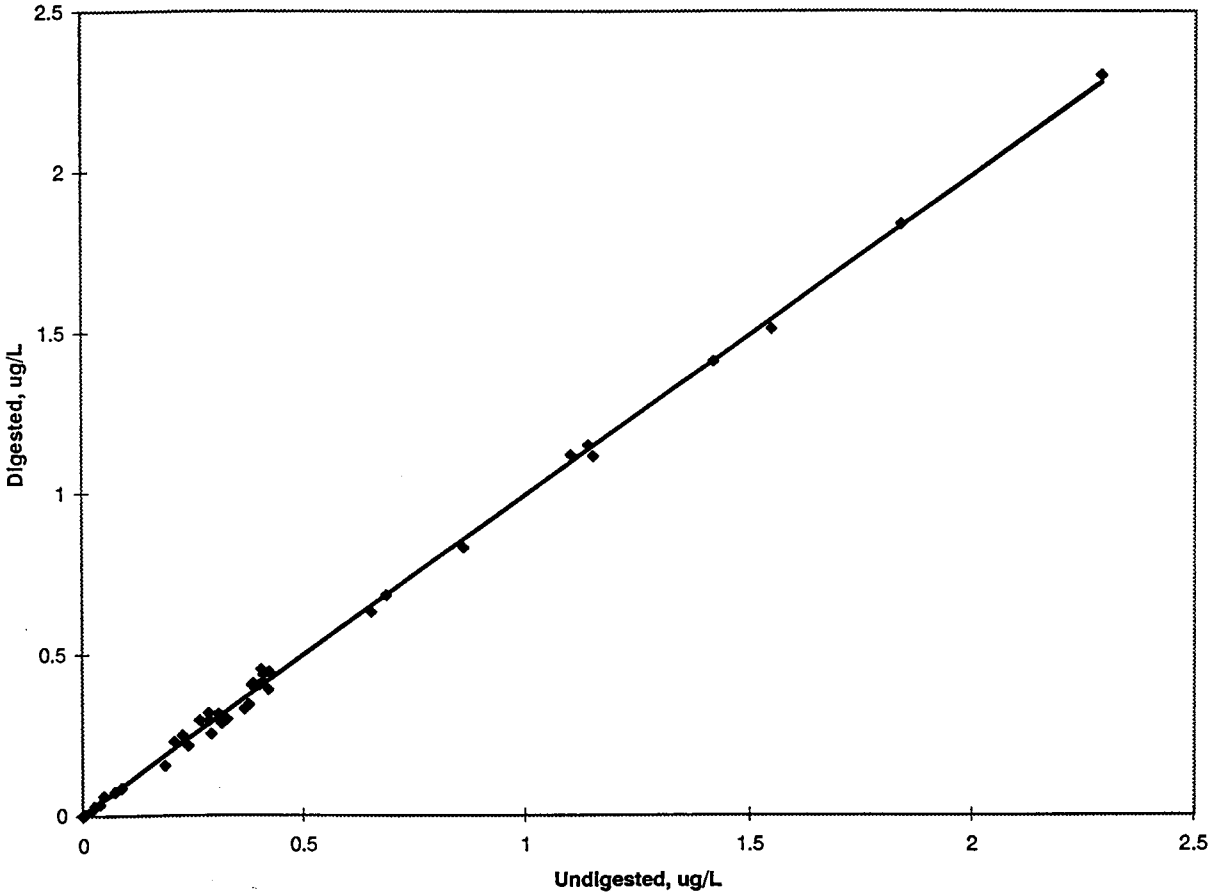

Fig. 5. Comparison of results for analyzing digested and undigested tap and ground water from different origins.

was used for removing acid fumes and water vapor and a flow meter was used for purge gas regulation. A piece of 1.2 mm i.d. stainless steel tubing was used to introduce the hydride into the graphite furnace through the sampling port. This introduction tubing was connected to the $CaCl_2$ trap with Teflon tubing. If a Zeeman AAS is used, teflon or other nonmagnetic tubing should be used for sample deposition.

2.3. Sample digestion materials

An aluminum block in which holes were drilled to a depth of 40 mm with a diameter of 30 mm to accommodate borosilicate glass tubes, 150 mm × 25 mm in size placed on a hot plate was used for sample digestion.

2.4. Standards, reagents, water, and gases

- Stock standard solutions were made by dissolving solid salts of As in DDW containing 10% HCl (Table 3).
- Working standard solutions, 10 ng ml^{-1}, were made by diluting stock solutions with DDW containing 5% HCl. The As^{3+} standard was traced to a commercial standard solution from an independent supplier, while other standard solutions were traced to the As^{3+} standard. This validation of standards was performed using CGF method and the program listed in Table 2.
- HCl, trace metal grade, 1 + 1.
- $NaBH_4$, reagent grade, 4% w/v in 0.2% NaOH, made fresh daily.

Table 4
Results of determination of As in typical water samples with different sample treatment, μg l^{-1}

Sample name	Unfiltered			Filtered		
	Digested	Undigested	R.P.D.	Digested	Undigested	R.P.D.
Lake water						
Green Lake, WA	5.92	5.27	11.6	5.21	4.95	5.1
Little Rock Lake Treatment Basin, WI	0.290	0.143	50.7			
Helmut Lake, WI	0.458	0.143	68.8			
Mud Lake, WI	0.379	0.166	56.2			
Little Rock Lake-Reference Basin, WI	0.330	0.116	64.9			
Sea water						
Puget Sound[a], Seattle, WA	2.79	2.69	3.4	2.62	2.58	1.5
River water						
Mississippi River, St. Paul, MN	2.03	1.76	14.2	1.67	1.70	1.8
Boulder Creek, CO	0.285	0.289	1.4			
Clear Creek, CO	0.654	0.630	3.7			
Fraser River, Vancouver B.C. Canada	0.349	0.339	2.9			
Sewage effluent						
Metropolitan Plant, St. Paul, MN	1.40	1.33	5.1	1.10	1.17	2.6
Ground water[b]						
Orcas Island, WA	0.686	0.681	0.7	0.682	0.687	0.7

[a] Collected from inner-tidal area.
[b] More data is shown in Fig. 5.

Table 5
Results for digestion and analyses of certified materials, μg g^{-1}

Sample name	Certified	HNO_3–$HClO_4$	Recovery (%)	HNO_3–$HClO_4$–H_2SO_4	Recovery (%)
DORM-2	18.0 ± 1.1	4.55 ± 0.59	25.3	17.7 ± 0.6	98.3
IAEA350	5.28 (3.36–5.75)	1.26 ± 0.11	23.9	5.09 ± 0.23	96.4
NIST 2709	17.7 ± 0.8	7.55 ± 0.83	42.7	17.0 ± 0.71	96.1

- BrCl, reagent grade, in a fume hood, dissolve 27 g reagent grade KBr in 2.5 l HCl. Place a clean magnetic stir bar in the bottle and stir for approximately 1 h in the fume hood. Slowly add 38 g reagent grade $KBrO_3$ to the acid while stirring.
- $K_2S_2O_8$, reagent grade, 2% w/v, made fresh daily.
- HNO_3, trace metal grade.
- $HClO_4$, trace metal grade.
- H_2SO_4, trace metal grade.
- Reagent double de-ionized water (DDW), 18 MΩ minimum,
- Argon, 5.0 grade.
- Pd solution, 600 μg ml^{-1}, made from commercial atomic absorption modifier solution, 100 g l^{-1} Pd, as $Pd(NO_3)_2$.

3. Procedures

3.1. Sample preparation

For tap, clean and low organic waters, sample digestion can be omitted. For organic rich waters, 10 ml of sample is put in a glass digestion tube with 1 ml HNO_3, 0.5 ml $HClO_4$, and 0.5 ml H_2SO_4. Add a few Teflon boiling chips to prevent bumping. The

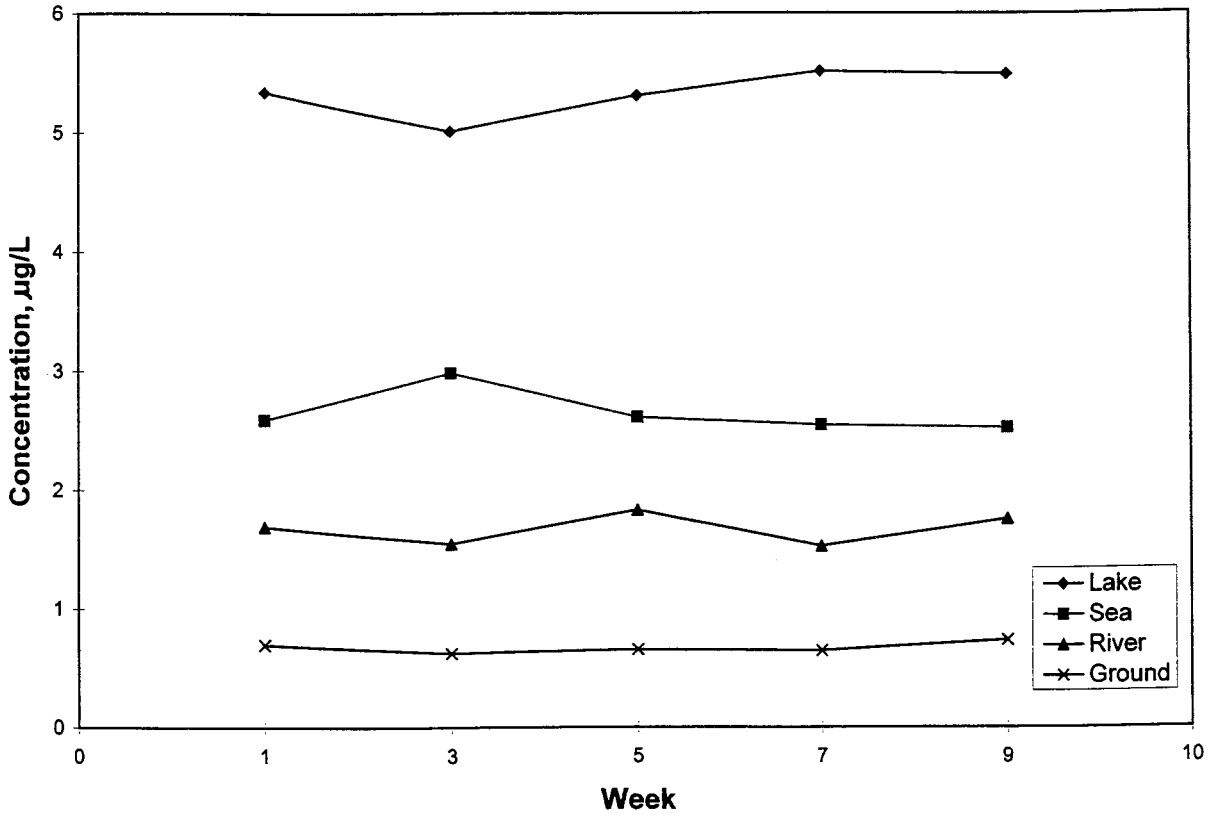

Fig. 6. Sample stability of storage.

glass tube is placed in the aluminum block and heated on a hot plate to 230°C to reach the fume stage of H_2SO_4. The tube contents were simmered for at least 20 min. The digestion takes about 2.5 h for a batch of samples. The samples are brought to a final volume of 10 ml.

3.2. Sample analysis

The instrument is made ready for analysis. 2.0 ml of 1 + 1 HCl, and a sample aliquot of up to 25 ml is added to the hydride generation vessel. If a sample aliquot less than 25 ml is used, DDW is added to bring the volume up to 25 ml. The 4-way valve cap is put in place, which is set to allow the purging gas at 100 ml min^{-1} to bypass the vessel. Before each hydride generation cycle, 30 µl Pd solution is injected onto the platform of the graphite furnace, and then the instrument is started. At the end of step 1, the introduction tubing is inserted through the sample introduction port to rest upon the center of the platform as shown in Fig. 1, and the four-way valve is switched to allow argon gas to purge the reaction vessel. The infusion pump is started to inject the borohydride solution for 2 min at a rate of 1.0 ml min^{-1}. The pump is stopped, while the purging gas continues to transport the residual hydride. In step 3 the introduction tubing is removed, the hydride trapped on the platform is atomized in step 4, and the absorbance of the sample is printed out. The furnace is cleaned in step 5 and the system is ready for the next analytical cycle.

3.3. Calibration curve.

Standard curves are generated using the same procedure as sample analysis with 0, 1, 2, and 4 ng of As^{3+} added to 25 ml DDW in the purge vessel.

4. Results and discussion

4.1. Optimization of instrument parameters

GFAAS has become a mature technique for analyses of trace elements since 1980 [20]. The instrument parameters and conditions are available in manuals from suppliers, however, these are for general analysis only. For specialized techniques, the instrument parameters and conditions must be optimized by the analyst.

Table 6
Typical As concentrations found in tap and domestic well water collected from different origins

Location	Concentration μg l^{-1}	Comments
City tap water		
Beijing, China	0.306	Single tap, single sample
Tianjing, China	0.344, 0.385	Single tap, duplicate samples
Vancouver B.C., Canada	0.084	Single tap, single sample
Seattle, WA	0.352–0.427	Single tap, 11 samples over 2 months
St. Paul, MN	0.298	Single tap, single sample
Louisville, CO	0.031, 0.026	Single tap, duplicate sample
Denver, CO	0.048	Single tap, single sample
Denver-Park Hill, CO	0.004	Single tap, single sample
Boulder, CO	0.073	Single tap, single sample
Lafayette, CO	0.208	Single tap, single sample
Municipal, Minocqua, WI	0.858	Single tap, single sample
Domestic well water		
Kempton, CO	1.104	Single tap, single sample
Boulder Junction, WI	2.300	Single tap, single sample
Presque Isle, WI	1.143	Single tap, single sample
Lake Tomahawk, WI	1.148	Single tap, single sample
Lac du Flambeau, WI	0.034	Single tap, single sample
Minocqua, WI	1.836	Single tap, single sample

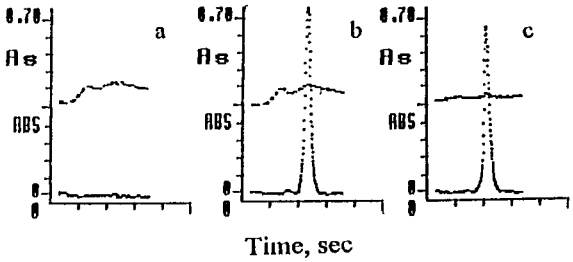

Fig. 7. Atomization profiles of As hydride from Pd coated platform for: (a) method blank, (b) 2 ng of As^{3+}, (c) 4 ml of tap water of Seattle corresponding to 0.392 μg l^{-1}.

The uniqueness of this study is that the analyte is converted into a metal hydride that is subsequently transferred and deposited on a Pd coated platform in the furnace of the instrument. This results in the separation of the metal from its background matrix. The sensitivity of GFAA can be taken advantage of with an effective sample size of 25 ml.

Atomization profiles by hydride generation GFAAS obtained at 2500°C are sharp and symmetrical, indicating higher sensitivities can be obtained using the peak height rather than the peak area of the absorbance signals. However, the sensitivity of this method was not an issue so that the peak area was used to improve precision and extend the linear calibration range.

An experiment for optimization of the temperatures of hydride deposition and atomization was conducted using the P-E 5000 GFAAS (Fig. 2) as hydrides can be collected at room temperature without a significant decrease of sensitivities. Slightly higher and constant sensitivities were found in the range of 120–900°C. At temperatures higher than 900°C, sensitivities decreased. When a Zeeman instrument is used, lower temperatures should be set because the Teflon introduction tubing can not withstand temperatures higher than 260°C. Higher temperatures can be used for non-Zeeman background correction instruments if necessary.

An examination of atomization efficiency was conducted. Very low sensitivity was found at 2100°C. As the atomization temperature was in-

creased an increase in sensitivity was found up to 2400°C above which sensitivity remained constant. An atomization temperature of 2500°C was used with an atomization time of 6 s. A temperature as low as 2300°C with an atomization time of 8 s can be used.

Pd has been extensively used as a modifier for conventional GFAAS. The data in Fig. 2 shows the importance of the use of Pd to coat the platform. Without the use of Pd, the hydride collection efficiency is very low making the analysis impossible.

4.2. Optimization of hydride generation, transportation, and collection

In the hydride generation vessel, many factors such as $NaBH_4$ concentration and injection rate, purging gas flow rate, purging time, solution acidity, and vessel size and geometric shape may affect the results. These parameters were tested and carefully adjusted.

Using this method, we found the concentrations of As in ambient water including tap water to be higher than expected, and since the method is very sensitive, typically, taking 0.5, 1, and 2 ml for most surface water, and 5, or 10 ml for tap water were enough for analyses. Therefore the method was designed to use 25 ml as a maximum. If samples less than this volume are used the final volume needs to be made up to 25 ml. A purging vessel of 60 ml works very well.

The purging gas flow rate may be as high as 200 ml min^{-1} without breakthrough because of the high affinity of the Pd coated platform for the As hydride. However, higher rates may bring more acid fumes and water vapor into the $CaCl_2$ trap, decreasing its efficiency, whereas lower rates need longer purging time. Since this procedure has not been automated, a shorter operation time to increase output has to be considered. Taking all of these factors into account, a purging rate of 100 ml min^{-1} was chosen.

The $CaCl_2$ trap is one of the key parts of the system. Without it, the acid fumes and solution drops may interfere with the analysis. After about 80 analysis cycles, the trap and transfer line may become wet. In order to ensure high precision and recovery, the trap and tubing should be replaced as necessary. Compared to previous studies based on the same technique, the method described in this paper provides the lowest MDL. It is believed that the trap plays an important role in this.

The efficiency of the hydride generation, transportation, and trapping was evaluated by comparison of characteristic amounts (m_o, pg/0.0044 A·S) obtained by hydride generation GFAAS and conventional GFAAS. This experiment was performed using P-E 5000 GFAAS. The m_o was found to be 17 and 16 pg for the two methods, respectively. Therefore, an efficiency close to 100% can be achieved. This efficiency can be achieved only when the $NaBH_4$ reagent solution is fresh. An m_o, 26 pg/0.0044 A·S was found using the Hitachi Zeeman GFAAS 9000, which was higher than the theoretical value of the Zeeman instrument due to using an internal gas flow rate during atomization.

4.3. Calibration and sample preparation

The method is based on hydride generation. If all species of the element occurring in ambient water can form hydrides quantitatively and efficiently transfer to the platform, the samples can be placed directly in the hydride generation vessel for analysis without the need of sample digestion.

It has been reported that As^{3+}, As^{5+}, MMA, and DMA are hydride forming species, however, it is unknown how many species, especially organo-As compounds occur in ambient water [27]. It is also unknown how the species composition is affected by factors such as oxidation potential (E_h), pH, temperature, organic contents, suspended solids, dissolved oxygen and other variables. Total arsenic determination may require a digestion method that will mineralize organo-As using an appropriate technique such as hot acid digestion [28], UV irradiation [25,29], or microwave digestion [25] prior to hydride generation. However, analyses of As at these ultra low levels, it is critical to avoid contamination, possible losses, or incomplete decomposition of some organic species. Sample preparation is an area that could use additional research. In order to explore the necessity for sample digestion, the

analytical behavior of major species, As^{3+}, As^{5+}, MMA and DMA were investigated individually using our method, and various environmental samples were analyzed with and without sample digestion.

Calibration curves of individual species were made by carrying standards through hydride generation and GFAAS detection (Fig. 3). Equivalent slopes of calibration curves were found for As^{3+}, As^{5+}, and MMA, suggests that As^{3+} can be used for calibration of As^{5+}, and MMA. However, a considerably lower slope was found for DMA, and the sensitivity of DMA decreased remarkably with increasing hydride generation cycles. This problem was not encountered when a flow injection system was used [25].

The calibration curve of DMA (Fig. 3) was made by analyzing 4 points of standards in the order of 1, 2, 3, and 4 ng standards. Recoveries calculated against As^{3+} were 75, 68, 60, and 53% for 1, 2, 3, and 4 ng standard respectively. After 8 cycles, the recovery dropped to 22%. This may be a major source of analytical error, and the magnitude of the error depends on how much DMA is contained in the sample. We attributed this to the higher boiling point of DMA hydride. The boiling points of As^{3+}, As^{5+}, MMA, and DMA hydrides are -55, -55, 2, and 35.6°C respectively. The boiling point of DMA hydride is higher than room temperature. As a result of this, it may condense on the wall of the tubing and on the $CaCl_2$ trap, especially when the trap becomes wet and the purging gas flow rate is lower. Even though, the curve was made under the most favorable conditions, a new $CaCl_2$ trap was used, and all the tubing was dry, the recovery of the first standard was only 75%, and sensitivity dropped after each analytical cycle, making the analysis difficult. The same problem has been reported by Crecelius et al. [9]. In order to eliminate this problem, the authors suggested that the transfer tubing be shortened and heated.

In order to determine total As accurately using our system, DMA must be mineralized. Several strong oxidants and combinations, BrCl [30], $K_2S_2O_8$ [29,31], HNO_3–$HClO_4$ [16], and HNO_3–$HClO_4$–H_2SO_4 [28] have been used for the decomposition of organo-metalic compounds including As. In this study these oxidants were compared for decomposition of DMA. Aliquots of 50 ng DMA in 5 ml of solution were digested by these methods and analyzed in groups of 4 replicates each using our method (Fig. 4). Recoveries of DMA digested with BrCl, $K_2S_2O_8$, and HNO_3–$HClO_4$ show the same pattern as non-digested DMA, low recovery which decreases run to run for replicate analyses. This indicates that these reagents and combinations do not effectively decompose DMA. Recovery of DMA digested with HNO_3–$HClO_4$–H_2SO_4 is close to 100%, and does not decrease run to run, indicating the DMA was completely decomposed. The digestion must reach the fume stage of H_2SO_4 and remain there for 20 min to achieve complete decomposition. This suggested that accurate total As analysis of samples containing DMA should therefore be digested with HNO_3–$HClO_4$–H_2SO_4 to the fume stage of H_2SO_4.

An evaluation of typical ambient water samples was made to determine the presence of DMA and/or non-hydride forming As compounds and the requirement for digestion to determine total As. These included 38 drinking and clean groundwater samples, and 11 surface water samples collected using ultra clean sampling technique [4]. They were analyzed as unfiltered and filtered with 0.45 μm filters, undigested and digested with HNO_3–$HClO_4$–H_2SO_4 (Fig. 5, Table 4). Each result is the mean of triplicate or duplicate analyses with R.P.D. within 5%. The mean concentrations of digested samples were obtained by analyzing 3 independent digestates.

Because certified reference water samples containing organo-As were not available in our laboratory, certified fish tissues, DORM-2(NRC) and IAEA350, and NIST2709 sediment were analyzed for validation of results. The materials were digested with mixtures of HNO_3–$HClO_4$ to the fume stage of $HClO_4$, and HNO_3–$HClO_4$–H_2SO_4 to the fume stage of H_2SO_4, respectively. The results are listed in Table 5.

Good agreement between certified and analytical results were obtained for digested samples with HNO_3–$HClO_4$–H_2SO_4. Recoveries were very low for HNO_3–$HClO_4$ digestates, suggesting the materials may contain high concentrations of

DMA and/or non-hydride forming species, especially fish tissues, and they require to be digested with HNO_3–$HClO_4$–H_2SO_4 to H_2SO_4 fume stage for complete decomposition. These results indicated that HNO_3–$HClO_4$–H_2SO_4 digestion is a reliable sample digestion method for total As analyses.

A comparison of the results in Table 4 and Fig. 5 for both filtered and unfiltered water, shows R.P.D. between the digested and undigested samples were below 14% for most samples. The exceptions were four lake samples from Wisconsin. The results suggest that sample digestion can be omitted for drinking and clean groundwater samples, however, for surface waters, digestion was unnecessary for most, but for some like Wisconsin lake waters, correct results for total-As can be obtained only when samples are digested. Only unfiltered samples were analyzed for the Wisconsin Lakes with digested samples considerably higher for total-As than undigested, suggesting the samples contained high concentration DMA and/or non-hydride forming species. These samples were from four small lakes (3 to 10 hectares) located in Vilas County, WI, with no human habitations on the shoreline. The samples were collected near the center of each lake from a depth of about 0.25 m using trace-metal-clean techniques. Except the sample from the Helmut Lake with a yellow color, other samples had no visible suspended matter or turbidity. Therefore, for samples with no previous data, several representative samples from the site should be tested to determine whether digestion is necessary. A comparison of filtered and unfiltered samples, indicates that dissolved As was 82–99% of total As for samples analyzed.

In order to minimize contamination, the hot acid digestion procedure was simplified. Since the hydride generation GFAAS method is very sensitive, a small volume of sample, typically, 10 ml of water was taken for digestion, making the use of glass test tubes in aluminum blocks possible. This made the digestion much easier and faster, 2–3 h per batch, and many more samples could be digested in the same space than our previous method [16], which utilized conical flasks combined with a glass funnel and glass balls in a sand bath and took 8 h per batch.

5. Sample storage stability

Typical samples listed in Table 4 were also used for observation of sample stability during storage. Samples acidified with an HCl concentration of 5 ml l^{-1} were stored for a period of 9 weeks at room temperature. The samples were analyzed without digestion 5 times (once per 2 weeks) over the period, and no significant decrease or increase in concentrations were observed. R.S.D. for all matrices were 6–8% over the storage period (Fig. 6).

6. Analytical performance of hydride generation GFAAS method

6.1. Method detection limit (MDL)

The MDL was determined using the procedure in 40CFR136, Appendix B to be 0.3 ng l^{-1} for a 25 ml water sample. This MDL is 60 times lower than the EPA's lowest health effect criteria. It is worth noting that the lamps used in this study were conventional hollow cathode lamps but a better MDL can be obtained by using a electrodeless discharge lamp. This is the lowest MDL among reported data so far.

6.2. Linearity of calibration curve

The Linearity is up to 4 ng of As at 193.7 nm wavelength, corresponding to 160 ng l^{-1} for 25 ml water, while 8,000 ng l^{-1} for 0.5 mL water sample. This range would cover concentrations of As in normal ambient waters. The linearity may expand by 20% at 197.3 nm wavelength.

6.3. Precision and accuracy

Within run precision of 5% R.S.D. and between run (day to day) R.S.D. of less than 10% are typical. For example, the sample stability experiment generated R.S.D. less than 10% for 5 measurements performed over 9 weeks for typical water samples. The accuracy of the method was evaluated by analyzing CRMs. Recoveries were above 96%. Moreover, typical water samples were

spiked and analyzed frequently during method development with As^{3+}, As^{5+}, MMA, and DMA. Analytical conditions, treatments, and procedures were determined to be acceptable for the method only when the spike recoveries were $>95\%$.

It is worth noting that samples from Beijing, and Tainjing (China), Colorado, and Wisconsin contained blind duplicates and blanks. Results for the duplicate samples were within the analytical precision reported and blanks were reported below the MDL.

7. Application of the method

The method described in this paper has been used for analyses of various ambient water samples including drinking, ground, lake, river, rain, sewage effluent, and seawater from different origins in three countries. None of the samples were below the MDL of this method. Concentrations in city drinking water ranged from 4–858 ng l^{-1}. The concentration of As in Seattle city tap water was higher. Considering the history of mining in this area [32], this is reasonable. Concentrations of domestic well water varied from ppt levels to ppb levels for the samples analyzed. Concentrations of most surface waters were 1–5 μg l^{-1}. Overall, except a tap water sample from Denver-Park Hill, CO, concentrations of As in all ambient water samples analyzed were far above the EPA's health effect criteria of 18 ng l^{-1}. Some of the results for drinking and domestic well waters are listed in Table 6. All drinking water was collected from cold taps that had been allowed to run for 10 to 20 min prior to collection.

Seattle tap water, collected from a tap in our laboratory, was monitored over 2 months. Concentrations were found to be 390 ± 37 ng l^{-1} for 11 samples. Typical atomization response signals for analysis of Seattle tap water are shown in Fig. 7.

Acknowledgements

This study was funded by Cebam Analytical, Incorporated, and supported in part by Superfund Basic Research grant ES046960 from the National Institute of Environmental Health Sciences. Authors thank colleagues, Micheal Ao, Steve Balogh, Andrew Nicholson, and Carl Watras for collecting samples using ultra clean sampling techniques. Thanks are also due to Raja Atallah for valuable discussion. Special thanks are due to Walter Slavin for direction in the development of this method.

References

[1] L. Nagymajtenyi, A. Selypes, G. Berencsi, J. Appl. Toxicol. 5 (1985) 61.
[2] A.H. Smith, R.C. Hopenhayn, M.N. Bates, et al., Environ. Health Perspect. 97 (1992) 259.
[3] G. Deknudt, A. Leonard, J. Arany, G.J. Du Buisson, E. Delavignette, Mutagenesis 1 (1986) 33.
[4] EPA Method 1669: Sampling ambient water for trace metals at EPA Water Quality Criteria Levels, Office of Water (4303), EPA 821-R-96-011, 1996.
[5] EPA, Guidance on establishing trace metal clean rooms in existing facilities, Office of Water (4303), EPA 821-B-96-001, 1996.
[6] EPA, Ambient water quality criteria for arsenic, EPA Rep. 440/5-80–021, 205 pp.
[7] R. Eisler, 1988, Arsenic hazards to fish, wildlife, and invertebrate: A synoptic review, US Fish Wildl. Serv. Biol. Rep. 85 (1.12) 92 pp.
[8] EPA Method 1632: Inorganic arsenic in water by hydride generation quartz furnace atomic absorption, Office of Water (4303), EPA 821-R-96-013, 1996.
[9] E.A. Crecelius, N.S. Bloom, C.E. Cowan, E.A. Jenne, Speciation of selenium and arsenic in nature water and sediments, vol. 2: Arsenic Speciation. Final Report. Prepared for Electric Power Research Institute, Palo Alto, CA by Battelle, Pacific Northwest Laboratories, Richland, WA, 1986.
[10] D.C. Gregoire, M.L. Ballinas, Spectrochim. Acta 52B (1997) 75.
[11] Z. Li, N. Zhe-ming, S. Xiao-quan, Spectrochim. Acta 44B (1989) 339.
[12] R.E. Sturgeon, S.N. Willie, G.I. Sproule, P.T. Robinson, S.S. Berman, Spectrochim. Acta 44B (1989) 667.
[13] Z. Li, N. Zhe-ming, S. Xiao-quan, Spectrochim. Acta 44B (1989) 751.
[14] J. Dédina, D.L. Tsalev, in: J.D. Winefordner (Ed.), Hydride Generation Atomic Absorption Spectrometry, Chemical Analysis, vol. 130, Wiley, Chichester, 1995
[15] G.A. Cutter, Anal. Chim. Acta 98 (1978) 59.
[16] L. Liang, P. Danilchik, Z. Huang, At. Spectrosc. 15 (4) (1994) 151.
[17] B.V. L'vov, Spectrochim. Acta 45B (1990) 633.
[18] M. Verlinden, H. Deelstra, E. Adriaenssens, Talanta 28 (1981) 637.

[19] W. Bernhard, P. Stauss, Spectrochim. Acta 48B (8) (1993) 951.
[20] W. Slavin, Graphite Furnace AAS, A source Book, The Perkin-Elmer Corporation, Norwalk, 1984.
[21] R.E. Sturgeon, S.N. Willie, S.S. Berman, Analyst 1 (1986) 115.
[22] S.N. Willie, R.E. Sturgeon, S.S. Berman, Anal. Chem. 58 (1986) 1140.
[23] Y. AN, S.N. Willie, R.E. Sturgeon, Spectrochim. Acta 47B (1992) 1403.
[24] Z. Li, S. McIntosh, R.G.R. Carnrick, W. Slavin, Spectrochim. Acta 47B (5) (1992) 701.
[25] S.N. Willie, Spectrochim. Acta 51B (1996) 1781.
[26] L. Liang, Spectrochim. Acta 47B (2) (1992) 239.
[27] D. W. Boening, Environ. Test. Anal. 18 (1997) September/October.
[28] W. Holak, J.J. Specchio, At. Spectrosc. 12 (4) (1991) 105.
[29] R.H. Atallah, D.A. Kalman, Talanta 38 (2) (1991) 167.
[30] G.A. Gill, W.F. Fitzgerald, Deep Sea Res. 32 (1985) 287.
[31] P.D. Goulden, P. Brooksbank, Anal. Chem. 46 (11) (1974) 1435.
[32] Bureau of Mines, Arsenic, A Charpter from Mineral Facts and Problems, 1989 ed., US Department of The Interior.

ELSEVIER

Talanta 47 (1998) 585–593

Talanta

A novel sorbent tube for ambient hydrogen sulfide determination

Mürvet Volkan [a,*], Tijen Eroğlu [a], Ahmet E. Eroğlu [a], O. Yavuz Ataman [a], Harry B. Mark Jr. [b]

[a] *Department of Chemistry, Middle East Technical University, 06531 Ankara, Turkey*
[b] *Department of Chemistry, University of Cincinnati, Cincinnati, OH 45221, USA*

Received 4 August 1997; received in revised form 16 February 1998; accepted 20 February 1998

Abstract

A novel tubular device has been developed for hydrogen sulfide determination in air. Several substrates such as commercial silica gel and alumina TLC plates, silica gel powder, alumina, $CaSO_4$, $CaCO_3$, $BaSO_4$, MgO, chalk, α-cellulose and ethyl cellulose were tested as solid substrates. 30–70-mesh silica gel was finally employed in glass tubes of 4.0 mm internal diameter. Silica gel is treated with 0.5 M aqueous $CdCl_2$ solution, dried, filled into the glass tube and sample gas is passed through the device using nitrogen as the carrier gas where 70% relative humidity is employed. The analyte reacts with the solid substrate to form a luminescent spot whose length in the tube is measured and correlated to concentration. The flow rate was 68 ml min^{-1}. The analytical system is linear in the range of 0.2–1.3 ppm H_2S for the specified conditions. The prepared devices are stable at least for 3 months prior to sampling; and after sampling, the luminescing spot is stable also at least for 3 months. © 1998 Elsevier Science B.V. All rights reserved.

Keywords: Hydrogen sulfide; Room temperature luminescence; Air pollution control

1. Introduction

Hydrogen sulfide is produced in nature primarily by decomposition of organic materials by bacteria. In addition, it is a constituent of natural gas, petroleum, sulfur deposits, volcanic gases and sulfur springs. The exposure limit value recommended by NIOSH (United States National Institute for Occupational Safety and Health) is 10 ppm/10 min. The immediately dangerous to life or health (IDLH) level is 300 ppm. Olfactory sensation is lost at 150–200 ppm where the unpleasant odor of rotten eggs ceases to be an insufficient warning for lethal exposure. Although the concentration of hydrogen sulfide in ambient air is not commonly so high to cause any health effects, it is necessary to monitor its concentration in certain locations since the presence of this gas has been one of the possible causes of casualties among people who work in sewers and similar environments. The most widely used fundamental tech-

* Corresponding author. Tel.: +90 312 2103228; fax: +90 312 2101280; e-mail: murvet@rorqual.cc.metu.edu.tr

0039-9140/98/$ - see front matter © 1998 Elsevier Science B.V. All rights reserved.
PII S0039-9140(98)00083-6

niques for H_2S determination have been compared by Bethea [1]. The chemical methods include collection of gas in liquid [2–4], collection on impregnated solid substrates [5–7], coulometry [8,9], gas chromatography [10–13] and ion chromatography [14].

This paper describes the development of a simple, low cost and sensitive method for the determination of H_2S concentration in air. The procedure has been developed by exploiting the room temperature luminescence signal obtained from the reaction of $CdCl_2$ with ambient H_2S. A $CdCl_2$-treated silica gel column was utilized as a dosimeter with proper calibration. The concentration of the analyte in air was simply correlated to the length of the tubular device which exhibits luminescence.

2. Experimental

2.1. Instrumentation

All the luminescence spectra were obtained by using a Perkin-Elmer Model LS50B Luminescence Spectrometer equipped with a 150-W xenon lamp as excitation source. A yellow cut-off optical filter was placed before the entrance slit of the emission monochromator. This spectrometer was used to characterize the luminescence spectra on different substrates. The final analytical measurements for the tubular device developed in this study relies on visual examination only. Standard gas concentrations were obtained by a Vici Metronics Dynacalibrator Model 230-14-C gas dilution system using permeation tubes obtained from the same company. Permeation tubes were used as needed, for both analyte and the interferant gases. In all the preparations, the permeation tube chamber temperature was set to 30°C for use and the calibration of the permeation tubes was done by measuring the weight loss versus time. N_2 was used as the carrier and dilution gas. The relative humidity was adjusted by mixing the analyte gas stream with a controlled humidity gas stream; the final relative humidity was determined by the relative amounts of the two streams. A humidity measuring box-type device (Fisher Scientific) was placed in the reaction chamber and its display was directly viewed through the transparent window of the chamber. The carrier gas stream with the desired humidity was obtained by using a washing bottle containing a saturated salt solution; $Pb(NO_3)_2$ was used to provide a final relative humidity of 70–74% in the reaction chamber.

2.2. Preparation of solid substrates by $CdCl_2$ treatment

Commercial silica gel and alumina TLC plates, silica gel powder, alumina, $CaSO_4$, $CaCO_3$, $BaSO_4$, MgO, chalk, α-cellulose and ethyl cellulose were tested as solid substrates. Approximately 0.5 g of the solid substrate material were immersed into 0.5 M aqueous solution of $CdCl_2$ and the contents were mixed well. After waiting for 5 min, the mixtures were filtered through a filter paper and the solid part was dried in an oven at 80°C. Since $CdCl_2$ is toxic, its handling was always carried out under a well-ventilated hood with extra care.

2.3. Measurements for luminescence characterization of the solid substrates

By using an IR pellet preparation kit, the solid materials which remained on the filter paper were pelletized and placed in the reaction chamber which has been described previously [7]. The luminescence signals on these solid substrates were then measured by the luminescence spectrometer utilizing a solid surface accessory.

2.4. Preparation and calibration of H_2S dosimeter

Silica gel, 30–70 mesh, which was treated by $CdCl_2$ as described above, was filled into a glass tube having an internal diameter of 4.0 mm and a length of 8.0 cm. The front end of this tubular device was connected to the output of the Vici Metronics system; the other end was connected to the exhaust. The flow rate of the sampling gas, 68 ml min^{-1}, and relative humidity, 70%, were kept constant throughout the calibration measurements. After exposure to the analyte gas for a measured duration and under controlled condi-

tions, the tubes were removed from the sampling system and placed in a dark location. For this purpose, a dark room or any place with subdued light may be used, but a simple box made from cardboard would also be sufficient. The tubes were illuminated under a portable UV lamp, Camag 29000. The length of the column that fluoresces was measured. Duplicate measurements were carried out for each concentration value.

3. Results and discussion

It was previously demonstrated that atmospheric hydrogen sulfide reacts with the surface of a filter paper treated with aqueous $CdCl_2$ and yields a luminescent species whose intensity can be correlated with the analyte concentration in ambient air [7]. It has also been shown that the luminescent species is CdS solid particles which were formed in a well-defined size [7]. In this study, the similar principles were employed for signal formation using a tubular device which is familiar to most users for monitoring toxic gases in a rapid, simple and inexpensive way.

3.1. Selection of the column material

In the literature [15–19], a variety of solid materials has been tested in room temperature luminescence (RTL) studies, and it has been concluded that one should select the most convenient substrate by considering the specific purpose of the determination, since no clear-cut guidelines could be developed. In the previous study [7], filter paper was chosen because of its low cost and high performance as a substrate. In this study, in order to make the measurements in a tubular device, a material consisting of particles of well-defined mesh size was sought for, so that it can be easily and conveniently filled into a glass tube. Some commercial TLC plates, in addition to the pellets prepared from various materials, were tried. The results are given in Table 1 and some typical background and sample fluorescence spectra obtained from these substrates are presented in Figs. 1–3. In these figures, the spectral features in the range of 350–500 nm are common to all the spectra; these peaks are the result of surface scattering of the Xe lamp emission. A cut-off filter of about 50% transmittance at 350 nm was used to prevent the background peak at 600 nm due to the scattering of excitation beam as the second order. As it can easily be understood from the table and the figures, the most satisfactory signal was obtained on the surface of the silica gel TLC plate. The relatively high homogeneity of the commercial silica gel TLC plate can be seen in Fig. 4. The silica gel was preferred as the column material because of its relatively high sensitivity and high signal/background value. Therefore, 30–70 mesh size silica gel was used as a column material; this material can be easily filled into the column and allows a large range of flow rates while the gas is sampled.

Table 1
Luminescence signals obtained on various substrates

Substrate[a]	Relative signal[b]	RSD (%)	(S/B)[c]
$CaSO_4$	58 ± 5	9	0.58
Chalk (dirty)	57 ± 3	5	0.57
Chalk (white)	73 ± 6	8	0.73
$BaSO_4$	85 ± 20	24	0.85
Silica gel 60G (for TLC)	97 ± 26[d]	27	0.97
Al_2O_3 (for column chrom.)	80 ± 14[d]	18	0.80
Al_2O_3 (for TLC)	45 ± 18	40	0.45
MgO	20 ± 3	15	0.20
$CaCO_3$	43 ± 18	42	0.43
α-Cellulose	28 ± 5	18	0.28
Ethyl cellulose	24 ± 7	29	0.24
Acetylated cellulose[e]	104 ± 17[f]	16	1.04
Silica gel[e]	164 ± 10	6	1.64

Treatment solution, 0.5 M $CdCl_2$; 0.870 ppm H_2S; 60 min collection; 68 ml min^{-1} flow rate; 70% relative humidity.
[a] Pelletized with an IR pellet preparation kit.
[b] Mean of five measurements $\pm$ standard deviations.
[c] Ratios of analyte signal at 620 nm to the background signal at 423 nm.
[d] Analyte signal was measured at 630 nm.
[e] Commercial TLC plates.
[f] Analyte signal was measured at 525 nm.

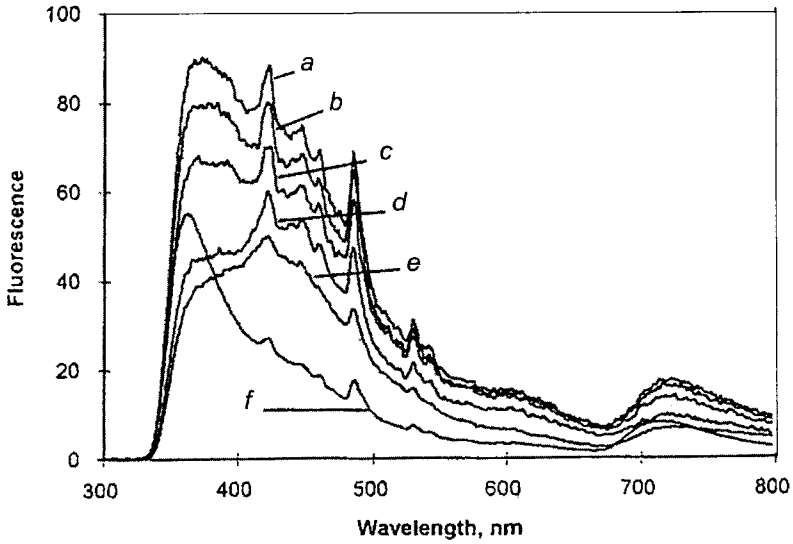

Fig. 1. Background signals from various solid surfaces. $\lambda_{ex} = 300$ nm. Slits are 10 and 5 nm for excitation and emission monochromators, respectively. (a) Silica gel TLC plate; (b) $CaCO_3$; (c) white chalk; (d) gray chalk; (e) ethyl cellulose; (f) nylon filter.

3.2. Variables affecting the luminescence signal

The concentration of $CdCl_2$ solution used for treatment of the solid substrate, and the relative humidity of the sampled gas are important parameters. Since they have been studied extensively in the previous paper [7], the optimum values obtained as 0.5 M $CdCl_2$ and 70% relative humidity were used throughout this study. It should be stressed that, although the presence of humidity is useful for sampling the gas, the normal laboratory temperature and ambient humidity could be employed during the visual examination and the length of the luminescent part is practically not affected by these parameters once it has been formed.

A careful interference study was undertaken; the details are shown in Table 2. These gases were chosen as interferants; because, except NO_2, they are the species expected to be found in the environments where H_2S is present. The effects of SO_2 and methyl mercaptan were explored in more detail since these gases have been known as the major interferants; both their concentrations and the ratio of interferant/analyte concentration were varied. In an initial set of experiments, the interferant gases, in concentrations as described in Table 2, were sent to the reaction chamber in the absence of analyte; no detectable signals were obtained. In the second set of experiments, the interferant and analyte were used together and the signals obtained were compared to those obtained by H_2S alone at the same concentration values; no significant differences were found. In another experiment, the total interference effect of some interferants was tested; 0.114 ppm methyl mercaptan, 0.289 ppm ethyl mercaptan and 0.090 ppm propyl mercaptan were sent to the reaction chamber without any analyte; no detectable signal was obtained. When exactly the same combination of interferants were tested together with 0.654 ppm H_2S, the signal obtained had no significant difference from that obtained by analyte alone at the mentioned concentration. A 95% confidence limit was employed for the significance tests. It can be concluded that the sampling procedure is free of interferences, at least for the most commonly known interferants at the mentioned conditions.

3.3. Monitoring H_2S concentrations in air

The H_2S dosimeter developed consists of a small glass tube filled with 30–70-mesh silica gel treated by $CdCl_2$, to be placed in a stationary

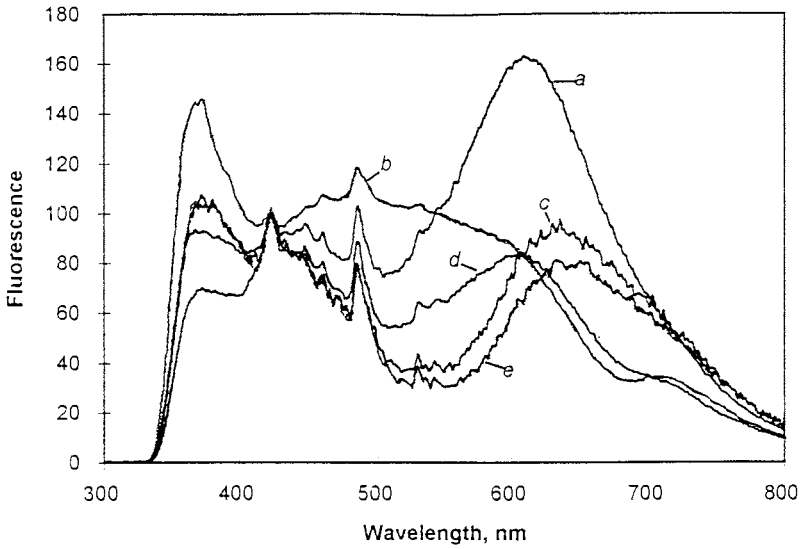

Fig. 2. Fluorescence emission spectra on various surfaces. $\lambda_{ex} = 300$ nm. Slits are 10 and 5 nm for excitation and emission monochromators, respectively. 0.870 ppm H_2S was collected for 1 h at 30°C and a relative humidity of 70%. All the spectra were normalized to a relative intensity of 100 at 423 nm. (a) Silica gel TLC plate; (b) acetylated cellulose TLC plate; (c) silica gel (pelletized); (d) cellulose acetate filter; (e) alumina (pelletized).

location for area monitoring. The monitoring procedure is based on the interaction of H_2S present in air of the working environment which is sampled through the tubular device.

The flow rate of the sampling system should be adjusted depending on analyte concentration. After exposure to analyte stream, the tube is illuminated by a portable UV source. At this stage, any blacklight source commonly used to view thin-layer chromatography plates can be employed. As can be seen in Figs. 2 and 3, the emission peak is located at around 600 nm; therefore the visual examination of the luminescence is possible. However, the visual examination is very difficult under daylight or in a well-illuminated room. Therefore, the measurement of the length of the column section which luminesces should best be done in a dark place or under subdued light. The concentration or absolute amounts of H_2S can be found from the calibration plot. The parameters such as the physical dimensions of the tube, particle size for silica gel, flow rate of sampling and humidity should be kept constant for calibration and measurement. The tubular dosimeter is a direct reading device, which reduces the total analysis time to a duration practically equal to that of sampling.

3.4. Calibration plots, reproducibility and detection limit

A typical calibration plot is shown in Fig. 5, where, after a linear response region, the saturation of the dosimeter at high analyte concentrations is illustrated. In this calibration graph, 1.00 ppm corresponds to 5.6 μg of H_2S collected in the tubular device for the conditions given. Under the same conditions, 1.00 ppm ambient concentration of H_2S can also be given as 1.37 mg m^{-3}; 1.00 ppm H_2S corresponds to 1.00 ml of H_2S in 1.00×10^6 ml or 1.00 m^3 of total gas. Using the ideal gas law at 303 K (30°C), it can be shown that H_2S (34.01 g mol^{-1}) concentration is equal to 1.37 mg m^{-3}. The duplicate set of tubular devices employed for the linear portion of calibration is shown in Fig. 6; the reproducibility among the duplicate samples are also illustrated in this figure. The photographs were taken in a dark room trying several exposure times for the camera in order to obtain the most realistic photographs.

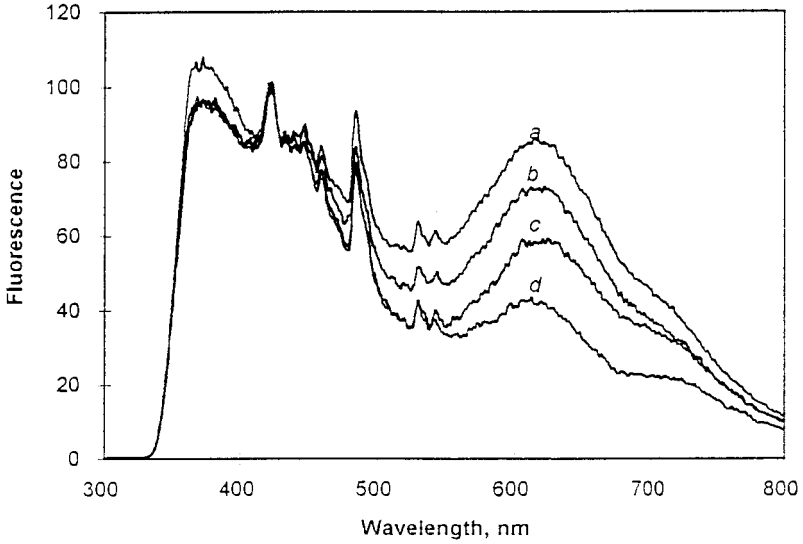

Fig. 3. Fluorescence emission spectra on various pelletized surfaces. $\lambda_{ex} = 300$ nm. Slits are 10 and 5 nm for excitation and emission monochromators, respectively. 0.870 ppm H_2S was collected for 1 h at 30°C and a relative humidity of 70%. All the spectra were normalized to a relative intensity of 100 at 423 nm. (a) $BaSO_4$; (b) chalk; (c) $CaSO_4$; (d) $CaCO_3$.

The tubes in couples correspond to the points on the calibration plot; two couples (four tubes) are shown for 1.30 ppm H_2S to show the typical reproducibility, which was 5.7% relative standard deviation for four tubes at 1.30 ppm H_2S. Most of the random error was caused by the physical disruption of the margins of the colored part when the tubes were removed from the chamber. The part which fluoresced was therefore measured by rotating the tube and recording the height at every 90° rotation; four measurements were averaged. The standard deviation was 0.06 cm corresponding to 20% relative standard deviation for 0.203 ppm. A 2s detection limit of 0.08 ppm H_2S was found which was based on these measurements.

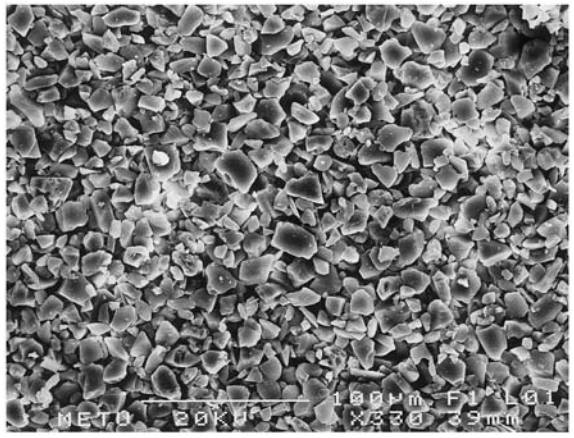

Fig. 4. SEM photograph (× 330) of commercial silica gel plate surface treated with 0.5 M $CdCl_2$ and exposed to 0.870 ppm H_2S for 60 min.

4. Conclusion

The advantages of the tubular device developed in this study may be summarized as follows:

Table 2
Compositions used in interference studies

Case no.	Interferant gas (ppm)	H_2S (ppm)
1	SO_2, 0.302	0.677
2	SO_2, 0.460	0.064
3	CH_3SH (methyl mercaptan), 0.119	0.679
4	CH_3SH (methyl mercaptan), 0.119	0.064
5	CH_3SH (methyl mercaptan), 0.055	0.018
6	CH_3CH_2 (ethyl mercaptan), 0.161	0.679
7	$(CH_3)_2S$ (dimethyl sulfide), 0.140	0.679
8	NO_2, 1.95	0.608

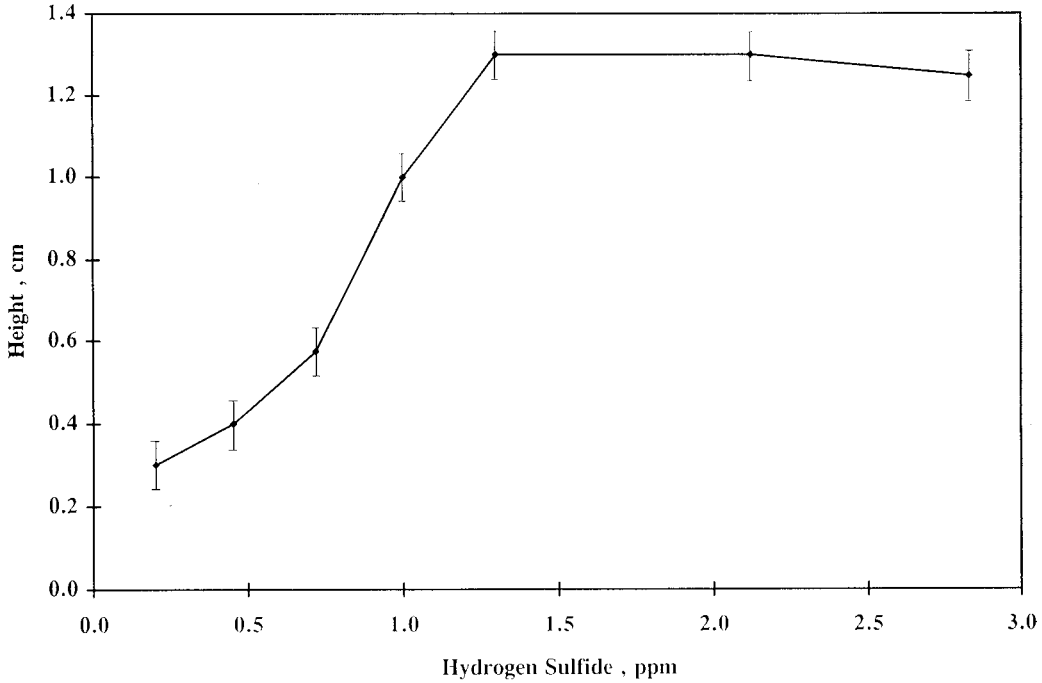

Fig. 5. Calibration plot for tubular devices. Height corresponds to the length of luminescent spot. Flow rate is 68 ml min^{-1}, 60 min sampling.

(1) During the studies done for characterization of the luminescence signals, solid sampling accessory of the luminescence spectrometer was employed and the excitation was performed directly on the solid substrates. Although the excitation wavelengths range between 290 and 350 nm, no quartz tubing was used during the experiments with visual examinations. Apparently, the low-cost glass tubes allow sufficient UV radiation to be transmitted through to induce the visible emission from the surfaces.

(2) The exposure limits, permissible concentrations of airborne contaminants are given as long-term (8 h) and short-term (10 min) as well as the time-weighted average (TWA) concentration. This tubular device is suitable for both types of measurements. For short periods, flow rate for sampling should be increased. Once the optimum flow rates are determined, the calibration plot can be prepared accordingly.

(3) The devices can easily be prepared by using a minimum amount of chemicals and time. Once the tubular devices are prepared, they can be stored for at least 3 months prior to use. It is suggested that a batch of devices be prepared exactly under the same conditions, a number of the tubes should be used to construct the calibration plot where the others can be employed for analyte measurements.

(4) The analytical signal is formed in the tubular device; no extraction or other involved chemical separations are needed.

(5) The examination is done visually, no instrumentation is necessary. A viewing place with subdued light and a portable UV lamp are all needed.

(6) During sampling, the reaction between H_2S and $CdCl_2$ is very rapid to form the stable luminescing product. The luminescence of material in the tubes after sampling is very stable and the devices can be stored on a lab bench for at least 3 months once the signal was formed. This may be useful for documentation and/or legal purposes.

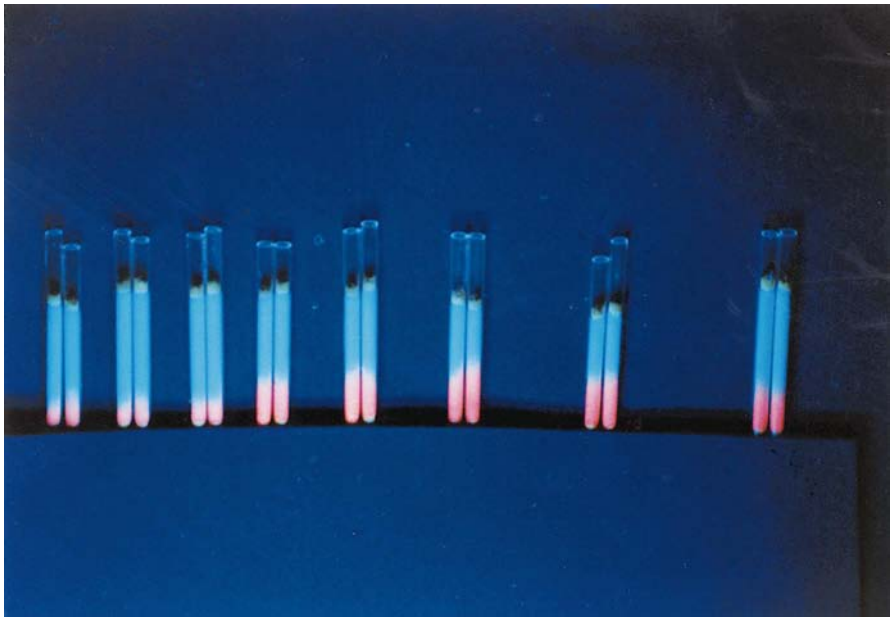

Fig. 6. Photograph of the tubular devices used for the calibration plot given in Fig. 5. From left to right, the tubes in couples correspond to 0.203, 0.454, 0.720, 1.00, 1.30, 1.30, 2.12 and 2.83 ppm H_2S.

(7) For routine purposes, the preparation and the calibration of the tubular devices can be realized in a qualified laboratory. The individual tubular devices can be conveniently marked on the glass surface for several concentration values with well-defined sampling parameters. A good cooperation between the workplace and the laboratory is needed for the assurance of the dosimeter performance.

Acknowledgements

We would like to acknowledge the financial support by the Middle East Technical University Research Fund through the funds AFP 94-01-03-07 and AFP 95-01-03-03 as well as the grant TBAG-1038 by TÜBITAK (The Scientific and Technical Research Council of Turkey).

References

[1] R.M. Bethea, J. Air Pollut. Control Assoc. 23 (1973) 710.
[2] M.B. Jacobs, M.M. Braverman, S. Hochheiser, Anal. Chem. 29 (1957) 1349.
[3] T. Pal, A. Ganguly, D.S. Maity, Analyst 111 (1986) 691.
[4] J.T. Purdham, L. Yongyi, Am. Ind. Hyg. Assoc. J. 51 (1990) 269.
[5] R. LaRue, O.Y. Ataman, D.P. Hautman, G. Gerhardt, H. Zimmer, H.B. Mark Jr., Anal. Chem. 59 (1987) 2313.
[6] E.T. Hayes, O.Y. Ataman, A.E. Karagözler, Y.L. Zhang, D.P. Hautman, R.T. Emerich, A.G. Ataman, H. Zimmer, H.B. Mark Jr., Microchem. J. 41 (1990) 98.
[7] A.E. Eroğlu, M. Volkan, E. Bayramlı, O.Y. Ataman, H.B. Mark Jr., Fresenius J. Anal. Chem. 355 (1996) 667.
[8] D.F. Adams, W.L. Bamesberger, T.J. Robertson, J. Air Pollut. Control Assoc. 18 (1968) 145.
[9] W.L. Bamesberger, D.F. Adams, Tappi 52 (1969) 1302.
[10] R.K. Stewens, J.D. Mulik, A.E. O'Keefe, K.J. Krost, Anal. Chem. 38 (1966) 760.
[11] R.S. Braman, J.M. Ammons, J.L. Briker, Anal. Chem. 50 (1978) 992.
[12] F.J. Sandalls, S.A. Penkett, Atmos. Environ. 11 (1977) 197.
[13] S. Jacobsson, O. Falk, J. Chromatogr. 479 (1989) 194.
[14] NIOSH Manual of Analytical Methods, 4th ed., US Department of Health and Human Services, Cincinnati, OH, USA, 1994.
[15] R.J. Hurtubise, in: G.G. Guilbault (Ed.), Solid Surface Luminescence Analysis: Theory, Instrumentation, Appli-

cations, Modern Monographs in Analytical Chemistry, vol. 1, Marcel Dekker, New York, 1981.
[16] R.J. Hurtubise, Phosphorimetry: Theory, Instrumentation and Applications, VCH, New York, 1990.
[17] R.J. Hurtubise, Molecular luminescence spectroscopy: methods and applications, Part II, in: S.G. Schulman, (Ed.), Chemical Analysis, vol. 77 (J.D. Winefordner (Ed.), Wiley, New York, 1988.
[18] T. Vo-Dinh, Room temperature phosphorimetry for chemical analysis, in: P.J. Elwing, J.D. Winefordner (Eds.), Chemical Analysis, vol. 68, Wiley, New York, 1984.
[19] M. Gunshefski, J.J. Santana, J. Stephenson, J.D. Winefordner, Appl. Spect. Rev. 27 (1992) 143.

ELSEVIER

Talanta 47 (1998) 595–604

Talanta

The effect of polymeric supports and methods of immobilization on the performance of an optical copper(II)-sensitive membrane based on the colourimetric reagent Zincon

Ines Oehme [a], Susanne Prattes [a], Otto S. Wolfbeis [b], Gerhard J. Mohr [a,c,*]

[a] *Institute of Organic Chemistry, Karl-Franzens University Graz, Heinrich St. 28, 8010 Graz, Austria*
[b] *Institute of Analytical Chemistry, University of Regensburg, 93040 Regensburg, Germany*
[c] *Department of Pharmacy, Centre for Chemical Sensors, ETHZ Technopark, Technopark St. 1, 8005 Zurich, Switzerland*

Received 20 August 1997; received in revised form 13 February 1998; accepted 20 February 1998

Abstract

A comparative study on the effect of different immobilization methods and matrix materials on the performance of copper(II)-sensitive membrane layers is presented. The indicator dye Zincon was immobilized in hydrophilic and hydrophobic polymers by various methods including: (a) physical entrapment of the Zincon-tetraoctylammonium ion pair in plasticized PVC, hydrogel, polystyrene, ethyl cellulose, poly-HEMA, AQ-polymer and in sol–gel glass; (b) electrostatic immobilization on an anion exchanger cellulose; and (c) covalent immobilization on cellulose via a sulfatoethylsulfonyl reactive group. The response to copper(II) ion was evaluated kinetically via the initial slope of the change in absorbance within 1 min. Layers made of hydrogel and PVC provide the highest sensitivity, while covalent immobilization is the most reproducible one, and sol–gel layers display the best mechanical stability. © 1998 Elsevier Science B.V. All rights reserved.

Keywords: Copper(II); Zincon; Optode membrane

1. Introduction

The growing activity in the field of ion-sensitive optical fibre devices and related optical methods for trace analysis of heavy metal ions has resulted in numerous sensing schemes, new indicator dyes, and in highly diversified methods of immobilization [1]. Both the method of immobilization and the type of polymer matrix exert a significant effect on the performance of ion-sensitive layers. Immobilization may shift spectra, pK_a values, luminescence lifetimes, and dynamic ranges, as well as binding or quenching constants of indicators. The proper choice of a polymer matrix for an ion-sensitive membrane layer is governed by

* Corresponding author. Tel.: +41 1 4451350; fax: +41 1 4451233; homepage: http://www.chemsens.ethz.ch

0039-9140/98/$ - see front matter © 1998 Elsevier Science B.V. All rights reserved.
PII S0039-9140(98)00084-8

parameters like permeability for the analyte, mechanical stability, and suitability for dye immobilization. From a manufacturing standpoint, the availability of the matrix, its compatibility with the mechanical support, and the toxicity of the chemicals and solvents needed for membrane preparation are of further significance.

Three general methods are widely applied for the preparation of chemically sensitive materials, namely physical, electrostatic and covalent immobilization [2]. In this context, the term physical immobilization may comprise: (a) adsorption of the reagent at the surface of the support; (b) entrapment of dyes in bulk matrices which they do not leave (e.g. due to their lipophilicity); and (c) inclusion into spheres (such as porous glasses). Electrostatic immobilization, in turn, is based on the Coulomb interaction of oppositely charged dye and support, while covalent immobilization is accomplished by forming a chemical bond between indicator and matrix.

Physical immobilization has been used, for example, in optodes for lead [3], silver and mercury [4], where lipophilic chromoionophores and selective neutral ion carriers were dissolved in plasticized PVC layers, also referred to as membranes. While such indicators and carriers readily dissolve in plasticized PVC, water-soluble indicators need to be made more lipophilic in order to render them soluble in plasticized PVC and related materials. This was accomplished in the case of 4-(2-pyridylazo)resorcinol by introducing an octadecyl chain [5], while hydrophilic porphyrins may be made lipophilic by ion pairing with tridodecylmethylammonium chloride [6]. More recently, sol–gel processes have attracted interest for the preparation of ion-sensitive layers and were used for the preparation of detectors for cobalt [7] using 1-nitroso-2-naphthol, and for iron [7,8] using 1,10-phenanthroline. Immobilization via the Langmuir–Blodgett technique was applied for a metal ion sensor based on fluorescence energy transfer using dioctadecyldithiocarbamate and *N′*,*N*-dioctadecyl-oxacyanine perchlorate [9]. In a copper(II)-selective membrane, the photometric reagent Zincon was lipophilized by ion pairing with tetraoctylammonium bromide and embedded in polyurethane hydrogel [10].

Electrostatic immobilization is the preferred method for immobilization of charged indicators. The cation exchanger Nafion™ is a frequently used matrix for immobilization of cationic dyes and was applied for a heavy metal-sensitive membrane based on the quenching of fluorescence of rhodamine [11] or porphyrins [12]. Xylenol orange, which is anionic at neutral pH, was immobilized on an anion-exchange resin and tested for lead sensing [13].

Numerous methods for covalent immobilization of indicators to polymeric supports via reactive functional groups have been presented [2]. Immobilization of chelating compounds onto cellulose [14] and silica glass [15] is well investigated and the resulting materials have been applied for the pre-concentration of heavy metal ions. For example, calcein covalently bound to cellulose was shown to respond to copper, nickel and cobalt [16].

In view of the complexity and poor comparability of the work reported so far, we have performed a study on the effect of different immobilization methods and matrix materials on the performance of an ion sensor based on a simple colourimetric indicator (Zincon) which was immobilized in various ways. This included: (a) physical entrapment of the lipophilic Zincon–tetraoctylammonium ion pair in both hydrophilic and hydrophobic organic polymers, and in sol–gel glass; (b) electrostatic immobilization on a cellulosic anion exchanger; and (c) covalent binding to cellulose. The immobilization methods presented here are generic in that they can be applied to many classical colourimetric and fluorescent indicators used in water analysis. Features like sensitivity, reproducibility of membrane preparation, leaching, and ease of immobilization were used to identify the most appropriate polymer matrix and immobilization method.

2. Experimental

2.1. Reagents

Zincon (2-carboxy-2′-hydroxy-5′-sulfoformazylbenzene, monosodium salt) and thick-layer chro-

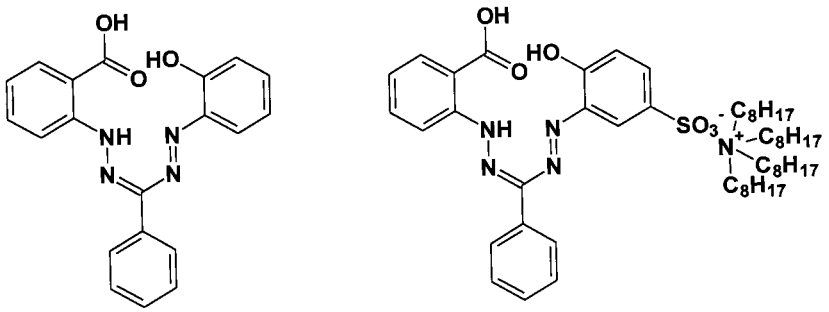

1 2

Fig. 1. Chemical structure of 2-carboxy-2′-hydroxy-formazylbenzene (**1**) and the Zincon–tetraoctylammonium ion pair (**2**).

matography plates (silica gel 60 F_{254}, layer thickness 1 mm, size 20×20 cm) were obtained from Merck (Darmstadt, Germany). Ethyl cellulose, polystyrene, tetramethoxysilane (TMOS) and trioctylphosphate (TOP) were from Aldrich (Steinheim, Germany). Tetraoctylammonium bromide (TOABr), 2-nitrophenyloctylether (NPOE), bis(2-ethylhexyl)-sebacate (DOS), poly(vinyl chloride) (PVC) high molecular weight, and 2-hydroxyethylmethacrylate (HEMA) were purchased from Fluka AG (Buchs, Switzerland). Polyurethane hydrogel D4 was obtained from Tyndall-Plains-Hunter Ltd. (Ringo, NJ), the hydroxylic plasticizer WM3 from Via Nova (Graz, Austria), and the AQ polymer from Eastman Kodak (Rochester, NY). 4-(β-Sulfatoethylsulfonyl)-2-aminophenol was a gift from Hoechst (Frankfurt, Germany). Quaternary ammonium cellulose anion exchanger QA52 was from Whatman (Maidstone, UK). Buffer components and copper nitrate were of analytical grade (Merck, Fluka). Triply distilled water was used throughout. Working solutions of copper nitrate were prepared by dilution of the stock solution (0.1 M) with 0.2 M acetic acid/acetate buffer of pH 6.0.

2.2. Syntheses

2-Carboxy-2′-hydroxy-formazylbenzene (compound **1**, Fig. 1) was prepared from 2-aminophenol and benzaldehyde-*ortho*-carboxyphenylhydrazone by analogy to a published procedure [17]. Elemental analysis: Calcd for $C_{20}H_{16}N_4O_3$ (360.37): C, 66.66; H, 4.48; N, 15.55; found: C, 66.40; H, 4.61; N, 15.50.

Zincon–tetraoctylammonium (Zincon–TOA) ion pair (compound **2**, Fig. 1) was prepared as described previously [10].

2.3. Immobilization protocols

2.3.1. Physical immobilization in polymers (M1–M9) and sol–gel (M10–M14)

Indicator dyes **1** and **2** were incorporated in different polymers. The membrane components for **M1**–**M9** were mixed in ratios given in Table 1. The solutions were cast onto a 175-μm polyester support (Mylar™, from Du Pont de Nemours) using a home-made coating device. The resulting layers had a thickness of approximately 2–4 μm and a dye content of 20 mmol kg^{-1} dry polymer. **M9** was prepared according to a given procedure [18] resulting in layers with a thickness of 25 μm. The thickness of the membranes was calculated from the amount of solvent and solute employed for the preparation of the layers.

The sol–gel components for **M10**–**M14** were mixed as given in Table 2 and then stirred for 30 min. The solutions were allowed to gelate in the dark at room temperature for 24h (**M13**), 36 h (**M11**, **M12**, **M14**) and 48 h (**M10**), respectively. The sol–gel layers were deposited on microscope slides of $11 \times 35 \times 0.15$ mm size by dip coating, stored at room temperature for 20 days and im-

Table 1
Composition of membrane cocktails

No.	Polymer	Solvent	Additive (mg)	Dye (mg)
M1	100 mg hydrogel	900 mg ethanol	10 WM3 (9%)	0.72 **1**
M2	100 mg hydrogel	900 mg ethanol	10 WM3 (9%)	1.82 **2**
M3	120 mg PVC	1.5 ml THF	240 DOS (65%)	6.55 **2**
M4	120 mg PVC	1.5 ml THF	240 NPOE (65%)	6.55 **2**
M5	120 mg PVC	1.5 ml THF	240 TOP (65%)	6.55 **2**
M6	120 mg ethylcellulose	1.5 ml chloroform	240 DOS (65%)	6.55 **2**
M7	290 mg polystyrene	2 ml methyl ethyl ketone	190 DOS (39%)	8.73 **2**
M8	2.5 g AQ-polymer (28% in water)	2.5 ml water	140 WM3	15.3 **2**
M9	2 ml HEMA	3 ml acetate buffer pH 6	5 azoisobutyronitrile	38.2 **2**

mersed in distilled water for 8 h before use. Sol–gel layers had a thickness of approximately 1 μm and a dye content of 40 mmol kg^{-1} silica.

*2.3.2. Electrostatic immobilization (**M15**)*

One gram of the anion exchange cellulose QA52 was soaked in 100 ml of a 10 mM aqueous solution of conventional Zincon for 3 h, filtered, washed with water and dried. As a result, ion pairs between the ammonium groups of QA52 and the sulfonate groups of Zincon were formed. The cellulose was placed as a thin film in a flow through cell behind a 20-μm cuprophane dialysis membrane.

*2.3.3. Covalent immobilization (**M16**)*

Transparent overhead foils (Hewlett-Packard, prod. no. 17703T) consisting of a 100-μm polyester support covered on both sides with a 10-μm layer of cellulose acetate were used as the immobilization matrix. One of the two cellulose layers was removed by treatment with acetone for a few minutes. To convert the cellulose acetate into cellulose, the membranes were treated with a 50 mM solution of sodium hydroxide for 5 min and then washed with distilled water.

Covalent coupling of Zincon to cellulose was accomplished via a vinylsulfonylgroup link according to published procedures [19–22]. For this purpose, 2-carboxy-2′-hydroxy-5′-(β-sulfatoethylsulfonyl) formazylbenzene (compound **5**) was prepared from 4-(β-sulfatoethylsulfonyl)-2-aminophenol and benzaldehyde-2-carboxyphenyl-hydrazone (compound **4**) by diazo coupling [17] (Fig. 2). Covalent immobilization of **5** onto cellulose was performed directly after synthesis in the reaction medium. The pH of the dye solution was adjusted to 8.5 with hydrochloric acid. The cellulose membranes were hung into this solution for 1 h and then washed with distilled water. In this process, the sulfatoethylsulfonyl group of compound **5** is converted into a vinylsulfonyl group by the alkaline medium, then to form a covalent link with the hydroxy group of the cellulose.

2.3.4. Apparatus

Optical spectra were measured on a UV-2101-PC photometer (Shimadzu, Kyoto, Japan). The copper(II)-sensitive membranes were placed in a self-machined flow-through cell, and sample solutions were passed through the cell at a rate of 2 ml min^{-1} using a peristaltic pump (Minipuls 3, Gilson Medical Electronics, Villiers-le-Bel, France). The light beam of the photometer was at first guided through the sensor membrane to form one wall of the flow-through cell, then through the sample solution and finally through another glass plate to form the second wall of the flow cell, and then to the detector [10]. For the reference signal, a membrane of the same polymer but without dye has been fixed in a reference flow through cell. The time dependence of the increase in absorbance due to formation of the blue Zincon-copper(II) complex was observed at 620 nm.

Reflectance measurements of the electrostatically immobilized Zincon were performed with an Oriel 3090 fibre optic universal photometer (L.O.T., Darmstadt, Germany) equipped with a

Table 2
Composition of sol–gel cocktails

No.	Silane (ml)	Ethanol (ml)	Catalyst	Dye (mg)
M10	1 TMOS	1.25	0.5 ml 0.1 M HCl	15 **2**
M11	1 TMOS	1.25	0.5 ml 1 mM HCl	15 **2**
M12	1 TMOS	1.25	0.5 ml 1 mM HCl	6 **1**
M13	1 TMOS	1.25	0.5 ml 1 mM NaOH	15 **2**
M14	1 TMOS+0.1 PhTMOS	1.25	0.5 ml 1 mM NaOH	6 **1**

TMOS, tetramethoxysilane; PhTMOS, phenyltrimethoxysilane.

150-W xenon arc lamp pulsed at 9 Hz. An interference filter of 625 nm with a bandwidth of 10 nm was used, when performing kinetic measurements. Light was guided through the input bundle of a bifurcated fibre to the flow-through cell and the reflected light was guided back via the output bundle to the photomultiplier Hamamatsu R 928. The area of illumination of the Oriel 3090 fibre on the membrane was approximately 5 mm in diameter.

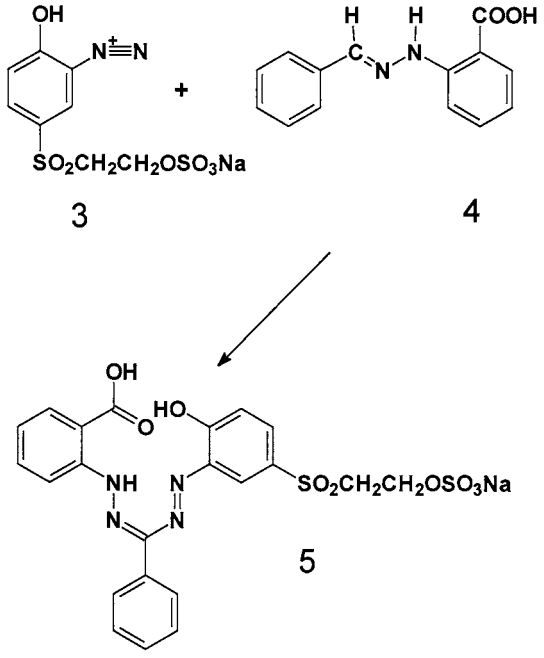

Fig. 2. Synthesis of 2-carboxy-2′-hydroxy-5′-(β-sulfatoethylsulfonyl) formazylbenzene (**5**) from **3** and **4** via diazo coupling.

3. Results and discussion

3.1. Spectral and sensing characteristics

Zincon is an established colourimetric reagent for the determination of copper and zinc. Because complexation is pH dependent, it can be applied as a relatively selective reagent for copper(II) at neutral pH. The proton dissociation equilibria of the conventional, water-soluble Zincon monosodium salt in aqueous solution are [23]:

$$\underset{\text{red}}{H_4L} \longleftrightarrow \underset{\text{pink}}{H_3L^-} \xleftrightarrow{pK_{a_1}=4-4.5} \underset{\text{yellow}}{H_2L^{2-}}$$

$$\xleftrightarrow{pK_{a_2}=7.9-8.3} \underset{\text{orange}}{HL^{3-}} \xleftrightarrow{pK_{a_3}=13} \underset{\text{violet}}{L^{4-}}$$

In order to use the dye as reagent phase in an optical copper(II)-sensitive layer, it was immobilized in the form of compound **1** (in membranes **M1**, **M12**, **M14**) and the Zincon–tetraoctylammonium ion pair (compound **2**, in membranes **M2** to **M11**, **M13**) in different polymers and in sol–gel. Zincon also was electrostatically immobilized on anion exchanger cellulose (**M15**). Furthermore, a sulfatoethylsulfonyl group was introduced into the dye (compound **5**) in order to covalently link it to cellulose (**M16**).

In contrast to the dye in aqueous solution, no dissociation in the pH range from 2 to 12 was observed in the case of membranes **M1** to **M16**. The spectra of the red membranes are similar in that they show a broad absorbance band between 500 and 575 nm. The spectra of the Zincon–TOA ion pair in a hydrogel layer (**M2**) before and after exposure to copper(II) are shown in Fig. 3.

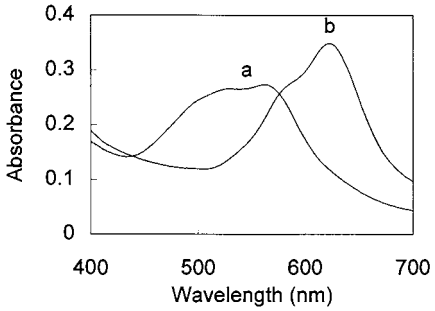

Fig. 3. Absorbance spectra of **M2** at pH 6.0; (a) before and (b) after saturation with copper(II).

On exposure to aqueous solutions of copper(II), layers **M1**–**M16** turn blue due to complex formation (Fig. 3), and the resulting absorbance maxima are summarized in Table 3. Bathochromic shifts ranging from 13 to 30 nm were observed when compared to Zincon in aqueous solution, where the absorbance maximum of the copper complex is at 600 nm.

We invariably found for all immobilization methods and polymers that copper(II) is extracted from the analyte solution until the reagent phase (the membrane) is saturated and all Zincon is present as the copper(II)-complex. As can be seen in Fig. 4, the slopes of the response curves ($\Delta A\ s^{-1}$) are concentration dependent and, therefore, can be used as the analytical information. Notwithstanding the differences in the slopes, all curves finally end up at the same absorbance. An exposure to the analyte for 1 min turned out to be adequate to calculate the initial slope. For all layers, the slope within the first minute was strictly linear. With increasing saturation, the response curves become more flatten and deviate from linearity.

Table 3
Figures of merit of the copper(II)-sensitive membranes

No.	Abs. max. of complex (nm)	Calibration plot[a] for the 1–100 μM copper range:		A[b] at 540 nm	Relative sensitivity[c] (%)
		Intercept	Slope		
M1	615	1.48E-6	5.10E-6	0.17	77
M2	620	8.54E-6	5.06E-6	0.18	76
M3	630	5.42E-6	6.21E-6	0.28	94
M4	630	1.70E-6	6.63E-6	0.28	100
M5	630	8.77E-6	6.21E-6	0.28	94
M6	625	6.27E-5[d]	0.15E-6	0.20	2
M7	620	1.82E-5	3.39E-6	0.16	51
M8	618	2.87E-5	4.06E-6	0.25	61
M9	630	3.75E-6	2.08E-6	0.60	31
M10	625	no response	no response	0.14	0
M11	625	2.43E-5	1.96E-6	0.14	30
M12	625	1.64E-5	2.36E-6	0.15	36
M13	625	8.22E-6	4.67E-6	0.20	70
M14	630	5.10E-5	4.88E-8	0.18	0.6
M15[e]	—	1.80E-6	5.06E-6	—	40
M16[f]	613	2.22E-6	5.03E-6	0.40	76
M16[g]	613	1.65E-6	1.32E-6	0.09	20

[a] For the 1–100 μM concentration range except for **M6**.
[b] Absorbance.
[c] Compared to membrane **M4** which is 100%.
[d] Working range 10–1000 μM copper(II).
[e] Reflectance measured at 625 nm.
[f] Shortly after immobilization.
[g] After a 50-day storage in buffer.

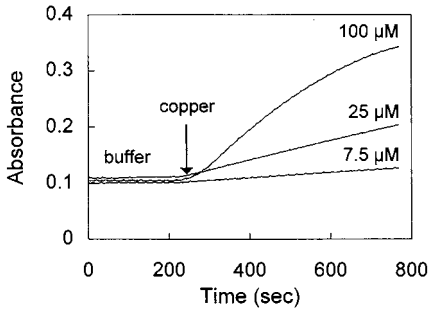

Fig. 4. Kinetics of the increase in absorbance at 620 nm as a result of exposure of membrane **M2** to different concentrations of copper(II).

3.2. Comparison of immobilization methods

For all membranes **M1**–**M16** the plots of initial slope ($\Delta A\ s^{-1}$) versus copper(II) concentration were found to be linear for the concentration range from 1 to 100 μM (i.e. from 63 ppb to 6.3 ppm) except for ethyl cellulose-based membrane **M6** whose dynamic range is from 10 to 1000 μM. Slope and intercept of the calibration functions of the membranes are summarized in Table 3. The variation in the absorbances at 540 nm (before use) reflects the variation in the reproducibility of the films whose thickness can vary by up to 15%.

Variations of **M2** in dye content from 20 to 30 mM and in membrane thickness from 2 to 8 μm correlate to variation in absorbance (A) at 540 nm between 0.15 and 0.22. As a result, the slope of the calibration function varies from 4.95×10^{-6} to 6.10×10^{-6} $\Delta A\ s^{-1}\ \mu M^{-1}$, because the response of the membrane to copper(II) is governed by its thickness and the concentration of the dye in the membrane.

Due to the high stability of the Zincon–copper complex, the response is irreversible throughout. Regeneration with 0.1 M HCl takes more than 1 h, and regeneration with 1.0 M HCl gave no reproducible results, probably because of decomposition of the dye. Therefore, a single use test appears to be the application of choice, and this requires a high reproducibility in the membrane preparation. Data on its reproducibility, expressed as the deviation in the absorbance at 540 nm for five membranes prepared from the same cocktail, are given in Table 4 which also gives data on dye leaching.

3.3. Physical immobilization in organic polymers

Zincon was made lipophilic by replacing the sodium ion of the sulfo group by tetraoctylammonium ion to give compound **2**. Zincon, similar to a wide range of indicator dyes for measurement of pH, cations, anions and neutral species, has been prepared and optimized for application in aqueous solutions. In general, these dyes contain sulfo or carboxy groups in order to make them water soluble. Their solubility in lipophilic polymer matrices is poor and crystallization in polymers can be observed after several hours. In order to make dyes such as Zincon polymer soluble, we have replaced the alkali ion by a quaternary am-

Table 4
Data on the reproducibility of the membrane preparation and dye leaching

No.	Reproducibility[a] (%)	Decrease in absorbance over time[b] (%)			
		17 h	7 days	14 days	50 days
M1	90	11	29	45	
M2	90	12	28	40	
M3	90	13	17	20	35
M11	94			4	
M12	94			70	
M13	94			44	
M16	97	12	31	51	78

[a] Defined as: 100%−standard deviation (in %) of the $A_{540\,nm}$ of five membranes.
[b] On storage in buffer of pH 6.0.

monium (QA) ion to form lipophilic ion pairs according to:

$$\text{Zincon} - SO_3^- Na^+ + QA^+ Br^-$$

$$\rightarrow (\text{Zincon} - SO_3^-)(QA^+) + NaBr$$

The quaternary ammonium halides exhibit long aliphatic alkyl chains which render them highly lipophilic. Consequently, the resulting ion pairs are highly lipophilic as well, and can be homogeneously dissolved in polymers such as plasticized poly(vinyl chloride), poly(vinyl acetate), ethyl cellulose, silicone or polyurethane hydrogel and spread as thin films on optical waveguides.

In order to evaluate whether there is any effect of the ammonium counter ion on the sensitivity of the copper(II)-sensitive layer, we also have synthesized compound **1**, which lacks the sulfo group of conventional Zincon. Compound **1** exhibits adequate lipophilicity to be entrapped in polymers without further derivatization. A comparison of the calibration plots of **M1** with **M2** and **M12** with **M11**, respectively, reveal, however, that there is no significant difference in sensitivity between **1** and **2**. Leaching, in contrast, is more pronounced in the case of **1**, obviously, because **2** is more lipophilic.

Highest sensitivity is provided by membranes based on hydrogel (**M1**, **M2**) or plasticized PVC (**M3**, **M4**, **M5**), while those based on ethyl cellulose (**M6**), polystyrene (**M7**) and AQ polymer (**M8**) display less sensitivity. Membranes **M3**–**M7** require up to 66% of plasticizer, since the plasticizer serves as solvent for the indicator dye and facilitates the transport of copper ion. As a result, 10% levels of plasticizer result in completely insensitive membranes. In order to warrant an adequate mechanical stability of polystyrene membrane **M7**, the maximum fraction of plasticizer must not exceed 40%, whereas PVC and ethyl cellulose membranes can be prepared with up to 66% plasticizer.

The polymers used display a good adhesion to polyester which was used as mechanical support, and homogeneous and flexible copper(II)-sensitive layers were obtained. Among the polymers applied, hydrogel is preferred since it dissolves in ethanol which is less toxic than tetrahydrofuran or chloroform which are required in the case of PVC and ethyl cellulose, respectively. In terms of resistance to mechanical stress, sol–gel layers are preferred.

3.4. Physical immobilization in sol–gel glass

The general performance of sol–gel-based layers strongly depends on the sol–gel protocol employed. The pH and the water-to-silane molar ratio (R) are the most significant process parameters [24,25]. The R value was kept constant at 4. The polymerization process may be divided into approximately three pH domains, viz. $pH < 2$ (the isoelectric point of silica is at pH 2), pH 2–7 and $pH > 7$. Polycondensation at below pH 2 yields dense and low-surface-area materials, which may be used for gas sensing, but are not suitable for ion sensing, as shown by **M10**, which is completely insensitive to copper(II) ions. Obviously, copper(II) ions were not able to penetrate the highly dense glass matrix and react with the indicator dye. The same is true for **M14**, which exhibits higher hydrophobicity due to the presence of phenyl groups in the sol–gel matrix. Alkaline catalysis at $pH > 7$ results in very porous sol–gel structures. Accordingly, a good sensitivity was obtained for **M13**, which is almost comparable to hydrogel membrane **M2**. However, the porous structure of the glass not only allowed the diffusion of copper(II) into the matrix but also a high leaching rate of the indicator dye. A compromise between leaching and sensitivity is found in **M12**, which was prepared by catalysis with hydrochloric acid around pH 3.

3.5. Electrostatic immobilization

Zincon readily binds to quaternary ammonium cellulose via the negatively charged sulfo-group. The electrostatic attraction is very strong, resulting in negligible leaching over a 17-h period of exposure to a flow of pH 6.0 buffer. However, it was difficult to reproducibly fix the cellulose fibres in the flow-through cell (**M15**). Complexation is irreversible and regeneration of the reagent phase by 1.0 M hydrochloric acid failed. The ease of preparation of this material is certainly advanta-

geous. The relative signal changes are significantly smaller than in the case of the hydrogel- and PVC-based membranes.

3.6. Covalent immobilization

Cellulose is an ideal support for ion sensing, because it is hydrophilic and ion permeable. In order to enable covalent immobilization of Zincon onto cellulose, the dye was modified by introducing a reactive group that covalently binds to the hydroxy groups of cellulose [19–22]. Neither the hydroxy nor the carboxy group of the Zincon can be used for covalent immobilization because they are required for complexation. Covalent immobilization was accomplished by synthesis of the reactive dye **5** which was attached to cellulose [19–22] as described in Section 2.

Two reactions occur in this process. The first is the elimination of a sulfate ion from **5** according to Eq. (1) to form a reactive vinyl intermediate:

$$\text{Zincon} - SO_2 - CH_2 - CH_2 - OSO_3Na + NaOH \rightarrow \text{Zincon} - SO_2 - CH{=}CH_2 \quad (1)$$

The second occurs between the reactive intermediate and cellulose (Cell-OH) to form the dye-cellulose conjugate:

$$\text{Zincon} - SO_2 - CH{=}CH_2 + \text{Cell} - OH \rightarrow \text{Zincon} - SO_2 - CH_2 - CH_2 - O - \text{Cell} \quad (2)$$

The resulting copper(II)-sensitive membrane **M16** was dark red and showed an average absorbance of 0.4 ± 0.012 ($n = 8$) at 540 nm. This indicates a very high reproducibility (97%) in the preparation of the membrane. The sensitivity is comparable to hydrogel membranes **M1** and **M2**. The storage stability on air and in the dark exceeds 6 months. On storage in buffer of pH 6.0, a continuous decrease in absorbance was observed (Table 4), which is attributed to slow hydrolysis.

4. Conclusions

Except for the ethyl cellulose based copper(II)-sensitive layers, all membranes display a working range from 1 to 100 μM copper(II). Highest sensitivity is found for hydrogel-based membranes, PVC membranes, and the covalently immobilized dye. The plasticizer had no effect on the sensitivity of PVC membranes. The reproducibility in the manufacturing of the copper(II)-sensitive membranes is a critical parameter with respect to precision. The standard deviation of the calibration points for polymer membranes, which is around $\pm 10\%$, is basically caused by the 90% reproducibility in making the membranes in the laboratory. The use of coating devices which are commonly used in photographic film production would allow a significant improvement in the reproducibility. The reproducibility is also found to be improved in the case of sol–gel membranes and if the dye is covalently immobilized, the resulting reproducibilities being 94 and 97%, respectively. However, covalent immobilization is more tedious and decomposition was observed during wet storage. Leaching was observed for all membranes, and is smallest for sol–gel copper(II)-sensitive membranes. Leaching is not expected to be a serious problem in case of single shot sensor membranes. If, however, applied for purposes of pre-concentration or continuous monitoring, leaching is likely to compromise any measurement.

Acknowledgements

This work was supported by the Austrian Science Foundation within project P-9869-TEC and P10,389-CHE which is gratefully acknowledged. We would also like to thank Dr. Michael Zevin from the Hebrew University of Jerusalem for co-operation in the preparation of sol–gel layers, and the Hoechst AG for providing 4-(β-sulfatoethylsulfonyl)-2-aminophenol.

References

[1] I. Oehme, O.S. Wolfbeis, Mikrochim. Acta 126 (1997) 177.
[2] O.S. Wolfbeis, E. Koller, in: O.S. Wolfbeis (Ed.), Fiber Optic Chemical Sensors and Biosensors, vol. 1, CRC Press, Boca Raton, FL, 1991, p. 303f.
[3] M. Lerchi, E. Bakker, B. Rusterholz, W. Simon, Anal. Chem. 64 (1992) 1534.

[4] M. Lerchi, E. Reitter, W. Simon, E. Pretsch, D.A. Chowdhury, S. Kamata, Anal. Chem. 66 (1994) 1713.
[5] K. Wang, K. Seiler, B. Rusterholz, W. Simon, Analyst 117 (1992) 57.
[6] R. Czolk, J. Reichert, H.J. Ache, Sensors Actuators A 25–27 (1991) 439.
[7] B.I. Kuyavskaya, I. Gigozin, M. Ottolenghi, D. Avnir, O. Lev, J. Non-Cryst. Solids 147–148 (1992) 808.
[8] O. Lev, B.I. Kuyavskaya, I. Gigozin, M. Ottolenghi, D. Avnir, Fresenius J. Anal. Chem. 343 (1992) 370.
[9] W. Budach, R.C. Ahuja, D. Möbius, W. Schrepp, Thin Solid Films 210–211 (1992) 434.
[10] I. Oehme, B. Prokes, I. Murkovic, T. Werner, I. Klimant, O.S. Wolfbeis, Fresenius J. Anal. Chem. 350 (1994) 563.
[11] F.V. Bright, G.E. Poirier, G.M. Hieftje, Talanta 35 (1988) 113.
[12] A. Morales-Bahnik, R. Czolk, J. Reichert, H.J. Ache, Sensors Actuators B 13–14 (1993) 424.
[13] I. Klimant, M. Otto, Mikrochim. Acta 108 (1992) 11.
[14] W. Wegscheider, G. Knapp, CRC Crit. Rev. Anal. Chem. 11 (1981) 79.
[15] D.E. Leyden, G.H. Luttrell, Anal. Chem. 47 (1975) 1612.
[16] L.A. Saari, W.R. Seitz, Anal. Chem. 56 (1984) 810.
[17] R.A. Brooks, N.J. Salem, US Patents 2,662,074 and 2,662,075, 1953.
[18] M.Y. Arica, V.N. Hasirci, Polym. Int. 32 (1993) 177.
[19] P. Burba, K.H. Lieser, Angew. Makromol. Chem. 50 (1976) 151.
[20] A. Holobar, B.H. Weigl, W. Trettnak, R. Benes, H. Lehman, N.V. Rodriguez, A. Wollschlager, P. O'Leary, P. Raspor, O.S. Wolfbeis, Sensors Actuators B 11 (1993) 425.
[21] G.J. Mohr, O.S. Wolfbeis, Anal. Chim. Acta 292 (1994) 41.
[22] G.J. Mohr, T. Werner, O.S. Wolfbeis, Dyes Pigments 24 (1994) 223.
[23] K.L. Cheng, K. Ueno, T. Imamura (Eds.), Handbook of Organic Analytical Reagents, CRC Press, Boca Raton, FL, 1982, p. 284.
[24] O. Lev, M. Tsionsky, L. Rabinovich, V. Glezer, S. Sampath, I. Pankratov, J. Gun, Anal. Chem. 67 (1995) 22A.
[25] C.J. Brinker, G.W. Scherer, Sol-Gel Science, Academic Press, San Diego, CA, 1990.

ELSEVIER

Talanta 47 (1998) 605–612

Talanta

Sequential extraction procedure for speciation of inorganic cadmium in emissions and working areas

Antonella Profumo [a,*], Giovanni Spini [a], Lucia Cucca [a], Ermenegildo Zecca [b]

[a] *Dipartimento di Chimica Generale, V.le Taramelli, 12, 27100 Pavia, Italy*
[b] *Dipartimento di Medicina Preventiva, Occupazionale e di Comunità, V.le Forlanini, 2, 27100 Pavia, Italy*

Received 18 December 1997; received in revised form 16 February 1998; accepted 20 February 1998

Abstract

A sequential extraction procedure for separating and concentrating soluble Cd(II) salts, CdO, Cd(0), CdS, CdSe and cadmium-aluminosilicates, has been developed for the cadmium speciation in samples such as particulate matter in emissions and working areas. The proposed procedure has been tested first on synthetic samples prepared in a laboratory with the different cadmium salts, then also in the presence of atmospherical particulate matter sampled in a laboratory of the Department of Analytical Chemistry, previously checked for the absence of cadmium. Finally the speciation was tested on particulate matter collected near the emission of a power plant fed by coal, after emission's treatment by electrostatic precipitator: matrix spiking and recovery analyses have been evaluated and the repeatability of the cadmium speciation was assessed by performing multiple analyses of the spiked samples. Quantitative determinations have been made by FAAS and GFAAS through the standard additions method. © 1998 Elsevier Science B.V. All rights reserved.

Keywords: Cadmium speciation; Emissions; Inorganic cadmium; Particulate matter

1. Introduction

The toxicity of cadmium is related to its chemical form, physical state and oxidation state; hence, the measurement of the different chemical forms is very important for a correct evaluation regarding the probable damage to human health caused by exposure to different species of cadmium. The main routes of human exposure to cadmium can be identified as acute exposure in the working environment (mainly involving inhalation of dusts and fumes and occasionally oral intake of cadmium) [1]. The 'non-effect' and lethal levels of cadmium administered in a single oral dose to adults has been estimated at 3 and 300–500 mg, respectively [2]. The lethal concentration of cadmium oxide fumes for man has been estimated to be about 5 mg m^{-3} for an 8 h exposure time [2]. The inorganic species of cadmium are more toxic than organic ones [3] and among the inorganic ones, the bivalent oxidation state is more toxic.

* Corresponding author. Tel.: +39 382 507581; fax: +39 382 578544; e-mail: aprofumo@ipv36.unipv.it

0039-9140/98/$ - see front matter © 1998 Elsevier Science B.V. All rights reserved.
PII S0039-9140(98)00088-5

Due to the different toxicity of cadmium compounds, hygienic level threshold for the individual species of Cd in working environments and emissions should be established by legislation, even if, at the moment, neither for emissions, nor for working areas this has been done. In Italy, nowadays, are taken into account the tolerable limits fixed by ACGIH (American Conference Governmental Industrial Hygienists) [4], for cadmium elemental and compounds, in 0.01 mg m^{-3} as Cd (T.W.A., Time Weighted Average). With regard to emissions, Italian law established a tolerable value for the total Cd and its compounds (as Cd) of 0.2 mg m^{-3} for a mass flow greater than 1 g h^{-1}, ignoring completely the need of speciation [5].

Many papers are reported in the literature regarding analytical procedures for the determination of Cd in air: the analyses of total cadmium in particulate matter have been made, for example, by flame atomic absorption spectrometry (FAAS) [6–9], inductively coupled argon plasma atomic emission spectrometry (ICP) [10], neutron activation analysis (NAA) [11,12]. In general, the available techniques for measuring cadmium in the atmosphere cannot differentiate among different compounds.

In the expectation that more detailed limits for the different chemical species of every toxic metal will be fixed by laws, in this paper a selective extraction procedure is proposed for determining in emissions and working places, soluble Cd(II) salts, CdO, Cd(0), CdS, CdSe (present as impurity in many minerals of cadmium) and cadmium aluminosilicates, the last ones may be present in ash from coal combustion or in other industrial productions.

Due to the fact that the proposed procedure needs extraction of the matrix, it cannot be applied to particulate matters of the vast majority of situations that will be encountered in environmental sampling: during the solubilization, in fact many reactions, not foreseeable a priori, among the cadmium compounds and some of the constituents of the complex matrix, can take place, such as redox changes, complexations, and so on. On the contrary the scenario of every emission or defined specific work place, can be reasonably expected, the possible interferences evaluated a priori and the speciation procedure adapted.

2. Experimental

2.1. Materials and methods

The determination of cadmium in the samples is done by FAAS and GFAAS, depending on the concentration level of cadmium.

A Perkin-Elmer model 1100 B atomic absorption spectrometer with an air-acetylene flame was used when the Cd concentration in samples was in the range of 0.05–2 mg l^{-1}.

For lower concentration levels of cadmium the measurements were performed on a Shimadzu AA-660 Spectrometer with a Graphite Furnace Atomizer Shimadzu GFA-4B, with the following thermal program: drying (ramp from ambient to 120°C for 30 s), pyrolysis (250°C ramp 30 s + hold 15 s), atomization (1400°C 4 s). In view of the standard addition method applied, the calibration curve exhibited a linear range between 0.1 and 5 mg l^{-1} of cadmium. During the Cd analysis of solutions with citrate buffer we have observed a matrix interference consisting in high blank values: this problem was overcome by a complexation of Cd by APCD (ammonium-pyrrolydine-dithiocarbamate) and its extraction in MIBK (methyl-isobutyl ketone), according to the procedure of Miyazaki et al. [13].

Particulate matter from the air of a laboratory was collected with two different kinds of samplers: (i) Tecora model Bravo low sampler equipped with flow meters from 0.1 to 1.0 l min^{-1} and from 1.0 to 10.0 l min^{-1}; (ii) Andersen Instrumental model 302, PM-10 high-volume sampler with 1.13 m^3 min^{-1} air flow.

All chemicals used through the experiments were of reagent grade; Cd(0), CdO, $CdSO_4$, CdSe from Aldrich Chemical Company, citric acid trisodium salt dihydrate and ammonium nitrate from Merck, ammonium-pyrrolydine-dithiocarbamate from BDH. CdS was prepared in laboratory from $Cd(NO_3)_2 \cdot 4H_2O$ solution and Na_2S.

Quantitative determinations are made by FAAS and GFAAS (Graphite Furnace Atomic Absorp-

Table 1
Selective sequential solubilization of Cd(II) soluble, CdO, Cd(0), CdS and CdSe in a synthetic mixture

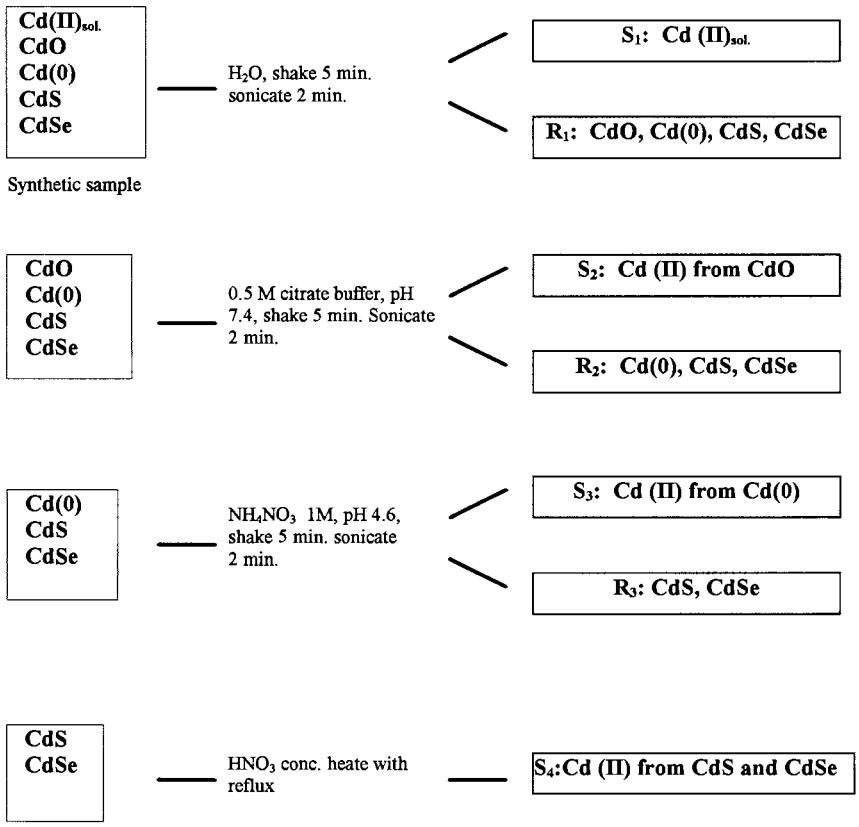

tion Spectrometry) by the standard additions method. The procedure has been tested at first on samples prepared from the pure cadmium salts, then in the presence of a matrix obtained from the particulate matter sampled from the air of a laboratory, not containing cadmium (<1 ng m^{-3}). Finally either on samples of particulates collected on filtering membranes near the emission of a power plant fed by coal, after emission's treatment by electrostatic precipitator, or on the same ones spiked with the different cadmium compounds.

All the experimental measures on the synthetic samples prepared in laboratory and reported in this paper are the average values of three independent determinations with a RSD $\leq 5\%$, except the values of the certified particulate which are the means of four determinations and whose standard deviations are reported singly.

The procedure for the sequential extraction of a mixture containing Cd(0), Cd(II) soluble salts, CdO, CdS, CdSe is illustrated below and the scheme is reported in Table 1. (It must be underlined that the procedure has been applied and verified first on each single compound).

Weighed amounts of $CdSO_4 \cdot 8/3\ H_2O$, CdO, Cd(0), CdS and CdSe were mixed and treated with 10 ml cold H_2O, sonicated for 2 min and then shaken for 5 min. Cd(II) soluble salts were recovered in solution [S_1], while Cd, CdO CdS and CdSe remain undissolved [R_1].

The residue [R_1] was treated with 10 ml of a 0.5-M citrate buffer pH = 7.4, sonicated for 2 min, shaken 5 min in order to dissolve CdO [S_2], while the other compounds remained undissolved [R_2]. Ten milliliters of Ammonium nitrate solu-

Table 2
(a) Cadmium speciation in a synthetic mixture containing: $Cd(II)_{sol.}$, CdO, Cd(0), CdS; (b) Cadmium speciation in a synthetic mixture containing $Cd(II)_{sol.}$, CdO, Cd(0), CdS, CdSe: in this case CdS and CdSe are given as sum

Species	Expected mg (as Cd)	Measured mg (as Cd)	Recoveries (%)
(a)			
$Cd(II)_{sol.}$	1.4	1.4	100
CdO	2.6	2.5	96
Cd(0)	4.2	3.9	93
CdS	2.3	2.3	100
(b)			
$Cd(II)_{sol.}$	1.1	1.0	91
CdO	2.1	2.1	100
Cd(0)	1.5	1.6	107
CdS	1.4	2.5	96
CdSe	1.2	(sum of Cd + CdSe)	

tion 1 M, pH 4.6 were then used to solubilize Cd metal [S_3] from residue [R_2], sonicated for 2 min and shaken for 5 min. The final residue [R_3] containing CdS and CdSe is treated with 3 ml of concentrated HNO_3 for 60 min with reflux, obtaining a solution [S_4] where Cd(II) is measured. After the treatment with nitric acid, in a real sample a possible residue can be expected, due to the presence in the particulate of cadmium aluminosilicates; in this case it is necessary to treat the residue with HF/H_2SO_4 in order to take in solution also this fraction of cadmium.

3. Results and discussion

The results of the speciation procedure on a mixture of Cd compounds synthetically prepared are shown in Table 2.

In relation to the scheme of Table 1, it is necessary to point out the fact that if the solubilization of a particulate sample gives a value of $pH < 4$, CdO and Cd(0) are partially dissolved in step 1, as a consequence, the Cd(II) concentration in [S_1] is higher than expected from Cd(II) soluble salts. Reducing the sonication and shaking times the Cd(0) and CdO species in solution diminish, but in this case only CdS or CdS + CdSe, if both are present, can be quantitatively separated and determined, while the separation of Cd(II), soluble and undissolved Cd(II) and Cd metal is partially verified.

It must be underlined that the good agreement between the measured and the expected values were obtained with samples composed by pure reagents: this situation does not represent real matrices. A first attempt to verify the efficiency of the procedure in more complex situations was done by repeating the speciation in presence of an environmental matrix. The matrix was constituted by the dust sampled from air of our laboratory. In order to verify the absence of cadmium in this matrix, 3000 m^3 of air were sampled through a glass fiber filter in high-volume Andersen sampler and checked for the total cadmium content. The analyses have been made by GFAAS, after 2 h reflux in conc. HNO_3, obtaining a value of 1.1 ng m^{-3} (total Cd), negligibly in relation to the limit of 1×10^{-2} mg m^{-3} established by ACGIH-TLV for Cd elemental and compounds in working areas.

A synthetic sample with the composition here reported has been accurately prepared and homogenized.

SiO_2: 1.011 g
$Cd(II)_{sol.}$: 3.7 mg, as Cd
CdO: 4.2 mg, as Cd
Cd(0): 2.5 mg
CdS: 2.8 mg, as Cd

SiO_2 acts as an inert powder in which to dilute weighed amounts of Cd compounds.

The homogeneity of the sample was confirmed by analyzing three sub-samples that gave a recovery between 85 and 100%.

Table 3
Results of speciation analysis of the mixture of cadmium salts dispersed in SiO_2, made in presence of a matrix of atmospherical particulate

	Cd concentration in solution (mg l^{-1})		Cd concentration in air (mg m^{-3})	
Species	Expected	Measured	Expected	Measured
Cd(II)	0.74	0.78	2.5	2.8
CdO	0.84	0.74	2.8	2.5
Cd(0)	0.50	0.44	1.7	1.5
CdS	0.56	0.62	1.9	2.1

From the laboratory room some air volumes have been sampled on cellulose acetate filters through low-volume TCR-Tecora Bravo sampler (10 l min^{-1}): to these matrix samples without cadmium, a weighed amount (2–4 mg) of the synthetic sample with known cadmium species, has been added and the sequential solubilization procedure applied. The results are listed in Table 3 and also in this case there is good agreement between found and expected values.

Finally, the procedure for cadmium speciation was applied to a real sample: urban atmospheric particulate certified by National Institute of Standards and Technology (NIST).

In the certified sample (1648) the reported total cadmium content is 75 mg g^{-1}. Our control GFAAS cadmium analysis on a weighed amount of the particulate sample, after acid digestion, yielded 72 mg g^{-1} (96%).

On three fractions (4–6 mg) of the certified particulate the proposed speciation procedure has been applied; cadmium quantitative determination has been done in GFAAS; CdO analyses have been made after solubilization in citrate buffer, APDC complexation and MIBK extraction. The relative percentage of the four cadmium compounds found in the sample and reported in the second column of Table 4, can be reasonably expected from this kind of emission. In order to verify the accuracy of the results, the extraction has been repeated on weighed amounts (40–50 mg) of the certified particulate sample spiked with 1 mg of the mixture of SiO_2 containing the different cadmium salts previously described. Recoveries are shown in the third column of Table 4.

In many industrial processes in which cadmium compounds are worked or produced, the cadmium raw materials contain other metals in percentage that can interfere during the solubilization steps of the proposed procedure, such as Cu(II) or Zn(0). The presence of Cu(II) may be expected in the emissions or in working places where the production processes are performed under oxidative conditions and Zn(0) in the case of reducing conditions. The relevant reactions that can take place during the various phases of the speciation are:

$$Cd(0) + Cu(II) \rightarrow Cd(II) + Cu(0);$$
$$Cd(II) + Zn(0) \rightarrow Cd(0) + Zn(II).$$

When Cu(II) is present, it is possible to measure more soluble Cd than there is really, due to oxidation of Cd(0); the opposite results would be obtained in the case of the presence of Zn(0) in the sample.

When the presence of one of these interferents is expected, the speciation can still be done but with a different approach: two independent extractions must be done, as reported in Tables 5 and 6.

Table 4
Cadmium speciation results

Species	Cd found (%)[a]	Recovery (%)[b]
$Cd(II)_{sol.}$	1.8 ± 0.4	120
CdO	64 ± 3	93
Cd(0)	10 ± 2	91
CdS	23 ± 2	93
Total cadmium	99 ± 2	

Cadmium speciation results (as percentage of each Cd compound on the total Cd) on: [a]a certified urban particulate NIST (1648); and [b]recoveries on the spiked samples.

Table 5
Selective sequential solubilization of $Cd(II)_{sol.}$, CdO, CdS and Cd(0) when Cu(II) is present.

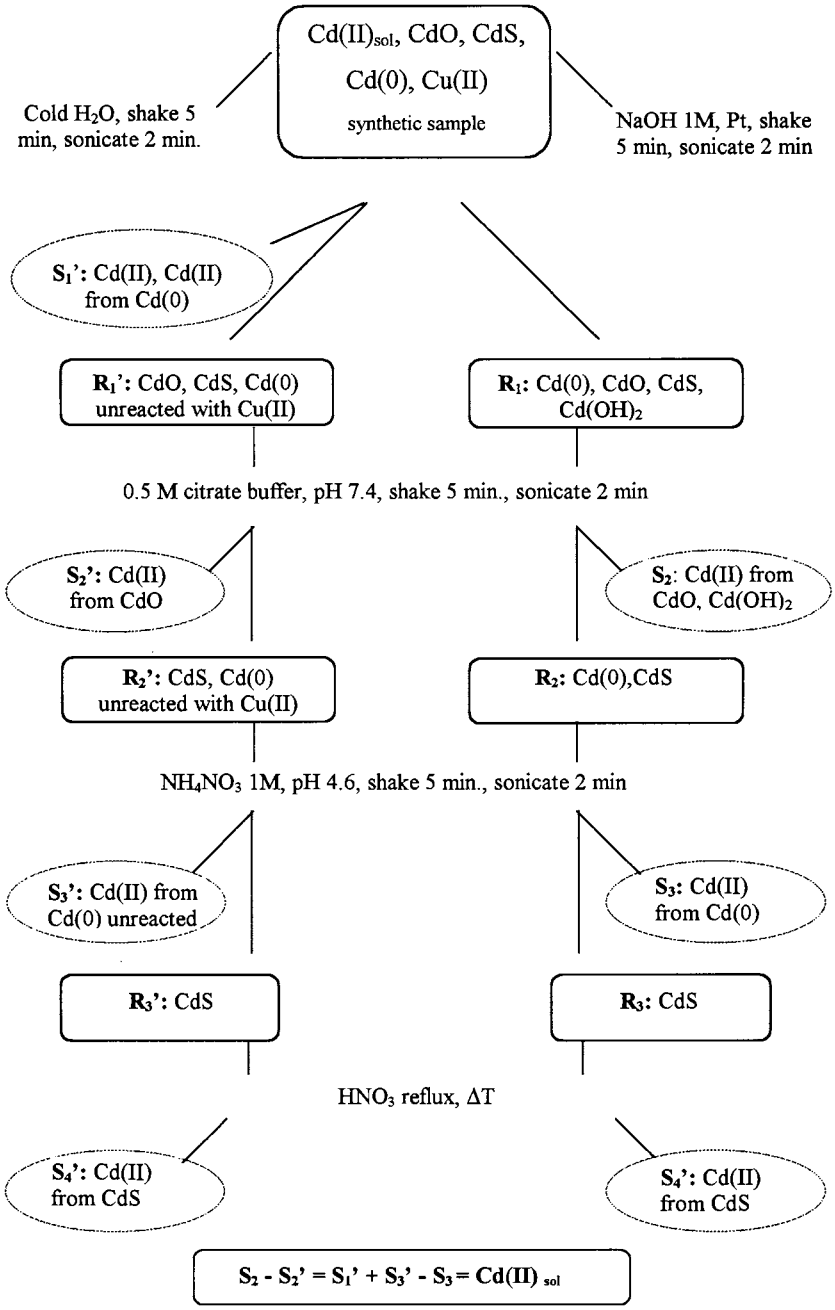

3.1. Selective solubilization when Cu(II) is present

Cu(II) salts can react with Cd(0)to produce Cu(0) and $Cd(II)_{sol.}$; the extraction with H_2O gives $Cd(II)_{sol.}$ in excess because of the reaction of Cd(0) with Cu(II), according to the left part of the scheme of Table 5. To eliminate the influence of Cu(II), the solubilization scheme of the right part

Table 6
Selective sequential solubilization of $Cd(II)_{sol.}$, CdO, CdS and $Cd(0)_i$ when Zn(0) is present. i, initial.

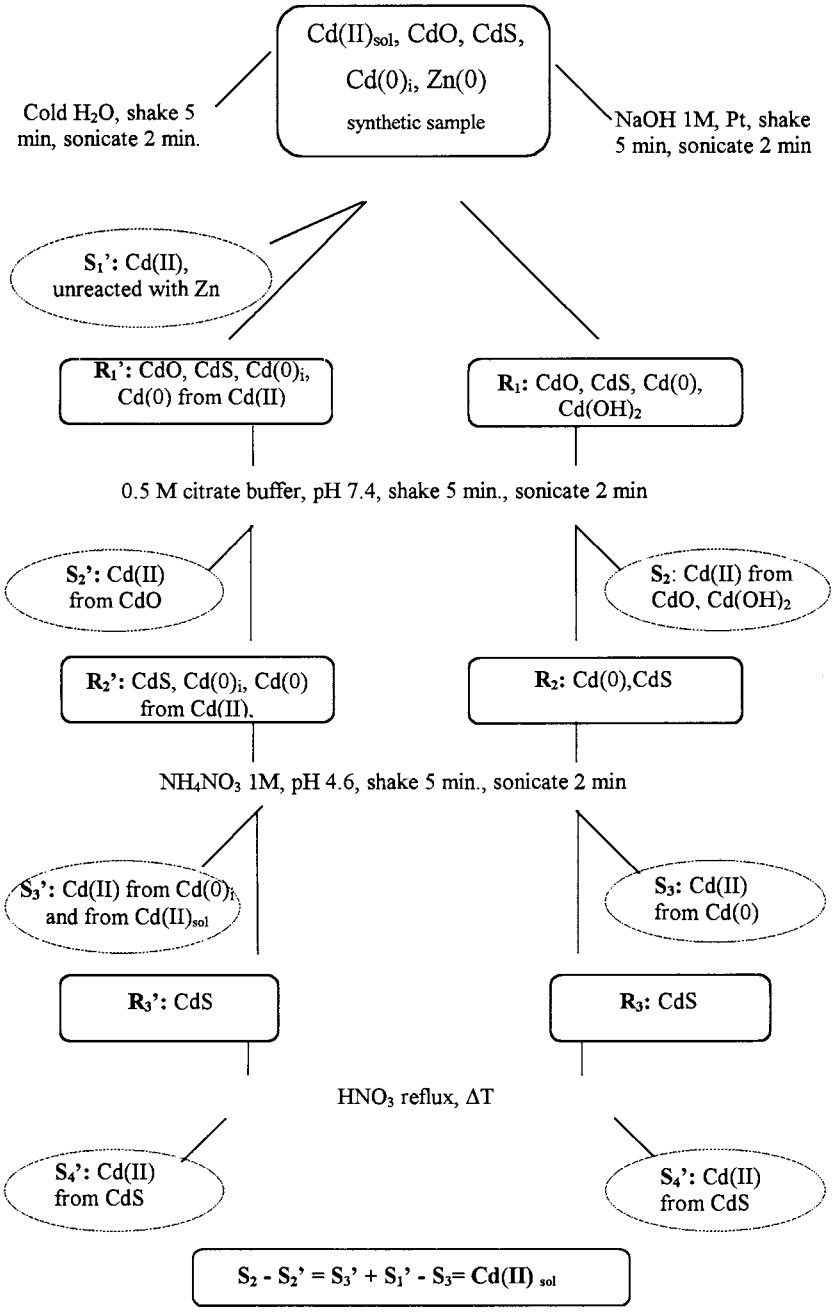

of Table 5, where the first step is the extraction in NaOH 1 M, in presence of Pt as a catalyst, must be done.

In order to verify the procedure of Table 5 the speciation in the synthetic mixture described in the table with Cu(II)/total Cd molar ratio = 10,

was done. The different species of cadmium are calculated as below described:

$Cd(II)_{sol.}$: $(S'_1) + (S'_3) - (S_3) = (S_2) - (S'_2)$: recovery 82%;

CdO from (S'_2): recovery 90%;

Cd(0) from (S_3): recovery 96%;

CdS either from (S'_4) or (S_4): recovery 94%.

3.2. Selective solubilization when Zn(0) is present

Zn(0) can react with $Cd(II)_{sol.}$ to form Cd(0).

In this case the scheme of the speciation is shown in Table 6.

Also for this situation, the speciation in the synthetic mixture described in the table, with Zn(0)/total Cd molar ratio = 10, was done. It is possible to distinguish $Cd(II)_{sol.}$ and Cd(0), through the combination of the results of the two schemes of solubilization of Table 6:

$Cd(II)_{sol.} = (S'_3) + (S'_1) - (S_3) = (S_2) - (S'_2)$: recovery 96%;

CdO from S'_2: recovery 92%;

Cd(0) from (S_3): recovery 89%;

CdS either from (S_4) or (S'_4): recovery 91%.

Also in these cases, if samples contain cadmium-aluminosilicates, they will remain undissolved after the nitric acid treatment: this fraction of cadmium can be determined by treating the residue with HF/H_2SO_4.

4. Conclusions

With the described procedure it is possible to speciate the different chemical species of inorganic Cd that can be air dispersed in emissions and working areas.

The method essentially based on sequential dissolutions of the sampled matrix, is easy to do, not time consuming and it is a preliminary answer to the need for improved analytical techniques for measuring cadmium species, as World Health Organization [14] strongly recommends.

Acknowledgements

The authors thank Roberto Miracca from Dip. Medicina Preventiva, Occupazionale e di Comunità of University of Pavia for his assistance in the experimental work. This work was principally supported by FAR (Fondi Ateneo per la Ricerca) of the Pavia University.

References

[1] K. Robards, P. Woisfold, Analyst 116 (1996) 549.
[2] G. Bressa, Chim. Oggi. 11 (1987) 23.
[3] IPCS Environmental Health Criteria 134. Cadmium. World Health Organization, Geneve, 1992.
[4] Threshold Limit Value for Chemical Substance in the Work Environment Adopted by ACGIH (American Conference of Governmental Industrial Hygienists) with included changes for 1995–1996, p. 12.
[5] G.U. of Repubblica Italiana no. 176, July 30, 1990; Suppl Ord.; D.M., July 12, 1990, no. 51.
[6] M. Vahter, L. Friberg, Fresenius Z. Anal. Chem. 332 (1988) 726.
[7] B. Lina, M. Vahter, B. Rahnter, U. Björs, Anal. Chem 332 (1988) 741.
[8] D.D. Siemer, R. Woodriff, Spectrochimica Acta. 29B (1974) 269.
[9] Method 1048, in: P.M. Eller (Ed.), NIOSH Manual of Analytical Methods, 3rd ed., suppl. 2, US Goverment Printing Office, Washington, 1987.
[10] C.D. Dretz, W. Lund, Anal. Chim. Acta. 262 (1992) 292.
[11] R. Cornelis, S. Dyg, B. Griepink, R. Dams, Fresenius Z. Anal. Chem. 338 (1990) 414.
[12] S. Landsberger, S. Larson, D. Wu, Anal. Chem 65 (1993) 1506.
[13] A. Miyazaki, A. Kimura, K. Bansho, Y. Umezaky, Anal. Chim. Acta 144 (1992) 213.
[14] Air Quality Guidlines for Europe, World Health Organization, Regional Office for Europe, Copenhaghen 1987; European series, vol. 23, pp. 200–209.

ELSEVIER

Talanta 47 (1998) 613–623

Talanta

Determination of ytterbium in animal faeces by tungsten coil electrothermal atomic absorption spectrometry

Éder C. Lima, Francisco J. Krug *, Joaquim A. Nóbrega [1], Ana Rita A. Nogueira [2]

Centro de Energia Nuclear na Agricultura, Universidade de São Paulo, Postal Box 96, 13400-970, Piracicaba SP, Brazil

Received 30 December 1997; received in revised form 23 February 1998; accepted 23 February 1998

Abstract

A method for ytterbium determination in animal faeces by tungsten coil electrothermal atomic absorption spectrometry (TCAAS) was developed. Faeces were dry-ashed in a muffle furnace, the ashes were treated with hydrochloric acid, and 10 μl of sample solution were delivered into 150-W tungsten coil atomizer. A matrix-matching procedure employing a 66-s heating program proved to be efficient for obtaining accurate results. Characteristic mass and detection limit were 7.1 pg and 0.35 μg g^{-1} Yb, respectively. The tungsten coil atomizer lifetime exceeded 300 firings with digested solutions and R.S.D. of measurements was 1.9% after ten consecutive injections of 10.0 μg l^{-1} Yb. Accuracy of the proposed method was assessed by employing a graphite furnace atomic absorption spectrometric procedure. Application of the paired *t*-test did not reveal any significant difference for ytterbium contents determined by both methods at 95% confidence level. It was demonstrated that the proposed procedure can successfully be used for evaluation of kinetic passage rate of feed through digestive tract of animals. © 1998 Elsevier Science B.V. All rights reserved.

Keywords: Ytterbium; Animal faeces; Tungsten coil atomizer; Electrothermal atomic absorption spectrometry

1. Introduction

Ytterbium salts have been recommended as particulate-phase markers in animal nutrition studies, as Yb fulfils the requirements of a good marker [1,2]. Recently a procedure for ytterbium determination in horse and cow faeces and digesta, validated by instrumental neutron activation analysis, was developed employing graphite furnace absorption spectrometry (GFAAS) with transversely heated graphite atomizer (THGA) and Zeeman-effect background correction [3]. It was demonstrated that this is an interference-free procedure for a wide range of concomitants, and the amounts of Yb added to the animal daily diet could be remarkably decreased. However, the overall cost of analysis is relatively expensive owing to the use of graphite tubes and other supplies, to the infrastructure required for the equipment installation, and to the high initial

* Corresponding author. Tel.: +55 19 4294646; fax: +55 19 4294610; e-mail: frajkrug@pira.cena.usp.br

[1] Present address: Departamento de Química, Universidade Federal de São Carlos, São Carlos SP, Brazil.

[2] Present address: Centro de Pesquisa de Pecuaria do Sudeste, Embrapa, São Carlos SP, Brazil.

0039-9140/98/$ - see front matter © 1998 Elsevier Science B.V. All rights reserved.
PII S0039-9140(98)00087-3

investments needed for installation of graphite furnace spectrometer.

Low mass metallic atomizers do not require a high power supply and a cooling system, diminishing the total instrumentation costs. These atomizers appear as an interesting complement to atomic absorption spectrometry, extending the applicability of electrothermal atomic absorption spectrometry (ETAAS) for elements not easily atomized from graphite surfaces, such as rare earth elements [4,5], and refractory species formed with barium [6] and chromium [7]. Additionally, metallic atomizers could be employed as an alternative atomizer for elements frequently determined in graphite surfaces, with comparable detection limits [8–10].

In recent years electrothermal atomizers with metal tubes [11–19] and coils [6–9,20–24] have been investigated owing to their simplicity and low cost, when compared to graphite atomizers.

Among metallic atomizers, tungsten has been the most frequently employed for analytical purposes due to its favorable physical properties, such as high boiling point, low specific heat, low vapor pressure, low thermal expansion and low resistivity [25]. It has been demonstrated that when argon-hydrogen mixtures were employed as purge gas for metallic atomizers, the analyte atomization efficiency was increased [6–9,20–24]. Also, the reducing atmosphere helps to extend the atomizer lifetime.

Although the previously reported method for ytterbium determination in digesta and faeces samples presents robustness and sensitivity [3], it could not be frequently applied in the ordinary veterinary laboratory due to the high costs of equipment acquisition (US$ 70000–100000), installation (at least 5 kW electrical power supply) and maintenance (graphite tubes and contacts). The aim of this work was to develop a new method for ytterbium determination in animals faeces, employing a low cost 150-W tungsten coil atomizer, with a significant decreasing in the amount of ytterbium added to animal daily diet when compared to the conventional flame atomic absorption spectrometry (FAAS) procedure [1,2].

2. Experimental

2.1. Instrumentation

A Varian SpectrAA-40 (Victoria, Australia) atomic absorption spectrometer coupled to a Varian DS-15 data station was used. An ytterbium hollow cathode lamp (part number 56-101286-00) from the same manufacturer was used. The analytical wavelength was set as 398.8 nm with a spectral bandpass of 0.2 nm. Measurements were based on peak height absorbance with a 50-ms time constant. In all experiments, 10 or 20 μl of the solutions were introduced into the atomizer using the GTA-96 autosampler from the same manufacturer.

The tungsten coil (OSRAM 150W, Munich, Germany) atomizer was fixed in two copper electrodes supported by a PTFE fitting, which was inserted into a 10-cm long flow-through cell mounted in a Perspex base. The whole assembly replaced the Varian GTA-96 graphite furnace as described by Silva et al. [6]. The coil was positioned 2 mm below the focal point, i.e. the beam passed tangentially to the bottom side of the coil without any physical obstruction. The tungsten coil was heated by a programmable power supply with a voltage feedback circuit (Anacom Equipments and Systems, São Bernardo do Campo, Brazil). Unless otherwise stated, a mixture con-

Table 1
Heating programs of tungsten coil atomizer

Step	Time (s)	Temperature (°C)
(A) With high pyrolysis temperature		
1	10	110
2	5	210
3	10	300
4	10	450
5	20	1100
6	1	2400
(B) With low pyrolysis temperature		
1	5	130
2	45	165
3	15	180
4	1	2400

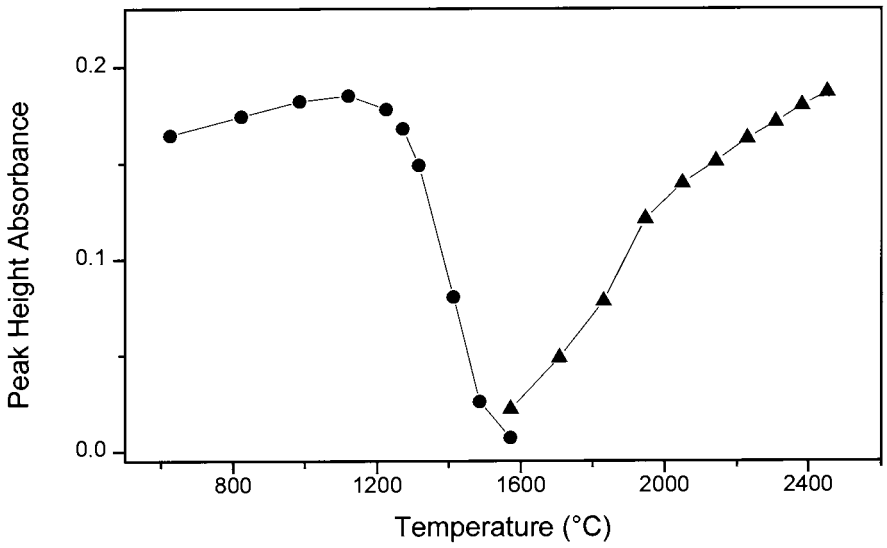

Fig. 1. Electrothermal behavior of 100 pg Yb in 0.12 mol l^{-1} HCl in tungsten coil atomizer. Heating program of Table 1(A). – ● –, pyrolysis temperature curve; – ▲ –, atomization temperature curve.

taining 90% (v/v) argon plus 10% (v/v) hydrogen flowing (AGA-Campinas, Brazil) at 1.1 l min^{-1} was used as purge gas.

A Perkin-Elmer 4100 ZL spectrometer (Überlingen, Germany) furnished with standard THGA (part number B050-4033) tube and ytterbium hollow cathode lamp (part number N305-0390) was used for accuracy assessment [3].

2.2. Procedure

2.2.1. Reagents and reference solutions

All solutions were prepared from analytical grade reagents and distilled-deionized water was used throughout.

A 1000-mg l^{-1} Yb stock solution was prepared from ytterbium oxide (Johnson and Matthey) in 2.0 mol l^{-1} HNO_3. Reference solutions containing from 5.00 to 60.0 μg l^{-1} Yb were prepared by appropriate dilution of the ytterbium stock solution in 0.12 mol l^{-1} HCl.

The effect of concomitants was investigated with solutions containing up to 1000 mg l^{-1} Na (NaCl, Merck), 1000 mg l^{-1} K (KCl, Merck), 1000 mg l^{-1} Ca ($CaCO_3$, Merck), 1000 mg l^{-1} Mg (MgO, Riedel), 100 mg l^{-1} Si ($Na_2SiO_3 \cdot 5H_2O$, Merck), 100 mg l^{-1} P (KH_2PO_4, Merck), 100 mg l^{-1} Fe (Fe_2O_3, Johnson and Matthey), 100 mg l^{-1} Al ($AlCl_3$, Titrisol, Merck), 100 mg l^{-1} Cr (Titrisol, Merck) and 100 mg l^{-1} Co (Titrisol, Merck), with and without 10.0 μg l^{-1} Yb in 0.12 mol l^{-1} HCl.

The following solutions were investigated for suppressing chemical interferences: 0.1 g l^{-1} Pd (Merck), 0.1 g l^{-1} La ($La(NO_3)_3$, Merck), 0.1 g l^{-1} Eu (Johnson and Matthey) and 1 g l^{-1} organic complexants solutions such as Eriochrome Black T (Merck), Eriochrome Blue Black B (Merck), Calcon (Merck, Germany), Murexide (Merck), 1-(2-pyridilazo)-2-naphthol (PAN, Sigma), 4-(2-pyridilazo)-resorcinol (PAR, Sigma), 4-(2-pyridialazo)-chromotropic acid (PAC), 8-hydroxiquinoline (Merck), EDTA disodium salt (Merck), all prepared in 2.0% v/v NH_3 (Merck).

2.2.2. Electrical measurements

A digital multimeter (Techmaster-DM-8700, Sperry Instruments) was employed for coil electric current intensity measurements at different applied voltages. The tungsten coil temperatures were calculated from the measured current through the atomizer within 0.2–15.0 V range. All measurements were carried out with five replicates

Table 2
Effect of concomitants on the atomization of 100 pg of Yb

Percentage of interference on atomization of 100 pg Yb										
μg	Ca	Mg	Na	K	Al	Cr	Co	Si	P	Fe
0.010	—	—	—	—	−36.0	−21.0	−12.0	−3.0	+1.0	6.0
0.025	—	—	—	—	−43.0	−26.0	−16.0	−7.0	+2.0	−10.0
0.050	—	—	—	—	−48.0	−34.0	−20.0	−14.0	0.0	−6.0
0.100	−52.0	−7.0	+3.0	0.0	−51.0	−42.0	−23.0	−22.0	+5.0	−8.0
0.250	−54.0	−12.0	+1.0	−2.0	−57.0	−46.0	−34.0	−38.0	0.0	−5.0
0.500	−60.0	−20.0	+7.0	−8.0	−61.0	−52.0	−44.0	−51.0	−4.0	−12.0
1.000	−68.0	−29.0	+6.0	−7.0	−67.0	−56.0	−48.0	−58.0	−18.0	−16.0
2.500	−69.0	−32.0	+4.0	0.0	—	—	—	—	—	—
5.000	−71.0	−39.0	+8.0	−20.0	—	—	—	—	—	—
10.00	−70.0	−56.0	−3.0	−22.0	—	—	—	—	—	—

Heating program of Table 1(A).

using four different coils (length 92.45 ± 0.03 mm; average mass 0.1102 ± 0.0002 g) to obtain the electric resistivities, which were converted in temperature values [25].

2.2.3. Pyrolysis and atomization temperature curves

The pyrolysis and atomization temperature curves were obtained with solutions containing 10.0 μg l^{-1} Yb in 0.12 mol l^{-1} HCl by using the heating program showed in Table 1(A). The pyrolysis curve was obtained within temperatures from 600 to 1500°C during 20.0 s, and the atomization step was kept constant at 2400°C for 1.0 s. The atomization curve was obtained by fixing the pyrolysis temperature at 1100°C and varying the atomization temperature from 1500 to 2500°C during 1 s.

2.2.4. Samples

The preparation of ytterbium-marked corn was adapted from reference [26]: 260 g of minced corn passed through 5 mm sieve were soaked for 24 h in ytterbium solution, prepared by dissolving 2.5 g of $YbCl_3 \cdot 6H_2O$ in 1 l of water. An acetate buffer solution (pH 5.5) was twice added to the reservoir containing the soaked corn in order to correct the water volume lost by evaporation. Afterwards, the suspension was filtered by suction and dried at 50°C for 48 h. The Yb-marked corn content was measured by GFAAS, resulting in about 2.0 mg g^{-1} Yb in corn.

Before performing the marking experiments, six animals Santa Ines sheeps (Ovis aries) were confined and fed with non-marked corn during 2 weeks, for feed conditioning where the non-marked samples were collected. Subsequently, the animals were fed with 3 g of Yb-marked corn (ca. 6.0 mg Yb per animal), and the faeces samples were collected at 6 h intervals over 5 days.

The samples were dry ashed in a muffle furnace, the ashes were treated with hydrochloric acid according to the procedure described elsewhere [3], and ytterbium in the resulting solutions was determined by tungsten coil electrothermal atomic absorption spectrometry (TCAAS) and GFAAS.

3. Results and discussion

3.1. General considerations

The ytterbium analytical signal did not change significantly when the flow rate of the 90% Ar + 10% H_2 purge gas mixture was varied from 0.6 to 1.4 l min^{-1}. It was observed that at flow rates below 0.9 l min^{-1} the tungsten coil lifetime was limited to 250 firings. As a compromise between purge gas consumption and atomizer lifetime, 1.1 l min^{-1} was used throughout.

The presence of hydrogen in purge gas composition was decisive for ytterbium atomization, in addition to its role in preventing oxidation of the

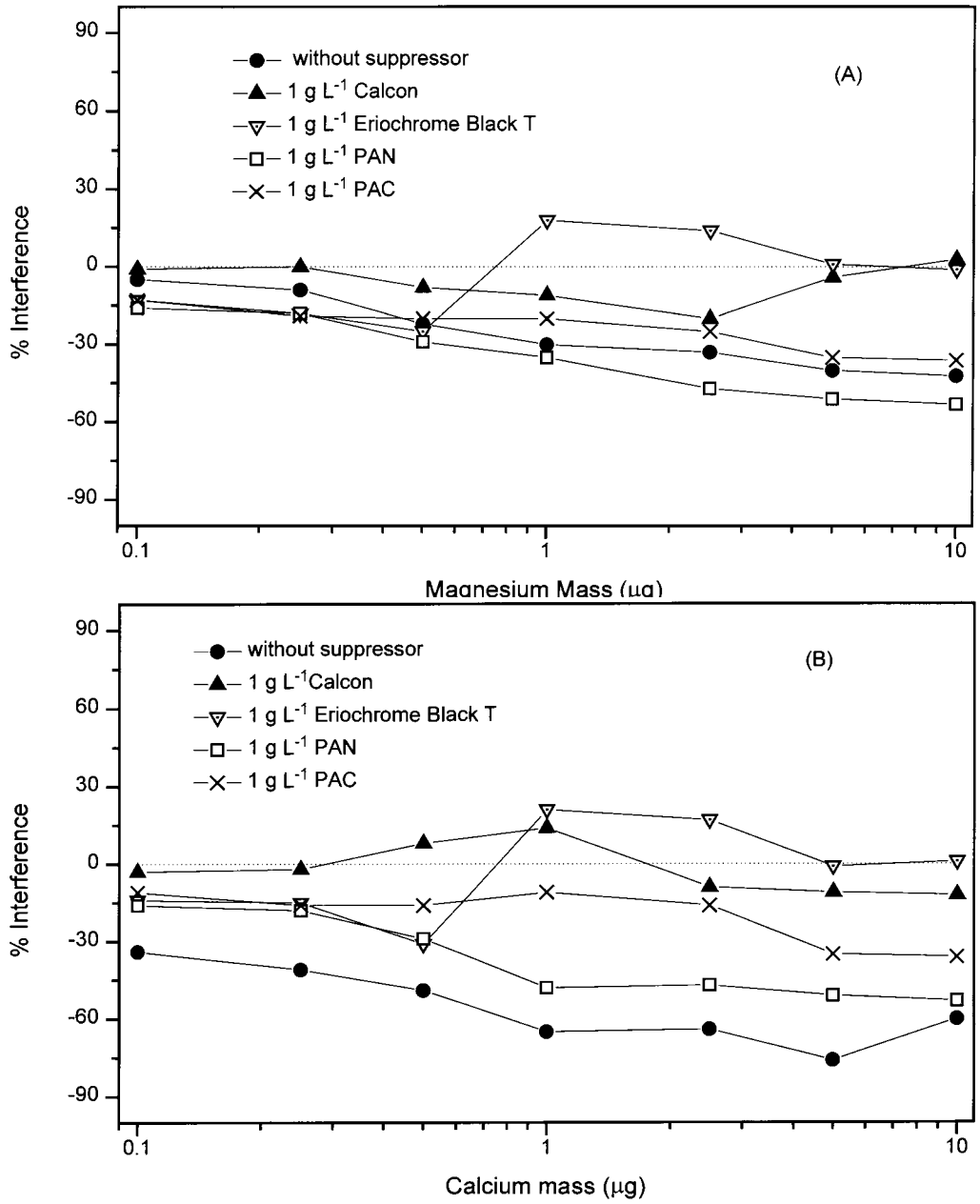

Fig. 2. (A) magnesium, (B) calcium and (C) aluminium interference curves on atomization of 100 pg Yb. Heating program of Table 1(B).

tungsten coil. The role of hydrogen in the atomization mechanisms of many other elements from tungsten surfaces has also been noted [6,9]. When the 90% Ar + 10% H_2 mixture was replaced by pure argon in all steps of the heating program (Table 1(A)), the peak height absorbance for 100 pg Yb decreased by 75%. Using the mixture only during the atomization step, the analytical signal decreased by 6%, indicating that hydrogen plays a decisive role on ytterbium atomization. Probably

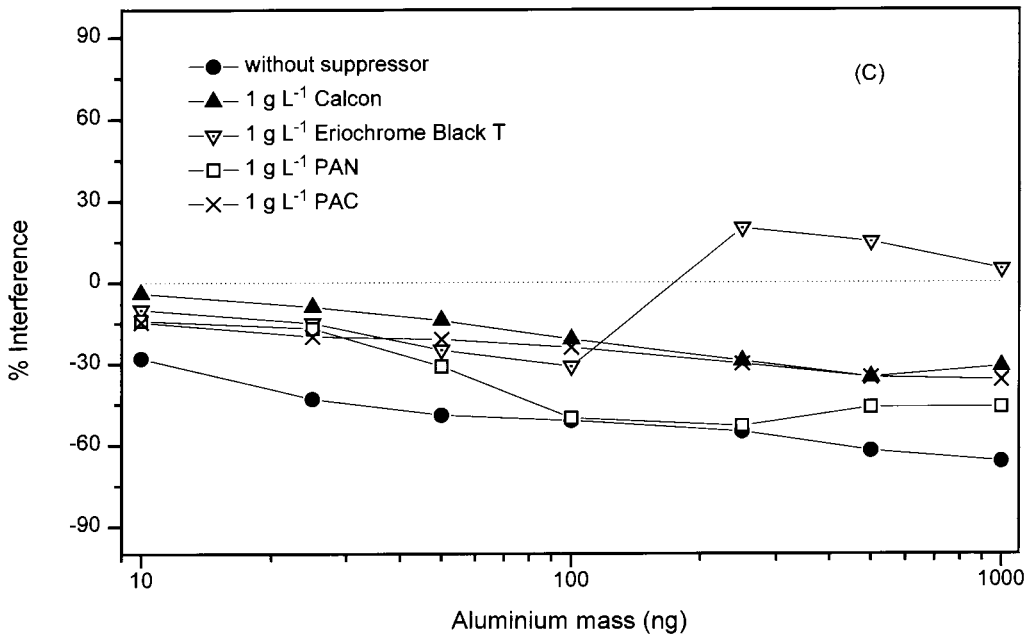

Fig. 2. (*Continued*)

hydrogen is mainly consumed by homogeneous reduction of ytterbium oxide in the gas phase according to Eq. (1):

$$Yb_mO_{n(s,l)} \rightleftharpoons Yb_mO_{n(g)} + nH_{2(g)} \rightleftharpoons mYb_{(g)} + nH_2O_{(g)} \quad (1)$$

The observation height could be essential for obtaining sensitive analytical signals for some elements, because there is a vertical temperature gradient above and below the atomizer center [21]; in this work it was observed that a 1-mm variation around the best position did not cause changes of more than 3% in the ytterbium analytical signals. Better sensitivity was obtained when geometric center of the tungsten coil was positioned between 1.0 and 2.0 mm below the radiation beam focal point. To get this, the coil height was initially positioned to intercept the center of the observation volume, and then the coil was moved downwards so that the most intense zone of the radiation beam was not obstructed by the coil.

The effect of concentration, within 0.1–5.0% v/v range, of HNO_3, HCl and H_2SO_4, on the atomization of 100 pg Yb was not critical and always lower than 8% for each mineral acid. Analytical signals obtained in HCl and H_2SO_4 medium were in average 10 and 20% lower, respectively, than the analytical signal obtained in HNO_3. However, to the purpose of this work, ytterbium reference solutions prepared in HCl were employed throughout, because better dissolution of the ashes was obtained in the dry-ashing procedure when this acid was employed, as previously reported [3].

3.2. Electrothermal behavior of ytterbium in tungsten coil atomizer

The pyrolysis and atomization temperature curves for 100 pg of ytterbium in 0.12 M HCl, obtained with the heating program of Table 1(A), are shown in Fig. 1. Ytterbium presented good thermal stability, maximum pyrolysis temperature not exceeding 1100°C being recommended. Although high, this temperature is not higher than those observed for calcium, aluminum and chromium [27] which are potential concomitants found in the samples. Although a plateau was not observed in the atomization temperature curve, it

Table 3
Recoveries of ytterbium in faeces

% Recovery			
Yb added (μg)	TCAAS (without Calcon)	TCAAS (with Calcon)	GFAAS
2.0	47.9 (0.7)	70.5 (1.2)	98.3 (0.7)
4.0	49.3 (0.7)	72.3 (1.5)	100.4 (0.8)
6.0	48.2 (0.8)	71.4 (1.3)	99.7 (0.6)

Heating program of Table 1(B). Standard deviation ($n = 3$) are given in parenthesis.

was decided to work at 2400°C where the highest signal to noise ratio was obtained. It should be pointed out that, at more elevated atomization temperatures, which means at greater heating rates of the tungsten coil atomizer, ytterbium peaks became sharper and higher, although the peak areas did not have any significant differences at temperatures higher than 2000°C. This means that the atomization efficiency is probably constant beyond this temperature. As previously mentioned, detection limit and sensitivity are much better when measurements are based on peak height absorbance when using tungsten coil atomizers [6,9,21].

3.3. Interferences

Effects on ytterbium atomization caused by ten elements, which could be present in the faeces samples, are shown in Table 2. It can be seen that the most severe interferences on ytterbium atomization were caused by aluminium and calcium, followed by chromium, cobalt and magnesium in this sequence. Changes in pyrolysis time, pyrolysis temperature, and atomization temperature were not effective to overcome these interferences. Probably the interference processes occur in the condensed phase, with formation of stable compounds such as mixed oxides between the analyte and the concomitant element [28]. Another possibility could be an analyte occlusion in the oxide/salt matrices [28]. The atomization efficiency would be affected by the non-dissociation of the refractory compounds and/or to difficulties for releasing the analyte from the matrix. A sound explanation of these effects is beyond the scope of this work, but it seems that the formation of refractory mixed oxides were the main cause for those interfering effects.

Attempts were carried out to correct these interferences with 0.1 g l^{-1} La, 0.1 g l^{-1} Eu, 0.1 g l^{-1} Pd, in 0.12 mol l^{-1} HCl. All these elements were considered unsuitable because they promoted a decrease of 35–70% on ytterbium signal without increasing the analyte thermal stability. In order to evaluate organic compounds that could form complexes with interferents and that could prevent the formation of metal oxides, a new heating program was implemented (Table 1(B)) with the temperature of the drying step not exceeding 200°C to avoid the thermal decomposition of the organic reagents. The pyrolysis step had no noticeable effect on concomitants volatilization and it was removed from the new heating program, but the elimination of this step promoted a decrease on interference levels up to 34% for all the interfering species. It is known that the formation of refractory mixed oxides of calcium, magnesium and aluminium occurs in the absence of carbon, at temperatures higher than 1000°C [29]. By analogy, keeping the temperature of condensed phase processes lower than 200°C, the formation of these refractory mixed oxide compounds would be minimized, which could explain the lowering of the interference level.

Interference curves of magnesium, calcium and aluminium on the atomization of 100 pg Yb, obtained in the presence of 1 g l^{-1} of several organic suppressors (Fig. 2(A–C)), indicate that Calcon presented the best suppression effect. It can be seen that the interferences were not noticeable up to 0.5 μg of Ca and Mg, and up to 25 ng Al. Based on these results, it would be advisable to keep the sample mass/sample volume ratio

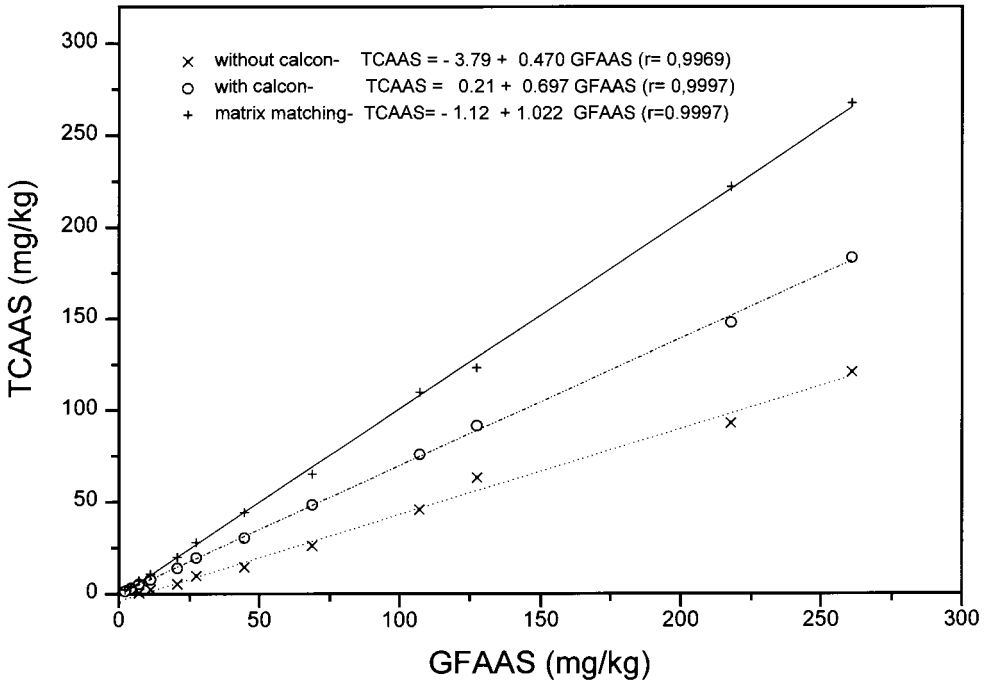

Fig. 3. Comparison of different procedures for analysis of animal faeces by TCAAS and GFAAS with THGA [3].

around 1/1000, lowering the concentration of these three elements and avoiding significant effects on ytterbium atomization. Ytterbium analytical signals obtained in the presence of concomitants with addition of Calcon revealed better recoveries than those obtained in the same chemical environment without the suppressor. The organic complexant would prevent the formation of ytterbium-concomitant oxides, by reacting with the interfering metals during the mild dry step of the modified heating program presented in Table 1(B). The greater the resistance to elevated temperature of the concomitant-suppressor or analyte-suppressor complexes the more selective the ytterbium atomization. Other complexants such as EDTA, 8-hidroxyquinoline and Murexide were also evaluated but they did not suppress the interferences. In addition, they caused high background signals (about 0.080 of absorbance) in the atomization of 100 pg Yb (0.140 of atomic signal).

3.4. Recovery tests

Recovery experiments (Table 3) were performed by adding 2.00, 4.00 and 6.00 mg Yb to non-marked dry-ashed sheep faeces obtained from 200 mg samples. Ashes were dissolved with 4 ml of 1 + 1 HCl and the volume made up to 200 ml. Ytterbium concentration was determined by TCAAS (with and without Calcon) and by GFAAS as previously reported [3].

The recovery test showed that use of the organic suppressor was not effective for completely correcting matrix effects, as obtained for isolated concomitants. The recoveries were on average 29 and 52% lower compared to GFAAS method, in the presence and absence of Calcon, respectively. However, a linear relationship between the absorbance and analyte concentration was obtained, indicating that there was a typical source of systematic interferences.

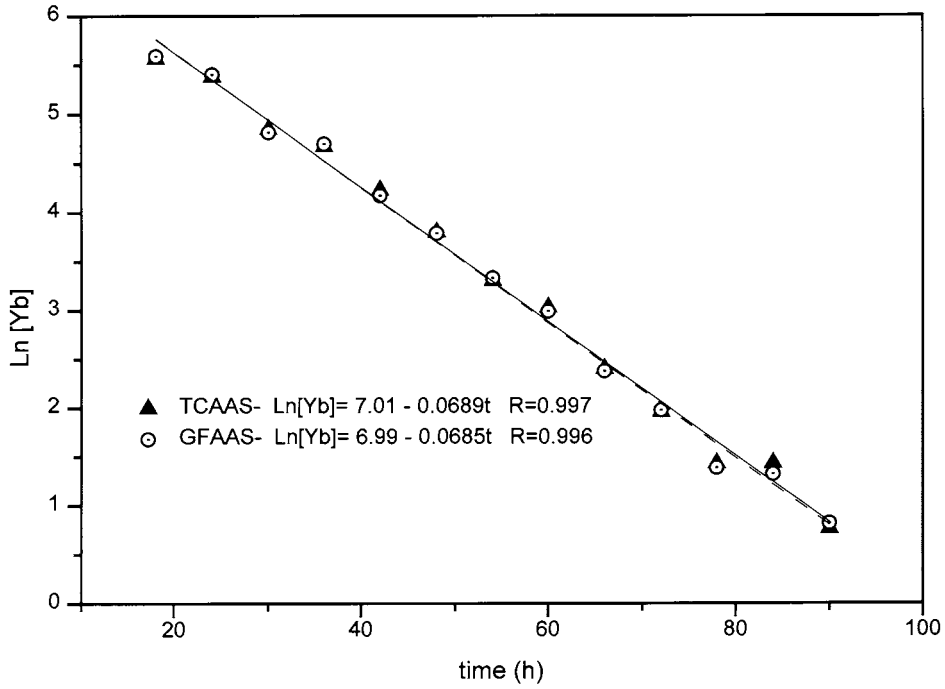

Fig. 4. Variation of ytterbium contents in faeces with time after feeding a single sheep with marked corn. Heating program of Table 1(B).

3.5. Figures of merit

The analytical curve within 5.0–60.0 μg l^{-1} Yb range was obtained by adding known amounts of ytterbium to a non-marked dry-ashed solutions (sample mass/sample volume ratio 1/1000) and using the heating program of Table 1(B). Characteristic mass based on peak height absorbance values was 7.1 ± 0.2 pg Yb (uncertainty based on ten average results obtained in different days) by using the tungsten coil atomizer with the matrix matching solutions. The coil lifetime exceeded 300 firings with 10 μl of digested solutions. The detection limit calculated according to IUPAC [30], based on 20 consecutive measurements of the blank solution (0.12 mol l^{-1} HCl), was 0.35 μg l^{-1} Yb which corresponded to 0.35 μg g^{-1} Yb in the sample. The relative standard deviation of measurements ($n = 10$) for typical samples containing 4.0–30.0 μg l^{-1} Yb was always lower than 5.0%.

3.6. Accuracy evaluation for ytterbium determination in animal faeces

Three TCAAS procedures were tested for analyzing faeces samples. When sample solutions were analyzed directly against analytical calibration curves made with ytterbium reference solutions in HCl medium, the results were systematically 53% lower than those obtained by GFAAS (Fig. 3) [3]. Even in the presence of Calcon, the results were systematically 30% lower than GFAAS (Fig. 3) confirming the results from the recovery tests. Based on these observations, a matrix method procedure was also tested, a close agreement with GFAAS results was obtained. The paired t-test showed that there is no significant differences at 95% confidence level between matrix matching-TCAAS and GFAAS. Matrix-matching procedure is very simple and has also been successfully applied to lead determination in blood samples by using TCAAS [9]. This proce-

dure can be easily implemented, because the animals were fed with the same daily diet starting 2 weeks before the marking experiment and consequently the concentration of inorganic constituents in the faeces samples is nearly constant.

The proposed method was also applied to evaluate the passage rate kinetic of corn on sheep gastrointestinal tract which was calculated from the slope of curve natural logarithm of the marker concentration against the time of sample collection (Fig. 4). The passage rate constants obtained from six animals were not statistically different from those obtained with GFAAS. The TCAAS procedure allowed a ten-fold diminution in the amount of marker added to the daily diet of the animals, when compared with the conventional flame atomic absorption spectrometry (FAAS) method [1]. Since 1 kg of ytterbium salts costs about US$3500.00, and field experiments carried out with cows could use up to 5–6 kg of ytterbium salts when the conventional FAAS procedure [1,2] is employed, the use of TCAAS could allow savings of about US$20000 for 1-year typical experiment. Taking into account the potentialities for producing a portable atomic absorption spectrometer with the same tungsten coil atomizer [31], a low cost equipment (US$15000) would also provide better costs per determination: from US$0.80 with GFAAS with THGA [3] to US$0.25 of the proposed method, performing 250 determinations per day [32].

Acknowledgements

We thank Gilberto B. Souza (EMBRAPA-CPPSE-São Carlos) for collecting and grinding the samples of faeces; Daniela C. Salvadori for sample preparation, Celso R. Almeida for his helpful assistance in electric measurements and Elias A.G. Zagatto for critical comments. We also thank Fundação de Amparo à Pesquisa do Estado de São Paulo (FAPESP Processo 1995/5782-7) and Financiadora de Estudos e Projetos (PRONEX) for financial support. We are grateful to Conselho Nacional de Desenvolvimento Científico e Tecnológico for fellowships of É.C. Lima, F.J. Krug, J.A. Nóbrega and A.R.A. Nogueira.

References

[1] L.D. Satter, D.K. Combs, J.M. Lopez-Guisa, W.F. Nelson, Nuclear and Related Techniques in Animal Production and Health, ed. IAEA, Proceedings of a Symposium, Viena, 1986, p. 469.
[2] R.C. Siddons, J. Paradine, D.E. Beever, P.R. Cornell, Br. J. Nutr. 54 (1985) 509.
[3] E.C. Lima, F.J. Krug, J.A. Nóbrega, E.A.N. Fernandes, J. Anal. At. Spectrom. 12 (1997) 475.
[4] B.V. L'vov, J. Anal. At. Spectrom. 3 (1988) 9.
[5] E. Krakovska, J. Anal. At. Spectrom. 5 (1990) 205.
[6] M.M. Silva, R.B. Silva, F.J. Krug, J.A. Nóbrega, H. Berndt, J. Anal. At. Spectrom. 9 (1994) 861.
[7] M. Knochem, E. Saritsky, I. Dol, Quim. Anal. 15 (1996) 184.
[8] M.F. Giné, F.J. Krug, V.A. Sass, B.F. Reis, J.A. Nóbrega, H. Berndt, J. Anal. At. Spectrom. 8 (1993) 243.
[9] F.J. Krug, M.M. Silva, P.V. Oliveira, J.A. Nóbrega, Spectrochim. Acta Part B 50 (1995) 1469.
[10] T. Cernohorsky, S. Kotrly, J. Anal. At. Spectrom. 10 (1995) 155.
[11] V. Sychra, D. Kolihova, O. VysKocilova, R. Hlavac, P. Püschel, Anal. Chim. Acta 105 (1979) 263.
[12] O. Vyskocilova, V. Sychra, D. Kolihova, P. Püschel, 105 (1979) 271.
[13] P. Püschel, Z. Formanek, R. Hlavac, D. Kolihova, V. Sychra, 127 (1981) 109.
[14] V. Sychra, J. Dolezal, R. Havlac, L. Petros, O. Vyskocilova, D. Kolihova, P. Püschel, 6 (1991) 521.
[15] S. Xiao-quan, B. Radziuk, B. Welz, V. Sychra, 7 (1992) 389.
[16] M. Suzuki, K. Ohta, Spectrochim. Acta Part B 39 (1984) 473.
[17] K. Ohta, W. Aoki, T.J. Mizuno, J. Anal. At. Spectrom. 3 (1988) 1027.
[18] K. Ohta, S.Y. Su, Anal. Chem. 59 (1987) 539.
[19] K. Ohta, T. Mizuno, Spectrochim. Acta Part B 44 (1989) 95.
[20] H. Berndt, G. Schaldach, J. Anal. At. Spectrom. 3 (1988) 709.
[21] C.G. Bruhn, F.E. Ambiado, H.J. Cid, R. Woerner, J. Tapia, R. Garcia, Anal. Chim. Acta 306 (1995) 183.
[22] P.J. Parsons, H. Qiao, K.M. Aldous, E. Mills, V. Slavin, Spectrochim. Acta Part B 50 (1995) 1475.
[23] C.G. Bruhn, F.E. Ambiado, H.J. Cid, R. Worner, J. Tapia, R. Garcia, Quim. Anal. 15 (1996) 191.
[24] M.M. Silva, F.J. Krug, P.V. Oliveira, J.A. Nóbrega, B.F. Reis, D. Penteado, Spectrochim. Acta Part B 51 (1996) 1925.
[25] R.C. Weast (Ed.), Handbook of Chemistry and Physics, 66th ed., CRC Press, Boca Raton, 1985.
[26] M.H. Poore, Rumen Passage Rates and Fiber Digestibilities for Wheat Straw, Alfafa Hay, and Flaked Sorghum Grain in Mixed Diets for Steers. PhD Thesis, University of Arizona, Tucson, 1987.
[27] F.J. Krug, manuscript in preparation.

[28] J. Carroll, N. Miller-ihli, J.M. Harnly, T.C. O'Haver, D. Littlejohn, J. Anal. At. Spectrom. 7 (1992) 533.
[29] N.N. Greenwood, A. Earnshaw, Chemistry of the Elements, Pergamon Press, Oxford, 1984, p. 1542.
[30] Commission on Spectrochemical and other optical procedures for analysis, Nomenclature, symbols, units and their usage in spectrochemical analysis—II, Spectrochim. Acta Part B 33 (1978) 241.
[31] C.L. Sanford, S.E. Thomas, B.T. Jones, Appl. Spectrosc. 50 (1996) 174.
[32] D.L. Massart, B.G.M. Vandeginste, S.N. Deming, Y. Michotte, L. Kaufman, Data Handling in Science and Technology—Chemometrics: A Textbook, vol. 2, Elsevier, Amsterdam, 1988, pp. 137–147.

ELSEVIER

Talanta 47 (1998) 625–630

Talanta

A comparative study using HPLC and packed column supercritical fluid chromatography for the assay of three anti-psychotic dosage forms

Yagnesh P. Patela, U.J. Dhorda [a], M. Sundaresan [b,*]

[a] *Ismail Yusuf College of Arts, Science and Commerce, Jogeshwari (East), Mumbai 400 060, India*
[b] *C.B. Patel Research Centre for Chemistry and Biological Sciences, 2nd Floor, Mithibai College Building, Vile Parle (West), Mumbai 400 056, India*

Received 3 November 1997; received in revised form 17 February 1998; accepted 25 February 1998

Abstract

A reproducible and selective method was developed for the analysis of three anti-pschycotics, i.e. haloperidol, trifluoperazine and trihexyphenidyl in bulk and dosage forms using packed column supercritical fluid chromatography (SFC). The analytes were resolved by elution with supercritical fluid carbon dioxide doped with 16.67% (v/v) methanol containing 0.8% isopropylamine. Parallel studies were performed by HPLC using ion pairing reagent and a comparison is discussed. The method was successfully used for the assay of three formulations containing a combination of: (1) haloperidol-trihexyphenidyl; (2) haloperidol-trifluoperazine; (3) trifluoperazine-trihexyphenidyl.
© 1998 Elsevier Science B.V. All rights reserved.

1. Introduction

Packed column supercritical fluid chromatography (PCSFC) using fluidic CO_2 has recently found applications in pharmaceutical analysis with analytical figures of merit equivalent to those obtained in RP HPLC. A spate of such applications has appeared during the last half decade. Berger has successfully used packed column SFC for the separation of 15 antipscyhotics [1], 11 stimulants [2], and five antidepressants [3]. Using this technique Bhoir et al. [4] separated and quantified a group of seven vasodilators. Other examples [5,6] can also be cited. Bari et al. [7], used this technique to assay chlorzoxazone, ibuprofen and acetaminophen in pharmaceutical dosage forms. Patel [8] used the technique of supercritical extraction and chromatography to determine the prostaglandin, misoprostol, in tablets. In SFC the problem of preparation of mobile phases is obviated and elution behaviour of the analyte can be changed by the three degrees of freedom it possesses, i.e. pressure, temperature and modifier concentration. The advantages of SFC over HPLC can be expressed in its speed, cost and eco-friendliness. The last mentioned factor can be reasoned out in the smaller amounts of organic

* Corresponding author. Tel: +91 226 119792; fax: +91 226 133400.

0039-9140/98/$ - see front matter © 1998 Elsevier Science B.V. All rights reserved.
PII S0039-9140(98)00110-6

solvent used, and the non-toxicity of CO_2 and hence in waste disposal. In order to illustrate the viability of PCSFC over HPLC for the assay of bulk drugs and dosage forms, the present work attempts at a comparison of HPLC and PCSFC methods, both developed in this laboratory, of three anti-psychotics, i.e. trifluoperazine, haloperidol and trihexyphenidyl in bulk and dosage forms. The method was utilized for the assay of three formulations containing a combination of: (1) haloperidol-trihexyphenidyl; (2) haloperidol-trifluoperazine; and (3) trifluoperazine-trihexyphenidyl.

Trifluoperazine and haloperidol are butyrophenones used in schizophrenia, mania and other pschycoses and for the control of severely disturbed or agitated behaviour [9]. Trihexyphenidyl is an anti muscarnic agent used in the treatment of parkinsonism and drug induced extra pyramidal reactions [9].

2. Experimental

Carbon dioxide, SFC grade, was obtained from Bombay Carbon Dioxide, Mumbai. Methanol used was from E. Merck, HPLC grade. Haloperidol, trifluoperazine and trihexyphenidyl were provided by M/s. Sigma Laboratories, Mumbai with certificate of analysis. Tetra butyl ammonium hydrogen sulphate was obtained from S.D. Fine Chem. Stock solutions containing 100 mg ml^{-1} of the drugs were prepared by diluting in a ten-fold stage initial solutions of 1 mg ml^{-1}.

A JASCO-900 series supercritical fluid chromatograph configured with two pumps was used for the chromatography. The instrument incorporates an on-line organic modifier addition facility to the supercritical fluid mobile phase. The facilities of varying pressures and temperatures and on-line addition of modifier have made SFC more reproducible, accurate and precise. The on-line modifier addition facility can be used in chromatography. The temperature of the column could be kept constant using a JASCO-CO-965 oven. A Rheodyne injector, model-7125 with a 20 ml external loop was used to introduce the sample into the column. A UV-vis spectrophotometric detector equipped with 16 ml high pressure flow cell of 5 mm path length was used for detection. The HPLC chromatograph used was from JASCO-900 series. Data integrations were performed using Borwin chromatographic software for both HPLC and SFC.

2.1. Supercritical fluid chromatography of three anti-pschycotics

Since the elution the three anti-pschycotics did not occur, with pure supercritical fluid CO_2 (7.18–44.88 MPa and 35–70°C), a modifier had to be used. All the three drugs are free bases and hence methanol alone did not suffice as modifier. In order to match the basicity of the three drugs, several bases, i.e. trimethylamine, triethylamine, isopropylamine etc. were added at different concentrations to methanol and relative elution of the

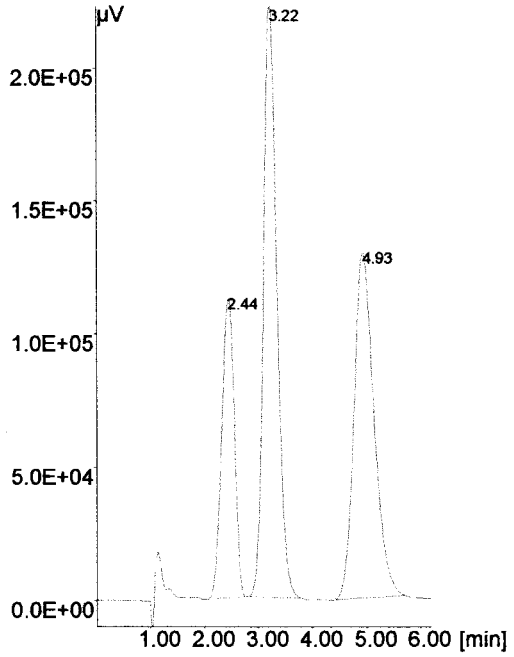

Fig. 1. Typical SFC separation of drugs eluted from a JASCO-ODS (250 × 4.6 mm) 5 µm column under steady conditions. The conditions were as follows: 16.67% modifier in CO_2, at a flow rate of 3.0 ml min^{-1}, at a temperature of 60°C and 29.4 MPa outlet pressure. Numbered solutes are indicated in the arbitrary mix and the number indicates retention order (min). (1) Haloperidol ~ 2.44. (2) Trifluoperazine ~ 3.22. (3) Trihexyphenidyl ~ 4.93.

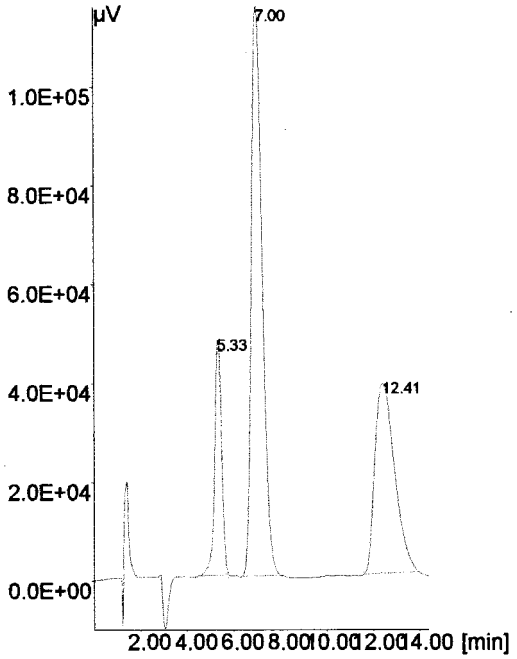

Fig. 2. Typical HPLC separation of drugs eluted from a JASCO-ODS (250 × 4.6 mm) 5 μm column under steady conditions. The mobile phase used was tetrabutyl ammonium sulphate (0.01 M) and the methanol in 1:1 ratio adjusted to pH 3.5 with triethylamine with a flow rate of 1.5 ml min^{-1}. Numbered solutes are indicated in the arbitrary mix and the number indicates retention order (min). (1) Haloperidol ~ 5.33. (2) Trifluoperazine ~ 7.00. (3) Trihexyphenidyl ~ 12.41.

three drugs. The most suitable secondary modifier was found to be isopropylamine. The column used for the assay was JASCO-ODS column (250 × 4.6 mm) 5 μm and detection was through absorptometry at 218 nm for HPLC and 210 nm for SFC. A mixture of the three drugs was prepared at 50 mg ml^{-1} and the injection volume was 20 ml. In all cases responses were measured as peak heights. For method development in SFC, chromatographic figures of merit like resolution (R), capacity factor (k'), selectivity (a), asymmetry factor (T) and the number of plates (N), (calculated as per USP [10]) as well as retention time (t_R min) of all the three compounds were determined at a minimum of five points in the range specified of the following parameters: (1) modifier concentration with respect to methanol (9.09–18.92% (v/v)) and 0.1–1.0% of isopropylamine in the above methanol concentration ranges, (2) temperature (35–70°C), (3) pressure (7.84–34.3 MPa) and (4) flow rate of SFC CO_2 with modifier concentration constant (1.5–3.5 ml min^{-1}). An assessment of the collected chromatographic data revealed that retention is only modestly affected by temperature for haloperidol and trihexyphenidyl. For trifluoperazine, however, a steep decrease in retention times was found. The asymmetry of the peaks increased above and below 60°C. The same effects were witnessed in changing pressures, too, with trifluoperazine showing a significant change in retention times with pressure. An examination of the effect of pressure showed that 29.4 MPa will be the optimum pressure, as below and above this value, symmetry and resolution are lost and as also efficiency. Modifier concentrations were found to have a profound effect on the chromatographic figures of merit. Variations of the concentration of isopropylamine in methanol from 0.1 to 1.0% (v/v) produced a series of chromatograms which revealed that 0.8% of isopropyalamine in methanol was the optimum concentration to obtain best resolution and symmetry. This modifier was then used for further studies. Further studies revealed that a modifier concentration of 16.67% (v/v) gave optimum chromatographic figures. The

Table 1
Comparative chromatographic figures of merit between HPLC and PCSFC

	SFC	HPLC
R_1 Resolution[a]	1.70	2.28
R_2	3.30	4.17
α_1 Selectivity coefficient[a]	1.56	0.87
α_2	1.87	1.96
k_1 Capacity factor[a]	1.17	5.00
k_2	1.83	4.33
k_3	3.42	8.50
T_1 Asymmetry[a]	0.95	1.20
T_2	1.00	1.14
T_3	1.12	1.20
N_1 No. of plates[a]	4160	3418
N_2	7111	3518
N_3	9720	4124

[a] Calculated as per USP [10].

Table 2
Linear regression (least squares fit) calibration data for SFC and HPLC

	Trifluoperazine	Trihexyphenidyl	Haloperidol
SFC			
Concentration range (μg ml^{-1})	12.50–0.05	10.00–0.04	3.00–0.01
Slope (*m*)	4076.32	4009.80	15217.39
Intercept (*b*)	−42.41	−5.20	−114.54
S.D. of slope (*Sm*)	8.15	3.50	128.85
S.D. of intercept (*Sb*)	39.21	13.47	148.78
Correlation coefficient (*r*)	1.00	1.00	1.00
S.E. (*Syx*)	96.11	3.34	364.64
LOQ (μg ml^{-1})	0.05	0.04	0.01
LOD (μg ml^{-1})	0.02	0.02	0.005
HPLC			
Concentration range (μg ml^{-1})	12.50–0.05	10.00–0.04	3.00–0.01
Slope (*m*)	4189.42	4029.17	15452.10
Intercept (*b*)	−36.02	−18.54	−107.24
S.D. of slope (*Sm*)	62.00	18.25	129.96
S.D. of intercept (*Sb*)	298.32	70.25	150.00
Correlation coefficient (*r*)	1.00	1.00	1.00
SE. (*Syx*)	701.23	172.50	367.57
LOQ (μg ml^{-1})	0.05	0.04	0.01
LOD (μg ml^{-1})	0.02	0.02	0.005

changes in the flow rate of CO_2 showed that the highest selectivity and resolution was at 3.0 ml min^{-1}. The selection of the optimum parameters on the basis of speed, efficiency and the most base line resolved chromatography led to the choice of a pressure of 29.4 MPa, temperature of 60°C, a modifier concentration of 16.67% (v/v) and a flow rate of 3.0 ml min^{-1}. A typical chromatogram of a mix of the three drugs containing each of the drugs at 50 mg ml^{-1} is shown in Fig. 1.

Simultaneously an HPLC method based on ion-pair chromatography was developed in the laboratory using the same column (JASCO-ODS (250 × 4.6 mm) 5 μm) for the isocratic, simultaneous assay of the three drugs. The mobile phase was tetrabutyl ammonium sulphate (0.01 M) and methanol in 1:1 ratio adjusted to pH 3.5 with triethylamine with a flow rate of 1.5 ml min^{-1}. The eluents were monitored at 218 nm. A typical chromatogram showing the separation of the three drugs in a mixture at 50 mg ml^{-1} concentration is shown in Fig. 2. The comparative chromatographic figures of merit for HPLC and SFC are given in Table 1.

For linearity studies eight different concentrations in the range 0.05–12.50 mg ml^{-1} of trifluoperazine, 0.04–10.00 mg ml^{-1} of trihexyphenidyl and 0.01–3.00 mg ml^{-1} of haloperidol were assayed. Peak responses were measured as peak heights. It was found that at the above ranges, the drugs exhibited linearity between concentration and peak heights. The data were analysed by the linear regression (least squares fit) method and the analytical figures of merit together with the statistical quantities are given in Table 2 for SFC and HPLC.

For studying performance data mixtures of the three drugs were assayed during the day and between days for a period of 7 days. For this the drug concentrations for the first two drugs, i.e. haloperidol and trifluoperazine were held at 3.00 and 4.00 mg ml^{-1}, respectively, while the concentration of trihexyphenidyl was low at 0.30 mg ml^{-1}. In the second experiment the first two were held at a low concentrations of 0.50 mg ml^{-1}, the concentration of trihexyphenidyl was 2.40 mg ml^{-1}. From the data given in Table 3 it is clear that SFC is highly reproducible, presenting excel-

Table 3
Performance data for the determination of three anti-psychotics by SFC

Drug	Concentration (μg ml^{-1})	CV within day	CV between day
Haloperidol	3.00	0.71	0.88
	0.50	1.88	2.68
Trifluoperazine	4.00	0.40	0.08
	0.50	2.80	2.90
Trihexyphenidyl	2.40	0.30	0.62
	0.30	3.04	1.28

lent column stability. The CV% were well within 3% for both inter-day and intra-day data.

2.2. Analysis in dosage forms by HPLC and SFC

Combination drug dosage forms containing: (1) haloperidol and trihexyphenidyl; (2) haloperidol and trifluoperazine; and (3) trifluoperazine and trihexyphenidyl were assayed using the packed column SFC method. The method of sampling of the combination drug forms were as per the US Pharmacopeia [10]. The peak responses obtained by SFC and HPLC related to slope and intercept values are given in Table 2. The comparative results obtained using the two methods are cited in Table 4.

3. Conclusions

The present work has shown the feasibility of replacing ion-pair HPLC with packed column supercritical fluid chromatography. PCSFC is faster, cheaper and generates less disposable waste problems. The run time for SFC is 6 min against 15 min for HPLC. While HPLC generates 90 ml of a mixture of aqueous and organic waste per hour of which 45 ml is organic, SFC generates 180 ml of waste of which only 30 ml are organic, the rest being CO_2 gas, which spontaneously evaporates and is eco-friendly. It is to be remembered that the above calculations pertain to ten determinations h^{-1} for SFC while HPLC determinations are only 4 h^{-1}. The LOQ and LOD values for SFC are compatible with HPLC values. The present work also shows that SFC obviates the necessity of preparation of mobile phases and increases the life of the column caused by frequent washings necessary for ion-pair chromatography.

Acknowledgements

The authors thank Shri C.P. Kelkar, Director (Admn.), Dr A.M. Bhagwat, Director, Dr R. Kalyanraman, Prof Emeritus, C.B. Patel Research Centre, Mumbai 56, Dr (Mrs) Devyani Dave, Principal, I.Y. College of Arts, Science and Com

Table 4
Comparative data on the assay of three formulations by HPLC and PCSFC

Drug	Labelled content (mg)	SFC		HPLC	
		Amount found (mg)	% Drug found	Amount found (mg)	% Drug found
Haloperidol	5.00	5.01	100.2	4.98	99.60
Trihexyphenidyl	2.00	1.99	99.50	2.01	100.5
Haloperidol	5.00	4.99	99.80	4.99	99.80
Trifluoperazine	2.50	2.51	100.4	2.49	99.60
Trifluoperazine	2.50	2.49	99.60	2.48	99.20
Trihexyphenidyl	1.00	1.01	101.0	1.01	101.0

merce, Mumbai 60 and co-workers Indravadan Bhoir, Viddesh Bari, Miss Nehal Shah and Miss Suvarna Patil for encouragement in carrying out this work.

References

[1] T.A. Berger, W.H. Wilson, J. Pharm. Sci. 83 (1994) 281.
[2] T.A. Berger, W.H. Wilson, J. Pharm. Sci. 84 (1995) 489.
[3] T.A. Berger, W.H. Wilson, J. Pharm. Sci. 83 (1994) 287.
[4] I.C. Bhoir, B. Raman, M. Sundaresan, A.M. Bhagwat, J. Pharm. Biomed Anal. (in press).
[5] K. Takaichi, T. Shinohara, T. Nagano, Hochudoku 13 (1995) 132.
[6] B.R. Simmons, N.K. Jagota, J.T. Steward, J. Pharm. Biomed. Anal. 13 (1995) 59.
[7] V.R. Bari, U.J. Dhorda, M. Sundaresan, Talanta 45 (1997) 297.
[8] Y.P. Patel, M. Sundaresan, U.J. Dhorda, Indian J. Pharm. Sci. 59 (1992) 132.
[9] Martindale The extra pharmacopeia, 31st edn., Royal Pharmaceutical Society, 1996.
[10] The United States Pharmacopeia USP XXII, Pharmacopieal Convention, Rockville, MD 20852 (1990).

ELSEVIER

Talanta 47 (1998) 631–637

Talanta

Selective and sensitive fluorometric determinations of cobalt(II) and hydrogen peroxide with fluorescein-hydrazide

Itsuo Mori *, Kenichi Takasaki, Yoshikazu Fujita, Takako Matsuo

Osaka University of Pharmaceutical Sciences, 4-20-1 Nasahara, Takatsuki Osaka 569-1094, Japan

Received 29 July 1997; received in revised form 24 February 1998; accepted 26 February 1998

Abstract

Fluorophotometric determinations of cobalt(II) and hydrogen peroxide were investigated by using the fluorescence reaction between fluorescein-hydrazide (fl-$NHNH_2$), and/or hydrogen peroxide, cobalt(II), respectively. The calibration graphs were liner in the range of 0–6.0 ng cobalt(II) and 0–1000 ng hydrogen peroxide per 10 ml at an emission wavelength (E_m) of 530 nm with an exicitation wavelength (E_x) of 508 nm, respectively. These proposed methods were selective and simple, and the effect of foreign ions was negligible in comparison with conventional reported methods such as nitroso *R*,4-(2-pyridylazo)resorcinol(PAR), alizarin, pyridine-2-aldehyde-2-pyridinehydrazone, stilbazo-cobalt(II), etc. © 1998 Elsevier Science B.V. All rights reserved.

Keywords: Cobalt(II); Fluorescein-hydrazide; Hydrogen peroxide

1. Introduction

Already, a number of spectro-or fluoro-photometric determinations of trace amounts of cobalt(II) or hydrogen peroxide using kinetic and catalytic reaction systems [1–7] have been reported. In addition, we have already recognized [8–13] that the coexisting of surfactants; cationic, anionic, nonionic, or amphoteric surfactant alone or combination had been effective in numerous spectrophotometric or fluorophotometric determinations of various metal ions with xanthene or aromatic amine derivatives as organic reagents.

In this time, the various fluorescence reactions among fluorescein (fl) derivatives such as fl, fluorescin (fl-H), fluorescein-hydrazide (fl-$NHNH_2$), oxidizing agents such as hydrogen peroxide and cobalt(II) as a kinetic action-metal ion were systematically investigated. Moreover, the coexisting effects of surfactant in these reactions were respectively examined. Then, the sensitive and selective fluorophotometric determinations of cobalt(II) and hydrogen peroxide by using the fluorescence reaction between fl-$NHNH_2$ and/or hydrogen peroxide, cobalt(II) were newly proposed in the presence of zephiramine (Zp) as a cationic surfactant.

* Corresponding author.

0039-9140/98/$ - see front matter © 1998 Elsevier Science B.V. All rights reserved.
PII S0039-9140(98)00118-0

Table 1
Fluorescence reaction among fl derivatives such as fl, fl-H, fl-$NHNH_2$, cobalt(II) and hydrogen peroxide in the presence of Zp

Fl derivative	Fl. Int		E_x (nm)	E_m (nm)	Diff. of Fl. Int.
	Solution A	Solution B			
Fl	982.1	1000	508	531	17.9
Fl-$NHNH_2$	63.9	23.6	508	531	40.3
Fl-H	428.6	410.4	508	531	18.2

Co(II) taken, 5.0×10^{-9} mol l^{-1}; hydrogen peroxide, 1.0×10^{-3} mol l^{-1}; Zp, 0.15%; fl derivatives, 1.0×10^{-4} mol l^{-1}; pH, 10.0.

2. Experimental

2.1. Apparatus and reagent

Fluorescence measurements were performed on an Hitachi, model F 3000 equipped with Ushio 150 W Xenon lamp and 10×10 mm quartz cells. An Hitachi-Horiba model F-7AD pH meter equipped with glass combined electrode, was used for all pH measurements.

All materials and reagents were of analytical grade and were used without further purification. De-ionized water was used throughout. A stock solution (1.0×10^{-2} mol l^{-1}) of cobalt(II) and hydrogen peroxide solutions were prepared by previous described methods [8,9,12–14] and were diluted as appropriate. A 1.0×10^{-3} mol l^{-1} fl-$NHNH_2$ solution was prepared by dissolving fl-$NHNH_2$ (prepared [15] by condensation of fl and hydrazine, and purified) in methanol containing concentrated hydrochloric acid. Sőrensen buffer (pH 10.0) was used for pH adjustments. A 1.5% Zp solution as a cationic surfactant was prepared by dissolving Zp in water.

2.2. Standard procedures

2.2.1. Determination of cobalt(II)

To a sample solution containing 0–6.0 ng cobalt(II) in a 10-ml calibrated flask, 1.0 ml of 1.5% Zp solution, 2.0 ml of pH 10.0 buffer solution, 1.0 ml of a 1.0×10^{-2} mol l^{-1} hydrogen peroxide solution, and 1.0 ml of a 1.0×10^{-3} mol l^{-1} fl-$NHNH_2$ solution, were added. The mixture was diluted to the mark with water (solution A), kept at 50°C for 30 min together with a reference solution without cobalt(II) (solution B), and cooled to room temperature for 10 min. The amount of cobalt(II) was calculated by measuring the difference of relative fluorescence intensities (R. fl. Int. ΔF) between solutions A and B at an emission wavelength (E_m) 530 nm with an excitation wavelength (E_x) of 508 nm.

2.2.2. Determination of hydrogen peroxide.

A hydrogen peroxide sample (0–1000 ng) was placed in a 10-ml calibrated flask, and 1.5 ml of 1.5% Zp solution, 2.0 ml of a Sőrensen buffer solution (pH 9.9), 1.0 ml of 5.0×10^{-5} mol l^{-1} cobalt(II) solution, and 1.0 ml of a 1.0×10^{-3} mol l^{-1} fl-$NHNH_2$ solution were added. The solution was diluted with water to 10 ml and mixed well (solution A). Solution A was kept at 50°C for 40 min and allowed to cool to room temperature(10–25°C) together with a reference solution without hydrogen peroxide (solution B). Then the difference of relative fluorescence intensities (R. fl. Int. ΔF) between solutions A and B was measured at an E_m of 530 nm with an E_x of 508 nm.

Table 2
Effect of oxidizing agents

Oxidizing agents	Fl. Int.		E_m (nm)
	Solution A	Solution B	
—	11.0	8.7	530
H_2O_2	63.9	23.6	530
$NaNO_2$	12.0	9.7	530
KIO_3	12.5	10.1	530
NaClO	11.8	8.9	530

Co(II) taken, 5.0×10^{-9} mol l^{-1}; fl-$NHNH_2$, 1.0×10^{-3} mol l^{-1}; Zp, 0.15%; E_x, 508 nm.

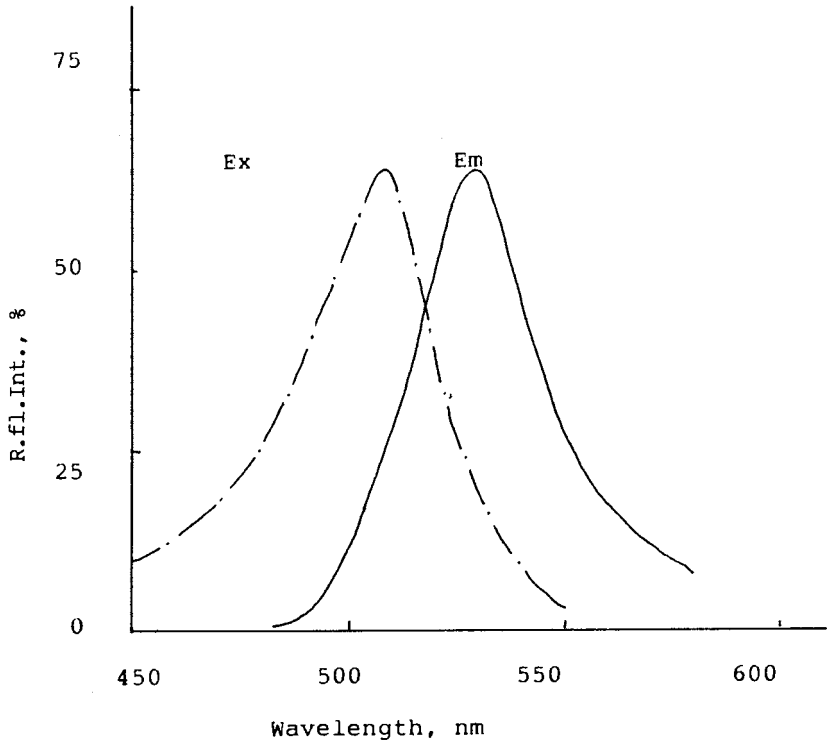

Fig. 1. Emission and excitation spectra of (fl-$NHNH_2$-cobalt(II)-hydrogen peroxide) solution in the presence of Zp: Co(II), 3.0 ng 10 ml^{-1}; fl-$NHNH_2$, 1.0×10^{-4} mol l^{-1}; hydrogen peroxide, 1.0×10^{-3} mol l^{-1}; Zp, 0.15%; pH, 10.

3. Results and discussion

3.1. Fluorescence reactions among fluorescein derivatives, oxidizing agent and cobalt(II)

Firstly, the fluorescence reactions among fl or fl-$NHNH_2$ or fl-H as fl-derivatives, hydrogen peroxide as an oxidizing agent and cobalt(II) were systematically investigated at weakly basic media in the presence of Zp as a cationic surfactant. Although the difference of fluorescences between fl derivatives-hydrogen peroxide-cobalt(II) solution (solution A) and fl derivatives-hydrogen peroxide solution (solution B) was scarcely recognized in the absence of Zp, these fluorescence reactions in the presence of cationic surfactant such as Zp were remarkable. Although the reaction at room temperature was very difficult to observe, the difference of R. fl. Int.(ΔF) between solutions A and B by using fl-$NHNH_2$ as a fl-derivatives was obvious and proportional to the coexisting of micro amount of cobalt(II), as shown in Table 1. Also the ΔF value in the presence of cationic surfactant was stable for 60 min, and abundant in reproducible.

Secondly, as shown in Table 2, the fluorescence reactions among fl-$NHNH_2$, oxidizing agent and cobalt(II) were systematically examined by changing the oxidizing agent such as hydrogen peroxide, sodium nitrate, potassium iodate etc. Of the various oxidizing agents tested, hydrogen peroxide was the most effective for the fluorescence reaction among fl-$NHNH_2$, oxidizing agent and cobalt(III).

3.2. Fluorescence spectra

Fl-$NHNH_2$ solution was easily converted to a strong fluorescence product by oxidizing agent

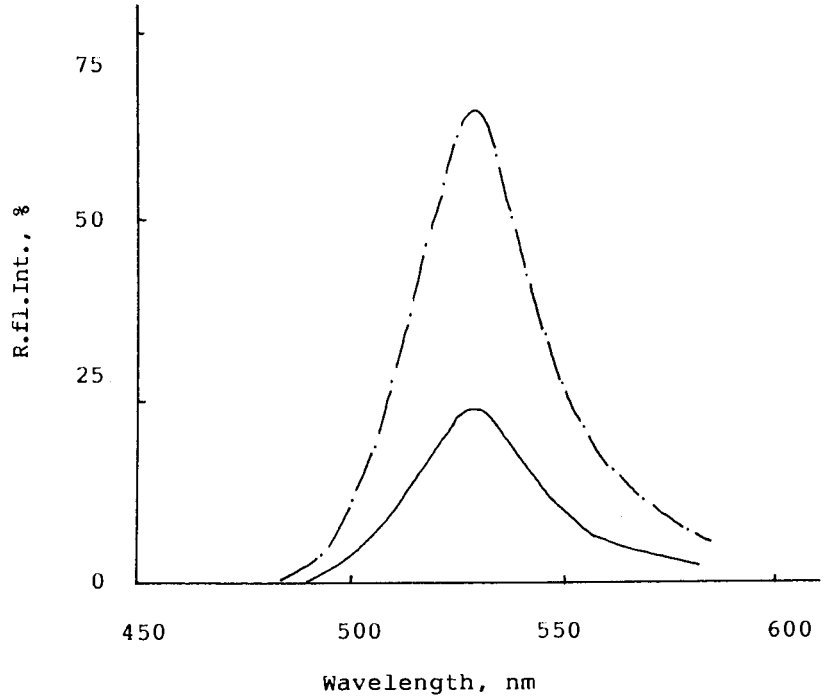

Fig. 2. Emission spectra of (fl-$NHNH_2$-cobalt(II)-hydrogen peroxide) and (fl-$NHNH_2$-hydrogen peroxide) solutions in the presence of Zp: ——, (fl-$NHNH_2$-hydrogen peroxide) solution; —·—·, (fl-$NHNH_2$-cobalt(II)-hydrogen peroxide) solution; cobalt(II), 5.0×10^{-9} mol l^{-1}; fl-$NHNH_2$, 1.0×10^{-4} mol l^{-1}; hydrogen peroxide, 1.0×10^{-3} mol l^{-1}; Zp, 0.15%; E_x, 508 nm; pH, 10.0.

such as hydrogen peroxide in the coexistence of trace amounts of cobalt(II) or palladium(II) represented the catalytic action. Fig. 1 shows the excitation (E_x) and emission (E_m) spectra of solution A at pH 9.9. The maximum, reproducible and stable difference of fluorescence intensities between solutions A and B was obtained at 530 nm as the maximum E_m with 508 nm as the maximum E_x, as shown in Fig. 2.

3.3. Effects of pH and oxidizing agent

The optima pH-ranges were 9.8–10.2, and Sőrensen borate buffer solution was effective for fluorescence reactions. The optimum amount of buffer solution was >2.0 ml per 10 ml.

As shown in Table 2, hydrogen peroxide as an oxidizing agent was most effective, and constant, maximum ΔF was obtained with 1.0–3.0 ml of 1.0×10^{-3} mol l^{-1} hydrogen peroxide solution in the final 10 ml for the assay of cobalt(II).

3.4. Effect of cationic surfactant

Already, the incorporations of various surfactant in the colouring or fluorescence reaction between various organic agent and polyvalent metal ions have offered many advantages in comparison with the colour or fluorescence system in the absence of surfactant [8–13]. Accordingly, the effect of surfactant was systematically investigated in the fluorescence-reactions between solutions A and B of the various tested surfactants; cationic, anionic, nonionic, amphoteric surfactants as shown in Table 3, Zp as a cationic surfactant was most effective for the fluorescence reaction. And the optimum amount of Zp solution was >1.0 ml of 1.5% Zp solution per 10 ml.

3.5. Effect of cobalt(II) concentration

Of the various tested kinetic metal ions such as cobalt(II), nickel(II), palladium(II), molybde-

Table 3
Effect of surfactants

Surfactants	E_x (nm)	E_m (nm)	Fl. Int.	
			Solution A	Solution B
—	500	520	9.9	7.2
Tween 20	500	520	165.3	156.0
Brij 35	500	520	95.6	86.3
Triton X 100	500	520	38.3	31.4
PVA	500	520	9.2	8.2
PVP	500	520	72.0	65.5
Benzethonium Cl	508	530	10.9	5.5
CPC	508	530	10.9	5.5
CTAC	508	530	62.8	24.3
STAC	508	530	55.2	20.8
Zp	508	530	63.9	23.6
SDS	500	520	5.3	5.3
AM-301	500	520	25.3	24.5

Co(II) taken, 5.0×10^{-9} mol l^{-1}; fl;-$NHNH_2$, 1.0×10^{-4} mol l^{-1}; hydrogen peroxide, 1.0×10^{-3} mol l^{-1}; surfactant, 0.15%; pH, 10.0; PVP, poly(*N*-vinylpyrrolidone); SDS, sodium dodecylsulphate; STAC, stearlyltrimethylammoium chloride; AM-301, laurylalcohol ether; Triton X 100, alkylarl polyethyleneglycol; Tween 20, polyoxyethylene sorbitanmonolaurate; PVA, (poly(*N*-vinylalcohol); CPC, cetylpyridinium chloride; CTAC, cetyltrimethylammonium chloride.

num(VI), manganese(II), etc. for the assay of hydrogen peroxide, cobalt(II) was most effective and the effect of its concentration was investigated. Constant and maximum ΔF in the fluorescence reaction was obtained with $4.0–6.0\times10^{-6}$ mol l^{-1} cobalt(II) final concentration.

3.6. Effects of fl-$NHNH_2$ concentration, temperature and stability

The effect of fl-$NHNH_2$ concentration on the standard procedure was examined by measuring the ΔF at E_m 530 nm for 2.0×10^{-3} mol l^{-1} cobalt(II) or hydrogen peroxide, respectively. Maximum and almost constant ΔF was obtained by using final 1.0×10^{-4} mol l^{-1} fl-$NHNH_2$ for the assay of cobalt(II) or hydrogen peroxide, respectively.

The effects of temperature and time were investigated in the ranges of 15–60°C and 0–50 min. Solutions A and B in the presence of Zp as a cationic surfactant were stable for at least 60 min, and gave a maximum, constant ΔF.

3.7. Calibration graph and reproducibility

The calibration graph were prepared according to the standard procedure, and were linear over the range of 0–6.0 ng cobalt(II) and 0–1000 ng hydrogen peroxide in a final volume of 10 ml, respectively. The precisions were calculated for 3.0 ng of cobalt(II) and 340 ng of hydrogen peroxide per 10 ml of aqueous solution; the relative standard deviations (RSD) were 3.6 and 32.4% ($n=8$), respectively.

3.8. Effect of foreign ions

Although small amount of several metal ions such as iron(III), nickel(II), copper(II), palladium(II) showed positive errors, these kinetic or catalytic active metal ions were permissible up to 100–500-fold excess over cobalt(II) by addition of masking agent such as sodium tartrate, sodium thiosulphate. The presence of pharmaceuticals such as thiamine, pyridoxine, tocopherol, nicotinamide did not interfere with the determination of cobalt(II).

Table 4
Effect of foreign ions for the assay of cobalt(II) and hydrogen peroxide

Foreign ions	Added as	Co(II)		H_2O_2	
		Molar ratio	Recovery (%)	Molar ratio	Recovery (%)
Ni(II)	Nitrate	200[a]	100.0	50[a]	99.1
Cu(II)	Sulphate	500[a]	98.7	20[a]	98.2
Pd(II)	Chloride	100[a]	98.2	20[b]	98.2
Mn(II)	Chloride	100	100.0	50	100.0
Al(III)	Nitrate	200	100.0	50	100.0
Fe(III)	Sulphate	500[a]	97.7	50[a]	99.1
Sn(IV)	Sulphate	200	99.8	50	99.1
Ti(IV)	Sulphate	500	100.0	100	100.0
V(V)	Vanadate	100	98.7	10	100.0
Mo(VI)	Molybdate	100	100.0	40	100.0
NO_2^-	Sodium	100	100.0	200	99.4
BrO_3^-	Potassium	200	100.0	50	100.0
F^-	Sodium	1000	100.0	200	100.0
S^{2-}	Sodium	200	99.5	100	99.5
$S_2O_3^{2-}$	Sodium	200	99.5	50	100.0
Citrate	Sodium	200	99.5	50	99.1
Tartrate	Sodium	500	100.0	100	99.6
Thiamine	Hydrochloride	750	99.5	—	—
Pyridoxine	Hydroxhloride	1000	100.0	—	—
Tocopherol	Acetate	1000	99.0	—	—
Nicotinamide	—	500	100.0	100	100.0
Ascorbate	—	100	100.0	100	100.0
Albumin	—	40[c]	99.2	20[c]	98.8
Urea	—	100	99.8	100	99.7

[a] Masked with 5.0×10^{-5} mol l^{-1} sodium tartrate solution.
[b] Masked with 5.0×10^{-5} mol l^{-1} sodium thiosulphate solution.
[c] Ratio of weight/weight.
Co(II) taken, 3.0 ng 10 ml^{-1}; hydrogen peroxide taken, 340 ng 10 ml^{-1}; fl-$NHNH_2$, 1.0×10^{-4} mol l^{-1}; Zp, 0.15%; E_x, 508 nm; E_m, 530 nm.

The presence of 1/50-fold copper(II) or 1/20-fold cobalt(II) excess over hydrogen peroxide gave a negative error for the assay of hydrogen peroxide. On the other hand, the presence of oxidizing or reductive agent such as bromate, L-ascorbate and citrate, glucose, urea, respectively, did not interfere with the assay for hydrogen peroxide.

The results of assay for cobalt(II) and hydrogen peroxide are shown in Table 4.

3.9. Applications

Although further investigations were necessary for the applications for pharmaceuticals or waste water samples containing cobalt(II) or hydrogen peroxide, the proposed method was applied to assay of cobalt or hydrogen peroxide in pharmaceuticals such as vitamine B_6, oxydol. The analytical results were satisfactory for cobalt-containing commercial pharmaceuticals such as 'Neuvita', 'Alinamin' tablets; analytical representative datas were 97.2–101.4% ($n=3$), as shown Table 5.

4. Conclusion

The fluorescence reactions among fl-$NHNH_2$, hydrogen peroxide and various metal ions such as cobalt(II), palladium(II) were systematically investigated, and the procedure for the assay of cobalt(II) and hydrogen peroxide was respectively proposed by using the fluorescence reaction

Table 5
Application for commercial pharmaceuticals (cobalt containing)

Sample	Cobalt content (μg)		
	Presentation	Proposed method	PR method[a]
'Neuvita ace' tab	16.275	16.752	16.666
'Alinamin' tab	4.340	4.564	4.691

[a] Mean of five determinations.

among fl-$NHNH_2$, hydrogen peroxide and cobalt(II). The fluorescence-reactions between fl-$NHNH_2$ and cobalt(II) in the presence of hydrogen peroxide, or fl-$NHNH_2$ and hydrogen peroxide in the presence of cobalt(II) was selective and sensitive in comparison with that using of fl-H alone as an organic agent, or previous reported methods [8,9,11,12,16].

References

[1] D. Pèrez-Bendito, Analyst 109 (1984) 891.
[2] F. Salinas, J.J. Berzas-Nevado, P. Valiente, Talanta 34 (1987) 321.
[3] D.G. Themelis, G.S. Vasilkiotis, Analyst 112 (1987) 791.
[4] M. Otto, J. Rentsch, G. Werner, Anal. Chim. Acta 147 (1983) 267.
[5] J. Medina, F. Hernandez, R. Marin, F.J. Lopes, Analyst 111 (1986) 235.
[6] E. Lebat-Esstells, A. Seillano-Cabeza, J. Medina-Escriche, Analyst 111 (1986) 193.
[7] T. Yamane, Mikrochim. Acta 1 (1984) 425.
[8] I. Mori, Y. Fujita, K. Kato, M. Toyoda, M. Akagi, Fresenius J. Anal. Chem. 343 (1992) 902.
[9] I. Mori, Y. Fujita, M. Toyoda, M. Akagi, Bull. Chem. Soc. Jpn. 62 (1989) 2536.
[10] F. Nanov', K. Stoyaok, Anal. Chim. Acta 183 (1982) 321.
[11] I. Mori, Y. Fujita, M. Toyoda, S. Kubo, Fresenius J. Anal. Chem. 342 (1992) 80.
[12] I. Mori, Y. Fujita, Y. Nakahashi, T. Tanaka, S. Isihara, Fresenius J. Anal. Chem. 330 (1988) 619.
[13] I. Mori, Y. Fujita, M. Toyoda, K. Kato, M. Akagi, Talanta 38 (1991) 683.
[14] Y. Fujita, I. Mori, M. Toyoda, T. Matsuo, Anal. Sci. 10 (1994) 827.
[15] T. Akita, Yakugaku Zasshi 81 (1961) 517.
[16] A. Seillano-Cabeza, M. Llobat-Estelles, J. Medin-Escriche, Analyst 110 (1985) 1333.

ELSEVIER

Talanta 47 (1998) 639–643

Talanta

Visible spectrophotometric and first-derivative UV spectrophotometric determination of rifampicin and isoniazid in pharmaceutical preparations

S.A. Benetton, E.R.M. Kedor-Hackmann *, M.I.R.M. Santoro, V.M. Borges

Departamento de Farmácia, Faculdade de Ciências Farmacêuticas, Universidade de São Paulo, Caixa Postal 66355, CEP 05389-970, São Paulo, Brazil

Received 6 October 1997; received in revised form 2 February 1998; accepted 26 February 1998

Abstract

Two methods are described for the determination of rifampicin and isoniazid in mixtures by visible spectrophotometry and first-derivative ultraviolet spectrophotometry. The absorbance at 475 nm in buffer solution pH 7.4 was employed to determine rifampicin after applying the three-point correction technique between 420 and 520 nm, while the amplitude of the first-derivative spectrophotometric spectrum at 257 nm in HCl 0.012 M was selected for the determination of isoniazid. The methods are rapid, simple and do not require any separation step. The recovery average was 99.03% for rifampicin and 100.01% for isoniazid. The methods were applied to determine the two compounds in commercial capsules and compared with the official method of the USP XXIII with good agreement between the results. © 1998 Elsevier Science B.V. All rights reserved.

1. Introduction

Since isoniazid (INH) and rifampicin (RIF) form one of the most effective antituberculosis regimens used in many countries, considerable effort has been spent on improving the efficacy of this therapy [1]. For most patients, regimens that contain these drugs can successfully be completed in 6 months if pyrazinamid is included in the regimen for the first 2 months. The most serious problem with tuberculosis therapy is patient non-adherence to the prescribed regimens and combined formulations of RIF and INH were introduced to improve patient acceptability and compliance. The combined formulation is official in the United States Pharmacopeia with the name rifampin and isoniazid capsules [2].

Although some procedures have been described for the assay of either RIF or INH in pharmaceutical preparations and in biological fluids, there are only a few methods reported to be able to analyse both drugs in combination [3,4]. These methods use high performance liquid chromatography (HPLC) and, although they are sensitive, they are laborious and expensive. The compendial method available (USP XXIII) for the assay of RIF–INH mixture in capsules employs a HPLC method for the determination of RIF and a titri-

* Corresponding author. Fax: +55 118154418.

0039-9140/98/$ - see front matter © 1998 Elsevier Science B.V. All rights reserved.
PII S0039-9140(98)00111-8

metric method, which requires a separation step, for the determination of INH [2].

The aim of this work was to investigate the utility of derivative spectrophotometry in the assay of RIF and INH in combination in pharmaceutical preparations without the necessity of sample pre-treatment. Derivative spectrophotometry [5] is a useful technique for the suppression of additive interference, and it has been used extensively for the simultaneous determination of substances in mixtures [6,7]. Two methods were developed and validated in this work: a visible spectrophotometric method using the three-point correction technique [8] for the determination of RIF and a derivative ultraviolet spectrophotometric method for the determination of INH. The methods had sufficiently good accuracy and precision and permitted a simple and time-saving assay of INH and RIF in mixtures.

2. Experimental

2.1. Apparatus

A Hewlett-Packard 8453 diode-array spectrophotometer fitted with a HP 845 UV-Visible ChemStation and a Hewlett-Packard 600 printer were used for all the measurements and treatment of data.

Chromatography was performed using a CG solvent delivery pump (model 480-C) and a CG variable UV detector set at 254 nm connected to a CG integrator (model CG-200) (Instrumentos Científicos CG, São Paulo, Brazil). The system was equipped with a Rheodyne 7125 injection valve fitted with a 20 μl loop. The analytical column was a Waters Nova-Pak® C8 (3.9×150 mm, 5 μm) column. The chromatographic conditions were the same described on the USP XXII under rifampin assay conditions [2]. A Digimed DM21-V6 pH meter was used for the determination of the end point in the titration of INH.

2.2. Materials and solutions

Rifampicin and isoniazid were kindly donated by a pharmaceutical industry and used without further purification. All solvents and reagents were of analytical grade. Phosphate buffer solution pH 7.4 was prepared according to the British Pharmacopoeia 1993 [9]. The commercial pharmaceutical formulations used in this work (capsules) contained 300 mg of rifampicin and 200 mg of isoniazid.

2.3. Procedures

2.3.1. Visible spectrophotometry

Standard solutions containing known quantities of RIF (20–70 μg ml^{-1}) in phosphate buffer pH 7.4 were prepared from a methanolic stock solution for the calibration curve.

The commercial capsules were emptied in a glass mortar and an amount of powder equivalent to 125 mg of RIF was accurately weighed out into a 100 ml amber volumetric flask. About 50 ml of methanol were added, sonicated for 5 min and the volume was made up with the same solvent. The methanolic solution was filtered through a Whatman No. 1 filter paper and further dilutions of the appropriate aliquots were made in phosphate buffer pH 7.4 to obtain a final solution containing 50 μg ml^{-1}. The absorbance of both the sample and the standard solutions were measured at 475 nm after applying the three-point correction technique between 420 and 520 nm. Phosphate buffer pH 7.4 was used in the reference cell.

2.3.2. First-derivative ultraviolet spectrophotometry

Standard solutions containing known quantities of INH (5–25 μg ml^{-1}) in HCl 0.012 M were prepared for the calibration curve.

The commercial capsules were emptied in a glass mortar and an amount of powder equivalent to 125 mg of INH was accurately weighed out into a 100 ml amber volumetric flask. About 50 ml of methanol were added, sonicated for 5 min and the volume was made up with the same solvent. After filtration through a Whatman No. 1 filter paper, a 5 ml aliquot was transferred to a 50 ml amber volumetric flask and diluted to volume with water. A 2 ml aliquot was transferred to a 25 ml amber volumetric flask and diluted to volume with HCl 0.012 M. The final concentra-

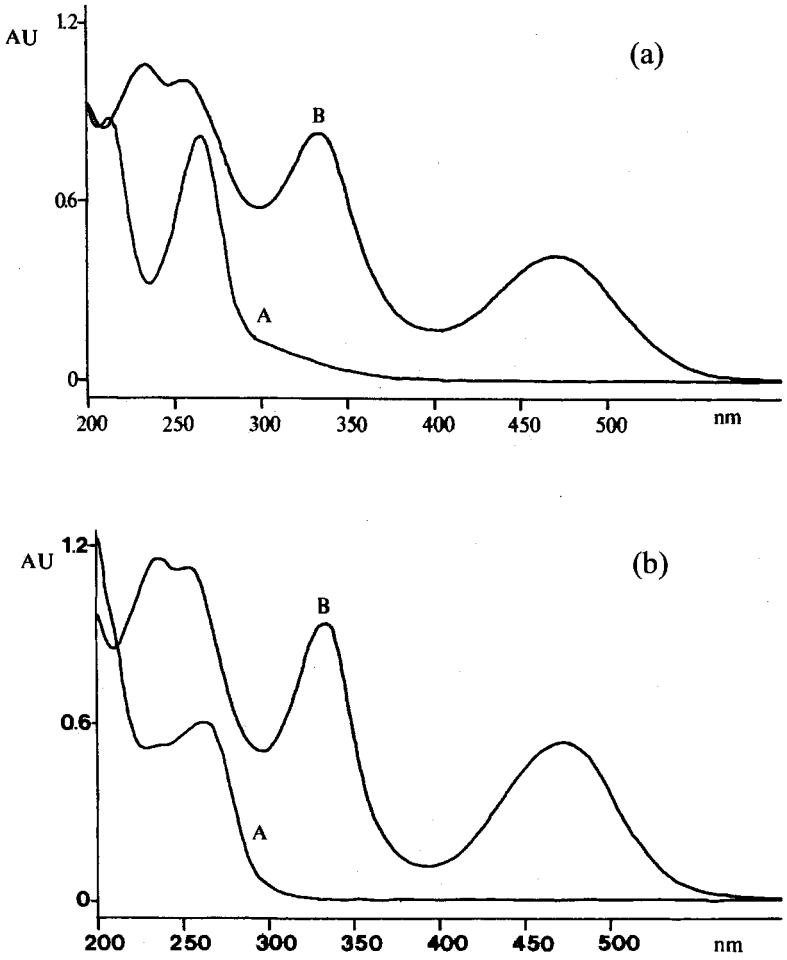

Fig. 1. Absorption spectra of (A) isonazid (20 μg ml^{-1}) and (B) rifampicin (30 μg ml^{-1}) in (a) HCl 0.012 M and (b) phosphate buffer solution pH 7.4.

tion was 10 μg of INH ml^{-1}. The amplitude of the first-derivative of both the sample and the standard solutions were measured at 257 nm. A solution of HCl 0.012 M was used in the reference cell.

The methods were validated as to precision (reported as the relative standard deviation, RSD %), linearity (evaluated by regression analysis), and accuracy. Accuracy was determined by recovery studies performed according to the USP XXIII guidelines [2]: the methods were applied to artificial samples which contained amounts of analyte both above (120%) and below (80%) the normal levels expected in the samples. The accuracy was then calculated from the test results as the percentage of analyte recovered by the assay.

3. Results and discussion

3.1. Method development

The influence of pH on the absorption spectra of RIF and INH was studied between pH 7.4 and 1.7. The pH value slightly affected the absorption spectra of RIF but exerted a profound influence on the quality and shape of the INH spectra (Fig. 1a, b). INH absorption spectra presented a shift

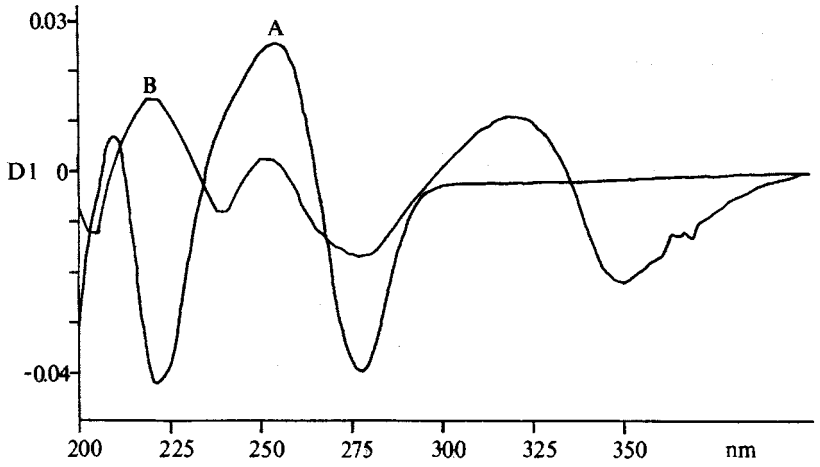

Fig. 2. First derivative spectra of (A) isonazid (20 μg ml^{-1}) and (B) rifampicin (30 μg ml^{-1}) in HCl 0.012 M.

to shorter wavelength as well as narrower and better-defined absorption spectra as the pH value of the medium decreased. The absorption spectrum of INH was completely overlapped with the spectrum of RIF in both acidic and alkaline conditions. Therefore, the determination of INH in the presence of RIF cannot be performed by direct absorbance measurements and derivative spectrophotometry was then employed. The improved resolution of overlapping absorption bands and the discrimination in favour of narrow bands against broader bands, which are the principal characteristic of derivative spectrophotometry, can result in the complete elimination of specific interference from the co-formulated compound (Fig. 2). The pH-induced shift of INH spectrum was exploited in this work and the best results for the analysis of INH by first order ultraviolet derivative spectrophotometry were obtained in HCl 0.012 M (pH 2.0), because the spectrum of INH is narrower in this medium than under less acidic conditions. The height (amplitude) of a derivative spectrum depends not only on the height of the normal spectrum but also on its width: for a given peak height, narrower peaks give larger derivative amplitudes. Therefore, the determination of INH was carried out by measuring the amplitude of the first-derivative spectrum of INH in HCl 0.012 M at 257 nm (zero-crossing wavelength of rifampicin).

In Fig. 1a it also can be seen that the absorption of RIF showed a large peak at 475 nm that can be used for direct absorbance measurement. However, the stability of RIF is very weak under these acid conditions (stable for less than 15 min) and the determination of RIF was carried out in phosphate buffer solution pH 7.4 (Fig. 1b). As the determination of RIF in capsules containing RIF–INH mixtures by direct visible spectrophotometry showed a small but systematic positive error, the three-point correction technique was employed in an attempt to avoid these biased results. The recovery tests showed improved results after the application of that correction technique.

3.2. Visible spectrophotometry (RIF analysis)

The precision (RSD %) of the results was of 0.56% as determined on ten replicate measurements of a commercial sample. The linearity of response, at a concentration range from 20 to 70 μg ml^{-1}, was evaluated by regression analysis and the regression equation ($Y = 0.0124X + 0.0026$) presented a correlation coefficient of 0.9999. The average percent recovery determined in the recovery test for RIF was 99.03%.

Table 1
Data obtained from the analysis of a commercial sample containing isoniazid (200 mg) and rifampicin (300 mg) in combination

Commercial sample (capsules)	Percentage of the declared amount	
	New method[a] (%)	USP XXIII method[b] (%)
Isoniazid	95.86 ± 0.53	95.02
Rifampicin	98.32 ± 0.34	97.13

[a] Mean value of ten determinations ± 95% confidence interval.
[b] Mean value of three determinations.

3.3. First-derivative ultraviolet spectrophotometry (INH analysis)

The precision (RSD %) of the results was of 0.78% as determined on ten replicate measurements of a commercial sample. The absorption spectrum of INH was completely overlapped with the spectrum of RIF (Fig. 1a). As the accuracy of absorbance measurements is low at high absorbance values, the addition of the absorbance of the two compounds limited the range of work for the analysis of INH by first-order derivative UV spectrophotometry (5–25 μg ml^{-1}). The linearity of response was evaluated by regression analysis and the regression equation ($Y = 0.121X - 0.003$) presented a correlation coefficient of 0.9999. The average percent recovery determined in the recovery test for INH was 100.01%.

3.4. Comparison of the developed methods with the USP XXIII methods

The commercial rifampicin capsules co-formulated with isoniazid were also assayed by the USP XXIII official methods and the results compared with those obtained using the developed methods. The results can be seen in Table 1.

4. Conclusion

It was concluded that first-derivative UV spectrophotometry is suitable as a rapid alternative to the official USP XXIII titration method for isoniazid in combination with rifampicin in pharmaceutical preparations. Rifampicin can also be determinated with good accuracy and precision by the visible spectrophotometric method employing the three-point correction technique. The short analysis time and low costs are the main advantages of these methods for routine analysis.

References

[1] C.A. Peloquin, S.E. Berning, Ann. Pharmacother. 28 (1994) 72–83.
[2] United States Pharmacopeia, 23 ed., United States Pharmacopeial Convention, Rockville, pp. 1381–1383, 1982 (1995).
[3] Y. Shah, S. Khanna, K.C. Jindal, V.S. Dighe, Drug Dev. Ind. Pharm. 18 (1992) 1589–1596.
[4] A. Walubo, P. Smith, P.I. Folb, J. Chromatog. B 658 (1994) 391–396.
[5] J.E. Cahill, F.G Padeka, Am. Lab. 12 (1980) 101–112.
[6] P. Levillain, D. Fompeydie, Analysis 14 (1986) 1–20.
[7] C.B. Ojeda, F.S. Rojas, J.M.C. Pavon, Talanta 42 (1995) 1195–1214.
[8] A.H. Becket, J.B. Stenlake (Eds.), Practical Pharmaceutical Chemistry, 4th ed., The Athlone Press, London, 1988, p. 288.
[9] British Pharmacopoeia London, Her Majesty's Stationery Office, 1993, p. A78.

ELSEVIER

Talanta 47 (1998) 645–649

Talanta

Flow injection determination of hydrazine with fluorimetric detection

Ali A. Ensafi *, B. Rezaei

College of Chemistry, Isfahan University of Technology, Isfahan, Iran

Received 9 October 1997; received in revised form 4 February 1998; accepted 26 February 1998

Abstract

A spectrophotometric flow injection system is described for the determination of hydrazine, involving oxidation of hydrazine by thallium(III) with concomitant formation of thallium(I). The optimum analytical conditions have been established. The linear range for hydrazine is 25–500 ng ml^{-1} with a detection limit of 20 ng ml^{-1}. The sampling frequency is 40 ± 5 samples h^{-1}. The relative standard deviation for 100, 250 and 500 ng ml^{-1} is 3.5, 2.6 and 1.8%, respectively. The method has been applied to the determination of hydrazine in water. © 1998 Elsevier Science B.V. All rights reserved.

Keywords: Fluorimetry; Hydrazine; Thallium

1. Introduction

Because of the environmental and toxicological significance of hydrazine compounds, a reliable method is required for their quantitation. Different methods have been proposed for the determination of hydrazine. These include spectrophotometric [1,2], coulometric [3], titrimetric [4] and amperometric [5,6] methods and ion-selective electrode [7,8].

Many automated flow injection techniques have been used for the determination of hydrazine [9–16]. Some of the sensitive methods are based on the construction of chemically modified electrodes [9–12] and thus require special equipment. Other spectrophotometric methods [13–15] are based on the reaction of hydrazine with dimethylbenzaldehyde and *n*-dimethyl-aminobenzaldehyde [14]; these methods have a high limit of detection and low precision. The other methods used expensive instrumentation (diode array detector) [13,15,16].

Only a few flow injection analysis (FIA) methods with fluorimetric detection have been used for the determination of hydrazine [17,18]. In this paper, a simple and rapid FIA method with spectrofluorimetric detection is proposed for the determination of hydrazine. The method is based on the oxidation of hydrazine by thallium(III) and monitoring of the fluorescence signal of thallium(I), as $TlCl_3^{2-}$, which is formed in the reaction.

* Corresponding author. Tel.: +98 31 8912351; fax: +98 31 8912350; e-mail: Ensafi@cc.iut.ac.ir

0039-9140/98/$ - see front matter © 1998 Elsevier Science B.V. All rights reserved.
PII S0039-9140(98)00113-1

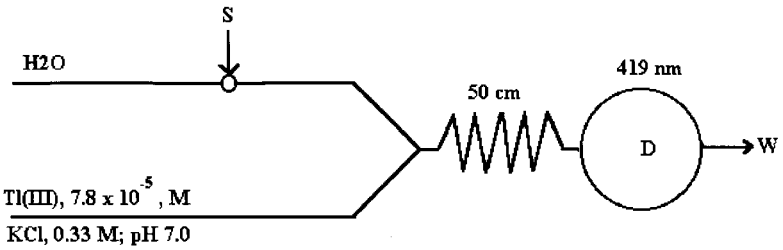

Fig. 1. Schematic diagram of the flow injection system.

2. Experimental

2.1. Apparatus

A Shimadzu spectrofluorimeter was used for recording excitation and emission spectra. The detector used in the flow system was a Shimadzu Model RF535 spectrofluorimeter with a 10-μl quartz flow cell and 1.0-cm path length. A 13-channel Desaga peristaltic pump was used to drive all flow streams at a constant flow rate in silicon rubber tubes (i.d. 1.0 mm). A Rheodyne sample injection system and Teflon mixing joint were also used. A Varian Model 9167 strip-chart recorder was used to record the peak heights.

2.2. Reagents

A stock solution of hydrazine (1000 μl ml^{-1}) was prepared by dissolving hydrazinium chloride (Merck) in water. The working solutions were prepared by diluting the stock solution with water.

Thallium(III) stock solution (1.0×10^{-3} M) in 10^{-3} M HCl was prepared from $TlCl_3$ (Merck). Solutions of lower concentration were prepared by diluting the stock solution with water.

2.3. Manifold and procedure

A schematic diagram of the instrumental set-up is shown in Fig. 1. Buffer solution and a mixture of thallium(III) with KCl chloride solution was pumped at a constant flow rate of 7.7 ml h^{-1} for each solution through silicon tubing with diameter of 1.0 mm, via a Teflon mixing chamber. The reaction was started by injection of the sample. Solution entered the flow-through cell of the spectrofluorimeter via a reaction coil of Teflon tubing (1.0 mm i.d.) and the fluorescence signal was monitored at 419 nm ($\lambda_{ex} = 227$ nm).

A mixture of 7.8×10^{-5} M thallium(III), 0.33 M KCl with buffer solution (phosphate buffer, 0.10 M, pH 7.0) and water were each pumped at a flow rate of 7.7 ml h^{-1}. A 50-μl sample volume containing between 25 and 500 μg ml^{-1} hydrazine was injected into the carrier (water). Solution entered the flow-through cell of the spectrofluorimeter via a 50-cm length of Teflon tubing, and the fluorescence intensity was monitored at 419 nm.

3. Results and discussion

Hydrazine is rapidly oxidized by thallium(III) in neutral media to produce thallium(I) and nitrogen. Thallium(I) forms $TlCl_3^{2-}$ in aqueous media in the presence of chloride ions. This thallium compound has a violet fluorescence [19], whereas thallium(III) does not have any fluorescence properties. Thus the fluorescence signal of $TlCl_3^{2-}$ was used for the determination of hydrazine. Fig. 2 shows the fluorescence spectra of a solution of thallium(III) with hydrazine. The excitation wavelength was 227 nm and the fluorescence wavelength was 419 nm.

3.1. Effect of reagent concentrations

The influence of pH, thallium(III) concentration and chloride concentration were investigated with 50 μl of 0.200 μg ml^{-1} hydrazine, using a reaction coil length of 25 cm and pump flow rate of 5.5 ml h^{-1} for each channel at 30°C.

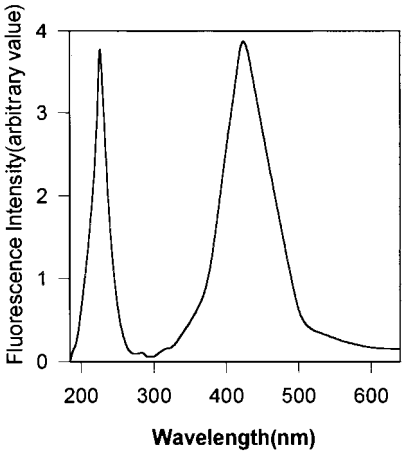

Fig. 2. Exitation (A) and emission (B) spectra of $TlCl_3^{2-}$. Thallium(III) concentration, 1.2×10^{-4} M; pH 7.0; KCl concentration, 0.33 M; hydrazine concentration, 300 ng ml^{-1}.

The effect of pH on the sensitivity was studied with 3.9×10^{-5} M thallium(III) in 0.16 M KCl solution. The results are shown in Fig. 3. The sensitivity increased up to pH 7.0 but decreased at greater pH values. The oxidation ability of thallium(III) decreased in alkaline solution, and the reduction ability of hydrazine decreased in acidic solution. Thus a pH of 7.0 was selected for the study.

The effect of KCl concentration on the sensitivity was studied with 3.9×10^{-5} M thallium(III) at pH 7.0. The fluorescence intensity increased with

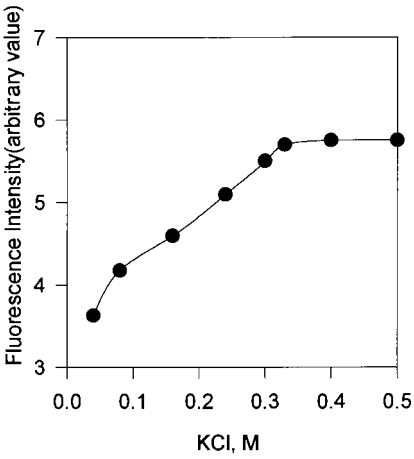

Fig. 4. Effect of KCl concentration on the sensitivity.

increasing KCl concentration from 0.04 to 0.33 M. This effect is due to the formation of $TlCl_3^{2-}$. Above 0.33 M chloride, the signals remained virtually constant (Fig. 4). Thus 0.33 M KCl was selected for the study.

The influence of thallium(III) concentration on the sensitivity was studied in the range $0.8–16 \times 10^{-5}$ M, with pH 7.0 in 0.33 M KCl solution. The intensity of the fluorescence signal increased slightly as the thallium(III) concentration increased up to 7.8×10^{-5} M, and was constant at higher concentration (Fig. 5). The thallium(III) concentration of the reagent was therefore chosen as 7.8×10^{-5} M.

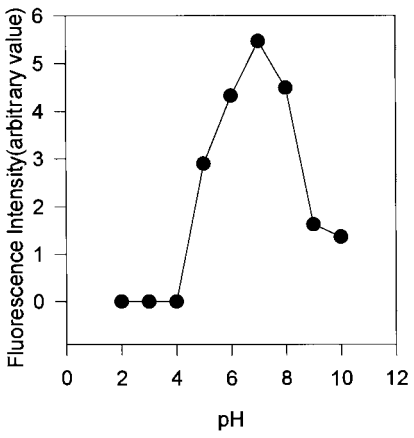

Fig. 3. Effect of pH on the sensitivity.

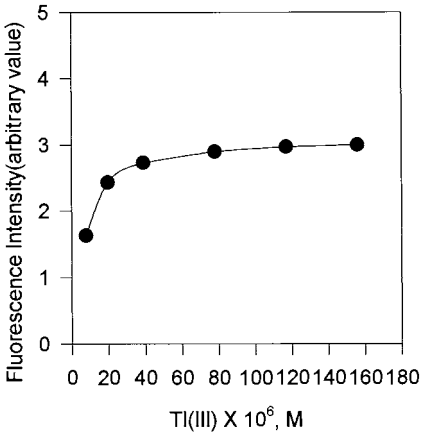

Fig. 5. Effect of thallium concentration on the sensitivity.

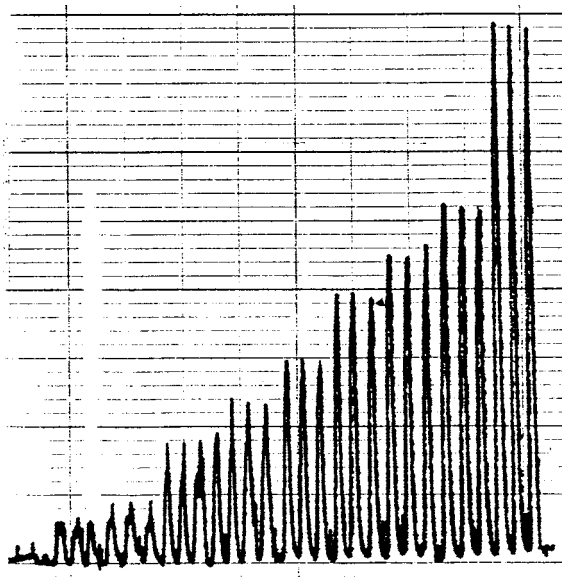

Fig. 6. Plot of the fluorescence signal obtained using the optimized conditions: (a) 25.6, (b) 38.4, (c) 64.0, (d), 100.0, (e) 135.0, (f) 192.0, (g) 256.0, (h) 320.0 and (i) 500.0 ng ml^{-1} hydrazine.

3.2. Influence of manifold variables

The effect of pump flow rate, sample loop volume and length of the reaction coil were studied with the optimum reagent concentration and pH 7.0 at 30°C, with 0.20 mg ml^{-1}.

The peak height obviously depends on the residence time of the sample zone in the system (on the flow rate and tube length). Low flow rates gave higher fluorescence intensities, although at a flow rate lower than 7.7 ml h^{-1} for each channel the peak height reproducibility was poor and the peaks were very broad and sample throughput was thus very low. Thus a flow rate of 7.7 ml h^{-1} for each channel was selected as the best compromise between reproducibility, sensitivity and throughput.

The influence of sample loop volume was studied with a pump flow rate of 7.7 ml h^{-1} and reaction coil length of 60 cm. The sample volume was varied between 10 and 180 μl. The peak heights increased with increasing volume injected up to 50 μl, above which they remained virtually constant. Thus a sample volume of 50 μl was chosen for further experiments.

The effect of reaction coil length on the fluorescence intensity was studied using the other optimized manifold parameters. Reaction coils measuring 10–200 cm were tested. There was an increase in sensitivity with increased reactor length up to 50 cm, above which the signal decreased slightly. Thus the length chosen for the reaction coil was 50 cm.

3.3. Calibration graph and precision

Under the optimum conditions described above, a series of standard solutions of hydrazine was injected into the manifold to test the linearity of the calibration system (Fig. 6). For the concentration range 25–500 ng ml^{-1} a linear relationship between hydrazine concentration and fluorescence intensity was obtained with correlation coefficient of 0.9970 and a standard deviation of 1.3×10^{-3} for the slope.

The experimental limit of detection for hydrazine is 20 ng ml^{-1}. The relative standard deviations for ten replicate analyses of 100, 250 and 500 ng ml^{-1} were 3.5, 2.6 and 1.8%, respectively. The sampling rate was about 40 ± 5 samples h^{-1}.

3.4. Interference study

In order to validate of the possible analytical applications of the method, the effects of various

Table 1
Influence of other substances on the determination of 0.100 μg ml^{-1} hydrazine

Substances	Tolerance limit ($W_{species}/W_{hydrazine}$)
Cl^-, SO_4^{2-}, PO_4^{3-}, acetate, citrate, CO_3^{2-}, $C_2O_4^{2-}$, ClO_3^-, BO_3^-, Zn^{2+}, NH_4^+, acetone, EDTA, tartrate, methanol, ethanol	500[a]
SO_3^{2-}, Br^-, IO_3^-, Ni(II), Co(II), Hg(II), acetaldehyde, NH_4OCl	200
Formaldehyde, $S_2O_8^{2-}$, Cu(II), phenylhydrazine	10

[a] Maximum tolerance limit that was checked.

Table 2
Determination of hydrazine in water (at optimum reagent concentration and manifold variables)

Sample	Hydrazine added (ng ml^{-1})	Hydrazine found (ng ml^{-1})		Recovery (%) for the proposed method ($n=5$)
		This method	Standard method [20]	
River water	100	102 ± 2.8	101 ± 4.0	102
	150	145 ± 2.1	–	97
	200	195 ± 2.9	–	98
	250	248 ± 3.4	–	99
Drinking water	100	102 ± 2.2	103 ± 3.3	102
	150	147 ± 2.8	–	98
	200	196 ± 3.0	–	98

compounds, cations and anions on the determination of 100 ng ml^{-1} hydrazine was investigated. The results are given in Table 1. The tolerance limit was defined as the concentration of added species causing less than 3% relative error. Most compounds did not interfere with the determination of hydrazine.

3.5. Determination of hydrazine in water samples

In order to test the reliability of the method, it was applied to the determination of hydrazine in water samples. The determinations were made by the standard addition procedure, because of the unknown matrix of the samples, using the spectrophotometric method of Gutierrez et al. [20]. The results are shown in Table 2. The values showed good agreement and good recoveries of added hydrazine and agree with the other spectophotometric method [20].

4. Conclusion

The proposed method is a simple, selective, rapid, automatic and inexpensive technique for the determination of ultra trace amounts of hydrazine as low as 20 ng ml^{-1}. The method was used for the determination of hydrazine in water samples and gave satisfactory results (Table 2). The results show that this method is a suitable method for determination of hydrazine in water without the need for any separation from interfering substances.

References

[1] F. Dias, A.S. Olojola, B. Joselskis, Talanta 26 (1979) 47.
[2] A. Safavi, A.A. Ensafi, Anal. Chim. Acta 300 (1995) 307.
[3] E.A. Maleki, M.K. Koupparis, Talanta 36 (1989) 431.
[4] J. Huamin, H. Weiying, W. Erkany, Talanta 39 (1992) 45.
[5] S. Ikeda, S. Sutake, Y. Kohri, Chem. Lett. 6 (1984) 873.
[6] W. Jeffrey, R. Rehrsson, L. Susan, L. Todd, Am. Ind. Hyg. Assoc. J. 54 (1993) 285.
[7] J. Wang, Z. Lu, Electroanalysis 1 (1989) 517.
[8] N.M. Raatcliffe, Anal. Chim. Acta 239 (1990) 257.
[9] W. Hou, E. Wang, Anal. Chim. Acta 257 (1992) 275.
[10] K.M. Korfhage, K. Ravichandran, R.P. Baldwine, Anal. Chem. 56 (1984) 1514.
[11] J. Wang, T. Golden, R. Li, Anal. Chem. 60 (1988) 1642.
[12] J. Wang, N. Naser, L. Angnes, Anal. Chem. 64 (1992) 1285.
[13] M.C. Gutierrez, A. Gomez-Hens, D. Prez-Benditto, Anal. Chim. Acta 225 (1989) 115.
[14] M.L. Balconi, F. Sigon, M. Bargarello, R. Ferraroli, F. Realint, Anal. Chim. Acta 234 (1990) 167.
[15] W.D. Basson, J.F. Staden, Analyst 103 (1978) 998.
[16] A.A. Ensafi, B. Naderi, Microchem. J. 56 (1997) 269.
[17] A. Rios, M.D. Luque De Castro, M. Valcarcel, Anal. Chim. Acta 187 (1986) 139.
[18] M.L. Balconi, F. Sigon, M. Borgarello, R. Ferraroli, F. Realini, Anal. Chim. Acta 234 (1990) 167.
[19] G.F. Kirkbright, T.S. West, C. Woodward, Talanta 12 (1965) 517.
[20] M.C. Gutierrez, A. Gomez-Hens, D. Prez-Bendito, Anal. Chim. Acta 225 (1989) 115.

ELSEVIER

Talanta 47 (1998) 651–658

Talanta

Amperometric detection with microelectrodes in flow injection analysis: theoretical aspects and application in the determination of nitrite in saliva

Vânia Mori, Mauro Bertotti *

Instituto de Química, Universidade de São Paulo, São Paulo SP 05599-970, Brazil

Received 14 November 1997; received in revised form 23 February 1998; accepted 26 February 1998

Abstract

The construction of a wall-jet cell with amperometric detection using a set of disc electrodes whose radii ranged from 5 to 750 μm has been proposed. The influence of some experimental parameters like flow rate and electrode radius on hydrodynamic voltammograms recorded for a 0.5 mmol dm^{-3} potassium ferrocyanide solution also containing 0.1 mol dm^{-3} KCl has been discussed. Some considerations regarding the current signals obtained from flow injection experiments using both a 5- and a 750-μm radius platinum electrode were carried out in order to achieve the lowest limit of detection, a value of 0.03 μmol dm^{-3} ferrocyanide being calculated by using the 5-μm radius microelectrode as amperometric detector. The wall-jet cell has been used in the determination of nitrite in saliva by quantifying the triiodide formed in the reaction of the analyte with excess iodide in acidic medium. A 12.5-μm platinum disc microelectrode maintained at + 0.2 V vs. Ag/AgCl was used as amperometric detector. Peaks obtained in fiagrams after injection of diluted saliva to the carrier stream containing 0.1 mol dm^{-3} sulphuric acid and 20 mmol dm^{-3} potassium iodide were compared to an analytical curve obtained in the same conditions ($r^2 = 0.997$) for a nitrite concentration in the range 1–10 μmol dm^{-3}. The concentration of nitrite in the saliva sample after the appropriate correction for dilution was found to be 2.3 ppm (0.05 mmol dm^{-3}), in a good agreement with results obtained by using a standard spectrophotometric procedure (2.5 ppm). The limit of detection of the method was calculated as 0.2 μmol dm^{-3}, and the reproducibility was checked by measuring the peak current for 19 injections of 10 μM nitrite, the standard deviation being 3.7%. © 1998 Elsevier Science B.V. All rights reserved.

Keywords: Flow injection analysis; Amperometric detection; Wall-jet cell; Microelectrode; Nitrite; Saliva

1. Introduction

Microelectrodes have been recently used in analytical determinations as amperometric detectors in flow cells, high-performance liquid chromatography and capillary electrophoresis, and they are particularly important when studies are to be performed in highly resistive media or without the deliberate addition of supporting electrolytes [1–4]. Also of importance is the possibility of introducing an extra domain for resolution of analytes

* Corresponding author. Fax: + 55 11 8155579; e-mail: mbertott@quim.iq.usp.br

0039-9140/98/$ - see front matter © 1998 Elsevier Science B.V. All rights reserved.
PII S0039-9140(98)00121-0

by recording consecutive voltammograms as the solution containing the electroactive species moves past the electrode [5,6]. This can only be attained at scan rates fast enough, justifying the need for microelectrodes since problems associated with both background increase and distortion in the wave shape are minimised. Another approach consists of using an assembly of independent microelectrodes parallel to the flowing solution, all of them held at a different potential by means of a multipotentiostat [7].

The present demand for the development of analytical methods for the quantification of chemical species in a variety of matrices of biological, clinical and environmental interest has contributed to the development of flow injection analysis (FIA). FIA utilises an unsegmented flowing stream into which reproducible sample volumes are injected [8]. With the advent of automation, some improvements concerning reproducibility, cost, simplicity and versatility have also been seen causing FIA to gain popularity in recent years. In spite of the relative lack of selectivity, FIA with amperometric detection is a field that has experienced growing attention because of the low cost of the instrumentation and its high sensitivity. In recent years, these advantages have been improved by using microelectrodes as amperometric detectors because of the possibility of using an easier instrumentation (a two-electrode configuration is sufficient for most of the cases) and the theoretical attainment of lower limits of detection. Accordingly, this work reports some studies concerning the electrochemical detection in a wall-jet cell where platinum disc microelectrodes were used as working electrodes. From an analytical point of view, the employment of microelectrodes in convective systems should lead to lower limits of detection, because in this approach higher mass-transfer rates are to be found under steady-state conditions where capacitive and resistive phenomena are alleviated. The chemical system chosen for the study was a solution containing ferrocyanide as electroactive species and potassium chloride as carrier solution, since in this medium the oxidation of ferrocyanide allows reversible one-electron voltammetric waves to be obtained owing to the high value for the heterogeneous electron transfer rate constant [9]. Some comparisons between the responses obtained with different sized microelectrodes and a conventional sized platinum electrode are made, as well as considerations regarding the influence of flow rate. We will also show that the constructed wall-jet cell with a microelectrode as amperometric detector offers advantages when measuring peaks for analytes at a sub-μmol dm^{-3} level, and some practical results of this association will be presented in a procedure developed for the determination of nitrite in saliva by flow injection analysis.

2. Experimental

2.1. Reagents

All chemicals used were of analytical reagent grade and no further purification step was carried out. Potassium ferrocyanide and sodium nitrite were obtained from Merck (Darmstadt, Germany), as were potassium iodide and potassium chloride (Rio de Janeiro, Brazil). Sulphanilic acid (Carlo Erba, Milan, Italy) and α-naphthylamine (Merck, Germany) were used in the spectrophotometric method for nitrite. Solutions were prepared by dissolving the respective salts in double-distilled water which was deionised in a Millipore system.

2.2. Apparatus

The flow cell was a wall-jet type, where the stream flows from a nozzle (0.5 mm i.d.) perpendicularly onto the working electrode surface. The body of the cell was made of plastic, the reference electrode being a silver wire covered by silver chloride immersed in a glass tube containing 3 mol dm^{-3} KCl. The auxiliary electrode was a steel wire. A platinum disc ($r = 0.75$ mm) and platinum disc microelectrodes ($r = 5$, 12.5 and 25 μm) were used as working electrodes, all of them positioned through the centre of the electrochemical cell in order that they sat well below the level of the running solution outlet. The best lateral positioning was achieved by measuring the steady-

state currents for all electrodes at a potential corresponding to the limiting region for the system ferrocyanide + potassium chloride ($E = +0.5$ V) as the displacement was carried out. Since the nozzle diameter was significantly larger than the radii of the microelectrodes, slight movements from the centred position were found not to lead to changes on the current signal. The distance from the tip of the nozzle to the electrodes surface was approximately 0.5 mm and, as reported by Macpherson et al. [10,11], we have noticed that a manual positioning was enough to achieve maximum and reproducible signals. Microelectrodes were constructed by sealing platinum microfibers (Goodfellow, Cambridge, UK) in glass pipettes, cutting perpendicular to the wire and polishing with emery paper and alumina (0.3 μm) on a very wet pad. In order to remove alumina particles, the cleaning of the microelectrodes was accomplished by rinsing the surface with a direct stream of water from a wash bottle and leaving them in an ultrasonic bath for 10 min. Electrical contact from the microfiber to a Ni/Cr wire was made by filling the glass pipette with conducting epoxy. The radii of the microelectrodes were checked by measuring the steady-state limiting currents from voltammograms recorded at slow scan rate (5 mV s^{-1}) in a standardised ferrocyanide solution in 1.0 mol dm^{-3} KCl medium and deviations not larger than 5% from the radii stated by the manufacturer were found assuming $D = 6.3 \times 10^{-6}$ cm^2 s^{-1} for the diffusion coefficient of ferrocyanide. For all microelectrodes the 'log plot' analysis of the voltammetric waves recorded at room temperature ($T = 23 \pm 2$°C) led to values from 58 to 60 mV, which are in agreement with the expected one for a reversible one-electron process under steady-state conditions (59.16 mV at 25°C). Current signals were recorded connecting the output of the potentiostat (CV-27, Bioanalytical Systems (BAS), West Lafayette, USA) to a strip-chart recorder (XYT, BAS). The cell was placed in a Faraday cage and the current signals were amplified by using a pre-amplifier (BAS low current module). The carrier flow was delivered by gravity and to achieve larger flow rate values it was also used a Gilson Minipuls 3 peristaltic pump. Samples were introduced to the carrier electrolyte with a home-made manual injection manifold. The injection loop was maintained constant in all experiments (100 μl) and the tube internal diameter was 1 mm (PTFE tubing). The tube length from the injection valve to the cell was 25 cm.

2.3. Analysis of saliva

Human saliva samples were collected and centrifuged at 1000 rpm for 20 min to separate insoluble materials. In order to minimise problems associated with poisoning the electrode surface by proteins contained in the matrix, saliva samples were 20-fold diluted in a calibrated flask. The solutions were analysed just after the dilution process.

2.4. Spectrophotometric analysis of nitrite [12]

To standards of nitrite and saliva samples, a sulphanilic acid solution prepared in 0.1 mol dm^{-3} HCl was added and the resulting solutions were let to stand for 5 min. Then, an α-naphthylamine solution in 0.3 mol dm^{-3} HCl was added and, after 10 min, the absorbance of the solutions was measured at 550 nm in a Micronal B382 spectrophotometer (São Paulo, Brazil).

3. Results and discussion

3.1. Voltammetric experiments in flowing system

The voltammogram for a 0.5 mmol dm^{-3} $Fe(CN)_6^{4-}$ + 0.1 mol dm^{-3} KCl solution was recorded at a slow scan rate (10 mV s^{-1}) in a quiescent solution for all set of electrodes and this procedure was repeated at increasing flow rate conditions, so a set of hydrodynamic voltammograms was recorded as well. Fig. 1 shows the voltammetric curves obtained for both the 5-μm radius microelectrode and the conventional sized electrode, and for this latter the effect of the enhanced mass transport on the shape of the voltammogram is clearly seen since it changes from the expected peaked shape in stationary solution to the sigmoidal one when steady-state conditions are attained. Moreover, the high flux

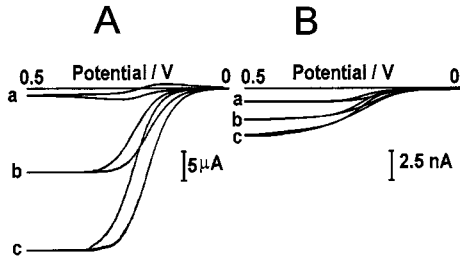

Fig. 1. Voltammogram for a 0.5 mmol dm^{-3} ferrocyanide solution in 0.1 mol dm^{-3} KCl at stationary solution (a) and the corresponding hydrodynamic voltammograms at 2.4 (b) and 3.8 ml min^{-1} (c). Working electrodes: 0.75-mm platinum disc electrode (A) and 5-μm platinum disc microelectrode (B).

of the electroactive material to the electrode when working at 3.8 ml s^{-1} causes a dramatic increase in the limiting current, which is not so pronounced for the microelectrode because the contribution of the convection is minimised due to the radial diffusion [13–16].

The limiting current for an electroactive species into a wall-jet detector depends on the flow rate of the running carrier, chemical properties of the system (concentration, viscosity, diffusion coefficient) and some physical parameters (the dimensions of both the nozzle and the electrode). Literature [17] reports that the current signal is influenced by the exponent of the flow rate, the power being 0.5 when the nozzle is much larger than the electrode and 0.75 in the opposite situation. In order for all data to be presented in the same figure, the ratio I_n/I_o was calculated, where I_n is the limiting current obtained for a voltammogram recorded at the nth flow rate and I_o is the limiting current for the voltammogram recorded at a quiescent solution. Fig. 2 shows a plot of the dependency of I_n/I_o on the square root of the flow rate. Data for three different sized microelectrodes are shown, as well as data for the conventional sized platinum electrode. For this latter, the

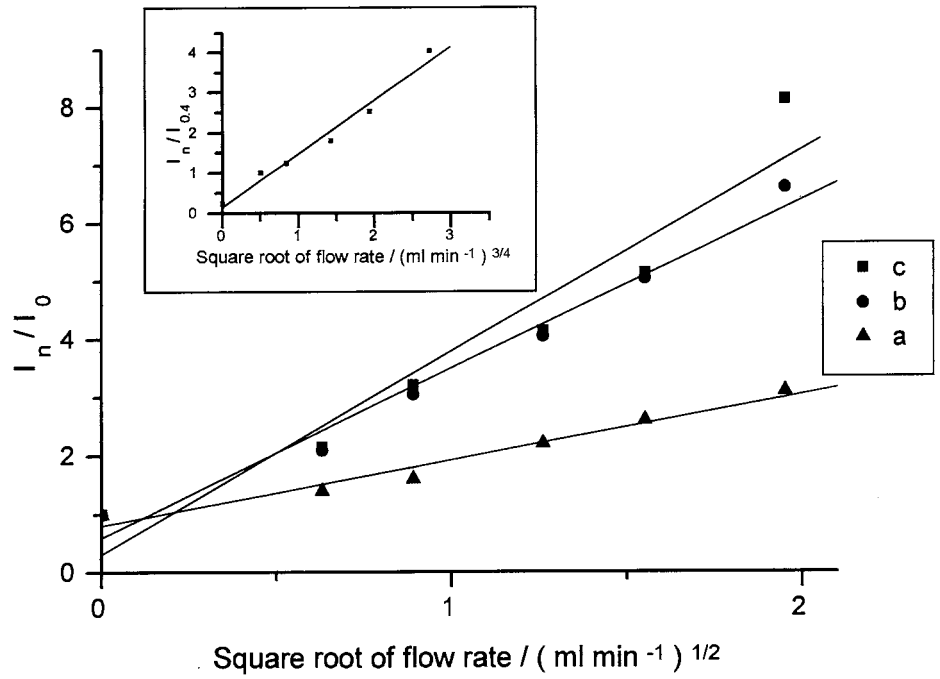

Fig. 2. Dependence of the ratio I_n/I_o on the square root of the flow rate for a 5- (a), 12.5- (b) and 25-μm (c) radius microelectrode. The inset shows the same dependence for a 0.75-mm radius electrode. I_n corresponds to the limiting current measured in the steady-state voltammograms for a 0.5-mmol ferrocyanide + 0.1 mol dm^{-3} KCl solution at the nth flow rate and I_o is the current value for a stationary solution, except that for the 0.75-mm radius electrode where I_o corresponds to the limiting current for the flow rate 0.4 ml min^{-1}.

I_o value adopted was the limiting current for the flow rate 0.4 ml min^{-1} where a steady-state situation was firstly obtained. For both the 5- and 12.5-μm radius microelectrodes the experimental data agree fairly well with the theory predictions, and for the 25-μm microelectrode a small deviation was observed. However, the exponential dependency is different from 0.5 for the 0.75-mm radius electrode, whereas the inset of Fig. 2 shows that the limiting current data for this electrode are nearly proportional to the 0.75 power flow rate dependency, in agreement with the theory.

3.2. Flow injection studies

Studies involving the current dependence on flow rate have already been reported for both flow through thin layer and wall-jet cells with a microelectrode used as electrochemical sensor [18–20]. In this work, systematic experiments in flowing solution were carried out by the injection of ferrocyanide solutions at different concentrations in a stream containing supporting electrolyte (0.1 mol dm^{-3} KCl) at 2.0 ml min^{-1}. We have observed the presence of very large spikes when diluted ferrocyanide solutions (below 1 μmol dm^{-3}) prepared in water were injected to the running solution, this phenomenon being presumably due to the significant change in the ionic medium when the sample reaches the electrode. Hence, ferrocyanide solutions were prepared in 0.1 mol dm^{-3} KCl to reduce the magnitude of the spikes. Fiagrams were recorded maintaining the potential of the electrodes at the limiting current region for the electroactive species (+0.5 V). Peak currents measured in triplicate for all electrodes were normalised to be compared in the same scale by calculating the respective current density (Table 1). As expected, current density values are much larger as the radius of the electrode decreases owing to the high mass transport rate inherent to electrodes of micrometer dimensions. Focusing on analytical aspects, the corrected sensitivity (ratio between peak current density and concentration) for both the 5-μm and the 0.75-mm radius electrodes was calculated by measuring current peaks in fiagrams obtained by injecting ferrocyanide in concentrations ranging from 0.2 to 1 μmol dm^{-3} to the carrier solution. Based on the slopes of both graphs the corrected sensitivity for the 5-μm radius microelectrode (21.4 mA m^{-2} μmol^{-1} dm^3) was calculated to be 5 times as many as the value for the conventional sized electrode, in accordance with the data shown in Table 1.

Table 1
Dependence of the current density on the radii of the electrodes

Electrode radius (μm)	Current density (mA m^{-2})
750	2.5
25	6.5
12.5	9.2
5	10.9

Currents at $E = +0.5$ V measured on fiagrams for the injection of 0.5 μmol dm^{-3} ferrocyanide to the wall-jet detector. Flow rate, 2.0 ml min^{-1}.

In order to find out the lower limit of detection with the proposed flow system configuration using ferrocyanide as electroactive species, experiments were carried out with all set of electrodes. Fig. 3 presents the results for triplicate injections of ferrocyanide solutions (from 0.05 to 1 μmol dm^{-3}) using both a 5-μm and a 0.75-mm radius electrode. At very large sensitivities, injection spikes attributable to the injector valve rotation are noticeable in some of the fiagrams but they did not interfere in the measuring of the analytical signals. It is clearly seen that a better discrimination be-

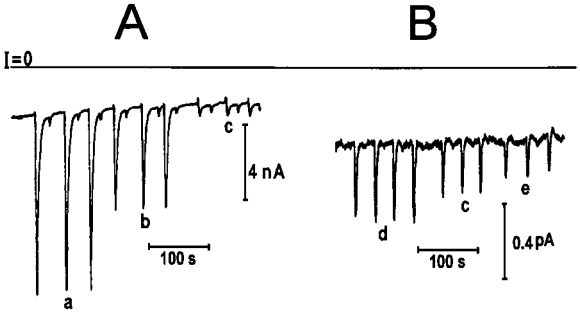

Fig. 3. Flow injection signals for injections of 1 (a), 0.5 (b), 0.2 (d), 0.1 (c) and 0.05 μmol dm^{-3} (e) ferrocyanide solutions also containing 0.1 mol dm^{-3} KCl to the wall-jet cell. Working electrodes: 750 (A) and 5 μm (B) platinum disc. Potential, +0.5 V; flow rate, 2.0 ml min^{-1}.

tween faradaic signal and background noise is obtained with the microelectrode, justifying its use as an amperometric detector in flow analysis when the concentration of the electroactive species is so low that the signal is not detectable by using a conventional sized electrode. Ferrocyanide concentrations as low as 0.03 μmol dm^{-3} were capable to be determined (calculated as 3 times the standard deviation of the blank) with this configuration and owing to the small microelectrode area, currents in the range of a few hundreds of fA were measured. This was found to be the lower limit of detection with the current instrumentation and it was only governed by the electronic noise since changes in the double layer capacity were minimised by injecting the electroactive species in a solution containing 0.1 mol dm^{-3} KCl. Therefore, even lower analyte concentrations could be measured with no pulse techniques with a further improvement in instrumentation to reduce even more the electronic noises.

A significant linear coefficient in the calibration plot was noticed using the data for the 5-μm radius microelectrode shown in Fig. 3 and we have no conclusive explanation for this fact. The following calibration plot was to be found in the mentioned ferrocyanide concentration range: I (pA) $= 1.06 C_{\text{ferrocyanide}}$ (μmol dm^{-3}) $+ 0.09$, the correlation coefficient r^2 being 0.998. At a more extended ferrocyanide concentration range (from 0.05 to 1.0 μmol dm^{-3}) the linear coefficient was less significant (0.04), the slope being 1.44 pA μmol^{-1} dm^3 ($r^2 = 0.998$).

3.3. Nitrite determination in saliva by FIA

Saliva constitutes one of the major sources of man's exposure to nitrite, a compound produced because of the microbial reduction of nitrate in the oral cavity [21]. Since nitrite can lead to the formation of various carcinogenic *N*-nitroso compounds after reaction with amines and amides, abundant in foods, its quantification is of concern and several methods have been proposed, the most used being the classical Griess method in which the absorbance of the products generated in the reaction of nitrites with an aromatic primary amine is measured and compared with a reference curve [12]. Besides spectrophotometric methods based on the formation of azo-dies compounds, other reported techniques for the determination of nitrite are also of importance including fluorimetry [22], chromatography [23] and chemiluminescence [24].

Electrochemical procedures for nitrite quantification based on its reduction have received attention in the last years but a very significant drawback is the highly acidic condition needed for the reduction to take place, which can cause some errors due to loss of the analyte [25]. On the other hand, methods based on the anodic oxidation of nitrite are lacking in selectivity since this process occurs at potentials so positive that much interference is to be expected [26]. Problems associated with high overpotential or passivation of bare electrodes have been overcome by covering the surface with some catalysts or by pre-treatment procedures [27,28].

A useful possibility for the amperometric analysis of nitrite is based on the stoichiometric oxidation of iodide by nitrite and further quantification of the generated triiodide at a more amenable potential [29,30]. The choice of the potential for monitoring the triiodide formed in the reaction involving the analyte and iodide was based on hydrodynamic voltammograms of iodide and iodine solutions, $+0.2$ V being a potential where neither the oxidation of iodide nor the reduction of dissolved oxygen are of great concern at the range of nitrite concentrations studied. The main reaction can be expressed as follows in acidic medium with excess of iodide:

$$2NO_2^- + 3I^- + 4H^+ \rightleftharpoons I_3^- + 2H_2O + 2NO$$

The flow injection procedure with a microelectrode detector (radius = 12.5 μm) was used in the analysis of nitrite by injecting conveniently diluted aliquots of saliva to a carrier stream containing iodide. In order to minimise the large spikes caused by the change in the ionic medium, saliva samples were diluted with a 20 mmol dm^{-3} KI solution. According to Abeledo and Kolthoff [31], no formation of iodine is expected to occur from the reaction between iodide and nitrite at neutral medium, but the chemical reaction is fully complete when the sample mixes with the running

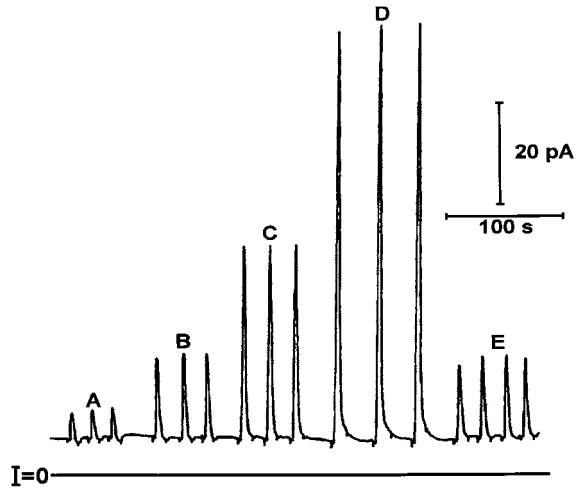

Fig. 4. Fiagrams for nitrite standard solutions (A–D) and saliva (E) obtained in the wall-jet flow system with amperometric detection (12.5 μm radius microeletrode). Potential, +0.2 V; concentration of nitrite in the standard solutions, 1 (A), 2.5 (B), 5 (C) and 10 μmol dm^{-3} (D); Flow rate, 1.4 ml min^{-1}.

solution (20 mmol dm^{-3} KI + 0.1 mol dm^{-3} sulphuric acid). Fig. 4 shows some fiagrams of nitrite additions (1–10 μmol dm^{-3} range) to the running solution and the fiagrams obtained after the injection of a diluted sample of human saliva, resulting in the following calibration plot: I (pA) = $8.6C_{nitrite}$ (μmol dm^{-3}) − 4.9, with a regression coefficient $r^2 = 0.997$. The negative linear coefficient may be explained by charging current effects due to the differences in the composition of the carrier solution and the sample, this problem having not been observed in the ferrocyanide system owing to the similar chemical composition of both solutions. The amount of nitrite contained in the saliva sample was found to be 2.5 μM (two determinations), in a good agreement with the results of the spectrophotometric analysis (2.7 μM). Taking into account the dilution of the saliva sample, the nitrite content in the original sample was calculated to be 2.3 ppm, which is consistent with other values reported in the literature [24]. In order to confirm that there was no interference from the matrix after the 20-fold dilution of saliva, samples were spiked with nitrite to check the recovery of the method. The average recoveries for addition of a standard solution of nitrite to volumetric flasks containing saliva were found to be 106% by measuring the current peaks in the fiagrams using the 5-μm radius microelectrode as detector. The reproducibility of the method was found to be 3.7% by measuring the peak current for 19 repetitive injections of 10 μM nitrite, with an optimum analytical throughput of 120 h^{-1} at a 1.4 ml min^{-1} flow rate. The limit of detection for nitrite determinations was calculated to be 0.2 μmol dm^{-3} (S/N = 3), this value being higher when compared to the ferrocyanide determination. This fact may be justified by the dispersion of the sample containing nitrite due to the chemical reaction of the analyte with iodide and sulphuric acid occurring at a lower flow rate value (1.4 ml min^{-1}).

The agreement between the results obtained by using the flow injection amperometric procedure and the spectrophotometric method shows that saliva contains no other oxidising species other than nitrite capable of reacting with iodide. Some metallic ions such as Cu(II) and Fe(III) could have this role in acidic medium but no variation in the current signal was observed after addition of EDTA to the diluted saliva samples.

Using microelectrodes as amperometric detectors in wall-jet systems presents some attractive features which include the possibility of reaching lower limits of detection owing to the increased faradaic to noise ratio. Also of importance is the fact that the proposed association makes unnecessary more expensive potentiostats where pulse techniques are available, so in an amperometric mode a simpler instrumentation could be used to apply the potential to the electrochemical cell. On the other hand, when the ionic environment of the sample and the carrier solution are very different the existence of relatively large current spikes are of concern and the faradaic signal may be distorted even by using microelectrodes at analyte concentrations in the sub-μmol dm^{-3} level. In these situations, a useful approach consists of injecting the sample in a solution with a chemical composition as close as possible to the running electrolyte.

Acknowledgements

This work was supported by CNPq (Conselho Nacional de Pesquisa e Desenvolvimento Tecnológico) and FAPESP (Fundação de Amparo à Pesquisa do Estado de São Paulo).

References

[1] J.E. Baur, E.W. Kristensen, R.M. Wightman, Anal. Chem. 60 (1988) 2334.
[2] C. Hua, K.A. Sagar, K. McLaughlin, M. Jorge, M.P. Meaney, M.R. Smyth, Analyst 116 (1991) 1117.
[3] R.J. Tait, P.C. Bury, B.C. Finnin, B.L. Reed, A.M. Bond, Anal. Chem. 65 (1993) 3252.
[4] F.-M. Matysik, A. Meister, G. Werner, Anal. Chim. Acta 305 (1995) 114.
[5] W.L. Caudill, A.G. Ewing, S. Jones, R.M. Wightman, Anal. Chem. 55 (1983) 1877.
[6] J.M. Slater, E.J. Watt, Analyst 119 (1994) 273.
[7] W.L. Caudill, J.O. Howell, R.M. Wightman, Anal. Chem. 54 (1982) 2533.
[8] J. Ruzicka, E.H. Hansen, Anal. Chim. Acta 78 (1975) 145.
[9] K. Winkler, J. Electroanal. Chem. 388 (1995) 151.
[10] J.V. Macpherson, S. Marcar, P.R. Unwin, Anal. Chem. 66 (1994) 2175.
[11] J.V. Macpherson, M.A. Beeston, P.R. Unwin, J. Chem. Soc. Faraday Trans. 91 (1995) 899.
[12] A.I. Vogel, A Textbook of Quantitative Inorganic Analysis, 4th ed., Longman, London, 1978.
[13] R.M. Wightman, Anal. Chem. 53 (1981) 1125A.
[14] A.G. Ewing, J.C. Bigelow, R.M. Wightman, Science 221 (1983) 169.
[15] S. Pons, M. Fleischmann, Anal. Chem. 59 (1987) 1391A.
[16] M. Fleischmann, S. Pons, D.R. Rolison, P.P. Schimdt, Ultramicroelectrodes, Datatech Systems, Morgantown, NC, 1987.
[17] K. Stulik, V. Pacakova, Electroanalytical Measurements in Flowing Liquids, Ellis Horwood, Chichester, UK, 1987.
[18] R.J. Tait, A.M. Bond, B.C. Finnin, B.L. Reed, Collection Czech. Chem. Commun. 56 (1991) 192.
[19] R.J. Tait, P.C. Bury, B.C. Finnin, B.L. Reed, A.M. Bond, J. Electroanal. Chem. 356 (1993) 25.
[20] W.W. Kubiak, M.M. Strozik, J. Electroanal. Chem. 417 (1996) 95.
[21] S.R. Tannenbaum, A.J. Sinskey, M. Weissman, W. Bishop, J. Natl. Cancer Inst. 53 (1974) 79.
[22] P. Damiani, G. Burini, Talanta 33 (1986) 649.
[23] T. Mitsuhashi, J. Chromatogr. 452 (1988) 295.
[24] N.P. Sen, P.A. Baddoo, S.W. Seaman, J. Chromatogr. 673 (1994) 77.
[25] B. Keilin, J.W. Otvos, J. Am. Chem. Soc. 68 (1946) 2665.
[26] S.M. Silva, C.R. Alves, S.A.S. Machado, L.H. Mazo, L.A. Avaca, Electroanalysis 8 (1996) 1055.
[27] A.P. Doherty, M.A. Stanley, D. Leech, J.G. Vos, Anal. Chim. Acta 319 (1996) 111.
[28] M. Bertotti, D. Pletcher, J. Braz. Chem. Soc. 8 (1997) 391.
[29] M. Trojanowicz, W. Matuszewski, B. Szostek, J. Michalowski, Anal. Chim. Acta 261 (1992) 391.
[30] M. Bertotti, D. Pletcher, Anal. Chim. Acta 337 (1997) 49.
[31] C.A. Abeledo, I.M. Kolthoff, J. Am. Chem. Soc. 53 (1931) 2893.

ELSEVIER

Talanta 47 (1998) 659–663

Talanta

The simple and rapid spectrophotometric determination of trace chromium(VI) after preconcentration as its colored complex on chitin

Suwaru Hoshi [a,*], Kiyotaka Konuma [a], Kazuharu Sugawara [a], Masayuki Uto [b], Kunihiko Akatsuka [a]

[a] *Department of Applied and Environmental Chemistry, Kitami Institute of Technology, 165 Koen-cho, Kitami-shi 090-8507, Japan*
[b] *Department of Functional Materials, Kitami Institute of Technology, 165 Koen-cho, Kitami-shi 090-8507, Japan*

Received 15 December 1997; received in revised form 18 February 1998; accepted 26 February 1998

Abstract

Preconcentration method with collection of metal complexes on a chitin has been applied to the spectrophotometric determination of chromium(VI) in water. The chromium(VI) is collected as its 1,5-diphenylcarbazide(DPC) complex on a column of chitin in the presence of dodecyl sulfate as counter-ion. The Cr-DPC complex retained on the chitin is eluted with a methanol-1 M acetic acid mixture (7:3, v/v), and the absorbance of the eluent is measured at 541 nm. Beer's law is obeyed over the concentration range of 0.05–0.6 μg of chromium(VI) in 1 ml of the eluent. The apparent molar absorptivity is 3.5×10^4 dm^3 mol^{-1} cm^{-1}. The tolerance limits for Fe(III) is low, i.e. ten times that of chromium(VI), but some metal ions and common inorganic anions do not interfere in concentration range of 100–10000 times that of chromium(VI). The present method can be applied to the determination of chromium(VI) in natural water samples. © 1998 Elsevier Science B.V. All rights reserved.

Keywords: The spectrophotometric determination of trace chromium(VI); Chitin; Chromium-1,5-diphenylcarbazide complex; Preconcentration

1. Introduction

A natural amino polysaccharide chitin is a hydrophilic polymer and has structural similarities to cellulose. However, chitin is stable over a wide pH range of aqueous solution due to the strong polysaccharide structure which is formed through intermolecular hydrogen bonds between its acetylamino groups. Therefore, the spectrophotometric, atomic absorption spectromeric and electroanalytical methods for a large number of inorganic ions have been developed by using the collection process on chitin after their ions convert into each suitable species such as colored metal complexes and anionic species [1–16]. Chitin has the excellent properties as the support for solid-phase extraction, in which the collection

* Corresponding author. Fax: +81 157247719; e-mail: HOSHI-suwaru/chem@king.cc.kitami-it.ac.jp

0039-9140/98/$ - see front matter © 1998 Elsevier Science B.V. All rights reserved.
PII S0039-9140(98)00112-X

and elution of species is rapid [1–4], and its protonated acetylamino groups act as an anion-exchanger for various types of anionic species in a weak acidic medium [5–15].

Chromium(VI) is one of the toxic elements in the environment. It is difficult, however, to determine chromium directly in natural water samples because of its very low concentration level. In an attempt to overcome such a limitation, numerous methods for separation and preconcentration methods for chromium have been developed [17]. The 1,5-diphenylcarbazide (DPC) is widely used as the spectrophotometric reagent for chromium(VI) because it is one of the most sensitive and selective reagents. Attention has also been paid to the preconcentration methods for trace chromium using solvent extraction [18–21] and solid phase extraction on ion-exchange resin [22–24] and Amberlite XAD resin [25] prior to the spectrophotometric determination by DPC method. We also showed that chromium(VI) could be collected as its DPC complex on chitin in the presence of dodecyl sulfate (ds) ion [1].

The aim of the present paper is to develop the spectrophotometric method for chromium(VI) after the collection and elution as the ion-associate of its DPC complex with ds on a chitin. The proposed method was applied to the determination of chromium(VI) in natural water samples.

1.1. Experimental

1.2. Reagents

A commercially available purified chitin powder(Funakoshi, Japan) was washed successively with a 1 M hydrochloric acid solution, distilled water and methanol; it was then kept at 50°C for 24 h in a vacuum drying oven.

Standard chromium(VI) solution (1 mg ml^{-1}) was prepared by dissolving accurately weighed 0.3734 g of analytical grade potassium chromate(Wako Pure Chemical, Japan) in water and diluting to volume in a 100 ml standard flask and was further diluted as required. The 1,5-diphenylcarbazide (DPC) (Wako) was used the special grade for determination of chromium(VI) and other chemicals used were of analytical grade.

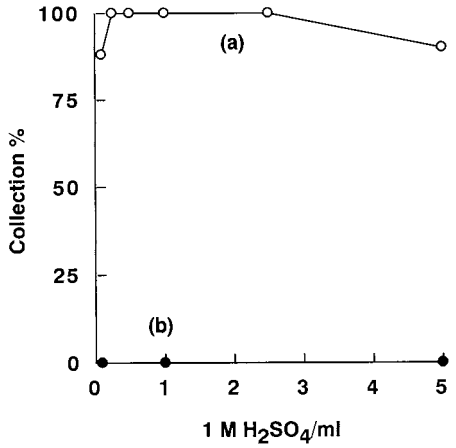

Fig. 1. Effect of sulfuric acid concentration on the collection: (a) In the presence of ds; (b) In the absence of ds. Condition as in standard procedure except for amount of 1 M H_2SO_4.

1.3. Apparatus

All absorbance measurements were made with a Shimadzu UV-2400 PC spectrophotometer with a black cell (light-path lengths 10 mm × light-path widths 2 mm, inner volume is about 1 ml). An Hitachi-Horiba Model F-7AD pH meter was used for all pH measurements.

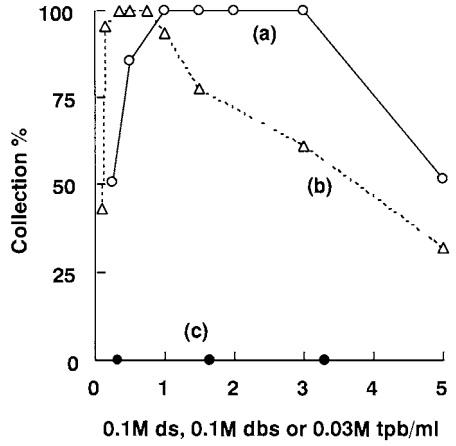

Fig. 2. Effect of counter-ion concentrations on collection: (a) 0.1 M ds; (b) 0.1 M dbs; (c) 0.03 M tpb. Condition as in standard procedure except for amounts of the counter-ions.

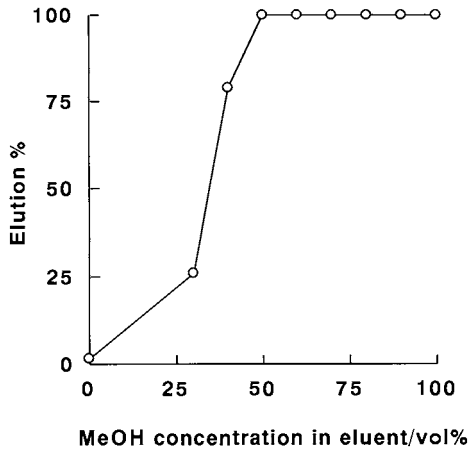

Fig. 3. Elution dependence of the chromium complex from chitin on methanol concentration in 1 ml of eluent. Condition as in standard procedure for 0.6 μg of chromium(VI) on the collection.

1.4. Standard procedure

To a 100 ml of solution containing up to 0.6 μg of chromium(VI) as chromate ion, add 1 ml of 1 M H_2SO_4 and 1 ml of 0.5(w/v)% DPC acetone solution, and after standing for 5 min, add 2 ml of 0.1 M Nads. Then pass the solution through a chitin column (polyethylene column, 6 mm i.d. × 60 mm long, 50 mg of chitin) fitted with a porous polyethylene disk with a 20 mm pore size at a flow-rate of 10 ml min^{-1}. Elute Cr-DPC complex with 1 ml of 7:3 v/v methanol–1 M acetic acid mixture, and measure the absorbance of the eluent at 541 nm against water.

Table 1
Effect of diverse ions on the determination of 0.3 μg of chromium(VI)

Ion added	Ion/Cr(VI) tolerated
F^-, Cl^-, ClO_4^-, NO_3^-, PO_4^{3-}	10 000
EDTA	5000
$Ca^{2+,a}$, $Mg^{2+,a}$, $Al^{3+,a}$, $Mn^{2+,a}$,MoO_4^{2-},WO_4^{2-}, VO_3^-	1000
$Co^{2+,a}$, $Ni^{2+,a}$, $Cu^{2+,a}$, $Zn^{2+,a}$, $Pb^{2+,a}$, $Ti^{4+,a}$, NO_2^-, $S_2O_3^{2-}$	100
$Fe^{3+,a}$	10

[a] 1500 μg of EDTA was added.

2. Results and discussion

2.1. Absorption spectra

The DPC method was selected for the determination of chromium(VI) because of simplicity for procedure and sensitivity for the determination of chromium(VI). The reagent conditions for the color reaction in sample solution were modified from the original DPC method [26], and chosen as described in the standard procedure. The Cr complex has absorption maximum at 541 nm in the eluent, where the reagent blank is almost negligible. Therefore, all absorbance measurements were carried out at 541 nm against water in this study.

2.2. Collection condition

Fig. 1 shows the effect of H_2SO_4 concentration on the collection of Cr-DPC complex on chitin. The quantitative collection of the Cr complex was obtained over a concentration range of 0.25–2.5 ml of 1 M H_2SO_4 in the presence of ds, but was not collected in the absence of counter-ion. The quantitative collection on the Cr complex was obtained over a concentration range of 0.25–2.5 ml of 0.5 (w/v)% DPC-acetone when 100 ml of sample solution contained 0.6 μg of chromium(VI) was used in the presence of ds. The effect of counter-ions on the collection was examined. Among the anions selected, tetraphenylborate (tpb) was not effective on the collection of the Cr complex. On the other hand, ds and dodecylbenzenesulfonate (dbs) were effective on the collection over a concentration range as shown in Fig. 2, respectively. It appears that the decrease of the collection percentage on chitin depends on the formation of the micelles in the higher concentration range of ds and dbs. It also seems that the difference between the collection behavior of ds and dbs, and tpb is due to the property of Cr-DPC complex formed, but the details are not presently clear. In this study, ds was mainly used because of its good reproducibility on the collection compared with that of dbs. The DPC and ds concentrations were decided as the standard procedure. Collection from a 100 ml of solution containing 0.6 μg of chromium(VI) on a column

Table 2
Analytical results for chromium(VI) in natural waters

Sample	Cr(VI) added (μg)	Cr(VI) found (μg)	Recovery (%)
Rain water	0.00	ND	—
	0.05	0.049	98.0
	0.10	0.102	102.0
	0.30	0.296	98.6
River water	0.00	0.019	—
	0.05	0.068	98.0
	0.10	0.117	98.0
	0.30	0.329	103.3
Spring water	0.00	0.017	—
	0.05	0.069	104.0
	0.10	0.122	105.0
	0.30	0.319	100.3

Sample volume for rain water: 50 ml; others: 100 ml; ND: not detected.

with various amounts (10–60 mg) of chitin was examined. The Cr complex was quantitatively collected on a column containing above 30 mg.

The effect of flow rate on the collection was examined. The flow rate of sample solution for the collection was varied from 5 to 30 ml min^{-1}. The column was aspirated over 5 ml min^{-1}. Chromium(VI) was quantitatively collected up to 20 ml min^{-1} of the flow rate.

Recoveries of 0.6 μg of chromium(VI) as Cr-DPC complex from various volumes over the range 100–500 ml. Chromium(VI) was quantitatively collected up to 300 ml of sample solution; up to 300-fold concentration could be easily achieved.

2.3. Eluent

From preliminary work [1], acetone, methanol, *N*,*N*-dimethylformamide (DMF) and their solvents mixture with 1 M acetic acid were tested as eluents. As results, the mixture of methanol with 1 M acetic acid (Fig. 3) was selected as eluent because of its reproducibility compared with those of acetone or DMF mixture, and 7:3 v/v methanol–1 M acetic acid mixture was used throughout in this study, because the absorbance of the eluent was not reproducible with over 90% of methanol concentration in the eluent. The Cr complex collected on the chitin was readily eluted with 1 ml of the eluent within 1 min. The absorbance of the eluent obtained was constant for at least 60 min.

Five successive collection and elution cycles with 0.6 μg of chromium(VI) on the same chitin gave almost identical results.

2.4. Calibration curve and precision

The calibration curve obtained by the standard procedure was linear over the concentration range of 0.05–0.6 μg of chromium(VI) in 1 ml of the eluent. The apparent molar absorptivity was 3.5×10^4 dm^3 mol^{-1} cm^{-1} at 541 nm. The relative standard deviation was 1.7% for 0.3 μg of chromium(VI) (five measurements).

2.5. Interferences

Table 1 shows the effect of diverse ions. The tolerance limit was taken as being the amount causing an error $\pm 3\%$ in the absorbance of the eluent for chromium(VI) alone. For the determination of 0.3 μg of chromium(VI), the tolerance limit for Fe^{3+} was low even in the presence of EDTA. The reducing agents, some metal ions in the presence of EDTA and oxoanions did not interfere in concentration up to 100–1000 times that of chromium(VI). The common anions and EDTA did not interfere in concentration up to 5000–10000 times that of chromium(VI).

2.6. Application

The method described was applied to the determination of chromium(VI) in natural water samples around our Kitami city. The samples were analyzed after filtration with a 0.45 μm cellulose acetate membrane filter. To each sample solution, a known amount of chromium(VI) was added and 1500 μg of EDTA was added to control metal ions in sample solutions. The percentage of recovery was estimated from the determination of chromium(VI) in the eluent. The results are summarized in Table 2. The recovery of chromium(VI) added for each water sample was almost complete. Thus, this method is particularly effective for the determination of chromium(VI) in natural water samples.

In conclusion, the collection of Cr-DPC complex on chitin is affected by counter-anions as shown in Fig. 3. The elution of the Cr complex from chitin is easily achieved by increasing the volume of methanol in the eluent. These facts suggested that most of the Cr complex is collected as the ion-associate with the counter-anions by hydrophobic interaction between the ion-associate and the surface of chitin. The presented method has the advantages of simplicity, rapidity and a high concentration factor on the preconcentration procedure, and makes it possible to determine chromium(VI) at sub ppb level.

References

[1] S. Hoshi, Y. Kamada, S. Inoue, M. Matsubara, Anal. Sci. 4 (1988) 227.
[2] S. Hoshi, M. Yamada, S. Inoue, M. Matsubara, Talanta 36 (1989) 606.
[3] S. Hoshi, Y. Tanaka, S. Inoue, M. Matsubara, Anal. Sci. 5 (1989) 471.
[4] S. Hoshi, M. Yamada, S. Inoue, M. Matsubara, Anal. Sci. 7 (1991) 657.
[5] S. Hoshi, S. Kanagami, M. Uto, M. Matsubara, Anal. Sci. 8 (1992) 103.
[6] S. Hoshi, T. Tomizuka, C. Enjo, Y. Haga, M. Uto, K. Akatsuka, Anal. Sci. 11 (1995) 729.
[7] S. Hoshi, K. Komuma, K. Sugawara, M. Uto, K. Akatsuka, Talanta 44 (1997) 1473.
[8] S. Hoshi, K. Komuma, K. Sugawara, M. Uto, K. Akatsuka, Anal. Sci. 13 (1997) 863.
[9] K. Komori, S. Igarashi, Y. Yotsuyanagi, Bunseki Kagaku 35 (1986) 890.
[10] H. Minamizawa, T. Hokazono, N. Arai, T. Okutani, Nippon Kagaku Kaishi (1993) 937.
[11] H. Minamizawa, N. Arai, T. Okutani, Bunseki Kagaku 42 (1993) 767.
[12] H. Minamizawa, N. Arai, Y. Tatehaba, T. Okutani, Nippon Kagaku Kaishi (1995) 512.
[13] H. Minamizawa, N. Arai, T. Okutani, Anal. Sci. 11 (1995) 961.
[14] H. Minamizawa, Y. Tatehaba, N. Arai, T. Okutani, Anal. Sci. 12 (1996) 947.
[15] Z-ping Bai, T. Nakamura, K. Izutsu, Anal. Sci. 6 (1990) 443.
[16] A. Hase, T. Kawabata, K. Terada, Anal. Sci. 6 (1990) 747.
[17] H. Onishi, Photometric Determination of Trace of Metals-Part IIA: Individual Metals Aluminium to Lithium, 4, Wiley, New York, 1986, p. 404.
[18] C.K. Mann, J.C. White, Anal. Chem. 30 (1958) 989.
[19] O. Kammori, A. Ono, Bunseki Kagaku 14 (1965) 1137.
[20] K. Shimokawa, H. Mori, H. Takada, Bunseki Kagaku 28 (1979) 437.
[21] K. Katsu, A. Ishibashi, Bunseki Kagaku 31 (1982) 191.
[22] K. Yoshimura, S. Ohashi, Talanta 25 (1978) 103.
[23] K. Ohzeki, T. Sakuma, T. Kambara, Bull. Chem. Soc. Jpn. 53 (1980) 2878.
[24] K. Yoshimura, Analyst 113 (1988) 471.
[25] S. Osaki, T. Osaki, Y. Takashima, Talanta 30 (1983) 683.
[26] H. Onishi, H. Koshima, Bunseki Kagaku 27 (1978) 727.

ELSEVIER

Talanta 47 (1998) 665–671

Talanta

Electrochemical detection of lectin using a galactosamine labeled with daunomycin

Kazuharu Sugawara [a,*], Hideki Kuramitsu [b], Suwaru Hoshi [a], Kunihiko Akatsuka [a], Shunitz Tanaka [b], Hiroshi Nakamura [b]

[a] *Kitami Institute of Technology, Kitami, Hokkaido 090, Japan*
[b] *Division of Material Science, Graduate School of Environmental Earth Science, Hokkaido University, Sapporo, Hokkaido 060, Japan*

Received 15 December 1997; received in revised form 25 February 1998; accepted 26 February 1998

Abstract

To detect a lectin from soybean, an electrochemical procedure was developed by the use of a labeling of galactosamine. Because the lectin has binding sites to galactosamine, galactosamine labeled with daunomycin having electroactivity was prepared. When labeled galactosamine (LG) combines with lectin, the part of daunomycin is taken in the binding sites of the lectin and becomes electroinactive. Therefore, the concentration of the lectin can be estimated by measuring the peak current of the LG. On the other hand, a competitive reaction to the lectin of galactosamine and the LG makes a detection of galactosamine possible. This method has merit that does not require a separation procedure of the free LG from the bound one. An effect of length of spacer between daunomycin and galactosamine was also investigated. It was found that adsorption of reagent on the electrode increased due to introduction of the spacer. Furthermore, the electrode response of the LG was influenced by the type of the spacer.
© 1998 Elsevier Science B.V. All rights reserved.

Keywords: Lectin; Galactosamine; Daunomycin-labeled galactosamine ligands; Voltammetric detection

1. Introduction

Lectin is glycoprotein or protein that has binding sites more than two per a molecular to sugar [1]. Recently, it has been discovered that lectin is widely distributed in unicellular and multicellular organisms [2–4]. Most of the lectins were discovered in plants, microorganisms and viruses. Several lectins are related to the aggregation of cell, catabolism of sugar in the blood, infection of bacterium, protection from infection, combination of the cellular and the formation of the cell organization. Lectin also forms precipitate of sugar residue of specific structure. Concanavalin A and phytohemagglutination as mitogens having the activity of division acceleration of lymphocyte are used to separate sugar from cell, based on specific binding [5–7]. Accordingly, the lectin is effective as a ligand to detect sugar and adsorbates to separate a sugar from sample matrix [8,9].

* Corresponding author. Tel.: +81 157269411; fax: +81 157247719; e-mail: sugawara/chem@king.cc.kitami-it.ac.jp

0039-9140/98/$ - see front matter © 1998 Elsevier Science B.V. All rights reserved.
PII S0039-9140(98)00114-3

Generally, the agglutination reaction of red cells is used to detect lectin. However, the method contains filtration and separation of reagent. Therefore, a more rapid and convenient method is needed to clear a biological function of the lectin in living body. This paper describes the voltammetric detection of lectin using labeled galactosamine (LG). In the previous study, avidin-biotin interaction that was known as one of the bindings strongly has been investigated by using biotin labeled with an electroactive compound [10–12]. The method can detect avidin and biotin on the basis of the binding between labeled biotin and avidin. This concept was applied to the sugar-lectin interaction. We prepared galactosamine labeled with electroactive daunomycin. From the structure, it is expected that daunomycin adsorbs on the electrode strongly and a sensitive accumulation voltammetry is achieved. When the LG reacts with lectin from soybean (SBA) that has specificity to galactosamine, the electroactive part is also covered with lectin. Because the molecular weight of lectin is larger than that of galactosamine, the covering makes the LG electroinactive. Consequently, lectin can be detected by the measurement of the peak current of LG indirectly. On the other hand, detection of galactosamine is possible when galactosamine competes with the LG to the binding sites of lectin. Furthermore, an effect of length (spacer) between daunomycin and galactosamine was discussed. The length of spacer of the LG brings steric hindrance to the binding. Therefore, voltammetric behavior of lectin was investigated by two LGs that the length of spacer was different.

2. Experimental

2.1. Reagents

Glycine max agglutinin from soybean (SBA), wheat germ agglutinin (WGA), peanut agglutinin (PNA), concanavalin A (Con A) were purchased from Sigma. SBA was dissolved in 0.1 M phosphate buffer (pH 7.0). D-Galactosamine hydrochloride was from WAKO Pure Chemicals, Japan. Ethylene glycolbis (sulfosuccinimidylsuccinate) (Sulfo-EGS) and bis(sulfosuccinimidyl)suberate (BS^3) (Pierce, USA) were used as spacer. Daunomycin was supplied from Sigma. Phosphate buffer was prepared with 0.1 M KH_2PO_4 and 0.1 M NaOH at pH 7.0. This buffer was used as an incubation solution and also as a supporting electrolyte for electrochemical measurement. High quality nitrogen gas was used for deaeration. All reagents were of analytical reagent grade, and water was deionized and distilled twice.

2.2. Apparatus

All voltammetric measurements were performed using a CV-50W voltammetric analyzer (Bioanalytical Systems (BAS), USA). The pH of the buffer solutions was measured with a Horiba D-13 pH-meter. Visible spectra of daunomycin and galactosamine labeled with daunomycin were measured with UV-2400 (PC) SGLP (Shimadzu, Japan).

2.3. Electrode

A glassy carbon electrode (model No. 11-2012, 3.0 mm diameter, BAS) was used as the working electrode. Before the experiments the electrode was washed in ethanol and 0.1 M nitric acid for 5 min and it was polished sequentially with 0.3, 0.05 mm. A platinum wire was used as a counter electrode and an Ag/AgCl electrode (model No. 3 11-2020, BAS) as a reference electrode. All potentials were measured against the Ag/AgCl electrode.

2.4. Preparation and separation of labeled galactosamine

LG was prepared by mixing 1.5 mM galactosamine, daunomycin and spacer in 500 μl of diethylformamide solution and 250 μl of 0.1 M phosphate buffer solution (pH 8.5) and incubating for 24 h at 4°C. The product was separated from unlabeled daunomycin and other by-products by thin-layer chromatography (silica gel 60

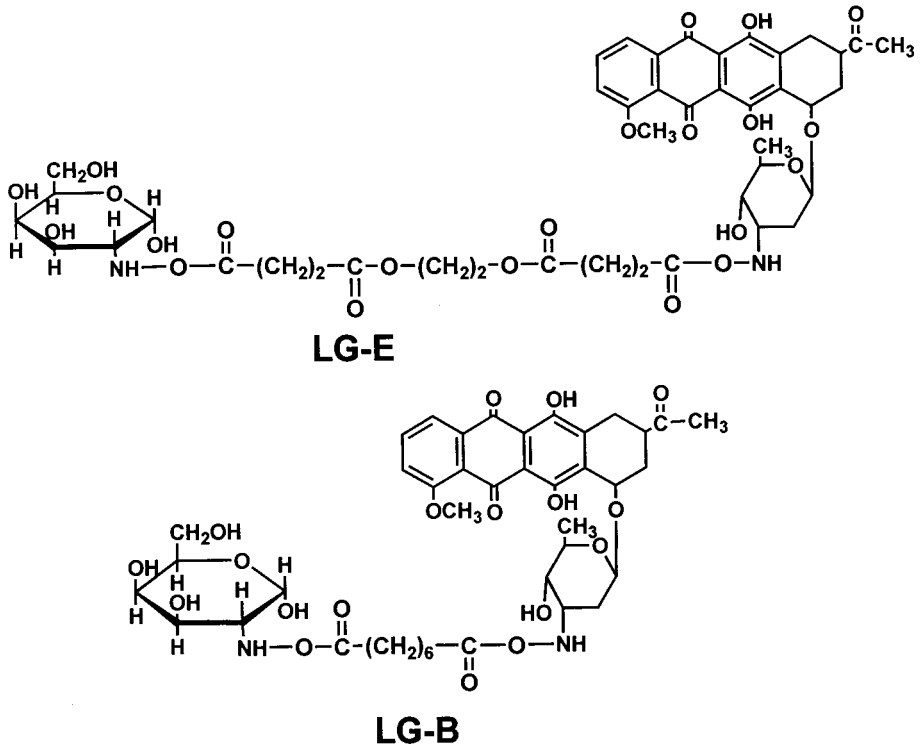

Fig. 1. Structure of labeled galactosamine prepared.

F_{254} alumina sheet, Merk). Developing solvent was used chloroform: ethanol (4:1(v/v)%). After developing, the portion of the silica gel adsorbing LG was stripped from the sheet and collected. The LG was dissolved in ethylalcohol, and then the solution was centrifuged to exclude silica gel. Since the visible spectrum of the product solution agrees with the spectrum of daunomycin the concentration was determined by the absorbance at 475 nm. Sulfo-EGS and BS[3] used as a spacer of LG are called LG-E and LG-B, respectively (Fig. 1). The structure of LG was confirmed by ^{1}H NMR.

2.5. Voltammetric measurement of interaction between lectin and labeled galactosamine

To react LG with lectin, the LG and lectin were mixed in 10 ml of 0.1 M phosphate buffer (pH 7.0), and the solution was stirred for 1 h at room temperature. Voltammetric measurement was performed after deaeration for 10 min with nitrogen gas. Then, a polished electrode was immersed in the solution, and the potential at -1.0 V was applied to the electrode for 5 min to accumulate the LG while stirring. After a rest period of 15 s, the oxidation response of LG was recorded by scanning the potential between -1.0 and -0.3 V by differential pulse voltammetry (scan rate, 5 mV s^{-1}; pulse amplitude, 50 mV; sample width, 2 ms; pulse width, 50 ms; pulse period, 200 ms). To investigate a competitive reaction between LG and galactosamine, galactosamine of various concentrations was added to the solution containing LG-E and lectin, and the solution was incubated for 1 h under the same conditions.

3. Results and discussion

3.1. Accumulation behavior of daunomycin and labeled galactosamine to the electrode

Cyclic voltammogram of 1.0×10^{-5} M daunomycin measured by linear sweep voltammetry (scan rate 50 mV s^{-1}) in 0.1 M phosphate buffer (pH 7.0) was shown in Fig. 2. Two redox pairs were observed. The more negative pair of peaks was due to quinone, and other pair of peaks was a redox based on two hydroxyl groups, respectively [13]. The voltammogram of LG was identical with that of daunomycin. On the other hand, difference in the absorption spectrum of LG and daunomycin was not observed. Therefore, it was confirmed that the electrode reaction was not affected by a labeling. In this study, the anodic peak at -0.60 V was used because a pair of peaks in positive potential was broad.

Fig. 3 shows the relationship between the peak current and accumulation time in a solution with 4×10^{-7} M LG-E, LG-B and daunomycin, respectively. These peak currents increased linearly up to 2 min with increasing the accumulation time and became a constant value over 10 min by the saturation of the reagent on the electrode. The peak currents of LG-E and LG-B were larger than that of daunomycin. Accordingly, it was found that LG adsorbed more than daunomycin on the electrode. This strong adsorbing property of the LG was because the hydrophilic amino group of daunomycin was converted into a hydrophobic imino group and an alkyl chain was introduced into the molecule. It was expected that the difference of peak current between LG-E and LG-B was based on the length of spacer. The relative standard deviation was 6.57% ($n = 5$) in the measurement of 4×10^{-7} M LG-E for 5 min.

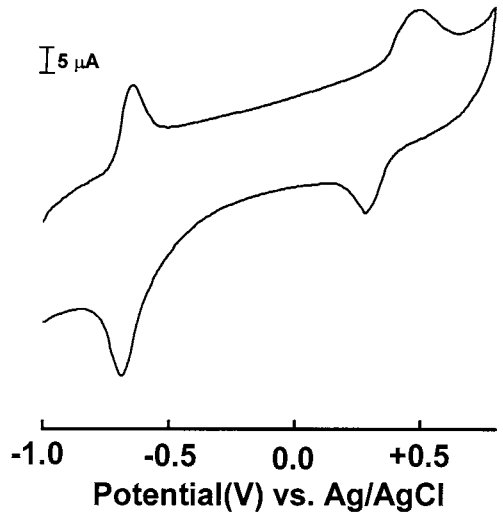

Fig. 2. Cyclic voltammogram of daunomycin. Glassy carbon electrode, 0.1 M phosphate buffer (pH 7.0), scan rate 50 mV s^{-1}, $E_a = -1.0$, $t_a = 5$ min, 1×10^{-5} M daunomycin.

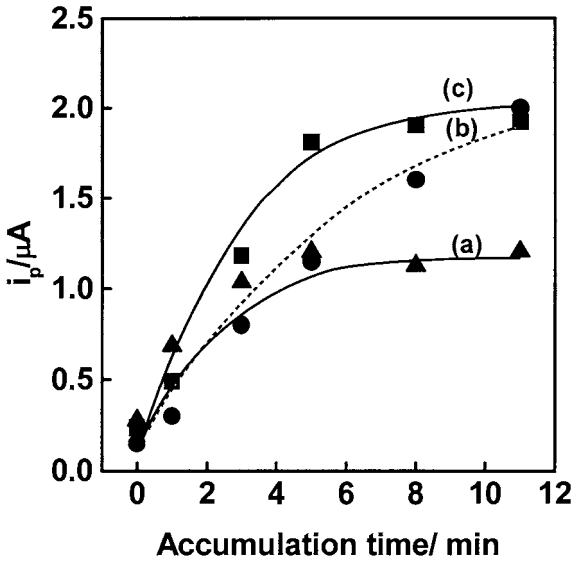

Fig. 3. Dependence of the peak current on the accumulation time. (a) 4×10^{-7}M daunomycin, (b) 4×10^{-7} M LG-B, (c) 4×10^{-7} M LG-E. Results obtained by differential pulse voltammetry (0.1 M phosphate buffer (pH 7.0), $E_a = -1.0$ V, scan rate = 5 mV s^{-1}).

3.2. Electrode response of LG by interaction with lectin

Voltammograms of 4×10^{-7} M LG-E and further adding SBA 5 μg ml^{-1} were investigated (Fig. 4). In the presence of SBA, the peak shape of LG-E did not change but the peak current decreased. For daunomycin, the peak current did not decrease. Therefore, it is suggested that decrease of the peak current is due to the galactosamine-lectin binding but not by interference such as the adsorption of

protein on the electrode. That is, a part of daunomycin was covered with a large volume of lectin so that it lost electroactivity. The changes of the peak current in the various concentrations of SBA were measured (Fig. 5a). Because the peak current decreases as a function of the concentration, SBA can be determined. When a sufficient amount of lectin was added to bind all the LG, the peak current became close to zero. The reason that the peak of the LB is not zero may be free ligand of LG. Otherwise, it is expected that the electroactive part is not perfectly covered with binding sites of the lectin.

The measurements of peak current for LG-B were also carried out (Fig. 5b). The peak current was a constant at value that was lower than that of LG-E. It is proposed that the LG-B is easily covered with the binding site comparing to the LG-E. Therefore, it is found that the LG-SBA binding is effected by difference of spacer. Because the change of peak current of LG-E was larger than that of LG-B, the LG-E was suitable to the detection of SBA. The detection of SBA using LG-E was possible in the range of 0.3–2 μg ml^{-1} SBA. The relative standard deviation at 1

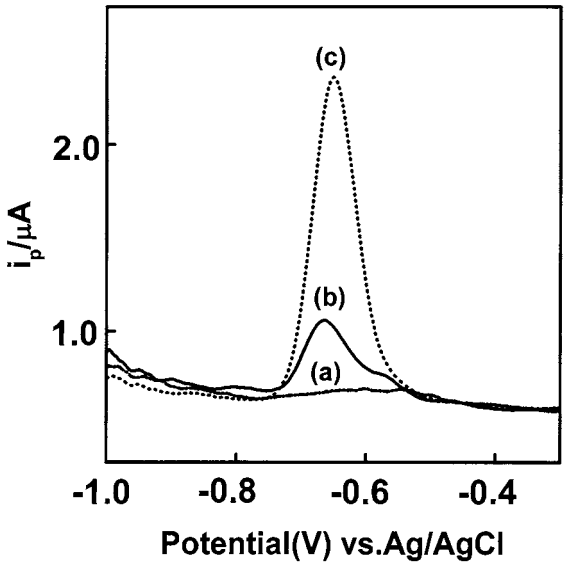

Fig. 4. Voltammograms of LG-E and adding SBA. (a) Blank, (b) 4×10^{-7} M LG-E, (c) 4×10^{-7} M LG-E + 5 μg ml^{-1} SBA.

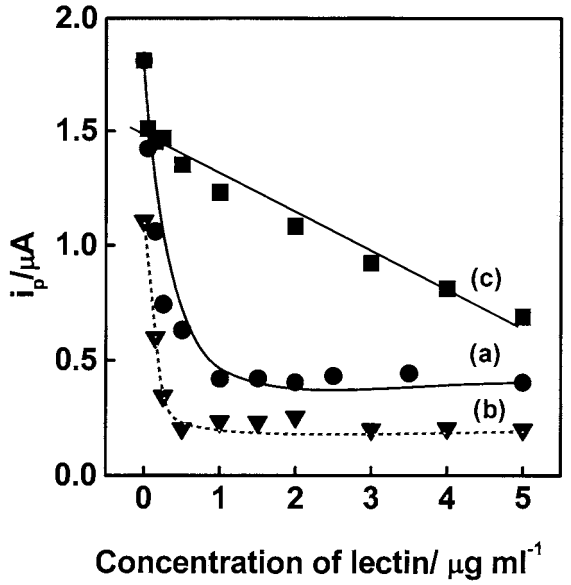

Fig. 5. Dependence on the interaction of the LG to SBA or WGA. (a) 4×10^{-7} M LG-E to SBA, (b) 4×10^{-7} M LG-B to SBA, (c) 4×10^{-7}M LG-E to WGA.

μg ml^{-1} SBA was about 5% ($n = 5$) with a detection limit of 0.2 μg ml^{-1}. Detection level of the method was compared. For erythrocyte agglutination in fresh human blood, investigation in the order of 10 μg ml^{-1} lectin was carried out [14]. In addition, the determination of lectin in similar concentrations has been reported by fluorescence quenching [15]. Accordingly, it is expected that the method is applied to practical samples although pretreatment is needed.

To clear the possibility of specific assay to sugar, the same procedure was performed to several lectins not having binding sites to galactosamine. As a result, the peak current of LG-E decreased with increases in the concentration of WGA lineally (Fig. 5c). For PNA and Con A, the same behavior was observed (not shown). The peak current decreased by non-specific adsorption of lectin on the electrode. The changes of peak current of LG-E to incubation time for several lectins were examined. For 4×10^{-7} M LG-E to 5 μg ml^{-1} SBA, the peak current decreased with increasing the incubation time exponentially and became a constant value up to 40 min. In 4×10^{-7} M LG-E to 5 μg ml^{-1} WGA non-specific lectin to

galactosamine, the peak current of LG-E was independent of incubation time. The results of PNA and Con A were similar to that of WGA. When the incubation time are enough, it is concluded that LG-E is selectively covered with the binding sites of SBA.

3.3. Influence of interfering substances

Table 1 indicates the concentration limits at which interfering substance give a relative error of $< 10\%$ in the peak current obtained after 5 min accumulation in 1 μg ml^{-1} SBA. The substances investigated were alanine, ascorbic acid, bovine serum albumin (BSA), cysteine, dopamine, histidine, glutathione, glycine and urea. Alanine, histidine, glutathione, glycine and urea of 5×10^{-4} M do not interfere to the peak current. Co-existing of 1×10^{-5} % BSA was allowed in the measurement. However, concentration of 7×10^{-5} M dopamine or 3×10^{-5} M ascorbic acid interfered to the detection of SBA. The influences occurred by the electroactive property of dopamine and ascorbic acid. These results show that the detection of SBA in the method is selective.

3.4. Detection of galactosamine

A galactosamine assay can be achieved by the competition reaction of LG and galactosamine for the limited binding sites of SBA. When concentration of galactosamine was changed from 5×10^{-10} to 5×10^{-3} M with 4×10^{-7} M LG-E and 1 μg ml^{-1} lectin, the peak current of LG increased with increasing the concentration of galactosamine. Shape of the response was a dose curve. This is because galactosamine occupies the binding sites of SBA. The change of peak current enables to detect galactosamine in the solution. The relative standard deviation at 1×10^{-7} M galactosamine was 6.5% ($n = 5$).

Table 1
Concentrations to which other substances can be present without causing interference

Substance	Concentration (10^{-4} M)
Alanine	5.0
Ascorbic acid	0.3
Cysteine	5.0
Dopamine	0.7
Histidine	5.0
Glutathione	5.0
Glycine	5.0
Urea	5.0
BSA	1×10^{-5} %

Measurement by glassy carbon electrode for 5 min in 0.1 M phosphate buffer (pH 7.0) with 1 μg ml^{-1} SBA.

4. Conclusions

In this study, it was found that lectin was detected on the basis of the interaction between LG and SBA electrochemically. On the other hand, it was shown that the adsorption of LG on the electrode and the interaction of the LG to SBA were attributed to the length of the spacer. The competition reaction to the limited binding sites of SBA between LG and galactosamine enabled the detection of galactosamine. A characteristic of this method is that it does not require separation of the free ligand from the bound one before the measurement. Therefore, it is expected that the proposed method can be applied to the detection of several lectins and sugar.

Acknowledgements

The authors thank the Ministry of Education, Science and Culture of Japan for support of this work under a Grant-in-Aid for Scientific Research (No. 08740567).

References

[1] I.E. Liener, N. Sharon, I.J. Goldstein (Eds), The Lectins: Properties, Functions and Applications in Biology and Medicine, Academic Press, Orlando, 1986, p. 600.
[2] H. Lis, N. Sharon, Ann. Rev. Biochem. 55 (1986) 35.
[3] M.E. Etzler, Ann. Rev. Plant. Physiol. 36 (1985) 209.
[4] J.C. Paulson, in: P.M. Conn (Ed.), Interaction of animal viruses cell surface receptors, The Receptors (Vol. 2), Academic Press, New York, p. 131.
[5] A. Cogoli, A. Tschopp, Immunology Today 6 (1985) 1.
[6] L.M. Hoffman, D.D. Donaldson, Biotechnol. 5 (1987) 157.
[7] M. Ueno, T. Arai, K. Kojima, J. Chromatogr. 597 (1992) 197.

[8] K.B. Lee, Y.S. Kim, R.J. Linhardt, Anal. Biochem. 203 (1992) 206.
[9] T. Mega, S. Hase, J. Biochem. 109 (1991) 600.
[10] K. Sugawara, S. Hoshi, K. Akatsuka, Fresenius J. Anal. Chem. 358 (1997) 755.
[11] K. Sugawara, S. Tanaka, H. Nakamura, Anal. Chem. 67 (1995) 299.
[12] K. Sugawara, S. Tanaka, H. Nakamura, Bioelectrochem. Bioenerg. 67 (1994) 205.
[13] E.N. Chaney, R.P Baldwin, Anal. Chem. 54 (1982) 2556.
[14] H. Lis, Biochim. Biophys. Acta 211 (1970) 582.
[15] P.K. Datta, S.C. Bera, Anal. Chim. Acta 220 (1989) 225.

ELSEVIER

Talanta 47 (1998) 673–679

Talanta

Use of a new type of 8-hydroxyquinoline-5-sulphonic acid cellulose (sulphoxine cellulose) for the preconcentration of trace metals from highly mineralised water prior their GFAAS determination

K. Zih-Perényi, A. Lásztity *, Zs. Horváth, Á. Lévai

Department of Inorganic and Analytical Chemistry, Eötvös L. University, P.O. Box 32, Budapest 112 H-1518, Hungary

Received 24 December 1996; received in revised form 23 February 1998; accepted 27 February 1998

Abstract

Sulphoxine cellulose microcolumn was used in an FI-GFAAS system for the preconcentration of trace metals, Cd, Co, Ni, Pb and V from water and from highly mineralised water and also in the presence of complexing agent, e.g. citrate. The recovery was quantitative at pH 5 for all of the elements from NIST 1643c trace elements in water SRM and from highly mineralised water samples. No significant difference was found in the sorption of V(IV) and V(V) during preconcentration. The preparation of the 8-hydroxyquinoline-5-sulphonic acid cellulose (sulphoxine-cellulose) by Mannich reaction from aminoethyl cellulose or via chlorodeoxy and ethylenediamine cellulose is also described.
© 1998 Elsevier Science B.V. All rights reserved.

Keywords: GFAAS determination; Sulphoxine cellulose; Trace metals

1. Introduction

From 1980 a great number of papers were published on the use of chelating cellulose exchangers for trace element preconcentration from various matrices. On the characteristics of cellulose exchangers a review was written in 1981 by Wegscheider and Knapp [1]. Some years later Myasoedova and Sawin gave a summary of chelating sorbents in analytical chemistry [2]. Chelating groups chemically bound to cellulose form stabile complexes with many transition metals while interfering matrix ions-usually alkali and alkaline earth metals-are either not complexed or complexed to a lesser extent and can be removed from the exchanger by washing. Chelating celluloses as solid sorbents for the separation of the analyte elements from interfering matrix components have been effectively used in flow injection on-line microcolumn preconcentration systems for atomic emission ICP-AES [3–5], ICP-MS [6] and atomic absorption FAAS [7], GFAAS [8] spectrometry.

The direct determination of trace elements in the low nanograms per liter range cannot be

* Corresponding author. Tel.: +36 1 2090555; fax: +36 1 2090602.

0039-9140/98/$ - see front matter © 1998 Elsevier Science B.V. All rights reserved.
PII S0039-9140(98)00106-4

executed in samples with high salt content as seawater (salinity 29.2 g l^{-1}) by ICP-MS [9] and in highly mineralised water (salinity 39.5 g l^{-1}) by GFAAS [10]. In that case the separation of the analyte from the matrix is a must.

A commercially available PC-controlled on-line preconcentration apparatus, TRACECON, supported with a microcolumn packed with oxine cellulose—a chelating cellulose with immobilised 8-hydroxyquinoline-5-sulphonic acid, was applied with good results for the determination of six elements from seawater matrix (6). The oxine cellulose was synthesised by Csanády et al. in 1989 [11]. For the synthesis the acid chloride prepared from carboxymethyl cellulose was reacted with tetraethylenepentamine and the formed aminocellulose was given into Mannich reaction with formaldehyde and 8-hydroxyquinoline-5-sulphonic acid. The product was an orange-yellow powder.

The optimisation of flow injection on-line microcolumn preconcentration of ultratrace elements at high Ca, Mg and sulphate concentrations and in the presence of citrate and oxalate complexing agents on iminodiacetic acid\ethylcellulose (IDAEC) chelating cellulose was published recently. Species distribution diagrams calculated in homogenous media could be used for the optimisation of the analysis of highly mineralised waters [8].

The aim of our present research work was to prepare a chelating cellulose with immobilised 8-hydroxyquinoline-5-sulphonic acid groups of unambiguous structure. In this paper the synthesis of a new type of 8-hydroxyquinoline-5-sulphonic acid cellulose (sulphoxine cellulose) is described. Then the application of sulphoxine cellulose for on-line flow-injection preconcentration and GF-AAS determination of trace Cd, Co, Ni, Pb and V in the presence of high salt content even if the sulphate content was also high (27 g l^{-1}) as in 'Hunyadi' a highly mineralised water for medicinal purposes and complexing agent (citrate) is discussed. At the work the experience of preconcentration on IDAEC [8] turned out to be useful. In natural waters vanadium principally exist as V(V) and V(IV). The sorption behaviour of the different oxidation states was examined as it was usually not investigated although this is important to prove the applicability of the preconcentration procedure for total vanadium determination.

2. Experimental

2.1. Reagents

Throughout the study high-purity water (distilled water purified on ion exchange celluloses) was employed. Ammonium acetate and citrate were purified on an IDAEC [12] column. Whatman cellulose powder, Whatman aminoethyl (AE) cellulose, *N*,*N*′-dimethylformamyde (DMF) (Reanal), $POCl_3$ (Aldrich), ethylenediamine (ED) (Reanal), formaldehyde (Reanal), 8-hydroxyquinoline-5-sulphonic acid (Merck, zur Synt.), tetraethylammonium-hydroxyde (20% aqueous solution, Merck, zur Synt,) were used for the synthesis of sulphoxine cellulose. All other reagents were of analytical grade purchased by Reanal. AAS standards including V(IV) supplied by Merck (Darmstadt, Germany) were used to prepare calibration solutions (0.2 M HNO_3). For vanadium(V) standard solution NH_4VO_3 (Reanal) was dissolved in hot high-purity water.

2.2. Instrumentation

A Perkin-Elmer model 3110 atomic absorption spectrometer with HGA-600 graphite furnace and AS-60 autosampler was applied. Perkin-Elmer analytical techniques for graphite furnace atomic absorption spectrometry were used as a basis for the operating conditions and analytical parameters.

2.3. Synthesis of chlorodeoxycellulose and reaction with ethylenediamine

The synthesis of chlorodeoxycellulose [13] and ethylenediamine-cellulose [14] was slightly modified. Whatman cellulose powder (10 g) is preswollen during 30–60 min in DMF. The mixture of 400 ml DMF and 12 ml $POCl_3$ is heated to 90°C. The preswollen cellulose powder is added to the solution and is heated at 90°C for 15 min. The

mixture is cooled down, filtered and washed successively with DMF (~ 100 ml), 5% NaOH (100–200 ml), water, 5% acetic acid and water again. Then the product is air-dried. The Cl-functional group is substituted by heating the prepared cellulose under appropriate stirring with 100 ml ethylenediamine in a water bath at 100°C for 2 h at reflux. After filtration the formed ED cellulose powder is washed with ethanol and water and air-dried. The capacity of the product is 0.50–0.60 mmol g^{-1}.

2.4. Synthesis of sulphoxine cellulose

For the immobilisation of oxine group the Mannich reaction [11] was used. Ten grams of dried ED-cellulose or AE-cellulose is suspended and preswollen in a mixture of 200 ml formaldehyde and 20 ml glacial acetic acid and reacted in an ultrasonic bath for 20 min, stirring for 40 min at room temperature and again 20 min in ultrasonic bath. After reaction the product is filtered and washed twice with 250 ml ethanol. The washed powder is suspended in a mixture of 8 g of 8-hydroxyquinoline-5-sulphonic acid, 45 ml tetraethyl-ammonium-hydroxyde and 125 ml ethanol and heated to 60°C. The suspension is stirred at 60°C for 2 h and filtered followed by washing successively with ethanol, 0.25 M NaOH, water, 0.25 M HCl, water and ethanol. The prepared sulphoxine cellulose is dried at 40°C. The product is a dark yellow powder. The yield is 10.4 g. The exchange capacity of sulphoxine cellulose for Cu-uptake (pH 6) is 0.6 mmol g^{-1} prepared from ED-cellulose, 0.2 mmol g^{-1} prepared from AE-cellulose. All the data of the results are on the sulphoxine cellulose prepared from ED-cellulose. The elemental analysis of this product gives 2.64% of N and 1.16% of S.

2.5. Characterisation of immobilised sulphoxine group on cellulose

The prepared chelating exchanger was converted to aluminium-form reacted with 0.01 M aluminium-sulphate solution at pH 4. The aluminium complex and/or H-form exchanger was suspended in CCl_4 and the fluorescence spectrum was recorded on an Hitachi F-4500 instrument. The excitation wavelength range was 200–500 nm, the emission range 400–600 nm.

2.6. Preconcentration

Multielement preconcentration and elusion of trace elements was performed by an on-line flow-injection dual four-way valve assembly [3] with a sulphoxine cellulose microcolumn. The column containing 40 mg of sulphoxine cellulose was converted to an NH_4-form with 0.1 M ammonium acetate. The sample buffered with 2 M ammonium acetate to pH 5 optimal for the preconcentration was passed through the microcolumn at a flow rate of 2.0 ml min^{-1}. The elution was carried out by 2 M HNO_3 with a flow rate of 2.5 ml min^{-1}. The eluates were collected into the vessels of the autosampler of the spectrometer. The sample volume loaded was 20.0 ml, the eluted volume was 0.80–0.95 ml. Usually at ~ 20–25 fold preconcentration was achieved.

If the loaded sample contained citric acid it was also buffered with ammonium acetate to pH 5 ± 0.1.

For the analysis of NIST 1643c trace elements in water standard reference material the solution was diluted 40 times before preconcentration.

3. Results and discussion

The sulphoxine cellulose was synthesised via chlorodeoxy and ethylenediamine cellulose [13,14] followed by Mannich reaction of the ethylenediamine cellulose, formaldehyde and 8-hydroxyquinoline-5-sulphonic acid [11]. The sulphoxine cellulose is a new type of oxine cellulose as the amine component is ethylenediamine.

The IR spectroscopy usually used for the verification of immobilised chelating groups could not be applied in this case because of low capacity and the interference of cellulose matrix. The fluorescence spectroscopy turned out to be suitable to prove the attaching of the 8-hydroxyquinoline-5-sulphonic acid group. The oxine ligand is very weakly fluorescent when uncomplexed but intensively fluorescent when is com-

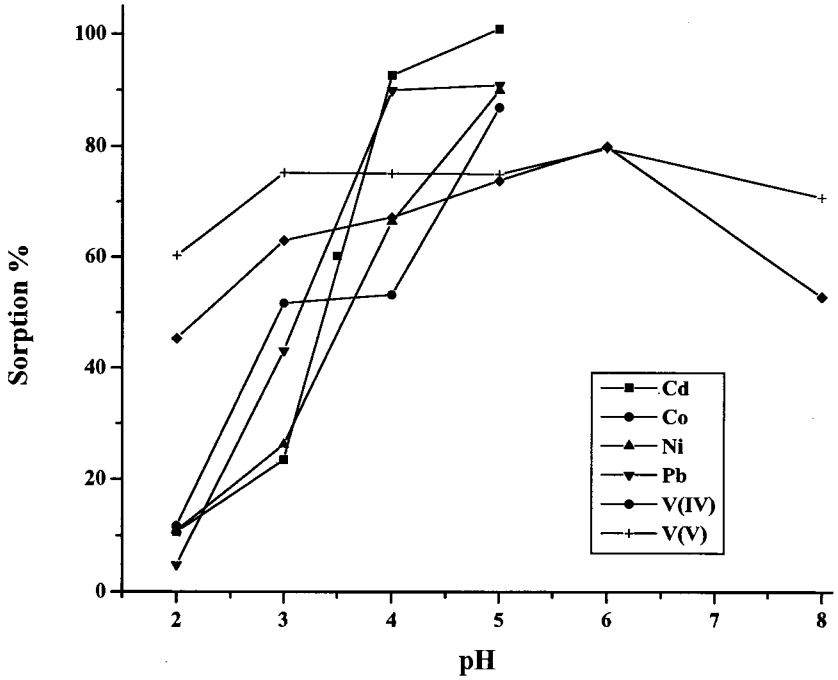

Fig. 1. Dependence of the sorption rates on the pH-values on sulphoxine cellulose microcolumn. Concentration before preconcentration (μg l^{-1}): Cd: 0.1; Co: 2.0; Ni: 5.0; Pb: 2.5; V(IV) and V(V): 5.0.

plexed by aluminium ion. The aluminium-oxine complex has an emission peak at 520 nm when the excitation wavelength is 405 nm [15]. The prepared sulphoxine-cellulose-aluminium complex in solid state dispersed in CCl_4 showed an emission maximum at 497 nm, while excited at 310 nm. The intensity decreased during sedimentation of particles. No emission was obtained in the case of an uncomplexed exchanger. The Mannich reation [11] also makes sure the linking of 8-hydroxyquinoline-5-sulphonic acid to the amine group of the cellulose.

The results of the experiments using sulphoxine cellulose microcolumn in an on line FI preconcentration system for Cd, Co, Ni, Pb and V can be seen in Fig. 1 and in Tables 1–5. The eluted elements were determined by GFAAS.

To find the optimal pH conditions the pH dependence of the sorption % (recovery of analyte spikes added to high purity water) of the elements investigated was studied in on-line mode on the sulphoxine cellulose microcolumn (Fig. 1). At pH 5 the sorption of Cd, Co, Ni and Pb ions was near 100%.

For the determination of total vanadium it is important to compare the sorption behaviour of the naturally occurring V(IV) and V(V) ions. Therefore the pH dependence of the sorption of both ions was studied. As a consequence of high stability of vanadium-sulphoxine complexes even at pH 3 the sorption is much higher for V(IV) (63%) and V(V) (75%) than for other elements. At pH 5 the sorption % of vanadium(IV) ions was 74%. The sorption of the two oxidation states agreed within the error of the analysis. Decreased sorption was found at pH 8. The same phenomena was observed on an inert type of 8 hydroxyquinoline-5-sulphonic acid based chelating ion-exchanger at pH > 7 [16]. The different sorption pattern of vanadium could be explained by its complex hydrolysis behaviour and slow decomposition of the formed species. In the extremely diluted solutions ($< 10^{-6}$ M) V(V) exists only in monomeric forms [17]: VO_2^+ (pH < 3.5)), $H_2VO_4^-$ (pH 3.5–7.5), HVO_4^{2-} (pH 7.5–13). The V(IV) species in the acidic pH range are [17]: VO^{2+},

Table 1
Calibration parameters for the FI-GFAAS preconcentration mode

Element	Concentration range[a] (μg l^{-1})	Slope (A-s μg l^{-1})	Intercept A-s	Regression coefficient	Sorption % (SD)[b]
Cd	0.03–0.60	3.037	0.0104	0.9998	101 (3.9)
Co	0.50–2.00	0.184	−0.007	0.9986	87 (2.9)
Ni	1.25–5.00	0.117	0.0014	0.9975	90 (3.6)
Pb	0.63–2.50	0.147	−0.003	0.9989	91 (3.4)
V(IV)	0.63–2.50	0.0398	−0.0040	0.9965	74 (4.5)

[a] Before preconcentration.
[b] Five calibrations.

$VO(OH)^+$, $(VO(OH))_2^{2+}$, $VO(OH)_2$. At $\sim 10^{-2}$ M alkaline V(1V) solution the formation of polyanionic species $V_4O_9^{2-}$ was found [18]. Although at the concentration of interest (10^{-7} M) the existence of $V_4O_9^{2-}$ was not proved nevertheless sorption depression occurred. The redox reactions make the complex chemistry of vanadium more difficult. In the sample solutions stored for analysis (pH 1–2) in the presence of reducing components (e.g. citrate) vanadium(V) can be spontaneously reduced to vanadium(IV) [19]. At higher pH V(IV) is exposed to slow oxidation to V(V) [18]

Considering the data pH 5 was chosen for the preconcentration throughout the experiments. There was no need to work at a higher pH which is not favourable for vanadium as well as for the cellulose fibres. The quantitative sorption of Cd, Co, Ni and Pb can be seen in Table 1. The analytical suitability of the on-line method using sulphoxine cellulose for the preconcentration of Cd, Co, Ni, Pb and V(IV) is apparent from the linearity of the calibration graphs presented by the data in Table 1. Since the sorption of the vanadium(IV) and (V) ions is equal at pH 5 vanadium(IV) standard solution was sufficient for calibration. The sorption % is equal to the ratio of measured concentration in the eluate and the expected concentration taking into account the preconcentration factor. The linearity of calibration graphs proves that the differences in the sorption % are within the experimental error in the concentration range used for calibration. For the construction of calibration graphs the solution with the same concentration can be used by increasing the preconcentration factors. A higher preconcentration factor increases the analysis time. A preconcentration of 20 was the most suitable one. The relative standard deviation of sorption % (five calibration graphs) was close to 4% for all measured elements except V(IV) for it was 6%.

Table 2
Analysis of NIST SRM 1643c trace elements in water

Element	Concentration (SD), μg l^{-1}	
	Found[a,b]	Certified value
Cd	11.6 (0.19)	12.2 ± 1
Co	24.1 (0.29)	23.5 ± 0.8
Ni	58.9 (2.5)	60.6 ± 7.3
Pb	35.6 (1.05)	$35.3 + 0.9$
V	32.6 (1.95)	31.4 ± 2.8

[a] Average of seven independent determinations.
[b] The sample was 40 times diluted before preconcentration.

In Table 2 the results of the FI-GFAAS analysis of NIST 1643c trace elements in water standard reference material are given. The 40 times diluted sample was on-line preconcentrated on sulphoxine cellulose microcolumn and analysed by external calibration. Table 2 shows the found and certified concentrations. It can be established that there was a good agreement with the certified values.

The analysis results of highly mineralised (total dissolved solids: 39.5 g l^{-1}) water 'Hunyadi' for medicinal purposes by FI-GFAAS preconcentration on sulphoxine cellulose at pH 5 is summarised in Table 3. For the analysis external calibration and standard addition methods were used. To check the validity of using external

Table 3
Analysis results and spike recoveries from 'Hunyadi' mineral water

Element	Addition range (μg l^{-1})	Spike average recovery (%)	Concentration by standard addition (μg l^{-1})	Concentration by external calibration (μg l^{-1}) (SD)[a]
Cd	0.08–0.18	104	0.250	0.259 (0.015)
Co	0.50–2.00	95	1.95	1.75 (0.085)
Ni	1.25–5.00	92	5.15	5.08 (0.600)
Pb	0.63–1.25	90	0.34	0.34(0.074)
V	0.63–1.25	80	0.8	0.7

'Hunyadi' mineral water matrix in g l^{-1}: $Na^+ = 5.2$; $Ca^{2+} = 0.54$; $Mg^{2+} = 3.2$; $Cl^- = 0.79$; $SO_4^{2-} = 27$; $HCO_3^{2-} = 1.0$.
[a] Three independent determinations from the same bottle.

calibration the spike recoveries were also determined. The results show that there is no need for standard addition except vanadium as there is a good agreement between the results by external calibration and standard addition. This type of mineral water was analysed previously on an IDAEC microcolumn [8]. The standard deviation and recovery of spikes were in the same range. It can be mentioned that the trace element concentrations could vary within the bottles of mineral waters. For example, the cobalt content fluctuated between 1–5 μg l^{-1}.

The effect of citrate was also examined on the sorption because the stability of metal-citrato complexes are close to those of humic acids. The effect of citrate and mineral water matrix was investigated by the construction of the species distribution diagrams. The sulphoxine cellulose-metal complex stability constants have not been determined. The critical stability constants of metal-8-hydroxyquinoline sulphonic acid complexes in homogenous solution were applied for computation [20]. For the construction of species distribution diagrams, SPEA a FORTRAN computer program was used [21]. The computed sorption % in the presence of citrate and mineral water matrix were 100 at pH 5 for all the elements even at 0.02 M citrate concentration. Table 4 gives the recovery % of elements from chelate forming solutions even in presence of matrix components of mineral acids. Recoveries were determined by external calibration preconcentrating aqueous standards. The measured recoveries are close to 100% in both matrices for Cd, Co, Ni, Pb and V(IV) at pH 5 showing negligible effect of the matrix. Addition of citrate to the aqueous solution also had no influence on the sorption of V(V) (recovery: 104%).

The detection limits shown in Table 5 are satisfactory as the measured concentrations in 'Hunyadi' are at least five times higher for most of the elements (see Table 3).

Table 4
Recovery of elements on sulphoxine cellulose at pH 5

Element	Recovery %[a]	
	0.002 M citrate solution	0.002 M citrate in mineral water solution
Cd	95	103
Co	107	97
Ni	105	94
Pb	91	104
V(IV)	101	101

Spike concentration in μg l^{-1}: Cd: 0.25; Co:2.00; Ni: 5.00; Pb: 2.50; V(IV): 5.00.
[a] Average of three independent determinations.

4. Conclusion

The use of FI-GFAAS in combination with sulphoxine cellulose microcolumn has provided a

Table 5
Detection limits

	Cd	Co	Ni	Pb	V
DL[a] (μg l^{-1})	0.004	0.134	0.350	0.063	0.244

[a] Refers to the original solution, 3σ criterion, preconcentration of seven blanks.

rapid and accurate technique for the determination of Cd, Co, Ni, Pb and V in water and in highly mineralised water. The oxidation state (IV and V) has no effect on the sorption of vanadium. The recovery of trace metals was quantitative in the presence of a complexing agent like citrate.

Acknowledgements

We would like to thank Toth Karolyne for her technical assistance. The research was sponsored by the National Foundation of Scientific Research (OTKA No. A 196/95/450).

References

[1] W. Wegscheider, G. Knapp, CRC Crit. Rev. Anal. Chem. 11 (1981) 79.
[2] G.V. Myasoedova, S.B. Sawin, Chelating sorbents in analytical chemistry, Crit. Anal. Chem. 17 (1986) 1.
[3] S. Caroli, A. Alimonti, F. Petrucci, Zs. Horvath, Anal. Chim. Acta 248 (1991) 241.
[4] N. Prakash, G. Csanady, M.R.A. Michaelis, G. Knapp, Microchim. Acta, [Wien], III (1989) 257.
[5] P. Schramel, L.O. Xu, G. Knapp, M. Michaelis, Fresenius J. Anal. Chem. 345 (1993) 600.
[6] K.S. Huang, S.J. Jiang, Fresenius J. Anal. Chem. 347 (1993) 238.
[7] E. Beinrohr, M. Cakrt, J. Garaj, M. Rapta, Anal. Chim. Acta 230 (1990) 163.
[8] Zs. Horvath, A. Lasztity, K. Zih-Perenyi, A. Levai, Microchem. J. 54 (1996) 391.
[9] K.E. Jarvis, A.L. Gray, R. S. Houk, Handbook of Inductively Coupled Plasma Mass Spectrometry, Blackie Academic Professional, London, 1992, p. 271.
[10] G. Bozsai, G. Schlemmer, Z. Grobenski, Talanta 37 (1990) 545.
[11] G. Csanady, P. Narayanan, K. Muller, W. Wegscheider, G. Knapp, Angew. Makromol. Chem. 170 (1989) 159.
[12] Zs. Horvath, A. Lasztity, O. Szakacs, G. Bozsai, Anal. Chim. Acta 173 (1985) 273.
[13] J.A. Smits, R.E. van Grieken, Anal. Chem. 52 (1980) 1479.
[14] T. Tashiro, Y. Shimura, J. Appl. Polym. Sci. 27 (1982) 747.
[15] W.T. Rees, Analyst 87 (1962) 202.
[16] K.L. Yang, S.J. Jiang, T.J. Hwang, J. Anal. At. Spectrom. 11 (1996) 139.
[17] C.F. Baes Jr., R.E. Mesmer, The Hydrolysis of Cations, Wiley Interscience, New York, 1976, p. 210.
[18] D.J. Labonette, Chem. Res. (S) (1988) 92.
[19] P.M. Ehde, I. Andersson, L. Petterson, Acta Chem. Scand. 43 (1989) 136.
[20] R.M. Smith, A.E. Martell, Critical Stability Constants, Vols. 1–5. Plenum, New York, 1974, 1975, 1976, 1977, 1982.
[21] A.E. Martell, R.J. Motekaitis, Determination and Use of Stability Constants, VCH, Weinheim/New York, 1992.

ELSEVIER

Talanta 47 (1998) 681–687

Talanta

Effect of electrolytes on the retention behavior of some benzenesulfonates in electrochemically modulated liquid chromatography

Monzir S. Abdel-Latif [a,*], Marc D. Porter [b]

[a] *Chemistry Department, The Islamic University, P.O. Box 108, Gaza, Israel*
[b] *Chemistry Department, Iowa State University, Ames, IA 50011, USA*

Received 7 July 1997; received in revised form 12 November 1997; accepted 27 February 1998

Abstract

The effects of electrolytes on the retention behavior of some benzenesulfonates in electrochemically modulated liquid chromatography were studied. Both cations and anions were found to have considerable effects on retention. As cation size increases, retention decreases, while anions show more complicated effects were anionic size and charge distribution contribute to the overall behavior of anions. Large anions with a delocalized negative charge on the whole species result in lower retention times, and vice versa. Also, electrolyte concentration plays an important role in the retention behavior observed. Initially, as electrolyte concentration was increased retention increased due to electrostatic interactions of cations with the negatively charged stationary phase. However, retention starts to slightly decrease or increase after some specific electrolyte concentration depending on the nature of the electrolytic species. Finally, an interesting behavior of double peak appearance of a single solute was observed at low electrolyte concentrations and was attributed to the presence of other active sites on the carbon stationary phase. © 1998 Elsevier Science B.V. All rights reserved.

Keywords: Electrochromatography; Supporting electrolyte; Carbonaceous stationary phases

1. Introduction

Electrochemically modulated liquid chromatography (EMLC) offers potential advantages in terms of the possibility of electrochemical manipulation and control of the stationary phase [1–6]. This feature of EMLC is of prime importance as in situ control of the stationary phase should result in highly improved chemical separations as well as decrease the risk of using toxic or dangerous chemicals as mobile phases. It had also been possible to carry out separations using potential gradients rather than conventional solvent gradients. This has significant impacts on the chromatographic system including the possibility of using a refractive index detector and excluding the need for column regeneration.

Most efforts in the field of electrochromatography, in general, were focusing on formulating

* Corresponding author. Tel.: +972 7863554; fax: +972 7863552; e-mail: mlatif@iugaza.edu

0039-9140/98/$ - see front matter © 1998 Elsevier Science B.V. All rights reserved.
PII S0039-9140(98)00107-6

procedures for potential applications as well as devising methods for the improvement of the carbon stationary phase [7–13], including pretreatment and particle size related problems. However, very little attention was devoted to studying mobile phase related aspects. Almost invariably, all electrochromatographic studies in the literature involved the use of either lithium, sodium, or tetraethylammonium perchlorate, at concentrations of usually 0.1 M, as mobile phase additives. A comparison study of these perchlorates (0.1 M each) to achieve improved separations of specific compounds had also been reported [14].

In this study, we report results obtained using a wide variety of electrolytes, at different concentrations, on the retention behavior of some benzenesulfonates in a EMLC system.

2. Experimental

2.1. Stationary phase packing material

The stationary phase was a 3–4 μm nonporous, spherical glassy carbon particulates. It was obtained by reseiving 0.4–12 μm Sigradur G glassy carbon particles, from HTW, Germany. The thus obtained packing material was used as the stationary phase and the working electrode as well. No pretreatment or modification of the carbon packing was conducted. However, it should be indicated that XPS analysis of this carbonaceous stationary phase revealed the presence of about 2% oxygen and 98% carbon. Oxygen was present as carboxylic acid, phenol, and quinone functionalities. These oxygen impurities imposed some problems as will be discussed later.

2.2. Column design and packing procedure

The general design of the EMLC column was the same as was discussed elsewhere [15]. About 0.9 g of the glassy carbon spheres were dispersed in a 50:50 dibromomethane/acetonitrile solution. The slurry was sonicated for 10 min and then packed into the column using pure acetonitrile at 5000 psi for 30 min followed by a solution of acetonitrile containing 0.1 M lithium perchlorate for, at least, 12 h. The Nafion tubing which holds the carbon spheres inside the column was pretreated by boiling in ethanol and 0.5 M lithium perchlorate for 10 min each, respectively.

2.3. Instrumentation

A HP HPLC 1050 series quaternary pump and a HP 1050 series diode-array detector were the essential components of the HPLC system. Both were controlled through a HP Chemstation software using a Pentium (100 MHz) processor and the output was displayed on a MicroScan 5AP/ADI monitor. A hard copy was obtained with a HP laser printer. The potential of the working electrode was controlled through a high power potentiostat from AMEL Instruments (Model 2055), Italy. A Ag/AgCl (satd NaCl) electrode was used as the reference electrode and the potential of the working electrode was adjusted with respect to this electrode. Injections were made using a Hamilton syringe via a Rheodyne injector (model 7125).

2.4. Reagents and chemicals

Benzenesulfonic acid, sodium salt dihydrate (BS), *p*-toluenesulfonic acid, sodium salt (TS), 4-hydroxybenzenesulfonic acid, sodium salt (HBS), *p*-chlorobenzenesulfonic acid, sodium salt (CBS), cesium chloride, lithium perchlorate, sodium perchlorate, trifluoroacetic acid (TFA), and potassium perchlorate were from Aldrich. Tetraethylammonium perchlorate (TEAP) was from GFS Chemicals. All other chemicals and reagents were from Fisher Scientific. HPLC grade acetonitrile and deionized water from a Milli-Q water purification system were used throughout this study. All reagents were filtered through a 0.2 μm filter paper from Alltech using a MFS microfiltration system.

About 100 ppm solutions of the different benzenesulfonates were prepared in deionized water and 5 μl were injected in each experiment.

Table 1
Effect of electrolytes on retention behavior[a]

Analyte	TEAP (min)	LiCl (min)	$NaClO_4$ (min)	K_2HPO_4 (min)
BS	0.73	1.25	0.78	0.92
HBS	0.73	1.81	0.98	1.44
TS	0.88	3.49	1.29	2.98
CBS	1.20	7.14	2.20	3.31

[a] Second peak retention time is selected.

2.5. Procedure

After column equilibration, as evident from baseline stability, 5 μl of the sulfonate solution of interest were injected. The flow rate was adjusted at 0.5 ml min^{-1} throughout the study and the mobile phase was always a 1% acetonitrile in water containing a specified amount of the electrolyte under investigation. The carbon stationary phase was the working electrode whose potential was adjusted at -0.5 V. This potential was arbitrarily selected due to the nature of the sulfonates studied and was kept constant throughout this study. It was essential to keep the potential constant in order to study the effect of variation of electrolytic components on retention. Detection was carried out at 220 nm unless otherwise indicated. Helium degassing was utilized throughout this work.

3. Results and discussion

3.1. Effect of electrolyte type

The effects of different electrolytes on the retention behavior of benzenesulfonates were studied in an attempt to find out which type of ions has more pronounced contribution to the retention behavior, if any. First, TEAP, lithium chloride, sodium perchlorate, and dipotassium hydrogenphosphate were used as mobile phase additives at the same concentration of 0.05 M each. Results of this study are summarized in Table 1. From the results presented in Table 1 and from data to be presented below it is obvious that electrolyte type affects the retention behavior. Therefore, a set of experiments were conducted to elucidate the actual contributions of both cations and anions of different electrolytes on retention.

3.2. The role of cationic species

The chloride form of sodium, potassium, and cesium were dissolved in deionized water containing 1% ACN to give a final concentration of 0.05 M solution of each. The retention times of the different sulfonates using these electrolyte additives were monitored and results are summarized in Table 2. It was evident from these data that cations have great influence on retention and a trend was clear, going from sodium to cesium, that retention decreased as cationic size was increased. Electrolytes containing lithium ions were excluded from the comparison of the effect of cationic size on retention since lithium ions would be highly hydrated due to their small ionic size. The hydrated lithium ions makes their effects on retention between sodium and potassium ions as shown in Tables 1 and 2.

The dependence of retention on the cationic size can be explained by the argument that as the cationic size increases, less positive charge per unit surface area of the cation, the number of species

Table 2
Effect of cationic size on retention[a]

Analyte	NaCl (min)	KCl (min)	CsCl (min)
BS	1.32	0.99	0.96
HBS	1.98	1.18	0.98
TS	3.91	2.02	1.88
CBS	9.11	3.71	3.11

[a] Second peak retention is selected.

Table 3
The role of anionic species[a]

Analyte	$LiClO_4$ (min)	LiCl (min)	NH_4Cl (min)	CH_3COONH_4 (min)[b]	NH_4NO_3 (min)[b]
BS	0.77	1.25	1.73	1.38	1.05
HBS	0.98	1.81	3.05	2.17	1.61
TS	1.19	3.49	5.47	4.17	2.55
CBS	2.01	7.14	10.96	9.63	NA[c]

[a] Second peak retention time is selected.
[b] Detection was done at 260 nm.
[c] Due to large shift in baseline.

that can be electrostatically adsorbed to the negatively charged carbon decreases. This results in low shielding of the sulfonate from the stationary phase which translates into lower retention times. The opposite process takes place for smaller cations, more positive charge per unit surface area, where larger numbers of these ions can be electrostatically adsorbed at the surface of the stationary phase resulting in more shielding of the negative charge of the stationary phase from the sulfonates leading to longer retention times. Therefore, it seems that adsorption and effective shielding account for the retention behavior effected by cations.

3.3. The role of anionic species

The nature of the anionic species available in the mobile phase turned out to have a tremendous effect on retention. This is obvious from comparison of retention times of sulfonates using lithium perchlorate and lithium chloride (0.05 M each in 1% ACN in water). Results can be seen in Table 3 where it is clear that the size of the anion is very important. Large increase in retention is observed when the anionic size becomes smaller. This may be attributed to the formation of a more compact electrical double layer of the small ions and the possibility that larger numbers of these ions can be close to the analyte and carbon surface. This decreases the possibility of free access and interaction between the negative charges on both analyte and stationary phase. Therefore, when the size of the anionic species decreases these species act as an effective barrier that retards sulfonates from accessing the negatively charged stationary phase. Perchlorate, on the other hand, is a large anion which means that a less compact electrical double layer is formed by fewer number of ions accommodated in the vicinity between the stationary phase and sulfonates allowing for easier access and thus lower retention.

In addition, it seems that charge distribution on anionic species has a very pronounced influence on retention. It was observed that when the negative charge is delocalized all over the anion, i.e. smallest surface charge at any point, this allows easier access of sulfonates to the stationary phase which translates into lower retention times. This can be further emphasized by looking at the data in Table 3 for some ammonium salts. The negative charge on the chloride is localized on this one atom species accounting for the observed longer retention time. While the negative charge on acetate is delocalized on the two oxygen atoms of the carboxylate. However, the nitrate ion has its negative charge delocalized on the three oxygen atoms, forming three arms of a tetrahedron while the fourth arm is the lone pair of electrons on the nitrogen. This can explain, in addition to the relatively large size of nitrate, the lower retention time observed in the case of nitrate. Of course, perchlorate has a larger size and less negative charge per unit surface area and thus has greater potential for reducing the retention times of sulfonates.

According to the explanation mentioned above, if the same cation is used, mobile phases containing chlorides will tend to give higher retention times than those containing acetates, nitrates, or perchlorates, respectively.

Table 4
Effect of electrolyte concentration on retention[a]

Analyte	Lithium perchlorate (t_R, min)				
	0.2 mM	1.0 mM	5.0 mM	10.0 mM	50.0 mM
BS	0.67	0.67	0.68	0.72	0.77
HBS	0.71	0.68	0.76	0.98	0.98
TS	0.83	0.98	1.33	1.36	1.18
CBS	0.98	1.47	2.35	2.33	2.01

[a] Second peak retention time is selected.

3.4. Effect of electrolyte concentration on retention

Based on the overall picture of the effects of anions and cations of different electrolytes mentioned previously, concentration effects can be easily understood. Retention is expected to increase at low electrolyte concentration as compared to the zero electrolyte retention times. This is because of the shielding resulting from the electrostatic adsorption of the cations to the carbon surface. On the other hand, when enough electrolyte concentrations are used, this saturates the carbon surface as well as exhibits high analyte solvation. This results in lower retention times when anionic species are large in size and have delocalized charges due to increased ease of analyte access and interaction with the stationary phase. This behavior is evident from the data in Table 4 which describes the change in retention as a function of lithium perchlorate concentrations. However, the effect of electrolyte concentration on retention should be looked at as combined cationic and anionic effects and generalizations should not be attempted for all types of electrolytes. Results presented in previous sections should be used as a guide to understand the overall influence of electrolytes on retention.

3.5. Electrolyte concentration and double peaks appearance

A very interesting effect of electrolyte concentration was probably that which resulted in double peaks, that are well characterized, for a single analyte. Regardless of the electrolyte used, double peaks were usually observed when electrolyte concentration was below some specific concentration (limiting concentration) characteristic of that solute and could approximately be determined from retention data. As the concentration of electrolyte was increased, the double peaks approached each other and, ultimately, merged into one single peak as the electrolyte concentration exceeded the limiting concentration (Fig. 1).

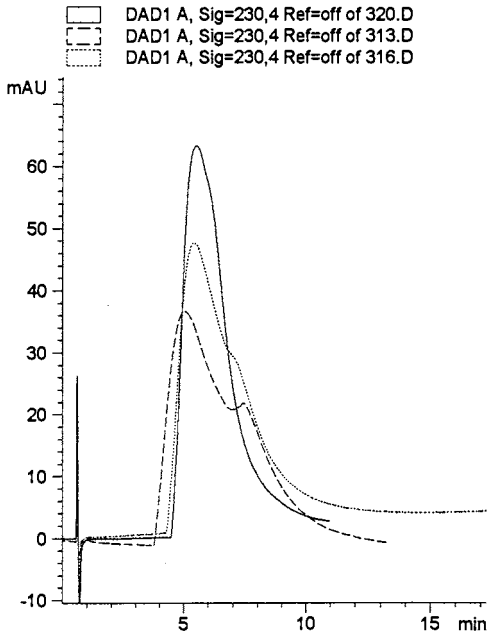

Fig. 1. Overlay chromatograms of CBS at the open circuit potential. The mobile phase was a 1% acetonitrile in water containing 0.05 M NH_4Cl (dashed line chromatogram), 0.15 M NH_4Cl (dotted line chromatogram), and 0.40 M NH_4Cl (solid line chromatogram).

The existence of double peaks can be attributed to the presence of other active sites on the carbon stationary phase. These active sites include the carbon surface with donor-acceptor types of interactions and the different types of oxygen functionalities covering some of the carbon surface. This argument of double peaks appearance due to the presence of oxygen functionalities was undoubtedly realized by running the same experiments using a porous graphitic carbon stationary phase which has a clean surface, with no oxygen residues as revealed by XPS. A single peak for each component was obtained. The presence of two forms of each sulfonate was rejected as a control experiment using a C_{18} column, at the same conditions, showed a single peak for each component. Also, the two species assumption declined as only one sharp peak is obtained at higher electrolyte concentrations.

Mobile phases containing ammonium chloride exhibited the most pronounced effects and resulted in well separated double peaks. However, it was possible to calculate the approximate ammonium chloride concentration that can result in single peaks chromatograms. This was accomplished by plotting the peak separation at the maxima, for each component, as a function of ammonium chloride concentration. It was observed that, at least, 0.25 M ammonium chloride was necessary. As a confirmation experiment, a 0.4 M ammonium chloride was used as the electrolyte in the 1% ACN in water mobile phase. Sharp peaks were obtained for all sulfonates, however it should be indicated that background increased as ammonium chloride concentration was increased, perhaps due to contamination by an absorbing impurity. Single peak separations were also obtained with a 0.25 M ammonium chloride. Fig. 2 shows that even with lithium perchlorate, a 0.05 M solution was necessary to achieve a separation that yields single peaks of CBS and TS. Therefore, it is possible to overcome the problem of double peaks in columns of similar stationary phases by simply increasing electrolyte concentration. The right concentration to use is dependent on the ionic species forming the electrolyte and is a characteristic of that electrolyte at the specific potential of the working electrode.

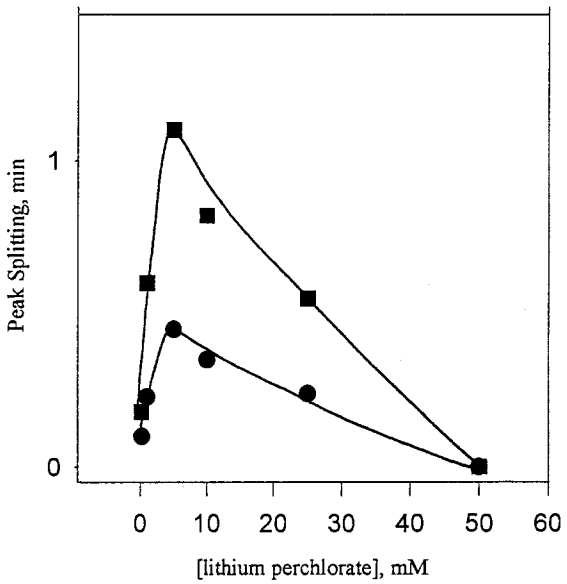

Fig. 2. Relationship between peak separation and lithium perchlorate concentration. Standard conditions are used (CBS, ■; TS, ●).

Fortunately, double peaks were also overcome by simply incorporating trifluoroacetic acid in the mobile phase (Fig. 3). We observed that incorporation of as little as 0.1% of TFA into the mobile phase was sufficient to achieve good looking chromatograms with well shaped peaks. The high affinity of TFA towards one of the active sites on the stationary phase can be the reason for the observed behavior. TFA adsorption to the stationary phase limits the interactions of benzenesulfonates to a single active site, and thus one migration mechanism, resulting in good looking peaks.

From these data, it should be evident that not only electrolyte type can affect retention behavior but electrolyte concentration affects it much as well.

3.6. Effect of electrolyte concentration on band broadening

Looking carefully at the column components, it seems fair to assume that some sulfonates can diffuse to the carbon surface close to the Nafion cation exchanger tubing. These sulfonates will

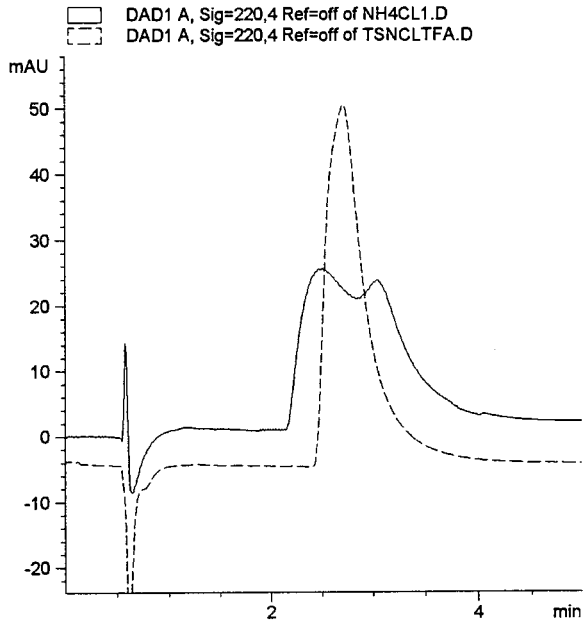

Fig. 3. A chromatogram of *p*-toluenesulfonate (TS), open circuit. Mobile phase: 6% acetonitrile in water containing 0.1 M ammonium chloride (solid line chromatogram) and 6% acetonitrile in water containing 0.1 M ammonium chloride as well as 0.1% TFA (dashed line chromatogram).

suffer lower shielding from the carbon surface than those present inside the column, especially at low electrolyte concentrations, and will also be repelled by the Nafion since it is impermeable to anions. Therefore, continuous diffusion to the surface as will as higher migration velocities of sulfonates close to the Nafion tubing may be a good reason for increased band broadening at low electrolyte concentrations.

At high electrolyte concentrations the carbon surface will be saturated with adsorbed ions as well as counter ions. Sulfonates, on the other hand, will be highly solvated and will suffer comparable shielding effects at the surface or inside the column which results in smaller band broadening and sharper peaks. Therefore, it is an advantage to incorporate an electrolyte at a high concentration to achieve better looking chromatograms.

References

[1] R.F. Antrim, R.A. Scherrer, A.M. Yacynych, Anal. Chim. Acta 164 (1984) 283.
[2] A.R. Ghatak-Roy, C.R. Martin, Anal. Chem. 58 (1986) 1574.
[3] H. Ge, P.R. Teasdale, G.G. Wallace, J. Chromatogr. 544 (1991) 305.
[4] R.S. Deinhammer, K. Shimazu, M.D. Rorter, Anal. Chem. 63 (1991) 1889.
[5] R.S. Deinhammer, E. Ting, M.D. Porter, J. Electroanal. Chem. 362 (1993) 295.
[6] R.S. Deinhammer, E. Ting, M.D. Porter, Anal. Chem. 67 (1995) 237.
[7] J.H. Stroll, K.L. Dunlop, Anal. Chem. 44 (1972) 2166.
[8] F.E. Woodard, D.E. McMackins, R.E. Jansson, J. Electroanal. Chem. 214 (1986) 303.
[9] R.S. Einsinger, R.C. Aikire, J. Electroanal. Soc. 130 (1983) 85.
[10] R.S. Einsinger, R.C. Aikire, J. Electroanal. Soc. 130 (1983) 93.
[11] P.J. Mayne, R. Shackleton, J. Appl. Electrochem. 15 (1985) 745.
[12] J. Koresh, A. Soffer, J. Electroanal. Chem. 147 (1983) 223.
[13] T. Nagaoka, T. Yoshino, Anal. Chem. 58 (1986) 1037.
[14] R.F. Antrim, A.M. Yacynych, Anal. Lett. 21 (1988) 1085.
[15] E. Ting, M. Porter, 1993 (Patent Pending).

ELSEVIER

Talanta 47 (1998) 689–696

Talanta

Determination of iron and nickel by flame atomic absorption spectrophotometry after preconcentration on *Saccharomyces cerevisiae* immobilized sepiolite

Hüseyin Bağ [a], Mustafa Lale [a], A. Rehber Türker [b,*]

[a] *Kırıkkale Üniversitesi Fen Edebiyat Fakültesi, 71450 Kırıkkale, Turkey*
[b] *Gazi Üniversitesi Fen Edebiyat Fakültesi, 06500 Ankara, Turkey*

Received 2 December 1997; received in revised form 19 February 1998; accepted 27 February 1998

Abstract

Iron and nickel have been preconcentrated on *Saccharomyces cerevisiae* immobilized sepiolite and determined by flame atomic absorption spectrophotometry (FAAS). Preconcentration studies were conducted by the column method. Effect of pH, amount of adsorbent, elution solution, flow rate and interfering ions on the recovery of the analytes have been investigated. Recoveries of Fe and Ni were 95 ± 1 and $99.5 \pm 0.1\%$, respectively, at 95% confidence level. The breakthrough capacities of analytes were also investigated and found to be 0.042 mmol g^{-1} for Fe and 0.055 mmol g^{-1} for Ni. The proposed method was applied to the determination of iron and nickel in brass (NBS SRM 37e). The detection limit of iron and nickel were found as 0.065 and 0.087 μg ml^{-1}, respectively. The direct determination of trace metals by flame atomic absorption spectrometry (FAAS) is limited and difficult because of low concentration and/or matrix interferences. The proposed method is excellent for the determination of trace metal in matrixes, such as metal alloys. © 1998 Elsevier Science B.V. All rights reserved.

Keywords: Trace metal determination; Preconcentration; *Saccharomyces cerevisiae*; Immobilization; Sepiolite; Flame atomic absorption spectrometry

1. Introduction

Many methods, such as extraction, coprecipitation, electrodeposition and ion exchange, have been used for preconcentration of trace metals. In recent years preconcentration by microorganisms has been widely used [1–6]. The use of microorganisms as biosorbent for metals has become a good alternative to the other preconcentration methods as regards higher recovery, economical advantages, simplicity and environmental protection. In general, microorganisms have the ability to selectively adsorb a specific element without preconcentrating the matrix [7–9].

Either living or nonliving microorganisms, such as yeast, fungi, bacteria and algae are capable of accumulating heavy metals and radionuclides from aqueous solution by a different chemical and biological mechanisms [10]. The products pro-

* Corresponding author. Tel: +90 312 2122900; fax: +90 312 2122279; e-mail: rturker@proton.fef.gazi.edu.tr

0039-9140/98/$ - see front matter © 1998 Elsevier Science B.V. All rights reserved.
PII S0039-9140(98)00104-0

duced by or derived from microbial cell such as metabolites, polysaccharides, and cell wall constituents are of effective in metal accumulating. Yeasts are considered to be more effective in heavy metal accumulation because of their great tolerance towards metals and their high binding capacity to the cell [11]. Maquieira et al. [6] have explained the specificity of microorganisms. According to their explanation, the binding sites of microorganisms have a diversity property. For that reason, if one element has an affinity to coordinate with one functional group, i.e. COO^-, and, if this element is present in a mixture of many other elements, each of them can form a stable complex with any of the other functional groups present in the cell wall of the microorganism. Therefore, by changing pH or elution conditions, selectivity can be obtained and this is well demonstrated in the interference effects where the elements in relatively high concentrations. There are many binding sites on the cell wall of microorganisms.

The physical confinement or localization of microbial cells to a certain region of a support material is defined as 'immobilization'. The use of immobilized cell systems has many advantages over the use of freely suspended cells. These include better capability of re-using the biomass, easy separation of cells from the reaction mixture, high biomass loadings and minimal clogging in continuous flow systems. In addition particle size can be controlled and high flow rates achieved with or without recirculation. Immobilized cell systems can be used in both batch and column experiments.

Nakajima et al. [8] have used *Saccharomyces cerevisiae* and some other microorganisms in a comparative study for metal uptake by immobilizing on calcium alginate gel. Maquieira et al. [12] have used *S. cerevisiae* by immobilizing covalently on controlled pore glass (CPG) for trace metal preconcentration. Gencer et al. [13] have immobilized *S. cerevisiae* on wood chips by adsorption using a medium of glucose nutrients for ethanol fermentation in a tubular fermenter. They had described a mathematical model for the kinetics of ethanol fermentation. Daugulis et al. [14] have immobilized *S. cerevisiae* on ion exchange resins by adsorption in glucose nutrients. Black et al. [15] have immobilized *S. cerevisiae* and *S. uvarum* on stainless steel and polyester foam for the production of ethanol.

In this study, *S. cerevisiae* has been immobilized on 'sepiolite' and used for the preconcentration of iron and nickel. Sepiolite is a hydrous magnesium mineral and has already been used for the adsorption of some gases [16], liquids [17] and as an adsorbent for preconcentration of trace elements alone [18], but not as an immobilization substrate.

2. Experimental

2.1. Apparatus

A Philips PU 9285 model flame atomic absorption spectrometer equipped with deuterium lamp background correction, hallow cathode lamps (HCL) and air acetylene burner was used for the determination of the metals. All absorption measurements were performed under the following conditions: wavelengths, 248.3 nm for Fe and 232 nm for Ni; fuel flow rate, 1.1 l min^{-1} for Fe and 0.9 l min^{-1} for Ni; HCL lamp current, 11.2 mA; bandpass, 0.5 nm; and integration time, 4 s for both elements. All pH measurements were performed with a JENWAY 3010 model digital pH meter.

2.2. Reagents

Doubly distilled deionized water and analytical grade reagent chemicals were used unless otherwise indicated. All metal stock solutions (1000 μg ml^{-1}) were prepared by dissolving the appropriate amounts of metals or compounds. The working solutions were prepared by dilution from the stock solutions.

2.3. Materials

The sepiolite used as a substrate for the immobilization of *S. cerevisiae* in this study was collected from the trances dug in the Türktaciri sepiolite deposit and ground and sieved to 35–60 mesh. Full details for the characterization of sepi-

olite have been given in the study [18] carried out before.

2.4. Procedures

A laboratory strain of *S. cerevisiae* was maintained on a medium comprising (g l^{-1}) malt extract (Difco) 3, yeast extract (Difco) 3, D-glucose (Carlo) 10, peptone (Difco) 5, and agar (Difco) 15. The yeast cultivated on the solid medium was stored in a refrigerator at 4°C before use, in order to extend their freshness and prevent contamination by the growth of other microorganisms. Liquid medium was prepared by mixing the substances mentioned above except agar. All the steps of every procedure were sterilized by autoclaving at 120°C for about 30 min. Firstly, starter culture was performed from the solid medium by loop-inoculating to 100 ml of liquid medium. Then, it is incubated for 24 h at 30°C on an orbital shaker (200 rpm). For experimental culture, 100 ml of liquid medium was prepared and inoculated with 5 ml of the starter culture and incubated on the orbital shaker for 24 h at 30°C. Then, the yeast grown in the experimental culture was separated from the growth media using centrifugation (5000 g for 5 min) to isolate the biomass. The biomass was treated according to the procedure described by Mahan et al. [19]. 10 ml of 0.1 mol l^{-1} HCl was added to the isolated biomass. After 10 min, the mixture was centrifuged and the acid solution was discarded. This procedure was repeated three times and then followed by rinsing the acid-washed biomass in distilled water. These rinsed yeast were again centrifuged and the resulting biomass lyophilized to yield a dry yeast powder.

The immobilization of *S. cerevisiae* was performed according to the procedure recommended by Mahan et al. [19]. 150 mg of dry yeast powder (*S. cerevisiae*) was mixed with 2 g of sepiolite. The mixture was wetted with 2 ml of doubly distilled deionized water and thoroughly mixed. After mixing, the paste was heated in an oven at 80°C for 24 h to dry the mixture. The wetting and drying step was repeated to maximize the contact between *S. cerevisiae* and sepiolite, thereby improving the immobilization efficiency. Then, the sepiolite-yeast briquette was broken to get original size (35–60 mesh).

S. cerevisiae immobilized sepiolite (0.2 g) was packed in a glass column (10 mm i.d and 200 mm length). Before use, 1 mol l^{-1} HCl solution and doubly distilled deionized water were passed through the column in order to condition and clean it. Then, the column was conditioned to the studied pH.

An aliquot of a solution (100 ml) of one or several elements containing 25 μg Ni, 50 μg Fe was taken and the pH was adjusted to the desired value with hydrochloric acid and ammonia. The resulting solution was passed through the column. By using a peristaltic pump, the flow rate was adjusted to the desired value. The retained metal ions were eluted from *S. cerevisiae* immobilized sepiolite with 10 ml of 1 mol l^{-1} hydrochloric acid solution. The eluate was aspirated into an air-acetylene flame for trace determination by AAS. The *S. cerevisiae* immobilized sepiolite was used repeatedly after washing with 1 mol l^{-1} HCl solution and distilled water, respectively. The recoveries of the elements were calculated from the ratio of the concentration found by FAAS to that calculated theoretically. All experiments done for the determination of the optimum conditions (pH, bed height, etc) were performed according to the general procedure described above.

2.5. Dissolution of standard reference material

As an application sample, standard reference brass material (NBS SRM 37e) was used. 0.5 g of the standard reference material were weighed and dissolved in 10 ml of doubly distilled deionized water and 10 ml of concentrated nitric acid. The solution was heated until the volume was one fourth of the beginning solution. Then, it was made up to 100 ml with doubly distilled deionized water and adjusted to pH 6 with hydrochloric acid and ammonia. Iron and nickel were determined after applying the general preconcentration procedure described above.

3. Results and discussion

3.1. Effect of pH

The retention of metal ions on the column containing *S. cerevisiae* immobilized sepiolite was studied as a function of pH. For that purpose, the pH values of element solutions were adjusted to a range of 2–10 with HCl or NH_3. As shown in Fig. 1, the optimum pH of the sample solution is 6 for nickel and 8 for iron. From the same figure, uptake of the metal ions was quantitative in part of the pH range 6–8. For the binding of metal ions, at least, two types of adsorption sites or two functional groups could be present in the yeast surface [21]. This causes the difference in metal binding to the surface with the pH of the medium. The decrease in binding at lower pH values was attributed to the protonation of weakly basic coordination groups on the yeast surface [22]. In a study [12], *S. cerevisiae* was immobilized on controlled pore glass (CPG) and the maximum uptake of iron was obtained at pH 6. The difference between the pH values may be due to the change of metal uptake mechanism according to the substrate used for the immobilization and killing process of yeast. In our previous study [18] in which sepiolite was used alone as an adsorbent the maximum retention of iron was at pH 2 with a recovery of 80%. But in the present study, the retention of iron was found extremely high and the maximum recovery was obtained at pH 8. This shows that the metal ions were adsorbed mainly by immobilized *S. cerevisiae* instead of sepiolite.

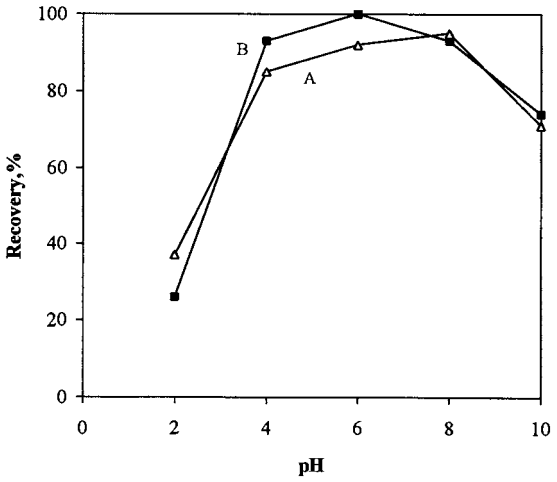

Fig. 1. The effect of pH on recovery of iron and nickel by *S. cerevisiae* immobilized sepiolite; A, iron; and B, nickel.

3.2. Effect of the amount of adsorbent (bed height)

The retention of the elements studied was examined in relation to the amount of *S. cerevisiae* immobilized sepiolite, which was varied from 0.05 to 0.4 g. It was found that above 0.15 g of adsorbent the recovery of Ni was gradually increased, but about 0.2 g of adsorbent that of Fe reached plateau. Therefore, 0.2 g of adsorbent was found to be optimum of all preconcentration purposes.

3.3. Effect of the type and volume of elution solutions

The elution studies were performed with 0.5 and 1 mol l^{-1} hydrochloric and nitric acid solutions. The eluate volume was 5, 10 and 15 ml. As can be seen in Table 1, for all elements studied 10 ml of 1 mol l^{-1} hydrochloric acid solution was found to be satisfactory.

3.4. Effect of flow rates of sample solutions

The retention of elements on an adsorbent depends upon the flow rate of the metal solution. Therefore, the effect of the flow rate of sample solution was examined under optimum conditions (pH, eluent type, etc.) by using a peristaltic pump. The solution was passed through the column with the flow rates adjusted in a range of 1–7.5 ml min^{-1}. As shown in Fig. 2, the optimum flow rates was found as 2.5 ml min^{-1} for both metal ions. The flow rate of elution solution used was 1 ml min^{-1}.

3.5. Effect of the volume of sample solution

The effect of changes in the volume of sample solution passed through the column on the reten-

Table 1
Effect of the type and volume of elution solutions on recovery of iron and nickel by *S. cerevisiae* immobilized sepiolite

Type of elution solution	Volume (ml)	Concentration (mol l^{-1})	Recovery (%)	
			Fe	Ni
HCl	5	0.5	81	85
	10		89	89
	15		90	89
HCl	5	1.0	87	90
	10		95	99
	15		95	99
HNO_3	5	0.5	79	83
	10		87	89
	15		88	92
HNO_3	5	1.0	87	89
	10		90	91
	15		91	94

tion of Fe and Ni was investigated. 100, 250, 500, 750 and 1000 ml of sample solutions containing 0.25, 0.10, 0.05, 0.033 and 0.025 μg ml^{-1} of Ni, 0.5, 0.2, 0.1, 0.066 and 0.05 μg ml^{-1} of Fe respectively, were passed through the column. It was found that iron and nickel up to 500 ml of sample solution could be recovered quantitatively. At higher sample volumes, the recoveries decreased gradually with increasing volume of sample. In this study, the elution volume was 10 ml and the preconcentration factors were 50 for both iron and nickel.

3.6. Precision of the method

For the precision of the method, the optimum conditions mentioned above were used. For this purpose, successive retention and elution cycles (with 0.25 μg ml^{-1} of Ni and 0.50 μg ml^{-1} of Fe) were performed and nickel and iron were determined in the solution by FAAS. As can be seen in Table 2, the recoveries of nickel and iron are quantitative and the precision of the method is very good.

3.7. Calibration graph and detection limit

The calibration graphs were linear up to 5 μg ml^{-1} for nickel and up to 8 μg ml^{-1} for iron. The detection limit (evaluated as the concentration corresponding to three times the standard deviation of the blank signal) were 0.065 μg ml^{-1} for iron and 0.087 μg ml^{-1} for nickel.

3.8. Capacity studies

The capacity study used was adapted from that recommended by Maquieira et al. [20]. 50 ml aliquots of a series of concentrations (5–80 μg ml^{-1}) was adjusted to the appropriate pH, then, preconcentrated and eluted. The amount of metal

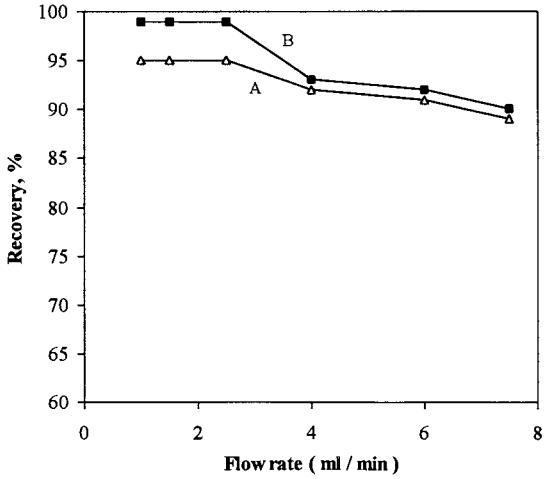

Fig. 2. The effect of flow rate of sample solutions on recovery of iron and nickel by *S. cerevisiae* immobilized sepiolite; A, iron; and B, nickel.

Table 2
Precision of the method

Element	Recovery[a] % $R \pm ts/\sqrt{N}$	N
Fe	95 ± 1	7
Ni	99.5 ± 0.1	7

[a] Average of N determinations with 95% confidence level.

adsorbed at each concentration level was determined from the following equation:

$$C = cv/w$$

where C is the capacity (in μg g^{-1}), c is the concentration (in μg ml^{-1}) of metal eluted, v is the volume (in ml) of solution used and w is the mass (in g) of the immobilized material. Evaluation of breakthrough capacity was made from a breakthrough curve by plotting the total metal concentration (μg ml^{-1}) versus the milimoles of metal adsorbed per gram.

The breakthrough capacity was evaluated from a breakthrough curve plot, which is shown in Fig. 3. As shown in Table 3, it was found that the breakthrough capacity of nickel was higher than that of iron. However, the breakthrough capacity of iron found in this study is higher than that obtained in a study [12] in which *S. cerevisiae* was immobilized on CPG and the breakthrough capacity of iron was found 0.020 mmol g^{-1}. As it is explained before, this difference in the breakthrough capacity of iron may be due to the change in the structure of the yeast during the killing, immobilization process and the type of immobilization substrate (sepiolite).

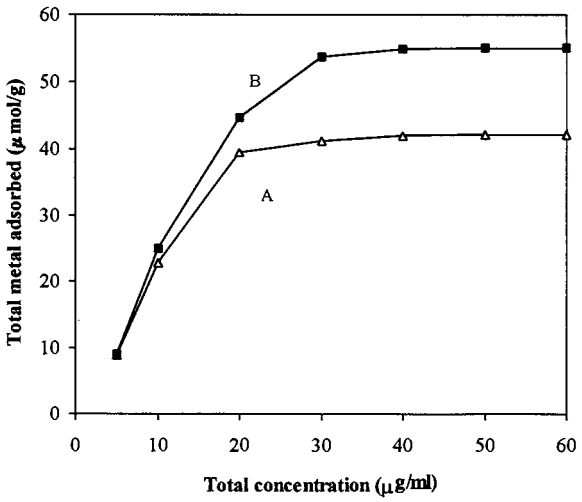

Fig. 3. The breakthrough curve of iron and nickel on *S. cerevisiae* immobilized sepiolite; A, iron; and B, nickel.

Table 3
Capacity for the metal ions and recovery

Metal ion	Capacity (mmol g^{-1})	Recovery (%)
Fe^{3+}	0.042	95
Ni^{2+}	0.055	99

Table 4
The effect of interfering ions on recovery

Interfering ions	Concentration (μg ml^{-1})	Recovery (%)	
		Fe[a]	Ni[b]
Cu^{2+}	—	95	99
	0.5	95	98
	1.0	92	98
	2.5	92	97
	5.0	90	94
	10.0	90	94
Zn^{2+}	—	95	99
	0.5	96	97
	1.0	96	97
	2.5	94	95
	5.0	93	94
	10.0	92	94
Fe^{3+}	—		99
	0.5		100
	1.0		100
	2.5		102
	5.0		103
	10.0		104
Ni^{2+}	—	95	
	0.5	89	
	1.0	91	
	2.5	97	
	5.0	99	
	10.0	102	

[a] 0.5 μg ml^{-1}.
[b] 0.25 μg ml^{-1}.

3.9. Effect of interfering ions

In order to investigate the effect of the interference of elements to each other on biosorption, the recoveries of elements was examined when they existed together in a same medium. The concentrations of interfering metal ions were adjusted in a range of 0.5–10 μg ml^{-1}. The results were given in Table 4. As can be seen, the effect of divers ions can be negligible. This shows that nickel and iron can be determined quantitatively in metal alloys although the matrix concentration is high.

3.10. The effect of column reuse

The stability and potential recyclability of the column were assessed by monitoring the change in the recoveries of iron and nickel ions through several adsorption-elution cycles. Each five runs were performed in the same day and the next five runs were made one day later. The columns were stored in doubly distilled deionized water. As shown in Fig. 4, a small decrease in the recoveries (~ 5 and 8% for iron and nickel, respectively) occurred. The columns seems to be relatively stable up to 20 runs.

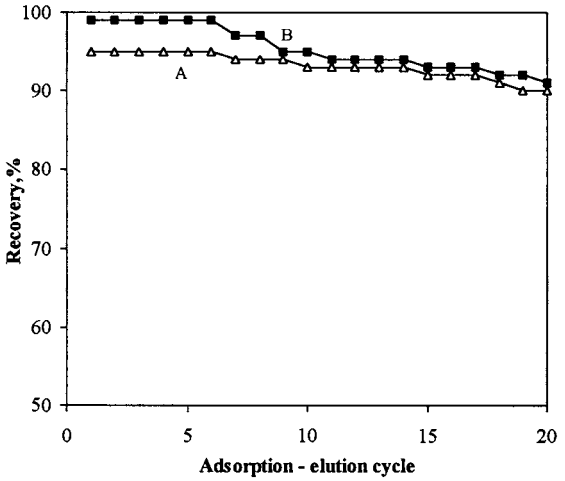

Fig. 4. The effect of column reuse on recovery of iron and nickel by *S. cerevisiae* immobilized sepiolite; A, iron; and B, nickel.

3.11. Application

Proposed preconcentration method was applied to the determination of Ni and Fe in standard reference material (NBS SRM 37e). Reference sample material was preconcentrated and analyzed as explained in Section 2. As shown in Table 5, it is clear that the calculated values for both metal agreed very well with the certified values. By using yeast immobilized sepiolite, nickel and iron were determined with high accuracy and precision although the matrix concentration (e.g. copper and zinc) was very high in standard reference material.

4. Conclusion

The method proposed by the use of *S. cerevisiae* immobilized sepiolite for the preconcentration of iron and nickel is simple, sensitive and accurate. Iron and nickel were quantitatively recovered from the column with a high precision. In conclusion, the proposed method is excellent as regards simplicity, sensitivity, selectivity, precision, accuracy and column stability.

Table 5
Analysis of standard reference material

Element	Concentration (% m/m)		Relative error (%)	LOD (μg ml^{-1})
	Calculated value[a]	Certified value[b]		
Fe	$(3.7 \pm 0.5) \times 10^{-3}$	0.004	−7.5	0.065
Ni	0.50 ± 0.01	0.53	−5.7	0.087

[a] Mean and S.D. of eight determinations.
[b] The composition of the brass (NBS SRM 37e) was Cu 69.61, Zn 27.85, Pb 1.00 and Sn 1.00% (m m^{-1}).

Acknowledgements

The support Gazi University Research Fund are gratefully acknowledged.

References

[1] V. Majidi, J.A. Holcombe, J. Anal. At. Spectrom. 4 (1989) 439.
[2] H.A.M. Elmahadi, G.A. Greenway, J. Anal. At. Spectrom. 8 (1993) 1011.
[3] H.A.M. Elmahadi, G.A. Greenway, J. Anal. At. Spectrom. 6 (1991) 643.
[4] C.A. Mahan, V. Majidi, J.A. Holcombe, Anal. Chem. 61 (1989) 624.
[5] L.C. Robles, C.G. Ollalla, A.J. Aller, J. Anal. At. Spectrom. 8 (1993) 1015.
[6] A. Maquiera, H. Elmahadi, R. Puchades, J. Anal. At. Spectrom. 11 (1996) 99.
[7] T. Sakaguchi, T. Tsuji, A. Nakajima, T. Horikoshi, Appl. Microbiol. Biotechnol. 8 (1979) 207.
[8] A. Nakajima, T. Sakaguchi, Appl. Microbiol. Biotechnol. 24 (1986) 59.
[9] V. Majidi, J.A. Holcombe, Spectrochim. Acta 43B (12) (1988) 1423.
[10] G.M. Gadd, C. White, L. de Rome, Biohydrometallurgy Sci. Technol. Lett., Kew Survey, UK (1988) 421.
[11] G.M. Gadd, C. White, J. Gen. Microbiol. 131 (1985) 1875.
[12] A. Maquieira, H.A.M. Elmahadi, R. Puchades, Anal. Chem. 66 (1994) 1462.
[13] M.A. Gencer, R. Mutharasan, Biotechnol. Bioeng. 25 (1983) 2243.
[14] A. J. Daugulis, N.M. Brown, W.R. Cluett, D.B. Dunlop, Biotechnol. Lett. 3 (1981) 651.
[15] G.M. Black, C. Webb, T.M. Mathews, B. Atkinson, Biotechnol. Bioeng. 26 (1986) 134.
[16] Y. Sarıkaya, S. Aybar, Comm. Fac. Sci. University d'Ankara 24 (1978) 33.
[17] B. Erdoğan, H.İ. Ünal, İ. Kayabalı, H. Öcal, Seventh National Clay Symposium, Ankara, 1985.
[18] A.R. Türker, H. Bağ, B. Erdoğan, Fresenius J. Anal. Chem. 357 (1997) 351.
[19] C.A. Mahan, J.A. Holcombe, Anal. Chem. 64 (1992) 1933.
[20] A. Maquieira, H.A.M. Elmahadi, R. Puchades, Anal. Chem. 66 (1994) 3632.
[21] L.C. Robles, C.G. Olalla, A.J. Aller, J. Anal. At. Spectrom. 8 (1993) 1015.
[22] B. Greene, M.T. Henz, M. Hosea, D.W. Darnall, Biotechnol. Bioeng. 28 (1986) 764.

ELSEVIER

Talanta 47 (1998) 697–709

Talanta

An investigation into the sorption of benzoic acids by polyurethane membrane

Kathy Rzeszutek, Art Chow *

Department of Chemistry, University of Manitoba, Winnipeg, Manitoba R3T 2N2, Canada

Received 15 December 1997; accepted 27 February 1998

Abstract

The extraction mechanism of organic compounds by ether- and ester-type polyurethane membrane has been investigated through a detailed study of sorption of monobromobenzoic acids. The effects of solution concentration, extraction time, surface area, pH, salts, and temperature on extraction were studied. It was found that monobromobenzoic acids are extracted in their neutral form, and that the extraction is controlled primarily by the relative strength of intra- and intermolecular hydrogen bonding. The ether-type polyurethane membrane allows a more efficient removal of monobromobenzoic acids from solution than the ester-type membrane. The extraction of benzoic acids with the ether-type membrane decreases as the temperature increases. When the ester-type polyurethane membrane is used, an extraction maximum is observed at room temperature with a decrease in extraction at lower and higher temperatures. © 1998 Elsevier Science B.V. All rights reserved.

Keywords: Polyurethane membrane; Extraction mechanism; Benzoic acids

1. Introduction

The strict regulations for waste disposal put forward in 1972 [1–3], forced the industries to become more environmentally responsible and created a need for more economical and efficient methods for purification of industrial waste effluents. Utilization of polymer membranes for purification has been actively researched during the last few years [4–10]. Even though the implementation of membrane separations for removal of organic contaminants from wastewater is still at its early stages of development, it has been shown to be a viable alternative to the conventional methods [4–10].

Polyurethane materials have been widely used as fibers, coatings, foams and polymer films. Polyurethanes are linear block polymers formed by reacting di- or poly-isocyanates with polyols [11]:

* Corresponding author. Tel.: +204 4749504; fax: +204 4747608.

0039-9140/98/$ - see front matter © 1998 Elsevier Science B.V. All rights reserved.
PII S0039-9140(98)00115-5

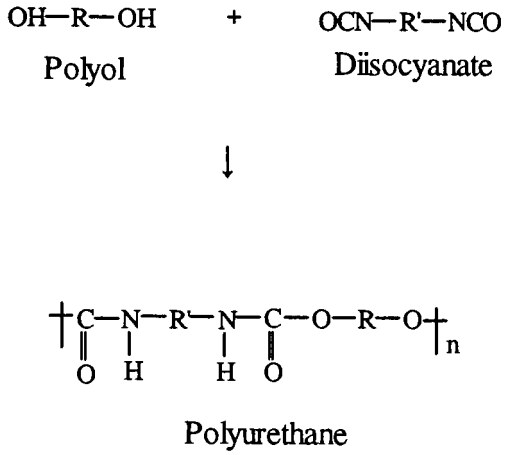

The most frequently used polyols are polyethers and/or polyesters (R) which make up the flexible segments of the polyurethane [12]. These flexible chains are joined by rigid polyurethane-polyurea segments containing an aromatic group (R′) [12]. The polyurethane-polyurea segments align as a result of strong hydrogen bonding, and agglomerate into hard domains. The ether or ester oxygen of the polyether or polyester chains also tends to align by hydrogen bonding with the NH-groups [12]. Because of its unique structure and extensive intermolecular interactions, polyurethane is very resistant to extreme pH conditions and temperatures, which makes it a good candidate for industrial membrane-separation applications.

Considerable research has been done on the extraction of inorganic and organic species by the polyurethane membrane [13–19]. There has been some discussion of the mechanism governing the extraction of inorganic species [13,14], but very little work has been done on the mechanism of extraction of organic compounds [15]. Through a detailed study of extraction of simple substituted phenolic compounds by the polyurethane membrane, we previously proposed a mechanism describing the sorption of phenols [15]. Because the overall process was found to be very complex, the suggested mechanism could not be generalized based only on data collected for such a narrow representative group of organic compounds. It was, however, shown that polyurethane membrane can be used to extract organic compounds which engage in hydrogen bonding with the membrane. Knowing how the sorption is affected by experimental conditions and compound characteristics is valuable from the industrial point of view as it will allow the creation of a more efficient purification system.

In order to obtain more detailed information regarding the mechanism, we have studied the role of functional groups and solution conditions on extraction by investigating the sorption of benzoic acids. Benzoic acids are representatives of a very broad class of carboxylic acids. The main industrial uses for benzoic acids are as a chemical raw material in the production of phenol, glycoldibenzoate esters, and sodium and potassium benzoates [20]. However, these acids have also some direct uses as anti-microbial agents in textile, leather, and cosmetic industries [21], corrosion inhibitors [22], polymer retarders [23] and stabilizers [24]. Because of the industrial importance of benzoic acids, knowledge on the extraction mechanism of these compounds by polyurethane membrane is important for membrane waste purification processes.

2. Experimental

2.1. Apparatus and reagents

Spectra and absorbance readings were taken using a Hewlett-Packard model 8452A diode-array spectrophotometer. Solution pH was measured with an Orion expandable ion analyser EA 940. A modified Burrell wrist-action shaker was used for sample agitation at room temperature. A Fisher Versa-Bath® shaking water bath was used for experiments at higher temperatures. Water was obtained from a Barnstead Nanopure II™ purification system fed with water purified by reverse osmosis. Polyurethane membranes, ether-type PT6310S and ester-type MP1495-SL were obtained from Deerfield Urethane and Stevens Elastomerics/Urethane Products, respectively. Three thicknesses of 0.025, 0.051, and 0.127 mm were used. All chemicals were reagent grade. The apparatus used for membrane testing was a 40 ml Kimble Glass amber glass vial (60960A-912) with a plastic cap and a Teflon™-faced silicone liner. For experiments

Table 1
Effect of concentration of monobromobenzoic acids on extraction

Compound	%E				
	'Natural' pH	3×10^{-6} M	3×10^{-5} M	1×10^{-4} M	3×10^{-4} M
o-Bromobenzoic acid	3.27				
Ether		***	0 ± 0	0 ± 0	2 ± 1
Ester		***	0 ± 0	0 ± 0	0 ± 0
m-Bromobenzoic acid	3.43				
Ether		***	0 ± 0	11 ± 1	27 ± 2
Ester		***	0 ± 0	6 ± 1	15 ± 2
p-Bromobenzoic acid	3.54				
Ether		3 ± 1	4 ± 1	10 ± 1	20 ± 2
Ester		7 ± 1	8 ± 1	8 ± 1	8 ± 1

Conditions: 25.0 ± 2.0°C, 10-ml aliquot of an aqueous monobromobenzoic acid solution, 0.051 mm ether- and ester-type membranes, active surface area of 2.54 cm^2.
*** Below instrumental detection limit.

involving different surface areas of membrane exposed to the sample solution, glass containers having larger caps were used.

2.2. Procedure

Sample solutions having concentrations of $\sim 3\times10^{-4}$ M (unless otherwise specified) were prepared by accurately weighing an appropriate amount of monobromobenzoic acid, dissolving it in the solvent and transferring to a 500 ml volumetric flask which was then filled to volume. Parameters such as salt, acid, or base concentrations were adjusted prior to dilution to volume. A 10 ml aliquot of the sample solution was then transferred, using a volumetric pipette, into the sample vial. The polyurethane membrane (ether- and ester-type 0.051 mm thick unless otherwise specified) was placed on the opening of the vial and covered with the Teflon™ silicone disk and a screw cap and carefully tightened. The vials were then inverted to put the sample in contact with the membrane and shaken for 24 h, except when extraction with time was investigated. The surface of the membrane exposed to the sample solution was 2.54 cm^2 (unless otherwise specified). For each experiment, triplicate samples were prepared and the experiment was repeated at least two times to establish reproducibility. The vials containing the samples were weighed prior to and after the extraction to determine if any leakage may have occurred. The UV-visible spectrum (190–820 nm) of the sample solution was taken and the absorbance (A_F) compared with the absorbance of the solution prior to extraction (A_I). The absorbance readings for the *ortho*, *meta* and *para* isomers of monobromobenzoic acid were taken at 280, 284 and 246 nm, respectively. The molar absorptivities at those wavelengths are approximately 1200, 2950, and 10660 l mol^{-1} cm^{-1} for the *ortho*, *meta* and *para* isomers. The degree of extraction is reported as the %E which is the % decrease of absorption from the solution assuming a Beer's Law dependence:

$$\%E = (A_I - A_F)/A_I \times 100\% \quad (1)$$

3. Results and discussion

3.1. Effect of benzoic acid concentration on extraction

The range of concentration of monobromobenzoic acids studied was $\sim 3\times10^{-6}$–3×10^{-4} M, which was dictated by the solubility of the compounds in water and the detection limit of the UV-visible spectrophotometer (Table 1). It was found that an increase in the concentration of *meta* monobromobenzoic acid resulted in increased extraction with both ether- and ester-type

polyurethane membranes. The increase in concentration of the *para* isomer resulted in increased extraction only when the ether-type polyurethane membrane was used; the extraction of this isomer with the ester-type membrane was basically constant with the increase in concentration. At the 'natural' pH of 3.27 (i.e. the pH of benzoic acid dissolved in only deionized water without adjustment), the *ortho* isomer is not extractable regardless of the concentration. For subsequent experiments, monobromobenzoic acid solutions having concentration of $\sim 3 \times 10^{-4}$ M were used.

Before benzoic acid enters the membrane, equilibrium between the benzoic acid molecules in solution and at the solution-membrane interface has to be established. This is followed by the transfer of benzoic acid from the membrane-solution interface onto the membrane surface and migration into the bulk of the membrane. The amount of benzoic acid removed from the solution is determined by the slowest of the above steps, which is either the transfer of benzoic acid into the membrane surface or its migration through the polymer.

For solvent extraction processes, the equilibrium distribution coefficient is the ratio of the equilibrium concentration of extractant in an aqueous phase to the concentration in an organic phase. For such processes, the equilibrium distribution coefficient remains the same regardless of the starting concentration of the extracting species. If sorption by the membrane is analogous to a solvent extraction, the ratio of the concentrations of the extractant in aqueous solution and in the membrane should not change as one would expect the extraction coefficient to be independent of the original concentration. However, it was found that the extractant concentration does affect the distribution coefficient (Table 1), and therefore the sorption by the polyurethane membrane cannot be considered a simple solvent extraction. We have shown that all of the sorption steps, i.e. onto the membrane surface, into the membrane, and through the membrane, plus the total capacity of the available membrane collectively determine the amount of the extracting species that will be removed from solution. Therefore, the distribution coefficient for the sorption by polyurethane membrane does not simply represent the transfer of the extractant from aqueous solution onto the surface of an organic phase as in the solvent extraction, but it also provides information about the transport properties of the bulk membrane.

The time needed to attain equilibrium in solution, at the solution-membrane interface and in the bulk of the membrane may vary, which can account for the change in sorption with the change in concentration. At lower benzoic acid concentrations, the concentration gradient is smaller than at the higher concentrations, which results in a slower migration of benzoic acid from the solution-surface interface into the polymer surface. Because fewer molecules are entering the membrane, fewer molecules are interacting with the polar groups of the membrane. As a result, less disruption of the intermolecular interactions between the membrane polar groups occurs, and migration deeper into the body of the polymer is slower than it would be at a higher benzoic acid concentration. Consequently, a lower percentage of benzoic acid is extracted. These results are consistent with the data obtained for the sorption of various phenols from solutions of differing concentrations [15]. The extraction of benzoic acids by the polyurethane membrane is governed to some extent by the strength and number of the intermolecular interactions formed between the polymer and the extracting species as is discussed later (Sections 3.2 and 3.6). The structures of the polymer and the *ortho* and *para* monobromobenzoic acids dictate the extent to which intermolecular interactions occur. This can account for the very low extraction of the *ortho* isomer with both membrane types, and the relatively low and level extraction of the *para* isomer with the ester-type polyurethane membrane.

3.2. Effect of extraction time and type of polyurethane membrane

To determine how much time is needed for the sorption process to reach equilibrium at room temperature, extraction over a range of 0.5 to 72 h using the ether- and the ester-type polyurethane

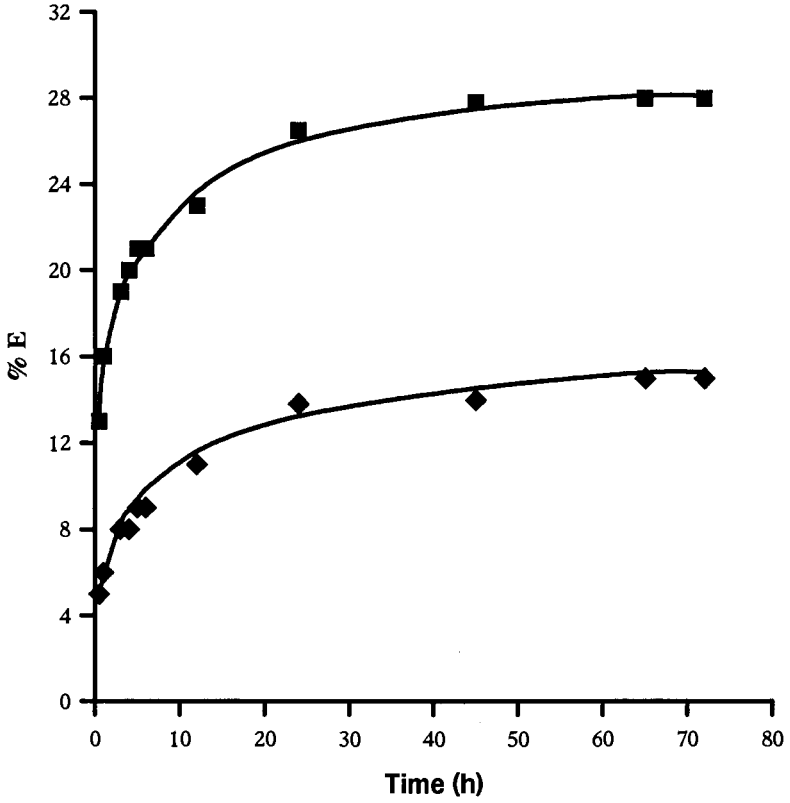

Fig. 1. Extraction of *m*-monobromobenzoic acid with time using the ether- and ester-type polyurethane membranes. Conditions: 25.0 ± 2.0°C, 10-ml aliquot of $\approx 3 \times 10^{-4}$ M aqueous monobromobenzoic acid solution, 0.051 mm ether- and ester-type membranes, active surface area of 2.54 cm^2. Extraction with the ether-type membrane, ■; extraction with the ester-type membrane, ◆.

membranes was measured. Sample solutions were mechanically shaken for the desired amount of time, and analysed after 0.5 h and subsequently at 1 h periods up to 12 h. Final readings were taken at 25, 45, 65, and 72 h.

The change in sorption of benzoic acid with time is illustrated by the extraction of *meta* monobromobenzoic acid shown in Fig. 1. Extraction with both the ether- and ester-type membranes increases very rapidly up to about 24 h, beyond which no further significant increase is observed. Therefore, we assumed that equilibrium was attained within approximately 24 h for solutions containing 3×10^{-4} M concentration of benzoic acids extracted with 0.051 mm thick ether- and ester-type polyurethane membranes.

It was also found that the ether-type polyurethane membrane extracts a greater amount of each benzoic acid than the ester-type membrane. We attribute this to the efficiency with which the benzoic acid molecules can disrupt the hydrogen bonding between the polar segments in each of the membranes. The ester-type membrane has a more compact and rigid internal structure than the ether-type membrane because the ester groups have a better probability of forming intermolecular hydrogen bonds than the ether groups [12]. Benzoic acid molecules entering the ester-type membrane will have to break more hydrogen bonds than in the ether-type membrane in order to move deeper into the polymer. This can account for the slower migration of benzoic acids through the ester-type membrane, and hence the lower extraction efficiency of this membrane.

3.3. Effect of surface area and thickness of the membrane

Sorption of benzoic acids with both membrane types can be increased by increasing the surface of the membrane exposed to the sample solution and/or by increasing the thickness of the membrane. When the surface area of the 0.051 mm thick membranes exposed to *meta* and *para* monobromobenzoic acid solutions was increased, a significantly greater extraction with both membrane types resulted (Table 2). Although, at the 'natural' pH of 3.27, the *ortho* isomer is extracted very poorly by the ether-type, an increase in extraction is still observed with an increase in the surface area (Table 2). However, when the ester-type polyurethane membrane is used, no extraction of the *ortho* isomer occurred regardless of the membrane surface area exposed to the sample solution. The thicker polyurethane membranes (0.051 and 0.127 mm) having identical surface area were found to have a higher sorptive capacity for the *meta* and *para* isomers than the thinner membranes (0.025 mm) (Table 3). The extraction of *ortho* monobromobenzoic acid with the ether-type membrane is very low, but also increases when a thicker membrane is used (Table 3).

Table 2
Effect of surface area on extraction of monobromobenzoic acids

Compound	%E		
	Active surface area (cm^2)		
	2.54	6.61	18.10
o-Bromobenzoic acid			
Ether	2 ± 1	3 ± 1	5 ± 1
Ester	0 ± 0	0 ± 0	0 ± 0
m-Bromobenzoic acid			
Ether	28 ± 3	47 ± 3	67 ± 3
Ester	15 ± 2	29 ± 3	58 ± 3
p-Bromobenzoic acid			
Ether	18 ± 2	34 ± 3	49 ± 3
Ester	8 ± 1	20 ± 2	36 ± 3

Conditions: 25.0 ± 2.0°C, 10-ml aliquot of $\approx 3 \times 10^{-4}$ M aqueous monobromobenzoic acid solution (pH 3.27, 3.43, and 3.54 for *o*-, *m*-, *p*-isomers respectively), 0.051 mm ether- and ester-type membranes.

Table 3
Extraction of monobromobenzoic acids by ether- and ester-type polyurethane membranes having thicknesses of 0.025, 0.051 and 0.127 mm

Compound	%E		
	Membrane thickness		
	0.025 mm	0.051 mm	0.127 mm
o-Bromobenzoic acid			
Ether	0 ± 0	2 ± 1	4 ± 1
Ester	0 ± 0	0 ± 0	0 ± 0
m-Bromobenzoic acid			
Ether	13 ± 2	25 ± 2	37 ± 3
Ester	3 ± 1	13 ± 2	17 ± 2
p-Bromobenzoic acid			
Ether	9 ± 1	21 ± 2	30 ± 3
Ester	4 ± 1	6 ± 1	12 ± 1

Conditions: 25.0 ± 2.0°C, 10-ml aliquot of $\approx 3 \times 10^{-4}$ M aqueous monobromobenzoic acid solution (pH 3.27, 3.43, and 3.54 for *o*-, *m*-, *p*-isomers, respectively), active surface area of 2.54 cm^2.

The above results can be explained by looking more closely at the initial transfer of benzoic acid onto the membrane surface and the subsequent migration through the membrane. After equilibrium between benzoic acid in solution and benzoic acid at the solution-membrane interface is achieved, the benzoic acid molecules will migrate into the surface and through the bulk of the membrane. The overall sorption process is absorption, but one can consider the first step in this process as Langmuir adsorption [25]. According to Langmuir, the extent of adsorption of, for example, gas molecules on a solid surface is determined by the equilibrium between the gas molecules on the surface and the gas molecules evaporating from the surface. The number of gas molecules on the surface is proportional to the area of the surface exposed to the gas [25]. Assuming that the first step in the sorption of benzoic acid in solution into the membrane surface is similar to the above example for gas adsorption onto a solid surface, we can use a modified Langmuir equation to describe it:

$$y = by_{\mathrm{m}}C/(1 + bC) \quad (2)$$

where y is the membrane surface, y_{m} is the

Table 4
Effect of acid addition on extraction

HCl final concentration (M)		%E		
		o-Bromobenzoic acid	*m*-Bromobenzoic acid	*p*-Bromobenzoic acid
0.0	Ether	2 ± 1	27 ± 2	19 ± 2
	Ester	0 ± 0	15 ± 1	7 ± 1
0.001	Ether	17 ± 2	45 ± 2	40 ± 2
	Ester	7 ± 1	24 ± 2	12 ± 2
0.010	Ether	20 ± 2	48 ± 2	40 ± 2
	Ester	9 ± 1	26 ± 2	22 ± 2
0.10	Ether	21 ± 2	47 ± 2	41 ± 2
	Ester	9 ± 1	26 ± 2	22 ± 2
0.50	Ether	20 ± 2	44 ± 2	40 ± 2
	Ester	8 ± 1	25 ± 2	20 ± 2
1.00	Ether	18 ± 2	48 ± 2	40 ± 2
	Ester	9 ± 1	26 ± 2	20 ± 2
2.00	Ether	12 ± 1	39 ± 2	40 ± 2
	Ester	9 ± 1	22 ± 2	20 ± 2

Conditions: 25.0 ± 2.0°C, 10-ml aliquot of $\approx 3 \times 10^{-4}$ M aqueous monobromobenzoic acid solution, 0.051 mm ether- and ester-type membranes, active surface area of 2.54 cm^2.

amount of benzoic acid adsorbed from solution when the monolayer is complete, C is the concentration of benzoic acid remaining in solution, and b is an adsorption coefficient which is constant at a given temperature. The adsorption of benzoic acid from solution onto the membrane surface would be expected to proceed rapidly, depending on the solubility of benzoic acid in water and its attraction to the membrane surface, until equilibrium is reached between benzoic acid in solution and that adsorbed on the surface of the membrane.

If we were to assume that the overall extraction is an adsorption process, such as the one described by Langmuir, all of the membranes would be expected to show identical removal of benzoic acid from solution because identical surface areas of each membrane were exposed to the sample solution. The results obtained from studying the effect of membrane thickness show a proportional relationship between the amount of benzoic acid extracted and the membrane thickness (Table 3). This indicates that although initially adsorption is taking place, the subsequent process responsible for further removal of benzoic acid cannot be accounted for by adsorption. One explanation is that benzoic acid, after being initially adsorbed onto the membrane surface, begins to migrate deeper into the polymer as a result of hydrogen bonding interactions with the polar segments of the membrane. Because of the migration, the concentration of benzoic acid at the solution-membrane interface and at the membrane surface will be depleted by a concentration gradient which is facilitated between the membrane surface and the bulk membrane. The benzoic acid molecules will continue to travel deeper into the membrane until the capacity of the membrane is reached. We have shown that for the 0.051 mm thick membrane equilibrium is attained within 24 h. A shorter time would be required for the extractions done with the 0.025 mm membrane and a longer time for extractions with the 0.127 mm membrane. Therefore, the thinner membranes extracted a lesser amount of benzoic acid because they have a smaller capacity. Because migration of benzoic acid follows the initial adsorption step, we shall refer to the overall extraction process as sorption.

3.4. Effect of pH on extraction

The effect of solution pH on extraction of monobromobenzoic acids was studied in order to confirm our hypothesis that neutral species extraction was occurring [15]. Benzoic acid solutions

having even slightly basic pH (0.001 M NH_4OH) do not show any extraction. In contrast, the slightly acidic solutions (0.001 M HCl) show significantly higher sorption that at the 'natural' pH (Table 4).

Benzoic acids are weak carboxylic acids which dissociate slightly in aqueous solution [26]. As a result, two forms will be present at the 'natural' pH, i.e. the undissociated neutral benzoic acid and the carboxylate anion of benzoic acid. The ratio of these two species is dependent on the dissociation constant, K_a, for the particular isomer (140×10^{-5}, 15.4×10^{-5}, 10.7×10^{-5} for *ortho*, *meta* and *para*, respectively) [27]. For example, because *ortho* monobromobenzoic acid has the highest K_a, it is more dissociated in solution than the *meta* and *para* isomers. The addition of base to the benzoic acid solutions results in formation of the carboxylate anion which is not extracted by the membrane. Conversely, the addition of acid, results in protonation of the benzoic acid molecules which may have been negatively charged at the 'natural' pH, and results in the observed increased extraction. However, when the solutions are made highly acidic (e.g. 2.0 M HCl final concentration), a positive charge may be placed on the carbonyl oxygen or the formation of carboxylic acid dimers and homoconjugated anions may take place [28] which would account for the decrease in extraction. These results strongly confirm the hypothesis that benzoic acids are efficiently removed from solution by the polyurethane membrane only if present as neutral molecules.

3.5. Effect of salts on extraction

The addition of salt to an aqueous solution of an organic compound increases the ionic strength of the solution, which has been shown to increase the efficiency of solvent extractions and extractions with polyurethane foam [29–31]. To determine the effect of salt on the sorption of benzoic acids, the sample solutions were first acidified prior to addition of salt and extraction to ensure that all of the benzoic acid molecules were in their 'neutral' form (Table 5). No change in extraction was observed for solutions having 0.5 M salt concentration. As the concentration of salt was increased from 0.5 to 2.0 M, the extraction efficiency slightly increased.

In high ionic strength solutions, the activity of species is different from that in low ionic strength solutions. If the addition of salt had an effect on extraction of benzoic acids by polyurethane membrane, we would expect to observe it even at 0.5 M NaCl concentration. The slightly higher extraction obtained at 1.0 and 2.0 M salt concentrations may have a large error associated with it because at high salt concentrations benzoic acids are known to form various dimers and homoconjugated species [28].

3.6. Effect of solvent type on extraction

The most important solvent effects originate from interactions between solvent and solute, such as hydrogen-bonding, dipole–dipole, and hydrophobic bonding interactions, which are related to the molecular structure of the solvent and the solute [32]. Information on extraction of monobromobenzoic acids from organic solvents having variable polarities may help to estimate the polarity of the membrane, and therefore allow prediction of the compounds which would be soluble in it. Comparison of the sorption of monobromobenzoic acids from water and polar and nonpolar organic solvents is shown in Table 6. *Ortho* and *para* monobromobenzoic acids extract much better from cyclohex-

Table 5
Effect of NaCl concentration on extraction

Compound	% E			
	NaCl final concentration (M)			
	0.0	0.50	1.0	2.0
o-Bromobenzoic acid				
Ether	20 ± 2	18 ± 2	25 ± 2	31 ± 3
Ester	8 ± 1	8 ± 1	11 ± 1	15 ± 2
m-Bromobenzoic acid				
Ether	48 ± 3	48 ± 3	54 ± 3	55 ± 3
Ester	26 ± 2	24 ± 2	29 ± 2	40 ± 3
p-Bromobenzoic acid				
Ether	40 ± 3	42 ± 3	49 ± 3	59 ± 3
Ester	22 ± 2	25 ± 2	31 ± 3	34 ± 3

Conditions: 25.0 ± 2.0°C, 10-ml aliquot of $\approx 3 \times 10^{-4}$ M monobromobenzoic acid solution having 0.01 M HCl final concentration, 0.051 mm ether- and ester-type membranes, active surface area of 2.54 cm^2.

Table 6
Extraction of monobenzoic acids from various solvents

Compound	% E				
	Water	Hexane	Cyclohexane	Acetonitrile	Ethyl acetate
o-Bromobenzoic acid					
Ether	2 ± 1	50 ± 3	38 ± 3	7 ± 1	$0+0$
Ester	0 ± 0	36 ± 3	26 ± 2	4 ± 1	$0+0$
m-Bromobenzoic acid					
Ether	28 ± 2	29 ± 2	30 ± 3	5 ± 1	$0+0$
Ester	15 ± 2	15 ± 2	16 ± 2	0 ± 0	$0+0$
p-Bromobenzoic acid					
Ether	18 ± 2	27 ± 2	30 ± 3	2 ± 1	$0+0$
Ester	8 ± 1	12 ± 1	21 ± 2	0 ± 0	$0+0$

Conditions: 25.0 ± 2.0°C, 10-ml aliquot of $\approx 3 \times 10^{-4}$ M organic and aqueous monobromobenzoic acid solutions (pH 3.27, 3.43, and 3.54 for *o*-, *m*-, *p*-isomers, respectively), 0.051 mm ether- and ester-type membranes, active surface area of 2.54 cm^2.

ane and hexane than from water. The *meta* isomer extracts equally well from the nonpolar organic solvents as it does from water. Extraction from acetonitrile is very low for all of benzoic acids. No extraction of monobromobenzoic acids occurred from ethyl acetate.

Acetonitrile is a polar aprotic solvent with a strong dipole. This solvent has a low hydrogen bond acceptor strength and promotes ionization of benzoic acids which results in ion pairing and formation of homoconjugated species such as RCOOH....$^-$OCOR [33]. The low extraction of monobromobenzoic acids from acetonitrile can therefore be accounted for by the formation of ionic and dimeric molecules. Ethyl acetate is also a polar aprotic solvent, but unlike the acetonitrile, it can engage in hydrogen bonding interactions. No extraction of the benzoic acids occurred out of this solvent probably due to the stronger intermolecular hydrogen bonding between the solvent and benzoic acids than between benzoic acids and the membrane.

Water is a protic solvent with a high dielectric constant. It can function in hydrogen bonding both as donor and acceptor, and its dielectric constant is high enough to exclude ion pair formation [34]. Because the benzoic acids are weak acids, they will dissociate in water to some extent. *Meta* and *para* monobromobenzoic acids have lower K_a values than *ortho* monobromobenzoic acid. These isomers were found to extract well from water probably because majority of the molecules are in their neutral form. *Ortho* monobromobenzoic acid is the strongest acid, and therefore it is dissociated to the highest extent which accounts for its very low sorption.

Cyclohexane and hexane are inert solvents of low dielectric constant which prevent ionization of benzoic acids [34]. These solvents are poor at solvating anions and forming hydrogen bonds. *Ortho* monobromobenzoic acid will be less ionized in hexane and cyclohexane than in water or in the polar organic solvents. Furthermore, because the *ortho* isomer carries more localized polarity, it will be less likely to interact with hexane through hydrophobic interactions. Consequently, it will preferably partition into the more polar membrane. *Para* monobromobenzoic acid also showed an increased extraction out of hexane and cyclohexane compared to that from water and the polar organic solvents. Again, this indicates that the hydrogen bonding interactions between benzoic acid and the membrane polar groups are stronger than the hydrophobic interactions with hexane or cyclohexane. Sorption of *meta* monobromobenzoic acid from water and from the nonpolar organic solvents is similar which suggests that the solubility of this benzoic acid in water and in hexane and cyclohexane is comparable.

3.7. Effect of temperature on extraction

During the sorption process, benzoic acid partitions between the solution (liquid phase) and the membrane (solid phase). The partitioning of benzoic acid between the two phases can be mathematically expressed as a distribution ratio, which is a ratio of the equilibrium concentration of benzoic acid in the liquid phase, K_s, to the concentration in the solid phase, K_m. This ratio will change with temperature because the solubility of benzoic acid in the two phases changes with temperature. Extraction of organic molecules from liquids into solids is conventionally represented as standard affinity, $\Delta\mu°$, and it is interchangeable with Gibbs free energy, ΔG [35]. The free energy of benzoic acid in the membrane and in aqueous solution can be represented as $\mu_m + RT \ln [K_m]$ and $\mu_s + RT \ln [K_s]$ respectively [35] and will be equal at equilibrium [35]:

$$\mu_m + RT \ln [K_m] = \mu_s + RT \ln [K_s] \quad (3)$$

A rearrangement of the above equation can give us the affinity of benzoic acid as a function of temperature, T:

$$-(\mu_m - \mu_s) = -\Delta\mu^0 = RT \ln [K_m] - RT \ln [K_s]$$
$$= RT \ln [K_m]/[K_s] = RT \ln K \quad (4)$$

where, K is the partition ratio.

The heat (ΔH^0) and entropy (ΔS^0) of sorption can be calculated from the partition ratios at two different temperatures or over a temperature range [36] with the assumption is that ΔH^0 and ΔS^0 are independent of temperature (i.e. if a plot of $\log K$ versus $1/T$ is a straight line). Therefore,

$$\Delta H^0 = -2.303RT_1T_2/(T_2 - T_1) \log K_1/K_2 \quad (5)$$

$$\Delta S^0 = -2.303R \log K_1/K_2 \quad (6)$$

where T_1 and T_2 are the two temperatures, and K_1 and K_2 are the partition ratios.

The percent removal of monobromobenzoic acids from solution by the polyurethane membrane was measured after 24 h (at which equilibrium was assumed to be attained) at 4, 10, 25, 37 and 55°C. The results of extraction by ester- and ether-type membranes are shown in Table 7. The plots of $\log K$ versus $1/T$ for *ortho*, *meta* and *para* monobromobenzoic acids extracted with the ether- and ester-type membranes at various temperatures are shown in Figs. 2 and 3, respectively. K, ΔH^0 and ΔS^0 calculated for extractions of

Table 7
Effect of temperature on extraction

Compound	% E				
	4°C	10°C	25°C	37°C	55°C
o-Bromobenzoic acid					
Ether	25 ± 3	21 ± 3	20 ± 2	17 ± 2	14 ± 2
Ester	2 ± 1	2 ± 1	6 ± 1	7 ± 1	2 ± 1
m-Bromobenzoic acid					
Ether	55 ± 2	50 ± 2	45 ± 2	36 ± 2	31 ± 2
Ester	15 ± 1	17 ± 1	23 ± 1	19 ± 1	14 ± 2
p-Bromobenzoic acid					
Ether	52 ± 2	48 ± 2	41 ± 2	32 ± 2	26 ± 2
Ester	14 ± 1	17 ± 1	23 ± 1	18 ± 1	14 ± 1

Conditions: 10 ml-aliquot of $\approx 3 \times 10^{-4}$ M aqueous monobromobenzoic acid solutions having 0.01 M HCl final concentration, 0.051 mm ether- and ester-type membranes, active surface area of 2.54 cm^2, temperature ± 1.0°C.

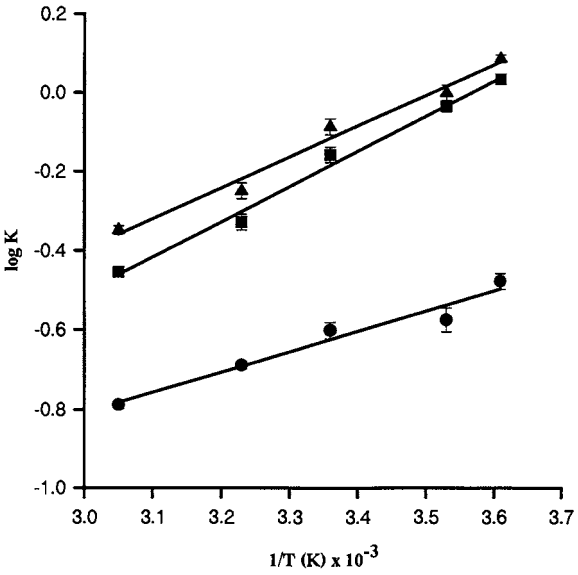

Fig. 2. Change in partition ratio with change in temperature for extraction of monobromobenzoic acids using the ether-type polyurethane membrane. Extraction equilibrium was reached after 24 h. Monobromobenzoic acids: ●, *ortho*-; ▲, *meta*-; ■, *para*-.

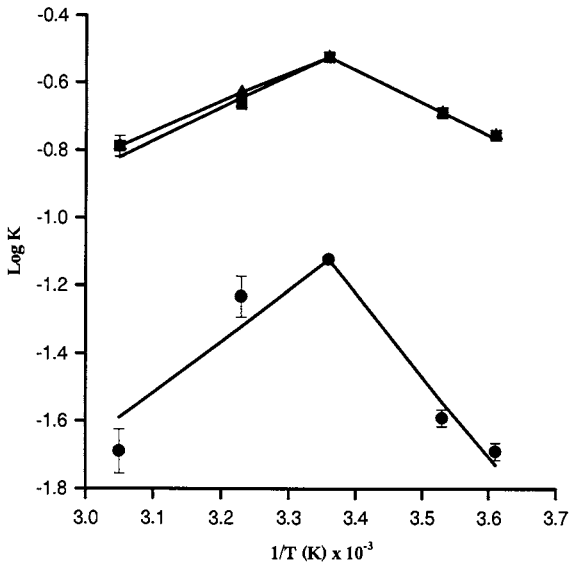

Fig. 3. Change in partition ratio with change in temperature for extraction of monobromobenzoic acids using the ester-type polyurethane membrane. Extraction equilibrium was reached after 24 h. Monobromobenzoic acids: ●, *ortho*-; ▲, *meta*-; ■, *para*-.

monobromobenzoic acids with both membrane types are shown in Table 8.

Extractions of all monobromobenzoic acid isomers with the ether-type membrane show a gradual decrease in $\%E$ with an increase in temperature (Table 7). Both ΔH^0 and ΔS^0 for these extractions are negative (Table 8). The negative entropy obtained for extraction of benzoic acids with the ether-type membrane indicates that the freedom of motion of benzoic acids is more restricted in the membrane than in solution. Because the sorption process involves a decrease in free energy, we would expect ΔH^0 to be also negative, which is confirmed by the data. Since the sorption of monobromobenzoic acids by the ether-type membrane is an exothermic process then, by applying Le Chatelier's principle, we would expect the extraction (under equilibrium conditions) to decrease with increasing temperature, which was observed. Furthermore, as the temperature increases, the physical structure of the membrane may be changing which can affect the strength of the intermolecular interactions between the membrane groups and benzoic acids. For example, the higher temperature may cause the membrane matrix to become more unstructured and affect the ability of the polar segments to engage in stable hydrogen bonding with benzoic acid molecules, which would result in a lower extraction.

Extractions of monobromobenzoic acids with the ester-type membrane show an extraction maximum at 25°C, and a slight decrease at higher and lower temperatures (Table 7; Fig. 3). Two sets of data were calculated corresponding to two straight line plots for which Eqs. (5) and (6) are valid at equilibrium (Table 8). The enthalpy and entropy for extractions performed over the 4–25°C range are positive and for the 25–55°C range, both are negative. One explanation is that at low temperatures, the ester membrane groups interact more strongly with each other, and therefore are not fully available for intermolecular interactions with benzoic acid molecules. As the temperature increases, some of the interactions

Table 8
Partition ratio, enthalpy, and entropy change for extraction of monobromobenzoic acids

Compound	K_1/K_2	ΔH^0 (KJ mol^{-1})	ΔS^0 (J mol^{-1} K^{-1})
o-Bromobenzoic acid			
Ether			
4–55°C	2.043	−11.56	−5.94
Ester			
4–25°C	0.271	42.68	10.86
25–55°C	3.691	−41.81	−10.86
m-Bromobenzoic acid			
Ether			
4–55°C	2.722	−16.20	−8.33
Ester			
4–25°C	0.589	17.30	4.40
25–55°C	1.834	−19.42	−5.04
p-Bromobenzoic acid			
Ether			
4–55°C	3.085	−18.22	−9.37
Ester			
4–25°C	0.589	17.30	4.40
25–55°C	1.834	−19.42	−5.04

Conditions: 10-ml aliquot of $\approx 3 \times 10^{-4}$ M aqueous monobromobenzoic acid solutions having 0.01 M HCl final concentration, 0.051 mm ether- and ester-type membranes, active surface area of 2.54 cm^2, temperature $\pm$ 1.0°C.

among the polar groups may be weakened due to increased energy of the individual segments. As a result, the polar groups are more available for interactions with benzoic acids in solution. Because hydrogen bonding interactions are weak and easily broken [37], at very high temperatures such interactions may not be stable, and therefore a decrease in extraction is observed. Similar conclusions were reached from our previous study on the extraction of substituted phenols by the polyurethane membrane [15].

4. Conclusion

The sorption process of *ortho*, *meta* and *para* monobromobenzoic acids by the polyurethane membrane is governed by the strength of intermolecular hydrogen bonding interactions. A combination of factors such as the physical structure of the membrane, solution conditions, the extracting species characteristics, and solvent and temperature effects were found to collectively influence the strength of the intermolecular interactions formed between the membrane polar groups and benzoic acids. All of the benzoic acids are sorbed to a higher extent by the ether-type polyurethane membrane than the ester-type membrane. This can be attributed to the stronger hydrogen bonding occurring between the benzoic acids and the polyether segments of the membrane than the polyester segments. It was found that benzoic acids must exist as neutral molecules in solution in order to be extracted by the membrane. This conclusion is supported by the study of the pH effects on extraction of benzoic acids from aqueous solution and by extraction from organic solvents. The extraction efficiency of the monobromobenzoic acid isomers from organic solvents was found to be comparable to that from water only when the interactions of benzoic acids with the solvents were weaker than with the membrane, and when no ionization of the benzoic acid was taking place. For example, all of the isomers extracted well from the nonpolar organic solvents, but very poorly for the polar organic solvents. Benzoic acid having the substituent in the *ortho* position extracted more poorly out of water than the *meta* and *para* isomers. We attribute this to the localized charge in the *ortho* compound which makes it more polar, and to the decreased possibility of interactions with the polar membrane groups due to steric effects. This is supported by the data for extractions of *ortho* monobromobenzoic acids from water and from polar and nonpolar organic solvents. Sorption by the ether-type membrane decreases with temperature, and sorption by the ester-type membrane reaches a maximum at room temperature and decreases at lower and higher temperatures. The differences in sorption with changes in the temperature result from the differences in the structure of the two membranes and changes in the strength of the intermolecular interactions among the polar membrane groups. The extraction of benzoic acids by the polyurethane membrane shows support for the mechanism proposed for the extraction of various phenols by the polyurethane membrane.

This study further clarified and confirmed the sorption mechanism we proposed for the extraction of phenols by the polyurethane membrane. Knowledge about the factors governing the sorption of organic compounds can allow easier developments in the useful applications of polyurethane membrane.

Acknowledgements

The authors would like to thank Dr Burchill for his assistance with the data analysis, and acknowledge the financial support of the University of Manitoba and the Natural Sciences and Engineering Research Council of Canada.

References

[1] L.H. Keith, W.A. Telliard, Env. Sci. Tech. 13 (4) (1979) 416.
[2] G. Altshuler, G. Belfort, in: M.J. McGuire, I.H. Suffet (Eds.), ACS Advances in Chemistry Series 202, ACS, Washington, DC, 1983, pp. 29–62.
[3] Water/Engineering and Management, Oct. 1987, 12.
[4] P. Aptel, Membrane pressure driven processes in water treatment, in: J.G. Crespo, K.W. Broddeker (Eds.), Mem-

brane Processes in Separation and Purification, NATO ASI Series, Series E: Applied Sciences, 272, Kluwer, Dordrecht, 1993, p. 263.
[5] Marcel Mulder, The use of membrane separation processes in environmental problems, in: J.G. Crespo, K.W. Broddeker (Eds.), Membrane Processes in Separation and Purification, NATO ASI Series, Series E: Applied Sciences, 272, Kluwer, Dordrecht, 1993, p. 233.
[6] W.S. Winston Ho, K.K. Sirkar, Membrane Handbook, Van Nostrand Reinhold, New York, 1992.
[7] Munir Cheryan, Ultrafiltration Handbook, Technomic, Lancaster Pennsylvania, USA, 1986.
[8] K. Scott, Handbook of Industrial Membranes, 1, Elsevier, New York, 1995.
[9] R.D. Noble, S.A. Stern, Membrane Separation Technology: Principles and Applications, Elsevier, New York, 1995.
[10] A. Reife, H.S. Freeman, Environmental Chemistry of Dyes and Pigments, Wiley–Interscience, New York, 1996.
[11] G. Woods, The ICI Polyurethanes Book, Polyurethanes and Wiley Publication, New York, 1987, p. 27.
[12] G. Woods, The ICI Polyurethanes Book, Polyurethanes and Wiley Publication, New York, 1987, pp. 27–54.
[13] R.D. Oleschuk, A. Chow, Talanta 42 (1995) 957.
[14] R.D. Oleschuk, A. Chow, Talanta 43 (1996) 1545.
[15] K. Rzeszutek, A. Chow, Talanta (in press).
[16] U.S. Aithal, T.M. Aminabhavi, J. Chem. Eng. Data 35 (1990) 298.
[17] U.S. Aithal, T.M. Aminabhavi, J. Appl. Polym. Sci. 42 (1991) 2837.
[18] S.B. Harogoppad, U.S. Aithal, T.M. Aminabhavi, J. Appl. Polym. Sci. 42 (1991) 3267.
[19] R.S. Khinnavar, T.M. Aminabhavi, J. Appl. Polym. Sci. 46 (1992) 909.
[20] Kirk-Othmer Encyclopedia of Chemical Technology, 4th edn., Wiley, New York, 1991, v. 4, p. 103.
[21] Kirk-Othmer Encyclopedia of Chemical Technology, 3rd edn., Wiley, New York, 1981, v. 14, p. 254.
[22] Kirk-Othmer Encyclopedia of Chemical Technology, 3rd edn., Wiley, New York, 1978, v. 3, p. 784.
[23] Kirk-Othmer Encyclopedia of Chemical Technology, 3rd edn., Wiley, New York, 1982, v. 20, p. 359.
[24] Kirk-Othmer Encyclopedia of Chemical Technology, 3rd edn., Wiley, New York, 1980, v. 12, p. 241.
[25] Gordon M. Barrow, Physical Chemistry, McGraw–Hill, New York, 1988, pp. 420–422.
[26] J. McMurry, Organic Chemistry, 3, Brooks/Cole, Monterey, CA, 1992, p. 770.
[27] E.H. Rodd, Chemistry of Carbon Compounds, IIIA Aromatic Compounds, Elsevier, New York, 1951, p. 572.
[28] S. Patai, The Chemistry of Functional Groups Series v.5: The Chemistry of Carboxylic Acids and Esters, Interscience, New York, 1969, p. 241.
[29] L. Shumack, A. Chow, Talanta 34 (1987) 957.
[30] P. Fong, A. Chow, Talanta 39 (1992) 497.
[31] R. Werbowesky, A. Chow, Talanta 43 (1996) 263.
[32] S. Patai, The Chemistry of Functional Groups Series, v. 5: The Chemistry of Carboxylic Acids and Esters, Interscience, New York, 1969, p. 238.
[33] S. Patai, The Chemistry of Functional Groups Series, v. 5: The Chemistry of Carboxylic Acids and Esters, Interscience, New York, 1969, p. 239.
[34] S. Patai, The Chemistry of Functional Groups Series, v. 5: The Chemistry of Carboxylic Acids and Esters, Interscience, New York, 1969, p. 236.
[35] C.L. Bird, W.S. Boston, The Theory of Coloration of Textiles, The Dyers Company Publications Trust, Bradford, UK, 1975, pp. 16–18.
[36] C.L. Bird, W.S. Boston, The Theory of Coloration of Textiles, The Dyers Company Publications Trust, Bradford, UK, 1975, pp. 175–179.
[37] C.L. Bird, W.S. Boston, The Theory of Coloration of Textiles, The Dyers Company Publications Trust, 1975, p. 54.

ELSEVIER

Talanta 47 (1998) 711–717

Talanta

Dual-phase gas-permeation flow-injection thermometric analysis for the determination of carbon dioxide

Shan-jun Liu [1], Matthieu Tubino *

Instituto de Química, Universidade Estadual de Campinas (UNICAMP), Caixa Postal 6154, CEP 13083-970, Campinas, SP, Brazil

Received 28 August 1997; received in revised form 28 February 1998; accepted 5 March 1998

Abstract

A flow-injection configuration based on a dual-phase gas-permeation system from a liquid donor to a gas acceptor stream with a thermistor flow-through detector is proposed for the direct analysis of the gas in the acceptor. This system was applied for the determination of carbon dioxide (in the form of carbonate) using the following chemical reaction: $CO_2(g) + 2NH_3(g) + H_2O(g) = (NH_4)_2CO_3(s)$, with a linear response from 1×10^{-3} to 50×10^{-3} mol l^{-1} of CO_3^{2-}. Carbon dioxide was produced in the liquid donor and permeated into the gaseous acceptor stream of air/water vapor. The detection limit is 1×10^{-3} mol l^{-1} of carbonate, and a sampling frequency of 60 h^{-1} is achieved with a relative standard deviation of 4.1% for replicate injections. The dual-phase gas-permeation flow-injection manifold, along with the membrane and phase separations, as well as the chemical reaction, provides enhanced selectivity when compared with the system employing a liquid acceptor stream, as serious interferents in this system, for instance, acetate and formate, among others, do not interfere in the proposed system. © 1998 Elsevier Science B.V. All rights reserved.

Keywords: Thermistor; Carbon dioxide; Gas permeation; Flow-injection analysis

1. Introduction

Gas diffusion/permeation flow-injection analysis (GD-FIA) has proved to be useful in the determination of volatile species, as an effective technique to increase the selectivity and sensitivity of an analytical method [1–4]. Due to the inherent selectivity of the membrane separation process, the selectivity of the detectors can be intrinsically enhanced [5]. These advantages have led to employing less or even non-selective detectors in GD-FIA, i.e. conductimetry [6–11] and potentiometry [11–13]. Thermistors were the probes of choice in this work because they are stable (± 0.05°C $year^{-1}$), inexpensive, sensitive, chemically inert, and small [14]. They have been applied as the detectors in the enzyme thermometric [15,16] and the enthalpimetric [17–20] analysis in FIA manifolds. Sampling frequencies up to 150 samples per hour can be realized [20]. Although conceived as a method for the determination of

* Corresponding author. Fax: +55 19 7883023; e-mail: tubino@iqm.unicamp.br

[1] On leave from Department of Chemistry, Nankai University, Tianjin, People's Republic of China.

0039-9140/98/$ - see front matter © 1998 Elsevier Science B.V. All rights reserved.
PII S0039-9140(98)00123-4

gaseous analytes, gas enthalpimetry has been applied primarily to the determination of analytes in solution [21].

In conventional GD-FIA the gas diffusing through the membrane is usually transferred into a liquid acceptor. One of the developments in GD-FIA was a dual-phase technique that involved a liquid donor and a gaseous acceptor [22–24] or the reverse [25]. The dual-phase GD-FIA has been used for the determination of metal hydride in AAS to enhance the selectivity [22], and as a sample introduction technique to MS [23,24]. As far as we know, no GD-FIA system has been designed to permit the separation of an analyte from a solution to a gaseous carrier for subsequent thermometric detection in the gas phase.

We reported the applications of a flow-through thermistor in various chemical systems and the effect of flow-rate on the flow thermometric analysis [26], which showed that the thermistor can be used as a detector of gas phase in flow injection analysis. The present work was to evaluate the analytical application of dual-phase gas-permeation flow-injection thermometric analysis with the thermistor detector for the determination of CO_2 in the gas phase. In the acceptor the reaction chosen for the study was the gas-phase chemical reaction of carbon dioxide, ammonia and water vapor:

$$CO_2(g) + 2NH_3(g) + H_2O(g) = (NH_4)_2CO_3(s) \quad (1)$$

A gas permeation unit was used to separate the sample and enhance the selectivity.

2. Experimental

2.1. Reagents

All reagents were of analytical grade. Distilled water from a glass distiller, further de-ionized with Milli-Q-plus reagent-grade water purification system (Millipore, Bedford, MA), was used for the preparation of the solutions.

Water vapor and ammonia gas: these gases were obtained by flowing clean air through the deionized water or the ammonia water solution. Before passing into the water or ammonia water solution, the air first passed through a filter packed with activated charcoal and sodium hydroxide to remove acidic gases.

Carrier streams: deionized water and air/water vapor were used in the donor and in the acceptor, respectively, as the carriers.

The sulfuric acid solution used was 2 mol l^{-1}.

Standard sodium carbonate solution: 26.4975 g of sodium carbonate were dissolved in deionized water to give 250 ml solution (1.0 mol l^{-1}). Working solutions were prepared by serial dilutions of the stock standard.

2.2. Apparatus

The arrangement of the thermistor flow-through detector was depicted in our previous paper [26]. The water vapor carrier and the ammonia gas stream met in the detection chamber at a relative angle of 180°. The product exited by the third tube. The volume of the reaction and detection chamber is about 35 μl. The thermistor in the flow-through cell formed one arm of a Wheatstone bridge circuit (Leeds & Northrup Co., Philadelphia, PA). The applied bridge potential was 1.5 V from a battery. At 298 K, the balance resistance of the thermistor arm was 9.67 kΩ and the sensitivity of the Wheatstone bridge was 5.08 mV K^{-1}.

The chart recorder used was a Modelo RB201 (Equipamentos Científicos do Brasil, Sao Paulo), using a 1-mV full scale and a linear speed of 10 cm h^{-1}.

The peristaltic pump used was an ISM 726 (Ismatec, Switzerland).

The pumping tubes used were Tygon® tubes (ENE 16; i.d. 1.42 mm, wall 0.80 mm; ENE 03, size, 0.015; Ismatec).

This sampling valve has been described previously [27].

The gas-permeation unit was made from two PVC half blocks on which were engraved channels that were mirror images of each other. The length and width of the channels were 110 and 4 mm.

Two types of membrane, polytetrafluoroethylene (PTFE) tape and silicone rubber, were tested.

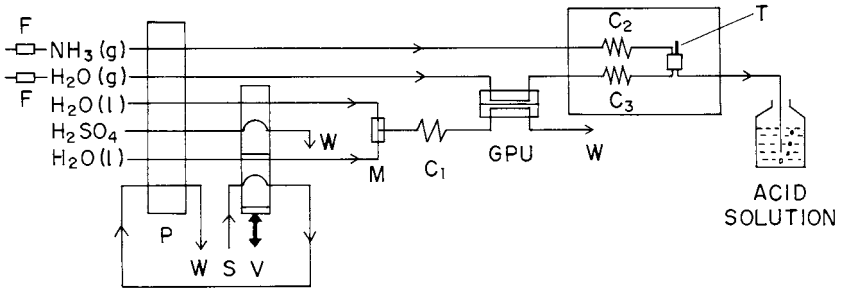

Fig. 1. Schematic diagram of the dual-phase gas-permeation flow-injection manifold for the thermometric determination of carbonate. F, air filter; T, thermistor flow-through detector; W, waste; P, peristaltic pump; V, sampling valve; M, mixing tee; GPU, gas-permeation unit; C_1, reaction tube; C_2 and C_3, temperature equilibration coils; S, Na_2CO_3 sample; g, gas; and l, liquid.

The thermostatic water bath used was a RCS 6 (MGW Lauda, Lauda-königshofen).

2.3. Manifold

A schematic diagram of the flow system is shown in Fig. 1. Reagent solutions and gases were pumped by a peristaltic pump. The flow-rate was 0.71 ml min^{-1} for each channel. A carbonate sample (200 μl; 0.025 mol l^{-1}) and 250 μl 2 mol l^{-1} of sulfuric acid solution were simultaneously injected into the water carriers, meeting at a mixing tee (M) and reacted in the tube C_1 (40 cm length), where CO_2 was produced. After passing through the gas permeation unit (GPU), the volatile analyte CO_2 permeated into the acceptor through the membrane and was carried by the stream of air/water vapor, passed through the equilibration coil C_3 and was transported to the thermistor detector, where it merged and reacted with the ammonia gas. The temperature equilibration coils C_2 and C_3, as well as the detection chamber, were immersed in a water bath maintained at 25.00 ± 0.01°C. The amount of heat evolved was monitored automatically using the unbalance potential of the Wheatstone bridge circuit. The signal was registered on a chart recorder.

3. Results and discussion

As seen in Fig. 1, the system designed allows the sample of carbonate to be mixed with the sulfuric acid solution, with the consequent formation of CO_2. The sample stream then passes through the gas-permeation unit where the gas diffuses across the gas-permeable membrane into the acceptor stream of air/water vapor. The CO_2 formed is carried by the water vapor to the reaction and detection chamber, where it meets and reacts with gaseous NH_3. The heat evolved is monitored by the thermistor, and the obtained peak height is used as the analytical signal. When CO_2 is no longer present in the sample stream, only NH_3, air and H_2O vapor streams pass through the thermistor detector and a rapid return to the base line is observed. In this proposed system, fundamental studies concerning the optimization of operating parameters were undertaken, and its enhancement of selectivity was evaluated.

3.1. Membrane materials

Since this system is based on a nonequilibrium process taking place within the gas-permeation unit, it is important to have the maximum transfer between the sample donor and the acceptor stream during the brief time that the sample actually spends in the permeation unit. PTFE tape and silicone rubber membranes were tested. The PTFE and the silicone rubber membrane gave similar results. The determinations were done by the relative peak heights observed for the same concentrations of Na_2CO_3 solutions. However, the PTFE tape is so thin and porous that drops of liquid water can pass across the membrane into

the acceptor even if the membrane is not much stretched. This liquid drops enters the detection chamber and causes serious noise or failures in measurements. The silicone rubber membrane can effectively avoid the leak of liquid water and also gives good sensitivity. Therefore the silicone rubber membrane was mainly used in this study.

3.2. Flow-rate

The effect of the flow-rate on the signal, maintained the identical flow-rate of the donor and the acceptor streams, is shown in Fig. 2. The signal first increases a little up to 0.71 ml min^{-1} and then decreases with the increase of the flow-rate. This can be explained by the contacting time of the sample with the permeation membrane and by the reacting time of CO_2 with the reactants in the detection chamber. The contacting time is shorter at higher flow-rate, thus less CO_2 passes across the membrane and gives lower signals. On the other hand, increasing the flow-rate has the advantage of the minimization of the residence time. Flow-rates also affected the analytical frequency (see Fig. 2). The sampling frequency achieved depends on the parameters chosen to perform the measurements and varied from 60 to 16 samples per hour.

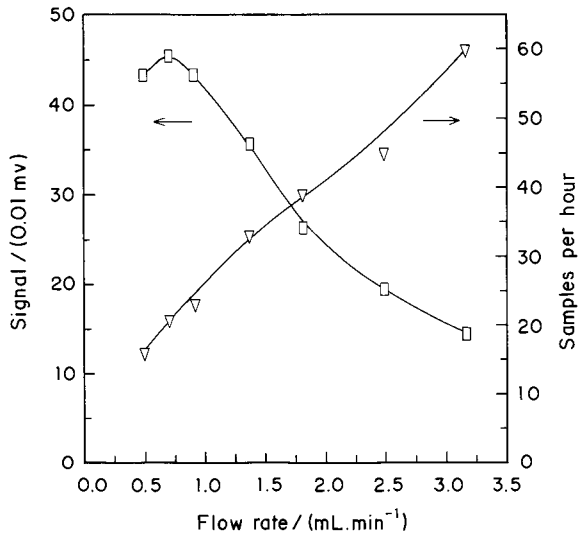

Fig. 2. Dependence of peak height (□) and sampling frequency (▽) on flow-rates. The conditions are the same as in Section 2.

3.3. Reagent concentrations

In the proposed configuration, CO_2 was generated by the merging of the carbonate solution with the H_2SO_4 solution, permeating in sequence through the membrane. The concentration of acid to achieve maximum conversion of carbonate to CO_2 was studied in the range from 1×10^{-3} to 2 mol l^{-1} (Fig. 3a). A dramatic increase in the signal from the H_2SO_4 concentration of 1×10^{-3} up to about 0.05 mol l^{-1} of H_2SO_4 was observed. After 0.25 mol l^{-1} the signal increases slowly with the increase of the concentration of sulfuric acid. Considering the gain in the signal the solution of 2 mol l^{-1} sulfuric acid was chosen for further experiments.

The effect of the concentrations of the ammonia gas was also examined, maintaining the concentrations of water vapor (at about 22°C) and CO_2 (2.5×10^{-2} mol l^{-1} Na_2CO_3) constant. The results are given in Fig. 3b. The increase of the ammonia concentrations gives higher sensitivity to the proposed method. It is easy to envisage that this method could be used to analyze ammonia in gaseous mixtures. It is probable that the use of gaseous NH_3 from a cylinder may improve the reproducibility and sensitivity of the method. However, the source of gaseous ammonia used in this work is quite inexpensive, easy to control, secure and gives good results.

3.4. Sampling volume

The dependence of the signal on the sample volume is shown in Fig. 4. The signal increases rapidly with respect to the sample volume up to 300 μl, then trends to a constant value at larger volumes. Larger sample volumes also imply a longer time interval for each analysis. Therefore, considering a good compromise of the signal with the sampling frequency, 200 μl was chosen as the injection volume of the sample.

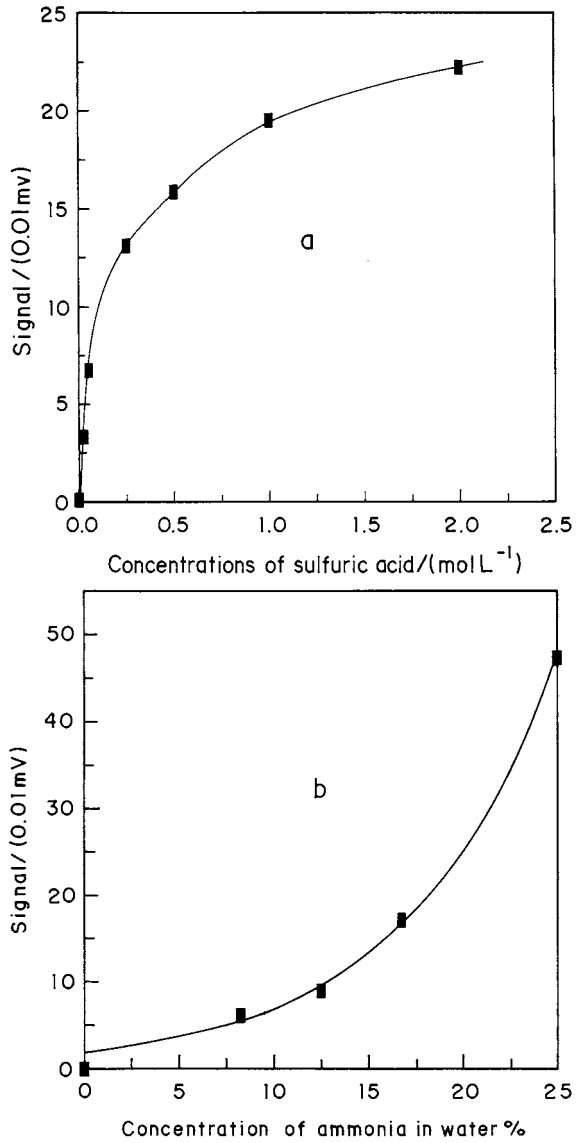

Fig. 3. Effect of reagent concentrations on peak height. (a) Sulfuric acid; (b) ammonia solution.

3.5. Length of the reaction tube

Fig. 5 depicts the dependence of the peak height on the length of the reaction tube C_1. It can be observed that the signal slowly decreases with the increase of the length of the reaction tube C_1. The signal decrease can be attributed to the increase of the dispersion of the sample as the length of the

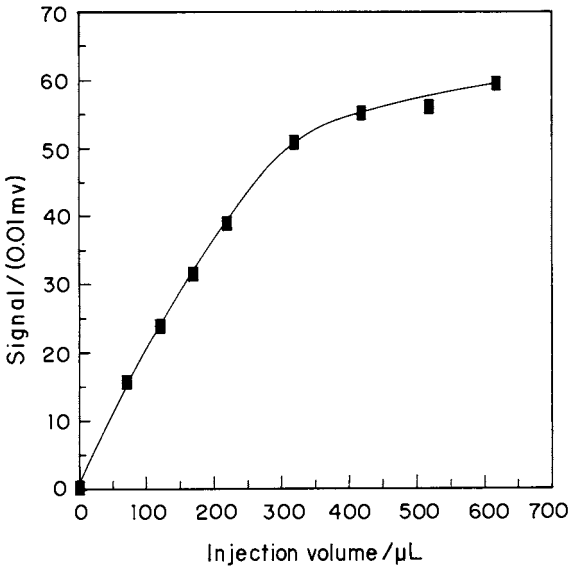

Fig. 4. Effect of sample volume on peak height.

reaction tube is enhanced. The augmentation of the length of the reaction tube also implies a decrease of the analytical frequency. The better length of reaction tube is between 0 and 60 cm,

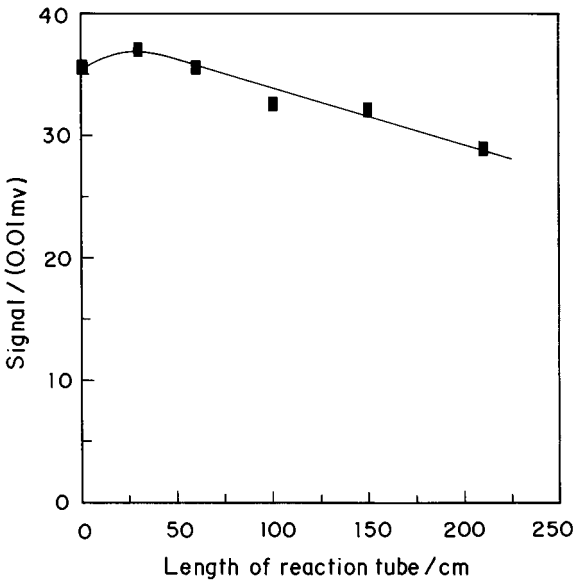

Fig. 5. Effect of the length of the reaction tube. Flow-rate, 0.50 ml min^{-1}; 240 µl of sample volume; 2.0×10^{-2} mol l^{-1} of Na_2CO_3 and 1 mol l^{-1} of H_2SO_4 for PTFE tape.

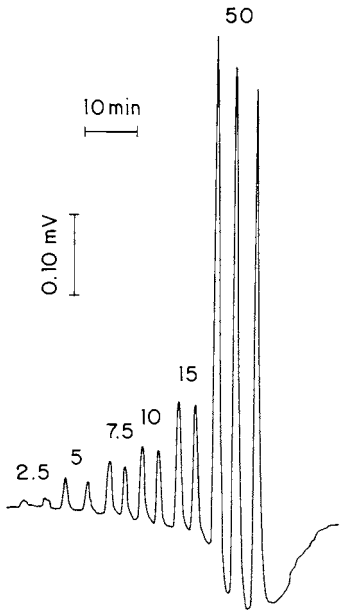

Fig. 6. A recording graph for the calibration curve. The numbers on the trace are the concentrations of carbonate in the sample in mol l^{-1}.

and in practical manipulation a tube of 40 cm was used.

3.6. Calibration curve

Under the above conditions a good linear relationship is obtained between the peak height and the concentrations of carbonate in the range of 2.5×10^{-3} to 50 $\times 10^{-3}$ mol l^{-1} with 200 μl of injection volume:

$$V\,(0.01\ \text{mV}) = (-3.42 \pm 0.54) + (1.33 \pm 0.02)C\ (10^{-3}\ \text{mol}\,l^{-1})\ r = 0.9993 \quad (2)$$

The detection limit is 1×10^{-3} mol l^{-1} of carbonate. The relative standard deviation is 4.1% for 1.0×10^{-2} mol l^{-1} of carbonate ($n = 7$). It can be observed from Fig. 6 that, with the increase of carbonate concentration, for example, 5.0×10^{-2} mol l^{-1} of carbonate, the signal goes below its initial baseline and then gradually returns to the baseline. Obviously this indicates the occurrence of an endothermic effect following the exothermic one, corresponding to the acid–base reaction. This endothermic signal could be attributed to the absorption of the water vapor by the formed salt and/or decomposition of the ammonium carbonate.

3.7. Effect of other ions

The response of the proposed system to a variety of ionic species that may be converted into volatile gases in acidic medium was studied, and the results are given in Table 1. One mol l^{-1} of NO_3^-, Cl^- (NaCl and NH_4Cl), S^{2-} (in the form of C_2H_5NS), HCO_2^- and $H_3CCO_2^-$, as well as 0.2 mol l^{-1} of NO_2^- and SO_3^{2-}, have the effect of less than 4% for 2.5×10^{-2} mol l^{-1} of CO_3^{2-}. Only higher concentrations of NO_2^- and SO_3^{2-} (1 mol l^{-1}) interfere seriously. Although the thermistor is a type of non-selective detector, its use in the proposed system of GD-FIA leads to very good selectivity for the analysis of carbonate. The dual-phase GD-FIA provides the possibility of selectivity enhancement due to: the chemical reaction in the donor stream before the membrane separation; the membrane separation; the phase change at the membrane separator; and the selective chemical reaction that was carried out in the acceptor stream. These combined selectivity enhancements can greatly increase the concentrations of interferents that can be tolerated [23].

4. Conclusions

The dual-phase gas-permeation flow-injection thermometric analysis has been shown to be a suitable technique for the determination of gaseous analytes. The thermistor can be used as a detector in the gas phase for flow-injection analysis, and it is a very simple, stable and low cost detector. The sensitivity is dependent on the reaction enthalpy change, on the reaction rate and on the experimental conditions. The selectivity of the thermistor detector can be significantly enhanced in combination with membrane separation and phase change. Compared with liquid donor/acceptor streams its selectivity is greatly enhanced, as in

Table 1
The response of other species

Species	Reagents	Concentrations (mol l^{-1})	Normalized signals to 0.363 mV
CO_3^{2-}	Na_2CO_3	0.025	1
NO_3^-	$NaNO_3$	1.0	0.038
NO_2^-	$NaNO_2$	0.020	0
		0.10	0
		1.0[a]	3.361
Cl^-	NaCl	1.0	0.041
	NH_4Cl	1.0	0.030
S^{2-}	$C_2H_5NS + NaOH$	1.0 + 1.0	0.045
SO_3^{2-}	Na_2SO_3	0.025	0.000
		0.20	0.041
		1.0	2.920
HCO_2^-	HCO_2Na	1.0	0
$H_3CCO_2^-$	H_3CCO_2Na	1.0	0

[a] Brown NO_2 gas was produced.

the liquid system ions such as S^{2-}, SO_3^{2-}, HCO_2^-, $H_3CCO_2^-$ and Cl^- are known as serious interferents.

Acknowledgements

The authors are grateful to Conselho Nacional de Desenvolviment Científico e Tecnológico (CNPq) and Fundação de Amparo à Pesquisa do Estado de São Paulo (FAPESP) for financial support.

References

[1] F. Lázaro, M.D. Luque de Castro, Analusis 16 (1988) 216.
[2] M.R. Straka, G. Gordon, G.E. Pacey, Anal. Chem. 57 (1985) 1799.
[3] D.A. Hollowell, G.E. Pacey, G. Gordon, Anal. Chem. 57 (1985) 2851.
[4] W.E. van der Linden, Anal. Chim. Acta 151 (1983) 359.
[5] V. Kubán, Crit. Rev. Anal. Chem. 23 (1992) 323.
[6] C. Pasquini, L. Cardoso de Faria, Anal. Chim. Acta 193 (1987) 19.
[7] J.J.R. Rohwedder, C. Pasquini, Analyst 116 (1991) 841.
[8] L. Cardoso de Faria, C. Pasquini, Anal. Chim. Acta 245 (1991) 183.
[9] F.G. Barros, M. Tubino, Analyst 117 (1992) 917.
[10] M. Tubino, F.G. Barros, J. Assoc. Off. Anal. Chem. 74 (1991) 346.
[11] W. Frenzel, C.Y. Liu, Fresenius J. Anal. Chem. 342 (1992) 276.
[12] W. Frenzel, C.Y. Liu, J. Oleksy-Frenzel, Anal. Chim. Acta 233 (1990) 77.
[13] W. Frenzel, Fresenius J. Anal. Chem. 336 (1990) 21.
[14] J. Janata, Principles of Chemical Sensors, Plenum, New York, 1989, p. 41.
[15] I. Satoh, T. Ishii, Anal. Chim. Acta 214 (1988) 409.
[16] U. Harborn, B. Xie, B. Danielsson, Anal. Lett. 27 (1994) 2639.
[17] W.A. de Oliveira, C. Pasquini, Analyst 113 (1988) 359.
[18] N. Kiba, Y. Ishida, M. Tsuchiya, M. Furusawa, Talanta 30 (1983) 187.
[19] C. Pasquini, W.A. de Oliveira, Anal. Chim. Acta 156 (1984) 307.
[20] W.E. van der Linden, M. Bos, H.H. Heskamp, H. Wilms, Fresenius J. Anal. Chem. 329 (1987) 440.
[21] J.K. Grime (Ed.), Analytical Solution Calorimetry, John Wiley, New York, 1985, pp. 276–278.
[22] G.E. Pacey, M.R. Straka, J.R. Gord, Anal. Chem. 58 (1986) 502.
[23] J.S. Canham, G.E. Pacey, Anal. Lett. 21 (1988) 1619.
[24] J.S. Canham, G.E. Pacey, Anal. Chim. Acta 214 (1988) 385.
[25] K.J. Smith, G.E. Pacey, Talanta 40 (1993) 1961.
[26] S.J. Liu, M. Tubino, Anal. Chim. Acta, 366 (1998) 5.
[27] M. Tubino, F.G. Barros, Quím. Nova 14 (1991) 49.

ELSEVIER

Talanta 47 (1998) 719–727

Talanta

Spectrophotometric determination of Mo(VI) in steel using a homogeneous ternary solvent system after single-phase extraction

João Carlos de Andrade [a,*], Cláudio José Cuelbas [a], Sebastiaõ de Paula Eiras [b]

[a] *Universidade Estadual de Campinas, Instituto de Química, CP6154, 13083-970, Campinas, SP, Brazil*
[b] *Universidade Federal de Uberlândia, Departamento de Química, CP422, 38400-057, Uberlândia, SP, Brazil*

Received 23 October 1997; received in revised form 28 February 1998; accepted 5 March 1998

Abstract

An alternative procedure for the determination of Mo(VI) with thiocyanate is proposed. According to this procedure, Mo(VI) is extracted with α-benzoinoxime by single-phase extraction in a water/ethanol/chloroform homogeneous ternary solvent system at a nominal pH of 2 and then is spectrophotometrically determined, after separation from the matrix in a similar solvent mixture. The determination is performed by forming a homogeneous phase using the solvent containing the extracted metal as one of the components of the reactional solvent system, eliminating the time-consuming metal complex destruction step. Under these experimental conditions, the calibration graph is linear up to 8.00 μg ml^{-1}, according to the equation $A = 0.005 + 0.143C_{Mo(VI)}$ ($r^2 = 0.9999$). Using the experimental conditions described, the absorbance readings are stable for periods up to 18 h. The interference of the most common interfering species for this method can be prevented by adding Fe^{2+} and $H_2PO_4^-$ to the solvent system prior to the extraction step. The accuracy of the proposed method was evaluated by comparing with standard samples determined by atomic absorption measurements with background correction. © 1998 Elsevier Science B.V. All rights reserved.

Keywords: Molybdenum; Spectrophotometry; Thiocyanate; Solvent mixture; Single-phase extraction

1. Introduction

Molybdenum is an essential element for both animals and plants and is also widely used in a variety of industrial processes, being an important constituent of metal alloys, pigments, lubricants and chemical catalysts, among others [1].

Due to its chemical importance, numerous analytical procedures for its determination can be found in the literature, either using static [2–7] or flow methods [8–11], with the thiocyanate method [12,13] one of the most used. This method makes use of the formation of an orange-red complex between molybdenum and thiocyanate ions in an acid medium in presence of appropriate reducing agents [12,13]. The reaction mechanism is quite complicated, apparently involving molybdenum

* Corresponding author. Fax: +55 19 7883023; e-mail: dandrade@iqm.unicamp.br

0039-9140/98/$ - see front matter © 1998 Elsevier Science B.V. All rights reserved.
PII S0039-9140(98)00125-8

species in the III, IV and V oxidation states [12–15].

On the other hand, several of the spectrophotometric procedures for molybdenum determination involve a prior separation step, usually by solvent extraction, followed by complex destruction prior to metal determination [8,9,12]. These steps are necessary to overcome chemical interferences from other species. One of the most used separation procedures for this purpose is conventional liquid–liquid extraction with α-benzoinoxime (ABO) [8,9,12], which is time-consuming, becoming the rate-determining step for most analytical methods for the determination of molybdenum by molecular absorption spectrometry.

Under this perspective, a reliable alternative procedure for the separation of Mo(VI) seems to be the use of the so called single-phase (SP) extraction technique, using an homogeneous ternary solvent system. This technique was first applied by Belcher et al. [16] for preparative purposes and more recently has been used as an analytical tool by da Silva and Martins [17] for the extraction of Fe(III), Cu(II), Co(II), Ni(II) and Pb(II).

According to this procedure [17], an aqueous solution is made totally miscible with an extractor solvent (such as benzene or chloroform) by the addition of a third solvent in which both are soluble (e.g. acetone or ethanol), known as the consolute. After the single-phase preparation, the homogeneous ternary solvent system is broken by the addition of an excess of water. Thus, differently from the conventional liquid–liquid extraction procedure, where the contact among the reactants occurs by mass transfer between the liquid phases, the metal ion-chelating agent contact in the single-phase extraction procedure is much more effective, rapid and complete, since it occurs in a homogeneous phase.

Thus, a procedure can be devised in which the metal could be determined spectrophotometrically after the single-phase separation, by forming another homogeneous phase using the solvent containing the extracted metal as one of the components of the new solvent system, eliminating the metal complex destruction step. This work reports an analytical procedure for the single-phase extraction of Mo(VI) with α-benzoinoxime in a mixture of water–ethanol–chloroform, followed by its spectrophotometric determination with thiocyanate in the same solvent system.

2. Experimental

2.1. Solutions and reagents

All chemicals were of analytical grade and distilled–deionized water was used throughout. The solutions were stored in high-density polyethylene bottles.

A Mo(VI) stock solution (1000 μg ml^{-1}) was prepared by dissolving 1.5019 g of oven dried (300°C) MoO_3 in 20 ml of concentrated HCl, under heating. After cooling, the solution was diluted to 1.000 l and stored. The Mo(VI) working solutions were prepared from stock as needed. The ammonium thiocyanate stock solution (1 mol l^{-1}), used as the color reagent, was prepared by dissolving appropriate amounts of the dried salt in ethanol. The working solutions were prepared as needed, keeping the composition of the mixture fixed as required by the experimental design or by the analytical procedure. An 1% m/v ferrous ammonium sulphate solution, employed as color stabilizer for the Mo–SCN complex [12], was prepared by dissolving an adequate amount of $(NH_4)_2Fe(SO_4)_2 \cdot 6H_2O$ in 0.1 mol l^{-1} H_2SO_4. The same acid solution was used to dilute the solution to volume.

Both stannous chloride and ascorbic acid were employed as reducing agents for the Mo(VI)–SCN reaction and were prepared as needed. For this, a 10% m/v stannous chloride stock solution was prepared by dissolving 2.5 g of $SnCl_2 \cdot 2H_2O$ in 2.5 ml of boiling concentrated HCl and diluting to 25 ml with water, after cooling. Stock solutions of ascorbic acid (4% m/v) were prepared by dissolving 4.0 g of the acid in a mixture of 10 ml of water and 60 ml of ethanol, completing the volume to 100.0 ml with ethanol.

Fresh α-benzoinoxime solution (2% m/v), commonly used as a Mo(VI) extractor in conventional extraction procedures [8,9,18,19], was obtained by dissolution of the solid compound in ethanol. In

Table 1
The water/ethanol/chloroform mixture experimental design, component and pseudocomponent compositions

Pseudocomponents (P)			Components (% m/m)		
Water[a]	Ethanol[b]	Chloroform[c]	Water	Ethanol	Chloroform
1	0	0	55	45	0
0	1	0	10	90	0
0	0	1	10	45	45
1/2	1/2	0	32.5	67.5	0
1/2	0	1/2	32.5	45	22.5
0	1/2	1/2	10	67.5	22.5
1/3	1/3	1/3	25	60	15
2/3	1/6	1/6	40	52.5	7.5
1/6	2/3	1/6	17.5	75	7.5
1/6	1/6	2/3	17.5	52.5	30

[a] $P_{water} = [C_{water}$ (% m/m) $- 10]/45$.
[b] $P_{ethanol} = [C_{ethanol}$ (% m/m) $- 45]/45$.
[c] $P_{chloroform} = C_{chloroform}$ (% m/m)/45.

this work it has been used in the single phase extraction procedure.

Stock solutions (5000 μg ml^{-1}) of Cr(VI), Fe(III), V(V) and W(VI), prepared for interferences studies, were used after appropriate dilutions. The Cr(VI), W(VI) and V(V) solutions were obtained simply by dissolving adequate amounts of dried $K_2Cr_2O_7$ and $Na_2WO_4 \cdot 2H_2O$ in water and $NaVO_3 \cdot H_2O$ in 10% v/v H_2SO_4, respectively. The Fe(III) stock solution was obtainned by heating a ferrous ammonium sulphate solution with a stoichiometric amount of $KMnO_4$ in sufficient H_2SO_4 to give a final acid concentration of 10% v/v, after dilution. The Mn^{2+} ions formed do not interfere in the analytical method.

2.2. The optimization of the solvent system composition for the reaction between Mo(VI) and thiocyanate

The optimization of this homogeneous solvent system, tested as a reaction medium for Mo(VI) determination with thiocyanate, was carried out by using a simplex centroid experimental design [20,21] with three verification points. The proportions of each mixture were in terms of % m/m, as described in Table 1, with a total mass of 15.0 g for each mixture. The limiting conditions of the solvent system were established by considering both the reagent solubilities in the homogeneous region and in the regions where biphasic mixtures began to be formed.

The procedure used for the optimization of the homogeneous ternary solvent system consisted of adding the reactants to 30 ml glass snap-cap type flasks, using the following addition order: 0.80 ml of water, 100 μl of a 300 μg ml^{-1} standard working Mo(VI) solution, 100 μl of the 1% m/v Fe(II) solution, 50 μl of concentrated hydrochloric acid, 2.00 ml of the 1 mol l^{-1} NH_4SCN solution, 0.20 ml of the 10% m/v $SnCl_2$ solution, 2.00 ml of the 4% m/v ascorbic acid solution and then appropriate amounts of water, ethanol and chloroform to follow the experimental design being tested. For operational simplicity, these amounts of solvents were transformed into volumes:

$$V_{water} = \left[C_{water} \frac{m_t}{(100 d_{water})} \right] - \sum V_{water}$$

$$V_{ethanol} = \left[C_{ethanol} \frac{m_t}{(100 d_{ethanol})} \right] - \sum V_{ethanol}$$

$$V_{chloroform} = \left[C_{chloroform} \frac{m_t}{(100 d_{chloroform})} \right]$$

where C_{water}, $C_{ethanol}$ and $C_{chloroform}$ are the (% m/m) values in Table 1 for each factorial point, d_{water}, $d_{ethanol}$ and $d_{chloroform}$ are the densities of the

pure solvents, m_t is the total mass (15.0 g), ΣV_{water} is the sumation of the volumes of the aqueous solutions and $\Sigma V_{ethanol}$ is the sumation of the volumes of ethanolic solutions already added. In this calculation, the ascorbic acid solution is 10% v/v water and 90% v/v ethanol. This approximation does not significantly affect the final results. The absorbance readings at 462 nm, taken as the system response, were obtained after a 2 h standing period.

After establishing the optimal reaction conditions in the homogeneous ternary system it was possible to devise a way to simplify the routine spectrophotometric determination of Mo(VI) with thiocyanate in this mixture by making use of a 'cocktail solution'. This solution was prepared by dissolving 10.00 g of ascorbic acid and 30.45 g of ammonium thiocyanate in 100 ml of water, which were then quantitatively transfered to a 1-l volumetric flask with an additional 48.0 ml of water, to which were also added 13.0 ml of the 1% m/v Fe^{2+} solution, 6.0 ml of concentrated HCl and 20.0 ml of the 10% m/v stannous chloride, followed by dilution to the mark with ethanol and solution homogenization.

2.3. The optimization of the single-phase extraction procedure

The single-phase extraction experiments were started with the construction of Gibbs–Rozemboon ternary diagrams [22] for the water–ethanol–chloroform solvent system, at a room temperature of 22 ± 3°C, to establish the composition ranges for complete miscibility. This was performed by phase titrations [17]. The results indicated that the mixture ratio of 6:12:4 for water:ethanol:chloroform should be the most appropriate one, since it presents the lowest opalescence upon phase breakdown.

With this solvent system and the conditions for the reaction between Mo(VI) and thiocyanate established, the development of the single-phase (SP) extraction procedure was then carried out by mixing 5.0 ml of water containing 75 μg of Mo(VI), 1.0 ml of hydrochloric acid 0.10 mol l^{-1}, 12.0 ml of ethanol containing 1.0 ml of the 2% m/v ABO solution and 4.0 ml of chloroform in 30 ml glass snap-cap flasks. The addition of 1.0 ml of 0.10 mol l^{-1} hydrochloric acid was necessary to provide an adequate hydrogen ion concentration to obtain the best extraction. Each of these homogeneous solutions were then separately poured over 50 ml of water contained in a pear shape separator funnel that had its top removed at the point of its maximum circumference [17]. After the phase separation, the lower $CHCl_3$ phase was quantitatively transferred to a 25.00 ml volumetric flask with 2.0 ml of ethanol and 1.0 ml of water, followed by the addition of 4.0 ml of chloroform, completing the volume with the cocktail solution described in the previous section.

2.4. The measurements

The volumes were delivered by using either variable volume Eppendorf micropipetes, microburets or precision dispensers, according to volume needed and the precision required. The absorbance readings were performed in a double-beam Hitachi U-2000 spectrophotometer using 10 mm optical path cells. The comparative atomic absorption measurements for evaluation of the method applicability were done by the standard addition method in a Perkin–Elmer Zeeman-5000 spectrophotometer, using an acetylene/N_2O flame at the 313.3 nm molybdenum resonance line, with background correction. All samples were run in triplicate and all readings were done in duplicate, at least.

2.5. Sample preparation

Using the optimal operational conditions, the method was tested using triplicate samples of 0.3000 g of stainless steel. These samples were placed in 250 ml erlenmeyers flasks and heated with agua-regia until complete dissolution. The volumes were then reduced to about 5 ml by slow evaporation. These solutions were then quantitatively transferred to 100 ml volumetric flasks and diluted to the mark with water.

2.6. Proposed analytical procedure

To 5.00 ml of the above sample solutions were added 5 ml of 0.02 mol l^{-1} HCl and the pH adjusted to 1.6 ± 0.2 with ammonia. After pH adjustment, the solutions were transferred to 50 ml volumetric flasks and the volume completed with 0.02 mol l^{-1} HCl solution. The final action for the determination of Mo(VI) was performed by transferring 5.00 ml of the resulting solutions to the 30 ml glass snap-cap type flasks to which a 0.5 ml of the 1% m/v Fe^{2+} solution and 0.5 ml of the 0.01 mol l^{-1} $H_2PO_4^-$ solution were added to prevent matrix interferences from Cr(VI) and W(VI), respectively. Then, 4.0 ml of chloroform and 12.0 ml of an ethanolic 7.3×10^{-3} mol l^{-1} α-benzoinoxime solution were added to each snap-cap flask. After a slight stirring, the homogeneous solutions ('single-phases') are then quantitatively transferred to separator funnels containing 50 ml of water. Each snap-cap flask was washed with small portions of both water and ethanol which were also transferred to the funnels. After stirring the organic phase in the funnel with a glass rod for about 5 s, the solvent system was left to settle. The organic phase was then transfered to 25 ml volumetric flasks. In sequence, enough cocktail solution was added to bring each volumetric flask to the mark and allowed to stand for at least 30 min to obtain for full color development. The absorbance was read at 462 nm against the blank. It is advisable to perform the SP extraction promptly after addition of the phosphate solution, to avoid the formation of a precipitate which often takes place a few minutes after of the phosphate addition to the solvent system.

3. Results and discussion

3.1. The reaction in the homogeneous phase

Screening experiments by spectral comparison indicated that the reaction between Mo(VI) and thiocyanate ions takes place in both aqueous media and in the homogeneous ternary water–ethanol–chloroform media, either in presence or in the absence of α-benzoinoxime. This indicates that, at least in principle, Mo(VI) could be determined in the homogeneous ternary solvent system after single-phase extraction, without the need of a Mo–ABO complex destruction step.

The limiting boundaries for the water–ethanol–chloroform system, under our experimental conditions, are shown in Fig. 1. By using the linear regression approach [20,21] it was possible to show that a second degree model best fits the results. Based on these results, a homogeneous ternary solvent system composed of 13% m/m of water, 42% m/m of chloroform and 45% m/m of ethanol was chosen as the best reaction medium. Considering then the measured mixture density at 25°C of (1.03 ± 0.01) g ml^{-1} and the individual solvent densities, the solvent composition located in the best response region (Fig. 1) is equivalent to a mixture of 3.4 ml of water, 14.7 ml of ethanol and 7.3 ml of chloroform. The final volume is very close to 25.0 ml, due to mixture volume contraction. Thus further quantitative determinations of Mo(VI) were performed in an homogeneous mixture prepared by adding 3.4 ml of water to 7.3 ml of chloroform and completing the volume to 25.00 ml in a volumetric flask with ethanol. This approximation also does not differ significantly from the optimized results and gives considerable operational simplicity. Smaller volumetric flasks can be used for this purpose, if the proportions are maintained.

The direct reaction between Mo(VI) and thiocyanate involve a Mo(VI) reduction step, usually performed by adding reducing agents, such as stannous chloride [3,12,18], ascorbic acid [2,23] or cuprous chloride [3]. These reducing agents induce a rapid $Mo(VI) \rightarrow Mo(IV)$ reduction, followed by a disproportioning of the Mo(IV) species to Mo(III) and Mo(V), where only quinquevalent molybdenum results in a colored thiocyanate complex [3]. The presence of small amounts of iron (or copper) increases the color intensity in the Sn(II) chloride–thiocyanate method, in immiscible or miscible organic solvents [24,25]. The formation of the $Mo_2^{III}[Mo^{V}O(SCN)_5]_3$ complex is postulated in the absence of iron, but it was also found that method sensitivity is increased in presence of Fe^{2+}, probably due to the formation of

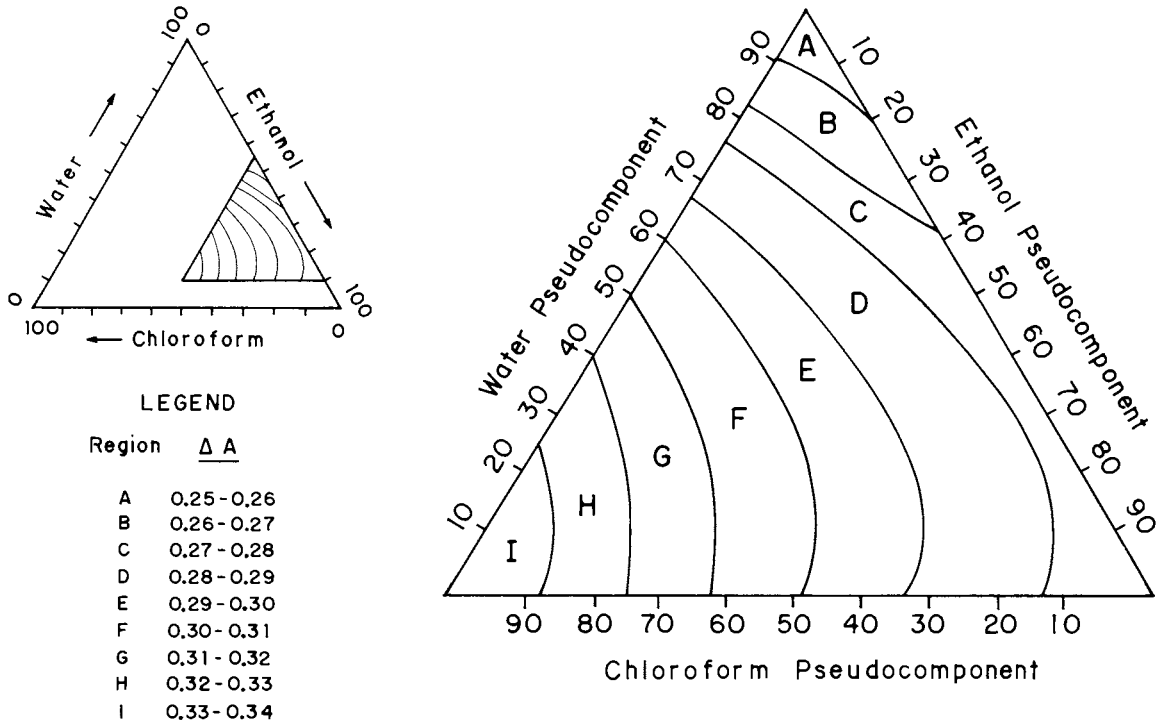

Fig. 1. Boundaries limiting the homogeneous ternary solvent system water/ethanol/chloroform. The smaller triangle represents the components system and the larger one amplifies the pseudocomponents region. The level curves represent the absorbance values range at each mixture region, adjusted by second degree equations.

$Fe^{II}[Mo^{V}O(SCN)_5]$ [12,24,25]. The maximum color intensity is obtained by mixing approximately equivalent concentrations of molybdenum and iron.

From our results it is possible to infer that the same chemical process should be taking place in the homogeneous water–ethanol–chloroform ternary system, including the known formation of color gradients when only $SnCl_2$ is used as reducing agent. This probably occurs because the reduction process takes place in a very short period of time, permitting re-oxidation of the $Fe^{II}[Mo^{V}O(SCN)_5]$ complex, resulting in the formation of Fe^{3+} ions which promptly complex with SCN^- ions present in solution [12,26]. Thus, an auxiliary reducing agent, such as ascorbic acid was shown to be necessary to keep the Fe–Mo–SCN complex stable in the homogeneous solution for a longer period of time, by slowing Fe^{3+} formation.

The effect of the reagent concentrations on the reaction between Mo(VI) and SCN^- in the ternary homogeneous phase was studied using univariate experiments, keeping constant both the Mo(VI) and the α-benzoinoxime concentrations at 1.00 mg ml^{-1} and 0.016 mol l^{-1}, respectively, and varying the proportions of HCl (0.03–0.17 mol l^{-1}), NH_4SCN (0.15–0.45 mol l^{-1}), $SnCl_2$ (0–0.018 mol l^{-1}) ascorbic acid (0–0.10 mol l^{-1}) and Fe^{2+} (0–4.0×10^{-2} mol l^{-1}) in the cocktail solution. The variation in the absorbance values were not significant (~0.150–0.170) after 30 min, except in the absence of $SnCl_2$, Fe^{2+} or ascorbic acid. Lower HCl concentrations led to the formation of a precipitade with time, probably due to Sn^{2+} hydrolysis, while color gradients are easily formed at higher acid concentrations. This resulted in the reagent concentrations proposed for the cocktail solution as mentioned in the experimental part, which led to good chemical stability of the Mo–SCN species.

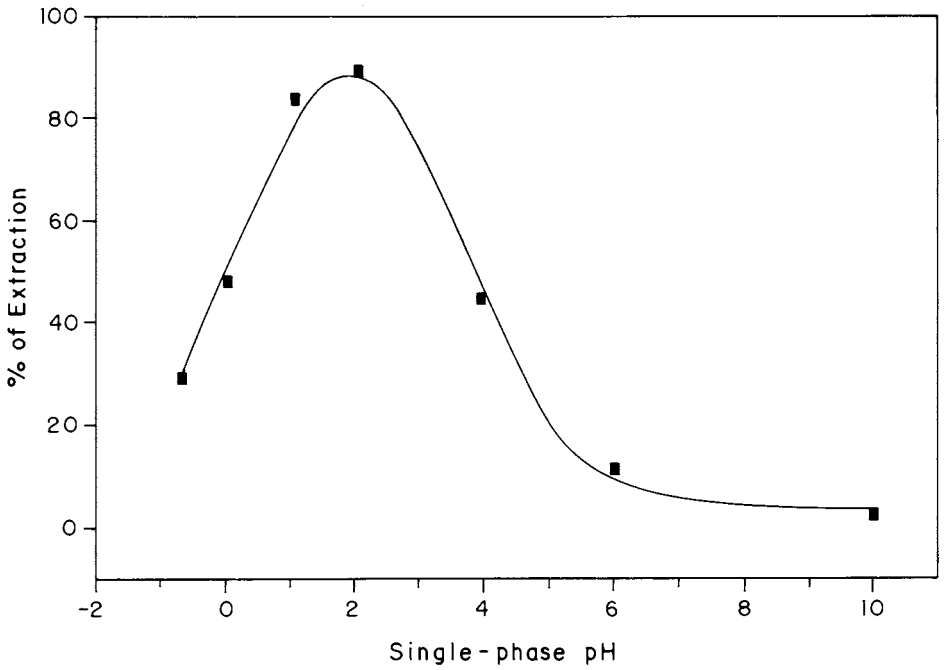

Fig. 2. Effect of the single-phase pH on the molybdenum extraction yield.

3.2. The single-phase extraction

The influence of the ABO concentration on the Mo(VI) extraction was observed under the extraction conditions stated in the experimental part. The extraction yield reaches its maximum level of about 90% at ABO concentrations higher than 3.0×10^{-3} mol l^{-1}, remaining constant up to 4.0×10^{-3} mol l^{-1}. Higher concentrations of ABO provoke the formation of a precipitate, probably a Mo–ABO complex, after a standing period of 1 h. Thus, for analytical purposes, the final analytical concentration of ABO should not exceed the limit of 4.0×10^{-3} mol l^{-1}.

The addition of 1.0 ml of 0.10 mol l^{-1} HCl to the solvent mixture used to obtain the single-phase gives a nominal pH value of 2.0, according to the Matkovich and Christian scale [27], herein called single-phase pH, or pHSP [17]. This corresponds to the best Mo(VI) extraction conditions, as can be seen from Fig. 2. In single-phase extraction, the addition of salts or acids to the water used for phase separation has frequently been utilized [17] to increase the extraction yield but in this work it was noted that the salting out effect is not effective.

3.3. The interferences

The action of Fe(III), Cr(VI), V(V) and W(VI) as potential interfering species were observed both in the SP extraction procedure and in the direct reaction between Mo(VI) and SCN^- ions in the chosen ternary homogeneous solvent system. As indicated in Table 2, the presence of a 100-fold excess of either Cr(VI) and Fe(III) in the reaction medium resulted in significative increases of the analytical signal, due to the reduction of Cr(VI) to the greenish Cr(III) species and by the formation of thiocyanate complexes with Fe(III). V(V) presented the smallest interference, as only a 100-fold excess in the extraction procedure presented a negative influence, while W(VI) induced a significative decrease in the signal, even at small excess, probably by competition with Mo(VI) in complexing with thiocyanate ions.

On the other hand, it was also noted that only V(V), Cr(VI) and W(VI) cause interference in the

Table 2
Interference factors[a] for the Molybdenum determination procedure in the water/ethanol/chloroform homogeneous ternary solvent system, before and after single-phase extraction

Interferences	Direct determination		After single-phase extraction	
	C_{mo}: 1.0 μg ml^{-1}	C_{mo}: 4.0 μg ml^{-1}	C_{mo}: 1.0 μg ml^{-1}	C_{mo}: 4.0 μg ml^{-1}
Cr(VI)				
1×	1.04	0.96	1.03	0.49
10×	1.02	1.02	0.92	0.44
100×	1.29	1.22	0.54	0.07
Fe(III)				
1×	1.09	0.99	1.01	1.00
10×	1.03	1.03	1.04	0.99
100×	1.20	2.58	0.94	—[b]
V(V)				
1×	0.99	1.00	1.09	1.00
10×	1.00	1.03	1.09	0.99
100×	1.07	1.06	0.39	—[b]
W(VI)				
1×	0.91	0.81	1.07	0.98
10×	0.85	0.58	1.00	0.88
100×	0.56	0.44	0.64	0.36

[a] An interference factor greater than 1.00 means an enhancement and a factor less than 1.00 means a depression of the expected value.
[b] Precipitation and phase breakdown always take place because it was not possible to adjust the single-phase pH to 2.0, due to the high acidity of the stock solutions.

Mo(VI) single-phase extraction process, due to interaction with α-benzoinoxime. Keeping Mo(VI) at the 1.0 μg ml^{-1} level, the changes in the observed analytical signal after the SP extraction do not exceed the ±10% range by using up to a ten-fold excess of the individualy interfering species, but a very significant decrease is observed at a 100-fold excess. In contrast to the direct procedure, the single-phase extraction procedure seems to be less sensitive to the presence of Fe(III). At the 4.0 μg ml^{-1} level of Mo(VI), severe interferences are observed for all metals tested.

To overcome the interference problems, an excess of both Fe^{2+} and phosphate was added to the reaction medium prior to the extraction procedure, as stated in the analytical procedure. The Fe^{2+} provokes the reduction of Cr(VI) to Cr(III) and phosphate is used to eliminate the interferences caused by tungsten [12,28,29]. Neither Cr(III) nor the tungsten–phosphate complex are extracted by ABO. Ni(II) and Mn(II) do not interfer, as they are also not extracted with ABO under the conditions described herein.

3.4. The method performance

The Sandell index for the proposed method corresponds to 0.007. The majority of methods involving thiocyanate found in the literature exhibit Sandell index values ranging from 0.005 to 0.009. However, the proposed method is more rapid and selective than comparative extraction methods [12].

The applicability of the method was tested by running two samples of stainless steel, as described in the experimental section. The calibration curve, prepared following the same procedure used for the actual samples, showed to be linear from 0.1 to 8.0 μg ml^{-1} of Mo(VI), according to the equation $A = 0.005 + 0.143C_{Mo(VI)}$ ($r^2 = 0.9999$). From ten replicate determination, the

Table 3
Determination of Mo(VI) in steel samples by atomic absorption spectrometry and by the proposed spectrophotometric method in the homogeneous water/ethanol/chloroform ternary solvent system, after single-phase extraction

Samples[a]	Atomic Absorption (standard addition) % m/m	Spectrophotometric (after SP extraction) % m/m
Steel 1	(2.3 ± 0.1)	(2.4 ± 0.1)
Steel 2[b]	(2.3 ± 0.2)	(2.2 ± 0.1)

[a] Samples run in triplicate.
[b] Reference standard material 160 b NBS (NIST): Mo (%) = 2.38.

relative standard deviation varied from 5.9% at the 0.1 μg ml^{-1} level to 0.9% at the 8.0 μg ml^{-1} level. Under these conditions, the absorbance readings remained stable for from 30 min to 18 h. As indicated in Table 3, the results compared favorably with those obtained by atomic absorption measurements when the complete procedure is followed.

Acknowledgements

Thanks are due to Prof. C.H. Collins for reading the manuscript and to CNPq for a fellwship to C.J.C.

References

[1] W.M. Jarrell, A.L. Page, A.A. Elseewi, Residue Rev. 74 (1980) 1.
[2] C.H. Kim, C.M. Owens, L.E. Smythe, Talanta 21 (1974) 445.
[3] C.E. Crouthamel, C.E. Johnson, Anal. Chem. 26 (1954) 1284.
[4] G. Hanson, A. Szabo, N.D. Chasteen, Anal. Chem. 49 (1977) 461.
[5] M. Sanchez, D. Gazquez, P. Garcia, Talanta 38 (1991) 747.
[6] I. Steffan, G. Vujicic, Mikrochim. Acta. 110 (1993) 89.
[7] C.L. Luke, Anal. Chim. Acta. 34 (1996) 302.
[8] E.G. Bradfield, J.F. Stickland, Analyst 100 (1975) 1.
[9] J.C. de Andrade, S.P. Eiras, R.E. Bruns, Analyst 118 (1993) 213.
[10] F.J. Krug, O. Bahia Filho, E.A.G. Zagatto, Anal. Chim. Acta 161 (1984) 245.
[11] L.C.R. Pessenda, A.O. Jacintho, E.A.G. Zagatto, Anal. Chim. Acta 214 (1988) 239.
[12] H. Onishi, Photometric Determination of Traces of Metals. Part II B: Individual Metals, Magnesium to Zirconium, 4th edn., John Wiley and Sons, New York, 1989.
[13] A.C. Basak, K.C. Ghosh, A.R. Paul, S. Bhattacharjee, L.P. Pandey, Talanta 42 (1995) 497.
[14] D.D. Perrin, J. Am. Chem. Soc. 80 (1958) 3540.
[15] O.W. Kolling, Anal. Chem. 37 (1965) 436.
[16] R. Belcher, R.J. Martin, W.I. Stephen, D.E. Henderson, A. Kamalizad, P.C. Uden, Anal. Chem. 45 (1973) 1197.
[17] J.F. da Silva, W. Martins, Talanta 39 (1992) 1307.
[18] F.D. Snell, Photometric and Fluorometric Methods of Analysis Metals Part 2, John Wiley and Sons, New York, 1978.
[19] P.G. Jeffery, Analyst 81 (1956) 104.
[20] J.A. Cornell, Experiments with Mixtures: Designs, Models and the Analysis of Mixture Data, 2nd edn., John Wiley and Sons, Nova York, 1990.
[21] J.A. Cornell, How to run mixture experiments for product quality, vol. 5, in: The ASQC Basic References in Quality Control: Statistical Techniques, American Society for Quality Control, Wisconsin—EUA, 1990.
[22] S. Siggia, J.G. Hanna, Anal. Chem. 21 (1949) 1086.
[23] K.N. Thimmaiah, W.D. Lloyd, Microchem. J. 32 (1985) 281.
[24] A.T. Dick, J.B. Bingley, J. Australian, Exptl. Biol. Med. Sci. 25 (1947) 193, Chem. Abstr. 42 (1948) 2307h.
[25] A.T. Dick, J.B. Bingley, Nature 158 (1946) 516, Chem. Abstr. 41 (1947) 1946d.
[26] L.P. Greenland, E.G. Lillie, Anal. Chim. Acta 69 (1974) 335.
[27] C.E. Matkovich, G.D. Christian, Anal. Chem. 46 (1974) 102.
[28] R. Caletka, V. Krivan, Fresenius J. Anal. Chem. 332 (1989) 866.
[29] P.Y. Peng, E.B. Sandell, Anal. Chim. Acta 29 (1963) 325.

ELSEVIER

Talanta 47 (1998) 729–733

Talanta

News analytical reagents for europium(III)

M.P. Montaña, N.B. Pappano, N.B. Debattista *

Department of Chemistry, San Luis National University, Chacabuco 917, 5700-San Luis, Argentina

Received 22 October 1997; accepted 13 March 1998

Abstract

The complexant reactions of 2′-hydroxychalcones with europium(III) are studied by the spectrophotometric method. The apparent formation constants are evaluated using a simple graphical linear method. The sequence of these constant values is explained and compared with aluminium(III) complexant reactions. © 1998 Elsevier Science B.V. All rights reserved.

Keywords: Europium(III); Reactions; Linear method

1. Introduction

Flavonoids are a group of phenolic compounds diverse in chemical structure and characteristics, widely distributed in nature. Particularly, 2′-hydroxychalcones are substances that exhibit an assorted chemical reactivity [1–3] and wide range of biological effects [4–6].

Due to the presence of α:β unsaturated carbonyl group, 2′-hydroxychalcones exhibit the ability of chelates formation [7–9]. They are much more reactive with metal ions than the ketones and benzaldehydes from which they are synthesized. The efficiency of 2′-hydroxychalcones for the spectrophotometric investigations of various metal cations such as U(VI), Fe(III), Al(III) has been observed [10–12].

Europium oxide is currently widely used as a phosphor activator and europium-activated ittrium vanadate exists in commercial use as the red phosphor in color TV tubes, being the most reactive and costly of the rare-earth metals. Besides, it is known that only important and stable complexes of lanthanides are those that make chelates.

In view of the analytical applications of orthohydroxychalcones and its ability by to form chelates, the present investigation is aimed at determining the composition and stability constants of europium(III) with substituted 2′-hydroxychalcones, which have not been studied so far. These reagents react instantaneously with europium ion and develop an intense yellow colour. The chelates have been shown to have definite chemical composition.

* Corresponding author. Tel.: +54 652 24689; fax: +54 652 30224; e-mail: ndea@uns1.edu.ar

0039-9140/98/$ - see front matter © 1998 Elsevier Science B.V. All rights reserved.
PII S0039-9140(98)00120-9

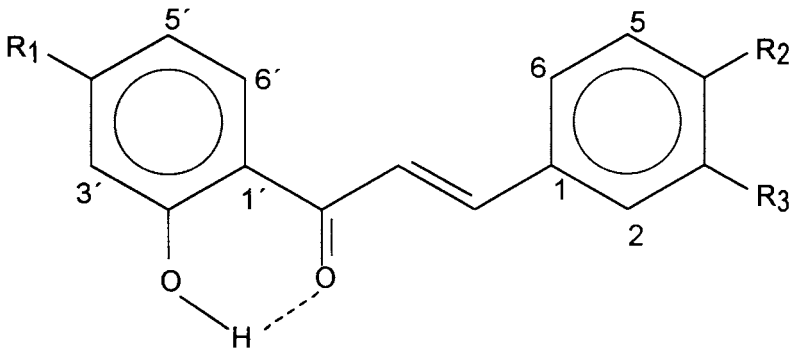

R1 = R2 = H; R3 = OH : 2',3 - DIHYDROXYCHALCONE

R1 = R3 = H; R2 = OH : 2',4 - DIHYDROXYCHALCONE

R2 = R3 = H; R1 = OH : 2',4' - DIHYDROXYCHALCONE

R2 = H; R1 = R3 = OH : 2',4',3 - TRIHYDROXYCHALCONE

Fig. 1. Structure and numbering system of substituted 2′-hydroxychalcones.

2. Experimental

2.1. Reagents

The substances studied were the following: I: 2′,3-dihydroxychalcone; II: 2′,4-dihydroxychalcone; III: 2′, 4′-dihydroxychalcone; IV: 2′,4′,3-trihydroxychalcone. Their structures and the numbering system are shown in Fig. 1. The compounds were prepared by condensation of 2-hydroxyacetophenone with substituted benzaldehydes [13].

They were purified by LH 20 Sephadex column chromatography with methanol as eluent and identified according to physical, chromatographic and spectroscopic properties.

2′,3-dihydroxychalcone: R_f (TLC): 0.26; mp: 166 C; UV_{max}^{MeOH} nm: 311, 253; IR ν ($CC1_4$) cm^{-1}: 1642 (C=O), 3605 (OH).

2′,4-dihydroxychalcone: R_f (TLC): 0.23; mp: 158–159 C; UV_{max}^{MeOH} nm: 365, 240; IR ν (CCl_4) cm^{-1}: 1641 (C=O), 3600 (OH).

2′,4′-dihydroxychalcone: R_f (TLC): 0.21; mp: 147 C; UV_{max}^{MeOH} nm: 315, 345, 222; IR ν ($CC1_4$) cm^{-1}: 1640 (C=O), 3590 (OH).

2′,4′,3-trihydroxychalcone: R_f (TLC): 0.185; UV_{max}^{MeOH} nm: 358, 314, 253, 210. ^1H NMR (200.13 Mhz, CD_3OD): δ 6.28 (d, $J = 2.3$ Hz, H3′); 6.4 (dd, $J = 9.0$, 2.3 Hz, H5′); 7.95 (d, $J = 9.0$ Hz, H6′); 7.66 (d, $J = 15.4$ Hz, Hα); 7.75 (d, $J = 15.4$ Hz, Hβ); 7.12 (br. t, $J = 2.1$ Hz, H2); 6.84 (dt, $J = 7.6$, 2.1, 2.1 Hz, H4); 7.21 (dt, $J = 7.6$, 2.1, 2.1 Hz, H5); 7.25 (dd, $J = 7.6$, 2.1 Hz, H6).

The complex solutions in methanol were prepared by mixing variable concentrations of 2′-hydroxychalcones and europium(III) (10^{-3}–10^{-4} M). The ligand: metal concentration relation (4:1), ionic strength (0.01) and temperature (29 C $\pm$ 0.1) were maintained constant. The absorbance measurements were made at a wavelength where only the complex absorbs.

2.2. Apparatus

Spectrophotometric measurements were performed using a Shimadzu UV-vis spectrophotometer UV-160A with standard 1.0 cm pathlength quartz cuvettes.

3. Results and discussion

The molar composition of the chelates was established by a molar-ratio method [14] and a 2:1 (ligand: metal) stoichiometry was found (Fig. 2).

The kinetic experiences allowed to establish that when the chelation reaction is completed only the L_2M species is present.

The chemical reaction is then:

$$nLH + M^{3+} \leftrightarrows L_nM + nH^+ \quad (1)$$

where LH is the complexant reagent, M^{3+} is the metallic ion and n is the stoichiometry coefficient (in this case $n = 2$). In the considered system, at constant ionic strength and pH, the apparent formation constant (K), is:

$$K = \frac{[L_2M^+]}{[LH]^2 \cdot [M^{3+}]} = \frac{K_c}{[H^+]^2} \quad (2)$$

where the brackets refer to the substance molar concentrations.

A linear spectrophotometric method, applicable to mono and polynuclear complexes was used to determine the values of the apparent formation constants [12]. This method is easy and of extensive applicability. Its application only requires: analytical concentrations of reactants, ligand molar absortivity and absorbances for equilibrium solutions.

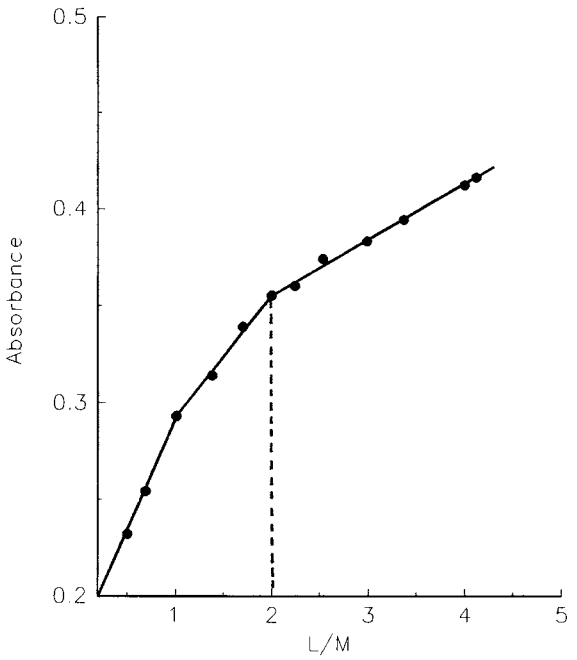

Fig. 2. Application of Yoe–Jones method to 2′,3-dihydroxychalcone.

Table 1
Concentration ranges and wavelength employed by 2′-hydroxychalcones-Eu(III) systems

System	Molar concentration		Wavelength (nm)
	$C_L \times 10^3$	$C_M \times 10^4$	
I-Eu(III)	0.273–2.169	0.670–5.333	460
II-Eu(III)	2.536–3.959	5.786–9.034	480
III-Eu(III)	1.952–4.893	4.816–12.07	460
IV-Eu(III)	4.112–6.425	9.980–15.60	480

The expression for complexes L_2M ($n = 2$) is:

$$a_j^2 + 4a_j b_j = \frac{(a_r + 4a_r b_r + K) \cdot (A - A_L)_r}{(a_r^2 \cdot b_r)} \cdot \frac{a_j^2 \cdot b_j}{(A - A_L)_j} - \frac{1}{K} \quad (3)$$

where a and b are the ligand and metal molar analytic concentrations, respectively, A is the reacting solution absorbance, A_L is the ligand absorbance (in this case $A_L = 0$); j and r indicate two equilibrium solutions and $K' = 1/K$.

In Table 1, the concentration ranges and the work wavelengths for the studied systems are listed.

The graphic representation of Eq. (3) allow estimated the apparent formation constant from the straight line slope and the intercept for all systems studied.

The values for the apparent formation constants of different complexes studied together with the apparent formation constants for complexes of these 2′-hydroxychalcones with Al(III), previously studied, are informed in Table 2.

Lanthanides are very electropositive and reactive metals. They form few complexes and usually oxygenates ones. Their reactivity apparently depends on size therefore europium, which has the largest metal radius, is the most reactive one. Due

to their large electropositivity, they have little tendency to form complexes with ligands that make 'pi' bonds [17].

The values for the apparent formation constants of the 2′-hydroxychalcones-Eu(III) studied decrease in the order:

$$2',3(OH)_2 > 2',4\text{-}(OH)_2 > 2',4'\text{-}(OH)_2 > 2',4',3\text{-}(OH)_3$$

This sequence and the lower K values obtained can be explained taking into account that:

- The 2′-hydroxychalcones constitute an extended planar system.
- The bond of the second ligand to voluminous europium is hindered by the existence of substituents close to the reaction center.

However, the chelation reactions with europium (III) are favored by the presence of substituents that cause a molecular torsion, thus hindering the electronic delocalization.

On the other hand, previous studies of the complexation of these 2′-hydroxychalcones with aluminium(III) allowed to establish the sequence:

$$2',4',3\text{-}(OH)_3 > 2',4'\text{-}(OH)_2 > 2',4\text{-}(OH)_2 > 2',3\text{-}(OH)_2$$

which is exactly inverse to that observed by Eu(III). This is due to:

- Lower aluminium size than europium.
- Non existence of steric impediments.
- The aluminium complexes are favored by an electronic density increase, being evident that this depends of the substituent effects present in the A or B ring.

Table 2
Apparent formation constants (K) for the complexes studied

System	$K \times 10^{-5}$ (Eu)	$K \times 10^{-5}$ (Al)[a]
I-M	6.45	1.00
II-M	3.48	2.69
III-M	2.12	3.55
IV-M	1.43	11.0

[a] [7,15,16].

4. Conclusions

Yoe–Jones method of molar ratio shows that the ligand:metal ratio is 2:1. The linear spectrophotometric method, used for evaluation of apparent formation constants, is easily applicable for the polynuclear complexes studied.

The 2′-hydroxychalcones could be used as analytical reagent for europium(III).

Considering the values for the apparent formation constants obtained for the compounds studied it can be concluded that 2′, 3-dihydroxychalcone is the most suitable one for Eu(III) complexation.

Moreover, this chalcone presents the advantage of being easily synthesized and purified with good yields.

Acknowledgements

The authors are thankful to San Luis National University for financial support.

References

[1] W. Tuly, L. Main, B.K. Nicholson, J. Organomet. Chem. 503 (1995) 75.
[2] R.R. Amaresh, P.T. Perumal, Tetrahedron Lett. 36 (1995) 7287.
[3] M. Shi, N. Itoh, I. Masaki, J. Chem. Res. (S) (1995) 304.
[4] R. Li, G.L. Kenyon, F.E. Cohen, X. Chen, B. Gong, J.N. Dominguez, E. Davidson, G. Kurzban, R.E. Miller, E.O. Nuzum, P.J. Rosenthal, J.H. McKerrow, J. Med. Chem. 38 (1995) 5031.
[5] B.S. Min, B.S. Ahn, K.H. Bal, Arch. Pharm. Res. 19 (1996) 543.
[6] H. Makita, T. Tanaka, H. Fujitsuka, N. Tatematsu, K. Satoh, A. Hara, H. Mori, Cancer Res. 56 (1996) 4904.
[7] N.B. Debattista, E.J. Borkowski, N.B. Pappano, J. Kavka, F.H. Ferretti, An. Assoc. Quim. Argent. 74 (1986) 179.
[8] T.S. Rao, K.L. Reddy, P. Lingaiah, Indian J. Chem. Sect A 27 (1988) 510.
[9] M. Palaniandavar, C. Natarajan, Aust. J. Chem. 33 (1980) 737.
[10] H. Sin, U.K. Rathi, J. Indian Chem. Soc. 56 (1979) 1028.
[11] M.L. Narwade, M.M. Chincholkar, S.W. Sathe, J. Indian Chem. Soc. 62 (1985) 194.
[12] N.B. Debattista, N.B. Pappano, Talanta (1997) En prensa.

[13] J.B. Harborne, T. Mabry, H. Mabry, The Flavonoids, Vol. 1, Academic Press, New York, 1975, p. 131.
[14] G.D. Christian, J.E. O'Reilly (Eds.), Instrumental Analysis, Allyn and Baconm, Boston, 1986, p. 186.
[15] N.B. Debattista, Doctoral thesis, Structure and reactivity of simple flavonoids, San Luis National University, Argentina, 1990.
[16] Personal communication, X Physical Chemistry Argentine Congress, Section B 89, 1997, p. 127.
[17] F.A. Cotton, G. Wilkinson, Química Inorgánica Avanzada, Ed. Limusa, México, 1990, pp. 1193–1194.

ELSEVIER

Talanta 47 (1998) 735–743

Talanta

Microfabricated glucose biosensor with glucose oxidase entrapped in sol–gel matrix

Saipeng Yang [a], Yunfeng Lu [a], Plamen Atanossov [a], Ebtisam Wilkins [a,*], Xiangchun Long [b]

[a] *Chemical and Nuclear Engineering Department, The University of New Mexico, Albuquerque, NM 87131-1341, USA*
[b] *Electrical Engineering and Computer Engineering Department, The University of New Mexico, Albuquerque, NM 87131-1341, USA*

Received 21 October 1997; received in revised form 9 March 1998; accepted 16 March 1998

Abstract

A microfabricated glucose biosensor based on an amperometeric hydrogen peroxide electrode has been developed. A sol–gel layer with 5 Å pore size and 2 μm thickness was used as the glucose oxidase entrapping matrix. The sol-gel matrix formed over the silicon-based sensor has good mechanical and chemical stability, and the ability to entrap a large amount of enzyme. The miniaturized electrode sensing system is composed of platinum as both working and counter electrodes and silver as a reference electrode. Nafion® coating was applied as the interference limiting layer. A series of technologies, such as standard photolithography, electron beam evaporation and image reverse lift-off were utilized for mass production allowing 143 electrodes to be produced at the same time. The effect of oxidable interferences was $< 10\%$ of the background value of the sensor response. Calibration tests of a series of individual sensors manufactured from the same silicon wafer and dip coated in the same conditions, showed a highly reproducible response characteristics (linear range up to 500 mg dl^{-1} and mean sensitivity of 0.54 ± 0.14 nA mg^{-1} dl^{-1} ($n = 10$)). © 1998 Elsevier Science B.V. All rights reserved.

1. Introduction

Biosensors are being intensively studied since Updike and Hicks proposed the first glucose enzyme electrode in 1967 [1]. Biosensors have become so important and widely used because they have various applications in many fields, such as clinical analysis, pharmaceutical, industry, food quality control, and biotechnology [2–8]. Of these biosensors, enzyme electrodes have been developed extensively due to their broad applications [9,10]. The areas of potential applications of electrochemical sensors are expanding rapidly. However, the greatest effort has been made in the biomedical area due to the need for devices that are potentially implantable, long-term operational, interference free and capable of rapid measurement of different biochemical species.

In biomedical, clinical and physiological analyses and bioprocess control areas, miniaturized sensors are strongly needed. The miniaturized sensor should be able to measure physiological parameters in vitro and in vivo [11,12]. Screen-

* Corresponding author. Tel.: +1 505 2775431; fax: +1 505 2775433; e-mail: plamen@unm.edu

0039-9140/98/$ - see front matter © 1998 Elsevier Science B.V. All rights reserved.
PII S0039-9140(98)00119-2

printing and photolithography [13,15] are currently the most convenient approaches for sensor miniaturization. Photolithographic technology has various applications in a wide range of materials and geometries [14]. It offers many interesting features for the fabrication of small analytical devices in general except the obvious reason of size and cost reduction [14], so their use in electrochemistry and electroanalysis is growing steadily and rapidly. Another reason for the success of photolithographically produced structures is that they can be considered disposable and display highly reproducible surface characteristics.

Most of the numerous in vivo glucose sensing devices suffer from the serious drawback of production processes which are rather delicate and therefore hard to integrate with other parts of the devices [16]. This fact not only increases the production costs but also causes serious problems with the reliability of such devices. The miniaturization and mass production technologies have been utilized to overcome this problem [17]. It can address some of the basic requirements of sensor miniaturization. In addition, it provides the possibility of integrating the transducer with some part of the associated electronic circuitry into a single chip [14].

The application of microfabricated sensors in clinical and biomedical areas can minimize the interaction between sensors and physiological subjects by using small size and mass. Due to the mass production based on thin film fabrication technology, the pre-calibration of one single sensor turns out to be accurately similar to the calibration of the others from the same wafer, the calibration test of each individual sensor can be avoided [18].

Due to the reduced size of the microfabricated electrode, the lifetime of the biosensor is affected by the enzyme-loading amount on the electrode. The approach of enzyme immobilization on the microfabricated electrode can increase the enzyme loading amount and enzyme lifetime. Enzyme layers can be applied by the main immobilization methods: (a) chemical cross-linking of glucose oxidase (GOD) [19]; (b) electrochemical codepositon with conductive polymers, such as polypyrrole etc. [20]; (c) direct galvanostatic codeposition of GOD and bovine serum albumin [21]; (d) coupling with semiconducting carbonaceous materials [22]; and (e) entrapment in water-dispersed anionic polymers [23]. Additional diffusion layers and interference barrier layers are needed to obtain sensor linearity and interference proofed signal.

The application of the sol–gel process in trapping organic molecules in the inorganic matrix has attracted a lot of attention in the last decade [24,25]. Organic molecules, such as enzymes, can be entrapped in the pore network of the sol–gel material. Compared to the other immobilization methods, such as polymer entrapment, using sol–gel glasses as enzyme immobilization matrices has many advantages, i.e. the ability to entrap large amounts of enzymes, thermal and chemical stability, simplicity of preparation without covalent modification, and flexibility of controlling pore size and geometry [24].

One of the most critical issues associated with biosensors is interference with body chemicals, such as ascorbic acid, uric acid, acetaminophen, etc. Most of the interferences are either due to the direct oxidation of electroactive species on the platinum working electrode at the applied potential, or to the oxidation of the interference species by a homogeneous chemical reaction with hydrogen peroxide formed in the enzymatic reaction [26,27]. Several approaches have been utilized to prevent interference effects, such as, additional electrodes to preliminarily oxidize the interference species in the much higher anodic current [28], the application of a barrier polymer and organic membranes to limit the interference substance flux from reaching the electrode [29], the application of a negative working potential to avoid the oxidation of interference species on the working electrode [30], or the application of a negatively charged membrane or coating to eliminate the interference of the substance with anonic charge such as ascorbic acid or uric acid [31].

The results from our previous in vitro and short-term in vivo implantations were obtained with a variety of hand-made glucose biosensors [14,32,33]. The reproducibility of the sensor fabrication and the size of the sensor are limiting factors for the long-term applications of such

sensor systems in animal or human experiments. In this study, we are describing a microfabricated glucose biosensor with GOD entrapped in the sol–gel matrix based on amperometric detection of hydrogen peroxide formed in the enzyme reaction to improve reproducibility of the sensor for mass production.

2. Experimental

2.1. Reagents

Glucose oxidase (GOD, EC.1.1.3.4, activity 200 EU mg^{-1}, purified from *Aspergillus niger*), β-D(+)-glucose, and the interference substances: ascorbic acid, uric acid and acetaminophen, were obtained from Sigma (St. Louis, MO). These substances were dissolved in 0.1 M sodium phosphate buffer (pH 7.4) to give stock solutions with the following average physiologic concentrations: 6 mM ascorbic acid, 15 mM uric acid, and 20 mM acetaminophen. In the interference tests the concentrations of these compounds in the measuring cell were: 0.125 mM for ascorbic acid, 0.33 mM for uric acid, 0.5 mM for urea, 0.5 mM for glycine and 0.13 mM for acetaminophen. Nafion® perfluorinated ionomer was obtained from Aldrich (Wilwaukee, WI) as 5 wt.% solution. Araldite-type epoxy was obtained from Fox Industries (Baltimore, MD).

All other chemicals were of analytical grade and used without further purification.

2.2. Instrumentation and measurement

The metal evaporator from Telemark Industries (Livermore, CA) was used to deposit the metal on silicon wafer. A bonding machine from West Bond (Anaheim, CA) was used to bind the electrode to the wires. A tempress dicing saw from Sola Basic Industries (Los Gatos, CA) was used to dice the silicon wafer.

The photo mask was designed by using 'Autocad®' program, printed on a transparency in MPC Design Technologies (Albuquerque, NM).

Potentiostat (voltammograph CV-1 B, Bioanalytical Systems, West Lafayette, IN) were used to maintain a potential of +0.7 V between the working and reference electrodes. The current passing through the working electrode was measured and recorded continuously using digital multimeters and X–Y chart recorders.

The glucose tests were conducted in a glass cell (volume 100 cm^3) thermostated at 25 or 37°C, under magnetic stirring. Phosphate buffer solution (pH 7.4) containing 0.1 M KCl was used in the tests and the glucose concentration was varied by consecutive additions of 1 ml glucose from the stock solution (20 g l^{-1} glucose, prepared at least 24 h before for maturation) so that the concentration step change is 40 mg dl^{-1} (2.2 mM). The anodic current of the sensor was continuously recorded.

A chemical interference test was performed by monitoring of the anodic current during the addition of ascorbic acid (0.125 mM), uric acid (0.33 mM), paracetamol (0.125 mM), glycine (0.5 mM) and urea (8.5 mM). These concentrations are selected to be within the physiological ranges for the particular chemicals.

3. Microfabricated sensor

3.1. Transducer design

Fig. 1 shows the schematic diagram of the electrode system design. The layout of the transducer was determined by several considerations. The transducers design should be simple and easy to fabricate. The working and counter electrodes were designed as rings surrounding the reference electrode. The working electrode (0.236 mm^2) and counter electrode (0.442 mm^2) are made from platinum, and the reference electrode is made from Ag/AgCl. The electrode system has a length of 2.0 mm, a width of 1.5 mm and thickness of 0.5 mm.

Two masks were designed to pattern Pt (working and counter electrode) and Ag (reference electrode) separately. The amount of the microelectrodes that can be produced at the same time is 143. The photo mask printed on the transparency was developed on a high-resolution plate in a dark room.

3.2. Transducer fabrication

The transducers were fabricated on a 76.2 mm diameter polycrystalline silicon wafer. The entire passivation layer, adhesion layer and metal layer are patterned by photolithography technology [14].

To obtain long-term performance of the silicon-based microelectrode in the aggressive body environment, passivation layers have to be applied before deposition of other layers. Two kind of layers were applied on the silicon wafer as the passivation layer. The wafer was thermally oxidized at 900°C over night to grow the first passivation layer of SiO_2. The layer was built to be ~ 1500 Å. SiO_2 films do not provide effective passivation for an aqueous or humid environment, since the silicon dioxide hydrates, forming a conductive hydrogel [17]. As such additional Al_2O_3 layer is needed to provide extra passivation. An electron-beam gun was used to deposit Al_2O_3 on the SiO_2 passivation layer.

Photolithography technology was used to pattern platinum and silver. After the cleaning of silicon wafer, photoresistor (AZ524) was span over the wafer. Two stages were utilized to pattern different metals (Pt and Ag) on the Si wafer by using different masks for Pt or Ag, respectively. Electron beam evaporation was used to deposit the metal (Pt and Ag) on the wafer. The mask designed for platinum was used first. Before the application of platinum, a 1500 Å Ti layer is applied on the passivation layers as an intermediary adhesive layer first to increase the adhesion between the deposited metals (Pt and Ag) which do not form oxide layers easily, and oxide passivation layers [14]. The electrode geometry was patterned using the 'image reverse lift-off' technique. Compared to the standard 'lift-off' technology, 'image reverse lift-off' gives a sharper edge of the patterned metal. During subsequent procedure of 'image reverse lift-off' technology, a platinum layer of 1500 Å corresponding to the working and the counter electrode geometry was obtained on the Si wafer. An additional stage was introduced to pattern the silver layer, which works as the reference electrode. 'Mask alignment' was followed to adjust the position of silver deposition. The same series of technologies, such as Ti deposition, photolithography, metal evaporation and lift-off etc. were utilized to prepare a silver layer of 1 μm thickness. In order to obtain an Ag/AgCl reference electrode, the wafer was placed in a 25 mM $FeCl_3$ solution to obtain the partial chloridation of the silver.

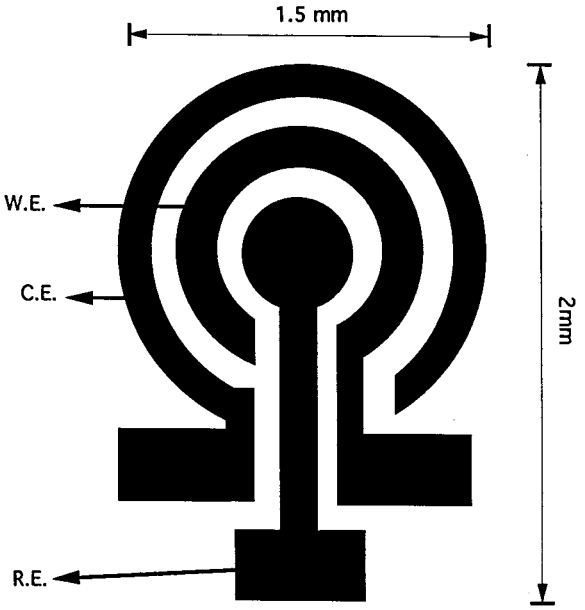

Fig. 1. Schematic of a designed microsensor system with working electrode (WE), reference electrode (RE) and counter electrode (CE).

After the microelectrode pattern by photolithography, individual electrodes were diced from the wafer by diamond dicing saw. Thereafter, the individual transducer chips will be bound to the electrical wires on the electrical board by using a binding machine. To work in the humidity and hostile environment of body, the microelectrodes were encapsulated in an araldite-type epoxy. Only the active area was left open.

3.3. Enzyme entrapment in sol–gel matrix

The sol was prepared using a two step acid-base catalyzed procedure [25]. Stock solution was prepared by reacting tetraethylorthosilicate (TEOS, from Kodak, Rochester, NY) with ethanol, H_2O, and HCl in a molar ratio of 1.0: 3.8: 2.0: $5.3 \times$

10^{-5} at 60°C for 90 min. Then, 10% (volume percent) of additional $NH_3.H_2O$ (0.125 N) and variable amounts of glucose oxidase were added to the stock solution. The sols containing glucose oxidase were placed in an ultrasonic bath for 1 min to help the dispersion of the enzyme, and aged at room temperature for 30 min. Then the sols were coated on the microsensor using dip-coating techniques and allowed to dry in air for 2 h before testing. The porous structure of the enzyme doped sol–gel membrane was investigated by adsorption experiments at 0°C using CO_2 volume matrix adsorption micromeritics ASAP 2010 (Norcross, GA) to investigate the average pore size of the enzyme containing matrix (5Å). The enzyme sol–gel membranes were prepared by casting the sols containing enzyme into the petri-dishes allowing it to dry in air.

3.4. Nafion® coating

After the microsensor was coated with enzyme entrapped in the sol–gel matrix, it was placed in 0.1M KCl to reach equilibrium with the electrolyte over night. Then 0.5% (w/v) solution of Nafion® in a 2-propanol and water (1:1) mixture was applied as the barrier layer to prevent the sensor from the interference species.

4. Results and discussion

4.1. Calibration test of the microsensor

The calibration tests of the microsensors (the dependence of the steady-state amperometric response on the concentration of glucose in the cell) were studied (calibration curves are not showing in the text). Two main characteristics of calibration curves are firstly, their extended range of linearity (the upper limit of the glucose concentration range over which the sensor response is linearly proportional to glucose concentration) and secondly, sensor sensitivity which is the slope of the linear part of the calibration curve.

Due to the reduced size of microsensors, the enzyme loading amount is important in obtaining sufficient signal values. Scanning electron microscopy (SEM) was used to test the thickness of the enzyme containing sol–gel matrix. The mean thickness of the sol–gel layer containing glucose oxidase is 2 μm, and average pore size is 5 Å. Fig. 2 shows the performance of microsensors with different enzyme loading. It can be seen from Fig. 2 that the signal sensitivity is increasing with increasing enzyme loading amount, and reaches a saturation at 3 mg GOD ml^{-1} sol–gel solution. At loading higher than this, the microsensor performance is controlled by the glucose diffusion through the enzyme layer. This fact is also evidenced by the dependence of the value of the saturated sensor response on the concentration of the enzyme in the coating solution which determines the enzyme loading (Fig. 2). When the enzyme loading increases, the signal sensitivity and the saturated signal increase also. They reached their saturated value after increasing the enzyme loading to a certain amount (2–3 mg GOD ml^{-1} sol–gel solution).

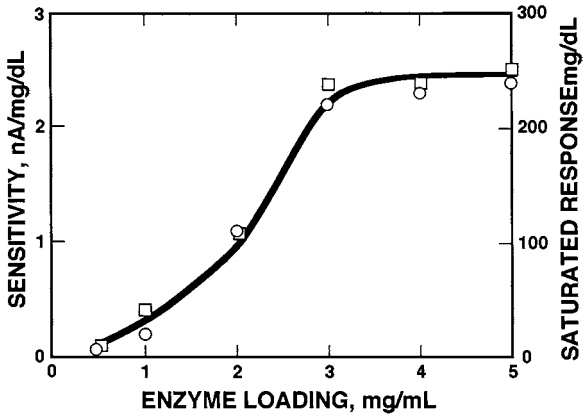

Fig. 2. Dependence of microsensor sensitivity (curve 1) and the value of the saturated sensor response (curve 2) on the concentration of the enzyme loading in the sol–gel layer.

An enzyme layer prepared from 3 mg GOD ml^{-1} sol–gel solution was used in the experiments for sensor evaluation.

4.2. Reproducibility test of microfabricated sensors

Twelve microsensors made from the same silicon wafer with exactly the same fabrication proce-

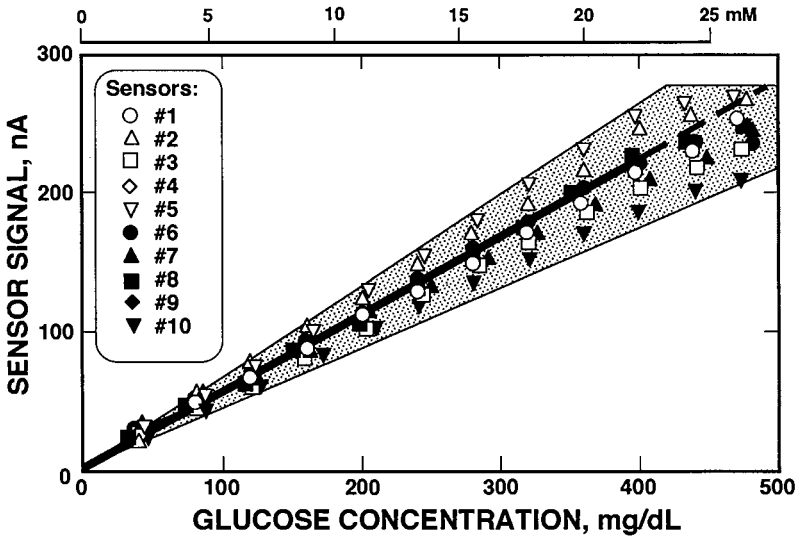

Fig. 3. Calibration performance of ten microsensors fabricated identically.

dures, including dicing, binding, epoxy encapsulation, enzyme layer coating and Nafion® interference layer coating were studied to test the production reproducibility. These twelve microsensors were coated at the same time by enzyme sol–gel solution and 0.5% Nafion® solution to obtain exactly the same coating.

Two of the 12 microsensors showed zero background current and no response to glucose. That was found to be due to loss of contact in the fine binding wire during the binding process.

The calibration performance of the other ten microsensors can be seen in Fig. 3. It is illustrated clearly from Fig. 3 that the ten microsensors showed highly reproducible response characteristics. The upper limit of the linear range is up to 500 mg dl^{-1} for all the sensors and the mean sensitivity is 0.54 ± 0.14 nA mg^{-1} dl^{-1} ($n = 10$).

4.3. Reproducibility of sensor response

A reproducibility test of the microsensor response in buffer solution was evaluated by continuous operation of the sensor during consecutive alternating of glucose concentration in buffer. After establishing the background current, the concentration of glucose in the cell is increased step-wise with 80 mg dl^{-1} and the sensor response to this concentration change is recorded (Fig. 4). After reaching a steady-state value of the amperometric current, the concentration of glucose in the cell is increased to the next level of 160 mg dl^{-1}. The alternating glucose concentration between these two levels (80 and 160 mg dl^{-1}) is further achieved by replacing the electrolyte in the cell. From the protocol of such an experiment, presented in Fig. 4, it can be seen that the amperometric response to alternating the glucose concentration attains the same signal value magnitude and response time with $\pm 2\%$ error. The sensors monitored the glucose level in the cell for 2 h between concentration changes. Continuous testing for > 5 days was performed; overnight sensors were left operating at the lowest glucose concentrations. There is no observable difference between the response times (estimated as time to reach 95% of the steady-state value of the current signal) for increasing concentration step, and for decreasing concentration step. The sensitivity of the sensor response to the alternation of the glucose concentration increased 6.5% daily. These results show that the sensors are able to respond to the varying glucose concentration in an acceptable time and with reproducible current values, which is important for the potential clinical application of such biosensors.

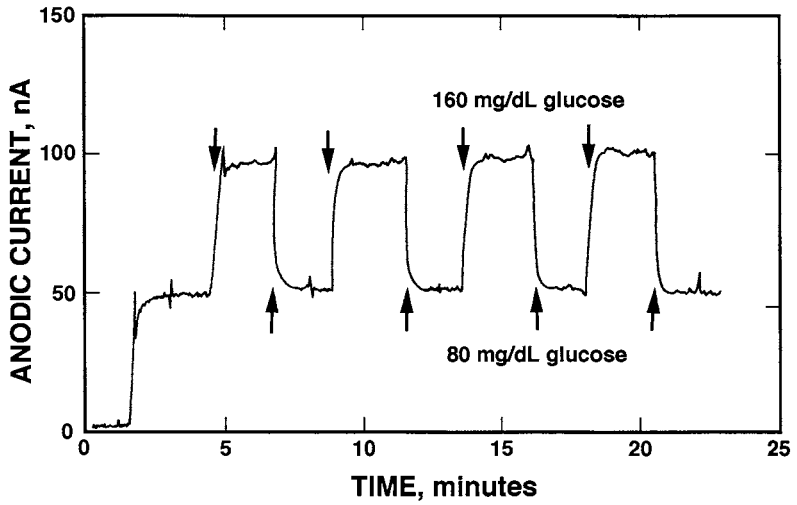

Fig. 4. Reproducibility test protocol of the microsensor: Transients of the amperometric response to glucose concentration alterations for glucose concentration changes between 80 and 160 mg dl^{-1}.

4.4. Interference test

The possible interference effect of several common body chemicals to the sensor has been studied. The experiments consist of monitoring of the microsensor's response to the interferences in the absence of glucose (background interference) and evaluation of the interference effect in the presence of glucose.

Fig. 5. presents protocols of the interference test obtained with the described microsensor. Protocol A corresponds to the experiment when interfering substrates (urea, glycine, ascorbic acid, paracetamol and uric acid) were added to the solution in the absence of glucose. Protocol B corresponds to the test of the interference effects in the presence of glucose, where the same sequence of interfering substrates were added to the solution after establishing the sensor response to 40 mg dl^{-1} of glucose. It can be seen from Fig. 5 that, in both cases, the interferences effect on the measured current is not significant, being $\sim 5\%$ (ascorbic acid: 5.4%; uric acid 4.1%; paracetamol: 3.9%; glycine:1.5%; urea: 1.8%) of the background signal (protocol A) and glucose response current value (Protocol B). The amperometric value of the sensor response to 40 mg dl^{-1} glucose before the addition of the interference substances (Fig. 5, protocol B) is the same as the response value to the same glucose concentration after the addition of interference substrates first (Fig. 5, protocol A).

It can be concluded from these tests that the microsensor can be used in the physiological conditions without the significant interference from the substances presented in body fluids.

5. Conclusion

A microfabricated glucose biosensor based on an amperometric hydrogen peroxide electrode has been developed. A sol–gel layer with 5Å pore size and 2 μm thickness was used as the glucose oxidase entrapping matrix. The miniaturized electrode sensing system is composed of platinum as both working and counter electrodes and silver as the reference electrode. These results demonstrate that the technology for sensor fabrication allows high reproducibility. Use of Nafion® as a protective layer results in diminished interference effects from the substances in body fluids. This sensor can be developed to be used for biomedical applications and can be applied as a disposable sensor.

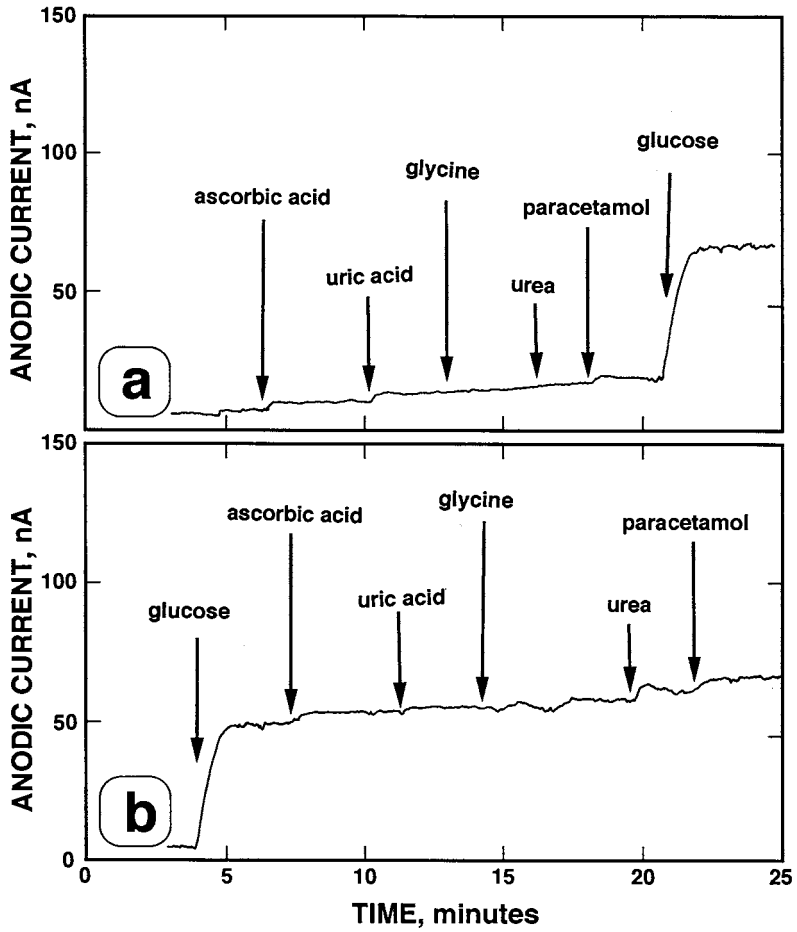

Fig. 5. Interference test protocols of the microsensor to the interferences in the absence of glucose (curve a), and in the presence of glucose (curve b).

References

[1] S.J. Updike, G.P. Hicks, Nature (London) 214 (1967) 986.
[2] P. Vadgama, P.W. Crump, Analyst 117 (1992) 1657–1670.
[3] B.H. Ginsberg, Clin. Chem. 38 (1992) 1596–1600.
[4] U. Fischer, S. Alcock, A.P.F. Turner, Biosens. Bioelectr. 10 (1995) 23–30.
[5] B. Bourrounet, T. Talou, A. Gaset, Sensors and Actuators Part B 27 (1995) 250–254.
[6] E. Marconi, G. Panfili, G. Palleschi, Anal. Lett. 29 (1996) 1125–1137.
[7] S.J. Alcock, A.P.F. Turner, IEEE Engineering In Medicine And Biology, June/July, 1994, 319–325.
[8] P. Connolly, Biosens. Bioelectr. 10 (1995) 1–6.
[9] E. Wilkins, P. Atanasov, Med. Eng. Phys. 18 (1996) 273–288.
[10] U. Fisher, Diabetic Med. 8 (1991) 309–321.
[11] V.V. Cosofret, M. Erdosy, T.A. Johnson, D.A. Bellinger, R.P. Buck, R.B. Ash, M.R. Neuman, Anal. Chim. Acta 314 (1995) 1–11.
[12] R. Hintsche, M. Paeschke, U. Wollenberger, U. Schnakenberg, B. Wagner, T. Lisec, Biosens. Bioelectr. 9 (1994) 697–705.
[13] H.D. Goldberg, R.G. Brown, M.E. Meyerhoff, Sensors and Actuators Part B 21 (1994) 171–183.
[14] M. Koudelka-Hep, F. Rohner-Jeanrenaud, E. Bobbioni-Harsch, J. Terrettaz, N.F. de Rooij, B. Jeanrenaud, Adv. Biosens. 2 (1992) 131–149.
[15] J. Zhou, J. Wu, C. Tian, W. Wu, H. Zhang, D. Lu, G. Zhang, Sensors and Actuators Part B 20 (1994) 17–22.
[16] S. Yang, P. Atanossov, E. Wilkins, J. Clin. Eng. 22 (1997) 55–63.

[17] M. Lambrechts, W. Sansen, Biosensors: Microelectrochemical Devices, Institute of Physics Publishing, IOP, Bristol, 1992, pp. 1–304.
[18] E. Lindner, V.V. Cosofret, R.P. Buck, T.A. Johnson, R.B. Ash, M.R. Neuman, W.J. Kao, J.M. Anderson, Electroanalysis 7 (1995) 864–870.
[19] Y. Murakami, T. Uchida, I. Karube, Electroanalysis 6 (1994) 735–739.
[20] M. Koudelka-Hep, D.J. Strike, N.F. de Rooij, Anal. Chim. Acta 281 (1993) 461–466.
[21] D.J. Strike, N.F. de Rooij, M. Koudelka-Hep, Sensors and Actuators Part B 13–14 (1993) 61–64.
[22] A.D. Clark, M.F. Chaplin, S.A. Roulston, L.J. Dunne, Biosens. Bioelectr. 10 (1995) 237–241.
[23] G. Fortier, J.W. Chen, D. Belanger, ACS Symposium Series, Biosensors and Chemical Sensors: Optimizing Performance through Polymeric Materials, 1992, pp. 22–30.
[24] S. Braun, S. Rappoport, R. Zusman, D. Avnir, M. Ottolenghi, Mater. Lett. 10 (1990) 1–5.
[25] Y. Lu, L. Han, C.J. Brinker, T. Niemczyk, G.P. Lopez, Sensors and Actuators Part B 35 (1996) 1–5.
[26] D.A. Gough, F.L. Anderson, J. Giner, C.K. Colton, J.S. Soeldner, Anal. Chem. 50 (1978) 941–944.
[27] J.P. Lowry, R.D. O'Neill, Anal. Chem. 64 (1992) 456–459.
[28] A. Koshy, E. Zilkha, T.P. Obrenovitch, H.P. Benetto, D.A. Richards, L. Symon, Anal Lett. 26 (1993) 831–849.
[29] C.Y. Chen, M. Gotoh, H. Makino, Y.C. Su, E. Tamiya, I. Karube, Anal. Chim. Acta. 265 (1992) 5–14.
[30] D.A. Gough, J.C. Armour, Diabetes 44 (1995) 1005–1009.
[31] F. Mizutani, S. Yabuki, T. Katsura, Anal. Chim. Acta. 274 (1993) 201–207.
[32] S. Yang, C. Salehi, P. Atanasov, E. Wilkins, Anal. Lett. 29 (1996) 1081–1097.
[33] S. Yang, P. Atanasov, E. Wilkins, Ann. Biomed. Eng. 23 (1995) 833–839.

ELSEVIER

Talanta 47 (1998) 745–752

Talanta

Iodimetric determination of 2-mercaptopyrimidines

Witold Ciesielski *, Robert Zakrzewski, Anna Krenc, Jolanta Zielińska

Department of Instrumental Analysis, University of Łódź, Lindleya 3, 90-131 Łódź, Poland

Received 18 November 1997; received in revised form 12 March 1998; accepted 16 March 1998

Abstract

A new method for the determination of 2-mercaptopyrimidines, using their reaction with iodine in neutral and alkaline medium, is presented. The determinability range in the volumetric titration, in phosphate buffer with starch as an indicator, was found to be equal to 40–1000 μmol for 2-mercaptopyrimidine (I) and 100–2000 μmol for 2-mercapto-4-methylpyrimidine (II), and 200–2000 μmol for 4,6-dimethyl-2-mercaptopyrimidine (III). In the volumetric titration in alkaline medium, with the potentiometric end-point detection, the determinability range is 50–250 μmol for 2-mercapto-4-methylpyrimidine (II), 50–500 μmol for 4,6-dimethyl-2-mercaptopyrimidine (III), 20–250 μmol for 4,5-diamino-2,6-dimercaptopyrimidine (IV), and 20–1000 μmol for 2-thioorotic acid (V). In the coulometric titration, using the biamperometric end-point detection, 0.1–4.0 μmol of 2-mercaptopyrimidine (I) and 0.1–5.0 μmol of 2-thioorotic acid (V) were successfully determined. © 1998 Elsevier Science B.V. All rights reserved.

Keywords: Iodimetric determination; Coulometric titration; Potentiometric titration; 2-Mercaptopyrimidines

1. Introduction

Pyrimidine derivatives have medical and biochemical properties. Compounds containing the 2- and 6-mercaptopyrimidine structure have been used for the treatment of hypothyroidism [1]. Heterocyclic thiols are used in vulcanisation processes [2] and as corrosion inhibitors [3]. 4,5-Diamino-2,6-dimercaptopyrimidine (IV) is used in chemical analysis for the determination of selenium [4]. 4,6-Dimethyl-2-mercapto-pyrimidine (III) [5] and 2-mercapto-4-methylpyrimidine (II) [6] are applied to the preparation of pesticides.

2-Mercaptopyrimidine (I) has been determined previously by titration using cerium [7] and dichromate [8] ions. 2-Mercaptopyrimidine (I) [9], 4,5-diamino-2,6-dimercaptopyrimidine (IV) [9] and 2-thioorotic acid (V) [9,10] were determined by the acid–base potentiometric or thermometric titration. A potentiometric method was used for determination of 2-mercaptopyrimidine (I) based on its oxidation with 1-chlorobenzotriazole [11]. The reaction between 2-mercaptopyrimidine (I) and *p*-diethylaminophenylmercuracetate [12] in an alkaline solution has been applied to the titrimetric determination of 2-mercaptopyrimidine (I) with diphenylcarbazole as an indicator. 2-Thioorotic acid (V) has been determined by mercuric (II) ions [13]. 2-Mercaptopyrimidine (I) has

* Corresponding author. Tel.: +48 42 6355808; fax: +48 42 6783958; e-mail: zai@chemul.uni.lodz.pl

0039-9140/98/$ - see front matter © 1998 Elsevier Science B.V. All rights reserved.
PII S0039-9140(98)00127-1

been determined using chloranil in dimethylsulphoxide as a solvent [14]. This compound reacts with the thiol and gives an equimolar amount of hydrogen chloride, which is titrated by the coulometric method. Spectrophotometric [15], chromatographic [16–18], polarographic [19,20], and voltamperometric [21–25] methods have also been proposed. The determination of 2-mercaptopyrimidines has been also carried out using the induced iodine–azide reaction [26–29].

It is known from the literature that the coulometric titration with iodine in alkaline medium is impossible because of positive errors, occurring due to disproportionation of iodine. In the present paper, the determination of 2-mercaptopyrimidines by direct titration with iodine in neutral and also in alkaline medium has been presented. In neutral medium reaction between 2-mercaptopyrimidines and iodine is based on the apparent stoichiometry:

$$2RSH + I_2 \rightleftharpoons R-S-S-R + 2HI \quad (1)$$

In alkaline medium the stoichiometry is changed:

$$R-S^- + 2I_2 + 4OH^- \rightarrow R-SO_2^- + 4I^- + 2H_2O \quad (2)$$

where:

R= 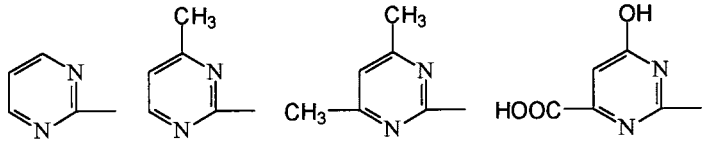

or

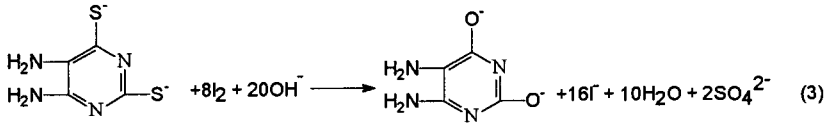

Similar reactions, which were applied to determinations of thiols, have been found in the literature [30–34].

In alkaline medium iodine disproportionates quickly to give iodide and hypoiodite ions, so hypoiodite is the actual oxidizing agent. The titration in alkaline medium is possible if the reaction rate of hypoiodite ions with thiol is higher than the reaction rate of the disproportionation of hypoiodite ions:

$$3IO^- \rightarrow 2I^- + IO_3^- \quad (4)$$

In determinations of larger quantities of 2-mercaptopyrimidines, with the visual or the potentiometric detection of the end-point, volumetric titrations were applied. Lower amounts were determined by the coulometric titration using the biamperometric detection of the end-point.

2. Experimental

2.1. Reagents and apparatus

Twice-distilled water in glass apparatus, potassium iodide, sodium hydroxide, acetic acid, 2-mercaptopyrimidine (I) (Aldrich), 2-mercapto-4-methylpyrimidine (II) (Aldrich), and 4,6-dimethyl-2-mercaptopyrimidine (III) (Aldrich) were employed. 4,5-Diamino-2,6-dimercaptopyrimidine (IV) (Aldrich) was purified by dissolving in 4 mol l^{-1} sodium hydroxide solution and reprecipitating with glacial acetic acid. 2-Thioorotic acid (V) was obtained according to earlier reported methods [35] and purified in the same way as the previous one. Standard solutions were taken by dissolving a weighed amount of the

reagent in water with addition of a similar amount of sodium hydroxide. Working solutions of 2-mercaptopyrimidine (I) or 2-thioorotic acid (V) used in the coulometric titration were obtained by suitable dilution of standard solutions: iodine, standard solutions 0.1, 0.05, 0.02 or 0.01 mol l^{-1}; phosphate buffer, pH 7 or 6; starch solution, 0.5% (m/m).

Titrations were done with an universal coulometric analyser 'Radelkis' (Hungary), type OH-404. The electrolysis cell [36] contained two platinum electrodes with an area of 5 cm^2 each, working in generating circuit, and with a OH-9381 double electrode in an amperometric indicator-circuit with two polarized electrodes. Also, a mechanical stirrer and pH-meter 'Radelkis' (Hungary), type OP-206 with a platinum electrode and a saturated calomel electrode were used.

2.2. Procedures

2.2.1. Volumetric titration with the starch indicator

A sample of 2-mercaptopyrimidine (I) (40–1000 μmol), a sample of 2-mercapto-4-methylpyrimidine (II) (100–2000 μmol) or a sample 4,6-dimethyl-2-mercaptopyrimidine (III) (200–2000 μmol) was dissolved in 50 ml of phosphate buffer (pH 7 or pH 6.0 in the case of 2-mercapto-4-methylpyrimidine (II)) and titrated with iodine to a blue starch end-point.

2.2.2. Potentiometric titration

A sample of 2-mercapto-4-methylpyrimidine (II) (50–250 μmol) or 4,6-dimethyl-2-mercaptopyrimidine (III) (50–500 μmol) was dissolved in 50 ml of 0.5 mol l^{-1} sodium hydroxide, a sample of 4,5-diamino-2,6-dimercaptopyrimidine (IV) (20–250 μmol) was dissolved in 50 ml of 3 mol l^{-1} sodium hydroxide, or a sample of 2-thioorotic acid (V) (20–1000 μmol) was dissolved in 50 ml of 2 mol l^{-1} sodium hydroxide and titrated with iodine, using the potentiometric detection of the end-point with a platinum indicator electrode and a saturated calomel electrode. The equivalence point of the reaction corresponded to the inflection point of the curve.

2.2.3. Coulometric titration

The coulometric titration was carried out in the reaction solution given in Table 3. A sample solution containing the determined compound was introduced into 20 ml of the reaction solution, which was placed in the anode part of the electrolysis cell. The cathode part of the electrolysis cell was filled up with the same solution. The polarization voltage applied to the indicator system electrodes was equal to 200 mV. After starting the mechanical stirrer, stabilized current [37] was passed through the solution. The current applied to the generating circuit (Table 3) depended on the quantity of the determined compound and was adjusted appropriately to maintain the titration time at several minutes. After completing the titration of 2-mercaptopyrimidine (the indicator current [38] was equal to 0.04 μA) the charge Q was noted. In the case of titration in neutral medium, the following samples were introduced into the same solution.

The 2-mercaptopyrimidine (I) content (μmol) in the tested sample was calculated according to Faraday's law:

$$n = \frac{Q}{z \cdot F} \cdot 10^3$$

where Q is charge, which passed through the solution (mC), z is number of electrons transferred in the reaction of 1 mol ($z = 1$), and F is the Faraday constant ($F = 96485$ C mol^{-1}).

In the case of coulometric titration in alkaline medium, each of the following samples was introduced into a fresh reaction solution and electric charge Q_0 was assigned. In order to compute Q_0, a suitable amount of water (instead of the particular compound) was introduced into the reaction solution.

The 2-mercaptopyrimidine contents (μmol) in the tested sample were calculated according to Faraday's law:

$$n = \frac{\Delta Q}{z \cdot F} \cdot 10^3$$

where $\Delta Q = Q - Q_0$ (mC), Q_0 is charge corresponding to blank titration, z is number of electrons transferred in the reaction of 1 mol ($z = 4$), and F is the Faraday constant ($F = 96485$ C mol^{-1}).

Table 1
Results of volumetric titration with starch indicator: $n = 6$; number of electrons transferred in the reaction of 1 mol (z) is 1

Compound	pH	Taken (μmol)	Found (μmol) $\bar{x} \pm t_{0,95} \cdot (s/\sqrt{n})$	Relative standard deviation, s_r
2-Mercaptopyrimidine (I)	7.0	42.00	42.1 ± 0.4	0.0086
		105.0	104.8 ± 0.3	0.0024
		496.0	495 ± 2	0.0037
		920.0	919 ± 3	0.0029
2-Mercapto-4-methylpyrimidine (II)	6.0	100.0	100.8 ± 0.1	0.0010
		200.0	200.8 ± 0.4	0.0020
		350.0	349 ± 1	0.0028
		1000.0	999 ± 4	0.0042
		2000.0	1991 ± 8	0.0038
4,6-Dimethyl-2-mercaptopyrimidine (III)	7.0	200.0	200.7 ± 0.4	0.0018
		350.0	352.5 ± 0.8	0.0022
		1000.0	1005 ± 3	0.0026
		2000.0	2008 ± 6	0.0030

3. Result and discussion

The results of iodimetric determination of 2-mercaptopyrimidine and its derivatives are presented in Tables 1–3. It has been shown that thiols, which react with iodine in neutral medium, can be successfully determined in alkaline media. Some thiols (2-thiobarbituric acid [33], 4,5-diamino-2,6-dimercaptopyrimidine (IV), 2-thioorotic acid (V)), which cannot be determined by the titration with iodine in neutral or light acid medium due to too low reaction rate, can be titrated in alkaline medium with high accuracy and precision. Potentiometric titration curves of 2-thioorotic acid (V) (as an example) are shown in Fig. 1. The course of reaction (2) between 2-mercaptopyrimidines and iodine depends on the concentrations of sodium hydroxide. It was found experimentally that the reaction rate of 2-mercaptopyrimidines with iodine increases with an increase in concentration of sodium hydroxide.

3.1. Volumetric titration

The optimum range of pH is 6.5–7.0 in the case of visual titration of 2-mercaptopyrimidine (I) with the starch indicator. The main direct reaction of iodine is observed with 2-mercapto-4-methylpyrimidine (II) at pH 2.0–6.5. A pH, within the range of 2.0–8.0, was found to be the most favourable for the reaction of iodine with 4,6-dimethyl-2-mercaptopyrimidine (III). Then the number of electrons transferred in the reaction of 1 mol was exactly 1. In the lower pH reaction (1) did not proceed stoichiometrically and the number of electrons transferred in the reaction of 1 mol was less than 1. An increase in pH of the reaction solution beyond the range given previously increases the number of electrons transferred in the reaction of 1 mol. A potentiometric detection of the end-point can be applied to titration with iodine in the neutral or acid medium and a sharp potentiometric end-point occurs in these media. But it is easier to employ the visual end-point. Comparing the iodimetric titration with the visual and the potentiometric detection of the end-point it may be concluded that the results are comparable.

The substitution of an amino group in the 2-mercaptopyrimidine ring increases the range of pH within which the tested compound reacts with iodine stoichiometrically according to Eq. (1). Iodimetric determination was applied to 2-thiocytosine [34]. The optimum range of pH is 6.5–8.0. The large value of pK_B (proton gained by the neutral molecule) of 2-thiocytosine (3.3) in comparison with pK_B of 2-mercaptopyrimidine (I) (1.35) confirms that the amino group activates the ring therefore it is easier to oxidise 2-thiocytosine than 2-mercaptopyrimidine (I).

The introduction of methyl groups into 2-mercaptopyrimidine (I) increases the range of pH within which the number of electrons transferred in

Table 2
Results of potentiometric titration in an alkaline medium: $n = 6$

Compound	Number of electrons transferred in the reaction of 1 mol (z)	Range of concentration of sodium hydroxide (mol l^{-1})	Taken (μmol)	Found (μmol) $\bar{x} \pm t_{0,95} \cdot (s/\sqrt{n})$	Relative standard deviation, s_r
2-Mercapto-4-methylpyrimidine (II)	4	0.4–0.6	50.00	49.7 ± 0.2	0.003
			125.0	124.4 ± 0.2	0.002
			250.0	248.6 ± 0.9	0.003
4,6-Dimethyl-2-mercaptopyrimidine (III)	4	0.4–0.6	50.00	50.06 ± 0.06	0.011
			100.0	100.7 ± 0.7	0.0027
			250.0	251.7 ± 0.7	0.0025
			500.0	504 ± 2	0.0040
2-Thioorotic acid (V)	4	1.5–2.5	20.00	20.01 ± 0.05	0.0023
			50.00	50 ± 0.2	0.0029
			100.0	99.3 ± 0.2	0.0021
			250.0	250 ± 1	0.0039
			500.0	500 ± 3	0.0050
			1000	995 ± 2	0.0022
5,6-Diamino-2,4-dimercaptopyrimidine (IV)	16	2.5–3.5	20.0	20.00 ± 0.03	0.0014
			60.0	60 ± 0.1	0.0020
			117.0	116.5 ± 0.3	0.0021
			250.0	248.1 ± 0.3	0.0012

the reaction of 1 mol (z) is exactly equal to 1. Methyl groups activate the ring as shown by higher pK_B values of 2-mercapto-4-methylpyrimidine (II) and 4,6-dimethyl-2-mercaptopyridine (III) (2.2 and 2.80, respectively) in comparison with 2-mercaptopyrimidine (I) (1.35). The basicity increases proportionally to the number of methyl groups in the molecule, increasing the range of pH within $z = 1$. The introduction of methyl groups into the 2-mercaptopyrimidine molecule increases the range of pH in the following order: 2-mercaptopyrimidine (I) < 2-mercapto-4-methylpyrimidine (II) < 4,6-dimethyl-2-mercaptopyrimidine (III).

3.2. Potentiometric titration in an alkaline medium

Good results in the potentiometric titration were achieved when the concentration of NaOH was varied within the range given in Table 2. Then, the number of electrons transferred in the reaction of 1 mol was exactly 4 or 16 (in the titration of 4,5-diamino-2,6-dimercaptopyrimidine (IV)). At the lower concentration of NaOH, reaction (2) did not proceed stoichiometrically and the number of electrons transferred in the reaction of 1 mol was less than 4 or 16 (in the case of 4,5-diamino-2,6-dimercaptopyrimidine (IV)). An increase in concentration of NaOH, over the range given in Table 2, caused an increase of the number of electrons transferred in the reaction of 1 mol because the product of reaction (2) reacted with iodine. Then the following reaction partially proceeds according to the equation:

$$R - SO_2^- + 2I_2 + 6OH^- \rightarrow R - O^- + 4I^- + SO_4^{2-} + 3H_2O \quad (5)$$

In case of the titration of 4,5-diamino-2,6-dimercaptopyrimidine (IV), o-amino group is oxidized in the next stage of the reaction with iodine [39] if the concentration of sodium hydroxide is higher than 4 mol l^{-1}.

Titrations of 2-mercaptopyrimidine (I) were carried out at different concentrations of sodium hydroxide, and the titration curves which were obtained are shown in Fig. 2. The shape of poten-

Table 3
Results of coulometric titration: $n = 6$

Compound	Number of electrons transferred in the reaction of 1 mol (z)	Reaction solution	Taken (μmol)	Found $\bar{x} \pm t_{0.95} \cdot \frac{s}{\sqrt{n}}$ (μmol)	Relative standard deviation, s_r	Current (μA)
2-Mercapto-pyrimidine (I)	1	$c(\mathrm{KI}) = 0.01$ mol l^{-1}, pH 7.0	4.000	3.99 ± 0.02	0.003	2.0
			2.000	1.998 ± 0.008	0.004	1.0
			1.000	1.004 ± 0.003	0.003	0.5
			0.4000	0.401 ± 0.002	0.005	0.2
			0.1000	0.101 ± 0.001	0.010	0.1
	4	$c(\mathrm{KI}) = 1$ mol l^{-1}; $c(\mathrm{NaOH}) = 0.5$ mol l^{-1}	4.000	3.98 ± 0.03	0.003	4.0
			2.000	1.996 ± 0.005	0.001	4.0
			1.000	1.00 ± 0.01	0.005	2.0
			0.4000	0.401 ± 0.007	0.007	1.0
			0.1000	0.102 ± 0.003	0.010	0.5
2-Thioorotic acid (V)	4	$c(\mathrm{KI}) = 1$ mol l^{-1}; $c(\mathrm{NaOH}) = 0.1$ mol l^{-1}	5.000	4.957 ± 0.001	0.0002	5.0
			2.500	2.489 ± 0.006	0.0025	5.0
			1.000	1.000 ± 0.001	0.0011	2.0
			0.5000	0.503 ± 0.001	0.0023	1.0
			0.2000	0.2017 ± 0.0001	0.0005	0.5
			0.1000	0.1014 ± 0.0001	0.001	0.5

tiometric titration curve is noteworthy (curves b and c). An introduction of iodine (oxidizer) results in a strong potential drop in the curve. The end-point of the titration corresponding to the inflection point of the curve and the shape of curve strongly depended on concentration of sodium hydroxide. Such a phenomenon also occurred during the titration of 4,6-dimethyl-2-mercaptopyrimidine (III) and 2-mercapto-4-methylpyrimidine (II). Similar curves were obtained in the titration of thiopental [33] and 2-thiocytosine [34]. The shape of the titration curves obtained at high sodium hydroxide concentration is associated to the electrochemical response of the indicator electrode to the redox couple present in the solution before and after the end-point.

2-Mercaptopyrimidines, which have amino [34] or hydroxide groups [33] in the 2-mercaptopyrimidine ring, demand greater concentration of sodium hydroxide in the titration with iodine in alkaline medium. Methyl groups do not have such influence.

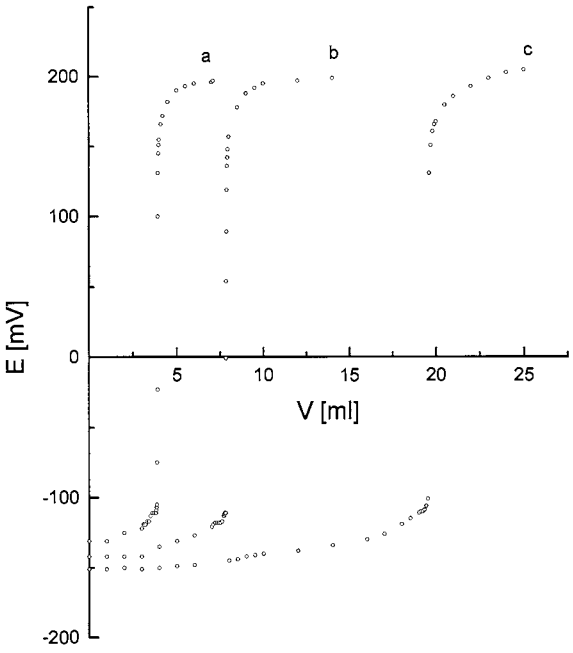

Fig. 1. Curves of potentiometric titration of 2-thioorotic acid in 2 mol l^{-1} NaOH with 0.05 mol l^{-1} iodine solution: (a) 50, (b) 100 and (c) 250 μmol.

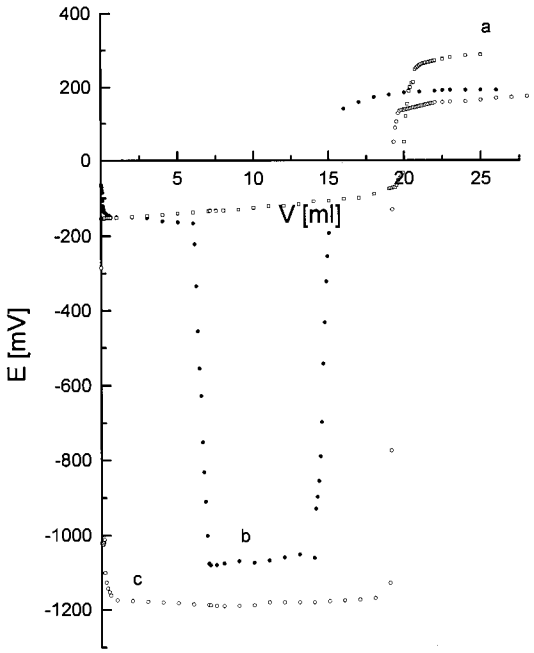

Fig. 2. Curves of potentiometric titration of 2-mercaptopyrimidine in alkaline medium with 0.05 mol l^{-1} iodine solution: (a) 250 μmol compound in 0.5 mol l^{-1} sodium hydroxide solution; (b) 125 μmol compound in 2 mol l^{-1} sodium hydroxide solution; (c) 125 μmol compound in 10 mol l^{-1} sodium hydroxide solution.

3.3. Coulometric titration

The potentiometric end-point detection in coulometric titration of lower amounts of 2-mercaptopyrimidines is not possible. The use of the biamperometric indicator system makes it possible to obtain correct results in the coulometric determination of 2-mercaptopyrimidine (I) and 2-thioorotic acid (V). The results are given in Table 3.

The reaction proceeding according to Eq. (1) is reversible [40]. An increase in the concentration of potassium iodide results in a shift of the reaction equilibrium towards parent compounds. Therefore, the coulometric titration in a neutral medium was carried out at low concentration of iodide ion solution (0.01 mol l^{-1}) to avoid this shifting of the reaction equilibrium. Studies, which were carried out by us, showed that the electric charge which was necessary to achieve the end-point of titration was lower by about 1% in

solution of 0.1 mol l^{-1} potassium iodide compared with the solution of 0.01 mol l^{-1} potassium iodide (in the 0.1 mol l^{-1} potassium iodide solution the end-point corresponding to detection of free iodine by the indicator system occurred before the equivalence point).

A high concentration of potassium iodide was used in the coulometric titration in an alkaline medium in order to obtain 100% current efficiency [32]. Moreover, such a solution is stable. Process of oxidation of iodide ions occurs only in the acidic solution and is not observed in an alkaline one.

4. Conclusions

Comparing the iodimetric determination of 2-mercaptopyrimidines with the methods previously reported [7–29], one may conclude that this method is characterised by a short analysis time, a high precision and accuracy, a simple procedure, commonly available reagents and the possibility of the determination over a wide order of magnitude. The coulometric method is partly automated and as an absolute one requires no use of standard solutions.

References

[1] D.T. Hurst, The Chemistry and Biochemistry of Pyrimidines, Purines and Pteridines, Wiley, New York, 1980.
[2] S.N. Korchemkin, V.M. Kharchevnikov, V.N. Krasovskii, E.N. Polivoda, Kauch. Rezina 6 (1979) 9; C. A. 91 (1979) 124662r.
[3] F. Zucchi, G. Trabanelli, G. Brunoro, C. Monticelli, G. Rocchini, Werkst. Korros. 44 (1993) 264; C. A. 119 (1993) 185696y.
[4] A. Izquierdo, M.D. Prat, L. Aragones, Analyst 106 (1981) 720.
[5] E. Baumann, J. Rheinheimer, U.J. Vogelbacher, M. Gerber, W. Rademacher, H. Walter, K.O. Westphalen, Ger. Offen. DE 4,335,950 (Cl. C07D239/46), 27 April 1995, Appl. 21 October 1993, 26 pp.; C. A., 123 (1995) P83384k.
[6] S. Fitzjohn, M.P. Robinson, M.D. Turnbull, PCT Int. Appl. WO 94 06,777 (Cl. CO7D239/38), 31 March 1994, GB Appl. 92/19,635, 16 September 1992, 78 pp.; C. A., 121 (1994) P157663h.
[7] M. Kucharski, H. Sikorska-Tomicka, T. Szumiło, Zeszyty Nauk. Politech. Białostockiej 7 (1981) 81.
[8] M. Kucharski, Zeszyty Nauk. Politech. Białostockiej 9 (1985) 125.
[9] E. Bosch, J. Guiteras, A. Izquierdo, M.D. Prat, Mikrochim. Acta II (1985) 339.
[10] A. Veveris, U. Mikstais, I. Jurgevica, Latv. PSR Zinat. Akad. Vestis Khim. Ser. 4 (1977) 498.
[11] Ch. Channegowda, S.M. Mayanna, Mikrochim. Acta III (1990) 271.
[12] I.U. Lipsbergs, V.Ya. Zaharans, Zh. Anal. Khim. 39 (1984) 1874.
[13] M. Shrivastava, G.S. Pandey, Indian J. Technol. 22 (1984) 115.
[14] S.I. Obtemperanskaya, M.M. Idilbi, N.V. Zhmurova, V.L. Antonovskii, Vestn. Mosk. Univ. Ser. 2 Khim 22 (1981) 414.
[15] R. Andrisano, G. Modena, Boll. Sci. Fac. Chim. Ind. Bologna 9 (1951) 100.
[16] P.R. Brandy, R.M. Hoskinson, J. Chromatogr. 54 (1971) 65.
[17] F. Baykut, O. Imregun, Istanbul Univ. Fen. Fak. Mecm. Ser. C 32 (1967) 131.
[18] K. Fink, R.E. Cline, R.M. Fink, Anal. Chem. 35 (1963) 389.
[19] A. Izquierdo, E. Bosch, M.D. Prat, Electrochim. Acta 27 (1982) 1465.
[20] J. Rodriguez, L. Calvo, C. Marin, A. Sanchez, Anal. Lett. 22 (1989) 2145.
[21] F. Lopez, M. Juan, P. Sanz Pedrero, C. Gonzalez Posa, J. Chim. Phys. Phys.-Chim. Biol. 77 (1980) 825.
[22] B. Lynch, M.R. Smyth, Anal. Chem. Symp. Ser. 25 (1986) 97.
[23] T.M. Florence, J. Electroanal. Chem. Interfac. Electrochem. 97 (1979) 219.
[24] J.T. Stock, R.E. Larson, Anal. Chim. Acta 138 (1982) 371.
[25] A. Fernandez, M. Jose, M.R. Smyth, Analyst 114 (1989) 1603.
[26] J. Kurzawa, Chem. Anal. (Warsaw) 32 (1987) 875.
[27] J. Kurzawa, Chem. Anal. (Warsaw) 33 (1988) 771.
[28] J. Kurzawa, Anal. Chim. Acta 173 (1985) 343.
[29] J. Kurzawa, Chem. Inz. Chem. 16 (1986) 41.
[30] J. Blażek, J. Kacmar, Z. Stejskel, Cesk. Farm. 6 (1957) 441.
[31] F. Jancik, B. Budesinsky, O. Cinkova, Cesk. Farm. 6 (1957) 108.
[32] W. Ciesielski, Chem. Anal. (Warsaw) 36 (1991) 555.
[33] W. Ciesielski, J. Kowalska, R. Zakrzewski, Talanta 42 (1995) 733.
[34] W. Ciesielski, R. Zakrzewski, Chem. Anal. (Warsaw) 41 (1996) 399.
[35] B.A. Ivin, A.I. D'yachkov, G.V. Rutkovskii, E.G. Sochilin, Zh. Org. Khim. 12 (1976) 1836.
[36] W. Jędrzejewski, W. Ciesielski, Chem. Anal. (Warsaw) 23 (1978) 781.
[37] K. Abresch, I. Claassen, Coulometric Analysis, Chapman & Hall, London, 1965, p. 29.
[38] C.L. Wilson, D.W. Wilson, Comprehensive Analytical Chemistry, Elsevier, Amsterdam, 1975, p. 416.
[39] R.M. Blanco, J. Palomas, Quim. Anal. 31 (1977) 97.
[40] J. Kurzawa, K. Janowicz, Acta Chim. Hung. 125 (1988) 147.

ELSEVIER

Talanta 47 (1998) 753–767

Talanta

Searching for heavy metals grouping roadside soils as a function of motorized traffic influence

A. Carlosena *, J.M. Andrade, D. Prada

Department of Analytical Chemistry, University of La Coruña, Campus A Zapateira s/n, E-15071 La Coruña, Spain

Received 18 December 1997; received in revised form 13 February 1998; accepted 16 March 1998

Abstract

Ninety two soil samples were collected in four sampling seasons in La Coruña, NW of Spain, and its surroundings to study the impact of vehicular traffic onto the metallic content of roadside soils in a medium-size city. Samples exhibited different levels of exposure and, therefore, sample groups should arise as a function of this anthropogenic impact. Surprisingly, this was not so when all the nine metals initially considered were subjected to multivariate analyses. Then, different unsupervised multivariate statistical techniques were used to discover those elements able to group the samples according to the level of road traffic. Such an objective was achieved only after removing the natural variability. Accordingly, Pb, Cd, Cu and Zn were found to satisfactorily conduct to this end, Pb being the most discriminant one. © 1998 Elsevier Science B.V. All rights reserved.

Keywords: Roadside soils; Heavy metals; Traffic intensity; PCA; Cluster analysis

1. Introduction

The concentration of heavy metals and toxic elements in roadside soils can provide valuable information about pollution levels in urban and industrial areas, since, in most cases, such concentrations reflect the extent of the emissions of these elements from anthropogenic sources [1,2]. Lead, in particular, is an ubiquitous environmental pollutant and its presence in soils has been extensively studied and attributed to the use of alkyl-lead compounds as antiknock additives in petrol [3,4]. However, in recent years, a number of publications have dealt with the pollution of the roadside environment with other elements, also. Metals, such as Cu, Fe, Cr and Zn, are essential components of many alloys, pipes, wires and tyres [5]. Lagerwerft and Specht [6] attributed Ni to gasoline, and Cd and Zn both to tires and motor oil. Mn, like Pb, is used as a vehicle fuel additive [7]. These elements are released into the roadside environment as a result of combustion, mechanical abrasion and normal wear and tear.

The toxic effects of heavy metals are well documented [8,9]. Heavy metals can be ingested directly by humans and animals through the inhalation of soil dust or they may enter the food chain as a result of their uptake by edible plants. Some studies have shown that a potentially sig-

* Corresponding author. Tel.: +34 981 167000; fax: +34 981 167065; e-mail: alatzne@udc.es

0039-9140/98/$ - see front matter © 1998 Elsevier Science B.V. All rights reserved.
PII S0039-9140(98)00117-9

nificant source of lead intake are children's playgrounds in urban communities, because of hand to mouth contact which is typical for children aged 1–3 years [10].

The total content of heavy metals in soils may be derived from two origins: natural and anthropogenic. Therefore, it is not easy to decide a priori which of these two contributions will 'decide' the main distribution patterns of the samples (i.e. groups caused by the different parent material of the soils, proximity to highways etc.). Accordingly, the detection of contamination patterns in an environmental study with multivariate, multiple-sample data involves both searching for groups of samples and determining which variables are producing such groups. In fact, it can occur that some variables would be mostly related to the natural origin and others to the anthropogenic one.

Finally, it is important to note that due to the complex soil matrices, it could happen that anthropogenic impacts could be masked by natural trends. In that case, it is of interest to use statistical methods to isolate only those effects which we are interested in.

These problems have to be addressed by using multivariate statistical procedures, typical for 'chemometrics'. Even though multivariate studies are broadly used in water, air or sediment studies [11,12] it is the authors' opinion that fewer applications have been made in studies of soils. One reason may be the inherent difficulty encountered in the interpretation of soil data.

Nevertheless, some interesting examples can be found in the literature (e.g. [13–15]). The issue of which variables should be considered when planning future monitoring in soils was recently addressed using Procrustes rotation [16]. In that case, a minimum set of variables (Pb and Co) was selected to describe the sample distribution with a minimum loss of information. The mathematical algorithms of Procrustes rotation aim to select redundant variables in raw data, which is equivalent to the identification of k variables which convey the main structure of the raw data. Each variable is deleted in turn from the data set and two subspaces are compared by rotation, translation and stretching. The variable giving the lower total residual can be discarded and the process is repeated until k variables remain (k is the optimum number of principal components). More details can be found elsewhere [16].

The first objective of the present work was to elucidate if the samples became grouped as a function of the natural origin or anthropogenic contribution. This work focused on the motorized vehicular traffic as the unique anthropogenic metallic source. Following, it was ascertained which metals defined each pattern. After the metals contributing to the anthropogenic influence were identified, the second objective was to determine if the new sample groups can be justified by the different traffic intensities (omitting the 'natural metals').

It has to be stressed that all the multivariate studies applied here are of the unsupervised type. This means that the information regarding the traffic density supported by each sample is only used to interpret the results achieved after each treatment. Supervised methods could be also applied as it was well pointed out by one referee. Such approximations would use methods as SIMCA, potential curves, discrimination analysis, etc. However, this work was focused on elucidating whether the groups obtained considering only the heavy metals attributed to vehicle emissions accurately reflect the traffic density supported by each sample. Therefore, it was preferred not to use the information regarding the traffic up to the interpretation stage of the multivariate analyses.

2. Sampling and analytical variables

The studied area comprises a highway, a medium-size city (La Coruña, 300000 inhabitants), an industrial area, and a main avenue. Sampling points were selected to reflect spatial variability (presumably, different parent soils) and traffic influence associated to each zone:

(a) along a highway (medium–high traffic intensity, ca. 20000 vehicles per day (vpd)),

(b) plots with uncultivated and cultivated soils along several perpendicular transects along the highway, where different distances—15–100 m—were considered (same number of vpd as the highway).

(c) In parks and gardens of the city (huge variability, from low-negligible traffic intensity to medium–moderate—5000–15000–vpd and high traffic levels—40000–60000 vpd).
(d) Along a pretty busy roadway (high intensity, ca. 80000 vpd).

Ninety two sampling points were established for each of the four sampling seasons (1st, fall; 2nd, winter; 3rd, spring; 4th, summer) made during one year. Soil samples were taken from 0 to 5 cm depth, air-dried, ground, and sieved through a 2 mm mesh sieve. After that, samples were dried at 60°C for 48 h and sieved to <0.2 mm. The fraction <2 mm was used to determine moisture content (at 105°C), pH (1:2.5 in water), and organic matter as loss on ignition (LOI) at 450°C for 6 h [17].

Aliquots (0.3 g) of <0.2 mm soil fractions were subjected to chemical extraction using concentrated HNO_3, and microwave-heated in PTFE (polytetrafluorethylene) vessels [18]. This digestion method was proved to extract potentially bioavailable metallic fractions instead of total quantities of native metals from soils [19,20]. This metallic fraction is considered as an useful parameter for characterizing the level of soil contamination.

Following Davies' ideas [21], the control scheme of the analytical procedure also involved analyzing by triplicate at least a 20% of the total number of samples (such subset was randomly selected). As the precision values were always satisfactory ($<10\%$ RSD), it seemed unnecessary to make replicate analyses for all the samples. In this way, the huge workload and high economical costs associated to the replication of 92 samples times four sampling seasons, are avoided without losses of precision. Additionally, sample throughput is quite improved.

Twelve variables were analyzed in each of the 92 samples. These were Cd, Co, Cu, Cr, Fe, Mn, Ni, Pb and Zn, moisture, pH, and LOI. Metals were analyzed using flame and/or graphite furnace atomic absorption spectrometry whenever concentrations were low. Accuracy was checked using certified reference materials (BCR, CRM141, calcareous loam soil; BCR, CRM277, estuarine sediment). The recovery obtained, expressed as obtained value/certified value, ranging between 86 and 108% for all metals, excepting for Cr where 73% was achieved.

3. Results and discussion

3.1. Principal component analysis (PCA)

PCA tries to reduce the original multidimensional space to a new one in which lower dimensions (principal components, PCs) are calculated to explain relationships and associations among variables. The new PC-space will account for sample distribution, as well.

Data analyses presented below were made on autoscaled data, after correcting outliers using the multivariate criteria from Stapanian et al. [22]. The multivariate analyses were made using both SCOUT (a program developed for the US-EPA, [22]) and MATLAB® built-in algorithms. The first approach was performed considering all twelve variables in each of the four sampling seasons in order to avoid the confounding effects of the different climatological conditions during the year.

Table 1 lists the loadings for the first two PCs in each sampling season. The PC1 explains about 35–40% of the initial variance and it is strongly related to Fe and Co, and, to a lesser extent to Zn. We have considered this factor as describing a natural pattern distribution. This same opinion is supported also by, e.g. Smith [13] and Hamilton [14] for whom Fe and Co are generally highly inter-related and linked to a geological origin.

The PC2 comprises about 20–22% of the variance and it is defined by Cd, Cu, Cr, Pb and Ni along the four sampling seasons. Those metals reveal the influence of the motor vehicles over roadside soils [3,5]. The PC3 (not shown here) explains about 11% of the information and although it is related to 'natural' variables (pH, moisture, Mn) it has no constant effect in the four sampling seasons.

Comparing the first two PCs, it can be deduced that the lithologic effect is more important for analyzing sample distribution than the anthropogenic one. Such influence was also identified by Macías et al. [23].

Table 1
PC1 and PC2 loadings, all sampling seasons

Variable	1st		2nd		3rd		4th	
	PC1	PC2	PC1	PC2	PC1	PC2	PC1	PC2
Cd	0.33	−0.33	0.38	−0.26	0.31	−0.36	0.35	−0.29
Co	−0.41	−0.28	−0.37	−0.35	−0.41	−0.22	−0.38	−0.30
Cu	0.31	−0.34	0.34	−0.32	0.24	−0.32	0.30	−0.30
Cr	−0.31	−0.39	−0.27	−0.43	−0.30	−0.43	−0.24	−0.47
Fe	−0.42	−0.15	−0.41	−0.27	−0.42	−0.14	−0.40	−0.19
Mn	−0.19	0.03	−0.22	−0.13	−0.22	0.01	−0.28	−0.05
Ni	−0.26	−0.35	−0.09	−0.42	−0.25	−0.43	−0.22	−0.44
Pb	0.28	−0.40	0.33	−0.35	0.25	−0.43	0.30	−0.32
Zn	0.35	−0.27	0.38	−0.27	0.32	−0.35	0.35	−0.25
Moisture	0.20	0.31	−0.19	−0.18	−0.22	−0.09	−0.06	0.18
LOI	−0.12	0.20	−0.08	0.02	−0.08	0.11	−0.00	0.25
pH	0.01	−0.20	0.13	−0.17	0.29	0.05	0.29	−0.10
% Variance	35.0	22.1	34.7	19.8	36.8	21.4	41.2	20.2
% Cum. var.	35.0	57.1	34.7	54.5	36.8	58.2	541.2	61.4

Fig. 1 presents the sample distribution in the PC1-PC2 subspace for each data set. PC1 grossly differentiates between two sample groups with two distinct geographical sample distributions, the city samples (including city gardens and the avenue) and the highway (including transects). PC2 allows reasonable differentiation between city gardens and avenue samples, and the highway itself and transect samples. In the figure, the four groups are identified using different symbols, highway samples (o), transect samples (x), main avenue (*) and city gardens (+).

These results show that the distribution pattern of the samples it is not defined by the different traffic intensities supported by them. Instead, it mostly follows the original characteristics of the soils. PC1 (associated to Fe, Co (natural) and Zn) is more relevant in discriminating geographical groups, than PC2 (associated to anthropogenic Cd, Cu, Cr, Pb and Ni) in discriminating samples more directly exposed to vehicle pressure (highway and main road) from less exposed ones (transect and gardens). A similar opinion was given by Dudka [15] studying metals in Polish soils. In his case, the natural factor (mainly defined by Co, Fe, Al, Ti, Ni, Cr, Na, Ba, Mg, K) comprised nearly 70% of the initial variance.

In order to elucidate anthropogenic influences, it was decided to consider only those variables which were directly linked to PC2, i.e. Cd, Cu, Cr, Ni, Pb, and Zn, all of them related to the roadside environmental pollution.

Fig. 2 reveals that an almost identical sample distribution is obtained using only those six selected metals rather than considering the overall initial variables. This was quite surprising since this means that the natural factor was not efficiently removed. Now, the first PC explains ca. 51% of the variance in all seasons and it is defined by Cd, Cu, Pb, and Zn. The second PC (ca. 27% variance) is related to Cr and Ni.

So, from this approach it can be deduced that the anthropogenic factor is now the dominating effect although there is still a significant natural factor responsible for the differences among the sample groups (exactly as before). Such supposition is justified by the fact that natural Ni and Cr soil contents are strongly related to each other and, both of them, to Fe (and to a lesser extent, to Co), reflecting the composition of the material from which they were originally derived [24]. Analyzing the correlation matrix, Ni and Cr are highly correlated (0.61–0.77), but not to the other metals.

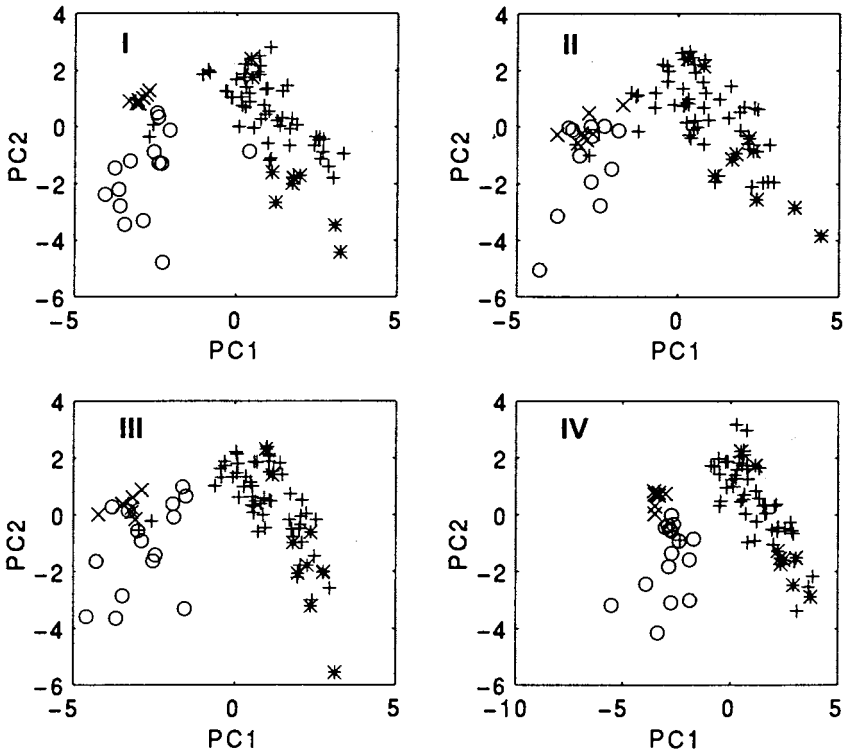

Fig. 1. Soils distribution in the PC1-PC2 score subspaces: (I), first; (II), second; (III), third; (IV), fourth sampling seasons. Highway samples (o), transect samples (x), main avenue with high traffic levels (*), and city gardens (+).

Keeping in mind that we are evaluating the anthropogenic effects over the samples, another variable reduction was made selecting only those variables which are clearly related to anthropogenic emissions i.e. Cd, Cu, Pb, Zn.

Fig. 3 shows the PC1–PC2 and PC1–PC2–PC3 subspaces for the first sampling season (fall). Amazingly, no sample groups were observed (neither in the other seasons); instead, just one swarm; even when almost no sample information is lost (PC1–PC2–PC3). This fact does not fulfil our second objective of differentiate sample groups according to traffic intensities. Therefore, more efforts have to be placed on studying which metals conduct to differentiated groups of samples interpretable as a function of traffic influences.

3.2. Cluster analysis

Cluster analysis looks for groups of samples according to their similarities. Due to the fact that there is no unique clustering or distance criterion, nor a sole way to consider initial data (original data, autoscaled data, PC-scores, etc.), several different combinations were tested. Best results were achieved using mean-centered data (when considering only heavy metals) and the *K*-means as the clustering criterion. If all the 12 variables are considered, data have to be autoscaled since not all the variables have the same units.

Though the *K*-means method is a typical non-hierarchical method, it has been addressed that there are iterative ways to construct a hierarchical clustering using the results of any non-hierarchical method providing it has been carried out for several values of *K*. More detailed discussions can be found at Massart and Kaufman [25]. This approach was applied by Wise and Gallagher to develop Matlab® algorithms [26] and it was applied here because neither the number of final

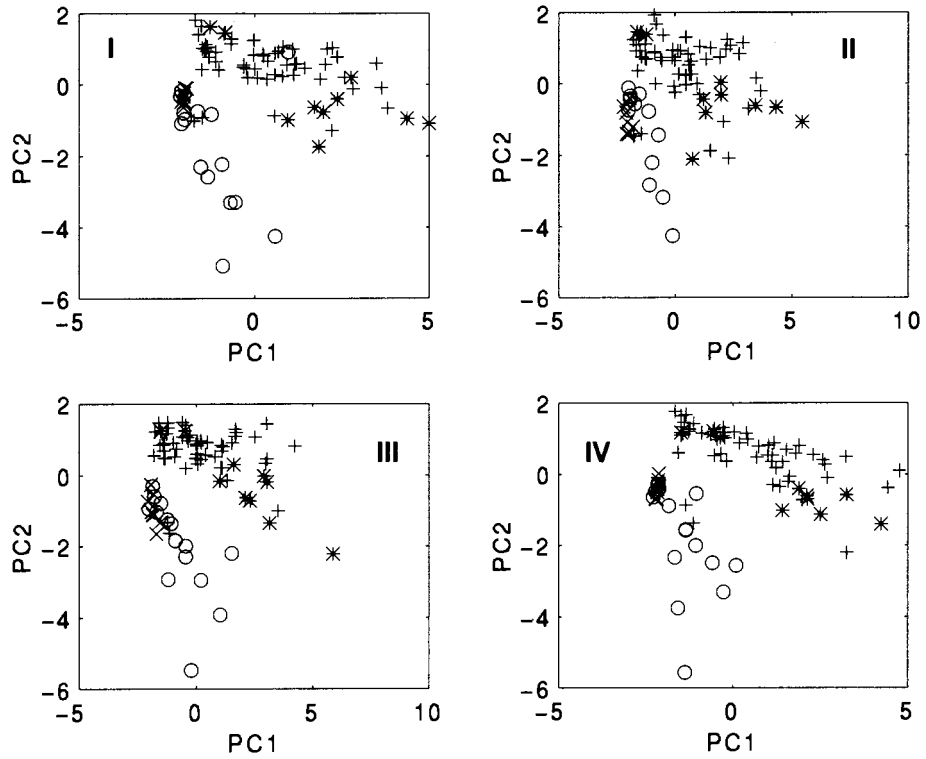

Fig. 2. Score plot for the first two PCs omitting natural pattern (see text): (I), first; (II), second; (III), third; (IV), fourth sampling seasons. Highway samples (o), transect samples (x), main avenue with high traffic levels (*), and city gardens (+).

clusters (K) nor the initial cluster centers could be anticipated (as it requires the non-hierarchical way). As in the PCA study, and for clarity of exposition, the same step by step approach will be followed.

We started by taking all 12 variables. A cluster analysis was made using the scores corresponding to the first two PCs as input values. The dendrogram corresponding to such analysis is presented in Fig. 4. The second column included in the dendrogram is intended to describe each sample according to the traffic intensity it supports. Thus, '1' means high levels of traffic (>40000 vpd); '2', medium–high (20000–40000 vpd); '3', medium 5000–15000 vpd) and '4', low–negligible (<5000 vpd). Accordingly, it can be observed that instead of getting sample groups as a function of traffic levels, two main groups grossly corresponding to the same sets shown in Fig. 1 can be seen: city samples (group A) and highway samples (group B). Each branch is divided into two new ones (named A′, A″; B′, B″) as it was in the PCA. Group A′ contained most of the gardens soil samples, and sample numbers 27 and 28 which were collected close to the avenue with high traffic levels. Their inclusion in this group is correct since they have lower metallic contents than those from their own geographical area. Both samples were collected not at the avenue edge, but at a 10–20 m distance from the edge. A′ samples have lower contents of Co (2–8 μg g^{-1}) and Fe (13–28 mg g^{-1}), Ni (8–20 μg g^{-1}), Cr (15–26 μg g^{-1}); with higher variability of Pb (50–300 μg g^{-1}), Zn (50–350 μg g^{-1}), Cd (0.04–0.29 μg g^{-1}) and Cu (9–60 μg g^{-1}).

The samples in Group A″ were from the avenue (symbols * in the PCA) with high traffic density as well as samples from the gardens surrounded by heavily travelled streets (e.g. samples # 48, 58, 61, 67). They contain high concentrations of Pb (200–600 μg g^{-1}), Cd (c.a 0.40 μg g^{-1}), and Cu (50–100 μg g^{-1}), low concentrations of Co (c.a. 5 μg g^{-1}), and medium concentrations of Fe (c.a. 20 mg g^{-1}). A″ branch concentrations of Ni (25–35 μg g^{-1}), Cr (20–35 μg g^{-1}) and Zn (200–400 μg g^{-1}) are higher than for the A′ branch.

Cluster B became separated into two different sets. Group B′ essentially combines soils from the highway border and several meadow samples (transect samples). This group has several distinct features: highest Co (16–25 μg g^{-1}), Ni (30–70 μg g^{-1}) and Cr (35–55 μg g^{-1}) levels, rather high Fe levels (27–37 μg g^{-1}), low Zn levels (c.a. 80 μg g^{-1}) and quite variable levels of Pb (40–300 μg g^{-1}) and Cd (0.01–0.33 μg g^{-1}), and medium for Cu (25–40 μg g^{-1}).

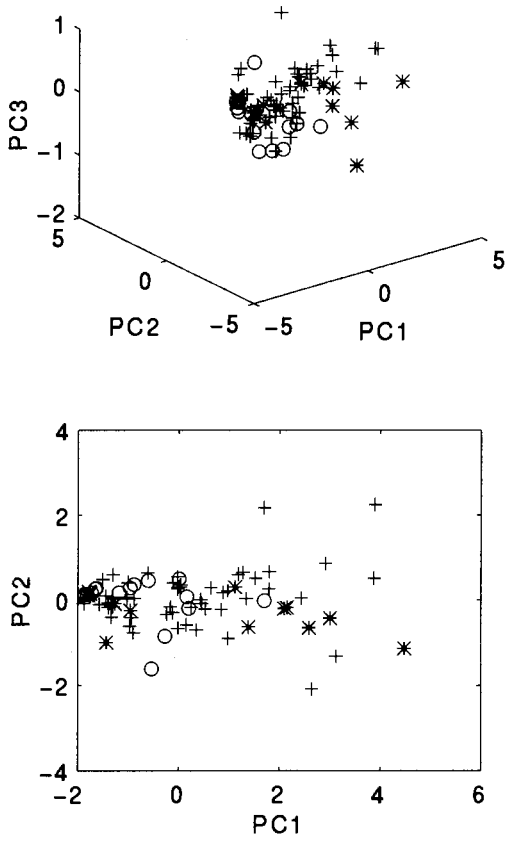

Fig. 3. Score plot for the PC1–PC2 and PC1–PC2–PC3 subspaces using selected metals (Cd, Cu, Pb, Zn), 1st sampling.

Group B″ is formed by cultivated soils and the remaining samples from the transects (i.e. away from the road edge; symbols x in the PCA). These samples are characterized by the lowest concentrations of Pb (17–50 μg g^{-1}), Zn (c.a 75 μg g^{-1}), Cd (< 0.1 μg g^{-1}), and Cu (c.a. 25 μg g^{-1}); medium–high concentrations of Ni (c.a. 20 μg g^{-1}) and Co (11–19 μg g^{-1}); high of Cr (c.a 40 μg g^{-1}) and the highest of Fe (35–40 mg g^{-1}). City garden samples # 69 and 70 included in B″ differ from the rest of the gardens (A′ cluster) because the gardens where they were taken were constructed very recently and, so, they exhibit only the natural characteristics of the soil without traffic influence already.

When considering the other three sampling seasons, similar dendrograms were obtained. The above explanations allow us to conclude that the main classification pattern is caused by the natural origin (Fe and Co) but not so clearly by the anthropogenic effects. The next step was to take only the heavy metals directly related with traffic emissions. Therefore, only Cd, Cu, Pb, Zn (linked to the PC1 from the final PCA study) were used to discover traffic contamination patterns in soils (following the second objective).

Outlying samples were not always the same along the four seasons and, consequently, the particular sample i.d. is not the same in all the dendrograms (the code level is maintained). This is not totally critical since, from here on, we are interested in the degrees of contamination rather than in particular location points. Special events are, without doubt, explained.

3.2.1. First sampling season

Fig. 5 shows two main groups X_1 and Y_1, and a minor one, Z_1 (hereby, the subscripts denote sampling season). Interesting subdivisions can be observed. Cluster X_1' contains type 1 samples (high motor vehicle influence) with high Pb (400–500 μg g^{-1}), Cu (70–100 μg g^{-1}) and Co (0.4–0.8 μg g^{-1}) values. Samples # 2, 56, 60 (type 2)

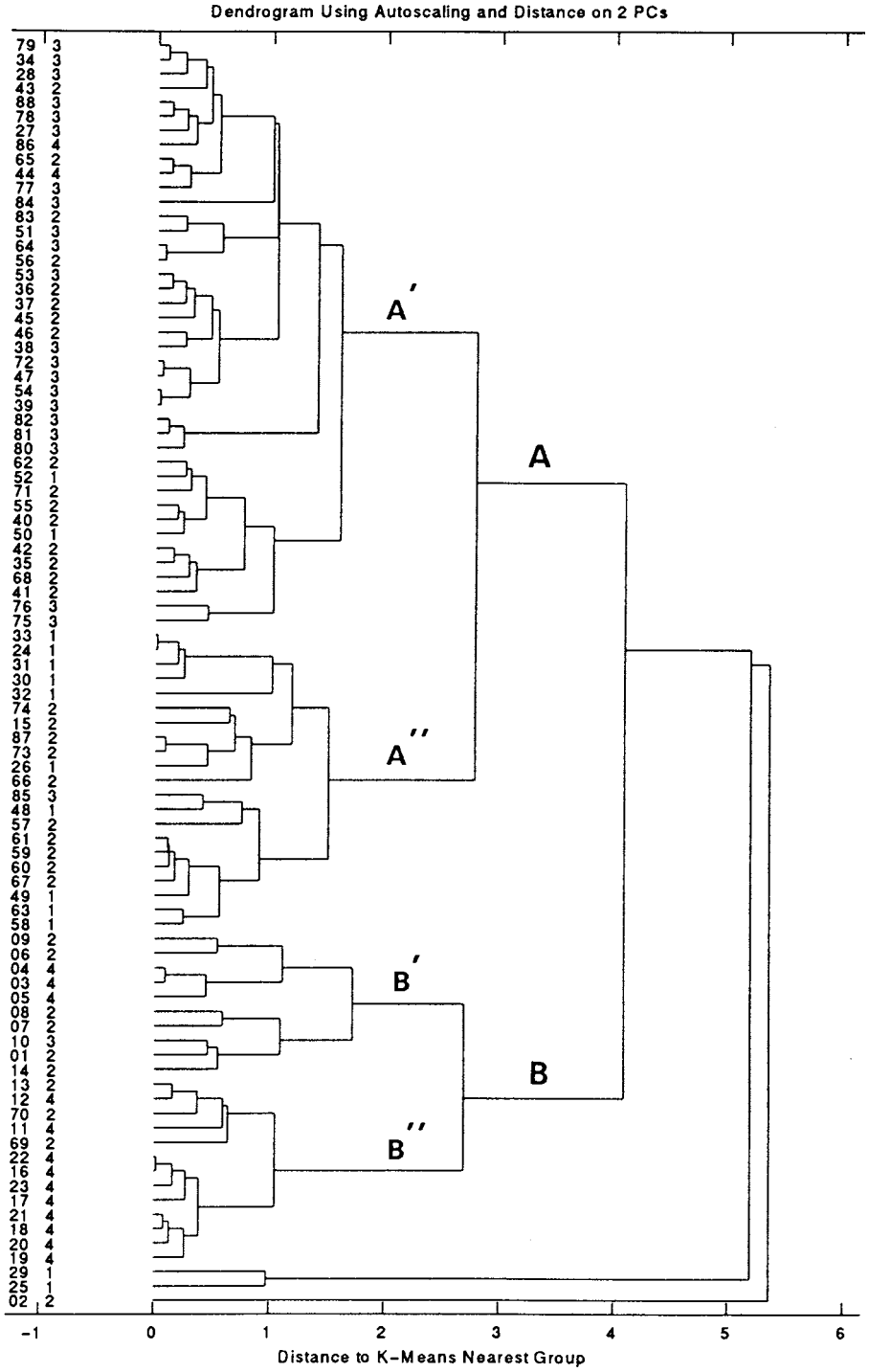

Fig. 4. Dendrogram for the first two PCs from all variables, 1st sampling season: A, city samples; B, highway samples; 1st column, sample i.d.; 2nd column codify traffic intensity (1, high; 2, medium-high; 3, medium; 4, low-negligible).

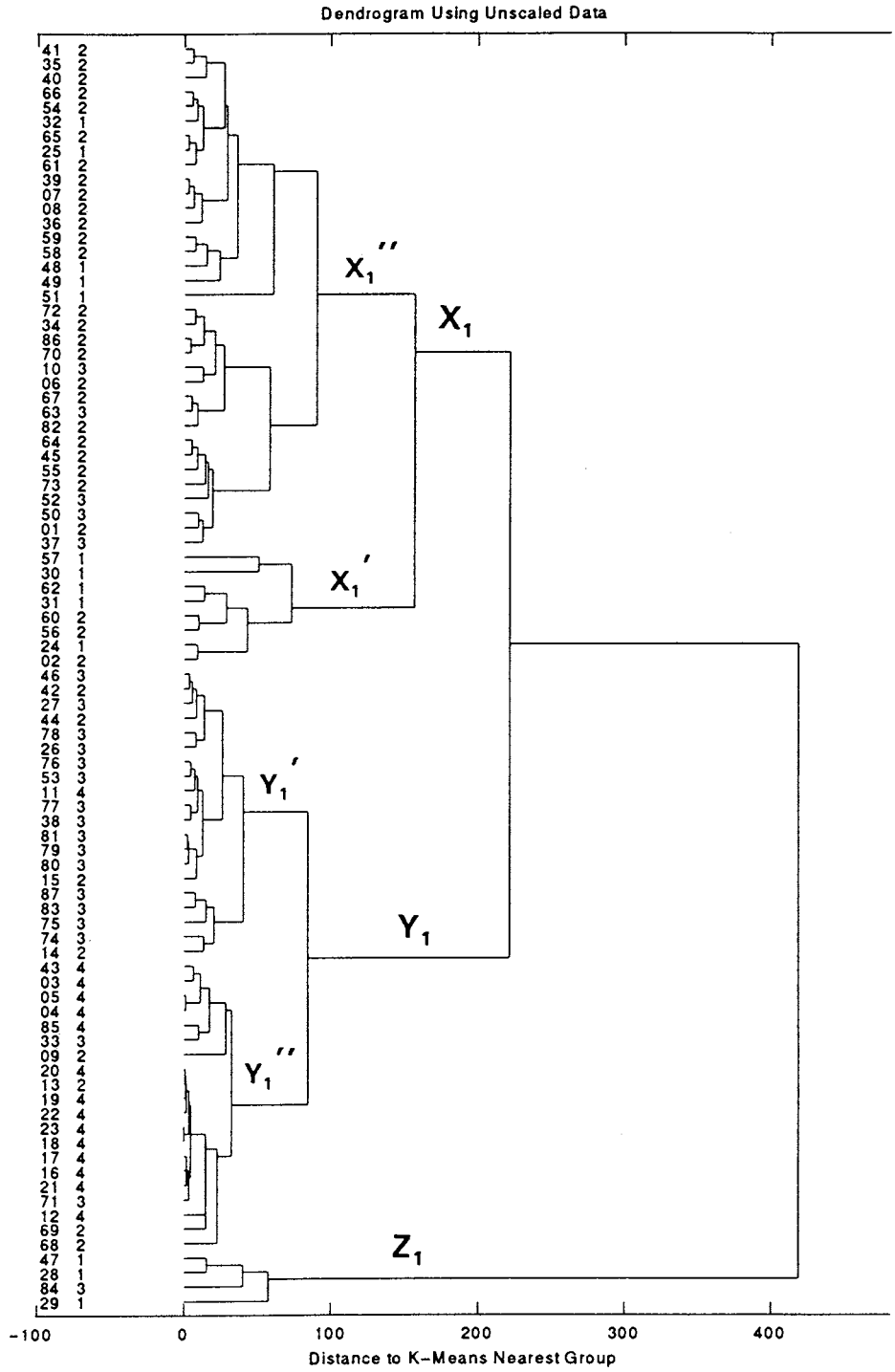

Fig. 5. Dendrogram 1st sampling season for selected metals: 1st column, sample i.d.; 2nd column codify traffic intensity (1, high; 2, medium-high; 3, medium; 4, low-negligible).

seem to be correctly included here due to a possible metallic accumulation caused by their particular location.

Cluster X_1'' (type 2 samples, medium–high influence) reveals medium–high Pb contents (c.a. 300 μg g^{-1}), Cu (40–80 μg g^{-1}) and quite variable Cd contents. Samples coded as 1 and 3 are properly included here owing to their metallic levels. Sample # 63 belongs to one garden which has a parking area and, therefore, presenting accumulation.

Cluster Y_1 shows two patterns. Group Y_1' contains most of the type 3 samples. Points # 14 and 15 (type 2, highway situation) were sited on a inclined plane, maybe producing metal leaching. Points 42 and 44 are situated in main streets (code 2), but in recently established gardens (low traffic influence). Sample # 11 (coded 4) presents low metal contents and, thus, it became wrongly emplaced since type 3 samples correspond to medium metallic contents. Group Y_1'' has the lowest metallic contents (type 4). Sample # 9 was misclassified because it has high Pb content (270 μg g^{-1}). Points # 68, 69, 71 (coded as 2, 2, 3) are grouped according to their recent construction (little exposure to emissions from motor vehicles).

Cluster Z_1 groups samples with the highest metallic concentrations (type 1). Sample # 84 (coded 3) is an abandoned garden, suffering from soil compaction and surface metal deposition.

3.2.2. Second and third sampling season

Fig. 6 and Fig. 7 show that the gross characteristics seen in the first sampling season are maintained both in the second and third sampling seasons. The main difference consists in the displacement of various samples towards clusters Zs (initially quite small). In this way, clusters Zs become the parent root for samples presenting the highest metallic levels. This means that concentration intervals for groups Zs are broadened, this is clearly seen for Pb (from 600–625 to 400–600 μg g^{-1}).

Clusters X_2 and X_3 are affected by the movement of samples type 1, achieving more homogenity between the Xs′ and Xs″ sets. They are formed mostly by samples suffering medium- high vehicle pressure and a few type 1 (high traffic) soils with lower figures than those contained in Zs′ groups.

Clusters Y_2 and Y_3 collect, again, samples taken from sites under medium and low–negligible road traffic (type 3 and 4) without that clear division noted in the first season. This can be attributed to the characteristically rainy weather in Galicia (winter and spring). The same argument can be used to explain why several samples (type 2) became included in clusters Y_2 and Y_3.

3.2.3. Fourth sampling season

The dendrogram in Fig. 8 is quite similar to that in Fig. 5 except group Z_4 which is larger than Z_1. Cluster Y_4 distinguishes quite well between type 3 and type 4 samples, as in the 1st season, what could be attributed to similar climate conditions (1st sampling, beginning of fall, 1993; 4th sampling, middle of summer, 1994).

It is interesting to note that samples # 69 and 70 in Fig. 8 discussed as # 68 and 69 in Fig. 5 joined group 3. The curious fact is that these newly constructed gardens migrated from a type 4 group (low influence) to a type 3 group, clearly revealing one year of traffic influence in soils (e.g. initial Pb was 18 μg g^{-1} and final values were 83 μg g^{-1}). This clearly demonstrates how important the effect of road traffic on soils placed in city gardens is and that, as expected, Pb can be used as an useful monitoring parameter.

Table 2 details the levels of Cd, Cu, Pb and Zn found for each of the groups cited above. It is quite clear that the concentration of the four metals increase with traffic density; although Cd, Cu and Zn present overlapping concentration intervals. On the contrary, each of the groups found in the four clusters show different, narrow concentrations of Pb, and they do not overlap.

4. Conclusions

When roadside soil pollution metal data sets were studied using PCA and cluster analyses to ascertain whether different pollution degrees can be sought, it was found that those metals linked to the natural soil variability (mostly Fe and Co, but also Ni, Mn and Cr) greatly mask the pollution trends. Therefore, they were split from the main data set and the multivariate studies were

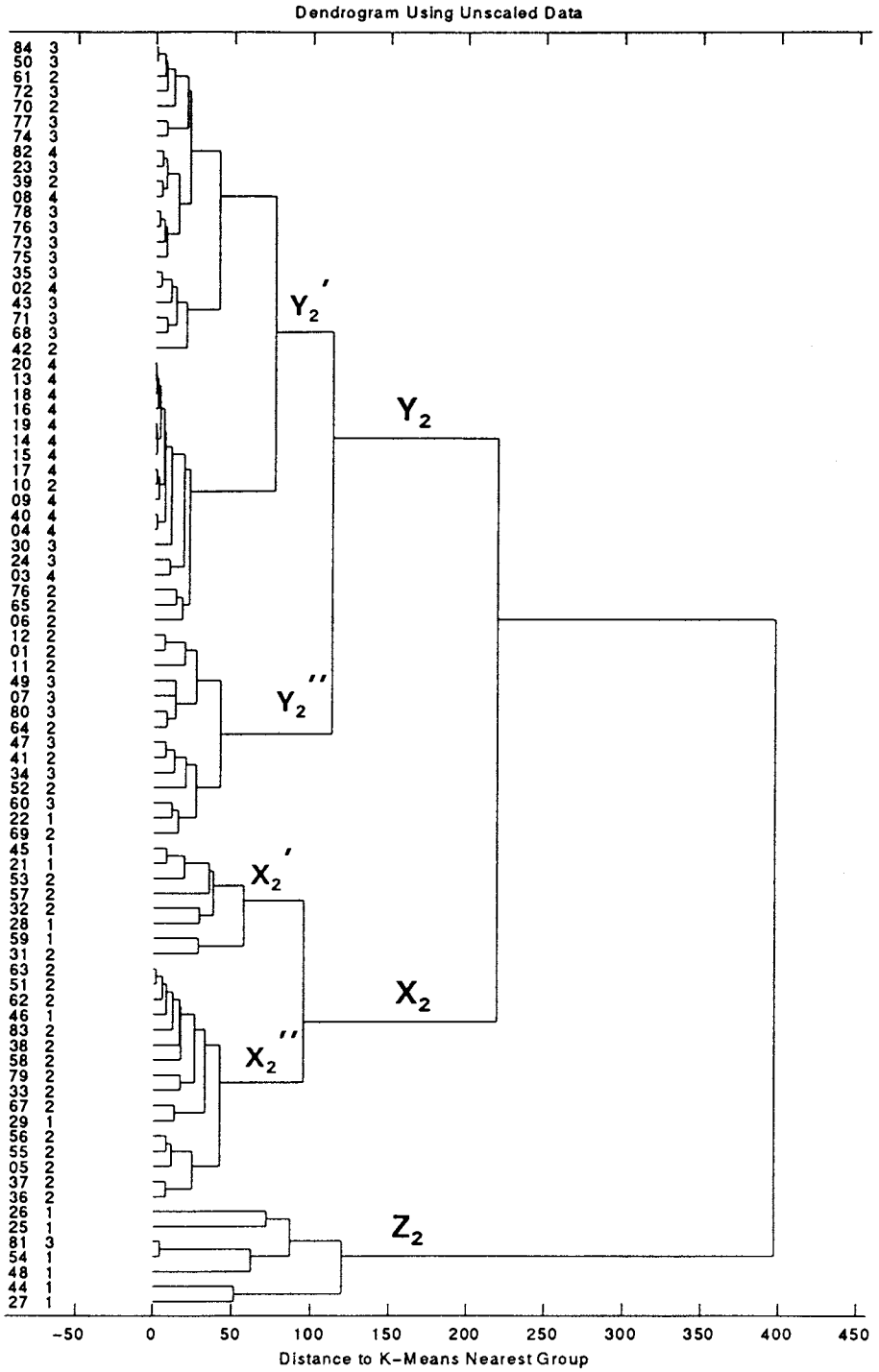

Fig. 6. Dendrogram 2nd sampling season for selected metals: 1st column, sample i.d.; 2nd column codify traffic intensity (1, high; 2, medium-high; 3, medium; 4, low-negligible).

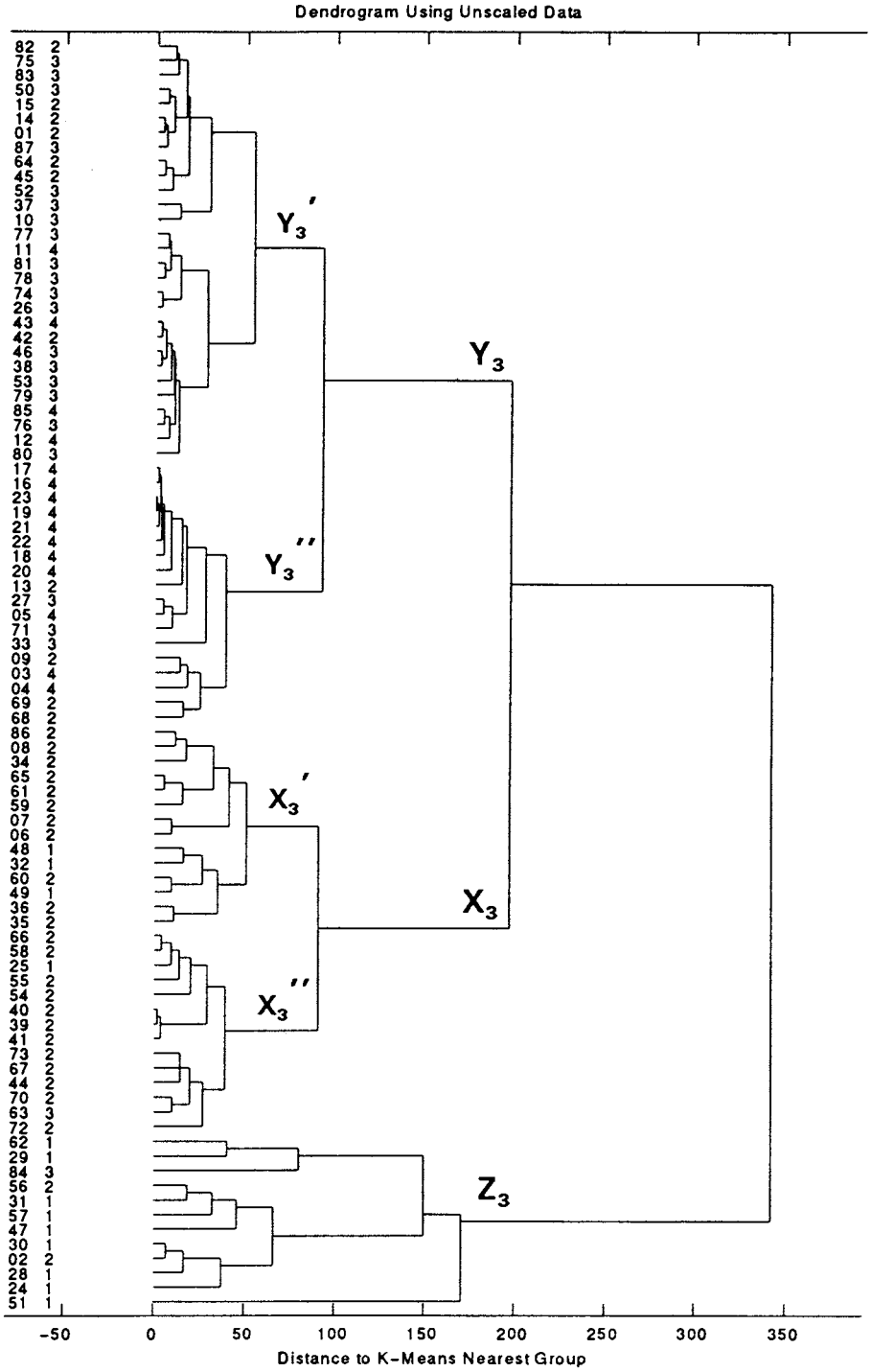

Fig. 7. Dendrogram 3rd sampling season for selected metals: 1st column, sample i.d.; 2nd column codify traffic intensity (1, high; 2, medium-high; 3, medium; 4, low-negligible).

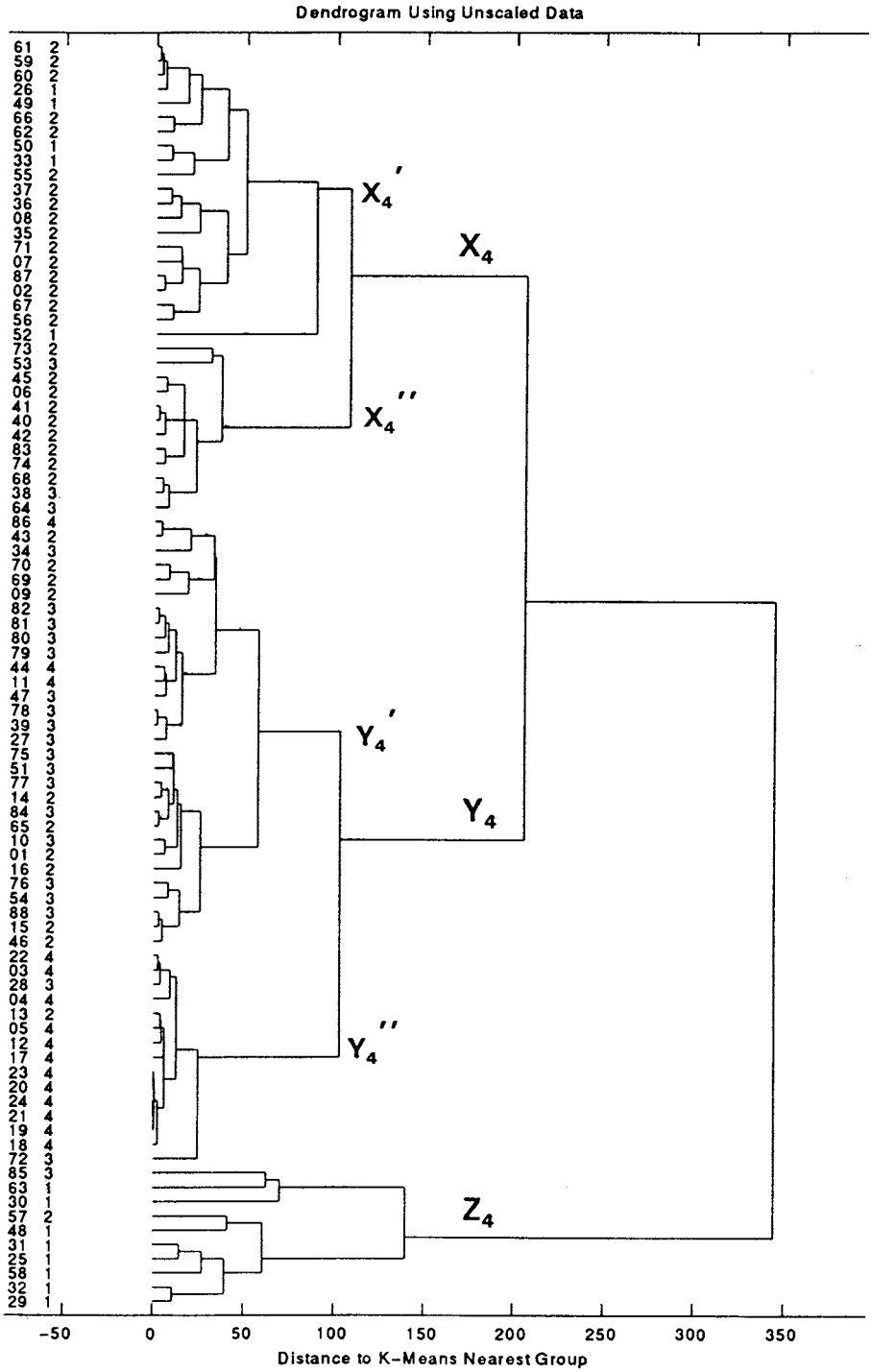

Fig. 8. Dendrogram 4th sampling season for selected metals: 1st column, sample i.d.; 2nd column codify traffic intensity (1, high; 2, medium-high; 3, medium; 4, low-negligible).

Table 2
Concentrations of Pb, Cd, Cu and Zn corresponding to each of the groups found in cluster analysis

Clusters	Concentration ± S.D. (μg g^{-1})			
	Pb	Cd	Cu	Zn
First Season				
$X_1'+Z_1$	512.7 ± 131.9	0.55 ± 0.20	88.63 ± 26.51	313.8 ± 61.3
X_1''	259.3 ± 61.4	0.25 ± 0.21	54.04 ± 20.32	217.0 ± 96.1
Y_1'	116.3 ± 21.8	0.16 ± 0.12	27.58 ± 8.40	145.0 ± 91.8
Y_1''	32.05 ± 16.86	0.03 ± 0.06	25.25 ± 10.08	78.68 ± 20.04
2nd Season				
Z_2	554.3 ± 67.8	0.57 ± 0.21	107.1 ± 37.5	297.1 ± 68.8
X_2	308.9 ± 51.1	0.34 ± 0.15	69.33 ± 17.54	247.5 ± 77.4
Y_2''	175.1 ± 23.7	0.27 ± 0.09	48.86 ± 15.32	169.8 ± 71.0
Y_2'	64.47 ± 41.8	0.11 ± 0.12	29.28 ± 8.44	104.9 ± 34.98
3rd Season				
Z_3	498.9 ± 74.3	0.43 ± 0.16	111.6 ± 55.6	285.1 ± 77.2
X_3	286.7 ± 52.8	0.25 ± 0.14	59.73 ± 15.38	212.2 ± 69.1
Y_3'	126.9 ± 30.5	0.14 ± 0.10	32.63 ± 8.02	144.2 ± 74.1
Y_3''	34.31 ± 19.44	0.06 ± 0.08	29.78 ± 10.47	80.35 ± 20.67
4th Season				
Z_4	532.2 ± 70.7	0.58 ± 0.21	85.03 ± 32.12	272.1 ± 108.4
X_4	295.5 ± 57.9	0.32 ± 0.18	62.88 ± 21.79	215.4 ± 79.8
Y_4'	126.8 ± 33.2	0.16 ± 0.11	32.03 ± 10.57	127.6 ± 52.0
Y_4''	24.01 ± 9.01	0.02 ± 0.03	24.73 ± 2.43	69.20 ± 12.13

performed again. Although this was not useful for the PCA assays in order to differentiate sample-groups, it succeeded when cluster analyses were performed. In this way, samples became grouped following several levels of metallic pollution caused by road traffic.

It was addressed that various pollution degrees appeared according to the different metal contents in soils. Most sample groups were differentiated by their contents of Pb which shows quite narrow intervals for the different groups and no overlap was observed. Just the opposite can be seen for the remaining metals. Their values are correlated to those of Pb (and so, to traffic characteristics) but their intervals overlap due to their broader range. Finally, Pb can be confirmed as the most distinctive metal from road traffic pollution though, without doubt, other metals (Cd, Cu, Zn) are important as well in the roadside soil environment.

References

[1] J.E. Fergusson, The Heavy Elements: Chemistry, Environment Impact and Health Effects, ch.9, Pergamon Press, Oxford, 1990.
[2] R.M. Harrison, D.P.H. Laxen, S.J. Wilson, Environ. Sci. Technol. 15 (1981) 1378.
[3] N.I. Ward, Sci. Total Environ. 93 (1990) 277.
[4] L. Gratani, S. Taglioni, M.F. Crescente, Chemosphere 24 (1992) 941.
[5] Y.B. Ho, K.M. Tai, Environ. Pollut. 49 (1988) 37.
[6] J.V. Lagerweff, A.W. Specht, Environ. Sci. Technol. 4 (1970) 583.
[7] S. Loranger, J. Zayed, Atmos. Environ. 9 (1994) 1645.
[8] O.J. Ogunsola, A.F. Oluwole, O.I. Asubiojo, M.A. Durosinmi, A.O. Fatusi, W. Ruck, Sci. Total Environ. 146/147 (1994) 111.
[9] J.E. Fergusson, N.D. Kim, Sci. Total Environ. 100 (1991) 125.
[10] M. Wilhelm, I. Lombeck, F.K. Ohnesorge, Sci. Total Environ. 141 (1994) 275.
[11] J.M. Andrade, D. Prada, S. Muniategui, E. Alonso, P. López, P. De la Fuente, M.A. Quijano, Anal. Chim. Acta 292 (1994) 253.

[12] B. Daus, H.W. Zwanziger, Fresenius J. Anal. Chem. 352 (1995) 444.
[13] K.A. Smith, in: B. J. Alloway (Ed.), Manganese and Cobalt in Heavy Metals in Soils ch. 10, Blackie and Son, London, 1990.
[14] E.I. Hamilton, Sci. Total Environ. 150 (1994) 7.
[15] S. Dudka, Sci. Total Environ. 121 (1992) 39.
[16] A. Carlosena, J.M. Andrade, M. Kubista, D. Prada, Anal. Chem. 67 (1995) 2373.
[17] American Association for Testing and Materials, Annual Book of ASTM Standards, ASTM, Philadelphia, Vol 4.8, 1993, 360–361.
[18] A. Carlosena, D. Prada, S. Muniategui, P. López, J.M. Andrade, E. González, 2nd International Conference on Polluted Soils, IHOBE Vitoria-Gasteiz, Spain, September 21–22, 1994.
[19] A. Cottenie, M. Verloo, Fresenius Z. Anal. Chem. 317 (1984) 389.
[20] A.D. Hewitt, C.M. Reynolds, At. Spectrosc. 11 (1990) 187.
[21] B.E. Davies, Water, Air, Soil Pollut. 63 (1992) 331.
[22] M.A. Stapanian, F.C. Garner, K.E. Fitzgerald, G.T. Flatman, J.M. Nocerino, J. Chemom. 7 (1993) 165.
[23] F. Macías, V.A. Veiga, R. Calvo de Anta, Cuaderno Lab. Xeolóxico de Laxe 18 (1993) 317.
[24] S.P. McGrathand, S. Smith, in: B.J. Alloway (Ed.), Chromium and Nickel in Heavy Metals in Soils ch.7, Blackie and Son, London, 1990.
[25] D.L. Massart, L. Kaufman, The Interpretation of Analytical Chemical Data by the use of Cluster Analysis ch.5, Krieger, Florida, USA, 1989.
[26] B.M. Wise, N.B. Gallagher, PLS_Toolbox for Matlab, User Manual v.1.5, Washington, USA.

ELSEVIER

Talanta 47 (1998) 769–778

Talanta

Spectroscopic investigations in molecularly organized solvent media. Part 5. Fluorescence behavior of polycyclic aromatic hydrocarbons dissolved in cetylpyridinium chloride + zwitterionic and cetyltrimethylammonium chloride + zwitterionic mixed surfactant systems

Siddharth Pandey [a], William E. Acree, Jr. [a,*], John C. Fetzer [b]

[a] *Department of Chemistry, University of North Texas, Denton, TX 76203-5070, USA*
[b] *Chevron Research and Technology Center, Richmond, CA 94802-0627, USA*

Received 15 December 1997; received in revised form 31 March 1998; accepted 3 April 1998

Abstract

Applicability of the cetylpyridinium (CPy^+) cation as a selective fluorescence quenching agent for discriminating between alternant versus nonalternant polycyclic aromatic hydrocarbons (PAHs) is examined for 25 representative solutes dissolved in two aqueous micellar cetylpyridinium chloride (CPC) + zwitterionic surfactant solvent media. Experimental results show that the CPy^+ cation effectively quenched fluorescence emission of all 10 alternant PAHs studied despite the presence of strong intramicellar coulombic interactions. Emission intensities of the 15 nonalternant PAHs also decreased upon addition of CPC to the zwitterionic surfactant solutions. Reduction in emission intensities for the nonalternant PAHs is rationalized in terms of changes in micellar structure caused by the coulombic interactions, rather than from loss of quenching selectivity by the CPy^+ cation. © 1998 Elsevier Science B.V. All rights reserved.

Keywords: Spectroscopy; Polycyclic aromatic hydrocarbons; Cetylpyridinium chloride; Cetyltrimethylammonium chloride; Zwitterionic mixed surfactant systems

1. Introduction

Selective fluorescence quenching agents facilitate chemical analysis by eliminating emission signals from undesired chemical interferences having only slightly different molecular structures. Sawicki et al. [1,2] introduced selective fluorescence quenching agents to thin-layer chromatographic analysis. Blümer and Zander [3] later extended the ideas to liquid chromatography. The authors noted that both nitromethane and nitrobenzene selectively quenched the fluorescence emission of perylene, dibenzo[*h*,*rst*]pentaphene and diben-

* Corresponding author. Fax: +1 940 5654318; e-mail: acree@unt.edu

0039-9140/98/$ - see front matter © 1998 Elsevier Science B.V. All rights reserved.
PII S0039-9140(98)00169-6

zo[*b*,*k*]chrysene dissolved in aqueous-acetonitrile (20:80% by volume) mixture. Emission intensities of the three nonalternant PAHs (e.g. naphtho[1,2*b*]fluoranthene, indeno[1,2,3*cd*]pyrene and acenaphthyleno[1,2*k*]-fluoranthene) were unaffected by nitromethane addition. Nitromethane (and nitrobenzene to a much lesser extent [4]) is a selective quenching agent for discriminating between alternant vs. nonalternant PAHs. Polycyclic aromatic hydrocarbons are classified as alternant PAHs if every alternant carbon atom in the aromatic ring system can be 'starred'. Nonalternant PAHs, on the other hand, would have at least one pair of adjacent starred atoms. [5,6] Fig. 1 illustrates the starring of the carbon atoms in the aromatic ring system for pyrene, fluoranthene and fluorene.

As part of a 7-year continuing spectroscopic investigation, we [7–26] have reported the fluorescence properties and quenching behavior of numerous PAH6 benzenoids, fluoranthenoids and fluorenoids, methylene-bridged cyclopenta-PAHs, acenaphthylene and acephenanthrylene derivatives, bi-PAHs, and polycyclic aromatic nitrogen heterocycles (PANHs) in organic nonelectrolyte and in aqueous micellar solvent media. In the later studies, we observed that nitromethane selectivity was lost in the case of the four anionic micellar solvent media studied. Nitromethane quenched the fluorescence emission of both alternant and nonalternant PAHs, which is contrary to the 'nitromethane selective quenching rule'. Unexpected fluorescence was found when we extended [27] our studies to include mixed cetyltrimethylammonium chloride (CTAC) + cetylpyridinium chloride (CPC) micelles. Here, it was learned that the cetylpyridinium cation also is a selective fluorescence quenching agent for alternant PAHs. Of the 41 PAH solutes examined, the only exceptions noted were four nonalternant PAHs (e.g. naphtho[2,3*b*]fluoranthene, benzo[*k*]fluoranthene, naphtho[1,2*b*]fluoranthene and benzo[*b*]fluoranthene) that are either known exceptions or borderline cases to the nitromethane selective quenching rule [10,16,28].

It should be noted that Ayala et al. [29,30] concurrently reported that the cetylpyridinium cation selectively quenches fluorescence emission of alternant polycyclic aromatic hydrocarbons. The authors' conclusions were based upon a study of the fluorescence behavior of only 14 PAH solutes. Unfortunately, three of the five listed nonalternant PAHs were completely misclassified. Acenaphthene, fluorene and acenaphthylene should be alternant PAHs as none of the five-membered ring systems are aromatic in nature. In fact, acenaphthene and fluorene have two CH_2 and one CH_2 group, respectively, on their five-membered ring systems. The only real nonalternant PAHs (fluoranthene and benzo[*b*]fluoranthene) in the Ayala et al. studies are known borderline exceptions to the nitromethane selective quenching rule. Our measurements showed that the selectivity of the cetylpyridinium cation for quenching the fluorescence emission of alternant vs. nonalternant PAHs is far better than reported in the two Ayala et al. studies.

Discovery of cetylpyridinium cation as a selective fluorescence quenching agent is important from a chemical analysis standpoint in that its solutions are optically transparent in the excitation spectral region of many of the PAHs. Primary inner-filtering corrections are minimized, and in many cases even eliminated. Inner-filtering

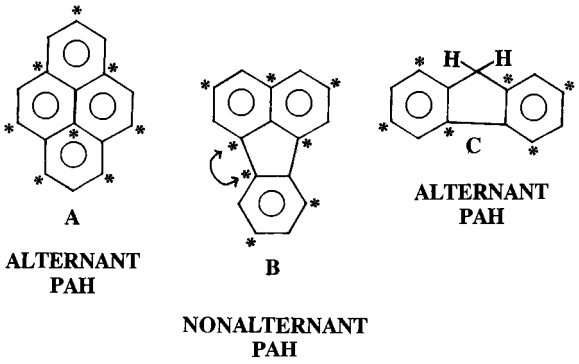

Fig. 1. Alternant vs. nonalternant polycyclic aromatic hydrocarbon classification. Pyrene (A) and fluorene (C) are classified as alternant PAHs because there are no pairs of adjacent starred carbon atoms in the aromatic ring system. The bridging carbon atom in the five-membered ring of fluorene is not considered to be part of the aromatic ring system. This carbon atom has two hydrogens bonded to it. Fluoranthene (B) is an example of a nonalternant PAH. The two adjacent starred carbon atoms are identified by arrows.

corrections are much larger for nitromethane solutions as a few drops of quenching agent results in appreciable absorbances. Accurate quantification of PAH concentrations requires both absorbance and fluorescence emission measurements when using the quenching agent nitromethane. To provide additional experimental data for micellar CPC solutions, we report in this communication the fluorescence behavior of 10 alternant and 15 nonalternant PAHs in aqueous micellar CPC + *N*-hexadecyl-*N*,*N*-dimethyl-3-ammonio-1-propanesulfonate (SB-16) and CPC + *N*-dodecyl-*N*,*N*-dimethyl-3-ammonio-1-propanesulfonate (SB-12).

These particular systems were judiciously selected because of the larger structural changes generally observed in mixtures which exhibit strong intra-micellar interactions, such as zwitterionic + cationic and anionic + cationic surfactant mixtures. The SB-16 and SB-12 zwitterionic surfactants have a positively-charged quaternary ammonium group and a negatively-charged sulfonate group, with the latter being further away from the micellar center than the former. As argued by Malliaris et al. [31] an electric field exists inside the Stern layer. The headgroup of the cationic surfactant, which in this case is the pyridinium electron acceptor site, will be attracted towards the negative outer part of the Stern layer. This will expose the CH_2 groups adjacent to the pyridinium headgroup to water, and in all likelihood will lead to a less rigid, more distorted micellar structure. Such intra-micellar interactions could adversely affect quenching selectivity through alteration of CPC conditional reduction potential or by providing a solubilization site not conducive to electron transfer. The increased water penetration might force the PAH molecule deeper within the hydrocarbon-like micellar interior, and away from the pyridinium group. If this does occur, then one should observe a noticeable difference in the extent of fluorescence quenching. For electron transfer to occur, the donor and acceptor sites must be in fairly close proximity. Moreover, the solvent media must be capable of supporting the newly-formed charged (or partially charged) species. This was the reason given for why nitromethane fails to quench the fluorescence emission of alternant PAHs dissolved in nonpolar solvents like cyclohexane and heptane [26]. Fluorescence spectra were also recorded in aqueous CTAC + SB-16 and CTAC + SB-12 solvent media. Here, no quenching agent is present and any decrease/increase in the observed PAH emission intensity should be related to changes in the micellar structure.

2. Materials and methods

The different aqueous micellar cetylpyridinium chloride (Aldrich, 98%) + SB-16 (Sigma), CPC + SB-12 (Sigma), cetyltrimethylammonium chloride (Aldrich, 25 wt% solution) + SB-16 and CTAC + SB-12 mixed surfactant solvent media were prepared by dissolving the commercial surfactants in doubly deionized water. Synthetic references and/or commercial suppliers for the PAH solutes contained in Tables 1–4 are listed in our earlier papers (for a single source listing see Tucker [21]). Stock solutions were prepared by dissolving the solutes in dichloromethane, and were stored in closed amber glass bottles in the dark to retard any photochemical reactions between the PAH solutes and dichloromethane solvent. Small 25-μl aliquots of each stock solutions were transferred by Eppendorf pipette into test tubes, allowed to evaporate, and diluted with 10 ml (graduate cylinder) of the micellar solvent media of interest. Solute concentrations were sufficiently dilute (10^{-6} molar) so as to prevent excimer formation. All solutions were ultrasonicated, vortexed and allowed to equilibrate for a minimum of 24 h before any spectrofluorometric measurements were made. Experimental results were unaffected by longer equilibration times.

Absorption spectra were recorded on a Milton Roy Spectronic 1001 Plus and a Hewlett-Packard 8450A photodiodearray spectrophotometer in the usual manner. The fluorescence spectra were measured on a Shimadzu RF-5000U spectrofluorimeter with the detector set at high sensitivity. Solutions were excited at the wavelengths listed in Table 1. Fluorescence data were accumulated in a

Table 1
List of alternant and nonalternant polycyclic aromatic hydrocarbons examined and their excitation wavelength

Letter	Polycyclic aromatic hydrocarbon	λ_{ex} (nm)
Alternant polycyclic aromatic hydrocarbons		
A	Naphtho[2,3*g*]chrysene	350
B	Benzo[*e*]pyrene	335
C	Pyrene	338
D	Naphtho[1,2,3,4*ghi*]perylene	316
E	Dibenzo[*def*,*p*]chrysene	310
F	Perylene	403
G	Benzo[*rst*]pentaphene	307
H	Anthranthrene	306
I	Coronene	334
J	Benzo[*a*]pyrene	350
Nonalternant fluoranthenoids and fluorenoids		
K	Naphtho[1,2*b*]fluoranthene	350
L	Benzo[*ghi*]fluoranthene	340
M	Benz[*def*]indeno[1,2,3*hi*]chrysene	406
N	Benzo[*a*]fluoranthene	406
O	Naphtho[2,1*k*]benzo[*ghi*]fluoranthene	368
P	Naphtho[1,2*k*]benzo[*ghi*]fluoranthene	366
Q	Benz[*def*]indeno[1,2,3*qr*]chrysene	408
R	Dibenzo[*a*,*e*]fluoranthene	390
S	Fluoreno[2,3,4,9*defg*]chrysene	315
T	Benzo[*j*]fluoranthene	315
U	Dibenzo[*ghi*,*mno*]fluoranthene	290
V	Naphtho[2,1*a*]fluoranthene	400
W	Benzo[*b*]fluoranthene	346
X	Benzo[*k*]fluoranthene	306
Y	Naphtho[2,3*b*]fluoranthene	316

1 cm^2 quartz cuvette at 21°C (ambient room temperature) with excitation and emission slit width settings of 15 and 3 nm, respectively. The fluorescence spectra represent a single scan which was then solvent blank corrected and verified by repetitive measurements.

Emission intensities associated with the quenching measurements were corrected for primary inner-filtering artifacts and self-absorption arising from the absorption of excitation radiation by solvent media and the PAH solute, respectively, according to the following expression: [32–34]

$$f_{prim} = F_{corr}/F_{obs} = 2.303A\,(y-x)/[10^{-Ax} - 10^{-Ay}] \quad (1)$$

which differs slightly from the approximate form [35]

$$f_{prim} \approx 10^{0.5A} \quad (2)$$

In the above equations F_{corr} and F_{obs} refer to the corrected and observed fluorescence emission signal, respectively, A is the absorbance per cm of pathlength at the excitation wavelength, and x and y denote distances from the boundaries of the interrogation zone to the excitation plane. For many of the fluorescence measurements primary inner-filtering correlations were relatively minor as the observed absorbance was often A $cm^{-1} <$ 0.05, even in the 300–320 nm spectral region.

Table 2
Relative emission intensities of alternant and nonalternant PAHs dissolved in aqueous micellar (CPC+SB-12) solvent media

Letter[a]	I[b]	II[c]	III[d]
Alternant polycyclic aromatic hydrocarbons			
A	640	44	31
B	1000	13	4.3
C	700	3.2	1.4
D	730	8.0	3.7
E	550	6.9	2.4
F	920	48	20
G	580	1.0	<1.0
H	880	23	9.5
I	870	16	9.8
J	560	5.6	1.7
Nonalternant fluoranthenoids and fluorenoids			
K	810	160	150
L	1020	990	1020
M	1130	80	77
N	250	230	220
O	870	250	250
P	750	550	520
Q	230	47	50
R	510	170	180
S	51	22	21
T	380	350	360
U	830	830	780
V	430	280	280
W	330	220	190
X	650	76	30
Y	640	50	26

[a] Letters refer to the compounds listed in Table 1.
[b] Solvent media was ca. 1.0×10^{-2} molar in SB-12.
[c] Solvent media was ca. 7.5×10^{-3} molar in SB-12+ca. 2.5×10^{-3} molar in cetylpyridinium chloride.
[d] Solvent media was ca. 5.0×10^{-3} molar in SB-12+ca. 5.0×10^{-3} molar in cetylpyridinium chloride.

Table 3
Relative emission intensities of alternant and nonalternant PAHs dissolved in aqueous micellar (CPC + SB-16) solvent media

Letter[a]	I[b]	II[c]	III[d]	IV[e]
Alternant polycyclic aromatic hydrocarbons				
A	980	77	40	43
B	890	24	6.3	1.9
C	740	4.4	<1.0	<1.0
D	570	98	24	5.6
E	660	16	4.0	2.2
F	640	120	34	13
G	450	<1.0	<1.0	<1.0
H	780	68	23	5.7
I	940	40	22	9.7
J	630	23	5.3	2.5
Nonalternant fluoranthenoids and fluorenoids				
K	760	260	210	130
L	1000	980	970	950
M	550	260	190	160
N	430	430	450	390
O	800	280	280	210
P	770	410	400	170
Q	830	210	180	170
R	730	220	210	270
S	55	26	21	17
T	670	660	630	600
U	840	780	730	680
V	860	400	370	370
W	470	380	300	230
X	750	190	80	42
Y	710	130	61	33

[a] Letters refer to the compounds listed in Table 1.
[b] Solvent media was ca. 4.0×10^{-3} molar in SB-16.
[c] Solvent media was ca. 3.0×10^{-3} molar in SB-16 + ca. 1.0×10^{-3} molar in cetylpyridinium chloride.
[d] Solvent media was ca. 2.0×10^{-3} molar in SB-16 + ca. 2.0×10^{-3} molar in cetylpyridinium chloride.
[e] Solvent media was ca. 1.0×10^{-3} molar in SB-16 + ca. 3.0×10^{-3} molar in cetylpyridinium chloride.

Secondary inner-filtering corrections were not necessary. Aqueous micellar CPC + SB-16, CPC + SB-12, CTAC + SB-16 and CTAC + SB-12 mixed surfactant solutions were 'optically transparent' in the PAH emission ranges. Computational procedures and interrogation zone dimensions are discussed in greater detail elsewhere [17–19,36,37].

3. Results and discussion

3.1. Experimental data for micellar CPC + zwitterionic surfactant systems

Table 2 and Table 3 summarize the fluorescence emission intensities of 25 representative polycyclic aromatic hydrocarbons dissolved in aqueous micellar CPC + SB-16 and CPC + SB-12 mixed surfactant solvent media. The first column of

Table 4
Relative emission intensities of alternant and nonalternant PAHs dissolved in aqueous micellar (CTAC + SB-12) solvent media

Letter[a]	I[b]	II[c]	III[d]	IV[e]
Alternant polycyclic aromatic hydrocarbons				
A	640	240	240	280
B	1000	940	890	790
C	700	650	630	540
D	730	160	150	180
E	550	360	290	430
F	920	640	800	720
G	580	120	100	140
H	880	560	440	540
I	870	160	190	270
J	560	550	570	570
Nonalternant fluoranthenoids and fluorenoids				
K	810	480	630	730
L	1020	990	860	940
M	1120	220	220	300
N	250	240	250	230
O	870	74	44	120
P	750	160	76	220
Q	230	25	36	87
R	510	51	43	55
S	51	57	41	46
T	380	270	250	370
U	830	750	740	670
V	430	140	150	160
W	330	370	330	320
X	650	530	590	600
Y	640	400	360	400

[a] Letters refer to the compounds listed in Table 1.
[b] Solvent media was ca. 1.0×10^{-2} molar in SB-12.
[c] Solvent media was ca. 7.5×10^{-3} molar in SB-12 + ca. 2.5×10^{-3} molar in cetyltrimethylammonium chloride.
[d] Solvent media was ca. 5.0×10^{-3} molar in SB-12 + ca. 5.0×10^{-3} molar in cetyltrimethylammonium chloride.
[e] Solvent media was ca. 1.0×10^{-2} molar in cetyltrimethylammonium chloride.

numerical values represents the measured emission intensities in the neat zwitterionic surfactant and the remaining three (or four) columns refer to the different mixed surfactant systems. For each series of measurements the stoichiometric concentration of the given PAH fluorophore was held constant. Careful examination of the numerical entries reveals that addition of CPC surfactant leads to a significant decrease in the emission signals of all ten alternant PAH molecules as would be expected based upon earlier studies [27,29,30] which showed that CPC is a selective fluorescence quenching agent. For many of the alternant PAHs the observed emission signal was reduced to less than 10% of its original value in the aqueous zwitterionic micellar solvent media (not shown). Experimental results clearly document that CPC still effectively quenches fluorescence emission of alternant PAHs, irrespective of the strong coulombic interactions between the positively-charged pyridinium cation and the negatively-charged sulfonate group on the zwitterionic cosurfactant. Readers will note that our methodology differs slightly from that used by Ayala et al. [29,30]. We calculate the extent of fluorescence quenching relative to the neat zwitterionic surfactant solvent media, and not relative to a deionized (distilled) water solution containing the dissolved polycyclic aromatic hydrocarbon. Our reference point allows us to study the much larger PAH solutes that are not very soluble in water.

More interesting quenching behavior is observed for the 15 nonalternant polycyclic aromatic hydrocarbons dissolved in both SB-12 + CPC and SB-16 + CPC solvent media. Here, the measured emission intensity generally does decrease with CPC addition, but not nearly to the extent as was observed in the case of alternant PAHs. Similar fluorescence behavior is observed with both zwitterionic surfactants. The larger nonalternant PAHs generally exhibited the larger reductions in emission intensity. For example, emission signals of benz[*def*]indeno[1,2,3*hi*]chrysene and benz[*def*]indeno[1,2,3*qr*]chrysene decreased to 10–20% of their initial emission intensities. Both solutes have 1 five-membered ring and 6 six-membered rings. Emission intensities of the smaller benzo[*a*]fluoranthene, benzo[*j*]fluoranthene, benzo[*ghi*]fluoranthene and dibenzo[*ghi*,*mno*]fluoranthene PAH solutes decreased by only a few percent. No special significance is given to these slight variations/reductions in emission intensities, which in all likelihood result from the fact that the solutions were prepared using a graduate cylinder. Method of sample preparation can not explain, however, the large reduction in emission signals of benz[*def*]indeno[1,2,3*hi*]chrysene, naphtho[2,1*k*]benzo[*ghi*]fluoranthene, dibenzo[*a*,*e*]-fluoranthene and benz[*def*]indeno[1,2,3*qr*]chrysene. Emission intensities of these latter four solutes decreased by a factor of two or more. Reduction in emission intensity is surprising in that only 4 of the 15 nonalternant PAH solutes studied were known exceptions (or border-line cases) to the selective quenching rule.

Apparent loss of CPC quenching selectivity could result from strong intramicellar interactions not related to the electron transfer process. Hashimoto and Thomas [38] established the quenching mechanism as electron transfer based upon an analysis of the time-dependent pyrene fluorescence decay in 0.1 M sodium lauryl sulfate + aqueous-ethylene glycol solvent mixture at both ambient room temperature and at 77 K. Malliaris et al. [39] later showed that the cetylpyridinium ion (CPy^+) behaved as an immobile quencher in time-resolved fluorescence quenching studies involving pyrene solubilized in CPC + CTAC mixed micelles. The residence time of CPy^+ inside the micelle was significantly longer than pyrene's fluorescence lifetime.

3.2. Experimental data for micellar CTAC + zwitterionic surfactant systems

To better understand how micellar structure affects the fluorescence process, emission spectra were recorded in two additional zwitterionic + cationic mixed surfactant systems. Both systems exhibited similar fluorescence behavior. Rationale for these measurements is that the coulombic interactions between CTAC positively-charged tetraalkylammonium headgroup and SB-12/SB-16

negatively-charged sulfonate group should mimic in part interactions present in the CPC + SB-12 and CPC + SB-16 solvent media. No quenching agent is present, however, in the two CTAC systems. Any decrease/increase in the observed PAH emission intensity should be related to changes in the micellar structure.

Measured fluorescence emission intensities of 25 representative PAH solutes dissolved in aqueous micellar CTAC + SB-12 and CTAC + SB-16 mixtures are reported in Table 4 and Table 5, respectively. Total surfactant concentration and CTAC/zwitterionic surfactant concentration ratios were identical to those used in the CPC quenching study. Examination of the numerical values reveals that the PAH solutes are more fluorescent in the aqueous micellar zwitterionic surfactant solvent media than in any of the seven cationic + zwitterionic surfactant mixtures. Emission intensities in the SB-12 and SB-16 micelles are even higher than those measured in CTAC micelles at comparable surfactant concentrations.

Alternant and nonalternant PAHs show a similar decrease in emission intensities, and as before in the case of the nonalternant PAHs the decrease in emission intensity is more pronounced for the larger benz[*def*]indeno- [1,2,3*hi*]chrysene and benz[*def*]indeno[1,2,3*qr*]chrysene PAH solutes. In many respects the nonalternant PAH fluorescence behavior in CTAC + SB-12 and in CTAC + SB-16 mixed micelles parallels the experimental data given in Table 2 and Table 3. This is not the case, however, for the alternant PAHs. Most of the alternant PAHs exhibited negligible fluorescence emission signals in the neat aqueous micellar CPC solutions, compared to fairly large emission signals in neat CTAC micelles. Based upon these observations, and in the absence of any experimental data to the contrary, we conclude that part (if not all) of the observed decrease in the measured emission intensity for nonalternant PAHs dissolved in micellar CPC + zwitterionic surfactant solvent media was a result of changes in micellar structure, rather than from loss of quenching selectivity by the cetylpyridinium cation.

Table 5
Relative emission intensities of alternant and nonalternant PAHs dissolved in aqueous micellar (CTAC + SB-16) solvent media

Letter[a]	I[b]	II[c]	III[d]	IV[e]	V[f]
Alternant polycyclic aromatic hydrocarbons					
A	980	420	330	490	360
B	890	820	740	470	730
C	740	660	620	580	510
D	570	120	140	160	200
E	660	600	530	590	550
F	640	460	470	480	500
G	450	49	53	49	36
H	780	400	490	490	480
I	940	150	120	160	180
J	630	520	520	520	550
Nonalternant fluoranthenoids and fluorenoids					
K	760	560	520	630	570
L	1020	980	970	970	930
M	550	90	95	95	100
N	430	430	420	410	400
O	800	100	71	69	150
P	770	110	100	110	130
Q	830	140	200	250	280
R	730	99	140	150	150
S	55	48	44	46	36
T	670	530	620	490	570
U	840	670	640	500	590
V	860	200	140	170	380
W	470	430	430	450	420
X	750	750	740	860	800
Y	710	510	380	340	350

[a] Letters refer to the compounds listed in Table 1.
[b] Solvent media was ca. 4.0×10^{-3} molar in SB-16.
[c] Solvent media was ca. 3.0×10^{-3} molar in SB-16 + ca. 1.0×10^{-3} molar in cetyltrimethylammonium chloride.
[d] Solvent media was ca. 2.0×10^{-3} molar in SB-16 + ca. 2.0×10^{-3} molar in cetyltrimethylammonium chloride.
[e] Solvent media was ca. 1.0×10^{-3} molar in SB-16 + ca. 3.0×10^{-3} molar in cetyltrimethylammonium chloride.
[f] Solvent media was ca. 4.0×10^{-3} molar in cetyltrimethylammonium chloride.

3.3. Fluorophore location in micelles and effect of micellar structure on observed emission intensities

A search of the chemical literature [40–47] reveals that select PAH molecules exhibit solvent polarity probe character as evidenced by a systematic enhancement of band I emission intensity with increasing solvent polarity. The I/III band

intensity ratio serves as a quantitative measure of the polarity of the solubilizing media in the immediate vicinity of the probe molecule. Published fluorescence investigations [48–54] have placed solubilized probes in the polar palisade region of the micelle in close proximity to the cationic/anionic surfactant headgroup. Measured I/III emission intensity ratios are generally larger in the case of quaternary ammonium surfactants, suggesting that the PAH molecule has a strong affinity for the positively-charged headgroup. This affinity provides an additional driving force in the solubilization of PAHs by quaternary ammonium surfactant micelles not present with anionic micelles.

Kamenka et al. [55] reported I/III band intensity ratios for pyrene in several aqueous micellar zwitterionic surfactant solutions, in both the absence and presence of added sodium chloride electrolyte. Intensity ratios were independent of surfactant and NaCl concentration, at least to within the experimental accuracy of the calculated values. For SB-12 micelles, the experimentally determined I/III ratio was I/III ≈ 1.48, which was slightly larger than values of I/III ≈ 1.41 and I/III ≈ 1.40 observed for pyrene dissolved in cetyltrimethylammonium bromide and cetyltrimethylammonium chloride, respectively [50]. We also observed similar results for the solvent polarity probes coronene, benzo[*ghi*]perylene and benzo[*e*]pyrene. Emission intensity ratios for all three PAHs were larger in SB-12 and SB-16 than in either aqueous CTAC or sodium dodecylsulfate (SDS) solutions.

Kamenka et al. interpreted the larger I/III value in SB-12 as an indication that pyrene resides, at least in part, in the fairly hydrated shell of thickness corresponding to the intercharge distance. In other words, pyrene is located between the positively-charged nitrogen atom and the sulfonate group (see Fig. 2). The authors went on to state that 'the intercharge groups bring about a rigidification of the micellar outer layer in the same manner as the chemical links between headgroups of amphiphilic repeat units in hydrophobic microdomains formed in solutions of polyamphiphiles'. A more rigid micellar structure would explain why PAH emission intensities are larger in the two aqueous micellar zwitterionic surfactant solvent media. There would be fewer collisions and less nonradiative pathways for the excited PAH fluorophore to return back to its ground electron state. From an analytical point-of-view, the larger emission intensities make the zwitterionic surfactant solvent media more suitable for spectrofluorometric analysis of PAH mixtures. Larger emission intensities lead to lower detection limits. Unfortunately, one cannot use the cetylpyridinium cation as a selective quenching agent in combination with zwitterionic surfactants because changes in micellar structure lead to decreased emission intensities for both alternant and nonalternant PAHs as shown in Table 2, Table 3, Table 4 and Table 5. Our published studies [26,56] have shown however, that nitromethane does retain its quenching selectivity in the presence of zwitterionic micelles.

The decreased fluorescence emission noted in mixed CTAC + SB-12 and CTAC + SB-16 micelles can be rationalized in terms of changes in micellar structure caused by the strong coulombic

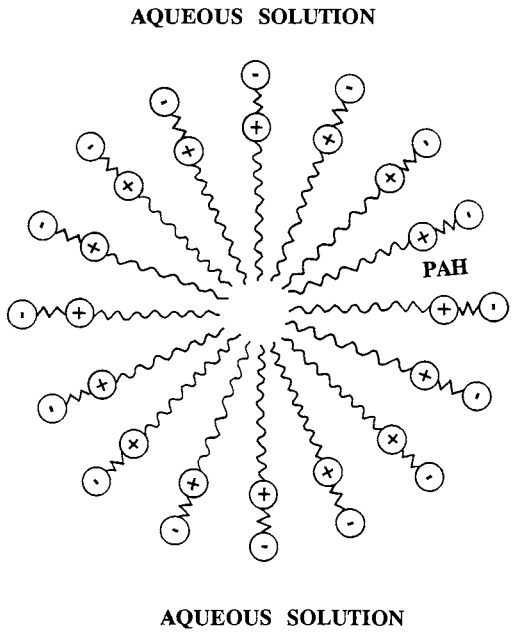

Fig. 2. Pictorial representation of a spherical zwitterionic micelle. The likely location of the PAH fluorophore is between the cationic and anionic charges of the zwitterionic surfactant.

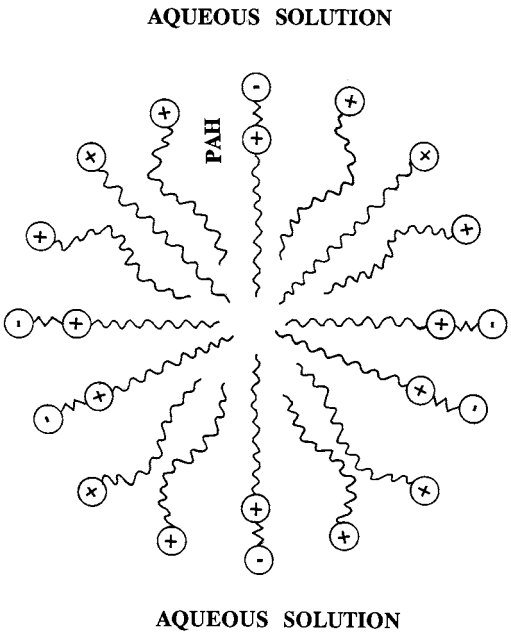

Fig. 3. Pictorial representation of a spherical micelle containing both cationic and zwitterionic surfactants. Strong coulombic interactions between dissimilar surfactant molecules are expected to place oppositely charged heard groups in close proximity to one another. Repulsive interactions should bend the alkylchain of the cationic surfactant away from the zwitterionic surfactant's inner positively-charged ammonium group. Such interactions should lead to a less rigid micellar structure for the solubilized PAH fluorophore.

interactions. Zwitterionic surfactants have a positively-charged quaternary ammonium group and a negatively-charged sulfonate group, with the latter being further away from the micellar center than the former. The zwitterionic surfactant is neutral overall, however, an electric field does exist inside the Stern layer. The headgroup of the CTAC cationic surfactant will be attracted towards the negative outer part of the Stern layer. This will expose the CH_2 groups adjacent to the tetraalkylammonium headgroup to water, and in all likelihood will lead to a less rigid, more distorted micellar structure whenever the long CTAC alkyl-chain comes in close proximity to the SB-12/SB-16 inner positive charge. An alkyl chain is hydrophobic in nature. To the extent possible, the CH_2 linkage will orient away from the zwitterionic surfactant's ionic functional groups as shown in Fig. 3. A less rigid micellar structure will provide for more collisions and for more radiationless pathways for the excited fluorophore to return to its ground electronic state. Moreover, the distorted micellar structure may allow greater oxygen penetration into the 'inner charge' region of the micelle, which in turn would further reduce PAH emission intensities. Oxygen is known to quench the fluorescence emission of polycyclic aromatic hydrocarbons [47,57], and is known to preferentially adsorb near a positively-charged quaternary ammonium surface as opposed to a negatively-charged anionic headgroup [58]. This would place the oxygen in close proximity to the solubilized polycyclic aromatic hydrocarbons. In the case of the more rigid zwitterionic micellar structure oxygen would not be able to penetrate as far into the 'inner charge' region, and in all likelihood would be adsorbed at the outer sulfonate group.

Acknowledgements

This work was supported in part by the University of North Texas Research Council.

References

[1] E. Sawicki, T.W. Stanley, W.C. Elbert, Talanta 11 (1964) 1435.
[2] E. Sawicki, W.C. Elbert, T.W. Stanley, J. Chromatogr. 17 (1965) 120.
[3] G.P. Blümer, M. Zander, Fresenius Z. Anal. Chem. 296 (1979) 409.
[4] F.K. Ogasawara, Y. Wang, V.L. McGuffin, Appl. Spectrosc. 49 (1995) 1.
[5] E. Zimmerman, Quantum Mechanics for Organic Chemists; Academic Press: New York, 1975, pp. 145–146.
[6] J. March, Advanced Organic Chemistry: Reactions, Mechanisms and Structure; McGraw-Hill: New York, 1968, pp. 46–48.
[7] S.A. Tucker, H. Darmodjo, W.E. Acree Jr., M. Zander, E.C. Meister, M.J. Tanga, S. Tokita, Appl. Spectrosc. 46 (1992) 1630.
[8] S.A. Tucker, W.E. Acree Jr., C. Upton, Appl. Spectrosc. 47 (1993) 201.
[9] S.A. Tucker, W.E. Acree Jr., C. Upton, Polycyclic Aromatic Compounds 3 (1993) 221.

[10] S.A. Tucker, W.E. Acree Jr., B.P. Cho, R.G. Harvey, J.C. Fetzer, Appl. Spectrosc. 45 (1991) 1699.
[11] V.L. Amszi, Y. Cordero, B. Smith, S.A. Tucker, W.E. Acree Jr., C. Yang, E. Abu-Shaqara, R.G. Harvey, Appl. Spectrosc. 46 (1992) 1156.
[12] S.A. Tucker, H. Darmodjo, W.E. Acree Jr., J.C. Fetzer, M. Zander, Appl. Spectrosc. 46 (1992) 1260.
[13] S.A. Tucker, W.E. Acree Jr., Appl. Spectrosc. 46 (1992) 1388.
[14] S.A. Tucker, W.E. Acree Jr., J.C. Fetzer, R.G. Harvey, M.J. Tanga, P.-C. Cheng, L.T. Scott, Appl. Spectrosc. 47 (1993) 715.
[15] S.A. Tucker, H.C. Bates, V.L. Amszi, W.E. Acree Jr., H. Lee, P. Di Raddo, R.G. Harvey, J.C. Fetzer, G. Dyker, Anal. Chim. Acta 278 (1993) 269.
[16] S.A. Tucker, H.C. Bates, W.E. Acree Jr., J.C. Fetzer, Appl. Spectrosc. 47 (1993) 1775.
[17] S.A. Tucker, J.M. Griffin, W.E. Acree Jr., M. Zander, R.H. Mitchell, Appl. Spectrosc. 48 (1994) 458.
[18] S.A. Tucker, J.M. Griffin, W.E. Acree Jr., P.P.J. Mulder, J. Lugtenburg, J. Cornelisse, Analyst 119 (1994) 2129.
[19] S.A. Tucker, J.M. Griffin, W.E. Acree Jr., J.C. Fetzer, M. Zander, O. Reiser, A. De Meijere, I. Murata, Polycyclic Aromatic Compounds 4 (1994) 141.
[20] S.A. Tucker, J.M. Griffin, W.E. Acree Jr., M.J. Tanga, J.E. Bupp, T.K. Tochimoto, J. Lugtenburg, K. Van Haeringen, J. Cornelisse, P.-C. Cheng, L.T. Scott, Polycyclic Aromatic Compounds 4 (1994) 161.
[21] S.A. Tucker, Ph.D. Dissertation, University of North Texas, Denton, Texas, 1994.
[22] J.R. Powell, S. Pandey, B.J. Miller, W.E. Acree Jr., P.E. Hansen, J.C. Fetzer, J. Lumin. 69 (1996) 27.
[23] S. Pandey, W.E. Acree Jr., J.C. Fetzer, Anal. Chim. Acta 324 (1996) 175.
[24] S. Pandey, J.R. Powell, W.E. Acree Jr., B.P. Cho, J. Kum, C. Yang, R.G. Harvey, Polycyclic Aromatic Compounds 12 (1997) 1.
[25] S. Pandey, K.A. Fletcher, J.R. Powell, M.E.R. McHale, A.-S.M. Kauppila, W.E. Acree Jr., J.C. Fetzer, Spectrochim. Acta 57A (1997) 165.
[26] S. Pandey, W.E. Acree Jr., B.P. Cho, J.C. Fetzer, Talanta 44 (1997) 413.
[27] S. Pandey, W.E. Acree, Jr., J. C. Fetzer, Talanta, 45 (1997) 39.
[28] H. Dreeskamp, E. Koch, M. Zander, Z. Naturforsch. 30A (1975) 1311.
[29] J.H. Ayala, A.M. Afonso, V. Gonzalez, Talanta 44 (1997) 257.
[30] J.H. Ayala, A.M. Afonso, V. Gonzalez, Appl. Spectrosc. 51 (1997) 380.
[31] A. Malliaris, N. Boens, H. Luo, M. Van der Auweraer, F.C. de Schryver, S. Reekmans, Chem. Phys. Lett. 155 (1989) 587.
[32] C.A. Parker, W.J. Barnes, Analyst 82 (1957) 606.
[33] J.F. Holland, R.E. Teets, P.M. Kelly, A. Timnick, Anal. Chem. 49 (1977) 706.
[34] M.C. Yappert, J.D. Ingle, Appl. Spectrosc. 43 (1989) 759.
[35] J.R. Lakowicz, Principles of Fluorescence Spectroscopy; Plenum Press: New York, 1983.
[36] S.A. Tucker, W.E. Acree Jr., J.C. Fetzer, J. Jacob, Polycyclic Aromatic Compounds 3 (1992) 1.
[37] S.A. Tucker, V.L. Amszi, W.E. Acree Jr., J. Chem. Ed. 69 (1992) A8.
[38] S. Hashimoto, J.K. Thomas, J. Am. Chem. Soc. 105 (1983) 5230.
[39] A. Malliaris, J. Lang, R. Zana, J. Chem. Soc., Faraday Trans. I 82 (1986) 109.
[40] D.C. Dong, M.A. Winnick, Photochem. Photobiol. 35 (1982) 17.
[41] D.C. Dong, M.A. Winnick, Can. J. Chem. 62 (1984) 2560.
[42] A.K. Mukhopadhyay, S. Georghiou, Photochem. Photobiol. 31 (1980) 407.
[43] P. Lianos, A.K. Mukhopadhyay, S. Georghiou, Photochem. Photobiol. 32 (1980) 415.
[44] R. Waris, M.A. Rembert, D.M. Sellers, W.E. Acree Jr., K.W. Street Jr., C.F. Poole, P.H. Shetty, J.C. Fetzer, Appl. Spectrosc. 42 (1988) 1525.
[45] R. Waris, M.A. Rembert, D.M. Sellers, W.E. Acree Jr., K.W. Street Jr., J.C. Fetzer, Analyst 114 (1989) 195.
[46] W.E. Acree Jr., S.A. Tucker, J.C. Fetzer, Polycyclic Aromatic Compounds (and references therein) 2 (1991) 75.
[47] D.S. Karpovich, G.J. Blanchard, J. Phys. Chem. 99 (1995) 3951.
[48] J.K. Thomas, Chem. Rev. (and references therein) 80 (1980) 283.
[49] J.K. Thomas, Acc. Chem. Res. 10 (1977) 133.
[50] P. Lianos, M.-L. Viriot, R. Zana, J. Phys. Chem. 88 (1984) 1098.
[51] P. Mukerjee, J.R. Cardinal, J. Phys. Chem. 82 (1978) 1620.
[52] R.A. Pyter, C. Ramachandran, P. Mukerjee, J. Phys. Chem. 86 (1982) 3206.
[53] R.A. Pyter, C. Ramachandran, P. Mukerjee, J. Phys. Chem. 86 (1982) 3198.
[54] M. Almgren, F. Grieser, J.K. Thomas, J. Am. Chem. Soc. 101 (1979) 279.
[55] N. Kamenka, Y. Chevalier, R. Zana, Langmuir 11 (1995) 3351.
[56] W.E. Acree, Jr., S. Pandey, S.A. Tucker, J.C. Fetzer, Polycyclic Arom. Compds., 12 (1997) 71.
[57] S.A. Tucker, L.E. Cretella, R. Waris, K.W. Street Jr., W.E. Acree Jr., J.C. Fetzer, Appl. Spectroscopy 44 (1990) 269.
[58] V.V. Bryukhanov, V.C. Laurinas, Zh. Priklad. Spektrosc. (English translation) 55 (1991) 275.

ELSEVIER

Talanta 47 (1998) 779–786

Talanta

A metallic cobalt electrode for the indirect potentiometric determination of calcium and magnesium in natural waters using flow injection analysis

ZuLiang Chen *, Mark A. Adams

Department of Botany, The University of Western Australia, Nedlands, WA 6907, Australia

Received 16 December 1997; received in revised form 30 March 1998; accepted 3 April 1998

Abstract

A flow injection analysis of Ca^{2+} and Mg^{2+} using indirect potentiometric detection in natural waters is proposed, where Ca^{2+} or Mg^{2+} are injected into a buffer carrier containing phosphate, resulting in the formation of $Ca_3(PO_4)_2$ or $Mg_3(PO_4)_2$. The consequent reduction in free phosphate in the carrier solution is detected using a metallic cobalt wire electrode. Indirect electrode response was used and the experimental conditions affecting electrode response were optimized. Responses were linear in the concentration range 5×10^{-4} to 5×10^{-3} M with a detection limit of 1×10^{-5} M in 20 mM phosphate buffer at pH 8.0. The relative standard derivation at 1 mM of Ca^{2+} and Mg^{2+} were 3.9 and 3.7% ($n = 10$), respectively. EGTA and 8-hydroxyquinoline were used as the masking agents for Ca^{2+} and Mg^{2+}, respectively. Concentrations of Ca^{2+} and Mg^{2+} in natural waters were successfully determined by the proposed method. © 1998 Elsevier Science B.V. All rights reserved.

Keywords: Indirect potentiometry; Cobalt electrode; Flow injection analysis; Calcium and magnesium

1. Introduction

The development of analytical methods for the determination of Ca^{2+} and Mg^{2+} has relevance to studies of soils, natural waters, fertilizers and plants [1]. There has been a considerable increase in demand for the development of simple, low cost and rapid analytical methods, such as flow injection analysis (FIA) which, when coupled with different detection techniques, can be employed for the determination of Ca^{2+} and Mg^{2+} in a wide variety of matrices. These detection techniques generally involve atomic spectroscopy and molecular spectroscopy. For example, atomic absorption spectrophotometry (AAS) has been successfully used in FIA for the determination of Ca^{2+} and Mg^{2+} in various matrices, including silica-based materials [2], vegetables [3] and soil [4,5]. Spectrophotometry with colour reagents [6–8] and fluorimetry with different fluorescence reagents [9,10] are also frequently used to monitor Ca^{2+} and Mg^{2+} concentrations in various matrices.

* Corresponding author. Fax: +61 8 93801108; e-mail: zchen@agric.uwa.edu.au

0039-9140/98/$ - see front matter © 1998 Elsevier Science B.V. All rights reserved.
PII S0039-9140(98)00170-2

Electrochemical methods, particularly potentiometry using ion-selective electrodes (ISEs), have been used relatively infrequently in FIA for the determination of Ca^{2+} and Mg^{2+}. Calcium ISE based on PVC membranes has been proposed for the potentiometric monitoring of Ca^{2+} and water hardness (the sum of Ca^{2+} and Mg^{2+}) [11–14]. However, most such electrodes suffer from interference by cations such as Mg^{2+} and Na^{+} [13] and there are thus few reports on the use of ISEs for the determination of Ca^{2+} and Mg^{2+}. Imato et al. [12] proposed a potentiometric determination of total hardness by FIA, which used both Cu^{2+} ISE and a Cu^{2+} buffer carrier containing a Cu-EDTA complex and free EDTA. A Cu^{2+} ISE was used to monitor the change of concentration of Cu^{2+} in the buffer carrier caused by the reaction of Ca^{2+} and Mg^{2+} with free EDTA. Unfortunately, this method does not discriminate between individual Ca^{2+} or Mg^{2+}. In addition, Cu^{2+} ISE have been known to suffer from interference by chloride ions, which are often present in high concentrations in natural waters [15].

Metallic cobalt wire may be used as a phosphate ISE [16,17] and for the potentiometric determination of phosphates in FIA [18]. Such electrodes exhibit a direct response to phosphates with high selectivity and sensitivity. In this paper, indirect potentiometric detection of Ca^{2+} and Mg^{2+} was investigated as a means of extending the application of cobalt wire electrodes which are simple and cheap to construct. Indirect potentiometric response to Ca^{2+} and Mg^{2+} was employed and we examined the theoretical basis for the mode of detection. Finally, the proposed method was demonstrated for the determination of Ca^{2+} and Mg^{2+} in natural waters using 8-hydroxyquinoline and EGTA for masking Mg^{2+} and Ca^{2+} respectively, in order to discriminate between Ca^{2+} and Mg^{2+}.

2. Experimental

2.1. Reagents and solutions

Analytical grade reagents (BHD, Chemical Pty, Australia) were used in all cases. Working standards were prepared daily from a stock solution of 10 mM prepared from $Ca(NO_3)_2$ and $Mg(NO_3)_2$ by appropriate dilution. Phosphate buffer carrier solutions were adjusted to the desired pH values through the addition of 1 mM potassium hydroxide or phosphoric acid solution. Interference studies were carried out with nitrate salts.

2.2. Equipment

The flow-injection potentiometric measurements were made using a FIA system as shown in Fig. 1, which consisted of a Waters (Milord, MA) 510 HPLC pump, a mixing coil (1 m × 1 mm ID) and a Rheodyne (Cotati, CA, USA) rotary injection valve fitted with an exchangeable sample loop. The metallic cobalt indicator and silver/silver chloride reference electrodes were 0.5 mm in diameter and 4.0 cm in length. A flow cell design was used as described previously [19]. The detector was connected to a pH/digital millivolt meter. The cobalt wire electrode was removed from the cell, briefly immersed in concentrated nitric acid and then rinsed with distilled water prior to use.

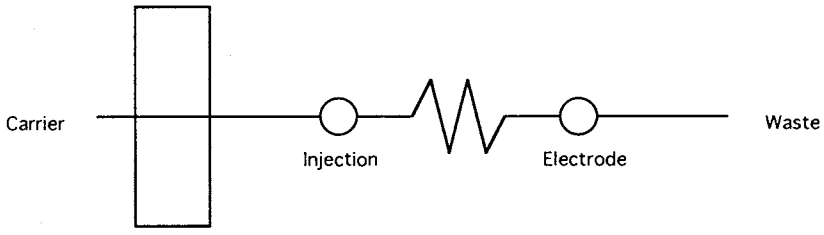

Fig. 1. Schematic of the potentiometric flow injection system.

Potentials were measured in a phosphate buffer solution and samples were manually injected using the rotary injection valve. Natural water samples were collected in 100 ml polyethylene bottle and preserved at 4°C. The natural water sample was filtered using a Millipore 0.45-μm membrane before injecting into the FIA system.

3. Results and discussion

3.1. Electrode response

In a previous paper [16–18], metallic cobalt wire electrodes were shown to have high sensitivity and selectivity towards phosphate ions. It is therefore of interest to examine the possibility of utilizing this electrode for indirect potentiometric detection of Ca^{2+} or Mg^{2+}. When a Ca^{2+} or Mg^{2+} solution is injected into a phosphate buffered carrier, precipitates of $Ca_3(PO_4)_2$ ($Ksp = 28.7$) or $Mg_3(PO_4)_2$ ($Ksp = 23.27$) are formed. Consequently, the reduction in free phosphate in carrier solutions may be detected using the metallic cobalt wire electrode. In this case, the cobalt wire electrode was oxdized to Co^{2+} at the electrode surface by brief immersion in concentrated nitric acid prior to use. The following equilibrium reactions are likely on the electrode surface [17].

$$3Co^{2+} + 2HPO_4^{2-} = Co_3(PO_4)_2\downarrow + 2H^+ \quad (1)$$

The equation is given by

$$K_1 = \frac{(H^+)^2}{(HPO_4^{2-})^2(Co^{2+})^3} \quad (2)$$

Where K_1 is the equilibrium constant based on the equilibrium (1), which can be derived in terms of the reaction (1) as,

$$K_1 = \frac{(k_3)^2}{ksp},$$

where k_3 represents the dissociation constant for HPO_4^{2-} and ksp is the solubility product constant for $Co_3(PO_4)_2$. H^+ is the carrier pH and HPO_4^{2-} is the concentration of phosphate in carrier.

At constant pH and flow rate, the potential of the metallic cobalt electrode in phosphate buffer carrier can be expressed by,

$$E_1 = C_1 + \frac{0.059}{3}\log(HPO_4^{2-}) \quad (3)$$

where C_1 is a constant and HPO_4^{3-} is the phosphate concentration in the buffered carrier.

On injection of Ca^{2+} or Mg^{2+} into a phosphate buffered carrier, precipitation of metallic phosphate salts at the electrode surface is described by:

$$Co_3(PO)_2 + 3M^{2+} = M_3(PO_4)_2 + 3Co^{2+} \quad (4)$$

Where M represents Ca^{2+} or Mg^{2+}, and the equilibrium can therefore be expressed by:

$$K_2 = \frac{(Co^{2+})^3}{(M^{2+})^3} \quad (5)$$

Where

$$K_2 = \frac{Ksp_{[Co_3(PO)_4]}}{Ksp_{[M_3(PO)_4]}},$$

and the potential of the metallic cobalt electrode is given:

$$E_2 = C_2 + \frac{0.059}{2}\log(M^{2+}) \quad (6)$$

Since the potentiometric response (peak height) in flow injection measurement is equal to the potential difference:

$$H = E_2 - E_1 \quad (7)$$

using Eqs. (6) and (3), one can obtain, at constant flow rate (constant dispersion factor):

$$H = \text{Const} + \left[\frac{0.059}{2}\log(M^{2+}) - \frac{0.059}{3}\log(HPO_4^{2-})\right] \quad (8)$$

Eqs. (3), (6) and (8) are of significance to the electrode response to Ca^{2+} and Mg^{2+}. They describe how electrode response depends on experimental conditions, such as buffer concentration and pH, on the conditional solubility product and on the flow rate. From Eq. (8), the response of the metallic cobalt wire electrode mainly depends on the concentration of the injected ions ($C_{M^{2+}}$) and the concentration of phosphate ($C_{H_2PO_4^-}$) in buffered carrier. A linear response between potential change and injected amount of tested ions

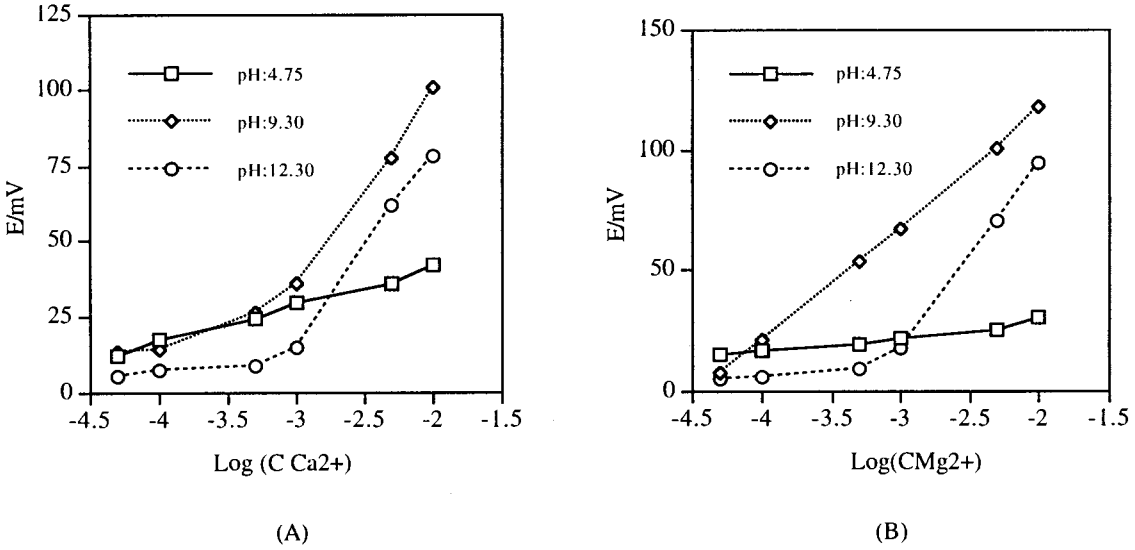

Fig. 2. Effect of pH on the electrode response using various phosphate buffer solutions (A) indirect response to Ca^{2+}; (B) indirect response to Mg^{2+}.

should be observed, e.g. if $C_{H_2PO_4^-} \gg C_{M^{2+}}$, a small change in potential should be observed. In contrast, a large change in potential would be obtained if the buffered carrier contained a low phosphate concentration.

3.2. Flow injection measurement

On the basis of Eq. (8), indirect potentiometric detection of Ca^{2+} or Mg^{2+} is influenced by the parameters: (1) the buffer solution pH; (2) the concentrations of phosphate in buffered carrier; (3) the ability of Ca^{2+} or Mg^{2+}, and Co^{2+} to react with PO_4^{3-}, HPO_4^{2-}; and (4) the flow rate. Nevertheless, initial studies were conducted to not only determine experimental conditions, but also to confirm the proposed response of the electrode as mentioned above. The influence of buffer pH on the electrode response was examined using 20 mM of different phosphate-buffered carriers, including NaH_2PO_4 (pH: 4.75), Na_2HPO_4 (pH: 9.30) and Na_3PO_4 (pH: 12.30). The results, shown in Fig. 2, demonstrate that electrode response to Ca^{2+} or Mg^{2+} significantly depends on buffer pH. Electrode response was most favourable in Na_2HPO_4 carrier and was unfavourable in NaH_2PO_4 and Na_3PO_4 carriers. A low pH buffer solution, e.g. NaH_2PO_4, lead to a decrease in electrode response due to the unfavoured formation of $Ca_3(PO_4)_2$ or $Mg_3(PO_4)_2$ as predicated in Eqs. (1) and (4). A decrease in electrode response using the a high pH carrier was also observed and may be due to side-reaction effects such as the formation of precipitates $Ca(OH)_2$ or $Mg(OH)_2$ [20] which block electrode function by forming a thin coating [21].

The influence of the phosphate concentration in the carrier on the electrode response was examined in NaH_2PO_4 solution adjusted to pH at 8.0. Fig. 3 shows the electrode response to Ca^{2+} and Mg^{2+} in 1, 10 and 100 mM phosphate carriers. The results show that an increase in phosphate concentration leads to a decrease in the electrode response. A linear relationship between the change in potential and concentrations of injected ions was found in 1 mM NaH_2PO_4 solution in a concentration range of 1×10^{-4}–1×10^{-2} M. In contrast, a low potential change was observed in a 100 mM phosphate carrier. This is in close agreement with the predication by Eq. (8). A low potential change would be observed; if $C_{H_2PO_4^-} \gg C_{M^{2+}}$ e.g. a slope of 30.2 mV per decade was obtained for Ca^{2+} and 28.7 mV per decade for Mg^{2+} in 1 mM phosphate carrier;

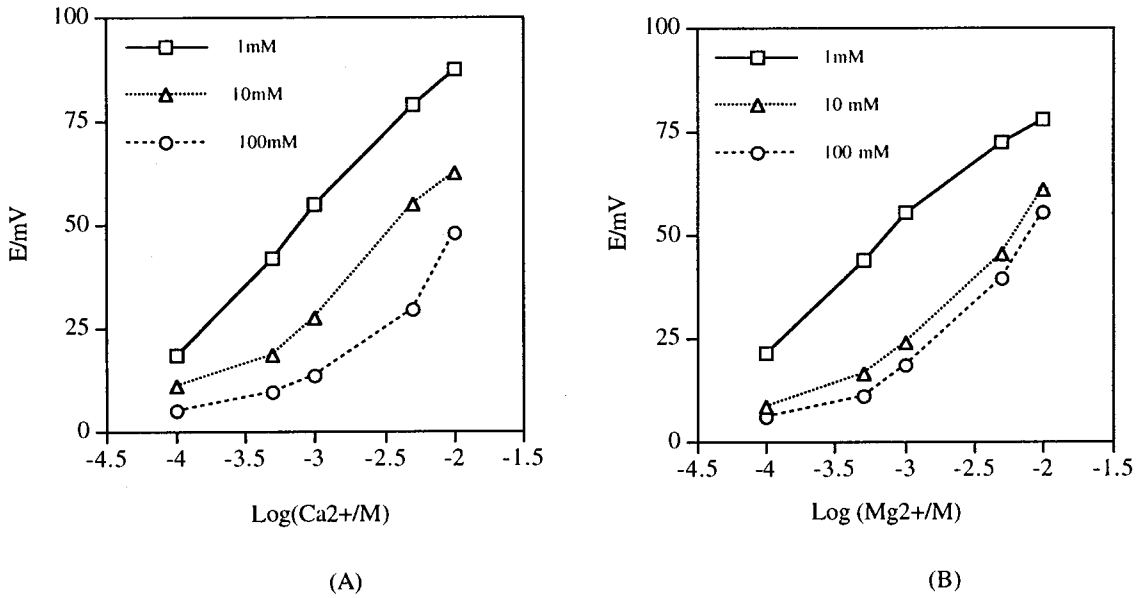

Fig. 3. Effect of phosphate concentration in buffer solution on the electrode response to Ca^{2+}; (B) indirect response to Mg^{2+}. The buffer carrier pH at 8.0, other conditions as described in Fig. 2.

these decreased to 8.1 mV per decade for Ca^{2+} and 7.3 mV per decade for Mg^{2+} in 100 mM carrier. The reductions can be attributed to the increase in phosphate concentration in carrier favouring the formation of $Co_3(PO_4)_2$ at the electrode surface as described in Eq. (1). In addition, ionic strength in the carrier buffer increases with increasing phosphate concentration, leading to an increasing background potential [22]. In view of both electrode sensitivity and buffer capacity, 20 mM phosphate buffer was used in subsequent studies.

As mentioned in the theoretical section, the electrode response also depends on the flow rate which affects sample dispersion and interaction with the electrode surface [23]. Fig. 4 shows such results from tests in a buffer carrier containing 20 mM potassium dihydrogen phosphate at pH 8.0, where the electrode response decreased as flow rate increased. Electrode potential decreased by 21 mV upon injection of a 80 μl × 1 mM Ca^{2+} or Mg^{2+} when the flow rate increased from 0.5 to 2.0 ml min^{-1} indicating that electrode response was controlled by the rate of reaction at the electrode surface. Fast rates of flow will cause the sample to pass the electrode too quickly to approach its equilibrium potential. A similar observation was reported previously for the indirect potentiometric analysis of sulfate in FIA system using lead ISE [24]. Hence, a flow rate of 1.0 ml

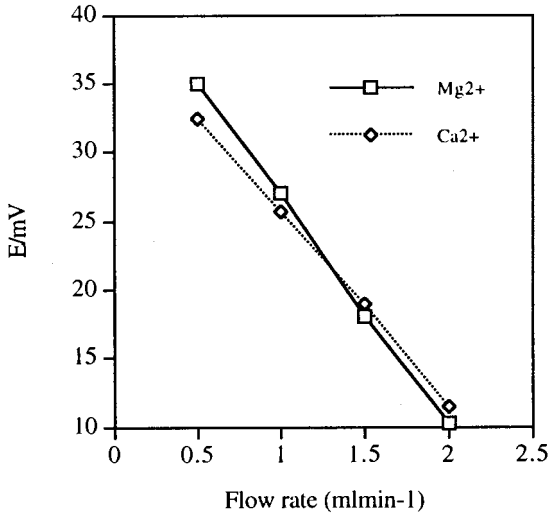

Fig. 4. Effect of flow rate on the electrode response. Other conditions as described in Fig. 2.

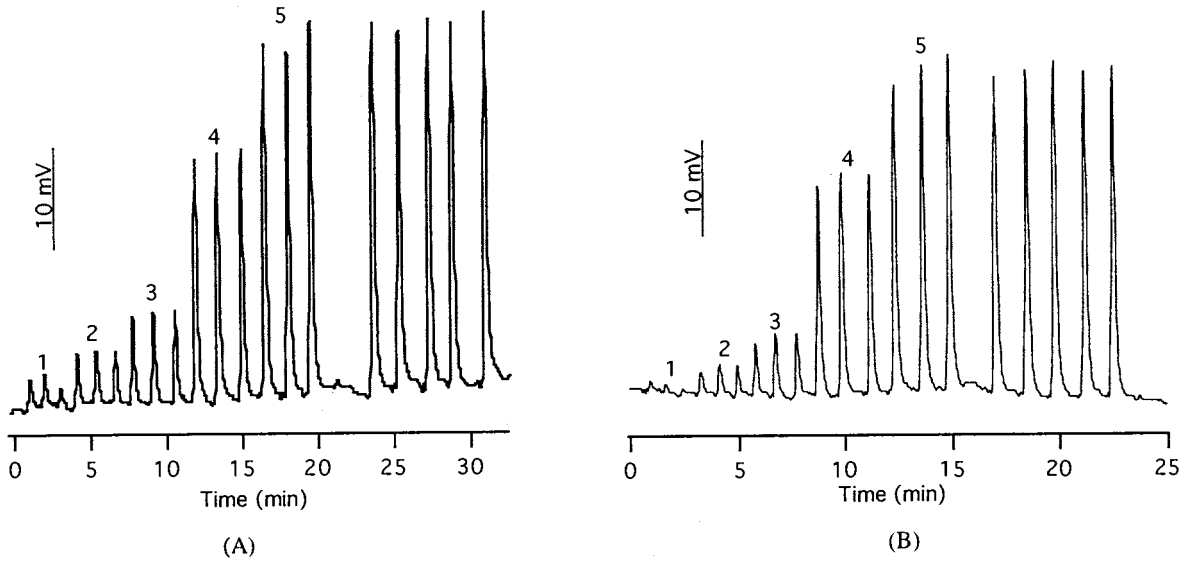

Fig. 5. Typical injection peak for the test injected in the following concentration. (A) Ca^{2+}, (1) 5×10^{-5}; (2) 1×10^{-4}; (3) 5×10^{-4}; (4) 1×10^{-3}; (5) 5×10^{-3} M. (B) Mg^{2+}, (1) 5×10^{-5}; (2) 1×10^{-4}; (3) 5×10^{-4}; (4) 1×10^{-3}; (5) 5×10^{-3} M. The buffer solution pH at 8.0, other conditions as described in Fig. 2.

min^{-1} was used in this study based on considerations of analysis speed and electrode sensitivity.

Fig. 5 shows a typical FIA recording for Ca^{2+} and Mg^{2+} obtained by injecting standards into 20 mM phosphate carrier at pH 8.0. Calibrations were based on triplicate injections of each standard. Concentrations of the tested ions ranged from 5×10^{-5} to 5×10^{-2} M. The slopes of 21.6 and 17.7 mV per decade for Mg^{2+} and Ca^{2+} were obtained with a detection limit (S/N = 3, signal to noise ratio equal to 3) of 1×10^{-5} M,. A linear relationship between injected ion and potential change was observed in the concentration range of 5×10^{-4}–5.0×10^{-3} M for Mg^{2+} and Ca^{2+}. The difference in slopes between Mg^{2+} and Ca^{2+} may result from different reaction kinetics, e.g. Ca^{2+} reacting with HPO_4^{2-} to form precipitates such as $CaHPO_4$ and $Ca_3(PO_4)_2$ [20]. Reproducibility was tested by a sequence of ten injections each of 80 $\mu l \times 1$ mM of Mg^{2+} or Ca^{2+}. Results indicate mean values of the potentiometric response of 27.0 ± 1.0 mV and 26 ± 1.0 with the relative standard deviations of 3.7 and 3.9%, respectively. The baseline potential exhibited little measurable drift and the noise level of the baseline was 0.2 mV.

3.3. Interference studies

According to Eqs. (1) and (4), cations forming a precipitate with phosphate or anions reacting with Mg^{2+} and Ca^{2+} are considered to interfere with determination of the Mg^{2+} and Ca^{2+}. Thus, ions usually present in soil and water, such as Ba^{2+}, Sr^{2+}, SO_4^{2-}, and HCO_3^- ions were tested in a 20 mM phosphate carrier at pH 8.0. In fact, the injection of standards of 1 mM Ba^{2+} and Sr^{2+} gave peak heights of 4.7 and 5.3 mV in the phosphate carrier due to formation of $Ba_3(PO_4)_2$ and $Sr_3(PO_4)_2$. In contrast, the electrode response towards SO_4^{2-} and HCO_3^- was smaller than that towards the cations tested. This agrees well with the proposed electrode response mentioned in previous section, where the potential change results in the formation of the precipitate at the electrode surface.

3.4. Determination of Ca^{2+} and Mg^{2+} in natural waters

Thuy et al. [10] suggested that Ca^{2+} and Mg^{2+} could be discriminated using masking reagents in their investigation of the fluorescence detection of

Table 1
Analysis of Ca^{2+} and Mg^{2+} in natural waters by the proposed FIA method and IC methods

Samples	Ca^{2+} (mM) ($n=5$)		Mg^{2+} (mM) ($n=5$)	
	FIA (RSD%)	IC (RSD%)	FIA (RSD%)	IC (RSD%)
1	0.53 (4.0)	0.51 (1.1)	0.12 (4.7)	0.11 (1.8)
2	0.37 (4.2)	0.36 (1.2)	0.18 (4.3)	0.17 (1.5)
3	0.15 (4.8)	0.15 (1.6)	0.13 (4.5)	0.14 (1.9)

calcein complexes of Ca^{2+} and Mg^{2+} in FIA, where 8-hydroxyquinoline was used as the masking agent for Mg^{2+} and EGTA for Ca^{2+}. Similarly, 8-hydroxyquinoline and EGTA were used for discrimination between Ca^{2+} and Mg^{2+} in this study. We tested the effects of additions of EGTA or 8-hydroxyquinoline on mixtures of Ca^{2+} and Mg^{2+} in various ratios.. For the masking of 2 mM Ca^{2+}, the best result was obtained with a 2 mM EGTA which fully eliminated Mg^{2+} interference. A similar result was obtained for the masking of 2 mM Mg^{2+} with 8-hydroxyquinoline solution, 2 mM Mg^{2+} completely disappeared upon addition of 4 mM 8-hydroxyquinoline solution. The results also show that sensitivity for Ca^{2+} or Mg^{2+} were unaffected by the presence of masking regents.

The usefulness of the proposed method was demonstrated for the analysis natural waters (samples of free soil water collected using vacuum micro-lysimeters). The results for the determination of Ca^{2+} and Mg^{2+} obtained using the proposed method, together with those from a more traditional technique such as ion chromatography with conductivity detection [25], are listed in Table 1. Results clearly indicate that the proposed FIA method is wholly comparable to the IC method and that coexisting ions in water samples show little interference with determination of Ca^{2+} and Mg^{2+}.

4. Conclusion

Concentrations of Mg^{2+} and Ca^{2+} in natural waters may be reliably quantified using an indirect potentiometric detector based on a metallic cobalt wire electrode in a flow injection analysis system. Detection depends on $Mg_3(PO_4)_2$ or $Ca_3(PO_4)_2$ precipitation when the tested ion is injected into a phosphate carrier. We have shown that the technique conforms to a theoretical understanding which was confirmed experimentally. The results obtained using a FIA system suggest the technique is characterized by a fast response, high sensitivity and selective determination of Ca^{2+} and Mg^{2+}. The proposed method is useful for the determination of Ca^{2+} and Mg^{2+} in natural waters in conjunction with masking reagents. Further research will concentrate on modifications to the FIA system to provide a masking-agent online which will assist in improving the discrimination between Ca^{2+} and Mg^{2+} while maintaining high rates of sample throughout.

Acknowledgements

The authors thank the Australian Research Council for financial support and the referees for their helpful suggestions for this article.

References

[1] R.E. Clement, G.A.Eicemen, C.J.Koester, Anal. Chem. 1985 67 (1995) 221R.
[2] I.L. Garcia, J.A. Cortez, M.H. Cordoba, Talanta 40 (1993) 1677.
[3] P. Vinas, N. Campillo, I.L. Garcia, M.H. Cordoba, Anal. Chim. Acta 283 (1993) 393.
[4] A.M.R. Ferreira, A.O.S.S. Rangeland, J.L.F.C. Lima, Commun. Soil Sci. Plant Anal. 26 (1995) 183.
[5] H. Elazouzi, M.Y. Perezjordan, A. Salvadoe, M. Delaguardia, Spectrochim. Acta Part B 51 (1996) 1747.
[6] W.D. Basson, J.F.van Staden, Analyst 103 (1981) 361.

[7] Y.A. Zolotov, E.I. Morosanova, S.V. Zhalovannaya, S.S. Dyukarev, Anal. Chim. Acta 308 (1995) 386.
[8] F. Blasco, M.J. Medina-Hernandez, S. Sagrado, F.M. Fernandez, Analyst 122 (1997) 639.
[9] H. Wada, H. Atsumi, G. Nakagawa, Anal.Chim. Acta 261 (1992) 275.
[10] D.F. Thuy, D.D. Weever, W.T. Kok, P. Luan, T.V. Nghi, Anal. Chim. Acta 295 (1994) 151.
[11] S.K.A.G. Hassan, G.J. Moody, J.D.R. Thomas, Analyst 105 (1980) 147.
[12] T. Imato, K. Ishii, N. Ishibashi, Anal. Sci. 8 (1989) 631.
[13] H. Wada, T. Ozawa, G. Nakagawa, Anal. Chim. Acta 211 (1988) 213.
[14] R.J. Forster, D. Diamond, Anal. Chem. 64 (1992) 1721.
[15] S.L. Beli, A. Zirino, Anal. Chem. 65 (1993) 2583.
[16] D. Xiao, H.Y. Hun, R.Q. Yu, Anal. Chem. 67 (1995) 288.
[17] R.K. Meruva, M.E. Meyerhoff, Anal. Chem. 68 (1996) 2022.
[18] Z.L. Chen, D.R. Marco, P.W. Alexander, Anal. Commun. 34 (1997) 93.
[19] P.W. Alexander, M. Trojanowicz, P.R. Haddad, Anal. Lett. 17 (1984) 309.
[20] J.A. Dean, Analytical Chemistry Handbook, Mcgraw-Hill, New York, 1995.
[21] D.E. Davey, D.E. Mulcahy, G.R. O' Connell, Talanta 37 (1990) 683.
[22] IUPAC Recommendation for Nomenclature of Ion Selective Electrodes, Pure Appl. Chem. 48 (1996) (1976) 127.
[23] J. Ruzicka, E.H. Hansen, Flow Injection Analysis, 2nd, Wiley, New York, 1988.
[24] T.C. Tang, H.J. Huang, Anal. Chem. 67 (1995) 2299.
[25] P.R. Haddad, P.E. Jackson, Ion Chromatography Principles and Application, Elsevier, Amsterdam, 1990.

ELSEVIER

Talanta 47 (1998) 787–796

Talanta

Low pressure chromatographic separation of inorganic arsenic species using solid phase extraction cartridges

Serife Yalçin, X. Chris Le *

Environmental Health Sciences Program, Department of Public Health Sciences, Faculty of Medicine, University of Alberta, Edmonton, AB T6G 2G3, Canada

Received 13 January 1998; received in revised form 6 April 1998; accepted 6 April 1998

Abstract

Routine water analysis of arsenic species requires simple, inexpensive, rapid and sensitive methods. To this end, we have developed two methods, which are based on the use of inexpensive solid phase extraction (SPE) cartridges as low pressure chromatographic columns for separation and hydride generation atomic absorption spectrometry (HGAAS) and hydride generation atomic fluorescence spectrometry (HGAFS) for detection of arsenic. Both anion exchange and reverse phase cartridges were successfully used to separate arsenite [As(III)] and arsenate [As(V)]. The composition, concentration, and pH of eluting buffers and the effect of flow rate were systematically investigated. Speciation of inorganic As(III) and As(V) were achieved within 1.5 min, with detection limits of 0.2 and 0.4 ng/ml, respectively. Both isocratic and step gradient elution techniques were suitable for the baseline resolution of As(III) and As(V) using anion exchange cartridges. Application of the methods to the speciation of As(III) and As(V) in untreated water, tap water, and bottled water samples were demonstrated. Results from the speciation of arsenic in a standard reference material water sample using these methods were in good agreement with the certified value and with inter-laboratory comparison results obtained using HPLC separation and inductively coupled plasma mass spectrometric detection (HPLC–ICPMS). © 1998 Elsevier Science B.V. All rights reserved.

Keywords: Solid phase extraction; Arsenic speciation; Liquid chromatography; Water analysis; Atomic spectrometry

1. Introduction

Arsenic occurs naturally in the environment in both organic and inorganic forms. In natural waters, the predominant forms of arsenic are arsenite [As(III)] and arsenate [As(V)]. The pentavalent form of arsenic dominates in oxygenated waters, but under reducing conditions, such as deep well waters, it may be present as the trivalent form [1].

Extensive epidemiological studies have been performed on a southwestern Taiwanese population [2,3], which was exposed to elevated levels of arsenic (up to mg/l concentration) from well water. There is sufficient epidemiological evidence suggesting that exposure to high levels of arsenic is associated with tumors of skin, lung, liver, and

* Corresponding author. Tel.: +1 403 4926416; fax: +1 403 4920364; e-mail: Xc.Le@UAlberta.CA

0039-9140/98/$ - see front matter © 1998 Elsevier Science B.V. All rights reserved.
PII S0039-9140(98)00171-4

bladder. There is growing concern over possible health risks associated with the chronic ingestion of low levels of arsenic in drinking water [4].

In the USA, the current maximum contaminant level (MCL) for arsenic in drinking water is 50 μg/l [5]. This level is being re-evaluated by the US Environmental Protection Agency (EPA). The alternative MCL expected in the new regulation may be as low as 2 μg/l and will likely set for total arsenic concentration [6]. US EPA is also required to develop a comprehensive study plan to reduce the uncertainty in assessing health risks associated with exposure to low levels of arsenic and to reexamine the revised MCL in year 2007 as appropriate. Because biochemical and toxicological behaviors of arsenic are strongly dependent upon the chemical species [7–9], incorporating arsenic speciation information into the health risk assessment would contribute to the reduction of uncertainty. In addition, processes for removal of arsenic from drinking water can be optimized according to actual arsenic species present in the water, arsenite or arsenate [10]. Therefore, there is a need to speciate inorganic arsenic in water.

Spectrophotometric measurement of colored arsenic complexes either with silver diethyldithiocarbamate (SDDC) [11–13], or ammonium molybdate [14,15] has been used for the determination of total inorganic arsenic. In the SDDC approach, arsenic is first reduced to arsine using zinc or $NaBH_4$. The arsine then reacts with SDDC to form a red colored complex, which is measured at the maximum absorption wavelength of 533 nm. In the molybdate method, a blue colored complex between arsenate ion and ammonium molybdate is measured.

During the last two decades, hydride generation (HG) atomic spectrometric detection techniques, e.g. atomic absorption spectrometry (AAS) and atomic fluorescence spectrometry (AFS), coupled with several separation techniques; e.g. liquid–liquid extraction [16–18], cold trapping [19–21], resin based low pressure ion exchange chromatography [22–24], selective derivatization [25], and HPLC [26,27], have brought a high level of sensitivity to speciation of arsenic compared to the colorimetric detection techniques. Many of these separation techniques, except chromatography, rely on selective detection of only one form of arsenic, usually As(III). A second aliquot of the same sample needs to be used in a separate analysis to obtain information on the other arsenic species, which is calculated from the difference between the two analyses. In some flow injection analysis applications, splitting of the sample zone allows the application of different treatment processes [28], e.g. on-line oxidation–reduction and selective sorption, to the various aliquots of the same sample, eliminating the need for separate analysis. However, this requires the use of either two detectors or detection with a time delay.

Solid phase extraction (SPE) is a convenient, inexpensive and time saving alternative to other extraction techniques. It has been often used for the clean-up and removal of organic contaminants [29–32].

Recently, SPE techniques have been applied to chemical speciation studies. Nixon and Moyer [33] and Hanna et al. [34] used cationic and/or anionic SPE cartridges, for the separation of organoarsenic species of seafood origin from others present in urine samples. Similarly, Lopez-Gonzalves et al. [35] used an anionic cartridge, placed before an HPLC column, for the retention of anionic species, and detected the cationic arsenobetaine and arsenocholine. More recently, the same group also investigated the use of anionic cartridges for preconcentration of arsenic followed by HPLC with HGAAS detection [36].

We have previously developed several analytical methods, based on HPLC separation with both atomic and mass spectrometric detection, for the speciation studies of more than a dozen arsenic compounds [26,37–40]. These methods have been successfully applied to studies of metabolism of arsenic compounds, urinary excretion of arsenic metabolites, and characterization of arsenic species in the environment. The present study focuses on arsenite and arsenate because these are two predominant arsenic species present in drinking water. The objective of the study is to develop a fast, simple and inexpensive method for the speciation of these two arsenic compounds in water.

Our approach is based on the use of a solid phase extraction (SPE) cartridge as a low pressure chromatographic separation column for the rapid

separation of arsenite and arsenate followed by hydride generation atomic spectrometric detection of arsenic. The use of inexpensive SPE cartridges eliminates the need of HPLC columns and HPLC pumps. The speciation of arsenite and arsenate in each sample is complete within 1.5 min, with a sub-ng/ml detection limit. These characteristics make the method suitable for routine arsenic speciation analysis in drinking water. In this paper, we describe the development of SPE cartridge-based techniques and demonstrate their application to the speciation of inorganic arsenite and arsenate in water samples.

2. Experimental

2.1. Instruments

The combination of SPE cartridge separation, hydride generation, and atomic spectroscopic detection is schematically shown in Fig. 1. An atomic absorption spectrophotometer (Varian, model SpectrAA-5) was used for detection unless otherwise stated. An arsenic ultra lamp (193.7 nm) was operated at 10 mA using an external control module (Varian). The spectral bandwidth was 0.5 nm. A T-shaped quartz absorption tube (Varian) heated to 925°C with a temperature controller module (Varian, model ETC-60) was used as the atomization cell. In several experiments, an atomic fluorescence detector (PS Analytical, model Excalibur 10.003) was also used. Hydride generation atomic fluorescence detection (HGAFS) was carried out using similar procedures as described previously [26,38]. A computer with a Varian Star Workstation ADC board and software was used to record and process signals from the atomic absorption or atomic fluorescence detector. Peak areas in chromatograms were used for quantitation.

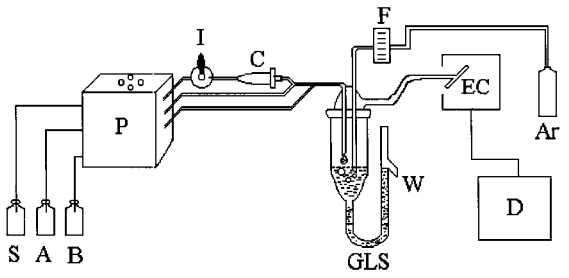

Fig. 1. A schematic diagram showing chromatographic separation on a solid phase extraction cartridge combined with hydride generation and atomic absorption detection. S, eluting buffer; A, 1 M HCl; B, 2% $NaBH_4$; I, sample injection valve; P, peristaltic pump; C, solid phase extraction cartridge; GLS, gas-liquid separator; EC, electrically heated quartz cell; Ar, argon gas; F, flowmeter; W, waste, D, atomic absorption detector. When an atomic fluorescence detector was used, have been used.

Strong anion exchange cartridges (QMA) and reverse phase cartridges (C_{18}) were obtained from Waters/Millipore (Mississauga, ON, Canada). These disposable cartridges are 2 cm in length and 1.2 cm in diameter. Each QMA cartridge contains 360 mg of hydrophilic, polar basic anion exchange phase as sorbent (pore size 300 A and particle size 37–55 μm). The C_{18} cartridges contain 360 mg of hydrophobic, non-polar bonded silica sorbent (pore size 125 A and particle size 55–105 μm). The cartridges were first preconditioned with 15 ml of methanol and then with 15 ml of the eluting buffer before being used for sample analysis.

The low pressure chromatographic separation unit utilized a four-channel peristaltic pump (Gilson, Minipuls 3) with adjustable speed. Typically, a sample was injected using a six port sample injection valve (Rheodyne) with either a 200 or 500 μl sample loop. A continuously flowing eluting buffer carried the sample to a SPE cartridge. Arsenic species were separated on the cartridge and sequentially eluted with the eluting buffer. Eluents were subsequently encountered with dilute hydrochloric acid (HCl) and sodium borohydride ($NaBH_4$) solutions. Gaseous arsenic hydrides produced from this reaction were separated from the liquid waste in a gas-liquid separator [41] and then carried by a continuous flow of argon to the atomic spectrometric detector, AAS or AFS. Hydride generation conditions were carefully optimized to achieve maximum signal to noise ratio. We found 80–100 ml/min argon flow, 1 M HCl and 2% $NaBH_4$ solution in 0.1 M NaOH to be optimum when the flow rate of these reagents were kept at 6 ml/min.

Direct flow injection analyses (FIA) were performed on the same experimental set-up except

without the use of SPE cartridges, and the same hydride generation conditions were used.

High performance liquid chromatography (HPLC) with inductively coupled plasma mass spectrometry (ICPMS) detection was also used for the speciation of arsenic in a water sample. An anion exchange column (Hamilton PRP-100X, 250 × 4.1 mm) with 50 mM phosphate buffer (pH 6.0) at a flow rate of 1.3 ml/min was used for separation. A PlasmaQuad 2 Turbo Plus ICPMS (VG Elemental) was used for the detection of arsenic at m/z 75, as described previously [37,39,40].

2.2. Standards and reagents

Sodium arsenite and sodium arsenate were obtained from commercial sources (Aldrich, Milwaukee, WI), and standard solutions were prepared through appropriate dilution with deionized water. All other reagents were of analytical grade or higher purity unless otherwise stated. Deionized water from a MAXIMA ultra-pure water system (ELGA) was used for the preparation of standard and reagent solutions. Sodium borohydride (Aldrich) in 0.1 M sodium hydroxide (Aldrich) solution was prepared fresh daily.

Ion chromatographic elution buffers, including Na_2HPO_4/NaH_2PO_4 (BDH), $Na_2B_4O_7$ (BDH), and $NaHCO_3$ (Aldrich) were prepared in deionized water. Reverse phase eluents, tetrabutylammonium chloride hydrate (TBAH) and malonic acid (Aldrich) were prepared by dissolving appropriate amounts of the reagents in deionized water. Dilute HCl or NaOH was used to adjust pH of the solution as necessary.

A standard reference material (SRM), Trace Elements in Water 1643-d, was obtained from National Institute of Standards and Technology (NIST, Gaithersburg, MD, USA). Raw water samples were obtained from a drinking water utility in Saskatchewan, Canada, and bottled waters were obtained from a local supermarket in Edmonton, Canada. One of the tap water samples was obtained from Los Angeles, California, and the other from Edmonton, Canada.

3. Results and discussion

3.1. QMA cartridge with a single eluent (method one)

The difference in dissociation constants between arsenious acid ($pKa = 9.29$) and arsenic acid ($pKa_1 = 2.25$, $pKa_2 = 6.76$ and $pKa_3 = 11.29$) [42] allows one to separate these two species on the basis of ion exchange. Their separation is pH dependent. At neutral pH, arsenious acid is not dissociated and is present as a neutral species, $As(OH)_3$. It is not expected to retain on an anion exchange cartridge. In contrast, arsenic acid is dissociated to $H_2AsO_4^-$ and is expected to elute later due to its retention on the anion exchange cartridge. Therefore, the separation of As(III) and As(V) can be achieved using an anion exchange cartridge with an ionic buffer solution as the eluent.

In order to find suitable composition and concentration of the eluting buffer, three eluents, bicarbonate, phosphate and borate were examined. Three different concentrations of each eluent, 5, 20 and 100 mM, were tested. Initially, the pH of eluents was kept at 9.0 and each eluent was used separately at a flow rate of 2 ml/min. Among the eluents used, 20 mM phosphate, 100 mM bicarbonate and 5 mM borate were found to be suitable for a baseline resolution of arsenite and arsenate. Under these conditions, the determination of arsenite and arsenate in each sample was complete in 4 min.

Further reduction of analysis time was achieved by optimizing the pH and flow rate of the eluting buffer. Three types of elution buffers, at predetermined concentrations, were used, each at several pH values between 5 and 10.5. The effect of eluent pH on signal intensity and resolution of arsenic signals is shown in Fig. 2, where 20 mM phosphate buffer was used. Both As(III) and As(V) are present as anionic species at pH 10.5, which is above pK_{a1} of both arsenic and arsenious acids. The two peaks are not well resolved. When the pH is reduced to below the pK_a of arsenious acid and above the pK_{a1} of arsenic acid, As(III) is present as a neutral species and elutes from the cartridge with the void volume, while As(V) is

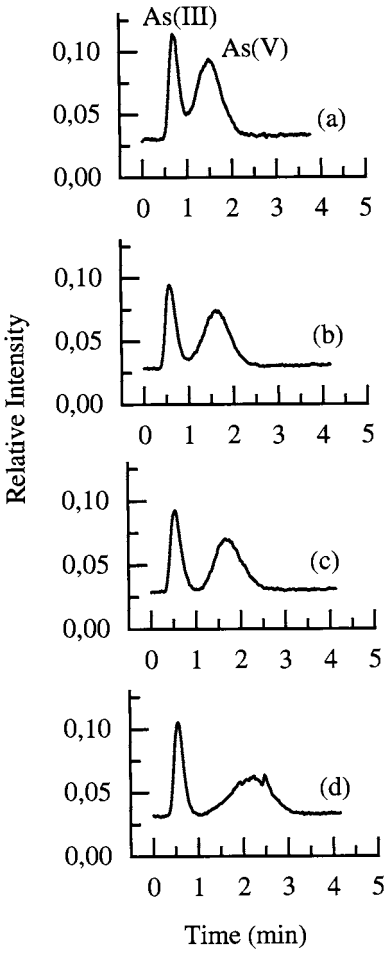

Fig. 2. The effect of pH on the separation of As(III) (4 ng/ml) and As(V) (5.2 ng/ml) using an anion exchange cartridge (QMA). Phosphate buffers with pH of 10.5 (a), 8.2 (b), 7.2 (c), and 6.0 (d) were used as eluents. The flow rate of the eluent was 4 ml/min.

dissociated as an anionic species. Thus, the difference in their ionic property is maximized, and the two peaks become better resolved from each other (Fig. 2b,c). This enhancement in resolution enabled us to increase the eluent flow rate to 4 ml/min. As a consequence, the total elution time was decreased to approximately 2 min. Further decrease of pH to 6.0 resulted in strong retention and broadening of arsenate peak (Fig. 2d). The use of bicarbonate and borate buffers in the same pH range did not improve the separation nor signal intensity over the use of phosphate buffer. Therefore, we chose to use 20 mM phosphate buffer at pH 7 for the isocratic separation of As(III) and As(V).

The flow rate of eluent was optimized to achieve baseline resolution within shortest analysis time. As expected, the analysis time was decreased almost to half when the eluent flow rate was increased from 2.5 to 5 ml/min. Flow rates outside this range were not suitable because a too slow flow rate resulted in peak broadening and longer analysis time while a too fast flow rate resulted in the loss of resolution and led to overlapping of the two peaks. We chose to use an optimum flow rate of 4 ml/min.

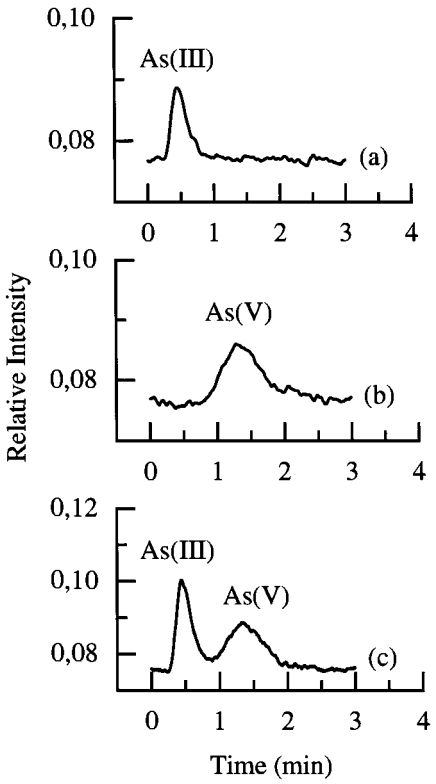

Fig. 3. Chromatograms showing the isocratic elution of As(III) and As(V) from an anion exchange (QMA) cartridge under the optimized conditions. A 20 mM phosphate buffer (pH 7) was used as the eluent at a flow rate of 4 ml/min. Atomic fluorescence detector was used for detection of (a) 1 ng/ml of As(III), (b) 1.3 ng/ml of As(V), and (c) a mixture containing 1 ng/ml of As(III) and 1.3 ng/ml of As(V).

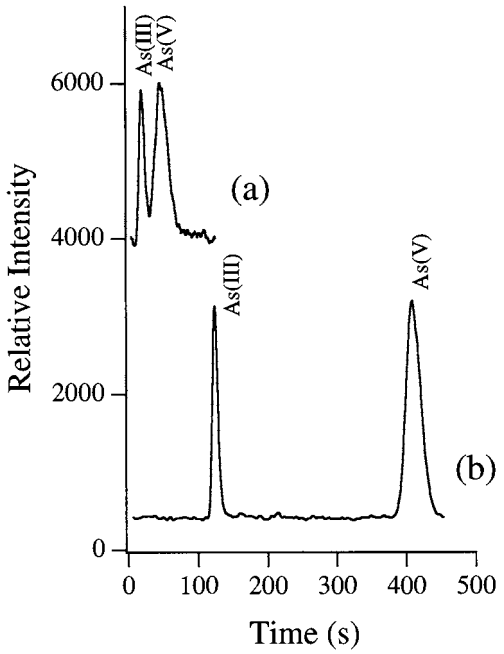

Fig. 4. Chromatograms obtained from analyses of a standard reference material, SRM 1643d water sample, using two methods. (a) QMA cartridge separation with HGAAS detection. (b) Anion exchange HPLC separation with ICPMS detection. A Hamilton PRP X-100 anion exchange column (250 × 4.1 mm, 10 μm particle size) was used for HPLC separation, with 50 mM $H_2PO_4^-$/HPO_4^{2-} buffer (pH 6.0) as the mobile phase.

Fig. 3 shows the elution of arsenate, arsenite and arsenite/arsenate mixture under optimum elution conditions: 20 mM phosphate buffer, pH 7, and flow rate 4 ml/min. At this pH, arsenious acid is fully protonated as a neutral species, [$As(OH)_3$] and eluted out first, without any appreciable interaction with the anion exchange sorbent. However, arsenate, which is highly ionized at this pH, was eluted at a later time due to its considerable ionic interaction with the QMA sorbent in the cartridge. The retention times of As(III) and As(V) remained constant whether the two species were analyzed separately (Fig. 3a,b) or in a mixture (Fig. 3c). The two arsenic species were almost baseline resolved within 2 min (Fig. 3c).

Fig. 4 shows chromatograms obtained from the analysis of a standard reference material, SRM 1643-d water, by using both the SPE cartridge separation with HGAAS detection (Fig. 4a) and HPLC–ICPMS (Fig. 4b). The HPLC–ICPMS method employed a 25-cm strong anion exchange column for chromatographic separation and ICPMS for detection of arsenic (m/z 75). The excellent resolution suggests that a much shorter column could be used for the speciation of these two arsenicals. Indeed, we have demonstrated that the separation of these species could be achieved with a 3-cm HPLC guard column [43]. The HPLC–ICPMS results show that As(III) and As(V) are the only major arsenic species present in this SRM water sample; no other arsenic species are detectable. The concentration of As(III) and As(V) obtained by using the HPLC–ICPMS method are 15.8 and 41.6 ng/ml, respectively.

The chromatogram obtained using the SPE cartridge separation and HGAAS detection method (Fig. 4a) is very similar to that by the HPLC–ICPMS method (Fig. 4b), except that much shorter time is needed using the SPE method. The SPE–HGAAS analysis of the SRM water sample also shows that As(III) and As(V) are the major arsenic species. Their concentrations are 15.2 ng/ml for As(III) and 39.9 ng/ml for As(V) from the SPE–HGAAS analysis, which are in excellent agreement with the HPLC–ICPMS results.

There is no certified value available for arsenic speciation from the SRM. However, the sum of As(III) and As(V) concentration, obtained by both SPE–HGAAS method (55.1 ng/ml) and the HPLC–ICPMS method (57.4 ng/ml) is in good agreement with the certified value of total arsenic concentration (56.02 ± 0.73 ng/ml).

The SPE–HGAAS method was further applied to the speciation of arsenic in several other water samples. Results from these analyses are summarized in Table 1. Calibration graphs constructed over the concentration range (1–10 ng/ml) of the water samples were linear with a regression coefficient of 0.999.

In addition to the speciation of As(III) and As(V), the samples were also analyzed by using a direct flow injection analysis method (FIA–HGAAS), which gives total concentration of hydride-forming arsenic species in the sample. The results are also summarized in Table 1. In all cases, the speciation results obtained by using the SPE–HGAAS method are in good agreement with the total arsenic concentration in the sample.

Table 1
Arsenic species in water samples (ng/ml)

Sample	Certified value[a]	SPE–HG–AAS/AFS*		FIA–HGAAS*
		As(III)	As(V)	Total arsenic
SRM-1643-d	56.02 ± 0.73	15.2 ± 0.9	39.9 ± 1.1	58.4 ± 1.3
Raw water[b]	—	1.8 ± 0.1	0.2 ± 0.1	—
Tap water II[c]	—	nd	3.4 ± 0.4	4.1 ± 0.2
Bottled water I[d]	9	1.6 ± 0.1	7.8 ± 0.3	9.1 ± 0.4

[a] There is no speciation information available for the reference material.
[b] From Saskatchewan, Canada.
[c] From Los Angeles, CA.
[d] Carbonated, bottled water. The label on the bottle showed reference value of arsenic concentration being 9 ng/ml.
nd, not detectable.
—, not available or not determined.
*, mean ± 1 S.D. from five replicate determinations.

3.2. QMA cartridge with two eluents (method two)

In this approach, separation of the two arsenic species on QMA cartridges was performed by using two eluents of increasing ionic strength. Several compositions and concentrations of eluents were tested in order to find a specific eluting buffer for each arsenic species. Among them, a 2–5 mM borate buffer at pH 9, and a 0.1 M bicarbonate/carbonate buffer at pH 9–11 were found suitable for the elution of arsenite and arsenate species, respectively. Arsenite was completely eluted from the QMA cartridge by using the borate buffer. Arsenate, on the other hand, was not eluted with borate in the first step and was only eluted with carbonate in the second step. Therefore, the two species were completely separated using sequential elution with the two eluting buffers. Switch of the eluting buffer from borate to carbonate immediately after As(III) was completely eluted allowed for the speciation of the two arsenic compounds within 1.5 min.

Applicability of the step gradient elution approach to the speciation of inorganic arsenic was demonstrated for water analyses. Fig. 5 shows chromatograms obtained from the analysis of a raw water sample (a) and a 5 ng/ml standard arsenic mixture (b). Eluting buffers were 2.6 mM borate (pH 9) for the first step and 0.1 M carbonate buffer (pH 11) for the second step. Switching between the buffers were made manually after the first peak (arsenite) returned to the baseline level. Therefore, a small shift observed in the retention time of arsenate in raw water with respect to that of the standard is acceptable. The amounts of arsenite and arsenate present in the raw water sample were determined to be 1.8 and 0.3 ng/ml, respectively. These results are in good agreement with those obtained by using isocratic eluting approach (Method one) as described above in Table 1.

Recovery studies were performed by applying the same speciation procedures to water samples which were spiked with known amounts of arsenic mixture. Peak shape and retention time of the arsenic species in the water samples and in the standard were consistent. Recoveries in the range of 82–104% were obtained for arsenite and arsenate, as summarized in Table 2.

Detection limits, based on three times the S.D. of blank signals, were 0.2 ng/ml for arsenite and 0.4 ng/ml for arsenate. These are similar to the detection limit obtained from the direct FIA–HGAAS analysis, which is approximately 0.3 ng/ml for both arsenic species.

3.3. Ion pair separation using C_{18} cartridges

Ion pair chromatographic separation of arsenite and arsenate was achieved on C_{18}-bonded phase silica cartridges. Ion pair chromatography is gen-

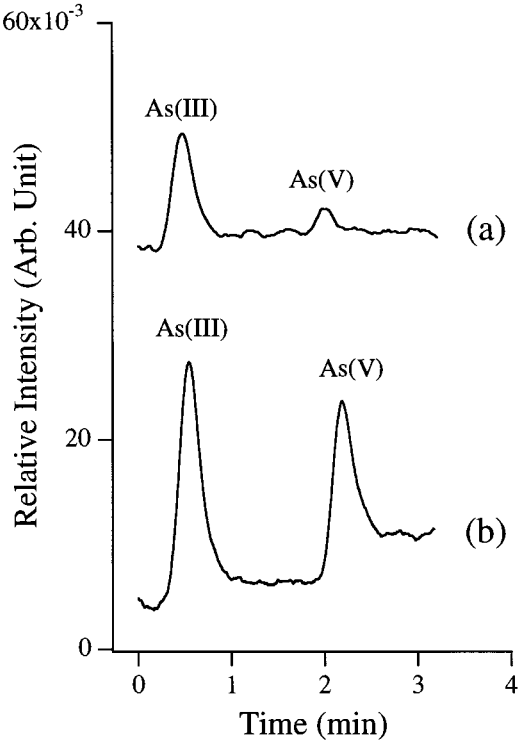

Fig. 5. Application of step gradient separation to the speciation of arsenic in a raw water sample. Elution buffers were 2.6 mM borate (pH 9) for the first step and 0.1 M carbonate (pH 11) for the second step. (a) Raw water sample and (b) 5 ng/ml As(III) and As(V) in a standard solution.

erally performed in mixed solvents. A counter ion added to the mobile phase allows for the retention of the analytes by a reverse phase mechanism. In this study, a mobile phase, which was previously used for the HPLC separation of seven arsenic species [26], consisting of tetrabutylammonium chloride (TBA), malonic acid and methanol (MeOH), was used. The effects of mobile phase pH and the composition of the reagents were investigated in the same manner as for ion exchange separation described above.

The effect of eluent pH on signal intensity, resolution and total analysis time was studied using an eluent containing 3 mM TBA, 2 mM malonic acid and 5% MeOH. As the eluent pH increased from 5.5 to 9.3, a decrease in signal intensity was observed due to the broadening in arsenate peak. Furthermore, retention times for As(III) and As(V) were increased by 25% and 150%, respectively. This may be attributable to the higher ionization ratio of the arsenic species at higher pH values. The higher ionization ratio resulted in a greater interaction between the ion pairing agent and the arsenic species; hence, the longer retention time and broader peak shape.

Fig. 6 shows chromatograms for arsenite, arsenate and arsenite-arsenate mixture. Elution of each species was complete, and there was no coelution from the two. Speciation of these two inorganic arsenic compounds can be achieved within 1.5 min. This further demonstrates the usefulness of low pressure chromatographic separation as a simple and rapid approach to the speciation of inorganic arsenic; both anion exchange and reversed phase cartridges are suitable.

Table 2
Recovery of arsenite and arsenate spiked into tap water and bottled water samples (concentration in ng/ml)

Sample	Amount present		Amount spiked		Amount determined		Recovery (%)	
	As(III)	As(V)	As(III)	As(V)	As(III)	As(V)	As(III)	As(V)
Tap water I[a]	nd	nd	2	2.7	1.7 ± 0.2	2.8 ± 0.1	85	104
Tap water II[b]	nd	3.4	2	2.7	1.8 ± 0.1	5.6 ± 0.4	90	82
Bottled water I[c]	1.6	7.8	2	2.7	3.3 ± 0.2	10.3 ± 0.3	85	92
Bottled water II[d]	nd	nd	4	—	3.5 ± 0.2	—	88	—

[a] From Edmonton, Canada.
[b] From Los Angeles, CA.
[c,d] Carbonated bottled water from a local supermarket, Edmonton, Canada.
nd, not detectable.
—, not determined.

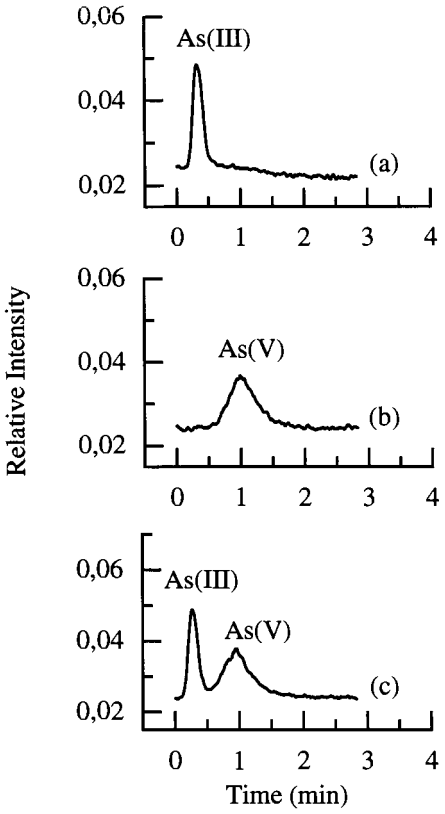

Fig. 6. Ion pair chromatographic elution of As(III) and As(V) on a C_{18} cartridge under optimized conditions. The eluent, flowing at 4 ml/min, contained 3 mM tetrabutylammonium chloride, 0.8 mM malonic acid, and 5% methanol (pH 6.0). (a) 10 ng/ml of As(III), (b) 13 ng/ml of As(V), and (c) a mixture containing 10 ng/ml of As(III) and 13 ng/ml of As(V).

4. Conclusion

The methods based on low pressure chromatographic analysis have several features in common with flow injection analysis methods, such as simplicity, low cost, and fast speed of analysis. The use of SPE cartridge separation provides necessary speciation information. The use of a larger sample loop (200–500 μl), as compared to conventional HPLC methods (10–50 μl), provides a higher concentration sensitivity. Like HPLC columns, these SPE cartridges can be reused for multiple sample analysis. We have carried out approximately 100 sample analyses using a single QMA cartridge without observing significant changes on the resolution and sensitivity. However, the cost of the SPE cartridges (approximately $3 each) is much lower than that of HPLC columns. In addition, there is no need to use high pressure HPLC pump; a peristaltic pump is sufficient to maintain a stable flow of eluent through SPE cartridges.

Acknowledgements

The authors thank Dr Jorg Feldmann of the University of British Columbia for providing HPLC–ICPMS results and Dr Joe Bergman of Buffalo Pound Water Administration Board, Saskatchewan, Canada for providing raw water samples. The authors also acknowledge American Water Works Association Research Foundation for its financial, technical, and administrative assistance in funding and managing the project (RFP 287) through which this information was discovered.

References

[1] W.R. Cullen, K.J. Reimer, Chem. Rev. 89 (1989) 713.
[2] W.P. Tseng, Environ. Health Perspect. 19 (1977) 109.
[3] C.-J. Chen, Y.-C. Chuang, S.-L. You, T.-M. Lin, H.-Y. Wu, Br. J. Cancer 53 (1986) 399.
[4] F.W. Pontius, K.G. Brown, C.-J. Chen, J. Am. Water Works Assoc. 86 (9) (1994) 52.
[5] United States Environmental Protection Agency Fed. Reg., 50:219:46936, Nov. 13, (1985).
[6] F.W. Pontius, J. Am. Water Works Assoc. 86 (9) (1994) 6.
[7] H.V. Aposhian, Rev. Biochem. Toxicol. 10 (1989) 265.
[8] M. Styblo, H. Yamauchi, D.J. Thomas, Toxicol. Appl. Pharmacol. 135 (1995) 172.
[9] H.B.F. Dixon, Adv. Inorg. Chem. 44 (1997) 191.
[10] M. Edwards, J. Am. Water Works Assoc. 86 (9) (1994) 64.
[11] W.H. Clement, S.D. Faust, Environ. Lett. 5 (1973) 155.
[12] A. Lopez, R. Torralba, M.A. Palacios, C. Camara, Talanta 39 (1992) 1343.
[13] A.G. Howard, M.H. Arbab-Zavar, Analyst 105 (1980) 338.
[14] P. Linares, M.D. Luque de Castro, M. Valcarcel, Anal. Chem. 58 (1986) 120.
[15] J.T. Van Elteren, N.G. Haselager, H.A. Das, C.L. De Ligny, J. Agterdenbos, Anal. Chim. Acta. 252 (1991) 89.
[16] T. Kamada, Talanta 23 (1976) 835.

[17] S.A. Amankwah, J.L. Fasching, Talanta 32 (1985) 111.
[18] D. Chakraborti, F. Adams, K.J. Irgolic, Fresenius Z. Anal. Chem. 323 (1986) 340.
[19] R.S. Braman, D.L. Johnson, C.C. Foreback, J.M. Ammons, J.L. Bricker, Anal. Chem. 49 (1977) 621.
[20] M.O. Andreae, Anal. Chem. 49 (1977) 820.
[21] A.G. Howard, M.M. Arbab-Zavar, Analyst 106 (1981) 213.
[22] G.E. Pacey, J.A. Ford, Talanta 28 (1981) 935.
[23] G.R. Ricci, L.S. Shepard, G. Colovos, N.E. Hester, Anal. Chem. 53 (1981) 610.
[24] M. Ochsenkuhn-Petropulu, K.M. Ochsenkuhn, I. Milonas, G. Parissakis, Can. J. Appl. Spectrosc. 40 (3) (1995) 61.
[25] R.K. Anderson, M. Thompson, E. Culbard, Analyst 111 (1986) 1143.
[26] X.C. Le, M. Ma, N.A. Wong, Anal. Chem. 68 (1996) 4501.
[27] A.G. Howard, J. Anal. At. Spectrom. 12 (1997) 267.
[28] L. Campanella, K. Pyrzynska, M. Trojanowicz, Talanta 43 (1996) 825.
[29] R.E. Majors, D.E. Raynie, LC-GC 15 (1997) 1106.
[30] Varian, Handbook of Sorbent Extraction Technology, 1993.
[31] J. Alberti, R. Rubio, G. Rauret, Fresenius Z. Anal. Chem. 351 (1995) 420.
[32] A. El Moll, R. Heimburger, F. Lagarde, M.J.F. Leroy, E. Maier, Fresenius Z. Anal. Chem. 354 (1996) 550.
[33] D.E. Nixon, T.P. Moyer, Clin. Chem. 38 (1992) 2479.
[34] C. Hanna, J.F. Tyson, S. McIntosh, Clin. Chem. 39 (1993) 1662.
[35] M.A. Lopez-Gonzalvez, M.M. Gomez, C. Camara, M.A. Palacios, J. Anal. At. Spectrom. 9 (1994) 291.
[36] M. Gomez, C. Camara, M.A. Palacios, A. Lopez-Gonzalvez, Fresenius Z. Anal. Chem. 357 (1997) 844.
[37] X.C. Le, M. Ma, J. Chromatog. A 764 (1997) 55.
[38] M. Ma, X.C. Le, Clin. Chem. 44 (1998) 539.
[39] X.C. Le, W.R. Cullen, K.J. Reimer, Environ. Sci. Technol. 28 (1994) 1598.
[40] X.C. Le, W.R. Cullen, K.J. Reimer, Talanta 41 (1994) 495.
[41] W.T. Corns, P.B. Stockwell, L.C. Ebdon, S.J. Hill, J. Anal. At. Spectrom. 8 (1993) 71.
[42] D.R. Lide (Ed.), Handbook of Chemistry and Physics, 77th Edition, CRC Press: New York, 1996, pp. 8–43.
[43] X.C. Le, M. Ma, Anal. Chem., 70 (1998) 1926.

ELSEVIER

Talanta 47 (1998) 797–801

Talanta

Short communication

Cathodic stripping voltammetry of 2,3-dichloroquinoxaline and 1,4-dichlorophthalazine reactive dyes and their hydrolysis products: Reactive Red 41 and Reactive Red 96

A. Rahim H.M. Yusoff [a], Arnold G. Fogg [a,*], Rahmalan Ahmad [b]

[a] *Chemistry Department, Loughborough University, Loughborough, Leicestershire LE11 3TU, UK*
[b] *Chemistry Department, Universiti Teknologi Malaysia, 80990 Johor Bahru, Malaysia*

Received 7 October 1997; received in revised form 17 February 1998; accepted 20 February 1998

Abstract

Preliminary studies of the feasibility of monitoring by cathodic stripping voltammetry the hydrolysis of two further types of reactive dyes have been made. The azo reduction peak in differential pulse cathodic stripping voltammograms of the 2,3-dichloroquinoxaline reactive dye, Reactive Red 41, and in those of its hydrolysis product are sufficiently separated for the hydrolysis of Reactive Red 41 to be followed using the heights of these peaks. In the case of the 1,4-dichlorophthalazine reactive dye, Reactive Red 96, the azo peaks of the reactive and hydrolysed dyes are too close to be used to monitor the hydrolysis reaction, but peaks associated with reduction of the 1,4-dichlorophthalazine group are present which could be used to monitor the hydrolysis of Reactive Red 96. © 1998 Elsevier Science B.V. All rights reserved.

Keywords: Cathodic stripping voltammetry; Reactive dyes; Hydrolysis; Reactive Red 41; Reactive Red 96

1. Introduction

Studies have been made in this laboratory of the cathodic stripping voltammetry (CSV) at a hanging mercury drop electrode (HMDE) of various types of reactive dye and their hydrolysis products, e.g. anthraquinone-based chlorotriazine reactive dyes [1–4], azotriazine reactive dyes with different leaving groups [5], and copper-complexed azosulfatoethylsulfone reactive dyes [6,7]. A main point of our work has been to show that CSV at an HMDE is a very convenient technique for determining these dyes at nanomolar levels and for monitoring their hydrolysis at these levels. The ability to monitor the hydrolysis of reactive dyes is important because hydrolysis is a major side reaction in the reaction of the dyes with cellulose or wool, i.e. in the dyeing process, and a major cause of pollution.

* Corresponding author. Tel.: +44 1509 222562; fax: +44 1509 223925; e-mail: a.g.fogg@boro.ac.uk

0039-9140/98/$ - see front matter © 1998 Elsevier Science B.V. All rights reserved.
PII S0039-9140(98)00089-7

Here a preliminary report on the cathodic stripping voltammetry and hydrolysis of Reactive Red 41 (**I**) and Reactive Red 96 (**II**) is presented. The reactive group in the former dye is the 2,3-dichloroquinoxaline ring and in the latter the 1,4-dichlorophthalazine ring, both of which have two active chlorine atoms.

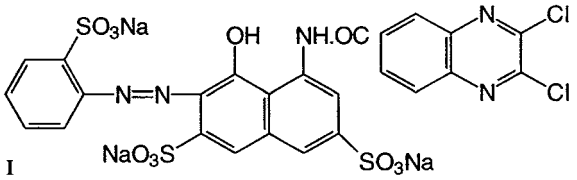

I

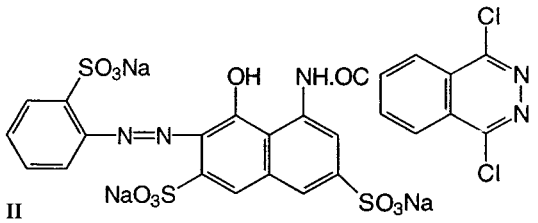

II

2. Experimental

Cathodic stripping voltammetry was carried out with a Metrohm 646/647 VA Processor, using a multi-mode electrode in the HMDE mode. The three-electrode system was completed by means of a glassy carbon auxiliary electrode and an Ag/AgCl (3 M KCl) reference electrode. All potentials are quoted relative to this reference electrode. Differential-pulse voltammetry was carried out with a pulse amplitude of 50 mV, a scan rate of 10 mV s^{-1} and a pulse interval of 1 s.

Britton Robinson buffer (BRB) was prepared by dissolving boric acid (2.47 g), orthophosphoric acid (2.7 ml) and glacial acetic acid (2.3 ml) in water and diluting to 1 l. Appropriate volumes of this solution were adjusted to the required pH with sodium hydroxide solution (3 M).

Samples of Reactive Red 41 and Reactive Red 96 were kindly provided by Zeneca Specialties (now BASF).

The general procedure used to obtain cathodic stripping voltammograms was as follows: a 20-ml aliquot of buffer was placed in the voltammetric cell and the solution was purged with nitrogen for 6 min with the stirrer on. After an initial blank run, the required volume of dye solution was added by means of a micropipette. After forming a new mercury drop accumulation was effected for the required time at the predetermined accumulation potential whilst the solution was stirred. The small mercury drop size was used on the Metrohm 647VA stand. At the end of the accumulation period the stirrer was switched off and after 10 s had elapsed to allow the solution to become quiescent a negative-going potential scan was initiated. When further volumes of sample or reagents were added the solution was deoxygenated for a further 20 s before producing further voltammograms.

Hydrolysis reactions were carried out at the 1.0×10^{-4} M level. Small aliquots were taken by micropipette at suitable time intervals and added to 20 ml of pH 7.0 Britton Robinson buffer in the voltammetric cell for analysis. Voltammetry was carried out at room temperature (about 20°C).

3. Results and discussion

3.1. Reactive Red 41

In differential pulse cathodic stripping voltammetry as well as in differential pulse polarography of this compound peaks corresponding to the reduction of the azo group predominate at relatively positive potentials. At pH 7.0 the peak of the reduction of the azo bond at -0.55 V is accompanied by another peak at about -1.0 V (Figs. 1 and 2), which corresponds probably to the reduction of the dichloroquinoxaline moiety.

In the course of hydrolysis at 80°C in 0.1 M sodium hydroxide solution the peak of the azo group of the reactive dye at -0.55 V rapidly decreases and is replaced by the azo peak of the hydrolysed dye at -0.68 V. The height of the latter peak increases even after the peak at -0.55 V decreases to zero (Fig. 1(a)). The peak at -1.0 V is decreased slightly and a new peak at about -1.07 V is formed.

When the hydrolysis is carried out at room temperature (about 20°C), the decrease in the azo

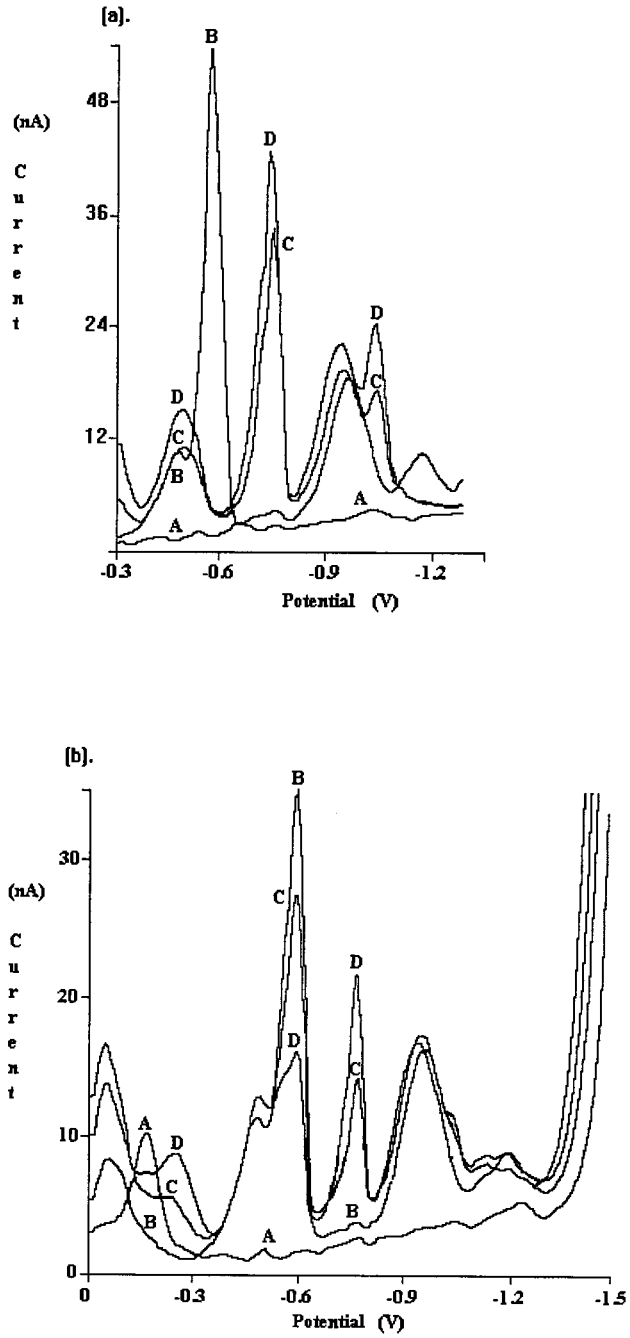

Fig. 1. Differential pulse cathodic stripping voltammograms at pH 7.0 (Britton-Robinson buffer) used to monitor the hydrolysis of Reactive Red 41 in 0.1 M sodium hydroxide solution. Initial dye concentration in voltammetric cell = 5.0×10^{-7} M. Accumulation time = 30 s. (a) Hydrolysis at 80°C. Accumulation potential = -0.3 V. A, buffer only. Hydrolysis time = B, 0; C, 2 and D, 4 min. (b) Hydrolysis at room temperature. Accumulation potential = 0 V. A, buffer only. Hydrolysis time = B, 0; C, 5 and D, 10 min.

peak at −0.55 V is slower and the increase in the reduction peak of the azo group in the hydrolysis product at −0.68 V seems to correspond to the decrease of the peak at −0.55 V. The peak at −1.0 V remains practically unchanged and the peak at −1.07 V is not formed.

Studies of the kinetics of hydrolysis are probably best studied by following either the decrease of the peak at −0.55 V or the increase of the peak at −0.68 V.

3.2. Reactive Red 96

Differential pulse cathodic stripping voltammograms of the dye show four peaks; at −0.45, −0.68, −0.85 and −1.05 V (Fig. 3). Both at 80°C and at room temperature (about 20°C) in 0.1 M sodium hydroxide solution the peaks at −0.45, −0.85 and −1.05 V decrease with time. At room temperature the decrease is relatively the same for all three peaks. At 80°C the peaks at −0.85 and −1.05 V decrease faster than the peak at −0.45 V.

It is assumed that the peak at −0.68 V corresponds to the reduction of the azo group and is somewhat greater for the hydrolysed dye compared with the reactive dye. The three peaks at

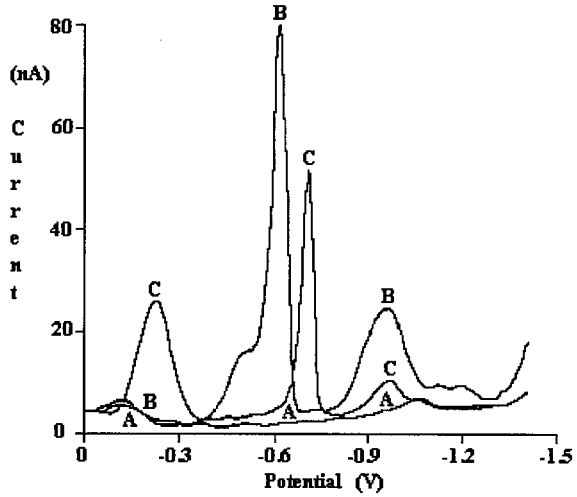

Fig. 2. Differential pulse cathodic stripping voltammograms for Reactive Red 41 (B) and hydrolysed Reactive Red 41 (C) in pH 7.0 Britton Robinson buffer. Dye concentration = 5×10^{-7} M. A, buffer only.

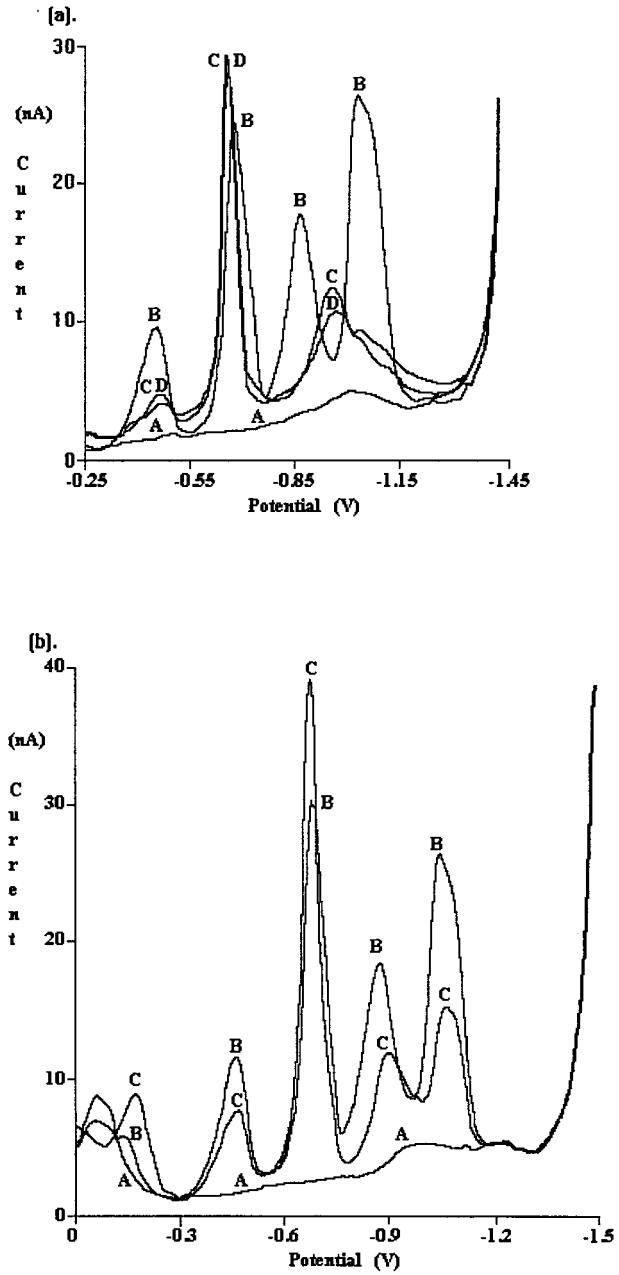

Fig. 3. Differential pulse cathodic stripping voltammograms at pH 7.0 (Britton-Robinson buffer) used to monitor the hydrolysis of Reactive Red 96 in 0.1 M sodium hydroxide solution. Initial dye concentration in voltammetric cell = 5.0×10^{-7} M. Accumulation time = 30 s. (a) Hydrolysis at 80°C. Accumulation potential = −0.25 V. A, buffer only. Hydrolysis time = B, 0; C, 2 and D, 4 min. (b) Hydrolysis at room temperature. Accumulation potential = 0 V. A, buffer only. Hydrolysis time = B, 0 and C, 3 h.

−0.45, −0.85 and −1.05 V were attributed to the reduction of the phthalazine moiety. The decrease of these peaks with time can be used for monitoring the hydrolysis of this dye.

The elucidation of the mechanism of the hydrolysis will involve the identification of the products and possible intermediates formed and the investigation of the kinetics over a wide pH range.

Acknowledgements

The authors thank Dr J.A. Taylor of BASF for his interest in this project and for providing the samples of dyes. A.R.H.M. Yusoff would like to thank the Universiti Teknologi Malaysia for financial support and leave of absence. The authors also thank Professor P. Zuman for helpful discussions.

References

[1] A.G. Fogg, M.V.B. Zanoni, Anal. Proc. 31 (1994) 173.
[2] M.V.B. Zanoni, A.G. Fogg, Anal. Proc. 31 (1994) 217.
[3] M.V.B. Zanoni, A.G. Fogg, J. Barek, J. Zima, Anal. Chim. Acta 315 (1995) 41.
[4] M.V.B. Zanoni, A.G. Fogg, J. Barek, J. Zima, Anal. Chim. Acta (in press).
[5] J. Barek, A.G. Fogg, J.C. Moreira, M.V.B. Zanoni, J. Zima, Anal. Chim. Acta 320 (1996) 312.
[6] A.G. Fogg, A.R.H.M. Yusoff, R. Ahmad, Talanta 44 (1997) 125.
[7] A.G. Fogg, A.R.H.M. Yusoff, R. Ahmad, Malaysian, J. Anal. Chem. (in press).

ELSEVIER

Talanta 47 (1998) 803–809

Talanta

Short communication

Purification of soluble fulvic acid low concentrations by a diafiltration technique

N. Calace, F. De Paolis, F. Minniti, B.M. Petronio *

Department of Chemistry, University of Rome 'La Sapienza', P.le Aldo Moro 5, 00185 Roma, Italy

Received 3 November 1997; received in revised form 13 March 1998; accepted 16 March 1998

Abstract

The purification of soluble fulvic acids (FA) based on a diafiltration technique is carried out on antarctic water and snow samples, characterised by low humic compound content (0.1–0.8 mg/l). Results are compared with those of FA purified with the dialysis technique that, together with ion-exchange resins, performs an often used purification process. With the adopted procedure it is possible to minimise the high content of inorganic salts deriving in part from the isolation method XAD-8 adopted, as shown by FTIR, elemental and thermogravimetric analysis. © 1998 Elsevier Science B.V. All rights reserved.

Keywords: Antarctica; Diafiltration; Purification; Soluble fulvic acids

1. Introduction

Humic substances, which constitute a ubiquitous class of naturally occurring polyelectrolytic organic compounds, are known to act as complexing agents for inorganic ions, and to aid in the movement of less-soluble organic compounds such as pesticides.

They are present both in solid matrices, such as soils and sediments, and in liquid matrices, such as seawater and freshwater. Extraction and purification procedures of humic compounds reported in the literature [1,2] for soils and sediments can be considered satisfactory; for waters, on the contrary, some problems can derive from the low concentration of dissolved organic matter. Adsorption chromatography into macroporous resins has been largely applied [3–5] to remove dissolved humic compounds, that are mainly constituted from fulvic acids; in particular, Thurman and Malcolm [6] have developed a procedure based on adsorption chromatography on XAD-8 resin, ion-exchange chromatography and lyophilisation, to recover aquatic humic compounds and to separate them from inorganic salts and non-acidic organic components. This method involves the use of multiple cycles of adsorption on XAD

* Corresponding author. Tel.: + 39 6 49913723; fax: + 39 6 49913723; e-mail: petroniobm@axrma.uniroma1.it

0039-9140/98/$ - see front matter © 1998 Elsevier Science B.V. All rights reserved.
PII S0039-9140(98)00128-3

resins and desorption both in acidic and basic medium to concentrate humic substances.

With this procedure we have treated antarctic water and snow samples. In this particular case it was necessary to employ very large quantities of sample (100 l), due to the low concentration of humic compounds in all kinds of antarctic matrices, because of the typical environmental conditions of Antarctica. Results concerning humic compounds obtained have not been satisfactory, especially with regard to thermogravimetric and elemental analyses data. It is our opinion that the purification procedure adopted is not adequate for samples with very low organic matter content, even if after adsorption of humic compounds on to XAD-8 resin, NaCl excess is removed by rinsing the column with one bed volume of deionised water and in the following step fulvic acids, recovered by a column with 0.1 N NaOH solution, are passed through a strong cation-exchange resin in the hydrogen-saturated form to convert the sodium salt of fulvic acids to its free-acid form. Same results are obtained when a dialysis technique is substituted for the ion-exchange resin treatment.

In this paper we present the results obtained on FA recovered by the Thurman procedure from antarctic water and snow samples and purified by the diafiltration technique. Results obtained by diafiltration are compared with those obtained with dialysis. Indeed, the aim of this paper is to point out that FA purification by dialysis, achieved by establishing concentration equilibrium across the membrane, is not complete.

Ultrafiltration experiments using Amicon cell and membranes have been previously conducted by Buffle et al. [7,8] for the separation and fractionation of organic ligands in fresh waters and for the separation of fulvic and humic acids from dissolved low-molecular weight compounds ($M_w < 200$), and by Shaw et al. [9] to evaluate the molecular size distribution of dissolved humic substances.

2. Materials and methods

2.1. Material

Soluble fulvic acids (FA) were obtained from superficial sea water and snow samples collected in Antarctica during Italian expeditions in 1994/95 and 1995/96. Antarctic samples have been selected owing to the low content of dissolved humic material.

Amberlite XAD-8 resin was obtained from Merck (Germany). In order to obtain the elimination of organic compounds (e.g. hydrolysed acrylic acid) bleeding of XAD-8 columns (500 and 36 ml) we performed, according to the literature [1–3,6], a resin cleaning by soxhlet sequential extractions for 24 h with methanol, diethyl ether, acetonitrile and methanol. Hence the resin is packed in glass columns and rinsed five times with 0.1 N NaOH and 0.1 N HCl alternatively, and then washed with deionised water until dissolved organic carbon (DOC) concentration is less than 0.3 mg l^{-1} (deionised water).

Millipore polycarbonate filters with diameter of 90 mm and pore size of 0.45 μm were used for filtration.

Spectra/Por Cellulose Ester tubular membranes with molecular weight cut off of 500 Da, diameter of 10 mm and volume of 0.79 ml per 1 cm of length were used for dialysis. Washing solution was deionised water.

2.2. Apparatus

An Amicon stirred ultrafiltration cell, model 8400, capacity 400 ml, equipped at the bottom with a 500-Da membrane disc (diameter 76 mm) was used. The cell is connected to a reservoir (5 l) containing washing solution (deionised water, pH 4.9) which is nitrogen pressurised (4 atm). Varying the operational conditions, the cell can be used under nitrogen pressure (3.5 atm) without interfacing with the reservoir. In this way it can work in preconcentration conditions. The system is shown in Fig. 1.

A Perkin-Elmer thermogravimetric balance model TGA 7, working in a nitrogen atmosphere at between 50 and 1300°C, with a heating rate of 10°C min^{-1}, and with 1.5 mg of sample, was used.

A Philips FTIR spectrometer model PU9800

was used, working in the diffuse reflectance mode. The samples have been prepared by mixing the dried residue (1 mg) with water-free KBr (100 mg); the spectrum was registered against a water-free KBr blank. Operating conditions were: 100 scans; resolution, 4 cm^{-1}; apodisation, normal; wavenumber range, 4000–400 cm^{-1}. The results were given in Kubelka Munk units deriving from a mathematical formula applied to diffuse reflectance spectra.

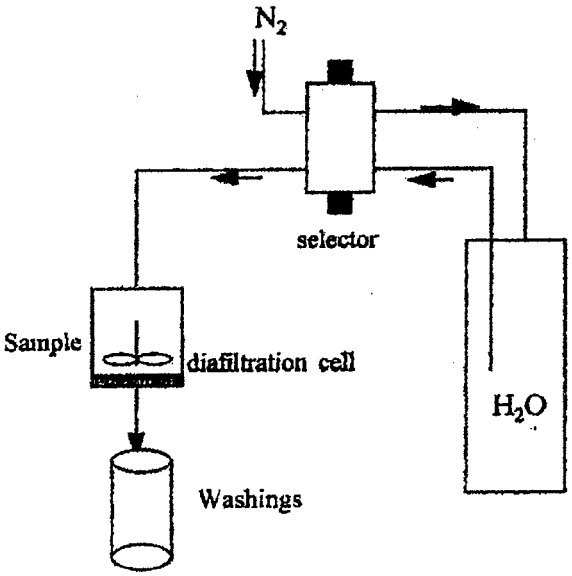

Fig. 1. Scheme of the diafiltration system.

Table 1
Concentrations of FA purified both with diafiltration and with dialysis

	FA (mg l^{-1})[a]	
	Dialysis	Diafiltration
Sea samples		
Sample 1	3.89	0.81
Sample 2	9.17	0.33
Sample 3	3.28	0.20
Sample 4	5.95	0.13
Snow samples		
Sample 5	3.14	0.14
Sample 6	1.89	0.14

[a] Determined by weighing of solid remainders.

Elemental analyses (Carlo Erba 240-B model) were carried out in the Microanalysis Laboratory of the Italian Research Council, Monte Libretti, Rome (Italy).

2.3. Recovery of fulvic acids (FA)

Liquid samples (100 l), after filtration on 0.45-μm polycarbonate filters, were acidified to pH 2 with concentrated hydrochloric acid and passed through two XAD-8 resin columns (500 and 36 ml, respectively). Humic material was recovered by eluting columns with 0.1 M NaOH, then the basic extract (150 ml) was acidified to pH 2 with hydrochloric acid in order to separate humic acids (precipitate) from fulvic acids (soluble in acid solution).

Some blanks on XAD-8 columns were carried out following the same procedure used to recover samples; organic blanks are not found in any cases.

2.4. Purification of fulvic acids

(a) Acid solution (12–28 mg DOC l^{-1}) containing fulvic acids (pH 2) was neutralised with concentrated NaOH and put in the ultrafiltration cell and the following steps were carried out.

Step one: the cell was not connected to the reservoir. Under nitrogen pressure the solution was concentrated to 10 ml. Under these conditions gas pressure was applied directly to cell. Solute greater than the molecular weight cutoff of the membrane (500 Da) is retained in the cell, and water and solutes smaller than the molecular weight cutoff pass into the filtrate (1.2–1.5 mg DOC l^{-1}).

Step two: the cell was connected to the reservoir. The pressurised diafiltrate solution, crossing through the cell, removes the remaining salts from the retentate without changing the volume of solution in the cell (washings, 0.5–0.8 mg DOC l^{-1}).

(b) Acid solution containing fulvic acids was concentrated with an IR lamp (60°C), put into dialysis tubes (molecular weight cutoff 500 Da)

Table 2
Elemental analysis data of FA purified both by diafiltration and by dialysis

Sample	Technique	N (%)	C (%)	H (%)	Ash (%) at 1300°C
1	Dialysis	1.92 ± 0.04	14.27 ± 0.22	2.01 ± 0.07	9.1
1	Diafiltration	<0.3	42.21 ± 1.68	5.04 ± 0.11	16.5
2	Dialysis	n.d.	1.71 ± 0.09	n.d.	4.2
2	Diafiltration	<0.3	43.89 ± 1.66	4.64 ± 0.05	11.3
3	Dialysis	n.d.	6.87 ± 0.18	1.00 ± 0.03	12.0
3	Diafiltration	<0.3	33.16 ± 1.19	3.96 ± 0.12	19.0
4	Dialysis	n.d.	n.d.	n.d.	0.5
4	Diafiltration	1.75 ± 0.04	32.51 ± 0.80	4.08 ± 0.08	11.8
5	Dialysis	n.d.	n.d.	n.d.	2.1
5	Diafiltration	2.50 ± 0.062	6.73 ± 0.65	2.54 ± 0.05	18.9
6	Dialysis	n.d.	2.55 ± 0.08	0.21 ± 0.00	10.0
6	Diafiltration	<0.3	41.22 ± 2.58	4.67 ± 0.32	17.2

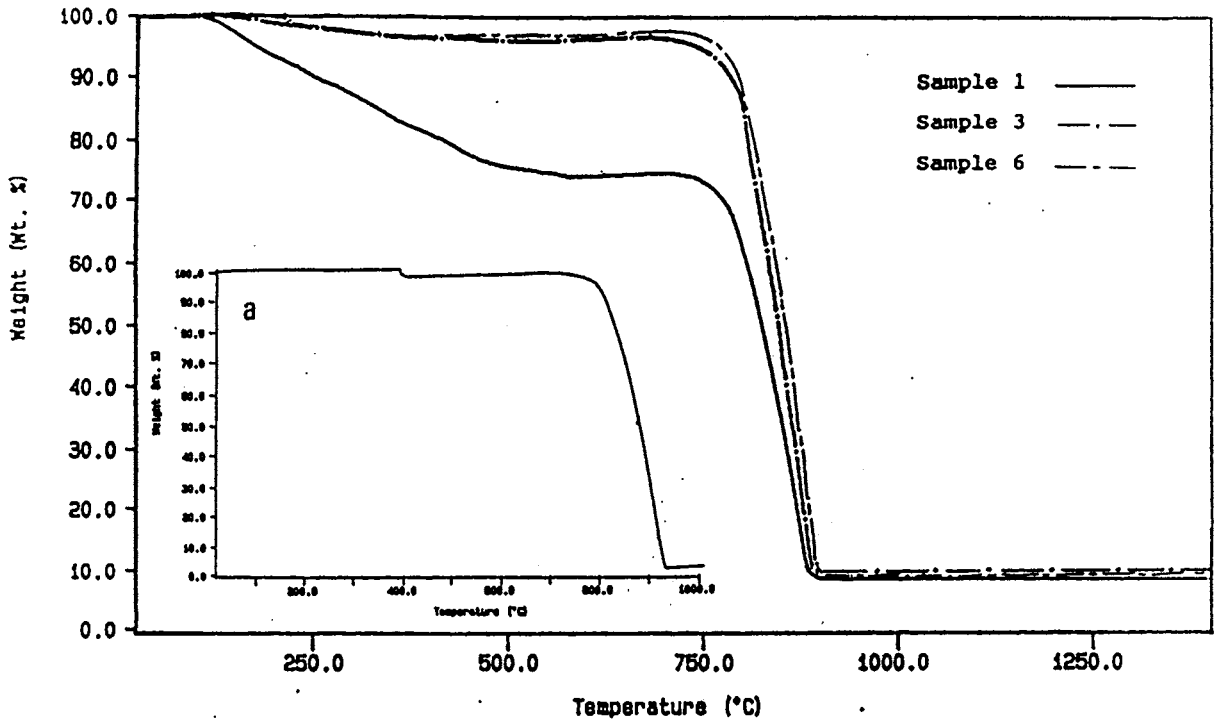

Fig. 2. Thermograms of dialysed fulvic acids and NaCl thermogram (a).

and dialysed against deionised water until chloride free.

In both cases purified solutions were lyophilised and fulvic acids characterised by the techniques reported above.

3. Results and discussion

Table 1 presents FA concentrations, determined by weighing of solid remainders of sea water samples (1–4) and snow samples (5 and 6). Data

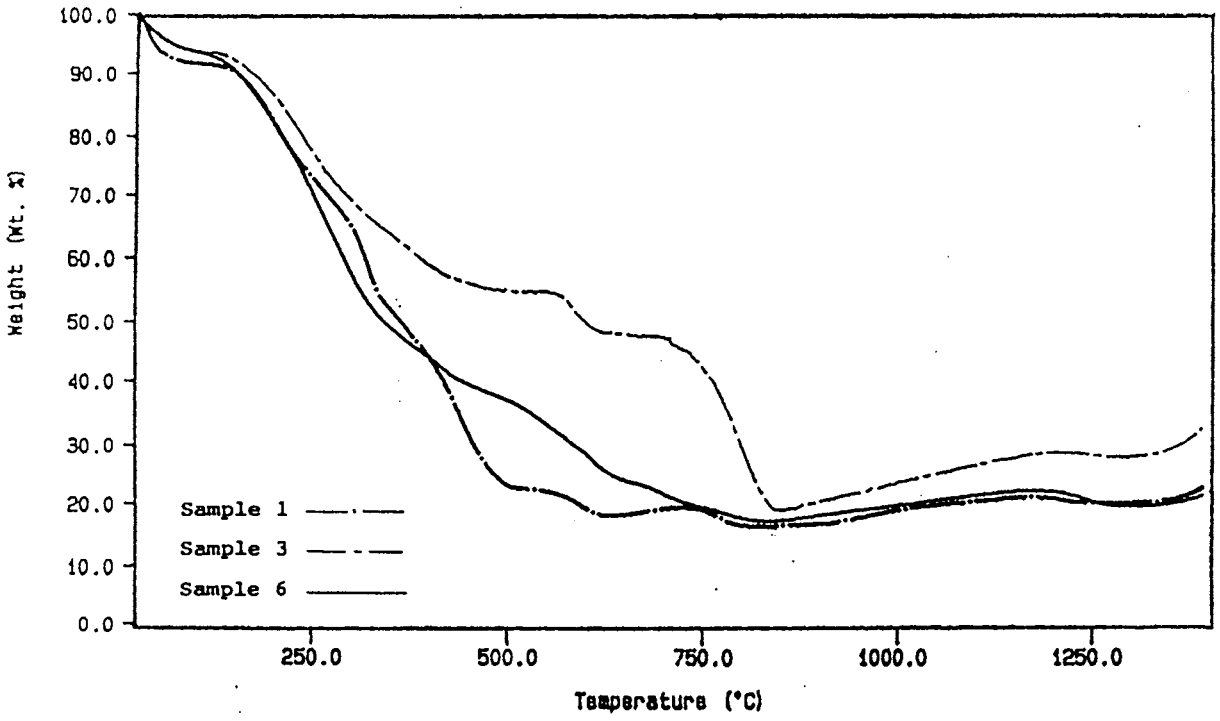

Fig. 3. Thermograms of diafiltered fulvic acids.

refer to different purification techniques. In the case of dialysed fulvic acids, the yield pattern is rather random because of the residual presence of inorganic salts. In particular Na^+ and Cl^- ions are present due to the extraction reagents used. On the other hand, data of FA yields recovered with the diafiltration technique are included in the same range.

Elemental analysis carried out on both dialysed and diafiltered fulvic acids (Table 2) highlights the negative effects of the inorganic salt presence. Indeed, as is shown by the weight loss at 800°C in the thermograms of Fig. 2, a great amount of residual inorganic salts is present in dialysed samples, even if the ash content percentage at 1300°C is lower than in diafiltered samples. The great amount of salts in dialysed samples, depressing the content organic substances, does not permit to evaluate the real content of C, N and H, and the percentage of metals bound to fulvic acids (ash contents).

The carbon, nitrogen and hydrogen content percentage in diafiltered samples, instead, approaches the literature data [10–14], showing the classical elemental distribution in dissolved fulvic substances (C 20–70%, N 0.1–5%, H 2–8% [13]). It must be emphasised that the analysed samples are from 'particular environments' such as snow and sea water, which is characterised by high ice coating and low temperature. These features decrease the fulvic acid solubility [15]; thus, the dissolved fulvic compounds are those having the highest functional group content (oxygenated groups in particular).

Thermograms (Fig. 2) obtained for dialysed samples only show a great weight loss (65% for sample 1, 90% for other samples) at about 800°C. This degradation step may be explained by thermal degradation of sodium chloride, whose thermogram (Fig. 2a) shows the same behaviour of dialysed samples. The losses of organic matter vary from 25% in sample 1 to 5% in other samples. On the contrary, thermograms carried out on diafiltered fulvic acids (Fig. 3) show a different

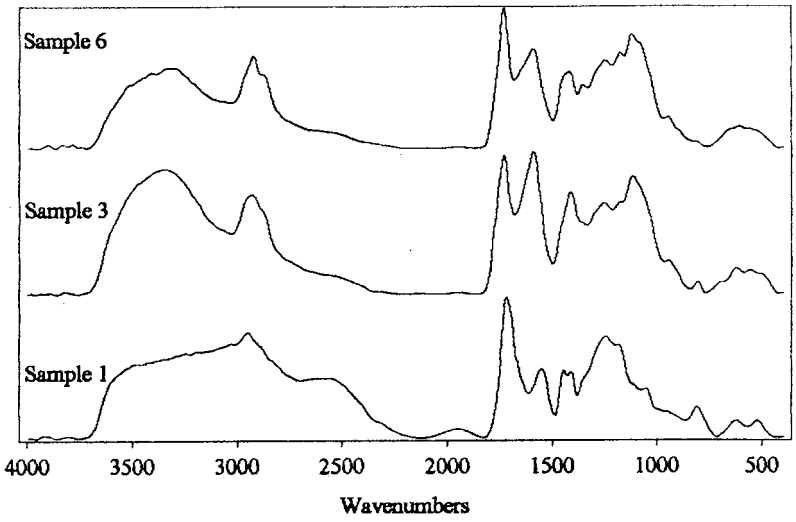

Fig. 4. FTIR spectra of fulvic acids purified with diafiltration technique.

pattern in which several steps of thermal degradation of organic matter can be noted (weight losses up to 800°C are between 80 and 90%). In this case, according to the literature data [16], weight losses below 350°C can be considered the result of thermal decomposition of carbohydrates, of the decarboxylation of acid groups, and the dehydration of hydroxylated aliphatic structures and the generation of low-molecular weight alcohols. Between 350 and 500°C the disassociation and breakdown of polyunsaturated structures and the elimination of hydrogen from the cracking of heterocyclic oxygen groups occur. After 500°C, up to 800°C, all the alicyclic carbon structures disappear. Only after 800°C can weight losses be attributed exclusively to inorganic species. FTIR spectra (Fig. 4) confirm the hydroxylated aliphatic structure and carboxyl group content with signals at 2930, 2880 and 1430 cm^{-1} due to stretchings and bendings of $-CH_2-$, signals at 3300 and 1250–1110 cm^{-1} due to –OH, and at 1730 and 1590 cm^{-1}, respectively, due to carboxylic acids and ionised carboxyl groups.

Using diafiltration technique, beyond inorganic salts, low-molecular weight compounds are removed. Spectroscopic analyses of preconcentration water (1.2–1.5 mg DOC l^{-1}) highlight the presence of alcohols and carbonyl compounds as impurities of samples. The amount of low-molecular weight compounds removed is so low that the preconcentration water thermogram does not present the losses of organic matter. The thermogravimetric analysis pattern only shows a weight loss at 800°C due to NaCl removed by FA solution confirming the high degree of purification obtained with diafiltration.

Summarising, the results reported above point out that, in the case of dialysis, fulvic acids are not completely purified. Indeed, the dialysis method cannot totally eliminate the high inorganic salt content, since the negatively charged species diffuse very slowly and the migration of other ionic species can be restricted by the development of a potential across the membrane. Moreover, the rate of diffusion for a small ion is determined by the concentration gradient existing across the membrane, and unless the gradient is maintained at near maximum value (by continually replacing the collecting solvent) the transfer process can be quite slow. On the other hand with diafiltration the FA solution obtained from elution of XAD-8 resin (see Section 2.3) can be efficiently processed in short times and the fulvic acid recovery is maximum (99%). In spite of these advantages, Buffle et al. [7] have pointed out that, because of the possibility of adsorption processes on membranes, and molecular association and/or coagulation phenomena during the filtration, the

concentration technique by ultrafiltration is not recommended, especially if the organic matter content retained in the cell is high. In our case this problem does not occur because of low macrosolute concentration.

4. Conclusions

In natural waters, fulvic acids, an important class of organic matter, are dissolved.

The extraction procedure has been studied in depth, whereas methods for their purification are not satisfactory.

In our laboratory, a diafiltration technique has been adopted. This method, based on dialysis under pressure (N_2) preceded by preconcentration, permits to obtain a increase in concentration and the purification of the fulvic acid solutions.

In this way, it is possible to: (1) work with a smaller volume of sample; (2) speedily obtain the purified samples; (3) obtain almost total recovery of samples; and (4) obtain almost total salt removal.

References

[1] E.M. Thurman, R.L. Malcolm, G.R. Aiken, Anal. Chem. 50 (6) (1978) 775.
[2] G.R. Aiken, E.M. Thurman, R.L. Malcolm, Anal. Chem. 51 (11) (1979) 1799.
[3] G.R. Aiken, in: G.R. Aiken, D.M. McKnight, R.L. Wershaw, P. MacCarthy (Eds.), Humic Substances in Soil, Sediment and Water: Geochemistry, Isolation and Characterization, John Wiley, New York, 1985, p. 692.
[4] G.R. Aiken, in: F.H. Frimmel, R.F. Christman (Eds.), Humic Substances and Their Role in the Environment, John Wiley, New York, 1988, p. 15.
[5] R.M. Town, K.J. Powell, Anal. Chim. Acta. 271 (1993) 195.
[6] E.M. Thurman, R.L. Malcolm, Environ. Sci. Technol. 15 (1981) 463.
[7] J. Buffle, P. Deladoey, W. Haerdi, Anal. Chim. Acta 101 (1978) 339.
[8] J. Buffle, D. Perret, M. Newman, in: J. Buffle, H. van Leeuwen (Eds.), Environmental Particles, vol. 1, Lewis Publishers, Boca Raton, 1992, p. 171.
[9] P.J. Shaw, R.I. Jones, H. De Haan, Environ. Tech. 15 (1994) 765.
[10] R.F.C. Mantoura, J.P. Riley, Anal. Chim. Acta. 76 (1975) 97.
[11] C. Steelink, in: G.R. Aiken, D.M. Mcknight, R.L. Wershaw, P. Maccarthy (Eds.), Humic Substances in Soil, Sediment and Water, John Wiley, New York, 1985, p. 457.
[12] B.M. Petronio, L. Campanella, N. Calace, N. Degli Innocenti, S. Tucci, Ann. Chim. 84 (1994) 81.
[13] W.D. Huffman, H.A. Stuber, in G.R. Aiken, D.M. Mcknight, R.L. Wershaw, P. Maccarthy (Eds.), Humic Substances in Soil, Sediment and Water, John Wiley, New York, 1985, p. 433.
[14] M. Krog, C. Grøn, Sci. Total Environ. 172 (1995) 159.
[15] V.E. Artemyev, Geochemistry of Organic Matter in River–Sea System, Kluwer Academic Publishers, Dordrecht, 1996, p. 56.
[16] J.D. Sheppard, D.W. Forgeron, Fuel. 66 (1987) 232.

ELSEVIER

Talanta 47 (1998) 815–821

Talanta

Hydrogen ion-selective membrane electrodes based on alkyldibenzylamines as neutral carriers

Dong-Hoe Cho *, Koo-Chun Chung, Myon-Yong Park

Department of Chemistry, Kon-Kuk University, Seoul 143-701, South Korea

Received 21 October 1997; received in revised form 2 March 1998; accepted 3 March 1998

Abstract

New synthetic hydrogen ion-selective carriers, derivatives of dibenzylamine, have been used as neutral carriers in liquid membrane electrodes to measure pH range from 2 to 10. A H^+-selective membrane electrode based on octyldibenzylamine gave a better linear response to pH than other alkyldibenzylamines as neutral carriers. It gave a linear response over the pH range 2–10 and a slope of 56.5 mV/pH at 20°C. The electrode had fairly low electrical resistance, good potential stability and reproducibility. The selectivity coefficients towards sodium, potassium and calcium ions as well as other characteristics of the membrane electrode have been studied. © 1998 Elsevier Science B.V. All rights reserved.

Keywords: Synthetic hydrogen ion-selective carriers; Dibenzylamine; Liquid membrane electrodes; Octyldibenzylamine; Selectivity coefficients

1. Introduction

After Cremer [1] found that a glass membrane had good selectivity to hydrogen ions, it was shown that the membrane was sensitive to alkali metal ions as well. Measurements of pH are most often made by using a glass electrode. It is the most popular electrode owing to its high selectivity, reliability and dynamic pH range. But there are limitations to its use under certain circumstances. Therefore, the disadvantage of glass electrodes for biological applications presents problems associated with their high resistance, fragility and instability in hydrofluoric acid solutions or acidic solutions of fluorides. In view of electric resistance, handling and preparation, there has been considerable interest in nonglass systems as substitutes for a glass membrane because they provide a lower electric resistance, easy handling and preparation, and they are neither rigid nor fragile, which is of crucial importance for the practical purpose, i.e. for the clinical application [2,3]. Liquid membrane electrodes responsive to pH have been studied by many researchers. Schulthess et al. [4] used TDDA (tri-*n*-dodecylamine) as a neutral carrier and showed a good selectivity but limited dynamic range of pH 4.5 and 11.0. Other various compounds have been studied as carriers of hydrogen ions (aliphatic,

* Corresponding author. Fax: +82 2 34365382; e-mail: dhcho@kkucc.konkuk.ac.kr

0039-9140/98/$ - see front matter © 1998 Elsevier Science B.V. All rights reserved.
PII S0039-9140(98)00122-2

heteroaromatic and their derivatives [5–11]), but they were limited a little in performance to pH response range. They are still inferior to glass electrodes. Organic membrane electrodes showed generally that the cation interference imposes limitations in their use at high pH, and the anion interference sets a limit at the lower end of the pH scale. Characteristics and response mechanism were briefly explained by Egorov and Lushchik [12].

Here we report on the new neutral carriers of H^+-ISE for an improvement, i.e. an extension of the applicable pH range and selectivity coefficient.

2. Experimental

2.1. Membrane materials

High-molecular weight polyvinylchloride (PVC, $n = 1100$), sodiumtetraphenylborate (NaTPB), ($\pm$)-bis(2-ethylhexyl)sebacate (BEHS) were obtained from Aldrich–Sigma. Alkyldibenzylamine derivatives as neutral carriers was synthesized by the *N*-alkylation of dibenzylamine [13]. Elemental analysis gave the following results: calculated for butyldibenzylamine (253.39), 85.32% C, 9.15% H, 2.83% N; found, 84.51% C, 9.23% H, 2.83% N; for hexyldibenzylamine (281.44), 85.35% C, 9.67% H, 4.98% N; found, 84.59% C, 9.73% H, 5.09% N; for octyldibenzylamine (309.49), 85.38% C, 10.10% H, 4.53% N; found, 84.65% C, 10.51% H, 4.18% N; for decyldibenzylamine (337.55), 85.40% C, 10.45% H, 4.15% N; found, 84.39% C, 10.81% H, 3.97% N; and for dodecyldibenzylamine (365.60), 85.42% C, 10.75% H, 3.83% N; found, 84.32% C, 10.98% H, 3.79% N. Deionized water and analytical reagent grade were used through the experiments.

2.2. Membrane and electrode preparation

The membrane components (1.00 wt.% neutral carrier, 31.1 wt.% PVC, 0.70 wt.% NaTPB and 67.2 wt.% BEHS as plasticizer, total 200 mg) were dissolved in 5 ml of freshly distilled THF. This solution was cast in a glass ring of internal diameter 30 mm resting on a glass plate. After evaporation of solvent overnight, the resulting membrane was peeled off from the glass ring and was cut into disks of 10 mm diameter. The membrane disks were mounted on electrode bodies for potential measurement. Ag/AgCl wire (0.5 mm in diameter) immersed in a internal filling buffer solution was used as reference electrode.

2.3. Potential measurement

All measurements were carried out at 20°C with cells of Hg, Hg_2Cl_2; KCl(sat'd)|test solution|membrane|citrate buffer solution (pH 5.6); Ag, AgCl. A citrate buffer of pH 5.6 (1 M citric acid, 2.73 M NaOH, 0.01 M NaCl) has been used as internal filling solution throughout. The sample solutions were stirred with a magnetic stirrer in a double-walled glass container with thermostated water circulating in the water jacket. For the stability of electrode potential, the electrodes were immersed in distilled water. The pH buffer solutions for the determination of the electrode functions was the universal Teorell buffer [14]. The selectivity coefficients were determined by the fixed interference method [15] by using solutions that were 0.01 M mol/l in chloride and 0.1 mol/l in the hydroxide of the respective interfering cations. The pH of the solutions was adjusted by the addition of 0.1 M hydrochloric acid. The electrical resistance of membranes was determined by current shunt method [16].

3. Results and discussion

3.1. Electric resistance of the membrane

The resistance of the electrode is much lower than that of a glass electrode and is favourable for electrode miniaturization. The amounts of alkyldibenzylamines as neutral carriers in membranes had no effect on the electric resistance of membrane electrodes. As the values of membrane thickness changed from 0.26 to 10.26($\pm$0.05) mm, electrical resistance varied from 5.4 to 8.8($\pm$ 5%) MΩ with a membrane area of 70 mm^2, but these variations of electrical resistance were small compared to input resistance. The membrane elec-

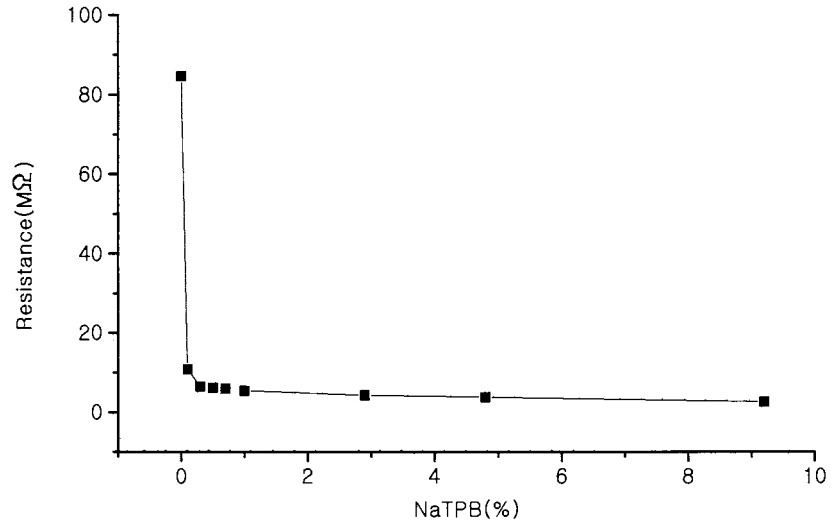

Fig. 1. Electrical resistance of hydrogen ion-selective membrane electrodes based on ODBA with varying amounts of NaTPB.

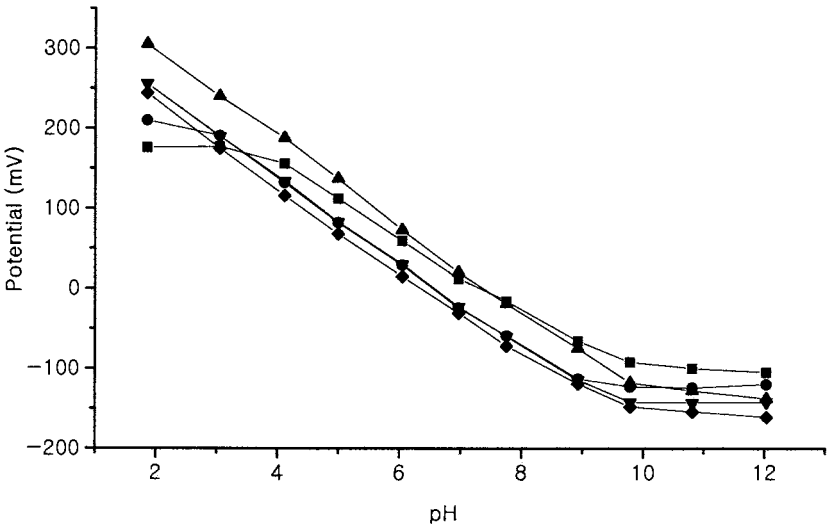

Fig. 2. Response of the hydrogen ion-selective membrane electrodes at 20°C to Teorell buffer solutions (Electrode nos. 1–5 refer to Table 1.) (■) Electrode no. 1; (●) electrode no. 2; (▲) electrode no. 3; (▼) electrode no. 4; (◆) electrode no. 5.

trodes to which NaTPB as lipophilic agent were not added did not respond selectively to hydrogen ions, and the membranes showed high electric resistance as much as 84.6(± 5%) MΩ. But more than 10 wt.% of NaTPB the composition of membranes could not use as electrodes by mechanical leaking because NaTPB is freely soluble in water. The data in Fig. 1 show, respectively, that the electrical resistance of polymer membranes based on ODBA were dependent on varying the amount of lipophilic agent.

3.2. Electrode potential

Five ion-selective electrodes were prepared by using membranes containing different hydrogen ion-selective carriers, alkyldibenzylamine (alkyl-, butyl-, hexyl-, octyl-, decyl- and dodecyl-), and

Table 1
Selectivity coefficients of hydrogen ion-selective membrane electrodes based on alkyldibenzylamine

Electrode no.	Neutral carriers	$K^{pot}_{H,M}$			pH range	Slope (mV/pH)
		M = Na	M = K	M = Ca		
1	BDBA	−8.6	−8.7	< −11.0	4–9	44.1
2	HDBA	−8.9	−9.0	< −11.2	3–9	52.5
3	ODBA	−9.8	−9.9	< −11.3	2–10	56.5
4	DDBA	−9.7	−9.8	< −11.5	2–10	51.0
5	DoDBA	−9.8	−9.7	< −11.4	2–10	49.7
6	TDDA [4]	−9.8	−10.4	< −11.1	4.5–11	57.8

Selectivity coefficients were determined by the fixed interference method using solutions that were 0.01 mol/l in chloride and 0.1 mol/l in the hydroxide of the respective interfering cations.

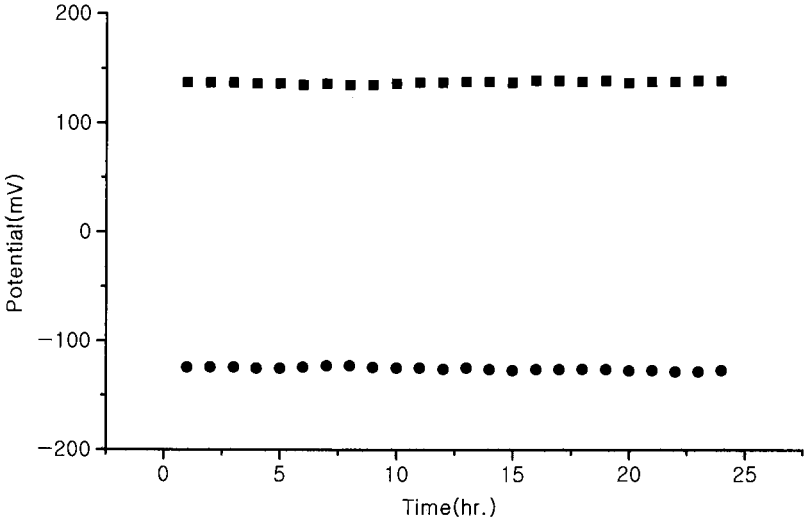

Fig. 3. Reproducibilities and stabilities of hydrogen ion-selective membrane electrode in phthalate and borax buffer solution. (Electrode no. 3 referred to Table 1.) (■) Phthalate-standard buffer solution; (●) borax standard buffer solution.

their potential response characteristics were compared. The neutral carriers we have been looking for are weak bases because they should exist in the unprotonated form in a membrane which is in permanent contact with strong acidic solutions. These compounds lead to lower acidity constants. The basicity and complexation behaviour arise from the free electron pair on the aromatic nitrogen atom. Fortunately, complexation is weak and limited to the transition metals. To increase the lipophilicity we applied *N*-alkylated derivatives of dibenzylamine with long hydrocarbon chains. The potentials of membranes based on amine derivatives as neutral carriers are due to selective transfer of hydrogen ions from the sample to the membrane phase. Neutral carriers with shorter (electrode nos. 1 and 2) and longer (electrode nos. 4 and 5) carbon chains showed inferior performance characteristics compared with the hydrocarbon of medium chain (electrode no. 3) (Fig. 2). As shown in Fig. 2. the linear pH ranges for the electrodes with different neutral carriers are 4–9, 3–9 and 2–10. And their Nernstian slopes show, respectively, 44.1, 52.5, 56.5, 51.0 and 49.7 mV/pH depending on the *N*-alkyl chains of butyl-, hexyl-, octyl-, decyl- and dodecyl. Electrode no. 3 showed a linear response to hydrogen ions in the range of pH 2–10 and a slope of 56.5 mV/pH at

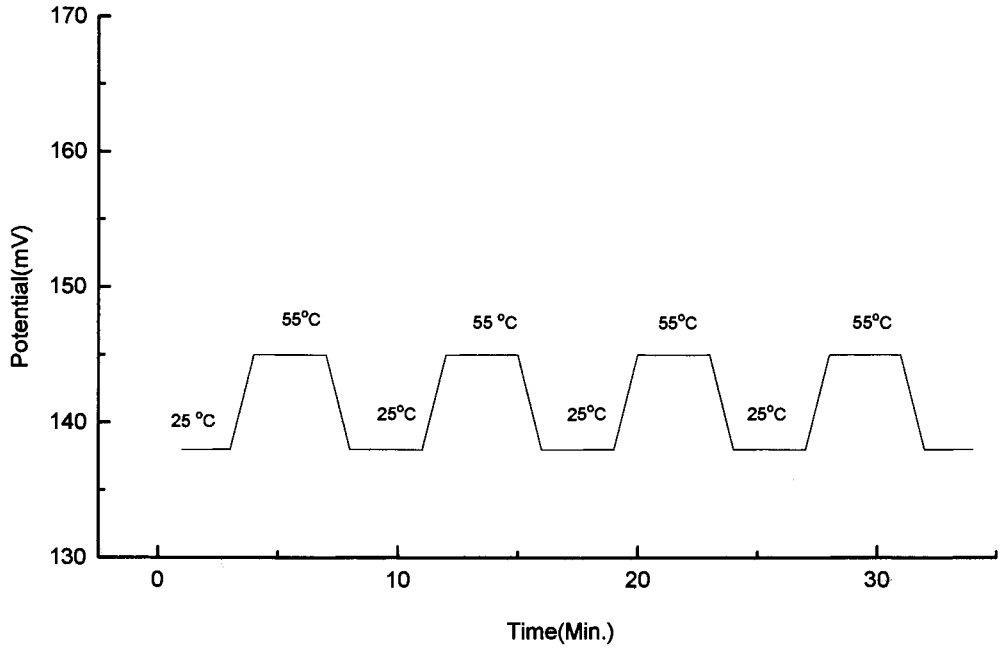

Fig. 4. Temperature effect on response time of hydrogen ion-selective membrane electrode in phthalate buffer solution. (Electrode no. 3 referred to Table 1.)

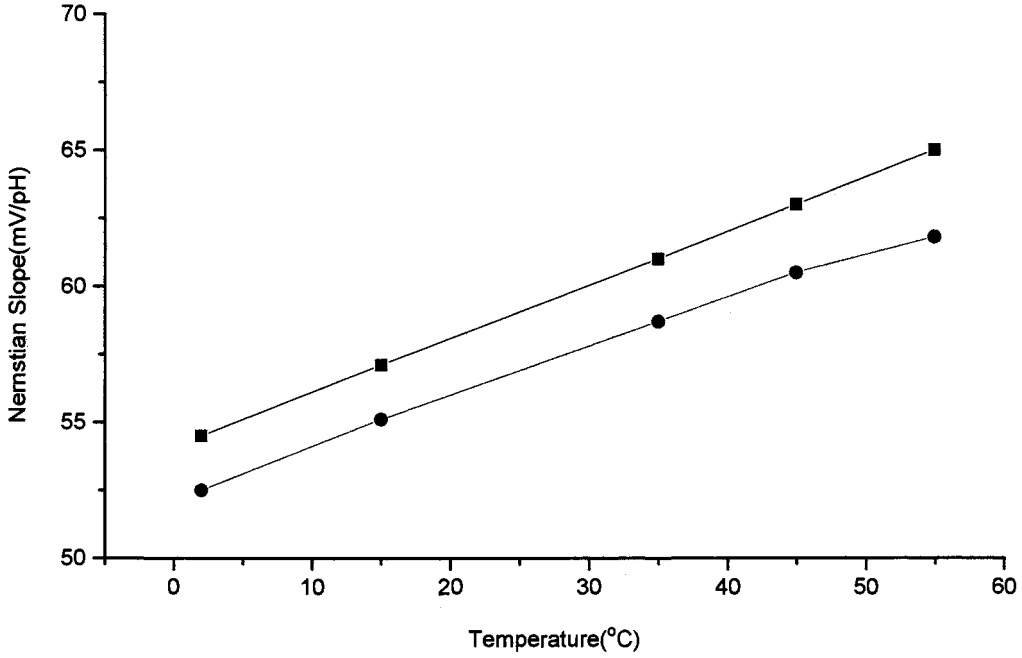

Fig. 5. Theoretical and experimental Nernstian slopes of hydrogen ion-selective membrane electrode. (Electrode no. 3 referred to Table 1.) (■) Theoretical; (●) experimental.

20°C. The stabilities and reproducibilities of the electrodes were quite satisfactory. As shown in Fig. 2, the deviations from the response curves were observed at lower and higher pH values. The detection limits in Teorell buffer solutions were found at pH 3 (electrode no. 1), pH 4 (electrode no. 2) and pH 2 (electrode nos. 3, 4 and 5), respectively. These lower pH limits were from anion interferences, such as halogen ions, and they showed lower potential value deviation from linearity. The detection limits in alkaline solutions caused by the interference of sodium, potassium, and calcium ions. Selectivities in respect to Na^+, K^+ and Ca^{2+} were determined by the fixed interference method.

3.3. Selectivity coefficients

In order to investigate the selectivities of the electrodes based on alkyldibenzylamines, the responses of pH electrodes were measured in the presence of sodium, potassium and calcium ions. Selectivity coefficients toward sodium, potassium and calcium ions were determined by the fixed interference method and they are shown in Table 1. The data are the selectivity coefficients with varying the *N*-alkyl chains of alkyldibenzylamine derivatives and they were compared with the reported data for the TDDA pH electrode [4]. Electrode nos. 1 and 2 have rather poor performance as a result of selectivity coefficients of $K^{pot}_{H,Na} = -8.6$ and -8.9, $K^{pot}_{H,K} = -8.7$ and -9.0, and less than $K^{pot}_{H,Ca} = -11.0$ and -11.2, respectively. Selectivity coefficients of Na^+ with regard to electrodes nos. 3, 4 and 5 were $K^{pot}_{H,Na} = -9.8$, -9.7 and -9.8, respectively. And these were similar to that of the TDDA electrode ($K^{pot}_{H,Na} = -9.8$). Electrode nos. 3, 4 and 5 provided high selectivity but the BDBA- and the HDBA-based electrodes were in short dynamic pH range.

3.4. Response time and stability

The stabilities and reproducibilities of the electrodes were satisfactory. The potential drift was shown at room temperatures in phthalate and borax standard buffer solutions. The standard deviation of absolute EMF value for the electrode was less than 0.5 mV over a 24-h period. The reproducibilities of the potential measurement with alternating phthalate and borax buffer solutions were 1.1 and 1.5 mV, respectively ($n = 10$). The results of potential drifts are shown in Fig. 3. To test the response time with varying temperature, from 25 to 55°C, we performed three measurements in phthalate buffer solution (shown in Fig. 4). Deviations of the variable temperatures were shown at ± 7 mV. It took 50–60 s response time to approach equilibrium potential. The electrode potentials in Figs. 3 and 4 indicated good response time, stabilities and reproducibilities, and slope values of experimental and theoretical curves were similar, as shown in Fig. 5. Therefore, these membrane electrodes were able to be used as commercial pH electrodes between 2 and 55°C.

4. Conclusions

For the hydrogen ion-selective membrane electrodes based on neutral carrier, the following points are important. The resistance of a membrane electrode is much lower than that of a glass electrode and is favourable for electrode miniaturization. The hydrogen ion-selective PVC membranes exhibit fast response, and a good reproducibility and stability. On the basis of the results presented here, the membrane electrodes made of octyldibenzylamine, which have the best results among the prepared electrodes, were shown to have pH values near the theoretical value, in the range of pH 2–10. Interfering ions, such as sodium, potassium and calcium ions, have less effect on these electrodes than glass electrodes. Works using such compounds should be carried out to improve the selectivity and wider pH range of hydrogen ion neutral carrier.

Acknowledgements

This study is supported by Korea Ministry of Education through Research Fund (BSRI 96-3444).

References

[1] M. Cremer, Z. Biol. 47 (1906) 562.
[2] D. Ammann, F. Lanter, R.A. Steiner, D. Schulthess, Y. Shijo, W. Simon, Anal. Chem. 53 (1981) 2267.
[3] W.R. Schlue, R.C. Thomas, J. Physiol. 364 (1985) 327.
[4] P. Schulthess, Y. Shijo, H.V. Pham, E. Pretsch, D. Ammann, W. Simon, Anal. Chim. Acta 131 (1981) 111.
[5] H.-L. Wu, R.-Q. Yu, Talanta 34 (1987) 577.
[6] S.M. Cobbe, P.A. Poole-Wilson, J. Physiol. 289 (1979) 3.
[7] S.C. Ma, N.A. Chaniotakis, M.E. Meyerhoff, Anal. Chem. 60 (1988) 2293.
[8] V.V. Cosofret, E. Lindner, R.P. Buck, R.P. Kusy, J.Q. Whitley, J. Electroanal. Chem. 345 (1993) 169.
[9] V.V. Cosofret, T.M. Nahir, E. Lindner, R.P. Buck, J. Electroanal. Chem. 327 (1992) 137.
[10] E. Lindner, V.V. Cosofret, R.P. Kusy, R.P. Buck, Talanta 40 (1993) 957.
[11] J. Chojnacki, J.F. Biernat, J. Electroanal. Chem. 277 (1990) 159.
[12] V.V. Egorov, Y.F. Lushchik, Talnata 37 (1990) 461.
[13] B.S. Furniss, A.J. Hannaford, P.W.G. Smith, Q.R. Tatchell, Vogel's Textbook of Practical Organic Chemistry, 5th ed., Longman Scientific & Technical, London, 1965, 901 pp.
[14] T. Teorell, E. Stenhagen, Z. Biochem. 299 (1938) 416.
[15] G.G. Guilbault, R.A. Drust, M.S. Frant, H. Freiser, E.H. Hansen, T.S. Light, E. Pungor, G. Rechnitz, N.M. Rice, T.J. Rohm, W. Simon, J.D.R. Thomas, Pure Appl. Chem. 48 (1976) 127.
[16] U. Oesch, W. Simon, Anal. Chem. 52 (1980) 692.

ELSEVIER

Talanta 47 (1998) 823–832

Talanta

Extraction and separation studies of platinum(IV) with *N*-n-octylaniline

T.N. Lokhande, M.A. Anuse *, M.B. Chavan

Department of Chemistry, Analytical Chemistry Laboratory, Shivaji University, Kolhapur-416004, India

Received 29 October 1997; received in revised form 8 April 1998; accepted 14 April 1998

Abstract

N-n-octylaniline in xylene is used for the extractive separation of platinum(IV) from acidic media. Platinum(IV) was extracted quantitatively with 10 ml of 3% reagent in xylene from 0.5 to 10 and 2.5 to 10 M hydrochloric and sulphuric acid, respectively. It was stripped from organic phase with water and estimated photometrically with stannous chloride. The effect of metal ion, acids, reagent concentration and of various foreign ions has been investigated. The method affords binary separation of platinum(IV) from iron(III), cobalt(II), nickel(II) and copper(II), and is applicable to the analysis of synthetic mixtures and alloys. The method is fast, accurate and precise.
© 1998 Elsevier Science B.V. All rights reserved.

Keywords: Platinum(IV); *N*-n-octylaniline; Solvent extraction

1. Introduction

Platinum is present in the earth's crust to the extent of 8×10^{-11} percent. Platinum is widely used as a catalyst in petroleum and chemical processes. It finds wide applications in automotive exhaust-gas control converters and is of immense importance to the electronics industry. Platinum is found in many items of jewellery and serves to an increasing extent as a form of investment. Hence the determination of platinum(IV) is of analytical importance.

Solvent extraction of precious metals is widely employed in chemistry and industry for many years. This technique has been used for separation of platinum metals [1–3]. These noble metals are recovered from a wide variety of sources that present metallurgical problems of a widely differing nature. The aqueous chemistry of these metals is extremely complex. The most prominent feature of the chemistry is the very great tendency of the metals to form chlorocomplexes in chloride media. In addition, the stabilities of the full chlorocomplexes are widely different. Two effects used to achieve separation by anion exchange [4] are: (i) the differing stabilities of chloro complex anions; and (ii) differences in structure, charge and size between different chlorocomplexes. The first effect is most useful in separating the precious metals from base metals; in moderately weak chloride medium most base metals will be present in solution in cationic forms, whereas the precious

* Corresponding author. Fax: +91 231 656133.

0039-9140/98/$ - see front matter © 1998 Elsevier Science B.V. All rights reserved.
PII S0039-9140(98)00172-6

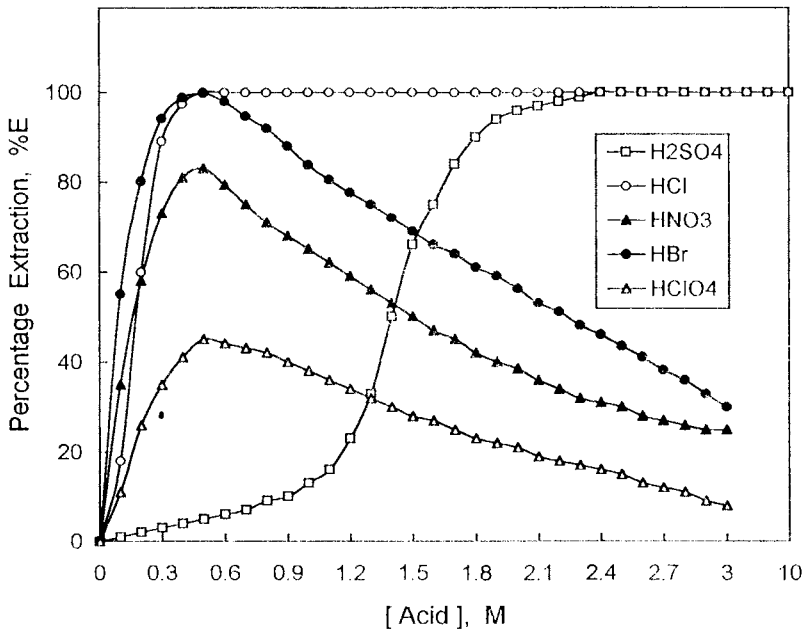

Fig. 1. Extraction of Pt(IV) with 3% *N*-n-octylaniline in xylene as a function of acid concentration. Pt(IV) = 200 μg.

metals chlorocomplexes are stable (or inert to substitution) at fairly low chloride concentrations. The second effect is very useful in achieving both group and individual precious metals separations.

Solvent extraction by high molecular weight organic bases has become increasingly popular in recent years in studying metal complexes. These are known as liquid anion exchangers, uniquely combine some of the advantages of liquid–liquid extraction and ion exchange. Further it was observed that acid binding property of high molecular weight amines depends on the fact that the acid salts of these bases are essentially insoluble in water but readily soluble in hydrocarbon solvent [5].

The use of n-octylaniline in the extraction of noble metals has been described in a number of papers [6–10]. The comparison can be made of the merits of *N*-n-octylaniline relative to n-octylaniline as an extractant. Pohlandt has reported that the effectiveness of n-octylaniline in these extractions depends on its method of preparation [9]. The difficulties were encountered in the extraction of noble metals are the formation of emulsions, equilibration time (30 min) and higher reagent concentration was required for the quantitative extraction of noble metals [7,9]. Further, the extraction method suffers from multiple extraction for quantitative recovery of the metal ion [7]. The number of factors that remained to be examined include the effect of varying amounts of extractant, varying phase ratios, different diluents and use of mineral acids other than hydrochloric acid. Tri-iso-octylamine [11] has been used as a group extractant for the noble metals from 1 M hydrochloric acid medium with 2 min shaking. The extraction of platinum(IV) by amine 304 [12] has been reported by measuring the percentage of metal extraction as a function of different amine and metal concentrations and aqueous ionic strengths. Other extractants reported for platinum(IV) are triphenylphosphine [13] and hexacyclen [14]. Triphenylphosphine in 1,2 dichloroethane extracts platinum(IV) with 60 min shaking. Hexacyclen was used for liquid–liquid extraction of platinum(II) and (IV) but the reaction solution was first heated at 90°C (water-bath) for 30 min and then extracted into methyl isobutyl ketone (MIBK). In *S*-(decyl)-*N*,*N*′-diphenyl isothiouronium bromide (DDTU) [15]

method, the time necessary for equilibrium to be reached is shorter for *N*-n-octylaniline, namely 30 s as compared with 90 min for DDTU.

N-n-octylaniline has been employed successfully in this laboratory for extractive separation of In(III), Tl(III), Zn(II), Bi(III) and Ga(III) [16–18]. Owing to generally greater solubility, primary amines are used less frequently than secondary amines. In addition, *N*-n-octylaniline, the presence of an octyl group attached to an amino group in aniline renders this amine less soluble in water. There is no emulsion formation and has the potential of being prepared in a large scale. Recently we have reported liquid–liquid extraction of palladium(II) with *N*-n-octylaniline from hydrochloric acid media [19]. An extension of this work has shown that *N*-n-octylaniline could also be used for solvent extraction separation of platinum(IV) from hydrochloric acid media. The method proposed here offers extraction separation and determination of platinum(IV) from associated elements.

Table 1
Extraction behaviour of platinum(IV) as a function of *N*-n-octylaniline concentration

HCl (M)	*N*-n-Octylaniline (% v/v)	% E	D
0.5	0.5	10.00	0.28
	1.0	25.00	0.83
	1.5	51.85	2.70
	2.0	66.67	5.00
	2.5	76.60	8.18
	3.0	99.9	2497.5
1.0	0.2	09.00	0.25
	0.5	45.00	2.05
	1.0	79.50	9.70
	1.5	90.00	22.50
	2.0	99.9	2497.5
	2.5	99.9	2497.5
	3.0	99.9	2497.5
2.0	0.5	47.30	2.24
	1.0	81.50	11.01
	1.5	91.80	28.00
	2.0	99.9	2497.5
	2.5	99.9	2497.5
	3.0	99.9	2497.5
2.5	0.5	49.90	2.49
	1.0	83.60	12.74
	1.5	92.65	31.51
	2.0	99.9	2497.5
	2.5	99.9	2497.5
	3.0	99.9	2497.5
3.0	0.5	54.25	2.96
	1.0	88.30	18.87
	1.5	96.50	68.90
	2.0	99.9	2497.5
	2.5	99.9	2497.5
	3.0	99.9	2497.5
5.0	0.5	57.70	3.4
	1.0	94.45	42.55
	2.0	99.9	2497.5
	2.5	99.9	2497.5
	3.0	99.9	2497.5

Pt(IV) = 200 μg; Aq:Org = 25:10.

2. Experimental

2.1. Apparatus

An Elico digital spectrophotometer model CL-27 with 1 cm quartz cells is used for absorbance measurement. pH measurements were carried out using Elico digital pH meter model LI-120.

2.2. Reagents

A stock solution of platinum(IV) is prepared by dissolving 100 mg of grade I platinum thermocouple wire (99.99%) in aqua-regia and evaporating almost to dryness. It was taken up with 2 ml of 1:1 HCl, and again evaporated to moist dryness. The hydrochloric acid treatment was repeated three times to remove all nitric acid and to destroy any nitrosoplatinic acid. After the final evaporation the material was transferred to a 100-ml volumetric flask. HCl (1 ml conc.) was added, and the solution was diluted to volume with distilled water. The solution was standardised gravimetrically [3] and found to be 1 mg ml^{-1} of platinum(IV). Working solution of 200 μg ml^{-1} was made from it by diluting stock solution with distilled water.

Other standard solutions of different metals used to study the effect of foreign ions are prepared by dissolving weighed quantities of their salts in distilled water or dilute hydrochloric acid. Solutions of anions are prepared by dissolving the

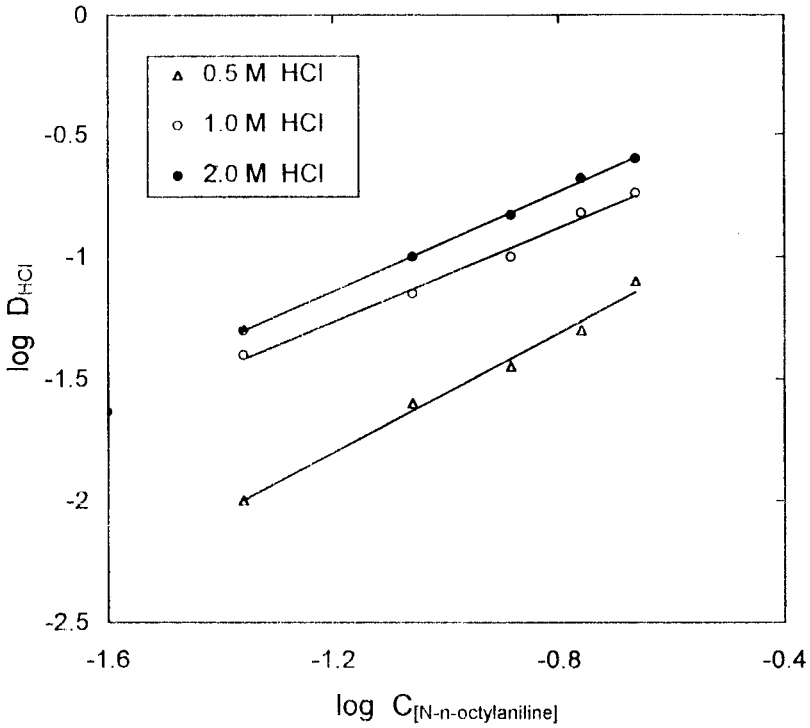

Fig. 2. HCl extraction by *N*-n-octylaniline.

respective alkali metal salts in water. All the chemicals used were of AR grade. Distilled water is used throughout. *N*-n-octylaniline is prepared by the method of Gardlund [20] and its solutions (% v/v) are prepared in xylene.

2.3. Procedure

To an aliquot of solution containing 200 μg platinum(IV) in 125 ml separatory funnel, enough hydrochloric acid and water were added to give a final concentration of 1 M with respect to hydrochloric acid in a total volume of 25 ml. The aqueous phase was equilibrated once with 10 ml of 3% *N*-n-octylaniline solution in xylene for 1 min. The phases were allowed to separate and the metal from the organic phase was stripped with two 10 ml portions of water. This solution was washed with 5 ml of petroleum ether (b.p. range 60–80°C) to remove the traces of dissolved amine and platinum(IV) was estimated spectrophotometrically by stannous chloride method [3].

3. Results and discussion

3.1. Effect of acidity

The extraction of 200 μg of platinum(IV) was carried out from different acid media with 3% *N*-n-octylaniline in xylene keeping the aqueous to organic volume ratio 2.5:1. The extraction was found to be quantitative from hydrochloric, sulphuric and hydrobromic acid media. The extraction is incomplete in nitric acid and perchloric acid (Fig. 1). Although the extraction is quantitative in sulphuric acid media over a wide range, it needs higher acid concentration while in hydrobromic acid medium a very narrow range of acidity is required but the equilibration time is more. The decreased extraction at high hydrobromic acid concentration is presumably due to preferential formation of the hydrobromide of the *N*-n-octylaniline. Hence the use of hydrochloric acid system is recommended for further studies.

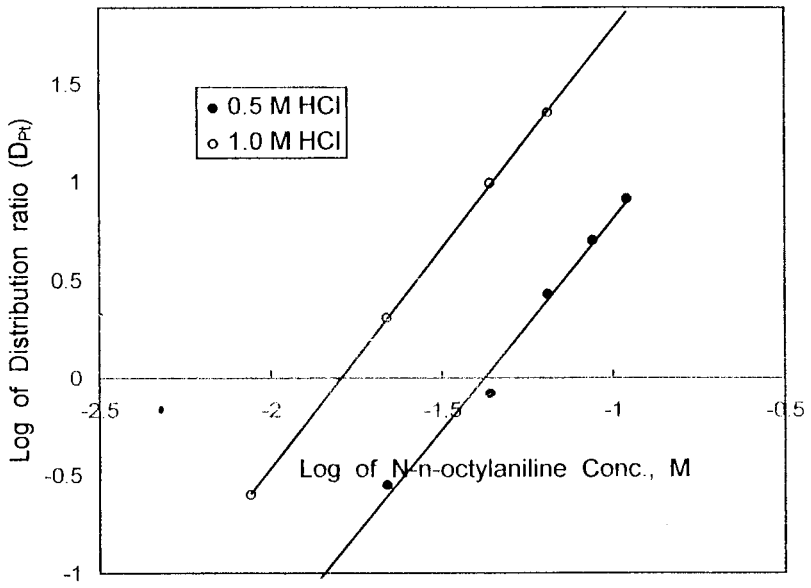

Fig. 3. Log–Log plot of distribution ratio (D_{Pt}) versus *N*-n-octylaniline concentration at 0.5 and 1.0 M HCl.

3.2. Distribution ratio as a function of N-n-octylaniline concentration

The concentration of *N*-n-octylaniline in xylene was varied from 0.5 to 3% over the acidity range of 0.5–10 M HCl. It was observed that extraction increases with an increase in acidity of the aqueous solution and becomes quantitative at 0.5 M HCl. It was found that 3% reagent in xylene was needed for quantitative extraction of metal ion from 1 M HCl (Table 1).

3.3. Nature of extracted species

In the extraction mechanism the species $[RR'NH_2^+Cl^-]$ is determined by plotting of log D_{HCl} against log $C_{[N\text{-n-octylaniline}]}$ (aq.:org. = 2.5). The results obtained for the extraction with 0.5, 1.0 and 2.0 M, hydrochloric acid solutions and various *N*-n-octylaniline concentration are shown in Fig. 2. The slopes obtained are 1.15, 1.05 and 1.05, thus indicating that the amine chloride is formed as in Eq. (1).

$$[RR'NH]_{(org)} + HCl_{(aq)} = [RR'NH_2^+Cl^-]_{(org)} \quad (1)$$

where $R = -C_6H_5$; and $R' = -CH_2(CH_2)_6CH_3$.

From these results it can also be seen that the lines do not coincide, indicating the possible formation of polynuclear complexes or aggregates.

Further, Log–log plot of the distribution ratio versus *N*-n-octylaniline concentration (Fig. 3) at 0.5 and 1 M hydrochloric acid gave slopes of 2.1 and 2.2, respectively indicating that the metal to amine ratio in the extracted species is 1:2. Hence probable extracted species is $[(RR'NH_2^+)_2\ PtCl_6^{2-}]$. The extraction mechanism is as follows in Eq. (2):

$$2[RR'NH_2^+Cl^-]_{(org)} + PtCl_{6(aq)}^{2-} = [(RR'NH_2^+)_2PtCl_6^{2-}]_{(org)} + 2Cl_{(aq)}^- \quad (2)$$

3.4. Period of extraction

Variation of the shaking period from 5 s to 15 min showed that the minimum of 30 s equilibration time was adequate for quantiative extraction of platinum(IV) from both hydrochloric acid and sulphuric acid media, and 2 min from hydrobromic acid medium. In the general procedure 1 min equilibration time was recommended in order to ensure the complete extraction of metal ion

Table 2
Effect of foreign ions on the extractive determination of Pt(IV) = 0.200 mg

Foreign ion	Added as	Amount tolerated (mg)	Foreign ion	Added as	Amount tolerated (mg)
Mn(II)	$MnCl_2 \cdot 6H_2O$	20	Rh(III)	$RhCl_3 \cdot 3H_2O$	1
Cd(II)	$CdCl_2 \cdot 2\frac{1}{2} H_2O$	15	Ru(III)	$RuCl_3 \cdot x\ H_2O$	1
Mg(II)	$MgCl_2 \cdot 6H_2O$	20	Sr(II)	$Sr(NO_3)_2$	20
Fe(II)	$FeSO_4 \cdot 7H_2O$	20	Sb(III)	Sb_2O_3	10
Fe(III)	$NH_4Fe(SO_4)_2 \cdot 12H_2O$	20	Ir(III)	$IrCl_3 \cdot xH_2O$	1.5
Pb(II)	$Pb(NO_3)_2$	20	Ti(IV)	$K_2TiF_6 \cdot H_2O$	5
Hg(II)[a]	$HgCl_2$	5	Th(IV)	$Th(NO_3)_4 \cdot 6H_2O$	5
V(V)	$NH_4VO_3 \cdot H_2O$	5	Re(VII)	$KReO_4$	1
U(VI)	$UO_2(NO_3)_2 \cdot 6H_2O$	10	Cr(III)	$CrCl_3$	10
Ni(II)	$NiCl_2 \cdot 6H_2O$	20	Pd(II)	$PdCl_2 \cdot xH_2O$	1
Bi(III)	$Bi(NO_3)_3 \cdot 5H_2O$	10	Tartrate	$C_4H_6O_6$	100
Tl(III)	$Tl(NO_3)_3$	2	Fluoride	NaF	100
Co(II)	$CoCl_2 \cdot 6H_2O$	20	Citrate	$C_6H_8O_7 \cdot H_2O$	100
Ce(IV)	$Ce(SO_4)_2$	2	Ascorbate	Ascorbic acid	100
Zn(II)	$ZnSO_4 \cdot 7H_2O$	20	Oxalate	$(COOH)_2 \cdot 2H_2O$	100
Be(II)	$BeSO_4 \cdot 4H_2O$	10	Acetate	CH_3 COONa	100
Ca(II)	$CaCl_2$	20	EDTA	EDTA(Disodium salt)	50
Ba(II)	$BaCl_2 \cdot 2H_2O$	20	Malonate	Malonic acid	20
Mo(VI)	$(NH_4)_6 Mo_7O_{24} \cdot 2H_2O$	20	Bromide	KBr	50
Cu(II)	$CuSO_4 \cdot 5H_2O$	20	H_2O_2	H_2O_2	100
Os(VIII)	OsO_4	1	Succinate	Succinic acid	20
Au(III)	$HAuCl_4 \cdot 4H_2O$	1	Iodide	KI	20
Ag(I)	$AgNO_3$	5	Sulphate	Na_2SO_4	>100
Se(IV)	SeO_2	5	Chloride	NaCl	>100
Te(IV)	Na_2TeO_3	5	Nitrate	KNO_3	50

[a] Masked with tartrate.

from hydrochloric acid medium. However, prolonged shaking of upto 15 min had no adverse effect on the extraction.

3.5. Effect of aqueous to organic volume ratio on extraction

Platinum(IV) was extracted from aqueous medium in the range of 10–250 ml at 1 M hydrochloric acid with 10 ml of 3% *N*-n-octylaniline in xylene. Platinum(IV) was stripped with water and estimated as described in the procedure. It was found that the extraction of platinum(IV) was quantitative when the aqueous to organic volume ratio was 1:1 to 3.5:1, while it decreased when the ratio was changed from 3.5:1 to 25:1. Hence, the aqueous to organic volume ratio recommended in the procedure is 2.5:1.

The loading capacity of 10 ml of 3% *N*-n-octylaniline is 6.5 mg of platinum(IV).

3.6. Extraction with various diluents

The suitability of several diluents such as benzene, toluene, xylene, amyl alcohol, n-butyl alcohol, 4-methyl-2-pentanol, chloroform, carbon tetrachloride, amyl acetate, n-butyl acetate and isobutyl methyl ketone (MIBK) for the extraction of platinum(IV) from chloride medium, using proposed method was investigated. It was found that a 3% (v/v) solution of *N*-n-octylamiline in benzene, toluene, xylene, amyl acetate, butyl acetate

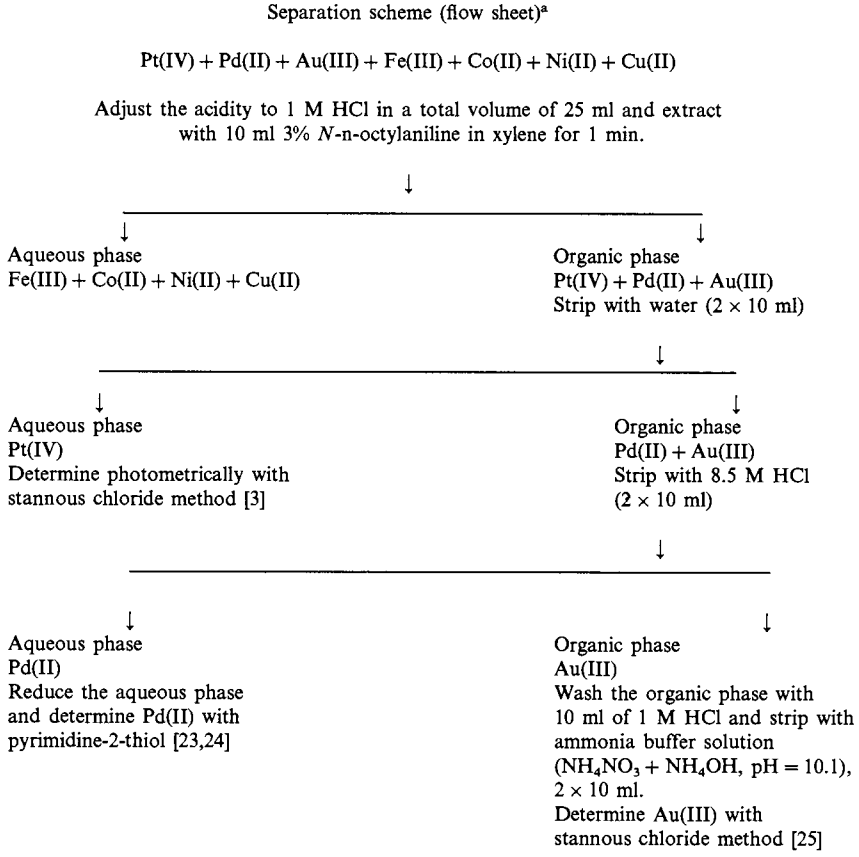

[a] Pt(IV), 200 μg + Pd(II), 200 μg + Au(III), 200 μg + 5000 μg each of Fe(III), Co(II), Ni(II) and Cu(II).

Scheme 1. Separation scheme (flow sheet)[a]

Pt(IV) + Pd(II) + Au(III) + Fe(III) + Co(II) + Ni(II) + Cu(II)

Adjust the acidity to 1 M HCl in a total volume of 25 ml and extract with 10 ml 3% *N*-n-octylaniline in xylene for 1 min.

Aqueous phase Fe(III) + Co(II) + Ni(II) + Cu(II)

Organic phase Pt(IV) + Pd(II) + Au(III) Strip with water (2 × 10 ml)

Aqueous phase Pt(IV) Determine photometrically with stannous chloride method [3]

Organic phase Pd(II) + Au(III) Strip with 8.5 M HCl (2 × 10 ml)

Aqueous phase Pd(II) Reduce the aqueous phase and determine Pd(II) with pyrimidine-2-thiol [23,24]

Organic phase Au(III) Wash the organic phase with 10 ml of 1 M HCl and strip with ammonia buffer solution (NH_4NO_3 + NH_4OH, pH = 10.1), 2 × 10 ml. Determine Au(III) with stannous chloride method [25]

[a] Pt(IV), 200 μg + Pd(II), 200 μg + Au(III), 200 μg + 5000 μg each of Fe(III), Co(II), Ni(II) and Cu(II).

Table 3
Binary separation of platinum(IV) from iron(III), cobalt(II), nickel(II) and copper(II)[a]

Composition of metal ion (μg)	Recovery of platinum(IV) (%)	RSD (%)	Recovery of added metal ion (%)	RSD (%)
Pt, 200; Fe, 10 000	99.4	0.17	99.6	0.32
Pt, 200; Co, 10 000	99.5	0.20	99.4	0.24
Pt, 200; Ni, 10 000	99.7	0.16	99.4	0.26
Pt, 200; Cu, 10 000	99.4	0.13	99.7	0.25

[a] Average of six determinations.

Table 4
Analysis of synthetic mixtures

Composition (μg)		Platinum(IV) found[a] (μg)	Recovery (%)	RSD (%)
1	Pt, 200; Pd, 1000	199.0	99.5	0.065
2	Pt, 200; Os, 1000	199.4	99.7	0.055
3	Pt, 200; Ru, 1000	199.2	99.6	0.060
4	Pt, 200; Rh, 500	199.4	99.7	0.055
5	Pt, 200; Ir, 1000	199.4	99.7	0.055
6	Pt, 200; Au, 1000	199.2	99.6	0.060
7	Pt, 200; Pd, 200; Au, 200	199.0	99.5	0.070
8	Pt, 200; Os, 200; Ru, 200; Ir, 200	198.8	99.4	0.090
9	Pt, 200; Pd, 200; Ru, 200; Os, 200; Rh, 200; Ir, 200	199.0	99.5	0.065
10	Pt, 200; Pd, 200; Ru, 200; Os, 200; Rh, 200; Ir, 200; Au, 200	198.8	99.4	0.090
11	Pt, 200; Pd, 200; Ru, 200; Os, 200; Rh, 200; Ir, 200; Au, 200; Fe, 5000; Co, 5000; Ni, 5000; Cu, 5000	198.8	99.4	0.090

[a] Average of six determinations.

and MIBK provides quantitative extraction of platinum(IV). While the extraction of platinum(IV) was incomplete in chloroform and carbon tetrachloride and zero extraction in amyl alcohol, n-butyl alcohol and 4-methyl-2-pentanol if amine is dissolved in these solvents. Inert solvent diluent such as xylene does not participate in the actual extraction process. However, *N*-n-octylaniline acts as a liquid anion exchanger for platinum(IV)—chloro complex [$PtCl_6^{2-}$] and promotes extraction.

3.7. Effect of foreign ion

Platinum(IV) was extracted in the presence of a large number of foreign ions. The tolerance limit was set at the amount of foreign ions causing an error of less than $\pm 2\%$ in the recovery of platinum(IV) (Table 2). It is observed that the method is free from interference from a large number of transition, non-transition metal ions and anions. The only species showing interference in the procedure are chromium(VI), manganese(VII), persulphate, thiosulphate, thiourea and thiocyanate. The persulphate ion keeps the platinum in (VI) oxidation state, which is not extractable. The thiosulphate, thiocyanate and thiourea are sulphur containing ligands, form very stable complexes with platinum(IV) and hence interfered.

3.8. Binary separation of platinum(IV) from iron(III), cobalt(II), nickel(II) and copper(II)

The method permits separation and determination of platinum(IV) from binary mixture containing either iron(III), cobalt(II), nickel(II) and copper(II).

Platinum(IV) is separated from iron(III), cobalt(II), nickel(II) and copper(II) by its extraction with 3% *N*-n-octylaniline in xylene from 1 M hydrochloric acid (Scheme 1). Under this condition

Table 5
Analysis of alloy

Alloy	Composition (%)	Platinum (μg)		Recovery (%)	RSD (%)
		Taken	Found[a]		
Alloy for electrical contacts	Pd, 35; Ag, 30; Pt, 10; Cu, 14; Au, 10; Zn, 1.0.	200	199.6	99.6	0.065
Solder alloy	Pd, 30; Pt, 10; Au, 60	200	199.8	99.8	0.055
Oakay alloy	Pt, 20; Pd, 10.5; Ni, 60; V, 9.5	200	199.4	99.7	0.060

[a] Average of six determinations.

all the base metals remain quantitatively in the aqueous phase in the cationic form where these are determined spectrophotometrically with thiocyanate [21], 1-nitroso-2-naphthol [21], DMG [21] and pyrimidine-2-thiol [22], respectively, and results are confirmed by atomic absorption spectroscopic method (AAS). Platinum(IV) is stripped from the organic phase with two 10 ml portions of water. The solution was washed with 5 ml of petroleum ether to remove the traces of dissolved amine and platinum(IV) was estimated spectrophotometrically with stannous chloride. The recovery of platinum(IV) and that of the added ions was 99.4%. The results are reported in Table 3.

3.9. Separation of platinum(IV) from multi component synthetic mixture

In natural occurrence platinum(IV) is always associated with the platinum group and base metals, hence its separation from these metals is of great importance. The proposed method allows the selective separation and determination of platinum(IV) from many metal ions (Table 4).

3.10. Extraction scheme for separation of platinum(IV), palladium(II), gold(III) and base metals and its application to alloys

The extraction study shows that it is possible to separate platinum(IV) from palladium(II), gold(III) and base metals from one another. The extraction scheme is presented in the form of a flow sheet (Scheme 1), while the results of analysis of the synthetic mixtures containing platinum(IV), palladium(II), gold(III) and base metals, corresponding to the various alloys are given in the Table 5.

The method is selective and permits rapid separation and determination of micro amounts of platinum(IV). The average recovery of platinum(IV) was greater than 99.5%.

4. Conclusion

The important features of this method are that: (i) it permits selective separation of platinum(IV) from other platinum groups and base metals which are generally associated with it; (ii) it is free from interference from large number of foreign ions which are associated with platinum(IV) in its natural occurrence; (iii) low reagent concentration is required; (iv) the time needed for equilibration is very short for *N*-n-octylaniline, namely 30 s as compared with 10 and 90 min for n-octylaniline [6] and DDTU [15], respectively; (v) the method is applicable to the analysis of platinum(IV) in synthetic mixtures with composition corresponding to alloys; and (vi) it is very simple selective, reproducible and rapid, requires only 25–30 min for separation and determination.

Acknowledgements

T.N. Lokhande is grateful to University Grants Commission, New Delhi for providing financial assistant. The authors express their gratitude to Professor K.J. Patil, Head of the Chemistry Department for providing laboratory facilities and kind encouragement.

References

[1] F.E. Beamish, The Analytical Chemistry of the Noble metals, Pergamon Press, Oxford, 1966.
[2] F.E. Beamish, J.C. Van Loon, Recent Advances in the Analytical Chemistry of the Noble Metals, Pergamon Press, Oxford, 1972.
[3] F.E. Beamish, J.C. Van Loon, Analysis of Noble Metals: Overview and Selected Methods, Academic Press, London, 1977.
[4] T.C. Lo, M.H.I. Baird, C. Hanson, Handbook of Solvent Extraction, Wiley–Interscience, New York, 1983.
[5] E.L. Smith, E.J. Page, J. Soc. Chem. Ind. 67 (1948) 48.
[6] A.A. Vasilyeva, I.G. Yudelevich, L.M. Gindin, T.V. Lanbina, R.S. Shulman, I.L. Kotlarevsky, V.N. Andrievsky, Talanta 22 (1975) 745.
[7] C. Pohlandt, Nat. Inst. Metallurgy, Randburg, S. Afr. Rept. No. 1881, 1977.
[8] C. Pohlandt, M. Hegetschweller, Nat. Inst. Metallurgy, Randburg, S. Afr. Rept. No. 1940, 1978.
[9] C. Pohlandt, Talanta 26 (1979) 199.
[10] R.N. Gedye, J. Bozic, P.M. Durbano, B. Williamsan, Talanta 36 (1989) 1055.
[11] M.Y. Mirza, Talanta 27 (1980) 101.
[12] F.J. Alguacil, A. Cobo, A.G. Coedo, M.T. Dorado, A. Sastre, Hydrometallurgy 44 (1997) 203.
[13] M. Mojski, Talanta 27 (1980) 7.
[14] S. Arpadjan, M. Mitcwa, P.R. Bontchev, Talanta 34 (1987) 953.
[15] E.A. Jones, T.W. Steele, Nat. Inst. Metallurgy, Johannesburg, Rept. No. 1569, 1973.
[16] G.N. Mulik, S.R. Kuchekar, M.B. Chavan, Indian J. Chem. 25A (1986) 1073.
[17] G.N. Mulik, S.R. Kuchekar, M.B. Chavan, J. Indian Chem. Soc. LXIV (1987) 68.
[18] N.B. Kadam-Patil, S.S. Sawant, G.N. Mulik, M.B. Chavan, Bull. Bismuth Inst. 64 (1992) 5.
[19] T.N. Lokhande, M.A. Anuse, M.B. Chavan, Talanta 46 (1998) 163.
[20] Z.G. Gardlund, R.J. Curtis, G.W. Smith, Liq. Crystals Ordered Fluids 2 (1973) 541.
[21] A.I. Vogel, Text Book of Quantitative Inorganic Analysis, 4th ed., ELBS/Longman, Edinburgh, 1978, pp. 741, 739, 747.
[22] S.R. Kuchekar, M.A. Anuse, M.B. Chavan, Indian J. Chem. 25A (1986) 1041.
[23] M.A. Anuse, N.A. Mote, M.B. Chavan, Talanta 30 (1983) 323.
[24] M.A. Anuse, M.B. Chavan, Chem. Anal. (Warsaw) 29 (1984) 409.
[25] E.B. Sandell, Colorimetric Determination of Trances of Metals, 3rd ed., Interscience, New York, 1965, pp. 503.

ELSEVIER

Talanta 47 (1998) 833–840

Talanta

Determination of nicotine by reagent-injection flow injection photometric method

Jingfu Liu *, Yingdi Feng

The First Light Industry Institute of Beijing, No. 7 Ju-Er Hutong, Beijing 100009, China

Received 19 November 1997; received in revised form 6 April 1998; accepted 14 April 1998

Abstract

Nicotine was determined by a reagent-injection flow injection photometric method making use of the Koing reaction. The applicability of four color reagents, aniline, barbituric acid, pyrazolone and sulfanilic acid, were evaluated and the sulfanilic acid was selected. The linear range, detection limit, R.S.D., and sample throughput of the established sulfanilic acid method were 0–10 mg l^{-1}, 0.12 mg l^{-1}, 0.7% and 50 h^{-1}, respectively. Background absorption from sample matrix was eliminated by the reagent-injection flow injection technique. The proposed method was applied to determine nicotine in tobacco and urine samples with satisfactory results. © 1998 Elsevier Science B.V. All rights reserved.

Keywords: Flow injection; Background absorption elimination; Nicotine; Tobacco; Urine

1. Introduction

The determination of total alkaloids and nicotine is of particular importance to the tobacco industry and toxicology. Various analytical methods, including thin-layer chromatography, gas chromatography, high-performance liquid chromatography and mass spectrometry, for their determination has been reviewed by Green et al. [1]. Though other methods such as near-infrared spectrometry [2], chromatography-tandem mass spectrometry [3], polarimetry [4], potentiometry [5], capillary electrophoresis [6] and radio-immunoassay [7,8] were reported, the most popular used were various spectrophotometric methods [9–15]. In particular most of these methods [9–13] are based on the Koing reaction [16] in which the pyridine ring was cleaved with cyanogen bromide or chloride and the resulting compound was condensed with a aromatic amine.

Because of the high toxicity of nicotine and the large numbers of samples which should be analyzed, air-segmented continuous flow analysis (CFA) methods are usually adopted in tobacco industry [17–19] thereby providing a closed-system with higher sample throughput and safer handing of the toxic sample and reagent. The CFA method was also applied to determine nicotine and its metabolites in urine samples [20]. Membrane dialysis unit was usually adopted in their system to eliminate the high background absorption from tobacco or urine sample matrix.

* Corresponding author.

0039-9140/98/$ - see front matter © 1998 Elsevier Science B.V. All rights reserved.
PII S0039-9140(98)00173-8

The study on flow injection (FI) determination of nicotine is very limited. Finster et al. [21] reported a flow injection method for the determination of nicotine in tobacco using aniline as the color reagent. Instead of using the dialysis technique, they successfully eliminated background absorption with stopped-flow flow injection technique, which significantly simplified the flow system, but the detection limit was relatively high (30 mg l^{-1}) and no detailed determination procedure was given in their report.

In this present study, chromogenic reagents, i.e. aniline, barbituric acid, pyrazolone and sulfanilic acid were evaluated for flow injection determination of nicotine. Reagent-injection flow injection technique was adopted to eliminate background absorption from sample matrix. The sulfanilic acid method was selected to determine nicotine in tobacco and urine samples.

2. Experimental

2.1. Reagents

All chemicals were of analytical grade except where specified and distilled water was used throughout.

Nicotine standard solution, a stock solution (1000 mg l^{-1}) was prepared by dissolving nicotine (Merck-Schuchardt) in water was kept in refrigerator. Working solutions were obtained by appropriately diluting the stock solution with water.

Potassium cyanide, 1.6% (w/v) aqueous solution (very toxic).

Chloramine-T, 4.8% (w/v) aqueous solution was prepared daily before use.

Buffer, 1 mol l^{-1} sodium dihydrogen phosphate/4% (w/v) citric acid solution.

Aniline solution, 2% (w/v). Ten grams of citric acid and 8 ml of glacial acetic acid were dissolved in 400 ml of water. With stirring 10 ml of aniline was added and 6 mol l^{-1} hydrochloric acid was added dropwise until the aniline was thoroughly dissolved. Then it was diluted to 500 ml. The pH of the solution was 4.3.

Barbituric acid solution, 1% (w/v). Five grams of barbituric acid was dissolved in a mixture of 200 ml water and 250 ml buffer solution. The solution was adjusted to pH 3.0 by adding 6 mol l^{-1} hydrochloric acid. Then it was diluted to 500 ml and filtered.

Pyrazolone (1-phenyl-3-methyl-5-pyazolone) solution, 0.08% (w/v). Zero point four grams of 1-phenyl-3-methyl-5-pyrazolone (chemically pure) was dissolved in 50 ml of ethanol, 200 ml of water and 250 ml of buffer solution were added. Then the solution was adjusted to pH 6.0 by adding 20% NaOH dropwise and diluted to 500 ml with water.

Sulfanilic acid solution, 4% (w/v). Twenty grams of sulfanilic acid and 3 g of sodium hydroxide were dissolved in 200 ml of water. Then 250 ml of buffer solution was added and mixed. The solution was adjusted to pH 6.0 by adding 20% NaOH dropwise and diluted to 500 ml with water.

Extracting solution, 5% (w/v) aqueous acetic acid.

2.2. Apparatus

A FAA-TI Tobacco Analyzer developed in this laboratory was used to conduct flow injection determination. The two analytical channel analyzer can analyse sugar, nicotine, total nitrogen and chloride in tobacco which consists of a sampler, a 12-channel peristaltic pump, two 16-port injection valves, a thermostatic bath, a 2-channel photometer with two 10 mm path length flow cells, a 586 computer and a printer. Self-developed FAAOS software was installed in the computer to administer the whole system automatically from introducing samples into the system to calculation of the results.

A digital pH meter (Orion Research, model 211) was used to measure the pH of the solutions.

2.3. Preparation of samples

2.3.1. Tobacco samples

To 0.5 g of cigarette sample, which was ground through a 0.5-mm screen using a mill, placed in a 250-ml flask was added 100 ml of extracting solution and the mixture was allowed to stand for 20 min with occasional shaking. Then it was filtered

and the filtrate was diluted appropriately with water before determination.

2.3.2. Urine samples

Urine samples obtained from smokers and non-smokers were analyzed 1 h after being sampled. Samples were diluted five times before determination.

3. Results and discussion

3.1. Optimization of the manifold

As this study is focus on developing a FI method to determine nicotine alkaloids and its metabolites in tobacco and urine samples which have high background absorbance, the established method must has the ability to eliminate it. It is well known that membrane dialysis and stopped-flow flow injection technique can be applied in FIA to eliminate background absorption. In this present study the reagent-injection FI technique was try to adopted to eliminate background absorption from sample matrix, as well as to simplify the flow system. In this on-line generation of cyanide chloride reaction system, there are two ways to get the simplest manifold for reagent-injection FI determination of nicotine, i.e. by injecting a mixture of KCN and chloramine-T into the chromogenic reagent or by injecting chromogenic reagent into the mixture of KCN and chloramine-T. If the latter was adopted, large volume of barbituric acid or pyrazolone should be injected to get high sensitivity as their aqueous solubility were very limited. This will result in low sampling rate which is unacceptable. Consequently the former was selected in this study. The FI parameters such as flow rates, injection volume and reaction coil length were optimized with the sulfanilic acid color system and results were shown in Fig. 1. Theoretically, the higher the flow rate ratio of sample (S) to chromogenic reagent (CR) the better to get high sensitivity. The value in Fig. 1 was selected as a compromise of sensitivity, sample throughput, buffer concentration needed and system stability. Though experiments show that a little longer reaction coil (RC2) is helpful for getting higher sensitivity in the barbituric acid and pyrazolone color system, the same reaction coil length was adopted in this study for simplicity.

3.2. Selection of chromogenic reagent

Though aniline, barbituric acid, pyrazolone and sulfanilic acid were all successfully applied to determine nicotine in CFA, it is still necessary to study in detail the applicability of these reagents in flow injection determination of nicotine as there are some difference between these two analytical technique.

3.2.1. Optimization of the chemical parameters

Using the above optimized manifold, the chemical parameters such as reagent concentration, pH of buffer solution and temperature were optimized, respectively, for each chromogenic reagent and the results are shown in Table 1.

As chloramine-T reacts with sulfanilic acid and aniline, the molar concentration of KCN must be a little higher than that of chloramine-T. The mass concentration ratio of KCN to chloramine-T was kept at 1:3 in the optimization of KCN and chloramine-T concentration. For all these four studied color reagents, peak heights increase with the increasing of KCN concentration in the range of 0.4–2.4%, but peak heights increase slowly when the concentration of KCN is above 1.6%. Considering that precipitation produced in the mixture of high concentration of KCN and chlo-

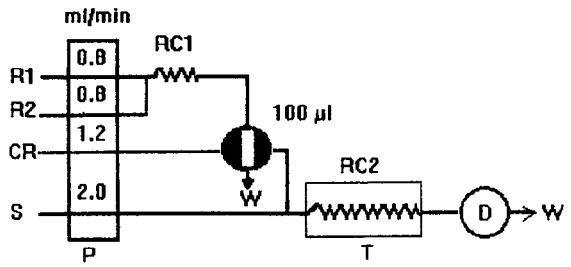

Fig. 1. Manifold optimized for the determination of nicotine. R1, potassium cyanide solution; R2, chloramine-T solution; CR, chromogenic reagent; S, sample solution; RC1, reaction coil (50 cm × 0.8 mm i.d.); RC2, reaction coil (300 cm × 0.8 mm i.d.); P, peristaltic pump; T, thermostatic bath; D, photometric detector; W, waste.

Table 1
Optimal detection conditions and analytical characteristics of the four studied methods

Method	Aniline	Barbituric acid	Pyrazolone	Sulfanilic acid
Detect wavelength (nm)	470	510	520	470
Reagent concentration				
Chloramine-T (%)	4.8	4.8	4.8	4.8
KCN (%)	1.6	1.6	1.6	1.6
Color reagent (%)	2.0	1.0	0.08	4.0
Buffer	Aniline-HAc	0.5 M NaH_2PO_4	0.5 M NaH_2PO_4	0.5 M NaH_2PO_4
Selected buffer pH	4.5	3.0	6.0	6.0
Reagent zone pH	7.5	7.0	8.0	8.0
Temperature (°C)	50	60	60	40
Linear range (mg l^{-1})	0–20	0–10	0–5	0–10
Regression equation				
Slope (Abs/mg l^{-1})	0.03206	0.06075	0.09434	0.06228
Intercept (Abs)	0.01013	0.01010	0.01420	0.01393
Correlation coefficient	0.9999	0.9999	0.9995	0.9998
Detection limit (mg l^{-1})	0.03	0.03	0.06	0.12
R.S.D. ($n=11$) (%)	1.0	0.8	1.1	0.7
Sample throughput (h^{-1})	50	50	50	50

ramine-T and the high toxicity of KCN, the adopted concentration of KCN and chloramine-T were 1.6 and 4.8%, respectively.

The influence of each color reagents concentration were studied by determining the peak heights of 10 mg l^{-1} nicotine under different concentration of color reagents. The concentration of sulfanilic acid and aniline were optimized in the range of 1–5% and the results indicate that the optimal value were 4 and 2%, respectively. Peak heights increase with the increasing of barbituric acid and pyrazolone concentration, the adopted concentration were 1% of barbituric acid and 0.08% pyrazolone, the highest concentration could be obtained in this study.

Peak heights decrease with the increasing of buffer concentration, but the concentration of buffer solution should not be too low owing to the low flow rate of chromogenic reagent solution compared with that of the sample solution and the high concentration of KCN and chloramine-T. Equal molar concentration of aniline-acetic acid buffer was used in the aniline system and 0.5 mol l^{-1} NaH_2PO_4 buffer solution was adopted in the other three color systems.

The effect of pH was studied by determining the peak heights of 10 mg l^{-1} nicotine under room temperature and by adding 6 mol l^{-1} HCl or 20% NaOH into the chromogenic reagent solutions to adjust different pH. Results shown in Fig. 2 indicate that these four color systems are all pH dependent. The selected pH in this study and the pH of the reagent zone under the selected pH are shown in Table 1.

The influence of temperature was investigated in the range of 20–60°C by determining 5 mg l^{-1} nicotine under the above optimized conditions. Results shown in Fig. 3 indicate that the best temperature for the sulfanilic acid and aniline color system were 40 and 50°C, respectively. Though higher temperature is helpful for obtaining higher sensitivity for the barbituric acid and pyrazolone color system, 60°C was adopted as many air bubbles formed in the flow system at higher temperature.

3.2.2. Evaluation of these four methods

Analytical characteristics such as sample throughput, linear range, regression equation, correlation coefficient, detection limit, and relative standard deviation of each color method were determined under the above optimized conditions and the results are shown in Table 1. Sample throughputs and relative standard deviations

(R.S.D.) were determined by repeated injection of a sample containing 2.5 mg l^{-1} nicotine (for sulfanilic acid, barbituric acid and pyrazolone system) or 5 mg l^{-1} nicotine (for aniline system). Detection limits were calculated as 3σ above the blank value (where σ is the S.D. ($n = 11$) for a blank solution). Regression equations and correlation coefficients were obtained by determining five nicotine standards covering the linear ranges.

The interference of several substance was studied by using a solution containing 5 mg l^{-1} nicotine and adding various concentrations of interferants up to the amounts where the relative error reached a value of about 5%. The errors were calculated by comparing the peak height with that obtained by introducing an solution of 5 mg l^{-1} nicotine containing no interferant as a reference. Citric acid was added into chromogenic reagents as masking agent of some metal ions. Experiments show that for all these four color system pyridine and isonicotinic acid interfere seriously, the tolerable concentrations were all < 1 mg l^{-1} except the aniline method can tolerate 5 mg l^{-1} of isonicotinic acid. The maximum permissible concentrations (mg l^{-1}) of Ca^{2+}, Cu^{2+} and Fe^{3+} were: Ca (500), Cu (5), Fe (100) for aniline; Ca (100), Cu (50), Fe (10) for barbituric acid; Ca (500), Cu (10), Fe (100) for pyrazolone; Ca (500), Cu (50), Fe (50) for sulfanilic acid. At least 500 mg l^{-1} of K^+, NH_4^+, Mg^{2+}, NO_3^-, glucose, sucrose, oxalic acid, triethanolamine, formaldehyde and phenol did not interfere.

The above study indicates that none of these color reagents has any significant superiority over the others at their own optimal temperature. The barbituric acid and the pyrazolone method have low detection limits and high slopes, but they need high temperature (60°C) which occasionally produces air bubbles. The aniline method has low detection limit, but its slope is low and what is more important the aniline reagent is toxic. The detection limit of the sulfanilic acid method is not as low as the barbituric acid and the aniline methods, but it has moderate reaction conditions and high tolerance to all interferants. Further experiments show that the sulfanilic acid method

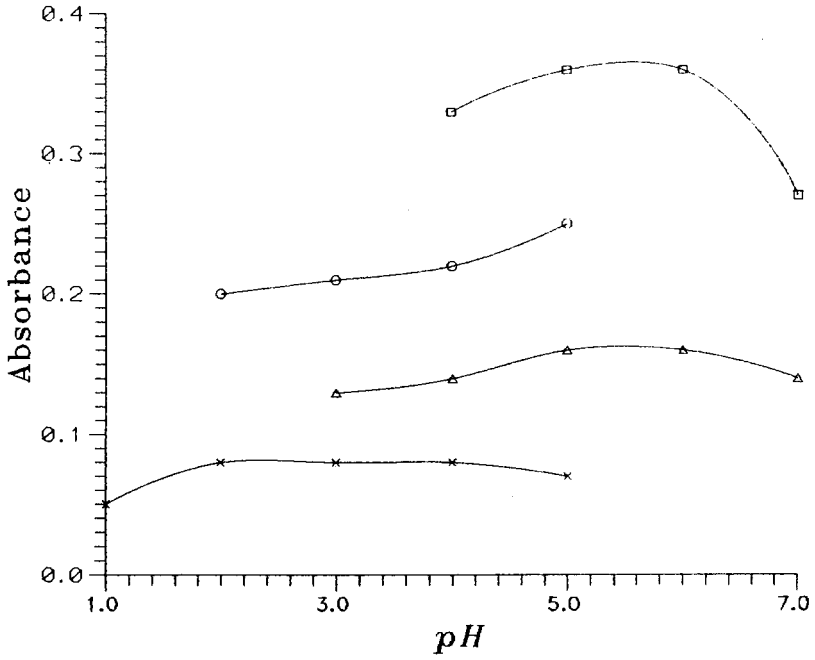

Fig. 2. Effect of pH on the determination of nicotine. 10 mg l^{-1} nicotine solution, room temperature, optimized reagent concentrations as shown in Table 1. Chromogenic reagent: (○), aniline; (×), barbituric acid; (△), pyrazolone; (□), sulfanilic acid.

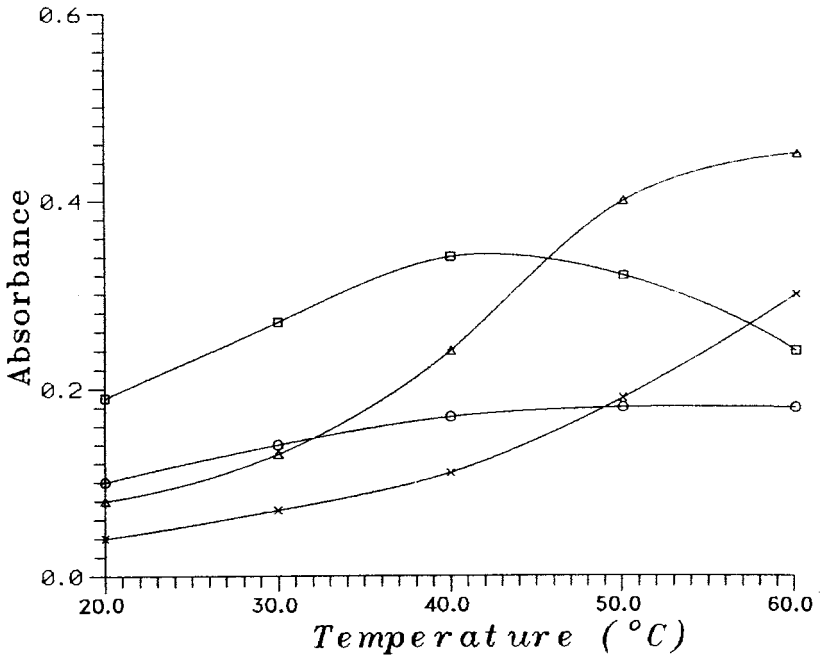

Fig. 3. Effect of temperature on the determination of nicotine. Five mg l^{-1} nicotine solution, optimized pH and reagent concentrations as shown in Table 1. Chromogenic reagent: (○), aniline; (×), barbituric acid; (△), pyrazolone; (□), sulfanilic acid.

is the best because of its highest slop and lowest detection limit under room temperature. This result also can be seen from Fig. 3 which indicates that the peak height of the sulfanilic acid method is about two to five times as high as the other three methods. The sulfanilic acid method was selected consequently in this study.

3.3. Applications

The sulfanilic acid method was applied to determine nicotine in tobacco and urine samples. Nine cigarette samples were analyzed by the above proposed sulfanilic acid method and the CFA sulfanilic method was adopted as reference method. The results shown in Table 2 indicates that results obtained by these two methods agree very well. The regression equation between the two sets of results was C (nicotine % by FI) = 1.005 C (nicotine % by CFA) + 0.01190, and the correlation coefficient was 0.9958. Paired t-test shows that $t = 1.29 < t_{0.05}(8) = 2.31$, which means that there are no significant difference between these two methods.

Six urine samples, three from smokers and three from non-smokers, was also analyzed by the proposed sulfanilic acid method. Samples were analyzed after diluting five times and standard addition experiment was conducted by detecting a solution prepared by mixing 10 ml of sample and 1 ml of 100 mg l^{-1} nicotine standard solution and diluted to 50 ml. Results shown in Table 3 indicate that the recoveries obtained by the proposed sulfanilic acid method are between 97–110%.

4. Conclusion

The applicability of aniline, barbituric acid, pyrazolone and sulfanilic acid in reagent-injection flow injection determination of nicotine were evaluated. Sulfanilic acid was selected for its relatively high sensitivity under room temperature, moderate reaction conditions and was applied successfully in determination of nicotine in both tobacco and urine samples. The present study also demonstrates that the reagent-injection FI technique can

Table 2
Determination of nicotine in cigarette with the FIA and CFA sulfanilic acid methods

Sample	Nicotine concentration (%)		Relative error (%)
	FIA sulfanilic acid[a]	CFA sulfanilic acid[b]	
1	1.23	1.25	−1.6
2	1.60	1.66	−3.6
3	2.48	2.48	0.0
4	1.20	1.16	3.4
5	1.31	1.30	0.8
6	2.12	2.10	1.0
7	2.22	2.17	2.3
8	1.56	1.46	6.8
9	2.33	2.28	2.2

[a] Average values ($n = 3$).
[b] Determined by the sample presenter using instrument produced by Alliance Instruments S.A.

Table 3
Determination of nicotine in urine by the proposed FIA sulfanilic acid method

Sample	Nicotine concentration (mg l^{-1})		Recovery (%)
	Added	Found	
Non-smoker			
1	0	1.04	
	10	12.04	110.0
2	0	0.88	
	10	10.88	100.0
3	0	0.79	
	10	10.45	97.0
Smoker			
4	0	21.55	
	10	31.75	102.0
5	0	15.60	
	10	25.50	99.0
6	0	11.40	
	10	21.30	99.0

be used to eliminate background absorption from sample matrix. As no dialysis unit was needed, the flow system of the proposed reagent-injection FI method is much simpler than that of the existed CFA methods. While the stopped-flow FI technique can be adopted to eliminate background absorption from sample matrix in only slow reactions, the reagent-injection FI technique can applied in all kinds chemical reactions, no matter it is fast or slow. The sampling throughput of the proposed method (50 h^{-1}) is a little higher than that of the existing CFA methods (40 h^{-1}).

References

[1] C.R. Green, D.A. Colby, P.J. Cooper, Recent Adv. Tob. Sci. 6 (1980) 123.
[2] M. Hana, W.F. McClure, T.B. Whitaker, M. White, D.R. Bahler, J. Near-Infrared Spectrosc. 3 (3) (1995) 133.
[3] A.S. Xu, L.L. Peng, J.D. Hulse, J. Chromatogr. B: Biomed. Appl. 682 (2) (1996) 249.
[4] H. Klus, H. Kuhn, Fachliche Mitt. Oestern. Tabakregie (C.A. 87 (1977) 180692e.) 17 (1977) 331.
[5] C.E. Efstathion, E.P. Diamandis, R.A. Hadjiioannon, Anal. Chim. Acta 127 (1981) 173.
[6] S. Ralapati, J. Chromatogr., B: Biomed. Appl. 695 (1) (1997) 117.
[7] J.J. Langone, H.K. Gjika, H. Van-Vunakis, Biochemistry 12 (1973) 5025.
[8] G.J. Knight, P. Wylie, M.S. Holman, J.E. Haddow, Clin. Chem. 31 (1985) 118.
[9] E. Werle, H.W. Becker, Biochem. Z. 313 (1942) 182.
[10] R.D. Barlow, R.B. Stone, N.J. Wald, E.V.J. Puhakainen, Clin. Chim. Acta 165 (1987) 45.
[11] G. Cope, P. Nayyar, R. Holder, J. Gibbons, R. Bunce, Clin. Chim. Acta 256 (2) (1996) 135.
[12] C.L. Smith, M. Cooke, Analyst 112 (1987) 1515.
[13] L.N. Markwood, J. Assoc. Off. Agric. Chem. 22 (1939) 427.
[14] M.A. El-Sayed, Y.A. Mohamed, Planta Med. (C.A. 83 (1975) 65509f) 27 (2) (1975) 140.
[15] Manish Rai, K.N. Ramachandran, V.K. Gupta, Analyst 119 (1994) 1883.
[16] W. Koing, J. Prakt. Chem. 69 (1904) 105.

[17] R.E. Davis, Tob. Sci. 20 (1976) 146.
[18] W.W. Sadler, R.R. Chesson, A.W. Schoenbaum, Tob. Sci. 4 (1960) 208.
[19] W.R. Harvey, B.M. Handy, Tob. Int. (C.A. 96 (1982) 159535g) 26 (1981) 183.
[20] E.V.J. Puhakainen, R.D. Barlow, J.T. Salonen, Clin. Chim. Acta 170 (1987) 255.
[21] P. Finster, J. Hollweg, E. Kausch, U. Burmester, Beitr. Tabakforsch. Int. (C.A. 110 (1989) 226704j) 14 (2) (1988) 105.

ELSEVIER

Talanta 47 (1998) 841–848

Talanta

Recent advances in solid-phase extraction of platinum and palladium

Krystyna Pyrzyńska *

Department of Chemistry, University of Warsaw, Pasteura 1, 02-093, Warsaw, Poland

Received 8 December 1997; received in revised form 27 February 1998; accepted 14 April 1998

Abstract

Increasing platinum concentrations have been detected in environmental samples since the introduction of catalytic converters used in cars. Also the intensive use of platinum-based anti-tumor drugs led to interest in the determination of trace amounts of platinum absorbed by the human body and of the physiological effect of its complexes on living organism. However, detection of Pt and Pd in environmental and biological samples with complex matrices, has to be generally preceded by a preconcentration/separation step. A brief overview of the application of solid sorbents for these procedures based on published data is presented. Attention is also paid to preparation of the samples and detection methods usually used for determination of platinum and palladium. © 1998 Elsevier Science B.V. All rights reserved.

Keywords: Platinum; Palladium; Solid sorbents; Preconcentration and separation

1. Introduction

With the introduction of Pt, Pd and Rh-containing catalytic converters in motor vehicles, the emission of these metals into the environment has increased. Platinum concentration in the road sediments collected in Sweden increased from 3.0 ng g^{-1} in 1984 to 8.9 ng g^{-1} in 1991 [1]. The emission of common catalytic converters, determined using laboratory-based car engines, is between 7 and 80 ng Pt per km [2]. Although platinum is emitted mainly in the elemental form as Pt(0) attached to alumina particles [3], in air-dust samples several percents of the total platinum content was determined as soluble species [4,5]. Moreover, the sequential extraction of Pt from road sediments yielded a significant exchangeable fraction [1]. An increased uptake of Pt and Pd by plants grown on polluted soils has been also found [6,7]. Some recent analytical data for platinum contents in environmental samples are given in Table 1.

Although palladium is also extensively used as catalyst in industrial chemical synthesis and in catalytic converters in cars, only the distribution of Pt in the environment has been intensively studied and so far only little information about Pd is available [14,15]. However, Pd is suspected to be one of the strongest allergens [16]. The

* Tel.: +48 22 8220211, ext. 398; fax: +48 22 8223532; e-mail: kryspyrz@chem.uw.edu.pl

0039-9140/98/$ - see front matter © 1998 Elsevier Science B.V. All rights reserved.
PII S0039-9140(98)00158-1

Table 1
Content of platinum in environmental samples

Sample	Detection method	Concentration range (ng l^{-1})	Ref.
Gullypot sediments	Voltammetry	2.4–13.6	[1]
Airbone dust	Voltammetry	1.10–5.91	[4]
Street dust	RNAA	14.5 ± 1.3	[8]
Corn	RNAA	642 ± 38	[8]
Beans	GFAAS	75 ± 5	[9]
Dust	GFAAS	12 ± 1	[10]
Soils	ICP–MS	0.3–8	[11]
Tabacco	IC–UV	1.52 ± 0.03 μg g^{-1}	[12]
Seawater (Atlantic Ocean)	ID–ICP–MS	55 ± 14	[13]

RNAA, radiochemical neutron activation analysis; GFAAS, graphite furnace atomic absorption spectrometry; ICP–MS, inductively coupled plasma-mass spectrometry; IC–UV, ion chromatography with UV absorption detection; ID, isotope dilution.

concentration of palladium in water from the river Rhein was estimated at 0.4 ± 0.1 ng l^{-1} [15], whereas deep-sea manganese nodules exhibit values in the range of 3.7–11.4 ng g^{-1} [14]. Unusually high Pd concentration of 0.3 μg g^{-1} in dust particles accumulated on plants near busy motorways were observed [15]. The average Pt/Pd ratio in these samples was 2.5.

Platinum complexes based on *cis*-dichlorodiamineplatinum(II) (cisplatin) have been widely used in cancer chemoteraphy for some years. These drugs are highly effective against a variety of solid tumours, however their use is associated with several toxic effects like nausea, neurotoxicity or nephrotoxicity [17]. A new generation of platinum based drugs, carboplatin and iproplatin, show a comparable activity against cancer together with less toxicity. One major field of interest has been interaction of cisplatin and related compounds with biological systems, especially DNA and its constituents. The interactions of palladium complexes and DNA have also been examined [18] due to the labile nature of Pd complexes. Platinum substitution reactions are known to be slow and palladium proves to be an ideal model because of its similar coordination properties.

Because of their inertness, platinum group metals have been considered harmless for a long time. Today it is known that they are present at elevated level in the environment, taken up by plants, such that and there is the possibility of the metals entering in the food chain. Chronic exposure to soluble platinum compounds may lead to toxic effects, which are known as a syndrome called *platinosis*. Employees exposed during the production and recycling of platinum-based catalytic converters revealed Pt levels in urine and blood up to 100 times higher compared to non-exposed control individuals [4]. For this reason, an adequate knowledge of the bioavalilability, bioaccumulation and evaluation of the toxic level of Pt and Pd to living organisms is necessary (Table 2).

In recent years the development of analytical methods for the determination of platinum and palladium contents in various matrices has attracted considerable interest [23,24]. Since the concentration of these metals, especially in environmental samples, is very low and often below the detection limits of common analytical techniques, a preconcentration/separation step usually precedes the determination. This process can also serve as a convenient method for interference removal. As solid phase extraction methods are most frequently used of matrix elimination and preconcentration of noble metals, its application in the determination of Pt and Pd is reviewed. Hereby, we focus on techniques that are particularly suitable for environmental analysis.

Table 2
Content of platinum and palladium in biological samples

Sample	Detection method	Concentration range	Ref.
Pd in urine	GFAAS	20–80 ng l^{-1}	[19]
Pt in urine	GFAAS	<70 ng l^{-1}	[19]
Pt in blood	ICP–MS	0.1–2.8 μg l^{-1}	[20]
Pt in plasma (after treatment)	ICP–MS	100–1000 μg l^{-1}	[21]
Pt in urine (after treatment)	ICP–AES	0.6–21.7 μg l^{-1}	[22]

ICP–AES, inductively coupled plasma–atomic emission spectrometry.

2. Sample preparation

The main goal of the first stage of analysis is the quantitative and, if possible, rapid dissolution of a sample. This step determines to a great extent the quality of the results and the duration of the complete analytical scheme. Special precautions for the purification of reagents, especially acids, and vessels are required in order to reduce the blank values [25–27].

The fire assay technique is especially useful for the collection of Pt and Pd from ores, rocks, concentrates and other industrial products, where large samples are required to insure homogenity. Lead, copper, antimony, bismuth, tin, nickel sulfide and copper–iron–nickel alloys have been used as collectors. Several reviews, discussing the potentials and limitations of this technique for the dissolution of platinum group metals and gold have been published [28,29].

Wet digestion techniques with acid mixtures in high-pressure PTFE bombs [10,12], microwave ovens [13,19], or using a high-pressure asher [4,30] were applied to decomposition of sediments, airborne particles and biotic materials. When samples of carbonate-rich sediments were decomposed using a mixture of HF and HNO_3, the precipitation of large amounts of calcium fluoride was observed [13]. It is therefore preferable to treat the samples first with HCl in order to dissolve the carbonate, while keeping calcium in solution. It is also necessary to remove the excess of the nitric acid from the sample solution after decomposition before any further preconcentration step, especially by liquid chromatography. Much of the work in sample preparation and subsequent analyses utilizes the properties of complex chlorides of Pt and Pd in aqueous solutions. Nitroso complexes may behave in different way than their chlorocomplexes [12,31] Therefore, their elimination should be carried out by several evaporation with hydrochloric acid.

Microwave digestion was applied to the mineralization of human blood samples prior to the determination of platinum by ICP–AES [32] and ICP–MS [33]. The concentrations of palladium and platinum in urine were determined by a GFAAS method without decomposition of the samples or by ICP–MS after UV photolysis [18]. In some biological materials with high concentrations of platinum, dilution with 1–2% nitric acid allowed direct abundance measurements using an ICP–MS method [26,34,35].

3. Detection methods

There are a variety of instrumental techniques reported in the literature for the determination of platinum and palladium, and this makes the selection of an appropriate method a crucial decision for the analyst. This is especially important for environmental samples, which contain very low contents of these analytes. One has to be beware that the detection limits presented by instrument manufacturers are generally obtained by analysis of dilute acid solutions containing low concentrations of metals. Such values are not valid for complex, real samples, in which detection limits are usually much poorer. Adsorptive cathodic stripping voltammetry, graphite furnace atomic absorption spectrometry (GFAAS), inductively coupled plasma-mass spectrometry (ICP–MS) and neutron activation analysis (NAA) are the

most sensitive methods used for the determination of platinum and palladium in a wide variety of biological and environmental samples.

The voltametric determination method uses the adsorption of the platinum formazone complex formed in situ on a hanging mercury drop electrode. This complex catalyzes the production of hydrogen and the reduction current associated with this reaction is related to the platinum concentration. However, this method is negatively affected even by a very low residual level of organic matrix in solution. Wei and Morrison [1] suggested that dry ashing is the most reliable digestion procedure for adsorptive voltammetry. In the analysis of Pt detection limits of 0.5 ng g^{-1} [1] and 0.1 ng g^{-1} [25] were achieved.

The detection limits offered by the GFAAS method are adequate for the determination of platinum concentration in blood from patients after cisplatin therapy [36]. The accuracy of the atomic absorption analysis for small concentrations of Pd and Pt strongly depends on the background absorption correction [14,37]. For environmental samples, this method requires a large-scale preconcentration step [9,10,19,37]. The combination of flow injection preconcentration using a microcolumn packed with activated carbon fibre and flame AAS has been applied to the determination of Pd [38]. Platinum in dust samples was enriched by electrodeposition into a graphite tube packed with reticulated vitreous carbon and then determined by atomic absorption directly from the packed tube used for preconcentration [10]. The lifetime of the tubes was at least 50 firings and the detection limit was found to be 0.07 ng ml^{-1}. The application of a flow system combined with a column preconcentration technique to GFAAS is more complicated due to the limited sample injection volume of 50–70 μl and the non-flow-through character of this method. This limitation was overcome in analysis of Pd and Pt by using different segmentation and fractionation techniques for the eluate collection [9,39]. Some efforts have been made using solid sample techniques, after preconcentration on ion exchange resins [37,40]. The stability of the suspensions can be improved by the use of surfactants, such as Triton X-100.

ICP–MS is one of the most suitable techniques for the determination of noble metals. Efficient sample introduction systems such as electrothermal vaporization, ultrasonic nebulization, direct injection and thermospray nebulization for the increase the sensitivity of this method. However, polyatomic ions originating from the plasma gas, reagents and components of the matrix can affect the measured signal to a large extent. Totlant et al. [41] reported a method for the direct measurement of platinum group metals in solid samples where the analyte is directly determined by slurry nebulization. Excellent detection limits (0.04–0.2 μg g^{-1}) were reported. Usually, however, a preconcentration of Pd and Pt is performed prior to the analysis of environmental samples, generally using ion exchange resins [13,27,42]. A detection limit of 20 pg g^{-1} was achieved for platinum, following enrichment in combination with thermospray nebulization [27].

Neutron activation analysis methods have been developed for determination of platinum in biological and environmental samples [8,43]. This technique offers very low detection limits, but is not suitable for routine analysis. It can be very useful as reference method.

Further improvements in detection limit, precision, reliability and selectivity of analytical methods are still a challenge to the analyst. The certified reference materials (CRM) provide a possibility to control the quality of analytical data. Unfortunately, there are only a few CRM for platinum and most of them have relatively high Pt contents. In Germany the project 'Emission of Precious Metals' was initiated with the purpose to prepare in the further new reference materials of environmental and biological origin. Several reference samples have been prepared with low and elevated platinum concentrations for interlaboratory studies with different analytical techniques and the results of these studies were reported by Wegscheider and Zischka [44].

4. Application of solid sorbents

Among the numerous techniques reported for the preconcentration and separation of platinum

and palladium the methods using ion exchange resins or sorbent extraction have proved to be especially effective. Separation of palladium and platinum from base metals can be obtained by means of cation exchange resins. Pd and Pt in the form of stable anionic chlorocomplexes pass through the column, while base metals with the exception of Fe^{3+}, which exist as cations under the same conditions, are retained on the column. Some disadvantages of cation exchange separations are the need to work at high concentrations of matrix components, and need for more than one pass of a sample through the column (or columns) to obtain satisfactory separations.

Strongly basic anion exchange resins with styrene or acrylic polymers cross-linked with divinylbenzene exhibit a high selectivity for platinum group metals and can remove them quantitatively from HCl solution [13,40,45–47]. However, there are difficulties in the complete elution of the complexes. The desorption is possible with hot nitric acid [13,40,48] or sulphur containing reagents, mainly thiourea by ligand substitution reaction [15,46]. The determination of palladium and platinum in the eluate solution can be a daunting task. It can lead to problems in GFAAS measurements due to the formation of stable but volatile species of the MeS type [37]. For ICP–AES and ICP–MS techniques the dilution of solutions was necessary to reduce the high levels of total dissolved solids from thiourea to level acceptable to each technique [46,49]. Moreover, it was observed that resin which had previously been in contact with thiourea solutions has a lower capacity for platinum metal complexes. Therefore reuse of such resin cannot be recommended. Elution of palladium can also be achieved with 1% ammonia solutions at ambient temperature, while 5% NH_3 at elevated temperature and slow flow rate elute platinum [47].

The comparison between anion exchangers with styrene-divinylbenzene (Varion AT 400) and cellulose matrix (Cellex T) for preconcentration and separation of palladium from other metals was reported [50]. Cellex T has lower ion exchange capacity towards chloride complexes of Pd than Varion AT 400. However this can be a factor facilitating the quantitative elution because less volume of eluent is needed for palladium recovery.

Many studies have been performed on the preconcentration of Pd and Pt from acidic media using resin containing selective chelating groups covalently attached to polymeric matrix. These groups include organophosphorus [51], dithizone derivatives [52,53], thiosemicarbazide [54], thiourea [55] and nitrogen containing compounds [56–60]. These resins display a high selectivity for platinum metals, fast sorption kinetics and good retention capacity. They were mainly used for the separation and preconcentration of Pd and Pt from synthetic solutions and only few of them were applied to real samples [55,58–60]. Some of theses resins have certain limitations. The elution of Pd and Pt from a resin containing S-bonded dithizone is strongly affected by the presence of Ir(IV) [53], whereas a resin containing thiosemicarbazide as a functional group appears suitable for column operation only if the flow rate is low enough [54]. Retention of palladium on the cellulose ion exchanger Hyphan with 1-(2-hydroxyphenyl-azo-)-2-naphtol groups depends on the pH values of the solution [56]. Maximum retention for Pd and Pt are achieved at pH 6.0–6.2, and pH 4.65, respectively. Palladium preconcentrated on chelating sorbent of the pyrazole type cannot be quantitatively eluted with acids or complexing agents [57]; digestion of the sorbent is therefore proposed for complete recovery. The desorption from imidazolinyl ethyl amino resin with a mixture of thiourea and sulfuric acid has to be performed immediately after preconcentration to achieve complete recovery of Pt and Pd [59]. In addition, the determination of these metals by ICP–AES had to be carried out within 2 h of elution. Otherwise, the results with errors may be obtained due to the reduction of the ions by thiourea.

Recently, new functional resins with chelating properties, prepared by simple immobilization of organic complexing reagents on different solid supports, have gained considerable attention. These resins can react with metal ions by complex formation, with complex stabilities depending on the experimental conditions. The use of such resins for trace metals preconcentration presents

numerous advantages. The same resin can be used for different analytical purposes by varying the type of organic reagent loaded. Generally, the organic reagent can be displaced out of the resin and easily recovered. By using an appropriate resin in combination with a selective complexing ligand and optimized experimental conditions, it is possible to obtain the desired selectivity with respect to a certain metal ion or a group of metal ions. Dimethyl glyoxime immobilized on microcrystalline naphthalene was applied to the preconcentration of Pd [61]. The adsorbed metal was stripped from the column with a DMF-*n*-butylamine mixture together with the naphthalene and was determined directly by flame AAS. A sorbent with thionalide loaded on silica gel [62] and the macroporous resin Bio-Beads SM-7 [63] can be useful for the rapid enrichment of palladium. 2,2′ - Dipyridyl - 3 - [(4 - amino-5-mercapto)-1,2,4triazolyl]-hydrazone supported on silica gel has also been reported as a useful chelating reagent for Pd preconcentration [64]. The retention was decreased in the presence of EDTA at concentrations above 10^{-6} mol l^{-1}. Schuster and Schwarzer proposed a fully automated preconcentration procedure for palladium using very selective reagents *N*,*N*-dialkyl-*N*′-benzoylthioureas loaded on C18 Polygosil [39]. These complexing agents have high resistance to hydrolysis and oxidation, thus enabling the determination of Pd even in strongly nitric acid solutions. For preconcentration of platinum Separon SGX C18 in the presence of cationic surfactants was proposed [65]. A sample matrix corresponding to 2.5 g of plant ash does not interfere with the separation. Amberlite XAD-7 resin coated with dimethylglyoxal bis(4-phenyl-3-thisomicarbazone was also studied [66]. While palladium reacts quantitatively at room temperature, it was necessary to heat Pt(II) with the reagent for 20 min at 80°C to ensure complete chelate formation. The presence of iodide ions accelerates the chelation of platinum. Platinum was preconcentrated with bis(carboxylmethyl)dithiocarbamate on Amberlite XAD-4 [9] and also using pyrrdidinedithiocarbamate on C18-bonded silica gel [67].

Te analytical performance of platinum collection using activated alumina was discussed by Cantarero et al. [68]. A flow-injection technique with on-line sample preconcentration was developed in an attempt not only to enhance sensitivity but also to decrease analysis time.

5. Conclusions

The importance of platinum and palladium has increased enormously as a result of technological developments in catalytic converters for automobiles, catalysts for petrochemical, chemical and pharmaceutical industries and anti-cancer therapy. Until now, Pt and Pd compounds have had little impact on the environment. However, some areas such as roadsides have experienced increasing Pt contamination in recent years. The low concentration of Pt and Pd in environmental and biological samples demands appropriate methods for their separation and preconcentration, prior to the analytical determination.

It has to be noted that reactivity, bioavailability and toxicity are not necessarily correlated with the total content of an element, but also depend on its chemical form, oxidation state, chemical bonds in which it is involved and the possible association with other components of given matrix. For example, the chlorocomplexes of platinum are potent sensitizing agents which can cause severe allergic reactions [16], whereas the insoluble platinum dioxide is rather non-toxic. In order to judge the actual health risk of platinum in the environment and to understand its transformation, methods for the determination of platinum species need be developed. So far only a few papers concerning platinum speciation in biological and environmental samples have been published [3,5,6,69–71]. The analytical methods necessary for such studies can be developed using hyphenated techniques, for example by coupling high performance liquid chromatography or capillary zone electrophoresis with a sensitive detection system such as mass spectrometry.

Acknowledgements

This research was carried out in the framework of the BW 1383/17/97 project.

References

[1] C. Wei, G.M. Morrison, Anal. Chim. Acta 284 (1994) 587.
[2] H.P. Köning, R.F. Hertel, W. Koch, G. Rosner, Atmos. Environ. 26A (1992) 741.
[3] R. Schlögl, G. Indlekofer, P. Oelhafen, Angew. Chem. 99 (1987) 312.
[4] F. Alt, A. Bambauer, K. Hoppstoch, B. Mergler, G. Tölg, Fresenius J. Anal. Chem. 346 (1993) 693.
[5] S. Lustig, S. Zang, B. Michalke, P. Schramel, W. Beck, Sci. Total Environ. 188 (1996) 195.
[6] J. Messerschmidt, F. Alt, G. Tölg, Anal. Chim. Acta 291 (1994) 161.
[7] E.L. Kothy, Plant Soil 53 (1979) 547.
[8] D. Wildhagen, V. Krivan, Anal. Chim. Acta 274 (1993) 257.
[9] M.L. Lee, G. Tölg, E. Beinrohr, P. Tschöpel, Anal. Chim. Acta 272 (1993) 193.
[10] E. Beinrohr, M.L. Lee, P. Tschöpel, G. Tölg, Fresenius J. Anal. Chem. 346 (1993) 689.
[11] M.L. Farago, P. Kavanagh, R. Blank, J. Kelly, G. Kazantzis, I. Thorton, P.R. Simpson, J.M. Cook, S. Parny, G.M. Hall, Fresenius J. Anal. Chem. 354 (1996) 660.
[12] U. Jerono, F. Alt, J. Messerschmidt, G. Tölg, Mikrochim. Acta 108 (1992) 221.
[13] D. Colodner, E.A. Boyle, J.M. Edmond, Anal. Chem. 65 (1993) 1419.
[14] R. Eller, F. Alt, G. Tölg, H.J. Tobschalt, Fresenius Z. Anal. Chem. 334 (1989) 723.
[15] V. Hodge, M. Stallard, Environ. Sci. Technol. 20 (1986) 1058.
[16] G. Rosner, R. Merget, in: A.D. Dayan (Ed.), Immunotoxicity of Metals and Immunotoxicology, Plenum, New York, 1979, p. 93.
[17] J. Redijk, Pure Appl. Chem. 59 (1987) 181.
[18] P. Watkins, E. Yuriew, Varian-Instruments at work vol. AA-118, 1995, p. 1.
[19] J. Bergerow, M. Turfeld, L. Duemann, Anal. Chim. Acta 340 (1997) 277.
[20] O. Nygren, G.T. Vaughan, T.M. Florence, G.M.P. Morrison, I.M. Warner, L.S. Dale, Anal. Chem. 62 (1990) 1637.
[21] P. Allain, S. Berre, A. Mauras, A. Le Bouil, Biol. Mass Spectrom. 21 (1992) 141.
[22] F.B. Lo, D.K. Aral, M.A. Nazar, J. Anal. Toxicol. 11 (1987) 242.
[23] Y.B. Qu, Analyst 121 (1996) 139.
[24] M. Balcerzak, Analyst 122 (1997) 67R.
[25] K. Hoppstock, F. Alt, K. Cammann, G. Weber, Fresenius J. Anal. Chem. 335 (1989) 813.
[26] P. Schramel, I. Wendler, S. Lusting, Fresenius J. Anal. Chem. 353 (1995) 115.
[27] M. Parent, H. Vanhoe, L. Moens, R. Dams, Fresenius J. Anal. Chem. 354 (1996) 664.
[28] J.C. Van Loon, R.R. Barefoot, in: Determination of the Precious Metals, Selected Instrumental Methods, Wiley, Chichester, 1991, pp. 106–151.
[29] S.J. Parry, in: Z.B. Alfassi, C.M. Wai (Eds.), Preconcentration Techniques for Trace Elements, CRC Press, Boca Raton, FL, 1992, pp. 401–415.
[30] F. Alt, U. Jerono, J. Messerschmidt, G. Tölg, Mikrochim. Acta III (1988) 299.
[31] D. Nachtigall, S. Artel, G. Wünsch, J. Chromatogr. 775 (1997) 197.
[32] V. Di Nioto, D. Ni, L. Dalla Via, F. Scomazzon, M. Vidali, Analyst 120 (1995) 169.
[33] J. Bergerow, L. Dunemann, J. Anal. At. Spectrom. 11 (1996) 303.
[34] B. Casetta, M. Roncadin, G. Martanarti, M. Furlanut, At. Spectrosc. 12 (1991) 81.
[35] L.J. Van Warmerden, O. Van Tellingen, R.A. Mares, J.H. Beijnen, Fresenius J. Anal. Chem. 351 (1995) 777.
[36] F.W. Sunderman, J. Sporn, S.M. Hopfer, K.R. Sweeney, N.G. Chakraborty, B. Grrnberg, Ann. Clin. Lab. Sci. 20 (1990) 379.
[37] I.V. Kubrakova, T.F. Kudinova, N.M. Kuzmin, I.A. Kovalev, G.I. Tsysin, Y.A. Zolotov, Anal. Chim. Acta 334 (1996) 167.
[38] S. Lin, C. Zheng, G. Yun, Talanta 42 (1995) 921.
[39] M. Schuster, M. Schwarzer, Anal. Chim. Acta 328 (1996) 1.
[40] V. Hodge, M. Stallard, M. Koide, E.D. Goldberg, Anal. Chem. 58 (1986) 616.
[41] M. Totland, I. Javis, R.E. Jarvis, Chem. Geol. 104 (1993) 175.
[42] G.E. Hall, J.C. Pelchat, J. Anal. At. Spectrom. 8 (1993) 1059.
[43] B. Rietz, K. Heydron, J. Radioanal. Nucl. Chem. 174 (1993) 49.
[44] W. Wegscheider, M. Zischka, Fresenius J. Anal. Chem. 346 (1993) 525.
[45] S.J. Al-Bazi, A. Chow, Talanta 31 (1984) 815.
[46] I. Jarvis, M.M. Totland, K.E. Jarvis, Analyst 122 (1997) 19.
[47] R. Gaita, S.J. Al-Bazi, Talanta 42 (1995) 249.
[48] M. Rehkämper, A.N. Halliday, Talanta 44 (1997) 663.
[49] I. Jarvis, K.E. Jarvis, Chem. Geol. 95 (1992) 1.
[50] K. Brajter, K. Słonawska, Mikrochim. Acta I (1989) 137.
[51] M. Fujiwara, T. Matsushita, T. Kobayashi, Y. Yamashoji, M. Tanaka, Anal. Chim. Acta 274 (1993) 293.
[52] M. Grote, A. Kettrup, Anal. Chim. Acta 172 (1985) 223.
[53] M. Grote, A. Kettrup, Anal. Chim. Acta 175 (1985) 239.
[54] S. Siddhanta, H.R. Das, Talanta 32 (1985) 457.
[55] X. Chang, Z. Su, G. Zhan, X. Luo, W. Gao, Analyst 119 (1994) 1445.

[56] I.M. Kenaway, M.E. Khalifa, M.M. El-Defrawy, Analysis 15 (1987) 314.
[57] E. Ivanova, O. Todorova, M. Stoimenova, Fresenius J. Anal. Chem. 344 (1992) 316.
[58] P. Di, D.E. Davey, Talanta 42 (1995) 685.
[59] Z.X. Su, Q.S. Pu, X.Y. Luo, X.J. Chang, G.Y. Zhan, F.Z. Ren, Talanta 42 (1995) 1127.
[60] A. Tong, Y. Akama, S. Tanaka, Anal. Chim. Acta 230 (1990) 1179.
[61] S. Usami, T. Fukami, E. Kinoshita, B.K. Puri, M. Satake, Anal. Chim. Acta 230 (1990) 17.
[62] K. Terada, K. Matsumoto, Y. Taniguchi, Anal. Chim. Acta 147 (1983) 411.
[63] J. Chwastowska, W. Żmijewska, E. Sterlińska, Anal. Chim. Acta 276 (1993) 265.
[64] C. Samara, Th.A. Konimtzis, Fresenius Z. Anal. Chem. 327 (1987) 509.
[65] V. Otruba, M. Strnadova, B. Skalnikova, Talanta 40 (1993) 221.
[66] S. Hoshi, K. Higashihara, M. Suzuki, Y. Sakurada, K. Sugawara, M. Uto, K. Akatsuka, Talanta 44 (1997) 571.
[67] N.K. Shah, C.M. Wei, J. Radioanal. Nucl. Chem. 130 (1989) 451.
[68] A. Cantarerro, M.M. Gomez, C. Camara, M.A. Palacios, Anal. Chim. Acta 296 (1994) 205.
[69] J. Bettmer, W. Buscher, K. Cammann, Fresenius J. Anal. Chem. 354 (1996) 521.
[70] J. Messerschmidt, F. Alt, G. Tölg, Electrophoresis 16 (1995) 161.
[71] B. Michalke, P. Schramel, Fresenius J. Anal. Chem. 357 (1997) 59.

ELSEVIER

Talanta 47 (1998) 849–859

Talanta

Determination of Mo, U and B in waters by electrothermal vaporization inductively coupled plasma mass spectrometry

Dirce Pozebon, Valderi L. Dressler, Adilson J. Curtius *

Departamento de Química da Universidade Federal de Santa Catarina, 88040-900 Florianópolis, S.C., Brazil

Received 5 January 1998; accepted 14 April 1998

Abstract

A method for the determination of Mo, U and B in waters by inductively coupled plasma mass spectrometry, using an electrothermal vaporizer for sample introduction, is described. For Mo and U, NH_4F was chosen as modifier and for B, synthetic sea water plus mannitol were used. The modifier effect was verified and the optimized pyrolysis and vaporization temperatures were obtained from pyrolysis and vaporization curves, together with the transient signals of the analytes. The masses of the modifiers added to the tube were also optimized. The detection limits were 0.018 or 0.30 ng ml^{-1} for Mo, 0.03 ng ml^{-1} for U and 0.68 ng ml^{-1} for B. The analytes were determined in certified waters and the obtained results agree with the certified or recommended values or, in the case of B in sea waters, with the values obtained by other methods. Uranium could not be measured in the sea water samples due to strong memory effect. © 1998 Elsevier Science B.V. All rights reserved.

Keywords: Electrothermal vaporization; Inductively coupled plasma mass spectrometry; Uranium; Molybdenum; Boron

1. Introduction

Several elements, such as V, Cr, As, Ba, Ta, W, B, U, Si, La, Mo and Nb are able to form refractory carbides with the carbon of the graphite tube, used in electrothermal vaporization or atomization [1–13]. The extend of the carbide formation by these elements depends, mainly, on the temperature of the graphite tube and on the matrix. The formation of carbides of As may be minimized by using Pd as a chemical modifier [14] and the carbides [1,4] of V and Cr decompose at temperatures below 2000°C. Consequently, for these three elements the loss in sensitivity due to carbide formation is not critical. For the other carbide forming elements, the effects on their determination are more severe, since the temperatures required for the decomposition of the carbides are around 3000°C or even 4000°C [4,8–11]. To reduce the carbide formation, besides the use of pyrolytic coated graphite tubes, several others

* Corresponding author. Tel.: +55 48 2319219; fax: +55 48 2319711; e-mail: adilsonc@fastlane.com.br

0039-9140/98/$ - see front matter © 1998 Elsevier Science B.V. All rights reserved.
PII S0039-9140(98)00174-X

possibilities were tested, such as the coating of the tube with ZrO_4, TaO_2 and W [7], flow of different gases through the tube [8–11], different chemical modifiers [10,11] and the use of filaments of W, Re and Ta or platforms coated with these elements [5,12,14].

The determination of W and Mo by electrothermal vaporization—inductively coupled plasma mass spectrometry (ETV-ICP-MS) was studied by Park and Hall [9] in 1987. More recently Goltz et al. [10] and Wanner et al. [11], studied the determination of Ta, U and B. These authors observed that the carbide formation is minimized when halocarbons or halides are introduced in the graphite furnace. These compounds decompose by heating the tube, producing free halogen that reacts with the analyte, forming more volatile compounds. Freon (CHF_3) mixed with Ar is frequently recommended, but several other modifiers containing halogen were also tested: NH_4F, NH_4Cl, NH_4Br, NaCl, NaF, CCl_2F_2 and HCl [10,11]. For B, the best tested modifier was NH_4F while for Ta, W and U, the halogenated hydrocarbon produced the best results. Freon was the only halocarbon tested for Mo [9].

Other chemical modifiers for the determination of B by electrothermal atomization atomic absorption spectrometry (ETAAS) were studied by Botelho et al. [13], who verified memory effect with all tested modifiers. Wei et al. [15] studied the effect of mannitol on the B determination by ETV-ICP-MS, verifying that the signal increases significantly due to the formation of complexes of B with mannitol, preventing the formation of carbides. Besides, mannitol also acts as a carrier for B from the vaporizer to the plasma. In spite of these positive effects, pyrolysis temperature higher than 400°C could not be used for the matrix separation, when only mannitol was present.

In this work, the determination of Mo, U and B in certified waters by ETV-ICP-MS, using modifiers, is studied. Ammonium fluoride, with or without NaCl, as modifier for Mo and U, and mannitol with synthetic sea water, as modifier for B, are tested. Sodium chloride and sea water act as carriers for the vapor from the vaporizer to the plasma. Related problems, as memory effects and tube life are considered.

2. Experimental part

2.1. Instrumentation

An inductively coupled plasma mass spectrometer from Perkin Elmer—Sciex ELAN 6000, equipped with an electrothermal vaporizer from Perkin Elmer HGA-600 MS and an autosampler AS-60, also from Perkin Elmer, was used. For the pneumatic nebulization a cross-flow nebulizer, a Scott type nebulization chamber and a Gilson peristaltic pump were used. The operational conditions for the ELAN 6000 are given in Table 1. The temperature programme for the HGA-600 MS, optimized in this study, is shown in Table 2. The connection from the HGA-600 MS to the ELAN 6000 was made using a poly(tetrafluorethylene) tube of 100 cm long and having an internal diameter of 0.6 cm. During the drying and pyrolysis stages, the internal argon flow was kept at 0.3 l min^{-1} to remove the vapor from the sample matrix. A graphite probe closes the sample introduction hole, 3 s before the ending of the second cooling stage, step 5 of Table 2. During vaporization, the carrier gas flow, 0.90 l min^{-1}, together with the internal gas flow of the furnace is directed in the sense to transport the sample vapor, produced in the graphite tube to the ICP-MS. The internal gas flow rate was kept at 0.3 l min^{-1} during all step 6 of the furnace temperature program for Mo and U when NaCl or sea water was used as modifier, and for the B deter-

Table 1
Instrumental conditions and data aquisition

RF power	1000 W
Argon flow rate	
Principal	15 l min^{-1}
Intermediate	1.2 l min^{-1}
Carrier	0.92 l min^{-1}
Nebulizator	1.0 l min^{-1}
Sampler and skimmer	Pt
Signal measurement	Peak area
Resolution	0.7 amu (at 10% of peak height)
m/z per reading cycle	2
Readings/replicate	75–100 (ETV)
Auto lens	On
Measurement mode	Peak hopping

Table 2
Furnace temperature program for the analysis of the certified waters

Step	Temperature (°C)	Ramp (s)	Hold (s)	Gas (ml min^{-1})
1	90	10	10	300
2	150	20	5	300
3	1200 (B, U), 1400 (Mo)	10	20	300
4	20	5	10	100
5	100	20	10	100
6[a]	2000 (B), 2400 (U), 2750 (Mo)	0.0 (Mo, B), 1.0 (U)	8 (Mo, B), 10 (U)	0[b], 300
7	2800	5	2	300
8	20	5	15	0

[a] Reading in this step.
[b] For Mo and U in Riverine Water.

minations. For all other situations, the internal gas flow was interrupted during the vaporization step. The maximum power heating (ramp 'zero') for the vaporization step was used for Mo and B while for U the ramp was 1 s. The reading time for Mo and B was 8 s and for U was 10 s. Pyrolytically graphite coated tubes, Perkin Elmer No. 091504, and probes made of electrolytically graphyte, Perkin Elmer I/N B0508371 were used. Argon with a purity of 99.996% (White Martins, Brazil) was used. The optimization of the ICP-MS parameters was done by adjusting the nebulizer gas flow and the alignment of the mass spectrometer in relation to the torch (x-y adjustment) in order to obtain the maximum production of ions M^+ and minimum signals for M^{2+}, MO^+ and background at m/z 220, using pneumatic nebulization. The carrier gas flow used in the electrothermal vaporization was optimized for maximum intensity of the analyte signals. The used instrumental conditions are given in Table 1. The vaporizer temperature program is given in Table 2. The cleaning step was used only when the vaporizer temperature was below 2650°C. The pyrolysis and vaporization temperatures for the analysis of the certified waters were 1400 and 2750°C for Mo, 1200 and 2400°C for U and 1200 and 2000°C for B, respectively.

2.2. Solutions and samples

Solutions were prepared from NH_4F (Merck), NaCl (Merck) and mannitol (VETEC, Brazil), all of analytical grade and HNO_3 (Suprapur, Merck). Milli-Q water with a resistivity of 18.2 MΩcm was used for the dilutions. A stock multielemental analytical solution (ICP-IV from Merck) containing 10 μg ml^{-1} of the analytes was used. The synthetic sea water was prepared based on the recipe used by Greenway et al. [16] dissolving products from SPEX (0.127 g of Mg + 2.4340 g of Na_2CO_3 + 1.8457 g of K_2CO_3 + 0.1023 g of $CaCO_3$ + 0.363 g of $(NH_4)_2SO_4$ + 6.2 ml of concentrated HCl) in 1% v/v HNO_3 and completing the volume to 100 ml.

Four certified waters were analyzed: Riverine Water SLRS 3; Nearshore Sea Water CASS-3; Open Ocean Sea Water NASS-4, all from the Nacional Research Council Canada (NRCC); and Water 1643d from the National Institute of Standards and Technology (NIST). The sea waters were diluted 1 + 9, 1 + 19 and 1 + 99 with 1% v/v HNO_3. The Water 1643d was diluted 1 + 1 and the SLRS 3 was analyzed without dilution.

2.3. Procedures

For the determination of Mo and U, 10 μl of the sample or of the analytical solution (0.05–1.0 ng ml^{-1} in 1% v/v HNO_3) were dispensed onto the graphite tube together with 5 μl of the 20000 μg ml^{-1} NaCl solution, when this carrier was used. After that, the temperature program shown in Table 2 was run up to step 3. Then, 5 (for Mo) or 10 μl (for U) of the 2.5% m/v solution of the NH_4F were introduced into the furnace and the

temperature program was run from step 5 to the end. For the determination of Mo in sea water samples, diluted 1 + 19, external calibration and matrix matching by pipetting 5 μl of 20000 μg ml^{-1} NaCl into the furnace, were used. Molybdenum and U were determined in the SLRS 3 sample without dilution and the analyte addition method was used for calibration, employing NH_4F as modifier. For the determination of B in the sea water samples when external calibration was used, 8 μl of 3% m/v mannitol plus 10 μl of the synthetic sea water were dispensed onto the graphite tube followed by 20 μl of the analytical solution (10–40 μg l^{-1}) or of the sample. For this element, when the analyte addition method was employed, only mannitol was added as modifier.

3. Results and discussion

3.1. Molybdenum and uranium

These two analytes can be determined in sea water by ICP-MS using the conventional pneumatic nebulization, after diluting the sample 1 + 19, since Mo is present in relatively high concentrations and U has a very low detection limit. Either external calibration with matrix matching with a NaCl solution or the analyte addition method can be employed. However, after about 50 measurements, the signal intensities decrease about 30%, probably due to solid deposition on the cones. Besides, for very small samples, or samples with a high concentration of dissolved solids or organic samples, the electrothermal vaporizer coupled to the ICP-MS may be advantageous.

The pyrolysis temperature curves for Mo, using NH_4F as modifier, depicted in Fig. 1, demonstrated that higher signals are obtained for pyrolysis temperature in the range from 1500 to 1700°C, the highest temperature tested, when NaCl is present. In the absence of NaCl, the signal decreases for pyrolysis temperatures higher than 1100°C, as also shown in Fig. 1. It is possible that, suppression effect is responsible for the lower signals in the presence of NaCl, for pyrolysis temperatures lower than around 1500°C. For higher pyrolysis temperature, less Na remains in the tube, before the vaporization, and less signal suppression is expected. This could explain the increase in the Mo signal intensities for pyrolysis temperature higher than 1300°C, when NaCl is present. Fig. 1 also shows that the signals are much lower when the internal Ar flow is interrupted during the vaporization. However, a flow rate of 0.3 l min^{-1} produces an irregular peak shape, with a higher relative standard deviation (RSD), when the Riverine Water was analyzed. For this reason, the internal flow rate was kept at 0.3 l min^{-1} for the sea water analysis, but was interrupted, during the vaporization, for the Riverine Water. The vaporization temperature curve for Mo, using NH_4F as modifier, depicted in Fig. 2, shows a steep increase up to 2750°C without reaching a plateau. For higher vaporization temperatures the signal intensity decreases probably because a more stable carbide is formed.

In the presence of NH_4F, the vaporization temperature curve for U, depicted in Fig. 2, shows that the signal intensities are already high at temperatures higher than 1700°C. According to Goltz et al. [10], the U signals increase significantly only after 2500°C, in the presence of HNO_3, HCl or NaCl, but without NH_4F, probably due to the decomposition of U oxides (UO_2 and UO) and, for temperature higher than 2600°C, probably to decomposition of the carbides. The different behavior found in this work should be attributed to the modifier, which facilitates the removal of U from the graphite tube, probably as UF_6, but does not avoid completely the memory effect. The best precision was obtained at 2400°C. The pyrolysis temperature curves, as can be seen in Fig. 1, show maxima at 1200°C in the presence of NaCl. The lower signal intensities for temperatures lower than 1200°C can be attributed to the formation of volatile uranium oxides [10]. In Fig. 3, it is shown that the signal intensities of U increases in function of the added mass of the modifier. For Mo, the increase is only up to 0.125 mg. The amounts of NH_4F used in this work were 0.125 and 0.25 mg for Mo and U, respectively.

The transient signals of U and Mo in sea water in different dilutions with 1% v/v HNO_3, with and

without NH_4F, using different vaporization temperatures, are shown in Fig. 4. At a vaporization temperature of 2700°C, the memory effect for U is very strong in the presence of sea water as shown by the tailing in Fig. 4(a, b and d). This effect could be confirmed by the blank signals. After 100 reading cycles the counts increased from 1000 to 7000. It seems that the NaCl favors the intercalation of U in the graphite [10], increasing the memory effect. Memory effect was also verified for U independently of the presence of sea water. The signals for U in Fig. 4(c and e), without using a modifier, are quite similar, although the dilutions in each case, are very different, showing that with the more concentrated sample, more U is retained in the graphite, as can be seen also by its tailing. In the absence of sea water and using a vaporization of 2400°C, Fig. 4(g), a tailing is not seen, which is not the case when the vaporization temperature is 2700°C,

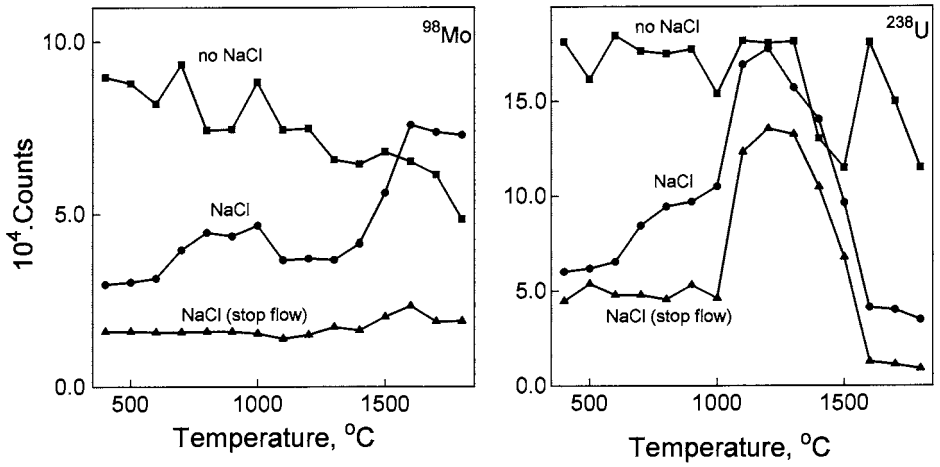

Fig. 1. Pyrolysis temperature curves for 0.01 ng of Mo and 0.01 ng of U in 1%, v/v, HNO_3, with NH_4F (0.125 mg for Mo and 0.25 mg for U), as modifier.

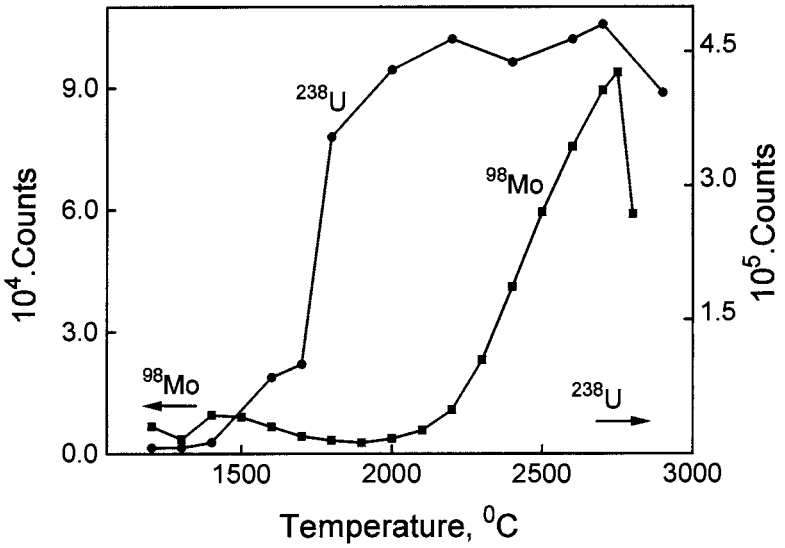

Fig. 2. Vaporization temperature curves for 0.01 ng of Mo and 0.01 ng of U in 1%, v/v, HNO_3, with NH_4F (0.125 mg for Mo and 0.25 mg for U), as modifier.

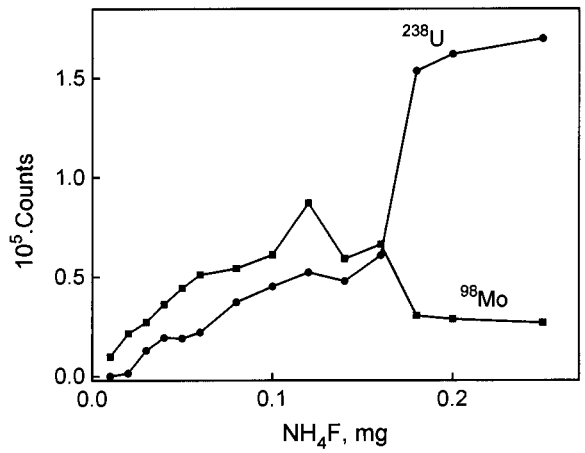

Fig. 3. Effect of NH_4F on the signal intensities of 0.01 ng of Mo and of 0.01 ng of U in 1%, v/v, HNO_3; pyrolysis and vaporization temperatures are 1200 and 2600°C, respectively.

Fig. 4(h). For Mo, the blank signal increases less than 20% after 100 cycles, showing that the memory effect is small. Also for Mo, the signal takes longer to return to the baseline, when sea water is present. A reading time of 12 s, using a vaporization temperature of 2700°C is necessary for the signal to return to the baseline. In this work a reading time of 8 s was adopted, since the loss in the signal intensity is small for this lower time and the tube may last longer. It is also shown, that for Mo, the modifier increases significantly the signal, specially if a high vaporization temperature is used (Fig. 4(a, b and h)). A double peak in the transient signal of Mo, using the modifier, was always observed when the sea water was present (Fig. 4(a, b and f)), indicating the vaporization of two Mo species. Without the modifier, only a single peak was observed. When the sea water was not present, the double peak appeared only for the higher vaporization temperature (Fig. 4(h)).

The analytical parameters obtained for Mo and U are shown in Table 3. The limit of detection (LD) was obtained from $3S/s$, where S is the slope of the analytical curve, and s is the standard deviation of five consecutive readings of the blank. The higher LD obtained for Mo, when the external calibration was used, is because the 20-fold dilution of the sample was considered in the analysis of sea water.

It should be emphasized that the analyte addition method was necessary for the determination of Mo and U in the Riverine Water, since accuracy was not achieved using external calibration, even when matrix matching with 1500 μg ml^{-1} NaCl was tested. For the Mo determination in sea water, when a ten-fold dilution was used, the RSD was higher than 10%, so a 20-fold dilution was adopted. The same amount of NaCl added in excess to the analytical solutions and to the samples corrected for the matrix and good results were obtained using external calibration.

In spite of the high amount of the salts (20000 μg ml^{-1} NaCl + 2.5% NH_4F) that were used in this work, up to 400 readings were possible with the same graphite tube, without visible deposits on the interface parts of the spectrometer. The use of NH_4F also improves linearity of the analytical curve and the sensitivity for Mo and U. For U, the addition of NH_4F does not prevent the carbide formation, even for the analyte in 1% v/v HNO_3 medium. However, by reading the blank after every three readings of the analytical or sample solutions, the U determination is possible when low amount of NaCl is present in the sample. For samples of high salt contents, the determination of U may be possible by ETV-ICP-MS, if freon is used since, as it was shown by Goltz et al. [10] when freon is mixed with the argon carrier gas, the U carbides are not formed. Freon was not tested in this work.

The obtained results for Mo in three certified waters are shown in Table 4. For U, only the Riverine Water could be analyzed and the result is also shown in Table 4. The agreement with the certified or recommended values is very good. The RSDs ranged from 2.9 to 10%. Uranium could not be determined in sea water. The memory effect is very high and increases from one cycle to the other, even when the sample was diluted 1 + 99 with 1% v/v HNO_3. With this dilution the NaCl concentration is less than 400 μg ml^{-1}. It was found that in the presence of 600 μg ml^{-1} of NaCl, the U signal is very similar to that in 1%

v/v HNO_3 and baseline displacement does not occur. Probably, the presence of other components of the sea water hinder the vaporization of U, making its direct determination very difficult.

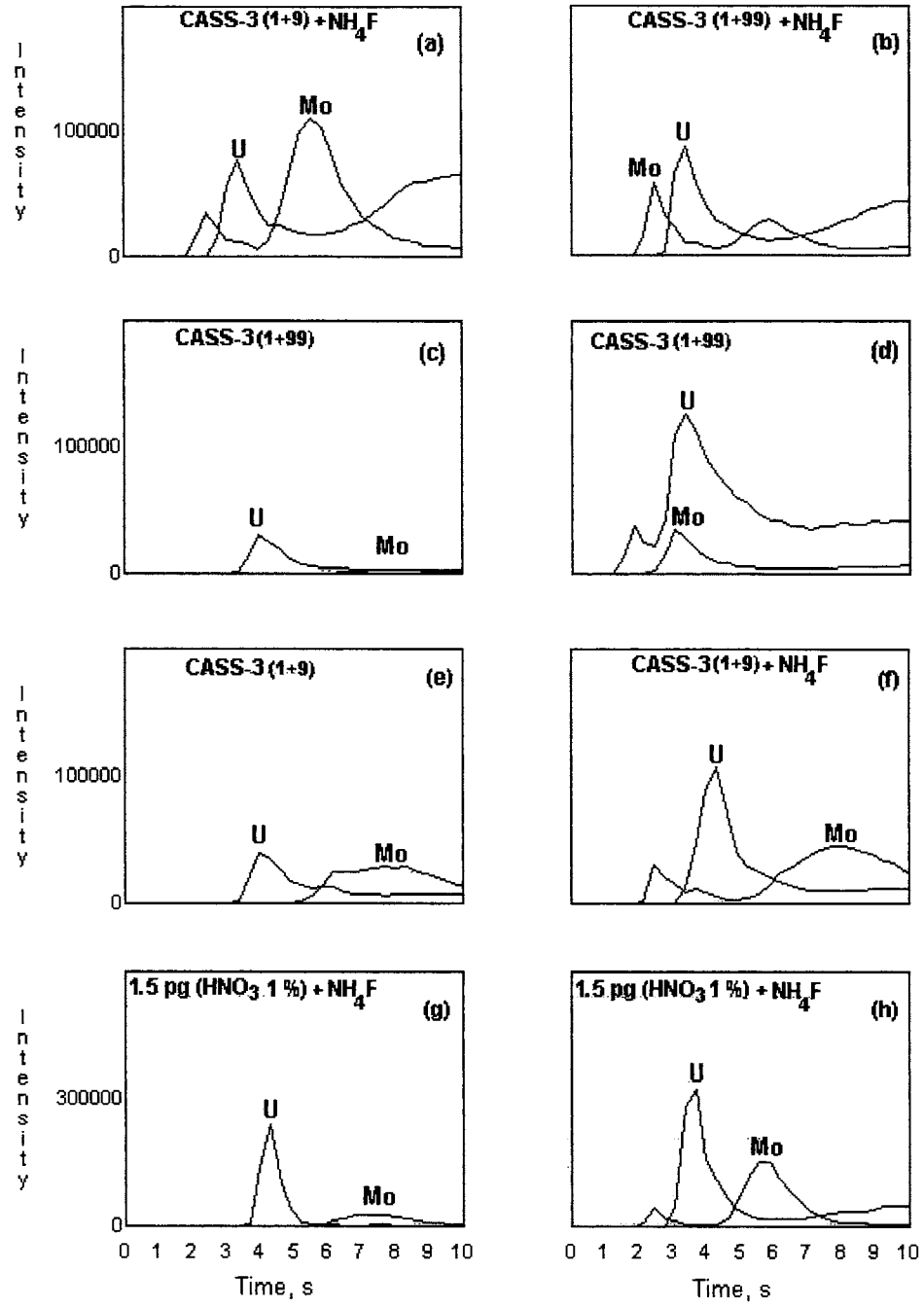

Fig. 4. Transient signals of ^{98}Mo and ^{238}U. For (a, b, d and h) the vaporization temperature is 2700°C and for (c, e, f and g) the vaporization temperature is 2400°C. For (c–e) no NH_4F was used. The informations in parentheses refer to the sample dilution.

Table 3
Figures of merit

Isotope	Parameters				
	LD (ng ml^{-1})	r^2		Analytical curve range (ng ml^{-1})	
		Analyte addition	External calibration	Analyte addition	External calibration
^{98}Mo	0.018; 0.30	0.9948	0.9992	0.1–0.4	0.1–0.75
^{238}U	0.03	0.9944	0.9991	0.05–0.2	0.1–0.75

Table 4
Determination of Mo and U ($n = 10$)

Sample	Certificated (ng ml^{-1})		Measured (ng ml^{-1})	
	^{238}U	^{98}Mo	^{238}U	^{98}Mo
CASS-3	—	8.95 ± 0.26	—	8.35 (0.47)
NASS-4	—	8.84 ± 0.60	—	8.32 (0.58)
SLRS 3	0.045[a]	0.19 ± 0.01	0.043 (0.010)	0.20 (0.02)

[a] Informed values in parentheses are the standard deviations.

3.2. Boron

The use of NH_4F, as modifier, was also tested for the B determination, but it was impossible to obtain analytical curves, as the signal intensity of the blank was very high. The blank intensity for mannitol was below 2000 counts, so it was chosen for the B determination. The pyrolysis temperature curves for B, with and without mannitol as modifier, are shown in Fig. 5(b and c). Without modifier, the sensitivity is quite low, probably because of the formation of volatile B compounds [13,15,17] and of a non-volatile boron carbide B_4C [17]. Also, no carrier is present in sufficient amount to transport the B vapor from the graphite tube to the plasma. In the presence of mannitol, the sensitivity is higher for all tested pyrolysis temperature. It was already shown by Wei et al. [15], that mannitol is a good modifier for B in ETV-ICP-MS, due to the formation of volatile complexes, avoiding the formation of boron carbides. However, mannitol alone does not allow the use of high pyrolysis temperatures. As shown in Fig. 5(a), the use of mannitol together with synthetic sea water, permits pyrolysis temperatures up to 1200°C, which was used in this work. Botelho et al. [13] have already observed, using ETAAS, that $Ca(NO_3)_2$, $CaCl_2$ and $MgCl_2$, components of the sea water, act as modifiers for B, allowing pyrolysis temperatures higher than 1000°C. In Fig. 6, the vaporization temperature curve for B is shown. The drop in the curve for temperatures higher than 2100°C, was also observed by Wanner et al. [11], using CHF_3 as modifier. These authors proposed that at higher temperatures, carbide formation as a competitive reaction could lead to signal decrease of B, while increasing the temperature even more, boron carbide can be vaporized independently of the modifier. These findings are also consistent with those of Byrne et al. [17], who have also shown that the drop is less severe in the presence of the modifier. In this work, 2000°C was used as the vaporization temperature. The used amounts of mannitol, 0.25 mg, and of synthetic sea water diluted $1 + 19$ with 1% v/v HNO_3, 5 μl, were taken from Fig. 7, which shows the signal intensities in function of the mannitol mass and of the synthetic sea water volume. The decrease of the signal intensities for masses higher than 0.3 mg,

probably is due to space charge effect, while the decrease of the signal for volumes higher than 6 μl of synthetic sea water is probably due to signal suppression by Na.

The transient signals of ^{10}B and ^{11}B, with and without mannitol, are shown in Fig. 8. A better peak shape was obtained when a pyrolysis temperature of 1200°C was used instead of 1100°C (Fig. 8(a and b)). The modifier effect of the mannitol on the signals obtained for sea water is also evident, when Fig. 8(b) is compared to Fig. 8(c). The internal Ar flow in the tube, increases the signals, favoring the transportation of the B vapor from the graphite tube to the plasma, as can be seen by comparing Fig. 8(d) to Fig. 8(e).

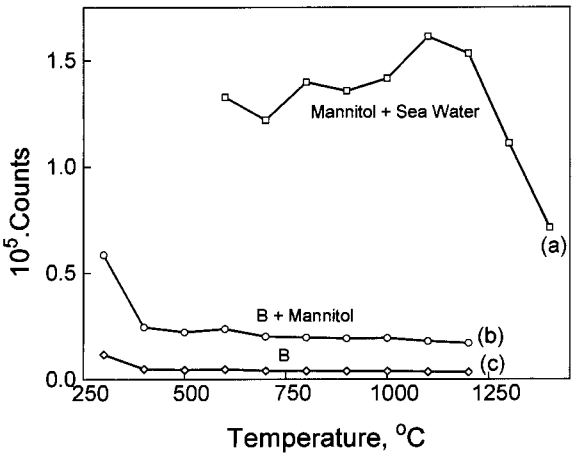

Fig. 5. Pyrolysis temperature curves for B; (a) 10 μl for CASS-3 ten-fold diluted; (b and c) 0.8 ng of B. The vaporization temperature was 2200°C.

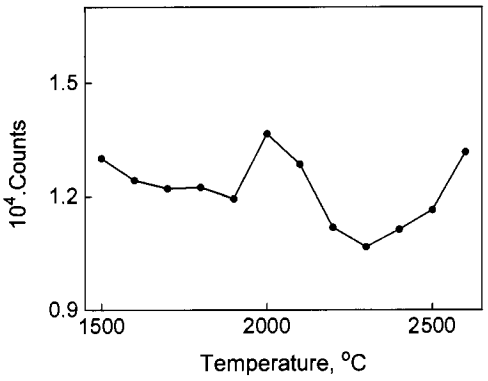

Fig. 6. Vaporization temperature curve for 0.6 ng of B in the presence of 0.125 mg of mannitol and 5 μl of synthetic sea water diluted 1 + 19. The pyrolysis temperature was 1200°C.

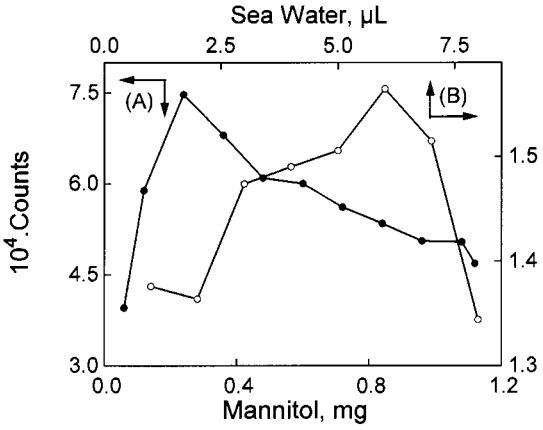

Fig. 7. Signal intensity of B in function of mannitol mass (A) and of synthetic sea water 20-fold diluted volume + 8 μl of 3% m/v mannitol (B). The pyrolysis temperature in (A) was 200°C and in (B) it was 1200°C.

The isotopic ratios of the two B isotopes are shown in Fig. 9 for 15 consecutive measurements of 0.8 ng of B in the presence of 0.24 mg of manitol and 10 μl of synthetic sea water diluted 1 + 99. The isotopic ratios do not change significantly, although they are somewhat different from the natural abundance, probably because of the superposition of the ^{12}C peak on the ^{11}B peak. In this work, the ^{10}B isotope was used for the determinations. The RSD for 15 consecutive measurements of this isotope was 2.9%.

To calculate the detection limit, the standard deviation of five measurements of the blank and the slope of the analytical curve (10–40 ng ml^{-1}), with $r^2 = 0.999$ were used. The obtained value was 0.68 ng ml^{-1}, not considering the dilution of the sample. The average results, in μg ml^{-1}, for ten determinations of B in the sea water samples (3.9 ± 0.10 and 3.78 ± 0.18 for CASS-3 and NASS-4, respectively) agree with those obtained by two other methods: analyte addition method by ETV-ICP-MS, using mannitol as modifier (3.98 ± 0.32 and 4.0 ± 0.24 for CASS-3 and NASS-4, respectively) and external calibration with matrix matching by ICP-MS with conventional nebulization (3.83 ± 0.12 and 3.78 ± 0.07

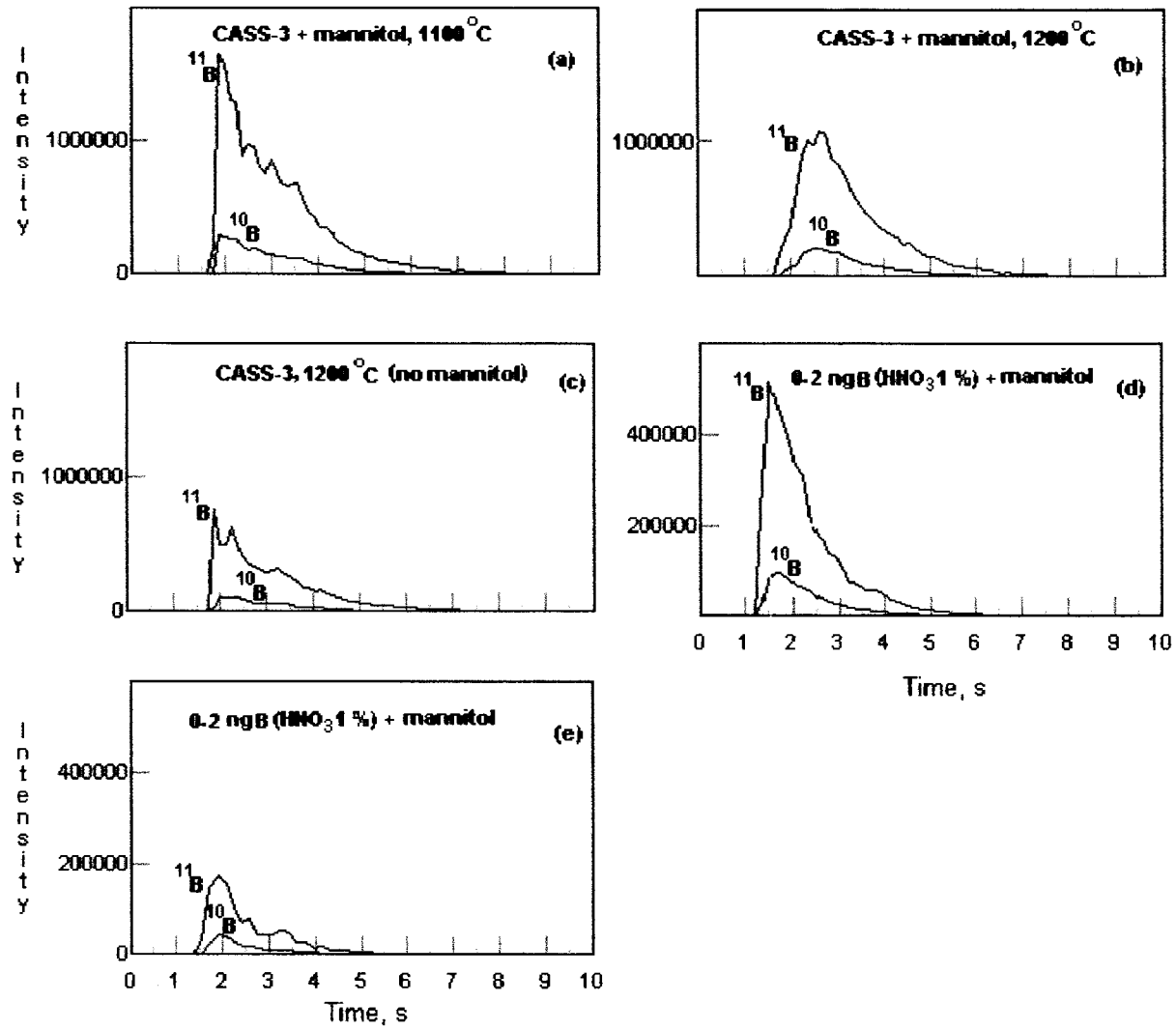

Fig. 8. Transient signals of B, for 20 μl of analytical solution or sea water 100-fold diluted in 1% v/v HNO_3; in (a–c), the shown temperature are of the pyrolysis step; the pyrolysis temperature in (d and e) is 300°C and the internal gas flow rate is 0.3 l min^{-1}, except in (e), where it was 0.1 ml min^{-1}. The vaporization temperature was 2000°C.

for CASS-3 and NASS-4, respectively). The values for the sea waters also agree with some values presented in the literature [18]. The obtained average concentration of B for ten determinations, 133.9 ± 11.7 ng ml^{-1} in the water NIST 1643d agrees with the certified value, 144.8 ± 5.2 ng ml^{-1}. The sea waters were diluted $1 + 99$ and the Water NIST 1643d was diluted $1 + 1$, before their analysis.

4. Conclusion

In conclusion, this work shows that Mo can be determined by ETV-ICP-MS in river and in sea water using NH4F, while U can only be determined in river water using this same modifier. For B, mannitol and synthetic sea water as modifiers, allows its determination in waters and in sea waters. It is possible to predict that these methods

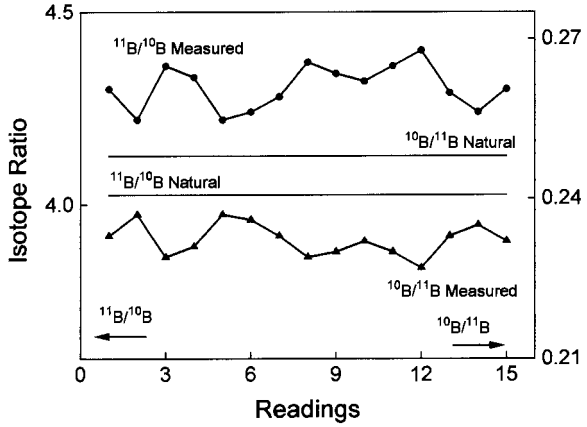

Fig. 9. Isope ratio of B in consecutive readings. The pyrolysis and vaporization temperatures were 1200 and 2000°C, respectively.

can also be applied to a variety of different complex samples.

Acknowledgements

We thank Financiadora de Estudos e Projetos (FINEP) for financial support. D. Pozebon and V.L. Dressler have doctorate scholarships from Conselho Nacional de Pesquisas e Desenvolvimento Tecnológico (CNPq).

References

[1] W. Wendl, G. Müller-Vogt, Spectrochim. Acta B 40 (1985) 527.
[2] D.A. Mohamed, Analyst 112 (1987) 209.
[3] C. Vellon, B.E. Guthrie, W.R. Wolf, Anal. Chem. 52 (1980) 457.
[4] W. Wendl, G. Müller-Vogt, Spectrochim. Acta B 39 (2/3) (1984) 237.
[5] A.J. Caruso, M.J. Carey, Crit. Rev. Anal. Chem. 23 (5) (1992) 397.
[6] J.R. Castillo, J.M. Mir, C. Bendicho, Frezenius Z. Anal. Chem. 332 (1988) 783.
[7] S. Arpadjan, V. Krivan, Fresenius Z. Anal. Chem. 329 (1988) 745.
[8] M.I.C. Monteiro, A.J. Curtius, J. Anal. At. Spectrom. 10 (1995) 329.
[9] C.J. Park, G.E.M. Hall, J. Anal. At. Spectrom. 2 (1987) 473.
[10] D.M. Goltz, D.C. Grégoire, J.P. Byrne, C.L. Chakrabarti, Spectrochim. Acta B 50 (8) (1995) 803.
[11] B. Wanner, P. Richner, B. Magyar, Spectrochim. Acta B 50 (1996) 817.
[12] C.J. Park, G.E.M. Hall, J. Anal. At. Spectrom. 3 (1988) 355.
[13] G.M.A. Botelho, A.J. Curtius, R.C. Campos, J. Anal. At. Spectrom. 9 (1994) 1263.
[14] I. Maravi, L.K. Olson, J. Wang, J.A. Caruso, J. Anal. At. Spectrom. 10 (1995) 7.
[15] W.-C. Wei, C.-J. Chen, M.-H. Yang, J. Anal. At. Spectrom. 10 (1995) 955.
[16] G.M. Greenway, S.M. Nelms, I. Skhosana, S.J.L. Dolman, Spectrochim. Acta B 51 (1996) 1909.
[17] J.P. Byrne, D.C. Grégoire, D.M. Goltz, C.L. Chakrabarti, Spectrochim. Acta B 49 (5) (1994) 433.
[18] A.M.T.C. Horta, A.J. Curtius, Anal. Chim. Acta 96 (1978) 207.

ELSEVIER

Talanta 47 (1998) 861–868

Talanta

Simultaneous determination of the colorants tartrazine, ponceau 4R and sunset yellow FCF in foodstuffs by solid phase spectrophotometry using partial least squares multivariate calibration

L.F. Capitán-Vallvey, M.D. Fernández, I. de Orbe, R. Avidad *

Department of Analytical Chemistry, University of Granada, E-18071, Granada, Spain

Received 16 December 1997; received in revised form 31 March 1998; accepted 15 April 1998

Abstract

A method is proposed for the simultaneous determination of the colorants tartrazine (TT), sunset yellow FCF (SY) and ponceau 4R (PR) in foods. The colorants were fixed in Sephadex DEAE A-25 gel at pH 2.0 and then packed in a 1-mm silica cell. The spectra of the analytes fixed in the solid support were recorded between 400 and 800 nm against a blank and the partial least squares (PLS) multivariate calibration was used to obtain the results. The linear dynamic ranges of the calibration graphs were from 50.0 to 650.0 ng ml^{-1} for the three colorants and these ranges were taking in account the optimisation of the calibration matrix using the PLS-1 algorithm. The experimental results showed that the optimum number of factors for the calibration matrix was four in all instances and the residual means standard deviation was 5.5267 for SY, 6.3878 for TT and 6.9816 for PR. The square of the correlation coefficients were 0.9977, 0.9978 and 0.9954 for SY, TT and PR respectively. The method was applied to the determination of the colorants in foods and results were compared with those obtained by means of HPLC as reference method. The results obtained can be considered as acceptable in most cases (eight of nine commercial samples). The relative standard deviations ranging between 0.5 and 10.8 for the commercial samples analysed. © 1998 Elsevier Science B.V. All rights reserved.

Keywords: Colorants determination; Partial least squares; Foods analysis; Solid phase spectrophotometry

1. Introduction

At present, single colorants or mixtures of two or three colorants are frequently used as additives in foods or pharmaceutical products to obtain attractive colours, to correct the colour or for the identification of a product. The substances use as colorants are commonly synthetic products added in small amounts to food or drug products [1–3]. However, the use and the amount of these chemicals must be controlled because they can occasionally produce allergy, asthma and other health disorders in sensitised individuals [4].

* Corresponding author. Tel.: +34 985 248436; e-mail: lcapitan@goliat.ugr.es

0039-9140/98/$ - see front matter © 1998 Elsevier Science B.V. All rights reserved.
PII S0039-9140(98)00159-3

4,5-Dyhidro-5-oxo-1-(4-sulfophenyl)-4-[(sulfophenyl)azo]-1H-pyrazole-3-carboxylic acid trisodium salt (CI 19140), commonly named Tartrazine (TT), 1-*p*-sulfophenylazo-2-naphthol-6-sulfonic acid disodium salt (CI 15985), also named sunset yellow FCF (SY), and the (4-sulpho-1′-naphthylazo)-1-hydroxy-2-naphthalene-6,8-disulphonic acid trisodium salt (CI 16255) know as Ponceau 4R (PR) are three of these synthetic colorants widely used as additives in non-alcoholic drinks, sweets, jellies and other foods and their legal maximum dose is 70.0 mg l^{-1} [3].

Chromatographic [5–8] and electroanalytical [9–11] methods have been proposed for the determination of these colorants, although spectrophotometric methods [12–14] have traditionally been the most widely employed. However, these methods present two significant drawbacks: the overlapping of the spectral absorption bands of the colorants and the influence of the matrix effect on the measurement of the analytical signal. These problems could be overcome by applying an appropriate statistical method, such as multivariate calibration, in the analysis of the results obtained [15,16]. In these methods, the calibration is carried out from the full-spectra or from a selected zone with a large amount of information. Its main advantages are: the ability to resolve complex mixtures of analytes whose spectra are strongly overlapping; speed in determining the components in a mixture; and the ability to perform the analysis without prior separations.

The PLS methods have been applied in several papers [17] for the calibration of spectrophotometric data in the determination of chemicals such as pesticides, sulphonamides, flavour enhancers in foods, or of mixtures of chemicals such as 2-furfuraldehyde and 5-hydroxymethyl-furfuraldehyde in solution [18].

In this paper we propose the application of PLS methods to resolve mixtures of colorants in foods by using solid-phase spectrophotometry. The method takes advantage of the sensitivity and selectivity of solid-phase spectrophotometry and also of the benefits of multivariate calibration methods, i.e. the fast determination of components of interest in a mixture without previous separation steps.

2. Experimental

2.1. Instruments and software

Absorbance measurements were carried out by using a Perkin–Elmer Lambda 2 spectrophotometer interfaced to an IBM SX-486 microcomputer for the spectral acquisition and subsequent manipulation of the experimental data. An Agitaser Model 2000 rotating-bottle (Tecnotrans, Barcelona, Spain), a Crison Digital pH-meter (Crison, Barcelona, Spain) equipped with a combined glass-calomel electrode, and a desk centrifuge (URA Technic mod. 2610, Barcelona, Spain) were also used. The absorbance measurements were carried out in two matching quartz cells (Starna, type 1, Essex, UK) with a 1-mm path length.

For the treatment of the spectral data the following programmes were used: Grams/386 Software Package ver. 1.0 and Add. Application PLS Plus ver. 2.1, Galactic Industries, Salem, MA and Data Leader Software Package, Beckman, Fullerton, CA, 1987.

2.2. Reagents

Stock solutions (100 mg l^{-1}) of sunset yellow FCF (Utter), (100 mg l^{-1}) of tartrazine FCF (Utter) and (100 mg l^{-1}) of Ponceau 4R (Aldrich) were prepared by the exact weighing of the standards and solution with reverse osmosis quality water. Working solutions were prepared from the stock solutions diluted with water. The solutions obtained were stable for at least one month in all instances.

To adjust the pH of the standards and samples a 0.5 M HCl aqueous solution was used and Sephadex DEAE A-25 gel (Sigma) without pretreatment was used as solid support. All solvents and reagents were of analytical grade unless stated otherwise.

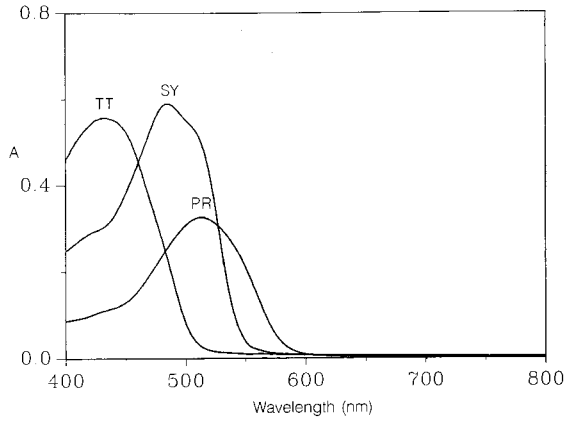

Fig. 1. Absorption spectra of Tartrazine (TT), Sunset Yellow (SY) and Ponceau 4R (PR) individually fixed in Sephadex DEAE A-25 gel, 10.0 μg ml^{-1} being the concentration level in the three cases.

2.3. Absorbance measurements

Absorbance spectra of the colorants fixed in the gel and packed in a cell of 1-mm path-length were recorded between 400 and 800 nm with an interval of 0.2 nm between each two points and were contrasted with the corresponding blanks. The spectra were smoothed taking 15 experimental points and using the Savitzky–Golay method, giving 1987 experimental points for each spectrum. The calibration matrix was prepared from 21 solutions containing mixtures of the three components in different ratios and optimised and calculated by using the PLS-1 algorithm both to analyse the spectra obtained and to calculate the concentrations of the analytes in the real samples.

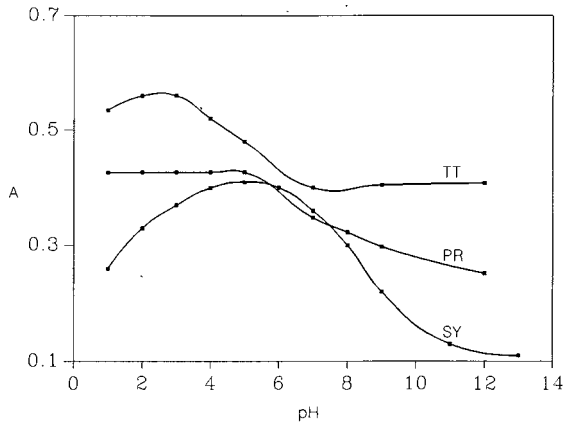

Fig. 2. Influence of the pH on the absorbances of Tartrazine (TT), Sunset Yellow (SY) and Ponceau 4R (PR) individually fixed in Sephadex DEAE A-25 gel. The concentration levels of the analytes were 10.0 μg ml^{-1} in all instances.

2.4. Procedures

2.4.1. Basic procedure

An aliquot of sample containing between 5.0 and 80.0 mg of SY, TT and PR (alone or in mixtures) was placed in a 100-ml calibrated flask and 2.2 ml of 0.5 M HCl were added, making the mark with water. The solution was transferred into a 1-l glass bottle and 50 mg of Sephadex DEAE A-25 gel were added. The mixture was shaken for 10 min and the gel beads were collected by filtration under suction and packed in a 1-mm cell. The cell was then centrifuged for 30 s at 2000 rpm (450 g). Blanks were prepared and treated in the same way as described for the standards and contained all the reagents except the colorants.

2.4.2. Procedure for real samples

An aliquot of the real sample containing between 5.0 and 80.0 μg of one, two or three colorants (typically from 2.0 to 10.0 g of commercial product) was introduced in a 100-ml calibrated flask together with 2.2 ml of 0.5 M HCl solution, making the mark with water. The solution was transferred into a 1-l glass bottle and 50 mg of Sephadex DEAE A-25 gel were added, after which the mixture was treated as described in the Section 2.4.1 and its absorbance was measured in the same way as described for the standards.

2.4.3. Treatment of the sample

The liquid samples [six soft drinks, two of orange, one of melon, one of banana, one of red-currant and one of lemon] were filtered through a cellulose acetate filter paper (Millipore HAWP 04700 filter type HA 0.45 μm size pore) and collected in a previously cleaned glass container. The solid or semisolid samples [honey sweet, alimentary additive and two jellies, one of pineapple and another of *tutti frutti*] were dis-

Table 1
Composition of the training set

Standards	SY (μg l^{-1})	TT (μg l^{-1})	PR (μg l^{-1})
1	0.0	50.0	0.0
2	0.0	250.0	0.0
3	0.0	600.0	0.0
4	50.0	0.0	0.0
5	0.0	0.0	50.0
6	0.0	0.0	250.0
7	0.0	0.0	600.0
8	200.0	100.0	250.0
9	300.0	200.0	100.0
10	100.0	100.0	400.0
11	50.0	200.0	100.0
12	150.0	250.0	200.0
13	100.0	300.0	100.0
14	150.0	80.0	250.0
15	200.0	200.0	200.0
16	100.0	250.0	150.0
17	150.0	150.0	200.0
18	80.0	200.0	100.0
19	80.0	250.0	150.0
20	150.0	100.0	300.0
21	50.0	80.0	100.0

solved in water with the aid of an ultrasonic bath, and then were filtered as in the preceding case. If a white precipitate (gum Arabian) appeared when the HCl solution was added, the sample was filtered, taking the usual precautions to avoid its contamination.

3. Results and discussion

As shown in Fig. 1, the spectra of the colorants SY, TT and PR in solid phase (same that in solution) are overlapped, so that the mixture of these colorants (in solution or fixed in Sephadex DEAE A-25 gel) is not easy to resolve with conventional spectrophotometric methods that use univariate calibration. However, this difficulty can be obviated by applying a multivariate calibration (PLS-1 algorithm) to perform the calculations. The experimental parameters that influence the fixation process of the colorants in the gel (pH of the solution equilibrated with the gel, amount of gel, etc.) must first be optimised before the calibration matrix is obtained.

3.1. pH-influence

To determine the influence of the pH on the retention of colorants in the gel, 0.1 M hydrochloric acid and 0.1 M sodium hydroxide solutions were used for the adjustment. The measurements of absorbance at different values of pH were performed at 487 nm for SY, 430 nm for TT and 525 nm for PR. As can be observed in Fig. 2, the influence of the pH on the absorbance of the colorants fixed in the gel was different according to the colorant. Tartrazine shows a maximum absorbance at pH values ranging between 1.0 and 3.0 and PR shows maximum absorbance at pH values from 1.0 and 4.5. However, the colorant SY shows a maximum absorbance when the pH values are between 4.0 and 6.0. A pH 2.0 was accepted as the working pH because the absorbances of the colorants TT and PR are maximum and the absorbance of the SY is 80% of the maximum value shown for this colorant when the pH is 5.0.

3.2. Other experimental parameters

To optimise other experimental parameters that influence the absorbance of the system in solid phase, we tested the amount of the gel used as solid support, the time and speed of equilibration, the ionic strength, the centrifugation time and the volume of sample. First, the influence of the amount of the gel equilibrated with the solution was studied because it was found that an increase of the amount of gel used was associated with an exponential decrease of the analytical signal. The

Table 2
Statistical parameters of the optimised matrix using the PLS-1 model

Colorant	No. of factors	RMSD[a]	RRMSD[b] (%)	R^{2c}
SY	4	5.5267	6.07	0.9977
TT	4	6.3878	4.00	0.9978
PR	4	6.9816	4.19	0.9954

[a] Residual mean standard deviation.
[b] Relative residual mean standard deviation.
[c] Square of the correlation coefficient.

optimum amount selected was 50 mg of Sephadex DEAE A-25 gel because this was the minimum required to fill the cell.

In order to determine the influence of the duration and speed of shaking on the absorbance of the system, 25 standards were prepared and measured as follows: five series of five standards each were shaken for different times in each series (5, 10, 15, 30 and 60 min) and each sample in the series at different speeds (20, 40, 60, 80 and 90 rpm). It was observed that 60 rpm and 10 min were the values that provide the best results, and these were selected as the working values.

The influence of the ionic strength on the absorbance of the system was tested by using NaCl and $KClO_4$ solutions at different concentration levels. The absorbance of the colorants-gel system showed a maximum value at concentration levels of NaCl or $KClO_4$ ranging between 0 and 2.0×10^{-2} mol l^{-1}, decreasing by around 12% at concentrations higher than 0.1 mol l^{-1}.

Six standards, all identically prepared and placed into the cell, were centrifuged for different time intervals (0, 30, 60, 120, 180 and 300 s) to study the influence on the absorbance of the system of the centrifugal time, i.e. the degree of compactness of the gel in the cell. The experimental data showed that the absorbance values were the same in all instances except in the non-centrifuged sample, whose absorbance decreased by 10%. We selected 30 s as the working value for centrifugation time.

Finally, the influence of the sample volume on absorbance was tested. In a previous study we found that the sensitivity of methods based on solid-phase spectrophotometry can be increased when the sample volume used for the analysis is also increased. In order to check the influence of this parameter, standards of different volumes (50, 100, 250, 500, 750 and 1000 ml) were prepared containing the same concentration of analyte and proportional amounts of the other reagents. It was found that for volumes ranging between 50 and 500 ml the measured absorbances were proportional to sample volumes but if volumes higher than 500 ml were used, the absorbance remained practically constant. According to the experimental data we selected 100-ml as working volume because the sensitivity obtained in this case was appropriate to our purposes. However, as mentioned above, the sensitivity of the method can be enhanced, if necessary, by increasing the volume of the standard solutions equilibrated with the gel, to a maximum of 500 ml.

4. Application of the PLS-1 algorithm

4.1. Optimising the data

A training set of 21 samples, randomly selected, was prepared to obtain the calibration matrix. This matrix was prepared with the experimental data obtained from ternary and binary mixtures and single solutions at low, medium and high concentrations of the three colorants. The concentrations of each colorant in each of the samples were selected to avoid the correlation of concentrations among the different samples that can produce underfitting in the PLS model. Table 1 shows the concentrations of each colorant in each sample of the set.

400–800 nm was the selected spectral band and 1987 experimental points per spectrum were recorded with an interval of 0.2 nm between consecutive points. The spectra were obtained in the previously optimised experimental conditions described above.

In order to select the optimum number of factors for the partial least squares algorithm, the cross-validation method [19] was used. As the training set comprised 21 spectra, the PLS calibration was performed on 20 of them and the concentration of the excluded sample was predicted. The process was repeated 21 time (one for each sample) and the predicted and known concentrations were compared. To test the fitness of the PLS model the prediction error sum of squares (PRESS) was calculated each time that a new factor was added to the PLS model, using *F*-statistic as signification test. Applying the Haaland and Thomas criterion [20], 11 factors (half of the standards plus one) were accepted as the maximum number of initial factors and the optimum number of factors was calculated for the

Table 3
Recovery study of mixtures TT, PR and SY in synthetic samples with one, two or three components

No.	TT			PR			SY		
	Taken[a]	Found[a]	(Rec %)	Taken[a]	Found[a]	(Rec %)	Taken[a]	Found[a]	(Rec %)
1	100.0	99.9	(99.9)	100.0	93.3	(93.3)	100.0	101.4	(101.4)
2	300.0	291.3	(97.1)	150.0	148.1	(98.7)	200.0	199.8	(99.9)
3	250.0	243.0	(97.2)	250.0	246.0	(98.4)	150.0	143.9	(95.9)
4	80.0	76.2	(95.2)	150.0	136.5	(91.0)	50.0	45.9	(91.8)
5	200.0	194.2	(97.1)	100.0	103.5	(103.5)	150.0	150.0	(100.0)
6	150.0	154.8	(103.2)	300.0	330.9	(110.3)	150.0	153.1	(102.1)
7	100.0	94.3	(94.3)	80.0	79.4	(98.8)	80.0	77.5	(96.9)
8	80.0	79.9	(99.9)	200.0	217.0	(108.5)	100.0	92.1	(92.1)
9	150.0	139.1	(92.7)	250.0	264.7	(105.9)	80.0	67.7	(84.6)
10	100.0	95.8	(95.8)	350.0	310.5	(88.7)	200.0	183.2	(91.6)
11	300.0	287.4	(95.8)	200.0	196.8	(98.4)	100.0	89.3	(89.3)
12	80.0	76.2	(95.2)	200.0	182.8	(91.4)	100.0	92.8	(92.8)
13	200.0	200.8	(100.4)	150.0	155.1	(103.4)	200.0	198.4	(99.2)
14	200.0	190.8	(95.4)	150.0	137.7	(91.8)	80.0	74.5	(93.1)
15	100.0	100.9	(100.9)	250.0	248.8	(99.5)	200.0	198.6	(99.3)
16	80.0	75.2	(94.0)	150.0	146.0	(97.3)	—	—	(1.2)
17	150.0	139.2	(92.8)	100.0	98.5	(98.5)	—	—	(−1.7)
18	500.0	476.0	(95.2)	200.0	199.0	(99.5)	—	—	—
19	100.0	100.0	(100.0)	—	—	(0.6)	200.0	196.2	(98.1)
20	150.0	149.4	(99.6)	—	—	(1.2)	250.0	239.8	(95.9)
21	300.0	296.4	(98.8)	—	—	(0.5)	80.0	77.2	(96.4)
22	—	—	(−1.2)	80.0	78.2	(97.7)	100.0	97.8	(97.8)
23	—	—	(0.1)	500.0	496.0	(99.2)	150.0	141.8	(94.5)
24	—	—	(2.2)	150.0	140.0	(93.3)	250.0	253.2	(101.3)
25	80.0	74.5	(93.1)	—	—	(−7.3)	—	—	(1.6)
26	150.0	137.7	(91.8)	—	—	(−8.8)	—	—	(−3.7)
27	500.0	481.0	(96.2)	—	—	(−9.5)	—	—	(2.1)
28	—	—	(1.2)	80.0	66.1	(82.6)	—	—	(−3.0)
29	—	—	(−2.5)	150.0	136.4	(90.9)	—	—	(−5.7)
30	—	—	(−3.9)	500.0	504.0	(100.8)	—	—	(−6.3)
31	—	—	(6.4)	—	—	(7.5)	80.0	76.7	(95.8)
32	—	—	(7.7)	—	—	(9.2)	150.0	142.7	(95.1)
33	—	—	(0.3)	—	—	(0.3)	500.0	502.5	(100.5)

The values between parenthesis are those measured by the method when this compound is not present.
[a] Concentrations expressed in mg l^{-1}.

first value of PRESS whose F-ratio probability fell below 0.75. The number of factors selected as optimum by this procedure was four. Table 2 shows the estimated values of residual mean standard deviation (RMSD absolute and relative RRMSD) independent of the values of R^2.

The values of RMSD and RRMSD were obtained from the expressions:

$$\mathrm{RMSD} = \sqrt{\frac{\sum_{i=1}^{N} (\hat{x}_i - x_i)^2}{N}} \quad \text{and}$$

$$\mathrm{RRMSD}(\%) = \frac{100\mathrm{RMSD}}{\bar{x}}$$

respectively, where N is the number of samples used in the prediction set, x_i is the true concentra-

Table 4
Simultaneous determination of SY, TT and PR in five replicated samples of commercial products by means of the PLS-1 model and using HPLC as reference method

No	SY (mg l^{-1})				TT (mg l^{-1})				PR (mg l^{-1})			
	PLS	RSD	HPLC	P(%)	PLS	RSD	HPLC	P(%)	PLS	RSD	HPLC	P(%)
1	3.68	3.5	3.74	87.8	10.67	1.6	10.24	24.8	0.45	4.1	0.58	27.5
2	3.68	3.5	3.74	87.8	9.40	21.3	9.30	84.8	4.00	80.0	0.91	99.3
3	3.20	4.7	3.50	44.9	15.68	2.1	14.36	39.8	ND	—	0.14	—
4	0.19	1.8	0.18	83.3	—	—	—	—	1.47	3.2	—	—
5	845.0	2.5	850.0	51.0	42 230	2.6	42 730	75.5	—	—	—	—
6	0.66	7.6	0.70	22.3	—	—	—	—	0.04	10.8	0.05	99.0
7	—	—	—	—	—	—	—	—	246.8	6.6	234.2	29.0
8	—	—	—	—	13.96	0.5	13.27	14.0	—	—	—	—
9	—	—	—	—	4.30	3.9	3.80	26.5	—	—	—	—
10	23.60	6.3	23.2	71.7	—	—	—	—	—	—	—	—

No.: 1 and 3 orange drinks, 2 pineapple jelly, 4 honey sweet, 5 alimentary colorant, 6 fruits jelly, 7 red currant soft drink, 8 lemon ice-pop, 9 banana drink, 10 melon drink.
ND: Not detected by this method.

tion of analyte in the sample, $\hat{x}_i$ is the estimated concentration of analyte in the sample, and $\bar{x}$ is the mean of the trues concentrations of the analytes in the prediction set. These values are indicative of the average error in the determination of each component.

On the other hand, the values of R^2, as indicative of the fit of the data to a straight line, were calculated from the expression: $R^2 = \Sigma_{i=1}^{N}(\hat{x}_i - \bar{x})^2 / \Sigma_{i=1}^{N}(x_i - \bar{x})^2$, obtaining the results summarised in Table 2.

In order to prove the applicability of this optimised calibration matrix, the concentration levels of TT, PR and SY were predicted in fifteen ternary mixtures, nine binary mixtures and nine single solutions. The results listed in Table 3 show that there is a good concordance between the true values and the predicted data experimentally obtained.

4.2. Application of the model to real samples

Next, the optimised matrix obtained by the PLS-1 model was applied to the analysis of ten real samples: two soft drinks of orange, one lemon ice-pop, one banana drink, one melon drink, one alimentary colorant, one red-currant soft drink, one honey sweet and two fruit jellies. These samples were also analysed by HPLC [21] to test the accuracy of the proposed method. Table 4 shows the results obtained with both the PLS-1 and the HPLC methods. The data that appear in this Table are: average values from five measurements of each sample by PLS-1 and HPLC, and the probability value (P_{val}) of the test used for the comparison of the measurements obtained by the two methods. As can be observed, the results obtained with both methods (PLS-1 and HPLC) were acceptably similar in most cases.

5. Conclusions

Solid-phase spectrophotometry can be used for the simultaneous determination of food colorants in mixtures, using the partial least squares (PLS-1) for the manipulation of the experimental data. Mixtures of sunset yellow FCF, tartrazine and Ponceau 4R have been simultaneously determined (at low, medium and high concentration levels) in different types of real samples, and the results obtained can be considered as acceptable. The proposed method is simple, quick, sensitive and inexpensive. The cost is low because the gel used as solid support can be recycled with an aqueous HCl solution, only conventional instruments are used, and the software is easy available.

References

[1] Diario Oficial de las Comunidades Europeas, (Madrid, Spain, Boletín Oficial del Estado), 13/vol. 01, 1962, pp. 3–12.
[2] Code of Federal Regulations, FDA (USA), Parts 1–99, Sec. 74.1710 (b), 1985, p. 307.
[3] Ministerio de Sanidad y Consumo, Lista positiva de aditivos alimentarios, vol. II, 1989, p. 20.
[4] M. Hanssen, J. Marsden, E for additives, Thorson, Northamptonshire, UK, 1984.
[5] A. Pnina, Y. Chain, M. Cais, Anal. Chim. Acta 248 (1991) 289.
[6] G.M. Greenway, N. Kometa, R. Macree, Food Chem. 43 (1992) 137.
[7] M.L. Putteman, L. Dryon, D.L. Massart, J. Assoc. Off. Anal. Chem. 64 (1981) 1.
[8] H.M. Salagoity, A. Bertrand, P. Sudran, Sci. Aliments 3 (1983) 127.
[9] A. Araujo Barros, Analyst 112 (1987) 1359.
[10] A.G. Fogg, A.A. Araujo Barros, J.O. Cabral, Analyst 111 (1986) 831.
[11] F. Becerro, F. Gonzalez, J. Hernandez, Talanta 37 (1990) 665.
[12] J.J. Berzas Nevado, J. Rodriguez, M.J. Villaseñor, Anal. Lett. 27 (1994) 1009.
[13] J.A. Jeransian, K.G. Sloman, A.K. Foltz, Anal. Chem. 57 (1985) 278R.
[14] R.B. Patel, M.R. Patel, A.A. Patel, A.K. Shah, A.G. Patel, Analyst 111 (1986) 577.
[15] H. Wold, Research papers, in: D.F. Willey (Ed.), Statistic, New York, 1966, pp. 411–444.
[16] S. Wold, in: H. Martens, H. Russwurm, (Eds.), Food Research and Data Analysis, Applied Science, London, 1983.
[17] S. Wold, H. Martens, H. Wold, in: A. Ruhe, B. Kagstrom (Eds.), The Multivariate Calibration Problem in Chemistry Solved by PLS, Springer, Heidelberg, 1983, pp. 286–293.
[18] A. Espinosa-Mansilla, F. Salinas, I. de Orbe, Fresenius J. Anal. Chem. 354 (1996) 245.
[19] M. Stone, J.R. Stat. Soc. B 36 (1974) 111.
[20] D.M. Haaland, E.V. Thomas, Anal. Chem. 60 (1988) 1193.
[21] J.F. Lawrence, F.E. Lancaster, B.S. Conacher, J. Chromatogr. 210 (1981) 168.

ELSEVIER

Talanta 47 (1998) 869–875

Talanta

Mixed micellar medium for the spectrophotometric determination of molybdenum in molybdenum/tungsten mixtures

Xirong Huang [a,*], Wenjuan Zhang [a], Guiying Xu [a], Shuhua Han [a], Ying Li [a], Cuiping Li [b]

[a] *Department of Chemistry, Shandong University, Jinan 250100, People's Republic of China*
[b] *Centre for Experiment, Shandong University, Jinan 250100, People's Republic of China*

Received 6 November 1997; received in revised form 14 April 1998; accepted 20 April 1998

Abstract

Effects of cetyltrimethylammonium bromide (CTAB) and/or nonylphenoxypolyethoxyethanol (OP) on the absorption spectra of the complexes of molybdenum and tungsten with bromopyrogallol red (BPR) were studied. Based on these effects, a mixture of CTAB and OP was thus selected as a medium for the selective and sensitive determination of Mo in Mo/W binary mixtures. Under the optimum conditions, Beer's law was obeyed over the range 0.06–0.8 μg ml^{-1} Mo with molar absorptivity being 1.3×10^5 l mol^{-1} cm^{-1} and detection limit 0.025 μg ml^{-1}. For 1.0 μg Mo, at least 20 μg W did not interfere in the determination of Mo with average recovery and relative standard deviation being 99.5% and $< 2\%$, respectively. The method developed maintained the features of simplicity and rapidity and, moreover, its selectivity and sensitivity enhanced greatly due to the use of CTAB/OP mixed micellar medium. When coupled with a compatible concentration method, the proposed method could be used for the determination of trace Mo in natural waters. © 1998 Elsevier Science B.V. All rights reserved.

Keywords: Mixed micellar medium; Molybdenum; Tungsten; Bromopyrogallol red; Spectrophotometry

1. Introduction

The spectrophotometric determination of Mo is often accompanied by the interference of W [1–3]. Although this problem is circumvented by means of various chemometric methods or by diverse spectrophotometric techniques such as multi-wavelength [4], extraction [5], derivative [6], etc. yet these techniques are, comparatively speaking, complicated or/and time-consuming. In addition, some of the above techniques lead to a loss of sensitivity [6]. Our previous studies showed that the mixed micellar medium prepared by ionic and non-ionic surfactants in an appropriate ratio was superior in analytical performance to the counterpart involving no non-ionic surfactant [7–9]. In this paper the effects of cetyltrimethylammonium (CTAB) or/and nonylphenoxypolyethoxyethanol

* Corresponding author. Fax: +86 531 8902167.

0039-9140/98/$ - see front matter © 1998 Elsevier Science B.V. All rights reserved.
PII S0039-9140(98)00175-1

(OP) on the absorption spectra of the complexes of Mo and W with bromopyrogallol red (BPR) and their application for the selective and sensitive determination of Mo in Mo/W mixtures were reported. The method developed here maintained the features of simplicity and rapidity (these features were sometimes as important to analysts as those of sensitivity and selectivity [10]) and, moreover, its sensitivity and selectivity enhanced greatly due to the use of CTAB/OP mixed micellar medium. When coupled with the concentration method developed by Yoshimura et al. [2], our method could be used for the determination of trace Mo in natural waters.

2. Experimental

2.1. Apparatus

A Shimadzu UV-240 spectrophotometer with a matched pair of 1.0-cm quartz cells was used for recording the UV-vis absorption spectra (the instrumental parameters were as follows: scan speed, fast; slit, 2 m; λ scale, 40 nm cm^{-1}; λ range, 400–700 nm). The cell compartment of the spectrophotometer was thermostated (to study the effect of temperature on the resolution and determination of Mo) by circulating water from its accessories. The pHs of solutions were measured using a model PHS-2 pH meter.

2.2. Reagents

Unless otherwise stated, all reagents used were of analytical grade and their solutions were prepared by weighing with distilled water as solvent.

The concentration of each reagent was as follows:

1. bromopyrogallol red (BPR), from Merck, 2×10^{-4} mol l^{-1}.
2. cetyltrimethylammonium bromide (CTAB), 2.75×10^{-3} mol l^{-1}.
3. Mo(VI), as $Na_2MoO_4 \cdot 2H_2O$, 10 μg ml^{-1} (At this concentration and pH = ca. 6, Mo could hardly polymerize. In addition, the loss of traces of Mo in glass vessels could almost be neglected in solutions at any pH values [2]).
4. W(VI), as $Na_2WO_4 \cdot 2H_2O$, 10 μg ml^{-1}.
5. nonylphenoxypolyethaxyethanol (containing approximately 10 moles of ethylene oxide) (OP), from Wuhan Tongxing Chemical Reagent Plant, China, 0.4% (m/v) (Because of high viscosity, preparation of its solution based on volume ratio was not reproducible).

2.3. General procedure

To a 10-ml test tube with stopper, add 0.8 ml of 0.4% OP, 0.2 ml of 2.75×10^{-3} mol l^{-1} (CTAB) and 2.5 ml of 2×10^{-4} mol l^{-1} BPR followed by mixing for a while, then add appropriate volumes of 10 μg ml^{-1} Mo(VI) or/and W(VI) and 3.0 ml of 0.05 mol l^{-1} H_2SO_4. After that, dilute the resulting solution to the mark (10 ml) with water and mix up the final solution. Finally, keep it for 15 min at room temperature and then record its absorption spectrum against corresponding reagent blank.

3. Results and discussion

3.1. Effect of surfactant

Without surfactant, the main peak position of Mo-BPR complex (486 nm) is in close proximity to that of W-BPR complex (488 nm) and their sensitivity is very low (Fig. 1). OP can, to some extent, augment their difference in sensitivity (Fig. 2). It inverts the main peak position of Mo-BPR complex, but the main peak of the Mo at 616 nm is still near to the peak of the W at 622 nm. In the presence of CTAB, however, not only the sensitivity of both complexes increases considerably (especially for Mo complex), but also their difference in peak position (632 nm for Mo and 600 nm for W) enlarges markedly (Fig. 3). Fig. 4 shows the absorption spectra of both complexes in the presence of CTAB/OP mixed surfactants. As we can see from Fig. 4, the absorbance value of the W complex at the absorption maximum of the Mo complex (at 637 nm) is zero. This indicates the mixed micellar medium prepared by CTAB and OP in an appropriate ratio could be used for the selective and sensitive determination of Mo in Mo/W mixtures.

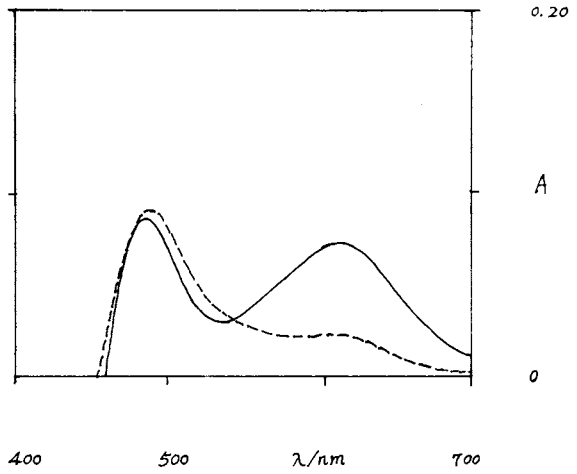

Fig. 1. Absorption spectra of Mo-BPR and W-BPR complexes in the absence of surfactants. Conditions: 20 μg Mo (solid line)/W (hyphenated line) + 2.5 ml of 2×10^{-4} mol l^{-1} BPR + 3.0 ml of 0.05 mol l^{-1} H_2SO_4.

3.2. Optimization of conditions

Conditions used for the selective and sensitive determination of Mo in Mo/W binary mixtures were optimized by studying the behavior of the Mo and/or W complexes on changing each experimental variable in turn while keeping others constant. Each optimal value met the following two requirements: (1) the absorbance value of the W at the absorption maximum of the Mo must be zero; and (2) the absorbance value of the Mo should be as high as possible.

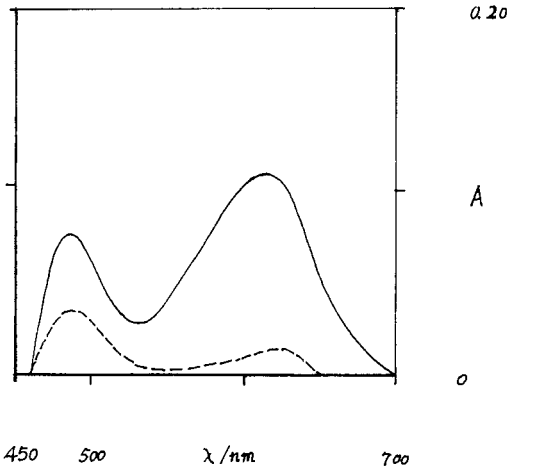

Fig. 2. Absorption spectra of Mo-BPR and W-BPR complexes in the presence of single nonionic surfactant. Conditions: 2.5 ml of 2×10^{-4} mol l^{-1} BPR + 1.0 ml of 0.04% OP + 20 μg Mo (solid line)/W (hyphenated line) + 3.0 ml of 0.05 mol l^{-1} H_2SO_4.

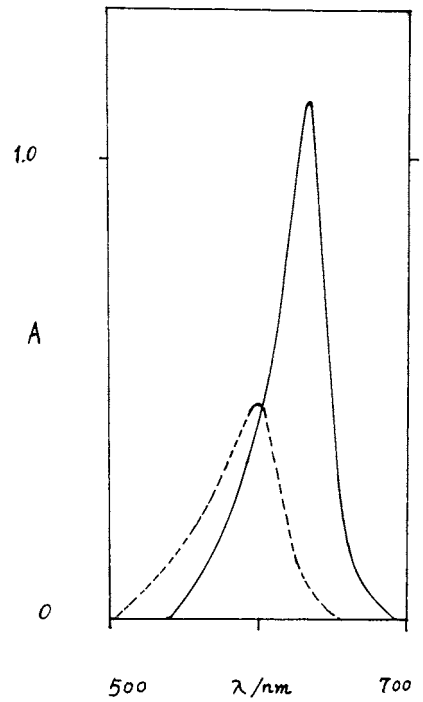

Fig. 3. Absorption spectra of Mo-BPR and W-BPR complexes in the presence of single cationic surfactant. Conditions: 2.5 ml of 2×10^{-4} mol l^{-1} BPR + 0.2 ml of 2.75×10^{-3} mol l^{-1} CTAB + 10 μg Mo (solid line)/W (hyphenated line) + 3.0 ml of 0.05 mol l^{-1} H_2SO_4.

3.2.1. Formula of the mixed surfactant solution and its volume

Let the total volume of 0.4% OP and 2.75×10^{-3} mol l^{-1} CTAB be 1.0 ml and their relative volumes change with an interval of 0.1 ml. With the decrease of the volume of the CTAB, the peak height of the Mo increased rapidly first (from 1.0 to 0.2 ml), which was accompanied by a small red shift of the peak (from 624 to 637 nm) and by a decrease of its half-band width (from 62 to 34 nm), then dropped rapidly (from 0.2 to 0.1 ml). After a slight increase in absorbance (ca. 3%) (from 1.0 to 0.8 ml), the peak height of the W decreased considerably (from 0.8 to 0.1 ml) with

the decrease of the CTAB, which was accompanied by a small red shift and occurrence of asymmetric peak shape (more steep right arm). According to the two requirements mentioned above, the optimum volume ratio should be 0.8 to 0.2 ml (the OP to the CTAB). In this ratio, the peak of the Mo located at 637 nm and W at 608 nm (Fig. 4). Small fluctuation in the volume of the CTAB (0.02 ml) or the OP (0.04 ml) had little influence on the resolution and determination.

The optimum volume of the mixed surfactant solution prepared in the optimum ratio was 1.0 ± 0.2 ml, 2.0 and 0.5 ml of the mixed surfactant solution produced 95% and 90% the height in 1.0 ml of such mixed surfactant solution, respectively.

The final concentration of CTAB in the optimum ratio was 5.5×10^{-5} mol l^{-1}, which was not only much lower than its CMC but also lower than the CMC of single OP. This result coincided with our theoretical prediction [7].

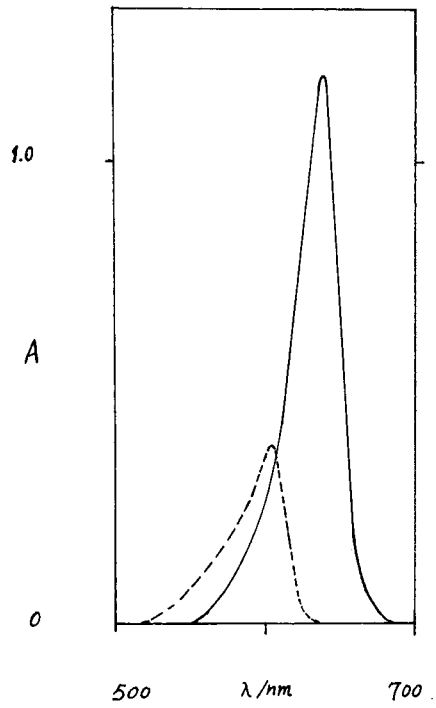

Fig. 4. Absorption spectra of Mo-BPR and W-BPR complexes in the presence of the mixed surfactants. Conditions: 0.2 ml of 2.75×10^{-3} mol l^{-1} CTAB + 0.8 ml of 0.4% OP + 2.5 ml of 2×10^{-4} mol l^{-1} BPR + 10 μg Mo (solid line)/W (hyphenated line) + 3.0 ml of 0.05 mol l^{-1} H_2SO_4.

3.2.2. Acidity under the optimum ratio

As the volume of 0.05 mol l^{-1} H_2SO_4 (used for adjusting pH) increased, the absorbance of the Mo system (composed of 1.0 ml of the mixed surfactant solution, 2.5 ml of 2×10^{-4}mol l^{-1} BPR and 5 μg Mo) increased first rapidly (from 1.0 to 1.5 ml), then slowly (from 1.5 to 2.5 ml). After that, it remained almost unchanged (from 2.5 to 3.0 ml). Further increase of the volume (from 3.0 to 4.0 ml) made the absorbance drop a little ($< 2\%$). Over the whole range of 1.0–4.0 ml, however, the change in the volume of 0.05 mol l^{-1} H_2SO_4 had almost no influence on the absorbance of the W system. So 2.0–3.5 ml of 0.05 mol l^{-1} H_2SO_4 was optimum for the resolution and determination of Mo. In subsequent experiments, 3.0 ml of 0.05 mol l^{-1} H_2SO_4 was added (the pH of the final solution was ca. 1.8).

3.2.3. Effect of BPR on the determination

With the increase of the volume of 2×10^{-4} mol l^{-1} BPR, the absorbance of the Mo system (aliquots of 2×10^{-4} mol l^{-1} BPR + 1.0 ml of the mixed surfactant solution + 5 μg Mo + 3.0 ml of 0.05 mol l^{-1} H_2SO_4) first increased (rapidly from 1.0 to 2.0 ml followed by slowly from 2.0 to 2.5 ml), then remained stable (from 2.5 to 3.0 ml), and finally decreased rapidly (> 3.0 ml). Considering BPR's absorption at 637 nm, 2.5 ml of 2×10^{-4} mol l^{-1} BPR was chosen as optimum in subsequent experiments.

3.2.4. Effect of ethanol on the determination

To increase the solubility of BPR and CTAB in water, their solutions were usually prepared in the literature with water/alcohol mixture. Here, the effect of ethanol on the determination of Mo was thus studied. We found that addition of ethanol reduced the absorbance of the Mo. The higher the content of ethanol, the greater the reduction of the absorbance (1.0 ml of 95% ethanol made the absorbance decrease by 5%). So no ethanol was added in our system.

3.2.5. Effect of temperature on the determination

The absorbance of the Mo system decreased with the increase of its temperature especially at higher temperatures (> 60°C). At room tempera-

ture, however, the fluctuation in temperature (± 5°C) did not cause any obvious changes in absorbance. For the sake of convenience, no thermostated equipment was incorporated. The temperature-dependent change of the absorbance was related to the temperature-dependent change of the relative contents of OP and CTAB in a OP/CTAB mixed micelle [11] (Note: the volume ratio of the mixed surfactant solution did not change).

3.2.6. Order of addition of the reagents and stability of the Mo system

The order in which the components of the reaction mixture were mixed had no influence on the sensitivity of the Mo system. However, the color development time would be shortened greatly if Mo was added after BPR and the mixed surfactant solution. At room temperature, formation of the Mo complex was virtually instantaneous and its absorbance remained stable for at least 24 h. To ensure reproducibility, a color development time of 15 min was recommended.

3.3. Analytical characteristics of the proposed method

Under the optimum conditions, Beer's law was obeyed over the range 0.06–0.8 μg ml^{-1} with molar absorptivity and detection limit being 1.3×10^5 l $mol^{-1}cm^{-1}$ and 0.025 μg ml^{-1} (calculated based on three times the standard deviation of the blank ($n = 11$)), respectively. For 5.0 μg Mo, the relative standard deviation (RSD) ($n = 7$) was 0.92%.

As compared with the literature system in which no OP was added [12–14], our Mo system was sensitive as well as selective. In addition, the present method still maintained the features of relative simplicity and rapidity of spectrophotometry. The operating conditions used for the resolution and determination were milder and easier to control than those of the thiocyanate method [15].

3.4. Composition ratio of the Mo complex

In the presence of OP, the ratio of Mo to BPR and the ratio of BPR to CTAB, obtained by the mole-ratio method with the final concentration of BPR fixed at 2×10^{-5} mol l^{-1}, were both 1:2. Thus the composition ratio of the Mo complex was 1:2:4 (Mo:BPR:CTAB). The difference between our result and a literature result of 1:2:2 (Mo:BPR:CTAB (CPC)) [12,13], obtained in the absence of OP, might be related to the oligomerization of BPR. To ascertain this deduction, the composition ratio of the ion-association complex, BPR-CTAB, was also studied by the mole-ratio method. For the complex formed between CTAB monomer and BPR oligomer, a result of 1:2 (BPR:CTAB) was obtained at pH = 1.8 (3.0 ml of 0.05 mol l^{-1} H_2SO_4 was added), $[BPR] = 4 \times 10^{-5}$ mol l^{-1} (a final concentration); for the complex formed by CTAB micelle and BPR monomer, however, a result of 1:1 (BPR:CTAB) was obtained at pH = 1.8, $[CTAB] = 1 \times 10^{-4}$ mol l^{-1} (a final concentration). These results confirmed our deduction.

3.5. Role played by OP

As we know, the Mo-BPR-CTAB ternary complex is not stable in water. Therefore, a stabilizing agent is usually needed to prevent the ion-association complex from precipitating. In order to obtain high sensitivity, it is necessary to ensure BPR oligomer against depolymerization [7]. CTAB micelles cause BPR oligomer to depolymerize, while OP micelles do not. In this sense, OP is a stabilizing as well as sensitizing agent. In addition, OP has a differentiating effect on Mo and W. It can enlarge, small as it is, their difference in sensitivity (discriminating in favor of Mo yet against W) (Figs. 1–4). Here, the role played by OP is much like that by crown ether (formed by the polyoxyethylene chains in an OP micelle). It was reported that Mo and W could be separated with crown ether [5,16]. Last but not least, OP lowers the symmetry of the absorption peak of the W complex, thereby favoring the resolution of Mo in Mo/W binary mixtures.

3.6. Interference study

In order to quantitatively examine the effect of W on the determination of Mo, five W/Mo binary

Table 1
Recovery assay of Mo in synthetic samples[a]

Composition (μg)	Found (μg)[b]	RSD (%)	Recovery (%)
Mo+W	Mo	Mo	Mo
1.0+5.0	1.0	1.2	100
1.0+10.0	1.0	0.9	100
1.0+15.0	1.0	1.3	100
1.0+20.0	0.98	1.8	98
1.0+25.0	0.95	2.1	95

[a] Measured under the same conditions as used for the calibration.
[b] Mean of five replicate determinations.

systems were selected (Table 1) as synthetic samples for the recovery assay of Mo in the samples. Results showed that at least 10-fold molar excess of W with respect to Mo did not interfere with the determination of Mo. No interference from W resulted from the steep right arm of the peak of the W as well as the position of the peak of the Mo (Fig. 4), which should be attributed to the mixed surfactants.

Effects of some other foreign ions, which often accompany Mo in real sample (hereafter, a certified steel sample and a seawater sample were selected to test and verify the reliability and the adaptability of our method, respectively), were also studied by analysing 5.0 μg Mo in the presence of increasing amounts of such foreign ions. The results, together with the effects of reducing agents and complexing agents, are summarized in Table 2. As we can see from Table 2, Zr, Sn, Ti, V, Sb, etc. interfere, in varying degree, with the determination of Mo. For a steel sample, the interference of Fe should also be taken into account. Also we can see from Table 2 that large amounts of EDTA and ascorbate (Vc) are tolerated. So most of above interferents can be easily masked with a mixture of EDTA and Vc. In addition, the amount of EDTA tolerated in the presence of OP is much larger than that in the absence of OP (Table 2). So the present determination method is compatible with the concentration method reported by Yoshimura et al. [2], the latter being needed for the determination of trace Mo in natural water samples.

3.7. Application

3.7.1. Certified steel sample (28Cr3SiNiMoWV)

A carbon steel sample composed of Mo (0.35%), W (0.80%), Ni (0.80%), V (0.05%), Cr (2.80%), Mn (0.50%), Si (0.90%) and C (0.25%) was analysed. The sample (0.25 g) was digested and large amount of Fe was separated in the same way as reported elsewhere [6]. Aliquots (2.0 ml) of the final solution, together with 0.5 ml of 0.01 mol l^{-1} Vc and 0.5 ml of 0.01 mol l^{-1} EDTA, were used for the spectrophotometric determination of Mo. The average Mo content in the sample, based on seven determinations, was 0.34% with RSD and average recovery being 2.3% and 98.4%, re-

Table 2
Effects of foreign ions on the determination of 5 μg Mo[a]

Foreign metal ions	Tolerance limits (μg)	Foreign nonmetal ions (0.01 M)	Tolerance limits (ml)
As(III)Cr(III)Ni(II)	>100	Nitrite	1.0
Co(II)Ca(II)Mg(II)	>100	Silicate	1.0
Cu(II)Pb(II)	80	Phosphate	1.0
Mn(II)	60	Oxalate	0.25
Zn(II)Al(III)	40	Citrate	0.5
Sb(V)Fe(II)	20	Flouride	>2.5
Sn(IV)Cr(VI)Fe(III)	10	Ascorbate	>2.5
Zr(IV)Sn(II)Ti(IV)	4	EDTA	>2.5 (1.0)[b]
V(V)	2		
Sb(III)	1		

[a] With a relative error being less than ±5%
[b] Data in parentheses obtained in the absence of OP.

spectively. The content obtained was in good agreement with the certified value.

3.7.2. Natural water sample

According to [2], a 500-ml seawater sample (provided by Shandong Bureau of Environmental Protection) was concentrated. After adsorption on Sephadex G-25 gel and elution with 20 ml of 0.01 mol l^{-1} EDTA solution (the first 5 ml of the effluent was discarded), aliquots (2.0 ml) of the effluent were used for the spectrophotometric determination. The average Mo content in the sample was 10.4 μg l^{-1} with RSD = 2.8% ($n = 7$). The content obtained was close to a value of 9.8 μg l^{-1} obtained by atomic absorption spectrometry (same conditions as in [2]).

4. Conclusion

(1) CTAB and OP has synergetic effects on the resolution of Mo in Mo/W binary mixtures. Under the optimum conditions, at least 10-fold molar excess of W with respect to Mo do not interfere with the determination of Mo. In addition, more EDTA (used as eluent and/or masking agent) is tolerated due to the presence of OP.

(2) The oligomer of BPR is responsible for the high sensitivity of the proposed method. OP favors the formation of BPR oligomer; therefore, it acts as both stabilizing and sensitizing agent in addition to its differentiating effect.

(3) The proposed method is superior in sensitivity and selectivity to the counterpart involving no OP. In addition, its operating conditions are mild and the results obtained are accurate and reproducible. When coupled with a concentration method, it can be used for routine determination of trace Mo in natural water samples.

Acknowledgements

The authors gratefully acknowledge financial support from the Key Laboratory for Colloid and Interface Chemistry of the State Education Commission of China.

References

[1] S. Hoshi, K. Konuma, K. Sugawara, M. Uto, K. Akatsuka, Talanta 44 (1997) 1473.
[2] K. Yoshimura, S. Hiraoka, T. Tarutani, Anal. Chim. Acta 142 (1982) 101.
[3] H. Shen, Y. Liu, Gaodeng Xuexiao Huaxue Xuebao 9 (9) (1988) 897.
[4] Y. Hu, Lihua Jianyan-Huaxue Fence 29 (6) (1993) 342.
[5] A.D. Barve, V.M. Shinde, Indian J. Chem. 33A (12) (1994) 1126.
[6] C. Cruces-Blanco, A.M. Garcia-Campana, F. Alez-Barrero, M. Roman-Ceba, Talanta 42 (1995) 1037.
[7] X. Huang, S. Han, W. Zhang, Y. Yin, G. Xu, Chin. Chem. Lett. 8 (6) (1997) 523.
[8] X. Huang, W. Zhang, S. Han, Y. Yin, G. Xu, X. Wang, Talanta 45 (1997) 127.
[9] X. Huang, N. Jie, S. Han, W. Zhang, J. Huang, Mikrochim. Acta 126 (1997) 329.
[10] S. Suryani, F. Theraulez, O. Thomas, Trends Anal.Chem. 14 (9) (1995) 457.
[11] G. Zhao, Physical Chemistry of Surfactants, Beijing University Press, Beijing, 1991.
[12] S.B. Savvin, R.K. Chernova, G.M. Beloliptseva, Zh. Anal. Khim. 35 (6) (1980) 1128.
[13] I.Y. Andreeva, L.I. Lebedeva, G.L. Kavelina, Zh. Anal. Khim. 37 (12) (1982) 2202.
[14] Deguchi, M. Iizuka, M. Yashiki, Bunseki Kagaku 23(1974)760.
[15] A.C. Basak, K.C. Ghosh, A.R. Paul, S. Bhattacharjee, L.P. Pandey, Talanta 42 (1995) 497.
[16] B.S. Mohite, D.N. Zambare, Anal. Lett. 27 (12) (1994) 2387.

ELSEVIER

Talanta 47 (1998) 877–881

Talanta

Determination of Mo and Bi in steels by electrothermal atomic absorption spectrometry after complexation and sorption on activated carbon

Maria Bertília Oss Giacomelli, José Bento Borba da Silva, Adilson José Curtius *

Departamento de Química da Universidade Federal de Santa Catarina, 88040-900 Florianópolis, S.C., Brazil

Received 23 December 1997; received in revised form 20 April 1998; accepted 20 April 1998

Abstract

A simple method for the preconcentration of Mo and Bi in steels is proposed. The analytes are complexed with the ammonium salt of dithiophosphoric acid *O*,*O*-diethyl ester and sorbed onto activated carbon. After desorption into a small volume of nitric acid at low pH, Mo and Bi are determined by electrothermal atomic absorption spectrometry. Iron(III) is reduced to Fe(II), which is not complexed and not significantly retained on the carbon. Enrichment factor of 23 and 26 were obtained for Mo and Bi, respectively. The method was applied to the analysis of four certified reference steels, after acid dissolution in a microwave system and good agreement was obtained with the certified or recommended values. © 1998 Elsevier Science B.V. All rights reserved.

Keywords: Electrothermal atomic absorption spectrometry; Dithiophosphoric acid *O*,*O*-diethyl ester; Molybdenum; Bismuth; Steel

1. Introduction

The determination of minor components of steels and other alloys is very important, since several characteristics of steels depend on their presence, even at very low concentrations. Elements like Sb, As, Bi, Se, Te, Pb and others [1] may affect their mechanical and magnetic properties and the homogeneity of the steel. Molybdenum increases the mechanical resistance of steels, facilitates thermal treatment by reducing its fragility and improves structural properties at higher temperatures [2]. On the other hand, Bi of higher than 0.0002% may induce breaking during cold working of the steel [3].

Electrothermal atomic absorption spectrometry (ETAAS) is a very sensitive technique for the determination of trace elements in alloys. In spite of the possibility of direct solid analysis [4], this technique has been more frequently used for the elemental determination after the dissolution of the sample. Separation of Fe have to be applied when a preconcentration is needed to lower the detection limits or when some interferents must be eliminated. It is also known that high concentra-

* Corresponding author. Tel.: +55 48 2319219; fax: +55 48 2319711; e-mail: adilsonc@fastlane.com.br

0039-9140/98/$ - see front matter © 1998 Elsevier Science B.V. All rights reserved.
PII S0039-9140(98)00176-3

tions of Fe limits the lifetime of the graphite tubes [5].

The sodium salt of dithiophosphoric acid *O*,*O*-diethyl ester (NaDDTP) was used by Bode and Arnswald [6,7] to complex a number of elements including Mo and Bi. Separation of Bi, Cd, Cu, In, Pb and Tl from high purity gallium and aluminum [8] and from high purity iron, chromium and manganese [9] have been reported. Complexes of the impurities with the ammonium salt of DDTP were formed in an acid solution and filtered through a small filter paper covered with a layer of activated carbon. After treating the carbon with a nitric acid, the traces were determined by flame AAS. A similar procedure was used to preconcentrate Mo in biological and geological reference materials [10] and Ag in waters and in soils solution [11]. This complexing agent was used for the on-line selective determination of Cd, Cu and Pb in digested solid environmental samples by flame AAS [12] and also of Pb in biological and environmental samples by ETAAS [13]. As the DDTP complexes As(III) and not As(V), a method for the on-line determination of these species in waters by ETAAS, using C_{18} as sorbent in a minicolumn and methanol as eluent, was also proposed [14].

In the present paper, the determination of Mo and Bi in steels after complexation with ammonium DDTP and sorption onto activated carbon is proposed. High enrichment factors were expected due to the small final volume. The DDTP complexes are stable in dilute mineral acid, which is a real advantage in many analytical applications. Also, this complexing agent is quite selective, since several metals are not complexed, including alkaline and alkaline earth elements Ga, Ge(IV) Ir, Mn(II), Nb, Pt(II and IV), Rh, Ru(III), Se(VI), Ta, Th, Ti, V(III), W(VI), Zn, Zr, Al and Fe(II) [6,7]. In this way, Fe(III) can be separated from the analytes, after reduction to Fe(II).

2. Experimental

2.1. Instrumentation

An atomic absorption spectrometer Perkin Elmer 3110 equipped with a HGA-600 furnace, an AS-60 Autosampler, and a deuterium-arc lamp background corrector, all from Perkin Elmer, was used for the integrated absorbance measurements. The operating conditions were those recommended by the manufacturer, unless otherwise specified. The sample volume used was 20 and 5 μl of the modifier solution, 3000 μg ml^{-1} of Pd and 2000 μg ml^{-1} of Mg were added for the Bi determinations. No modifier was used for Mo. Argon (99.996%, White Martins, Brazil) was used as the purge gas. Mo and Bi hollow cathode lamps from Hitachi, were operated at 15 and 18 mA, respectively. The analytical wavelength for Mo and Bi were 313.3 and 223.1 nm, respectively. For Mo determinations, pyrolytic graphite coated tube (Perkin Elmer Part No. B010-9322) was used, whereas, the same tube with a totally pyrolytic graphite platform (Perkin Elmer Part No. B 010-9324) was used for Bi. The temperature program is given in Table 1.

A microwave dissolution system MLS-1200 from Milestone, was used to dissolve the samples.

Table 1
Temperature program for Mo and Bi

Step	Temperature (°C)	Ramp (s)	Hold (s)	Argon flow rate (ml min^{-1})
1	90	10	10	300
2	140	5	15	300
3	1600 (Mo), 1000 (Bi)	10	15	300
4[a]	2650 (Mo), 2000 (Bi)	0	5	0
5	2650	1	5	300
6	20	10	10	300

[a] Read in this step.

2.2. Samples and solutions

Four certified reference steels from the National Institute of Standards and Technology (NIST) were analyzed: SRMs 361, 362, 363 and 364.

All chemicals used were of analytical-reagent grade, unless otherwise specified. The water was de-ionized in a Milli-Q system (resistivity of 18.2 MΩ cm). The hydrochloric and nitric acids were Suprapur from Merck.

Molybdenum, 1000 mg l^{-1}. Prepared from a Titrisol ampoule from Merck.

Bismuth, 1000 mg l^{-1}. Analytical solution from Aldrich (No. 20.699-7) in 5% v/v nitric acid.

Dithiophosphoric acid O,O-diethyl ester, ammonium salt, 1%, m/v. Dissolved the commercial reagent (Aldrich, No. 17779-2, 95% purity) in water.

Ascorbic acid, 20 g l^{-1}. Prepared from the Merck reagent in 1 M hydrochloric acid aqueous solution.

Magnesium nitrate solution, modifier for graphite furnace AAS, 10.0 ± 0.2 g l^{-1} (Merck No. B593213 431).

Palladium nitrate solution, modifier for graphite furnace AAS, 10.0 ± 0.2 g l^{-1} (Merck No. B936989 710).

Iron, 10 g l^{-1}. Prepared by dissolving iron as metal powder (Merck No. K21526019, 99.5% purity) in nitric acid.

Activated carbon, 0.5% suspension in water. From Merck, No. 2186.

2.3. Sample dissolution

About 0.25 g of the steel sample was weighed in triplicate in a PTFE flask. Hydrochloric acid of 4 ml and nitric acid of 2 ml were added and the flask was subjected to a power program in the microwave oven. Four heating steps with a duration of 5 min each, with 250, 400, 650 and 250 W, were applied. The program was repeated twice to obtain a clear solution.

2.4. Preconcentration procedure

A filter-paper of 2.5 cm diameter was covered with 50 mg of activated carbon by filtering 10 ml of the activated carbon suspension through it, using a water vacuum system, which was operated only after placing the suspension onto filter. Different volumes of the dissolved sample, depending on the analyte and on the steel, were placed into a 50-ml volumetric flask and 1 M hydrochloric acid was added. For Bi, the sample volumes varied from 1 to 5 ml, whereas for Mo, the sample solutions were first diluted before taking aliquots, except for SRM 363, as shown in Table 2. Ascorbic acid, 5 ml of the 20 g l^{-1} solution, was added to reduce the Fe(III) to Fe(II). Then 10 ml of DDTP solution was added. The total volume was adjusted to 50 ml with 1 M hydrochloric acid. After stirring for about 5 min, the solution containing the complexes was passed through the filter with the activated carbon. After drying at 110°C for about 15 min, the carbon was scraped into a 50-ml beaker, then 1 ml of concentrated nitric acid was added. The solution was evaporated to dryness. The residue was treated with 1 ml of 20% v/v nitric acid. The metals were measured in the supernatant [10,11]. A blank, not containing the sample, was always taken through the whole procedure. The standard solutions for calibration were prepared in 1 M hydrochloric acid and submitted to the preconcentration procedure as described above.

Table 2
Volumes of the steel solutions used in the preconcentration procedure

Steel	Bi (ml)	Dilution for Mo[a]	Mo (μl)
SRM 361	5	1+4	25
SRM 362	1	3+47	250
SRM 363	2.5	—	40
SRM 364	2.0	4+46	25

[a] Before taking an aliquot for the preconcentration.

3. Results and discussion

3.1. Furnace temperature program

The optimized pyrolysis and atomization temperatures were obtained from experimental pyrolysis and atomization curves. The optimum

pyrolysis temperature was 1700°C for Mo. For atomization, the maximum temperature of 2650°C was recommended by the manufacturer for a plateau was not reached. Using the mixture of palladium and magnesium nitrates as modifier, the optimum pyrolysis and atomization temperatures for Bi were 1000 and 2000°C, respectively. For Mo, the same tube could be used for at least 90 heating cycles without loss in sensitivity. For Bi, the lifetime of the tube was about 200 cycles.

3.2. Iron interference

In Fig. 1, the integrated absorbances for Mo and Bi are shown, for solutions subjected to the preconcentration procedure used in this work, as a function of the concentration of Fe(III) in the initial solution. For Bi, the signal decreases at Fe(III) concentrations higher than 10 μg ml^{-1}, while for Mo, at 10 μg ml^{-1}, the signal is already lower than that obtained in the absence of the interferent. For 1000 μg ml^{-1} of Fe(III), the signals for both analytes are very low. According to Bode and Arnswald [7], Fe(III) is partially complexed and the compound decomposes to Fe(II) and disulfide, $\{(C_2H_5O)_2PSS\}_2$. It was observed that in the presence of Fe(III), the solution becomes green with a gray precipitate, after the addition of the DDTP solution. Ascorbic acid was used to reduce Fe(III) to Fe(II) which is not complexed and does not interfere with the complexation of the analytes. As shown in Fig. 2, an ascorbic acid concentration of 0.15% m/v is sufficient to compensate for the effect of 1000 μg ml^{-1} of Fe(III). For the steels analyzed in this work, a concentration of 0.2% m/v was used. In the presence of the reducing agent, the solution is clear. An initial concentration of 2000 μg ml^{-1} of Fe(III) is reduced to about 160 μg ml^{-1} in the final solution, showing that Fe is not significantly extracted (the final concentration would be 100 μg ml^{-1} if all Fe was extracted).

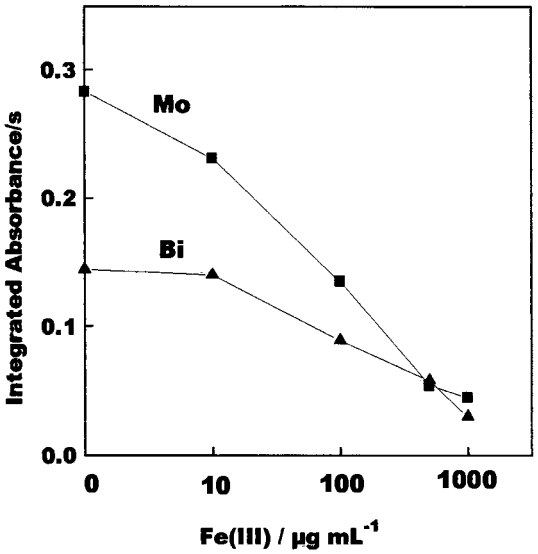

Fig. 1. Effect of Fe(III) on the preconcentration of Mo and Bi. Molybdenum initial concentration: 0.8 ng ml^{-1}; and Bi initial concentration: 1.8 ng ml^{-1}.

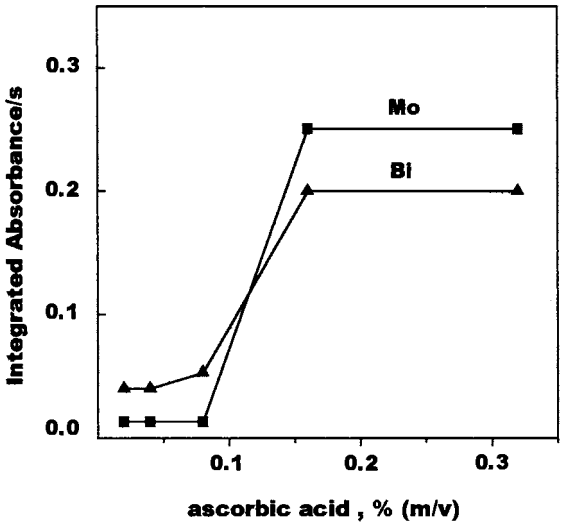

Fig. 2. Effect of ascorbic acid on the preconcentration of Mo and Bi in the presence of Fe(III). Initial concentrations: 1000 μg ml^{-1} Fe(III); 0.8 ng ml^{-1} Mo; and 1.8 ng ml^{-1} Bi.

3.3. Analytical curves

The linear regression of analytical curves obtained with and without preconcentration gave slopes for Mo of 0.185 and 0.00811 $s \cdot (ng/ml)^{-1}$, respectively and for Bi, 0.130 and 0.00495 $s \cdot (ng/ml)^{-1}$, respectively. The working concentration ranges were 0.0–0.8 ng ml^{-1} for Mo and 0.0–1.8 ng ml^{-1} for Bi. The correlation factors were higher than 0.99 for both elements. The enrich-

Table 3
Analytical results for Mo and Bi in certified reference steels of NIST ($n = 3$)

Sample	Found (μg g^{-1})		Certified (μg g^{-1})	
	Mo	Bi	Mo	Bi[a]
SRM 361	1890 (7.5)	3.6 (0.2)	1900 ± 19	4.0
SRM 362	710 (14)	17.4 (0.33)	680 ± 6.8	20
SRM 363	273 (5.5)	7.3 (1.02)	280 ± 2.8	8
SRM 364	4920 (20)	9.8 (0.8)	4900 ± 49	9

Values in parenthesis are the standard deviations. [a] Not certified.

ment factor is defined as the ratio of the slopes of the two analytical curves, that is, with and without preconcentration. The factor is determined not only by the yield of the extraction but also by possible interferences from impurities in the carbon and residues of the complexation agent on the analyte signals. The expected enrichment factor would be 50 assuming 100% recoveries, because the initial volume was 50 ml and the final volume was 1 ml. The obtained enrichment factors were 23 ± 1 and 26 ± 2 for Mo and Bi, respectively, however, the recoveries are quite reproducible.

3.4. Analysis of certified steel samples

Four certified reference materials were analyzed after acid dissolution. For Mo, the acid solution was diluted in order to bring the concentrations within the working range of the analytical curve. For Bi, the solution resulting from the dissolution was directly subjected to the preconcentration procedure. The results in Table 3 demonstrate the accuracy of the proposed method. The relative standard deviation for Mo was ranging from 0.4 to 2%, which was better than that for Bi of 2–14%.

In conclusion, the method is adequate for the determination of Mo and Bi in steels. It is also very flexible, since different initial volumes can be used resulting in different enrichment factors and detection limits. Another advantage of the procedure is that most of the Fe(III) is separated from the analytes, avoiding early destruction of the graphite tube and interferences. The procedure may also be used in the determination of other trace elements in steels and in other samples.

Acknowledgements

The authors are thankful to Conselho Nacional de Pesquisas e Desenvolvimento Tecnológico (CNPq) and to Coordenação de Aperfeiçoamento de Pessoal de Nível Superior (CAPES). M.B.O. Giacomelli and J.B.B. Silva have doctorate scholarships from CAPES and CNPq, respectively.

References

[1] A. Osojnick, M. Renko, T. Drglin, Z.J. Torkar, J. Physique IV 5 (1995) C7–189.
[2] V. Chiaverini, Aços e Ferros Fundidos, 6st ed., Associação Brasileira de Metais, São Paulo, 1988, p. 209.
[3] W. Frech, Anal. Chem. 275 (1975) 353.
[4] R. Irwin, A. Mikkelsen, R.G. Michel, J.P. Dougherty, F.R. Preli, Spectrochim. Acta (Part B) 45 (1990) 903.
[5] H.M. Ortner, W. Birzer, B. Welz, G. Schlemmer, A.J. Curtius, W. Wegscheider, V. Sychra, Fresenius Z. Anal. Chem. 323 (1986) 681.
[6] H. Bode, W. Arnswald, Fresenius Z. Anal. Chem. 185 (1962) 99.
[7] H. Bode, W. Arnswald, Fresenius Z. Anal. Chem. 185 (1962) 179.
[8] H. Berndt, J. Messerschmidt, Fresenius Z. Anal. Chem. 308 (1981) 104.
[9] H. Berndt, J. Messerschmidt, Fresenius Z. Anal. Chem. 310 (1982) 230.
[10] V.L.A. Monte, A.J. Curtius, J. Anal. At. Spectrom. 5 (1990) 21.
[11] A.K. Avila, A.J. Curtius, J. Anal. At. Spectrom. 9 (1994) 543.
[12] R. Ma, F. Adams, Spectrochim. Acta (Part B) 51 (1996) 1917.
[13] X.-P. Yan, F. Adams, J. Anal. At. Spectrom. 12 (1997) 459.
[14] D. Pozebon, V.L. Dressler, J.A. Gomes Neto, A.J. Curtius, Talanta 45 (1998) 1167.

ELSEVIER

Talanta 47 (1998) 883–890

Talanta

Spectrophotometric determination of some aromatic amines

Nidal A. Zatar *, Ali Z. Abu-Zuhri, Asma A. Abu-Shaweesh

Chemistry Department, An-Najah N. University, P.O. Box 7, Nablus, Palestine

Received 6 January 1998; received in revised form 13 April 1998; accepted 20 April 1998

Abstract

A method for spectrophotometric determination of four aromatic amines is described. The method is based on the reaction between the amine and the colorless Fe(III)-ferrozine complex. The amine reduces iron from Fe(III) to Fe(II) which forms a violet colored complex with ferrozine. The method is suitable for to the determination of 1,4-phenylenediamine, 2,4-diaminotoluene, 8-aminoquinoline and 2-amino-3-hydroxypyridine. The effect of different factors such as; pH, stability of the complex, temperature, ferrozine concentration, Fe(III) concentration and methanol concentration have been studied. The composition of the complex as well as the tolerance amount of other amines have been reported. Maximum absorbance is at 562 nm and Beer's law is obeyed over the ranges 0.17–1.6 ppm for 1,4-phenylenediamine, 0.45–3.7 ppm for 2,4-diaminotoluene, 0.51–3.4 ppm for 8-aminoquinoline and 0.53–4.4 ppm for 2-amino-3-hydroxypyridine. The obtained molar absorbtivities were 4.7×10^4, 2.0×10^4, 1.6×10^4, 1.5×10^3 l mol^{-1} cm^{-1} respectively. © 1998 Elsevier Science B.V. All rights reserved.

Keywords: Spectrophotometric determination; Fe(III) complex; Aromatic amines; UV-visible spectroscopy

1. Introduction

The wide distribution of aromatic amines in nature, their importance in industry as raw materials, intermediate and finished products, their toxic and carcinogenic properties and their use in variety of chemical researches provide the need for simple fast and reproducible method for the determination of these amines.

Several methods have been reported for spectrophotometric determination of amines. Bubnis et al. [1] presented a procedure for the determination of ϵ-amino groups of insulin and bovine albumin. Gaur et al. [2] described a simple sensitive method for the determination of free amino groups on solid supports using spectrophotometric method. Sakai [3] developed a spectrophotometric method for the determination of berberine in pharmaceuticals. Falco et al. [4] proposed a method for the determination of amphetamine and methamphetamine in urine by H-poit standard addition method (HPSAM) using a UV-visible spectrophotometric technique. The method was applied for the analysis of some drugs extractions. On the other hand, Gunduz et al. [5] developed conductometric and spectrophotometric methods for the determination of methyl-, n-propyl- and n-butylamines. The end points of the conductometric titrations are fairly sharp and can be used in the determination of these amines.

* Corresponding author. Tel.: +972 9 2370042; fax: +972 9 2387982.

0039-9140/98/$ - see front matter © 1998 Elsevier Science B.V. All rights reserved.
PII S0039-9140(98)00177-5

Our literature survey showed that no work has been published on the quantitative determination of 1,4-phenylenediamine (**I**), 2,4-diaminotoluene (**II**), 8-aminoquinoline (**III**) and 2-amino-3-hydroxypyridine (**IV**). The aim of the present work is to develop a spectrophotometric method for the determination of aforementioned four aromatic amines. The method is based on the reduction of Fe(III)-ferrozine complex [Fe(III)-Fz] to Fe(II)-ferrozine complex [Fe(II)-Fz] using the investigated amines. The produced Fe(II)-Fz complex from this oxidation–reduction process exhibits a stable violet color which absorb at 562 nm. The intensity of the violet colored complex was found to be directly proportional to the amine concentration. On the other hand Fz–Fe(III) complex did not show any absorption at this wavelength.

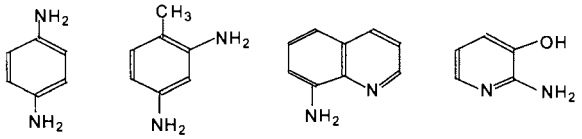

2. Experimental

2.1. Chemicals

Unless otherwise stated, all chemicals and solvents used were of analytical reagent grade.

Ferrozine (Fz) 10^{-2} M: prepared from 3-(2-pyridyl)-5,6-bis(4-phenylsulfonic acid)-1,2,3-tartrazine $C_{20}H_{13}N_4O_6Na.2H_2O$ (Sigma lot no. 25H0345). A 0.528 g sample was weighed out accurately and dissolved in distilled water in 100-ml volumetric flask.

Ferric sulfate 10^{-2} M: prepared from $Fe_2(SO_4)_3$, pure chemical (Riedel-de-Haen). A 0.399 g sample was weighed out accurately and dissolved in distilled water in 100-ml volumetric flask and standardized using 1,10-phenanthroline.

1,4-phenylenediamine 10^{-2} M: prepared from $C_6H_5(NH_2)_2$ (Aldrich lot no. 0416ML). A 0.0265 g sample was weighed out accurately and dissolved in absolute methanol in 25-ml volumetric flask.

2,4-Diaminotoluene 10^{-2} M: prepared from $CH_3C_6H_3(NH_2)_2$, (Aldrich lot no. 0301TK). A 0.0299 g sample was weighed out accurately and dissolved in absolute methanol in 25-ml volumetric flask.

8-Aminoquinoline 10^{-2} M: prepared from $C_9H_8N_2$ (Merck Schuchardt lot no. 173033). A 0.0272 g sample was weighed out accurately and dissolved in absolute methanol in 25-ml volumetric flask.

2-Amino-3-hydroxypyridine 10^{-2} M: prepared from $C_5H_6N_2O$ (Riedel-de-Haen lot no. 90230). A 0.0263 g sample was weighed out accurately and dissolved in absolute methanol in 25-ml volumetric flask.

Buffer solutions: The buffer solutions in the range 2.0–12.0 were prepared from acetic acid, phosphoric acid, boric acid and sodium hydroxide solutions.

2.2. Apparatus

All spectrophotometric measurements were carried out using a UV-2, Unicam UV-visible spectrophotometer. The cell used for measurements were 1×1 cm glass cells. A hanna 8521 model pH meter was used for pH measurements.

2.3. Procedure

A portion of solution containing an amount of the desired amine in the range 1.6–4.4 ppm was transferred into a 10-ml volumetric flask. Then 3.0 ml of 10^{-4} M Fe(III) and 1.0 ml of 10^{-2} M Fz were added. The final solution was completed to 10.0 ml using buffer solution. The absorbance of the reaction mixture was measured after 3 min at 562 nm and at room temperature against a reagent blank containing Fe(III), Fz and buffer solution.

3. Results and discussion

The method is based on the reduction of Fe(III) to Fe(II) using the investigated amines. The produced Fe(II) from this oxidation–reduction process reacts with ferrozine (Fz) ligand to form a stable violet colored Fz–Fe(II) complex which

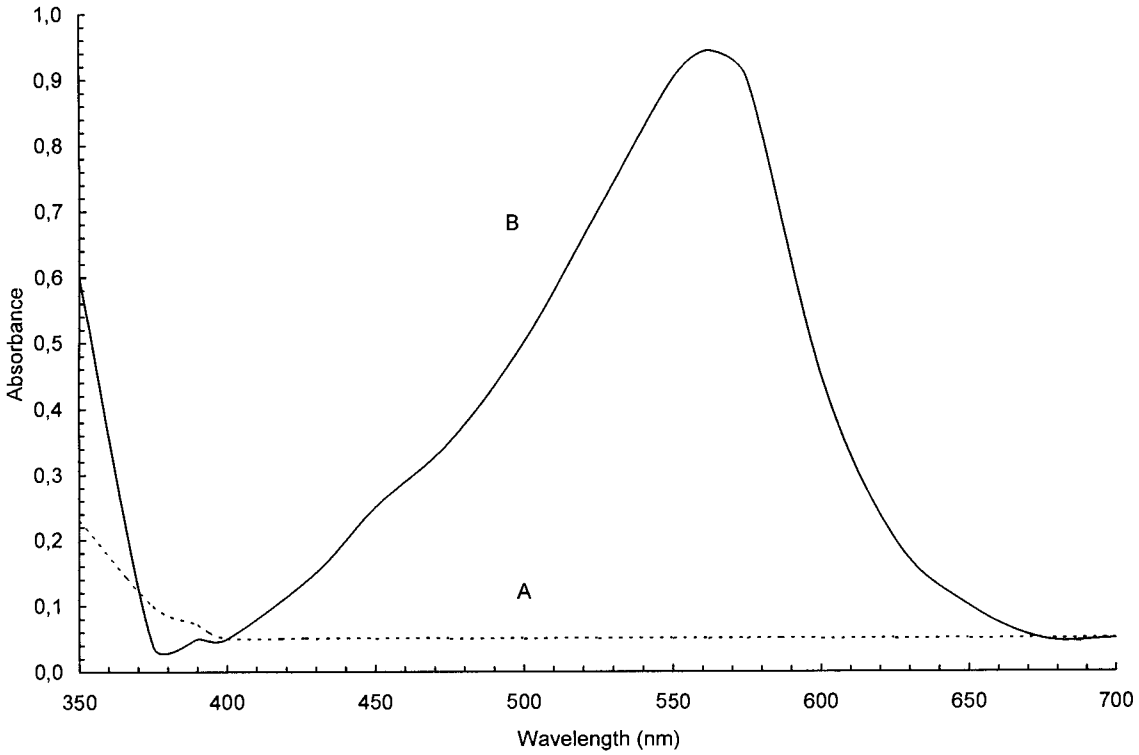

Fig. 1. Absorption spectra of: (A) 1.0×10^{-4} M 1,4-phenylenediamine solution vs buffer solution; (B) Mixture of 1.0×10^{-4} M 1,4-phenylenediamine, 3.0×10^{-4} M Fe(III) and 1.0×10^{-3} M Fz against a reagent blank as a reference. pH is 5, temperature 25°C.

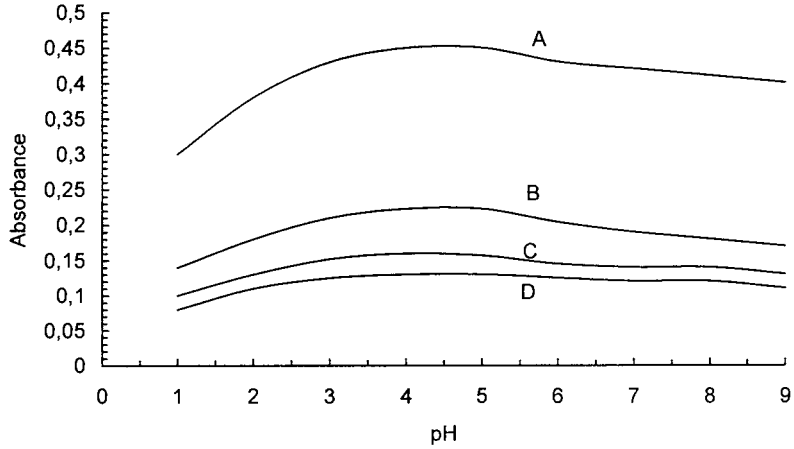

Fig. 2. Effect of pH on absorbance of 1.0×10^{-4} M for (A) 1,4-phenylenediamine, (B) 2,4-diaminotoluene, (C) 8-aminochinoline, (D) 2-amino-3-hydroxypyridine. Conditions: $[Fe(III)] = 3.0 \times 10^{-4}$ M, $[Fz] = 1.0 \times 10^{-3}$ M, wavelength 562 nm, temperature 25°C.

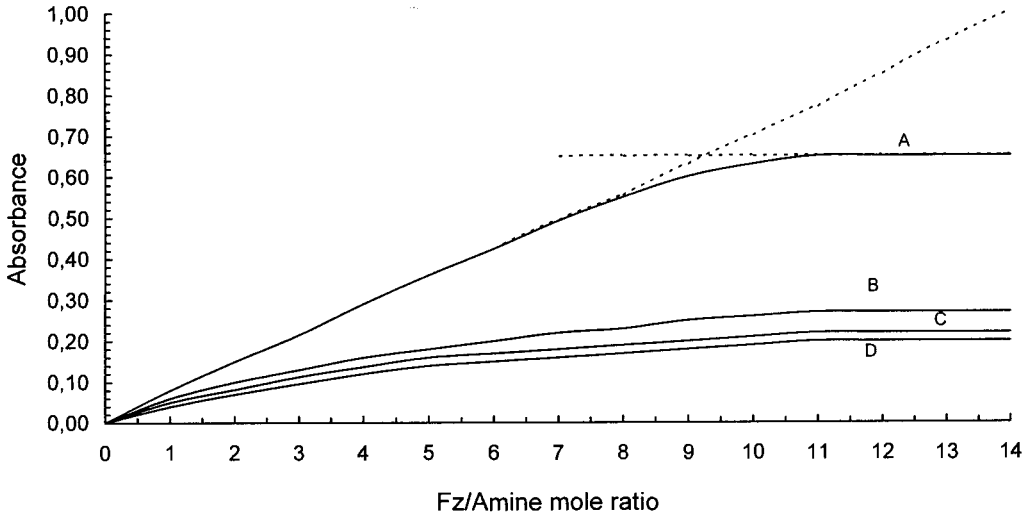

Fig. 3. Effect of ferrozine concentration on maximum absorbance at 562 nm for solution containing (A) 1.0×10^{-4} M 1,4-phenylenediamine, (B) 2,4-diaminotoluene, (C) 8-aminochinoline, (D) 2-amino-3-hydroxypyridine. Conditions: [Fe(III)] = 3.0×10^{-4} M, temperature 25°C.

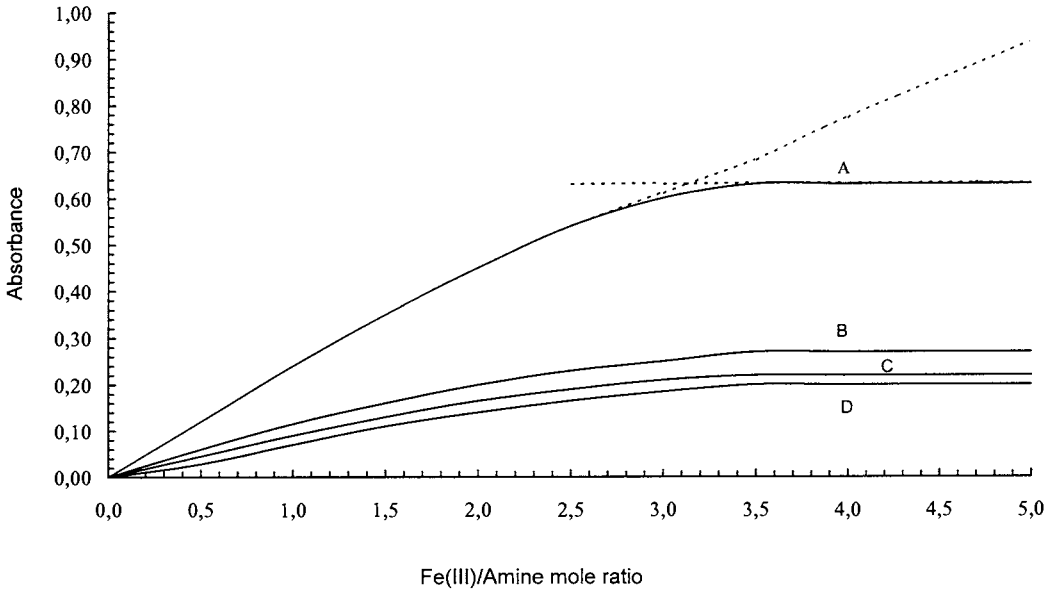

Fig. 4. Effect of iron(III) concentration on maximum absorbance at 562 nm for solution containing 1.0×10^{-4} M: (A) 1,4-phenylenediamine, (B) diaminotoluene, (C) 8-aminochinoline, (D) 2-amino-3-hydroxypyridine. Conditions: [Fz] = 1.0×10^{-3} M, temperature 25°C.

exhibit an absorbance maxima at 562 nm. The intensity of the violet colored complex was found to be directly proportional to the amine concentration. The proposed mechanism of the reactions is shown below:

$$H_2Fz \leftrightarrow 2H^+ + Fz^{2-}$$

$$3Fz^{2-} + Fe^{3+} \leftrightarrow [Fe(III)Fz_3]^{3-}$$

$$\text{Amine (colorless)} + 3[Fe(III)Fz_3]^{3-}\ \text{(colorless)} \leftrightarrow \text{Imine (colorless)} + 3[Fe(II)Fz_3]^{3-}\ \text{(violet)}$$

Many parameters such as pH, effect of time, temperature, ferrozine concentration, Fe(III) concentration, methanol concentration and the effect of other amines might affect the color intensity and the sensitivity of the proposed method. The effect of these parameters was investigated in order to optimize the conditions for spectrophotometric determination of amines.

3.1. Absorption spectra

The absorption spectra of the four amines systems under investigation are studied in the wavelength range 300–700 nm. The solutions are prepared as described in the general procedure. The results obtained showed similar absorption spectra for the four amine solutions with maximum absorbance at 562 nm. Typical spectra for 1,4-phenylenediamine is shown in Fig. 1. Spectral interference of the reagent can be eliminated by measurements against a reagent blank solution.

3.2. Effect of pH

The effect of pH on the absorption maxima at 562 nm was studied for solutions containing fixed concentration of amine and prepared as described in the general procedure in the pH range 2.0–11.0

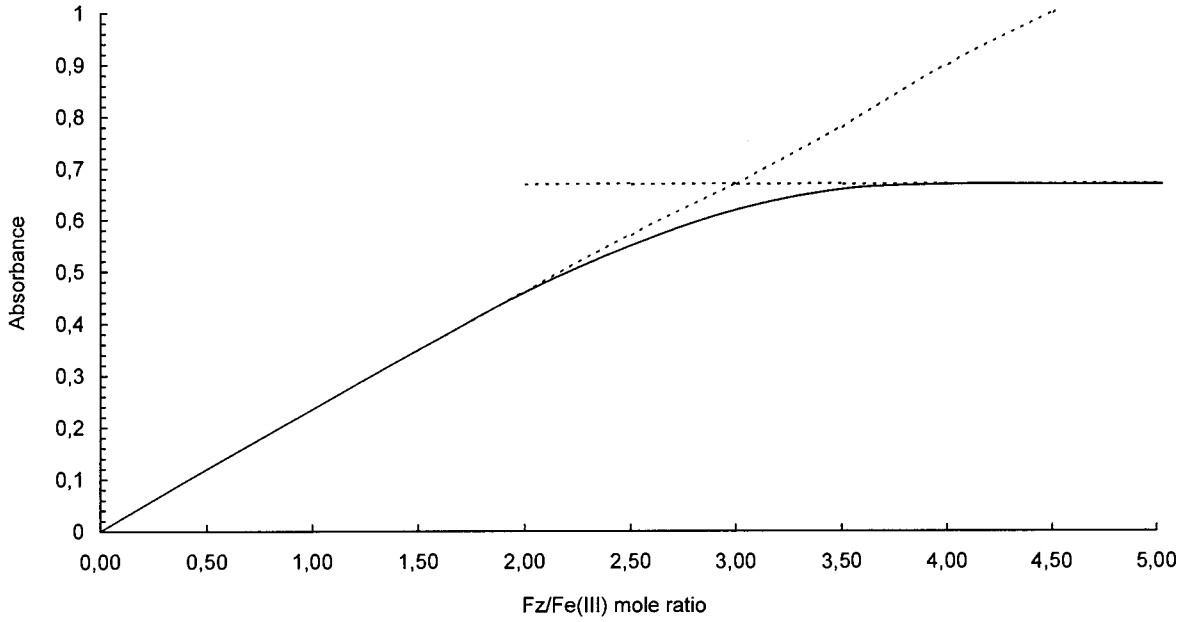

Fig. 5. Effect of ferrozine to Fe(III) mole ratio on absorbance at 562 nm for solution containing 1.0×10^{-4} M 1,4-phenylenediamine at pH 5 and at 25°C.

Table 1
The linear range, the molar absorptivity and the relative standard deviation for the four amines systems

Amine	Linear range (ppm)	Molar absorptivity (l mol^{-1} cm^{-1})	R.S.D.*
1,4-Phenylenediamine	0.17–1.60	4.7×10^4	3.1% for 1.1 ppm
2,4-Diaminotoluene	0.45–3.70	2.0×10^4	5.1% for 2.4 ppm
8-Aminoquinoline	0.51–3.40	1.6×10^4	5.8% for 2.3 ppm
2-Amino-3-hydroxypyridine	0.53–4.40	1.5×10^3	3.0% for 2.2 ppm

Conditions: [Ferrozine] = 1.0×10^{-3} M, [Iron(III)] = 3.0×10^{-4} M, pH 5, temperature = 25°C, λ_{max} = 562 nm.
* Five measurements in each case.

Table 2
Effect of other amines on the determination of 1.0×10^{-4} M of the investigated amine

Investigated amine	Investigated amines: (other amines)	Interfering amines (error, %)								
	Mole ratio	3,4-DAP	2-ACP	2-AMP	2-AP	2-APIC	1,4-PDA	8-AC	2,4-DAT	2-AHP
1,4-PDA	1:0.1	a	a	a	a	a	—	+16.3	+20.8	+17.0
	1:0.2	a	a	a	a	a	—	+42.5	+31.8	+27.9
	1:10	±0.2	±0.2	±0.5	±3.7	±0.4	—	h	h	h
	1:30	±3.7	±1.6	±2.7	±6.4	±1.4	—	h	h	h
	1:50	±5.6	±3.2	±6.3	±5.5	±4.0	—	h	h	h
8-AC	1:0.1	a	a	a	a	a	+8.3	—	+5.4	+10.3
	1:0.2	a	a	a	a	a	+14.5	—	+7.4	+19.1
	1:10	±0.4	±0.2	±1.2	±5.7	±0.5	h	—	h	h
	1:30	±2.6	±3.7	±2.8	±3.3	±3.5	h	—	h	h
	1:50	±4.8	±5.6	±3.9	±4.4	±4.4	h	—	h	h
2,4-DAT	1:0.1	a	a	a	a	a	+4.3	+40.1	—	+16.3
	1:0.2	a	a	a	a	a	+13.1	+61.5	—	+40.4
	1:10	±0.9	±0.4	±2.6	±3.0	±0.4	h	h	—	h
	1:30	±1.8	±2.6	±1.2	±3.9	±2.2	h	h	—	h
	1:50	±3.9	±4.8	±1.3	±2.6	±4.4	h	h	—	h
2-AHP	1:0.1	a	a	a	a	a	+10.3	+4.2	+3.2	—
	1:0.2	a	a	a	a	a	+13.5	+9.7	+9.2	—
	1:10	±0.9	±0.1	±0.6	±1.1	±0.4	h	h	h	—
	1:30	±1.9	±2.9	±3.4	±4.4	±1.5	h	h	h	—
	1:50	±4.4	±4.6	±6.6	±6.2	±4.9	h	h	h	—

1,4-PDA, 1,4-phenylenediamine; 2-ACP, 2-amino-5-chloropyridine; 8-AC, 8-aminoquinoline; 2-AMP, 2-amino-3-methylpyridine; 2,4-DAT, 2,4-diaminotoluene; 2-AP, 2-amimopyridine; 2-AHP, 2-amino-3-hydroxypyridine; 2-APIC, 2-aminopicoline; 3,4-DAP, 3,4-diaminopyridine.
Conditions, $[Fz] = 1.0 \times 10^{-3}$ M; $[Fe^{3+}] = 3.0 \times 10^{-4}$ M; pH 5; $\lambda = 562$ nm; temp. = 25°C; h, higher interference; a, no interference.

for the four amines. Similar results were obtained for all the above mentioned amines. The results obtained showed that the absorbance increases gradually by increasing the pH up to pH 5. At pH above this value a slight decrease in the absorbance was observed. Therefore, pH 5 was selected as optimum pH for further work. Fig. 2 shows the results obtained for 1,4-phenylenediamine system. Similar results are obtained for the other three amines.

3.3. Effect of time

The effect of time on absorption maxima at 562 nm was studied for the four amine solutions prepared as described in the general procedure. The results obtained showed that full color development was attained after 3 min. The intensity of the color stayed constant for at least 24 h after preparation of the samples.

3.4. Effect of temperature

The effect of temperature on color development was investigated. There was no detectable change in the absorbance at 562 nm in the temperature range 20–50°C. Any further increase in the temperature beyond 50°C resulted in a decrease in the absorbance. In the present work, all absorbance measurements were done at 25°C. Similar results were obtained for the four studied amines.

3.5. Effect of ferrozine concentration on absorbance

The absorbance of the amine systems under investigation exhibit dependence on ferrozine concentration. The results obtained showed that increasing the ferrozine concentration and keeping the concentrations of Fe(III) and amine constant, produced an increase in the absorbance up to a ferrozine to amine mole ratio of 9:1, beyond which any further increase did not affect the absorbance up to at least 100:1. The effect of ferrozine concentration in the four amines systems is almost similar. Typical results for the effect of ferrozine concentration on the absorbance is presented in Fig. 3 for 1,4-phenylenediamine system.

3.6. Effect of Fe(III) concentration on absorbance

The effect of increasing the Fe(III) concentration on the absorbance of the four amines systems is studied for solutions prepared as described in the general procedure and measured at 562 nm. The results obtained are similar for the four systems. It was found that keeping the amine concentration fixed and increasing the concentration of Fe(III) produced an increase in the absorbance up to an Fe(III) to amine mole ratio of 3:1. Any further increase in the Fe(III) concentration did not effect the absorbance. Typical results for the effect of Fe(III) concentration on the absorbance is presented in Fig. 4 for 1,4-phenylenediamine system.

3.7. Composition of Fe(II)-ferrozine complex

From the data obtained from the effect of ferrozine and Fe(III) concentrations on the absorbance of the amine solutions, the ferrozine to Fe(II) mole ratio can be obtained. Since Fe(III) is reduced by the amine present in the solution to Fe(II) then it is more convenient to plot Fe(II) to ferrozine mole ratio rather than Fe(III) to ferrozine mole ratio. The results obtained (Fig. 5) showed a ferrozine to Fe(II) mole ratio of 3:1.

It can be concluded that one mole of aromatic amine was required to react with three moles of Fe(III)-Fz complex. The amine oxidized into the corresponding imine [6] and the Fe(III)-Fz complex is reduced into Fe(II)-Fz complex which absorbs at 562 nm. These results are in good agreement with that obtained by Lopez-Cueto et al. [6] and support our proposed mechanism.

3.8. Effect of methanol concentration on absorbance

The reason for studying the effect of methanol concentration on the absorbance is because the amines under investigation are prepared in methanolic solutions since they are insoluble in water. It was found that the minimum methanol content required for solubilizing amine is 5% (v/v) methanolic solution. The effect of methanol is studied in the range 5–50% (v/v) for solutions

containing fixed amounts of amines, Fe(III) and ferrozine. The absorbance is measured as described in the general procedure. The results obtained showed that increasing the concentration of methanol in the studied range did not affect the absorbance.

3.9. Beer's law and sensitivity

From the investigation of the variables that effect the absorbance, the conditions for the color development and the absorbance measurements were selected. Following the recommended procedure, linear relationships were obtained between amines concentration and the corresponding absorbance. The ranges of linearity and the molar absorptivities are presented in Table 1. It can be seen that the 1,4-phenylenediamine system is the most sensitive followed by 2,4-diaminotoluene, 8-aminoquinoline and 2-diamino-3-hydroxypyridine which shows the lowest sensitivity. The precision of the determination of the four amines were checked using five replicates at fixed concentration levels. The R.S.D.s are given in Table 1. The difference in the molar absorptivity and the sensitivity of the four amine systems might be due to the difference in their molecular structure and the ability of the amine to reduce Fe(III)-Fz complex into Fe(II)-Fz complex.

3.10. Interference studies

The effect of other amines on the determination of the four amines under investigation has been studied. The results obtained are presented in Table 2. It was found that the amines 2-aminopyridine, 3,4-diaminopyridine, 2-amino-5-chloropyridine, 2-aminopicoline, 2-amino-3-methylpyridine did not interfere up to at least 50-fold molar excess of any of them relative to the studied four amines. On the other hand it was found that 1,4-phenylenediamine, 2,4-diaminotoluene, 8-aminoquinoline, 2-amino-3-hydroxypyridine interfere seriously in the determination of each of them in the presence of the other three, and greater than 0.1-fold molar excess of any of them can not be tolerated. The reason why some amines interfere and some do not might be due to the difference in their molecular structure and the reduction power of the amines.

References

[1] W.A. Bubnis, C.M. Ofner, Anal. Biochem. 207 (1992) 129–133.
[2] R.K. Gaur, S. Paliwal, P. Sharma, C.S.K. Gupta, J. Biochem. Biophys. Methods 18 (1989) 323–329.
[3] T. Sakai, J. Pharm. Sci. 68 (1979) 875–877.
[4] P.C. Falco, F.B. Riego, A.S. Gabeza, C.M. Legua, Anal. Chim. Acta 287 (1994) 41–48.
[5] T. Gunduz, M. Tastekin, Anal. Chim. Acta 286 (1994) 247–251.
[6] G. Lopez-Cueto, S. Maspoch, J.F. Rodriguez-Medina, C. Ubide, Analyst (and references therein) 121 (1996) 407–412.

ELSEVIER

Talanta 47 (1998) 891–898

Talanta

Reversed-phase liquid chromatographic determination of isoniazide in human urine as a test of the genetically predetermined type of biotransformation by acetylation

M.I. Evgen'ev [a,*], S.Yu. Garmonov [a], I.I. Evgen'eva [a], S.M. Goryunova [b], V.I. Pogorel'tsev [b], F.S. Levinson [a]

[a] *Department of Analytical Chemistry, Kazan State Technological University, 420015, K. Marx str. 68, 420015 Kazan, Russia*
[b] *Department of Clinical Pharmacology, Kazan State Medical University, 420012, Butlerov str. 49, Kazan, Russia*

Received 22 July 1997; received in revised form 30 January 1998; accepted 21 April 1998

Abstract

A new method of determination of genetically predetermined type of biotransformation by acetylation rate using reversed-phase liquid chromatography (RP-HPLC) was described. The method is based on determination of isonicotinic hydrazide (INH) which is excreted with the patient's urine during 24 h period after oral administration of 0.4 g of the drug. INH is used as pharmacogenetic marker. Precolumn derivatization of 4-chloro-5,7-dinitrobenzofurazan is used at RP-HPLC determination of INH and a new drug phosphabenzide (diphenylphosphinylacetic hydrazide, DPPAH) with specrtophotometric detection in urine. The limit of INH detection was 0.27 μg ml^{-1} and the one of DPPAH was 0.82 μg ml^{-1}. As a result of pharmacokinetic investigation it was discovered that bimodal distribution by acetylation rate for DPPAH is less apparent than in the case of INH. It is shown, that immunomodulator xymedone (*N*-(β-oxyethyl)-4,6-dimethyldihydropirimidon-2) is the acetylation inductor of xenobiotics. © 1998 Elsevier Science B.V. All rights reserved.

Keywords: RP-HPLC; Derivatization; 4-Chloro-5,7-dinitrobenzofurazan; Drugs

1. Introduction

Clarification of the connection between concentration of xenobiotics, their metabolites and pharmacological effect is the base of effective and secure application of drugs as well as diagnostics and treatment of personnel exposed to industrial toxicants [1–4]. In connection with this, the task of the development of sensitive and selective methods of determination of drugs and other xenobiotics in biological substrates of a human being is very urgent. The availability of relatively simple and clinically applicable methods for the determination of drugs in biological substrates for diagnostics of genetically predetermined type of

* Corresponding author. Tel.: +7 8432 399566; fax: +7 8432365768; e-mail: evgen@cnit.ksu.ras.ru

0039-9140/98/$ - see front matter © 1998 Elsevier Science B.V. All rights reserved.
PII S0039-9140(98)00166-0

their biotransformation in the organism is of particular importance. Such diagnostics allows us to prescribe an individual dosage of drugs [1,2,4]. Hydrazide of isonicotinic acid (isoniazide, INH) is one of such drugs, which brings about individually different reactions in the organism. Two types of INH metabolism (fast and slow) are determined due to genetic differences in the activity of acetylating enzyme of *N*-acetyltransferaze [1,2]. Determination of acetylation phenotype of this drug can also be used for establishing the optimal dosage of other xenobiotics. In addition, comparison of pharmacogenetic peculiarities of INH excretion from the organism is very useful in the investigation of new drugs similar to INH in chemical properties, such as phosphabenzide (hydrazide of diphenylphosphinilacetic acid, DPPAH). Methods of INH determination in biological substrates and drugs by means of ionexchange chromatography [5], HPLC with spectrofluorimetric detection [6,7], spectrophotometric [8,9], spectrofluorimetric [10] and voltamperometric [11,12] methods have already been described in the literature.

Earlier we showed the possibility of selective INH determination in the mixtures as 5,7-dinitrobenzofurazan (DNBF) derivatives by spectrophotometric method [13,14], in the system of flow-injection analysis [15].

In this work we describe the method of determination of genetically predetermined rate of acetylation at drug biotransformation based on precolumn derivatization of INH and DPPAH 4-chloro-5,7-dinitrobenzofurazan at RP-HPLC determination in biological substrates. In this case isoniazide was used as pharmacogenetic marker, allowing us to determine a patient's *N*-acetyltransferaze activity.

2. Experimental

2.1. Apparatus

Chromatography was performed using a model Milichrom-1 pump (Analytpribor, Orjol, Russia), and a UV-VIS absorbance detector (Carl Zeis Yena Specol 210 as detector with variable wavelength) containing a 6 μl flow cell (path length 5 mm). The detector signal was monitored by TZ 4100 Line Recorder (Laboratorni Pristroye, Praga, Czech Republic). Detection of urine samples was performed at 510 nm wavelength for INH and 495 nm wavelength for DPPAH. Spectrophotometric measurements were performed by SF-26 spectrophotometer (LOMO, Sankt-Petersburg, Russia).

The analytical columns were made of stainless steel (120×2.0 mm^2 I.D.) Silasorb C-18 (10 μm) and Silasorb 600 (10 μm) (Biochimmack, Moskow, Russia). A quard column (50×2 mm^2 I.D.) (Elsiko, Moskow, Russia) was packed with Diasorb-130-C4 (10 μm).

Chromatography was performed at a flow rate of 0.1 ml min^{-1}. The mobile phase was composed of acetonitrile-3 mM acetate buffer (pH 5,5) (25:75, v/v) for INH; acetonitrile-5 mM acetate buffer (pH 5.5)-methanol (28:67:5, v/v) for DPPAH.

2.2. Reagents

INH, DPPAH, calcium panthotenate, xymedone of pharmacopoeic purity were obtained from different pharmaceutical laboratories. DNBF, 4-hydroxy-5,7-dinitrobenzofurazan was prepared as previously described [13]. All solvents (methanole, acetonitrile, dimethylsulfoxide, methylene chloride, chloroform, propanole-2) were of analytical-reagent grade from Khimprom (Novocheboksarsk, Russia). In necessary cases they were dehydrated above molecular sieves. Doubly-distilled water was used throughout. Reanal buffer solutions were used (Hungary).

2.3. Procedure

Urine samples were collected in polyethylene vessels at appropriate time intervals. The samples were immediately centrifuged at 4°C at $1000 \times g$ for 10 min, decanted and stored at -18°C until thawing for subsequent analysis. Acetylation phenotype was determined in the group of 26 patients with normal kidney and liver functions. The patients were not previously medically treated. The Pharmacokinetics were studied after oral administration of 0.4 g of INH or DPPAH.

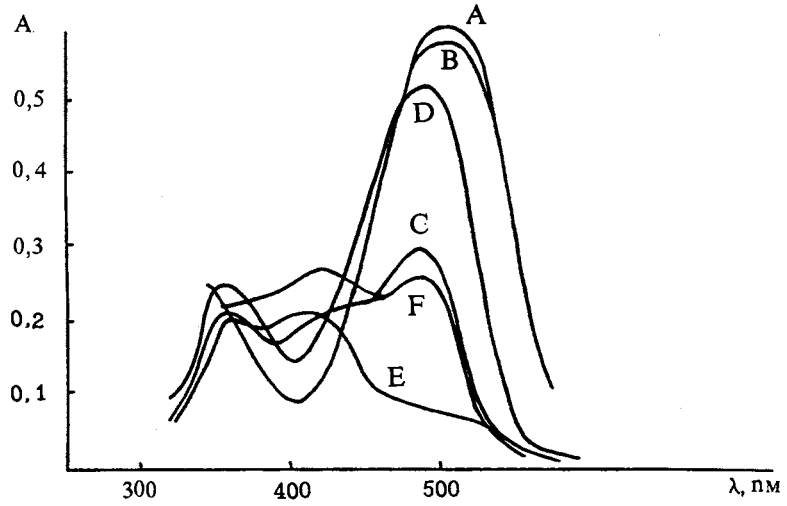

Fig. 1. Absorption spectra of the DNBF derivatives (2×10 mol l^{-1}) of: (A) INH in dimethylsulfoxide; (B) INH in dimethylsulfoxide–water mixture (30:70, v/v); (C) DPPAH in methanole; (D) DPPAH in methanole–water mixture (pH 6.76; 50:50, v/v); (E) DPPAH in methanole–tetrachloromethane (30:70, v/v); and (F) DPPAH in methanole–water mixture (pH 1.68; 50:50, v/v).

A total of 2 ml of urine under analysis in a 50 ml standard flask is diluted to the mark with distilled water. A 1 ml portion of 0.01 M DNBF solution in acetonitrile and 2 ml of 0.05 M acetate buffer solution (pH 5.5) are added to an aliquat (8 ml) of a resulting solution, mentioned above. After stabilization for 5 min an aliquot of 4 μl was injected into the LC system.

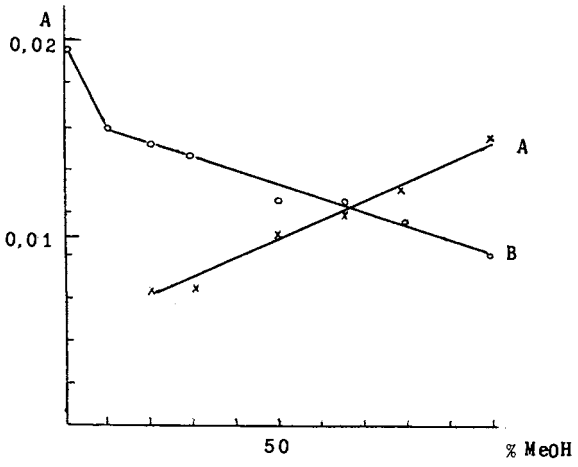

Fig. 2. Effect of methanole percentage in mobile phase (methanole–methylene chloride mixture) on peak height of INH derivative. (A) ion, (B) ion pair.

Stock standards were prepared by weighing 0.1 and 0.2 g of INH and DPPAH into volumetric flask and dissolving with water to active solutions containing approximately 100 and 200 mg ml^{-1}. Calibration curve standards were diluted from the two stock solutions using volumetric glassware to yield working standard concentrations of about 200–100 μg ml^{-1}. Standard solutions were prepared daily immediately before the analysis.

Concentrated initial INH (DPPAH) solutions were prepared by dissolving the drug in blank human urine. Working urine control samples containing 200–100 mg ml^{-1} of INH and DPPAH were prepared with blank human urine. Freshly prepared INH and DPPAN solutions were used.

3. Results and discussion

In organic and water–organic mediums interaction of DNBF with INH and DPPAH is taking place rapidly with the formation of intensively coloured products (Fig. 1).These products were isolated and the molar absorbance was found to be 30000 l mol^{-1} cm^{-1} at 510 nm for INH in water–dimethylsulfoxide (70:30, v/v) and 24400 l mol^{-1} cm^{-1} at 490 nm for DPPAH in water–

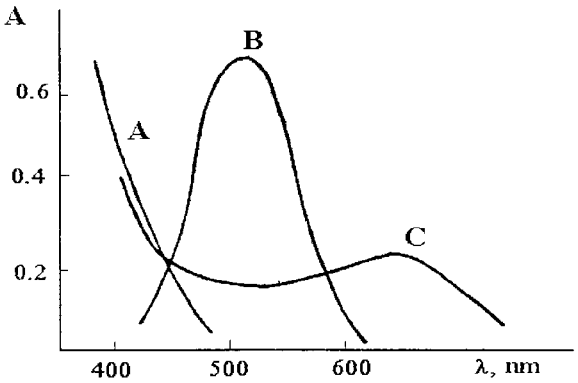

Fig. 3. Effect of urine pretreatment on absorption spectra: (C) DNBF derivatives of the urine biogenic components (urine diluted 1:25), (A) DNBF derivatives of the urine biogenic components. Urine pretreatment by threechloroacetic acid (reagent blank), (B) INH derivatives in urine (2.1×10^{-5} mol l^{-1}).

methanol (90:10, v/v). Comparison of these data with the molar absorbance of the products of analytical reactions under the same conditions (29500 l mol^{-1} cm^{-1} for INH, 24000 l mol^{-1} cm^{-1} for DPPAH) points out at quantitative interaction of DNBF with nucleophiles. The composition of resulting products [16,17] indicates that the reaction takes place according to the following scheme:

The DPPAH derivative dissolves well in non-aqueous and mixed mediums, in biological fluids, while INH derivative is slightly soluble in alcohols, acetonitrile and their water mixtures. Its solubility is good in biological fluids. The Beer's law plots are easily reproducible and are linear over the whole concentration range of 2×10^{-6}–10^{-4} mol l^{-1}.

Spectral characteristics of INH and DPPAH derivatives do not depend on medium acidity at a pH above 4. They undergo strong changes in more acidic solutions (Fig. 1F).

The influence of composition of solvent mixtures typical for NP-HPLC and RP-HPLC on absorption spectra of INH, DPPAH derivatives and hydrolyzed reagent form (OH DNBF) was studied.

Influence of non-aqueous and water–organic composition of mediums on absorption spectra of INH derivative is small. At the same time, for DPPAH derivative the change in medium polarity, due to addition of non-polar (methylene chloride, chloroform, tetrachloromethane) solvents or water, influences strongly the absorption spectra of dissolved substance (Fig. 1C,D,E). When polar properties of solvent mixtures are diminished, the absorption band with $\lambda_{max} = 490$ nm is practically

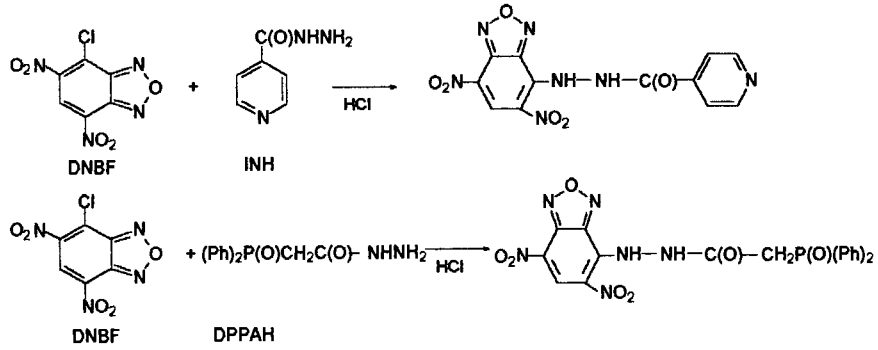

Excess of reagent (DNBF) in water solutions undergoes hydrolysis with the formation 4-hydroxy-5,7-dinitrobenzofurazan (OH DNBF) according to the scheme

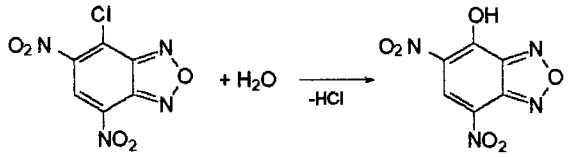

OH DNBF

non-existent and instead there appears a new band with $\lambda_{max} = 420$ nm. It can lead to non-reproducibility of results under conditions of NP-HPLC at spectrophotometric detection. Besides, ionic equilibriums 5,7-dinitrobenzofurazan derivatives of amino compounds and OH DNBF influence the results of spectrophotometric detection. It is connected with the fact, that the above compounds (NH- or OH-acids) in proton and non-proton dipolar solvents can exit as molecular (non-ionizing) forms, ion pairs of different type and free ions, which are in equilibriums

$$(HX)_s \rightarrow \{(H^+X^-)_s \simeq (H^+//X^-)_s\} \rightarrow H^+{}_s + X^-{}_s$$

This equilibrium can be shifted with the change in concentration of the substance or composition of the solvents and cause strong changes in absorption spectra of compounds [18,19].

It turned out that under conditions of NP-HPLC these equilibriums for the studied substances manifest themselves in the fact, that INH, DPPAH and OH DNBF derivatives are eluated by two peaks

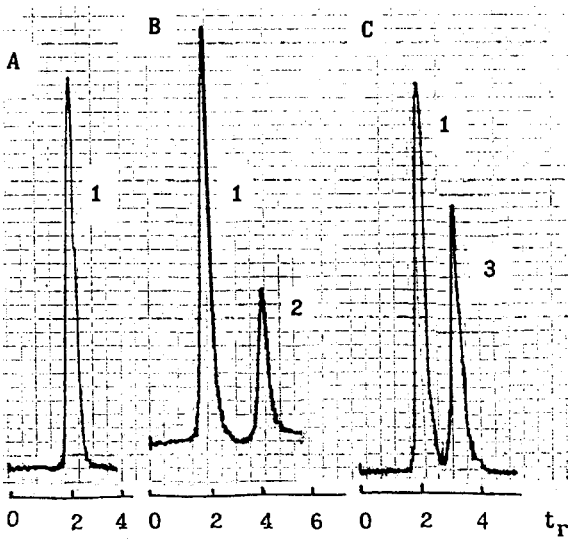

Fig. 4. RP-HPLC chromatograms of blank urine (A), urine with INH (B), urine with DPPAH (C). Column (120 × 2 mm), Silasorb C-18, flow rate 100 mkl min^{-1}. 1-DNBF derivatives of the urine biogenic components, 2-INH derivative (mobile phase CH_3CN-0.03 M acetic buffer (pH 5.5) 25:75 (v/v)), 3-DPPAH derivative (mobile phase CH_3CN-MeOH-0.05 M acetic buffer (pH 5.5) 28:67:5 (v/v)).

(Fig. 2). At this, intensity correlation of the peaks depends on the composition of mobile phase and the solvent, which was used for preparation of the solution of investigated substance and the time of its exposure in the solution. As seen from Fig. 2, peak intensity, corresponding to the part of free ions ($V_r = 6.5$ min), grows with the increase of MeOH content in the mixture. In CH_2Cl_2 the substance is eluated as molecular form. Similar results were obtained in the chromatographic investigation of potassium salts of INH, DPPH and OH DNBF derivatives. With the addition of dibenzo-18-crown-6 to the solution, the equilibrium was shifting to the formation of ions. It allowed us to correlate chromatographic peaks with the corresponding forms of the substance. The above mentioned effects impede the usage of NP-HPLC for determination of INH and DPPH derivatives in biological fluids. Under the same conditions, these effects in RP-HPLC are not observed and the substance is eluated in one peak.

The possibility of spectrophotometric detection of INH (510 nm) and DPPAH (495 nm) in urine was verified with consideration of a complex composition of a biological fluid [20]. The essential biogenic amino containing urine components (urea, uric acid, creatine, creatinine and others) also react with DNBF and form colored derivatives. However, compared to DNBF derivatives of INH and DPPAH the maximums of absorption spectra of these derivatives are shifting [16]. For example, derivatives of aliphatic amino compounds and amino acids have bands with maximum absorption between 410 and 450 nm. It allows us to conduct selective spectrophotometric detection of INH and DPPAH in the presence of these biogenic amines without chromatographic separation. The main INH metabolite (acetylisoniazide, $\lambda_{max} = 430$ nm) and other metabolites do not influence the spectrophotometric detection of drugs.

At the same time, the interaction of DNBF with urine without INH and DPPAH results in the formation of intensive blue–green solution (Fig. 3). The change in pH in 5-6,8 range doesn't influence the intensity of coloring.

As the main biogenic amino containing components of urine do not form derivatives with DNBF absorbing at 480–700 nm, the observed absorption

Table 1
Determination of isoniazide and phosphabenzide in urine

Drugs	Added (μg ml^{-1})	Found (μg ml^{-1})[a]	S_r[b]
Isoniazide	1.30	1.36 ± 0.09	0.05
Isoniazide	3.10	3.28 ± 0.20	0.05
Isoniazide	5.00	4.90 ± 0.24	0.04
Isoniazide	10.25	9.95 ± 0.46	0.04
Isoniazide (patient sample)		4.55 ± 0.28	0.05
Phosphabenzide	2.80	2.87 ± 0.18	0.05
Phosphabenzide	4.25	4.15 ± 0.26	0.05
Phosphabenzide	9.55	9.14 ± 0.45	0.04
Phosphabenzide	14.20	13.95 ± 0.69	0.04
Phosphabenzide (patient sample)		8.25 ± 0.41	0.04

$n = 5$; $P = 0.95$.
[a] Mean ± confidence limit.
[b] Standard deviation.

cannot be regarded as the reaction of a certain component of biosubstrate with the reagent. The absorption spectrum is likely to be due to the effect of cooperative interaction of different components of analyzed matrix with DNBF. The influence of pretreatment of urine on absorption spectra also points out at this. If the urine sample is pretreated by 0.5 ml of 10% trichloroacetic acid, then by DNBF solution and then its pH is returned to the initial level (5.5), the absorption in the range of 480–700 nm completely disappears. This effect is due to the fact that biogenic compounds are bases and nucleophilic properties of amino group decrease as a result of the formation of protonated forms when reacting with trichloroacetic acid. Due

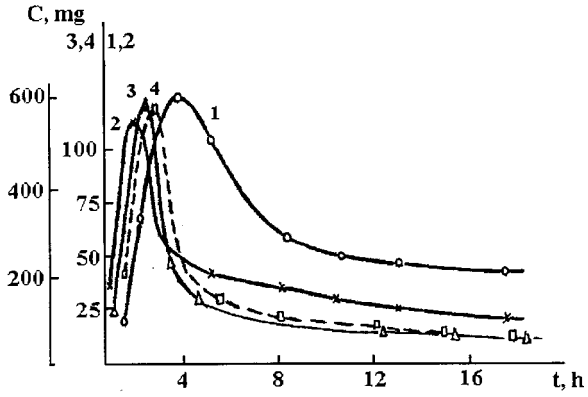

Fig. 5. Pharmacokinetic excretion with urine: 1,2-INH; 3,4-DPPAH.

to the same effect, the analysis of urine not pretreated with trichloroacetic acid under RP-HPLC conditions (mobile phases: mixtures of acetonitrile–water, methanole–water at different pH), does not reveal the separation of biogenic amino compounds (Fig. 4). Hydrolized reagent form OHDNBF which is quickly formed in water medium [21] is eluated with the same biogenic amino derivatives of urine and doesn't impede the determination of INH and DPPAH. At the same time, analyte derivatives are separated from the rest of the components of urine by using mobile phase, containing 25% of acetonitrile, 75% of 0.03 M acetate buffer solution (pH 5.5) for INH and 28% of acetonitrile, 5% of methanole, 67% of 0.05 M acetate buffer solution (pH 5.5) for DPPAH. Such simplification of urine chromatograms after DNBF reaction is greatly advantageous for conducting routine monitoring of drugs in biological substrate.

Comparison of molar absorbance of drug solutions in urine (24200 l mol^{-1} cm^{-1} for DPPAH and 29600 l mol^{-1} cm^{-1} for INH) after DNBF addition and solutions of synthetically isolated derivatives of the same compounds in urine (24800 l mol^{-1} cm^{-1} for DPPAH and 30300 l mol^{-1} cm^{-1} for INH) shows practically complete drug derivatization in urine.

Results of the experimental investigation were used for diagnostics of biotransformation phenotype of drugs by acetylation. For diagnostics, it is necessary to determine a free INH content excreted

Table 2
Parameters INH and DPPAH with urine excretion

Analyte	Time of half excretion ($t_{1/2}$, h)	Amount of excreted dose (%)	Excretion rate constant (1 h^{-1})
INH (fast acetylators, 14 patients)	2.5 ± 0.5	6.5 ± 1.6	0.28 ± 0.06
INH (slow acetylators, 12 patients)	4.5 ± 0.6	16.0 ± 2.4	0.15 ± 0.02
DPPAH (for fast acetylator by INH)	2.9	23.9	0.24
DPPAH (for slow acetylator by INH)	1.4	30.2	0.50

$P = 0.95$.

with human urine within 24 h after peroral administration of 0.4 g of the drug. Fast acetylation takes place if there is less than 10% of original dosage; the higher drug content corresponds to slower acetylation.

Upon investigation of drug stability in urine at 25°C, it was discovered that there is a 60% decrease of free DPPAH and a 52% decrease of INH in the biosubstrate within 10 h, while the 5,7-dinitrobenzofurazan derivative of INH is stable for 5 days. This last fact is very important for routine drug analysis.

The linearity of the method was obtained when analysing urine samples, containing fixed INH (DPPAH) quantities in the concentration ranging from 200 ng ml^{-1} to 150 mg ml^{-1}. The calibration equation for peak height on INH determination is recorded as:

$$H(mm) = Cx(\mu g\ ml^{-1})*9.13 + 1.2\ (r = 0.9987,\ n = 50),$$

for DPPAH as

$$H(mm) = Cx(\mu g\ ml^{-1})*5.04 + 1.1\ (r = 0.9982,\ n = 43).$$

Analytical possibilities of the method are in Table 1.

The limit of INH detection is 0.270 μg ml^{-1} and the one for DPPAH—0.82 μg ml^{-1}.

Excretion curves of INH and DPPAH with urine are presented in Fig. 5. Pharmacokinetic parameters (Table 2) are calculated by INH content in urine of 26 patients. It is seen that parameters have bimodal distribution and differ both in time of half excretion and the quantity of excreted free drug. It allows us to estimate genetically predetermined activity of *N*-acetyltransferaze of separate patients. The level of excreted free INH for slow acetylators is twice higher than for fast acetylators. The difference in time of half excretion and the quantity of excreted drug for the patients of the same group depends on variations of functional condition of the alimentary canal.

The excretion rate of a new DPPAH drug with urine was checked on patients with fast and slow type of acetylation of INH. Comparison of pharmacokinetic parameters shows bigger DPPAH content in urine. For DPPAH the bimodality of rate of drug excretion is less apparent, in contrast with INH metabolism, which takes place with the formation of acetyl derivative. It shows that there is another mechanism of xenobiotic biotransformation.

The influence of such drugs as calcium pantothenate, immunomodulator xymedone on INH acetylation rate was studied. The experimental data show that INH acetylation rate increases greatly during oral administration of these drugs. It is expressed in INH level decrease in urine, which is 40.7% in the case of calcium pantothenate (0.2 g per os), 21.4% in the case of xymedone (1.0 g per os). This effect for calcium pantothenate and pyridoxine hydrochloride has been described earlier [1,4], while the properties of xymedone as *N*-acethyltransferaze inductor are described for the first time. Besides, xymedone shows antimutagene properties as an inhibitor of induced SOS-answer of the cells [22]. Considering this fact, the data obtained in our experiment allow us to use this method for antimutagene screening.

Therefore, we conclude that our method allows us to diagnose biotransformation phenotype of xenobiotics by acetylation rate.

References

[1] I. Szoradi, Pharmacogenetics, Principles and Paediatric Aspects, Akadémiai Kiadó, Budapest, 1984, p. 82.
[2] L.E. Cholodov, V.P. Yakovlev, Clinical Pharmacokinetics, Medicine, Moskow, 1985, pp. 191 (in Russian).
[3] Ian I. Tinsley, Chemical Concepts in pollutant behavior, Mir, Moskow, 1982, pp. 89 (in Russian).
[4] Hooker, K.D., Yost, P.M., in: E.T. Herfindal, D.R. Gourley, L.A. Hart, (Eds.), Clinical Pharmacy and Therapeutics, fifth ed. Williams and Wilkins, Baltimore, 1992, pp. 1098.
[5] Y. Abiko, K. Onaue, Y. Yamamara, I. Nakazona, I. Yoshiga, J. Biochem. 48 (1960) 838.
[6] Ch. Gaitonde, P.V. Pathak, J. Chromatogr. Biomed. Appl. 532 (1990) 418.
[7] Ken-ichi Mawatari, F. Iinuma, M. Watanabe, Anal. Sci. 6 (1990) 515.
[8] M.E. El-Kommos, A.S. Yanni, Analyst 113 (1988) 1091.
[9] C. Andras, Acta Pharm. Hung. 59 (1989) 205.
[10] P.C. Ioannou, Talanta 34 (1987) 857.
[11] G.V. Prochorova, E.A. Osipova, A.R. Barabanova, Zh. Anal. Khim. 45 (1990) 2246.
[12] S.T. Suliman, I.O. Hameed, Anal. Chim. Acta 206 (1988) 379.
[13] M.I. Evgen'ev, I.I. Evgen'eva, N.G. Nikolaeva, N.A. Moskva, F.S. Levinson, B.I. Demchenko, Khim.-Farm. Zh. 25 (1991) 80.
[14] M.I. Evgen'ev, N.G. Nikolaeva, I.I. Evgen'eva, F.S. Levinson, H.C. Budnicov, Zh. Anal. Khim. 47 (1992) 1123.
[15] M.I. Evgen'ev, S.Y. Garmonov, I.I. Evgen'eva, H.C. Budnicov, Talanta 42 (1995) 1465.
[16] M.I. Evgen'ev, S.Y. Garmonov, G.G. Trubnikova, I.I. Evgen'eva, V.I. Pogorel'tsev, V.P. Emelianov, H.C. Budnicov, D.A. Valimuhametova, Khim.-Farm. Zh. 29 (1995) 59.
[17] M.I. Evgen'ev, I.I. Evgen'eva, N.G. Nikolaeva, S.Y. Garmonov, J.D. Samuilov, H.C. Budnicov, Zh. Anal. Khim. 50 (1995) 642.
[18] V.M. Tsentovskij, L.V. Petuchova, M.I. Evgen'ev, Zh. Obsch. Khim. 55 (1984) 679.
[19] V.M. Tsentovsij, M.I. Evgen'ev, I.V. Schulaeva, F.S. Levinson, Zh. Obsch. Khim. 59 (1989) 405.
[20] Y.V. Hmelevskij, O.K. Usatenko, Basic biochemical constants of Human, Zdorovje, Kiev, Ukraine, 1987 (in Russian).
[21] M.I. Evgen'ev, I.I. Evgen'eva, Izv. Vuzov@, Khim. i. Khim. Technol. 37 (1994) 41.
[22] G.V. Czerepnev, Proceeding of the Russian Conference, Mutagenes and Cancerogenes in Environmental, Problems of the Anti-Mutagenesis, Kazan, Russia, May 1996, pp. 36.

ELSEVIER

Talanta 47 (1998) 899–905

Talanta

Influence of interfering dissolved organic matter on the determination of hydrogen peroxide by a colorimetric method based on the peroxidase catalyzed oxidation of *N*,*N*-diethyl-*p*-phenylenediamine

Masami Fukushima *, Kenji Tatsumi

Department of Hydrospheric Environmental Protection, National Institute for Resources and Environment (NIRE), 16-3 Onogawa, Tsukuba 305-8569, Japan

Received 8 December 1997; received in revised form 20 April 1998; accepted 21 April 1998

Abstract

The influence of dissolved organic matter (DOM), such as humic acid (HA) and hydroxybenzoic acids, on the determination of H_2O_2 via a colorimetric method using *N*,*N*-diethyl-*p*-phenylenediamine (DPD) was examined. The influence of DOM on absorbance decay at 551 nm, which represents the wavelength for maximum absorption of the oxidized species of DPD (DPD^+), were investigated in detail. Significant decrease in the absorbance at 551 nm was observed in the presence of HA and gallic acid. This resulted in a fadeout of the purple color of DPD^+, which, in term, created great difficulties in the measurement of H_2O_2 in solutions which contain DOM. To remove DOM prior to the addition of coloring reagents, a diethylaminoethyl Sephadex A-25 ion exchanger was used prior to the analysis for pre-separation. It was found that this pre-separation was useful in the DPD colorimetric determination of H_2O_2 the solution which contain DOM. © 1998 Elsevier Science B.V. All rights reserved.

Keywords: Hydrogen peroxide; DPD colorimetry; Humic acid; Hydroxybenzoic acids

1. Introduction

Hydrogen peroxide (H_2O_2) formation in natural waters is of interest relative to photochemical oxidation of dissolved organic matter (DOM) since the latter involves the generation of H_2O_2 [1,2]. The decomposition of H_2O_2 in natural waters causes the production of hydroxyl radicals, which contribute to the degradation of organic pollutants [3,4]. Therefore, the determination of H_2O_2 in aqueous systems which contain DOM is of crucial importance in our understanding of the fate of organic pollutants in natural waters.

Several methods exist for the analysis of H_2O_2 e.g. electrochemical detection [5–7] and chemiluminescence [8,9]. In addition, a variety of colorimetric methods have been reported [10–14]. It was noteworthy that Barder et al. [13] reported a colorimetric method, based on the peroxidase

* Corresponding author. Tel.: +81 298 588328; fax: +81 298 588308; e-mail: fukusima@nire.go.jp

0039-9140/98/$ - see front matter © 1998 Elsevier Science B.V. All rights reserved.
PII S0039-9140(98)00178-7

(POD) catalyzed oxidation of *N*,*N*-diethyl-*p*-phenylenediamine (DPD), in which the purple color of the oxidized species of DPD (DPD^+) was used for the detection of H_2O_2. Because of the high absorption coefficient ($\varepsilon = 21{,}000$ at 551 nm), H_2O_2 could be detected in a variety of water samples, such as lake waters at the ppb level [13]. However, Zepp et al. [14] pointed out that some DOM species, such as humic substances, interfered with the determination as the result of the peroxidase catalyzed oxidation of trialylmethane derivatives. Although Barder et al. [13] also commented on the influence of DOM as it affects the calibration factor for the DPD method, detailed data were not presented in their reports. In fact, when we determined H_2O_2 in solutions which contained several-tens ppm of humic substances using the DPD method, H_2O_2 could not be determined because of a remarkable fadeout of the DPD^+ chromophore. As a result, it is necessary to obtain detailed information relative to the influence of DOM on the color stability of DPD^+ as well as methods for preventing interference by DOM. However, the specific reasons for why DOM interfere with the colorimetric determination of H_2O_2 based on the peroxidase catalyzed oxidation remain unknown. In addition, the magnitude of this interference by DOM, such as humic substances, also remains unknown. In studies involving $KMnO_4$ degradation and gas chromatography, a variety of hydroxybenzoic acids, such as salicylic and gallic acids, have been identified as structural components of humic substances [15,16]. This paper describes an investigation of the influence of DOM, such as humic substances and hydroxybenzoic acids, on the determination of H_2O_2 using the DPD colorimetric method.

2. Experimental

2.1. Reagents and materials

An aqueous solution of H_2O_2 (31%, Wako Pure Chemicals) was diluted with pure water to the required concentration, which was then calibrated by titration with $KMnO_4$. *N*,*N*-diethyl-*p*-phenylenediammonium sulfate (DPD) (0.1 g) (Wako Pure Chemicals) was dissolved in 10 ml of a solution of 0.1 M H_2SO_4. An aqueous solution of horseradish peroxidase (POD) was prepared by dissolving 10 mg POD in 10 ml of pure water. This solution was stored at 5°C and replaced with a fresh solution at weekly intervals. The hydroxybenzoic acids used in this study were gallic acid (GA), 3,5-dihydroxylbenzoic acid (DHBA) and *m*-hydroxylbenzoic acid (HBA) (Tokyo Kasei Ltd). A diethylaminoethyl Sephadex A-25 (A-25) (Pharmacia LKB Biochemistry) ion exchanger was used for the pre-separation of DOM. One milliliter of the resin was packed into a polypropylene mini-column (Bio-Rad). A humic acid fraction (HA) was extracted from Bibai peat soil (Hokkaido, Japan) according to the protocol described by the International Humic Substances Society (IHSS) [17]. The pH of the alkaline extract (0.1 M NaOH) was adjusted to below pH 1 with dilute HCl. The resulting precipitated fraction was separated by centrifugation, and dialyzed against distilled water. The HA was obtained as a powder by lyophylization. The elemental composition of the preparation was: C 57.3, H 5.7, N 2.9, and O 34.1%.

2.2. Preparation of the test solutions

The purpose of the study was to investigate the behavior of the photosensitized generation of H_2O_2 in the presence of DOM. Therefore, the test solutions which contained the DOM were irradiated prior to use. A total of 15 ml of the solution (pH 4 adjusted with 0.05 M phosphate buffer), containing GA or HA, were pipetted into a quartz cuvette ($10 \times 24 \times 40$ mm), and the solution subjected to light irradiation using a 500 W Xenon short arc lamp (Ushio Denki, KK) in conjunction with a quartz filter. A UV-29 and UV-31 quartz filter (Toshiba Glass), which removed light below 290 or 310 nm, was used for this purpose. Oxygen gas, which was first passed through pure water, was bubbled into the solution during the light irradiation. The temperature of the solution was maintained at 25 ± 1°C. In order to remove DOC prior to the addition of the chromophore reagents, the test solution was passed through the

A-25 ion exchange column and the effluent was then used for the determination of H_2O_2.

2.3. Procedures

A 5 ml aliquot of the test solution was pipetted into a 10-ml test tube, and then mixed with 500 μl of 0.5-M phosphate buffer (pH 6). A 50 μl of the DPD solution was then added, followed by 50 μl of the POD solution and the solution was then vigorously mixed. The absorbance at 551 nm was measured using a Jasco V-550 type spectrophotometer (Japan Spectroscopic Co.) with a quartz cell (1×1 cm) after 40 ± 5 s.

The absorbance decay at 551 nm was observed by using the kinetic program supplied with the spectrophotometer. A 3 ml aliquot of a solution, containing 10 μM H_2O_2 and DOM, was pipetted into the quartz cell, which contained a micro-magnetic stirring bar. After adding the DPD and POD, absorbance at 551 nm was continuously monitored over a period of 300 s.

The time-dependent variation of the absorption spectra of DPD was also observed. A 3 ml aliquot of the solution, containing 10 μM H_2O_2, 10 mg l^{-1} POD and DPD, was pipetted into the quartz cell, and the absorption spectrum was measured in the range of 600–220 nm. Subsequently, after adding 30 μl of 0.01 M GA to the quartz cell, the UV-VIS absorption spectra were measured at 30 s intervals at a wavelength scan rate of 4000 nm min^{-1}.

3. Results and discussion

3.1. Influence of DOM on the absorbance at 551 nm

The test solutions used in the present work contain a variety of DOM, such as humic substances and hydroxybenzoic acids, since the calibration factor for the DPD method may be affected by such contaminants. Since the degree of the interference by DOM has not been described, we initially investigated the degree of the interference by measuring the absorbance decay at 551 nm in the presence of DOM, such as HA and hydroxybenzoic acids. Fig. 1 shows the influence of the presence of HA, GA, DHBA and HBA on the absorbance decay at 551 nm. In the absence of DOM, the absorbance at 551 nm was rapidly increased up to 25 s and then maintained plateau for a period of 300 s. In the presence of HA, the rate of the absorbance decay increased with increasing HA concentration (Fig. 1a). For the case of hydroxybenzoic acids (Fig. 1b), a decrease in absorbance was not observed, but absorbance decay was observed in the presence of 10 μM GA and DHBA. These results indicate that the presence of contaminants such as HA, DHBA and GA are capable of causing a fadeout of the color of DPD^+.

In order to clarify the reasons for why the color of DPD^+ faded in the presence of DOM, the

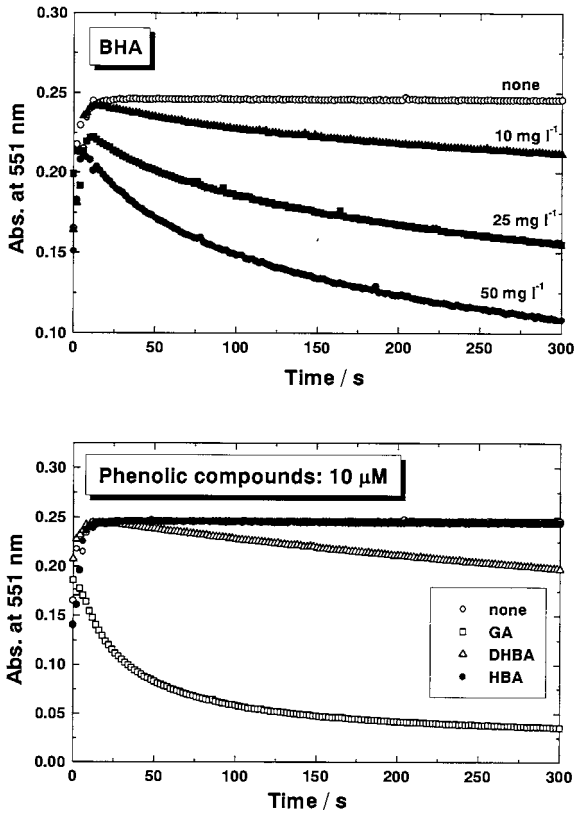

Fig. 1. Influence of HA (a) and hydroxybenzoic acids (b) on the absorbance decay at 551 nm. Hydroxybenzoic acids: 10 μM; pH: 6.0 (0.05 M phosphate buffer); DPD: 0.1 g l^{-1}; POD: 10 mg l^{-1}; 25°C.

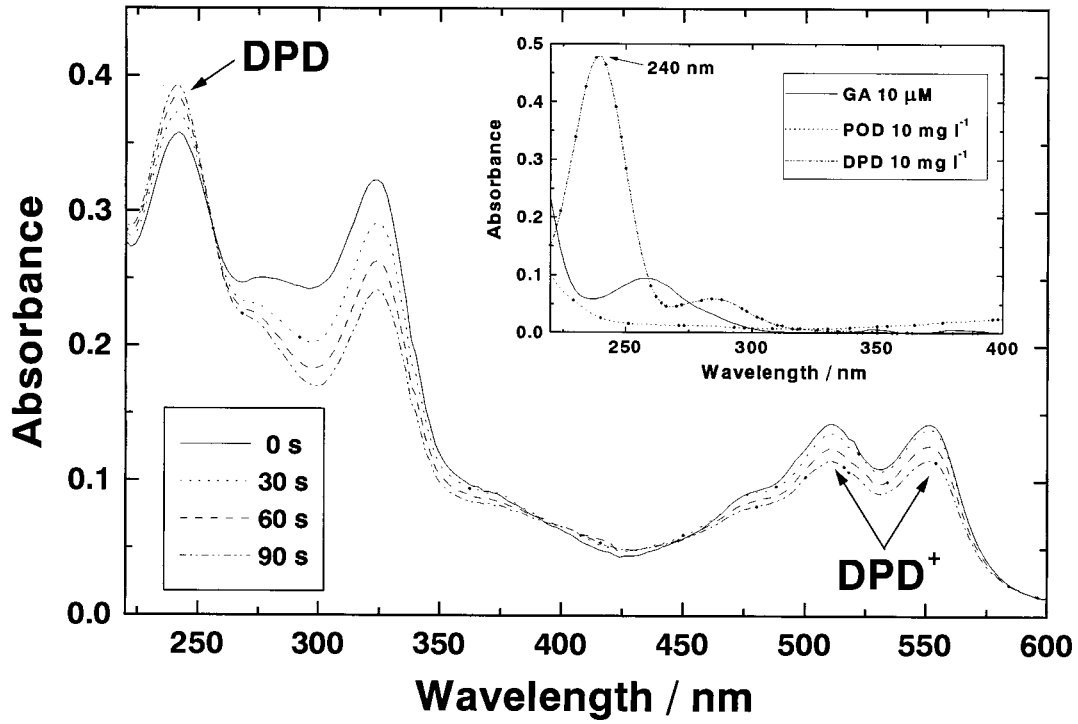

Fig. 2. Time-dependent variation of the UV-VIS absorption spectra of DPD in the presence of GA. pH: 6.0 (0.05 M phosphate buffer); POD: 10 mg l^{-1}; DPD: 10 mg l^{-1}; GA: 10 μM, 25°C. Insertion figure shows the absorption spectra of DPD, POD and GA, respectively.

UV-VIS absorption spectra of DPD, in the presence of 10 μM H_2O_2 and 10 mg l^{-1} POD, in the range 600–220 nm were determined (Fig. 2). In the absence of GA, four peaks at 551, 510, 324 and 240 nm were observed. The insert in Fig. 2 shows the spectrum for DPD without H_2O_2 and POD. This spectrum has a major peak at 240 nm, which represents the reduced species of DPD. Therefore, the peaks at 551, 510 and 324 nm can be assigned to DPD^+ (the oxidized form) by comparison of the spectra of DPD in Fig. 2 with that in the insert. In Fig. 2, the absorbance values at 551, 510 and 324 nm were decreased with time after the addition of GA, but the peak at 240 nm, which represents the reduced DPD, increased. These results show that the color of DPD^+ fades as a result of the addition of GA, and that the level of reduced DPD is increased. This can be attributed that DPD^+ is reduced in parallel with the oxidation of GA. Moreover, in our previous work [18], the oxidation reaction of GA was confirmed by NMR spectroscopy as shown below:

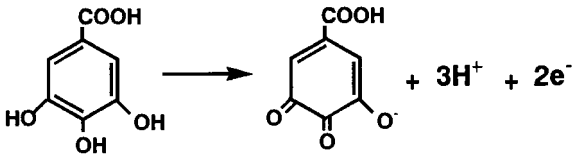

Hence, the series of reactions, which account for the fadeout of color of DPD^+ in the presence of GA, can be represented as Scheme 1.

It is therefore concluded that the fadeout of color of DPD^+ is due to the reduction of DPD^+ by GA. As shown in Fig. 1, the rate of fadeout in the presence of HA and GA was very rapid. This

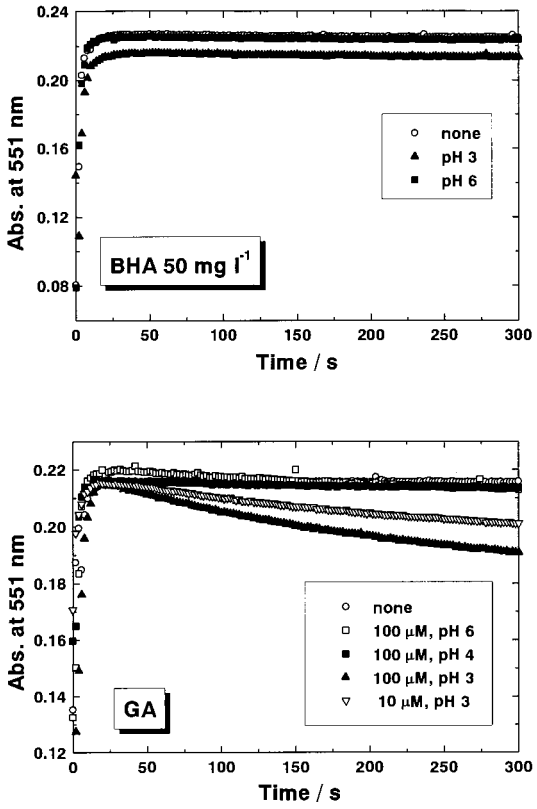

Fig. 3. Effect of pre-separation by the A-25 column on the absorbance decay at 551 nm. pH: 6.0 (0.05 M phosphate buffer); DPD: 0.1 g l^{-1}; POD: 10 mg l^{-1}; 25°C.

poses a serious problem for the determination of H_2O_2 by the DPD colorimetric method.

3.2. Removal of DOM by an anion-exchanger

The rapid fadeout of the color of DPD^+ is inconvenient for the precise determination of H_2O_2 with the DPD method and DOM, such as HA and hydroxybenzoic acids, represent interfering concomitants for this determination. One of the methods for preventing such interference is the removal of DOM prior to the addition of coloring reagents. In order to remove DOM, we examined the use of an anion-exchanger, A-25, which has been successfully used for the separation of a variety of low-molecular-weight organic acids, such as amino acids, citric acid and tannic acid, as well as humic substances in natural waters [19–22].

When an aqueous solution of H_2O_2 without DOM (10 μM, pH 4) was passed through the A-25 column, the absorbance at 551 nm was unchnged. This shows that H_2O_2 is not adsorbed on the A-25 resin, and that the use of the A-25 column is suitable for the pre-separation of DOM. Fig. 3 shows the effects of pre-separation by the A-25 column on absorbance decay. In the case of HA, the absorbance at pH 3 was slightly lower than the samples without HA and at pH 6.

Scheme I

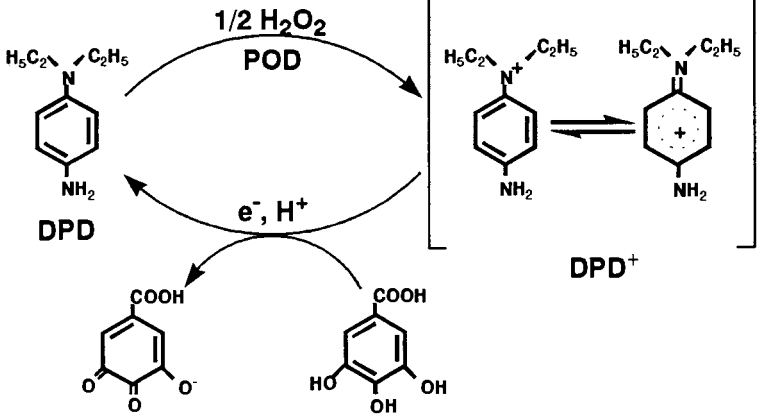

Scheme 1.

This can be attributed to the inefficient uptake of HA on the A-25 column because of its weak negative charge. The majority of the carboxy groups in HA are undissociated at pH 3. In the presence of 10 and 100 μM GA, an absorbance decay was observed at pH 3. However, no absorbance decay was observed at pH 4 and 6. Since it is known that the pK_a value of carboxy groups of GA is 4.4 [23], a negatively charged species can be obtained in sufficient quantities only at higher pH. Therefore, pre-separation by the A-25 column must be carried out at higher pH values, in which the carboxy groups are sufficiently dissociated. As a result, the pH of the test solution was adjusted at pH 6, which was sufficient to obtain negatively charged HA or hydroxybenzoic acids, by using 0.05 M phosphate buffer prior to the pre-separation.

3.3. Determination of H_2O_2 in the test solutions containing HA or hydroxybenzoic acids

The pre-separation of DOM by the A-25 column was then applied to the determination of H_2O_2 in the test solutions, which were prepared by UV irradiation. Fig. 4 shows the standard curves for the DPD method. For the case of pure water (Fig. 4a), the relative standard deviation (RSD) for five replications, using 10.7 μM H_2O_2 was within 1%. A straight line was obtained up to 16 μM H_2O_2 (slope 0.0205, $r = 0.999_8$). The absorption coefficient (ε) calculated from the slope ($20\,500 \pm 200$) is in good agreement with that of the literature ($21\,000 \pm 500$) [13].

Fig. 4b shows a standard addition plot in the presence of GA, in which it was not separated by the A-25 column. In this case, since the fadeout of the DPD^+ color as a result of GA was dramatic, considerably smaller absorbance values were observed for all data points. Moreover, a linear relationship between absorbance and H_2O_2 concentration could not be obtained ($r = 0.779_1$). Thus, H_2O_2 in the sample solution could not be determined by the standard addition method without the separation of GA. However, a linear relationship was obtained by the adoption of the pre-separation technique ($r = 0.999_5$) (Fig. 4c), and the slope (0.0209) was in good agreement with that for the case of pure water (0.0205). This shows that pre-separation using an A-25 column is useful for the DPD colorimetric determination of H_2O_2 for test solutions containing GA.

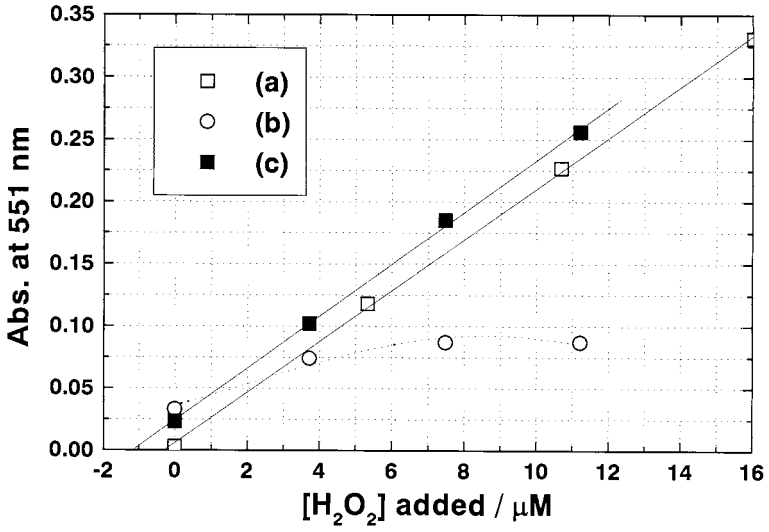

Fig. 4. Comparison of standard addition curves with and without pre-separation by the A-25 column. (a) without GA (b) with 10 μM GA before pre-separation (c) with 10 μM GA after pre-separation. Wavelength range of light irradiation: 290 nm <, light irradiation time: 90 min; pH 4.0 (0.05 M phosphate buffer).

Table 1
Determination of H_2O_2 generated in the sample solution after the light irradiation

Samples (concentration)	Wavelength range for irradiation (irradiation time)	$[H_2O_2]$ generated μM ($n = 4$)	
		Standard addition	Calibration
GA (10 μM)	290 nm<(1.5 h)	2.6 ± 0.3	2.9 ± 0.4
DHBA (100 μM)	290 nm<(1.0 h)	30 ± 3	27 ± 3
HA (50 mg l^{-1})	310 nm<(3.0 h)	37 ± 3	32 ± 5
HA (10 mg l^{-1})[a]	310 nm<(2.5 h)	16 ± 3	14 ± 4

[a] Fe(III) (10 μM) was added.

Table 1 shows comparisons of the analytical values between the calibration curve method and the standard addition method for a variety of test solutions. In this case, the DPD colorimetric determinations of H_2O_2 were carried out after pre-separation by the A-25 column. In Table 1, the measurement values obtained by the standard addition method were in good agreement with those obtained by the calibration curve method. This shows that pre-separation by the A-25 column is suitable for the DPD colorimetric determination of H_2O_2 in solutions which contain DOM.

For the case of an HA solution containing 10 μM Fe(III) ion, 1 mM ethylenediaminetetraacetic acid (EDTA) was added as a masking agent in a study reported by Voelker and Sulzberger [24]. Although the presence of Fe(III) brought about coloring prior to the addition of POD, this was preventable by the addition of EDTA. We also investigated the influence of Fe(III) and found that the presence of 100 μM Fe(III) caused a positive error ($< 5\%$) for 10 μM H_2O_2. It was therefore concluded that, although interference by Fe(III) was observed, this error was not significant.

The determination of H_2O_2 in solutions containing DOM is difficult because the color of DPD^+ faded rapidly. However, the precise determination of H_2O_2 by the DPD method can be carried out after pre-separation of DOM using an A-25 column.

References

[1] W.J. Cooper, R.G. Zika, Science (Washington, DC) 220 (1983) 711.
[2] R.G. Zepp, A.M. Braum, J. Hoigné, J.A. Leenheer, Environ. Sci. Technol. 21 (1987) 485.
[3] C.-H. Liao, M.D. Gurol, Environ. Sci. Technol. 29 (1995) 3007.
[4] S.H. Lin, C.C. Lo, Water Res. 31 (1997) 2050–2056.
[5] H. Lundbäck, G. Johansson, Anal. Chim. Acta 128 (1981) 141.
[6] J.E. Harr, Anal. Chem. 35 (1963) 893.
[7] R.J. Kieber, G.R. Helz, Anal. Chem. 58 (1986) 2312.
[8] A.L. Lazrus, G.L. Kok, S.N. Gitlin, J.A. Lind, S.E. McLaren, Anal. Chem. 57 (1985) 917.
[9] G.L. Kok, K. Thompson, A.L. Lazrus, S.E. McLaren, Anal. Chem. 58 (1986) 1192.
[10] A.O. Allen, C.J. Hochanadel, J.A. Ghormley, T.W. Davis, J. Phys. Chem. 56 (1952) 575.
[11] H.A. Mottala, B.E. Simpson, G. Gorin, Anal. Chem. 42 (1970) 410.
[12] J.E. Frew, P. Jones, G. Scholes, Anal. Chim. Acta 155 (1983) 139.
[13] H. Bader, V. Sturzenegger, J. Hoigné, Water Res. 22 (1988) 1109.
[14] R.G. Zepp, Y.I. Skurlatov, L.F. Rittmiller, Environ. Technol. Lett. 9 (1988) 287.
[15] M. Schnitzer, S.U. Kahn, Humic Substances in the Environment, Marcel Dekker, New York, 1972, pp. 137–201.
[16] L.B. Sonnenberg, J.D. Johnson, R.F. Christman, in: I. H. Suffet, P. MacCarthy (Eds.), Aquatic Humic Substances: Influence on Fate and Treatment of Pollutants, American Chemical Society, Washington, DC, 1989, pp. 1–23.
[17] International Humic Substances Society (IHSS), Outline of Extraction Procedures, 1982.
[18] M. Fukushima, K. Tatsumi, Toxic. Environ. Chem. (in press).
[19] M. Hiraide, S.P. Tillekeratne, K. Otsuka, A. Mizuike, Anal. Chim. Acta 172 (1985) 215.
[20] M. Hiraide, M. Ishi, A. Mizuike, Anal. Sci. 4 (1988) 605.
[21] M. Taga, S. Tanaka, M. Fukushima, Anal. Sci. 5 (1989) 597.
[22] M. Taga, S. Tanaka, M. Fukushima, Anal. Sci. 6 (1990) 455.
[23] D.D. Perrin, Stability Constants of Metal-Ion Complexes Part B, Pergamon Press, New York, 1979, p. 511.
[24] B.M. Voelker, B. Sulzberger, Environ. Sci. Technol. 20 (1996) 1106.

ELSEVIER

Talanta 47 (1998) 907–919

Talanta

Laser-induced fluorescence of pyrene and other polycyclic aromatic hydrocarbons (PAH) in seawater

Steven M. Rudnick *, Robert F. Chen

Environmental Coastal and Ocean Sciences Program, University of Massachusetts Boston, Boston, MA 02125, USA

Received 20 January 1998; received in revised form 13 April 1998; accepted 21 April 1998

Abstract

Polycyclic aromatic hydrocarbons (PAH) in the marine environment are currently of great concern due to their potential carcinogenicity. The standard methods of detection and quantification of PAH in seawater and sediments are costly, time-consuming and do not account for the heterogeneous nature of their distribution and sources. Laser-induced, time-resolved fluorescence spectroscopy may help to overcome these limitations. Several PAH have relatively long-lived stimulated fluorescence emissions, which allow them to be detected among a background of more intense but shorter-lived chromophores. Using time-delayed techniques we have shown an ability to detect PAH, principally pyrene, at environmental levels (ng l^{-1}) both in the laboratory and in situ in Boston Harbor and other study areas. Further development may lead to the rapid determination of several PAH in typical near-shore marine environments. © 1998 Elsevier Science B.V. All rights reserved.

Keywords: PAH; Fluorescence; Spectroscopy; Boston Harbor; Marine

1. Introduction

Polycyclic aromatic hydrocarbons (PAH) in the environment have long been suspected to be human carcinogens [1]. While there is strong evidence linking airborne PAH with various cancers [2,3] and while several PAH mixtures (e.g. shale-oils and soots) and exposure circumstances (e.g. aluminum and coke production) have been determined to be carcinogenic to humans [4], only a few individual PAH have been listed as probable (not definite) human carcinogens. Furthermore, the relationship between PAH in aqueous media and carcinogenicity is less well-established [5]. Nevertheless, the Environmental Protection Agency (EPA) determined in the 1980 Document Ambient Water Quality Criteria for Polynuclear Aromatic Hydrocarbons that there was sufficient concern to promulgate a standard of 311 ng l^{-1} for total PAH in surface water. Levels of PAH close to and exceeding this level have been found in estuarine waters [6–9].

Recent efforts by the EPA have been aimed at establishing sediment quality criteria in an effort to further reduce human exposure to PAH, espe-

* Corresponding author. Tel.: +1 617 2877440; fax: +1 617 2877474; e-mail: 7001srudn@umbsky.cc.umb.edu

0039-9140/98/$ - see front matter © 1998 Elsevier Science B.V. All rights reserved.
PII S0039-9140(98)00160-X

cially via ingestion of shellfish. Sediments may be a significant source of PAH to the overlying water column particularly in areas where historical PAH input to the sediments has been high [10–12]. Such fluxes are determined in part by the availability of PAH to partition into porewater and thus exchange into overlying waters [11,13]. Because some of the PAH in sediments are not readily available to partition (i.e. PAH associated with soot) and are therefore not bioavailable [14], measuring the PAH in the overlying water may provide a better indication of exposure of marine organisms to PAH than discrete sediment sampling. Also, the distribution of PAH in the sediments may be quite heterogeneous and small numbers of samples may not provide a representative distribution [15,16] while overlying water measurements can be made much more extensively in a short period of time. Previous studies have also shown that dissolved PAH comprise 70–90% of the total PAH (dissolved plus particulate) in estuarine regions [9,17,18]. Because particle bound PAH may not be as bioavailable, and because particle bound PAH is significantly quenched [11], water column PAH fluorescence may be a particularly good measure of bioavailable PAH.

Relatively few investigations of PAH levels in the marine water column have been undertaken. This may be a consequence of generally low levels of PAH in the marine water column (ng l^{-1} or less) and the time-consuming protocols, usually gas chromatography (GC) or gas chromatography–mass spectrometry (GC–MS), necessary to quantify their presence. Ultra-violet fluorescence has been used to determine the presence of fossil fuel components in the water column. Erhardt and Knap [19] describe the use of fluorescence for detecting oil residues in solvent extracted samples; Katz et al. [8] describe a bulk fluorescence technique for total PAH at 50 μg l^{-1} concentrations; Carr and Harris [20] showed sub-ng l^{-1} detection limits using preconcentration on silica; and Eastwood et al. [21] describe a field spectrofluorometer using extraction and synchronous fluorescence to determine PAH in oils at environmental levels (<1 mg l^{-1}). The system upon which this work builds was first used by Lieberman et al. [22] to detect petroleum hydrocarbons in seawater. We extend that work by detecting and quantifying specific PAH.

In situ measurement of organic substances in the marine water column is possible by using a laser as the source of UV stimulation and optical fibers to deliver the radiation and return the induced emission. The major optical interference with the fluorescence determination of PAH in the marine environment is the fluorescence of dissolved humic substances. The concentration of humics is typically three to four orders of magnitude greater than that of PAH. Humic substances have comparatively short fluorescence lifetimes (the time required for a bulk fluorescence signal to decay to $1/e$ of its initial amplitude). Using a single exponential to fit the data, Milne found a lifetime of <4 ns for humic substances [23]. Later work using a multi-component model found dominant lifetime components in humic substances of 1–3, and 6–8 ns. The fluorescence quantum efficiency of humic substances is relatively low, typically about 0.1% [24]. PAH have fluorescence lifetimes of 4–130 ns in seawater [25] and fluorescence quantum efficiencies in the range of 5–50% when excited by specific wavelengths. In addition, many of the PAH have distinctive wavelength emission signatures that occur in the range of 360–420 nm while the humic substances tend to have broad, less well-defined spectra with peaks in the 430–530 nm range [26]. By time gating the fluorescent measurement, spectral signatures of substances such as PAH with much longer fluorescent lifetimes, but which are usually masked by the large humics signal, can be studied [27–32]. A pulsed nitrogen laser with a narrow pulse width (600 ps) is used as an excitation source allowing deconvolution of ns response signals. This work combines a state-of-the-art, time-resolved, laser-induced fluorescence system with a data analysis method to detect and quantify PAH at ambient levels in seawater at significantly improved levels of detection compared with previous works. While the majority of PAH in coastal waters is of pyrolytic origin [33,34], specific point sources and spill sources of petrogenic PAH can be readily identified with this system. This is discussed in the conclusions.

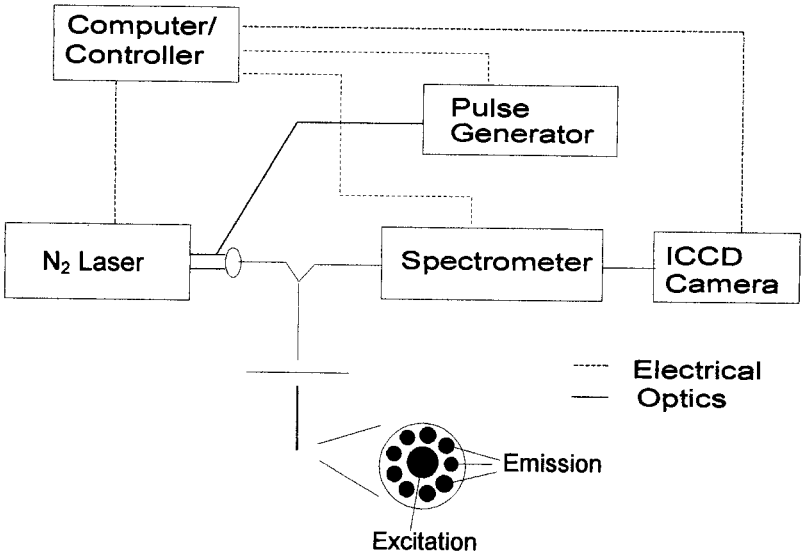

Fig. 1. Schematic representation of the time-resolved, laser-induced fluorescence (LIF) system as deployed in situ.

2. Experimental section

2.1. System description

We have developed a time-resolved, laser-induced fluorescence spectrometer system (Fig. 1) capable of detecting PAH in situ in the presence of natural fluorophores. The system consists of a pulsed nitrogen laser ($\lambda = 337$ nm, 600 ps pulse width, 1.3 mJ pulse^{-1}, Photon Technology, Model PL2300) lens focused onto a 400 mm diameter silica clad silica optical delivery fiber. The collection fibers, a concentric ring of 9×200 mm diameter fibers at the sensor end, (Fig. 1), deliver the emission radiation in a slit geometry to a 1/4-m imaging spectrograph (SPEX, Model 270M) whose output is focused on the input lens of a gated, intensified 1024×256 pixel charge-coupled camera (Princeton, Model ICCD-1024). The camera is thermo-electrically cooled and controlled by a Princeton Instruments Model ST130 controller and CSMA software. A Princeton Instruments Model PG-200 time delay unit controls the time gating. The trigger signal for the time gating is derived from a 100 μm diameter fiber placed directly in the laser beam before the focusing lens and routed to the optical trigger on the delay unit. Time delays of 0, 2, 4, 8, 16, 32, 64 and 128 ns were routinely used for these studies.

The fiber cable that has been used for these investigations is 22 m long, for a total optical path length of 44 m. Silica fiber has an index of refraction of 1.48 at 337 nm, which results in a theoretical down and back propagation time of about 218 ns. Subtracting the trigger propagation time of about 3 ns, a delay of about 215 ns is required to turn on the camera just at the leading edge of the response (scattered laser light and induced fluorescence). Some variation in timing has been noted as a result of temperature variations of the trigger unit during field deployments. The optical fibers disperse the laser pulse and the emission signal so that both have a Gaussian shaped spreading centered at approximately 2 ns for a 22-m fiber. The spreading in the excitation fiber is due to different path lengths through the fiber (0.4 ns) and the spreading in the emission fiber is due both to this effect (0.4 ns) and to the spectral dispersion from the fiber's wavelength dependent index of refraction (1.1 ns difference in transit time between 350 and 550 nm light for this fiber). This spreading is of little consequence when measuring PAH with long fluorescence decay times but can give an incorrect estimate of the

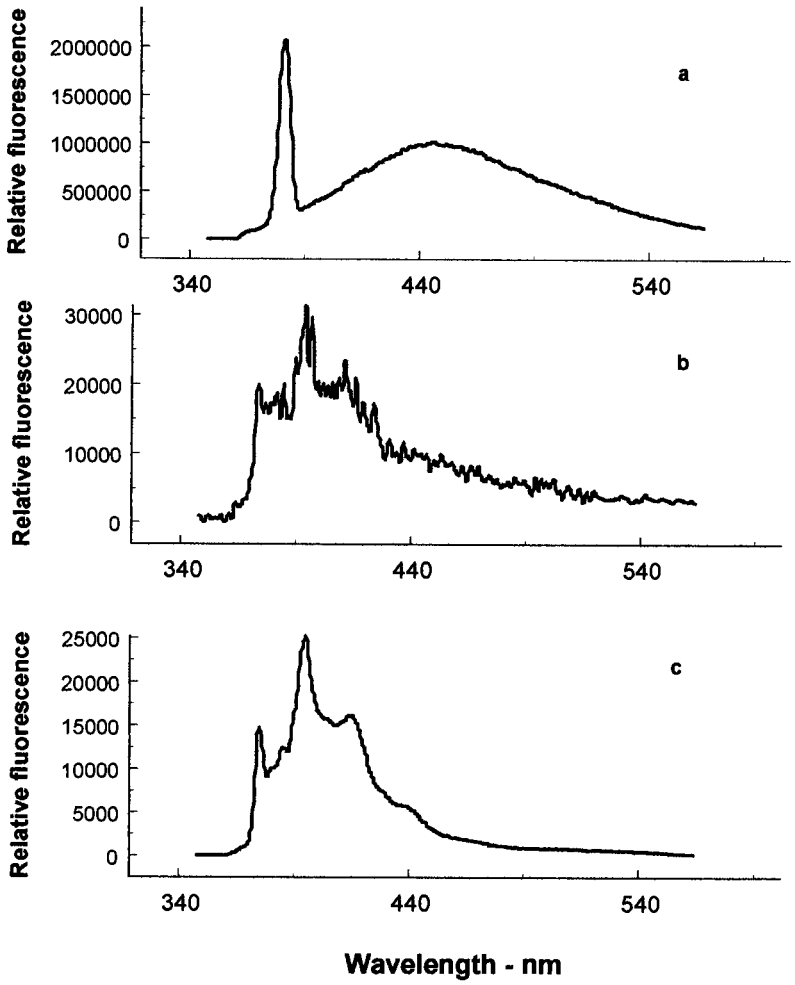

Fig. 2. (a) Seawater plus 100 ng l^{-1} pyrene 0 ns delay. The peak at 381 nm is the Raman scattering signal of water. (b) 64 ns delayed signal. (c) Pure pyrene in water (10 μg l^{-1} scaled to 100 ng l^{-1}) at 64 ns delay.

lifetime of fast fluorophores such as humic substances and some PAH. A similar timing consideration applies to the amplitude of the detected signals as a function of the base delay of the system. A 1 ns shift of the base delay can cause a 20% change in the response to humics fluorescence (assuming a 4 ns lifetime) while affecting longer-lived fluorophores such as quinine sulfate (16 ns decay) by only a few percent. During system operation, these effects can be minimized by periodically adjusting the timing to obtain a consistent Raman amplitude and normalizing the amplitude of the detected signals to a relatively long decay time standards such as pyrene or quinine sulfate. The exponential decays can be correctly estimated by examining the successive time frames.

The width of the pulse that gates the camera intensifier has a major effect on the fluorescence that is recorded. While the start of the gate signals allows discrimination against short time decay fluorophores, a short gate width reduces the response to long-lived fluorophores. A gate width of 50 ns was used for most of our investigations since we were most interested in the longer-lived fluorophores. For some investigations, however,

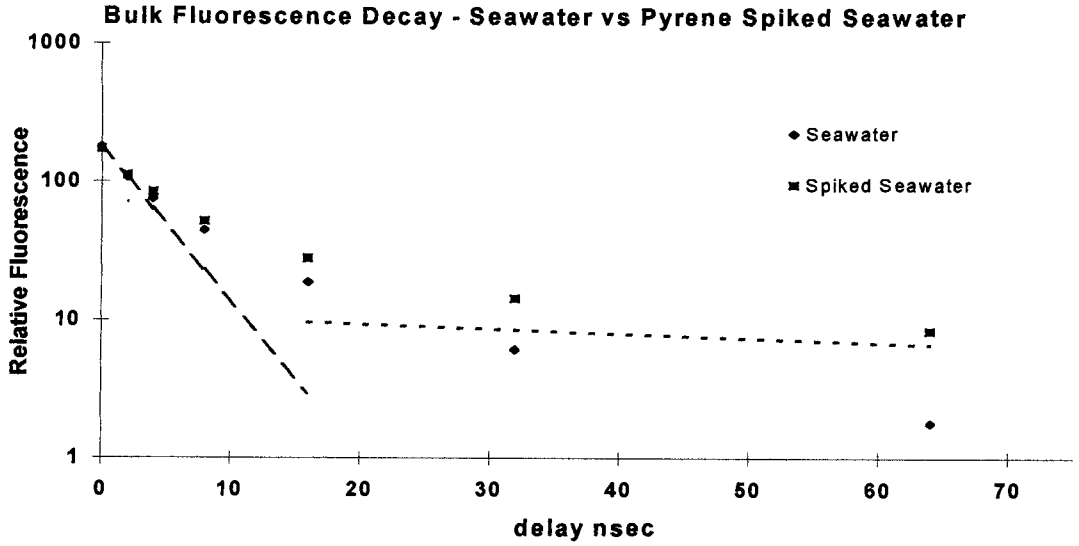

Fig. 3. Logarithmic decay characteristics of seawater and pyrene in Fig. 2. Multiple decay constants are implied by the curvature of the graph. The pyrene decay constant dominates at long delays for the spiked sample. See text for discussion of lines.

where we were interested in relative bulk decay time constants, this was shortened to 20 ns. Each complete sample is the sum of the fluorescence responses to 50 pulses from the laser. The CCD is read after each pulse and summation is performed in software.

The optical setup provided a spectral display of emission fluorescence from 350 to 550 nm with a resolution of approximately 0.3 nm. The data is extracted from the CSMA files to a flat ASCII format using a C-program written by the authors. This allows calculation and presentation in a variety of programs and formats.

Table 1
PAH parameters and system limits of detection

Compound	Sol.[a]	Abs.[b]	TC ns[c]	LOD[d]
Phenanthrene	640	0.015	16	900
Fluoranthene	250[e]	0.71	32	50
Pyrene	132	5.5	128	8
Anthracene	23	0.60	4.0	6000

[a] Solubility in seawater, mg l^{-1}.
[b] Molar absorption coefficient at 337 nm l mol^{-1} cm^{-1} 10^{-4} [46].
[c] Fluorescence lifetime [25]. Phenanthrene is from this work.
[d] System limit of detection, ng l^{-1}.
[e] Fluoranthene value is in fresh water [5].

At the start of each series of investigations, usually once each day, a complete time-resolved set of spectra was acquired for milli-q water, quinine sulfate, and 4 PAH standards: pyrene, anthracene, phenanthrene, and fluoranthene (Sigma). This was done both for laboratory and field studies. PAH standards were prepared in GC grade ethanol (Burdick and Jackson) to provide stock solutions of approximately 10 mg l^{-1}. These solutions were further diluted in milli-q water to prepare working standards of 10 μg l^{-1} for pyrene, fluoranthene and anthracene and 100 μg l^{-1} for phenanthrene. By adjusting the spectral position to the Raman peak at 381 nm and the amplitude to the pyrene response, we were able to standardize our investigations against changes in field conditions and instrument response. Small volumes (1–100 μl $^{-1}$) of the stock solutions were added to seawater to generate training sets for principal component regression. Replicated runs consistently indicate a short-term variability of ± 5% of nominal values for any sample. This may be due to laser power variations or intensifier noise. All field and laboratory data presented below from our laser-induced fluorescence (LIF) system have implied error bars of this magnitude.

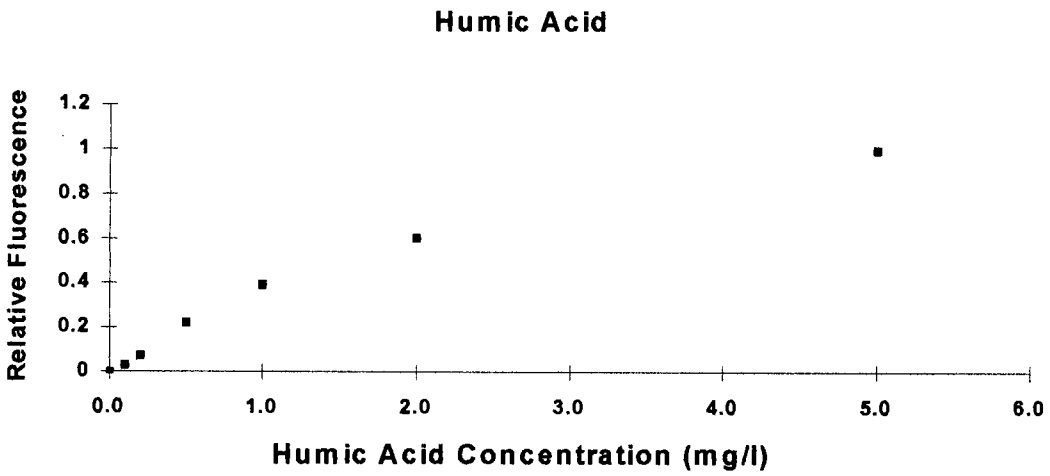

Fig. 4. Fluorescence of IHSS Suwannee River humic acids vs. concentration. A non-linear response indicates an inner filter effect. The curve is normalized to maximum fluorescence.

2.2. Laboratory studies

Laboratory fluorescence investigations were conducted with the fiber optic probe held in a silicone rubber stopper at the top of amber bottles with capacities of 250 ml or greater. Clear bottles or smaller bottles can create problems as a result of fluorescence of the glass, fluorescence of materials outside the bottle, and reflections.

Seawater samples were collected in 4-l amber bottles and their fluorescence determined by our LIF system. The samples were then filtered through precombusted (4 h at 350°C) 0.7 μm glass fiber filters, and their fluorescence was again determined by the LIF system. Filtered and unfiltered samples show little difference ($< 5\%$ in peak amplitude) for our estuarine, samples suggesting that filterable particles have little effect on the fluorescence signal. We would expect some fluorescence quenching due to colloids, particles with diameters less than 10 μm, to occur in both the filtered and unfiltered samples [35,36] and we discuss this effect below. An internal standard of 4 μg of dihydroanthracene (Sigma) from a 10 mg l^{-1} stock solution prepared as above, was added to the 4-l samples which were then extracted using dichloromethane (DCM) (Burdick and Jackson Company; $50 + 25 + 25$ ml l^{-1}). The 400-ml extracts were concentrated to near dryness with a rotary evaporator, dried under nitrogen and reconstituted with 100 μl of hexane (Burdick and Jackson). No additional cleanup steps were performed. The residual seawater fluorescence for each sample was determined with the LIF system.

Gas chromatography–mass spectroscopy determinations were performed on a Finnigan 4510B GC–MS (30 m $\times$ 0.25 mm I.D., 25 mm film thickness DB-5 column—J and W). Injections were 1 μl of the 100-μl extracts. PAH concentrations were corrected for extraction efficiencies as determined by the internal standard. A 100 ng μl^{-1} 16 PAH (Ultra, # PM612) was used as an external standard to determine mass response factors for the GC–MS.

Suwannee River humic acid (International Humic Substances Society- # IS101H) was used to study the effects of humic substances on PAH detection by LIF. In this and the other investigations of environmental variables described later, the method of successive addition with stirring in a single bottle was used. The fluorescence was continuously monitored using the LIF system in these investigations. The humic acid was prepared as a 100 mg l^{-1} in milli-q stock solution. Small aliquots were successively added to PAH solutions. A similar procedure was used for ionic strength investigations using weighed amounts of sodium chloride added to milli-q solutions of

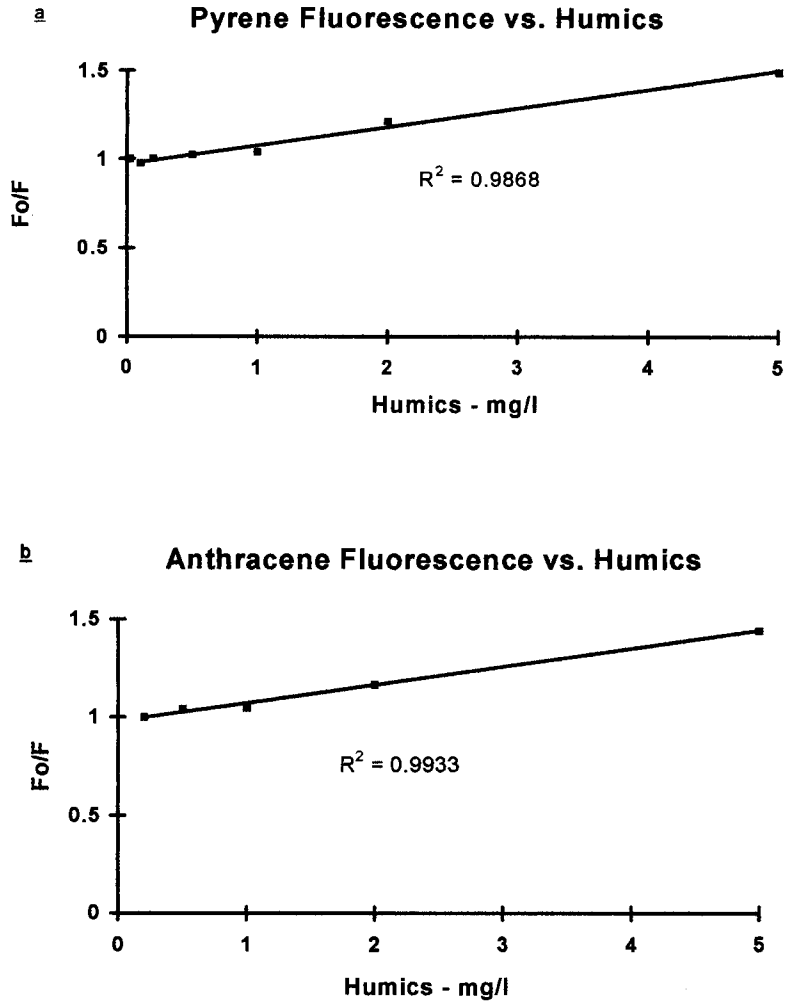

Fig. 5. Stern–Volmer plots of (a) pyrene and (b) anthracene fluorescence vs. humic acid concentration showing static quenching effects of humic acid. Data are corrected for inner filter effect.

pyrene and anthracene at concentrations of 10 μg l^{-1}. Investigations of pH effects were conducted using successive additions of hydrochloric acid or sodium hydroxide in 0.01 M sodium chloride solutions of pyrene and anthracene.

For oxygen studies, the bottle was flushed with nitrogen and a dissolved oxygen meter was used to monitor the replenishment of oxygen with stirring in air. For temperature studies, the fluorescence was monitored by first cooling the bottle in an ice bath and then heating the bottle slowly (~1°C min^{-1}) on a hot plate to 40°C.

2.3. Field studies

Three different probe deployments have been used for field studies. In Boston Harbor, the probe was mounted on the support rack of a Seabird 911 Conductivity, Temperature and Depth (CTD) system and was towed just beneath the surface (~1/2 m) for continuous transects, or the fiber cable was payed out by hand for vertical profiling with the CTD. The system has also been deployed three times on large research vessels (3–10 days of continuous operation). For these

Table 2
Environmental variable effects on PAH fluorescence

Interfering variable	Correction factor	Boston harbor range	Correction range (%)
pH	none	7.6–8.5	none
Salinity	none	15–32 psu	none
Temperature	−1%/°C	2–20°C	0–20
Dissolved oxygen	−3%/mg l^{-1}	2–10 mg l^{-1}	0–20
Humic substances	~−6%/mg l^{-1}	1–5 mg l^{-1}	6–30

deployments the probe was placed in the bottom of a 1/4 m long, 4-cm diameter glass column in which bow-pumped 'clean' seawater flows vertically upward to minimize scattering due to bubbles. The probe has also been inserted in the sidewall of a benthic chamber to measure sediment flux processes [37].

3. Results and discussion

3.1. Time-resolved fluorescence

Petroleum products have been found in both water and soils using similar laser-induced fluorescence systems [29,31,32]. This investigation extends these results to the detection of petroleum components, PAH, at relatively low levels (1–100 ng l^{-1}) in situ in the marine water column.

Long-lived fluorophores such as PAH can be detected even in the presence of the much higher fluorescence produced by natural organic matter. Fig. 2 shows the non-delayed and 64 ns delayed signals for a spiked sample of Boston Harbor surface water (28 PSU), filtered and extracted as described earlier to remove ambient PAH. Pyrene has been added to produce a nominal concentration of pyrene in the sample of 100 ng l^{-1}. While there is no indication of pyrene in the non-delayed signal (Fig. 2(a)), the characteristic fluorescence spectrum of pyrene (Fig. 2(c)—scaled from concentrated standard) is seen in the delayed signal (Fig. 2(b)). Previous studies have shown that pyrene concentration in estuarine surface waters ranges up to 200 ng l^{-1} [7,9,38] and concentrations in the range of 10–130 ng l^{-1} have been observed in Boston Harbor waters in this study.

The ability to detect compounds such as PAH using time-resolved spectroscopy depends on the fluorescent lifetimes of the PAH of interest relative to those of other fluorophores present in the sample. The bulk (spectrally integrated) fluorescence of the samples of Fig. 2 is shown in Fig. 3 as a function of delay time. A detectable difference between the spiked and unspiked samples can be seen beginning at about the 8-ns delay point. The figure also shows that solvent extraction (DCM) does not remove all of the long-lived fluorophores from the seawater sample. The fluorescence in the residue samples indicates that some long-lifetime fluorophores are hydrophilic. The residue bulk fluorescence at 64 ns is generally less than 10% of the original 64 ns bulk fluorescence in estuarine water samples and the residue spectra have broad, featureless characteristics. The curvature of the semi-log plot suggests the presence of a number of fluorophores with different lifetimes. The fast early decay is thought to be mostly humic substances and an exponential curve fitted to the two shortest time delays of the spiked seawater sample (dashed line) has a decay time of 3.9 ns. As indicated in the introduction, actual humic substance lifetimes may consist of more than a single exponential decay. For detection of PAH with lifetimes much shorter than that of pyrene, such multiple exponentials are a complicating factor in deconvolving the data. (Additional work is in progress in our laboratory to better characterize the humic substance lifetimes in seawater samples.) An exponential curve fitted to the difference of the curves at the two longest time delays (dotted line) should approximately plot the decay of the added pyrene in the seawater matrix and indicates a lifetime of 129 ns which is

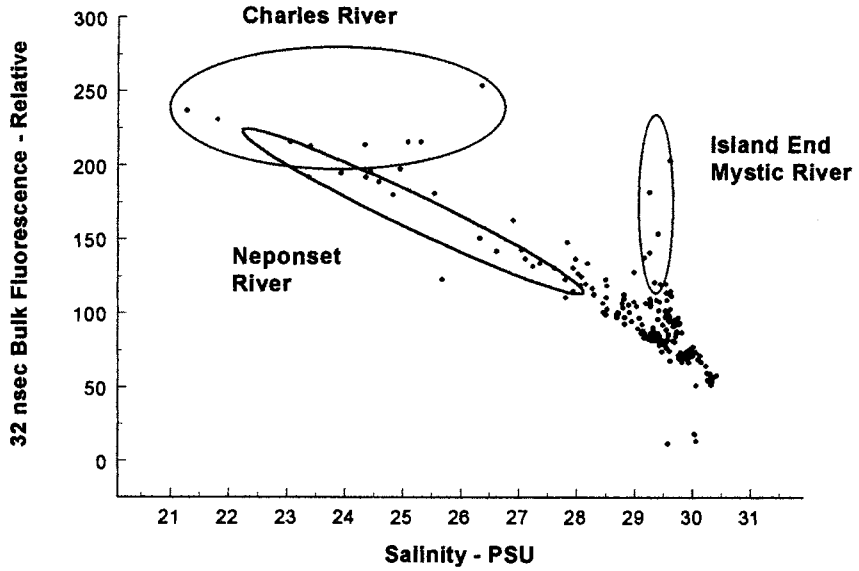

Fig. 6. Long-lived fluorophores (32 ns delay) vs. salinity in Boston Harbor. Several distinct sources can be inferred from the data. See text.

similar to that measured for pyrene in water by other investigators [25,36].

The majority of fluorophores in near-shore waters are usually comprised of humic substances and these can be expected to be the major interferences with the fluorescent determinations of PAH [39]. Dissolved humic substances exhibit a broad fluorescence emission peak centered between 420 and 460 nm [26], bulk fluorescence lifetimes of 1–8 ns (Section 1), and fluorescence quantum efficiencies of about 0.1–1% (quinine sulfate = 55%) [40]. With a fluorescence lifetime of approximately 4 ns, typical estuarine humic fluorescence would decay to our system noise level in about 30 ns. The detection levels of various PAH in seawater are therefore dependent upon their fluorescence lifetime, their quantum efficiency, and their molar absorption at the excitation wavelength. The PAH of interest in this study have lifetimes between 4 and 128 ns, and quantum efficiencies of between 25 and 50% and molar absorptions at 337 nm excitation that vary over a wide range. Table 1 indicates the theoretical detection limits for this system for 4 PAH based on current signal to noise performance and a masking humics substance signal equivalent to typical Boston Inner Harbor seawater. The detection limit is taken as the level of PAH which would yield a bulk fluorescence signal (integrated spectral data) equal in energy to the humics signal over the wavelength range and time delay most appropriate to the specific PAH. For pyrene, for example, this is the spectral range of 360–420 nm and a delay of 128 ns. (For a fluorophore as long-lived as pyrene, system noise levels are the limiting factor, not the residual humics signal.) Pyrene is typically found in urban estuaries at concentration of 10–200 mg l^{-1} [6,9,18]. The 8 ng l^{-1} detection limit of this system provides sufficient sensitivity for the reliable detection of pyrene in these areas. Fluoranthene concentrations are similar [6,9] and the 50 ng l^{-1} detection limit for fluoranthene suggests possible detection capability in the estuarine environment. The application of correlation and regression techniques to the data can improve this performance as we discuss later in the paper. The detection limits numbers are derived from responses and time decay constants that were determined with the LIF system on pure PAH dissolved in milli-q water. The concentrations used were typically about 25% of their saturation levels in seawater.

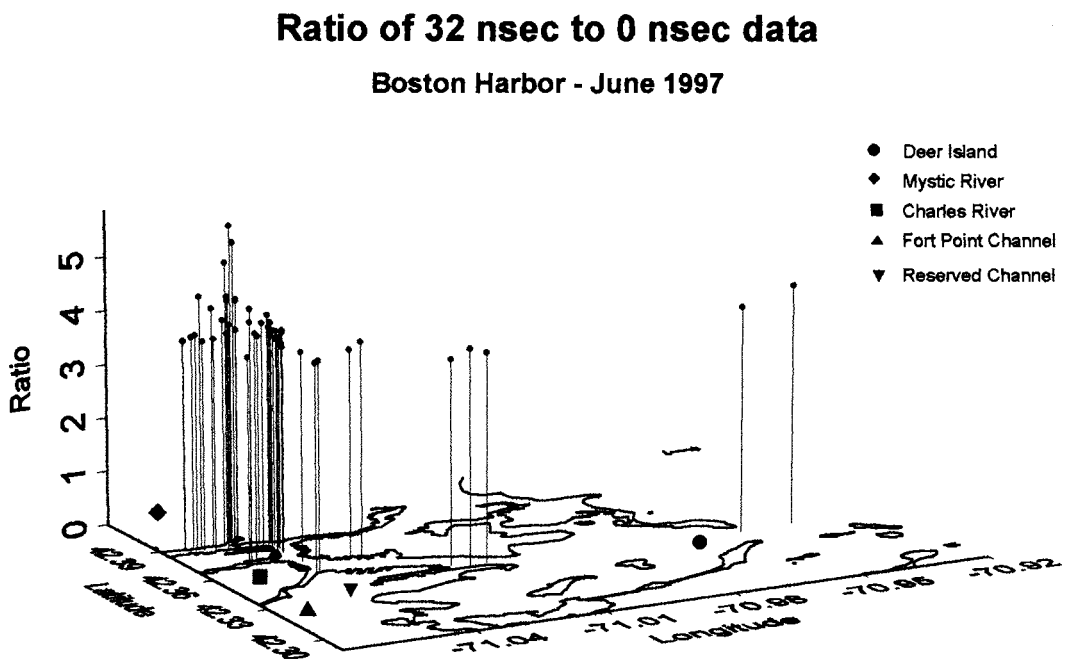

Fig. 7. Excess long-lived fluorophores during a Boston Harbor Deployment (June, 1997)—32 ns delay/0 ns delay. For clarity, only a subset of the samples is shown.

The humics signals used for comparison were typical signals from Boston Harbor samples.

The low sensitivity for anthracene is due to its short fluorescence lifetime and that for phenanthrene is a result of its low absorption at 337 nm excitation. Fluoranthene detection is limited by the similarity of its emission spectrum to that of humic substances. Further development of our system utilizing different excitation wavelengths should lower the detection limits for phenanthrene considerably.

3.2. Environmental variables

In addition to their masking effect, humic substances have been shown to reduce the induced fluorescence response of PAH by static quenching processes [36,41]. This and the effects of other environmental variables as described below have been studied utilizing the LIF system in a laboratory setting to enable environmental corrections to be made to our field data.

Static quenching of PAH fluorescence is caused by the formation of a non-fluorescent complex [41]. If this complexation can be characterized by a single binding coefficient, Kb, a Stern-Volmer equation can be derived to describe the fluorescence:

$$F_0/F = 1 + K_b[\mathrm{Hu}] \quad (1)$$

where F_0 is the fluorescence in the absence of quenching, F is the quenched fluorescence, and [Hu] is the concentration of humics.

Our early investigations did not show this linear dependence indicating that either other quenching mechanisms (e.g. dynamic) or inner filter effects were present. Observed decreases in the Raman signal with increasing humics concentrations were suggestive of the latter mechanism. Fig. 4 shows the bulk fluorescence with increasing concentration of Suwannee River humic acid in milli-q water as measured by the LIF system confirming the non-linear effect. By measuring the absorption of the humic acid at the wavelengths used to examine the quenching behavior, the pyrene peak

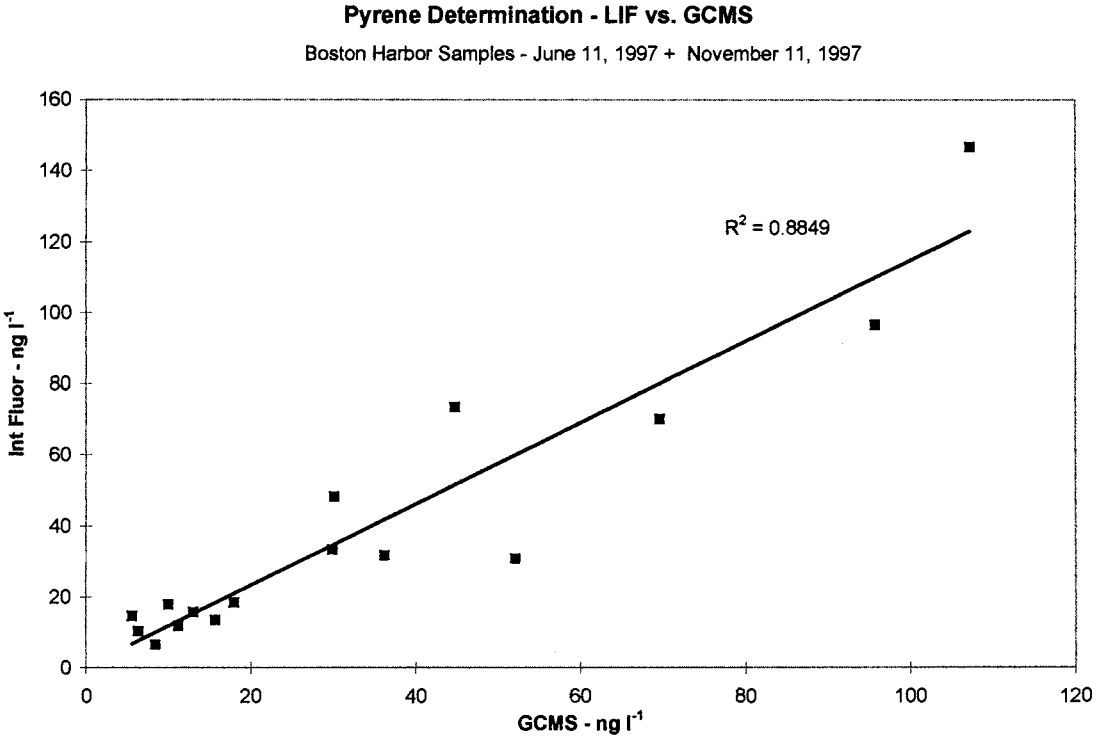

Fig. 8. Pyrene comparisons. Laser-induced fluorescence versus gas chromatography–mass spectroscopy pyrene concentrations for discrete marine samples.

at 393 nm and the anthracene peak at 399 nm, correction factors for the inner filter effects were derived. Fig. 5 (a) and (b), show the Stern–Volmer curves for pyrene and anthracene after these corrections have been applied. The linear relationships are consistent with static quenching by the humic acid. The results also indicate that a correction for humic acid concentration is necessary for fluorescence measurements taken in an estuarine environment.

We have found PAH fluorescence as measured by our system to vary linearly with concentration for all of the PAH of interest over ranges in which the compounds might be found in natural waters (1–200 ng l^{-1}). Other environmental variables that we have investigated are temperature, salinity, pH and dissolved oxygen. Over ranges that are encountered in the estuarine environment, only temperature and dissolved oxygen would appear to have significant effects on PAH fluorescence (Table 2). Quenching by oxygen molecules is a dynamic process that has the effect of decreasing the fluorescence lifetimes and intensities of the PAH [42]. These results suggest that corrections are required for interpreting PAH fluorescence signals collected in waters with varying temperatures and dissolved oxygen such as in depth profiles in stratified waters.

3.3. Field studies

We have deployed this system in situ in Boston Harbor, the Mid-Atlantic Bight and San Diego Bay. Figs. 6 and 7 show some results of the deployment of our system in the surface waters in Boston Harbor. Fig. 6 reveals apparent conservative mixing between high fluorescence freshwater end members and low fluorescence seawater throughout most of the Inner Harbor and from the Neponset River. The Charles River is the major source of fresh water to the Inner Harbor area but the opening of the dam just above its

mouth controls its flow. As a result, the mixing regime of the Charles River is both tidally and temporally dependent. The Charles River samples show a high long-lived fluorescence signature from areas at the mouth of the Charles where a number of docks and marinas are located. The samples marked Island End Mystic River show the impact of a marina and an industrial area in the mouth of the Mystic River. The Mystic River is a minor fresh water flow into Boston Harbor and the fluorescent material indicated here is mixed out of the area by tidal action.

A higher ratio of the delayed fluorescence emission signal to the non-delayed signal is suggestive of relatively higher concentrations of PAH. Fig. 7 is a plot of the ratio of the spectrally integrated 32-ns delayed signal to that of the integrated non-delayed signal along one of our harbor transects. Only about one quarter of our 32-ns measurements, those with the highest value of this ratio, are shown for clarity. The highest points are in proximity to marinas and docks, the Constitution Wharf area, Fort Point Channel, Reserved Channel and the Island End marina indicated above. In addition, a high ratio is seen in the vicinity of the Deer Island Publicly Owned Treatment Works.

With its long fluorescence lifetime, moderate aqueous solubility and significant quantum efficiency at 337-nm excitation, pyrene is an excellent compound through which we can explore the capabilities of our system as indicated above by the spiked sample. Fig. 8 is a plot of estimated pyrene levels in the 4 l filtered water samples as determined by LIF fluorescence spectra at 128 ns delay versus pyrene concentration determined by GCMS analysis of the samples. The LIF results were quantified by principal component regression using the Chemometrics Toolbox in the MATLAB Program, Version 5.0 (The MathWorks, Natick, MA) and a training set of 4 PAH in seawater. Not surprisingly, principal component analysis indicates that only two components, the pyrene spectrum and the seawater (humics) spectrum, are required for the regression. This particular regression set uses only the spectral data in the range of 360–425 nm. The dissolved organic carbon values for these filtered samples were in the range of 1.8–4 mg l^{-1} suggesting a humic substance concentration of less than 2 mg l^{-1}. Humic substances comprise 25–50% of the DOC in coastal waters [43] and humic substances are thought to be responsible for fluorescence quenching in natural waters [35,36]. As we have previously discussed, this could imply a correction of up to 10% in the LIF values. This correction is not applied to this data, primarily because the training set was produced in similar seawater, significantly reducing this potential correction. The results suggest that determination of pyrene in situ using time-resolved, laser-induced fluorescence spectroscopy is entirely feasible. As we develop the system further, advanced spectral analysis techniques will be examined and employed to further extend the PAH detection capabilities of our system.

As indicated above, the TR–LIF system has a limit of detection more than adequate for detecting pyrene at typical ambient environmental levels in urban estuaries. Oil spills in coastal regions are an issue of acute concern. Pyrene concentrations in crude oils are typically 0.1% by weight [44,45]. At 8 ng l^{-1} pyrene sensitivity, the TR–LIF system may be able to trace crude oil spills to a dilution exceeding 10^8:1, or ten parts per billion.

Acknowledgements

Financial support for this work was provided by MIT Sea Grant, Massachusetts Water Resources Authority and the U.S. Department of Energy.

References

[1] G. Grimmer, Environmental Carcinogens: Polycylic Aromatic Hydrocarbons, CRC Press, Boca Raton, FL, 1983.
[2] J. Misfield, Epidemiology, in: G. Grimmer (Ed.), Environmental Carcinogens: Polycylic Aromatic Hydrocarbons, CRC Press, Boca Raton, FL, 1983.
[3] P. Boffetta, N. Jourenkova, P. Gustavsson, Cancer Causes Control 8 (1997) 444–472.
[4] International Agency for Research on Cancer, IARC Monogr Eval Carcinog Risk Chem Humans, vols. 1–65, IARC, Lyon, France, 1971–1996.

[5] M.C. Mix, Polycyclic aromatic hydrocarbons in the aquatic environment: occurrence and biological monitoring, in: E. Hodgson (Ed.), Reviews in Environmental Toxicology, vol. I, Elsevier, Amsterdam, 1984, pp. 51–102.
[6] T.F. Bidleman, A.A. Castleberry, W.T. Foreman, M.T. Zaranski, D.W. Wall, Estuarine Coastal Shelf Sci. 30 (1990) 91–109.
[7] I. Bouloubassi, A. Saliot, Mar. Pol. Bull. 22 (12) (1991) 588.
[8] C.N. Katz, D.B. Chadwick, G.S. Douglas, Oceans '91, 1992.
[9] R.J. Law, V.J. Dawes, R.J. Woodhead, P. Matthiessen, Mar. Pol. Bull. 34 (5) (1997) 306–322.
[10] H.W. Chen, MS Thesis, MIT, 1993.
[11] Y.-P. Chin, P.M. Gschwend, Environ. Sci. Technol. 26 (8) (1992) 1621–1626.
[12] G. Lei, R.F. Chen, 1997, in preparation.
[13] S.E. McGroddy, J.W. Farrington, Environ. Sci. Technol. 29 (6) (1995) 1542–1550.
[14] O. Gustafsson, F. Haghseta, C. Chan, J. Macfarlane, P.M. Gschwend, Environ. Sci. Technol. 31 (1) (1997) 203–209.
[15] P.D. Boehm, J.W. Farrington, Environ. Sci. Technol. 18 (11) (1984) 641–645.
[16] K.A. Maruya, R.W. Risebrough, A.J. Horne, Environ. Sci. Technol. 30 (10) (1996) 2942–2947.
[17] I. Bouloubassi, A. Saliot, Fresenius J. Anal. Chem. 339 (1991) 765–771.
[18] J. Dachs, J.M. Bayona, C. Raoux, J. Albaiges, Environ. Sci. Technol. 31 (3) (1997) 682–688.
[19] M. Ehrhardt, A. Knap, Mar. Chem. 26 (1989) 179–188.
[20] J.W. Carr, J.M. Harris, Anal. Chem. 60 (7) (1988) 698–702.
[21] D. Eastwood, R.L. Lidberg, J.H. Zimmerman, M.E. Dominguez, SPIE Proceedings, 1993.
[22] S.H. Lieberman et al., Second International Symposium—Filed Screening Methods for Hazardous Wastes and Toxic Chemicals, Las Vegas, NV, 1991.
[23] P.J. Milne, D.S. Odum, R.G. Zika, Time-resolved fluorescence measurements on dissolved organic matter, in Zika, Cooper (Eds.), Photochemistry of aquatic systems, American Chemical Society, 1987, pp. 132–140.
[24] S.M. Rudnick, R.F. Chen, Ocean Sciences, San Diego, CA, American Geophysical Union, 1996.
[25] S.M. Inman, P. Thibado, G.A. Theriault, S.H. Lieberman, Anal. Chim. Acta 239 (1990) 45–51.
[26] S.A. Visser, Fluorescence Phenomena of Humic Matter of Aquatic Origin and Microbial Cultures, in: R.F. Christman, E.T. Gjessing (Eds.), Aquatic and Terrestrial Humic Materials, Ann Arbor Science, Ann Arbor, MI, 1983, pp. 183–202.
[27] S.E. Apitz, L.M. Borbridge, K. Bracchi, S.H. Lieberman, J. Soil Contaminat. 1 (3) (1992) 197–216.
[28] J. Bublitz, M. Dickenhausen, M. Grätz, S. Todt, W. Schade, Appl. Optics 34 (18) (1995) 3223–3233.
[29] S.H. Lieberman, S.M. Inman, G.A. Theriault, SPIE, Boston, MA, 1989.
[30] R. Niessner, W. Robers, A. Krupp, Fresenius J. Anal. Chem. 341 (1991) 207–213.
[31] U. Panne, R. Niessner, Sens. Actuators B 13–14 (1993) 288–292.
[32] W. Schade, J. Bublitz, Environ. Sci. Technol. 30 (1996) 1451–1458.
[33] K.T. Benlahcen, A. Chaoui, H. Budzinski, J. Bellocq, P. Garrigues, Mar. Pol. Bull. 34 (5) (1997) 298–305.
[34] G. Brown, W. Maher, Org. Geochem. 18 (5) (1992) 657–668.
[35] D.A. Backus, P.M. Gschwend, Environ. Sci. Technol. 24 (1990) 1214–1223.
[36] M.U. Kumke, H.-G. Lohmannsroben, T. Roch, Analyst 119 (1994) 997–1001.
[37] R.F. Chen, D.B. Chadwick, S.H. Lieberman, Org. Geochem. 26 (1/2) (1997) 67–77.
[38] M.J. Wade, Sources, Fate and Effects of Polycyclic Aromatic Hydrocarbons in Massachusetts Bays: The Science Behind the Management Issues, Boston, Massachusetts Bays Program, 1995.
[39] M.M. De Souza Sierra, O.F.X. Donard, M. Lamotte, V. Belin, M. Ewald, Mar. Chem. 47 (1994) 127–144.
[40] S.A. Green, N.V. Blough, Limnol. Oceanogr. 39 (8) (1994) 1903–1916.
[41] T.D. Gauthier, E.C. Shane, W.F. Guerin, W.R. Seitz, C.L. Grant, Environ. Sci. Technol. 20 (11) (1986) 1162–1166.
[42] I.B. Berlman, Handbook of Fluorescence Spectra of Aromatic Molecules, Academic Press, New York, 1971.
[43] G.R. Harvey, D.A. Boran, Geochemistry of humic substances in seawatter., in: Aiken, McKnight, Wershaw (Eds.), Humic substances in soil, sediment and water: geochemistry, isolation and characterization, Wiley, New York, 1985, pp. 233–247.
[44] A.G. Requejo, et al., Org. Geochem. 24 (10) (1996) 1017–1033.
[45] J.W. Short, R.A. Heintz, Environ. Sci. Technol. 31 (8) (1997) 2375–2384.
[46] W. Karcher, R.J. Fordham, J.J. Dubois, P.G.J.M. Glaude, J.A.M. Ligthart (Eds.), Spectral Atlas of Polycyclic Aromatic Compounds, vol. D. Reidel, Boston, MA, 1985.

ELSEVIER

Talanta 47 (1998) 921–927

Talanta

Syntheses of three new derivatives of 8-aminoquinoline and its applications for fluorimetric determination of copper(II)

Qiu-E Cao [a], Ketai Wang [a], Zhide Hu [a,*], Qiheng Xu [b]

[a] *Department of Chemistry, Lanzhou University, Lanzhou, 730000, People's Republic of China*
[b] *Department of Chemistry, Yunnan University, Kunmin, 650091, People's Republic of China*

Received 20 January 1998; received in revised form 20 April 1998; accepted 21 April 1998

Abstract

Three new 8-aminoquinoline-5-azo derivatives: 5-(3-fluo-4-chlorophenylazo)-8-aminoquinoline (FCPAQ), 5-(3-fluo-4-chlorophenylazo)-8-benzenesulfonamidoquinoline (FCPBSQ), 4,4′-bis(8-aminoquinoline-5-azo)-biphenyl (BAQABP) have been synthesized, and were found to be good fluorescence reagents for the determination of copper(II). In slightly acidic or basic medium, copper(II) reacts with FCPAQ, FCPBSQ or BAQABP to form a chelate, which exhibits an intensive fluorescence in ultraviolet region. The fluorescence intensity is proportional to the concentration of copper(II) over the range of 4.0–140, 1.0–200 and 3.0–150 μg l^{-1} with the detection limits of 0.80, 0.20 and 0.50 μg l^{-1} for the FCPAQ, FCPBSQ and BAQABP systems, respectively. The methods have been successfully applied to the determination of trace amount of copper in ore, alloy, water and hair samples. © 1998 Elsevier Science B.V. All rights reserved.

Keywords: 8-Aminoquinoline derivatives; Copper; Spectrofluorimetry

1. Introduction

8-Hydroxyquinoline (8-HQ) and 8-mercaptoquinoline (8-MQ) are well known reagents which are widely used as chelating agents in analytical chemistry [1]. The 8-amino derivative of quinoline (8-AQ) has been received little analytical attention, resulting in only a few published paper [2,3]. The 8-AQ derivatives with (*N*,*N*) as its chelating atom is more selective than 8-HQ (*N*,*O*) and 8-MQ (*S*,*O*). In recent years, a series of 8-aminoquinoline-5-azo derivatives have been synthesized and found to be good chromogenic and fluorescence reagents for the determination of some metal ions [4–7].

As part of an investigation of the 8-aminoquinoline-5-azo derivatives chelating systems, this paper reports the syntheses of the three derivatives of 8-aminoquinoline-5-azo: 5-(3-fluo-4-chlorophenylazo)-8-aminoquinoline (FCPAQ), 5-(3-fluo-4-chlorophenyl-azo)-8-benzenesulfonami-

* Corresponding author. Fax: +86 931 89112578; e-mail: chem@lzu.edu.cn

0039-9140/98/$ - see front matter © 1998 Elsevier Science B.V. All rights reserved.
PII S0039-9140(98)00161-1

doquinoline (FCPBSQ), 4,4′-bis(8-aminoquinoline-5-azo) biphenyl (BAQABP), their fluorescence reactions with copper(II) and the use of the spectrofluorimetric determination of trace amounts of copper(II).

Due to the inherent sensitivity of the fluorescence technique, the fluorescence methods are being used increasingly in biochemical, medical and chemical research. The methods suitable for the fluorimetric detection of copper are not many [8–14], and some of them are catalytic kinetic spectrofluorimetric methods, fluorescence quenching methods and extraction spectrofluorimetric methods, the directly aqueous spectrofluorimetric methods are scarce. In the paper, three simple aqueous spectrofluorimetric methods for the determination of copper with high sensitivity and more selectivity, based on the reaction of three new reagents with copper in the presence of Tween-80, are proposed. They are used to determine copper in industrial, environmental and biological samples with satisfactory results.

2. Experimental

2.1. Reagents and chemicals

All chemicals were of analytical reagent grade, and double-distilled water was used throughout.

FCPAQ and FCPBSQ solutions were 2.0×10^{-4} mol l^{-1} in ethanol.

BAQABP solution was 2.0×10^{-4} mol l^{-1} in *N*,*N*-dimethylformamide (DMF).

Copper(II) standard solution, 1.000 mg ml^{-1}, was prepared by dissolving 0.1000 g of pure copper (99.9%, Beijing Chemical Plant, China) in 10 ml of 1:1 (v/v) nitric acid. The solution was then heated gently to remove nitrogen oxide. After cooling, it was transferred to a 100-ml volumetric flask and diluted to volume with water. A working solution of 2.0 mg l^{-1} was prepared by diluting the standard solution with water daily.

A buffer solution was prepared with 0.1 mol l^{-1} $Na_2B_4O_7$ solution and 0.1 mol l^{-1} HCl or NaOH solution.

Tween-80 aqueous solution 2.0% (v/v) was used in this work.

2.2. Apparatus

Fluorescence measurements were performed on a Hitach (Japan) M-850 fluorescence spectrometer with an 150W Xenon lamp and an 1-cm quartz cell. All of the fluorescence data were given with correction. The pH measurements were made with a model pHs-2 pH meter (Shanghai, China). Elemental analyses were done with a PE model PE-2400 analyzer. A Mattson model PK-6000 infrared spectrophotometer and a Bruker model AM-400 NMR spectrometer were used for recording IR and NMR spectra. The splitting patterns for NMR spectra were designated as follows: s, singlet; d, doublet; m, multiplet; br, broad.

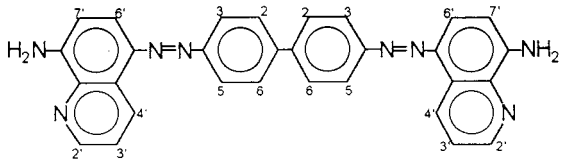

1

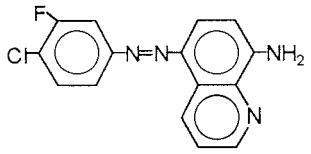

2

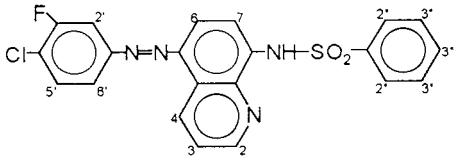

3

Fig. 1. The structures of BAQABP, FCPAQ and FCPBSQ. 1. BAQABP. 2. FCPAQ. 3. FCPBSQ.

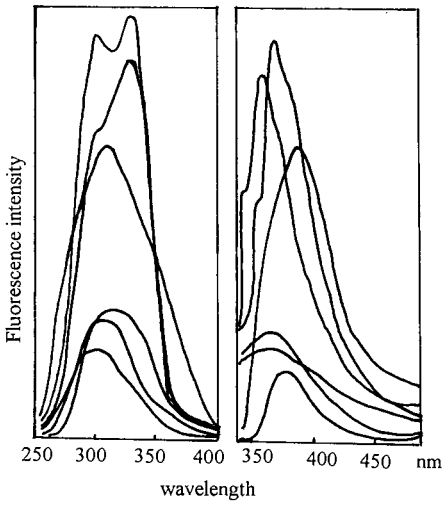

Fig. 2. Excitation (left) and emission (right) spectra of the complexes and the corresponding reagent blanks (from top to bottom, the spectra represent in turn FCPAQ-Cu(II), FCPBSQ-Cu(II), BAQABP-Cu(II), FCPAQ, FCPBSQ and BAQABP, respectively.

2.3. Syntheses of FCPAQ, FCPBSQ and BAQABP

8-Aminoquinoline was synthesized from quinoline [15].

Table 1
Tolerance limits of the foreign ions (μg) in the determination of 2.0 μg of copper(II) in the three systems

Ion added	FCPAQ	FCPBSQ	BAQABP
Ca^{II}, Mg^{II}, Ba^{II}, NH_4^+, PO_4^{3-}, F^-	2000	2000	2000
Cr^{VI}	600	1000	400
Pb^{II}	200	200	200
W^{V}, SiO_3^{2-}	200	300	200
Sb^{III}, Sn^{IV}, Bi^{III}	200	100	100
Mo^{VI}, Al^{III}, V^{V}, Ni^{II}, Hg^{II}	100	100	100
Zn^{II}, Mn^{II}, Cd^{II}	100	200	100
Co^{II}	10	40	40
Pt^{II}, Pd^{II}	10	20	10
Ga^{IV}, In^{III}, Th^{IV}, Ti^{IV}, Ce^{IV}	40	20	20
Fe^{III}	10 (200[a])	10 (200[a])	10 (200[a])

[a] After removed as described in the text.

Table 2
The analytical characteristics of the three methods

Quality Parameters	FCPAQ	FCPBSQ	BAQABP
LOD[a] (10^{-3} mg l^{-1})	0.8	0.2	0.5
RSD[b] (%)	1.15	1.02	1.32
Linear reagression equations[c]			
Linear range(10^{-3} mg l^{-1})	4–140	1–200	3–150
A (intercept)	1.4504	0.3051	5.2570
B (slope)	453.01	240.78	314.23
r	0.9993	0.9990	0.9992

[a] LOD: limit of detection, calculated from three times the standard deviation of nine blank measurements.
[b] RSD: relative standard deviation (for 1.0 mg/l Cu(II), $n = 9$).
[c] Linear regression equation: $F = A + BC$, where C expressed as mg l^{-1}.

2.3.1. Preparation of BAQABP

A sample of 0.01 mol of benzidine was dissolved in 25 ml ice-cold hydrochloric acid solution (1:3), and slowly diazotized with a solution of 0.02 mol of sodium nitrite in 20 ml of water. The diazotized solution was then added dropwish with stirring to an ice-cold solution of 8-AQ (0.02 mol) in 150 ml of 2 mol l^{-1} acetic acid. A 2 mol l^{-1} solution of sodium hydroxide was used to keep pH constant throughout. After the procedure was finished, the mixture was left for 2 h with stirring at room temperature, then neutralized with sodium hydroxide and filtered. The red precipitate was recrystallized twice from *N*,*N*-dimethylformamide (DMF) aqueous solution (1:3) to give a yield of 30% (m.p. > 240°C). The structure has been verified as shown in Fig. 1 by elemental analysis, IR and ^{1}H-NMR. Elemental analysis was as follows: calculated 72.86% C, 4.48% H, 22.66% N; found 72.42% C, 4.69% H, 22.98% N. ^{1}H-NMR (solvent: acetone-d_6) (ppm), 6.75 (br, 4H, $J = 9.00$ Hz, H-2 and H-4), 7.66 (dd, 2H, $J = 8.2$, 4.1 Hz, H-3′, 8.06 (d, 4H, $J = 9.50$ Hz, H-3 and H-5), 8.07 (d, 2H, $J = 8.2$ Hz, H-6′, 8.83 (dd, 2H, $J = 8.2$, 1.6 Hz, H-4′, 9.33 (dd, 2H, $J = 4.1$, 1.6 Hz, H-2′. IR (KBr) (cm^{-1}), 3457, 3330 (ν_{NH2}), 1663,1609, 1560, 1505 ($\nu_{C=C}$, $\nu_{C=N}$ and δ_{NH2}), 1427 ($\nu_{N=N}$), 1378, 1333 (ν_{Ar-N}), 1170, 1122, 818, 787 (δ_{Ar-H}).

Table 3
Determination of copper in the samples by the three methods

Samples[a]	FCPAQ method		FCPBSQ method		BAQABP method	
	Found[b]	Recovery	Found[b]	Recovery	Found[b]	Recovery
Cu-ore 72-Cu-01	0.46 ± 0.0011	96	0.47 ± 0.0091	98	0.48 ± 0.0095	104
Al-alloy(ZL9)	0.31 ± 0.0072	101	0.30 ± 0.0048	105	0.29 ± 0.0081	95
Running water	26.50 ± 0.49	101	25.50 ± 0.46	97	26.00 ± 0.53	97
Human hair 1	3.01 ± 0.033	96	2.99 ± 0.030	102	3.12 ± 0.062	103
Human hair 2	3.93 ± 0.038	105	3.83 ± 0.030	101	3.91 ± 0.052	95

[a] The standard value of the copper ore (72-Cu-01) is 0.48% and of the aluminum-alloy(ZL9) is 0.30%, the composition (%) of copper ore are Pb (0.018) Zn (0.064), Cd (0.0016) and of aluminum alloy are Si (12.98), Fe (0.63), Mn (0.12), Mg (0.72), Zn (0.11). The value of running water expressed as 10^{-3} mg l^{-1}.
[b] Mean $\pm$ standard deviation.

2.3.2. Preparation of FCPAQ

Synthesis of FCPAQ was the same as that of BAQABP exception of using 0.1 mol of 3-fluo-4-chloroaniline and 0.1 mol of 8-AQ. The red powders were recrystallized two times from 95% ethanol with the melting point of 210–212°C. Elemental analysis was as follows: calculated (%): C, 59.91, H, 3.35, N, 18.63; found (%): C, 59.59, H, 3.01, N, 19.02. The data obtained from IR and ^{1}H-NMR confirmed the structure of FCPAQ as shown in Fig. 1.

2.3.3. Syntheses of FCPBSQ

FCPBSQ was synthesized by the following procedure according to the literature [3]. A 0.03 mol sample of FCPAQ was placed in a 100-ml three-necked flask, which was fitted with a motor stirrer and immersed in an ice water bath. A 0.03 mol sample of benzene sulfochloride was added in small portions over 2 h with the solution being stirred throughout. The reaction mixture was then poured into 200 ml of cold water with vigorous stirring. A red solid separated out and was filtered. The solid was recrystallized twice from 95% ethanol, and the red powdery substance (m.p. 223–225°C) with the yield of 40% was obtained. The structure in Fig. 1 has been verified by elemental analysis, IR and ^{1}H-NMR. Elemental analysis: calculated 57.27% C, 3.20% H, 12.71% N; found 57.01% C, 3.02% H, 13.20% N. ^{1}H-NMR (solvent: acetone-d_6) (ppm): 7.05 (d, 1H, $J = 8.30$ Hz, H-7), 7.58–7.54 (m, 3H, H-3″), 7.66 (dd, 1H, $J = 8.94$, 4.10 Hz, H-3), 7.64 (d, 1H, $J = 6.20$ Hz, H-5′, 7.96 (dd, 1H, $J = 2.20$, 6.70 Hz, H-6′, 7.95 (dd, 2H, $J = 8.90$, 2.30 Hz, H-2″), 8.05-8.02 (m, 2H, H-2′ and H-6), 8.83 (dd, 1H, $J = 8.82$, 1.58 Hz, H-4), 9.31 (dd, 1H, $J = 4.10$, 1.59 Hz, H-2), 10.91 (s, 1H, –NH–). IR (KBr) (cm^{-1}): 3327 (ν_{N-H}), 1617, 1591, 1512, 1483 ($\nu_{C=C}$, $\nu_{C=N}$), 1433 ($\nu_{N=N}$), 1380, 1336 (ν_{Ar-N}), 1258, 1132 ($\nu_{S=O}$), 1217, 1177, 890, 814, 790 (δ_{Ar-H}), 1044 (ν_{N-S-C}), 686 (ν_{S-C}).

2.4. Procedure for FCPAQ method

Transfer an appropriate amount of sample solution or standard copper(II) solution to a 25 ml volumetric flask. Add 2.0 ml of FCPAQ solution, 4.0 ml of buffer solution (pH = 5.4) and 2.0 ml of Tween-80 solution. Dilute to volume with water and mix well. The mixture was heated for 15 min in a boiling-water bath. After the solution was cooled to room temperature, the fluorescence intensity was measured at $\lambda_{ex}/\lambda_{em} = 328/368$ nm.

2.5. The procedures for FCPBSQ and BAQABP methods

The procedure for the FCPBSQ and BAQABP methods are similar to that for the FCPAQ method, except that 2.0 ml of FCPBSQ or 1.0 ml of BAQABP solution, 4.0 ml of buffer solution (pH = 6.4 or 8.2), 4.0 or 2.0 ml of Tween-80 were added, and then heated for 5 or 20 min in a

Table 4
Comparison of the main characteristics for fluorimetric determination of copper with several organic reagents

Reagent[a]	$\lambda_{ex}/\lambda_{em}$ (nm)	Linear range (μg l^{-1})	Experimental condition	Interfering ions[b]	Ref.
BSTMED	370/440	0–2000	pH = 8, heated, extracted	Fe^{III}, Co^{II}, Ni^{II}	[9]
Neocuprorine	560/570	1–6	pH = 9, extracted	No	[10]
Vc-OPDA	350/420	0–8	pH = 6.9	Hg^{II}, Cr^{VI}, Sn^{IV}, V^{V}	[8]
BPTNCAP	308/403	0.4–64	pH = 5.6, boiled for 30 min	Pb^{II}, Fe^{III}, Bi^{III}, Ag^{I}	[11]
BPRCAP	305/405	0–48	pH = 5.6, boiled for 25 min	Pb^{II}, Fe^{III}, Bi^{III}, Ag^{I}	[12]
SDBH	300/410	0–80	pH = 9.0, boiled for 45 min	Pb^{II}, Fe^{III}, Al^{III}, Co^{II}, Ni^{II}	[13]
Thiamine	370/440	0.24–400	pH = 12, stood for 30 min	Fe^{III}, Co^{II}, Mn^{II}, Fe^{II}	[14]
CFPAQ	328/368	4–140	pH = 5.4, boiled for 15 min	No	[c]
FCPBSQ	326/362	1–200	pH = 6.4, boiled for 5 min	No	[c]
BAQABP	296/382	3–150	pH = 8.4, boiled for 20 min	No	[c]

[a] The abbreviation of the reagents represented as follows: BSTMED: bis-(salicyadehyde)tetramethyl-ethylenediimine; Vc-OPDA: ascorbic acid and *o*-phenylenediamine; 3PTNCAP: 3-tolyl-5-(4-nitro-2-carboxylphenylazo)-2-thioxo-4-hiazolidone; 3PRCAP: 3-phenyl-5-(2′-carboxylphenylazo)-2-thioxo-4-hiazolinone; SDBH: salicyladehydebenazalhydrazone.
[b] Could produce interference at the same concentration of copper(II).
[c] This work.

boiling-water bath for FCPBSQ or BAQABP systems. The fluorescence intensity was measured at $\lambda_{ex}/\lambda_{em} = 326/362$ or 298/382 nm for the two methods, respectively.

3. Results and discussion

3.1. Fluorescence spectra

The fluorescence spectra of the reagent blanks and the corresponding complexes are shown in Fig. 2. The shapes of the fluorescence spectra of BAQABP and its complex are similar. The maximum excitation wavelengths are all at 298 nm, but the maximum emission wavelength shifts from 370 nm (for BAQABP) to 382 nm for its complex. The peak form and position of fluorescence spectra of FCPAQ and FCPBSQ changed after adding Cu(II) to the solutions. The maximum excitation and emission wavelengths are at 302 and 359, 302 and 356 nm for the reagent blanks of FCPAQ and FCPBSQ and 328 and 368, 326 and 362 nm for their complexes, respectively.

3.2. Effect of solution acidity

The qualitative description of the effect of solution acidity could be expressed by the three quantitative fitting polynomials: $F = -2.2863 - 5.9436X + 3.3159X^2 - 0.2734X^3$ ($r = 0.9961$), $F = 61.9660 - 47.3380X + 12.0221X^2 - 0.8666X^3$ ($r = 0.9945$), $F = -58.4282 + 18.8225X - 0.9758X^2 - 0.00137X^3$ ($r = 0.9958$) in the pH range of 3.0–7.5, 2.0–7.0 and 4.5–9.0 for the FCPAQ, FCPBSQ and BAQABP systems, where X is pH and r is the correlation coefficient. It can be seen that in strongly alkaline or acidic medium, the fluorescence intensities of the three systems are very low. The optimum pH ranges for the FCPAQ, FCPBSQ and BAQABP systems were found over 6.5–7.5, 5.5–7.0 and 7.4–9.0, respectively. So further works were carried out at pH = 7.0, pH = 6.4 and pH = 8.2, obtained with a $Na_2B_4O_7$–HCl buffer solution, for the FCPAQ, FCPBSQ and BAQABP systems, respectively.

3.3. Effects of reagent concentration

In the certain concentration range, the fluorescence intensity of the systems increased with increasing the concentration of the reagents, then reached maximum and remained constant. The relationship between the concentration of the reagents and the fluorescence intensity could also be

expressed by the quantitative fitting polynomials: $F = 11.7200 + 5.3000X + 0.4125X^2 - 0.0562X^3$ ($r = 0.9852$), $F = -1.6000 + 12.9095X - 0.9161X^2 + 0.0146X^3$ ($r = 0.9942$), $F = -1.5524 + 4.6369X + 1.5779X^2 - 0.2246X^3$ ($r = 0.9932$) over the concentration range of $(1.5–10.0) \times 10^{-6}$ mol l^{-1} for FCPAQ and FCPBSQ systems and $(1.0–7.5) \times 10^{-6}$ mol l^{-1} for BAQABP system, where X is the concentration of the reagents expressed as 10^{-6} mol l^{-1} and r is correlation coefficient. The optimum concentration ranges of reagents are as follows: $(6.0–10.0) \times 10^{-6}$ mol l^{-1} FCPAQ and FCPBSQ, $(3.0–7.5) \times 10^{-6}$ mol l^{-1} BAQABP. Therefore, 8.0×10^{-6} mol l^{-1} FCPAQ and FCPBSQ and 4.0×10^{-6} mol l^{-1} BAQABP were used in this work.

3.4. Effect of surfactant

In the absence of surfactant or presence of an anionic surfactant, the complexes will precipitate out of aqueous solution, but in the presence of a non-ionic or a cationic surfactant, such as the emulsifying agent OP, poly(vinyl alcohol)(PVA), Triton X-100, Tween-80 or CTAB, the solubility and the fluorescence intensity increased. Tween-80 was found to be the best additive for all of the three systems. The concentration of the Tween-80 over 0.12–0.56, 0.30–0.56 and 0.08–0.30% gave good results for FCPAQ, FCPBSQ and BAQABP systems. So 0.16, 0.32 and 0.16% of Tween-80 were recommended for the three systems, respectively.

3.5. Effect of heating time

The complexes of copper with three reagents are difficult to form at room temperature. The fluorescence intensity reached maximum by heating in a boiling-water bath for at least 10 min for FCPAQ system, 3 min for FCPBSQ system, and 15 min for BAQABP system. Thus 15, 5 and 20 min were selected for the three systems, respectively. When the maximum fluorescence intensity of the systems are reached, they all can remain constant at least 12 h at room temperature.

3.6. Composition of the complexes

The excitation and emission spectra of the reagent blanks and their corresponding systems (in Fig. 2) shown that the peak position of the excitation and emission of the reagent blanks shift after adding Cu(II) to its solutions. The fluorescence intensity were enhanced remarkably at the same time, which indicate that the complex has formed between the Cu(II) and the reagents. From IR spectra of the solid complex (prepared by the employed procedure but omitting Tween-80), it was found that the vibrational bands of $\nu_{C=N}$ and ν_{Ar-N} in IR spectra of all the complexes shift slightly to higher frequency. The vibrational band of ν_{N-H} at about 3300 cm^{-1} in IR spectra of FCPBSQ-Cu(II) complex disappeared, and in IR spectra of FCPAQ-Cu(II) and BAQABP-Cu(II) complexes, it shift to lower frequency, this could be taken as the evidences for the involvement of quinoline nitrogen and amino nitrogen in the complex formation with the copper(II), and one hydrogen in the amino group dissociated in the formation of the complex [16].

The composition of the complex was determined by Job's method of continuous variation and by the molar ratio method. The molar ratio of copper to the reagent is 1:2 for the FCPAQ and FCPBSQ systems and 1:1 for the BAQABP system. The apparent stability constant (k) of the three complexes, calculated from the results of the molar ratio and Job's method, are $\text{Log}\, k = 12.95 \pm 0.10$, 14.02 ± 0.10 and 7.81 ± 0.10 for the FCPAQ-Cu(II), FCPBSQ-Cu(II) and BAQABP-Cu(II) complexes. respectively.

3.7. Effect of foreign ions

The effects of foreign ions on the determination of 2.0 μg of copper in the three systems were all summarized in Table 1. The tolerance limit was taken as the maximum concentration of the foreign ions causing about a $\pm 5\%$ error in the determination. For all the systems, many kinds of foreign ions did not interfere at 10–1000-fold concentration of copper, and no foreign ions caused interference under five-fold concentration of copper. Main interference for all the systems

were found for Fe(III) at five-fold concentration of copper, but it could be removed by adding excessive amount of NH_4OH and then precipitating it as hydroxide.

3.8. The calibration graph

The calibration graphs for the three systems were investigated under the optimum conditions described above. The results were shown in Table 2. It can be seen from the results that all the three methods are of high sensitivity and precise.

3.9. Applications

3.9.1. Determination of copper in ore and alloy samples

An appropriate amount of copper ore or alloy was dissolved in 15 ml of *aqua regia*, the mixture was heated gently and evaporated to nearly dry. The residue was heated to near dryness with 1:1 hydrochloric acid solution. The residue was dissolved in water, then an excessive amount of NH_4OH was added under agitation to precipitate iron and aluminum as hydroxide. The mixture was filtered and the filtrate was heated to get rid of NH_3. The solution was allowed to be cooled, then diluted to 50 ml with water and analyzed directly. The results were presented in Table 3.

3.9.2. Determination of copper in hair and water samples

After the hair sample was washed with water, it was immersed in acetone for a while, then washed with water and dried under an infra-red lamp. After cooling, an appropriate amount of the sample was firstly carbonized at low temperature, then burned in the muffle furnace at 700°C for 30–60 min. When the residue was cooled to room temperature, it was extracted by heating in 1.0 ml of 9 mol l^{-1} H_2SO_4. The solution was finally transferred to a 50-ml volumetric flask and diluted to volume with water and analyzed directly. The results were offered in Table 3.

A sample of 100 ml of the running water was concentrated to 10 ml, then analyzed directly. The results were given in Table 3.

4. Conclusion

The comparison (in Table 4) of the FCPAQ, FCPBSQ and BAQABP methods with others shows that FCPAQ, FCPBSQ and BAQABP are more selective and sensitive fluorescence reagents for copper. The three methods are relatively simple, selective, sensitive and of wide concentration range for the determination of copper. They have been used for the determination of copper in ore, water, alloy and hair samples with satisfactory results.

Acknowledgements

The project was supported by Natural Science Foundation of China.

References

[1] K. Burger, Organic Reagents in Metal Analysis, Pergamon, Oxford, 1973.
[2] M. Blanco, S. Maspoch, Talanta 31 (1984) 85.
[3] J.H. Billman, R. Chernin, Anal. Chem. 34 (1962) 408.
[4] J.W. Zhao, Q.H. Xu, Talanta 38 (1991) 909.
[5] Ch.M. Ruan, Q.H. Xu, Analyst 116 (1991) 99.
[6] Q.E. Cao, J.W. Zhao, Q.H. Xu, Fenxi Hauxue 21 (1993) 682.
[7] Z.T. Zheng, Q.H. Xu, Anal. Lett. 25 (1992) 1573.
[8] S. Kawakubo, H. Kato, M.I. Watsuki, Analyst 119 (1994) 2119.
[9] M.Y. Khuhawar, S.N. Lanjwani, Q.G. Khaskhely, J. Chem. Soc. Pak. 17 (1995) 28.
[10] B.W. Bailey, R.M. Dagnall, T.S. West, Talanta 13 (1966) 1661.
[11] H.J. Shi, Z.Y. Wang, H.X. Shi, Fenxi Huaxue 24 (1996) 312.
[12] H.J. Shi, Z.Y. Wang, H.X. Shi, Anal. Lett. 28 (1995) 1287.
[13] C.Q. Jiang, B. Tang, H.Y. Fu, H. Cao, X.G. Zhang, Gaodeng Xuexiao Huaxue Xuebao 17 (1996) 49.
[14] Z.L. Wang, J.Zh. Li, Z.Y. Zhang, Fenxi Huaxue 22 (1994) 472.
[15] N.N. Vorozhtzov, I.M. Kogan, Chem. Ber. 65B (1932) 142.
[16] J. Fujita, K. Nakamoto, M. Kobayashi, J. Am. Chem. Soc. 78 (1956) 3295.

ELSEVIER

Talanta 47 (1998) 929–941

Talanta

Quantitative determination of trace amounts of Al-citrate by anion-exchange FPLC-ETAAS

Tjaša Bantan [a], Radmila Milačič [a,*], Boris Pihlar [b]

[a] *Department of Environmental Sciences, Jožef Stefan Institute, Jamova 39, 1000 Ljubljana, Slovenia*
[b] *Faculty of Chemistry and Chemical Technology, University of Ljubljana, Aškerčeva 5, 1000 Ljubljana, Slovenia*

Received 21 January 1998; received in revised form 20 April 1998; accepted 21 April 1998

Abstract

An anion-exchange fast protein liquid chromatographic-electrothermal atomic absorption spectrometric procedure (FPLC-ETAAS) was developed for determination of trace amounts of negatively charged Al-citrate in the pH range 3.5–8.0. Aqueous-4 mol dm^{-3} NH_4NO_3 linear gradient elution at a flow rate of 1 cm^3 min^{-1} was applied for 10 min to separate Al-citrate on a FPLC Mono Q HR 5/5 column. The separated aluminium species were determined 'off line' by ETAAS in 0.5 cm^3 fractions. After separation the column was regenerated for 5 min with 4 mol dm^{-3} NH_4NO_3 and equilibrated with water. All reagents used in the separation procedure were cleaned with a silica based LiChrosorb RP-18 HPLC column to remove traces of aluminium. The main advantage of NH_4NO_3 as eluent lies in its ability to decompose quantitatively in the graphite tube during the ashing step, which enables reproducible analysis of aluminium in the separated fractions. Using the procedure developed reproducible (RSD $\pm$ 2.0%) and quantitative determination of negatively charged Al-citrate at a retention time of 4.5 min was obtained. The LOD was found to be 2.0 ng cm^{-3} of Al-citrate. The technique was successfully applied for the determination of Al-citrate in human serum. Spiked samples (50–150 ng Al^{3+} cm^{-3}) were microultrafiltered through a membrane filter (cut-off 30000 Da) to separate aluminium bound to transferrin from low molecular weight aluminium complexes. It was found that 15–19% of aluminium in spiked samples from healthy volunteers passed through the membrane. By applying FPLC separation it was proved that all the aluminium in the filtrate corresponded to Al-citrate. The analytical technique developed enabled quantitative and reproducible determination (RSD $\pm$ 3.0%) of Al-citrate in spiked human serum at levels which could be found in patients undergoing long term haemodialysis. © 1998 Elsevier Science B.V. All rights reserved.

Keywords: Speciation of Al-citrate; Spiked serum samples; Anion-exchange fast protein liquid chromatography—electrothermal atomic absorption spectrometry

1. Introduction

Al-citrate plays an important role in the environment and in biological systems. It is presumed to exist in plant leaves and in the soil solution of

* Corresponding author. Tel: +386 611773900; fax: +386 61219385; e-mail: radmila.milacic@ijs.si

0039-9140/98/$ - see front matter © 1998 Elsevier Science B.V. All rights reserved.
PII S0039-9140(98)00167-2

acid forest soils [1]. It was demonstrated that citric acid is the most important organic ligand able to chelate aluminium from plants intoxicated with aluminium [2]. Jorge and Arruda exposed aluminium tolerant and aluminium sensitive plants to toxic concentrations of Al^{3+} [3]. After exposure, penetration of aluminium into plant roots occurred. Later the exudation of citric and malic acid was induced, in which toxic ions were exuded from the root tip cells of aluminium tolerant plants. These effects were not observed in aluminium sensitive roots. Organic acid excretion was demonstrated to be a mechanism of aluminium tolerance in higher plants. The most important role in these processes is played by citric acid [4]. In contrast to its beneficial role in the inhibition of aluminium absorption in plants, the gastrointestinal absorption of aluminium was markedly enhanced in the presence of citrate in rats [5–8] and in humans [9,10]. Serum, bone and tissue aluminium concentrations were considerably increased. It was presumed that citrate acts as a chelator for aluminium and that the Al-citrate complex in serum may play an important role in intracellular accumulation, and consequently in the toxicity of aluminium. In order to appraise the Al-citrate equilibrium complexes, the equilibrium reactions of citrate ion with aluminium have been studied by potentiometry and the ^{13}C NMR technique [11]. Due to its biological importance, the distribution of Al-citrate in biological samples was also frequently investigated by computer simulation. On the basis of known thermodynamic equilibrium constants, aluminium speciation was calculated in serum [12–15], blood plasma and in the gastrointestinal tract [16]. There have been many experimental studies performed on the binding of aluminium to serum constituents [17–23]. The reported data indicate that transferrin is the main high molecular weight aluminium complex, while Al-citrate was presumed to be the predominant low molecular weight serum species. The most frequently applied separation techniques in these studies were ultrafiltration and microultrafiltration [17,18], which were later combined with gel electrophoresis [20] and various chromatographic techniques [20,21]. On the basis of the systematic investigations of Medel's group [17,19–21] it was proved that approximately 88% of aluminium in spiked human serum is bound to transferrin and presumed that the remaining 12% of aluminium is bound as Al-citrate. In a recent publication quantitative determination of Al bound to transferrin in human serum was reported employing the anion-exchange FPLC-ETAAS technique [21]. Analogous observations were made by D'Haese et al. [22] who used a polymer-based weak anion-exchange column with ETAAS detection for speciation of aluminium in the serum of a dialysis patient. Aluminium speciation in serum from a patient with chronic renal failure was also investigated by FPLC gel chromatography with ETAAS detection [23]. The chromatographic peak which was presumed to correspond to Al-citrate was significantly increased when an excess of citric acid was added to serum. Speciation of Al-citrate was investigated employing the HPLC-ETAAS technique as well [24]. Various normal, reversed phase and mixed phase (ODS/-NH_2) columns were used, but the recoveries for Al-citrate were moderate and the method was not suitable for quantitation of Al-citrate in biological samples.

Since Al-citrate is very important in the understanding of aluminium bioavailability, there is a need to incorporate more detailed speciation data into studies of aluminium bioavailability and toxicity in biological systems [25,26]. Therefore, reliable and sensitive analytical procedures for determination of Al-citrate should be developed. In our recent investigation [27] a systematic study was performed of the quantitative determination of Al-citrate and some other negatively charged low molecular weight aluminium complexes by FPLC separation on a Mono Q HR 5/5 strong anion-exchange column with ICP-AES detection, using $NaNO_3$ as eluent. The applicability of the developed technique for speciation of Al-citrate in the majority of biological samples was limited due to its moderate sensitivity. The aim of the present work was therefore to lower the detection limits for speciation of Al-citrate to the low ng cm^{-3} concentration level. For this purpose the choice of an appropriate eluent which would enable quantitative separation of Al-citrate on a Mono Q HR 5/5 strong anion-exchange FPLC column and reli-

able determination of separated species by ETAAS, played a critical role. Gradient elution with NH_4NO_3 was investigated and the applicability of the method developed tested for the speciation of Al-citrate in spiked human serum samples.

2. Experimental

2.1. Apparatus

A strong anion-exchange FPLC column (Pharmacia, Sweeden) of Mono Q HR 5/5 (column dimensions 5 × 50 mm, 10 μm beaded hydrophilic polyether resin substituted with quaternary amine groups, pH stability 2–12) was employed for the separation of Al species. The column was connected to a Varian Star gradient high pressure pump, equipped with a Rheodyne Model 7161 injector (0.5 cm^3 loop). Separated aluminium species, as well as total aluminium, were determined by ETAAS on a Hitachi Z-8270 polarized Zeeman atomic absorption spectrophotometer equipped with an autosampler. An Iskra MA 5740 pH Meter with combined glass electrode was employed to determine the pH of samples. A Heraeus (Osterode, Germany) Model 17S Sepatech biofuge was used for centrifugation of human serum.

2.2. Reagents

Merck suprapur acids and water doubly distilled in quartz were used for the preparation of samples and standard solutions. All other chemicals were of analytical reagent grade.

A stock aluminium solution (100 μg Al cm^{-3}) was prepared in a 0.5 dm^3 calibration flask by dissolving 0.6952 g of $Al(NO_3)_3 \cdot 9H_2O$ (Riedel-de Haën) in water. A stock Al-citrate solution (100 μg of total Al cm^{-3}) was made weekly by mixing 0.6952 g of $Al(NO_3)_3 \cdot 9H_2O$ salt and 35.5 g of citric acid (Merck) (100:1 citric acid to Al molar ratio) in a 0.5 dm^3 calibration flask. The same stock solutions were used either for the preparation of standards for calibration in ETAAS determinations or for the preparation of synthetic standard solutions which were used in the investigations of aluminium speciation on the FPLC column. Solutions for spiking serum samples were prepared daily by dilution of an appropriate amount of stock Al^{3+} solution ($Al(NO_3)_3 \cdot 9H_2O$) with water. The concentrations of spiking solutions ranged from 2.0 to 10.0 μg Al cm^{-3}. The pH of spiking solutions was 5.5.

Imidazole ($C_3H_4N_2$) (0.2 mol dm^{-3}) (Merck) buffer solution with the addition of an appropriate amount of hydrochloric acid (0.1 mol dm^{-3}) (Merck) was used to adjust the pH of samples in the range 3.5–8.0. pH values higher than 8.0 were obtained by the addition of an appropriate amount of potassium hydroxide (0.5 mol dm^{-3}).

A total of 8 mol dm^{-3} ammonium nitrate eluent was prepared by dissolving 640.32 g of NH_4NO_3 in 1 dm^3 of water. Lower concentrations of NH_4NO_3 were prepared by dilution with water.

Chelex 100 (Na^+ form, 100–200 mesh) chelating ion-exchange resin (Sigma) and a silica based LiChrosorb RP-18 HPLC column (150 × 4.6 mm i.d.) were used for cleaning the reagents.

Centricon 30 concentrators (Amicon, Germany) with a nominal cut-off of 30000 Da were used in the ultramicrofiltration procedure of human serum.

2.3. Recommended cleaning procedures

To avoid contamination by extraneous aluminium, polyethylene or Teflon ware was used. Sample preparation, chromatographic separations and determination of aluminium by ETAAS were carried out under clean-room conditions (class 10000). Before use plastics were treated with 10% HNO_3 for 24 h, rinsed well with water and dried at room temperature.

In order to lower the blank in FPLC separations, the NH_4NO_3 solution which was used as eluent and the FPLC column itself was purified before use. Cleaning of the reagent was performed by a batch chelating ion-exchange procedure. A total of 5 g of Chelex 100 (Na^+ form, 100–200 mesh) was added to 1 dm^3 of 8 mol dm^{-3} ammonium nitrate solution and stirred for 24 h. After that the solution was decanted and passed through a silica based LiChrosorb RP-18 HPLC

column (flow rate 1 cm^3 min^{-1}) to remove traces of aluminium from the reagent. Applying this procedure the concentration of aluminium in the eluent was below 1 ng Al cm^{-3}. It was found experimentally that the supplied FPLC column contained trace amounts of aluminium as well. Namely, when samples with an excess of citrate (synthetic standard solutions, serum samples) were analysed, the recoveries obtained for Al-citrate were found to be much higher than 100%. Therefore, to obtain reliable results, efficient cleaning of the FPLC column before use in separation of Al-citrate at the ng cm^{-3} level, was of critical importance. For that purpose 0.5 cm^3 of 5 mol dm^{-3} citric acid was injected onto the column and the recommended separation procedure applied. The cleaning was repeated five times until the concentration of aluminium eluted under the chromatographic peak of Al-citrate was below 1 ng Al cm^{-3}.

A similar cleaning procedure was applied to remove traces of aluminium from the microultrafiltration membranes of Centricon 30 concentrators. A total of 2 cm^3 of 2 mol dm^{-3} citric acid was added to the microultrafiltration tubes and centrifuged for 60 min at 3000 rev min^{-1}. Then 2 cm^3 of 0.1 mol dm^{-3} citric acid was centrifuged under the same conditions. Application of 0.1 mol dm^{-3} citric acid was repeated twice. Using this cleaning procedure the concentration of aluminium in the filtrate was found to be below 1 ng Al cm^{-3}. Then followed washing of citric acid from membranes with water under the same centrifugation conditions. It was found experimentally that water efficiently removed traces of citric acid from the microultrafiltration membranes, when five repetitive centrifugations were applied.

2.4. Sample preparation

2.4.1. Synthetic solutions of Al-citrate

In the study of the distribution of aluminium species over a wide pH range the following procedure was applied for preparation of synthetic Al-citrate solutions. Buffer solution was first adjusted to the required pH. 45 cm^3 of buffer solution was then transferred to a 50 cm^3 volumetric flask. An appropriate amount of stock Al-citrate solution was added and the flask was filled to the mark with buffer solution.

2.4.2. Human serum

Blood from healthy volunteers was collected into aluminium/free Becton-Dickinson vacutainers without additives. Samples were immediately centrifuged for 10 min at 3000 rev min^{-1}. Serum was transferred into a Teflon flask with a polyethylene pipette to prepare a pooled sample and stored at 4°C. Analyses were done within 3 days.

2.5. Recommended FPLC-ETAAS procedure

A total of 0.5 cm^3 of the sample was injected onto the Mono Q HR 5/5 strong anion-exchange column. Separation of Al-citrate was performed by aqueous—(0–100% 4 mol dm^{-3} NH_4NO_3) linear gradient elution for 10 min at a flow rate of 1.0 cm^3 min^{-1}. The eluate was collected in 0.5 cm^3 fractions in Eppendorf polyethylene cups and the concentration of aluminium determined 'off line' by ETAAS at optimum measurement conditions (Table 1), using calibration with aqueous standard solutions. After each separation the column was regenerated for 5 min with 4 mol dm^{-3} NH_4NO_3 at a flow rate of 1 cm^3 min^{-1} and equilibrated with water firstly for 20 min at a flow rate of 2.0 cm^3 min^{-1} and in the following 5 min at a flow rate of 1.0 cm^3 min^{-1}.

3. Results and discussion

3.1. Development of the FPLC-ETAAS procedure

The method which has previously been developed in our laboratory [27] for quantitative determination of Al-citrate and some other negatively charged low molecular weight aluminium complexes by FPLC separation on a Mono Q HR 5/5 strong anion-exchange column with ICP-AES detection, was of limited application for speciation of Al-citrate in the majority of biological samples because of its moderate sensitivity. In order to lower the detection limits for speciation of Al-citrate to the low ng cm^{-3} concentration level, a

Table 1
Measurement parameters for determination of aluminium by ETAAS with Zeeman backround correction

Stage number	Stage	Temperature (°C)		Time (s)		Gas flow (cm^3 min^{-1})
		Start	End	Ramp	Hold	
1	Dry	60	90	15	5	200
2	Dry	90	100	10	10	200
3	Dry	100	150	20	10	200
4	Ash	150	1000	20	20	100
5	Atom	2700	2700	0	4	0
6	Clean	2800	2800	0	4	200
7	Cool			0	5	200

Wavelength, 309.3 nm; spectral bandwidth, 1.30 nm; lamp current, 10.0 mA; sample volume, 10 μl.

more sensitive technique, e.g. ETAAS needed to be applied for determination of separated aluminium species. For this purpose the choice of an appropriate eluent which would enable quantitative separation of Al-citrate on a Mono Q HR 5/5 strong anion-exchange FPLC column and reliable ETAAS determination of the separated species was of critical importance. $NaNO_3$ which was used as eluent in ICP-AES detection [27] was found to be a difficult matrix in ETAAS determinations due to the residual deposit in the graphite tube. The sensitivity of measurements changed during successive determinations, making the reliability of the results questionable. In addition, it was found that the purity of commercially available $NaNO_3$ was insufficient and the reagent was not easy to purify. Therefore, the use of other eluents was examined. $Mg(NO_3)_2$ was very clean and could be used without performing a cleaning procedure. Quantitative separation of Al-citrate was obtained applying aqueous-4 mol dm^{-3} $Mg(NO_3)_2$ linear gradient elution, but the same problems in ETAAS determinations as with $NaNO_3$ were observed. In addition, the column pressure was considerably increased due to the high density of the eluent which could shorten the column lifetime. So, the applicability of NH_4NO_3 as eluent was also investigated. It was found experimentally that to obtain quantitative separation of Al-citrate, at least 4 mol dm^{-3} NH_4NO_3 should be used in aqueous-NH_4NO_3 linear gradient elution, and efficient washing of the column with water applied before the next separation, as described under Section 2. During the chromatographic run the pH of the water-NH_4NO_3 eluent ranged from 7.0 to 6.0. The pH of the eluent did not influence the separation of Al-citrate either in synthetic samples or in human sera, since the former were buffered and the latter have their own buffer capacity. The NH_4NO_3 eluent also offered some important advantages. The column pressure was very low. The reagent could be efficiently purified when the recommended cleaning procedure was performed (Section 2). The main advantage of NH_4NO_3 lies in its ability to quantitatively decompose in the graphite tube to N_2O and H_2O at 210°C. So, careful drying and ashing of samples by a slow temperature ramp was performed as presented in Table 1. As very low amounts of NH_4NO_3 were introduced into the pyrolitically coated graphite tube, there was no possibility for a microexplosion during the heating period. Integrated absorbances were used for the calculation of aluminium concentrations. Although the concentration of NH_4NO_3 increased during the chromatographic run (gradient elution), determination of aluminium in the separated fractions was interference-free, due to the efficient matrix decomposition, and very reproducible measurements were obtained. Excellent agreement between the results was found when either the standard addition method or aqueous standard calibration was applied. Therefore, all determinations of aluminium in the eluted fractions were performed using calibration with aqueous standard solutions. A typical chro-

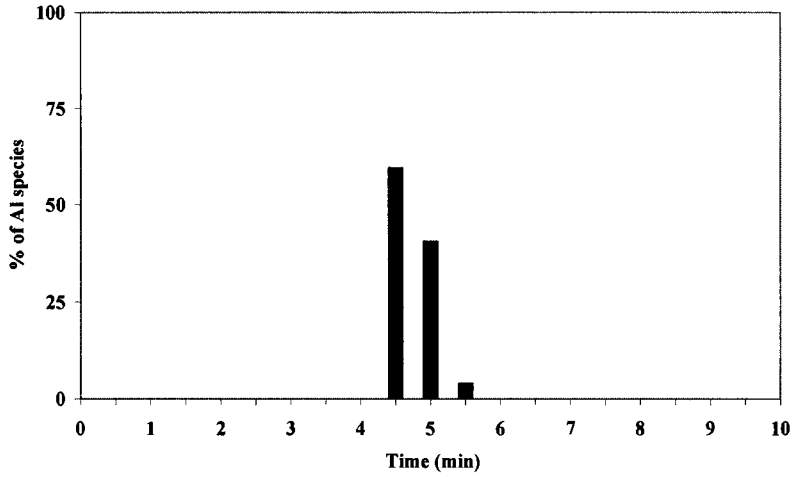

Fig. 1. Typical chromatogram of Al-citrate (100 ng Al cm^{-3}, 100 molar excess of citric acid) at pH = 7.4, separated on an anion-exchange FPLC Mono Q HR 5/5 column and detected by ETAAS with Zeeman correction. Sample volume 0.5 cm^3, aqueous-NH_4NO_3 (4 mol dm^{-3}) linear gradient elution, flow rate 1 cm^3 min^{-1}, fraction collection 0.5 cm^3, $n = 3$.

matogram for Al-citrate at pH 7.4, separated on an FPLC Mono Q HR 5/5 anion-exchange column with ETAAS detection is presented in Fig. 1. It is evident that negatively charged Al-citrate species are quantitatively eluted at this pH between 4.5 and 5.5 min with a maximum peak at a retention time of 4.5 min.

3.2. Validation of the FPLC-ETAAS procedure

In order to obtain reproducible results, the recommended cleaning, separation and detection procedures should be followed exactly. The reproducibility of measurements was tested for six consecutive separations of Al-citrate (100 ng Al cm^{-3}, pH = 7.4) and the results are presented in Table 2. From these data it can be seen that Al-citrate was quantitatively and reproducibly eluted at a retention time of 4.5 min. The recoveries were calculated on the basis of ratio between found and added aluminium concentrations and ranged from 96 to 101%. The reproducibility of the measurements was found to be $\pm 2\%$. The efficiency of Al-citrate separation was also tested in wide concentration range from 10.0 to 100 ng Al-citrate cm^{-3}. The results are summarized in Table 3. It is evident that reproducible and quantitative measurements were obtained even in the low concentration range (10 ng Al-citrate cm^{-3}). From the present data it is also evident that measurements are linear up to 100 ng Al-citrate cm^{-3}. When applying the recommended cleaning procedures the blank in the eluted fractions was found to be below 1.0 ng Al cm^{-3}. The limit of detection (LOD), calculated on a 3s basis (a value of three times the standard deviation of the blank), for separated Al-citrate species was 2.0 ng cm^{-3}.

3.3. Influence of pH on the distribution of aluminium species in synthetic samples of Al-citrate

In order to study the distribution of Al-citrate in the pH range from 3.5 to 8.0, synthetic solutions of Al-citrate were prepared at different pH values and chromatographic separations performed. The results are presented in Fig. 2. It is evident that negatively charged Al-citrate species were separated quantitatively at a retention time of 4.5 min in the pH range from 5.0 to 7.5. At pH values lower than 5.0 the percentage of negatively charged species decreased since a neutral Al-citrate complex fraction in the solution increased and was eluted at the retention time of 1.5 min. At pH 8.0 the percentage of negatively charged

Table 2
Reproducibility of measurements and efficiency of Al-citrate separation[a]

Synthetic solution of Al-citrate	Al-citrate added (ng cm^{-3})	Anion-exchange FPLC-ETAAS (ng cm^{-3})						Al-citrate found (ng cm^{-3})	Recovery %
		$t = 3.5$[b]	$t = 4.0$	$t = 4.5$	$t = 5.0$	$t = 5.5$	$t = 6.0$		
1. Replicate	99 ± 0.5	<LOD[c]	<LOD	67 ± 0.5	25 ± 0.5	4.5 ± 0.5	<LOD	97 ± 1	98 ± 1
2. Replicate	99 ± 0.5	<LOD	2.5 ± 0.5	58 ± 0.5	36 ± 0.5	3.5 ± 0.5	<LOD	100 ± 1	101 ± 1
3. Replicate	99 ± 0.5	<LOD	3.0 ± 0.5	53 ± 0.5	36 ± 0.5	3.0 ± 0.5	<LOD	95 ± 1	96 ± 1
4. Replicate	99 ± 0.5	<LOD	6.0 ± 0.5	52 ± 0.5	35 ± 0.5	3.0 ± 0.5	<LOD	96 ± 1	97 ± 1
5. Replicate	99 ± 0.5	<LOD	5.0 ± 0.5	51 ± 0.5	37 ± 0.5	4.0 ± 0.5	<LOD	97 ± 1	98 ± 1
6. Replicate	99 ± 0.5	<LOD	5.0 ± 0.5	50 ± 0.5	39 ± 0.5	5.5 ± 0.5	<LOD	99.5 ± 1	100 ± 1

[a] Al-citrate (100 ng Al cm^{-3}, 100:1 citric acid to Al molar ratio) at pH 7.4, tested for six consecutive determinations by employing anion-exchange FPLC with ETAAS detection (fraction collection 0.5 cm^3). Mono Q HR 5/5 column, sample volume 0.5 cm^3, aqueous-NH_4NO_3 (4 mol dm^{-3}) linear gradient elution, flow rate 1 cm^3 min^{-1}.
[b] t, time (min).
[c] LOD, limit of detection (0.8 ng cm^{-3}).
$\bar{x} = 98 \pm 2$; RSD = $\pm 2\%$.

Table 3
Linearity of measurement[a]

Al-citrate added (ng Al cm^{-3})	Anion-exchange FPLC-ETAAS (ng cm^{-3})						Al-citrate found (ng Al cm^{-3})	Recovery %
	t[b] = 3.5	t = 4.0	t = 4.5	t = 5.0	t = 5.5	t = 6.0		
9.5 ± 1	<LOD[c]	2.0 ± 0.5	4.0 ± 0.5	2.0 ± 0.5	<LOD	<LOD	9.0 ± 1	95 ± 1
27.5 ± 1	<LOD	8.0 ± 0.5	12.5 ± 0.5	6.0 ± 0.5	<LOD	<LOD	26.5 ± 1	96 ± 1
52 ± 1	<LOD	11.0 ± 0.5	28.0 ± 0.5	10.5 ± 0.5	<LOD	<LOD	50.0 ± 1	96 ± 1
72.5 ± 1	<LOD	9.5 ± 0.5	41.0 ± 0.5	23.5 ± 0.5	<LOD	<LOD	73.0 ± 1	101 ± 1
98 ± 1	<LOD	6.0 ± 0.5	50.0 ± 0.5	38.0 ± 0.5	5.0 ± 0.5	<LOD	99.0 ± 1	101 ± 1

[a] Determination of different Al-citrate concentrations in synthetic samples (100:1 citric acid to Al molar ratio) at pH 7.4, by employing anion-exchange FPLC with ETAAS detection (fraction collection 0.5 cm^3). Mono Q HR 5/5 column, sample volume 0.5 cm^3, aqueous-NH_4NO_3 (4 mol dm^{-3}) linear gradient elution, flow rate 1 cm^3 min^{-1}.
[b] t, time (min).
[c] LOD, limit of detection (0.8 ng cm^{-3}).

Al-citrate is slightly decreased due to the appearance of an $Al(OH)_4^-$ species which is eluted at the retention time of 2.0 min. The distribution of aluminium species versus pH from Fig. 2, in the presence of a 100 molar excess of citric acid, agreed with the reported calculated data of Martin [12,13] and of Venturini and Berthon [16] who performed their calculations based on thermodynamic equilibrium constants for the same aluminium concentrations and aluminium to citrate molar ratios.

It was found experimentally that in the pH range examined, positively charged monomeric aluminium species were strongly adsorbed on the resin column. These adsorbed species did not influence the following separations and were removed only by the recommended cleaning procedure.

3.4. Applicability of the developed FPLC-ETAAS procedure for determination of Al-citrate in spiked human serum

A pooled sample of human serum was used in the experiments. For determination of the total aluminium concentration in serum, a similar procedure as described by Wang et al. [28] was applied. Prior to analysis the sample was diluted 1:1 with a 0.2% (v/v) aqueous solution of TRITON X-100. Then the concentration of aluminium was determined by ETAAS at optimal measurement conditions (Table 1) employing the standard addition calibration method. The total aluminium concentration in the pooled serum was found to be 3.5 ± 0.5 ng cm^{-3} and was too low for speciation investigations. To perform speciation studies, samples were therefore spiked with various concentrations of aluminium. To 2 cm^3 of serum 0.05 cm^3 of an appropriate aqueous aluminium spiking solution was added, so that the final concentrations in spiked serum samples were 52 ± 3, 108 ± 3 and 130 ± 3 ng Al cm^{-3}. After spiking of samples the pH of the serum did not change. The concentrations of aluminium in spiked serum samples were similar to those which could be found in serum of haemodialysis patients [29]. The spiked serum samples were then microultrafiltered. In order to get enough sample for determination of ultrafiltrable aluminium by ETAAS and Al-citrate by FPLC-ETAAS, four filtrates of same spikes were combined. Separation and determination of aluminium species were performed under the recommended procedures. The results of these experiments are presented in Table 4. It is evident that in samples analysed about 15.5% of aluminium was ultrafiltrable, regardless of the total concentration of aluminium in the spiked serum. Ultrafiltrable aluminium was separated on the resin column and as evident a complete amount appeared at the retention time of Al-citrate, that is, the concentration of Al-citrate corresponded to the concentration of ultrafiltrable

Table 4
Determination of Al-citrate in spiked human serum by FPLC-ETAAS, $n = 2$

Concentration of Al in spiked serum (ng cm^{-3})	Concentration of ultrafiltrable Al[a] (ng cm^{-3})	% Of ultrafiltrable Al	Anion-exchange FPLC-ETAAS (ng cm^{-3})					% Of Al-citrate in spiked serum
			$t = 3.5$[b]	$t = 4.0$	$t = 4.5$	$t = 5.0$	$t = 5.5$	
52 ± 3	8 ± 1	15.4 ± 1	<LOD[c]	<LOD	6.0 ± 0.5	2.5 ± 0.5	<LOD	16.3 ± 1
108 ± 3	17 ± 1	15.7 ± 1	<LOD	5.5 ± 0.5	8.5 ± 0.5	2.5 ± 0.5	<LOD	15.2 ± 1
130 ± 3	20 ± 1	15.3 ± 1	<LOD	<LOD	17.5 ± 0.5	3.5 ± 0.5	<LOD	16.0 ± 1

[a] Microultrafiltration (cut off 30 000 Da), 1.5 h 3000 rev min^{-1}.
[b] t, time (min).
[c] LOD, limit of detection (0.8 ng cm^{-3}).

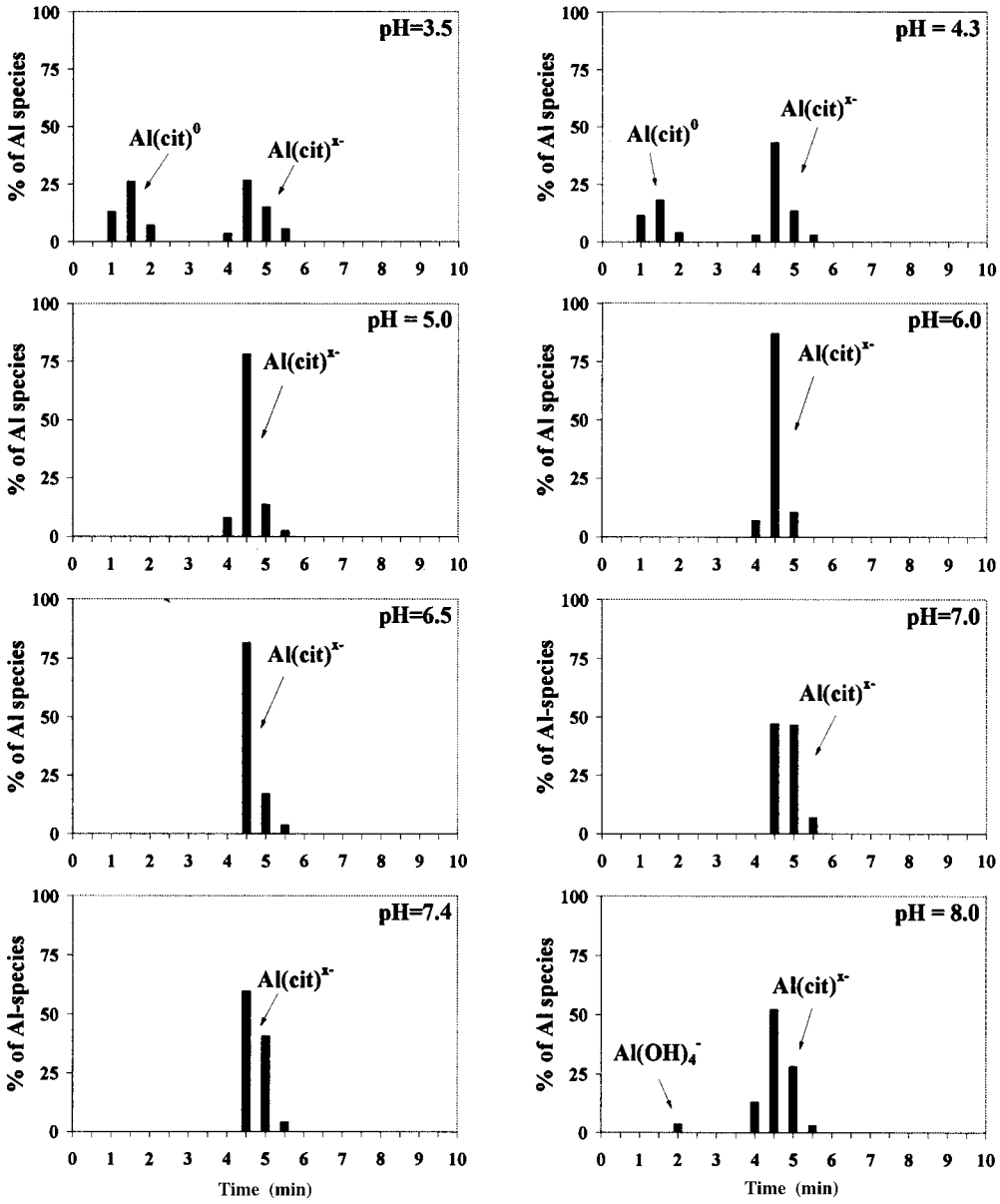

Fig. 2. Influence of pH on the distribution of Al species (100 ng Al cm^{-3}, 100 molar excess of citric acid) employing anion-exchange FPLC with detection by ETAAS with Zeeman correction (fraction collection 0.5 cm^3). The percentage of monomeric Al species in synthetic samples of Al-citrate was determined. The conditions were: Mono Q HR 5/5 column, sample volume 0.5 cm^3, aqueous-NH_4NO_3 (4 mol dm^{-3}) linear gradient elution, flow rate 1 cm^3 min^{-1}, $n = 3$.

aluminium. On the basis of these observations it can therefore be concluded that aluminium in spiked serum samples exists as citrate complex and was quantitatively determined. Its concentration matched with that of theoretical predictions [14,15].

In order to test the reproducibility of measurements in serum, another pooled sample was

Table 5
Reproducibility of measurement of Al-citrate in spiked human serum[a]

Spiked human serum (156 ± 2 ng Al cm^{-3})	Concentration of ultrafiltrable Al (ng cm^{-3})	% Of ultrafiltrable Al	Anion-exchange FPLC-ETAAS (ng cm^{-3})					% Of Al-citrate in spiked serum
			$t = 3.5$[b]	$t = 4.0$	$t = 4.5$	$t = 5.0$	$t = 5.5$	
1. Replicate	30 ± 1	19.2 ± 1	<LOD[c]	4.4 ± 0.5	18.5 ± 0.5	5.5 ± 0.5	<LOD	18.2 ± 1
2. Replicate	30 ± 1	19.2 ± 1	<LOD	5.1 ± 0.5	20.1 ± 0.5	4.5 ± 0.5	<LOD	19.0 ± 1
3. Replicate	30 ± 1	19.2 ± 1	<LOD	3.8 ± 0.5	23.5 ± 0.5	3.2 ± 0.5	<LOD	19.5 ± 1
4. Replicate	30 ± 1	19.2 ± 1	<LOD	3.6 ± 0.5	23.0 ± 0.5	2.8 ± 0.5	<LOD	18.8 ± 1
5. Replicate	30 ± 1	19.2 ± 1	<LOD	<LOD	26.5 ± 0.5	2.6 ± 0.5	<LOD	18.7 ± 1

RSD, $\pm 3\%$.
[a] Concentration of Al-citrate in spiked human serum (156 ± 2 ng Al cm^{-3}), tested for five consecutive determinations after microultracentrifugation (cut off 30 000 Da) by employing anion-exchange FPLC with ETAAS detection.
[b] t, time.
[c] LOD, limit of detection (0.8 ng cm^{-3}).

analysed. The total aluminium concentration in this serum sample was also found to be 3.5 ± 0.5 ng cm^{-3}. The sample was spiked (156 ± 2 ng Al cm^{-3}), microultrafiltered and speciation of Al-citrate was performed in the filtrate by injecting five consecutive sample aliquots on the resin column. The results of these measurements are presented in Table 5. It is evident from these data that reproducible retention times and good reproducibility of measurements (RSD $\pm$ 3%) were obtained after consecutive determinations. The percentage of ultrafiltrable aluminium and Al-citrate in spiked serum was about 19% and was slightly higher than that found in the sample which was used in the experiments presented in Table 4. Although only two different pool samples were analysed, it can be concluded that the percentage of ultrafiltrable aluminium and consequently of Al-citrate is not constant and could slightly vary in different samples. Similar observations were reported in the literature [20] where ultrafiltrable aluminium in spiked serum was found to be about 12 ± 5%.

The LOD for Al-citrate in serum samples ($3s$ basis) was found to be 2.0 ng cm^{-3}.

4. Conclusions

A method was developed for separation and quantitative determination of negatively charged Al-citrate at ng cm^{-3} concentration level. Separation was done on a Mono Q HR 5/5 strong anion-exchange column, using aqueous-4 mol dm^{-3} NH_4NO_3 gradient elution. Al-citrate was quantitatively and reproducibly separated at a retention time of 4.5 min. Separated aluminium species were determined 'off line' by ETAAS. Since NH_4NO_3 decomposed quantitatively in the graphite tube during the ashing step, very reproducible measurements of aluminium were obtained. The analytical procedure developed was successfully employed in speciation of Al-citrate in spiked human serum. It was experimentally proved that microultrafiltrable (cut-off 30000 Da) aluminium in spiked serum corresponds to Al-citrate, which until now was only theoretically predicted.

Acknowledgements

The authors would like to thank the Ministry of Science and Technology of Slovenia for financial support of the present work.

References

[1] G. Sposito, The Environmental Chemistry of Aluminium, CRC Press, Boca Raton, FL, 1989, p. 125,126.
[2] J.D. Ownby, H.R. Popham, J. Plant Physiol. 135 (1989) 588.
[3] R.A. Jorge, P. Arruda, Phytochemistry 45 (1997) 675.
[4] J.M. de la Fuente, V. Ramírez-Rodríguez, J.L. Cabrera-Ponce, L. Herrera-Estrella, Science 276 (1997) 1566.
[5] P. Slanina, Y Falkeborn, Food Chem. Toxicol. 22 (1984) 391.
[6] J.W. Coburn, M.G. Mischel, W.G. Goodman, I.B. Salusky, Am. J. Kidney Dis. 16 (1991) 708.
[7] B. Quartley, G. Esselmont, A. Taylor, M. Dobrota, Food Chem. Toxic. 31 (1993) 543.
[8] M.F. van Ginkel, G.B. van der Voet, P.C. D'Haese, M.E. De Broe, F.A. de Wolff, J. Lab. Clin. Med. 121 (1993) 453.
[9] J.S. Lindberg, J.B. Copley, K.G. Koenig, H.M. Cuhner, South. Med. J. 86 (1993) 1385.
[10] D.C. Ackley, R.A. Yokel, Toxicology 120 (1997) 89.
[11] J.E. Gregor, H. Kipton, J. Powell, Aust. J. Chem. 39 (1986) 1851.
[12] R.B. Martin, Clin. Chem. 32 (10) (1986) 1797.
[13] R.B. Martin, J. Inorg. Biochem. 28 (1986) 181.
[14] W.R. Harris, Clin. Chem. 38 (9) (1992) 1809.
[15] L.O. Öhman, R.B. Martin, Clin. Chem. 40 (4) (1994) 598.
[16] M. Venturini, G. Berthon, J. Inorg. Biochem. 37 (1989) 69.
[17] J. Pérez Parajón, E. Blanco González, J.B. Cannata, A. Sanz-Medel, Tr. Elem. Med. 6 (1989) 41.
[18] H.B. Röllin, C.M.C.A. Nogueira, Eur. J. Clin. Chem. Clin. Biochem. 35 (1997) 215.
[19] J.I. García Alonso, A. López García, J. Pérez Parajón, E. Blanco González, A. Sanz Medel, J.B. Cannata, Clin. Chim. Acta 189 (1990) 69.
[20] Kat. Wróbel, E.B. González, Kaz. Wróbel, A. Sanz-Medel, Analyst 120 (1995) 809.
[21] A.B. Soldado Cabezuelo, E. Blanco González, A. Sanz Medel, Analyst 122 (1997) 573.
[22] P.C. D'Haese, G.F. Van Landeghem, L. V. Lamberts, M.E. De Broe, Mikrochim. Acta 120 (1995) 83.
[23] F.Y. Leung, A.E. Niblock, C. Braadley, A.R. Henderson, Sci. Total Environ. 71 (1988) 49.
[24] A.K. Datta, P.J. Wedlund, R.A. Yokel, J. Trace Elem. Electrolytes Health Dis. 4 (1990) 107.

[25] W.R. Harris, G. Berthon, J.P. Day, C. Exley, T.P. Flaten, W.F. Forbes, T. Kiss, C. Orvig, P.F. Zatta, J. Toxicol. Environ. Health 48 (1996) 543.
[26] T.P. Flaten, A.C. Alfrey, J.D. Birchall, J. Savory, R.A. Yokel, J. Toxicol. Environ. Health 48 (1996) 527.
[27] T. Bantan, R. Milacic, B. Pihlar, Talanta 46 (1998) 227.
[28] S.T. Wang, S. Pizzolato, H.P Demshar, J. Anal. Toxicol. 15 (1991) 66.
[29] E. Kaneko, H. Hoshino, T. Yotsuyanagi, N. Gunji, M. Sato, T. Kikuta, M. Yuasa, Anal. Chem. 63 (1991) 2219.

ELSEVIER

Talanta 47 (1998) 943–969

Talanta

Monitoring and characterization of polyaromatic compounds in the environment

T. Vo-Dinh [a,*], J. Fetzer [b], A.D. Campiglia [c]

[a] *Oak Ridge National Laboratory, Advanced Monitoring Development Group, Oak Ridge, TN 37831-6101, USA*
[b] *Chevron Research and Technology Co., Richmond, CA 94802, USA*
[c] *North Dakota State University, Fargo, ND 58105-5516, USA*

Received 17 February 1998; received in revised form 15 April 1998; accepted 21 April 1998

Abstract

This paper provides an overview of analytical techniques and instruments used to monitor and characterize polycyclic aromatic compounds (PACs) in the environment. The basic operating principles of various analytical approaches and systems are presented. The review deals specifically with spectroscopic methods, chromatographic and hyphenated techniques, and field monitoring devices. Emphasis is given to portable devices that can be used under field conditions. Specific examples of analytical techniques and instruments developed in the authors's laboratories will be discussed to illustrate the usefulness and potential of these approaches for environmental monitoring and characterization of PACs. © 1998 Elsevier Science B.V. All rights reserved.

Keywords: Polyaromatic compound; Polyaromatic hydrocarbon; Chromatography; Hyphenated technique; Vapor dosimeter; Multispectral imaging; Biosensor

1. Introduction

Polycyclic aromatic compounds (PACs), which comprise a complex class of condensed multi-ring benzenoid compounds, are important environmental pollutants originating from a wide variety of natural and anthropogenic sources. PACs are generally formed during incomplete combustion or pyrolysis of organic matter containing carbon and hydrogen. Because combustion of organic materials is involved in countless natural processes or human activities, PACs are omnipresent and abundant pollutants in air, soil and water. Among energy-related products, fossil fuels are the major sources of PACs. The primary sources of airborne PACs are associated with combustion, coal coking, and petroleum catalytic cracking. Coal and shale conversion also contribute to production of PACs. Production, transportation and, use of synthetic fuels and petroleum products provide emission sources for PACs. In urban environments an important source of PACs is diesel exhaust. Food cooking and cigarette smoking activities contribute to PAC occurrence in indoor environments.

* Corresponding author. Tel.: +1 615 5746249; fax: +1 615 5767651; e-mail vodinht@ornl.gov

0039-9140/98/$ - see front matter © 1998 Elsevier Science B.V. All rights reserved.
PII S0039-9140(98)00162-3

The parent homocyclic species, which contain only carbon and hydrogen, are the familiar polyaromatic hydrocarbon (PAH) compounds. In addition to the PAH compounds, there are thousands of substituted compounds that could have various substitutuent groups, such as alkyl, amino, chloro, cyano, hydroxy, oxy, or thio groups. Also there is a wide spectrum of PAH heterocyclic derivatives that contain one or several heteroatoms such as nitrogen, oxygen, or sulfur in the aromatic structure. Over the past few decades, the family of PACs has been called by various names, e.g. polycyclic organic compounds (POCs), polycyclic organic matter (POM), polynuclear aromatic (PNA) compounds. Historically, the term 'PAH' has been most widely used because the early interest was devoted to carcinogenic activities of the basic homocyclic system. Benzo[*a*]pyrene (BaP), which has been extensively investigated, is the most familiar PAH compound. In this review the term PAC is used to include both heterocyclic and homocyclic compounds whereas the term PAH is used to designate only homocyclic hydrocarbons.

Chemical analysis of PACs is of great environmental and toxicological interest because many of them have been shown to be mutagens and/or potent carcinogens in laboratory animal assays [1,2]. More than two centuries ago, skin cancer was observed in chimney sweeps, and later on in workers at tar factories. It was earlier observed that frequent contact with soot and tar materials were correlated with the incidence of skin cancer. The carcinogenic activity of these soot and tar materials was later associated with their PAC contents. Dibenz[*a*,*h*]anthracene and benzo[*a*]pyrene were among the first polyaromatic compounds identified as chemical carcinogens. Now, a wide variety of polycyclic hydrocarbons were synthesized and tested for carcinogenicity, and the toxicity of PAC is no longer in question. The parent class of homocyclic polyaromatic hydrocarbons was first investigated in the 1960 and 1970s. The research focus on polyaromatics has subsequently evolved from investigation of the parent PAHs to the study of PAC systems. The change of focus from the basic homocyclic polyaromatic compounds to heterocyclic PACs is due to the realization that not only homocyclic aromatic compounds but also heterocyclic systems contribute to the biological activities encountered in many environmental samples. Many heterocyclic PACs are produced in conjunction with their parent PAH compounds. From both epidemiological and experimental studies, many heterocyclic PACs are highly suspect as etiologic agents in human cancer.

This paper provides an overview of analytical techniques and instruments used to monitor and characterize PACs in the environment. The basic operating principles of various analytical approaches and systems are presented. The review deals specifically with spectroscopic methods, chromatographic and hyphenated techniques, and field monitoring devices. Emphasis is given to portable devices that can be used under field conditions. Specific examples of analytical techniques and instruments developed in the authors's laboratories will be discussed to illustrate the usefulness and potential of these approaches for environmental monitoring and characterization of PACs.

2. Spectroscopic analysis of polyaromatic compounds

Due to the intrinsically strong fluorescence emission from the rigid π-electron systems of PACs, fluorescence spectroscopy has been utilized extensively for PAC identification and quantification in environmental samples [3]. Ultraviolet (UV) absorption spectroscopy, which has been widely used in conjunction with chromatographic separations, will be discussed in Section 3 on hyphenated techniques.

2.1. Fluorescence spectroscopy

Fluorimetry at room temperature is a simple method of analysis which offers the advantages of inexpensive instrumentation, excellent dynamic ranges, and limits of detection at the ng ml^{-1} level [4]. In most analyses, deoxygenation of the sample is not critical and fluorescence measurements are rapidly performed. The sample is

placed in a quartz cell and excited with ultraviolet or visible light in a spectrofluorimeter. The excitation source is usually a xenon arc lamp operated at high pressure for continuous radiation between 200 and 800 nm. The appropriate excitation wavelength may be selected by means of an excitation monochromator. The detection system consists of an emission monochromator, which selects the luminescence wavelength region of interest; the photodetector—usually a photomultiplier tube—which converts the luminescent radiance flux to an electrical signal; and the amplifier-readout system, which amplifies and processes the signal as required and displays it in a convenient fashion. A computer may be interfaced to the spectrofluorimeter for data acquisition and instrument control.

A spectrofluorimeter with a dual sample-reference measurement capability may be used to compensate for instrumental distortions such as source intensity fluctuations and wavelength dependence, efficiency of the excitation wavelength selector and optical components, and wavelength dependence of detector response. Several accessories are commercially available, which can be used to collect corrected excitation spectra [5].

Conventional fluorimetric methods—in which either the excitation or emission wavelength is set at its maximum position while the other is scanned—present limited selectivity. The similarity and/or overlapping of broad fluorescence bands at room temperature usually interferes in the characterization process of single components. Several luminescence techniques have been developed to improve the selectivity of fluorescence measurements. These include temporal (lifetime) resolution [6], analysis of excitation-emission matrices (EEM) of fluorescence intensity [7], and narrowing of fluorescence peaks with the use of supersonic jets [8], matrix isolation [9], and Shpolskii effect [10].

A relatively simple and rapid approach for the simultaneous analysis of multicomponent mixtures is the synchronous excitation technique. This approach consists of varying simultaneously both the excitation (λ_{ex}) and emission (λ_{em}) wavelengths while keeping a constant wavelength interval $\delta\lambda(=\lambda_{em}-\lambda_{ex})$ between them. The advantages of synchronous excitation include narrowing of spectral bandwidth, simplification of emission spectra, reduction of the spectral range for a given analyte, and easy compensation for Rayleigh and Raman scatter. Unlike EEM methods, synchronous excitation can be performed with any commercial spectrofluorimeter in which excitation and emission monochromators can be interlocked.

Originally proposed by Lloyd for spectral fingerprinting of oil samples in forensic analysis [11], synchronous excitation was further developed by Vo-Dinh for the determination of PACs in multicomponent mixtures [12,13]. The technique was demonstrated to be an attractive alternative for the preliminary screening of environmental samples [14–16], and for on-site luminescence analysis of contaminated samples [17–20].

The use of laser sources in molecular luminescence has several advantages over traditional spectrofluorimeters. Since the radiance of a laser is greater than that of a conventional source with typical excitation bandpass values, laser excitation increases the sensitivity of fluorimetric methods and often improves the limits of detection. Laser-induced fluorescence, therefore, has been employed as a detection technique for monitoring of trace organic pollutants in a wide variety of environmental samples. Recent applications include the determination of chlorinated hydrocarbons in gas mixtures [21], the analysis of petroleum hydrocarbons in natural waters [22], and real-time measurement of dioxins in combustion sources [23].

Stevenson and Vo-Dinh [24,25] demonstrated the advantage of using laser excitation for the analysis of PACs by synchronous luminescence spectroscopy. Because of the small value of the wavelength interval ($\delta\lambda$) usually employed in synchronous excitation [12,13], the use of large excitation slits with commercial spectrofluorimeters may create undesired scattering and stray light interferences. The sensitivity of the synchronous method, therefore, is usually limited by the use of narrow slits. The high irradiance of the laser source—associated to the narrow linewidth of the laser beam—allows one to use small $\delta\lambda$ values

and still achieve high sensitivities without loss of spectral resolution. Limits of detection at the zeptomole (10^{-21} mole) level were estimated for several PACs without previous separation from complex matrices.

The high coupling efficiency of lasers to fiber optics can be useful in remote sensing applications. Laser-induced fluorimetry with optical fibers is a promising approach for the detection of PACs in environmental samples [26–32]. A highly selective sensor towards pyrene and other PAHs was obtained by immobilizing β-cyclodextrin at the tip of an optical fiber [26]. Fluorescence from PAHs excited with a He–Cd laser (325 nm) was detected with limits of detection at the nanomolar level. The high selectivity of the device towards PAHs resulted from the hydrophobic nature of the β-cyclodextrin tip, which did not form stable complexes with other heterocyclic compounds usually present in contaminated samples.

The selectivity of fluorescence sensors can be improved by time-resolved fluorimetry [27–32]. The addition of an independent parameter such as time to the emission spectra of complex PACs mixtures reduces the overlapping of fluorescence bands. By using a pulsed nitrogen laser as excitation source, limits of detection at the pg ml^{-1} level are usually obtained.

2.2. Phosphorescence spectroscopy

According to the experimental procedure, phosphorimetry can be divided in four different techniques, which include solution low-temperature phosphorimetry (LTP), micelle-stabilized room-temperature phosphorimetry (MS–RTP), sensitized room-temperature phosphorimetry in liquid solutions (sensitized-RTPL), and solid-surface room-temperature phosphorimetry (SS–RTP).

Until 1975, most work involving phosphorescence was carried out at low temperature (e.g. 77 K). By the use of cryogenic equipment, the solutions were frozen to form a rigid matrix to minimize collisions competing with phosphorescence for the deactivation of the triplet state. Since then, very little has been done in the area of LTP. The lack of widespread use can be attributed to three major reasons. The high cost of cryogenic equipment and liquid coolant, the time-consuming deoxygenation of the solvent in order to avoid quenching effects, and the inconvenient procedure to introduce the sample into the cooling system.

Micelle-stabilized room-temperature phosphorimetry in aqueous solution was first applied as an analytical method by Cline-Love and co-workers [33,34]. Micellar solutions consist of colloidal aggregates of surfactants or detergents which protect the phosphorescing triplet state of the analytes from external quenchers and vibrational deactivation. The use of MS–RTP in routine analysis is restricted by the long sample processing time resulting from the necessity of thorough sample deoxygenation. There are, nevertheless, considerable advantages in the use of the micellar method. The RTP analysis of large polycyclic aromatic non-polar compounds in aqueous solutions is facilitated by the high solubility of this species in the micellar environment. In addition, MS–RTP offers a means to conduct phosphorescence analysis in flow systems and liquid chromatography.

RTP detection in continuous flows and chromatographic systems can be also performed by means of sensitized RTPL [35–37]. In this technique, the weakly or non-phosphorescent analyte (donor) transfers its triplet energy to a given acceptor. A suitable acceptor should have a triplet energy lower than that of a donor, a high quantum phosphorescence yield, and a lower molar absorption in the excitation region of the donor. In addition, the energy gap between the triplet states of the donor and the acceptor should be large enough to prevent significant reverse mechanisms. So far, the most appropriate acceptor tested for the technique has been biacetyl [35]. Limits of detection in the nanomolar range were obtained by flow injection of several poly-halogenated naphthalenes and biphenyls, and liquid chromatography analysis of mixtures of chlorinated naphthalenes, biphenyls, and dibenzofurans [36]. Several advantages justify the use of sensitized-RTPL as a detection technique. It is inherently more sensitive than ultraviolet absorption, the background noise due to scattering and fluorescing impurities is negligible at the emission of biacetyl (522 nm), and it is particularly selective

since all the constituents of the sample do not produce the sensitized phosphorescence signal of the acceptor. Further research, however, is necessary to develop new acceptor systems and extend the application potential of sensitized-RTPL.

In the early 1970s, Schulman and Walling [38,39] reported the emission of phosphorescence from analyte solutions deposited on solid substrates. In contrast to LTP, the sample preparation procedure was very simple and required no more than 10 min per sample. Following these early reports, a large number of studies dealing with the optimization of experimental parameters affecting the sensitivity and selectivity of SS–RTP have appeared in the literature [40,41]. Depending on the analyte, solid surface, and experimental conditions, calibration curves with linear dynamic ranges of 10^2–10^3 fold change in analyte concentration, limits of detection in the nanogram or sub-nanogram level, and relative standard deviations from 5 to 15% can be obtained with commercial spectrofluorimeters. To distinguish between fluorescence and phosphorescence emission, the instrument should have a phosphoroscope or a pulsed-source gated detection system. The simplicity of the sampling procedure, elimination of the need for cryogenic equipment, and the possibility of automation have turned SS–RTP into the most popular phosphorimetry technique of the last two decades.

In the specific case of PACs, SS–RTP has shown to be a sensitive and selective technique [42–54]. In general, filter paper has been the substrate of choice, and thallium(I) appears to be the most effective phosphorescence enhancer [42,43,47,50]. In certain cases, the sensitivity of the technique has been improved by the use of matrix-modified filter paper substrates. Diethylene triaminepentaacetic acid, cyclodextrin, and sodium dodecyl sulfate are just a few of the many compounds used to modify the surface of the filter paper and induce—or enhance—PACs RTP emission [47,52–54].

If selective monitoring of targeted components in complex matrices is of interest, selective external heavy-atom perturbation (SEHAP) [45,49], second-derivative [46], and synchronous excitation [44] techniques can be employed to reach the desired selectivity.

SEHAP was first developed by Vo-Dinh and Hooyman [45] for the analysis of targeted PACs in complex mixtures. It is based on the appropriate choice of a heavy atom salt and a set of measurement wavelengths to enhance the phosphorescence emission of the target compound and minimize the spectral interference from other components of the mixture. By using lead(II) acetate and 390/690 nm as a set of wavelengths ($\lambda_{ex}/\lambda_{em}$), the authors [45] were able to determine benzo[*a*]pyrene at the nanogram level in a synthetic mixture containing acridine, carbazole, dibenzocarbazole, and fluoranthene in about 200-fold excess.

Spectral interferences can be considerably reduced by synchronous phosphorimetry. Vo-Dinh and Gammage [44] introduced the synchronous excitation technique to phosphorescence analysis on solid substrates. The technique was employed to facilitate the differentiation between dibenzanthracene (DBA) isomers—1,2,3,4-DBA and 1,2,5,6-DBA—which is made difficult by spectral overlapping in conventional SS–RTP. It was possible to detect 4.2 ng of 1,2,5,6-DBA in a binary mixture containing ten-fold excess of 1,2,3,4-DBA.

Other alternatives to improve the selectivity of SS–RTP analysis include the use of a separation technique prior to RTP detection. Several workers have proposed paper (PC) and thin-layer chromatography (TLC) prior to SS–RTP detection [55,56]. The unique possibility of complete analysis of a complex mixture using the same substrate turns PC–SS–RTP and TLC–SS–RTP combinations into relatively simple and useful tools for analytical purposes.

SS–RTP has also been employed as a detection technique for high performance liquid chromatography (HPLC) [40,57]. Filter paper discs were utilized by Vo-Dinh and Hiromoto [40] to quantitatively determine benzo[*a*]pyrene and benzo[*e*]pyrene in coal liquid samples. Ford and Hurtubise [57] used silica chromatoplates to identify benzo[*f*]quinoline and phenanthridine in shale oil sample. In both cases [40,57], the HPLC fractions were manually collected and spotted onto the substrates for RTP detection.

An SS–RTP automated system [58,59] was later developed for HPLC detection which completely eliminated the manual steps of previous procedures [60]. The eluent from the chromatographic column was sprayed onto a moving filter paper strip with a concentric nebulizer. An autoanalyzer continuous filter was employed to pull the filter through the sample compartment of the spectrofluorimeter. A laboratory-constructed filter paper guide was used to perform all RTP measurements in a continuous mode. A kinetic program permitted plotting the phosphorescence intensity as a function of time. By selecting the appropriate set of measurement wavelengths (λ_{ex}/λ_{em}), it was possible to characterize a single component of a mixture of PAHs partially resolved by HPLC. This feature, associated to SEHAP and synchronous excitation, makes the SS–RTP detector a useful tool for liquid chromatographic operations. Complex systems can be separated into simpler ones, and the individual components of a simple mixture can be selectively determined by choosing the appropriate set of experimental conditions. Furthermore, the SS–RTP detector allows the identification of compounds either from the retention times or from their phosphorescence characteristics. An additional parameter for identification is certainly valuable for qualitative purposes.

A novel approach for the analysis of complex mixtures was recently developed [61]. It consists of an acousto-optic tunable filter (AOTF)-based imaging spectrometer for SS–RTP analysis. A He–Cd laser was used as an excitation source, and a cooled two dimensional CCD was employed as a detector. The new system will be valuable in the analysis of complex mixtures involving paper and thin-layer chromatography. By imaging phosphorescence spots of partially separated mixtures, overlapped compounds with similar R_f ratios can be identified at their maximum wavelengths of emission. Further identification can be performed by spectral characterization of a selected section of the chromatogram. Using this approach, complex mixtures can be separated into simpler ones, and the individual characterization of target compounds can be accomplished on the solid substrate without further elution or extraction procedures. The quantitative determination of a target compound can be performed by comparing the phosphorescence intensity of its area of deposition with those from standard solutions spotted on the same solid substrate. This aspect is of valuable use in the analysis of complex mixtures without previous separation. The developed system, however, did not have the capability of performing lifetime discrimination among short-lived phenomena and phosphorescence emission. Future improvements of the original system should include: (i) the use of an intensified CCD to increase the analyte-to-background signal ratios for short analysis times; and (ii) the introduction of lifetime measurement capability. These additional features will turn the SS–RTP imaging spectrometer into a powerful instrument for fundamental and applied studies.

Very few attempts have been made to improve the sensitivity of SS–RTP analysis with the use of lasers as excitation sources. Laser-induced SS–RTP was first reported by Vo-Dinh and Uziel [62]. A He–Cd continuous-wave laser was used to detect benzo[*a*]pyrene-*r*-7-*t*-8,9,10-tetrahydrotetrol (a benzo[*a*]pyrene–DNA adduct derivative) on filter paper substrates. Trace levels of derivative were detected without previous separation from the biological mixture.

Laser-induced SS–RTP was later employed for the analysis of PACs in complex mixtures [63,64]. A nitrogen laser and a dye laser were employed as the excitation source. For all the studied compounds, the limits of detection obtained with the laser system were at the pg level. The levels of detection estimated with a commercial spectrofluorimeter were at the ng level. The drastic improvement obtained by laser-induced SS–RTP was due to the high irradiance of the laser source, and the small area probed by the laser beam on the solid substrate. This combination results in the capability of measuring nl volumes of sample with good reproducibility. Within the linear dynamic ranges of the studied PACs, the relative standard deviations varied between 7 (phenanthrene) and 9.5% (chrysene). The precision of measurements obtained with a spectrofluorimeter for the same analyte mass deposited on the paper substrate varied from 31 (phenanthrene) to 41%

(1,2-benzofluorene). The high values obtained with the commercial system were the result of the simultaneous detection of analyte signal and background emission from the solid substrate. Although a relatively small excitation slit was used for the measurements (10 nm), the irradiated area on the paper substrate was still larger than the analyte spot. When smaller excitation slits were employed (5 nm), very weak or no phosphorescence signals were observed. By focusing the laser beam on the solid substrate, one can selectively excite the sample spot and avoid excitation of background materials.

The low limits of detection and good reproducibility obtained by laser-induced SS–RTP resulted in a simple experimental procedure for the analysis PACs in a contaminated soil sample [64]. Since the evaporation of the extracting solvent was not necessary to pre-concentrate the sample, the direct deposition of the extract on the paper substrate was sufficient to determine several PACs at the ng level. The RTP detection technique, which has been used in a fiberoptic RTP sensor [65,66] developed for PAC monitoring, will be described in Section 4.3.

3. Chromatography and hyphenated techniques

Environmental analysis of PACs by chromatographic methods remains a very active area, both in the development of new methodologies and new instrumental approaches, and in the examination of different types of samples. The predominant problem in PAC analyses is the determination of the species. With the wide variety of structural types and the large numbers of isomeric compounds, this is a demanding challenge. Often neither the separation or detection method alone can accomplish this; both a very structurally selective separation and a detection method that gives some additional information in the identification of the chromatographic peaks are necessary. For the purposes of this section of the review, hyphenated techniques will refer to the use of sequential chromatographic steps or to the use of detectors that have historically not been widely used as chromatographic detectors.

3.1. Gas chromatography

Gas chromatography (GC) has in the past been limited by column stability to only the more volatile PACs. This translated into the smaller PAHs of up to around 300 molecular weight. Sulfur-containing hydrocarbon species, such as thiophenes, and aromatic sulfides and mercaptans, are also as volatile as the PAHs because the sulfur atom is only weakly polarizable and does not form strong hydrogen bonds. For the other heteroatom-containing PACs, the need for volatility often meant that only species having molecular weights smaller than that of the parent homocyclic compoundscouyld be used for analysis. For the more polar, and stronger hydrogen bonding, oxygen- and nitrogen-containing PACs, volatility is very small.

The development of higher-temperature columns has greatly extended the range of PACs for GC analysis. These columns rely either on the separation occurring on the activated wall of the fused silica column or with special cross-linked polymeric phases. High-temperature GC has been used for PAHs of up to 424 molecular weight, $C_{34}H_{14}$, in a coal tar pitch standard reference material [67,68]. At these temperature, and with the high resolution of GC, many isomers are seen. The lack of authentic standard compounds limited the identification of the peaks to only a small number.

The most dramatic improvement in separation selectivity in GC has been the development of phases that differentiate the shapes of the analytes. Liquid-crystal stationary phases have shown a high degree of selectivity in separating PAH isomers [69,70]. The orderly nature of this phase is the key to separating isomers. Structural features such as the length-to-width ratio and the presence of internal features that induce non-planarity have been shown to control the separation. It is thought that these structural features determine the permeation of the PAHs into the stationary phase and the subsequent degree of interaction between the PAH and the liquid crystal. This separation mechanism is thought to be identical to that found in the separation of PAHs on polymeric reversed-phase HPLC columns, which

will be discussed in detail below. These phases have been used successfully to determine isomeric PAHs of environmental interest [71,72].

For nitrogen-containing PACs, the chemiluminescence nitrogen detector (CLND) has been shown to provide selective and sensitive detection [73]. Fig. 1 shows a pair of chromatograms of a liquid chromatographic fraction of a river sediment sample. The upper curve is the FID trace, showing both the PAHs and the nitrogen PACs. This chromatogram is complex and peak identification is difficult. The lower curve is a simultaneous trace from a CLND (the sample flow was split before detection). The individual nitrogen PACs are easily resolved, making retention time comparison to standard compounds much easier.

Two detectors are now commonly used for the sulfur-containing PACs, the flame photometric detector (FPD) and the chemiluminescence detector. The FPD was used to determine thiophenic PACs in crude oils and refined petroleum products [74,75]. This detector has a severe nonlinear response, which is due to the fact that the light-emitting process is induced by a two-sulfur-atom mechanism. The chemiluminescence sulfur detector does not suffer from this problem, and has been used to detect sulfur PACs in refined petroleum products [76].

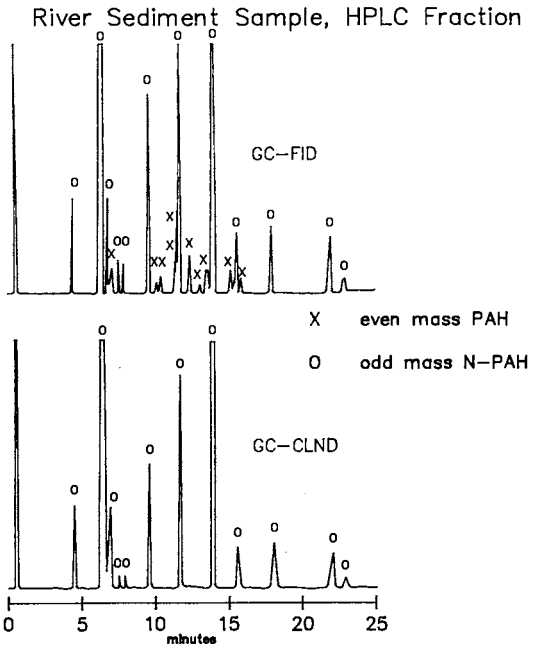

Fig. 1. Chromatograms showing the FID and CLND responses for a river sediment extract (Courtesy of Antek, Houston, TX).

For laboratory analyses mass spectrometry (MS) remains as the most widely used GC detector in characterization of PACs. In two recent symposia on PACs, of the 26 papers presented that used GC as the chromatographic methods, 22 used MS detection (either solely or in combination with other detectors), three used FID alone, and one used FTIR detection [77,78]. It is the mandated regulatory method for determination of PAHs in ambient air and in effluent water samples. It also gives some structural information, particularly if the chemical ionization mode is used. For PAHs, the ratio of the M and $M+1$ has been shown to be specific for isomers and correlates to the ionization potential. Simonsick and Hites [79,80] used molecular modeling to predict ionization potentials for the GC peaks in which no standard compound was available, and gave tentative identifications to several eight- and nine-ring PAHs. They used a variety of standards to check this approach. Daishima and Iida used a similar approach to differentiate PAC isomers [81].

Gas chromatography with an atomic emission detector (AED) provides monitoring of GC peaks for almost any heteroatom. The atomic emission is provided by a plasma source, usually a microwave induced plasma. The atomic emission of several elements is monitored simultaneously with a diode array. The AED can also detect carbon and hydrogen, giving it universal detection capabilities like FID. It can also detect deuterium, so the use of deuterated compounds as surrogates for recovery determination in sample extraction and preparation is comparable to MS. The ability to determine several elements makes identification of unknown peaks easier. In two similar studies, Boduszynski and co-workers [82] and Andersson and Sielex [83] have used GC-AED to characterize sulfur-containing PACs in crude oil fractions.

3.2. Liquid chromatography

For laboratory analyses HPLC has become the most widely applicable mode of chromatography for PACs because it is amenable for a separation range from the very non-polar PAHs and sulfur-containing PACs to the very polar classes such as the phenolics and those with sulfur and nitrogen in higher oxidation states (i.e. nitro-PAHs, sulfoxides, sulfones, etc.).

Normal-phase HPLC is sometimes used as a fractionation step before subsequent separation by reversed phase. This mode of chromatography can separate polar PACs from the PAHs, and even separate the PAHs by the number of bonds. These phases, however, only have moderate success at separating isomers [84]. Normal-phase HPLC was used to isolate three- and four-ring fractions from a variety of sediment samples. Subsequent separation by reversed phase yielded fractions that were analyzed for specific methyl-substituted phenanthrenes and chrysenes [85].

3.2.1. Shape-selective separations

The HPLC mode that has found to be the best at separating isomers is the use of a shape-selective reversed-phase column. The mechanisms that control PAH retention in reversed-phase HPLC, and particularly the ability of a phase to separate isomers, have been widely studied. Briefly, the bonded-phase moieties are structured to be large. Steric effects between adjacent moieties limits their movements, and they tend to orient themselves into very structured phases. Typically the commonly used octadecyl (ODS) moiety is bound to the silica surface through the use of a monochlorosilane. The shape-selective phases, however, use di-and trichlorosilanes. Under controlled conditions, these result in oligomeric moieties in which each segment contains an ODS side chain. These very large, bulky moieties array themselves into sheets of hydrocarbon material, parallel to each other and perpendicular to the silica surface. This type of phase has become commonly called a polymeric ODS phase, to differentiate it from the monomeric (monofunctionally derived) ODS phases. The separation mechanisms of PAHs on polymeric ODS have been widely investigated [86–98].

Recent work has extended this approach to include very long-chain phases of thirty carbons or more (at these high carbon numbers, the phases give very ordered structures for monochlorosilanes), and rigid planar moieties, such as the pyrenyl bonded phase. These phases exhibit the same selectivities for non-planar versus planar and length-to-breadth ratio as the polymeric ODS phase. Fig. 2 shows chromatograms of the PAHs found in a carbon black extract. It shows both the wide-range of ring numbers and the good resolution between isomers that a polymeric ODS column can achieve [73].

3.2.2. Detection in HPLC

The area of research and development in HPLC that has advanced the greatest in the past decade is the availability of multi-dimensional detectors. In the past, UV absorbance detection at a single wavelength or fluorescence detection at fixed excitation and emission wavelengths were the only trace level detection approach. Although these were often useful, they were also very frequently prone to interferences or a lack of selectivity or sensitivity. Several of the following sections will describe multi-dimensional detection methods that are now possible.

3.2.2.1. 'Full spectrum' UV detectors. Some PACs, and in particular the PAHs, exhibit characteristic UV absorbance spectra. The UV spectra arise from electronic transitions. The intensities of these transitions and their energies are predominantly determined by the arrangement of the aromatic rings in the molecules. Fig. 3 shows an example of the very different spectra obtained for similar nine-ring isomeric structures of formula $C_{32}H_{16}$. Since the arrangement of the rings in a PAH is unique, the UV absorbance spectrum for each PAH is a fingerprint.

Ring substitution, particularly by alkyl groups, effects the location of the UV absorbance bands only slightly, resulting in a red-shift of only a few nanometers for each alkyl linkage. Typically an alkyl group red-shifts the spectrum 1–2 nm. A saturated ring causes a shift of 5–10 nm, depending on whether the saturated ring consists of two, three, or four additional carbon atoms. Alkyl

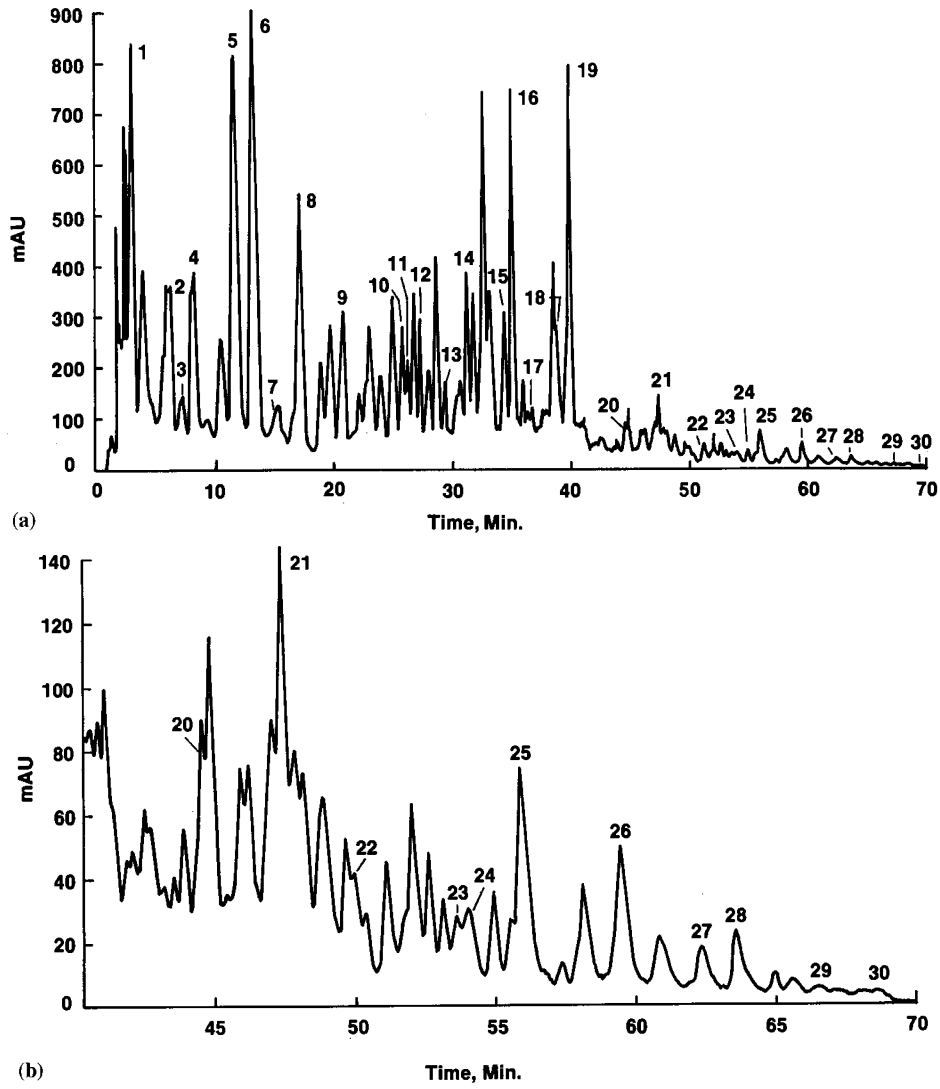

Fig. 2. HPLC Chromatogram of a carbon black extract separated on a polymeric ODS phase. (The numbers of the chromatographic peaks correspond to those of the PAC species.)

substitution has no effect on the pattern of the spectral bands.

These spectral characteristics of PAHs have led to the wide use of a new type of UV absorbance detector in the past decade. An HPLC detector that can obtain the complete UV spectra of eluents has become readily available. The photodiode array detector (PDA), often referred to as the diode array detector (DAD), relies on a very different optical arrangement than the older single-wavelength detectors. Single wavelength detectors operate through dispersion of a light source into the full spectrum, and transmission of a single wavelength through the detector flow-cell. The resulting chromatogram is a monitoring of the absorbance at that single wavelength. The PDA passes the total light through the flow-cell, with dispersion into the individual wavelengths afterwards. The dispersed light is focused on an array of photosensitive diodes that are spatially

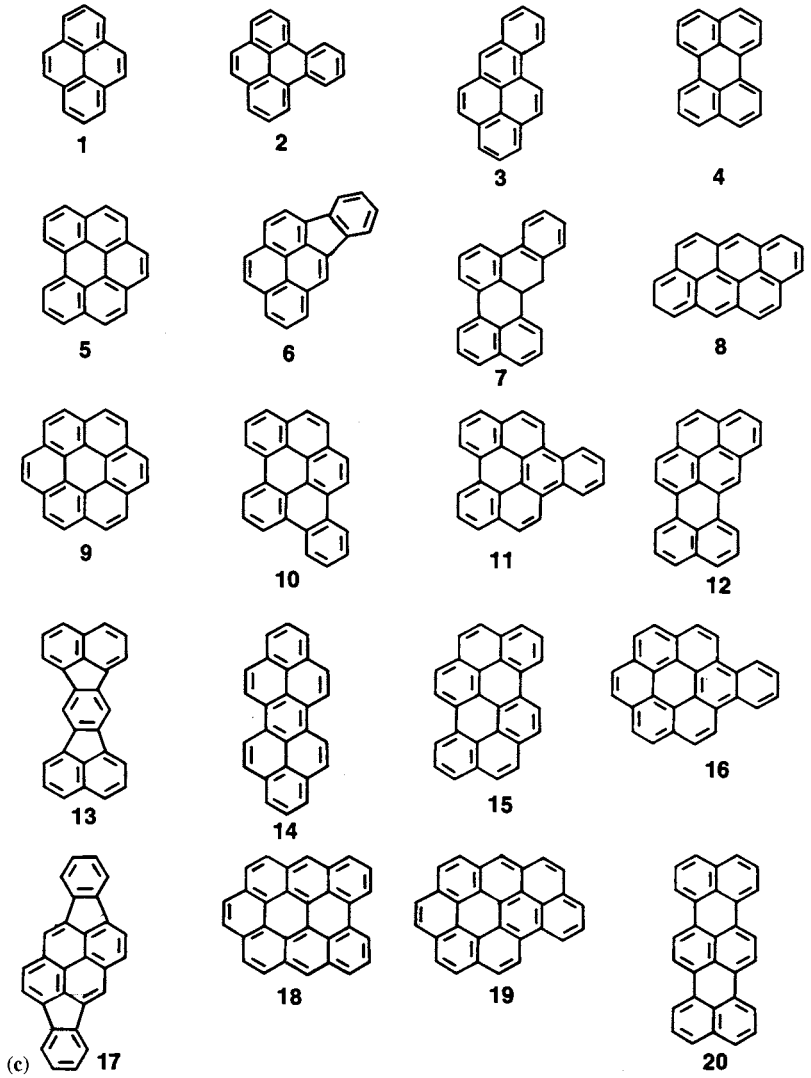

Fig. 2. (*Continued*)

arranged in order to simultaneously detect light at different wavelengths. Thus, the amount of light absorbed by eluents can be monitored across the whole spectral range.

With spectral resolutions typically of 1 nm or less, and a spectral range from 200 to 800 nm in some cases, the DAD can be used to identify a wide variety of PACs. The dynamic intensity range in which interpretable spectra can be collected is from a few thousandths of an absorbance unit (AU) up to 2 or 3 AU.

The HPLC–DAD was used to determine the PAHs present in a coal tar pitch [99] and the PAHs and fullerenes produced in acetylene-rich flames, and in the electrolytic condensation of benzene and toluene [100–102]. These uses highlight both the capabilities of HPLC–DAD and the ease that PAHs are produced. HPLC DAD was used to identify the PAHs present in fumes from asphalts used in roofing and road paving under normal operations [103]. A similar method was used to determine the PAHs found in refinery

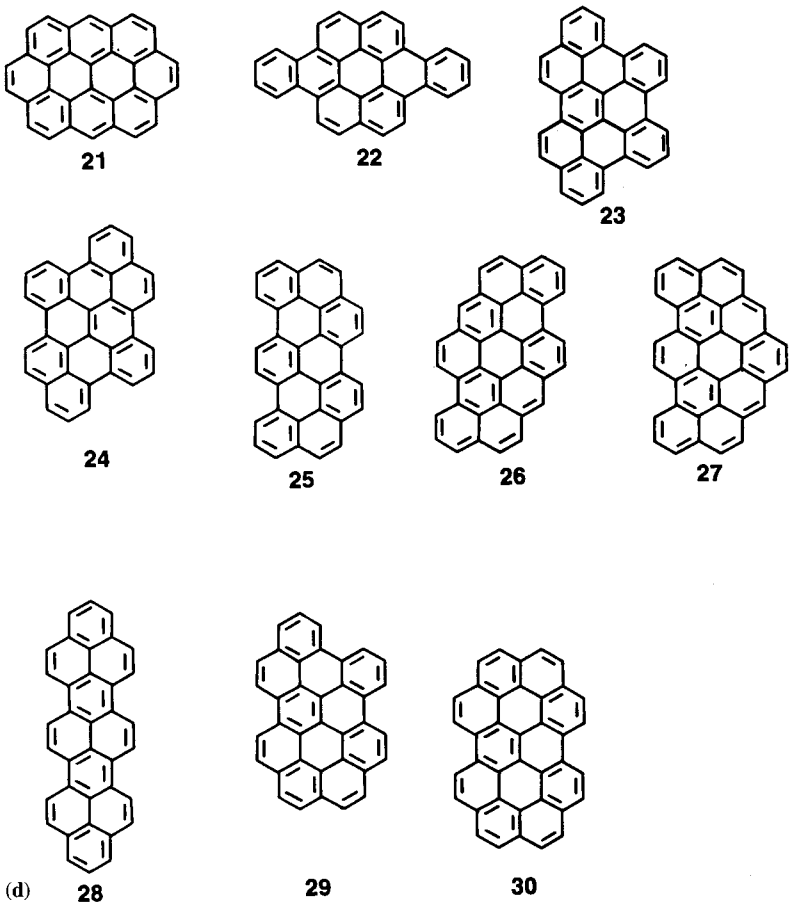

Fig. 2. (*Continued*)

effluent waters that had been treated by bioremediation [104].

Large PAHs were found in samples collected from areas of hydrothermal activity using HPLC–DAD [105,106]. The deep-sea rift areas, such as in the Middle Valley area near the Juan de Fuca trench and the Escanaba Trough in the northeastern Pacific Ocean and in the Guaymas Basin in the Gulf of California, had benzo[*ghi*]perylene, coronene, ovalene, and several other PAHs of six through ten rings. Less geothermally active areas, such as Yellowstone Park in Wyoming had smaller PAHs such as pyrene and coronene. In some cases the peaks were collected and additionally characterized by low-temperature Shpolskii spectrometry. It is thought that the PAHs are formed through the action of the super-heated water on the organic sediment.

3.2.2.2. Use of mobile-phase modifiers in fluorescence detection. For environmental analysis of PACs, fluorescence detection is widely used. The high sensitivity inherent to fluorescence, has been augmented over the years by the commercial availability of programmable detectors. These detectors allow the excitation and emission wavelengths to be changed throughout the chromatographic run, allowing the analyst to specifically target certain compounds during windows around its retention time. This type of detection, although very useful in many cases, does not always work. This section, and those following, will describe certain alternate approaches.

Selective fluorescence quenching has been used to detect alternant structures (i.e. containing only six-member rings) or non-alternant PAHs (structures containing also five-member, seven-member rings, etc.) [107,108]. A quenching reagent, such as nitromethane, is added to the mobile phase. The fluorescence of alternant PAHs is totally quenched, while that of non-alternant PAHs is unaffected. Micelle-forming reagent modifiers have been used in aqueous reversed-phase to both increase sensitivity and selectivity [109–112]. The sensitivity improvement is due to partitioning into the lipophilic micelles, which increases the effective concentrations. Selective quenching reagents can also be added to micellar solutions.

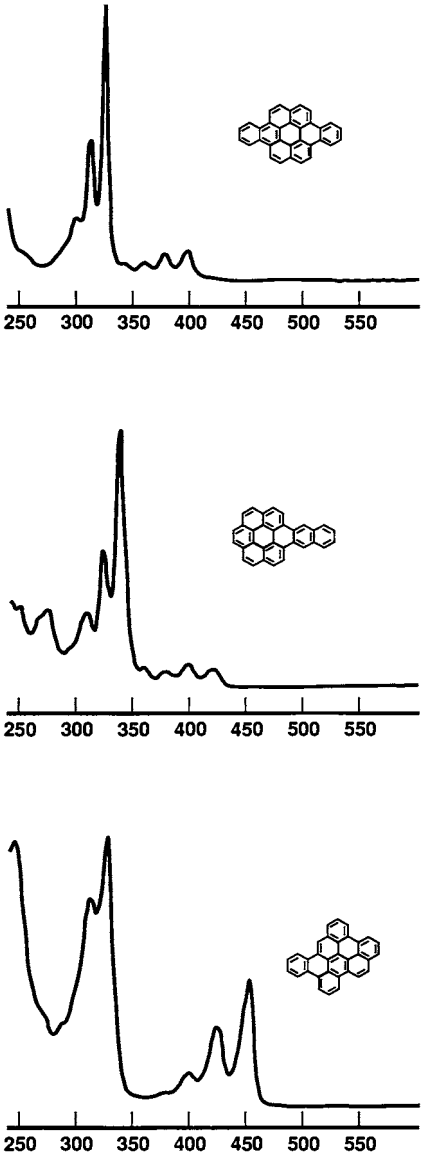

Fig. 3. UV Spectra of three nine-ring PAHs of 400 molecular weight illustrating the spectral selectivity for the different isomeric structures.

3.2.2.3. Multi-dimensional fluorescence detection. A variety of sophisticated fluorescence detectors have recently been used for PAHs. These include detection of the fluorescence lifetimes and collection of the full 3-dimensional spectra of each eluting species. In order to understand the unique capabilities of each of these types of detectors, relevant background on some principles of fluorescence spectrometry will be briefly mentioned here.

As discussed previously in Section 2, the complete fluorescence spectra of a compound is also called its excitation–emission matrix (or EEM, for short) or 3-D spectrum. It consists of an array of emission spectra collected a various incrementally increasing excitation wavelengths (or vice versa). The resulting contour map is a fingerprint for that PAH [113]. Spectrally the EEMs for individual PAHs are independent of each other and total intensities are additive (in the case of possible co-elution).

The low levels of emitted light are an inherent problem in this type of detection. In normal fluorescence spectrometers, photomultipliers greatly increase the signal. This approach is not amenable to simultaneous detection of hundreds of wavelengths because of the size of a photomultiplier

An early study used an optical multichannel analyzer to collect the emission spectra of eluents [114]. Data was collected by photographing the images on an oscilloscope. The aromatics in a petroleum spill sample were examined. Hershberger, Callis, and Christian [115] used a videofluorimeter, based on a Vidicon television-type camera, to collect emission spectra.

Other studies have used a photodiode array in an analogous mode to that described for UV absorbance detection. Fogarty et al. [116] used a

videofluorometer to collect the EEMs of standard mixtures of PAHs. They used a dye laser as the excitation source, and an intensified diode array as the detector. This more elaborate detection apparatus can collect the total EEM as a function of time. Data manipulation software can then display the data in one of several modes including individual EEMs, the excitation spectra as a function of retention time, or the emission spectra as a function of retention time.

Gluckman et al. [117] used spectral subtraction to determine the PAHs in extracts of carbonaceous materials. They collected the emission spectra of eluting PACs under constant excitation. Charge-coupled devices have also been used for this type of detection.

A much less expensive and commercially available alternative has arisen in the past few years. Fluorescence spectrometers can now scan at rates of many hundreds of nanometers per second. This allows collection of the on-the-fly spectra of chromatographic peaks if a flow cell is used. Ferrer et al. [118] used this approach to collect full EEMs of PAHs in a standard mixture and a variety of water samples. They used retention time windows for certain target compounds, and scanned small (50×50 nm) EEM ranges that were optimized for each of the various PAHs. This approach is now readily possible with commercial fluorometers (Hitachi Instruments, personal communication).

Additionally another dimension to fluorescence detection is applicable. The excited states of fluorescent molecules are very short lived. Emission of the light occurs in the picosecond to microsecond range. This is much, much less than the time scale of the chromatography. Pulsed laser sources and fast detection optics allow the fluorescence decay of the molecules to be monitored as each peak elutes through the flow cell. This novel area of fluorescence detection was reviewed by Smalley and McGown [119]. It has been applied to the ultra-trace level determination of PAHs in a variety of environmentally related samples [120].

3.3. Supercritical fluid chromatography

The supercritical fluid chromatography (SFC) has been used in a variety of separations. This mode of chromatography has both the narrow peaks and fast analysis times inherent to GC (because of the large diffusion coefficients of analytes in the mobile phase) and the separation variables of mobile and stationary phase common in HPLC. Additionally, supercritical fluid extraction (SFE) as an initial sample preparation step can be fully integrated so that SFE-SFC is commonly used [121]. This allows efficient sample preparation, under automation, as an integral part of the chromatographic run. SFC-DAD is now commercially available as an SFC detector (with the use of high-pressure flow cells), and has been used for trace level determination of PAHs in a variety of matrices.

Other detector types, such as MS, FTIR, and atomic-emission detector (AED), have not yet been applied much to environmental analyses. The basic principles of these methods were recently reviewed in a volume edited by Jinno [122]. In the case of MS, the biggest hurdles are the coupling of the large volumes of vaporized carbon dioxide in the column eluent to the MS vacuum system and the effect of the carbon dioxide on the mass spectra. There have been few chemical ionization reference spectra collected with carbon dioxide as the reagent gas, so the spectra collected in SFC–MS must be compared to those of standards. In SFC–FTIR, the supercritical fluid is usually not transparent in many spectral regions of interest. One report uses capillary SFC with xenon as the fluid to get around this problem [123]. Post-column collection of the peaks for off-line FTIR is also a solution to this problem [124].

4. Environmental monitors for PACs

4.1. Vapor dosimeter

Various vapor monitoring devices have been developed for personnel dosimetry [125]; many devices are based on the earlier studies by Palmes and Lindenboom [126]. Some of these vapor monitors operate via gaseous diffusion, generally employing some sorbent materials such as activated charcoal for vapor adsorption. The adsorbed spe-

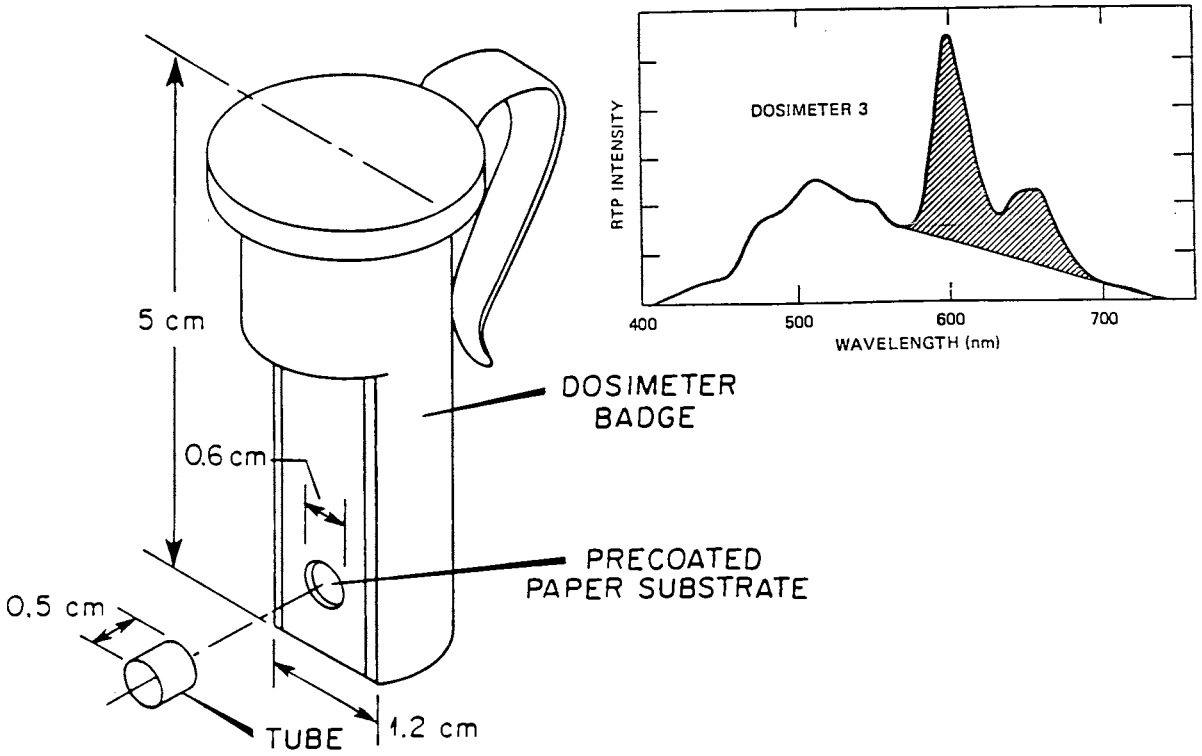

Fig. 4. The vapor dosimeter for polyaromatic compounds. The insert (upper right curve) shows the RTP spectrum of pyrene vapor (shaded area) detected at an industrial site.

cies are subsequently extracted from the charcoal using an appropriate organic solvent; the resulting solution is then concentrated and analyzed generally by chromatographic procedures. A direct-reading personal dosimeter have been developed to detect vapors of PACs [127]. This dosimeter for PAC is different from the previous vapor monitoring devices. The device employs the room temperature phosphorescence (RTP) technique for direct measurement of the amount of analyte collected on the dosimeter, requiring no sample desorption or wet-chemical extraction procedure. The time-weighted average exposure to the chemical vapors can be determined on the dosimeter substrate.

The RTP dosimeter is a self-contained, badge-size passive monitor. The device weighs about 30 g and can be conveniently worn by a person or placed at a stationary location. The operating principle of the RTP dosimeter is based on the combination of three processes: 1) sample collection via a diffusion controlled process, 2) adsorption of the analyte molecule on a substrate, and 3) direct detection using the RTP technique.

Fig. 4 shows a schematic illustration of the dosimeter. The dosimeter is designed to be compatible with the Raman spectrophotometers currently used for measuring the RTP signal. The dosimeter shown in Fig. 4 basically consists of a badge-size sample holder, a RTP-active substrate, and an interchangeable diffusion tube. The dosimeter body is a 4.0-cm long and 1.0-cm wide pen-size badge made of aluminum. The sample collection area is a circle having 0.5 cm diameter.

The screen device serves to prevent air turbulence from affecting the diffusion process within the dosimeter. The type of diffusion chamber used in the version of the dosimeter investigated here consists of a honeycomb tube which is composed of parallel cylindric holds of 0.01 m diameter and

0.04 m length. The use of a honeycomb is effective in preventing artifacts caused by turbulent mass transport in windy environments. The honeycomb decreases the effective value of the sample collection area, S, and therefore the sampling rate, but increases the reproducibility of the method of sampling. With the honeycomb tube, it is not necessary to cover the open end of the diffusion tube with a windscreen since the honeycomb geometry can effectively prevent disruption of the diffusion process by ambient air movements. Vapor collection of the dosimeter is based on molecular diffusion. A solid sorbent material is placed at the closed end ($x = 0$) of the tube while the open inlet of the tube ($x = L$) is exposed to the outside concentration, C_0 of analyte vapor molecules. The heart of the RTP dosimeter is the sample collection material that consists of RTP-active substrate. One of the unique features of this dosimeter involves the combined use of the sample substrate as a sample holder for in situ detection, a sorbent medium for diffusion and a phosphorescence signal amplifier for direct measurement. The sorbent material maintains the concentration of the analyte compounds at the collection surface at zero or near-zero concentration, C_s, while the air outside the dosimeter is at ambient concentration. A concentration gradient is therefore maintained, which serves as a driving force inducing the diffusion of the analyte molecules from the outside of the dosimeter onto the RTP-active surface.

The unique feature of this dosimeter is the dual mode of the RTP substrate that serves both as a sample collector/sorbent and as a phosphorescence signal amplifier using the external heavy-atom effect [128]. A variety of solid heavy-atom salts have been found to increase the RTP signal of many organic compounds by several orders of magnitude. The procedures developed for analyzing the dosimeters are extremely simple since the dosimeters can be inserted into a detector for direct reading of the integrated exposure immediately after exposure.

Measurements were conducted to detect vapors of a variety of PAC compounds including acridine, chrysene, fluorene, phenanthrene and pyrene [127]. The RTP spectrum of pyrene vapor at 1 ppb can be easily detected after only 1 h exposure. The presence of pyrene can be clearly detected in the vapors emitted by a complex sample such as a coal liquefaction product. In an 8-h exposure study, the dosimeter response was linear over the entire time period, with no indication of substrate saturation, even at 8 h. The results demonstrated that the dosimeter can be designed to produce a response linear to the exposure time for over 8 h under saturated equilibrium vapor conditions. This feature is important for quantitative applications where daily occupational exposure of workers for 8 h work day shifts is generally monitored.

There is a strong need for practical monitoring devices for personal exposure to PAC vapors and aerosols. An important factor in health effects assessment is our knowledge of personnel exposures to pollutants. Until the development of the RTP dosimeter, there was no practical device suitable for large-scale monitoring of chemical vapors or aerosols. Conventional procedures to monitor these species generally involves time-consuming sample collection and extraction procedures, and laboratory identification and quantification of the extracted materials. These procedures are usually elaborate, costly, and not suitable for routine applications of field measurements. The passive RTP monitor could provide a simple and low-cost approach for monitoring chemical vapors and obtain the much needed information on human exposure to potentially hazardous pollutants.

4.2. Portable field monitors

There is an increase in demand for portable environmental instruments for PACs, particularly for ground water monitoring and hazardous waste site assessment. This demands has led to increased efforts for the development of practical techniques and instrument capable of rapid screening contaminants under field conditions. This approach leads to shorter turnaround analysis time and improved cost effectiveness for environmental monitoring and remediation. A battery-operated portable synchronous luminescence monitor has been developed to address this

environmental screening need [129]. Developed for on-site analysis of ground water and hazardous waste sites, this instrument is capable of emission, excitation and synchronous luminescence measurements. The device is suited for trace analysis of important pollutants such as PACs, creosotes and polychlorinated biphenyls (PCBs). One important application of the device is the characterization of gasoline and petroleum oil spills. A commercial system of the device (Environmental Systems, Knoxville, TN) has been successfully used to assess contaminated soils and underground gasoline leaks. The usefulness of the monitor is illustrated by comparing the SL scan of an actual spill oil with its source oil provided by the US Coast Guard. The same characteristic peaks at 285, 308, 332, 397, and 441 nm appear in the oil spill sample as well as in the source oil sample.

A portable luminescence spectrometer based on a dual acousto-optic tunable filters (AOTF) system has been developed [130,131]. In contrast to a grating monochromator, an AOTF offers the advantage of having no moving parts and can be scanned at very high rates (millisecond time scale) without the possibility of error due to gear backlash or other mechanical problems. These characteristics, combined with the small size of these devices, make AOTFs an important new alternative to conventional monochromators, especially for field instrumentation.

4.3. Remote in situ sensors

The development of remote in situ monitors for detection of trace quantities of toxic chemicals is critical to the achievement of environmentally viable and safe technologies. In order to detect minute amounts of a compound in a complex 'real-life' sample, sensors must be able not only to differentiate compounds having different molecular sizes but also to identify specific substituents and/or derivative chemical groups attached to the basic structure. Contaminants in environmental samples frequently encompass a wide variety of chemical species. Due to the generally complex nature of hazardous wastes, several techniques are often required to provide unambiguous identification and accurate quantification of the trace contaminants.

4.3.1. Fluorescence monitors

A remote fiberoptic fluorescence monitor has been developed in our laboratory to detect PAHs on a real-time basis. The device, which was based on a pulsed nitrogen laser and gated CCD detector, was used to evaluate the efficacy of autotropic biofilms for removing PAH contaminants from industrial wastewater. This portable system could detect anthracence at ppb concentration levels in 10 μs [132]. Another monitor using the laser-based synchronous luminescence (LSL) technique has been developed for detection of PAC contaminants [133]. The LSL system was designed to allow several different laser dyes to be used in a single scan (a 'multi-dye scan'), thereby extending the wavelength range of the scan. When the laser wavelength reached the edge of the lasing region of one dye, the control program paused to allow a manual insertion of a new dye solution before continuing the scan. The process of dye exchange was rapid; only a few seconds elapsed before scanning was resumed. Due to the simplicity of the dye laser used, no realignment was necessary when switching between dyes. The wavelength regions scanned by different laser dyes in a multi-dye scan need not be continuous, and can use different wavelength separation ($\delta\lambda$) values. In the multi-dye scanning mode, the same $\delta\lambda$ values are used for all laser dyes, and the different dyes 'overlap' at the extremes of their scanning ranges [133].

The LSL monitor could employ standard cuvette sample holders as well as fiberoptic probes for remote sensing. When the fiber probe was used, the cuvette holder was replaced with a flat mirror with a small hole in its center. The end of the 3-m fiber probe was mounted behind the mirror so that the laser light passed through the hole in the mirror and onto the fiber's proximal end (Fig. 5). The probe consisted of a single fiber, which was used to transmit laser light to the sample and to collect the fluorescence. The fluorescence emitted from the fiber was reflected by the mirror toward the monochromator's collection optics. Only a small fraction (5%) of

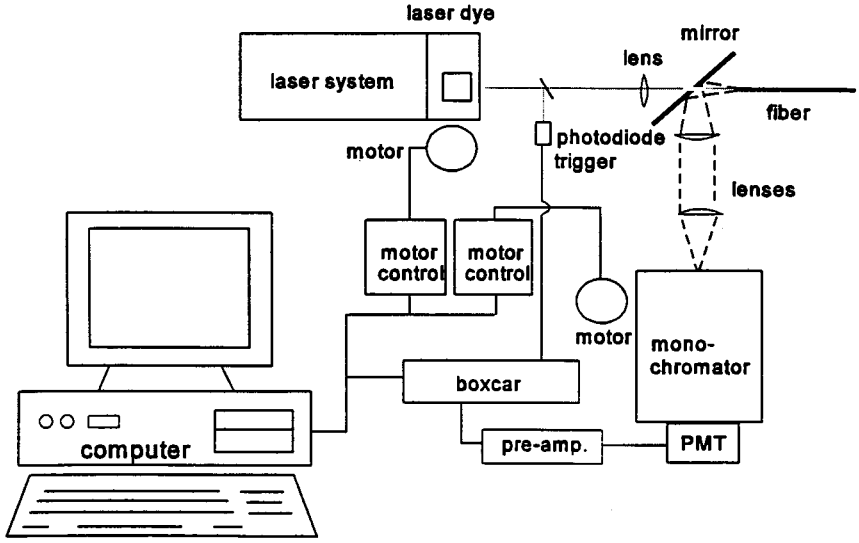

Fig. 5. Schematic diagram of the laser synchronous fluorescence fiberoptic sensor.

fluorescence was lost through the hole in the mirror. The position of the lenses was adjusted to optimize for the best laser-to-fiber coupling efficiency (~85%) and fluorescence collection efficiency.

An illustration of the usefulness of the LSL monitor involved analysis of multi-component mixtures using the fiberoptic probe [133]. In this analysis, the mixture consisted of 1.8 ppb of benzo[*a*]pyrene (BaP) and 10-ppb perylene in water. A $\delta\lambda = 25$ nm was used to achieve optimal BaP fluorescence; if a smaller dl were used perylene would exhibit a single peak. A boxcar gate delay of 5 ns was used to avoid most of the laser scatter from the ends of the fiber. Three laser dyes were required to scan the range between 385 and 510 nm. The dye cuvettes were rapidly changed after each section of the scan. No dye-laser realignment was required, but the alignment of the laser beam and optical fiber coupling lens was checked after each dye exchange. The current availability of wide-range tuning lasers equipped with optical parametric oscillators will make the operation of LSL instruments simpler. The examples discussed here demonstrate the usefulness of laser-based luminescence monitors for remote sensing of PAC in hazardous wastes.

4.3.2. RTP fiberoptic sensor

The development of an RTP sensor for the analysis of PACs in contaminated waters was recently pursued in our laboratory [65,66]. A block diagram of the laser system and the RTP sensor is shown in Fig. 6. Basically, the RTP device consists of two cylindrical parts (a stainless-steel sheath and a Teflon stud) easily attached by concentric incised threads. The fiber optic bundle passed through the center of the sheath and reached the sample compartment of the RTP sensor located between the two cylindrical parts. A hole (0.3-cm diameter) at the distal end of the Teflon stud allowed the entry of solution into the sample cavity. By dipping the sensor into the sample, the paper substrate in the cavity is imbibed with the solution. The sample collected by the filter paper is then excited by the laser irradiation from the fiber optic. Several PAHs and nitrogen heterocyclic compounds of environmental importance were determined at the ng ml^{-1} level of concentration.

From the selectivity point of view, fiber optical sensing based on phosphorescence emission offers several advantages over fluorescence optosensing. The higher selectivity is based on the nature of the phosphorescence phenomenon, which is less common than fluorescence at ambient temperatures.

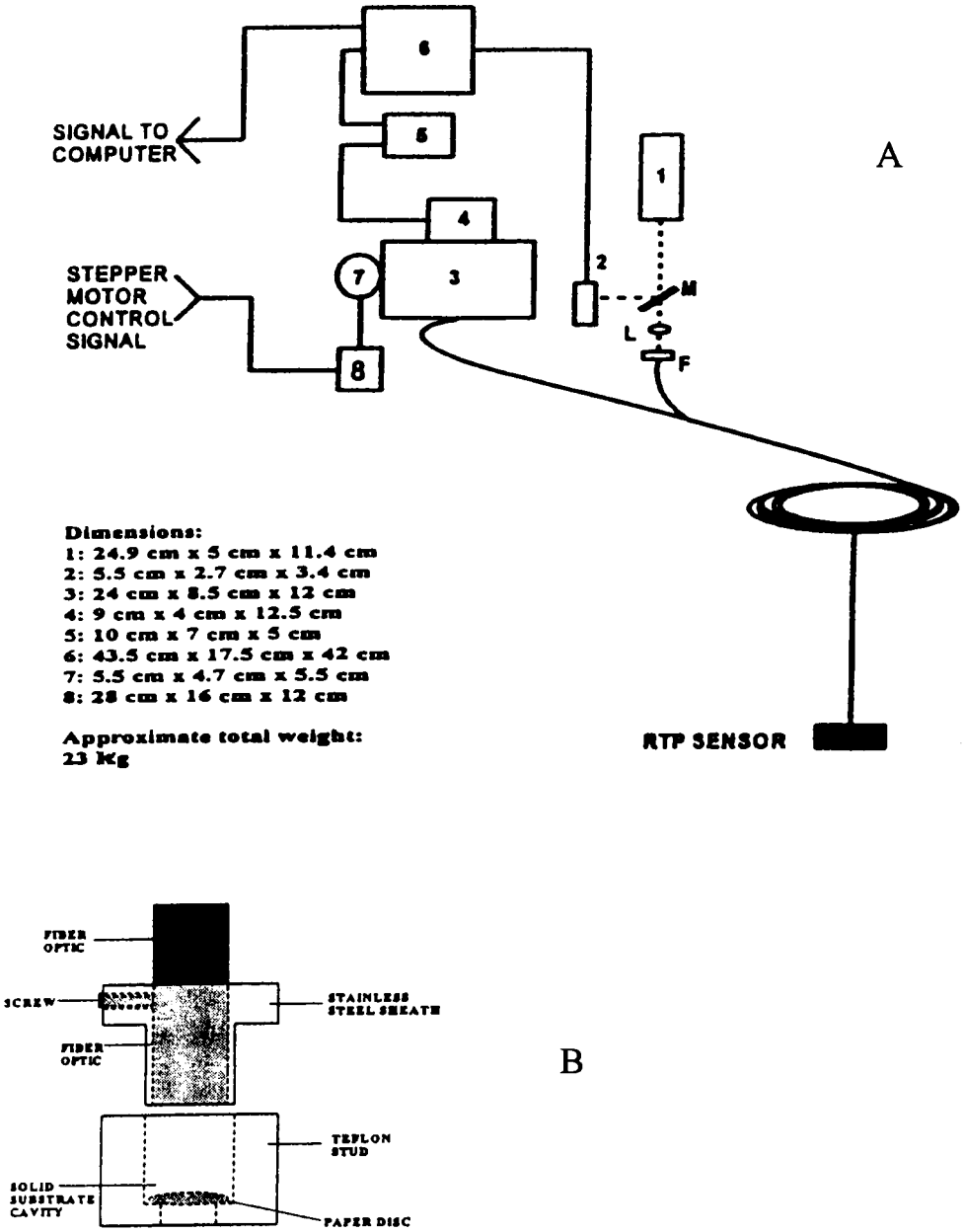

Fig. 6. (A) Block diagram of the laser system employed with the laser-induced RTP sensor. 1 = Nitrogen laser; 2 = photodiode trigger; 3 = monochromator; 4 = PMT; 5 = preamplifier; 6 = boxcar; 7 = motor; 8 = motor control; L = lens; M = reflecting surface; F = fiber optic mount. (B) Cross-section of the RTP sensor.

In addition, the interference from short-lived scattering and possible fluorescence signals can be avoided by using appropriate delay times. This feature will be particularly useful in minimizing or even eliminating the spectral interference of humic materials, a problem often related to fluorescence optosensing of PAHs [134]. In the analysis of complex mixtures with several phosphorescent

concomitants, the selectivity toward a target compound can be enhanced by SEHAP.

The proposed sensor also presents significant instrumental advantages. RTP emission usually occurs at longer wavelength regions than fluorescence, which allows the use of low-cost fiber optics for measurements beyond 450 nm. The measurements of triplet excited lifetimes (μs to s) require less expensive instrumentation than fluorescence lifetimes, which are usually in the ns range.

The RTP sensor is an attractive alternative for field applications. The laser system is very simple to operate, relatively small and requires minimum alignment. The design of the laser device minimizes the contact of the analyte with quenching species such as oxygen and moisture, eliminating the need for the flow of dry gas usually employed in conventional SS–RTP procedures. By using appropriate heavy-atom salts, the excitation wavelengths of compounds of interest can be shifted to overlap the excitation line of the nitrogen laser and avoid the change in excitation source [66]. By spotting standard solutions on the paper substrates previously imbibed with the sample, on-site identification of compounds can be easily performed. Finally, by changing the paper substrate in the sample compartment, the SS-RTP sensor can be used for an infinite number of measurements. This represents a valuable feature for the analysis of large numbers of environmental samples.

4.3.3. Surface-enhanced Raman scattering (SERS) fiberoptic sensor

Another analytical monitor of great promise is the SERS sensor [135–137]. The application of Raman spectroscopy for the study of environmental systems is rapidly expanding because of the specificity of this analytical technique for chemical identification. Conventional Raman spectroscopy, however, has limited applicability for trace organic detection because of the inherently weak Raman scattering cross section. The SERS effect, whereby an enhancement factor of up to 10^7 in Raman signals from molecules adsorbed on rough metallic surfaces [138,139], has recently generated increasing interest in the Raman technique [137]. For aqueous environmental samples, conventional Raman spectroscopy has the disadvantage of requiring large samples (usually 10–100 mg of the bulk pure specimens). The increased sensitivity provided by the SERS effect has eliminated this major limitation.

The development of SERS-active substrates that allow direct measurements in liquid samples is critical for in situ analysis. SERS has been observed using different solid substrates such as metal electrodes, metal islands, films, glass or cellulose coated with silver-covered nanoparticles. However, with the exception of metal electrodes and colloidal solutions, most of the SERS studies performed with solid substrates to date have been performed in the dry state. Recently, we have developed the technique of measuring SERS in solution using probes covered with silver-coated substrates mounted in fiberoptic sensors.

Fig. 7 shows a schematic diagram of a prototype fiberoptic remote SERS monitor. A preliminary version of a SERS fiberoptic probe has been developed and described previously [140,141]. A single optical fiber was used to transmit the laser excitation into the SERS probe, and a second fiber was used to collect the scattered radiation from the sample. The laser beam transmitted through a bandpass filter was focused into one end of the excitation fiber with the use of a microscope objective lens. This end of the excitation fiber was held by a fiberoptic holder. The terminus end of the excitation fiber was positioned close to the SERS substrate in order to contain the laser beam to a very small spot on the substrate. The SERS probe was prepared with a glass backing (microscope slide, 1-mm thick) so that the excitation and collection fibers could be positioned either head on, with the fibers positioned on opposite sides of the SERS substrate, or side-by-side, with the two fibers on the same side of the substrate. The terminus end of the collection fiber was positioned next to the entrance slit of a spectrometer. Since the f/number of the fiber and that of the spectrometer were different, it was necessary to focus the input radiation from the collection fiber with lenses. An $f/1$ lens was used to collect and collimate the output beam from the collection fiber. A second lens with an f/number

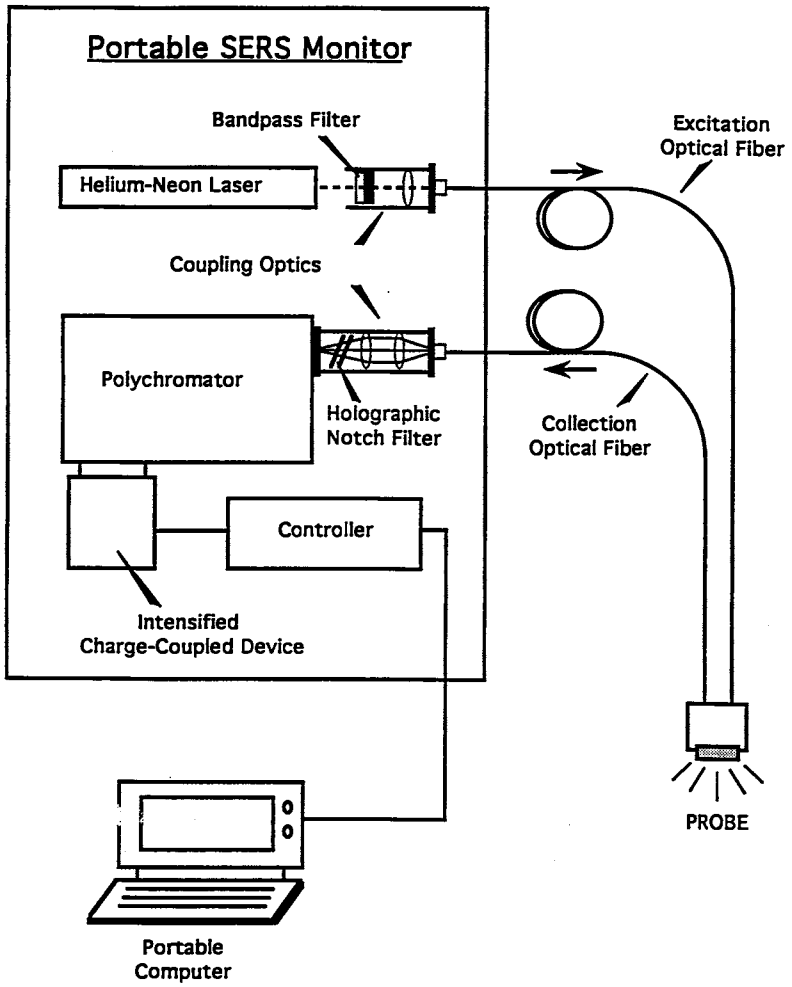

Fig. 7. The Portable SERS fiberoptic sensor.

matching that of the spectrometer ($f/7$) was then used to focus the collected SERS signal into the slit of the spectrometer equipped with a red-enhanced intensified charge-coupled device (ICCD).

4.4. Multispectral imaging and sensing systems

Since AOTFs with high spatial resolution (typically 100 lines mm^{-1}) and large optical apertures are available, they can be applied for spectral imaging applications. Several remote spectral imaging systems have recently been developed, which combine a two-dimensional CCD detector, an AOTF device and optical imaging fiberoptic probe (IFP) technology [142]. These devices can have useful applications in remote sensing and imaging of hazardous waste samples.

AOTF devices consist of a piezoelectric transducer bonded to a birefringent crystal. The transducer is exited by a radio frequency (rf) (50–200 MHz) and generates acoustic waves in a birefringent crystal. Those waves establish a periodic modulation of the index of refraction via the elasto-optic effect [142]. Under proper conditions, the AOTF will diffract part of the incident light within a narrow frequency range. This is the basis of an electronically tuned optical filter using the Bragg diffraction of light by periodic modulations

in the index of refraction in the crystal established by the acoustic waves. Only light that enters the crystal such that its angle to the normal of the crystal surface is within a certain range can be diffracted by the Bragg grating. This range is called the acceptance angle of the AOTF. The percentage of light diffracted is the diffraction efficiency of the device. This parameter greatly depends on the incidence angle, the wavelength selected and the power of the rf signal.

In a non-collinear AOTF, the diffracted beam is separated from the undiffracted beam by a diffraction angle. The undiffracted beam exits the crystal at an angle equal to the incident light beam, while the diffracted beam exits the AOTF at a small angle with respect to the original beam. A detector can be placed at a distance so that the diffracted light can be monitored, while the undiffracted light does not irradiate the detector. In addition, when the incident beam is linearly polarized and aligned with the crystal axis, the polarization of the diffracted beam is rotated 90% with respect to the undiffracted beam. This can provide a second means to separate the diffracted and undiffracted beams. One polarizer is placed before the AOTF, and is aligned with the crystal. At the exit of the AOTF, a second polarizer is rotated 90% with respect to the first. The undiffracted light is blocked by the crossed polarizers, while most of the diffracted beam escapes.

A prototype AOTF-based multispectral imaging instrument was developed for spectral imaging [142]. The light emitted from the output end of the IFP was collected by an imaging lens, filtered by the AOTF, and then imaged onto a CCD. By changing the wavelength of the AOTF, a spectrum could be acquired as a series of images (one for each wavelength). The device has multiple sensor probes that can be used to detect different analytes simultaneously. We have developed several devices that take advantage of recent advances in several technologies, including a two-dimensional CCD detector, imaging fiberoptic, and AOTFs. The integration of these technologies leads to versatile and powerful imaging systems that can remotely detect and analyze fluorescent objects. This imaging system could find useful applications in environmental monitoring areas where the detection of multiple components in complex media is required. The results demonstrate the potential of the AOTF technology to be used for remote imaging spectroscopy and simultaneous spectrum acquisition of different contaminants in hazardous waste samples.

4.5. Biosensors

For the past few years, biosensor technology has been at the forefront of analytical instrumentation research. The integration of biological methods, laser systems and advanced optical sensor technology promises to open new horizons in environmental and biological monitoring of PACs and related bioindicators. Immunoassay techniques are very powerful monitoring tools because of their excellent specificity and reasonable sensitivity. The immunological principle can be combined with laser and fiberoptic technology to develop a new generation of sensors for PACs and related biomarkers [143–150]. A limitation of immunochemical techniques is the need to produce and characterize the antibody for each specific compound of interest. The specificity of the antibodies is not always perfect and some degree of cross-reactivity occurs, especially for situations involving complex mixtures.

Antibodies are polymers of hundreds of individual amino acids arranged in a highly ordered sequence. Antibodies are the product of immune system cells (B cells) when those cells are exposed to antigenic substances or molecules. The antibodies produced following antigen exposure have recognition/binding sites for specific molecular structures (or substructures) of the antigen. Just as specific configurations of a unique key enable it to enter a specific lock, so in an analogous manner, an antigen-specific antibody 'fits' its unique antigen. Thus, an antigen-specific antibody interacts with its unique antigen in a highly specific manner, so that hollows, protrusions, planes, ridges, etc. (i.e. the total three-dimensional structure) of antigen and antibody are complementary. This molecular recognition feature of antibodies is the key to their usefulness in immunosensors; molecular structural recognition allows one to develop antibodies that can bind specifically to

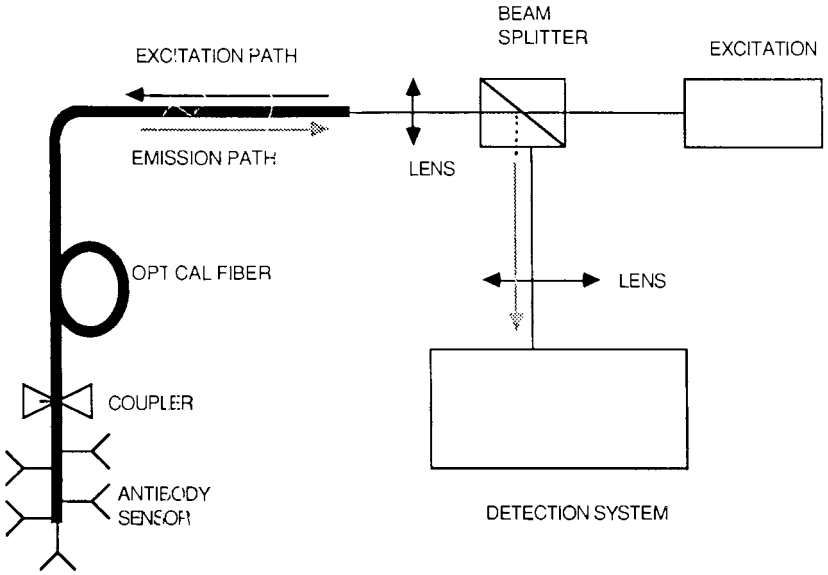

Fig. 8. The anibody-based biosensor for benzo[*a*]pyrene.

chemicals, biomolecules, microorganism components, etc. Such antibodies may then be used as specific 'probes' to identify an analyte of interest that is often present in extremely small amounts, among a myriad of other chemical substances.

Fiberoptic antibody-based fluoroimmunosensors (FISs) have been developed for BaP and related adducts [143]. Polyclonal or monoclonal antibodies produced against BaP are immobilized at the terminus of a fiberoptics probe or contained in a microsensing cavity within the FIS for use both in in vitro and in vivo fluorescence assays (Fig. 8). High sensitivity is provided by laser excitation and optical detection. The FIS device utilizes the back-scattering of light emitted at the remote sensor probe. A single fiber is used to transmit the excitation radiation into the sample and collect the fluorescence emission from the antigen. The laser radiation reaches the sensor probe and excites the BaP bound to the antibodies immobilized at the fiberoptics probe. The excellent sensitivity of this device illustrates that it has considerable potential to perform trace analyses of chemical and biological samples in complex matrices. Measurements are simple and rapid (approximately 12 min), and the technique is applicable to other compounds provided appropriate antibodies are used. The FIS instrument can detect 1 fmol of BaP and 40 amol of BP-tetrol.

Another type of immunosensors have membrane-enclosed antibody probes. The FIS sensing tip has a membrane-enclosed cavity (containing antibodies) constructed with 200/300-mm diameter core/cladding plastic-clad fused silica fiber [145]. Very fast cellulose dialysis membrane (7-mm thick, molecular weight cutoff = 10000) was stretched across the face of a piece of plastic heat-shrink tubing and positioned with a band of heat shrink. The tip was assembled so that it could slide on and off the fiber and, when in place, a tight seal would form between the fiber jacket and the plastic tubing. Approximately 2–3 mm of bare fiber core was exposed. The plastic heat-shrink tip was tapered, resulting in an inner diameter of roughly 300 mm. The distance between the membrane and the fiber face was adjusted to about 0.5 mm, yielding an approximate sensor volume of 40 nl.

One of the following criteria must be met if a fiber optic immunosensor is to be used in a continuous fashion: (a) the interaction of the antigen/hapten with the antibody must be rapid and reversible, thereby permitting competitive-equilibrium-binding operation; (b) the immunoreagent

reservoir must not be appreciably depleted during the measurement process; or (c) the sensor must be capable of in situ regeneration, hence, repetitive (i.e. pseudo-continuous) operation is possible. Devices that do not satisfy any of these criteria are more appropriately called probes rather than sensors. The regenerable immunosensor is versatile with regard to the immunoassay protocols that can be utilized. Moreover, excellent sensitivity is possible by performing heterogeneous assays. The regenerable immunosensor combines typical fiberoptic sensor instrumentation (see above) with a reagent delivery system that employs capillary columns [145–147]. Several narrow-bore capillary columns surround a single optical fiber. This assembly is contained by a hollowed-out frit that defines a sample chamber. Typically the capillaries have internal diameters of 200 μm and the entire tip is only approximately 2 mm in diameter with a chamber volume 1 μl. The capillaries are connected to syringes and serve specific functions (delivery of immunobeads, aspiration of sample, etc.).

5. Conclusion

The development of effective methods and instrumentation for trace detection of PACs in the environment and assessment of their potential hazards, ecological impacts, and human health risks is necessary for the achievement of environmentally viable and safe technologies. Problem areas pertaining to identification of specific compounds or classes of compounds, i.e. analysis of complex mixtures, estimation of realistic dose regimes, and determination of biological effects continue to create new challenges to chemical analysis of PACs.

The monitoring and characterization of PAC species in complex environmental systems require a battery of analytical methods and instrument. For example, chromatography and mass spectrometry techniques are useful laboratory techniques that can provide complete characterization of complex samples after sample clean-up and treatment. On the other hand, luminescence, Raman and SERS spectroscopies are spectrochemical techniques that have a number of important advantages to remote sensing of hazardous wastes under field conditions. The examples shown in this overview illustrate the different uses of these techniques for monitoring a wide variety of chemical species. Laser-based luminescence is well known for its high sensitivity for polyaromatic compounds. On the other hand, Raman spectroscopy can be used for weakly luminescing compounds, and can provide an analytical tool having figures of merit that complement luminescence. The Raman technique is well known for its high selectivity. With the advances of fiberoptic technology, the SERS technique, which can amplify the Raman signal by several orders of magnitude, can provide a remote sensing technique with the added merit of improved sensitivity due to the surface-enhanced effect. Advanced multisensor systems using phosphorescence detection and acousto-optic tunable filters are currently being developed in our laboratory to further extend the capabilities of remote sensing technologies.

Finally, an area of great importance to PAC research is the application of analytical techniques to 'biological monitoring' of human exposure to PACs. This is a challenging area for research and development, and advances in analytical methodology and instrumentation are critically needed to analyze complex biochemical systems in the attempt not only to monitor the presence of PACs in the environment but also to assess the ultimate human health effects associated with PACs.

Acknowledgements

This research is sponsored by the Office of Biological and Environmental Research, U.S. Department of Energy under contract DE-AC05-960R22464 with Lockheed Martin Energy Research Corporation, and the ETPI Project (Autotropic Biofims) is acknowledged.

References

[1] T. Vo-Dinh (Ed.), Chemical Analysis of Polycyclic Aromatic Compounds, Wiley-Interscience, New York, 1989.

[2] G. Grimmer (Ed.), Environmental Carcinogens: Polycyclic Aromatic Hydrocarbons, CRC Press, Boca Raton, FL, 1983.
[3] I.M. Warner, S.A. Soper, L.B. McGown, Anal. Chem. 68 (1996) 73R.
[4] A. Jurgensen, E.L. Inman Jr., J.D. Winefordner, Anal. Chim. Acta 131 (1981) 187.
[5] J.D. Ingle, Jr., S.R. Crouch, Spectrochemical Analysis, Prentice-Hall, Englewood Cliffs, NJ, 1988.
[6] L.B. McGown, F.V. Bright, CRC Crit. Rev. Anal. Chem. 18 (1987) 245.
[7] I. Warner, G. Patonay, M.P. Thomas, Anal. Chem. 57 (1985) 463A.
[8] J.M. Hayes, G.J. Small, Anal. Chem. 55 (1983) 565A.
[9] E.L. Wehry, G. Mamantov, Anal. Chem. 51 (1979) 643A.
[10] C. Gooijer, I. Kozin, N.H. Velthorst, Mikrochim. Acta 127 (1997) 149.
[11] J.F. Lloyd, Nature Phys. Sci. 231 (1971) 64.
[12] T. Vo-Dinh, Anal. Chem. 50 (1978) 396.
[13] T. Vo-Dinh, Appl. Spectrosc. 36 (1982) 576.
[14] T. Vo-Dinh, in: D. Eastwood, (Ed.), New Directions in Molecular Luminescence, ASTM, Philadelphia, PA, 1983, p. 5.
[15] T. Vo-Dinh, P.R. Martinez, Anal. Chim. Acta 125 (1981) 13.
[16] T. Vo-Dinh, R.B. Gammage, P.R. Martinez, Anal. Chem. 53 (1981) 253.
[17] T. Vo-Dinh, R.B. Gammage, in: G. Choudhar (Ed.), Chemical Hazards in the Workplace: Measurement and Control, American Chemical Society, Washington, DC, 1981, p. 269.
[18] T. Vo-Dinh, R.B. Gammage, Am. Ind. Hyg. Assoc. J. 42 (1981) 112.
[19] T. Vo-Dinh, Am. Ind. Hyg. Assoc. J. 48 (1987) 594.
[20] T. Vo-Dinh, D.A. White, M.A. O'Malley, P.J. Seligman, R.C. Beier, J. Agric. Food Chem. 36 (1988) 333.
[21] C.S. McEnally, R.F. Sawyer, C.P. Koshland, D. Lucas, Appl. Opt. 33 (1994) 3977.
[22] E.M. Filippova, V.V. Chubarov, V.V. Fadeev, Can. J. Appl. Spectrosc. 38 (1993) 139.
[23] D.J. Funk, R.C. Oldenborg, D.P. Dayton, J.P. Lacosse, J.A. Draves, T.J. Logan, Appl. Spectrosc. 49 (1995) 105.
[24] C.L. Stevenson, T. Vo-Dinh, Appl. Spectrosc. 47 (1993) 430.
[25] C.L. Stevenson, T. Vo-Dinh, Anal. Chim. Acta 303 (1995) 247.
[26] J.P. Alarie, T. Vo-Dinh, Talanta 38 (1991) 529.
[27] W.A. Chudyk, M.M. Carraba, J.E. Kenny, Anal. Chem. 57 (1985) 1237.
[28] S.M. Inmam, P. Thibado, G.A. Theriault, S.H. Lieberman, Anal. Chim. Acta 239 (1990) 45.
[29] A. Miuone, B.W. Smith, J.D. Winefordner, Talanta 37 (1991) 111.
[30] R. Niessner, U. Panne, H. Schroder, Anal. Chim. Acta 255 (1991) 231.
[31] U. Panne, R. Niessner, Sens. Actuators B 13–14 (1991) 288.
[32] A. Robbat, L. Tyng-Yun, B.M. Abraham, Anal. Chem. 64 (1992) 1477.
[33] L.J. Cline-Love, M. Skriec, J.G. Hobarta, Anal. Chem. 52 (1980) 754.
[34] M. Skrilec, L.J. Cline-Love, Anal. Chem. 52 (1980) 1559.
[35] J.J. Donkerkbroek, J.J. Elzas, C. Gooijer, R.W. Frei, N.H. Velthorst, Talanta 28 (1981) 717.
[36] J.J. Donkerkbroek, C. Gooijer, N.H. Velthorst, R.W. Frei, Anal. Chem. 54 (1982) 891.
[37] J.J. Donkerkbroek, N.J.R. van Eikema Hommes, C. gooijer, N.H. Velthorst, R.W. Frei, Chromatographia 15 (1982) 218.
[38] E.M. Schulman, C. Walling, Science 178 (1972) 53.
[39] E.M. Schulman, C. Walling, J. Phys. Chem. 77 (1973) 902.
[40] T. Vo-Dinh, Room Temperature Phosphorimetry for Chemical Analysis, Wiley, New York, 1984.
[41] R.J. Hurtubise, Phosphorimetry: Theory, Instrumentation, and Applications, VCH, New York, 1990.
[42] T. Vo-Dinh, E. Lue Yen, J.D. Winefordner, Talanta 24 (1977) 146.
[43] E. Lue-Yen Bower, J.D. Winefordner, Anal. Chim. Acta 102 (1978) 1.
[44] T. Vo-Dinh, R.B. Gammage, Anal. Chem. 50 (1978) 2054.
[45] T. Vo-Dinh, J.R. Hooyman, Anal. Chem. 51 (1979) 1915.
[46] T. Vo-Dinh, R.B. Gammage, Anal. Chim. Acta 107 (1979) 261.
[47] R.T. Parker, R.S. Freelander, E.M. Schulman, R.B. Dunlap, Anal. Chem. 51 (1979) 1921.
[48] T. Vo-Dinh, R.B. Gammage, P.R. Martinez, Anal. Chim. Acta 118 (1980) 315.
[49] T. Vo-Dinh, P.R. Martinez, Anal. Chim. Acta 125 (1981) 13.
[50] S.Y. Su, J.D. Winefordner, Michrochem. J. 27 (1982) 151.
[51] H.T. Karnew, S.G. Schulman, J.D. Winefordner, Anal. Chim. Acta 164 (1984) 257.
[52] G. Ramis Ramos, M.C. Garcia Alvarez-Coque, A.M. O'Reilly, I.M. Khasawneh, J.D. Winefordner, Anal. Chem. 60 (1988) 416.
[53] A.M. Alak, T. Vo-Dinh, Anal. Chem. 60 (1988) 596.
[54] L.M. Perry, A.D. Campiglia, J.D. Winefordner, Anal. Chem. 61 (1989) 2328.
[55] C.D. Ford, R.J. Hurtubise, Anal. Chem. 50 (1978) 610.
[56] G.C. de Lima, M. de Nicola, Anal. Chem. 50 (1978) 1658.
[57] C.D. Ford, R.J. Hurtubise, Anal. Lett 13 (1980) 485.
[58] A.D. Campiglia, L.M. Perry, J.D. Winefordner, Appl. Spectrosc. 43 (1989) 1341.
[59] A.D. Campiglia, L.M. Perry, J.D. Winefordner, Appl. Spectrosc. 44 (1989) 729.
[60] A.D. Campiglia, A. Berthod, J.D. Winefordner, J. Chromatogr. 508 (1990) 37.

[61] A.D. Campiglia, D.M. Hueber, F. Moreau, T. Vo-Dinh, Anal. Chim. Acta 346 (1997) 361.
[62] T. Vo-Dinh, M. Uziel, Anal. Chem. 59 (1992) 239.
[63] A.D. Campiglia, D.M. Hueber, T. Vo-Dinh, Appl. Spectrosc. 50 (1996) 252.
[64] A.D. Campiglia, D.M. Hueber, T. Vo-Dinh, Polyc. Arom. Comp. 8 (1996) 117.
[65] A.D. Campiglia, J.P. Alarie, T. Vo-Dinh, Anal. Chem. 68 (1996) 1599.
[66] A.D. Campiglia, T. Vo-Dinh, Talanta 41 (1996) 1805.
[67] A. Bemgard, B.O. Lundmark, A. Colmsjo, in: P. Garrigues (Eds.), Polycyclic Aromatic Compounds: Synthesis, Properties, Analytical Measurements, Occurrence, and Biological Effects (Proceedings of the 13th International Symposium on PAHs, Bordeaux, France) Gordon and Breach, London, 1993, p. 603.
[68] A. Bemgard, A. Colmsjo, J. Chromatogr. Sci. 30 (1992) 23.
[69] J.M. Janini, G.M. Muschik, W. Zelinski Jr., Anal. Chem. 48 (1978) 323.
[70] R.C. Kong, M.L. Lee, Y. Tominaga, R. Pretap, M. Iwao, R.N. Castle, J. Chromatogr. Sci. 20 (1982) 502.
[71] B.A. Jones, J.S. Bradshaw, M. Nishioka, M.L. Lee, J. Org. Chem. 49 (1984) 4947.
[72] K.E. Markides, M. Nishioka, B.J. Tarbet, J.S. Bradshaw, M.L. Lee, Anal. Chem. 57 (1985) 1296.
[73] J.C. Fetzer, in: T. Vo-Dinh (Ed.), Chemical Analysis of Polycyclic Aromatic Compounds, Wiley-Interscience, New York, 1989, p. 59.
[74] C.M. White, L.J. Douglas, M.B. Perry, C.B. Schmidt, Energy Fuels 1 (1987) 222.
[75] M. Nishioka, Energy Fuels 2 (1988) 214.
[76] M.K. Andari, H. Bebhehani, A. Stanislaus, Fuel Sci. Technol. 14 (1996) 939.
[77] Polycyclic Aromatic Compounds, vol. 5, Proceedings of the 14th International Symposium on Polycyclic Aromatic Compounds, Tan-Tara, USA, 1994.
[78] Polycyclic Aromatic Compounds, vol. 9, Proceedings of the 15th International Symposium on Polycyclic Aromatic Compounds Belgerate, Italy, 1996.
[79] W.J. Simonsick Jr., R.A. Hites, Anal. Chem. 56 (1984) 2749.
[80] W.J. Simonsick Jr., R.A. Hites, Anal. Chem. 58 (1986) 2114.
[81] S. Daishima, Y. Iida, Anal. Sci. Supp. Proc. Int. Congr. Anal. Sci. 1 (1991) 439.
[82] M.M. Boduszynski, D.A. Grudoski, C.E. Rechsteiner, R.M. Angus, in: Proceedings of the 6th UNITAR International Conference, vol. 2 1995, p. 335.
[83] J.T. Andersson, K.J. Sielex, J. High Resolut. Chromatogr. 19 (1996) 49.
[84] J.C. Fetzer, W.R. Biggs, J. Chromatogr. 346 (1985) 81.
[85] P. Garrigues, H. Budzinski, M.P. Manitz, S.A. Wise, Polycyclic Arom. Cmpds. 7 (1995) 275.
[86] J.C. Fetzer, W.R. Biggs, J. Chromatogr. 295 (1984) 161.
[87] J.C. Fetzer, W.R. Biggs, J. Chromatogr. 322 (1985) 275.
[88] J.C. Fetzer, W.R. Biggs, J. Chromatogr. 386 (1987) 87.
[89] S.A. Wise, W.E. May, Anal. Chem. 55 (1983) 1479.
[90] S.A. Wise, L.C. Sander, J. High Resolut. Chromatogr. Chromatogr. Commun. 8 (1985) 248.
[91] L.C. Sander, S.A. Wise, in: J.C. Giddings, E. Grushka, J. Cazes, P.R. Brown (Eds.), Advances in Chromatography, vol. 25, Marcel Dekker, New York, 1986, p. 139.
[92] L.C. Sander, S.A. Wise, Anal. Chem. 59 (1987) 2309.
[93] L.C. Sander, S.A. Wise, Anal. Chem. 61 (1989) 1749.
[94] P. Shah, L.B. Rogers, J.C. Fetzer, J. Chromatogr. 388 (1987) 411.
[95] H. Ohta, K. Jinno, Y. Saito, J.C. Fetzer, W.R. Biggs, J.J. Pesek, M.T. Matyska, Y.-L. Chen, Chromatographia 42 (1996) 56.
[96] K. Jinno, T. Nagoshi, N. Tanaka, M. Okamoto, J.C. Fetzer, W.R. Biggs, J. Chromatogr. 386 (1987) 123.
[97] K. Jinno, N. Anazawa, N. Tanaka, M. Okamoto, J.C. Fetzer, R.W. Biggs, J. Chromatogr. 402 (1987) 173.
[98] K. Jinno, in: J.C. Giddings, E. Grushka, P.R. Brown (Eds.), Advances in Chromatography, vol. 30, Marcel Dekker, New York, 1989, p. 65.
[99] J.C. Fetzer, J.R. Kershaw, Fuel 10 (1995) 1533.
[100] H. Richter, K. Taghizadeh, W.J. Grieco, A.L. Lafleur, J.B. Howard, J. Phys. Chem. 100 (1996) 19603.
[101] M.T. Beck, J.C. Fetzer, S. Keki, Carbon 32 (1994) 795–799.
[102] M.T. Beck, Z. Dinya, A. Dombi, J.C. Fetzer, S. Keki, L. Papp, P. Szabo, J. Szepvolgyi, M. Zsuga, in: K.M. Kadish, R.S. Ruoff (Eds.), Fullerenes: Recent Advances in the Chemistry and Physics of Fullerenes and Related Materials, The Electrochemical Society, Pennington, NJ, 1994, pp. 80–91.
[103] M.L. Machado, P.W. Beatty, J.C. Fetzer, A.H. Glickman, A. Kreich, E.L. McGinnis, Fundam. Appl. Toxicol. 21 (1993) 492–499.
[104] J.M. Moldowan, J. Dahl, J.C. Fetzer, Energy Fuels 9 (1995) 155–162.
[105] J.C. Fetzer, B.R.T. Simoneit, H. Budzinski, P. Garrigues, Polycyclic Arom. Cmpds. 9 (1996) 109.
[106] B.R.T. Simoneit, J.C. Fetzer, Org. Geochem. 24 (1996) 1065.
[107] W.E. Acree Jr., S. Pandey, S.A. Tucker, J.C. Fetzer, Polycyclic Arom. Compounds 12 (1997) 71.
[108] S. Pandey, W.E. Acree Jr., J.C. Fetzer, Talanta 45 (1997) 39.
[109] M.N. Kayali, S. Rubio-Barroso, L.M. Polo-Diez, J. Liq. Chromatogr. 17 (1994) 3623.
[110] M.R. Hadjmohammadi, M.H. Fatimi, J. Liq. Chromatogr. 18 (1995) 2568.
[111] M.N. Kayali, S. Rubio-Barroso, L.M. Polo-Diez, J. Liq. Chromatogr. 19 (1996) 759.
[112] M.A. Garcia, M.L. Mariana, J. Liq. Chromatogr. 19 (1996) 1757.
[113] J.R. Kershaw, J.C. Fetzer, Polycyclic Arom. Compounds 7 (1995) 253–268.
[114] J.R. Jadamec, W.A. Saner, Y. Talmi, Anal. Chem. 49 (1977) 1316.

[115] L.W. Hershberger, J.R. Callis, G.D. Christian, Anal. Chem. 53 (1981) 971.
[116] M.P. Fogarty, D.C. Shelly, I.M. Warner, HRC CC, J. High Resol. Chromatogr. Chromatogr. Commun. 4 (1981) 561.
[117] J.C. Gluckman, D.C. Shelly, M.V. Novotny, Anal. Chem. 57 (1985) 1546.
[118] R. Ferrer, J. Guiteras, J.L. Beltran, J. Chromatogr. A 779 (1997) 123.
[119] M.B. Smalley, L.B. McGown, in: P.R. Brown, E. Grushka (Eds.), Advances in Chromatography, vol. 37, Marcel Dekker, New York, 1997, p. 50.
[120] R. Kotzick, S. Haaszio, R. Niessner, Proc. SPIE Int. Soc. Op. Eng. 2504 (1995) 107.
[121] W. Yao, P. Spitzauer, A. Kettrup, Environ. Sci. (China) 7 (1995) 224.
[122] K. Jinno (Ed.), Hyphenated Techniques in Supercritical Fluid Chromatography and Extraction, J. Chromatogr. Ser., v.53, Elsevier, Amsterdam, 1992.
[123] S.B. French, M.V. Novotny, Anal. Chem 58 (1986) 164.
[124] M.W. Raynor, K.D. Bartle, I.L. Davies, A. Williams, A.A. Clifford, J.M. Chalmers, B.W. Cook, Anal. Chem. 60 (1988) 427.
[125] L.A. Wallace, W.R. Ott, J. Air Pollut. Control Assoc. 32 (1982) 601.
[126] E.D. Palmes, A.F. Gunnison, Am. Ind. Hyg. Assoc. J. 34 (1973) 78.
[127] T. Vo-Dinh, Environ. Sci. Technol. 19 (1984) 997.
[128] T. Vo-Dinh, Industrial Hygiene Application: a Personal Dosimeter Badge for Polyaromatic vapors, in: T. Vo-Dinh (Ed.), Room Temperature Phosphorimetry for Chemical Analysis, Wiley, New York, 1984, p. 244.
[129] J.P. Alarie, T. Vo-Dinh, G. Miller, M.N. Ericson, S.R. Maddox, W. Watts, D. Eastwood, R. Lidberg, M. Dominguez, Rev. Sci. Instr. 64 (1993) 2541.
[130] D. Hueber, C.L. Stevenson, T. Vo-Dinh, Appl. Spectrosc. 49 (1995) 1624.
[131] F. Moreau, S. Moreau, D.M. Hueber, T. Vo-Dinh, Applied Spectrosc. 50 (1996) 1295.
[132] T. Vo-Dinh, J.P. Alarie, G.D. Griffin, R.S. Burlage, W. Hill, in: FY-97 Report for the ETPI Project on Autotropic Biofilms: Technical Development for Removing Contaminants from Industrial Wastewater, Oak Ridge National Laboratory, Oak Ridge, TN, 1998.
[133] C.L. Stevenson, T. Vo-Dinh, Appl. Spectrosc. 47 (1993) 430.
[134] U. Panne, F. Lewitzka, R. Niessner, Analusis 20 (1992) 533.
[135] T. Vo-Dinh, Sens. Actuators B 29 (1995) 183.
[136] T. Vo-Dinh, Surface-enhanced Raman scattering, in: P. Halevi (Ed.), Photonic Probes of Surfaces, Elsevier, New York, 1995.
[137] T. Vo-Dinh, Surface-enhanced Raman spectroscopy, in: T. Vo-Dinh (Ed.), Chemical Analysis of Polycyclic Aromatic Compounds, Wiley, New York, 1989, p. 451.
[138] D.J. Jeanmaire, R.P. Van Duyne, J. Electroanal. Chem. 84 (1977) 1.
[139] R.K. Chang, T.E. Furtak (Eds.), Surface-Enhanced Raman Scattering, Plenum, New York, 1982.
[140] J.M. Bello, V.A. Narayana, D.L. Stokes, T. Vo-Dinh, Anal. Chem. 62 (1990) 2437.
[141] J.P. Alarie, D.L. Stokes, W.S. Sutherland, A.C. Edwards, T. Vo-Dinh, Appl. Spectr. 1608 (1992) 46.
[142] F. Moreau, D.M. Hueber, T. Vo-Dinh, Instrum. Sci. Technol. 24 (1996) 179.
[143] T. Vo-Dinh, B.J. Tromberg, G.D. Griffin, K.R. Ambrose, M.J. Sepaniak, E.M. Gardenhire, Antibody-based Fiberoptics Biosensor for the Carcinogen Benzo(a)pyrene, Appl. Spectrosc. 41 (1987) 735.
[144] T. Vo-Dinh, T. Nolan, Y.F. Cheng, M.J. Sepaniak, J.P. Alarie, Appl. Spectrosc. 44 (1990) 128.
[145] T. Vo-Dinh, J.P. Alarie, R.W. Johnson, M.J. Sepaniak, R.M. Santella, Clin. Chem. 37 (1991) 532.
[146] T. Vo-Dinh, M.J. Sepaniak, G.D. Griffin, in: O.S. Wolfbeis (Ed.), Fiber Optics Chemical Sensors and Biosensors ch. 17, CRC Press, Boca Raton, FL, 1991, p. 217.
[147] T. Vo-Dinh, M.J. Sepaniak, G.D. Griffin, J.P. Alarie, Immunomethods 3 (1993) 85.
[148] J.P. Alarie, J.R. Bowyer, M.J. Sepaniak, A.M. Hoyt, T. Vo-Dinh, Anal. Chim. Acta 236 (1990) 237.
[149] J.R. Bowyer, J.P. Alarie, M.J. Sepaniak, T. Vo-Dinh, R.Q. Thompson, Analyst 116 (1991) 117.
[150] J.P. Alarie, M.J. Sepaniak, T. Vo-Dinh, Anal. Chim. Acta 229 (1990) 169.

ELSEVIER

Talanta 47 (1998) 971–979

Talanta

Oxygen sensor via the quenching of room-temperature phosphorescence of perdeuterated phenanthrene adsorbed on Whatman 1PS filter paper

S.M. Ramasamy, R.J. Hurtubise *

Department of Chemistry, University of Wyoming, Laramie, WY 82071-3838, USA

Received 23 February 1998; received in revised form 20 April 1998; accepted 21 April 1998

Abstract

Perdeuterated phenanthrene (d-phen) exhibits strong room-temperature phosphorescence (RTP) when adsorbed on Whatman 1PS filter paper. An oxygen sensor was developed that depends on oxygen quenching of RTP intensity of adsorbed d-phen. The system designed employed a continuous flow of nitrogen or nitrogen–air onto the adsorbed phosphor. The sensor is simple to prepare and needs no elaborate fabrication procedure, but did show a somewhat drifting baseline for successive determinations of oxygen. Nevertheless, very good reproducibility was achieved with the RTP quenching data by measuring the RTP intensities just before and at the end of each oxygen determination. The calibration plots gave a nonlinear relationship over the entire range of oxygen (0–21%). However, a linear range was obtained up to 1.10% oxygen. A detection limit of 0.09% oxygen in dry nitrogen was acquired. Also, carbon dioxide was found to have a minimal effect on the RTP quenching. Thus, oxygen could be measured accurately in relatively large amounts of carbon dioxide. The performance of the oxygen sensor was evaluated by comparing data obtained with a commercial electrochemical trace oxygen analyzer. Also, additional information on the quenching phenomena for this system was obtained from the RTP lifetime data acquired at various oxygen contents. © 1998 Elsevier Science B.V. All rights reserved.

Keywords: Phosphorescence; Oxygen; Quenching

1. Introduction

There is considerable interest in the development of novel and sensitive oxygen sensors [1–5], and numerous oxygen sensors have been developed based on fluorescence detection [2,4,5]. However, very few oxygen sensors have been described that stem from solid-matrix room-temperature phosphorescence (RTP). Wolfbeis [6] has reviewed earlier work where RTP was used for oxygen sensing. Charlesworth [7] reported the details of a RTP method to monitor oxygen concentrations in a gas stream using camphorquinone as the phosphor. He was able to determine oxygen in the range of 0.1–25%. Liu et al. [8] evaluated immobilized room-temperature phosphorescent metal chelates as sensing materials for oxygen. They were able to developed an oxygen transducer based on the RTP quenching of Al-ferron

* Corresponding author. Tel.: +1 307 7664363; fax: +1 307 7663807; e-mail: Hurtubis@uwyo.edu

0039-9140/98/$ - see front matter © 1998 Elsevier Science B.V. All rights reserved.
PII S0039-9140(98)00163-5

chelate. Garcia et al. [9] showed that Erythrosin B gives a strong RTP signal when adsorbed on non-ionic resins or when encapsulated in silicone films. Oxygen transducers based on RTP quenching of the immobilized erythrosin B were evaluated by the previous authors. In addition, phosphorescent complexes of porphyrin ketones have been employed in oxygen sensing [10]. In particular, platinum(II) octaethylporphine ketone was dissolved on a polystyrene layer to give an oxygen-sensitive film. A detection limit of 1.5 hPa was obtained for oxygen. In later work, Hartmann and Trettnak [11] studied the effects of polymer matrices on calibration functions of luminescent oxygen sensors that were based on porphyrin ketone complexes. Also, Lee and Okura [12] developed an oxygen sensor which depended on the RTP quenching of platinum octaethylporphyrin in polymer films. Recently, Alava-Moreno et al. [13] reported on oxygen sensing by the RTP quenching of some lead 8-hydroxyquinoline complexes. The sensors developed were shown to be useful for the determination of dissolved oxygen in tap water.

In this work, a very simple solid-matrix RTP method was developed for sensing oxygen in which the phosphor, perdeuterated phenanthrene (d-phen), adsorbed on Whatman 1PS paper acted as the sensor. Several analytical figures of merit were obtained for the sensor and detailed consideration was given to the experimental conditions for obtaining RTP.

2. Experimental

2.1. Instrumentation

Spex Fluorolog 2 and Perkin Elmer LS50B spectrofluorimeters were used to obtain the solid-matrix RTP intensity and RTP lifetime (τ_p) data of d-phen adsorbed on Whatman 1PS and No.1 filter papers.

2.2. Reagents

Absolute ethanol was purified by distillation. Perdeuterated phenanthrene (D_{10}) (99.5 atom % D, MSD Isotopes, Montreal, Canada) was used as received. Cylinders of nitrogen (ultrahigh purity), compressed air (U.S.P.) and carbon dioxide (U.S.P.) were purchased from United States Welding, Denver, CO. Oxiclear was obtained from Labclear, Oakland, CA. Whatman No. 1 and 1PS filter paper circles were developed in ethanol to collect impurities at one end.

2.3. Measurements

A 1 μg sample of d-phen in ethanol–water (90:10) was spotted onto a Whatman No.1 or 1PS filter paper circle of 6.4 mm diameter. The sample was dried at 110°C for 30 min. A sample holder was made from a rectangular teflon block which fit tightly inside a 1-cm fluorescence cell. As shown in Fig. 1, holes were made in the teflon block which permitted gas to flow in and out of the 1-cm^2 fluorescence cell. As indicated in the Fig. 1, a section of teflon was cut from the teflon block, and a circular depression was made in the flat part of the teflon that remained after the removal of the section of the teflon. Four pieces of blank filter paper were placed in the depression, and then the piece of filter paper with the d-phen was placed on top of the blank filter paper samples. The sample holder was inserted into the quartz cell and wrapped at the top with parafilm to prevent entry of ambient air. In the Spex spectrofluorimeter, the following phosphorimetric parameters were used to get the maximum RTP intensity from the sample: excitation and emission maxima of 287 and 498 nm, respectively; delay time of 10 ms and zero time between flashes; 10 flashes per data point; a window of 100 ms was chosen to obtain a strong RTP intensity.

2.4. Gas flow manifold and measurements

As shown in Fig. 1, nitrogen or carbon dioxide gases were passed through Drierite and Oxiclear to remove traces of moisture and oxygen, respectively. Compressed air was passed through Drierite to minimize its moisture content. An environment with various concentrations of oxygen was maintained in the cell by varying the relative flow rates of nitrogen, compressed air, or

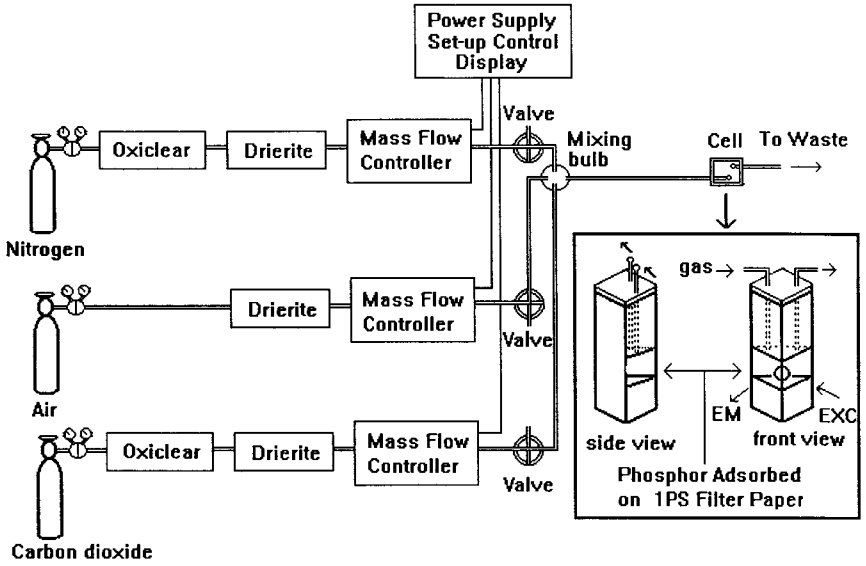

Fig. 1. Experimental system for continuous gas-flow for oxygen sensing.

carbon dioxide. A mass flow meter/controller (Model 201, Porter, Hatfield, PA) was used to control and measure the flow rate of each gas. Tygon tubing of 1/4′ inner diameter was employed to carry the gases, and two-way brass valves (Whitey) were used to select the gas or gas mixture that would flow to the sample. The gas flow over the sample was maintained at a constant flow rate of 200 ml min^{-1} for both nitrogen and nitrogen–air mixtures with or without carbon dioxide. The oxygen concentration (% v/v) was calculated by dividing the flow rate of air by the sum of flow rates of nitrogen and air, and considering that pure air has 20.95% oxygen. All the RTP measurements were made at 23 ± 1°C.

Initially, nitrogen was passed into the sample cell for 15 min to cool it to room temperature after drying the filter paper sample. Then, either nitrogen, a nitrogen–air, or nitrogen–air–carbon dioxide mixture was allowed to flow through the sample holder for about 7–9 min at each percentage of oxygen. The solid-matrix RTP intensity data were acquired with the phosphorimeter collecting data for 25 s under optimized conditions. The recovery time for the sensor was 7.5 min. For the RTP lifetime measurements, nitrogen and nitrogen–air mixtures were passed successively over the sample for 5 min before collecting a decay curve. RTP decay data were processed for a single exponential decay, which resulted in a correlation coefficient value of 0.991, or greater, in an environment of pure air and 0.997 or greater in the nitrogen atmosphere.

A Teledyne (Model 316RB) trace oxygen analyzer was first calibrated with compressed air at the recommended flow rate of 2 scfh (944 ml min^{-1}), and then the analyzer in the instrument was flushed with ultrahigh purity nitrogen for 1 h to remove traces of oxygen. Each nitrogen–air mixture was passed into the analyzer at a flow rate of 200 ml min^{-1} for 15 min. This much time was allowed for the oxygen in the nitrogen–air mixture to reach a steady state of diffusion to the electrochemical fuel cell of the analyzer because this flow rate was less than the flow rate recommended by the instrument manufacturer. The analyzer showed a constant analog reading after 5 min for all the gas mixtures studied. The oxygen contents of these mixtures, calculated from the relative flow rates of gases, showed essentially a perfect linear relationship with the values obtained from the Teledyne analyzer.

3. Results and discussion

3.1. Choice of solid matrix and phosphor

Filter paper is one of the most widely used solid-matrices for obtaining room-temperature fluorescence (RTF) and RTP from adsorbed organic compounds. The ability to obtain RTP from numerous types of organic compounds, low limits of detection, small sample size, and relative ease of sample application are some of the factors responsible for its popularity [14,15]. Recent studies have shown that Whatman 1PS filter paper has several advantages for obtaining RTF and RTP signals compared to Whatman No. 1 filter paper [16–18]. According to the technical information available from the manufacturer, the 1PS filter paper has been impregnated with a heat cured coating of silicone and a proprietary tin complex [19]. This coating imparts stability and hydrophobic character to the 1PS filter paper. The 1PS filter paper is normally employed in the separation of aqueous and organic phases. However, when a small drop of a phosphor in ethanol:water (1:1) was spotted onto the 1PS filter paper, it formed a tiny droplet that spread very little on the filter paper surface [17]. As the solvent evaporated, the phosphor was adsorbed on a very small area of the filter paper. The localization of phosphor to a small area on the 1PS paper, in contrast to diffusion of the sample with Whatman No. 1 filter paper, is largely responsible for an increase in the sensitivity of solid-matrix RTP [17]. It is quite likely that the tin complex in the filter paper also exerts a heavy-atom effect to enhance the RTP from phosphors [17].

In a search for a suitable phosphor in this study, the following compounds were first tested on Whatman No. 1 filter paper for their potential to give strong RTP: acriflavine, benzo[*f*]quinoline hydrobromide, 9-bromoanthracene, 6-bromocoumarin-3-carboxylic acid, 9-bromophenanthrene, bromophenol blue, bromotriphenylethylene, coumarin-3-carboxylic acid, decacyclene, eosin B (spirit soluble), eosin B, fluoranthene, β-naphthoflavone, potassium 1-bromonaphthyl sulfate, phenanthrene, d-phen, and triphenylene. Of these compounds, d-phen, followed by triphenylene, were found to have the strongest RTP emissions and long RTP lifetimes. In this work, d-phen was chosen because it gave not only a strong RTP signal, but it also gave the maximum RTP quenching for a given oxygen content with the phosphor adsorbed on 1PS filter paper. Recently, Ramasamy and Hurtubise [20] reported a detailed comparison of the solid-matrix luminescence properties of d-phen and phenanthrene adsorbed on several solid matrices. For example, they showed that d-phen gave a RTP lifetime of 9.7 s on Whatman No.1 filter paper.

3.2. Oxygen quenching of RTP signals

Fig. 2 shows a typical quenching pattern of the RTP intensity of d-phen adsorbed on Whatman 1PS filter paper for sequential flows of nitrogen and nitrogen–air at numerous oxygen contents. The duration of the measurement of the RTP signal was found to be important in getting reproducible results. In this study, average RTP values were obtained over a 25 s time period. For a given oxygen content, a shorter measurement period resulted in lower RTP values, and therefore, lower sensitivity. By using a fixed measurement time, very accurate results were obtained. An important observation about the quenching results in Fig. 2 is that the RTP intensity in the presence of nitrogen remained essentially steady before oxygen was introduced into the system, but decreased after successive nitrogen–air flows. However, the decrease in these RTP values did not affect the accuracy of the method because equal increments of time were used between each oxygen measurement.

Continuous passing of nitrogen for more than 1 h over the phosphor, after the phosphor had been exposed to several percentages of oxygen, did not restore the original RTP intensity. Also, the RTP intensity, after the introduction of oxygen, changed somewhat with time as indicated in Fig. 2. Thus, it was necessary to measure the RTP after a fixed time period. The changes in RTP did not greatly affect the accuracy and precision of the oxygen determinations as discussed in the next section. The RTP intensity versus time plot in Fig. 2 shows RTP signals over a wide time frame.

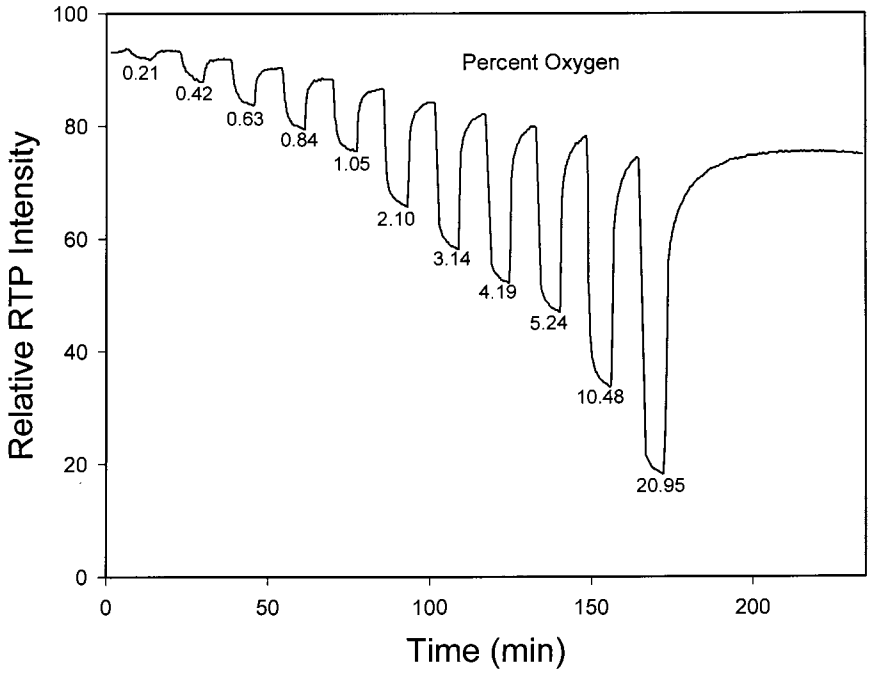

Fig. 2. RTP intensity versus time plot for several percentages of oxygen passed sequentially into the experimental system.

Thus, the phosphor was exposed to several oxygen levels over this time period. For a typical RTP measurement with an unknown sample, the phosphorimeter would be on for a 25 s period to measure the RTP of the sample after the gaseous mixture was passed over the sample for a fixed time period (7–9 min). In addition, a calibration curve most likely would be prepared from much fewer percentages of oxygen compared to the ones in Fig. 2.

3.3. Analytical figures of merit

Since the baseline changed for successive oxygen determinations, the P_0 values for each oxygen quenching measurement were obtained in the presence of dry nitrogen just before each oxygen determination. The RTP signal (P) during the quenching step was measured as described in the previous section. Fig. 3 shows a typical Stern–Volmer plot for the oxygen quenching of the RTP of d-phen adsorbed on 1PS filter paper (average of three runs). The calibration plot over the entire range of percent oxygen investigated (0–21% oxygen) followed a nonlinear relationship. However, a linear range was obtained from 0 to 1.10% oxygen with a linear correlation coefficient of 0.995 (Fig. 3). The limit of detection (LOD) using the 0–1.10% oxygen range was 0.09% oxygen. The LOD was calculated from the equation, LOD = 3 (standard deviation of the blank)/(slope of the calibration plot). The RTP quenching values, (P_0/P), were reproducible with 95% confidence limits of ± 0.01, ± 0.22, and ± 0.57 at 0.21, 3.00 and 21.00% oxygen levels, respectively. Also, six successive determinations of 0.54% oxygen showed a 95% confidence interval of ± 0.007 for P_0/P (a relative standard deviation of 0.6%).

Whatman 1PS filter paper samples without any phosphor adsorbed showed a very weak RTP quenching pattern for the range of oxygen percentages shown in Fig. 2 compared to the quenching pattern observed for d-phen. To account for the contribution from the blank signals, the blank P_0 and P values from Whatman 1PS paper were subtracted from the corresponding d-phen P_0 and P values. The blank corrected RTP values were used in another calibration plot. The overall

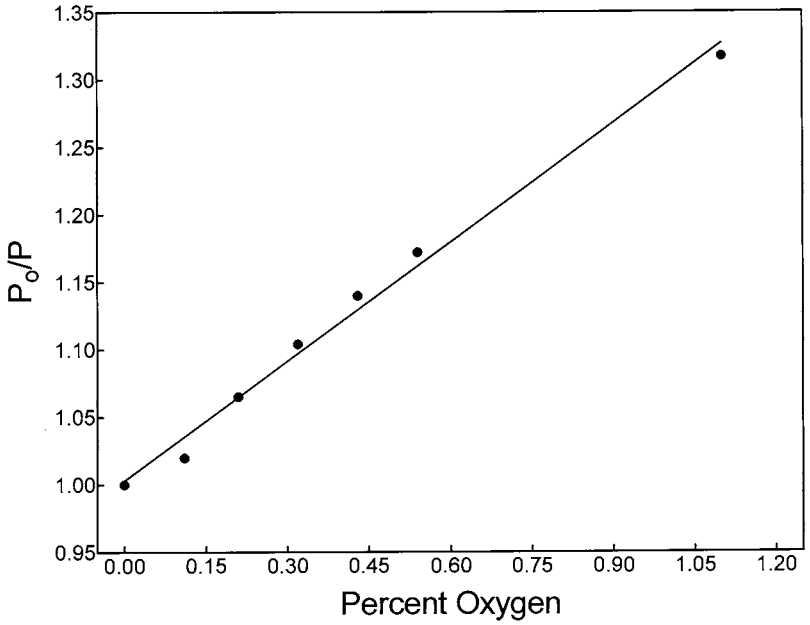

Fig. 3. Plot of the ratio of RTP intensity without oxygen (P_0) to RTP intensity with oxygen (P) versus percent of oxygen from 0 to 1.10% oxygen.

shape and the linear range of the calibration plot did not change compared to plots without blank subtraction. Generally, the phosphor signals for the phosphor adsorbed on 1PS paper were 43 times greater than the RTP background signals of the 1PS paper from 0.10 to 21% oxygen. By using each P_0/P value without blank subtraction and the corresponding P_0/P value with blank subtraction in the range of 0.10–1.10% oxygen, the average percentage error was calculated as 0.84%. In the range of 1.70–21.0% oxygen, the average percentage error for P_0/P without blank subtraction was 3.78%. Thus, for highly accurate results, it would be necessary to correct the P_0 and P values for d-phen with the corresponding P_0 and P values from blank Whatman 1PS filter paper. Also, the ratio of the slopes for plots of P_0/P vs. $\%O_2$ from 0 to 1.10% O_2 without and with blank subtraction was 1.09. For the ranges of 0–1.70% O_2 and 0–2.33% O_2, the ratios of slopes without and with blank subtraction were 1.09 and 1.10, respectively. If there were no effect due to the blank, then the ratio of slopes would be 1.00. This is so because the blank phosphorescence signals would be quenched to different extents with increasing % O_2.

3.4. Baseline change

Whatman 1PS filter paper was exposed to polychromatic UV radiation from a 450 W xenon lamp for 1 h to photochemically decompose the phosphorescent impurities so as to minimize the phosphorescence background signals [15]. However, d-phen adsorbed on the UV treated 1PS filter paper gave a calibration plot and linear range similar to the non-UV treated filter paper sample. Thus, there was no major advantage to using the UV-treated 1PS filter paper. Also, samples of the phosphor adsorbed on 1PS filter paper, after oxygen quenching, were reheated and cooled in nitrogen. However, the RTP intensity prior to exposure to oxygen was not restored. The exact reason for this has not been established. However, different samples of phosphor spotted on 1PS filter paper and heated to 110°C for 30, 45, and 60 min gave similar phosphorescence lifetime (τ_p) values after 15 min cooling in a nitrogen atmo-

sphere. Thus, moisture was absent in the filter paper matrix after drying, otherwise it could have been another potential source for the change in the baseline.

The baseline decrease that occurred with time (Fig. 2) happened after quenching, whether the sample was continuously exposed to the exciting radiation or exposed only during the RTP measurement. The previous result suggests that little photodecomposition of the phosphor occurred while the sample was exposed to the exciting radiation. This was supported by the fact that no decrease in RTF intensity was observed when d-phen in ethanol was subjected to the repeated cycle of quenching with air and regeneration with nitrogen.

3.5. Effects of moisture and carbon dioxide on the quenching of RTP

Moist nitrogen and moist air were found to cause significant quenching of the RTP intensity of d-phen adsorbed on 1PS filter paper. This was most likely due to the breaking of hydrogen bonds in the cellulose network of the filter paper by moisture and thus causing the phosphor to be held less rigidly in the matrix [14,15]. It is well known that moisture can quench RTP.

Carbon dioxide in the presence of nitrogen and air had little effect on the quenching of the RTP of the phosphor. For instance, 10–95% carbon dioxide (v/v) in nitrogen–air mixtures with 1.05% oxygen caused an error of only 0.6–4% for the RTP quenching measurements. Similarly, for 5.24 and 10.45% oxygen in air with 10–75% carbon dioxide and 10–50% carbon dioxide produced an error of 2–3% and 2–5%, respectively. Thus, oxygen can be determined in the presence of a wide range of carbon dioxide concentrations with a relatively small error in the determination.

3.6. Comparison of RTP results with Teledyne trace oxygen analyzer

The percent oxygen of five nitrogen–air mixtures ranging from 0.21 to 1.05% were obtained with a Teledyne trace oxygen analyzer and compared to the percent oxygen obtained from the RTP quenching method. Table 1 compares the data from the two methods. As indicated in Table 1, the percent oxygen obtained by the RTP method gave values that were much closer to the accepted values of oxygen. The accepted values were calculated as described in the Section 2. In fact, the results from the Teledyne system were all lower compared to the corresponding values obtained by RTP. The data in Table 1 show that the RTP method is very reliable.

3.7. RTP lifetime before and during oxygen quenching

The phosphorescence lifetime (τ_p) values of d-phen adsorbed on Whatman 1PS filter paper were obtained. The τ_p values were measured after a 5 min equilibration period for each nitrogen–air mixture, and the τ_p^0 values were acquired before each oxygen quenching measurement by passing nitrogen through the cell for a 5 min time period between the measurement steps. Fig. 4 illustrates the change of τ_p^0/τ_p values with oxygen content. As indicated, the τ_p^0/τ_p plot showed a nonlinear relationship over the entire percent oxygen range. Because the plot was not linear, a simple diffusion controlled oxygen quenching mechanism was not occurring over the range of % oxygen investigated. For all the different oxygen contents studied, the P_0/P values were considerably greater than the τ_p^0/τ_p values. Thus, P_0/P was used in the determination of the percentage oxygen. Studies are continuing to develop a detailed understanding of the RTP quenching mechanism of oxygen with d-phen adsorbed on 1PS paper.

Table 1
Comparison of the % oxygen from the RTP method and the from a Teledyne analyzer

Accepted value (% oxygen)	RTP method (% oxygen)	Teledyne analyzer (% oxygen)
0.21	0.17	0.15
0.42	0.42	0.33
0.63	0.69	0.51
0.84	0.89	0.69
1.05	1.14	0.87

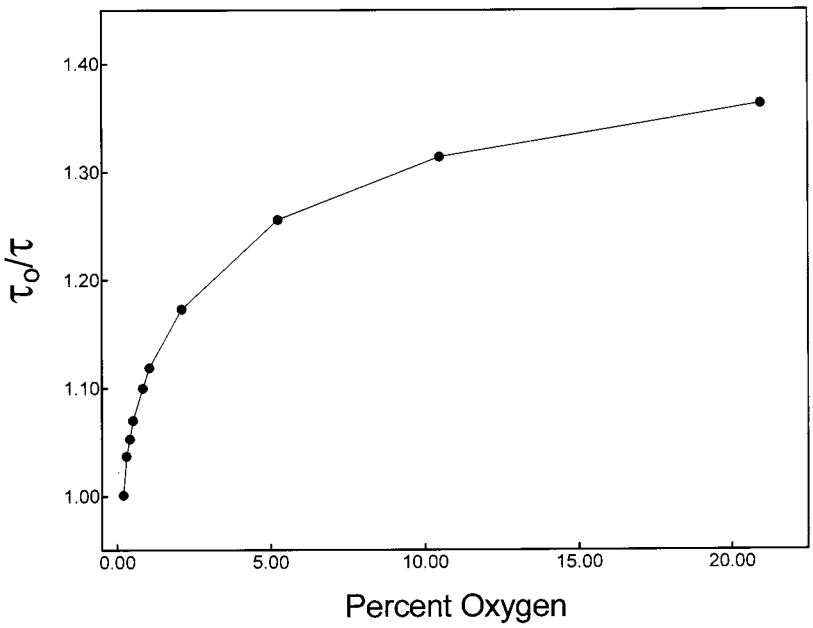

Fig. 4. Plot of the ratio of RTP lifetime without oxygen (τ_0) to RTP lifetime with oxygen (τ) versus the percent of oxygen.

4. Conclusion

A solid-matrix RTP oxygen sensor was developed that is inexpensive and easy to use. The basis of the sensor is the oxygen quenching of the RTP of a phosphor adsorbed on filter paper. It is a simple matter to prepare the sensor. One adsorbs the phosphor on filter paper, drys the filter paper with the adsorbed phosphor, and then the dried paper is placed in a spectroflurometric cell. Oxygen can be determined over a wide range, the reproducibility and accuracy of the sensor were very good, and the limit of detection for oxygen was very low (0.09%). One disadvantage of the sensor is that the RTP of the phosphor is sensitive to moisture, but if moisture is minimized very accurate data can be obtained from the sensor. However, a major advantage of the sensor would be for the determination of oxygen in samples that contain large amounts of carbon dioxide.

Acknowledgements

Financial support for this project was provided by the United States Department of Energy, Grant No. DE-FG06-95ER14551.

References

[1] D.M. Oglesby, B.T. Upchurch, B.D. Leighty, J.P. Collman, X. Zhang, P.C. Herrmann, Anal. Chem. 66 (1994) 2745.
[2] Z. Rosenzweig, R. Kopelman, Anal. Chem. 67 (1995) 2650.
[3] M.F. Choh, P. Hawkins, Talanta 42 (1995) 483.
[4] K.A. Kneas, W. Xu, J.N. Demas, B.A. DeGraff, Appl. Spectrosc. 51 (1997) 1346.
[5] A. Mills, A. Lepre, B.R.C. Theobald, E. Slade, B.A. Murrer, Anal. Chem. 69 (1997) 2842.
[6] O.S. Wolfbeis, in: S.G. Shulman (Ed.), Molecular Luminescence Spectroscopy: Methods and Applications, Part 2, Wiley, New York, 1988, pp. 154–155.
[7] J.M. Charlesworth, Sens. Actuators B 22 (1994) 1.
[8] Y.M. Liu, R.P. Garcia, J.V. Gonzalez, M.E.D. Garcia, A.S. Medel, Anal. Chem. 66 (1994) 836.
[9] M.E.D. Garcia, R.P. Garcia, N.V. Garcia, Analyst 120 (1995) 457.
[10] D.B. Papkovsky, G.V. Ponomarev, W. Trettnak, P. O'Leary, Anal. Chem. 67 (1995) 4112.
[11] P. Hartmann, W. Trettnak, Anal. Chem. 68 (1996) 2615.
[12] S.K. Lee, I. Okura, Anal. Sci. 13 (1997) 535.

[13] F. Alava-Moreno, M.J. Valencia-Gonzalez, A. Sanz-Medel, M.E. Diaz-Garcia, Analyst 122 (1997) 807.
[14] T. Vo-Dinh, Room Temperature Phosphorimetry for Chemical Analysis, Wiley, New York, 1984.
[15] R.J. Hurtubise, Phosphorimetry: Theory, Instrumentation, and Applications, VCH/Wiley, New York, 1990.
[16] S.W. Tjioe, R.J. Hurtubise, Anal. Lett. 26 (1993) 557.
[17] S.W. Tjioe, R.J. Hurtubise, Talanta 41 (1994) 595.
[18] S.W. Tjioe, R.J. Hurtubise, Talanta 42 (1995) 59.
[19] Whatman Technical Publication 811 PS A.
[20] S.M. Ramasamy, R.J. Hurtubise, Appl. Spectrosc. 50 (1996) 1140.

ELSEVIER

Talanta 47 (1998) 981–986

Talanta

Detection of 2-chloroethylethyl sulfide on soil particles using ion trap-secondary ion mass spectrometry

Gary S. Groenewold *, Anthony D. Appelhans, Jani C. Ingram, Garold L. Gresham, Anita K. Gianotto

Idaho National Engineering and Environmental Laboratory, Idaho Falls, ID 83415-2208, USA

Received 18 March 1998; received in revised form 20 April 1998; accepted 21 April 1998

Abstract

2-Chloroethylethyl sulfide (CEES) is used as a simulant for mustard (HD) in a study to develop secondary ion mass spectrometry (SIMS) for rapid, semi-quantitative detection of mustard on soil. Selectivity and sensitivity are markedly improved employing multiple-stage mass spectrometry (MS^n) using an ion trap SIMS. $C_2H_5SC_2H_4^+$ from CEES eliminates C_2H_4 and H_2S, which are highly diagnostic. CEES was detectable at 0.0012 monolayer on soil. This corresponds to approximately 15 ppm (mass/mass) for a soil having a surface area of 12 m^2 g^{-1}. A single analysis could be conducted using only 2 mg of soil in under 5 min. © 1998 Elsevier Science B.V. All rights reserved.

Keywords: Spectrometry; Mustard; Soil

The detection of chemical warfare agent residues on environmental surfaces is an important analytical activity because of the potential for proliferation of these weapons, and for environmental monitoring in areas where they are stored. Historically, one of the most widely used agents has been bis(2-chloroethyl) sulfide, also known as mustard gas and HD. It was initially used in combat in 1917; by the end of the First World War, more than 16% of all casualties were due to chemicals, in most cases mustard [1]. Manufacture of mustard is continuing to this day; consequently, there are ongoing opportunities for exposure [2–5].

Under some conditions, detection of mustard can be challenging. The compound is a semivolatile liquid under ambient conditions, and can strongly adsorb to many surfaces [5]. These factors can serve to confound many detection approaches; nevertheless several analytical schemes have been successfully adopted. Among these are a variety of chromatographic methods [5,6], some of which utilize mass spectrometry as a detector [5,7] All of these techniques rely on getting the compound into the gas phase.

An alternative approach is presented in this paper, which directly targets strongly sorbed organosulfides. Static secondary ion mass spectrometry (SIMS) can be used to analyze adsorbed contaminants on soil, and has been applied to the detection of organic phosphates [8–12] and amines [13] in our laboratory. When SIMS is

* Corresponding author. Tel. +1 208 5262803; fax: +1 208 5268541; e-mail gsg@inel.gov

0039-9140/98/$ - see front matter © 1998 Elsevier Science B.V. All rights reserved.
PII S0039-9140(98)00165-9

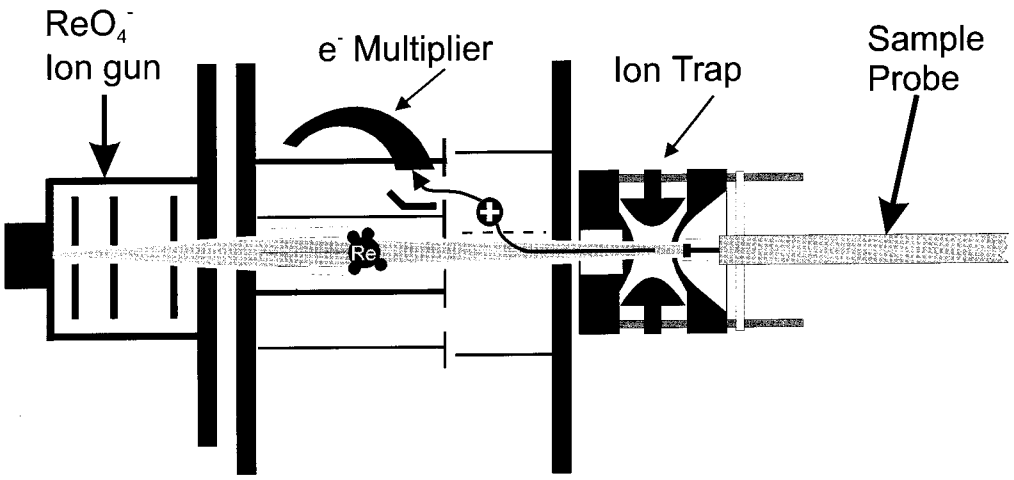

Fig. 1. Schematic diagram of the ion trap SIMS instrument.

combined with the MS/MS capability of an ion trap mass spectrometer, remarkable improvements in detectability have been realized [14]. In this report, the SIMS behavior of the mustard surrogate compound 2-chloroethyl ethyl sulfide (CEES) is explored. It is found that the fragmentation behavior of CEES permits the compound to be distinguished from background, which in turn enables detection at concentrations of one thousandth of a molecular layer. The work builds upon a previous study conducted in our laboratory which showed that SIMS could be used to detect ionic condensation products (organosulfonium ions) originating from CEES degradation [15].

1. Experimental

1.1. Sample

A clean soil sample obtained from the Rocky Mountain Arsenal (CO), was used in the present study. The sample was predominantly silicate in nature, with minor contributions from aluminum and iron, as determined using scanning electron microscopy and energy dispersive X-ray analysis. The soil was sieved and the $0.0049'' < x < 0.0098''$ mesh fraction was used. The surface area of this fraction was measured at 12 $m^2\ g^{-1}$ using N_2 adsorption (BET method) [16].

The samples were exposed to CEES, by wetting the soil surface with methylene chloride solutions of the compound, 1 μl solution to 1 mg soil. This ratio just wets the soil, but does not leave a lot of standing solution. The monolayer coverage on the soil particles could be calculated using the mass of CEES in the wetting solution, the mass of the soil, the surface area, and assuming 20 $Å^2$ per molecule. This method has been used successfully for generating samples having known surface coverages [8,9]. The wetted soil samples were allowed to dry, and were then prepared for SIMS analysis by attaching particles to a sample holder using double-sided tape.

1.2. Ion trap SIMS

The instrument used in this study was a Finnigan ITMS instrument modified for SIMS with a ReO_4^- primary ion gun, on offset dynode with multichannel plate detector and an insertion lock for introducing the sample (Fig. 1) [14,17]. As illustrated in Fig. 1 the high energy ReO_4^- beam is directed through the ion trap, striking the sample which is located behind one of the ion trap end caps. The ReO_4^- primary particle provides enhanced production of molecular secondary ions, which is advantageous when probing surface adsorbates [18,19]. Secondary ions emitted from the sample are focused into the ion trap where

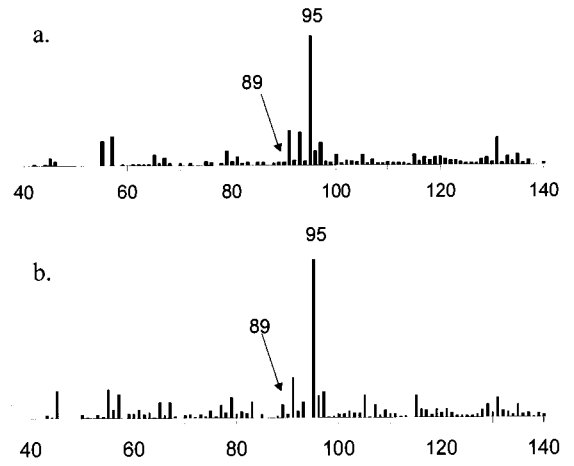

Fig. 2. Partial cation SIMS spectra acquired using the ion trap SIMS. (a) Unexposed soil. (b) Soil exposed to 0.03 monolayer CEES, acquired using the ion trap SIMS instrument; ions at m/z 89, 61, 55 and 45 are partially derived from CEES; other ions are background.

they undergo collisions with a He bath gas present in the trap and lose sufficient kinetic energy that they are trapped by the dynamic electrostatic field. In addition, by applying the appropriate oscillating fields (filtered noise field) to the end caps during the ion-trapping sequence, all ions except those within a narrow mass range can be kept out of the trap. This makes it possible to fill the trap with only the ions of interest, greatly improving the signal to noise and resultant sensitivity.

Once trapped, the ions can either be mass selectively ejected out to the detector region (single MS), or they can be collisionally dissociated by applying a high frequency oscillating field to the end caps (MS/MS). The ionic fragments from the dissociation remain trapped and can then either be further dissociated (MS^3), or mass selectively ejected to the detector.

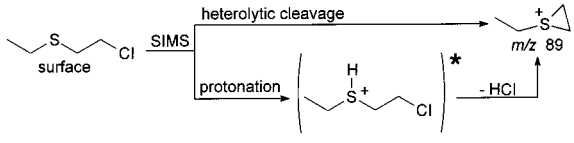

Fig. 3. Possible formation mechanism for m/z 89^+, observed in the cation spectrum of CEES on soil.

In a typical MS experiment, the ion trap was operated at $a_z = 0$, and $q_z = 0.9078$, which corresponds to a low mass cutoff of 40 amu ($\beta = 0.9802$). Ionization time was typically 20 ms, after which the mass spectrum was recorded using a mass selective instability scan with axial modulation [20]. A single 'scan' consisted of ten summed spectra.

For MS/MS experiments, the ionization time was typically longer (100–1000 ms), during which time a filtered noise field [20] was applied to the end caps, such that m/z 89 was isolated. After forming and isolating the ion, it was then fragmented and the daughter ions were scanned out for measurement. A typical MS/MS acquisition resulted in a primary ion beam dose of 1.0×10^{13} ions cm^{-2} to the sample.

The MS^3 experiments were identical to the MS/MS experiments for CEES-derived m/z 89, except that a filtered noise field was added subsequent to the first fragmentation period, which had the effect of isolating m/z 61 as the daughter ion from m/z 89. m/z 61 was then further dissociated to produce its daughter ion spectrum.

2. Results and discussion

The strategy employed in these analyses is based on the CEES ion fragment at m/z 89, thus contributions to m/z 89 not arising from CEES must be identified. The SIMS spectrum of 'clean' soil contains a wide variety of ions (Fig. 2). Most of the ion signal originates from hydrocarbon background, which is present on virtually every sample. It has been speculated that this originates from background contaminants present in the instrument, although paraffinic contamination from the ambient atmosphere certainly occurs, particularly if the contaminant molecules also contain heteroatom functionality [13]. This chemical background limits the sensitivity of detection and obscures specificity. In the spectra of our 'clean' soil there are peaks at m/z 89 and 91 and MS/MS analyses of m/z 91 and 89 indicates that they are hydrocarbon in nature: both ions undergo loss of C_2H_2 to form m/z 65 and 63, respectively, which is what would be expected

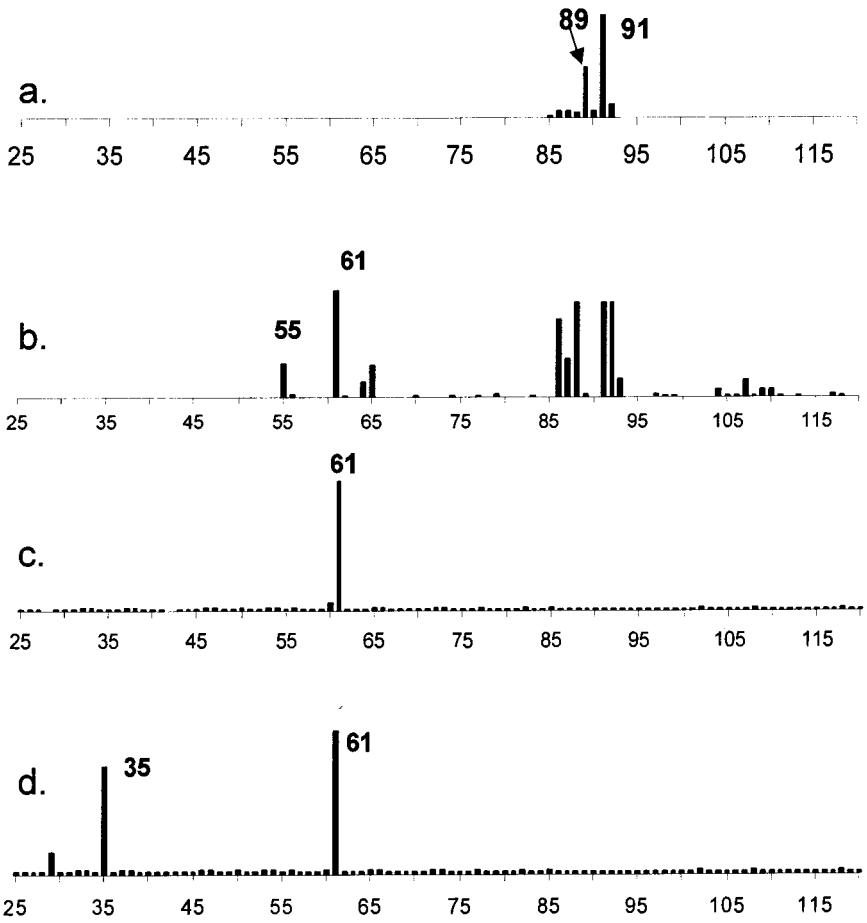

Fig. 4. MS^n fragmentation of m/z 89 from SIMS analysis of CEES. (a) Isolation of m/z 89 (and 91). (b) Fragmentation of m/z 89 to form 61 and 55. (c) Isolation of m/z 61. (d) Fragmentation of m/z 61 to form m/z 35.

from ions having compositions of $C_7H_7^+$ and $C_7H_5^+$.

When soil samples doped with CEES were analyzed, the spectra collected were similar to the undoped benchmark, but contained a more abundant ion at m/z 89, which corresponds to [CEES-Cl]$^+$. Ions corresponding to the protonated, intact molecule were not observed above background. We can envision two mechanisms for the formation of m/z 89 upon SIMS activation: 1) heterolytic cleavage of the C–Cl bond, or 2) protonation of CEES to form an unstable cation which rapidly eliminates HCl (Fig. 3). We favor the heterolytic cleavage mechanism at this time, since the He bath gas in the ion trap serves to stabilize gas-phase ion species [21], and stable protonated mustard species have been reported [22]. This explanation is also consistent with the idea that the S-lone pairs provide anchimeric assistance for the elimination of the β-chloro substituent [23,24].

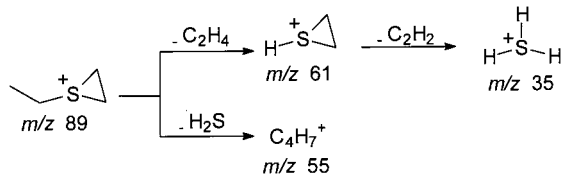

Fig. 5. Fragmentation of ethyl thiiranium$^+$ ($C_2H_5SC_2H_4^+$) formed from CEES.

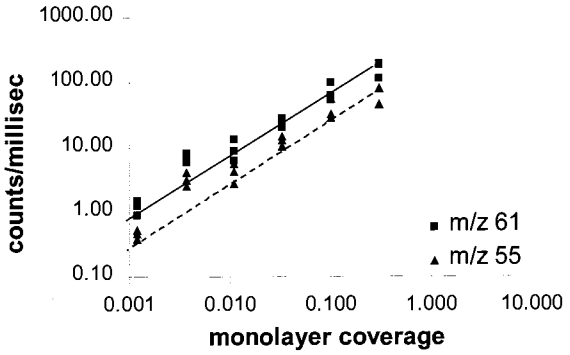

Fig. 6. Absolute abundance of the m/z 89 daughter ions 61 and 55 versus surface concentration of CEES.

Other ions derived from CEES are observed in the SIMS spectrum at m/z 61, 55, and 45. m/z 61 and 55 could be observed using MS/MS, and are discussed below. m/z 45 was not observed as a daughter ion from m/z 89 using the ion trap; we believe that the fragmentations leading to m/z 45 compete unfavorably with those producing 61 and 55. The composition of m/z 45 is probably CH_3S^+; in related work recently completed in our laboratory, we have shown that CH_3S^+ is produced from $C_4H_7S^+$.

The identity of m/z 89 was proven by MS/MS and MS/MS/MS experiments. m/z 89 was isolated using a filtered noise field and then fragmented. Abundant daughter ions were observed at m/z 61 and 55, representing the loss of 28 (C_2H_4) and 34 (H_2S) mass units, respectively (Figs. 4 and 5). It was noted that these losses were significantly different than those observed from the endogenous m/z 89, which only eliminated C_2H_2 to produce m/z 63. Further, the elimination of 34 amu is highly diagnostic for a sulfur bearing ion. This reaction must involve substantial rearrangement to produce the $C_4H_7^+$ daughter ion at m/z 55; in fact, extensive rearrangement of $C_3H_7S^+$ prior to elimination of H_2S has been observed [25]. The composition of the m/z 61 daughter ion was further probed by adding another ion isolation and fragmentation step to the experiment. This showed the elimination of C_2H_2 to form m/z 35; this unusual cation is certainly H_3S^+. Starting from an initial parent ion composition of $C_4H_9S^+$, no other elemental compositions are possible for this ion. The structure proposed for m/z 89 is the ethyl thiiranium ion, and is consistent with structures proposed for other sulfur bearing species [26,27].

The quantitative potential of this approach was assessed by analyzing a series of soil samples that were generated such that the concentration of CEES on the surface of the soil ranged over three decades. The instrument was then set to isolate m/z 89, and detect the daughter ions subsequent to fragmentation. The daughter ions could be clearly observed at the lowest concentration studied, which was 0.0012 monolayer (for a 12 $m^2\ g^{-1}$ soil sample, this corresponds to 15 ppm on a mass/mass basis). When ion abundance was plotted versus surface concentration (monolayers), a linear relationship was observed from 0.0012 to 0.3 monolayers (Fig. 6).

The sensitivity plot in Fig. 6 implies that some level of analytical precision is achievable, and in fact, under carefully controlled conditions, sample-to-sample ion abundances can be reproduced to within 30% (one standard deviation). However, analytical imprecision arising from sample preparation (factors such as fraction of the tape covered by the soil sample) and variation in primary ion beam intensity prohibits a higher precision on a day-to-day basis. Another factor which influences day-to-day precision is the longevity of CEES on the soil surface. It was observed that after 5 months of standing, CEES could just barely be detected on a soil sample initially exposed to 0.3 monolayer. The mechanism for the disappearance of the compound is not known, but evaporation from the surface, or degradation (perhaps to the hydroxy derivative) are the most likely possibilities and will be dependent on the local environmental conditions and the chemistry of the soil.

3. Conclusions

This research demonstrates that organosulfide adsorbates can be easily characterized on soil surfaces using an ion trap SIMS. An MS/MS approach provides the necessary specificity for detection of the analyte ions, which is achieved

primarily through the diagnostic loss of H_2S. This elimination is unique compared to other elimination reactions common to endogenous hydrocarbon ions originating from the vacuum system or the environment. The abundance of the analyte signal was clearly demonstrated to be proportional to the analyte surface coverage, which makes a semiquantitative assessment of contaminant concentration possible. The limit of detection corresponded to 0.001 monolayer of CEES on the soil, corresponding to approximately 15 ppm (mass/mass) for a soil having a surface area of 12 $m^2\ g^{-1}$.

Acknowledgements

The authors gratefully acknowledge the funding provided by the United States Department of Energy NN-20 Office. The authors also gratefully acknowledge the technical assistance of Marnie Cortez.

References

[1] J.A.F. Compton, Military Chemical and Biological Agents, The Telford Press, Caldwell, NJ, 1987, p. 9.
[2] L. Ember, Chem. Eng. News, May 3, (1993) 8–9.
[3] Nature breaks up Iraqi toxic trail, New Scientist, January 23, (1993) 6.
[4] Chemical, biological arms pose grave threat, Chem. Eng. News, March 1, (1993) 9.
[5] R.M. Black, R.J. Clarke, R.W. Read, M.T.J. Reid, J. Chromatogr. 662 (1994) 301.
[6] Z. Witkiewicz, M. Mazurek, J. Szulc, J. Chromatogr. 503 (1990) 293.
[7] P.A. D'Agostino, L.R. Provost, J. Chromatogr. 589 (1992) 287.
[8] J.C. Ingram, G.S. Groenewold, A.D. Appelhans, D.A. Dahl, J.E. Delmore, Anal. Chem. 68 (1996) 1309.
[9] J.C. Ingram, G.S. Groenewold, A.D. Appelhans, J.E. Delmore, D.A. Dahl, Anal. Chem. 67 (1995) 187.
[10] J.C. Ingram, G.S. Groenewold, A.D. Appelhans, J.E. Delmore, J.E. Olson, D.L. Miller, Environ. Sci. Technol. 31 (1997) 402.
[11] G.S. Groenewold, J.C. Ingram, J.E. Delmore, A.D. Appelhans, D.A. Dahl, J. Haz. Mats. 41 (1995) 359.
[12] G.S. Groenewold, J.C. Ingram, J.E. Delmore, A.D. Appelhans, J. Am. Soc. Mass Spectrom. 6 (1995) 165.
[13] G.S. Groenewold, J.C. Ingram, A.K. Gianotto, A.D. Appelhans, J.E. Delmore, J. Am. Soc. Mass Spectrom. 7 (1996) 168.
[14] A.D. Appelhans, G.S. Groenewold, J.C. Ingram, J.E. Delmore, D.A. Dahl, in: A. Benninghoven, B. Hagenhoff, H.W. Werner (Eds.), Secondary Ion Mass Spectrometry SIMS X, Wiley, New York, 1997, p. 935.
[15] G.S. Groenewold, J.C. Ingram, A.D. Appelhans, J.E. Delmore, D.A. Dahl, Environ. Sci. Technol. 29 (1995) 2107.
[16] A.W. Adamson, Physical Chemistry of Surfaces, Wiley, New York, 1990, p. 609.
[17] G.S. Groenewold, A.D. Appelhans, J.C. Ingram, J. Am. Soc. Mass Spectrom. 9 (1997) 35.
[18] J.E. Delmore, A.D. Appelhans, E.S. Peterson, Int. J. Mass Spectrom. Ion Processes 146/147 (1995) 15.
[19] J.E. Delmore, A.D. Appelhans, E.S. Peterson, Int. J. Mass Spectrom. Ion Processes 108 (1991) 179.
[20] J.F.J. Todd, in: R.E. March, J.F.J. Todd (Eds.), Practical Aspects of Ion Trap Mass Spectrometry, vol. I, CRC Press, New York, 1995, p. 4.
[21] D. Goeringer, S. McLuckey, Proceedings of the 45th ASMS Conference on Mass Spectrometry and Allied Topics, June 1–5, 1997, Palm Springs, CA, p. 793.
[22] E. Ali-Mattila, K. Siivinen, H. Kenttamaa, P. Savolahti, Int. J. Mass Spectrom. Ion Phys. 47 (1983) 371.
[23] O. Bortolini, M. Fogagnolo, Mass Spectrom. Rev. 14 (1995) 117.
[24] M.C. Carreno, J.C. Carretero, J.L. Garcia Ruano, M.C. Martinez, Org. Mass Spectrom. 25 (1990) 339.
[25] W.J. Broer, W.D. Weringa, Org. Mass Spectrom. 14 (1979) 36.
[26] W.J. Broer, W.D. Weringa, Org. Mass Spectrom. 15 (1980) 229.
[27] N.M.M. Nibbering, S. Ingemann, L.J. de Koning, in: S. Patai, Z. Rappoport (Eds.), The chemistry of sulphur-containing functional groups, Suppl. S, Wiley, Chichester, 1993, p. 293.

ELSEVIER

Talanta 47 (1998) 987–999

Talanta

Conducting polymer ion sensor electrodes–III. Potentiometric sulfide ion selective electrode

Nada F. Atta [a], Ahmed Galal [1,a,*], Harry B. Mark Jr.[b], T. Yu [c], Paul L. Bishop [c]

[a] *Department of Chemistry, Faculty of Science, University of Cairo, Giza, Egypt*
[b] *Department of Chemistry, University of Cincinnati, PO Box 210172, Cincinnati, OH 45221-172, USA*
[c] *Department of Civil and Environmental Engineering, University of Cincinnati, PO Box 210071, Cincinnati, OH 45221-0071, USA*

Received 21 August 1997; received in revised form 30 April 1998; accepted 4 May 1998

Abstract

A new potentiometric sensor electrode for sulfide based on conducting polymer films is introduced. The electrode is formed by electrochemically depositing a film of poly(3-methylthiophene) and poly(dibenzo-18-crown-6) onto an alloy substrate. Different methods were used for the electrode preparations. The alloy used has a low melting point, which allowed its use for manufacturing a microsize version of this electrode. The electrode response is stable for 3 days. The working temperature range for this electrode is between 10 and 40°C. The linear dynamic range is 1.0×10^{-7}–1.0×10^{-2} M and measures total sulfide concentration over a range of pH from 1 to 13. The polymer electrode showed high selectivity for sulfide in the presence of many common interfering anions. The electrode is useful for the measurement of total sulfide in biological environments and can be manufactured in the micron scale. Therefore, it will be useful for the measurement within biofilms. © 1998 Elsevier Science B.V. All rights reserved.

Keywords: Conducting polymers; Sensor electrodes; Hydrogen sulfide; Environmental pollution; Selective electrodes

1. Introduction

Hydrogen sulfide is created by the decomposition of metal sulfides and organic matter. Sulfur-reducing bacteria, which use sulfur as an energy source, are the primary producers of large quantities of hydrogen sulfide [1]. These bacteria change sulfates in aqueous media to hydrogen sulfide. Another problem caused by hydrogen sulfide in the environment is its corrosive nature to metals and other materials. The effect on metals spans the gamut from tarnishing, as with silver, to deterioration by corrosion, as in the case of iron and copper [2]. It rapidly attacks many construction materials, such as concrete. Moreover, relatively high concentrations of sulfides can cause biofouling of the ion exchangers in the water softening process and to water distribution pipes.

The sulfide ion-selective electrodes are produced in different versions [3] and have been applied for measuring sulfide in various sample

* Corresponding author. Fax: +971 3 671291; e-mail: Helmyag@nyx.uaeu.ac.ae

[1] Current address: Department of Chemistry, Faculty of Science, University of United Arab Emirates, PO Box 17551, Al-Ain, United Arab Emirates.

0039-9140/98/$ - see front matter © 1998 Elsevier Science B.V. All rights reserved.
PII S0039-9140(98)00182-9

systems [4]. The liberation of hydrogen sulfide is a significant indication of flourishing and multiplying of sulfate-reducing bacteria in biofilms [1]. Commercial sulfide ion-selective electrodes have been used for studying the production of sulfide in cultures of *Desulfovibrio desulfuricans* [1] and slurries of estuarine marshland [5]. Several research groups reported the fabrication of different sulfide ion-selective electrodes for the study of microbial environments and biofilms [6–8]. The amounts of sulfide expected in these environments from aerobic and anaerobic bacteria species are in the ranges of 1.5×10^{-6}–6.0×10^{-4} M.

In situ measurement of sulfide activity was introduced by the use of the sulfide ion-selective membrane electrodes [9]. However, the determination of total sulfide can be accomplished only after the samples are buffered to high pH by a high ionic strength buffer [10]. The direct determination of total sulfide is also possible using a sulfide ion selective electrode coupled to a pH electrode [11]. The previous electrodes, cited in the literature, are limited for use in solutions with pH values < 6.0 and have some interference problems. There are a wide variety of commercially available electrodes fabricated in standard dimensions. The pH of most waters as well as treated and untreated wastewater are above pH 6.0 [12,13]. These commercial electrodes are, thus, generally limited with respect to interfering ions, with pH limits, and are relatively expensive [8].

In this work, we are continuing our attempts toward developing solid state ion selective electrodes based on polymer technology [14–18]. The sensing matrix is a conducting polymer film deposited electrochemically on an alloy substrate. We studied different parameters of preparation affecting the response behavior and lifetime of the conducting polymer sulfide selective electrode. The effect of pH and several interfering ions are also studied. The morphology of the conducting polymer film is examined using scanning electron microscopy (SEM). We suggest a possible mechanism for the response of this electrode to sulfide ion. Moreover, the advantage of using the alloy substrate with a relatively low melting point allows the fabrication of an ultramicro-version of this sensor.

2. Experimental

2.1. Reagents and solutions

Sodium fluoride, chloride, bromide, iodide, bicarbonate, acetate, citrate, thiocyanate, nitrate, nitrite, perchlorate, borate, thiosulfate, sulfate, phosphate and sulfide were of analytical grade and were purchased from Fisher Scientific. Dibenzo-18-crown-6, 3-methylthiophene, acetonitrile, tetrabutyl ammonium tetrafluoroborate and other chemicals were purchased from Aldrich, and were treated as previously described [15]. All solutions were made up with double glass-distilled and de-ionized water. Electrode calibrations were performed on 25 ml solution in 0.1 M phosphate buffer (NaH_2PO_4/Na_2HPO_4, pH 7.0) to which concentrated (1 M) Na_2S solution was incrementally added. The pH change at the neutral pH used varied between 7.0 and 7.4 for the concentration range studied, ca. 5.0×10^{-8} to 8.0×10^{-3} M sulfide, respectively. Incremental addition of the 1 M Na_2S to the solution containing the phosphate buffer where as low as 1.0–200 μl from the stock solution. The pH change was adjusted with 1 M NaOH and 1 M HNO_3 to the pH 7. In order to check whether the preparation of the conducting polymer electrode and its pretreatment steps were successful, the response of the electrode was tested when immersed in two different concentrations of Na_2S, ca. 1.0×10^{-5} and 1.0×10^{-3} M sulfide solutions (pH 7.0), respectively. Initial calibration of the conducting polymer electrode was compared simultaneously with that of an Orion Sulfide Electrode Model 94-16.

2.2. Potentiometric measurement

Potential measurements were made with an Orion model 601A ionalyzer using an Orion model 90-02 double-junction reference electrode with a 10% KNO_3 solution in its outer chamber. All measurements were conducted in the presence of 1.00×10^{-3} M KNO_3 as an ionic strength adjuster (except in the experiments where the interference and pH effects were investigated). The measurements were carried out at 25 ± 0.5°C in de-aerated solutions, unless otherwise stated. We

used the injection method [19] in which a volume of concentrated solution of primary ion, smaller than the cell volume, is injected by means of a micro-pipette into the rapidly stirred test solution in which the cell assembly had been previously conditioned. The chart-recorder (and timer) is started at the instant of injection of the concentrated sample and the response time is recorded as the time after which a stable reading of ± 5 mV is reached.

2.3. Electrode fabrication

A lead glass micropipette (1.5 mm o.d, and 0.75 mm i.d.) was used as the housing body for a low melting-point alloy (44.7% Bi, 22.6% Pb, 19.1% In, 8.3% Sn and 5.3% Cd). The alloy wire was fused into a heat-pulled glass pipette. The size of the electrode tip was controlled by the speed of pipette pulling and heating temperature. This electrode can be used for the measurement within the biofilm. The tip was then polished in order to eliminate the excess glass edges and to obtain an average exposed disc area of the alloy of ~ 0.50–0.70 mm diameter electrode surface. The electrode surface was carefully polished and rinsed. This is followed by the electrochemical deposition of poly(3-methylthiophene).

2.4. Electropolymerization step

The electrode surface was polished using Alpha A cloth and alumina slurry. The conducting polymer films were electrochemically grown potentiostatically at 1.65 V from a solution containing 50 mM 3-methylthiophene and 100 mM tetrabutylammonium tetrafluoroborate (TBATFB) in acetonitrile (AcN) for 30 s. The electrode was then transferred to a solution containing 50 mM dibenzo-18-crown-6 and 100 mM TBATFB in AcN; a constant potential of 2.0 V was then applied to the poly(3-methylthiophene) layer for 5 min. The electrode was rinsed and dried in air for the following step. The electrode was then conditioned for use in the determination of sulfide by cycling in 50–150 mM ammonium sulfide solutions. Cycling potential limits were between 0.0 and 1.6 V (unless otherwise stated). Typically, the electrode was cycled for 10 times at a scan rate of 50 mV s^{-1}. The number and speed of scans affected the response of the electrode. The total charge accumulated during the positive cycles (0–+1.6 V) was ~ 2670 μC and the final anodic peak current was ~ 65 μA. Presumably, the polymer film is 'doped' with sulfide anion, at this stage. The electrode was then rinsed with deionized water and inserted in a diluted sulfide solution (ca. 10 mM) until a constant potential value was reached.

3. Results and discussion

3.1. Effect of electrode preparation and pretreatment method

The response of the electrode towards sulfide ions differed according to the method used for its preparation and the pretreatment step. We have examined five different methods for electrode preparation. The methods used in this study are:

1. the base alloy is mechanically polished as described above, and then immersed in 2 M $(NH_4)_2S$ solution for different time intervals (ca. 1–15 min),
2. the base alloy is immersed in the $(NH_4)_2S$ solution and subjected to electrochemical oxidation at different positive potentials,
3. the base alloy is coated with silver by electrochemical deposition, and then treated with $(NH_4)_2S$,
4. the base alloy is coated with poly(dibenzo-18-crown-6) [17], and
5. the base alloy is coated with poly(3-methylthiophene) and a thin layer of poly(dibenzo-18-crown-6) and treated with $(NH_4)_2S$ as described above.

Figs. 1–4 show the effect of the preparation schemes on the response of the electrode towards sulfide. Fig. 1 shows the response of an $(NH_4)_2S$-treated alloy electrode in the concentration range 5.0×10^{-8}–5.0×10^{-3} M sulfide. A linear response was only observed between 5.0×10^{-4} and 5.0×10^{-3} M. This electrode showed a relatively high standard variation for twenty measurements and its lifetime was short, ca. 15 min. Reactivat-

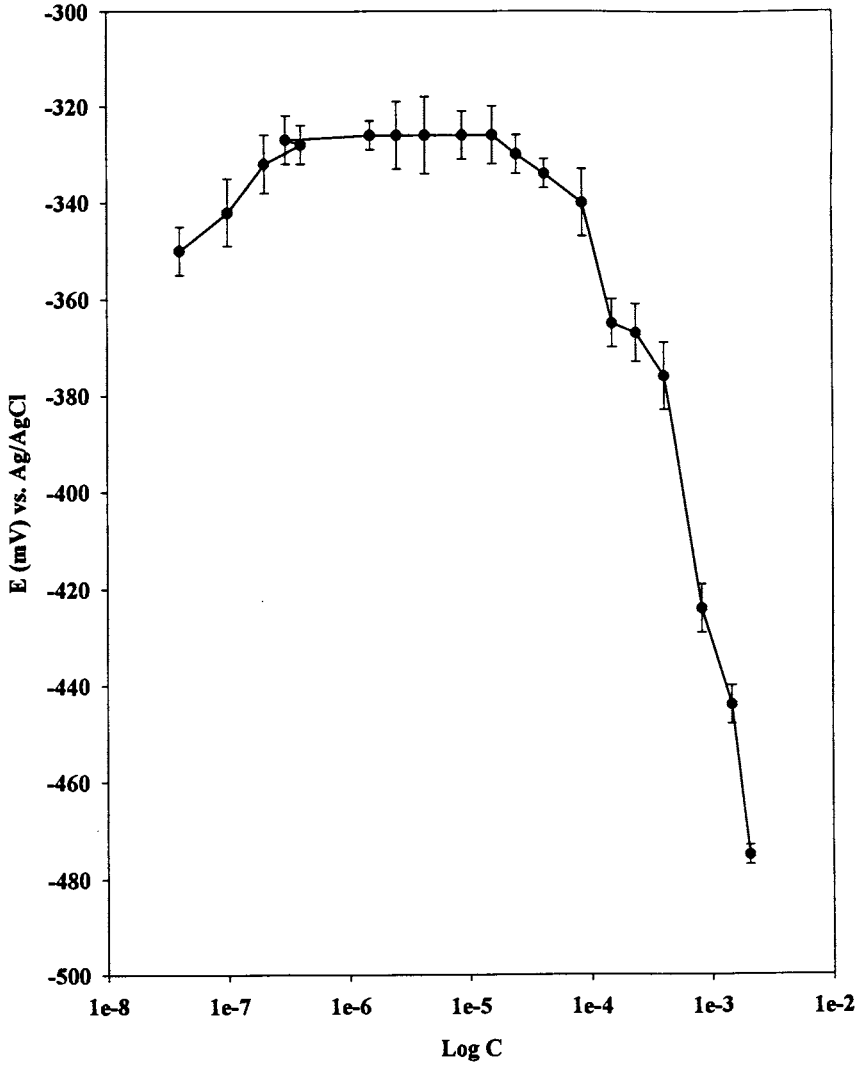

Fig. 1. Potentiometric response of $(NH_4)_2S$ treated alloy electrode to sulfide. The electrode was prepared by immersing the alloy in 2 M $(NH_4)_2S$ solution for 10 min.

ing the surface was, therefore, necessary between successive measurements.

Fig. 2 shows the potentiometric response for an electrochemically treated alloy in $(NH_4)_2S$. In this case, the electrode is subjected to repeated cycles between 0.2 and 1.5 V, with a scan rate of 100 mV s^{-1}. It was observed that the electrode response changed somewhat upon varying the limits of the potential intervals for cycling and the number of cycles, during the preparation step of the electrode. The data in Fig. 2 for an electrode cycled 10 times between a 0.2 and 1.5 V potential limit is a typical example. It shows that:

1. The calibration curve exhibits two distinctly different linear portions in the concentration ranges of 5.0×10^{-8}–5.0×10^{-6} M and 5.0×10^{-6}–5.0×10^{-3} M, respectively, and
2. The standard deviation of the potential response at low concentrations of sulfide is relatively high compared to the electrode response at higher concentrations.

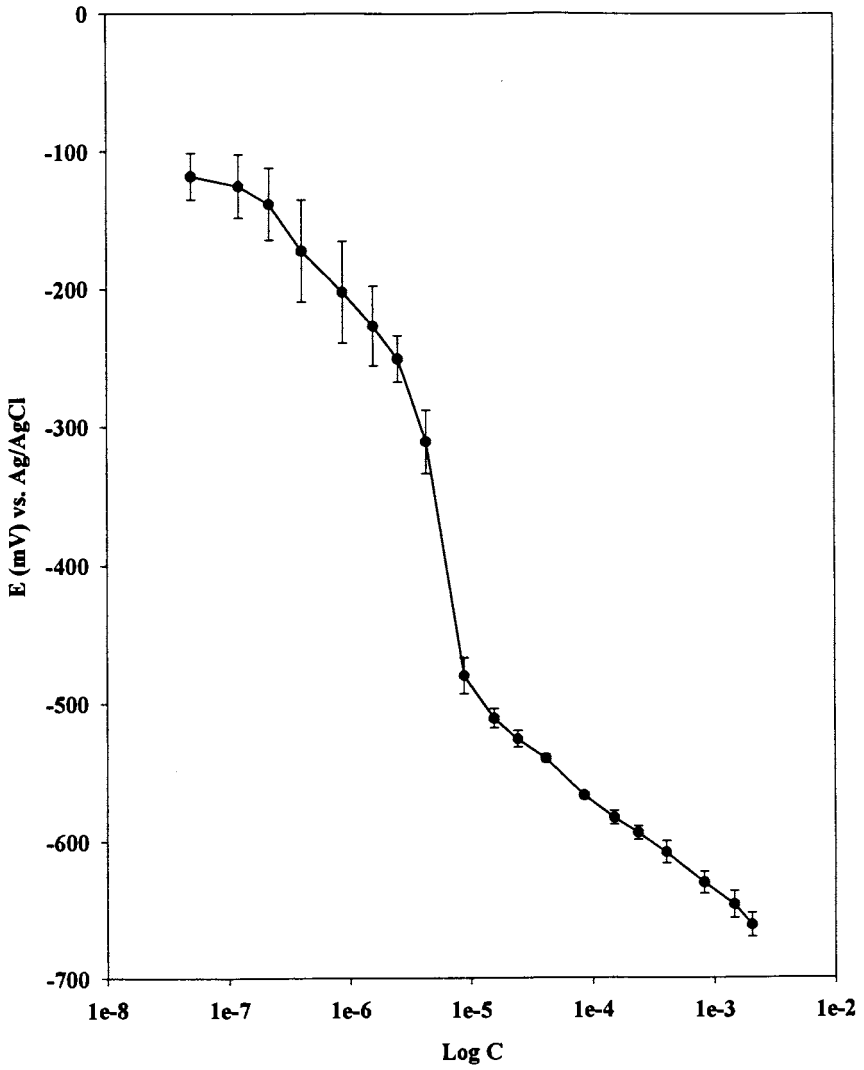

Fig. 2. Potentiometric response of $(NH_4)_2S$ electrochemically treated alloy electrode. The electrode was prepared by immersing the alloy in 2 M $(NH_4)_2S$ and subjected to constant potential of 1.4 V for 2 min.

This behavior is may be the result of the mixed composition of the base alloy that, upon exposure to $(NH_4)_2S$, forms different corresponding metal sulfides. Moreover, SEM examination of the surface of the alloy after melting and insertion into the capillary pipette shows that the surface is highly irregular with possible structure differences at the interface after the heating process (cf. Fig. 5). However, it is hard to rationalize this as the reason for the discontinuity in the two response regions, nor the high variation in the response of the electrode at low concentrations of sulfide. Also, the stability of the electrode response for extended times, even at relatively high concentrations of sulfide, was poor. This can be explained in terms of a poor adherence of the metal sulfide layer at the surface of the electrode.

The data given in Fig. 3 show the potentiometric response of a silver-modified alloy substrate. The silver was first electrochemically deposited at the surface of the alloy. The surface was then washed with water, dried and treated with

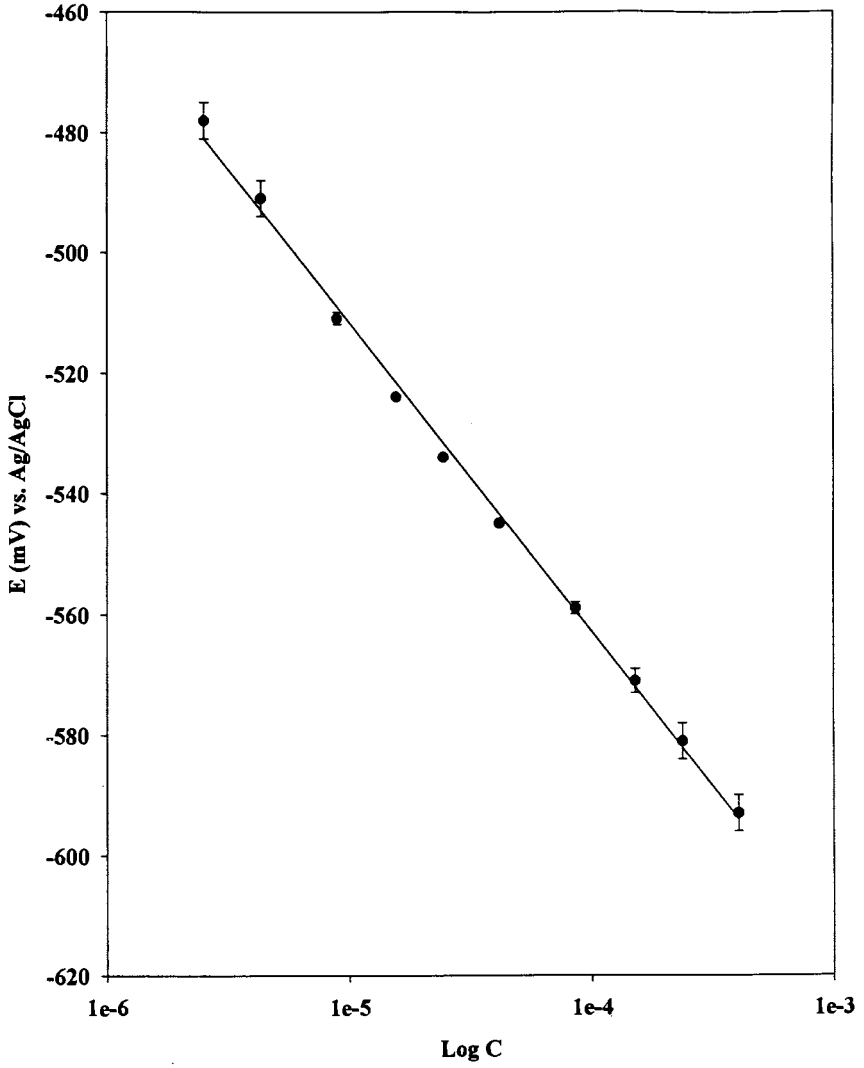

Fig. 3. Potentiometric response of Ag-coated alloy treated with $(NH_4)_2S$. The electrode was prepared by electrochemically depositing silver over the alloy substrate and then immersed in 2 M $(NH_4)_2S$ for 5 min.

$(NH_4)_2S$. The electrode showed a linear response in the range 5.0×10^{-6}–8.0×10^{-4} M sulfide. However, the response of the electrode changed considerably after 24 h of use. We noticed, upon examination with optical microscopy, that the morphology and color of the electrode surface had changed markedly. It appears that the adherence of the silver sulfide layer to the alloy substrate is weak or it dissolves over the period of 1 day.

Procedure (iv), which was previously described by Ma et al. [20], consisted of electropolymerizing dibenzo-18-crown-6 directly on the surface of a platinum electrode. The potentiometric response of this alloy electrode after the electrodeposition of the crown was unstable and irreproducible. Thus, changing the nature of the substrate from platinum to the alloy affected considerably the electrode behavior. However, the reason for using the alloy substrate rather than platinum is its relatively low melting point and the ease of con-

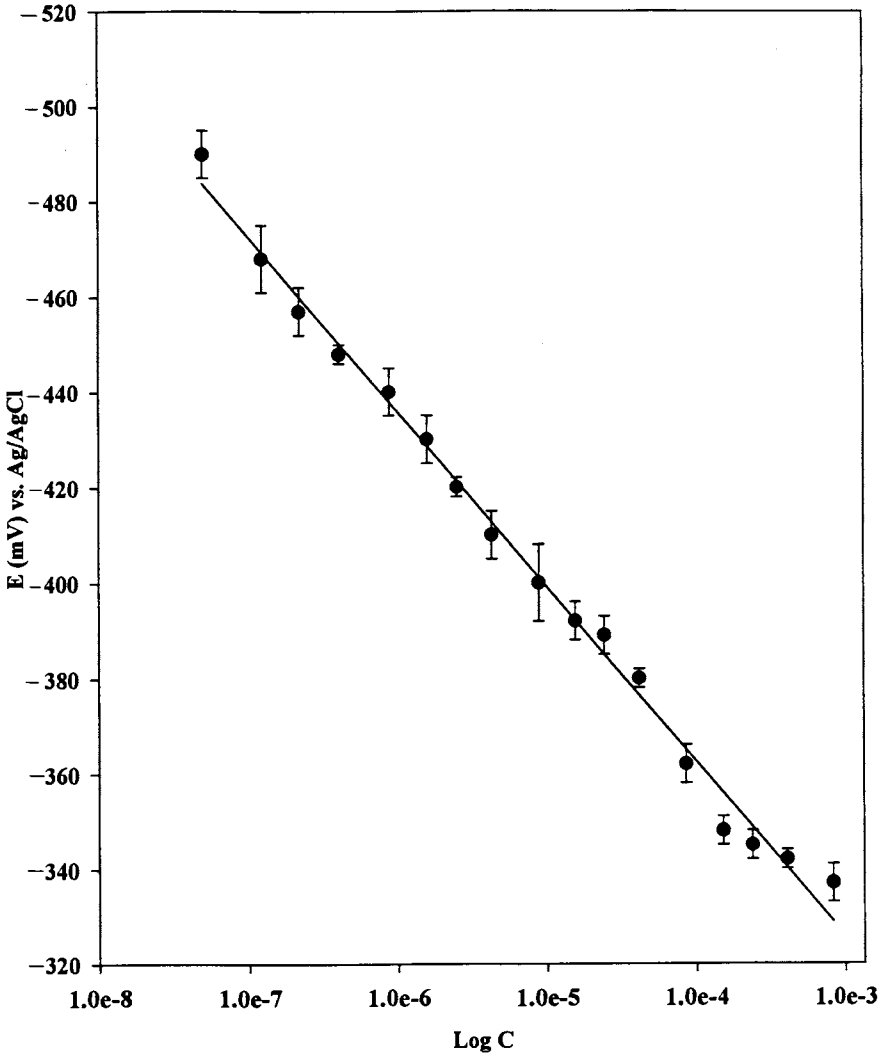

Fig. 4. Potentiometric response of conducting polymer sulfide electrode treated with $(NH_4)_2S$. The electrode was prepared as described in procedure (v) of Section 3.

structing a sulfide selective microelectrode and even ultramicroelectrode [8]. Pt and Ag could also be used to fabricate the microelectrode. However, a vertical puller, which has special heating specifications was needed for this purpose. Therefore, we used the alloy, which met the available horizontal puller heating conditions and requirements.

The response of electrodes prepared by depositing a layer of poly(3-methylthiophene), followed by the electropolymerization of the dibenzo-18-crown-6, and then electrode treatement in $(NH_4)_2S$, as described in Section 3, procedure (v), is shown in Fig. 4. The slope for the calibration curve shown in Fig. 4 is -35.7 mV decade^{-1}, with a correlation coefficient of 0.992. The calibration curve has a linear response range between 5.0×10^{-8} and 1.0×10^{-3} M. This will allow its application for measurements in biofilms and other environmentally hazardous systems.

3.2. Optimization of the conducting polymer preparation conditions

The response of the conducting polymer sulfide electrode varied with the conditions of the electropolymerization steps. Fig. 6 shows the effect of changing the electropolymerization times for the deposition of poly(3-methylthiophene) and poly-(dibenzo-18-crown-6). The performance of the electrode was based on the Nernstian slope obtained and the lifetime of the electrode. The following conclusions are observed from the data obtained:

1. A relatively low slope is observed for the crown films formed at 5–15 min as compared to those deposited between 15 and 30 min,
2. The expected theoretical Nernstian slope is 29.5 mV decade^{-1}. Poly(3-methylthiophene) films deposited for 25 s (as indicated on the x-axis of Fig. 6) and crown films then deposited, for 20 or 30 min, gave the closest slopes to theoretical. The slopes calculated for these electrodes are in the range of -27.4 to -33.4 mV decade^{-1},
3. The pH-studies (Section 4 below) suggest that the polymer electrode responds to the total concentration of sulfide. A suggested mechanism is illustrated in Fig. 7. The polymer film electrode is formed under oxidative conditions. In this case, the resulting oxidized polymer is doped by the counter-anions used as a supporting electrolyte during the polymerization step (TFB^-). The final applied potential to the polymer film in the synthesis step determines the level of doping of the film. The treatment of this polymer film in $(NH_4)_2S$ resulted in the exchange of the preparation-step dopant (TFB^-) with that of the treatment-step, S^{2-} and/or HS^-. The number of positive 'sites' at which the exchange might take place, which in turn determines the concentration level and nature of the sulfide species within the film, is a function of several factors such as: the thickness of the polymer film, the potential used for polymerization, the level of initial doping with the TFB^-, the method of treatment with $(NH_4)_2S$, and the poly(3-methylthiophene) to poly(dibenzon-18-crown-6) ratio. The level of doping within the polymer film affects these factors as recently described [21].
4. We were not able to polymerize directly the crown ether onto the base alloy surface. On the other hand, we were able to polymerize the crown over the poly(3-methylthiophene) surface. Therefore, the poly(3-methylthiophene) is considered as the working substrate for the poly(crown ether). The role of poly(crown ether) films in solid state ion sensors was described by Ma et al. [20]. It was suggested [20] that the response mechanism of this electrode is due to the formation of hydrogen bonds and mononegative charged anions between poly-(crown ether) and guest molecules on the electrode surface. A similar hydrogen bond model is suggested in the present study. In this respect, ion-exchange or diffusion between the membrane phases and the solution phase leads to an unbalanced charge distribution. Thus, monovalent or divalent ionic species, HS^- or S^{2-}, in this case, is adsorbed within the membrane. This process should predominantly take place by an ion-exchange process in order to account for the observed response. Kliza and Meyerhoff [22] proposed possible potentiometric anion response mechanisms of poly(por-

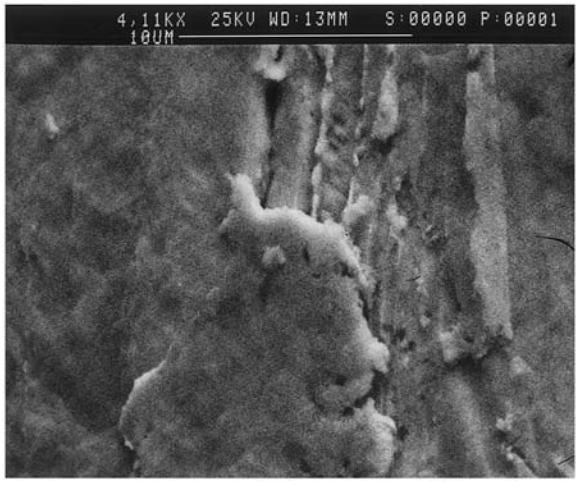

Fig. 5. Scanning electron micrograph of the alloy substrate after heating and insertion in the micropipette.

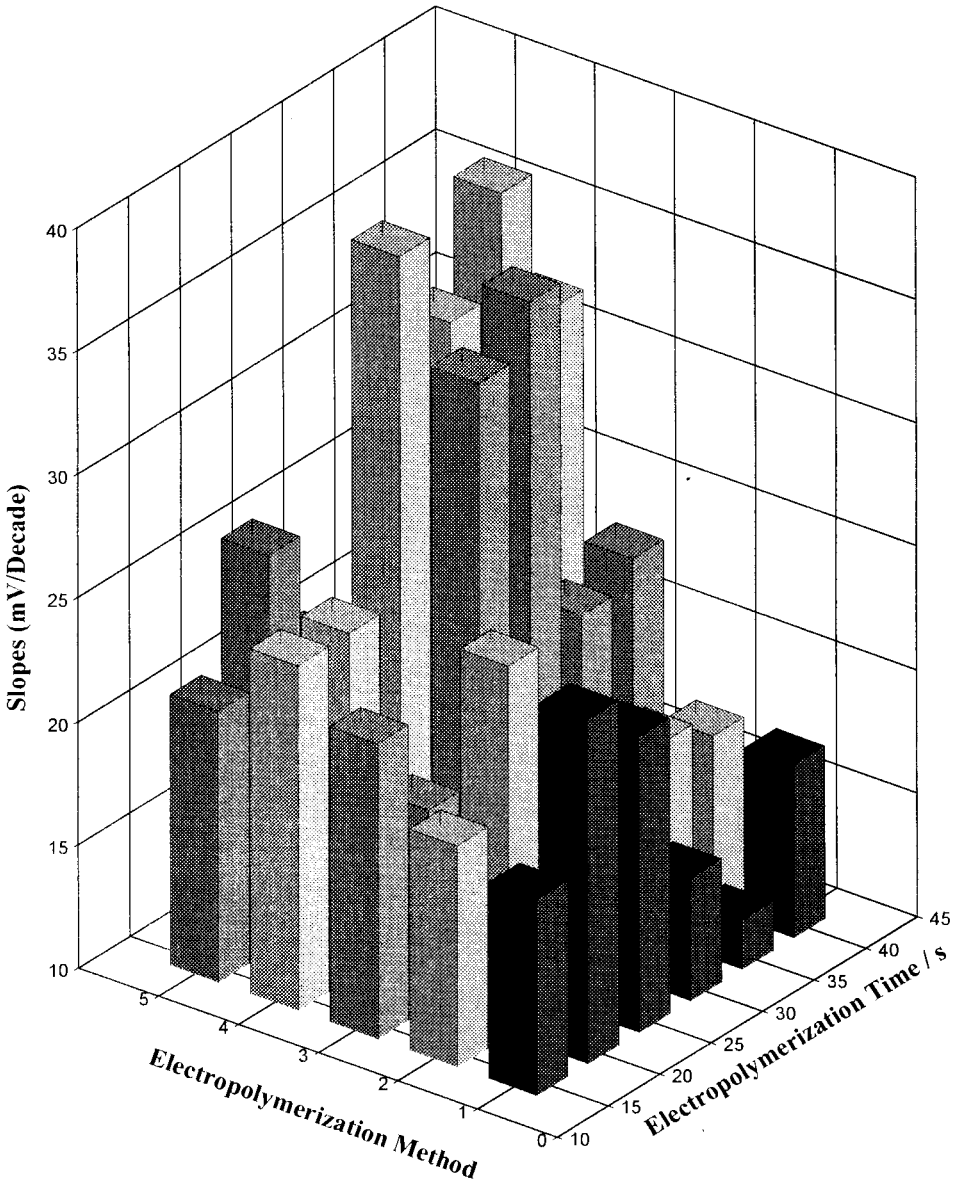

Fig. 6. Effect of varying the electropolymerization conditions of the conducting polymer sulfide electrode on the potentiometric response. Bars indicate the deposition time for crown ether (a) 5, (b) 10, (c) 15, (d) 20 and (e) 30 min.

phyrin) derivatives electrodes. Among the suggested mechanisms was a 'redox response' due to redox reaction within the conducting polymer and ion-exchange process with the anion-doped polymer backbone.

3.3. Selectivity coefficients

The electrode behavior can be represented by an equation first used by Nicolsky [23] for the glass electrode showing a mixed response to hy-

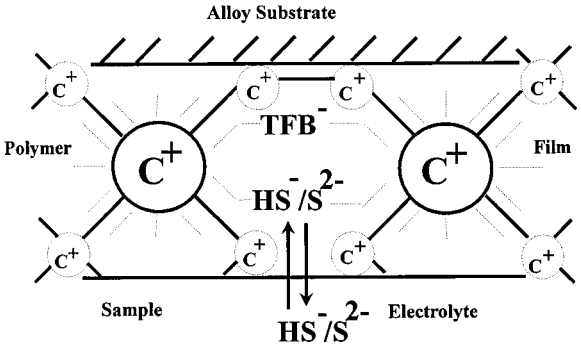

Fig. 7. Response mechanism of the conducting polymer sulfide electrode. C's represent the organic polymer film formed from the polymerization of poly(3-methylthiophene) and poly(-dibenzo-18-crown-6) in the oxidized state.

drogen and sodium ions, which can be adopted for the study of the interference effects on the conducting polymer sulfide sensor electrode:

$$E = \text{const.} \pm k \log(C_i + k_{ij}C_j)$$

and for the case of other interferents and sulfide ions as:

$$E = \pm \frac{RT}{zF} \ln\left[a_i + \sum_j K_{ij}^{Pot} a_j\right] + \text{const.}$$

where i and j are two similarly charged ions, K_{ij} is the selectivity coefficient, and K_{ij}^{Pot} is the ratio of the solubility products and activity coefficients. The selectivity coefficient of the electrode formed by procedure (v) was evaluated by the 'fixed interference method' described by Srinivasan and Rechnitz [24]. In this method, a fixed interferent concentration of 1.0×10^{-2} M was used. The results for common interfering anions are summarized in Table 1. It shows that for the large majority of anions, the selectivity coefficients are of the order of 5.0×10^{-4} or smaller. This electrode can be used successfully for the measurement of sulfide in the presence of high concentrations of sulfate ions, where the following equilibria hold:

$$2S + 3O_2 + 2H_2O = 2H_2SO_4$$

and,

$$SO_4^{2-} + 4H_2 = S^{2-} + 4H_2O$$

in the presence of aerobic and anaerobic bacteria, respectively.

Table 1
Selectivity coefficients of the conducting polymer sulfide electrode

Anion	log K	Anion	log K
F^-	−5.78	SCN^-	−4.21
Cl^-	−5.12	NO_3^-	−3.84
Br^-	−4.61	NO_2^-	−3.55
I^-	−3.83	ClO_4^-	−4.05
HCO_3^{2-}	−3.55	$B_4O_7^{2-}$	−5.33
$C_2H_3O_2^-$	−4.87	$S_2O_3^{2-}$	−3.31
$(OH)(CO_2H)CH_2CO_2^{2-}$	−5.32	SO_4^{2-}	−4.18

Table 2
Technical parameters of the polymer sulfide selective electrode

Parameter	Value
Linear concentration range (M)	1.0×10^{-7} to 1.0×10^{-1}
pH range	4–10
Detection limit (M)	2.00×10^{-9}
Temperature range (°C)	10–40
Resistance[a] (Ohm $\times 10^{-6}$)	<1
Internal reference	Solide
Reproducibility[b](mV)	2%
Response time[c] (s)	<60
Size (o.d, i.d) (mm)	1.5, 0.70
Check point[d] (mV)	−420

[a] The ohmic resistance of the electrode after forming the polymer onto the alloy.
[b] Twenty successive preparations and measurements.
[c] Depends on the thickness of the polymer film.
[d] Measured for a freshly prepared electrode in 5.0 x 10^{-6} M sulfide.

A summary of the performance parameters for the sulfide conducting polymer electrode is given in Table 2. The data shows relatively low detection limit, fast response and a wide linear dynamic range.

3.4. pH effect

The total sulfide concentration in solution can be expressed by the following:

$$S_T = [S^{2-}]\left(1 + \frac{a_{H^+}^2}{K_1' K_2'} + \frac{a_{H^+}}{K_2'}\right)$$

and

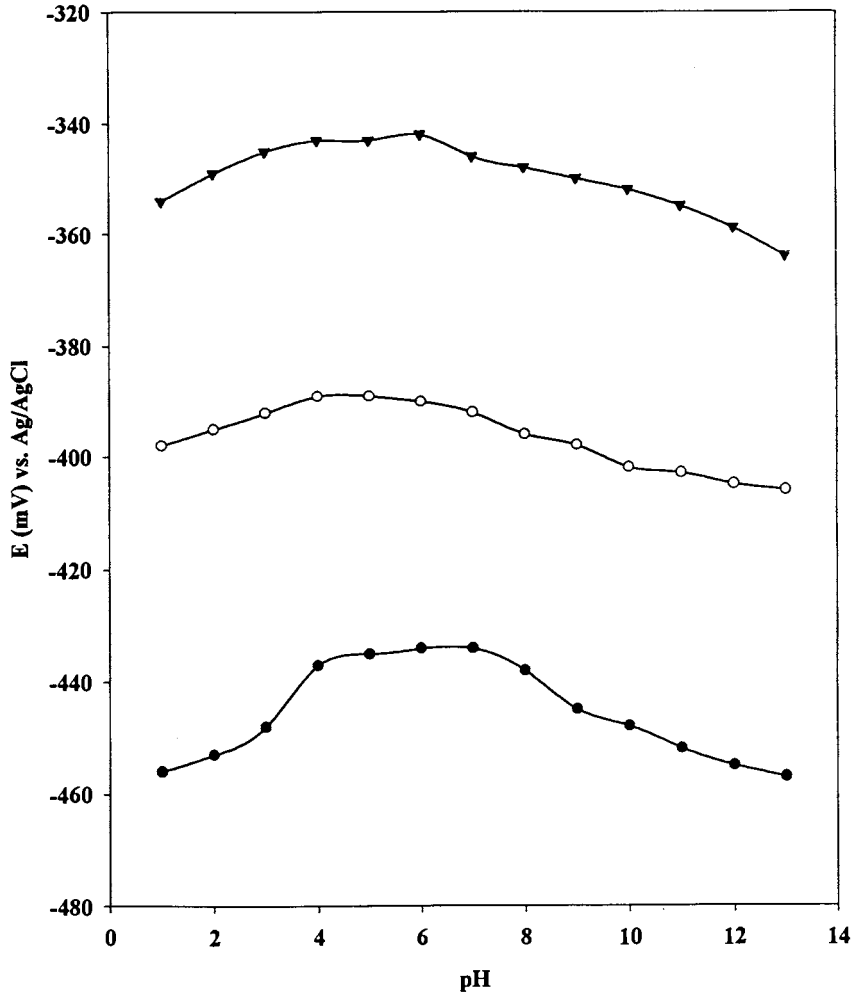

Fig. 8. Effect of varying the pH on the potentiometric response of the polymer sulfide electrode. (▲) 4.0×10^{-4} M, (○) 2.5×10^{-5} M, (●) 1.6×10^{-6} M sulfide.

$$S_T = [S^{2-}][HS^-] + [H_2S]K_1' = \frac{a_{H+}[HS]}{[H_2S]}K_1'$$

$$= \frac{a_{H+}[S^{2-}]}{[HS^-]}$$

S_T denotes the total sulfide in solution, and K_1' and K_2' are the apparent equilibrium constants, which are expressed in both activity and concentration terms [25]. The effect of changing the pH was examined over the range of 1.0–13.0 for 4.0×10^{-4} to 1.5×10^{-6} M sulfide concentrations. The data shown in Fig. 8 shows unexpectedly that the electrode prepared according to scheme (v) has a relatively constant response over a wide range of pH, except at low sulfide concentration. Most of the commercially available sulfide electrodes responses are strongly affected by the change of the pH and essentially respond to S^{2-} ions [26]. At pH > 7 or so, measurements with commercial electrodes must be used simultaneously with a pH electrode to obtain total sulfide concentration. The obtained slope values are not close to those theoretically reported for a dianion which should suggest that the electrode would respond to the total sulfide concentration. Thus, we can not explain why the electrode has almost same response at pH < 7.

3.5. Response time; temperature effects; life time and morphology

The response time of the sulfide polymer electrode is a function of the film thickness. Thin films give a response time of < 60 s, while thicker films (~ 2000 Å or higher) have a response time of 120 s or higher. The response is, therefore, partly controlled by the rate of diffusion of the active species within the polymer film. The working temperature range was determined from the calibration curves of the electrode measured at different temperatures. The values obtained from the slopes of the calibration curves were compared to the expected theoretical values reported earlier [27,28]. The working temperature of this electrode was found to be 10–40°C. As the response of the electrode is affected by the amount of sulfide present within the film, loss of sulfide with time is important. The electrode can be used for successive measurements for a period of ten hours without regeneration. By storing the electrode overnight in a solution containing 1.0×10^{-4} M sulfide, it can be used continuously for 3 days, after which significant degradation was then observed. The readiness of oxidation of the sulfide ions trapped within the polymer film to the corresponding sulfate ions should affect the performance and lifetime of the sensor electrode. For instance, a limited lifetime of 10 h was observed with this electrode when stored in air.

Scanning electron micrographs of the surface of the alloy substrate and the polymer-covered alloy are given in Figs. 5 and 9, respectively. Fig. 5 shows the surface of the alloy substrate after heating and insertion in the capillary glass tube. The irregularity of the surface is a key factor with respect to adherence in the deposition of successive layers. However, the polymer film response was not affected by the roughness of the alloy surface. Fig. 9, on the other hand, shows the surface of the polymer layer after treatment with the $(NH_4)_2S$. The morphology of the polymer film deposited on the alloy surface is not significantly different from that deposited on platinum [29].

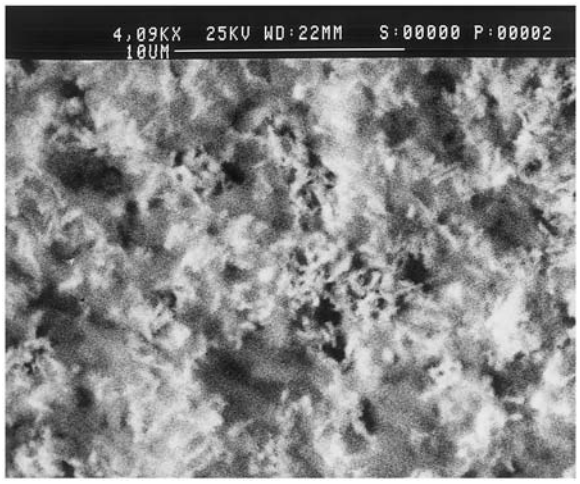

Fig. 9. Scanning electron micrograph of the alloy substrate covered with treated polymer layer (according to method V).

4. Conclusions

We prepared a sulfide selective electrode based on conducting polymer electrochemically deposited on an alloy substrate. The electrode showed high selectivity towards many common interfering anions. The optimum preparation conditions were based on electrochemically depositing a poly(3-methylthiophene) layer followed by electrodepositing a poly(dibenzo-18-crown-6) film. The film thickness and method of preparation affected the response and performance of the electrode. The electrode response was stable and reproducible for 3 days, after which the regeneration of the polymer film was necessary. The electrode can be fabricated in the micrometer dimensions [8].

Acknowledgements

The authors would like to thank the National Science Foundation for supporting this work (Grant No INT-95054978).

References

[1] D.J. Crombie, G.J. Moody, J.D.R. Thomas, Lab. Pract. 29 (1980) 259.
[2] G. Castello, A. Baccaria, G. Poggi, Analyst 112 (1987) 1093.
[3] J. Koryta, Anal. Chim. Acta 61 (1972) 329.
[4] J. Gulens, K. Jessome, C.K. Macneil, Anal. Chim. Acta 96 (1978) 23.
[5] D.B. Nedwell, I.M. Barat, Microb. Ecol. 7 (1981) 305.
[6] D.C. Nelson, B.B. Jørgensen, N.P. Revsbech, Appl. Environ. Microbiol. 52 (1986) 225.
[7] M. Khül, B.B. Jørgensen, Appl. Environ. Microbiol. 58 (1992) 1164.
[8] T. Yu, P.L. Bishop, A. Galal, H.B. Mark, Jr., ACS Symposium Series 690 Polymers in Sensors, Theory and Practice, Chapter XIX, 1998.
[9] Standard Methods for the Examination of Water and Wastewater, 15th edn.; APHA-AWWA-WPCF, (1980) 442.
[10] Determination of the Total Sulfide Content in Water, Orion: Cambridge, MA, Application Note A12.
[11] V.T. Frevert, H. Galster, Z. Schweis, Hydrol. 40 (1978) 199.
[12] R.W. Fairbridge (Ed.), The Encyclopedia of Geochemistry and Environmental Sciences, Van Nostrand Reinhold, New York, 1972.
[13] P. Gerhardt, R.G.E. Murray, W.A. Wood, N.R. Krieg (Eds.), Methods for General and Molecular Bacteriology, American Society for Microbiology Series, Washington, DC, 1994.
[14] A.E. Karagözler, O.Y. Ataman, A. Galal, Z. Xue, H. Zimmer, H.B. Mark Jr., Anal. Chim. Acta 248 (1991) 163.
[15] A. Galal, Z. Wang, H. Zimmer, P.L. Bishop, H.B. Mark Jr., Anal. Chim. Acta 299 (1994) 145.
[16] N. Akmal, S.K. Lunsford, A. Galal, A.E. Karagözler, H.B. Mark Jr., Croat. Chem. Acta 68 (1995) 403.
[17] Y.L. Ma, A. Galal, S.K. Lunsford, H. Zimmer, H.B. Mark Jr., Z.F. Huang, P.L. Bishop, Biosens. Bioelect. 10 (1995) 705.
[18] S.K. Lunsford, Y.L. Ma, A. Galal, C. Striely, H. Zimmer, H.B. Mark Jr., Electroanalysis 7 (1995) 420.
[19] W.E. Morf, E. Lindner, W. Simon, Anal. Chem. 47 (1975) 1596.
[20] Y.L. Ma, A. Galal, H. Zimmer, H.B. Mark Jr., Z.F. Huang, P.L. Bishop, Anal. Chim. Acta 298 (1994) 21.
[21] A. Michalska, A. Travaska, A. Lenenstam, Anal. Chem. 69 (19) (1997) 4060.
[22] D.M. Kliza, M.E. Meyerhoff, Electroanalysis 4 (1992) 841.
[23] B.P. Nicolsky, Acta Physicochim., URSS 7 (1937) 507.
[24] K. Srinivasan, G.A. Rechnitz, Anal. Chem. 41 (1969) 1203.
[25] V.T. Frevet, H. Galster, H. Schweiz, Z. Hydrol. 40 (1978) 199.
[26] V.M. Jovanovic, M.S. Jovanovic, Anal. Chim. Acta 233 (1990) 329.
[27] R.J. Simpson, In: A.K. Covington (Ed.), Ion-selective Electrode Methodology, CRC Press, Baco Raton, Fl., Vol. 1, 1980.
[28] M.J.D. Brand, G.A. Rechnitz, Anal. Chem. 42 (1970) 616.
[29] A. Galal Abdo, Ph.D. thesis, Cincinnati, OH, USA, 1992.

ELSEVIER

Talanta 47 (1998) 1001–1012

Talanta

Practice and mechanism of HPLC oligosaccharide separation with a cyclodextrin bonded phase

Alain Berthod [a,*], Samuel S.C. Chang [1,b], John P.S. Kullman [b], Daniel W. Armstrong [b]

[a] *Laboratoire des Sciences Analytiques, UMR CNRS 5619, Université de Lyon 1, Bat. 308-D, 69622 Villeurbanne, France*
[b] *Department of Chemistry, University of Missouri-Rolla, Rolla MO 65401, USA*

Received 26 November 1997; received in revised form 30 April 1998; accepted 4 May 1998

Abstract

A series of six oligosaccharides: linear arabinosides, cellosides, isomaltosides, mannosides, maltosides and xylosides containing up to 15 sugar units, as well as α, β and γ-cyclodextrins, were separated without derivatization with acetonitrile-water mobile phases and a β-cyclodextrin bonded phase column using both UV (195 nm) and refractive index detection. The mobile phases contained more than 60%v/v acetonitrile to separate the oligosaccharides with baseline resolution with practical retention times. The chromatographic mode is intermediate between normal-phase chromatography and hydrophilic interaction chromatography. Sugar retention occurs through partition exchange and polar interactions. The saccharide-stationary phase interaction was studied through retention behavior and peak efficiency. It is shown that partitioning interactions and hydrogen bonding interactions between the hydroxyl groups of the stationary phase and those of the sugars are the two possible mechanisms responsible for sugar retention. The sugar retention times are dramatically reduced when the mobile phase water content is increased. The conformation of the oligosaccharides also affects retention. Excellent and rapid separation of the saccharide components of commercial corn syrup and dextrin are shown. The plots of the log retention factor versus degree of polymerization (DP) were linear. The slope of these plots was related to the solute-stationary phase interaction energy. This energy is directly related to the mobile phase water content. The kinetics of the interaction is slow. At 1 ml min^{-1}, the peak efficiencies were in the 10000–15000 plate m^{-1} range (70–100 d_p). The efficiency maximum was not reached at 50 µl min^{-1} indicating slow interactions between large molecules. © 1998 Elsevier Science B.V. All rights reserved.

Keywords: Oligosaccharides; Refractive index detection; Hydrophilic interaction chromatography; Degree of polymerisation

1. Introduction

Carbohydrates have long been recognized for their role as structural material (cellulose) in plants and as energy and carbon sources in the biological world. Sugars have a low volatility and

* Corresponding author. Tel.: + 33 4 78949510; fax: + 33 4 72431078; e-mail: berthod@univ-lyon1.fr

[1] Present address: Novartis Pharmaceutical Corp., East Hannover, NJ 07936, USA.

0039-9140/98/$ - see front matter © 1998 Elsevier Science B.V. All rights reserved.
PII S0039-9140(98)00179-9

thermal stability that hinders the use of gas chromatography in their study. High performance liquid chromatography (HPLC) was early used for sugar identification and quantization [1,2]. The main drawback was the detection problem since sugars do not absorb UV light with wavelength longer than 200 nm. Improvements in refractive index detectors and the availability of high quality HPLC solvents (transparent down to 190 nm) resulted in an increase in the use of HPLC for sugar analysis [3–8].

Oligosaccharides are short-chain carbohydrates made by glycosidic linkage of several simple sugars of monosaccharides. Although there is no established boundary between oligo- and polysaccharides, the term oligosaccharide is usually applied to carbohydrate made of 2–10 monosaccharide units. The number of simple sugar units is called degree of polymerization (DP) [9]. HPLC was used to separate oligosaccharides found in natural products [10–12], glycoproteins or glycolipids [13–15], pharmaceuticals [16–19] and, of course, food products [20–25].

Four different chromatographic modes are used to separate the underivatized form of carbohydrates. They are (i) cation-exchange chromatography [26–29], (ii) anion-exchange chromatography [30–34], (iii) chromatography with amino-bonded stationary phases [35–40] and (iv) classical reversed phase chromatography with alkylated silica gels [41–45]. Table 1 gathers the advantages and drawbacks of the four chromatographic modes and give some application examples and the corresponding available column hardware and manufacturers. Alcohol bonded stationary phases appeared more recently [46,47]. The separation mechanism seems to resemble that of the amino-bonded phase's without the glycosamine formation problem [48,49]. Cyclodextrin (CD) bonded phases were designed for the separation of isomers. However, they can be listed in the alcohol or so-called 'diol' bonded phase category. They proved to be very effective in the separation of monosaccharides, deoxysaccharides, oligosaccharides [50], cyclodextrins [51,52] and also anomeric forms of saccharides [53].

In this work the separation of homologous series of different oligosaccharides is examined. Commercially available pure oligosaccharides with degree of polymerization (DP) ranging from 2 to 10 were used to study the retention mechanism of the hydrophilic interaction chromatography mode. This mode, intermediate between normal phase and partition chromatography, was first introduced by Alpert in 1990 [54]. Examples of separation of natural mixtures of vegetal origin are also presented.

2. Experimental

2.1. Chemicals

The seven oligosaccharide series investigated were (i) the malto-oligosaccharides, DP = 1, glucose; DP = 2, maltose; DP = 3, maltotriose; DP = 4 to 7, maltotetraose, pentaose, hexaose and heptaose, respectively; (ii) the cyclodextrins, DP = 6, α-CD; DP = 7, β-CD and DP = 8, γ-CD; (iii) the cello-oligosaccharides, DP = 1, glucose; DP = 2, cellobiose; DP = 3 to 5, cellotriose, cellotetraose and cellopentaose, respectively; (iv) the isomalto-oligosacchaides, DP = 1, glucose; DP = 2, isomaltose; DP = 3 and 4, isomaltotriose and isomaltotetraose, respectively; (v) the manno-oligosaccharides, DP = 1, mannose; DP = 2, mannobiose; DP = 3 to 6, mannotriose, tetraose, pentaose and hexaose, respectively; (vi) the arabino-oligosaccharides, DP = 1, arabinose; DP = 2 to 8, arabinobiose, triose, tetraose, pentaose, hexaose, heptaose and octaose, respectively; and (vii) xylo-oligosaccharides, DP = 1, xylose; DP = 2 to 6, xylobiose, triose, tetraose, pentaose and hexaose, respectively. Fig. 1 shows the configuration of the unit making the seven series studied. It should be pointed out that simple arabinose has a six atom ring (with 5 C-atoms and 1 O-atom) and arabinobiose and the higher members of this series are made by duplicating with 1–5 linkage the five atom ring (4 C and 1 O) shown in Fig. 1.

CDs were obtained from Advanced Separation Technologies (Astec, Whippany, NJ). The simple sugars and the malto, isomalto and cello-oligosaccharides were obtained from Sigma (St Louis, MO). The other saccharides were bought from Megazyme

Table 1
Comparison of the HPLC methods for carbohydrate separation

Column	Advantages	Drawbacks	Examples	Column (supplier)	Ref.
Diol or polyol bonded silica gel	Stable		Oligosaccharides	Cyclobond 2000 (Astec)	[50], This work
	No reactions with sugars		Maltosides and CDs	Cyclobond I (Astec)	[48,49]
			Maltosides	LiChrospher Diol (Merck)	[45]
				Polyol-RSil (Alltech)	[44]
Alkyl-bonded silica gel	Stable	Resolve	Cellosides and CDs	ODS-2 (Whatman)	[42]
	Low cost	Anomers	Maltosides	Spherisorb (Waters)	[40,41]
			Cello and xylosides	Dextro Pak (Waters)	[39]
Amine-bonded silica gel	Strong commercial support	React with sugards, fragile low reproducibility	Cellosisdes	μBondapak (Waters)	[38]
			Maltosides	μBondapak (Waters)	[36,37]
			Isomaltosides	Lichrosorb-NH_2 (Merck)	[35]
			CDs	Partisil PAC (Whatman)	[33,34]
Anion exchange phase (+electro-chemical detection)	High resolution and sensitivity	Costly (metal-free systems) low capacity, high pH	Arabinosides	CarboPac (Dionex)	[32]
			Maltosides	CarboPac (Dionex)	[28,31]
			Mannosides	CarboPac (Dionex)	[30]
Cation exchange resin	Durable wide pH range	High operating temperature, costly	Malto, xylo, cellosides	Aminex HPX Ca (BioRad)	[26,27]
			Maltosides + CDs	Aminex 50W Ca (BioRad)	[23–25]
			Maltosides	Aminex HPX Ag (BioRad)	[22]

Astec, Advanced Separation Technologies, Whippany, NJ 07981. Alltech, Alltech Associates, Deerfield, IL 60015. BioRad, Life Science Group, Hercules, CA 94547. Dionex, Dionex Corporation, Sunnyvale, CA 94088. Merck, Merck GmBH, Munchen, Germany. Waters, Waters Corporation, Milford, MA 01757. Whatman, Clifton, NJ 07014.

Pty. (Sidney, Australia). HPLC grade acetonitrile (ACN) was from Fisher Scientific (Fairlawn, NJ).

2.2. Chromatographic system

Two HPLC systems were used. A Shimadzu HPLC system had a model LC-6A pump with an SPD-6A UV detector set at 195 nm and a CR-2AX Chromatopac integrator. A Waters model R401 differential refractometer was added in series with the UV detector. The second system consisted of a BioAnalytical System (BAS, West Lafayette, IN) with a model PM-80 solvent delivery module, a BAS UV-116A detector and a Gateway 2000 computer interfaced by a BAS AD-5 ChromGraph Analog/Digital converter.

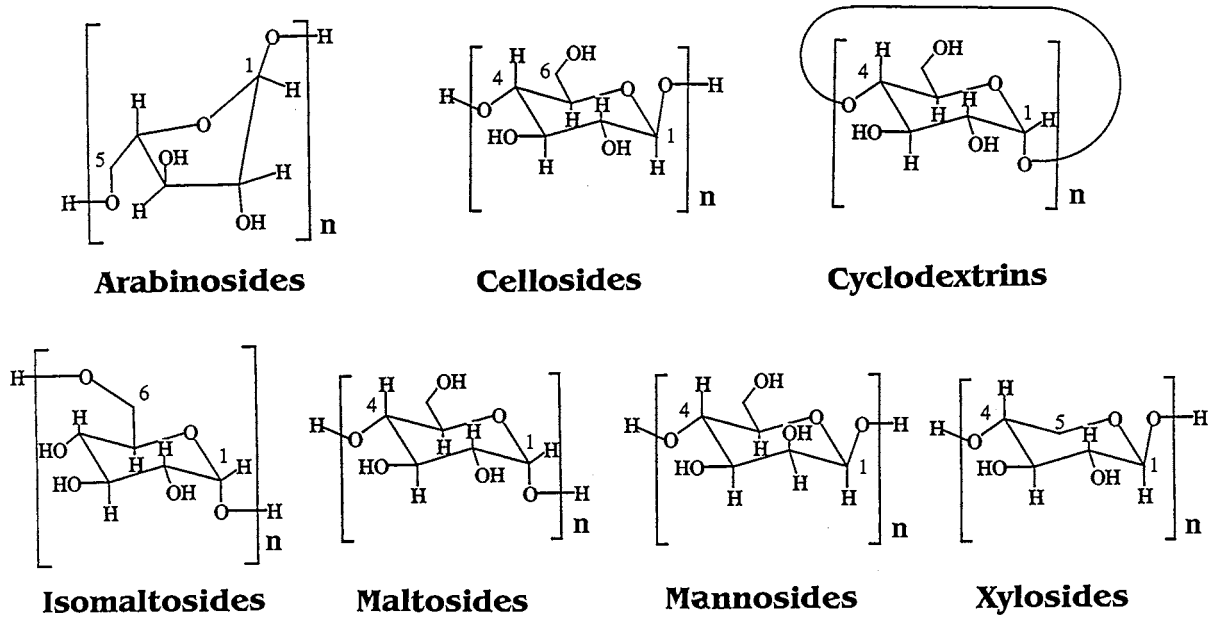

Fig. 1. Structure of the incremental group in the seven oligosaccharides series studied. The linkage is shown.

A 250×4.6 mm i.d. stainless steel column packed with 5 μm Cyclobond 1-2000 silica particles (β-CD bonded phase from Astec) was used with ACN–water mobile phases. The flow rate was 1 ml min^{-1} unless otherwise indicated. The UV detection wavelength was 195 nm.

3. Results and discussion

3.1. Water content and retention factor

Table 2 lists the retention and resolution factors along with the peak efficiency obtained for the seven series of oligosaccharides using an acetonitrile (ACN)–water 70–30%v/v at 1 ml min^{-1}. Fig. 2 shows the separation of linear oligosaccharides with DP ranging from 1 to 7 and the three α, β and γ-CDs. The separation of the 10 different underivatized sugars was performed in < 16 min with baseline resolution. Fig. 3 shows the separation of the manno-oligosaccharides with DP ranging from 1 to 6. The effect of the mobile phase water content is shown. The seven mannosides are separated in < 8 min when the 35% water containing mobile phase is used (Fig. 3A). The separation time almost doubles with the 70–30%v/v ACN–water mobile phase (Fig. 3B). Fig. 4 shows the retention factor of the xylosides (DP = 1 to 6) plotted versus the mobile phase water content. A rapid decrease of the oligosaccharide retention factors was observed when the mobile phase water content was increased. This trend was already described by Armstrong [52]. The opposite trend is observed in reversed phase LC where hydrophobic interaction largely control retention. The plots of $\log k'$ versus the mobile phase water content were not linear as it is observed in classical reversed phase liquid chromatography (RPLC).

The plots of $\log k'$ versus DP were linear for all mobile phase compositions studied as illustrated by Fig. 5 for the same oligosaccharides as in Fig. 4 (xylosides). The increasing retention factors with decreasing water content in this acetonitrile–water system indicates that polar and/or hydrogen bonding interactions with the stationary phase control retention. Such a chromatographic mode with a polar stationary phase and a less polar,

Table 2
Chromatographic data for oligosaccharides separation on a β-CD phase

Series	DP	1	2	3	4	5	6	7	8
Arabinosides (ACN–water 80–20%v/v)	k'	1.00	1.04	1.54	2.09	2.78	3.67	4.82	6.25
	Rs	—	0.3	3.0	2.6	2.6	2.5	2.5	2.2
	N	—	3700	3100	2900	2700	2300	2100	1600
Cellosides	k'	0.69	0.93	1.25	1.63	2.11			
	Rs	—	3.0	2.9	2.7	2.6			
	N	7000	7800	5700	4700	4000			
Cyclodextrins	k'						2.48	3.17	3.91
	Rs						—	3.0	3.0
	N						4600	4800	5200
Isomaltosides	k'	0.70	1.11	1.50	2.04				
	Rs	—	2.5	2.4	1.8				
	N	4000	3500	2200	1400				
Maltosides	k'	0.71	1.18	1.62	2.15	2.83	3.57	4.42	5.20
	Rs	—	3.3	3.2	3.2	3.1	3.0	3.0	2.9
	N	5400	5300	5000	4900	4200	4500	4500	4000
Mannosides	k'	0.69	1.04	1.48	2.03	2.77	3.75		
	Rs	—	2.9	2.9	2.7	2.6	2.5		
	N	4000	3800	3500	3000	2400	1900		
Xylosides	k'	0.87	1.11	1.43	1.76	2.17	2.65		
	Rs	—	2.9	2.6	2.3	2.4	2.5		
	N	2300	2400	2600	3000	3200	3000		

The mobile phase composition is ACN–water 70–30%v/v except for the arabinoside series.
DP, degree of polymerisation; k,' retention factor $= (t_r - t_o)/t_o$, average value of 2 experiments; accuracy $\pm$ 3%; Rs, resolution factor; N, efficiency in plates for 25 cm; accuracy $\pm$ 15%.

ACN rich, mobile phase can be seen as normal phase chromatography. It was termed hydrophilic intercation chromatography (HILIC) [54]. In HILIC, the polar solutes are retained by partitioning between the mobile phase and a water rich layer on the stationary phase [54,55] and/or by direct interaction with polar sites of the stationary phase [54,56]. As reviewed by Churms [57], numerous studies yielded evidence that the mechanism governing oligosaccharide separations on cyclodextrin-bonded phases is HILIC. Interactions involving the hydrophilic exterior of cyclodextrins rather than the formation of inclusion complexes with the cavity are responsible for sugar retention [50,52,57].

A linear relationship between the log of retention factors and DPs was sometimes noted [57,58]. This relationship is commonly obtained with hydrophobic homologues series in RPLC. A simple retention theory was early developed by Martin and Synge [59]. The logarithms of the retention factor k' can be related to the differences in free energy between the solute/stationary phase interaction and the solute/mobile phase interaction, $\Delta G°$, by

$$\log k' = \Delta G°/RT + \log \phi \quad (1)$$

where R, T, and ϕ are the gas constant, the absolute temperature, and the phase ratio of the column, respectively [60,61]. The free energy of retention of a molecule can be regarded as a linear combination of retention energies that are assigned to each segment of the molecule. For members of a homologous series of solutes, differing only in the number of structurally identical groups (i.e. sugar units, Fig. 1) Eq. (1) can be written as [62]:

$$\log k' = \Delta G°_{ms}/RT + (DP - 1)\Delta G°_{s}/RT + \log \phi \quad (2)$$

in which the subscripts 'ms' and 's' refer to the retention energy contribution of the monosaccha-

ride and the incremental sugar group, respectively. Eq. (2) shows that the slopes of the $\log k'$ versus DP number are proportional to ΔG°_{s}, the incremental sugar contribution to the interaction energy difference for a given mobile phase composition.

Table 3 lists the hydration number, the number of carbon atoms and hydroxyl groups in the monomer sugar unit, the slopes, A, and intercepts, B, of the $\log k'$ versus DP for the ACN–water 70–30%v/v mobile phase and the slopes, C, and intercepts, D, of the regression lines of the interaction energy difference versus mobile phase water content. The maximum percentage of water in the mobile phase is also listed. With a mobile phase containing more water than the listed maximum percentage, the sugars were not retained enough to be reliably separated. The oligosaccharides were separated with mobile phases containing amounts of water increasing from 20%v/v to the maximum value listed in Table 3 (in steps of 5%).

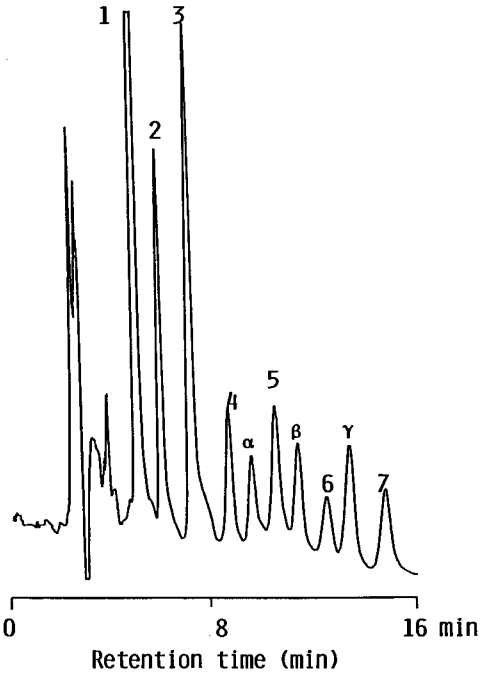

Fig. 2. Chromatogram of the separation of malto-oligosaccharides and cyclo-dextrins. The numbers are the DP of the maltosides, the greek letters correspond to α-CD DP = 6, β-CD DP = 7 and γ-CD DP = 8. Mobile phase: ACN–water 70–30%v/v at 1 ml min^{-1}. Injection volume 20 μl. Detection: UV at 195 nm.

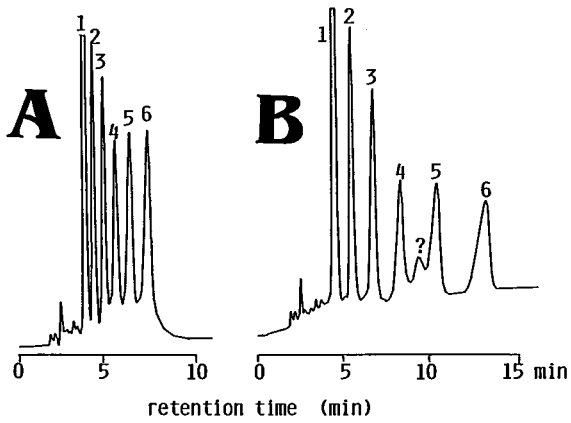

Fig. 3. Chromatogram of the separation of manno-oligosaccharides. The numbers are the DP of the mannosides. A-mobile phase: ACN–water 65–35%v/v, B-mobile phase: ACN–water 70–30%v/v both at 1 ml min^{-1}. Injection volume 20 μl. Detection: UV at 195 nm.

For every mobile phase composition and every oligosaccharide series, the $\log k'$ versus DP plots were linear with regression coefficients higher than 0.992. The fact that equations derived for a hydrophobic partition mechanism in RPLC can fit our results suggests that the sugar retention mechanism on CD stationary phase is also a partition mechanism. In the HILIC description, it was shown that a partition mechanism between two phase could exist [54]. A water enriched stationary phase with the CD moieties could be the first phase. The less polar ACN/water mobile phase could be the second phase [50,54,55,63]. Although the $\log k'$ versus DP relationship has not been used in HILIC by any other authors, the trend can be seen clearly on their chromatograms obtained using stationary phases such as a polyhydroxyethyl phase (figure 10 in [64]), amino-bonded phases (figures 3, 4 and 5 in [58], figure 4 in [64]) or a CD-bonded phase (figure 1 in [50]).

Using further the partition model, from Eq. (2), the B intercept can be expressed as

$$B = (\Delta G^{\circ}_{ms} - \Delta G^{\circ}_{s})/RT + \log \phi \quad (3)$$

The phase ratio is independent of the water content. But the energy difference between the monosaccharide (ms) and the incremental sugar

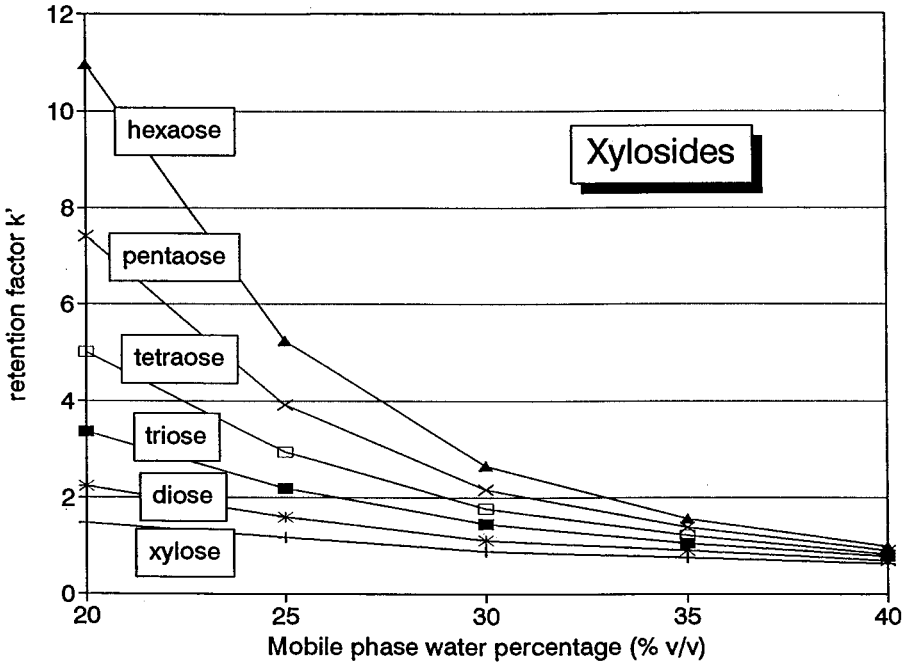

Fig. 4. Plots of the xyloside (DP = 1 to 6) retention factors versus the mobile phase water content. Column 25 cm, 4.6 mm i.d., cyclobond I-2000 (β-CD bonded 5 μm silica particles).

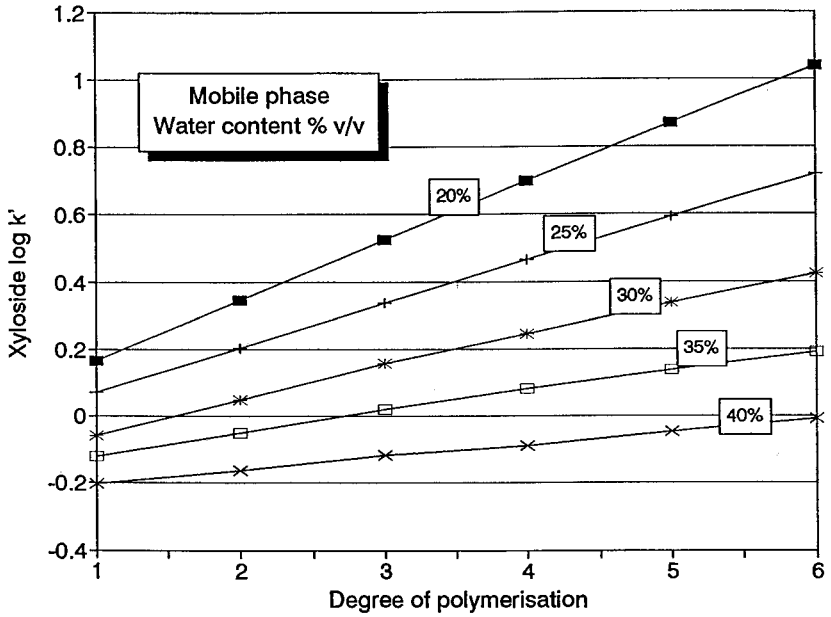

Fig. 5. Plots of the results shown in Fig. 4 for the xyloside saccharides as log k' versus the sugar degree of polymerisation (DP) for the different mobile phase compositions.

group (an ether link is created and two hydroxyl groups are eliminated) is not negligible and depends on the water content. From Eq. (2), the slope A of the $\log k'$ versus DP plots is related to the solute-stationary phase interaction energy by

$$A = \Delta G^{\circ}_{s}/RT \quad (4)$$

The experimental data of Table 3 shows that this energy decreases as the water mobile phase content increases. The decrease is not linear. However, the plot of the logarithm of the energy (A values) versus the mobile phase water content was linear with regression coefficient higher than 0.985 (Table 3). Furthermore, the slopes, C, of the later plots were almost identical, within experimental errors, for all oligosaccharides, except the arabinose series for which the retention vanished with as low as 25%v/v mobile phase water content. The average value was $C = -0.0333 \pm 0.0009$. This result indicates that the retention mechanism for all the oligosaccharide series studied is comparable with similar polar interactions and/or partitioning between the stationary phase hydrated cyclodextrin units and the sugars.

Stretching the model to its limits, the D intercepts correspond to the log of the theoretical slope that would be obtained in pure ACN (0% water) for the $\log k'$ versus DP plots. For example, the value $D = -0.102$ obtained for the CD series means that the slope A of the $\log k'$ versus DP plot for CDs in pure ACN would be $10^{-0.102} = 0.8$. Ignoring the contribution of the B term, the k' value of α-CD (DP = 6) would be close to $10^{0.8 \times 6} = 63000$ (theoretical retention time ~ 4 months at 1 ml min^{-1}). The same calculation done with the celloside series produce a A slope of $10^{1.15} = 14$ (Table 3). The estimated cellose (DP = 1) k' value would be about 10^{14} in pure ACN, a purely theoretical value since the corresponding retention time would be in the 0.6 billion year range! Furthermore, the injection would be difficult since the sugars cannot be solubilized in pure ACN. These values show that, with dry ACN, i.e. no possible hydration of the stationary phase CD-hydroxyl groups, the hydrogen bindings between the CD stationary phase and any sugar solute would be so strong that the sugar would be adsorbed and blocked on the column. These results show that the sugar retention mechanism in HILIC mode is due to partitioning and hydrogen bonding. It is not possible to separate the two causes because they are related. The formation of a hydrated later on the CD-bonded stationary phase is due to hydrogen bonding between water and stationary phase-hydroxyl groups. However, direct hydrogen bonding between the sugar solutes and that stationary phase cannot be excluded.

The sugar conformation also plays a role in the overall retention. The cyclodextrin, maltoside and xyloside series have all three similar 'A' energy values (Table 3). The incremental xylose unit bears only two hydroxyl groups while the incremental glucose unit has three. This suggests that the interaction of the primary alcohol hydroxyl group in maltosides and CDs is weaker than the interaction of the two other hydroxyl groups that are secondary alcohols. The cellosides have an incremental unit that differs from the maltosides and CDs only in the equatorial position of the acetal linkage which is in the axial position for the maltoside and CD series (Fig. 1). This changes only the conformation of the saccharide and makes the celloside retention resemble that of the isomaltoside. As a result of the 1–6 linkage of the glucose units in the isomaltoside saccharides there are three secondary hydroxyl groups in each incremental unit, but this also produces a different conformation for the individual sugars. This conformation effect is seen in the intercept values (B Eq. (3), and D). It was demonstrated that the conformation of a sugar molecule affects its hydration number [55]. A high hydration number means that the sugar will be readily water soluble and vice versa. Table 3 lists the hydration number of the first sugar (DP = 1) and of cellobiose and maltose (DP = 2) [55]. The hydration number is not clearly related to the regression parameters of Table 3. However, the three parameters, hydration number, number of hydroxyl groups and conformation do have an effect on the experimental retention factors. This is illustrated by Fig. 2 were the linear malto-oligosaccharides are well separated from their cyclodextrin homologues (i.e. of the same DP). The cyclization eliminates two hydroxyl groups making the CDs less retained than the linear malto-saccharide of the same DP.

Table 3
Chromatographic data for the study of the retention mechanism of saccharides

Saccharides	In sugar unit			$\log k' = f(\mathrm{DP})$ for water 30%v/v		$\log A = f(\%\mathrm{Water})$		%Water max
	Hydration number	Hydroxyl groups	Carbon atoms	Slope A	Intercept B	Slope C	Intercept D	
Arabinosides[a]	3.5	2	5	0.127[a]	−0.207[a]	—	—	25%
Cellosides	3.5, 4.8	3	6	0.121	−0.276	−0.0343	1.15	35%
Cyclodextrins	—	3	6	0.086	−0.109	−0.0328	−0.102	40%
Isomaltosides	3.5	3	6	0.152	−0.287	−0.0330	1.13	35%
Maltosides	3.5, 4.2	3	6	0.084	0.020	−0.0349	−0.041	40%
Mannosides	3.4	3	6	0.148	−0.293	−0.0321	0.133	35%
Xylosides	2.3	2	5	0.096	−0.145	−0.0325	−0.079	40%

The hydration numbers were taken from [55].
[a] *A* and *B* values are given for the ACN–water 70–30%v/v composition, except for the arabinosides separated with a ACN–water 80–20%v/v mobile phase.
The regression coefficients of the $\log k'$ versus DP were higher than 0.992. The regression coefficients of the $\log A$ versus % water were higher than 0.985. '% Water max.' corresponds to the mobile phase water content above which the saccharides were not retained enough.

Also the molecular rigidity induced by the macrocycle blocks some hydrogen bonding interactions so that the α-CD (DP = 6, 18 hydroxyl groups) is less retained than the DP = 5 linear malto-saccharide with only 17 hydroxyl groups (Fig. 2).

3.2. Kinetics of the sugar-stationary phase interaction

The retention factors, k', are related to the thermodynamic behavior of the solute-stationary phase interaction. The kinetics of these exchanges are studied by efficiency measurements. Table 2 lists the peak efficiency obtained with the water 70–30%v/v at 1 ml min^{-1}. The efficiency seems to decrease when the retention time increases. The chromatographic system was not optimized to reduce brand broadening. All efficiencies were measured by the half-height method assuming perfectly gaussian peaks. The accuracy of the plate numbers given is in the 15% range. The coupling of the refractive index detector after the UV detector produced an ~10% efficiency loss on the RI peaks compared to the UV peak efficiency. This loss is due to the UV cell and the connecting tubing volume that introduced extra-column band broadening. It should be pointed out that the RI cell volume (38 μl) was five times larger than the UV detector cell (8 μl). If the RI detector had preceded the UV detector, the loss of efficiency observed on UV peaks compared to RI peaks would have exceeded 10%. Also an RI detector cell should never be pressurized, then the RI detector had to be the last detector. Band-broadening cannot explain the decrease in efficiency observed for long retained peaks. Oppositely, an efficiency increase is observed with increased elution time when extra-column band broadening is significant. The variance due to the column increases with retention time. The extra-column variance is constant. Since variances are additive, the extra-column variance contribution becomes less and less significant as the column variance increases: the peak efficiency seems to increase.

The highest efficiencies obtained with the smallest sugars were in the 5000 plate range (Table 2). This produced a 20000 plates m^{-1} or 50 μm HETP (10 d_p). The common efficiencies obtained with most saccharides were in the 2000

plate range (8000 plates m^{-1}, 125 μm HETP or 25 d_p) which is a low value for a modern HPLC column. Plate efficiencies of 6000 to 19000 (25000 to 76000 plates m^{-1} or 40 down to 13 μm HETP or 8 to 2.6 d_p) were obtained for small carbohydrates on CD-bonded columns [51]. Verzele et al. [46] established that the efficiency obtained with a polyol-bonded phase and large carbohydrate solutes was intrinsically low and could be significantly increased by reducing the flow rate. Fig. 6 shows the chromatogram evolution obtained when decreasing the flow rate. The α-CD peak efficiency shows 3100, 5500 and 7200 plates at flow rates of 1, 0.1 and 0.05 ml min^{-1}, respectively. The maximum efficiency was not reached at 0.05 ml min^{-1} (100 min retention time). The sugar-CD-stationary phase interaction are slow and become even slower when the number of hydrogen bonds increases (larger saccharides) [46]. It should be pointed out that the studied oligosaccharides exist as anomeric mixtures. Slight differences in the retention of the α- or β-pyranosides or open-chain forms may be responsible for peak broadening. Fig. 2 and Table 2 show that decent resolution factors, in the 2.5 range, can be obtained with the practical 1 ml min^{-1} flow rate producing acceptable separations within 20 min.

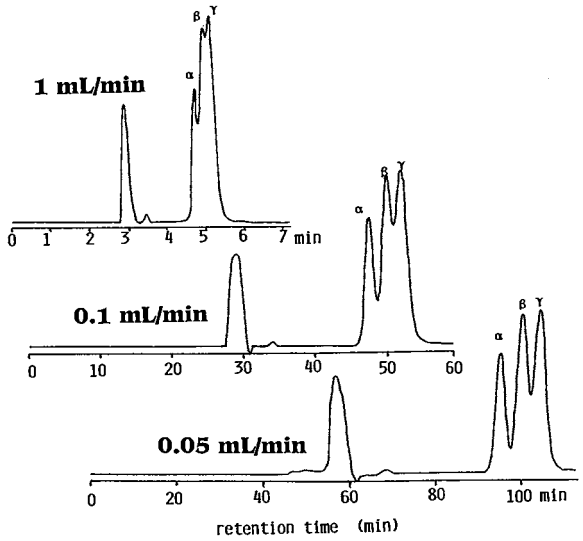

Fig. 6. Chromatograms of the separation of α, β, and γ-CD at different flow rates. Mobile phase: ACN–water 60–40%v/v. Flow rate 1 ml min^{-1}, efficiency in the 3000 plate range ($h \sim 17$ d_p); flow rate 0.1 ml min^{-1}, efficiency in the 5000 plate range ($h \sim 10$ d_p); flow rate 0.05 ml min^{-1}, efficiency in the 7000 plate range ($h \sim 7$ d_p). Refractive index detection.

The peak efficiency of the same compound was found to increase by about 20–25% when the mobile phase water content was decreased by 5%. This is a rough estimate of this variation due to the low accuracy in efficiency measurement (± 15%) and to the change in retention times associated with changes in water content. However, the resolution did increase significantly when the mobile phase water content was decreased (Fig. 3A,B).

3.3. CD-bonded phases and saccharide separation

Oligosaccharide separations on a β-CD-bonded stationary phase are effective. The solutes are injected without derivatization. No buffers are needed in the mobile phase and the system is operated at room temperature. The resolution obtained compares favorably to those obtained with the methods listed in Table 1. The CD-column produces sharp peaks without broadening or doubling due to the resolution of the anomeric forms of the sugars. The standard alkylated silica (e.g. C18) columns often produce such broad, doubled or complex peaks. It was shown that the CD-bonded phases were able to separate anomers of sugars if desired by specially tuning the mobile phase composition, the flow rate and the column temperature [52]. This is true for any polar column.

As exposed in the hydrophilic interaction study, the solute retention decreases when the mobile phase water content is increased. Resolution and selectivity are interrelated. The selectivity, α, can be expressed from Eq. (2) as

$$\log \alpha = \log(k'_{DP+1}/k'_{DP}) = \Delta G^{\circ}_{s}/RT = A \qquad (5)$$

The selectivity factor is constant for a given ACN–water mobile phase composition and saccharide series. The retention study has shown that the 'A' term increased rapidly when the mobile phase water content was decreased. Also the selectivity factor, α, increases exponentially when the water content is decreased. However, the reten-

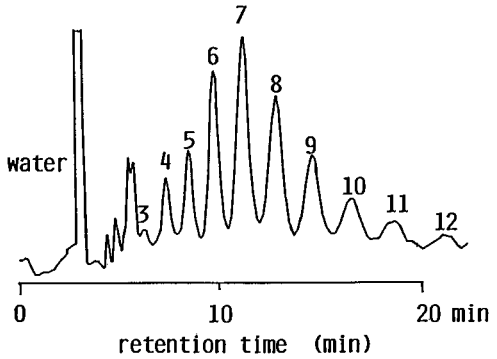

Fig. 7. Separation of the oligosaccharides of a corn syrup food additive. The numbers correspond to the DP of the maltosaccharides. Mobile phase: ACN–water 65–35% at 1 ml min^{-1}. Refractive index detection.

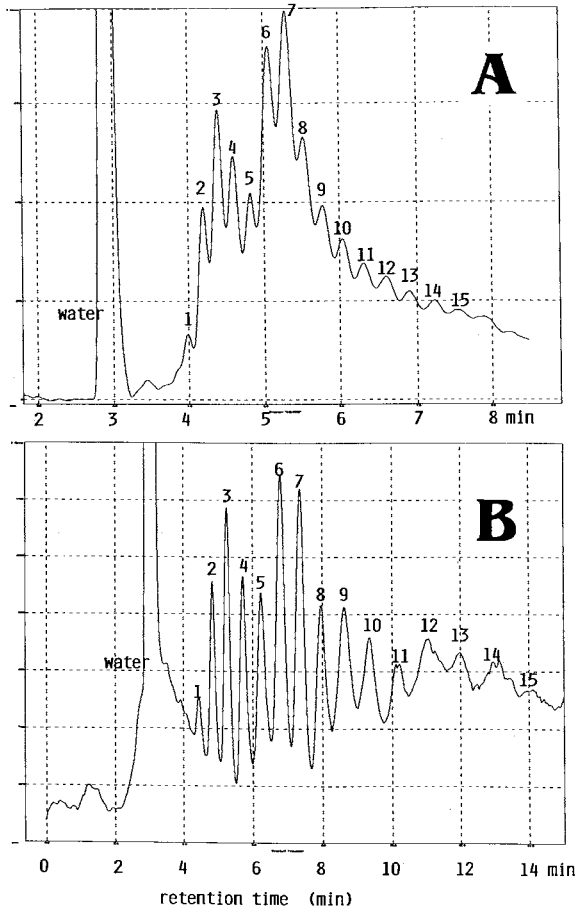

Fig. 8. Chromatograms of Fluka compound 31410, Dextrin 10 (hydrolyzed maize starch). The numbers correspond to the DP of the maltosides. A-mobile phase: ACN–water 60–40%v/v; B-mobile phase 65–35%v/v. Refractive index detection.

tion factors and the duration of the analysis increase as well. Since the efficiency increases somewhat, the resolution factor should be greatly increased by small decreases of the mobile phase water content. Consequently, the optimization of a given saccharide analysis is usually straightforward.

Two examples illustrates the use of the cyclodextrin stationary phase in saccharide analysis. Fig. 7 shows the separation of the malto-oligosaccharides contained in a commercial corn syrup solution. This separation was obtained on the first try without optimization. Fig. 8 shows the chromatograms of the Dextrin 10 sample (Fluka 31410) from maize starch with two mobile phases, ACN–water 60–40 and 65–35%v/v. The 5% decrease in mobile phase water content produced a dramatic resolution improvement but obtained at the cost of a doubled analysis duration. A 70–30% mobile phase would produce a baseline separation of the oligosaccharides in about 40 min (not shown).

Acknowledgements

The National Institutes of Health, NIH R01GM53825-01 and the Centre National de la Recherche Scientifique, UMR 5619, are gratefully acknowledged for their financial support to DWA and AB, respectively.

References

[1] J.C. Linden, C.L. Lawhead, J. Chromatogr. 105 (1975) 125.
[2] J.K. Palmer, Anal. Lett. 8 (1975) 215.
[3] S.C. Churms, J. Chromatogr. 500 (1990) 555.
[4] K.B. Hicks, in: R.S. Tipton, D. Horton (Eds.), Advances in Carbohydrate Chemistry and Biochemistry, vol. 46, Academic Press, San Diego, 1988, pp. 17–72.
[5] S.C. Churms, Carbohydrates, CRC Handbook of Chromatography, I, CRC Press, Boca Raton, FL, 1982.
[6] S.C. Churms, Carbohydrates, CRC Handbook of Chromatography, II, CRC Press, Boca Raton, FL, 1991.
[7] S. Honda, Anal. Biochem. 140 (1984) 1.
[8] L.A. Th. Verhear, B.F.M. Kuster, J. Chromatogr. 220 (1981) 313.

[9] R.W. Binkley, Modern Carbohydrate Chemistry, Marcel Dekker, New York, 1988, pp. 7–12.
[10] V.M.B. Cabalda, J.F. Kennedy, K. Jumel, in: Biotechnology of Amylodextrin Oligosaccharides, R.B. Friedman (ed.), ACS Symposium Series, American Chemical Society, Washington, DC, 1991, Vol. 458, pp. 140–170.
[11] C. Taylor, N.W.H. Cheetham, G.J. Walker, Carbohydr. Res. 137 (1985) 1.
[12] B.S. Valent, A.G. Darvill, M. McNeil, B.K. Robertsen, P. Albershiem, Carbohydr. Res. 79 (1980) 165.
[13] E.F. Hounsell, in: D. Horton (Ed.), Advances in Carbohydrate Chemistry and Biochemistry, vol. 50, Academic Press, San Diego, 1994, pp. 311–350.
[14] K. Kakehi, S. Honda, J. Chromatogr. 379 (1986) 27.
[15] T. Takahashi, P.G. Schmidt, J. Tang, J. Biol. Chem. 258 (1983) 2819.
[16] M.J. Bionkowski, H.E. Conard, J. Biol. Chem. 260 (1985) 356.
[17] P. Nebinger, J. Chromatogr. 320 (1985) 351.
[18] S.R. Delaney, H.E. Conard, J.H. Glaser, Anal. Biochem. 108 (1980) 25.
[19] P. Nebinger, M. Koel, A. Franz, E. Werries, J. Chromatogr. 265 (1983) 19.
[20] J.F. Pirisino, in: J.F. Lawrence (Ed.), Food Constituents and Food Residues, Their Chromatographic Determination, Marcel Dekker, New York, 1984, pp. 159–193.
[21] R. Macrae, in: G. Birch (Ed.), Analysis of Food Carbohydrates, Elsevier, London, 1985, pp. 61–89.
[22] V.K. Dua, C.A. Bush, Anal. Biochem. 133 (1983) 1.
[23] T.V. Den, C.J. Biermann, J.A. Marlett, J. Agric. Food Chem. 34 (1986) 421.
[24] J. Bouchard, E. Chornet, R.P. Overend, J. Agric. Food Chem. 36 (1988) 1188.
[25] L.E. Fitt, W. Hassler, D.E. Just, J. Chromatogr. 187 (1980) 381.
[26] K. Brunt, J. Chromatogr. 246 (1982) 145.
[27] H. Hokse, J. Chromatogr. 189 (1980) 98.
[28] J. Schmidt, M. John, C. Wandrey, J. Chromatogr. 213 (1981) 151.
[29] H.D. Scobell, K.M. Brobst, J. Chromatogr. 212 (1981) 51.
[30] S. Tabata, Y. Dohi, Carbohydr. Res. 230 (1992) 179.
[31] R.N. Ammeraal, G.A. Delgado, F.L. Tenbarge, R.B. Friedman, Carbohydr. Res. 215 (1991) 179.
[32] N. Torto, T. Buttler, L. Gorton, G. Marko-Varga, H. Stalbrand, F. Tjerneld, Anal. Chim. Acta 313 (1995) 15.
[33] N. Torto, T. Buttler, L. Gorton, G. Marko-Varga, H. Stalbrand, F. Tjerneld, J. Chromatogr. A 725 (1996) 165.
[34] M.P.H. Dunkel, R. Amado, Carbohydr. Res. 268 (1995) 151.
[35] F.M. Rabel, A.G. Caputo, E.T. Butts, J. Chromatogr. 126 (1976) 731.
[36] G. White, T. Katona, J.P. Zodda, M.N. Eakins, J. Chromatogr. 625 (1992) 157.
[37] W.M. Blanken, M.L.E. Bergh, P.L. Koppen, D.H. Van den Eijnden, Anal. Biochem. 145 (1985) 322.
[38] K. Kainuma, T. Nakakuki, T. Ogawa, J. Chromatogr. 212 (1981) 126.
[39] K.L. Smiley, M.E. Slodki, J.A. Boundy, R.D. Plattner, Carbohydr. Res. 108 (1982) 279.
[40] E.K. Gum Jr., R.D. Brown Jr., Anal. Biochem. 82 (1977) 372.
[41] K. Koizumi, Y. Okada, S. Horiyama, T. Utamura, M. Hisamatu, A. Amemura, J. Chromatogr. 265 (1983) 89.
[42] N.W.H. Cheetham, P. Sirimanne, W.R. Day, J. Chromatogr. 207 (1981) 439.
[43] J.F. Franco, J.L. Garrido, Chromatographia 23 (8) (1987) 557.
[44] G.D. McGinnis, S. Prince, J. Lowrimore, J. Carbohydr. Chem. 5 (1) (1986) 83.
[45] C. Brons, C. Olieman, J. Chromatogr. 259 (1983) 79.
[46] M. Verzele, F. Van Damme, J. Chromatogr. 362 (1986) 23.
[47] B. Herbreteau, M. Lafosse, L. Morin-Allory, M. Dreux, Chromatographia 33 (1992) 325.
[48] D. Kariesky, D.C. Shelly, I. Warner, Anal. Chem. 53 (1981) 2146.
[49] M. Lafosse, B. Herbreteau, M. Dreux, L. Morin-Allory, J. Chromatogr. 472 (1989) 209.
[50] P.J. Simms, R.M. Haines, K.B. Hicks, J. Chromatogr. 648 (1993) 131.
[51] H.L. Jin, A.M. Stalcup, D.W. Armstrong, J. Liq. Chromatogr. 11 (1988) 3295.
[52] D.W. Armstrong, H.L. Jin, J. Chromatogr. 462 (1989) 219.
[53] D.W. Armstrong, H.L. Jin, Chirality 1 (1989) 27.
[54] A.J. Alpert, J. Chromatogr. 499 (1990) 177.
[55] Z.L. Nikolov, P.J. Reilly, J. Chromatogr. 325 (1985) 287.
[56] K.E. Bij, C. Horvath, W.R. Melander, A. Nahum, J. Chromatogr. 203 (1981) 65.
[57] S.C. Churms, J. Chromatogr. 720 (1996) 75.
[58] K. Koizumi, T. Utamura, Y. Okada, J. Chromatogr. 321 (1985) 145.
[59] A.J.P. Martin, R.L.M. Synge, Biochem. J. 35 (1941) 1358.
[60] P.C. Sadek, P.W. Carr, M.J. Ruggio, Anal. Chem. 59 (1987) 1032.
[61] L.R. Snyder, J.J. Kirkland, Introduction to Modern Liquid Chromatography, 2nd edn, Wiley, New York, 1979, pp. 579–583.
[62] G. Guichon, in: Cs. Horvath (Ed.), HPLC: Advances and Perspectives, vol. 2, Academic Press, NY, 1980, p. 2.
[63] L.R. Snyder, J.L. Glajch, J.J. Kirkland, Practical HPLC Method Development, 2nd edn, Wiley, New York, 1979, pp. 278–282.
[64] H. Kutsuna, H. Otsu, K. Yamagushi, J. Chromatogr. 635 (1993) 187.

ELSEVIER

Talanta 47 (1998) 1013–1020

Talanta

First and second dissociation constants and related thermodynamic functions of adipic acid in various binary methanol/solvent systems

G.A. El-Naggar *

Chemistry Department, Faculty of Education, (Damanhour Branch) Alexandria University, P.O. Box 426 Ibrahimia, Alexandria 21321, Egypt

Received 11 December 1997; received in revised form 30 April 1998; accepted 4 May 1998

Abstract

The First and second dissociation constants of adipic acid were determined by EMF measurements in water/methanol mixtures with 0, 30, 50 and 70 wt% organic cosolvent. Measurements were made at four different temperatures (ranging from 30 to 60°C) using the cell: glass electrode/HCL (m_1), H_2L (m_2), Na_2CO_3 (m_3)/AgCl $_{(S)}$, Ag. The computations of these dissociation constants were based on the method of successive approximation by means of basic programmes. The thermodynamic properties (ΔG°, ΔH°and ΔS°) for first and second dissociation reactions of the acid under study, were computed, analyzed and discussed in terms of solute–solvent interactions.
© 1998 Elsevier Science B.V. All rights reserved.

Keywords: Solvent effect; Dissociation constant; Dicarboxylic acid; EMF measurements and thermodynamic parameters

1. Introduction

This work is part of continuing research on the ionization of mono- and dibasic acids in various water–organic solvent systems, in which the introduction of an organic solvent to water changes the degree of dissociation of the examined acids [1–10]. In previous work we [3,4,8–11] examined the dissociation of some dicarboxylic acid in mixed solvent media of varying dielectric constants. These studies reflected the superposition of medium effects and indicated that these acids which have different structures were markedly different in ionic behaviour [9–11]. In an attempt to provide further experimental data about the ionization of dicarboxylic acids, we have extended our investigation to include adipic acid the molecule which has the formula $(CH2)_4(COOH)_2$.

In this paper the first and second ionization constants of the acid understudy were computed in media of varying methanol composition up to 70 wt% methanol which allow for a wide range of dielectric constant and the measurements were made at four different temperatures (ranging from

* Fax: +20 3 5862184.

0039-9140/98/$ - see front matter © 1998 Elsevier Science B.V. All rights reserved.
PII S0039-9140(98)00183-0

Table 1
Some EMF Data used for the determination of the first and second ionization constants

30% Adipic acid; 40°C					50% Adipic acid; 50°C				
$10^{-3}\ m_1 = 4.396 - E_1$ (mv) = 254.1; $-E_0$ (mv) = 552.25					$10^{-3}\ m_1 = 4.452 - E_1$ (mv) = 235.8; $-E_0$ (mv) = 544.6				
$10^{-3}\ m_2$	$10^{-3}\ m_3$	$-$E (mv)	$10^{-3}\ I$	$10^{-5}\ K_1$	$10^{-3}\ m_2$	$10^{-3}\ m_3$	$-E$ (mv)	$10^{-3}\ I$	$10^{-5}\ K_1$
20.644	5.159	152.1	10.583	3.981	21.750	5.429	123.2	11.006	3.131
28.885	7.219	144.1	14.846	3.924	30.942	7.724	114.2	15.639	3.069
38.430	9.605	140.1	19.808	4.119	40.350	10.072	110.6	20.399	3.262
46.966	11.738	138.1	24.244	4.358	46.746	11.669	108.8	23.639	3.378
53.830	13.453	137.2	27.800	4.616	54.517	13.609	107.9	27.569	3.635
60.104	15.022	136.7	31.038	4.895	60.697	15.152	107.1	30.695	3.811
30% Adipic acid; 30°C					70% Adipic acid; 60°C				
$10^{-3}\ m_1 = 4.678 - E_1$ (mv) = 282.2; $-E_0$ (mv) = 567.6					$10^{-3}\ m_1 = 3.429 - E_1$ (mv) = 293.9; $-E_0$ (mv) = 629.2				
$10^{-3}\ m_2$	$10^{-3}\ m_3$	$-E$ (mv)	$10^{-3}\ I$	$10^{-6}\ K_2$	$10^{-3}\ m_2$	$10^{-3}\ m_3$	$-E$ (mv)	$10^{-3}\ I$	$10^{-8}\ K_2$
11.381	9.102	107.5	21.920	2.379	8.346	6.675	23.3	15.231	3.473
17.421	13.934	99.5	35.026	2.579	12.288	9.828	13.4	23.907	4.198
22.138	17.706	96.2	45.249	2.727	16.396	13.114	9.4	32.948	4.630
25.844	20.670	93.6	53.203	2.742	20.137	16.105	7.5	41.176	4.933
29.669	23.729	91.8	61.989	2.707	24.366	19.488	5.8	50.467	5.163
33.526	26.814	90.1	69.624	2.906	27.069	21.650	4.7	56.399	5.251

30 to 60°C at interval of 10°C). This study is likely to enable us to determine the effects of solvent on the ionization processes of adipic acid and consequently of the thermodynamic functions of dissociation which can add useful information to the field of acid dissociations.

2. Experimental

Adipic acid (B.D.H) was recrystallized and dried. Methyl alcohol (from Prolabo) was purified as described previously [12]. Stock solutions HCl ($\cong 0.2$ (mmole kg^{-1})) were analysed by AgCl weighings. Stock buffer solutions made of adipic acid and Na_2CO_3 (dried at 300°C for 3h) were prepared by weight, from B.D.H. Analar samples.

K_1 and K_2 determinations were based on EMF measurements of the cell: glass electrode/HCl (m_1) H_2L (m_2), Na_2CO_3 (m_3)/$AgCl_{(s)}$/Ag; where H_2L = adipic acid; m_1, m_2 and m_3 are the molal concentrations of HCl H_2L and Na_2CO_3, respectively. The practical work has been simplified by adopting a practice [13,14] which prevents movements of the electrode between its calibration and usage. This is preferable to the technique [15,16] of transferring the glass electrode from an HCl solution to an acid ligand solution followed by extrapolation of timed reading to compensate for any EMF drifts. This procedure is considerably faster than that required with a Pt/H_2 electrode where each measurement necessitates refilling with a fresh buffer solution. Moreover several values of K_1 and K_2 could be computed from a single run. The buffer compositions were taken as $[H_2L]:[Na_2CO_3] \cong 3:1$ for K_1 determinations and 1.2:1 for K_2 determinations. About 230 g of the required wt% methyl alcohol (to ± 0.01 g) was weighed into the cell together with sufficient dilute HCl containing the required wt% methyl alcohol ($\cong 0.035$ m) to make $\cong 0.0015$ to 0.0025 m (addition by weight pipette to ± 0.1 mg). With the electrodes in positions, the cell was equilibrated at the desired temperature, the temperature was controlled to ± 0.01°C. This could take up to three h the HCl solution was then given a short stir (5 s)

Table 2
pK_1 and pK_2 values of adipic acid in media of different dielectric constant (ε) at different temperatures

T (°c) wt/wt%		30	40	50	60
0	pK_1	4.41 ±0.03	4.31 ±0.01	4.28 ±0.01	4.19 ±0.02
	pK_2	5.11 ±0.02	5.27 ±0.02	5.33 ±0.03	5.40 ±0.01
	ε	78.73	73.12	69.85	66.63
30	pK_1	4.62 ±0.02	4.55 ±0.04	4.46 ±0.02	4.37 ±0.04
	pK_2	4.72 ±0.03	5.79 ±0.04	5.81 ±0.01	5.92 ±0.03
	ε	62.71	59.33	56.59	53.94
50	pK_1	4.85 ±0.01	4.74 ±0.04	4.66 ±0.04	4.55 ±0.03
	pK_2	6.28 ±0.02	6.32 ±0.02	6.49 ±0.02	6.59 ±0.02
	ε	53.47	50.40	47.82	45.28
70	pK_1	5.15 ±0.05	4.93 ±0.01	4.87 ±0.05	4.80 ±0.03
	pK_2	7.36 ±0.05	7.42 ±0.01	7.59 ±0.03	7.63 ±0.03
	ε	43.63	41.04	38.81	36.68

by a fitted microstirer and left to settle untile EMF (E) was constant (30 min). Up to six additions of stock buffer were then added by weight pipette. In the first addition about 15 g of stock buffer solution were added while in the latter addition, about 8 g of this solution were added in each case. After each addition the solution was stirred and EMF of the cell then monitored to constancy. The time needed could vary from 1 ≅ h for the first addition for a K_2 series (the point of the greatest EMF change) down to ≅ 15 min for the latter addition and also for all K_1 series. The constancy of the EMF values was checked by the difference between the first and the last readings which never more than ±0.1 mv. Measurements to ±0.1 mv were made with a digital PH meter (Backman 4500 type). The AgCl electrode was made by plating a thin spiral Pt wire with Ag in 0.5% KAg $(CN)_2$ for ≅ 1h with a 9-V battery followed by eletrolysis for AgCl in 0.05 M HCl with a 9-V battery for 20 s.

3. Results and discussion

3.1. Treatment of data for the determination of pK values

The thermodynamic pK value for the first and second ionization reactions of adipic acid were calculated in methyl alcohol water media of varying solvent compositions (0–70 wt% methyl alcohol) within the temperature range (30 to 60°C). The expressions used for calculating pK_1 and pK_2 are,

$$K_1 = [H^+][HL^-]\gamma_H\gamma_{\bar{HL}}/[H_2L] \quad (1)$$

$$K_2 = [H^+][L^{2-}]\gamma_L/[HL^-] \quad (2)$$

$$K_{NaL} = [Na^+][L^{2-}]\gamma_L/[NaL^-] \quad (3)$$

$$-\log \gamma_I = AZ_i^2[I^{1/2} + /(1 + BI^{1/2}) - QI] \quad (4)$$

$$E_{cell} = E^\circ_{cell}{}^- K^- \log([H^+][CL^-]\gamma_H\gamma_{CL} \quad (5)$$

$$K^- = 2.3026\ RT/F$$

Where I and γ represent ionic strength and activity coefficient, respectively (γ_{H2L} was negligible i.e. close to 1). The Debye–Huckel constant 'A' was calculated for each temperature and each solvent composition while the constants 'B' and 'Q', the values of which were taken as 1.3 and 0.3, respectively [14]. Firstly $E^\circ_{(cell)}$ was calculated from Eqs. (4) and (5) by knowing $E^\circ_{(cell)}$ of the diluted HCl solution (I = [HCl]). If the stoichiometric molal concentrations of HCl, H_2L, Na_2CO_3 are m_1, m_2, and m_3, respectively, the following equations are used (with Eqs. (1)–(5)) for calculating K_1.

$$[H_2L] = m_1 + m_2 - 2m_3 - [H^+] + [L^{2-}] + [NaL^-] \quad (6)$$

$$[HL^-] = m_2 - [H_2L] - [L^{2-}] - [NaL^-] \quad (7)$$

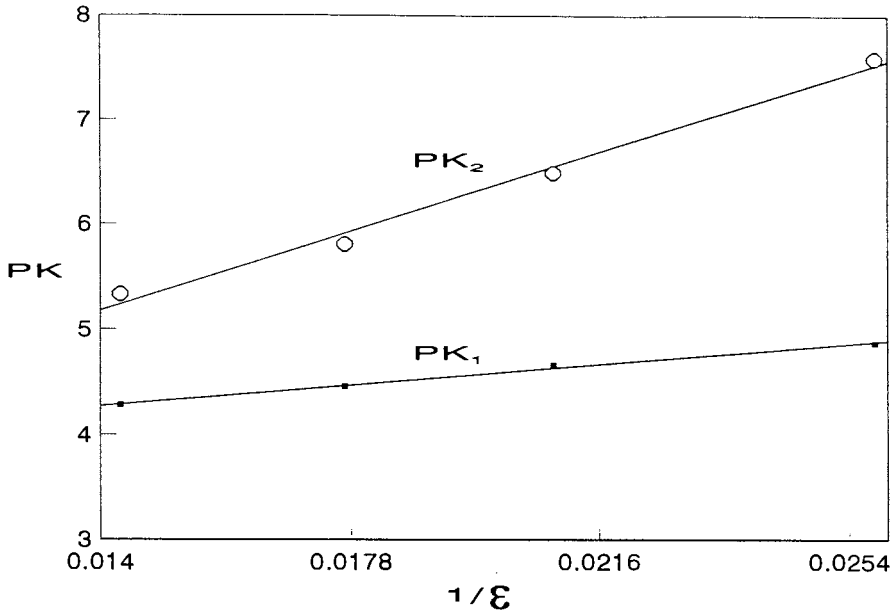

Fig. 1. Variation of PK_1 and PK_2 with ε^{-1} at 50°C.

Approximate values of $[H^+]$ on the addition of buffer solution were calculated from Eqs. (4) and (5) with $I = m_1$ followed by use of Eqs. (6) and (7) with $[L^{2-}] = 0$ and $[NaL^-] = 0$ in the first cycle. The subseqent value of I was used to recalculated $[H^+]$ followed by calculation of $[L^{2-}]$ via Eq. (2) with published or estimated values of K_2 [17]. $[NaL^-]$ was calculated from Eq. (3) using $K^{(3)}_{NaL} = 0.2$. If present estimates of K_2 were significantly different the calculations were repeated until the difference between successive values of $[H^+]$ agreed to $|\Delta[H^+]| \leq 1 \times 10^{-9}$ m, K_1 was then obtained from Eqs. (1) and (4).

For $K_2[H^+]$ was calculated as described above and then by applying Eqs. (8) and (9) found,

$$[HL^-] = m_1 + 2m_2 - 2m_3 - [H^+] - 2[H_2L] \quad (8)$$

$$[L^{2-}] = m_2 - [H_2L] - [HL^-] - [NaL^-] \quad (9)$$

with $[H_2L] = 0$ and $[NaL^-] = 0$ in the first cycle followed by the use of Eqs. (1) and (3) for calculating $[H_2L]$ and $[NaL^-]$, respectively. K_2 was calculated from Eqs. (2) and (4) when the difference between two successive of $[H^+]$ agreed to $|\Delta[H^+]| \leq 1 \times 10^{-9}$ m. All computations were made by means of BASIC programmes with IBM Computer.

Some of the obtained K_1 and K_2 values for the different ionic strengths and temperatures are represented in Table 1. It is obvious that most of the K_1 and K_2 values for a one run are varied with ionic strength. Accordingly the extrapolated K_1 and K_2 at zero ionic strength were computed by the least square method. This method based on extrapolation, for the determination of K_1 and K_2 was used earlier [13,14] and was found to be valid and efficient under different experimental conditions. The computed pK_1 and pK_2 values at zero ionic strength for different solvent compositions and temperatures are shown in Table 2 together with their respective estimates of errors, from which it can be readily seen influence of the composition of the medium on the first and second ionization constants.

This effect can be easily described by the relation between the pK and the inverse of the bulk dielectric constant of the medium (ε), based on Born's electrostatic model [17].

$$\frac{dpK_n}{d(1/\varepsilon)} = \frac{e^2}{2KT(\text{lin } 10)} \Phi_n$$

where Φ_n is expressed in terms of the reciprocal of the radii of the ions taking part on the equilibria,

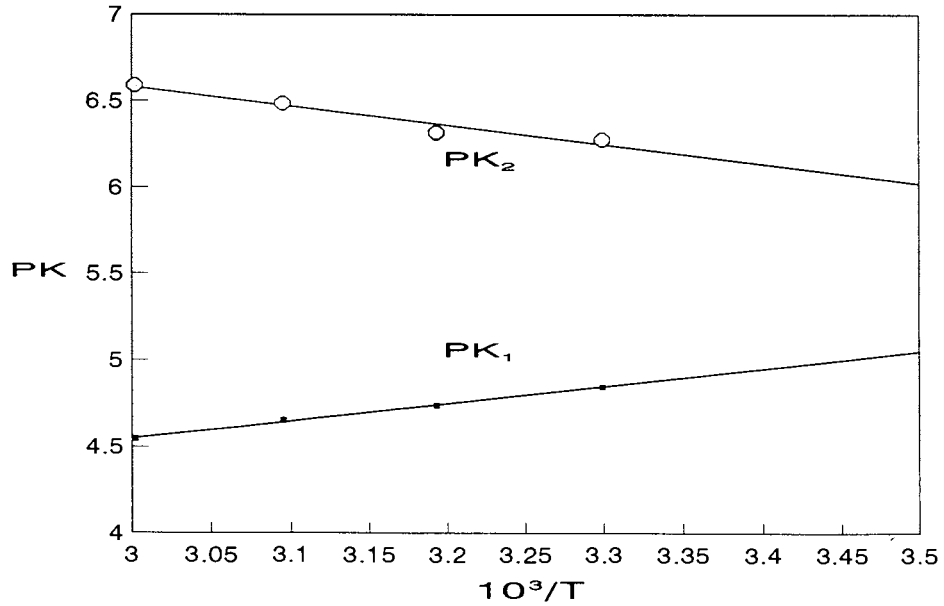

Fig. 2. Van't Hoff plots of the first and second dissociation reactions on 50 wt% methanol.

K is the Boltzmann constant, T the absolute temperature. For n equal 1 to 2 we have [17]

$$\Phi_1 = 1/r_H + 1/r_1;\ \Phi_2 = 1/r_H + 4/r_2 - 1/r_1$$

r_H, r_1 and r_2 being the radii of H^{+}, HL^{-} and L^{2-}, respectively.

This equation predicts linear relationship between pK_n and $1/\varepsilon$, in all cases for which the change in pK_n after a change of medium can be attributed to electrostatic phenomena. In such case, it is assumed that all non-electrostatic solute–sovent interaction remain constant, regardless of the solvent composition. It was found indeed that the plots of pK_n versus $1/\varepsilon$ were linear. This finding lead to the conclusion that the non-electrostatic-solvent interaction remains invariable in methanol–water binary mixtures. 'ε' values were obtained from the data of Akerlof [18] and were listed in Table 2. It is also obvious from Table 2, that the ratio of K_1/K_2 increases gradually with increasing the organic solvent content of the medium and the largest value of K_1/K_2 has been obtained for 70 wt% methanol ($K_1/K_2 =$ 307.97). This behaviour was observed before [19] in many dicarboxylic acids and was attributed to intramolecular hydrogen bonding which causes the first ionization constant to increase at the expense of the second one. In accordance with this interpretation it was stated [19] that strain as a result of sterric crowding of carboxyl groups is relieved to some extent by formation of the intramolecularly hydrogen bonded mono-anion. In aqueous medium [20] there is strong hydrogen bonding of the carboxylate and, to a much smaller extent, of the carboxyl group to the solvent. The addition of methanol to water causes the basicity of the medium to be changed gradually, so the hydrogen bonding of the carboxylate ion with solvent appears to decrease gradually [20] giving chance to such intramolecular hydrogen bonding to increase.

4. Thermodynamics of acid dissociations

The thermodynamic functions for the first and second ionization processes were computed from the well known equations. The plots of $pK_{(1\text{ or }2)}$

Table 3
Thermodynamic parameters ΔH°, ΔG°, ΔS° for the first and second ionization constants in different solvent composition and at different temperatures (ΔH°, ΔG°, kj. mol^{-1} and ΔS° in $jmol^{-1}$ K^{-1})

wt/wt%	T°c	30	40	50	60		30	40	50	60
	ΔH_1°	12.91	12.91	12.91	12.91	$-\Delta H_2^\circ$	18.34	18.34	18.34	18.34
		±0.08	±0.08	±0.08	±0.08		±0.11	±0.11	±0.11	±0.11
0	ΔG_1°	25.58	25.84	26.49	26.75	ΔG_2°	29.65	31.59	32.99	34.46
		±0.15	±0.07	±0.08	±0.12		±0.12	±0.11	±0.18	±0.25
	$-\Delta S_1^\circ$	41.80	41.29	42.02	41.55	$-\Delta S_2^\circ$	158.30	159.42	158.82	158.48
		±0.60	±0.30	±0.34	±0.40		±0.5	±0.5	±0.7	±0.1
	ΔH_1°	16.03	16.03	16.03	16.03	$-\Delta H_2^\circ$	12.44	12.44	12.44	12.44
		±0.09	±0.09	±0.09	±0.09		±0.08	±0.08	±0.08	±0.08
30	ΔG_1°	26.80	27.28	27.57	27.88	ΔG_2°	33.17	34.72	35.95	37.79
		±0.10	±0.23	±0.13	±0.24		±0.15	±0.22	±0.06	±0.49
	$-\Delta S_1^\circ$	35.52	35.91	35.69	35.57	$-\Delta S_2^\circ$	150.47	150.60	149.75	150.78
		±0.50	±0.80	±0.50	±0.80		±0.5	±0.7	±0.3	±1.5
	ΔH_1°	19.58	19.58	19.58	19.58	$-\Delta H_2^\circ$	20.01	20.01	20.01	20.01
		±0.11	±0.11	±0.11	±0.11		±0.12	±0.12	±0.12	±0.12
50	ΔG_1°	28.17	28.45	28.83	28.98	ΔG_2°	36.45	38.26	40.15	42.04
		±0.06	±0.25	±0.25	±0.20		±0.09	±0.11	±0.12	±0.12
	$-\Delta S_1^\circ$	28.34	28.32	28.61	28.22	$-\Delta S_2^\circ$	186.24	186.05	186.14	186.23
		±0.40	±0.90	±0.90	±0.64		±0.5	±0.5	±0.5	±0.5
	ΔH_1°	13.76	13.76	13.76	13.76	$-\Delta H_2^\circ$	19.13	19.13	17.13	19.13
		±0.08	±0.08	±0.08	±0.08		±0.12	±0.12	±0.12	±0.12
70	ΔG_1°	29.12	29.50	30.13	30.60	ΔG_2°	42.69	44.48	46.97	48.66
		±0.33	±0.62	±0.36	±0.50		±0.28	±0.09	±0.18	±0.22
	$-\Delta S_1^\circ$	50.67	50.27	50.65	50.54	$-\Delta S_2^\circ$	203.92	203.12	204.53	20.47
		±1.10	±1.90	±1.10	±1.40		±1.0	±0.5	±0.7	±0.80

versus $1/T$ gave straight lines for each solvent composition, as can be seen from Figs. 1 and 2 (representative figure) which shows that ΔH_1° and ΔH_2° may be treated as sensibly constant over the temperature range studied. The obtained values of ΔH°, ΔG° and ΔS° for both ionization reactions at different temperatures are listed in Table 3. It is clear from Table 3 that both ΔG_1° and ΔG_2° have positive values which indicates the preferential stabilization of H_2L in the first dissociation process and of the species HL^- in the second dissociation process by the mixed solvent. The positive values of ΔG°, for both dissociation processes increase with increasing the organic content of the solvent mixture. This trend is consistent with effect of the lowered dielectric constant of the mixed solvent and it is caused by the increase of the electrostatic free energy of the ions produced in the dissociation process.

The standard entropy of dissociation of adipic acid has large negative values for both ionization reactions which can be explained on the basis of electrostatic action of the carboxylic groups transmitted through CH_2-groups and through solvent molecules (field effect). The charged anions of this acid impose order on the surrounding solvent molecules, which in turn interfere with the internal rotation of the alkyl chain of the acid. Adipic acid has long chain length consists of four CH_2 groups and hence the partial molal entropies of its anions decrease noticeably (relative to the neutral acid). ΔS_1° and ΔS_2° becomes more negative with increasing the proportion of methanol in the solvent mixture as opposed to pure water [21]. The qualitative expla-

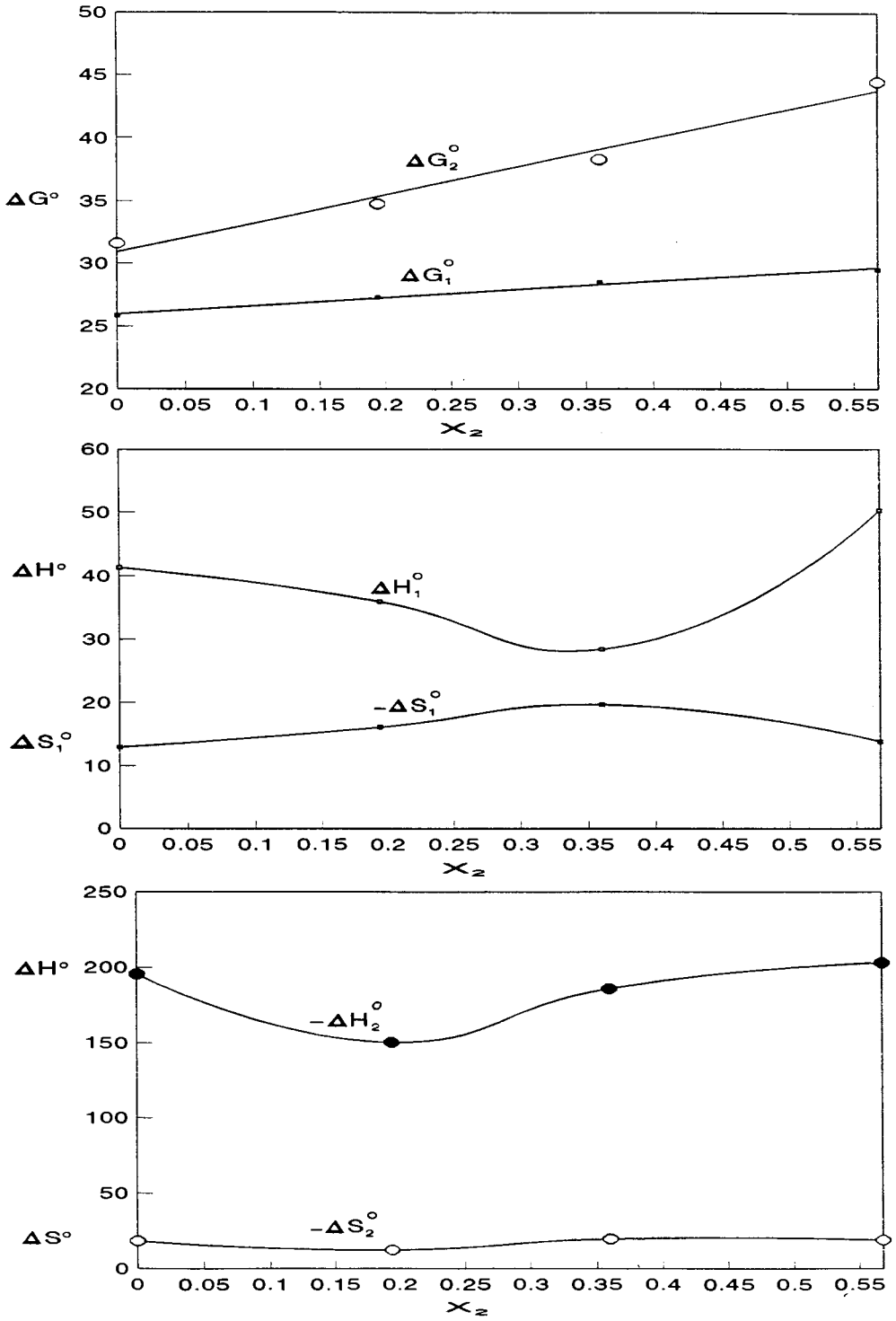

Fig. 3. of ΔH°, ΔG° and ΔS° with the mole fraction of methyl alcohol at 40°.

nations of this trend is that the methyl alcohol–water mixtures are less structured than pure water [20], hence the species (such as H^+, HL^- and L^{2-}) will orient solvent molecules to a greater extent in methyl alcohol–water media. Consequently, this greater degree of orientation results in a more negative entropy of dissociation. Fig. 3 represents the variation of $\Delta H°$, $\Delta S°$ and $\Delta G°$ for both ionization reactions with the mole fraction of methanol at 40°C. The profile of $\Delta H°$ (and $\Delta S°$) mole fraction curves predicts that a compensation effect may exist between $\Delta H°$ and $\Delta S°$. The true explanation of this compensation effect must lie in terms of solvent–solute interactions. Any effect, for example that leads to a stronger binding between the solute species and solvent molecules will lower the enthalpy, it also will lower entropy by restricting the freedom of vibration and rotation of solvent. Application of more exact theories leads to the result that they generally will give rise to a fairly exact compensation.

References

[1] W.J. Albery, Ann. Rev. Phys. Chem. 31 (1980) 227.
[2] R.W. Taft, Prog. Phys. Org.-Chem. 14 (1982) 247.
[3] M.F. Amira, Sh. A-El-shazly, M.M. Khalil, Thermochim. Acta 115 (1987) 1.
[4] M.T. Mohamed, A.A. Zaghloul, M.F. Amira, Bull. Fac. Sci. Alex. Univ. 31 (1991) 116.
[5] Y. Kondo, W. Sugitani, M. Tokui, J. Chem. Soc. Faraday Trans. 88 (20) (1992) 3019.
[6] G. Papanastasiou, I. Zigas, Talanta 36 (1989) 977.
[7] J. Barbosa, J.L. Beltran, V. Sanz-Nebot, Anal. Chim. Acta 288 (1994) 271.
[8] A.A. Zaghloul, Afinidad 462 (1996) 123.
[9] A.A. Zaghloul, G.A El-Naggar, M.F Amira, Gazz-Ital. 126 (1996) 735.
[10] A.A. Zaghloul, G.A. El-Naggar, Sh.A. El-Shazly, M.F. Amira, Talanta 45 (1997) 189.
[11] M.T. Mohamed, A.A. Zaghloul, A.M. Saad, A.M. El-Bahnasawy, M.F. Amira, Afinidad accepted for publication (1997).
[12] V.I. Vogel, A Text Book of Practical Organic Chemistry, third, Longmans, London, 1971.
[13] C.B. Monk, M.F. Amira, J. Chem. Soc. Faraday Trans. 1 (74) (1978) 1170.
[14] C.B. Monk, M.F. Amira, J. Chem. Soc. Faraday Trans. 76 (1980) 1773.
[15] A. Zielen, J. Phys. Chem. 67 (1963) 1474.
[16] B.M. Low, D.G. Smith, J. Chem. Soc. Faraday Trans. 1 (69) (1973) 1939.
[17] M.K. Chantooni Jr., I.M. Kolthoff, J. Phys. Chem. 79 (1975) 1176.
[18] G. Akerlof, J. Am. Chem. Soc. 54 (1932) 4125.
[19] L. Hunter, Chem. Ind. (1953) 155.
[20] I.M. Kolthoff, M.K. Chantooni, J. Am. Chem. Soc. 97 (1975) 1376.
[21] E.J. King, J. Am. Chem. Soc. 73 (1951) 155.

ELSEVIER

Talanta 47 (1998) 1021–1031

Talanta

Study of the determination of acetylcholine after enzymatic hydrolysis by triangle programmed coulometric flow titration

Róbert E. Gyurcsányi [a,*], Zsófia Fehér [b], Géza Nagy [c]

[a] *Institute of General and Analytical Chemistry, Technical University of Budapest, Gellért tér 4, H-1111 Budapest, Hungary*
[b] *Technical Analytical Research Group of the Hungarian Academy of Sciences, Technical University of Budapest, Gellért tér 4, H-1111 Budapest, Hungary*
[c] *Department of General and Physical Chemistry, Jannus Pannonius University, Ifjuság u. 6, H-7601 Pécs, Hungary*

Received 3 February 1998; received in revised form 28 April 1998; accepted 4 May 1998

Abstract

A new method for the determination of acetylcholine is introduced and studied. The method uses enzymatic hydrolysis of acetylcholine carried out in a flow-through analytical reactor column, while for the detection triangle programmed coulometric flow titration is employed. The flow-through coulometric titration system and the preparation of the enzyme reactor are described. The operation conditions for the hydrolysis and for the titration were optimized. The flow-through coulometric titration technique offers a better precision for the determination of acetylcholine in small concentration ranges than methods based on the detection of pH change. Working conditions of the system can be easily adjusted for different sample concentration ranges. The limit of detection for the determination of acetylcholine was found to be 8×10^{-5} M. The method described could be advantageously used for indirect determination of acetylcholinesterase inhibitors. © 1998 Elsevier Science B.V. All rights reserved.

Keywords: Coulometric titration; Enzyme reactor; Flow analysis; Acetylcholine

1. Introduction

Acethylcholine (ACH) is the first described and most abundant neurotransmitter in the animal world. It is the primary neurotransmitter between neurons and muscles.

Because of its biological importance a wide variety of different methods have been worked out for the quantitative determination of ACH in different samples [1–4]. Among them, because of their high selectivity, quantitative enzymatic reactions are frequently used. The acetylcholinesterase enzyme (ACHE) catalyzed hydrolysis of ACH is usually the selective analytical reaction. However often a second enzymatic step, the cholineoxidase catalyzed oxidation of the choline, obtained in the hydrolysis, follows. The product of this reaction, H_2O_2, is detected using amperometric or colorimetric technique [5,6].

* Corresponding author. Tel.: +36 1 4631592; fax: +36 1 4633408; e-mail: robi.aak@chem.bme.hu

0039-9140/98/$ - see front matter © 1998 Elsevier Science B.V. All rights reserved.
PII S0039-9140(98)00185-4

Considering electrochemical transducers for detection, the amperometric method offers a lower detection limit. However its drawback is that needs the use of another enzyme and thus of a more complex bienzymatic system [7–14]. Moreover the activity of the cholineoxidase is generally lower than the activity of acetylcholinesterase, thus the second reaction catalyzed by the cholineoxidase is the conversion limiting step [15].

Although most of the reports on determination of ACH deal with amperometric detection, some describe methods with potentiometric detection. Potentiometric biosensors worked out for ACH determination often use pH detection [16–19], however ion selective electrodes for the determination of choline have also been reported [20]. The first potentiometric enzymatic sensor based on pH detection was made by Mosbach and co-workers [21]. The potentiometric method based on pH detection is much simpler than the amperometric one, but suffers from the lack of sensitivity and precision. It was expected that this disadvantage could be reduced using a titration technique, because the titration is one of the most precise and reliable methods of quantitative analysis. Acid–base titrations can be performed with high reproducibility and reliability.

In this laboratory a coulometric flow titration technique [22–24] as well as titration systems [23,25–27] have been developed. The coulometric reagent addition has well-accepted advantage in the practice of acid–base titrations.

Several analytical tasks were successfully solved performing titrations in flow media using triangle programmed coulometric reagent addition [24,28–33].

In these measurements a flow manifold is used in which the stream of the sample solution-flowing at a constant rate-merges with the reagent. The reagent is generated coulometrically in a flow-through electrolysis cell placed upstream from the merging zone. By changing the reagent generating current intensity, the mass flow of the reagent can be changed just as well as the degree of titration downstream of the confluence. Using a triangle shaped reagent generating current–time program the titration degree increases for a while, after it decreases. With a proper program two of the easy to detect equivalence points show up. The higher the sample concentration the nearer are the two equivalence points to each other. This can be easily explained by the degree of over-titration of the sample. For samples with low concentrations the extent of over-titration is larger, as well as the distance—translated in time units—between the two equivalence points. Comparing the reagent generating program to the flow parameters, the sample concentration can be obtained from the time difference between the two equivalence points (see later).

The aim of the present work was to design and study a flow titration system for ACH determination. It was expected that coulometric acid–base titration with a better precision and reliability can be more advantageous than direct pH measurement for this purpose. Regarding this we prepared flow-through analytical reactors containing immobilized acetylcholinesterase enzyme and designed a flow titration apparatus for the determination of the acetic acid liberated in the enzyme catalyzed reaction. In the course of our work we studied the analytical performance of the reactor–titrator combination of acetylcholine determinations. This paper is about our findings.

1.1. Theory

The working principle of the triangle programmed flow titration has been described in details earlier [22,30]. Only a brief outline is given below. The titration is performed by coulometric generation of the reagent from a suitable solution. A triangle shaped current–time program is employed for reagent generation, which results in a corresponding mass flow change of the reagent. The constant sample and reagent flow are merged and due to the special design of the titration cell, the titration is performed practically in one drop. If the conditions are well selected two titration curves can be observed in time using an appropriate detector downstream. The time Q, elapsed between the apparition of the two equivalence points (inflection points, forward and backward) of the titration curves provides the quantitative analytical information.

$$Q = 2\tau - \frac{2a}{b}\frac{\mu F \tau V_s}{i_{max}} c_s, \quad (1)$$

where 2τ is the duration of the entire reagent addition program, a and b are stoichiometric constants, V_s is the flow rate of the sample solution, c_s is the concentration of the sample solution, i_{max} is the maximum value of the reagent generating current, F is the Faraday constant, μ is the number of electrons taking part in the reagent generating reaction. As it can be seen from Eq. (1). a linear relationship with negative slope exists between the Q value and the concentration of the sample.

In this work the ACH is hydrolyzed by catalytic action of ACHE enzyme immobilized in the analytical flow-through column according to Eq. (2). The liberated acetic acid is titrated by the coulometrically generated reagent. In our studies hydroxide ions were generated with close to 100% current efficiency on the surface of a negatively polarized platinum electrode with current intensity control.

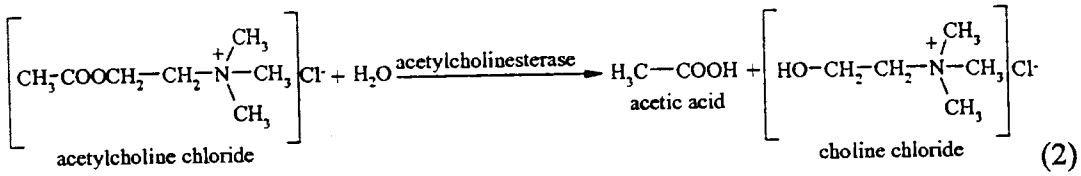

(2)

2. Experimental

2.1. Chemicals

Acetylcholinesterase (type III, from electric eel), acetylcholine and glutaraldehyde were obtained from Sigma.

3-propylamino(triethoxy)Silane was obtained from Merck (Germany). Controlled pore glass (CPG) was obtained from BDH Chemicals. All the other reagents: potassium dihydrogen phosphate, disodium hydrogen phosphate, acetic acid (Reanal, Hungary), and potassium nitrate (Fluka Chemicals, Switzerland) were of analytical grade.

The acetylcholine and acetic acid solutions for calibration were prepared by serial dilution method using freshly boiled deionized water. This was a result of preliminary investigations, which were carried out in order to establish the effect of the buffer capacity of the sample on the determination of acetylcholine. Although with the unbuffered acetylcholine samples the conversion of the enzyme reactor was lower, the linear range of the determination was much larger than with the buffered sample solutions.

2.2. The preparation of the enzyme reactor

The acetylcholinesterase enzyme was immobilized on alkylaminated CPG following a slightly modified recipe of [34]. Firstly the alkylaminated CPG was activated with glutaric aldehyde. The reaction was carried out by reacting the 4 g of alkylaminated CPG beads with a solution of 2.5% glutaraldehyde in 0.1 M phosphate buffer at pH 7. The reaction vessel was kept for 45 min under vacuum and for another 45 min at atmospheric pressure. After filtering, the glass beads were washed thoroughly with deionized water, to get rid of the excess of glutaraldehyde. Then the glass beads were introduced in a small vial which contained 400 μl acetylcholinesterase enzyme solution ($\sim$400 U) diluted with 750 μl 0.1 M pH 8.2 phosphate buffer. The vial was kept at first for 45 min under vacuum and for another 2 h and 45 min under atmospheric pressure while it was frequently shaken up. The beads obtained with the immobilized enzyme on their surface were used in our experiments as column packing.

While not in use the beads were stored in refrigerator at 4°C in 0.1 M pH 8.2 phosphate buffer.

To prepare the flow through analytical column, 0.7 g portion of the CPG beads with enzyme immobilized on it were introduced into the lumen

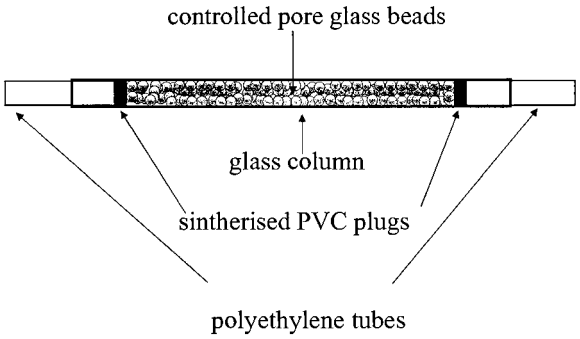

Fig. 1. Schematic design of the enzyme reactor.

of a 2.5 mm internal diameter glass capillary to form a 83 mm long packed section. Both ends of the glass capillary were closed with sintherized PVC plugs. These plugs allowed solution passage but held back the beads. The schematic design of the enzyme reactor is shown in Fig. 1.

While not in use the reactor column was stored in refrigerator at 4°C in 0.1 M pH 8.2 phosphate buffer. During 2 months of continuous use we found no significant change in the activity of the enzyme reactor.

2.3. Apparatus and procedure

The coulometric flow titration system used in our experiments was made of four main parts, as it is shown in Fig. 2.

The enzyme reactor, where the hydrolysis of acetylcholine content of the streaming sample solution took place.

The titrant (OH^-) is produced in the reagent generation part. This contain a special flow-through electrolysis cell, made of plexi glass. Both half cells of it, separated from each other with a dialysis membrane, contain platinum electrodes. The electrodes were connected to a Triangle Current Source (OH-409 Radelkis, Hungary). 0.3 M KNO_3 solution was streamed with a flow rate of 2 ml min^{-1} through the reagent generating half cells. During the triangle current program the electrolysis of the reagent generating solution took place in the cell. As result in one of the half cells H^+ and in the other OH^- ions are generated. The OH^- ions are conducted in the titration vessel while the H^+ ions are let to go to the waste.

The third part of the apparatus is the titration cell (drip vessel), where the reaction between the acetic acid and the reagent takes place.

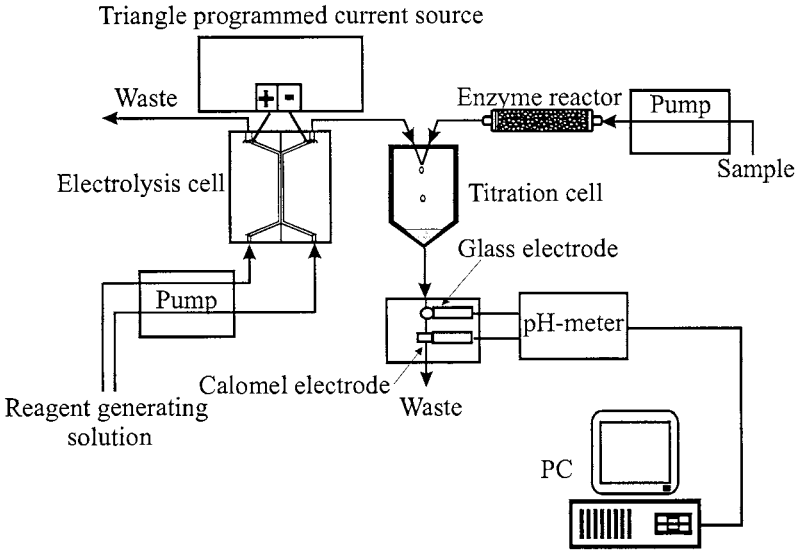

Fig. 2. The schematic design of the triangle programmed coulometric flow titration system.

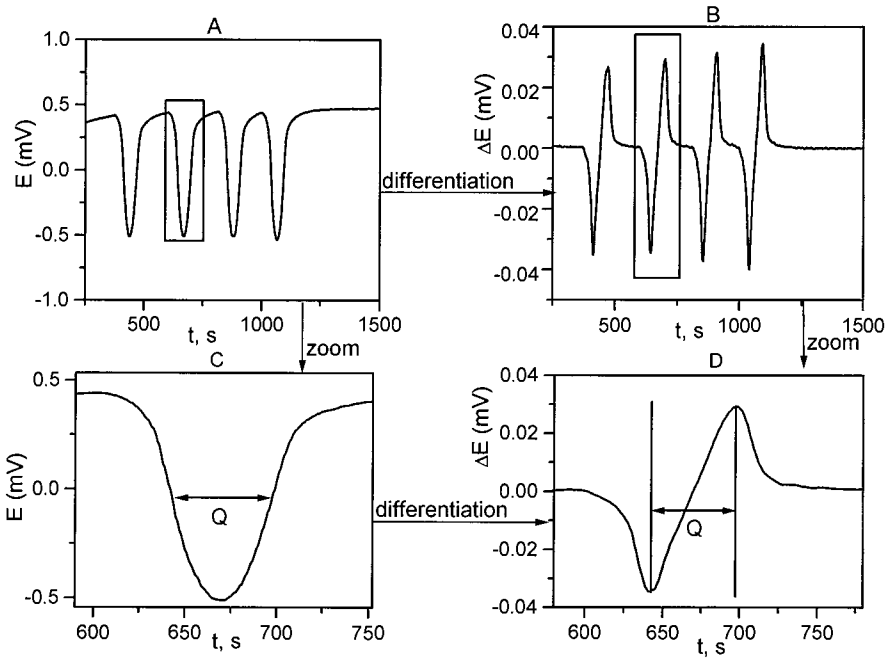

Fig. 3. Triangle programmed titration curves obtained in case of acetylcholine solution; $c_s = 7.5 \times 10^{-4}$ M, $2\tau = 80$ s, $i_{max} = 0.5$ mA, $V_s = 1.87$ ml min^{-1}; (A) original curves in the case of replicate samples; (B) selected titration curve; (C) and (D) differential titration curves for replicate and individual sample.

The fourth part is the detection and evaluation part. The pH in the detection cell was followed with a microcapillary pH-sensitive glass electrode (OP-0753P, Radelkis, Hungary). A microcapillary saturated calomel electrode (OP-0837P, Radelkis, Hungary) was used as reference electrode. The electrodes were connected to a Precision Digital pH-meter (OP-208/1, Radelkis, Hungary), the data was acquired through an analog-digital converter interface by a personal computer.

The solutions were flown by a multichannel peristaltic pump, model OL-602, (LaborMIM, Hungary).

The acetylcholine samples were flown through the enzyme reactor where—due to the enzymatic hydrolysis—acetic acid was produced. In the titration cell the acetic acid was merged with the base generated in the reagent generating cell and the titration occurred. When acetic acid samples were titrated, the enzyme reactor was disconnected.

The electrode potential of a pH-sensitive electrode in time was recorded during the titration. The special triangle current program used for the reagent generation resulted in a bell shape potential–time response curve. The difference in time between the appearance of the inflection points (Q) was used for evaluation. The inflection points usually can easily be located on the electrode potential–time recordings by observation. However, converting the curves to $(\Delta E/\Delta t) - t$ differential titration curves the end points show up clearly as peaks. So for automatic end point location the derivative curves were used. To avoid false peaks we used the simultaneous differentiation and smoothing algorithm of the Savitzky–Golay method [35]. Usually one smoothing step made the automatic end point location safe. In this case noise generated local maxima were not falsely taken as end points. We found the Savitzky–Golay method very suitable for our purpose because it preserves the features of the data such as peak height and width. The extreme values (maximum and minimum) on the derivative curves correspond to the inflection points on the E–t curves. A triangle programmed titration

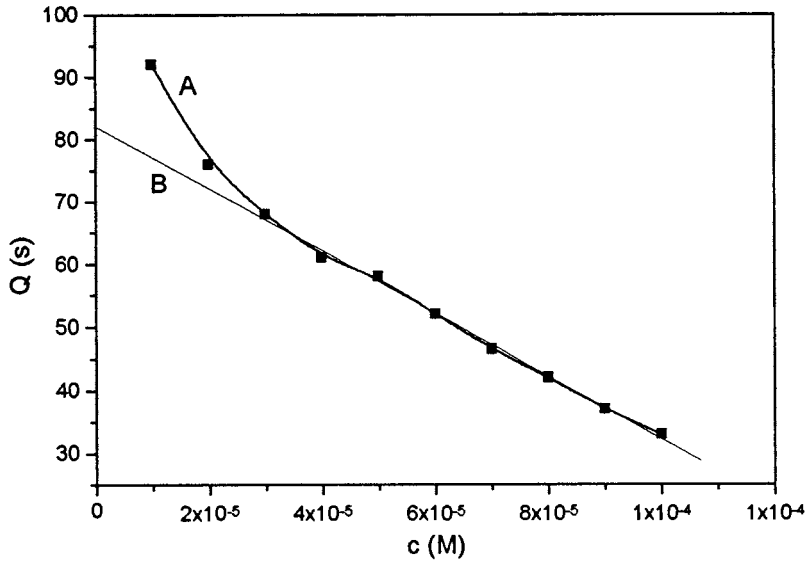

Fig. 4. Calibration curve for acetic acid obtained by triangle programmed coulometric flow titration in the concentration range of 10^{-4}–10^{-5} M (A), the calibration curve is linear in the concentration range of 3×10^{-4}–10^{-5} M ($R = -0.999$); (B) $2\tau = 80$ s, $i_{max} = 0.7$ mA, $V_s = 1.87$ ml min^{-1}.

curve and the way of its evaluation can be seen in Fig. 3.

3. Results and discussion

3.1. Preliminary investigations

3.1.1. Determination of current efficiency

In case of coulometric titration the reagent generating current efficiency must be very close to 100%. When the triangle programmed reagent generating program is used, it is more difficult to achieve since the current intensity changes by time. For checking the current efficiency of the reagent generating cell in the course of the titration program, constant current levels in the range 0.2–5 mA were applied for a given time interval on the electrodes. The solution flowing through the investigated half-cell was collected (originally 0.1 M KNO_3 solution) and titrated in the classical way with 0.01 M HCl. It was found that in the current interval mentioned, hydroxide ions are generated with a current efficiency of 100%, within the error limit of the determination (0.1%).

3.1.2. Determination of acetic acid by coulometric flow titration technique

Before performing the quantitative determination of the acetylcholine we found important to investigate the conditions in which the acetic acid can be titrated by coulometric flow titration. Originating from the nature of the coulometric flow titration one can analyze solutions in relative small concentration ranges (usually less than one order of magnitude) with very good precision. However, extending the concentration range, the precision and the sensitivity of the determination decreases. To analyze solutions in different concentration ranges the adjustment of i_{max} value of the reagent addition program as well as the flow rate of the sample have special importance, because these parameters determine the concentration of the reagent. The maximum concentration of the reagent (corresponding to i_{max} on the triangle current–time program) should be high enough to achieve a certain level of over-titration but not as high to decrease the sensitivity of the determination. The selection of the appropriate values of these two parameters can be done by calculation using Eq. (1). After adjusting the appropriate

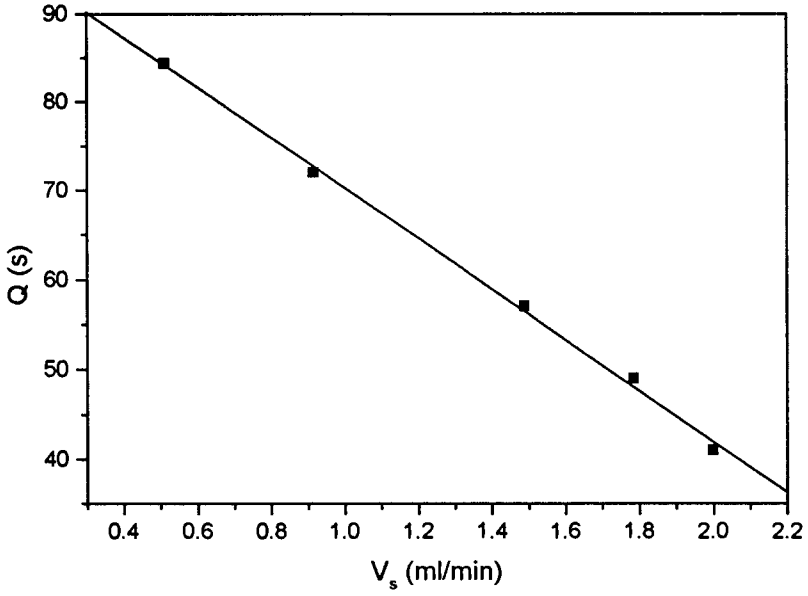

Fig. 5. The linear relationship between the Q value and the flow rate in the case of acetic acid solutions ($R = -0.998$); $c_s = 5 \times 10^{-4}$ M, $2\tau = 80$ s, $i_{max} = 3.5$ mA.

parameters, titrations were performed using acetic acid solutions and the potential–time curves were recorded. The results obtained are shown in Fig. 4.

From Fig. 4. one can see that the calibration curve is linear for acetic acid concentrations between 3×10^{-5} and 10^{-4} M ($R = -0.998$). At smaller concentrations, the Q values are larger than theoretically predicted ones because of tailing of the concentration profile (in the direction of the flow) in the flow channel. In this case the titration curve is not symmetrical. The electrode response which is slow due to the small acid concentrations and unbuffered media can be responsible for this.

The dependence of the Q value on the sample flow rate is also an important parameter of the triangle programmed titrations. In order to study this a 5×10^{-4} M acetic acid solution was titrated at different flow rates. The Q values obtained at this experiment are plotted against the sample flow rate as it is shown in Fig. 5. From Fig. 5. it can be seen that the relationship between the Q values and the flow rate is linear in agreement with the theory.

3.2. Determination of acetylcholine by coulometric flow titration technique

3.2.1. The effect of the flow rate on the analytical signal

To study the dependence of acetylcholine response on the flow rate in the flow through reactor–titrator system, titration were performed in case of acetylcholine samples streaming at different flow rates. The Q value-flow rate dependence obtained is shown in Fig. 6. As it can be seen the curve has a minimum. The theory of the coulometric flow titration predicts a linear function with negative slope. The minimum can be explained by flow rate dependence of the conversion degree in the enzyme reactor. The increase of the flow rate can decrease the conversion degree of the ACH in the enzyme reactor which results in a decrease in the concentration of the produced acetic acid thus the Q value increases. The flow

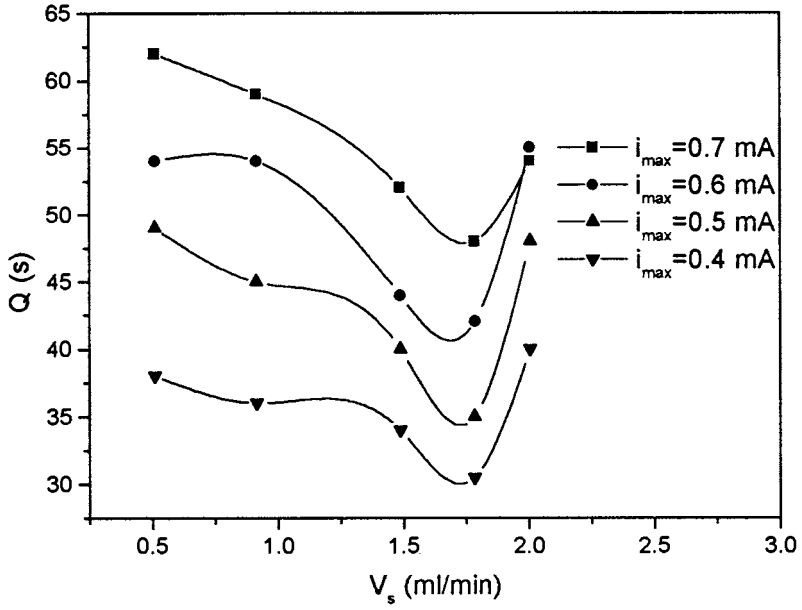

Fig. 6. Dependence of the analytical signal Q on the sample (ACH) flow rate at different i_{max} values, when the enzyme reactor (ACHE) is included in the system; $c_s = 10^{-3}$ M, $2\tau = 80$ s.

rate corresponding to the minimum of the Q value was mostly chosen for further work.

3.2.2. Estimation of the conversion of the enzyme reactor

The well established theory of the coulometric flow titration can offer a possibility to determine the efficiency of the enzyme reactor. An acetylcholine solution of given concentration was titrated using different i_{max} values. By plotting the Q values versus the reciprocal value of the corresponding i_{max}, a linear relationship can be obtained. From the slope of the curve $(2a\mu F\tau V_s c_s/b)$, the concentration of the acetic acid can be calculated (Eq. (1).). All the parameters included in the mathematical expression of the slope with the exception of the acetic acid concentration produced in the enzymatic titration are known. By comparing this value with the original concentration of the acetylcholine the conversion can be estimated. In the calculation the experimentally determined value of $2\tau =$ 137.75 s was used.

$$\text{Conversion} = \frac{c_{\text{acetic acid}}}{c_{\text{acetylcholine}}} \times 100 \quad (3)$$

The linear relationship of the analytical signal, Q on the reciprocal value of i_{max} is shown in Fig. 7.

The conversion value achieved with the enzyme reactor used, calculated by the method described above, was approximately 12%. The value of the conversion was useful for establishing the i_{max} value, necessary for the experiments.

3.2.3. Determination of acetylcholine

The reactor column was connected to the flow channel and the flow rate, as well as the other titration parameters were adjusted. The titration of acetylcholine after enzymatic hydrolysis was carried out as it was described at the acetic acid measurement. The calibration obtained for the acetylcholine in these measurements was linear but only for a concentration range of at most one order of magnitude. The triangle current programmed coulometric flow titration has the advantage that adjusting properly the i_{max} value, smaller concentrations and concentration ranges can be determined with good precision. The optimal working conditions for different concentration ranges were easily established varying the

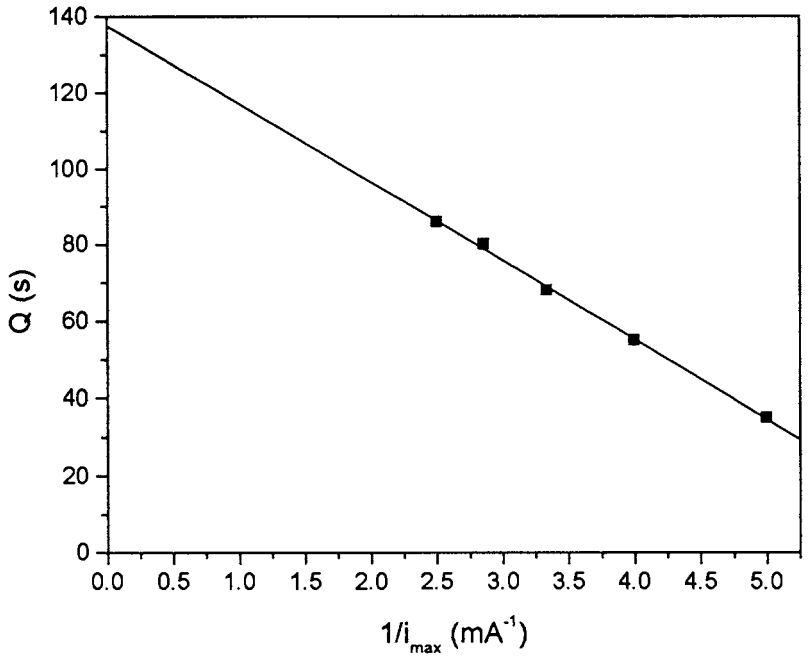

Fig. 7. Dependence of the analytical signal on the reciprocal value of the current maximum applied during the triangle programmed reagent generation in the case of acetylcholine sample; $c_s = 9 \times 10^{-5}$ M, $2\tau = 120$ s, $V_s = 0.94$ ml min^{-1}.

parameters of the system. One calibration curve in the range of 10^{-4}–10^{-3} M acetylcholine concentration is presented in Fig. 8. The calibration curve is linear ($R = -0.999$) in the concentration range of 3×10^{4}–10^{-3} M acetylcholine. After a careful adjustment of i_{max}, calibration curves could be taken for acetylcholine concentrations between 10^{-4}–5×10^{-4} M. Further experiments have shown that the lowest acetylcholine concentration that can be measured by this technique is 8×10^{-5} M (with an enzyme reactor having a conversion of 12%). Lower than this concentration the Q values, were not only higher than the theoretical ones but also a second inflection point could be observed, which made the reading of the Q values uncertain.

4. Conclusion

As it was mentioned in the introduction the principal advantage of the triangle programmed coulometric flow titration relies in the precision of the method. Although the detection limit (8×10^{-5} M) is much lower than in the case of classical titrations, it is higher than that of amperometric determinations (the other electrochemical technique widely used for the determination of acetylcholine). The linear range is at most one order of magnitude, which is lower than for amperometric detection, but it can be easily adjusted for different sample concentration ranges by changing the experimental parameters. Difficulties may be encountered in case of real samples where the eventual presence of inhibitors or activators of the acetylcholinesterase enzyme can interfere. Thus a practical application of this method can be the indirect determination of organophosphoric pesticides. In this case the high precision offered by this method is very important. In our laboratories research for pesticide determinations based on pH measurement are in progress.

Acknowledgements

The support of the Hungarian Science Foundation (OTKA, T 022507) is gratefully acknowledged.

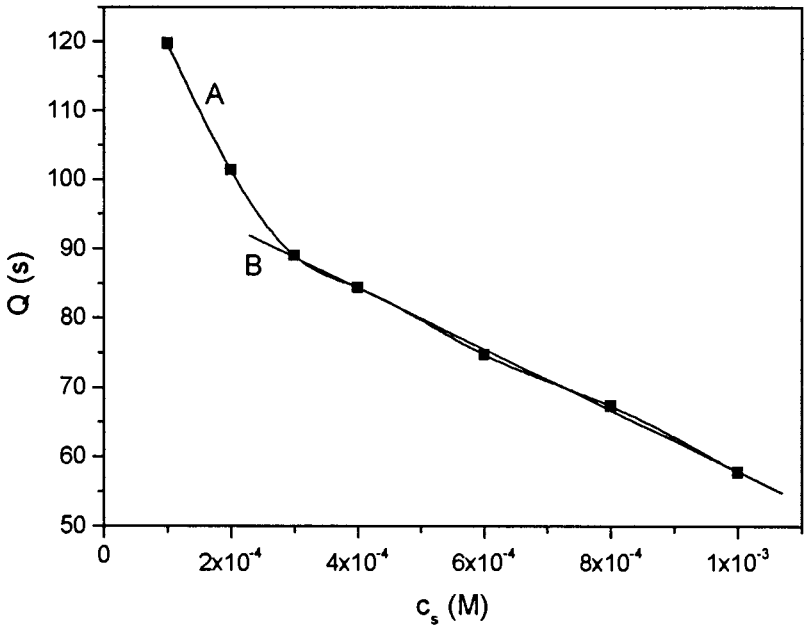

Fig. 8. Calibration curve for acetylcholine in the concentration range of 10^{-4}–10^{-3} M (A), the calibration curve is linear in the concentration range of 3×10^{-4}–10^{-3} M ($R = 0.999$) (B); $2\tau = 120$ s, $i_{max} = 0.47$ mA, $V_s = 1.87$ ml min^{-1}.

References

[1] W. Stavinoha, S.T. Weintraub, Anal. Chem. 46 (1974) 757.
[2] H. Stadler, T. Nesselhut, Neurochem. Int. 9 (1986) 127.
[3] O. Niwa, T. Horiuchi, M. Morita, T. Huang, P.T. Kissinger, Anal. Chim. Acta 318 (1996) 167.
[4] M. Gotoh, E. Tamiya, M. Momoi, Y. Kagawa, I. Karube, Anal. Lett. 20 (1987) 857.
[5] K. Honda, K. Miyaguchi, H. Nishino, H. Tanaka, T. Yao, K. Imai, Anal. Biochem. 153 (1986) 50.
[6] J.R. Wetherell, M.C. French, Biochem. Soc. Trans. 14 (1986) 1148.
[7] J.-L. Marty, K. Sode, I. Karube, Anal. Chim. Acta 228 (1989) 49.
[8] R.M. Morelis, P.R. Coulet, Anal. Chim. Acta 231 (1990) 27.
[9] U. Loeffler, U. Wollenberger, F. Scheller, W. Goepel, Fresenius Z. Anal. Chem. 335 (1989) 295.
[10] M. Mascini, D. Moscone, Anal. Chim. Acta 179 (1986) 439.
[11] M. Masoom, Anal. Chim. Acta 214 (1988) 173.
[12] A. Guerrieri, G.E. De Benedetto, F. Palmisano, P.G. Zambonin, Analyst 120 (1995) 2731.
[13] A. Riklin, I. Willner, Anal. Chem. 67 (1995) 4118.
[14] E.N. Navera, K. Sode, E. Tamiya, I. Karube, Biosens. Bioelectron. 6 (1991) 675.
[15] R. Rouillon, N. Mionetto, J.-L Marty, Anal. Chim. Acta 268 (1992) 347.
[16] P. Durand, A. David, D. Thomas, Biochim. Biophys. Acta 527 (1978) 277.
[17] R. Tor, A. Freeman, Anal. Chem. 58 (1986) 1042.
[18] C. Tran-Minh, P.C. Pandey, S. Kumaran, Biosens. Bioelectron. 5 (1990) 461.
[19] K. Stein, G. Schwedt, Anal. Chim. Acta 272 (1993) 73.
[20] C. Eppelsheim, N. Hampp, Analyst 119 (1994) 2167.
[21] H. Nilsson, A.-C. Akerlund, C. Mosbach, Biochem. Biophys. Acta 304 (1973) 217.
[22] G. Nagy, Zs. Fehér, K. Tóth, E. Pungor, Anal. Chim. Acta 91 (1977) 87.
[23] G. Nagy, Zs. Fehér, K. Tóth, E. Pungor, Anal. Chim. Acta 91 (1977) 97.
[24] G. Nagy, Zs. Fehér, K. Tóth, E. Pungor, Anal. Chim. Acta 100 (1978) 181.
[25] G. Nagy, Zs. Fehér, K. Tóth, E. Pungor, Hung. Sci. Instrum. 46 (1979) 5.
[26] G. Nagy, Zs. Fehér, K. Tóth, J. Havas, É. Kiss, E. Pungor, Hung. Sci. Instrum. 59 (1985) 11.
[27] U. Spohn, G. Nagy, E. Pungor, Anal. Sci. 2 (1986) 423.
[28] Zs. Fehér, G. Nagy, K. Tóth, E. Pungor, A. Tóth, Analyst (London) 104 (1979) 560.

[29] G. Nagy, Zs. Fehér, K. Tóth, E. Pungor, in: E. Pungor (Ed.), Modern Trends in Analytical Chemistry, Akadémiai Kiadó, Budapest, 1984, pp. 285–296.
[30] Zs. Fehér, I. Kolbe, E. Pungor, Analyst 113 (1988) 881.
[31] Zs. Fehér, I. Kolbe, E. Pungor, Fresenius Z. Anal. Chem. 332 (1988) 345.
[32] U. Spohn, G. Nagy, E. Pungor, Anal. Sci. 2 (1986) 431.
[33] M. Becker, B. Fuhrmann, U. Spohn, Anal. Chim. Acta 324 (1996) 115.
[34] M. Masoom, A. Townshend, Anal. Chim. Acta 166 (1984) 111.
[35] A. Savitzky, M.J.E. Golay, Anal. Chem. 36 (1964) 1627.

ELSEVIER

Talanta 47 (1998) 1033–1042

Talanta

Determination of metals in used lubricating oils by AAS using emulsified samples

Irene M. Goncalves, Miguel Murillo *, Angela M. González

Centro de Química Analítica, Escuela de Química, Facultad de Ciencias, Universidad Central de Venezuela, Apartado Postal 47102, Caracas 1041-A, Venezuela

Received 4 March 1998; received in revised form 22 April 1998; accepted 22 April 1998

Abstract

An efficient method was developed for the determination of metals in used lubricating oils, by atomic absorption spectrometry. Oil samples were treated with an acid mixture and then emulsified in water (10% w/w) using ethoxy nonylphenol (6% w/w) as surfactant. Emulsion characteristics (oil, surfactant content and acid mixture) were optimized to obtain the best AAS signal. Good agreement was found between calibration curves of aqueous and emulsified standard solutions when a peristaltic pump was used to introduce the solutions into the flame. The emulsion methodology was comparable, within 95% of confidence, to traditional ashing methodologies when a standard reference oil and a used lubricating oil were analyzed. Precision between 0.4 and 5% RSD was obtained when real sample was analyzed using emulsions. © 1998 Elsevier Science B.V. All rights reserved.

Keywords: Atomic absorption spectrometry; Surfactant; Emulsion methodology

1. Introduction

The determination of metals in lubricating oils has always been a challenge in analytical chemistry. Metals, such as Ba, Ca and Mg are added to the new oil, as organometallic compounds, to improve the oil performance under severe conditions. In addition, metals, such as Fe, Al and Ni, are present in used oils due to the wear of the lubricated area. Therefore, determination of the metal content in used oils is important to identify and repair any possible defective functioning area of the oil-lubricated equipment and to plan maintenance. Hence, an easy and accurate procedure is needed for quality and maintenance control [1,2].

Modern instrumental techniques such as inductively coupled plasma-optical emission spectrometry (ICP-OES) [3–7] and atomic absorption spectrometry (AAS) [8–16] have been widely used for this analysis.

AAS has been one of the most commonly used techniques in the analysis of lubricating oils, requiring aqueous solutions. However, the oil high organic content and viscosity make the determina-

* Corresponding author. Fax: +58 2 6627121; e-mail: mmurillo@strix.ciens.ucv.ve

0039-9140/98/$ - see front matter © 1998 Elsevier Science B.V. All rights reserved.
PII S0039-9140(98)00186-6

tions inaccurate and difficult. The need to have the sample in aqueous solution has been solved by ashing the oil and analyzing the residue dissolved in inorganic acids [17–19]. These procedures solve the problems associated with the sample matrix and they need inorganic aqueous solutions as standards. However, these treatments require considerable sample pre-treatment (usually several hours) increasing the risks of contamination and sample loss.

Another approach that has been proposed to simplify the analysis is the dilution of the sample in an appropriate organic solvent [8–11,13–15]. The methodology is fast, simple and accurate, however the high organic content produces high noise levels and fluctuations of the instrumental signal reducing the sensitivity of the determination. In addition, it requires the use of organometallic standards increasing analysis costs.

An alternative methodology to avoid those problems is to use emulsions. In an emulsion the oil is incorporated in an aqueous phase, and can be directly introduced into the burner. Its application does not require destroying the organic matter or the use of large amounts of organic solvent. When the oil is evenly dispersed in the water phase, the sample similarly behaves to an aqueous solution, so it is possible to use inorganic water soluble standards to prepare calibration curves, minimizing the time and cost of the analysis [20–25]. Stable emulsions are the only requirement needed to use this methodology, and therefore the use of surfactants to prepare the emulsion is important [26–29].

This work proposes a fast, accurate and precise methodology for the analysis of used lubricating oils by AAS with the use of emulsions. The optimization of emulsion conditions and comparison of the methodology with traditional methodologies such as ashing and direct dilution with organic solvent are presented. Metals such as Mg, that is used as an additive, and Al, Cr, Cu, Ni, Pb and Si, that are associated with the wear out of the lubricated machinery, were determined in a used lubricating oil, comparing the results with those from traditional methods too.

2. Experimental

2.1. Instrumentation

A Varian Techtron model AA6 atomic absorption spectrophotometer was used with hollow cathode lamps of each element. The optimal instrumental settings to produce the highest sensitivity for each element were used.

The aqueous and emulsion solutions were introduced into the burner by a peristaltic pump (Pharmacie). Homogenization of the emulsions was carried out using a Cole Palmer Model 8850 ultrasonic device (IL, USA).

2.2. Reagents

All chemicals used were analytical reagent grade. Deionized water (Milli-Q, Millipore, USA) was used to prepare samples and standards.

Standard aqueous solutions were prepared from the appropriate 1000 mg l^{-1} stock solution of each metal, (BDH and Aldrich), and diluted to obtain working solutions.

Multielemental organometallic standards in oil solution (Jarrel Ash) (Al, Cr, Cu, Pb, Mg, Ni, Si) of 50, 100 and 250 mg l^{-1}, were used (Jarrel-AS Division, Fisher Scientific) to optimize and calibrate the methods, either for direct dilution or for emulsions. Working solutions were prepared by direct dilution with water, organic solvent or emulsion mixture.

Ethoxy nonylphenol (average condensation of 10 mol) was used as surfactant (Etoxil Venezuela).

A new base oil free of metals, (Corpoven) was used to determine the optimal proportion of oil and to prepare emulsified standards and blanks.

2.3. Cleaning of material

Glass and polyethylene bottles were used to prepare emulsions. Each one was treated overnight with HNO_3 (10%) and then rinsed with abundant deionized water.

2.4. Samples

Used lubricating oil (Supradiesel, S.F., Corpoven, Venezuela) was obtained at a local service station.

2.5. Emulsion preparation

2.5.1. With acid treatment

The used lubricating oil was shaken before any treatment to homogenize it and heated (100°C) until constant weight was obtained, in order to eliminate water residue present. Emulsions were prepared in polyethylene flasks by weighing 5 g of the used oil. Each sample was mixed with 10.0 g of an acid mixture (HNO_3/HCl 1:3; or HF/HCl/HNO_3 1:8:1) and heated, at 65°C for 5 min. Each sample was then mixed with 3 g of ethoxy nonylphenol and stirred by ultrasonic agitation for 5 min. Deionized water was then added up to the final appropriate dilution. This procedure took $\sim$15 min.

Standard solutions of organometallics in oils, aqueous standards in metal free oil and blank solutions were treated in a similar way.

2.5.2. Without acid treatment

The procedure was the same, excluding the adding of the acids and heating.

2.6. Reference methods

2.6.1. Dry ashing

Three ashing methods were used to destroy the organic matter in the samples; all of them were carried in open vessels.

The sample (5 g) was heated until dry and no more smoke appeared. The residue was then heated in a muffle at 250°C (1 h) and at 600°C (4 h) to eliminate any visible carbon residue. The final residue was then dissolved in 1.5 ml concentrated HCl and diluted with deionized water [8].

2.6.2. Wet ashing

The oil ($\sim$5 g) was heated in 5.0 ml concentrated H_2SO_4 solution, to dryness. The residue was then heated in the muffle and dissolved in HCl, following the same procedure as for dry ashing [19].

2.6.3. Modified wet ashing

The oil (5 g) was mixed with 1g of silica gel and 5.0 ml of H_2SO_4. The mixture was reduced to carbon by heating. The residue was heated in a muffle with the same temperature program described for dry ashing. The residue was dissolved in concentrated HCl (1–2 ml). A 10% $CaCl_2$ solution (1 ml) was added to the solution to

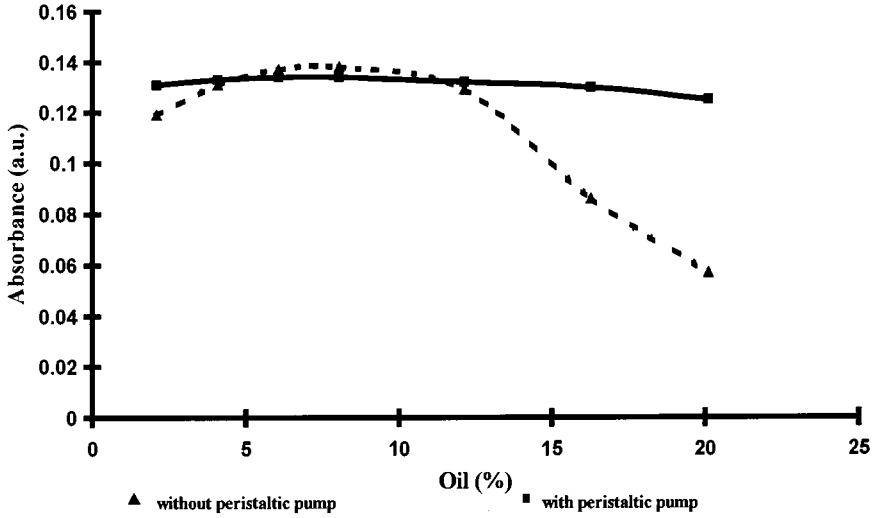

Fig. 1. Absorption signal of Fe in emulsions with different oil content.

Table 1
Line equation of calibration curves obtained with different standard solutions by AAS and using or not peristaltic pump to introduce sample

	Without PP			With PP		
	Aqueous	Aqueous emulsion	Oil emulsion	Aqueous	Aqueous emulsion	Oil emulsion
	Al			Al		
Slope	0.005	0.0033	0.003	0.0022	0.0022	0.0021
Intercept	0.0002	−0.001	−0.001	−0.0003	−0.0006	−0.0001
r^2	0.9997	0.9983	0.9901	0.989	0.9961	0.9997
	Mg			Mg		
Slope	0.0653	0.041	0.0409	0.0361	0.0349	0.0343
Intercept	0.0002	0.0016	−0.001	0.0016	−0.0002	0.0031
r^2	0.9997	0.9934	0.9997	0.996	0.9991	0.9968
	Ni			Ni		
Slope	0.0088	0.0039	0.0039	0.0029	0.0027	0.0028
Intercept	−0.0087	−0.0021	−0.019	0.0005	0.0011	0.0002
r^2	0.991	0.9967	0.9967	0.9992	0.997	0.9993
	Cr			Cr		
Slope	0.0207	0.0116	0.0098	0.0083	0.0084	0.0081
Intercept	9.00E-05	0.0007	0.0008	−0.0002	0.0015	0.0016
r^2	0.9982	0.9725	0.9916	0.9989	0.9983	0.9991
	Cu			Cu		
Slope	0.0424	0.0309	0.0295	0.0212	0.0202	0.0202
Intercept	0.0306	−0.0016	0.0072	−0.0025	−0.0027	0.0023
r^2	0.9781	0.999	0.9987	0.9997	0.9993	0.9996
	Pb			Pb		
Slope	0.0073	0.0035	0.0032	0.0029	0.0028	0.0029
Intercept	−0.0036	−0.0036	0.0002	−0.0004	0.0002	0.0006
r^2	0.9966	0.9966	0.9992	0.9987	0.9986	0.9991
	Si			Si		
Slope	0.0013	0.0007	nd	nd	nd	nd
Intercept	−0.0007	0.0008	nd	nd	nd	nd
r^2	0.9996	0.9716	nd	nd	nd	nd
	Fe			Fe		
Slope	0.0071	0.0043	0.0048	0.0031	0.0031	0.003
Intercept	−0.0011	0.0012	0.0001	−0.001	−0.0016	−0.0002
r^2	0.9997	0.999	0.9996	0.9954	0.9987	0.9985

Without PP: without peristaltic pump; With PP: with peristaltic pump; aqueous: inorganic aqueous standards; aqueous emulsion: inorganic emulsionated standards; oil emulsion: oil standard emulsionated; nd: no determined.

reduce interference by silica on the absorption response, especially for Fe and Mg [19]. The solution was then filtered and diluted with deionized water.

2.6.4. Direct dilution with organic solvent

Xylene was used as solvent to dilute the oil samples and the multielemental oil standard used in the calibration.

Used lubricating oil, new base oil free of metals, and the multielemental oil standard were treated with the same procedures to compare results and to identify any possible interference due to the procedure.

3. Results and discussion

3.1. Study of emulsification conditions

Since the amount of oil, surfactant, water and acid mixture may affect the conditions of the emulsions; those factors were studied before applying the methodology to the real samples.

To choose a surfactant two factors were considered. First, Becher [26] reported that a non-ionic emulsifying agent with a hydrophile lipophile balance (HBL) between 8 and 18 is a good option to obtain stable oil in water emulsions. Ethoxy nonylphenol is a non-ionic surfactant, water soluble with HLB of 14, which is not affected by the presence of Ca, Mg or Fe salts [27]. Second, ethoxy nonylphenol has been successfully used by Murillo et al. to prepare emulsions of lubricating oils [4,6] and crude oils [7] in the determination of metals by ICP-AES.

It is well known that stability of the emulsions depends on the amount of surfactant present. In this work, different emulsions were prepared using 10% metals free base oil, water and different amounts of surfactant (1.0–10%). The optimum amount of surfactant in the emulsion was the highest one that produced a visually stable and homogeneous emulsion, in our case 6% w/w. This

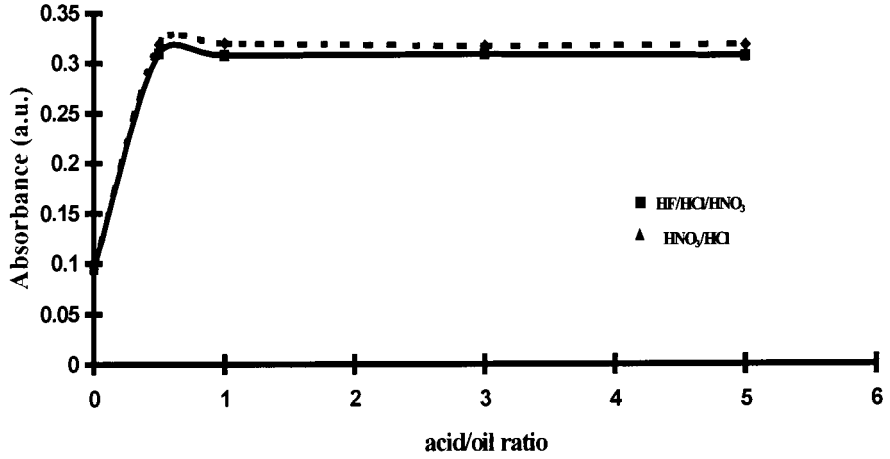

Fig. 2. Effect of the acid content on the Cu absorption signal, for emulsified solutions with different acid content.

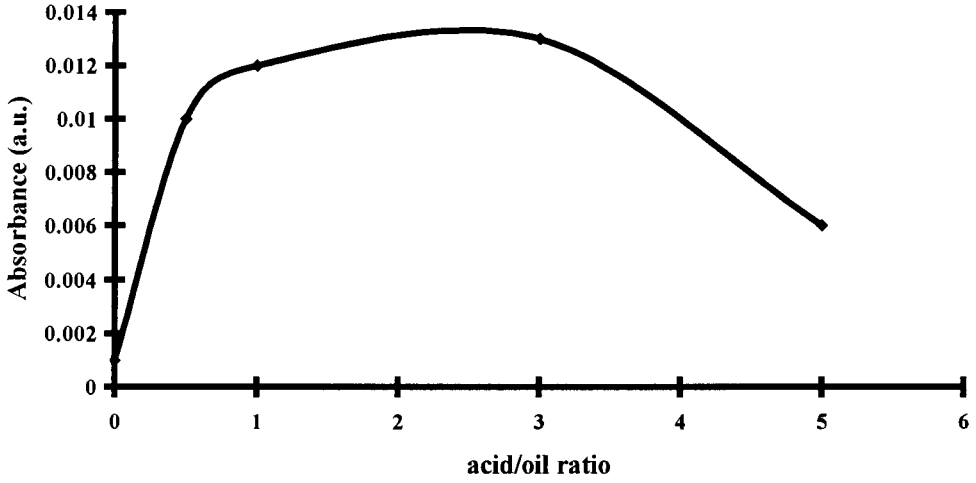

Fig. 3. Effect of the acid content on the Si absorption signal for emulsified solutions with different HF/HNO_3 content.

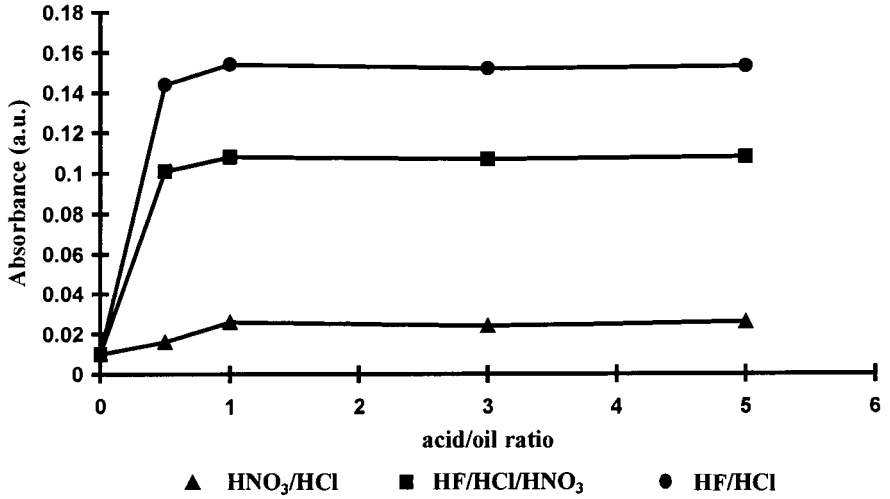

Fig. 4. Effect of the acid content on the Cr absorption signal for emulsified solutions with different acid mixtures.

Table 2
Concentrations of metals in standard lubricating oil (100 mg l^{-1} of each element) by different methodologies

Metal	Emulsions mg $l^{-1} \pm s$	Dry ash mg $l^{-1} \pm s$	Modified dry ash mg $l^{-1} \pm s$
Pb	103 ± 2	103 ± 2	106 ± 4
Cr	101 ± 2	101 ± 2	111 ± 1
Al	102 ± 3	98 ± 2	95 ± 2
Cu	106 ± 2	105 ± 3	103 ± 2
Ni	97 ± 1	95 ± 3	96 ± 1
Fe	107 ± 1	103 ± 2	96.3 ± 0.5
Si	95 ± 3	ND	ND
Mg	102 ± 2	94 ± 3	102.1 ± 0.1

Number of replicates = 3.
ND = no determined.

result was in agreement with results from previous studies done in this laboratory [4,6].

Optimization of the best amount of oil in the sample was the next step. Standard solutions with 5 mg l^{-1} of each metal (1 mg l^{-1} for Mg), 6% w/w of surfactant and water were prepared using different amounts of metals free base oil. Amounts of oil in the samples ranged from 2 to 25% w/w. Each solution was analyzed by AAS. The solution that produced the highest AAS signal was chosen as optimum. Results for Fe are given in Fig. 1; similar results were obtained for Al, Mg, Cr, Cu, Fe, Pb and Si. The solutions that produced higher AAS signal had oil content between 6 and 12% w/w of oil, and that behavior was independent of the element determined.

Solutions with $> 12\%$ w/w of oil gave significantly lower signals, probably the increase of viscosity in the emulsions, could be affecting efficiency of the sample introduction into the flame. To examine that theory, the same solutions were fed into the flame using a peristaltic pump, expecting to reduce sample introduction inefficacy [6]. Results in Fig. 1 for Fe show that the use of the peristaltic pump mitigated the depression of the signal of solutions with $> 12\%$ of oil. In addition, when no pump was used, emulsions with low amounts of oil ($< 6\%$) produce low signals; this also was improved with the use of the pump. Similar results were observed for the other elements studied.

Table 3
Metal content of the used oil by different methodologies

Element	Dry ash method (mg $l^{-1} \pm s$)	Wet ash method (mg $l^{-1} \pm s$)	Emulsion with HF/HCl/HNO_3 (mg $l^{-1} \pm s$)	Emulsion with HCl/HNO_3 (mg $l^{-1} \pm s$)	Emulsion without acid treatment (mg $l^{-1} \pm s$)	Oil dilution in xylene (mg $l^{-1} \pm s$)
Pb	1315 ± 34	1402 ± 41	1384 ± 62	1357 ± 17	194 ± 1	ND
Cr	17.7 ± 0.2	21.3 ± 0.5	12.1 ± 0.3	19.7 ± 0.22[a]	<5	ND
Al	76 ± 3	72.6 ± 0.6	80.6 ± 0.5	70.2 ± 0.7	10.6 ± 0.3	ND
Cu	23.1 ± 0.1	25 ± 1	28.6 ± 0.4	28.4 ± 0.6	8.6 ± 0.3	ND
Ni	115 ± 4	115.0 ± 0.8	122 ± 3	130 ± 4	34 ± 1	ND
Fe	383 ± 15	389 ± 1	385 ± 4	382 ± 13	59 ± 2	126.4 ± 0.3 [#]
Si	ND	92 ± 3[b]	91 ± 2	ND	ND	ND
Mg[c]	1127 ± 7	1159 ± 25	1098 ± 5	1081 ± 13	826 ± 16	785 ± 2 [#]

Number of replicates: 3.
ND: no determined.
[#] Number of replicates: 5.
[a] Using HF/HCl acid mixture.
[b] Using HF/HNO_3 instead of H_2SO_4.
[c] Mg was also determined in a new lubricating oil by (a) wet ashing method: 796 ± 11 mg l^{-1} (b) Emulsions without acid treatment: 809 ± 16 mg l^{-1}.

3.2. Comparison of the emulsified solutions with aqueous solutions

Calibration curves made with standard inorganic emulsions, standard oil emulsions and aqueous solutions were prepared to evaluate the possibility of using aqueous solutions to calibrate the AAS when emulsions are being analyzed. Table 1 presents slope, intercept and regression coefficients for each calibration curve. Clear differences in sensitivity were found between aqueous and emulsified standards calibration curves. When aqueous solutions were used, appreciable higher sensitivity was obtained, whereas emulsified ones had similar slopes among them. These results were also element independent, indicating possible inefficient sample introduction. Those differences were not surprising since there are important differences in the viscosity between the aqueous and emulsified solutions. Therefore, under these conditions aqueous solutions could not be recommended for calibration.

Table 4
Variance analysis of results obtained with different methodologies for the analysis of the used oil

Metal	Tabulated F (95% confidence)	Calculated F
Pb	$F_{3,8} = 5.32$	$F_{a,b,c,d} = 2.70$
Cr	$F_{1,4} = 7.71$	$F_{b,f} = 3.72$
Al	$F_{2,6} = 5.14$	$F_{a,b,d} = 3.32$
Cu	$F_{3,8} = 5.32$	$F_{a,b,c,d} = 4.07$
Ni	$F_{2,6} = 5.14$	$F_{a,b,c} = 3.41$
Fe	$F_{3,8} = 5.32$	$F_{a,b,c,d} = 1.04$
Si	$F_{1,4} = 7.71$	$F_{c,e} = 0.01$
Mg	$F_{2,6} = 5.14$	$F_{a,b,c} = 4.91$ F_b (blank), $_g$ (blank,sample) = 4.07

a = Dry ash method.
b = Wet ash method.
c = Emulsion with $HF/HCl/HNO_3$.
d = Emulsion with HCl/HNO_3
e = Emulsion with HF/HNO_3.
f = Emulsion with HF/HCl.
g = Emulsions without acid treatment.
Since all of the F calculated < F tabulated: No significative differences were found among the content of metals obtained by the different methodologies.

When a peristaltic pump was used to control the amount of sample that reached the flame, there were no differences in sensitivities among calibration curves using aqueous and emulsified standards (Table 1, with PP), behavior that was also element independent. The three calibration curves were similar within a 95% of confidence, therefore when a peristaltic pump is used; calibration curves with aqueous standards could be recommended for our working range of concentrations, when emulsified oil samples are being analyzed.

3.3. Effect of the amount and type of acid mixture used in the treatment of the used lubricating oil

It is widely known that used lubricating oil has a lot of metal particles due to regular wear of the machinery lubricated, therefore a previous acid treatment is needed to dissolve those metals. For the present work, a standard reference oil was emulsified with the optimized conditions and added an acid mixture. Two commonly used acid mixtures were tried HNO_3/HCl (1:3) and $HF/HCl/HNO_3$ (1:8:1) [19]. Different acid/oil ratios were used. Results for Cu are presented in Fig. 2. Two main observations were possible:

- The signal increases with the amount of acid mixture present up to a 1:1 w/w acid: oil ratio. Between 1 and 5 acid/sample ratio, the signal remains almost constant, except for Si in which case the signal decreased when a w: w ratio of acid to sample oil of 3 was used, (Fig. 3). From that consideration, a ratio of acid to oil of 2 was chosen as optimum.
- There were no significant differences among the responses of the metals using either of the acid mixtures, except for Cr. Low absorption signals for Cr were observed when HCl/HNO_3 (3:1) or $HF/HCl/HNO_3$ (1:8:1) mixtures were used, (Fig. 4). However, when a mixture HF/HCl (1:9) larger signals were observed, possibly because of the absence of HNO_3 in the solution [16], therefore HF/HCl (1:9) was selected as best acid mixture for determination of Cr.

3.4. Accuracy of the methodology

A standard lubricating oil (Jarrel Ash 100 mg l^{-1} of each element) was analyzed using emulsions, dry ashing and modified dry ashing methods, and aqueous inorganic standards to prepare calibration curves. A peristaltic pump was used to introduce the samples. Results range from 94 to 110 mg l^{-1} with standard deviations between 1 and 4. (Table 2). No significant differences were detected among reported value for the standard (100 mg l^{-1}) and values obtained using those methodologies, within a 95% confidence level. The main difference in applying those methodologies was the time needed for each one.

To evaluate the applicability of the proposed methodology, several replicates of a used lubricating oil was analyzed. Each replicate was analyzed by traditional methods (digestion), and by emulsions, determining Pb, Cr, Al, Cu, Ni, Fe, Si and Mg. Results are presented in Table 3.

The importance of the acid treatment in the emulsions of the used oil was evident. The sample was analyzed with the acid treatment and without it. Results show that higher amounts of metals were obtained when acid treatment and ashing techniques were used than when emulsions of the samples did not have acids present. Lower amounts of metals Fe and Mg were also obtained, when direct dilution of the sample with xylene was tried (Table 3). This may be due to the presence of metal particles in suspension in the oil, which reduce the efficiency of the nebulization–atomization process in the flame.

Comparable results from traditional methods and emulsions were obtained with 95% confidence (Table 4), showing that the use of emulsions is as accurate and precise as traditional established methods, but also easier, faster and cheaper.

4. Conclusions

The sensitivity of the determination of metals by AAS in lubricating oils proved to be very dependent on the sample matrix. Important differences in sensitivity between calibration with aqueous standards and with emulsified standards were found. However, the use of a peristaltic pump solved those differences.

The use of acids in the preparation of emulsified used oil proved to be a requirement. This fact was not surprising because it is well known that used lubricating oils have high levels of particles that come from the wear of the metal surfaces that are lubricated. Results were shown to be independent to the mixture of acids used, except for Cr, where HNO_3 has a depressing effect on the signal. The amount of acid mixture in the emulsions did not affect the homogeneity of the emulsion up to when a ratio of 5:1 of acid to oil was used.

Comparison of the proposed methodology using emulsions, with traditional ashing methods showed that they are significantly similar, within a 95% confidence. The main differences among them are that emulsions methodology does not require a long time sample pretreatment or large amounts of organic solvent, is easy to follow and shows a reproducibility that ranges between 0.5 and 4.5% RSD.

Acknowledgements

This study was supported by Centro de Química Analítica, CQA-UCV, BID-CONICIT project QF-33 and Consejo de Desarrollo Científico y Humanístico de la Universidad Central de Venezuela, CDCH N: 03-12-3650.95 and 03-12-3527.95. We thank Peter C. Uden for his assistance in the preparation of this paper. Thanks also to the two referees for their constructive comments on the manuscript.

References

[1] A. King, D. Hilligoss, G. Wallace, At. Spectrosc. 5 (1984) 189.
[2] J.D. Algeo, Spectrochim. Acta 40B (1985) 1447.
[3] A. Salvador, M. de la Guardia, V. Berenguer, Talanta 30 (1983) 986.
[4] E. Pinto, Undergraduate thesis, Universidad Central de Venezuela, Caracas, 1992.
[5] M. Hassan, At. Spectrosc. 6 (1993) 170.

[6] M. Murillo, A. Gonzalez, A. Ramirez, N. Guillen, At. Spectrosc. 3 (1994) 90.
[7] M. Murillo, J. Chirinos, J. Anal. At. Spectrom. 9 (1994) 237.
[8] J. Burrows, J. Heerdt, J. Willis, Anal. Chem. 37 (1965) 579.
[9] S. Holding, J. Noar, Analyst 95 (1970) 1041.
[10] J. Guttenberger, M. Harold, Z. Anal. Chim. 262 (1972) 102.
[11] M. Kabanova, D. Loseva, Z. Turkinky, Prikl. Spectrosk. 18 (1973) 378.
[12] C. Saba, K. Eisentraut, Anal. Chem. 49 (1977) 454.
[13] C. Saba, K. Eisentraut, Anal. Chem. 51 (1979) 1927.
[14] Z. Wittmann, Analyst 104 (1979) 156.
[15] P. Hon, O. Law, S. Mok, Analyst 105 (1980) 919.
[16] J. Brown, C. Saba, W. Rhine, K. Eisentraut, Anal. Chem. 52 (1980) 2365.
[17] O. Milner, J. Glass, P. Kirchner, Anal. Chem. 24 (1952) 1728.
[18] R. Muter, L. Nice, Trace elements in fuels, in: Suresh P. Babú (Ed.), Advances in Chemistry Series 141, American Chemical Society, Washington, 1975, Chapter 5, 57.
[19] M. Barbooti, N. Zaki, S. Baha-Uddin, E. Hassan, Analyst 115 (1990) 1059.
[20] L. Westwood, Dev. Appl. Spectrosc. 9 (1971) 235.
[21] J. Hernánadez, L. Polo-Diez, A. Bernal, Anal. Chim. Acta 108 (1979) 39.
[22] M. de la Guardia, A. Carreño, V. Berenguer, Analusis 8 (1980) 448.
[23] M. de la Guardia, A. Salvador, V. Berenguer, Analusis 9 (1981) 74.
[24] A. Salvador, M. de la Guardia, V. Berenguer, Talanta 30 (1985) 986.
[25] J. Beferull, M. de la Guardia, A. Carreño, Anal. Chim. Acta 174 (1985) 353.
[26] P. Becher, Emulsiones: Teoría y Práctica, 2nd edn., Editorial Blume, Barcelona, 1972.
[27] A. Martínez, Introducción a la Química de Superficies y Coloides, Editorial Alhambra, Madrid, 1977.
[28] J. Mora, A. Canals, V. Hernández, J. Anal. At. Spectrom. 6 (1991) 139.
[29] A. Ruiz, A. Canals, V. Hernández, J. Anal. At. Spectrom. 8 (1993) 109.

ELSEVIER

Talanta 47 (1998) 1043–1051

Talanta

Prognostication criterion of potential and practical use of analytical reagents in titrimetria of individual substances

V.K. Chebotarev *, Y.K. Kraev, I.V. Voronkina, E.G. Iljina, L.E. Cherdantseva

Department of Analytical Chemistry, Altai State University, Barnaul, Russia

Received 4 February 1998; received in revised form 28 April 1998; accepted 4 May 1998

Abstract

Various possible criterion in titrimetric methods have been discussed in this paper and more informative, visual and universal criterion—the degree of proceeding of individual reaction at the equivalence point have been chosen. The equation for the degree of proceeding of individual analytical reaction suited for any chemical reactions under real conditions with an allowance made for both component and titrant concentration have been deduced. This criterion allows us to make a prognosis of any parametres of a titrimetric procedure of an individual substance determination and the procedure as a whole, not having carried out the experiment. © 1998 Elsevier Science B.V. All rights reserved.

Keywords: Prognostication; Titrimetry; Proceeding degree

1. Introduction

Methods of titrimetric analysis, especially the method of instrumental electrochemical titrimetry, are the most widely used in analytical practice. These methods have high metrologycal characteristics, simplicity of apparatus and operations, possibility of automation of both titrimetric procedures and the whole analysis. Therefore these methods will not lose their significance during the long period of time, in spite of the development of new approaches and methods in analytical chemistry connected with instrumental determination and physical methods of analysis.

The possibility of theoretical calculation (prognosis) is the top of research work. It is especially important because it allows the reduction of the time for the development of procedures. In the field of prognostication of analytical reagents used in titrimetric methods of analysis in the last 20 years a tremendous progress has been made from the application of prognostication spontaneous elements to elaboration of prognostication theory principles when acid-base, complex formation [1–6] and precipitation reactions are used [7–9]. The prognostication is rendered possible by a plot of theoretical curves of titration and estimation of errors of potentiometric titration with the equilibrium constants using [10–14]. In particular,

* Corresponding author. Tel. +385 2228561; fax: +385 2228561; e-mail:iljina@biogeo.dcn-asu.ru.

0039-9140/98/$ - see front matter © 1998 Elsevier Science B.V. All rights reserved.
PII S0039-9140(98)00184-2

valuable investigations in this field were carried out by Meites et al. [14–17]. Gulyantski uses for the prognostication of a titration possibility and a calculation of errors an index of a titration curve slope [18]. Some articles are devoted to the prognostication and calculation of titration errors with nomogram [7–9,19–21].

Prognostication in different titrimetric methods of analysis allows us to solve some problems and determine many characteristics of procedures for the short period of time not having carried out any experiments, calculate all the necessary parameters of procedures and the optimal conditions of analysis.

The equilibrium constants of reactions and the degrees of proceeding at the equivalence point are the basis of prognostication of titration with the use of any methods of the equivalence point fixing.

All the main aspects of prognostication will be exemplified by the precipitation reactions because they will differ little from the rest of the reaction. Our approach differs slightly from the method of nomogram which is worked out comfortably to acid–base reaction at the same time and then the method of nomogram was used to other reactions [7–9,19–21].

2. Theoretical

Possible criterion for the prognostication of individual substances titration for precipitation reaction may be being:

1. theoretical titration curves,

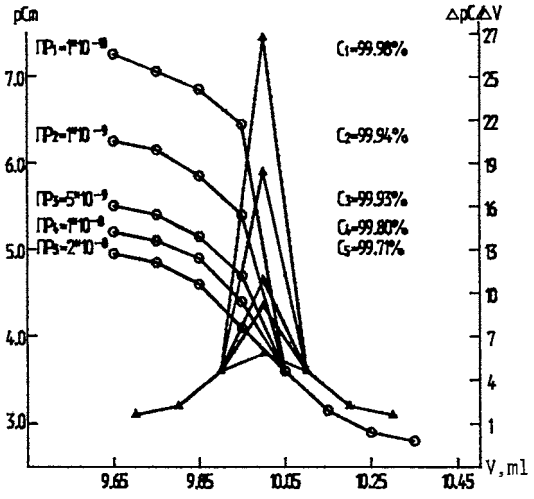

Fig. 1. Theoretical titration curves (integral and differential).

2. solubility products (SP),
3. degree of proceeding at the equivalence point (C%)

The degree of proceeding of an individual reaction shows which part of determined substance have reacted with the titrant at the equivalence point. It is expressed as a percentage and found to be the difference between the initial amount of determined substance (100%) and the amount of substance not reacted at the equivalence point (X%).

The value of the titration jump is dependent on the degree of proceeding. The equation for the calculation of the degrees of proceeding of analytical reactions with the formation of a binary compound is

Table 1
The proceeding degrees of reactions at the e.p. in argentometry titrations of inorganic ions

Ag_nA_m SP[30] C%	Ag_3AsO_3 1.00×10^{-17} 99.90	Ag_3AsO_4 1.00×10^{-22} 99.98	AgBr 5.30×10^{-13} 100.0	AgCN 1.40×1^{-16} 100.0
Ag_2CO_3 1.20×10^{-12} 99.73	AgCl 1.78×10^{-11} 99.97	Ag_2CrO_4 1.10×10^{-12} 99.74	$Ag_3Co(CN)_6$ 3.90×10^{-21} 100.0	$Ag_3Fe(CN)_6$ 1.00×10^{-22} 100.0
$Ag_4Fe(CN)_6$ 8.50×10^{-45} 100.0	Ag_2HVO_4 2.00×10^{-14} 99.93	AgJ 8.30×10^{-17} 100.0	Ag_3PO_4 1.30×10^{-20} 99.98	Ag_2S 6.30×10^{-50} 100.0
AgCNS 1.10×10^{-12} 100.0	Ag_2SO_3 1.50×10^{-14} 99.94	AgSeCN 4.00×10^{-16} 100.0	Ag_2SeO_3 4.80×10^{-16} 99.97	AgN_3 2.90×10^{-9} 99.89
AgOH 1.95×10^{-8} 99.72	$AgJO_3$ 3.00×10^{-8} 99.65	$AgVO_3$ 5.00×10^{-7} 99.58	$Ag_2C_2O_4$ 3.50×10^{-11} 99.18	$AgReO_4$ 7.95×10^{-5} 82.17

$C>99.99=100.0$%.

Table 2
The ionic products of iethyldithiophosphates and the proceeding degrees of reactions at the eq.p.

Ma_n	SP [18,19]	C%	IP_{poten}	C%	IP_{linear}	C%
HgA_2	1.15×10^{-32}	100.0	1.41×10^{-31}	100.0	1.00×10^{-30}	100.0
HgA	—	—	4.82×10^{-16}	100.0	1.19×10^{-15}	100.0
AgA	1.30×10^{-16}	100.0	1.23×10^{-15}	100.0	1.57×10^{-15}	100.0
CuA	1.10×10^{-16}	100.0	6.27×10^{-11}	99.98	1.77×10^{-10}	99.97
TlA_3	—	—	2.23×10^{-33}	100.0	1.08×10^{-33}	100.0
PdA_2	6.91×10^{-18}	100.0	4.27×10^{-20}	100.0	9.37×10^{-21}	100.0
BiA_3	1.04×10^{-22}	100.0	8.54×10^{-21}	100.0	1.41×10^{-21}	100.0
SbA_3	—	—	4.90×10^{-19}	99.93	2.40×10^{-19}	99.94
PbA_2	7.50×10^{-12}	99.57	3.63×10^{-13}	99.82	—	—
CdA_2	1.50×10^{-10}	98.66	1.51×10^{-9}	97.11	—	—

$$C = 100 - \frac{M^*_{\text{e.p.}}(V_{\text{det}} + V_{\text{tit}})*100}{M^*_{\text{det}}V_{\text{tit}}}\% \quad (1)$$

where M_{det} * V_{det} is the initial quantity of the determined substance (100%)$M_{\text{e.p}}$ *$(V_{\text{det}} + V_{\text{tit}})$ is the quantity of the determined substance at the equivalence point (X%)

Eq. (1) is good for calculating the degree of proceeding of any reaction. For the precipitation reaction of any stoichiometry

$$\text{m}A^{\text{n}-} + \text{n}M^{\text{m}+} = M_{\text{n}}A_{\text{m}}$$

$$C = 100 - \frac{m^*S_{\text{M}_\text{n}}\text{A}^*_{\text{m}}(V_{\text{det}} + V_{\text{tit}})*100}{M^*_{\text{det}}M_{\text{tit}}}\% \quad (2)$$

$$C = 100 - \frac{S_{M_n}A^*_m(n^*M_{\text{det}} + m^*M_{\text{tit}})*100}{M^*_{\text{det}}M_{\text{tit}}}\% \quad (3)$$

M_{det}, M_{tit}, $M_{\text{e.p}}$ represent the molarity of the determined component, the titrant and the determined component at the equivalence point, respectively; m, n are the stoichiometric coefficients in the precipitation reaction; ${}^{\text{S}}M_{\text{n}}A_{\text{m}}$ is the solubility and $V_{\text{det}}, V_{\text{tit}}$ represent the volume of the determined component and titrant, respectively.

Eqs. (1)–(3) take into account the real conditions of titration, i.e. concentration changes in titration as a result of using different concentrations of the titrant and determined component and different volumes of aliquot of the determined component.

It should be use the real and conditional solubility products for the calculation SP if there are the large ionic strength in solution or competitive reactions in titration.

In order to conclude which criterion of prognostication is the most simple-graphic, visual, universal, informative, easy calculated it is necessary to compare these criterion. First of all we will calculate and plot differential and integral titration curves of individual substances for precipitation reactions with the formation of binary compound using hypothetical $\text{SP}_{\text{MA}} = 1.00\times10^{-10}$, 5.00×10^{-9}, 1.00×10^{-8}, 2.00×10^{-8}. The conditions of titration are standard ($M_{\text{det}} = M_{\text{tit}} = 0.1$ mol l^{-1}, $V_{\text{det}} = V_{\text{tit}}$ 10 ml, grad of volume addition near equivalence point is 0.1 ml).

Fig. 1 shows that in the case when a binary compound is formed in titration all the mentioned above criterion of prognostication may be used.

1. Theoretical curves of titration—they are visual and more universal, but insufficiently informative and labour-consuming in calculations.
2. Solubility products. These criterion do not demand calculations, rather visual, but less informative, universal as its threshold value ($\text{SP}_{\text{MA}} = 1.00\times10^{-8}$, ${}^{\text{SP}}MA_2 = 5.00\times10^{-13}$, ${}^{\text{SP}}MA_3 = 3.33\times10^{-17}$, ${}^{\text{SP}}M_2A_3 = 1.39\times10^{-22}$, ${}^{\text{SP}}M_2A_5 = 1.25\times10^{-31}$) depends on composition of insoluble compounds.
3. The reaction proceeding degree at the equivalence point. It is calculated easy, visual, rather universal, informative, threshold value is the same for any compound compositions [22].

Thus, the reaction proceeding degree at the e.p. (C) is the best prognostication criterion. Its threshold value is 99.80%, under this value of C_{lim}

Table 3
Dependence of the proceeding degrees of reactions at the e.p. on concentration of substances

M_{det} mol l^{-1}	0.005	0.005	0.007	0.001	0.01	0.01	0.1	0.2
M_{tit} mol l^{-1}	0.005	0.05	0.007	0.01	0.01	0.1	0.1	0.2
C%	99.66	99.78	99.71	98.90	99.80	99.89	99.98	99.99

concentration jump at the end point of titration is may be detected, but lower this value of C jump is not observed. $C_{lim} = 99.71\%$—the limit analytical reaction proceeding degree under which we must not carry out determination. The determinations were carried out under standard conditions. Titrations are possible up to $C_{lim} = 99.80\%$ at any detecting the end point (visually, if indicator will be chosen, by conductometry, if the change of electrical conductance in titration will be observed; by amperometry, if electrochemical reaction on the indicator electrode will be go, by potentiometry, if indicator electrode will be chosen and so on).

Integral and differential potentiometric titration curves of anions by argentometry with a silver indicator electrode and chloride–silver reference electrode under standard conditions of titration were calculated. These curves do not differ from the curves in Fig. 1.

3. Experimental

The synthesis of dithiophosphoric acid derivatives (potassium dimetyl- and diamyl-dithiophosphates) was made by a more generally used procedure [23]. The potentiometric measurements were made with model 121 pH-meter with a silver indicator electrode and chloride–silver reference electrode. Stirring was carried out magnetically. All the measurements were made at room temperature. Aqueous solutions of $AgNO_3$, $PdCl_2$, $Bi(NO_3)_3$, $Hg_2(NO_3)_2$, $Cu(NO_3)_2$ were used in our studies. Potassium dimetyl-, diethyl- and diamyldithiophosphates solutions were prepared by dissolving a precisely weighed amount in water. Their concentrations were checked by potentiometric method with standard solutions of KI and $AgNO_3$. The determination of the solubility products of dithiophosphate complexes were conducted at temperature $+25 \pm 1$°C by potentiometric method and calculated by the linearization method [24–27]. Solution volume and electrode potential in calculations of SP were measured with error ± 0.05 ml and ± 0.001 B.

4. Results and discussion

On the examples of argentometry and others we will discuss if it is possible to make a prognosis of the parametres of procedures and optimal conditions of analysis stated before.

(1) The calculation of the proceeding degree at the equivalence point allows the evaluation of the possibility of titration of any substance with this reagent up to $C = 99.80\%$. Table 1 shows that the determination of many inorganic anions is possible ($[Fe(CN)_6]^{4-}$, AsO_3^{3-}, CrO_4^{2-}, Br^- and so on).

(2) Table 1 allows us to expose the complete possibilities of using argentometry.

From more than 40 difficult soluble silver salts with inorganic anions, 17 have the proceeding degree at the equivalence point more than 99.80%, i.e. they may be determined individually on practice, but not all of them were titrated by argentometry and if we take into consideration that very many organic anions form difficult soluble salts or complexes with silver ions we may arrive at the conclusion that the possibilities of argentometry are highly great.

Let us take nickel diethyldithiophosphate, the famous titrant at present. This reagent was used only for copper determination in potentiometry before we began investigate its possibilities as a titrant [31]. Based on published data of diethyldithiophosphates solubility products [28,29], theory of analogy [32], assumptions have been made, that ions of elements which give the least soluble sulphides (Hg(I), Hg(II), Ag(I), Tl(III),

Table 4
Dependence of the limit proceeding degree of reaction on titration gradient (f = 2)

Grad%	0.1	0.5	1.0	2.0	3.0	5.0	7.0	10.0
C_{lim}%	99.97	99.86	99.71	99.43	99.13	98.55	97.97	97.13

Cu(I), Pd(II), Bi(III), Sb(III), probably Pb(II)) will be titrated individually. It should be noted that IP not SP is the equilibrium constant for organic chelate difficult soluble compounds. Inorganic difficult soluble compounds have an ionic crystal structure and are partly soluble in water, only ions migrate in solution, in this case SP = IP is the degree of solubility.(SP is used for the calculation of the proceeding degree of reaction in the case of inorganic difficult soluble compounds).

Chelate difficult soluble compounds with organic ligands have a molecular crystal structure and under partly dissolving come into the solution both in the form of ions and of molecules and it is necessary to use IP, which is the degree of durability of the chelate compound [33] (and is used for the calculation of the reaction proceeding degree). We could not find the solubility products and ionic products of Hg(I), Tl(III), Sb(III) diethyldithiophosphates in literature, they were determined by potentiometry and the rest solubility products were defined more exactly.

The proceeding degree of all ions mentioned above with nickel diethyldithiophosphate have been calculated in Eq. (2) (Table 2).

The data in Table 2 allows us to make the conclusion that all the ions except Cd(II) will be titrated up to $C = 99.80\%$. Complete possibilities of using nickel diethyldithiophosphate as a potentiometric reagent made on the basis of our prognostication have been confirmed experimentally [27].

(3) Table 3 shows that the titration of determined substances over the range 0.2–0.005 mol l^{-1} (M_{det}) and the use of titrant over the concentration range 0.2–0.005 mol l^{-1} (M_{tit}) under $SP_{MA} = 1 \times 10^{-10}$ is possible. Thus, we made a prognosis of the optimal concentration of both the determined substance and the titrant.

(4) It is possible to make a prognosis of threshold concentration of a determined component under given concentration of titrant and vice versa, based on the equation

$$M_{thresh} = \frac{m^* S_{M_nA_m}}{0.002 - \frac{n^* S_{M_nA_m}}{M_{tit}}} \quad (4)$$

M_{thresh} is the threshold concentration of the determined substance; m, n are the stoichiometric coefficients; ${}^{S}M_nA_m$ is the solubility and M_{tit} is the titrant concentration.

In the case of chlorides titration with 0.1 M silver nitrate ($SP_{AgCl} = 1.78 \times 10^{-10}$), $M_{thresh} =$ 0.007124 mol l^{-1} for chloride and for difficult soluble compounds with $SP_{MA} = 1 \times 10^{-8}$, $M_{thresh} = 0.1$ mol l^{-1}.

(5) The errors in titrimetric methods of analysis are conditioned theoretically by the difference between 100% procedure degree and the practically turned out one. The main error in titrimetry is connected with the precision of determination of the titrant equivalent volume.

Two new parametres in prognostication and the development of titrimetric procedures are proposed to aid the management of titration, i.e. to regulate the titration errors in wanted range: titration gradient (grad) and dilution coefficient or dilution degree (f).

The titration gradient is the amount of determined component reacted with added titrant portion near the equivalence point (e.p.)

$$\text{grad} = \frac{V^*_{ad.tit} 100}{V_{det}}\% \quad (5)$$

$$\text{grad} = \frac{m^* M^*_{tit} V^*_{ad.tit} 100}{n^* M^*_{det} V_{det}}\% \quad (6)$$

$V_{ad.tit}$ is the volume of the portion of added titrant near the e.p., the rest of the symbols are the same in Eqs. (1) and (2). Eq. (5) is valid for compounds of type AB, under the condition $M_{tit} = M_{det}$.

Table 5
Dependence of C_{lim} on dilution coefficient (grad = 1%)

f	1.1	1.3	1.5	1.8	2.0	4.0	5.0	11.0
C_{lim}	99.09	99.48	99.60	99.67	99.71	99.83	99.85	99.89

Dilution coefficient shows how many times titrating volume at the eq.p. more than volume of determined substance and can be calculated:

$$f = \frac{V_{det} + V_{tit}}{V_{det}} \quad (7)$$

$$f = 1 + \frac{n^* M_{det}}{m^* M_{tit}} \quad (8)$$

The limit proceeding degree and possibility of titration with limiting error (Table 4) depend on titration gradient (under certain value off).

Table 4 shows that C_{lim} (Section 2) is decreased with increasing gradient and the titration possibilities are extended. C_{lim} depends on the dilution coefficient (Table 5) under certain value of grad. Using Table 5 you can see that C_{lim} is increased with increasing f and the titration possibilities are decreased. C_{lim} dependence on the titration gradient under certain value of dilution coefficient is expressed graphically by a direct line, and the dependence of C_{lim} on dilution coefficient under determined grad is expressed by hyperbola (Fig. 2).

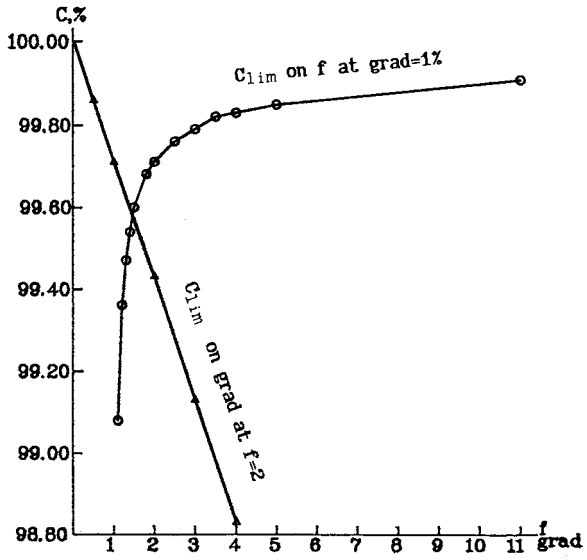

Fig. 2. Dependence of the limit proceeding degree on the dilution coefficient.

The limit proceeding degree of analytical reaction is the function of two variables—titration gradient and dilution coefficient. Using Fig. 2 you can find C_{lim} (Tables 4 and 5) obtained on the basis of the theoretical titration curves and from the deduced equation:

$$f = 2.0 \; C_{lim} = 100.0 - 0.283 \; \text{grad} \quad (9)$$

$$f = 1.1...1.5$$

$$C_{lim} = 100.0 - \text{grad}[100.0 - (92.096 + 10.130f - 3.426f)] \quad (10)$$

$$f = 1.5...2.5$$

$$C_{lim} = 100.0 - \text{grad}[100.0 - (100.023 - 0.629/f)] \quad (11)$$

$$f = 2.5...11.0$$

$$C_{lim} = 100.0 - \text{grad}[100.0 - (99.930 - 0.414/f)] \quad (12)$$

It is possible to calculate C from Eqs. (9)–(12) under any values of grad and f. Difference between C and f obtained on the basis of theoretical

Table 6
Potentiometric titration of IO_3^- in dependence on grad

IO_3^- taken (g)	IO_3^- found (g)	IO_3^- found (%)	grad (%)
0.08713	0.08721	100.09	2.30
0.06971	0.06979	100.12	2.80
0.03485	0.03477	99.78	5.7

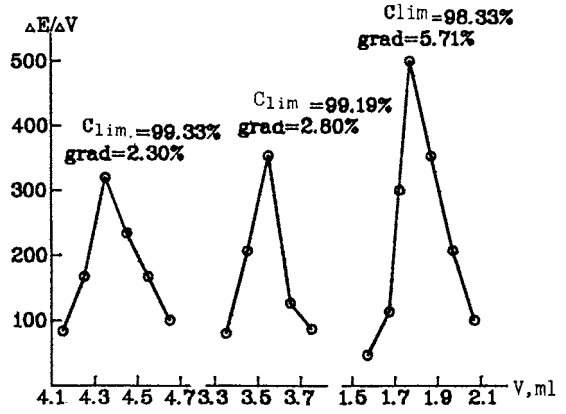

Fig. 3. Potentiometric titration curves of KIO_3 by argentometry in the dependence of titration gradient.

titration curves and equations do not exceed ± 0.08%.

The main error of determination of the titrant equivalent volume in the visual and potentiometric method of determination of the end point of titration is connected with the titration gradient. The error of determination of titrant volume at the eq.p. is over the range from zero to titrant gradient. Thus, we can make a prognosis of the error of individual determination, based on the chosen titration gradient (Table 6).

(6) Under different volumes of determined component and the same (or different) titrant concentrations, added with certain volume gradient, values of concentration jump at the end point will be different because the different amounts of determined components will react with titrant portion. The reaction proceeding degree depends on titrant gradient (Table 5). C_{lim} is decreased with the grad increasing and the determination of individual substance which is not titrated under standard conditions becomes possible. For instance, KIO_3($SP = 3.00 \times 10^{-8}$) under standard conditions is not titrated because concentration jump is not observed on theoretical titration curve ($C =$ 99.65%, grad = 1%). We observed concentration jump with increasing of titration gradient and we succeed in detecting end point of titration. Fig. 3Table 6 show that it is possible to conduct potentiometric titration with satisfactory error.

(7) Based on prognosis of the possibility of the practical using of nickel diethyldithiophosphate we can make conclusion on necessity of synthesis of dithiophosphoric acid derivatives with pre-programmed properties, which possess, firstly, greater selectivity, i.e. form stable complexes with a smaller number of ions, secondly, form stable complexes with a greater number of ions, which in its turn decreases the selectivity of determinations and increases the number of ions, determined individually and widens the possibilities of multicomponent mixtures titrations. For the synthesis of reagents with pre-programmed properties we based on phenomenon 'effect of weighting' [34], i.e. dependence of analytical properties on number of carbon atoms in reagent molecules and based on the introduction of different radicals not concerning functional analytical group. So the first alkylderivative of dithiophosphoric acid-potassium dimethyldithiophosphate, must give less stable complexes than diethyldithiophosphate, as shown in Tables 2 and 7 the number of ions, determined individually, are the same. Potassium diamyldithiophosphate and more high-molecular derivatives must give more stable complexes with greater number of ions; and the number of ions, titrated individually really increases in comparison with dimethyl- and diethyldithiophosphates titration (Tables 2 and 7).

Fig. 4 shows that the durability of forming complexes (SP is decreased) and potential jumps of electrode in potentiometric titrations are increased up to their certain values with the number of carbon atoms in reagent molecules in the investigated dithiophosphates row, and the tendency to of SP to decrease is observed. As mentioned above parameters are changed differently for various metal ions.

(8) It is clear that it is possible to reduce the time for evolving titrimetric procedures of analysis, made all the preliminary calculations, i.e. made the prognosis.

(9) Is it possible to make complete prognosis of titration procedure (for instance, potentiometric titration of chlorid-ions by argentometry)? Yes, it is. Because all the necessary data exist ($SP_{AgCl} = 1.78 \times 10^{-10}$) and silver nitrate is the salt of strong acid and weak base). For compounds MA

Table 7
Ionic products of dimetyl-(I) and diamyldithiophosphates(2) and the proceeding degrees of reaction at the eq.p.

Ma_n	HgA HgA_2 AgA	TlA_3 PdA_2 CuA	TeA_4 BiA_3 SbA_3	PbA_2 CdA_2 SeA_4	TlA InA_3 NiA_2
IP1	1.20×10^{-30} 4.79×10^{-15} 3.63×10^{-15}	6.46×10^{-29} 3.09×10^{-18} 1.74×10^{-10}	1.66×10^{-23} 1.82×10^{-18} 1.66×10^{-17}	1.05×10^{-12} 1.29×10^{-8} 6.17×10^{-19}	4.17×10^{-5} 2.24×10^{-12} 7.24×10^{-7}
C%	100.0 100.0 100.0	100.0 100.0 99.97	99.93 99.90 99.83	99.74 95.55 99.40	87.08 96.78 77.37
IP2	7.57×10^{-34} 3.24×10^{-18} 1.35×10^{-16}	3.89×10^{-36} 7.08×10^{-25} 1.05×10^{-12}	4.57×10^{-35} 2.09×10^{-27} 6.03×10^{-22}	1.35×10^{-15} 1.78×10^{-11} 1.62×10^{-37}	1.91×10^{-6} 6.03×10^{-18} 2.82×10^{-10}
C%	100.0 100.0 100.0	100.0 100.0 100.0	100.0 100.0 99.87	99.97 99.36 100.0	97.24 99.87 98.35

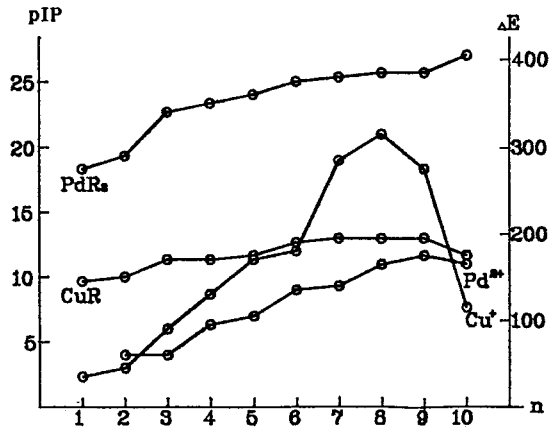

Fig. 4. Dependence of pIP and jump of electrode potential on number of carbon ions in copper(I) and palladium(II) dithiophosphate.

($SP_{MA} = 1.00\times10^{-10}$) all the main characteristics have already been determined above, we must only determine the optimal pH range in titrations. Upper pH limit will depend on hydrolysis beginning of silver ions (it is calculated from SP) and under standard conditions it will equal 7.29; lower pH limit is in very acid media, as there will not be competitive reaction in this media, it is in good agreement with work [35].

5. Conclusions

Various prognostication criterion of the potential and practical uses of analytical reagents in titrimetria of individual substances are discussed and more visual, rather informative and universal criterion—the proceeding degree of individual reaction at the equivalence point-has been chosen. We determined the threshold proceeding degree of the reaction $C = 99.80\%$ and its limit value $C = 99.71\%$ under which titration jump are not observed. New notion-titration gradient-has been introduced on which the limit proceeding degree of reaction is depend. The prognosis of the possibilities of individual titrations of various sulphide forming ions by some dithiophosphoric acid derivatives have been made on the basis of the reaction proceeding degrees. Prognosis have been confirmed in both literature and experimental data. It is possible to make prognosis of any procedure parameters of individual substance titration. Using derivatives with different length of carbon radical we can regulate the number of ions, determined individually.

References

[1] V.K. Chebotarev, A.I. Chebotareva, Z.I. Ivanova, Tez. dokl. nauch.-tehn. kon. po metodam analiza, Sverdlovsk (1972) S. 126–127.
[2] V.K. Chebotarev., A.V. Butakova, N.E. Chechushkova, Tez. dokl. Vsesouznoy kon. po electrohim. metodam analiza, Tomsk (1981) S. 263.
[3] V.K. Chebotarev, V.D. Chigirinzev, N.N. Artuhova, Tez. dokl. V Vsesouznoy kon., Organ. reagenti v analiticheskoi chimii, Kiev (1983) H.2 S. 185.
[4] V.K. Chebotarev, N.N. Artuhova, L.V. Yakovleva, Tez. dokl. II Vsesouznoi kon. po electrohim. metodam analiza, Tomsk (1985) S. 209.
[5] V.K. Chebotarev, N.N. Artuhova, G.D. Krutikova, Fiziko-chemicheskie metodi issledovaniya chimicheskih prozessov. Meshvuz. sb. Altaiskii gosuniversitet, Barnaul (1988) S. 108–113.
[6] V.K. Chebotarev, Y.K. Kraev, I.V. Voronkina, Tez. dokl. II Vses. kon. Matematicheskie metodi i EVM v analitich-eskoi chimii, Moskva (1991) S. 152.

[7] T.A. Hudyakova, A.P. Arbatskii, T.N. Tarasova, Zavod Lab. 49 (1983) 912.
[8] T.A. Hudyakova, A.P. Arbatskii, A.V. Fedyai, GGU, Gorkii (1987) 29. S., Dep. V VINITI., 26.07.77., 3063–77.
[9] T.A. Hudyakova, A.P. Arbatskii, Kislotno-osnovnie svoistva elektrolitov i kriterii ih analiza, M, Chimiya (1988) S. 31–42.
[10] J. Ricci, Hydrogen ion concentration, Princenton Univ. Press, Princenton, 1952, p. 459.
[11] J. Zsaco, Stud. Univ. Bades. Baluat Chem. 2 (1960) 13.
[12] T.A. Khudyakova, A.P. Kreshkov, J. Electroanal. Chem. 29 (1971) 181.
[13] E. Wänninen, Talanta 10 (1962) 221.
[14] M.D. Barry, L. Meites, Anal. Chim. Acta 68 (1974) 435.
[15] S. Young, E. Matijevic, L. Meites, J. Phys. Chem. 78 (1974) 2626.
[16] G. Kateman, H.C. Smith, L. Meites, Anal. Chim. Acta 152 (1983) 61.
[17] L. Meites, N. Fanelli, P. Papoff, Anal. Chim. Acta 192 (1987) 33.
[18] A. Gulyanickiy, Acids and Bases Reactions on Analytical Chemistry, Mir, Moscow, 1975, p. 240.
[19] E. Wänninen, Talanta 27 (1980) 22.
[20] M.N. Bulatov, Zurn. Anal. Chem. 296 (1984) 1980.
[21] M.N. Bulatov, Izv. Vuzov. Chimiya i Chim. Tekhnol. 30 (1987) 25.
[22] N.N. Artuhova, V.K. Chebotarev, B.M. Maryanov, Zurn. Anal. Chem. 154 (1989) 273.
[23] P.S. Pischimuka, Russ. Zurn. Fiz.-Chim. Ob. 44 (1912) 1406.
[24] F.M. Tulupa, L.M. Tkacheva, Y.I. Usatenko, Zurn. Neorg. Chem. 13 (1968) 2058.
[25] F.M. Tulupa, Y.I. Usatenko, V.S. Barkalov, Zurn. Neorg. Chem. 13 (1968) 3227.
[26] B.M. Maryanov, Zurn. Anal. Chem. 41 (1968) 1698.
[27] N.N. Artuhova, V.K. Chebotarev, B.M. Maryanov, Izv. Vuzov. Chimiya i Chim. Tekhnol. 31 (1988) 29.
[28] A.I. Busev, M.I. Ivanutin, Tr. Komis. Po Anal. Chim. AN SSSR. 11 (1960) 172.
[29] A.I. Kakovskii, Tr. Inst. Gorn. Dela 3 (1956) 55.
[30] Y.Y. Lurie, Spravochnik po analiticheskoi chimii, M, Chimiya (1989) 69–70.
[31] A.I. Busev, M.I. Ivanutin, Zurn. Anal. Chim. 11 (1956) 523.
[32] V.I. Kuznezov, Zurn. Anal. Chim. 2 (1947) 67.
[33] F.M. Tulupa, Chim. Tekhnol. 15 (1969) 114.
[34] K.B. Yazimirskii, Zurn. Anal. Chim. 8 (1953) 312.
[35] V.J. Shiner, M.L. Smith, Anal. Chem. 28 (1956) 1043.

ELSEVIER

Talanta 47 (1998) 1053–1061

Talanta

Short communication

Closure of analytical chemical data and multivariate classification

Roberto Aruga *

Department of Analytical Chemistry, University of Turin, via Giuria 5, 10125 Turin, Italy

Received 23 December 1997; received in revised form 9 March 1998; accepted 10 March 1998

Abstract

When it is not possible to analyze an exactly reproducible amount of sample (or whenever samples contain indefinite amounts of extraneous materials) it is customary to normalize the data by making, for example, the sum of the concentrations obtained for each sample equal to 100. Although the data normalized (or 'closed') in such a manner have been criticized, it is empirically shown that closure is appropriate in order to compare and classify samples of the type indicated above © 1998 Elsevier Science B.V. All rights reserved.

Keywords: Closure of data; Multivariate classification; Normalization to 100 of data

1. Introduction

Carrying out quantitative analyses on samples the amount of which is not exactly determinable (or not exactly reproducible) is a fairly common event in analytical chemistry.

In chromatography, for example, there is the problem of uncontrolled variations in the amount of sample injected or pyrolyzed [1,2]. Other cases may occur in the analytical determination of typical constituents on a set of similar samples, for the sake of evaluation or comparison. It could happen in fact, that samples, besides their typical constituents, contain extraneous materials (which are not quantified).

Archaeological ceramics, the basic constituent of which is clay, can be cited as an example. An extraneous substance, generally of a nonplastic nature (the so called 'temper') could have been added to the original clay, in order to improve the properties of the manufactured product [3].

Another case, also related with cultural heritages, occurred recently in this laboratory. It concerned the determination of amino acids on samples of ancient proteinaceous pictorial ligands relating to mural paintings [4]. Samples of this kind, in fact, can contain indefinite amounts of plaster or mortar.

In such cases the presence of a dilution process of an indefinite magnitude, which affects the concentration of the constituents analyzed can be assumed.

* Fax: +39 11 6707615; e-mail: aruga@ch.unito.it

0039-9140/98/$ - see front matter © 1998 Elsevier Science B.V. All rights reserved.
PII S0039-9140(98)00126-X

As analytical data are increasingly multivariate (in the sense that they consist of the determination of several variables on each sample), particular normalizations are commonly used in the cases mentioned above. For example, it is customary in chromatography to make the sum of the concentrations obtained for each sample equal to 100 or to 1, and to express the amount of each constituent determined in terms of a percentage (or of unit fraction) of the total amount. Data normalized in such a manner are also defined as 'closed'.

Data closure has been repeatedly criticized [1,5], incurring the most unfavourable consequences when multivariate methods based on the concept of principal component (PC) are used, such as principal component analysis (PCA) and factor analysis (FA; see the following section). The main effects of data closure can be summarized as follows: (1) introduction of spurious negative correlations between major variables and alteration of the covariance and correlation matrices; (2) a consequent reduction in the number of significant PCs and alteration of the results obtained with the above multivariate methods.

As a consequence (see e.g. Ref. 1) minimization of the effects of closure was attempted, but the problem is considered, from the broadest point of view, as not yet completely resolved [5].

It must also be noted that multivariate data processing with PCA or FA is often carried out on analytical data with the aim of studying provenances of objects, evaluating the quality of products, etc. [6]. For this reason the problem of closure, though mainly considered in geochemistry and geology [7], is also of interest in analytical chemistry.

In this paper, some simple observations of a practical, empirical nature have been drawn about the problem of closure of analytical data in relation to multivariate classification.

2. Methods of multivariate data processing

As they have come into widespread use, only a brief account will be given on the chemometric techniques used on the data of this study, together with references to specific texts for mathematical details.

A first, preliminary step consisted of the normalization (or standardization) of the raw data, to avoid misclassifications due to different orders of magnitude and ranges of variation of the variables. Autoscaling, or z-transform (which is one of the most commonly used data pretreatments), was carried out for this purpose. The values of each variable, after this scaling procedure, are characterized by zero as the mean value and by unit variance [6].

Principal component analysis determines, from the covariance matrix of the data, a set of new variables called principal components (PCs). The directions of PCs correspond with the directions of the largest data spread (or variance). It is usually possible to represent objects (even from different categories) on only a few PCs (i.e. dimensions) with sufficient accuracy or, in other words, without excessive loss of the information contained in all the original experimental variables [6].

Factor analysis allows one to define groups of mutually correlated variables by means of the matrix of loadings obtained by PCA and, as a consequence, to find the latent factor corresponding to each group. In other words, the latent factors determined by FA can be considered as a set of a few causes that explains the whole set of experimental data [8].

Hierarchical agglomerative clustering was also performed, in order to subdivide the samples into categories. This measures dissimilarities between objects and displays the results in the form of dendrograms, in which objects are represented on one axis and the corresponding mutual agglomeration levels (i.e. dissimilarities between objects) on the other axis [6].

3. Discussion

The effect of closure of experimental data can be visualized in an elementary manner. Let us consider, for example, four hypothetical samples (represented by points 1–4 in Fig. 1) and the determination of two constituents represented by variables X_1 and X_2. The values of X_1 and X_2 (in wt.%) for objects 1–4, respectively, are the follow-

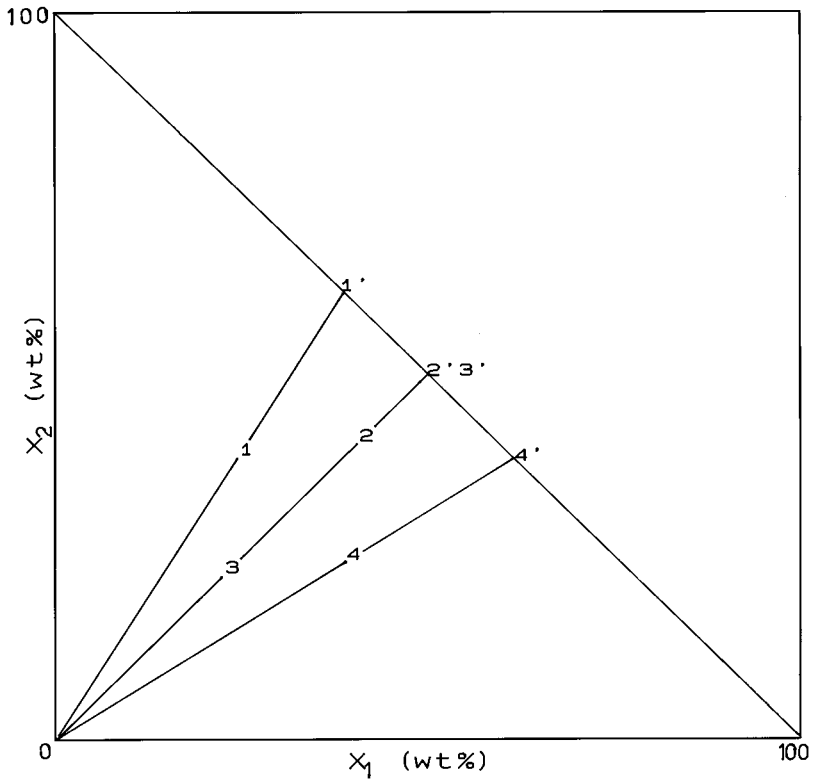

Fig. 1. Bivariate representation of four hypothetical samples with raw data (1–4) and after closure to 100 (1′–4′). The values are in wt.%.

ing: X_1, 22, 40, 20, 38; X_2, 38, 40, 20, 22. A closure to 100 of the data causes a constraint, in the sense that it subjects the data to an equation of the type: $X'_1 + X'_2 = 100$ or $X'_2 = 100 - X'_1$ (primed symbols are used for the variables after closure). Therefore, the points representing the four samples after closure (1′–4′ in Fig. 1) are situated on a straight line with slope and intercept -1 and 100, respectively. This justifies, firstly, the introduction of a negative correlation between the variables, as X_1 and X_2, which before closure are positively correlated with $r = +0.22$ (r, linear correlation coefficient), appear clearly anticorrelated in Fig. 1 after closure ($r = -1$). Secondly, the reduction in the number of significant PCs is justified. More precisely, two significant PCs (i.e. two orthogonal scattering directions of the points) are present in this case before closure, with variances of 61 and 39%, respectively, in comparison with only one PC, corresponding to the straight line $X'_2 = 100 - X'_1$, after closure.

In an analogous manner, if three variables are considered, closed samples are constrained in a plane ($X'_3 = 100 - X'_1 - X'_2$) and, if three PCs were originally present, they are now reduced to only two, and so on.

It can be noted that the same problem occurs in the study of mixtures, when the ratios between their constituents are considered [7,9].

Moreover, it can be noted that samples 2 and 3 are mutually correlated, in the sense that they show the same ratio between the two constituents. Samples 1 and 4, on the contrary, show different X_1/X_2 ratios both between each other and in comparison with samples 2 and 3.

To sum up, the following two kinds of straight lines can be considered in a diagram such as that of Fig. 1. (1) Parallel lines defined by equation $X'_2 = \beta_o - X'_1$ ($\beta_o = 100, 1$). They are the lines of closed data, i.e. of constant sum of constituents.

Table 1
Metal concentration data (wt.%) for 22 samples of Roman pottery (Terra Sigillata) belonging to three categories of provenance (A, B, G in the sample name) [10]

Sample name	K	Mg	Ca	Ti	Mn	Fe	Al
A1	3.60[a]	5.32	1.78	0.96	0.15	8.93	19.8
	1.80[a]	2.66	0.89	0.48	0.07	4.47	9.90
A2	3.25	7.43	1.65	0.89	0.11	9.05	19.8
	1.63	3.71	0.82	0.44	0.55	4.53	9.90
A3	3.13	8.45	1.81	0.91	0.14	9.12	20.0
	1.57	4.22	0.90	0.45	0.07	4.56	10.0
A4	3.09	6.20	1.81	0.93	0.15	9.39	20.3
	1.54	3.10	0.90	0.46	0.07	4.70	10.1
A5	2.96	7.80	1.69	0.88	0.12	9.24	19.6
	2.96	7.80	1.69	0.88	0.12	9.24	19.6
A6	3.18	8.08	1.73	0.89	0.12	9.22	19.2
	3.18	8.08	1.73	0.89	0.12	9.22	19.2
A7	2.97	8.59	1.78	0.86	0.11	8.90	18.9
	2.97	8.59	1.78	0.86	0.11	8.90	18.9
A8	3.15	8.00	1.85	0.92	0.14	8.88	19.1
	3.15	8.00	1.85	0.92	0.14	8.88	19.1
B1	1.94	3.17	9.99	0.95	0.15	7.32	18.8
	0.97	1.59	4.99	0.47	0.07	3.66	9.40
B2	2.24	4.09	8.70	0.86	0.09	6.81	17.4
	1.23	2.25	4.78	0.47	0.05	3.75	9.57
B3	1.98	3.51	8.98	0.91	0.16	7.30	18.4
	1.19	2.11	5.39	0.55	0.10	4.38	11.0
B4	1.88	3.33	9.52	0.93	0.13	7.07	18.2
	1.22	2.16	6.19	0.60	0.08	4.60	11.8
B5	2.10	3.37	9.00	0.94	0.16	7.39	17.4
	1.47	2.36	6.30	0.66	0.11	5.17	12.2
B6	1.96	3.57	10.1	0.89	0.17	7.48	18.3
	1.57	2.86	8.08	0.71	0.14	5.98	14.6
B7	2.02	3.24	11.1	0.93	0.14	7.18	17.3
	1.82	2.92	9.99	0.84	0.13	6.46	15.6
B8	1.92	3.22	12.5	0.93	0.15	7.76	17.0
	1.92	3.22	12.5	0.93	0.15	7.76	17.0
G1	2.86	2.10	10.9	1.28	0.06	6.05	23.3
	1.43	1.05	5.45	0.64	0.03	3.03	11.6
G2	3.20	1.94	9.71	1.21	0.05	5.76	22.3
	1.76	1.07	5.34	0.67	0.03	3.17	12.3
G3	3.03	2.00	11.6	1.18	0.06	5.90	23.3
	1.82	1.20	6.96	0.71	0.04	3.54	14.0
G4	3.19	2.01	12.3	1.32	0.07	6.30	21.7
	2.07	1.31	7.99	0.86	0.04	4.09	14.1
G5	3.06	1.78	9.53	1.20	0.05	6.62	20.9
	2.14	1.25	6.67	0.84	0.03	4.63	14.6
G6	2.88	2.02	11.5	1.10	0.07	6.33	22.2
	2.30	1.62	9.20	0.88	0.05	5.06	17.8

[a] The upper value refers to the original sample (to which no temper seems to have been added); the lower value to the sample after a simulated temper addition (see text).

(2) Lines of the type $X_2 = \beta_1 X_1$, i.e. of constant ratios between constituents. Samples, in consequence of a 'dilution' with extraneous substances, move along these latter lines towards the origin, as the concentrations represented by X_1 and X_2 undergo a proportionally constant decrease. On

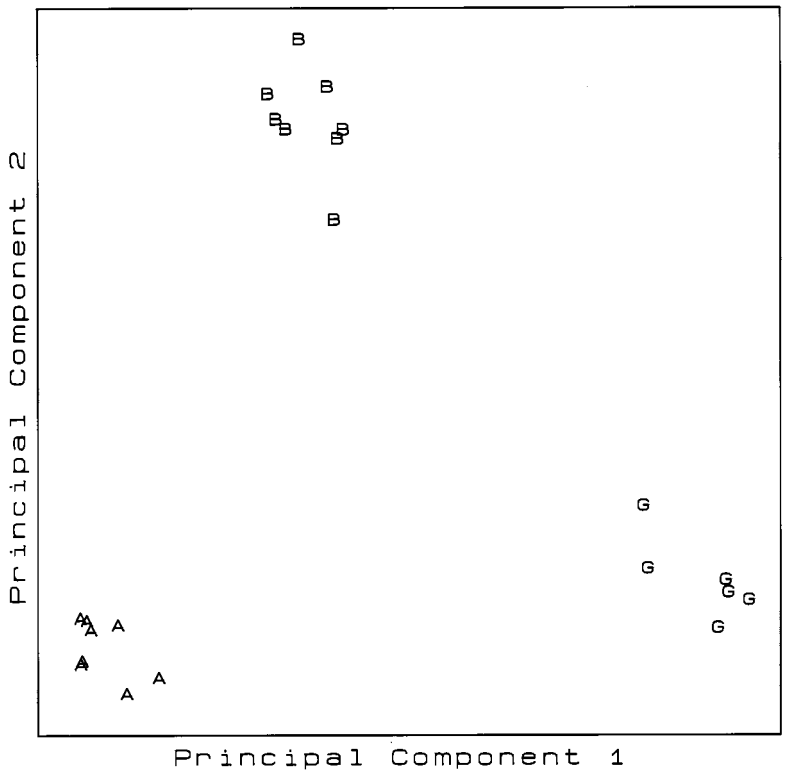

Fig. 2. Representation of 22 samples of Roman pottery belonging to three categories of provenance (A, B, G) on the first two principal components (92% of the total variance) by means of the original data (i.e. without temper addition).

the contrary, they move in the opposite direction when the data are closed (see above).

As a consequence of the preceding considerations, it can be said that data closure to 100 joins all mutually correlated samples and differentiates, along the straight line $X'_2 = 100 - X'_1$, samples with different X_1/X_2 ratios. In other words, closure of data leads to a classification of objects based on correlation and not on distance [6]. This appears correct: as the actual amounts of the samples under study are unknown, only ratios of constituents within each sample and not absolute quantities between samples can be compared.

In order to clarify the consequences of this fact on sample classifications we may consider, for example, samples 1–4 of Fig. 1 as archaeological ceramic wares which must be classified on the basis of provenance. Moreover, let us suppose that samples of different provenances are characterized by different ratios between constituents [3]. Samples 2 and 3, if data are not closed, are represented in very different positions on the diagram, and then could be attributed to different classes of provenance. Indeed, it seems probable that the two samples, having the same X_1/X_2 ratio, come from the same clay quarry and that sample 3 derives from sample 2 after addition to the latter of a temper containing negligible amounts of X_1 and X_2. After closure, on the contrary, the diagram appears more readily interpretable, in the sense that samples $2'$ and $3'$ are clearly attributed to the same category.

As the above conclusions refer to a merely theoretical and bivariate elementary case, it seems appropriate to check them by means of a real case, taking into account that, in general, real cases are characterized by a higher number of variables.

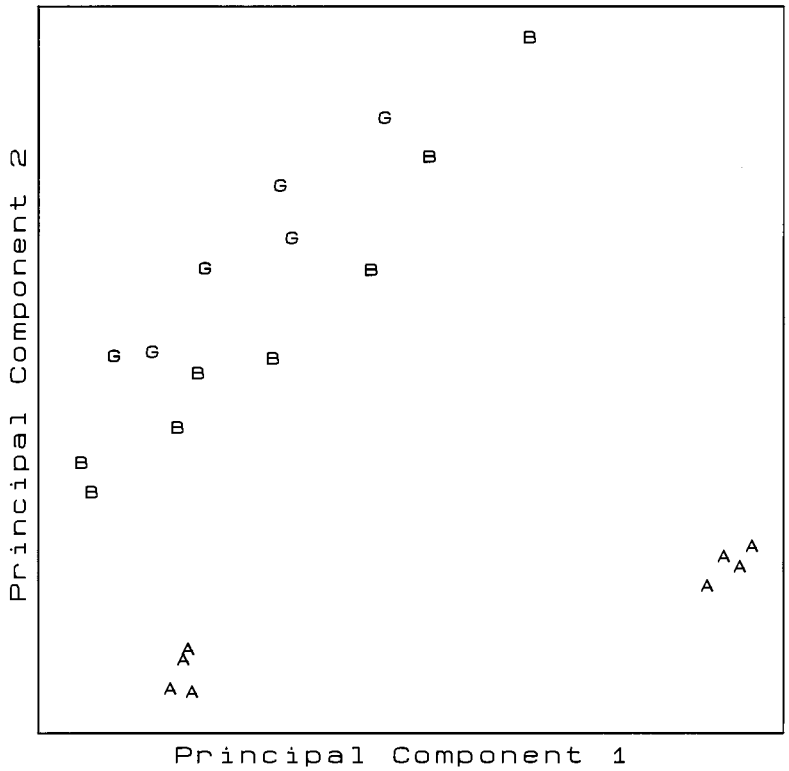

Fig. 3. Representation of the 22 samples of Fig. 2 on PC(1,2) (variance, 87%), after simulated additions of variable amounts of temper (see Table 1).

More precisely, the concentration data of seven metals obtained previously by spectroscopic techniques [10] have been considered. They refer to archaeological pottery of the Roman epoch found in excavation campaigns carried out in the town of Aosta (north-western Italy). The samples belong to the following three categories of provenance. Category A: eight samples of 'Terra Sigillata' (a high-quality ceramic ware, the name of which comes from the fact that in most cases the ware was stamped with a sigillum, peculiar to the workmanship which produced it) manufactured in north-western Italy. Category B: eight samples of 'Terra Sigillata' manufactured in another region of Italy (probably in Central Italy). Category G: six samples of 'Terra Sigillata' from Gaul. The above categories were identified both by chemists, on the basis of chemical and statistical techniques, and by archaeologists, by means of stylistic–visual techniques. It must be noted that the study of these samples did not show any evidence of temper additions to original clay. The original data, which are collected in Table 1, have been processed according to the following three procedures.

(1) Autoscaling and PCA on the original data of Table 1 (reported in the upper positions in the table). The representation of the 22 objects on the first two PCs (92% of the total variance) is reported in Fig. 2.

The real situation is correctly represented in Fig. 2, as the three classes are clearly discriminated.

(2) In a second study it was simulated that various amounts of temper had been added to the samples under investigation, and the data have been modified according to this. The values of the eight samples of class A have been corrected as to

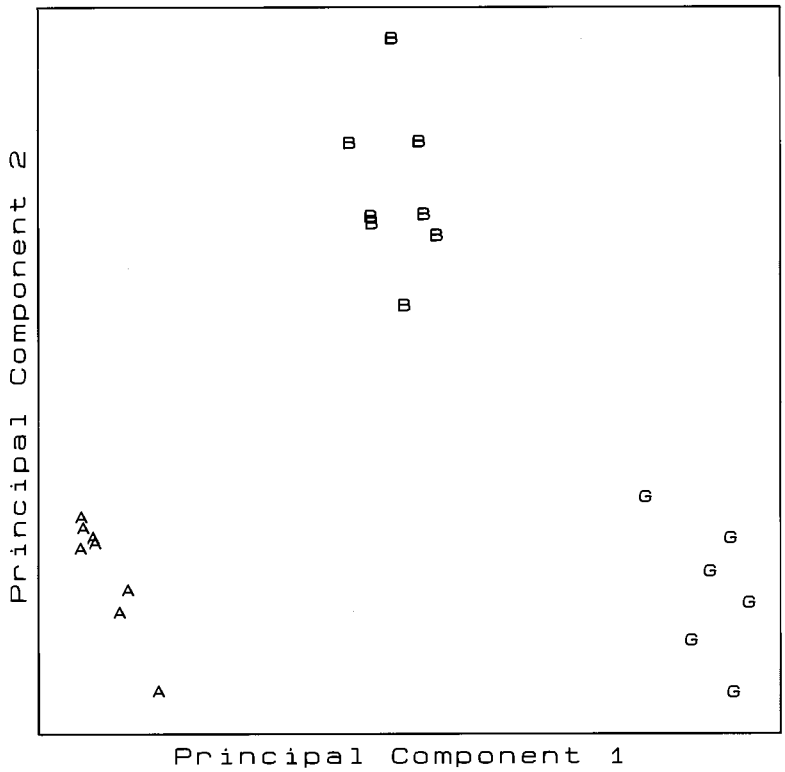

Fig. 4. Representation of the 22 samples of Fig. 2 on PC(1,2) (variance, 91%), after simulated temper additions and closure to 100.

whether the same amount of temper had been added to four of them, and not added to the others. The modified concentration values (i.e. after temper addition) are reported in the lower positions in Table 1. More precisely, a temper addition equal to the mass of the sample has been considered for samples A1–A4 (i.e. (values in the second row) = 0.5 × (values in the first row) of Table 1). For samples A5–A8, for which no temper addition has been considered, the two values are equal. On the other hand, gradually different temper additions have been imagined for the samples of classes B and G. They range from zero (i.e. unaltered clay) for sample B8, to a maximum value for samples B1 and G1. The amount of temper added, in this case too, can be easily derived from the ratio between the two concentration values, upper and lower, for each sample. It has also been supposed that a temper consisting of a relatively pure material, such as quartz, had been added to clay [3], so that the decrease in the concentrations of the seven metals was proportionally constant.

After performing autoscaling and PCA on the modified data of Table 1, Fig. 3 was generated (87% of the total variance). It can be observed, in this representation, that class A has been split into two groups, while classes B and G become indistinguishable. It can then be concluded that the presence of extraneous materials, if data are not closed, can make a classification impossible (classes B and G) or wrong (class A).

(3) A third PCA was carried out autoscaling the modified data of Table 1 after closure to 100 (Fig. 4). As it can be seen in this representation, closure leads to a correct classification analogous to that of Fig. 2.

The three sets of data listed above have been also processed using cluster analysis ('complete linkage' method [6]). The dendrograms obtained showed groups of objects analogous to those of

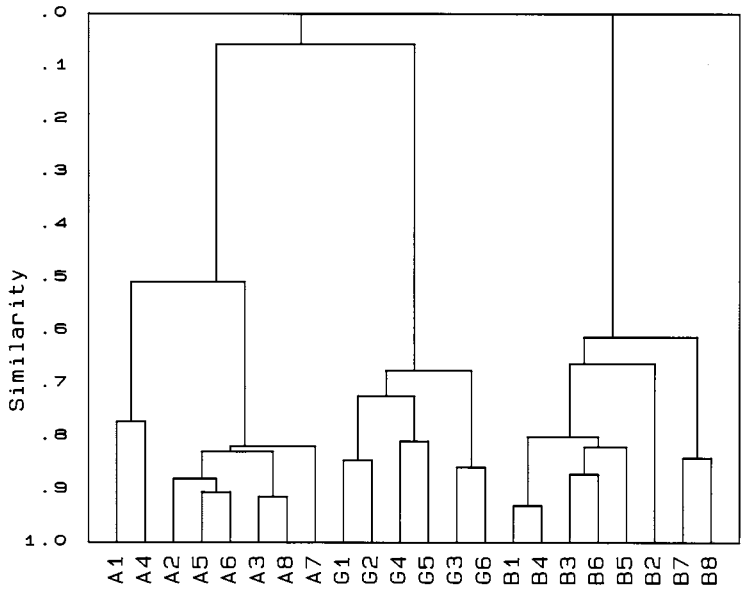

Fig. 5. Representation of the 22 samples of Fig. 2 by a dendrogram ('complete linkage'), after simulated temper additions and closure to 100.

Figs. 2–4. As an example, the dendrogram obtained after data closure to 100 is reported in Fig. 5. It shows a disposition of the 22 samples quite similar to that of Fig. 2.

4. Conclusions

On the basis of the preceding discussion, the following main conclusions can be listed in a summary.

(1) Closure of data leads to a sample classification based on correlation, i.e. on the ratios between constituents for each sample.

(2) The introduction of negative correlations between variables as well as the elimination of one significant PC caused by closure appear necessarily connected with this kind of classification.

(3) When samples contain indefinite amounts of extraneous material, comparisons and classifications based on correlation (and, therefore, data closure) conduct to good results. It is interesting to note that in the case, for example, of archaeological ceramics with possible temper additions, classifications are sometimes made using Q-mode PCA, which is typically based on correlation between samples [3,5,10]. This fact seems to greatly support the empirical approach followed in this work.

(4) Also, from the point of view of FA, the elimination of one PC does not necessarily appear as a negative event. For example, in the study of provenances of archaeological ceramics with possible temper additions, closure eliminates the direction of variance corresponding to 'temper addition' or 'technological' factor, which can be seen as a fortuitous and disturbing factor while, on the other hand, it leaves the other unaltered (i.e. geochemical) factors, useful for studying provenances.

References

[1] E. Johansson, S. Wold, K. Sjödin, Anal. Chem. 56 (1984) 1685.
[2] G. Blomquist, E. Johansson, B. Söderström, S. Wold, J. Chromatogr. 173 (1979) 7.
[3] R.L. Bishop, H. Neff, Compositional data analysis in archaeology, in: R.O. Allen (Ed.), Archaeological Chemistry IV, American Chemical Society, Washington, 1989.

[4] A. Casoli, P. Mirti, G. Palla, Fresenius J. Anal. Chem. 352 (1995) 372.
[5] J.C. Davis, Statistics and Data Analysis in Geology, Wiley, New York, 1986.
[6] D.L. Massart, L. Kaufman, The Interpretation of Analytical Chemical Data by the Use of Cluster Analysis, Wiley, New York, 1983.
[7] G.S. Koch, R.F. Link, Statistical Analysis of Geological Data, vol. 2, Dover Publications, New York, 1971.
[8] E.R. Malinowski, Factor Analysis in Chemistry, Wiley, New York, 1991.
[9] J.A. Cornell, Experiments with Mixtures, Wiley, New York, 1990.
[10] R. Aruga, P. Mirti, A. Casoli, Anal. Chim. Acta 276 (1993) 197.

ELSEVIER

Talanta 47 (1998) 1065–1069

Talanta

Liquid–liquid distribution of ion associates of hexabromotellurate (IV) with quaternary ammonium counter ions

Koichi Yamamoto *, Keisuke Adachi

Department of Materials Science, Yonago National College of Technology 4448, Hikona-cho, Yonago-shi, Tottori 683, Japan

Received 16 January 1998; received in revised form 11 March 1998; accepted 12 March 1998

Abstract

The distribution behavior of ion associates $(Q^+)_2$. $TeBr_6^{2-}$ of $TeBr_6^{2-}$ with quaternary ammonium cations (Q^+) between aqueous phase and two organic phases (1,2-dichloroethane (DCE) and chloroform (CF)) was examined, and the extraction constants (log K_{ex}) were determined. The extractability with long-chain alkyltrimethylammonium cations (group I) is greater than that with symmetrical tetraalkylammonium cations (group II) in the 1,2-dichloroethane extraction system and the difference in log K_{ex} for two cations (one of each type) with the same number of carbon atoms was about 3 on the average. The contributions of a methylene group in the cations of groups I and II to log K_{ex} were found to be $0.43 \sim 1.10$ and about 0.74 on the average. Among the ion associates examined, the extractability of the extracting solvent was in the DCE > CF; the difference in log K_{ex} was about 5 on the average.
© 1998 Elsevier Science B.V. All rights reserved.

Keywords: Liquid–liquid distribution; Hexabromotellurate (IV); Quaternary ammonium ion

1. Introduction

An extraction of tellurium from an aqueous halide medium into an organic solvent has been frequently used for both the separation and spectrophotometric determination of tellurium. The extraction behavior of tellurium with high molecular weight amines in various media, i.e. with dodecyl(trialkylmethyl)amine [1], trioctylamine [2,4] and tribenzylamine [3] or with quaternary ammonium salts such as trioctylmethylammonium bromide [4] and cetyltrimethylammonium bromide [5] from hydrochloric acid [1–3], hydrobromic acid [2,4], hydroiodic acid [2], sodium iodide-perchloric acid [2] solution or potassium iodide-sulphuric acid [5] solution, has been examined for the separation or the determination of tellurium. The methods for the solvent extraction–photometric determination of tellurium (IV) based on the extraction of the ion-association complexes of the halide-complexes ($TeCl_6^{2-}$, $TeBr_6^{2-}$, TeI_6^{2-}) of tellurium (IV) with cations of some dyes [6,7] such as Rhodamine 4G [8], Victoria Blue 4R [9] have been reported. Tanaka et al.

* Corresponding author.

0039-9140/98/$ - see front matter © 1998 Elsevier Science B.V. All rights reserved.
PII S0039-9140(98)00188-X

[10] proposed the atomic absorption spectrophotometric method for the determination of tellurium by an extraction into nitrobenzene as an ion associate of tellurium (IV), halide ion and 1,10-phenanthroline.

In this work, the extraction constants (log K_{ex}) for the ion associates of hexabromotellurate (IV) ion with various quaternary ammonium ions distributed between an aqueous and two organic phases (1,2-dichloroethane and chloroform) were determined and correlated with the number of carbon atoms in the quaternary ammonium ions. The extractability of hexabromotellurate (IV) was also discussed.

2. Experimental

2.1. Apparatus

The apparatus for recording spectra and absorbance measurements and for horizontal shaking were as described in the previous paper [26]. A Kubota Model 5010 tabletop laboratory centrifuge was used to ensure complete phase separation after extraction.

2.2. Reagents

Hexyltrimethylammonium bromide (purity, > 98%) was obtained from Tokyo Kasei Co. Ltd. The supplier and purity of other quaternary ammonium ions, and the preparation of the quaternary ammonium ion solutions were as described in the previous paper [25,26].

A standard tellurium (IV) solution (1.57×10^{-3} M) was prepared by diluting 20 ml of a 1000 ppm standard tellurium (IV) solution (7.84×10^{-3} M tellurium tetrachloride in 6 M hydrochloric acid solution, Wako Pure Chem.) to 100 ml with distilled water.

Hydrobromic acid was used for the formation of a tellurium (IV)-bromo complex.

Commercially available 1,2-dichloroethane and chloroform were used without further purification, and were saturated with distilled water before use.

2.3. Standard procedure for stoichiometry measurement

A total of one milliliter of a 1.57×10^{-3} M tellurium (IV) solution was transferred to a 25 ml stoppered test-tube; then 2 ml of a concentrated hydrobromic acid solution and an appropriate amount of aqueous quaternary ammonium salt solution were added. The solution was diluted to 5 ml with distilled water. The aqueous solution was mechanically shaken with 5 ml of an extracting solvent for 30 min at 25°C. After centrifugation of the mixture, the absorbance of the aqueous phase was measured at 442 nm against distilled water as a reference; the concentration of tellurium in the aqueous phase was then calculated from the molar absorptivity of the hexabromotellurate (IV).

3. Results and discussion

3.1. Absorption spectrum

In the aqueous phase at 3.43 M bromide concentration, tellurium (IV) reacts with bromide to form $TeBr_6^{2-}$ [10,11]. The absorption spectrum of the hexabromotellurate (IV) ion in aqueous solution is shown in Fig. 1. The maximum absorbances of the hexabromotellurate (IV) ion were

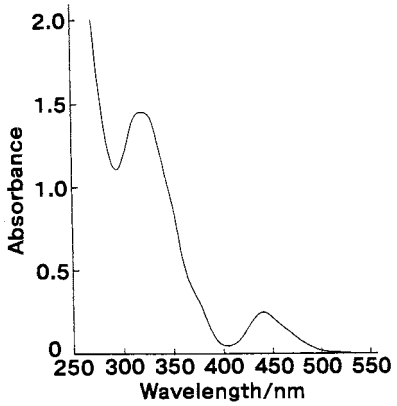

Fig. 1. Absorption spectrum of the tellurium (IV)-bromo complex in water. Tellurium(IV): 7.84×10^{-5} M; bromide ion, 3.43 M; reference, distilled water.

at 319 and 442 nm, where the absorbances of the reagent blank were negligibly small. The absorbance at 442 nm was used for the determination of tellurium because of the good reproducibility. The molar absorptivity for tellurium was about 3.4×10^3 l mol^{-1} cm^{-1} at 442 nm.

3.2. Determination of extraction constants and some considerations of extractability of ion associates

Hexabromotellurate (IV) anion, $TeBr_6^{2-}$ distributes between the aqueous and organic phases:

$$TeBr_6^{2-} + 2Q^+ \rightleftharpoons ((Q^+)_2 \cdot TeBr_6^{2-})org \quad (1)$$

and

$$K_{ex}(TeBr_6^{2-}) = \frac{[(Q^+)_2 \cdot TeBr_6^{2-}]\,org}{[Q^+]^2[TeBr_6^{2-}]} \quad (2)$$

where K_{ex} is the extraction constant: the subscript 'org' refers to the organic phase and the absence of a subscript indicates the aqueous phase. The distribution ratio of tellurium between the aqueous and organic phases (D_{Te}) is given by

$$D_{Te} = \frac{[(Q^+)_2 \cdot TeBr_6^{2-}]\,org}{[TeBr_6^{2-}]} \quad (3)$$

Hence, the following equation can be derived from Eqs. (2) and (3):

$$D_{Te} = K_{ex}(TeBr_6^{2-}) \cdot [Q^+]^2 \quad (4)$$

where

$$\log D_{Te} = \log K_{ex}(TeBr_6^{2-}) + 2 \log [Q^+] \quad (5)$$

The quaternary ammonium ions will form ion associates with a foreign anion, as shown in Eq. (6), and these are also extracted into the organic phase:

$$Q^+ + X^- \rightleftharpoons (Q^+ \cdot X^-)\,org;$$

$$K_{ex}(X^-) = [Q^+ \cdot X^-]\,org/[Q^+][X^-] \quad (6)$$

where X^- is Br^- and $C1^-$.

The side-reaction coefficient for the quaternary ammonium ion ($a\,(Q^+(X^-))$ is given by

$$\alpha(Q^+(X^-)) = \frac{[Q^+]'}{[Q^+]}$$

$$= \frac{[Q^+] + [Q^+ \cdot Br^-]\,org + [Q^+ \cdot Cl^-]\,org}{[Q^+]}$$

$$= 1 + K_{ex}(Br^-) \cdot [Br^{-1}] + K_{ex}[Cl^-] \cdot [Cl^-] \quad (7)$$

where $[Q^+]'$ is the total concentration of the quaternary ammonium ion that is not bound in ion associates with hexabromotellurate (IV), and $K_{ex}(Br^-)$ and $K_{ex}(C1^-)$ are the extraction constants of a quaternary ammonium ion with bromide and chloride ions, respectively. $[Q^+]$ can be calculated by

$$[Q^+] = [Q^+]'/a(Q^+(X^-)) \quad (8)$$

In the extraction of hexabromotellurate (IV), the distribution ratios of tellurium at different concentrations of the quaternary ammonium ions were determined. The plots for all quaternary ammonium cations were linear with slopes almost equal to two. This means that the extraction equilibrium shown in Eq. (1) holds and that the extracted species was $(Q^+)_2 \cdot TeBr_6^{2-}$. The extraction constants calculated from Eq. (5) are summarized in Table 1; the standard deviation is very small.

3.3. Relationship between the extraction constants and the number of carbon atoms in the quaternary ammonium ion and effect of the extracting solvent

The values of the extraction constants ($\log K_{ex}$) were plotted against the number of carbon atoms in the quaternary ammonium ion (Nc). The result obtained for the 1,2-dichloroethane extraction system is shown in Fig. 2. For the same carbon number, the extractability ($\log K_{ex}$) with long-chain alkyltrimethylammonium cations (group I) is larger than that with symmetrical tetraalkylammonium cations (group II) for the 1,2-dichloroethane extraction system, and the difference in $\log K_{ex}$ values between these groups is about 3 for an identical carbon number. This indicates that the electrostatic attraction of the cations in group I for the anionic complex is

Table 1
Extraction constants (log K_{ex}) obtained between aqueous and organic phases

Extracting solvent	Q^+ cation[a]	log K_{ex}			Slope of log D_{Te} vs. log $[Q^+]$ plots
		$TeBr_6^{2-}$[b]	Br^- [12]	Cl^- [12]	
1,2-Dichloroethane	HTMA	5.24 ± 0.05 (6)	−0.28	−1.47	1.94
	OTMA	9.63 ± 0.02 (6)	0.90	−0.29	2.03
	DTMA	13.11 ± 0.07 (5)	2.08	0.89	2.15
	DDTMA	15.56 ± 0.08 (4)	3.26	2.07	2.22
	TDTMA	18.17 ± 0.06 (5)	4.44	3.25	2.00
	CTMA	20.97 ± 0.06 (5)	5.62	4.43	2.12
	STMA	22.68 ± 0.11 (4)	6.59	5.40	1.94
	TPA	7.63 ± 0.23 (7)	0.29	−0.90	1.84
	TBA	14.16 ± 0.10 (5)	2.65	1.46	2.09
	TAA	20.06 ± 0.06 (6)	5.01	3.82	1.82
	Zeph	24.15 ± 0.11 (4)	7.17	5.98	2.26
Chloroform	Zeph	19.15 ± 0.07 (6)	5.87	4.68	2.16

[a] HTMA, hexyltrimethylammonium bromide; OTMA, octyltrimethylammonium chloride; DTMA, decyltrimethylammonium chloride; DDTMA, dodecyltrimethylammonium chloride; TDTMA, tetradecyltrimethylammonium chloride; CTMA, cetyltrimethylammonium chloride; STMA, stearyltrimethylammonium chloride; TPA, tetrapropylammonium chloride; TBA, tetrabutylammonium chloride; TAA, tetraamylammonium chloride; Zeph, tetradecyldimethylbenzylammonium chloride.
[b] Mean value ± SD. The figures in parentheses are the numbers of measurements.

larger than that of the cations in group II. By dividing the slope of the line in Fig. 2 by two, the contribution of a methylene group to the extraction constants (log K_{ex}) was found to be 0.43 ~ 1.10 and about 0.74 on the average, in good agreement with the value previously reported [13–26].

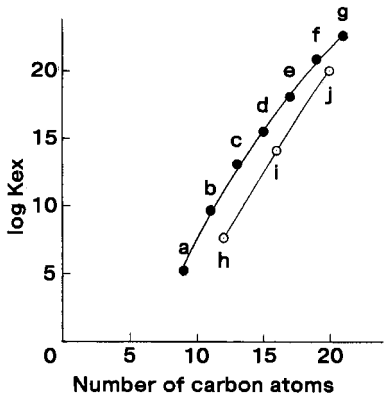

Fig. 2. Relation between log K_{ex} and number of carbon atoms in the quaternary ammonium ion. Q^+: (a) HTMA, (b) OTMA, (c) DTMA, (d) DDTMA, (e) TDTMA, (f) CTMA, (g) STMA, (h) TPA, (i) TBA, (j) TAA; extracting solvent: 1,2-dichloroethane.

Among the ion associates examined, the extractability of the extracting solvent was in the 1,2-dichloroethane > chloroform; the difference in the log K_{ex} was about 5 for Zeph.

3.4. Extractability of hexabromotellurate (IV)

The extraction constants (log K_{ex}) for the 1:2 ion associates of halogeno complex anions with $Zeph^+$ into the chloroform extraction are listed in Table 2. From these values, it was found that the extractability of halogeno complex anions was in

Table 2
Extraction constants of ion associates of various metal-halogeno complex anions with tetradecyldimethylbenzylammonium cation in chloroform-extraction

X^-	Metal-halogeno complex	log K_{ex}	Δ log K_{ex}
Cl^-	$PdCl_4^{2-}$	14.79[a]	1.32
	$PtCl_6^{2-}$	16.11[b]	
Br^-	$PdBr_4^{2-}$	17.27[a]	1.88
	$TeBr_6^{2-}$	19.15	
I^-	PdI_4^{2-}	22.45[a]	

[a] Ref [15].
[b] Ref [25].

the order $PdI_4^{2-} > TeBr_6^{2-} > PdBr_4^{2-} > PtCl_6^{2-} > PdCl_4^{2-}$; the differences in log Kex between two halogeno complex anions in this order were 3.30, 1.88, 1.16 and 1.32. The extractability of $TeBr_6^{2-}$ is about 76 times that of $PdBr_4^{2-}$ with respect to the divalent bromo complex anion.

The linear relationship was obtained between the extraction constants (log Kex) for 1:2 ion associates of $TeBr_6^{2-}$ with quaternary ammonium ions and the number of carbon atoms in quaternary ammonium ion, and the contribution of a methylene group to the extraction constant was the almost same as those for 1:2 ion associates of other divalent halogeno complex anions [15,25] and 1:1 ion associates of monovalent halogeno complex anions [14,16–18,26]. The result of the extractability of $TeBr_6^{2-}$ obtained in this work is useful for developing a sensitive extraction-spectrophotometric method of tellurium. The molar absorptivity of the tellurium (IV)–bromo complex anion is small (about 3.4×10^3 l mol^{-1} cm^{-1} at 442 nm), and no increase in the sensitivity has been achieved. Combining the method utilizing the light-absorption of the tellurium (IV)–bromo complex anion with the solvent extraction may make a sensitive spectrophotometric method for tellurium: for example, we recommend the 1,2-dichloroethane extraction of the ion associate of $TeBr_6^{2-}$ with tetradecyldimethylbenzylammonium cation.

References

[1] G. Nakagawa, Nippon Kagaku Zasshi 81 (1960) 446.
[2] T. Suzuki, T. Sotobayashi, S. Koyama, Bunseki Kagaku 23 (1974) 999.
[3] G. Nakagawa, Nippon Kagaku Zasshi 81 (1960) 1258.
[4] I. Tsukahara, T. Yamamoto, Talanta 28 (1981) 585.
[5] M. Vijayakumar, T.V. Ramakrishna, G. Aravamudan, Talanta 26 (1979) 323.
[6] L.S. Alekseeva, V.I. Murashova, L.I. Bakunina, V.G. Skripchuk, Zavodsk. Lab. 37 (1971) 1299.
[7] V.I. Murashova, V.G. Skripchuk, Zh. Analit. Khim. 27 (1972) 340.
[8] Z.M. Khvatkova, A.P. Golovina, N.B. Zorov, N.K. Belova, I.P. Alimarin, Vestn. Mosk. Univ. Khim. 13 (1972) 355.
[9] P.P. Kish, S.G. Kremeneva, Zh. Analit. Khim. 25 (1970) 2200.
[10] S. Tanaka, Y. Takabatake, I. Hayashida, H. Yoshida, Bunseki Kagaku 38 (1989) 245.
[11] I. Havezov, N. Jordanov, Talanta 21 (1974) 1013.
[12] S. Motomizu, Dojin News 38 (1987) 3.
[13] S. Motomizu, S. Hamada, K. Toei, Bunseki Kagaku 32 (1983) 648.
[14] K. Yamamoto, S. Motomizu, Talanta 36 (1989) 561.
[15] K. Yamamoto, T. Fujibayashi, S. Motomizu, Solvent Extr. Ion Exch. 10 (1992) 459.
[16] K. Yamamoto, M. Endo, Anal. Sci. 10 (1994) 755.
[17] K. Yamamoto, S. Inada, Anal. Sci. 11 (1995) 643.
[18] K. Yamamoto, M. Endo, Anal. Sci. 12 (1996) 739.
[19] I. Kasahara, Y. Ohgaki, K. Matsui, K. Kano, S. Taguchi, K. Goto, Nippon Kagaku Kaishi (1986) 894.
[20] H. Matsunaga, T. Yotsuyanagi, Nippon Kagaku Kaishi (1982) 785.
[21] R. Modin, G. Schill, Acta Pharm. Suecica 7 (1970) 585.
[22] G. Schill, Acta Pharm. Suecica 2 (1965) 13.
[23] K.O. Borg, D. Westerlund, Z. Anal. Chem. 252 (1970) 275.
[24] B.-A. Persson, S. Eksborg, Acta Pharm. Suecica 7 (1970) 353.
[25] K. Yamamoto, S. Katoh, Talanta 43 (1996) 61.
[26] K. Yamamoto, A. Matsumoto, Talanta 44 (1997) 2145.

ELSEVIER

Talanta 47 (1998) 1071–1076

Talanta

Dual-analyte spectroscopic sensing in sol–gel derived polyelectrolyte–silica composite thin films

Yining Shi, Carl J. Seliskar *, William R. Heineman

Department of Chemistry, University of Cincinnati, P.O. Box 210172, Cincinnati, OH 45221-0172, USA

Received 2 December 1997; received in revised form 24 March 1998; accepted 25 March 1998

Abstract

Ferrozine (3-(2-pyridyl)-5,6-diphenyl-1,2,4-triazine-*p,p′*-disulfonic acid, monosodium salt hydrate), an iron indicator, and HTPS (8-hydroxyl-1,3,6-pyrenetrisulfonic acid, trisodium salt), a pH indicator, were immobilized in sol–gel derived PDMDAAC-SiO_2 (where PDMDAAC stands for poly(dimethyldiallylammonium chloride), composite thin films via ion-exchange. The two indicators were immobilized in two adjacent sections of the same PDMDAAC-SiO_2 film which was supported on a glass optical substrate. The spectroscopic response of the film to both Fe^{2+} and H^+ in solutions was investigated by attenuated total reflection (ATR) spectrometry at two well-separated wavelengths, 562 nm for Fe^{2+} and 460 nm for H^+. The Ferrozine/HPTS immobilized PDMDAAC-SiO_2 films had the following characteristics: linear range, 2.5×10^{-6}–5.0×10^{-5} M for Fe^{2+}, pH 4.1–6.8 for H^+; sensitivity, 2.2×10^4 ΔA/M for Fe^{2+}, 0.583 ΔA/pH for H^+. © 1998 Published by Elsevier Science B.V. All rights reserved.

Keywords: Attenuated total reflection; Chemical sensing; Indicators; Polyelectrolyte; Sol–gel

1. Introduction

Organically modified sol–gel derived materials have been of interest for the construction of optical chemical and biochemical sensors in recent years [1–4]. The organic modifiers incorporated in the sol–gel processed inorganic matrices can be organic dyes, synthetic polymers, and biomacromolecules [1]. We have been interested in developing synthetic polyelectrolyte-containing sol–gel derived materials that are suited for the fabrication of indicator-based and preconcentration-based optical chemical sensors.

Recently we have prepared a series of optically transparent polyelectrolyte-containing silica composite materials by the sol–gel method [5]. The polyelectrolytes incorporated in the silica matrices can be either polycations (e.g. poly(dimethyldiallylammonium chloride), PDMDAAC) or polyanions (e.g. Nafion® perfluorinated ionomer). Of these composites, the PDMDAAC-SiO_2 composite can be processed into crack-free thin films with variable thickness ($0.1 \sim 3.5$ mm) by spin-coating. Our studies have shown that these thin films are highly ion-exchangeable while retaining the nanoscale porosity and optical transparency of the parent sol–gel glass [5]. These unique properties make PDMDAAC-SiO_2 composite films at-

* Corresponding author. Tel: +1 513 5569213; fax: +1 513 5569239; e-mail: seliskcj@ucbeh.san.uc.edu

0039-9140/98/$ - see front matter © 1998 Published by Elsevier Science B.V. All rights reserved.
PII S0039-9140(98)00140-4

tractive host matrices for the electrostatic immobilization of ionizable dye molecules and chemical reagents, as well as for the preconcentration of dilute anionic solution species. Using the PDMDAAC-SiO_2 thin films, we have developed an indicator immobilization-based pH sensing platform [5] and a preconcentration-based spectroelectrochemical sensor [6,7].

In this paper we report on a new spectroscopic sensing platform for dual-analyte determination of two ions (i.e. Fe^{2+} and H^+) with PDMDAAC-SiO_2 films. While pH sensing in a single pass transmission geometry at normal incidence has been demonstrated in our previous study[5], we describe here a dual-analyte sensing scheme for the determination of pH and Fe^{2+} concentration in an attenuated total reflection (ATR) device.

2. Experimental

2.1. Materials

The following chemicals were used: tetraethoxysilane (Aldrich), poly(dimethyldiallylammonium chloride) (PDMDAAC, 20 wt.% aqueous solution; Polysciences), 3-(2-pyridyl)-5,6-diphenyl-1,2,4-triazine-*p,p′*-disulfonic acid, monosodium salt hydrate (Ferrozine®; Aldrich), 8-hydroxyl-1,3,6-pyrenetrisulfonic acid, trisodium salt (HPTS; Molecular Probes) and ferrous chloride hydrate (Sigma). All reagents were used without further purification. Reagent solutions were all made by dissolving the appropriate amounts of chemicals in deionized water (Barnstead water purification system). pH buffer solutions were prepared by making 0.08 M NaH_2PO_4 (Aldrich) and 0.25 M K_2HPO_4 (Fisher Scientific) in 500 ml of deionized water, followed by adjustment, with HCl or NaOH, to the desired pH values. Indium–tin-oxide (ITO) tin float glass (indium tin oxide layer, 11–50 W/sq. inch, 150 nm thick, over tin float glass) was purchased from Thin Film Devices. This ITO tin float glass was cut into 1×3 inch slides, scrubbed with Alconox, and rinsed thoroughly with deionized water and then 1-propanol prior to use.

2.2. Preparation of the indicator-immobilized PDMDAAC-SiO_2 composite thin films

The PDMDDAC-SiO_2 films were prepared according to the same general procedure described previously [6]. In brief, 4.0 ml of tetraethylorthosilicate, 2.0 ml of deionized water and 0.1 ml of 0.1 M HCl were combined in a sealed vial and stirred at room temperature. After 3 h of stirring, the resulting sol solutions were blended with a 10% (wt.) PDMDAAC aqueous solution in volume ratio of 2:3 (PDMDAAC/sol). This PDMDAAC-containing sol solution was then diluted with 2/7 vols of water and spin-coated on ITO glass slides at 3000 rpm for 30 s. (Although we have used ITO glass as the substrate out of convenience, the same results can be obtained with a 1×3-inch microscope slide [5]). Both ends of the ITO glass slides were masked with tape prior to spin-coating, leaving these sections of the ITO surface uncoated for prism coupling. The tape present on the slides during spin-coating did not interfere significantly with the formation of a uniform coating as verified by thickness measurements and sensing performance. The films (≈ 0.75 μm thick) were dried under ambient conditions for at least 2 days. Film thicknesses were measured by an interference fringe method [5]. These aged films were then immersed in deionized water for 8 h or overnight to ensure sufficient equilibration with water. These water-treated films were then partially masked with a masking glass slide (0.5×3 inch) and immersed in HTPS aqueous solution (0.02 mM) for about 20 min. Then the masking glass slide was moved to, and fixed onto, the HTPS-loaded film section. This remasked slide was then immersed in the Ferrozine aqueous solution (2 mM) for about 3 h. A longer immersion time for the Ferrozine immobilization was used since the Ferrozine anion showed slower uptake kinetics than the HTPS anion. The resulting pattern of the indicator-immobilized ITO glass slides is shown schematically in Fig. 1.

2.3. ATR spectrometry

The ATR sensing measurements were performed using a modification of a home-made cell

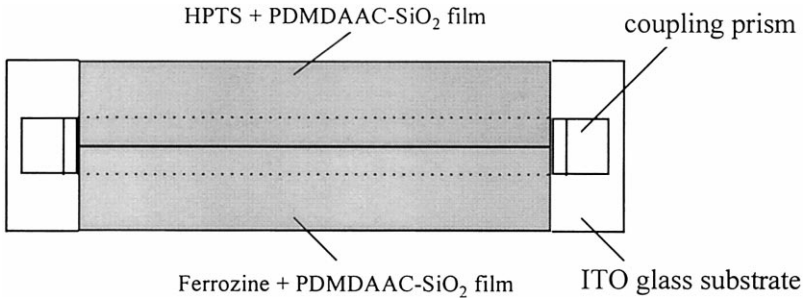

Fig. 1. Schematic pattern of the Ferrozine and HPTS immobilized PDMDAAC-SiO_2 film for dual-analyte (Fe^{2+} and pH) sensing. The dashed lines indicate the path of the interrogating light that undergoes multiple internal total reflection within the glass substrate as a result of prism coupling.

designed for the ATR-based spectroelectrochemical sensing purposes, as shown in Fig. 2. The instrumental set-up for performing the ATR spectrometry is standard [6,7]. The spectroscopic response curves for the Fe^{2+} sensing measurements were acquired by introducing ferrous solutions in the order of increasing Fe^{2+} concentration and recording the change in transmittance of the light at 562 nm propagating through the ATR device. The spectroscopic response curves for the pH sensing measurements were obtained sequentially in the same manner as that for the Fe^{2+} sensing measurements by switching the monitoring wavelength from 562 to 460 nm. Although not done for measurements reported here, simultaneous dual sensing is possible with this configuration by using two wavelengths of light simultaneously.

3. Results and discussion

Two ionizable reagents, Ferrozine and HTPS, were used as colorimetric indicators for the sensing of Fe^{2+} and H^+, respectively. Both reagents in aqueous solutions carry negative charge ($HPTS^{3-}$, $Ferrozine^{2-}$) and thus partition into the anion-exchangeable PDMDAAC-SiO_2 films via electrostatic interactions. It was found that HPTS showed a faster partition kinetic than Ferrozine. Factors which might cause this difference in partitioning rate include differences in negative charge, molecular size, and polarity. HPTS is a widely used pH indicator [6] which has a pH-dependent absorption maximum at 460 nm (yellow colored) in its basic form. Ferrozine is a colorimetric indicator for iron [8,9], which by itself is transparent in the visible region (>400 nm) while demonstrating a metal-to-ligand charge transfer absorption maximum at 562 nm (purple colored) upon coordination with Fe^{2+}. Fig. 3 shows the visible absorption spectra of the HTPS-loaded film and of the Ferrozine-loaded film exposed to Fe^{2+}. Owing to these widely separated absorption wavelengths ($\Delta\lambda_{max} > 100$ nm), these two indicators can be immobilized into two adjacent sections of the PDMDAAC-SiO_2 films supported on the same glass substrate, and function to sense H^+ and Fe^{2+}, respectively, without significant optical interference between the two sections of the sensing film.

Fig. 4 shows the pH response of HTPS immobilized in the PDMDAAC-SiO_2 film using ATR spectrometry at 460 nm. Similar to their pH sensing in the transmission geometry with normal incidence [5], these films also responded rapidly to the pH changes in the ATR geometry. The response time is approximately 8 s for 90% of the full-range response of one unit of pH change. Compared with the single indicator immobilized films for transmission geometry measurements [5], these HPTS and Ferrozine immobilized films in the ATR geometry showed a wider linear pH range (≈ 0.4 pH units wider) which was shifted to lower pH values, as shown in Fig. 5.

Fig. 6 shows the Fe^{2+} response of Ferrozine immobilized in the PDMDAAC-SiO_2 film performed also in the ATR mode but using a different wavelength, 562 nm. It is obvious that the

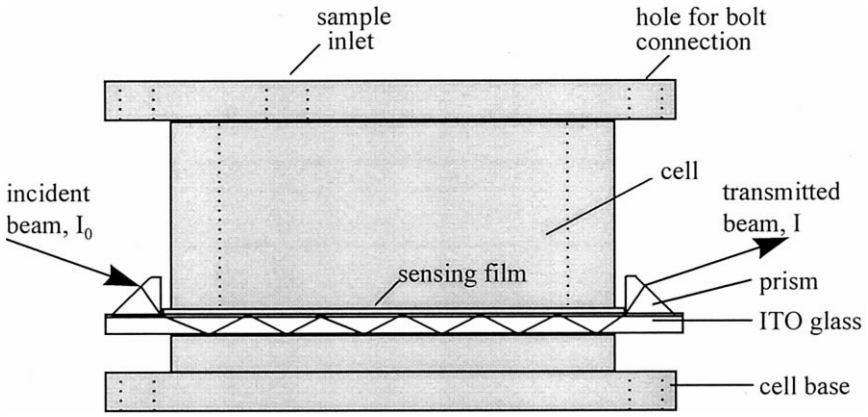

Fig. 2. Experimental arrangement for ATR spectrometry.

response time for sensing Fe^{2+}, about 10 min for 90% of the full response, was much slower than that for pH sensing. The reason for these sluggish response kinetics may possibly be attributed to (1) the sterically hindered chelating reactions which involve re-orientation of the multiple ligands immobilized in the micro-heterogeneous environments for binding to the Fe^{2+} ion (note that the colored product for sensing is an octahedral complex formed by one Fe^{2+} and three molecules of Ferrozine), and (2) slower diffusion of Fe^{2+} into the anion-exchangeable film structure due to its larger size and greater positive charge in comparison with H^+. (Note also that the ion-exchange site in the PDMDAAC-SiO_2 films is a positively charged quaternary ammonium.) Fig. 7 illustrates the calibration curve for the sensing of Fe^{2+} in the concentration range between 2.5 and 50 mM. Sensitivity down to 1.0 mM was determined from the background. The relatively small linear range for Fe^{2+} is mainly due to the low Ferrozine concentration in the film. This range can be slightly increased by increasing the Ferrozine concentration in the film. However, we have not been able to improve this linear range significantly by doing this.

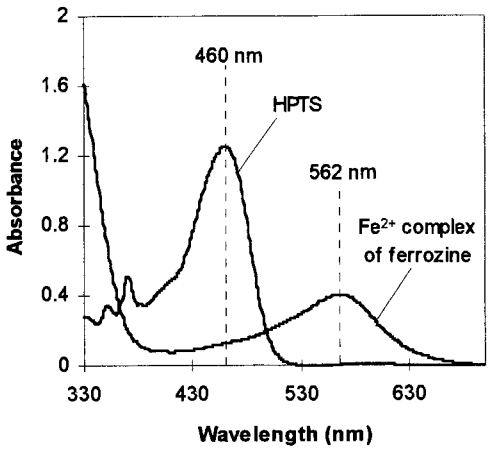

Fig. 3. UV–visible absorption spectra of HPTS (basic form) and ferrous complex of Ferrozine immobilized in the PDMDAAC-SiO_2 films. Measurement wavelengths are indicated by dashed vertical lines.

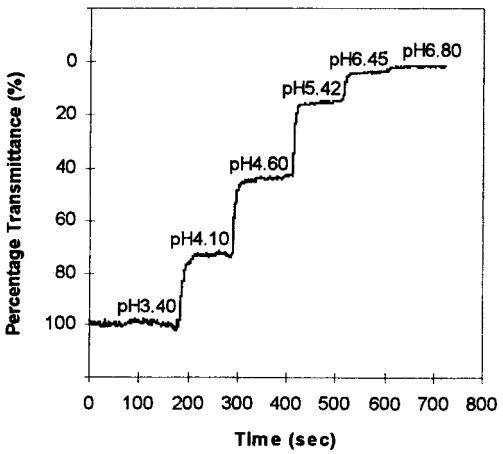

Fig. 4. Optical pH response of the Ferrozine and HPTS immobilized PDMDAAC-SiO_2 films. $\lambda = 460$ nm.

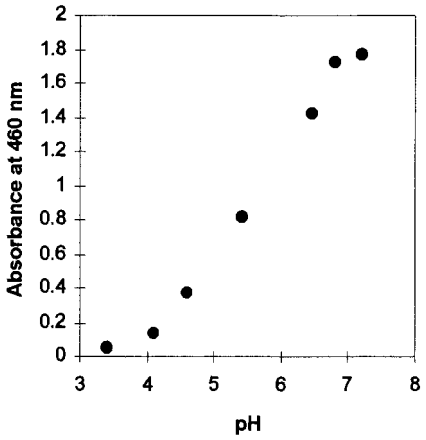

Fig. 5. Calibration curve of absorbance vs. pH for the Ferrozine and HPTS immobilized PDMDAAC-SiO_2 films. Linear range ($R^2 = 0.993$): pH 4.1–6.8.

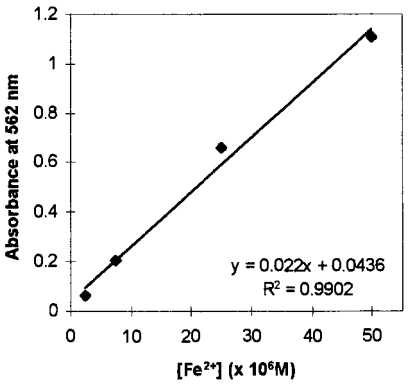

Fig. 7. Calibration curve of absorbance versus concentration of Fe^{2+} for the Ferrozine and HPTS immobilized PDMDAAC-SiO_2 films.

It should be noted that ITO-coated glass, instead of plain glass (e.g. lime soda glass), was used as the ATR optical element. The reason for this choice is that an ITO-coated glass is a semiconducting glass and can serve as an optically transparent electrode, thus possessing the potential for developing spectroelectrochemical sensors with multimode selectivity [6,7]. Although Ferrozine is a highly selective indicator for Fe^{2+}, it also forms colored complexes with metal ions such as Co^{2+} and Cu^{+}. The Ferrozine complexes of the two metal ions show broad absorbance bands at 450–520 nm for cobalt and 470 nm for copper [9]. In order to improve further the selectivity of Ferrozine towards Fe^{2+}, an attempt to incorporate electrochemical potential modulation (as another mode of selectivity) into the sensing system was made but was unsuccessful. The lack of success was simply because the spectral absorbance property of the Fe(II) Ferrozine complex is not electrochemically modulated under the present experimental conditions. An attempt to co-immobilize the two indicators in the same region of the sol–gel films was also made using a physical entrapment method where both indicators were mixed in the sol before spin-coating. However, the resulting films responded to Fe^{2+} more slowly than the films described above, presumably due to a more narrow pore structure of the films prepared in this manner. Investigations of other iron complex systems which are promising for the development of indicator-based spectroelectrochemical sensor are currently underway.

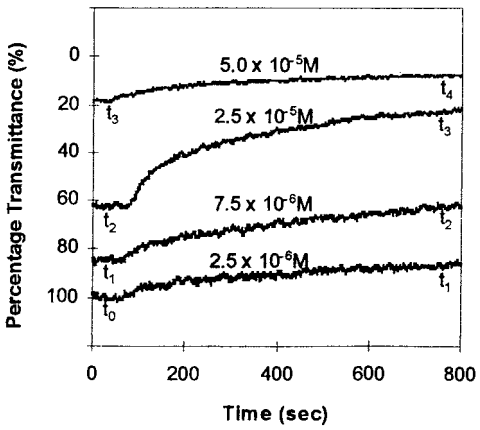

Fig. 6. Optical Fe^{2+} response of the Ferrozine and HPTS immobilized PDMDAAC-SiO_2 films. $\lambda = 562$ nm. The response curves were recorded in the following time sequence: $t_0 \rightarrow t_1 \rightarrow t_2 \rightarrow t_3 \rightarrow t_4$.

In addition, the limit of detection (LOD) for Fe^{2+} found in this study is at the level of micromoles, which could be enhanced by orders of magnitude by replacing the presently used 1-mm thick ATR optical element with a micron-thick integrated optical waveguide (IOW). The IOW-ATR configuration supports a much higher total

reflection number per unit length of beam propagation in the slide [10] and this produces typically lower LODs. Work on the IOW-ATR sensor for ultrasensitive determination of Fe^{2+} based on immobilization of Ferrozine in the PDMDAAC-SiO_2 films is under current investigation.

Acknowledgements

Financial support provided by the Department of Energy (Grant DE-FG07-96 ER62331) is gratefully acknowledged.

References

[1] O. Lev, M. Tsionsky, L. Rabinovich, V. Glezer, S. Sampath, I. Pankratov, J. Gun, Anal. Chem. 67 (1995) 22A.
[2] B.C. Dave, B. Dunn, J.S. Valentine, J.I. Zink, Anal. Chem. 66 (1994) 1120A.
[3] D. Avnir, S. Braun, O. Lev, M. Ottolenghi, Chem. Mater. 6 (1994) 1605.
[4] L.S. Ellerby, C.R. Nishida, F. Nashida, S.A. Yamanaka, B. Dunn, J.S. Valentine, J.I. Zink, Science 255 (1992) 1113.
[5] Y. Shi, C.J. Seliskar, Chem. Mater. 9 (1997) 821.
[6] Y. Shi, A.F. Slaterbeck, C.J. Seliskar, W.R. Heineman, Anal. Chem. 69 (1997) 3679.
[7] Y., Shi, C.J., Seliskar, W.R. Heineman, Anal. Chem. 69 (1997) 4819.
[8] L.L. Stookey, Anal. Chem. 42 (1970) 779.
[9] M.V. Dawson, S.J. Lyle, Talanta 37 (1990) 1189.
[10] L. Yang, S.S. Saavedra, Anal. Chem. 67 (1995) 1307.

ELSEVIER

Talanta 47 (1998) 1077–1084

Talanta

Complex formation equilibria of some β-amino-alcohols with lead(II) and cadmium(II) in aqueous solution

Silvia Canepari [a], Vincenzo Carunchio [b], Paola Castellano [b], Antonella Messina [b,*]

[a] *CIMS-Bioanalytical Chemistry Section, University of Rome 'La Sapienza', P. le Aldo Moro, 5-00185 Rome, Italy*
[b] *Department of Chemistry, University of Rome 'La Sapienza', P. le Aldo Moro, 5-00185 Rome, Italy*

Received 23 September 1997; received in revised form 18 March 1998; accepted 2 April 1998

Abstract

A study of complex formation equilibria of some β-amino-alcohols with lead(II) and cadmium(II) ions at 25°C and in 0.5 M KNO_3 is reported. The amino-alcohols considered are 2-amino-1-propanol, 2-amino-1-butanol, 2-amino-1-pentanol and 2-amino-1,3-propanediol. *sec*-Buthylamine and 2-amino-1-methoxy-propane have been also considered for comparison. The results are discussed in terms of ligand structure, paying attention to the number of hydroxyl groups and to the length of the alkyl residual. A weak contribution of the alcoholic oxygen in the coordination of cadmium(II) and the presence of a mixed hydroxyl species in lead(II) containing systems are hypothesized. © 1998 Elsevier Science B.V. All rights reserved.

Keywords: β-Amino-alcohols; Complex formation equilibria; Lead(II); Cadmium(II)

1. Introduction

β-Amino-alcohols and related derivatives are employed in various industrial fields, like the synthesis of high polymers and plastics or the production of detergents or even as gas purifiers. Furthermore, they are present in living organisms and are frequently employed in the pharmaceutical field; aminoethanol is in fact the characteristic moiety of several medicines, like various antibiotics, antiseptics and anesthetics, and natural occurring substances like adrenaline and some sphingoids.

Considering that the interaction of these substances with metal ions, which can occur by means of both the amino and the hydroxyl groups, can be responsible of a substantial modification of their pharmacological and biological behavior, the complexation equilibria of β-amino-alcohols has not been extensively studied and only a few data have been reported until now [1–15].

The aim of the present work is the study of complex formation equilibria of some aliphatic β-amino-alcohols with lead(II) and cadmium(II). The ligands considered, whose protonation and

* Corresponding author. Tel: +39 6 49913695; fax: +39 6 490631; e-mail messina@axrma.uniroma1.it

0039-9140/98/$ - see front matter © 1998 Elsevier Science B.V. All rights reserved.
PII S0039-9140(98)00147-7

complex formation equilibria with silver(I) ion have been recently studied [15], are *sec*-butylamine (L_I), 2-amino-1-propanol (L_{II}), 2-amino-1-methoxy-propane (L_{III}), 2-amino-1-butanol (L_{IV}), 2-amino-1-pentanol (L_V) and 2-amino-1,3-propanediol (L_{VI}). They differ in the number and the position of the hydroxyl groups and for the length of the alkyl residual. L_I and L_{III}, in which the OH group is not present, have been also considered in order to check the possibility of chelate formation with a deprotonated alcoholic group, which was hypothesized in some complexes of β-amino-alcohols [13,16–18].

As regards the metals involved in this study, cadmium(II) and lead(II) are, as is well known, between the most toxic polluting ions, so that a knowledge of their interaction with biological active substances can also help to clarify the role of these ions in environmental problems. Until now with the exception of a few reports regarding monoethanolamine [9,10,19,20] and some alkanol-substituted ethilenediamines [18], their complex with β-amino-alcohols have never been considered.

2. Experimental

2.1. Materials and apparatus

All the ligands, with the exception of 2-amino-1-methoxy-propane, were from Sigma, analytical grade and were used without further purification. 2-Amino-1-methoxy-propane was a synthesis product from Aldrich and was purified by distillation under a nitrogen atmosphere. The purity grade of all the ligands has been controlled by potentiometric titration as described elsewhere [15].

Water used for preparing all solutions was purified with a Millipore Milli-Q RG Ultra-Pure water system. All the other reagents were obtained in high purity. Ultra pure KNO_3 (Suprapur, Merck) was used as an ionic strength buffer.

Temperature control (25 ± 0.1°C) was achieved by means of water circulation in the jacketed vessel from a water thermocryostat (thermostat HAAKE DC3 and cryostat HAAKE K15).

The KOH solution was put into the titration vessel by a Metrohm Dosimat 655 digital burette with a total volume of 1 ml. In order to have CO_2-free potassium hydroxide, the solution was preserved in a bottle stopped by a soda lime plug and kept under argon atmosphere. In these conditions the solution was stable for up to 1 month.

Potentiometric titrations were carried out using a Metrohm model 665 pH/mV meter, with a glass combined micro-electrode (Metrohm). The potentiometric apparatus was made completely automatic by using an IBM model 30 personal computer with a parallel interface and an appropriate software program (G. Arena and G. Maccarrone, Department of Chemistry, University of Catania, personal communication).

2.2. Metal ions stock solutions

Lead(II) and cadmium(II) nitrate (Carlo Erba) solutions were standardized by a 0.01 M EDTA (Titrisol, Merck) solution and using xylenol orange as the indicator [21].

2.3. Ligand stock solutions

All the ligands considered are highly hygroscopic and easily uptake CO_2 so that, for the preparation of their solutions, direct weighing was not possible. Stock solutions were prepared and handled in strictly air-free conditions, as already described in a previous paper [15].

2.4. Potassium hydroxide

KOH 0.1 M (CO_2-free solution, Merck) was standardised by potentiometric titrations against a solution of potassium hydrogen phthalate dried at 120°C for 24 h (Merck pro analysis) using the Gran method [22] for the evaluation of the end point.

2.5. Nitric acid

A solution 0.1 M HNO_3 was prepared by diluting the pure concentrated standardized product (Titrisol, Merck) and the titre was controlled by potentiometric titrations against tris(hydrox-

Table 1
Initial analytical C_L, C_M and C_H, and C_L/C_M ratios and pH ranges employed in potentiometric titrations of cadmium(II)–2-amino-1-propanol

Experiment No.	C_L	C_M	C_L/C_M	C_H	pH ranges
1, 2, 3	2.00	0.60	3.3	2.20	7.6–8.8
4, 5, 6	4.80	0.95	5.0	5.28	7.4–9.0
7, 8, 9	7.61	1.52	5.0	8.37	7.6–9.0
10, 11, 12	6.06	0.60	10.1	6.61	6.5–9.2
13, 14, 15	10.00	0.95	10.5	11.00	6.6–9.1

Data in mM.
$I = 0.5$ M KNO_3; $T = 25$°C.

Table 2
Formation constants of complexes formed between L_I, L_{II}, L_{III}, L_{IV}, L_V, L_{VI}, with cadmium(II) and related statistical parameters obtained by overall evaluation of data at $I = 0.5$ M KNO_3 and $T = 25$°C.

	L_I	L_{II}	L_{III}	L_{IV}	L_V	L_{VI}
pK_a^a	10.599 (3)	9.450 (6)	9.424 (2)	9.554 (5)	9.766 (3)	8.786 (1)
Log $\beta_{1,1,0}$ (log K_1)	—	2.27 (8)	—	2.48 (4)	2.66 (4)	2.32 (4)
Log $\beta_{2,1,0,}$	—	4.32 (7)	—	4.75 (9)	5.01 (8)	4.35 (7)
Log K_2	—	2.05	—	2.27	2.35	2.03
χ_2	—	15.32	—	17.89	18.37	7.86
σ	—	3.31	—	3.46	3.63	2.99

[a] [15]

ymethyl)-aminomethane (Merck), and dried at 100°C for 24 h.

An independent check of the analytical procedure was also carried out weekly by direct titration of KOH solution against the HNO_3 one. The results were controlled by the Gran method [22] in order to ensure titre maintenance and the absence of carbon dioxide absorption.

3. Methodology

The alkalimetric titrations were carried out by adding KOH to the test solution placed in a thermostatic vessel, kept under a stream of purified argon presaturated with a 0.5 M KNO_3 solution.

The electrode standard potentials $E°$ were determined every day from the acid region of the titration run of a 0.005 M HNO_3 solution (0.5 M ionic strength buffer) against 0.1 M KOH. The $E°$ values were accepted only if their daily variation was within ± 0.2 mV and if the C_H (initial hydrogen ion amount inside the titration cell) calculated by HYPERQUAD [23,24] was in agreement with the analytical value within a 1% error. The response of the glass electrode was checked every week evaluating the pK_w value from the whole calibration curve (pH range 2.3–11.1). Values lower than 13.68 were considered not acceptable.

The linearity of $E°$ versus pH function was also checked; the slope of the straight line obtained was, within the experimental errors, coincident with the Nernst value ($r^2 > 0.9999$; slope = 59.18 ± 0.02).

For the determination of complexes formation constants, solutions of various metal and ligand concentrations were titrated with KOH. Before the titrations all the solutions were acidified with a known excess of nitric acid. The ionic strength was kept constant at 0.5 M by adding solid KNO_3. The initial volumes were 25 ml for cadmium(II) containing systems and 5 ml for the lead(II) ones.

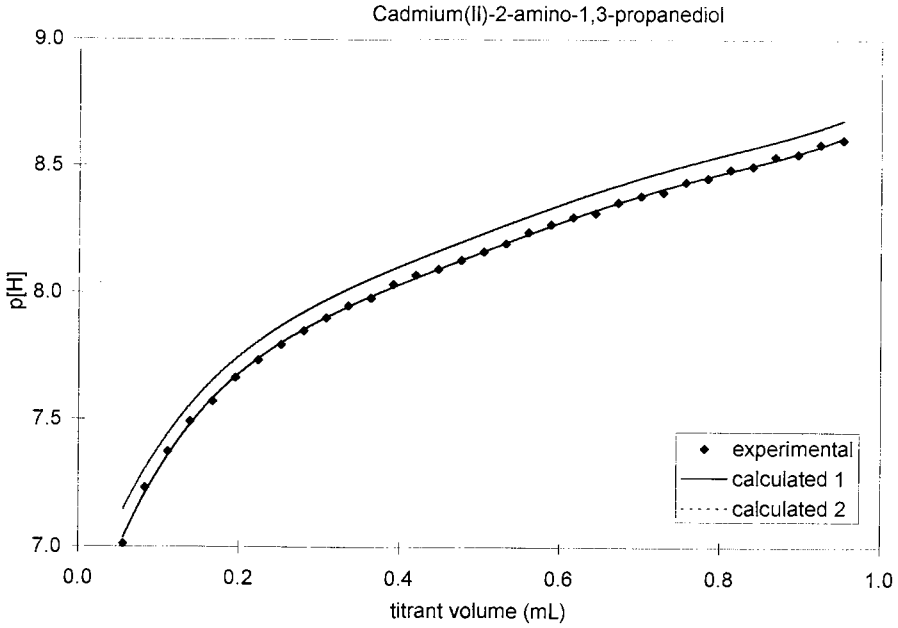

Fig. 1. Comparison between experimental and calculated curves related to either the ML, ML_2 model (calculationd 1) or to a model in which only the hydrolysis constants [25] are considered (calculation 2). $C_L = 10.00$ mM; $C_M = 0.95$ mM; $C_H = 10.00$ mM; $I = 0.5$ M KNO_3; $T = 25$°C.

All the calculations for the calibration of the glass electrode and for the determination of the complex formation constants were carried out by employing the HYPERQUAD least squares computer program [23,24]. The errors of e.m.f. and titrant volume were estimated as 0.2 mV and 0.002 ml respectively. During the refinement of $\log \beta$ values the protonation constants were fixed and the hydroxyl species formation constants were considered as known [25] and no attempts were made to adjust their values.

4. Results

In the study of lead(II) and cadmium(II) complexation equilibria with the selected amino-alcohols, the first problem that needed to be dealt with was the competition between complex and hydroxyl-species formation equilibria, whose presence is not negligible in the systems examined. The occurrence of precipitate formation in fact causes, especially for cadmium(II) systems, severe limitations for the pH ranges, and the ligand and metal analytical concentrations (C_L and C_M, respectively) in which the potentiometric measurements are possible. For the choice of optimal operative conditions, a preliminary study had to be carried out for each system. Semi-quantitative titrations were performed outside the titration cell in order to make clearer the occurrence of precipitate formation. The C_L and C_M values were varied within 2.00–10.00 and 0.60–2.00 mM ranges, respectively.

4.1. Cadmium(II) complexes

In Table 1 the experimental conditions for the potentiometric runs of the cadmium(II)-2-amino-1-propanol system, are reported as an example. Similar conditions have been employed for all the other ligands. For all the cadmium systems the acceptable pH ranges are extremely narrow and potentiometric titrations were possible only at high C_L/C_M ratios. In order to obtain a number of experimental points sufficient for evaluation

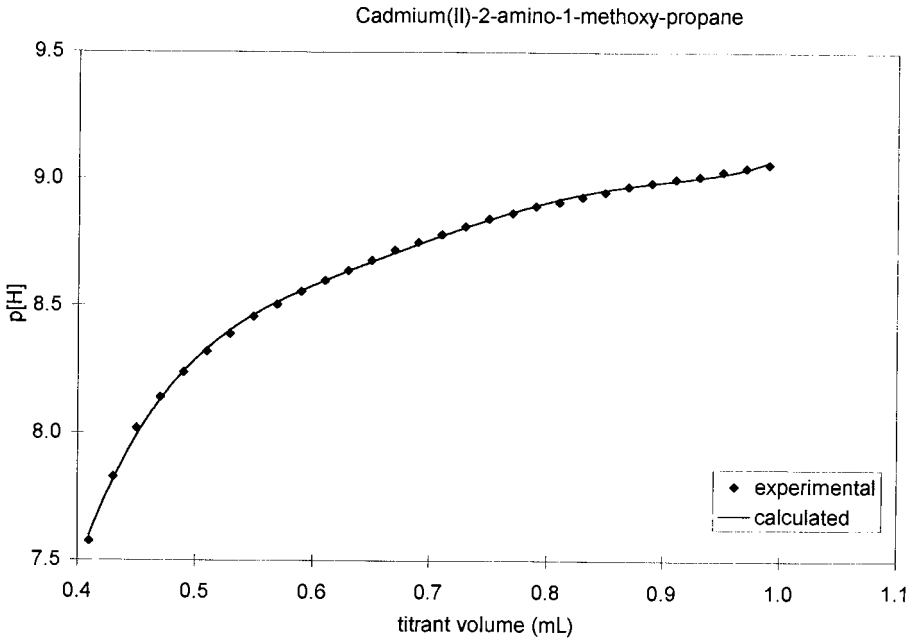

Fig. 2. Comparison between experimental and calculated curves related to a model in which only the hydrolysis constants [25] are considered. $C_L = 9.20$ mM; $C_M = 0.95$ mM; $C_H = 11.00$ mM; $I = 0.5$ M KNO_3; $T = 25$°C.

without decreasing too much the titrant addition volumes (which were maintained at values of ≥ 5 μl) the use of 25 ml cell has been preferred and each titration has been replicated three times. The calculations were made considering one by one each set of replicate runs and then an overall data evaluation was performed. The hydrolysis constants $\log \beta_{01-1} = -9.65$ and $\log \beta_{01-2} = -19.8$ were used for all the calculations.

The $\log \beta$ values resulted from the overall evaluation of data related to cadmium(II) complexes, together with statistical parameters χ_2 and σ supplied by HYPERQUAD [23,24], are reported in Table 2. As can be noted the resulting errors are higher than the usual ones. In fact, due to the complex weakness, even at the highest C_L/C_M ratios, no more than 30% of the metal had been complexed before precipitation occurred. In these conditions, the errors due to the analytical concentrations and the protonation constants inaccuracies became considerable and are heavily reflected on the $\log \beta$ S.D.s. Furthermore, in these adverse conditions, the speciation study was also hampered, and only the most probable species (ML and ML_2) have been looked for.

Notwithstanding the high S.D. of the constants values, the reliability of the data reported is ensured by the reproducibility of the results and by the satisfactory agreement of the experimental and calculated data (Fig. 1).

The complex species related to the ligands L_I and L_{III} were systematically rejected by the elaboration program. In Fig. 2 the experimental and calculated curves related to the system containing cadmium(II) and L_{III} ($C_L/C_M = 10$) are reported. The same behavior has been observed in the presence of L_I. From the examination of Fig. 2, in which, in spite of the behavior shown in Fig. 1, the experimental data agree with the curve calculated considering only the hydroxyl species, it is evident that, in the experimental conditions examined, no complex species are formed in detectable amounts.

4.2. Lead(II) complexes

Experimental conditions chosen for potentiometric runs of lead(II)–2-amino-1-propanol sys-

Table 3
Initial analytical C_L,C_M and C_H, C_L/C_M ratios and pH ranges employed in potentiometric titrations of lead(II)–2-amino-1-propanol

Experiment No.	C_L	C_M	C_L/C_M	C_H	pH ranges
1	1.51	0.99	1.5	1.60	6.45–7.89
2	2.00	0.99	2.0	2.20	6.20–8.67
3	4.80	1.97	2.4	5.28	6.33–8.73
4	4.80	1.58	3.0	5.28	6.64–8.66
5	3.20	0.99	3.2	3.52	6.02–8.82
6	2.00	0.59	3.4	2.20	6.84–8.61
7	4.80	0.99	4.8	5.28	6.19–8.83
8	7.61	1.46	5.2	8.37	6.20–8.80
9	10.00	1.98	5.0	11.00	6.18–8.88
10	7.61	0.99	7.7	8.37	6.13–9.05
11	10.00	1.46	6.8	11.00	6.15–8.99
12	10.00	0.99	10.1	11.00	5.90–9.02
13	6.06	0.59	10.3	6.61	5.87–9.08

Data is in mM.
$I = 0.5$ M KNO_3; $T = 25$°C.

Table 4
Formation constants of complexes formed between L_I, L_{II}, L_{III}, L_{IV}, L_V, L_{VI}, with lead(II) and related statistical parameters obtained by overall evaluation of data at $I = 0.5$ M KNO_3 and $T = 25$°C.

	L_I	L_{II}	L_{III}	L_{IV}	L_V	L_{VI}
pK_a^a	10.599 (3)	9.450 (6)	9.424 (2)	9.554 (5)	9.766 (3)	8.786 (1)
Log $\beta_{1,1,0}$ (log K_1)	5.42 (3)	4.20 (3)	4.12 (4)	4.30 (5)	4.49 (2)	—
Log $\beta_{2,1,0,}$	10.30 (1)	8.25 (1)	8.19 (3)	8.35 (3)	8.65 (3)	—
Log K_2	4.88	4.05	4.07	4.05	4.16	—
χ_2	8.94	8.70	12.00	11.79	9.60	—
σ	1.04	0.95	1.11	1.00	0.88	—

[a] [15]

tem are reported in Table 3. Similar conditions have been employed for all the other ligands. For the lead(II)–2-amino-1,3-propandiol system, precipitation readily occurs even at the highest C_L/C_M ratios in slightly acidic conditions (pH ≈ 6) so that the allowable pH range is so narrow that the potentiometric study of the complexation equilibria is not possible.

For the other lead(II) systems, the study was possible in a quite wide range of pH values. The hydrolysis constants $\log \beta_{01,-1} = -7.75$, $\log \beta_{01,-2} = -17.2$, $\log \beta_{03,-4} = -23.3$, $\log \beta_{04,-4} = -19.90$ and $\log \beta_{06,-8} = -42.60$ [25] were used in all the calculations. In addition to the ML and ML_2 complexes, species like MLOH, ML_2OH, $ML(OH)_2$, ML_3, M_2L, M_2L_2 and M_2LOH were tried one at a time and in different combinations.

Due to the presence of the hydrolitic species PbOH, $Pb_3(OH)_4$ and $Pb_6(OH)_8$, which in these conditions are predominant, the results related to experimental runs at $C_L/C_M \leq 3$ were unsatisfactory. The respective experimental runs were then not considered in the successive evaluations. The results of the calculations, which allowed the rejection of all the species tried, with the exception of the ML and ML_2 ones, are reported in Table 4. The values of the statistical parameters obtained indicate the good reliability of the results.

5. Discussion

From a first examination of the formation constant values reported in Tables 2 and 4, it is

evident that the strength of the complexes, for both metal ions, generally follows the ligand basicity order. In particular, the insertion of hydroxyl groups into the ligand structure causes a general decrease of the complexes strength, in agreement with the lowering of the pK_a values due to the withdrawing effect discussed previously [15]. It is then presumed that the coordination occurs mainly by means of the amino group. The dependence is stronger for lead(II) systems with respect to the cadmium(II) ones, according with the stronger 'hard' character of the first metal. However, it is worth noting that, while for the lead(II) systems, the difference between the pK_a and $\log \beta_{1,1,0}$ values remains roughly constant, when the cadmium(II) ion is involved in the coordination, that difference decreases with the increase in the number of hydroxyl groups present in the ligand structure. The behaviour of systems containing L_{VI} is, it is proposed, particularly representative. The interaction of this ligand with lead(II) is too weak to efficiently compete with precipitation equilibria, accordingly with the low amino group basicity. This fact supports the hypothesis that lead(II) complexes are formed via NH_2 coordination. On the other hand, in the presence of cadmium(II), the complexes formed with the same ligand are stronger than expected on the basis of the pK_a values. Furthermore, considering that no complexes are formed between cadmium(II) and L_I, in spite of its basicity, and that, as already noted, complexes between cadmium(II) and L_{III}, which has a pK_a and a structure similar to the L_{II} ones, are too weak to be detected, it seems probable that the OH groups are also involved in the complexation of cadmium(II). The contribution of neutral OH groups has already been proposed by other authors [9] in similar systems.

As for the lead(II) systems, the absence of a neutral OH contribution in the complex formation, is confirmed also by the $\log \beta$ values related to L_{II} and L_{III}, which, according to their pK_a values, are very similar.

As regards the length of the alkyl residual, an increase of the number of C-atoms causes an increase of complex strength, which follows the variation of NH_2 basicity due to the field effect [15]. As suggested by the value of $\log \beta_{110}/\log \beta_{210}$ ratio, which is almost independent on the ligand structure, the steric hindrance of the ligands does not seem to influence the complex strength. This is not surprising for large ions as cadmium(II) and lead(II), also considering that no more than two ligands per metal ions are bounded.

Acknowledgements

This work was financially supported by a National Project of Italian M.U.R.S.T., Rome, Italy.

References

[1] A. Braibanti, G. Mori, F. Dallavalle, L. Leporati, J. Chem. Soc. Dalton Trans. (1975) 1319.
[2] A. Braibanti, G. Mori, F. Dallavalle, J. Chem. Soc. Dalton Trans. (1976) 826.
[3] A. Braibanti, G. Mori, F. Dallavalle, J. Chem. Soc. Dalton Trans. (1979) 1050.
[4] C. Van Poucke, Z. Eeckhaut, Bull. Soc. Chim. Belg. 81 (1972) 363.
[5] B.A. Timini, D.H. Everett, J. Chem. Soc. B (1968) 1380.
[6] D.J. Alner, R.C. Lansbury, A.G. Smeeth, J. Chem. Soc. A (1968) 417.
[7] J.J. Christensen, R.M. Izatt, D.P. Wrathall, L.D. Hansen, J. Chem. Soc A (1969) 1212.
[8] A.Y. Sychev, A.P. Gerbeleu, P.K. Migal, Russ. J. Inorg. Chem. 8 (1963) 1081.
[9] I. Cukrowski, F. Marsicano, R.D. Hancock, P.T. Tshetlho, W.A.L. Van Otterlo, Polyhedron 14 (1995) 1661.
[10] P.K. Migal, A.N. Pushnyak, Russ. J. Inorg. Chem. 5 (1960) 293.
[11] J.M. Antelo, F. Arce, J. Casado, M.C. Regal, A. Varela, J. Chem. Res (1982) 144.
[12] L. Bologni, A. Sabatini, A. Vacca, Inorg. Chim. Acta 69 (1983) 71.
[13] K.S. Bai, E. Martell, J. Inorg. Nucl. Chem. 31 (1969) 1697.
[14] W. Forsling, Acta Chem. Scand. A 32 (1978) 57.
[15] S. Canepari, V. Carunchio, P. Castellano, A. Messina, Talanta 44 (1997) 2059.
[16] D. Masi, C. Mealli, M. Sabat, A. Sabatini, A. Vacca, F. Zanobini, Helv. Chim. Acta 67 (1984) 1818.
[17] J.L. Hall, J.A. Swisher, D.G. Brannon, T.M. Liden, Inorg. Chem. 1 (1962) 409.
[18] J.L. Hall, W.E. Dean, E.A. Pacofsky, J. Am. Chem. Soc. 82 (1960) 3303.
[19] F. Arce, C. Blanco, J. Casado, Talanta 33 (1986) 1031.

[20] J.A. Santaballa, C. Blanco, F. Arce, J. Casado, Talanta 32 (1985) 931.
[21] A.I. Vogel, A Text Book of Quantitative Inorganic Analysis, 3rd ed., chap. 4, Longmans, London, 1961.
[22] G. Gran, Analyst 77 (1952) 661.
[23] P. Gans, A. Sabatini, A. Vacca, Coord. Chem. Rev. 120 (1992) 389.
[24] P. Gans, A. Sabatini, A. Vacca, J. Chem. Soc. Dalton Trans. (1985) 1195.
[25] R.M. Smith, A.E. Martell, Critical Stability Constants, vol.4, Plenum, New York, 1976 (and references therein).

ELSEVIER

Talanta 47 (1998) 1085–1092

Talanta

A simple method for the spectrophotometric determination of atrazine using *p*-aminoacetophenone and its application in environmental and biological samples

Ritu Kesari, V.K. Gupta *

School of Studies in Chemistry, Pt. Ravishankar Shukla University, Raipur (M.P.), 492010, India

Received 22 October 1997; received in revised form 30 March 1998; accepted 3 April 1998

Abstract

A spectrophotometric method is described for the determination of the widely used herbicide, atrazine. Atrazine reacts with pyridine and forms a quaternary halide which adds a hydroxyl group in the presence of alkali to form a carbinol base. The heterocyclic ring of the resulting carbinol breaks forming a glutaconic dialdehyde which is subsequently coupled with *p*-aminoacetophenone (PMP) to form a yellow orange polymethine dye. Beer's law is obeyed in the range 0.16–1.6 ppm of atrazine at 470 nm. The method is sensitive and free from the interference of most of the foreign species. The analytical parameters have been optimised and the method has been successfully applied to the determination of atrazine in various environmental and biological samples. © 1998 Elsevier Science B.V. All rights reserved.

Keywords: Spectrophotometric determination; Atrazine; *p*-Aminoacetophenone

1. Introduction

Atrazine (2-chloro-4-ethylamino-6-isopropylamino-*S*-triazine) is widely used as a selective, pre- and post-emergence herbicide on many crops including corn, coriander, sugarcane, sorghum, pineapple, orchards, etc. It is also used as a non-selective herbicide for vegetation control on non-crop land. Atrazine is toxic to animals and man. It produces strong eye irritation, weakness, lethargy, anorexia, diarrhoea, spasticity of muscles of mouth and limbs etc. [1–3]. Its toxic properties also include mutagenic and embryotoxic effects [4]. The acute oral LD_{50} value for rats proposed for atrazine is 3080 mg/kg [2,5]. A workplace airborne control limit, i.e. TLV of 5 mg/m^3 has been recommended by ACGIH [3].

Because of wide uses and toxicity of atrazine, a large number of instrumental methods such as GLC [6], HPLC [7], TLC [8], LC [9], enzyme immunoassay [10], etc. are reported for its determination. Very few reagents such as *p*-aminobenzoic acid [11], ethylcyanoacetate [12], and picric

* Corresponding author.

0039-9140/98/$ - see front matter © 1998 Elsevier Science B.V. All rights reserved.
PII S0039-9140(98)00168-4

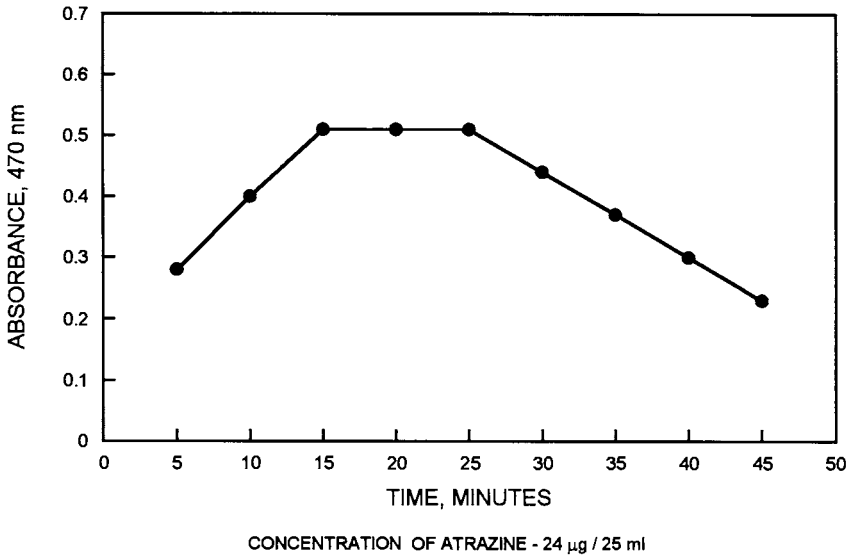

Fig. 1. Effect of time of heating with pyridine reagent on colour reaction.

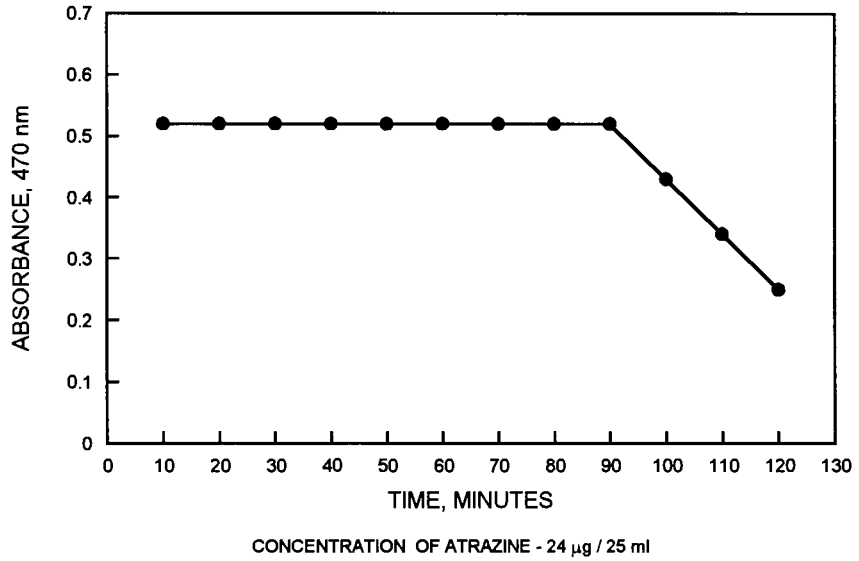

Fig. 2. Effect of time on stability of dye.

acid [13] are reported for the spectrophotometric determination of atrazine.

In this communication a simple and sensitive method based on Konig's reaction is discussed for the determination of atrazine. Atrazine is first reacted with pyridine and converted into a quaternary pyridinium halide, subsequently it adds a hydroxyl group in the presence of alkali to form a carbinol base. In the second step a glutaconic dialdehyde is formed due to breaking of the heterocyclic linkage of the carbinol. Finally the glutaconic dialdehyde couples with *p*-aminoacetophenone in acidic medium to form a yellow-orange polymethine dye which showed maximum

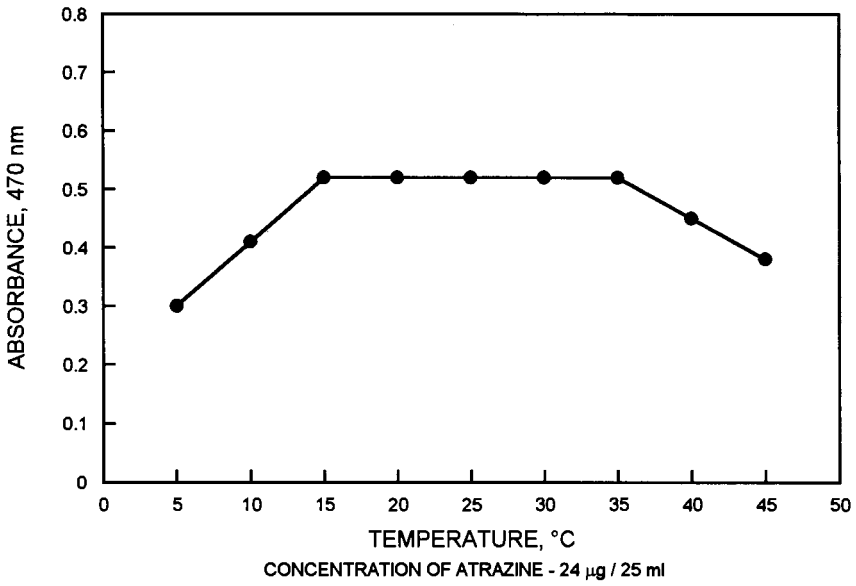

Fig. 3. Effect of temperature on colour reaction.

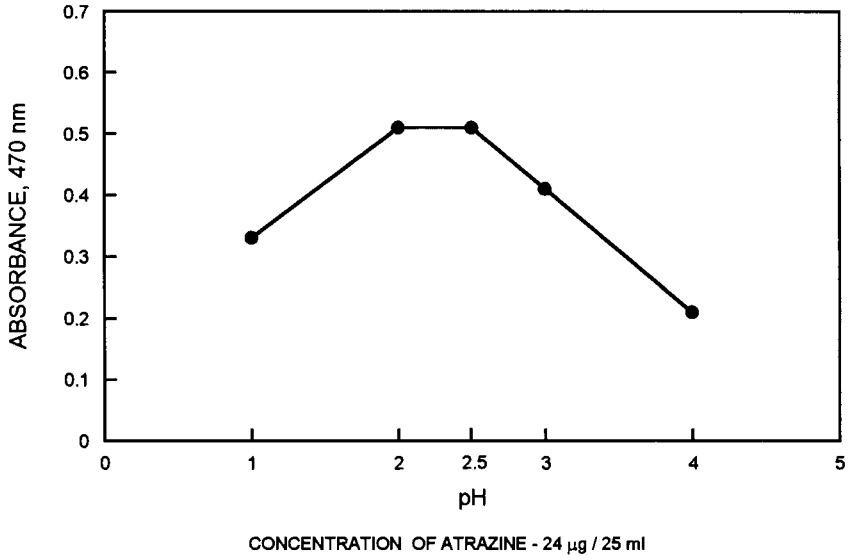

Fig. 4. Effect of pH on colour reaction.

absorbance at 470 nm. Different analytical parameters, i.e. time, pH, reagent concentration and temperature have been investigated for optimum sensitivity. The method has been successfully applied for the determination of atrazine in grains, fruits, vegetables, soil, water and biological samples.

2. Experimental

2.1. Apparatus

A UV–vis Spectrophotometer model 108 with matched silica cells was used for all spectral measurements. pH measurements were made with Systronics pH meter model 331.

Table 1
Effect of foreign species on the determination of atrazine (concentration of atrazine—10 μg/25 ml)

Foreign species	Tolerance limit* (ppm)	Foreign	Tolerance limit* (ppm)
Ethanol	2000	Mg^{2+}, Ca^{2+}	700
Carbaryl	1500	Al^{3+}, Cd^{2+}	300
Propoxure		Cu^{2+}, Fe^{2+}, Fe^{3+}	
Paraquot	750	PO_4^-, NO_3^-	200
Parathion		SO_4^{2-}	50
Aldrin	500		
BHC, dimethoate	400		
Kelthane	250		
Phenol	200		
Formaldehyde	80		
Ammonia	50		

*The amount causing the error of $\pm 2\%$ in the absorbance values.

2.2. Reagents

All chemicals used were of AnalaR grade or similar. Demineralised, doubly distilled water was used throughout the experiment.

2.3. Atrazine (Northern Minerals Ltd.)

A stock solution of 1 mg ml^{-1} was prepared in methanol. A working standard of 10 μg ml^{-1} was prepared by appropriate dilution of the stock solution with water.

2.4. Pyridine reagent (BDH)

3 ml of concentrated hydrochloric acid was mixed with 18 ml of freshly distilled pyridine and 12 ml of water were mixed into it [11].

2.5. p-Aminoacetophenone (PAAP) (Ferak Berlin)

A 1% (w/v) solution was prepared in 1:4 hydrochloric acid.

2.6. Sodium hydroxide

A 2 M aqueous solution was used.

2.7. Procedure

An aliquot of standard solution containing 4–40 μg of atrazine was taken in a graduated tube. To it, 0.2 ml pyridine reagent was added. This solution was placed on a boiling water bath for 15 min and then allowed to cool at room temperature. Now 1 ml of 2 M sodium hydroxide and 2 ml of *p*-aminoacetophenone solutions were added. The solution was kept for 5 min for complete colour development and then made up to the mark with water. The absorbance was measured at 470 nm against demineralised water as reference.

3. Results and discussion

3.1. Spectral characteristics

The colour system shows the maximum absorbance at 470 nm whereas the reagent blank has negligible absorbance at this wavelength. The colour system obeys Beer's law over the range 4–40 μg of atrazine per 25 ml of final solution (0.16–1.6 ppm) at 470 nm. The molar absorptivity and Sandell's sensitivity were found to be 1.1×10^5 (± 100) 1 mol^{-1} cm^{-1} and 0.001 μg cm^{-2}, respectively.

3.2. Effect of reagent concentration

The effect of various reagent concentration on the colour reaction was studied. It was found that under optimum conditions 0.2 ml of pyridine reagent and 1 ml of 2 M sodium hydroxide solution were required for the reaction. It was also found

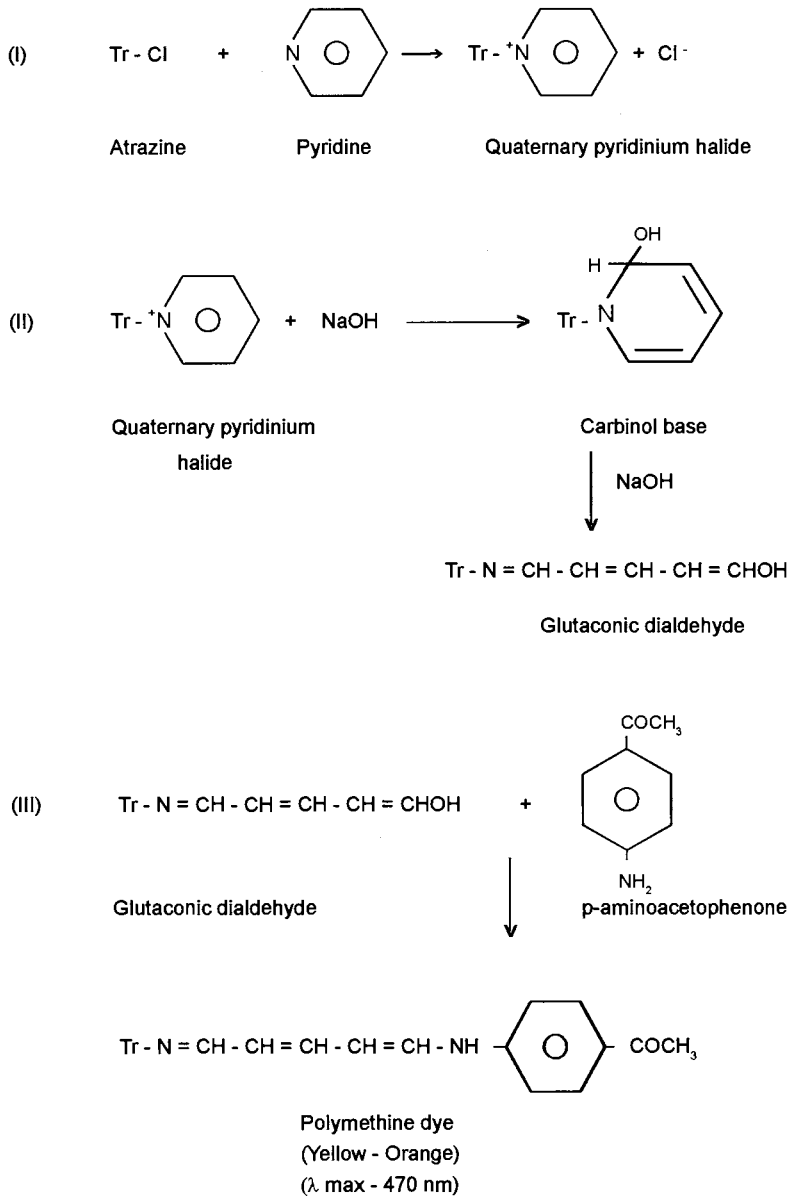

Scheme 1.

found that 2 ml of *p*-aminoacetophenone was sufficient for complete colour development. It was observed that if the proposed reagent concentration is decreased the absorbance value is also decreased.

3.3. Effect of time and temperature

Maximum colour intensity was observed when the solution containing pyridine reagent was heated for 15 min on a boiling water bath and then allowed to cool at room temperature. The coloured dye was found to be stable for 90 min in the temperature range 15–35°C. (Fig. 1, Fig. 2, Fig. 3).

3.4. Effect of pH

The effect of pH on the colour reaction was studied and it was found that the polymethine dye

Table 2
Application of the method for the determination of atrazine in plant materials and grain

Sample	Amount of atrazine (μg)			Recovery %	
	Added	Found*		(A)	(B)
		(A)	(B)		
Pineapple**	5	4.89 (±0.01)	4.80	97.8 (±0 3)	96.00
	10	9.90 (±0.02)	9.70	99.0 (±0.2)	97.00
	15	14.85 (±0.02)	14.50	99.0 (±0.1)	96.00
Potato**	5	4.90 (±0.01)	4.85	98.1 (±0.3)	97.00
	10	9.79 (±0.02)	9.50	97.9 (±0.2)	95.00
	15	14.82 (±0.01)	14.30	98.8 (±0.1)	95.33
Corn**	5	4.90 (±0.03)	4.75	97.9 (±0.5)	95.00
	10	9.88 (±0.01)	9.88	98.8 (±0.1)	98.80
	15	14.79 (±0.02)	14.60	98.6 (±0.2)	97.35

* Mean of seven replicate analysis.
** Amount of samples—25 g.
A, proposed method; B, reported method [11].

was formed only under acidic conditions. The pH of the final solution was between 2 and 2.5 (Fig. 4).

3.5. Effect of foreign species

To assess the validity of the method, the effect of various common species and other pesticides was studied on the determination of atrazine. Known amount of foreign species and pesticides was added to a standard solution containing 10 μg of atrazine per 25 ml, prior to analysis and the solution was analysed by the proposed method. The tolerance limit of some pesticides and common ions are listed in Table 1.

3.6. Precision

Precision of the method was checked by analysing 10 μg of atrazine in 25 ml of final solution for a period of 7 days. The S.D. and R.S.D. were found to be ±0.006 and 3.0%, respectively.

3.7. Colour reaction

The probable colour reaction is shown in Scheme 1 and it can be explained in three steps—

1. Atrazine is reacted with pyridine and converted into a quaternary pyridinium halide;
2. Pyridinium halide further undergoes addition of hydroxyl group in the presence of alkali to form a carbinol base, which further undergoes breaking of heterocyclic ring forming glutaconic dialdehyde;
3. Glutaconic dialdehyde couples with *p*-aminoacetophenone in acidic medium to give a yellow-orange polymethine dye.

3.8. Application

The proposed method has been satisfactorily applied for the determination of atrazine in various environmental and biological samples.

3.8.1. Determination of atrazine in plant materials

Different samples of fruits and vegetables, free from atrazine were taken. The samples were weighed, crushed and spiked with known amounts of atrazine and kept for 1 day. The samples were washed with 100 ml of water. From this water atrazine was extracted with two 10-ml portions of chloroform. The chloroform extract was evaporated to dryness and the residue was dissolved in 25 ml of methanol. Aliquots of the above solution

Table 3
Application of the method for the determination of atrazine in water and soil

Sample	Amount of atrazine (μg)			Difference	Recovery %
	Originally found*	Added	Total found*		
	(a)	(b)	(c)	(c−a)	(c−a)×100/b
Water**	4.14 (±0.02)	5	9.08 (±0.04)	4.94	98.9 (±0.9)
	4.44 (±0.03)	10	14.10 (±0.03)	9.66	96.5 (±0.5)
	4.46 (±0 02)	15	19.00 (±0.03)	14.54	96.9 (±0.2)
Soil**	4.31 (±0.02)	5	9.15 (±0.02)	4.84	96.9 (±0.4)
	3.95 (±0.01)	10	13.79 (±O.03)	9.84	98.4 (±0.2)
	3.97 (±0.01)	15	18.77 (±0.02)	14.80	98.6 (±0.2)

* Mean of seven replicate analysis.
** Amount of water sample—100 ml.
*** Amount of soil sample—50 g.

were taken and analysed by the proposed and the reported method [11] (Table 2).

3.8.2. Determination of atrazine in grains

Since the grain samples obtained from the market were found to be free from atrazine, known amount of atrazine was added to the samples to check the recovery. The samples were kept for 1 day and atrazine was extracted with two 10-ml portions of chloroform. The chloroform extract was evaporated to dryness and the residue was dissolved in 25 ml of methanol. Aliquots were taken and analysed by the proposed and the reported method [11] (Table 2).

Table 4
Application of the method for the determination of atrazine in biological samples

Sample	Amount of atrazine (μg)		Recovery %
	Added	Found*	
Blood**	5	4.89 (±0.01)	97.9 (±0.3)
	10	9.80 (±0.02)	98.0 (±0.2)
	15	14.89 (±0.02)	99.2 (±0.2)
Urine**	5	4.85 (±0.01)	96.8 (±0.3)
	10	9.79 (±0.02)	97.9 (±0 3)
	15	14.90 (±0.02)	99.3 (±0.2)

*Mean of seven replicate analysis.
**Amount of samples—2 ml.

3.8.3. Determination of atrazine in soil samples

Various soil samples were collected from an agricultural field where atrazine was sprayed as herbicide. Samples were weighed and finely ground. These samples were washed with two 10-ml portions of methanol. The washing was collected and made up to 25 ml with methanol. Aliquots were then analysed as described above (Table 3).

3.8.4. Determination of atrazine in water

Water samples were collected from an agricultural field where atrazine was sprayed. The samples were extracted with two 10-ml portions of chloroform. The extract was then evaporated to dryness and the residue was dissolved in 25 ml of methanol. Aliquots were then analysed as described above (Table 3).

3.8.5. Determination of atrazine in biological samples

Since the presence of atrazine in biological samples has been reported [14], synthetic samples were prepared by adding known amount of atrazine to blood and urine samples, which were found to be free from atrazine. Two ml aliquots of blood and urine samples were taken and deproteinised by adding 2 ml of 1% trichloroacetic acid [15]. After 15 min the mixture was centrifuged and the supernatant solution was transferred in to a 25 ml graduated tube and analysed as described above. The results of the analysis are shown in Table 4.

4. Conclusion

The present method provides simple, sensitive and rapid spectrophotometric procedure for the quantitative determination of atrazine. The method is fairly reproducible and free from the interference of a large number of foreign species. The method has also been compared with recently reported spectrophotometric method and found to be more sensitive. The proposed method can be applied for the determination of atrazine in various environmental and biological samples.

Acknowledgements

The authors are grateful to Pt. Ravishankar Shukla University for providing facilities. One of them (Ritu Kesari) is thankful to Pt. Ravishankar Shukla University for providing a research scholarship.

References

[1] G.S. Gruzdev, The Chemical Protection of Plants, Mir Publishers, Moscow (1983) p. 401.
[2] H. Martin, Pesticide Manual, Basic Information on the Chemical Used as Active Components of Pesticides, 1st Ed., British Crop Protection Council (1968) p. 23.
[3] G.D. Clayton, E.E. Clayton, Industrial Hygiene and Toxicology, Vol. ll, Part E, 4th Ed., Wiley, New York (1994) p. 3405.
[4] V. Mersch-Sundermann, U. Schneider, G. Klopman, H.S. Rosenkranz, Mutagenesis 9 (1994) 205.
[5] R.W. Stewens, Pesticide in the Environment, Vol. 1, Part 1, Marcel Dekker Inc., New York (1977) p. 57.
[6] D.S. Gamble, M.l. Haniff, R.H. Zienus, Anal. Chem. 58 (1986) 732.
[7] A. Dandkwrdt, S. Pullen, S. Rauchalles, K. Kramer, F. Just, B. Hock, Anal. Lett. 28 (1995) 621.
[8] H. Zahradnickova, P. Simek, P. Horicova, J. Triska, J. Chromatogr. A 688 (1994) 383.
[9] D.C. Holland, R.K. Munns, J.E. Roybal, J.A. Hurlbet, A.R. Long, J. AOAC Int. 78 (1995) 25.
[10] B. Grussener, N.C. Shambaugh, W.C. Watzin, Environ. Sci. Technol. 29 (1995) 1067.
[11] J.V. Das, V.K. Gupta, J. lndian Chem. Soc. 72 (1995) 765.
[12] T.M. Vickrey, D.L. Karlesky, G.L. Blackmer, J. AOAC Int. 63 (1980) 506.
[13] V. Nastasa, R. Cuciureanu, Rev. Med. Chir. 88 (1984) 319 (Rom.); CA 103 (1985) 225.
[14] Lu Chensheng, L.C. Anderson, R.A. Fenske, J. Toxicol. Environ. Health 50 (1997) 101.
[15] M. Rai, K.N. Ramchandran, V.K. Gupta, Analyst 119 (1994) 1883.

ELSEVIER

Talanta 47 (1998) 1093–1098

Talanta

Kinetic-catalytic determination of traces of iron by the oxidative coupling reaction of 3-methyl-2-benzothiazolinone hydrazone with *N*,*N*-dimethylaniline

Takashi Tomiyasu [1,a], Norio Teshima [a], Shigenori Nakano [b], Takuji Kawashima [a,*]

[a] *Laboratory of Analytical Chemistry, Department of Chemistry, University of Tsukuba, Tsukuba, 305-8571, Japan*
[b] *Chemical Institute, Faculty of Education, Tottori University, Koyama-cho, Tottori, 680-0945, Japan*

Received 5 March 1998; received in revised form 20 April 1998; accepted 21 April 1998

Abstract

A new kinetic-catalytic method by the initial rate procedure for the determination of nanogram level of iron(III) is developed, which is based on its catalytic effect on the oxidative coupling of 3-methyl-2-benzothiazolinone hydrazone (MBTH) with *N*,*N*-dimethylaniline (DMA) to form an indamine dye ($\lambda_{max} = 590$ nm) in the presence of hydrogen peroxide. Iron(II) is also determined, being oxidized to iron(III) by hydrogen peroxide. Calibration graphs obtained by the initial rate method are linear in the range 1–1000 ng ml^{-1} Fe and as low as 10^{-8} M Fe(II, III) can easily be determined. The relative standard deviations are 6.6, 2.5 and 1.5% for ten determinations of 1, 20 and 60 ng ml^{-1} of Fe(III), respectively. The method is applicable to the determination of iron in natural waters without preconcentration and separation. © 1998 Published by Elsevier Science B.V. All rights reserved.

Keywords: Catalytic method; Initial rate; Iron determination; 3-Methyl-2-benzothiazolinone hydrazone; *N*,*N*-dimethylaniline; Oxidative coupling

1. Introduction

Determination of iron is important, because it plays an important role in an ecological system. Iron is widely distributed at various concentration levels throughout the environment and it occurs at low concentration in various natural waters [1,2]. Thus a sensitive method having a wide determinable range is required for the determination of iron in environmental waters. For this purpose, the kinetic-catalytic method has become an attractive procedure because of high sensitivity and sufficient accuracy without expensive and special equipments. Many kinetic-catalytic methods have been reported for the iron determination. Some of them were applied to water samples, but were less reproducible at lower concentrations of iron [3–7]. Methods, utilizing the oxidative cou-

* Corresponding author. Tel.: +81 298 536503; e-mail: kawasima@staff.chem.tsukuba.ac.jp

[1] On research leave from Kagoshima University, Japan.

0039-9140/98/$ - see front matter © 1998 Published by Elsevier Science B.V. All rights reserved.
PII S0039-9140(98)00164-7

pling of *p*-anisidine [8,9], *N*-phenyl-*p*-phenylenediamine [10] and 4-aminoantipyrine [11] with *N*,*N*-dimethylaniline (DMA) in the presence of hydrogen peroxide, the oxidation of *N*,*N*-dimethyl-*p*-phenylenediamine by hydrogen peroxide [12], the oxidation of chlorpromazine by hydrogen peroxide [13] as indicator reactions have been proposed and these methods have sufficient sensitivity to determine iron at the ng level. However, their determinable ranges are not wide enough and higher temperature such as 50°C [8,9] is needed to accelerate the reaction. Thus simple, rapid and reliable methods are still required from the practical point of view.

3-Methyl-2-benzothiazolinone hydrazone (MBTH) couples with DMA to form a violet compound ($\lambda_{max} = 590$ nm) in the presence of hydrogen peroxide. The reaction has already been utilized for the catalytic determinations of copper(II) [14,15], chromium(III) [16], manganese(II) [17,18] and cobalt(II) [19]. The present authors found that iron(II, III) also catalyzed this coupling reaction and the initial rate increased linearly with iron concentration. The initial rate procedure has some advantages and is sometimes preferable to the fixed time method [20]. In addition, the use of the initial rate as a parameter can be obtained a wider determinable range, i.e. two or three order of magnitude and a rapidity of the method [21]. This paper describes a new catalytic method employed the initial rate measurement for the determination of trace amounts of iron by means of the oxidative coupling of MBTH with DMA in the presence of hydrogen peroxide. The proposed method is rapid and highly sensitive, and has a wide dynamic range; only 30 s is required for a single run and 1–1000 ng ml^{-1} of iron can be determined with reasonable reproducibility. The method has been successfully applied to the determination of low levels of iron in natural water samples.

2. Experimental

2.1. Apparatus and reagents

A Japan Spectroscopic V-530 UV/VIS spectrophotometer installed with a thermostated cell holder (40 ± 0.1°C) was used for the absorbance measurements. The temperature was controlled with a Shibata control unit (CU-85) circulating thermostat bath. For the reaction, 1-cm glass cells were used. The reaction was initiated by the injection of a hydrogen peroxide solution from a Gilson Pipetman (Model P-200). For mixing, a remote-controlled magnetic Acrobat stirrer (MS, Osaka, Japan) was installed at the side of cell holder in the spectrophotometer.

The water used to prepare the solutions was purified with a Milli-Q PLUS water system (Millipore). Reagent-grade chemicals were used throughout.

An MBTH solution (0.045 M) was prepared by dissolving 1.05 g of 3-methyl-2-benzothiazolinone hydrazone hydrochloride, monohydrate in water and diluting to 100 ml with water. A DMA solution (2.0 M) was prepared in 2.0 M nitric acid solution: the equimolar acid was required to dissolve DMA in water. A hydrogen peroxide solution (3.0 M) was prepared by suitably diluting commercial 31% solution with water. An iron(III) standard solution (1000 mg l^{-1}) was obtained from Wako ($Fe(NO_3)_3$ in 0.1 M HNO_3). Working solutions were prepared by suitably diluting this solution with 0.1 M nitric acid. A stock solution of iron(II) (1000 mg l^{-1}) was prepared by dissolving 0.702 g of ammonium iron(II) sulfate hexahydrate (Mohr's salt) in 10 ml of 1 M hydrochloric acid and diluted to 100 ml with water. Working solutions were prepared by suitably diluting the stock solution with 0.1 M hydrochloric acid.

2.2. Recommended procedure

To 10.0 ml of sample solution in a glass-stoppered tube, 2.0 ml of DMA solution and 0.5 ml of 0.08 M nitric acid were added. The solution was thoroughly mixed. The mixed solution was then kept at 40°C in a water bath for about 15 min to achieve the required temperature. Then a 1.8 ml aliquot of the solution was taken into a 1-cm glass cell. The cell was placed in the holder at 40°C and the solution was magnetically stirred. To the solution in the cell, 0.13 ml

of MBTH solution (40°C) was added and the reaction was initiated by the injection of 0.07 ml of hydrogen peroxide solution (40°C). The increase in absorbance at 590 nm of the product was recorded against a pure-water reference for 30 s. The time can be reduced at higher concentrations of iron: for the determination of 200–1000 ng ml^{-1} iron, only 10 s is required to follow the reaction. The initial slope of absorbance/time curves, $R_0[=\Delta(abs)/\Delta(s)]$, was used as a parameter for the iron determination.

3. Results and discussion

3.1. Oxidative coupling reaction of MBTH with DMA by hydrogen peroxide and the accelerating effect of iron on the color development

In the presence of hydrogen peroxide, MBTH couples with DMA to form a violet compound ($\lambda_{max} = 590$ nm). The reaction is accelerated by trace amounts of iron(III) and can be followed by measuring the increase in absorbance at 590 nm (Fig. 1). The initial slopes of the absorbance/time curves [$\Delta(abs)/\Delta(s)$] were determined and then used as a measure of the initial reaction rate. As the slope, R_0, increases with an increase in the concentration of iron(III), it was used as the parameter for the iron determination. Iron(II) is also determined, being oxidized to iron(III) by hydrogen peroxide.

3.2. Effect of reaction variables

The influence of temperature on R_0 was studied over the range 25–50°C. Although higher sensitivity was obtained at higher temperatures, the rate of the uncatalyzed reaction became higher at temperatures higher than 40°C. A temperature of 40°C was thus chosen for the procedure. Nitric, hydrochloric, sulfuric and perchloric acids were examined as acidic media. Iron(III) showed the same catalytic effect in each acid medium, except sulfuric acid. An interference of copper(II) became larger in hydrochloric acid medium. Thus, nitric acid was used for adjustment of the pH of the reaction mixture. As shown in Fig. 2, the R_0 values in the presence of iron(III) increased with increasing pH, while the blank value kept low. However, the influence of interfering substances

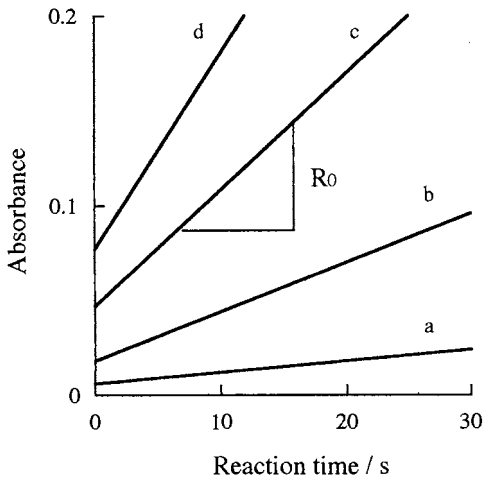

Fig. 1. Absorbance/time curves for the oxidative coupling of DMA with MBTH. Concentration of iron(III) (ng ml^{-1}): (a) 0, (b) 20, (c) 60, (d) 100. Conditions as in the recommended procedure (3×10^{-3} M MBTH, pH 2.2, 0.3 M DMA, 0.1 M hydrogen peroxide, 40°C). Initial slope of absorbance/time curve, $R_0(\Delta(abs)/\Delta(s))$, was used as a measure of the initial reaction rate.

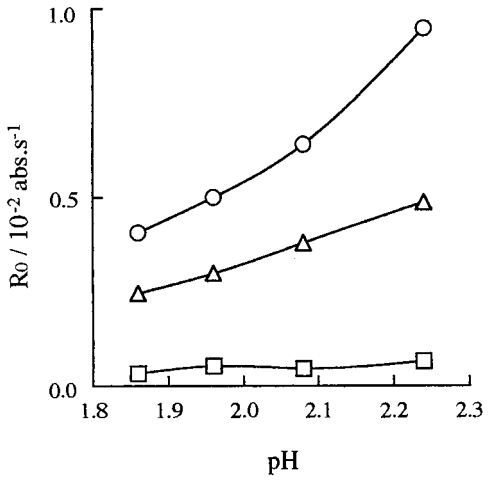

Fig. 2. Effect of pH. Concentration of iron(III) (ng ml^{-1}): (□) 0, (△) 50, (○) 100. Conditions as in Fig. 1, except for pH.

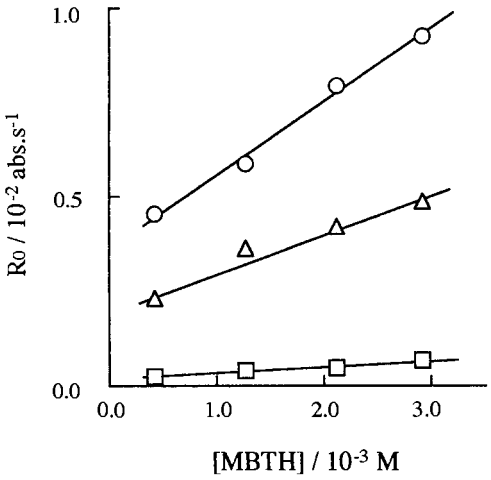

Fig. 3. Effect of MBTH concentration. Concentration of iron(III) (ng ml^{-1}): (□) 0, (△) 50, (○) 100. Conditions as in Fig. 1, except for the MBTH concentration.

such as copper(II) increased significantly at higher pH. A pH of 2.2 was chosen by considering the sensitivity and less interference of other ions. Fig. 3 shows the effect of MBTH concentration on R_0. The R_0 value increased with an increase in MBTH concentration in the presence of iron(III). A higher sensitivity can be realized at higher MBTH concentrations. A 3×10^{-3} M MBTH concentration was chosen by considering the sensitivity and the solubility of this reagent. The effect of DMA concentration was studied in the range 0.03–0.3 M. The higher sensitivity was obtained at higher DMA concentrations (Fig. 4). A 0.3 M DMA concentration was chosen, since it gave a higher sensitivity and a lower blank value. The effect of hydrogen peroxide concentration was examined in the range 0.02–0.13 M and the R_0 values of both blank and iron solutions remained constant over the concentration range examined. A 0.1 M hydrogen peroxide concentration was used for further investigations.

3.3. Calibration graph and reproducibility

The calibration graphs for iron(III) up to 1000 ng ml^{-1} were obtained by the recommended procedure. The equation of the line is represented as $R_0[= \Delta(\text{abs})/\Delta(s)] = 9.0 \times 10^{-5}[\text{Fe}] + 7.9 \times 10^{-4}$ from the graphs and the correlation coefficient is $r = 0.999$ ($n = 6$). The relative standard deviations for ten determinations of 2, 20, 60 ng ml^{-1} of iron(III) are 4.9, 2.5 and 1.5%, respectively; the lower limit of determination is 1 ng ml^{-1} with 6.6%. Since iron(II) showed the same catalytic effect as iron(III), the total iron concentration can be determined: 1–1000 ng ml^{-1} of iron(II, III) can be determined by the proposed method with good reproducibility.

3.4. Effect of foreign ions

The effect of various foreign ions on the determination of 50 ng ml^{-1} of iron(III) was examined by the proposed method. The following ions showed no interference up to at least the concentrations (μg ml^{-1}) indicated in parentheses: Cl^- (500); SO_4^{2-} (300); NO_3^- (200); Li(I), Na(I), K(I), Ca(II), Mg(II), Ni(II), Pb(II), Mn(II), Zn(II), Ba(II), ClO_3^-, Br^-, CH_3COO^- (100); NH_4^+, Co(II), Al(III) (50); Cr(III), BrO_3^-, CO_3^{2-} (10); V(V), IO_3^-, IO_4^-, SCN^-, PO_4^{3-} (1). The interfering ions at the amounts of 1000 ng ml^{-1} are listed in Table 1. Copper(II) and chromium(VI) seem to act as catalysts on the color formation reaction. Tartrate and citrate cause negative error for the iron determination, probably because these or-

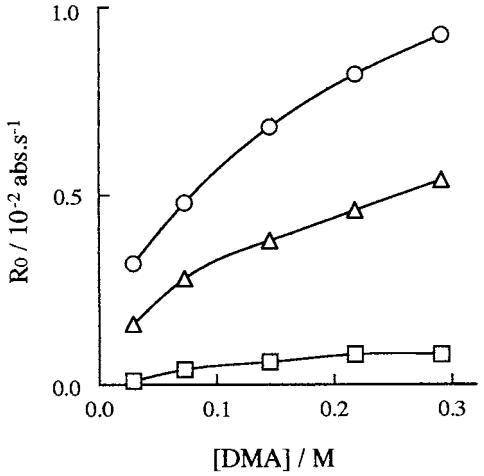

Fig. 4. Effect of DMA concentration. Concentration of iron(III) (ng ml^{-1}): (□) 0, (△) 50, (○) 100. Conditions as in Fig. 1, except for the DMA concentration.

Table 1
Effect of interfering ions on the determination of 50 ng ml^{-1} iron(III)

Ion	Added (ng ml^{-1})	Found (ng ml^{-1})	Error (%)
Cr(VI)	1000	87.0	+74.0
Cu(II)	1000	65.2	+30.4
Mo(VI)	1000	40.3	−19.4
W(VI)	1000	34.9	−30.2
$S_2O_3^{2-}$	1000	44.7	−10.6
$C_6H_5O_7^{3-}$	1000	28.1	−43.8
$C_4H_4O_6^{2-}$	1000	44.8	−10.4

ganic acids act as masking agents for iron(III). The formation of precipitate was observed in the presence of molybdenum(VI) and tungsten(VI). However, these interfering ions showed no interference at 100 ng ml^{-1} levels. Furthermore, the contents of these ions are usually very low in natural waters, thus no separation, preconcentration and masking processes are required for the iron determination. In the presence of V(V), Cr(VI), IO_3^-, IO_4^- and BrO_3^-, some coloration reactions occured before the addition of hydrogen peroxide. When an absorbance at a given reaction

Table 2
Determination of iron in water samples

Dilution (times)	Added (ng ml^{-1})	Found (ng ml^{-1})	In sample (ng ml^{-1})	Recovery (%)
Tap water				
1	0	15.0	15.0	—
2	0	8.0	16.1	—
2	10	17.0	—	94.4
2	20	26.1	—	93.2
5	0	3.3	16.6	—
5	10	13.7	—	103
5	20	23.1	—	99.1
10	0	1.5	14.5	—
Ave.			15.5	97.5
Ground water[a]				
1	0	11.6	11.6	—
2	0	6.4	12.8	—
2	10	15.4	—	93.7
2	20	24.4	—	92.5
5	0	2.5	12.4	—
5	10	12.2	—	97.3
5	20	22.7	—	101
10	0	1.0	10.1	—
Ave.			11.7	96.1
Pond water[a]				
1	0	394.3	394	—
2	0	191.2	382	—
2	10	203.5	—	101
2	20	216.2	—	102
5	0	77.1	385	—
5	10	87.0	—	99.9
5	20	93.1	—	95.8
10	0	38.4	384	—
Ave.			386	99.8

[a] Tap, ground and pond waters were collected at Tsukuba City.

time was used as a parameter, this color formation may cause a positive error for the iron determination. By using the initial reaction rate as a parameter, such interferences from these ions could be effectively avoided.

3.5. Application to water analysis

The present method was applied to the determination of iron in ground, pond and tap water samples without pretreatment. The determinations were made by diluting the water samples at different times. To examine the recovery of iron(III), known amounts of iron(III) were added to the samples. The results are given in Table 2. The values corrected for dilution showed good agreement, and good recoveries of added iron(III) were obtained, ranging from 93 to 103% (mean 98%).

4. Conclusions

A spectrophotometric method using the initial rate procedure is proposed for the trace amounts of iron(II, III) by their catalytic effects on the oxidative coupling of MBTH with DMA in the presence of hydrogen peroxide. Owing to the initial rate measurement, the present method has three order of magnitude of the determinable range 1–1000 ng ml^{-1} iron as well as high sensitivity: as little as 10^{-8} M iron(III) can be determined. The method is applicable to the determination of iron in natural waters without preconcentration and separation.

Acknowledgements

We gratefully acknowledge support of a grant for Scientific Research No.09640715 from the Ministry of Education, Science, Sports and Culture, Japan. T. Tomiyasu wishes to thanks the Ministry of Education, Japan, for financial support.

References

[1] V.A. Elrod, K.S. Johnson, K.H. Coal, Anal. Chem. 63 (1991) 893.
[2] D.W. King, J. Lin, D.R. Kester, Anal. Chim. Acta 247 (1991) 125.
[3] T.J. Cardwell, D. Caridi, R.W. Cattrall, Anal. Chim. Acta 192 (1987) 129.
[4] J. Alonso, J. Bartroli, M.D. Valle, R. Barber, Anal. Chim. Acta 226 (1989) 137.
[5] S. Abe, M. Endo, Anal. Chim. Acta 226 (1989) 137.
[6] T. Tomiyasu, H. Sakamoto, N. Yonehara, Anal. Sci. 10 (1994) 761.
[7] S.H. Wang, L.Y. Du, A.M. Zhang, B. Li, Anal. Lett. 30 (1997) 2099.
[8] T. Kawashima, Y. Kozuma, S. Nakano, Anal. Chim. Acta 106 (1979) 355.
[9] T. Kawashima, N. Hatakeyama, M. Kamada, S. Nakano, Nippon Kagaku Kaishi 1981 (1981) 84.
[10] S. Nakano, M. Odzu, M. Tanaka, T. Kawashima, Mikrochim. Acta [Wien] I (1983) 403.
[11] S. Nakano, M. Sakai, M. Kurauchi, T. Kawashima, Microchem. J. 49 (1994) 298.
[12] K. Hirayama, N. Unohara, Anal. Chem. 60 (1988) 2573.
[13] T. Tomiyasu, H. Sakamoto, N. Yonehara, Anal. Sci. 12 (1996) 507.
[14] F. Holz, Fresenius Z. Anal. Chem. 313 (1984) 29.
[15] S. Nakano, H. Ihara, M. Tanaka, T. Kawashima, Mikrochim. Acta [Wien] II (1985) 455.
[16] S. Nakano, S. Hinokuma, T. Kawashima, Chem. Lett. (1983) 357.
[17] S. Nakano, A. Ohta, T. Kawashima, Mikrochim. Acta [Wien] II (1985) 273.
[18] Y. Miyata, T. Hirano, S. Nakano, T. Kawashima, Anal. Sci. 7 (1991) 97.
[19] Z.-Y. Yu, N. Teshima, S. Nakano, T. Kawashima, Talanta 43 (1996) 1519.
[20] D. Perez-Bendito, M. Silva, Kinetic Methods in Analytical Chemistry, Ellis Horwood, Chichester, 1988, pp. 43–44.
[21] T. Tomiyasu, Anal. Chim. Acta 312 (1995) 179.

ELSEVIER

Talanta 47 (1998) 1099–1106

Talanta

Electrochemical behaviour of gold, silver, platinum and palladium on the glassy carbon electrode modified by chitosan and its application

Xianzeng Ye *, Qinghua Yang, Yan Wang, Nanqiang Li

Department of Chemistry,Peking University, Beijing 100871, People's Republic of China

Received 21 August 1997; received in revised form 5 January 1998; accepted 28 April 1998

Abstract

The chitosan-modified glassy carbon electrode can be used as a working electrode for the determination of precious metal elements: Au, Ag, Pt, Pd. In low pH medium, the complex anions of these precious elements combine with the protonated group $-NH_3^+$ in the chitosan molecule in the form of an ion-association complex. These metal ions were selectively enriched and we got sensitive anodic stripping current. These elements content in ore, welding material have been determined by this method. The results were consistent with those from standard sample and ICP atomic emission spectrometry method. The possible mechanism of electrochemical reaction has been proposed by the study of CV, UV and FT-Raman spectrometry. © 1998 Elsevier Science B.V. All rights reserved.

Keywords: Chemically modified electrode; Chitosan; Precious metal element; Glassy carbon electrode; Anodic stripping voltammetry

1. Introduction

Chitosan is the main component of the shell of shrimps, crabs and insects, with the following structure:

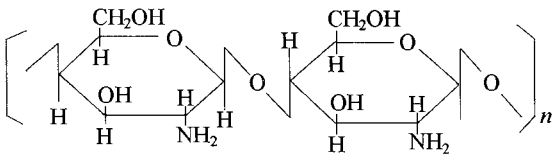

It has not only hydrophilic and hydrophobic groups but also complex groups such as $-NH_2$ and –OH. It is chemically stable and is widely used in medicine, agriculture, sewage treatment and fibre manufacture etc. [1,2]. In analytical chemistry, it is used to separate and enrich trace amounts of Ni(II), Cu(II), Cd(II) [3]. It can be used as a modifying reagent to prepare chemically modified electrode. Its application to determine trace Fe(III) [4] and Pb(II) [5] has been reported. So far, there are few electrochemical studies on the analysis of precious metal elements. Therefore, we attempted to use the chitosan-modified glassy carbon electrode to assay trace Au, Ag, Pt,

* Corresponding author. Fax: +86 10 62751708; e-mail: yexz@chemms.chem.pku.edu.cn

0039-9140/98/$ - see front matter © 1998 Elsevier Science B.V. All rights reserved.
PII S0039-9140(98)00189-1

Pd by anodic stripping voltammetry in the present paper. We got a good result and the mechanism of electrode process for this chemically modified electrode has been investigated in detail.

2. Experimental

2.1. Apparatus

The electrochemical experiments were carried out by using a PAR M270A electrochemical system (EG&GPARC, USA). A three-electrode system was used for all experiments. A glassy carbon electrode with chitosan coating is used as a working electrode. A saturated calomel electrode and a platinum electrode are used as reference electrode and counter electrode, respectively. The Raman spectra were recorded by means of Nicolet 910 FT-Raman spectrometer with YAG laser source (1064 nm).

2.2. Reagents

1% chitosan solution was prepared by dissolving 0.01996 g chitosan in 2 ml of 2 mol l^{-1} HAc solution; Au(III) standard solution was prepared by dissolving 0.7458 g $AuCl_3 \cdot HCl \cdot 4H_2O$ in 6 mol l^{-1} HCl solution, transferring to 100 ml volumetric flask, and diluting to volume. The concentration was 3.567 mg ml^{-1}. Before use, dilute the stock solution with 6 mol l^{-1} HCl to get 0.10 mg ml^{-1} solution; Ag(I) standard solution was prepared by dissolving 0.0540 g pure silver wire in 5% HNO_3 solution, transferring to 50 ml volumetric flask, diluting to volume. It's concentration was 1.08 mg ml^{-1}; Pt(IV) standard solution was prepared by dissolving 0.0402 g pure platinum wire in 10 ml aqua regia, heating to boiling. HCl was added gradually in order to eliminate HNO_3. Finally, it was dissolved in 10 ml of 1.0 mol l^{-1} HCl solution and transferred to 100 ml volumetric flask. The concentration was 400 μg ml^{-1}; Pd(II) standard solution was prepared by dissolving 0.1000 g $PdCl_2$ in 10 ml 1.0 mol l^{-1} HCl solution, transferring to 100 ml volumetric flask. The concentration was 600 μg ml^{-1}. More dilute metal solutions were prepared from these standard solution.

All other reagents were of analytical grade. Water was quartz-distilled twice. High purity nitrogen was used for deaeration for 15 min, and the measurements were carried out under an atmosphere of nitrogen at 20 ± 2°C.

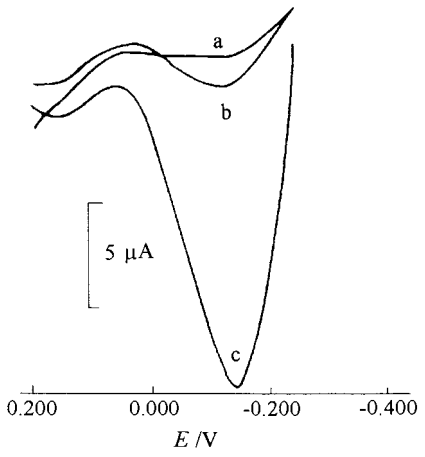

Fig. 1. Anodic stripping votammogram of Pt(II). HCl–KCl (0.04 mol l^{-1}), pH 2.2, 3 μg ml^{-1} Pt(IV), $v = 0.2$ V s^{-1}, DT = 2 min, DP = −0.3 V. (a) Base solution (b) bare glassy carbon electrode (c) glassy carbon electrode modified with chitosan.

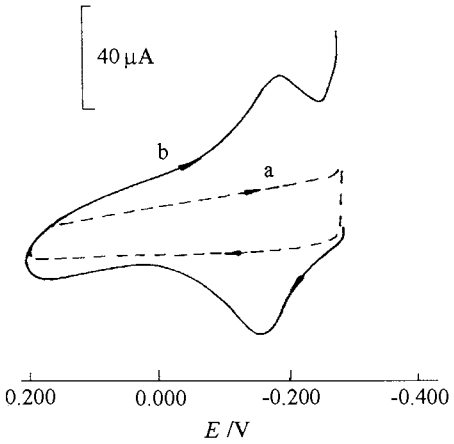

Fig. 2. Cyclic voltammogram of Pt(II). Pt(IV) (4 μg ml^{-1}), (a) DP = 0.2 V (b) DP = −0.3 V, other conditions are the same as in Fig. 1c.

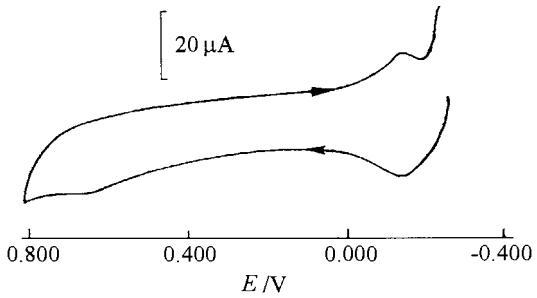

Fig. 3. Cyclic voltammogram of Pt(II). Pt(II) (20 μg ml^{-1}), DT = 0.0 s. Glassy carbon electrode modified with chitosan.

2.3. Preparation and regeneration of CME

The surface of glassy carbon electrode was polished with alumina slurry and sonicated with deionized water and ethanol, respectively, for 3 min. After sonication, the electrode was rinsed with deionized water and allowed to dry in the air. Then the electrode was coated by injecting 4.0 μl of 1% chitosan solution with a microinjector. The CME was placed under infrared light for 30 min and the chitosan CME was acquired. The electrode was permitted to be used for a new run after it had been dipped in 2 mol l^{-1} NaCl solution for 5 min and washed with distilled water. The durability of the chitosan CME was more than a month. The real surface area of the CME was determined to be 0.285 cm^2 by small amplitude triangular potential scanning method [6] (a method to calculate the real surface area by determining differential capacitance). The film thickness is 1.1 μm according to the density of chitosan (1.29 g cm^{-3}).

3. Results and discussion

3.1. Voltammetric behaviours of Pt on the chitosan/GC CME

The working electrode was dipped into Pt solution and deposited for two min at -0.3 V (versus SCE). The anodic stripping voltammetric curve at the CME and bare glassy carbon electrode in 0.04 mol l^{-1} KCl–HCl supporting electrolyte (pH 2.2, $v = 200$ mV s^{-1}) are shown in Fig. 1. The peaks are observed at a potential of -0.16 V. However, the peak current at the modified electrode is 10 times higher than that of the bare electrode. Therefore, the use of chitosan CME made it possible to improve the sensitivity for the determination of Pt greatly.

The cyclic voltammograms at different deposit potential are shown in Fig. 2. The stripping peak current is proportional to v over the range of $10 \sim 100$ mV s^{-1} is not proportional to $v^{1/2}$. The potential difference between reduction and oxidation peaks (ΔE_p) is 40 mV. These data indicate that the redox of electroactive material in the film belongs to a surface-confined quasi-reversible wave [7]. The differential pulse voltammetric curve of Pt have been made in 0.04 mol l^{-1} HCl–KCl (pH 2.2) solutions at 293 K, where the pulse height is 50 mV, the pulse width is 40 ms, the scan rate is 5 mV s^{-1} and the scan range is $-0.3 \sim 0.20$ V. The peak half-width $W_{1/2} = 65$ mV was acquired from the plot and it was increased with the pulse height. The value of $W_{1/2} = 65$ mV was approximate to 60 mV (paper value), and the electron transfer number was equal to two [8].

The cyclic voltammogram of Pt(II) also shows that there is no redox peaks when the CME is deposited at $+0.2$ V (Fig. 2a). It means $PtCl_6^{2-}$ cannot be enriched in the coating film. The redox peaks appear when the CME is deposited at -0.3 V (Fig. 2b).This illustrates that it is $PtCl_4^{2-}$ which can be enriched in the coating film. Generally, Pt(II) is active enough to react with the reagent, but Pt(IV) cannot. So we concluded that $PtCl_4^{2-}$ combined with chitosan.

The $-NH_2$ group of chitosan is protonated in low pH solution. Based on the above results, the electrode process can be expressed as follows:

enriching process: $C_6H_{11}O_4N|_{ed} + H^+$

$= C_6H_{11}O_4NH^+|_{ed}$

$PtCl_6^{2-} + 2e = PtCl_4^{2-} + 2Cl^-$

$C_6H_{11}O_4NH^+|_{ed} + PtCl_4^{2-}$

$= C_6H_{11}O_4NH^+PtCl_4^{2-}|_{ed}$

Table 1
The content of platinum in ore and recovery

Sample	Pt content (μg ml^{-1})	Recovery		
		Added amount (μg ml^{-1})	Detected amount (μg ml^{-1})	Recovery (%)
1	0.32			
2	0.31	0.70	0.68	98
3	0.34	1.40	1.43	102
Mean	0.32			100

stripping process: $C_6H_{11}O_4NH^+PtCl_4^{2-}|_{ed} + 2Cl^- - 2e = C_6H_{11}O_4NH^+|_{ed} + PtCl_6^{2-}$

The following experiments prove the mechanism further.

We have used $SnCl_2$ reducing Pt(IV) to Pt(II) and scanned directly (not having been electroenriched). The oxidation peak current can also be obtained. The peak potential is in good agreement with the above plot (Fig. 3). It indicates that Pt(IV) is reduced to Pt(II) first, then enriched and oxidized.

We compared the UV spectra of chitosan + $PtCl_6^{2-}$ and chitosan + $PtCl_4^{2-}$ system. The former has an absorption peak at 224 nm which is consistent with the absorption peak of chitosan, but the latter has a strong absorption peak at 251 nm. This illustrates that $PdCl_4^{2-}$ combined with chitosan and produced a new component $C_6H_{11}O_4NH^+PtCl_4^{2-}$. The Raman spectrogram also proves this point. There is a vibrational peak of N–H bond at 3300 ~ 3500 cm^{-1} in chitosan + $PtCl_6^{2-}$, but it disappears in chitosan + $PtCl_4^{2-}$ system. This indicates that new component of $C_6H_{11}O_4NH^+PtCl_4^{2-}$ was produced.

Under the above conditions, the anodic stripping peak current is proportional to the concentration of Pt(IV) over the range of 0.5 ~ 5.0 μg ml^{-1}, i_{pa} (μA) = 0.557 − 5.98c[Pt(IV)], correlation coefficient r = 0.9984. The method can assay 0.025 μg ml^{-1} Pt(IV) if the electrode preconcentrates for 10 min.

We have used this technique to assay the platinum content in ore without separation. The determination results is consistent with the standard sample. The method is as follows: The ore sample

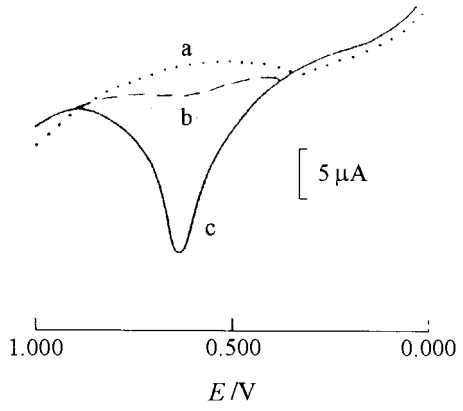

Fig. 4. Anodic stripping voltammogram of Pd(II). HCl–KCl (0.02 mol l^{-1}), pH 2.0; 1.5 mg l^{-1} Pd(II), v = 0.1 V s^{-1}, DT = 60 s, DP = 0.0 V. (a) Base solution (b) bare glassy carbon electrode (c) glassy carbon electrode modified with chitosan.

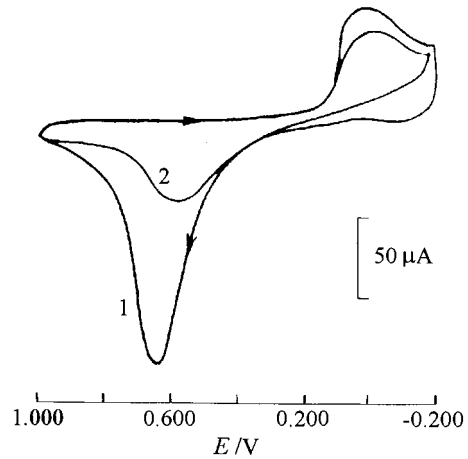

Fig. 5. Cyclic voltammogram of Pd(II). DP = − 0.2 V, 3.3 mg l^{-1} Pd(II); 1, First scanning; 2, second scanning; other conditions are the same as in Fig. 4.

Table 2
The determination results of Pd in 105 deoxycatalyst and recovery

No.	Pd content (%)	Recovery		
		Added amount (mg l^{-1})	Detected amount (mg l^{-1})	Recovery (%)
1	1.4	0.075	0.071	95
2	1.4	0.15	0.14	93
3	1.1	0.22	0.21	95
4	1.5	0.30	0.29	97
Mean	1.4			95

was incandesced at 600 ~ 650°C. Then the sample was washed with 4 mol l^{-1} HCl to eliminate Cu and Ni. The residue was dissloved with aqua regia, adding HCl to eliminate HNO_3. Finally transferred to 10 ml volumetric flask with 0.01 mol l^{-1} HCl. The determination results are shown in Table 1 under the above conditions.

The standard deviation is 0.015 μg g^{-1}, the relative standard deviation is 4.7%. Compared with the standard sample (0.35 μg g^{-1}, China Academy of Geology Research 72-Pt-02 sample) the relative error is −8.6%. The coexisting element in ore 20 times of Os(VIII), 10 times of Au(III), 5 times of Ru(III), Ag(I) did not interfere with determination.

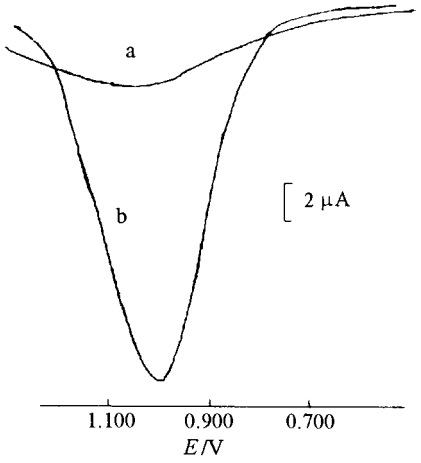

Fig. 6. Anodic stripping voltammogram of Au(III). KCl–HCl (0.1 mol l^{-1}), pH 2.0, 0.1 μg ml^{-1} Au(III), $v = 0.1$ V s^{-1}, DP = 0.0 V, DT = 5 min. (a) Bare glassy carbon electrode (b) glassy carbon electrode modified with chitosan.

3.2. Pd(II)

In palladium solution (0.02 mol l^{-1} KCl–HCl as supporting electrolyte, pH 2), the working electrode was deposited at 0.0 V for 1 min and scan positively. At potential of 0.65 V the anodic stripping peak was observed. The peak current at modified electrode was 15 times higher than that at bare electrode (Fig. 4).

The amount of modifying reagent was selected for 4.0 μl of 1% chitosan solution. The stripping peak current increases proportionally with the increase of scanning rate over the range of 0.02 ~ 0.12 V s^{-1} at the concentration of 3.3 μg ml^{-1} of Pd(II). In cyclic voltammograms of Pd(II) (Fig. 5), the potential difference between anodic peak potential (0.65 V) and cathodic peak potential (0.041 V) is about 600 mV and the anodic peak current and cathodic peak current is intended to be equal when scanning for the second time. So the reversibility of the electrode reaction of Pd(II) is worse than that of Pt(II). Similarly to Pt(II), $PdCl_4^{2-}$ in solution combined with the protonated group $-NH_3^+$ in chitosan molecule and was enriched selectively at electrode surface in the form of $C_6H_{11}O_4NH^+PdCl_4^{2-}$. This point can also be proved by UV spectra. The chitosan + Pd(II) system produced a new absorption peak at 263 nm compared with the chitosan system. A new component was produced. $PdCl_4^{2-}$ reacts with chitosan and produces an ionpair, so it can be adsorbed and enriched at the electrode surface. But when we deposited at 0.0 V for 60 s, it was electroreduced to Pd(0). In such way we get a more sensitive anodic stripping voltammetric current. If we enrich it only by static charge adsorp-

Table 3
The determination results of Au in ore and recovery

No.	Au content (g T^{-1})	Recovery		
		Added amount (μg ml^{-1})	Detected amount (μg ml^{-1})	Recovery (%)
1	3.48	1.00	1.04	104
2	3.59	2.00	1.94	97
3	3.49	3.00	2.89	96.3
4	3.52	4.00	4.06	101.5
Mean	3.52			99.7

tion, its anodic stripping current is smaller than that electroreduced. As seen in Fig. 5, the anodic stripping current of the second scan is obviously smaller than the first scan. (We have deposited 60 s for the first scan, then scan directly for the second circle).

The electrode process can be described as follows:

enriching process: $C_6H_{11}O_4N|_{ed} + H^+ = C_6H_{11}O_4NH^+|_{ed}$

$C_6H_{11}O_4NH^+|_{ed} + PdCl_4^{2-} = C_6H_{11}O_4NH^+PdCl_4^{2-}|_{ed}$

$C_6H_{11}O_4NH^+PdCl_4^{2-}|_{ed} + 2e = C_6H_{11}O_4NH^+ \cdot Cl^- \cdot Pd|_{ed} + 3Cl^-$

stripping progress: $C_6H_{11}O_4NH^+ \cdot Cl^- \cdot Pd|_{ed} + 3Cl^- - 2e = C_6H_{11}O_4NH^+|_{ed} + PdCl_4^{2-}$

Under above conditions we have determined palladium in 105 deoxidized catalyst. The results and percent recovery are shown in Table 2. The standard deviation is 0.017%, the relative standard deviation is 12%. The result is consistent with that from the ICP-AES method. 150 times of Ru(III), large amount of Mn(II), Ni(II), NO_3^- did not interfere with determination. 0.1 times of Cu(II), 0.75 times of Pt(IV) had no interference with determination.

3.3. Au

Gold anodic stripping peak was observed at 1.00 V when the working electrode was deposited at 0.2 V for 5 min and scan positively in 0.1 mol l^{-1} KCl–HCl solution (pH $1 \sim 2$, $v = 100$ mV s^{-1}). The peak current at the modified electrode is 5 times higher than that at the bare electrode (Fig. 6). The anodic stripping current is proportional to the concentration of Au(III) over the range of $0.01 \sim 1.0$ μg ml^{-1}. The correlation coefficient $r = 0.9983$.

We have used this method to determine the content of gold in ore. A sample of ore (10.0050 g) was incandesced at $600 \sim 650$°C for 1 h to eliminate C and S elements. The sample was first leached with 6 mol l^{-1} HCl several times, then filtered and the residual sample was dissolved with 40 ml aqua regia. After filtering, the residual sample was washed with 0.1 mol l^{-1} HCl until the filtrate was colourless and transparent. The filtrate was heated to dryness, HNO_3 was eliminated, it was dissolved in 0.01 mol l^{-1} HCl solution and transferred to 25 ml volumetric flask. The determination results are shown in Table 3 with the above method. The standard deviation is 0.0497, the relative standard deviation is 2.0%. The results are consistent with 3.60 ± 0.12 g T^{-1} of the standard sample (GBW(E) 070023, China Academy of Geology Resarch).

Au(III) exits in the form of $AuCl_4^-$ in HCl medium (pH $1 \sim 2$). It combines with the protonated group NH_3^+ in chitosan group and can be enriched selectively. However, this kind of combination is more relaxed than that of Pt(II) and Pd(II). So no obvious change is observed in UV and Raman spectra.

The electrochemical reaction process is like that of Pd. The ionpair of $AuCl_4^-$ and chitosan is more relaxed than that of $PtCl_4^-$. It must be

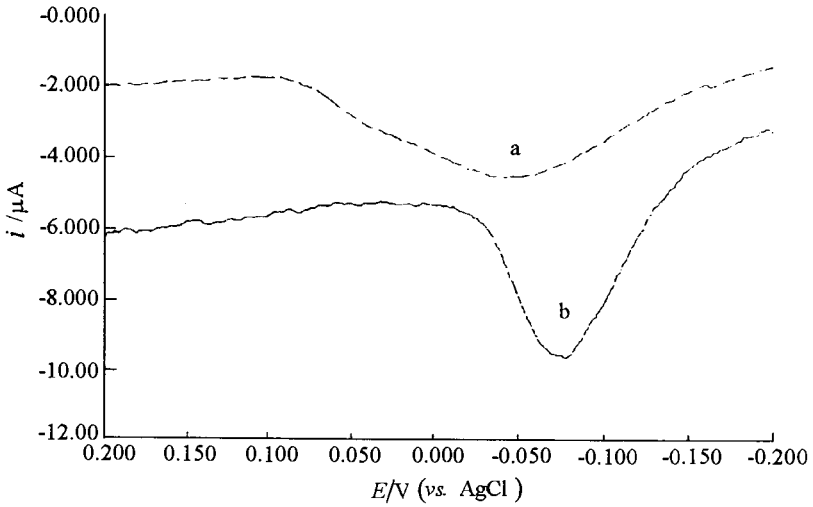

Fig. 7. Anodic stripping voltammogram of Ag(I). Potassium hydrogen benzene bicarboxylic acid (0.1 mol l^{-1}), 0.1 mol l^{-1} NH_4SCN, pH 4.0, 0.1 μg ml^{-1} Ag(I), DP = −0.8 V, DT = 180 s, $v = 0.1$ V s^{-1}. (a) Bare glassy carbon electrode (b) glassy carbon electrode modified with chitosan.

electroreduced in order to get more sensitive anodic stripping current.

3.4. Ag

Ag(I) also has a good anodic stripping peak in potassium hydrogen benzene bicarboxylic acid + 0.1 mol l^{-1} NH_4SCN system (pH 4.0). The potential is at −0.075 V. The peak current is obviously higher than that at the bare electrode (Fig. 7). The concentration of Ag(I) is proportional to the anodic stripping peak current over the range of $0.02 \sim 1.0$ μg ml^{-1}. The correlation coefficient $r = 0.9989$.

We have determined silver in standard solution by this method with the average (9872 ± 16) μg ml^{-1}. The reality is 1000 μg ml^{-1}. The relative standard deviation is 1.6% and percent recovery is $97 \sim 101\%$. The Ag content in the welding material was also determined with the results of 0.92% while the reality was 1.0%.

The mechanism is that $Ag(SCN)_2^-$ combined with the protonated group in chitosan molecule, then electroreduced to Ag. The combination is relax which is similar to Au(III). No obvious change is observed in UV spectra.

4. Conclusion

Because chitosan has a wider range of potential window in positive potential with complexing capacity group. It is ideal to be used as the modifying reagent for CME to determine precious elements such as Au, Ag, Pt, Pd. In low pH medium, the correlated complex anionic ions of the precious metal combine with the protonated group $-NH_3^+$ in chitosan molecule when scanning positively. So the metal ions can be enriched selectively and produce sensitive anodic stripping peak current. The results of determination are consistent with standard sample. These metal ions combine in different way with chitosan according to UV and Raman spectra. The ion-association complex of Pt(II) and Pd(II) with chitosan is tighter than that of Au(III) and Ag(I). Its dissociation degree is smaller than that of Au(III) and Ag(I).

References

[1] J.P. Zikakis, (Ed.), Chitin, Chitosan and Related Enzymes, London, Academic Press, 1984, p. 77.
[2] Jian Xu, XinRong Jin, University Chemistry 9 (3) (1994) 22.

[3] Komori Kazunori, Igarashi Shukuro, Yotsuyanagi Takao, Bunseki Kagaku 35 (10) (1986) 890.
[4] Bai Zu-Ping, Nakamura Tosbio, Izutsu Kosuke, Electroanalysis 2 (1990) 75.
[5] X. Jin-Rui, L. Bin, C. Chuan-quan, Proceedings of the Fifth National Conference in Electroanalytical Chemistry, Wu Han, 262, 1993.
[6] Yonghui Liu, Technology of Electrochemical Determination, Beijing Aviation College Press, Beijing, 1987, p. 117.
[7] R.W. Murray, in: A.J. Bard (Ed.), Electroanalytical Chemistry, 13, Marcel Dekker, New York, 1984, p. 200.
[8] E.P. Parry, R.A. Osteryoung, Anal. Chem. 37 (1965) 1634.

ELSEVIER

Talanta 47 (1998) 1107–1119

Talanta

Electrochemical polymerization of toluidine blue o and its electrocatalytic activity toward NADH oxidation

Chen-Xin Cai *, Kuan-Hong Xue

Department of Chemistry, Nanjing Normal University, Nanjing 210097, People's Republic of China

Received 15 December 1997; accepted 7 May 1998

Abstract

A stable electroactive thin film of poly(toluidine blue o) (PTOB) has been deposited on the surface of a glassy carbon electrode by cyclic voltammetry from an aqueous solution containing toluidine blue o (TOB). Cyclic voltammograms of PTOB indicate the presence of two redox couples and the formal potential shifts linearly in the negative direction with increasing solution pH with a slope of 58 and 54 mV per pH unit for couple I and couple II, respectively. The PTOB modified glassy carbon electrode shows electrocatalytic activity toward NADH oxidation in phosphate buffer solution (pH 7.0), with an overpotential ca. 470 mV lower than that of the bare electrode. The catalytic rate constant of the modified glassy carbon electrode for the oxidation of NADH is determined by cyclic voltammetry and rotating disk electrode measurements. The experimental results indicate that the electrode can be used as a detector for NADH determination with a linear range of 5.0×10^{-6} to 2.0×10^{-3} mol l^{-1} and the detection limits of $(5.0 \pm 0.3) \times 10^{-7}$ mol l^{-1} at optimal conditions. © 1998 Elsevier Science B.V. All rights reserved.

Keywords: Electrocatalysis; Chemically modified electrode; Mediator; NADH; Toluidine blue o

1. Introduction

The electrochemical oxidation of dihydronicotiamide adenine dinucleotide (NADH) to the corresponding oxidized form (NAD^+) at a bare electrode surface is highly irreversible and take place at considerable overpotential, that is increased further by the presence of the enzyme [1]. Although some effects of the electrochemical oxidation pathway of NADH are not clear, a multistep (ECE) transfer scheme is usually proposed to describe the oxidation reaction of NADH [1–3]. It is assumed that the oxidation of NADH at a solid electrode proceeds via two successive one-electron transfer steps involving radical intermediates, which often cause side reactions, electrode fouling and interfering background currents in real samples [4]. In addition, the process of electrochemical oxidation of NADH is not very reproducible since it has been shown to depend on the history and pretreatment of the electrode surface.

One way to overcome these problems is to modify the electrode surface with mediators. The mediated electron transfer enables efficient electrocatalytic oxidation of NADH [5–7]. Many

* Corresponding author. E-mail: cxcai@pine.njnu.edu.cn

0039-9140/98/$ - see front matter © 1998 Elsevier Science B.V. All rights reserved.
PII S0039-9140(98)00190-8

compounds, when modified on the electrode surface, were found to enhance the electron transfer rate and reduce the overpotential for the oxidation of NADH [8–23]. These compounds include adsorbed aromatic compounds containing catechol functionalities and adsorbed phenoxazines [15–21], conducting organic salt [22], and nickel hexacyanoferrate [23] etc. Using the cyclic voltammetry and scanning electrochemical microscopy (SECM), Grundig et al. [24] studied the NADH oxidation on the composite electrodes, containing *N*-methyl phenazine (NMP^+) methosulfate, 1-methoxy-5-methyl phenazine (M-NMP^+) methosulfate and Meldola blue etc. Electrocatalytic oxidation of NADH at the conducting polymers modified electrodes were also reported recently [25–33].

Among the many mediators, the conducting polymers have certain advantages. Karyakin et al. [29] reported that the long-term operational stability of poly(methylene blue) film was much higher than that of the adsorbed mediator. Moreover, electropolymerization yields modified electrode with a three-dimensional distribution of mediators. Such an electrode should be preferable because of the much larger catalytic response of polymer coatings than monolayers, the catalytic activity and sensitivity can be improved and miniaturization for in vivo sensor devices should also be possible.

Many compounds have even been found to mediate the electron transfer for NADH oxidation, there is still a great deal of interest in the development of new materials for the electrocatalytic oxidation of NADH or especially alternative approaches for immobilization of the mediator on the electrode surface in order to further lower the overpotential for NADH oxidation and also to find more efficient and stable chemically modified electrodes for the electrocatalytic oxidation of NADH.

In the previous paper, we have reported the electrocatalysis of NADH at a glassy carbon electrode modified with poly(azure I) (PAI) [34] and poly(nile blue A) (PNB) [35]. The aim of the present work was to investigate the electropolymerization of the toluidine blue o (TOB, the structure is shown in Scheme 1), characterize of poly(toluidine blue) (PTOB) and test the electrocatalytic activity of PTOB toward NADH oxidation. The experimental results indicated that the PTOB films have two redox couples, which were similar to the PAI [34] and PNB [35], in the potential range of -0.6 to $+0.4$ V, suggesting the existence of two redox reaction processes. The electrocatalytic activity of the PTOB films (couple II) for electrooxidation of NADH is more efficient than that of PAI and PNB films.

2. Experimental

2.1. Chemicals

NADH and toluidine blue o (cat. no. 119444, dye content $\sim 85\%$) were obtained from Sigma and Merck, respectively. They were used as received without further purification. All other chemicals were of analytical grade. The 0.1 mol l^{-1} phosphate buffer (pH 7.0) solution was always employed. The electropolymerization of TOB was performed in 0.1 mol l^{-1} Britton–Robinson (B–R) buffer solution (pH 9.7). The composition of the B–R solution is a liter of water containing 3.92 g H_3PO_4, 2.40 g CH_3COOH and 2.47 g H_3BO_3. The 0.1 mol l^{-1} NaOH solution was used to control the solution at different pH's. Water, twice distilled from a quartz apparatus, was used in all experiments.

2.2. Apparatus

A three-electrode system with a coiled platinum wire serving as the counter electrode, a saturated calomel electrode (SCE) as a reference electrode and a PTFE-shrouded glassy carbon electrode (5 mm diameter) as the working electrode was employed. The working electrode was polished with metallographic abrasine paper (6 #, Shanghai,

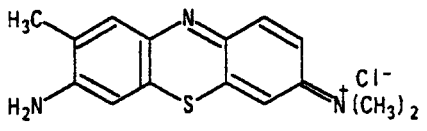

Scheme 1.

China) firstly, then progressively with fine slurries of 1, 0.5 and 0.05 μm alumina in order to obtain a mirror-like surface. After thorough rinsing, the electrode was cleaned in an ultrasonic bath, first with ethanol and finally with doubly distilled water. Prior to use, the electrode was treated electrochemically by a continuous cyclic potential sweep from -0.5 to 1.5 V at sweep rate 50 mV s^{-1} in phosphate buffer solution (pH 7.0) until a stable voltammogram was obtained (this process was completed in about 10 min).

A PAR M270 electrochemical system (EG&G) was used to carry out the electrochemical experiments. Rotating disk electrode measurements were carried out with a PAR M616 disk electrode system (EG&G) using a glassy carbon electrode (4 mm diameter). The stability of the PTOB film was tested using a ZF-3 potentiostat programmed by a ZF-4 waveform generator and an LZ 3-204 recorder (Shanghai, China) was used to record the cyclic voltammograms. A type 501 thermostat (Shanghai, China) was used to control the experimental temperature to 25 ± 0.1°C.

2.3. Procedures

The electropolymerization of TOB was carried out by cyclic voltammetry in the potential range of -0.6 to 1.2 V at a sweep rate of 100 mV s^{-1} in B–R buffer solution (pH 9.7). The monomer concentration was usually 5×10^{-4} mol l^{-1}. The film thickness was dependent on the number of cycles. Usually, the PTOB film was formed by cycling the potential in above potential range for 30 min, this corresponds to a surface coverage, Γ, of about 6.8×10^{-10} mol cm^{-2}. After the PTOB film had formed on the electrode surface, the electrode was rinsed thoroughly with water, and dipped into the buffer solution to test its electrochemical responses and examine the electrocatalytic activity toward NADH oxidation in the potential range of -0.6 to $+0.4$ V.

All tested solution were deaerated by passing through highly pure nitrogen for 20 min before the electrochemical experiments, and a continuous flow of nitrogen was maintained over the sample solution during experiments.

3. Results and discussion

3.1. Electropolymerization of TOB and electrochemical responses of the PTOB modified glassy carbon electrode

The cyclic voltammetry was used to form the PTOB, this allows the potential range necessary for electrode modification to be determined more readily than the other methods, for example, the constant potential technique. Furthermore, modification can be recognized and monitored easily by the progressive nature of the cyclic voltammetric curves.

The cyclic voltammograms taken in TOB aqueous solution indicate the formation of the PTOB film on the electrode surface (Fig. 1). The potential sweep range, especially the upper limit, is the most important factor for preparing the PTOB modified electrode. If the potential sweep is confined within the region of -0.6 to $+0.4$ V, a simple cyclic voltammogram corresponding to the redox reaction of TOB with the formal potential of -0.26 V is observed (Fig. 1A). This steady state cyclic voltammogram persists indefinitely provided that the anodic upper potential is not taken too positive. The potential sweep in this potential range results in no substantial film formation.

However, electropolymerization was observed when the value of anodic upper potential reached 1.2 V. During this process, the redox peaks corresponding to the redox reaction of TOB monomer decrease quickly with an increase of the scan number. A new redox peak appears around 0 V in the cyclic voltammogram (Fig. 1 B). The peak currents increase with successive scanning, indicating an increase in the quantity of electroactive species on the electrode. With increasing the scan number, the anodic peak potential shifted in the positive and cathodic peak potential in the negative direction, respectively. These peaks cannot be related to a monomer redox couple. These indicated that electropolymerization of TOB has taken place on the electrode surface and formed the PTOB films. The effect of the solution pH on the PTOB films growth was studied. The results indicated that the rate of the films growth in-

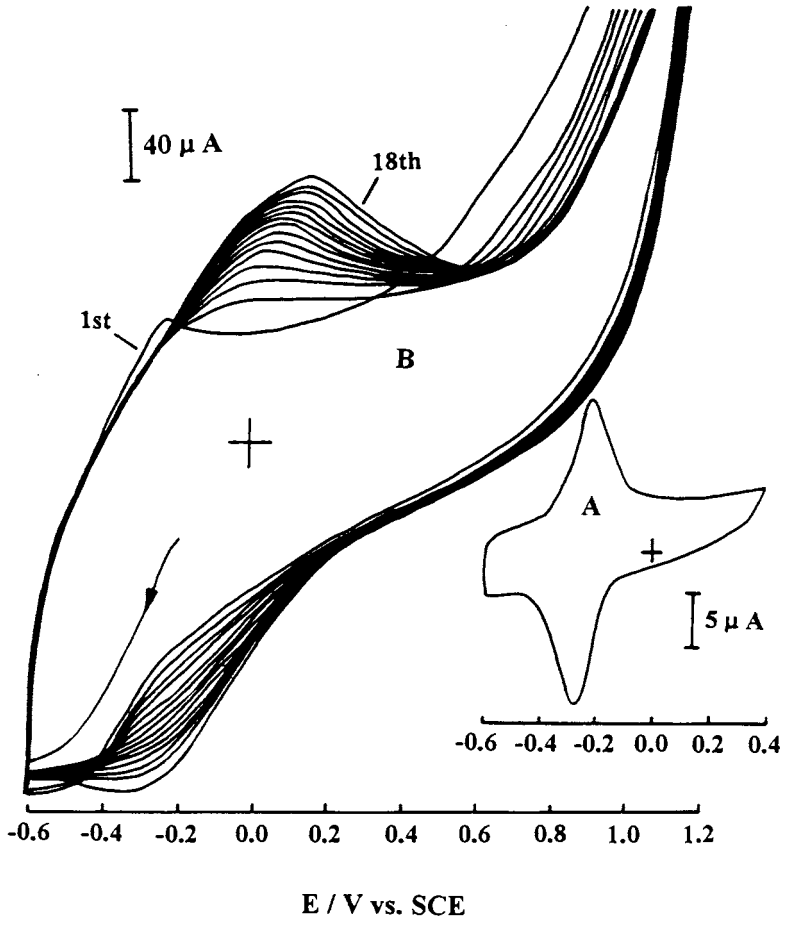

Fig. 1. Cyclic voltammograms of 5×10^{-4} mol l^{-1} TOB at glassy carbon electrode in 0.1 mol l^{-1} B–R buffer solution (pH 9.7) at 100 mV s^{-1}. Scan limits, -0.6 to $+0.4$ V (A) and -0.6 to $+1.2$ V (B).

creased with an increase of the buffer solution pH.

If the electrode is subsequently removed from the cell, rinsed with water, and placed in phosphate buffer solution (pH 7.0) containing no TOB, two couples with well-defined redox peaks can be observed (Fig. 2). The peak currents of the two redox couples are linearly proportional to the scan rates (shown in the inset of Fig. 2), confirming a surface confined redox couples. The formal potential, $E^{0\prime}$, which is taken as the mid-point of the anodic and cathodic potential, is -277 and 5 mV for couple I and couple II, respectively, at a scan rate of 20 mV s^{-1}. The values of the $E^{0\prime}$ shift slightly in the negative direction with an increase of the scan rate. These values change to -292 and -3 mV, respectively, at a scan rate of 100 mV s^{-1}. The separations between the anodic and cathodic peaks are 41 and 72 mV for couple I and couple II, respectively, at a scan rate of 20 mV s^{-1}. The value of separations are increased with increasing scan rates.

We tried several washing procedures to eliminate the monomer-type redox activity. Washing thoroughly with buffer solution, treatment in an ultrasonic bath or cycling in buffer solution did not affect the redox peaks. This indicated that the monomer type redox peaks cannot be explained through the inclusion of the TOB monomer into the PTOB films. If the redox couple I were caused

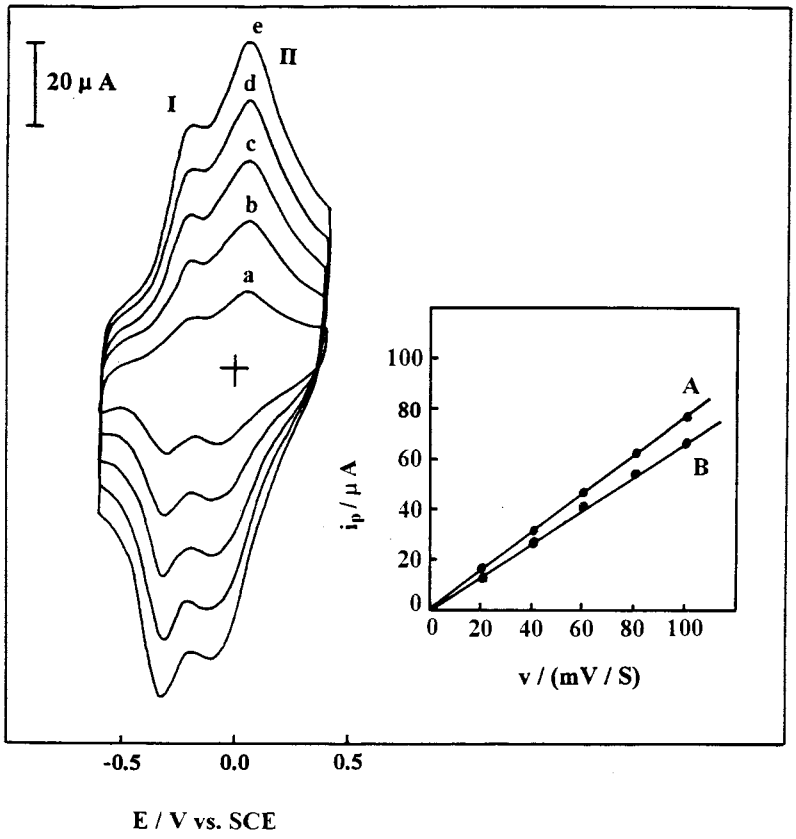

Fig. 2. Cyclic voltammograms of PTOB modified glassy carbon electrode in 0.1 mol l^{-1} phosphate buffer solution (pH 7.0) at scan rate of (a) 20, (b) 40, (c) 60, (d) 80 and (e) 100 mV s^{-1}. The inset shows the plot of the cathodic current versus scan rates for redox couple I (A) and II (B).

by the inclusion of the monomer into the PTOB films, the redox peaks would decrease after washing thoroughly the modified electrode with buffer solution. Furthermore, long time ultrasonication can remove the PTOB from the electrode surface because the two couples of redox peaks decrease simultaneously.

Bauldreay and Archer [36] studied polymerized mechanism of thionine, nile blue etc. According to their results, the initial step for the TOB polymerization is one-electron oxidation of NH_2 group and forms a cation radical when the potential is scanned to 1.2 V. The unpaired electron can be delocalization through the TOB molecule, but the unpaired electron may be sited with high probability on either amine group and at position ortho to them [36]. Radical dimerization can occur via carbon–nitrogen coupling routes as shown in Scheme 2. The oxidation of the NH_2 group in the dimer can occur again, the polymerization can take place readily to form the PTOB.

From the structure of PTOB, the film contains monomer units and each monomer unit retains its electroactive heterocyclic nitrogen atom. Moreover, the PTOB film also contains the nitrogen bridges between monomer units. These nitrogen bridges should be electroactive like those in polyaniline films. The redox potential for the heterocyclic nitrogen atom and the nitrogen bridges must be different. So, two couple of redox peaks appeared on the cyclic voltammograms of PTOB (as shown in Fig. 2). Because the formal potential of redox couple I is closed to that for redox reaction of TOB monomer, we ascribe the redox

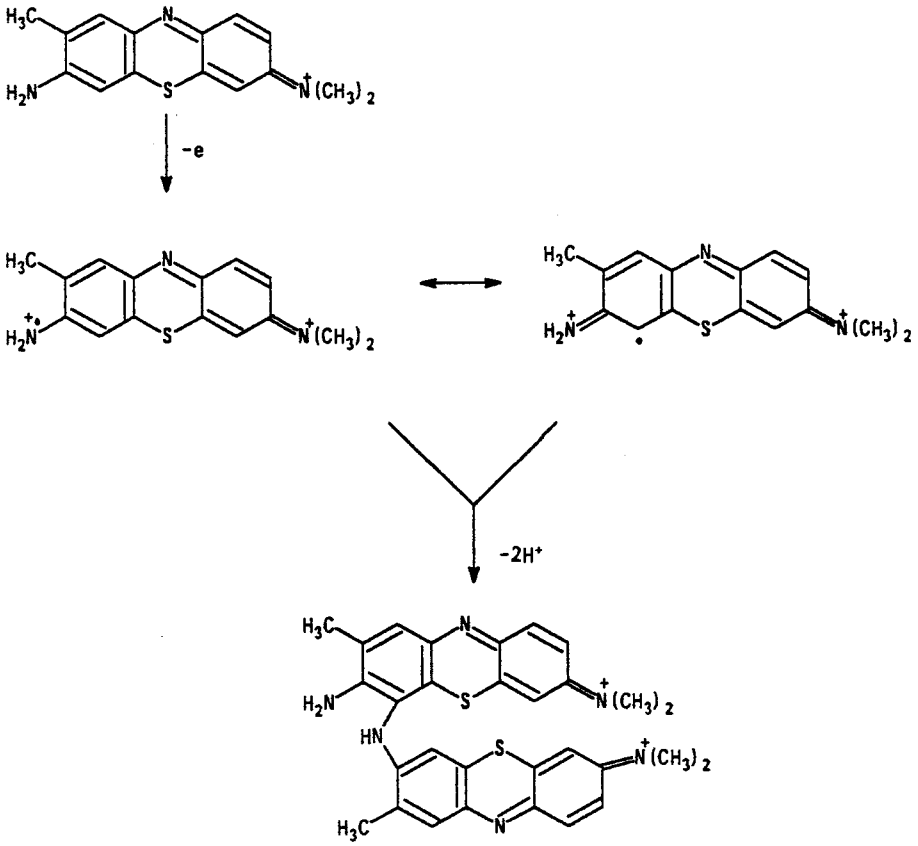

Scheme 2.

couple I to the redox reaction of the monomer units existed in PTOB film, the redox couple II to redox reaction of the nitrogen bridges.

Karyakin et al. [37] also obtained two redox couples in studying the polymer of methylene blue modified glassy carbon electrode. They pointed out that the monomer-type conjugation may be present in the polymer of methylene blue. They also ascribed the redox couple at negative redox couple, which corresponds to the redox peaks I in the present case, to the monomer-type redox activity.

3.2. Stability of PTOB

The PTOB modified electrode was rather durable, i.e. they withstood removal from the solution and washing with distilled water. The stability of the PTOB was also examined by repetitive scans the modified glassy carbon electrode in the potential range of -0.6 to $+0.4$ V in phosphate buffer solution (pH 7.0). For the first few scans (about five cycles), the peak currents decrease on the continuous scanning. Then, no changes in height and separation of cyclic voltammetric peaks were observed after 6 h repetitive scans (more than 500 cycles). The modified electrode showed no appreciable loss of electroactivity after storing in the phosphate buffer solution for 1 week.

3.3. pH dependence of PTOB

In order to test the effects of solution pH on the electrochemical behaviour of PTOB, the voltammetric responses of a PTOB modified

glassy carbon electrode were obtained in solutions of pH's varying from 2.6 to 10.2. Fig. 3 shows the cyclic voltammograms of the PTOB in three solutions of different pH. All the cyclic voltammograms have two redox couples. As can be seen in Fig. 3, the anodic and cathodic peak potential for two redox couples are pH dependent, they shift in the negative direction with an increase of the solution pH. The formal potentials of two redox couples shift to the negative direction with the slope of 58 and 54 mV per pH unit for couple I and couple II (not shown here), respectively, which is very close to the anticipated Nernstian value of 59 mV. It can therefore be concluded that an equal number of electrons and protons is involved in the two electrode reactions.

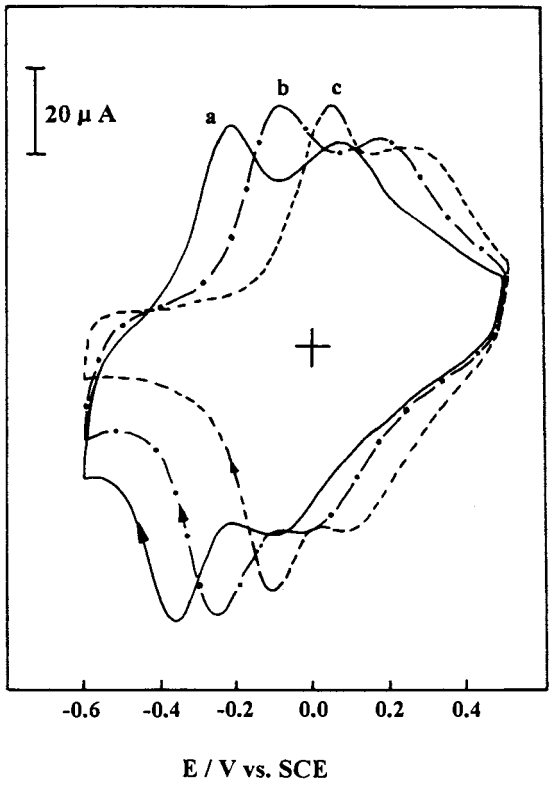

Fig. 3. Cyclic voltammograms of glassy carbon electrode modified with PTOB in 0.1 mol l^{-1} B–R buffer solution at pH value of (a) 6.8, (b) 4.8 and (c) 2.6. Scan rate: 50 mV s^{-1}.

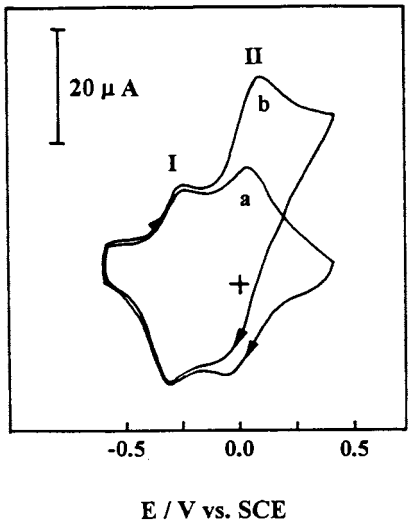

Fig. 4. Cyclic voltammograms of PTOB modified glassy carbon electrode in 0.1 mol l^{-1} phosphate buffer solution (pH 7.0) in the absence (a) and presence (b) of 1.0×10^{-3} mol l^{-1} NADH. Scan rate: 50 mV s^{-1}, surface coverage $\Gamma = 6.8 \times 10^{-10}$ mol cm^{-2}.

3.4. Electrochemical oxidation of NADH at PTOB modified electrode

One of the objectives of our study was the development of a modified electrode capable of the electrocatalytic oxidation of NADH. Since the poly(azure I) [34], poly(nile blue A) [35] and poly(methylene blue) [29] have been proved to act as active electron-transfer mediators for the electrocatalytic oxidation of NADH, it was expected that PTOB covered glassy carbon electrode may similarly be used to catalyze the oxidation of NADH. In order to test the electrocatalytic activity of the PTOB film, the cyclic voltammograms were obtained in the absence and presence of NADH, and the curves are presented in Fig. 4. In the absence of NADH (Fig. 4a), two couples of well-behaved redox peaks for PTOB film on the electrode can be observed. Upon the addition of 1.0×10^{-3} mol l^{-1} NADH, there is a great enhancement of the anodic current and almost no cathodic current is observed in the return wave for redox couple II (Fig. 4b), which indicates a strong electrocatalytic effect. Simultaneously, the anodic peak potential shifts to the positive direc-

Table 1
The formal potentials (versus SCE) of PTOB, PAI, PMB and PNB film (at scan rate of 20 mV s^{-1})

Polymer	$E^{0\prime}$ (I) mV^{-1}	$E^{0\prime}$(II) mV^{-1}	Solution pH	Reference
PTOB	−256	5	7.0	This work
PAI	−267	−70	7.0	[34]
PMB[a]	−300	−80	8.5	[29]
PNB	−404	−67	6.8	[35]

[a] The value of the PMB was obtained at scan rate of 1 mV s^{-1}.

tion by about 50 mV after addition of NADH, indicating a kinetic limitation existing in the reaction between PTOB films and NADH. The anodic peak potential for the oxidation of NADH at PTOB modified electrode is about +80 mV, while NADH is oxidized at about +550 mV at an unmodified glassy carbon electrode under identical conditions. A decrease in overpotential of approximately 470 mV is achieved.

A small enhancement of the anodic currents for the redox couple I was found after addition of NADH compared with the voltammogram in a buffer solution without NADH, indicating that the electrocatalytic activity of the redox couple I is small. The different electrocatalytic activity toward NADH oxidation between the redox couple I and II is probably due to the difference of the formal potential existing between couple I and II. The redox couple II is more efficient for NADH oxidation than the redox couple I because the formal potential of couple II is much more positive than that of couple I [5].

Comparing the electrocatalytic activity of the PTOB films (couple II) toward NADH electrooxidation with that of PAI [34], PNB [35] and poly(-methylene blue) (PMB) [29], one can find that the PTOB film is more efficient because the electrocatalytic current for NADH electrooxidation is larger in the case of PTOB. This can be explained again through the different formal potential among them, the formal potential (couple II) of the PTOB film is more positive than that of PAI [34], PNB [35] and PMB [29]. The formal potential of these polymerized films is shown in Table 1.

The amount of the PTOB modified on the glassy carbon electrode surface (Γ) can be controlled by the scan number during the electrpolymerization process of TOB. The surface coverage, Γ, can be calculated from the following equation

$$\Gamma = Q/\mathrm{nFA} \quad (1)$$

where Q is the amount in coulombs of consumed charge obtained from integrating the peak area in cyclic voltammograms under the background correction, the other symbols have their usual meanings. Although the surface of the glassy carbon electrode is microscopically rough, it is difficult to estimate the roughness factor, so in all calculations, the geometric area of the electrode was employed. The effect of Γ on the electrocatalytic peak current (for couple II) for NADH oxidation was studied. The catalytic current increases with increasing Γ up to about 6.0×10^{-10} mol cm^{-2} (for 1.0×10^{-3} mol l^{-1} NADH), whereas the catalytic current levels off for the Γ above the 6.0×10^{-10} mol cm^{-2}. Based on these results and in order to ensure that the electrocatalytic current for NADH oxidation at PTOB modified electrode was independent of the Γ, a value of 6.8×10^{-10} mol cm^{-2}, which corresponds to about 30 min cycling the glassy carbon electrode in TOB solution in the potential range of −0.6 to 1.2 V (100 mV s^{-1}), was employed in the following experiments.

Fig. 5 shows the cyclic voltammograms of PTOB modified glassy carbon electrode at various scan rates obtained in 0.1 mol l^{-1} phosphate buffer solution (pH 7.0) containing 1.0×10^{-3} mol l^{-1} NADH. It can be noted in Fig. 5 that the catalytic oxidation peak potential (peak II) for NADH shifts slightly to positive potentials with increasing the scan rate, suggesting a kinetic limitation existing in the reaction process between the

PTOB film and NADH. The oxidation currents for NADH increase linearly with the square root of the scan rate, suggesting that at sufficient overpotential the reaction is transport limited.

These results show that the overall electrochemical oxidation of NADH at the PTOB modified glassy carbon electrode might be controlled by the diffusion of NADH in solution and the cross-exchange process between NADH and the redox site of the PTOB. Andrieux and Saveant [38] derived a relation between the peak current and the concentration of the substrate for the case of slow scan rate and large k, where k is the catalytic reaction rate constant between the PTOB and NADH in the present case.

$$i_{cat} = 0.496\ nFAD^{1/2}v^{1/2}c^*(nF/RT)^{1/2} \quad (2)$$

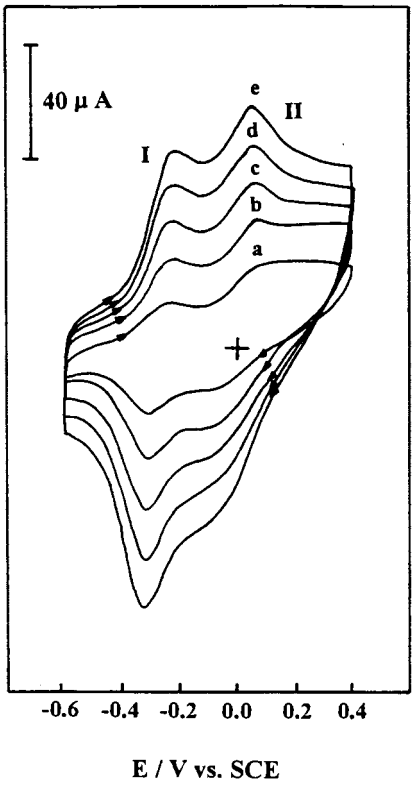

Fig. 5. Cyclic voltammograms of glassy carbon electrode modified with PTOB in 0.1 mol l^{-1} phosphate buffer solution (pH 7.0) containing 1.0×10^{-3}mol l^{-1} NADH at scan rate of (a) 20, (b) 40, (c) 60, (d) 80 and (e) 100 mV s^{-1}.

where D and c^* are the diffusion coefficient (2.4×10^{-6} cm^2 s^{-1} [2]) and the bulk concentration of the NADH, respectively, and the other symbols have their usual meanings. Low values of k result in the values of the coefficient lower than 0.496. For low scan rates (2 to 10 mV s^{-1}), a average value of this coefficient was found to be 0.38 for a PTOB modified electrode with a coverage of $\Gamma = 6.8 \times 10^{-10}$ mol cm^{-2}. According to the approach of Andrieux and Saveant, an average value of k could be calculated to $(2.4 \pm 0.2) \times 10^3$ l $mol^{-1}.s^{-1}$. This reaction rate is controlled by both the kinetic process between NADH and the PTOB films and the mass transfer process of the NADH in solution.

3.5. Rotating disk electrode measurements

Kinetic parameters also obtained from rotating disk electrode (RDE) measurements, which were carried out by sweeping the potential at 2 mV s^{-1} from -0.20 to $+0.35$ V (for peak II). The catalytic current, which taken as the plateau current under the background correction at the low scan rate for each rotational speed, for NADH oxidation at the PTOB modified electrode was measured in phosphate buffer solution (pH 7.0) containing 1.2×10^{-3} mol l^{-1} NADH. The results are shown in Fig. 6. The currents increase with increasing rotational speed. A plot of i_{Cat} versus $\omega^{1/2}$ was found to be nonlinear, and the lack of linearity suggests that the reaction is limited by kinetics and not by transport limitations. The catalytic currents i_{Cat} corresponding to the mediated reaction is a function of the Levich current i_{Lev} representing the mass transfer of NADH in the solution and the kinetic current i_K corresponding to the electron cross-exchange between NADH and the PTOB redox site. The value of k can be obtained from the Koutecky–Levich plot using the following expression [39]:

$$1/i_{Cat} = 1/i_{Lev} + 1/i_K \quad (3)$$

and

$$i_{Lev} = 0.62\ nFAD^{2/3}v^{-1/6}c^*\omega^{1/2} \quad (4)$$

$$i_K = nFAk\Gamma c^* \quad (5)$$

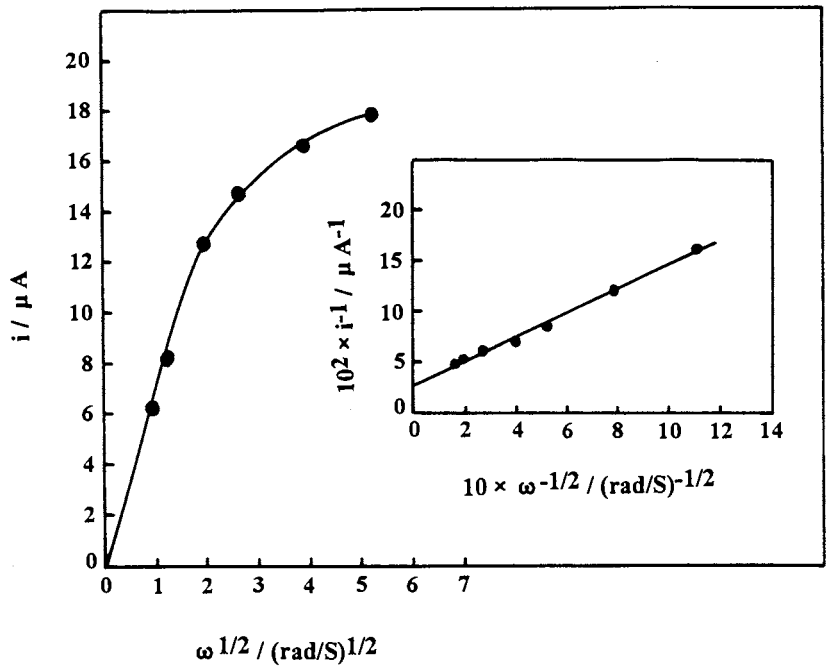

Fig. 6. Levich plot for the oxidation of NADH at a PTOB modified glassy carbon electrode in 0.1 mol l^{-1} phosphate buffer solution (pH 7.0) with a $\Gamma = 6.8 \times 10^{-10}$ mol cm^{-2} and the NADH concentration of 1.2×10^{-3} mol l^{-1}. The inset shows the plot of $1/i$ versus $1/\omega^{1/2}$ (Kouctecky–Levich plot).

where c^* is the bulk concentration of NADH, ω is the rotational speed, v is the kinematic viscosity, Γ is the surface coverage of PTOB, k is the catalytic reaction rate constant between the PTOB and NADH and all other parameters have their usual meanings. The Koutecky–Levich plot, obtained from the data in the main panel of Fig. 6, is shown in the inset of Fig. 6. Such a plot shows the anticipated linear dependence between the $1/i_{Cat}$ and the $1/\omega^{1/2}$. From the intercept of the plot, the value of the k was found to be $(1.8 \pm 0.3) \times 10^3$ l mol^{-1} s^{-1}, which is similar to that determined from cyclic voltammetric measurements.

The value of k, which was obtained by using RDE method, was decreased as the NADH concentration increased (the data are shown in Table 2). The value of k is larger than that obtained at PNB modified electrode [35] and is the same order as that at PAI [34].

Table 2
The electrocatalytic rate constant (k) at various NADH concentration

10^3 C_{NADH}/mol l^{-1}	1.0	1.5	2.0	2.5	3.0	3.5
10^{-3} k/l mol^{-1} s^{-1}	2.2	1.7	1.5	1.2	1.1	0.83

A similar observation, the k decreased with increasing of the NADH concentration, has been previously reported for the electrooxidation of NADH at electrodes modified with different mediators [16,17,40]. In order to rationalize such a concentration dependence of the rate constant, Gorton et al. [17] has suggested that the process involves a charge transfer complex between NADH and the mediator in a mechanism similar to Michaelis–Menten kinetics. Although we have not explored this specific aspect in this study, it is plausible that a similar mechanism might be operative.

3.6. Calibration of NADH detection at PTOB modified electrode

To optimize the response of PTOB modified electrode for NADH determination, the effect of

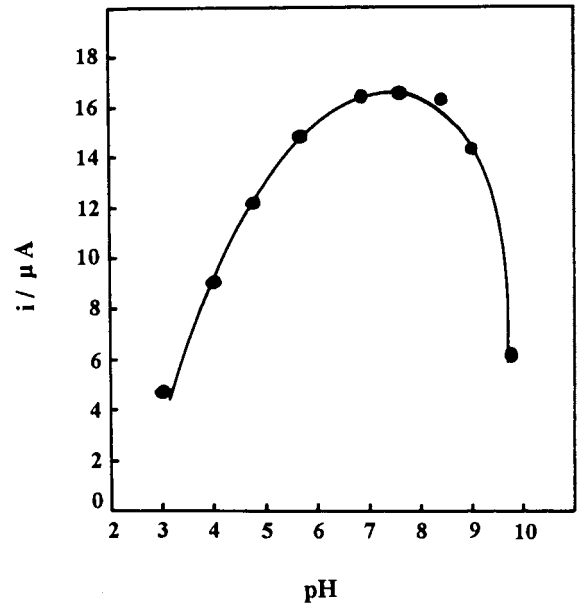

Fig. 7. Effect of solution pH on the electrocatalytic current for NADH oxidation at PTOB modified electrode.

solution pH on the electrocatalytic activity of the electrode toward NADH oxidation was examined. The results are shown in Fig. 7. The catalytic current changes with solution pH and reaches a maximum value between pH 6.8 and 8.3. It decreases markedly with increase in pH above 8.5. So, the solution pH 7.0 was selected in NADH determination.

The steady-state current of oxidation NADH at PTOB modified glassy carbon electrode was measured amperometrically in phosphate buffer solution (pH 7.0). The applied potential is +0.1 V. Once the background current has decayed to a constant value, the NADH was added. After stirred briefly, the steady-state currents was recorded. The dependence of the steady-state currents (under background correction) on NADH concentration is shown in Fig. 8. The response currents depends linearly on NADH concentration in the range of 5.0×10^{-6} to 2.0×10^{-3} mol l^{-1}. At higher concentration, the steady-state currents appears to be a levelling off, this probably due to the kinetic limitations. The detection limits is $(5.0 \pm 0.3) \times 10^{-7}$ mol l^{-1} (at $S/N = 3$). The value is similar to the result obtained by Abruña et al. [30], using flow injection method, at glassy carbon electrode midified with films derived from 3,4-dihydroxybenzaldehyde (5.0×10^{-7} mol

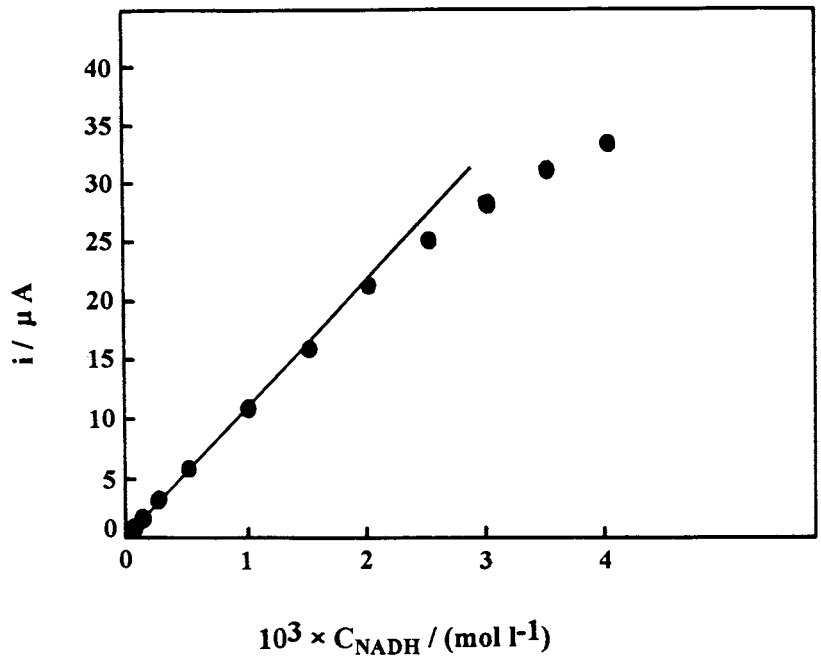

Fig. 8. The dependence of the catalytic current, obtained at PTOB modified electrode in 0.1 mol l^{-1} phosphate buffer solution (pH 7.0), on NADH concentration.

dm^{-3}), but one order larger than the result obtained by Dong and Chi [9], also using flow injection, at glassy carbon electrode modified with polypyrrole films contained methylene blue (4.0×10^{-8} mol dm^{-3}). The lower detection limits are expected to be obtained at the PTOB modified glassy carbon electrode under flow injection conditions, because the flow injection method possesses a much higher current sensitivity than cyclic voltammetry. The results indicate that the PTOB modified glassy carbon electrode is an excellent detector for NADH, because a wide linear range and low detection limits can be achieved. The reproducibility was examined by using separately prepared PTOB modified electrode to determine 1.0×10^{-3} mol l^{-1} NADH ten times, an average of 11.6 μA was obtained, the relative standard deviation was 2.8%, which shows the modified electrode can be used to determine NADH precisely.

4. Conclusions

The oxidation of the toluidine blue o (TOB) on glassy carbon electrode gives rise to stable redox active electropolymerized films. Cyclic voltammograms of the resulting poly(toluidine blue o) (PTOB) indicate the presence of two couple of redox reactions with the formal potential of −277 and 5 mV for redox couple I and II, respectively, at scan rate of 20 mV s^{-1}. The formal potential shifts toward negative direction with increasing the solution pH with a slope of 58 and 54 mV per pH unit for couple I and couple II respectively, which is very close to the anticipated Nernstian dependence of 59 mV per pH unit. The PTOB modified glassy carbon electrode exhibits electrocatalytic activity toward NADH oxidation and the electrode can be used as a detector for NADH determination with a linear range of 5.0×10^{-6} to 2.0×10^{3} mol l^{-1} and detection limits of $(5.0 \pm 0.3) \times 10^{-7}$ mol l^{-1} (at $S/N = 3$).

References

[1] J. Moiroux, P.J. Elving, J. Am. Chem. Soc. 102 (1980) 6533.
[2] W.J. Blaedel, R.G. Haas, Anal. Chem. 42 (1970) 918.
[3] B.W. Carlson, L.L. Miller, J. Am. Chem. Soc. 105 (1983) 7453.
[4] P.J. Elving, W.T. Bresenahan, J. Moiroux, Z. Samec, Bioelectrochem. Bioenerg. 9 (1982) 365.
[5] L. Gorton, J. Chem. Soc. Faraday Trans. 1 82 (1986) 1245.
[6] I. Katakis, E. Domínguez, Mikrochim. Acta 126 (1997) 11.
[7] M. Jesus Lobo, A.J. Miranda, P. Tunon, Electroanalysis 9 (1997) 191.
[8] E. Lorenzo, L. Sanchez, F. Pariente, J. Tirado, H.D. Abruña, Anal. Chim. Acta 309 (1995) 79.
[9] Q. Chi, S. Dong, Analyst 119 (1994) 1063.
[10] K. Essaadi, B. Keita, L. Nadjo, J. Electroanal. Chem. 367 (1994) 275.
[11] M. Somasundrum, J. Hall, J.V. Bannister, Anal. Chim. Acta 295 (1994) 47.
[12] E. Katz, T. Lotzbeyer, D.D. Schlereth, W. Schuhmann, H.L. Schmidt, J. Electroanal. Chem. 373 (1994) 189.
[13] K. Hajizadeh, H.T. Tang, H.B. Halsall, W.R. Heineman, Anal. Lett. 24 (1991) 1453.
[14] B. Persson, L. Gorton, J. Electroanal. Chem. 292 (1990) 115.
[15] B. Persson, J. Electroanal. Chem. 287 (1990) 61.
[16] L. Gorton, G. Johansson, A. Torstensson, J. Electroanal. Chem. 196 (1985) 81.
[17] L. Gorton, A. Torstensson, H. Jaegfeldt, G. Johansson, J. Electroanal. Chem. 161 (1984) 103.
[18] H. Jaegfeldt, A. Torstensson, L. Gortona, G. Johansson, Anal. Chem. 53 (1981) 1979.
[19] H. Jaegfeldt, T. Kuwana, H. Johansson, J. Am. Chem. Soc. 105 (1983) 1805.
[20] F. Ni, H. Feng, L. Gorton, T.M. Gorton, Langmuir 6 (1990) 66.
[21] L. Gorton, G. Bremle, E. Csoregi, G. Jonsson-Pettersson, B. Persson, Anal. Chim. Acta 249 (1991) 43.
[22] W.J. Albery, P.N. Bartlett, J. Chem. Soc. Chem. Commun. (1984) 234.
[23] B.F. Yon, C.R. Lower, Anal. Chem. 59 (1987) 2111.
[24] B. Grundig, G. Wittstock, U. Rudel, B. Strehlitz, J. Electroanal. Chem. 395 (1995) 143.
[25] N.F. Atta, A. Galal, A.E. Karagözler, H. Zimmer, J.F. Rubinson, H.B. Mark Jr., J. Chem. Soc. Chem. Commun. (1990) 1347.
[26] F. Xu, H. Li, S.J. Cross, T.F. Guarr, J. Electroanal. Chem. 368 (1994) 221.
[27] T. Ohsaka, K. Tanaka, K. Tokuda, J. Chem. Soc. Chem. Commun. (1993) 222.
[28] M. Somasundrum, J.V. Bannister, J. Chem. Soc. Chem. Commun. (1993) 1629.
[29] A.A. Karyakin, E.E. Karyakina, W. Schuhmann, H.L. Schmidt, S.D. Varfolomeyev, Electroanalysis 6 (1994) 821.
[30] F. Pariente, E. Lorenzo, H.D. Abruña, Anal. Chem. 66 (1994) 4337.
[31] B. Persson, H.S. Lee, L. Gorton, T. Skotheim, P. Bartlett, Electroanalysis 7 (1995) 935.

[32] Z. Huan, B. Persson, L. Gorton, S. Sahni, T. Skotheim, P. Bartlett, Electroanalysis 8 (1996) 575.
[33] H. Shu, B. Mattiasson, B. Persson, G. Nagy, L. Gorton, S. Sahni, L. Geng, L. Boguslavsky, T. Skotheim, Biotechnol. Bioeng. 46 (1995) 270.
[34] C.C. Cai, K.H. Xue, J. Electroanal. Chem. 427 (1997) 147.
[35] C.C. Cai, K.H. Xue, Anal. Chim. Acta 343 (1997) 69.
[36] J.M. Bauldreay, M.D. Archer, Electrochim. Acta 28 (1983) 1515.
[37] A.A. Karyakin, E.E. Strakhova, E.E. Karyakina, S.D. Varfolomeyev, A.K. Yatsimirsky, Bioelectrochem. Bioenerg. 32 (1993) 35.
[38] C.P. Andrieux, J.M. Saveant, J. Electroanal. Chem. 93 (1978) 163.
[39] A.J. Bard, L.R. Faulker, Electrochemical Methods Fundaments and Applications, Chapter 8, Wiley, New York, 1980.
[40] F. Pariente, F. Tobalina, G. Moreno, L. Hernandez, E. Lorenzo, H.D. Abruña, Anal. Chem. 69 (1997) 4065.

ELSEVIER

Talanta 47 (1998) 1121–1127

Talanta

Adsorbed resin phase spectrophotometric determination of vanillin or/and its derivatives

Rong Li [a,*], Zitao Jiang [a], Luyuan Mao [b], Hanxi Shen [b]

[a] *Department of Food science and Engineering, Tianjin University of Commerce, Tianjin 300400, People's Republic of China*
[b] *Department of Chemistry, Nankai University, Tianjin 300071, People's Republic of China*

Received 28 August 1997; accepted 8 May 1998

Abstract

The reactive mechanism, stability and interrelating properties, and thermodynamic constants of β-cyclodextrin polymer (β-CDP) including vanillin, 4-hydroxybenzaldehyde and piperonal were investigated. The effects of pH, temperature, time and solvent concentration on the inclusion reaction were determined. The optimum conditions were determined (pH, 3.0; temperature, normal atmospheric temperature; time, 90 min; ethanol concentration, $<1\%$). The method was applied for the direct ultraviolet solid phase spectrophotometric determination of vanillin in peanut toffee and toffee, and the other aromatic aldehydes using β-CDP adsorbed resin with satisfactory results. The β-CDP resin has less background absorbance in ultraviolet region compared to other ion-exchanger resins. © 1998 Elsevier Science B.V. All rights reserved.

Keywords: Vanillin; 4-Hydroxybenzaldehyde; Piperonal; β-Cyclodextrin polymer; Resin phase spectrophotometry

1. Introduction

The diameter of β-cyclodextrin (β-CD) cavity is 7.5 angstrom, and is fairly hydrophobic. β-CD includes organic compounds containing the hydrophobic aromatic group to form inclusion complexes [1–9]. Several possible or already realized applications of β-CD have been reviewed by Szejtli [10]. β-cyclodextrin polymer (β-CDP), which was synthesized via use of epoxy chloropropane as a cross linking agent [11], still retains the inclusion property of β-CD. It can be applied to separate and concentrate organic compounds containing the hydrophobic aromatic group from solution to form inclusion complexes. Several methods have been developed recently to remove the butter components from citrus by treatment of the juice with β-CDP [12–18]. In earlier studies, β-CDP was found to be effective in adsorbing naringin, which is an intermediate for vanillin [19], limonin and nomilin from grapefruit juice. Shaw and Yu discussed in some details the inclusion compounds between β-CDP and either naringin or limonin [13–17].

Vanillin is an important material used in the food industry. It is also widely used in dairy and artificial dairy products. Because of its volatility,

* Corresponding author.

0039-9140/98/$ - see front matter © 1998 Elsevier Science B.V. All rights reserved.
PII S0039-9140(98)00191-X

instability, and indissoluble properties in water, it is not easily directly determined in solution. In this paper the reaction mechanism of β-CDP including vanillin, 4-hydroxybenzaldehyde and piperonal was examined. The thermodynamic constants and effect of experimental factors of inclusion reactions were determined. The present paper gives an outline of adsorbed resin phase spectrophotometric determination of vanillin and its derivatives based upon the ability of β-CDP to selectively include and adsorb these compounds.

2. Experimental

2.1. Reagents

Standard vanillin, 4-hydroxybenzaldehyde and piperonal solutions. An appropriate amount of analytical reagent grade vanillin, 4-hydroxybenzaldehyde and piperonal was dissolved in ethanol respectively. Their stock standard solutions were about 1.0 mg ml^{-1} and were standardized as described earlier [20,21]. Working standard solutions of 10 and 100 μg ml^{-1} were prepared before use by serial dilution.

2.1.1. Buffer solutions

The mixed solutions of sodium citrate-hydrochloric acid (pH-ranges 1.5–4.0), acetic acid-sodium acetate (pH-ranges 4.0–5.5), or sodium hydroxide-potassium dihydrogen phosphate (pH-ranges 6.0–12.0), were used as buffer solutions.

2.1.2. β-CDP resin

The resin was synthesized as described previously [11], which is transparent and insoluble in water. The quantity of β-cyclodextrin (β-CD) existing in β-CDP resin was determined as described earlier [22]. Before use, the resin first was ground into 80–100 mesh and immersed in deionized water so as to remove any remaining metallic ions. It was dried under vacuum and stored in a desiccator.

All chemicals used were of analytical reagent grade.

2.2. Apparatus

The spectrophotometer used was a Shimadzu model UV-240 fitted with matched 5-mm quartz cell, the bottom of which has a small hole in order to release the excess of solution when the resin was packed into a sample cell. The pH-meter used was a Shanghai model pHs-2. The thermostatic shaker used was a Peking model SHZ-2.

2.3. General procedure

Selection of conditions for β-CDP including vanillin and its derivatives. To a 25-ml stoppered conical flask add 1.0 ml of solution of each compound in ethanol (100 μg ml^{-1}), 5.0 ml of buffer solution and 1.0 ml of 1.0 mol l^{-1} sodium chloride. Dilute the solution to 10.0 ml with deionized water, add 0.2 g of β-CDP resin and shake mechanically for 90 min. Transfer 1.0 ml of the solution into a 10-ml volumetric flask and add 5.0 ml of buffer solution. Dilute to the mark with deionized water and mix well. Measure the absorbance respectively at 279 nm (vanillin), 282 nm (4-hydroxybenzaldehyde) and 315 nm (piperonal) against a reference blank solution that does not contain any analyte, e.g. vanillin, 4-hydroxybenzaldehyde and piperonal. Calculate Ks and Q on the basis of follows [23]:

$$Ks = \{[G]_0 - [G]_{eq}\}/\{[G]_{eq} \times ([\beta\text{-CD}]_0 - [G]_0 + [G]_{eq})\}$$

$$Q = \{[G]_0 - [G]_{eq}\} \times V\ m^{-1}$$

In formulas: $[G]_0$ is the initial concentration of analyte, $[G]_{eq}$ is the equilibrium concentration of analyte, $[\beta\text{-CD}]_0$ is the initial concentration of β-CD in β-CDP, V is the volume of solution and m is the weight of β-CDP resin used.

2.3.1. Determination of vanillin and its derivatives

To a 25-ml stoppered conical flask add 5.0 ml of buffer solution (pH 3.0), 1.0 ml sodium chloride (1.0 mol l^{-1}) and an appropriate amount of the sample solution of vanillin, 4-hydroxybenzaldehyde and piperonal respectively. Dilute the solution to 10 ml with deionized water, add 0.5 g of β-CDP resin and shake mechanically at normal

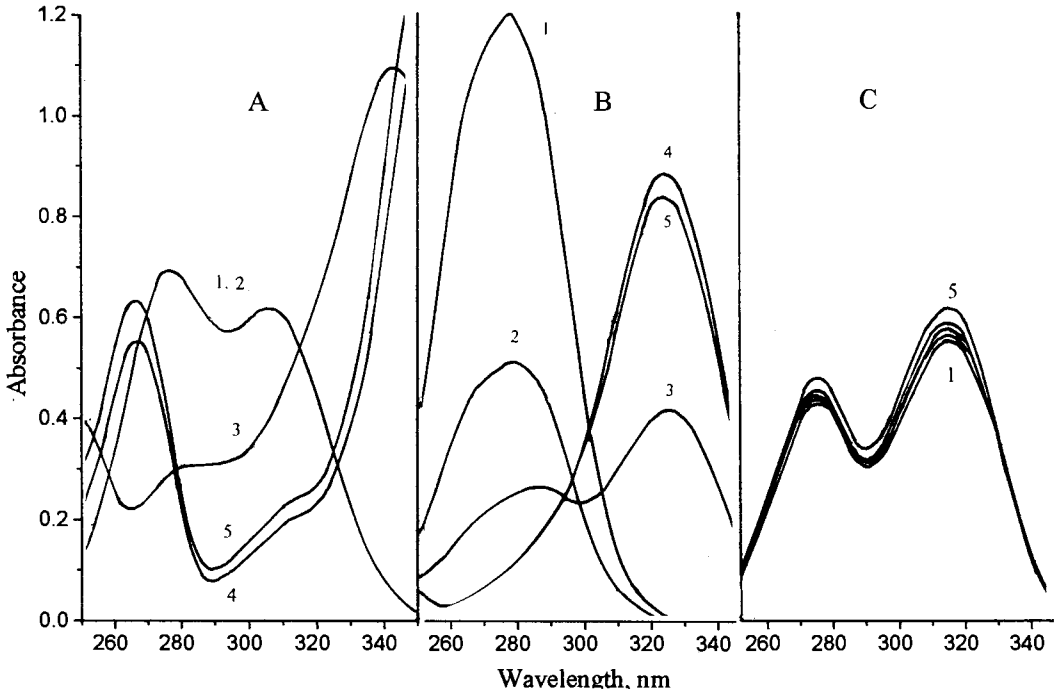

Fig. 1. Absorption spectra of vanillin (A), 4-hydroxybenzaldehyde (B) and piperonal (C). Cell path length, 10 mm; the sample solution, 10 μg ml^{-1}; pH, 1: 3.0; 2: 4.5; 3: 7.5; 4: 10.0; 5: 12.0.

atmospheric temperature (20°C) for 90 min. After allowing to stand for a few minutes so that β-CDP including vanillin or its derivatives resin (β-CDP-vanillin) that is insoluble solid beads can perfectly drop to the bottom of the conical flask, suck β-CDP-vanillin resin and a small amount of solution using a sucker and transfer them into a 5-mm quartz cell whose bottom has a small hole, from which the solution sucked can be released, but β-CDP-vanillin resin can remain, again and again until the cell is stuffed with β-CDP-vanillin resin. Measure the absorbance of β-CDP -vanillin resin at 295 nm (vanillin), 299 nm (4-hydroxybenzaldehyde) and 328 nm (piperonal), against a β-CDP resin blank as reference.

2.3.2. Determination of vanillin in candy

A sample of candy (2.0 g) that was obtained from local market, was immersed after it was ground, in an appropriate amount of 95% ethanol at normal atmospheric temperature for 1 h. The solution was filtrated and made up the volume of filtrate to 50 ml with 0.001 mol l^{-1} hydrochloric acid and mixed well [27]. A 3 ml aliquot was transferred into a 25-ml conical flask and vanillin was determined as described previously.

Table 1
The equilibrium constants in different pH-values (*K*s: l mol^{-1})[a]pH

Compounds	pH			
	2.0	3.0	6.6	12.0
Vanillin	58.3	99.4	65.4	56.4
4-Hydroxybenzaldehyde	110.4	225.9	156.4	73.5
Piperonal	218.2	230.4	226.6	194.6

[a] The ionic strength: 0.1 mol l^{-1}; $[G]_0$: 10 μg ml^{-1}; $[\beta\text{-CD}]_0$: 1.02×10^{-2} mol l^{-1}; β-CDP: 0.2 g; mean of three determinations.

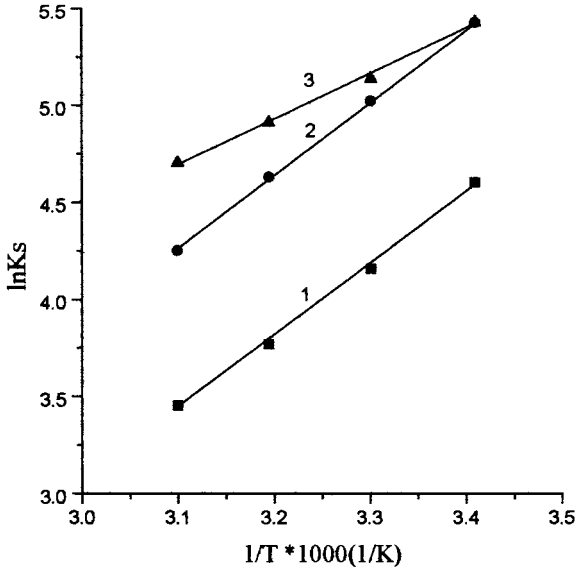

Fig. 2. Effect of temperature on Ks. The sample solution, 10 μg ml^{-1}; pH, 3.0; β-CDP, 0.2 g; 1, vanillin; 2, 4-hydroxybenzaldehyde; 3, piperonal.

3. Results and discussion

3.1. Effect of pH on inclusion reaction

Vanillin, 4-hydroxybenzaldehyde, and piperonal all contain benzene ring whose size and geometry are suitable for the hydrophobic cavity of β-CDP. Their shapes that existed in solution were changeable except piperonal as pH-values of solution because of hydroxyl group. The absorption spectra of three compounds in different pH-ranges are shown in Fig. 1.

Table 2
The thermodynamic constants of inclusion reaction (kJ mol^{-1})[a]

Compounds	ΔH	ΔG_{293}	ΔS_{293}
Vanillin	−29.1	−11.2	−0.061
4-Hydroxybenzaldehyde	−33.7	−13.4	−0.069
Piperonal	−18.7	−13.3	−0.019

[a] The ionic strength, 0.1 mol l^{-1}; pH, 3.0; $[G]_0$, 10 μg ml^{-1}; $[\beta\text{-CD}]_0$: 1.02×10^{-2} mol l^{-1}; β-CDP, 0.2 g; mean of three determinations.

Table 1 shows that the equilibrium constants (Ks) of β-CDP including the neutral molecules of vanillin and 4-hydroxybenzaldehyde are larger than those of their phenyl salts in strong basic medium and those of their oxonium salts in strong acidic medium. The results show clearly that β-CDP includes neutral molecule easily because its cavity is hydrophobic. Weak polar and no-polar compounds are easily included to form complexes in general conditions. The molecular structure of piperonal is not changeable as pH changes. Thus, its Ks almost is a constant in different pH-ranges. When pH >12, because of ionization of β-CDP, its inclusion ability decreases and results in Ks of three compounds decreasing. Vanillin, 4-hydroxybenzaldehyde, and piperonal exist in different pH-values:

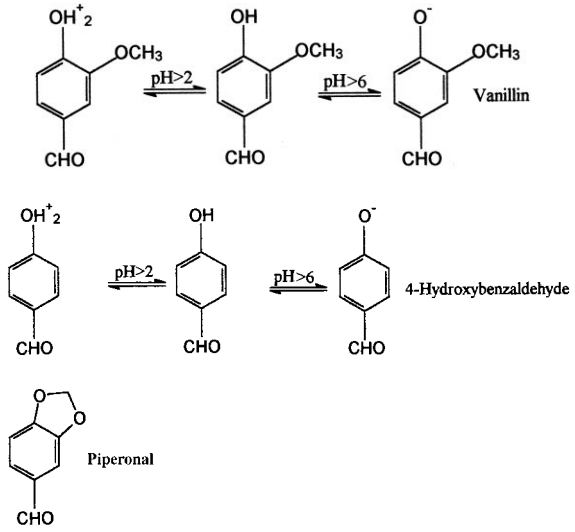

Though three compounds all contain benzaldehyde group, the stability of their β-CDP inclusion complexes is distinctly different. It is well documented that the stability of β-CD inclusion complexes results from the size/geometry of the solute and its ability to properly fit into the β-CD cavity. Moreover, hydrogen bonding between the solute and the secondary hydroxyl groups of the cyclodextrin, van der Waals interaction, and/or hydrophobic interactions are important to strength of binding. Piperonal whose molecule is the most suitable for β-CD cavity in three com-

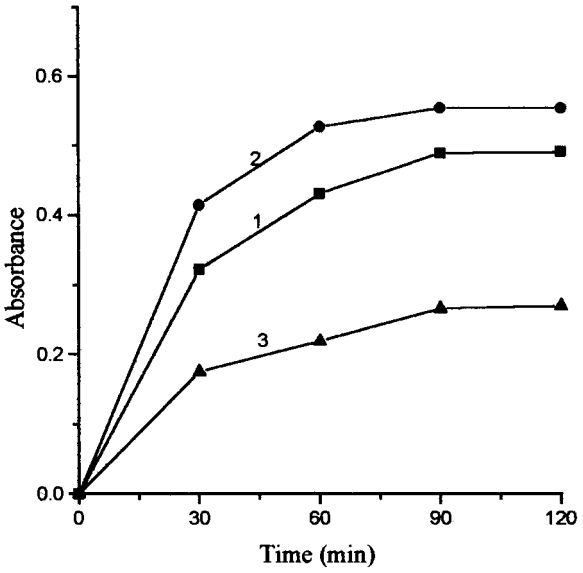

Fig. 3. Effect of time on the inclusion reaction. The sample solution, 10 μg ml^{-1}; pH, 3.0; β-CDP, 0.2 g; 1, vanillin; 2, 4-hydroxybenzaldehyde; 3, piperonal.

pounds is included the most easily and its complex is the stablest, too. Vanillin, which has an *o*-substituent and the others do not, is included the most difficult of the three compounds and its complex is the unstablest, too. Therefore, the order of inclusion complexes' stability is: piperonal > 4-hydroxybenzaldehyde > vanillin. On the basis of the results of Fig. 1 and Table 1, the pH 3.0 was selected for our analysis.

3.2. Effect of temperature on inclusion reaction

There is such relationship between *K*s and temperature: $\ln Ks = -\Delta H/RT + B$. A plot of $\ln Ks$ versus $1/T$ will provide a straight line whose slope is equal to $-\Delta H/R$, on the basis of which, $\Delta G = \Delta H - T\,\Delta S$, and $\Delta G_0 = -RT \ln Ks$ the thermodynamic constants of inclusion reaction can be obtained. The results are shown in Fig. 2 and Table 2.

These show that the inclusion reaction was exothermal. It was desirable that the temperature of inclusion reaction was as low as possible, which is in agreement with the findings of Gelb et al. [24,25]. Normal atmospheric temperature (20°C) was used for our analysis.

Table 3
Effect of ethanol concentration[a]

Ethanol (%, v/v)	1	20	40	80
*K*s (l mol^{-1})	99.4	84.6	53.5	21.9
Q (μmol g^{-1})	14.9	9.7	6.9	3.4

[a] The ionic strength, 0.1 mol l^{-1}; pH, 3.0; $[G]_0$, 10 μg ml^{-1}; $[\beta\text{-CD}]_0$, 1.02×10^{-2} mol l^{-1}; β-CDP, 0.2 g; mean of three determinations.

3.3. Effect of time on inclusion reaction

Under the conditions of normal atmospheric temperature and pH 3.0, the equilibrium time of β-CDP including vanillin, 4-hydroxybenzaldehyde and piperonal was 90 min, as shown in Fig. 3. For this reason, 90 min was selected for our analysis.

3.4. Effect of ethanol concentration on inclusion reaction

The *K*s and *Q* of vanillin were determined in different ethanol concentration and the results are shown in Table 3.

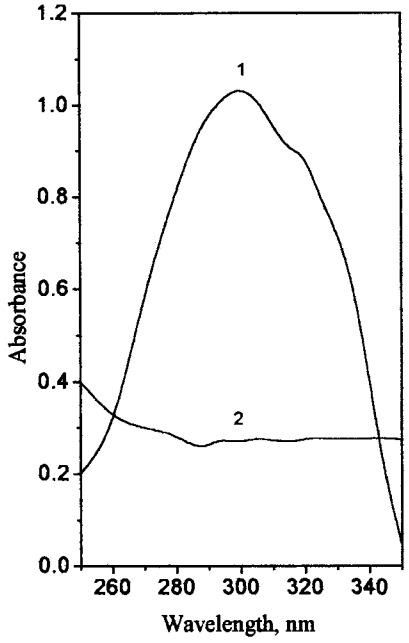

Fig. 4. Absorption spectra of β-CDP and vanillin in β-CDP resin phase. Cell path length, 5 mm; Vanillin, 10 μg ml^{-1}; pH, 3.0; β-CDP, 0.5 g; 1, β-CDP-vanillin; 2, β-CD.

Table 4
Determination of vanillin in candy[a]

Samples	Vanillin (mg g^{-1})			Recovery
	Found	Added	Recovered	
Peanut toffee	0.340	1.000	1.301	96.1
Toffee	0.311	1.000	1.236	92.5

[a] Mean of five determinations.

Thus it can be seen that Ks and Q were in relation to the property and concentration of solvent. In the concentration of ethanol medium, vanillin, 4-hydroxybenzaldehyde and piperonal did not easily enter into the hydrophobic cavity of β-CDP because ethanol can bind to the β-CDP cavity as they noted [26]. A more important reason is that bulk solvent, ethanol, is much less polar compared to water, in fact, the polarity of ethanol is very similar to that of the interior of the β-CDP. Therefore, Ks and Q decreased gradually as the concentration of ethanol rose. Finally, the solution of 1% ethanol was used for our analysis.

3.5. Determination of vanillin, 4-hydroxybenzaldehyde and piperonal

3.5.1. Absorption spectra of the resin phase

Maximum absorbances of vanillin, 4-hydroxybenzaldehyde and piperonal in β-CDP resin were respectively at 295, 299 and 328 nm where the absorbance of the β-CDP blank was fairly small, and at 279, 282 and 315 nm in ethanol solution of 1%, moved 16, 17 and 13 nm toward the longer wavelength region than in solution. Fig. 4 shows the absorption spectra of β-CDP and vanillin included in β-CDP resin.

3.5.2. Calibration

The calibration curves were reasonably linear and might be expressed by the equations:

$$A_{(295\ nm)} = 0.0578X\ (\mu g\ ml^{-1}) + 0.0880,\ \gamma$$
$$= 0.9986,\ N = 5,\ \text{vanillin}$$

$$A_{(299\ nm)} = 0.0549X\ (\mu g\ ml^{-1}) + 0.0078,\ \gamma$$
$$= 0.9985,\ N = 5,\ \text{4-hydroxybenzaldehyde}$$

$$A_{(328\ nm)} = 0.0266X\ (\mu g\ ml^{-1}) + 0.0040,\ \gamma$$
$$= 0.9977,\ N = 5,\ \text{piperonal}$$

Where, X is the concentrations of vanillin, 4-hydroxybenzaldehyde and piperonal in sample solution.

3.5.3. Determination of vanillin in candy

The results for two samples are given in Table 4. The recovery of added vanillin is in the range of 92.5–96.1%.

Acknowledgements

This work was supported by the National Natural Science Foundation of China.

References

[1] S. Harata, Bull. Chem. Soc. Jpn. 48 (1975) 2409.
[2] J. Szejtli, Z. Budai, Acta Chim. Acad. Sci. Hung. 99 (1979) 433.
[3] J. Szejtli, L. Szente, E. Banky-Elod, Acta Chim. Acad. Sci. Hung. 101 (1979) 27.
[4] W.L. Hinze, Separation and Purification Methods, vol. 10, Marcel Dekker, New York, 1981, p. 159.
[5] M. Tardy-Lengyel, J. Szejtli, J. Inclusion Phenom. 35 (1982) 127.
[6] S. Hamai, Bull. Chem. Soc. Jpn. 55 (1982) 2721.
[7] J. Szejtli, Cyclodextrin and Their Inclusion Complexes, Akademiai Kiado, Budapest, 1982.
[8] L.X. Song, Q.J. Meng, X.Z. You, Chem. Res. App. 6 (1994) 99.
[9] X.F. Lu, Z. Xia, F.P. Xu, M.G. Xie, Chin. J. Anal. Chem. 24 (1996) 621.
[10] J. Szejtli, Starch 34 (1982) 379.
[11] M. Komiyama, H. Hirai, Polym. J. 19 (1987) 773.
[12] R.L. Johnson, B.V. Chandler, J. Sci. Food Agric. 33 (1982) 287.
[13] P.E. Shaw, C.W. Wilson, J. Food Sci. 48 (1983) 646.
[14] P.E. Shaw, C.W. Wilson, J. Food Sci. 50 (1985) 1205.
[15] P.E. Shaw, J.H. Tatum, C.W. Wilson, J. Agric. Food Chem. 32 (1984) 832.
[16] P.E. Shaw, B.S. Buslig, J. Agric. Food Chem. 34 (1986) 837.
[17] E.K.C. Yu, Appl. Microbiol. Biotechnol. 28 (1988) 546.
[18] C.W. Wilson, C.J Jr. Wagner, P.E. Shaw, J. Agric. Food Chem. 37 (1989) 14.
[19] C.S. Su, C.P. Yang, J. Agric. Food Chem. 54 (1991) 635.

[20] H.A.A. Medien, Anal. Lett. 27 (1994) 983.
[21] M. Tarek, M. Zaki, A.M. Soliman, Anal. Lett. 22 (1989) 3091.
[22] X.D. Su, L.Z. Liu, H.X. Shen, Fenxi Kexue 13 (1997) 102.
[23] R. Li, Z.T. Jiang, X.H. Lin, L.Y. Mao, H.X. Shen, Anal. Lett. 30 (1997) 1685.
[24] R.I. Gelb, L.M. Schwartz, R.F. Johnson, D.A. Laufer, J. Am. Chem. Soc. 101 (1979) 1869.
[25] R.I. Gelb, L.M. Schwartz, B. Cardelino, H.S. Fuhrman, R.F. Johnson, D.A. Laufer, J. Am. Chem. Soc. 103 (1981) 1750.
[26] Y. Matsui, K. Mochida, Bull. Chem. Soc. Japan 52 (1979) 2808.
[27] Z.T. Jiang, L. Ren, L.H. Liu, Tangye Shipin Keji 10 (1992) 30.

ELSEVIER

Talanta 47 (1998) 1129–1137

Talanta

Detection of TMV with ODA-H_2O_2-HRP voltammetric enzyme-linked immunoassay system

Kui Jiao [a,*], Shusheng Zhang [a], Lu Wei [a], Chengfan Liu [a], Chenliang Zhang [b], Zhofang Zhang [b], Jingyu Liu [c], Peng Wei [c]

[a] *Department of Applied Chemistry, Qingdao Institute of Chemical Technology, 53 Zhengzhou Road, 266042 Qingdao, People's Republic of China*

[b] *Institute of Plant Quarantine, Ministry of Agriculture, 100029 Beijing, People's Republic of China*

[c] *Beijing Institute of Geology, Nuclear Industry, 100029 Beijing, People's Republic of China*

Received 22 December 1997; received in revised form 29 April 1998; accepted 8 May 1998

Abstract

o-Dianisidine (ODA)-H_2O_2-horseradish peroxidase (HRP) voltammetric enzyme-linked immunoassay system has firstly been used for the detection of tobacco mosaic virus (TMV). HRP catalyzes strongly the oxidation reaction of ODA by H_2O_2, the product of which produces a sensitive second order derivative linear sweep voltammetric peak at potential of -0.56 V (versus SCE) in Britton–Robinson (BR) buffer. HRP activity has been measured with this voltammetric peak and TMV detected through immunoreaction. The detection limit for HRP is 9.25×10^{-7} mU l^{-1} and the linear range is 2.5×10^{-6}–5.0×10^{-4} mU l^{-1}. The detection limit for the clarified TMV is 0.25 ng ml^{-1} and the highest dilution ratio detected for the infected leaf sap is $1{:}8 \times 10^5$. The sensitivity for TMV detection with this method is higher than that with the enzyme-linked immunosorbent spectrophotometric assay (ELISA) using ODA-H_2O_2-HRP system. The processes of the enzyme-catalyzed reaction and the electro-reduction of the product of the enzyme-catalyzed reaction have been described. © 1998 Elsevier Science B.V. All rights reserved.

Keywords: Tobacco mosaic virus (TMV); Horseradish peroxidase (HRP); *o*-Dianisidine; Electrochemical immunoassay; Voltammetry

1. Introduction

Tobacco mosaic virus (TMV) is an important plant virus, which has a number of plant strains and a widespread hosts, and makes inroads on several hundreds plants such as *Nicotiana tobacco*, *Lycopersicon esculentum*, *Capsicum frutescens*, *Brassica pekinensis*, *Raphanus gativus*, *Humumlupulus*, *Cucumis sativus*, *Spinacia oleracca* and so on. The early detection for TMV in various plants and seeds for the purpose of the provention and control of plant disease is very important. Hence, the sensitive assay for TMV is needed. ELISA method is now the mostly employed method for the detection of TMV [1–5].

* Corresponding author. Tel.: +86 532 4851401; fax: +86 532 4856613; e-mail: faoe@mail.qtd.com.cn

0039-9140/98/$ - see front matter © 1998 Elsevier Science B.V. All rights reserved.
PII S0039-9140(98)00192-1

The detection limit for TMV with stephylococal protein A-ELISA method is 0.5 ng ml^{-1}, but that with indirect ELISA method is 10 ng ml^{-1}.

In indirect ELISA method, *o*-dianisidine (ODA) was sometimes used as the substrate [6–8] with a detection limit of 7.5×10^{-5} mU l^{-1} for HRP and 10 ng ml^{-1} for TMV. Enzyme-linked immunoassay with electrochemical detection is a sensitive method [9–11]. In this work, ODA is used as the substrate of voltammetric emzyme-linked immunoassay for the detection of TMV. The detection limit for HRP is 9.25×10^{-7} mU l^{-1} and that for TMV is 0.25 ng ml^{-1}, the determined highest dilution ratio for the infected leaf sap is $1{:}8 \times 10^5$.

2. Experimental

2.1. Apparatus

MP-1 voltammetric analyser, produced by Shandong no. 7 Electric Communication Factory, with three-electrode system composed of a dropping mercury electrode or a hanging mercury drop electrode as working electrode, a platinum electrode as auxiliary electrode and a saturated calomel electrode (SCE) as reference electrode; JM-01 hanging mercury drop electrode was made by Jiangsu Electric Analysis Apparatus Factory; Philips 8700 spectrophotometer, manufactured by British Philips Company and model SA720 pH meter by American Orion Company.

2.2. Antigen and antibody

Tobacco mosaic virus (TMV) and its antiserum (TMV-As) were offered by The Institute of Plant Quarantine, Ministry of Agriculture, China. TMV was purified from infected Nicotiana tobacco leaf. The procedure of purification involves precipitation with polyethylene glycol (PEG), two differential centrifugation cycles and 10–40% sucrose density-gradient centrifugation. The infected leaf sap was obtained from following procedure: Added 2 ml 0.2 mol l^{-1} phosphate buffer of pH 7.2 into 1 g of fresh infected leaf, ground and filtered.

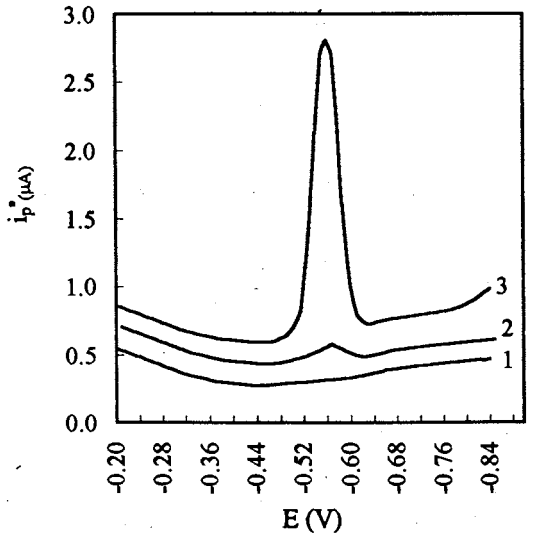

Fig. 1. Second order derivative linear sweep voltammograms. (1) Phosphate buffer, (2) Reaction without HRP: $1 + 1.0 \times 10^{-4}$ mol l^{-1} ODA + 3.0×10^{-4} mol l^{-1} H_2O_2, (3) Reaction with HRP: $2 + 2.5 \times 10^{-5}$ mU l^{-1} HRP.

Purified TMV was used to immunize a rabbit for the preparation of antiserum TMV-As.

2.3. Reagents

HRP solution: Dongfeng Biochemical Technique, Shanghai Institute of Biochemistry, 250

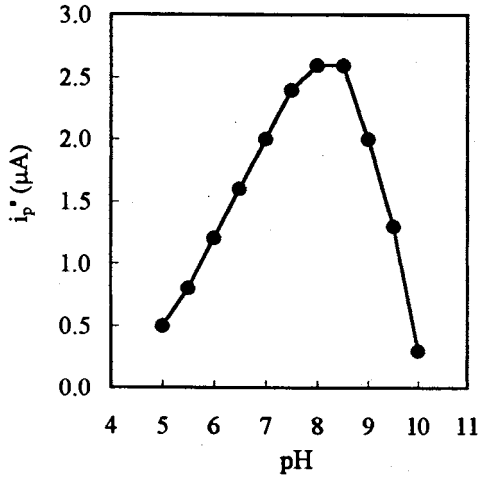

Fig. 2. Dependence of the voltammetric peak height on the pH value of BR buffer. Conditions are as curve 3 in Fig. 1

Table 1
The comparison results of this method with ELISA method for the detection of TMV infected leaf sap

Dilution ratio of sap	1:10	1:250	1:1250	1:2500	1:5000	1:10 000	1:20 000	1:40 000	1:80 000	1:160 000	1:800 000	Blank
i_p''(μA)	4.50	4.40	2.80	2.50	2.10	1.80	1.60	1.40	1.15	0.90	0.65	0.30
A_{420}	0.370	0.182	0.016	0.014	0.014	0.014	0.015	0.014	0.014	0.014	0.000	0.000

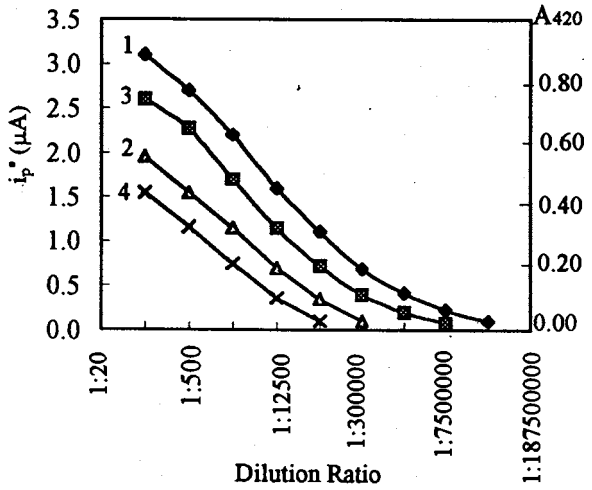

Fig. 3. Dilution curves of detection of IgG-HRP. (1) Free IgG-HRP with this method, (2) Free IgG-HRP with ELISA method, (3) IgG-HRP adsorbed on the solid phase carrier with this method, (4) IgG-HRP adsorbed on the solid phase carrier with ELISA method.

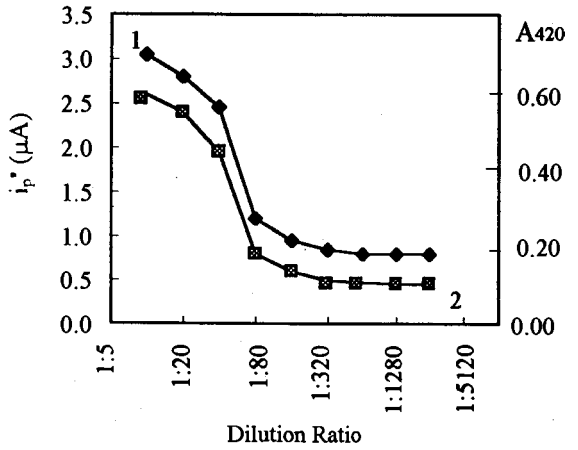

Fig. 5. Dependence of the height of the voltammetric peak (i_p) and the absorbance (A_{420}) for the detection of TMV on the dilution ratio of IgG-HRP. (1) This method, (2) ELISA method.

units per mg enzyme ($RZ > 3.0$); 2.5×10^8 mU l^{-1} stock solution of HRP was prepared by dissolving 0.0500 g of HRP in 50 ml H_2O, which was stored in a refrigerator at 4°C. The goat anti-rabbit IgG-HRP was purchased from the Military Medical Science Academy of China. ODA solution: Fluka, 1.0×10^{-2} mol l^{-1} ODA stock solution was prepared by dissolving 0.2443 g ODA in 100 ml methanol. H_2O_2 solution: 1.0×10^{-3} mol l^{-1}, was prepared before using. BR buffer (0.2 mol l^{-1}): pH 8.4. Tween 40 solution: 0.16 g l^{-1}. KH_2PO_4-Na_2HPO_4 buffer (PBS): pH 6.4. Substrate solution: To a colorimetric tube of 10 ml are in turn added 1.0 ml 1.0×10^{-2} mol l^{-1} ODA solution, 3.0 ml 1.0×10^{-3} mol l^{-1} H_2O_2 solution, 1.0 ml pH 6.4 PBS buffer, and 1.0 ml 0.16 g l^{-1} Tween 40 solution, diluted to the scale with dideionized water. 0.1 mol l^{-1} carbonate buffer: 8.58 g $Na_2CO_3 \cdot 10H_2O + 5.88$ g $NaHCO_3$, diluted to 1000 ml, pH 9.6. PBS–Tween 20 solution: 2.90 g $Na_2HPO_4 \cdot 12H_2O + 0.20$ g $KH_2PO_4 + 8.00$ g $NaCl + 0.20$ g $KCl + 0.5$ ml

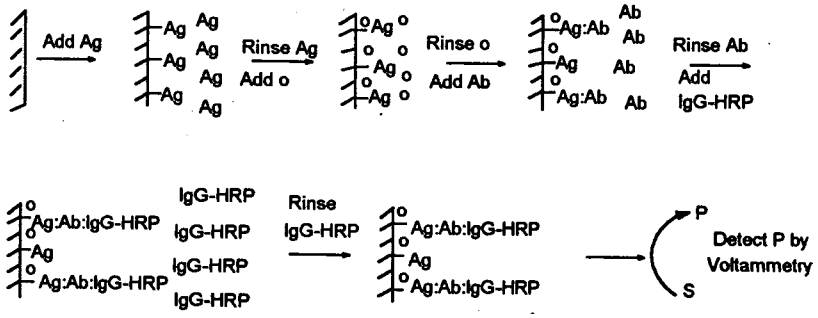

Fig. 4. Principle of detection of plant virus with the indirect method. Polystyrene cuvette; O, bovine serum albumin; Ag, TMV-Ag; S, substrate; P, product.

Tween 20, diluted to 1000 ml, pH 7.4. 1% bovine serum albumin.

2.4. Procedures

2.4.1. Measurement of HRP activity

ODA 1.0 ml (1.0×10^{-2} mol l^{-1}) + 3.0 ml (1.0×10^{-3} mol l^{-1}) H_2O_2 + 1.0 ml (2.5×10^{-4} mU l^{-1}) HRP + 1.0 ml pH 6.4 PBS buffer + 1.0 ml (0.16 g l^{-1}) Tween 40, diluted to 10.0 ml with dideionized water. Then set it in a 37°C water-bath for 10 min, remove, 5.0 ml of the above solution is transferred into a colorimetric tube of 10 ml and 5.0 ml of pH 8.4 BR buffer solution is subsequently added, then shaken to uniform solution and transferred into a 10 ml electrolytic cell. The second order derivative linear sweep voltammogram is recorded with the MP-1 voltammetric analyser.

2.4.2. Determination of TMV

The purified TMV of 5000 ng ml^{-1} and the TMV infected leaf sap of 1:10 are successively diluted with 0.1 mol l^{-1} pH 9.6 carbonate buffer. Coat the polystyrene cuvette, which is 96-well, with the above diluted antigens of 200 μl per well, incubate at 37°C for 2 h, place it in a refrigerator of 4°C for 24 h. Empty the well and then add 300 μl PBS–Tween 20 per well, set it for 3 min and repeat this manipulation three times. Coat the cuvettes with 200 μl 1% bovine serum albumin and incubate at 37°C for 30 min. Wash the cuvettes with PBS–Tween 20 as above manipulation. Add 200 μl of 1:6400 TMV-As per well and incubate at 37°C for 2 h. Wash the cuvettes as above. Add 200 μl goat anti-rabbit IgG-HRP to each well and incubate it at 37°C for 2 h. Wash the cuvettes as above and wash them twice more with dideionized water. Add 500 μl substrate solution per well, set at 37°C for 10 min, transfer the reaction solution into an electrolytic cell of 5 ml, add 100 μl 0.2 mol l^{-1} pH 8.4 BR buffer and 400 μl dideionized water to the cell and record the 2nd order derivative linear-sweep voltammogram. The ELISA detection to the immuno-reaction solutions prepared as above is carried out with Philips 8700 spectrophotometer.

3. Results and discussion

3.1. The second order derivative linear sweep voltammetric peak of the product of the enzyme-catalyzed reaction

The product of the HRP-catalyzed reaction has well-defined voltammetric peak. Fig. 1 is the results of the second order derivative linear sweep voltammograms. Curve 1 is the voltammogram of the PBS, which has no voltammetric peak. Curve 2 is that of PBS + ODA + H_2O_2 solution, which has a small voltammetric peak at −0.56 V. The small peak is due to a slow oxidation of ODA by H_2O_2 as well as the high sensitivity of this method. Curve 3 is that of the enzyme-catalyzed reaction solution. Owing to the presence of HRP, which quickens greatly the reaction of oxidizing ODA by H_2O_2, the reaction product produces a well-defined voltammetric peak at −0.56 V. Although the HRP content is as low as 9.25×10^{-7} mU l^{-1}, a distinctive increase of this peak can still be measured.

3.2. Conditions of the enzyme-catalyzed reaction

HRP catalyzes strongly the reaction of the oxidation of ODA by H_2O_2 in KH_2PO_4-Na_2HPO_4. In a pH range from 5.0 to 9.0, the effect of the pH value of the KH_2PO_4-Na_2HPO_4 buffer solution on the voltammetric peak was investigated. In a pH range from 6.2 to 6.6, a sensitive and stable voltammetric peak appears and pH 6.4 is chosen as the reaction pH. The concentrations of the buffer solution, ODA and H_2O_2 were also experimented. The voltammetric peak is the highest and stable in 0.01 mol l^{-1} KH_2PO_4-Na_2HPO_4 buffer, 1.0×10^{-3} mol l^{-1} ODA and 3.0×10^{-4} mol l^{-1} H_2O_2 solution.

The experiments of the influence of the reaction time and the reaction temperature on the voltammetric peak indicate that the peak rises to the highest at 2 min and 37°C. The peak height has no change within 2 h and the small blank peak has also no change. A reaction time of 10 min and a reaction temperature of 37°C are selected.

Some surfactants have certain sensitivity-increasing effects on the voltammetric peak, at the

same time some suppression effects on the blank. Among them, non-ionic surfactants such as Tween 40, Tween 20, Tween 80, and Triton X-100 have the more distinctive promoting effect than ionic surfactants such as cetyl trimethyl ammonium bromide (CTMAB) and sodium dodecyl sulfonate (SDS). The Tween 40 has the most remarkable effect. The peak height increases 400% at the Tween 40 concentration of 1.6×10^{-2} g l^{-1}. Surfactant dissolved in water forms micellar system, which is the fine medium for the organic electrochemical investigation. The solubility of some water-slightly soluble organic compounds may increase in micellar system while the electro-conductivity has no change. In this experiment, the solubility of the azo product of the enzyme-catalyzed reaction in water is poor. The surfactant increases the solubility of the azo product, as well as ODA. Furthermore, micelle can reduce the bonding action of some intermediates with catalyst and the electrostatic action of the micelle can concentrate the opposite charge ions and the hydrophobic species, so there are more chances of reaction. Hence, surfactants have sensitivity-increasing effect.

Owing to the existence of various metal elements such as Zn, Cu, Fe, Mn, Pb etc. in plant tissues, the effect of more than 20 metal ions on the determination of TMV by proposed voltammetric enzyme-linked immunoassay method was investigated. The results demonstrate that all ions tested have no influence on the voltammetric peak when their concentrations are lower than 10^{-6} mol l^{-1}. The peak height decreases slightly when concentrations are higher than 10^{-6} mol l^{-1}. According to the mean contents of metal elements in plant, they have no remarkable effect on the detection of TMV in plant.

3.3. Detection conditions

A fine second order derivative linear sweep voltammetric peak of the product of the enzyme-catalyzed reaction can be obtained in some buffer solutions such as BR, HOAc-NaOAc, $NH_3.H_2O$-NH_4Cl, H_3BO_3-KCl-NaOH and KH_2PO_4-Na_2HPO_4. In this work, BR buffer solution is selected as the supporting electrolyte. Fig. 2 is the dependence of the peak height on the pH value of BR buffer. The peak height increases with the increase of pH and with a relative stability, before it decreases with the further increase of pH. The peak is the highest at pH 8.4. BR buffer solution of pH 8.4 (1.0 ml) in 10.0 ml of the overall solution is selected as the concentration of BR buffer.

The selected instrumental conditions are -0.1 V as the initial potential, 10.4 s as the mercury drop stand time and 798 mV s^{-1} as the potential scanning rate.

3.4. Determination of HRP and labelled HRP

The peak height in the BR buffer solution has a good linear relationship with the HRP content in the range from 2.5×10^{-6} to 5.0×10^{-4} mU l^{-1}. The relative standard deviation for 11 parallel determinations to 1.0×10^{-5} mU l^{-1} HRP is 3.2%, and the detection limit of HRP is 9.25×10^{-7} mU l^{-1}.

The free IgG-HRP of different dilution ratio was detected under the optimum experimental conditions. The result is shown in curve 1 of Fig. 3, and that of the ELISA method in curve 2 of Fig. 3. The highest dilution ratio detected by this method is $1:2 \times 10^7$ and by ELISA method $1:2 \times 10^5$. The effect of the solid-phase carrier on the determination was studied in order to apply this system to the detection of TMV. The results of this method and the ELISA method are shown in curve 3 and 4 of Fig. 3 respectively. The highest dilution ratios of this method and the ELISA method are $1:6 \times 10^6$ and $1:6 \times 10^4$, respectively.

The substrate of the enzyme-catalyzed reaction is *o*-dianisidine (ODA), namely 3,3′-dimethoxybenzidine (I). In buffer solution of proper pH value, HRP can strongly catalyze H_2O_2 oxidation of ODA [6]. In the case of pH < 3.7, oxidation of ODA at low concentration yields free radical, which is unstable and further produces free *o*-dianisidine quinonediimine, two-equivalent oxidized form (II). Neutralization of the acidic solution of pH < 3.7 leads to an azo product bisazobiphenyl (III). If the enzyme-catalyzed reaction is carried out at pH > 6, the main product will be (III). Azo product (III) can easily be detected by voltammetry. So, HRP activity can be measured.

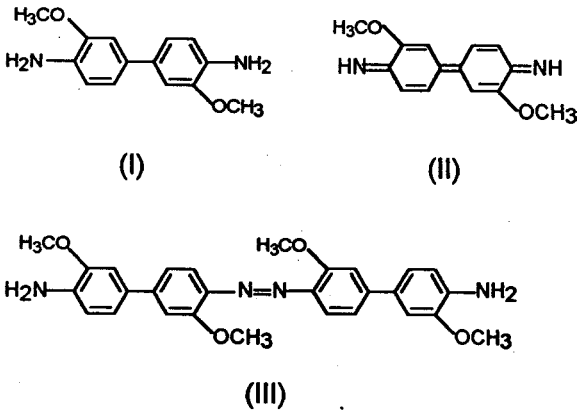

The process of the electro-reduction of the azo product has been investigated by cyclic voltammetry. The cyclic voltammograms of the azo product were recorded in pH 4.0–10.0 BR buffer solution.

When pH < 5.0, there is no cyclic voltammetric peak. Between pH 5.0 and 6.5, there is only the cathodic peak but no corresponding anodic peak. Between pH 6.5 and 8.4, both the cathodic peak and anodic peak appear, but the height of the anodic peak is lower than that of the cathodic peak. The heights of these two peaks increase with the increase of pH value, and the ratio of the anodic to the cathodic increases. At pH 8.4, the heights of the two peaks reach the highest and are almost equal. Between pH 8.4 and 8.6, the heights of the two peaks have a little decrease but they are still almost equal. Between pH 8.6 and 10.0, the cathodic peak is obviously divided into two peaks, and the anodic peak remains one. Both the cathodic peak and the anodic peak disappear when pH > 10.0.

According to the cyclic voltammetry, azo compound (III) undergoes the following electro-reduction reaction in the pH range from 5.0 to 10.0:

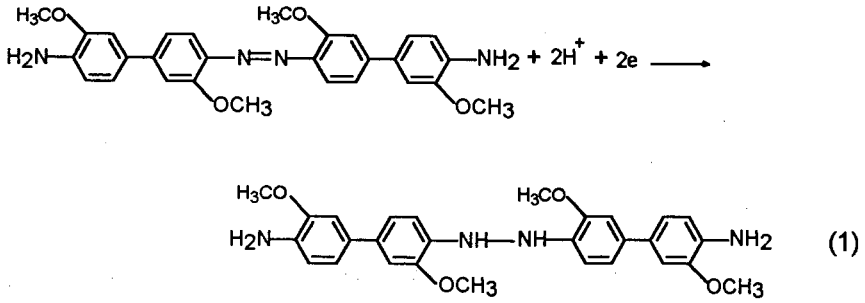

From the literatures [12,13], the product of reaction (1) will further undergo a disproportionation, which is catalyzed by acid:

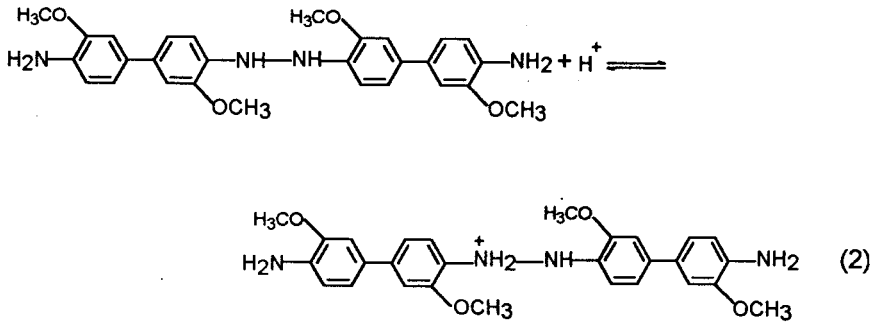

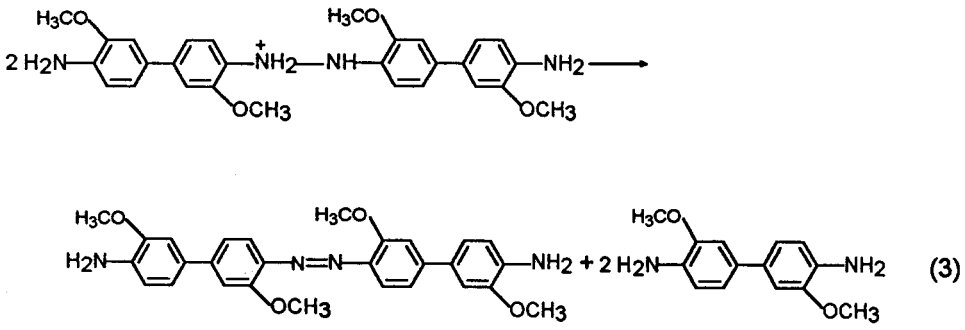

Because the acid catalysis disproportionation is very quick, the rates of reactions (2) and (3) are so fast that there is no anodic peak of the azo product if pH < 6.5. At pH 6.5, the anodic peak is observable. With the increase of pH, the concentration of H^+ decreases, and reactions (2) and (3) slow down, and the anodic peak appears, which increases with the increase of pH. At pH 8.4, the height of the anodic peak almost equals to that of the cathodic, which demonstrates that the disproportionation no longer takes place. If pH > 8.6, the two peaks produced by the separation of the cathodic peak can be seen, which indicates that the azo product gains electrons step by step in alkaline solution. There is a similar mechanism in [13].

3.5. Determination of TMV

The determination of TMV was carried out with indirect method, the advantages of which are that the common enzyme label suitable for various viruses, e.g. goat antirabbit IgG-HRP, is adopted, and preparation of enzyme labelled-antibody for each detected virus is not necessary, so the manipulation is simpler, the detection cost lower and application easier. The essential principle of detecting plant virus with the indirect method of voltammetric enzyme-linked immunoassay is shown in Fig. 4. The more the detected virus (Ag) is, the more the IgG-HRP combined on the solid phase carrier, the more the azo product, the higher the voltammetric peak.

3.5.1. The optimum working concentrations of TMV-As (namely Ab) and IgG-HRP

Coat the polystyrene cuvettes with 10 μg ml^{-1} purified TMV. Dilute the TMV-As with PBS-Tween 20. Conduct the experiment according to the procedure with the commodity working concentration 1:40 of IgG-HRP and different dilution ratios of TMV-As. The peak height is the highest when the dilution ratio of TMV-As is 1:6400. So select 1:6400 TMV-As as the working concentration of TMV-As.

Coat the polystyrene cuvettes with 10 μg ml^{-1} purified TMV. Conduct the experiment according to the procedure with 1:6400 TMV-As and different dilution ratios of IgG-HRP. The product of IgG-HRP catalyzed reaction is detected by voltammetry and spectrophotometry, respectively. The results are shown in Fig. 5. According to the principle that the labelled antibody concentration should be at the upper point of the one third of the linear portion of the concentration curve of the labelled antibody [14], the selected working concentration of IgG-HRP is 1:40.

3.5.2. The linear range, the detection limit and the precision of the purified TMV determination

Under the optimum conditions, the linear range of the purified TMV determination is 0.25–5000 ng ml^{-1} and the lowest detection concentration is 0.25 ng ml^{-1}. The relative standard deviation for 11 parallel determinations to 1.0 ng ml^{-1} TMV is 4.8%. Under the same conditions, the linear range and the lowest detection concentration with ELISA method are 25–5000 and 25 ng ml^{-1}, respectively.

3.5.3. The determination of the TMV-infected leaf sap

Dilute the infected leaf sap prepared according to 2.2 with 0.1 mol l^{-1} pH 9.6 carbonate buffer.

Detect the TMV according to the experimental procedure. The results of this method and the ELISA method are listed in Table 1. The highest dilution ratio detected with this method is 1:800000 and the detection range 1:250–1:800000. The highest dilution ratio detected with ELISA method is 1:160000 and the detection range 1:10–1:2500.

Acknowledgements

This work was supported by the National Natural Science Foundation of China.

References

[1] J.L. Pellequer, M.H.V. Van Regenmortel, J. Immunol. Methods 166 (1993) 133.
[2] M.K. Clark, Annu. Rev. Phytopathol. (1981) 83.
[3] L. Torrance, Plant Pathol. 30 (1981) 1.
[4] J.P. Chen, S. Song, C.L. Zhang, Z.F. Zhang, Agric. Sci. Zhejiang 2 (1989) 81.
[5] J.L. Pellequer, M.H.V. Van Regenmortel, Mol. Immunol. 30 (1993) 955.
[6] A. Claiborne, I. Fridovich, Biochemistry 18 (1979) 2324.
[7] A. Claiborne, I. Fridovich, Biochemistry 18 (1979) 2329.
[8] H.W. Hofmann, R. Schuessig, Med. Laborasoriums Diagn. 24 (1983) 155.
[9] H.B. Halsall, W.R. Heineman, J. Int. Fed. Clin. Chem. 2 (1990) 179.
[10] K. Jiao, S.S. Zhang, L. Wei, Sci. China (Series B) 39 (1996) 135.
[11] K. Jiao, S.S. Zhang, M. Zhang, L.Q. Zhang, Fenxi Huaxue (Chin. J. Anal. Chem.) 23 (1995) 1211.
[12] T.M. Florence, J. Electroanal. Chem. 52 (1974) 115.
[13] K. Jiao, Xiaoxia Gao, Sci. Sinica (Series B) 28 (1985) 1121.
[14] C.L. Zhang, Z.F. Zhang, Plant Quarantine 2 (1982) 8.

ELSEVIER

Talanta 47 (1998) 1139–1147

Talanta

Enzyme-less amperometric biosensor for L-ascorbate using poly-L-histidine-copper complex as an alternative biocatalyst

Yasushi Hasebe *, Tatsushi Akiyama, Toshimitsu Yagisawa, Shunichi Uchiyama

Department of Environmental Engineering, Faculty of Engineering, Saitama Institute of Technology, 1690, Fusaiji, Okabe, Saitama, 369-0293, Japan

Received 8 April 1997; received in revised form 5 May 1998; accepted 11 May 1998

Abstract

A poly-L-histidine(PLH)-copper(II) complex can be used as an alternative biocatalyst in an O_2 detection-type amperometric enzyme-less L-ascorbate (AsA) sensor. The PLH–Cu(II) membrane was simply prepared by entrapping the PLH in polyacrylamide gel and subsequent treatment of the gel with $CuCl_2$ solution. This enzyme-less biosensor can be used over a relatively wide pH region from 4 to 11 and enables precise determination of AsA (RSD less than 3%, $n = 10$) at pH 7.0. The fundamental performance characteristics (sensitivity, response time, and linear range) of this PLH–Cu(II)-based sensor is comparable to those of a native ascorbate oxidase-based sensor. Unfortunately, the selectivity is inherently rather low and, as a result, the response was degraded in the presence of higher concentrations (more than mM order) of quinones. However, reducing sugars caused no interference and the sensor could be used to detect AsA in some fruits and drinks. This enzyme-less sensor has excellent stability for at least 3 months of repeated analysis (more than 300 samples) without loss of ordinal activity. © 1998 Elsevier Science B.V. All rights reserved.

Keywords: Enzyme-less biosensor; Amperometry; Poly-L-histidine-copper complex; Ascorbic acid

1. Introduction

Because of their specificity and selectivity, enzymes have great potential usefulness in analytical chemistry [1], and a number of enzyme-based biosensors have been proposed so far [2–5]. Ascorbate oxidase (AO_x, EC.1.10.3.3) that catalyzes the oxidation of L-ascorbate (AsA, the reduced form of vitamin C) to dehydroascorbate (the oxidized form of vitamin C) by dissolved oxygen has been used in an enzyme sensor for the determination of vitamin C, in which purified enzymes [6–12] and/or cucumber tissue [13,14] that contains AO_x have been utilized as the biorecognition elements. However, in these systems, the optimal measurement conditions are limited by the properties of the native enzyme; further, the native enzyme generally loses its catalytic activity after repeated measurements. Conse-

* Corresponding author. Fax: +81 485 856004; e-mail: hasebe@sit.ac.jp

0039-9140/98/$ - see front matter © 1998 Elsevier Science B.V. All rights reserved.
PII S0039-9140(98)00193-3

quently, improvement in the stability of the responses would be required in the native enzyme-based vitamin C sensor, particularly for practical applications such as food analysis.

It is well-known that the Cu(II) ion catalyzes the air oxidation of AsA [15], and its catalytic activity is significantly enhanced by complexation with poly-L-histidine (PLH). The PLH–Cu(II) complex catalyzes the oxidation of AsA by molecular oxygen according to Michaelis–Menten kinetics [16,17]. In this enzyme-mimic reaction, the PLH backbone contributes to the generation of broad specificity of the reaction toward AsA. Consequently, if the PLH–Cu(II) complex immobilized in some membranes retains its catalytic activity, the PLH–Cu(II) complex would be utilized for effecting an artificial biocatalyst in an enzyme-less vitamin C sensor. In this study, the PLH–Cu(II) complex was entrapped in polyacrylamide gel and coupled to an oxygen electrode as the catalytic layer of the enzyme-less vitamin C sensor. The fundamental responsive characteristics of the PLH–Cu(II) complex membrane electrode have been evaluated and compared with that of the native-enzyme electrode. Further, this enzyme-less electrode was applied to the determination of AsA in food samples such as fruits and drinks.

2. Experimental

2.1. Chemicals

Poly-L-histidine (PLH, mol. wt. 15600; Sigma, St. Louis, MO) and ascorbate oxidase (AO_x, EC 1.10.3.3, from *Cucurbita* sp. 232 U mg^{-1}; Wako Pure Chemicals, Osaka Japan) were used as received. Sodium L-ascorbate (AsA) and 2,6-dichlorophenolindophenol sodium salt dihydrate (analytical grade) were obtained from Wako. All other chemicals were of analytical reagent grade and used without further purification. The standard solution of AsA was prepared daily by dissolving the reagent grade AsA into buffer and appropriately diluting this solution for sample preparations.

2.2. Preparation of the membranes

The PLH was entrapped in polyacrylamide gel according to the usual method [18–20]. The PLH (0 to 10 mg), acrylamide monomer (375 mg) and *N*,*N*′-methylenebisacrylamide (20 mg) were dissolved in 2 ml 0.1 M phosphate buffer (pH 7.0), and dissolved oxygen was removed by introducing nitrogen (N_2) gas through the mixture for 5 min. Next, the solution was transferred into a flat Petri dish (50 mm diameter), and then the solution was polymerized by adding 0.2 ml 1% potassium persulphate and 0.2 ml 5% 3-dimethylaminopropionitrile solution. The thickness of the membrane thus prepared was ca. $0.2 \sim 0.3$ mm. The PLH-entrapping gel, which was cut into a circle (5 mm diameter) with a microchip, was immersed in each concentration of $CuCl_2$ solution for 10 min for formation of the PLH–Cu(II) complex. After the membrane was well rinsed with double-distilled water, the membrane was placed on the gas permeable membrane of a Clark type oxygen electrode (Denki Kagaku Keiki). Native enzyme (AO_x)-entrapping gel was prepared in a similar manner using 2 mg (ca. 500 U) of AO_x in place of the PLH and coupled with the oxygen electrode. These biosensors were placed in 0.1 M phosphate buffer (pH 7.0) for 30 min before amperometric measurements.

2.3. Amperometric measurements

Amperometric measurements were conducted using a potentiostat (NPOT-1, Nikko Keisoku), one pen recorder (U-228, Nippon Denshi Kagaku) and the oxygen electrode modified with the PLH–Cu(II)-entrapping gel or AO_x-entrapping gel. The potential of the Au working electrode of the oxygen electrode was maintained at -0.7 V versus a reference electrode (Ag/AgCl) with a potentiostat, and the current response based on the electrochemical reduction of dissolved oxygen was monitored. The electrodes were immersed into a constantly stirred (200 rpm) 20-ml 0.1 M buffer solution in a 50-ml beaker, which was open to the atmosphere, and the buffer was allowed to equilibrate with atmospheric oxygen during the measurements. The temperature of the buffer so-

lution was maintained at 25 ± 0.1°C with a thermostatted water bath (ELYRA, RC-12, Tokyo Rika Kikai). After the steady-state current baseline had been obtained, the AsA standards (5–100 μl) and/or real samples (0.1–1.5 ml) were added with an Eppendorph micropipete, and the response was recorded as a current decrease resulting from the addition of the samples.

2.4. Assay of real samples

The samples of fruit extracts were prepared as follows. First, each fruit was squeezed to obtain the juice. Next, 5 ml of this juice was centrifuged at 2500 rpm for 10 min, and the clear supernatant of this solution was filtered on a membrane filter (Advantec, 200 nm) and diluted twice with 0.1 M phosphate buffer solution (pH 7.0) in advance. The drinks and fruit juices were used as samples. Under the amperometric measurements, these real samples were automatically diluted 10 to 200 times in the buffer solution in which the electrode is immersed. The AsA concentration in the food samples was estimated by fitting the average current values for three measurements of the samples to the calibration curve of AsA which was made daily using the AsA standards. The analytical results of the sensor were compared with those obtained by the 2,6-dichlorophenolindophenol titration method. For titration, the sample solutions of the fruits or juices were appropriately (2–100 times) diluted with 0.05% metaphosphoric acid solution and were titrated with 5×10^{-4} M indophenol standard solution (factor: 0.95–1.08).

3. Results and discussion

3.1. The steady-state current responses for AsA

Fig. 1 shows typical current response curves of an immobilized PLH–Cu(II) membrane oxygen electrode upon the addition of each concentration of the AsA standards. The steady-state current, where the rate of decrease in dissolved oxygen would be equal to the rate of oxygen supply from the bulk solution through the membrane layer, was apparently shifted by the addition of AsA, and the current reached another steady-state value within 5 min. The difference between the steady-state current values before and after the AsA addition, ΔI, was found to be dependent on the concentration of AsA added. Rinsing the membrane by immersing the electrode in fresh buffer returned the original baseline within 10 min and subsequent measurements were possible. The responsive behavior (current–time profile) of the PLH–Cu(II)-based electrode is quite similar to that of the AO_x-based electrode. These results suggest the possibility of using the PLH–Cu(II)-electrode as an enzyme-less AsA sensor.

To verify that these responses arise from the catalytic action of the PLH–Cu(II) complex, we prepared different membranes by varying the amount of the PLH and copper. Table 1 summarizes the response to 1×10^{-4} M AsA using various membranes. The magnitude of the ΔI depends essentially upon the amount of PLH in the gel and the copper concentration in the membrane preparation. These results strongly indicate that the amperometric response of the PLH–Cu(II)-electrode originates from the AsA oxidation by molecular oxygen catalyzed by the PLH–Cu(II) complex in the gel. The slight response of a blank membrane without the PLH may be caused by a

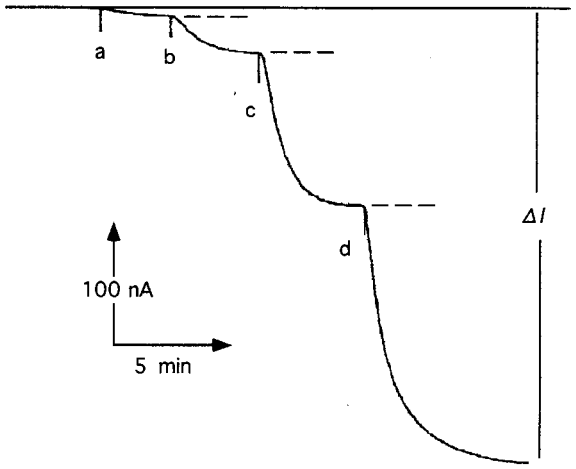

Fig. 1. Steady-state current–time responses of the PLH–Cu(II) membrane electrode on successive additions of increasing concentrations of AsA. AsA addition: (a) 3×10^{-5}, (b) 1×10^{-4}, (c) 3×10^{-4}, and (d) 5×10^{-4} M. Air-saturated 0.1 M phosphate buffer (pH 7.0) kept under constant stirring.

Table 1
The current response to AsA (1×10^{-4} M) with various PLH–Cu(II) membranes

Membrane	[PLH][a]	[$CuCl_2$][b]	ΔI (nA)	Relative response (%)
1	10	10	72	100
2	5	10	48	67
3	1	10	27	38
4	0.1	10	18	25
5	0	10	6	8
6	10	5	60	83
7	10	1	46	64
8	10	0.1	20	28
9	10	0.01	5	7

[a] The amount of PLH in the membrane preparation.
[b] The concentration of the $CuCl_2$ solution in which the PLH-entrapping membrane is immersed for membrane preparation.

Cu(II) ion-catalyzed air oxidation of AsA, because polyacrylamide gel possesses possible coordination sites for copper. Because it has been reported that the binding constant of copper to the PLH is remarkably large, (10^{19} M^{-1} at pH 5) [17], it is reasonable to assume that most of the copper binds to the PLH in the gel layer, even if polyacrylamide possesses possible coordination sites for copper. The maximum response was observed with membrane 1, so the remaining experiments were carried out using membrane 1.

3.2. Effect of pH

In general, the response of a native enzyme-based biosensor is usually limited in the acidic and/or alkaline pH region due to the limitation of the catalytic property of the enzymes [6,8]. The effect of pH on the current response of the PLH–Cu(II)-electrode is shown in Fig. 2. At pH 3, ΔI was strongly suppressed to less than 10 nA, whereas ca. 80–100 nA of the ΔI were induced over a relatively wide pH range 4–11. This observation indicates that the present PLH–Cu(II)-based sensor can be used for the measurement of various pH samples which is an advantage over native-AO_x-based sensors [6,10]. The pH dependence behavior over the pH range below 6 is nearly consistent with the literature results obtained in sodium acetate buffer, in which the catalytic activity of the PLH–Cu(II) increased with pH to about pH 5 and then leveled off, reaching limiting values [16].

It has been reported that the coordination structure of a copper-binding site is different under acidic and alkaline conditions [17]. Fig. 3 illustrates the ESR spectra of the PLH–Cu(II) complex at each pH. It is clear that the coordination chemistry of the PLH–Cu(II) complex is different at each pH. At pH 3, the hyperfine structure and asymmetry of the ESR signal decreased compared with that at pH 7 and 10,

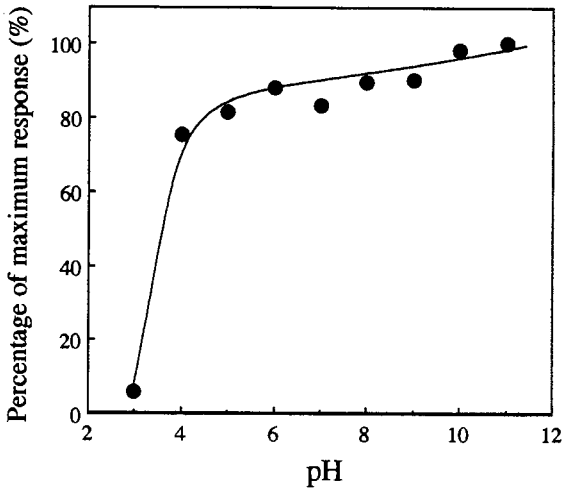

Fig. 2. Effect of pH upon the PLH–Cu(II) membrane electrode response at 1×10^{-4} M AsA. The pH of the solution was adjusted using 0.1 M Britton–Robinson buffer; other experimental conditions as in Fig. 1.

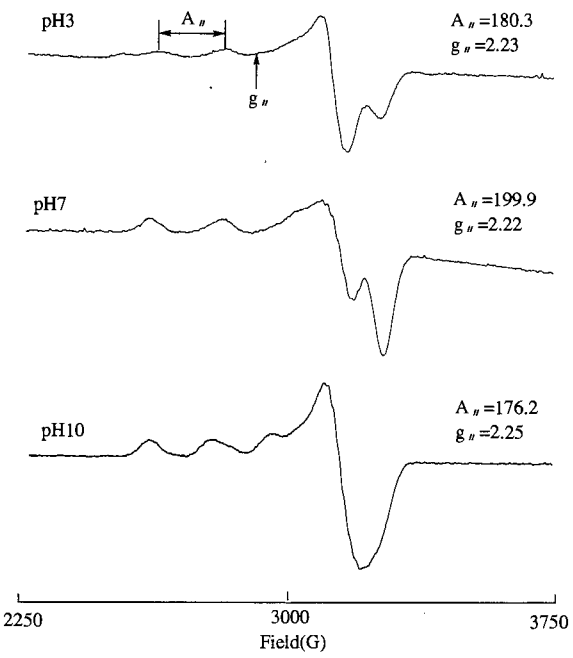

Fig. 3. ESR spectra of the PLH–Cu(II) complex in the 0.1 M Britton–Robinson buffer ($[PLH] = 1 \times 10^{-4}$ M, $[CuCl_2] = 1 \times 10^{-4}$ M) at 77 K and pH 3 (A), pH 7 (B), and pH 10 (C). Measurement conditions; Frequency 9.011 (A), 9.015 (B), and 9.011 GHz (C). Power 4 mW, Sweep time 2 min, modulation width 1.0000 mT, time constant 0.3 s.

suggesting that the binding of copper to the PLH may be limited and that the amount of aquo–copper-complex could be increased. Thus, a rapid decrease in the sensor response occurred at pH 3.0 presumably due to the limitation of the formation of the PLH–Cu(II) complex. On the other hand, at pH 7 and 10, the ESR signal exhibited a typical type II copper resonance and the change in ESR spin Hamiltonian parameters (the $A_{//}$ value was decreased and the $g_{//}$ value was increased with pH increase) suggests that the coordination chemistry is distorted varying from a square-planer to pseudotetragonal geometry with increased pH [21,22]. Although the ternary structure and copper-binding site of the PLH–Cu(II) complex entrapped in the gel is not identified at present, it is safe to say that, at least, the catalytic activity of the PLH–Cu(II) membrane electrode is not significantly influenced by pH over the wide pH range of 4–11.

3.3. Kinetic parameters

If the reaction catalyzed by the PLH–Cu(II) complex in the gel proceeds according to Michaelis–Menten kinetics, the K_m constant could be calculated from the rate of the reaction v and the substrate concentration. In this case, v corresponds to the rate of the oxygen consumption, namely, the change in the steady-state current, ΔI. Fig. 4 shows an electrochemical Lineweaver–Burk plot, which plots the reciprocal of ΔI as a function of the reciprocal of the AsA concentration, and fitting the following equation [23,24]:

$$\frac{1}{I_s} = \frac{1}{I_{max}} + \frac{1}{S}\frac{K_m}{I_{max}} \quad (1)$$

The plot represents an essentially straight line ($r^2 > 0.990$), indicating that the AsA oxidation by molecular oxygen catalyzed by the PLH–Cu(II) complex in the gel follows Michaelis–Menten kinetics. From the intercept of this line and its slope, the $K_{m\ obs}$ and the $I_{max\ obs}$ at pH 7.0 and 25°C were calculated at 1.35 mM and 788 nA, respectively. This result is further evidence that

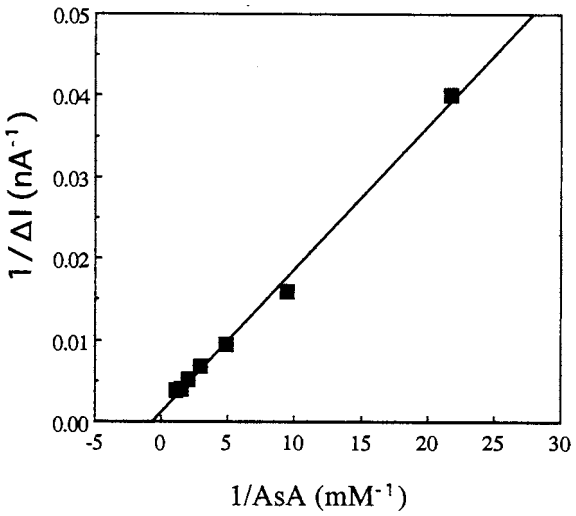

Fig. 4. The electrochemical Lineweaver–Burk plot of the PLH–Cu(II) complex membrane electrode. The plots were based on the ΔI at each concentration of AsA, except for the data at low AsA concentration of less than 3×10^{-5} M, because ΔI was relatively small and the S/N level significantly deceased at lower concentration of AsA.

Table 2
The current responce of the PLH–Cu(II) membrene electrode for 2×10^{-4} M AsA and other interfering substances

Analyte	ΔI (nA)	Relative response (%)
L-Ascorbate	134	100
Hydroquinone	65	48
Epinephrine	57	47
L-Dopa	53	40
Dopamine	43	32
Norepinephrine	22	16
Catechol	14	10
D-Glucose	nr[a]	0
D-Fructose	nr	0
D-Galactose	nr	0
Sucrose	nr	0

[a] nr, No response.

the polyacrylamide gel does not have any undesirable influence on the reaction kinetics of the PLH–Cu(II) complex and that the PLH–Cu(II) acts as an enzyme-mimic catalyst in which the substrate–PLH–Cu(II) complex exists as an intermediate.

3.4. Specificity

Because the PLH–Cu(II) complex is known to act as a catalyst in different oxidations of organic substrates by molecular oxygen [16], the responsiveness of these compounds was next investigated. Table 2 summarizes the relative response toward AsA and other oxidizable compounds. Whereas no response was observed to reducing sugars, hydroquinone and some polyphenolic compounds induced responses at less than half the magnitude of that for AsA. It has been reported that the oxidation rate of an anionic substrate is higher than that of neutral and cationic substrates due to the electrostatic effect of the PLH which is positively charged [16]. In this sensor, the responsiveness was in the order of AsA > hydroquinone > L-dopa > dopamine > norepinephrine > catechol. This tendency is basically concomitant with the interpretation that the electrostatic interaction of the polycationic PLH with the substrates leads to the broad specificity of the PLH–Cu(II) complex [16]. Because the polyacrylamide gel also has a cationic side chain (–CO–NH_3^+) under the pH range studied, it can be considered that the electrostatic interaction between the substrates and the positively charged gel matrix also contributes to the increase in specificity for anionic L-ascorbate over the other organic compounds studied.

3.5. Calibration curve

Fig. 5 illustrates calibration graphs of AsA with the PLH–Cu(II) and native enzyme-based electrodes. The calibration profile of both electrodes is basically similar under the present measurement conditions, and the PLH–Cu(II)-based sensor showed a useful calibration at AsA concentrations ranging from 3×10^{-6} to 3×10^{-4} M with a detection limit of 3×10^{-6} M (S/N = 3, ca. 8 nA). The precision of the measurement of 0.1 mM AsA at pH 7.0 was found to be less than 3% in 10 successive assays. This observation suggests that the catalytic activity of the PLH–Cu(II) complex is comparable to that of native ascorbate oxidase. Compared with native ascorbate oxidase, a broad specificity toward other oxidizable compounds such as quinone and polyphenols would disturb the accurate determination of AsA. In this con-

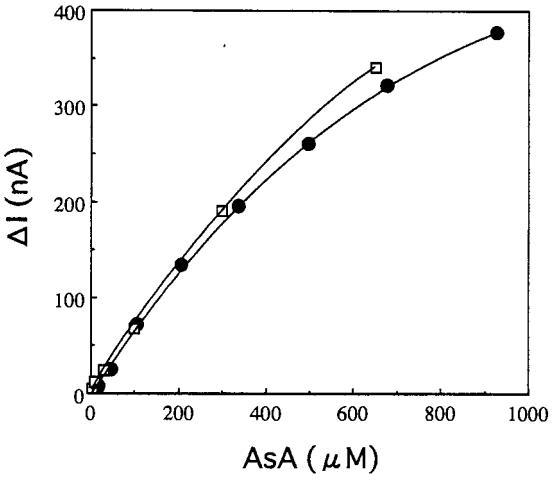

Fig. 5. Calibration graphs for AsA with the PLH–Cu(II) membrane electrode (●) and the native-enzyme membrane electrode (□). Other experimental conditions as in Fig. 1.

Table 3
Comparison of the parameters of the calibration curves of the PLH–Cu(II)-electrode in the absence and presence of some interference

Interference	[Interference][a] (M)	Dynamic range (M)	Detection limit[b] (M)
None		3×10^{-6}–$\sim1\times10^{-3}$	3×10^{-6}
Hydroquinone	1×10^{-4}	2×10^{-5}–$\sim1\times10^{-3}$	2×10^{-5}
	1×10^{-3}	1×10^{-5}–$\sim2\times10^{-3}$	1×10^{-5}
Catechol	1×10^{-3}	1×10^{-5}–$\sim1\times10^{-3}$	1×10^{-5}
D-Glucose	2×10^{-2}	3×10^{-6}–$\sim1\times10^{-3}$	3×10^{-6}

[a] These compounds were dissolved in the buffer in which the electrode is immersed.
[b] The values were estimated as S/N = 3, (ca. 8 nA).

text, the effects of various sources of interference on the AsA responses were studied. Table 3 summarizes the calibration parameters of the PLH–Cu(II)-electrode with and without interference. Unfortunately, in the presence of 2 mM hydroquinone, the dynamic range became narrow and the detection limit decreased from 3×10^{-6} to 1×10^{-5} M. Consequently, if the PLH–Cu(II)-based sensor is used for determination of AsA in samples containing a higher concentration of these interfering substances, some treatment of the samples to eliminate these interfering substances (i.e. catalytic and enzymatic decomposition) would be required in advance for an accurate AsA assay. However, the concentration level of these interferents in many food samples is usually lower than that of AsA. On the other hand, the current response was scarcely affected by excess amounts (up to 100 mM) of reducing sugars (i.e. D-glucose). This feature may be desirable for an AsA assay in food samples which contain large amounts of sugars as well as AsA.

3.6. Applicability for real sample analysis

Although higher concentrations (more than mM order) of quinone and polyphenolic compounds interfere with the response, the concentration of these compounds in some fruits and drinks is known to be smaller than that of AsA. In this context, we next tested the effectiveness of the PLH–Cu(II) membrane electrode for food analysis. Table 4 summarizes the analytical results of AsA in fruit extracts and some juices. The results of the sensor were compared to those by the conventional titration method. The RSD ($n=3$) for real samples were found to be below 4.2%, and passable agreement was observed between the sensor and the conventional titration method. Even if the real samples contain interfering species, the inhibitory effects of the interference could be eliminated because the real samples were automatically diluted a maximum of 200 times in the buffer solution in which the electrode is immersed. These results suggest that the PLH–Cu(II)-based electrode has the potential to determine AsA in some food samples.

3.7. Stability

To test the long-term stability of the PLH–Cu(II)-based sensor, measurements of 1×10^{-4} M AsA were performed every $2\sim4$ days for 3 months, and the average output signals for 3 measurements were compared with those of the AO_x-based electrode. As shown in Fig. 6, the response of the AO_x-based sensor decreased to less than 50% after 3 weeks, while the PLH–Cu(II) membrane electrode retained its activity for 3 months after repeated measurements of more than 300 samples (about a 10% decrease in the output signal was observed). No serious leakage of the PLH–Cu(II) complex from the gel lattice occurred during the repeated measurements and storage time in spite of its smaller molecular size (mol. wt. 15600) to that of the native enzyme. It can be assumed that the intermolecular interaction of the PLH through the copper-binding site

Table 4
Analytical results of the real sample analysis with the PLH–Cu(II) membrane electrode and the conventional method

Samples	Sensor				Titration[a]
	Sample volume[b] (ml)	ΔI (nA)	[AsA][c] (mM)	RSD ($n=3$) (%)	[AsA] (mM)
Kiwi	1.5	25	1.7	3.5	1.6
Lemon	1.5	37	2.0	4.1	1.8
Strawberry	0.2	80	4.3	3.7	4.0
Green tea	0.2	20	1.0	3.1	1.6
Orange juice	0.2	34	2.0	4.2	2.9
Vitamin drink	0.1	246	53	3.1	56

[a] The indophenol titration method was carried out using appropriately diluted samples.
[b] The volume of the samples which were added to the buffer (25 ml) in which the sensor is immersed.
[c] The AsA concentration is calculated using the calibration curve in Fig. 5.

leads to enhancement of the net molecular size of the PLH–Cu(II) complex in the gel. Additionally, the simplicity of the structure of the catalytic site compared to that of the native enzyme may contribute to the retention of its catalytic activity for long-term periods. From this result, it can be emphasized that the stability of the native-enzyme-based vitamin C sensor could be markedly improved by the use of the PLH–Cu(II) complex as an artificial biocatalyst. From a practical point of view, this would be one of the important advantages of this system.

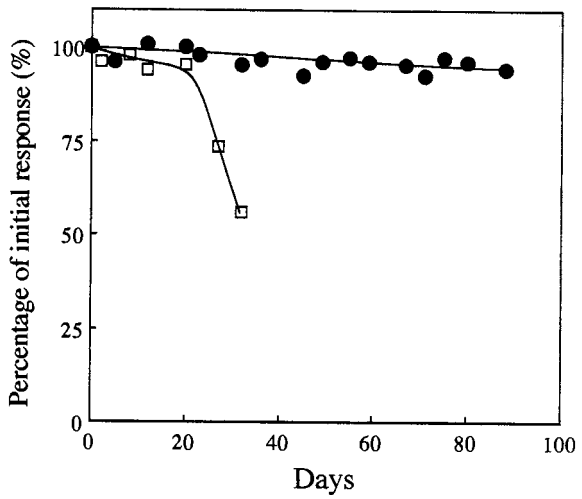

Fig. 6. The long-term storage stability of the 2×10^{-4} M of AsA response using the PLH–Cu(II) membrane electrode (●), and the native-ASOD based electrode (□).

4. Conclusions

The PLH–Cu(II) complex-entrapping polyacrylamide gel could be exploited as a novel artificial biocatalytic layer for an AsA sensor, which enables repeated and precise measurements of AsA over a relatively wide pH region from 4 to 11. The fundamental performance characteristics (sensitivity, response time and linear range) of the PLH–Cu(II)-based biosensor are comparable to those of a native ascorbate oxidase-based sensor. Unfortunately, the selectivity is rather low and a high concentration of quinone and polyphenolic compounds interferes with the AsA response. However, reducing sugars cause no interference, and this enzyme-less sensor can be used to detect AsA in some fruit extracts and drinks. Furthermore, this sensor has excellent stability for at least 3 months of repeated analysis (more than 300 samples) without loss of ordinal activity.

Acknowledgements

The authors are grateful to the Ministry of Education, Science and Culture of Japan for partial support of this work through a Grant-in-Aid for Scientific Research. (No 07772138).

References

[1] G.G. Guilbault (Ed.), Handbook of Enzymatic Methods of Analysis, Marcel Dekker, New York, 1976.
[2] A.P.F. Turner, I. Karube, G.S. Wilson (Eds.), Biosensors, Fundamentals and Applications, Oxford Science Publications, 1987.
[3] P.R. Coulet (Ed.), Biosensor Principles and Applications, Marcel Dekker, New York, 1991.
[4] Aizawa (Ed.) Chemical Sensor Technology, Vol. 4, Kodansha Ltd./Elsevier, 1994.
[5] F.W. Scheller, F. Schubert, F. Fedrwitz (Eds.), Frontiers in Biosensorics I, II, Birkhäuser, Basal, 1997.
[6] K. Matsumoto, K. Yamada, Y. Osajima, Anal. Chem. 53 (1981) 1974.
[7] B.J. Vincke, M.J. Devleesshouwer, G.J. Patriarche, Anal. Lett. 18 (1985) 1593.
[8] G.J. Patriarche, J.-M. Kauffmann, J.C. Vire, B.J. Vincke, in: G.G. Guilbault, M.M. Mascini (Eds.), Analytical Uses of Immobilized Biological Compounds for Detection, Medical and Industrial Uses, Reidel, Dordrecht, 1988, pp. 62–63.
[9] B. Mattiasson, B. Danielsson, Carbohydr. Res. 102 (1982) 273.
[10] H. Endo, C. Matsunaga, M. Hoshi, T. Hayashi, R. Takai, E. Watanabe, Biosens. Bioelectron. 9 (1994) 501.
[11] S. Uchiyama, Y. Hasebe, S. Suzuki, Electroanalysis 5 (1993) 535.
[12] S. Uchiyama, Talanta 39 (1992) 1289.
[13] S. Uchiyama, Y. Umetsu, Anal. Chim. Acta 208 (1988) 291.
[14] S. Uchiyama, Y. Hasebe, M. Tanaka, Electroanalysis 9 (1997) 176.
[15] M.M. Taqui Khan, A.E. Martell, J. Am. Chem. Soc. 89 (1967) 4176.
[16] I. Pecht, A. Levizki, M. Anbar, J. Am. Chem. Soc. 89 (1967) 1578.
[17] A. Levizki, I. Pecht, A. Berger, J. Am. Chem. Soc. 94 (1972) 6844.
[18] Y. Hasebe, S. Toda, K. Aoki, H. Tonobe, S. Uchiyama, Anal. Biochem. 251 (1997) 32.
[19] Y. Hasebe, K. Oshima, O. Takise, S. Uchiyama, Talanta 42 (1995) 2079.
[20] Y. Hasebe, K. Yokobori, K. Fukasawa, T. Kogure, S. Uchiyama, Anal. Chim. Acta 357 (1997) 51.
[21] H. Yokoi, A.W. Addison, Inorg. Chem. 16 (1977) 1341.
[22] K.D. Karlin, Z. Tyekár (Eds.), Bioinorganic Chemistry of Copper, Chapman and Hall, London, 1993.
[23] F.R. Shu, G.S. Wilson, Anal. Chem. 48 (1976) 1679.
[24] R.A. Kamin, G.S. Wilson, Anal. Chem. 52 (1995) 1198.

ELSEVIER

Talanta 47 (1998) 1149–1155

Talanta

Strontium ion-selective electrodes based on the diamides with pyridine ring as ionophores

Guoying Qian [a], Michael Bin Wu [1,a], Guoliang Wu [a,*], Shu Huang [b], Yunjiang Yan [b], Baozhi Tian [b]

[a] *Institute of Salt Lake, Chinese Academy of Sciences, Xining 810008, People's Republic of China*
[b] *Department of Chemistry, Sichuan University, Chengdu 610064, People's Republic of China*

Received 16 December 1997; accepted 12 May 1998

Abstract

Poly(vinyl chloride) membrane strontium ion-selective electrodes were developed by using three lipophilic diamides containing pyridine ring as ionophores. The relationship between the structure of the ionophores and the performance of these electrodes, as well as the effects of the plasticizers and additives, were investigated. The Sr^{2+}-electrode based on *N*,*N*,*N*′,*N*′-tetracyclohexyl-2,6-pyridine-bis(methyleneoxy acetamide) as neutral carrier, potassium tetrakis (*p*-chlorophenyl) borate (KTpClPB) as additive, and *o*-nitrophenyloctyl ether (*o*-NPOE) as plasticizing solvent. It exhibits excellent properties with a Nernstian slope of 29 mV/pSr^{2+} and a linearity range of 2×10^{-5} to 1×10^{-2} M at 25°C, $K^{Pot}_{Sr,Ba} = 2 \times 10^{-2}$. © 1998 Elsevier Science B.V. All rights reserved.

Keywords: Strontium ion-selective electrode; Diamide; Ionophore

1. Introduction

The performance and preparation of the heterogeneous membrane and liquid membrane type strontium ion-selective electrodes have been documented [1–6], but the selectivity of Sr^{2+}-selective electrodes is unsatisfactory. In particular, they reject other alkaline-earth-metal cations poorly. Recently, more attention has been paid to ionophore ligands as sensing materials for neutral carrier type ion-selective electrodes due to the high selectivity of the compounds. The behavior of Sr^{2+} electrode based on neutral carrier [7] is better than that of the others, however the interference of Ba^{2+} is still highly significant.

Electrically neutral lipophilic ligands containing the appropriate number of binding sites of high dipole moment and/or high polarizability could be employed as ionophores for alkaline-earth-metal cations. The lipophilic diamides as the ionophores of calcium and barium ions have been reported [8–10]. We report here the performance of the Sr^{2+} electrodes using three synthesized

* Corresponding author. Present address: Xian Branch of Institute of Salt Lake, Chinese Academy of Sciences, Xian, 710043, People's Republic of China. Tel.: +86 29 5520383.

[1] Present address: Department of Biophysics and Physiology, Mount Sinai School of Medicine, 1 Gustave Levy Place, New York, NY 10029, USA.

0039-9140/98/$ - see front matter © 1998 Elsevier Science B.V. All rights reserved.
PII S0039-9140(98)00194-5

lipophilic diamides with pyridine ring as neutral carriers. The PVC membrane electrode based on *N*,*N*,*N*′,*N*′ - tetracyclohexyl - 2,6 - pyridine - bis-(methyleneoxy acetamide) as ionophore, *o*-NPOE as plasticizing solvent, and KTpClPB as additive, exhibit significantly high selectivity for Sr^{2+}.

2. Experimental section

2.1. Reagents

Sodium tetraphenyl borate (NaTPB) of analytical grade, poly(vinyl chloride) (PVC) powder and dioctylphthalate (DOP) of chromatographic grade were purchased from Shanghai Chemical. Potassium tetrakis(*p*-chlorophenyl)borate (KTpClPB) and *o*-nitrophenyloctyl ether (*o*-NPOE) were the products of Fluka (Switzerland). Tri(2-ethylhexyl) phosphate (TEHP) was a product of BDH (England). Dioctylphenylphosphate (DOPP) was a product of Beijing Chemical Reagent Factory. Redistilled deionized water was used, and all other reagents were analytical grade.

2.2. Syntheses of ionophores

The ionophores (1–3) used in this work were synthesized by the reaction of 2,6-pyridine dimethanol with appropriate chloroacetamide and NaH in tetrahydrofuran(THF) as shown in Scheme 1 [11].

N,*N*′ - dibenzyl - 2,6 - pyridine - bis(methyleneoxy acetamide) (ionophore 1) was obtained as a white solid (36%), mp 95–96°C; $C_{25}H_{27}N_3O_4$: C 69.13 (69.27), H 6.31 (6.28), N 9.70 (9.69); IR (KBr): 1653 cm^{-1} (C=O); ^1H NMR ($CDCl_3$, TMS): 4.08 (S, 4H, $2 \times OCH_2CO$), 4.47 (S, 4H, $2 \times ArCH_2O$), 4.52 (S, 6H, $2 \times NHCH_2$), 7.19–7.78 (m, 13H, ArH) ppm; MS (*m*/*z*): 435 (M + 2, 50%), 434 (M + 1, 13%).

N,*N*′-diphenyl-*N*,*N*′-dibenzyl-2,6-pyridine-bis-(methyleneoxy acetamide) (ionophore 2) was obtained as a light yellow viscous liquid (51%), $C_{37}H_{35}N_3O_4$: C 75.76 (75.88), H 5.99 (6.02), N 7.11(7.17); IR (KBr): 1673 cm^{-1} (C=O); ^1H NMR ($CDCl_3$, TMS): 3.95 (S, 4H, $2 \times OCH_2CO$), 4.62 (S, 4H, $2 \times ArCH_2O$), 4.88 (S, 4H, $2 \times NCH_2$), 6.95–7.73 (m, 23H, ArH) ppm; MS (*m*/*z*): 587 (M + 2, 54%).

N,*N*,*N*′,*N*′ - tetracyclohexyl - 2,6 - pyridine - bis-(methyleneoxy acetamide) (ionophore 3) was obtained as a white solid (70%), mp 129–130°C; $C_{35}H_{55}N_3O_4$: C 72.51 (72.35), H 9.74 (9.53), N 7.09 (7.22); IR (KBr) 1642 cm^{-1} (C=O); ^1H NMR ($CDCl_3$, TMS): 1.20–3.43 (m, 44H, $4 \times C_6H_{11}$), 4.21 (S, 4H, $2 \times OCH_2CO$), 4.70 (S, 4H, $2 \times ArCH_2O$), 7.42, 7.64 (m, 3H, C_5H_3N) ppm; MS (*m*/*z*): 582 (M + 1, 100%).

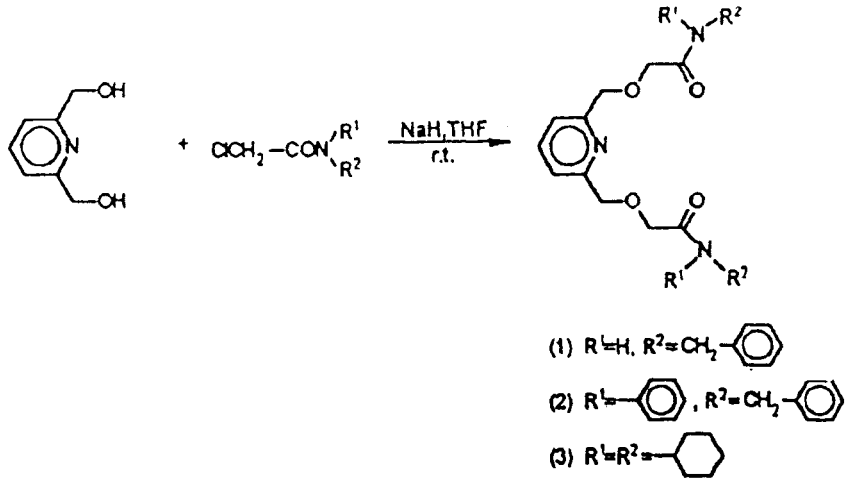

Scheme 1. Syntheses if ionophores (1–3) used in this report.

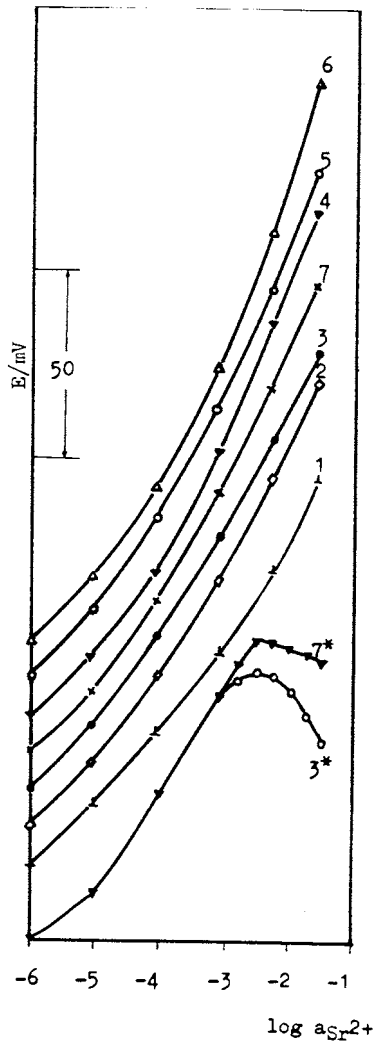

Fig. 1. Response curves of Sr^{2+}-electrodes. Electrodes: (1) ionophore 1/*o*-NPOE/PVC; (2) ionophore 2/*o*-NPOE/PVC; (3) 3* ionophore 3/*o*-NPOE/PVC; (4) ionophore 3/DOP/PVC; (5) ionophore 3/DOPP/PVC; (6) ionophore 3/TEPH/PVC; (7) 7* ionophore 3/*o*-NPOE/KTpClPB/PVC.

2.3. Apparatus

Potentiometric measurements were made with a model 901 microprocessor ionalyzer (Orion, Cambridge, MA) and pH measurements were made with a model PHM 84 Research pH meter (Radiometer, Copenhagen). A saturated calomel electrode was used as a reference. Potentiometric titration was made with a model 2Z-3 recording potentiometric titrator (Rex, Shanghai).

2.4. Membranes and electrodes fabrication

The polymeric membranes used in this study were prepared as follows [9]: ionophore, plasticizer and (or not) additive were dissolved in 5 ml 4% (w/v) PVC solution of THF. The solution was poured into a glass ring ($\sim$31 mm in diameter) on a glass plate and kept for 2 days at room temperature to yield an elastic translucent (or transparent) sensing membrane with $\sim$0.2 mm thickness. The electrode was made by fixing a disk (8 mm diameter) of the membrane to the PVC tubing with THF solution of the membrane. The internal aqueous solution was 10^{-2} M $SrCl_2$ saturated with AgCl. Before use, the electrodes were conditioned in the 10^{-2} M $SrCl_2$ aqueous solution for 1 day. The composition of membrane (w/w) was 1.7% ionophore, 32.8% PVC, and 65.5% plasticizer. The composition of the membrane containing additive (w/w) was 1.7% ionophore (3), 0.3% additive, 32.6% PVC, and 65.4% *o*-NPOE.

2.5. EMF measurements

Measurements were performed by the following cell: Hg, Hg_2Cl_2, KCl (saturated) // sample solution/membrane/$SrCl_2$ (10^{-2} M), AgCl, Ag. The performance of the electrodes was examined by measuring the EMFs of $SrCl_2$ solutions prepared with a concentration range of 10^{-1} to 10^{-6} M by successive dilution. The activities of metal ions were based on activity coefficient (γ) data calculated by using the extended Debye–Huckel equation. The individual activity coefficients for $SrCl_2$ were treated as Baumman [5].

The selectivity coefficients $K^{Pot}_{Sr,M}$, (M is the interfering ion) were calculated by the modified Nernst equation according to the recommendations of IUPAC [12].

$$K^{Pot}_{Sr,M} = a_{Sr}/(a_M)^{Z_{Sr}/Z_M}$$

(fixed interfering method) (1)

$$\log K^{\mathrm{Pot}}_{\mathrm{Sr,M}} = \frac{E_{\mathrm{M}} - E_{\mathrm{Sr}}}{2.303RT/Z_{\mathrm{Sr}}F} + \left(1 - \frac{Z_{\mathrm{Sr}}}{Z_{\mathrm{M}}}\right) \log a_{\mathrm{Sr}} \quad \text{(separate solution method)} \qquad (2)$$

Z_{Sr} is the charge of strontium ion ($+2$), Z_{M} is an integer with sign and magnitude corresponding to the charge of interfering ion M.

3. Results and discussion

The calibration curves of the strontium ion-selective electrodes are shown in Fig. 1, curves 1–7 are responses to $SrCl_2$ solution, curves 3* and 7* are responses to $Sr(NO_3)_2$ solution. The electrodes 3 and 7 show near-Nerstian potentiometric response for 2×10^{-5} to 10^{-2} M $SrCl_2$ with the slope of ~ 27.6 and 29.3 mV/pSr^{2+} (determined by linear regression) at 25°C, respectively. In 0.05 M $Mg(Ac)_2$ pH adjusted to 6 with HCl as ionic strength adjustment buffer (ISAB), the linear response concentration range of electrode 3 is from 3×10^{-5} to 5×10^{-2} M, and from 3×10^{-5} to 1×10^{-1} M $SrCl_2$ for electrode 7. Their limits of detection are 8×10^{-6} M, which determined from the crossing point between the Nernstian asymptote and the horizontal asymptote. The selectivity coefficients as shown in Fig. 2 were determined by the fixed interference method [12] except for H^+, Cu^{2+}, Cd^{2+}, Zn^{2+}, and Pb^{2+}. The background concentrations of the interference ions employed were 0.1 M for LiCl, NaCl, KCl, NH_4Cl, $MgCl_2$, and 10^{-2} M for $CaCl_2$, $BaCl_2$. The selectivity coefficients of the electrodes for strontium over hydrogen, copper, cadmium, zinc and lead ions were determined by the separate solution method [12]. The solutions were prepared as 10^{-2} M

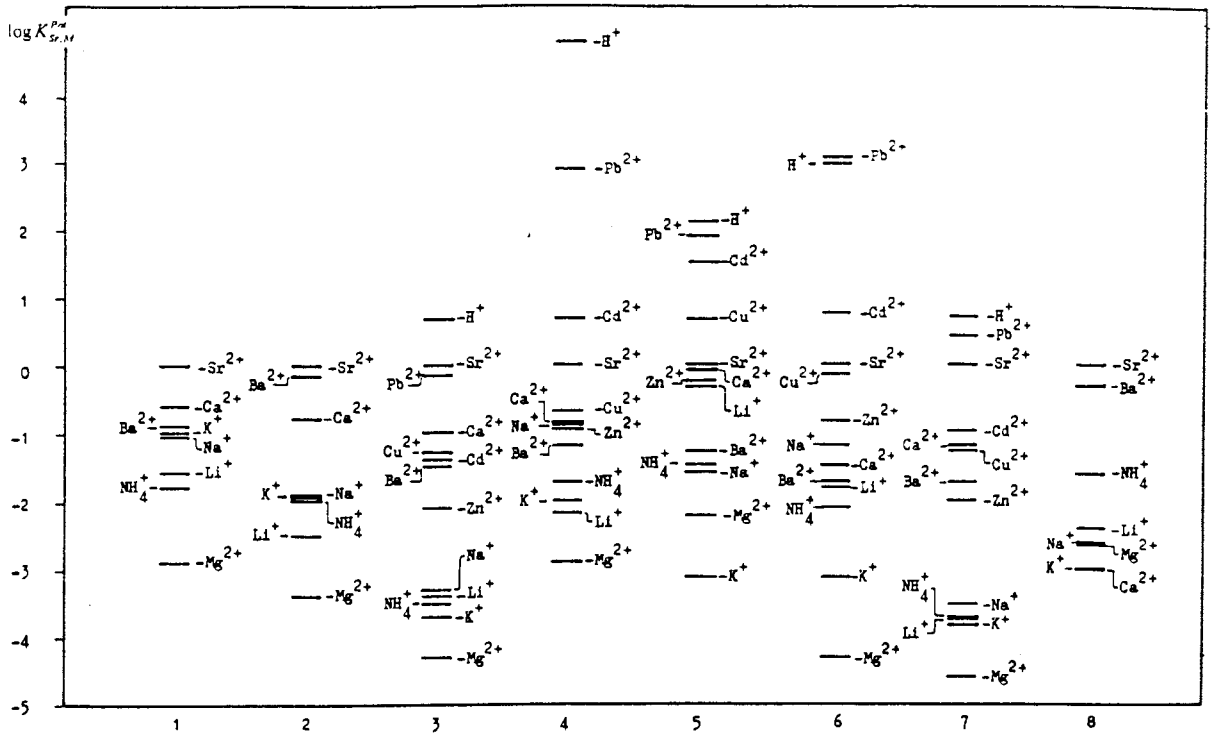

Fig. 2. Selectivity coefficients of Sr^{2+}-electrodes. Electrodes: (1) ionophore 1/*o*-NPOE/PVC; (2) ionophore 2/*o*-NPOE/PVC; (3) ionophore 3/*o*-NPOE/PVC; (4) ionophore 3/DOP/PVC; (5) ionophore 3/DOPP/PVC; (6) ionophore 3/TEPH/PVC; (7) ionophore 3/*o*-NPOE/KTpCIPB/PVC; (8) poly(dibenzo-18-crown-6) [7].

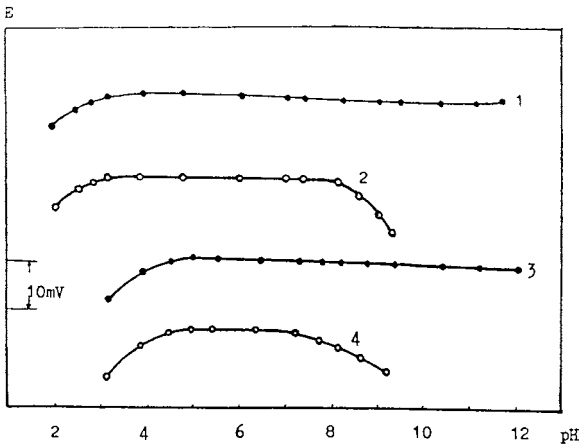

Fig. 3. Effect of pH on response of Sr^{2+}-electrodes. ○: Electrode 3, ionophore 3/*o*-NPOE/PVC; ●: Electrode 7, ionophore 3/KTpCIPB/*o*-NPOE/PVC. 1 and 2: 10^{-3} M $SrCl_2$; 3 and 4: 10^{-4} M $SrCl_2$.

chlorides except for lead nitrate. The selectivity coefficients of the electrodes 1, 2 and 3 determined by separate solution method approximated to the values of columns one to three in Fig. 2. The selectivity coefficients of the strontium ion-selective electrode 8 based on a poly(dibenzo-18-crown-6) film [7] are illustrated in Fig. 2 to allow some comparison with the results.

The electrodes 1, 2 and 3 in Figs. 1 and 2 showed clearly that the three compounds used in this study provided functionally active strontium ion-selective electrodes, and all neutral carrier electrodes exhibited a marked selectivity for strontium over alkali-metal and other alkaline-earth-metal ions. The ionophores are selective for strontium ion, due to the ideal size of the C-shaped cavity of the compounds. The radius of the pseudo ring containing two amide O-atoms, two ether O-atoms, and one aromatic N-atom approximates to 1.20 A which fits Sr^{2+} (radius 1.13A) better than Mg^{2+} (0.66 A), Ca^{2+} (0.99 A), and Ba^{2+} (1.35 A), according to the CPK (Cory–Pauling–Koltum) model. It is therefore expected that the electrodes based on the ionophores show better selectivity for Sr^{2+} than other alkaline-earth-metal ions, but ions with radii approximately equal to 1.20 A such as Pb^{2+} (1.21 A) and Ag^{+} (1.25 A) interfere seriously.

It is obvious that the response slope and selectivity for the strontium ion both decrease in the following order: ionophore (3) > ionphore (2) > ionophore (1). Different substituents of the amide N-atom result in the difference of performance. The stereoeffect of the cyclohexyl group with the chair conformation is better than that of the other substituents. The reason why ionophore (3) exhibits the best performance among three ionophores may be due in part to the lipophilicity and electron-donating of the cyclohexyl group. The enhancement of electron density for amide O-atom through the conjugate effect contributes to the coupling with strontium ion.

The electrodes 3 and 7 in Figs. 1 and 2 demonstrated the effect of additive on the performance of the electrode. The response of the electrode containing additive was better than that of the electrodes without additive, but the overtheoreti-

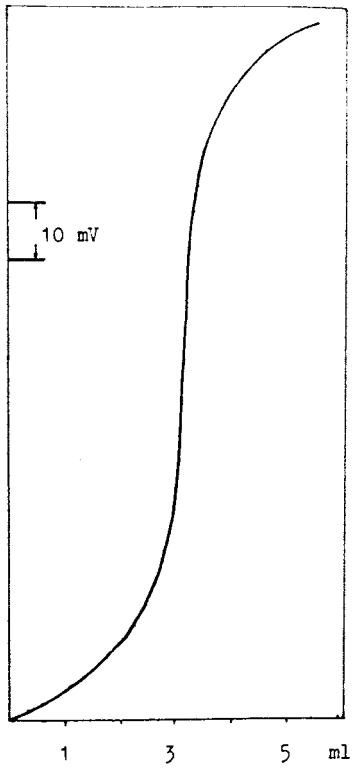

Fig. 4. The titration curve of 10^{-2} M strontium chloride solution (30 ml) with 10^{-1} M sodium carbonate solution using electrode 7.

cal slope of the former electrode to high concentration ($>10^{-2}$ M) $SrCl_2$ solutions became obvious. The effects of additives KTpClPB on the selectivity of electrode was relatively better than that of KTPB or NaTPB, though there was only little difference caused by them. The selectivity for Sr^{2+} over the OH^- especially lipophilic anions such as NO_3^- as shown in Fig. 1, and to a smaller extent over the alkali and other alkaline-earth-metal interference ions is improved by the addition of an appropriate amount of KTpClPB, but the interference of Pb^{2+} and Cd^{2+} increased slightly. The additive lowers the resistance of electrode membrane and the resistance of the electrode 7 measured by the parallel resistance method [13] approaches 0.1 MΩ.

The performance of the electrodes 3, 4, 5 and 6 were found to depend on the particular plasticizer used which displayed the cooperative effect of the plasticizer as shown in Figs. 1 and 2. The response to high concentration aqueous $SrCl_2$ solutions ($>10^{-2}$ M) showed evidently overtheoretical slope and increasingly striking in sequential order of the electrode and concentration of $SrCl_2$. The interference of Pb^{2+}, Cd^{2+}, Cu^{2+}, and other alkaline-earth-metal ions for Sr^{2+}-electrodes 4, 5 and 6 has become very serious. The d-c resistances of electrode membranes vary with different plasticizer used. The typical resistance of electrode 4 is ~ 10 MΩ, electrode 5 and 6 is ~ 8 MΩ, electrode 3 is ~ 0.3 MΩ (25°C, ~ 0.2 mm thickness). Obviously, *o*-NPOE, as the plasticizing solvent of Sr^{2+} electrode membrane, is better than the others. Electrode with pure NPOE membrane show no obvious response to alkaline metal ions [14]. Electrode with pure DOP membrane has better response to alkaline metal ions [14]. Pure TEHP and DOPP membrane electrodes have better response and selectivity to Li^+ [14]. Pure DOPP membrane electrode has very good response and selectivity to Ca^{2+} [14]. As shown in Fig. 2, the selectivities of electrodes 3, 4, 5 and 6 are caused by the effect of the plasticizer. The above results illustrate that the role of plasticizer, in addition to its proper function, also partly behaves as an ionophore. Because the response slopes of electrode three and seven to alkaline metal ions and H^+ are much lower than Nernstian responses, the selectivity coefficients of electrodes 3 and 7 are lower than that is shown in Fig. 2. For example, the response to H^+ has a slope of ~ 31 mV pH^{-1}, is almost same as the response to Sr^{2+}. The assumption is $Z_{Sr} = Z_H$, according to Eq. (2) (separate solution method), $K^{Pot}_{Sr,H} = -1.3$, where in Fig. 2, $K^{Pot}_{Sr,H} = +0.7$ is calculated based on $Z_{Sr} = +2$, $Z_H = +1$.

The pH effect in $SrCl_2$ solution was determined by additions of HCl or LiOH to adjust the pH of the solution. In Fig. 3, the change in potential is given as a function of the measured pH. The useful pH range in 10^{-3} M $SrCl_2$ is 3.0 to 8.2 for the electrode three, and 3.0 to 11.5 for electrode seven; in 10^{-4} M $SrCl_2$, the useful pH range is 4.1 to 7.8 for electrode 3, and 4.0 to 12.0 for electrode 7. Strontium precipitated as hydroxide and/or carbonate at high pH (>11.5 for 10^{-3} M $SrCl_2$, and >12 for 10^{-4} M $SrCl_2$), resulting in the solution interference. The membrane electrode containing additive can be used in a wide pH range.

The standard deviations of the electrode potential readings over a period of 10 h in 10^{-3} M $SrCl_2$ solution were 1.0 mV for electrode 3, and 0.9 mV for electrode 7 (take readings every 6 min in the beginning, then every 30 min, total 29 readings, $n = 29$) at room temperature. Potential readings for electrodes dipped alternately into stirred solution of 10^{-4} and 10^{-3} M $SrCl_2$ showed 45.2 ± 0.4 mV, 72.8 ± 0.3 mV for electrode 3, and 40.8 ± 0.3 mV, 70.1 ± 0.3 mV for electrode 7, respectively, over 2 h (repeat five readings, $n = 5$). The performance characteristics of electrode 7 did not show detectable change after using it for about 90 days.

The response times of electrodes 3 and 7 were within 20 s which tested by measuring the time required to achieve a 95% steady potential for a 10^{-3} M $SrCl_2$ solution when $SrCl_2$ concentration was rapidly increased 10-fold from 10^{-4} to 10^{-3} M or for a 5×10^{-4} M $SrCl_2$ solution when $SrCl_2$ concentration was rapidly decreased a half from 10^{-3} to 5×10^{-4} M.

4. Application

Electrode 7 was applied to the determination of strontium ions in some chemical products con-

taining strontium by the direct potentiometry and the potentiometric titration with $Mg(Ac)_2$ as ISAB. The titration curve of strontium chloride with sodium carbonate is shown in Fig. 4 by using electrode 7 as an indicator. Nice agreement was obtained between the procedures of potentiometric titration and the EDTA volumetric analysis [15].

In conclusion it has been shown that the derivatives of 2,6-pyridine-bis(methyleneoxy acetamide) are good strontium ion ionophores due to the ideal size of the C-shaped cavity of the compounds. The lipophilic and electron-donating substituents of amide N-atom improve obviously the behavior of the ionophores. The strontium ion-selective electrode using *N*,*N*,*N*′,*N*′-tetracyclohexyl-2,6-pyridine-bis(methyleneoxy acetamide) as neutral carrier, KTpClPB as additive, *o*-NPOE as plasticizing solvent is recommended.

References

[1] A.K. Jain, S.K. Srivastava, R.P. Singh, S. Agrawal, J. Appl. Chem. Biotechnol 27 (1977) 680.
[2] S.K. Srivastava, C.K. Jain, Bunseki Kagaku 33 (1984) 525.
[3] N. Faizan, M.C. Chattopadhyaya, J. Inst. Chem. (India) 62 (1990) 95.
[4] E.A. Materova, V.V. Muzhovikov, Elektrokhimiya 7 (1971) 1741.
[5] E.W. Baumann, Anal. Chem. 42 (1975) 959.
[6] V.N. Golubev, B.A. Purins, A.D. Gutsol, V.I. Panteleev, I.A. Sobolev, L.M. Khomchik, USSR SU987, 499, 7 Jan, 1983.
[7] N. Akmal, H. Zimmer, H.B. Jr. Mark, Anal. Lett. 24 (1991) 1431.
[8] D. Erne, N. Stojanac, D. Ammann, E. Pretsch, W. Simon, Helv. Chim. Acta 63 (1980) 2264.
[9] G.L. Wu, C.M. Lu, X.Y. Du, G.Z. Tan, J.Z. Xu, Huaxue Tongbao (Chinese) 18 (1985) 19.
[10] V.P.Y. Gadzepko, J.M. Hungerford, A.M. Kadry, Y.A. Ibrahim, R.Y. Xie, G.D. Christian, Anal. Chem. 58 (1986) 1948.
[11] S. Huang, Y.J. Yan, B.Z. Tian, Hecheng Huaxue (Chinese) 2 (1994) 230.
[12] IUPAC, Recommendations for Nomenclature of Ion-Selective Electrodes, Pure Appl. Chem. 48 (1976) 127.
[13] E.L. Eckfeldt, G.A. Perley, J. Electrochem. Soc. 98 (1951) 37.
[14] G.Y. Qian, R.L. Wang, G.L. Wu, Chem. Sens. (Chinese) 9 (4) (1989) 43.
[15] People's Republic of China Standard, GB 669-77.

ELSEVIER

Talanta 47 (1998) 1157–1163

Talanta

Applicability of 0.05 mol kg^{-1} potassium hydrogen phthalate as reference value pH standard in water–organic solvent mixtures

Kosuke Izutsu *, Hiroki Yamamoto

Department of Environmental Sciences, Faculty of Science, Shinshu University, 3-1-1 Asahi, Matsumoto 390-8621, Japan

Received 17 February 1998; received in revised form 8 May 1998; accepted 12 May 1998

Abstract

The applicability of 0.05 mol kg^{-1} potassium hydrogen phthalate (KHPh(S), S = the solvent under study) as reference value pH standard (RVS) was studied in water–organic solvent mixtures. Phthalic acid in various aqueous organic solvent mixtures was titrated potentiometrically with Bu_4NOH (MeOH), using a pH-ISFET and a glass electrode as pH-sensors, and the buffer capacity of the HPh^- solution was roughly estimated from the difference between the first and second half-neutralization potentials. The influence of potassium ion to the buffer capacity was also studied, titrating KHPh and Et_4NHPh with CF_3SO_3H and Bu_4NOH (MeOH) and comparing the titration curves. The KHPh solution loses its buffer capacity if the solvent mixture has an aprotic property. For aqueous mixtures of protophilic aprotic solvents (e.g. DMSO and DMF), it is unsuitable as RVS if the water content is less than ca. 40 (v/v)%. The necessity of selecting subsidiary pH standard(s) is suggested for the solvent systems in which KHPh is inapplicable. © 1998 Elsevier Science B.V. All rights reserved.

Keywords: Potassium hydrogen phthalate; Reference value pH standard; pH-ISFET; Buffer capacity; Aqueous solvent mixtures; Protophilic aprotic solvents

1. Introduction

A criteria for the standardization of pH measurements in organic solvents and water–organic solvent mixtures of moderate to high permittivities was proposed in 1985 from the Commission on Electroanalytical Chemistry of IUPAC [1]. According to it, the pH is conceptually defined by $pH = -\log a(H^+)$, where $a(H^+)$ is the activity on molality basis of proton in the solution under study. In the operational definition, however, the relation between the EMFs of cells (I) and (II) and the pH values of solutions s (standard) and x (sample) in solvent S is given by $pH(x) - pH(s) = \{E(s) - E(x)\}/2.303RT$,

Reference electrode/salt bridge (S)//solution s(S)

/H^+-sensing electrode (I)

* Corresponding author. Tel.: +81 263 351085; fax: +81 263 351085; e-mail: kizutsu@gipac.shinshu-u.ac.jp

0039-9140/98/$ - see front matter © 1998 Elsevier Science B.V. All rights reserved.
PII S0039-9140(98)00196-9

Reference electrode/salt bridge (S)//solution x(S)

/H^+-sensing electrode (II)

and 0.05 mol kg^{-1} potassium hydrogen phthalate in S (KHPh(S)) is designated the reference value pH standard (RVS). If the pH value of 0.05 mol kg^{-1} KHPh(S) (pH_{RVS}) or some other primary pH standard is known, we get the pH of the sample solution from the above relation. The pH_{RVS} data now available are for binary mixtures between water and the following eight organic solvents [2]: methanol (10, 20, 50, 64, 84.2) [1], ethanol (10, 20, 40, 70) [3], 2-propanol (10, 30, 50, 70) [4], 1,2-ethanediol (10, 30, 50, 70) [5], 2-methoxyethanol (20, 50, 80) [6], acetonitrile (5, 15, 30, 50, 70) [7], 1,4-dioxane (10, 30, 50) [8] and DMSO (20, 30) [9]. The figures in parentheses show the (m/m)% of organic solvent in the mixtures for which pH_{RVS} values have been given. The pH measurement based on this definition is very reliable and convenient, directly giving pH values. It is noted, however, that no pH_{RVS} data are available for water–poor solvent mixtures and for neat organic solvents. Especially for H_2O–DMSO, pH_{RVS} is not available at $H_2O < 70$ (m/m)%.

The authors of [1] pointed out the restricted use of 0.05 mol kg^{-1} KHPh(S) as the RVS in water–poor solvent mixtures, i.e. 90 to 100 (m/m)%-pure organic solvents, attributing its main reason to the low solubility of KHPh. But the selection of a subsidiary RVS was deferred, because, at that time, the response of pH electrodes was also problematic in such water-poor systems. We show in this report that the KHPh(S) solution loses its buffer capacity in aqueous solvent mixtures with an aprotic property. In aqueous mixtures of protophilic aprotic solvents such as DMF and DMSO, the lack of buffer capacity begins at relatively high water contents (ca. 40 (v/v)%). (Note: The water content of a (v/v)% is equal to $100a/[a+(100-a)d]$ (m/m)%, where d is the density of organic solvent (0.7765 for AN, 0.7864 for MeOH, 0.9439 for DMF, and 1.095 for DMSO at 25°C.) Nowadays, the needs for pH measurements in water-poor and water-free solvent systems, including ones with aprotic properties, are increasing both in pure and applied fields of chemistry. As we reported recently [10,11], the introduction of pH-ISFETs and an iridium oxide pH sensor has considerably improved the problematic situation of pH-sensors in such solvent systems. Now it is very desirable to develop subsidiary pH standard(s) for the solvent systems in which KHPh is not applicable.

2. Experimental

2.1. Apparatus

As pH-sensors, an Si_3N_4-type pH-ISFET from the Shindengen Industrial and a glass electrode (Horiba model 1076A-10C, for nonaqueous solutions) were used [11]. The potentials of these sensors were measured simultaneously against a single $Ag/Ag^+(S)$ or aqueous Ag/AgCl reference electrode [11]. To measure the potential of the glass electrode, a high-impedance voltage-follower, constructed using an OP amplifier (Burr–Brown OPA129), was used, while, to measure the potential of the ISFET, a BAS ISFET mV/pH meter was used. They were connected between the cell and a Yokogawa model LR4100 two-pen recorder. The potential-time relations were recorded with the recorder but, at the same time, the data were stored in a memory card and processed with a personal computer. In the acid-base titration, a Metrohm 665 Dosimat automatic burette equipped with an exchange-unit 552-5BC was used. The dissolved carbon dioxide was not purged before titration, because its influence on the results was negligible. All measurements were carried out at room temperatures between 20 and 25°C.

2.2. Reagents

Potassium hydrogen phthalate and o-, m- and p-phthalic acids were Nacalai Tesque reagent grade products. Mono- and di-tetraethylammonium phthalates were kindly supplied by Mitsubishi Chemical Corporation. Tetrabutylammonium hydroxide (1.0 M, here M = mol dm^{-3}) in methanol was the Aldrich product. Acetonitrile (AN), dimethyl sulfoxide

(DMSO), *N*,*N*-dimethylformamide (DMF) and methanol (MeOH) were Wako reagent grade products and were used after further purification by distillation.

3. Results and discussion

3.1. Buffer capacity of hydrogen phthalate solutions

The curves in Fig. 1 were obtained by titrating 20 ml of (3 mM phthalic acid (H_2Ph) + 2 mM CF_3SO_3H) in various AN–water mixtures with 1.0 M Bu_4NOH (MeOH). The water content is shown on each curve in (v/v)% (hereafter, % means (v/v)%). The indicator electrode was the Si_3N_4-ISFET and the titration speed was 0.005 ml min^{-1}. The ISFET was confirmed to respond with 55 ± 1 mV pH^{-1} in both aqueous and non-aqueous (MeOH, AN, DMF and DMSO) solutions (see [10] for the method of calibration). Thus we assumed the same slope also for aqueous–organic solvent mixtures. The curve for 1% H_2O has three potential jumps: the first jump is for the neutralization of CF_3SO_3H, and the second and third ones are for the two-step neutralization of H_2Ph. The curve for pure (100%) H_2O, on the other hand, does not show the first jump and the second one is also very small. The mark x on each curve corresponds to the point where all phthalic acid is in the HPh^- form. In 100% H_2O, the slope of the curve at mark x is small, showing that the buffer capacity of the HPh^- solution is appreciable. With the decrease in H_2O content, however, the slope at mark x increases, corresponding to the gradual decrease in buffer capacity.

Fig. 2(A, B) shows the titration curves of (3 mM H_2Ph + 2 mM CF_3SO_3H) and (0.05 M H_2Ph + 0.02 M CF_3SO_3H), respectively, in 99% DMSO–1% H_2O with 1.0 M Bu_4NOH (MeOH). The titrations were at 0.005 ml min^{-1} for Fig. 2(A) and at 0.05 ml min^{-1} for Fig. 2(B); taking 40 and 60 min, respectively, from the start to the end. In Fig. 2(A), the response of the pH-ISFET was fast enough but that of the glass electrode was seriously delayed. In order to get a satisfactory titration curve with the glass electrode, it took too long. This situation is the same as what we reported previously [10,11]. Though the response of the glass electrode was fairly improved in Fig. 2(B), it was due to the influence of MeOH

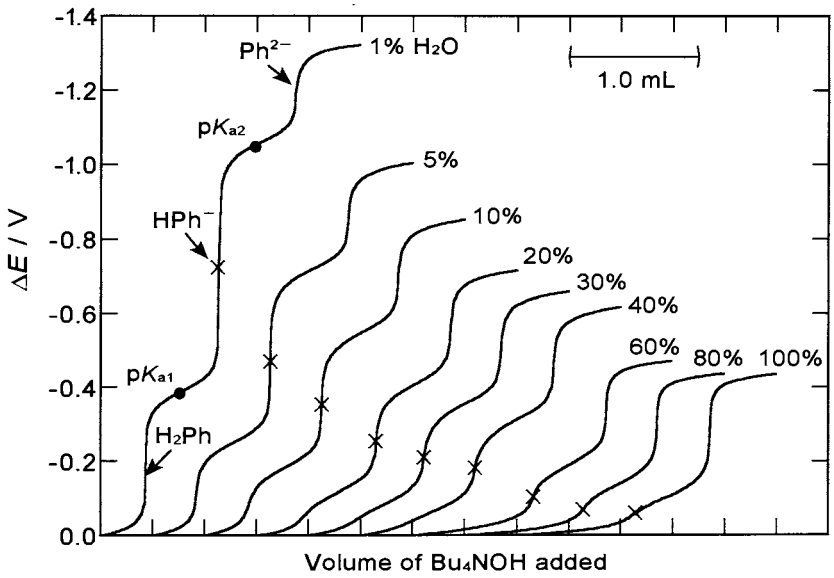

Fig. 1. Titration curves of 20 ml of (3 mM phthalic acid (H_2Ph) + 2 mM CF_3SO_3H) in various AN–water mixtures with 1.0 M Bu_4NOH(MeOH). The water content in (v/v)% is shown on each curve. pH-sensor, Si_3N_4-ISFET; titration speed, 0.005 ml min^{-1}.

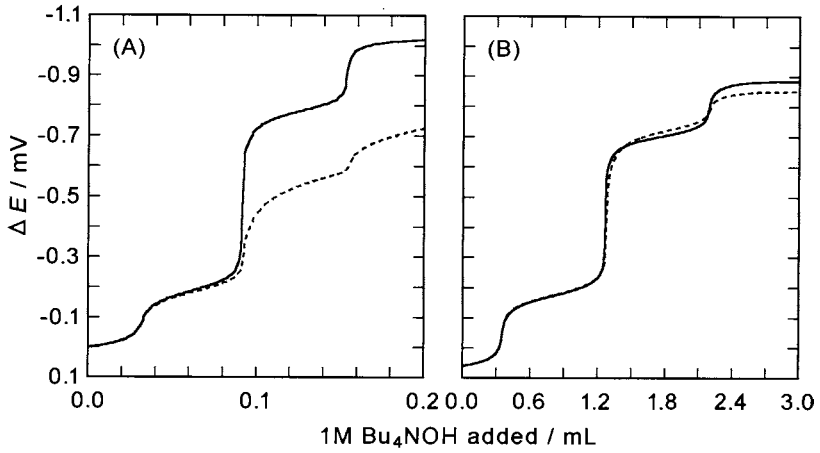

Fig. 2. Titration curves of 20 ml of (3 mM $H_2Ph + 2$ mM CF_3SO_3H) (A) and (0.05 M $H_2Ph + 0.02$ M CF_3SO_3H) (B) in 99% DMSO–1% H_2O with 1.0 M Bu_4NOH(MeOH). Titration speed: (A) 0.005 ml min^{-1}, (B) 0.05 ml min^{-1}. pH-sensor: Si_3N_4-ISFET (solid curve) and glass electrode (dashed curve).

introduced with the titrant (0.72 ml MeOH for 1 ml titrant). Thus, except in Fig. 2, only the results obtained with the pH-ISFET are described.

From the curves similar to those in Fig. 1, the difference between the first and second half-neutralization potentials ($\Delta E_{1/2}$) were obtained for 3 mM H_2Ph in aqueous mixtures of AN, DMSO, DMF and MeOH and for 0.05 M H_2Ph in aqueous mixtures of AN, DMSO and MeOH. The results are shown in Fig. 3(A, B). For 1% H_2O mixtures of AN and DMSO, the values of $\Delta E_{1/2}$ in Fig. 3(B) are somewhat smaller than those in Fig. 3(A) (see also $\Delta E_{1/2}$'s in Fig. 2(A, B). Here again, it is due to the influence of MeOH introduced with the titrant [12,13]: the MeOH introduced between the two half-neutralization potentials was 0.048 ml in Fig. 3(A) but 0.72 ml in Fig. 3(B). For the first and second dissociations of H_2Ph in neat solvents, pK_{a1} and pK_{a2} have been reported to be 14.2 and 29.8 in AN [12,13], 6.2 and 16.0 in DMSO [12,13], 6.7 and 16.5 in DMF [14], and 7.4 and 12.1 in MeOH [12,13]. If the ISFET responds at 55 mV pH^{-1}, we get, from these values, $\Delta E_{1/2}$ of 858 mV for AN, 539 mV for DMSO and DMF, and 259 mV for MeOH. These values roughly agree with the $\Delta E_{1/2}$ values for pure organic solvents in Fig. 3(A), indicating that the effect of MeOH introduced with the titrant was not so serious in this case.

According to [15], the buffer capacity (β), as defined by $\beta = db/dpH$ (db: the amount of strong base (in mole for 1 dm^3) needed for the increase of dpH), of the solution of an acid salt (M^+HA^-) can be estimated by $\beta \fallingdotseq 2 \times 2.3C(K_{a2}/K_{a1})^{1/2}/\{1 + 2(K_{a2}/K_{a1})^{1/2}\}$, where C is the molar concentration of MHA. We apply this relation to estimate the buffer capacity of the 0.05 M HPh^- solution. We also assume the relation $\Delta E_{1/2} \fallingdotseq 55(pK_{a2} - pK_{a1})$ for the results in Fig. 3 (55 = sensitivity of the pH-ISFET in mV pH^{-1}), even though, in water-rich regions, some deviation from this relation occurs because the K_{a1} of H_2Ph is not small enough. Then, we get $\beta \fallingdotseq 0.073C$, $0.0082C$ and $0.0010C$ for $\Delta E_{1/2} = 200$, 300 and 400 mV, respectively. It means that, when $\Delta E_{1/2} = 300$ mV, the pH of 0.05 M HPh^- solution is varied by 0.1 unit if a strong acid or base of 4×10^{-5} M is added. The acid or base impurities of this level are often contained in high-grade organic solvents, unless they are purified with much effort [13]. Thus, it is appropriate to consider that the buffer capacity of the HPh^- solution is too low when $\Delta E_{1/2} \geqq 300$ mV. In Fig. 3(A), $\Delta E_{1/2} \geqq 300$ mV if the water content is $<$ 30% for DMF and DMSO and $<15\%$ for AN. For MeOH, $\Delta E_{1/2} < 300$ mV holds over the entire range. In Fig. 3(B), $\Delta E_{1/2} \geqq 300$ mV if the water content is $<40\%$ for DMSO and $<25\%$ for AN.

Again for MeOH, $\Delta E_{1/2} < 300$ mV holds over the entire range.

3.2. Effect of potassium ions

In the above, we studied the buffer capacity of HPh^- in water–organic solvent mixtures, but in the absence of potassium ion. Actually however, the RVS is 0.05 mol kg^{-1} KHPh(*S*) and the potassium ion may influence the above results.

In order to see the influence of the potassium ion, we titrated each of 0.05 M Et_4NHPh and 0.05 M KHPh in various water–organic solvent mixtures using 1 M CF_3SO_3H(*S*) and 1 M Bu_4NOH(MeOH) as titrants and compared the titration curves for the two hydrogen phthalates. The results for DMSO–H_2O mixtures are shown in Fig. 4. For the mixture containing 1% H_2O, the curve for KHPh deviated considerably from that for Et_4NHPh, the potential (pH) on the first half during the neutralization of HPh^- to Ph^{2-} markedly being suppressed. This is due to the formation of K_2Ph precipitate. We confirmed it by potentiometric titrations of $(Et_4N)_2Ph$ with $KClO_4$ and of $KClO_4$ with $(Et_4N)_2Ph$, using a potassium ion-sensitive glass electrode. As in Fig. 5, two potassium ions reacted with Ph^{2-} to form a K_2Ph precipitate ($2K^+ + Ph^{2-} \rightarrow K_2Ph$). The potential (pH) suppression became less pronounced with the increase in water content and almost disappeared in the mixture of 30% H_2O. Similar influence of the potassium ion was also observed in AN–H_2O (by formation of K_2Ph, Fig. 5) and to a lesser degree in MeOH–H_2O mixtures. Though the potassium ion somewhat depressed the potential (pH) jump of the HPh^- solution in water–poor solvent mixtures (Fig. 4), it does not mean the increase in the buffer capacity. We consider that the results in Section 3.1 also apply to the KHPh solutions.

The minimum water content needed to dissolve 0.05 M KHPh at 25°C was found to be 11% for AN–H_2O, 10% for MeOH–H_2O, 1% for DMSO–H_2O, and 0% for DMF–H_2O. Thus, in MeOH-H_2O mixtures, the use of 0.05 M KHPh is limited at $H_2O \leqq 10\%$ due to the insufficient solubility of KHPh. In AN–H_2O mixtures, in addition to the insufficient solubility at $H_2O \leqq 11\%$, the lack in buffer capacity occurs at $H_2O \leqq 25\%$. In DMSO– and DMF–H_2O mixtures, the solubility is not a problem, but the lack in buffer capacity occurs at $H_2O \leqq 40\%$ and it is a serious problem. These results are for 0.05 M KHPh(*S*), but will apply, almost without modification, to the 0.05 mol kg^{-1} KHPh(*S*) as RVS.

It is well known that, in neat aprotic solvents, the difference between pK_{a1} and pK_{a2} is very big for *o*-phthalic acid, though it is not the case for

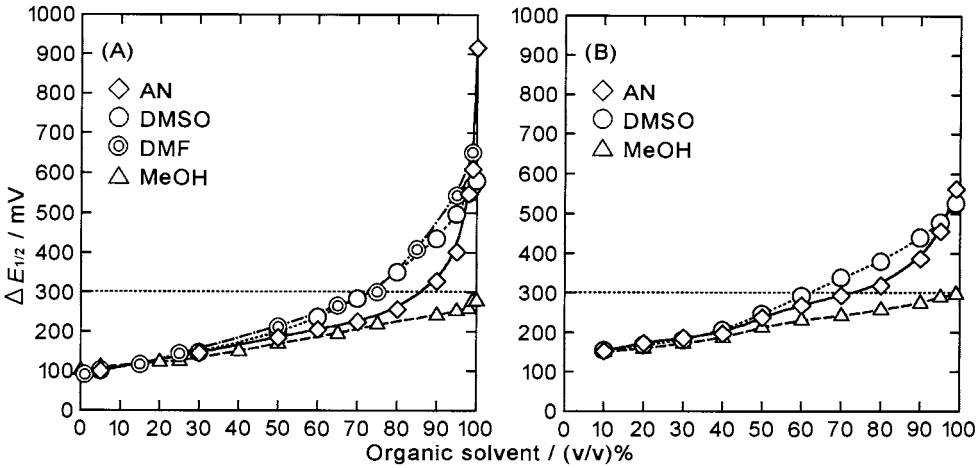

Fig. 3. Difference between the first and second half-neutralization potentials ($\Delta E_{1/2}$) for 3 mM H_2Ph (A) and 0.05 M H_2Ph (B) against the (v/v)% of organic solvents. Titration speed: (A) 0.005 ml min^{-1} and (B) 0.05 ml min^{-1}. pH-sensor: Si_3N_4-ISFET.

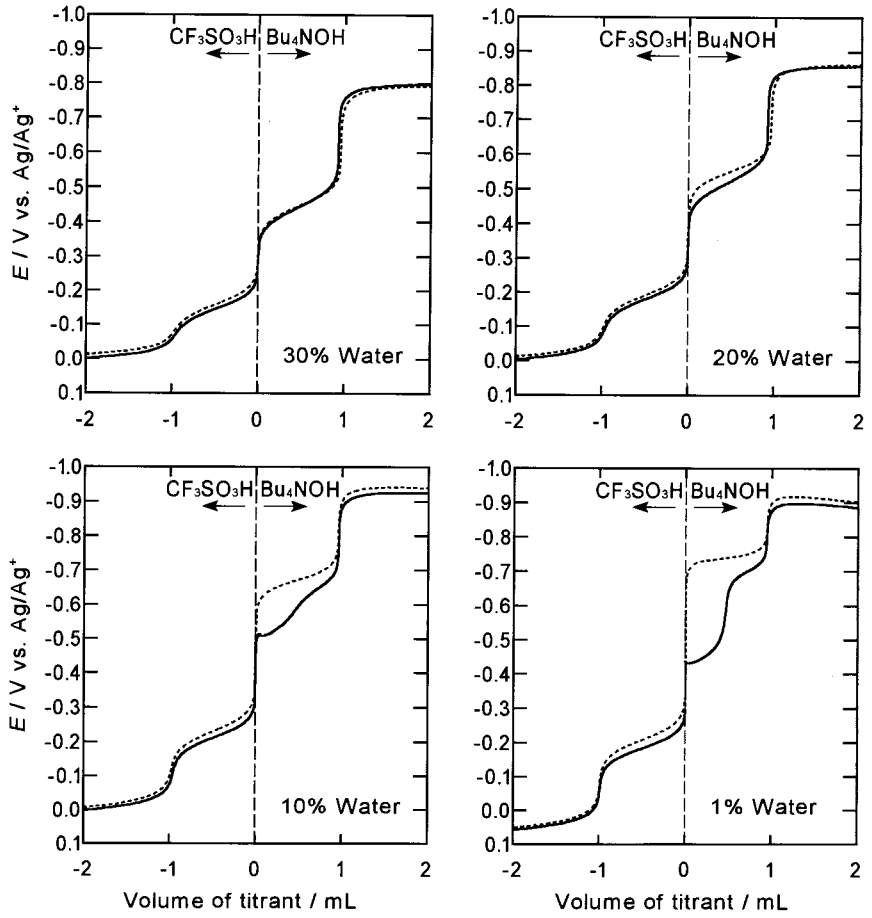

Fig. 4. Titration curves of 20 ml of 0.05 M KHPh (solid curve) and 0.05 M Et_4NHPh (dashed curve) in various DMSO–H_2O mixtures with 1 M $CF_3SO_3H(S)$ (from 0 to the left) and 1 M Bu_4NOH(MeOH) (from 0 to the right). pH-sensor: Si_3N_4-ISFET. Titration speed: 0.05 ml min^{-1}.

m- and *p*-phthalic acids [12,13] (Fig. 6). It is because, for *o*-phthalic acid in aprotic solvents, the HPh^- form is very stable (due to intramolecular hydrogen bonding), while the Ph^{2-} form is very unstable. In DMSO– and DMF–H_2O mixtures, protophilic DMSO and DMF molecules strongly interact with H_2O molecules to retain their aprotic nature even when the water content is fairly high (30–40%). Some data are available for pK_{a1} and pK_{a2} of *o*-phthalic acid in water–aprotic solvent mixtures, but only of fairly high water contents [16]. This report is the first to point out the problem of the lack of buffer capacity of 0.05 mol kg^{-1} KHPh in water–aprotic solvent mixtures.

As described above, the needs for pH measurements in water-poor and water-free solvent systems, including ones with aprotic properties, are increasing. It is necessary to select appropriate (and authorized) pH standard(s) for solvent systems in which KHPh is not applicable. The pH_{RVS} data for 0.05 mol kg^{-1} KHPh(*S*) have been given in four digits [1–9]. But, in water-poor and water-free solvent systems, such a high precision will be difficult to get. The most urgent need is to increase the number of solvent systems for which pH standards are available.

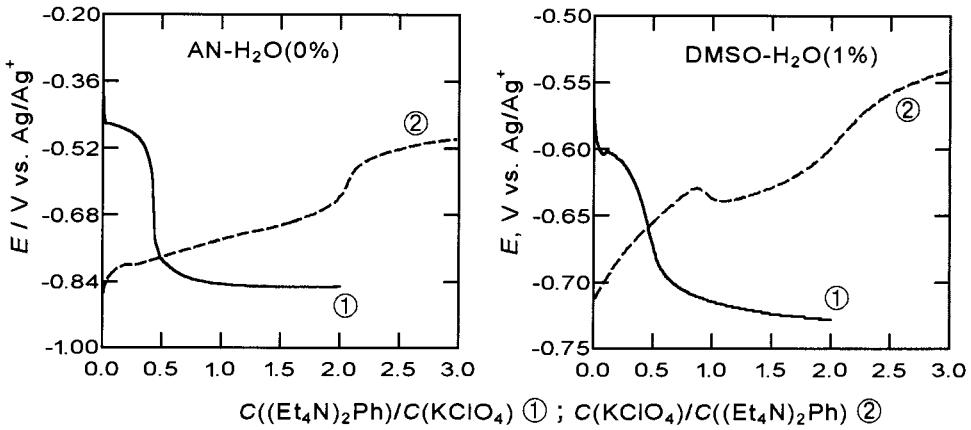

Fig. 5. Titration curves of 3 mM $KClO_4$ (20 ml) with 60 mM $(Et_4N)_2Ph$ (curve 1) and 3 mM $(Et_4N)_2Ph$ (20 ml) with 60 mM $KClO_4$ (curve 2), using a K^+-sensitive glass electrode. In the left figure, curve 2, 60 mM $KClO_4$ in 90% AN–10% H_2O was used as titrant. Titration speed; 0.05 ml min^{-1}.

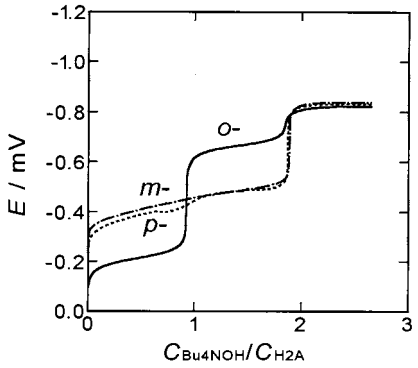

Fig. 6. Titration curves of *o*-, *m*- and *p*-phthalic acids (0.05 M, 20 ml) in 99% DMSO–1% H_2O with 1.0 M Bu_4NOH(MeOH). pH-sensor: Si_3N_4-ISFET. Titration speed; 0.05 ml min^{-1}.

Acknowledgements

The authors are grateful to S. Ida and S. Narita for their preliminary studies on this subject. This work was supported in part by a Grant-in-Aid for Scientific Research from the Ministry of Education, Science, Sports and Culture, Japan.

References

[1] T. Mussini, A.K. Covington, P. Longhi, S. Rondinini, Pure Appl. Chem. 57 (1985) 865; S. Rondinini, P.R. Mussini, T. Mussini, Pure Appl. Chem. 59 (1987) 1549.
[2] P.R. Mussini, T. Mussini, S. Rondinini, Pure Appl. Chem. 69 (1997) 1007.
[3] P. Longhi, P.R. Mussini, T. Mussini, S. Rondinini, J. Chem. Eng. Data 34 (1989) 64.
[4] S. Rondinini, P. Longhi, P.R. Mussini, A. Nese, M. Pozzi, G. Tiella, Anal. Chim. Acta (and literature cited therein) 207 (1988) 211.
[5] P.R. Mussini, I. Marcolungo, S. Rondinini, P. Longhi, Chim. Ind. (Milan) 73 (1991) 262.
[6] F. Arrigoni, P.R. Mussini, T. Mussini, S. Rondinini, J. Solution Chem. 24 (1995) 1265.
[7] S. Rondinini, A. Nese, Electrochim. Acta 32 (1987) 1499.
[8] T. Mussini, A.K. Covington, M. Cicognini, P. Longhi, S. Rondinini, Anal. Chim. Acta 162 (1984) 103.
[9] M.J. Taylor, J. Chem. Eng. Data 24 (1979) 230.
[10] K. Izutsu, T. Nakamura, S. Hiraoka, Chem. Lett. (1993) 1843; K. Izutsu, M. Ohmaki, Talanta 43 (1996) 643.
[11] K. Izutsu, H. Yamamoto, Anal. Sci. 12 (1996) 905.
[12] I.M. Kolthoff, M.K. Chantooni Jr., J. Am. Chem. Soc. 98 (1976) 7465.
[13] K. Izutsu, Acid-Base Dissociation Constants in Dipolar Aprotic Solvetns, IUPAC Chemical Data Series No. 35, Blackwell, Oxford, 1990.
[14] E. Roletto, A. Vanni, V. Zelano, Ann. Chim. (Rome) 70 (1980) 147.
[15] J.E. Ricci, Hydrogen Ion Concentration, Princeton University Press, Princeton, NJ, 1952, p. 249; H.A. Laitinen, Chemical Analysis, 1st ed., McGraw-Hill, New York 1960, p. 38.
[16] U. Mandai, S. Bhattacharya, S. Sen, K.K. Kundu, J. Chem. Soc. Parkin Trans II (1985) 853.

ELSEVIER

Talanta 47 (1998) 1165–1174

Talanta

Studies on optimization of a platinum catalyst and porphine modified, pyrolytic graphite, amperometric, glucose sensor by sequential level elimination experimental design

Li-Xian Sun [1], Fen Xu[1], Tatsuhiro Okada *

National Institute of Materials and Chemical Research, 1-1, Higashi, Tsukuba Ibaraki 305-8565, Japan

Received 19 February 1998; received in revised form 8 May 1998; accepted 12 May 1998

Abstract

A new amperometric glucose sensor based on the glucose oxidase immobilized on pyrolytic graphite (PG) modified with tetraammineplatinum(II) chloride (TAPtCl) and 5,10,15,20-tetrakis (4-methoxy-phenyl)-21*H*,23*H*-porphine cobalt(II) (TMPPCo) as well as Nafion was studied. The performances amongst the glucose sensors with or without TAPtCl or/and TMPPCo measured with oxygen present in the solution were compared. The compositions of the membranes of the glucose sensors were optimized by a new orthogonal experimental design technique–sequential level elimination method according to chemometric approaches. Our studies show that the prepared sensor with optimal membrane composition in this study gives satisfactory performance in terms of long-term stability, fast amperometric response, good detection limits and satisfactory recovery. The study provides a useful basis for developing other sensors with corresponding optimal membranes. © 1998 Elsevier Science B.V. All rights reserved.

Keywords: Biosensor; Pyrolytic graphite modified electrode; Glucose; Porphine; Platinum catalyst; Nafion; Chemometrics; Membrane optimization

1. Introduction

Glucose sensors play an important role in clinical analyses. There have been, therefore, a lot of literature [1–8] on the development of glucose sensors. Cobalt protoporphyrin has been used to catalyze the decomposition of H_2O_2 [9]. Becker et al. have reported catalytic decomposition of hydrogen peroxide using a platinum catalyst [10]. Wang and Wu [11] and Mizutani et al. [2] have previously realized the anion-excluding function of Nafion (perfluorosulfonic acid ionomer). So far there are no reports on glucose sensors using a combination of catalysts as mediators incorporated in Nafion as a covering membrane which can avoid the interference from out side anions with the

* Corresponding author. Fax: +81 298 544678; e-mail: tokada@home.nimc.go.jp

[1] On leave from the Department of Chemistry, Hunan Normal University, Changsha, 410081, People's Republic of China.

0039-9140/98/$ - see front matter © 1998 Elsevier Science B.V. All rights reserved.
PII S0039-9140(98)00195-7

intention of increasing the life time of a sensor.

Chemometric methods have found wide applications in various fields [12–15] and are particularly useful for the design of experiments [16,17]. There are several methods such as simplex optimization and traditional orthogonal experimental design which can be used for the optimization of various methods. Unfortunately, the simplex optimization may converge to local optimal solutions [18]. Traditional orthogonal experimental designs sometimes fail to obtain the global optimal solution [19]. Mao et al. [19] have suggested a new orthogonal experimental design technique, sequential level elimination. As its name suggests, the worst level of each factor, corresponding to the minimum/maximum (depends on the aim of optimization) average value (as the statistic) in the experiment, was eliminated step by step. Compared with other methods, Mao et al. [19] found that the sequential level elimination has many advantages. First, it showed satisfactory characteristics in finding the optimal solution while serious model interactions exist in the system. Second, it can save on the number of experiments over the traditional multifactor-turn design. Finally, the analysis algorithm for the experimental data is very simple. In this study the authors will skip the comparisons between the sequential level elimination and the other methods as Mao et al. have already done so [19]. Moreover, the authors have used the sequential level elimination to optimize the membrane composition of a sulbenicillin PVC (poly(vinyl chloride)) membrane electrode with satisfactory results as compared with traditional factorial design [16]. The membrane composition of the glucose electrode was therefore optimized by the sequential level elimination in this study. The electrodes thus prepared were studied for the optimal membrane composition in view of the excellent performances such as high sensitivity and long-term stability.

2. Experimental

2.1. Reagents and apparatus

Glucose oxidase (GOD) type II (EC1.1.3.4, 193 U mg^{-1}), glucose and tetraammineplatinum(II) chloride (TAPtCl) were obtained from Wako. 5,10,15,20-Tetrakis (4-methoxy-phenyl)-21*H*,23*H*-porphine Cobalt(II) (TMPPCo) and a solution of Nafion (5 wt.%) were obtained from Aldrich. KH_2PO_4, K_2HPO_4, and 2-propanol were of analytical reagent grade. Deionized doubly distilled water was used throughout.

Phosphate buffer solution (PBS) was prepared by mixing 0.1 M KH_2PO_4 and 0.1 M K_2HPO_4 to a pH of 7.0 using a pH meter in the presence of dissolved oxygen. Unless otherwise noted, all experiments were performed in phosphate buffer solution in the presence of oxygen.

A standard solution of GOD (10 mg ml^{-1}) in phosphate buffer (pH 7.0) was prepared and stored at 4°C.

Amperometric measurements and cyclic voltammetry were performed with a BAS CV-50W electrochemical instrument (Bioanalytical Systems, West Lafayette, IN) connected with a Hewlett-Packard 7400A ColorPro printer.

The electrochemical cell was composed of a Pt wire as an auxiliary electrode, a Ag/AgCl reference electrode, and a 5 mm ∅ basal plane pyrolytic graphite (PG) electrode coated with a specific membrane composition as the working electrode (for its preparation see Section 2.2). All the potentials are referred to Ag/AgCl. During the electrochemical measurements, the solutions in the electrochemical cell were stirred using a MS-1613 magnetic stirrer (Toyo) in the presence of oxygen. A pH meter (Horiba) was used for the phosphate buffer solution preparations. Personal computers were used for data processing.

2.2. Enzyme electrode fabrication

The PG electrodes were first conditioned according to the procedure of Wang and Tuzi [20]. The electrodes were first polished on 0.05 μm alumina slurry and then rinsed in distilled water with sonication. The working electrode (apparent surface area = 0.20 cm^2) was put in the above electrochemical cell containing a phosphate buffer blank solution (pH 7.0), and the potential was held at + 1.5 V versus Ag/AgCl for 30 min. After

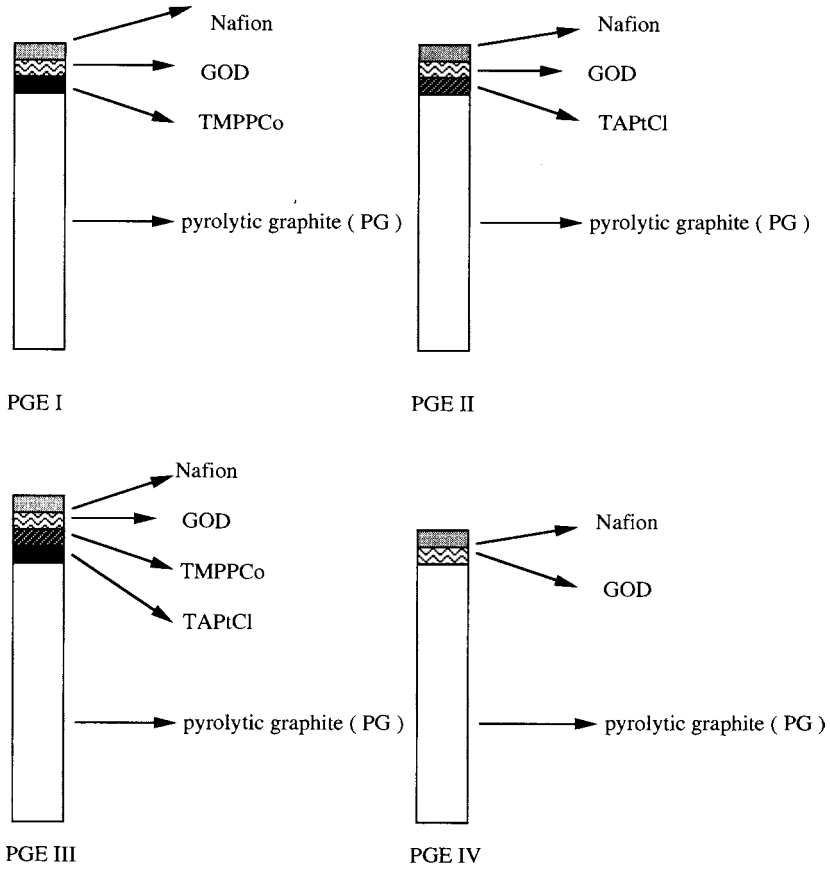

Fig. 1. Schematic graph of the composition of the four kinds of glucose electrodes.

the preanodization, as shown in Fig. 1, four kinds of glucose PG electrodes, PGE I (containing TMPPCo, GOD, Nafion), PGE II (containing TAPtCl, GOD, and Nafion), PGE III (containing TAPtCl, TMPPCo, GOD, and Nafion), and PGE IV (containing GOD and Nafion) were prepared by the following method. In the preparation of PGE I, first 10 μl of TMPPCo solution (1.0 mM in benzene) was put on the surface of the PG. After the benzene evaporated at room temperature, 10 μl GOD solution was placed on the PG electrode surface, and the phosphate buffer solvent (pH 7.0) was also allowed to evaporate at room temperature. Finally, a Nafion membrane coating on the PG was made by dropping a 0.5% (w/v) Nafion solution (50 μl) onto the electrode, where the Nafion solution was prepared by diluting the 5% solution as received with a mixture of 2-propanol (50%) and water [9]. The electrode was allowed to dry with the surface facing up at room temperature. Similarly, the PGE II was prepared by substituting TMPPCo with TAPtCl in PGE I. The TAPtCl coatings were formed by immersing the PG electrode into 1.0 mM TAPtCl solution for a fixed time (see Table 1 for details). PGE III was prepared by first dipping the PG electrode into a 1.0 mM TAPtCl solution for a fixed time (see Table 1 for detail), the solvent was allowed to evaporate at room temperature. The other procedures for making the remaining coatings of TMPPCo, GOD, and Nafion were the same as those described for PGE I. For PGE IV,

Table 1
The electrode membrane compositions of the orthogonal design using the $L_9(3^4)$ table

Electrode No.	TAPtCl	TMPPCo	Enzyme	Nafion
	Level[a] (min)[b]	Level[a] (μl)[c]	Level[a] (μl)d	Level[a] (μl)[e]
1	1 (10)	1 (10)	1 (10)	1 (50)
2	1 (10)	2 (10)	2 (10)	2 (50)
3	1 (10)	3 (10)	3 (10)	3 (50)
4	2 (20)	1 (15)	2 (15)	3 (60)
5	2 (20)	2 (15)	3 (15)	1 (60)
6	2 (20)	3 (15)	1 (15)	2 (60)
7	3 (30)	1 (20)	3 (20)	2 (70)
8	3 (30)	2 (20)	1 (20)	3 (70)
9	3 (30)	3 (20)	2 (20)	1 (70)

[a] Levels of the factors to be optimized for the membrane composition of the glucose electrode.
[b] Dipping time (min) in 1.0 mM TAPtCl.
[c] Amount (μl) of 1.0 mM TMPPCo in benzene.
[d] Amount (μl) of 10 mg ml^{-1} GOD in phosphate buffer solution.
[e] Amount (μl) of 0.5% Nafion in 2-propanol–water (50:50 v/v).

all the procedures utilized were the same as those adopted in PGE I except for containing neither TMPPCo nor TAPtCl in the membrane. As TAPtCl and GOD are light sensitive, the whole process of preparation of the membranes was carried out in the dark.

2.3. Measurement of response of the electrode to glucose

As mentioned above, an electrochemical cell composed of a three-electrode configuration was used for the amperometric measurements. The prepared enzyme electrode (i.e. the working electrode), an Ag/AgCl reference electrode and a platinum auxiliary electrode were immersed in a cylindrical cell containing 10 ml of a test solution of 0.1 M phosphate buffer solution (pH 7) with oxygen. The solution was stirred with a magnetic stirrer. The current response of each enzyme electrode to glucose addition in the presence of dissolved oxygen was recorded by holding the electrode potential at 0.90 V (versus Ag/AgCl).

Unless otherwise stated, all measurements throughout were carried out in phosphate buffer solution in the presence of dissolved oxygen at room temperature.

During the measurements, suitable amounts of 1 M glucose stock solution were added to the electrochemical cell containing phosphate buffer in the presence of oxygen. The current of each glucose electrode increased immediately after the addition of glucose and reached a steady state within a few seconds. As the Nafion layer is thin, the added glucose is expected to diffuse quickly through the layer, and is available to be oxidized by the GOD reaction:

$$\text{Glucose} + O_2 \overset{\text{GOD}}{\rightarrow} \text{gluconolactone} + H_2O_2$$

$$H_2O_2 \rightarrow 2H^+ + O_2 + 2e^-$$

The hydrogen peroxide produced near the electrode surface is immediately oxidized to give an anodic current response. Cobalt protoporphyrin [9] and a platinum catalyst [10] have been used to catalyze the decomposition of H_2O_2. In addition, TMPPCo can effectively adsorb the oxygen present in the phosphate buffer solution [21], and it can therefore stimulate the oxidation of glucose by GOD. Both TAPtCl and TMPPCo were used as the mediators for the glucose electrode (discussed in the following section) as they improve the interface characteristics of the glucose electrode.

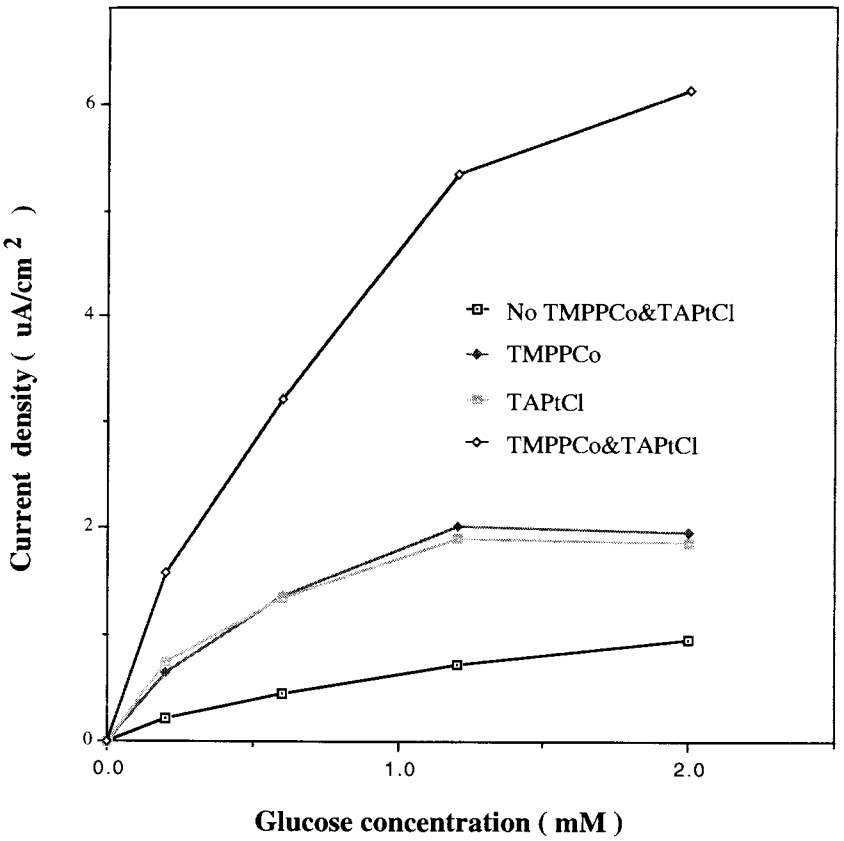

Fig. 2. Comparison of the amperometric response curves of the glucose electrodes with or without mediators (before optimization of the membrane compositions).

3. Results and discussion

3.1. Comparison of different electrode mediators

Many researchers have studied the effects of electrode mediators on the corresponding electrode performances. Jiang et al. [9] and Becker et al. [10] have studied the mechanisms of decomposition of H_2O_2 catalyzed by cobalt protoporphyrin and a platinum catalyst, respectively. The anion-excluding function of Nafion in a glucose sensor has been realized by Wang and Wu [11] and Mizutani et al. [2]. In the present paper, the authors use TAPtCl and TMPPCo as the electrode mediators, and Nafion as the anion-excluding membrane of glucose sensor, to investigate the relationship between the amperometric response characteristics of the glucose electrodes with and without TAPtCl and TMPPCo. Here we do not discuss the mechanism of the catalytic decomposition of H_2O_2 by TAPtCl and TMPPCo in detail as the functions of TAPtCl and TMPPCo are the same as those reported in Refs.[9,10].

Table 2
Average initial slope of each level for each factor of the electrode in Table 1

Level	TAPtCl	TMPPCo	Enzyme	Nafion
1	0.3630	0.4696	0.4855	0.7194
2	0.4573	0.3630	0.5708	0.3909
3	0.6090	0.5967	0.3730	0.3190

Values are in $\mu A\ cm^{-2}\ mM^{-1}$.

Fig. 2 shows the amperometric responses of several kinds of glucose electrodes. As shown in

Table 3
The electrode membrane compositions of the orthogonal design using the $L_8(2^7)$ table*

Electrode No.	TAPtCl	TMPPCo	Enzyme	Nafion
1′	2	1	1	1
2′	2	1	2	2
3′	2	3	1	2
4′	2	3	2	1
5′	3	1	1	2
6′	3	1	2	1
7′	3	3	1	1
8′	3	3	2	2

[a] Each number in columns 2–5 represents the level of each factor corresponding to Table 1.

Fig. 2, the electrodes with mediators give higher responses than those without mediators. It is further noted that the combination of TAPtCl and TMPPCo in the electrode membrane has the greatest sensitivity. The reason may be that the functions of the mediators have some non-linearity additivity. Furthermore, it seems that the electrode was more stable and sensitive with a sandwich structure membrane as described in Section 2.2. TMPPCo was adopted as the middle layer to separate TAPtCl and GOD because both TAPtCl and GOD are hydrophilic compounds as compared with TMPPCo. In addition, the order of making the membrane layers was very important. The best way is to use TAPtCl as the first layer, TMPPCo as the second layer, GOD as the third layer and Nafion as the last layer (Fig. 1). It is obvious that the proportions of TAPtCl, TMPPCo, GOD, and Nafion in the electrode membrane will strongly affect the performance of the electrodes. Therefore, the optimal proportion of the four components in the electrode membrane will be sought for by a new orthogonal experiment design—sequential level elimination.

Table 4
The average initial slope of each level corresponding to each factor of the electrodes in Table 3

Level	TAPtC	TMPPCo	Enzyme	Nafion
1		1.4541	1.2764	1.7255
2	1.3215		1.2470	0.7978
3	1.2018	1.0692		

Values are in $\mu A\ cm^{-2}\ mM^{-1}$.

3.2. Optimization of the glucose electrode membrane composition

The so called sequential level elimination method, as a new optimization method, [19] was used for optimization of the membrane composition in this study. Firstly, a suitable orthogonal design table, $L_9(3^4)$ was selected in the light of the initial experiments and a priori knowledge. This table is for an experimental design with 4 columns (factors), 3 levels for each factor and 9 experiments altogether. In the context of the present paper 4 factors were chosen: the glucose oxidase, the TAPtCl, the TMPPCo, and the Nafion, each having 3 levels (Table 1). Three levels of 4 factors were decided after a number of initial exploratory experiments. The initial experiments showed that an electrode prepared using too small amounts of GOD, and/or TAPtCl, and/or TMPPCo, and/or Nafion, exhibited a poor amperometric response performance. According to the results of these initial experiments, it appears that taking the values of Table 1 for each level of each factor was reasonable.

The experiment was carried out according to the $L_9(3^4)$ table in Table 1. The amperometric response characteristics of the corresponding electrodes were measured. Several parameters should be considered such as the initial slope (S), the linear dynamic range (L), the detection limit (D), and the and response time (T) in the objective function (F) in order to make it more useful and effective. The objective function (F) may be expressed as follows:

$$F = w_1 S + w_2 L + w_3 \frac{1}{D} + w_4 \frac{1}{T} \quad (1)$$

where w_i ($i = 1,\sim2,\ldots,\sim4$) is the weighting of the ith factor. It should be that the greater the F value, the better the sensor performance. This method, however, will make the optimization process more complicated as it is not easy to assign a

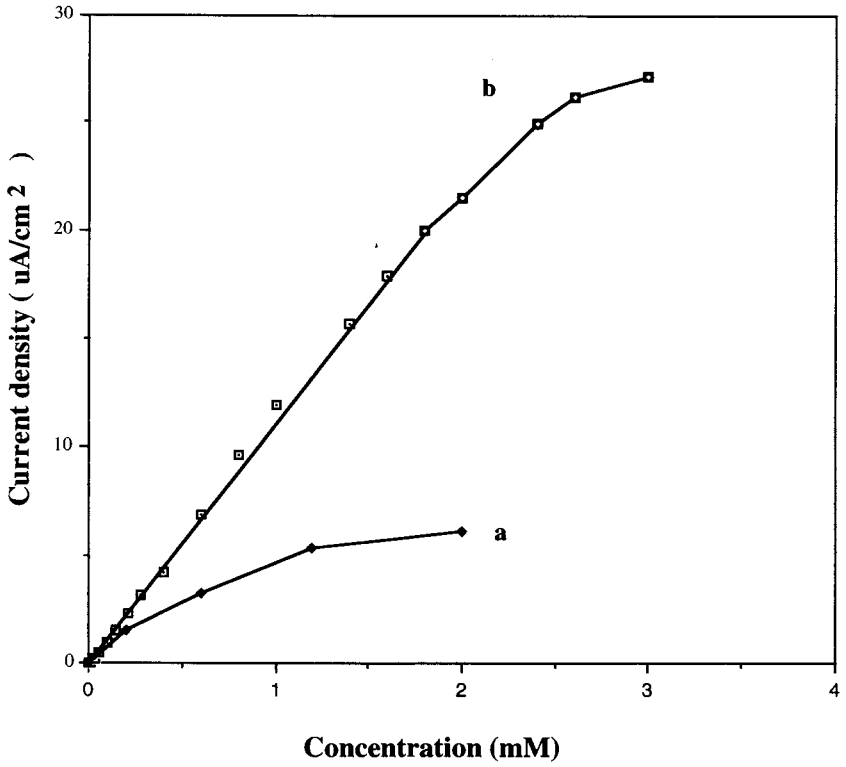

Fig. 3. Calibration curves of the glucose electrodes: (a) the response characteristics of the electrode prior to optimization; (b) the response characteristics of the electrode with the optimal membrane after optimization.

suitable weighting to the each of the above parameter. Some electrodes may exhibit relatively high slopes but relatively narrow linear dynamic ranges while other electrodes may show the opposite. How to select the proper weighting for each parameter is a project to be further studied. The authors noticed that the differences in the response times and the detection limits between different glucose electrodes were not quite large enough in this study. At the same time, they considered that the priority for a wider linear dynamic range comes after that for a larger initial slope for the glucose electrodes. Therefore, the initial slope of the electrode was used as the object function for quantitative optimization and for its simplicity in this study. The average initial slope for each factor at each level was calculated and used as the statistic (Table 2). At this step, the level corresponding to the least initial slope for each factor was eliminated, i.e. the levels 1, 2, 3, and 3 were eliminated for factors TAPtCl, TMPPCo, GOD, and Nafion, respectively. Two levels remained for each factor at this time.

A new orthogonal design $L_8(2^7)$ was selected for the remaining 2 levels of 4 (not 7) factors, the results are shown in Table 3. In fact, one needs to only carry out seven new experiments because experiment No 3 in Table 3 is the same as No. 6 in Table 1. Now, the average initial slope for every factor at each level from Table 3 was calculated and the results are shown in Table 4. Here again the level corresponding to the least initial slope for each factor was eliminated, i.e. the levels 3, 3, 2 and 2 were eliminated for factors TAPtCl, TMPPCo, GOD, and Nafion, respectively.

The best level of factors corresponding to the optimum membrane composition of the electrode in this study were 2, 1, 1 and 1 for TAPtCl, TMPPCo, GOD, and Nafion, respectively, i.e. the optimum membrane composition of the electrode

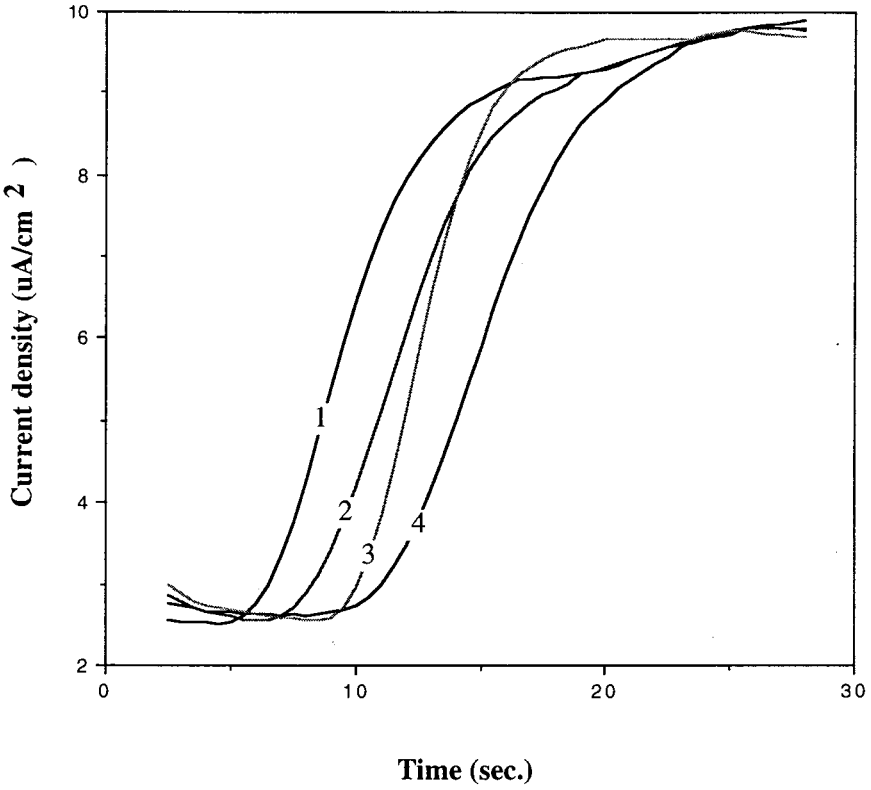

Fig. 4. Repeatability of the glucose sensor. The amperometric response to four independent 0.6 mM glucose additions from fresh phosphate buffer is plotted as a function of time (s).

was: TAPtCl (20 min.), TMPPCo (10 μl), GOD (10 μl), and Nafion (50 μl). The surface density of each component was: TMPPCo (0.04 mg cm^{-2}), GOD (0.5 mg cm^{-2}) and Nafion (0.005 mg cm^{-2}). The authors noted that the amount of Nafion forcefully affected the life time of the glucose sensor. The life time was about several hours without Nafion in the electrode membrane. The amount of TAPtCl could be used for increasing the sensitivity. TMPPCo was specifically useful for improving both the sensitivity and the reproducibility.

3.3. The response characteristics of the glucose sensor

From Fig. 3b, the glucose sensitive electrode prepared according to the optimum membrane composition in the above study shows an amperometric response with a linear response of up to 2 mM with an average initial slope of 10.6 μA cm^{-2} mM^{-1}. The detection limit was about 0.5 μM when the signal to noise ratio was 3. Moreover, the electrode has a relatively good linearity even in quite low glucose concentration measurements. It is vital to perform optimization of the membrane of the glucose electrode to increase both sensitivity and linear range.

3.4. Repeatability of the glucose sensor

As shown in Fig. 4, the prepared sensor displayed good repeatability for four repetitive measurements of 0.6 mM glucose additions from phosphate buffer (pH 7), with a RSD of 2.66%. The response time of the glucose electrode which reached 90% maximal current density during the measurements was about 6 s. Therefore, the response of the electrode was very fast.

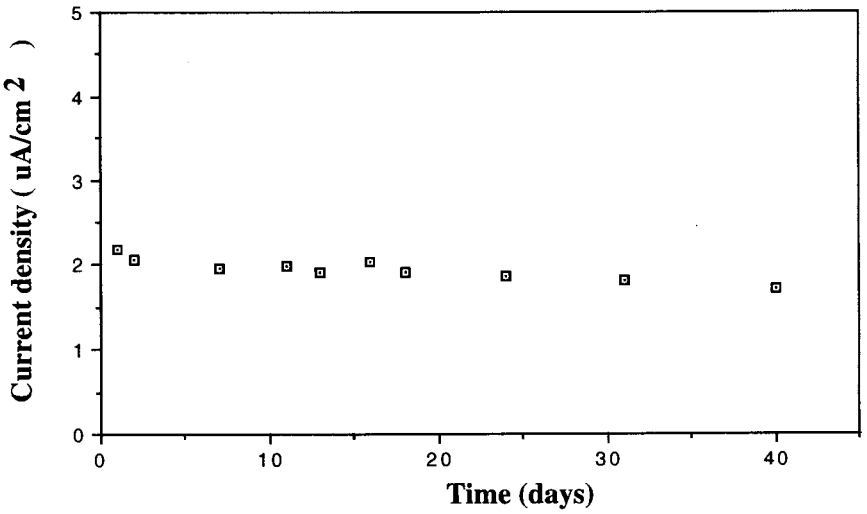

Fig. 5. A long-term stability test of the glucose electrode. The amperometric response to 0.2 mM glucose is plotted as a function of time (days).

3.5. Stability of the glucose sensor

The glucose sensor was stored by keeping it in phosphate buffer (pH 7) which was placed in a refrigerator at a temperature of 4°C when not in use. The long-term stability of the sensor was checked by detecting the current response of 0.2 mM glucose within certain time intervals. The result of the long-term stability of the sensor is shown in Fig. 5 which shows that the glucose electrode could be continuously used for at least 40 days without obvious loss of activity. Further investigations will be carried out to improve the life time of the glucose sensors.

3.6. Recovery of the sensor

The prepared glucose electrode was used to determine glucose using the calibration curve in Fig. 3. The results are listed in Table 5. The recovery was from 91.9–111.2%. This shows that the prepared electrode can be used for the determination of glucose.

4. Conclusion

The results obtained from the experiments described above demonstrate a simple, rapid, and sensitive approach for preparation of a glucose biosensor including immobilization of TAPtCl, TMPPCo, glucose oxidase, and Nafion. The new experimental design technique, i.e. the sequential level elimination method, is very useful for finding the optimal membrane composition. Therefore, it can be utilized for optimization of other electrode membranes. The prepared sensor displayed good performances in regard to sensitivity, reproduci-

Table 5
Recovery of the glucose sensor with the optimal membrane composition

No.	1	2	3	4	5	6	7	8
Added (mM)	0.100	0.400	0.600	0.800	1.000	1.40	1.80	2.00
Found (mM)	0.0919	0.4048	0.6161	0.798	1.1125	1.4575	1.8711	2.0155
Recovery (%)	91.9	101.2	102.7	99.8	111.2	104.1	104.0	100.8

bility, good recovery, and a long life time. Further studies on using similar electrode membrane configurations and experimental design methods is under way in our laboratory and will be reported when completed.

Acknowledgements

LXS would like to thank the AIST fellowship for their support for a research visit to NIMC.

References

[1] H. Liu, J. Qian, Y. Liu, T. Yu, J. Deng, Bioelectrochem. Bioenerg. 39 (1996) 303.
[2] F. Mizutani, S. Yabuki, T. Katsura, Amperometric glucose-sensing electrodes with the use of modified enzyme, in: A.M. Usmani, N. Akmal (Ed.), Diagnostic Biosensor Polymers, ACS Symposium Series 556, Maple Press, York, PA, 1994, pp. 41– 46.
[3] D.J. Harrison, R.F.B. Turner, H.P. Baltes, Anal. Chem. 60 (1988) 2002.
[4] R. Rajagopalan, A. Aoki, A. Heller, J. Phys. Chem. 100 (1996) 3719.
[5] G.F. Khan, W. Wernet, J. Electrochem. Soc. 143 (1996) 3336.
[6] S.D. Kumar, A.V. Kulkarni, R. Kalyanraman, T.S. Krishnamoorthy, Anal. Chim. Acta 338 (1997) 135.
[7] P.N. Bartlett, S. Booth, D.J. Caruana, J.D. Kilburn, C. Santamaria, Anal. Chem. 69 (1997) 734.
[8] M.C. Shin, H.S. Kim, Anal. Lett. 28 (1995) 1017.
[9] R. Dong, S. Jiang, J. Electroanal. Chem. 291 (1990) 11.
[10] A. Becker, J. Schilm, M. Sell, Ger. Offen. DE 19507678 A1, 1996.
[11] J. Wang, H. Wu, J. Electroanal. Chem. 395 (1995) 287.
[12] L.X. Sun, K. Danzer, J. Chemom. 10 (1996) 325.
[13] L.X. Sun, K. Danzer, G. Teiel, Fresenius' Anal. Chem. 359 (1997) 143.
[14] S.D. Brown, R.S. Bear Jr., CRC Crit. Rev. Anal. Chem. 24 (1993) 99.
[15] W.P. Carey, K.R. Beebe, B.R. Kowalski, Anal. Chem. 59 (1987) 1529.
[16] L.X. Sun, Y.C. Li, R.Q. Yu, Chem. J. Chin. Univ. 14 (1993) 1363.
[17] J. Goupy, Chemom. Intell. Lab. Syst. 35 (1996) 145.
[18] Y.L. Xie, R.Q. Yu, PhD Thesis, Hunan University, China, 1992.
[19] S.S. Mao, F.S. Ma, J.F. Wu, Appl. Probab. Stat. 6 (1990) 185.
[20] J. Wang, P. Tuzhi, Anal. Chem. 58 (1986) 1787.
[21] S. Röösli, E. Pretsch, W.E. Morf, E. Tsuchida, H. Nishide, Anal. Chim. Acta 338 (1997) 119.

ELSEVIER

Talanta 47 (1998) 1175–1189

Talanta

Protonation constant of monoaza-12-crown-4 ether and stability constants with selected metal ions in aqueous solution in the presence of an excess of sodium ion: a potentiometric and differential pulse polarographic study at fixed ligand to metal ratio and varied pH

Ewa Cukrowska [a], Ignacy Cukrowski [b,*]

[a] *Department of Chemistry and Biochemistry, Medical University of Southern Africa, MEDUNSA 0204, Box 235, Pretoria, South Africa*

[b] *Department of Chemistry, University of the Witwatersrand, Private Bag 3, WITS 205O, Johannesburg, South Africa*

Received 10 July 1997; received in revised form 18 December 1997; accepted 14 May 1998

Abstract

The ligand monoaza-12-crown-4 ether (A12C4) was studied in aqueous solution at 298 K and an ionic strength of 0.5 mol dm^{-3} in the presence of an excess of sodium ion (0.5 mol dm^{-3} $NaNO_3$). The protonation constant of A12C4, determined by glass electrode potentiometry (GEP) in the same background electrolyte, was found to be $\log K = 9.36 \pm 0.03$. Polarographic experimental and calculated complex formation curves (ECFC and CCFC) for labile metal–ligand systems, studied at a fixed total ligand (L_T) to total metal (M_T) concentration ratio and varied pH, were used for the modelling of the metal species formed and the refinement of their stability constants. The metal–ligand model and formation constants are optimised by solving mass-balance equations written for the assumed model and by fitting the CCFC to the ECFC. The CCFC can be generated for any metal–ligand model, including polynuclear metal species, for any L_T:M_T ratio, and for more than one ligand competing in the complex formation reaction. Three lead complexes with the ligand A12C4, viz. PbL^{2+}, $PbL(OH)^{+}$ and $PbL(OH)_2$, were found and their overall stability constants from differential pulse polarography (DPP), as $\log \beta$, were estimated to be 3.75 ± 0.03, 9.30 ± 0.05 and 12.70 ± 0.05, respectively. Two copper complexes CuL^{2+} and $CuL(OH)_2$ are reported and their stability constants (from DPP) were estimated to be 6.00 ± 0.05 and 21.77 ± 0.1, respectively. Two cadmium complexes CdL^{2+} and $CdL(OH)^{+}$ are reported. The stability constant for CdL^{2+} was estimated from DPP and GEP as 2.80 ± 0.05 and 2.68 ± 0.03 (the latter value was obtained from a few potentiometric experimental points), respectively, and the stability constant for $CdL(OH)^{+}$ from DPP was estimated to be 7.88 ± 0.05. GEP could not be used for the stability constants determination of other metal complexes studied because of precipitation occurring prior the completion of a complex formation reaction. © 1998 Elsevier Science B.V. All rights reserved.

Keywords: Differential pulse polarography; Speciation; Complex formation curves

* Corresponding author. Tel.: +27 11 7162119; fax: +27 11 3397967; e-mail: IGNACY@AURUM.CHEM.WITS.AC.ZA

0039-9140/98/$ - see front matter © 1998 Elsevier Science B.V. All rights reserved.
PII S0039-9140(98)00203-3

1. Introduction

The ligands aza-crowns, crown ethers and cryptands have become of interest recently [1,2] because of their numerous applications in the selective removal and concentration of metal ions [3]. A huge amount of data has been collected for these ligands [2,3] but relatively few are regarded as stability constants which meet the criteria required for incorporation in the compilation by Martell and Smith [4]. In addition, there is very little known about the binding power of the ligand monoaza 12-crown-4 ether (A12C4) [2,4]. For example, in the recent review by Izatt et al. [2] only stability constants for Na^+ in anhydrous MeOH or MeOH:H_2O (95:5 v/v) are reported.

The Lingane [5] and DeFord and Hume [6] techniques of speciation are possibly the most frequently used in speciation studies by polarography. It has been shown that the classic expression derived by DeFord and Hume can be used after simple modification for the determination of stability constants of complex metal ions by a.c. [7,8] or differential pulse [9] polarography. However, the original DeFord and Hume equation as well as its modifications were, more often than not, used by applying the same analytical procedure (measurements performed at fixed pH) and mathematical model of the calculations [6–9] as introduced by DeFord and Hume [6]. Differential pulse polarography (DPP) was recently found to be a very useful tool in the field of ligand design strategies [10–14]. A speciation study by DPP, where the experiment was performed at a fixed total ligand (L_T) to total metal (M_T) concentration ratio and varied pH, was found particularly advantages [10–20] in studying complex formation reactions with heavy post-transition metal ions such as Pb^{II}, Cd^{II} and Bi^{III}. DPP was recommended for the study of relatively strong complexes of very acidic metal ions such as Bi^{III} [10–12] and relatively weak complexes of metal ions, such as Pb^{II} [13,17,18]. The former one has to be studied at extremely low pH and both these metal ions often require a large L_T:M_T ratio and a low total metal ion concentration to suppress metal ion hydrolysis. This is why it is often impossible [21] to employ a classic approach [5,6] based on the measurements performed at fixed pH and varied L_T:M_T ratio. Moreover, when metal complexes with ligands H_nL (ligands with ionizable hydrogens) are of interest, as is the case in the ligand design strategies, then one can expect simultaneous formation of several, and often protonated, metal complexes at a particular pH. Some of the metal complexes might be minor metal species shadowed by the presence of other metal species. In addition, the contribution of different species to the overall composition of the solution vary dramatically with the change in pH. In such a case, recently derived equations [22–25] do not seem to be suitable either.

Recently, experimental and calculated polarographic complex formation curves have been defined [17,18], used for the prediction of a metal–ligand model and the refinement of stability constants for metal complexes studied with protonated ligands at a fixed L_T:M_T ratio and varied pH [17–20]. The corrected shift in the peak potential was used [17–20], instead of the experimentally observed one [5–9], for generating the experimental complex formation curve (ECFC). The calculated complex formation curve (CCFC) was obtained from mass-balance equations written for the assumed metal–ligand model and solved for the free metal ion concentration. The refinement process was based on a curve fitting procedure. The way in which one could come up with a reasonable model of species and initial guesses for their stability constants was also proposed. This new approach to speciation study by polarography was successfully applied for metal–ligand systems where relatively strong [19,20] as well as weak metal complexes [17,18] were formed. Where possible, glass electrode potentiometry (GEP) (this technique produced over 80% [26] of all stability constants reported in the literature [4]) was used to verify polarographic results. The aim of this study was to investigate the binding power of the ligand A12C4 in aqueous solutions in the presence of an excess of sodium ion by use of a newly developed polarographic speciation technique. Where possible, potentiometric investigation was also used to support the polarographic results.

2. Experimental

2.1. Instrumentation

All experiments were performed in a Metrohm jacketed glass purlvessel, equipped with a magnetic stirrer, and thermostatted at 298 K by water circulating from a constant temperature bath. The pH of solutions was measured to ± 0.1 mV ($\pm$ 0.001 pH unit) with a pHI 72 pH meter and combination glass electrode (cat. no. 39536) (both Beckman). Differential pulse polarograms were obtained with the use of a computer controlled instrumental setup [12] and a model 663 VA stand (Metrohm). A multi mode electrode (Metrohm, cat. no. 6.1246.020) was employed as the working electrode and used in the dropping mercury electrode mode with a drop time of 2 s. A silver/silver chloride electrode and a platinum electrode (both Metrohm) were used as reference and auxiliary electrodes, respectively. A pulse height of 50 mV and step height of 4 mV were used. Pulse width and integration time were set to 200 and 60 ms, respectively. High purity nitrogen was used for deaeration of the sample solutions.

2.2. Materials

The ligand A12C4 was obtained from Aldrich and used as received. All other reagents used were of analytical grade (Merck). Pure water was obtained by passing deionised water through a Milli-Q-water purification system. The metal nitrate stock solutions, about 1×10^{-2} mol dm^{-3}, were prepared in 1×10^{-2} mol dm^{-3} nitric acid.

2.3. Procedure

2.3.1. Polarography

In a typical run, the first polarogram was recorded for a solution containing about 5×10^{-5} mol dm^{-3} of metal ion in 0.45 mol dm^{-3} $NaNO_3$ + 0.05 mol dm^{-3} HNO_3. Several different L_T:M_T ratios were used and were prepared by addition of the appropriate amount of the solid ligand A12C4 to the vessel containing a metal ion solution. After recording a polarogram, the pH of the solution was increased in steps of about 0.100–0.150 pH units, by addition of a standard NaOH solution from a microburette graduated to 0.01 ml, and after each addition a new polarogram was recorded. In this way a set of between 30 and 40 polarograms was obtained for each L_T:M_T ratio as a function of pH. Polarograms of the ligand alone as a function of pH were also run in a similar way. The ligand appeared to be polarographically inactive. It has been checked that equilibration of the metal–ligand solutions occurred within a few minutes. All polarograms were recorded on solutions adjusted to $\mu = 0.5$ mol dm^{-3}.

2.3.2. Potentiometry

To establish the protonation constant of the ligand A12C4 two titrations were performed. The first titration involved addition of 0.0820 mol dm^{-3} NaOH in 0.4205 mol dm^{-3} $NaNO_3$ to the cell containing 0.0530 mol dm^{-3} HNO_3 in 0.445 mol dm^{-3} $NaNO_3$, from which the E° and response slope of the glass electrode was calculated. Next, a titration of a solution containing the ligand (at about 0.015 mol dm^{-3}) was performed. The potential of the cell was measured to within ± 0.1 mV for each addition of the titrant. The ionic strength was maintained at 0.5 mol dm^{-3}. To establish the stability constants of metal ions with the ligand a similar procedure was employed to establish the E° and response slope of the glass electrode before each titration of a solution containing a metal ion and a ligand. The metal ion concentrations were kept as low as possible, to delay precipitation of metal hydroxides. In a typical run, the metal ion concentration was about 1×10^{-3} mol dm^{-3} (or slightly lower) and a ligand to metal ratio of about 1.3:1.

2.3.3. Treatment of polarographic data

It has been demonstrated [17–20] that labile metal–ligand equilibria, when the polarographic experiment is performed at a fixed L_T:M_T ratio and varied pH, can be related to experimentally available data by the following equation provided that a single and well shaped DPP peak is observed:

$$\Delta E_p(i) - \frac{RT}{nF} \ln \frac{I_p(M_{Comp})(i)}{I_p(M_{Free})(i)} = \frac{RT}{nF} \ln \frac{[M_T](i)}{[M_{Free}](i)}. \quad (1)$$

In Eq. (1) $\Delta E_p(i)$ represents a shift in a peak potential observed from the DPP experiment at each ith pH(i) value to which the metal–ligand system was adjusted in a polarographic cell, $[M_T](i)$ and $[M_{Free}](i)$ stand for the total and free metal ion concentration, respectively, at each ith pH(i) value, $I_p(M_{Comp})(i)$ is the height of the DPP peak recorded at an ith pH(i) value and represents all labile metal species in a solution, $I_p(M_{Free})(i)$ is a calculated DPP peak height of the metal ion M(aq) one would observe at an ith pH(i) value with an assumption that complexes of the metal M were not formed.

Eq. (1) was tested on metal–ligand systems where weak cadmium [17] and lead [18] complexes were formed with a ligand *N*,*N*,*N*′*N*′-tetramethylethylenediamine (TMen). The results obtained from DPP [17,18] could not be verified by GEP because precipitation of metal hydroxide species occurred prior to the complex formation reaction with TMen under the conditions of a potentiometric experiment. However, the use of Eq. (1) has been verified successfully by GEP on metal ligand systems where strong and labile Pb^{II} [19] and Cd^{II} [20] complexes were formed with a ligand *N*,*N*′ - bis(2 - pyridylmethyl) - 1,2 - diaminoethane (DPA-2). Modelling of the species formed and optimisation of the stability constants was achieved by the use of polarographic experimental and calculated complex formation curves [18]. The ECFC is simply the left hand side of Eq. (1) when plotted versus pH:

$$\Delta E_p(i) - \frac{RT}{nF} \ln \frac{I_p(M_{Comp})(i)}{I_p(M_{Free})(i)} = f(\text{pH}). \quad (2)$$

It is called the experimental complex formation curve because all the terms in Eq. (2) are available from polarographic experiment. The CCFC is obtained by varying the metal–ligand species formed (modelling of a metal–ligand system) and optimisation of their stability constants in such a way that the calculated corrected shift in the peak potential best fits the experimental corrected shift. The CCFC is obtained when the right-hand side of Eq. (1) is plotted versus pH:

$$\frac{RT}{nF} \ln \frac{[M_T](i)}{[M_{Free}](i)} = f(\text{pH}). \quad (3)$$

It is important to note that each DPP peak represents all labile metal species present in a solution. All metal complexes are assumed to be polarographically active. The written representation of the reduction process is normally given in the following form [27]:

$$\{M^{n+} \Leftrightarrow ML \Leftrightarrow ML_2 \Leftrightarrow \cdots \Leftrightarrow ML_j\} \Leftrightarrow M(Hg);$$

$$(E^\circ, n).$$

The above notation is used to emphasise the fact that, for reversible reductions, it is impossible to determine which of the species actually reacts with the electrode in the electron transfer process [27] (this assumption is opposite to that made in recently developed speciation techniques by polarography [22–25]). This implies that the free metal ion concentration $[M_{Free}](i)$ at any pH, where metal complexes are formed, is not directly available from the DPP experiment. However, it can be calculated from the mass-balance equations written for the assumed metal–ligand model. In this model all known metal complexes, such as $M_x(OH)_y$, and all metal–ligand complexes thought to be present in the solution must be incorporated. For each datum point, obtained at each ith pH(i) value to which the metal–ligand system was adjusted in a polarographic cell by the addition of a standard hydroxide solution, the total metal ion $M_T(i)$ and total ligand $L_T(i)$ concentrations are known. By the use of the appropriate mass-balance equations:

$$[M_T](i) = [M_{Free}](i) + \sum\sum x[M_xL_yH_z](i) \quad (4)$$

$$[L_T](i) = [L_{Free}](i) + \sum\sum y[M_xL_yH_z](i) \quad (5)$$

solved simultaneously for each datum point for the assumed metal–ligand model one can obtain the free metal ion concentration $[M_{Free}](i)$ used further by Eq. (3) to generate the CCFC. The known constants (for example for all known $M_x(OH)_y$ complexes) are kept fixed during the solution of the mass-balance equations. The metal–ligand model and the calculated stability constants are varied until the CCFC best fits the

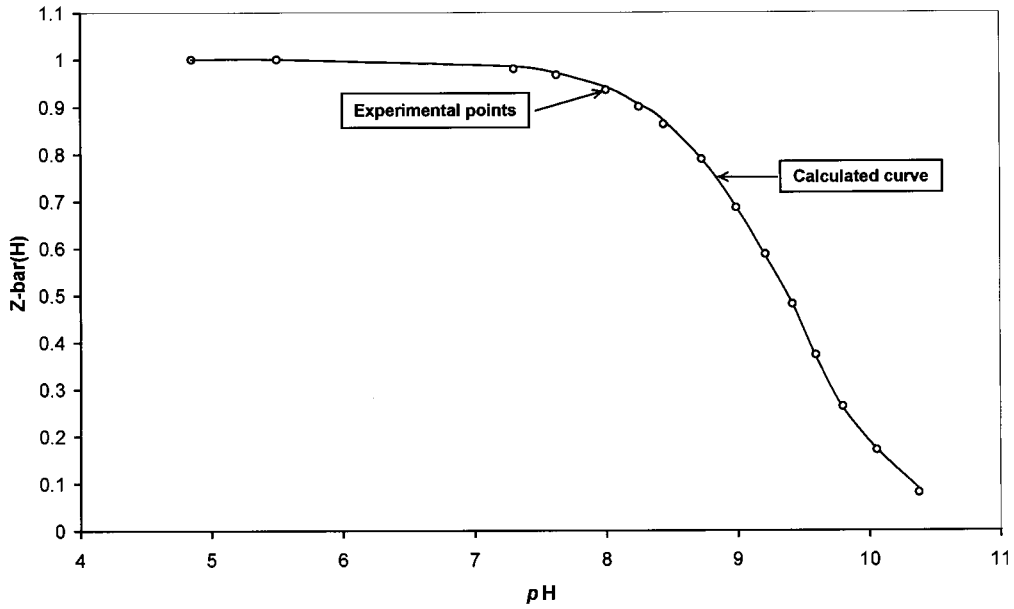

Fig. 1. Experimental (○) and theoretical (solid line) protonation curves for the protonation of the ligand A12C4 in a background of 0.5 mol dm^{-3} $NaNO_3$.

ECFC for the metal–ligand system studied at a particular L_T:M_T ratio. Note that the CCFC may be calculated for any metal–ligand model, including polynuclear metal complexes with a ligand or competing polynuclear hydroxy metal species.

3. Results and discussion

3.1. Potentiometric study

The protonation of the ligand A12C4 (L) was studied by GEP carried out using a cell containing a glass indicating electrode calibrated for measurements of hydrogen ion concentration (see Section 2). A solution of A12C4, which was initially acidic and made up in a background of 0.45 mol dm^{-3} $NaNO_3$ ($L_T = 1.495 \times 10^{-2}$ mol dm^{-3}; $H_T = 0.0508$ mol dm^{-3}), was titrated with NaOH, also made up in a background of $NaNO_3$ ($OH_T = 8.20 \times 10^{-2}$ mol dm^{-3}). Values of the protonation function, Z-bar(H), defined [28] as:

$$Z - \text{bar(H)} = \frac{H_T - [H] + [OH]}{L_T} \quad (6)$$

were calculated for each datum point and are plotted (○) versus observed values of $p[H] = -\log_{10}[H]$ in Fig. 1.

The protonation function can be interpreted as the average number of protons coordinated per ligand molecule. It is clear that the ligand accepts, as expected, one proton, is virtually completely protonated at pH below 7.5 and is completely deprotonated at pH values above about 11. The program ESTA [29] was used to calculate the protonation constant of A12C4. In this calculation no account was taken of the fact that the ligand forms a complex with the sodium ion. The stability constants for the complex formation reaction of Na^+ with A12C4 have been reported [2] in non-aqueous media ($\log K_1 \approx 2$). In addition, it has been observed that stability constants of crown ethers and aza-crowns are smaller in aqueous than in anhydrous solutions by 2–3 log units [3]. Based on this information we have concluded that the value of $\log K_1$ for Na^+ with the ligand A12C4 must be fairly low, most likely less than 1. Because of that the protonation constant of the ligand A12C4 ($\log K = 9.36 \pm 0.03$, see Table 1) obtained in the presence of Na^+ has

been used for further calculations without any correction. When the stability constant of Na^+ with a ligand aza-crown or cryptand is relatively large then the appropriate correction has to be made [15].

It is well known that GEP works well provided that metal complexes are formed in the pH range between 2 and 10 and when one can work with a metal ion concentration of about 1×10^{-3} mol dm^{-3} and above. This requirement made it impossible to collect reliable data for all metal ions studied in this study because precipitates were observed prior the completion of a complex formation reaction with the ligand A12C4. Only in the case of Cd^{II} it was possible to collect a few experimental points ($M_T = 9.434 \times 10^{-4}$ mol dm^{-3}; $L_T = 1.148 \times 10^{-3}$ mol dm^{-3}) prior to precipitation. The stability constant for the complex CdL^{2+} obtained from GEP and calculated by the program ESTA [29] is included in Table 3.

3.2. Polarographic study

3.2.1. Reversibility, evaluation of E_p and I_p

The shift in the peak potential in Eq. (1) is assumed to be caused by the fully reversible reduction of complexed metal species. Since the experiment was performed over the full pH range and the formation of hydroxy metal species was also expected to occur, it was important to examine the DPP peaks recorded at different pH values. In Fig. 2 a set of selected DPP peaks are seen which were obtained for the Pb–A12C4 system studied at $L_T:M_T = 250$. These peaks are not plotted along the real potential scale to facilitate the discussion that follows but they are seen as recorded at the indicated pH values to which the solution sample was adjusted by the addition of a standard NaOH solution. The full analysis of peaks recorded at pH 3.807 and 11.360 is also indicated in Fig. 2.

The empty circles (Fig. 2D) represent the experimentally recorded differential current at a particular value of an applied step potential. The equation describing a gaussian curve was modified to the following form:

$$I_r = I_p \exp\{-(E_{Appl} - E_p)^2/[2 \times (w_{1/2}/2.345)^2]\} \quad (7)$$

where I_r stands for the reduction current of electrochemically active species, E_{Appl} stands for the applied step potential at which a single measurement of differential current is performed, and I_p, E_p and $w_{1/2}$ have the usual meaning in a DPP experiment. The background current I_b was approximated by the use of a linear equation

$$I_b = aE_{Appl} + b \quad (8)$$

and the overall and recorded differential current was calculated by the addition of I_r and I_b. In this way all the DPP peaks for all the metal ions studied were analysed and from that the values of E_p and I_p (used further in Eq. (2) for the calculation of the ECFC) and $w_{1/2}$ were estimated. Curves A, B and C seen in Fig. 2 represent the calculated I_r (from Eq. (7)), I_b (from Eq. (8)) and the overall current ($I_r + I_b$), respectively. The values of I_p, E_p and $w_{1/2}$ for the DPP peaks recorded at pH 3.807 and 11.360 were estimated to be 3.253 ± 0.009 and 1.864 ± 0.009 (arbitrary units), -320.98 ± 0.08 and $-0.482.61 \pm 0.10$ mV, and 61.0 ± 0.1 and 64.4 ± 0.4 mV, respectively. The estimated standard deviation of the overall fit of the calculated into the observed DPP peaks was 2.28×10^{-2} and 2.34×10^{-2} for the above DPP peaks, respectively. For all other DPP peaks, the values of $w_{1/2}$ were in the range of about 63.0 ± 1

Table 1
Dissociation constant for water and the overall stability constants for lead^{II} complexes with OH^- from Ref. [4]

Equilibrium	Log β
$H^+ + OH^- \Leftrightarrow H_2O$	13.74
$Pb^{2+} + OH^- \Leftrightarrow Pb(OH)^+$	6.0
$Pb^{2+} + 2OH^- \Leftrightarrow Pb(OH)_2$	10.3
$Pb^{2+} + 3OH^- \Leftrightarrow Pb(OH)_3^-$	13.3
$2Pb^{2+} + OH^- \Leftrightarrow Pb_2(OH)^{3+}$	7.6[a]
$3Pb^{2+} + 4OH^- \Leftrightarrow Pb_3(OH)_4^{2+}$	31.7
$4Pb^{2+} + 4OH^- \Leftrightarrow Pb_4(OH)_4^{4+}$	35.2
$6Pb^{2+} + 8OH^- \Leftrightarrow Pb_6(OH)_8^{4+}$	67.4
$L + H^+ \Leftrightarrow HL^+$	9.36 ± 0.03

The protonation constant for the ligand A12C4 was determined in this study. All log β values are reported at 298 K and an ionic strength of 0.5 mol dm^{-3}, if not indicated otherwise.
[a] At an ionic strength of 0.0 mol dm^{-3}.

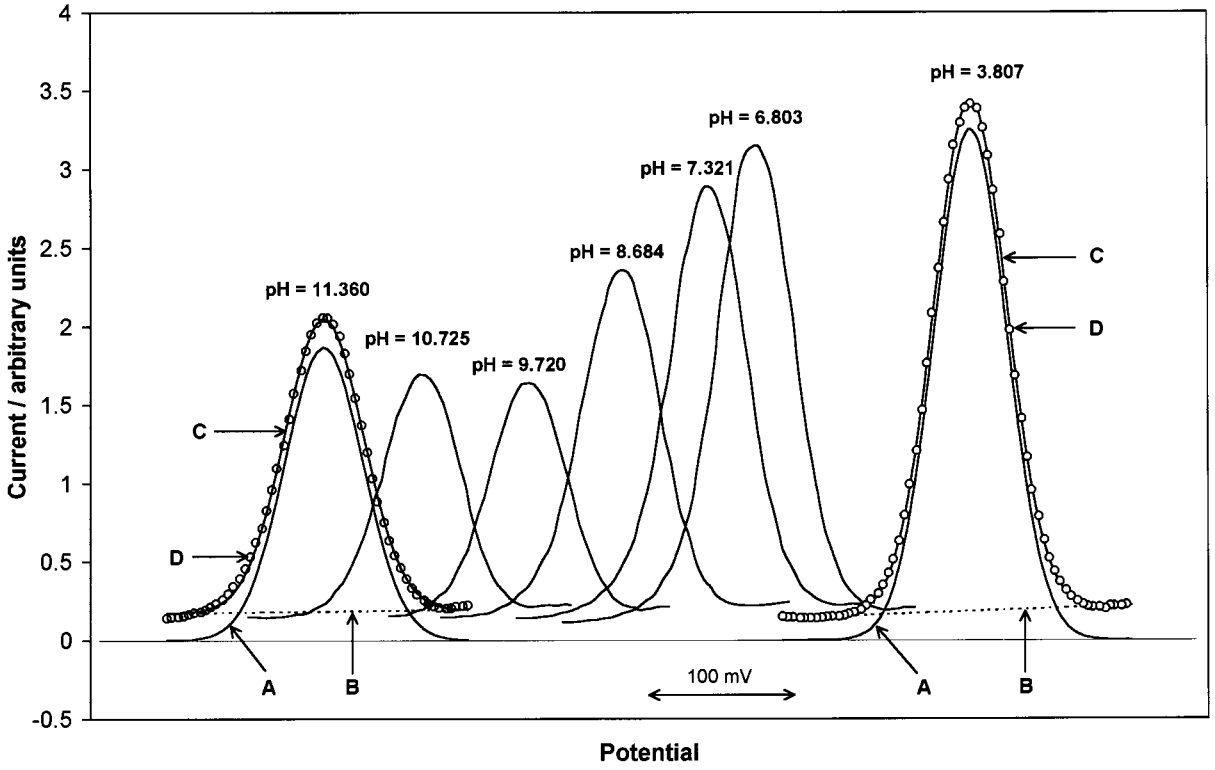

Fig. 2. A set of selected DPP peaks of the Pb–A12C4–OH system recorded at 298 K in a single solution containing initially 4.959×10^{-5} mol dm^{-3} Pb^{2+}. L_T:$M_T = 250$. A, the calculated peak from Eq. (7); B, the calculated background current from Eq. (8); C, the calculated overall DPP current; D, the experimental points obtained at a particular value of the step potential.

mV. It is well known that the reversibility of a DPP peak is most conveniently assessed by its half peak width $w_{1/2}$. Parry and Osteryoung [30] have derived a general expression for the half peak width of a DPP peak which predicts a value of 62 mV for a fully reversible two-electron reduction with an applied pulse of 50 mV (as is the case in this study). From the above calculated values one can conclude that the Pb–A12C4 system shows a high degree of reversibility. The above analysis of the DPP peaks can also be used as a successful test of the computer controlled instrumental setup [12] built in our laboratory and employed in this study.

3.2.2. Modelling of the metal species formed

DPP can work well at a relatively low total metal ion concentration and a high L_T:M_T concentration ratio. This often allows us to avoid precipitation at all or makes it possible to collect enough experimental data to estimate the stability constants for at least one ML complex. It is obvious that one can expect simultaneous formation of several metal species including, in particular, hydroxy metal species when relatively weak metal complexes are expected to form. In such a case Eq. (1) proved [17–20] to be a reliable method for polarographic data evaluation for labile metal complexes.

The use of Eq. (1), in the form of polarographic complex formation curves from Eqs. (2) and (3), is a curve fitting procedure which requires two good guesses, namely the number of metal species formed over the whole pH range studied and trial values for their stability constants. It has been shown [17–20] that three relationships can be of great help in the prediction of the metal species formed, viz. $\Delta E_p(i)$ or $E_p(i)$ plotted versus pH,

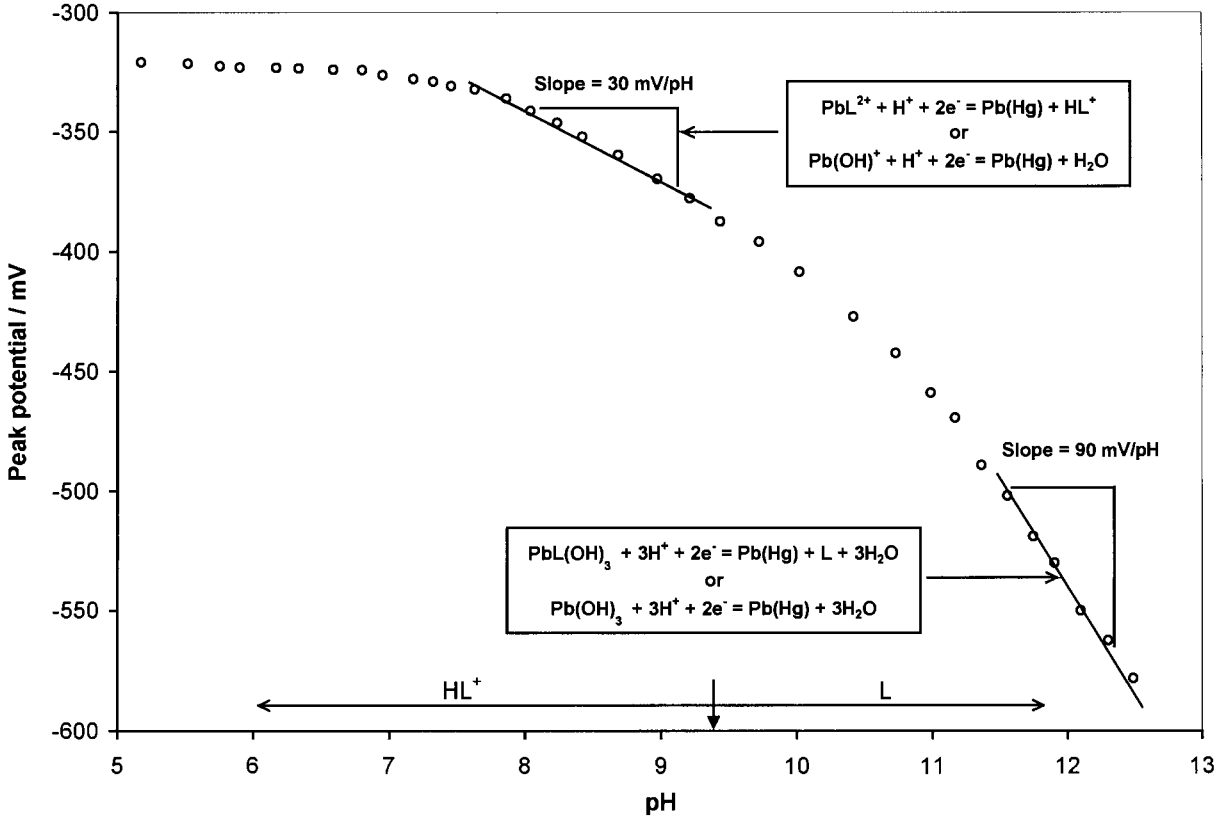

Fig. 3. The observed DPP peak potential for the Pb–A12C4–OH system plotted vs. pH. All polarograms were recorded in one solution sample, at 298 K and an ionic strength of 0.5 mol dm^{-3}, containing initially 4.959×10^{-5} mol dm^{-3} Pb^{2+} and a L_T:M_T ratio of 250, adjusted to a particular pH to give the data points indicated by (○). The vertical arrow indicates the protonation constant of the ligand.

$\Delta E_p(i)$ or $E_p(i)$ plotted versus $\log[L_{Free}]$ and $I_p(M_{Comp})(i)/I_p(M_{Free})(i)$ plotted versus pH. Usually, the first relationship appeared to be the most informative from which one could conclude the major metal species formed and suggest minor metal species for further consideration. As an example, a shift in the peak potential versus pH for the Pb–L system studied at a L_T:M_T ratio of 250 is seen in Fig. 3. The experimental points are indicated by circles. The protonation constant for the ligand A12C4 (an arrow at pH = 9.36) and the regions in which particular forms of the ligand L are the predominant ligand species are also marked in Fig. 3.

For metal–ligand systems where there is a pH range over which one metal species is a major metal complex one can identify a particular and constant slope. From the value of this slope it is possible to predict the number of protons involved in the electrochemical reaction and, further, the kind of metal complex formed [13]. Unfortunately, for all metal ions studied the relationships, such as that seen in Fig. 3 and plotted for the Pb–L–OH system, appeared to be of little use since a continuous variation in the peak potential was observed. However, several important conclusions can be drawn. A significant shift was observed only above pH 7. At this pH a shift caused by the formation of $Pb(OH)^+$ is also expected. This observation clearly indicates that if a lead complex ML is formed then it must be a weak complex which can hardly compete with the formation of $Pb(OH)^+$ (see Fig. 3—the slope of about 30 mV per pH and two electrochemical

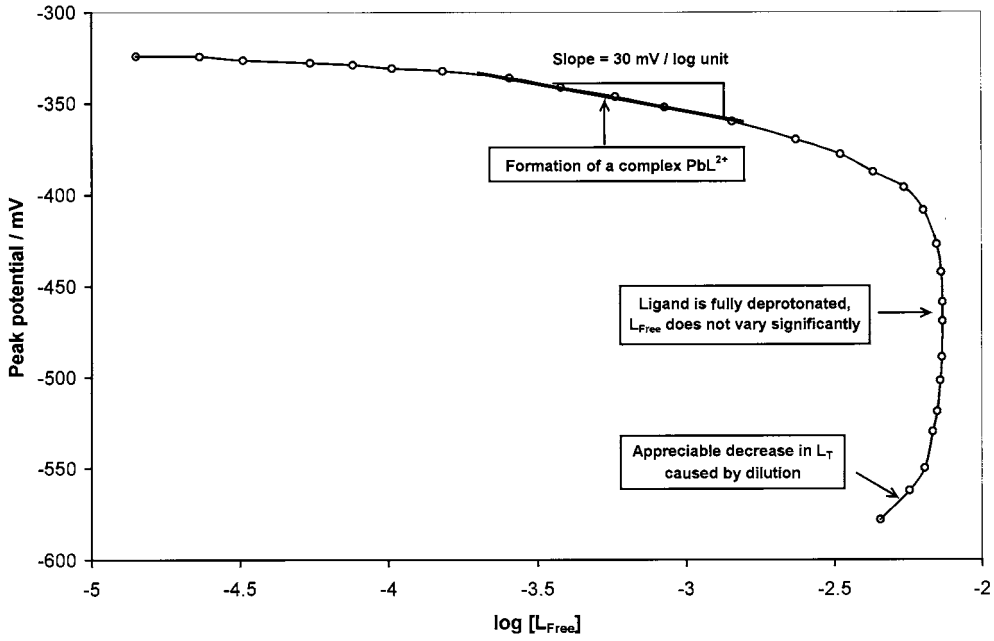

Fig. 4. The observed DPP peak potential for the Pb–A12C4–OH system plotted vs. log $[L_{Free}]$. Experimental parameters as in Fig. 3.

processes to be considered in which one proton per electrochemical reaction is involved). The observed shift in the peak potential approaches a value of about 90 mV per pH which indicates the involvement of three protons per electrochemical process. This observation supports the formation of either $PbL(OH)_3^-$ or $Pb(OH)_3^-$ at the highest pH studied (see the electrochemical processes in Fig. 3). From the above, it is clear that the lead species $ML(OH)_n$ (where n varies from 0 to 3) and $M_x(OH)_y$ (all known lead hydroxy species) have to be included in the initial M–L–OH model. None of these species can be considered, at this stage, as a major metal species.

The shift in the peak potential plotted versus the free ligand concentration is seen in Fig. 4. There is a narrow range where the slope of about 30 mV per log unit, expected for the formation of the ML complex, is observed. It occurs just prior to the pH range where the ligand is fully deprotonated and its concentration does not vary significantly—see the vertical part of the relationship in Fig. 4. A 'back-fanning' feature seen in Fig. 4 at higher values of $-\log [L_{Free}]$ occurs over the pH range where the ligand is fully deprotonated and is related to an appreciable decrease in L_T caused by the dilution of the sample studied by the addition of a standard hydroxide solution. One has to remember that, under the experimental conditions employed in this study, the shift in the peak potential versus $\log [L_{Free}]$ provides valuable information only about the formation of ML_n complexes and if they are formed over the pH range where the protonated forms of the ligand are still present. Here, the observed shift of about 30 mV per log unit supports the formation of the complex ML. It is quite clear, from the above, that a full M–L–OH model can only be obtained by the use of the polarographic complex formation curves for labile metal–ligand systems [17–20].

3.2.3. Trial values of stability constants

It has been shown that the Lingane equation in its modified form [12,13,15]:

$$\Delta E_p(i) - \frac{RT}{nF}\ln\frac{I_p(M_{Comp})(i)}{I_p(M_{Free})(i)} = \frac{RT}{nF}\ln\beta_{ML_j(OH)_b} + j\frac{RT}{nF}\ln[L_{Free}](i) + b\frac{RT}{nF}\ln[OH](i) \quad (9)$$

(which allows for the calculation of the stability constants for $ML_n(OH)_m$ complexes from data obtained under the experimental conditions applied in this study) generates reasonable values for the calculated formation constants provided that the particular complex is the predominant metal species in the solution for the particular pH region considered. Eq. (9) was also used for the calculation of the protonated species [13] when [OH] in this equation was replaced by [H]. For minor species or for species which are formed simultaneously it generates stability constants which are always slightly greater than expected [17–20]. This is because in this equation the observed shift in the peak potential is attributed only to a single metal species. However, Eq. (9) is very convenient in the calculation of trial values for the stability constants [17–20] of species predicted from the relationships such as are seen in Figs. 3 and 4, or for any species which is considered as likely to be formed. The stability constants, as $\log\beta$, for ML, ML(OH), $ML(OH)_2$ and $ML(OH)_3$ were estimated from Eq. (9) and are shown in Table 2 together with pH ranges where they were fairly constant. These trial values were used for further refinement by solving the mass-balance equations (Eqs. (4) and (5)) for M_{Free} and fitting the CCFC to the ECFC.

Table 2
The overall stability constants, obtained from the modified Lingane equation, for lead species with the ligand A12C4 and pH ranges for which reasonable constancy in $\log\beta$ was observed

Equilibrium	Log β	pH range
$Pb^{2+} + L \Leftrightarrow PbL^{2+}$	4.22 ± 0.06	7.5–8.4
$Pb^{2+} + L + OH^- \Leftrightarrow PbL(OH)^+$	9.50 ± 0.07	8.6–9.7
$Pb^{2+} + L + 2OH^- \Leftrightarrow PbL(OH)_2$	13.17 ± 0.05	10.4–11.5
$Pb^{2+} + L + 3OH^- \Leftrightarrow PbL(OH)_3^-$	15.40 ± 0.07	11.4–12.5

These values are regarded as not reliable and were used only as the trial values for further refinement by Eqs. (3)–(5).

3.2.4. ECFC and CCFC for the Pb–A12C4–OH model

The experimental corrected shift in the peak potential was calculated for each datum point from Eq. (2) and plotted versus pH to give the experimental complex formation curves for the Pb–A12C4–OH system studied at a L_T:M_T ratio of 250:1 (empty circles in Fig. 5).

To make sure that the observed shift in the peak potential has not only been caused by the formation of $Pb_x(OH)_y$ species, the theoretical complex formation curve for the Pb–OH system was calculated (see empty squares linked with dashed line in Fig. 5). In the calculation of the CCFC for the Pb–OH system all known [4], including polynuclear, lead species with OH^- were included (see Table 1). It is seen that the experimental corrected shift in the peak potential (○) is greater than the calculated corrected shift (□) for all species of $Pb_x(OH)_y$. The observed difference between the experimental (circles) and the theoretical (squares) data points clearly indicates the formation of lead complexes with the ligand A12C4. One must realise that the calculated corrected shift in the peak potential for the Pb–OH system is the maximum expected corrected shift from the experiment when reversible reduction processes occur at the DME. It is because the free metal ion concentration required in Eq. (3) cannot be smaller than the value obtained from the appropriate mass-balance equations solved for the Pb–OH system. One can see that the corrected shift caused by $Pb_x(OH)_y$ starts to be significant only above a pH of about 7. The observed difference between the circles and the squares in the pH range between 7 and 8 is small which supports the supposition drawn from earlier relationships (Figs. 3 and 4) that the complex ML is indeed formed and that this is a weak complex. In the pH range between 8 and 11 a significant difference in the corrected shifts (circles and squares) is observed. This supports the for-

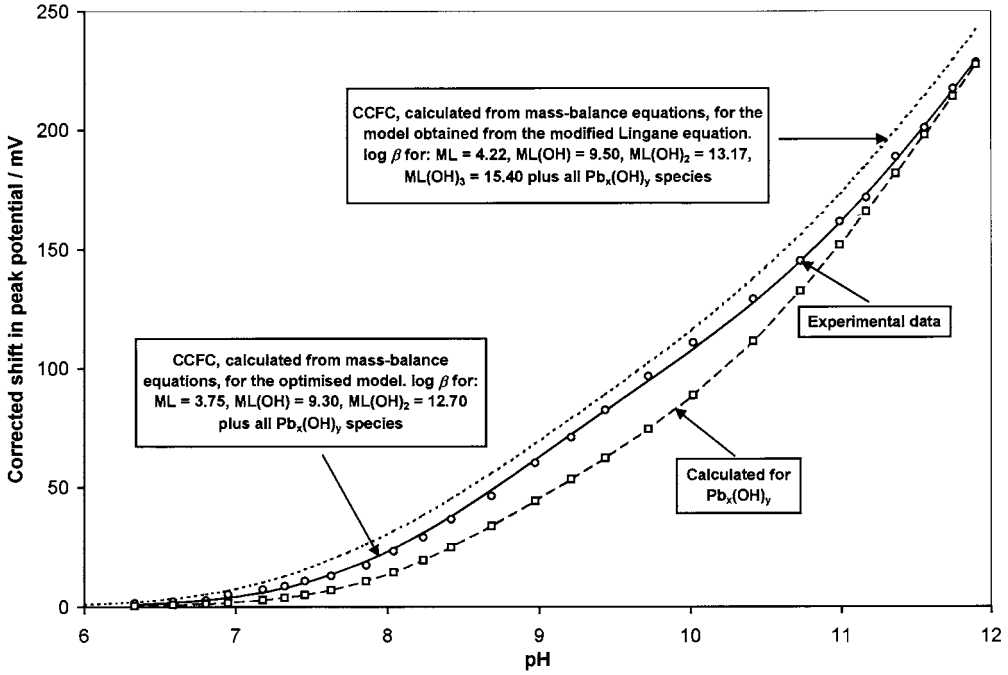

Fig. 5. Experimental and calculated complex formation curves for the Pb–A12C4–OH system in a background of 0.5 mol dm^{-3} $NaNO_3$ at 298 K for a L_T:M_T ratio of 250. (○) represents the experimental corrected shift in the DPP peak potential calculated from Eq. (2) for each datum point obtained at an *i*th pH(*i*) value. The solid line represents the CCFC for the metal–ligand system composed of the refined model ML, ML(OH), $ML(OH)_2$ (see Table 3) and all known species $Pb_x(OH)_y$ (see Table 1). The dashed line with (□) represents the CCFC obtained for species $Pb_x(OH)_y$ only. The dotted line represents the CCFC for the metal–ligand model obtained from the modified Lingane equation (see Table 2) and all species of $Pb_x(OH)_y$. The protonation constant for the ligand A12C4, the stability constants for the Pb^{II} complexes with OH^- and the protonation constant for water are from Table 1.

mation of $ML(OH)_n$. At the highest pH studied the calculated corrected shift for the species $Pb_x(OH)_y$ approaches the experimental values. This clearly indicates that the species $Pb_x(OH)_y$ become the predominant lead complexes at high pH. The dotted line seen in Fig. 5 was obtained when the stability constants calculated from the modified Lingane equation (Eq. (9)) were used for the calculation of the corrected shift. The dotted line is significantly above the circles (experimental points) which means that the stability constants obtained from Eq. (9) are too large and/or that the model for the Pb–L–OH system is not correct. The most suspicious lead species is $PbL(OH)_3^-$ because the observed difference between the dotted line and the circles is the greatest at highest pH values where this complex is expected to form. From the above it is clear that the modified Lingane equation cannot be used for the calculation of the stability constants when several metal complexes are formed simultaneously in a solution. Next, a number of CCFCs were generated from Eqs. (3) and (5) for different Pb–L–$(OH)_n$ models including all known lead complexes with OH^- (see Table 1 (note that the formation constants for the $Pb_x(OH)_y$ species were kept fixed during the refinement process)). The solid line seen in Fig. 5 represents the CCFC for the model for which the best fit was obtained. In this model PbL^{2+}, $PbL(OH)^+$, $PbL(OH)_2$, and all known $Pb_x(OH)_y$ were incorporated and the refined stability constants for the lead species with the ligand A12C4 are seen in Table 3. Note, that the species $ML(OH)_3$, suggested from the modified Lingane equation, is not included in the final metal–ligand model. Also, the refined stability constants (obtained from Eqs. (2) and (3)) are significantly smaller than those obtained from Eq.

(9) except for the stability constant of ML(OH). This suggests that the complex ML(OH) should be a major lead species in the solution. The fact, that the dotted line is relatively close to the circles in Fig. 5 over the pH range where the complex ML(OH) is expected to form, can also be used in a support of the above supposition.

3.2.5. Species distribution diagram for the Pb–L–OH model

In Fig. 6 a species distribution diagram is presented. It was calculated for the refined Pb–L–OH model for which the best fit was obtained (solid line in Fig. 5). It is seen that the lead complexes with the ligand L start to form above a pH of about 6 and only above pH 7 are they are at a significant concentration level (above 15% of the total metal ion concentration). This is why a noticeable shift in the peak potential is observed above pH 7 in Fig. 3. Over the whole pH range studied the species $Pb_x(OH)_y$ are predicted to form together with lead species formed with the ligand A12C4.

This is why in Fig. 3 the shift in the peak potential varies continuously rather than having a definite slope over a particular and easily identifiable pH range. It is clear now that the solid lines seen in Fig. 3 indicate the average number of protons involved in a number of electrochemical processes occurring simultaneously at DME. The only major lead species formed with A12C4 is the complex $PbL(OH)^+$ which is in accord with the predictions made above. The maximum slope of about 90 mV per pH unit seen in Fig. 3 correlates well with the pH region in Fig. 6 where the complex $Pb(OH)_3^-$ becomes a major species in the solution. This is in accord with the calculated corrected shift for the $Pb_x(OH)_y$ species seen in Fig. 5 over the pH region where $Pb(OH)_3^-$ is a major lead species (the pH region where the dashed line (□) approaches the observed corrected shift in the peak potential (circles) and the calculated shift (solid line) for the proposed Pb–L–OH model). Also the increase in the peak height at greatest pH where $Pb(OH)_3^-$ becomes a major metal species (see Fig. 2) is in support of the proposed Pb–L–OH model. It is seen in Fig. 6 that the formation of all polynuclear species except $Pb_3(OH)_4^{2+}$ is fully suppressed. The fact, however, that the polynuclear species is predicted to exist in the solution, even though the L_T:M_T ratio was high and $[M_T]$ was as low as 3×10^{-5} mol dm^{-3}, indicates that the lead complexes with the ligand A12C4 are very weak and that they can hardly compete with the formation of the hydroxy complexes of lead. In general, the species distribution diagram correlates well with the model proposed and the stability constants obtained. This indicates that the curve fitting procedure is a powerful tool in speciation studies by polarography. Even very small differences between the experimentally observed and the calculated corrected shifts in the peak potential for $Pb_x(OH)_y$ (see the pH range between 6.5 and 7.5 in Fig. 5) can be accounted for and give reasonable results.

Table 3
The refined stability constants for Pb^{II}, Cd^{II} and Cu^{II} with the ligand A12C4 obtained in this study in a background of 0.5 mol dm^{-3} $NaNO_3$ at 298 K and an ionic strength 0.5 mol dm^{-3}

Equilibrium	Log β	Technique
$Pb^{2+} + L \Leftrightarrow PbL^{2+}$	3.75 ± 0.03	DPP
$Pb^{2+} + L + OH^- \Leftrightarrow PbL(OH)^+$	9.30 ± 0.05	DPP
$Pb^{2+} + L + 2OH^- \Leftrightarrow PbL(OH)_2$	12.70 ± 0.05	DPP
$Cd^{2+} + L \Leftrightarrow CdL^{2+}$	2.80 ± 0.05	DPP
$Cd^{2+} + L \Leftrightarrow CdL^{2+}$	2.68 ± 0.03	GEP
$Cd^{2+} + L + OH^- \Leftrightarrow CdL(OH)^+$	7.88 ± 0.05	DPP
$Cu^{2+} + L \Leftrightarrow CuL^{2+}$	6.00 ± 0.05	DPP
$Cu^{2+} + L + 2OH^- \Leftrightarrow CuL(OH)_2$	21.77 ± 0.1	DPP

3.2.6. ECFC and CCFC for other metal ions studied

An attempt to employ GEP for the determination of the stability constants of zinc, copper and lead have failed because of the precipitation of, most likely, hydroxy species of these metal ions. As has been mentioned above, few potentiometric experimental data were obtained for cadmium

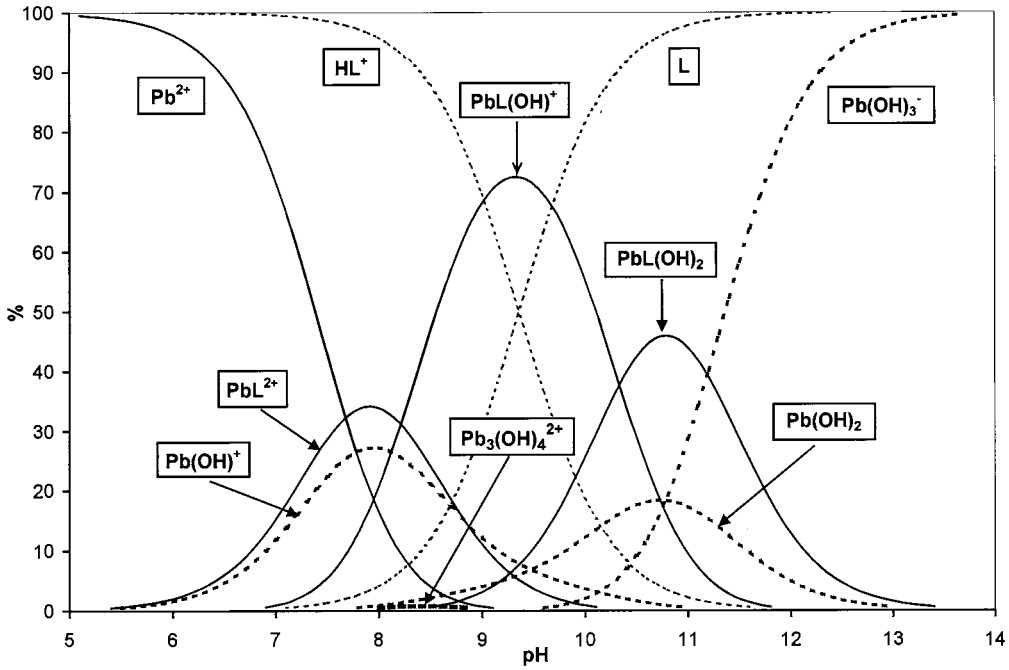

Fig. 6. The species distribution as a function of pH calculated for the Pb–A12C4–OH model, based on the polarographic results reported in this study at 298 K and an ionic strength of 0.5 mol dm^{-3} in a background of 0.5 mol dm^{-3} $NaNO_3$. $M_T = 3.30 \times 10^{-5}$ mol dm^{-3}; L_T:$M_T = 250$. The solid lines represent the fractions of the total lead concentration M_T for lead complexes with the ligand A12C4. The dashed thick lines represent the fractions of the total lead concentration M_T for the lead complexes $Pb_x(OH)_y$. The dotted lines represent the fractions of the total ligand concentrations L_T in solution.

and the stability constant of the complex ML obtained from GEP is seen in Table 3. It is pleasing to note that the values of the stability constants of CdL^{2+} from GEP and DPP do not differ significantly. This can be used to support the polarographic refinement procedure used here and allows us to assume that the stability constants obtained from polarography of other metal ions can be regarded as reliable. The metal ions Cd^{2+}, Zn^{2+} and Cu^{2+} were studied by DPP. The experimental conditions, as well as the mathematical approach used, were similar to those described above for the determination of the lead species with the ligand A12C4. The polarographic procedure was not successful in the case of zinc but it worked, to some extend, for copper and cadmium—here again precipitation has not allowed data collection over the full pH range. The stability constants obtained from the refinement of the polarographic data are shown in Table 3 and the fit of the CCFCs to the ECFCs for these metal ions is shown in Fig. 7. For comparison, the corrected shifts (experimental and calculated) for lead is also incorporated in the same Figure.

The analysis of the polarographic complex formation curves seen in Fig. 7 is of interest now. It is seen that each metal ion has generated a different polarographic complex formation curve. The shape and the position (along the pH scale) of the complex formation curve are a function of the metal–ligand model and the strengths of the complexes formed. The bigger the value of the stability constant for the ML complex the smaller the pH value at which the recorded and corrected shifts in the peak potential are observed. The biggest $\log K_1$ was obtained for CuL^{2+} and the ECFC and CCFC for this metal–ligand system are observed at the lowest pH. The opposite applies to cadmium which gave the smallest value of $\log K_1$ and, as a result, its complex formation curves were recorded at greatest pH values. From the above one can conclude that the complex

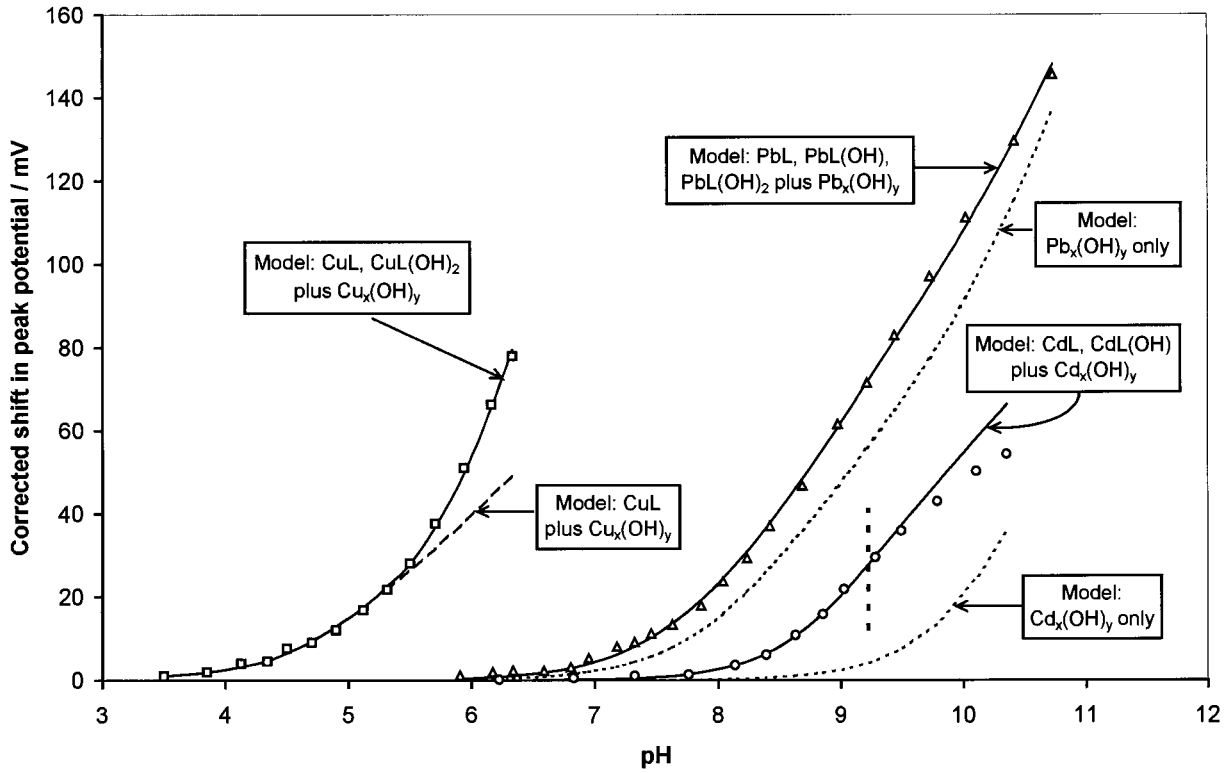

Fig. 7. The experimental and calculated (solid lines) complex formation curves for the Cu–A12C4–OH (□), Pb–A12C4–OH (△) and Cd–A12C4–OH (○) systems. For all metal–ligand models all known hydroxy metal species [4] were included. The dashed vertical line represents the pH at which precipitation of $Cd(OH)_2$ is predicted. The refined stability constants are shown in Table 3.

formation curves, defined by Eqs. (2) and (3), are characteristic relationships for the particular metal–ligand system studied. On the other hand, when 'traditional' techniques of speciation are used (the Lingane [5] or DeFord and Hume [6] technique) and ΔE_p is plotted versus $[L_{Excess}]$ then, regardless of the metal–ligand system studied, a slope of about 30 mV per log $[L_{Excess}]$ is observed for the complex ML provided that this complex is the predominant metal species in the solution. An additional disadvantage of the Lingane [5], DeFord and Hume [6], and more recent speciation techniques [22–25] is that they are all designed for speciation studies at a fixed pH value and varied excess of the ligand. It is quite clear that these techniques can not be used successfully for the metal–ligand systems studied in this study. In addition, none of the above polarographic speciation techniques (in their original form) allow us to account for the simultaneous formation of hydroxy metal species.

Acknowledgements

The authors thank the University of the Witwatersrand and the Foundation for Research Development for generous financial support for this study.

References

[1] G. Gokel, Crown Ethers and Cryptands, The Royal Society of Chemistry, Thomas Graham House, Science Park, Cambridge, 1991.
[2] R.M. Izatt, K. Pawlak, J.S. Bradshaw, R.L. Bruening, Chem. Rev. 91 (1991) 1721.
[3] J.S. Bradshaw, K.E. Krakowiak, B.J. Tarbet, et al., Pure Appl. Chem. 61 (1989) 1619.

[4] NIST Standard Reference Database 46, NIST Critically Selected Stability Constants of Metal Complexes Database, version 3.0, compiled by R.M. Smith and A.E. Martell, U.S. Department of Commerce, National Institute of Standards and Technology, Gaithersburg, MD 20899, USA.
[5] J.J. Lingane, Chem. Rev. 29 (1941) 1.
[6] D.D. DeFord, D.N. Hume, J. Am. Chem. Soc. 73 (1951) 5321.
[7] A.M. Bond, J. Electroanal. Chem. 20 (1969) 223.
[8] A.M. Bond, J. Electroanal. Chem. 23 (1969) 227.
[9] G.A. Heath, G. Hefter, J. Electroanal. Chem. 84 (1977) 295.
[10] R.D. Hancock, I. Cukrowski, J. Baloyi, J. Mashishi, J. Chem. Soc. Dalton Trans. (1993) 2895.
[11] R.D. Hancock, I. Cukrowski, I. Antunes, E. Cukrowska, J. Mashishi, K. Brown, Polyhedron 15 (1995) 1699.
[12] I. Cukrowski, E. Cukrowska, R.D. Hancock, G. Anderegg, Anal. Chim. Acta 312 (1995) 307.
[13] I. Cukrowski, F. Marsicano, R.D. Hancock, P.T. Tshetlho, W.A.L. van Otterlo, Polyhedron 14 (1995) 1661.
[14] R. Luckay, R.D. Hancock, I. Cukrowski, J.H. Reibenspies, Inorg. Chim. Acta 246 (1996) 1.
[15] I. Cukrowski, F. Marsicano, R.D. Hancock, E. Cukrowska, Electroanalysis 7 (1995) 763.
[16] I. Cukrowski, R.D. Hancock, R.C. Luckay, Anal. Chim. Acta 319 (1996) 39.
[17] I. Cukrowski, Anal. Chim. Acta 336 (1996) 23.
[18] I. Cukrowski, M. Adsetts, J. Electroanal. Chem. 429 (1997) 129.
[19] I. Cukrowski, Electroanalysis, 9, No. 9 (1997) 699.
[20] I. Cukrowski, Analyst 122 (1997) 827.
[21] A.M. Bond, R.J. Taylor, J. Electroanal. Chem. 28 (1970) 207.
[22] H.G. de Jong, H.P. van Leeuwen, K. Holub, J. Electroanal. Chem. 234 (1987) 1.
[23] H.G. de Jong, H.P. van Leeuwen, J. Electroanal. Chem. 234 (1987) 17.
[24] H.G. de Jong, H.P. van Leeuwen, J. Electroanal.Chem. 35 (1987) 1.
[25] J. Puy, J. Salvador, J. Galceran, M. Esteban, J.M. Diaz-Cruz, F. Mas, J. Electroanal. Chem. 360 (1993) 1.
[26] A.E. Martell, R.D. Hancock, in: J.P. Fackler, Jr. (Ed.), Metal Complexes in Aqueous Solutions, Modern Inorganic Chemistry Series, Plenum, New York, 1996.
[27] D.R. Crow, in: Polarography of Metal Complexes, Academic Press, London, 1969, p. 64.
[28] F. Marsicano, C. Monberg, B.S. Martincigh, K. Murray, P.M. May, D.R. Williams, J. Coord. Chem. 16 (1988) 321.
[29] P.M. May, K. Murray, D.R. Williams, Talanta 35 (1988) 825.
[30] E.P. Parry, R.A. Osteryoung, Anal. Chem. 37 (1965) 1634.

ELSEVIER

Talanta 47 (1998) 1191–1198

Talanta

Automated determination of tin and nickel in brass by on-line anodic electrodissolution and electrothermal atomic absorption spectrometry

José Bento Borba da Silva *, Maria Bertília Oss Giacomelli, Ivan Gonçalves de Souza, Adilson José Curtius

Departamento de Química, Universidade Federal de Santa Catarina, 88040-900-Florianópolis SC, Brazil

Received 30 December 1997; received in revised form 14 May 1998; accepted 15 May 1998

Abstract

The application of an on-line metallic alloy dissolution system using anodic electrodissolution in a flow injection system for the determination of tin and nickel in copper alloys is described. After the electrolyzed material was collected in the autosampler cup, determination was carried out using electrothermal atomic absorption spectrometry (ETAAS). Using specific software developed in Turbo Pascal 7.0, it is possible to control electrolysis time, intensity of the applied current, and triggering of the three-way solenoid valves that push the fluids. Through manipulation of these variables, it is possible to adjust the analytical signal to within the working range of the spectrometer. Calibration of the spectrometer was accomplished by processing reference material. For tin, relative standard deviations for a series of measurements ($n = 5$) performed on the same point and on different points of the sample was smaller than 2 and 4%, respectively; for nickel, 2 and 5%, respectively. The results for tin and nickel were in good agreement with those obtained through application of the classical methodology, as well as with data obtained by optical emission spectrometry. The detection limit for tin was 0.001% (w/w), whereas for nickel it was 0.003% (w/w). The analytical throughput is 30 samples h^{-1}. © 1998 Elsevier Science B.V. All rights reserved.

Keywords: Anodic electrodissolution; Flow injection analysis; Electrothermal atomic absorption spectrometry; Tin; Nickel

1. Introduction

Monitoring the composition of different classes of metallic alloys is a routine procedure in the metallurgical industry, given the need to produce alloys with a very well-known composition in terms of certain constituents. Elements often found in extremely low concentrations can affect the final quality and the desirable characteristics of alloys. In this sense, tin is frequently added to copper alloys because it acts as an anti-corrosive agent. The addition of tin can minimize the corrosion of the zinc component which affects metal

* Corresponding author. Tel.: + 55 48 3319219; fax: 55 48 3319711; e-mail: bentojb@hotmail.com

0039-9140/98/$ - see front matter © 1998 Elsevier Science B.V. All rights reserved.
PII S0039-9140(98)00197-0

parts that are destined for nautical use and are subjected to prolonged contact with sea water. Tin also increases mechanical resistance, promotes homogenization, and improves distribution of lead in copper alloys [1].

Atomic absorption spectrometry has been used since about 1960 for the determination of the metallic composition; metallurgy is one of the main fields where this technique has been employed. The determination of tin by electrothermal atomic absorption spectrometry (ETAAS) can, similarly to the flame technique, present a series of difficulties. A number of studies can be found in the literature regarding the determination of tin in iron, copper and zinc alloys using the standard addition method. In these studies, the authors simply dissolve the samples in nitric acid [2]. Another study concluded that only nitric acid solutions can be used to determine tin in steels; hydrochloric acid suppresses the tin signal completely, while sulfuric and perchloric acids cause depression and severe dispersion of the signal. That study also reported interferences due to Cr, Ni, Ti and Nb [2,3].

The methods usually employed by ETAAS for the determination of alloy components either use the method of standard addition or involve the use of analytical solutions with matrix matching for the major alloy components. Alternatively, indirect methods in which the analyte is separated from the matrix by some kind of extraction can be employed. With the standard addition method, the problem of matrix matching is minimized; however, this technique also restricts the linear range. This can be a problem for samples which contain a high concentration of the analyte, close to the end of the linear range. In addition, this method is usually tedious and time-consuming. The extraction technique is equally tedious, because it involves many steps and reagents. It can also introduce contamination or loss of the analyte [4].

Barnett et al. [5] have determined various elements, one of which was tin, in zinc, iron, and copper alloys. Calibration was performed using analytical curves with adjustment of the matrix only for the major elements of the alloy. According to these authors, the presence of iron, zinc or copper results in an enhancement of signals for certain analytes. For example, the lead signal in a solution with 0.1% zinc is about 10% enhanced compared to a solution containing only HNO_3. In copper solutions, the enhancement of the Pb analytical signal can reach 35%. Since the levels of the elements varied in the different samples, corrections for enhancements due to the major element in the alloy only, was considered sufficient by the authors [5].

The technique of hydride generation (HG) has often been employed in the analysis of alloys by flame and ETAAS methods for the determination of tin, among other elements that form hydrides. In more recent works, the generated hydrides have been determined by the flow injection technique (FIA) [3,6,7]. Welz et al. [7] investigated the determination of tin in steels using FIA-HG-AAS. According to these authors, under the best study conditions it was possible to determine tin in steels within a 0.008–0.1% range, using calibration with matrix-free solutions. McIntosh et al. [3] studied techniques in which the generated hydrides were trapped at low temperatures on a L'Vov platform coated with Pd, with an efficiency of about 80% and a precision ranging between 3 and 5%. The method was employed, for example, for the analysis of Sn, Ge, Te, Sb, and Se in steels, with results that were in good agreement with reference materials. Haug et al. [6] have also studied the determination of tin using hydride generation in the FIA system. In that paper, these authors present an automatic system for trapping the hydride generated on the graphite tube or on the L'Vov platform at a temperature of 500–600°C. The tube (or platform) was coated with carbide-forming elements, such as Zr, Nb, Ta, or W. A precision of about 2% was observed.

When determining nickel in steels and ores by ETAAS using NH_4VO_3 as matrix modifier, Gao et al. [8] obtained linear analytical curves within a concentration range of 0.01–0.16 μg ml^{-1} Ni. The sensitivity was 0.002 μg ml^{-1}. The relative error observed in the determination of the element in standard samples was $< 3.5\%$. The authors emphasize how simple and fast this method is.

A common factor in most determinations employing the atomic absorption technique is the

need to use the sample in its liquid form. The dissolution of metallic samples is generally carried out using acid mixtures or fusion mixtures of salts and peroxides. The selection of the appropriate procedure for dissolution must take into account the chemical composition and the physical structure of the material, as well as the analytical technique to be employed for the quantification of the dissolved species. In any event, these processes are generally very slow and require high quantities of reagents. These methods can also be sources of contamination and errors, and, in many cases, an experienced technician is required for the work [9,10].

Other alternative processes have been suggested, employing closed systems using several different reagents and reaction times, as well as microwave ovens [11]. Currently, a number of procedures aiming towards the elimination of steps in the chemical dissolution of metallic alloys are being used. Noteworthy among them are arc/spark sources of discharge with ac/dc currents, glow discharge and laser ablation [12]. However, these procedures require calibration with a material whose composition is very similar to that of the sample to minimize errors in the determination. Besides, these techniques require expensive equipments and, in most cases, equipment which is not available in many laboratories that analyze metallic alloys. One advantage of this type of technique, however, is the possibility of using the sample in its solid form, with almost no prior preparation.

Alternatively, anodic electrodissolution has been employed as a technique that uses the sample in its solid form and at the same time offers the advantages of low cost and simple operation [9,10,13]. In short, these procedures are based on using the conducting sample as an anode. With the help of an appropriate cathode, and having both anode and cathode inside an electrolytic solution, a given electric current is applied during a given time interval. After electrolysis, the electrodissolved analyte is determined through an adequate spectrometric technique.

Chirnside et al. [14] introduced the use of anodic electrodissolution as a technique for dissolving alloys for analytical purposes, in a study to determine boron traces in nickel. The sample was electrodissolved with sequential deposition of the generated nickel ions over the cathode. Subsequently, the boron ions in solution were spectrophotometrically determined with curcumin.

Later, Coutinho et al. [15] developed a method to determine soluble aluminium in killed steels, employing anodic electrodissolution as the procedure for dissolving the sample. Tolg et al. [16] have determined Al in high purity iron after anodic electrodissolution of the alloy, followed by electrodeposition in a mercury cathode. The detection system used by the authors was ETAAS. In a more comprehensive article, Ohls and Koch [17] determined Al, Si, Mn, Cr, Ni and Co in low-alloy steels using an electrolytic procedure. The ions, electrodissolved in a chloridric acid solution, were subsequently determined by inductively coupled plasma atomic emission spectrometry (ICP-AES).

Bergamin et al. [18,19], first applied solubilization of metallic samples by anodic electrodissolution procedures in flow injection systems. They designed an electrolysis chamber attached directly to the flow injection system. In that work, a spectrophotometric determination of soluble aluminium [18] and molybdenum [19] was carried out in steels. The samples were polished and then electrodissolved with the application of a continuous electric current. These studies were later extended to determine Cr, Ni, Mn, Si, and Fe in ferrous and austenitic steels by ICP-AES. Ohls and Flock [20] have also focused on anodic electrodissolution of metallic samples in flow injection systems with ICP-AES detection. The basic arrangement, common to all these FIA systems, involves the use of an electrolytic cell, a stabilized source of current, a peristaltic pump, and a system for introduction of the electrolyte, usually through a proportional injector.

The work described in the present paper is aimed at determining the levels of tin and nickel in copper alloys by employing an automated on-line sample dissolution system and quantification by ETAAS. After anodic electrodissolution of the sample, the electrodissolved material is collected into the cups of the spectrometer autosampler.

2. Experimental

2.1. Instrumentation

The work being described was carried out using an Ismatec 73315-15 peristaltic pump, equipped with Tygon tubing of several diameters and polyethylene tubing with a 0.8 mm internal diameter; Cole Parmer 983000-62 three-way solenoid valves with connectors; a 486 DX-2 (66 MHz) personal computer; a Perkin Elmer atomic absorption spectrometer (AAnalyst 100) with a deuterium background correction system, equipped with an HGA 800 furnace and an AS-72 autosampler. Instrument operating conditions were those recommended by the manufacturers, unless otherwise stated.

Argon 99.996% (White Martins, Brazil) was employed as the purge gas. All measurements were performed in peak areas always with a 20 μl sample. For Sn determination, 5 μl of $Pd(NO)_3$/$Mg(NO)_3$ were added as modifier.

The electrochemical dissolution chamber used was similar to that described in previous studies [9,10,21]. It was built in acrylic with a silver needle which functions as the cathode. The support electrolyte is introduced inside this needle. The electrolyte and the electrodissolved material pass through a drain located at the base of the chamber. A rubber disk, placed on the surface of the cell, is used to insulate the system when the sample is placed on the chamber.

The electrochemical dissolution of the samples was performed with a continuous current source manufactured in our laboratory. This source enables application of 16 levels of current from 0 to approximately 500 mA. A 486-DX2 (66 MHz) personal computer and software written in Turbo Pascal 7.0 are used to control electrolysis time, intensity of the applied current, and triggering of the three-way solenoid valves [21].

2.2. Reagents

All experiments employed analytical-grade chemicals and distilled/deionized water. Nitric acid (0.5 mol l^{-1}) was prepared by dilution of Merck reagent in deionized water (Milli-Q System).

For the determination of Sn a mixed palladium nitrate-magnesium nitrate chemical modifier [7] solution was used. The modifier solutions was prepared by dilution of appropriate aliquots of a Pd nitrate solution (Merck) and a solution of $Mg(NO_3)_2.6H_2O$ (Merck) in de-ionized water to give 15 μg Pd + 10 μg $Mg(NO_3)_2$ in 5 μl.

For the conventional determination method, solutions for the tin and nickel analytical calibration curves were prepared from stock solutions (1000 mg l^{-1}) in (Merck) HNO_3 1% (v/v). All solutions contained 200 μg l^{-1} copper and 50 μg l^{-1} zinc for matrix matching. The analytical curve for Sn spanned from 0 to 80 μg l^{-1}, and for Ni, from 0 to 50 μg l^{-1}. The tin stock solution was 985 mg l^{-1} and was 8% (v/v) in HCl; nickel stock solution was 1000 mg l^{-1}, prepared from a Merck titrisol solution, according to the manufacturer's recommendations.

2.3. Operational conditions

The operational conditions for each determination are shown in Table 1.

The temperature programs for Sn and Ni in the presence of the matrix and of the electrolyte are shown in the Table 2.

Table 1
Instrumental parameters and operating conditions of ETAAS

	Sn	Ni
Wavelength (nm)	286.3	232.0
Slit (nm)	0.7	0.2
Light source (mA)	HCl, 14	HCl, 15
Measurement mode	Peak area	Peak area
Graphite tube	Pyrolytically coated B0-109322	Pyrolytically coated B0-105197
L'Vov platform	With	Without
Chemical modifier	Pd/Mg nitrate	Without
Modifier volume (μl)	5	—
Sample volume (μl)	20	20

Table 2
Graphite furnace temperature program for Sn and Ni determinations

Step	Temperature (°C)	Ramp (s)	Hold (s)	Argon flow rate (ml min^{-1})
1	90	10	10	250
2	140	5	15	250
3	800(Sn), 1000(Ni)	10	15	250
4[a]	2200(Sn), 2300(Ni)	0	5	0
5	2500	1	5	250
6	20	10	5	250

[a] Read step.

2.4. Flow injection diagram

The used system, shown in Fig. 1, contains two three-way solenoid valves, a peristaltic pump, a control unit for the valves (home-built), containing an ULN 2004 integrated circuit, an electrolytic cell (home-built) and a current source (home-built). Firstly, the solenoid valve V1 is actuate for 2 s, assuring that the cell is filled with the electrolyte during the electrolysis. Then, the current source is actuated, after selecting a current and a time. When the electrolysis is finished, valve V1 is turned off while valve V2 is actuated. An air flow pushes the electrolyte, containing the dissolved sample, to the autosampler cup.

2.5. Calibration procedures, samples and standard materials

The calibration of the instrument is performed by submitting a certified reference material, having a composition similar to the sample, to the same process used for the sample. In this way, matrix matching is obtained.

Samples of the brass alloys, containing known quantities of Sn and Ni were used in all experiments. These samples were characterized by optical emission spectrometry. The elements of interest in these samples were also determined by ETAAS after conventional chemical dissolution with matrix matching for cooper and zinc.

For determinations using the traditional method, three 0.1000 g replicates of each sample were weighed and dissolved in 5 ml concentrated HNO_3. The volume was then adjusted to 100 ml. For determination of the analytes, adequate dilutions in HNO_3 1% (v/v) were done. The determinations by optical emission spectrometry were obtained using an Jarrel-Ash spectrometer.

Since the samples for electrodissolution had been pretreated, only one surface was polished with 400 grit sandpaper. After having been polished, the samples were thoroughly washed with deionized water and dried with tissue paper.

2.6. Optical emission spectrometry (OES) determinations

All analysis by OES were performed in a Jarrel Ash A-300 spectrometer equipped with a spark generator. The used operating conditions were: voltage of 220 V; current of 2 A; inter-electrode gap de 1.5 mm; slit of 0.05 nm and exposition time of 1 min. Calibrations was performed with previously analysed samples.

3. Results and discussion

As the support electrolyte, HNO_3 0.5 mol l^{-1} was chosen due to its excellent performance in studies of anodic electrodissolution of non-ferrous alloys [13]. According to Yuan et al. [13] who have investigated electrolysis in aluminium alloys with six different electrolyte compositions, the highest absorbance signals for copper using peak height were obtained with HNO_3. Using HNO_3 these authors observed that at low or high concentrations (below 0.2 mol l^{-1} or above 1.0 mol l^{-1}), the signals were lower in relation to the intermediate concentration values. Thus, these authors recommended that this acid concentration

range (0.2–1.0 mol l^{-1}) be used. In the present study with copper alloys, the results of the preliminary assays with 0.5 mol l^{-1} HNO_3 were satisfactory. Nitric acid was therefore used as the working electrolyte in later investigations.

The electrolyte flow rate was chosen based on the intensity of the analytical signal and on the minimization of precipitate occurring in the analytical path. For flow rates lower than 5 ml min^{-1}, the occurrence of a dark precipitate was observed around the cathode. This effect can be attributed to the occurrence of secondary reactions such as the formation of cupric and cuprous oxides and hydroxides around the anodic surface. High electrolyte flow rates result in a lower residence time of the electrolysis products inside the chamber and thus favor a continuous renewal of the anodic surface. At flow rates higher than 6 ml min^{-1}, the formation of solid products was not observed. The chosen flow rate for electrolyte propulsion was 9 ml min^{-1}.

Optimization of electrolysis time was achieved through attenuation of the support electrolyte flow, so that the volume of the electrodissolved material would fit into the cups of the autosampler. A 10 s interval was chosen. The smooth surface observed in the cavities that were formed in the alloys due to the electrolysis, under any of the conditions applied, suggests that there is no preferential dissolution related to the various oxidation potentials of the constituents. This effect also suggests that the electrolytic process occurs in a potential transpassive region, confirming the minimization of the occurrence in parallel reactions. It is also important to stress that, under optimized conditions, we did not observe the formation of bubbles due to gas evolution.

In determinations which employ acid mixtures for dissolution, the necessary amount of analyte for the detection system is obtained through the dissolution of a given sample mass. With anodic electrodissolution in the flow injection system, this amount is obtained by means of an electrolysis. Thus it becomes necessary to establish electrolysis conditions that enable the liberation of a sufficient amount of the analyte in solution. The completion of the anodic process to produce adequate analyte in solution depends, among other factors, on the composition of the electrolytic solution, the alloy constituents, the potential applied to the electrodes, and the density of the current employed for the electrolysis [9,13].

The integrated absorbances of tin and nickel (Y) are linearly correlated with the applied current (X). The obtained equations are $Y = 0.02 + 0.00071\ X$ ($r = 0.99962$) and $Y = 0.079 + 0.0022\ X$ ($r = 0{,}99986$), for tin and nickel, respectively. The integrated absorbance (Y) is given in s and the current (X) is in mA; r is the correlation coefficient. The absorbance values refer to a sample containing 0.010% (w/w) tin and 0.005% (w/w) nickel. The currents used for this experiment varied from 0 to about 500 mA.

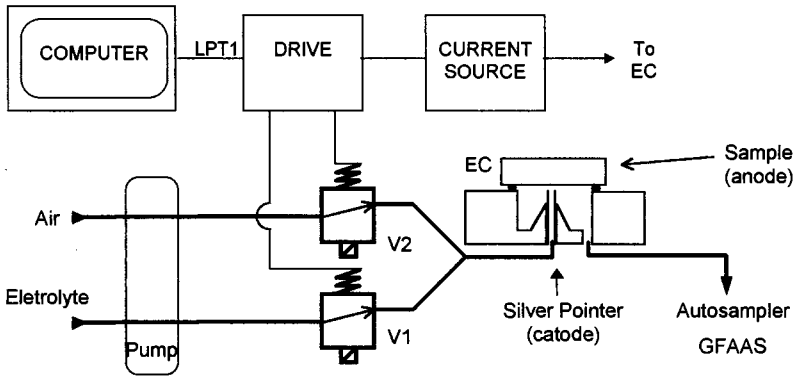

Fig. 1. Flow diagram of the proposed system. Three-way solenoid valves (V1 and V2); electrolytic cell (EC); exit to printer (LPT1); polyethylene tubes (—) and electric contacts (—).

Table 3
Sn and Ni concentrations, % (w/w) in brass

Sample	Optical emission spectrometry	Chemical dissolution and atomic absorption spectrometry[a]	Anodic dissolution and flow injection analysis
Sn			
1	0.050 ± 0.003	0.057 ± 0.006	0.054 ± 0.008
2	0.058 ± 0.003	0.060 ± 0.005	0.061 ± 0.007
3	0.075 ± 0.004	0.066 ± 0.008	0.064 ± 0.002
4	0.082 ± 0.004	0.083 ± 0.004	0.081 ± 0.006
5	0.105 ± 0.005	0.110 ± 0.003	0.108 ± 0.007
Ni			
1	0.031 ± 0.002	0.039 ± 0.009	0.036 ± 0.0040
2	0.013 ± 0.001	0.022 ± 0.003	0.010 ± 0.0010
3	0.020 ± 0.001	0.027 ± 0.002	0.032 ± 0.0009
4	0.080 ± 0.004	0.084 ± 0.010	0.079 ± 0.0006
5	0.032 ± 0.002	0.031 ± 0.0009	0.035 ± 0.0015

[a] With matrix matching for Cu and Zn.

The analytical calibration curves for Sn and Ni, showed linear variations as $Y = 0.02 + 7.06\ X$ and $Y' = 0.016 + 9.34\ X'$, where X and X' are the concentrations of Sn and Ni in % (w/w), respectively and Y e Y' are the integrated absorbances. In both situations, the electrolyses were carried out using 150 mA currents for 10 s with the electrolyte being pumped at 9 ml min^{-1}. The correlation coefficient was always higher than 0.998.

In all experiments, for Sn and for Ni, blanks were obtained in a similar manner to that employed for obtaining signals for the calibration curve, except that the current source was turned off. The ideal way of obtaining blanks would be by performing a calibration in a similar manner and by applying the same current level to an alloy sample that did not contain the analytes. Since this is impossible in pratice, the system used only estimates the contribution in the analytical signal originated from any chemical dissolution. For Sn in all concentration levels studied, the blanks were lower than 0.008 (in units of integrated absorbance/s), while for nickel a value as 0.028 was obtained.

Table 3 presents the results obtained for tin and nickel using the proposed system. For comparison, this table also shows data obtained through the usual sample chemical dissolution technique, by graphite furnace and optical emission spectrometry. As can be observed from Table 3, the results obtained for Sn and Ni with the proposed system are in agreement with the data obtained using the other techniques employed for comparison. In relation to the precision of the measurements, the proposed system gave a relative deviation (three replicates) generally below 5%.

The detection limit was calculated using the equation $DL = 3\ s/a$, where s is the standard deviation for ten measurements of the first point in the analytical curve for each metal and a is the slope of the analytical calibration curve. The detection limit obtained for tin was 0.001% (w/w), while for nickel it was 0.003% (w/w). However, by increasing the current level these detection limits can be improved.

For tin, the relative standard deviation to the measurements performed in the same point of the alloy was below 2%, whereas for different points in the sample it was always below to 4%.

For nickel, on the other hand, the relative standard deviation was below 2 and 5%, for the same situations, respectively.

The working range for tin and nickel, using a current of the 150 mA, was from the DL to about 0.1% (w/w). One of the main advantages of the proposed system, is the possibility of using all of the 16 computer-controlled current levels offered by the source. The adequate combination of current level and electrolysis time facilitates the adjustment of the analytical signal to within the working range of the spectrometer. Above a given concentration of the element in the sample, it is necessary to reduce sensitivity, so as to enable the direct alloy analysis. This can be carried out, for example, by using secondary absorption lines [22]. This possibility is being investigated.

High sampling frequency, low chemical consumption, no need for glassware or heating systems, low contamination risks, and a high automation level are some of the advantages of the proposed system. Besides, only a small part of the sample is dissolved.

4. Conclusions

The automatic method employed for on-line dissolution of the samples with anodic electrodissolution in the flow injection system was shown to be an adequate method for the determination of tin and nickel in brass by electrothermal atomic absorption spectrometry (ETAAS). Calibration of the spectrometer was done with reference materials of similar composition of the samples. The microcontroled triggering of the source and of the solenoid valves used for directing the flows allow for the automation of the process. Appropriate selection of valve opening times, levels of applied current, and the duration time of electrolysis makes it easier to bring the analytical signal within the spectrometer working range. The accuracy and precision of the measurements was comparable to that of conventional acid dissolution followed by AAS or by optical emission spectrometry. The procedure described in this paper can be extended to the determination of other elements in non-ferrous alloys.

Acknowledgements

We gratefully acknowledge the financial support of the following Brazilian research agencies: CNPq (Conselho Nacional de Desenvolvimento Científico e Tecnológico); CAPES (Fundação Coordenação de Aperfeiçoamento de Pessoal de Nível Superior); and FINEP (Financiadora de Estudos e Projetos). Details of construction of the current source were not included, but are available on request.

References

[1] A. Phillips, Metais e Ligas não Ferrosas, Propriedades e Empregos, Editora Politécnica, São Paulo, 1945.
[2] B. Welz, Atomic Absorption Spectrometry, 2, VHC, Weinheim, 1985, pp. 331–334.
[3] S. McIntosh, L. Zhang, G.R. Carnrick, W. Slavin, Spectrochim. Acta 47B (1992) 897.
[4] B. Mile, C.C. Rowlands, A.V. Jones, J. Anal. At. Spectrom. 7 (1992) 1069.
[5] W.B. Barnett, E.A. MacLaughlin Jr., Anal. Chim. Acta 80 (1975) 285.
[6] H.O. Haug, L. Yiping, Spectrochim. Acta 50 (1995) 1311.
[7] B. Weltz, M. Schubert-Jaccobs, T. Guo, Talanta 9 (1992) 1097.
[8] Z.Z. Gao, Y.Q. Li, Metallurgical Analysis 2 (1992) 18.
[9] I.G. Souza, H. Bergamin Fº, J. Krug, P.V. Oliveira, B.F. Reis, M.F. Gine, Anal. Chim. Acta 245 (1991) 211.
[10] I.G. Souza, H. Bergamin Fº, F.J. Krug, B.F. Reis, P.V. Oliveira, J.A. Nóbrega, Quím. Nova 15 (1992) 204.
[11] S. Kotot, G.M. Kimber, Trends Anal. Chem. 9 (1990) 203.
[12] T.R. Dulski, Anal Chem. 65 (1993) 29R–39R.
[13] D. Yuan, X. Wang, P. Yang, B. Huang, Anal. Chim. Acta 243 (1991) 65.
[14] R.C. Chirnside, H.J. Cluley, P.M.C. Proffitt, Analyst 82 (1957) 18.
[15] C.A. Coutinho, J.C. Azevedo, G.S.P. Etrusco, Metalurgia ABM 39 (1983) 87.
[16] G. Tölg, M. Hiraide, P. Tschöpel, Anal. Chim. 186 (1986) 261.
[17] K. Ohls, K.H. Koch, Frezenius Z. Anal. Chim. 326 (1987) 520.
[18] H. Bergamin Fº, F.J. Krug, B.F. Reis, E. Zagatto, E.C. Arruda, CA. Coutinho, Anal. Chim. Acta 190 (1986) 177.
[19] H. Bergamin Fº, F.J. Krug, B.F. Reis, J.A. Nóbrega, M. Mesquita, I.G. Souza, Anal. Chim. Acta 214 (1988) 397.
[20] J. Ohls, K. Flock, Frezenius Z. Anal. Chem. 331 (1988) 408.
[21] J.B.B. Silva, M.B.O. Giacomelli, A. Lehmkuhl, A.J. Curtius, R.R.U. Queiróz, I.G. Souza, Quím. Nova. (in press).
[22] M.A. Belarra, M. Resano, J.R. Castillo, Spectrochim. Acta, B 51 (1996) 697.

ELSEVIER

Talanta 47 (1998) 1199–1213

Talanta

Seventeen new 14- and 15-crown-formazans: their synthesis and evaluation in spectrophotometric determination of lithium[1]

Yehia A. Ibrahim *, Ahmed H.M. Elwaby, Barsoum N. Barsoum, Ashraf A. Abbas, Suzan K. Khella

Department of Chemistry, Faculty of Science, Cairo University, Giza, Egypt

Received 11 May 1998; accepted 18 May 1998

Abstract

A number of new crown-formazans with 14 and 15 membered rings have been synthesized, characterized and investigated as selective spectrophotometric chelating agents for lithium. The effect of sodium ion concentration on the background lithium signal was studied. A comparative study for the sensitivity of these new crown-formazans in spectrophotometric determinations was studied and compared with those reported previously. The three new 14- and 15-crown-formazans **4a**–**c** containing the pyridyl *N*-oxide at the formazyl carbon showed the highest selectivity to lithium determination in the presence of sodium ion. © 1998 Elsevier Science B.V. All rights reserved.

Keywords: New crown-formazans; Selective spectrophotometric chelating agents; Lithium

1. Introduction

Lithium is used in the treatment of manic depression psychosis. The lithium level in blood must be maintained between 0.5 and 2 mM. A higher level is toxic and a level of 5 mM can be lethal [1]. Hence, the level of lithium in the patient's blood must be frequently monitored [1,2]. The determination of lithium is performed by the use of flame photometry or atomic absorption spectrophotometry [1,2]. Also, several ion selective electrodes were reported for the determination of lithium [3]. The difficulty in determining lithium in blood or serum is their high content of sodium (ca. 140 mM). The success of any method of such determination is assessed by the possibility of accurate microdetermination in the presence of high concentrations of sodium and other interfering ions present in blood serum. Several crown-formazans were recently investigated for determination of lithium spectrophotometrically [4–13]. Since improvements in easy and accurate methods for determination of lithium is still a subject of current interest, we performed a comparative study for the spectrophotometric deter-

* Corresponding author. E-mail: Yehia_AI@FRCU.EUN.EG

[1] Dedicated to Professor Gary D. Christian on the occasion of his 60th birthday.

0039-9140/98/$ - see front matter © 1998 Elsevier Science B.V. All rights reserved.
PII S0039-9140(98)00205-7

mination of lithium ion using the twenty crown-formazans **2a**–**c**–**7a**–**d**. The aim of this work was to study the effect of two structural factors namely, the ether part of these macrocycles and the substituent at the formazyl carbon, on the sensitivity of lithium determination. For this comparative study, data for the ligands **5a**, **b**, and **c** were taken from previously published studies [6,13]. Since the cyano substituent at the formazyl carbons was shown to enhance the ability of the crown-formazans towards lithium determination, our aim in the present study was to compare the presence at the formazyl carbon of other electron withdrawing groups such as aryl, arylsulfonyl, 4-pyridyl-*N*-oxide and *p*-cyanophenyl groups. The last represents an interesting extended cyano substituted formazan through the phenyl group.

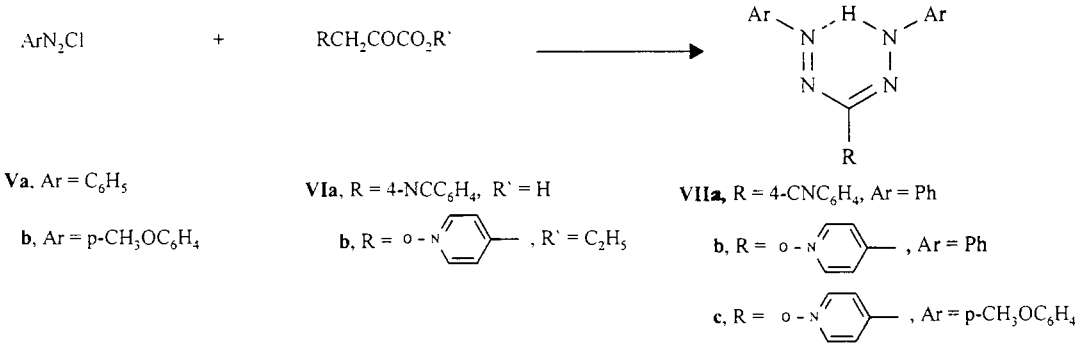

2. Experimental

2.1. Reagents and chemicals

The crown-formazans **2**–**7** used in the present study were prepared according to the procedure described below. Acetone, analytical grade, was used as received. Chlorides of sodium and lithium were of the highest purity available. Doubly distilled water was used. The following solutions were prepared:

Solution I: 0.05 mM of each of the formazans and 50 mM NaOH in 85% acetone and 15% water.

Solution II: 0.05 mM of each of the formazans and 50 mM NaOH in 70% acetone and 30% water, with a total sodium ion concentration of 440 mM from added NaCl.

Solution III: 0.05 mM of each of the formazans and 50 mM NaOH in 50% acetone and 50% water, with a total sodium ion concentration of 1050 mM from added NaCl. Higher water ratios were used at high sodium concentration to avoid turbidity from limited solubility.

2.2. Apparatus

Electronic absorption spectra were measured with a Perkin-Elmer Lambda 4B spectrophotometer.

2.3. Synthesis of the crown-formazans

We describe in the present investigation the synthesis of a number of new crown-formazans **1**–**7** as outlined in Scheme 1. Thus, the bis-*o*-aminophenoxy derivatives **III** (obtained by alkylation of *o*-acetamidophenol **I** with the appropriate dihalo-compound or epichlorohydrin to give **II**, followed by hydrolysis) were bis-diazotized to give the bis-diazonium salts **IV**. The latter were then coupled with the appropriate pyruvic acid derivatives, ethyl cyanoacete, malonic acid or sulfonylacetic acid derivatives to give the corresponding crown-formazans **1**–**7** following the procedure reported recently for the synthesis of the crown-formazans [14,15]. Moreover, the yield has been improved in some cases by using the phase transfer catalytic procedure reported recently by Katritzky et al. [16]. Also, in a preliminary

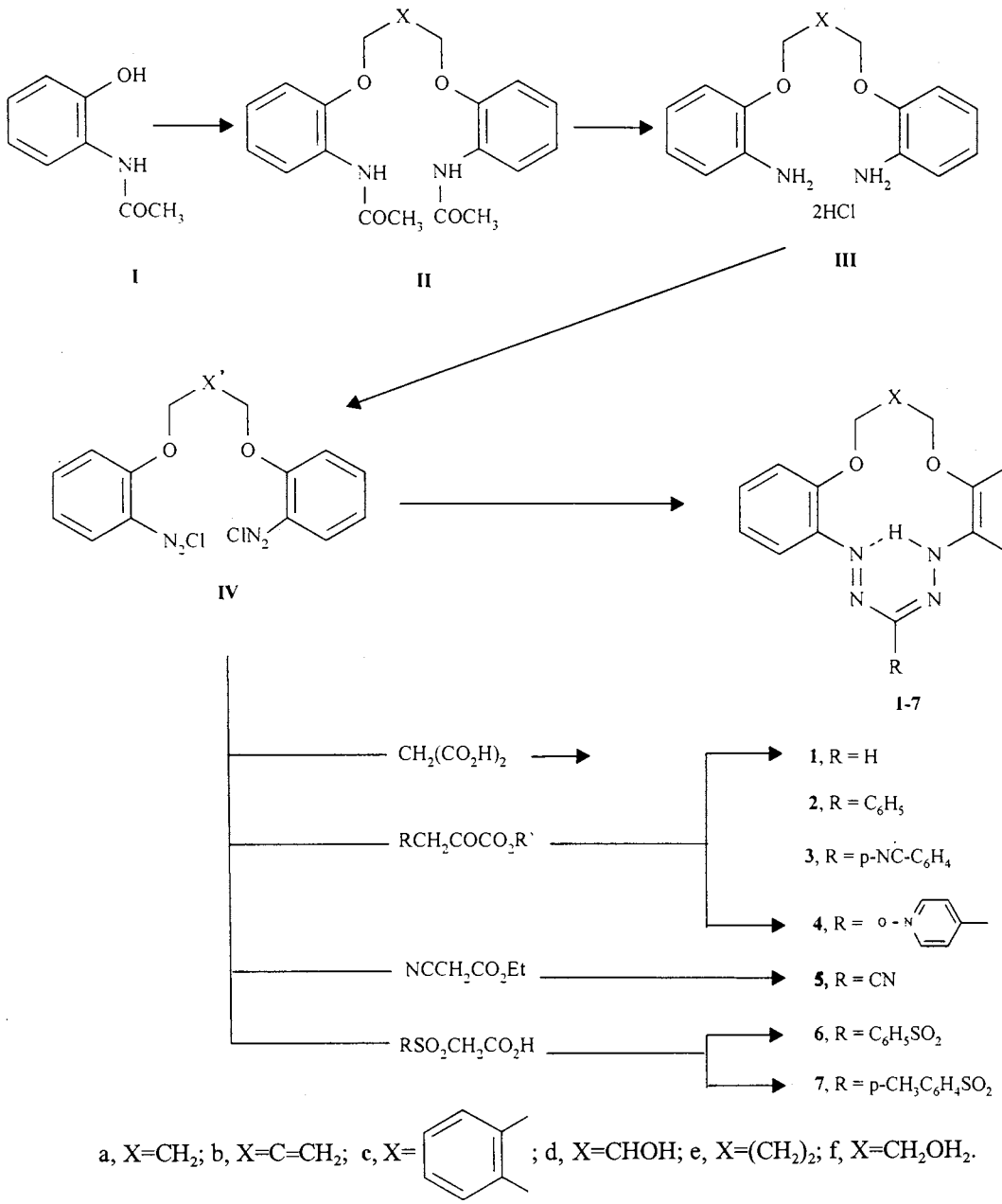

Scheme 1.

investigation the behavior of *p*-cyanophenylpyruvic acid **VIa** and ethyl 4-pyridylpyruvic acid 1-oxide **VIb** toward arenediazonium salts was studied. Thus, the latter reaction using benzenediazonium chloride **Va** and *p*-methoxybenzene-diazonium chloride **Vb** led to the direct formation of the corresponding formazans **VIIa–c** with good yields.

2.4. Procedure

For spectrophotometric studies of lithium in the presence of sodium ion an aliquot of lithium standard was added to give concentrations ranging between 0.5–3; 0.5–3.5 and 1.5–5 mM when dissolved in solutions I, II and III, respectively. The absorbance of these solutions was measured using the solvent solution as a blank. The absorbance of 3 mM lithium in solution I with an increasing level of sodium ranging from 50 to 200 mM (by addition of sodium chloride) was measured; the reference was a solution of 85% acetone, 15% water, containing 50 mM NaOH, but no crown-formazan. The absorbance of solution I for each crown-formazan was also measured at different time intervals, up to 90 min.

3. Results and discussions

All investigated crown-formazans in solutions I showed an absorption band around $\lambda_{max} = 488–535$ nm and on adding lithium this band also appeared almost at the same position, however, with a hyperchromic effect (Fig. 1a–d show some representative examples). Interestingly, with the crown-formazans **4a**–**d** (containing the pyridyl *N*-oxide group) a new absorption band appeared at $\lambda_{max} = 450–460$ nm only in the presence of lithium (cf. Fig. 1b–d). Calibration graphs for lithium were made in solutions I, II and III with the crown-formazans **2**, **3**, **4**, **5**, **6** and **7** using the band at their corresponding λ_{max} at 488–535 nm and also with the crown-formazans **4** using the band at $\lambda_{max} = 450–460$ nm which were found to be more sensitive in this respect. Table 1 shows the slopes of the calibration graphs obtained for the investigated crown-formazans **2**–**7** at the specified λ_{max} (Fig. 2a–d show some representative calibration graphs). This Table also contains the reported [6,13] data for compounds **5a**–**c** for comparison. From this comparison it is apparent that:

(1) Out of all the investigated new crown-formazans **2**, **3**, **4**, **6** and **7** only compounds **4** (with the pyridyl *N*-oxide substituent) showed the highest sensitivity for lithium determination comparable to those reported for the cyano derivatives [6,13].

(2) Moreover, the new pyridyl derivatives have interesting and important advantages over all other crown-formazans in lithium ion determination which consists in the fact that in the presence of lithium a new characteristic band appears at $\lambda_{max} = 450–460$ nm in addition to the band at $\lambda_{max} = 530–535$ nm which was originally present in the absence of lithium. Both bands could be used to obtain a good calibration graph for lithium although the shorter $\lambda max = 450–460$ nm band is more sensitive as is indicated from the slopes of these graphs at both λ_{max} (cf. Table 2).

(3) The substituent (X) at the ether part of these crowns has almost no effect on the position of λ_{max} of these crown-formazans whether in the presence or absence of lithium ion. However, with $X = C{=}CH_2$ the highest sensitivity for lithium was obtained in each case. In the case of compound **4c**, with $X = o–C_6H_4$, good sensitivity for lithium was also obtained (cf. Table 1).

(4) Replacing the cyano group in compounds **5a**–**c** by the *p*-cyanophenyl group as in compounds **3a**–**c** was thought to enhance the sensitivity for lithium as it might have a better conjugative effect through the benzene ring. However, the results in Table 1 indicate that compounds **3a**–**c** are among the least sensitive towards lithium determination and they are almost identical to the phenyl derivatives **2a**–**c**.

(5) The phenylsulfonyl derivatives **6a**–**d** showed better sensitivity than the phenyl **2a**–**c** or cyanophenyl **3a**–**c** derivatives. This could be explained by the increased electron withdrawing effect of the directly attached SO_2 group to the formazyl carbon. However, compounds **6a**–**d** showed less sensitivity than the cyano derivatives **5a**–**c**. Also, substituting the phenyl group in **6a**–**d** by the *p*-methylphenyl group decreased the sensitivity of the crown-formazans **7a**, **c** and **d** towards lithium. Such an effect may be attributed to the electron releasing effect of the methyl group.

3.1. Effect of sodium

It has been found that the effect of sodium differs in each case according to the crown-formazan used. Table 2 (column B) shows the percent effect of 10 mM sodium ion on 1 mM lithium in

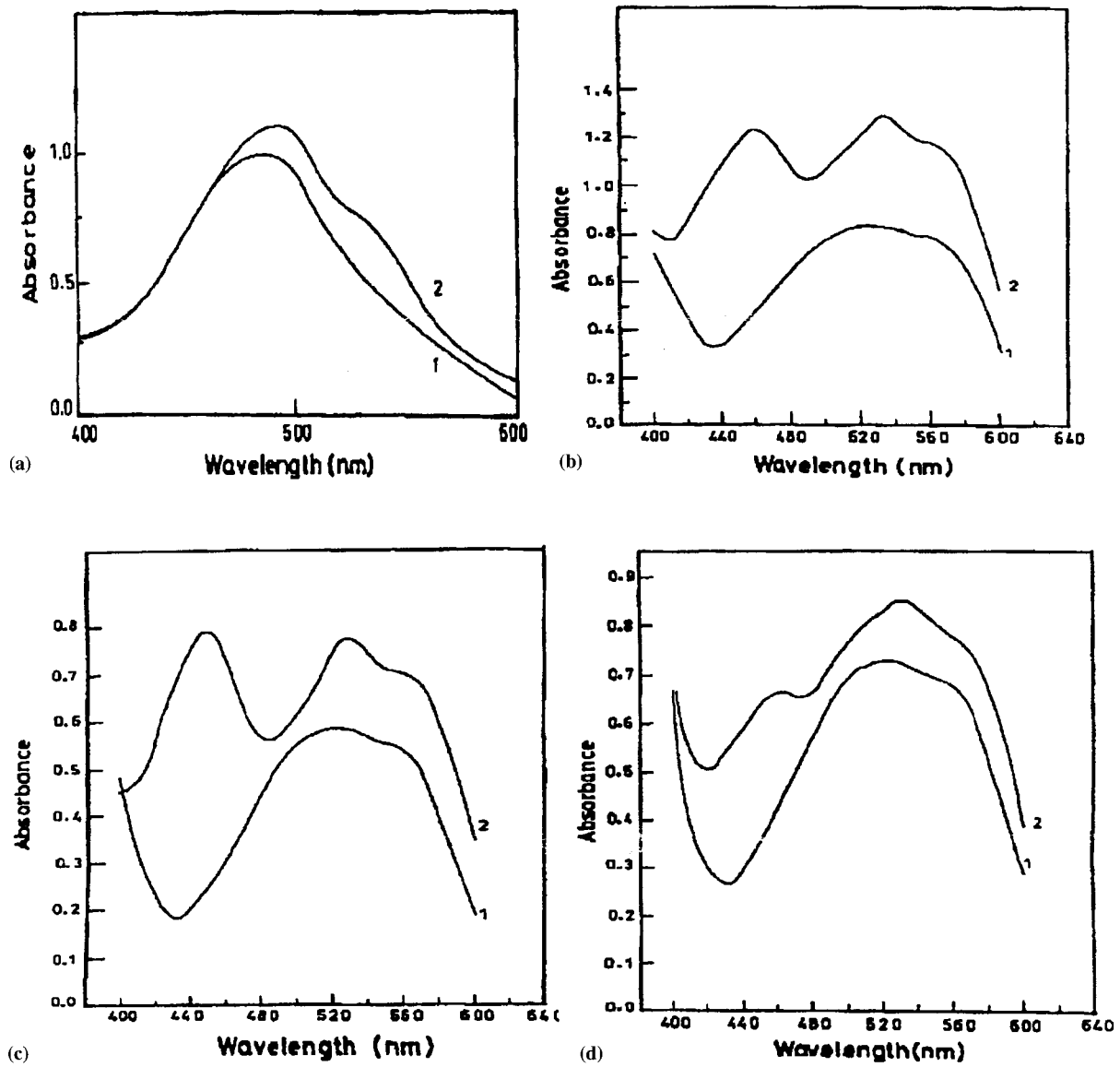

Fig. 1. (a): (1) The absorption spectra of **6c** in solution I; (2) the same in the presence of 3 mM Li; (b): as for (a) but for **4a**; (c): as for (a) but for **4b**; (d): as for (a) but for **4c**.

the range of 140–160 mM sodium ion concentration, (which is the sodium ion concentration in biological fluids) for the different crown-formazans (Fig. 3a–d shows the effect of sodium for some representative examples). Thus, the absorbance of the 3 mM lithium at the λ_{max} is affected by the sodium ion concentration for each crown-formazan in the following ways:

(a) Decrease from 50–200 mM of sodium for crowns **6c**, **4b**, **4c** and **4d**.

(b) Increase up to 60 mM of sodium and then decrease for crowns **2a**, **b**, **3a**–**c**, **4a**–**d**.

(c) Increase up to 70 mM of sodium and then decrease for crowns **2c**, **6a**.

(d) Increase up to 80 mM of sodium and then decrease for crowns **5b**, **7a**, **c**.

Table 1
Slope of the calibration graphs obtained by plotting the concentration of lithium (mol l^{-1}) against absorbance at the indicated λ_{max} in solutions I, II, III containing the different ligands **2–7**

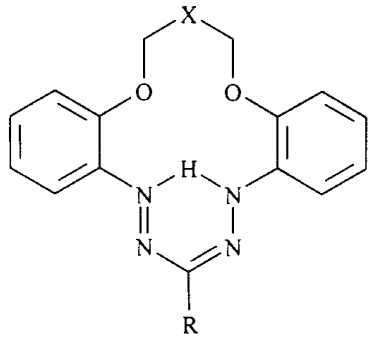

Compound No.	R	a, X = CH_2			b, X = C=CH_2			c, X = 0–C_6H_4			d, X = CHOH		
		I[a]	II[a]	III[a]	I[a]	II[a]	III[a]	I[a]	II[a]	III[a]	I[a]	II[a]	III[a]
5a–c	CN	97.5	25	6.7	37.5	135	33	19.3	38.4	2.6			
		λ_{max} 496.5 nm			λ_{max} 504 nm			λ_{max} 495 nm					
2a–c	Ph	22	3.6	—[b]	22	5	—[b]	26	0	---[b]			
		λ_{max} 520 nm			λ_{max} 514 nm			λ_{max} 512 nm					
3a–c	*p*-CNC_6H_4	26	14	2.6	25	11	—[b]	36	0	—[b]			
		λ_{max} 510 nm			λ_{max} 510 nm			λ_{max} 508 nm					
6a–d	$PhSO_4$	40	32	14	78	60	—[b]	60.8	44	16	29.3	17	14.3
		λ_{max} 488 nm			λ_{max} 487 nm			λ_{max} 490 nm			λ_{max} 490 nm		
7a, c, d	*p*-$CH_3C_6H_4SO_2$	37.3	8.8	1.2				46	35.2	3	40	17	17
		λ_{max} 488 nm						λ_{max} 489 nm			λ_{max} 487 nm		
4a–d	4-Pyridyl-*N*-oxide	84	30	11	136	30	18	122	42	40	50	9	8
		λ_{max} 460 nm			λ_{max} 450 nm			λ_{max} 460 nm			λ_{max} 450 nm		
		52	25	8.4	58	23	13	81	47	42	33	9	7.5
		λ_{max} 535 nm			λ_{max} 530 nm			λ_{max} 530 nm			λ_{max} 530 nm		

[a] I, II, and III refer to solutions I, II, and III.
[b] Precipitate is formed.

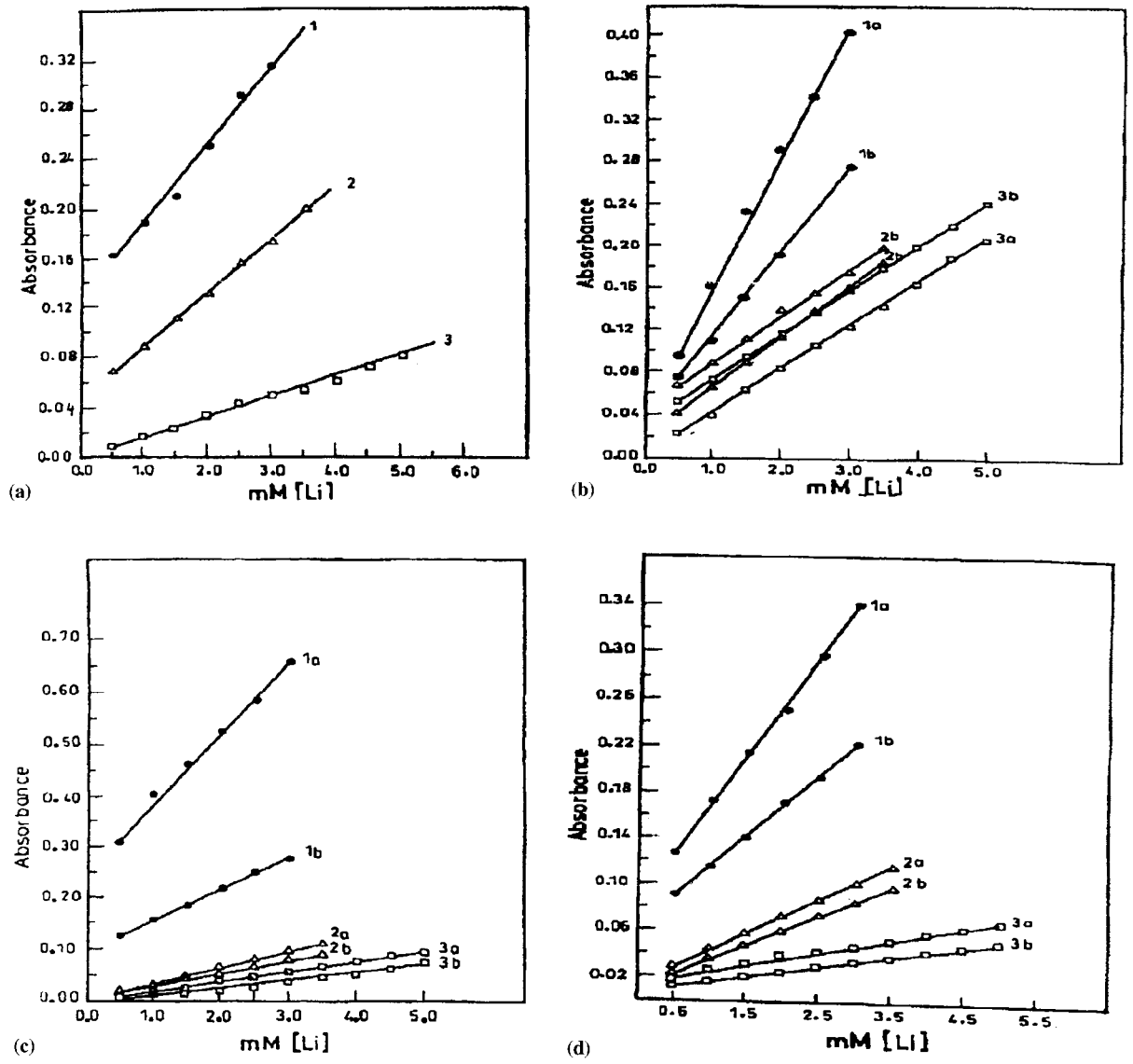

Fig. 2. (a): Calibration graphs of Li in solution I (1), in solution II (2), and in solution III (3) for the crowm-formazan **6c**; (b): calibration graphs of Li in solution I (1a, b), in solution II (2a, b), and in solution III (3a, b) for the crowm-formazan **4a** (1a, 2a, and 3a at $\lambda_{max} = 460$ nm; 1b, 2b, and 3b at $\lambda_{max} = 530$ nm); (c): as for (b) but for the crowm-formazan **4b** (1a, 2a, and 3a at $\lambda_{max} = 450$ nm; 1b, 2b, and 3b at $\lambda_{max} = 530$ nm); (d): as for (b) but for the crowm-formazan **4c** (1a, 2a, and 3a at $\lambda_{max} = 460$ nm; 1b, 2b, and 3b at $\lambda_{max} = 535$ nm).

(e) Increase up to 90 mM of sodium and then decrease for crown **7d**.

(f) Increase up to 100 mM of sodium and then decrease for crown **5a**.

(g) Increase up to 110 mM of sodium and then decrease for crown **5c**.

(h) Increase up to 120 mM of sodium and then decrease for crown **7b**.

The effects of 10 mM sodium on 1 mM lithium are generally in the 2–5% range, which corresponds to a relative selectivity for lithium of 500–200 at equal concentration changes.

Table 2
Reaction time and the influence of sodium for 1 mM lithium

Compound No.	R	a, X = CH_2		b, X = C=CH_2		c, X = 0–C_6H_4		d, X = CHOH	
		A	B	A	B	A	B	A	B
5a–c	CN	30	0.7	50	0.53	60	0.23		
2a–c	Ph	50	5.0	70	3.2	60	5.7		
3a–c	*p*-CNC_6H_4	70	2.9	70	4.1	50	1.4		
6a–d	$PhSO_4$	70	2.3	60	0.9	50	4.9	50	0.72
7a, c, d	*p*-$CH_3C_6H_4SO_2$	50	4.0			50	4.5	40	4.0
4a–d	4-Pyridyl-*N*-oxide	30[a]	12	40[a]	1.5	30[a]	5.7	60[a]	32
		30[b]	5.4	40[b]	5.9	30[b]	2.7	60[b]	15

A, the time (in min) to reach stability where the measurements were made, and B, percent effect of sodium ion on 1 mM lithium caused by adding 10 mM sodium in the range 140–160 mM sodium ion concentration for the different ligands **2–7**, (percent changes are negative).
[a] λ_{max} 450–460 nm, [b] λ_{max} 530–535 nm.

3.2. Effect of time

The absorbance of solution I was measured at different intervals of time up to 90 min. It was noticed that a slight increase or decrease in the absorbance occurs with time for most of the formazans under investigation, probably due to the rate of complexation and exchange with sodium. The state of stability is reached from 30–70 min as shown in Table 2 (Fig. 4a–d show the effect of time for some representative examples).

4. Conclusion

It is interesting to notice that crown-formazans containing the pyridyl *N*-oxide groups (compounds **4a–c**) showed the best results having the highest sensitivity to lithium determination, little affected by sodium and reaching stability in a relatively shortest time.

5. Experimental procedure for the synthetic part

All melting points are uncorrected. IR spectra were recorded on a Perkin-Elmer 1430 spectrophotometer. NMR spectra were measured with a Varian GEMINI 200 spectrometer (200 MHz ^1H NMR; 50 MHz ^{13}C NMR). ^{13}C NMR spectra were recorded using the APT pulse sequence. Mass spectra were recorded on a Finigan Mat312 (70 eV) or a Finigan Mat 1125 (70 eV) spectrometer. Elemental analyses were carried out at the Microanalytical Centre, Cairo University.

1,2-Dibromoethane, 1,3-dibromopropane, 1,4-dibromobutane, 2 - chloromethyl - 3 - chloropropene, α,α-dibromo-*o*-xylene, epichlorohydrin, 2,2-dichloroethylether, tetrabutylammonium iodide, tetrabutylammonium hydrogensulphate and benzyltriethylammonium chloride were used as purchased from Aldrich. The arylpyruvic acids [17,18], arenesulfonylacetic acids [19], ethyl 4-pyridylpyruvate 1-oxide [20] were prepared as reported.

6. Synthesis of bis(acetamido) ethers IIIiv–vi

*6.1. 2-Hydroxy-1,3-bis(2-acetamidophenoxy) propane (**IId**)*

To a solution of 2-acetamidophenol (**I**) (10 mmol) in DMF (10 ml) containing 10 mmol potassium carbonate, was added epichlorohydrin (5 mmol). The reaction mixture was heated on a

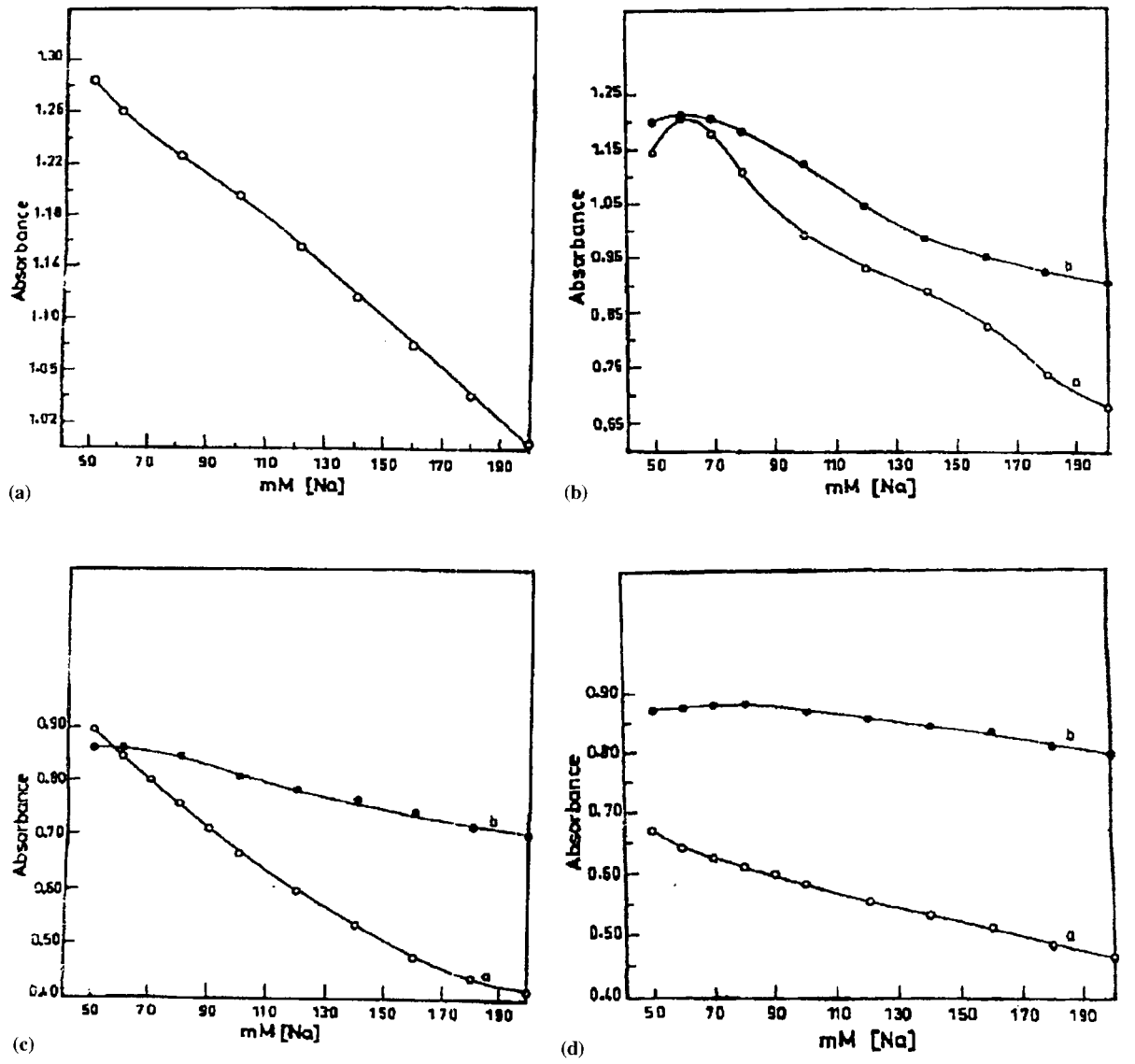

Fig. 3. (a): Effect of sodium ion concentration on the absorbance of 3 mM Li in solution I for the crowm-formazan **6c**; (b): as for (a) but for the crown-formazan **4a** (a, at $\lambda_{max} = 450–460$ nm; b, at $\lambda_{max} = 530–535$ nm); (c): as for (a) but for the crown-formazan **4b** (a, at $\lambda_{max} = 450–460$ nm; b, at $\lambda_{max} = 530–535$ nm); (d): as for (a) but for the crown-formazan **4c** (a, at $\lambda_{max} = 450–460$ nm; b, at $\lambda_{max} = 530–535$ nm).

steam bath for 2 h. Water (50 ml) was added and the reaction mixture was kept in the refrigerator over night. The solid obtained was collected and crystallized from ethanol as yellow crystals of **IId** (95%), m.p. 126–128°C; IR: 3348, 3229 (OH, NH), 1685 (C=O) cm^{-1}; ^1H NMR (DMSO) δ 2.1 (s, 6H, $COCH_3$), 4.05–4.36 (m, 5H, OCH_2, CHOH), 5.77 (d, 1H, OH), 6.88–7.99 (m, 8H, ArH's), 9.12 (s, 2H, NH). Anal. Calc. for $C_{19}H_{22}N_2O_5$ (358.39): C, 63.68; H, 6.19; N, 7.82. Found: C, 63.70; H, 6.30; N, 8.10%.

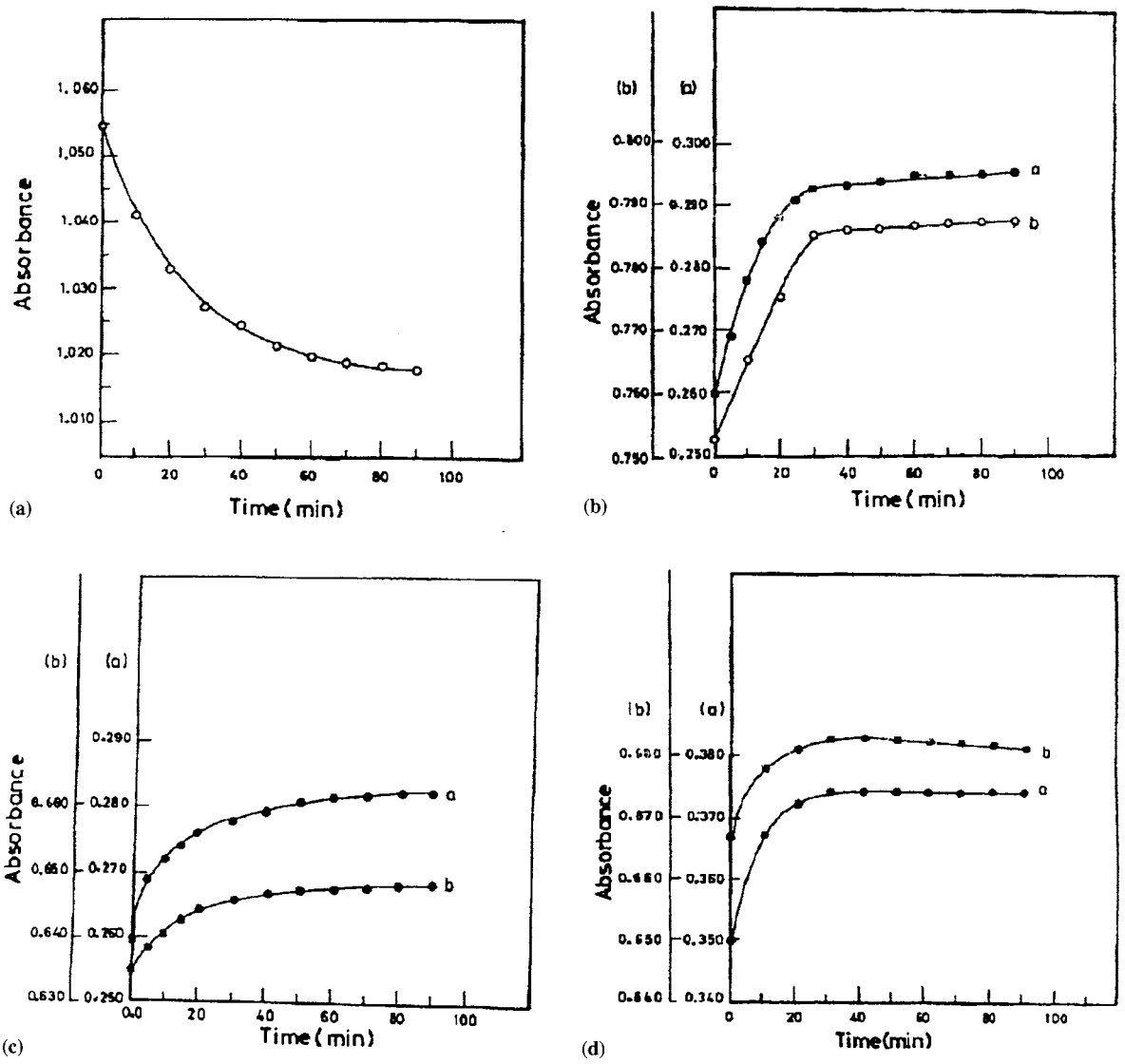

Fig. 4. (a): Effect of time on the absorbance signal of the crowm-formazan **6c** in solution I; (b): as for (a) but for the crown-formazan **4a** (a, at $\lambda_{max} = 450–460$ nm; b, at $\lambda_{max} = 530–535$ nm); (c): as for (a) but for the crown-formazan **4b** (a, at $\lambda_{max} = 450–460$ nm; b, at $\lambda_{max} = 530–535$ nm); (d): as for (a) but for the crown-formazan **4c** (a, at $\lambda_{max} = 450–460$ nm; b, at $\lambda_{max} = 530–535$ nm).

*6.2. 1,4-Bis(2-acetamidophenoxy)butane (**IIe**), 1,5-bis(2-acetamidophenoxy)-3-oxapentane (**IIf**)*

To a solution of the potassium salt of *o*-acetamidophenol (**I**) (10 mmol) in DMF (10 ml) was added each of 1,4-dibromobutane (for **IIe**) and/or 2,2′-dichlorodiethylether (for **IIf**) (5 mmol). The reaction mixture was heated under reflux for 15 min. The solvent was then removed in vacuo, and the remaining residue was washed with water and crystallized from the proper solvent to give **IIe**, **IIf**.

Compound **IIe** was crystallized from ethanol as colorless crystals (60%), m.p. 172°C; ^{1}H NMR

($CDCl_3$) δ 2.06 (t, 4H, $OCH_2\underline{CH_2}$), 2.13 (s, 6H, $COCH_3$), 4.14 (t, 4H, CH_2O), 6.86–8.35 (m, 10H, ArH's, NH). Anal. Calc. for $C_{20}H_{24}N_2O_4$ (356.42): C, 67.46; H, 6.79; N, 7.86. Found: C, 67.56; H, 6.82; N, 7.76%.

Compound **IIf** was crystallized from toluene as colorless crystals (59%), m.p. 133°C; ^1H NMR ($CDCl_3$) δ 2.07 (s, 6H, $COCH_3$), 3.92 (t, 4H, $\underline{CH_2}O\underline{CH_2}$), 4.23 (t, 4H, $OCH_2\underline{CH_2}OAr$), 6.90–8.36 (m, 10H, ArH's, NH). Anal. Calc. for $C_{20}H_{24}N_2O_5$ (372.42): C, 64.50; H, 6.50; N, 7.52. Found: C, 64.56; H, 6.42; N, 7.56%.

7. Synthesis of bis(*o*-aminophenoxy)ether dihydrochloride III

7.1. General procedure

To a solution of each of an appropriate **II** (10 mmol) in absolute ethanol (20 ml) was added concentrated hydrochloric acid (6 ml). The reaction mixture was heated under reflux for 1 h and the solvent was then removed in vacuo. The remaining solid was collected, washed with ether to give colorless crystals of the corresponding **III**

7.1.1. 2-Hydroxy-1,3-bis(2-aminophenoxy)propane dihydrochloride (IIId)

With the use of the general procedure, **IId** gave colorless crystal of **IIId** (92%), m.p. > 300°C. Anal. Calc. for $C_{15}H_{20}N_2Cl_2O_3$ (347.24): C, 51.88; H, 5.81; N, 7.07; Cl, 20.42. Found: C, 51.90; H, 6.00; N, 8.30; Cl, 20.10%.

7.1.2. 1,4-Bis(2-aminophenoxy)butane dihydrochloride (IIIe)

With the use of the general procedure, **IIe** gave colorless crystals of **IIIe** (90%), m.p. 269°C. Anal. Calc. for $C_{16}H_{22}Cl_2N_2O_2$ (345.27): C, 55.66; H, 6.42; N, 8.11; Cl, 20.54. Found: C, 55.69; H, 6.39; N, 8.22; Cl, 20.64%.

7.1.3. 1,5-Bis(2-amino phenoxy)-3-oxapentane dihydrochloride (IIIf)

With the use of the general procedure, **IIf** gave colorless crystals of **IIIf** (91%) m.p. 241–242°C. Anal. Calc. for $C_{16}H_{22}N_2Cl_2O_3$ (361.27): C, 53.19; H, 6.14; N, 7.75; Cl, 19.63. Found: C, 53.09; H, 6.10; N, 7.70; Cl, 20.01%.

8. Synthesis of macrocyclic crown-formazans 1–7

8.1. General procedure A

A solution of the appropriate diamine dihydrochloride **III** (1 mmol) in water (5 ml) and concentrated hydrochloric acid (3 ml) was diazotized at −5°C with a solution of sodium nitrite (0.14 g in 5 ml water) over 30 min. Stirring was continued for 30 min at −5°C. The solution was then added dropwise with stirring to a cold (0°C) solution containing (1 mmol) of each of the appropriate arylpyruvic acids, arylsulphonylacetic acid, ethyl 4-pyridylpyruvate 1-oxide, malonic acid, sodium pyruvate and cyanoacetic acid (1 mmol) in water (10 ml) containing NaOH (2.2 g) over a period of 1 h. The reaction mixture was then kept in the freezer overnight. The solid precipitate was collected and purified on preparative TLC using silica gel (60 F_{254}) with the proper eluent for each derivative.

8.2. General orocedure B

A solution of the appropriate diamine dihydrochloride **III** (1 mmol) in water (5 ml) and concentrated hydrochloric acid (3 ml) was diazotized at −5°C with a solution of sodium nitrite (0.14 g in 5 ml water) over 30 min. Stirring was continued for 30 min at −5°C. The solution was then added dropwise with stirring to a cold (0°C) solution of water–methylene chloride (20 ml each) containing the appropriate phase transfer catalyst (0.2 g), sodium pyruvate (1 mmol), arylsulfonylacetic acid (1 mmol) and sodium hydroxide (1.2 g). Stirring was continued for 12 h at 0°C and the reaction mixture was kept in the freezer overnight. The product was then extracted with methylene chloride. The solvent was then removed in vacuo and the remaining residue was purified as described in general procedure A.

*8.2.1. 16-Hydroxy-16,17-dihydro-5H, 7H,15H-dibenzo[b,i][1,11,4,5,7,8]dioxa-tetraazacycloteteradecine (**1d**)*

(a) With the use of general procedure A **IIId** was diazotized and coupled with sodium pyruvate to give, after chromatographic purification using a mixture of chloroform–petroleum ether (40–60) 5:1 as an eluent ($R_f = 0.42$), deep red crystals of **1d** (7%), m.p. 198°C; Ms: m/z 312 (M^+, 93.6%), 212 (12.5%), 170 (12.2%), 120 (100%), 108 (53%), 94 (60.5%), 80(59.5%); ^{1}H NMR ($CDCl_3$) δ 3.32 (d, 1H, OH), 4.25–4.66 (m, 5H, OCH_2, CHOH), 6.95–7.92 (m, 8H, ArH's), 8.32 (s, 1H, CH=N), 15.6 (s, 1H, NH). Anal. Calc. for $C_{16}H_{16}N_4O_3$ (312.33): C, 61.53; H, 5.16; N, 17.94. Found: C, 61.70; H, 5.10; N, 18.10%.

(b) With the use of general procedure B compound **1d** was obtained in an 18% yield using tetrabutylammonium iodide, in a 16% yield using tetrabutylammonium hydrogen sulfate and in a 22% yield using benzyltriethylammonium chloride as PTC.

(c) With the use of general procedure A **IIId** was diazotized and coupled with malonic acid in a pyridine–ethanol mixture (30:10) containing $CuSO_4$ (1 mmol) and sodium acetate (3 g) following the same sequence used for the general procedure to give, after chromatographic purification, deep red crystals of **1d** (6%).

*8.2.2. 16,17-Dihydro-5H,15H-7-phenyldibenzo-[b,i][1,11,4,5,7,8]dioxatetraazacyclotetra-decine (**2a**)*

With the use of general procedure B **IIIa** was diazotized and coupled with phenylpyruvic acid to give, after chromatographic purification using a mixture of methylene chloride–petroleum ether (40–60) 1:3 as an eluent, deep red crystals of **2a** (20%) using tetrabutylammonium iodide as PTC, m.p. 178°C (lit.[14], yield 4%, m.p. 178–180°C).

*8.2.3. 7-(4-Cyanophenyl)-16,17-dihydro-5H,15H--dibenzo[b,i][1,11,4,5,7,8]dioxatetraazacyclotetra-decine (**3a**)*

With the use of general procedure A **IIIa** was diazotized and coupled with 4-cyanophenylpyruvic acid to give, after chromatographic purification using chloroform as an eluent ($R_f = 0.63$), deep red crystals of **3a** (10%), m.p. 259–262°C; Ms: m/z 397 (M^+, 66.25%), 212 (13.6%), 120 (64.18%), 77 (37.79%), 41 (100%); ^{1}H NMR ($CDCl_3$) δ 2.49 (quintet, 2H, OCH_2–$\underline{CH_2}$). 4.45 (t, 4H, OCH_2), 7.0–8.35 (m, 12H, ArH's), 15.94 (s, 1H, NH). Anal. Calc. for $C_{23}H_{19}N_5O_2$ (397.434): C, 69.51; H, 4.82; N, 17.62. Found: C, 69.70; H, 4.80; N, 17.52%.

*8.2.4. 7-(4-Cyano phenyl)-16-methylene-16,17-dihydro-5H,15H-dibenzo[b,i][1,11,4,5,7,8]dioxa-tetreazacyclotetradecine (**3b**)*

With the use of general procedure A **IIIb** was diazotized and coupled with 4-cyanophenylpyruvic acid to give, after chromatographic purification using chloroform as an eluent ($R_f = 0.81$), deep red crystals of **3b** (11%); m.p. 250°C; Ms: m/z 409 (M^+, 53.92%), 235 (18.11%), 160 (28.27%), 145 (100%), 131 (65.85%), 120 (53.22%); ^{1}H NMR ($CDCl_3$) δ 4.84 (s, 4H, OCH_2), 5.58 (s, 2H, $\underline{CH_2}$=C), 7.0–8.30 (m, 12H, ArH's), 15.99 (s, 1H, NH). Anal. Calc. for $C_{24}H_{19}N_5O_2$ (409.44): C, 70.40; H, 4.68; N, 17.10. Found: C, 70.55; H, 4.62; N, 17.02%.

*8.2.5. 13-(4-Cyanophenyl)-5,21-dihydro-11H-tribenzo[b,i,m][1,11,4,5,7,8]dioxatetreazacyclo-pentadecine (**3c**)*

With the use of general procedure A **IIIc** was diazotized and coupled with 4-cyanophenylpyruvic acid to give, after chromatographic purification using a mixture of chloroform–petroleum ether (40–60) 1:1 as an eluent ($R_f = 0.61$), deep red crystals of **3c** (9%); m.p. 278–280°C; Ms: m/z 459 (M^+, 57.63%), 367 (12.25%), 235 (21.11%), 195 (91.25%), 181 (75.75%), 104 (78.22%), 44 (100%); ^{1}H NMR ($CDCl_3$) δ 5.37 (s, 4H, OCH_2Ar), 7.04–8.25 (m, 16H, ArH's), 16.03 (s, 1H, NH). Anal. Calc. for $C_{28}H_{21}N_5O_2$ (459.506): C, 73.19; H, 4.61; N, 15.24. Found: C, 73.28; H, 4.71; N, 15.28%.

*8.2.6. 7-(4-Cyanophenyl)-16-hydroxy-16,17-dihydro-5H,15H-dibenzo[b,i][1,11,4,5,7,8]dioxa-tetraazacyclotetradecine (**3d**)*

With the use of general procedure A **IIId** was diazotized and coupled with 4-cyanophenylpyruvic acid to give, after chromatographic purifica-

tion using chloroform as an eluent ($R_f = 0.18$), deep red crystals of **3d** (8%), m.p. 297–299°C; Ms: m/z 413 (M^+, 62.29%), 235 (15.53%), 212 (13.96%), 128 (29.69%), 120 (100%), 94 (57.51%); ^{1}H NMR (DMSO) δ 4.49 (m, 5H, OCH_2, CHOH), 5.53 (d, 1H, OH), 7.12–8.33 (m, 12H, ArH's), 15.88 (s, 1 H, NH). Anal. Calc. for $C_{23}H_{19}N_5O_3$ (413.43): C, 66.82; H, 4.63; N, 16.94. Found: C, 65.99; H, 4.66; N, 16.83%.

*8.2.7. 7-(4-Cyanophenyl)-5H-15,16,17,18-tetrahydrodibenzo[b,i][1,11,4,5,7,8]dioxatetra-azacyclopentadecine (**3e**)*

With the use of general procedure A **IIIe** was diazotized and coupled with 4-cyanophenylpyruvic acid to give, after chromatographic purification using chloroform as an eluent ($R_f = 0.75$), deep red crystals of **3e** (9%), m.p. 208–210°C; Ms: m/z 411 (M^+, 100%), 275 (5.87%), 212 (10.68%), 162 (15.17%), 120 (49.22%), 55 (34%); ^{1}H NMR ($CDCl_3$) δ 2.14 (t, 4H, OCH_2-CH_2), 4.14 (t, 4H, OCH_2), 6.95–8.32 (m, 12H, ArH's), 14.78 (s, 1H, NH). Anal. Calc. for $C_{24}H_{21}N_5O_2$ (411.46): C, 70.06; H, 5.14; N, 17.02. Found: C, 70.16; H, 5.15; N, 16.91%.

*8.2.8. 7-(4-Cyanophenyl)-5H-15,16,18,19-tetrahydrodibenzo[b,i][1,11,14,4,5,7,8]trioxa-tetraazacyclohexadecine (**3f**)*

With the use of general procedure A **IIIf** was diazotized and coupled with 4-cyanophenylpyruvic acid to give. after chromatographic purification using chloroform as an eluent ($R_f = 0.44$), deep red crystals of **3f** (14%); m.p. 187–189°C; Ms: m/z 427 (M^+, 52%), 399 (13.5%), 212 (28.87%), 120 (100%), 91 (41.51%); ^{1}H NMR ($CDCl_3$) δ 4.07 (t, 4H, CH_2OCH_2), 4.33 (t, 4H, $OCH_2\ CH_2OAr$), 6.97–8.29 (m, 12H, ArH's), 14.49 (s,1H, NH). Anal. Calc. for $C_{24}H_{21}N_5O_3$ (427.46): C, 67.44; H, 4.95; N, 16.38. Found: C, 67.94; H, 5.0; N, 16.48%.

*8.2.9. 16,17-Dihydro-5H,15H-dibenzo[b,il-[1,11,4,5,7,8]dioxatetraazacyclotetra-decine-7-(4-pyridyl 1-oxide) (**4a**)*

With the use of general procedure A **IIIa** was diazotized and coupled with ethyl 4-pyridylpyruvate 1-oxide to give, after chromatographic purification using a mixture of methylene chloride/methanol (20:1) as an eluent ($R_f = 0.36$), deep red crystals of **4a** (20%), m.p. 242°C; Ms: m/z 389 (M^+, 13.5%), 373 (63.8%), 212 (26.7%), 184 (21.4%), 148 (17.8%), 78 (72.7%) 52 (89.8%); ^{1}H NMR (DMSO) δ 2.30 (br s, 2H, OCH_2-CH_2), 4.43 (br s, 4H, OCH_2), 7.06–8.24 (m, 12H, ArH's), 15.70 (s, 1H, NH). Anal. Calc. for $C_{21}H_{19}N_5O_3$ (389.41): C, 64.77; H, 4.92; N, 17.98. Found: C, 64.69; H, 4.90; N, 17.90%.

*8.2.10. 6-Methylene-16,17-dihydro-5H,15H-dibenzo[b,i][1,11,4,5,7,8]dioxate-treazacyclotetradecine-7-(4-pyridyl 1-oxide) (**4b**)*

With the use of general procedure A **IIIb** was diazotized and coupled with ethyl 4-pyridylpyruvate 1-oxide to give, after chromatographic purification using a mixture of chloroform–methanol (20:1) as an eluent ($R_f = 0.4$), deep red crystals of **4b** (20%), m.p. 257°C; Ms: m/z 401 (M^+, 12.7%), 385 (47.2%), 211 (14.1%), 160 (20.8%), 131 (87.0%), 79 (68.9%), 52 (100%); ^{1}H NMR ($CDCl_3$) δ 4.85 (s, 4H, OCH_2), 5.58 (s, 2H, C=CH2), 7.06–8.21 (m, 12H, ArH's), 15.92 (s, 1H, NH). Anal. Calc. for $C_{22}H_{19}N_5O_3$ (401.42): C, 65.83; H, 4.77; N, 17.45. Found: C, 65.80; H, 4.74; N, 17.40%.

*8.2.11. 5,21-Dihydro-1 1H-tribenzo[b,i,m][1,11,4,5,7,8]dioxatetreazacyclopentadecine-13-(4-pyridyl 1-oxide) (**4c**)*

With the use of general procedure A **IIIc** was diazotized and coupled with ethyl 4-pyridylpyruvate 1-oxide to give, after chromatographic purification using a mixture of methylene chloride—methanol (100:6) as an eluent ($R_f = 0.43$), deep red crystals of **4c** (17%), m.p. 270°C; Ms: m/z 451 (M^+, 9.5%), 435 (44.7%), 212 (25.6%), 196 (81.5%), 121 (14.1%), 104 (100%), 78 (98.7%); ^{1}H NMR (DMSO) δ 5.50 (s, 4H, OCH_2), 7.05–8.23 (m, 16H, ArH's), 15.81 (s, 1H, NH). Anal. Calc. for $C_{26}H_{21}N_5O_3$ (451.48): C, 69.17; H, 4.69; N, 15.51. Found: C, 69.13; H, 4.60; N, 15.43%.

*8.2.12. 16-Hydroxy-16,17-dihydro-5H,15H-benzot[b,i][1,11,4,5,7,8]dioxatetreazacyclotetra-decine-7-(4-pyridyl 1-oxide) (**4d**)*

With the use of general procedure A **IIId** was

diazotized and coupled with ethyl 4-pyridylpyruvate 1-oxide to give, after chromatographic purification using a mixture of chloroform–methanol (40:3) as an eluent ($R_f = 0.40$), deep red crystals of 4d (15%), m.p. 266°C; Ms: m/z 405 (M^+, 12.9%), 389 (16.9%), 211 (17.2%), 170 (17.4%), 146 (10.4%), 120 (100%), 79 (65.1%), 52 (81.8%); ^{1}H NMR could not be obtained because the compound is insoluble in DMSO. Anal. Calc. for $C_{21}H_{19}N_5O_4$ (405.41): C, 62.22; H, 4.72; N, 17.27. Found: C, 62.10; H, 4.68; N, 17.22%.

*8.2.13. 16-Hydroxy-16,17-dihydro-5H,15H-dibenzo[b,i][1,11,4,5,7,8]dioxatetraazacyclotetradecine-7-carbonitrile (**5d**)*

With the use of general procedure A **IIId** was diazotized and coupled with cyanoacetic acid in pyridine (10 ml) and ethanol (10 ml) containing $CuSO_4$ (1 mmol) and sodium acetate (3 g) following the same reaction sequence used for the general procedure to give, after chromatographic purification using chloroform as an eluent ($R_f =$ 0.62), deep red crystals of **5d** (40%); m.p. 274°C; Ms: m/z337 (M^+, 100%), 312 (3.5%), 212 (14.2%), 120 (100%), 108 (81.2%), 44 (44.7%); IR: 2227 cm^{-1}, (CN), 3465 cm^{-1}, (OH); ^{1}H NMR (DMSO) δ 4.16 (s, 5H, OCH_2, CHOH), 5.54 (d, 1H, OH), 7.067.85 (m, 8H, ArH's), 15.89 (s,1H, NH). Anal. Calc. for $C_{17}H_{15}N_5O_3$ (337.33): C, 60.53; H, 4.48; N, 20.76. Found: C, 60.70; H, 4.60; N, 21.00%.

*8.2.14. 16-Hydroxy-16,17-dihydro-5H,15H-7-phenylsulphonyldibenzo[b,i][1,11,4,5,7,8]dioxatetraazacyclotetradecine (**6d**)*

(a) With the use of general procedure A **IIId** was diazotized and coupled with phenylsulphonylacetic acid to give, after chromatographic purification using chloroform as an eluent ($R_f = 0.72$), deep red crystals of **6d** (8%); m.p. 320°C; Ms: m/z 452 (M^+, 36%), 311 (8.8%), 283 (7%), 212 (8.2%), 120 (100%); IR: 3510 cm1^{-}, (OH), 1159, 1314 cm^{-1}, (SO_2); ^{1}H NMR (DMSO) δ 4.15–4.47 (m, 5H, OCH_2, CHOH), 5.50 (d, 1H, OH), 7.06–8.12 (m, 13H, ArH's), 15.46 (s, 1H, NH). Anal. Calc. for $C_{22}H_{20}N_4O_5S$ (452.49): C, 58.40; H, 4.46; N, 12.38; S,7.30. Found: C, 58.60; H, 4.70; N, 12.60; S, 7.30%.

(b) With the use of general procedure B compound **6d** was obtained in a 16% yield using tetrabutylammonium iodide, in a 23% yield using tetrabutylammonium hydrogen sulfate and in a 17% yield using benzyltriethylammonium chloride as PTC.

*8.2.15. 5,21-Dihydro-11H-13-p-tolylsulphonyltribenzo[b,i,m][1,11,4,5,7,8]dioxatetraazacyclopentadecine (**7a**)*

With the use of general procedure B **IIIa** was diazotized and coupled with *p*-tolylsulphonylacetic acid to give, after chromatographic purification using a mixture of methylene chloride–petroleum ether (40-60) 1:3 as an eluent, deep red crystals of **7a** (30%) using tetrabutylammonium iodide as PTC, m.p. 228-229°C (lit.[15], yield 11%, m.p. 227–229°C).

*8.2.16. 16-Hydroxy-16,17-dihydro-5H,15H-7-p-tolylsulphonyldibenzo[b,i][1,11,4,5,7,8]dioxatetraazacyclotetradecine (**7d**)*

(a) With the use of general procedure A **IIId** was diazotized and coupled with *p*-tolylsulfonylacetic acid to give, after chromatographic purification using chloroform as an eluent ($R_f = 0.8$), deep red crystals of **7d** (12%); m.p. 228°C; Ms: m/z 466 (M^+, 37%), 311 (10.5%), 383 (10.5%), 212 (7%), 120 (85.2%), 108 (75%), 91 (100%); IR: 3476 cm^{-1}, (OH), 1313–1160 cm^{-1}, (SO_2); ^{1}H NMR ($CDCl_3$) δ 2.4 (s, 3H, C_6H_4 $\underline{CH_3}$), 3.1 (d, 1H, OH), 4.25–4.33 (m, 3H, OCH_2, CHOH), 4.6 (dd, 4.2 Hz, 9.6 Hz, 2H, OCH_2), 6.95–8.05 (m, 12H, ArH's), 15.65 (s, 1H, NH). Anal. Calc. for $C_{23}H_{22}N_4O_5S$ (466.56): C, 59.22; H, 4.75; N, 12.01; S, 6.87. Found: C, 58.90; H, 4.90; N, 11.70; S, 7.0%.

(b) With the use of general procedure B compound **7d** was obtained in a 23% yield using tetrabutylammonium iodide, in an 18% yield using tetrabutylammonium hydrogen sulfate and in a 24% yield using benzyltriethylammonium chloride as PTC.

*8.3. Synthesis of 1,5-diarylformazans **VIIa–c***

8.3.1. General procedure

A solution of aniline and/or *p*-anisidine (1

mmol) in water (5 ml) and concentrated hydrochloric acid (3 ml) was diazotized at −5°C with a solution of sodium nitrite (0.14 g in 5 ml water) over 5 min. Stirring was continued for 30 min at −5°C. The solution was then added dropwise with stirring to a solution containing (1 mmol) of each of the appropriate 4-cyanophenylpyruvic acids and/or ethyl 4-pyridylpyruvate 1-oxide (1 mmol) in water (10 ml) containing NaOH (2.2 g) over a period of 10 min. The reaction mixture was then kept in the freezer overnight. The solid obtained was collected and crystallized from the proper solvent to give corresponding formazan **VIIa**–**c**.

*8.3.2. 1,5 Diphenyl-3-(4-cyanophenyl)formazan **VIIa***

With the use of the general procedure aniline was diazotized and coupled with 4-cyanophenylpyruvic acids to give crude **VIIa** which was crystallized from DMF to give (69%) deep red crystals, m.p. 224°C (lit.[21] m.p. 203–204°C]. ^{1}H NMR ($CDCl^3$) δ 7.69–8.23 (m, 14H, Ar H's), 15.67 (s, 1H, NH). Anal. Calc. for $C_{20}H_{15}N_5$ (325.37): C, 73.83; H, 4.65; N, 21.52. Found: C, 73.72; H, 4.55; N, 21.40%.

*8.3.3. 1,5-Diphenyl-3-(4-pyridyl 1-oxide)formazan **VIIb***

With the use of the general procedure aniline was diazotized and coupled with ethyl 4-pyridylpyruvate 1-oxide to give crude **VIIb** which was crystallized from toluene to give (70%) deep red crystals, m.p. 215°C (lit.[22] m.p. 203–204°C).

*8.3.4. 1,5-Di-p-methoxyphenyl-3-(4-pyridyl 1-oxide)formazan **VIIc***

With the use of the general procedure *p*-anisidine was diazotized and coupled with ethyl 4-pyridylpyruvate 1-oxide to give crude **VIIc** which was crystallized from ethanol to give (52%) deep red crystals, m.p. 130°C. ^{1}H NMR ($CDCl_3$) δ 3.87 (s, 6H, OCH_3), 6.97–8.22 (m, 12H, ArHs), 15.72 (s, 1H, NH). Anal. Calc. for $C_{20}H_{19}N_5O_3$ (377.40): C, 63.65; H, 5.07; N, 18.56. Found: C, 63.32; H, 4.99; N, 18.40%.

References

[1] A. Kaplan, L. Szabo, Clinical Chemistry: Interpretation and Techniques, Lea and Febiger, Philadelphia, PA, 1979, pp. 362–363.
[2] N.W. Tietz (Ed.), Fundamentals of Clinical Chemistriy, Saunders, Philadelphia, PA, 1970, pp. 878, 899–900.
[3] Y.A. Ibrahim, A.H.M. Elwahy, H.R. Hanna, S.K. Khella, Supramol. Chem. 4 (1994) 83.
[4] V.M. Dziomko, V.M. Ostrovskaya, T.E. Zhukova, Khim. Geterotsikl. Soedin. 8 (1979) 1039.
[5] R.V. Sitnikova, A.N. Krylova, S.L. Zelichenok, et al., Zh. Anal. Khim. 37 (1982) 611.
[6] A.S. Attiyat, Y.A. Ibrahim, G.D. Christian, Microchem. J. 37 (1988) 114.
[7] R.V. Sitnikova, A.N. Krylova, Lab. Delo 3 (1980) 142.
[8] E.Y. Misionzhnik, M.G. Uzbekov, V.M. Ostrovskaya, et al., Lab. Delo 7 (1990) 19.
[9] M.S. Kravchenko, V.M. Ostrovskaya, M.S. Fumarova, Vysokochist. Veshchestva 6 (1990) 152.
[10] V.M. Ostrovskaya, G.I. Sitnikova, I.A. D'yakonova et al., USSR Pat. No. 1495714, 1989; Chem. Abstr. 111 (1989) 224523.
[11] C.I. Lin, M. Pirio, USA Pat. No. 4742010, 1988; Chem. Abstr. (1988) 110, 88600.
[12] G.D. Christian, Lithium 3 (1990) 181.
[13] Y.A. Ibrahim, B.N. Barsoum, A.H.M. Elwahy, S.K. Khella, Supramol. Chem. 9 (1997) 5.
[14] Y.A. Ibrahim, A.H.M. Elwaby, A.A. Abbas, Tetrahedron 50 (1994) 11489.
[15] Y.A. Ibrahim, A.H.M. Elwahy, A.A. Abbas, Heteroatom. Chem. 7 (1996) 215.
[16] A.R. Katritzky, S.A. Belyakova, H.D. Durst, Tetrahedron Lett. 35 (1994) 6465.
[17] A.G.L. Cooper, J.Z. Ginos, A. Meister, Chem. Rev. 83 (1983) 2188.
[18] E. Erlenmeyer, F. Wittenberg, Liebigs Ann. 337 (1904) 299.
[19] S. Gabriel, Chem. Ber. 14 (1881) 833.
[20] N.Y. Ivashchenko, O.N. Yakovleva, S.D. Moshchitskii, A.F. Pavlenko, L.M. Shvydak, Fiziol. Aktiv. Veshchestva (1969) 150 (in Russian) Chem. Abst. 73 (1970) 35719.

ELSEVIER

Talanta 47 (1998) 1215–1222

Talanta

Evaluation of some new 14- and 15-crown-formazans as carriers in cesium ion selective electrodes[1]

Barsoum N. Barsoum, Suzan K. Khella, Ahmed H.M. Elwaby, Ashraf A. Abbas, Yehia A. Ibrahim *

Department of Chemistry, Faculty of Science, Cairo University, Giza, Egypt

Received 11 May 1998; accepted 18 May 1998

Abstract

A number of new crown-formazans with 14 and 15 membered rings have been investigated as selective neutral carriers in cesium ion selective electrodes. Two plasticizers (NPOE and NPBnE) were studied. The new 14-crown-formazan **4a** containing the 4-pyridyl *N*-oxide at the formazyl carbon exhibited the highest selectivity in cesium ion selective electrodes, especially towards the two low selectivity monovalent ions K^+ and $NH4^+$. Also, membranes containing the plasticizer NPBnE showed better cesium selectivity relative to most ions than those containing NPOE. Membranes containing **4a** and variable compositions of plasticizers, potassium tetrakis-(*p*-chlorophenyl)borate (KTpClPB), and trioctylphosphine oxide (TOPO) were studied in order to prepare an electrode with the optimum cesium selectivity. The highest selectivity for cesium was achieved with the two electrodes designated d and e with membranes containing the ionophore **4a**, NPBnE and KTpClPB with and without TOPO. Selectivities are reported relative to sodium, potassium, barium, calcium, ammonium, lithium, cobalt, and magnesium. © 1998 Elsevier Science B.V. All rights reserved.

Keywords: Cesium ion selective electrodes; 14-Crown-formazans; 15-Crown-formazans; Carriers

1. Introduction

More stringent requirements are needed for the monitoring and microdetermination of cesium in mineral rocks, thermal water in nuclear and industrial wastes, soil, plants, biological, and botanical samples. The methods reported for cesium ion microdetermination in aqueous and nonaqueous solutions include spectrophotometric [1] atomic absorption [2–21] radioanalysis [22–36], and potentiometric [37–45] methods. Among the two crown compounds reported as ionophores in the potentiometric methods [44,45] the cyanodibenzo-14-crown-4 **1a** showed the highest selectivity in cesium ion selective electrodes [45]. In the present study the authors undertook the evaluation of the

* Corresponding author. E-mail: Yehia_Al@FRCU.EUN.EG

[1] Dedicated to Professor Gary D. Christian on the occasion of his 60th birthday.

0039-9140/98/$ - see front matter © 1998 Elsevier Science B.V. All rights reserved.
PII S0039-9140(98)00204-5

12 new 14- and 15-crown-formazans **1**–**4** as ionophores in cesium ion selective electrodes. The aim of this research was to study the effect of two structural factors, namely the ether part of these macrocycles and the substituent at the formazyl carbon on enhancing the selectivity of the crown-formazans in cesium ion selective electrodes.

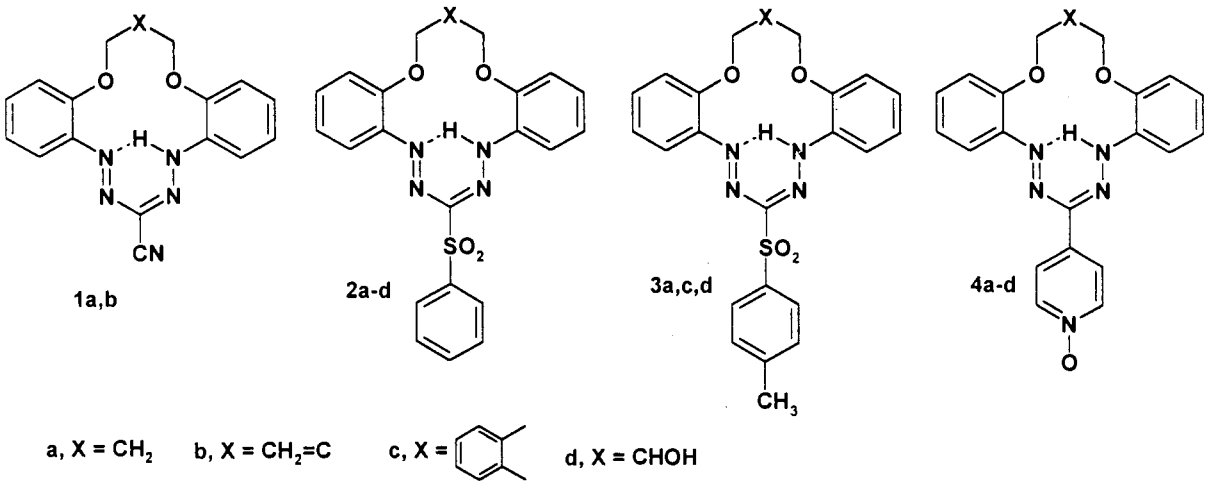

2. Experimental

2.1. Reagents and chemicals

The crown-formazans **1c**, **2**–**4** used in the present study were prepared according to the procedure described in the preceding article. High molecular weight polyvinyl chloride (PVC) was obtained from Fluka. The plasticizers *o*-nitrophenyloctyl ether (NPOE) and *o*-nitrophenylbenzyl ether (NPBnE) were prepared following the procedures previously described [46]. Potassium tetrakis-(*p*-chlorophenyl)borate (KTpClPB) was obtained from Specialty Organics, Irwindale, CA. Trioctylphosphine oxide (TOPO) was obtained from Aldrich. All salt solutions were prepared from reagent grade chlorides using deionized water.

2.2. Electrode measurement system

Measurements were made by the use of the following cell:

Hg, Hg_2Cl_2, KCl (sat′d)

/sample solution/membrane/AgCl, Ag.

A Beckman digital pH meter (model 4500) was used for monitoring the voltage.

2.3. Electrode membrane solution preparation

PVC (33.0 mg), individual crown-formazan **1**–**4** corresponding to a minimum of 4% (w/w) (4.1 mg) of neutral carrier in the membrane, a plasticizer (NPOE or NPBnE) (65.0 mg) and KTpClPB (0.5 mg) were dissolved in 350 μl tetrahydrofuran. Membranes a–g containing the crown-formazan **4a** were prepared as outlined in Table 5.

2.4. Electrode fabrication

Two aliquots of 25 μl of the above membrane solution were carefully deposited on a compact Ag/AgCl plug of a Beckman threaded ion selective electrode tip. The second aliquot was deposited after the first aliquot had almost dried. The tip was left to stand for 24 h to allow the THF solvent to evaporate and then it was soaked in 0.1 M CsCl solution for 24 h before use following the recommended procedure [47].

Table 1
Reciprocals of the selectivity coefficient ($1/K^{pot}_{Cs,M}$) for cesium ion with respect to other metal cations, with ionophores **2a**, **3a**, and **4a** using NPOE and NPBnE plasticizers

Ionophore	Plasticizer	Slope	$1/K^{pot}_{Cs,Na}$	$1/K^{pot}_{Cs,K}$	$1/K^{pot}_{Cs,Ba}$	$1/K^{pot}_{Cs,Ca}$	$1/K^{pot}_{Cs,NH_4}$	$1/K^{pot}_{Cs,Li}$	$1/K^{pot}_{Cs,Co}$	$1/K^{pot}_{Cs,Mg}$
2a	NPOE	50	240	5.3	300	300	18	420	1300	1300
2a	NPBnE	53	250	5.7	410	630	25	920	1500	1900
3a	NPOE	44	79	2.9	130	69	4.2	250	460	460
3a	NPBnE	50	140	24	390	200	7.7	330	660	660
4a	NPOE	50	360	8.7	260	300	8.7	260	700	900
4a	NPBnE	47	680	31	660	520	25	360	1400	1100

Table 2
Reciprocals of the selectivity coefficient ($1/K^{pot}_{Cs,M}$) for cesium ion with respect to other metal cations, with ionophores **2b**, and **4b** using NPOE and NPBnE plasticizers

Ionophore	Plasticizer	Slope	$1/K^{pot}_{Cs,Na}$	$1/K^{pot}_{Cs,K}$	$1/K^{pot}_{Cs,Ba}$	$1/K^{pot}_{Cs,Ca}$	$1/K^{pot}_{Cs,NH_4}$	$1/K^{pot}_{Cs,Li}$	$1/K^{pot}_{Cs,Co}$	$1/K^{pot}_{Cs,Mg}$
2b	NPOE	50	110	3.5	170	83	4.4	330	500	700
2b	NPBnE	50	180	4.8	200	115	6.6	480	830	1000
4b	NPOE	53	150	21	240	330	34	140	660	1020
4b	NPBnE	51	260	24	330	280	27	390	710	1020

2.5. Procedure

Selectivity coefficients were determined by the separate solution method as previously described [45]. Standard solutions of 0.2, 0.5, 2, 5, 10, 20, 50, 100 and 200 mM CsCl (the primary ion) in deionized water were used. The signals from 100 mM pure solutions of the chlorides of sodium, potassium, cobalt, barium, lithium, magnesium, calcium, and ammonium were also recorded for all the electrodes.

2.6. Selectivity coefficient determination

$K^{pot}_{Cs,M}$ was determined according to the separate solution method [48,49]. In this method the selectivity coefficient is calculated from the measured potentials of the primary ion and the secondary ion at equal concentrations of the pure solutions of these ions.

$$\log K^{pot}_{Cs,M} = \frac{E_2 - E_1}{S} + (1 - \frac{1}{Z_M}) \log [A]$$

Z_M is the charge of the secondary ion, [A] is the concentration of the primary ion (Cs), S is the slope of the cesium (primary ion) calibration curve.

3. Results and discussions

The electrodes were fabricated as described for the best selective electrodes containing the crown-formazan **1a** [45] except that the plasticizer NPBnE was used in the present study instead of *o*-nitrophenylpentyl ether (NPPE) which was shown to have poor selectivity [45]. Tables 1–4 list the slope and selectivity coefficient ($K^{pot}_{Cs,M}$) of the different membranes investigated using the separate solution method. All the membranes gave linear calibration curves over the concentration range measured for the primary ion with a slope ranging from 43–55 as shown in Tables 1–4. The calibration plots for the electrodes based on the investigated carriers **1**–**4** showed a near Nernstian response slope (43–55 mV decade^{-1}) for Cs^+ and their minimum detection for Cs^+ was approximately 2×10^{-4} M. The response time of the electrode to changes in Cs^+ concentration was less than 5 min. The life time of the membranes is long enough for practical use. The same calibration curves were obtained after two weeks. The crown-formazans investigated in the present study differ from compound **1a** either in the ether part or in the substituent at the formazyl

Table 3
Reciprocals of the selectivity coefficient ($1/K^{pot}_{Cs,M}$) for cesium ion with respect to other metal cations, with ionophores **2c**, **3c**, **4c**, and **1c** using NPOE and NPBnE plasticizers

Ionophore	Plasticizer	Slope	$1/K^{pot}_{Cs,Na}$	$1/K^{pot}_{Cs,K}$	$1/K^{pot}_{Cs,Ba}$	$1/K^{pot}_{Cs,Ca}$	$1/K^{pot}_{Cs,NH_4}$	$1/K^{pot}_{Cs,Li}$	$1/K^{pot}_{Cs,Co}$	$1/K^{pot}_{Cs,Mg}$
2c	NPOE	47	80	1.0	130	160	4.4	320	570	800
2c	NPBnE	55	96	4.2	230	170	6.9	310	590	830
3c	NPOE	45	36	1.5	100	76	3.6	100	420	360
3c	NPBnE	47	86	2.9	160	110	6.8	140	520	730
4c	NPOE	47	95	2.2	220	180	4.1	410	840	1020
4c	NPBnE	50	190	6.6	480	260	8.3	280	1000	910
1c	NPOE	50	150	9.1	400	200	5.8	210	910	1200
1c	NPBnE	43	76	2.5	140	60	1.3	60	390	440

Table 4
Reciprocals of the selectivity coefficient ($1/K^{pot}_{Cs,M}$) for cesium ion with respect to other metal cations, with ionophores **2d**, **3d**, and **4d** using NPOE and NPBnE plasticizers

Ionophore	Plasticizer	Slope	$1/K^{pot}_{Cs,Na}$	$1/K^{pot}_{Cs,K}$	$1/K^{pot}_{Cs,Ba}$	$1/K^{pot}_{Cs,Ca}$	$1/K^{pot}_{Cs,NH_4}$	$1/K^{pot}_{Cs,Li}$	$1/K^{pot}_{Cs,Co}$	$1/K^{pot}_{Cs,Mg}$
2d	NPOE	50	66	3.0	130	115	5.8	210	420	580
2d	NPBnE	44	48	2.6	71	71	3.3	120	350	380
3d	NPOE	48	65	5.9	120	87	2.4	160	300	460
3d	NPBnE	50	40	1.9	66	63	2.6	115	320	290
4d	NPOE	50	83	1.7	182	120	3.8	330	480	1000
4d	NPBnE	50	63	1.7	170	100	1.7	290	480	690

carbon. The first variable affects the ring size and the second affects the electron availability inside the crown ring. Comparison of data in Tables 1–4 indicates that the selectivity is very sensitive to the ring size which is controlled by the ether part (OCH_2XCH_2O), and the optimum size selectivity was achieved for crowns having different substituents at the formazyl carbon with the trimethylene group in the ether part (i.e $OCH_2CH_2CH_2O$, compounds **2a**, **3a** and **4a**) (Table 1). With a slight decrease in the cavity size as shown in Table 2 for **2b**, **4b** containing the methylene derivative ($OCH_2C(=CH_2)CH_2O$), the selectivity for cesium decreases with respect to most metals investigated. Also, the slight increase in the crown cavity size as shown in Table 3 for compounds **1c**, **2c**, **3c**, and **4c** (containing the *o*-xylenyl group in the crown ring) caused a decrease in the cesium selectivity. A dramatic drop in cesium selectivity towards most cations was observed (Table 4) for crowns **2d**, **3d**, and **4d** containing the hydrophilic hydroxyl group in the ether part ($OCH_2CH(OH)CH_2O$). Regarding the substituent at the formazyl carbon, crown-formazans containing the 4-pyridyl-1-oxide showed the highest selectivity, especially towards the two low selectivity monovalent ions potassium and ammonium. Also, the membranes containing the plasticizer NPBnE showed better cesium selectivity relative to most ions than those containing NPOE.

Thus, from Tables 1–4 it is apparent that the electrode composed of the ionophore **4a** in a membrane containing the NPBnE as a plasticizer exhibits the best selectivity, especially toward potassium and ammonium ions. In an attempt to optimize the selectivity of this electrode, the authors studied variable membrane compositions containing this ionophore, as shown in Table 5. Table 6 shows the slope and the selectivity coefficients, for cesium with respect to sodium, potassium, barium, calcium, ammonium, lithium, cobalt, and magnesium, of these different electrodes. Fig. 1 shows the cesium calibration graphs

Table 5
Composition of the electrode membrane matrices, with the slopes of the cesium calibration graphs

Number	Crown-formazan (mg)	Electrode composition						Slope of the linear portion of the calibration curve (mV decade^{-1})
		NPOE (mg)	NPBnE (mg)	KTpClPB (mg)	TOPO (mg)	PVC (mg)	THF (μl)	
a	4.1	65	0	0.5	0	33	350	50
b	4.1	0	65	0.5	0	33	350	47
c	4.1	0	65	0.5	1.0	33	350	33
d	4.1	0	65	4.6	0	33	350	47
e	4.1	0	65	4.6	1.0	33	350	47
f	4.1	0	65	0	0	33	350	44
g	4.1	0	65	0	1.0	33	350	30

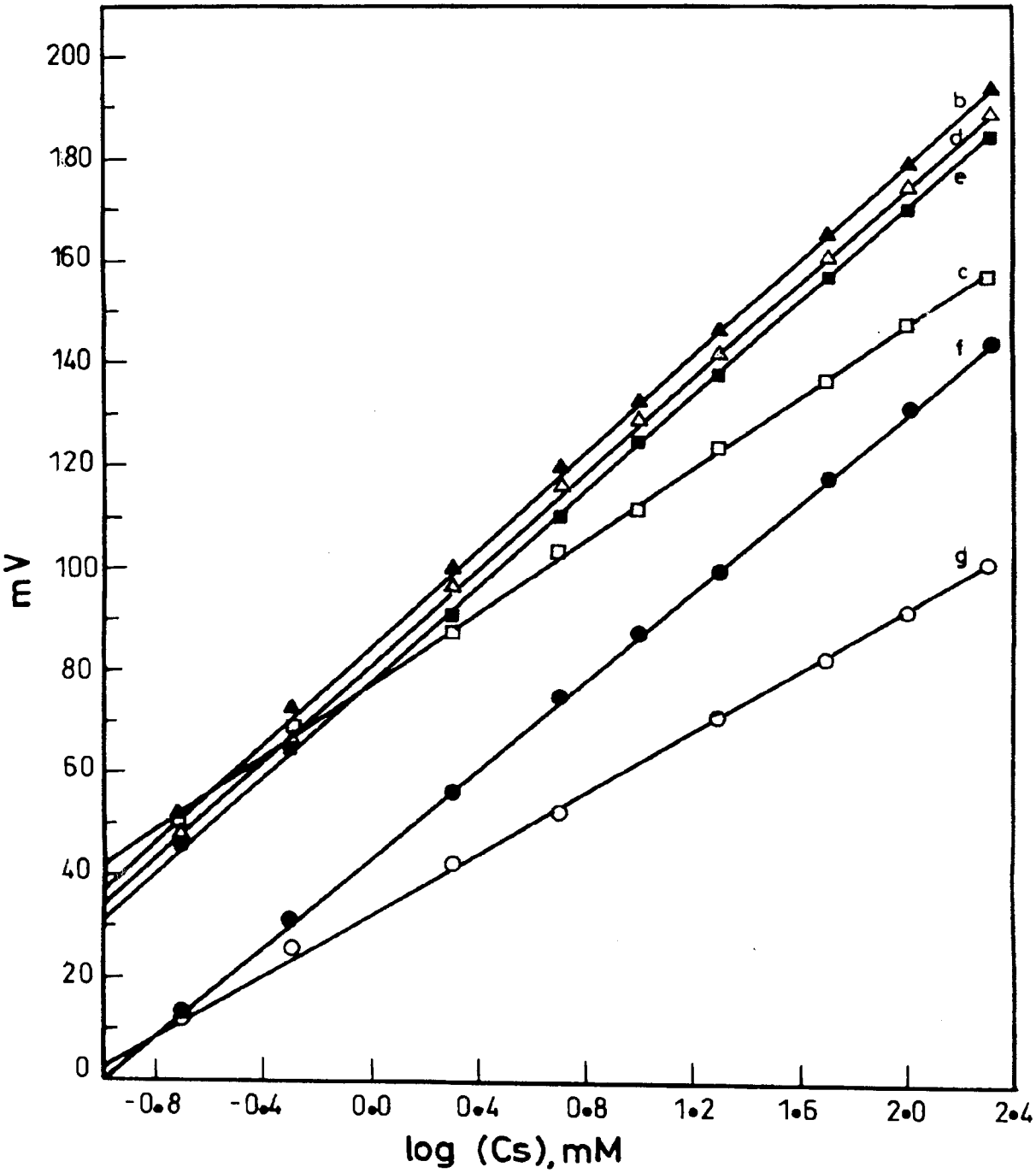

Fig. 1. The calibration graphs for cesium using electrodes b–g.

Table 6
Reciprocals of the selectivity coefficient ($1/K^{pot}_{Cs,M}$) for cesium ion with respect to other metal cations, with ionophore **4a** using different electrode membrane matrices composition shown in Table 5

Electrode matrices	$1/K^{pot}_{Cs,Na}$	$1/K^{pot}_{Cs,K}$	$1/K^{pot}_{Cs,Ba}$	$1/K^{pot}_{Cs,Ca}$	$1/K^{pot}_{Cs,NH_4}$	$1/K^{pot}_{Cs,Li}$	$1/K^{pot}_{Cs,Co}$	$1/K^{pot}_{Cs,Mg}$
a	360	8.7	260	230	8.7	260	690	910
b	680	31	660	520	25	360	1400	1100
c	570	25	190	120	14	330	210	640
d	740	38	1080	1100	60	570	2900	2400
e	950	39	630	570	27	710	2900	2400
f	13	0.9	7.3	3.0	1.0	4.6	4.1	14
g	18	7.4	6.8	0.1	6.3	2.5	0.8	5.0

of the electrodes b–g (Table 5). All curves are linear over the concentration ranges used and the slopes of these curves range from 30 mV decade^{-1} for electrode g, 33 for electrode c, 44 for electrode f, 47 for electrodes b, d, e, and f to 50 for electrode a. Thus, all electrodes have a slope of 44–50 mV decade^{-1} except electrodes c and g where TOPO was used. Table 6 shows that electrodes d and e are good candidates as cesium selective electrodes with good selectivity, especially towards the small interfering ions. Fig. 1 shows the calibration graphs for cesium using electrodes b–g (Table 5).

3.1. Effect of KTpClPB and TOPO

From Tables 5 and 6 it is clear that in the absence of TOPO (electrodes b, d, and f) an increase in the KTpClPB causes an increase in the selectivity for cesium over all the other ions investigated. The cesium calibration curves of both electrodes b and d containing KTpClPB have the same slope (47 mV decade^{-1}). The slope is slightly lower (44 mV decade^{-1}) for electrode f which does not contain KTpClPB. In the presence of 1 mg TOPO an increase of KTpClPB (electrodes c and e) from 0.5 to 4.6 mg (22 and 200% molar ratio of KTpClPB to **4a**) causes an increase in the selectivity for cesium over the other ions. Also, for electrodes c and e the slope increases from 33 to 47 mV decade^{-1}. In absence of KTpClPB and presence of TOPO (electrode g), the selectivity for cesium is poor and the slope is also low (30 mV decade^{-1}). In the absence of both TOPO and KTpClPB (electrode f) the selectivity is very poor.

4. Conclusion

The present research offers a comparative study for the construction of good cesium ion selective electrodes. The highest selectivity for cesium was achieved with the two electrodes d and e (Tables 5 and 6) with membranes containing the ionophore **4a**, NPBnE, and KTpClPB with and without TOPO.

References

[1] K. Boguslawska, M. Cieplinski, A. Cyganski, Chem. Anal. (Warsaw) 30 (1985) 281.
[2] B.P. Bermejo, G.E. Beceiro, B.A. Bermejo, M.F. Bermejo, Microchem. J. 40 (1989) 103.
[3] N.V. Bondareva, E.S. Zolotoviskaya, Zavod. Lab. 57 (1991) 36.
[4] H. Huang, J. Zhu, Guangpuxue-Yu-Guangpu-Fenxi 10 (1990) 26.
[5] Z. Shen, P. Li, Fenxi-Huaxue 14 (1986) 55.
[6] Y.M. Samoilov, S.S. Shatskaya, Izv.-Sib.-Otd.-Akad.-Nauk-SSSR,-Ser.-Khim.-Nnauk 2 (1989) 119.
[7] D. Wagley, G. Schmiedel, E. Mainka, H.J. Ache, At. Spectroscr. 10 (1989) 106.
[8] U. Voelkopf, Z. Grobenski, R. Tamm, B. Weiz, Analyst 110 (1985) 573.
[9] V. Otruba, J. Kalacek, Chem. Listy 87 (1993) 64.
[10] M. Zhang, J. Hu, Yankuang-Ceshi 7 (1988) 119.
[11] E.D. Prudnikov, Y.S. Shapkina, Zh. Anal. Khim. 45 (1990) 1740.
[12] Z. Grobenski, D. Weber, B. Weiz, J. Wolff, Analyst 108 (1983) 925.

[13] R. Goguel, Anal. Chim. Acta 169 (1985) 179.
[14] V. Otruba, J. Jambor, L. Sommer, Chem Listy 77 (1983) 994.
[15] A. Hatterer, S. Walter, Analusis 15 (1987) 552.
[16] X. Chen, K. Wang, Fenxi-Huaxue 11 (1983) 277.
[17] F. Hu, Z. Wang, Q. Liu, Chin. Sci. Bull. 36 (1991) 560.
[18] Q. Bao, Y. Wang, Fenxi-Shiyanski 6 (1987) 59.
[19] L.A. Pelieva, Z.V. Lakiza, V.P. Nagorskii, Zavod. Lab. 52 (1986) 32.
[20] V.I. Chaplygin, N.B. Zorov, Y.Y. Kuzyakov, Talanta 30 (1983) 505.
[21] V.I. Chaplygin, N.B. Zorov, Y.Y. Kuzyakov, O.I. Matveev, Zh. Anal. Khim. 38 (1983) 802.
[22] E. Taskaev, J. Radioanal. Nucl. Chem. 118 (1987) 319.
[23] J.R.W. Woittiez, ECN (Rep.), ECN-147, 1984 pp. 241.
[24] H.K. Wankhade, A.N. Garg, J. Radioanal. Nucl. Chem. 91 (1985) 149.
[25] F. Chisela, P. Braetter, Anal. Chim. Acta 188 (1986) 85.
[26] I.G. Gokmen, G.E. Gordan, N.K. Aras, J. Radioanal. Nucl. Chem. 113 (1987) 453.
[27] D.H. Oughton, J.P. Day, J. Radioanal. Nucl. Chem. 174 (1993) 177.
[28] K. Bibow, H.H. Mundal, Clin. Chem. 36 (1990) 1902.
[29] D. Behne, H. Juergensen, J. Radioanal. Nucl. Chem. 42 (1978) 447.
[30] M.B. Shiryaeva, L.N. Lyubimova, Y.P. Salmin, K.N. Ryumina, N.A. Levina, M.A. Tatarkin, Zh. Anal. Khim. 38 (1983) 984.
[31] R.H. Mitchell, M. Artist, J. Radioanal. Nucl. Chem. 81 (1984) 255.
[32] D. Van-Renterghem, R. Cornelis, R. Vanholder, Anal. Chim. Acta 257 (1992) 1.
[33] M.G. Davydov, N.P. Dobrynina, V.V. Kishel'gof, S.A. Mareskin, A.P. Naumov, Zh. Anal. Khim. 39 (1984) 237.
[34] M.G. Davydov, V.V. Kishel'gof, V.G. Magera, S.A. Mareskin, Zh. Anal. Khim. 43 (1988) 297.
[35] K.H. Theimer, V. Krivan, Anal. Chem. 62 (1990) 2722.
[36] N.A. Shubina, G.M. Kolesov, Zh. Anal. Khim. 48 (1993) 889.
[37] G. Eisenman, in: G. Eisenman (Ed.), Glass Electrodes for Hydrogen and Other Cations, Edward Arnold, London 1967, pp. 281.
[38] C.J. Coetzee, A.J. Basson, Anal. Chim. Acta 57 (1971) 478.
[39] C.J. Coetzee, A.J. Basson, Anal. Chim. Acta 83 (1976) 361.
[40] C.J. Coetzee, A.J. Basson, Anal. Chim. Acta 92 (1977) 399.
[41] S. Vlasselaer, W. D'Olieslager, M. D'Hont, J. Radioanal. Chem. 35 (1977) 211.
[42] W. D'Olieslager, L. Heerman, J. Electrochem. Soc. 126 (1979) 347.
[43] E.W. Baumann, Anal. Chem. 48 (1976) 548.
[44] A.S. Attiyat, G.D. Christian, J.L. Hallman, R.A. Bartsch, Talanta 35 (1988) 789.
[45] A.S. Attiyat, Y.A. Ibrahim, G.D. Christian, Microchem. J. 37 (1988) 122.
[46] C.H.F. Allen, J.W. Gattes, Organic Synthesis, Collective Vol. III, Wiley, New York, 1955, pp. 140, 141.
[47] K. Kimura, H. Yano, T. Shono, J. Chem. Soc. Perkin Trans 2 (1988) 1945.
[48] R.Y. Xie, V.P.Y. Gadzekpo, A.M. Kadry, Y.A. Ibrahim, J. Ruzicka, G.D. Christian, Anal. Chim. Acta 184 (1986) 259.
[49] V.P.Y. Gadzekpo, G.D. Christian, Anal. Chim. Acta 164 (1984) 279.

ELSEVIER

Talanta 47 (1998) 1223–1229

Talanta

Investigation of the interaction between acridine orange and bovine serum albumin

Xi-Zeng Feng, Zhang Lin, Lin-Jin Yang, Chen Wang, Chun-li Bai *

Institute of Chemistry, Academia Sinica, Beijing, 100080, China

Received 26 January 1998; received in revised form 19 May 1998; accepted 20 May 1998

Abstract

The results from the measurement of the fluorescence spectrum showing the binding characteristics of acridine orange (AO) and bovine serum albumin (BSA) are reported. It was found that the equilibrium constant $k = 4848.64$ l mol^{-1}, and the number of binding sites $n = 0.82$. Based on the mechanism of the Forster energy transference, the transfer efficiency of energy and distance between the acceptor AO and BSA were found. The interaction between AO and BSA have been verified as consistent with the static quenching procedure and the quenching mechanism is related to the energy transfer. © 1998 Elsevier Science B.V. All rights reserved.

Keywords: Acridine orange; Bovine serum albumin; Equilibrim constant; Binding sites; Energy transfer

1. Introduction

Acridine orange (AO) is a kind of cationic basic fluorescent dye. As a proton-acceptor, this neutral molecule can penetrate into the membrane of acid cystbubbles or cell-organs and accept protons. On the other hand, the cationic molecule with H^+ can not penetrate the membrane, and, therefore, would remain within the cell and would cause a variation in local concentration. The absorption maximum and fluorescence maximum of this compound is blue-shifted and red-shifted, respectively, depending on the aggregation of this compound. These characteristics can be used to detect the dynamic state of H^+ transfer between membranes, such as the mitochondrion [1], the turtle urinary bladder [2], the plasma membrane vesicles from *Avena saliva* L. (cv Rhiannon) [3], and the lysosome [4–6]. As the spectra are closely related to the varying concentrations, the measured shift of the spectra could help to determine the sensitivity of the H^+ transfer. Extensive investigations into the interaction between the serum protein and internal compound or pharmaceutical molecule have been made [7–9]. The information obtained of the emission wavelength, the fluorescent polarization, the energy transfer and the fluorescent longevity are useful in analyzing the structure and the site of the fluorophore in the protein. We have previously reported [10] on the aggregation and dissociation equilibrium of actinide orange, and spectroscopic studies [11] to evaluate the interactions between acridine orange and alcohol.

* Corresponding author. Tel.: +86 010 62568158; fax: +86 010 62557908; e-mail: clbai@infoc3.icas.ac.cn

0039-9140/98/$ - see front matter © 1998 Elsevier Science B.V. All rights reserved.
PII S0039-9140(98)00198-2

In this paper we investigate the binding reaction and the effect of the energy transfer between AO and bovine serum albumin (BSA), by fluorescence spectra methods. It was demonstrated that the reaction constant and the number of binding sites could be explicitly derived. Furthermore, as a probe for the biomolecule, the binding reaction of AO to BSA and the AO transfer between membranes in vivo are discussed. In addition, the relationship between AO aggregation and its spectra were studied, the influence of the micelle to the aggregated AO state and its influence on the sensitivity of the fluorescence spectra of AO were studied.

2. Experimental

AO and SDS were from Fluka, BSA was from Huamei Biotechnological, Beijing. The water used was triple-distilled. The absorption spectra were obtained by using a U3200 spectrophotometer. Fluorescence measurements were made on a Hitachi MPF4 spetrofluorometer.

The following reagents were added to a 5 ml tube in the order indicated: BSA, AO, and SDS. After adding tripled-distilled water to the 5 ml tube and stirring, the absorption spectra and fluorescence spectra were measured at room temperature. Fluorescence measurements were taken at excitation and emission wave-lengths of 280 and 300–500 nm, respectively, with a resolution of 8 and 10 nm respectively.

3. Results and discussions

3.1. The binding properties of AO and BSA

For the static quenching interaction, if it is assumed that there are similar and independent binding sites in the biomolecule, the relationship between the fluorescence intensity and the quenching medium can be deduced from the following formula:

$$nQ + B = Qn + B \quad (1)$$

where B is the biomolecule with a fluorophore, Q is the quenchable pharmaceutical molecule, $Qn+$ B is the quenched biomolecule whose resultant constant is K_a. Here:

$$K_a = \frac{[Qn + B]}{[Q^n][B]} \quad (2)$$

If the overall amount of biomolecules (bound or unbound with the quenchable molecule) is B_0, then $[B_0] = [Qn + B] + [B]$, here [B] in the concentration of unbound biomolecule, then the relationship between fluorescence intensity and the unbound biomolecule as $[B]/[B_0] = F/F_0$ that is:

$$\log \frac{(F_0 - F)}{F} = \log K + n \log [Q] \quad (3)$$

With Eq. (3), the binding constant K and binding sites n can be found. The fluorescence quenching of BSA with varying concentrations of AO is shown in Fig. 1. The best fit to the fluorescence data using Eq. (3) was found by setting $n = 0.82$ and $K = 4848.64$ l mol^{-1}.

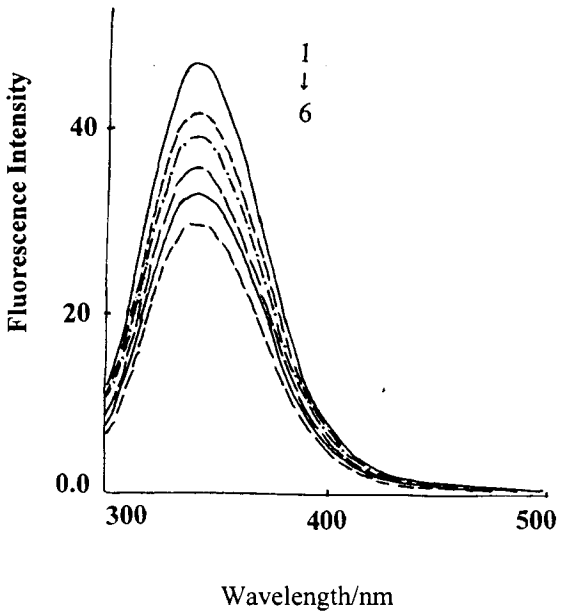

Fig. 1. Fluorescence spectra of BSA in the presence of AO in aqueous solution. [BSA] = 1×10^{-5} mol dm^{-3}; [AO]: (1) 0.0, (2) 0.1, (3) 0.3, (4) 0.5, (5) 0.8, and (6) 1.2×10^{-5} mol dm^{-3}.

3.2. The energy transfer between AO and biomolecule

If we assume the binding reaction in the BSA molecule happens in a sequential manner, the distance between the binding site and the fluorophore in the protein can be evaluated according to the Forster mechanism of non-radiation energy transfer [12]. According to Forster's theory [13], the energy transfer effect is related not only to the distance between acceptor and donor (r), but also to the critical energy transfer distance (R_0), that is:

$$E = \frac{R_0^6}{R_0^6 + r_0^6} \tag{4}$$

Where R_0 is the critical distance when the transfer efficiency is 50%,

$$R_0^6 = 8.8 \times 10^{-25} K^2 N^{-4} \phi J \tag{5}$$

In Eq. (5), K^2 is the spatial orientation factor of the dipole, N is the index of refraction of the medium, ϕ is the fluorescence quantum yield of the donor, J is the overlap integral of the fluorescence emission spectra of the donor and the absorption spectra of the acceptor. Therefore:

$$J = \sum F(\lambda)\varepsilon(\lambda)\lambda^4 \Delta\lambda / \sum F(\lambda)\Delta\lambda \tag{6}$$

where $F(\lambda)$ is the fluorescence intensity of the fluorescent donor of wavelength λ, $\varepsilon(\lambda)$ is the molar absorption coefficient of the acceptor of wavelength λ, then the energy transfer efficiency is:

$$E = 1 - \frac{F}{F_0} \tag{7}$$

The overlapping spectra of the absorption spectra of AO and BSA (AO/BSA = 1:1) and the fluorescence spectra of BSA are shown in Fig. 3. So J can be evaluated by integrating the spectra in Fig. 3 for $\lambda = 300 \sim 500$ nm. Under these experimental conditions, we found $R_0 = 1.5$ nm from Eq. (5) using $K^2 = 2/3$, $N = 1.336$, $\phi = 0.15$ [14], and the energy transfer effect $E = 0.3148$ from Eq. (7). At last, the distance between AO and the amino-acid residue in BSA can be evaluated from Eq. (4) where $r = 1.65$ nm.

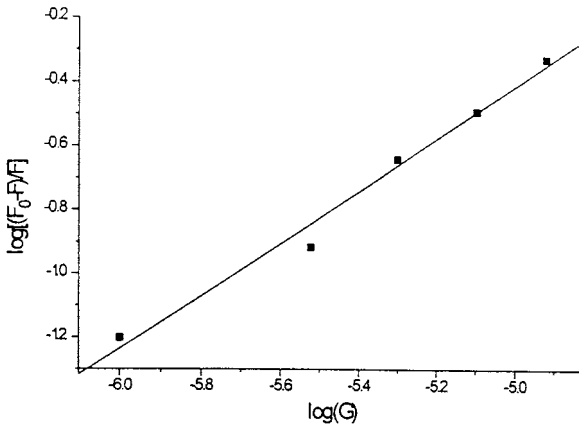

Fig. 2. Plots of $\log((F_0 - F)/F)$ vs. $\log[G]$.

The quenching curve of AO to BSA shows (not shown here) a fine linear relationship in the overall concentration range of BSA. The correlation coefficient is 0.9973 (25°C), indicating the static quenching interaction. At high concentrations of AO, the quench curve is linear because the two tryptophan residues in BSA can inlay into the biomolecule finely, indicating the quenching that the interaction between AO and BSA is a single quenching course. In Fig. 2, the calculated binding constant ($K = 4848.68$ l mol^{-1}, indicating that the binding reaction of AO to BSA is strong) and the binding sites ($n = 0.82$, indicating that the binding site is one) show that AO can bind with albumin. According to the Forster non-radiation energy transfer (Fig. 3) it was calculated that the energy transfer efficiency of AO and BSA is $E = 0.3184$ and the distance between AO and the tryptophan residue is $r = 1.65$ nm. These data, which is corresponding to the theory of energy transfer [15], indicate further that the binding reaction of AO to BSA is through an energy transfer which will quench the fluorescence of the protein. The mechanism of the interaction between AO and DNA is regarded as essential for use as a probe of the biomolecule, the aggregation state and DNA will be further investigated in future work.

3.3. The spectrum of AO dimer in different concentrations

Fig. 4 shows the absorption spectra (Fig. 4a) and fluorescence spectra (Fig. 4b) of AO for different concentrations in neutral solution. In Fig. 4a, there is an absorption maximum at 492 nm, which corresponds to the monomer state of AO at low concentration. The absorption spectra changes with increasing concentrations of AO. The 492 nm peak becomes lower whereas the 465 nm peak appears higher. We interpret this result as being due to the aggregation of the monomer caused by concentration. As previously reportedly by Tan and Schnelder [16] and Robinson et al. [17], similar absorption results showed maxima at 492 and 370 nm for low and high concentration solutions of AO, respectively, which is assumed to be the monomer and dimer.

In the fluorescence spectra, the monomer AO has a fluorescence maximum at 530 nm (λ_{em}^{max}). With increasing concentration of AO in solution, an increasing of AO dimers results in the red-shift of this peak [18]. Fig. 4b shows the fluorescence spectra of AO at different concentrations. At a low concentration (2×10^{-6} mol dm^{-3}), the fluorescence maximum is at 530 nm. A moderate AO concentration (2×10^{-5} mol dm^{-3}) causes the coexistence of monomer and dimer AO, though the monomer is the major component.

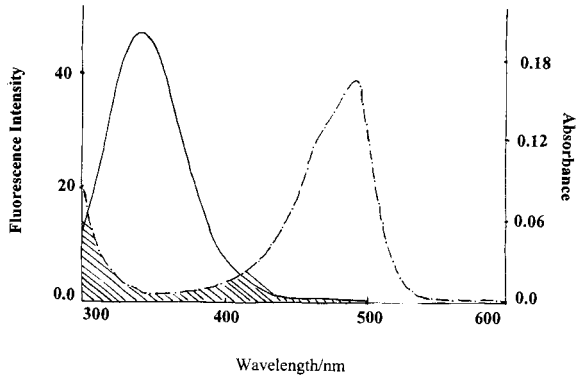

Fig. 3. The overlap of the fluorescence emission spectra (1) and the absorption spectra (2) when the molar ratio of AO is 1:1. [BSA] = 1×10^{-5} mol dm^{-3}; [AO] = 1×10^{-5} mol dm^{-3}.

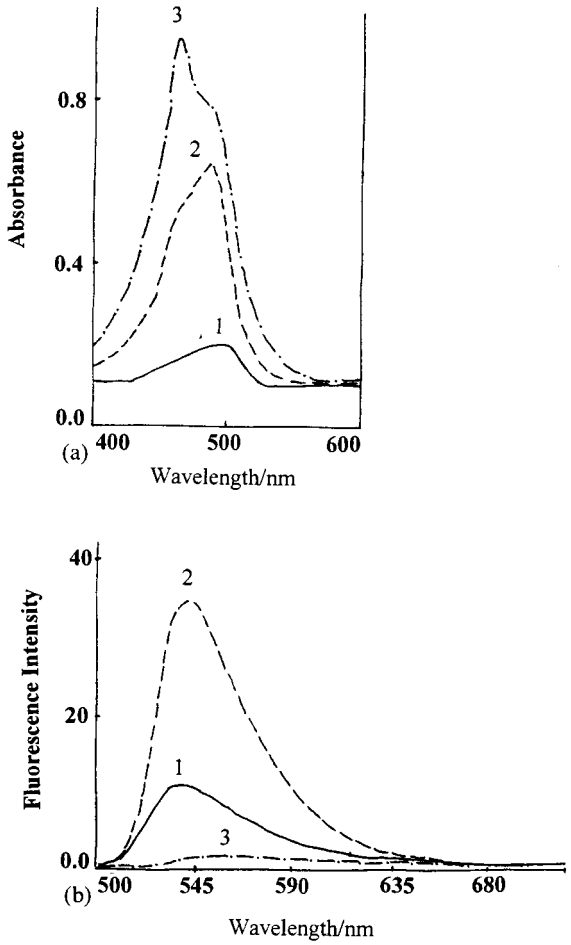

Fig. 4. (a) Absorption spectrum of AO in aqueous solution at different concentrations: (1) $2 \times 10 - 6$ mol m^{-3}, cell = 10 mm; (2) 2×10^{-5} mol m^{-3}, cell = 5 mm; (3) 2×10^{-4} mol dm^{-3}, cell = 1 mm. (b) Fluorescence spectrum of AO in aqueous solution at different concentrations: (1) 2×10^{-6} mol dm^{-3}, cell = 10 mm; (2) 2×10^{-5} mol dm^{-3}, cell = 10 mm; (3) 2×10^{-4} mol m^{-3}, cell = 10 mm.

Correspondingly, the fluorescence spectra shows a 530 nm maximum and the peak is higher than before, which indicates that the quantum yield of AO is related to its concentration. At a higher concentration (2×10^{-3} mol dm^{-3}), as the dimer becomes the major component, the spectrum shows a red-shift of 530 nm maximum and the maximum fluorescence intensity decreases rapidly. The above results indicate that the change in the absorption spectra and the fluorescence spectra

are closely related to the aggregation of AO which depends on the concentration in the solution.

3.4. The influence of the micelle on the AO dimer

The absorption spectra and fluorescence spectra of AO (1×10^{-4} mol dm^{-3}) with or without the cationic surfactant SDS were studied (Fig. 5). The absorbency (A) and the ratio of the two absorption maxima (A^{492}/A^{465}), which change with varying concentrations of SDS, are listed in Table 1.

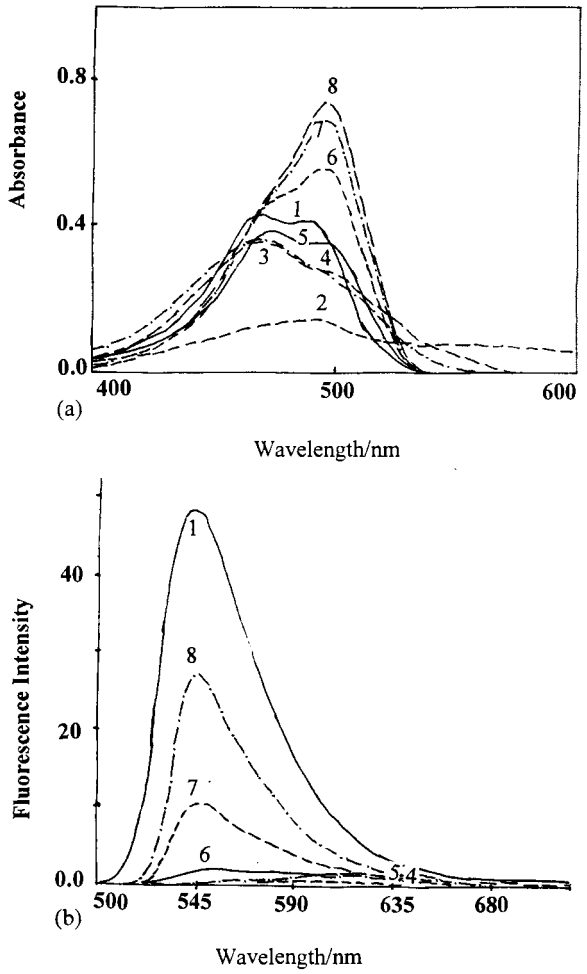

Fig. 5. (a) Addition effect of SDS on the absorption spectrum of AO. [AO] = 1×10^{-4} mol dm^{-3}; [SDS]: (1) 0.0, (2) 0.1, (3) 0.5, (4) 1.0, (5) 3.0, (6) 5.0, (7) 7.0, and (8) 9.0×10^{-3} mol dm^{-3}. (b) Addition effect of SDS on the fluorescence spectrum of AO. [AO] = 1×10^{-4} mol dm^{-3}; [SDS]: (1) 0.0, (2) 0.1, (3) 0.5, (4) 1.0, (5) 3.0, (6) 5.0, (7) 7.0, (8) 9.0×10^{-3} mol dm^{-3}.

Table 1
Absorbance of the AO dimer and monomer

AO (mol l^{-1})	SDS (mol l^{-1})	A^{456}	A^{492}	A^{492}/A^{465}
2×10^{-6}	0	0.155	0.200	1.290
2×10^{-5}	0	0.526	0.625	1.240
2×10^{-4}	0	0.884	0.788	0.891
1×10^{-4}	0	0.403	0.400	0.993
1×10^{-4}	1×10^{-4}	0.114	0.142	1.246
1×10^{-4}	5×10^{-4}	0.306	0.207	0.667
1×10^{-4}	1×10^{-3}	0.304	0.268	0.882
1×10^{-4}	3×10^{-3}	0.308	0.306	0.991
1×10^{-4}	5×10^{-3}	0.401	0.506	1.260
1×10^{-4}	7×10^{-3}	0.401	0.608	1.516
1×10^{-4}	9×10^{-3}	0.401	0.703	1.751

Fig. 5 shows that the absorption maximum of AO decreases rapidly when SDS at low concentrations were added. We interpret this result as the association of the cation from AO and the anion from SDS, and with increasing concentrations of SDS in the system, AO formed a dimer at first, then dissolved into a monomer. This phenomena occurred continuously until the concentration of SDS reached its critical value (9×10^{-3} mol dm^{-3}). At this point, the absorption maximum of the AO monomer achieved its greatest value. In addition, Fig. 5b shows that the fluorescence maximum of the AO monomer decreased sharply when SDS at low concentration was added, the fluorescence maximum of the AO dimer appeared at 640 nm when SDS of high concentration was added to the solution. The maximum of the AO monomer (540 nm) reached the strongest intensity when the concentration of SDS reached its critical value.

These results indicate: (1) When the concentration of AO is 1×10^{-4} mol dm^{-3}, the monomer and dimer simultaneously exist in the solution (Fig. 5a, curve 1). When SDS of low concentrations ($0 \sim 1 \times 10^{-3}$ mol dm^{-3}) was added, the dimer concentration in the solution increases correspondingly (Fig. 5a, curves 2–4), whilst the concentration of SDS is between 1×10^{-3} and 5×10^{-3} mol dm^{-3}, the formation of a great deal of 'pre-micelle' in the system can help to disperse AO into the micelle medium (Fig. 5a, curves 5 and 6), which will reduce the dimer in the solution

(the ratio of A^{492}/A^{465} decreases). When the concentration of SDS increases further ($5 \times 10-3$–9×10^{-3} mol dm^{-3}), the dimer disappear because of the formation of the micelle (Fig. 5a, curves 7 and 8). (2) The fluorescence spectra showed that there is a fluorescence peak of the AO monomer at 545 nm, when the concentration of AO is 1×10^{-4} mol dm^{-3} (Fig. 5b, curve 1). When SDS at low concentration is added in the solution, the fluorescence peak of the AO monomer primarily vanishes, namely, AO forms dimers in this solution which produce much weak fluorescence (not shown in the Figure). When the SDS concentration is 1.0–3.0×10^{-3} mol dm^{-3}, the AO dimer produces weak fluorescence peaks at 635 nm (as shown in Fig. 5b, curves 4 and 5). When the SDS concentration further increases (5.0–9.0×10^{-3} mol dm^{-3}), the fluorescence of the AO monomer is also enhanced as shown in Fig. 5b, curves 6–8. The results show that the association state of AO vary with the increase in SDS concentration. Therefore we postulate that the existence of the micelle can change the aggregation state of AO into the monomer state. The introduction of the micelle to the system could probably raise the sensitivity of the H^+ transfer.

Previous papers [4,6] have discussed the relationship between the spectra and the concentration of AO, but the relationship to the concentration range has been investigated for the first time in this paper. Therefore, the key to raising the measurement sensitivity of the H^+ transfer is to choose a suitable concentration range where the spectra can change markedly. Fig. 5, where the increasing concentration of AO caused an increase of AO aggregation and the fluorescence quenching of the AO monomer (540 nm) arose due to the aggregation, shows why AO can be used as a sensitivity index of the H^+ transfer. From Fig. 5, we know that the aggregation of AO in solution is influenced by the cationic surfactant SDS. Especially, when the concentration of SDS is near or reaching its critical concentration, the maximum fluorescence intensity of the AO monomer is sensitized. This phenomena indicates that the micelle can change the existing state of the AO dimer to the monomer. Therefore we predict the that introduction of the micelle can raise the measurement sensitivity of the H^+ transfer, this aspect will be verified in further studies.

4. Summary

It was demonstrated by measuring the fluorescence spectrum that the binding characteristics of AO and BSA can be identified. It was found that the equilibrium constant $k = 4848.64$ l mol^{-1}, and the number of binding sites $n = 0.82$. Based on the mechanism of Forster energy transference, the transfer efficiency of energy and the distance between the acceptor AO and BSA was found to be 0.3184 and 1.65 nm, respectively. We further investigated the effect of the micell on the AO association state. The results showed that AO is induced into the dimer state by SDS at low concentration. When SDS is at a higher concentration, it induced the dissociation of AO. The special characteristic of this AO association is used to detect the dynamic state of H^+ transfer between the membranes. The introduction of the micell can greatly improve the sensitivity of this detecting method.

Acknowledgements

This work was supported by the National Natural Science Foundation of China and the Foundation of the Chinese Academy of Science.

References

[1] P. Dell'Antone, R. Colonna, G.F. Azzone, Biochim. Biophys. Acta. 234 (1971) 541.
[2] S. Gluck, S. Kelly, Q. Al-Awqati, J. Biol. Chem. 257 (16) (1982) 9230.
[3] M.G. Palmgren, Plant Physiol. 94 (1990) 882.
[4] P. Dell'Antone, Biochem. Biophys. Res. Commun. 86 (1) (1979) 180.
[5] J. Cuppoletti, D. Aures-Fischer, G. Sachs, Biochim. Biophys. Acta 899 (1987) 276.
[6] P. Dell'Antone, FEBS Lett. 168 (1) (1984) 15.
[7] U. Kragh-Hansen, Pharmacol. Rev. 33 (1) (1981) 17.
[8] J.A. Squella, Biochem. Pharmacol. 36 (20) (1987) 3531.
[9] H. Ogata, Biochem. Pharmacol. 39 (9) (1990) 1495.

[10] X.-Z. Feng, X.-W. He, H.-X. Shen, Chem. Soc. Jpn. 10 (1997) 680.
[11] X.-Z. Feng, X.-W. He, H.-X. Shen, Chem. Soc. Jpn. 10 (1997) 720.
[12] L.A. Sklar, B.S. Hudson, R.D. Simoni, Biochemistry 16 (23) (1977) 5100.
[13] T. Forster, Ann. Phys. 437 (1948) 55.
[14] L. Cyril, J.K. Earl, W.M. Sperry, Biochemists Handbook, E.&F.N. Epon. Led. Press, London, 1961, p. 83.
[15] W. Marty, M. Boiret, M. Deumie, J. Chem. Edu. 63 (4) (1986) 365.
[16] J.S. Tan, R.L. Schnelder, J. Phys. Chem. 79 (1975) 1380.
[17] B.H. Robinson, A. Loffler, Z.G. Schwar, Biochemistry 16 (25) (1977) 5100.
[18] J.V. Adelsberg, J. Barasch, Q. Al-Awqati, Methods Enzymol. 172 (1989) 85.

ELSEVIER

Talanta 47 (1998) 1231–1236

Talanta

Flow injection potentiometric determination of paraquat in formulations and biological samples

Bahruddin Saad *, Marinah Ariffin, Muhammad Idiris Saleh

School of Chemical Sciences, Universiti Sains Malaysia, 11800 Penang, Malaysia

Received 24 March 1998; accepted 21 May 1998

Abstract

A flow injection potentiometric method for the rapid determination of paraquat in herbicide formulations and biological samples is described. It is based on the utilization of a flow-through potentiometric detector containing polyvinyl chloride-immobilised octamethylcyclotetrasiloxane, a lipophilic plasticizer (tetra-*n*-undecyl 3,3′,4,4′-benzophenone tetracarboxylate) and membrane additive potassium tetrakis(4-chlorophenyl)borate. The detector was minimally interfered by the presence of constituents such as Na^+, K^+, Ca^{2+}, Mg^{2+}, glucose, urea, lactic and citric acids at physiological levels, respectively. Good correlation between results of the proposed method and HPLC for the formulation samples was found, while results for the determination of paraquat in biological samples such as urine, vomitus and stomach washout was less satisfactory. © 1998 Elsevier Science B.V. All rights reserved.

Keywords: Sensor; Ion-selective electrodes; Potentiometry; Flow injection analysis; Paraquat; Formulations; Biological samples

Paraquat is a popular weedicide that is extensively used throughout the world [1–5].

The incidence of paraquat poisoning, often through suicidal intent rather than accidental ingestion, is still a major problem in many countries. Malaysia is no exception, and although the trend is declining, yet the estimate that more than 400 deaths per year [6] is sufficient case for concern.

As an effort to minimise this fatality, manufacturers have introduced several strategies, including the use of more effective labelling, the use of enmetics to induce vomiting if minimum lethal dose was swallowed, and also the use of less concentrated active ingredients [7]. A pesticide formulation analysis is important for quality assurance purposes in a formulation plant and also to ensure the stability of a formulated product which may be stored for years before use. Due to its widespread use, and sometimes abused, much attention has been devoted to studies on analytical methods for a rapid and reliable method for their determinations in samples such as environmental [3,5,8] and body fluids [2,9,10]. A review of the analytical methods was presented earlier [4,5].

We have reported an interesting paraquat sensor based on octamethylcyclotetrasiloxane [4,5].

* Corresponding author. Tel.: +60 4 6577888; fax: +60 4 6574854; e-mail: bahrud@usm.my

0039-9140/98/$ - see front matter © 1998 Elsevier Science B.V. All rights reserved.
PII S0039-9140(98)00213-6

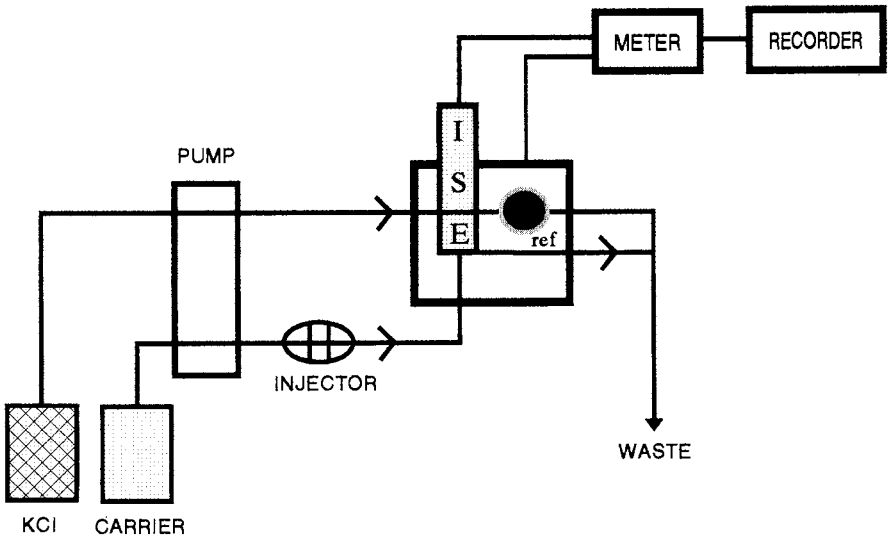

Fig. 1. FIA manifold and experimental set-up used in the study. Carrier stream consisted of 0.001 mM paraquat dichloride in Trizma base buffer (pH 5.5); reference stream was 10 mM KCl solution.

The promising features exhibited by the sensor such as high selectivity and resistance to interference from surfactants are sufficient impetus for us to extend the application of the sensor to the determination of paraquat in other real samples such as biological fluids and weedicide formulations. The results are compared and discussed in relation to a HPLC method. The performance of the sensor in mock samples containing a fixed background concentration of paraquat and other constituents such as Na^+, K^+, Ca^{2+}, Mg^{2+}, glucose, urea, lactic acid and citric acid at physiological levels are also assessed.

1. Experimental

1.1. FIA Set-up, materials and reagents

The FIA manifold used is shown in Fig. 1. Solutions were propelled by a multi-channel peristaltic pump (Gilson Minipuls 3) through PTFE tubing (0.8 mm i.d.). Samples were injected into a Rheodyne type 500 Teflon rotary injection valve. Sampling volume and carrier flow-rate of 50 μl and 2.5 ml min^{-1}, respectively, were used. The distance between the injection valve and the flow-cell was 5 cm. The carrier stream consisted of 0.001 mM paraquat dichloride in Trizma base buffer (pH 5.5). The instrumentation, flow-through detector, experimental conditions, chemicals and reagents used were as described earlier [5]. Paraquat formulations of different brands were purchased from outlets around Penang. Biological samples were taken from patients at the General Hospital in Penang and sent to the Chemistry Department, Penang for positive identification of paraquat. An aliquot of these samples were sent to us and kept refrigerated at 4°C before use.

1.2. Solid phase extraction

Some urine samples were subjected to the solid phase extraction (SPE) procedure as described by Gill et al. [11]. Extract Clean C18 cartridges, purchased from Altech, USA, with negative pressure elution were used for the clean-up of 1 ml urine sample that was made alkaline by adding concentrated ammonia. The final solution from the elution was evaporated to dryness and the residue was dissolved in 1 ml water before finally injecting into the HPLC column.

1.3. HPLC

Reversed phase ion-pair HPLC separation was carried out on a Hitachi L-4250 unit using a Phenomenex Spherisorb 10 ODS (250 × 4.60 mm) column at room temperature, in conjunction with a Hitachi L-6200 intelligent pump. Data were collected and integrated with a Hitachi D-2500 Chromato Integrator. The detection wavelength was at 257 nm and the volume of sample injected was 20 μl. An aqueous solution consisting of 10 mM sodium heptanesulphonic acid, 22 mM sodium dihydrogen orthophosphate, 35 mM disodium hydrogen dodecahydrate and 100 mM triethylamine that were mixed with acetonitrile at a ratio of 78:22 (v/v) was used as mobile phase. The solutions were passed through a 0.45-μm filter (Millipore, Bedford) before degassed for 15 min in an ultrasonic bath (Mettler Electronics, USA).

2. Results and discussion

Calibrations of the flow-through paraquat sensor under the optimised conditions [5] revealed that the peaks were not only reproducible but there were no noticeable carryover even when injecting from high to lower concentrations of paraquat. Key characteristics of the FIA detection system are as follows: detection limit, 0.01 mM; relative standard deviation for the determination of 0.5 mM paraquat that were spiked to urine sample, 0.12% ($n = 5$); sample throughput, 85 samples per hour. The detector response remained unchanged for 4 h when the system was continuously pumped with the carrier stream.

Table 1
% increase/decrease in peak heights between solutions containing species at physiological levels in a background of 0.10 mM paraquat when compared to 0.10 mM paraquat standards ($n = 4$)

Species	Fortified concentrations (mM)	% Increase/decrease in peak heights
Na^+	150	+7.78
K^+	100	−0.33
NH_4^+	50	−0.33
Ca^{2+}	12	+0.33
Mg^{2+}	8	+7.78
Citric acid	25	−1.44
Glucose	5	−0.33
Lactic acid	25	−0.78
Urea	400	−1.44

Before the determinations of paraquat in real biological samples were carried out, an assessment of the performance of the electrode in the presence of Na^+, K^+, Ca^{2+}, Mg^{2+}, glucose, urea, lactic acid and citric acid, respectively, were studied. This was done by preparing 0.10 mM paraquat in the interferent ions and comparing the peak heights of 0.10 mM paraquat standards. Percent increase/decrease in peak heights as well as the levels of interferents studied are summarized in Table 1. The results further supports the good selectivity characteristics of the paraquat sensors [5]. The presence of these constituents, even at concentrations many times more than the primary ion, did not seem to affect the electrode performance. However, slight positive interference from sodium and magnesium ions, at 150 and 8 mM concentrations, respectively, was noted (Table 1).

Control serum and urine from a normal student volunteer were fortified with known quantity of paraquat and directly determined using the proposed FIA procedure. The results obtained were compared to a HPLC method (Table 2) where in the latter technique, the samples were subjected to the solid-phase extraction pretreatment step. Recoveries for the proposed method for most samples were better than the HPLC method.

Table 3 shows the results for the direct determination of paraquat in some real biological samples such as urine, stomach washout and vomitus. Due to small quantities in most of these samples (except samples no. 5 and 6), a solid phase extraction step was not done before the injection into the HPLC column. With the exception of samples no. 8 and 10, there was poor agreement between the direct FIA and the HPLC results. Positive interference from unidentified constituents in some of these samples (samples no. 9 and 12) on the sensor response should not be ruled out. When an aliquot of the urine samples (samples no. 5 and 6) were subjected to the SPE treatment, after which it was analysed using the HPLC

Table 2
Recoveries of paraquat added to urine and control serum samples

Sample no.	Sample type	Fortified Paraquat concentration (mM)	Recovery (%)	
			FIA	HPLC[a]
1	Urine	0.05	91.20 ± 0.03	90.50 ± 0.09
2	Urine	0.10	93.10 ± 0.00	97.50 ± 0.35
3	Urine	0.50	92.80 ± 0.11	91.90 ± 0.81
4	Control Serum	0.10	95.70 ± 0.08	89.60 ± 0.39

Results are means ± standard deviations.
[a] Samples were subjected to SPE step before the analysis.

Table 3
Comparison of results[a] for the determination of paraquat dichloride concentration in real biological samples[b]

Sample no.	Sample type	Paraquat concentration (mM)		
		FIA[c] (without SPE pretreatment)	HPLC[d] (without SPE pretreatment)	HPLC (with SPE pretreatment)
5	Urine	0.30 ± 0.00	0.56 ± 0.11	0.23 ± 0.01
6	Urine	0.21 ± 0.01	0.43 ± 0.07	0.27 ± 0.03
7	Stomach washout	0.90 ± 0.01	0.15 ± 0.04	—
8	Stomach washout	0.08 ± 0.01	0.09 ± 0.02	—
9	Stomach washout	11.10 ± 0.01	3.80 ± 0.09	—
10	Stomach washout	0.33 ± 0.01	0.30 ± 0.08	—
11	Stomach washout	0.22 ± 0.01	0.29 ± 0.07	—
12	Vomitus	6.70 ± 0.01	2.00 ± 0.25	—

[a] Results are means ± standard deviations.
[b] All samples, except no. 9 were not diluted. Sample no. 9 was diluted 100 times.
[c] $n = 4$.
[d] $n = 3$.

method, paraquat concentrations of 0.23 and 0.27 mM, respectively, were obtained (Table 3). This was in good agreement with the FIA values, and was consistent with the observation that a pretretment step for biological samples prior to the HPLC separation was mandatory [2,10].

Seven paraquat formulations of different brands were determined using the FIA method, and the results compared to the HPLC methods. The data indicated there was reasonable agreement between the two methods (Table 4). All these formulations samples, except sample no. 16, contained paraquat as the sole active ingredient. The good agreement between the two methods especially for sample no. 16 which was a dual active ingredient formulation with a claimed paraquat dichloride and 2,4-D at 16.6% and 28.0% (w/w) respectively was a further testimony of the good selectivity feature of the proposed sensor. The presence of surfactants and other ingredients did not seem to affect the sensor performance, thus further supporting the earlier observation that the sensor was negligibly affected by the presence of surfactants [5]. A student *t*-test

Table 4
Comparison of results[a] for the determination of paraquat dichloride concentration in weedicide formulations[b] using the proposed (FIA) and HPLC methods

Sample no.	Sample brand	Paraquat dichloride concentration (% w/w)	
		FIA[c]	HPLC[d]
13	Action	30.60 ± 1.70	36.00
14	Contact	34.50 ± 1.60	34.40 ± 8.70
15	Gramoxone	40.70 ± 2.20	36.80 ± 5.40
16	Paramine	15.20 ± 0.01	15.70 ± 5.90
17	Paraquat Extra	39.70 ± 1.90	38.80 ± 6.40
18	Silverquat	35.20 ± 0.01	35.40 ± 6.90
19	Superzone	34.50 ± 1.60	30.80 ± 0.50

[a] Results are means ± standard deviations. All samples were not subjected to SPE treatment.
[b] All formulations except sample no. 16 contain only paraquat dichloride as active ingredients. Sample no. 16 was claimed to contain paraquat dichloride and 2,4-D at 16.6% and 28% (w/w), respectively.
[c] $n = 4$.
[d] $n = 3$, except for sample 13, $n = 2$.

perform on the results indicated that there was no significant difference in the means of the results obtained from the two methods ($t_{calculate} = 0.41$; $t_{critical} = 2.447$ at 95% confidence level) [12].

3. Conclusion

A rapid analytical method for the determination of paraquat using flow injection analysis incorporating a flow-through paraquat selective membrane developed earlier [5] was described. Under the optimized conditions, a sample throughput of about 85 samples per hour can be achieved.

Recoveries of paraquat that were spiked to urine and control serum samples were good. There was also a good agreement of the results obtained between the FIA and HPLC method for the determination of paraquat in weedicide formulations. Indeed what was most encouraging was the ability of the FIA method to determine paraquat in a dual-active ingredient formulation containing paraquat and a higher amount of 2,4-D. The good agreement of results between the proposed FIA and HPLC method was partly attributed to the good selectivity characteristic of the paraquat sensor but also to the complementary features of the FIA technique itself such as short exposure period of the sensor surface to potential interferents.

However, there was poor agreement in results of the FIA as compared to the HPLC method for the determination of paraquat in biological samples such as stomach washout and vomitus, indicating that more studies need to be conducted on such samples. Attention should also be directed towards improving the FIA/HPLC correlation by paying attention to calibrant system as reflected in the activities of the International Federation of Clinical Chemists [13].

On the whole, the proposed FIA procedure was superior to the HPLC method in terms of better reproducibility, speed and did not seem to require pretreatment steps prior to the analysis.

Acknowledgements

Support of the Ministry of Science, Technology and Environment of Malaysia through its Intensification of Research in Priority Areas via grant 123/2304/2504 is acknowledged. Financial support to Marinah Mohd. Ariffin in the form of a postgraduate scholarship from the Universiti Sains Malaysia is also very much appreciated. We are also grateful to Shaharudin Hasan of the Chemistry Department, Penang for his kind assistance and cooperation in providing the biological fluid samples.

References

[1] G.R. Sagar, Human Toxicol. 6 (1987) 7.
[2] M.T. Corasaniti, G. Nistico, J. Chromatogr. 643 (1993) 419.
[3] I. Kambhampati, K.S. Roinestad, T.G. Hartman, J.D. Rosen, E.K. Fukuda, R.L. Lippincott, R.T. Rosen, J. Chromatogr. A 688 (1994) 67.
[4] B. Saad, M. Tahir, M.N. Ahmad, M.I. Saleh, M.S. Jab, A.H. Hussin, Anal. Chim. Acta 285 (1994) 271.

[5] B. Saad, M.M. Ariffin, M.I. Saleh, Anal. Chim. Acta 338 (1997) 89.
[6] Anon., Chemistry Department of Malaysia, Yearly Report 1994.
[7] L.J. Onyon, G.N. Volans, Human Toxicol. 6 (1987) 19.
[8] M.C. Carneiro, L. Puignou, M.T. Galceran, J. Chromatogr. A 669 (1994) 217.
[9] S. Kawase, S. Kanno, S. Ukai, J. Chromatogr. 283 (1984) 231.
[10] I. Nakagiri, K. Suzuki, Y. Shiaku, Y. Kuroda, N. Takasu, A. Kohama, J. Chromatogr. 481 (1989) 434.
[11] R. Gill, S.C. Qua, A.C. Moffet, J. Chromatogr. 255 (1983) 483.
[12] G.D. Christian, Analytical Chemistry, 5th edn, Wiley, New York, 1994, p. 35.
[13] Proceedings International Federation of Clinical Chemist, 1-8, European Working Group on ISEs, A.H.J. Maas (Ed.), Private Press, Copenhagen, 1979–1987.

ELSEVIER

Talanta 47 (1998) 1237–1243

Talanta

Co-precipitative pre-concentration with sodium diethyldithiocarbamate and ICP-AES determination of Se, Cu, Pb, Zn, Fe, Co, Ni, Mn, Cr and Cd in water

D. Atanassova [a,*], V. Stefanova [a], E. Russeva [b]

[a] *Centre of Analytical Chemistry and Applied Spectroscopy, Plovdiv University, 24 Tsar Assen Steet, 4000 Plovdiv, Bulgaria*
[b] *Institute of General and Inorganic Chemistry, Bulgarian Academy of Sciences, 1113 Sofia, Bulgaria*

Received 25 February 1997; received in revised form 19 May 1998; accepted 22 May 1998

Abstract

Sodium diethyldithiocarbamate in the presence of a weak oxidizing agent is used as a co-precipitative agent for the pre-concentration of Se, Cu, Pb, Zn, Fe, Co, Ni, Mn, Cr and Cd. A procedure was developed for ICP-AES determination of these elements after pre-concentration in river and waste water (an enrichment factor of 40). The recovery of all the elements tested for was more than 98%. The limits of determination (mg l^{-1}) (10 S.D. blank) are 0.001 (Cu, Co, Cr, Mn), 0.0007 (Zn, Cd), 0.003 (Se), 0.004 (Fe), 0.007 (Ni), and 0.01 (Pb). © 1998 Elsevier Science B.V. All rights reserved.

Keywords: Co-precipitation; Sodium diethyldithiocarbamate; ICP-AES; Water

1. Introduction

Trace elements such as Pb, Cu, Cd, As, Se, etc. are present in natural water at very low levels. Hence, it is necessary to develop contamination-free sampling techniques and to adapt suitable analytical methods to these low concentrations. Some novel analytical techniques allow direct analysis of very low concentrations [1–3], but most of the common methods available still require a pre-concentration step.

Co-precipitation is one of the oldest approaches to concentration and separation of the elements to be analysed which is still used in the analysis of trace elements. Co-precipitation is widely applied in the analysis of water—fresh, sea, tap, and waste water [4–10]. As the precipitation agents used are Ga [5,7], Pd [8,9], Fe [9], as well as different dithiocarbamates (DTC): APDC [6], Na-dibenzyl-DTC [11] and Co-DTC [12]. The optimal conditions for co-precipitation with 5,8-polyquinolyl polysulfide of 21 elements are reported in Ref. [13].

The present study aimed at developing a suitable pre-concentration procedure for Se, Pb, Cu, Zn, Ni, Fe, Cd, Co, Cr, and Mn based on co-precipitation with sodium diethyldithiocarbamate and subsequent ICP-AES analysis. Most of the

* Corresponding author. E-mail: vstef@uni-plovdiv.bg

0039-9140/98/$ - see front matter © 1998 Elsevier Science B.V. All rights reserved.
PII S0039-9140(98)00211-2

elements studied are toxic and harmful to human health and their allowable concentration in waters is strictly regulated.

2. Experimental

2.1. Apparatus and reagents

A Spectroflame atomic emission spectrometer (Spectro Analytical Instruments, Germany) was used through the experiments. The optimized operating parameters are listed in Table 1.

Reagents of extra pure or of AR grade and redistilled water (RDW) were used throughout. The solution of sodium diethyldithiocarbamate (Na-DTC) at a concentration 1.10^{-1} mol l^{-1} was prepared by dissolving 2.253 g of the reagent (from E. Merck) in 100 ml RDW. Stock solutions (1000 mg l^{-1}) of the elements to be studied (from E. Merck) were used.

Hydrogen peroxide (1%) was prepared from 30% H_2O_2 (from E. Merck).

Table 1
ICP-AES operating parameters

Incident power (kW)	1.5	
Nebulizer pressure (bar)	2.0	
Plasma gas (l min^{-1})	16	
Auxiliary gas (l min^{-1})	3.5	
Sample flow rate (ml min^{-1})	1.0	
Observation height (mm)	14	
Type of optic system/ wavelength (nm)	As (VP) 193.76	Cd (M) 214.42
	Se (VP) 196.09	Co (M) 228.60
	Zn (P) 213.856	Cr (M) 267.706
	Mn (P) 257.610	Mg (M) 279.792
	Cu (P) 324.75	Sr (M) 421.548
	Al (M) 308.202	Ba (M) 230.415
	Ca (M) 317.929	Ni (P) 231.604
	Mo (M) 284.814	FE (p) 259.95
		Pb (P) 220.34

VP, vacuum polychromator; P, air polychromator; M, monochromator.

2.2. Procedures

2.2.1. Pre-concentration procedures

All samples were acidified to pH 4.5–5.0 with concentrated nitric acid prior to co-precipitation.

2.2.1.1. Co-precipitation of the elements studied in a model solution. To a 250-ml beaker were added 150 ml of RDW and 50 μl of the stock standard solutions of the elements to be studied (for a final concentration of the working solution of 2 mg l^{-1}). Then a 1 ml 0.1 mol l^{-1} HNO_3 and 60 ml 1.10^{-1} mol l^{-1} solution of Na-DTC was added and the mixture allowed to stand for 30 min. Then 1 ml 1% H_2O_2 was added and the precipitate allowed to stand for 5–6 h. Then it was filtered in a Büchner funnel through a dense narrow pore filter paper, washed with 400–500 ml of RDW and finally mineralized.

2.2.1.2. Co-precipitation of the elements studied in waste water samples. An aliquot (500-ml) of the water sample was acidified with 4 ml 1.10^{-1} mol l^{-1} HNO_3. To this was added 180 ml 1.10^{-1} mol l^{-1} Na-DTC with continuous mixing. The solution was allowed to stand for 30 min and then 3 ml 1% H_2O_2 was added. It was processed further as described above. Standard additions (1 mg l^{-1}, calculated to a final solution of 25 ml) were introduced prior to precipitation.

When the analysed water sample volume was 1000 ml all the reagent volumes were increased 2-fold.

2.2.2. Mineralization

The filter paper with the precipitate was transferred into a 250-ml beaker. Conc. HNO_3 (5 ml) and several glass beads were added. The beaker was covered with a watch glass and heated carefully on a sand bath until evaporation of nitrogen oxide finished and the solution became clear. After the solution was cooled, 20 ml RDW were added and the solution again heated until white fumes appeared. Then approximately 15 ml RDW was added. The sample was transferred quantitatively into a 25-ml volumetric flask (it was filtered if necessary) and diluted RDW.

2.2.3. Calibration

Calibration and was carried out with standard solutions of the elements containing 0.25, 0.50, 1.00, 1.50, and 2.0 mg l^{-1}. Standard solutions for calibration were prepared by spiking a blank solution (the model matrix) with stock solutions of the elements.

3. Results and discussion

The pre-concentration procedure by oxidation of K-pyrrolidine-1-carbodithoinat was successfully applied for the spectrophotometric determination of trace amounts of Cu [14]. The authors discuss producing thiuram disulphide in the solution by oxidising of the reagent mentioned by adding iodine.

In the present study Na-DTC is used both as a complex forming agent and as a collector. This is the main advantage of the proposed approach. The co-precipitation runs according to the following scheme:

Stage A—chelate formation

$$\underset{\textbf{(I)}}{(C_2H_5)_2\text{–}NC(S)SNa} + Me^{n+} \rightarrow \underset{\textbf{(II)}}{[(C_2H_5)_2 - NC(S)S]_n Me}$$

Stage B—'in situ' preparation of the collector [15]

$$(C_2H_5)_2\text{–}NC(S)SNa + H_2O_2 \rightarrow \underset{\textbf{(I)}}{(C_2H_5)_2NC(S)S\text{–}S(S)CN(C_2H_5)_2}$$

bis(ethanol) thiuram disulphide (**III**)

Stage C—co-precipitation

$$\underset{\textbf{(II)}}{[(C_2H_5)_2NC(S)S]_n Me} + \underset{\textbf{(III)}}{[(C_2H_5)_2NC(S)S\text{–}S(S)CN(C_2H_5)_2]} \Downarrow$$

In the region $2 < pH < 6$ Na-DTC transforms to disulphide.

3.1. Optimization of operating conditions

3.1.1. Precipitation

A number of parameters have been studied with a view to provide quantitative precipitation, namely, the order of addition of reagents, the effect of the amount of Na-DTC, the optimum pH, etc.

It was established that the reagents should be added in the following order: nitric acid to adjust the required pH, Na-DTC, and H_2O_2.

The effect of the amount of Na-DTC on the precipitation and subsequent ICP-AES analysis was studied according to the procedure described in Section 2.2.1.1. The concentration of all the elements studied was kept constant at 2 mg l^{-1}. The concentration of Na-DTC was varied in the range 0.009–21.6 g l^{-1}. The results obtained are shown in Fig. 1a and b. The retention versus the Na-DTC concentration shows that the quantitative sorption of all the elements studied was achieved at 5.4 mg ml^{-1} Na-DTC. Further increasing the Na-DTC concentration did not significantly affect the retention—R exceeded 95%.

The effect of pH is demonstrated in Fig. 2a and b. No co-precipitation could be achieved at a pH below 1.7 since Na-DTC was decomposed in the acid medium. The best retention with good reproducibility of the results was observed at pH 5–7 for all the elements studied. Apart from the title elements the retention of As and Mo has been investigated as well. Experiments revealed that Mo(VI) was quantitatively sorbed at pH 1.7 (90% retention). Our results are in good agreement with Ref. [12], where $R > 94\%$ was achieved for Mo at pH ~ 1.5. The retention of As(III) did not exceed 2.4% over the whole pH interval studied.

The effect of time on co-precipitation was studied. The precipitate was allowed to stand from 1 up to 48 h. It was established that 5 h was sufficient to produce results of good precision.

The effect of the sample volume has been studied as well. The results obtained are listed in Table 2. It is seen that the elements studied can be successfully concentrated by a factor of 8–80 depending on the sample volume. This concentration factor is sufficient to ensure the analysis of the elements in real water samples.

3.1.2. Mineralization of the precipitate

Mineralization with various acids or acid mixtures (e.g HNO_3:$HClO_4$ 1:1, 2:1, 3:1, etc.) was carried out. It was established that mineralization

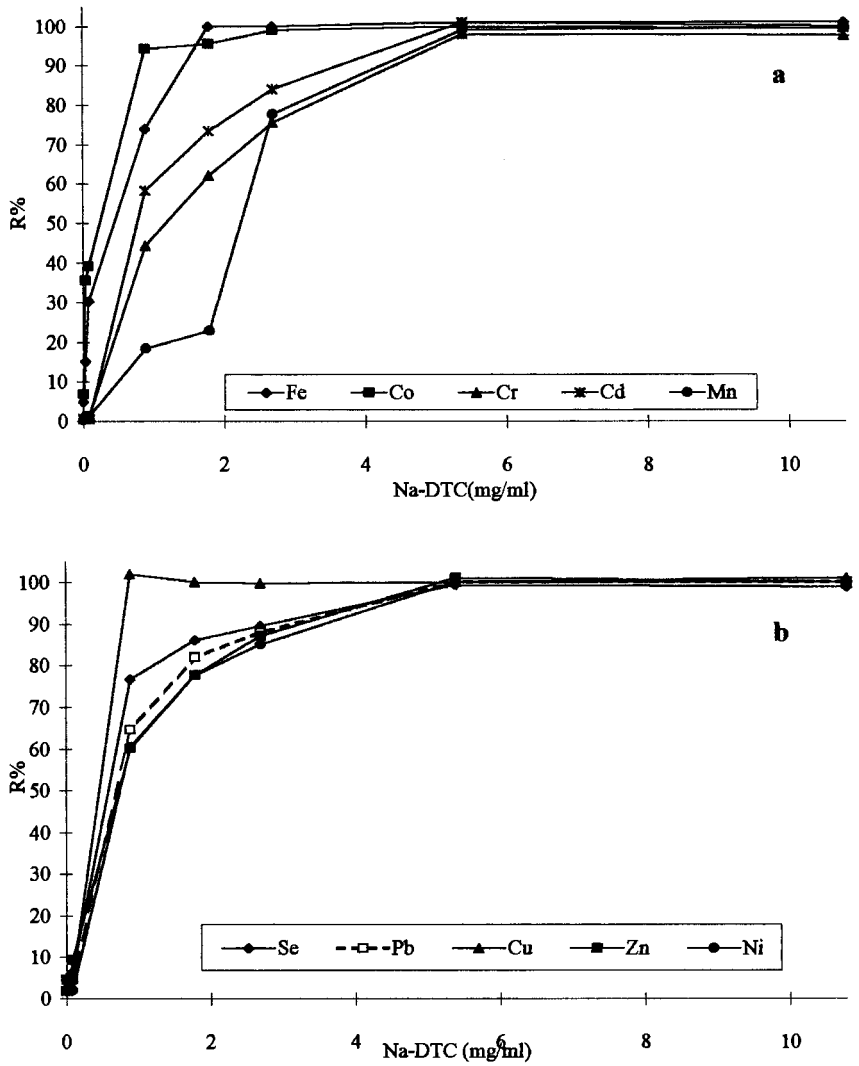

Fig. 1. Effect of the amount of sodium diethyldithiocarbamate on the quantitative co-precipitation of the elements studied.

with HNO_3 was best for the purpose of the present study. The possible loss of the micro-components during the mineralization step were investigated. Experiments were carried out as follows. A precipitate of thiuram disulfide was prepared in RDW. It was spiked with the elements under study and treated as described in section Section 2.2.2. The results of the ICP-AES determination showed no loss of the analysed elements in the course of analysis.

3.1.3. Effect of matrix components on co-precipitation and subsequent ICP-AES determination

Experiments were carried out with model solutions containing the micro-components to be studied and Ca (100 mg l^{-1}) and Sr, Mg, Ba, and Al (10 mg l^{-1}). The results obtained are presented in Table 3. It is seen that matrix components do not interfere with the ICP-AES determination.

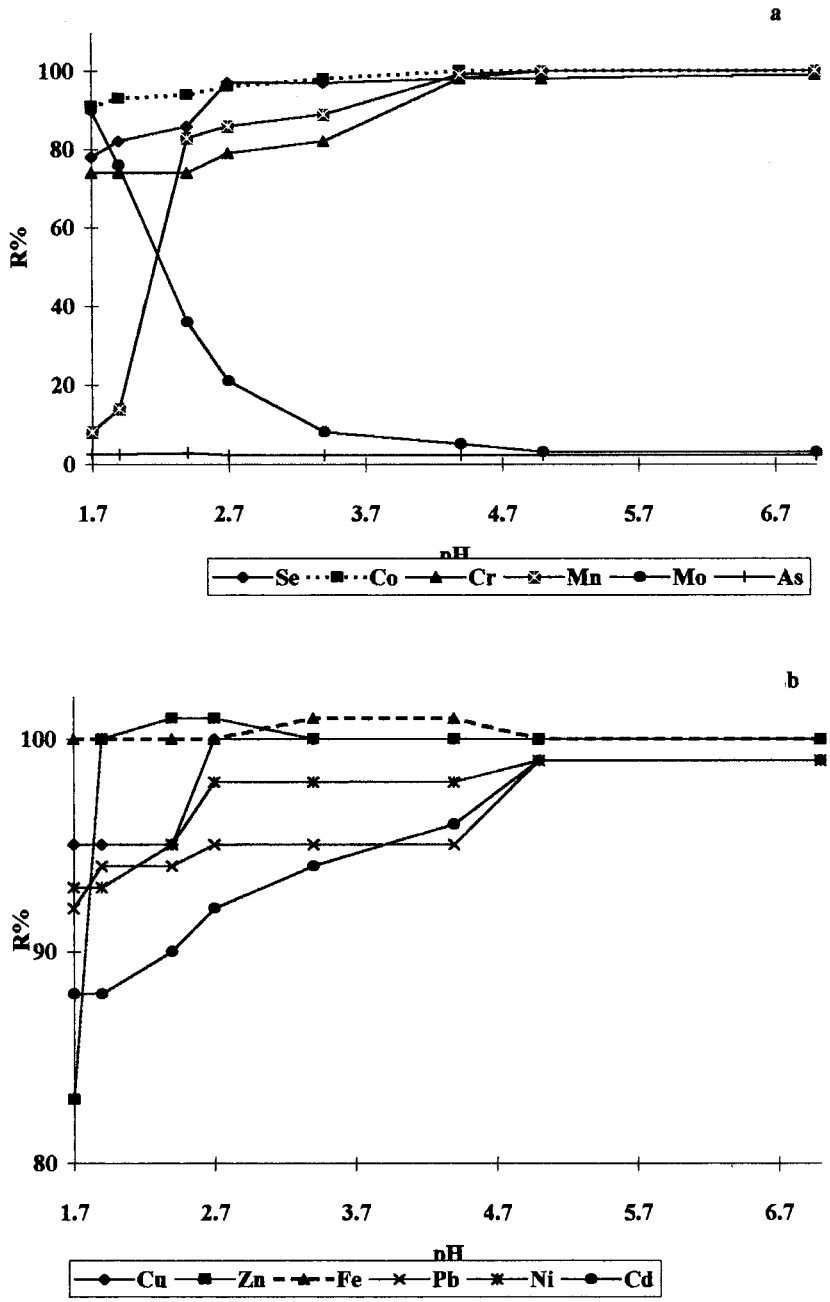

Fig. 2. Effect of pH on the quantitative co-precipitation of the elements studied.

3.1.4. Optimization of ICP-AES analysis

It was established that Na-DTC caused a 20–40% decrease in the analytical signals of the majority of the elements studied as compared to the signals produced by aqueous standard solutions. The excitation conditions were improved by increasing the incident power. The matrix effect was eliminated using a calibration with standard solu-

Table 2
Effect of the enrichment factor on the retention of the elements studied

Element	Retention (%)			
F ($V_{sample}/V_{concentrate}$)	10	20	40	80
Se	100	100	99	98
Pb	98	95	99	98
Cu	99	100	99.5	99
Zn	100	100	97	97.5
Ni	98	99	96	98
Fe	99	101	98	99
Cd	98	99	99	98
Co	100	101	100	97
Cr	98	97	96	97
Mn	99	101	97	98

tions containing the same amount of Na-DTC as that in the samples analysed.

The limits of determination were calculated according to the formula:

$$\text{DL (mg l}^{-1}) = \frac{10 \cdot \text{S.D.}_{\text{blank}} \cdot V_{\text{concentrate}}}{\text{Sensitivity} \cdot V_{\text{sample}}}$$

where $\text{S.D.}_{\text{blank}}$ is the S.D. of the blank solution (10 replicates), $V_{\text{concentrate}}$ is the volume of the concentrated sample (25 ml), and V_{sample} is the volume of the analysed sample (500 ml).

Table 3
Effect of the matrix components on quantitative co-precipitation of the elements studied

Element	Retention (%)	
	In RDW with addition of standards	In the model matrix[a]
Se	99	98.4
Pb	100	100
Cu	100	100
Zn	100	100
Ni	100	100
Fe	98.5	100
Cd	100	98
Co	98.5	100
Cr	98.5	98
Mn	100	98

[a] Ca (100 mg l^{-1}); Ba, Sr, Mg and Al (10 mg l^{-1}).

Table 4
Analysis of waste water by ICP-AES and ICP-MS

Element	Content (mg l^{-1})	
	ICP-AES	ICP-MS reference method
Se	<0.006	<0.001
Pb	0.56 ± 0.006	0.53 ± 0.002
Cu	0.047 ± 0.0008	0.05 ± 0.003
Zn	3.6 ± 0.05	3.25 ± 0.05
Ni	<0.014	<0.002
Fe	0.32 ± 0.002	0.29 ± 0.02
Mn	0.24 ± 0.004	0.26 ± 0.002
Cd	0.16 ± 0.002	0.13 ± 0.005
Co	0.003 ± 0.0005	0.003 ± 0.0008
Cr	<0.003	<0.001

$n = 10$, $P = 0.95$.

The following values were obtained (mg l^{-1}): 0.001 (Cu, Co, Cr, Mn), 0.0007 (Zn, Cd), 0.003 (Se), 0.004 (Fe), 0.007 (Ni), and 0.01 (Pb).

3.2. ICP-AES analysis of waste water

Experiments showed that no preliminarily sample preparation was necessary except for addition of HNO_3 to adjust the pH to 4.5. Waste water samples (500 ml) from a non-ferrous metallurgical plant near Plovdiv were analysed by the proposed procedure. The results are presented in Table 4. They are in good agreement with that obtained by the reference ICP-MS method.

4. Conclusions

A method for the pre-concentration of toxic metals (10 elements) in waste water and their determination by ICP-AES was developed. It is based on complex formation with sodium diethyldithiocarbamate, co-precipitation of the complexes with collector bis(ethanol) thiuram disulfide produced 'in situ' by oxidation of the excess of sodium diethyldithiocarbamate with H_2O_2. The sediment was dissolved with HNO_3 and the concentrated elements were determined by ICP-AES. The method was applied for multielemental analysis of river and waste water with an enrichment factor of 40.

References

[1] S.J. Yeh, J.C. Wei, C.N. Ke, C.Y. Yang, J. Radioanal. Nucl. Chem. 172 (1994) 221.
[2] M.A. Bolshov, V.G. Koloshnikov, S.N. Rudnev, C.F. Boutron, U. Gorlach, C.C. Patterson, J. Anal. At. Spectrom. 7 (1992) 99.
[3] R.E. Sturgeon, S.N. Willie, J. Zheng, A. Kudo, D.C. Gregoire, J. Anal. At. Spectrom. 8 (1993) 1053.
[4] Z. Zhuang, X. Wang, P. Yang, C. Yang, B. Huang, J. Anal. At. Spectrom. 9 (1994) 779.
[5] T. Akagi, H. Haraguchi, Anal. Chem. 62 (1990) 81.
[6] X. Shan, J. Tie, G. Xie, J. Anal. At. Spectrom. 3 (1988) 259.
[7] T. Akagi, K. Fuwa, H. Haraguchi, Anal. Chim. Acta 177 (1985) 139.
[8] Z.X. Zhuang, C. Yang, X. Wang, P. Yang, B.L. Hung, Fresenius' J. Anal. Chem. 355 (1996) 277.
[9] R.K. Skogerboe, W.A. Hanagan, H.E. Taylor, Anal. Chem. 57 (1985) 2815.
[10] H. Sawatari, T. Hayashi, E. Fujimori, A. Hirose, H. Haraguchi, Bull. Chem. Soc. Jpn. 69 (1996) 1925.
[11] C.L. Smith, J.M. Motooka, W.R. Willson, Anal. Lett. 17 (1984) 1715.
[12] J. Zucheng, P. Schramel, Fresenius' J. Anal. Chem. 343 (1992) 600.
[13] M. Vircavs, V. Rone, A. Pelne, D. Vircava, Anal. Chim. Acta. 299 (1994) 291.
[14] E. Beinrohr, J. Garaj, Analyst 111 (1986) 979.
[15] V.M. Birko, Dithiocarbamates, Science, Moscow, 1984, p. 22 (in Russian).

ELSEVIER

Talanta 47 (1998) 1245–1254

Talanta

A common method for the determination of several calcium channel blockers using an HPLC system with ultraviolet detection

M.A. García [a,*], C. Soláns [a], J.J. Aramayona [b], L.J. Fraile [b], M.A. Bregante [b], J.R. Castillo [c]

[a] *Department of Analytical Chemistry, Veterinary Faculty, University of Zaragoza, Miguel Servet 177, 50013 Zaragoza, Spain*
[b] *Department of Pharmacology and Physiology, Veterinary Faculty, University of Zaragoza, Miguel Servet 177, 50013 Zaragoza, Spain*
[c] *Department of Analytical Chemistry, Sciences Faculty, University of Zaragoza, Plaza San Francisco, 50009 Zaragoza, Spain*

Received 24 September 1997; received in revised form 23 February 1998; accepted 22 May 1998

Abstract

We report a common HPLC method for the single or simultaneous determination of four calcium channel blockers (CCB), namely diltiazem (DTZ), verapamil (VER), nifedipine (NIF) and nitrendipine (NIT) and their active metabolites demetildiltiazem and deacetildiltiazem (MA and M1), norverapamil (NOR), and dehydronifedipine (DHN). DHN was first synthesised in our laboratory and different pH values of the mobil phase were subsequently prepared and tested for chromatographic separation. The detection system and the environmental light conditions were optimised. The best separations of all analytes were obtained using a C_{18} column and a mobile phase of methanol, 0.04 M ammonium acetate, acetonitrile and triethylamine (2:2:1:0.04 v/v). Quantitation was performed using imipramine (IMI) as the internal standard. For DTZ and its metabolites (M1 and MA), the wavelength chosen was 237 nm; for VER and its metabolite NOR, it was 210 nm; and, finally for NIF and its metabolite DHN and NIT it was 216 nm. When a simultaneous analysis was carried out the wavelength was of 230 nm. The optimum pH were 7.90 and 7.10 when the separation of NIT and DTZ or VER and NIF were carried out, respectively, and 7.90 when a simultaneous separation was carried out. The detection limit of the assay was less than 8 ng ml^{-1} for all compounds, with coefficients of variation less than 7% (for inter- and intra-day) over the concentration range of 1–1000 ng ml^{-1}. The retention times were less than 11 min. When NIF or NIT were studied, it was necessary to use a sodium vapour lamp in order to avoid the photodegradation which takes place under daylight conditions. © 1998 Elsevier Science B.V. All rights reserved.

Keywords: Calcium channel blockers; HPLC; Ultraviolet detection

* Corresponding author. Tel.: +34 976 761658; fax: +34 976 761612.

0039-9140/98/$ - see front matter © 1998 Elsevier Science B.V. All rights reserved.
PII S0039-9140(98)00210-0

1. Introduction

Calcium channel blockers (CCB) are widely used in the treatment of hypertension, angina pectoris and cardiac arrythmias [1–4]. These drugs display similar pharmacologic activity, but have heterogeneous chemical structures and physicochemical properties. They have been shown to be extensively metabolised by the mixed-function oxidase system. Some of the metabolites that are formed retain a potent pharmacological activity [5–7]. For this reason, an optimal analytical method allows for the analysis of the parent drug and their active metabolites.

Various methods have been reported for the determination of CCB, namely spectrofluorimetric [8–11], voltametric [12–14], thin-layer chromatographic [15,16], radio receptor assay [17], radio immunoassay [18], gas chromatographic [19–25] and liquid chromatographic methods [26–32]. These methods have been developed to allow for the analysis of individual drugs. However, combined therapy has been reported to be markedly effective for some clinical cases [33–35], for which reason the analytical method must allow for a simultaneous determination of several CCB.

Our objective has been to obtain and to validate a common method to separate and quantify selected drugs that are representative of classical CCB groups: diltiazem (DTZ) (the benzothiazepine group) and its active metabolites, demetildiltiazem (MA) and deacetildiltiazem (M1); verapamil (VER) (the difenilaquilamine group) and its active metabolite, norverapamil (NOR) and, as pyridine representatives, nitrendipine (NIT) and nifedipine (NIF) with its metabolite dehydronifedipine (DHN). This method has to allow for the analysis of a compound and its metabolite or to separate all CCB compounds studied when a simultaneous determination is being carried out.

2. Experimental

2.1. Apparatus

Spectroscopic analyses were carried out using a Varian Unity 300, a mass spectroscopic VG Autospec, an IR Perkin-Elmer 1600 series FTIR, an HP89530A diode array (Hewlett-Packard) and a luminiscence spectrometer LS50 (Perkin-Elmer).

The HPLC system consisted of a Waters 501 pump and a Waters M717 autosampler. Separations were performed using a C_{18} reversed-phase column (Novapack; 150×3.9 mm. i.d.) packed with 4×10^{-6} m particles. A pre-column (Novapack C_{18}-guard-pack) was used between the injector and the analytical column to effectively minimise accumulation of matter in the analytical column. Analysis was carried out at room temperature (ca. 22°C).

Detection was performed with a tunable UV–vis detector (Waters 484). FGS 602N2 sodium vapour lamps and SOX-55, 55W lamps (Philips, Spain) were also used.

Height integrations, peak height measurements, calculations and the plotting of the chromatograms were all carried out using an integration pack program (Kontron Instrument).

2.2. Chemical, reagents and solutions

NIF, DTZ and the internal standard imipramine (IMI) were purchased from Sigma, whilst NIT was purchased from Research Biochemical International. MA and M1 were gifts from the Institute Mario Negri (Milan, Italy). VER and NOR were kindly supplied by Knoll Laboratories (Spain) (Fig. 1).

All reagents were of reagent or HPLC grade and were obtained from Scharlau. Water was glass-distilled and purified through a Milli-Q purification system (Millipore).

Stock solutions, 100 mg ml^{-1} (as base) of DTZ, MA, M1, VER, NOR, and IMI in water, and NIF, NIT and DHN in methanol, were prepared. They were kept protected from light with an aluminium foil covering and stored at 4°C in a dark room. The solutions were stable for a period of at least 3 months.

2.3. Preparation of DHN

DHN was synthesised in our laboratory by oxidation of the 1,4-dihydro derivative, which was

obtained from *o*-nitrobenzaldehyde, ethylacetoacetate and NH_3 by Hantzsch synthesis, according to the procedure reported by Kamal et al. [36]. The powder was recrystallised from ethyl acetate to produce yellow needles. The yield obtained by this method was close to 85%.

The structure of the metabolite was elucidated by combined IR, ^1H RMN, ^{13}C RMN and MS. IR: 1615.1, 1531.0 cm^{-1} (aromatic). ^1H RMN ($CDCl_3$) (ppm): 2.26 (6H, s, CH_3), 3.45 (6H, s, CH_3), 7.16, 7.57 and 8.19 (4H, aromatic protons). ^{13}C RMN ($CDCl_3$): 23.61 (CH_3), 52.13 (CH_3), 124, 132.85, 145.15 (aromatic) and 167.22 ($-COO^-$). EI-MS *m*/*z*: 230 molecular ion.

2.4. HPLC procedure

A Novapack C_{18} reversed-phase column was used as the stationary phase. The mobile phase consisted of a mixture of methanol, 0.04 M ammonium acetate, acetonitrile and triethylamine (2:2:1:0.04 v/v). The pH was adjusted to 7.90 by the addition of 0.1 M acetic acid in order to separate DTZ, M1 and MA. The same pH was used for the analysis of NIT. However, the pH was adjusted to 7.10 in order to separate VER and NOR or NIF and DHN. The detections were 237, 210 and 216 nm for DTZ and its metabolites,

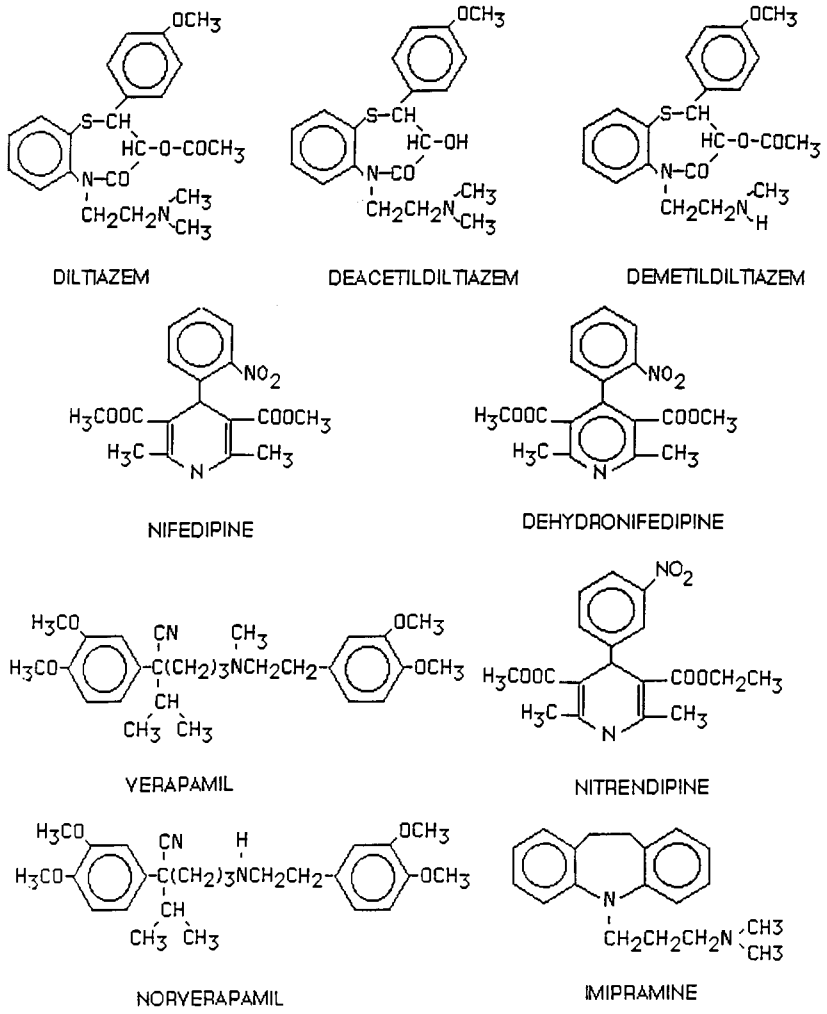

Fig. 1. Structure of CCB and its metabolites and IMI.

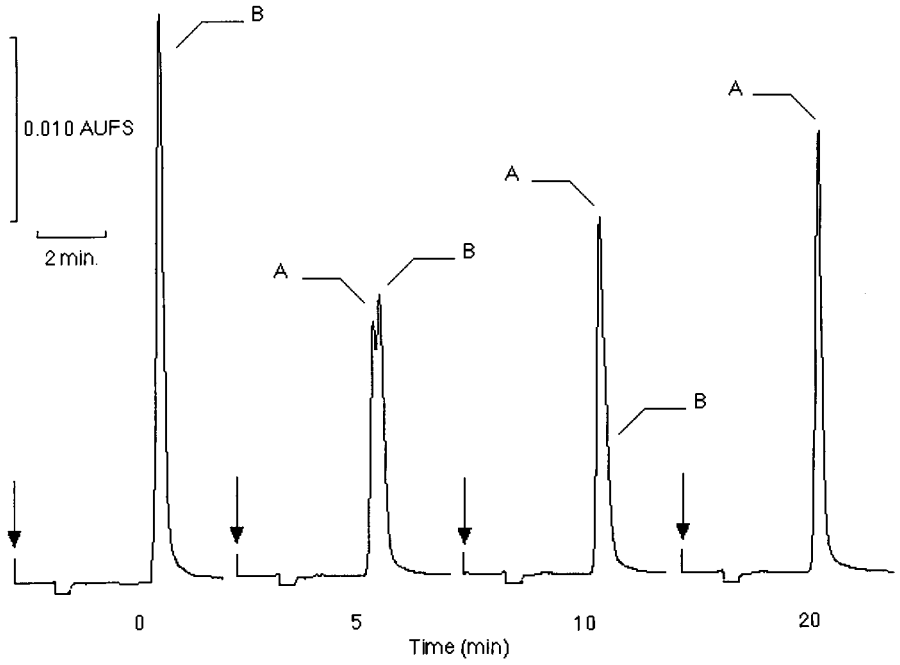

Fig. 2. Evolution time of NIF dissolution allowed to decompose at room temperature and exposed to daylight. A: unidentified decomposition product; and B: NIF.

for VER and its metabolite and for NIF and NIT, respectively.

When a simultaneous analysis was carried out, the pH was adjusted to 7.90 and detection was achieved at 230 nm. In all cases, the HPLC–UV system was operated isocratically at room temperature, the effluent flow rate was 1.2 ml min^{-1} and quantification was performed using IMI as the internal standard

2.5. Effect of light conditions

Solutions of NIF, DHN and NIT in methanol and DTZ, MA, M1, VER and NOR in water were exposed to laboratory-light, daylight and a sodium vapour lamp over a period of 12 h. During this time, serial samples (at 0, 2, 4, 5, 10, 20, 30, 60, 90, 120, 180, 240, 360, 480, 600 and 720 min) were taken and analysed by HPLC.

2.6. Luminescence and wavelengths used

Samples of DTZ, MA, M1, VER, and NOR in water, and NIF, NIT and DHN in methanol (1000 ng ml^{-1} for each compound), were prepared and kept protected from light. Spectral analyses were carried out using a diode array (200–300 nm) and a luminescence spectrometer. The samples were diluted to obtain a signal in the range 0–1 U_{abs}.

3. Results and discussion

3.1. Effect of light conditions

When working with photolabile compounds, the light conditions should be studied. We have not found any reports on the photolability of

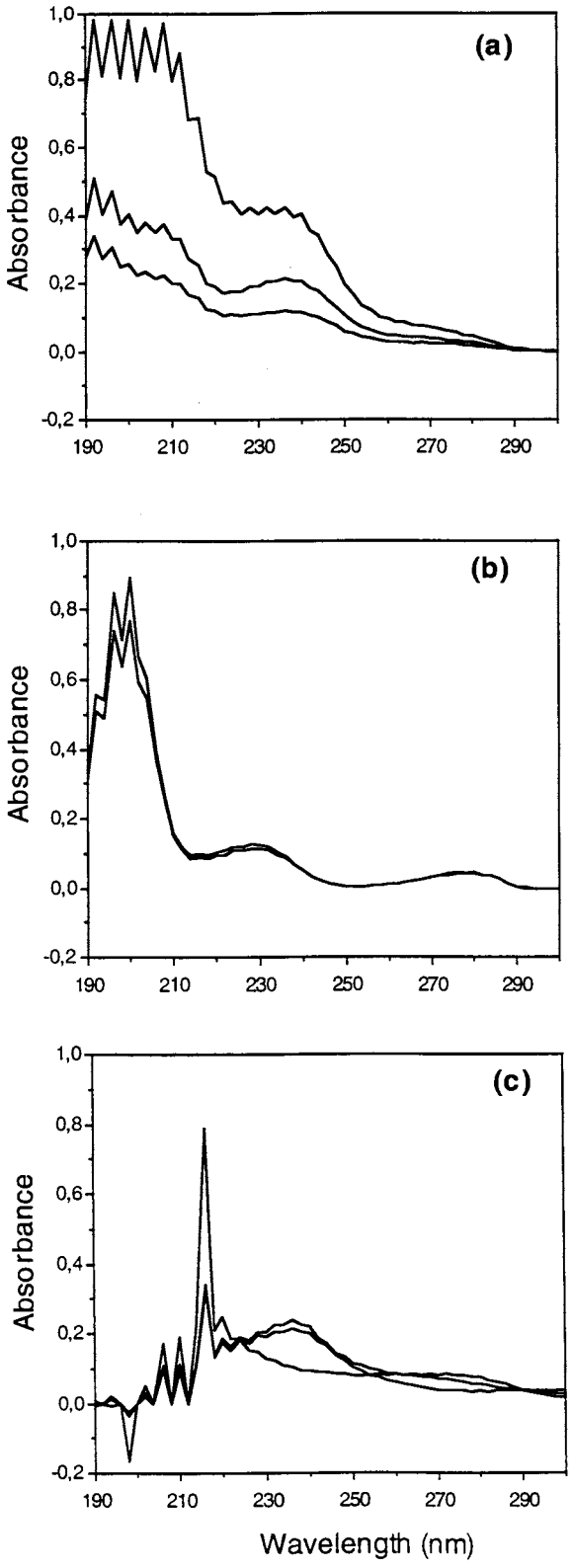

DTZ, VER and NIT. However, it is known that NIF is extremely light sensitive [37,38], decaying in daylight to the nitroso derivative by an intramolecular photochemical reaction, with a half-life of around 1–2 h, depending upon the solvent. Moreover, photolabile of NIF in methanol solutions has not been studied, so far as we are aware, and this has encouraged us to carry out this study.

When the samples of DTZ, MA, M1, VER, NOR and DHN were exposed to laboratory light, daylight or sodium light, we found that none of the compounds showed any decay of concentration over time.When the samples of NIT in methanol were exposed to laboratory light or sodium light no decay of concentration was observed, but when they were exposed to daylight a linear decay was detected. Under these light conditions, NIT disappeared by about 22% at 720 min. Moreover, we could extrapolate a half life of 1625.8 min.

Finally, when the samples of NIF were exposed to sodium light, NIF showed no decay of concentration. However, we could observe a linear monophasic decay with daylight, with a half-life of 5.2 min and a linear monophasic decay with laboratory light, with a half-life of 128.8 min. A new peak related to the photochemical degradation of NIF could be detected in the chromatographic analysis. This degradation product eluted at a retention time that was shorter than the original compound and interfered with the peak resolution (Fig. 2).

It must be concluded therefore that NIF is highly photolabile in methanol solution and clear glass and also under normal daylight, but less sensitive under laboratory light. Our estimation of its half-life is in the same order as the values previously reported [39–41] in aqueous and toluene solution. Moreover, we have concluded that NIT is poorly photolabile in methanol solution under daylight.

We wish to emphasize that our experiments were carried out in the summer time, and for this reason, the daylight sensitivity of NIF or NIT

Fig. 3. Absorbtion spectra of: (a) DTZ and its metabolites M1 and MA in water; (b) VER and NOR in water; (c) NIF, DHN and NIT in methanol.

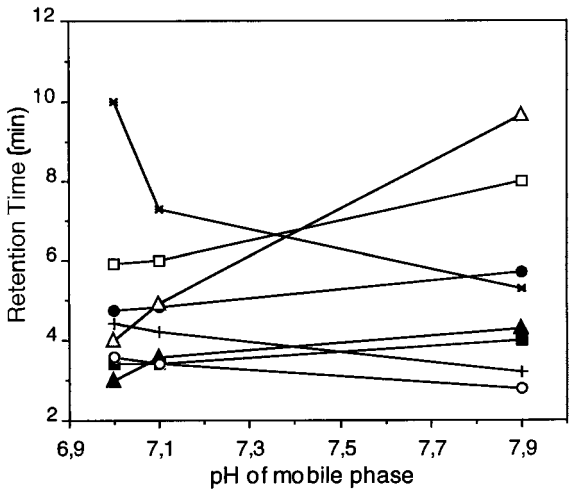

Fig. 4. Retention time of all compounds studied vs. pH of the mobile phase. DTZ (□) and its metabolites MA (■), M1 (●); VER (△) and its metabolite NOR (▲); NIF (+) and its metabolite DHN (○); and NIT (∗)

might be different to other laboratories. Nevertheless, all experiments with NIF or NIT should be carried out under a sodium lamp.

3.2. Luminescence and wavelengths used

The detection system is an important aspect when it is necessary to employ a method for the simultaneous separation and quantification of broad groups of compounds with heterogeneous chemical structures. Systems with UV and luminescence detection have been used extensively in HPLC methods in order to minimise costs as compared to electrochemical or MS detection systems. For this reason we have carried out spectral analysis.

We were unable to find luminescence in any of the compounds tested, except in VER and NOR. For this reason, the luminescence method was discarded as a detection technique in this study.

The detection wavelength was chosen following a UV spectral study. For DTZ and its metabolites, M1 and MA (Fig. 3a), several maximum absorption values were observed. To minimise the possible spectrum interferences induced by the matrix, the wavelength chosen was 237 nm. For VER and its metabolite NOR (Fig. 3b), the wavelength selected was 210 nm, as a compromise to

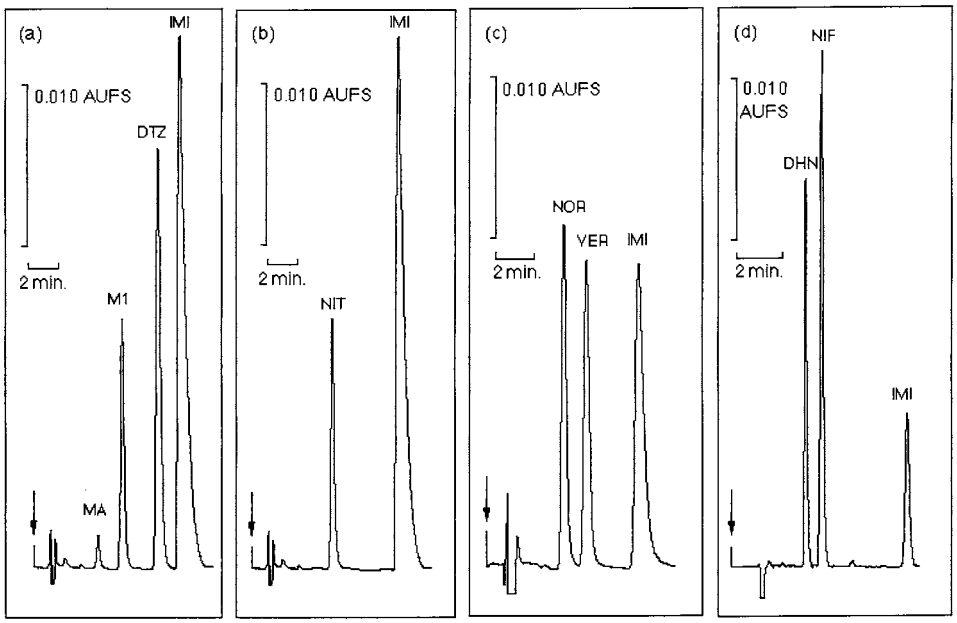

Fig. 5. Typical chromatograms for: (a) DTZ and its metabolites M1 and MA; (b) NIT; (c) VER and its metabolite NOR; and (d) NIF and it metabolite DHN. The standard peaks were obtained by injecting 300 ng of each compound.

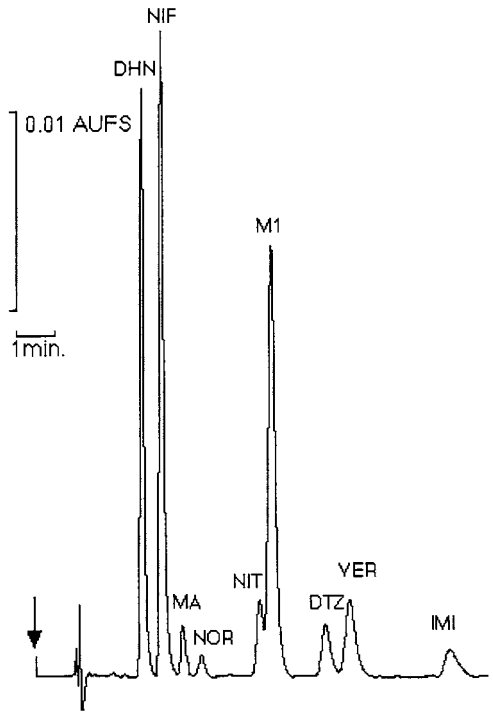

Fig. 6. Typical chromatogram of a standard mixture of DTZ and its metabolites M1 and MA; NIT; VER and its metabolite NOR; and NIF and it metabolite DHN. The standard peaks were obtained by injecting 200 ng of each compound.

Table 1
Standard curves for DTZ and its metabolites MA and M1; VER and its metabolite NOR; NIF and its metabolite DHN; and NIT

Analyte	Curve ($y = ax + b$)			
	a	b	r^2	n
DTZ	0.1883	−0.3815	0.999	6
M1	0.2432	+2.1448	0.999	6
MA	0.1427	−0.6660	0.999	6
VER	0.1251	−0.7076	0.999	6
NOR	0.1512	−0.4595	0.999	6
NIF	0.3319	−0.4992	0.999	6
DHN	0.4460	−0.3365	0.999	6
NIT	0.1473	−1.9829	0.999	6

Range 0–1000 ng ml^{-1}.

avoid interference and make good use of the maximum absorption zones. The spectroscopic analyses of the pyridines showed two typical maximum spectra (Fig. 3c), one with a maximum absorption at 238 nm, exhibited by NIF and NIT and the other, corresponding to a maximum absorption at 216 nm, exhibited by all three compounds (NIF, DHN and NIT).

When a simultaneous analysis was performed, the wavelength was 230 nm.

3.3. pH of the mobile phase and retention times

The chromatographic separation of the calcium channel blockers was further investigated by changing the pH of the mobile phase. Various mobile phases for the separation of several CCB have been described by different authors [26–32]. After carrying out previous experiments (data not shown) with these phases, the mobile phase was held constant in methanol, 0.04 M ammonium acetate, acetonitrile and triethylamine (2:2:1:0.04 v/v) and a pH ranged between 7.00 and 7.90.

pH variations in the aqueous phase do not significantly affect the chromatographic profile of neutral substances [28]. Nevertheless, this factor plays an important role in the separation of acidic and basic compounds. Fig. 4 shows the effect of increasing the pH of the mobile phase on the separation of each analyte.

Compounds having ionisable amino functional groups undergo ion-pairing with an undefined number of strongly acidic silanol groups. These interactions are controlled directly by pH. We found that the ionised forms (DTZ, M1, MA, VER and NOR) were less well retained in a reversed-phase column (typical of partition chromatography). However, the pH effect on the chromatographic profile of pyridines (NIF, NIT, and DHN) could not be explained by the same mechanism. For these compounds, factors other than simple partition between the mobile phase and stationary phase, for example aromatic interactions with siloxane groups, could be more important.

The optimum pH to separate NIT (Fig. 5b) or DTZ and its metabolites, M1 and MA (Fig. 5a) was 7.90. However, the pH to separate VER and its metabolite (Fig. 5c) or NIF and its metabolite DHN (Fig. 5d), was 7.10. These pH values provide optimum resolutions of the different

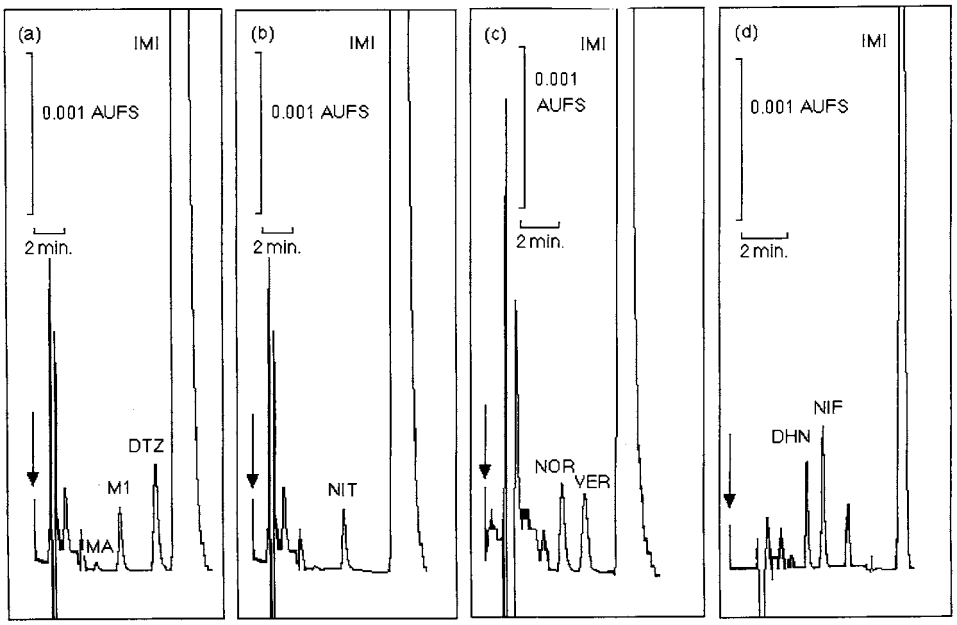

Fig. 7. Typical chromatograms for: (a) DTZ and its metabolites deacetildiltiazem M1 and MA; (b) NIT; (c) VER and its metabolite NOR; and (d) NIF and it metabolite DHN. The standard peaks were obtained by injecting 8 ng of each compound.

Table 2
Accuracy and precision of the HPLC method for the determination of all compounds

Analyte added (ng ml^{-1})	Concentration	Concentration found (ng ml^{-1})[a]	Accuracy (%)	Precision CV (%)[b]
DTZ	100	96.12 ± 3.59	96.1	3.73 (3.40)
	200	203.60 ± 4.22	101.8	2.07 (3.52)
	500	519.00 ± 3.10	103.8	0.59 (1.59)
M1	100	95.79 ± 4.23	95.8	4.41 (4.23)
	200	213.79 ± 7.39	106.8	3.46 (4.12)
	500	510.30 ± 7.30	102.1	1.73 (2.05)
MA	100	90.83 ± 6.14	90.8	6.76 (4.35)
	200	219.25 ± 9.44	109.6	4.30 (3.45)
	500	495.27 ± 7.74	99.1	1.56 (2.67)
VER	100	98.78 ± 1.76	98.8	1.79 (2.01)
	200	208.61 ± 0.75	104.3	0.35 (1.34)
	500	497.31 ± 5.58	99.5	1.12 (1.45)
NOR	100	101.13 ± 0.98	101.1	0.97 (2.09)
	200	211.89 ± 1.00	105.9	0.47 (0.67)
	500	496.02 ± 4.64	99.2	0.93 (1.23)
NIF	100	93.70 ± 0.66	93.7	0.71 (1.03)
	200	191.56 ± 1.71	95.8	0.90 (1.24)
	500	496.38 ± 2.09	99.3	0.42 (0.67)
DHN	100	98.53 ± 1.19	98.5	1.47 (2.20)
	200	202.77 ± 0.82	101.4	1.38 (1.67)
	500	498.97 ± 2.27	99.8	0.20 (0.78)
NIT	100	97.79 ± 2.42	97.8	2.47 (3.02)
	200	197.62 ± 3.66	98.8	1.85 (2.78)
	500	501.59 ± 4.87	100.3	0.97 (1.23)

[a] Each value represents the mean of six independent determinations.
[b] The intrassay variations were the mean CV of the peak height ratios calculated on each day of analysis ($n = 6$), whereas the interassay variations were calculated using the mean peak height ratios obtained on each day of analysis. Interassay variations appear in parentheses.

chromatographic peaks. The retention times were less than 11 min for all the compounds studied and the peak with the lowest retention time leaves enough room for possible interference induced by the matrix. To obtain simultaneous separation for all the compounds and their metabolites, the pH of the mobile phase was adjusted to 7.90 (Fig. 6).

To study the selectivity and robustness of the analytical method, in addition to the lighting conditions and pH of the mobile phase, we also studied other factors such as the concentration of the ion and the concentration of triethylamine. Although they also affected the retention of these drugs, they did not, in general, alter its selectivity. Overall, the compounds analysed showed a decrease in their retention time when the ionic strength of the mobile phase was increased. This fact has also been described for these compounds [28] by other authors. The optimal concentration of the ammonium acetate was 0.04 M. Concentration of triethylamine ranged between 0.01 and 0.08%. It was found that triethylamine reduced the retention time and greatly improved the peak shapes at a concentration of up to 0.04%. No further improvements were detected when that concentration was higher. Other ions, including ammonium bromide, ammonium perchlorate and sodium bromide were also investigated during the development of the method. However, they were not chosen because, when compared with ammonium acetate, they required a long time to reach stable assay conditions.

3.4. Internal standard

Ideally, an internal standard should have physicochemical properties similar to the analyte. However, because of the variety in the physicochemical properties of the different CCBs, it is extremely difficult to find one. Five compounds were investigated as a possible internal standard, namely clomipramine, loxapine, amitriptyline, alprazolam and imipramine. Clomipramine, loxapine and amitriptyne had retention times that were too long (>20 min), whilst that of alprazolam was too short (<2.5 min). IMI was the only one clearly separated from all the CCBs and their metabolites and its retention time was within a tolerable limit for routine analysis. For these reasons, it was selected as the internal standard.

3.5. HPLC detection limits and calibration curve

The various CCBs and their metabolites were weighed and diluted in water or methanol to obtain the proper concentrations for the HPLC calibration curve. Nine concentrations were conducted (0, 5, 10, 25, 50, 100, 200, 500 and 1000 ng ml^{-1}), and linear regression was used to analyse the suitability. The analysis of the standard solutions showed a good linear correlation (Table 1) between concentration and peak height (range 0–1000 ng ml^{-1}).

The concentration that could be detected (calculate by the Miller method [42]) was less than 8 ng ml^{-1} in every case (Fig. 7). The limit of detection and linearity range allows this method to be applied in pharmacokinetic studies.

3.6. Accuracy and precision (intra- and inter-day)

The precision (intra- and inter-day) of the method was calculated at three concentrations (100, 200 and 500 ng ml^{-1}). The precision of the assay was determined using the variability in the peak-height ratios at each concentration, while the accuracy was determined by comparing the measured concentration with the added concentration (Table 2). Both accuracy and precision showed satisfactory levels in all cases.

4. Conclusions

A sensitive reversed-phase high-performance liquid chromatographic method has been developed and validated for the individual or simultaneous separation and determination of CCB and their metabolites, using IMI as the internal standard and UV as the detection method.

All operations with NIF and NIT should be carried out in a dark room using sodium vapour lamps.

References

[1] E.M. Sorkin, S.P. Clisold, R.N. Brogden, Drugs 30 (1985) 182.
[2] H. Echizen, M. Eichelbaum, Clin. Pharmacokinet. 11 (1986) 425.
[3] M.M.T. Buckley, S.M. Grant, K.M. Goa, D. McTavish, E.M. Sorkin, Drugs 39 (1990) 757.
[4] D. McTavish, E.M. Sorkin, Drugs 38 (1989) 19.
[5] G. Neugebauer, Cardiovasc. Res. 12 (1978) 247.
[6] N. Yabana, T. Nagao, N. Sato, J. Cardiovasc. Pharmacol. 7 (1985) 152.
[7] F.P. Guengerich, M.V. Martin, P.H. Beaune, P. Kremers, T. Wolf, D.J. Waxman, J. Biol. Chem. 246 (1986) 5051.
[8] P. Hubert, J. Crommen, J. Liq. Chromatogr. 17 (1994) 2147.
[9] Y. Koike, K. Shimamura, I. Shudo, H. Saito, Res. Commun. Chem. Pathol. Pharmacol. 24 (1979) 37.
[10] R.G. McAllister, S.M. Howel, J. Pharm. Sci. 65 (1976) 431.
[11] K. Schlobmann, Arznei. Forsch-Drug Res. 22 (1972) 60.
[12] A. Alvarezlueje, L.J. Nunezvergara, J. Squella, Electroanalysis 6 (1994) 259.
[13] A. El-Jammal, J.C. Vire, G.J. Patriarche, O. Palmeiro, Electroanalysis 4 (1992) 57.
[14] J. Squella, J. Mosre, M. Blaquez, L.J.J. Nunezvergara, Electroanal. Chem. 319 (1991) 177.
[15] K. Kohno, U. Takeuchi, A. Etoh, K. Noda, Arzneim. Forsch. 27 (1977) 1424.
[16] S. Ebel, H. Schutz, A. Hornitschek, Arzneim. Forsch. 28 (1978) 2188.
[17] R.J. Gould, K.M.M. Murphy, S.H. Snyder, Life Sci. 33 (1983) 2665.
[18] K.P. Campbell, A. Sharp, M. Strom, S.D. Kahl, Proc. Natl. Acad. Sci. USA 83 (1986) 2792.
[19] E. Braunwald, New Engl. J. Med. 307 (1982) 1618.
[20] J.P. Clozel, Y. Caille, P. Taeyamens, P.B. Theroux, J.G. Begner, J. Pharm. Sci. 73 (1984) 207.
[21] G.D. Todd, D.W.A. Bourne, R.G. McAllister, Ther. Drug. Monit. 2 (1980) 411.
[22] C. Fischer, F. Schonberger, W. Muck, K. Heuck, M. Eichelbaum, J. Pharm. Sci. 82 (1993) 244.
[23] B. Marciniec, E. Kujawa, Chem. Anal. 40 (1995) 511.
[24] A. Kazuki, S. Baba, S. Aoki, Chem. Pharm. Bull. 36 (1988) 3000.
[25] S. Kondo, A. Kuchiki, K. Yamamoto, K. Akimoto, K. Takahaski, Chem. Parm. Bull. 28 (1980) 1.
[26] R. Bernasconi, S. Caliari, R. Latini, D. Leopaldi, S. Porzio, A. Salimbeni, Eur. J. Drug Metab. Pharmacokinet. 17 (1992) 269.
[27] D.R. Abernethy, J.B. Schwartz, E.L. Todd, J. Chromatogr. 342 (1985) 216.
[28] R.S. Bradley, J.T. Stewart, J. Liq. Chromatogr. 171 (1994) 2675.
[29] D. Romanova, E. Brardsteterova, D. Klalikova, L. Bozekova, Pharmazie 49 (1994) H10.
[30] T. Ohkubo, H. Noro, K. Sugawara, J. Pharm. Biomed. 10 (1992) 67.
[31] J.S. Grundy, R. Kherani, R. Foster, J. Chromatogr. 654 (1994) 146.
[32] J.M. El-Sayed, E.M. Niazy, S.H. Khidr, J. Clin. Pharm. Ther. 18 (1993) 325.
[33] T. Tateishi, K. Ohashi, T. Sudo, et al., J. Clin. Pharmacol. 29 (1989) 994.
[34] K. Ohashi, T. Tateishi, T. Sudo, et al., J. Cardiovasc. Pharmacol. 15 (1990) 96.
[35] K. Ohashi, T. Sudo, K. Sakamoto, et al., J. Clin. Pharmacol. 33 (1993) 222.
[36] A. Kamal, M. Ahmad, M. Mohd, A.M. Hamid, J. Chem Soc. 37 (1963) 610.
[37] P.A. Soons, J.H.M. Schellens, M.C.M. Roosemalen, D.D.J. Breimer, Pharm. Biomed. 9 (1991) 475.
[38] F. Barbato, B. Cappello, L. Grumetto, P. Morrica, Farmaco 48 (1993) 417.
[39] B.J. Schmid, H.E. Perry, J.R. Idle, J. Chromatogr. 425 (1988) 107.
[40] C.H. Kleinbloesem, J. Van Harten, J. Chromatogr. 308 (1984) 209.
[41] F.A. Tucker, P.S.B. Minty, G.A. MacGregor, J. Chromatogr. 342 (1985) 193.
[42] J.C. Miller, J.N. Miller, Estadistica Para Química Analítica, Addison Wesley Iberoamericana, Wilmington, DE, 1993.

ELSEVIER

Talanta 47 (1998) 1255–1261

Talanta

Flow-through fluorescence immunosensor for atrazine determination

E. Turiel, P. Fernández, C. Pérez-Conde, A.M. Gutiérrez, C. Cámara *

Departamento de Química Analítica. Facultad de Ciencias Químicas, Universidad Complutense de Madrid, 28040 Madrid, Spain

Received 19 February 1998; received in revised form 13 May 1998; accepted 22 May 1998

Abstract

A new flow-through fluoroimmunosensor for atrazine determination based on the use of protein A immobilized on controlled pore glass as immunoreactor is reported. The support, placed in the optical path of the flow cell, allows the 'in situ' quantification of atrazine by on-line antigen–antibody binding upon successive injections of both substances. The immunosensor has a detection limit of 2.1 μg l^{-1}, a sample speed of about 10 samples per hour, and provides high reproducibility both within-day (3.2% for 5 μg l^{-1} and 2.2% for 30 μg l^{-1}) and between days. The optimum working concentration range was 2.1–50 μg l^{-1}. Possible interferences of other triazines like simazine, desethylatrazine (DEA) and desisopropylatrazine (DIA) were evaluated. Simazine and DIA were not cross-reactive; however, the cross-reactivity for DEA was CR = 7.7%. The proposed immunosensor was successfully applied to the determination of atrazine in drinking water and citrus fruits. © 1998 Elsevier Science B.V. All rights reserved.

Keywords: Flow-through fluoroimmunosensor; 'In-situ' detection; Atrazine

1. Introduction

The pesticide atrazine (2-chloro-4-ethylamine-6-isopropylamine-1,3,5-triazine) is used extensively as a preemergent herbicide for corn, sorghum, nursery conifers, as well as inforest conservation [1]. In fact, this herbicide is a common contaminant in surface and ground water.

In general, triazines are mainly determined by chromatographic methods, GC-MS being the most usual [2]. Several LC methods for pesticides determination in water, which require the use of preparative and extractive methods to separate the target pesticide from other herbicides with similar structures, have been described [3].

Immunological methods can be applied as an alternative to these high time consuming methods for the determination of these substances. Flow injection coupled to immunoassays is arising as a powerful tool for the development of analytical procedures [4]. Minimal sample clean-up, high selectivity, relatively simple handling and low detection limits are some important advantages of immunoassays for pesticide determination.

Fluorescence immunoassay, which is widely applied in clinical, environmental and related areas, combines the high selectivity inherent to an anti-

* Corresponding author. Tel.: +34 91 3944318; Fax: +34 91 3944329.

0039-9140/98/$ - see front matter © 1998 Elsevier Science B.V. All rights reserved.
PII S0039-9140(98)00206-9

body binding interaction with the sensitivity and hazard-free analysis of the fluorescence detection methods.

Some flow-through fluorescence immunosensors have been developed for triazine herbicides (atrazine, cyanazine, propazine, simazine and terbutryn), using an Eu (III) complex as a tracer [5]. The immunological reaction is carried out in a column, and requires 2 h for antigen-antibody complex incubation. Furthermore, a complete assay needs at least two operation steps. Recently, Gascon et al. [6] and Bjarnason et al. [7], developed a new sensitive enzyme-linked immunosorbent assay for atrazine determination by flow injection analysis, in which the detection limit were 0.075 and 0.02 μg l^{-1}, respectively, and the total assay time was around 30 min per cycle.

Kramer et al. [8] described the first results with a prototype instrument for the determination of pesticides in water using flow injection immunoanalysis and enzyme-linked immunosorbent assay. It was possible, with this device, the pesticides determination in the concentration of 0.1 μg l^{-1}, but the process is complex and requires a high steps number, and a large analysis time.

The development of 'in situ' detection methods with on-line incubation, where the reaction is integrated in the detection, has made the assay very fast, because no further preparation and incubation steps are required.

Consequently, sensitive and selective flow-through fluorescence immunosensors are a new analytical tool which allows rapid direct determination using low sample volumes. An immunosensor for atrazine was developed by Bier [9] using a grating coupler, which requires a detergent to avoid air bubbles in the narrow incubation cell. The detection limit was 15 μg l^{-1}, the analysis time around 90 min, but it was not applied to real samples.

In a previous paper [10] we developed a flow-trough fluorescence immunosensor for theophyline with 'in-situ' detection.

This paper describes a new flow-through fluorescent immunosensor for atrazine determination. In the assay, protein-A immobilized on controlled pore glass (Pr-A-CPG) was used as a support for the immunological reaction, the antigen was labelled with fluoresceine isothiocyanate (FITC), and the antibody was a sheep polyclonal antiserum.

The proposed immunosensor was applied to the determination of atrazine in drinking water and citrus fruits.

2. Experimental

2.1. Apparatus

- Perkin Elmer LS50 spectrofluorimeter controlled by an IBM model 55SX computer and the FLDM (fluorescence data manager) software.
- The gas chromatograph used was a HP-5890-II with nitrogen-phosphorous detection (NPD) from Hewlett Packard.
- 19 μl Hellma (Jamaica, NY) flow cell (optical path 1 cm).
- Flow injection system consisting of a Gilson Microplus 2 peristaltic pump, an Omnifit injection valve (six way) and PTFE tubes (0.5 mm id).
- Crison 2001 pH meter.
- Glass column (10 cm × 10 mm).
- Rotavapor system.

2.2. Reagents

- Protein A immobilized on controlled-pore glass (Pr-A-CPG) supplied by Bio-Processing (Consett, Co Durham, UK).
- Atrazine, simazine, desisopropylatrazine and desethylatrazine were obtained from Riedel-de-Häen. Stock standard solutions (1000 mg l^{-1}) were prepared in acetonitrile and stored at −18°C.
- Atrazine polyclonal antibody and atrazine–FITC supplied by Immunogen International (Tyne and Wear, UK).
- Phosphate buffer solution (PBS) pH = 7 (1 l of Milli-Q water containing: 8 g NaCl, 0.2 g KH_2PO_4, 0.2 g KCl, 2.9 g Na_2HPO_4 and 1 g $MgCl_2$), and 0.5 M citric acid (Merck, Darmstadt, Germany) containing 0.5 M NaCl.
- Fluorosil (Carlo Erba).

- RS-grade acetone, *n*-hexane and acetonitrile (Carlo Erba).
- Analytical-reagent grade chemicals were used.

2.3. Procedures

2.3.1. Flow-through immunosensor design.

The immunoreactor used is shown in Fig. 1A. It was a flow cell whose optical path was filled with Pr-A-CPG for in-situ fluorescence detection. A frit was placed at the end of the optical path of the flow cell, to prevent the carrier sweep away the protein A.

An empty space of few millimeters was left below the top of the optical path to ensure that all the immuno-reaction took place in the excitation path of the spectrofluorimeter and that the fluorescence emission was therefore detected properly.

A diagram of the flow injection system is shown in Fig. 1B. The device consists of a peristaltic pump, a six way injection valve and the detection system, which is a spectrofluorimeter containing the immunoreactor.

2.3.2. Assay procedure

The developed method was based on the principle of a heterogeneous competitive fluorescence immunoassay with on-line incubation.

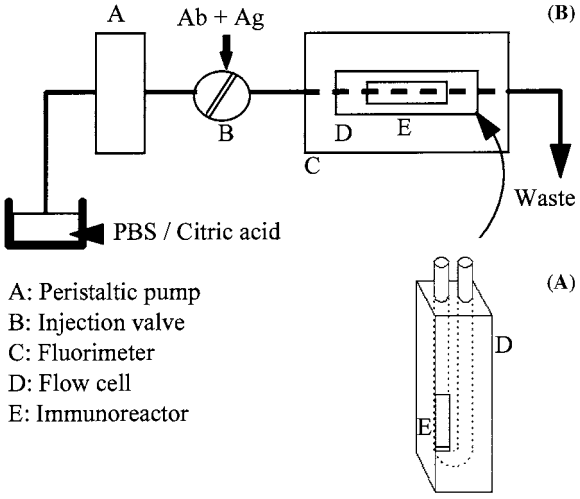

Fig. 1. (A) Flow-cell, (B) flow injection system.

The immunological process used was as follows: into a carrier solution flowing at 0.2 ml min^{-1} (10 mM PBS, pH = 7), 30 μl of anti-atrazine (diluted 1/100 in PBS) was injected and retained on the support (Pr-A-CPG). After 80 s, 30 μl of a mixture of labelled-antigen (atrazine–FITC, 332 nmol l^{-1}) and antigen (atrazine) was injected. The two antigens compete for the active sites of the antibodies, and antigen–antibody complex is formed. The excess of antigen (labelled and unlabelled) was eliminated from the immunoreactor by the carrier solution. The fluorescence signal, which corresponded to the antibody–atrazine–FITC complex was measured 'in-situ' in the immunoreactor. Finally, a citric acid solution (0.5 M pH = 2) was pumped to the flow cell to regenerate the reactor (for about 1 min), followed by a preconditioning step with PBS. The atrazine concentration for the competitive calibration curve was varied within the range 2.1–50 μg l^{-1}.

2.3.3. Sample preparation for immunological method

2.3.3.1. Water sample. About 0.5 g of freeze-dried water residue [11] was placed in a 0.50 l flask and dissolved in 10^{-3} mol l^{-1} HCl solution.

The sample injected in the flow-through immunosystem was prepared with 980 μl of reconstituted water and 20 μl of atrazine–FITC (332 nmol l^{-1}).

2.3.3.2. Orange sample. To 75 g of whole ground orange (peel and pulp), 10 g of NaCl and 100 ml of acetonitrile were added and mixed in a beater for 4 min. After settling for 1 min, 7.5 g of Na_2SO_4 were added to 75 ml of the acetonitrile solution and the mixture centrifuged for 5 min; 100 μl of this solution were added to 20 μl of atrazine–FITC and 880 μl of PBS. Samples were analysed using the assay procedure.

2.3.4. Sample preparation for GC

The solution obtained in the above procedure was evaporated and solvent evaporation was hastened flushing with helium to give a final volume of 50 ml.

Clean up: these 50 ml were cleaned using a column (10 cm length and 10 mm id) filled with 0.8 g of fluorosil and 0.5 g of Na_2SO_4 previously activated with 5 ml of 15% acetone in n-hexane and 5 ml of *n*-hexane. Atrazine was desorbed from the column with 5 ml of 15% acetone in *n*-hexane. The solvent was evaporated in a rotavapor system to a final extract volume of 1 ml. This final solution was analyzed by gas chromatography coupled to nitrogen–phosphorous detection.

3. Results and discussion

3.1. Immunosensor optimization

To improve the immunoassay performance, the influence of parameters such as pH, concentration of regeneration solutions, flow rates, etc. was studied.

A study of the influence of pH on the antigen–antibody binding and on the immunosensor regeneration was carried out varying carrier and regeneration solution pH within the range 6.0–8.5 and 1–4, respectively. The optimum pH range of antigen–antibody binding was 7.0–7.5 in 10 mM PBS solution (in 0.1 M NaCl), and the optimum pH for the regeneration solution (0.5 M citric acid solution containing 0.5 mol l^{-1} [10]) was 2.0.

The effect of carrier flow rate on the antibody–protein A binding step and on the on-line incubation of the antigen–antibody complex was tested. For the antibody binding step five different flow rates were tested (0.1, 0.2, 0.3, 0.4 and 0.5 ml min^{-1}) for an injection volume of 30 μl of antiserum solution (1/100 dilution). The fluorescent signal was monitored at the maximum emission intensity of the antibody ($\lambda_{exc} = 273$ nm, $\lambda_{em} = 340$ nm).

The results are shown in Fig. 2. The highest intensity, which means the maximum amount of antibody bound to protein A, was obtained within the range 0.2 to 0.3 ml min^{-1}.

The study of the on-line incubation was monitored at the maximum emission of atrazine–FITC ($\lambda_{exc} = 495$ nm, $\lambda_{em} = 514$ nm), using both 0.2 and 0.3 ml min^{-1} rates. A rate of 0.2 ml min^{-1} was chosen as optimum.

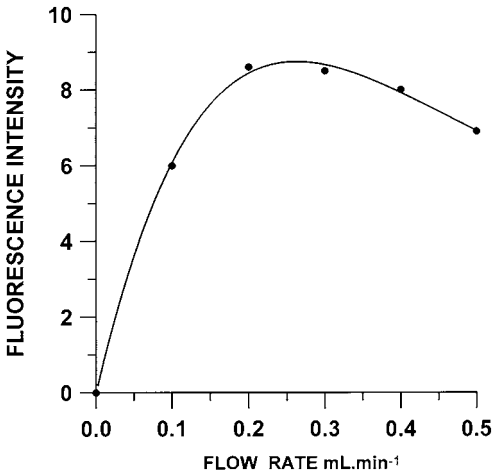

Fig. 2. Effect of carrier flow rate on the antibody–protein A binding step.

The time between the antibody and antigen injections should be enough to allow that the antibody has settled when the antigen arrives, but not longer, so as avoid increasing the analysis time. Four times between injections were tested: 40, 60, 80 and 100 s, and the results showed that at times over 80 s the analytical signal did not improve. Therefore 80 s was chosen as the optimum value.

The effect of the antigen–FITC concentration was evaluated at four different values (166, 332, 498 and 664 nmol l^{-1}) using an antibody dilution of 1/100. The results showed that from 498 nmol l^{-1} the immunosensor was saturated, so 332 nmol l^{-1} was chosen for further assays.

Antibody dilution is a critical variable in immunoassays because it has a strong influence on both detection limit and calibration range.

Three calibration curves were studied using antibody dilutions of 1/75, 1/100, and 1/200. The atrazine-FITC concentration was 332 nmol l^{-1} and the atrazine concentration was varied up to 0.3 mg l^{-1}. A 1/100 antibody dilution was chosen because it provided high sensitivity of detection and a wide useful calibration range.

The presence of acetonitrile, used as extraction solvent in the orange samples preparation, do not disturb the analytical signal, at least until the ratios 1:10 solvent: PBS employed.

The optimum experimental conditions for this atrazine immunosensor are summarized in Table 1.

3.2. Analytical performance

Under the optimum conditions, the useful concentration of the atrazine immunoassay calibration was up to 50 μg l^{-1} (Fig. 3). The detection limit was 2.1 μg l^{-1} calculated as the least detectable dose (LDD), commonly used to define sensitivity, which is measured assesing replicates of zero standard and calculating the mean signal and standard deviation (SD). The response, analytical signal-2 SD, read in mass or concentration from the standard curve is the LDD, that is, the smallest concentration that can be distingued from zero with 95% confidence [12]. A detection limit of 2.1 μg l^{-1}, however, is high for the application of this sensor for monitoring of atrazine in drinking water given that the highest permissive concentration in this kind of samples is 0.1 μg l^{-1} [13]. Some enzyme immunoassays described [7,8] show very high sensitivity for atrazine, but these methods involve multiple steps, are complicated and time consuming.

Table 1
Summary of optimum conditions for atrazine fluoroimmunosensor

Parameter	Optimum value
Excitation wavelength	495 nm
Emission wavelength	514 nm
Excitation and emission slits	10 nm, 12.5 nm respectively
Carrier solution	10 mmol PBS in 0.1 M NaCl
Carrier solution pH	7.0
Regeneration solution	0.5 M citric acid in 0.5 M NaCl
Regeneration solution pH	2.0
Antibody dilution	1/100
Antibody binding flow rate	0.2–0.3 ml min^{-1}
Antigen binding flow rate	0.2 ml min^{-1}
Time between injections	80 s
Labelled antigen concentration	332 nmol l^{-1}
Fluorescence measurement time	150 s

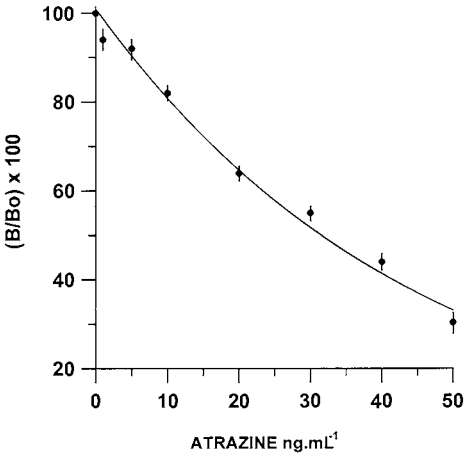

Fig. 3. Calibration curve obtained for atrazine. A three-parameter equation was used to fit the standard curve. Represented experimental points corresponding to the mean ± standard deviation of five determinations. (B/Bo)% is the fluorescence intensity of atrazine expressed as a percentage of the intensity of an atrazine-free sample.

The developed immunosensor can be applied with success to the atrazine determination in citrus fruits. With the purpose of improving detection limit different strategies will be carried out: using a stop flow, in order to increase the incubation time, or increasing the sample volume injected [7].

The within-day precision study was carried out at two different analyte concentrations: 5 and 30 μg l^{-1}. Each concentration was injected six times under the same conditions. The RSD value obtained was 3.2% for 5 μg l^{-1} and 2.2% for 30 μg l^{-1}.

The competitive calibration curve was repeated on 3 days in order to test its reproducibility (Table 2). Calibration between days were reproducible (Fig. 4), and no significant differences at the 95% confidence level were found.

The life-time of the immunosensor was about 25 immunoassays, and it allowed a sample speed about 10 samples h^{-1}.

The antibody specificity was determined by measuring the cross-reactivity of three structurally related compounds: simazine, desethylatrazine (DEA) and desisopropylatrazine (DIA). The cross-reactivity (CR) of a compound is defined as:

Table 2
Calibration curve reproducibility

Atrazine (μg l^{-1})	0	1	5	10	20	30	40	50
Curve 1	100	94	92	86	64	55	44	30
Curve 2	100	92	92	84	67	56	46	32
Curve 3	100	93	91	85	62	54	42	29

Values of B/Bo (%) obtained from calibration curve prepared on 3 different days.

$$\% \text{ CR} = \frac{\text{mass of the analyte at midpoint}}{\text{mass of the interferent at midpoint}} \times 100$$

The experiment was carried out by performing a competitive calibration for each substance under the same conditions [12].

The calibration curves for the atrazine and interferents are shown in Fig. 5. Simazine and DIA were not cross-reactive. However, cross-reactivity for DEA was CR = 7.7%, which suggests that the isopropyl group is the epitope recognized for the antibody.

3.3. Analysis of real samples

The flow-through immunosensor was successfully applied to determine atrazine in orange samples and drinking water.

The freeze-dried water samples was prepared as is described by Martín-Esteban et al. [11]. Besides atrazine, these samples contain simazine, carbaryl, propanil, linuron, fenamiphos and permethrin. Its content has being proposed for certification.

The water and orange samples were treated as described in the procedure and subsequently analyzed using the flow-through optimized immunosensor. The results are shown in Table 3.

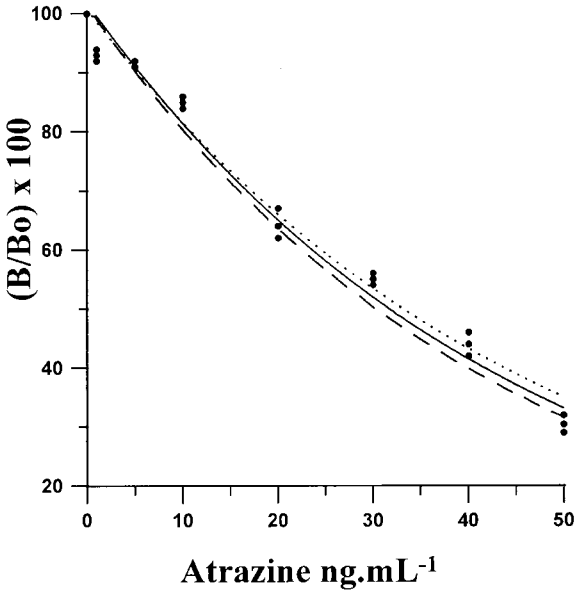

Fig. 4. Calibration curves obtained in different days. Experimental points are fitted to a three parameter ecuation. Day one (—), day two (----), day three (.....).

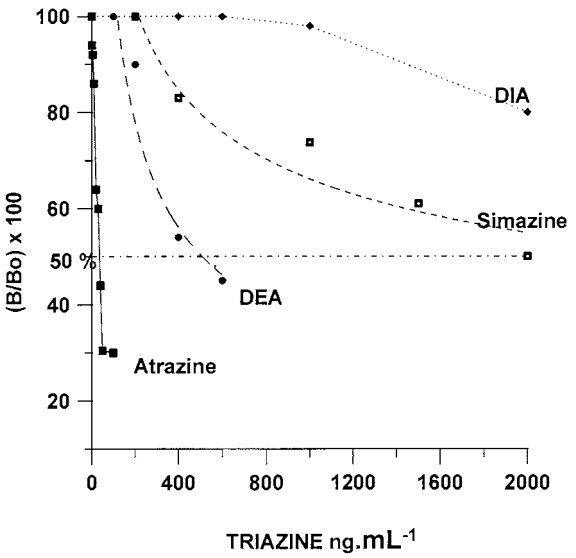

Fig. 5. Calibration curves obtained for atrazine and interferents.

Table 3
Results of immunosensor determinations

Sample	Fluoroimmunosensor $X \pm S$ ($\mu g\ l^{-1}$)	Interlaboratory value[a] $X \pm S$ ($\mu g\ l^{-1}$)	Gas chomatograph $X \pm S$ ($\mu g\ l^{-1}$)
Drinking water 1	11.9 ± 1.0	11.4 ± 1.5	—
Drinking water 2	7.9 ± 1.1	7.5 ± 0.6	—
Orange	224 ± 5	—	210 ± 4

[a] Data obtained from [11].

The value obtained for atrazine in the orange sample using the immunosensor was compared with that obtained using GC-NPD, and the results obtained for drinking waters with the values proposed for certification. In both cases good agreement was observed and there were not significant differences at the 95% confidence level.

4. Conclusions

The flow-through fluoroimmunosensor described has demostrated to be very appropriate for atrazine determination in drinking water and citrus fruit samples. It is considered to be highly selective, because no significant interferences from other triazines of similar structure, such as simazine and desisopropylatrazine, were detected, although a high concentration of desethylatrazine can interfere.

This biosensor has major advantages over chromatographic techniques, namely better sensitivity provided reaction-detection integration, it is faster, it requires minimal sample handling, and no clean-up and preconcentration steps are needed.

Acknowledgements

This work received financial support from CICYT (AMB 95-0689-C02-02). The authors wish to thank Max Gorman for revising the manuscript.

References

[1] R.A. Leonard, in: R. Grover (Ed.), Environmental Chemistry of Herbicides, CRC Press, Boca Raton, Fl, 1988, pp. 45–87.
[2] J.J. Vreuls, A.J. Bulterman, R.T. Ghijsen, U.A. Brinkman, Analyst 117 (1992) 1701.
[3] U.A.Th. Brinkman, J. Chromatogr. A 665 (1994) 217.
[4] R. Puchades, A. Maquieira, Crit. Rev. Anal. Chem. 26 (1996) 195.
[5] M. Wortberg, C. Middendorf, A. Katerkamp, T. Rump, K. Cammann, Anal. Chim. Acta 289 (1994) 177.
[6] J. Gascón, A. Oubiña, B. Ballesteros, D. Barceló, F. Camps, M. Marco, M.A. González-Martínez, S. Morais, R. Puchades, A. Maquieira, Anal. Chim. Acta 347 (1997) 149.
[7] B. Bjarnason, N. Bousios, S. Eremin, G. Johansson, Anal. Chim Acta 347 (1997) 111.
[8] P.M. Kramer, B.A. Baumann, P.G. Stoks, Anal. Chim. Acta 347 (1997) 187.
[9] F.F. Bier, R. Jockers, R.D. Schmid, Analyst 119 (1994) 437.
[10] C.M. Rico, P. Fernández, A.M. Gutiérrez, C. Pérez-conde, C. Cámara, Analyst 120 (1995) 2589.
[11] A. Martín-Esteban, P. Fernández, C. Cámara, G.N. Kramer, E.A. Maier, Intern. J. Environ. Anal. Chem. 67 (1997) 125.
[12] D.W. Chan, Immunoassay: a practical guide, Ed Academic Press, 1987.
[13] EEC Drinking Water Directive, 80/778/EWG. L229, Commission of the European Communities, Brussels, 1980, p. 11.

ELSEVIER

Talanta 47 (1998) 1263–1270

Talanta

Comparative determination of Ba, Cu, Fe, Pb and Zn in tea leaves by slurry sampling electrothermal atomic absorption and liquid sampling inductively coupled plasma atomic emission spectrometry

J. Mierzwa *, Y.C. Sun, Y.T. Chung, M.H. Yang

Department of Nuclear Science, National Tsing-Hua University, 30043 Hsinchu, Taiwan

Received 20 January 1998; received in revised form 14 May 1998; accepted 26 May 1998

Abstract

The comparative determination of barium, copper, iron, lead and zinc in tea leaf samples by two atomic spectrometric techniques is reported. At first, slurry sampling electrothermal atomization atomic absorption spectrometry (ETAAS) was applied. The results of Ba and Pb determination were calculated using the method of standard additions, and results of Cu, Fe and Zn from the calibration graphs based on aqueous standards. These results were compared with the results obtained after microwave-assisted wet (nitric + hydrochloric + hydrofluoric acids) digestion in closed vessels followed by inductively coupled plasma-atomic emission spectrometric (ICP-AES) determination with the calibration by means of aqueous standards. The exception was lead determined after a wet digestion procedure by ETAAS. The accuracy of the studied methods was checked by the use of the certified reference material Tea GBW-07605. The recoveries of the analytes varied in the range from 91 to 99% for slurry sampling ETAAS, and from 92.5 to 102% for liquid sampling ICP-AES. The advantages of slurry sampling ETAAS method are simplicity of sample preparation and very good sensitivity. Slurry sampling ETAAS method is relatively fast but if several elements must be determined in one sample, the time of the whole microwave-assisted digestion procedure and ICP-AES determination will be shorter. However, worse detection limits of ICP-AES must also be taken into the consideration in a case of some analytes. © 1998 Elsevier Science B.V. All rights reserved.

Keywords: Electrothermal atomic absorption spectrometry; Inductively coupled plasma-atomic emission spectrometry; Slurry sampling; Microwave-assisted wet digestion; Tea leaves; Heavy metals determination

1. Introduction

Tea is a liquor prepared from the leaves of the tea plant (*Camellia sinensis*). Hot or cold, tea remains one of most popular beverages in the world. The chemical composition of tea and tea

* Corresponding author. Tel.: + 886 3 5723883; fax: + 886 3 5723883; e-mail: jmierzwa@yahoo.com

0039-9140/98/$ - see front matter © 1998 Elsevier Science B.V. All rights reserved.
PII S0039-9140(98)00214-8

leaves is the object of broad scientific studies from, e.g. a medical, toxicological or environmental point of view.

During the past several years, some researchers analyzed the tea leaf and reported the determination of heavy metals (mostly aluminum) in various brands of tea leaves [1–9]. Different analytical techniques (including also Al, Ba and Mn determination by slurry sampling ICP-AES [9]; a disadvantage of this method is sensitivity to particle size) were used but the method of combining ultrasonic slurry sampling with electrothermal AAS has not been reported until now. The microwave-assisted wet digestion of plant samples is now a well established and efficient technique [10] of sample preparation prior to the determination of metals but it was concluded after our preliminary experiments [11] that such a procedure for tea leaves cannot simply follow literature data and need some more optimization.

The main analytical task was to develop and evaluate sensitive, reliable and relatively rapid techniques for the determination of some heavy metal impurities in tea leaves or plant samples of a similar matrix.

The first aim of the present work was to study the applicability of slurry sampling ETAAS for the determination of Ba, Cu, Fe, Pb and Zn in samples of tea leaves. Of these elements lead is a very volatile element and a common problem is the thermal stabilization of this metal in graphite furnace up to the atomization stage. The application of the STPF (stabilized temperature platform furnace) concept, especially a proper chemical matrix modification is necessary. The second aim was to check and optimize the performance of microwave-assisted wet mineralization using a closed vessel system. The more risky application of perchloric acid was excluded in this study. The digested tea leaves samples were then analyzed by ICP-AES.

2. Experimental

2.1. Instrumentation

The measurements were carried out using PE model 5100 Zeeman atomic absorption spectrometer, HGA-600 electrothermal atomizer and AS-60 autosampler (all instrumentation from Perkin-Elmer, Norwalk, CT). The high intensity hollow cathode lamps of Intensitron® type were used. All experiments were carried out with pyrolytic graphite coated graphite tubes (Perkin-Elmer, Part no. B010-9322) with pyrolytic graphite platforms (Perkin-Elmer, Part no. B010-9324). Argon (5N purity) was used as the purge gas at 300 ml min^{-1}, except in the atomization stage (gas stop excluding iron and zinc). The samples were weighed using an electronic balance Mettler AT-201 (Mettler, Switzerland). Tea slurries were mixed by means of an automated ultrasonic slurry sampler USS-100 (Perkin-Elmer) equipped with a titanium probe. The analytical measurements were based on the absorbance peak areas. The basic instrumental and experimental conditions for ETAAS determinations are shown in Table 1.

A simultaneous ICP-AES spectrometer Optima 3000 DV (Perkin-Elmer) equipped with the standard nebulization system (cross-flow nebulizer and Scott-type spray chamber made from Ryton®) was used for the comparative measurements. The main operational conditions of the spectrometer and the analytical wavelengths are listed in Table 2.

Tea leaf samples were digested in the MDS-2000 (CEM, Matthews, NC) microwave oven equipped with the internal pressure and temperature control system. This oven has a variable power range (up to 630 W) adjustable in 1% increments and a programmable timer. The lined Teflon vessels with a volume of 100 ml and a pressure-relief valve were employed. The temperature and pressure in the vessel during wet digestion were monitored and recorded.

2.2. Samples and reagents

A sample of commercially available tea (Oolong type, i.e. partially fermented; manufactured by Tea Ren, Taiwan) and one certified reference material (Tea GBW 07605 from National Research Centre for Certified Reference Materials, Peking, People's Republic of China) were studied.

Table 1
Basic instrumental parameters of electrothermal AAS determination of Ba, Cu, Fe, Pb and Zn in tea leaves

Element	Ba	Cu	Fe	Pb	Zn
Wavelength (nm)	553.6	324.8	248.3	283.3	213.9
Slit (nm)	0.4	0.7	0.2	0.7	0.7
Purge gas	Ar	Ar	Ar	Ar	Ar
Drying temp. (°C)	115	115	115	115	115
Ramp, hold (s)	12/30	12/30	12/30	12/30	12/30
Ashing temp (°C)	1200	1350	1400	1000	750
Ramp, hold (s)	10/30	10/30	10/30	10/30	10/30
Atomization temp (°C)	2550	2400	2350	1900	1750
Ramp, hold (s)	0/5	0/10	0/8	0/5	0/4
Clean-up (°C)	2650	2600	2600	2500	2400
Hold (s)	4	3	3	3	3
Gas stop	Yes	Yes	No[a]	Yes	No[b]
Cool down step	Yes	No	No	Yes	No
L'vov platform	Yes	Yes	Yes	Yes	Yes
Integration time (s)	5	10	8	5	4
Injected: sample volume (μl)	20	20	20	20	15
modifier volume (μl)	10[c]	—	—	10[d]	—

[a] Argon flow rate of 50 ml min^{-1} was used.
[b] Argon flow rate of 20 ml min^{-1} was used.
[c] Palladium nitrate modifier was applied.
[d] Nickel + phosphate modifier was applied.

All the acids used, i.e. nitric, hydrochloric and hydrofluoric of special purity (Tracepure®) were from E. Merck, Darmstadt, Germany. Palladium nitrate and ammonium phosphate modifiers, and nickel nitrate of spectral purity were also obtained from E. Merck, Germany. A surfactant Triton X-100 was purchased from Fluka A.G. (Switzerland). Single- (for AAS) or multi-element (for ICP-AES) working standards of Ba, Cu, Fe, Pb and Zn were prepared from 1 g l^{-1} stock solutions (Spectrosol®, E. Merck, Germany) and doubly-distilled, deionized water was used for all further dilutions. All standards were acidified to obtain a proper concentration of acids.

2.3. Slurry preparation and sampling

At first, the analytical sample of Oolong tea was ground for 20 min in a mixer mill MM-2000 type (K.F. Retsch, Germany) with the use of an additional liquid nitrogen cooling system. It was observed that the additional cooling improved the efficiency of grinding. The diameter of the particles of the ground sample was examined several times by scanning electron microscopy (SEM) and optical microscopy, and it was verified that the average particle diameter was < 60 μm. The tea sample of certified reference material was not ground, and the bottle containing this sample was simply shaken five to six times prior to its further sampling.

All tea leaf slurries were prepared by the balance method (in 2.5 ml polyethylene vessels) in the concentration range 0.4–3.6% m m^{-1}. A 0.04 and/or 4.0% v/v HNO_3 with 0.005% (final concentration of the surfactant in the liquid phase) of Triton X-100 were used as a liquid medium for slurry preparation. Ultrasonic mixing (for 15 s at ca. 55% of the ultrasonic probe power setting) was performed in the same vessels placed into an autosampler, before the sampling of slurry in the electrothermal atomizer. All measurements were repeated three times for three individual slurries of the same tea sample.

2.4. Microwave assisted digestion

Typically, 0.3 g of a tea leaf sample was weighed into the Teflon PFA lined vessel, a proper volume of concentrated acids was dispensed and the vessel was closed tightly. A pure nitric acid and three different acid combinations were tested, i.e. a mixture of nitric acid and hydrofluoric acid (9 + 1 ml), mixtures of nitric and hydrochloric acid (9 + 1 ml, 9 + 2 ml and 9 + 3 ml), and mixtures of nitric, hydrochloric and hydrofluoric acid (9 + 1 + 1 ml, 8 + 2 + 1 ml and 7.5 + 2.5 + 1 ml). The microwave oven heating program was optimized to be as short as possible. Finally, the time of the sample microwave treatment was 10 min at maximum oven power (630 W) and the recorded pressure was up to 180 psi. Samples were cooled after the microwave treatment for ~30 min, and then transferred into the calibration flasks and made up to 20 or 50 ml with water of high purity.

Table 2
Operating conditions of ICP-AES spectrometer and the analytical wavelengths

Spectrometer	Echelle with a simultaneous detection (SCD detector)
ICP RF power	1.5 kW
Radiofrequency	40.68 MHz
Carrier gas flow rate	1.0 l min^{-1}
Auxiliary gas flow rate	1.2 l min^{-1}
Plasma gas flow rate	15.0 l min^{-1}
Plasma observation	Radial[a]
Nebulizer type	Gem tip, cross-flow
Pump uptake	1.5 ml min^{-1}
Analytical wavelengths (nm):	Ba 455.40
	Cu 324.75
	Fe 239.56
	Pb 220.35[b]
	Zn 213.85

[a] For lead radial and axial plasma observations were done.
[b] Measurements were close to the limit of detection.

2.5. ICP-AES determination

The measurement conditions were optimized on signal-to-background ratio. The main operational conditions of the ICP-AES spectrometer are presented in Table 2. The radial only direction of plasma observation was used, except lead measurements. A one-point background correction was applied. Analytical results were calculated using the straight calibration graphs based on acidified multielement standard solution.

All measurements were repeated three to five times for three individual digests.

3. Results and discussion

3.1. ETAAS measurement optimization

The ashing and atomization temperatures were optimized experimentally for all the studied elements, using both aqueous solutions and slurried samples, and the temperatures chosen are listed in Table 1. The maximum power heating prior to the atomization step and L'vov platform atomization were always employed. The cool-down step was included in the temperature-time programs for barium and lead determination.

In spite of the above mentioned optimization, some losses of lead were observed. For lead atomization the shift of peak shape and appearance time was also observed for the investigated tea slurries. The application of a chemical matrix modifier was necessary to obtain good analytical recoveries. A mixed modifier containing nickel nitrate and ammonium phosphate (adopted from [12], where the authors employed it for the determination of lead in water) was used. It was confirmed that this modifier (100 μg ml^{-1} $Ni(NO_3)_2$ + 10 mg ml^{-1} $NH_4H_2PO_4$) was effective to stabilize lead up to ~1000°C. The use of a chemical matrix modifier (palladium nitrate alone) was also very advantageous in the case of barium determination, especially for the improvement (symmetrization) of the shape of analytical peaks. A slightly better average characteristic mass (7.6 instead of 8.4 pg/0.0044 As) was also observed. It was experimentally found, that the

Table 3
Metal partitioning in slurries (for Oolong tea sample, slurry ~2.5% m m^{-1})

Element	% Metal extracted into the liquid phase[a]	
	0.04% HNO_3	4.0% HNO_3
Ba	12	17
Cu	88	90
Fe	39	48
Pb	ca. 3	ca. 2
Zn	23	74

[a] Liquid phase concentration was determined by ETAAS after 12 min of slurry centrifuging.

optimum concentration of the palladium matrix modifier was 2.0 g l^{-1}. Practically the same peak shapes and analytical results were obtained (for lead and barium) for the tea slurries pre-mixed with modifier or for separate addition of chemical modifier into the graphite furnace. The addition of chemical matrix modifiers was not necessary for the reliable determination of copper, iron and zinc.

The influence of the ultrasonic mixing time for the repeatability of analytical signal of analytes was also investigated. However, almost the same repeatability (RSD 1.2%) was observed for ultrasonication time in the range 15–35 s, thus the shortest possible time (15 s) was chosen to decrease time of the whole analytical procedure.

3.2. Metal partitioning

The partitioning of determined metals between the solid and liquid phases of slurry is generally (except zinc) similar (Table 3) for both 0.04 and 4% HNO_3 solutions, respectively. The repeatability of the analytical results was also almost the same for slurries prepared in these media. This result indicates a lack of more significant slurries agglomeration in spite of the change of the solution pH value. A 0.04% medium of slurry preparation is more convenient, because a slightly longer life-time of the pyrolytically coated graphite platform was observed. The amount of lead leached into the liquid phase (this fact can be fortunate for tea drinkers) is very small (below 5%) and it practically does not depend on the concentration of nitric acid (0.04 versus 4% acid). Very similar behavior of this element was formerly reported for the other plant slurries prepared in a similar way, i.e. slurried cabbage leaves and cabbage roots [13]. The extraction of barium, zinc and iron can be qualified as moderate. On the other hand almost a total extraction of copper was observed, both for the more diluted and for the more concentrated acidic medium.

3.3. Microwave-assisted digestion

A concentrated nitric acid was initially used but this method was not very effective (see also [7]) and recoveries were not very good. Three combinations of acids (i.e. nitric + hydrofluoric, nitric + hydrochloric and nitric + hydrochloric + hydrofluoric) were then investigated in a more detailed manner. It was observed that a mixture of nitric, hydrochloric and hydrofluoric acid was more efficient and gave better recoveries (as checked for certified reference material) than the mixtures of nitric and hydrochloric, or nitric and hydrofluoric acids only.

It was stated experimentally that after even a relatively short digestion of 10 min (at temperature up to 180°C) a clear (sometimes only slightly yellow) solution was obtained. Fig. 1 illustrates changes of the temperature and pressure during sample treatment. At microwave heating times longer than 10 min no more changes in digestion were observed. For the mixture containing $HNO_3 + HCl + HF$ (in volumes: 9 + 1 + 1 ml) good recoveries of the analytical results for certified reference material were noted, generally in the range of 100–6%, except iron. In this case recoveries only in the range of 86–88.5% were observed. The use of the same acids in a volume proportion of 7.5 + 2.5 + 1 ml ($HNO_3 + HCl +$ HF) improved the recovery of iron, i.e. up to 93.9%. The average recoveries of iron and barium (as the element which is least susceptible to some changes of digestion medium) measured after microwave assisted digestion with diverse acidic media are graphically summarized in Fig. 2.

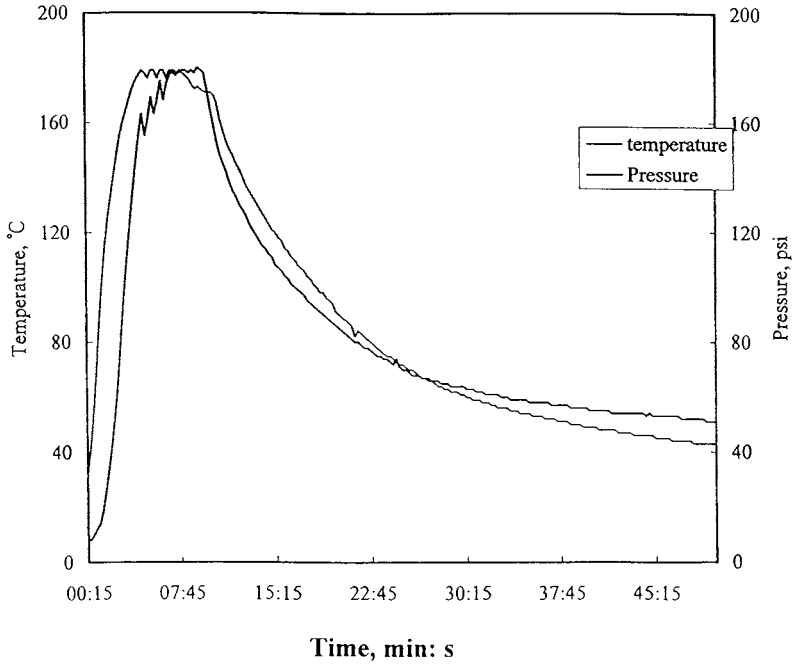

Fig. 1. Relationship between time of microwave assisted digestion and temperature and/or pressure inside of microwave vessel.

3.4. Analytical results

The integrated absorbance measurements were used to quantify the atomic signals and then to calculate the concentration of metals in the tested samples. The standard addition method was applied for barium determinations by ETAAS to improve analytical accuracy because some matrix effects on analytical signal value were observable. For the other analytes straight calibration curves based on aqueous standards were adequate. The characteristic masses (sensitivities) were 7.6, 9.0, 6.2, 14 and 0.6 pg/0.0044 As for Ba, Cu, Fe, Pb and Zn, respectively, for their spectral resonance lines listed in Table 1. The spiked recoveries (for slurries ca. 2% mm^{-1}) were in the range from 93.8% for iron to 102.5% for copper. The over-all reproducibility of slurry ETAAS results calculated from the values of five replicates of each sample was acceptable for this analytical technique (RSD $< 9.8\%$). The within-batch precision of the slurry sampling, obtained for nine replicates of three slurries of different concentration was good (RSD's obtained for all elements were between 1.8 and 4.2%).

The linearity of the ICP-AES calibration curves was very good (correlation coefficients in the range of 0.9999–1.0000 were obtained). The over-all reproducibility of ICP-AES results calculated as RSD for five replicates of each sample was always $< 7.0\%$. The recoveries of the analytes determined by liquid sampling ICP-AES (for the samples spiked with 0.4, 0.1, 1.0 and 0.2 ppm of Ba, Cu, Fe and Zn, respectively) were 96, 95, 93.5 and 101% for Ba, Cu, Fe and Zn, respectively.

The more troublesome analytical case is the determination of lead. Its level in tea leaf samples is usually relatively low and the direct use of ICP-AES technique (even with modern ICP-AES instrumentation) cannot be recommended. We tested ICP-AES measurement for a real tea (Oolong) sample both in radial and axial observation mode, and with not very good analytical effects. In this case (measurements in a concentration region near ICP-AES detection limit) the determination of lead by means of electrothermal

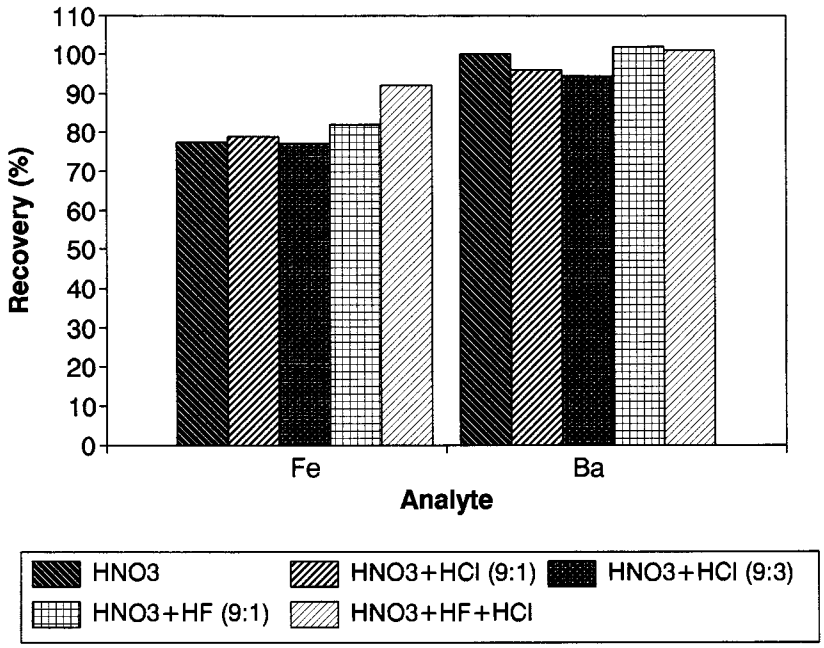

Fig. 2. Average recoveries of iron and barium after the procedure of microwave assisted wet digestion ICP-AES determination using different digestion media (CRM, Tea Leaves GBW 07605).

atomization AAS with solution or slurry sampling could still be preferable.

The analytical results obtained by slurry sampling ETAAS and liquid sampling ICP-AES for a real tea sample are listed in Table 4 and they are very similar (maximum difference is ca. 5%). The results of both tested and compared analytical techniques are in good agreement with the certified values (Table 5). The elevated contents of Ba and Pb in the certified reference material and in the real tea sample may be attributed, e.g. to the plant uptake of these elements from a polluted soil.

Table 4
Results of metal determinations in the sample of Oolong tea

Sample	Concentration (mg kg^{-1}) $\pm$ SD ($n = 5$)	
	Liquid sampling ICP-AES	Slurry sampling ETAAS
Ba	50.1 ± 4	48 ± 4.1
Cu	12.4 ± 0.5	12.6 ± 1.0
Fe	232 ± 14	242 ± 18
Pb	2.72 ± 0.25[a]	2.86 ± 0.26
Zn	21.5 ± 1.0	20.8 ± 1.1

[a] Microwave-assisted wet digestion followed by ETAAS determination.

4. Conclusion

The analytical repeatability of slurry sampling ETAAS is slightly less efficient but, summing up, both analytical methods are reliable and very good recoveries are obtained.

Slurry sampling ETAAS can be successfully used for the simple, rapid and reproducible determination of single metals in tea leaf samples, whereas microwave-assisted acid digestion in a closed system followed by simultaneous ICP-AES determination offers a fast alternative for multi-element determination, except the determination of some trace (or ultra-trace) elements in tea leaves, e.g. lead.

Acknowledgements

The financial support of the National Science

Table 5
Results of metal determination in the certified reference material Tea Leaves GBW 07605

Sample	Concentration (mg kg^{-1}) $\pm$ SD ($n = 5$)		
	Certified value	Slurry sampling ETAAS	Liquid sampling ICP-AES
Ba	58 ± 3	52.8 ± 5	59.1 ± 4
Cu	17.3 ± 1.0	17.1 ± 1.4	17.0 ± 0.8
Fe	264 ± 10	250 ± 18	248 ± 12
Pb	4.4 ± 0.2	4.15 ± 0.32	4.36 ± 0.28[a]
Zn	26.3 ± 0.9	25.0 ± 1.7	25.4 ± 1.4

[a] ICP-AES with axial plasma observation.

Council of Taiwan (Taipei, Taiwan) is greatly acknowledged by one of the authors (Jerzy Mierzwa).

References

[1] N.S. Saleh, J. Radioanal. Chem. 74 (1982) 191.
[2] S. Ahmad, M.S. Chaudhary, A. Mannan, I.H. Qureshi, J. Radioanal. Chem. 78 (1983) 375.
[3] I. Kojima, T. Uchida, C. Iida, Anal. Sci. 4 (1988) 211.
[4] K.R. Koch, M.A.B. Pougnet, S.D. De Villiers, Analyst 114 (1989) 911.
[5] C.F. Wang, C.H. Ke, J.Y. Yang, J. Radioanal. Chem. 173 (1993) 195.
[6] R.G. Sud, R. Prasad, M. Bhargava, J. Sci. Food Agric. 67 (1995) 341.
[7] K. Lamble, S.J. Hill, Analyst 120 (1995) 413.
[8] R. Liu, A. Zhang, D. Liu, S. Wang, Analyst 120 (1995) 1195.
[9] C.K. Manickum, A.A. Verbeek, J. Anal. At. Spectrom. 9 (1994) 227.
[10] H.M. Kingston, L.B. Jassie, Introduction to Microwave Sample Preparation. Theory and Practice, American Chemical Society, Washington, DC, 1988.
[11] J. Mierzwa, Y.C. Sun, M.H. Yang, Asianalysis IV Conference, Fukuoka, Japan, 1997 (abstract 2P10).
[12] Y. Xu, Y. Liang, J. Anal. At. Spectrom. 12 (1997) 471.
[13] R. Dobrowolski, J. Mierzwa, Fresenius J. Anal. Chem. 346 (1993) 1058.

ELSEVIER

Talanta 47 (1998) 1271–1278

Talanta

Ion-pair extraction of uranyl ion from aqueous medium using crown ethers

P.K. Mohapatra, V.K. Manchanda *

Radiochemistry Division, Bhabha Atomic Research Centre, Trombay, Bombay-400085, India

Received 1 February 1998; received in revised form 29 April 1998; accepted 26 May 1998

Abstract

Ion-pair extraction behaviour of uranyl ion from aqueous solutions was studied at pH 3.0 employing crown ethers viz. benzo 15 crown 5 (B15C5), 18 crown 6 (18C6), dibenzo 18 crown 6 (DB18C6), and dibenzo 24 crown 8 (DB24C8) in chloroform as the organic phase and picric acid as the organophilic counter anion. The stoichiometry of the extracted species corresponded to $[UO_2(\text{crown ether})_n]^{2+} \cdot [\text{pic}^-]_2$ where $n = 1.5$ for benzo 15 crown 5 and 1 for 18 crown 6 as well as dibenzo 18 crown 6. Adducts of DB24C8 could not be observed as practically no extraction was possible using this reagent. The separation behaviour of fission products from an irradiated uranium target was also studied. An interesting observation on the separation of trivalent lanthanides from uranyl ion is reported. © 1998 Elsevier Science B.V. All rights reserved.

Keywords: Uranyl; Crown ethers; Separation; Solvent extraction

1. Introduction

The cyclic polyethers better known as crown ethers are a unique class of compounds with hyrophilic interior and lipophilic exterior capable of metal ion transport across non-aqueous barriers [1–3]. Due to their size selective nature these compounds have gained importance as specific cation binding agents. The solvent extraction technique has been employed as a convenient and useful method for understanding the complexation as well as extraction characteristics of metal ion crown ether systems [4]. Takeda et al. [5,6] have reported 'size-selective extraction' of alkali metal ions employing crown ethers where picrate is used as the organophilic counter anion. Similarly, McDowell et al. [7,8] have studied the extraction behaviour of alkali and alkaline earth ions using crown ethers and a liquid cation exchanger such as di(2-ethyl hexyl) phosphoric acid. Though the extraction behaviour of alkali and alkaline earth ions have been extensively studied in the presence of crown ethers, data on the actinide ions is relatively scarce.

Due to its importance as nuclear fuel material,

* Corresponding author. Fax: +91 22 5560750; e-mail: acsrcd@magnum.barct1.ernet.in

0039-9140/98/$ - see front matter © 1998 Elsevier Science B.V. All rights reserved.
PII S0039-9140(98)00215-X

the chemistry of uranium has gained importance over the years. The extraction behaviour of uranium, is therefore, of interest to the chemists engaged in the study of its hydrometallurgy, recovery from sea water as well as separation from fission products. Reports on the extraction of uranium using crown ethers are very limited and concern those from strongly acidic solution of HCl and HNO_3 [9–13]. The strong complexing nature of the anions like Cl^- and NO_3^- result in the formation of anionic complexes which are extracted along with the protonated forms of the crown ethers [9–11]. The extraction studies from HNO_3 solution [11–13] involved solvated species, similar to those encountered in TBP extraction and follow a different mechanism altogether. The choice of the counter anions in such systems do not permit the formation of innersphere complexes with crown ethers which could result in size selectivity.

The present work involves the ion-pair extraction of uranyl ion in the presence of crown ethers of varying cavity size and substituents. The motivation for carrying out extraction work at pH medium is to explore the possibility of size selective extraction under these conditions. Studies involving the separation of fission products from irradiated targets are also carried out in order to understand their separation behaviour which could be of great use in recovery processes.

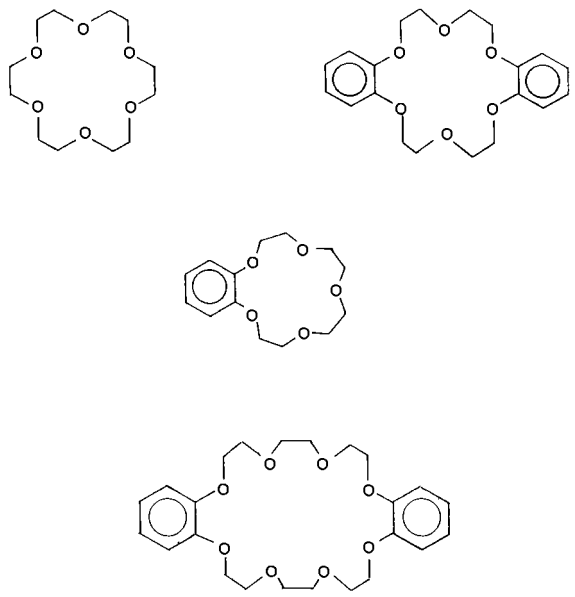

Fig. 1. Structures of the crown ethers used in the present work.

2. Experimental

2.1. Reagents

The crown ethers employed in the present work (Fig. 1) such as benzo 15-crown-5 (B15C5), 18-crown-6 (18C6), dibenzo 18-crown-6 (DB18C6) and dibenzo 24-crown-8 (DB24C8) were procured

Table 1
Ranges of variation of the variable parameters in the experiments to determine the species extracted

Variable parameter	Range of variation	Conditions for other parameters
Crown ether concentration	$[B15C5] = 2.85\times10^{-1}-5.70\times10^{-2}$ M; $[18C6] = 2.34\times10^{-1}-4.86\times10^{-2}$ M; $[DB18C6] = 1.06\times10^{-1}-2.12\times10^{-2}$ M; $[DB24C8] = 1.93\times10^{-1}-3.86\times10^{-2}$ M	[picric acid] = 0.02 M; pH = 3.0; ionic strength = 0.1 M
Picric acid concentration	$2.00\times10^{-2}-6.67\times10^{-3}$ M[a]; $2.00\times10^{-2}-4.00\times10^{-3}$ M[b]	$[18C6] = 2.53\times10^{-1}$ M; $[B15C5] = 4.00\times10^{-1}$ M; $[DB18C6] = 1.81\times10^{-1}$ M; $[DB24C8] = 3.89\times10^{-1}$ M; pH = 3.0; ionic strength = 1.00×10^{-1} M
pH	1.90–3.15	$[18C6] = 2.82\times10^{-1}$ M; [picric acid] = 2.00×10^{-2} M; ionic strength = 1.00×10^{-1} M

All experiments are carried out at 25°C.
[a] 18C6.
[b] B15C5, DB18C6 and DB24C8.

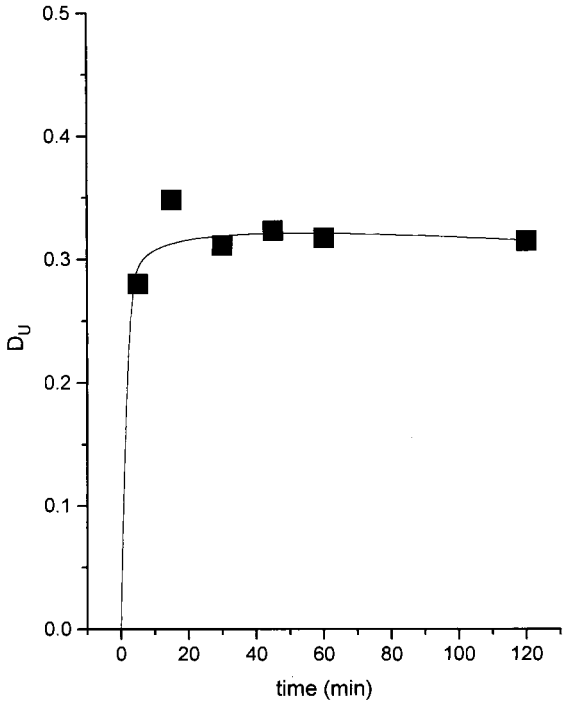

Fig. 2. Extraction of uranyl ion as a function of equilibration time. [18C6] = 3.75×10^{-1} M; [picric acid] = 0.02 M; pH = 3.00.

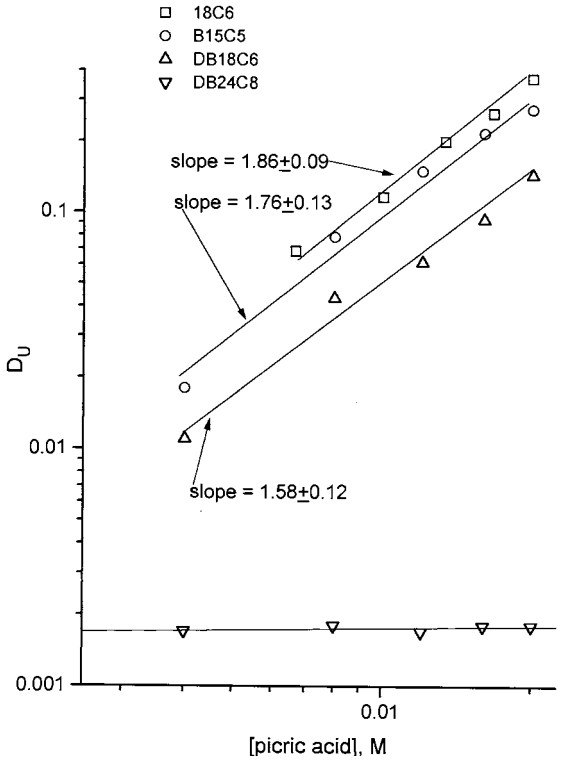

Fig. 3. Effect of picric acid concentration on uranyl ion extraction. [B15C5] = 4.00×10^{-1} M; [18C6] = 2.53×10^{-1} M; [DB18C6] = 1.81×10^{-1} M; [DB24C8] = 3.89×10^{-1} M; pH = 3.00.

from E. Merck and were used without further purification. Laboratory grade picric acid supplied by B.D.H. (Bombay) was recrystallized prior to use. Tetramethyl ammonium chloride and tetramethyl ammonium hydroxide were procured from Fluka Chemie AG and were used for ionic strength and pH adjustment, respectively.

^{233}Uranium was obtained by the neutron irradiation of ^{232}thorium and was subsequently purified from its daughter product ^{229}Th by an anion exchange method [14].

Table 2
pH variation for uranyl ion

pH	D_U	pH	D_U
1.90	0.464	2.82	0.512
2.08	0.449	2.90	0.511
2.25	0.522	2.94	0.502
2.48	0.510	3.06	0.521
2.60	0.510	3.12	0.518
2.63	0.508	3.15	0.508
2.66	0.503	—	—

Temperature = 25°C, ionic strength = 0.1 M, conc. of 18-crown-6 = 0.273 M.

2.2. Procedure

In order to identify the species extracted into the organic phase, separate experiments were carried out by varying one of the variable parameters such as picric acid concentration in the aqueous phase, crown ether concentration in the organic phase, pH of the aqueous phase etc., while maintaining the rest of them constant. Table 1 lists the variable parameters and the range in which they are varied.

It may be noted here, that the aqueous phase pH is fixed at 3.0 for most of the experiments due to the fact that higher pH values could result in the hydrolysis of the metal ion and lower pH

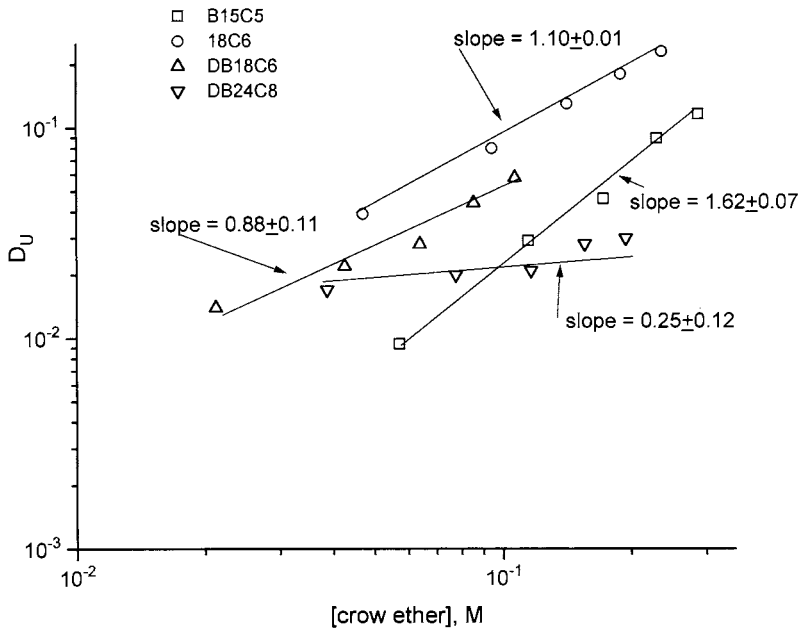

Fig. 4. Extraction as a function of crown ether concentration. [picric acid] = 0.02 M; pH 3.00.

values caused the protonation of crown compounds and made the deprotonation of picric acid difficult. The pH values at equilibrium were measured by using a miniaturised combination glass electrode in the extraction tube itself.

Distribution studies were carried out by equilibrating equal volumes (generally 1 ml) of the two phases (organic and aqueous phase) for 1 h in a thermostated water bath and ^{233}U was assayed subsequently by liquid scintillation counting. The distribution ratio (D_u) is defined as:

$$D_U = \frac{\text{concn. of uranium in the organic phase per unit volume}}{\text{concn. of uranium in the aqueous phase per unit volume}}$$

Distribution ratio values were measured with a precision of $\pm$ 5%.

3. Calculations

The data treatment of the uranyl ion-crown ether extraction system is carried out in a manner similar to the americium-crown ether system described earlier [15]. The two phase extraction equilibrium is given as:

$$UO_2^{2+} + nL_{(o)} + 2A^- \overset{K_{ex}}{\rightleftharpoons} [UO_2(L)_n]^{2+}[A^-]_{2(o)} \quad (1)$$

Therefore,

$$K_{ex} = \frac{[UO_2L_nA_2]_{(o)}}{[UO_2][L]_o^n[A]^2} \quad (2)$$

The charges on the species are ignored for simplicity. The subscript 'o' indicates species in the organic phase while those without any subscript indicate in the aqueous phase. The partition coefficient P_L of the crown ether (L) and the dissociation constant (K_{LH}) of the conjugated acid (LH) are represented as:

$$P_L = [L]_o/[L] \quad (3)$$

$$K_{LH} = [L][H]/[LH] \quad (4)$$

As the tracer concentration of U is employed in the present work, the ligand bound to the uranyl ion can be neglected in the ligand balance equation and with equal volumes of the organic and aqueous phases:

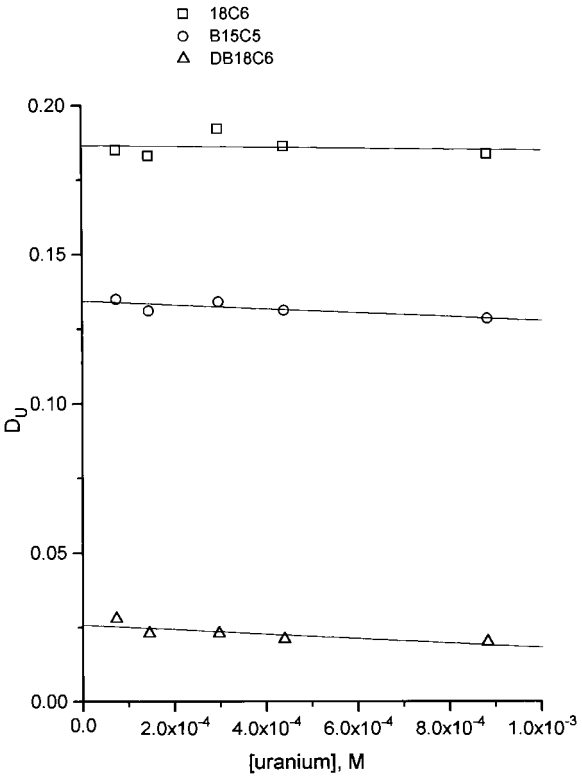

Fig. 5. Effect of uranium concentration on uranyl ion extraction. [B15C5] = 2.70×10^{-1} M; [18C6] = 2.53×10^{-1} M; [DB18C6] = 6.11×10^{-2} M; pH = 3.00, [picric acid] = 0.02 M.

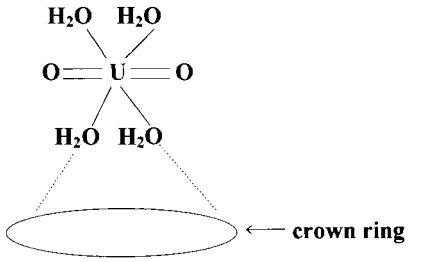

a) The side-way model for the 1:1 complex

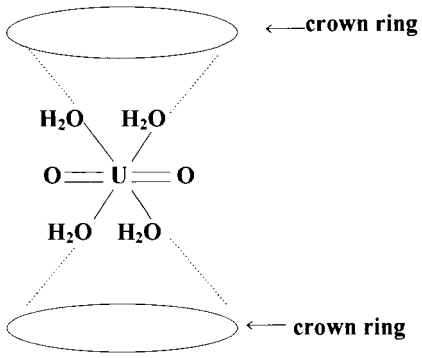

b) The sandwitch model for 1:2 complex

Fig. 6. Proposed models for the extracted species.

$$[L]_{total} = [L]_o + [L] + [LH] \quad (5)$$

where $[L]_{total}$ is the total ligand concentration. From Eqs. (4) and (5)

$$[L]_o = [L]_{total}/(1 + P_L^{-1} + [H]P_L^{-1} \cdot K_{LH}^{-1}) \quad (6)$$

Substituting $[L]_o$ from Eq. (6) into Eq. (2)

$$K_{ex} = \frac{D(1 + P_L^{-1} + [H]P_L^{-1} \cdot K_{LH}^{-1})^n}{[L]_{total}^n [A]^2} \quad (7)$$

Since $[HA]_{total} \gg$ total uranyl ion concentration ($\sim 1 \times 10^{-5}$ M), the equilibrium of picrate anion

Table 3
The extraction constant (log K_{ex}) and distribution ration (D_U) values for UO_2^{2+}-crown ether-picric acid extraction system

Ligand	Extraction constant (log K_{ex})		Distribution ratio (D)[b]	
	Am^{3+}	UO_2^{2+}	Am^{3+}	UO_2^{2+}
15C5	5.18	—	0.064	—
B15C5	—	2.47, 3.55[a]	—	0.116[c]
18C6	5.93	3.46	0.115	0.092
DB18C6	—	3.22	—	0.058

pH 3.0; ionic strength = 0.1 M and temperature = 25°C.
Data on Am^{3+} extraction system are included for comparative purposes [15].
[a] 1:2 complex formation.
[b] [ligand] = 0.11 M.

Table 4
Diluent effect on the extraction of UO_2^{2+} from 0.02 M picric acid (ionic strength = 0.1 M and pH 3.0) using 0.08 M 18C6[a]

Diluent	Dielectric constant	D_U
n-Dodecane	2.0	$<1\times10^{-3}$
Carbon tetrachloride	2.23	$<1\times10^{-3}$
Toluene	2.38	8.411×10^{-3}
Chloroform	4.81	0.07
Dichloromethane	9.08	0.10
Nitrobenzene	34.8	0.62

[a] Data obtained at 25°C.

is represented as:

$$[A] = [HA]_{total}/\{1 + [H](P_{HA}K_a^{-1} + K_a^{-1})\} \quad (8)$$

where P_{HA} and K_a are the partition coefficient (97.5) and dissociation constant ($pK_a = 0.29$) of picric acid, respectively. The complex formation constant values can be computed from the distribution ratio data by Eq. (9):

$$\frac{1}{D} = \frac{1}{K_{ex}[L]_o^n[A]^2} + \frac{\beta_1^{ML}\cdot P_L^{-1}}{K_{ex}[L]_o^{n-1}[A]^2} + \frac{\beta_2^{ML}\cdot P_L^{-2}}{K_{ex}[L]_o^{n-2}[A]^2} \quad (9)$$

Due to the weak complexation of uranyl ion with crown ethers in aqueous phase, attempts to compute the complex formation constants employing Eq. (9) did not succeed as large errors are associated with these values.

Table 5
Separation factors (SF)[a] of fission products from irradiated uranium target

Radionuclide	B15C5[b]	18C6[c]	DB18C6[d]
^{147}Nd	24.6	3.2	4.3
^{99}Mo	–	–	2.1
^{143}Ce	21.0	2.8	1.6
^{140}Ba	86.7	268.0	618.0
^{112}Pd	16.7	1.2	28.6
^{97}Zr	5.5	1.0	31.5
^{140}La	8.8	2.8	7.6
^{115}Cd	7.1	–	1.4
^{103}Ru	2.2	0.42	3.1
^{153}Gd	42.0	4.1	–

[a] $SF = D_{\text{radionuclide of interest}}/D_U$.
[b] [B15C5] = 0.29 M.
[c] [18C6] = 0.25 M.
[d] [DB18C6] = 0.11 M.
Picrate conc. = 0.02 M; IS = 0.1 M; pH 3.0.

4. Results and discussion

Fig. 2 shows the effect of time of equilibration for the extraction system UO_2^{2+}-18C6-picric acid at pH 3.0. Though 5 min were required for getting an equilibrium D_U value, an equilibrium time of 30 min was maintained throughout this work. The fast attainment of equilibrium is a characteristic of ion-pair extraction [15].

The dissociation constant values (pK_a) of picric acid (HA) and HL^+ (where L = 18-crown-6) are reported to be 0.29 [16] and 1.46 [17], respectively. To ensure that these species exist in their unprotonated form, and to avoid hydrolysis, pH 3.0 was considered as a compromise in the present work.

The picrate-extraction behaviour of uranyl ion using crown ethers was similar to that of trivalent americium as reported earlier [15]. Table 2 lists the distribution ratio values in presence of 0.273 M 18C6 and 0.02 M picric acid and at different pH values (ionic strength = 0.1 M). The hydrogen ion concentration independent extraction was observed in the pH range 2.25–3.15 during the extraction process. Similar acidity independent extraction behaviour was also observed for the other crown ethers viz. B15C5, DB18C6 studied.

The experiments to determine the number of picrate ions extracted, were carried out using 0.400 M B15C5, 0.253 M 18C6, 0.181 M DB18C6 and 0.389 M DB24C8, pH 3.0 and ionic strength of 0.1 M. Slopes of the log *D* versus log[picric acid] plots in the range of 1.58 to 1.86 were obtained for B15C5, 18C6 as well as DB18C6 (Fig. 3) suggesting the extraction of two picrate ions. On the other hand, the picrate ion variation experiment in case of DB24C8 yielded a straight line parallel to the abscissa with $D \sim 1.7\times10^{-3}$ suggesting the inefficiency of the ligand (DB24C8) for uranyl ion extraction.

The results of the experiments at different concentrations of crown ether but fixed picric acid concentration (0.02 M), pH (3.0) and ionic strength (0.1 M) revealed the extraction of 1:1 as well as 1:2 M:L species (Fig. 4) for benzo 15 crown 5 (B15C5) while 1:1 species for 18C6 and DB18C6. A dependence of 0.25 ± 0.12 was seen in case of DB24C8 which conformed to the observation made during the picrate concentration varia-

tion experiments above. The possibility of the extraction of polynuclear species in the case of DB24C8 was ruled out as the metal ion concentration variation experiments did not show any dependence of D_U on uranyl ion concentration (Fig. 5).

Table 3 gives the extraction constant ($\log K_{ex}$) values obtained for all the crown ethers studied in the present work. For comparison purposes extraction constants for a trivalent americium involving similar extractants are also included. $\log K_{ex}$ values suggested that similar to Am(III), the large hydration energy of uranyl ion did not permit replacement of the inner-sphere water molecules by the crown ether moieties. Since the species extracted into the organic phase appeared to contain varying numbers of crown ether and water molecules, their partition coefficient values are likely to vary significantly. For comparison of the relative extractability, the D values are also listed in Table 3. The higher extraction of Am^{3+} as compared UO_2^{2+} was also reported by us earlier [18] using TBP (tri-*n*-butyl phosphate) and DOSO (di-*n*-octyl sulphoxide). It was observed that the 18 membered ligands (18C6 as well as DB18C6) were better extractants than B15C5 and the larger (24 membered) DB24C8 which was very poor extractant. The 1:1 complex formation with both 18C6 and DB18C6 were represented by the side-way model while B15C5 formed by a sandwich model [4] (Fig. 6).

Table 4 shows the effect of the nature of diluent on the extraction process. Polar diluents such as CH_2Cl_2, $CHCl_3$ and nitrobenzene were found to be much better extractants than non-polar diluents such as carbon tetracholoride and *n*-dodecane. Such behaviour is typical of a solvent extraction system involving ion-pairs.

The aqueous phase complex formation constants of uranyl ion with the crown ethers were too low to be reported accurately. This trend is similar to that observed in our study involving trivalent actinide ion [15] suggesting outersphere interaction through hydrogen bonding to be dominant in the complexation process. Earlier attempts by Izatt et al. [19,20] to determine the complexation constants of uranyl ion with 18C6 in a methanol medium using calorimetry were not successful. According to Costes et al. [21–23] and Bombieri et al. [24] no interaction of uranyl ion with crown ethers was feasible and in the solid state the latter only co-crystallize with the former. However, Brighli et al. [25] had observed the formation of 'inclusion' complexes with cryptands as well as crown ethers in propylene carbonate medium.

4.1. Separation studies

The separation of fission products from uranium was accomplished by the picrate extraction method at pH 3.0 by employing the crown ethers studied in the present work. The results (Table 5) showed excellent separation for ^{140}Ba ($SF > 100$) with all the ligands employed. The separation factors for trivalent ions were relatively much lower. Nevertheless, the higher extractability of the trivalent lanthanide ions compared to uranyl ion was in sharp contrast to the extraction behaviour observed with well-known extractants.

In extraction systems involving extractants like β-diketones, bis-2-ethylhexyl phosphoric acid, TBP and amines the uranyl ion is extracted to a much greater extent than the trivalent ions under identical experimental conditions [26–31]. The greater extraction of trivalent lanthanides compared to the uranyl ion in the present work for 18C6 system was probably due to the greater organophilicity of the extractable complex of the trivalent ions (containing two crown moieties and three picrate ions) than that of the uranyl ion (containing one crown moiety and two picrate ions) [19]. Possibility of smaller number of associated water molecules with Ln^{3+} ions as compared to UO_2^{2+} might also favour lanthanide extraction. Mo possibly formed anionic species under the prevailing experimental conditions and was therefore not extracted into the $CHCl_3$ phase.

It can be said in conclusion that though extraction of uranyl ion from picric acid medium using crown ethers was possible, no size selectivity was observed. In fact, increasing the crown ether ring size decreased the metal ion extractability i.e. the K_{ex} values followed the trend B15C5 $>$ 18C6 $>$ DB18C6 $>>$ DB24C8. The unusual separation behaviour of trivalent lanthanide ions was ex-

plained on the basis of a more organophilic extracted species compared to that for the uranyl ion.

Acknowledgement

The authors sincerely express their gratitude to Dr S.B. Manohar, Head, Radiochemistry Division for his keen interest in this work.

References

[1] G.W. Gokel, Crown Ethers and Cryptands, Royal Society of Chemistry, London, 1992.
[2] J.D. Lamb, R.M. Izatt, J.J. Christensen, D.J. Eatough, in: G.M. Nelson (Ed.), Co-ordination Chemistry of Macrocyclic Compounds, Plenum Press, New York, 1979, pp. 145–217.
[3] I.M. Kolthoff, Anal. Chem. 51 (1979) 1.
[4] Y. Takeda, Top. Curr. Chem. 121 (1984) 1.
[5] Y. Takeda, Bull. Chem. Soc. Jpn. 54 (1981) 526.
[6] Y. Takeda, H. Kato, Bull. Chem. Soc. Jpn. 52 (1979) 1027.
[7] W.J. McDowell, Sep. Sci. Technol. 23 (1988) 1251.
[8] W.J. McDowell, G.N. Case, D.W. Alrup, Sep. Sci. Technol. 18 (1983) 1983.
[9] W.J Wang, B. Chen, P. Zheng, B. Wang, M. Wang, Inorg. Chim. Acta 117 (1986) 81.
[10] W.J. Wang, J. Lin, A. Wang, P. Zheng, M. Wang, B. Wang, Inorg. Chim. Acta 149 (1988) 151.
[11] V.V. Yakshin, B.N. Laskorin, Dok. Akad. Nauk SSR 241 (1978) 159.
[12] J.P. Shukla, K.V. Lohitakshan, Chem. Script. 29 (1989) 341.
[13] J.P. Shukla, R.K. Singh, A. Kumar, Radiochim. Acta 54 (1991) 73.
[14] P.K. Mohapatra, Ph. D. thesis, University of Bombay, 1993.
[15] P.K. Mohapatra, V.K. Manchanda, Radiochim. Acta 55 (1991) 193.
[16] G. Kortun, W. Vogel, K. Andrussov, Dissociation Constants of Organic Acids in Aqueous Solutions, Butterworth, London, 1961.
[17] A.A. Majumdar, A.R. Gupta, Ind. J. Chem. 25A (1986) 861.
[18] V.K. Manchanda, P.K. Mohapatra, Radiochim. Acta 69 (1995) 81.
[19] R.M. Izatt, J.D. Lamb, J.J. Christensen, B.L. Haymore, J. Am. Chem. Soc. 99 (1977) 8344.
[20] R.M. Izatt, R.E. Terry, B.L. Haymore, L.D. Hansen, N.K. Dalley, A.G. Avondet, J.J. Christensen, J. Am. Chem. Soc. 98 (1976) 7620.
[21] R.M. Costes, G. Folcher, P. Plurien, P. Rigny, Inorg. Nucl. Chem. Lett. 11 (1975) 13.
[22] G. Folcher, P. Chardin, R.M. Costes, N. Keller, G. de Villardi, Inorg. Chim. Acta 34 (1979) 87.
[23] R.M. Costes, G. Folcher, P. Plurien, P. Rigny, Inorg. Nucl. Chem. Lett. 12 (1976) 491.
[24] G. Bonbieri, G. De Paoli, A. Cassol, A. Immirzi, Inorg. Chim. Acta. 18 (1976) L23.
[25] M. Brighli, P. Fux, J. Lagrange, P. Lagrange, Inorg. Chem. 24 (1985) 80.
[26] T.H. Siddall, in: J.F. Flagg (Ed.), Solvent Extraction: General Principles in Chemical Processing of Reactor Fuels, Academic Press, New York, 1961.
[27] J. Stràv, The Extraction of Metal Chelates, Pergamon, Oxford, 1964.
[28] V.V. Ramakrishna, S.K. Patil, Structure and Bonding, vol. 6, Springer, Heidelberg, 1984, p. 35.
[29] H.A.C. McKay, D. Scargill, A.G. Wain, Gmelin Handbook of Inorganic Chemistry, 8th edn, Suppl. Ser., Transuranium, Springer-Verlag, Berlin, Part D2, 1975, p. 177.
[30] J. Stràv, H. Frieser, Equilibrium constants of Liquid–Liquid Distribution Reactions, Part 4, Chelating Extractants, Pergamon, Oxford (IUPAC Chemical Data Series No. 18) 1978.
[31] A.S. Kertes, Y. Marcus, E. Yanir, Alkylammonium salt extractants, Equilibrium Constants of Liquid–Liquid Distribution Reactions Part 2, Butterworths, London, 1974, p. 1974.

ELSEVIER

Talanta 47 (1998) 1279–1286

Talanta

Spectrophotometric determination of azathioprine in pharmaceutical formulations

Chilukuri S.R. Lakshmi, Manda N. Reddy *

Department of Pharmaceutical Sciences, Andhra University, Visakhapatnam-530 003, India

Received 9 February 1998; received in revised form 26 May 1998; accepted 27 May 1998

Abstract

Four simple and sensitive visible spectrophotometric methods (A–D) have been described for the assay of azathioprine (ATP) either in pure form or in pharmaceutical formulations. Methods A and B are based on the oxidation of ATP with excess *N*-bromosuccinimide (NBS) or chloramine-T (CAT) and determining the consumed NBS or CAT with a decrease in colour intensity of celestine blue (CB) (method A) or gallocyanine (GC) (method B), respectively. Methods C and D are based on the diazotisation of reduced azathioprine (RATP) with excess nitrous acid and estimating either the consumed nitrous acid (HNO_2) with cresyl fast violet acetate (CFVA) (method C) or by coupling reaction of the diazonium salt formed with *N*-1-naphthyl ethylene diamine dihydrochloride (NED) (method D). All of the variables have been optimized and the reactions presented. The concentration measurements are reproducible within a relative standard deviation of 1.0%. Recoveries are 99.2–100.3%. © 1998 Elsevier Science B.V. All rights reserved.

Keywords: Azathioprine; *N*-Bromosuccinimide; Chloramine-T; Nitrous acid; Celestine blue; Gallocyanine; Cresyl fast violet acetate; *N*-1-naphthylethylene diamine; Spectrophotometry

1. Introduction

Azathioprine (ATP) is primarily an immuno suppressive agent, used mainly in allotransplantation procedures. It is also used in systemic anti-inflammatory states, such as rheumatoid arthritis, lupus erythematosus, polymyosites and Crohn's disease. It is chemically known as 6-[(1-methy1-4-nitroimidazol-5-yl) thiol] purine and is official in the United States Pharmacopeia [1] and British Pharmacopeia [2]. A survey of the literature revealed that only a single visible [3] and three UV spectrophotometric [4–7] methods have been reported. Other methods include polarography [3], high performance liquid chromatography [8] and titrimetry [9,10]. The reported spectrophotometric methods suffer deficiencies such as low λ_{max} value or low sensitivity. It is, therefore, of interest to develop simple and sensitive procedures with higher λ_{max} for the determination of ATP in pure and pharmaceutical formulations.

This paper describes four visible spectrophotometric methods for the determination of ATP making use of its ability to react with NBS and

* Corresponding author. Tel.: +91 555547.

0039-9140/98/$ - see front matter © 1998 Elsevier Science B.V. All rights reserved.
PII S0039-9140(98)00216-1

CAT directly and with HNO_2 after reduction. Azine dyes are well known for their high absorptivity and they have been utilised for estimating excess NBS (with CB, (1-aminocarbony1-7-dimethylamino)-3-4-dihydroxyphenoxazin-5-ium chloride; C.I. No. 51050) [11], CAT (with GC, (phenoxazin-5-ium, 1-carboxy-(2-dimethylamino)-3,4-dihydroxychloride; C.I. No. 51030) [12] and HNO_2 (with CFVA (Benzo (α) phenoxazin-7-ium, 5-imino 9-amino, acetate) [13] in the indirect determinations of bioactive compounds. The NED reagent was preferred as a coupler by a number of workers for visible spectrophotometric determination of drugs containing primary amino group in aromatic or heterocyclic moiety during diazocoupling process [14].

We have applied these sensitive visible spectrophotometric procedures in the determination of ATP in bulk samples and pharmaceutical formulations. Methods A, B and C involve the addition of excess oxidant to ATP (NBS or CAT) or reduced ATP (HNO_2) and unreacted oxidant in each case (NBS with CB, method A; CAT with GC, method B; HNO_2 with CFVA, method C) is determined by measurement of the decrease in absorbance of the dye. Method D describes the determination of reduced ATP with NED coupler after diazotisation.

2. Experimental

2.1. Instruments

A Systronics model 106 digital spectrophotometer with 1 cm matched glass cells was used for all the absorbance measurements. An Elico LI-120 digital pH meter was used for pH measurements.

2.2. Reagents

All chemicals were of analytical grade and all of the solutions were prepared with double distilled water. Freshly prepared solutions were always used.

Aqueous solutions of 100 μg ml^{-1} NBS (Loba), 50 μg ml^{-1} CB (E. Gurr) and 5 M HCl (E. Merck) were prepared for method A. Aqueous solutions of 200 μg ml^{-1} CAT (Loba), 100 μg ml^{-1} GC (E. Gurr) and 5 M HCl were prepared for method B. Aqueous solutions of 20 μg ml^{-1} $NaNO_2$ (Sarabhai), 50 μg ml^{-1} CFVA (Chroma) and 5 M HCl (E. Merck) were prepared for method C. Aqueous solutions of 0.25% $NaNO_2$ (Sarabhai), 2 M HCl (E. Merck) and 2.5% ammonium sulphamate (Loba), 0.1% NED (E. Merck) and 2.5 M sodium acetate (BDH) were prepared for method D.

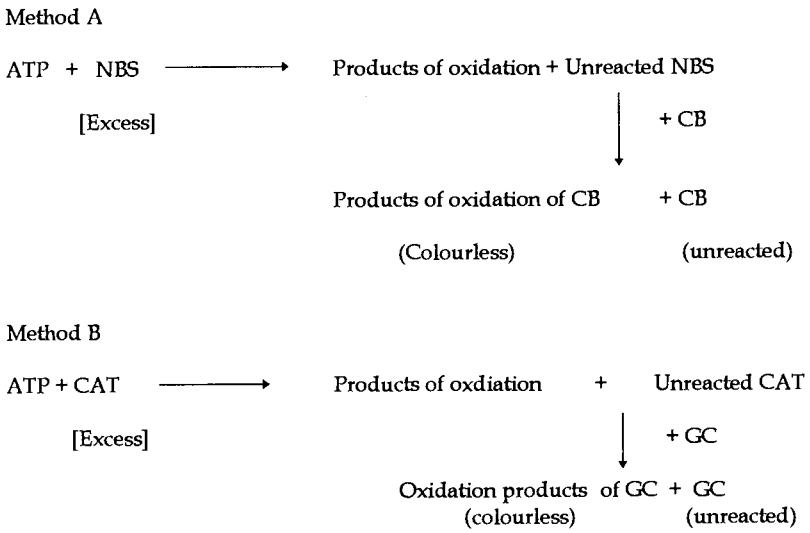

Scheme 1. Methods A and B for preparation of standard drug solution.

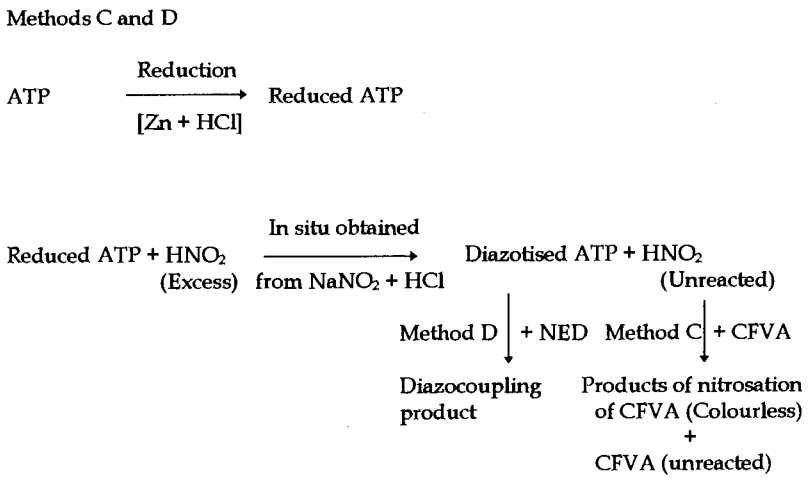

Scheme 2. Methods C and D for preparation of standard drug solution.

2.3. Preparation of standard drug solution

2.3.1. For methods A and B

ATP (20 mg) was dissolved in 10 ml of 0.1 M NaOH solution and diluted to 100 ml with distilled water (200 μg ml^{-1}) (Scheme 1).

2.3.2. For methods C and D

About 50 mg of ATP was dissolved in MeOH and treated with 10 ml of 1 M HCl and 0.25 g of Zn dust added in portions. After standing for 45 min at room temperature, the solution was filtered through cotton wool, the residue was washed with 3×5 ml portions of methanol and the filtrate was neutralised with NaOH and diluted with MeOH stepwise to prepare working solutions of 100 and 500 μg ml^{-1} for methods C and D, respectively (Scheme 2).

2.4. Analysis of pure samples

2.4.1. Methods A and B

To each of 25 ml graduated test tubes containing standard ATP solution (0.2–1.2 ml of 200 μg ml^{-1} for method A; 0.25–1.0 ml of 200 μg ml^{-1} for method B), 1.25 ml of 5 M HCl (for methods A and B) and 2.5 ml of 100 μg ml^{-1} NBS (for method A) or 2.0 ml of 200 μg ml^{-1} CAT (for method B) were added and the solutions diluted to 15 ml with distilled water. After 10 min, 10 ml of dye solution (50 μg ml^{-1} CB for method A; 100 μg ml^{-1} GC for method B) was added, mixed thoroughly and the absorbances were measured after 5 min at 540 nm (for methods A and B) against distilled water. The blank (omitting drug) and dye (omitting drug and oxidant) solutions were prepared in a similar manner and their absorbances were measured against distilled water. The decrease in absorbance corresponding to consumed oxidant and in turn to ATP content was obtained by subtracting the decrease in absorbance of the test solution (dye-test) from that of the blank solution (dye-blank). The amount of ATP in a sample was obtained from the Beer–Lambert plot.

2.4.2. Method C

Aliquots of standard reduced ATP solution (0.5–3.0 ml, 100 μg ml^{-1}) were placed in a series of 25 ml calibrated tubes. Then 1.25 ml of 5 M HCl and 2.0 ml of 20 μg ml^{-1} $NaNO_2$ solutions were added successively and the volume in each tube was brought to 15.0 ml with distilled water. After 5 min 10.0 ml of 50 μg ml^{-1} CFVA solution was added, mixed thoroughly and the absorbance was measured after 5 min at 565 nm against distilled water. A blank experiment was carried out in a similar manner omitting drug. The decrease in absorbance corresponds to consumed HNO_2 which in turn to ATP concentration

was obtained by subtracting the absorbance of the blank solution from that of the test solution. The amount of ATP in a sample was obtained from the Beer–Lambert plot.

2.4.3. Method D

An aliquot of reduced ATP solution containing 0.25–1.25 ml (500 μg ml^{-1}) was delivered in to a series of 20 ml graduated test tubes and the volume was adjusted to 2.0 ml with distilled water. Then 1 ml of 0.25% $NaNO_2$ and 1 ml of 2 M HCl solutions were added and kept aside for 5 min, to complete the diazotisation. Then 2 ml of ammonium sulphamate and after 5 min 1 ml each of 2.5 M sodium acetate and 0.1% NED solutions were added and made up to 20 ml with distilled water. The absorbance of the coloured species was read at 515 nm against a reagent blank. The amount of ATP in a sample was computed from Beer–Lambert plot.

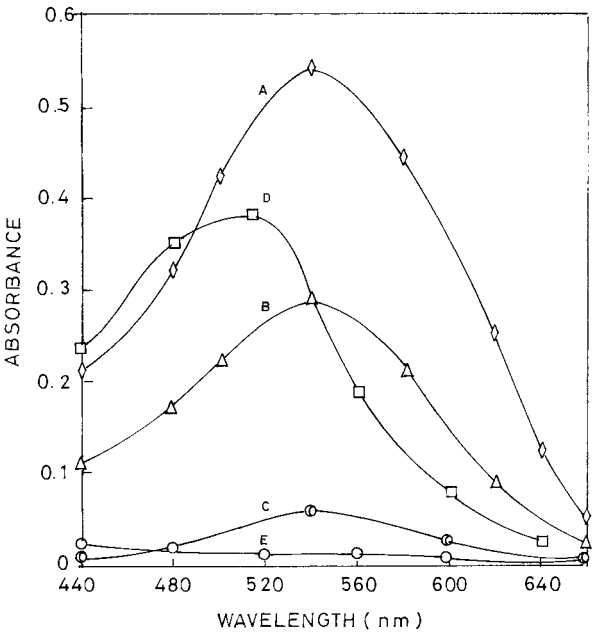

Fig. 1. Absorption spectra of ATP/NBS-CB system (B) or reagent blank (C) or dye (CB in 0.25 M HCl) (A) against distilled water. (Concentration of ATP: 2.88×10^{-5} M, NBS: 5.62×10^{-5} M, CB: 5.49×10^{-5} M, HCl: 0.25 M); ATP/HNO_2-NED system (D) against reagent blank (E) versus distilled water. (Concentration of ATP: 7.21×10^{-5} M, $NaNO_2$: 1.8×10^{-3} M, HCl: 0.1 M, Ammonium sulphamate: 1.75×10^{-2} M, NED: 1.93×10^{-4} M).

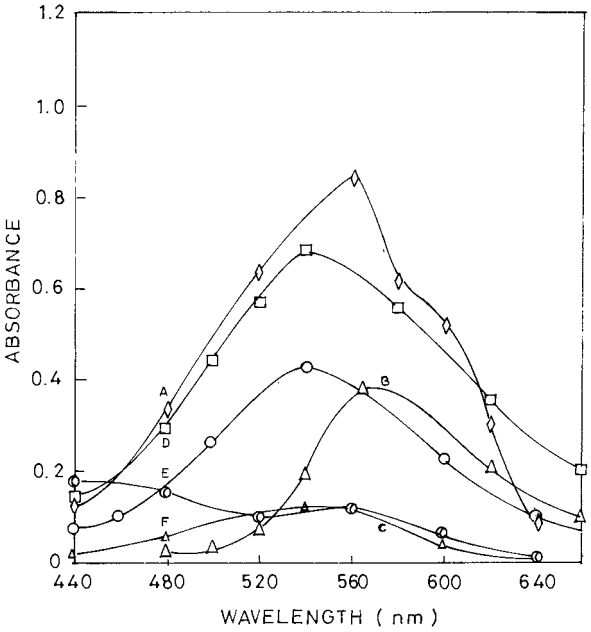

Fig. 2. Absorption spectra of ATP/HNO_2-CFVA system (B) or reagent blank (C) or dye (CFVA in 0.25 M HCl) (A) against distilled water. (Concentration of ATP: 3.60×10^{-5} M, $NaNO_2$: 2.32×10^{-5} M, CFVA: 6.23×10^{-5} M, HCl: 0.25 M); ATP/CAT-GC system (E) or reagent blank (F) or dye (GC in 0.25 M HCl) (D) against distilled water. (Concentration of ATP: 2.16×10^{-5} M, CAT: 5.68×10^{-5} M, GC: 1.19×10^{-5} M, HCl: 0.25 M).

2.5. Analysis of pharmaceutical formulations

Table powder equivalent to 20 mg (for methods A and B) and 50 mg (for methods C and D) were separately taken and the sample solution prepared as described for the standard solutions and filtered if insoluble materials were present prior to analysis as described for pure samples.

3. Results and discussion

The optimum conditions for the development of methods A–D were established by varying parameters one at a time [15] and observing the effect produced on the absorbance of the coloured species.

Table 1
Optical and regression characteristics, precision and accuracy of the proposed methods

Parameters	Methods			
	A	B	C	D
λ_{max} (nm)	540	540	565	515
Beer's law limit (μg ml^{-1})	1.6–9.6	1.0–8.0	2.0–12.0	5.0–25.0
Detection limit (μg ml^{-1})	0.048	0.024	0.046	0.112
Molar absorptivity (1 mol^{-1} cm^{-1})	0.991×10^{4}	1.97×10^{4}	1.05×10^{4}	0.266×10^{4}
Sandell's sensitivity (μg cm^{-2}/0.001 absorbance unit)	0.028	0.014	0.026	0.052
Regression equation (Y)[a]				
Slope (b)	3.58×10^{-2}	7.11×10^{-2}	3.77×10^{-2}	1.93×10^{-2}
Standard deviation on slope (S_b)	6.25×10^{-5}	1.53×10^{-4}	7.64×10^{-5}	2.0×10^{-5}
Intercept (a)	-3.0×10^{-4}	-9.14×10^{-5}	1.01×10^{-4}	-3.0×10^{-4}
Standard deviation on intercept (S_a)	3.31×10^{-4}	7.54×10^{-4}	5.06×10^{-4}	3.32×10^{-4}
Standard error of estimation (S_e)	3.16×10^{-4}	8.77×10^{-4}	4.83×10^{-4}	3.16×10^{-4}
Correlation coefficient (r)	0.9999	0.9999	0.9999	0.9999
Relative standard deviation (%)[b]	0.36	0.26	0.30	0.52
% Range of error[b] (95% confidence limit)	0.38	0.27	0.32	0.55

[a] With respect to $Y = a + bC$, where C is concentration (μg ml^{-1}) and Y is absorbance.
[b] Six replicate samples.

3.0.1. Methods A–C

These methods involve two steps, namely reaction of ATP (or its reduction product) with an excess of oxidant (NBS, CAT or HNO_2) and the estimation of unreacted oxidant using a known excess of dye (CB, GC or CFVA). The excess dye remaining is then measured with a spectrophotometer at appropriate λ_{max} (540 nm for methods A and B; 565 nm for method C) (Figs. 1 and 2). The effect of oxidant concentration and acidity for a different time intervals in first step and dye concentration in second step, waiting period in each step with respect to maximum sensitivity, minimum blank, adherence to Beer's law, reproducibility and stability of final colour were studied through control experiments. The obtained optimum conditions are incorporated in the procedures recommended.

3.0.2. Method D

This method involves the reduction of the nitro group in ATP to amino group and subsequent diazotisation with nitrous acid, followed by coupling with NED. The effect of the essential parameters for reduction (concentration of HCl and amount of zinc, waiting period), diazotisation (concentration of HCl and $NaNO_2$, waiting period) and coupling (concentration of ammonium sulphamate and waiting period for destroying excess HNO_2; concentrations of sodium acetate and NED, waiting period) to ascertain optimum conditions were studied by means of controlled experiments varying one parameter at a time. The obtained optimum conditions are incorporated in the procedure recommended.

3.1. Analytical data

The Beer's law limits, molar absorptivity, Sandell's sensitivity, detection limits [16], regression equation and correlation coefficients obtained by least squares treatment of these results are given in Table 1. The precision of each method was tested by analysing six replicate samples containing 8, 6, 8 and 20 μg ml^{-1} of pure drug for methods A, B, C and D, respectively. The percent standard deviation and the percent range of error at 95% confidence level of each method are given in Table 1.

Commercial formulations (Tables) containing ATP were successfully analysed by the proposed methods. The values obtained by the proposed and reference [4] methods for formulations were compared statistically by the t- and F-tests and

Table 2
Assay and recovery of ATP in pharmaceutical formulations

Pharmaceutical formulations	Labelled amount found (mg)	Amount found[a] (mg) using proposed methods				Found by reference method	% Recovery by proposed methods[b]			
		A	B	C	D		A	B	C	D
Tablet I	25	24.7 ± 0.39 $t = 1.02$ $F = 2.64$	24.8 ± 0.22 $t = 1.63$ $F = 1.19$	24.9 ± 0.32 $t = 0.18$ $F = 1.78$	24.9 ± 0.20 $t = 1.72$ $F = 1.44$	24.97 ± 0.24	99.3 ± 0.48	99.7 ± 0.74	99.6 ± 0.53	99.8 ± 0.31
Tablet II	25	24.4 ± 0.32 $t = 0.45$ $F = 0.43$	25.3 ± 0.43 $t = 0.79$ $F = 2.73$	24.7 ± 0.37 $t = 1.06$ $F = 2.02$	24.9 ± 0.30 $t = 1.28$ $F = 1.33$	24.77 ± 0.26	99.2 ± 0.64	99.6 ± 0.43	100.6 ± 0.49	100.1 ± 0.63
Tablet I	50	49.93 ± 0.27 $t = 2.02$ $F = 1.40$	49.9 ± 0.28 $t = 1.30$ $F = 1.31$	50.01 ± 0.48 $t = 2.33$ $F = 2.25$	49.48 ± 0.29 $t = 1.31$ $F = 1.21$	49.54 ± 0.32	100.3 ± 0.74	99.8 ± 0.48	98.9 ± 0.28	99.6 ± 0.64
Tablet II	50	49.73 ± 0.31 $t = 0.92$ $F = 0.93$	49.70 ± 0.27 $t = 1.56$ $F = 1.40$	49.85 ± 0.16 $t = 0.38$ $F = 4.0$	49.93 ± 0.27 $t = 1.51$ $F = 1.40$	49.70 ± 0.33	99.6 ± 0.54	100.2 ± 0.19	99.2 ± 0.49	99.9 ± 0.27

[a] Average $\pm$ standard deviation of six determinations; the F and t-values refer to comparison of the proposed method with the reference method. Theoretical values at 95% confidence limits $F = 5.05$, $t = 2.57$.
[b] Recovery of 10 mg added to the pharmaceutical formulations (average of three determinations).

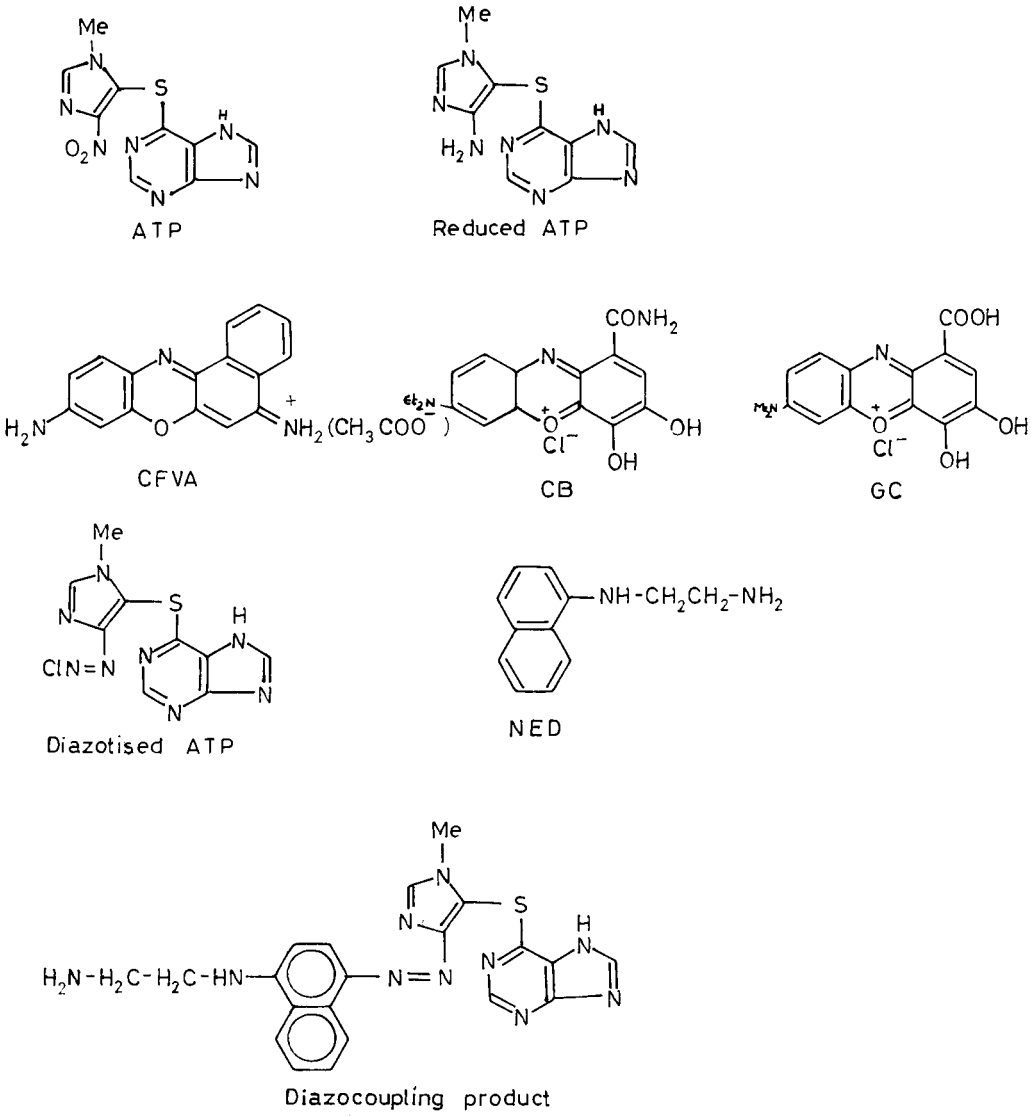

Scheme 3.

found not to differ significantly. As an additional demonstration of accuracy, recovery experiments were performed by adding a fixed amount of the drug to the preanalysed formulations. These results are summarised in Table 2. The ingredients usually present in formulations of ATP did not interfere with the proposed analytical methods.

3.2. Chemistry of coloured species

In method A, NBS provides molecular bromine at low concentration in polar media [17]. This reacts with ATP (mole ratio 4.3: 1) resulting in either oxidation, substitution or addition depending upon the functional groups present in ATP. Probably a mixture of reproducible products are

produced. The remaining molecular bromine is involved in bromination reaction with the dye (CB) to form a brominated dye which is colourless [11].

In method B, CAT undergoes hydrolysis in aqueous acidic medium to give sodium hypochlorite followed by hypochlorous acid [18]. This reacts with ATP (mole ratio 2.6:1) to form the relevant oxidation products, probably a mixture which appears to be reproducible under the specified experimental conditions. The remaining hypochlorous acid may be responsible for the bleaching of the colour of GC through disruption of the extended chromophore system in it [12].

As the stability of nitrous acid is poor, it is produced in situ by the addition of sodium nitrite to dilute hydrochloric acid solution in method C. This reacts with reduced ATP (mole ratio 1:1) giving the diazonium salt. The remaining HNO_2 reacts with CFVA with involvement of primary and secondary amino groups in dye due to nitrosation [13].

In method D, reduced ATP reacts with HNO_2 giving diazonium salt which inturn involves in coupling reaction with NED to produce coloured azo dye.

All these reactions are presented in Scheme 3.

4. Conclusion

Methods A–D possess higher λ_{max} and ε_{max} values than the reported lone visible spectrophotometric method and have the advantage of wider range in Beer's law limits. Thus all the proposed methods are simple, sensitive, selective and useful for the routine determination of ATP in pure samples and pharmaceutical formulations.

Acknowledgements

One of the authors (C.S.R Lakshmi) is grateful to the U.G.C. for providing J.R.F.

References

[1] United States Pharmacopeia, Vol. XXII, USP Convention, Rockville, 1990.
[2] British Pharmacopoeia, Vol. I: HMSO, London, 1993, p. 59.
[3] P. Stanislaw, G. Wladyslaw, W. Tadeusz, Chem. Anal. (Warsaw) 21 (1976) 475.
[4] A. Abu-shady Hamed, T. Hassib Sonia, F. Youssef Nadia, Egypt. J. Pharm. Sci. 32 (1991) 363.
[5] J. Kracmar, J. Kracmarova, T.N. Bokovikova, V.E. Ciciro, G.A. Nesterova, A.V. Suranova, N.V. Trius, Pharmazie 44 (1989) 768.
[6] H. Tadeusz, S. Lech, Chem. Anal. (Warsaw) 29 (1984) 429.
[7] A.H. Chalmers, Biochem. Med. 12 (1975) 234.
[8] B. HansJoachim, Z.K. Rudolf, J. Chromatogr. 137 (1977) 61.
[9] J. Schnekenburger, M. Quade-Heukel, Dtsch. Apoth-Ztg 124 (1984) 1167.
[10] P.K. Teresa, Acta Pol. Pharm. 38 (1981) 1313.
[11] C.S.P. Sastry, K.R. Srinivas, K.M.M. Krishna Prasad, Mikrochim. Acta 122 (1996) 77.
[12] C.S.P. Sastry, K. Rama Srinivas, K.M.M. Krishna Prasad, Talanta 43 (1996) 1625.
[13] C.S.P. Sastry, K. Rama Srinivas, K.M.M. Krishna Prasad, Anal. Lett. 29 (1996) 1329.
[14] J.W. Daniel, Analyst 86 (1961) 640.
[15] D.L. Massart, B.G.M. Vendegingte, S.N. Deming, Y. Michotte, L. Kaufman, Chemometrics T Text book, Elsevier, Amsterdam, 1988, p. 293.
[16] IUPAC, Spectrochim Acta 33 (1978) 241.
[17] R.D. Tiwari, U.C. Pande, J. Ind. Chem. Soc. 51 (1974) 112.
[18] M.M. Campbell, C. Johnson, Chem. Rev. 78 (1987) 65.

ELSEVIER

Talanta 47 (1998) 1287–1296

Talanta

Determination of trace amounts of beryllium using derivative spectrophotometry in non-ionic micellar medium

Har Bhajan Singh [a,*], Narinder Kumar Agnihotri [b], Vinay Kumar Singh [c]

[a] *Department of Chemistry, University of Delhi, Delhi 110007, India*
[b] *Department of Chemistry, Motilal Nehru College, Benito Juarez Road, New Delhi-110021, India*
[c] *Department of Chemistry, Sri Aurobindo College, Malviya Nagar, New Delhi-110017, India*

Received 8 December 1997; received in revised form 20 May 1998; accepted 1 June 1998

Abstract

A rapid and sensitive method for the trace level determination of beryllium based on the formation of a 1:2 complex (λ_{max} 560 nm) with 1,4-dihydroxy-9,10-anthracenedione in an aqueous medium containing Triton X-100 is reported. Beer's law is followed in the range 3.60–360 ng ml^{-1} of Be(II). The molar absorptivity and Sandell's sensitivity are 1.68×10^4 l $mol^{-1}cm^{-1}$ and 0.54 ng cm^{-2}, respectively; detection limit is 0.23 ng ml^{-1} of Be(II). Analysis of synthetic mixtures of composition similar to that of alloys and spiked samples of distilled water, gave results that are in agreement with their beryllium content. © 1998 Elsevier Science B.V. All rights reserved.

Keywords: Beryllium(II) determination; Non-ionic surfactant; Derivative spectrophotometry; 1,4-Dihydroxy-9,10-anthracenedione; Peak height; Trough depth

1. Introduction

Beryllium, one of the most toxic non-radioactive elements [1], is an insidious poison and exhibits latent toxicity i.e. symptoms appear several years after exposure. Use of beryllium and its compounds in metallurgy, aerospace, nuclear installations besides their emission during combustion of coal and oil, makes this element a serious environmental hazard [2]. Sensitive analytical methods are, therefore, necessary to monitor it.

Methods commonly used for the micro determination of Be(II) include spectrofluorimetric [3–5], spectrophotometric [6–8], atomic absorption spectrometric (AAS) [9–11], inductively coupled plasma-atomic emission spectrometric (ICP-AES) [12–15], and inductively coupled plasma-mass spectrometric (ICP-MS) [16] methods. The majority of these analytical procedures involve formation of a soluble/insoluble complex which has to be subsequently extracted, usually with CCl_4, $CHCl_3$ etc. before determination. Atomic spectrometric methods for the determination of Be(II), though generally selective, lack sensitivity [9] be-

* Corresponding author. Tel.: +91 725-7794/725-6538.

0039-9140/98/$ - see front matter © 1998 Elsevier Science B.V. All rights reserved.
PII S0039-9140(98)00217-3

cause of numerous interferences in the flame [17,18], and in the graphite furnace [19,20]. The determination of Be(II) in a wide range of samples by ICP-AES/ ICP-MS is now widely accepted with the limit of detection (LOD) well below the ppb level [12–16]. As the concentration of analyte in real samples is low, a pre-concentration/extraction step generally precedes the analysis using ICP [12,13]. Important photometric reagents include hydroxy-acids, chromotropic acids, β-diketones, azo dyes and derivatives of hydroxyquinone and triphenylmethane. Though the reactions with ligands of the above classes are in general not specific, acetylacetone is suggested as a reagent for the extractive spectrophotometric determination of Be(II) [6]. The interferences in these methods can be over-come using different techniques such as masking [3,5], ion-exchange [4], chromatography [8], liquid–liquid extraction [11,17] and co-precipitation [21]. However, most of these are tedious and time consuming [3]. Sometimes, an incomplete separation may appear to give a significant improvement in the sensitivity though yielding erroneous results. This makes such procedures impractical for routine analysis. In the absence of a suitable specific method, there is an ever increasing need to develop newer methods for the accurate and sensitive determination of beryllium(II) [3–5,11].

In this work, we report a sensitive method for the trace level determination of Be(II) using 1,4-dihydroxy-9,10-anthracenedione (1,4-dihydroxy-9,10-anthraquinone, H_2AQ), a hydrophobic complexone and well known acid–base indicator capable of forming polychelate(s) [22]. H_2AQ and its Be(II) complex get solubilized in micellar medium produced by adding Triton X-100, a non-ionic surfactant, to water. The use of surfactant not only simplifies the procedure by avoiding the extraction step with toxic organic solvents but also enhances the sensitivity and selectivity of the method [23]. Further, the sensitivity and selectivity of the method are improved by derivatization of spectra as closely overlapped absorption bands of interfering ions get well resolved [24]. Analytical parameters of the complex are evaluated. The method is successfully applied to determine Be(II) in synthetic mixtures of alloy composition and spiked samples of water using first/second order derivative spectral profiles, without any preconcentration.

2. Experimental

2.1. Instruments

The absorption spectra were recorded, against water as reference, on a Shimadzu UV-260 spectrophotometer (Kyoto, Japan) using 10 mm fused silica cells, selecting spectral band width of 1.0 nm and a scanning speed of 40 nm min^{-1}. First and second order derivative spectra were obtained with $\Delta\lambda = 2$ and 4 nm, respectively. An ECIL digital pH-meter (model PH 5662, India) equipped with a combined glass electrode was used for pH measurements.

2.2. Reagents

All reagents used were of analytical-reagent grade unless stated otherwise; double distilled water was used to prepare solutions. Stock solution (0.01 M) of Be(II) was prepared in decimolar sulphuric acid using $BeSO_4 \cdot 4H_2O$ (E. Merck, Darmstadt, Germany). Working solutions were prepared by appropriate dilution of the stock solutions every 2 weeks.

1,4-Dihydroxy-9,10-anthracenedione, H_2AQ (Fluka, Switzerland) (9.61 mg) was first dissolved, with stirring at 70°C, in minimum amount of 0.2 M sodium hydroxide. 5.0 g Triton X-100 (polyethylene glycol *tert*-octylphenyl ether; Aldrich, USA), was then added to it. The solution was later acidified with 0.1 M H_2SO_4 and diluted to 100 ml.

2.3. Procedure

2.3.1. Determination of experimental variables

In all working solutions, the final concentration of Be(II), H_2AQ, ammonium acetate, and Triton X-100 was kept at 2.0×10^{-5}, 2.0×10^{-4}, 1×10^{-2} M and 2.50% (m/v), respectively, unless stated otherwise.

Two sets of solutions, one with and the other without the metal ions, but each containing H_2AQ and ammonium acetate, were prepared in the pH range 1.0–12.0 to study the effect of variation of pH on the absorbance of the ligand as well as its beryllium(II) complex.

In order to study the impact of varying surfactant/ligand/metal concentration on the absorbance of the system, solutions of the ligand and complex were prepared, at optimum pH. All parameters were kept constant except the concentration of the component under investigation.

An interference study has been carried out by measuring the absorbance profiles in normal mode and derivative amplitudes in first/second order derivative mode of a set of solutions containing 7.2 ng ml^{-1} of Be(II) ions and varying the amount of interfering ions.

2.3.2. Determination of beryllium(II) in standard samples

Calibration curves for the determination of beryllium(II) were prepared by measuring absorbance (at 560 nm, normal mode)/derivative amplitudes (at 596 nm, in first derivative mode; at 588 and 605 nm, in second derivative mode).

Alloy (Be–Cu or Be–Ni) sample solution was prepared by dissolving 0.5 g of the sample in 8.0 ml of dilute hydrochloric acid (1 + 1) and by adding 2–3 ml of 30% H_2O_2 as the solution was heated. The sample solution was diluted in order to bring the beryllium(II) concentration within the linear range of the calibration graph. In the case of copper-based alloys copper is masked by sodium thiosulphate solution. Be(II) concentration in the sample solutions is then determined by measuring the absorbance (560 nm) or trough depth at 596 nm in first order derivative amplitude and using the respective calibration curve.

3. Results and discussion

3.1. Effect of pH

The absorbance of H_2AQ and its Be(II) complex is pH dependent in the pH range 1.0 to 11.0 whereas the absorption maxima of the complex at 560 nm is not (Fig. 1). The optimum pH of the complex formation was determined by calculating the difference in the absorbance of the ligand and the complex at 560 nm as a function of pH as spectra recorded against water. A constant (± 2.0%) and maximum relative change in the absorbance of the complex with respect to the ligand was observed in the pH range 6.1 to 7.2, but this decreased above pH 7.2 due to ionization of the phenolic groups of unbound H_2AQ, present; pH 6.4 was taken as optimum pH of maximum complex formation during all subsequent studies. Ammonium acetate is found to be the most suitable buffer to regulate H^+ ions during this study.

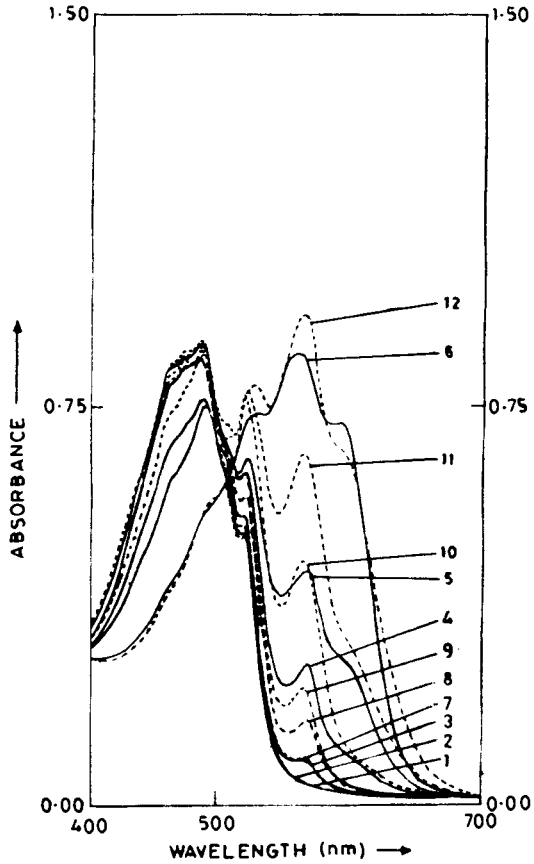

Fig. 1. Absorption spectra at different pH (given in parenthesis) values of: (i) ligand, curve No. 1–6 ($C_{H_2AQ} = 2.0 \times 10^{-4}$ M + Triton X-100 2.5% (m/v)), and (ii) Be(II) complex, curve No. 7–12 ($C_{H_2AQ} = 2.0 \times 10^{-4}$ M + $C_{Be(II)} = 1.0 \times 10^{-5}$ M + Triton X-100 2.5% (m/v)), curve No. 1 and 7 (3.50); 2 and 8 (5.00); 3 and 9 (6.50); 4 and 10 (8.00); 5 and 11 (9.50), 6 and 12 (11.00).

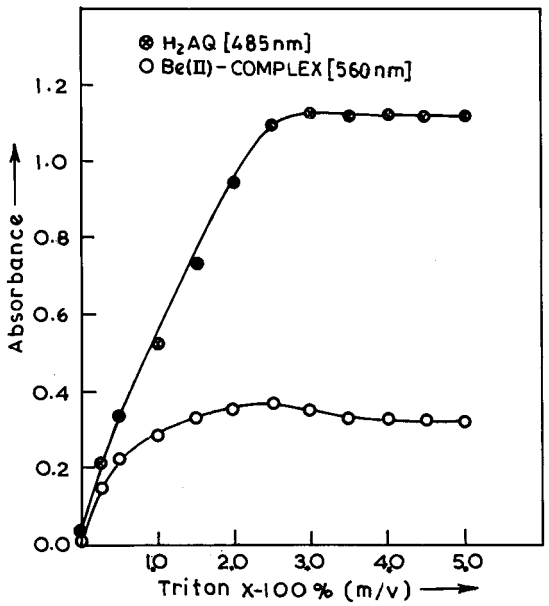

Fig. 2. Effect of increasing amount of Triton X-100 on the absorption of: ligand, ($C_{H_2AQ} = 2.0 \times 10^{-4}$ M), (—●—) and complex ($C_{H_2AQ} = 2.0 \times 10^{-4}$ M + $C_{Be(II)} = 2.0 \times 10^{-5}$ M), (—○—).

3.2. Effect of surfactant

Cationic surfactants, cetylpyridinium chloride and cetyltrimethylammonium bromide increase the ionization of H_2AQ which increases the concentration of mono basic species, HAQ^{-1} at optimum pH. Consequently, λ_{max} of the complex at 560 nm merges into the peak of the ligand species, HAQ^- at 555 nm as H_2AQ is present in excess to that of the metal ion in the system. In the case of anionic surfactant, sodium laurylsulphate, the increase in absorbance due to complex formation is not high as formation of the complex is hindered [23]. Since the maximum increase in absorbance in the case of Be(II) complex and the ligand is observed in the presence of a non-ionic surfactant Triton X-100 because of their increased solubilization, it is used for micelle formation during present study. The concentration of Triton X-100 is maintained at 2.50% (m/v), an amount greater than the CMC (critical micelle concentration) (3.2×10^{-3} M) so as to obtain maximum absorbance (Fig. 2). At concentrations $\geq 2.50\%$ (m/v), a decrease in the absorbance is observed due to a decrease in the concentration of chromophores per micelle.

3.3. Effect of time

The colour of H_2AQ and its Be(II) complex, in the presence of Triton X-100, is stable up to 8.0 and 5.0 h, respectively, at room temperature (20–25°C). Turbidity appears in both cases due to reprecipitation of the ligand in aqueous phase at temperature ≤ 15°C as solid micelles are formed. All absorbance measurements at room temperature (20–25°C) in the aqueous phase, therefore, are to be completed within 5 h.

3.4. Effect of the amount of the ligand

The absorbance at 560 nm increases with increasing H_2AQ concentration, partly due to the absorbance of the free ligand at λ_{max} of the complex and partly due to the increasing concentration of the complex. Therefore, correction due to absorbance of free ligand has been made to calculate the correct absorbance value due to complex, and hence concentration of the complex. An increase in the absorbance due to the complex is observed when the ligand concentration is increased up to 8 times the concentration of Be(II). The concentration of H_2AQ is kept between 10–45 times the Be(II) concentration wherever possible, as the contribution of the complex to the absorbance at its λ_{max}, 560 nm remains constant in this range of ligand concentration.

3.5. Number of coloured species and their composition

The number of coloured species in the solutions of the ligand and its beryllium(II) complex has been determined based on matrix rank determination of the absorbance matrix, prepared by using absorbance data at different wavelengths (at interval of 20–40 nm) of a series of solutions having different pH or varying composition. The rank is determined by triangularizing the absorbance matrix, based on the method of Gaussian elimination and comparison of the diagonal elements with an

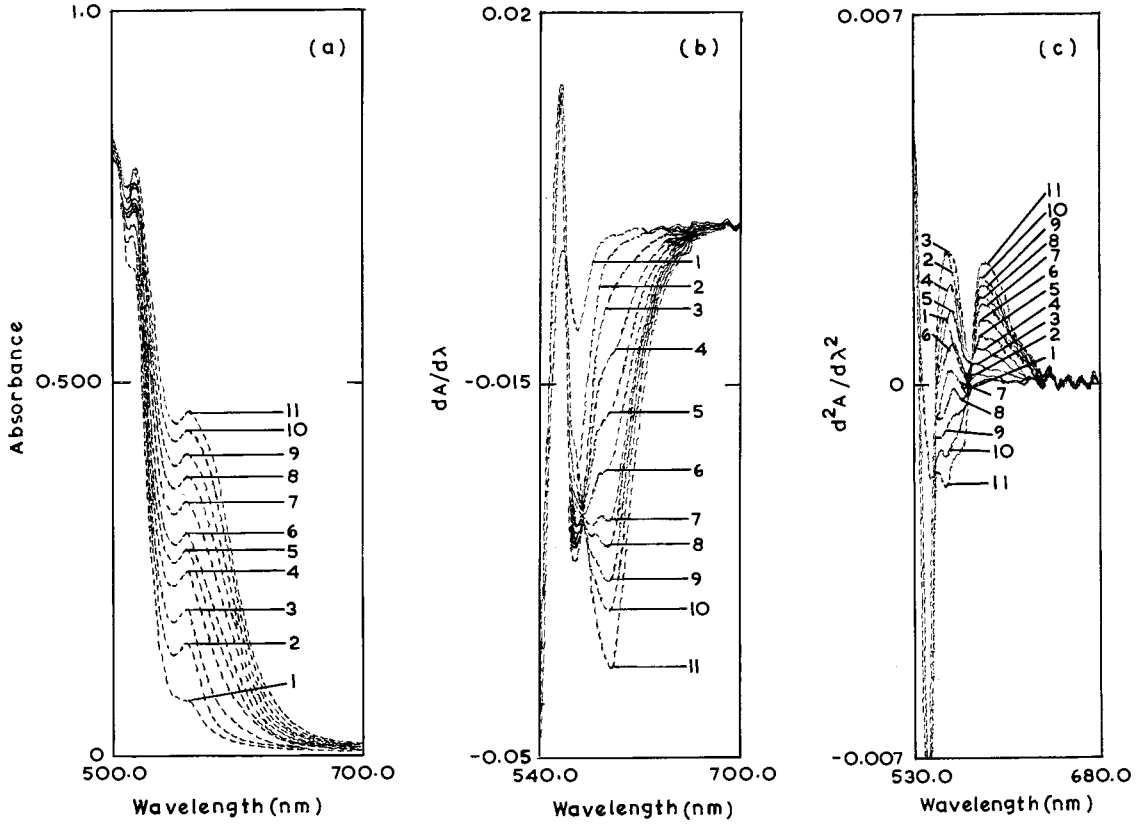

Fig. 3. Effect of increasing Be(II) ion concentration on the absorption of the solution containing $C_{H_2AQ} = 2.0 \times 10^{-4}$ M and Triton X-100 2.5% (m/v); increment of $C_{Be(II)}$ in each step is 36.0 ng ml^{-1} starting with curve No. 1 (0.0 ng ml^{-1}) to curve No. 11 (360 ng ml^{-1}). (a) Zero-order, (b) first-order and (c) second-order derivative absorption spectra.

assumed error matrix [25]. Three coloured species viz., H_2AQ, HAQ^- and AQ^{2-} are inferred to be present in the solution containing H_2AQ and Triton X-100 in the pH range 1.0–12.0; the first two exist under the experimental conditions (pH 5.00–7.60), when the value of assumed error matrix is ≥ 0.0024 absorbance units. Since three chromogenic species have been inferred in the Be(II) complex; in the pH range 5.00–7.60, the third chromogenic species i.e. $[Be(HAQ)_2]$ besides H_2AQ and HAQ^{-1} must be the product of the complexation of Be(II).

The stoichiometry of the complex, ascertained by plotting the absorbance of the complex at 560 nm versus mole fraction of the metal ion, shows a maximum at 0.33, corresponding to the formation of a 1:2 (M:L) complex. Considering the effect of pH on the complexation reaction, the complex is represented as $[Be(HAQ)_2]$, where HAQ^-, is the mono-basic species of the dibasic ligand, 1,4-dihydroxy-9,10-anthracenedione (H_2AQ).

3.6. Calibration graphs

An increase in absorbance at 560 nm is found to be directly proportional to the concentration of the beryllium complex (Fig. 3a). Linear regression of absorbance, A_{560nm}, on the metal ion concentration (ng ml^{-1}of Be(II) ions) shows a good fit (Eq. (1)) with a residue square value of 0.9971.

$$A_{560nm} = 1.073 \times 10^{-3}\,[Be] + 1.781 \times 10^{-2} \qquad (1)$$

The corrected absorbance, A_{corr} has been calculated using Eq. (2), as the free ligand shows some

Table 1
Analytical evaluation of different absorptiometric modes of determination of Be(II) using H_2AQ

Photometric parameters	Normal mode (560 nm)	1st Derivative mode (596 nm)	2nd Derivative mode (588 nm)
Analytical sensitivity S_A (ng ml^{-1})	0.15	0.08	0.18
Limit of quantitation $C_Q(k=10)$ (ng ml^{-1})	1.50	0.80	1.80
Detection limit $C_L(k=3)$ (ng ml^{-1})	0.45	0.23	0.55
Linear dynamic range (ng ml^{-1})	1.50–360	0.80–396	1.80–360
RSD% ($n=6$)	1.12	0.67	4.38

absorbance at λ_{max} of the complex (560 nm) and spectra are recorded against water as reference. The linear regression of A_{corr} on the metal ion concentration shows an improved fit as shown by an enhanced value of residue square i.e. 0.9972 (Eq. (3)).

$$[A_{corr}]_{560nm} = [A_{obs}]_{560nm} - [V_L - R(V_M)] \times \left(\frac{(A_{obs})_{560nm}}{V_L}\right)_{Ligand\ blank} \quad (2)$$

$$[A_{corr}]_{560nm} = 1.106 \times 10^{-3}\ [Be] - 1.209 \times 10^{-2} \quad (3)$$

R is a stoichiometric constant of the complex, whereas V_L and V_M are the equimolar volumes of the ligand and the metal ion solutions, respectively.

A study of the absorption spectra in derivative modes is of great analytical value as λ_{max} of the complex corresponds to the cross-over point at 560 nm in first derivative mode. The distance measured from the base line (or zero line) of the ligand to the trough, at 596 nm (TD) and to the peak, at 588 nm (PH), in first and second-order derivative modes, respectively (Fig. 3b, c), shows good linear fit with the metal ion concentration (in ng ml^{-1}), giving residue square value (r) of 0.9921 and 0.9931, respectively.

$$[Be] = 4.863\ [TD]_{596nm} + 7.069 \times 10^{-1} \quad (4)$$

$$[Be] = 18.68\ [PH]_{588nm} + 18.67 \quad (5)$$

The molar absorption coefficient (ε), specific absorptivity (a) and Sandell's sensitivity (S) of the resulting complex (w.r.t. metal ion) calculated using corrected absorbance values, are found to be 1.68×10^4 l mol^{-1} cm^{-1}, 1.86 ml g^{-1} cm^{-1} and 0.54 ng cm^{-2}, respectively. Beer's law obeys from 3.60–360 ng ml^{-1} of beryllium(II) ions under the conditions specified above.

3.7. Detection limit and sensitivity

The sensitivity of a method can be reported as calibration sensitivity, $S_c = m$ or as analytical sensitivity, $S_A = S_s/m$; where S_s is the standard deviation of the analytical signal at any particular concentration of the analyte, and m is the slope of the calibration graph. The limit of detection, $C_L(k=3)$, and limit of quantitation, $C_Q(k=10)$, are reported in Table 1, where k is a numerical factor chosen according to the confidence level desired [26]. As recommended by IUPAC, the latter is used to establish the lower limit of the linear dynamic range. The precision (RSD%) of the absortiometric studies in different modes evaluated for six samples containing 7.2 ng ml^{-1} Be(II) ions and other analytical parameters are listed in Table 1. The results show that the determination of Be(II) ions in the first order derivative mode at 596 nm is more precise and sensitive than in the normal mode. Besides, lower detection limit of 0.23 ng ml^{-1} and wider linear dynamic range of 0.80–396 ng ml^{-1} of Be(II) ions is also observed.

3.8. Conditional stability constant

The conditional stability constant, k' [27–29] of the complex formed above is calculated using A_{corr} values and concentration instead of activity according to the following equilibrium.

$$Be^{2+} + 2\ H_2AQ \rightleftharpoons [Be(HAQ)_2] + 2\ H^+$$

An average (of eight values) of k' is found to be 2.15×10^4 l mol^{-1} with a relative standard deviation of 1.25%.

3.9. Interference study

The extent of interference of various cations and anions in the trace level determination of beryllium(II) was examined in detail. A maximum error of $\pm$ 4.0% in the absorbance value/derivative amplitude was considered tolerable. The precipitate, if formed, was removed by centrifugation. The tolerance limit of interfering ions studied is given in Table 2. Ions of Al, Au, Ce, Cu, Fe, Sn and UO_2 interfere when present at concentrations higher than that of the analyte. The presence of citrate and EDTA at concentrations higher than the analyte, masks the formation of the complex as indicated by a marked decrease in absorbance. Attempts were made to overcome the interferences of the above mentioned metal ions using masking agents such as oxalate, fluoride, thiocyanate, ascorbate, phosphate, and thiosulphate. Oxalate, ascorbate and thiosulphate were found suitable in the present case. A 50-fold excess of Fe(III) and UO_2(II) and 300-fold excess of Ni(II) could be tolerated using oxalate as masking agent. The interference due to Cu(II) ions up to 200-folds can be eliminated by using a 2×10^{-2} M of thiosulphate as a masking agent. On the other hand interference from Co(II) ions (300-fold excess) can be eliminated with 1.5% (m/w) of ascorbate.

The derivatization of the absorption spectra has also been utilized to improve the selectivity of the method as it resolves the overlapping absorption profiles of the analyte and the interfering ion in the normal mode into well separated peaks, troughs and cross-over points in the derivative modes. In the present case, interferences due to the presence of Au(III) (λ_{max} at 565 nm) and UO_2(II) (λ_{max} at 596 nm) could be easily overcome by carrying out the measurement in the derivative modes. Using first-order derivative spectral profiles at 596 nm, Be(II) can be determined in the presence of Au(III) (30-fold excess) or UO_2(II) (40-fold excess) without any preseparation.

UO_2(II) complex shows peaks at 560 and 596 nm in the normal mode and a cross-over point at 596 nm, a peak at 586 nm and troughs at 612 and 665 nm in the first order derivative mode. The cross-over point of the UO_2(II) complex at 596 nm is used to determine Be(II) in the presence of UO_2(II), whereas trough depth at 665 nm, zero-

Table 2
Tolerance limits[a] of diverse ions (DI) in the photometric determination of Be(II) using H_2AQ in presence of Triton X-100

Diverse ions	Ratio, [DI:M]*	Diverse ions	Ratio, [DI:M]*
Cations			
Mo(VI)	1000	UO_2(II)	4.0[c]
Ce(IV)	2.0	W(VI)	2000
VO(II)	100[e]	Zr(IV)	150[e,f]
B(III)	200	Ga(III)	10[e,f]
Al(III)	4.0	Tl(III)	300[f]
In(III)	15[e]	Bi(III)	30[e,f]
As(III)	100[e,f]	Fe(III)	1.0[c,f]
Cr(III)	5.0[e,f]	Au(III)	3.0
Ca(II)	500	Sn(II)	2.0[e,f]
Mg(II)	30	Mn(II)	200[e]
Pb(II)	30[e]	Fe(II)	5.0
Cu(II)	5.0[d,f]	Co(II)	10[b,f]
Cd(II)	15	Zn(II)	100
Ni(II)	100[c]	Hg(II)	30
Ag(I)	150[f]	Na(I)	3000
Li(I)	10	K(I)	1500
Tl(I)	2500		
Anions			
Fluoride	100	Chloride	600
Bromide	600[e]	Iodide	1500
Thiocyanate	1000	Ascorbate	2500
Tartrate	200[e]	Citrate	2.0[e]
Oxalate	2000	EDTA	5.0[e]
Phosphate	100	Acetate	800
Thiosulphate	1500		

* $C_{Be} = 7.2$ ng ml^{-1}, C_{DI} = ng ml^{-1}.
[a] $\leq$4.0% Deviation (in the absence of masking agents).
[b] Masked by ascorbate.
[c] Masked by oxalate.
[d] Masked by thiosulphate.
[e] Negative deviation.
[f] Precipitation observed at high concentration of DI.

Table 3
Comparison of spectrophotometric reagents for Be(II) determination in micellar medium

Reagent	pH	λ_{max} (nm)	Surfactant	Linear range (ng ml^{-1})	Reference
Eriochrome cyanine R	6.7–7.2	595	Zephiramine	18–55	[30]
Chrome azurol S	5.1	610	Zephiramine	1–40	[31]
Chrome azurol S	4.5	605	POEDA	$\leq$80	[32]
Chrome azurol S	5.0	605–615	CTMB	80[a]	[33]
Pyrocatechol Violet	8.0	680	CPC	—	[34]
1,4-Dihydroxy-9,10-anthracenedione	6.1–7.2	560	Triton X-100	3.6–360 (0.23)[a]	Present work

POEDA, Polyoxyethylenedodecylamine.
CTMB, Cetyltrimethylammonium bromide.
CPC, Cetylpyridinium chloride.
[a] Detection limit

crossing point of Be(II) complex is used to determine UO_2(II) in the presence of Be(II). Be(II) (0.03–0.30 μg ml^{-1}) and UO_2(II) (0.5–12.0 μg ml^{-1}) can be simultaneously determined without any masking and pre-separation utilizing first-order derivative spectrum. Data given in Table 2 indicates that the method has adequate selectivity for the determination of beryllium(II) in real samples.

3.10. Comparison with other reagents

A comparison of various photometric reagents commonly employed for beryllium determination in micellar medium is given in Table 3. The superiority of H_2AQ in terms of a wider determination range (0.80–396 ng ml^{-1}) and higher sensitivity (0.23 ng ml^{-1}) is evident.

4. Applications

4.1. Determination of Be(II) in standard samples

In order to confirm the usefulness of the proposed method, it has been applied to determine trace amounts of Be(II) in alloys of copper and nickel using first-order derivative spectral profiles (trough depth, TD) at 596 nm. As standard samples of beryllium were not available, synthetic samples with similar compositions to the alloys were prepared [35]. The sample containing a total metal ion concentration of 0.5 g was treated in the same way as the standards. An appropriate amount of thiosulphate was used to give its final concentration of 2.0×10^{-2} M, wherever necessary. The composition of the simulated alloys, their most important industrial applications, and the results of determination of Be(II) obtained from a series of six replicates, are given in Table 4.

4.2. Recovery test

The utility of the method was evaluated by investigating the recovery of Be(II) from water samples spiked with known amounts of beryllium. The recoveries lay within the range 97–102% (Table 5).

5. Conclusions

A simple, sensitive and inexpensive derivative spectrophotometric method for the determination of beryllium(II) by means of 1,4-dihydroxy-9,10-anthracenedione and Triton X-100, is reported. It consists of direct measurement of absorbance/derivative amplitudes of the analyte solution. Compared with other highly sensitive methods such as fluorimetric (detection limit, 7 ng ml^{-1}) [3], spectrophotometric (100–800 ng ml^{-1}) [7], atomic absorption spectrometry (detection limit 2 ng ml^{-1}) [11], electrothermal atomization-atomic absorption spectrometry (2–20 ng ml^{-1}) [36], flame-atomic ab-

Table 4
Determination of beryllium in synthetic mixtures of alloy composition

Alloy/uses	Composition (%)				Be found(%)[a]
	Be	Co	Ni	Ag	
Copper-based:					
Master alloy	4.00	—	—	—	4.03 ± 0.06
Welder bar	3.40	0.24	—	—	3.59 ± 0.06
Casting alloy	2.45	—	1.10	—	2.47 ± 0.08
Casting alloy	2.10	0.50	—	—	2.09 ± 0.06
Electric terminals, springs	1.90	0.24	—	—	1.90 ± 0.04
Good electrical conductor	0.50	2.50	—	—	0.506 ± 0.009
Bearings	0.40	1.60	—	0.95	0.401 ± 0.006
Welding equipment	0.40	—	1.50	—	0.401 ± 0.007
Nickel-based:					
Springs	1.80	—	—	—	1.84 ± 0.03
Castings	2.70	—	—	—	2.72 ± 0.02

[a] ± Standard deviations ($n = 6$).

Table 5
Recovery of beryllium from spiked water samples

Sample	Be added (ng ml^{-1})	Be found[a] (ng ml^{-1})	RSD (%)
Distilled water	None	—	—
	10	10.10 ± 0.17	1.73
	20	20.16 ± 0.41	2.06
	50	50.40 ± 0.86	1.71
	100	100.41 ± 0.95	0.94

[a] ± Standard deviations ($n = 6$).

sorption spectrometry (4 ng ml^{-1}) [17] and inductively coupled plasma-atomic emission spectrometry (ICP-AES) (0.2 ng ml^{-1}, 0.15–80 and 0.1 μg g^{-1}) [13–15], it provides a high sensitivity with a detection limit of 0.23 ng ml^{-1} which brings the developed method in the class of highly sensitive methods. The method provides a selective determination of Be(II) in the presence of Au(III) or UO_2(II) as well as simultaneous determination of Be(II) and UO_2(II) in solution without prior separation using derivative spectral profiles. The method has been successfully applied for the determination of beryllium in standard samples.

Acknowledgements

We gratefully acknowledge the financial assistance received from Ministry of Defence, Government of India, New Delhi, through their Grants-in-Aid scheme.

References

[1] The Guinness Book of Records 1992, D. McFarlan (Ed.), Guinness Publishing, London, 1991, p. 107.
[2] L. Friberg, G.F. Norberg, V.B. Vouk, Handbook on the Toxicology of Metals, Elsevier, Amsterdam, 1979.
[3] A. Petidier, S. Rubio, A. Gomez-Hens, M. Valcarcel, Talanta 32 (1985) 1041.
[4] F. Capitán, E. Manzano, A. Navalón, J.L. Vilchez, L.F. Capitán-Vallvey, Analyst 114 (1989) 969.
[5] M. Torre de la, F. Fernández-Gámez, F. Lázaro, M.D. Luque de Castro, M. Valcárcel, Analyst 116 (1991) 81.
[6] E.B. Sandell, H. Hnishi, Photometric Determination of Traces of Metals, Part 1, vol. 3, Wiley, New York, 1978.
[7] M.A. Bello López, M. Callejón Mochón, J.L. Gómez Ariza, A. Guiraúm Pérez, Analyst 111 (1986) 1293.
[8] M.Y.Y. Vin, S.M. Khopkar, Analyst 113 (1988) 175.
[9] H. Vanhoe, C. Vandecasteele, B. Desmet, R. Dams, J. Anal. At. Spectrom. 3 (1988) 703.
[10] H. Haraldsen, M.A. Bruno Pougnet, Analyst 114 (1989) 1331.
[11] L.C. Robles, C. García-Olalla, M.T. Alemany, A.J. Aller, Analyst 116 (1991) 735.

[12] M. Yamamoto, Y. Obata, Y. Nitta, F. Nakata, T. Kumamaru, J. Anal. At. Spectrom. 3 (1988) 441.
[13] F. Buhl, W. Galas, Fresenius Z. Anal. Chem. 332 (1988) 366.
[14] L. Halicz, I.B. Brenner, O.J. Yoffe, J. Anal. At. Spectrom. 8 (1993) 475.
[15] H. Van Veen Eric, T.C. De Loos-Vollebregt Margaretha, P. Wassink Alex, H. Kalter, Anal. Chem. 64 (1992) 1643.
[16] D.E. Kimbrough, I.H. Suffet, Analyst 121 (1996) 309.
[17] J.R. Castillo, M.A. Belarra, M. Domingurez, J. Aznárez, Talanta 29 (1982) 485.
[18] W.G. Ellis, V.F. Hodge, D.A. Darby, C.L. Jones, T.A. Hinners, At. Spectrosc. 9 (1988) 181.
[19] P. Lagas, Anal. Chem. Acta 98 (1978) 261.
[20] D.L. Styris, D.A. Redfield, Anal. Chem. 59 (1987) 2897.
[21] J. Ueda, T. Kitadani, Analyst 113 (1988) 581.
[22] H.D. Coble, H.F. Holtzclaw Jr., J. Inorg. Nucl. Chem. 36 (1974) 1049.
[23] G.L. McIntire, Crit. Rev. Anal. Chem. 21 (1990) 257.
[24] F.S. Rojas, C.B. Ojeda, J.M.C. Pavon, Talanta 35 (1988) 753.
[25] L.P. Varga, F.C. Veatch, Anal. Chem. 39 (1967) 1101.
[26] G.L. Long, J.D. Winefordner, Anal. Chem. 55 (1983) 712A.
[27] A. Ringbom, J. Chem. Educ. 35 (1958) 282.
[28] L.G. Sillen, A.E. Martell, Stability Constants of Metal Complexes, Vol. 1–2, Chemical Society, London, 1964, 1971.
[29] L. Sommer, M. Langová, Crit. Rev. Anal. Chem. 19 (1988) 225.
[30] H. Kohara, N. Ishibashi, F. Fukamachi, Bunseki Kagaku 17 (1968) 1400.
[31] Y. Horiuchi, H. Nishida, Bunseki Kagaku 18 (1969) 180, 1401.
[32] H. Nishida, T. Nishida, H. Ohtomo, Bull. Chem. Soc. Jpn. 49 (1976) 571.
[33] Z. Marczenko, H. Kalowska, Chem. Anal. (Warsaw) 23 (1977) 935.
[34] R.K. Chernova, L.N. Kharlamova, V.V. Belousova, E.G. Kulapina, E.G. Sumina, Zh. Anal. Khim. 33 (1978) 858.
[35] B.R.F. Kjellgren, C.W. Schwenzfeier Jr., E.S. Melick, in: I.M. Kolthoff, P.J. Elving (Eds.), Treatise on Analytical Chemistry, Part 2, vol. 6, 1st edn, Wiley, New York, 1964, pp. 12–13.
[36] N. Goyal, P.J. Purohit, A.G. Page, M.D. Sastry, Talanta 39 (1992) 775.

ELSEVIER

Talanta 47 (1998) 1297–1301

Talanta

Short Communication

Potentiometric titration of Co(II) in presence of Co(III)

Eugenijus Norkus *

Department of Catalysis, Institute of Chemistry, A. Goštauto 9, LT-2600 Vilnius, Lithuania

Received 11 February 1998; received in revised form 6 May 1998; accepted 22 May 1998

Abstract

A potentiometric titration for cobalt(II) determination in the presence of Co(III) based on the oxidation of Co(II) with Na_2CrO_4 in ethylenediamine medium and back-titration of the oxidant excess with $(NH_4)_2Fe(SO_4)_2$ in acid medium is described. The titration is monitored with a Pt indicator electrode and carried out until the greatest jump of potential from one drop of titrant appears. A RSD smaller than 1.5% has been obtained for 50–300 μmol Co(II). The method proposed was applied in the analysis of a new type electroless copper plating solutions containing Co(II)-ethylenediamine complex compounds as reducing agents. Cu(II), Co(III) and Cr(III) do not interfere in the determination of Co(II). © 1998 Elsevier Science B.V. All rights reserved.

Keywords: Cobalt(II); Potentiometric titration; Pt indicator electrode

1. Introduction

The determination of Co (II) in the presence of other metal ions, especially in the presence of Co(III), is of great importance in many areas of chemistry. One of the most widely applied methods for the determination of Co(II) is potentiometric titration. Most of the methods of Co(II) redox titration that have been proposed are based on direct titration with an oxidant [1–3].

It should be noted that a part of Co(II) may be oxidized by dissolved oxygen in this case. Hence, the results of the analysis may be diminished.

Therefore, the aim of this work was to develop a sufficiently simple, accurate, and rapid method of reverse redox titration to determine Co(II) concentration in solutions containing both Co(II) and Co(III).

2. Experimental

2.1. Reagents

All reagents were of analytical grade. The $(NH_4)_2Fe(SO_4)_2$ solutions were standardized by potentiometric titration with $K_2Cr_2O_7$ in an acid medium in the usual way [1]. The $CoSO_4 \cdot 7H_2O$ solution was standardized by EDTA titration, with Murexyde as an indicator [4].

* Tel.: +370 2 611731; fax: +370 2 617018; e-mail: Norkus@ktl.mii.lt

0039-9140/98/$ - see front matter © 1998 Elsevier Science B.V. All rights reserved.
PII S0039-9140(98)00208-2

2.2. Apparatus

The potential of the indicator electrode (Pt) was measured by using a universal ionometer EV-74 (Belarus). The reference electrode was an Ag/AgCl electrode with a saturated KCl solution. In some experiments the solutions were deaerated by bubbling Ar.

2.3. Recommended procedure of Co(II) determination

The procedure recommended for titrimetric determination of Co(II) under the optimum operating conditions selected is as follows. Ca. 1 ml of the test solution containing 0.05–0.30 M Co(II) is added into a 50-ml beaker containing a deaerated mixture of 10 ml of 0.1 M En solution and 4 ml of 0.033 mol l^{-1} Na_2CrO_4 solution. The test solution is added carefully along the beaker wall. The solution is kept unagitated for 1 min. Then, 5 ml of 1:1 H_2SO_4 solution is added and the Cr(VI) unreacted is titrated with 0.1 M $(NH_4)_2FeSO_4$ solution until the greatest jump of the potential from one drop of titrant appears. The jump of the potential reaches ca. 300 mV. Magnetic stirring was employed in the titrations.

3. Results and discussion

The calculations performed by using values of the stability constants of Co(II), Co(III), Cr(III) complex compounds with ethylenediamine (En), ethylenediamine protonation constants [5–8] and standard potentials of Co(III)/Co(II) and Cr(VI)/Cr(III) redox couples [9,10] showed that the initial process of Co(II) oxidation with Na_2CrO_4 should occur in an alkaline medium. En supporting solution 0.1 M (pH ~ 11.7) was used for this purpose.

The back-titration of Cr(VI) excess with a reducing solution ($(NH_4)_2Fe(SO_4)_2$) was carried out in an acid medium (H_2SO_4 was used).

The general procedure for the determination of Co(II) was as follows: the solution under study containing Co(II) compounds was added into a 50-ml beaker containing 10 ml of 0.1 M En solution and excess of Na_2CrO_4 solution. The excess of the H_2SO_4 solution was added after the oxidation and the Cr(VI) unreacted was titrated with 0.1 M $(NH_4)_2FeSO_4$ solution until the greatest jump of the potential from one drop of titrant appeared.

The calculation of Co(II) concentration in the solutions was performed taking into account the stoichiometry of the reactions that have occurred:

$$3Co^{2+} + CrO_4^{2-} + 4H_2O \rightarrow 3Co^{3+} + Cr^{3+} + 8OH^- \quad (1)$$

$$2CrO_4^{2-} + 2H^+ \rightleftarrows Cr_2O_7^{2-} + H_2O \quad (2)$$

$$6Fe^{2+} + Cr_2O_7^{2-} + 14H^+ \rightarrow 6Fe^{3+} + 2Cr^{3+} + 7H_2O \quad (3)$$

Preliminary investigations have shown that the results of analysis depend on the amount of the oxidant, time and oxidation conditions. The final procedure for Co(II) determination was developed after the optimization of those variables.

3.1. Influence of the amount of oxidant

The investigations carried out under the conditions of oxidation in an En solution showed that the molar ratio of $[CrO_4^{2-}]$:$[Co^{2+}]$ should be in the range of 0.4–1.4, i.e. in our case it corresponded to 4 ml of 0.033 M Na_2CrO_4 solution. Additional experiments were performed with the aim of investigating the influence of Co(III)-En complex compounds formed during the titration of Cr(VI) unreacted with $(NH_4)_2FeSO_4$ in an acid medium. The results obtained showed that Co(III) complexes do not influence the results of analysis.

3.2. Influence of the oxidation time

To prevent the oxidation of Co(II) with dissolved oxygen in the En solution the sample was added carefully along the beaker wall. The optimal time of oxidation was found to be 1 min. When the subsequent procedure was carried out without waiting for a while the results were 6% lower. Similar lower results were obtained when the oxidation was carried out for a longer period of time (5 min).

Table 1
Influence of dissolved oxygen on the recovery of Co(II)[a]

Co(II) taken (μmol)	Co(II) found (μmol)	Error (%)	SD (μmol)	RSD (%)	Co(II) taken (μmol)	Co(II) found (μmol)	Error (%)	SD (μmol)	RSD (%)
Co(II) determination without oxygen remotion					Co(II) determination in deaerated solutions				
50	48	−4	1.2	2.3	50	49	−2	0.9	1.5
75	71	−5	1.3	2.4	75	75	0	1.1	1.5
100	92	−8	0.9	1.0	100	102	+2	1.2	1.1
125	121	−3	1.1	0.9	125	127	+2	0.9	0.7
150	149	−1	2.2	1.5	150	150	0	2.2	1.5
175	173	−1	1.7	1.0	175	176	+1	0.9	0.5
225	217	−4	1.1	0.5	200	202	+1	1.7	0.8
250	241	−4	1.1	0.5	225	227	+1	2.0	0.9
300	283	−6	1.1	0.4	250	254	+2	1.6	0.6
					300	300	0	0.8	0.3

[a] Average of five determinations.

Table 2
Influence of the pH on Cu(II) reduction[a]

pH of the electroless plating solution	The total amount of the copper reduced after 2 h (mmol)	
	Calculated from the Co(II) analysis	Calculated from the Cu(II) analysis
5.45	0.7	0.7
5.78	1.0	1.0
6.05	1.3	1.3
6.11	1.5	1.5
6.35	2.1	2.0
6.73	3.3	3.4

[a]Initial electroless copper plating solution containing (M): Cu(II)-0.05, Co(II)-0.15, En-0.60. Plating conditions: loading 1.2 $dm^2\ l^{-1}$; temperature 50°C.

3.3. Influence of the medium acidity

It was determined that the back-titration of Cr(VI) with $(NH_4)_2FeSO_4$ should occur under the optimal acidity conditions in the system under investigation, i.e. they corresponded to ca. 2–2.5 M H_2SO_4 in our case. To prevent decomposition of Co(III) complex compounds with concentrated H_2SO_4, 5 ml of diluted (1:1) H_2SO_4 solution was used.

3.4. Influence of the dissolved oxygen

The calculated redox potentials of O_2 and Na_2CrO_4 in 0.1 M En solution were 0.54 and 1.17 V, respectively. Although CrO_4^{2-} is a stronger oxidizing agent than O_2, the results of the analysis showed that a slight part of Co(II) was oxidized by dissolved oxygen. To prevent the dissolved oxygen influence, the procedure of Co(II) oxidation with Na_2CrO_4 was carried out in deaerated solutions (Ar was bubbled through the solution). The results obtained (Table 1) showed that the procedure of Co(II) oxidation must be carried out in deaerated solutions to obtain more exact results of analysis.

It must be noted that the end-point detection is well-defined. The jump of the potential from one drop of titrant reaches ca. 300 mV.

4. Application

The method proposed was applied in the analysis of a new type electroless copper plating solutions.

Polyvalent metal ions are in some cases strong reducing agents enough to reduce other metal ions to the metallic state. The autocatalytic electroless process of Cu(II) reduction to metallic Cu by Co(II) ions takes place in the ethylenediamine (En) solutions [11]:

$$CuEn_2^{2+} + 2CoEn_3^{2+} \xrightarrow{Cu} + 2CoEn_3^{3+} + 2En \qquad (4)$$

In order to investigate the kinetics of Eq. (4) at various pH it is of great importance to observe the changes in Co(II) concentration. The system under investigation is rather complicated. The initial solution contains 0.05 M Cu(II) salt, 0.15 M Co(II) salt and 0.60 M En (pH adjusted to 5–7 at 50°C). Concentrations of Cu(II) and Co(II) decrease in the course of the electroless plating process (Eq. (4)) with the increase in the amount of Cu deposited and Co(III) formed [12]. The calculations show that $CuEn_2^{2+}$, $CoEn_2^{2+}$ and $CoEn_3^{2+}$ complex compounds predominate in the solution [13]. However, the μ-peroxy or μ-peroxy-μ-hydroxy complex compounds having very high molar extinction coefficients may be formed during the interaction of $CoEn_2^{2+}$ and $CoEn_3^{2+}$ with air oxygen [14,15].

It has been established that to determine Co(II) in the above system the method of Co(II) redox titration is applicable.

By using the method proposed the amount of copper deposited was calculated from the Co(II) analysis data taking into account the stoichiometry of Eq. (4). To check-up the method and to compare the results obtained with the data of another kind

of analysis the investigation of the amount of copper deposited was carried out by using a modified iodimetric method [16].

The results obtained showed a good agreement of both methods (Table 2).

Acknowledgements

The author is most thankful to Prof A. Vaškelis for helpful discussion and Mrs Jūrate Vaičiūnienė for assistance in titration experiments.

References

[1] I.M. Kolthoff, R. Belcher, V.A. Stenger, G. Matsuyama, Volumetric Analysis, Vol. 3, Titration Methods: Oxidation–Reduction Reactions, New York, 1957.
[2] J. Cihalik, Potentiometrie, Nakladatelstvi Cekoslovenski Akademie Ved, Praha, 1961.
[3] E-Siya Chang, J. Dolezal, J. Zyka, Zh. Analit. Khim. 16 (1961) 308.
[4] G. Schwarzenbach, H. Flaschka, Die Komplexonometrische Titration, Ferdinand Enke, Stuttgart, 1965.
[5] L.G. Sillen, A.E. Martell (Eds.), Stability Constants of Metal-Ion Complexes, Special Publication No 17, Supplement No 1, Chemical Society, London, 1964.
[6] L.G. Sillen, A.E. Martell (Eds.), Stability Constants of Metal-Ion Complexes, Special Publication 25, Supplement No 1, Chemical Society, London, 1971.
[7] J. Bjerrum, Metal Amine Formation in Aqueous Solution, Haase, Copenhagen, 1941.
[8] J. Inczedy, Analytical Applications of Complex Equilibria, Akadémiai Kiadó, Budapest, 1976.
[9] D. Dobos, Electrochemical Data: A Handbook for Electrochemists in Industry and Universities, Akadémiai Kiadó, Budapest, 1978.
[10] A.M. Sukhotin (Ed.), Handbook of Electrochemistry, Khimiar, Leningrad, 1981 (in Russian).
[11] A. Vaškelis, J. Jaciauskiene, E. Norkus, Chemija (Vilnius) N3 (1995) 16.
[12] A. Vaškelis, E. Norkus, G. Rozovskis, J. Vinkevicius, Trans. Inst. Met. Fin. 75 (1997) 1.
[13] E. Norkus, A. Vaškelis, J. Reklaitis, A. Griguceviciene, Chemija (Vilnius) N3 (1995) 21.
[14] R.D. Jones, D.A. Summerville, F. Basolo, Chem. Rev. 79 (1979) 139.
[15] E.C. Niederhoffer, J.H. Timmons, A.E. Martell, Chem. Rev. 84 (1984) 137.
[16] E. Norkus, P. Norkus, J. Vaiciuniene, J. Jaciauskiene, Chemija (Vilnius) N1 (1998) 68.